A. GRIESBECK

HANDBOOK OF ORGANIC PHOTOCHEMISTRY AND PHOTOBIOLOGY

AXEL GRIESBECK
MICHAEL OELGEMÖLLER
FRANCESCO GHETTI

HANDBOOK OF ORGANIC PHOTOCHEMISTRY AND PHOTOBIOLOGY

Contents

Preface

The third edition of the *Handbook of Organic Photochemistry and Photobiology* follows a new concept of topical articles and has evolved to a state-of-the-art collection of modern aspects of photochemistry and photobiology.

This compilation of topical reviews comprises very different fields of photochemistry and photobiology. With 67 contributions written by leading experts, this handbook provides leading-edge information on the applications of photochemical and photobiological principles, techniques, and methodologies.

It is a trivial though pivotal fact that natural photosynthesis is the photochemical reaction that integrates photocatalysis and well-balanced steps of energy and electron transfers initiated from electronically excited states. It is the original basis of life on Earth and continues to support us with food, fuel, and oxygen. This process demonstrates that photochemistry can develop into a highly valuable tool for modern organic synthesis. In the history of modern chemistry, there has been a very strong first period of success when numerous light-induced reactions were discovered, modified, and applied to synthetic problems. The organic chemistry community became aware of the reactivity potential of electronic excited states of a molecule. Indeed, photochemistry refers, in many cases, to a multiplication of reactivity options, i.e., in addition to the ground state, electronically excited states show different chemical behavior and often differ so remarkably that they behave as completely new molecules. The modern and powerful techniques of time-resolved spectroscopy approaching new fascinating time domains ("femtochemistry") in the last decades have enabled the photochemistry community to describe a photophysical process in full detail and also to predict photochemical reactivity by application of theoretical methods.

As spectroscopic and analytical tools become more and more sophisticated and theoretical methods develop rapidly, photochemistry and photobiology are merging, and for both areas, interdisciplinary research is essential. Photochemistry is a perfect example of a powerful bridge among chemistry, physics, and biology, and between material science and life science. Chemists worldwide are now aware of the fascinating opportunities that electronically excited molecules present, and this will definitely lead to a new period of exciting developments. Photochemical reactions can be performed at low temperatures, in solid or liquid state or under gas-phase conditions, with spin-selective direct excitation or sensitization, and even multiphoton processes have started to be used in synthetic methods. This handbook provides an overview of these opportunities and tracks the actual developments.

The compilation of this handbook was made possible by the strong cooperation between the editors and the editorial staff at CRC Press, a highly professional and trusting relationship. More importantly, we are deeply indebted to all the contributors for their time and intellectual input that made this compilation possible. We express our sincere thanks to all of them.

Axel G. Griesbeck
Köln, Germany

Michael Oelgemöller
Townsville, Australia

Francesco Ghetti
Pisa, Italy

Editors

Axel G. Griesbeck studied political science and chemistry at the University of Munich, Germany, where he received his doctoral degree in 1984 for work on singlet oxygen. After postdoctoral positions in Würzburg, ETH Zürich, and the Weizmann-Institute in Rehovot, he finished his habilitation in 1991 at the University of Würzburg. Since 1995, he has been a professor of organic chemistry and photochemistry in the Department of Chemistry at the University of Cologne, Cologne, Germany. He was a visiting professor at Wisconsin (Madison, Wisconsin), Tsukuba (Japan), and Tapei (Taiwan) and received the Grammaticakis-Neumann prize in 1997 and the Honda–Fujishima award in 2009. His current research activities are focused on using organic molecules as substrates and as catalysts for photoinduced reactions, either directly excited or generated by energy transfer as well as by electron transfer processes. The reactions are performed in solution phase, in gas phase, or in nanocompartments. Recent applications of these processes are the syntheses of antimalaria-active peroxides by photooxygenation.

Michael Oelgemöller received his diploma from the University of Münster, Germany in 1995 and his PhD from the University of Cologne, Germany in 1999. He was a researcher at the Inoue Photochirogenesis Project in Osaka (1999–2001) and at Bayer CropScience Japan in Yuki (2001–2004). From 2004 to 2008 he held a position as a lecturer in organic and medicinal chemistry at Dublin City University in Ireland. In February 2009, he joined James Cook University in Australia as an associate professor in organic chemistry. In 2000, he received the Kurt-Alder award of the University of Cologne. He was a visiting professor at the University of Pau in France in 2009 and at Osaka Prefecture University in Japan in 2011. His research activities include synthetic organic photochemistry, solar photochemistry, the development of new photochemical synthesis tools, and photochemical water treatment.

Francesco Ghetti graduated with a degree in physics from Pisa University in 1980 and has been a researcher at the Institute of Biophysics (Pisa section) of the Italian National Research Council (CNR) since 1985. His main research topics are photomotile reactions in microorganisms and related primary events of phototransduction and biological effects of environmental ultraviolet radiation on microorganisms and plants. He has served as treasurer of the European Society for Photobiology (1999–present), as president of the Italian Society for Photobiology (2002–2007), and as one of the vice presidents of the International Union for Photobiology (2004–2009). He has also organized several international photobiology congresses, directed NATO advanced study institutes, and chaired numerous symposia.

Contributors

Hans-Werner Abraham
Institute of Chemistry
Humboldt-Universität
zu Berlin
Berlin, Germany

Maryam Afshar
Division of Genetics and
Molecular Medicine
St John's Institute of
Dermatology
King's College London School
of Medicine
King's College, London

Igor V. Alabugin
Department of Chemistry and
Biochemistry
Florida State University
Tallahassee, Florida

Mariza N. Alberti
Laboratory of Organic Chemistry
Department of Chemistry
University of Crete
Crete, Greece

Angelo Albini
Department of Chemistry
University of Pavia
Pavia, Italy

Joakim Andréasson
Department of Chemical
and Biological
Engineering
Chalmers University of
Technology
Göteborg, Sweden

Mariachiara Arisi
Dermatology Department
University of Brescia
Brescia, Italy

Kerrie A.B. Austin
Lehrstuhl für Organische
Chemie I
Technische Universität
München
Garching, Germany

Thorsten Bach
Lehrstuhl für Organische
Chemie I
Technische Universität
München
Garching, Germany

Akos Banyasz
CNRS, IRAMIS, SPAM,
URA2453
Laboratoire Francis Perrin
Gif-sur-Yvette, France

Shaik Basha
Discipline of Marine
Biotechnology and Ecology
Central Salt and Marine
Chemicals Research Institute
Council of Scientific
and Industrial Research
Bhavnagar, Gujarat, India

Kristian Berg
Department of Radiation
Biology
Oslo University Hospital
and
Norwegian Radium Hospital
Oslo, Norway

Ranieri Bizzarri
The National Enterprise
for nanoScience and
nanoTechnology
Scuola Normale Superiore
and
Consiglio Nazionale delle
Ricerche
Istituto Nanoscienze
Pisa, Italy

Aurélien Blanc
Laboratoire de Synthèse et
Réactivité Organiques
Institut de Chimie
University of Strasbourg
Strasbourg, France

Christian G. Bochet
Department of Chemistry
University of Fribourg
Fribourg, Switzerland

Cornelia Bohne
Department of Chemistry
University of Victoria
Victoria, British Columbia, Canada

Stephen G. Bown
Division of Surgery and Interventional Science
National Medical Laser Centre
UCL Medical School
University College London
London, United Kingdom

André M. Braun
Engler-Bunte-Institut
Karlsruher Institut für Technologie
Karlsruhe, Germany

Stanley B. Brown
Faculty of Biological Sciences
University of Leeds
and
Photopharmica Ltd.
Leeds Innovations Centre
Leeds, United Kingdom

Götz Bucher
Department of Chemistry
The University of Glasgow
Glasgow, Scotland, United Kingdom

Maria E. Budén
Facultad de Ciencias Químicas
Departamento de Química Orgánica
Instituto de Investigaciones en Físico-Química de Córdoba
Universidad Nacional de Córdoba
Córdoba, Argentina

Piergiacomo Calzavara-Pinton
Dermatology Department
University of Brescia
Brescia, Italy

Flavio Cermola
Department of Organic Chemistry and Biochemistry
University of Naples "Federico II"
Naples, Italy

Giovanni Checcucci
Consiglio Nazionale delle Ricerche
Istituto di Biofisica
Pisa, Italy

Edward L. Clennan
Department of Chemistry
University of Wyoming
Laramie, Wyoming

Clare Conway
Photopharmica Ltd.
Leeds Innovations Centre
Leeds, United Kingdom

Thomas P. Coohill
Department of Physics and Astronomy
Siena College
Loudonville, New York

Alexander J. Cowan
Department of Chemistry
Imperial College London
London, United Kingdom

Emma E. Coyle
School of Chemical Sciences
Dublin City University
Dublin, Ireland

Rosalie K. Crouch
Department of Neuroscience
and
Department of Ophthalmology
Medical University of South Carolina
Charleston, South Carolina

Maurizio D'Auria
Dipartimento di Chimica
Università della Basilicata
Potenza, Italy

Valentina Dichiarante
Department of Chemistry
University of Pavia
Pavia, Italy

and

CEA, iBiTecs
Service de Bioénergétique
Biologie Structurale et Mécanismes
Gif-sur-Yvette, France

Thierry Douki
Laboratoire "Lésions des Acides Nucléiques"
INAC/SCIB UMR-E3 CEA/UJF CEA
Grenoble, France

Patrick Z. El-Khoury
Department of Chemistry
Bowling Green State University
Bowling Green, Ohio

Maurizio Fagnoni
Department of Chemistry
University of Pavia
Pavia, Italy

Luis Manuel Frutos
Departamento de Química Física
Universidad de Alcalá
Alcalá de Henares (Madrid), Spain

Wolfgang Gärtner
Department of Biophysical Chemistry
Max-Planck-Institute for Bioinorganic Chemistry
Mülheim, Germany

Niall W.A. Geraghty
School of Chemistry
National University of Ireland Galway
Galway, Ireland

Francesco Ghetti
Consiglio Nazionale delle Ricerche
Istituto di Biofisica
Pisa, Italy

Beverley Glass
School of Pharmacy and Molecular Sciences
James Cook University
Townsville, Queensland, Australia

Helmut Görner
Max-Planck-Institute for Bioinorganic Chemistry
Mülheim, Germany

Samer Gozem
Department of Chemistry
Bowling Green State University
Bowling Green, Ohio

Anna D. Gudmundsdottir
Department of Chemistry
University of Cincinnati
Cincinnati, Ohio

Thomas Gustavsson
CNRS, IRAMIS, SPAM, URA2453
Laboratoire Francis Perrin
Gif-sur-Yvette, France

Donat-P. Häder
Möhrendorf, Germany

Yun-Jeong Han
Department of Biotechnology and
Kumho Life Science Laboratory
Chonnam National University
Gwangju, Korea

Andreas Hebert
Institut für Chemie
Technische Universität Berlin
Berlin, Germany

Klaas J. Hellingwerf
Laboratory for Microbiology
Swammerdam Institute for Life Sciences
University of Amsterdam
Amsterdam, the Netherlands

Johnny Hendriks
Laboratory for Microbiology
Swammerdam Institute for Life Sciences
University of Amsterdam
Amsterdam, the Netherlands

Norbert Hoffmann
Institut de Chimie Moléculaire de Reims
Université de Reims Champagne Ardenne
Reims, France

Marijke Hospes
Laboratory for Microbiology
Swammerdam Institute for Life Sciences
University of Amsterdam
Amsterdam, the Netherlands

Mark Huntress
Department of Chemistry
Bowling Green State University
Bowling Green, Ohio

Maria Rosaria Iesce
Department of Organic Chemistry and Biochemistry
University of Naples "Federico II"
Naples, Italy

Yoshihisa Inoue
Department of Applied Chemistry
Osaka University
Suita, Japan

Giulio Jori
Department of Biology
University of Padova
Padova, Italy

David Keane
School of Biotechnology
Dublin City University
Dublin, Ireland

Jeong-Il Kim
Department of Biotechnology and
Kumho Life Science Laboratory
Chonnam National University
Gwangju, Korea

Horst Kisch
Department Chemie und Pharmazie
Universität Erlangen-Nürnberg
Erlangen, Germany

Petr Klán
Department of Chemistry
Research Centre for Toxic Compounds in the Environment
Masaryk University
Brno, Czech Republic

Virginie Lhiaubet-Vallet
Consejo Superior de Investigación Científicas
Instituto de Tecnología Química
Universidad Politécnica de Valencia-CSIC
Valencia, Spain

Edward D. Lipson
Department of Physics
Syracuse University
Syracuse, New York

Robert S.H. Liu
Department of Chemistry
University of Hawaii
Honolulu, Hawaii

Mary Treasa Lohan
School of Chemistry
National University of Ireland Galway
Galway, Ireland

Aba Losi
Department of Physics
University of Parma
Parma, Italy

Matthew Lukeman
Department of Chemistry
Acadia University
Wolfville, Nova Scotia, Canada

Alexander J. MacRobert
Division of Surgery and Interventional Science
National Medical Laser Centre
UCL Medical School
University College London
London, United Kingdom

Hajime Maeda
Division of Material Sciences
Graduate School of Natural Science and Technology
Kanazawa University
Kanazawa, Japan

Michela Magaraggia
Department of Biology
University of Padova
Padova, Italy

Dimitra Markovitsi
CNRS, IRAMIS, SPAM, URA 2453
Laboratoire Francis Perrin
Gif-sur-Yvette, France

Péter Maróti
Department of Medical Physics
University of Szeged
Szeged, Hungary

Sandra E. Martín
Facultad de Ciencias Químicas
Departamento de Química Orgánica
Instituto de Investigaciones en Físico-Química de Córdoba
Universidad Nacional de Córdoba
Córdoba, Argentina

Kerstin Mayer
Institut für Chemie
Technische Universität Berlin
Berlin, Germany

Katherine L. McGilvray
Department of Chemistry
Centre for Catalysis Research and Innovation
University of Ottawa
Ottawa, Ontario, Canada

Federico Melaccio
Department of Chemistry
Bowling Green State University
Bowling Green, Ohio

and

Dipartimento di Chimica
Università degli Studi di Siena
Siena, Italy

Fabian Michalik
Institut für Chemie
Technische Universität Berlin
Berlin, Germany

Miguel Angel Miranda
Consejo Superior de Investigación Científicas
Instituto de Tecnología Química
Universidad Politécnica de Valencia-CSIC
Valencia, Spain

Dariusz Mitoraj
Department Chemie und Pharmazie
Universität Erlangen-Nürnberg
Erlangen, Germany

Kazuhiko Mizuno
Department of Applied Chemistry
Graduate School of Engineering
Osaka Prefecture University
Osaka, Japan

Tadashi Mori
Department of Applied Chemistry
Graduate School of Engineering
Osaka University
Osaka, Japan

Anne Morrissey
Oscail
Dublin City University
Dublin, Ireland

Gillian M. Murphy
Dermatology Department
Beaumont Hospital
Dublin, Ireland

Carlo Musio
Consiglio Nazionale delle Ricerche
Istituto di Biofisica
Fondazione Bruno Kessler
Trento, Italy

and

Consiglio Nazionale delle Ricerche
Istituto di Cibernetica "Eduardo Caianiello"
Napoli, Italy

Riccardo Nifosì
The National Enterprise for nanoScience and nanoTechnology
Pisa, Italy

Kieran Nolan
School of Chemical Sciences
Dublin City University
Dublin, Ireland

Michael Oelgemöller
School of Pharmacy and Molecular Sciences
James Cook University
Townsville, Queensland, Australia

Esther Oliveros
Laboratoire des Intéractions Moléculaires et Réactivité Chimique et Photochimique
Université Paul Sabatier (Toulouse III)
Toulouse, France

Massimo Olivucci
Department of Chemistry
Bowling Green State University
Bowling Green, Ohio

and

Dipartimento di Chimica
Università degli Studi di Siena
Siena, Italy

Thomas Oppenländer
Faculty of Mechanical and Process Engineering
Hochschule Furtwangen University
Villingen-Schwenningen, Germany

Michael Orfanopoulos
Laboratory of Organic Chemistry
Department of Chemistry
University of Crete
Crete, Greece

Bernhard Ortel
Section of Dermatology
University of Chicago Medical Center
Chicago, Illinois

Tamara C.S. Pace
Department of Chemistry
University of Victoria
Victoria, British Columbia, Canada

Runa Pal
Department of Chemistry and Biochemistry
Florida State University
Tallahassee, Florida

Günther H. Peschl
UV-Consulting Peschl
Mainz, Germany

Uwe Pischel
Facultad de Ciencias Experimentales
Departamento de Ingeniería Química
Química Física y Química Orgánica
Universidad de Huelva
Huelva, Spain

Luca Pretali
Department of Chemistry
University of Pavia
Pavia, Italy

Stefano Protti
Department of Chemistry
University of Pavia
Pavia, Italy

and

CEA, iBiTecs
Service de Bioénergétique
Biologie Structurale et Mécanismes
Gif-sur-Yvette, France

V. Jayathirtha Rao
Organic Chemistry Division II,
Indian Institute of Chemical Technology
and
Medicinal Chemistry Department
National Institute of Pharmaceutical Education and Research
Hyderabad, India

Davide Ravelli
Department of Chemistry
University of Pavia
Pavia, Italy

Vivienne E. Reeve
Faculty of Veterinary Science
The University of Sydney
Sydney, New South Wales, Australia

Lesley E. Rhodes
School of Translational Medicine
Salford Royal NHS Foundation Hospital
University of Manchester
Manchester, United Kingdom

Mariateresa Rossi
Dermatology Department
University of Brescia
Brescia, Italy

Roberto A. Rossi
Facultad de Ciencias Químicas
Departamento de Química Orgánica
Instituto de Investigaciones en Físico-Química de Córdoba
Universidad Nacional de Córdoba
Córdoba, Argentina

Karola Rück-Braun
Institut für Chemie
Technische Universität Berlin
Berlin, Germany

Evelyne Sage
CNRS UMR3348
Institut Curie-Centre de Recherche
Centre Universitaire
Orsay, France

Silvia Santillo
Consiglio Nazionale delle Ricerche
Istituto di Cibernetica "Eduardo Caianiello"
Napoli, Italy

J.C. Scaiano
Department of Chemistry
Centre for Catalysis Research and Innovation
University of Ottawa
Ottawa, Ontario, Canada

Igor Schapiro
Department of Chemistry
Bowling Green State University
Bowling Green, Ohio

Mathias O. Senge
SFI Tetrapyrrole Laboratory
School of Chemistry
and
Institute of Molecular Medicine
Trinity Centre for Health Sciences
Trinity College Dublin
Dublin, Ireland

Natalia N. Sergeeva
SFI Tetrapyrrole Laboratory
School of Chemistry
and
Institute of Molecular Medicine
Trinity Centre for Health Sciences
Trinity College Dublin
Dublin, Ireland

Oksana Shvydkiv
School of Chemical Sciences
Dublin City University
Dublin, Ireland

Pill-Soon Song
Faculty of Biotechnology and Subtropical Horticulture Research Institute
Jeju National University
Jeju, Korea

Kolupula Srinivas
Medicinal Chemistry Department
National Institute of Pharmaceutical Education and Research
Hyderabad, India

Yuki Sudo
Division of Biological Science
Graduate School of Science
Nagoya University
Nagoya, Japan

and

Precursory Research for Embryonic Science and Technology
Japan Science and Technology Agency
Saitama, Japan

Junwang Tang
Department of Chemical Engineering
University College London
London, United Kingdom

Peter H. Tang
Department of Neuroscience
and
Department of Ophthalmology
Medical University of South Carolina
Charleston, South Carolina

John Tobin
School of Biotechnology
Dublin City University
Dublin, Ireland

Massimo Trotta
Consiglio Nazionale delle Ricerche
Istituto per i Processi Chimico-Fisici
Bari, Italy

Rex M. Tyrrell
Department of Pharmacy and Pharmacology
University of Bath
Bath, United Kingdom

Saroj M. Verma
Dermatology Department
Beaumont Hospital
Dublin, Ireland

Vadim R. Viviani
Laboratory of Biochemistry and Biotechnology of Bioluminescence
Department of Chemistry, Physics, and Mathematics
and
Department of Evolutive Genetics and Molecular Biology
Federal University of São Carlos, Sorocaba
São Carlos, Brazil

Jacek Waluk
Institute of Physical Chemistry
Polish Academy of Sciences
Warsaw, Poland

Julie Tzu-Wen Wang
Division of Surgery and Interventional Science
National Medical Laser Centre
UCL Medical School
University College London
London, United Kingdom

Ann R. Webb
School of Earth Atmospheric and Environmental Sciences
University of Manchester
Manchester, United Kingdom

Pablo Wessig
Institut für Chemie
Universität Potsdam
Potsdam, Germany

Uta Wille
ARC Centre of Excellence for Free Radical Chemistry and Biotechnology
School of Chemistry
The University of Melbourne
Parkville, Victoria, Australia

Jakob Wirz
Departement Chemie der Universität Basel
Basel, Switzerland

Josephine H. Woodhams
Division of Surgery and Interventional Science
National Medical Laser Centre
UCL Medical School
University College London
London, United Kingdom

Cheng Yang
Precursory Research for Embryonic Science and Technology
Japan Science and Technology Agency
Saitama, Japan

and

Department of Applied Chemistry
Osaka University
Suita, Japan

Lan-Ying Yang
Department of Chemistry
University of Hawaii
Honolulu, Hawaii

Wang-Yong Yang
Department of Chemistry and Biochemistry
Florida State University
Tallahassee, Florida

Antony R. Young
Division of Genetics and Molecular Medicine
St John's Institute of Dermatology
King's College London School of Medicine
King's College, London

Yao-Peng Zhao
Department of Chemistry
University of Hawaii
Honolulu, Hawaii

Howard E. Zimmerman
Department of Chemistry
University of Wisconsin
Madison, Wisconsin

1

Industrial Photochemistry

André M. Braun
Karlsruher Institut für Technologie

Günther H. Peschl
UV-Consulting Peschl

Esther Oliveros
Université Paul Sabatier (Toulouse III)

1.1 Introduction

Tempora mutantur, nos et mutamur in illis—The times change, and we change with them. As progress in physics opened the way to new radiation sources and optical applications, and chemical physics showed the way into micro- and nanoscale technology, awareness grew that photophysical and photochemical processes may lead to new products and more economic manufacturing. At the same time, it was also officially realized that the material and energetic resources of our planet are limited and that the capacity of the planet's ecosystem to digest all kinds of xenobiotic waste is getting to its limits. In this context, different domains of photophysics and photochemistry are receiving more attention and support from both governmental and industrial operators, as they offer the prospect to master key technologies for the development and production of new materials and to lead to new processes that may be qualified as "environmentally friendly" (keyword: green chemistry [1]). This situation fosters research in general but also the technical development of products and processes for a large variety of applications.

It should be recalled that industrial photochemistry comprises a large variety of domains in which compounds are used (i) for their photophysical properties (e.g., fluorescence: optical brighteners [2]; phosphorescence: optical sensors [3]; photochromism [4]: optical sensors and data storage; and energy transfer: photodynamic therapy (PDT sensitizers [5]) or (ii) for their photochemical reactivity (e.g., homolysis: radical initiators [6], surface functionalization [7], and ablation [8]; heterolysis: ionic initiators [6a]; and electron transfer: photocatalysis [9]) to be exploited for the preparation of chemical compounds, materials, and products (e.g., polymers and composite materials of all kinds and shapes). With the same technique, organic compounds, e.g., pollutants in water [10a,b,d,e] and air [10c–e], may also be degraded.

This chapter on "industrial photochemistry" is meant to focus on the domain of preparative photochemistry developed for the industrial production of chemicals and materials of all kinds. In general, the photochemical production of large amounts of chemicals per unit of time demands powerful light sources and corresponding reactors of rather big dimensions and special geometries. Special geometries of irradiation equipments are also needed for the production of, for example, polymer foils and polymer-coated surfaces, small polymer parts, and functionalized nanoparticles. Interdependences

of the many factors that decide on an efficient transfer of radiative to chemical energy were only identified within the last two or three decades. As a consequence, the technical development and exploitation of preparative photochemistry was for a long time disfavored or discarded by prejudices originating from the bad results of too many inadequate and hazardous upscaling efforts [11]. However, after World War II, a number of photochemical processes were successfully developed [12,13], but the work of industrial chemists and engineers involved in these developments was mostly ignored in academic research or kept secret. The publication of a first comprehensive textbook on photochemical technology focusing on the industrial preparative chemistry [14] may mark the renewal of interest in large-scale photochemistry. Considered by many as the reference, it does however not cover all the facets of this vast domain, and a number of reference and textbooks concentrating on some special topics must also be cited [6b,15–17].

Photochemistry was considered for a long time a "playground" for academics doing highly valuable fundamental research but demonstrating little interest in its applicatory potential. For more than 40 years, a quasi-total absence of teaching devoted to the growing interest in photochemical technology left research and development efforts in this domain to a few academic and industrial teams. Industrial chemists, making use of a more or less qualitative knowledge about electronic excited states and multiplicity, and chemical engineers with a solid knowledge in physical chemistry developed large-scale photochemical processes. Their designs are still valid references for new plant constructions [14]. Some very important technical developments, such as digital photography [18], micro- and nanoscale lithography [19], ablation and etching for the production of all kinds of electronic devices [8], optical sensors [3], photoelectrochemical devices [20], and light emitting diodes (LEDs) [21], were mostly developed outside the mainstreams of research in academia. Most recent developments in the domains of renewable energies, medicine (e.g., diagnostic devices, therapeutic equipment), communications, etc., are for a large part based on the use of photophysical and photochemical processes, and the present exponentially growing need of specialized scientists and engineers is finally answered with the most recent implementation of a number of curricula in the domain of photonics at well-known academic institutions.

Preparative photochemistry is mostly applied by chemical companies that produce intermediate and/or fine chemicals (e.g., pharmaceutical, agrochemical, food processing, and fragrance industries) and by companies producing basic or final products, for example, food, electronic, automotive, furniture, building, and packaging industries. It is impossible to establish a complete list of products that are prepared on a large scale by photochemical processes, and nondisclosure agreements prohibit to relate products with industries involved. However, given the large diversity of products, a nonexhaustive list of companies may be cited for their interest in photochemical synthesis without divulging details of their activities: Astra Zeneca, Balmer Lawrie, BASF, Bayer, Bristol Myers Squibb, Clariant, CSS Almac, Leo Pharmaceutical Products, Monsanto, Rhishiroop, Sanofi-Aventis, Sasol, Solvay, Symrise, Tata Chemical, and Toray. Table 1.1 summarizes the most important photochemical reactions and classes of products prepared or the processes relying on the first.

In the domain of photochemical environmental techniques, Areva, Suez, and Véolia are certainly among those mostly known in Europe.

The importance of industrial scale preparative photochemistry may be demonstrated by the electrical power installed for the radiation sources of the photochemical reactors. Table 1.2 shows those data for the preparative photochemical equipment installed and maintained in western Europe as far as the authors contributed to its installation.

Published information about corresponding installations in eastern Europe and Russia, but also on the American continent is not available to the authors. Industries in Korea and Japan make use of photochemical reactions since many decades, and there are no signs that these activities would decrease. In addition, new demands from China and India reflect a rapidly growing interest, and for Asia, the total electrical power installed in preparative photochemical equipment may be largely underestimated. Based on the information available to the authors, 30 MW of worldwide installed electrical power in

TABLE 1.1 Most Important Photochemical Reactions Used in Industrial Photochemistry

Photochemical Reaction	Products and Processes
Chlorination	Acylchlorides
	Alkylchlorides
	Arylchlorides
	(Poly)Chlorinated polymers
	Chlorination of organic surfaces
Electrocyclic reactions	Vitamin D derivatives
Isomerization	Vitamin A precursors and derivatives
	Stilbene derivatives
Nitrosylation	Lactams
Oxychlorination	Oxidative functionalization of polymers
	Oxidative degradation of organic pollutants
Oxidation	Oxidative degradation of organic pollutants
	Alkylchlorides
	Activation of inorganic surfaces
	Functionalization of organic surfaces
Catalyzed oxidation	Treatment of polluted air
Initiated oxidation	Treatment of waste water
Sensitized oxidation	Terpenoids
	O-Heterocyclic compounds
Cationic polymerization	Vinyl-type (pre)polymers
	Surface coating and polymer materials
Radical polymerization	Vinyl-type (pre)polymers
	UV curing (surface coating and printing)
Sulfochlorination	Alkylsulfonylchlorides
Sulfoxidation	Alkylsulfonic acids

TABLE 1.2 Preparative Photochemical Activities in Western Europe Represented by the Electrical Power of the Radiation Sources Installed[a]

Location	Electrical Power of Radiation Sources Installed (kW)
France	1800
The Netherlands	1250
Belgium	190
Germany	2700
Italy	650
Others	160
Total western Europe	6750

[a] Data refer only to photochemical equipment, where the authors contributed to its design and/or installation.

preparative photochemical equipment seem realistic. Observing over the last two decades a slightly decreasing activity in western Europe, these estimates reflect the delocalization of modern production facilities to emerging countries, whereas small units for highly specialized applications remain at the traditional centers of research and development. This trend will most probably be amplified within the European Union by new regulations that restrict the activity of the chemical industries with arguments

propagating lowest risks for the environment of its inhabitants and improved levels of health and life expectancy. Saving on costs of transportation and environmental regulations and taking advantage of cheap labor on all levels, photochemical techniques aiming at new products by the transformation of materials will be developed in regions where raw materials are available and intermediate chemicals are already prepared.

It must be emphasized that a combination of the data shown in Tables 1.1 and 1.2 and of other estimates mentioned reveal that the production of highly priced fine chemicals (e.g., fragrances, pharmaceutically active compounds) does not represent the major fraction of installed electrical power, and this fact invalidates the old prejudice that preparative photochemistry may only be applied for the production of compounds and materials of high added value.

Using very similar equipment, photochemical environmental techniques [10] should also be mentioned in this chapter. Several multinational companies use photochemical processes for the abiotic treatment of waste water, and facilities with up to 200 kW of installed electrical power are known. Organic pollutants dissolved or suspended in water are partially or entirely oxidized by using H_2O_2- or O_3/H_2O_2-photolysis or the photochemically enhanced Fenton reaction [23], in the presence or absence of an additional enhancement by Fe(III) oxalate photolysis [23b]. TiO_2-photocatalyzed oxidative degradation of organics in condensed aqueous phase is a frequently cited topic of research, but there is so far no information available that would confirm its successful large-scale application.

Vacuum-ultraviolet (VUV) photolysis and/or TiO_2 photocatalysis are most efficient for the *treatment of polluted air* [10c–e], and reactor modules based on the latter process are emerging rapidly, as TiO_2-functionalized surfaces (glass, quartz, zeolites, etc.) become commercially available. Different designs of reactor modules are offered by mostly newly founded companies, and some time will be needed to see this promising market structured.

UV-C irradiation for water disinfection [10a,b,24] is a still growing market, and the electrical power of the corresponding photochemical equipment reached certainly more than 100 MW. The domain of water disinfection is a large-scale photochemical application and is mentioned here, because equipment similar to that needed for preparative photochemistry is used. Since a few years, dye-sensitized singlet oxygen production is proposed as an alternative means of water disinfection. Such a process might show an economic advantage in cases where water can be recirculated and sunlight could be used for electronic excitation (e.g., fish ponds, cooling circuits) [24b,c].

1.2 State of the Art in Industrial Photochemistry

Due to many adverse factors, large-scale preparative photochemistry for the syntheses of chemicals did not show signs of progression until recently. The industrial use of photochemistry focused primarily on the evolution of microelectronics (Figure 1.1) and on large-scale surface treatment [17] (Figure 1.2) as spin-offs of new inventions and fast developments in the domain of polymer photochemistry [6,19]. Until the mid-1980s, silver halogenide photography found its peak in a last refined development of large dimensioned and brilliantly colored pictures [25] as well as in the instant picture development [26], but industrial laboratories were turning already toward digital alternatives [18].

1.2.1 Radiation Sources

Preparative photochemistry was more or less limited to the use of low and medium-pressure mercury and sodium arcs, and some processes were developed with tungsten lamps and fluorescent tubes [14]. Usually, this restricted choice did not allow an optimal selection of the spectral domain of electronic excitation, and mostly liquid filters were used to limit irradiation in particular toward higher photonic energies [14,28]. Glass filters [29] were and are not always available at affordable costs for pilot

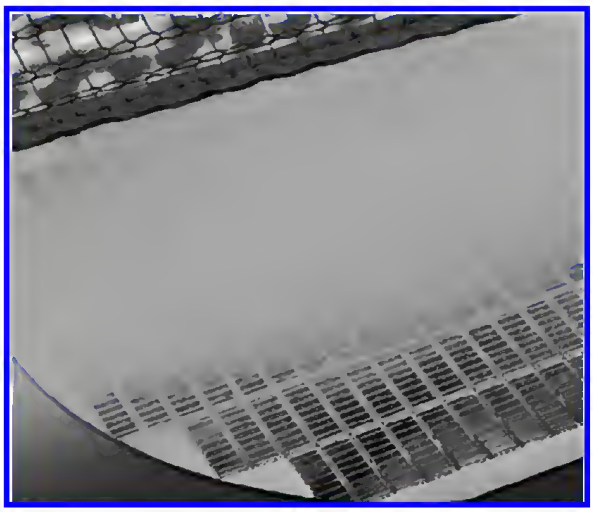

FIGURE 1.1 **(See color insert.)** Photochemical surface treatment in wafer manufacturing. (From Heraeus Noblelight GmbH, *Ultraviolet, High Power Cold UV*, Hanau, Germany, 2005. With permission.)

FIGURE 1.2 Equipment for ink drying and UV curing. (From UV-Consulting Peschl, *Ultraviolet-Technology, Product Overview*, Mainz, Germany, 2010. With permission.)

or production scale equipment. With the implementation of a variety of doped medium-pressure mercury arcs, the relatively widespread spectral distribution of the mercury lines could be concentrated to given spectral domains (Figure 1.3 [29]) with the corresponding benefits in energy costs and restricted side reactions.

In the mid-1980s, the first excimer radiation sources became available [30], and it was expected that this new class of radiation source would boost the technical applications of preparative photochemistry for three reasons: (i) the quasimonochromatic emissions of these sources would lead to more specific electronic excitations and therefore to higher yields of pure products [31], (ii) "lamps" without electrodes fixed to their envelope ("electrode-free lamps") would allow to adapt their forms and dimensions to those of the photochemical reactors and therefore to the given characteristics of the photochemical processes [32], and (iii) excimer "lamps" can be used in a pulsed mode that may induce higher yields and better product qualities [33]. Excimers were already generated earlier by microwave-driven excitation of

the emitting gas phase, a technique that might show advantages due to a rate-enhancing effect attributed to a simultaneous microwave excitation of the reaction system [34]. However, such radiation sources lose the advantage of "electrode-free lamps," since the microwave conduction between generator and "lamp" restricts the reactor design possibilities.

In retrospect, excimer radiation sources could not substitute the conventional arcs, although some very interesting applications in preparative photochemistry became known [35]. Main reasons include (i) the lack of a product line of commercially available excimer radiation sources of different electrical power reaching from laboratory to pilot scale, (ii) the spectral domain of useful excimer emissions, which is restricted to the VUV, UV-C to UV-B spectral regions, and (iii) the very high costs for "lamp" and corresponding power supply. Nevertheless, XeCl excimer (λ_{em}: 308 nm) could successfully replace the conventional medium-pressure mercury arc in printing processes (UV, curing ink drying [36]) due to the lower operational temperature of the former.

The Xe_2 excimer radiation source (λ_{em}: 172 nm) must be mentioned for its impact on vacuum-ultraviolet (VUV) photochemistry, a domain rarely mentioned outside fundamental research in spectroscopy and radiation chemistry. In fact, the development of these radiation sources brought a revival to water homolysis, reported since long with photonic energies higher than 6.2 eV [37], and therefore to environmental techniques [10b–d]. Xe_2 excimer emission might be produced with efficiencies as high as 40% of the input electrical power [38] and was used successfully in processes of surface activation and functionalization (Figure 1.4) of films [39] and aerosols [7] due to the photochemical reactivity of C–C bonds.

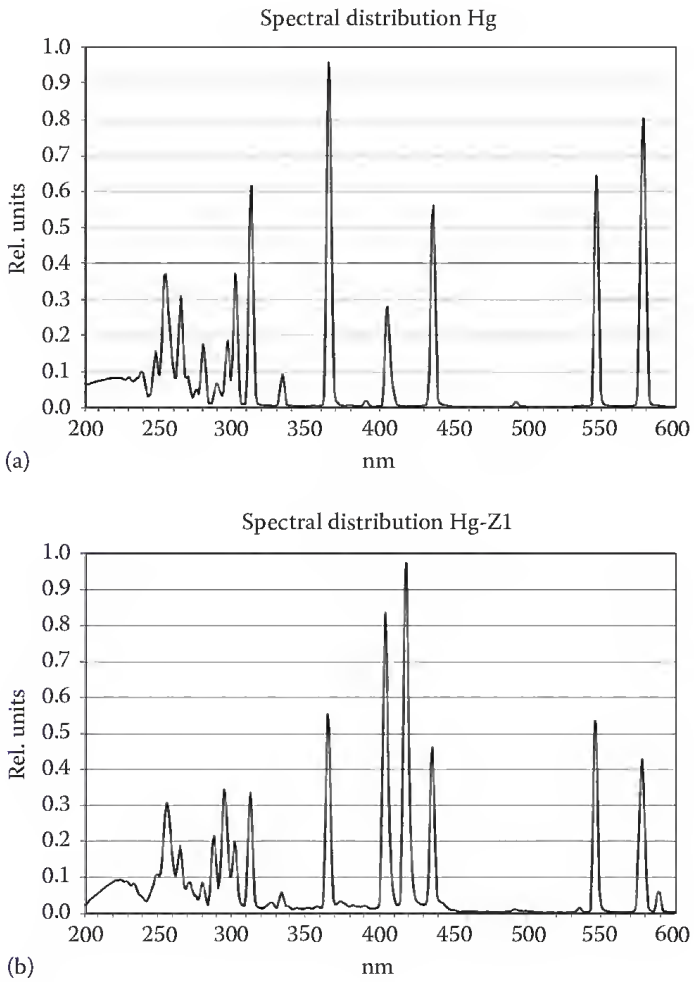

FIGURE 1.3 Examples of emission spectra of nondoped (a) and doped medium-pressure mercury arcs (b) Z1.

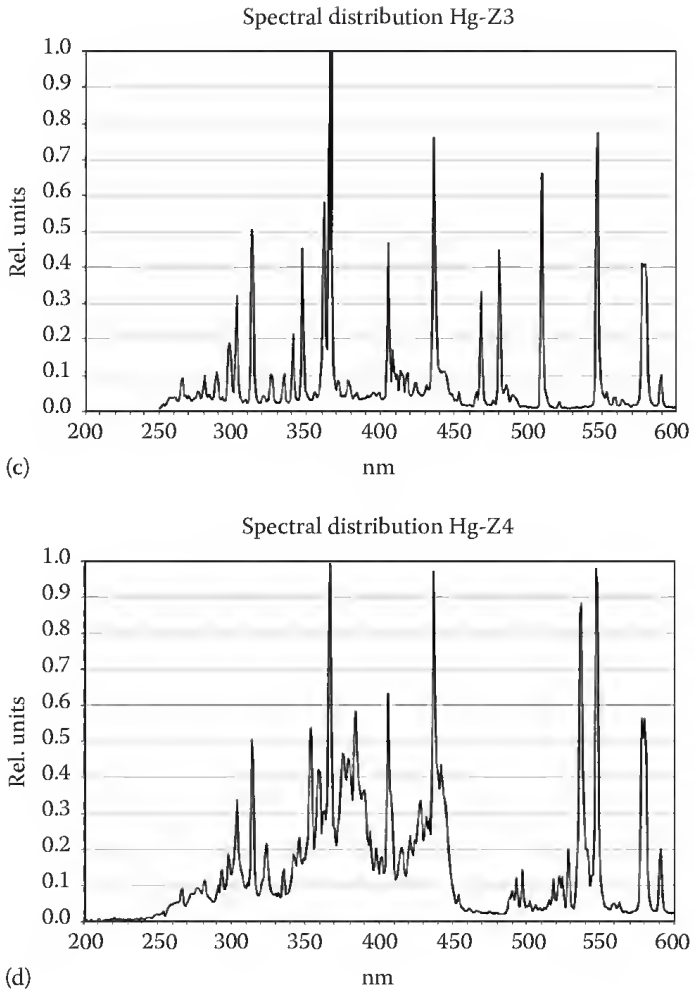

FIGURE 1.3 (continued) (c) Z3, (d) Z4. Spectra taken from arcs manufactured by Heraeus Noblelight GmbH, Hanau, Germany. (From UV-Consulting Peschl, *Photochemistry, Product Overview*, Mainz, Germany, 2009. With permission.)

FIGURE 1.4 (See color insert.) Xe_2 excimer radiation source (Xeradex, 20 W, Radium, Wipperfürth, Germany) used for the surface functionalization of polystyrene films.

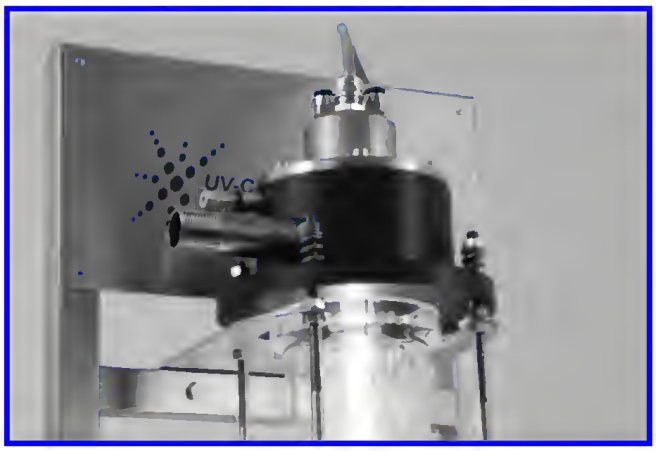

FIGURE 1.5 Pilot installation dedicated for waste water treatment with an "amalgam lamp." (Reactor manufactured by UV-Consulting Peschl and located at the Université Paul Sabatier, Toulouse, France. With permission.)

In condensed aqueous phases, the absorption cross section of H_2O is quite high at $\lambda_{exc} = 172$ nm, and limitations in upscaling [40] can be avoided with the use of O_3-producing doped low-pressure mercury arcs ("amalgam lamps") with main lines of emission at 185 and 254 nm. The two lines exhibit radiation powers of <10% and approximately 40%, respectively, of the electrical power [29] (Figure 1.5). These arcs became very rapidly a standard in environmental techniques and water disinfection. All "lamps" emitting in the VUV spectral region may be mounted in installations, for example, for the treatment of off-gases originating from chemical production units, biological water treatment stations, large kitchen units (Figure 1.6, e.g., fast food providers), and spray-dyeing workshops. VUV-driven TiO_2-photocatalytic processes might show higher efficiencies than those installed with UV-C and/or UV-A and UV-B excitation [41]. Care must be taken that O_3 is eliminated before treated off-gases are leaving such installations.

The introduction of LEDs provides an even larger choice of radiation sources. LEDs combine the advantage of a quasi-monochromatic emission, at present in the UV-A and VIS spectral domain, with those of long lifetime and the possibility of pulsed operation. However, LEDs do not exhibit design advantages of "electrodeless lamps," but may represent an optimal choice, when used in more or less large arrays in equipment for surface reactions (Figure 1.7) or in all kinds of immersion-type reactors. LEDs are also the perfect choice in combination with mini- or microreactors.

Solar irradiation is, of course, limited to photochemical processes with electronic excitations in the UV-A and VIS regions. Such processes should also be thermally insensitive. Large variations in incident photon fluxes, in particular day/night cycles, might be compensated by the installation of a series of reactors by which excitation by solar and artificial radiation can be combined.

FIGURE 1.6 Oxylight-HD unit [27] for the posttreatment of aerosols and aerosolates in the off-gas in large kitchen hoods.

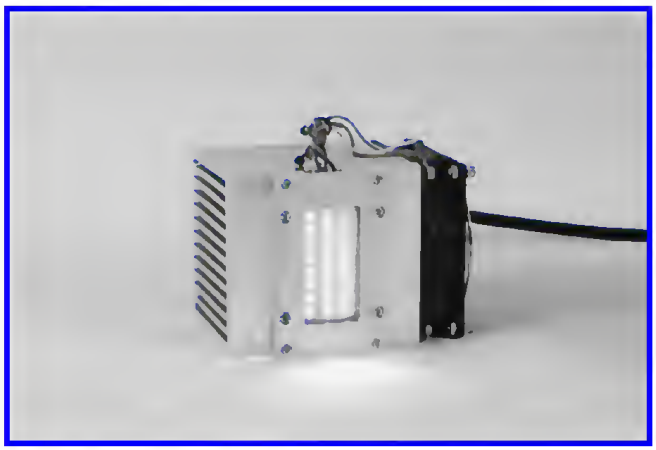

FIGURE 1.7 LED array used for surface treatment. (Array developed by Heraeus Noblelight GmbH and UV-Consulting Peschl, located at the Université de Haute Alsace, Mulhouse, France. With permission.)

1.2.2 Reactor Design

Mini- and microreactors might be used more frequently in future projects of preparative photochemistry, when chemicals of up to a few 100 kg/year are to be produced. However, immersion-type reactors of all kinds are still a standard in large-scale preparative photochemistry as well as for photochemical environmental techniques. They range from large volume multilamp installations, built in most cases for heterogeneous gas/liquid reaction mixtures (e.g., photosulfoxidations) and showing surprisingly high efficiencies, to one-lamp tubular reactors. Earlier, most production-scale photochemical processes were made in reactors that contained the volume of an entire batch. Experience taught, however, that semibatch installations, where the reaction medium circulates between a large central reservoir and a number of smaller reactors, present a number of mostly technical advantages [14]. Such installations ensure a rate of production largely independent of maintenance and repair and flexible to the needs of the market. They also provide better conditions for the optimization of flux (turbulence) and gas saturation. In addition, further development to a continuous process mode is made easier since the performance of one photochemical reactor in use is already known, and a parallel reactor configuration may be changed into an "in series" configuration without great difficulties. The efficiency of an immersion-type reactor depends primarily on the ratio between the irradiated and the reactor volumes, and, generally, ratios of 1/1.2–1/1.5 should be chosen. The irradiated volume may be evaluated knowing the absorbance of the photochemically reactive substrate, that is, its concentration and molar absorption coefficient at a given wavelength of excitation, and the dimensions of the radiation source. As the length or height of the reactor is given by the length of the radiation source, the volume of the reactor may be varied by changing the diameter of the cooling or protection tube representing the inner wall of the reactor volume (Figure 1.8). Several academic research groups focused their interest on model calculations of shape and dimension of an irradiated volume that depend on the dimensions and the spectral and operational characteristics of the radiation source as well as on the spectral absorption characteristics and the concentrations of the components of the reaction system [42,43]. Beside volume considerations, incident photon flux density, optimized flux of the reaction system, temperature control, gas saturation, and the probability of secondary reactions (e.g., filming) are usually the main factors affecting reactor design. In most cases, design work is made empirically, although some of the parameters might be calculated or pictured under assumed constraints with the use of specialized software.

As already mentioned, photochemical mini- and microreactors are a recent topic in industrial preparative photochemistry. Photochemical minireactors and irradiation equipment are already commercially available. The example of a production-scale application shown in Figure 1.9 uses thin-film minireactors positioned into the parallel beam of incident photons.

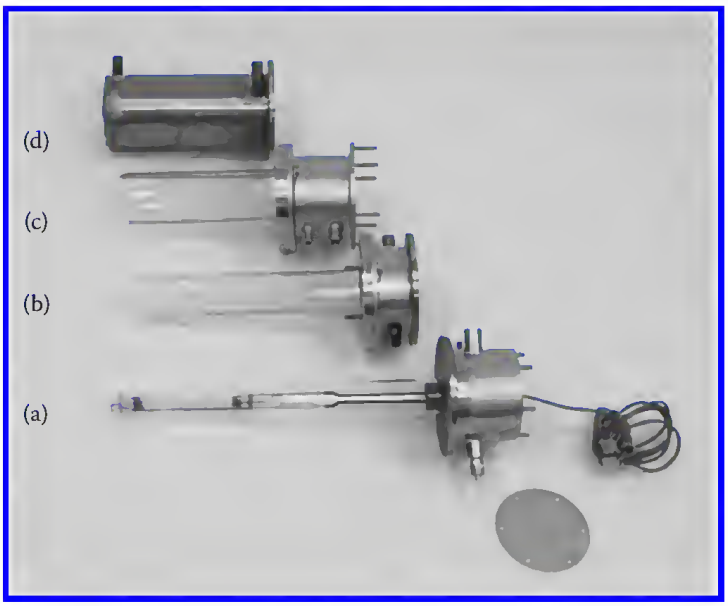

FIGURE 1.8 Constituents of an immersion well (a) through (c). From below: (a) radiation source (TQ 718, Heraeus Noblelight) with immersion tube, (b) cooling tube, (c) protection tube (optional), and (d) reactor (PTQ 1,5 KGS). (From UV-Consulting Peschl, *Photochemistry, Product Overview*, Mainz, Germany, 2009. With permission.)

FIGURE 1.9 **(See color insert.)** Photochemical mini-(thin-film) reactors of a production unit installed in a ventilated closet. (Picture shown with the kind permission of Heraeus, owner of IP rights of the pictured installation.)

Quite a number of academic and industrial research groups work at the implementation of photochemical microreactors. Microreactors represent at present the ultimate solution for problems of mass and photonic energy transfers encountered in larger reactor units. The material of the reactor body, its combination with a glass or quartz window, channel design, and dimensions depend strongly on the photochemical process to be developed, and some specialized equipment builders propose interesting solutions, but so far, no application became known.

As the photochemical reactor design depends on the reaction system to be treated, new challenges arise with the use of (micro)heterogeneous systems. Special designs are also needed for photochemical bioreactors [44], and new developments make use of combinations of differently emitting LEDs tuned on maximum growth of biomass.

Positive reaction geometries, where "lamps" are positioned outside and their emission focalized on a reactor tube [14], are no longer used for water disinfection but still represent simple and cheap solutions for chain reactions exhibiting high quantum yields and exothermicity (e.g., photochlorination), as they are now exploited in developing and emerging countries.

1.2.3 Upscaling/Downscaling

Upscaling means to change all process parameters determined for an optimized laboratory-scale reaction to achieve production of a previously fixed mass of product per unit of time in an installation adapted accordingly. In the course of developing a given photochemical process, care must be taken that only equipment is used that may be upscaled without technical problems. Such problems are primarily linked to the availability of large radiation sources and filters. For laboratory-scale photochemical processes, batch or semibatch equipment is most frequently chosen, but semibatch or continuous modes are definitely favored for technically developed processes. Such a change calls in most cases for an intermediate pilot phase in which process parameters are again optimized using a pilot reactor of the same or at least similar design than that foreseen for the reactor(s) of the production unit. Development on a laboratory scale concerns primarily the operational mode, the type of radiation source, the design of the photochemical reactor for a given class of reaction, and the absorption cross section of the substrate(s) within the actinic important spectral range, and incident photon flux density and residence time are the primary parameters to be optimized. Based on the results of optimized laboratory experiments, the electrical power needed for the radiation sources to be used to fabricate a previously fixed mass of product per unit of time can be evaluated by linear extrapolation. Radiation density, size, commercial availability, and replacement costs on one side and economic considerations (space to be attributed, investment including accessory equipment, operational period of reactor(s), costs of maintenance, costs of safety measures, availability and costs of specialized working force, etc.) on the other are the top priorities to decide on the power of the radiation sources and the number of reactors to be installed. As the rate of the photochemical reaction depends primarily on the rate of absorbed photons, upscaling is much simplified, if the absorbed (spectral) photon flux density [45] is kept constant within a limit of ±10%. For that purpose, the absorption conditions are kept constant, and radiation sources of increasing electrical power but similar incident photon flux density are used. Some brands of radiation sources are now commercially available in series that ensure similar radiation densities over a large range of electrical power.

Quantitative analyses of a number of pilot and production-scale reactors installed over a period of some 20 years show that practically all installations operate at the upper limit of radiation density ("over-irradiation"), hence producing high concentrations of excited states and reactive intermediates that are difficult to be trapped quantitatively within their lifetimes. Deviations from optimal process conditions (e.g., concentrations, flux) may therefore favor different reaction channels leading to secondary products and reactor filming. In sensitized processes, where a chemically inert sensitizer is excited and highly reactive intermediates should be quantitatively trapped, high radiation densities may simply lead to a strong decrease of substrate concentration within a fraction of the time of residence and, therefore, to a waste of energy. While the radiation density in the actinic important spectral region of a given process is primarily determined by the power and the dimensions of a given type of radiation source, fine-tuning is always possible by varying the diameter of the inner wall of the reactor. The problem of "over-irradiation" may, however, also be solved by pulsed excitation of suitable radiation sources. The incident photon energy per time of residence may then be optimized by varying the frequency of the exciting flashes.

As already mentioned earlier, the flow characteristics of the reaction system through the photochemical installation are a very important process parameter. Low fluxes may result in a depletion of substrate(s) at times inferior of the time of residence, and bimolecular reactions require turbulent flow conditions to ensure acceptable efficiencies. In falling film reactors [14], the dimension of the

FIGURE 1.10 Microreactor module made of silicium. (Picture taken at the Lehrstuhl für Umweltmesstechnik, University Karlsruhe, Germany. Reactor module developed by IMTEC, University of Freiburg, Germany. With permission.)

photochemical reactor and the flux of the reaction medium determine the volume and therefore the thickness of the falling film. Since this thickness can only be varied within a small range, efficient trapping of reactive intermediates depend on the turbulence and enhanced gas absorption due to the tumbling of the falling film, but may also be affected by the incident radiation density and, where necessary, by increased gas pressures.

For smaller production levels (up to a few 100 kg/year), upscaling may in fact consist of downscaling and multiplying reactor units operating in parallel. On first sight, such installations appear complicated, implying large numbers of pumps, complex piping, and gas supplies and may therefore also call for additional means as far as safety is involved. Total costs of investment and maintenance seem higher, but there are a number of economical and technical advantages to consider. Such installations need less space and the rate of production may be more rapidly adapted to the needs of the market. The combination of mini- or microreactors with the appropriate radiation source provides optimum conditions of electronic excitation, and gas dissolution/saturation and turbulence reach maximum levels in microchannels (Figure 1.10), hence ensuring best results (efficiency, quality of product) for processes in which electronically excited states or highly reactive intermediates have to be trapped by photochemically inactive reactants. Once a process is optimized on a mini- or microreactor scale, upscaling is a simple operation of multiplication. For safety reasons, processes might require confined spaces with special atmospheric treatment, and arrays of mini- or microreactors can be rapidly installed in such an environment.

Recently, a similar principle was adapted for larger scale photochemical reactors by conceiving a laboratory-scale tubular reactor module that may be simply multiplied in its length depending on the dimensions of the radiation source [46]. The optimized performance of the laboratory-scale module being determined for a given process, the elongated pilot or production reactor is rapidly optimized by adapting the reactant concentrations. The new design found already first applications in photochemically advanced oxidation processes.

1.3 Large-Scale Preparative Photochemistry and Means of Safety

In addition to the measures of safety imposed by the handling of chemical compounds in a given process, the use of photochemical equipment demands a special means of safety that concern radiation, electrical incidents, glass or quartz tube failures, hotspot-initiated explosions, and/or fire and temperature control.

1.3.1 Radiation

The effects of radiation may be roughly divided into those damaging the skin and those damaging the eye. In addition, polymer composite materials that might be used within the radiation field will be photolyzed and damaged, and resulting leaks of gases or liquids must be avoided by periodic inspection of such parts.

Photodermatology differentiates three spectral domains generating different degrees of skin irritation and damage: UV-C (200–280 nm), UV-B (280–320 nm), and UV-A (320–380 nm) [14]. Using radiation sources emitting these kinds of radiation, danger is imminent, when these "lamps" are used without being positioned inside adequate protection tubes or reactor vessels. Immersion, cooling tube, and protection tubes (Figure 1.8) that are made of synthetic or natural quartz do not provide protection, but those made of borosilicate protect at least against radiation at wavelengths <320 nm. The same holds for reactor vessels that are made of borosilicate. UV radiation transmitted through a reactor filled with reaction medium is mostly negligible (depending on the absorption of the medium), and VIS radiation (light, wavelengths >380 nm) is at the present state of knowledge of no concern for the skin. UV radiation at wavelengths <200 nm is absorbed by molecular oxygen contained in air, hence its penetration through air depends on the wavelength-dependent absorption cross section of molecular oxygen. Safety rules for VUV radiation sources should be the same as those imposed for UV-C sources.

It must be emphasized that the most sensitive organ exposed to radiation is the eye. Wanting to see what is happening, it is usually forgotten that damage to the eye may be fast and in most cases irreversible. Eye protection is not only required when dealing with UV radiation, exposure to intense VIS radiation may lead to mostly reversible blindness, but at higher doses to retina damage. Therefore, protection glasses should be worn when performing all kinds of photochemical experiments, and dark protection glasses when radiation sources are used that emit at wavelengths >320 nm.

Protection against radiation is already necessary for laboratory-scale experiments and is mostly accomplished with shields made of black tissue or aluminum foil. On large-scale reactors (enameled) stainless steel equipment provides best protection but cannot always be used, because reaction systems might be sensitive to metal ions contained in and leached from the reactor wall. Where reactors are made of borosilicate, protection against VIS radiation may consist of shields or curtains preferably made of blackened aluminum or aluminum foil.

1.3.2 Electrical Incidents

With the exception of tungsten lamps, fluorescence tubes, and some halogen lamps, radiation sources must be operated with a power supply. The power supply is necessary to ignite the arc through the gas phase containing the emitting atoms or clusters of atoms (e.g., mercury, sodium) and to maintain a constant operating voltage. Igniting voltage peaks may vary between 2000 and 6000 V, and, for example, low- and medium-pressure Hg arcs are driven between 30 and 100 and between 100 and 3500 V, respectively. From these data result considerable currents and care should be taken that all electrical connections (plugs and cables) are protected. Commercially available lamps are equipped with special plugs to avoid false connections. Power supplies are usually located outside the range of potentially spilled areas, and when handling flammable solvents or when working in an environment that must be kept explosion proof, special ventilated rooms are an advantage or may even be required.

Particular care for sufficient insulation must be taken when operating excimer radiation sources. These sources are driven with potentials of 3000–8000 V at frequencies in the range of 80–200 kHz. Under these conditions, insufficient or damaged insulation may cause the propagation of high-frequency potentials over the entire surface of an installation. Clamps, usually provided with protection sheets made of cork or plastic, do not provide sufficient insulation, and entire mounting racks may show St. Elmo's fire. Since damages on plugs or cables might not be readily detected, connections of all the different parts of an installation to the ground are certainly providing best levels of safety. Commercially available combinations of power supply, radiation source, and connections are equipped to avoid electromagnetic fields even at close

distance from the installation. This is not necessarily the case for self-made or assembled equipment, and at higher powers, means of protection (e.g., Faraday cages) are recommended.

1.3.3 Glass or Quartz Tube Failures

The probability that immersion, cooling, and/or protection tubes (Figure 1.8) made of quartz and/or borosilicate would break is very small, as long as fundamental safety rules are maintained. Quartz is more resistant to thermal shocks than borosilicate and is usually chosen for the most inner (immersion) tube of the well into which the radiation source is mounted. In accord with the required conditions of irradiation, temperature, and pressure, the outer tubes of the well might or must be made of borosilicate. Filter glasses (e.g., mixtures of quartz and borosilicate, colored borosilicates) might be mechanically fragile, and their use as material of construction has to be tested. Diameter and wall thickness of these tubes depend on the radiation source chosen (type, dimension), the incident photon flux density to be implemented, the flux of the cooling medium (if any), and the pressure required for a given process. Well tubing should be periodically inspected for cracks and cleaned from all kinds of stain developing on the surface exposed to the reaction and to the cooling medium as well as inside the cavity of the radiation source.

Most of the very large photochemical production units are made of stainless steel. In most cases, this is a matter of mechanical and thermal stability. Over the last decades, equipments made of borosilicate gained in importance, in particular for smaller reactors ($\leq$20 kW), because the material exhibits excellent chemical inertness, and glass reactors require much smaller investments. However, it cannot be denied that mechanical and thermal shocks are the biggest threat to such installations. In development, glass reactors are highly appreciated, because they provide optimal conditions to observe the effect of most important factors of process optimization, such as fluid dynamics, gas introduction, and distribution as well as field and absorption of radiation.

1.3.4 Hotspot-Initiated Explosions and/or Fire

All radiation sources produce heat. While heat production by fluoerscence tubes might be negligible, low-pressure arcs and excimer radiation sources may reach maximum surface temperatures of 120°C–150°C, The mostly used medium-pressure mercury arcs require an optimal operational surface temperature of 850°C; consequently, the temperature of the electrodes may reach 1350°C. Gaseous organic compounds entering the lamp cavities may be ignited, hence initiating explosion and fire within the space of a production unit. This danger can be averted by introducing an inert and UV-transparent gas into and to the bottom of the cavity and by maintaining a slight overpressure within the cavity that prevents other gases from penetrating into the space, where the hotspot is located. The absence of molecular oxygen from the cavity also diminishes considerably the rate of electrode oxidation at elevated temperatures, and maintaining a nitrogen atmosphere within the cavity is affecting favorably the lifetime of the radiation source and therefore one of the most important factors of maintenance: lamp replacement. Depending on the type of radiation source, the introduction of nitrogen into its cavity might be mandatory in order to prevent ozone generation. Usually, a flow control system regulating the inert gas flow is linked to the controls of the power supply of the radiation source.

1.3.5 Temperature Control

Depending on (i) the radiation source to be used, (ii) the photochemical process, and (iii) the thermodynamics of the process, cooling circuits must be installed. Water is usually taken as a cooling liquid circulating through an outer layer of the well limited by the immersion and the cooling tubes (Figure 1.8). But other cooling liquids may be used, as long as they are transparent in the spectral region of interest, photochemically stable, and complying with all safety regulations. For reasons of environmental protection and increasing costs of clean water, closed cooling circuits with tap water may be installed. Pure deionized

water should not be used, because it will corrode metal and borosilicate surfaces. Water cooling through the well of a radiation source serves two purposes: (i) maintaining an optimal operational temperature of the radiation source and (ii) absorbing the infrared radiation emitted by the radiation source, hence contributing to an efficient thermoregulation of the reaction system. Liquid filter systems that restrict the emitted polychromatic radiation to the spectral region of interest may be used as well. It is most important that the flow control system of the cooling circuit can interrupt the irradiation in case of failure.

Water absorbs VUV radiation and corresponding cooling circuits cannot be installed in the outer layers of a well protecting a VUV-emitting radiation. Some radiation sources may comprise an internal cooling circuit using the cavity of the potential-bearing electrode. In these cases, the use and periodic control of distilled (deionized) water is mandatory. Commercially available radiation sources may not require additional cooling or comprise an internal cooling circuit and corresponding controls.

1.3.6 ATEX or NEC Certification

Integral safety measures may be installed with ATEX- (ATmosphère EXplosible) or NEC-certified equipment. The EU regulation 94/9/EG (ATEX 100a) and the US regulations NEC 500/505 classify the requirements imposed on the equipment and on the safety measures necessary in order to ensure safe operational conditions in potentially hazardous areas. Consequently, only ATEX- or NEC-certified equipment can be installed and used in photochemical processes on an industrial scale, where organic solvents are to be used. ATEX-certified irradiation equipment from 2 to 40 kW is commercially available, and large-scale photochemical processes can nevertheless be realized.

ATEX certification is based on a risk analysis and on the corresponding tests of all parts in interaction with the irradiation equipment: radiation source, metal parts, quartz or glass tubing (wells) as well as electric supply and electronic controls. Besides measures to prevent explosion of gases in hotspot zones, special attention is given to the safety of the irradiation system. Radiation sources might implode provoking short circuits as well as cracks and breakage of the surrounding quartz or glass tubes. Leaks in the well might lead to an immersion of the lamp cavity by the cooling liquid and/or the reaction system, but a destruction of the well should never be the origin of a fire under these safety conditions. Certified radiation sources are sold with a minimum lifetime guarantee and a tested breaking behavior reducing considerably the threat of damaging the surrounding quartz or glass tubes. Transparent materials used for the construction of the well must be tested (Figure 1.11) to ensure their stability in case (i) of fast rising

FIGURE 1.11 Setup of tests for a photochemical reactor comprising a 40 kW medium-pressure mercury arc. (Picture from UV-Consulting Peschl. With permission.)

FIGURE 1.12 Electric and electronic control systems for the installation of 5 × 20 kW medium-pressure mercury arcs. (Picture from UV-Consulting Peschl. With permission.)

temperatures within the operational limits of the radiation equipment, (ii) of mechanical stress (impact of fragments, temperature-dependent dimension variations), and (iii) of sudden drops of temperature (e.g., in case of emergency cooling). Special tests are required for processes under pressure. The loss of pressure and/or flow of the cooling medium and the increase of temperature must be permanently controlled for a given irradiation system.

The risk analysis as well as all tests results must be documented and serve as a basis for the operating manual. Finally, the classification of the irradiation system must correspond to the requirements imposed by a given chemical process. ATEX-certified electrics and electronics (Figure 1.12) control the safe operation of radiation sources autonomously, through permanent voltage measurements, ground fault monitoring, and links between the flow controls of inert gas and water and the safety switches of the power supply.

1.4 Summary

This chapter focuses on and describes the present state of the art of large-scale preparative photochemistry and is meant to be a brief update of the presentations given in a number of earlier textbooks and reviews. New developments of radiation sources (excimer and LED) and the introduction of photochemical mini- and microreactors confirm the actual interest and open new domains of industrial applications. Safety requirements and respective costs are most often critical factors in deciding for or against the implementation of a photochemical process, and corresponding frequently evoked problems are discussed.

References

1. P.T. Anastas, J.C. Warner, *Green Chemistry: Theory and Practice*, Oxford University Press, New York, 1998.
2. R. Anliker, G. Müller, Fluorescent whitening agents, in *Environmental Quality and Safety* (F. Coulston, F. Korte, eds.), Suppl. Vol. 4, Thieme, Stuttgart, 1975.
3. B. Lee, Review of the present status of optical fiber sensors, *Opt. Fiber Technol.*, 9 (2003) 57–79.
4. H. Dürr, H. Bouas-Laurent, *Photochromism, Molecules and Systems*, Elsevier, Amsterdam, 1990.
5. R.R. Allison, G.H. Downie, R. Cuenca, X. Hu, J.H. Childs Carter, C.H. Sibata, Photosensitizers in clinical PDT, *Photodiag. Photodyn. Ther.*, 1 (2004) 27–42.

6. (a) N.S. Allen, M. Edge, I.R. Bellobono, E. Selli, *Current Trends in Polymer Photochemistry*, Ellis Horwood, New York, 1995, and references cited therein; (b) G. Bradley, J.V. Crivello, K. Dietliker, *Photoinitiators for Free Radical Cationic & Anionic Photopolymerisation*, Wiley, Chichester, 1999.
7. J. Salas Vicente, J. López Gejo, S. Rothenbacher, S. Sarojiniamma, E. Gogritchiani, M. Wörner, G. Kasper, A.M. Braun, Oxidation of polystyrene aerosols by VUV-photolysis and/or ozone, *Photochem. Photobiol. Sci.*, 8 (2009) 944–952.
8. R. Larciprete, M. Stuke, Direct observation of excimer-laser photoablation products from polymers by picosecond-uv-laser mass spectroscopy, *Appl. Phys. B: Lasers Opt.*, 42 (1987) 181–184.
9. (a) N. Serpone, E. Pellizzetti, *Photocatalysis, Fundamentals and Applications*, Wiley, Chichester, 1989; (b) M. Chanon, ed., *Homogeneous Photocatalysis, Wiley Series in Photoscience and Photoengineering*, Vol. 2, Wiley, Chichester, 1997; (c) M. Schiavello, ed., *Heterogeneous Photocatalysis, Wiley Series in Photoscience and Photoengineering*, Vol. 3, Wiley, Chichester, 1997.
10. (a) M. Doré, *Chimie des Oxydants et Traitement des Eaux*, Lavoisier, Paris, 1989; (b) O. Legrini, E. Oliveros, A.M. Braun, Photochemical processes for water treatment, *Chem. Rev.*, 93 (1993) 671–698; (c) F. Benoit-Marquié, U. Wilkenhöner, V. Simon, A.M. Braun, E. Oliveros, M.-T. Maurette, VOC photodegradation at the gas–solid interface of a TiO_2 photocatalyst: Part I: 1-butanol and 1-butylamine, *J. Photochem. Photobiol. A: Chem.*, 132 (2000) 225–232; (d) T. Oppenländer, *Photochemical Purification of Water and Air*, Wiley, Weinheim, 2003, and references cited therein; (e) P. Boule, D. Bahnemann, P. Robertson, eds., *Environmental Photochemistry*, Part II, Springer, Heidelberg, 2005.
11. R. Roberts, M.A. Muradaz, R.F. Cozzens, *Photochemistry in the Chemical Process Industries*, MITRE Corporation, McLean, VA, 1982, Chapter 7 and Appendix A.
12. R.J. Marcus, J.A. Kent, G.O. Schenck, Applied aspects of organic photochemistry, *Ind. Eng. Chem.*, 54 (1962) 20–28.
13. M. Fischer, Industrial applications of photochemical syntheses, *Angew. Chem. Intl. Ed.*, 17 (1978) 16–26.
14. (a) A.M. Braun, M.-T. Maurette, E. Oliveros, *Technologie Photochimique*, Presses Polytechniques Romandes, Lausanne, 1986; (b) A.M. Braun, M.-T. Maurette, E. Oliveros, *Photochemical Technology*, D.F. Ollis, N. Serpone, transl., Wiley, Chichester, 1991.
15. Jan F. Rabek, *Experimental Methods in Photochemistry and Photophysics*, Part I and II, Wiley, Chichester, 1982.
16. (a) A.G. Griesbeck, J. Mattay, *Synthetic Organic Photochemistry*, Dekker, New York, 2005; (b) S. Protti, D. Dondi, M. Fagnoni, A. Albini, Photochemistry in synthesis: Where, when, and why? *Pure. Appl. Chem.*, 79 (2007) 1929–1938.
17. (a) N.S. Allen, *Photopolymerisation and Photoimaging Science and Technology*, Kluwer, Norwell, MA, 1989; (b) J.-P. Fouassier, *Photoinitiation, Photopolymerization, and Photocuring: Fundamentals and Applications*, Hanser Gardner, Cincinnati, OH, 1995; (c) R. Stowe, A. Berejka, R. Mehnert, A. Pincus, I. Janorsky, *Uv & Eb Curing Technology & Equipment*, Wiley, Chichester, 1999; (d) R. Dessauer, *Photochemistry, History and Commercial Applications of Hexaarylbiimidazoles*, Elsevier, Amsterdam, 2006.
18. (a) http://www.cambridgeincolour.com/tutorials/camera-sensors.htm; (b) http://www.dpreview.com/learn/?/Glossary/Camera_System/sensors_01.htm
19. N.S. Allen, ed., *Handbook of Photochemistry and Photophysics of Polymeric Materials*, Wiley, Hoboken, NJ, 2010.
20. M. Grätzel, Dye-sensitized solar cells, *J. Photochem. Photobiol., C: Rev.*, 4 (2003) 145–153.
21. E.F. Schubert, *Light-Emitting Diodes*, Cambridge University Press, Cambridge, 2006.
22. Heraeus Noblelight GmbH, *Ultraviolet, High Power Cold UV*, Hanau, 2005.
23. (a) E. Oliveros, O. Legrini, A.M. Braun, M. Hohl, T. Müller, Large scale development of a light-enhanced Fenton reaction by optimal experimental design, *Water Sci. Technol.*, 35 (1997) 223–230.

(b) J.J. Pignatello, E. Oliveros, A. MacKay, Advanced oxidation processes for organic contaminant destruction based on the Fenton reaction and related chemistry, *Crit. Rev. Environ. Sci. Technol.*, 36 (2006) 1–84.

24. (a) Figawa (Firmen im Gas- uznd Wasserfach) Working Group on UV-Water Treatment, *Ultraviolet Disinfection in Water Treatment*, Techn. Report 01 | 08, Rev. Vers. of Techn. Report No. 20/98, Köln, 2009 (from http://www.heraeus-noblelight.com/fileadmin/user_upload/PDF/disinfection/UV_Disinfection__in_Water_Treatment72x_ok.pdf); (b) A. Acra, M. Jurdi, H. Mu'allem, Y. Karahagopian, Z. Raffoul, *Water Disinfection by Solar Radiation, Assessment and Application*, International Development Research Centre (IDRC), Ottawa, Ontario, 1990 (from http://almashriq.hiof.no/lebanon/600/610/614/solar-water/idrc/); (c) M.E. Jiménez-Hernández, F. Manjón, D. García-Fresnadillo, G. Orellana, Solar water disinfection by singlet oxygen photogenerated with polymer-supported Ru(II) sensitizers, *Solar Energy*, 80 (2006) 1382–1387.
25. (a) M.R. Peres, Silver dye-bleach photography, in *Focal Encyclopedia of Photography*, 4th edn., Focal Press, Elsevier, Burlington, VT, 2007; (b) e.g., http://www.lorenadams.com/PURPLE/DIRLINKS/cibachrome.html
26. L.K. Mills, *Photographic System, Apparatus and Cassette for Processing a Self-Developing Film Unit*, US 4183651, January 15, 1980 (Polaroid Corp., Waltham, MA, 1980).
27. UV-Consulting Peschl, *Ultraviolet-Technology*, Product Overview, Mainz, 2010.
28. S.L. Murov, I. Carmichael, G.L. Hug, *Handbook of Photochemistry*, 2nd rev. edn., Dekker, New York, 1993.
29. UV-Consulting Peschl, *Photochemistry, Product Overview*, Mainz, 2009.
30. B. Eliasson, U. Kogelschatz, UV excimer radiation from dielectric-barrier discharges, *Appl. Phys. B*, 46 (1988) 299–303.
31. E. Oliveros, A.M. Braun, G. Drivon, J. Kervennal, *Synthesis of Perfluoroalkyl Bromide by Photochemical Bromination of Corresponding Iodide*, EU 92401674.4, June 16, 1992 (Atochem).
32. A.M. Braun, L. Jakob, E. Oliveros, C.A. Oller de Nascimento, Up-scaling photochemical reactions, *Adv. Photochem.* (D.H. Volman, G.S. Hammond, D.C. Neckers, eds.), 18 (1993) 235–313.
33. A. Ferreira de Mattos Silvares, C.A. Oller do Nascimento, E. Oliveros, S.H. Bossmann, A.M. Braun, Pulsed XeCl excimer excitation for optimizing the polydispersity of methyl methacrylate pré-polymers, *Ind. Eng. Chem. Res.*, 46 (2007) 7436–7447.
34. S. Horikoshi, A. Tsuchida, H. Sakai, M. Abe, S. Sato, N. Serpone, Microwave discharge electrodeless lamps (MDEL), Part IV. Novel self-ignition system incorporating metallic microwave condensing cones to activate MDELs in photochemical reactions, *Photochem. Photobiol. Sci.*, 8 (2009) 1618–1625.
35. (a) T. Oppenländer, G. Baum, W. Egle, T. Hennig, Novel vacuum-UV-(VUV) and UV-excimer flow-through photoreactors for waste water treatment and for wavelength-selective photochemistry, *J. Chem. Sci.*, 107 (1995) 621–636; (b) G. Tröscher, *Die Photochemische Herstellung von Prävitamin D3: Untersuchungen zum Einsatz von Xenonbromid-Excimerstrahlern und Senbsibilisatoren*, PhD Thesis, Fakulty of Chemical and Process Engineering, Universität Karlsruhe (TH), Karlsruhe, 2002.
36. A. Peled, ed., *Photo-Excited Processes, Diagnostics and Applications*, Kluwer, Boston, MA, 2003.
37. M.C. Gonzalez, E. Oliveros, M. Wörner, A.M. Braun, Vacuum-ultraviolet photolysis of aqueous reaction systems, *J. Photochem. Photobiol., C: Rev.*, 5 (2004) 225–246.
38. Radium, Higher efficiency, higher profitability; the revolution in excimer radiation: Radium XERADEX® systems, Radium Lampenwerk, Wipperfürth, 2010.
39. J. López Gejo, N.P. Manoj, S. Sumalekshmy, H. Gliemann, T. Schimmel, M. Wörner, A.M. Braun, Vacuum-ultraviolet photochemically initiated modification of polystyrene surfaces: Morphological changes and mechanistic investigations, *Photochem. Photobiol. Sci.*, 5 (2006) 948–954.
40. G. Heit, A.M. Braun, VUV photolysis of aqueous systems: Spatial differentiation between volumes of primary and secondary reactions, *Water Sci. Technol.*, 35 (1997) 25–30.

41. (a) W. Han, P. Zhang, W. Zhu, J. Yin, L. Li, Photocatalysis of p-chlorobenzoic acid in aqueous solution under irradiation of 254 nm and 185 nm UV light, *Water Res.*, 38 (2004) 4197–4203; (b) J. Biomorgi, M. Haddou, E. Oliveros, M.T. Maurette, F. Benoit-Marquié, Coupling of adsorption on zeolite and V-UV irradiation for the treatment of VOC containing air streams: Effect of TiO_2 on the VOC degradation efficiency, *J. Adv. Oxid. Technol.*, 13 (2010) 107–115.
42. (a) Preface: In Honor of Dr. Alberto Cassano, *Ind. Eng. Chem. Res.*, 46 (2007) 7393; (b) R.L. Romero, O.M. Alfano, A.E. Cassano, Radiation field in an annular, slurry photocatalytic reactor. 2. Model and experiments, *Ind. Eng. Chem. Res.*, 42 (2003) 2479–2488.
43. A. Ferreira de Mattos Silvares, *Desenvolvimento experimental e simulação matemética do processo de pré-polimerição fotoiniciada de metacrilato de metila* (*MMA*), Tese, Escola Politécnica de Universidade de São Paulo, São Paulo, 2006.
44. C. Posten, Design principles of photo-bioreactors for cultivation of microalgae, *Eng. Life Sci.*, 9 (2009) 165–177.
45. S.E. Braslavsky et al., Glossary of terms used in photochemistry, 3rd edn. (IUPAC recommendations 2006), *Pure Appl. Chem.*, 79 (2007) 293–465.
46. A.M. Braun, A. Peschl, Modularer Photo-Röhrenreaktor, EU 10 20190 014 712.5, April 12, 2010 (UV-Consulting Peschl, Mainz, 2010).

2

Excilamp Photochemistry

Thomas Oppenländer
Hochschule Furtwangen University

2.1 Vacuum-Ultraviolet and UV Excilamps in Photoscience

During the past two decades, the development of modern excilamps initiated an enormous number of laboratory investigations in photochemistry and related fields, and it also led to various industrial applications. The interdisciplinary aspects of these developments were summarized in several recent reviews [1–6]. The current presentation highlights tendencies and developments of future significance in this area of research and development.

The organization of this contribution follows the sequence of keywords presented in Table 2.1: initially, some industrial and medical applications and the development of mercury-free artificial lighting systems will be mentioned. Thereafter, photochemical processes of surface modification and surface cleaning that are of utmost industrial importance in material sciences and nanotechnology will be presented. Subsequently, applications of excilamps in analytical instrumentation and the development of novel actinometric procedures for the measurement of the photon flux q_p of excilamps will be discussed. Also, the use of excilamps in synthetic photochemistry will be briefly described. Another part of this review will deal with destructive photochemical processes that are under active investigation, for example, surface disinfection, vacuum ultraviolet (VUV) or UV disinfection of aqueous systems, and advanced oxidation processes (AOPs) for water and air treatment. All processes mentioned in Table 2.1 are based on photo-induced changes of chemical entities.

The reason for the worldwide interest in the use of this lamp generation is related directly to its extraordinary characteristics: excilamps are mercury-free gas-discharge sources of noncoherent VUV or UV radiation with high radiant power of up to 700 W cm^{-2} [7]. The spontaneous emission of radiation is based on the formation of short-lived excimers or exciplexes, which can be either produced by dielectric barrier discharges (DBDs, silent discharges) [8,9], by capacitive discharges (CDs) [10], or by other techniques [11] including corona discharges [12,13]. Excilamps are nonlaser sources of radiation. In contrast to lasers they

TABLE 2.1 Areas of Research and Application of Excilamps

Industrial Applications	Process Technologies	Analytical Photochemistry	Synthetic Photochemistry	Destructive Photochemistry	
Plasma displays	Photo-CVD	Instrumentation	Production of fine chemicals	Surface disinfection	
Artificial lighting	UV curing	Actinometry		Aqueous phase	Gaseous phase
Photomedicine	Photolithography			VUV/UV Disinfection	
Surface modification				Advanced oxidation processes (AOPs)	
Surface cleaning					

CVD, chemical vapor deposition; VUV, vacuum-UV radiation (100 nm ≤ λ ≤ 200 nm); UV, ultraviolet radiation (200 nm ≤ λ ≤ 400 nm).

TABLE 2.2 Matrix of Gases Applied in Excilamps[a], the Corresponding Emission Maxima and Molar Photon Energies

	Ng[b]					
X_2[c]	—	He	Ne	Ar	Kr	Xe
	Emission Maximum λ_{max}/nm/Molar Photon Energy Q_λ/kJ mol^{-1}[d]					
—	—	74/1616.6	83/1441.3	126/949.4	146/819.4	172/695.5
F_2	157/762.0	—	108/1107.7	193/619.8	248/482.4	354/337.9
Cl_2	259/461.9	—	—	175/683.6	222/538.9	308/388.4
Br_2	289/413.9	—	—	165/725.0	207/577.9	282/424.2
I_2	342/349.8	—	—	—	190/629.6	253/472.8

[a] *Source:* Data from Gallert, B. and Kogelschatz, U., *Appl. Phys. B.*, 52, 14, 1991.
[b] Ng: noble gas.
[c] X_2: halogen.
[d] Calculated using the Planck law of radiation: $Q_\lambda = N_A hc_0/\lambda$.

provide almost monochromatic (narrow-band) and noncoherent radiation with a full width at half maximum (FWHM) of less than 15 nm. The wavelength of the emission maximum depends on the nature of the gas-filling components (Table 2.2). Thus, excilamps cover a broad range of radiant energy (Table 2.2) that can be used for selective initiation of photochemical reactions and processes.

The acronym "excilamp" describes two kinds of noncoherent VUV or UV sources. It was first introduced by Tarasenko [15]. An excimer or exciplex is an electronically excited dimer (e.g., a xenon excimer, Xe_2^*) or an electronically excited complex (e.g., a krypton chloride exciplex, KrCl*), respectively [16]. These electronically excited molecules are short-lived species that decompose within nanoseconds with the formation of the electronic ground states of the participating atoms accompanied by emission of radiation. Some representative emission spectra of excilamps are presented in Figure 2.1.

Excilamps are so-called cold lamps that exhibit almost no infrared (IR) emission. Thus, they are ideally suited for low-temperature photoprocessing of temperature-sensitive materials. The variable power adjustment enables instant start at full radiation output. In addition, the so-called electrodeless configuration guarantees a long lifetime of several thousand hours of operation [17,18]. Possible mechanisms for the limitation of the lifetime of CD-driven exciplex lamps were discussed by Sosnin et al. [18].

Interestingly, excilamps exhibit an unprecedented variation in geometrical design of the lamp's body. Due to the "electrodeless" configuration (Figure 2.2) of the setup, the lamp body of excilamps may be designed as tubular structures radiating outward or inward. In this context, "electrodeless" means that the hot and the ground electrode are not in contact with the plasma producing gas or gas mixture. Additionally, special geometries, flat panels [19–23] or excilamps with a large emitting surface [24,25], and windowless or open systems are possible [9,26–30] (Figure 2.3). This enormous variability of geometrical options of

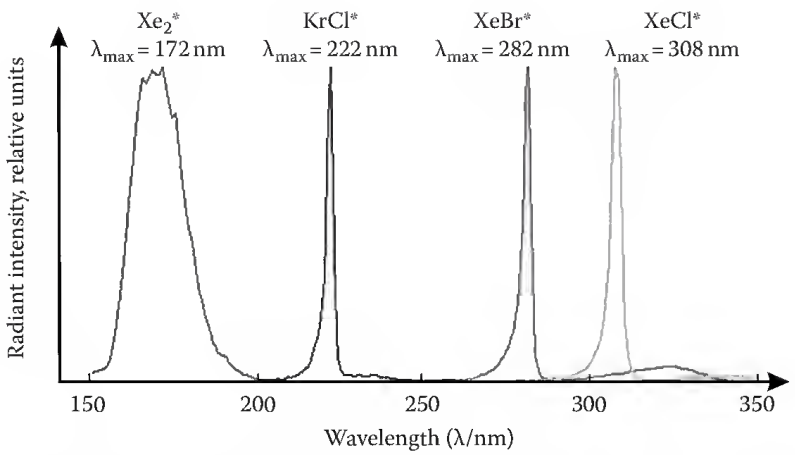

FIGURE 2.1 Representative emission spectra of some commercially available excilamps. (Excimer lamp spectra by courtesy of Heraeus Noblelight GmbH, Hessen, Germany.)

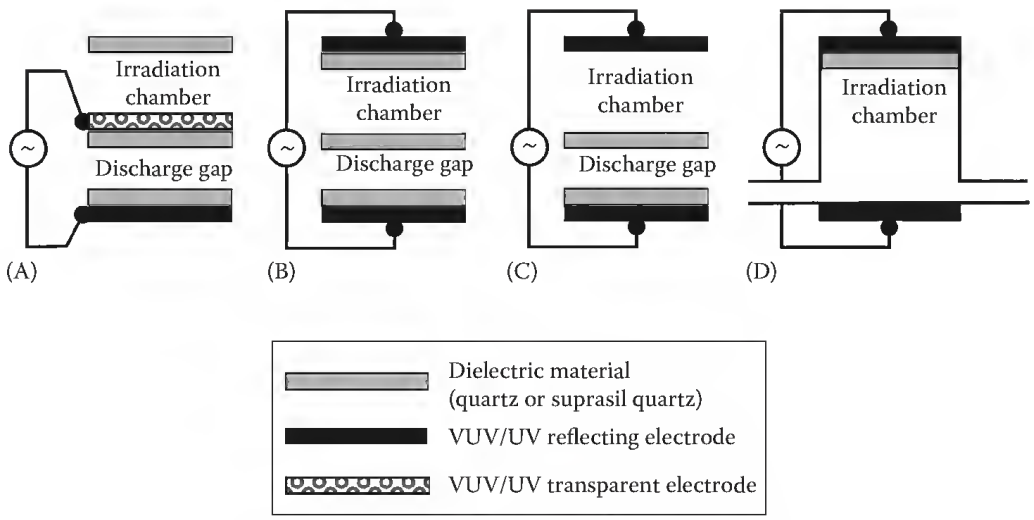

FIGURE 2.2 Examples of electrode configurations of the setup of excilamp systems: (A–C) closed and (D) open lamp designs.

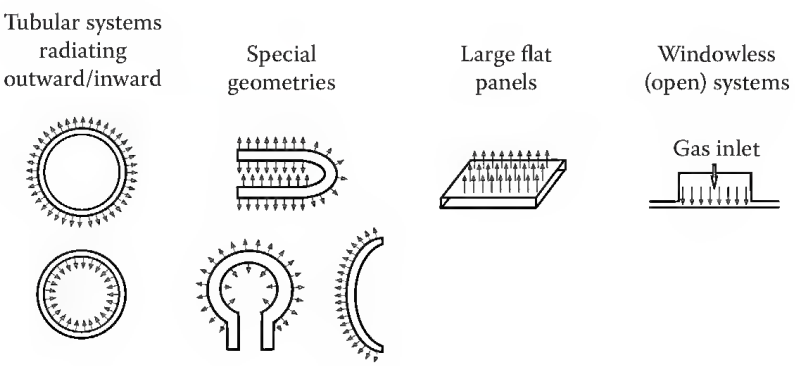

FIGURE 2.3 Possible geometries of excilamp systems.

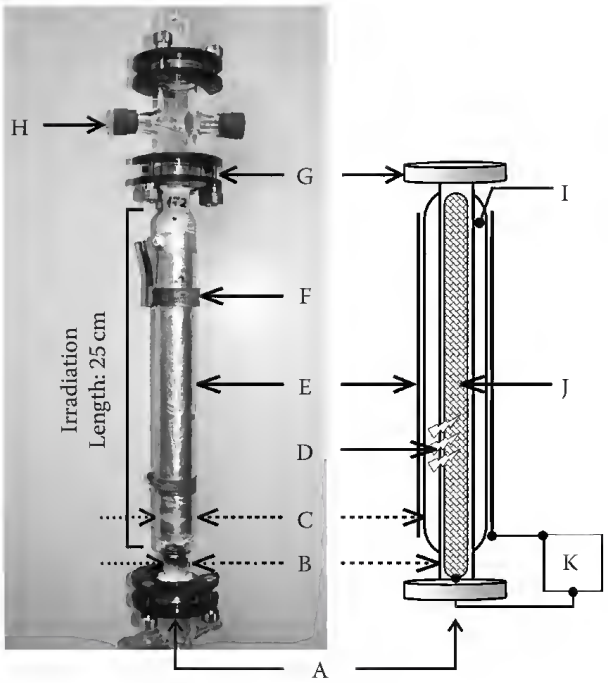

FIGURE 2.4 Photograph and schematic representation of an excilamp flow-through photoreactor. A: flow of medium; B: inner tube (Suprasil or quartz); C: outer tube (Suprasil or quartz); D: radiation directed inward; E: outer electrode (ground) consisting of aluminum; F: connection to the plasma generator, ground electrode; G: flange connectivity; H: connection to the plasma generator, hot inner electrode; I: sealed discharge gap containing the excimer gas or gas mixture; J: hot inner electrode; K: plasma generator. (Photo courtesy of T. Oppenländer, Hochschule Furtwangen University.)

excilamp design enables engineers for the first time in photochemical engineering to adapt the geometry of the lamp to the reactor system or to the photochemical reaction conditions [31]. Furthermore, an upscaling [32,33] and the miniaturization [34] of excilamps are easily possible.

A typical flow-through photoreactor configuration for the irradiation of aqueous or gaseous media [35–38] is shown in Figure 2.4. In this example, the excilamp is used with its radiation directed inward by applying VUV/UV-reflecting aluminum as the outer electrode.

The tubular excilamp configuration allows the variation of inner electrodes and inserts. For example, the inner electrode may consist of a spiral metal wire or of a metallic static mixer (Figure 2.5A) [39]. Furthermore, inserts like semipermeable ceramics can be axially mounted within the flow of the medium to introduce gases locally into the irradiation zone (Figure 2.5B) [40].

The electrical behavior of excilamps is still under active investigation [41] with the objective to enhance the radiant efficiency (η), i.e., the ratio of radiant energy Q_λ to the input of electrical energy W_{el}^{in}, $\eta = Q_\lambda / W_{el}^{in}$. For example, Merbahi et al. [41] confirmed a VUV efficiency of a single xenon microdischarge of about 55%–60%, and Shiga et al. [19] calculated that almost 80% of the electron energy is deposited in the electronic excitation of Xe. Under their experimental conditions, most of this energy is converted to VUV radiation. Salvermoser and Murnick [13] reported a conversion efficiency of their Xe_2^* excilamp of greater than 50% using a corona discharge in xenon gas. However, typical commercial excilamps exhibit radiant efficiencies between 5% and 40% [1]. The most efficient Xe_2^* excilamp that is currently available on the market is the Xeradex* VUV excimer lamp system

* http://www.osram.com/_global/pdf/Professional/Display_Optic/Semiconductor_Medical/Xeradex/Xeradex%252020W_175_S45_95.pdf (latest access: 12/06/2009).

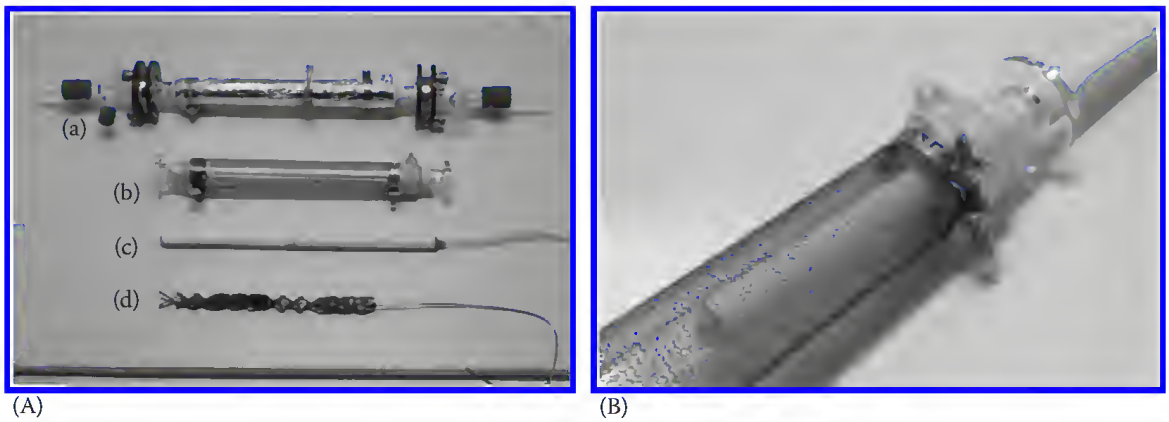

FIGURE 2.5 (A) Excilamp flow-through photoreactors and examples of inserts. (a) Excilamp with axially mounted quartz tube; (b) quartz body of an excilamp with flanges; (c) ceramic oxygenator; (d) metallic static mixer. (B) An axially mounted ceramic oxygenator within the flow channel of the excilamp. (Photo by B. Müller, Augsburg, Germany. Courtesy of Hochschule Furtwangen University.)

with a stated radiant efficiency (η) of 40% at an electrical input power of 20, 50, or 100 W. Figure 2.6 shows a photo of a DBD-driven tubular XeCl* excilamp that demonstrates typical discharge phenomena constituted either of thin current filaments (microdischarges) or of homogeneous discharges. The complex physical phenomena that trigger these different discharge modes were discussed explicitly by Kogelschatz [42].

FIGURE 2.6 **(See color insert.)** The emission characteristics of a cylindrical and outward radiating DBD-driven XeCl* excilamp exhibiting thin micro- and homogeneous discharges. (Photo by B. Müller, Augsburg, Germany. Courtesy of Hochschule Furtwangen University.)

2.2 Industrial Applications

Low- and medium-pressure mercury lamps are widely used UV sources. They are extensively applied in various industrial areas, for example, for the disinfection of water, air, and surfaces; for UV curing of lacquers, resins, adhesives, and paints; for photochemically initiated advanced oxidation processes (AOPs) for water (e.g., [43]) and air purification and detoxification; and for therapeutic treatment of skin diseases, for example, phototherapy of psoriasis. Especially, the lighting industry uses low-pressure mercury gas-discharge tubes for illumination purposes. They contain additional luminescent material (so called phosphors [44,45]) for the conversion of the 254 nm radiation to visible light, for example, modern fluorescent energy-saving lamps. However, mercury is a toxic element and therefore the disposal of fluorescent lamps is hazardous and dangerous for the environment and human health.* Fortunately, the development of mercury-free excilamps led to new developments and prospects in these fields of R&D. Further, it opened up novel possibilities of applications in emerging scientific areas like nanotechnology, photolithography, photochemical vapor deposition (photo-CVD), modification of surface properties, or contact-free surface cleaning.

2.2.1 Plasma Displays and Artificial Lighting

During the past decade, the sales of AC plasma displays (PDPs) emerged as a multibillion market [46–48]. PDPs are used as large flat television screens, which also can generate three-dimensional (3D) images [49] by the field-sequential technique. They utilize the radiation emission of noble gas excimers (usually a Xe/Ne mixture) at high partial pressure that are produced in microstructured stripe barrier rips [48] by DBDs. The VUV radiation excites red, green, and blue luminescent phosphors that are located within the ribs and that convert the VUV radiation to visible light via photophysical mechanisms. Conventional PDPs use Zn_2SiO_4:Mn^{2+} or YBO_3:Tb^{3+}, (Y,Gd)BO_3:Eu^{3+} or Y(V,P)O_4:Eu^{3+}, and $BaMgAl_{10}O_{17}$:Eu^{2+} (barium magnesium aluminate (BAM [50,51]) to produce green, red, and blue colors, respectively [49]. These energy transfer mechanisms are under active investigation.

It is of utmost environmental interest to develop powerful mercury-free lighting systems that use the Xe_2^* excimer fluorescence followed by conversion to visible light applying selective phosphors. One of the first outcomes of intensive R&D in this field was the development of the flat panel lamp PLANON®† based on the DBD technology using xenon as excimer gas. This tile-like lamp has a maximum visual area of 320 × 320 mm and a thickness of only 10 mm. It exhibits a constant and bright and high luminance over the whole area, and a long lifetime. Therefore, it is unprecedentedly qualified for backlighting of LCD displays [19] that are used, for example, for GPS systems or for medical monitoring applications [52–54]. On the same basis, the development of the tubular lamp system Linex®‡ was described recently. This lamp generation represents an important milestone for the future application of mercury-free luminescent excilamp systems in general lighting [2]. Its fast response without any warm-up phase makes it ideally suitable for application in scanners, fax, and photocopy machines.

The main problems of the satisfactory development of luminescent excilamp systems for use as powerful lighting devices or as PDPs are directly related to the stability, absorption, and emission characteristics of the kind of luminescent material used. Up to date, most UV-emitting phosphors (e.g., BAM) have been optimized for excitation by the 254 nm line of low-pressure mercury fluorescence. However, recently Guivan et al. [55] reported on experimental results concerning the excitation of green, red, and blue phosphors by XeI* excilamp radiation.

The Xe/Ne plasma discharge generates high-energy photons (λ = 147 and 172 nm) that cause degradation reactions and color shifts of BAM. Thus, main challenges of future research concentrate on the optimization of

* http://www.mercury2009.org (latest access: 12/06/2009).

† http://www.osram.ch/_global/pdf/osram_de/produkte/display_optic/planon/PLANON_TechnikInfos.pdf (latest access: 12/06/2009).

‡ http://www.osram.com/_global/pdf/Professional/Display_Optic/Display_Systems/123D005GB_PI_LINEX.pdf (latest access: 12/06/2009).

the phosphors for use under VUV excitation. An intensive search for VUV-stable phosphors is still in progress. For example, a promising candidate as a blue-emitting phosphor is $Ba_5SiO_4Cl_6:Eu^{2+}$ [56], with its maximum of emission at 440 nm. A thulium cation–doped lanthanum phosphate phosphor (LPTM, $LaPO_4:Tm^{3+}$) exhibits a narrow band emission with its maximum at $\lambda = 452$ nm and several additional bands in the UV region of the electromagnetic spectrum [57]. The emission spectra of this material were studied by excitation with a Kr_2^* and a Xe_2^* excilamp, respectively. LPTM showed much higher stability against VUV-induced degradation compared to BAM. An europium cation–doped barium aluminate ($BaAl_2O_4:Eu^{2+}$) phosphor [58] exhibited a broad emission band between 425 and 650 nm, peaking at 500 nm under 172 nm excitation. Recently, Yuan et al. [59] investigated the VUV spectroscopic properties and the emission characteristics of a series of lanthanide cation–doped alkali rare earth diphosphates of the type $AREP_2O_7:Ln^{3+}$ (A: Na, K, Rb, Cs; RE: Y, Lu, La, Gd; Ln^{3+}: Ce, Pr, Tb, Eu, Tm). As a result of this study, they demonstrated that Tb^{3+}-doped $NaREP_2O_7$, with RE being La or Gd, are potential candidates for green PDP phosphors under excitation by 172 nm. For 3D PDPs, short decay times of the phosphors and bright luminescence are essential. Thus, Zang et al. [49] presented a series of short-decaying phosphors of the types $Y_3Al_5O_{12}:Ce^{3+}$ (green), $(Y,Gd)Al_3(BO_3)_4:Tb^{3+}$ (green), and $(Y,Gd)_2O_3:Eu^{3+}$ (red), enabling for the first time switchable 3D/2D PDP television. The conversion of 172 nm radiation by UV-C emitting phosphors to germicidal radiation is also under active investigation [60]. Considerable research interests have focused on the so-called quantum cutting (QC) process (e.g., [61]). In this process, the absorption of a single VUV photon by the phosphor results in a cascade emission of two photons of lower energy (down conversion) [45]. Since the energy of a VUV photon is more than twice the energy of a visible photon, it should be possible to obtain two visible photons for each VUV photon absorbed. Special phosphors (two-photon phosphors) utilizing this effect are under development. Quantum efficiencies close to 200% have already been demonstrated with red ($LiGdF_4:Eu^{3+}$) and green ($K_2GdF_5:Tb^{3+}$) phosphors [62,63]. The combination of using efficient Xe_2^* excimer radiation with quantum cutting phosphors could further improve the efficiency of mercury-free fluorescent lamps and plasma displays.

2.2.2 Photomedicine

The mechanistic aspects, photochemical and photobiological effects of phototherapy and of photochemotherapy are areas of modern research in photoscience [64]. Sunlight therapy for skin diseases, for example, psoriasis, alopecia areata, vitiligo, atopic dermatitis, and eczema, has been applied empirically since antiquity [65]. Psoriasis is a skin condition that is characterized by red, scaly plaques covered with silvery scales. Alopecia areata is a disease that causes round patches of hair loss. Vitiligo describes a leucodermal condition, that is, white areas of skin from congenital or acquired absence or loss of melanin pigmentation. Phototherapy or photochemotherapy (i.e., psoralen + UVA, PUVA-therapy) for the treatment of such diseases use conventional medium-pressure mercury lamps with or without metal halide additives and/or optical filter systems, or mercury containing fluorescent tubes like the Philips TL01. The latter lamp emits a narrow band of UVB radiation around 311–312 nm [65]. In modern phototherapy, 308 nm xenon excimer lasers are successfully applied for the treatment of localized psoriasis [66]. However, recently a research group [67] of Osram Sylvana Inc. described a novel Xe_2^* excilamp with a gadolinium cation–doped strontium magnesium aluminate phosphor ($Sr(Al,Mg)_{12}O_{19}:Gd^{3+}$) that emits a narrow band of UVB radiation with its maximum at 310 nm. Thus, this fluorescent excilamp seems ideally suited for UVB phototherapy. In addition, since several years the XeCl* excilamp with its emission maximum at 308 nm is extensively evaluated for these purposes [68,69]. It is applied in novel dermatological instruments called Excilite* (DEKA, Italy) [70] or VTRAC† (PhotoMedex, USA), which are under active investigation [71–77]. In fact, spectral measurements of the XeCl* excilamp demonstrated that 50% of its radiant energy is located between 306 and 309.5 nm, whereas 90% is delivered by a narrow band between 298 and 312 nm [68]. An advantage of this XeCl* excilamp apparatus over expensive laser systems is the possibility of treatment of large areas [78] of up to 504 cm^2 with a high irradiance of

* http://www.dekalaser.com/uploaded/pr1/25ENG.pdf (latest access: 12/06/2009).
† http://www.photomedex.com/product.php?pid=131 (latest access: 12/06/2009).

50 mW cm^{-2}. This situation is accompanied by a significant shortening of the patient's sessions. Thus, perhaps the long-term risk of UV-induced carcinogenicity can be reduced significantly.

2.2.3 Surface Modification

VUV/UV irradiation of polymers is interesting for fundamental and applied sciences [79,80], materials processing [81], and nanofabrication technologies [82]. For example, polymeric materials are used as photoresists in semiconductor technology in combination with VUV radiation. Further, polymers are widely used in spacecraft technology. Thus, they are exposed to solar VUV/UV radiation in space and undergo specific photo-induced degradation reactions, for example, mass loss by ablation or etching. In addition, modern research concentrates on the VUV-induced modification of surface properties of polymers that are used extensively in medicine or biology to enhance their biocompatibility.

2.2.3.1 Biomaterials

Already in 1998, Cezeaux et al. [83] demonstrated that the VUV irradiation of expanded poly(tetrafluoro ethylene) (ePTFE Teflon) vascular grafts using an excilamp provides a better surface for endothelial cell proliferation. However, no effect of VUV treatment of the polymer on cell adhesion was observed. It is also possible to chemically modify polymer surfaces by the combined treatment with VUV photons and a reactive gas atmosphere [84]. Thus, the adhesion of smooth muscle cells from human aorta [85] and of human endothelial cells [86] on PTFE could be significantly enhanced by 172 nm irradiation with a Xe_2^* excilamp under an ammonia (NH_3)-containing atmosphere. This result is due to the creation of new polar functional groups (–C–NH_2, –C=O, –C–OH, –C–OOH) on the surface of the polymer by photochemically induced cleavage of C–F bonds followed by incorporation of N and O atoms. The changes of the surface structure of the PTFE sample were analytically established by x-ray photoelectron-, UV-Vis-, IR-spectroscopy, secondary ion mass spectrometry [86], and laser-induced fluorescence measurements [84,87]. It was also demonstrated that the VUV/NH_3 treatment of PTFE led to an enhanced surface polarity of the sample, which is correlated with its wettability by water. Contact angle measurements of water on the VUV/NH_3-treated PTFE surface verified this result. Additionally, grafting of the PTFE surface with amino acids directly after the VUV/NH_3 treatment supports the adhesion and proliferation of aortic smooth muscle cells and mouse 3T3 fibroblasts [87]. Thus, the VUV/NH_3-modified or amino acid–grafted PTFE was proposed as useful material for vascular prostheses [86] or for percutaneous implants or substrates for skin cultivation [88]. Similar techniques were used by Olbrich et al. [89] to improve the cytocompatibility of a novel nanocomposite polymer material that may have applications in tissue engineering. Interestingly, Mikulikova et al. [90] could produce cell microarrays on PTFE after VUV/NH_3 processing through thin nickel contact masks with holes of a diameter of only 100 μm and seeding of the cells on the surface. The cell adhesion and proliferation occurred only on the photochemically modified spots. This procedure may be useful for microarray techniques in advanced genomics and proteonomics [90].

Hozumi et al. [91] described a method for the spatially defined immobilization of bovine serum albumin (BSA) onto a microstructured surface of poly(methyl methacrylate) (PMMA). This was achieved after the VUV-initiated ablation of PMMA through a photomask using a Xe_2^* excilamp with generation of microwells of a depth of less than 400 nm and a diameter of less than 20 μm. The wells could be selectively filled with an aminosilane, which increases the bioaffinity to BSA. Catalase from bovine liver functionalized with an allyl group could be successfully immobilized on poly(ethylene terephthalate) after irradiation of the polymer with a KrCl* excilamp [92].

2.2.3.2 Polymers

VUV photons are eligible for the treatment of polymer surfaces at low process temperatures [93]. The penetration depth of VUV photons into the polymer material is low due to the high absorbance of the latter. Thus, the bulk of the irradiated polymer is not affected by VUV radiation and morphological and chemical changes are limited to the surface of the material [30]. These changes are initiated by homolytic bond cleavages with formation of radicals or other transient species in the surface layers of the polymeric substrate. Table 2.3

TABLE 2.3 Examples of Treatment of Polymer Surfaces with Excilamp Radiation

Polymer Material	Excilamp Used	Analytical Methods[a]	Effects Observed	References
Fabrics: Acetate, Nylon 6, PET[b], Acrylic, PP[c]	Xe_2^*/air	CAM, CWM, MAM, SRM	Increase of wettability, improvement of serviceability properties	[96]
LDPE[d], BOPP[e], PS[f], PMMA[g]	Kr_2^*, Xe_2^* NH_3 atmosphere	QCM, XPS, ATR-FTIR	VUV absorption spectra, ablation, incorporation of N atoms	[94,97]
Mulberry silk fabric	Xe_2^*	CAM, AFM, SEM	Enhanced hydrophilicity, wickability	[98,99]
PC[h]	Xe_2^*	AFM, XPS, TR-IR	Increasing roughness, chemical degradation	[100]
PE[i], PS[f], PVA[j]	Xe_2^*/N_2, air	CAM, XPS, IR	Chemical changes, degradation, wettability	[101]
PET[b]	KrCl*/1,5-hexadiene, perfluoro-4-methyl-pent-2-ene, polyethylene glycol 200, monosilane, polyethylene, methane	CAM, XPS, AFM, FTIR, SEM, PA-FTIR	Grafting, formation of thin films, chemical changes, coloration with dyes	[95,102]
PET[b]	Xe_2^*/1-octene, *n*-nonane, heptafluorodecene	XPS, ToF/SIMS, AFM, CAM, DSC	Grafting	[103]
PET[b]	Xe_2^*	XPS, ToF/SIMS, AFM	Enhanced roughness, decrease of O/C ratio, generation of mass fragments	[104]
PI[k]	Ar_2^*, Xe_2^*	SEM, AFM, XPS	Increasing roughness, degradation	[105]
PMMA[g]	Ar_2^* (windowless)	IR, EPR, XPS, SEM, WLRS, SHG, CAM,	Etching, ablation, degradation of surface residues, activation, change of permeability, control of wettability	[30,106]
PMMA[g]	Xe_2^*	CAM	Etching, ablation, formation of microwells	[107]
PP[c]	Xe_2^*/N_2/O_2	XPS	Etching, electroless plating of Pd/Sn films, adhesiveness	[108]
PS[f]	Xe_2^*/O_3	ATR-FTIR, OM, AFM, FLS, CAM, GC/MS of washing solutions	Microstructuring, oxidative functionalization, chemical changes	[109,110]
PS[f]	Xe_2^*/air	CAM, XPS, AFM,	Wettability, chemical changes, increase of O/C ratio, photooxidation, etching, hydrophilic stability	[111]

(*continued*)

TABLE 2.3 (continued) Examples of Treatment of Polymer Surfaces with Excilamp Radiation

Polymer Material	Excilamp Used	Analytical Methods[a]	Effects Observed	References
PS[f] submicron particles, aerosol	$Xe_2^*/O_2/O_3$, gas phase	ATR-FTIR, SMPS	Surface functionalization (–OH, –CO), diminution of particle size and concentration by degradation	[112]
PTFE[l]	Xe_2^*	XPS, SIMS	Enhanced adhesive properties	[113,114]
PTFE[l]	Kr_2^*, Xe_2^* NH_3 atmosphere	CAM, ATR-FTIR, XPS, SIMS	Increase in hydrophilicity, incorporation of N atoms	[84,115]
SiOCH-layers	Xe_2^*, KrCl*	ToF/SIMS, FTIR, XRR, laser-SAW, PUVSE	Curing, porogen removal	[116]

Abbreviations:

[a] AFM, atomic force microscopy; ATR-FTIR, attenuated total reflectance Fourier transform infrared spectroscopy; CAM, contact angle measurement; CWM, capillary wetting measurement; DSC, differential scanning calorimetry; EPR, electron paramagnetic resonance spectroscopy; FLS, fluorescence spectroscopy; FTIR, Fourier transform infrared spectroscopy; GC/MS, gaschromatography mass spectrometry; IR, infrared spectroscopy; MAM, moisture absorption measurement; OM, optical microscopy; PA-FTIR, photoacoustic FTIR; PUVSE, purged UV spectroscopic ellipsometry; QCM, quartz crystal microbalance; laser-SAW, laser-induced surface acoustic waves spectroscopy; SEM, scanning electron microscope; SHG, surface hydroxyl groups, determination by reaction with trifluoroacetic anhydride; SIMS, secondary ion mass spectrometry; SMPS, scanning particle mobility sizer; SRM, surface reflectance measurement; ToF/SIMS, time-of-flight secondary ion mass spectrometry; TR-IR, total reflection-IR; WLRS, white light reflection spectroscopy; XPS, x-ray photoelectron spectroscopy; XRR, x-ray reflectrometry.

[b] Poly(ethylene terephthalate), Mylar®.

[c] Polypropylene.

[d] Low-density polyethylene.

[e] Biaxially oriented poly(propylene).

[f] Polystyrene.

[g] Poly(methyl methacrylate).

[h] Polycarbonate.

[i] Polyethylene.

[j] Poly(vinyl alcohol).

[k] Polyimide.

[l] Poly(tetrafluoroethylene).

summarizes significant contributions to this field of research. The extent of ablation (etching), for example, depends strongly on the absorbance characteristics of the polymer and the intensity and the wavelength of the impinging VUV radiation [94]. Of special interest in materials processing are methods of grafting a surface by photochemical generation of active sites on the polymer followed by exposure to gaseous reagents [95].

2.2.4 Surface Cleaning

VUV-induced cleaning of materials, for example, glasses for the manufacturing of liquid crystal displays (LCDs), mirrors for space applications, reticles used for photolithography, or silicon (Si) wafers used for semiconductor manufacturing can easily be performed by use of VUV excilamps, normally in Ar with traces of O_2 and H_2O. The mechanisms of this process for the removal of residual organic contaminants on the surface of a substrate include direct VUV photolysis of the organic matter, which is accompanied by formation of a highly oxidative atmosphere induced by photolysis of oxygen and water vapor, and further by photolysis of ozone. This atmosphere contains a series of reactive oxygen species ($O(^1P)$, $O(^1D)$, •OH, O_3). Thus, the chemical reaction scheme of advanced oxidation of hydrocarbons on surfaces was outlined by Falkenstein [117]. The complete oxidation of the organic matter results in the products H_2, H_2O, CO, and CO_2, which are removed by the carrier gas stream. Tode et al. [118] used

the direct irradiation of Si wafers with the VUV radiation of an Ar_2^* excilamp to remove surface-bound hydrocarbons in an argon atmosphere. Organic contamination on the surface of Si wafers could be eliminated by exposure to a Xe_2^* excilamp under ambient air conditions [119]. Alkyl monolayers on p-type Si wafers were decomposed by irradiation with a Xe_2^* excilamp [120]. Similarly, oxygen atoms could be removed from an oxidized silicon surface (SiO_2) on a Si wafer in a vacuum chamber using an Ar_2^* excilamp, thus enabling ultraprecise SiO_2 processing with formation of elemental Si [121]. On the other hand, silicon was oxidized with formation of SiO_2 dielectric films by Ar_2^* excilamp irradiation in the presence of O_2 [122].

2.3 Process Technologies

A large variety of modern technological applications use polymers or polymer-based materials covered by thin films of metals or dielectrics, for example, solar cell structures, printed circuit boards, silicon and semiconductor microelectronics, and optoelectronics. Thus, the demand for low-temperature processing of these polymers is evident. Consequently, excilamps are especially qualified for photo-CVD, UV curing, and photolithographic processes.

2.3.1 Photo-CVD

Metallic or nonmetallic thin films on various substrates may be produced by photo-induced chemical vapor deposition (photo-CVD) [123–125]. Already in 1989, Esrom et al. [126] demonstrated the deposition of palladium layers on Al_2O_3 or quartz by 172 nm irradiation of palladium acetate films using a Xe_2^* excilamp. Table 2.4 summarizes some recent developments in this area of research.

TABLE 2.4 Recent Examples of Photo-CVD Using Excilamp Radiation

Substrate	Precursor	Excilamp Used	Network Produced	Reference
Glass	Silicon	Xe_2^*/dry air	SiO_2	[127]
n-type Si(100) wafers	MPEOPS[a]	Xe_2^*	PEG[b]-based monolayer	[128]
n-type Si(100) wafers	ODS[c], FAS[d], CMPhS[e], AphS[f]	Xe_2^*	Organosilane self-assembled monolayers	[129]
PET[g]	P(DMS*co*MS)[h] P(MS*co*MVS)[i]	Xe_2^*, KrCl*	$H_3C–Si–O–Si–$	[130]
p-type Si(001) wafer	—	Ar_2^*, Xe_2^*, KrCl*/O_2	Ultrathin SiO_2 film	[131]
Si wafers	SiH_4/O_2, H_2O/O_2, H_2O_2	Xe_2^*	SiO_2	[132]
Si(100) wafers, quartz	Palladium acetate	Xe_2^*	Pd^0 films and nanoparticles	[133]
Si(100) wafers	$Ti(OC_3H_7)_4$[j]	Xe_2^*	TiO_2 films	[134]
Silver nanoparticles	TEOS[k]	Xe_2^*	SiO_2	[135]

Abbreviations:
[a] 2-(methoxypoly[ethyleneoxy]propyl)trimethoxy-silane.
[b] Poly(ethylene glycol).
[c] Octadecyltrimethoxy-silane.
[d] Heptadecafluoro-1,1,2,2-tetrahydro-decyl-1-trimethoxy-silane.
[e] (*p*-Chloromethyl)phenyltrimethoxy-silane.
[f] (*p*-Aminophenyl)trimethoxy-silane.
[g] Poly(ethylene terephthalate).
[h] Poly(1,1-dimethylsilazane-*co*-1-methylsilazane).
[i] Poly(1-methylsilazane-*co*-1-methyl-1-vinylsilazane).
[j] Titanium(IV) isopropoxide.
[k] Tetraethylorthosilicate.

2.3.2 UV Curing and Photolithography

UV curing of polymeric precursors is a typical part of "green" technology that uses photons of distinct energy for initiation of polymerization. A large variety of UV-curable materials, for example, inks, coatings, and adhesives, are available on the market. Research activities try to increase the curing efficacy, increase the speed of the process, and improve the physical-chemical properties of the curables. The use of excilamps in printing processes for UV curing was established by Mehnert [136]. A powerful XeCl* excilamp with a maximum irradiance of 200 mW cm^{-2} was used in this study to cure offset inks with medium- to high-cure speed and without thermal stress for the material [32]. The lamp was developed by Heraeus Noblelight (Germany) [137]. Recent research focused on the radiation-induced polymerization of acrylates using a KrCl* excilamp [138] without addition of any photoinitiator. Consequently, this process was scaled up by using a KrCl* excilamp with an electrical input power of 10 kW and an irradiance of 175 mW cm^{-2} [139]. On the other hand, a new reaction concept was recently reported by Silvares et al. [140]. This research group validated a photoreaction system that applies a pulsed XeCl* excilamp for the production of prepolymer methyl metacrylate (MMA) of low polydispersity by photochemically initiated polymerization using benzoin as the photoinitiator. From a series of experiments, they concluded that the pulse frequency of the XeCl* excilamp is an important factor for the polydispersity and the rate of production of the prepolymer MMA material. Photochemical matt finishing of acrylate coatings using a dual-lamp setup consisting of a Xe_2^* excilamp and a medium-pressure mercury lamp was described by Bauer et al. [141]. This technique produced a very natural optical appearance of the coating. Therefore, it seems to be predestinated for the finishing of durable parquet or PVC flooring.

Chip manufacturing relies on the development of photolithographic methods. The optical resolution (R) of these techniques is defined by the Rayleigh equation ($R = k_1 \times \lambda/NA$, NA: numerical aperture). Thus, as the wavelength of the radiation applied decreases, the optical resolution on a wafer decreases significantly. For example, Xe_2^* excilamps have been used for submicrometer patterning of photoresist films [142], monolayers of alkyl- and fluoroalkylsilanes on Si wafers [143,144], monolayers of chloromethylphenylsiloxane (CMPhS) [145], and polystyrene surfaces [110] and for the microfabrication of metal oxide films on polymer substrates [146,147].

2.4 Analytical Photochemistry

Trends of applications of excilamps as radiation sources in analytical instruments and of actinometric procedures for the measurement of their photon flux were summarized by Oppenländer [148]. Recent developments include the use of an Ar_2^* excilamp for the soft single photon ionization of organic molecules in an orthogonal acceleration time-of-flight mass spectrometer (oaToFMS) [149]. Batalova et al. [150,151] and Noskova et al. [152] reported on the use of XeBr* and KrCl* excilamps for the photochemical pretreatment of foodstuffs or urine to quantitatively determine the Hg^{2+} or the iodine content by polarographic analyses. Batalova et al. [153] also described an electrochemical version of the well known ferrioxalate actinometer [154] for the measurement of the photon fluxes of a KrCl* and a XeBr* excilamp. Sosnin et al. [155] presented an electrochemical version for the quantitative determination of the concentration of formaldehyde using the known methanol actinometer [156,157] in the photolysis of water with a Xe_2^* excilamp at 172 nm. Bark et al. [158] used the amount of H_2O_2 formed by irradiation of pure water for the calculation of the photon flux of their lamp system at wavelengths below 190 nm. Shen et al. [159] recently presented a model for the measurement of germicidal UV radiation of KrCl* and XeBr* excilamps in photoreactors by applying the photoconversion of (E)-5-[2-(methoxycarbonyl)ethenyl]cytidine to the violet fluorescent product 3-β-D-ribofuranosyl-2,7-dioxopyrido[2,3-*d*]pyrimidine. The concentration of the photoproduct was quantitatively monitored by fluorescence spectroscopy.

Actinometry with production of ozone by irradiation of oxygen with a Xe_2^* excilamp was applied by Laszlo et al. [160]. Recently, this method was optimized for the measurement of incident 172 nm

photons in an experimental setup used for aerosol functionalization [112]. In their experiments, Vicente et al. [112] reported that the generation of the photostationary O_3/O_2 composition was independent of the addition of H_2O using their Xe_2^* excilamp configuration. However, this result is in strict contrast to the work reported by Salvermoser et al. [161,162]. This group demonstrated a significant influence of trace amounts of water during 172 nm irradiation of oxygen in air on the stationary state concentration of ozone. Presumably, the formation of hydroxyl radicals (HO•) and of hydroperoxyl radicals (HO_2•) by 172 nm photolysis of water vapor initiates a catalytic cycle of O_3 destruction. These results were verified by a quantitative kinetic model that describes the influence of humidity on the photochemical production of O_3 [162]. The 172 nm photolysis of dry air yields very clean O_3 with high yield and without any NO_x impurities. Consequently, several sustainable applications of these novel Xe_2^* excilamp ozone generators for sterilization or odor control in food storage were proposed [162].

2.5 Synthetic Photochemistry

Unfortunately, the enormous potential of excilamps in synthetic photochemistry is still limited to some practical examples that were demonstrated by Griesbeck et al. [163,164] and Oelgemöller [165]. These authors concentrated on the use of a powerful XeCl* excilamp (electrical input power $P_{el}^{in} = 3$kW) in a falling film photoreactor. They performed photodecarboxylations, [2 + 2]-photocycloadditions, and Type III photooxygenations with high yields and isolation of gram quantities of photoproducts. On the other hand, industrial photochemical engineering successfully established the use of a XeBr* excilamp for the technical synthesis of Vitamin D3 by photolysis of 7-dehydrocholesterol [166] (see also [148]). An interesting paper from Terasaki et al. [167] deals with the photosynthesis of trace amounts of aspartic acid by 172 nm irradiation of an aqueous solution of urea and maleic acid. This is probably the first contribution of excilamp VUV photochemistry to studies elucidating the mechanisms of the formation of biomolecules on the primitive earth, that is, a contribution to prebiotic chemistry dealing with origin of life studies.

2.6 Destructive Photochemistry

In contrast to photochemically induced synthesis of complex structures, destructive photochemistry uses the energy of VUV or UV radiation to initiate the change or destruction of structural entities like organic molecules in water or air, or to inactivate microorganisms in these media. Several books describe the enormous efforts in advanced oxidation processes (AOPs) and advanced oxidation technologies (AOTs) [168–171], and in UV-disinfection technologies [172] to gain insight into the different aspects of the underlying complex mechanisms. Interestingly, excilamps are still not yet part of industrial applications in this area, with one exception: Triton Thalassic Technologies, Inc. $(T^3I)^*$ claims the development of an almost monochromatic light source for applications in the industrial UV disinfection of fluids [173]. This lamp possibly resembles a XeBr* [174,175] excilamp.

2.6.1 Surface Disinfection

Infection control by surface treatment is of utmost importance for public health in hospitals, vehicles, and public transportation including airplanes. Heise et al. [176] described a hybrid process by combination of flat KrCl* or XeBr* excilamps and a reactive DBD plasma to successfully inactivate spores of *Bacillus subtilis* and *Aspergillus niger* on PET foils. Similarly, Christofi et al. [177] reported the UV inactivation of *Staphylococcus aureus*, *Streptococcus pyogenes*, *Bacillus subtilis*, and *Aspergillus awamori*

* http://t3i-uv.com/uv.html (latest access: 12/06/2009).

spores, and clumps of *Mycobacterium phlei* deposited on membrane filters using a XeBr* excilamp. The energy needed to kill 99.9% (log 3 reduction) of film populations (3.4×10^5 to 9.5×10^5 colony forming units (CFU)/cm^2) were 22, 18, 47, 387, and 27 mJ cm^{-2}, respectively.

2.6.2 UV Disinfection

UV-disinfection techniques rely on the damage of the DNA [178] of microorganisms by absorption of germicidal UV radiation (200 nm < λ < 300 nm) [172,179]. As a consequence, the microorganisms cannot replicate and thus cannot cause disease [180]. Recently, DNA damage was directly detected by an approach based on polymerase chain reaction (PCR) [181] during standardized UV disinfection with low-pressure mercury lamps. Several recent studies applied modern excilamps for UV-disinfection of aqueous media using various indicator microorganisms. One of the most widely studied candidates for this purpose is the XeBr* excilamp [175,182–187]. Its emission maximum is bathochromically shifted from the absorption maximum of DNA (λ_{max} = 260–265 nm [188]) by several nanometers. Fortunately, it also exhibits a hypsochromic tailing down to 260 nm [185]. The maximum germicidal effectiveness of UV-C radiation is located around 260 nm [172]. Thus, the efficiency of inactivation of microorganisms with a XeBr* excilamp compares to that of a low-pressure mercury lamp (λ = 253.7 nm). Several recent studies deal with the effect of 222 nm radiation of KrCl* excilamps on microorganisms [189–192] or on enzyme systems [193]. Two separate studies demonstrated the effect of short wavelength UV-C radiation on microorganisms using a KrBr* excilamp [194] and the iodine atomic emission of an I_2^* excilamp at 206 nm [195]. Wang et al. [196,197] compared the effectiveness of a Xe_2^* and a KrCl* excilamp to that of a low-pressure mercury lamp on *Bacillus subtilis* spores. They found that the 222 nm radiation was more effective for the inactivation of *B. subtilis* spores than 254 and 172 nm. The two log reductions (i.e., by 99%) of *B. subtilis* required fluences of 21.6, 40.4, and 870 mJ cm^{-2} at these individual wavelengths, respectively. The VUV exposure at 172 nm is much less efficient than at 222 and at 254 nm. This is due to a completely different mechanism that is active in 172 nm irradiation of water. Due to the high absorbance of water at this wavelength, only water absorbs the incident VUV radiation of the Xe_2^* excilamp, which leads to homolytic cleavage of water molecules and subsequent formation of •OH radicals and hydrogen atoms (see Section 2.6.3). The latter are immediately scavenged by dissolved molecular oxygen with formation of hydroperoxyl radicals (HO_2•) that enter the oxidative radical cycle. Thus, in the case of the Xe_2^* excilamp, the inactivation of *B. subtilis* spores seems to be due to the highly oxidative conditions of the radical species cocktail that is generated by water photolysis. However, this process of *B. subtilis* inactivation is inefficient in comparison to the photochemical reactions of DNA and of other cell components at 254 and 222 nm irradiation. Interestingly, *B. subtilis* spores did not show any inactivation under conditions of the H_2O_2-UV AOP [198]. Psychrophilic and mesophilic microorganisms of an opaque graywater were sensitive to VUV and UV radiation from Xe_2^* and KrCl* excilamps [199].

2.6.3 Advanced Oxidation Processes

In 1987, Glaze et al. [200] introduced the term advanced oxidation processes (AOPs). It refers to the oxidation of contaminants in water or air that relies on the formation and reactivity of hydroxyl radicals (HO•). Several reviews describe the underlying hydroxyl radical–induced mechanisms of AOPs [201–207]. The understanding of the mechanisms of AOPs may be improved significantly by distinct modeling of the kinetic regimes that are involved [208,209]. In recent years, many experimental studies demonstrated the enormous potential of excilamps in AOPs. Especially, the complex reaction scheme that is initiated by water photolysis (H_2O-VUV, Reactions 1, 2; Table 2.5) at 172 nm with Xe_2^* excilamps was investigated comprehensively during the past two decades. The results of these investigations were reviewed and critically judged by Gonzalez et al. [210]. Hydroxyl radicals are short-lived, highly reactive, and nonselective powerful oxidants. They exhibit electrophilic

TABLE 2.5 Some Relevant Reactions Leading to *Oxidation* and *Mineralization* of Organic Substrates by 172 nm Irradiation of Aqueous Solutions with a Xe_2^* Excilamp and the Corresponding Second-Order Rate Constants of Elementary Reactions

Reaction	Quantum Efficiencies (Φ) or Rate Constants (k)
(1) $H_2O + h\nu_{VUV} \longrightarrow H_2O^* \longrightarrow H\bullet + \bullet OH$	$\Phi(\bullet OH) = 0.42$[a]
(2) $H_2O + h\nu_{170-200\,nm} \longrightarrow H_2O^* \longrightarrow H^+ + \bullet OH + e^-_{aq}$	$\Phi(e^-_{aq}) = 0.05$[b]
(3) $RH_{saturated} + \bullet OH \longrightarrow R\bullet + H_2O$ (substrate oxidation: hydrogen abstraction)	[c]
(4) $RH_{unsaturated} + \bullet OH \longrightarrow (RHOH)\bullet$ (substrate oxidation: electrophilic addition)	[c]
(5) $H\bullet + {}^3O_2 \longrightarrow HO_2\bullet$ (scavenging of hydrogen atoms)	$1.2 \times 10^{10}\,M^{-1}\,s^{-1}$ [d]
(6) $e^-_{aq} + {}^3O_2 \longrightarrow O_2^{\bullet -}$ (scavenging of hydrated electrons)	$1.9 \times 10^{10}\,M^{-1}\,s^{-1}$ [d]
(7) $R\bullet + {}^3O_2 \longrightarrow R\text{-}O_2\bullet$ (scavenging of carbon-centered radicals)	[c]
(8) $(RHOH)\bullet + {}^3O_2 \longrightarrow (RHOH)\text{-}O_2\bullet$ (scavenging of carbon-centered radicals)	[c]
(9) $R\text{-}O_2\bullet + R\text{-}O_2\bullet \longrightarrow R\text{-}O\text{-}O\text{-}O\text{-}O\text{-}R$ (formation of intermediary tetroxides)	[c,e]
(10) $R\text{-}O\text{-}O\text{-}O\text{-}O\text{-}R \longrightarrow R_2C{=}O, RCHO, R_2CHOH + \cdots$ (decomposition of tetroxides)	[c,e]
(11) $R\text{-}O_2\bullet, (RHOH)\text{-}O_2\bullet + nO_2 \rightarrow\rightarrow\rightarrow\rightarrow CO_2 + H_2O + \cdots$ (mineralization)	$>10^9\,M^{-1}\,s^{-1}$ [e]
(12) $R\bullet + R\bullet \longrightarrow R\text{-}R$ (recombination of carbon-centered radicals)	[c]
(13) $\bullet OH + \bullet OH \longrightarrow H_2O_2$ (recombination of hydroxyl radicals)	$5.5 \times 10^9\,M^{-1}\,s^{-1}$ [d]

Note: A Comprehensive Discussion is Presented by Gonzalez et al. [203,210].

[a] Heit et al. [156].

[b] Hart and Anbar [220].

[c] These rate constants are dependent on the molecular structure of the radicals and intermediates but often they are in the order of diffusion control.

[d] http://kinetics.nist.gov/solution/

[e] von Sonntag and Schuchmann [221].

character, are easy to produce, and are ubiquitous in nature. Most important, their reactivity is kinetically controlled (Table 2.5). Thus, as a rule of thumb, the overall rate of oxidation of a contaminant in water or air is approximately proportional to the second-order rate constant of the elementary reaction of hydroxyl radicals with this specific contaminant [204]. The second-order rate constants of hydroxyl radicals with many substrates are freely available on the Internet* or from Buxton et al. [211]. Some examples are summarized in Table 2.5. The reactivity of hydroxyl radicals toward organic substrates includes hydrogen abstraction (Reaction 3, Table 2.5) or electrophilic addition to double bonds (Reaction 4, Table 2.5) with the formation of carbon-centered radicals, and in some cases also electron transfer reactions [201]. Interactions of hydroxyl radicals with S-, N-, or P-atom containing functional groups in aqueous phase may lead to the formation of intermediary two center–three electron adducts [212]. These groups also affect the efficacy of hydrogen atom abstractions at adjacent carbon atoms [209]. Hydrogen atoms or solvated electrons formed by VUV photolysis of water are immediately scavenged by dissolved molecular oxygen (Reactions 5, 6; Table 2.5). A complex chain-like mechanism that involves the scavenging of carbon-centered radicals by dissolved molecular oxygen with formation of peroxyl radicals [213,214] (Reactions 7, 8, Table 2.5) leads to the formation of oxidized intermediary products like aldehydes, carboxylic acids, and alcohols. This series of reactions occurs on the way to the complete mineralization of the organic substrates (Reactions 9–12; Table 2.5). Hydroxyl radicals also efficiently recombine with formation of hydrogen peroxide (Reaction 13, Table 2.5). The concentration of H_2O_2 formed during 172 nm irradiation of contaminated water depends strongly on the nature of the organic contaminant that is present in water [215]. However, the efficacy of the oxidation of organic substrates (i.e., diminution of substrate concentration) or their mineralization (i.e., diminution of the total organic

* The Radiation Chemistry Data Center of The Notre Dame Radiation Laboratory; http://kinetics.nist.gov/solution/ (latest access: 08/22/2011).

carbon content, TOC) by VUV photolysis of aqueous reaction systems is extremely limited by the high absorbance A_λ of water below 190 nm. The linear absorption coefficient $\alpha_{172} = A_{172}/d$ of pure liquid water is 550 cm^{-1} [216] (d = optical pathlength or penetration depth). Due to the low penetration depth of 172 nm radiation into water, which is less than 100 µm, the photoreaction takes place in a tiny photoreaction volume at the quartz–water interface. The production of a high local concentration of hydroxyl radicals subsequently leads to a high local concentration of carbon-centered radicals according to Reactions 3 and 4 (Table 2.5). The scavenging of these carbon-centered radicals by dissolved molecular oxygen generates an oxygen deficit within the irradiated volume. As a consequence, the efficacy of the TOC diminution according to Reactions 7–11 (Table 2.5) is inherently low. It is strongly dependent on the concentration of O_2 in the radical reaction zone. Two solutions for this problem have been proposed: a combination of a Xe_2^* photochemical irradiation unit with an electrochemical reactor to produce oxygen within the irradiation zone by water electrolysis was described by Braun et al. [210,217]. A much simpler technical concept was introduced by Oppenländer et al. [40]. This group used an axially mounted ceramic oxygenator for the injection of molecular oxygen or air directly into the irradiated volume of the Xe_2^* excilamp flow-through photoreactor (see Figure 2.5A and B). With this simple reactor concept, the efficacy of the TOC diminution by 172 nm irradiation of contaminated water samples could be increased drastically [40]. The use of a static mixer electrode (SME, Figure 2.5A), which was axially centered within the water flow of a Xe_2^* flow-through photoreactor, had almost no influence on the TOC diminution kinetics. But the SME enhanced the efficacy of the substrate oxidation by about 20%–30% compared to a spiral metal wire electrode. The substrate decrease (i.e., the oxidation) and the TOC diminution (i.e., the mineralization) during 172 nm irradiation of solutions of Rhodamine B and of methanol were independent of the temperature of the water in the range from 20°C to 60°C [218]. The present results of VUV photolysis of water with Xe_2^* excilamps open up a miniaturization strategy of photoreactor design similar to that described by Coyle and Oelgemöller [219].

The problems of VUV water photolysis are in contrast to VUV photolysis of gaseous media (Reactions 14–20, Table 2.6) where the absorbance is much lower and the diffusion coefficients are much higher than in aqueous media. Some of the relevant 172 nm initiated reactions of gaseous media are summarized in Table 2.6.

The enormous progress of research in AOPs of aqueous and gaseous systems using the excilamp technology is illustrated by various examples presented in Table 2.7.

TABLE 2.6 Some Relevant Reactions during VUV Irradiation of Air[a]

Reaction	Quantum Efficiencies (Φ) or Rate Constants (k)
(14) $^3O_2 + h\nu_{<200\,nm} \rightarrow O(^3P) + O(^1D)$	$\Phi(-O_2) = 1.0$[b]
(15) $O(^1D) + H_2O \rightarrow 2\,{\bullet}OH$	2.2×10^{-10} cm^3 $molecule^{-1}$ s^{-1} [c,d]
(16) $^3O_2 + O(^3P) \rightarrow O_3$	2.8×10^{-12} cm^3 $molecule^{-1}$ s^{-1} [d]
(17) $HO_2{\bullet} + O_3 \rightarrow 2\,^3O_2 + {\bullet}OH$	2×10^{-15} cm^3 $molecule^{-1}$ s^{-1} [c,d]
(18) ${\bullet}OH + O_3 \rightarrow HO_2{\bullet}$[e] $+ {}^3O_2$	7.3×10^{-14} cm^3 $molecule^{-1}$ s^{-1}[d]
(19) $CO_2 + h\nu_{140-170\,nm} \rightarrow CO + O(^1D)$	$\Phi(CO) = 1.0$[f]
(20) $CO + {\bullet}OH \rightarrow CO_2 + H{\bullet}$	1.44×10^{-13} cm^3 $molecule^{-1}$ s^{-1} [d]

[a] Gas kinetic data, freely available at: www.iupac-kinetic.ch.cam.ac.uk/past_summary.html (latest access: 08/27/2009).

[b] See Bolton and Cater [202].

[c] c.f. Salvermoser et al. [161].

[d] Atkinson et al. [222–224].

[e] Second-order rate constants for gas phase elementary reactions of the hydroperoxyl radical with various substrates of interest were critically evaluated by Lloyd [225].

[f] Yang and Servedio [226], at λ = 147 nm.

TABLE 2.7 Selected Examples of Applications of Excilamp-Initiated AOPs in Aqueous and Gaseous Media

Substrate	Excilamp	Analytical Method[a]	References
1,1,1-Trichloroethane	Xe_2^*, Xe_2^* + KrCl*, KrCl*	TOC, GC/MS, IC: [Cl^-], GC/ECD, [H_2O_2], p.s.	[227,228]
1,1,2-Trichloroethane (groundwater sample)	Xe_2^*	GC/MS, p.s.	[229]
1,1,2-Trichlorotrifluoroethane	Xe_2^*, gas phase	GC	[230]
1,2,4-Trichlorodibenzo-*p*-dioxin	Xe_2^*, KrCl*	HPLC, GC/MS, p.s.	[231]
1,2-Dichloroethane	Xe_2^*	TOC, [Cl^-]	[232]
1,2-Dichloroethene (groundwater sample)	Xe_2^*	GC/MS, p.s.	[227]
1,2-Ethanediol	Xe_2^*	TOC	[233]
1-Butanol	Xe_2^*, gas phase XeCl* + TiO_2, gas phase	GC, IR, p.s. GC, IR, p.s.	[234]
1-Butylamine	Xe_2^*, gas phase XeCl* + TiO_2, gas phase	GC	[234]
2,4-Dichlorophenol	Xe_2^*, Xe_2^* + SME, KrCl* + H_2O_2, Cl_2^* + H_2O_2, XeBr*	TOC, HPLC	[39,229,233,235–238]
2-Amino-1-naphthalenesulfonate	KrCl* + H_2O_2	HPLC	[239,240]
2-Chlorodibenzo-*p*-dioxin	Xe_2^*, KrCl*	HPLC, GC/MS, p.s.	[231]
2-Propanol	Xe_2^*, gas phase	GC/MS, p.s.	[241]
3,4-Dimethoxynitrobenzene	XeCl*	UV/VIS	[242]
3-Amino-5-methylisoxazole	Xe_2^*	HPLC, IC, DOC, p.s.	[243]
4,4′-Diaminostilbene-2,2′-Disulfonate	KrCl* + H_2O_2	HPLC	[240]
4-Chloro-3,5-dinitrobenzoic acid	Xe_2^*	HPLC, IC, DOC	[244]
4-Chlorophenol	Xe_2^*, Xe_2^* + O_3, KrCl*, KrCl* + H_2O_2, XeBr*	HPLC, TOC, COD, UV/VIS, [Cl^-]	[232,233,238,245–251]
Acetic acid	Xe_2^*	TOC	[233]
Alcohols (C_1–C_3)	Xe_2^*, gas phase	GC, CO_2/CO ratio	[252]
Alcohols[b] (C_1–C_8)	Xe_2^*	TOC	[233]
Anatoxin-a	Xe_2^*	HPLC	[253,254]
Atrazine	Xe_2^*, KrCl*	GC/MS, HPLC, TOC, p.s., [NO_3^-], [NO_2^-], [NH_4^+], [Cl^-]	[255,256]
Azo dyes[c]	Xe_2^*	TOC, UV/VIS, GC, LC/MS	[257,258]
Benzoic acid	Xe_2^*	TOC, HPLC, IC	[40,210,259]
Bromate ion (BrO_3^-)	KrCl*	n.s.	[260]
Carbon dioxide	Xe_2^*, Kr_2^*, gas phase	FT-IR	[261]
Chlorinated ethenes[d]	KrCl*, gas phase	FT-IR, p.s.	[262]
Chlorophenols	XeBr*	HPLC/MS	[263]
Citric acid	Xe_2^*	HPLC, TOC, influence of O_2/N_2	[264]
Cresols, Amino-cresol	KrCl*, XeBr*, XeCl*	UV/VIS, FLS, bio-degradation	[265,266]
Cyanide (CN^-)	Xe_2^*	HPLC, IC, DOC, pH, p.s.	[243]

(*continued*)

TABLE 2.7 (continued) Selected Examples of Applications of Excilamp-Initiated AOPs in Aqueous and Gaseous Media

Substrate	Excilamp	Analytical Method[a]	References
Cyclopropane	Xe_2^*, gas phase	GC	[267]
Dimethylamine	Xe_2^*, gas phase	GC, GC/MS, FT-IR	[268]
Diphenyl-4-sulfonate	$KrCl^* + H_2O_2$	HPLC	[240]
Dissolved molecular oxygen	Xe_2^*	OSO	[269,270]
EDTA	$KrCl^* + H_2O_2$	HPLC	[240,271]
Fe(III)-EDTA	Xe_2^*, $KrCl^* + H_2O_2$	TOC, pH, $[O_2]$, ICP: $[Fe^{n+}]$, HPLC	[240,272]
Formaldehyde	Xe_2^*, $KrCl^*$, $Xe_2^* + KrCl^*$	[HCHO], TOC	[257]
Formic acid	Xe_2^*	TOC	[233]
Gallic acid	Xe_2^*	HPLC, TOC, influence of O_2/N_2	[264]
Galvanic waste water	Xe_2^*	TOC, $[Ni^{2+}]$	[273]
Ground water: PAH, Cyanide (CN^-)	Xe_2^*	[PAH], $[CN^-]$, pH	[274]
Hexacyanoferrate (II), Hexacyanoferrate (III)	Xe_2^*	UV/VIS	[275]
Humic acid	Xe_2^*, $KrCl^*/O_3$	TOC, ASV, FT-IR, exhaust gas analysis	[276,277]
Hydrogen bromide	$XeCl^*$, gas phase	UV/VIS	[278]
Hydrogen sulfide (H_2S)	I_2^*, gas phase	IC, $[H_2S]$, p.s.	[279]
Landfill leachate	$Xe_2^* + KrCl^*$	TOC	[36]
Methanol, Methanol + NO_3^-	Xe_2^*	GC, IC, HPLC, DOC, p.s., temperature effects	[156,157,218, 280,281]
n-Heptanol	Xe_2^*, O_2, air, N_2	GC, TOC	[40]
Nitrate (NO_3^-)	Xe_2^*	IC, GC, UV/VIS, p.s.	[282]
Nitrite (NO_2^-)	Xe_2^*	IC, GC, UV/VIS, p.s.	[282]
Nitrobenzene	Xe_2^*	UV/VIS, GC-TOF/MS, p.s.	[283]
Nitrogen dioxide (NO_2)	Xe_2^*, gas phase	FT-IR	[284]
Organic dyes[e]	Xe_2^*, $KrBr^*$	UV/VIS, COD, ESI-MS	[258,285]
Oxalic acid	Xe_2^*, O_2, N_2	HPLC/ESI-MS, TOC, $[H_2O_2]$	[215]
Oxygen	Xe_2^*, gas phase	UV/VIS, O_3–actinometry	[112,160–162,247, 286,287]
Phenol, Phenol + NO_3^-, Phenol + humic substance	Xe_2^*, Xe_2^* gas phase, $XeCl^* + TiO_2$, gas phase, $KrCl^*$, $XeCl^*$	TOC, HPLC, IC, DOC, GC, UV/VIS, FLS, p.s.	[233,234,248,288–291]
Polystyrene particles	Xe_2^*, gas phase	FT-IR, SMPS	[112]
Propanone (Acetone)	Xe_2^*	TOC	[233]
Rhodamine B	Xe_2^*, SME, $Xe_2^* + KrCl^*$, $KrCl^*$, $KrCl^* + H_2O_2$, Cl_2^*, $XeCl^*$, $I_2^* + TiO_2$	UV/VIS, TOC, GC, temperature effects	[36,39,218,236,237, 272,274]
Sulfur dioxide (SO_2)	Xe_2^*, Kr_2^*, gas phase	FT-IR	[261]
Tetrachloroethene	$KrCl^*$, gas phase, Xe_2^*	IR, p.s., TOC, GC/MS, IC	[227,262]
Tetrachloroethene (ground water sample)	Xe_2^*	GC/MS, p.s.	[229]

TABLE 2.7 (continued) Selected Examples of Applications of Excilamp-Initiated AOPs in Aqueous and Gaseous Media

Substrate	Excilamp	Analytical Method[a]	References
Tetrachloromethane	Xe_2^*, gas phase	GC/MS, p.s.	[231,241]
Tetrahydrofurane (THF)	Xe_2^*, gas phase	GC/MS, FT-IR, TOC, $[CO_2]$, p.s.	[267,292]
Textile waste water	Xe_2^*	TOC, UV/VIS	[273]
Thiophene	Xe_2^*, gas phase	GC, FT-IR	[293]
Trichloroacetic acid	Xe_2^*	$[Cl^-]$	[232]
Trichloroethene	Xe_2^*, $KrCl^*$, gas phase	GC/MS, p.s.	[241,294]
Trichloroethene, ground water sample	Xe_2^*	TOC, GC/MS, IC	[227,229]
Trichloromethane	Xe_2^*, gas phase	GC/MS, IC, IR, p.s.	[38,227,230]
Urea + maleic acid	Xe_2^*	LC/MS	[167]
Uridine (1-β-D-ribofuranosyl-uracil)	$KrCl^*$	UV/VIS	[242]

Abbreviations:

[a] ASV, anodic stripping voltammetry; COD, chemical oxygen demand; DOC, dissolved organic carbon; ESI-MS, electrospray ionization MS; FLS, fluorescence spectroscopy; FT-IR, Fourier transform IR spectroscopy; GC, gas chromatography; GC/ECD, GC/electron capture detector; GC/MS, GC/mass spectrometry; GC-TOF-MS, GC-time of flight-MS; HPLC, high-performance liquid chromatography; IC, ion chromatography; ICP, inductively coupled plasma; IR, infrared spectroscopy; LC, liquid chromatography; MS, mass spectrometry; n.s., not stated; OSO, oxygen-sensitive optode; PAH, polycyclic aromatic hydrocarbons; p.s., product study; SME, static mixer electrode; SMPS, scanning particle mobility sizer; TOC, total organic carbon; UV/VIS, ultraviolet/visible spectroscopy.

[b] Primary alcohols: methanol, ethanol, 1-propanol, 1-butanol, 1-pentanol, 1-hexanol, 1-heptanol, 1-octanol; secondary alcohols: 2-propanol, 2-butanol, 2-hexanol, cyclohexanol; tertiary alcohol: 2-methyl-2-propanol (t-butanol).

[c] Azo dyes: naphthol blue black B, orange 1, orange G.

[d] Perchloroethylene (PCE), trichloroethene (TCE), 1,2-dichloroethenes (DCE), vinyl chloride (VC), and saturated chlorinated hydrocarbons (CHC).

[e] Organic dyes: C. I. acid red, basic violet, food yellow, basic fuchsin.

2.7 Epilogue

The excilamp technology became mature during the past two decades. Although this modern lamp generation is still tested and improved, its potentials are obvious. In several cases, it moved out of researcher's laboratories to produce commercially useful applications. Unfortunately, everyday realities attest that the excilamps have not yet reached the standard photochemical laboratory. Up to date, the greatest hurdle of this development seems to be the fact that relatively cheap mercury containing low- or medium-pressure lamps are generally used in these laboratories (possibly with conventional filter systems). Therefore, a huge challenge of the future development of excilamps includes their cheap mass production. As with the development of other forms of lamps (e.g., LEDs), this way is influenced massively by economical aspects and by the environmental legislation related to the use or ban of mercury in lighting and UV-disinfection applications. Nevertheless, the author is confident that excilamps will play a significant role in several modern and sustainable photochemical and technological applications. Undoubtedly, excilamps are lamps of the future.

Acknowledgments

The author thanks Eszter Szakács (University of Szeged, Hungary) and Dr. Ulrich Kogelschatz for having read the chapter. The critical comments of Dr. Kogelschatz on the content and his stimulating suggestions are greatly acknowledged and appreciated. Further, he is grateful to Heraeus Noblelight GmbH (Hanau) for the emission spectra of the excilamps.

References

1. Boyd, I. W., Zhang, J.-Y., Kogelschatz, U., in *Photo-Excited Processes, Diagnostics and Applications (PEPDA)*, A. Peled, ed. 2003, Kluwer Academic Publishers: Dordrecht, the Netherlands. pp. 161–199.
2. Dirks, J., Müller, S., *Photonik*, 2003(4): 38–40.
3. Kogelschatz, U., *Proc. SPIE*, 2004. **5483**: 272–286.
4. Lomaev, M. I., Sosnin, E. A., Tarasenko, V. F., Shits, D. V., Skakun, V. S., Erofeev, M. V., Lisenko, A. A., *Instrum. Exp. Tech.*, 2006. **49**(5): 595–616.
5. Sosnin, E. A., Oppenländer, T., Tarasenko, V. F., *J. Photochem. Photobiol. C*, 2006. **7**: 145–163.
6. Sosnin, E. A., Sokolova, I. V., Tarasenko, V. F., in *Photochemistry Research Progress*, A. Sanchez, Gutierrez, S. J., eds. 2008, Nova Science Publishers, Inc.: Hauppauge, New York. pp. 225–269.
7. Erofeev, M. V., Tarasenko, V. F., *J. Phys. D: Appl. Phys.*, 2006. **39**: 3609–3614.
8. Eliasson, B., Kogelschatz, U., *Appl. Phys. B*, 1988. **46**: 299–303.
9. Kogelschatz, U., *Appl. Surf. Sci.*, 1992. **54**: 410–423.
10. Sosnin, E. A., Erofeev, M. V., Tarasenko, V. F., Shitz, D. V., *Instrum. Exp. Tech.*, 2002. **45**(6): 838–839.
11. Panchenko, A. N., Tarasenko, V. F., Belokurov, A. N., Mendoza, P., Rios, I., *Phys. Scr.*, 2006. **74**: 108–113.
12. Salvermoser, M., Murnick, D. E., *Appl. Phys. Lett.*, 2003. **83**(10): 1932–1934.
13. Salvermoser, M., Murnick, D. E., *J. Appl. Phys.*, 2003. **94**: 3722–3731.
14. Gellert, B., Kogelschatz, U., *Appl. Phys. B*, 1991. **52**: 14–21.
15. Tarasenko, V. F., *Pure Appl. Chem.*, 2002. **74**(3): 465–469.
16. Braslavsky, S. E., *Pure Appl. Chem.*, 2007. **79**(3): 293–465.
17. Zhang, J.-Y., Boyd, I. W., *Appl. Surf. Sci.*, 2000. **168**: 296–299.
18. Sosnin, E. A., Erofeev, M. V., Tarasenko, V. F., *J. Phys. D: Appl. Phys.*, 2005. **38**: 3194–3201.
19. Shiga, T., Pitchford, L. C., Boeuf, J.-P., Mikoshiba, S., *J. Phys. D: Appl. Phys.*, 2003. **36**: 512–521.
20. Guivan, N. N., Janca, J., Brablec, A., Stahel, P., Slavicek, P., Shimon, L. L., *J. Phys. D: Appl. Phys.*, 2005. **38**: 3188–3193.
21. Panchenko, A. N., Tarasenko, V. F., *Quantum Electron.*, 2006. **36**: 169–173.
22. Zhu, W., Takano, N., Schoenbach, K. H., Guru, D., McLaren, J., Heberlein, J., May, R., Cooper, J. R., *J. Phys. D: Appl. Phys.*, 2007. **40**: 3896–3906.
23. Schitz, D. V., Erofeev, M. V., Skakun, V. S., Tarasenko, V. F., Avdeev, S. M., *Instrum. Exp. Tech.*, 2008. **51**(6): 886–889.
24. Boyd, I. W., Zhang, J. Y., *Nucl. Instrum. Methods B*, 1997. **121**: 349–356.
25. Shishatskaya, L. P., Yakovlev, S. A., Volkova, G. A., *J. Opt. Technol.*, 1998. **65**(12): 1026–1028.
26. Kogelschatz, U., in *Twentieth International Conference on Phenomena in Ionized Gases, Invited Talks.* 1991: Pisa, Italy. pp. 218–227.
27. Esrom, H., Kogelschatz, U., *Appl. Surf. Sci.*, 1992. **54**: 440–444.
28. Lenk, M., Mehnert, R., in *Proceedings of the RadTech Europe*. 2001: Basle, Switzerland, October 8–11. pp. 153–158.
29. Mehnert, R., Lenk, M., Prager, L. in *Fifth International Symposium on Ionizing Radiation and Polymers, Invited Talk*. 2002. Sainte-Adele, Quebec, Canada.
30. Elsner, C., Lenk, M., Prager, L., Mehnert, R., *Appl. Surf. Sci.*, 2006. **252**: 3616–3624.
31. Braun, A. M., Jakob, L., Oliveros, E., *J. Water SRT-Aqua*, 1993. **42**(3): 166–173.
32. Mehnert, R., Pincus, A., Janorsky, I., Stowe, R., Berejka, A., in *Chemistry & Technology of UV & EB Formulation for Coatings, Inks & Paints*, P.K.T. Oldring, ed. 1998, Wiley: Chichester, U.K. pp. 83–105.
33. Erofeev, M. V., Lomaev, M. I., Sosnin, E. A., Tarasenko, V. F., Shitz, D. V., *Tech. Phys.*, 2001. **46**(10): 1341–1344.
34. Erofeev, M. V., Sosnin, E. A., Tarasenko, V. F., *J. Appl. Spectrosc.*, 2003. **70**(5): 807–810.
35. Oppenländer, T., *Eur. Photochem. Assoc. Newslett.*, 1994(50): 2–8.
36. Oppenländer, T., Baum, G., *Chem. Ing. Tech.*, 1994. **66**(11): 1523–1527.

37. Oppenländer, T., Baum, G., Egle, W., *gwf Wasser Abwasser*, 1995. **136**(6): 311–316.
38. Oppenländer, T., *Chem. Ing. Tech.*, 1997. **69**(1 + 2): 134–138.
39. Oppenländer, T., Baum, G., Sreiff, F., Mathys, P., Schneider, G., *Chem. Ing. Tech.*, 1996. **68**(1 + 2): 155–158.
40. Oppenländer, T., Walddörfer, C., Burgbacher, J., Kiermeier, M., Lachner, K., Weinschrott, H., *Chemosphere*, 2005. **60**: 302–309.
41. Merbahi, N., Ledru, G., Sewraj, N., Marchal, F., *J. Appl. Phys.*, 2007. **101**: 123309-1–123309-9.
42. Kogelschatz, U., *IEEE Trans. Plasma Sci.*, 2002. **30**(4): 1400–1408.
43. Kruithof, J., *IUVA News*, 2005. **7**(2): 21–24.
44. Yen, W. M., Shionoya, S., Tokyo, S.-K., Yamamoto, H., in *Phosphor Handbook*. 2006, CRC Press: Boca Raton, FL.
45. Lakshmanan, A., in *Luminescence and Display Phosphors, Phenomena and Applications*. 2008, Nova Science Publishers: New York.
46. Kogelschatz, U., *J. Phys. IV France*, 1997. **7**: C4-47–C4-66.
47. Bischoff, M., Bieri, M., in *14. Electronic Displays '99*. 1999, Network GmbH: Hagenburg, Berlin, Germany. pp. 127–134.
48. Mikoshiba, S., in *Proceedings of the International Conference on Phenomena in Ionized Gases (ICPIG XXVI)*. 2003. Greifswald, Germany.
49. Zang, D. S., Song, J. H., Park, D. H., Kim, Y. C., Yoon, D. H., *J. Lumin.*, 2009. **129**: 1088–1093.
50. Zachau, M., Schmidt, D., Mueller, U., Chenot, C., in *USP6045721*. 2000, Patent-Treuhand-Gesellschaft, Für Elektrische Glühlampen mbH, Munich, Germany.
51. Jung, K. Y., Kang, Y. C., *Mater. Lett.*, 2004. **58**(16): 2161–2165.
52. Lecheler, R., Dichtl, J., in *14. Electronic Displays '99*. 1999, Network GmbH: Hagenburg, Berlin, Germany. pp. 66–69.
53. Fiegler, M., Ziemssen, K., Homberg, B., *SID Symposium Digest*, 2003. **34**(172).
54. Trampert, K. E., Daub, H. P., Neiger, M., Heering, W., in *Proceedings of the 10th International Symposium on the Science and Technology of Light Sources (LS-10)*. 2004, IoP: Toulouse, France. pp. 509–510.
55. Guivan, M. M., Malinin, A. N., Brablec, A., Janca, J., Stahel, P., Slavicek, P., *Czech. J. Phys.*, 2006. **56**(Suppl. 2): B659–B664.
56. Zeng, Q., Tanno, H., Egoshi, K., Tanamachi, N., Zhang, S., *Appl. Phys. Lett.*, 2006. **88**: 051906-1–051906-3.
57. Rao, R. P., *J. Lumin.*, 2005. **113**: 271–278.
58. Xing, D.-S., Gong, M.-L., Qiu, X.-Q., Yang, D.-J., Cheah, K.-W., *Mater. Lett.*, 2006. **60**: 3217–3220.
59. Yuan, J. L., Wang, J., Xiong, D. B., Zhao, J. T., Fu, Y. B., Zhang, G. B., Shi, C. S., *J. Lumin.*, 2007. **126**: 717–722.
60. Marking, G. A., Snyder, T. M., in *USP7435358*. 2008.
61. Tzeng, H.-Y., Cheng, B.-M., Chen, T.-M., *J. Lumin.*, 2007. **122–123**: 917–920.
62. Wegh, R. T., Donker, H., van Loef, E. V. D., Oskam, K. D., Meijerink, A., *J. Lumin.*, 2000. **87–89**: 1017–1019.
63. Lee, T.-J., Luo, L.-Y., Diau, E. W.-G., Chen, T.-M., Cheng, B.-M., Tung, C.-Y., *Appl. Phys. Lett.*, 2006. **89**: 131121-1–131121-3.
64. Krutmann, J., Hönigsmann, H., Elmets, C. A., eds., in *Dermatological Phototherapy and Photodiagnostic Methods*, 2nd edn. 2009, Springer-Verlag GmbH: Heidelberg, Germany.
65. Green, C., Diffey, B. L., Hawk, J. L. M., *Phys. Med. Biol.*, 1992. **37**(1): 1–20.
66. Rodewald, E. J., Housman, T. S., Mellen, B. G., Feldman, S. R., *Dermatol. Online J.*, 2001. **7**(2): 4.
67. Marking, G. A., Snyder, T. M., in *EP1832642 (A2)*. 2007, Osram Sylvana Inc.: Lake Zurich, IL
68. Di Lazzaro, P., Murra, D., Felici, G., Fu, S., *Rev. Sci. Instrum.*, 2004. **75**(5): 1332–1336.
69. Köllner, K., Wimmershoff, M. B., Hintz, C., Landthaler, M., Hohenleutner, U., *Br. J. Dermatol.*, 2005. **152**: 750–754.
70. Muzzi, F., Baldesi, A., in *WO 03/024526 A1*. 2003, EL.EN S.P.A.: Italy.

71. Cappugi, P., Mavilia, L., Mavilia, C., Brazzini, B., Rossi, R., Hercogova, J., Lotti, T. M., Campolmi, P., Andreasi, L., *Int. J. Immunopathol. Pharmacol.* 2002. **15**(3): 14–19.
72. Bianchi, B., Campolmi, P., Mavilia, L., Danesi, A., Rossi, R., Cappugi, P., *J. Eur. Acad. Dermatol. Venereol.*, 2003. **17**: 408–413.
73. Leone, G., Iacovelli, P., Paro Vidolin, A., Picardo, M., *J. Eur. Acad. Dermatol. Venereol.*, 2003. **17**: 531–537.
74. Mori, M., Campolmi, P., Mavilia, L., Rossi, R., Cappugi, P., Pimpinelli, N., *J. Am. Acad. Dermatol.*, 2004. **50**(6): 943–945.
75. Aubin, F., Vigan, M., Puzenat, E., Blanc, D., Drobacheff, C., Deprez, P., Humbert, P., Laurent, R., *Br. J. Dermatol.*, 2005. **152**(1): 99–103.
76. Mavilia, L., Mori, M., Rossi, R., Campolmi, P., Puglisi Guerra, A., Lotti, T., *G. Ital. Dermatol. Venereol.*, 2008. **143**(5): 329–337.
77. Chimento, S. M., Newland, M., Ricotti, C., Nistico, S., Romanelli, P., *J. Drugs Dermatol.*, 2008. **7**(3): 258–263.
78. Mavilia, L., Campolmi, P., Rossi, R., Mori, M., Pimpinelli, N., Cappugi, P., *Br. J. Dermatol.*, 2005. **152**: 1376–1377.
79. Esrom, H., Kogelschatz, U., *Thin Solid Films*, 1992. **218**: 231–246.
80. Skurat, V., *Nucl. Instrum. Methods B*, 2003. **208**: 27–34.
81. Takezoe, N., Yokotani, A., Kurosawa, K., *Mem. Fac. Eng., Miyazaki Univ.*, 1999. **28**: 1–16.
82. Liaw, I. I., Boyd, I. W., in *Functionalized Nanoscale Materials, Devices and Systems*, A. Vaseashta, Mihailescu, I. N., eds. 2008, Springer: the Netherlands. pp. 61–76.
83. Cezeaux, J. L., Romoser, C. E., Benson, R. S., Buck, C. K., Sackman, J. E., *Nucl. Instrum. Methods B*, 1998. **141**: 193–196.
84. Heitz, J., Niino, H., Yabe, A., *Jpn. J. Appl. Phys.*, 1996. **35**: 4110–4116.
85. Svorcik, V., Walachova, K., Heitz, J., Gumpenberger, T., Bacakova, L., *J. Mater. Sci. Lett.*, 2001. **20**: 1941–1942.
86. Gumpenberger, T., Heitz, J., Bäuerle, D., Kahr, H., Graz, I., Romanin, C., Svorcik, V., Leisch, F., *Biomaterials*, 2003. **24**: 5139–5144.
87. Svorcik, V., Rockova, K., Ratajova, E., Heitz, J., Huber, N., Bäuerle, D., Bacakova, L., Dvorankova, B., Hnatowicz, V., *Nucl. Instrum. Methods B*, 2004. **217**: 307–313.
88. Heitz, J., Svorcik, V., Bacakova, L., Rockova, K., Ratajova, E., Gumpenberger, T., Bäuerle, D., Dvorankova, B., Kahr, H., Graz, I., Romanin, C., *Biomaterials*, 2003. **24**: 5139–5144.
89. Olbrich, M., Punshon, G., Frischauf, I., Salacinski, H. J., Rebollar, E., Romanin, C., Seifalian, A. M., Heitz, J., *J. Biomater. Sci. Polym. Edn.*, 2007. **18**(4): 453–468.
90. Mikulikova, R., Moritz, S., Gumpenberger, T., Olbrich, M., Romanin, C., Bacakova, L., Svorcik, V., Heitz, J., *Biomaterials*, 2005. **26**: 5572–5580.
91. Hozumi, A., Saito, T., Shirahata, N., Yokogawa, Y., Kameyama, T., *J. Vac. Sci. Technol. A*, 2004. **22**(4): 1836–1841.
92. Opwis, K., Knittel, D., Schollmeyer, E., *Biotechnol. J.*, 2007. **2**: 347–352.
93. Kogelschatz, U., Esrom, H., Zhang, J.-Y., Boyd, I. W., *Appl. Surf. Sci.*, 2000. **168**: 29–36.
94. Truica-Marasescu, F.-E., Wertheimer, M. R., *Macromol. Chem. Phys.*, 2005. **206**: 744–757.
95. Praschak, D., Bahners, T., Schollmeyer, E., *Appl. Phys. A*, 2000. **71**: 577–581.
96. Gotoh, K., Hayashiya, M., *Text. Res. J.*, 2008. **78**(1): 37–44.
97. Truica-Marasescu, F., Wertheimer, M. R., *J. Appl. Polym. Sci.*, 2004. **91**: 3886–3898.
98. Periyasami, S., Gulrajani, M. L., Gupta, D., *Surf. Coat. Tech.*, 2007. **201**: 7286–7291.
99. Periyasamy, S., Gupta, D., Gulrajani, M. L., *Eur. Polym. J.*, 2007. **43**: 4573–4581.
100. Geretovszky, Z., Hopp, B., Bertoti, I., Boyd, I. W., *Appl. Surf. Sci.*, 2002. **186**: 85–90.
101. Tanaka, S., Naganuma, Y., Kato, C., Horie, K., *J. Photopolym. Sci. Tech.*, 2003. **16**(2): 165–170.
102. Praschak, D., Bahners, T., Schollmeyer, E., *Appl. Phys. A*, 1998. **66**: 69–75.
103. Zhu, Z., Kelley, M. J., *Appl. Surf. Sci.*, 2005. **252**: 303–310.
104. Zhu, Z., Kelley, M. J., *Appl. Surf. Sci.*, 2004. **236**: 416–425.

105. Chen, W., Zhang, J., Fang, Q., Hu, K., Boyd, I. W., *Thin Solid Films*, 2004. **453–454**: 3–6.
106. Hozumi, A., Shirahata, N., Nakanishi, Y., Asakura, S., Fuwa, A., *J. Vac. Sci. Technol. A*, 2004. **22**(4): 1309–1314.
107. Hozumi, A., Masuda, T., Hayashi, K., Sugimura, H., Takai, O., Kameyama, T., *Langmuir*, 2002. **18**(23): 9022–9027.
108. Charbonnier, M., Romand, M., *Int. J. Adhes. Adhes.*, 2003. **23**: 277–285.
109. Lopez-Gejo, J., Gliemann, H., Schimmel, T., Braun, A. M., *Photochem. Photobiol.*, 2005. **81**: 777–782.
110. Gejo, J. L., Manoj, N., Sumalekshmy, S., Glieman, H., Schimmel, T., Wörner, M., Braun, A. M., *Photochem. Photobiol. Sci.*, 2006. **5**: 948–954.
111. Hozumi, A., Inagaki, H., Kameyama, T., *J. Colloid. Interface Sci.*, 2004. **278**: 383–392.
112. Vicente, J. S., Gejo, J. L., Rothenbacher, S., Sarojiniamma, S., Gogritchiani, E., Wörner, M., Kasper, G., Braun, A. M., *Photochem. Photobiol. Sci.*, 2009. **8**: 944–952.
113. Niino, H., Miyabo, A., Yanese, H., Yabe, A., *J. Photopolym. Sci. Tech.*, 2002. **15**(1): 65–70.
114. Hopp, B., Geretovszky, Z., Bertoti, I., Boyd, J. W., *Appl. Surf. Sci.*, 2002. **186**: 80–84.
115. Heitz, J., Niino, H., Yabe, A., *Appl. Phys. Lett.*, 1996. **68**(19): 2648–2650.
116. Prager, L., Marsik, P., Wennrich, L., Baklanov, M. R., Naumov, S., Pistol, L., Schneider, D., Gerlach, J. W., Verdonck, P., Buchmeiser, M. R., *Microelectron. Eng.*, 2008. **85**: 2094–2097.
117. Falkenstein, Z., *Proc. SPIE*, 2001. **4440**: 246–255.
118. Tode, M., Takigawa, Y., Iguchi, T., Matsuura, H., Ohmukai, M., Sasaki, W., *Metall. Mater. Trans. A*, 2007. **38A**: 596–598.
119. Strein, E., Allred, D., *Thin Solid Films*, 2008. **517**: 1011–1015.
120. Shirahata, N., Oda, K., Asakura, S., Fuwa, A., Yokogawa, Y., Kameyama, T., Hozumi, A., *J. Vac. Sci. Technol. A*, 2004. **22**(4): 1615–1619.
121. Ohtsubo, T., Azuma, T., Takaura, M., Higashiguchi, T., Kubodera, S., Sasaki, W., *Appl. Phys. A*, 2003. **76**: 139–141.
122. Zhang, J.-Y., Boyd, I. W., *Appl. Surf. Sci.*, 2002. **186**: 64–68.
123. Boyd, I. W., Zhang, J. Y., *Mater. Res. Soc. Symp.*, 2000. **617**: J4.4.1–J4.4.12.
124. Boyd, I. W., Zhang, J. Y., *Proc. SPIE*, 2000. **4070**: 275–283.
125. Boyd, I. W., Zhang, J. Y., Kogelschatz, U., A. Peled, ed. 2003, Kluwer Academic Publishers: Dordrecht, the Netherlands. pp. 161–199.
126. Esrom, H., Demny, J., Kogelschatz, U., *Chemtronics*, 1989. **4**: 202–208.
127. Kato, C., Tanaka, S., Naganuma, Y., Shindo, T., *J. Photopolym. Sci. Tech.*, 2003. **16**(2): 163–164.
128. Shirahata, N., Hozumi, A., *J. Nanosci. Nanotechnol.*, 2006. **6**: 1695–1700.
129. Furukawa, T., Takai, O., *Meas. Sci. Technol.*, 2006. **17**: 1247–1253.
130. Prager, L., Wennrich, L., Heller, R., Knolle, W., Naumov, S., Prager, A., Decker, D., Liebe, H., Buchmeister, M. R., *Chem. Eur. J.*, 2009. **15**: 675–683.
131. Fukano, A., Oyanagi, H., *J. Appl. Phys.*, 2003. **94**(5): 3345–3349.
132. Pfeifer Roland, R., Bolle, M., Anderson, R. W., *Chem. Mater.*, 2001. **13**: 2493–2500.
133. Fang, Q., He, G., Cai, W. P., Zhang, J.-Y., Boyd, I. W., *Appl. Surf. Sci.*, 2004. **226**: 7–11.
134. Kaliwoh, N., Zhang, J.-Y., Boyd, I. W., *Surf. Coat. Tech.*, 2000. **125**: 424–427.
135. Boies, A. M., Roberts, J. T., Girshick, S. L., Zhang, B., Nakamura, T., Mochizuki, A., *Nanotechnology*, 2009. **20**: 295604.
136. Mehnert, R., in *Proceedings of the Exhibition and Conference on Radiation Curing*, A. Milton-Thompson, ed. 1999: Berlin, Germany. pp. 303–310.
137. Roth, A., Radtech Report, 1996. **10** (5): 21–22.
138. Knolle, W., Naumov, S., Madani, M., von Sonntag, C., *Nucl. Instrum. Methods B*, 2005. **236**: 195–200.
139. Scherzer, T., Prager, L., Knolle, W., Naumov, S., in *RadTech Conference Proceedings*, Chemistry Part Two. 2006, Chicago, IL.
140. Silvares, A. F. M., do Nascimento, C. A. O., Oliveros, E., Bossmann, S. H., Braun, A. M., *Ind. Eng. Chem. Res.*, 2007. **46**: 7436–7447.

141. Bauer, F., Decker, U., Czihal, K., Mehnert, R., Riedel, C., Riemschneider, M., Schubert, R., Buchmeiser, M. R., *Proc. Org. Coat.*, 2009. **64**: 474–481.
142. Tanabe, H., Seki, Y., Yano, J., Ushioda, J., Ogura, Y., *Proc. SPIE*, 1996. **2726**: 866–869.
143. Sugimura, H., Ushiyama, K., Hozumi, A., Takai, O., *Langmuir*, 2000. **16**: 885–888.
144. Hong, L., Sugimura, H., Furukawa, T., Takai, O., *Langmuir*, 2003. **19**: 1966–1969.
145. Sugimura, H., Hong, L., Lee, K.-H., *Jpn. J. Appl. Phys.*, 2005. **44**(7A): 5185–5187.
146. Shirahata, N., Hozumi, A., *Chem. Mater.*, 2005. **17**: 20–27.
147. Shirahata, N., Sakka, Y., Uchikoshi, T., Hozumi, A., *J. Vac. Sci. Technol. A*, 2005. **23**(4): 1146–1151.
148. Oppenländer, T., *Trends Chem. Eng.*, 2003. **8**: 123–136.
149. Mühlberger, F., Saraji-Bozorgzad, M., Gonin, M., Fuhrer, K., Zimmermann, R., *Anal. Chem.*, 2007. **79**(21): 8118–8124.
150. Batalova, V. N., Zakharova, E. A., Slepchenko, G. B., Malygina, M. V., *J. Anal. Chem.*, 2004. **59**(5): 468–473.
151. Batalova, V. N., Bylatskaya, O. A., Sosnin, E. A., *Proc. SPIE*, 2004. **5483**: 323–327.
152. Noskova, G. N., Sosnin, E. A., Ivanova, E. E., Merzha, A. N., Tarasenko, V. F., *Atmos. Oceanic Opt.*, 2004. **17**(2–3): 208–210.
153. Batalova, V. N., Sosnin, E. A., Zakharova, E. A., Tarasenko, V. F., *Instrum. Exp. Tech.*, 2003. **46**(1): 73–76.
154. Kuhn, H. J., Braslavsky, S. E., Schmidt, R., *Pure Appl. Chem.*, 2004. **76**(12): 2105–2146.
155. Sosnin, E. A., Zakharova, E. A., Moskalyeva, M. L., Batalova, V. N., in *Proceedings of the PhysCon.*, 2005: St. Petersburg, Russia. pp. 786–789.
156. Heit, G., Neuner, A., Saugy, P.-Y., Braun, A. M., *J. Phys. Chem.*, 1998. **102**: 5551–5561.
157. Oppenländer, T., Schwarzwälder, R., *J. Adv. Oxid. Technol.*, 2002. **5**(2): 155–163.
158. Bark, Y. B., Barkhudarov, E. M., Kozlov, Y. N., Kossyi, I. A., Silakov, V. P., Taktakishvili, M. I., Temchin, S. M., *J. Phys. D: Appl. Phys.*, 2000. **33**: 859–863.
159. Shen, C., Fang, S., Bergstrom, D. E., Blatchley III, E. R., *Environ. Sci. Technol.*, 2005. **39**: 3826–3832.
160. Laszlo, Z., Ilisz, I., Peintler, G., Dombi, A., *Ozone Sci. Eng.*, 1998. **20**: 421–432.
161. Salvermoser, M., Murnick, D. E., Kogelschatz, U., *Ozone Sci. Eng.*, 2008. **30**: 228–237.
162. Salvermoser, M. J., Kogelschatz, U., Murnick, D. E., *Eur. Phys. J. Appl. Phys.*, 2009. **47**: 22812-p1–6.
163. Griesbeck, A. G., Kramer, W., Oelgemöller, M., *Green Chem.*, 1999. **1**(4): 205–207.
164. Griesbeck, A. G., Maptue, N., Bondock, S., Oelgemöller, M., *Photochem. Photobiol. Sci.*, 2003. **2**: 450–451.
165. Oelgemöller, M., *Eur. Photochem. Assoc. Newslett.*, 2000. **69**: 11–23.
166. Jansen, M., Braun, A. M., Troscher, G., Popp, H.-P., in *EP0967202 B1*. 2003, F. Hoffmann-LaRoche AG: Basel, Schweiz.
167. Terasaki, M., Nomoto, S., Mita, H., Shimoyama, A., *Origins Life Evol. B.*, 2002. **32**: 91–98.
168. Halman, M. M., in *Photodegradation of Water Pollutants*. 1996, CRC Press: Boca Raton, FL.
169. Oppenländer, T., in *Photochemical Purification of Water and Air. Advanced Oxidation Processes (AOPs): Principles, Reaction Mechanism, Reactor Concepts*. 2003,Wiley-VCH: Weinheim, Germany.
170. Tarr, M. A., in *Chemical Degradation Methods for Wastes and Pollutants*. 2003, CRC Press : Boca Raton, FL.
171. Parsons, S., ed., in *Advanced Oxidation Processes for Water and Wastewater Treatment*. 2004, IWA Publishing: London, U.K.
172. Bolton, J. R., Cotton, C. A., in *The Ultraviolet Disinfection Handbook*. 2008, American Water Works Association: Denver, CO.
173. Ressler, B., in *USP7217936*. 2007.
174. Falkenstein, Z., Coogan, J. J., *J. Phys. D: Appl. Phys.*, 1997. **30**: 2704–2710.
175. Coogan, J. J., *Photochem. Photobiol.*, 2005. **81**: 1511–1517.
176. Heise, M., Neff, W., Franken, O., Muranyi, P., Wunderlich, J., *Plasmas Polym.*, 2004. **9**(1): 23–33.
177. Christofi, N., Misakyan, M. A., Matafonova, G. G., Barkhudarov, E. M., Batoev, V. B., Kossyi, I. A., Sharp, J., *Chemosphere*, 2008. **73**: 717–722.
178. Sinha, R. P., Häder, D.-P., *Photochem. Photobiol. Sci.*, 2002. **1**: 225–236.

179. Sonntag von, C., Kolch, A., Gebel, J., Oguma, K., Sommer, R., in *European Conference on UV Radiation, Effects and Technologies*. 2004: Karlsruhe, Germany.
180. Bolton, J. R., in *Ultraviolet Applications Handbook*, 3rd ed., 2010, Bolton Photosciences Inc., Published by ICC Lifelong Learn Inc.: Edmonton, Alberta, Canada.
181. Süß, J., Volz, S., Obst, U., Schwartz, T., *Water Res.*, 2009. **43**: 3705–3716.
182. Sosnin, E. A., Lavrent'eva, L. V., Yusupov, M. R., Masterova, Y. V., Tarasenko, V. F., in *Second International Workshop on Biological Effects of Electromagnetic Fields*. 2002: Rhodes, Greece. pp. 953–957.
183. Sosnin, E. A., Stoffels, E., Erofeev, M. V., Kieft, I. E., Kunts, S. E., *IEEE Trans. Plasma Sci.*, 2004. **32**(4): 1544–1550.
184. Sosnin, E. A., Lavrent'eva, L. V., Erofeev, M. V., Masterova, Y. V., Kuznetzova, E. N., Tarasenko, V. F., *Proc. SPIE*, 2004. **5483**: 317–322.
185. Avdeev, S. M., Sosnin, E. A., Velichevskaya, K. Y., Lavrent'eva, L. V., *Proc. SPIE*, 2007. **6938**: 13-1–13-5.
186. Naunovic, Z., Pennell, K. G., Blatchley III, E. R., *Environ. Sci. Technol.*, 2008. **42**(5): 1605–1614.
187. Naunovic, Z., Lim, S., Blatchley III, E. R., *Water Res.*, 2008. **42**: 4838–4846.
188. Sonntag von, C., in *Process Technologies for Water Treatment*, S. Stucki, ed. 1987, Plenum Press: New York.
189. Clauß, M., Mannesmann, R., Kolch, A., *Acta Hydroch. Hydrob.*, 2005. **33**(6): 579–584.
190. Clauß, M., *Acta Hydroch. Hydrob.*, 2006. **34**: 525–532.
191. Matafonova, G. G., Batoev, V. B., Astakhova, S. A., Gomez, M., Christofi, N., *Lett. Appl. Microbiol.*, 2008. **47**(6): 508–513.
192. Clauß, M., Grotjohann, N., *Mutat. Res.-Gen. Tox. EN*, 2009. **673**(2): 83–86.
193. Clauß, M., Grotjohann, N., *Clean*, 2008. **36**(9): 754–759.
194. Sosnin, E. A., Avdeev, S. M., Kuznetzova, E. A., Lavrent'eva, L. V., *Instrum. Exp. Tech.*, 2005. **48**(5): 663–666.
195. Sosnin, E. A., Lavrent'eva, L. V., Masterova, Y. V., Erofeev, M. V., Tarasenko, V. F., Tech. *Phys. Lett.*, 2004. **30**(7): 615–617.
196. Wang, D., Oppenländer, T., Gamal El-Din, M., Bolton, J. R., *Photochem. Photobiol.*, 2010. **86**: 176–181.
197. Wang, D., Oppenländer, T., Gamal El-Din, M., Bolton, J. R., in *Proceedings of the IOA and IUVA 2009 North American Conference*. 2009: Boston, MA, May 4–5. pp. S16-2.
198. Mamane, H., Shemer, H., Linden, K. G., *J. Hazard. Mater.*, 2007. **146**: 479–486.
199. Oppenländer, T., Baum, G., *Gwf Wasser Abwasser*, 1996. **137**(6): 321–325.
200. Glaze, W. H., Kang, J.-W., Chapin, D. H., *Ozone Sci. Eng.*, 1987. **9**: 335–352.
201. Legrini, O., Oliveros, E., Braun, A. M., *Chem. Rev.*, 1993. **93**: 671–698.
202. Bolton, J. R., Cater, S. R., in *Aquatic and Surface Photochemistry*, G.R. Helz, ed. 1994, Lewis Publishers: Boca Raton, FL. pp. 467–490.
203. Gonzalez, M. C., Martiere, D. O., Braun, A. M., in *Recent Res. Dev. Photochem. Photobiol.*, S.G. Pandalai, ed., 1998. **2**: 25–45.
204. Munter, R., *Proc. Estonian Acad. Sci. Chem.*, 2001. **50**(2): 59–80.
205. Gogate, P. R., Pandit, A. B., *Adv. Environ. Res.*, 2004. **8**: 501–551.
206. Gogate, P. R., Pandit, A. B., *Adv. Environ. Res.*, 2004. **8**: 553–597.
207. Cooper, W. J., Cramer, C. J., Martin, N. H., Mezyk, S. P., O'Shea, K. E., von Sonntag, C., *Chem. Rev.*, 2009. **109**: 1302–1345.
208. Li, K., Crittenden, J., *Environ. Sci. Technol.*, 2009. **43**(8): 2831–2837.
209. Minakata, D., Li, K., Westerhoff, P., Crittenden, J., *Environ. Sci. Technol.*, 2009. **43**(16): 6220–6227.
210. Gonzalez, M. G., Oliveros, E., Wörner, M., Braun, A. M., *J. Photochem. Photobiol. C*, 2004. **5**: 225–246.
211. Buxton, G. V., Greenstock, C. L., Helman, W. P., Ross, A. B., *J. Phys. Chem. Ref. Data*, 1988. **17**: 513–886.
212. Asmus, K., Bonifacic, M., in *S-Centered Radicals, the Chemistry of Free Radicals*, Z. B. Alfassi, ed. 1999, John Wiley & Sons: Chichester, U.K.

213. Sonntag von, C., Dowideit, P., Xingwang, F., Mertens, R., Xianming, P., Schuchmann, M. N., Schuchmann, H.-P., *Water Sci. Technol.*, 1997. **35**(4): 9–15.
214. Alfassi, Z. B., ed., in *The Chemistry of Free Radicals: Peroxyl Radicals* 1997, John Wiley & Sons: Chichester, U.K.
215. Azrague, K., Bonnefille, E., Pradines, V., Pimienta, V., Oliveros, E., Maurette, M.-T., Benoit-Marquie, F., *Photochem. Photobiol. Sci.*, 2005. **4**: 406–408.
216. Weeks, J. L., Meaburn, G. M. A. C., Gordon, S., *Rad. Res.*, 1963. **19**: 559–567.
217. Reid, V., Bailleux, C., Braun, A., Wörner, M., Schnabel, C., in *EP1160203 (A1)*. 2001.
218. Oppenländer, T., Xu, F., *Ozone Sci. Eng.*, 2008. **30**: 99–104.
219. Coyle, E. E., Oelgemöller, M., *Photochem. Photobiol. Sci.*, 2008. **7**: 1313–1322.
220. Hart, E. J., Anbar, M., in *The Hydrated Electron* 1970, Wiley-Interscience: New York.
221. Sonntag von, C., Schuchmann, H.-P., *Angew. Chem. Int. Ed. Engl.*, 1991. **30**: 1229–1253.
222. Atkinson, R., Baulch, D. L., Cox, R. A., in *CRC Handbook of Chemistry and Physics*, D.R. Lide, ed. 1991–1992, CRC Press: Boca Raton, FL.
223. Atkinson, R., Baulch, D. L., Cox, R. A., Crowley, J. N., Hampson, R. F., Hynes, R. G., Jenkin, M. E., Rossi, M. J., Troe, J., *Atmos. Chem. Phys.*, 2004. **4**: 1461–1738.
224. Atkinson, R., Baulch, D. L., Cox, R. A., Crowley, J. N., Hampson, R. F., Hynes, R. G., Jenkin, M. E., Rossi, M. J., Troe, J., *Atmos. Chem. Phys.*, 2006. **6**: 3625–4055.
225. Lloyd, A. C., *Int. J. Chem. Kinet.*, 1974. **6**(2): 169–228.
226. Yang, J. Y., Servedio, F. M., *Can. J. Chem.*, 1968. **46**: 338–341.
227. Oppenländer, T., Baum, G., *Chem. Ing. Tech.*, 1995. **67**(1): 96–99.
228. Loraine, G. A., Glaze, W. H., *J. Adv. Oxid. Technol.*, 1999. **4**(4): 424–433.
229. Baum, G., Oppenländer, T., *Chemosphere*, 1995. **30**(9): 1781–1790.
230. Loraine, G. A., *Hazard. Waste Hazard. Mat.*, 1993. **10**(2): 185–194.
231. Nohr, R. S., MacDonald, J. G., Kogelschatz, U., Mark, G., Schuchmann, H.-P., von Sonntag, C., *J. Photochem. Photobiol. A*, 1994. **79**: 141–149.
232. Wörner, M., Schnabel, C., Hashem, T. M., Zegenhagen, F., Gieser, J., Braun, A. M., *J. Inform. Rec.*, 1998. **24**: 455–460.
233. Oppenländer, T., Gliese, S., *Chemosphere,* 2000. **40**: 15–21.
234. Benoit-Marquie, F., Wilkenhörner, U., Braun, A. M., Oliveros, E., Maurette, M.-T., *J. Phys. IV France*, 1999. **9**: 113–116.
235. Oppenländer, T., *Chem. Ing. Tech.*, 1997. **69**: 1245.
236. Oppenländer, T., Waizmann, J., *Chem. Ing. Tech.*, 1997. **69**(10): 1470–1474.
237. Oppenländer, T., *Chem. Ing. Tech.*, 1998. **70**(8): 1013–1016.
238. Christofi, N., Matafonova, G. G., Batoev, V. B., Misakyan, M. A., Barkhudarov, E. M., Kossyi, I. A., in *Water Resources Research Progress*, L.N. Robinson, ed. 2008, Nova Science Publishers: Hauppauge, New York. pp. 101–126.
239. Sörensen, M., Tanner, U., Sagawe, G., Frimmel, F. H., *Acta Hydroch. Hydrob.*, 1996. **24**: 132–136.
240. Sörensen, M., Frimmel, F., *Water Res.*, 1997. **31**: 2885–2891.
241. Falkenstein, Z., *J. Adv. Oxid. Technol.*, 1997. **2**(1): 223–238.
242. Zhang, J.-Y., Esrom, H., Boyd, I. W., *Appl. Surf. Sci.*, 1999. **138–139**: 315–319.
243. Gonzalez, M. C., Hashem, T. M., Jakob, L., Braun, A. M., *Fresenius J. Anal. Chem.*, 1995. **351**: 92–97.
244. Lopez, J. L., Garcia Einschlag, F. S., Gonzalez, M. C., Capparelli, A. L., Oliveros, E., Hashem, T. M., Braun, A. M., *J. Photochem. Photobiol. A*, 2000. **137**: 177–184.
245. Jakob, L., Hashem, T. M., Bürki, S., Guindy, N. M., Braun, A. M., *J. Photochem. Photobiol. A*, 1993. **75**: 97–103.
246. Kreysig, D., Ritter, K., Karger, R., in *CUTEC-Schriftenreihe, Oxidation Technologies for Water and Waste Water Treatment*, A. Vogelpohl, ed. 1996, Clausthaler Umwelttechnik-Institut GmbH, Clausthal-Zellerfeld, Germany. pp. 1–5.
247. Hashem, T. M., Zirlewagen, M., Braun, A. M., *Water Sci. Technol.*, 1997. **35**(4): 41–48.

248. Bazyl, O. K., Kopylova, T. N., Sokolova, I. V., Sosnin, E. A., Svetlitchnyi, V. A., Tarasenko, V. F., Tchaikovskaya, O. N., *Proc. SPIE*, 2002. **4147**: 240–244.
249. Sokolova, I. V., Chaikovskaya, O. N., Svetlichnyi, V. A., Kuznetsova, R. T., Kopylova, T. N., Maier, G. V., Sosnin, E. A., Lipatov, E. A., Tarasenko, V. F., *High Energy Chem.*, 2002. **36**(4): 272–275.
250. Murcia, M. D., Gomez, M., Gomez, E., Gomez, J. L., Christofi, N., *World Acad. Sci. Eng. Tech.*, 2009. **55**: 249–253.
251. Gomez, M., Matafonova, G., Gomez, J. L., Batoev, V., Christofi, N., *J. Hazard. Mater.*, 2009. **169**: 46–51.
252. Oppenländer, T., *J. Environ. Eng. Sci.*, 2007. **6**: 253–264.
253. Afzal, A., Ikehata, K., Oppenländer, T., Bolton, J. R., Gamal El-Din, M., in *Proceedings of the International Ozone Association-Pan American Group 2008 Annual Conference*, Orlando, FL, August 24–27, 2008: pp. 574–579.
254. Afzal, A., Oppenländer, T., Bolton, J. R., El-Din, M. G., *Water Res.*, 2010. **44**: 278–286.
255. Rehberg, K., Mannschott, P., Erdinger, L., Sonntag, H. G., Schramm, B., *Vom Wasser*, 1994. **83**: 139–156.
256. Gonzalez, M. C., Braun, A. M., Prevot, A. B., Pelizzetti, E., *Chemosphere*, 1994. **28**(12): 2121–2127.
257. Oppenländer, T., Baum, G., Egle, W., Hennig, T., *Proc. Indian Acad. Sci. (Chem. Sci.)*, 1995. **107**: 621–636.
258. Feng, X., Zhu, S., Hou, H., *Environ. Technol.*, 2006. **27**: 119–126.
259. Wörner, M., Eggers, J., Nunes, M., Schnabel, C., Rudolph, S., Zegenhagen, F., Workman, A., Braun, A. M., in *Oxidation Technologies for Water and Wastewater Treatment*, A. Vogelpohl, ed. 2003, Papierflieger Verlag: Goslar, Germany. pp. 843–848.
260. Metzger, W., Falkenstein, Z., in *Conference Proceedings of the First International Congress on Ultraviolet Technologies*. 2001, International Ultraviolet Assoc. (IUVA), electronic release: Washington, DC.
261. Tsuji, M., Kawahara, T., Kawahara, M., Kamo, N., Hishinuma, N., *Jpn. J. Appl. Phys.*, 2008. **47**: 8943–8949.
262. Prager, L., Hartmann, E., *J. Photochem. Photobiol. A*, 2001. **138**: 177–183.
263. Matafona, G., Christofi, N., Batoev, V., Sosnin, E., *Chemosphere*, 2008. **70**: 1124–1127.
264. Quici, N., Litter, M. I., Braun, A. M., Oliveros, E., *J. Photochem. Photobiol. A*, 2008. **197**: 306–312.
265. Sokolova, T. V., Chaikovskaya, O. N., Sosnin, E. A., Sokolova, I. V., *J. Appl. Spectrosc.*, 2006. **73**(5): 632–639.
266. Chaikovskaya, O. N., Sokolova, I. V., Karetnikova, E. A., Maier, G. V., *J. Appl. Spectrosc.*, 2008. **75**(2): 261–267.
267. Gassiot, I., Baus, C., Schaber, K., Braun, A. M., *J. Inform. Rec.*, 1998. **24**: 129–132.
268. Fethi, F., Lopez-Gejo, J., Köhler, M., Braun, A. M., *J. Adv. Oxid. Technol.*, 2008. **11**(2): 208–221.
269. Heit, G., Braun, A. M., *J. Inform. Rec.*, 1996. **22**: 543–546.
270. Heit, G., Braun, A. M., *Water Sci. Technol.*, 1997. **35**(4): 25–30.
271. Sörensen, M., Frimmel, F. H., *Acta Hydroch. Hydrob.*, 1996. **24**(4): 185–188.
272. Oppenländer, T., *Chem. Ing. Tech.*, 1997. **69**: 1782–1786.
273. Oppenländer, T., Baum, G., *Umwelt*, 1995. **25**: 100–101.
274. Oppenländer, T., Waizenegger, K., Baum, G., in *Proc. IOA-Internat. Ozone Assoc., International Conference on Ozonation and Related Oxidation Processes in Water and Liquid Waste Treatment.* 1997: Berlin, Germany.
275. Laszlo, Z., Dombi, A., *Chemosphere*, 2002. **46**: 491–494.
276. Grichetschkina, M. V., Zaitsev, N. K., Braun, A. M., *Toxicol. Environ. Chem.*, 1996. **53**: 143–151.
277. Ikematsu, T., Hayashi, N., Ihara, S., Satoh, S., Yamabe, C., *Vacuum*, 2004. **73**: 579–582.
278. Pfeifer Roland, R., Bolle, M., Anderson, R. W., *J. Phys. D: Appl. Phys.*, 1998. **31**: 1336–1342.
279. Xia, L.-Y., Gu, D.-H., Tan, J., Dong, W.-B., Hou, H.-Q., *Chemosphere*, 2008. **71**: 1774–1780.
280. Gonzalez, M. C., Braun, A. M., *J. Photochem. Photobiol. A*, 1996. **95**: 67–72.
281. Sosnin, E. A., Erofeev, M. V., Tarasenko, V. F., *Russ. Phys. J.*, 2006. **49**(10): 1145–1148.
282. Gonzalez, M. C., Braun, A. M., *Res. Chem. Intermed.*, 1995. **21**: 837–859.

283. Li, Q.-R., Gu, C.-Z., Di, Y., Yin, H., Zhang, J.-Y., *J. Hazard. Mater.*, 2006. **B133**: 68–74.
284. Tsuji, M., Kawahara, M., Noda, K., Senda, M., Sako, H., Kamo, N., Kawahara, T., Kamarudin, K. S. N., *J. Hazard. Mater.*, 2009. **162**: 1025–1033.
285. Feng, X., Zhu, S., Hou, H., *Water SA*, 2006. **32**(1): 43–48.
286. Eliasson, B., Kogelschatz, U., *Ozone Sci. Eng.*, 1991. **13**(3): 365–373.
287. Ivanov, V. V., Popov, N. A., Proshina, O. V., Rakhimova, T. V., Rulev, G. B., Saenko, V. B., *Tech. Phys. Lett.*, 2001. **27**(1): 29–31.
288. Gonzalez, M. C., Braun, A. M., *J. Photochem. Photobiol. A*, 1996. **93**: 7–19.
289. Oppenländer, T., Fradl, M., *Chem. Eng. Technol.*, 1999. **22**(11): 951–954.
290. Dombi, A., Ilisz, I., Laszlo, Z., Wittmann, G., *Ozone Sci. Eng.*, 2002. **24**: 49–54.
291. Chaikovskaya, O. N., Sokolov, I. V., Svetlichnyi, V. A., Kudryasheva, N. S., Fedorova, E. S., *J. Appl. Spectrosc.*, 2006. **73**(6): 829–833.
292. Baus, C., Schaber, K., Gassiot-Pintori, I., Braun, A., *Sep. Purif. Technol.*, 2002. **28**: 125–140.
293. Lopez-Gejo, J., Köhler, M., Brand, N., Betzwieser, T., Braun, A. M., Poon, B. C. Y., Lock Yue, P., Benoit-Marquie, F., Maurette, M. T., in *European Conference on UV Radiation*. 2004: Karlsruhe, September 22–24, Paper 4.3.
294. Scheytt, H., Esrom, H., Prager, L., Mehnert, R., von Sonntag, C., in *Non-Thermal Plasma Techniques for Pollution Control*, Part B, B. M. Penetrante, S. E. Schultheiss, eds. 1993, Springer-Verlag: Berlin, Germany. pp. 91–101.

3

Microphotochemistry: Photochemical Synthesis in Microstructured Flow Reactors

Oksana Shvydkiv
Dublin City University

Michael Oelgemöller
James Cook University

3.1 Introduction

Over the last decades, microtechnology has received a great deal of attention. Its application rapidly grows in many areas, as evident, for example, in electronics and engineering. The development of microstructured devices for chemical reactions was observed only within the last 10 years.[1–12] Miniaturization of chemical reactors offers many practical advantages of relevance to the pharmaceutical and fine chemicals industry.[13,14] Also, the possibility of preparing chemicals in the required volume at the point of use neglects the need to store and transport hazardous materials. The small scales of microreactions make them additionally advantageous for green chemistry.[15–19] Since light is regarded as a "clean reagent," organic photochemistry can likewise serve as a green synthetic method.[20–23] The potential of organic photochemistry as a powerful synthesis method is furthermore well documented, and a number of elegant chemo- and enantioselective transformations with high chemical and quantum yields have been realized.[24–26] The combination of microtechnology and photochemistry, that is, microphotochemistry, thus represents a promising and appealing new concept (Figure 3.1).[27–29]

3.2 From Conventional (Batch) to Micro (Flow) Photoreactors

Immersion well reactors or chamber reactors (Figure 3.2) are most commonly used in conventional laboratory-scale photochemistry.[30] The total volume of such laboratory batch systems is typically limited to 1 L. As common light sources, single low-, medium-, or high-pressure mercury lamps are used in immersion well reactors, while an array of fluorescent lamps is used for chamber reactors.

The application of batch systems for photochemical reactions has a number of disadvantages. Depending on the spectroscopic properties of the chromophoric reagent, complete light absorption is

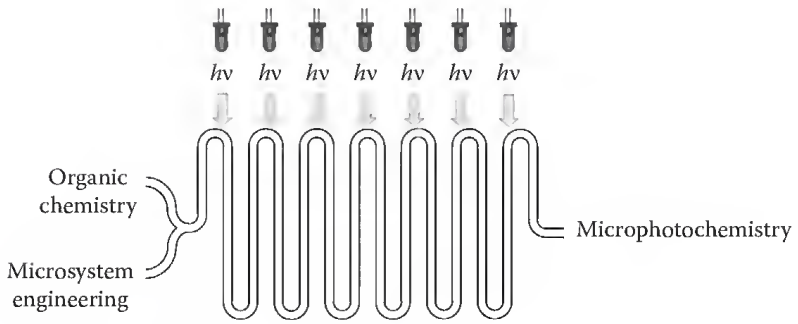

FIGURE 3.1 **(See color insert.)** The concept of microphotochemistry.

FIGURE 3.2 **(See color insert.)** Immersion well reactor (with courtesy of UV-consulting Peschl), chamber reactor (Rayonet) with Schlenk flask, and top-irradiation chamber reactor (Luzchem) with petri dishes.

typically observed within a narrow layer of the reaction solution (as expressed in the Beer–Lambert law). High dilutions are thus commonly applied to reduce this effect. In addition, photochemical processes occur most effectively closest to the light source, which limits the total irradiation volume of the reaction. Common lamps typically show emission of numerous wavelengths or of broad emission (±50 nm) at the chosen wavelength. Therefore, optical filters must be frequently applied, which reduce the energy efficiency of the lamps. Electric losses due to the generation of heat further lower the energy efficiency and require the usage of intensive water or air cooling during operations. The limited lifetime of lamps (~2000 h) additionally causes significant installation, maintenance, and operation costs. Batch processes with fixed volumes cannot be easily automated and follow-up reactions or decompositions are frequently observed. The formation of polymeric films and iron deposits on immersion wells is also common. Some novel reactor types, for example, falling-film[31,32] or spinning-disc reactors,[33,34] can reduce these effects but have not been adopted widespread.

Many of these disadvantages can be overcome by carrying out photochemical transformations in microreactors or microchips (Figure 3.3), on demand equipped with miniaturized light sources. Many microreactor devices, including complete systems as the KeyChem-Lumino reactor, are now commercially available, although many researchers continue to custom build their own devices.

Microstructured reactors are (generally, but not absolutely) reactors with three-dimensional structures, the inner parameters of which are under 1 mm in size.[1] There are two main types of "closed" microreactors, namely serpentine reactors and falling-film reactors. These reactors consist of a solid support with one or more microchannels. "Open" reactors without solid base use flexible microcapillaries instead.

The main feature of "closed" serpentine reactors is the long channel length, which can range from several centimetres to over a meter. Longer channels can be used to increase residence times, thus

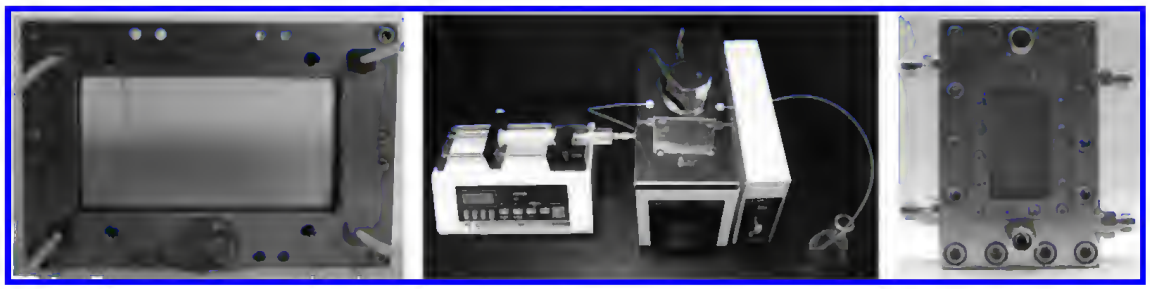

FIGURE 3.3 (See color insert.) Dwell device (Microglas), KeyChem-Lumino system (with courtesy of YMC), and falling-film reactor (IMM).

making them advantageous when prolonged irradiation is needed. On-chip mixing of reagents can be achieved using separate inlets. Multilane microreactors have also been developed and can be used for scale-up.

Falling-film reactors were specifically designed for gas–liquid reactions.[35] The central element of its design is the reaction plate on which parallel microchannels are arranged. In these channels, the liquid phase generates thin falling films that move by gravity force. The large interfacial area of up to 20,000 m^2/m^3 guarantees efficient saturation of the film with reactant gas that is flowing over the liquid phase. In contrast, closed channel devices require presaturation of the reaction mixture with reagent gas. Scale-up can be realized using cylindrical falling-film reactor models or larger channel plates.

The advantages of photochemical synthesis in microdimensioned reaction vessels were first discussed by Porter and Volman, although for batch systems.[36] Microstructured flow systems have additional characteristics, which make them beneficial for photochemical processes. The thin layers of the microchannels (100–1000 μm) ensure extensive penetration of light throughout the reaction mixture, even for relatively concentrated solutions. Microstructured devices also have a large surface-area-to-volume ratio that provides fast heat and mass transfer. The typically continuous flow mode circumvents undesired side reactions or decompositions caused by follow-up reactions. The starting reagents may be mixed directly online in a mixing channel preceding the actual reaction channel. The reagents can also be introduced to the reaction region in a specific sequence, thus removing the necessity for premixing. The irradiation time in a microreactor is easily changed, as it is directly proportional to the flow rate of the system. By changing the flow rate, product formation can be precisely controlled. The small experimental scale of microreactions reduces the total amount of waste and only requires small amounts of solvents and chemicals. The microreactor design also allows online UV[37] or IR monitoring[38] of the reaction. The small reactor size enables employing miniaturized or compact energy-saving light sources such as light-emitting diodes (LEDs).[39,40] The processes in microreactors and the microreactor itself are safer in operation and can be automated. Likewise, the reactions proceeding in a small volume can be controlled much more easily with respect to pressure, temperature, and residence time.[41] Thus, the risk of highly exothermic or explosive reactions can be reduced drastically. Microreactors can be operated in series or in parallel clusters for scale-up or optimization studies. Parallel networks of microreactors offer an efficient route to generate product volume on demand at the point of use.

3.3 Photochemical Reactions in Microreactors

A number of examples concerning photochemical performances in microreactors already exist in the literature.[27,28] Based on the conditions required, these reactions can be divided into three basic categories: homogeneous reactions (the reagents are all in the same phase, i.e., in solution), heterogeneous reactions (reactions between liquid and gaseous reagents), and catalytic reactions (reactions that involve heterogenic catalysis).

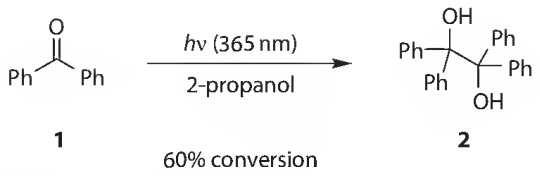

SCHEME 3.1 Photopinacolization of benzophenone.

3.3.1 Homogeneous Reactions

3.3.1.1 Photopinacolization

The photopinacolization is one of the earliest photochemical reactions that was investigated in microstructured reactors with online UV detection. Jensen and coworkers studied the transformation of benzophenone **1** using isopropanol as solvent in two house-made microreactors (Scheme 3.1).[37] One reactor was fabricated by bonding a patterned silicon wafer to a Pyrex plate. The second reactor had a sandwich structure of a silicon wafer between two quartz wafers and allowed irradiation with lower wavelengths. In this investigation, a miniaturized fluorescent UV lamp was used as a light source.

For greater conversions to benzopinacol **2**, longer residence times or lower flow rates were required. No detectable product formation was obtained for flow rates greater than 10 μL min^{-1}. With reduced flow rates, the conversion improved. An adequate flow rate was established to be 4 μL min^{-1} and showed conversions of up to 60%. At flow rates lower than 3 μL min^{-1} product **2** tended to crystallize in the microchannel, thus clogging the device. The progress of the reaction was monitored off-chip using HPLC analysis and online using UV spectroscopy. The concentration of benzophenone was 0.5 M, which is relatively high for photochemical reactions. The use of these concentrated solutions effectively demonstrated the general advantage of microstructured reactors, as the shallow channel depth of 500 μm enabled complete irradiation of the reaction mixture.

3.3.1.2 Barton Reaction

The preparation of the steroidal product **4** from substrate **3** via the Barton reaction (Scheme 3.2) was selected as a model reaction for microreactor testing.[42,43] This reaction is of importance because product **4** is a key intermediate for the synthesis of myriceric acid A (an endothelin receptor antagonist). The experiments were carried out in a glass-covered stainless steel microreactor Type A or Type B (manufactured by Dainippon Screen Mfg). Microreactor Type A had a one-lane channel of 1000 μm width, 107 μm depth, 2.2 m length, and a hold-up volume of 0.2 mL. It was used for the initial process optimization. Microreactor Type B had 16 lanes with a channel 1000 μm wide, 500 μm deep, 0.5 m long, and a hold-up volume of 4 mL. This reactor type was used for multigram-scale production.

The initial work was concentrated on increasing reaction output through an optimized and energy-saving experimental setup. Therefore, the application of three different types of transparent glass covers (quartz, soda lime glass, and Pyrex) and two light sources (300 W high-pressure Hg lamp and 15 W

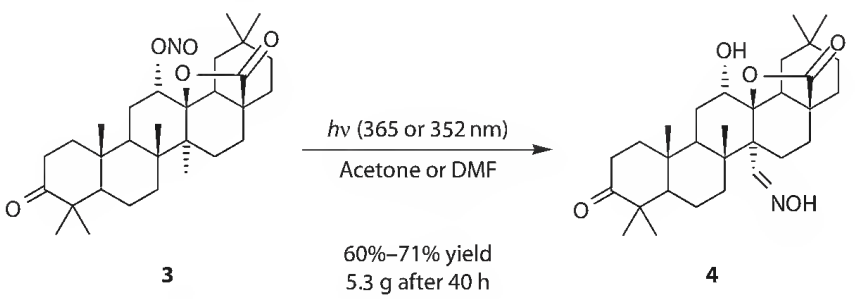

SCHEME 3.2 Barton reaction.

black light) were investigated. It was determined that Pyrex was most suited to the desired 15 W black light source. Due to the thermal instability of product **4** at temperatures greater than 50°C, the authors also examined the temperature dependence and the distance between the microreactor and the light source. Under optimized conditions, a residence time of 12 min furnished the desired product **4** in a yield of 71%. In an extension of this study, the same authors examined a UV-LED panel (48 pieces × 35 mW) as a light source suitable in combination with microreactor Type A. After a residence time of 12 min, the desired product **4** was isolated in a yield of 70%. This result clearly demonstrated that UV-LEDs, despite their low intensity (compared to high-pressure mercury lamp), have sufficient strength to initiate photochemical processes. The authors also reported a gram-scale synthesis of the target compound using two microstructured reactors Type B connected in series and coupled with 8 × 20 W black lights. After constant operation for 20 h, the amount of product **4** isolated was 3.1 g (60% yield). Encouraged by the successful gram-scale synthesis, Sugimoto and coworkers focused their forthcoming work on the development of practical and automated multigram-scale synthesis.[43] For this research, they used an automated photomicroreactor system, DS-AMS-1 (manufactured by Dainippon Screen Mfg). This system provided operation monitoring via PC software and moreover had important safety functions. It employed one set of a Type B microreactor and six small (15 W) black light lamps. After continuous operation for 40 h, product **4** was obtained in an amount of 5.3 g (61% isolated yield). This clearly demonstrated the potential for numbering up of microstructured reactors and process optimization for the larger scale production of chemicals.

3.3.1.3 Photocycloaddition Reactions

3.3.1.3.1 Photochemical [2 + 2] Cycloaddition of Cyclohex-2-Enone with Vinyl Acetate

The photochemical [2 + 2] cycloaddition reaction is one of the most powerful and versatile methods for the formation of four-membered rings and has been extensively applied in organic synthesis.[24–26] Fukuyama and coworkers selected the photochemical [2 + 2] cycloaddition of cyclohex-2-enone **5a** with vinyl acetate **6a** as a model reaction (Scheme 3.3) for testing in a commercially available microreactor dwell device (FOTURAN® glass, manufactured by mikroglas).[44] This reactor has a channel of 500 μm depth, 1000 μm width, and 1.4 m length.

A regular 300 W high-pressure mercury lamp was used as a light source in this study. After 2 h of irradiation (flow rate of 0.5 mL h^{-1}) a GC yield of 88% for the desired product **7a** was obtained. Under the same conditions, the batch reactor (10 mL Pyrex flask) furnished only 8% of **7a**. The same reaction was repeated with two microreactors in series at a flow rate of 1 mL h^{-1}, which resulted in a similar isolated yield of 85%. Thus, microstructured reactors can shorten irradiation times and increase yield at the same time.

In an extension of the work, the suitability of the photochemical [2 + 2] cycloaddition for microflow conditions was further verified and two additional cyclohexenones, **5b** and **5c**, and two additional alkenes, **6b** and **6c**, were examined (Scheme 3.4).

In all cases examined, the corresponding cycloaddition products **7b–e** were obtained in yields of 47%–70% as regioisomeric mixtures.

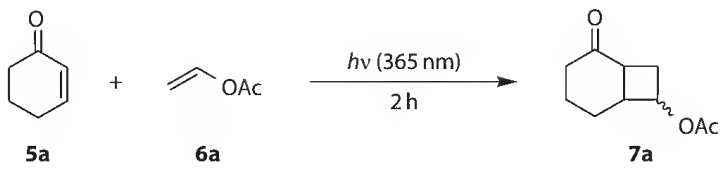

SCHEME 3.3 Photochemical [2 + 2] cycloaddition of cyclohex-2-enone with vinyl acetate.

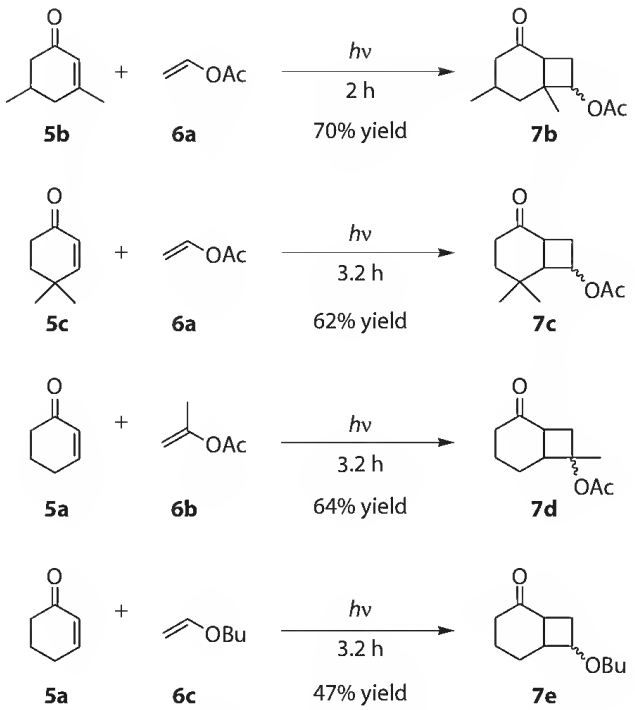

SCHEME 3.4 Photochemical [2 + 2] cycloaddition of cyclohexenones with alkenes.

3.3.1.3.2 Diastereoselective [2 + 2] Photocycloaddition of a Chiral Cyclic Enone with Cyclopentene

Asymmetric photoreactions are of special importance due to the formation of potentially biologically active natural products and unique structural compounds.[45,46] Hence Ryu and colleagues explored the utility of a microflow system in photoinduced asymmetric reactions and compared the results with those obtained using a larger volume batch reactor.[47] The model reaction examined was the reaction of the cyclohexenonecarboxylate derivative **8**, which incorporated a (–)-8-(phenyl)menthyl group as a chiral auxiliary, with cyclopentene **9** (Scheme 3.5).

A microreactor with a single channel of 1000 μm × 100 μm × 2.2 m (width × depth × length) and a hold-up volume of 0.2 mL (Dainippon Screen Mfg) was employed. A simple Pyrex test tube with an inner diameter (ID) of 13 mm was used for the batch comparison test. Both systems were irradiated simultaneously by a common high-pressure Hg lamp. The photoreaction in the microflow system reached completion in 0.5 h, which was two times faster than in the batch system (1 h). However, the ratios of stereoisomers **10** and **11** were almost identical in both systems. Additionally, the authors investigated the

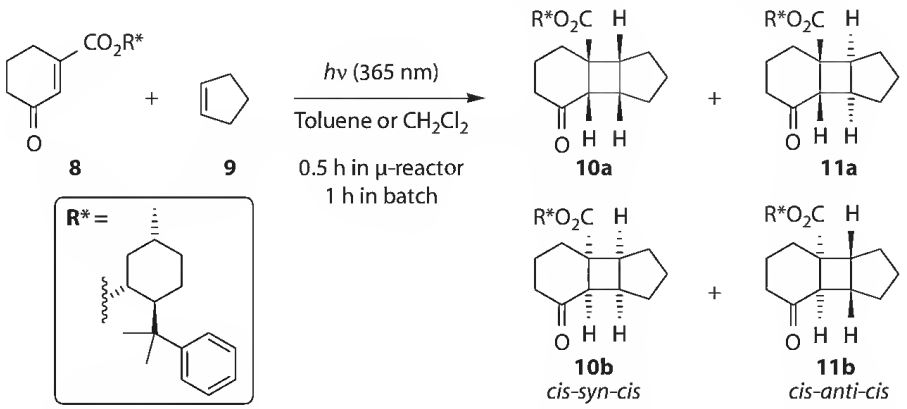

SCHEME 3.5 Diastereoselective [2 + 2] cycloaddition of a chiral cyclic enone and cyclopentene.

effect of temperature on the diastereoselectivity. The highest diastereoisomeric excess values of **10** (82%) and **11** (54%) were observed in the microflow reaction at −40°C. This was explained by a more accurate temperature control in the microflow system associated with a very large surface-area-to-volume ratio of the reaction chamber. In summary, this study has shown that a flow microreactor can be used for asymmetric photoreactions.

3.3.1.3.3 Intramolecular [2 + 2] Photocycloaddition of a 1-Cyanonaphthalene Derivative

Continuous flow microreactors have also been used in regioselectivity studies. The intramolecular [2π + 2π] photocycloaddition of 1-cyano-2-((3-methyl-2-butenyloxy) methyl) naphthalene **12** in acetonitrile has been reported by Maeda et al. (Scheme 3.6).[48] The authors in particular compared the regioselectivity and efficiency for batch and microstructured reactor conditions.

The transformation was performed in custom-built reactors made from poly(dimethylsiloxane) with channels 300 μm wide, 50 μm deep, and 45 or 202 mm long. The reaction mixture was pumped through the microchannel at two flow rates of 0.03 and 0.05 mL h^{-1} and was irradiated by a xenon lamp coupled with a UV-29 filter. The channel pathlength of 202 mm afforded prolonged reaction time and was found as optimal. After an irradiation time of 3.4 min, the intramolecular photocycloadduct at the 1,2-position of the naphthalene ring **13** and the photocycloadduct at the 3,4-position **14** were detected in a ratio of 55:7 in the microreactor, respectively. In contrast, only 5% of photocycloadduct **13** and traces of photocycloadduct **14** were noticed under batch conditions after the same reaction time. This reaction was also investigated in the batch system with a longer residence time of 180 min and photocycloadducts **13** and **14** were detected in a ratio of 56:17, respectively, but the regioselectivity was still not as good as in the microreactor. The improved regioselectivity in the microreactor was explained by the flow mode. The initially formed cycloadduct **13** is continuously removed from the system, therefore reducing photocycloreversion to **12**. Extended irradiation times gave higher yields of **14** since reversion to the starting material does not take place for this compound. The enantioselectivity was also investigated using $Eu(hfc)_3$ and a small but significant enantiomeric excess of 2% (e.e.) was determined.

3.3.1.3.4 Intramolecular [2 + 2] and [2 + 3] Photocycloadditions of 2-(2-Alkenyloxymethyl)-Naphthalene-1-Carbonitriles

Mizuno and coworkers examined other intramolecular photocycloadditions of 2-(2-alkenyloxymethyl)-naphthalene-1-carbonitriles **15a–c** (Scheme 3.7).[49] This investigation included a comparison to a batch reaction (Pyrex tube with a diameter of 8 mm) and a study on the effects of substituents, solvent, residence time, flow rate, and the microchannel dimensions.

Two microreactor types were utilized. The first (Type A) microreactor was commercially available (ICCDI05, Institute of Microchemical Technology), and was made from Pyrex glass with a channel of 100 μm width, 40 μm depth, and 120 mm length. A second (Type B) microreactor was made in-house from Pyrex plates and had a channel width of 2.5 mm, a depth of 50 μm, and a length of 60 mm. A 500 W xenon lamp was used as a light source.

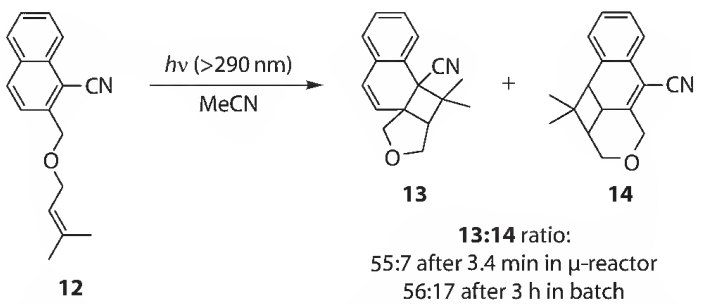

SCHEME 3.6 Intramolecular [2π + 2π] photocycloaddition of 1-cyano-2-((3-methyl-2-butenyloxy)methyl) naphthalene.

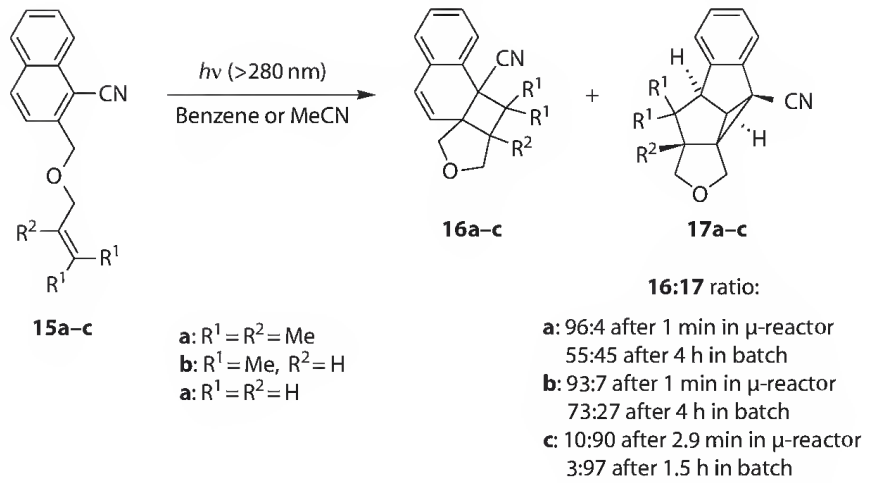

SCHEME 3.7 Intramolecular photocycloaddition of 2-(2-alkenyloxymethyl)-naphthalene-1-carbonitriles.

The irradiations performed in the microreactors allowed for increased regioselectivity and the initial photoproducts **16a–c** were selectively formed, while undesirable photocycloreversions yielding **17a–c** were suppressed. Additionally, higher conversions of 69%–75% were achieved in the microreactors after just 1 min, while the batch reactor showed a lower conversion of 74% after 3 h of irradiation. The increase in efficiency was explained by the better light penetration through the reaction medium in the microreactors compared to the batch system. It was also demonstrated that wider channels can significantly increase output while maintaining a shallow channel depth.

3.3.1.3.5 Intramolecular [2 + 2] Photocycloaddition of a Coumarin Derivative

Abbott Laboratories have recently designed a convenient flow-based photochemical microreactor named LOPHTOR.[50] The unique aspect of this new tool was its integration with an autosampler that enabled a set of conditions to be programmed and executed without human intervention. The reaction microchannels of 1000 μm width, 250 μm depth, and 3.93 m length were fabricated from stainless steel that contained integrated cooling channels on the back side. The total volume of the serpentine flow cell channels was 0.98 mL and it was sealed during operation by a fluorinated ethylene propylene (FEP) membrane using nitrogen. This membrane also created a transparent cover of the channel. A medium pressure mercury arc lamp (450 W) with concentrator and cold integral mirror was used for irradiation. On demand, selective wavelength filtering could be provided by a set of uranium-doped quartz plates.

The utility of LOPHTOR for photochemical synthesis was evaluated by the authors using the known intramolecular [2 + 2] cycloaddition of coumarin derivative **18** (Scheme 3.8) as model reaction. For comparison purposes, the same transformation was attempted in a batch mode, that is, in the roundbottom flask fitted with a magnetic stirring bar and condenser.

Initially, Vasudevan and coworkers investigated the dependency between product yields and residence time. Complete conversion of starting material **18** was achieved after 2 h in the microreactor and product **19** was isolated in a yield of 98%. In contrast, a much lower product yield of 30% was obtained

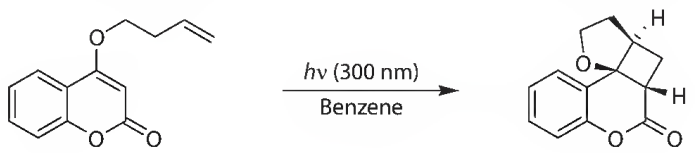

SCHEME 3.8 Intramolecular enone photocycloaddition.

in the batch system even after prolonged irradiation for 24 h. The substrate portfolio was subsequently expanded and the reaction procedure was applied to other coumarin derivatives. In all cases examined, a similar tendency was established. The product yields were significantly lower using the conventional batch photochemical setup, despite longer reaction times, and were characterized by extensive formation of side products.

The effect of the reactant concentration on the conversion of **18** to **19** was also evaluated. Five different concentrations of **18** in the range from 0.085 to 0.425 M were tested and no decrease in conversion rate was observed. This provides a convenient manner for scale-up of this process to generate hundreds of milligrams of material that will ideally suit early drug discovery applications.

3.3.1.3.6 Photochemical [2 + 2] Cycloaddition of Maleimide with 1-Hexyne and Intramolecular [5 + 2] Photocycloaddition of 3,4-Dimethyl-1-Pent-4-Enylpyrrole-2,5-Dione

The application of continuous flow technology to perform organic photochemistry on large scale was investigated by Booker-Milburn et al.[51] The main focus of this research was to show the superiority of a continuous flow system over a batch reactor with respect to the product quality, 24 h isolated yield, and nonstop functionality. This is one of the first research studies on photochemistry where simple UV-transparent FEP tubing was used as the reaction vessel. The authors described this system as a flow reactor rather than a microreactor. However, during the reactor design optimization FEP tubing with an inner diameter of 700 μm and an outer diameter (OD) of 1100 μm was used, which defines the reactor as a microchannel. Four different flow reactors were constructed with hold-up volumes from 60 up to 280 mL, which were entirely determined by the tubing length and dimensions. In two of these designs, FEP tubing with the aforementioned diameter was employed. Being interested in multigram output, Booker-Milburn and coworkers considered wider tubing with the dimensions 2700 μm ID × 3100 μm OD as optimal. One to five layers of this tubing were wrapped around a standard Pyrex or Vycor filter. An immersion well equipped with a 400 or a 600 W medium pressure Hg lamp as light sources was used as a base for this construction.

These reactors were assessed using the [2 + 2] photocycloaddition of maleimide **20** with 1-hexyne **21** to the cyclobutene product **22** and the intramolecular [5 + 2] photocycloaddition of 3,4-dimethyl-1-pent-4-enylpyrrole-2,5-dione **23a** to the bicyclic azepine **24a** as model systems (Scheme 3.9). Using an

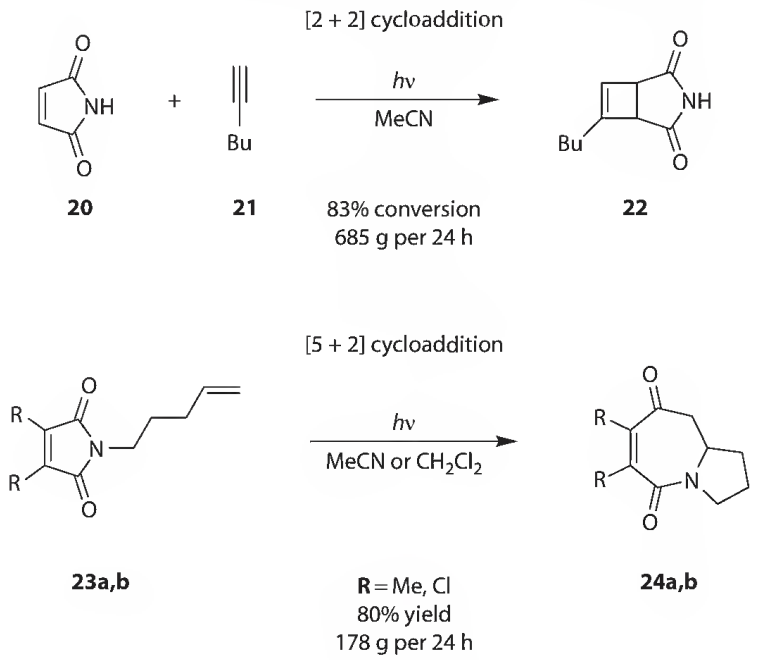

SCHEME 3.9 [2 + 2] and [5 + 2] cycloaddition reactions of maleimide and its derivatives.

optimized system with three layers of FEP tubing and a Vycor filter, these reactions were performed with outstanding results compared to common batch reactors. A 0.4 M solution of the maleimide **20** underwent 83% conversion at 0.8 mL min^{-1} flow rate representing a projected yield of the desired cyclobutene **22** of over 685 g/day. At the same flow rate a 0.1 M solution of compound **23a** was irradiated and the bicyclic azepine **24a** was isolated in a yield of 80%. This remarkable result represents a 24 h yield of 178 g of **24a**.

Using flow reactors, the residence time could be tuned by adjusting the volume of the reactor and the flow rate. Following this strategy, problematic photochemical reactions could be performed continuously, achieving the highest possible yield of product and limiting by-product formation. To demonstrate this principle, the authors selected the intramolecular [5 + 2] photocycloaddition reaction of 3,4-dichloro-1-pent-4-enyl-pyrrole-2,5-dione **23b** to the bicyclic azepine **24b** and tested it in flow and batch setups. As expected, the desired azepine **24b** was obtained in significantly higher yield in the flow reactor (45 g) compared to the batch system (0.5–1 g). The reactor was also applied to the protecting-group-free synthesis of (±)-neostenine using the [5 + 2] photocycloadditions as a key step.[52]

3.3.1.4 Photodimerization of Maleic Anhydride

An important example of a problematic photochemical reaction is the photodimerization of maleic anhydride **25** (Scheme 3.10). It is known that this reaction yields the insoluble cyclobutane tetracarboxylic dianhydride (CBTA) **26**, which is used as raw material for polyimide and for alignment films for liquid crystal displays. This reaction was selected by Yoshida and coworkers as a model reaction for a novel liquid/gas slug flow microreactor.[53]

The microreactor approach demonstrated that the clogging problem within the reactor can be overcome by a combination of slug flow and ultrasonication. Inert N_2 gas introduced into the solution flow as a spacer swept through the reactor tube and transported precipitated products in the liquid segments. At the same time, ultrasound vibrations inhibited the adhesion and sedimentation of precipitate within the reactor tube. FEP tubes of various sizes were used as the reaction vessel and the impact of the tube dimensions on product conversion was examined. Additionally, the effects of maleic anhydride concentration and residence time were also investigated. A standard 400 W high-pressure Hg lamp was employed as a light source. The experimental results showed that a 10% solution of maleic anhydride **25** underwent a satisfactory conversion of 70% after a residence time of 22 min in a FEP tube of 1.4 mm OD and 0.8 mm ID, respectively. The quality of the desired product **26** in the microreactor was of higher purity when compared to that from the batch system (cylindrical glass vessel with an ID of 75 mm and a height of 300 mm). Moreover, the unique design of the slug flow microreactor made it adaptable for continuous circulation and recycle operation. This allowed for an improvement of conversions and reduction in maleic anhydride waste. The slug flow microreactor was operated continuously for over 16 h without clogging.

3.3.1.5 Diastereodifferentiating Addition of Methanol to (*R*)-(+)-(*Z*)-Limonene

Another example of asymmetric synthesis performed in microreactors was the toluene-sensitized photoaddition of methanol to (*R*)-(+)-(*Z*)-limonene **27** (Scheme 3.11) as reported by Sakeda et al.[54] This transformation occurs with the formation of three addition products: *cis*- and *trans*-4-isopropenyl-1-methoxy-1-methylcyclohexane (*cis* **28** and *trans* **29** isomers) and exocyclic isomer **30**. Compared to

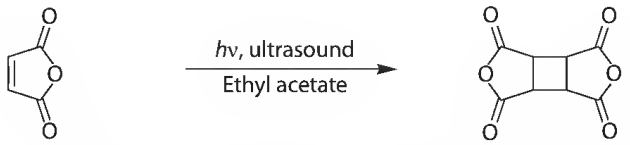

25 26% conversion after 10 min in μ-reactor **26**
26% conversion after 6 h in batch

SCHEME 3.10 Photodimerization of maleic anhydride.

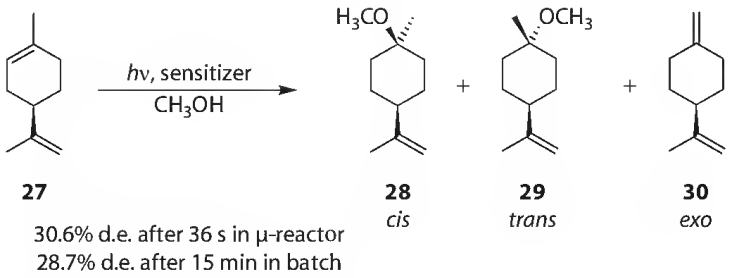

SCHEME 3.11 Diastereodifferentiating photosensitized addition of methanol to (*R*)-(+)-(*Z*)-limonene.

a microbatch cell, the authors found faster reactions and higher diastereomeric excess (d.e.) values in microchanneled reactors.

Three kinds of quartz microreactors (Shimadzu Co.) with channel sizes of 500 μm × 300 μm × 60 mm, 400 μm × 40 μm × 100 mm, and 200 μm × 20 μm × 100 mm (width × depth × length) and a quartz batch cell with a total volume of 1 mL (light passlength of 3 mm) were utilized for this study. Irradiations were conducted using a low-pressure mercury lamp (40 W, 254 nm). The irradiation time within the microchannels was controlled by the injection rate of the syringe pump. The yield of *cis* and *trans* isomers increased linearly during the examined irradiation period of 135 s within the microreactors. In contrast, the yield in the batch cell increased linearly only up to 20 min and reached a plateau. Furthermore, the diastereomeric excess value was 30.6% (36 s of irradiation) in the microreactor while it was 28.7% (15 min of irradiation) in the batch cell. The origin of the difference observed for the d.e. value in the MR versus the batch cell was clarified by the estimated reaction constants for *cis* and *trans* isomer formation. These constants were significantly higher for the microchannels than for the batch chamber. In addition, a comparison study on the effect of the channel size on the photon efficiency was performed. Photon efficiency increased with decreasing channel size and was greater for the microreactors (0.11–0.29) than the batch system (0.06). The superior performance of the microreactor was explained by a better light penetration, the higher spatial illumination homogeneity, short exposure times, and a fast and continuous product removal from the irradiated area, which suppressed side reactions.

3.3.1.6 Continuous-Flow Synthesis of Vitamin D_3

The first example of a combined photochemical and thermal reaction in a microreactor was described recently by Takahashi et al.[55] The two-step conversion of provitamin D_3 **31** to vitamin D_3 **33** via previtamin D_3 **32** was selected as a model transformation in this study (Scheme 3.12).

The first step of this transformation is a photochemical one and was carried out in a custom-made quartz microreactor with a channel 200 μm deep, 1 mm wide, 250 mm long, and with a volume of 50 μL. For the second step, a microreactor that enabled simultaneous photo- and thermal reactions was utilized. Its microchannel was 200 μm deep, 1 mm wide, and 500 mm long and had an internal volume of 100 μL.

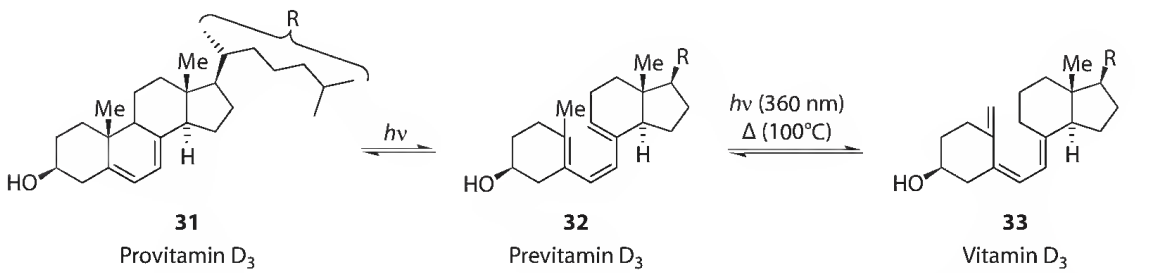

SCHEME 3.12 Two-step conversion of provitamin D_3 to vitamin D_3.

Those two microreactors were connected via polyetheretherketone (PEEK) tubing and employed a single 400 W high-pressure mercury lamp. The first reactor was irradiated through a Vycor filter (313–578 nm). The second reactor was irradiated through a combination of a Vicor and glass UV filters (360 nm) and was placed in a hot oil bath (100°C). Using this setup, an optimization study on the reaction conditions, in particular the solvent, concentration, and flow rate, was carried out. A fairly concentrated 30 mM solution of provitamin D_3 in 1,4-dioxane was introduced at a flow rate of 5 μL min^{-1} with a syringe pump. After chromatographic purification, the desired vitamin D_3 **33** was obtained in a yield of 32% (HPLC-UV yield: 60%), which was significantly higher compared to the existing industrial process, where the yield of vitamin D_3 is below 20%.[30] The parallel application of photo- and thermal conditions within the second step of the vitamin D_3 synthesis shifted the equilibrium of the competing photoisomerization of the side product tachysterol (not shown) toward previtamin D_3 **32**. Moreover the generation of second undesired product lumisterol (not shown) was suppressed to less than 10%. Consequently, the microflow synthesis of vitamin D_3 did not require any purification of intermediates or high-dilution conditions, thereby reducing the amounts of waste.

3.3.1.7 Photodecarboxylative Benzylations of Phthalimide

Recently, Oelgemöller et al. have studied photodecarboxylative benzylations of phthalimide under batch and microflow conditions.[56] The benzylated hydroxyphthalimidines **36a** and **36b** were synthesized from the corresponding phenylacetates **35a** or **35b** and phthalimide **34** (Scheme 3.13), respectively.

Conventional batch transformations were performed in a Pyrex Schlenk tube (volume 100 mL) that was irradiated in a Rayonet chamber reactor equipped with 16 UVB fluorescent lamps (8 W each, λ = 300 ± 25 nm). The dwell reactor (mikroglas) was made from Foturan™ glass and consisted of a (bottom) serpentine reaction channel (0.5 mm depth, 2 mm width, and 1.15 m length) and a top heat-exchanging channel. The microreactor was placed under a UV panel (Luzchem) fitted with five UVB lamps. Only two reactions were tested under micro conditions and improved yields of 97% (**36a**) and 98% (**36b**) were achieved after 2 h. Despite its larger lamp power, the batch reactor gave somewhat lower yields of 92% (**36a**) and 80% (**36b**) after an extended irradiation period of 3 h. The cosolvent acetone (50 Vol-%) functioned as a sensitizer and the improved performance in the microreactor was thus explained by a better light penetration through the solution. The same authors extended their study to other intra- and intermolecular photodecarboxylation reactions involving phthalimides and alkyl phenylglyoxolates.[57,58]

3.3.1.8 Photoaddition of Isopropanol to Furanones

Oelgemöller and coworkers have also investigated the 4,4′-dimethoxybenzophenone (DMBP)-sensitized addition of isopropanol **38** to furanones **37a–c** (Scheme 3.14).[59–61] The reaction was chosen as a model for a microreactor comparison study. Three types of microstructured reactor setups were examined; the dwell device (described in Section 3.3.1.7) under a UVA-panel (5 × 8 W), a microchip (Micronit

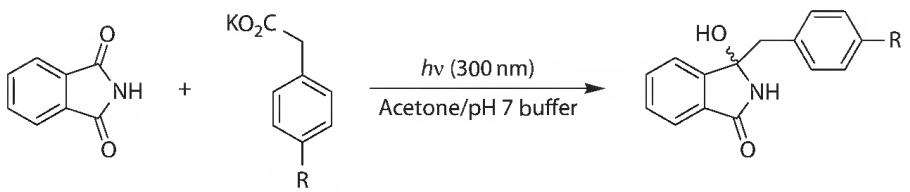

34 **35a,b** **36a,b**

a: R = Me
b: R = F

a: 97% yield after 2 h in μ-reactor
92% yield after 3 h in batch
b: 98% yield after 2 h in μ-reactor
80% yield after 3 h in batch

SCHEME 3.13 Photodecarboxylative addition of phenylacetates to phthalimide.

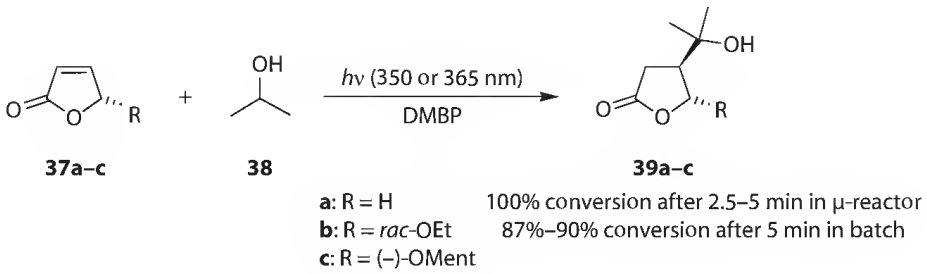

SCHEME 3.14 Sensitized isopropanol addition to furanones.

Microfluidics) incorporating a panel of 365 nm high-power UV-LEDs (6 × 75 mW), and an in-house microreactor that consisted of two parallel PTFE capillaries wrapped around a Pyrex tube containing a single UVA-lamp (1 × 8 W) in its center. Conversion rates of **37a–c** were determined by NMR spectroscopy. The results from the microflow systems were compared to those in a conventional test tube irradiated in a batch chamber reactor (Rayonet, 16 × 8 W).

The batch system, the dwell device, and the microcapillary reactor gave high to almost complete conversions to **39a–c** after just 5 min of irradiation. Despite its weaker light sources, the microchip reached high conversions already after 2.5 min. Based on the conversion rates, reactor geometries and energy efficiency calculations the microreactor systems gave superior results compared to the batch process. Of the three microreactor designs examined, the LED-driven microchip gave the best overall results. This was explained by the highest light transmission through the very shallow reaction channel of the microchip (150 μm depth), compared with the wider channel of the dwell device (500 μm depth) and the inner diameters of the microcapillary (558 μm) and the test tube (9 mm), respectively. However, the capillary reactor was seen as the best setup in terms of handling and improvement potential.

3.3.1.9 Photocyanation of Pyrene

The photocyanation of pyrene **40** (Scheme 3.15) across an oil/water interface has been described by Ueno and coworkers.[62] This transformation was performed in microchips made in-house from polystyrol substrate, with channel width of 100 μm, depth of 20 μm, and length of 350 mm. The reactors had either two or three inlets to the serpentine reaction channels. This allowed for a separate introduction of the oil and water phases, with equal flow rates, thus ensuring formation of stable water/oil or water/oil/water interfaces, respectively. The microchips were irradiated with light from a high-pressure mercury lamp (300 W) through a copper sulfate solution filter (>330 nm).

An aqueous solution of sodium cyanide (1 M) and a solution of pyrene **40** (20 mM) and 1,4-dicyanobenzene (DCB, 40 mM) in propylene carbonate were pumped through the reactors. The product, 1-cyanopyrene **41**, remained in the oil layer. After a residence time of 210 s, the photoproduct **41** was obtained in yields of 28% for the oil/water system and 73% for the water/oil/water system, respectively. Below a flow rate of 0.2 μL min^{-1} no stable oil/water interface could be obtained, which prevented further improvement of conversion rates and consequently yields.

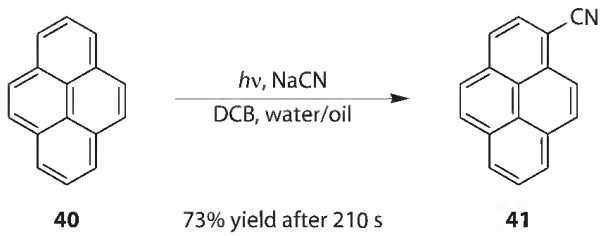

SCHEME 3.15 Photocyanation of pyrene.

3.3.2 Heterogeneous Reactions

The heterogeneous reactions are characterized by interactions between liquid and gaseous reagents. It is thus necessary to continuously provide a supply of reagent gas to the reaction media. The falling-film-type reactor was especially designed for the purpose, but other reactor systems have been utilized as well.

3.3.2.1 Photooxygenation Reactions

3.3.2.1.1 Photochemical Generation and Addition of Singlet Oxygen to α-Terpinene

The first study concerning the safe synthesis of the potentially explosive endoperoxide in a microreactor was reported by Wootton et al.[63] The photochemical synthesis of ascaridole **43** proceeds via addition of singlet oxygen to α-terpinene **42** in the presence of an organic dye as sensitizer (Scheme 3.16). This reaction requires sufficient oxygen saturation and therefore large quantities of oxygenated organic liquids with explosive nature are often formed in conventional conditions.

The reactor was built in-house from a glass substrate and consisted of two inlets at the start of the serpentine irradiation area (total length 50 mm, average depth of 50 μm, and average width of 150 μm) and an outlet channel. A methanol solution of α-terpinene and Rose Bengal was introduced via a divergent inlet channel with a flow rate of 1 μL min^{-1} and mixed with oxygen on-chip (flow rate of oxygen of 15 μL min^{-1}). This design made presaturation of the α-terpinene solution with oxygen unnecessary. Irradiation was performed using an unfiltered tungsten lamp (20 W, 6 V). The small volume of aerated solvent in the system together with nitrogen degassing of the product mixture at the outlet avoided accumulation of oxygenated solvents. The conversion of ascaridole **43** after workup was determined by GC and was 85% at a residence time of only 5 s.

3.3.2.1.2 Photochemical Generation and Addition of Singlet Oxygen to Cyclopentadiene

A further example for the safe conduction of a potentially explosive reaction in a microstructured reactor has been described by Jähnisch and Dingerdissen.[64] These authors showed that the falling-film microreactor (FFMR by IMM) is also suitable for the continuous photochemical generation of singlet oxygen in the presence of dissolved Rose Bengal. The photooxygenation of cyclopentadiene **44** by singlet oxygen, followed by the reduction to 2-cyclopenten-1,4-diol **46**, has been chosen as a model reaction (Scheme 3.17). The initially generated endoperoxide **45** is potentially explosive, which represents a safety concern for the large-scale conventional synthesis.

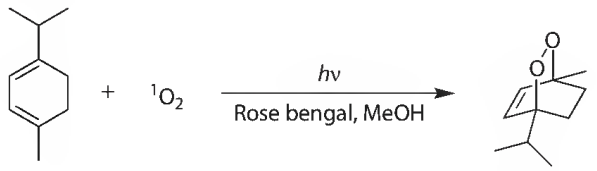

42 **43**

85% conversion after 5 s in μ-reactor
67% isolated yield after 4 h in batch

SCHEME 3.16 Photoaddition of singlet oxygen to α-terpinene.

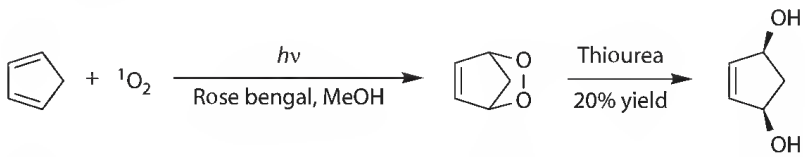

44 **45** **46**

SCHEME 3.17 Photoaddition of singlet oxygen to cyclopentadiene and subsequent reduction.

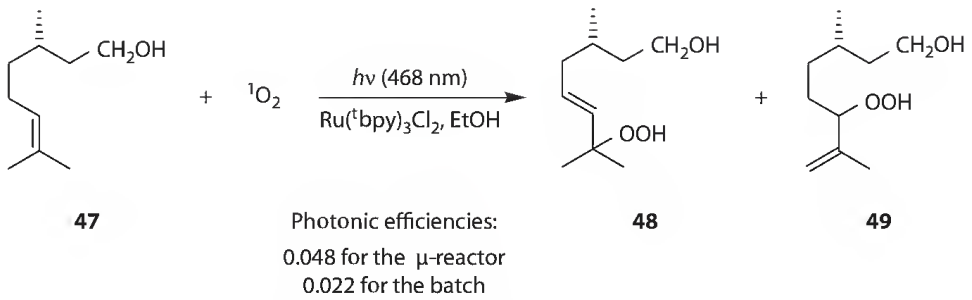

SCHEME 3.18 Sensitized photooxygenation of (*S*)-(−)-β-citronellol.

The photooxygenation step of this transformation took place in the reaction plate of the falling-film microreactor, which had 32 parallel microchannels of 66 mm length, 600 μm width, and 300 μm depth. A methanol solution of cyclopentadiene was pumped through the microreactor at a flow rate of 1 mL/min, thus creating a very thin layer of liquid. The reactor was additionally cooled to 10°C–15°C. The effluent containing the endoperoxide **45** was passed into a solution of thiourea in methanol at 10°C. The aforementioned techniques and short holdup insured that the quantity of the endoperoxide and the oxygenated solution was always kept at a safe level. As light source, a xenon lamp (1000 W) was used. The oxygen was fed to the reactor counter currently to the liquid with a flow rate of 15 L h^{-1}. Under nonoptimized conditions, the desired product 2-cyclopenten-1,4-diol **46** was obtained in a yield of 20% (0.95 g). This study proved that a falling-film microreactor is suitable for photooxygenation reactions on a preparative scale.

3.3.2.1.3 Photosensitized Oxidation of Citronellol

The photochemical oxidation of (*S*)-(−)-β-citronellol **47** is used in the fragrance industry to produce (−)-rose oxide.[65,66] The Schenck-ene reaction of **47** with singlet oxygen yields a mixture of the peroxides **48** and **49** (Scheme 3.18). This transformation was selected by Meyer and coworkers as a model reaction for a reactor comparison study based on space–time yields (STY) and photonic efficiencies.[67]

The microscale oxidation of **47** was carried out in a commercially available microstructured reactor (Little Things Factory GmbH) that was made of HT-residence glass and consisted of a single half-round serpentine channel with a width of 1 mm, depth of 0.5 mm, and a total volume of 270 μL. The reaction mixture was saturated with compressed air in a double-wall storage container outside the microreactor and was continuously pumped through the microreactor in a loop. The illumination took place for about 60–70 h using an LED array (4 × 10 LEDs, λ_{max} = 468 nm) with light intensities from 1 to 7.98 mW/cm^2. The batch experiments were performed in the modified Schlenk-tube reactor with an illuminated volume of 7.46 mL (total volume 40 mL). A LED-stick (2 × 15 LEDs, λ_{max} = 468 nm) with a light intensity of 6.5 mW/cm^2 was placed at the center of this reactor. Prior to irradiation for 5–8 h, the ethanol solution of (−)-β-citronellol was purged with compressed air for 20 min. The progress of the reaction was monitored by HPLC. The photonic efficiency for the LTF-microreactor was 0.048, which was two times higher than for the Schlenk reactor. Likewise, the STY was about one order of magnitude higher in a microreactor than in a Schlenk reactor. In contrast to the industrial process, a ruthenium complex (tris(4,4′-*tert*-butyl-2,2′-dipyridyl)-ruthenium(II)-dichloride) was used as photosensitizer. While the ruthenium complex has a higher photostability and quantum yields of singlet oxygen formation compared to Rose Bengal, a sensitizer comparison study with 450 W xenon lamp (λ = 50–1600 nm) showed that Rose Bengal is about twice as efficient as the ruthenium complex.

3.3.2.2 Photochlorination Reaction

The portfolio of heterogeneous reactions is not limited to photooxygenations.[35,68,69] The selective photochlorination of toluene-2,4-diisocyanate **50** (TDI, Scheme 3.19) was examined by Jähnisch et al. in a falling-film reactor (IMM).[68] The main product of this transformation, 1-chloromethyl-2,4-diisocyanatobenzene **51** (1Cl-TDI), is used industrially as an intermediate in the synthesis of polyurethanes.[30]

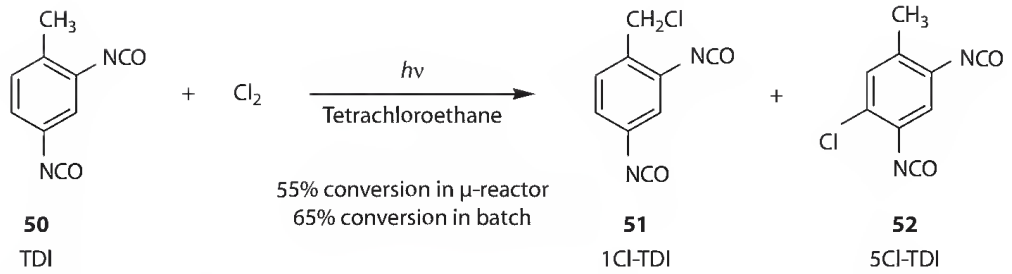

SCHEME 3.19 Photochlorination of toluene-2,4-diisocyanate.

The experiments were carried out using a reaction plate with 32 parallel channels of 600 μm width, 300 μm depth, and 66 mm length each. A relatively concentrated solution of toluene-2,4-diisocyanate **50** (100 mmol in 30 mL of tetrachloroethane) was introduced to the reactor at flow rates ranging from 0.12 (residence time of 14 s) to 0.57 mL/min (residence time of 5 s) and was irradiated by the xenon lamp (1000 W, unfiltered) through the quartz window of the reactor. The backside of the reaction plate was kept at a temperature of 130°C to reduce the undesired side reaction to the ring chlorinated product toluene-5-chloro-2,4-diisocyanate (5Cl-TDI) **52**. The conversion of TDI **50** drastically increased from 30% to 81% when increasing the residence time from 5 to 14 s, while the selectivity of the target product 1Cl-TDI **51** decreased somewhat from 80% to 67%. The yield of 1Cl-TDI **51** improved from 24% after 5 s to 54% after 14 s. The effect of the reactor material was investigated by using different reaction plates, one nickel and one iron. The selectivity of the desired product **51** was affected notably by the plate material (50% for iron, 67% for nickel) and this was explained by the formation of $FeCl_3$, which functions as a Lewis acid.

For comparison, batch reactions were carried out in the glass flask using a high-pressure mercury lamp as a light source. At similar conversion rates of toluene-2,4-diisocyanate **50** (55% in FFMR, 65% in batch), the selectivity for the target product 1Cl-TDI **51** was 80% under micro- and only 45% under batch conditions. In addition, the selectivity to the ring-chlorinated by-product (5Cl-TDI) **52** was significantly higher in the batch reactor (54%) compared to the FFMR (5%). The space–time yield achieved in the microstructured reactor (401 mol L^{-1} h^{-1}) for the formation of product **51** was orders of magnitude higher compared to the conventional reactor (1.3 mol L^{-1} h^{-1}). The advanced performance of photochlorination reaction in falling-film microreactor was explained by the better penetration of photons and the higher mass-transfer rates in the thinner liquid films. Also the chlorine radicals are located over the total film volume and high local concentration, which leads to recombination, are avoided. In a conventional reactor, the radical concentration near the light source is high, while at the center of the reactor it is very low. As a result, the selectivity of the desired side-chain chlorinated derivatives decreases and prefers to take place at the aromatic core instead.

Recently, Ryu and coworkers have studied the photochlorination of cycloalkanes using various microflow reactors.[70] Monochlorination of cyclohexane to chlorocyclohexane was achieved using natural light and molecular chlorine. Likewise, the reactions of various cycloalkanes with sulfuryl chloride were successfully realized with high monochlorination selectivity using a 15 W black light.

3.3.3 Catalytic Reactions

Due to their large surface-to-volume ratios, microreactors are especially interesting for use in catalytic reactions. Immobilization of a catalyst on the channel walls consequently increases the specific illuminated surface area of the photocatalyst and subsequently maximizes interactions of catalyst material with light and reagents. The product is simply separated from the catalyst by the flow and this feature can also improve the selectivity of the process. One of the most widely used heterogeneous photocatalyst is titanium dioxide (TiO_2).[71]

Catalytic microphotoreactors have been particularly studied for the treatment of waste water and exhaust air,[40,72–79] while synthetic applications are rather rare.

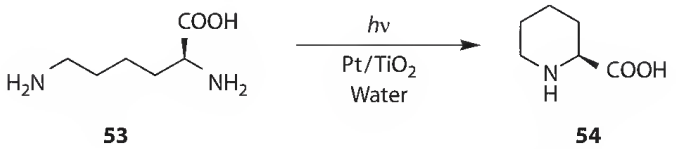

SCHEME 3.20 Photocatalytic synthesis of L-pipecolinic acid.

3.3.3.1 Photocatalytic Synthesis of L-Pipecolinic Acid

The first application of a photocatalytic microsystem in organic synthesis has been reported by Takei et al.[80] The authors studied the photocatalytic synthesis of L-pipecolinic acid **54** (L-PCA) from L-lysine **53** (Scheme 3.20) in a home-made microchip. The titania-modified microchannel chip (TMC) used in this study was composed of two Pyrex glass substrates. One substrate with branched channels of 700 μm wide and 3.5 μm deep was fused to another substrate with a 300 nm thick coating of TiO_2. The TiO_2 coating served as catalyst and was made of particles with a diameter of 100 nm. The film contained platinum as reducing agent at 0.2 wt%. A high-pressure mercury lamp with a UV transmitting filter was used for irradiations.

A 2 mM aqueous solution of L-lysine was pumped through the microchip at different flow rates. The crude product mixture was collected from the reactor outlet and was analyzed by HPLC. The results were compared to a batch system comprising a bulk cuvette and TiO_2 particles (diameter 25 nm) in suspension. It is notable that the ratio of illuminated surface area to the solution volume was comparable in both setups (0.29 m^2/mL for the TMC and 0.25 m^2/mL for suspended particles). The conversion of L-lysine **53** to L-pipecolinic acid **54** in the microchip reached 87% after a residence time of less than 1 min (0.86 min). In the batch experiment the same conversion rate of 86% was achieved only after 1 h. Analysis of selectivity and enantiomeric excess (e.e.) revealed that these parameters were independent of reaction time and were similar in the micro- and bulk setup (selectivity was 22% and e.e. was 50% and 47%).

In contrast, the productivity for L-PCA **54**, that is, the amount produced per minute, was much lower in the microchip (2.8×10^{-10} mol/min) compared to the bulk system (1.9×10^{-8} mol/min). This was due to the larger volume of the batch cuvette (4 mL), but this disadvantage may be overcome through numbering up of microreactors in the future. A significant advantage of the catalytic microstructured reactor is the exclusion of the separation step, as the immobilized photocatalyst remains in the microchannel while the product is eluted.

3.3.3.2 Photocatalytic N-Alkylation of Amines

Synthetic photocatalysis in microstructured reactors has been intensively studied by Matsushita and Ichimura et al.[72,81] In their work they used not only miniaturized reactors but also miniaturized light source such as UV-LED arrays. A remarkable example was the TiO_2-catalyzed N-ethylation of benzylamine **55** (Scheme 3.21).

This reaction was studied in three house-made quartz microreactors with specific illuminated surface areas per unit of volume of 7.3×10^3, 6.0×10^3, and 4.0×10^3 m^2/m^3, respectively. These large areas

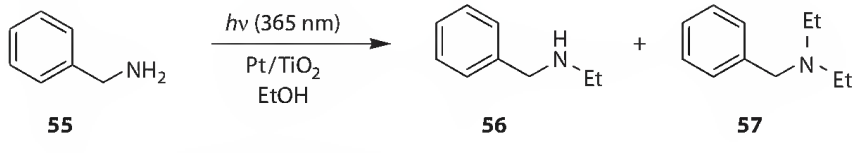

SCHEME 3.21 *N*-ethylation of benzylamine.

were realized in reactor channels with a width of 500 μm, length of 40 mm, and depth of 300, 500, or 1000 μm, respectively. The sides and bottom of the channels were coated with TiO_2 catalyst (Pt-loaded and Pt-free). A 1 mM alcohol solution of benzylamine **55** was fed into the microreactors at a flow rate between 2 and 40 μL/min and was irradiated with an UV-LED array (λ_{max} = 365 nm) with a total optical power output of 9.8 mW. The product solutions were analyzed by GC or HPLC methods. Benzylamine **55** could be converted in high selectivity to the N-alkylated product **56** in yields of 43% after just 90 s or 85% after 150 s, respectively.

Ethanol was found to be the most suitable solvent for this transformation due to the kinetic stability of its ethoxy radical intermediate. Consequently, ethanol was applied for alkylation reactions of other amines. Aniline and butylamine were tested and gave the corresponding N-ethylated products in yields of 11% and 36%, respectively, after a residence time of 180 s.

The effect of the depth of the microchannel was also examined and showed that the efficiency of N-alkylation was enhanced with decreasing channel depth. This observation was attributed to the increased illuminated surface-to-volume ratio.

Remarkably, this reaction proceeded in the presence of titanium dioxide photocatalyst, even without cocatalyst platinum and yields of up to 98% of N-alkylated product **56** were achieved after 90 s. In contrast to other studies,[82] N-alkylation did not occur under batch conditions without the presence of platinum. Selectivity was high in the microreactors and no N,N-dialkylated product **57** was obtained in the presence or absence of platinum. This was achieved by the continuous-flow mode and monochromatic irradiation, which prevented the undesired follow-up reaction. In contrast, bis-alkylation is frequently observed under batch conditions.

The authors further expanded their study on the N-alkylation of amines by optimizing the irradiation and flow conditions.[83] A novel photocatalytic microreaction system with a microchannel 500 μm wide, 25 μm deep, and 50 mm long was developed. The high surface area of TiO_2/Pt photocatalyst ($4.0 \times 10^3 m^2/m^3$) achieved was irradiated with a more powerful LED array (total optical power output 490 mW). In this microsystem, the alkylation of amines (benzylamine, aniline, and piperidine) proceeded faster compared to the previously described model. For example, *N*-ethylbenzylamine **56** was obtained in a yield of 62% after 6 s, however, the bis-alkylated product *N*,*N*-diethylbenzylamine **57** was also detected in 3.8% yield. The same trend was noticed for aniline. At a shorter residence time (5 s), the formation of the main product **56** increased with increasing light intensity, whereas at a prolonged residence time (60 s), the formation of the tertiary amine **57** enhanced with increasing light intensity. These results clearly demonstrate that the outcome of the reaction (mono- vs. bis-alkylation) can be controlled by precise control of the irradiation and flow conditions.

3.3.3.3 Photocatalytic Reduction in Microreactors

Another example of a synthetically useful transformation has been also reported by Matsushita et al.[84] The authors examined the photocatalytic reduction of benzaldehyde **58** and nitrotoluene **60** (Scheme 3.22) in microreactors.

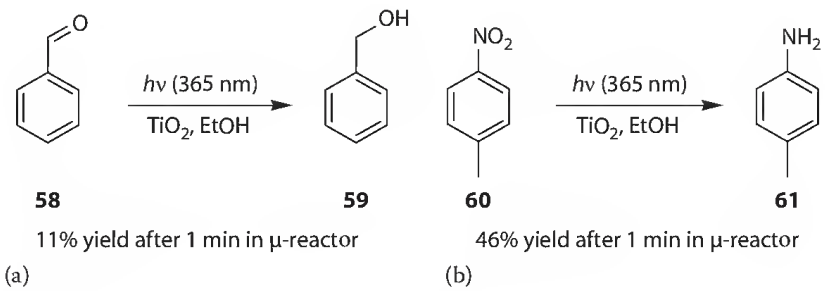

SCHEME 3.22 Photocatalytic reduction of (a) benzaldehyde and (b) nitrotoluene.

For this study, photocatalytic quartz microreactors with immobilized photocatalyst were fabricated. These reactors contained a microchannel of 500 µm width, 100 µm depth, and 40 mm length with a total specific illuminated surface area per unit of liquid of approximately $1.4 \times 10^4 m^2/m^3$. The bottom and side walls of the microchannel were coated with a TiO_2 layer. An array of 365 nm UV-LEDs with an optical power output of 1.4 mW was employed as a light source.

Alcoholic solutions of benzaldehyde **58** (0.1 mM) saturated with nitrogen were used. Ethanol was found to be the most efficient solvent and gave a yield of benzyl alcohol **59** of 11% after 60 s. Photoreduction of *p*-nitrotoluene **60** gave *p*-toluidine **61** in yields of 46% after 60 s. Although the reactions were not further optimized, they demonstrated that microstructured reactor can be utilized for the efficient reduction of organic compounds.

3.3.4 Microphotochemistry in Industry

The reactions described earlier have been performed on laboratory scales. However, isolated examples of gram-scale synthesis have been achieved.[42,43,51] In contrast, photochemical processes realized on industrial scale are still rare. There are several contributing factors for this neglect. Microreactors are generally made from expensive materials, such as stainless steel or quartz glass. The fabrication of reactor microchannels is also costly and complicated. Despite the increased utilization of energy-efficient LEDs as light sources for photochemical reactions, medium- and high-pressure mercury lamps are still predominantly used in industry. These conventional lamps are costly to run, have a limited lifetime, and additionally tend to generate a large amount of heat and therefore require additional cooling systems. In contrast, product synthesis in kilograms quantity using microreactor clusters requires complex automation and control devices.

Nevertheless, the proven advantages of photochemical synthesis in microreactors make it an interesting synthesis tool for low-volume processes.

3.3.4.1 Synthesis of 10-Hydroxycamptothecin and 7-Alkyl-10-Hydroxycamptothecin

The first industrial production of camptothecin derivatives using a microphotoreactor plant was realized by Heraeus.[85] The synthesis of 10-hydroxycamptothecin **63a** and 7-ethyl-10-hydroxycamptothecin **63b** from camptothecin-*N*-oxide **62a** or 7-ethyl camptothecin-*N*-oxide **62b** (Scheme 3.23) was performed in this plant. Compounds **63a** and **63b** are precursors in the synthesis of the anticancer drugs irinotecan and topotecan.

The developed plant consisted of twelve microreactors operated in parallel and irradiated by individual light sources (Figure 3.4). The microreactors themselves are characterized by their simple design. They comprise of two parallel quartz glass separated by a spacer, which creates a gap from 40 to 100 µm. The design produces a very thin film of the reaction solution. As light source, mercury high-pressure emitters (Heraeus Noblelight) with a UV emission wavelength range from 350 to 400 nm and an optical power output of 250 W were used. These lamps also comprised spectral filters with a specific band pass and coating on both sides.

The productivity of the microreactor plant was evaluated using the amount of 10-hydroxycamptothecin **63a** produced within 24 h. At conversion rate of 95% of **62a**, the desired product **63a** is produced in

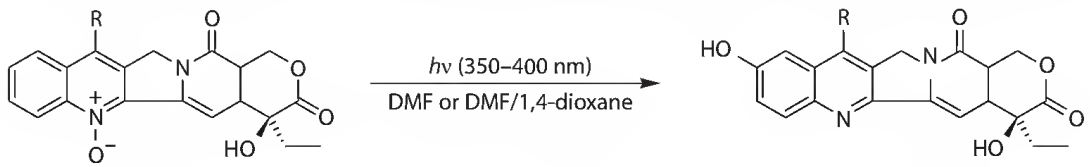

62a,b
Camptothecin-*N*-oxide

a: R = H 2 kg/day
b: R = Et

63a,b
10-hydroxycamptothecin

SCHEME 3.23 Synthesis of camptothecin derivatives.

FIGURE 3.4 **(See color insert.)** Photochemical production plant. (Courtesy of Heraeus.)

an amount of 2 kg/day (yield 90%). In contrast, the batch system reached a maximum conversion of only 85% and a much lower product yield of 50%. Moreover, the concentration of the camptothecin-*N*-oxide solution used in the microsystem (0.6 wt%) was six times higher than in the batch system (0.1 wt%).

This remarkable process represents the first example of a photochemical production in a microreactor array.

3.4 Concluding Remarks

The examples presented in this chapter clearly demonstrate the versatility and potential of microphotochemistry as a synthesis tool. Microstructured reactors have been successfully used for a broad range of photochemical reaction types. The technology takes full advantage of the small dimensions and flow condition of microtechnology. This results in the reduction or complete elimination of side reactions, enhanced selectivity, increased photonic efficiency, and reduction of hazards and wastes. The large area-to-volume ratio within the microchannels is especially advantageous for photocatalytic applications. It is hoped that microphotochemistry will emerge as an important future R&D tool, for example in modern lead development processes, and ultimately as a production technology. The Heraeus process clearly demonstrates this potential. Consequently, microphotochemistry may emerge as "the new photochemistry of the future." This statement refers to Giacomo Ciamician's visionary lecture, presented before the International Congress of Applied Chemistry in New York in 1912.[86]

Acknowledgments

Financial support for our work on microphotochemistry was provided by Science Foundation Ireland (SFI, 07/RFP/CHEF817), the Environmental Protection Agency (EPA, 2008-ET-MS-2-S2), and the Department of Environment, Heritage and Local Government (DEHLG, 2008-S-ET-2). We also thank Dr. Thomas Dietrich (mikroglas chemtech), Prof. André Braun (Quantapplic), Günther Peschl (UV-Consulting Peschl), and Dr. Silvia Werner (Heraeus) for useful discussions and support.

References

1. K. Jähnisch, V. Hessel, H. Löwe, and M. Baerns, Chemistry in microstructured reactors, *Ang. Chem., Int. Ed.*, 2004, 43, 406–446.
2. B. Ahmed-Omer, J. C. Brandt, and T. Wirth, Advanced organic synthesis using microreactor technology, *Org. Biomol. Chem.*, 2007, 5, 733–740.

3. T. Van Gerven, G. Mul, J. Moulijn, and A. Stankiewicz, A review of intensification of photocatalytic processes, *Chem. Eng. Process*, 2007, 46, 781–789.
4. P. Watts and C. Wiles, Recent advances in synthetic micro reaction technology, *Chem. Commun.*, 2007, 443–467.
5. P. Watts and C. Wiles, Micro reactors: A new tool for the synthetic chemist, *Org. Biomol. Chem.*, 2007, 5, 727–732.
6. P. D. I. Fletcher, S. J. Haswell, E. Pombo-Villar, B. H. Warrington, P. Watts, S. Y. F. Wong, and X. Zhang, Micro reactors: Principles and applications in organic synthesis, *Tetrahedron*, 2002, 58, 4735–4757.
7. K. Geyer, J. D. C. Codée, and P. H. Seeberger, Microreactors as tools for synthetic chemists—The chemists' round-bottomed flask of the 21st century? *Chem. Eur. J.*, 2006, 12, 8434–8442.
8. V. Hessel and H. Löwe, Organic synthesis with microstructured reactors, *Chem. Eng. Technol.*, 2005, 28, 267–284.
9. P. Watts and S. J. Haswell, The application of microreactors for small scale organic synthesis, *Chem. Eng. Technol.*, 2005, 28, 290–301.
10. D. Webb and T. F. Jamison, Continuous flow multi-step organic synthesis, *Chem. Sci.*, 2010, 1, 675–680.
11. H. Pennemann, P. Watts, S. J. Haswell, V. Hessel, and H. Löwe, Benchmarking of microreactor applications, *Org. Proc. Res. Dev.*, 2004, 8, 422–439.
12. T. Fukuyama, M. T. Rahman, M. Sato, and I. Ryu, Adventures in inner space: Microflow systems for practical organic synthesis, *Synlett*, 2008, 151–163.
13. A. E. Rubin, S. Tummala, D. A. Both, C. C. Wang, and E. J. Delaney, Emerging technologies supporting chemical process R & D and their increasing impact on productivity in the pharmaceutical industry, *Chem. Rev.*, 2006, 106, 2794–2810.
14. A. de Mello and R. Wootton, But what is it good for? Applications of microreactor technology for the fine chemical industry, *Lab Chip*, 2002, 2, 7N–13N.
15. B. P. Mason, K. E. Price, J. L. Steinbacher, A. R. Bogdan, and D. T. McQuade, Greener approaches to organic synthesis using microreactor technology, *Chem. Rev.*, 2007, 107, 2300–2318.
16. V. Hessel, D. Kralisch, and U. Krtschil, Sustainability through green processing—novel process windows intensify micro and milli process technologies, *Energy Environ. Sci.*, 2008, 1, 467–478.
17. D. Kralisch and G. Kreisel, Assessment of the ecological potential of microreaction technology, *Chem. Eng. Sci.*, 2007, 62, 1094–1100.
18. S. J. Haswell and P. Watts, Green chemistry: Synthesis in micro reactors, *Green Chem.*, 2003, 5, 240–249.
19. J. J. Lerou, A. L. Tonkovich, L. Silva, S. Perry, and J. McDaniel, Microchannel reactor architecture enables greener processes, *Chem. Eng. Sci.*, 2010, 65, 380–385.
20. S. Protti, D. Dondi, M. Fagnoni, and A. Albini, Assessing photochemistry as a green synthetic method. Carbon–carbon bond forming reactions, *Green Chem.*, 2009, 11, 239–249.
21. C. L. Ciana and C. G. Bochet, Clean and easy photochemistry, *Chimia*, 2007, 61, 650–654.
22. M. Oelgemöller, C. Jung, and J. Mattay, Green photochemistry: Production of fine chemicals with sunlight, *Pure Appl. Chem.*, 2007, 79, 1939–1947.
23. A. Albini and M. Fagnoni, Green chemistry and photochemistry were born at the same time, *Green Chem.*, 2004, 6, 1–6.
24. N. Hoffmann, Photochemical reactions as key steps in organic synthesis, *Chem. Rev.*, 2008, 108, 1052–1103.
25. M. Demuth and G. Mikhail, New developments in the field of photochemical syntheses, *Synthesis*, 1989, 145–162.
26. P. Magaretha, Preparative organic photochemistry, *Top. Curr. Chem.*, 1982, 103, 1–89.
27. E. E. Coyle and M. Oelgemöller, Micro-photochemistry: Photochemistry in microstructured reactors. The new photochemistry of the future, *Photochem. Photobiol. Sci.*, 2008, 7, 1313–1322.

28. M. Oelgemöller and O. Shvydkiv, Recent advances in microflow photochemistry, *Molecules*, 2011, 16, 7522–7550.
29. Y. Matsushita, T. Ichimura, N. Ohba, S. Kumada, K. Sakeda, T. Suzuki, H. Tanibata, and T. Murata, Recent progress on photoreactions in microreactors, *Pure Appl. Chem.*, 2007, 79, 1959–1968.
30. A. M. Braun, M. Maurette, and E. Oliveros, *Photochemical Technology*, Wiley: Chichester, U.K., 1991.
31. A. G. Griesbeck, W. Kramer, and M. Oelgemöller, Photoinduced decarboxylation reactions. Radical chemistry in water, *Green Chem.*, 1999, 1, 205–207.
32. A. G. Griesbeck, N. Maptue, S. Bondock, and M. Oelgemöller, The excimer radiation system: A powerful tool for preparative organic photochemistry. A technical note, *Photochem. Photobiol. Sci.*, 2003, 2, 450–451.
33. B. Dunk and R. Jachuck, A novel reactor for UV irradiated reactions, *Green Chem.*, 2000, 2, G13–G14.
34. H. C. Yatmaz, C. Wallis, and C. R. Howarth, The spinning disc reactor—studies on a novel TiO_2 photocatalytic reactor, *Chemosphere*, 2001, 42, 397–403.
35. K. Jähnisch, M. Baerns, V. Hessel, W. Ehrfeld, V. Haverkamp, H. Löwe, Ch. Wille, and A. Cuber, Direct fluorination of toluene using elemental fluorine in gas/liquid microreactors, *J. Fluorine Chem.*, 2000, 105, 117–128.
36. K. Porter and D. H. Volman, Microphotochemistry in liquid systems. The photolysis of propionaldehyde in aqueous solutions, *Bull. Soc. Chim. Belg.*, 1962, 71, 831–836.
37. H. Lu, M. A. Schmidt, and K. F. Jensen, Photochemical reactions and on-line UV detection in microfabricated reactors, *Lab Chip*, 2001, 1, 22–28.
38. U. Bentrup, L. Küpper, U. Budde, K. Lovis, and K. Jähnisch, Mid-infrared monitoring of gas-liquid reactions in Vitamin D analogue synthesis with a novel fiber optical diamond ATR sensor, *Chem. Eng. Technol.*, 2006, 29, 1216–1220.
39. S. Landgraf, Application of semiconductor light sources for investigations of photochemical reactions, *Spectrochim. Acta, Part A*, 2001, 57, 2029–2048.
40. G. Kreisel, S. Meyer, D. Tietze, T. Fidler, R. Gorges, A. Kirsch, B. Schäfer, and S. Rau, Leuchtdioden in der Chemie—eine Hochzeit verschiedener Technologien, *Chem. Ing. Tech.*, 2007, 79, 153–159.
41. S. Marre, J. Baek, J. Park, M. G. Bawendi, and K. F. Jensen, High-pressure/high-temperature microreactors for nanostructure synthesis, *J. Assoc. Lab. Autom.*, 2009, 14, 367–373.
42. A. Sugimoto, Y. Sumino, M. Takagi, T. Fukuyama, and H. Ryu, The Barton reaction using a microreactor and black light. Continuous flow synthesis of a key steroid intermediate for an endothelin receptor antagonist, *Tetrahedron Lett.*, 2006, 47, 6197–6200.
43. A. Sugimoto, T. Fukuyama, Y. Sumino, M. Takagi, and I. Ryu, Microflow photo-radical reaction using a compact light source: Application to the Barton reaction leading to a key intermediate for myriceric acid A, *Tetrahedron*, 2009, 65, 1593–1598.
44. T. Fukuyama, Y. Hino, N. Kamata, and I. Ryu, Quick execution of [2 + 2] type photochemical cycloaddition reaction by continuous flow system using a glass-made microreactor, *Chem. Lett.*, 2004, 33, 1430–1431.
45. Y. Inoue, Asymmetric photochemical reactions in solution, *Chem. Rev.*, 1992, 92, 741–770.
46. A. G. Griesbeck and U. J. Meierhenrich, Asymmetric photochemistry and photochirogenesis, *Angew. Chem. Int. Ed.*, 2002, 42, 3147–3154.
47. K. Tsutsumi, K. Terao, H. Yamaguchi, S. Yoshimura, T. Morimoto, K. Kakiuchi, T. Fukuyama, and I. Ryu, Diastereoselective [2 + 2] photocycloaddition of chiral cyclic enone and cyclopentene using a microflow reactor system, *Chem. Lett.*, 2010, 39, 828–829.
48. H. Maeda, H. Mukae, and K. Mizuno, Enhanced efficiency and regioselectivity of intramolecular ($2\pi + 2\pi$) photocycloaddition of 1-cyanonaphthalene derivative using microreactors, *Chem. Lett.*, 2005, 34, 66–67.
49. H. Mukae, H. Maeda, S. Nashihara, and K. Mizuno, Intramolecular photocycloaddition of 2-(2-alkenyloxymethyl)naphthalene-1-carbonitriles using glass-made microreactors, *Bull. Chem. Soc. Jpn.*, 2007, 80, 1157–1161.

50. A. Vasudevan, C. Villamil, J. Trumbull, J. Olson, D. Sutherland, J. Pan, and S. Djuric, LOPHTOR: A convenient flow-based photochemical reactor, *Tetrahedron Lett.*, 2010, 51, 4007–4009.
51. B. D. A. Hook, W. Dohle, P. R. Hirst, M. Pickworth, M. B. Berry, and K. I. Booker-Milburn, A practical flow reactor for continuous organic photochemistry, *J. Org. Chem.*, 2005, 70, 7558–7564.
52. M. D. Lainchbury, M. I. Medley, P. M. Taylor, P. Hirst, W. Dohle, and K. I. Booker-Milburn, A protecting group free synthesis of (±)-neostenine via the [5 + 2] photocycloaddition of meleimides, *J. Org. Chem.*, 2008, 73, 6497–6505.
53. T. Horie, M. Sumino, T. Tanaka, Y. Matsushita, T. Ichimura, and J. Yoshida, Photodimerization of maleic anhydride in a microreactor without clogging, *Org. Process Res. Dev.*, 2010, 14, 405–410.
54. K. Sakeda, K. Wakabayashi, Y. Matsushita, T. Ichimura, T. Suzuki, T. Wada, and Y. Inoue, Asymmetric photosensitized addition of methanol to (*R*)-(+)-(*Z*)-limonene in a microreactor, *J. Photochem. Photobiol., A*, 2007, 192, 166–171.
55. S. Fuse, N. Tanabe, M. Yoshida, H. Yoshida, T. Doi, and T. Takahashi, Continuous-flow synthesis of vitamin D_3, *Chem. Commun.*, 2010, 46, 8722–8724.
56. V. Belluau, P. Noeureuil, E. Ratzke, A. Skvortsov, S. Gallagher, C. A. Motti, and M. Oelgemöller, Photodecarboxylative benzylations of phthalimide in pH 7 buffer: A simple access to 3-arylmethyleneisoindolin-1-ones, *Tetrahedron Lett.*, 2010, 51, 4738–4741.
57. O. Shvydkiv, S. Gallagher, K. Nolan, and M. Oelgemöller, From conventional to microphotochemistry: Photodecarboxylation reactions involving phthalimides, *Org. Lett.*, 2010, 12, 5170–5173.
58. S. B. Tan, O. Shvydkiv, J. Fiedler, F. Hatoum, K. Nolan, and M. Oelgemöller, Photodecarboxylative additions of α-thioalkyl-substituted carboxylates to alkyl phenylglyoxolates, *Synlett*, 2010, 2240–2243.
59. O. Shvydkiv, A. Yavorskyy, K. Nolan, A. Youssef, E. Riguet, N. Hoffmann, and M. Oelgemöller, Photosensitized addition of isopropanol to furanones in a 365 nm UV-LED microchip, *Photochem. Photobiol. Sci.*, 2010, 9, 1601–1603.
60. A. Yavorskyy, O. Shvydkiv, K. Nolan, N. Hoffmann, and M. Oelgemöller, Photosensitized addition of isopropanol to furanones in a continuous-flow dual capillary microreactor, *Tetrahedron Lett.*, 2011, 52, 278–280.
61. O. Shvydkiv, A. Yavorskyy, S. B. Tan, K. Nolan, N. Hoffmann, A. Youssef, and M. Oelgemöller. Microphotochemistry—a reactor comparison study using the photosensitized addition of isopropanol to furanones as a model reaction, *Photochem. Photobiol. Sci.*, 2011, 10, 1399–1404.
62. K. Ueno, F. Kitagawa, and N. Kitamura, Photocyanation of pyrene across an oil/water interface in a polymer microchannel chip, *Lab Chip*, 2002, 2, 231–234.
63. R. C. R. Wootton, R. Fortt, and A. J. de Mello, A microfabricated nanoreactor for safe, continuous generation and use of singlet oxygen, *Org. Proc. Res. Dev.*, 2002, 6, 187–189.
64. K. Jähnisch and U. Dingerdissen, Photochemical generation and [4 + 2]-cycloaddition of singlet oxygen in a falling-film microreactor, *Chem. Eng. Technol.*, 2005, 28, 426–427; K. Jähnisch and U. Dingerdissen, Photochemische Erzeugung und [4 + 2]-Cycloaddition von Singulett-Sauerstoff im Mikrofallfilmreaktor, *Chem. Ing. Tech.*, 2004, 76, 630–632.
65. K. Gollnick, Photooxygenation and its application in chemistry, *Chim. Ind.*, 1982, 63, 156–166.
66. W. Rojahn and H.-U. Warnecke, Die photosensibilisierte Sauerstoffübertragung—eine Methode zur Herstellung hochwertiger Riechstoffe, *DRAGOCO-Report*, 1980, 27, 159–164.
67. S. Meyer, D. Tietze, S. Rau, B. Schäfer, and G. Kreisel, Photosensitized oxidation of citronellol in microreactors, *J. Photochem. Photobiol. A*, 2007, 186, 248–253.
68. H. Ehrich, D. Linke, K. Morgenschweis, M. Baerns, and K. Jähnisch, Application of microstructured reactor technology for the photochemical chlorination of alkylaromatics, *Chimia*, 2002, 56, 647–653.
69. N. Steinfeldt, R. Abdallah, U. Dingerdissen, and K. Jähnisch, Ozonolysis of acetic acid 1-vinyl-hexyl ester in a falling film microreactor, *Org. Process Res. Dev.*, 2007, 11, 1025–1031.
70. H. Matsubara, Y. Hino, M. Tokizane, and I. Ryu, Microflo photo-radical chlorination of cyclohexanes, *Chem. Eng. J.*, 2011, 167, 567–571.

71. J.-M. Herrmann, Heterogeneous photocatalysis: State of the art and present applications, *Top. Catal.*, 2005, 34, 49–65.
72. Y. Matsushita, N. Ohba, S. Kumada, K. Sakeda, T. Suzuki, and T. Ichimura, Photocatalytic reactions in microreactors, *Chem. Eng. J.*, 2008, 135, S303–S308.
73. R. Gorges, S. Meyer, and G. Kreisel, Photocatalysis in microreactors, *J. Photochem. Photobiol. A: Chem.*, 2004, 167, 95–99.
74. H. Nakamura, X. Li, H. Wang, M. Uehara, M. Miyazaki, H. Shimizu, and H. Maeda, A simple method of self assembled nano-particles deposition on the micro-capillary inner walls and the reactor application for photo-catalytic and enzyme reactions, *Chem. Eng. J.*, 2004, 101, 261–268.
75. N. Kitamura, K. Yamada, K. Ueno, and S. Iwata, Photodecomposition of phenol by silica-supported porphyrin derivative in polymer microchannel chips, *J. Photochem. Photobiol. A: Chem.*, 2006, 184, 170–176.
76. T. Kirner, J. Albert, M. Günther, G. Mayer, K. Reinhäckel, and J. M. Köhler, Static micromixers for modular chip reactor arrangements in two-step reactions and photochemical activated processes, *Chem. Eng. J.*, 2004, 101, 65–74.
77. Y. Matsushita, M. Iwasawa, T. Suzuki, and T. Ichimura, Multiphase photocatalytic oxidation in a microreactor, *Chem. Lett.*, 2009, 38, 846–847.
78. M.-Y. Ye, B.-X. Li, R.-M. Ye, and J.-H. Liu, Photodegradation of organics with titanium oxide/hydrogen peroxide catalyst system in microreactor and its application in environmental analysis, *Chin. J. Anal. Chem.*, 2010, 38, 643–647.
79. Z. He, Y. Li, Q. Zhang, and H. Wang, Capillary microchannel-based microreactors with highly durable ZnO/TiO_2 nanorod arrays for rapid, high efficiency and continuous-flow photocatalysis, *Appl. Catal. B: Environ.*, 2010, 93, 376–382.
80. G. Takei, T. Kitamori, and H.-B. Kim, Photocatalytic redox-combined synthesis of L-pipecolinic acid with a titania-modified microchannel chip, *Catal. Commun.*, 2005, 6, 357–360.
81. Y. Matsushita, N. Ohba, S. Kumada, T. Suzuki, and T. Ichimura, Photocatalytic N-alkylation of benzylamine in microreactors, *Catal. Commun.*, 2007, 8, 2194–2197.
82. B. Ohtani, H. Osaki, S. Nishimoto, and T. Kagiya, A novel photocatalytic process of amine N-alkylation by platinized semiconductor particles suspended in alcohols, *J. Am. Chem. Soc.*, 1986, 108, 308–310.
83. Y. Matsushita, N. Ohba, T. Suzuki, and T. Ichimura, N-Alkylation of amines by photocatalytic reaction in a microreaction system, *Catal. Today*, 2008, 132, 153–158.
84. Y. Matsushita, S. Kumada, K. Wakabayashi, K. Sakeda, and T. Ichimura, Photocatalytic reduction in microreactors, *Chem. Lett.*, 2006, 35, 410–411.
85. S. Werner, R. Seliger, H. Rauter, and F. Wissmann, Quarzglas-Mikrophotoreaktor und Synthese von 10-Hydroxycamptothecin und 7-Alkyl-10-hydroxycamptothecin, *EP-2065387A2*, 2009 [*Chem. Abstr.*, 2009, 150, 376721].
86. G. Ciamician, The photochemistry of the future, *Science*, 1912, 36, 385–394.

4

Photolabile Protecting Groups in Organic Synthesis

Christian G. Bochet
University of Fribourg

Aurélien Blanc
University of Strasbourg

4.1 Introduction

It is well known that, for the time being, certain functional groups need a temporary inactivation of their intrinsic chemical properties in order to allow transformations elsewhere in a molecule. This inactivation is achieved by protecting groups, the use of which has been frequently reviewed, commented, and criticized.[1,2] When the original reactivity of a functional group has to be restored, the protecting group needs to be removed by a reagent, which should be strong enough to induce the detachment of the protecting moiety, but mild enough to keep the rest of the molecule intact—including possibly other protecting groups that must be maintained for further transformations. This compatibility between different protecting groups, that is, the possibility of their selective removal in any given sequence, is often called *orthogonality*, and this is highly desirable in order to give to the synthetic plan a certain flexibility. However, the number of orthogonal sets of hydrolysis conditions is unfortunately rather small (e.g., acidic, basic, reductive, oxidizing, and nucleophilic conditions), and thus any additional dimension would be welcome.

In this context, light is an interesting "reagent," as only a few functional groups are photosensitive (at reasonable intensities and photon energies). Therefore, the availability of protecting groups that can be removed by mild irradiation (say, for a few minutes at wavelengths between 300 and 450 nm) might help to solve various synthetic problems. Such photolabile protecting groups (PPGs) do indeed exist, and a certain degree of orthogonality between them, exploiting different excitation wavelengths, has been demonstrated (*chromatic* orthogonality).[3–6]

The field of PPGs has been reviewed by many on several occasions,[7–13] including us.[14,15] Some of these reviews were either focused on certain applications or grouped according to their mechanisms. In this

chapter, in order to give the reader a useful overview on what can be achieved using PPGs and to help the synthetic chemist to choose the appropriate one, we decided to sort them according to the type of functional groups that can be protected, with only a brief listing of the main families. Later consultation of more focalized articles is nevertheless advised.

4.2 Main Families of PPGs

A very large number of different PPGs have been developed since the initial work published by Barltrop and Schofield in 1962,[16–18] and soon after by Barton et al.[19,20] but they are frequently variations of a common core structure. The main families are listed hereafter.

4.2.1 o-Nitrobenzyl Derivatives

These compounds are by far the most popular PPGs, since their early application by Patchornik, Amit, and Woodward in 1970.[21] They are based on the abstraction of a benzylic hydrogen by a neighboring excited nitro group, followed by a cascade of reactions that lead eventually to the release of the Y group (Scheme 4.1). This family of PPGs is quite versatile, as Y can range from an alcohol to a carboxylic acid, an amine, an amide, a phosphate, and even a masked carbonyl group.

4.2.2 Benzyl Alcohol Derivatives

A benzylic carbon–Y bond (Y being frequently an oxygen-bound moiety) has been shown to undergo photolytic cleavage,[22] possibly by heterolysis, as the benzylic carbocation is stabilized in the excited state (the *meta* effect), although this mechanism has been disputed.[23,24] Various substituents on the aromatic ring, in particular methoxy groups at both *meta* positions, greatly accelerate the reaction (Scheme 4.2). Diverse variations on the aromatic part itself have also been proposed, such as polyaromatics or heterocycles (vide infra).

4.2.3 Norrish Type II

Similar to the *ortho*-nitrobenzylic-based PPGs, the abstraction of a benzylic hydrogen atom by a nearby excited carbonyl group (i.e., a Norrish-type II reaction) has been exploited (Scheme 4.3).[25] It is worth noting that, in some cases, the released group has an oxidation state higher than before irradiation. This has to be taken into account in the synthetic planning:

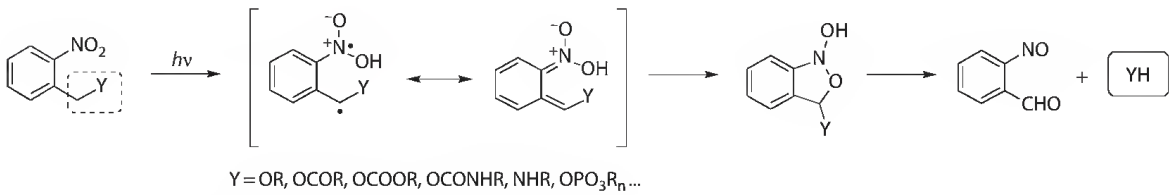

SCHEME 4.1 Photolysis of *o*-nitrobenzyl derivatives.

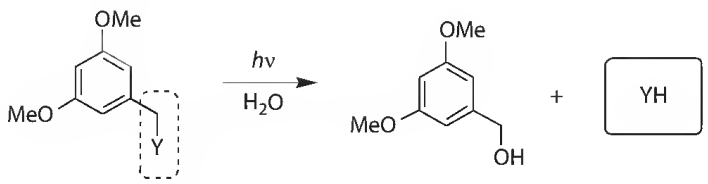

SCHEME 4.2 Photolysis of benzyl alcohol derivatives.

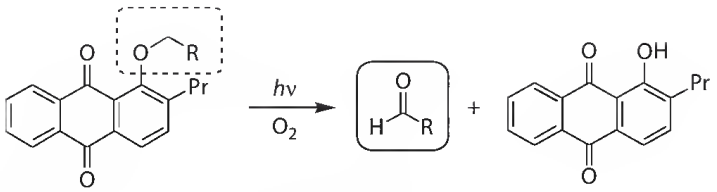

SCHEME 4.3 Photolysis of PPGs by a Norrish-type II mechanism.

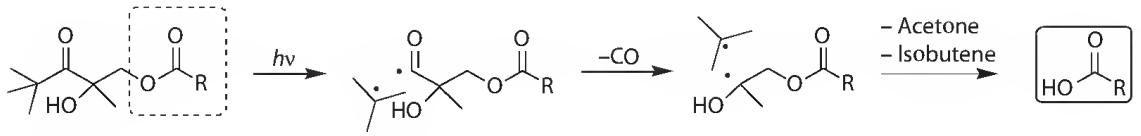

SCHEME 4.4 Photolysis of PPGs by a Norrish-type I mechanism.

4.2.4 Norrish Type I

A completely different approach is used on pivaloyl derivatives, where the photoinduced homolysis of the C–C bond adjacent to a carbonyl group (Norrish-type I reaction) is followed by a cascade of reactions leading to the liberation of a carboxylic acid (Scheme 4.4).[26–28]

4.2.5 Cinnamyl Esters

Cis–trans isomerization of alkenes is a common photochemical reaction, and it was exploited in cinnamate esters, where photoisomerization to the *Z*-isomer allowed an intramolecular transesterification, which leads to the release of an alcohol (Scheme 4.5).[29,30]

4.2.6 Coumarin Derivatives

The coumarin chromophores, released as side products in the photolysis of cinnamyl esters (see Section 4.2.5), have also been employed to protect a broad variety of functional groups (Scheme 4.6).[31–34] The postulated mechanism involves a heterolytic cleavage of the C–Y, leading to the formation of an ion pair.[35]

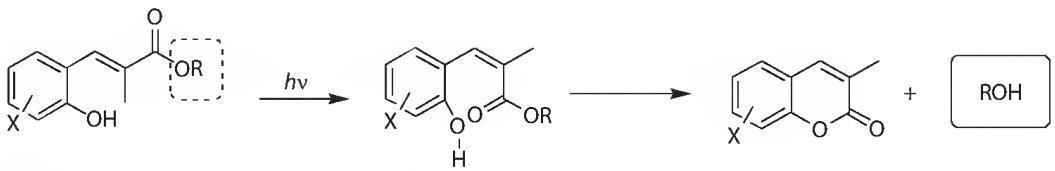

SCHEME 4.5 Photolysis of (*E*)-cinnamyl esters.

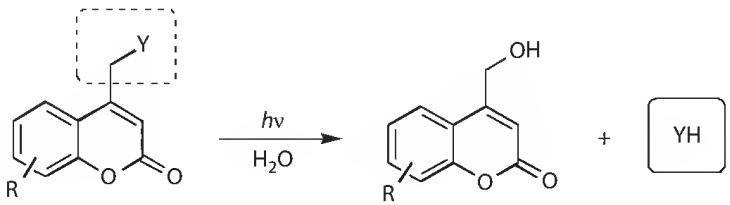

Y = –OCOR, –OCO_2R, –$OCONR_2$, –$OPOOR^1OR^2$ ...

SCHEME 4.6 Photolysis of coumarin derivatives.

Low-energy irradiation (>320 nm or two-photon absorption), solubility in aqueous media, and nontoxicity of coumarin derivates have made them ideal candidates for "caging compounds" despite their relatively low quantum yields.[10]

4.2.7 Phenacyl Derivatives

Phenacyl groups containing a leaving group in the α-position can be efficiently photolyzed, particularly if a *para*-hydroxy group in present on the aromatic ring.[36–46] The exact mechanism can vary depending on the particular substituents; either a radical pair or an intramolecular S_N2 attack by the *ipso* carbon atom is involved (Scheme 4.7).

A related core structure was recently developed by Klan et al. for the protection of a wide variety of functional groups. However, despite the structural similarities, the mechanism follows different pathways, depending on the nature of the solvent in which the photolysis is conducted (Scheme 4.8).[47–52]

4.2.8 Benzoin Derivatives

Structurally close compounds, benzoin esters, with an additional aromatic group α to the carbonyl group also react very efficiently upon irradiation. However, the mechanism follows a different path, as benzofuran derivatives are the common side products. Again several routes have been proposed, involving a radical cyclization, an intramolecular Paterno-Büchi [2 + 2] cycloaddition or a cationic intermediate (Scheme 4.9).[53–61]

4.2.9 7-Nitroindolines

Acylated 7-nitroindolines smoothly transfer the acyl group to an incoming nucleophile upon irradiation, and this feature as been exploited in a series of PPGs (Scheme 4.10).[62–70] The photolysis mechanism involves the photoinduced migration of the *N*-acyl group to one of the oxygen atoms from the nitro group, generating a very electrophilic *O*-acyl intermediate, then trapped by the nucleophile. Time-resolved infrared spectroscopic studies confirmed this mechanism.[71]

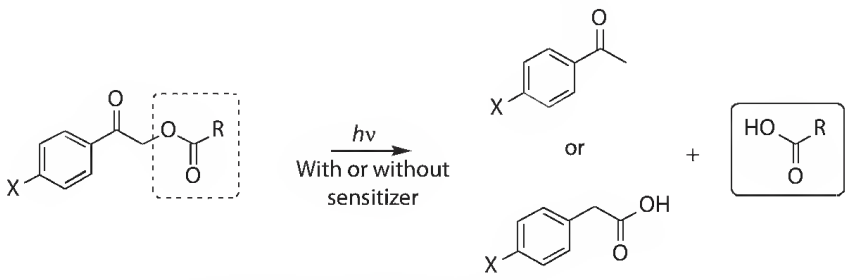

SCHEME 4.7 Photolysis of phenacyl derivatives.

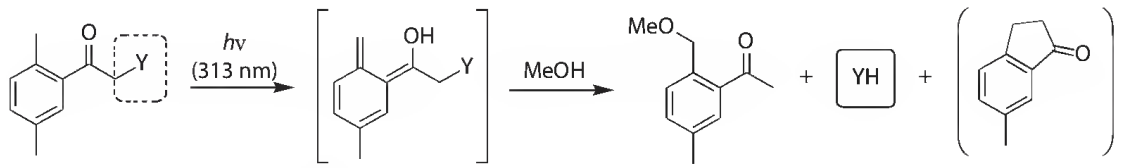

SCHEME 4.8 Photolysis of *o*-methylated phenacyl derivatives.

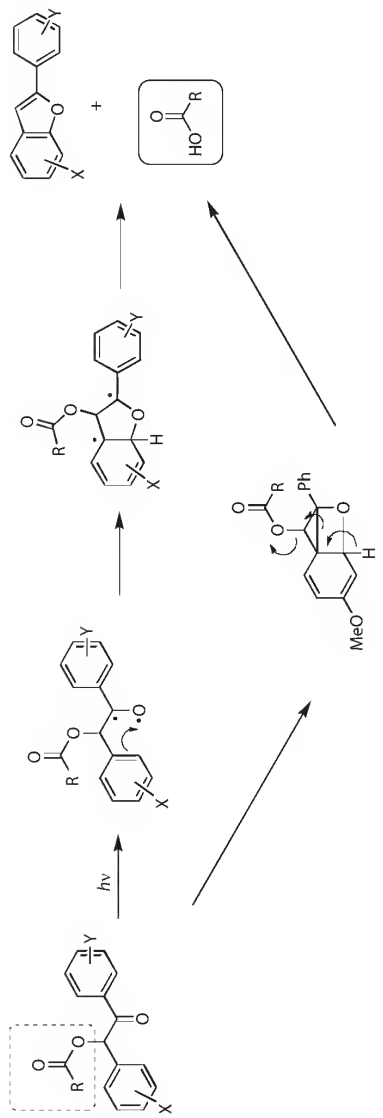

SCHEME 4.9 Photolysis of benzoin esters.

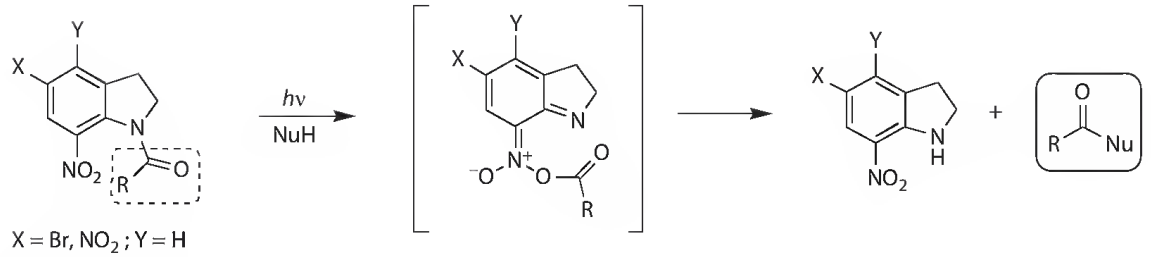

SCHEME 4.10 Photolysis of 7-nitroindoline derivatives.

4.3 PPGs for Specific Functional Groups

4.3.1 PPGs for Carboxylic Acids

Carboxylic acids are probably the most easily protected groups, as esters of most photoreactive alcohols can be used. Very common are *ortho*-nitrobenzyl alcohol esters such as **1**, which can be prepared by simple esterification procedures (e.g., DCC-type coupling). Among the multitude of example, the following is interesting, because the released carboxylic acid is itself strongly absorbing, but without significant detrimental interference (Scheme 4.11).[72]

ortho-Nitroanilides such as **2** are interesting (Scheme 4.12), because their photolysis in water-containing media lead to carboxylic acids,[70] whereas in amine-containing media it leads to amides (ammonia furnishes carboxamides, but—more interestingly—aminoacids lead to dipeptides).[62,73] In methanol, a methyl ester is obtained, and a stoichiometric amount of a large variety of alcohols (even tertiary) in anhydrous acetonitrile leads to esters.[74] It is thus a very versatile PPG, despite its relatively difficult acylation, which requires acid chlorides activated by aluminum trichloride; otherwise, acylation of indoline, followed by nitration is required. If these harsh conditions are incompatible with sensitive parts on the carboxylic side, an indirect route is necessary.[68,75]

Very efficient release is observed in the photolysis of benzoin esters, with a relatively harmless by-product (a benzofuran derivative).[53,54,57,61] A combination of benzoin esters (sensitive to short wavelength) and *ortho*-nitrobenzylic esters (sensitive to longer wavelength) was used in the initial

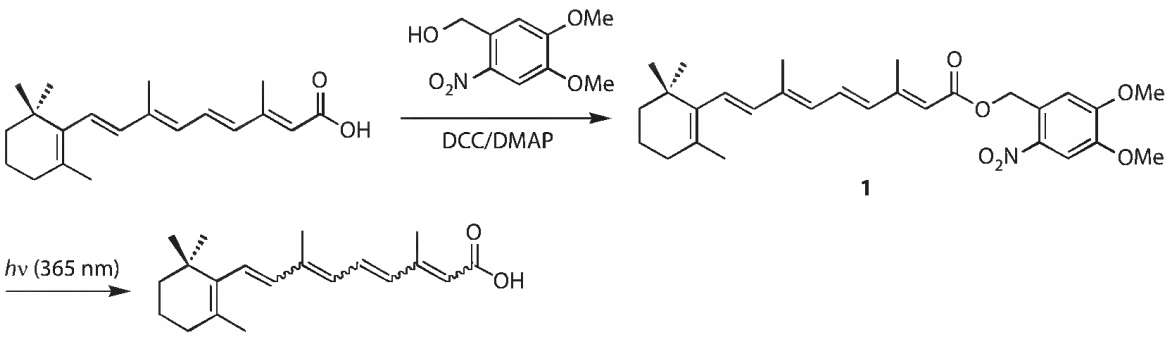

SCHEME 4.11 Release of carboxylic acids from *o*-nitrobenzylic esters.

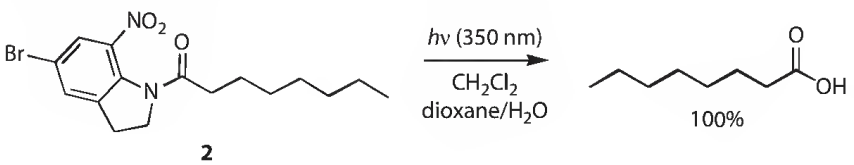

SCHEME 4.12 Release of carboxylic acids from 7-nitroindoline amides.

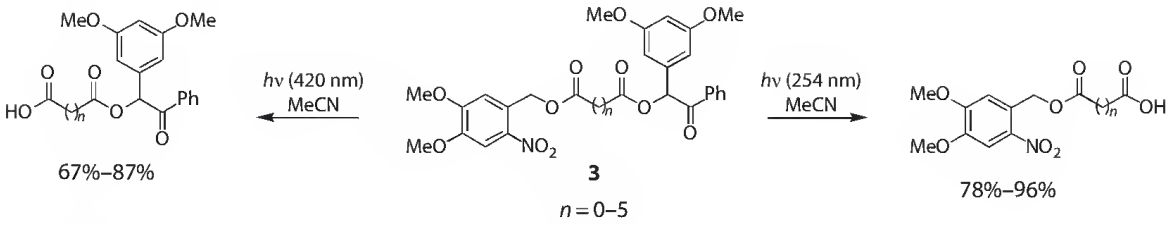

SCHEME 4.13 Example of chromatic orthogonality.

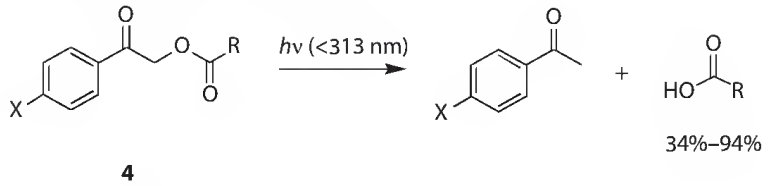

SCHEME 4.14 Release of carboxylic acids from phenacyl esters.

description of chromatic orthogonality (**3**, Scheme 4.13).[4,6,76] Despite their very high photolysis quantum and chemical yields, benzoin esters suffer from a relatively high sensitivity to common organic reagents (e.g., hydrides or most organometallic reagents) and sometimes from difficulties in making the esters themselves (benzoin is prone to α-ketol rearrangement).

Also suffering from significant sensitivity toward common organic reagents, phenacyl esters **4** remain interesting candidates for specific applications, particularly in biochemistry (Scheme 4.14).[37]

The Norrish-type I fragmentation of pivaloyl derivatives has been introduced as part of a photolabile linker, but it proceeds as well for conventional solution-phase chemistry (**5**, Scheme 4.15).[28] Despite the presence of a carbonyl group, pivaloyl esters show remarkable stability toward a series of chemical conditions (such as acids, bases, or transition-metal catalysis). The by-products are gaseous or volatile molecules (isobutene, carbon monoxide, and acetone), and the photolysis quantum yield is very high; on the other hand, it requires irradiation with a relatively short wavelength (280–340 nm).

4.3.2 PPGs for Amines

Historically, amines were among the first functional groups for which PPGs were developed, as part of a strategy for peptide synthesis.[11,77] The nitrogen atom is protected as a carbamate, which is conveniently formed by the reaction of the free amine with the corresponding photolabile chloroformiate. The most common PPGs are variations of the *ortho*-nitrobenzylic motif (**7**, Scheme 4.16), such as

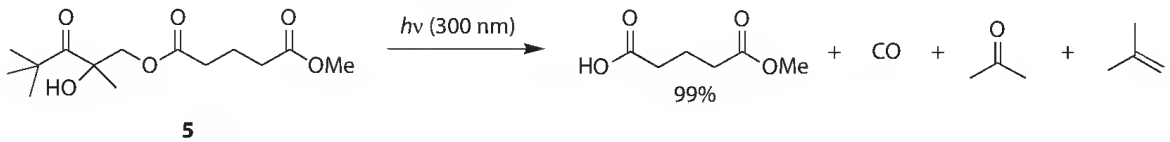

SCHEME 4.15 Traceless release of carboxylic acids.

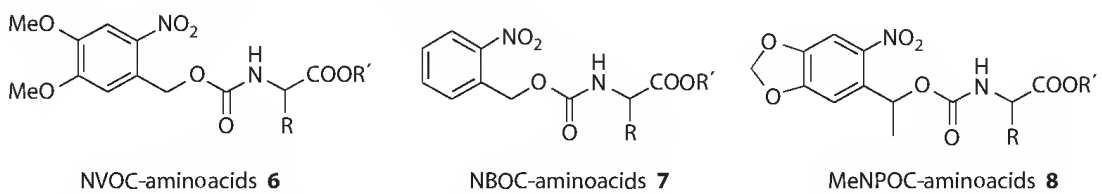

SCHEME 4.16 Example of *o*-nitrobenzyl derivatives of amino acids.

4,5-dimethoxy-2-nitrobenzyl carbamates **6** (nitroveratryloxycarbonyl, or NVOC). The two methoxy groups were introduced to shift the irradiation to longer wavelengths (up to 420 nm), as deep UV light can be harmful to some amino acids (such as tryptophan) or nucleic acids. This redshift occurs at the cost of a decrease in quantum yield, but unless very specific performances are expected, this has no practical consequences. An improved version was introduced a decade ago, by adding an additional methyl group at the benzylic position and a methylenedioxy group on the aromatic ring (**8**). This group, called MeNPOC, is photolyzed more efficiently than its unsubstituted NBOC counterpart **7**, also at longer wavelengths, but it is not widely accessible commercially, and an enantiopure version is essential to avoid the formation of diastereomeric pairs with chiral compounds.[78,79]

A related PPG bearing a nitrodibenzofuran core was recently introduced. Interestingly, it shows a high two-photon cross section, thus allowing deprotection at wavelengths as long as 710 nm, using a focused laser beam (**9**, Scheme 4.17).[80,81]

A significant drawback of such PPGs is the release of a dark-colored nitroso side product, which progressively limits the light availability over time, and which needs to be separated from the released product. Cleaner, but also requiring a purification step, are derivatives of the simple 3,5-dimethoxybenzyl alcohol, such as carbamate **10**; on the other hand, shorter wavelengths are required, and compatibility tests should be performed before including such PPGs in longer syntheses.[22] An improved version includes two methyl groups at the benzylic site (Ddz, **11**).[82] Interestingly, the α-methyl styrene side product undergoes a [2 + 2] cyclodimerization, but this process is normally not detrimental to the overall reaction (Scheme 4.18). Ddz derivatives are, however, very acid sensitive, about three orders of

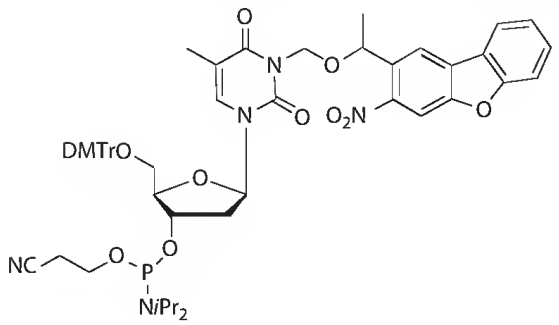

9

SCHEME 4.17 Example of a nitrodibenzofuran derivative of thymidine phosphoramidite.

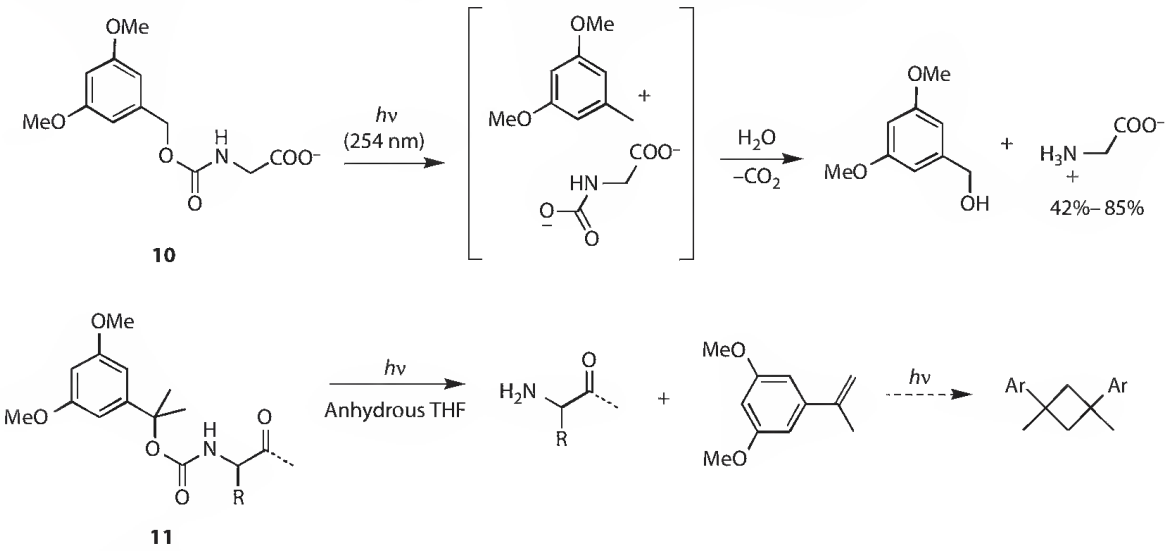

SCHEME 4.18 Release of amino acids from benzyl alcohol derivatives.

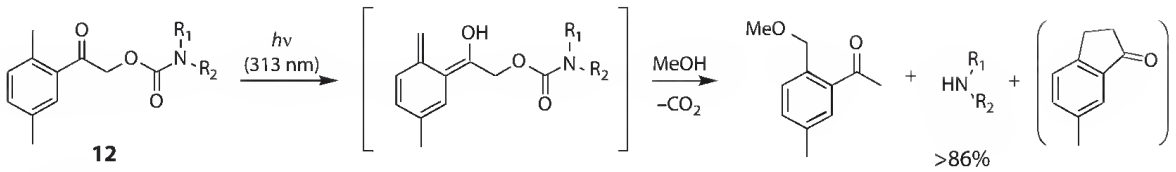

SCHEME 4.19 Release of amines from *o*-methylated phenacyl derivatives.

magnitude more than the Boc group. It is also worth noting that the cleavage of the 3,5-dimethoxybenzyloxycarbonyl group requires water to proceed (the reaction is a solvolysis), whereas the Ddz variant can be cleaved in anhydrous media.

Variations of the phenacyl group can be used in carbamates (**12**) to protect amino groups, and the photodeprotection proceeds in high yields. Interestingly, in nucleophilic solvents such as methanol, the release mechanism does not follow the usual route for phenacyl groups, but rather proceeds through a photoenol (Scheme 4.19).[52]

4.3.3 PPGs for Alcohols

There are numerous ways to protect alcohols with PPGs, as ethers, carbonates, and mixed acetals. It should however be pointed out that, although simple by principle, this sort of protection can pose certain synthetic problems, as the formation of such derivatives is sometimes cumbersome to optimize.

Although formally part of a carbonyl group, but more alcoholic from the reactivity point of view, the anomeric hydroxyl group of sugars has been protected as a mixed acetal with a nitrobenzyl alcohol derivative in the early days of PPGs. For example, the derivatives of glucose **13** in Scheme 4.20 were photolyzed in a 100% yield.[83] This strategy is also compatible with more complex structures, such as a precursor for Aplysiatoxin (**14**, Scheme 4.20).[84]

Another very important field where PPGs are used is in the light-directed automated synthesis of oligonucleic acids or peptides (Scheme 4.21).[85,86]

A structurally related group, the 2-(2-nitrophenyl)propyloxycarbonyl (NPPOC), has been shown to be quite efficient in releasing alcohols upon irradiation.[87–93] Despite the similarity, the reaction proceeds by a photoelimination (Scheme 4.22). For example, cytosine derivative **15** or thymine derivative **16** was deprotected almost quantitatively.

The benzylic photosolvolysis that we cited in the introduction has been widely used with a series of variations (Scheme 4.23), such as the Pixyl derivative **17** and its *S*-Pixyl analogue **18**,[94–96] the Aqmoc **19**, Pmoc **20**, Phmoc **21**, and Mcmoc **22**.[97] The naphthalene derivative **23**, although also bearing a benzylic leaving group, apparently reacts via a different mechanism, as a quinone methide intermediate was observed.[98,99] The Bhc derivative **24** and the BHQ derivative **25** are promising candidates for biological applications, as they exhibit significant two-photon absorptions.[100–103]

A convenient family of PPGs, by virtue of the ease of their preparation, is the hydroxycinnamyl derivatives, such as ester **26**. Irradiation triggers the isomerization of the *trans*-olefin to its *cis*-isomer, which

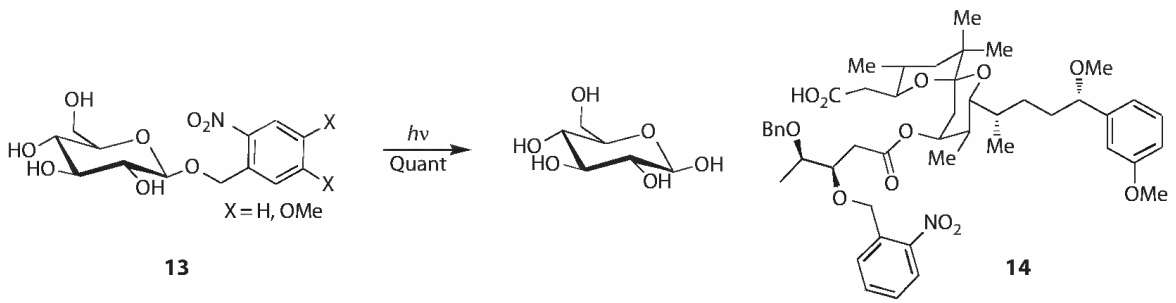

SCHEME 4.20 Release of alcohols from *o*-nitrobenzyl derivatives.

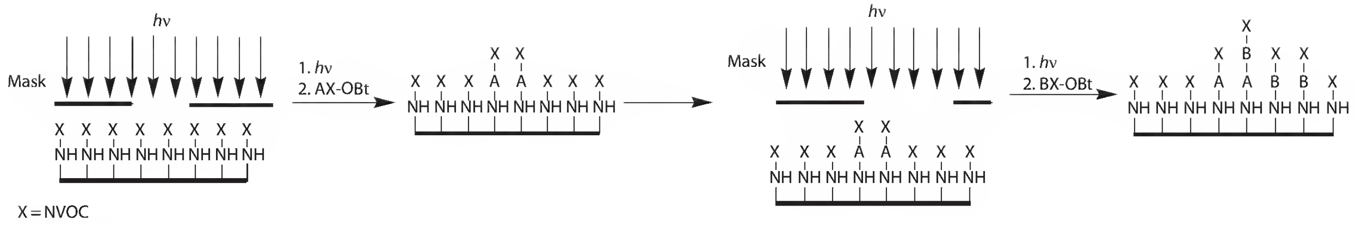

SCHEME 4.21 Light-directed solid-phase synthesis of bio-oligomers.

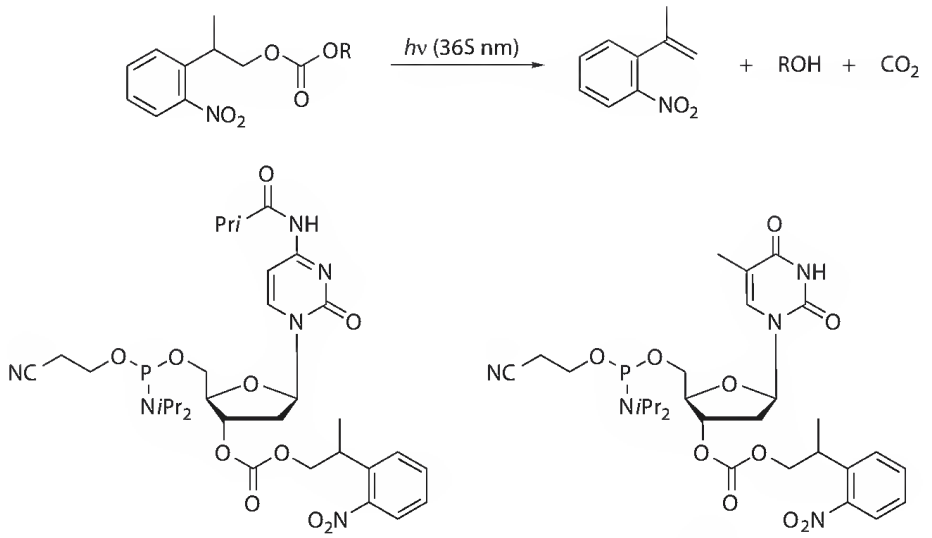

15 **16**

SCHEME 4.22 Release of alcohols from NPPOC derivatives.

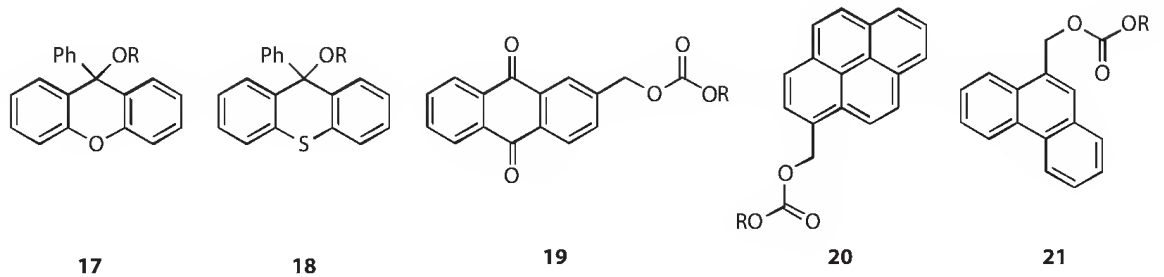

17 **18** **19** **20** **21** **22** **23** **24** **25**

SCHEME 4.23 Release of alcohols from benzylic-type methylene groups.

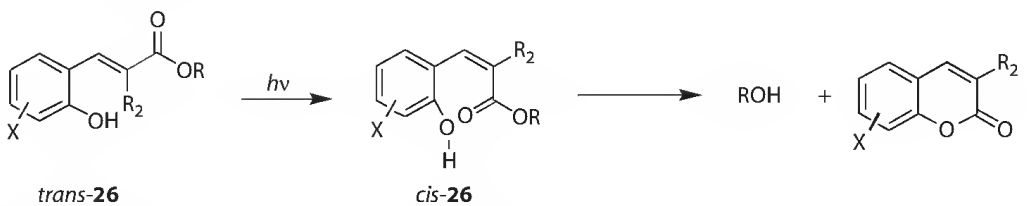

trans-**26** *cis*-**26**

SCHEME 4.24 Release of alcohols from (*E*)-cinnamyl esters.

can undergo an intramolecular transesterification, thus liberating the alcohol (Scheme 4.24). However, with regard to robustness, the numerous chemically sensitive functions (phenol, olefin, ester) make this group more appropriate for specific uses where *release* is more important than *protection*, as it can be the case in biochemistry or particular technologies (e.g., fragrance release).[29,104–109]

Glycols can be protected as ketals and photochemically released, as illustrated by a salicylaldehyde derivative (**27**, Scheme 4.25).[110]

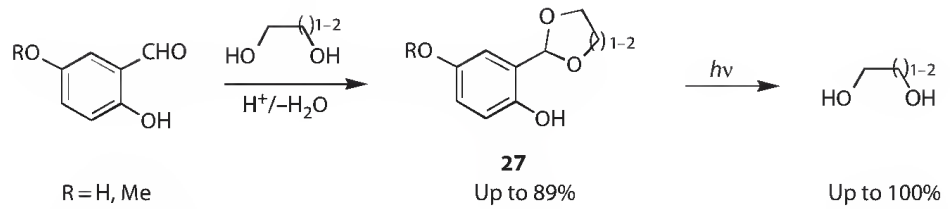

SCHEME 4.25 Release of diols.

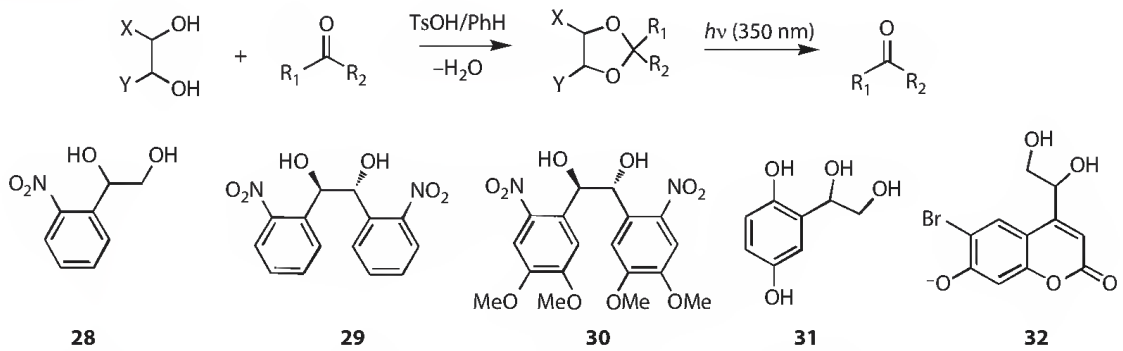

SCHEME 4.26 Release of ketones.

4.3.4 PPGs for Carbonyl Groups

The most commonly used strategy to mask a carbonyl group is to convert it into an acetal or ketal. Variants of the *ortho*-nitrobenzylic core have been developed over the years, with derivatives like **28**, **29**, or **30** (Scheme 4.26). **28** was the first of such groups, which was remarkably robust under acidic conditions, but quite labile in basic media.[111] The homochiral version **29** improved the stability toward bases, and allowed the protection of chiral carbonyl compounds without the formation of diastereomeric pairs.[112] Derivative **30** was later introduced for an improved absorption at longer wavelengths (up to 400 nm).[113] A different type of diol (**31**) was recently developed, the ketal of which releases a ketone by an excited state proton transfer, in yields ranging between 59% and 100%.[114] The coumarin derivative **32** is particularly interesting for its high two-photon cross section.[115]

Although it is not strictly speaking a protection, the photoinduced release of a carbonyl compound using a Norrish-type II reaction has been used, in particular for the release of fragrances (e.g., **33** and **34**).[116–119] It is based on the abstraction of a hydrogen *ipso* to an oxygen atom, making it formally an oxidative process (Scheme 4.27).

A completely different approach exploits the photofragmentation of α-hydroxy-*ortho*-thioesters (**35**). The reaction can be sensitized, thus allowing the use of nonabsorbing substituents and the possibility of working a relatively long wavelengths (Scheme 4.28).[120–123]

The *meta* effect operating in the photolysis of benzylic esters has been invoked in the development of phenol-derived ketals **36** (Scheme 4.29).[124,125]

4.3.5 PPGs for Thiols

Thiols can be protected with PPGs, and most of the standard cores have been used, in a similar fashion as for alcohols. As photoliberation of thiols frequently involves biomolecules (e.g., cysteine derivatives), water solubility can be an issue, and various substituents on the cores have been introduced.[60,126–128] Thiols can be either directly attached to the reacting center, such as in *ortho*-nitrobenzylic derivative **37**, or via a thiocarbonate, such as in **38** (Scheme 4.30).[129]

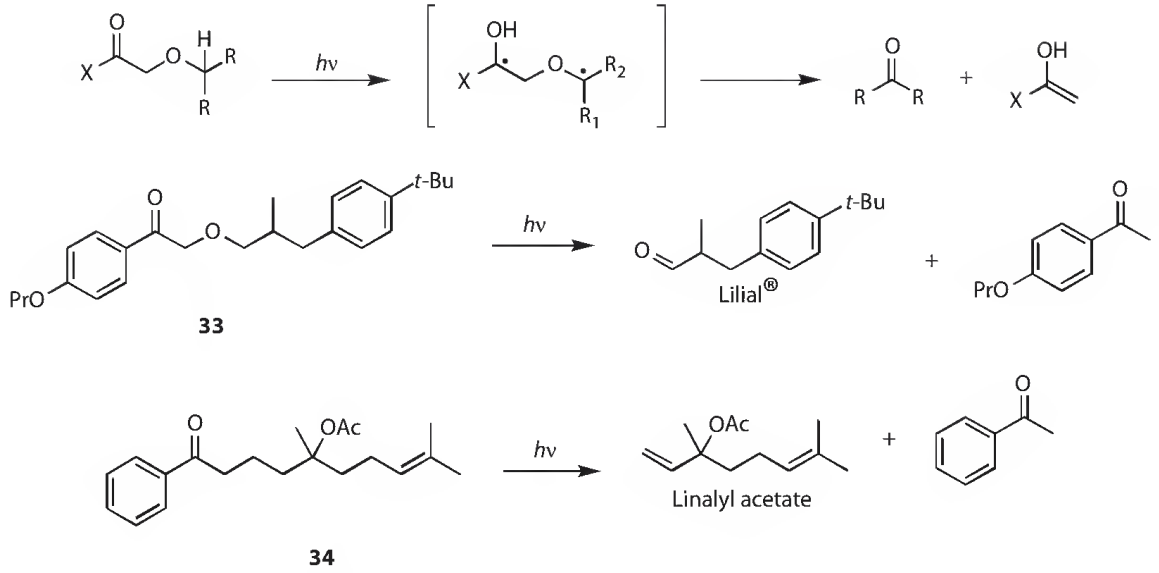

SCHEME 4.27 Oxidative release of fragrances.

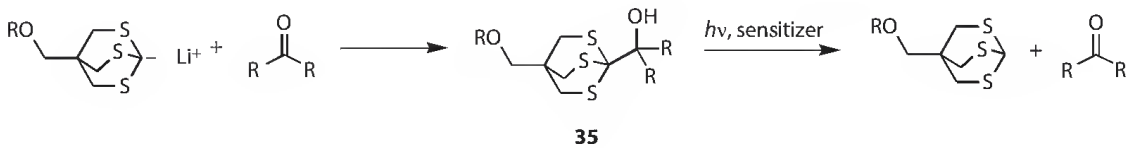

SCHEME 4.28 Photolysis of *o*-thioesters.

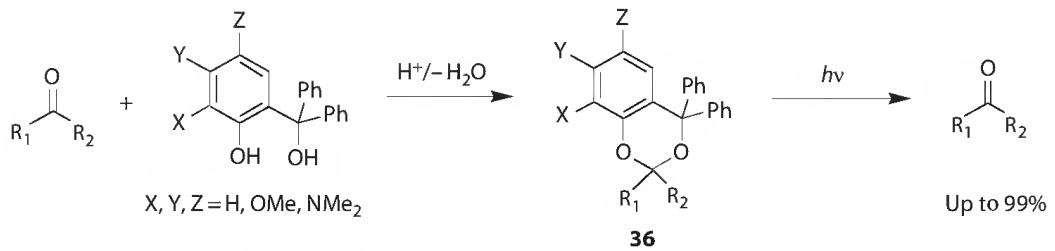

SCHEME 4.29 Photolysis of phenol-derived ketals.

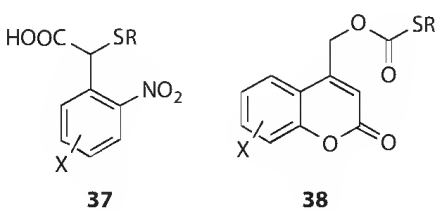

SCHEME 4.30 Examples of protected thiols.

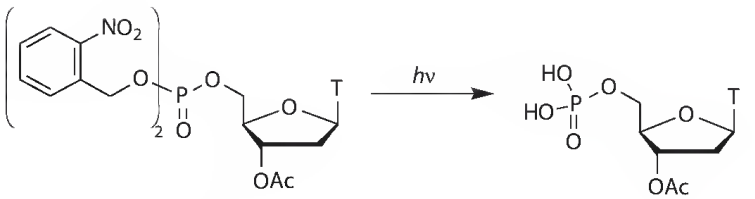

39

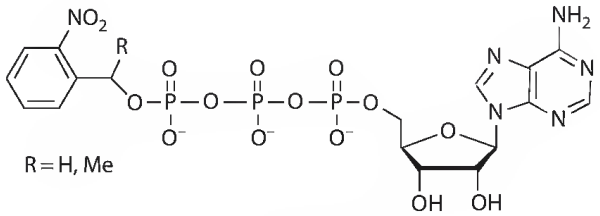

Caged-ATP **40**

SCHEME 4.31 Release of phosphates from *o*-nitrobenzyl derivatives.

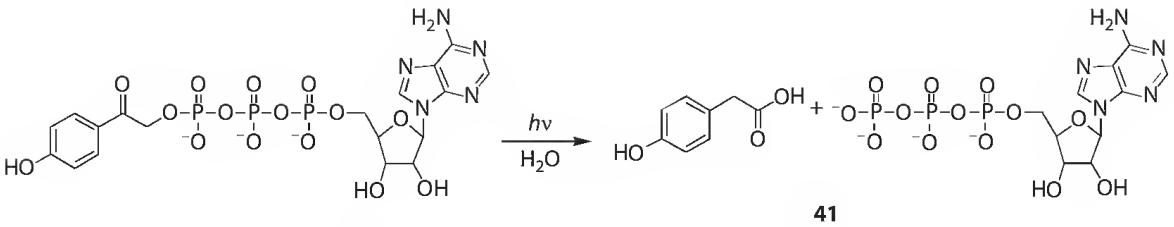

41

SCHEME 4.32 Release of phosphates from *p*-hydroxyphenacyl derivatives.

4.3.6 PPGs for Phosphates

In an early example, the phosphate group of a nucleotide was protected by an *ortho*-nitrobenzylic group (**39**, Scheme 4.31).[130] Shortly thereafter, ATP was protected (**40**) and photochemically released:[131]

Phenacyl phosphate esters release phosphates upon irradiation very efficiently, in particular derivatives bearing a *para*-hydroxy group (**41**, Scheme 4.32).[132] The key feature of this group is the very high release rate, crucial in several biochemical applications. An additional interesting feature is the lower absorbance of the nonconjugated *para*-hydroxy-phenylacetic by-product (avoiding the darkening of NVOC-type irradiated solutions, as mentioned earlier), which does not interfere in the photolytic process.

4.4 Conclusion

Other types of functional groups can of course be protected and later photochemically released; many of the specific applications are derived from the larger families presented in this overview. Apart from that, there are a series of very ingenious, though specific, methods, such as the protection/photodeprotection of the silyl group.[133–135] At the moment, there are few uses for this kind of PPG in general organic synthesis, but its mere availability might orient choices in a future synthetic scheme or technological development.

This book shows the breadth of reactions promoted by light, as well as their sometimes discouraging sensitivity to substituents and experimental conditions. The photolysis of PPGs are, however, part of a privileged class of reactions, which are quite tolerant to different reaction conditions and structural patterns, provided that the core motifs adhere to the general reactivity of the groups seen in Section 4.2, and that the incident light wavelengths coincide at least partially with those of the relevant chromophore's absorptions. This tolerance might actually be the reason why PPGs find increasing uses in a wide variety of fields, ranging from lithography to biology, material science, or organic synthesis.

References

1. Kocienski, P. *Protecting Groups* (Thieme, Stuttgart, Germany, 1994).
2. Schelhaas, M. and Waldmann, H. Protecting group strategies in organic synthesis. *Angewandte Chemie, International Edition* 35, 2056–2083 (1996).
3. Bochet, C. G. Photochemical release of various functional groups. *Pure and Applied Chemistry* 78, 241–247 (2006).
4. Bochet, C. G. Orthogonal photolysis of protecting groups. *Angewandte Chemie, International Edition* 40, 2071–2073 (2001).
5. Bochet, C. G. Wavelength-selective cleavage of photolabile protecting groups. *Tetrahedron Letters* 41, 6341–6346 (2000).
6. Blanc, A. and Bochet, C. G. Wavelength-controlled orthogonal photolysis of protecting groups. *Journal of Organic Chemistry* 67, 5567–5577 (2002).
7. Pillai, V. N. R. Photolytic deprotection and activation of funtional groups. *Organic Photochemistry* 9, 225–321 (1987).
8. Pillai, V. N. R. Photoremovable protecting groups in organic synthesis. *Synthesis*, 1–26 (1980).
9. Pelliccioli, A. P. and Wirz, J. Photoremovable protecting groups: Reaction mechanisms and applications. *Photochemical & Photobiological Sciences* 1, 441–458 (2002).
10. Loudwig, S., Specht, A., and Goeldner, M. Caged compounds, the photolabile precursors of bioactive molecules. Developments and prospects. *Actualité Chimique* 1, 7–12 (2002).
11. Gug, S. et al. Photolabile glutamate protecting group with high one- and two-photon uncaging efficiencies. *ChemBioChem* 9, 1303–1307 (2008).
12. Givens, R. S., Weber, J. F. W., Jung, A. H., and Park, C.-H. New photoprotecting groups: Desyl and p-hydroxyphenacyl phosphate and carboxylate esters. *Methods in Enzymology* 291, 1–29 (1998).
13. Givens, R. S. and Kueper, L. W. Photochemistry of phosphate esters. *Chemical Reviews* 93, 55–66 (1993).
14. Bochet, C. G. Photolabile protecting groups and linkers. *Journal of the Chemical Society, Perkin Transactions* 1, 125–142 (2002).
15. Bochet, C. G. and Blanc, A. Photolabile protecting groups in organic synthesis, in *Handbook of Synthetic Photochemistry* (eds. Albini, A. and Fagnoni, M.) pp. 417–447 (Wiley-VCH, Weinheim, Germany, 2010).
16. Barltrop, J. A. and Schofield, P. Photosensitive protecting groups. *Tetrahedron Letters* 3, 697–699 (1962).
17. Barltrop, J. A. and Schofield, P. Organic photochemistry. Part II. Some photosensitive protecting groups. *Journal of the Chemical Society*, 4758–4765 (1965).
18. Barltrop, J. A., Plant, P. J., and Schofield, P. Photosensitive protective groups. *Journal of the Chemical Society, Chemical Communications* 22, 822–823 (1966).
19. Barton, D. H. R., Chow, Y. L., Cox, A., and Kirby, G. W. Photochemical transformations. Part XIX. Some photosensitive protecting groups. *Journal of the Chemical Society*, 3571–3578 (1965).
20. Barton, D. H. R., Chow, Y. L., Cox, A., and Kirby, G. W. Photosensitive protection of functional groups. *Tetrahedron Letters* 3, 1055–1057 (1962).
21. Patchornik, A., Amit, B., and Woodward, R. B. Photosensitive protecting groups. *Journal of the American Chemical Society* 92, 6333–6335 (1970).
22. Chamberlin, J. W. Use of the 3,5-dimethoxybenzyloxycarbonyl group as a photosensitive N-protecting group. *Journal of Organic Chemistry* 31, 1658–1660 (1966).
23. Zimmerman, H. E. The meta effect in organic photochemistry: Mechanistic and exploratory organic photochemistry. *Journal of the American Chemical Society* 117, 8988–8991 (1995).
24. Pincock, J. A. Photochemistry of arylmethyl esters in nucleophilic solvents: Radical pair and ion pair intermediates. *Accounts of Chemical Research* 30, 43–49 (1997).
25. Brinson, R. G. and Jones, P. B. Caged trans-4-hydroxy-2-nonenal. *Organic Letters* 6, 3767–3770 (2004).

26. Peukert, S. and Giese, B. The pivaloylglycol anchor group: A new platform for a photolabile linker in solid-phase synthesis. *Journal of Organic Chemistry* 63, 9045–9051 (1998).
27. Glatthar, R. and Giese, B. A new photocleavable linker in solid-phase chemistry for ether cleavage. *Organic Letters* 2, 2315–2317 (2000).
28. Kessler, M., Glatthar, R., Giese, B., and Bochet, C. G. Sequentially photocleavable protecting groups in solid-phase synthesis. *Organic Letters* 5, 1179–1181 (2003).
29. Porter, N. A. and Bruhnke, J. D. Acyl thrombin photochemistry: Kinetics for deacylation of enzyme cinnamate geometric isomers. *Journal of the American Chemical Society* 111, 7616–7618 (1989).
30. Porter, N. A., Thuring, J. W., and Li, H. Selective inhibition, separation, and purification of serine proteases: A strategy based on a photoremovable inhibitor. *Journal of the American Chemical Society* 121, 7716–7717 (1999).
31. Suzuki, A. Z. et al. Coumarin-4-ylmethoxycarbonyls as phototriggers for alcohols and phenols. *Organic Letters* 5, 4867–4870 (2003).
32. Piloto, A. M., Rovira, D., Costa, S. P. G., and Goncalves, M. S. T. Oxobenzo[f]benzopyrans as new fluorescent photolabile protecting groups for the carboxylic function. *Tetrahedron* 62, 11955–11962 (2006).
33. Hagen, V. et al. [8-[Bis(carboxymethyl)aminomethyl]-6-bromo-7-hydroxycoumarin-4-yl]methyl moieties as photoremovable protecting groups for compounds with COOH, NH_2, OH, and C[n.58875]O functions. *Journal of Organic Chemistry* 75, 2790–2797 (2010).
34. Lin, W. and Lawrence, D. S. A strategy for the construction of caged diols using a photolabile protecting group. *Journal of Organic Chemistry* 67, 2723–2726 (2002).
35. Schade, B. et al. Deactivation behavior and excited-state properties of (Coumarin-4-yl)methyl derivatives. 1. Photocleavage of (7-methoxycoumarin-4-yl)methyl-caged acids with fluorescence enhancement. *Journal of Organic Chemistry* 64, 9109–9117 (1999).
36. Anderson, J. C. and Reese, C. B. Photo-induced rearrangement involving aryl participation. *Tetrahedron Letters* 3, 1–4 (1962).
37. Sheehan, J. C. and Umezawa, K. Phenacyl photosensitive blocking groups. *Journal of Organic Chemistry* 38, 3771–3774 (1973).
38. Givens, R. S., Jung, A., Park, C.-H., Weber, J., and Bartlett, W. New photoactivated protecting groups. 7. *p*-Hydroxyphenacyl: A phototrigger for excitatory amino acids and peptides. *Journal of the American Chemical Society* 119, 8369–8370 (1997).
39. Park, C.-H. and Givens, R. S. New photoactivated protecting groups. 6. *p*-Hydroxyphenacyl: A phototrigger for chemical and biochemical probes. *Journal of the American Chemical Society* 119, 2453–2463 (1997).
40. Banerjee, A., Lee, K., Yu, Q., Fang, A. G., and Falvey, D. E. Protecting group release through photoinduced electron transfer: Wavelength control through sensitized irradiation. *Tetrahedron Letters* 39, 4635–4638 (1998).
41. Conrad, P. G., II, Givens, R. S., Weber, J. F. W., and Kandler, K. New phototriggers: Extending the *p*-hydroxyphenacyl p-p* absorption range. *Organic Letters* 2, 1545–1547 (2000).
42. Givens, R. S. et al. New phototriggers 9: p-Hydroxyphenacyl as a C-terminal photoremovable protecting group for oligopeptides. *Journal of the American Chemical Society* 122, 2687–2697 (2000).
43. Conrad, P. G., II et al. p-Hydroxyphenacyl phototriggers: The reactive excited state of phosphate photorelease. *Journal of the American Chemical Society* 122, 9346–9347 (2000).
44. Rajesh, C. S., Givens, R. S., and Wirz, J. Kinetics and mechanism of phosphate photorelease from benzoin diethyl phosphate: Evidence for adiabatic fission to an a-keto cation in the triplet state. *Journal of the American Chemical Society* 122, 611–618 (2000).
45. Givens, R. S. et al. The photo-Favorskii reaction of p-hydroxyphenacyl compounds is initiated by water-assisted, adiabatic extrusion of a triplet biradical. *Journal of the American Chemical Society* 130, 3307–3309 (2008).

46. Stensrud, K. F., Heger, D., Sebej, P., Wirz, J., and Givens, R. S. Fluorinated photoremovable protecting groups: The influence of fluoro substituents on the photo-Favorskii rearrangement. *Photochemical & Photobiological Sciences* 7, 614–624 (2008).
47. Zabadal, M., Pelliccioli, A. P., Klan, P., and Wirz, J. 2,5-Dimethylphenacyl esters: A photoremovable protecting group for carboxylic acids. *Journal of Physical Chemistry A* 105, 10329–10333 (2001).
48. Pelliccioli, A. P., Klan, P., Zabadal, M., and Wirz, J. Photorelease of HCl from o-methylphenacyl chloride proceeds through the Z-xylylenol. *Journal of the American Chemical Society* 123, 7931–7932 (2001).
49. Klan, P., Zabadal, M., and Heger, D. 2,5-Dimethylphenacyl as a new photoreleasable protecting group for carboxylic acids. *Organic Letters* 2, 1569–1571 (2000).
50. Klan, P., Pelliccioli, A. P., Pospisil, T., and Wirz, J. 2,5-Dimethylphenacyl esters: A photoremovable protecting group for phosphates and sulfonic acids. *Photochemical & Photobiological Sciences* 1, 920–923 (2002).
51. Literak, J., Wirz, J., and Klan, P. 2,5-Dimethylphenacyl carbonates: A photoremovable protecting group for alcohols and phenols. *Photochemical & Photobiological Sciences* 4, 43–46 (2005).
52. Kammari, L., Plistil, L., Wirz, J., and Klan, P. 2,5-Dimethylphenacyl carbamate: A photoremovable protecting group for amines and amino acids. *Photochemical & Photobiological Sciences* 6, 50–56 (2007).
53. Sheehan, J. C., Wilson, R. M., and Oxford, A. W. The photolysis of methoxy-substituted benzoin esters. A photosensitive protecting group for carboxylic acids. *Journal of the American Chemical Society* 93, 7222–7228 (1971).
54. Sheehan, J. C. and Wilson, R. M. Photolysis of desyl compounds. A new photolytic cyclization. *Journal of the American Chemical Society* 86, 5277–5281 (1964).
55. Routledge, A., Abell, C., and Balasubramanian, S. The use of a dithiane protected benzoin photolabile safety catch linker for solid-phase synthesis. *Tetrahedron Letters* 38, 1227–1230 (1997).
56. Rock, R. S. and Chan, S. I. Synthesis and photolysis properties of a photolabile linker based on 3′-methoxybenzoin. *Journal of Organic Chemistry* 61, 1526–1529 (1996).
57. Pirrung, M. C., Ye, T., Zhou, Z., and Simon, J. D. Mechanistic studies on the photochemical deprotection of 3′,5′-dimethoxybenzoin esters. *Photochemistry and Photobiology* 82, 1258–1264 (2006).
58. Pirrung, M. C. and Huang, C.-Y. Photochemical deprotection of 3′,5′-dimethoxybenzoin (DMB) carbamates derived from secondary amines. *Tetrahedron Letters* 36, 5883–5884 (1995).
59. Pirrung, M. C., Fallon, L., and McGall, G. Proofing of photolithographic DNA synthesis with 3′,5′-dimethoxybenzoinyloxycarbonyl-protected deoxynucleoside phosphoramidites. *Journal of Organic Chemistry* 63, 241–246 (1998).
60. Pirrung, M. C. and Bradley, J.-C. Dimethoxybenzoin carbonates: Photochemically-removable alcohol protecting groups suitable for phosphoramidite-based DNA synthesis. *Journal of Organic Chemistry* 60, 1116–1117 (1995).
61. Peach, J. M., Pratt, A. J., and Snaith, J. S. Photolabile benzoin and furoin esters of a biologically active peptide. *Tetrahedron* 51, 10013–10024 (1995).
62. Pass, S., Amit, B., and Patchornik, A. Racemization—Free photochemical coupling of peptide segments. *Journal of the American Chemical Society* 103, 7674–7675 (1981).
63. Papageorgiou, G., Ogden, D. C., Barth, A., and Corrie, J. E. T. Photorelease of carboxylic acids from 1-acyl-7-nitroindolines in aqueous solution: Rapid and efficient photorelease of L-glutamate. *Journal of the American Chemical Society* 121, 6503–6504 (1999).
64. Papageorgiou, G., Ogden, D., Kelly, G., and Corrie, J. E. T. Synthetic and photochemical studies of substituted 1-acyl-7-nitroindolines. *Photochemical & Photobiological Sciences* 4, 887–896 (2005).
65. Papageorgiou, G. and Corrie, J. E. T. Regioselective nitration of 1-acyl-4-methoxyindolines leads to efficient synthesis of a photolabile L-glutamate precursor. *Synthetic Communications* 32, 1571–1577 (2002).

66. Papageorgiou, G. and Corrie, J. E. T. Effects of aromatic substituents on the photocleavage of 1-acyl-7-nitroindolines. *Tetrahedron* 56, 8197–8205 (2000).
67. Helgen, C. and Bochet, C. G. Photochemical protection of amines with Cbz and Fmoc groups. *Journal of Organic Chemistry* 68, 2483–2486 (2003).
68. Helgen, C. and Bochet, C. G. Preparation of secondary and tertiary amides under neutral conditions by photochemical acylation of amines. *Synlett*, 1968–1970 (2001).
69. Hassner, A., Yagudayev, D., Pradhan, T. K., Nudelman, A., and Amit, B. Light-sensitive protecting groups for amines and alcohols: The photosolvolysis of N-substituted 7-nitroindolines. *Synlett* 15, 2405–2409 (2007).
70. Amit, B., Ben-Efraim, D. A., and Patchornik, A. Light-sensitive amides. The photosolvolysis of substituted 1-acyl-7-nitroindolines. *Journal of the American Chemical Society* 98, 843–844 (1976).
71. Cohen, A. D., Helgen, C., Bochet, C. G., and Toscano, J. P. The mechanism of photoinduced acylation of amines by *N*-acyl-5,7-dinitroindoline as determined by time-resolved infrared spectroscopy. *Organic Letters* 7, 2845–2848 (2005).
72. Neveu, P. et al. A caged retinoic acid for one- and two-photon excitation in zebrafish embryos. *Angewandte Chemie, International Edition* 47, 3744–3746 (2008).
73. Nicolaou, K. C., Winssinger, N., Pastor, J., and DeRoose, F. A general and highly efficient solid phase synthesis of oligosaccharides. Total synthesis of a heptasaccharide phytoalexin elicitor (HPE). *Journal of the American Chemical Society* 119, 449–450 (1997).
74. Debieux, J.-L., Cosandey, A., Helgen, C., and Bochet, C. G. Photoacylation of alcohols in neutral medium. *European Journal of Organic Chemistry*, 2073–2077 (2007).
75. Debieux, J. L. and Bochet, C. G. Preparation of photoactivable amino acid derivatives. *Journal of Organic Chemistry* 74, 4519–4524 (2009).
76. Bochet, C. G. Chromatic orthogonality in organic synthesis. *Synlett* 13, 2268–2274 (2004).
77. Goissis, G., Erickson, B. W., and Merrifield, R. B. Synthesis of protected peptide acids and esters by photosolvolysis of 1-peptidyl-5-bromo-7-nitroindolines. *Proceedings of American Peptide Symposium*, 5, 559–561 (1977).
78. Holmes, C. P. and Jones, D. G. Reagents for combinatorial organic synthesis: Development of a new o-nitrobenzyl photolabile linker for solid phase synthesis. *Journal of Organic Chemistry* 60, 2318–2319 (1995).
79. Holmes, C. P. Model studies for new o-nitrobenzyl photolabile linkers: Substituent effects on the rate of photochemical cleavage. *Journal of Organic Chemistry* 62, 2370–2380 (1997).
80. Lusic, H., Uprety, R., and Deiters, A. Improved synthesis of the two-photon caging Group 3-nitro-2-ethyldibenzofuran and its application to a caged thymidine phosphoramidite. *Organic Letters* 12, 916–919 (2010).
81. Momotake, A., Lindegger, N., Niggli, E., Barsotti, R. J., and Ellis-Davies, G. C. R. The nitrodibenzofuran chromophore: A new caging group for ultra-efficient photolysis in living cells. *Nature Methods* 3, 35–40 (2006).
82. Birr, C., Lochinger, W., Stahnke, G., and Lang, P. The a,a-dimethyl-3,5-dimethoxybenzyloxycarbonyl (Ddz) residue, an N-protecting group labile toward weak acids and irradiation. *Justus Liebigs Annalen der Chemie* 763, 162–172 (1972).
83. Zehavi, U., Amit, B., and Patchornik, A. Light-sensitive glycosides. I. 6-Nitroveratryl b-D-glucopyranoside and 2-nitrobenzyl b-D-glucopyranoside. *Journal of Organic Chemistry* 37, 2281–2285 (1972).
84. Ireland, R. E., Thaisrivongs, S., and Dussault, P. H. An approach to the total synthesis of aplysiatoxin. *Journal of the American Chemical Society* 110, 5768–5779 (1988).
85. McGall, G. H. et al. The efficiency of light-directed synthesis of DNA arrays on glass substrates. *Journal of the American Chemical Society* 119, 5081–5090 (1997).
86. Fodor, S. P. A. et al. Light-directed, spatially addressable parallel chemical synthesis. *Science* (Washington, DC) 251, 767–773 (1991).

87. Hasan, A. et al. Photolabile protecting groups for nucleosides: Synthesis and photo-deprotection rates. *Tetrahedron* 53, 4247–4264 (1997).
88. Pirrung, M. C., Wang, L., and Montague-Smith, M. P. 3′-Nitrophenylpropyloxycarbonyl (NPPOC) protecting groups for high-fidelity automated 5′→3′ photochemical DNA synthesis. *Organic Letters* 3, 1105–1108 (2001).
89. Berroy, P., Viriot, M. L., and Carre, M. C. Photolabile group for 5′-OH protection of nucleosides: Synthesis and photo-deprotection rate. *Sensors and Actuators B* B74, 186–189 (2001).
90. Buehler, S., Lagoja, I., Giegrich, H., Stengele, K.-P., and Pfleiderer, W. New types of very efficient photolabile protecting groups based upon the [2-(2-nitrophenyl)propoxy]carbonyl (NPPOC) moiety. *Helvetica Chimica Acta* 87, 620–659 (2004).
91. Woell, D. et al. On the mechanism of intramolecular sensitization of photocleavage of the 2-(2-nitrophenyl)propoxycarbonyl (NPPOC) protecting group. *Journal of the American Chemical Society* 129, 12148–12158 (2007).
92. Smirnova, J., Woell, D., Pfleiderer, W., and Steiner, U. E. Synthesis of caged nucleosides with photoremovable protecting groups linked to intramolecular antennae. *Helvetica Chimica Acta* 88, 891–904 (2005).
93. Yi, H., Maisonneuve, S., and Xie, J. Synthesis, glycosylation and photolysis of photolabile 2-(2-nitrophenyl)propyloxycarbonyl (NPPOC) protected glycopyranosides. *Organic & Biomolecular Chemistry* 7, 3847–3854 (2009).
94. Coleman, M. P. and Boyd, M. K. S-Pixyl analogues as photocleavable protecting groups for nucleosides. *Journal of Organic Chemistry* 67, 7641–7648 (2002).
95. Coleman, M. P. and Boyd, M. K. The S-pixyl group: An efficient photocleavable protecting group for the 5′ hydroxy function of deoxyribonucleosides. *Tetrahedron Letters* 40, 7911–7915 (1999).
96. Misetic, A. and Boyd, M. K. The pixyl (Px) group: A novel photocleavable protecting group for primary alcohols. *Tetrahedron Letters* 39, 1653–1656 (1998).
97. Furuta, T., Hirayama, Y., and Iwamura, M. Anthraquinone-2-ylmethoxycarbonyl (Aqmoc): A new photochemically removable protecting group for alcohols. *Organic Letters* 3, 1809–1812 (2001).
98. Kostikov, A. P. and Popik, V. V. 2,5-Dihydroxybenzyl and (1,4-dihydroxy-2-naphthyl)methyl, novel reductively armed photocages for the hydroxyl moiety. *Journal of Organic Chemistry* 72, 9190–9194 (2007).
99. Kulikov, A., Arumugam, S., and Popik, V. V. Photolabile protection of alcohols, phenols, and carboxylic acids with 3-hydroxy-2-naphthalenemethanol. *Journal of Organic Chemistry* 73, 7611–7615 (2008).
100. Fedoryak, O. D. and Dore, T. M. Brominated hydroxyquinoline as a photolabile protecting group with sensitivity to multiphoton excitation. *Organic Letters* 4, 3419–3422 (2002).
101. Furuta, T. et al. Brominated 7-hydroxycoumarin-4-ylmethyls: Photolabile protecting groups with biologically useful cross-sections for two photon photolysis. *Proceedings of the National Academy of Sciences of the United States of America* 96, 1193–1200 (1999).
102. Zhu, Y., Pavlos, C. M., Toscano, J. P., and Dore, T. M. 8-Bromo-7-hydroxyquinoline as a photoremovable protecting group for physiological use: Mechanism and scope. *Journal of the American Chemical Society* 128, 4267–4276 (2006).
103. Davis, M. J. et al. Substituent effects on the sensitivity of a quinoline photoremovable protecting group to one- and two-photon excitation. *Journal of Organic Chemistry* 74, 1721–1729 (2009).
104. Turner, A. D., Pizzo, S. V., Rozakis, G. W., and Porter, N. A. Photochemical activation of acylated a-thrombin. *Journal of the American Chemical Society* 109, 1274–1275 (1987).
105. Turner, A. D., Pizzo, S. V., Rozakis, G., and Porter, N. A. Photoreactivation of irreversibly inhibited serine proteinases. *Journal of the American Chemical Society* 110, 244–250 (1988).
106. Koenigs, P. M., Faust, B. C., and Porter, N. A. Photochemistry of enzyme-bound cinnamoyl derivatives. *Journal of the American Chemical Society* 115, 9371–9379 (1993).

107. Gagey, N. et al. Two-photon uncaging with fluorescence reporting: Evaluation of the o-hydroxycinnamic platform. *Journal of the American Chemical Society* 129, 9986–9998 (2007).
108. Gagey, N., Neveu, P., and Jullien, L. Two-photon uncaging with the efficient 3,5-dibromo-2,4-dihydroxycinnamic caging group. *Angewandte Chemie, International Edition* 46, 2467–2469 (2007).
109. Derrer, S., Flachsmann, F., Plessis, C., and Stang, M. Applied photochemistry - light controlled perfume release. *Chimia* 61, 665–669 (2007).
110. Kostikov, A. P. and Popik, V. V. Photolabile protection of 1,2- and 1,3-diols with salicylaldehyde derivatives. *Organic Letters* 10, 5277–5280 (2008).
111. Gravel, D., Hébert, J., and Thoraval, D. o-Nitrophenylethylene glycol as photoremovable protective group for aldehydes and ketones: Syntheses, scope, and limitations. *Canadian Journal of Chemistry* 61, 400–410 (1983).
112. Blanc, A. and Bochet, C. G. Bis(o-nitrophenyl)ethanediol: A practical photolabile protecting group for ketones and aldehydes. *Journal of Organic Chemistry* 68, 1138–1141 (2003).
113. Kantevari, S., Narasimhaji, C. V., and Mereyala, H. B. Bis(4,5-dimethoxy-2-nitrophenyl)ethylene glycol: A new and efficient photolabile protecting group for aldehydes and ketones. *Tetrahedron* 61, 5849–5854 (2005).
114. Kostikov, A. P., Malashikhina, N., and Popik, V. V. Caging of carbonyl compounds as photolabile (2,5-dihydroxyphenyl)ethylene glycol acetals. *Journal of Organic Chemistry* 74, 1802–1804 (2009).
115. Lu, M., Fedoryak, O. D., Moister, B. R., and Dore, T. M. Bhc-diol as a photolabile protecting group for aldehydes and ketones. *Organic Letters* 5, 2119–2122 (2003).
116. Rochat, S., Minardi, C., De Saint Laumer, J.-Y., and Herrmann, A. Controlled release of perfumery aldehydes and ketones by Norrish type-II photofragmentation of a-keto esters in undegassed solution. *Helvetica Chimica Acta* 83, 1645–1671 (2000).
117. Levrand, B. and Herrmann, A. Light induced controlled release of fragrances by Norrish type II photofragmentation of alkyl phenyl ketones. *Photochemical & Photobiological Sciences* 1, 907–919 (2002).
118. Levrand, B. and Herrmann, A. Controlled light-induced release of volatile aldehydes and ketones by photofragmentation of 2-oxo-(2-phenyl)acetates. *Chimia* 61, 661–664 (2007).
119. Herrmann, A. Controlled release of volatiles under mild reaction conditions: From nature to everyday products. *Angewandte Chemie, International Edition* 46, 5836–5863 (2007).
120. McHale, W. A. and Kutateladze, A. G. An efficient photo-SET-induced cleavage of dithiane-carbonyl adducts and its relevance to the development of photoremovable protecting groups for ketones and aldehydes. *Journal of Organic Chemistry* 63, 9924–9931 (1998).
121. Vath, P., Falvey, D. E., Barnhurst, L. A., and Kutateladze, A. G. Photoinduced C–C bond cleavage in dithiane-carbonyl adducts: A laser flash photolysis study. *Journal of Organic Chemistry* 66, 2887–2890 (2001).
122. Valiulin, R. A. and Kutateladze, A. G. 2,6,7-Trithiabicyclo[2.2.2]octanes as promising photolabile tags for combinatorial encoding. *Journal of Organic Chemistry* 73, 335–338 (2008).
123. Kurchan, A. N., Mitkin, O. D., and Kutateladze, A. G. Dithiane and trithiane-based photolabile molecular linkers equipped with amino-functionality: Synthesis and quantum yields of fragmentation. *Journal of Photochemistry and Photobiology A: Chemistry* 171, 121–129 (2005).
124. Wang, P., Hu, H., and Wang, Y. Novel photolabile protecting group for carbonyl compounds. *Organic Letters* 9, 1533–1535 (2007).
125. Wang, P. et al. Sequential removal of photolabile protecting groups for carbonyls with controlled wavelength. *Journal of Organic Chemistry* 73, 6152–6157 (2008).
126. Jones, P. B., Pollastri, M. P., and Porter, N. A. 2-Benzoylbenzoic acid: A photolabile mask for alcohols and thiols. *Journal of Organic Chemistry* 61, 9455–9461 (1996).
127. Specht, A., Loudwig, S., Peng, L., and Goeldner, M. *p*-Hydroxyphenacyl bromide as photoremoveable thiol label: A potential phototrigger for thiol-containing biomolecules. *Tetrahedron Letters* 43, 8947–8950 (2002).

128. Clarke, K. M., La Clair, J. J., and Burkart, M. D. A three-component photoreversible tag for thiols. *Journal of Organic Chemistry* 70, 3709–3711 (2005).
129. Kotzur, N., Briand, B., Beyermann, M., and Hagen, V. Wavelength-selective photoactivatable protecting groups for thiols. *Journal of the American Chemical Society* 131, 16927–16931 (2009).
130. Rubinstein, M., Amit, B., and Patchornik, A. Use of a light-sensitive phosphate protecting group for mononucleotide syntheses. *Tetrahedron Letters* 16, 1445–1448 (1975).
131. Kaplan, J. H., Forbush, B., III, and Hoffman, J. F. Rapid photolytic release of adenosine 5′-triphosphate from a protected analog: Utilization by the sodium: Potassium pump of human red blood cell ghosts. *Biochemistry* 17, 1929–1935 (1978).
132. Givens, R. S. and Park, C.-H. Hydroxyphenacyl ATP: A new phototrigger. V. *Tetrahedron Letters* 37, 6259–6262 (1996).
133. Pirrung, M. C., Fallon, L., Zhu, J., and Lee, Y. R. Photochemically removable silyl protecting groups. *Journal of the American Chemical Society* 123, 3638–3643 (2001).
134. Brook, M. A., Gottardo, C., Balduzzi, S., and Mohamed, M. The sisyl (tris(trimethylsilyl)silyl) group: A fluoride resistant, photolabile alcohol protecting group. *Tetrahedron Letters* 38, 6997–7000 (1997).
135. Brook, M. A., Balduzzi, S., Mohamed, M., and Gottardo, C. The photolytic and hydrolytic lability of sisyl ($Si(SiMe_3)_3$) ethers, an alcohol protecting group. *Tetrahedron* 55, 10027–10040 (1999).

5

Photochemical Key Steps in Organic Synthesis

Norbert Hoffmann
Université de Reims Champagne Ardenne

5.1 Introduction

Photochemical reactions are characterized by the transformation of electronically excited molecules that are generated by light absorption.[1,2] Compared to their ground state, such excited molecules possess completely different electronic configurations. Consequently, their chemical reactivity completely changes. Frequently, complementary reactions are observed for molecules at the ground and the excited states.[3] Thus, using photochemical reactions, the spectrum of chemical transformations of a compound family is significantly enlarged. Total syntheses can be shortened, and frequently complex, polycyclic, or highly functionalized structures can easily be obtained from simple substrates.[4] New product families or product libraries difficult to achieve with ground-state reactions are thus available, opening new perspectives in the search of biologically active compounds. Catalytic reactions are also affected by light irradiation. Either ground-state reactions become more efficient or new catalytic reactions are observed. Such reactions also enrich the methodology in organic synthesis. After a period of stagnation, activity in the field of organic photochemical reactions and their application to synthesis has started to grow again in academic and industrial research. In the two preceding editions of this handbook[5] as well as in other books,[1,6,7] large collections of organic photochemical reactions are presented. Many books deal with experimental conditions and equipment.[1,8] This chapter briefly discusses some selected examples predominantly chosen in the field of total synthesis and synthesis of biologically active compounds. The examples have been manly taken from recent literature.

5.2 Photocycloadditions

5.2.1 [2 + 2] Photocycloadditions

Among the photochemical reactions, the [2 + 2] photocycloaddition of α,β-unsaturated carbonyl compounds with alkenes, allenes, or alkynes leading to cyclobutanes or cyclobutenes, respectively,[9] is certainly the most applied reaction in organic synthesis.[10,11] The reaction can be performed either by using direct excitation of the α,β-unsaturated carbonyl chromophore or by sensitization. In the latter case, acetone is most frequently used as sensitizer to transform α,β-unsaturated carboxylic compounds. Acetone absorbs light and after intersystem crossing, the triplet energy is transferred onto the substrate. The intramolecular version of these reactions was frequently applied to complex multistep syntheses of natural products. In such a reaction, the bisfuranone compound **1** is transformed into the cyclobutane derivative **2** (Scheme 5.1, Equation 5.1).[12] Principally, the [2 + 2] photocycloaddition can take place at both furanone moieties. Obviously, only excitation of the less conjugated and thus more reactive furanone leads to cycloaddition. Although 1,4-biradical intermediates are involved in these reactions, the

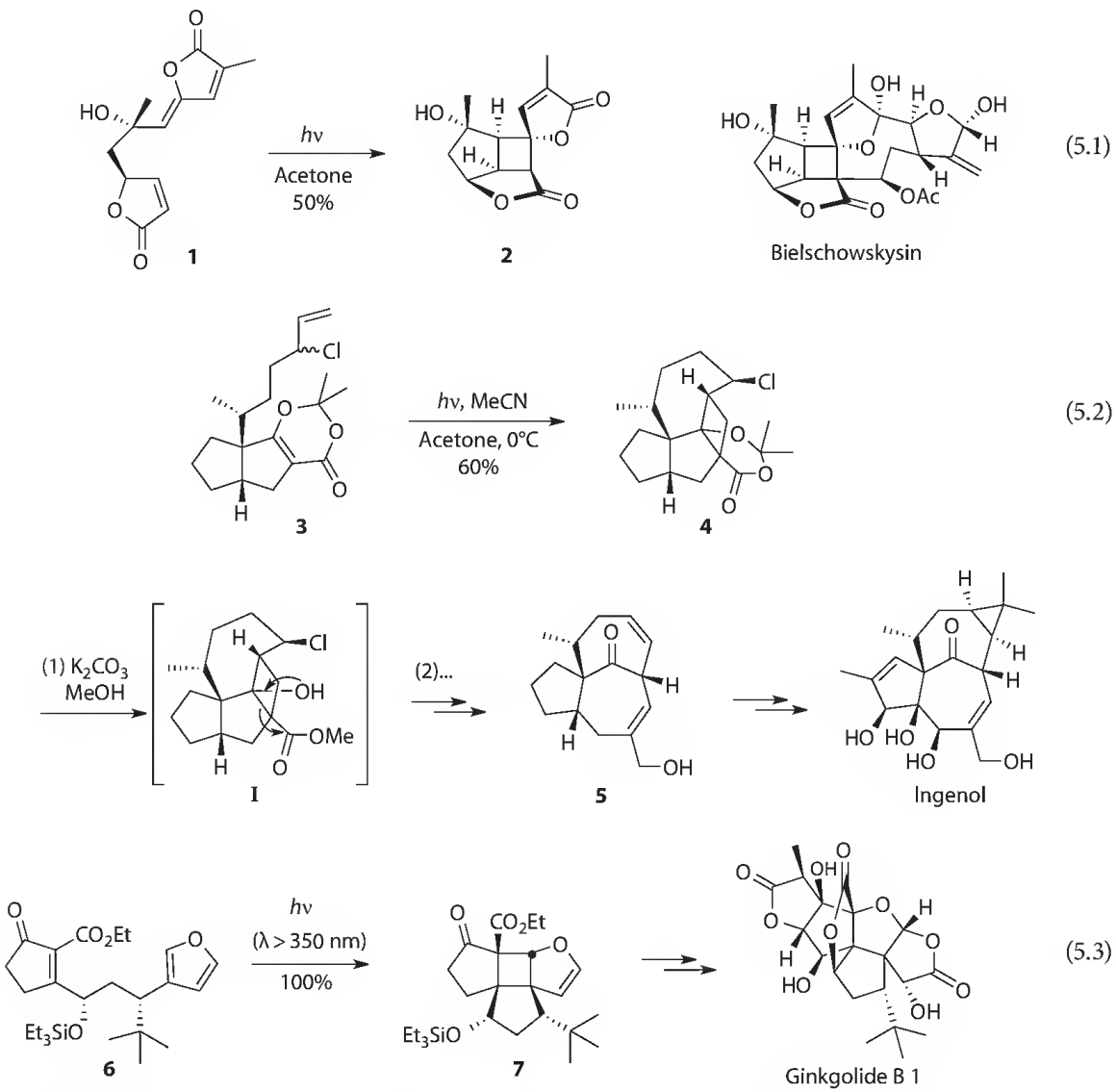

SCHEME 5.1 Intramolecular [2 + 2] photocycloaddition of α,β-unsaturated carbonyl compounds.

transformation is highly stereoselective.[9] Particularly in intermolecular reactions, these intermediates often diminish the stereo- and regioselectivity.[13] Compound **2** is a partial structure of the diterpene, bielschowskysin, which is isolated from corals *Pseudopterogorgia kallos*. Bielschowskysin possesses cytotoxic and antiplasmodial activities. A similar strategy but using the intramolecular [2 + 2] photocycloaddition of allenes to furanones has been applied to the synthesis of this compound[14] and other natural products.[15]

The same acetone sensitized [2 + 2] photocycloaddition was applied to the synthesis of ingenol. The challenge of this synthesis is to build up, in a straightforward way, a bicyclo[4.4.1]undecan-11-one moiety with *trans* junction of the two seven-membered rings. The intramolecular cycloaddition of the tricyclic dioxygenone derivative **3** yields the cyclobutane derivative **4** possessing already one seven-membered ring (Scheme 5.1, Equation 5.2).[16] The stereochemistry of the *trans* linkage of the bicyclo[4.4.1]undecan-11-one system is established in this step. It is controlled by the presence of the chlorine atom in the allyl position of the alkene side chain of **3**. Elimination of the isopropylidene group intermediately generates the aldol **I**. A retroaldol reaction leads to the second seven-membered ring of the target. Further in situ transformations lead to compound **5**, which is transformed into the final product ingenol. β-Diketones often exists in equilibrium with a β-hydroxyenone (mono enolized biacetyle chromophore). After [2 + 2] photocycloaddition with an alkene, the resulting aldole undergoes retroaldol cleavage.[17] The combination of these two reaction steps is also called de Mayo reaction. The [2 + 2] photocycloaddition in combination with a retro Mannich reaction was also applied to synthesis.[18]

The intramolecular transformation of the cyclopentenone derivative **6** is induced by direct excitation (Scheme 5.1, Equation 5.3).[19] The enone moiety is added to a furan ring leading to the cyclobutane derivative **7**, which is obtained in quantitative yield. It should also be pointed out that the reaction is completely stereoselective. Electronic effects such as the electron-rich olefinic partner and the substitution at the linking group (allylic 1,3-strain[20]) contributes to the efficiency of the reaction. Compound **7** was transformed into ginkgolide B1. Derivative **7** possesses already significant structural elements of the target.

Chiral induction in photochemical reactions is extensively studied also with the aim to apply such transformations to organic synthesis.[21,22] Frequently, the intermolecular version of the reaction is less stereoselective.[23] Nevertheless, if the resulting stereoisomers can easily be separated, such transformations become interesting for application in organic synthesis. The acetone-sensitized transformation compound **8** obtained from uracil with ethylene yields a mixture of diastereoisomers **9a,b** (Scheme 5.2, Equation 5.4).[24] After chromatographic separation, the isomers were transformed into the cyclobutane amino acids **10** and ***ent*-10**, respectively. Cyclobutane amino acids possessing an additional hydroxymethyl group are also available in a similar way.[25] These are β-amino acids that significantly affect secondary and tertiary structures when incorporated in polypeptides.[26] Thus the rigidity caused by the cyclobutane ring may favor the formation of a helix structure. The same kind of reaction was also applied to several cyclobutane containing natural products.[27]

Using chiral templates[22,28] such as lactame **13** derived form Kemp's acid, the intramolecular reaction of quinolone **11** with olefine **12** is performed in high yield and complete dia and regioselectivity (Scheme 5.2, Equation 5.5).[29] In the template structure, the two lactame functions of **13** and **11** are linked together via hydrogen bonds. Such catalysts can also be considered as organocatalysts.[30] Under basic reaction conditions, a rearrangement (**II**) takes place leading to the tricyclic compound **15**. This compound was further transformed into the alkaloid (+)-meloscine.

[2 + 2] Photocycloaddition between two alkenes is catalyzed by Cu(I) salts.[31] This reaction was frequently applied to the synthesis of natural products possessing a cyclobutane ring. When the enolether **16** was irradiated in the presence of a copper (I) salt, the cyclobutane derivative **17** was obtained in high yields (Scheme 5.3).[32] The high stereoselectivity of the transformation is explained by the complexation of both olefin moieties by a copper ion. Compound **17** was transformed into (–)-grandisol, which is a component of the aggregation pheromone of the male boll weevil (*Anthonomus grandis*). This product was frequently synthesized using photochemical reactions as key steps.[33]

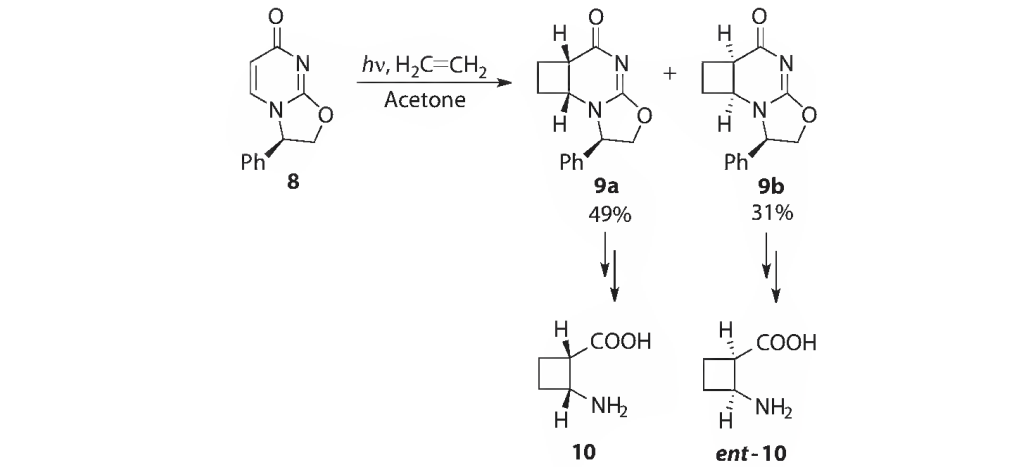

(5.4)

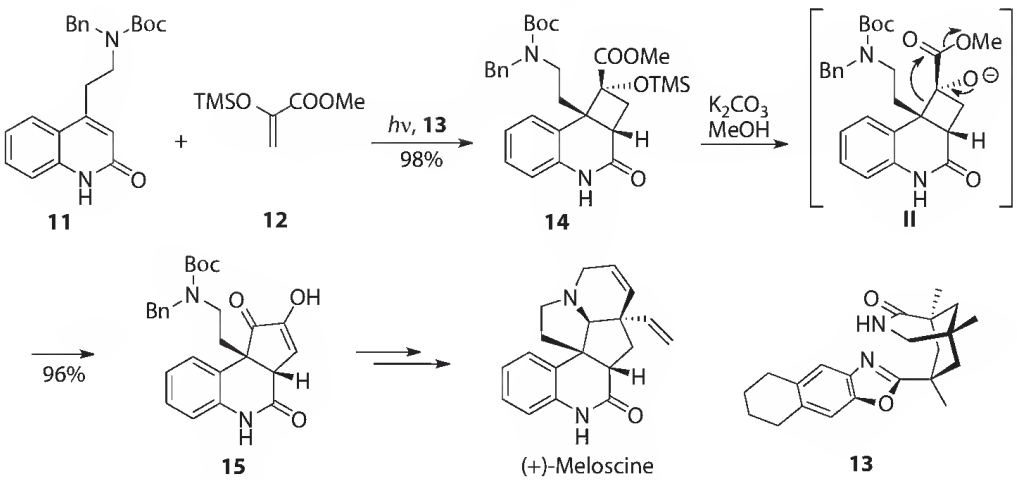

(5.5)

SCHEME 5.2 Intermolecular [2+2] photocycloaddition of α,β-unsaturated carbonyl compounds.

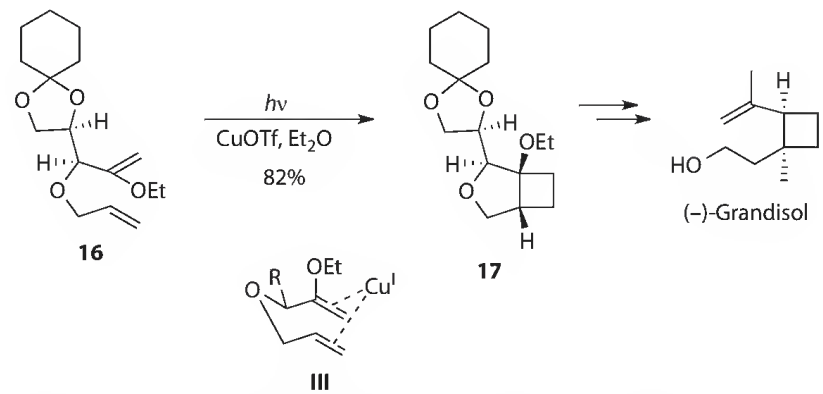

SCHEME 5.3 Intramolecular Cu(I)-catalyzed [2+2] photocycloaddition of alkenes.

Small heterocycles such as oxetanes can also be obtained via [2 + 2] photocycloaddition. Electronically excited carbonyl compounds react with alkenes (Paternò–Büchi reaction).[11,34] Many investigations have been carried out on various stereochemical aspects of this reaction.[35] The transformation of dihydropyrrole **18** with benzaldehyde yielded the two diastereomeric oxetanes **19a,b** (Scheme 5.4).[36] It should be indicated that the reaction is stereospecific as far as the relative configuration of the three chiral centers

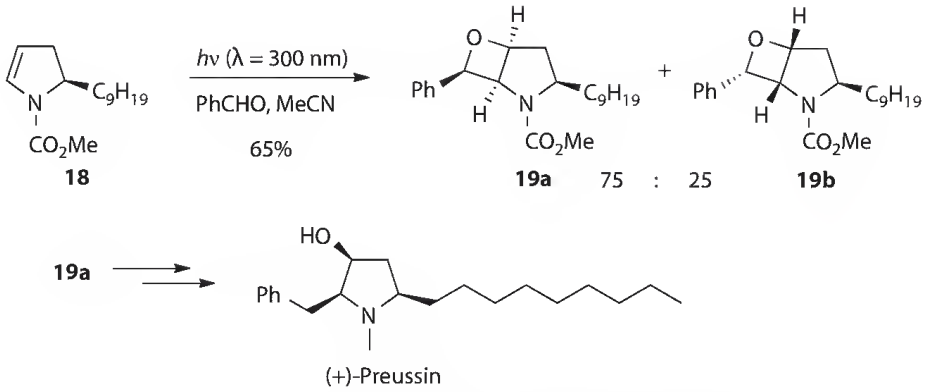

SCHEME 5.4 Paternò–Büchi reaction of benzaldehyde with the dihydropyrrole derivative **18**.

in the oxetane ring is concerned. Only the *syn*-isomer is formed.[37] The two diastereomers isolated from the reaction mixture resulted from the induction of the chiral center at the position of the *n*-nonyl substituent. The major isomer **19a** was transformed into the pyrrolidine alkaloid (+)-preussin.

5.2.2 Photocycloadditions of Higher Order

In accordance with the Woodward–Hoffmann rules[38] and for concerted reactions, photochemical excitation induces a reactivity that is complementary to that at the ground state. Thus, [4 + 4] cycloadditions can be easily carried out under photochemical conditions.[39] Intermediates such as biradicals are also frequently involved in higher order cycloadditions. An example is depicted in Scheme 5.5.[40] Irradiation of the maleimide derivative **20** leads to the formation of the biradical **IV**.[41] Intramolecular addition yielded the tetracyclic compound **21**. This step is a formal [5 + 2] cycloaddition. It should be mentioned that product **21** is also photoreactive, which diminishes the yield of the reaction. However, when the transformation is carried out in a "high flow-rate/low volume continues photochemical FEP reactor,"[42] the yield can be considerably increased. This technique also allows large-scale transformations and can be considered for industrial applications. Further transformations of **21** led to (±)-neostenine, which belongs to the family of *Stemona* alkaloids.

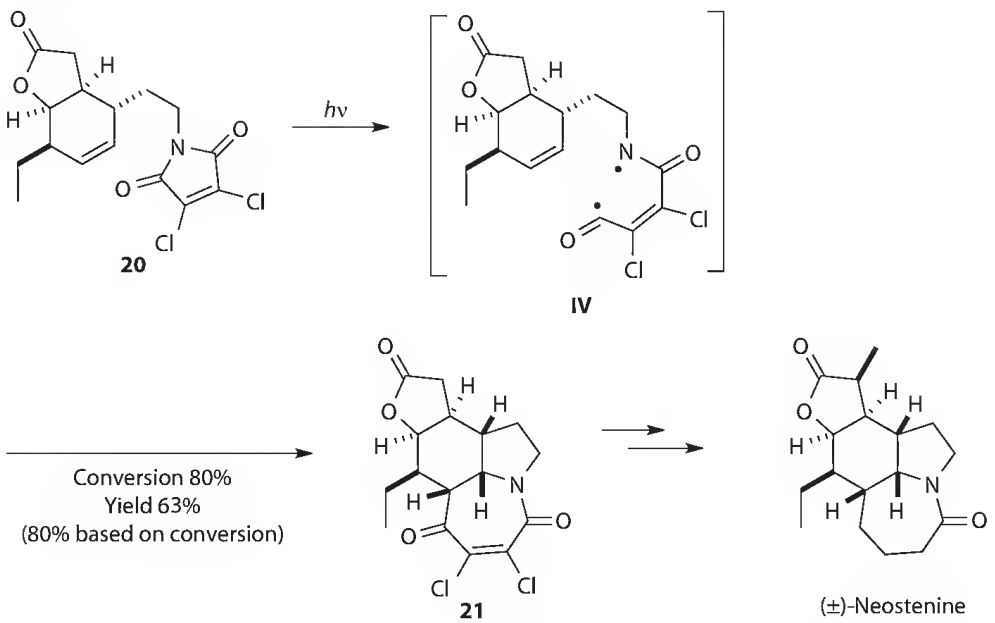

SCHEME 5.5 Intramolecular formal [5 + 2] photocycloaddition of a maleimide moiety with an alkene.

Generally, singlet excited states are highly polarized. In the case of tautomeric equilibria, the formation of the more polar one is favored at the excited state, which is in contrast to the ground-state reactivity. Upon irradiation, hydroxyflavone **22** yields intermediately the oxidopyrrillium ion **V**, which, in the presence of an excess of methyl cinnamate **23**, is trapped by a [2 + 3] cycloaddition, leading to compound **24** (Scheme 5.6).[43] The intermediate **V** is already localized on the potential energy surface of the ground state. Similar compounds can also be generated with ground-state reactions.[44] During workup

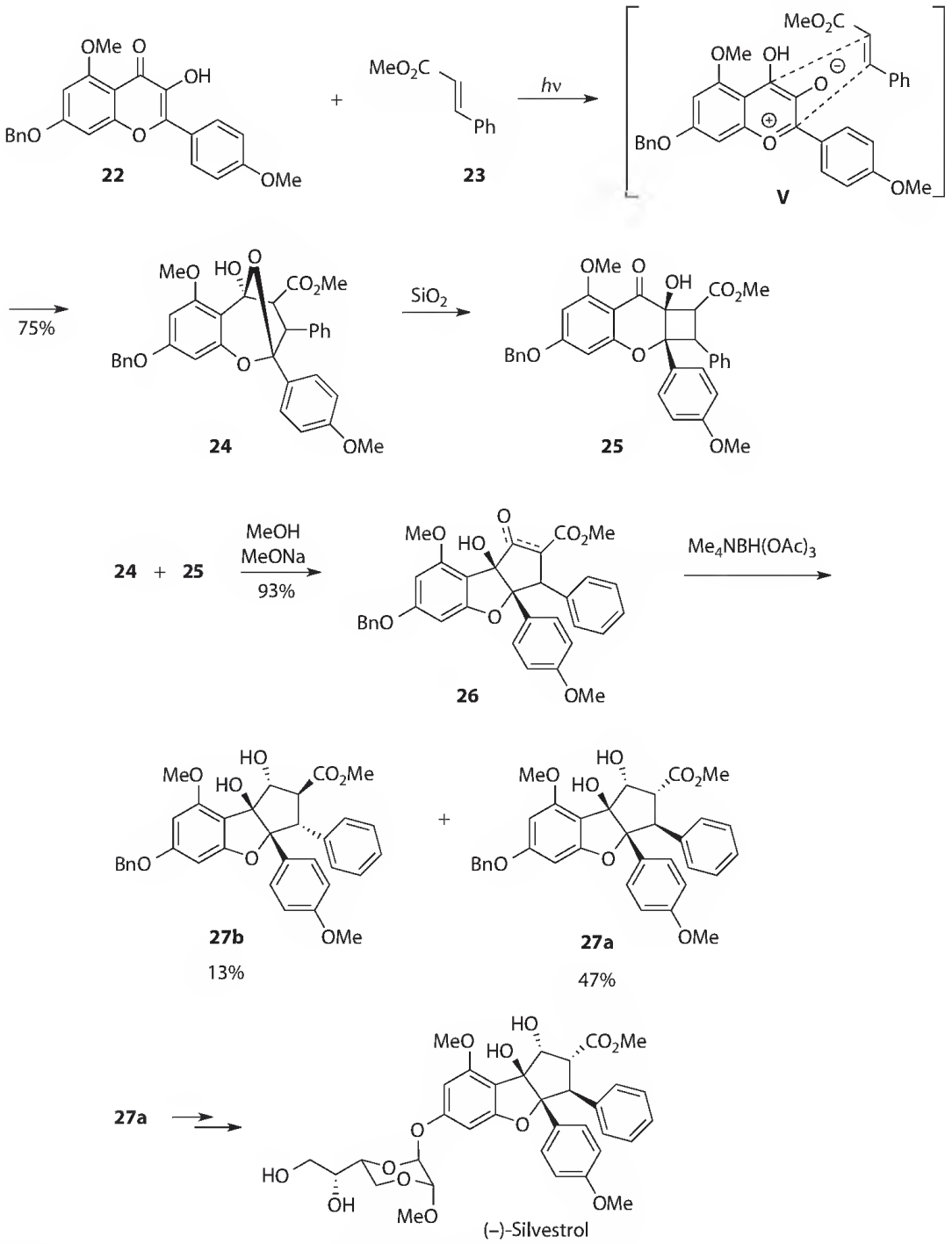

SCHEME 5.6 [2 + 3] Photocycloaddition of a hydroxyflavone derivative.

and in particular during chromatography on silica gel, **24** is partially transformed into the cyclobutane **25**. The latter compound was not detected in the crude reaction mixture. It does not therefore result from a [2 + 2] photocycloaddition. Basic treatment of the mixture of compounds **24** and **25** yields **26** as a mixture of keto-enol tautomers. After reduction, the diastereoisomers **27a,b** are obtained. The major isomer **27a** was transformed into (–)-silvestrol. During these steps, an optical resolution was performed. An asymmetric synthesis using a TADDOL as chiral template was also described.[45] Various derivatives of this compound have been synthesized in the same way. It should be pointed out that the photochemical key step is essential in these syntheses since numerous ground-state reactions, in particular 1,4 addition cyclizations to the highly substituted α,β-unsaturated carbonyl system, were unsuccessful. The target compounds are particularly interesting due to their cytotoxic activity.

5.2.3 Photocycloadditions of Aromatic Compounds

Most ground-state reactions of aromatic compounds are characterized by a great tendency to regenerate aromaticity in the products. For instance, electrophilic substitution is certainly the most characteristic transformation of benzene-type aromatic compounds. Photochemical reactions however possess a strong tendency to yield nonaromatic products. Typical examples that have been applied to organic synthesis are photocycloadditions with alkenes.[46,47] Three modes can be distinguished: [2 + 2] (*ortho*-photocycloaddition), [2 + 3] (*meta*-photocycloaddition), and [2 + 4] (*para*-photocycloaddition or photo-Diels–Alder reaction) (Scheme 5.7). The [2 + 3] photocycloaddition[48] of benzene derivatives was most frequently applied to organic synthesis.

When irradiated, the benzene derivative **28** yielded a mixture of the angular (**29**) and the linear (**30**) photocycloadduct (Scheme 5.8).[49] This regioselectivity is not controlled since both isomers were isolated in almost equal proportions.[47] However, both products **29** and **30** are in photostationary equilibrium so that the desired angular isomer **29** can be prepared in an excess. The transformation is stereospecific. The approach of the olefinic side moiety to the electronically excited benzene ring is controlled by an allylic 1,3-strain effect in the transition state **VI**.[20] Only one stereoisomer of the intermediate **VII** is formed. Since the reaction occurs at the singlet state, **VII** possesses zwitterionic character. Charge or radical combination occurs in two ways, leading either to the angular (**29**) or the linear (**30**) compound. Product **29** was transformed into the sesquiterpenoid penifulvin A, which is isolated from the fungus *Penicillium griseofulvum*. It belongs to the structure family of fenestranes[50] and possesses significant insecticidal activity. The fact that the reaction occurs at the singlet state also avoids *cis/trans* isomerization at the olefinic side chain. Thus the *trans* isomer **31** was transformed into penifulvin B and the *cis* isomer **32** into penifulvin C.[51]

The [2 + 2] photocycloaddition frequently occurs in competition to the [2 + 3] one.[52] Depending on the substituents, one of the two modes is favored. Despite the fact that also in this case, complex polycyclic compounds are obtained starting form simple substrates, few applications to organic synthesis have

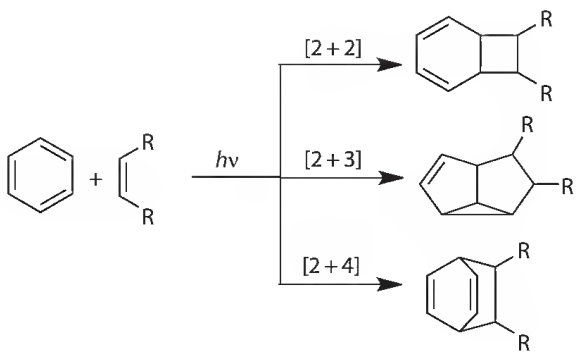

SCHEME 5.7 Photocycloadditions of benzene derivatives.

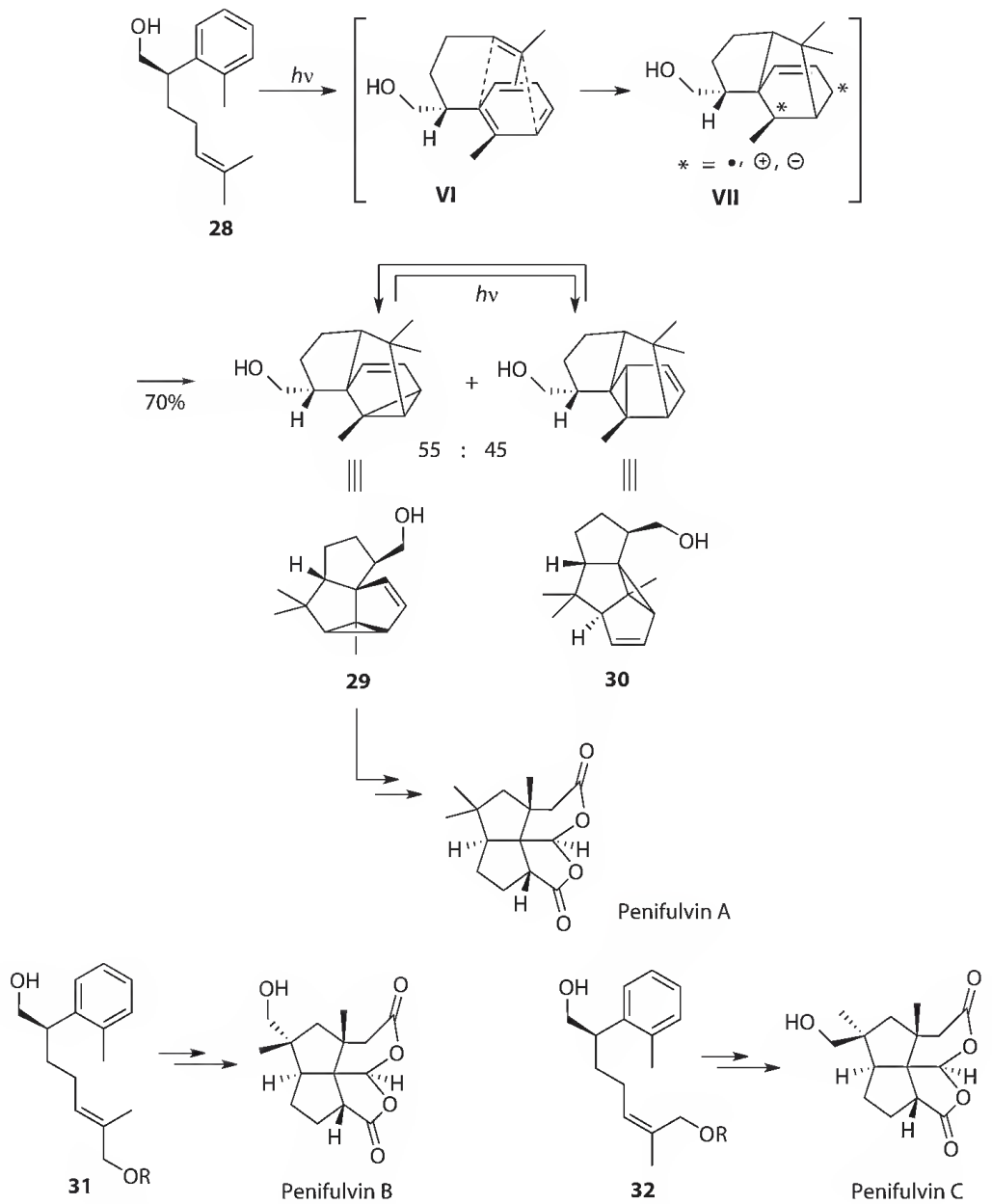

SCHEME 5.8 Intramolecular [2 + 3] photocycloaddition of aromatic compounds.

been described. Recently, such reactions were applied to the synthesis of neurotransmitter analogues[53] and to the synthesis of intermediates for the production of herbicides.[54]

5.3 Photochemical Rearrangements

Among the photochemical rearrangements, the oxa-di-π-methane rearrangement has been applied to the synthesis of complex polycyclic natural products. This rearrangement is observed with β,γ-unsaturated carbonyl compounds (Scheme 5.9, Equation 5.6).[55] Most frequently, the reactions is observed at the triplet state possessing ππ* character. This means that the transformations can easily be carried out using triplet sensitization. Under these reaction conditions with acetophenone as sensitizer, the tricyclic compound **33** was transformed into compounds **34**, **35**, and **36** (Scheme 5.9, Equation 5.7).[56] In a second photochemical reaction, the diastereomer **34** is transformed into **35**. Under optimized conditions, the

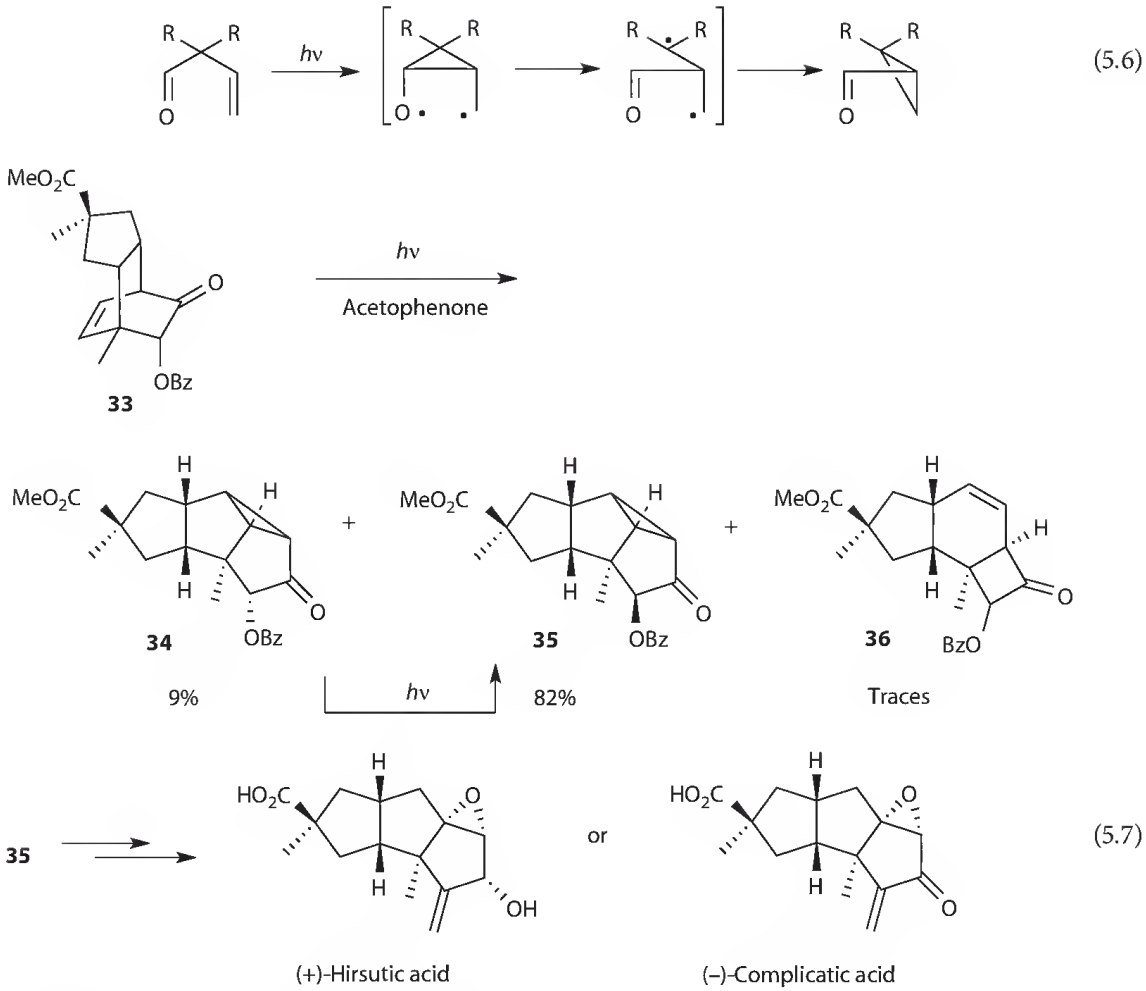

SCHEME 5.9 Oxa di-π-methane rearrangement.

latter compound can be obtained in high selectivity. Compound **36** presumably results from a 1,3-acyl rearrangement at the singlet state. Under the optimized conditions, this compound is only obtained in traces. Compound **35** was transformed into the triquinane-type natural products (+)-hirsutic acid and (–)-complicatic acid. The latter compound could act as seretonin 5-HT6 receptor antagonist. This pharmacological activity is interesting in the context of the treatment of Alzheimer disease.

Photodeconjuation of α,β-unsaturated carbonyl and carboxyl compounds is a versatile reaction to modify a functional group.[57] The transformation was also applied to the synthesis of natural products. Recently, a corresponding diester (**37**) has been transformed (Scheme 5.10, Equation 5.8).[58] After light absorption, the dienol **VIII** is generated via 1,5-hydrogen shift. Protonation of this intermediate in the presence of an amino alcohol leads to the deconjugated product **38** as mixture of *cis/trans* isomers. These compounds have been transformed into amphiasterin B4 and its epimer **39**. Amphiasterin B4 is isolated from the sponge *Plakortis quasiamphiaster* and possesses cytotoxic activity. The reaction was also applied to asymmetric synthesis. The dienol intermediate can be protonated by a chiral amino alcohol.[59] Chirality can also be induced by a chiral auxiliary attached as alcohol part of the ester function.[60]

A similar photochemical reaction is observed with benzaldehyde derivatives. Irradiation of compound **40** leads to the intermediate **IX** in which the aromatic character is suppressed (Scheme 5.10, Equation 5.9).[61] As in the previous case, this reaction step can be considered as a 1,5-hydrogen shift. The intermediate is trapped by an intramolecular Diels–Alder reaction. Thus starting from a relatively simple substrate, a complex polycyclic molecule (**41**) is obtained in high yield and complete stereoselectivity.

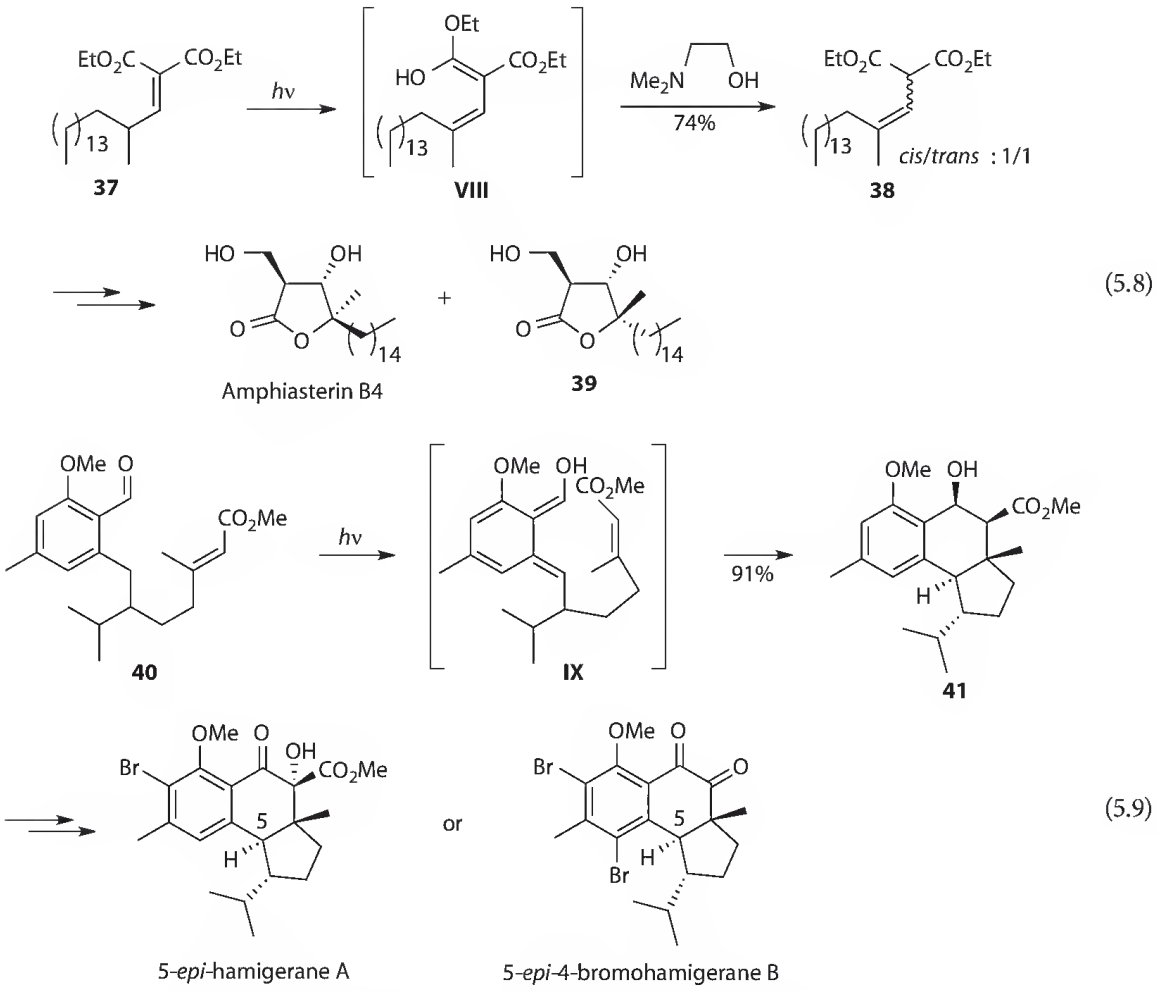

SCHEME 5.10 Photochemical generation and reactions of dienol intermediates.

The stereochemical course of reaction is explained by an allylic 1,3-strain effect (compare Schemes 5.1 and 5.8, Equation 5.1). A very similar reaction with almost complete chiral induction was carried out in a template structure.[62] Compound **41** was transformed into 5-*epi*-hamigerane and 5-*epi*-4-bromohamigerane B. Similar examples have been reported.[63] In a more general context, the intermediate **IX** contains a *ortho*-quinodimethane structure. Such structures are generated in many syntheses of polycyclic compounds.[64]

Photochemical cylization reactions are frequently observed. In particular, many reports exist on application of electrocyclic reactions to organic synthesis.[65] These reactions occur at the ground and the excited states. The stereochemical course is determined by the Woodward–Hoffmann rules and it is complementary for both electronic states.[38,65] As far as the application to organic synthesis is concerned, such reactions can also be successfully carried out with highly functionalized substrates. Upon irradiation, compound **42** undergoes photocylization, leading to the intermediate **X** in the sense of a 6π electrocyclization, which involves the polar mesomeric form of the amide function (Scheme 5.11).[66] This process is certainly favored by the presence of a hydrogen bond from an adjacent phenol to the amide oxygen. Furthermore, an additional substituent on the amide nitrogen is necessary to establish a favorable conformation for the cyclization step. The final product **43** is generated by a 1,5-hydrogen shift. Compound **43** was transformed into (+)-narciclasine and (+)-pancratistatin. These alkaloids have been isolated from the roots of *Pancratium littorale* and possess antitumor activity. Compared to corresponding ground-state transformations, the photochemical reaction conditions are much milder. Therefore, this kind of photocyclization was applied as a versatile step to the total synthesis of natural products

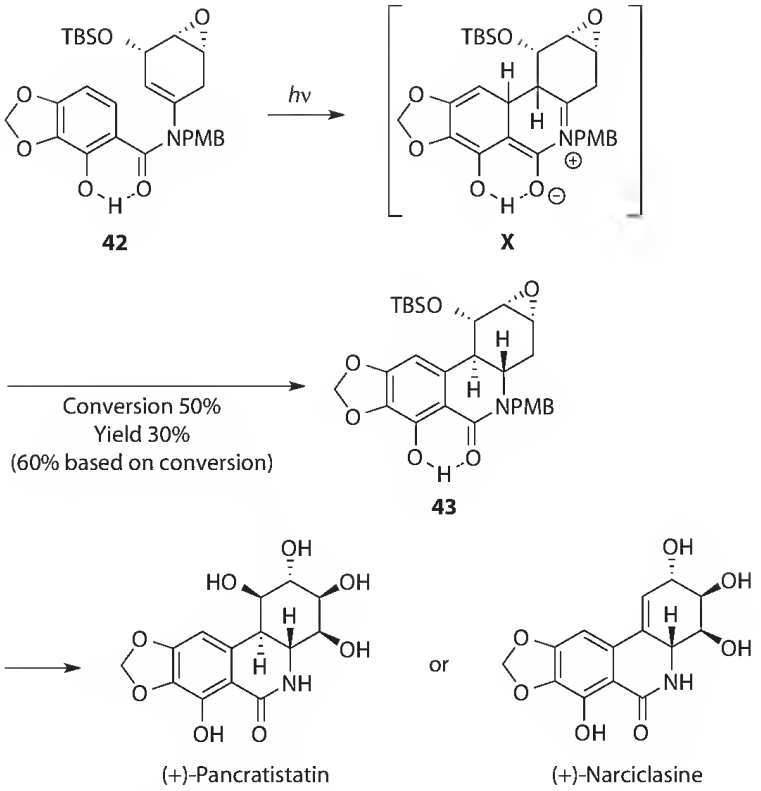

SCHEME 5.11 Photochemical cyclization of an aromatic enamide.

of various alkaloid families and other biologically active compounds.[67] Derivatives of narciclasine and pancratistatin have been synthesized in a similar cyclization step but with a photochemical electron transfer as key step (see the following).[68]

5.4 Photochemical Electron Transfer–Mediated Transformations

Electron transfer–mediated reactions play also an important role in organic synthesis. At the ground state, electron transfer is controlled by the redox potentials of the substrate molecules and the redox reaction is only possible when the LUMO of the acceptor molecule is energetically lower than the HOMO of the donor molecule. Due to electronic excitation by light absorption, the redox potential changes and the exothermicity of photochemically induced electron transfer is quantified by the Rehm–Weller equation.[69] The redox chemistry of organic molecules is considerably enriched by the photochemical electron transfer. Numerous synthetic applications have been reported.[70,71]

In compound **44**, an intramolecular photochemically induced electron transfer takes place from an indol to a dihydroindol moiety (Scheme 5.12).[72] After deacylation, the radical anion **XI** is generated. The presence of a lithium salt increases the polarity of the reaction medium, which stabilizes the radical ion pair with respect to back electron transfer. The lithium ion particularly stabilizes the radical anion **XI**. The presence of an OAc on the donor indole fragment facilitates the electron transfer, and yields are increased when compared to transformations of derivatives without this substituent.[73] Debromination at the dihydroindole moiety and radical combination lead to the intermediate **XII**. After tautomerization, the final product **45** is isolated in good yields. **45** was transformed in seven additional steps into (–)-diazonamide A.

Many photochemical electron transfer–induced reactions have been carried out with phthalimide derivatives.[71,74] A phenomenon of chiral memory[75] has been observed in such reactions of a phthalimide derivative. The L-proline compound **46** was transformed into the benzodiazepine derivative **47** (Scheme 5.13).[76] Eighty-six percent of the chiral information was preserved in the final product **47**. In this case, the electron

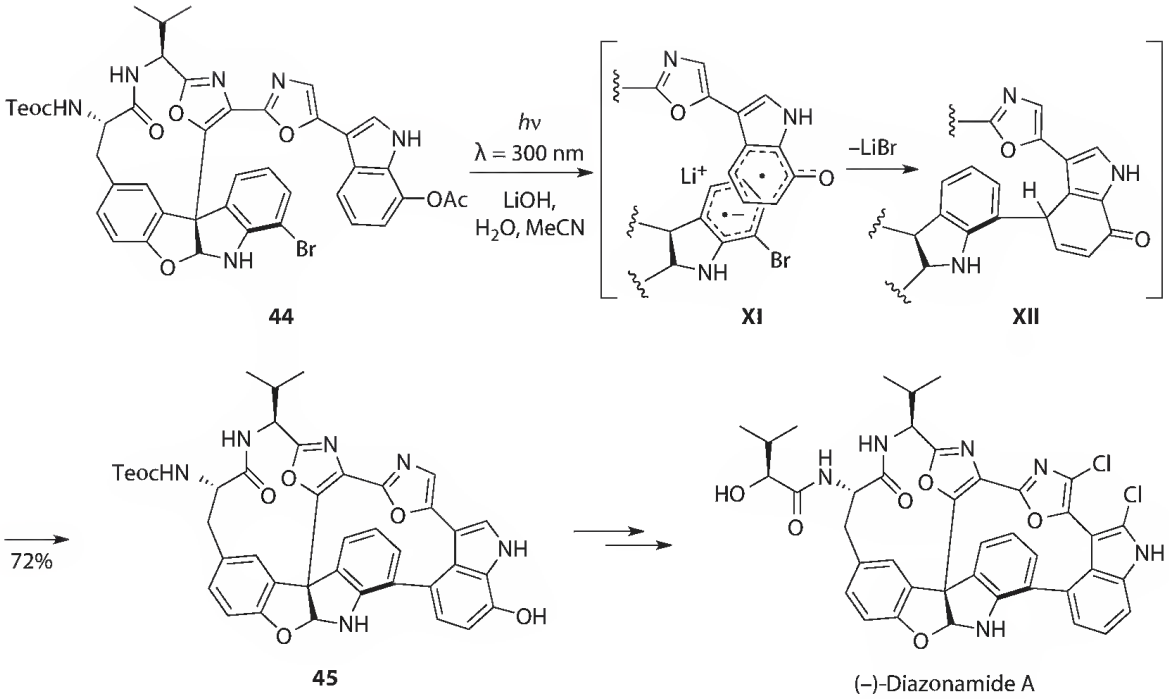

SCHEME 5.12 Intramolecular photochemical electron transfer–induced macrocyclization.

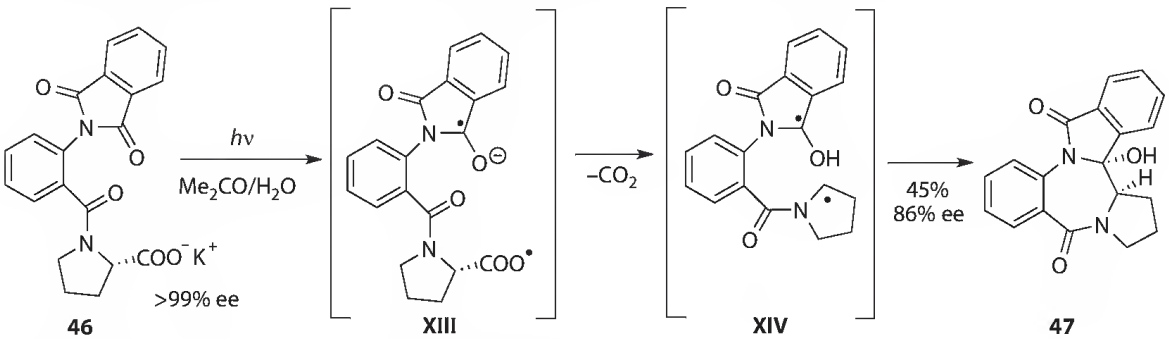

SCHEME 5.13 Chiral memory effect in a photosensitized cyclization.

transfer occurs between a carboxylate function and the phthalimide moiety, which is directly excited to its triplet state (T_1) via acetone sensitization (energy transfer). Thus intermediate **XIII** is generated. For classification of this reaction, it should be added that the electron transfer itself is not sensitized. No electron transfer occurs from or to the sensitizer (acetone). The configuration of the pyrrolidine moiety in **47** has been inverted with respect to the substrate **46.** This result was explained by an enhanced barrier of the rotation around the central C–N bond of an atropisomer of intermediate **XIV** before cyclization. The biradical **XIV** also possesses triplet character. The photochemical electron transfer–induced reactions of phthalimides have been widely applied to the synthesis of macrocyclic compounds[77].

Recently, a lot of photochemically catalyzed reactions using electron transfer have been applied to organic synthesis.[78] In this case, the sensitizer is involved in photochemical electron transfer and acts as redox catalyst.[79]

Electron-rich alkenes such as the silyl enol ether in compound **48** are oxidized by the photochemical excited sensitizer DCA (Scheme 5.14).[80] A cascade reaction is induced by the addition of the resulting radical cation in **XV** to an alkene. Thus the rings B and C of a steroid system are constructed. The final products **49a,b** are obtained in moderate yields. Only two stereo isomers have been obtained since the relative configuration of the created chiral centers at the junctions of rings A,B and B,C is identical in

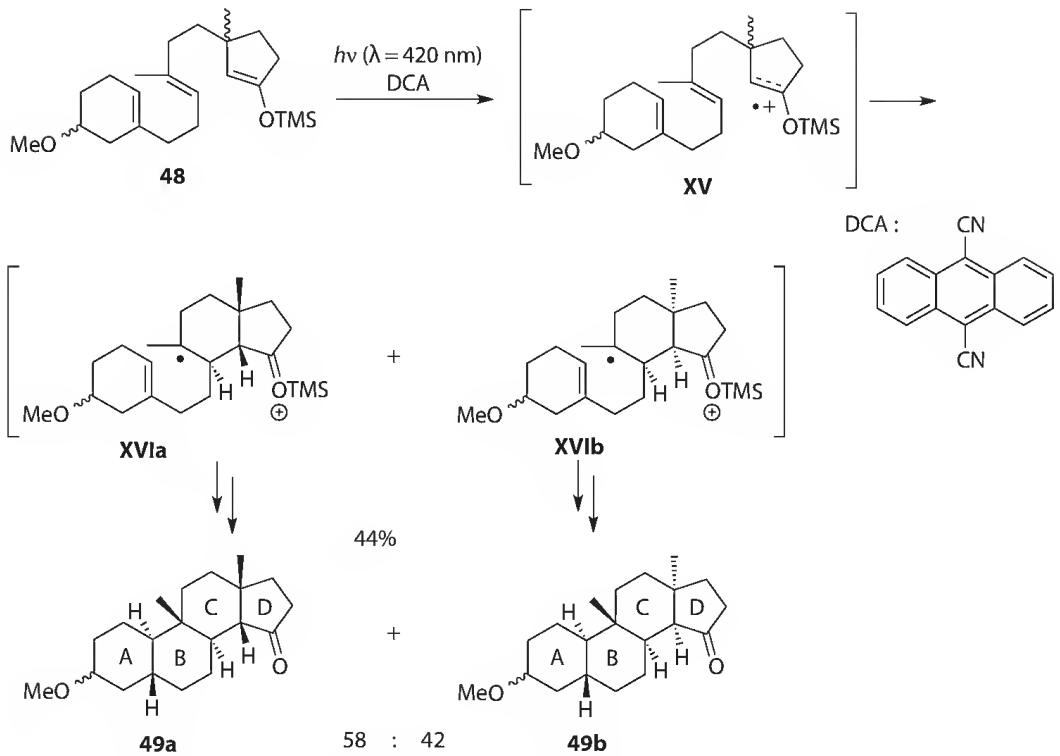

SCHEME 5.14 Cascade reaction induced by photochemical electron transfer.

both isomers. The first cyclization leading to the formation of ring C in **XVIa,b** is unselective while the second cyclization leading to the formation of ring B is stereospecific. The same reaction was applied to the asymmetric synthesis of a triterpene derivative of damarane type.[81]

Despite its interest for organic synthesis, in particular for a convenient synthesis of nitrogen-containing heterocycles, the radical addition of simple tertiary amines to olefinic double bonds could not be easily carried out. Numerous side reactions such as polymerization were frequently observed. The process has therefore been applied to photochemically induced radical polymerization.[82] However, several transformations with silylated amines have been successfully carried out.[83] α-Aminoalkyl radicals[84] can be produced by photochemical electron transfer. In such a case, an electron acceptor, for example, an aromatic ketone **50**, is photochemically excited (Scheme 5.15). Electron transfer form the tertiary amine (**51**) to the ketone takes place, leading to a radical ion pair **XVII** and **XVIII**. After proton transfer, neutral radicals **XIX** and **XX** are generated. α-Aminoaminoalkyl radicals **XX** obtained in this way form pyrrolidine **51** have been added in high yields to the electron-deficient double bond of α,β-unsaturated lactones such as **52**.[85,86] The radical addition occurred stereospecifically *anti* with respect to the alkoxy substituent but the configuration of a second chiral center in the α-position of the nitrogen atom was not controlled and two diastereoisomers **53a,b** have been isolated in high yields. The efficiency of the transformation was achieved because electron donor–substituted aromatic ketones such as **54** were used as sensitizer. The corresponding ketyl radicals (**XIX**) are particularly stable and can regenerate the sensitizer during a radical chain reaction, which considerably diminishes side reactions. Furthermore, the sensitizer is used in catalytic amounts and remains stable during the transformation. The adducts **53a** and **53b** have been transformed into the pyrrolizidine alkaloids (–)-isoretronecanol and (+)-laburnine, respectively. Under similar reaction conditions, radical tandem reactions have been carried out with unsaturated tertiary amines.[86,87] Using inorganic semiconductors such as TiO_2 or ZnS as photochemical electron transfer sensitizers, the same transformations have been performed with heterogeneous photocatalysis.[88] An intramolecular version was performed in a template structure (compare Scheme 5.2).[89]

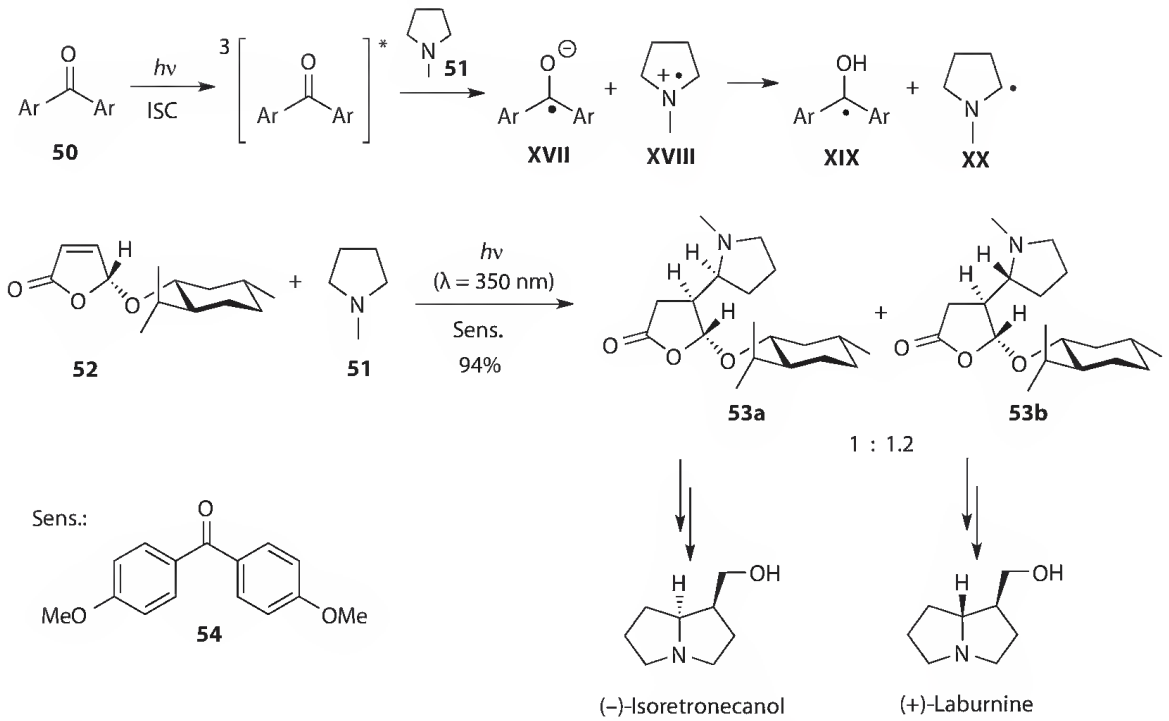

SCHEME 5.15 Photochemical electron transfer–induced addition of tertiary amines to alkenes.

Alcohols, cyclic ethers, or acetals are added in a similar way to alkenes although the corresponding α-hydroxy of α-alkoxy radicals are not generated via electron transfer.[78,90] In these cases, benzophenone is frequently used as sensitizer and the radicals are generated via hydrogen abstraction by the electronically excited sensitizer. The proton and the electron of the hydrogen atom are transferred almost simultaneously. With such a reaction, 1,3-dioxolane **56** was added stereoselectively to the α,β-unsaturated lactone **55** (Scheme 5.16).[91] The adduct **57** was transformed into the bistetrahydrofurane **58**. Further transformations led to UIC-94017 (now also named TMC-114), which is an efficient HIV protease inhibitor. In particular, the bis-tetrahydrofurane core structure contributes as a P2 ligand.

Recently, ruthenium complexes have been used for photochemical electron transfer catalysis in [2 + 2] photocycloadditions between two α,β-unsaturated carbonyl moieties[92] and dehalogenations.[93] This reaction step has been combined with organocatalysis in an efficient asymmetric alkylation of aldehydes.[94] Using an iridium catalyst (**59**$^+$), an asymmetric α-fluoromethylation of various aldehydes has been performed (Scheme 5.17).[95] By addition of the organocatalyst **61**, the aldehyde **60** is transformed into the

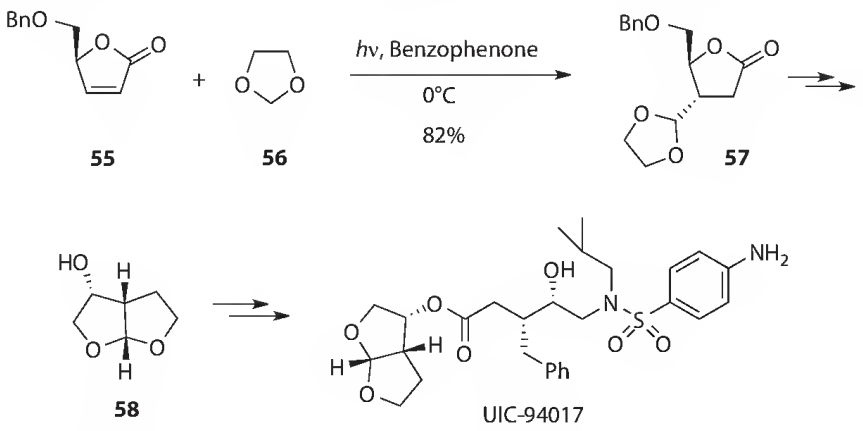

SCHEME 5.16 Addition of 1,3-dioxolane **56** induced by photochemical hydrogen abstraction.

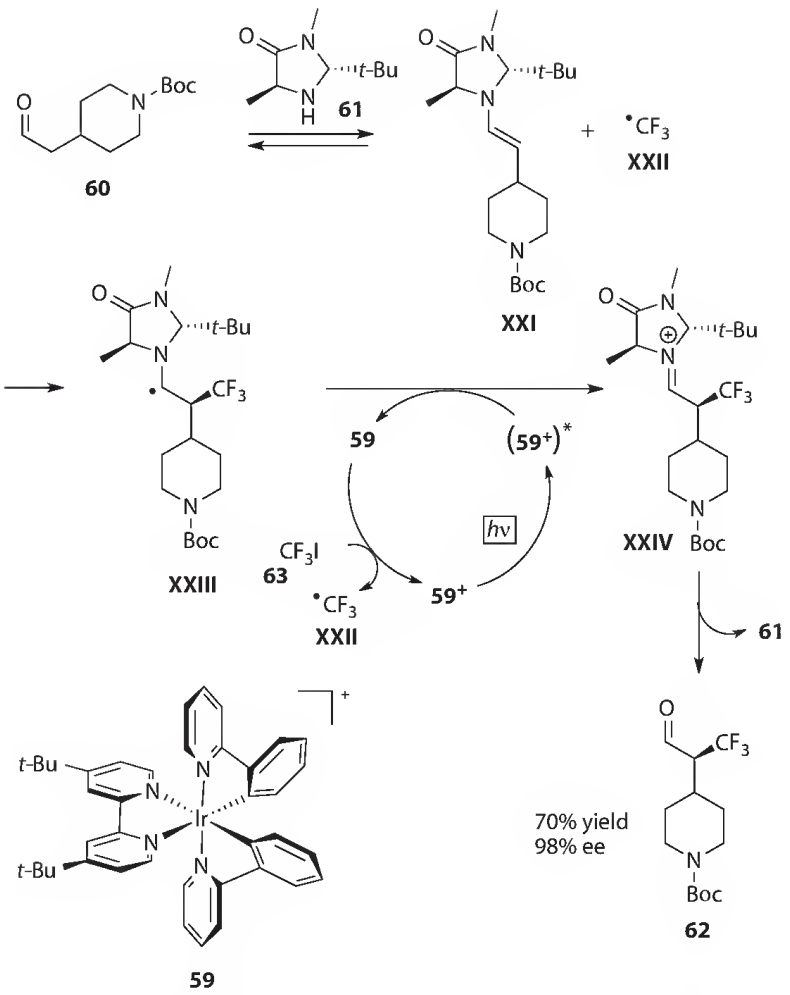

SCHEME 5.17 Photochemical electron transfer catalysis combined to organo-catalysis.

enamine **XXI**. The α-aminoalkyl radical **XXIII** is then obtained by addition the trifluoromethyl radical **XXII**. The first one is oxidized by the photochemical excited iridium complex (**59**$^+$)*, leading to the iminum ion **XXIV**. Sponification leads to the trifluoromethylated aldehyde **62** in high yield and enantioselectivity. The organocatalyst **61** is regenerated, which closes the organocatalytic cycle. The neutral Ir complex **59** is a powerful reductand and by electron transfer to trifluoromethyl iodide **63**, the corresponding radical **XXII** for the addition to the enamine **XXI** is produced. The positively charged iridium complex is regenerated and the photoredox catalytic cycle is thus closed. Only 0.5 mol% of the photocatalyst **59**$^+$ was added while 20 mol% of the organocatalyst **61** was needed. The reaction has also been performed with various aldehydes and higher fluoralkyl iodides as well as with fluoralkyl iodides carrying functional groups.

5.5 Photo-Oxygenation

Molecular oxygen belongs to the small family of compounds possessing triplet multiplicity at the ground state. The reactivity, in particular with organic molecules at the singlet ground state, is therefore reduced. Singlet oxygen in contrast is very reactive also due to the high electronegativity of oxygen. Nevertheless, photo-oxygenations are often highly selective. Most frequently, the photo-oxygenation of alkenes have been applied to organic synthesis (Scheme 5.18).[96] Singlet oxygen is most conveniently produced via photochemical sensitization. Due to the low excitation energy of the S_1 state (22.5 kcal mol^{-1}), dyes are used as sensitizers, and the excitation can also be carried out with visible light. After light

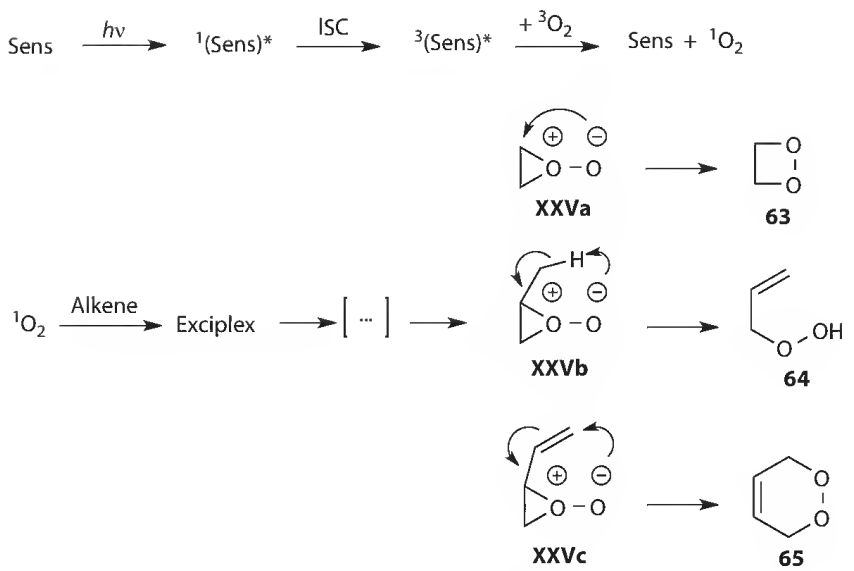

SCHEME 5.18 Generation of singlet oxygen and reaction with alkenes.

absorption of the sensitizer, intersystem crossing (ISC) occurs. Possessing triplet multiplicity (T_1), the sensitizer can now easily interact with oxygen in the triplet ground state (T_0). The oxygen is thus exited at the S_1 state and the dye sensitizer returns to its singlet ground state (S_0).

The first intermediate in the reaction of singlet oxygen with alkenes is an exciplex. Various other intermediates are described in the literature. The most significant ones used to explain the formation of the final products are **XXVa,b,c**. Depending on the structure of the alkene, three main types of products are obtained: dioxetanes **63**, hydroperoxides **64** from an ene reaction, and endoperoxides **65** from a pseudo Diels–Alder reaction. Aside these reactions, singlet oxygen also induces electron transfer leading to $O_2^{\bullet -}$.[97]

Recently, the ene reaction was applied to the synthesis of 1,2,4-trioxanes. This functional group is a partial structure of artemisinine and structural analogues (Scheme 5.19). These compounds originate from traditional Chinese medicine and possess antimalarial activity, which is essentially linked to the 1,2,4-trioxane moiety.[98] This structure can be easily built up using photo-oxygenation of ally alcohols followed by acetalization with a ketone. For example, allyl alcohol **66** was transformed into hydroxyhydroperoxide **67a,b**, which was obtained as a mixture of diastereoisomers.[99] Acetalization with adamantone **68** yielded the final product **69**, which possesses high in vitro antimalarial activity.[100] A large variety of 1,2,4-trioxane can easily be synthesized in this way.[101] Homoallyl alcohols were photo-oxygenated in the same way. Thus, 1,2,4-trioxepanes such as compound **70** are available.[102] This product possesses interesting in vivo antimalarial activity, which is certainly also favored by the presence of the polar amino group. A 1,2,4-trioxane was also attached to artemisinine as in **71**.[103] Such compounds may also possess cytostatic activity. Dihydroxyhydroperoxides have been transformed into 1,2,4-trioxane possessing an additional orthoester group.[104] These fragments were also attached to artemisinine.

Many pseudo-Diels–Alder reactions of singlet oxygen with furans have been applied to organic synthesis. Thus, addition of singlet oxygen to furfural **72** leads to the corresponding adduct **XXVI** (Scheme 5.20). The formation of this adduct occurs via an intermediate of type **XXVc** (Scheme 5.18). Addition of methanol used as solvent leads to hydroxyfuranone **73** in high yields.[105] When the reaction is carried out at $T > 40°C$, acetalization is completed and methyloxyfuranone is obtained.[106] The reaction was also efficiently carried out with visible light, in particular sunlight.[107] The acetalization can also be carried out with chiral alcohols such as (–)-menthol **74**.[87,108] Two diastereoisomers of menthyloxyfuranone **75a,b** are thus obtained in a 1:1 ratio. The isomer **75a** possessing 5*R* configuration crystallized preferentially and the isomer **75b** can partially be transformed into **75a**. When the acetalization of **73** is carried out with (+)-menthol **ent-74**,[109,110] the menthyloxyfuranone **ent-75a** possessing 5*S* configuration is obtained. Both isomers of the chiral synthon

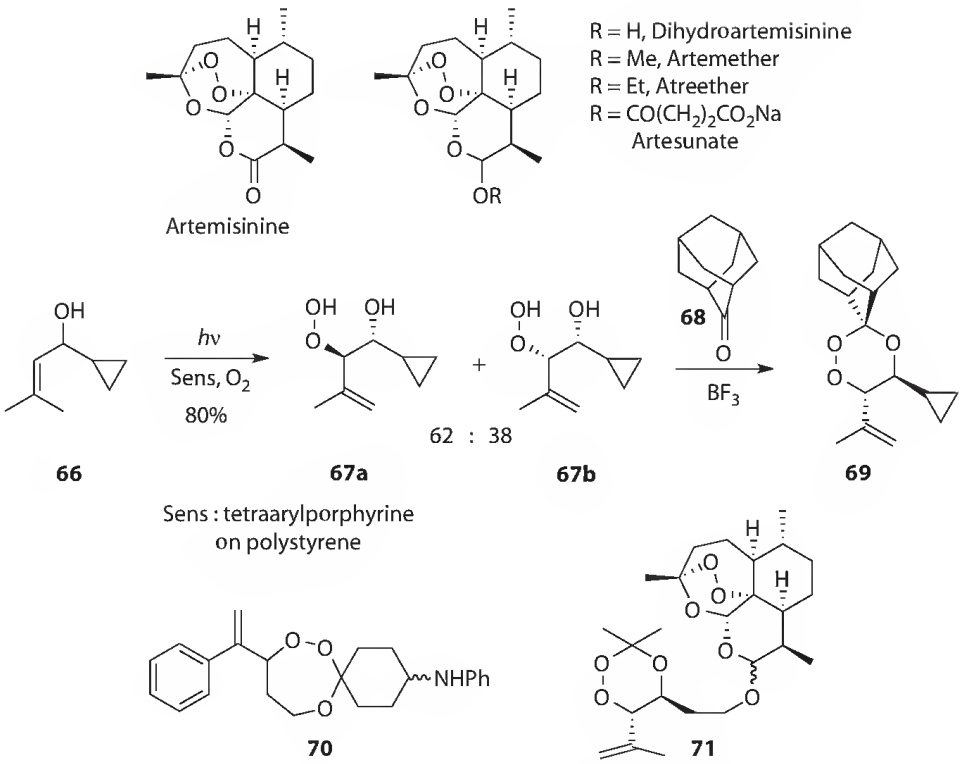

SCHEME 5.19 Synthesis of 1,2,4-trioxanes using photo-oxygenation of alkenes.

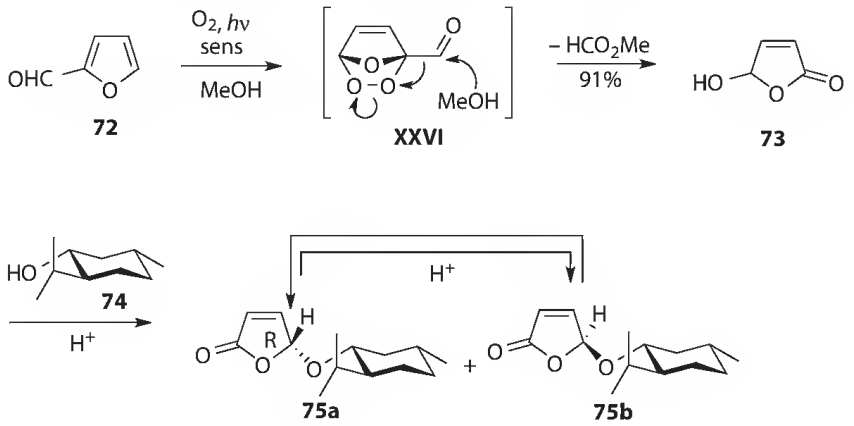

SCHEME 5.20 Synthesis of menthyloxyfuranone.

are thus available, which permits a versatile application to asymmetric synthesis. The reason is that almost all reactions are highly or completely diastereoselective and the configuration of the chiral center generated in the β-position of the α,β-unsaturated lacton can be predicted.[87] The chiral synthons **75** or **ent-75** were widely applied to asymmetric synthesis. Natural products, nitrogen-containing heterocycles, various amino acid derivatives, aromatic and pheromone derivatives, chiral ligands for asymmetric catalysis, and products possessing a biological activity of pharmaceutical or agrochemical interest have been synthesized.[110,111]

The 5-hydroxyfuranone moiety is a partial structure of numerous natural terpene compounds belonging to various product families such as labdanes[112] or eremophilanolides.[113] Generally, this partial structure is built up by photooxygenation of a furane moiety. A lot of such syntheses are reported in the literature. For example, the furan derivative **76** was successfully photooxidized to hydroxyfuranone **77** (Scheme 5.21, Equation 5.10).[114] The reaction is regioselective. After, saponification, the labdane compound sibiricinone

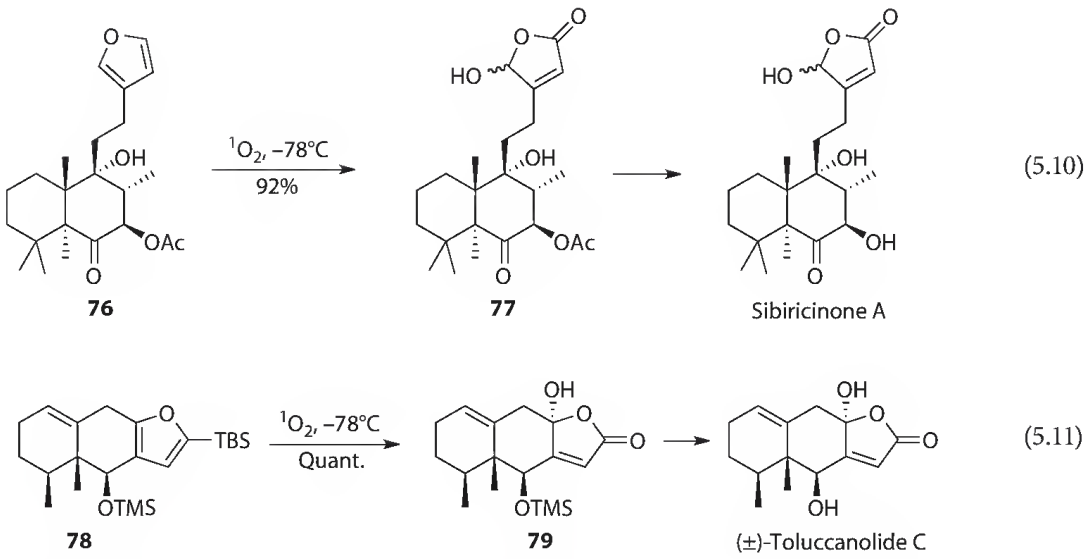

SCHEME 5.21 Selective photo-oxygenation of furan moieties.

A was obtained. Frequently, these reactions are performed in methylene chloride at low temperature with rose bengal as sensitizer and the isolated yields are generally higher than 90%.[115] In the same way, the silylated furan **78** was transformed into hydroxyfuranone **79** (Equation 5.11).[116] The presence of the tributylsilyl group (TBS) at the furan ring increases the efficiency so that **79** was isolated in quantitative yield. Furthermore in many transformations, this substituent determines the regioselectivity.[117] After deprotection in **79**, the eremophilane compound (±)-toluccanolide C was obtained.

The hydroxyfuranone moiety is in equilibrium with the γ-keto-α,β-unsaturated butyric acid form. Under particular reaction conditions, the second form can be targeted. This transformation was applied to complex total syntheses. The silylated furan derivative **80** was photooxygenated (Scheme 5.22).[118] Intermediately, the hydroxyfuranone **XXVII** was formed. In a second transformation, this compound was transformed into the unsaturated ketoester **81**. The overall yield of these two reactions was almost quantitative. The α,β-unsaturated ketone in **81** was then transformed into a dienolsilylether (**82**). A Diels–Alder reaction was carried out under thermolysis conditions leading to the tricyclic compound **83** as a mixture of regioisomers. Desilylation of the latter compound yielded the tricyclic diketone **84**, which was transformed into the alkaloids, zoanthamine and norzoanthamine. Such compounds possess several interesting pharmaceutical activities. For example, norzoanthamine derivatives strongly inhibit the growth of murine leukemia cells and possess antiplatelet activities. Compound **84** constitutes the tricyclic partial structure of rings A, B, and C of the target compounds with the correct relative configuration. Numerous other transformations the hydroxyfuranone fragment can be envisaged as key steps in total syntheses. Thus, the carbonyl function of the open structure was transformed in a Wittig reaction. This strategy was successfully applied to the synthesis of milbemycin G and (6*R*)-6-hydroxy-3,4-dihydromilbemycin E.[119]

5.6 Photochemically Supported Organometallic Reactions

Although carried out under thermic conditions, organometallic reactions are frequently accelerated under photochemical conditions.[120] Heating and concomitant irradiation become standard reaction conditions as in the case of the Vollhardt reaction.[121] This [2 + 2 + 2] photocycloaddition of three acetylene functions leads to aromatic compounds and is carried out with cheap cobalt catalysts. The reaction was also used for the synthesis of pyridines from two alkyne and one nitrile moiety.[122] In this case, detailed investigations on the influence of light irradiation on the efficiency was carries out[123] and the reaction was, for example, applied to the synthesis of axial chiral biaryl compounds containing a naphthalene and a pyridine moiety.[124] Asymmetric catalysis was used to induce chirality.

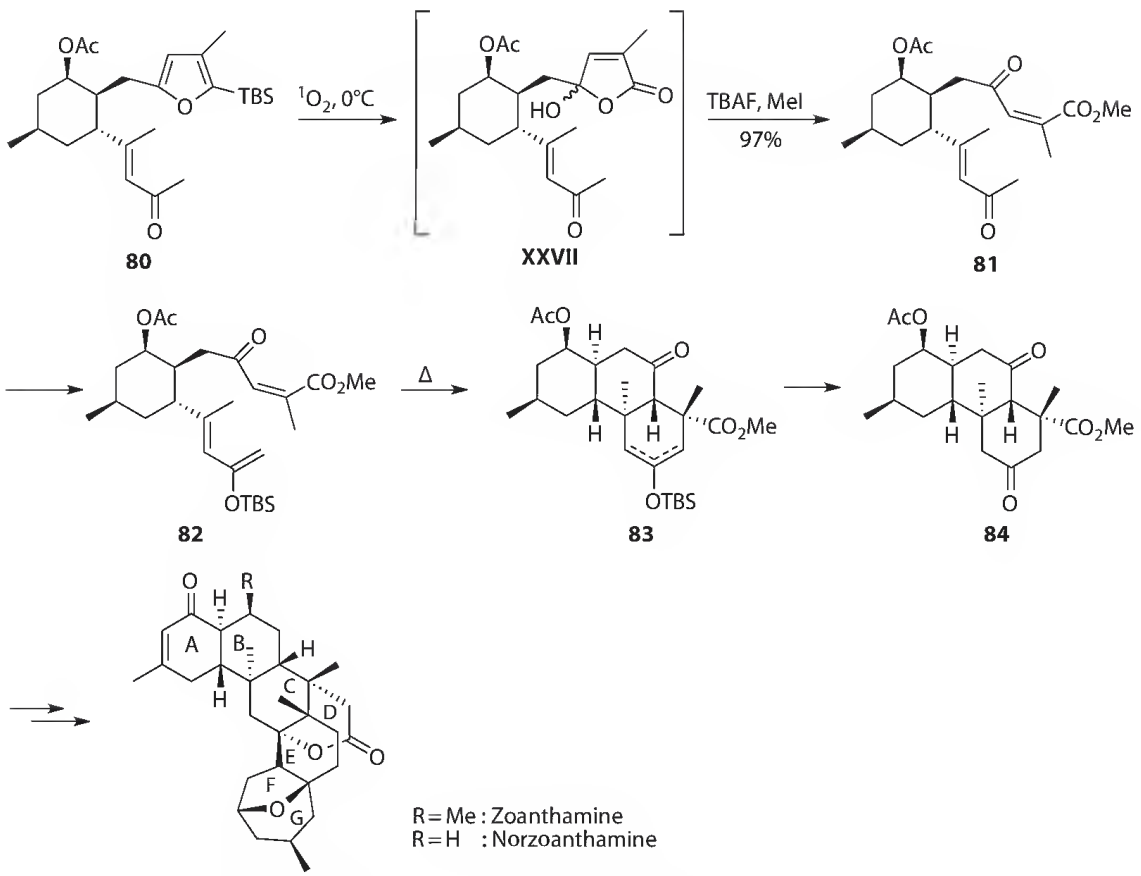

SCHEME 5.22 Photo-oxygenation of a furan moiety and transformation into a γ-keto-α,β-unsaturated butyric acid derivative.

A similar reaction is observed between two alkyne and one alkene moiety. In this manner, cyclohexadienes are obtained. This reaction was used to build up the tricyclic system of pasteurestin B by the transformation of unsaturated compound **85** into **86** (Scheme 5.23).[125] Cobalt remains attached to the cyclohexadiene partial structure. Treatment with Cu^{2+} at the end of the reaction leads to demetallation. With the same strategy, pateurestin A was synthesized. These compounds are potential antibiotics for veterinary applications. This method as well as the cyclotrimerization of alkynes

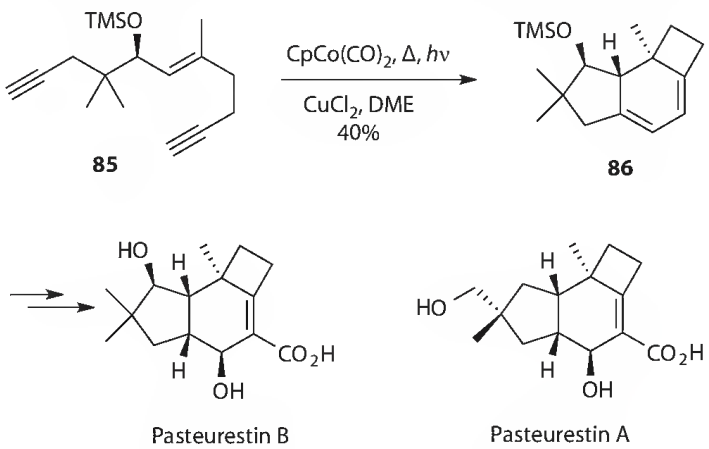

SCHEME 5.23 Intramolecular cobalt-catalyzed [2 + 2 + 2] cycloaddition.

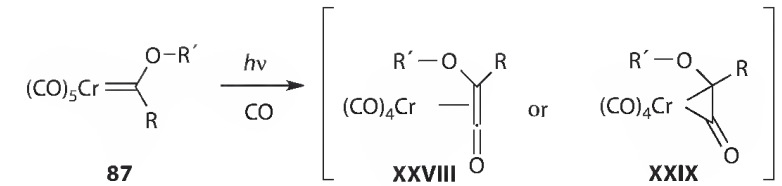

(5.12)

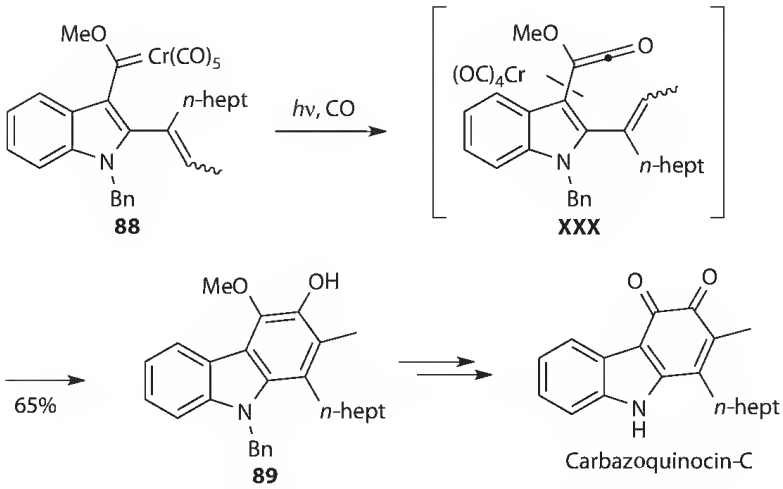

(5.13)

SCHEME 5.24 Photochemical transformation of Fischer-type carbene complexes.

provides a general approach to polycyclic systems, for example, steroid- or taxane-like structures.[126] Complex benzocyclobutenes structures are also easily available.[127]

Numerous photochemical transformations of Fischer-type carbene complexes have been applied to organic synthesis.[128,129] Upon irradiation, chromium carbon complexes of type **87** are transformed into ketenes, which are linked to the chromium atom **XXVIII** (Scheme 5.24, Equation 5.12).[129] A cyclopropane **XXIX** structure is also discussed. These intermediates readily react, for instance, with nucleophiles, undergo [2 + 2] cycloaddition with different unsaturated compounds such as alkenes or imines or they undergo electrocyclizations. The latter reaction was carried out with the indol derivative **88** (Equation 5.13).[130] Upon irradiation under carbon monoxide, compound **88** yields first the ketene intermediate **XXX**. Electrocyclization and loss of the chromium carbonyl complex leads to the final product **89**.[131] The catecol derivative **89** was transformed into the alkaloid carbazoquinocin-C possessing an *ortho*-quinone moiety. This compound family possesses activity against lipid oxidation and neuronal protecting properties.

Similar reactions were successfully carried out with tungstenhexacarbonyl.[132] In most of these cases, no intermediate metal complex is isolated. Thus the reaction was applied to the synthesis of substructures of altromycin B, a pluramycin antibiotic.[133]

Metal-catalyzed oxidations are also improved by light irradiation. Thus the oxidation of primary alcohols to aldehydes using TEMPO and Cu^+ as catalytic system and air as oxidant was accelerated by irradiation with visible light.[134] The reaction was selectively carried out with hexoses derivatives and applied to the efficient synthesis of tetrahydroxyazepanes. These compounds are interesting due to numerous pharmaceutical activities such as the inhibition of glycosidases or glycosyltransferases. Similar effects of light irradiation on the aerobic oxidation kinetics have been observed with ruthenium catalysts.[135] Osmium tetroxide catalyzed *cis*-hydroxylation is easily carried out with a large variety of alkenes.[136] Due to the aromatic stability in benzene-type aromatics, these compounds cannot be hydroxylated under standard reaction conditions. However, when the reaction mixture is irradiated, aromatic compounds such as benzene or toluene are stereoselectively oxidized.[137] Although the yields remained low, this reaction considerably simplified the synthesis of insositols such as (±)-pinitol. Optimizing this transformation would significantly enrich the synthetic chemistry associated to *cis*-dihydrodiol.[138]

Studies of mechanistic details of the organometallic reactions such as the Suzuki or the Sonogashira reaction led to the conclusion that some partial steps may be photochemially carried out thus avoiding the use of metal catalysts.[139] Such transformations have been carried out; they are based on a photo-S_N1 reaction of aromatic compounds involving phenyl cation intermediates.

5.7 Further Reactions

Photochemical excitation is involved in numerous other transformations of interest in organic synthesis. Many radical reactions are photochemically induced. In most cases, the photochemical step is not particularly studied since the radical intermediates are also generated by thermal reaction.[140] The interest is mostly focused on the radical reaction steps. Recently, photochemical reaction conditions have been applied to the transformation of thiocarbonyl compounds. This functional group is able to add reversibly to radical intermediates and thus control the overall reaction. In this function, they have been applied to organic synthesis[141] and to radical polymerization (RAFT).[142] In the present example, the dithiocarbamate **90** was irradiated with visible light leading to fragmentation of a C–S bond (**XXXI**) (Scheme 5.25).[143] Intramolecular addition of the acyl radical and trapping with the dithiocarbamyl radical leads to the bicylic lactame **91**. In a second photochemical step using UV light and in view of an oxidation, the dithiocarbamate function in **91** was exchanged by TEMPO (**92**). Treatment with *meta*-chloroperbenzoic acid led to keto lactame **93**. Further transformations led to the tricyclic compound **94**, which can be transformed into (–)-aphanorphine as previously described. The method was applied to the synthesis of numerous nitrogen-containing cyclic and isocyclic compounds.[144] The presence of thiocarbamates in the reaction mixture also accelerates photochemical-induced radical addition of amines to alkenes.[145]

In the multistep synthesis of complex polyfunctional compounds, protecting groups are often necessary and must be meticulously chosen. On one hand, they must resist the transformation conditions of other functional groups and on the other, they must be removed without damaging the core structure. In most cases, acidic or basic reagents are used for deprotection. Metal and enzymatic catalysis have also been used. The major advantage of photochemical protecting groups is that no chemical reagents are needed for deprotection and removal is rapid and clean in most cases.[146] These properties are particularly suitable for applications in the fields of biochemistry and microbiology and other application domains can easily be prospected.[147] In a recent example of a total synthesis, an *ortho*-nitrobenzyl protecting

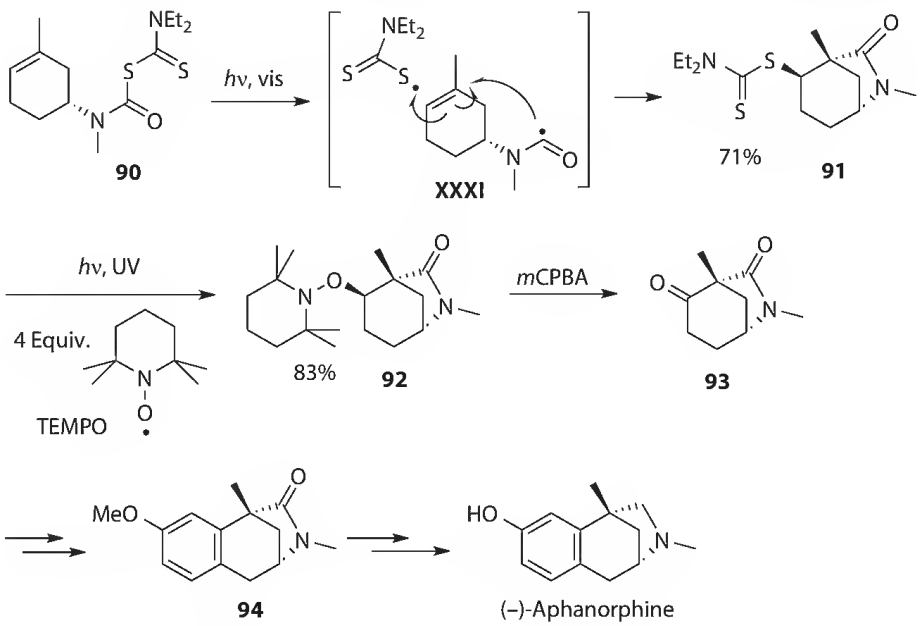

SCHEME 5.25 Photochemically induced radical reaction.

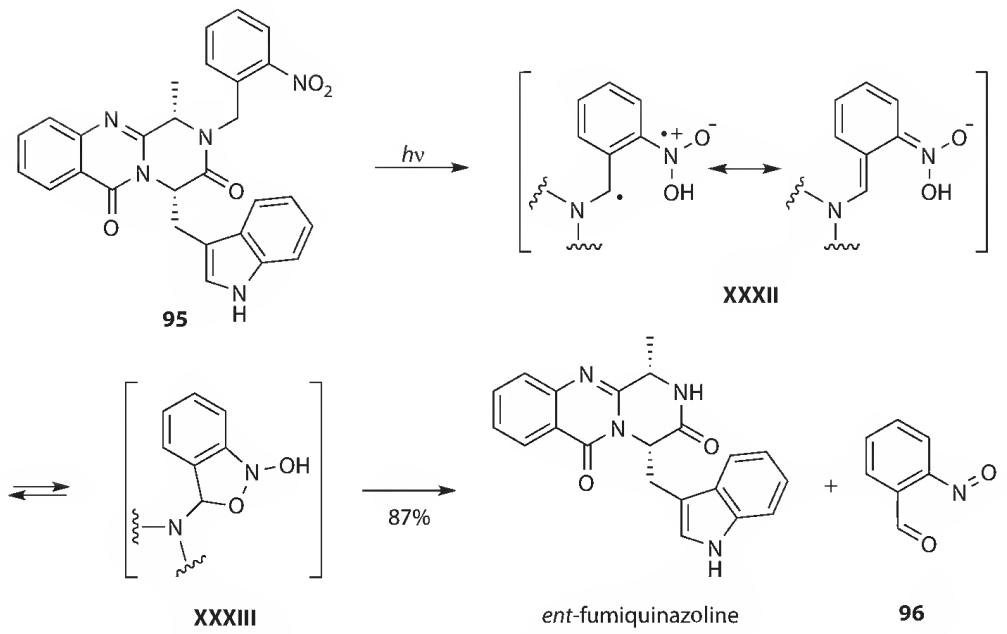

SCHEME 5.26 Photochemical removal of a protecting group.

group is efficiently eliminated from the substrate **95** in the last step of the synthesis of *ent*-fumiquinazoline (Scheme 5.26).[148] After photochemical excitation, hydrogen transfer occurs from the benzyl position to the nitro function yielding intermediate **XXXII**. This species is in equilibrium with the bicyclic intermediate **XXXIII**. *ortho*-Nitrobenzaldehyde **96** is now eliminated from these intermediates. Recently, ruthenium complexes have been used for photochemical electron transfer catalysis and deprotection with photolabile protecting groups have been carried out in this manner (compare Section 5.4).[149]

Despite the advantages that photochemical reactions present when used as key steps in numerous organic syntheses, organic chemists sometimes hesitate to make use of them. Sometimes it is assumed that photochemical reactions are difficult to reproduce or to scale up. However, as any other chemical transformation, these reactions are well reproducible and can easily be scaled up when the reaction parameters are well chosen and optimized. For example, changing the scale often needs an adaptation of concentrations and geometry of the reaction vessel in order to fulfill the conditions of optimal absorption according to the Lambert–Beer law. The very broad scale of photochemical transformations applied to organic synthesis is best illustrated by industrial processes[150] such as the preparation of rose oxide using photo-oxygenation of citronellol as a key step[107,150,151] or the synthesis of vitamin D using a photochemical electrocyclic rearrangement of 7-dehydrocholesterol (provitamin D)[152] as a key step. On the other hand, a large variety of photochemical reactions are very successfully performed in microreactors.[153] Very delicate transformations in which, for example, both the substrate and the product are photoreactive have been can also be carried out with particularly adapted and easily constructed equipment.[40,42]

Photochemical transformations are frequently discussed in the context of green chemistry since often chemical activation is avoided and thus waste can be diminished.[154,155] In this context, photochemical reactions are particularly attractive when they can be carried out with sunlight as renewable energy source.[107,151,154,156]

5.8 Conclusions

Photochemical reaction steps are applied in almost all fields of organic synthesis. The present chapter manly focuses on total syntheses of natural products and compounds possessing biological activity. Photochemical excitation changes completely the properties of a chemical compound. Under these conditions, transformations can be carried out, which are not possible at the ground state. Thus starting form easily available

products, complex and highly target related structures are built up in only one step. In many cases of complex syntheses, the number of steps is considerably reduced. Often no chemical activation (acids, bases, metal catalysts,...) is needed and optimized irradiation apparatus also facilitates an industrial application. In some fields of organic synthesis such as radical reactions, photochemical conditions are well established. In other fields such as organometallic reactions, it is less the case. However, many of these reactions are performed under drastic conditions or with expensive catalysts, which also limit the tolerance of functional groups. Under photochemical conditions, often the reactions are accelerated, yields and selectivity are increased, and the transformations can be performed with simple and cheap catalytic systems. A more systematic study of these reactions and their application to synthesis is therefore highly recommended.

References

1. Klán, P.; Wirz, J. *Photochemistry of Organic Compounds*, Wiley, Chichester, U.K., 2009.
2. Turro, N. J.; Ramamurthy, V.; Scaiano, J. C. *Principles of Molecular Photochemistry—An Introduction*, University Science Books, Sausalito, CA, 2010. Gilbert, A.; Beggott, J. *Essentials of Molecular Photochemistry*, Blackwell Scientific Publications, Oxford, U.K., 1991. Kopecky, J. *Organic Photochemistry—A Visible Approach*, VCH, Weinheim, Germany, 1992.
3. Turro, N. J. *Angew. Chem. Int. Ed. Engl.* 1986, *25*, 882–901. Olivucci, M.; Santoro, F. *Angew. Chem. Int. Ed.* 2008, *47*, 6322–6325. Robb, M. A.; Olivucci, M. *J. Photochem. Photobiol. A: Chem.* 2001, *144*, 237–243.
4. Hoffmann, N. *Chem. Rev.* 2008, *108*, 1052–1103; Bach, T.; Hehn, J. P. *Angew. Chem. Int. Ed.* 2011, *50*, 1000–1045.
5. Horspool, W.; Lenci, F.; eds. *CRC Handbook of Organic Photochemistry and Photobiology,* 2nd Edn., CRC Press, Boca Raton, FL, 2004. Horspool, W.; Song, P.-S.; eds. *CRC Handbook of Organic Photochemistry and Photobiology,* 2nd Edn., CRC Press, Boca Raton, FL, 1995.
6. Nalwa, H. S.; ed. *Handbook of Photochemistry and Photobiology, Vol. 2: Organic Photochemistry*, American Scientific Publishers, Stevenson Ranch, CA, 2003. Albini, A.; Fagnoni, M.; eds. *Handbook of Synthetic Photochemistry*, Wiley-VCH, Weinheim, Germany, 2009.
7. Ramamurthy, V.; Schanze, K. S.; eds. *Molecular and Supramolecular Photochemistry*, Marcel Dekker, New York, *Vol. 1: Organic Photochemistry*, 1997; *Vol. 2: Organic and Inorganic Photochemistry*, (Ramamurthy, V.; Schanze, K. S.; eds.) 1998; *Vol. 3: Organic Molecular Photochemistry*, (Ramamurthy, V.; Schanze, K. S.; eds.) 1999; *Vol. 6: Organic, Physical and Materials Photochemistry*, (Ramamurthy, V.; Schanze, K. S.; eds.) 2000; *Vol. 8: Understanding and Manipulating Excited-State Processes*, (Ramamurthy, V.; Schanze, K. S.; eds.) 2001; *Vol. 9: Photochemistry of Organic Molecules in Isotropic and Anisotropic Media*, (Ramamurthy, V.; Schanze, K. S.; eds.) 2003; *Vol. 11: Chiral Photochemistry*, (Inoue, Y.; Ramamurthy, V.; eds.) 2004; *Vol. 12: Synthetic Organic Photochemistry* (Griesbeck, A. G.; Mattay, J.; eds.) 2005. Horspool, W.; Armesto, D. *Organic Photochemistry—A Comprehensive Treatment,* Ellis Horwood PTR Prentice Hall, New York, 1992. Kagan, J. *Organic Photochemistry: Principles and Applications*, Academic Press, London, U.K., 1993.
8. Mattay, J.; Griesbeck, A.; eds. *Photochemical Key Steps in Organic Synthesis*, VCH, Weinheim, Germany, 1994. Ninomiya, I.; Naito, T. *Photochemical Synthesis*, Academic Press, London, U.K., 1989. *Einführung in die Photochemie* (Becker, H. G. O.; ed.), Deutscher Verlag der Wissenschaften, Berlin, Germany, 1991. Braun, A.; Maurette, M.-T.; Oliveros, E. *Technologie Photochimique*, Presses Polytechniques Romandes, Lausanne, Switzerland, 1986. Wöhrle, D.; Tausch, M. W.; Stohrer, W.-D. *Photochemie—Konzepte, Methoden, Experimente*, Wiley, VCH, Weinheim, Germany, 1998.
9. Schuster, D. I.; Lem, G.; Kaprinidis, N. A. *Chem. Rev.* 1993, *93*, 3–22.
10. Crimmins, M. T.; Reinhold, T. L.; *Org. React.* 1993, *44*, 297–588. Winkler, J. D.; Bowen, C. M.; Liotta, F. *Chem. Rev.* 1995, *95*, 2003–2020. Lee-Ruff, E.; Mladenova, G. *Chem. Rev.* 2003, *103*, 1449–1484. Namyslo, J. C.; Kaufmann, D. E. *Chem. Rev.* 2003, *103*, 1485–1538. Magareta, P. *Molecular and Supramolecular Photochemistry* (Ramamurthy, V.; Schanze, K. S.; eds.), *Vol. 12: Synthetic Organic Photochemistry* (Griesbeck, A. G.; Mattay, J.; eds.), Marcel Dekker, New York, 2005, pp. 211–237.

11. Mattay, J.; Conrads, R.; Hoffmann, R. *Methoden der Organischen Chemie (Houben-Weyl)*, 4th Edn., Vol. 5 E21 (Helmchen, G.; Hoffmann, R. W.; Mulzer, J.; Schaumann, E.; eds.), Thieme Verlag, Stuttgart, Germany, 1996, pp. 3085–3178. Iriondo-Alberdi, J.; Greaney, M. *Eur. J. Org. Chem.* 2007, 4801–4815.
12. Doroh, B.; Sulikowski, G. A. *Org. Lett.* 2006, *8*, 903–906.
13. Andrew, D.; Weedon, A. C. *J. Am. Chem. Soc.* 1995, *117*, 5647–5663.
14. Miao, R.; Gramani, S. G.; Lear, M. J. *Tetrahedron Lett.* 2009, *50*, 1731–1733.
15. See for example: Hue, B. T. B.; Dijkink, J.; Kuiper, S.; Larson, K. K.; Guziec, F. S., Jr.; Goubitz, K.; Fraanje, J.; van Maarseveen, J. H.; Hiemstra, H. *Org. Biomol. Chem.* 2003, *1*, 4364–4366. Lutteke, G.; AlHussainy, R.; Wrigstedt, P. J.; Hue, B. T. B.; de Gelder, R.; van Maarseveen, J. H.; Hiemstra, H. *Eur. J. Org. Chem.* 2008, 925–933.
16. Winkler, J. D.; Rouse, M. B.; Greaney, M. F.; Harrison, S. J.; Jeon, Y. T. *J. Am. Chem. Soc.* 2002, *124*, 9726–9728. See also: Winkler, J. D.; Harrison, S. J.; Greaney, M. F.; Rouse, M. B. *Synthesis* 2002, *14*, 2150–2154; Winkler, J. D.; Lee, E. C. Y.; Nevels, L. I. *Org. Lett.* 2005, *7*, 1489–1491.
17. For recent examples see: Minter, D. E.; Winslow, C. D. *J. Org. Chem.* 2004, *69*, 1603–1606.
18. (a) White, J. D.; Ihle, D. C. *Org. Lett.* 2006, *8*, 1081–1084; (b) Winkler, J. D.; Axten, J. M. *J. Am. Chem. Soc.* 1998, *120*, 6425–6426.
19. Crimmins, M. T.; Pace, J. M.; Nantermet, P. G.; Kim-Meade, A. S.; Tomas, J. B.; Watterson, S. H.; Wagman, A. S. *J. Am. Chem. Soc.* 2000, *122*, 8453–8463.
20. Hoffmann, R. W. *Chem. Rev.* 1989, *89*, 1841–1860.
21. Rau, H. *Chem. Rev.* 1983, *83*, 535–547. Inoue, Y. *Chem. Rev.* 1992, *92*, 741–770. Pete, J.-P. *Adv. Photochem.* Vol. 21 (Neckers, D. C.; Volman, D. H.; von Bünau, G.; eds.), John Wiley & Sons, New York, 1996, pp. 135–216. Griesbeck, A. G.; Meierhenrich, U. J. *Angew. Chem. Int. Ed.* 2002, *41*, 3147–3154. Inoue, Y. *Nature* 2005, *436*, 1139–1140.
22. Müller, C.; Bach, T. *Aust. J. Chem.* 2008, *61*, 557–564.
23. For a comprehensive discussion see: Hoffmann, N.; Buschmann, H.; Raabe, G.; Scharf, H.-D. *Tetrahedron* 1994, *50*, 11167–11186. See also: Bertrand, S.; Hoffmann, N.; Pete, J.-P. *Tetrahedron* 1998, *54*, 4873–4888.
24. Fernandes, C.; Gauzy, C.; Yang, Y.; Roy, O.; Pereira, E.; Faure, S.; Aitken, D. J. *Synthesis* 2007, 2222–2232.
25. Mondière, A.; Peng, R.; Remuson, R.; Aitken, D. J. *Tetrahedron* 2008, *64*, 1088–1093.
26. Fernández, D.; Torres, E.; Avilés, F. X.; Ortuño, R. M.; Vendrell, J. *Bioorg. Med. Chem.* 2009, *17*, 3824–3828. Ortuño, R. M.; Moglioni, A. G.; Moltrasio, G. Y. *Curr. Org. Chem.* 2005, *9*, 237–259.
27. See for example: Alibés, R.; de March, P.; Figueredo, M.; Font, J.; Racamonde, M.; Parella, T. *Org. Lett.* 2004, *6*, 1449–1452. Inoue, M.; Sato, T.; Hirama, M. *J. Am. Chem. Soc.* 2003, *125*, 10772–10773.
28. Svoboda, J.; König, B. *Chem. Rev.* 2006, *106*, 5413–5430.
29. Selig, P.; Herdtweck, E.; Bach, T. *Chem. Eur. J.* 2009, *15*, 3509–3525. Selig, P.; Bach, T. *Angew. Chem. Int. Ed.* 2008, *47*, 5083–5084.
30. Wessig, P. *Angew. Chem. Int. Ed.* 2006, *45*, 2168–2171. List, B. (ed.) *Chem. Rev.* 2007, Issue 12 (Special Issue Organocatalysis).
31. Ghosh, S. *CRC Handbook of Organic Photochemistry and Photobiology,* 2nd Edn. (Horspool, W.; Lenci, F.; eds.), CRC Press, Boca Raton, FL, 2004, pp. 18/1–18/15. Langer, K.; Mattay, J. *CRC Handbook of Organic Photochemistry and Photobiology* (W. M. Horspool, P.-S. Song, eds.), CRC Press, Boca Raton, FL, 1995, pp. 84–104. R. G. Salomon, *Tetrahedron* 1983, *39*, 485–575.
32. Sarkar, N.; Nayet, A.; Ghosh, S. *Org. Lett.* 2004, *6*, 1903–1905.
33. Marotta, E.; Righi, P.; Rosini, G. *Org. Process Res. Dev.* 1999, *3*, 206–219. Hoffmann, N.; Scharf, H.-D. *Liebigs Ann. Chem.* 1991, *12*, 1273–1277.
34. Bach, T. *Synlett* 2000, 1699–1707. D'Auria, M.; Emanuele, L.; Racioppi, R. *Adv. Photochem.* 2005, *28*, 81–127.

35. Griesbeck, A. G.; Abe, M.; Bondock, S. *Acc. Chem. Res.* 2004, *37*, 919–928. Kutateladze, A. G. *J. Am. Chem. Soc.* 2001, *123*, 9279–9282. Abe, M.; Kawakami, T.; Ohata, S.; Nozaki, K.; Nojima, M. *J. Am. Chem. Soc.* 2004, *126*, 2838–2846. Griesbeck, A. G.; Bondock, S. *Photochem. Photobiol. Sci.* 2002, *1*, 81–83. Griesbeck, A. G.; Bondock, S.; Gudipati, M. S. *Angew. Chem. Int. Ed.* 2001, *40*, 4684–4687. Buschmann, H.; Scharf, H. D.; Hoffmann, N.; Plath, M. W.; Runsink, J. *J. Am. Chem. Soc.* 1989, *111*, 5367–5373. Buschmann, H.; Scharf, H. D.; Hoffmann, N.; Esser, P. *Angew. Chem. Int. Ed. Eng.* 1991, *30*, 477–515. D'Auria, M.; Emanuele, L.; Racioppi, R. *Photochem. Photobiol. Sci.* 2003, *2*, 904–913.
36. Bach, T.; Brummerhop, H.; Harms, K. *Chem. Eur. J.* 2000, *6*, 3838–3848.
37. See also: Griesbeck, A. G.; Mauder, H.; Stadtmüller, S. *Acc. Chem. Res.* 1994, *27*, 70–75.
38. Woodward, R. B.; Hoffmann, R. *Angew. Chem. Int. Ed.* 1969, *8*, 781–853.
39. Sieburth, S. McN. *Synthetic Organic Photochemistry* (Griesbeck, A. G.; Mattay, J.; eds.), Marcel Dekker, New York, 2005, pp. 239–268. Bouas-Laurent, H.; Castellan, A.; Desvergne, J.-P.; Lapouyade, R. *Chem. Soc. Rev.* 2000, *29*, 43–53. Bouas-Laurent, H.; Castellan, A.; Desvergne, J.-P.; Lapouyade, R. *Chem. Soc. Rev.* 2001, *30*, 248–263. Becker, H.-D. *Chem. Rev.* 1993, *93*, 145–172.
40. Lainchbury, M. D.; Medley, M. I.; Taylor, P. M.; Hirst, P.; Dohle, W.; Booker-Milburn, K. I. *J. Org. Chem.* 2008, *73*, 6497–6505.
41. Davies, D. M. E.; Murray, C.; Berry, M.; Orr-Ewing, A. J.; Booker-Milburn, K. I. *J. Org. Chem.* 2007, *72*, 1449–1457.
42. Hook, B. D. A.; Dohle, W.; Hirst, P. R.; Pickworth, M.; Berry, M. B.; Booker-Milburn, K. I. *J. Org. Chem.* 2005, *70*, 7558–7564.
43. Adams, T. E.; El Sous, M.; Hawkins, B. C.; Hirner, S.; Holloway, G.; Khoo, M. L.; Owen, D. J.; Savage, G. P.; Scammalls, P. J.; Rizzacasa, M. A. *J. Am. Chem. Soc.* 2009, *131*, 1607–1616. Gerard, B.; Cencic, R.; Pelletier, J.; Porco Jr., J. A. *Angew. Chem. Int. Ed.* 2007, *46*, 7831–7834. Gerard, B.; Jones II, G.; Porco Jr., J. A. *J. Am. Chem. Soc.* 2004, *126*, 13620–13621.
44. Singh, V.; Krishna, U. M.; Vikrant, V.; Trivedi, G. K. *Tetrahedron* 2008, *64*, 3405–3428.
45. Gerard, B.; Sangji, S.; O'Leary, D. J.; Porco Jr., J. A. *J. Am. Chem. Soc.* 2006, *128*, 7754–7755.
46. Wender, P. A.; Siggel, L.; Nuss, J. M. *Comprehensive Organic Synthesis*, Vol. 5 (Trost, B. M.; Fleming, I.; Paquette, L. A.; eds.), Pergamon Press, Oxford, U.K., 1991, pp. 645–673; Gilbert, A.; *CRC Handbook of Organic Photochemistry and Photobiology,* 2nd Edn. (Horspool, W. M.; Lenci, F.; eds.), CRC Press, Boca Raton, FL, 2004, pp. 41/1–41/11. Mattay, J. *Angew. Chem. Int. Ed.* 2007, *46*, 663–665. Streit, U.; Bochet, C. G. *Chimia* 2008, *62*, 962–966.
47. Hoffmann, N. *Synthesis* 2004, 481–495.
48. Wender, P. A.; Ternansky, R.; deLong, M.; Singh, S.; Olivero, A.; Rice, K. *Pure Appl. Chem.* 1990, *62*, 1597–1602. Cornelisse, J. *Chem. Rev.* 1993, *93*, 615–669. Chappell, D.; Russell, A. T. *Org. Biomol. Chem.* 2006, *4*, 4409–4430.
49. Gaich, T.; Mulzer, J. *J. Am. Chem. Soc.* 2009, *131*, 452–453.
50. Keese, R. *Chem. Rev.* 2006, *106*, 4787–4808.
51. Gaich, T. PhD Thesis, Universität Wien, Vienna, Austria, 2009.
52. Vízvárdi, K.; Toppet, S.; Hoornaert, G. J.; De Keukeleire, D.; Bakó, P.; Van der Eycken, E. *J. Photochem. Photobiol. A: Chem.* 2000, *133*, 135–146.
53. Verrat, C.; Hoffmann, N.; Pete, J.-P. *Synlett* 2000, 1166–1168. Verrat, C. PhD Thesis, Université de Reims Champagne-Ardenne, Reins, France, 2000.
54. Hoffmann, N.; Pete, J.-P. *Synthesis* 2001, 1236–1242.
55. Demuth, M. *Org. Photochem.* 1991, *11*, 37–109. Zimmerman, H. E.; Armesto, D. *Chem. Rev.* 1996, *96*, 3065–3112. Rao, V. J.; Griesbeck, A. G. *Molecular and Supramolecular Photochemistry* (Ramamurthy, V.; Schanze, K. S.; eds.), *Vol. 12: Synthetic Organic Photochemistry* (Griesbeck, A. G.; Mattay, J.; eds.), Marcel Dekker, New York, 2005, pp. 189–210.
56. Banwell, M. G.; Austin, K. A. B.; Willis, A. C. *Tetrahedron* 2007, *63*, 6388–6403.
57. Piva, O. *CRC Handbook of Organic Photochemistry and Photobiology,* 2nd Edn. (Horspool, W.; Lenci, F.; eds.), CRC Press, Boca Raton, FL, 2004, pp. 70/1–70/18.

58. Salim, H.; Piva, O. *J. Org. Chem.* 2009, *74*, 2257–2260.
59. Hénin, F.; Letinois, S.; Muzart, J. *Tetrahedron Asymm.* 2000, *11*, 2037–2044. Piva, O.; Mortezaei, R.; Hénin, F.; Muzart, J.; Pete, J.-P. *J. Am. Chem. Soc.* 1990, *112*, 9263–9273.
60. See for example: Comesse, S.; Piva, O. *Tetrahedron Asymm.* 1999, *10*, 1061–1067. Bargiggia, F.; Dos Santos, S.; Piva, O. *Synthesis* 2002, 427–437. Pelotier, B.; Holmes, T.; Piva, O. *Tetrahedron Asymm.* 2005, *16*, 1513–1520. Bach, T.; Höfer, F. *J. Org. Chem.* 2001, *66*, 3427–3434.
61. Nicolaou, K. C.; Gray, D.; Tae, J. *Angew. Chem. Int. Ed.* 2001, *40*, 3679–3683.
62. Gorsch, B.; Orlebar, C. N.; Herdtweck, E.; Massa, W.; Bach, T. *Angew. Chem. Int. Ed.* 2003, *42*, 3693–3696.
63. Nicolaou, K. C.; Gray, D.; Tae, J. *Angew. Chem. Int. Ed.* 2001, *40*, 3675–3678. Nicolaou, K. C.; Gray, D.; Tae, J. *J. Am. Chem. Soc.* 2004, *126*, 613–627.
64. Segura, J. L.; Martín, N. *Chem. Rev.* 1999, *99*, 3199–3246. Charlton, J. L.; Alauddin, M. M. *Tetrahedron* 1987, *43*, 2873–2889.
65. Beaudry, C. M.; Malerich, J. P.; Trauner, D. *Chem. Rev.* 2005, *105*, 4757–4778.
66. Rigby, J. H.; Maharoof, U. S. M.; Mateo, M. E. *J. Am. Chem. Soc.* 2000, *122*, 6624–6628.
67. For some examples see: Kametani, T.; Takagi, N.; Toyota, M.; Honda, T.; Fukumoto, J. *J. Chem. Soc. Perkin Trans. 1* 1981, 2830–2834. Naito, T.; Hirata, Y.; Miyata, O.; Ninomiya, I. *J. Chem. Soc. Perkin Trans. 1* 1988, 2219–2225. Benchekroun-Mounir, N.; Dugat, D.; Gramin, J.-C.; Husson, H.-P. *J. Org. Chem.* 1993, *58*, 6457–6465. Nozulak, J.; Kalkman, H. O.; Floersheim, P.; Hoyer, D.; Schoeffter, P.; Buerki, H. R. *J. Med. Chem.* 1995, *38*, 28–33. Higuchi, R. I.; Edwards, J. P.; Caferro, T. R.; Ringgenberg, J. D.; Kong, J. W.; Hamann, L. G.; Arienti, K. L.; Marschke, K. B.; Davis, R. L.; Farmer, L. J.; Jones, T. K. *Bioorg. Med. Chem. Lett.* 1999, *9*, 1335–1340. Fürstner, A.; Domostoj, M. M.; Scheiper, B. *J. Am. Chem. Soc.* 2005, *127*, 11620–11621.
68. Pandey, G.; Murugan, A.; Balakrishnan, M. *Chem. Commun.* 2002, 624–625. See also: Pandey, G.; Karthikeyan, M.; Murugan, A. *J. Org. Chem.* 1998, *63*, 2867–2872.
69. Rehm, D.; Weller, A. *Isr. J. Chem.* 1970, *8*, 259–271. Kavarnos, G. J. *Fundamentals of Photoinduced Electron Transfer*, VCH Publishers Inc., New York, 1993. For a recent treatment of photochemical electron transfer in connection with Marcus theory see: Rosspeintner, A.; Kattnig, D. R.; Angulo, G.; Landgraf, S.; Grampp, G. *Chem. Eur. J.* 2008, *14*, 6213–6221. Rosspeintner, A.; Kattnig, D. R.; Angulo, G.; Landgraf, S.; Grampp, G.; Cuetos, A. *Chem. Eur. J.* 2007, *13*, 6474–6483.
70. Cossy, J.; Belotti, D. *Tetrahedron* 2006, *62*, 6459–6470. Fagnoni, M. *Heterocycles* 2003, *60*, 1921–1958. Pandey, G. *Molecular and Supramolecular Photochemistry, Vol. 1: Organic Photochemistry* (Ramamurthy, V.; Schanze, K. S.; eds.), Marcel Dekker, New York, 1997, pp. 245–294. Cossy, J.; Pete, J.-P. *Adv. in Electron Transfer Chem.* 1996, *5*, 141–195. Mattay, J. (ed.) *Top. Curr. Chem.* 1990, *156* (Photoinduced Electron Transfer I). Mattay, J. (ed.) *Top. Curr. Chem.* 1990, *158* (Photoinduced Electron Transfer II). Mattay, J. (ed.) *Top. Curr. Chem.* 1991, *159* (Photoinduced Electron Transfer III). Mattay, J. (ed.) *Top. Curr. Chem.* 1992, *163* (Photoinduced Electron Transfer IV). Mattay, J. (ed.) *Top. Curr. Chem.* 1993, *168* (Photoinduced Electron Transfer V).
71. Griesbeck, A. G.; Hoffmann, N.; Warzecha, K.-D. *Acc Chem. Res.* 2007, *40*, 128–140.
72. Burgett, A. W. G.; Li, Q.; Wei, Q.; Harran, P. G. *Angew. Chem. Int. Ed.* 2003, *42*, 4961–4966.
73. Li, J.; Jeong, S.; Esser, L.; Harran, P. G. *Angew. Chem. Int. Ed.* 2001, *42*, 4765–4769. Nicolaou, K. C.; Bella, M.; Chen, D. Y.-K.; Huang, X.; Ling, T.; Snyder, S. A. *Angew. Chem. Int. Ed.* 2002, *43*, 3495–3499. Nicolaou, K. C.; Chen, D. Y.-K.; Huang, X.; Ling, T.; Bella, M.; Snyder, S. A. *J. Am. Chem. Soc.* 2004, *126*, 12888–12896.
74. Yoon, U. C.; Mariano, P. S. *Acc. Chem. Res.* 2001, *34*, 523–533. Oelgemöller, M.; Griesbeck, A. G. *J. Photochem. Photobiol. C: Photochem. Rev.* 2002, *3*, 109–127. McDermott, G.; Yoo, D. J.; Oelgemöller, M. *Heterocycles* 2005, *65*, 2221–2257.
75. Zhao, H.; Hsu, D. C.; Carlier, P. R. *Synthesis* 2005, 1–16. Fuji, K.; Kawabata, T. *Chem. Eur. J.* 1998, *4*, 373–376.
76. Griesbeck, A. G.; Kramer, W.; Lex, J. *Angew. Chem. Int. Ed.* 2001, *40*, 577–579.

77. See for example: Yoon, U. C.; Jin, Y. X.; Oh, S. W.; Park, C. H.; Park, J. H.; Campana, C. F.; Cai, X.; Duesler, E. N.; Mariano, P. S. *J. Am. Chem. Soc.* 2003, *125*, 10664–10671. Griesbeck, A. G.; Heinrich, T.; Oelgemöller, M.; Molis, A.; Heidtmann, A. *Helv. Chim. Acta* 2002, *85*, 4561–4578. Griesbeck, A. G.; Heinrich, T.; Oelgemöller, M.; Lex, J.; Molis, A. *J. Am. Chem. Soc.* 2002, *124*, 10972–10973. Griesbeck, A. G.; Oelgemöller, M.; Lex, J. *J. Org. Chem.* 2000, *65*, 9028–9032.
78. Fagnoni, M.; Dondi, D.; Ravelli, D.; Albini, A. *Chem. Rev.* 2007, *107*, 2725–2756.
79. Hoffmann, N. *J. Photochem. Photobiol. C: Photochem. Rev.* 2008, *9*, 43–60.
80. Bunte, J. O.; Rinne, S.; Mattay, J. *Synthesis* 2004, 619–633.
81. Heinemann, C.; Demuth, M. *J. Am. Chem. Soc.* 1999, *121*, 4894–4895.
82. See for example: Lalevée, J.; Allonas, X.; Genet, S.; Fouassier, J.-P. *J. Am. Chem. Soc.* 2003, *125*, 9377–9380.
83. Yoon, U. C.; Mariano, P. S. *Acc. Chem. Res.* 1992, *25*, 233–240. Pandey, G. *Synlett* 1992, 546–552. Pandey, G.; Dumbre, S. G.; Pal, S.; Khan, M. I.; Shabab, M. *Tetrahedron* 2007, *63*, 4756–4761.
84. Renaud, P.; Giraud, L. *Synthesis* 1996, 913–926
85. Bertrand, S.; Hoffmann, N.; Pete, J. P. *Eur. J. Org. Chem.* 2000, 2227–2238.
86. Bertrand, S.; Hoffmann, N.; Humbel, S.; Pete, J. P. *J. Org. Chem.* 2000, *65*, 8690–8703.
87. Marinković, S.; Brulé, C.; Hoffmann, N.; Prost, E.; Nuzillard, J. M.; Bulach, V. *J. Org. Chem.* 2004, *69*, 1646–1651.
88. Marinković, S.; Hoffmann, N. *Chem. Commun.* 2001, 1576–1577. Marinković, S.; Hoffmann, N. *Int. J. Photoenergy* 2003, *5*, 175–182. Marinković, S.; Hoffmann, N. *Eur. J. Org. Chem.* 2004, 3102–3107.
89. Bauer, A.; Westkämper, F.; Grimme, S.; Bach, T. *Nature* 2005, *436*, 1139–1140.
90. For some examples see: Benko, Z.; Fraser-Reid, B.; Mariano, P. S.; Beckwith, A. L. J. *J. Org. Chem.* 1988, *53*, 2066–2072. Mann, J.; Weymouth-Wilson, A. *Synlett* 1992, 67–69. Hoffmann, N. *Tetrahedron Asymm.* 1994, *5*, 879–886. Graalfs, H.; Fröhlich, R.; Wolff, C.; Mattay, J. *Eur. J. Org. Chem.* 1999, 1057–1073. Mosca, R.; Fagnoni, M.; Mella, M.; Albini, A. *Tetrahedron* 2001, *57*, 10319–10328. Doohan, R. A.; Hannan, J. J.; Geraghty, N. W. A. *Org. Biomol. Chem.* 2006, *4*, 942–952. Geraghty, N. W. A.; Hernon, E. M. *Tetrahedron Lett.* 2009, *50*, 570–573.
91. Ghosh, A. K.; Leshchenko, S.; Noetzel, M. *J. Org. Chem.* 2004, *69*, 7822–7829.
92. Ischay, M. A.; Anzovino, M. E.; Du, J.; Yoon, T. P. *J. Am. Chem. Soc.* 2008, *130*, 12886–12887. Du, J.; Yoon, T. P. *J. Am. Chem. Soc.* DOI: 10.1021/ja903732v
93. Narayanam, J. M. R.; Tucker, J. W.; Stephenson, C. R. J. *J. Am. Chem. Soc.* 2009, *131*, 8756–8757.
94. Nicewicz, D. A.; MacMillan, D. W. C. *Science* 2008, *322*, 77–80.
95. Nagib, D. A.; Scott, M. E.; MacMillan, D. W. C. *J. Am. Chem. Soc.* 2009, *131*, 10875–10877.
96. Foote, C. S.; Clennan, E. L. *Structure Energetics and Reactivity in Chemistry Series* 1995, *2* (Active Oxygen in Chemistry), 105–140. Clennan, E. L. *Tetrahedron* 2000, *56*, 9151–9179. Prein, M.; Adam, W. *Angew. Chem. Int. Ed. Engl.* 1996, *35*, 477–494. Prein, M.; Adam, W. *Acc. Chem. Res.* 1996, *29*, 275–283. Schweitzer, C.; Schmidt, R. *Chem. Rev.* 2003, *103*, 1685–1758. Stratakis, M.; Orfanopoulos, M. *Tetrahedron* 2000, *56*, 1595–1615. *Tetrahedron Symposium in Print Number 126, Organic Chemistry of Singlet Oxygen* (Greer, A.; ed.), *Tetrahedron* 2006, *62* (46). Greer, A. *Acc. Chem. Res.* 2006, *39*, 797–804. Montagnon, T.; Tofi, M.; Vassilikogiannakis, G. *Acc. Chem. Res.* 2008, *41*, 1001–1011. Richard, J.-A. *Synlett* 2009, 1187–1188. Sheppard, A. N.; Acevedo, O. *J. Am. Chem. Soc.* 2009, *131*, 2530–2540.
97. For an application to organic synthesis see: Gomez, J.-M.; Gil, L.; Ferroud, C.; Gateau-Olesker, A.; Martin, M.-T.; Marazano, C. *J. Org. Chem.* 2001, *66*, 4898–4903.
98. Robert, A.; Dechy-Cabaret, O.; Cazelles, J.; Meunier, B. *Acc. Chem. Res.* 2002, *35*, 167–174. Wu, Y. *Acc. Chem. Res.* 2002, *35*, 255–259.
99. Griesbeck, A. G.; El-Idreesy, T. T. *J. Chin. Chem. Soc.* 2006, *53*, 1469–1476. See also: Griesbeck, A. G.; El-Idreesy, T. T.; Fiege, M.; Brun, R. *Org. Lett.* 2002, *4*, 4193–4195.
100. Griesbeck, A. G.; El-Idreesy, T. T.; Höinck, L.-O.; Lex, J.; Brun, R. *Bioorg. Med. Chem. Lett.* 2005, *15*, 595–597.

101. For some other example see for instance: Singh, C.; Kanchan, R.; Sharma, U.; Puri, S. K. *J. Med. Chem.* 2007, *50*, 521–527. Singh, C.; Verma, V. P.; Naikade, N. K.; Singh, A. S.; Hassam, M.; Puri, S. K. *J. Med. Chem.* 2008, *51*, 7581–7592. Kumar, L.; Kaushik, N.; Malik, A.; Kumar, P. *Asian J. Chem.* 2009, *21*, 3540–3546.
102. Singh, C.; Pandey, S.; Kushwaha, A. K.; Puri, S. K. *Bioorg. Med. Chem. Lett.* 2008, *18*, 5190–5193.
103. Griesbeck, A. G.; Neudörfl, J.; Hörauf, A.; Specht, S.; Raabe, A. *J. Med. Chem.* 2009, *52*, 3420–3423.
104. Griesbeck, A. G.; Raabe, A. *Synlett* 2009, 1514–1516.
105. Bolz, G.; Wiersdorff, W.-W. (BASF) DE 2111119 A1, 1972.
106. Schenck, G. O. *Liebigs Ann. Chem.* 1953, *584*,156–176. Cottier, L.; Descotes, G.; Nigay, H.; Parron, J.-C.; Grégoire, V. *Bull. Soc. Chim. Fr.* 1986, 844–850
107. Esser, P.; Pohlmann, B.; Scharf, H.-D. *Angew. Chem. Int. Ed. Engl.* 1994, *33*, 2009–2023.
108. Martel, J.; Tessier, J.; Demoute, J.-P. (ROUSSEL-UCLAF) EP 0023454 B1, 1983. Moradei, O. M.; Paquette, L. A.; Peschko, C.; Danheiser, R. L. *Org. Synthesis* 2003, *80*, 66–73.
109. (+)-Menthol **ent-74** is also obtained in the Haarmann & Reimer (Symrise) process: Fleischer, J.; Bauer, K.; Hopp, R. (Haarmann & Reimer) DE 2109456 A1, 1971.
110. Oertling, H.; Reckziegel, A.; Bertram, H.-J. *Chem. Rev.* 2007, *107*, 2136–2164.
111. Feringa, B. L.; de Jong, J. C. *Bull. Soc. Belg.* 1992, *101*, 627–640. Feringa, B. L.; de Lange, B.; Jansen, J. F. G. A.; de Jong, C.; Lubben, M.; Faber, W.; Schudde, E. P. *Pure Appl. Chem.* 1992, *64*, 1865–1871. Hashem, A.; Kleinpeter, E. *Adv. Heterocycl. Chem.* 2001, *81*, 107–165. Hoffmann, N.; Bertrand, S.; Marinkovic, S.; Pesch, J. *Pure Appl. Chem.* 2006, *78*, 2227–2246.
112. Hanson, J. R. *Nat. Prod. Rep.* 2007, *24*, 1332–1341.
113. Fraga, B. M. *Nat. Prod. Rep.* 2008, *25*, 1180–1209.
114. Marcos, I. S.; Castañeda, L.; Basabe, P.; Diez, D.; Urones, J. G. *Tetrahedron* 2008, *64*, 10860–10866.
115. Kernan, M. R.; Faulkner, D. J. *J. Org. Chem.* 1988, *53*, 2773–2776.
116. Mace, L. H.; Shanmugham, M. S.; White, J. D.; Drew, M. G. B. *Org. Biomol. Chem.* 2006, *4*, 1020–1031.
117. Adam, W.; Rodriquez, A. *Tetrahedron Lett.* 1981, *22*, 3505–3508. Katsumura, S.; Hori, K.; Fujiwara, S.; Isoe, S. *Tetrahedron Lett.* 1985, *26*, 4625–4628.
118. Yoshimura, F.; Sasaki, M.; Hattori, I.; Komatsu, K.; Sakai, M.; Tanino, K.; Miyashita, M. *Chem. Eur. J.* 2009, *15*, 6626–6644.
119. Helliwell, M.; Karim, S.; Parmee, E. R.; Thomas, E. J. *Org. Biomol. Chem.* 2005, *3*, 3636–3653. Bailey, S.; Helliwell, M.; Teerawutglrag, A.; Thomas, E. J. *Org. Biomol. Chem.* 2005, *3*, 3654–3677.
120. Hennig, H. *Transition Metals for Organic Synthesis,* Vol. 2 (Beller, M.; Bolm, C.; eds.), Wiley-VCH, Weinheim, Germany, 1998, pp. 412–419.
121. Vollhardt, K. P. C. *Angew. Chem. Int. Ed. Engl.* 1984, *23*, 539–556. Saito, S.; Yamamoto, Y. *Chem. Rev.* 2000, *100*, 2901–2915. Kotha, S.; Brahmachary, E.; Lahiri, K. *Eur. J. Org. Chem.* 2005, 4741–4767. Agenet, N.; Busine, O.; Slowenski, F.; Gandon, V.; Aubert, C.; Malacria, M. *Org. React.* 2007, *68*, 1–302. Galan, B. R.; Rovis, T. *Angew. Chem. Int. Ed.* 2009, *48*, 2830–2834.
122. Varela, J. A.; Saá, C. *Chem. Rev.* 2003, *103*, 3787–3801. Heller, B.; Hapke, M. *Chem. Soc. Rev.* 2007, *36*, 1085–1094.
123. Heller, B.; *Nachr. Chem. Tech. Lab.* 1999, *47*, 9–14. Heller, B.; Heller, D.; Wagler, P.; Oehme, G. *J. Mol. Catal. A: Chem.* 1998, *136*, 219–233. Heller, B.; Heller, D.; Oehme, G. *J. Mol. Catal. A: Chem.* 1996, *110*, 211–219. See also: Geny, A.; Agenet, N.; Iannazzo, L.; Malacria, M.; Aubert, C.; Gandon, V. *Angew. Chem. Int. Ed.* 2009, *48*, 1810–1813.
124. Gutnov, A.; Heller, B.; Fischer, C.; Drexler, H.-J.; Spannenberg, A.; Sundermann, B.; Sundermann, C. *Angew. Chem. Int. Ed.* 2004, *43*, 3795–3797.
125. Kögl, M.; Brecker, L.; Warrass, R.; Mulzer, J. *Eur. J. Org. Chem.* 2008, 2714–2730.
126. Petit, M.; Aubert, C.; Malacria, M. *Org. Lett.* 2004, *6*, 3937–3940. Chouarqui, G.; Petit, M.; Phansavath, P.; Aubert, C.; Malacria, M. *Eur. J. Org. Chem.* 2006, 1413–1421.

127. See for example: Han, S.; Bond, A. D.; Disch, R. L.; Holmes, D.; Schulman, J. M.; Teat, S. J.; Vollhardt, K. P. C.; Whitener, G. D. *Angew. Chem. Int. Ed.* 2002, *41*, 3223–3227. Han, S.; Anderson, D. R.; Bond, A. D.; Chu, H. V.; Disch, R. L.; Holmes, D.; Schulman, J. M.; Teat, S. J.; Vollhardt, K. P. C.; Whitener, G. D. *Angew. Chem. Int. Ed.* 2002, *41*, 3227–3230. Bruns, D.; Miura, H.; Vollhardt, K. P. C.; Stanger, A. *Org. Lett.* 2003, *5*, 549–552.
128. Dötz, K. H.; Stendel Jr., J. *Chem. Rev.* 2009, *109*, 3227–3274. Barluenga, J.; Santamaria, J.; Tomás, M. *Chem. Rev.* 2004, *104*, 2259–2284.
129. Hegedus, L. S. *Tetrahedron* 1997, *53*, 4105–4128. Hegedus, L. S. *Acc. Chem. Res.* 1995, *28*, 299–305.
130. Rawat, M.; Wulff, W. D. *Org. Lett.* 2004, *6*, 329–332.
131. For mechanistic details see also: Merlic, C. A.; Xu, D. *J. Am. Chem. Soc.* 1991, *113*, 7418–7420. Merlic, C. A.; Xu, D.; Gladstone, B. G. *J. Org. Chem.* 1993, *58*, 538–545.
132. For some recent examples see: Ohe, K.; Yokoi, T.; Miki, K.; Nishino, F.; Uemura, S. *J. Am. Chem. Soc.* 2002, *124*, 526–527. Miura, T.; Kiyota, K.; Kusama, H.; Iwasawa, N. *Org. Lett.* 2005, *7*, 1445–1447. Sangu, K.; Fuchibe, K.; Akiyama, T. *Org. Lett.* 2004, *6*, 353–355.
133. Koo, B.; McDonald, F. E. *Org. Lett.* 2005, *7*, 3621–3624.
134. Gassama, A.; Hoffmann, N. *Adv. Synth. Catal.* 2008, *350*, 35–39.
135. Masutani, K.; Uchida, T.; Irie, R.; Katsuki, T. *Tetrahedron Lett.* 2000, *41*, 5119–5123. Egami, H.; Onisuka, S.; Katsuki, T. *Tetrahedron Lett.* 2005, *46*, 6049–6052. Shimizu, H.; Onisuka, S.; Egami, H.; Katsuki, T. *J. Am. Chem. Soc.* 2005, *127*, 5396–5413.
136. Kolb, H. C.; VanNieuwenhze, M. S.; Sharpless, K. B. *Chem. Rev.* 1994, *94*, 2483–2547.
137. Motherwell, W. B.; Williams, A. S. *Angew. Chem. Int. Ed. Engl.* 1995, *34*, 2031–2033. Jung, P. M. J.; Motherwell, W. B.; Williams, A. S. *Chem. Commun.* 1997, 1283–1284.
138. Hudlicky, T.; Reed, J. W. *Synlett* 2009, 685–703.
139. Fagnoni, M.; Albini, A. *Acc. Chem. Res.* 2005, *38*, 713–721. Freccero, M.; Fagnoni, M.; Albini, A. *J. Am. Chem. Soc.* 2003, *125*, 13182–13190. Dichiarante, V.; Fagnoni, M.; Albini, A. *Angew. Chem. Int. Ed.* 2007, *46*, 6495–6498.
140. Renaud, P.; Sibi, M. P.; eds. *Radical in Organic Chemistry,* Vol. 1, Wiley-VCH, Weinheim, Germany, 2001.
141. Quiclet-Sire, B.; Zard, S. Z. *Chem. Eur. J.* 2006, *12*, 6002–6016.
142. Moad, G.; Rizzardo, E.; Thang, S. H. *Aust. J. Chem.* 2005, *58*, 378–410. Moad, G.; Rizzardo, E.; Thang, S. H. *Acc. Chem. Res.* 2008, *41*, 1133–1142. Perrier, S.; Takolpuckdee, P. *J. Polym. Sci. Part A: Polym. Chem.* 2005, *43*, 5347–5393.
143. Grainger, R. S.; Welsh, E. J. *Angew. Chem. Int. Ed.* 2007, *46*, 5377–5380.
144. Grainger, R. S.; Innocenti, P. *Angew. Chem. Int. Ed.* 2004, *43*, 3445–3448. Ahmet, S.; Baker, L. A.; Grainger, R. S.; Innocenti, P.; Quevedo, C. E. *J. Org. Chem.* 2008, *73*, 8116–8119.
145. Harakat, D.; Marinković, S.; Pesch, J.; Hoffmann, N. *Org. Biomol. Chem.* 2006, *4*, 1202–1205. Gassama, A.; Ernenwein, C.; Hoffmann, N. *ChemSusChem* DOI 10.1002/cssc.200900150.
146. Kocieński, P. J. *Protecting Groups,* 3rd Edn., Georg Thieme Verlag, Stuttgart, Germany, 2005.
147. Goeldner, M.; Givens, R.; eds. *Dynamic Studies in Biology,* Wiley-VCH, Weinheim, Germany, 2005. Pillai, V. N. R. *Synthesis* 1980, 1–26. Guillier, F.; Orain, D.; Bradley, M. *Chem. Rev.* 2000, *100*, 2091–2157. Bochet, C. G. *J. Chem. Soc., Perkin Trans. 1* 2002, 125–142. Pelliccioli, A. P.; Wirz, J. *Photochem. Photobiol. Sci.* 2002, *1*, 441–458. Bochet, C. G. *Synlett* 2004, 2268–2274. Falvey, D. E.; Sundararajan, C. *Photochem. Photobiol. Sci.* 2004, *3*, 831–838. Mayer, G.; Heckel, A. *Angew. Chem. Int. Ed.* 2006, *45*, 4900–4921.
148. Snider, B. B.; Busuyek, M. V. *Tetrahedron* 2001, *57*, 3301–3307.
149. Borak, J. B.; Falvey, D. E. *J. Org. Chem.* 2009, *74*, 3894–3899.
150. Braun, A.; Maurette, M.-T.; Oliveros, E. *Photochemical Technology*, Wiley, Chichester, U.K., 1991.
151. Monnerie, N.; Ortner, J. *J. Solar Energy Engineering* 2001, *123*, 171–174.

152. Quinkert, G.; Eis, K. *Essays in Contemporary Chemistry, From Molecular Structure to Biology* (Quinkert, G.; Kisakürek, M. V.; eds.), Verlag Helvetica Chimica Acta, Zürich, Switzerland, 2001, pp. 189–282. Schäfer, B. *Naturstoffe in chemischen Industrie*, Elsevier Spektrum Akademischer Verlag, München, Germany, 2007. Saltiel, J.; Cires, L.; Turek, A. M. *CRC Handbook of Organic Photochemistry and Photobiology*, 2nd Edn. (Horspool, W.; Lenci, F.; eds.), CRC Press, Boca Raton, FL, 2004, pp. 27/1–27/22.
153. Coyle, E. E.; Oelgemöller, M. *Photochem. Photobiol. Sci.* 2008, *7*, 1313–1322. Fukuyama, T.; Rahman, M. T.; Sato, M.; Ryu, I. *Synlett* 2008, 151–163. Matsushita, Y.; Ichimura, T.; Ohba, N.; Kumada, S.; Sakeda, K.; Suzuki, T.; Tanibata, H. *Pure Appl. Chem.* 2007, *79*, 1959–1968.
154. Ciamician, G. *Science* 1912, *36*, 385–394.
155. Albini, A.; Fagnoni, M. *ChemSusChem* 2008, *1*, 63–66. Protti, S.; Dondi, D.; Fagnoni, M.; Albini, A. *Pure Appl. Chem.* 2007, *79*, 1929–1938.
156. Oelgemöller, M.; Jung, C.; Mattay, J. *Pure Appl. Chem.* 2007, *79*, 1939–1947.

6

Photochirogenesis

Cheng Yang
Osaka University

Yoshihisa Inoue
Osaka University

6.1 Introduction

The term "photochirogenesis" was coined by one of the present authors in 1996 when the ERATO Photochirogenesis Project[1] was launched and is conceptually synonymous to more traditional "asymmetric photochemistry" or "chiral photochemistry" with some emphasis on the creation of molecular chirality by photon. A photochirogenic reaction may involve the enantioselective destruction of a racemic mixture or the enantio- or diastereodifferentiating creation of a new stereogenic center in prochiral or chiral substrate through the electronically excited state.

Synthesis of chiral compounds that are difficult to obtain by thermochemical reactions but readily accessible by photochemical reactions is certainly one of the major motivations for promoting the study on photochirogenesis. The photochemical routes to chiral compounds are particularly efficient or even essential for the construction of such compounds that are thermally unstable, highly constrained, and/or polycyclic. The switching of chemo- and stereoselectivity, often observed upon photoexcitation as a consequence of the promotion of an electron to the antibonding orbital and the subsequent alterations in reactivity and redox properties, renders the photochirogenic route an attractive alternative to the conventional catalytic and enzymatic counterparts. Indeed, the photochirogenesis has now become an indispensable and practical protocol for synthesizing molecules of complex structures, such as naturally occurring and bioactive complex organic compounds.[2]

The very wide range of temperature available for most photochemical processes is obviously another crucial advantage for photochirogenesis over the conventional catalytic and enzymatic asymmetric syntheses that work only in much narrower temperature regions. Executing photoreactions at a lower temperature not only enhances the chemo- and stereoselectivities in general but also makes easier the detection and trapping of reaction intermediates as well as the elucidation of reaction mechanisms.

The use of pulsed laser irradiation enables us to directly observe the transient species and reaction intermediates of very short lifetimes and obtain the information about rapidly occurring excited-state events.[3] It is also to be noted that photochirogenesis has an inherent advantage for mechanism elucidation over usual achiral photoreactions, as the stereochemical outcomes contain rich information about the conformational and/or configurational changes experienced in a photochirogenic process.

As a result of the intensive studies particularly in the last two decades, this highly interdisciplinary area of photochemistry and asymmetric synthesis has seen a considerable growth in the numbers of researchers and publications and also the expansion of its scope and limitations. Nevertheless, it is also true that the studies so far do not cover the whole of the photochirogenic reactions, the optical yields reported hitherto are not fully satisfactory, and the factors and mechanism controlling the stereodifferentiation process in the excited state are not completely elucidated.

In this chapter, we will only briefly mention about the historical background and the earlier studies but rather focus on the most recent developments in photochirogenesis research published in the last 10 years, which are classified in terms of the source of chirality and the reaction media employed. For the earlier work in photochirogenesis, readers are directed to the excellent reviews published previously.[4–7]

6.2 Photochirogenesis with Circularly Polarized Light

The use of circularly polarized light (CPL) in chiral photochemistry is based on the fact that an enantiomeric compound exhibits the circular dichroism or ellipticity, possessing distinctly different molar extinction coefficients for left- and right-handed CPL (ε_l and ε_r), and therefore, one of the enantiomeric pairs can be preferentially phototransformed upon CPL irradiation at an appropriate wavelength where the circular dichroism intensity ($\Delta\varepsilon = \varepsilon_l - \varepsilon_r$) is not zero. This process may be called as photochemical kinetic resolution or deracemization. Since the enantiomeric enrichment is achieved by physical chiral source (i.e., CPL) without using any chiral reagent, auxiliary, or catalyst, CPL-induced chirogenic photoreaction is sometimes referred as "absolute" asymmetric synthesis. However, this may be misleading as CPL does not create any stereogenic center but simply induce an enantiomeric imbalance in the chiral, but racemic, substrate used as a starting material.

The possible use of CPL for inducing molecular chirality was proposed by van't Hoff[4] and le Bel[8] as early as mid-nineteenth century, but it took half a century until the Kuhn's first experimental proof of CPL photochirogenesis using a racemic mixture of α-azidopropionamide and bromopropionate.[9] The mechanistic studies on a variety of CPL-induced photochirogenic reactions flourished in 1970s. However, the use of CPL has never been considered as a practical tool for preparative asymmetric synthesis, simply because the generally low anisotropy factors ($g = \Delta\varepsilon/\varepsilon$) reported so far hinder the efficient photochemical enantiomeric enrichment by CPL.

Intriguingly, CPL photochemistry may be related to the origin of the terrestrial homochirality, or the extreme enantiomer imbalance. The origin of homochirality in biosphere is still a target of intensive researches and debates, and hence attracts much attention of scientists.[10–13] Of several hypothetical theories and potential mechanisms that have been proposed to explain the terrestrial homochirality, the one proposed originally by Bonner and Rubenstein in mid-1980s[14] and further developed by others[13,15] is directly related to the CPL photochemistry, claiming that the enantioselective photodecomposition of racemic organic compounds such as amino acid was induced by the CPL from a neutron star or a star formation region to leave the enantiomerically enriched compounds, which were ultimately delivered to the primitive earth. This theory was supported by the facts that (1) a variety of natural and non-natural amino acids were found in the organic mantle of the Murchison meteorite, some of which were enantiomerically enriched, (2) the extraterrestrial origin of these amino acids was confirmed by the deviation of the $^{13}C/^{12}C$ and $^{15}N/^{14}N$ ratios from those found on earth, and (3) the off-plane radiation from an electron storage ring is elliptically polarized and indeed the circularly polarized infrared radiation was observed from the reflection nebulae in the star formation regions.[13,16]

In this relation, it is crucial that a variety of nonaromatic amino acids were found in a photolyzate from the vacuum-UV irradiation of a 2:1:1:1:1 mixture of water, methanol, ammonia, carbon monoxide, and carbon dioxide at 12 K, despite the low combined quantum yield ($\Phi \sim 10^{-4}$).[13,16] Furthermore, in the CPL photolysis of racemic leucine in 0.1 M aqueous HCl solution, it was shown that the use of l-CPL at 212.8 nm, which is preferentially absorbed by (*S*)-leucine, enriches (*R*)-leucine to give an enantiomeric excess (ee) of 2.5% at 75% conversion.[17] These results support the Bonner–Rubenstein theory that the CPL photolysis of racemic amino acids in the outer space is a source of chirality imbalance in biomolecules occurring on the earth.

More recently, the chiroptical property, CPL photolysis, and photodecomposition mechanism of several aliphatic amino acids were comparatively studied in aqueous solutions at different pH values.[18–21] These studies revealed that (1) the chiroptical properties, particularly anisotropy (*g*) factor, of amino acid are highly sensitive to solution pH, with the *g* factor maximizing at pH 1, (2) glycine and alanine photodecompose only slowly to give ammonia and the corresponding α-hydroxycarboxylic acid, and (3) in sharp contrast, higher amino acids with γ-hydrogen, such as valine, leucine, and isoleucine, efficiently photodecompose to give glycine as a major, common product at acidic pH values via the Norrish type II mechanism, but more slowly to α-hydroxycarboxylic acid through an α-lactone intermediate at neutral pH. The ee values obtained upon photolysis with synchrotron-generated CPL at 215 nm are also pH-dependent, and L-leucine of 1.3% ee was obtained after 55% of the racemic leucine used was decomposed by l-CPL irradiation.

Then, amplification or self-replication of the enriched enantiomer becomes critical for further validating the Bonner and Rubenstein's theory. At present, no chirality amplification is known for photochemical reaction, but autocatalytic reactions have been reported by Soai et al.[22] They demonstrated that the small initial imbalance of molecular chirality generated by CPL can be significantly amplified.[23,24] Thus, racemic pyrimidyl alcohol **1** was subjected to photolysis with r- or l-CPL to give slightly (*R*)- or (*S*)-enriched **1**,[23] which was added to a solution containing 2-alkynylpyrimidine carbaldehyde **2** and diisopropylzinc without purification as a "seed of chirality" for self-catalytic synthesis of **1**. Excellent ee's >99.5% were achieved after three rounds of consecutive asymmetric autocatalysis.

On the other hand, the different physical properties of conglomerate *versus* racemate could be another possible cause of chiral amplification. For example, Breslow et al. demonstrated that conglomerate crystals of some L-amino acids show much higher solubilities in aqueous solution than more stable racemate crystals, allowing chiral discrimination upon crystallization/dissolution process.[25] Soloshonok et al. reported the enantiomeric self-purification of nonracemic α-trifluoromethyl lactic acid through sublimation[26] and of β-amino acid derivatives through disproportionation in the achiral phase of chromatography.[27]

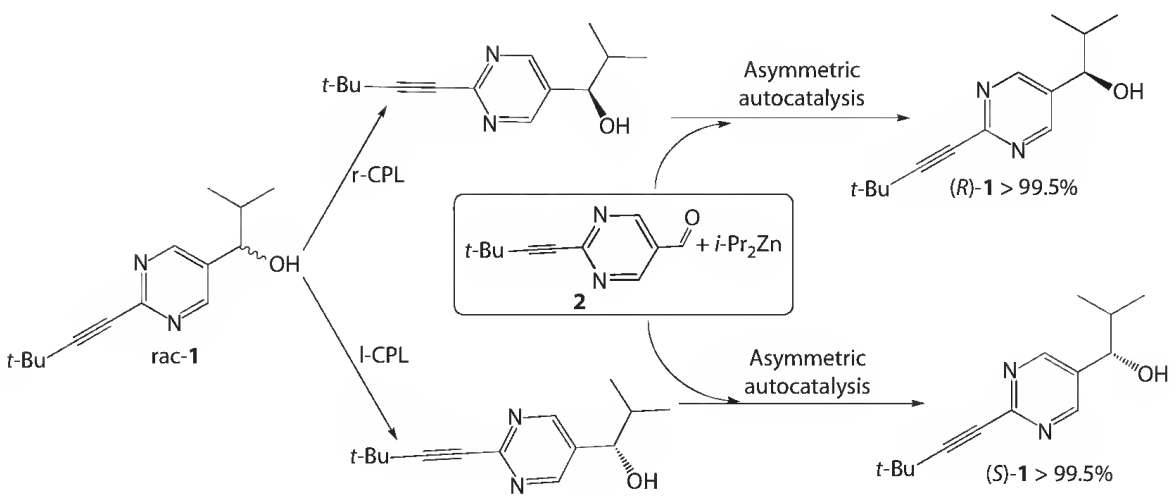

An interesting application of CPL has recently been reported for the preparation of chiral polydiacetylene films by Iwamoto et al.[28–31] CPL irradiation of monomer films of 10,12-tricosadiynoic acid derivatives **3** and **4** deposited on a fused silica substrate gave polydiacetylene films **5** and **6**, respectively. The polydiacetylene films obtained by irradiating r- and l-CPL showed the apparent CD signals at 500–700 nm of opposite sign, which was ascribed to the helical structure of the opposite chiral sense. The strong CD signals remained even after the polymer suffered a thermochromic change upon heating at 80°C for 10 min. Although a chiral LB film of polydiacetylene has been obtained previously under specific conditions from achiral monomers, its formation was rather unintended and the sign of chirality was uncontrollable.[32]

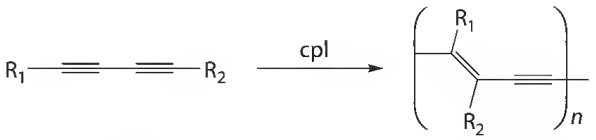

3: $R_1 = -(CH_2)_9CH_3$, $R_2 = -(CH_2)_8COOH$
4: $R_1 = -(CH_2)_{11}CH_3$, $R_2 = -(CH_2)_8COOH$

5: $R_1 = -(CH_2)_9CH_3$, $R_2 = -(CH_2)_8COOH$
6: $R_1 = -(CH_2)_{11}CH_3$, $R_2 = -(CH_2)_8COOH$

6.3 Photochirogenesis in Fluid Solution

Of various reaction media ever examined for photochirogenesis, fluid solutions have been most frequently and extensively employed, enabling less substrate- or conformation-dependent, more comprehensive, and chiral-source efficient photochemical transformations as well as the dynamic and external control of chemo- and stereoselectivities, when compared with the solid state. An important progress has been made in solution-phase photochirogenesis by using the unconventional media, such as supercritical fluid and ionic liquid, which possess novel intriguing properties distinctly different from those of conventional solvents.

6.3.1 Photochirogenesis in Organic Solution

6.3.1.1 Intramolecular Photochirogenesis in Organic Solution

Diastereodifferentiating photoreaction necessitates a stoichiometric amount of chiral auxiliary attached to the photoreactive prochiral moiety of substrate, but generally affords one of the two possible diastereomeric photoproducts in good-excellent selectivity, particularly for [2 + 2], [4 + 2], and [4 + 4] photocycloaddition.[33] This is simply because the intramolecular steric and electronic interactions of the chiral auxiliary with the photoreactive moiety are stronger, more effective, and long-lived in general than those attained upon intermolecular diastereodifferentiation or enantiodifferentiating photosensitization described in Sections 6.3.1.2 and 6.3.1.3.

Some of diarylethenes are typical photochromic compounds at ambient temperatures, which are highly durable for the reversible photoconversion between the "open" and "closed" forms upon irradiation at specific wavelengths.[34] Generation of new chiral centers in the closed-ring isomer is one of the characteristic properties of diarylethene derivatives. This feature makes the diarylethenes potentially useful for nondestructive readout in optical memories by detecting the change in optical rotation.[35,36] Yokoyama et al. investigated the diastereodifferentiating photoinduced ring-closure reaction of chiral diarylethenes **7O**–**11O**.[37–40] The ring-closure reactions of **7O**, **8O**, and **9O** carried out in ethyl acetate at room temperature are highly diastereodifferentiating, affording **7C**, **8C**, and **9C** in 98%, 98%, and 95% diastereomeric excess (de), respectively. The diastereoselectivity was manipulated moderately by changing the reaction temperature. Upon irradiation at −67°C, the de values were enhanced to 100% for **7C**

and 99% for **8C**, but decreased to 89% for **9C**. Photolysis of **10O** gave **10C** in a much lower 47% de, which however showed a remarkable difference (1300°) in specific rotation from the open form at the photostationary state. Photoirradiation of **11O** with UV light in ethyl acetate led to highly diastereoselective photocyclization (90% de) and a large change (950°) in specific rotation at 633 nm.

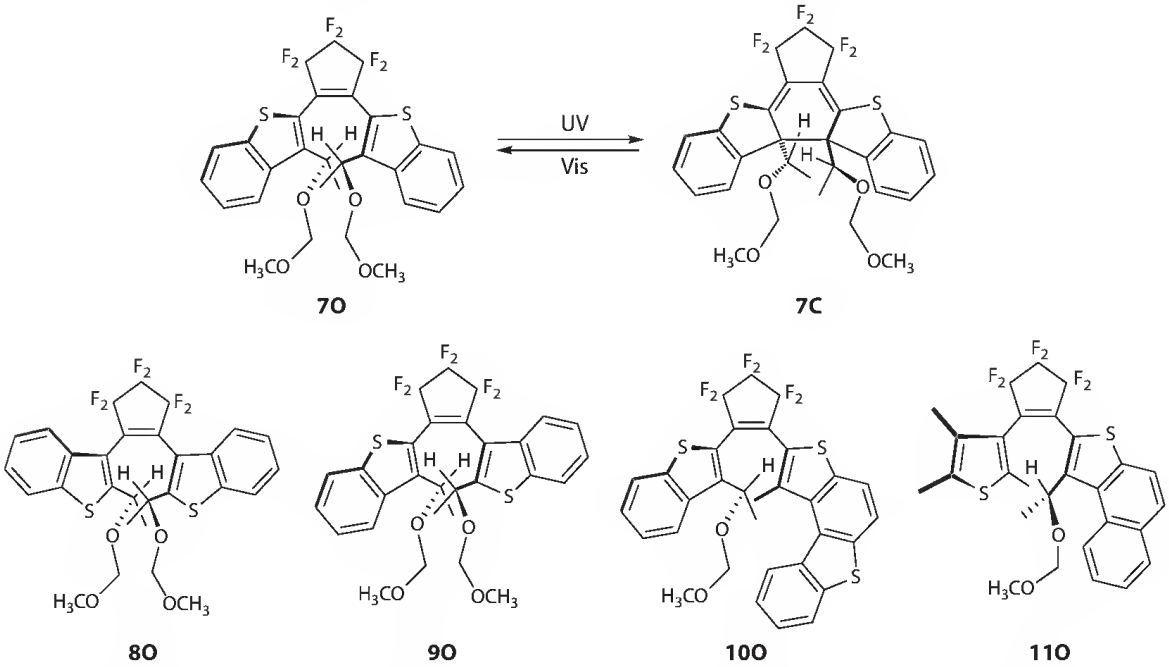

7O **7C**

8O **9O** **10O** **11O**

West et al. have recently reported the diastereodifferentiating intramolecular [4 + 4] photocycloaddition of 4-mesyloxypyran-2-one derivatives.[41] Photocycloaddition of **12** gave **13** and **14** in a diastereomeric ratio (dr) of 1.4:1 (58% de) in 69% combined yield in aqueous methanol at 0°C. In toluene at −78°C, the dr was improved to 4.2:1 (81% de) with keeping the chemical yield at 64%.

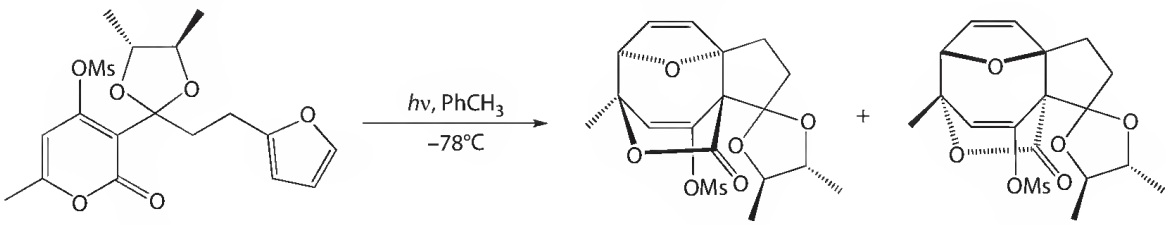

12 **13** **14**

One of the intriguing topics in photochirogenesis study is the memory of chirality.[42–44] Griesbeck et al. reported the stereoselective synthesis of pyrrolo[1,4]benzodiazepines **16a–d** through decarboxylative photocyclization of **15a–d**.[45] The reaction involves a photoinduced intramolecular electron transfer process from the carboxylate anion to the electronically excited phthalimide, followed by CO_2 extrusion and subsequent recombination of the resulting radical pair. Photolysis of proline derivatives **15a,b** led to the exclusive formation of *trans*-photoproducts **16a,b**. Despite the intermediacy of a triplet 1,7-diradical, the photocyclization proceeded highly enantioselectively to give **16a** in 86% ee. Moreover, photodecarboxylation of **15c,d** proceeded with a complete inversion of the configuration at the stereogenic center to give **16c,d** as sole products. The high degree of chirality memory was interpreted in terms of the high activation barriers for the rotation about the central C–N bond, which helped preserving the absolute axial chirality during the course of the reaction.

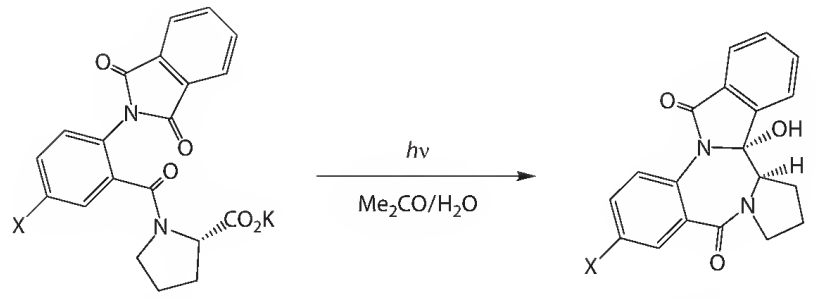

15a: X = H
15b: X = Cl

16a: X = H
16b: X = Cl

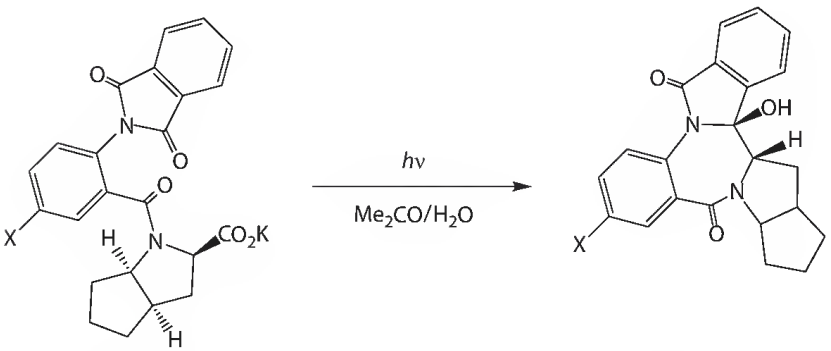

15c: X = H
15d: X = Cl

16c: X = H
16d: X = Cl

Garcia-Garibay et al. reported the memory of chirality upon recombination of a radical pair produced in the photolysis of chiral bis(phenylpyrrolidinonyl)ketone **17** in solution.[46,47] Ketone **17** was photodecomposed in a low quantum yield of 0.05, suggesting that the geminate recombination of ketyl radical is much faster than decarbonylation. On the other hand, the rate of decarbonylation k_{-CO} should be faster than the rotation rate of radicals formed in the first step, as no epimerization was observed for ketone. Photolysis of enantiopure (*S*,*S*)-**17** gave stereo-retained (*S*,*S*)-**18**, single inverted (*R*,*S*)-**18**, and double inverted (*R*,*R*)-**18** in 70%, 21%, and 9% yield, respectively. The solvent-caged effect appears to be responsible for the efficient chirality memory. At a higher temperature, the yield of (*S*,*S*)-**18** decreased to 50%, while those of (*R*,*S*)- and (*R*,*R*)-**18** increased to 35% and 15%, respectively. These results are satisfactorily rationalized in terms of the accelerated rotation of radicals at the higher temperature; the rotation time constants ($1/k_{rot}$) for the radicals generated by the photolysis were estimated to be 6.5 ps at 25°C and 3.2 ps at 69°C.

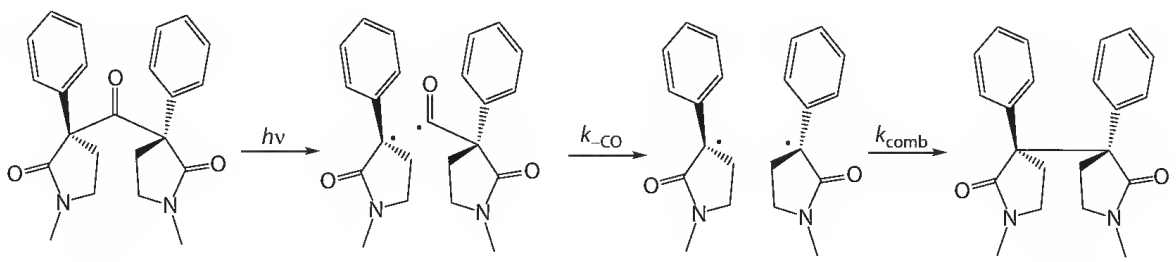

(*S*,*S*)-**17**

(*S*,*S*)-**18**

Sakamoto et al. investigated the chiral memory effect observed in the β- and γ-hydrogen abstraction reactions of thioimides.[48,49] Photochemical reactions of thioketones are known to proceed through S_2 ($\pi\pi^*$) and T_1 ($n\pi^*$) state. Similar to thioketone, excited thioimides are prone to abstract intramolecular hydrogens. Upon photoexcitation, **19** abstracts a β-hydrogen to give a 1,3-biradical intermediate, which in turn rearranges to give **20** with accompanying conversion of the chiral tertiary carbon to a chiral quaternary carbon. Thus, the irradiation of enantiopure **19a–d** with a high-pressure mercury lamp leads to the formation of the corresponding thioketones **20a–d** in quantitative yields and 97%–100% ee. The extremely high level of chirality memory suggests that the photoreaction proceeds through a singlet excited state and the resulting singlet 1,3-biradical is short-lived and hence rapidly rearranges to **20** without accompanying racemization at the original stereogenic center. No hydrogen abstraction reaction was observed for monothioimide **19e**, presumably due to the lack of stabilizing phenyl group as well as the presence of destabilizing ester group. The chiral memory effect has also been examined with optically pure thioimide **21**, which undergoes the γ-hydrogen abstraction reaction to give **22** and **23**. Photoirradiation of (*S*)-**21** yielded a mixture of (3*R*,4*S*)-**22** (>50% yield) and a small amount of (3*R*,4*R*)-**22** (10%–13% yield) and **23** (15%–23% yield). Both (3*R*,4*S*)-**22** and (3*R*,4*R*)-**22** were obtained in significantly high ee's (>85%).

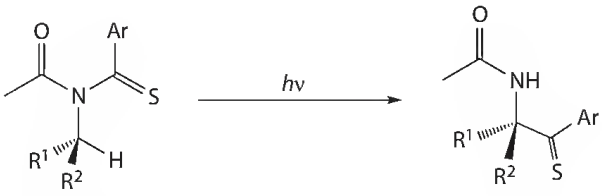

19 **20**

a: R^1 = Me, R^2 = Ph, Ar = Ph
b: R^1 = Me, R^2 = Ph, Ar = *p*-Tol
c: R^1 = Me, R^2 = Ph, Ar = *p*-Anis
d: R^1 = Me, R^2 = Ph, Ar = *p*-ClPh
e: R^1 = CO_2Me, R^2 = Pr^i, Ar = Ph
f: R^1 = CO_2Me, R^2 = Ph, Ar = Ph

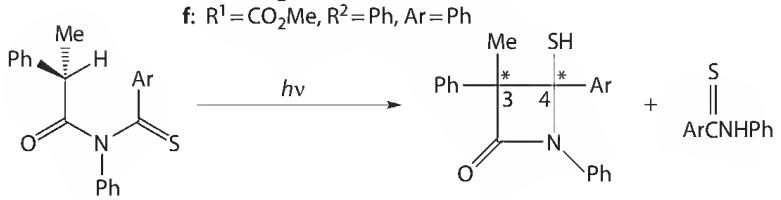

21 **22** **23**

Sivaguru et al. have recently examined the enantiospecificity in the Norrish/Yang type II reaction of α-oxoamides **24** and the photocyclization of acrylanilides **27**.[50–52] These compounds exhibit the non-biaryllic atrop isomerism as a consequence of the restricted rotation about the N–C(aryl) bond and are axially chiral. The isolated enantiomers of axially chiral α-oxoamides **24** can be stored at 0°C for months without racemization. Photolysis of **24** gave cyclization product **25** in >95% yield, along with a small amount of demethylation product **26**.[51] Good enantiospecificity was observed for **25**, showing an efficient chirality delivery from axial to point chirality. The enantiomer ratio of **25a** was found to depend on the reaction temperature, displaying an increase from 74:26 (48% ee) at 40°C to 90:10 (80% ee) at −40°C.

The memory of chirality was also examined with the photolysis of acrylanilide **27**.[52] The rotation about the N–C(aryl) bond in **27** is hindered by the steric bulk of the vinyl moiety. The constraint around the N–C bond leads to two atropisomers of opposite optical activity, which slowly interconvert in the ground state but not in the excited state. Upon photoirradiation, acrylanilide **27** undergoes conrotatory 6π-photocyclization to yield *cis*-**28** and *trans*-**29**. Acrylanilide **27d** bearing a β-CH_3 substituent gave **29d** in 94% ee in methanol, while **27f** with a β-H afforded racemic **29f**. Thus, the β-substituent R_1 serves as an important "messenger" or "commander" for transferring the axial chirality in reactant to the point chirality in photoproduct.

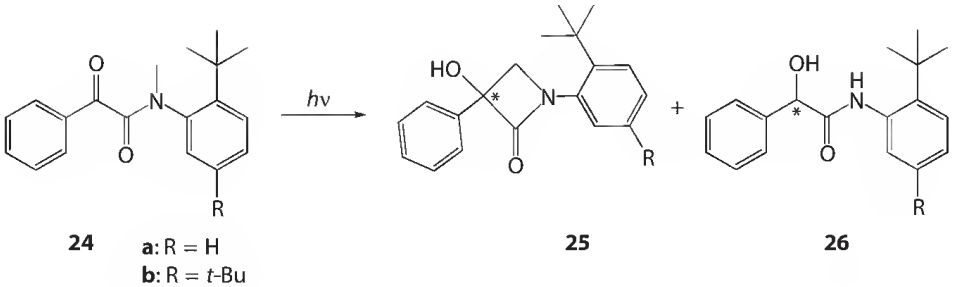

24 **a**: R = H
b: R = *t*-Bu

25 **26**

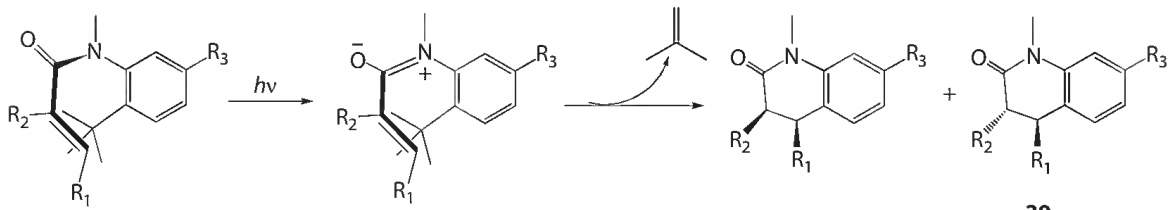

27 **28** **29**

R_1	R_2	R_3=H	R_3=*t*-Bu
CH_3	CH_3	**27a**	**27d**
H_2C—CH_2		**27b**	**27e**
H	CH_3	**27c**	**27f**

Compared to the aforementioned diastereodifferentiating photoreactions that are controlled by a chiral auxiliary covalently bonded to the substrate moiety, the photochemical enantiodifferentiation to manipulate the formation of two energetically equivalent enantiomeric products is obviously much more challenging, relying only on the weak noncovalent interactions of prochiral substrate with chiral source. Indeed, most of the enantiodifferentiating photoreactions in solution give only poor enantioselectivities.[5,7] The supramolecular approach,[53,54] which utilizes the noncovalent interactions in both ground and excited states, has proven a convenient, versatile methodology for controlling thermodynamically the molecular assembly and kinetically the subsequent photochirogenic reaction.

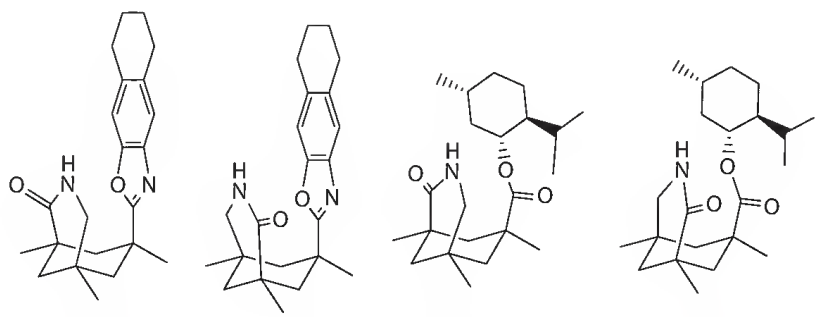

30a **30b** **30c** **30d**

Bach et al. synthesized a series of Kemp's acid derivatives **30a–d** as chiral hydrogen-bonding templates for the use in various intra- and intermolecular enantiodifferentiating photoreactions. The enantiodifferentiating intramolecular photocycloaddition of prochiral 2-quinolone allyl ether **31** was studied in the

presence of chiral template **30a–c**. Although hydrogen-bonding templates may often self-aggregate to yield hydrogen-bonded homodimers, this is not the case with **30a,b** ($K_{dim} \sim 0\,M^{-1}$) as a consequence of the steric hindrance of the bulky tetrahydronaphthalene fence. Instead, the amide moiety of **30a,b** efficiently forms dual hydrogen bonds with **31**. One of the enantiofaces of **31** is shielded by the tetrahydronaphthalene fence, and therefore, the intramolecular attack of the allyl is allowed only from the open face. Photoirradiation of **31** in the presence of template **30b** at −60°C yielded **32** in 93% ee.[55,56] By using **30a** as a chiral hydrogen-bonding template, similar intramolecular [2 + 2] photocycloaddition reactions of **33** and **35** in toluene at −60°C afforded **34** in 59%–75% ee and **36** in 74%–92% ee.[57] The stereochemical outcomes were significantly enhanced by increasing the amount of template, lowering the temperature, and decreasing the polarity of solvent.

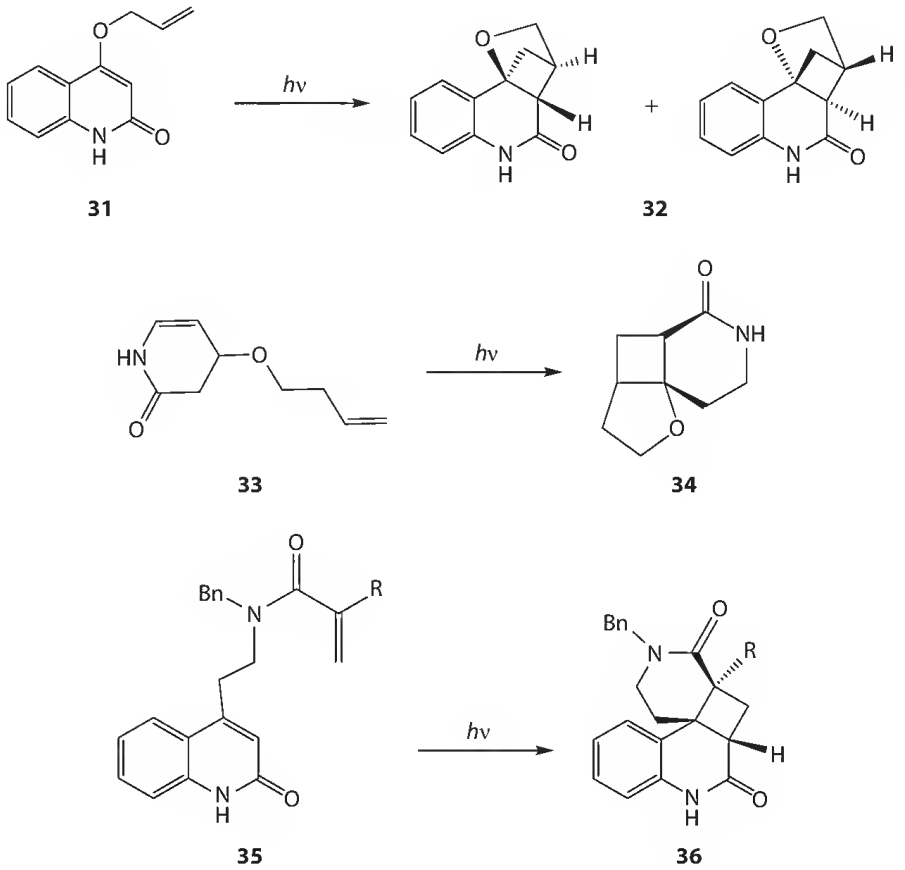

In the presence of chiral template **30a**, enantiodifferentiating 6π-photocyclization of acrylanilides **37a–c** afforded photoproducts **38** and **39** in ratios ranging from 48:52 to 27:73. The ee's of **38** and **39** were enhanced up to 57% and 39%, respectively, by increasing the template/guest ratio and lowering the temperature.[58,59] The Norrish–Yang cyclization of imidazolidinones **40** to *endo*- and *exo*-products **41** and **42** was carried out in the presence of chiral templates **30a–d**.[56,60] The *exo*/*endo* ratio of the products formed from **40c** was dramatically switched from 38/62 in the absence of chiral template to 90/10 in the presence of **30c**. The photocyclization of **40** in the presence of chiral template **30a,b** afforded **41** in up to 60% ee.[56]

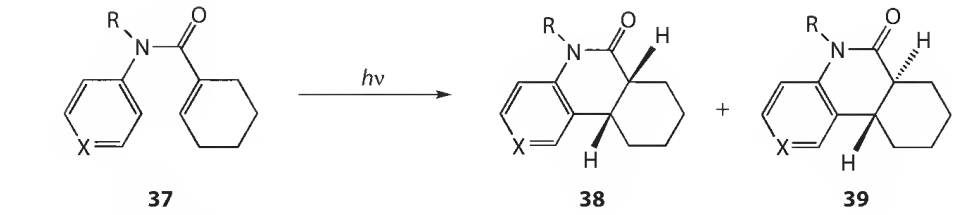

37 **38** **39**

a: X = CH, R = H
b: X = CH, R = CH
c: X = N, R = H

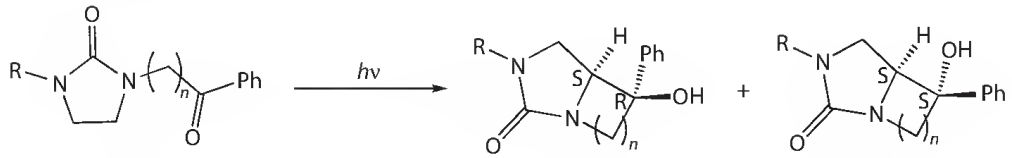

40 **41** **42**

a: R = H, *n* = 1
b: R = Ac, *n* = 1
c: R = H, *n* = 2
d: R = Ac, *n* = 2

6.3.1.2 Intermolecular Photochirogenesis in Organic Solution

Stereochemical control in photochirogenesis is tricky in general and sensitive to substrate geometry. Therefore, photochirogenesis with singlet oxygen, the smallest possible cyclophile, is considered as a great challenge. Recently, an efficient stereochemical control was achieved in [2 + 2] photocycloaddition of $^1O_2$ to oxazolidinon-functionalized enecarbamates **43** possessing chiral auxiliary. Oxazolidinone-substituted chiral enecarbamates (*Z*)/(*E*)-**43** are versatile substrates for investigating the conformational, stereoelectronic, and steric effects on the stereodifferentiating singlet oxygenation of the alkene functionality.[61–66] No enantioselectivity was observed upon cycloaddition of $^1O_2$ to unsubstituted enecarbamate **43a** and **b**. However, the singlet oxygenation of (4*R*)-**43b** and (4*R*)-**43c** afforded (1*S*,2*S*)-**44b** and (1*S*,2*S*)-**44c** in >90% ee, irrespective of the configuration at the C-3 position. The carbonyl group does not appear to play a significant role in the determination of the stereochemical course of cycloaddition, as the diastereomer ratio did not show any dependence on the solvent polarity. The π-face selectivity observed upon $^1O_2$ attack was reasonably attributed to the effective shielding by the *R*-substituent at C-4 of enecarbamate **43**. Interestingly, the photolysis of a diastereomeric mixture of (3*R*,4*R*)- and (3*S*,4*R*)-**43c** to a low conversion (<30%) and the subsequent decomposition of the resulting dioxetane gave enantiomerically enriched methyldesoxybenzoin (MDB) in ca. 33% ee. At higher conversions, the ee of MDB was reduced.[61] These results indicate that the photocycloaddition reaction rate is influenced by the configuration at C-3. Quenching experiments suggested that the major pathway upon interaction of **43** with $^1O_2$ is not the reaction but the quenching.

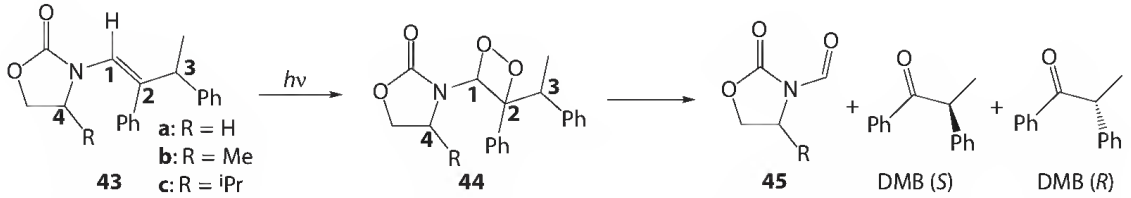

43 **44** **45** DMB (*S*) DMB (*R*)

a: R = H
b: R = Me
c: R = ^{i}Pr

Further investigation demonstrated that the photocycloaddition reaction is also affected by the alkene geometry, as the (*E*)-isomers of **43b,c** produce MDB in higher ee's than the (*Z*)-isomers. For example, a 1:1 mixture of (3*R*,4*R*)- and (3*S*,4*R*)-(*Z*)-**43c** give (*R*)-MDB in 27 ± 4% ee, while the same diastereomer pair of (*E*)-**43c** gave an almost doubled ee value.[63] This chiral photoreaction was revealed to be sensitive to solvent and temperature, and (*R*)-MDB of 97% ee was obtained in CD_3OD at –70°C at 8% conversion.

Tung et al. investigated the photodimerization of 2-naphthoates **46a–g** with chiral ester auxiliaries.[67] Photodimerization of alkyl 2-naphthoates **46a–g** resulted in *anti*^{HH}-**47a–g** as main products. For substrates **46a–f** with α-chiral ester moieties, relatively high diastereoselectivities of up to 59% de were achieved. In contrast, substrate **46g** with a β-chiral auxiliary gave the photodimers in <5% de, revealing the critical role of the proximate chiral center. The de of photodimer **47** was also affected by the solvent used, as evidenced by the fact that *anti*^{HH}-**47** was given in −54% de (88% yield) in cyclohexane but in −44% de (83% yield) in methanol.

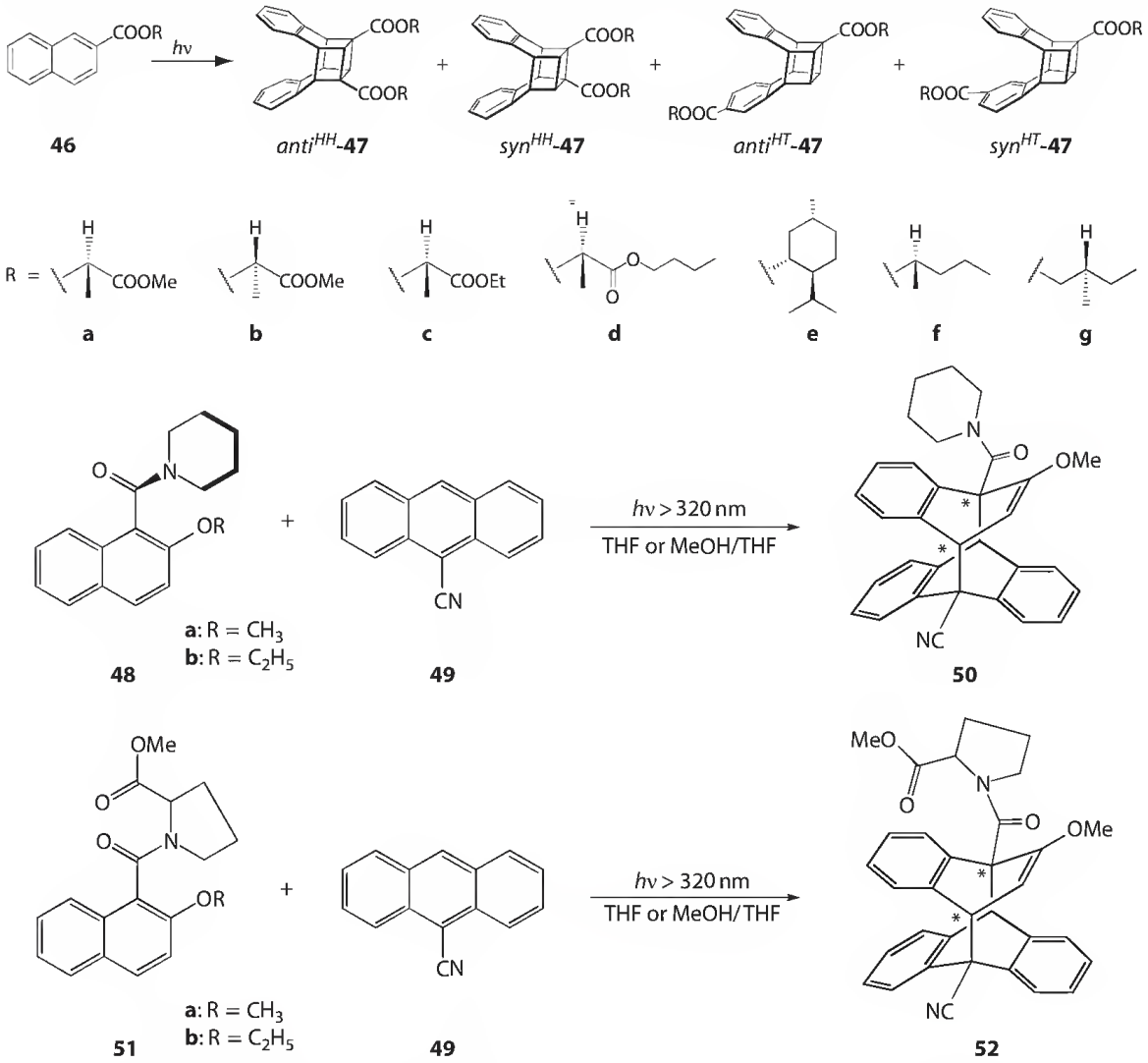

Sakamoto et al. reported a highly enantiodifferentiating cross-photocycloaddition of 2-alkoxyl-1-naphthamides **48** and **51** with 9-cyanoanthracene **49** in solution.[68–71] In these naphthamides, the free rotation about the aryl-carbonyl bond is more or less hindered as a consequence of the steric bulk of the *N*-substituent and the enantiomeric atropisomers are conformationally fixed at low temperatures and in the solid state. In the case of **48a** and **48b**, the relatively compact amide group allows racemization to occur in solution at room temperature. The racemization half-lives of **48a** in THF are 11.8, 19.4, and 36.7 min at 15°C, 10°C, and 5°C, respectively, but can be elongated to 128.3 min by using a mixed solvent of MeOH and THF at 15°C, which may be rationalized by the increased bulk of the amide moiety solvated by methanol. Interestingly, naphthamide **48a** (R = Me) forms chiral crystals of $P2_12_12_1$ space group, while **48b** (R = Et) gives racemic $P2_1/c$ crystals. Photolysis of a cooled solution of crystalline **48a** and **49** gave cross-cycloadduct **50** of 95% ee in quantitative yield, achieving the memory of labile chirality. Naphthamides **51a,b** that carry proline methyl ester as a chiral handle were synthesized for

further investigating the chiral memory effect in diastereodifferentiating photocycloaddition. Bearing an (*S*)-proline moiety, amides **51a,b** adopt the (*S*, *aR*)-conformation in the crystals of $P2_1$ space group. The activation free energy required for the conformational transformation between the two diastereomeric isomers in solution was determined as 22.2–22.3 kcal mol^{-1}. Photocycloaddition of amides **51a,b** to **49** in solution at –20°C gave **52a** and **52b** in 63% and 53% de, respectively. However, the photoirradiation of the chiral crystals gave the same products in up to 100% de.

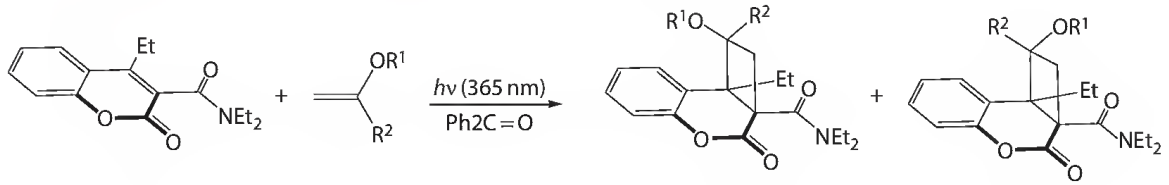

53 **54** *endo*-**55** *exo*-**55**

a: R^1 = Et, R^2 = H
b: R^1 = R^2 = Me

Achiral *N,N*-diethyl-4-coumarin-3-carboxamide **53** crystallizes in chiral space group $P2_12_12_1$, where the amide carbonyl is twisted almost orthogonally to the coumarin plane. The activation free energy for the racemization of **53** in solution varies in a range 20.5–22.4 kcal mol^{-1}, depending on the solvent used.[72] The intermolecular [2 + 2] photocycloaddition of alkenes **54** to temporary chiral amide **53** performed by direct irradiation in methanol at –20°C gave *endo*-**55** and *exo*-**55** in 82% and 86% ee, respectively. However, the use of benzophenone as a triplet sensitizer afforded *endo*-**55a** of 98% ee and *exo*-**55a** of 97% ee in 99% combined yield. The lower ee observed upon direct irradiation was ascribed to the racemization of the starting amide accelerated in the singlet excited state. Using **54b** as substrate for the photocycloaddition to **53**, *endo*-**55b** was given as a sole product in 99% ee.

Inoue et al. have recently reported the wavelength control of diastereoselectivity of Paternó-Büchi reaction of **56a,b** by choosing the direct and charge-transfer (CT) band excitation.[73] The CT complex of **56a** with **57** has a modest binding constant of 0.04 M^{-1} at 25°C. Direct excitation of **56** at 290 nm gave **58a** and **58b** in 64% and 71% de, respectively, while much lower de's of 4% and 22% were obtained upon CT band excitation at 330 nm, suggesting that the conventional exciplex and the excited CT complex do not share a common intermediate but have distinctly different structures and reactivities in the excited state. Intriguingly, the oppositely signed differential activation enthalpy change $\Delta\Delta H^{\ddagger}$ and entropy change $\Delta\Delta S^{\ddagger}$ were obtained for direct and CT excitations. The magnitude of $\Delta\Delta S^{\ddagger}$ is appreciably larger for the direct excitation than for the CT excitation, possibly due to the better stacked CT complex that is less flexible in the excited state than the exciplex.

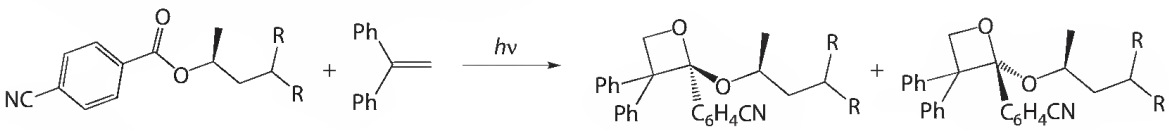

56 **57** (1'*S*, 2*R*)-**58** (1'*S*, 2*S*)-**58**

a: R = H
b: R = Me

Inoue et al. examined the photocyclodimerization of 2-anthracenecarboxylic acid (AC) in the presence of chiral templates **60** and **61**. Photocyclodimerization of AC gives four stereoisomeric dimers, that is, *anti*- and *syn-head-to-tail* (HT) dimers **59a** and **59b** and *anti*- and *syn-head-to-head* (HH) dimers **59c** and **59d**, of which **59b** and **59c** are chiral. The enantiodifferentiating photocyclodimerization of AC was firstly studied in organized media by using native γ-CD as chiral host.[74] The gastroprokinetic agent **60** and its epimer **61** were found to strongly bind AC by forming a nine-membered dual hydrogen-bonding motif between the prolinol's amino and hydroxyl groups.[75] One of the enantiofaces of AC was blocked by the 2-methoxybenzamide

moiety of **60** upon stacking complexation, and the photocyclodimerization of AC can occur only from the opposite side of bound AC. In the presence of chiral template **60**, photocyclodimerization of AC affords HT dimer **59b** in −36% ee and HH dimer **59c** in −40% ee in CH_2Cl_2 at −50°C. In contrast, epimer **61**, which forms an extended, rather than stacked, complex with AC leading to poor enantioselectivity (<3% ee). Detailed photophysical and photochemical studies of the system revealed that the ee is not simply determined by the ratio of diastereomeric *re*- and *si*-AC-**60** complexes but also affected by the relative lifetime of these diastereomeric complexes.[76] The *re*-complex has a lifetime of 3.7 ns, which is much shorter than that of *si*-complex (10 ns). The encounter complexes are proposed to have a perpendicular geometry, where electrostatic repulsion is minimized, and the enantioselectivity lies on the relative rotation of two perpendicularly contacted AC molecules. By taking the relative lifetimes of complexes into account, the relative population of the diastereomeric complexes was successfully calculated from the ee values of dimers.

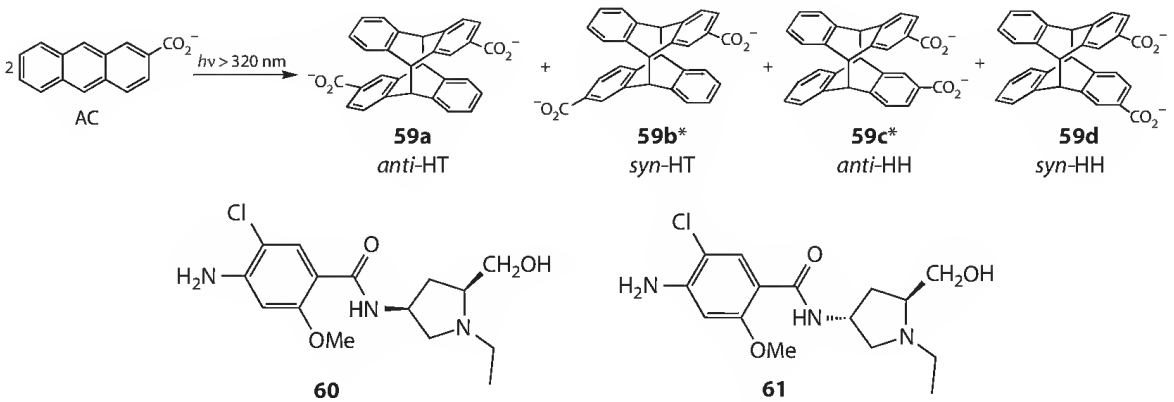

Bach et al. examined a number of enantiodifferentiating intermolecular photoreactions in the presence of chiral templates **30**. When complexed by these chiral templates, one enantioface of the bound photosubstrate is shielded by the chiral template and the subsequent photoreaction occurs only from the unshielded face. Photoirradiation of aromatic aldehyde **62** yields dienol intermediates firstly as a result of intramolecular γ-hydrogen abstraction. The (*Z*)-dienol returns to the starting material quickly but the (*E*)-isomer has a longer lifetime to process a Diels–Alder reaction with a dienophile. The photoinduced cycloaddition of **62** to alkene in the presence of **30a** prefers the exo product **63** and furnishes photoproducts in up to 94% ee.[77]

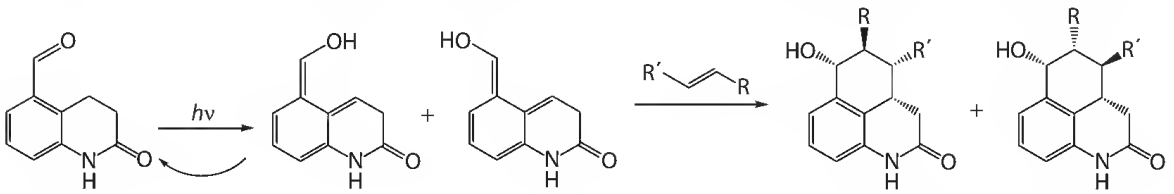

Intermolecular [4 + 4] photocycloaddition of 2-pyridinone to cyclopentadiene affords racemic **65** and **66** in a ratio of 2:3 in the absence of chiral template. However, the photocycloaddition in the presence of **30a** gave **65** and **66** in remarkable 84%–87% ee's.[78]

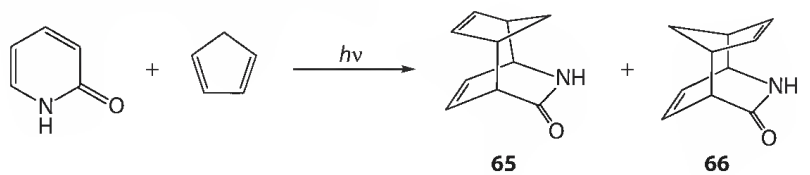

6.3.1.3 Sensitized Photochirogenesis in Organic Solvent

An essential advantage of sensitized photochirogenesis over other photochirogenic strategies is the inherently "catalytic" nature of the chirality transfer process, which enables us to photochemically multiply the molecular chirality with a minimal amount of chiral sensitizer as is the case with catalytic or enzymatic asymmetric synthesis. On the other hand, the intermolecular chirality transfer process in the excited state is difficult to control or design and the enantioselectivity reported for sensitized photochirogenesis has not been very high in general until recently. Thus, as a modification or expansion of the concept of traditional chiral photosensitization via exciplex intermediate, a couple of inventions have been proposed to assure the chirogen–substrate interactions in the excited state, while keeping the "catalytic" nature. These include the selective excitation of the charge-transfer or other complexation-induced absorption emerged at longer wavelengths upon formation of chirogen–substrate complex in the ground state and the photoredox reaction–mediated by chiral donor or acceptor. In all of these strategies, it is essential that an appropriate wavelength should be chosen for selectively activating the chiral sensitizer, mediator, or complex derived therefrom while avoiding the direct excitation of substrate, and also that strong and intimate interactions should be maintained between chirogen and substrate for an appropriate period of time to effectively transfer the chiral information to the substrate in the excited state. In this context, the singlet sensitization via the Förster mechanism does not appear to be suitable for the chirality transfer in the excited state, since no steric interaction is expected to occur during the coupled energy transfer.

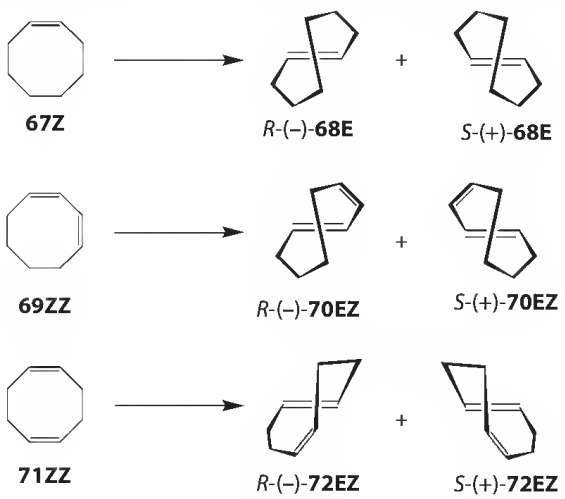

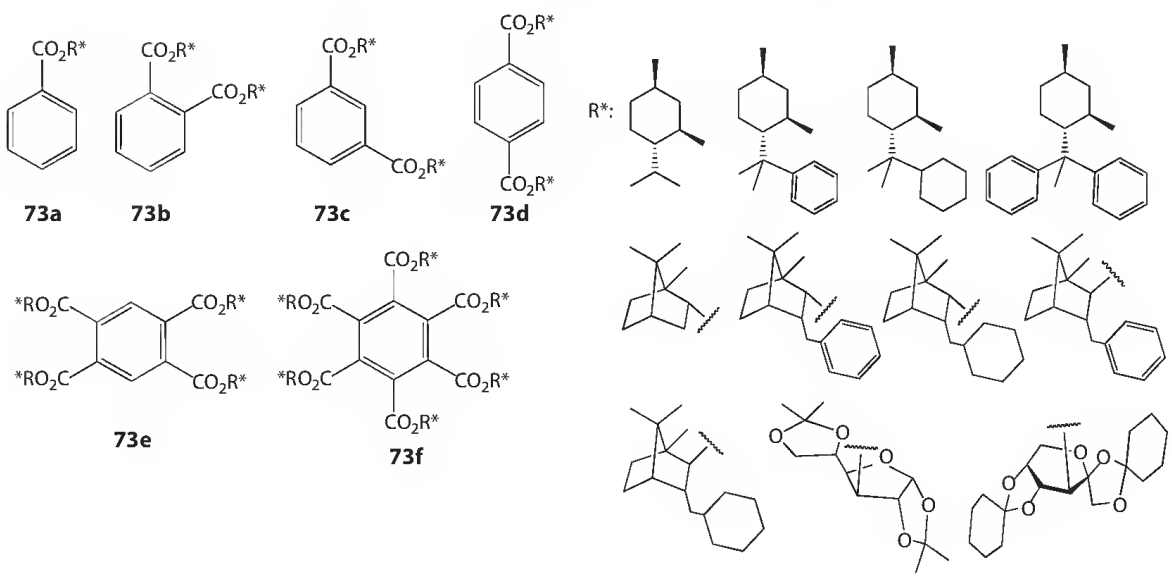

Photosensitized isomerization of 1,2-diphenylcyclopropane, the very first example of enantiodifferentiating photosensitization reported by Hammond and Cole, has been extensively investigated.[79–82] However, the photoisomerization sensitized by conventional chiral sensitizers in solution affords *trans*-1,2-diphenylcyclopropane in only 10% ee at the best.[83]

Inoue et al. investigated the sensitized enantiodifferentiating photoisomerization of cycloalkenes, which has now become a sort of benchmark test system for studying photochirogenesis.[84–96] Representative examples include the *Z-E* photoisomerization of cyclooctene **67Z** and 1,3- and 1,5-cyclooctadienes **69ZZ** and **71ZZ** to the corresponding planar chiral (*E*)-isomers **68E, 70EZ** and **72EZ.** A series of benzene(poly)carboxylates **73a–f** with a variety of ester groups were synthesized as chiral singlet sensitizers to explore the effects of internal and external factors on the enantiodifferentiating photoisomerization of cycloalkenes. By analyzing the behavior of ee obtained upon sensitized photoisomerization of cyclooctene **67Z** at various temperatures, they unequivocally revealed the essential roles of entropy in the critical enantiodifferentiating process occurring in an exciplex intermediate. Thus, the chiral sense of product **68E** was dramatically inverted by simply changing the reaction temperature in several cases.[85–87] It was further demonstrated that the other entropy-related factors, such as solvation and hydrostatic pressure, also significantly affect the enantiodifferentiation process not only to increase the product's ee but also to switch the chiral sense of the product. Therefore, by optimizing these environmental factors, the enantioselectivity was enhanced up to 73% ee for **68E** and 75% ee for **72EZ**, although the enantioselectivity remained low at 14.3% ee for **70EZ.**[97]

Bach et al. reported the chiral photocyclization of pyrrolidine-appended quinolone **75** mediated by chiral template **74a**, in which a hydrogen-bonding motif, the Kemp's acid derivative, was covalently grafted with a photoinduced electron transfer (PET) sensitizer, benzophenone.[98,99] Upon complexation with the chiral template through dual hydrogen bonds, one of the enantiofaces of **75** is cover by the benzophenone moiety of **74a**. Photoirradiation of **74a** causes the electron transfer from the pyrrolidine nitrogen in **75** to the benzophenone in **74a**, which is followed by the migration of a hydrogen from the carbon α to nitrogen to the radical anionic benzophenone. The resulting pyrrolidyl radical attacks the *ipso*-carbon to form the spiro skeleton preferentially from the open face of quinolone, and therefore the photocyclization of **75** in the presence of 0.1 equivalent of **74a** gave **76** in 52%–64% yield with up to 70% ee.

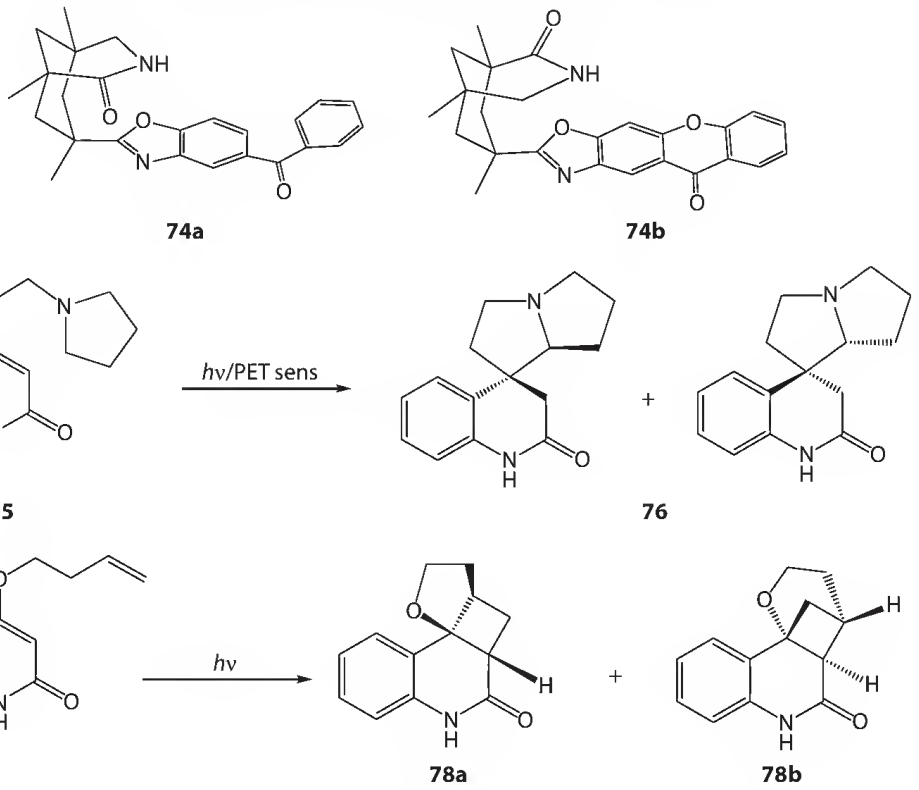

For PET reactions, polar solvents are commonly employed for better stabilizing the generated radical ion pair and also discouraging the back electron transfer through the formation of solvent-separated or free radical ion pair. However, this is obviously disadvantageous for transferring the chiral information from sensitizer to substrate, lacking any intimate interaction between them. Inoue et al. proposed an interesting approach that circumvents this trade-off by performing the photochirogenic PET reaction with a polar saccharide-modified photosensitizer in nonpolar solvents. Thus, the PET process can be facilitated by the microenvironmental polarity around the sensitizer, while solvent separation is prevented due to the low bulk polarity of nonpolar solvent.[100] By applying this approach to the anti-Markovnikov addition of alcohol to 1,1-diphenyl-2-alkoxypropene **79** sensitized by chiral naphthalene(di)carboxylates **81–85**, they obtained photoadduct **80** in up to 58% ee for **82h**.

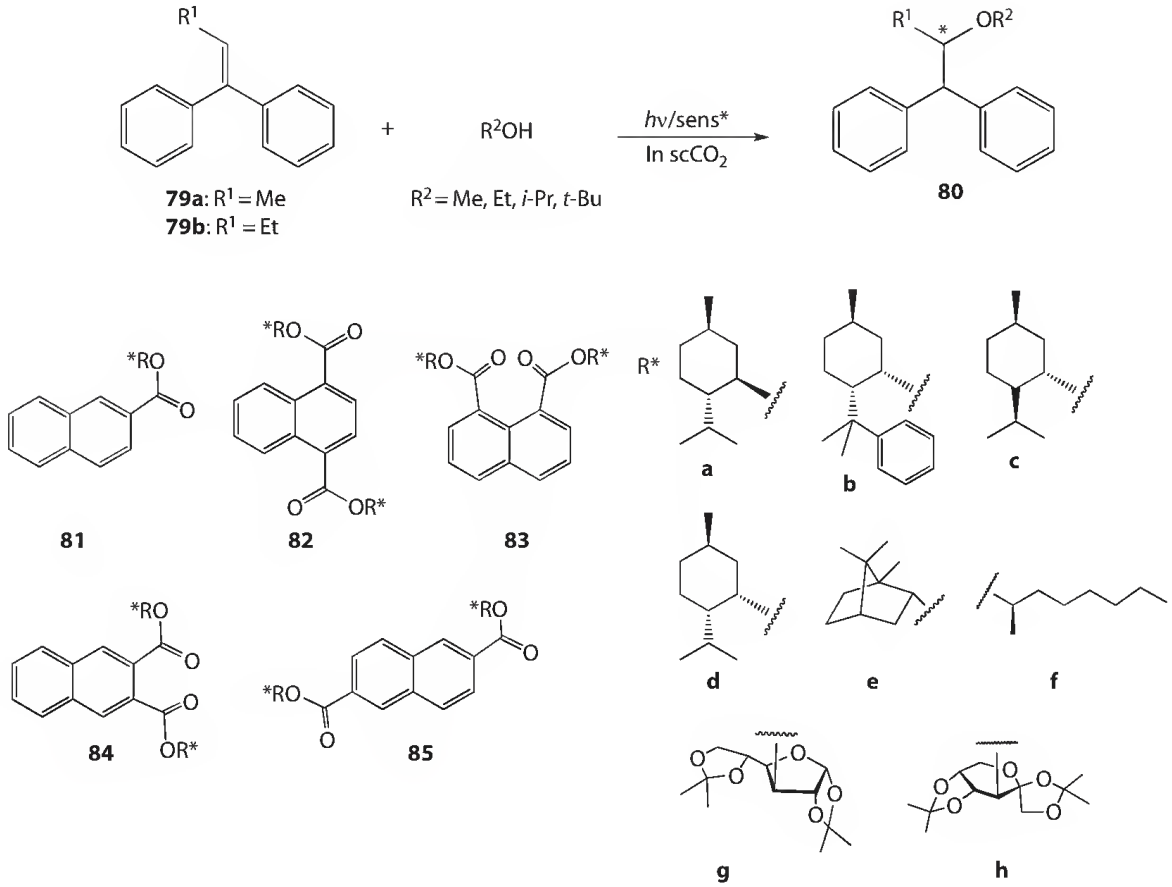

More recently, Bach et al. employed chiral template-sensitizer **74a,b** for the intramolecular [2 + 2] photocycloaddition of prochiral 4-(3′-butenyloxy)quinolone **77** to obtain tricyclic adduct **78a** and **78b**.[101] In the presence of 0.1 equivalent of benzophenone-appended chiral template **74a**, cycloadducts **78a** and **78b** were given in a ratio of 75:25 with 39% and 17% ee, respectively. No reaction took place at temperatures lower than −25°C, for which the relatively low triplet energy of the sensitizer would be responsible. However, xanthone-bearing template **74b** with a higher triplet energy of 310 kJ mol^{-1} and a more effective shielding group gave **78a** and **78b** in much higher 94% ee.

MacMillan et al. recently reported a photoinduced asymmetric alkylation of aldehydes **86**.[102] The chiral reaction involves the addition of electron-deficient alkyl radical, formed via the reduction of alkyl bromide by photoredox catalyst $Ru(bpy)_3^{2+}$, to an electron-rich enamine generated by the condensation of aldehyde **86** and organocatalyst **87**. The photoexcited $^*Ru(bpy)_3^{2+}$ is thought to efficiently remove a single electron from a sacrificial quantity of enamine to provide the electron-rich $Ru(bpy)_3^{2+}$, which electron transfers to alkyl bromide with an electron-withdrawing group (EWG) to furnish the electron-deficient alkyl radical. Attack of the alkyl radical to the enamine proceeds in a highly enantioselective fashion to eventually give the adduct, and therefore **88**, in high ee's of up to 99%. Due to the intensive absorption of $Ru(bpy)_3^{2+}$, the photoreaction was readily initiated and efficiently underwent even by using a 15 W fluorescent lamp as a light source. In a common chiral photosensitization, sensitizer is covalently attached to a chiral substituent in order to ensure chiral environment for the sensitized photochirogenic process. In contrast, $Ru(bpy)_3^{2+}$ was used as a sensitizer without a chiral substituent in this case, as the photogenerated alkyl radical reacts with the chiral enamine rather than aldehyde directly. Thus, **87** functions as an efficient chiral auxiliary for the diastereodifferentiating addition of alkyl radical generated photochemically.

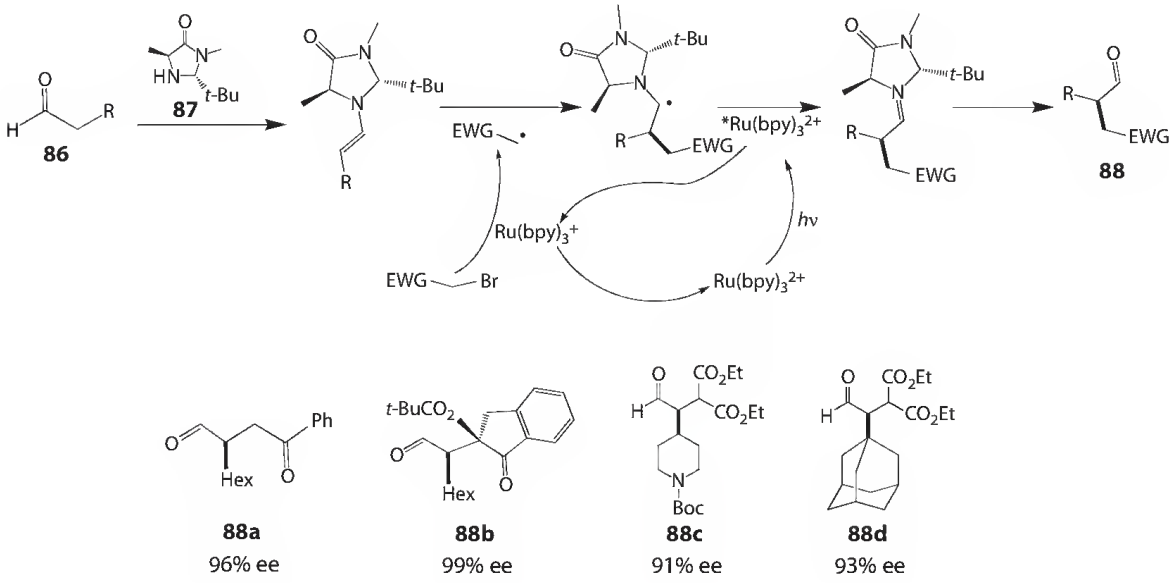

The same photoredox organocatalysis strategy was employed in α-trifluoromethylation of aldehydes.[103] The photoinduced enantiodifferentiating α-trifluoromethylation of aldehydes **86** was carried out in the presence of chiral organocatalyst **87** and photocatalyst $Ru(bpy)_3^{2+}$ or $Ir(ppy)_2(dtb\text{-}bpy)^+$. Employing **87** as chiral organocatalyst, the photoaddition of **86c** at –20°C afforded **89c** in 87% ee by $Ru(bpy)_3^{2+}$ but 99% ee by $Ir(ppy)_2(dtb\text{-}bpy)^+$, implying a possible involvement of the photocatalyst in the enantiodifferentiating process. Exclusion of light from this protocol resulted in an almost complete loss of catalyst efficiency (<5% yield). Photoreaction of **86a–d** with different substituents sensitized by $Ir(ppy)_2(dtb\text{-}bpy)^+$ in the presence of **87** at –20°C gave α-trifluoromethyl ketones **89a–d** in >90% ee.

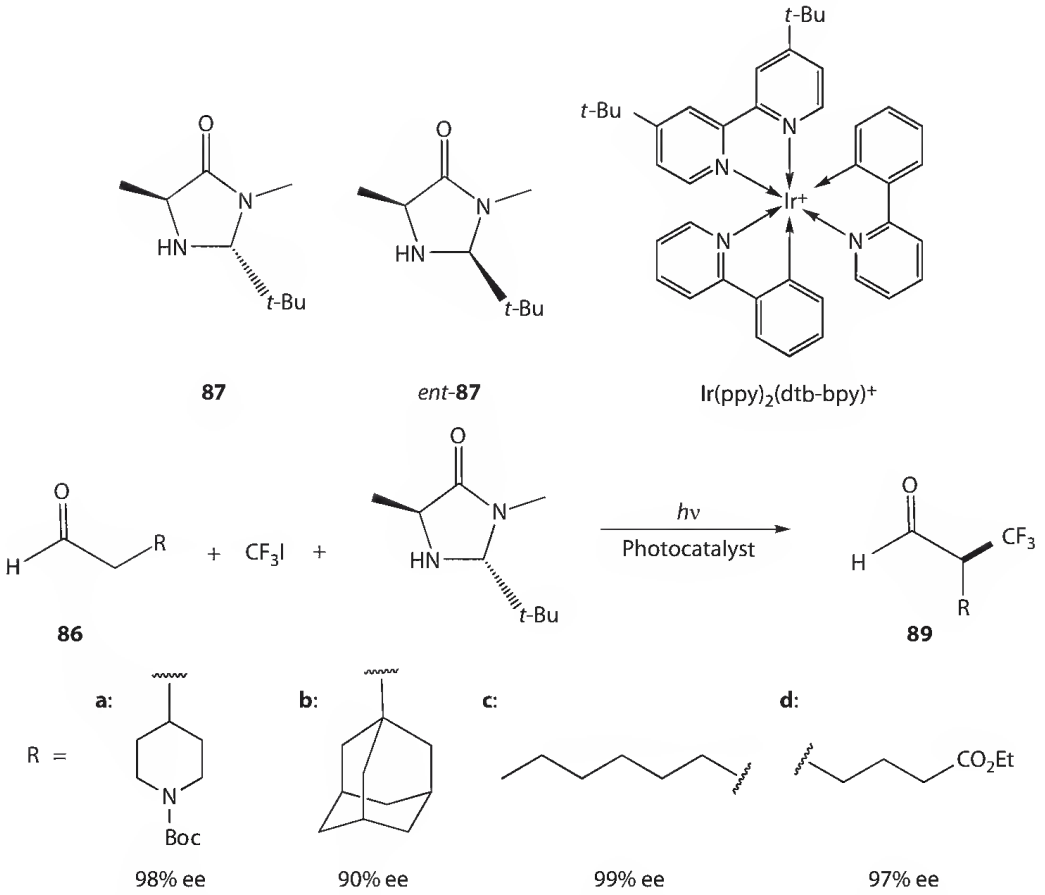

Yoon et al. reported that $Ru(bpy)_3^{2+}$ serves as an excellent photocatalyst for the intra- and intermolecular anion radical-mediated [2 + 2] enone cycloadditions.[104,105] For example, photoirradiation of a solution containing **90**, **91** and $Ru(bpy)_3^{2+}$ with visible light for 4 h affords the [2 + 2] cross-cycloadduct **92** in 84% isolated yield, while direct irradiation of the mixture of **90** and **91** at 300 nm failed to produce any observable cycloadducts but isomers originated from E/Z isomerization of enone **90**. In this work, no attempt has been done to control the enantioselectivity, but an excellent diastereoselectivity for **92** was observed with dr >10:1 (>91% de).

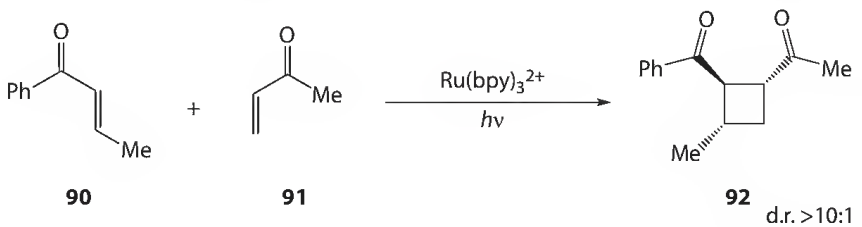

6.3.2 Photochirogenesis in Chiral Ionic Liquid

Chiral solvents have been employed as a source of chirality for photochirogenic reactions. An inherent disadvantage of this strategy is the use of a large excess amount of costly enantiopure compound as chiral solvent. Despite the low chirogen efficiency and cost performance, the efficiency of photochemical chirality transfer is poor in general, with the highest ee values of <10%.[106]

As a new medium for photochirogenesis, chiral ionic liquid, room-temperature molten salt, has been used recently. The use of chiral ionic liquid is beneficial not only from the environmental but also from

the photochirogenic viewpoints, since some chiral ionic liquids are readily available (or easily prepared), can be removed from the reaction mixture, and hence recyclable. The easy access to antipodal ionic liquids would be an additional benefit.

Armstrong et al. investigated the enantiodifferentiating di-π-methane photorearrangement of dibenzobicyclo[2.2.2]octatrienedicarboxylic acid derivatives **93a–c** to the corresponding tricyclic compounds **94a–c** in chiral ionic liquids **95a–d**.[107] Photoirradiation of methyl ester **93b** in chiral ionic liquids **95a–d** led to the formation of racemic **94b** without exception. In contrast, the photorearrangement of carboxylic acid **93c** in **95b** gave **94c** in modest 6% ee, while no enantiodifferentiation was observed upon irradiation in other three chiral ionic liquids. The observed enantioselectivity is possibly due to the interaction of the acid substrate with the ionic liquid. Interestingly, in the presence of added base, such as *N*-methylephedrine, *N,N*-dimethylbenzylamine and sodium hydroxide, the photorearrangement of **93c** performed in all of the chiral ionic liquids provided **94c** in appreciable enantioselectivities. Nevertheless, the chiral induction is considered to originate not from the added base but from the chiral medium, as the addition of antipodal *N*-methylephedrines gave similar ee values in the same ionic liquid and the antipodal chiral ionic liquid gave the antipodal product, irrespective of the chiral amines added. This may indicate that the added base simply facilitates the dissociation of **93c** to carboxylate for better interaction with chiral imidazolium cation.

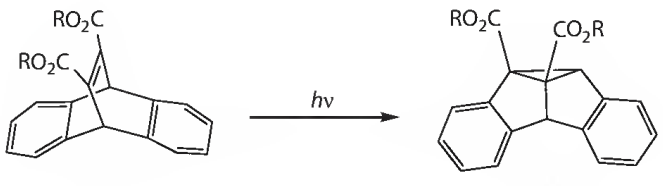

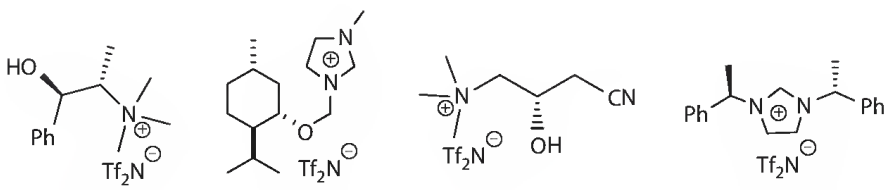

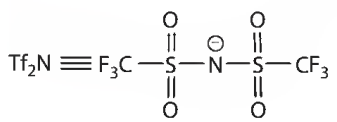

Apart from the photochemical reactions, some photophysical properties have also been investigated in chiral ionic liquids. Enantiodifferentiating fluorescence quenching by intramolecular PET was studied in chiral ionic liquid.[108] The lifetime of *N*-methyl-2-pyrrolidinemethyl (*S*)-(6-methoxy-2-naphthyl) propionate was 8.9 ns in D-tartrate ionic liquid, but became 10% longer in L-tartrate ionic liquid. The observed differences in fluorescence lifetime and steady-state fluorescence quantum yield became more evident at higher temperatures.

6.3.3 Photochirogenesis in Supercritical Fluid

In contrast to conventional organic solvents, supercritical carbon dioxide ($scCO_2$) possesses several advantages, such as inflammability, low toxicity, low density, low viscosity, and low cost. Photochirogenesis in $scCO_2$ was firstly reported for the enantiodifferentiating photoisomerization

of cyclooctene **67Z** sensitized by chiral benzene(poly)carboxylates **73**.[93] Since the sensitized photoisomerization of **67Z** is highly sensitive to solvation,[92] it is particularly interesting to examine the photoreaction near the critical point, where the solvent properties such as viscosity, density, and dielectric constant changed drastically in narrow ranges of pressure and temperature. Indeed, a sudden change of enantioselectivity was observed near the critical density ($\rho_C = 0.468\,g/cm^3$; $P = 9.8\,MPa$ at 45°C). The differential activation volume ($\Delta\Delta V^{\ddagger}_{S-R} = \Delta V^{\ddagger}_{S} - \Delta V^{\ddagger}_{R}$) obtained for the near-critical region ($-5.6\,cm^3/mol$) was much greater than that for the same photoisomerization performed in pentane ($3.5\,cm^3/mol$), suggesting that the transition-state structure and/or enantiodifferentiation mechanism in near critical (nc) CO_2 are completely different from those in $scCO_2$ and conventional organic solvents.

The scope of photochirogenesis in $scCO_2$ was expanded to bimolecular reaction systems through investigating the enantiodifferentiating polar photoaddition of alcohol to 1,1-diphenylpropene **79** sensitized by chiral naphthalenecarboxylates **81–85**.[109–112] The reactivity and enantioselectivity were critically correlated by the bulkiness of the attacking agent, alcohol. Thus, the enantioselectivity increases with the size of alcohol and gives the best ee for 2-propanol, while the bulkiest *t*-butanol yields no adduct. For all the sensitizers, a large leap of ee was observed around the critical density at the narrow pressure range of 9–10 MPa, while the pressure dependence of ee is continuous in the subcritical region of $P < 9\,MPa$ and supercritical region of $P > 10\,MPa$.

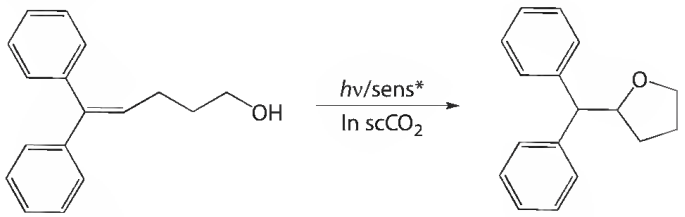

96 **97**

The sudden leap of ee in the narrow pressure range transferring from the near-critical to supercritical state implies a significant difference in clustering mechanism and/or cluster structure between both states. Recently, the effect of entrainer (organic solvent added to $scCO_2$) on the intramolecular photoaddition of **96** in $ncCO_2$ and $scCO_2$ has been examined.[112] In organic solvents, the enantioselectivity is known to critically depend on the microenvironmental polarity around the exciplex intermediate, and the addition of a small amount of ether to methylcyclohexane appreciably enhances the ee of **97** as a result of the selective solvation. Hence, the effect of methanol clustering to sensitizer **82h** was examined in $scCO_2$ to reveal the appreciable bathochromic shift and band broadening induced by lowering the pressure from 10 to 9 MPa, which were accounted for in terms of the enhanced clustering of methanol to the saccharide moiety. In the photoaddition of methanol to **96** in the presence of **82h**, the differential activation volumes $\Delta\Delta V^{\ddagger}_{S-R}$ were determined as 60, 530, and $22\,cm^3\,mol^{-1}$ for the pressure regions 7.7–9, 9–10, and 10–18 MPa, respectively, which are much larger than those in organic solvents. The anomalously large $\Delta\Delta V^{\ddagger}_{S-R}$ value obtained near the critical density may reflect the dynamic nature and the density fluctuation of this critical region.

6.4 Photochirogenesis in Organized Media

6.4.1 Photochirogenesis in Nanosized Cavity of Zeolite and Mesoporous Silica

Zeolites are aluminosilicates with well-defined mesoporous structures.[113,114] They are attractive as supramolecular hosts for photoreactions, being transparent to UV/Vis lights and possessing supercages, the size of which is tunable by changing the countercations compensating the negative charge

of $[AlO_4]^{5-}$ tetrahedra. Indeed, the diastereodifferentiating photoreactions conducted in zeolite supercage show remarkable differences from those in homogeneous solution. Thus, photoirradiation of (*S*)-tropolone-2-methylbutyl ether **98** in hexane leads to the formation of a 1:1 mixture of diastereomers **99a** and **99b**, while the same photoreaction conducted in NaY zeolite affords **99a** in up to 68% de.[115] In contrast, the photocyclization of **98** on silica gel surface gave **99a** without any diastereodifferentiation, confirming the important role of confinement played by the zeolite supercages.

Similarly, only negligible diastereoselectivities were observed upon photoirradiation of 2,2-dimethyl-(2*H*)-naphthalenone-4-carboxylates **100** either in hexane solution or on silica gel surface. In contrary, **101b** and **101c** were given in 57% and 47% de, respectively, upon photoirradiation of **100** in supercage of NaY zeolite.

The oxa-di-π-methane rearrangement of 2,4-cyclohexadienones-4-carboxylate and -carboxamide **102** in trifluoroethanol solution afforded **103** in a low de (<5%). However, **103b** and **103e** were formed in up to 59% and 73% de, respectively, when the photoreaction was carried out within NaY zeolite.[116] Interestingly, the diastereoselectivity was switched to give the epimeric product by changing the zeolite host from LiY or NaY to KY, RbY or CsY, suggesting that the stereochemical fate is highly sensitive to the size of supercage and is tunable by the cation species in zeolites.

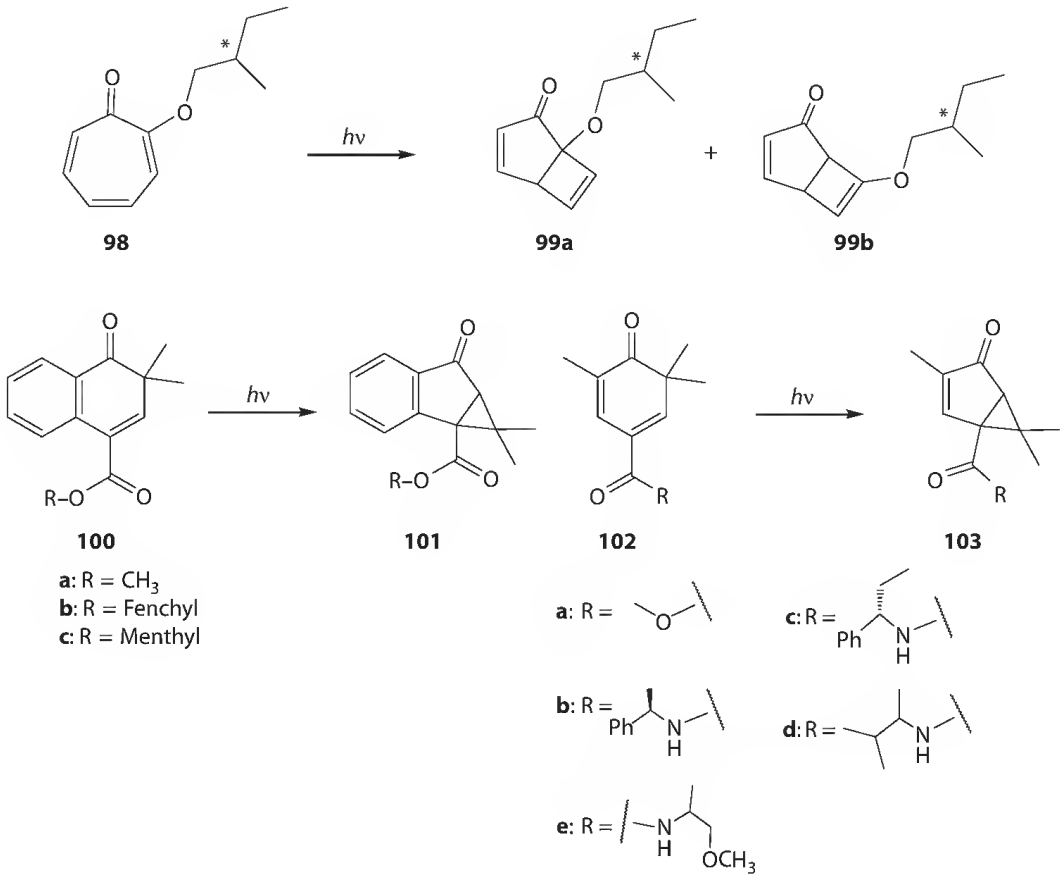

Diastereodifferentiating photoisomerization of chiral *cis*-2,3-diphenyl-1-benzoylcyclopropane derivatives **104** was examined in the supercage of zeolite. Photoisomerization of **104** is implemented through the C1–C2 or C1–C3 cleavage, the bond rotation about C2–C3, and the ring closure to diastereomeric *trans*-isomers.[117,118] The photolysis of **104** in zeolite supercage led to much higher diastereoselectivity than that in organic solvent, and the *meta*- rather than *para*-substituted substrates consistently afforded higher de's of up to 71% for **104g**.[119–121] Irradiation period and temperature were found to have only minor effects on the diastereoselectivity, probably due to the rigidity of zeolite supercage.

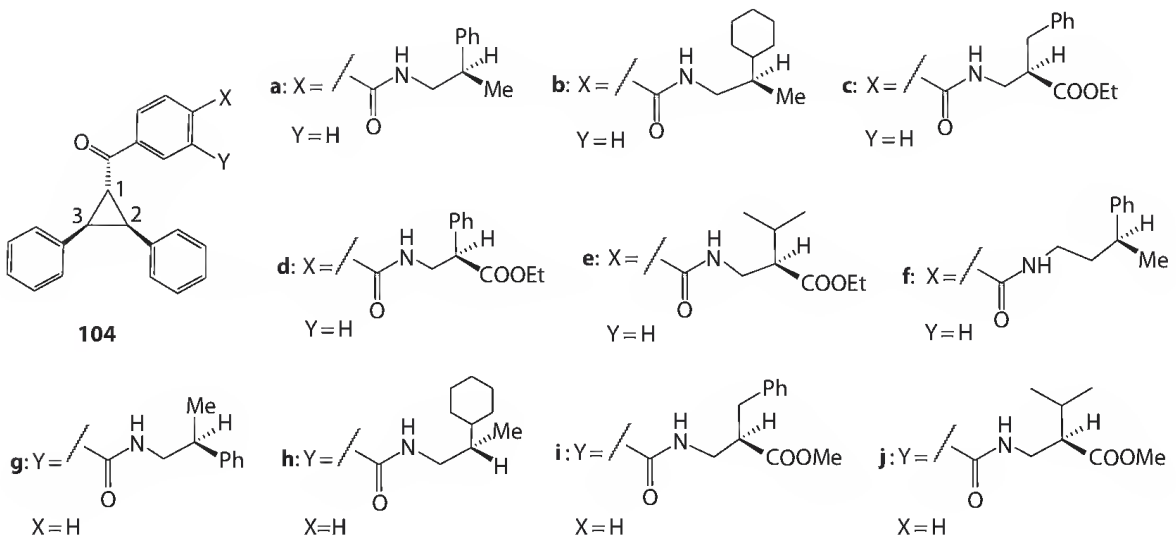

Direct and triplet-sensitized diastereodifferentiating photoisomerizations of chiral 2β,3β-diphenylcyclopropane-1α-carboxylates **105** was investigated in LiY, NaY, KY, RbY, and CsY zeolites.[117] Direct irradiation of **105a** adsorbed in zeolite gave **106a** and **107a** in up to 55% de. Photolysis of **105c** in homogeneous solution gave a low de of <5%, while the epimeric product was obtained in 50% de upon irradiation in zeolite. The stereochemical outcomes upon direct irradiation considerably differed from those from the triplet sensitization by 4-methoxyacetophenone,[122] and the chiral auxiliaries possessing an aromatic or carbonyl substituent performed better than those with alkyl substituents.

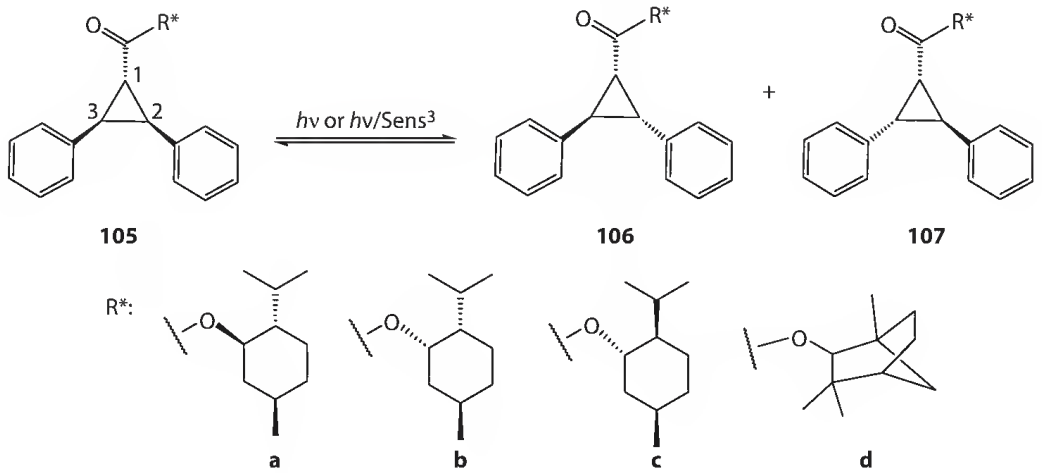

Zeolite supercages are not inherently chiral and should be modified with chiral inductors for the use in enantiodifferentiating photoreactions. This is made possible by adsorbing chiral organic molecules into zeolite supercage or by replacing the inorganic cations in supercage with chiral organic ammonium ions. Indeed, several thermochemical asymmetric reactions have been carried out in chirally modified zeolite supercage prepared by using these methods.[123–127]

The enantio- and diastereodifferentiating photoisomerization of diphenylcyclopropane derivatives in chirally modified zeolites were comprehensively studied in recent years.[128–132] Upon direct excitation or triplet sensitization, the *cis*-to-*trans* photoisomerization of **108a** did not occur in the supercage of MY zeolite, probably due to the strong cation-π interaction that stabilizes the sandwich-type conformation of *cis*-diphenylcyclopropane. In contrast, the cations in supercage prefer to coordinate to the amide or

ester moiety of **108b–f,** and hence, the photoisomerization underwent smoothly to give the *trans*-isomer in a *cis:trans* ratio ranging from 12:88 to 58:42 at the photostationary state. By using ephedrine as a chiral inductor, photoisomerized product **109c** was obtained in 20% ee.[122,133]

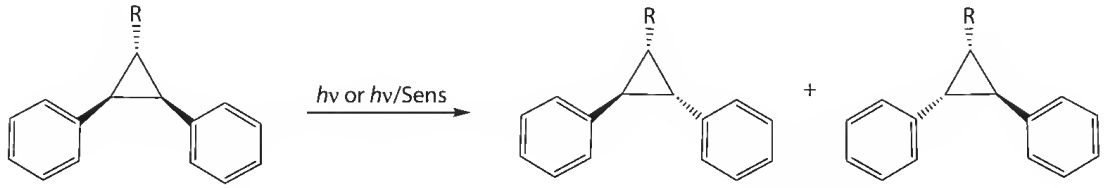

108 **109**

a: R = H **b**: R = COOH **c**: R = $CONHCH_2CH_2CH_2CH_3$ **d**: R = $CONHCH_2Ph$
e: R = $COOCH_3$ **f**: R = $COOCH_2CH_3$

The enantiodifferentiating photocyclizations of tropolone derivatives **110** and pyridone derivatives **112** were performed in zeolites modified with chiral inductor such as ephedrine, norephedrine, and pseudoephedrine.[134–141] The ee's of up to 69% were obtained for chiral photoproduct **111c** in the photocyclization of tropolone **110c** using ephedrine-modified zeolite.[140] Similarly, the enantiodifferentiating photocyclization of pyridone derivative **112e** using norephedrine-modified KY zeolite afforded cyclization product **113e** in 55% ee, demonstrating that the chiral organic compounds absorbed in the cavity of supercage can efficiently effect the chirality induction of the photosubstrate located nearby.

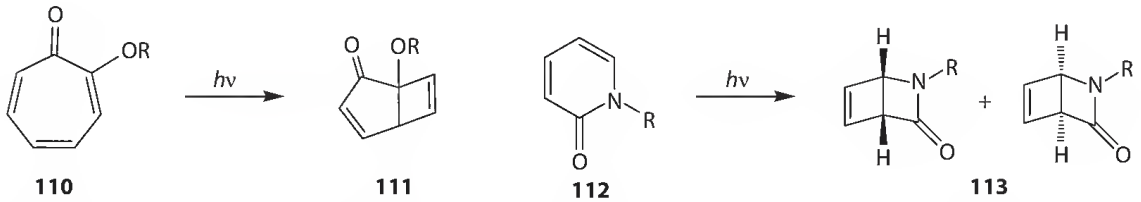

110 **111** **112** **113**

a: R = CH_3
b: R = CH_2CH_2Ph
c: R = CH_2COOCH_3
d: R = CH_2CH_3

e: R = $CH_2CH_2CH_3$
f: R = CH_2Ph
g: R = $CH_2CH_2CH_2Ph$

a: R = CH_3
b: R = CH_2CH_3
c: R = $CH_2CH_2CH_3$

d: R = CH_2Ph
e: R = CH_2CH_2Ph
f: R = $CH_2CH_2CH_2Ph$

Turro et al. investigated the photolysis of racemic benzoin methyl ether **114** immobilized in chirally modified zeolites. The geminate radical pair derived from the Norrish type I (α–cleavage) reaction of **114** was shown to recombine with enantiodifferentiation in the chiral cavity, regenerating enantiomerically enriched starting material **114**. Upon photolysis in solution, **115a** and **115b** were formed as major product in 23% and 70% yield, respectively. However, **115c** became the major product (79% yield), when the photoreaction was performed in zeolite. Photolysis of racemic **114** in the NaY zeolite modified with diethyl tartrate gave **114** in 9.2% ee. [142]

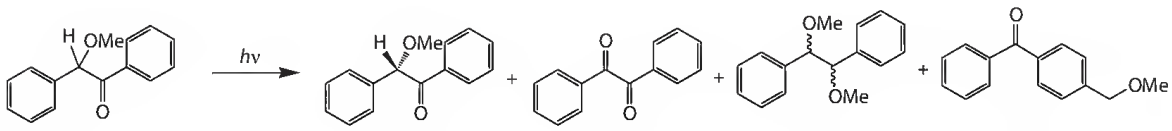

114 **114** **115a** **115b** **115c**

Di-π-methane rearrangement of benzonorbornadiene **116** is photochemically silent upon direct irradiation, but **117** is produced smoothly upon triplet sensitization.[143,144] Photolysis of **116** in TlY zeolite, which is known to accelerate the intersystem crossing of adsorbed compound due to the heavy atom effect, afforded **117** efficiently.[145] By using (+)-ephedrine hydrochloride as a chiral inductor, the photolysis of **116** within the chirally modified TlY zeolite provided **117** in 14% ee.

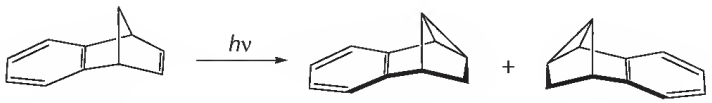

116 **117**

Most of the photoreactions in chirally modified zeolites were done in the solid state and inevitably necessitate a stoichiometric, or even more, amount of chiral inductor. Inoue et al. tried to enhance the chirogen efficiency by using a substrate that is not adsorbed in zeolite and a catalytic amount of chiral sensitizer immobilized in zeolite. They comparatively studied the enantiodifferentiating photoisomerization of **67Z** sensitized by chiral sensitizer dissolved in homogeneous solution[93,96] and the same photoisomerization mediated by chiral sensitizer-immobilized NaY zeolite performed in hexane suspension.[146] In homogenous solution, optically active 1-methylheptyl benzoate sensitizer afforded **68E** as a racemic mixture, while a modest ee of 4.5% was given in the photosensitization with NaY zeolite modified by methylheptyl benzoate.

Y-type zeolites were employed as confining media for the photooxygenation of chiral enecarbamates **43**, which is sensitive to the configuration around the double bond. In solution, the (*E*)-isomers consistently gave higher stereoselectivities than the corresponding (*Z*)-isomers. Moreover, the photoirradiation of chiral enecarbamates in zeolite in the absence of a $^1O_2$-generating sensitizer led to very low conversions (<3%) with poor mass balances (<35%).[61] Methylene blue was immobilized in zeolite as a $^1O_2$-generating sensitizer for photooxidizing the enecarbamate.[64] Thus, photooxygenation of (*Z*)-(3*R*/*S*,4*S*)-**43c** in methylene blue-bearing NaY zeolite gave (*S*)-MDB in good yield and up to 80% ee, and (*Z*)-(3*R*/*S*,4*R*)-**43c** gave the same product in 71% ee, while (*E*)-(3*R*/*S*,4*R*)-**43c** afforded (*R*)-MDB in 63% ee in NaY zeolite modified with methylene blue. These results indicate that the stereoselectivity of the singlet oxygenation to give MDB relies on the configuration at the C4 position of the oxazolidinone moiety, and the zeolite provides a path favorable for the attack of $^1O_2$ to the C=C double bond of the substrate.

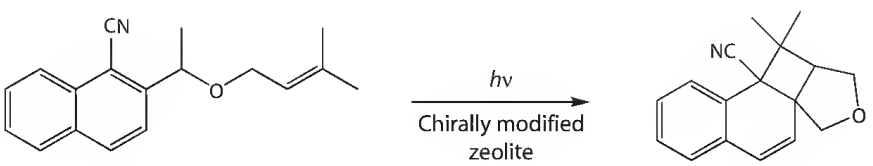

118 **119**

Chiral inductors:

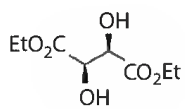

120a

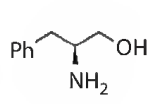

120b

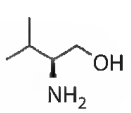

120c

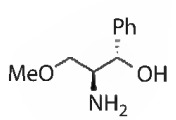

120d

120e

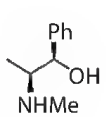

120f

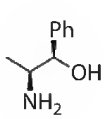

120g

The intramolecular [2 + 2] photocycloaddition of 1-cyano-2-(5-methyl-2-oxa-4-hexenyl)naphthalene **118** was carried out in the supercages of chirally modified NaY zeolite.[147] Chiral inductors **120a–g** and substrate **118** were completely adsorbed by zeolite after stirring the suspension for 3 h in hexane, while only the adsorbed substrate was readily extracted from the zeolite by treating with acetonitrile. Irradiation of a cyclohexane slurry of dry NaY zeolite containing **118** and l-(+)-diethyl tartrate **120a** gave cycloadduct **119** in 10% ee, while other chiral inductors provided the same product in smaller ee's (<2%). The enantioselectivity was highly sensitive to the composition of zeolite, and the ee's of up to 15% were observed when NaY zeolites modified by enantiomerically pure amino alcohols **120b** and **120c** were used as chiral host.

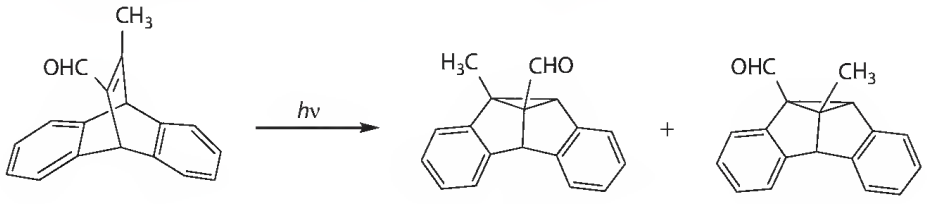

121 **122a** **122b**

(1*R*,2*S*)-*trans*-1,2-Diaminocyclohexane was covalently introduced to the surface of mesoporous silica MCM-41 to give a chiral mesoporous organosilica. The photoinduced di-π-methane rearrangement of 11-formyl-12-methyldibenzobarrelene **121** performed in these chiral mesoporous materials led to the formation of **122a** in 24% ee at a conversion of 11%.[148]

Inoue et al. recently investigated the photocyclodimerization of 2-anthracenecarboxylic acid (AC) in γ-CD-modified mesoporous silica.[149] The mesostructured silica was prepared by co-condensing silica-modified γ-CD with triethoxysilane tethered to triblock polymer $EO_{20}PO_{70}EO_{20}$. The γ-CD-modified mesoporous silica thus prepared was shown to have a 2D-hexagonal structure with an average pore size of 3.4 nm, a surface area of 287.6 m^2/g, and a total pore volume of 0.201 cm^3/g. In aqueous solution, AC was adsorbed or complexed by the CD-modified mesoporous silica and gave the cyclodimers **59a–d** upon photoirradiation. In contrast to the results obtained upon photoirradiation of free AC in aqueous solution, where the HT dimers **59a** and **59b** were formed in >80% combined yield, the photocyclodimerization of AC in the mesoporous silica gave HH dimers **59c** and **59d** as major products in 73% combined yield. The HH preference is possibly due to the hydrogen-bonding interaction between AC's carboxylate and the walls of mesoporous silica as well as the modified microenvironment around γ-CD grafted on the walls of mesoporous silica. Photodimer **59c** was given in up to 45% yield in 24% ee by performing the photocyclodimerization of AC in γ-CD modified the mesoporous silica. On the other hand, much lower conversion of AC was obtained for the γ-CD modified mesoporous silica prepared by the postsynthesis method.

6.4.2 Cyclodextrin-Mediated Photochirogenesis

The enantiodifferentiating *Z-E* photoisomerization of (*Z*)-cyclooctene **67Z** included and sensitized by sensitizer-attached β-CDs represents one of the pioneering works in supramolecular photochirogenesis.[150–156] Direct photolysis of solid-state complex of native β-CD and **67Z** with vacuum UV at 185 nm afforded (*E*)-isomer **67E** in negligible ee, revealing that the cavity of native β-CD is not efficient in transferring the supramolecular chirality to molecular chirality through a photochemical process.[82] However, it was demonstrated that appropriate modification of β-CD with a chromophore can drastically improve the enantioselectivity of photoisomerization of **67Z** sensitized by the chromophore attached to CD. The sensitizer moiety is self-included and shielded in the CD cavity and therefore the energy transfer from the sensitizer to unbound **67Z** located outside the cavity is prohibited. Only **67Z** that is included within the CD cavity can efficiently form an exciplex with the sensitizer to undergo isomerization. Indeed, the first attempt of this concept with **123b** as supramolecular chiral sensitizer affords **67E** in 15% ee, which is remarkably higher than that obtained upon direct irradiation of **67Z**•β-CD complex.[152] Later, the ee of **67E** was enhanced up to 24% ee by using 6-*O*-(methylphthaloyl)-β-CD **123c** as a chiral sensitizing host.[157]

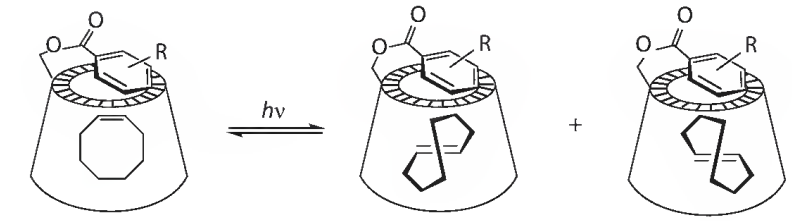

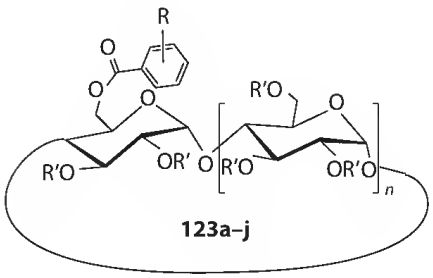

123a: R = H, *n* = 5, R′ = H
123b: R = H, *n* = 6, R′ = H
123c: R = *o*-CO_2Me, *n* = 6, R′ = H
123d: R = *m*-CO_2Me, *n* = 6, R′ = H
123e: R = *p*-CO_2Me, *n* = 6, R′ = H
123f: R = *o*-OMe, *n* = 6, R′ = H
123g: R = *m*-OMe, *n* = 6, R′ = H
123h: R = *p*-OMe, *n* = 6, R′ = H
123i: R = H, *n* = 6, R′ = Me
123j: R = H, *n* = 7, R′ = Me

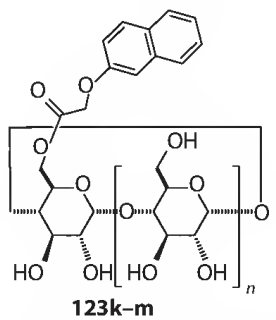

123k: *n* = 5 (α-CD)
123l: *n* = 6 (β-CD)
123m: *n* = 7 (γ-CD)

The photosensitizer structure appears to critically influence the stereochemical outcomes of the enantiodifferentiating photoisomerization. Thus, the photoisomerization of **67Z** sensitized by 6-*O*-(*m*-methoxybenzoyl)-β-CD **123g** afforded **67E** in 46% ee, which is the highest enantioselectivity ever reported with CD-based sensitizers.[153] The *ortho*- and *para*-analogues **123f** and **123h** gave much lower ee's of less than 15% under the identical reaction conditions.[154]

It was found that the entropy factor does not play a significant role in photoisomerization of **67Z** with **123a–h** because of the rigid β-CD framework, which is in contrast to the significant entropy contribution observed in conventional photosensitization.[85,96] However, when the photoisomerization of **67Z** is sensitized by *O*-permethylated 6-*O*-benzoyl-β-CD **67i**, which has a more flexible skeleton than nonmethylated CD derivatives due to the diminished hydrogen-bonding network at the secondary rim, the entropy-related factors become crucial as the enantioselectivity is strongly temperature-dependent.

Despite the apparent analogy to cyclooctene, (*Z,Z*)-1,3-cyclooctadiene **69ZZ** is much more difficult to photoisomerize to planar chiral (*E,Z*)-isomer **70EZ** in good ee. Thus, the enantiodifferentiating photoisomerization of **70ZZ** sensitized by naphthalene-substituted CDs **123k-m**[158] gave **70EZ** in modest enantioselectivities of up to 4.6% ee. Although only a faint effect of the entropy-related factors was observed with α- and β-CD-based sensitizer **123k** and **123l**, the entropy factor is much more effective for the photoisomerization mediated by γ-CD-based sensitizer **123m**, to which the more flexible framework of γ-CD is most likely attributed.

The intramolecular meta photocycloaddition of olefin to benzene ring is a highly effective approach for creating complex polycyclic molecules.[159,160] Solid-state complexes of 4-phenoxy-1-butene derivatives **124** with β-CD, prepared by mixing the two components in hot aqueous solution, have host:guest stoichiometries of 2:1 for **124a** and **124c–e** but 1:1 for the others.[161] Photolysis of the CD complexes of **124a**, **124b**, and **124e** gave only negligible enantioselectivities, while the rest of the complexes afforded modest enantioselectivities, with the highest ee of 17% for **125c**. It is deduced that one of the enantiotopic faces of the included benzene ring is better shielded by the CD walls when **124** is included in the β-CD cavity, favoring the attack of the vinyl from the opposite side.

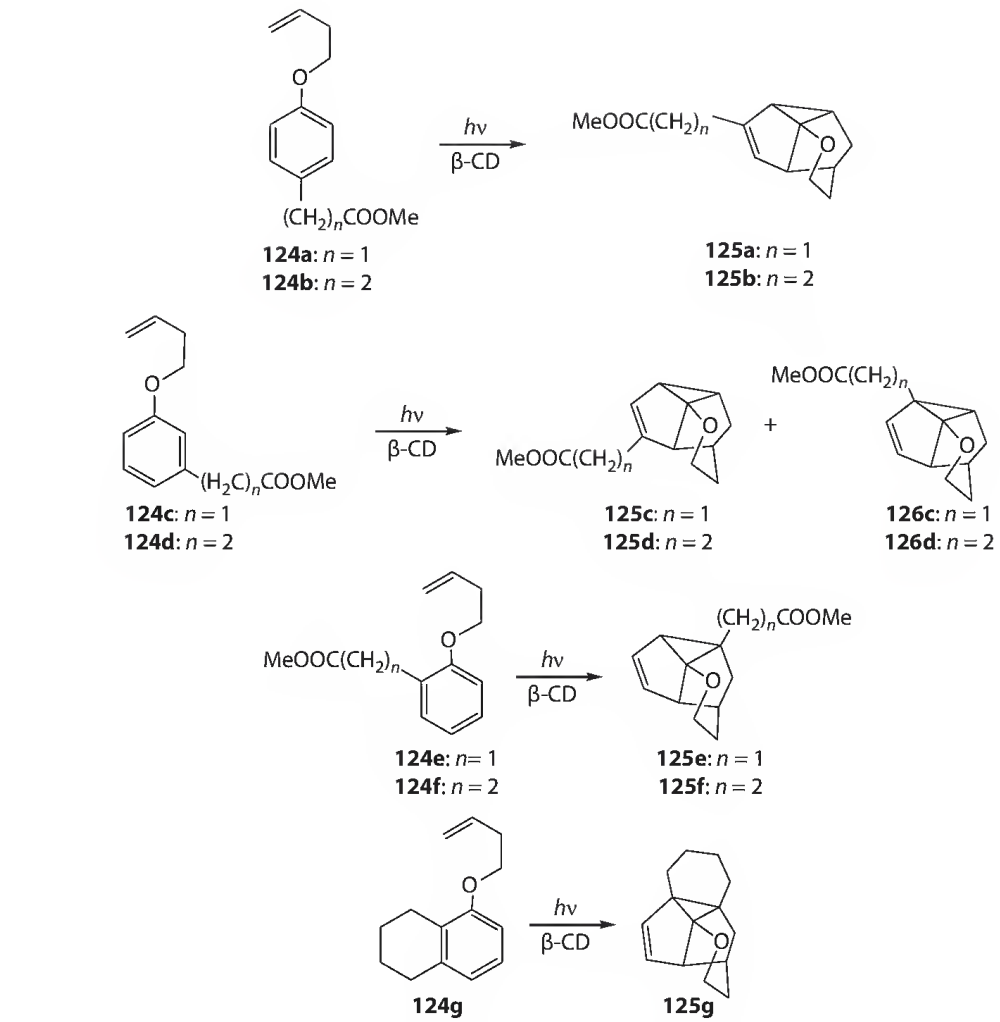

Photolysis of chiral aryl ester **127** leads to the concerted elimination of carbon dioxide through a spirolactonic transition state to afford decarboxylation product **128**.[162–166] The photodecarboxylation of enantiopure **127** in solution gave **128** with complete stereoretention (>99% ee). To investigate the relatively rigid and well-organized environment of CD on the concerted process, a racemic mixture of **127** was photolyzed in the presence of β-CD in aqueous solution. Up to 14.1% ee biasing (*R*)-enantiomer was given for **128**, indicating that one of enantiomeric **127** reacts faster than its antipodal isomer in the cavity of β-CD.

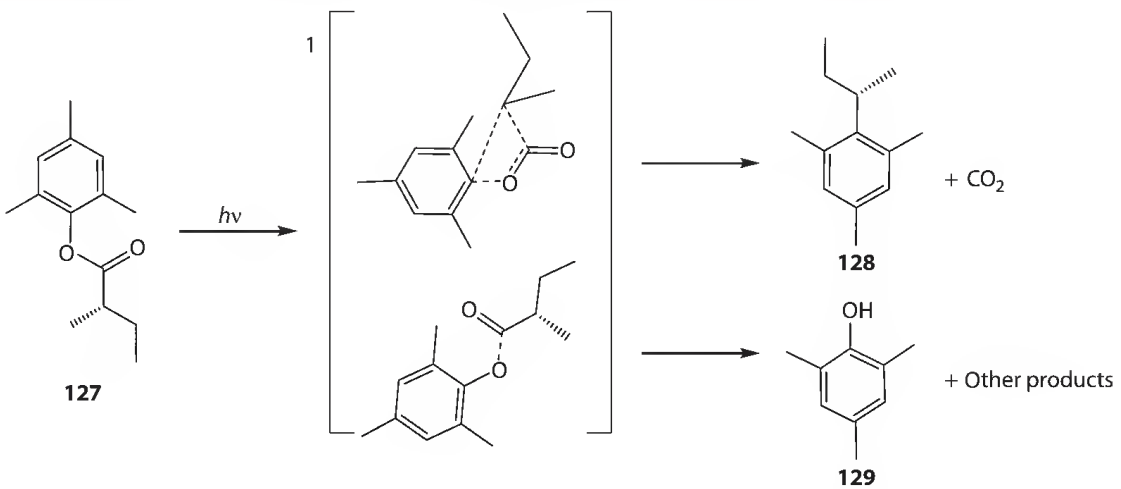

The [4 + 4] photocyclodimerization of AC with native γ-CD was firstly studied by Tamaki et al. in 1984.[167,168] They demonstrated that the photodimerization quantum yield is significantly improved from 0.05 to 0.4 upon addition of γ-CD to the reaction mixture and the chemical yields of HT dimers **59a,b** are considerably increased at the expense of HH dimers **59c,d**. In contrast, β-CD forms a 2:2 complex with AC, which turned out to give exclusively achiral HT dimer **59a**. Inoue et al. reinvestigated the photoreaction in detail from the chirogenic point of view by using chiral HPLC for separating all of the six stereoisomers **59a–d**.[74] The binding behavior of AC with γ-CD was evaluated by spectral titration to give the stepwise association constants in aqueous solution at 25°C: K_1 = 161 M^{-1} and K_2 = 38,500 M^{-1}. The much larger K_2 value was ascribed to the intimate contacts of two ACs with the CD walls in the 1:2 complex. Photocyclodimerization of AC in the presence of native γ-CD yielded HT dimer **59b** in up to 41% ee at 0°C, but HH dimer **59c** was given in <5% ee.

In order to improve the stereoselectivity of AC photocyclodimerization, a series of γ-CD derivatives have recently been designed and synthesized. Secondary rim-modified γ-CDs **130a–d** gave cyclodimer **59b** in ee's comparable to that obtained with native γ-CD, while 3^A-amino-3^A-deoxy-*altro*-γ-CD **130e** greatly enhanced the enantioselectivity. Such contrasting behavior was interpreted in terms of the electrostatic interaction between the cationic ammonium and anionic carboxylate as well as the distorted cavity due to the presence of the altrose unit.[169] The stereochemical outcomes of the supramolecular photocyclodimerization of AC with native and modified γ-CDs are sensitive to temperature and pressure. Hydrostatic pressure is rarely applied to the study of supramolecular systems but was found quite effective in controlling the supramolecular complexation and subsequent photochirogenic processes. In supramolecular photochirogenesis conducted in aqueous solutions, high pressure plays the primary role to discriminate the volume differences of two or more competing complexes, intermediates, and/or transition states and also the secondary role to reduce the freezing point of water down to –25°C at 200 MPa. Indeed, the ee of cyclodimer **59b** was enhanced up to 71%, when the photocyclodimerization of AC complexed with **130e** was carried out in aqueous solution at –21°C under a pressure of 210 MPa.

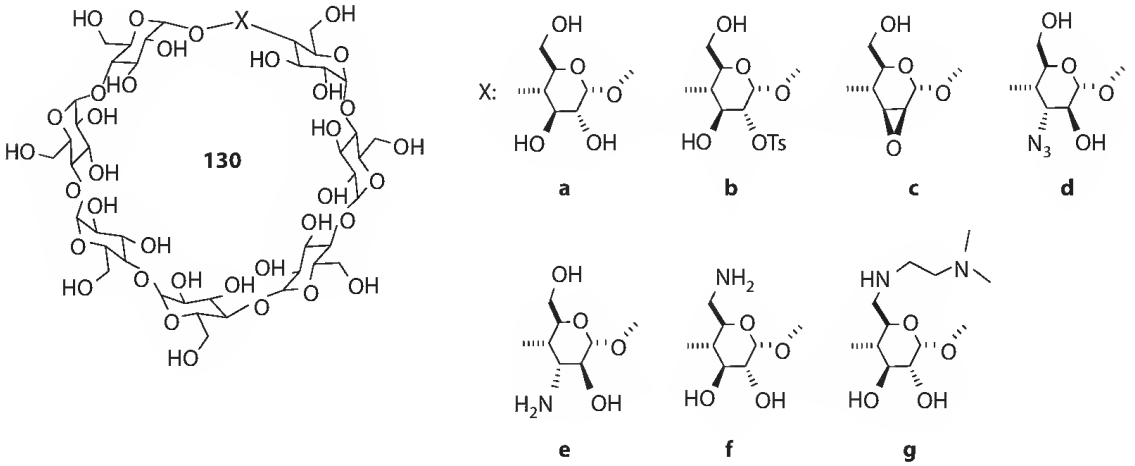

γ-CD derivatives **130g**, **131a–d**, and **132a–d** with two cationic groups on the primary rim were designed and synthesized for obtaining the HH cyclodimers as major products in the photocyclodimerization of AC.[170,171] The two positively charged groups in the host were expected to attract two AC molecules to preferentially form the HH-oriented 1:2 complexes. Indeed, the yields of HH dimers were significantly improved by the use of the dicationic CDs, and the *anti/syn* ratio of HH dimers was gradually increased by increasing the interamino distance, exhibiting a good structure–function relationship in the supramolecular system. Up to 35% ee was given for **59c** by using host **132b** and optimizing the reaction temperature and solvent. On the other hand, the photocyclodimerization of

AC mediated by **130g** in aqueous methanol solution at a low temperature afforded **59c** of 41% ee in 42% yield, which is much higher than those obtained with **132a–d**, suggesting that two ammonium ions on a single flexible chain are more effective in manipulating the enantioselectivity. The yield and enantioselectivity of HH dimers were also significantly enhanced upon photolysis of a solid-state complex of AC with di-3,6-anhydro-γ-CDs **133a–d** with distorted cavities.[172]

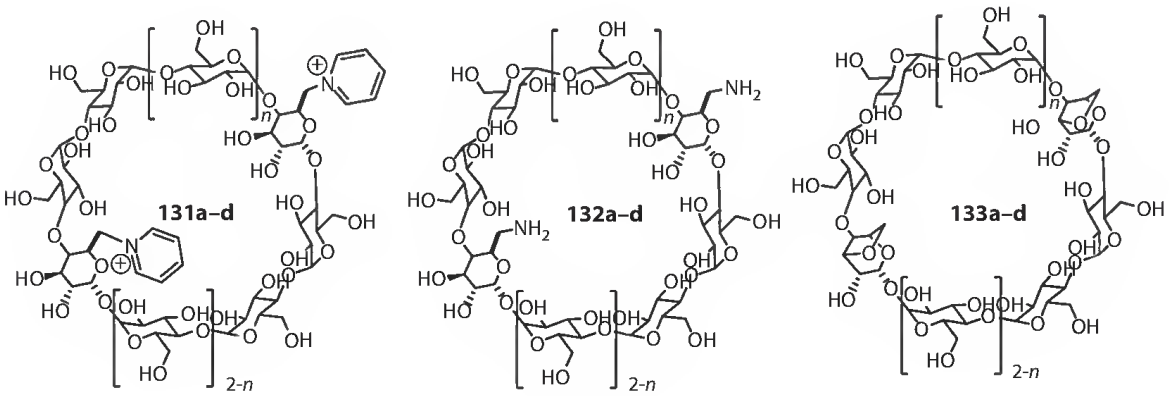

a: $n=1$; **b**: $n=2$; **c**: $n=3$; **d**: $n=4$

As the host structure was shown to greatly affect the stereochemical outcomes of photoreactions, a series of γ-CDs modified with various bridging substituents were synthesized to explore the effect of the aromatic cap on the photocyclodimerization of AC. Ditosylated γ-CD **134** gave the photocyclodimers in such yields and ee's that are comparable to those obtained with native γ-CD, indicating that the flexible capping does not appreciably alter the chiral environment of native γ-CD. Although diphenyl ether-capped γ-CD **136** and **137** gave **59b** in ee's lower than that obtained with native γ-CD, biphenyl-capped **135** afforded antipodal **59b** in a much enhanced ee of −56%. The seemingly tiny structural difference between **135** and **136** (by merely one oxygen) led to dramatic changes in chiral sense and ee of the photoproduct, unequivocally revealing the crucial role played by the rigid capping.[173,174] γ-CDs **138** and **139** with a *p*-cresolbisbenzimidazole cap suffered pH-dependent conformational changes of the capping moiety with accompanying inversion of the enantioselectivity for HH dimer **59c** by changing the solution pH.[175]

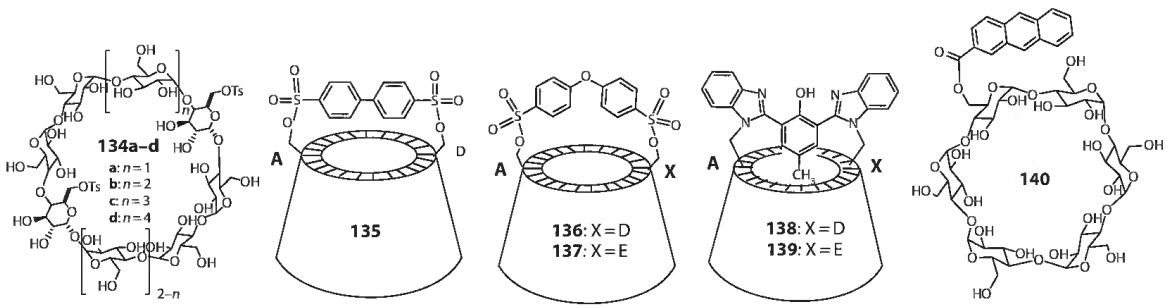

It was examined how and to what extent a bulky component located outside the cavity can affect the photoreaction occurring inside the cavity by using the supramolecular photocyclodimerization of α-CD-tethered AC **140** mediated by γ-CD and cucurbit[8]uril (CB[8]). Photolysis of **140** in water gave a mixture of α-CD-tethered AC dimers corresponding to **59a–d**, in which the HT dimers were favored. Photocyclodimerization of **140** included in native γ-CD resulted in γ-CD-wheeled rotaxane **141** in 68% yield at 210 MPa and −20°C, which was hydrolyzed to give HT dimer **59b** in 91% ee.[176] Strikingly, when

achiral CB[8] was used as a host, the major photoproduct was completely switched from HT to HH dimers and **59c,d** were obtained in 99% combined yield. It is thus demonstrated that a bulky group located outside the binding site can critically influence the reaction occurring inside.

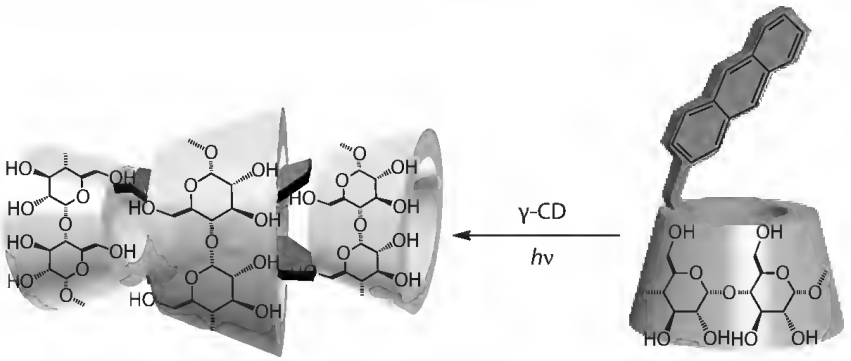

141 **140**

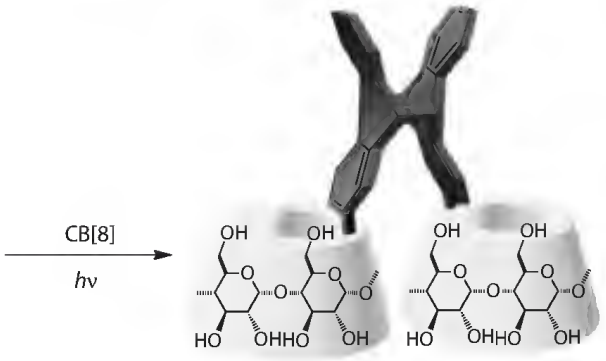

142

Up to now, photosensitization is the only method to realize "catalytic" photochirogenesis. However, Inoue et al. have recently established a novel strategy for conducting catalytic photochirogenesis mediated by nonsensitizing metallosupramolecular hosts **143**–**145** that are coordinated with Cu^{2+}. Thus, in the presence of 0.1 equivalent of γ-CD-Cu^{2+} complex, photocyclodimerization of AC in aqueous methanol solution at −50°C gave **59c** in 52% yield and up to 70% ee, which are the highest enantioselectivity ever reported for CD-mediated photochirogenesis.

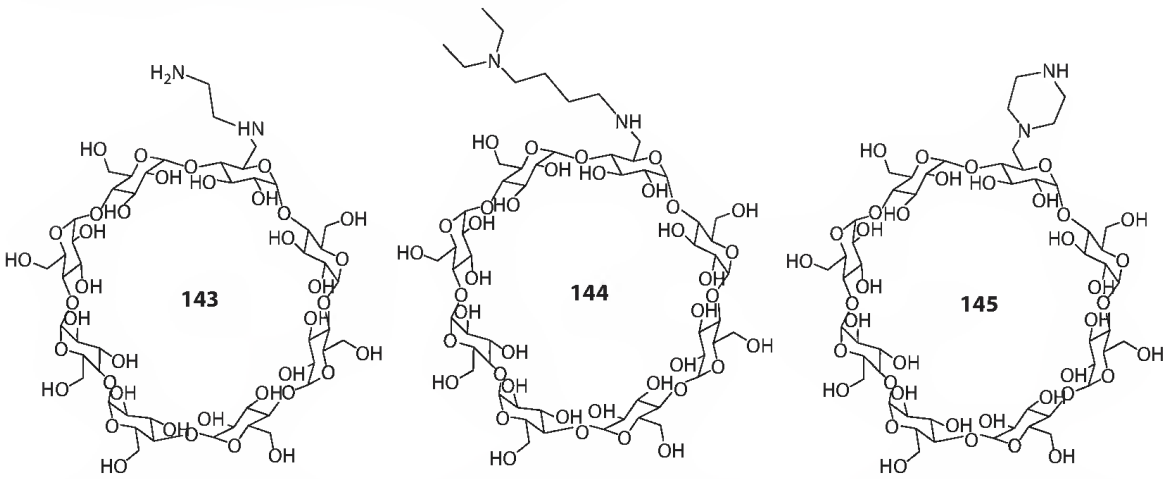

143 **144** **145**

6-(5-Cyanonaphthyl-1-carboamido)-6-deoxy-β-CD **146** was employed as an electron-accepting sensitizer for effecting the anti-Markovnikov photoaddition of methanol to 1,1-diphenylpropene **79a**.[177,178]

The appended naphthalene component in **146** was demonstrated to perch laterally on the CD rim and shallowly included in the cavity in aqueous solution. The naphthalene fluorescence of **146** was efficiently quenched by **79a** in aqueous solution of low methanol contents but less efficiently in more hydrophobic solvents. Methanol adduct **80a** and water adduct **147** were competitively produced upon photosensitization of **79a** by **146** in aqueous solutions of different methanol contents, where **80a** is favored by a factor of 2.5 as a result of higher nucleophilicity of methanol. The enantioselectivity is generally low in solution of high methanol content, but is significantly improved by increasing water content to give 18% ee for **147** and 13% ee for **80a** in 10% methanol solution at −10°C. Being different from other supramolecular photochirogenesis with β-CD-based sensitizers, the enantioselectivity obtained with **146** was highly sensitive to the temperature change, and the ee value varied from −2.1% to 5.8% by lowering the reaction temperature from 45°C to −40°C in a 1:1 water–methanol mixture. By applying high pressure and low temperature, the ee of water adduct **147** was enhanced to 24%–26%.

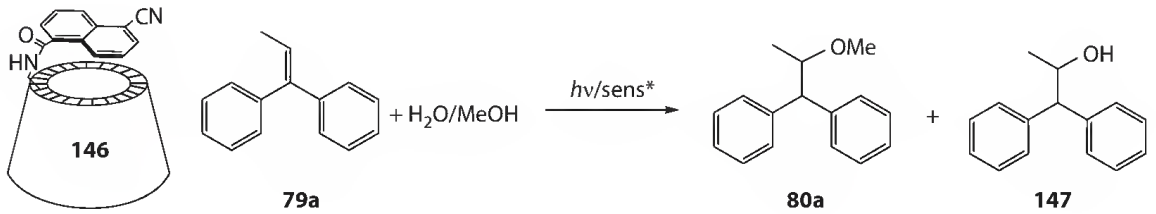

Wu et al. reported the enantiodifferentiating photocyclodimerization of methyl 3-methoxyl-2-naphthoate **148** mediated by native γ-CD.[179] The photocyclodimerization of **148**–**150** is not a concerted but a stepwise process, requiring two photons to give [4 + 4] cycloadduct **149** as an intermediate, which is converted to cubane-like cyclodimer **150** upon absorption of a second photon. Native γ-CD was shown to form 1:2 host–guest complex with **148** with a binding constant of $6.7 \times 10^6 M^{-2}$. The formation of the host–guest complex significantly improved the efficiency of the photocyclodimerization of **148**. Interestingly, the chirality delivery from γ-CD to the cube-like photodimer also occurs in a two-step fashion. Thus, the intermediate **149** was formed in only 39% ee, but the enantioselectivity of cube-like photodimer **150** was improved to 48% ee.

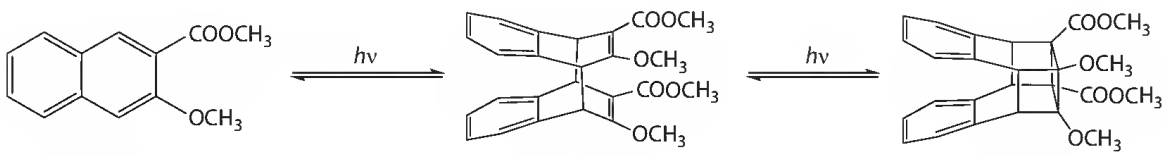

6.4.3 Photochirogenesis with Biomolecule

Biomolecules, such as protein and DNA, behave as naturally occurring chiral supramolecular hosts, possessing well-organized binding site(s) suitable for accommodating and orientating a variety of organic molecules in a stereospecific fashion. Photochemistry is environmentally benign and highly compatible with biomolecules, necessitating no harsh thermal activation or biohazardous heavy/transition metal catalyst. Thus, biomolecule-mediated photochirogenesis is normally carried out in aqueous solution under mild conditions. Nevertheless, the photosubstrate to be used in biosupramolecular photochirogenesis should be water-soluble at least to some extent.

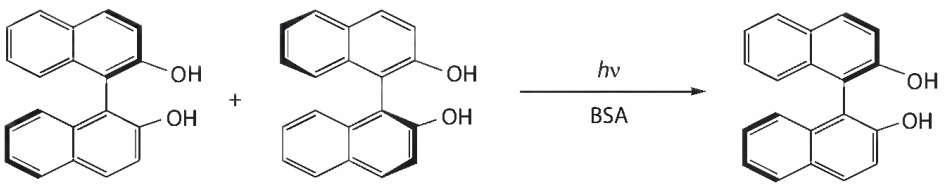

(*R*)-(+)-**151** (*S*)-(−)-**151** (*R*)-(+)-**151**

Serum albumin is the most frequently used protein in photochirogenesis study, partly due to their high affinity to various organic compounds and commercial availability. Zandomeneghi et al. reported the first photochemical kinetic resolution of racemic 1,1′-binaphthol **151** with bovine serum albumin (BSA). Since the enantiomers of **151** showed distinctly different affinities to BSA and the bound species absorbed light at longer wavelengths, it was possible to selectively photodecompose the preferentially bound enantiomer. By applying such a strategy, they obtained (*R*)-(+)-**151** in 99.5% ee at 77% conversion upon photolysis of racemic **151** in the presence of BSA.[180–182]

Inoue et al. investigated the enantiodifferentiating photoisomerization of cyclooctene **67Z** to **68E** sensitized by a series of nucleosides and nucleotides.[183] Photoisomerization of **67Z** sensitized by pyrimidine and purine nucleosides afforded **68E** in up to 5.2% ee at the photostationary state. By using calf thymus DNA (ctDNA) as chiral sensitizer, **68E** was yielded in −15.2% ee with an *E*/*Z* ratio of 0.008. The enantioselectivity was considerably reduced by carrying out the photoreaction at higher temperatures. Supramolecular interaction plays an important role in the enantiodifferentiating process, as indicated by the fact that the photoisomerization of **67Z** in 50% aqueous methanol, where ctDNA keeps its B-form but the supramolecular interaction between **67Z** and ctDNA is significantly reduced, gave **68E** in a negligible ee of −0.9%.

Inoue et al. have comprehensively studied the enantiodifferentiating photocyclodimerization of AC mediated by different proteins.[76,183–186] Bovine serum albumin (BSA) was revealed to have four binding sites that accommodate one, three, two, and three AC molecules in the order of binding affinity.[183,185] Somewhat unexpectedly, AC in the first unimolecular binding site gave dual fluorescence lifetimes of 4.8 and 2.1 ns, suggesting the existence of two binding modes that may differ in position and/or orientation. A much longer lifetime of 13.2 ns was obtained for ACs bound to the second site of BSA, and ACs bound to sites 3 and 4 showed a single lifetime of 15.8 ns, which is indistinguishable from that in bulk water. Nitromethane quenched the fluorescence of unbound AC, while ACs bound to sites 1 and 2 were nicely protected from the attack of nitromethane. Photocyclodimerization of AC in the presence of BSA dramatically switched the product distribution from HT for free AC to HH, affording *anti*-HH dimer **59c** in 40% yield. At the AC/BSA ratio of 3.6, *syn*-HT dimer **59b** was obtained in up to 38% ee in the presence of 18 mM nitromethane, while *anti*-HH dimer **59c** was given in up to 58% ee in the absence of nitromethane.[185]

Human serum albumin (HSA), differing from BSA by only 26 (out of *ca.* 600) amino acid residues, exhibited totally different complexation, photophysical and photochemical behaviors with AC.[187,188] Extensive spectroscopic studies on complexation behavior suggested that HSA possesses five different binding sites for AC. ACs complexed to the unimolecular binding sites 1 and 2 were unreactive due to the isolation from other ACs, but could be replaced by inhibitors, such as 4-iodobenzoate and warfarin, from which the exact positions of AC-binding sites 1 and 2 were pinpointed on the x-ray crystallographic structure. AC in site 3 was demonstrated to be moderately protected from the attack from species in bulk solution but still able to give chiral photoproducts with high ee.[186] In sharp contrast to the BSA case, the HT dimers were favored in the photocyclodimerization of AC in the presence of HSA. Significantly high ee's of 82% and 90% were obtained for **59b** and **59c**, respectively, upon irradiation of AC with HAS in aqueous buffer solution at 5°C.[183]

6.4.4 Photochirogenesis in Liquid Crystal

Ishida et al. have studied enantiodifferentiating photocyclodimerization of AC and 1-anthracenecarboxylic acid **152** by using liquid crystals as chiral organized media for photochirogenesis.[189] The salt formed by mixing equimolar amounts of amphiphilic amino alcohol **154** and AC afforded liquid crystal (LC) of two

smectic phases with a transition temperature at 65°C and an isotropic phase at >100°C. The AC-containing LC was photolyzed and the resulting mixture was analyzed after the treatment with trimethylsilyldiazomethane to give the corresponding esters. The photoreaction in the smectic phases afforded the HH dimers exclusively. In particular, **59c** was obtained in 72% yield and up to 78% ee upon irradiation of AC with **154** at 30°C. The very high preference for the HH photodimers was attributed to the alignment of ACs in the LC. The packing mode of the liquid crystalline matrix was deduced to significantly influence the *syn/anti* selectivity, since the **59d/59c** ratio changed greatly in the different smectic phases. High combined yield (>98%) of HH dimers **153c** and **153d** was obtained also in the photocyclodimerization of **152** in the smectic phase, but a poor ee value of <2% was observed for chiral *anti*-HH dimer **153c**.

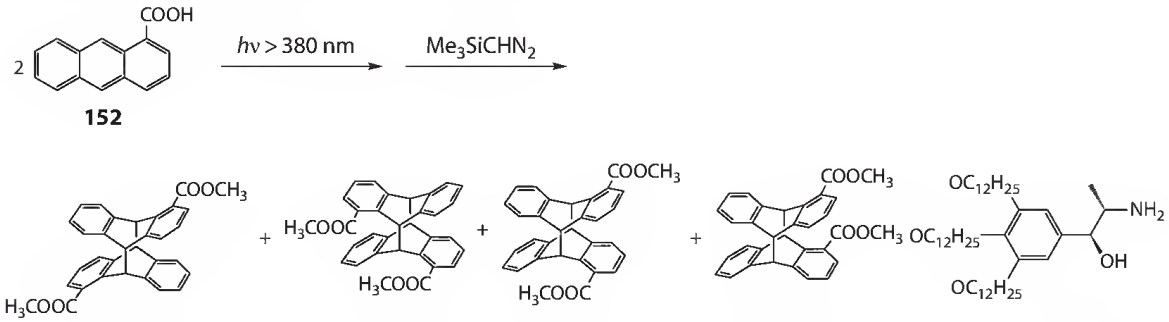

Tung et al. have examined the photocyclization of tropolone ethers **110a** in chiral inductor-modified lyotropic LCs prepared by dissolving chiral inductor in organic solvent following by the addition of sodium dodecyl sulfate (SDS) and water to the solution.[190] Lamellar LC phase was given by mixing pentanol, SDS, and water in a weight ratio of 1:1.5:1.5, while hexagonal LC was formed at a ratio of 1:6:9. Photoirradiation of **110a** in (1*R*,2*S*)-(−)- or (1*S*,2*R*)-(+)-norephedrine-doped hexagonal LC gave **106a** in up to 40% ee at −10°C, but a much lower enantioselectivity was given in lamellar LC phase. The good enantioselectivity was ascribed to the chelate complex of the substrate with the inductor formed through hydrogen-bonding interactions. Menthol, which has only one hydroxyl group and thus cannot form a chelate structure with the photosubstrate, gave only a poor enantioselectivity of <5% ee. The same lyotropic LCs were used for mediating the photochemical reduction and cleavage of cyclohexyl phenyl ketone **155** to chiral alcohol **156** *via* intermolecular hydrogen abstraction and to **157** *via* intramolecular hydrogen abstraction.[191] The ratio of **156/157** was sensitive to the chiral inductor doped. Thus, a **156**:**157** ratio of 1:3 was given in the hexagonal LC phase in the presence of proline, while a 12:1 ratio was given in the presence of prolinol. Modest ee's of up to 5% were found for **156** in the photoreaction in norephedrine-doped LC.

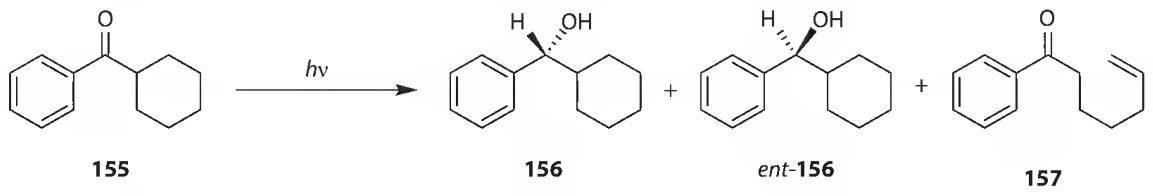

Inoue et al. recently investigated the enantiodifferentiating photoisomerization of cyclooctene **67E** sensitized by different LCs, including lyotropic LCs of poly(γ-benzyl-L-glutamate) and difluorobenzene derivatives and thermotropic cholesteryl oleyl LCs.[192] The as-employed LCs in general afforded only low enantioselectivities, but the lyotropic LCs of poly(γ-benzyl-L-glutamate) showed contrasting results in cholesteric and nematic mesophases. Photoisomerization in achiral difluorobenzene LC sensitized by doped chiral sensitizers suggests that the chiral spatial arrangement of the LC is not suitable to induce appreciable ee, but an optically active product can be photochemically derived from the molecular chirality of chiral sensitizer.

6.4.5 Photochirogenesis in Polymer

Ramamurthy et al. examined the effect of Nafion polymer on the diastereoselectivity of three different photoreactions, that is, the geometrical isomerization of *trans,trans*-2,3-diphenyl-cyclopropanecarboxylic acid derivatives **158a,b**, the electrocyclization of 2-oxo-1,2-dihydropyridine-1-acetic acid derivatives **159a,b**, and the oxa-di-π-methane rearrangement of dimethylnapthalenone derivative **100c**.[193,194] Nafion is a block copolymer of sulfonated tetrafluoroethylene, which forms a cluster of *ca.* 5 nm diameter with narrow channels (*ca.* 1 nm in diameter) interconnecting the clusters. In Nafion channels, the photochemical behavior of the aforementioned substrates was significantly altered from that observed in solution. Although these intramolecular photoreactions generally give a 1:1 mixture of diastereomeric products in organic solvent, the product's de varied from 5% to 21% upon photolysis in the nanoclusters of alkali ion-exchanged Nafion. Of particular interest, the product distribution was a critical function of the countercation of Nafion. Na^+ Nafion was found to give relatively high diastereoselectivity than Li^+ Nafion. The moderately enhanced asymmetric induction may be ascribed to the combined effects of the different conformation of the reactant molecule within the ionic clusters of Nafion due to the cation–substrate interaction and the confinement provided by the Nafion's interior walls.

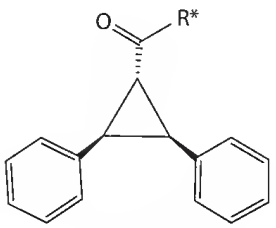

158a,b

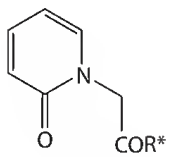

159a,b

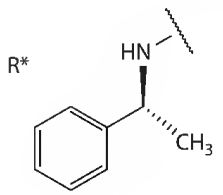

a

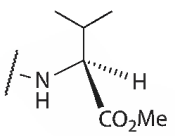

b

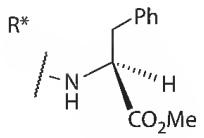

a

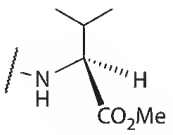

b

Inoue et al. investigated the photodecarboxylation of **127** in polyethylene (PE) films, including PE0, PE46, PE50, PE68, and PE74, as anticipated that the PE films can significantly influence both the ground-state conformations of photosubstrate and the diffusion rates of the intermediate(s) derived therefrom.[166] In all polymers examined, the near-perfect retention of stereochemistry (>98% ee) was observed for **128**. However, the ratio of **128/129** was highly dependent on the polymer employed. Two unstreched high-density PE films, PE68 and PE74, give **128** almost exclusively with a trace amount of **129**, suggesting that the cavities of these two PE films either force all of the **127** molecules to adopt *s-cis* conformations or prevent the escape of the radical pair to form **129**.

Polymer-supported catalysts have major advantages in product purification and catalyst reuse. Bach et al. used the chiral hydrogen-bonding agent immobilized on Wang resin and methoxypolyethylene glycol (MPEG) to examine the enantiodifferentiating intramolecular [2 + 2] photocycloaddition of **31**.[195] Photolysis of **31** in toluene in the presence of template polymer **160** gave **32** in an enantiomer ratio of 93:7 at conversions ranging from 24% to 31%, with **160** being recovered >90%. A much higher conversion of >96% was obtained with polymer **161** due to the good solubility of the polymer in toluene. Photoadduct **31** was given in an enantiomer ratio >95:5 and the chiral template was recovered >97%, when **161** was used as template.

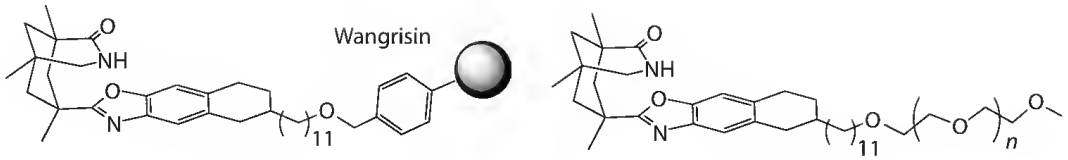

160 **161**

6.4.6 Photochirogenesis in Other Organized Media

Fujita et al. reported the asymmetric [2 + 2] photocycloaddition of **162** to **163** within the cage of metal-mediated self-assembly **165** and **166**. Photochemical and thermal reactions carried out in the confined M_6L_4 cages led to remarkably acceleration and significantly high selectivity.[196–198] In hosts **165** and **166**, chiral ligands are coordinated to the cage peripheries to provide the chiral environment. Up to 50% ee was obtained for **164b** in the photocycloaddition mediated by **165b**.[199] This study demonstrates that significantly chiral environment can be induced by the peripheral chiral auxiliaries located outside the cage.

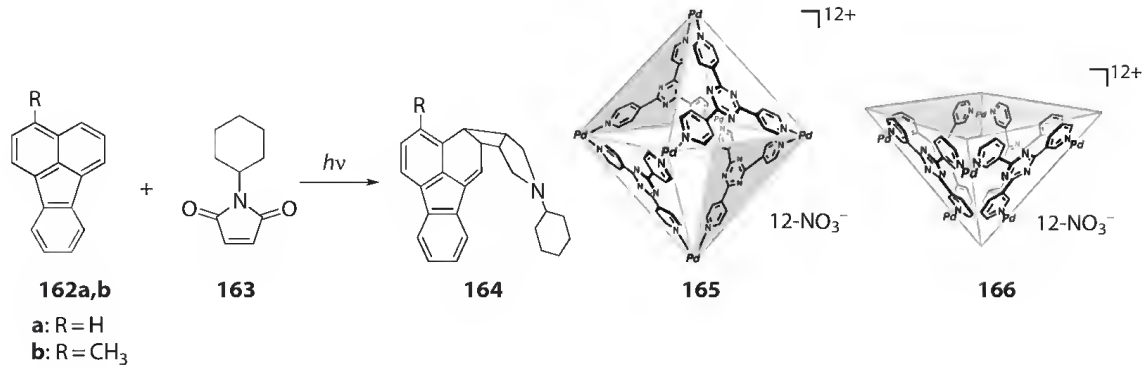

162a,b **163** **164** **165** **166**

a: R = H
b: R = CH_3

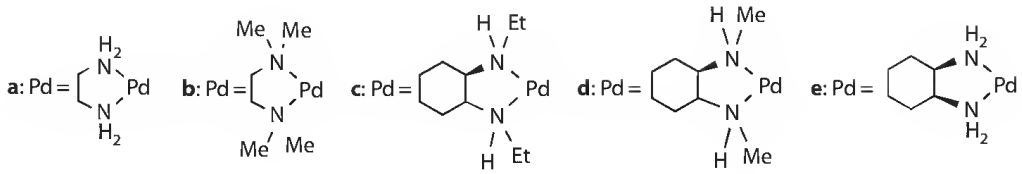

Inoue et al. reported the photoisomerization of **67Z** in homochiral metal–organic POST-1 nanopores, which was composed of tartaric acid derivative **167** and zinc nitrate.[156,200] Photoisomerization of **67Z** sensitized by POST-1 give **68E** with a modest ee of 5.4%, which is comparable to that observed in the photoisomerization of **67Z** sensitized by **168** (4.9% ee). The low enantioselectivity is possibly due to the large chiral channel of POST-1, which has a diameter much larger than the size of **67Z** and therefore is inefficient to constrain the movement of **67Z**.

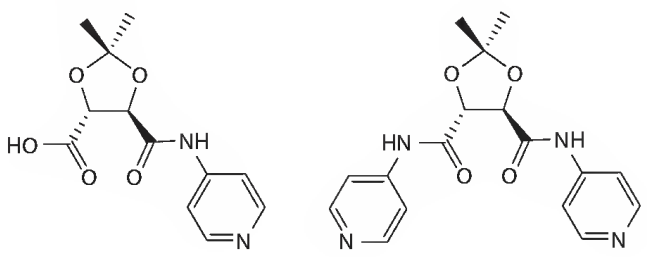

167 **168**

Diastereodifferentiating photoreactions of **170**, **171**, and **173** mediated by octa acid **169**, which forms capsule-like structure through self-aggregation, were investigated by Ramamurthy et al.[201,202] Photolysis of **170a–d** in acetonitrile gave cycloadducts in de less than 2%. However, in the presence of octa acid **169**, the diastereoselectivity was greatly improved. Up to 92% de was observed in the photoreaction of **170b**. Controlling free space and rotational freedom of photosubstrate in the capsule was deduced to be crucial in deciding the efficiency of chirality transfer. Moderately diastereodifferentiating photoreactions of **171** and **173** were observed when complexed to the synthetic cavitand **169**. Photoreaction of **171** and **173** in the presence of octa acid yielded **172** in 35% de at 298 K and **174** in 36% de at 178 K.

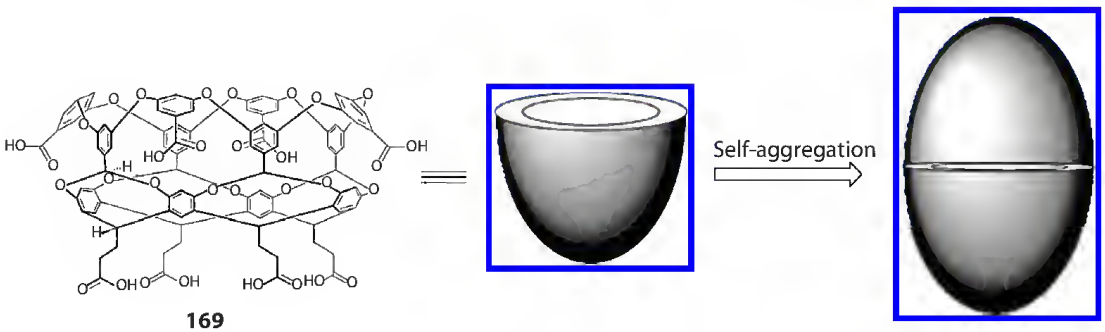

169

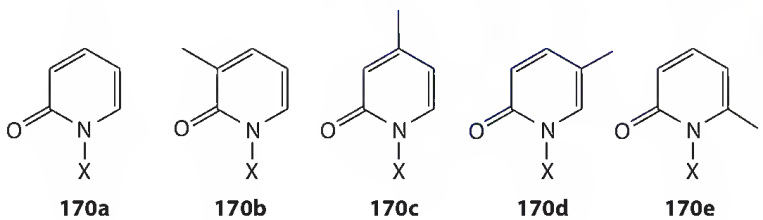

170a **170b** **170c** **170d** **170e**

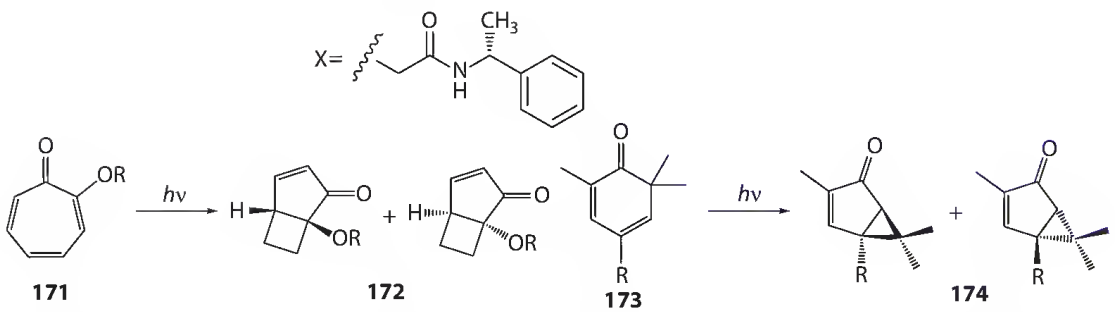

171 **172** **173** **174**

Shinkai et al. have studied the photocyclodimerization of AC in the gel formed by mixing D-alanine derivative **175** bearing 3,4,5-tris(*n*-dodecyloxy)benzoylamide moiety and nonpolar solvents such as cyclohexane.[203] HH photodimers **59c** and **59d** were exclusively formed by performing the photocyclodimerization of AC in the gel thus formed. However, only poor ee of less than 10% was observed for chiral HH dimer **59c**.

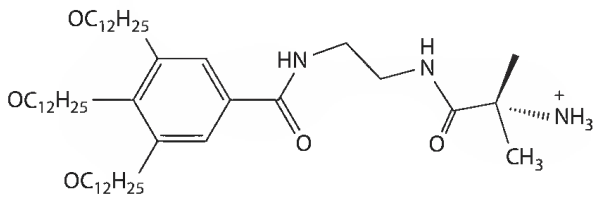

175

6.5 Photochirogenesis in Single Crystal

Photochirogenesis in single crystal may be divided into three categories in terms of the chiral source employed, that is, chiral auxiliary introduced to photosubstrate, co-crystallization of achiral photosubstrate with chiral inductor, and chiral crystal formed from achiral photosubstrate. In this section, we will concisely introduce only the recent progresses in the solid-state photochirogenesis in single crystals. For bimolecular photoreactions in crystalline state, readers are directed to Chapters 12 and 13 of Ref. [7].

The chiral auxiliary strategy is commonly employed in solution-phase photochirogenesis. At present, there are only several reports concerning the asymmetric induction by chiral auxiliary tethered to photosubstrate in the crystalline state. Ramamurthy et al. compared the Yang photocyclizations of a series of α-oxoamides **176** performed in solution phase and crystal.[204,205] Photoirradiation of α-oxoamide in solution led in general to poor chemo- and diastereoselectivities, affording a mixture of β-lactam and oxazolidinone with negligible de's for the former product. Interestingly, β-lactam was exclusively obtained upon photoirradiation of **176** in the crystalline state, and the de's as high as >80% were obtained for all of the α-oxoamide crystals at conversions <20%. In most cases, the de became lower upon prolonged irradiations, possibly due to the distortion or collapse of the original crystal structure caused by photoreaction. Significantly, the photolysis of crystalline **176a** quantitatively gave the corresponding β-lactam in 100% de even after 100% conversion.

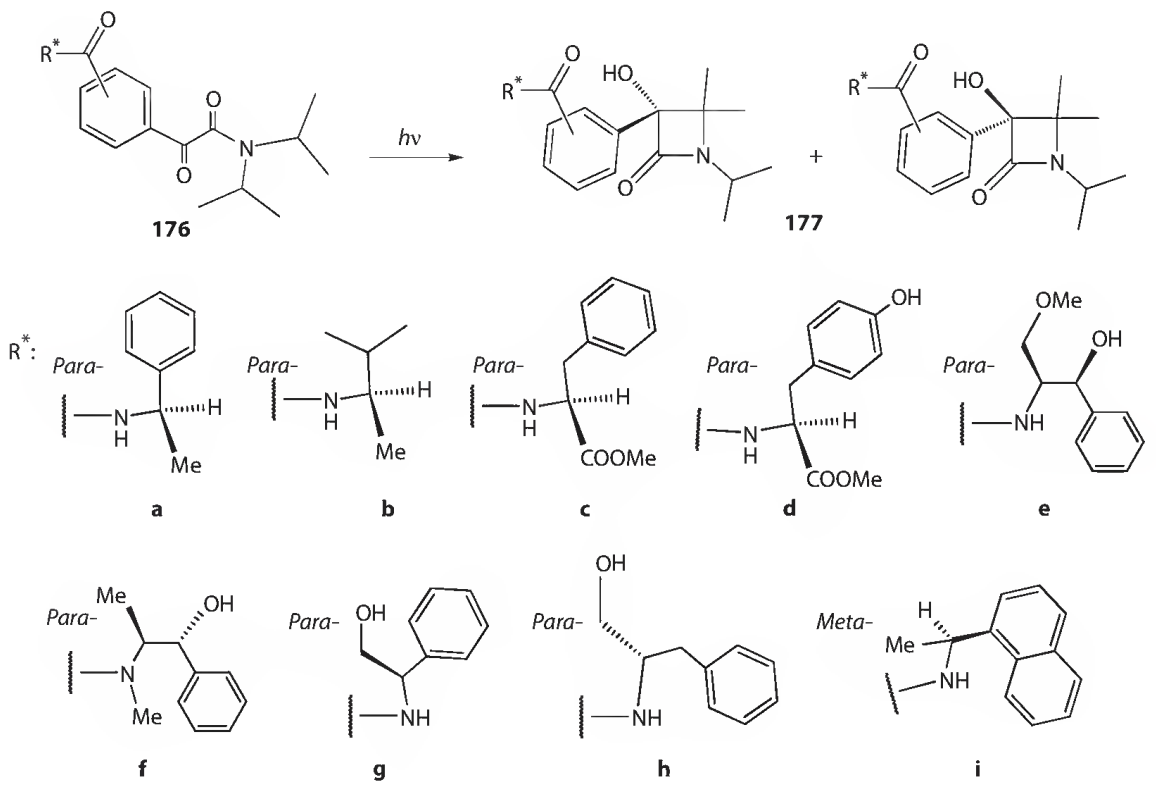

For photosubstrates without any covalently bonded chiral auxiliary, co-crystallization with chiral inductor may be a method of choice for efficient photochirogenesis. Scheffer et al. investigated the solid-state photochirogenesis of a series of aryl ketones **178** co-crystallized with various chiral inductors.[206–208] In solution, all of 4-carboxylphenyl cycloalkyl ketones **178a–c** gave the corresponding Yang cyclization product **179** upon irradiation. However, the photoreactivity turned out to be critically dependent on the size of cycloalkane ring in **178**. Thus, co-crystals of **178a** (n = 0) with chiral amines did not show

any photoreactivity in the solid state, while co-crystals of **178c** (n = 2) with chiral amines underwent the Norrish type I cleavage but no Yang cyclization upon irradiation. Only co-crystals of **178b** (n = 1) yielded cyclobutanol **179b** in the solid-state photoreaction. Of ten chiral amines examined, four gave **179b** in >90% ee. The salts of (*R*)-(–)-1-aminoindan and (*S*)-(–)-1-(*p*-tolyl)ethylamine afforded essentially the quantitative ee at 100% conversion. The distance between the carbonyl oxygen and one of the enantiotopic γ-hydrogens in the co-crystal of **178b** was shown to be 2.7 ± 0.2 Å, nicely satisfying the requirement for the Norrish type II reaction.

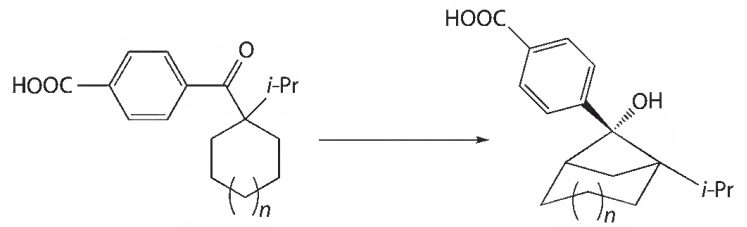

178
a: $n=0$
b: $n=1$
c: $n=2$

179

A series of *endo*-7-benzoylnorbornene derivatives **180** were photolyzed in co-crystals with various optically pure amines.[209] In solution phase, retro-Claisen photorearrangement dominated the reaction to yield *cis*-fused dihydrofuran derivatives **181** in excellent chemical yields. Chiral crystals were given for **180i** by forming a salt bridge between the *para*-carboxylic substituent and chiral amine. The use of (*R*)- and (*S*)-1-phenylethylamine as chiral inductors led to the formation of antipodal dihydrofuran **181b** in ee as high as 95%. The ee of photoproduct decreased with increasing conversion, presumably due to the breakdown of the crystal lattice as the photoreaction proceeded.

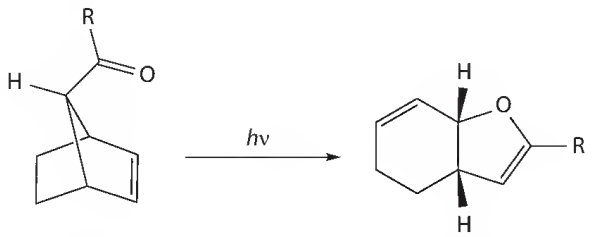

180 **181**

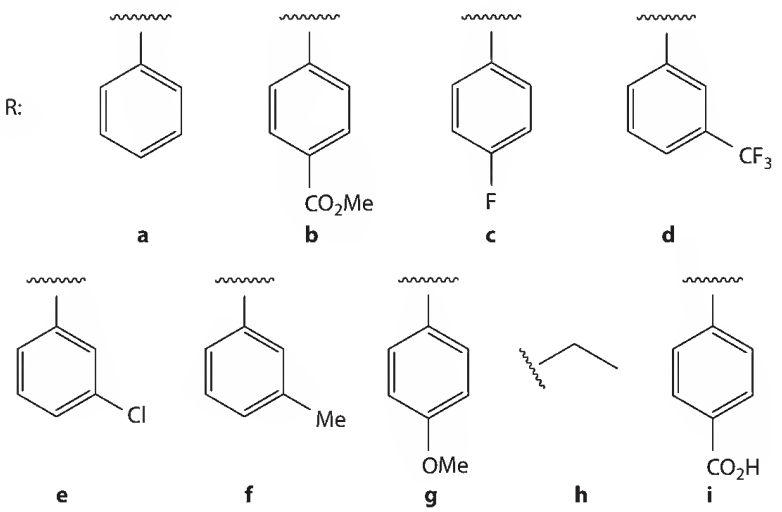

a **b** **c** **d**

e **f** **g** **h** **i**

Photoirradiation of *cis*-bicyclo[4.3.0]non-8-ylacetophenone **182** exclusively gave chiral *cis*-3a,4,5,6,7,7a-hexahydro-1H-indene **183** via the Norrish type II reaction both in solution and in the solid state.[210] The yields of **183** obtained upon irradiation of co-crystals of **182** with chiral amines **184a-e** were comparable to those obtained in solution, but the ee's were not very high (≤44%).

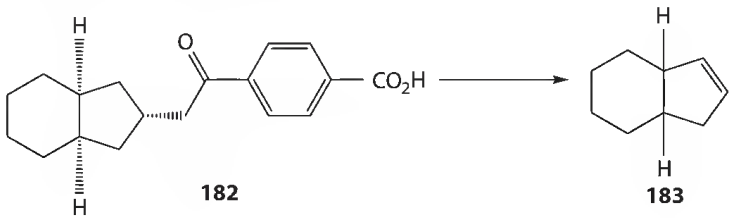

182 **183**

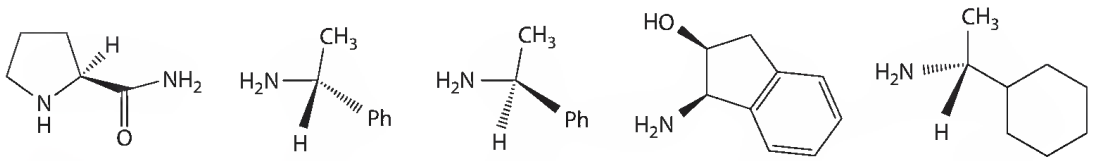

184a **184b** **184c** **184d** **184e**

Solid-state photolysis of co-crystals of **185** with optically pure amines, such as 1-phenylethylamine, 1-cyclohexylethylamine, 2-phenylpropylamine, and 1-(*p*-tolyl)ethylamine, afforded cyclobutanols **186** in good yields.[211] Up to 96% ee was obtained at 22% conversion in the photolysis of co-crystal of **185** with 1-(*p*-tolyl)ethylamine at −40°C. A prolonged irradiation only slightly reduced the ee to 92% at 91% conversion.

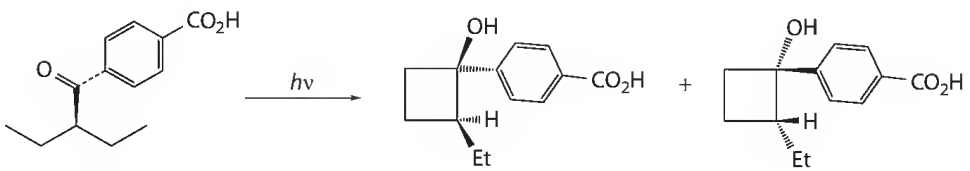

185 **186**

Achiral compounds occasionally crystallize in chiral space groups, which can be transferred to molecular chirality and preserved in the photoproduct obtained upon irradiation. This strategy, not necessitating any chiral source and hence sometimes called absolute asymmetric synthesis, may provide chiral photoproducts with high enantioselectivity.[70] However, not all achiral compounds can form chiral crystals and usually crystals of both enantiomorphs may be formed in a given batch of crystals, although it is not uncommon that crystals of the same chiral sense are preferred upon careful crystallization. Also, the chiral sense of obtained crystal is difficult to predict. It usually needs to consult x-ray crystallographic analysis to determine whether the crystal is in a chiral form or not. With careful precautions, solid-state CD may be used as a convenient alternative tool for check the crystalline chirality.

Koshima et al. investigated the photocyclization of isopropylbenzophenone derivatives employing the co-crystallization approach.[212] Three chiral salt crystals of carboxylic acid derivatives **187** with achiral amines were prepared by spontaneous crystallization. Photoirradiation of salt **187** at >290 nm led to a single crystal-to-single crystal transformation to a mixture of hydrogen-abstraction photoproducts. Three optically active products **190**, **191**, and **192** were given in a 6:3:1 ratio with ee's ranging from 78% to 87%. Interestingly, irradiation of the same crystal at 350 nm afforded the cyclopentanol **190** as the sole product, but the mechanism for the wavelength-dependent behavior is not yet clear. In contrast, photoirradiation of chiral crystals of salts **188** and **189** afforded the corresponding cyclobutanols in ee's <10%.

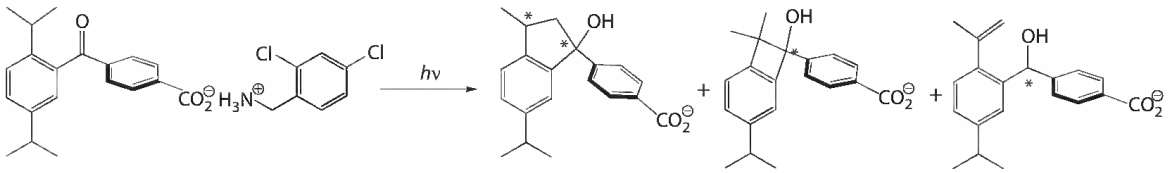

187 190 191 192

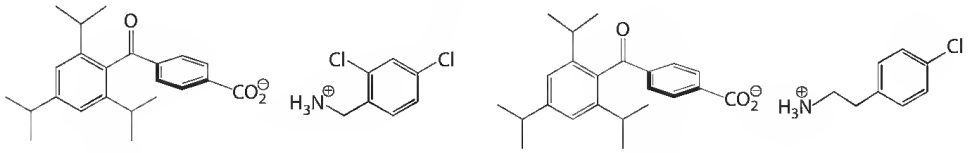

188 189

Irie et al. investigated the chiral co-crystal of diarylethene **193** with octafluoronaphthalene **195**.[213] Recrystallization of a 1:2 mixture of **193** and **195** in hexane afforded chiral monoclinic crystals containing **193** and **195** in 1:2 ratio. Photoirradiation of the chiral co-crystal gave (*R,R*)-**194** from the crystal of (*P*)-helical conformer and (*S,S*)-**194** from that of (*M*)-helical conformer both in >99% ee at conversions <11%. The significant enantioselectivity was ascribed to the naphthalene–octafluoronaphthalene stacking that was not greatly affected during the photochemical conversion.

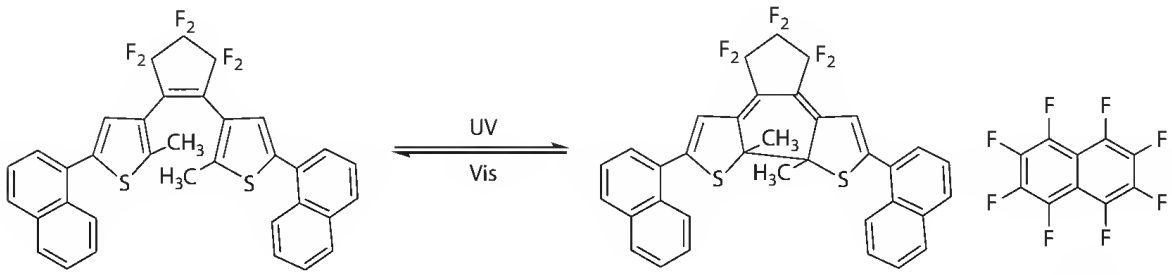

193 194 195

6.6 Conclusions

In this chapter, we reviewed the recent development in photochirogenesis, a field that is relatively new and still rapidly growing, in terms of the reaction media adopted. The novel intriguing findings in unconventional media, such as $scCO_2$, ionic liquids, liquid crystals, and other well-confined host cavity, started to unveil their unique properties and great potentials. The importance of highly ordered media for efficiently manipulating photochirogenic process is underscored by the significant enantioselectivities observed for the photoreactions performed in chiral liquid crystals. Chiral ionic liquids, which are not sufficient from the viewpoint of chiral-source efficiency alone, afforded only low optical yields in the limited attempts, but may become attractive chiral media from the green chemical point of view in the future, when further experimental attempts and mechanistic considerations can improve the stereochemical outcomes. The observation of the rapid leap of enantioselectivity in the near-critical region of $scCO_2$ is unprecedented and needs further clarifications of the effects of density fluctuation on photochirogenesis.

The chiral auxiliary strategy has met a considerable success. However, the consumption of equimolar amount of chiral source and the synthetic labor in covalently attaching the chiral auxiliary to photosubstrate and removing it after photoreaction reduces the value of the method to some degree. Photochirogenesis with chiral crystal is an attractive approach to optically active compounds without using any chiral source and often gives significantly high stereoselectivities, is limited to those

photosubstrates that crystallize in chiral space group, which is however difficult to predicate. The use of three-dimensionally well-organized chiral supramolecular hosts appears to be a highly efficient and promising strategy for inducing high stereoselectivity through the confinement of guest substrate in chiral supramolecular host cavity by manipulating the multiple noncovalent interactions.

Catalytic photochirogenesis is one of the most intriguing and challenging tasks in this area. Photochirogenesis with a catalytic amount of chiral source has been realized by enantiodifferentiating photosensitization, where only the excited-state interactions between chiral sensitizer and substrate contribute to the stereochemical outcomes. However, recent development in supramolecular chemistry provides another possibility to achieve a photochirogenic reaction with a catalytic amount of supramolecular chiral source at an accelerated rate through complexation of photosubstrate with chiral host.

Obviously, photochirogenesis has left its infancy, but is still rapidly growing and far away from maturity with many important aspects to be uncovered. The major tasks in this challenging area include the enhancement of chemo- and stereoselectivity in general and the achievement of catalytic photochirogenesis through supramolecular methodologies, for both of which interdisciplinary approaches would be most useful.

References

1. Nishino, H.; Inoue, Y. Photochirogenesis. Directed toward optical formation and increase of chirality, *Kokagaku*, *24*, 54 (1997).
2. Nicolaou, K.; Snyder, S.; Corey, E. *Classics in Total Synthesis II: More Targets, Strategies, Methods*; Wiley-VCH: Weinheim, Germany (2003).
3. Zewail, A. *Femtochemistry: Ultrafast Dynamics of the Chemical Bond*; World Scientific Publishing Company, Inc.: Singapore (1994).
4. Rau, H. Asymmetric photochemistry in solution, *Chem. Rev.*, *83*, 535 (1983).
5. Inoue, Y. Asymmetric photochemical reactions in solution, *Chem. Rev.*, *92*, 741 (1992).
6. Axel, G. Griesbeck; Meierhenrich, U. J. Asymmetric photochemistry and photochirogenesis, *Angew. Chem. Int. Ed.*, *41*, 3147 (2002).
7. Inoue, Y.; Ramamurthy, V.; Eds. *Chiral Photochemistry*; Marcel Dekker: New York (2004).
8. Le Bel, J. Sur les relations qui existent entre les formules atomiques des corps organiques, et le pouvoir rotatoire de leurs dissolutions, *Bull. Soc. Chim. Paris*, *22*, 337 (1874).
9. Kuhn, W.; Braun, E. Photochemische erzeugung optisch aktiver stoffe, *Naturwissenschaften*, *17*, 227 (1929).
10. Pagni, R. M.; Bartmess, J. A photochemical mechanism for homochirogenesis, *J. Phys. Chem. A*, *111*, 10604 (2007).
11. Nuevo, M.; Meierhenrich, U. J.; Caro, G. M. M.; Dartois, E.; d'Hendecourt, L.; Deboffle, D.; Auger, G.; Blanot, D.; Bredehoeft, J. H.; Nahon, L. The effects of circularly polarized light on amino acid enantiomers produced by the UV irradiation of interstellar ice analogs, *Astron. Astrophys.*, *457*, 741 (2006).
12. Nahon, L.; Garcia, G.; Powis, I.; Meierhenrich, U.; Brack, A. Advanced search for the origin of life's homochirality: Asymmetric photon induced processes on chiral compounds with far UV circularly polarized synchrotron radiation, *Proc. SPIE Int. Soc. Opt. Eng.*, *6694*, 1 (2007).
13. Bonner, W. A.; Rubenstein, E. Supernovae, neutron stars and biomolecular chirality, *Biosystems*, *20*, 99 (1987).
14. Rubenstein, E.; Bonner, W.; Noyes, H.; Brown, G. Supernovae and life, *Nature*, *306*, 118 (1983).
15. Bailey, J.; Chrysostomou, A.; Hough, J.; Gledhill, T.; McCall, A.; Clark, S.; Menard, F.; Tamura, M. Circular polarization in star-formation regions: Implications for biomolecular homochirality, *Science*, *281*, 672 (1998).
16. Caro, G.; Meierhenrich, U.; Schutte, W.; Barbier, B.; Segovia, A.; Rosenbauer, H.; Thiemann, W.; Brack, A.; Greenberg, J. Amino acids from ultraviolet irradiation of interstellar ice analogues, *Nature*, *416*, 403 (2002).

17. Flores, J.; Bonner, W.; Massey, G. Asymmetric photolysis of/RS/-leucine with circularly polarized ultraviolet light, *J. Am. Chem. Soc.*, *99*, 3622 (1977).
18. Nishino, H.; Kosaka, A.; Hembury, G. A.; Aoki, F.; Miyauchi, K.; Shitomi, H.; Onuki, H.; Inoue, Y. Absolute asymmetric photoreactions of aliphatic amino acids by circularly polarized synchrotron radiation: Critically pH-dependent photobehavior, *J. Am. Chem. Soc.*, *124*, 11618 (2002).
19. Nishino, H.; Nakamura, A.; Inoue, Y. Synchronous enantiomeric enrichment of both reactant and product by absolute asymmetric synthesis using circularly polarized light. Part I. Theoretical and experimental verification of the asymmetric photoisomerization of methyl norbornadiene-2-carboxylate to methyl quadricyclane-1-carboxylate, *J. Chem. Soc. Perk. Trans., 2*, 1693 (2001).
20. Nishino, H.; Nakamura, A.; Shitomi, H.; Onuki, H.; Inoue, Y. Synchronous enantiomeric enrichment of both reactant and product by absolute asymmetric synthesis using circularly polarized light. Part III. Numerical simulation and experimental verification of the reversible asymmetric photoisomerization between methyl norbornadiene-2-carboxylate and methyl quadricyclane-1-carboxylate, *J. Chem. Soc. Perk. Trans., 2*, 1706 (2001).
21. Nishino, H.; Kosaka, A.; Hembury, G.; Shitomi, H.; Onuki, H.; Inoue, Y. Mechanism of pH-dependent photolysis of aliphatic amino acids and enantiomeric enrichment of racemic leucine by circularly polarized light, *Org. Lett.*, *3*, 921 (2001).
22. Soai, K.; Shibata, T.; Sato, I. Enantioselective automultiplication of chiral molecules by asymmetric autocatalysis, *Acc. Chem. Res.*, *33*, 382 (2000).
23. Kawasaki, T.; Sato, M.; Ishiguro, S.; Saito, T.; Morishita, Y.; Sato, I.; Nishino, H.; Inoue, Y.; Soai, K. Enantioselective synthesis of near enantiopure compound by asymmetric autocatalysis triggered by asymmetric photolysis with circularly polarized light, *J. Am. Chem. Soc.*, *127*, 3274 (2005).
24. Sato, I.; Sugie, R.; Matsueda, Y.; Furumura, Y.; Soai, K. Asymmetric synthesis utilizing circularly polarized light mediated by the photoequilibrium of chiral olefins in conjunction with asymmetric autocatalysis, *Angew. Chem. Int. Ed.*, *43*, 4490 (2004).
25. Breslow, R.; Cheng, Z.-L. On the origin of terrestrial homochirality for nucleosides and amino acids, *Proc. Natl. Acad. Sci. USA*, *106*, 9144 (2009).
26. Soloshonok, V.; Ueki, H.; Yasumoto, M.; Mekala, S.; Hirschi, J.; Singleton, D. Phenomenon of optical self-purification of chiral non-racemic compounds, *J. Am. Chem. Soc.*, *129*, 12112 (2007).
27. Soloshonok, V. Remarkable amplification of the self-disproportionation of enantiomers on achiral-phase chromatography columns, *Angew. Chem.*, *118*, 780 (2006).
28. Kohn, H.; Ohshima, Y.; Manaka, T.; Iwamoto, M. Optical chirality induced in evaporated poly(diacetylene) film by circularly polarized light, *Macromol. Symp.*, *268*, 77 (2008).
29. Kohn, H.; Ohshima, Y.; Manaka, T.; Iwamoto, M. Induced optical chirality of poly(diacetylene) film by circularly polarized light and its control by changing substrate temperature, *Jpn. J. Appl. Phys.*, *47*, 1359 (2008).
30. Manaka, T.; Kon, H.; Ohshima, Y.; Zou, G.; Iwamoto, M. Preparation of chiral polydiacetylene film from achiral monomers using circularly polarized light, *Chem. Lett.*, *35*, 1028 (2006).
31. Zou, G.; Kohn, H.; Ohshima, Y.; Manaka, T.; Iwamoto, M. Fabricating chiral polydiacetylene film by monolayer compression and circularly polarized ultra-violet light, *Chem. Phys. Lett.*, *442*, 97 (2007).
32. Huang, X.; Liu, M. Chirality of photopolymerized organized supramolecular polydiacetylene films, *Chem. Commun.*, *2003*, 66 (2003).
33. Hoffmann, N.; Pete, J.-P. Diastereodifferentiating photoreactions, *Mol. Supramol. Photochem.*, *11*, 179 (2004).
34. Irie, M. Diarylethenes for memories and switches, *Chem. Rev.*, *100*, 1685 (2000).
35. Yamaguchi, T.; Uchida, K.; Irie, M. Asymmetric photocyclization of diarylethene derivatives, *J. Am. Chem. Soc.*, *119*, 6066 (1997).
36. Yamaguchi, T.; Nomiyama, K.; Isayama, M.; Irie, M. Reversible diastereoselective photocyclization of diarylethenes in a bulk amorphous state, *Adv. Mater.*, *16*, 643 (2004).

37. Yokoyama, Y. Chiral photochromism based on 6pi-electrocyclization system, *Kokagaku*, *39*, 162 (2008).
38. Yokoyama, Y.; Shiozawa, T.; Tani, Y.; Ubukata, T. A unified strategy for exceptionally high diastereoselectivity in the photochemical ring closure of chiral diarylethenes, *Angew. Chem. Int. Ed.*, *48*, 4521 (2009).
39. Okuyama, T.; Tani, Y.; Miyake, K.; Yokoyama, Y. Chiral helicenoid diarylethene with large change in specific optical rotation by photochromism, *J. Org. Chem.*, *72*, 1634 (2007).
40. Tani, Y.; Ubukata, T.; Yokoyama, Y.; Yokoyama, Y. Chiral helicenoid diarylethene with highly diastereoselective photocyclization, *J. Org. Chem.*, *72*, 1639 (2007).
41. Li, L.; Bender, J. A.; West, F. G. Diastereocontrol in [4 + 4]-photocycloadditions of pyran-2-ones: Effect of ring substituents and chiral ketal, *Tetrahedron Lett.*, *50*, 1188 (2009).
42. Abe, M.; Nojima, M. Memory of chirality in photochemical reactions, *Kokagaku*, *31*, 28 (2000).
43. Griesbeck, A. G. Spin-selectivity in photochemistry: A tool for organic synthesis, *Synlett*, *34*, 451 (2003).
44. Zhao, H.; Hsu, D. C.; Carlier, P. R. Memory of chirality. An emerging strategy for asymmetric synthesis, *Synthesis*, *36*, 1 (2005).
45. Griesbeck, A.; Kramer, W.; Lex, J. Diastereo-and enantioselective synthesis of pyrrolo [1, 4] benzodiazepines through decarboxylative photocyclization, *Angew. Chem. Int. Ed.*, *40*, 577 (2001).
46. Resendiz, M. J. E.; Family, F.; Fuller, K.; Campos, L. M.; Khan, S. I.; Lebedeva, N. V.; Forbes, M. D. E.; Garcia-Garibay, M. A. Radical reactions with double memory of chirality (2MOC) for the enantiospecific synthesis of adjacent stereogenic quaternary centers in solution: Cleavage and bonding faster than radical rotation, *J. Am. Chem. Soc.*, *131*, 8425 (2009).
47. Resendiz, M.; Natarajan, A.; Garcia-Garibay, M. Diastereoselective synthesis and spin-dependent photodecarbonylation of di (3-phenyl-2-pyrrolidinon-3-yl) ketones: Synthesis of nonadjacent and adjacent stereogenic quaternary centers, *Chem. Commun.*, *39*, 193 (2008).
48. Sakamoto, M.; Kawanishi, H.; Mino, T.; Kasashima, Y.; Fujita, T. Photochemical asymmetric synthesis of phenyl-bearing quaternary chiral carbons using chiral-memory effect on beta -hydrogen abstraction by thiocarbonyl group, *Chem. Commun.*, 4608 (2006).
49. Sakamoto, M.; Kawanishi, H.; Mino, T.; Fujita, T. Asymmetric synthesis of beta -lactams using chiral-memory effect on photochemical gamma -hydrogen abstraction by thiocarbonyl group, *Chem. Commun.*, 2132 (2008).
50. Ayitou, A.; Ugrinov, A.; Sivaguru, J. 6-Photocyclization O-tert-butylacrylanilides. N-substitution dictates the regiochemistry of cyclization, *Photochem. Photobiol. Sci.*, *8*, 751 (2009).
51. Ayitou, A. J.-L.; Jesuraj, J. L.; Barooah, N.; Ugrinov, A.; Sivaguru, J. Enantiospecific photochemical Norrish/Yang type II reaction of nonbiaryl atropchiral alpha -oxoamides in solution-axial to point chirality transfer, *J. Am. Chem. Soc.*, *131*, 11314 (2009).
52. Ayitou, A. J.-L.; Sivaguru, J. Light-induced transfer of molecular chirality in solution: Enantiospecific photocyclization of molecularly chiral acrylanilides, *J. Am. Chem. Soc.*, *131*, 5036 (2009).
53. Lehn, J. M. *Supramolecular Chemistry: Concepts and Perspectives*; VCH: Weinheim, Germany (1995).
54. Schneider, H. J.; Duerr, H.; Eds. *Frontiers in Supramolecular Organic Chemistry and Photochemistry*; VCH: Weinheim, Germany (1991).
55. Bach, T.; Bergmann, H.; Harms, K. Enantioselective intramolecular [2 + 2]-photocycloaddition reactions in solution, *Angew. Chem. Int. Ed.*, *39*, 2302 (2000).
56. Bach, T.; Bergmann, H.; Grosch, B.; Harms, K. Highly enantioselective intra- and intermolecular [2 + 2] photocycloaddition reactions of 2-quinolones mediated by a chiral lactam host: Host-guest interactions, product configuration, and the origin of the stereoselectivity in solution, *J. Am. Chem. Soc.*, *124*, 7982 (2002).
57. Selig, P.; Bach, T. Photochemistry of 4-(2′-aminoethyl)quinolones: Enantioselective synthesis of tetracyclic tetrahydro-1aH-pyrido[4′,3′:2,3]- cyclobuta[1,2-c] Quinoline-2,11(3H,8H)-diones by Intra- and intermolecular [2 + 2]-photocycloaddition reactions in solution, *J. Org. Chem.*, *71*, 5662 (2006).

58. Auerbach, S. M.; Carrado, K. A.; Dutta, P. K.; Eds. *Handbook of Zeolite Science and Technology*; Marcel Dekker: New York (2003).
59. Bach, T.; Grosch, B.; Strassner, T.; Herdtweck, E. Enantioselective [6pi]-photocyclization reaction of an acrylanilide mediated by a chiral host. Interplay between enantioselective ring closure and enantioselective protonation, *J. Org. Chem.*, *68*, 1107 (2003).
60. Bach, T.; Bergmann, H.; Brummerhop, H.; Lewis, W.; Harms, K. The [2 + 2]-photocycloaddition of aromatic aldehydes and ketones to 3,4-dihydro-2-pyridones: Regioselectivity, diastereoselectivity, and reductive ring opening of the product oxetanes, *Chem. Eur. J.*, *7*, 4512 (2001).
61. Poon, T.; Turro, N.; Chapman, J.; Lakshminarasimhan, P.; Lei, X.; Jockusch, S.; Franz, R.; Washington, I.; Adam, W.; Bosio, S. Stereochemical features of the physical and chemical interactions of singlet oxygen with enecarbamates, *Org. Lett.*, *5*, 4951 (2003).
62. Adam, W.; Bosio, S. G.; Turro, N. J.; Wolff, B. T. Enecarbamates as selective substrates in oxidations: Chiral-auxiliary-controlled mode selectivity and diastereoselectivity in the [2 + 2] cycloaddition and ene reaction of singlet oxygen and in the epoxidation by DMD and mCPBA, *J. Org. Chem.*, *69*, 1704 (2004).
63. Poon, T.; Sivaguru, J.; Franz, R.; Jockusch, S.; Martinez, C.; Washington, I.; Adam, W.; Inoue, Y.; Turro, N. J. Temperature and solvent control of the stereoselectivity in the reactions of singlet oxygen with oxazolidinone-substituted enecarbamates, *J. Am. Chem. Soc.*, *126*, 10498 (2004).
64. Sivaguru, J.; Poon, T.; Franz, R.; Jockusch, S.; Adam, W.; Turro, N. Stereocontrol within confined spaces: Enantioselective photooxidation of enecarbamates inside zeolite supercages, *J. Am. Chem. Soc.*, *126*, 10816 (2004).
65. Sivaguru, J.; Poon, T.; Hooper, C.; Saito, H.; Solomon, M. R.; Jockusch, S.; Adam, W.; Inoue, Y.; Turro, N. J. A comparative mechanistic analysis of the stereoselectivity trends observed in the oxidation of chiral oxazolidinone-functionalized enecarbamates by singlet oxygen, ozone, and triazolinedione, *Tetrahedron*, *62*, 10647 (2006).
66. Sivaguru, J.; Saito, H.; Solomon, M. R.; Kaanumalle, L. S.; Poon, T.; Jockusch, S.; Adam, W.; Ramamurthy, V.; Inoue, Y.; Turro, N. J. Control of chirality by cations in confined spaces: Photooxidation of enecarbamates inside zeolite supercages, *Photochem. Photobiol. Sci.*, *82*, 123 (2006).
67. Xu, H.-X.; Chen, B.; Zhang, L.-P.; Wu, L.-Z.; Tung, C.-H. Diastereodifferentiating photodimerization of alkyl 2-naphthoates with chiral auxiliaries, *Tetrahedron Lett.*, *50*, 4965 (2009).
68. Sakamoto, M.; Unosawa, A.; Kobaru, S.; Saito, A.; Mino, T.; Fujita, T. Asymmetric photocycloaddition in solution of a chiral crystallized naphthamide, *Angew. Chem. Int. Ed.*, *44*, 5523 (2005).
69. Sakamoto, M.; Iwamoto, T.; Nono, N.; Ando, M.; Arai, W.; Mino, T.; Fujita, T. Memory of chirality generated by spontaneous crystallization and asymmetric synthesis using the frozen chirality, *J. Org. Chem.*, *68*, 942 (2003).
70. Sakamoto, M. Absolute asymmetric photochemistry using spontaneous chiral crystallization, *Mol. Supramol. Photochem.*, *11*, 415 (2004).
71. Sakamoto, M. Spontaneous chiral crystallization of achiral materials and absolute asymmetric photochemical transformation using the chiral crystalline environment, *J. Photochem. Photobiol. C*, *7*, 183 (2006).
72. Sakamoto, M.; Kato, M.; Aida, Y.; Fujita, K.; Mino, T.; Fujita, T. Photosensitized 2 + 2 cycloaddition reaction using homochirality generated by spontaneous crystallization, *J. Am. Chem. Soc.*, *130*, 1132 (2008).
73. Matsumura, K.; Mori, T.; Inoue, Y. Wavelength control of diastereodifferentiating Paterno-Buchi reaction of chiral cyanobenzoates with diphenylethene through direct versus charge-transfer excitation, *J. Am. Chem. Soc.*, *131*, 17076 (2009).
74. Nakamura, A.; Inoue, Y. Supramolecular catalysis of the enantiodifferentiating [4 + 4] photocyclodimerization of 2-anthracenecarboxylate by gamma -cyclodextrin, *J. Am. Chem. Soc.*, *125*, 966 (2003).
75. Mizoguchi, J.-i.; Kawanami, Y.; Wada, T.; Kodama, K.; Anzai, K.; Yanagi, T.; Inoue, Y. Enantiodifferentiating photocyclodimerization of 2-anthracenecarboxylic acid using a chiral N-(2-hydroxymethyl-4-pyrrolidinyl)benzamide template, *Org. Lett.*, *8*, 6051 (2006).

76. Kawanami, Y.; Pace, T. C. S.; Mizoguchi, J.-i.; Yanagi, T.; Nishijima, M.; Mori, T.; Wada, T.; Bohne, C.; Inoue, Y. Supramolecular complexation and enantiodifferentiating photocyclodimerization of 2-anthracenecarboxylic acid with 4-aminoprolinol derivatives as chiral hydrogen-bonding templates, *J. Org. Chem.*, *74*, 7908 (2009).
77. Grosch, B.; Orlebar, C. N.; Herdtweck, E.; Kaneda, M.; Wada, T.; Inoue, Y.; Bach, T. Enantioselective [4 + 2]-cycloaddition reaction of a photochemically generatedo-quinodimethane: Mechanistic details, association studies, and pressure effects, *Chem. Eur. J.*, *10*, 2179 (2004).
78. Bach, T.; Bergmann, H.; Harms, K. Enantioselective photochemical reactions of 2-pyridones in solution, *Org. Lett.*, *3*, 601 (2001).
79. Hammond, G. S.; Cole, R. S. Asymmetric induction during energy transfer, *J. Am. Chem. Soc.*, *87*, 3256 (1965).
80. Murov, S. L.; Cole, R. S.; Hammond, G. S. Mechanisms of photochemical reactions in solution. LIV. A new mechanism of photosensitization, *J. Am. Chem. Soc.*, *90*, 2957 (1968).
81. Ouannes, C.; Beugelmans, R.; Roussi, G. Asymmetric induction during transfer of triplet energy, *J. Am. Chem. Soc.*, *95*, 8472 (1973).
82. Inoue, Y.; Kosaka, S.; Matsumoto, K.; Tsuneishi, H.; Hakushi, T.; Tai, A.; Nakagawa, K.; Tong, L. Vacuum UV photochemistry in cyclodextrin cavities. Solid state z-e photoisomerization of a cyclooctene -b- CD inclusion complex, *J. Photochem. Photobiol. A: Chem.*, *71*, 61 (1993).
83. Inoue, Y.; Yamasaki, N.; Shimoyama, H.; Tai, A. Enantiodifferentiating cis-trans photoisomerizations of 1, 2-diarylcyclopropanes and 2, 3-diphenyloxirane sensitized by chiral aromatic esters, *J. Org. Chem.*, *58*, 1785 (1993).
84. Inoue, Y.; Daino, Y.; Tai, A.; Hakushi, T.; Okada, T. Synchrotron-radiation study of weak fluorescence from neat liquids of simple alkenes: Anomalous excitation spectra as evidence for wavelength-dependent photochemistry, *J. Am. Chem. Soc.*, *111*, 5584 (1989).
85. Inoue, Y.; Yokoyama, T.; Yamasaki, N.; Tai, A. An optical yield that increases with temperature in a photochemically induced enantiomeric isomerization, *Nature*, *341*, 225 (1989).
86. Inoue, Y.; Yokoyama, T.; Yamasaki, N.; Tai, A. Temperature switching of product chirality upon photosensitized enantiodifferentiating cis-trans isomerization of cyclooctene, *J. Am. Chem. Soc.*, *111*, 6480 (1989).
87. Inoue, Y.; Yamasaki, N.; Yokoyama, T.; Tai, A. Highly enantiodifferentiating photoisomerization of cyclooctene by congested and/or triplex-forming chiral sensitizers, *J. Org. Chem.*, *58*, 1011 (1993).
88. Inoue, Y.; Matsushima, E.; Wada, T. Pressure and temperature control of product chirality in asymmetric photochemistry. Enantiodifferentiating photoisomerization of cyclooctene sensitized by chiral benzenepolycarboxylates, *J. Am. Chem. Soc.*, *120*, 10687 (1998).
89. Shi, M.; Inoue, Y. Geometrical photoisomerization of (Z)-cyclooctene sensitized by aromatic phosphate, phosphonate, phosphinate, phosphine oxide and chiral phosphoryl esters, *J. Chem. Soc. Perk. Trans.*, *2*, 2421 (1998).
90. Inoue, T.; Matsuyama, K.; Inoue, Y. Diastereodifferentiating Z-E photoisomerization of 3-benzoyloxycyclooctene: Diastereoselectivity switching controlled by substrate concentration through competitive intra- vs intermolecular photosensitization processes, *J. Am. Chem. Soc.*, *121*, 9877 (1999).
91. Matsuyama, K.; Inoue, T.; Inoue, Y. Self-sensitized diastereodifferentiating Z-E photoisomerization of 3-, 4-, and 5-benzoyloxycyclooctenes: Intra- versus intermolecular photosensitization, *Synthesis*, *2001*, 1167 (2001).
92. Shi, M.; Inoue, Y. Enantiodifferentiating photoisomerization of (Z)-cyclooctene sensitized by chiral C2-symmetric phosphoramide, *Aust. J. Chem.*, *54*, 113 (2001).
93. Saito, R.; Kaneda, M.; Wada, T.; Katoh, A.; Inoue, Y. First asymmetric photosensitization in supercritical fluid. Exceptionally high pressure/density dependence of optical yield in photosensitized enantiodifferentiating isomerization of cyclooctene, *Chem. Lett.*, *31*, 860 (2002).
94. Oelgemoeller, M.; Inoue, Y. Photosensitized asymmetric isomerization and cycloaddition of cycloalkenes and cycloalkadienes, *J. Photosci.*, *10*, 71 (2003).

95. Pirrung, M. C.; Bleecker, A. B.; Inoue, Y.; Rodriguez, F. I.; Sugawara, N.; Wada, T.; Zou, Y.; Binder, B. M. Ethylene receptor antagonists: Strained alkenes are necessary but not sufficient, *Chem. Biol.*, *15*, 313 (2008).
96. Inoue, Y.; Ikeda, H.; Kaneda, M.; Sumimura, T.; Everitt, S. R. L.; Wada, T. Entropy-controlled asymmetric photochemistry: Switching of product chirality by solvent, *J. Am. Chem. Soc.*, *122*, 406 (2000).
97. Inoue, Y.; Tsuneishi, H.; Hakushi, T.; Tai, A. Optically active (E,Z)-1,3-cyclooctadiene: First enantioselective synthesis through asymmetric photosensitization and chiroptical property, *J. Am. Chem. Soc.*, *119*, 472 (1997).
98. Inoue, Y. Synthetic chemistry: Light on chirality, *Nature*, *436*, 1099 (2005).
99. Bauer, A.; Westkaemper, F.; Grimme, S.; Bach, T. Catalytic enantioselective reactions driven by photoinduced electron transfer, *Nature*, *436*, 1139 (2005).
100. Asaoka, S.; Wada, T.; Inoue, Y. Microenvironmental polarity control of electron-transfer photochirogenesis. Enantiodifferentiating polar addition of 1,1-diphenyl-1-alkenes photosensitized by saccharide naphthalenecarboxylates, *J. Am. Chem. Soc.*, *125*, 3008 (2003).
101. Mueller, C.; Bauer, A.; Bach, T. Light-driven enantioselective organocatalysis, *Angew. Chem. Int. Ed.*, *48*, 6640 (2009).
102. Nicewicz, D. A.; MacMillan, D. W. C. Merging photoredox catalysis with organocatalysis: The direct asymmetric akylation of aldehydes, *Science*, *322*, 77 (2008).
103. Nagib, D. A.; Scott, M. E.; MacMillan, D. W. C. Enantioselective alpha -trifluoromethylation of aldehydes via photoredox organocatalysis, *J. Am. Chem. Soc.*, *131*, 10875 (2009).
104. Ischay, M.; Anzovino, M.; Du, J.; Yoon, T. Efficient visible light photocatalysis of [2 + 2] enone cycloadditions, *J. Am. Chem. Soc.*, *130*, 12886 (2008).
105. Du, J.; Yoon, T. Crossed intermolecular [2 + 2] cycloadditions of acyclic enones via visible light photocatalysis, *J. Am. Chem. Soc.*, *131*, 14604 (2009).
106. Seebach, D.; Oei, H. Mechanism of electrochemical pinacolization. The first asymmetric synthesis in a chiral medium, *Angew. Chem. Int. Ed.*, *14*, 634 (1975).
107. Ding, J.; Desikan, V.; Han, X.; Xiao, T. L.; Ding, R.; Jenks, W. S.; Armstrong, D. W. Use of chiral ionic liquids as solvents for the enantioselective photoisomerization of dibenzobicyclo[2.2.2]octatrienes, *Org. Lett.*, *7*, 335 (2005).
108. Bose, S.; Wijeratne, A. B.; Thite, A.; Kraus, G. A.; Armstrong, D. W.; Petrich, J. W. Influence of chiral ionic liquids on stereoselective fluorescence quenching by photoinduced electron transfer in a naproxen dyad, *J. Phys. Chem. B*, *113*, 10825 (2009).
109. Nishiyama, Y.; Kaneda, M.; Saito, R.; Mori, T.; Wada, T.; Inoue, Y. Enantiodifferentiating photoaddition of alcohols to 1,1-diphenylpropene in supercritical carbon dioxide: Sudden jump of optical yield at the critical density, *J. Am. Chem. Soc.*, *126*, 6568 (2004).
110. Nishiyama, Y.; Kaneda, M.; Asaoka, S.; Saito, R.; Mori, T.; Wada, T.; Inoue, Y. Mechanistic study on the enantiodifferentiating anti-Markovnikov photoaddition of alcohols to 1,1-diphenyl-1-alkenes in near-critical and supercritical carbon dioxide, *J. Phys. Chem. A*, *111*, 13432 (2007).
111. Nishiyama, Y.; Wada, T.; Mori, T.; Inoue, Y. Critical control by temperature and pressure of enantiodifferentiating anti-Markovnikov photoaddition of methanol to diphenylpropene in near critical and supercritical carbon dioxide, *Chem. Lett.*, *36*, 1488 (2007).
112. Nishiyama, Y.; Wada, T.; Asaoka, S.; Mori, T.; McCarty, T. A.; Kraut, N. D.; Bright, F. V.; Inoue, Y. Entrainer effect on photochirogenesis in near- and supercritical carbon dioxide: Dramatic enhancement of enantioselectivity, *J. Am. Chem. Soc.*, *130*, 7526 (2008).
113. Breck, D. W. *Zeolite Molecular Sieves: Structure, Chemistry, and Use*; Krieger Pub. Co.: Malabar, FL (1984).
114. Davis, M. E.; Lobo, R. F. Zeolite and molecular sieve synthesis, *Chem. Mat.*, *4*, 756 (1992).
115. Joy, A.; Uppili, S.; Netherton, M. R.; Scheffer, J. R.; Ramamurthy, V. Photochemistry of a tropolone ether and 2,2-dimethyl-1-(2H)-naphthalenones within a Zeolite: Enhanced diastereoselectivity via confinement, *J. Am. Chem. Soc.*, *122*, 728 (2000).

116. Natarajan, A.; Joy, A.; Kaanumalle, L. S.; Scheffer, J. R.; Ramamurthy, V. Enhanced enantio- and diastereoselectivity via confinement and cation binding: Yang photocyclization of 2-benzoyladamantane derivatives within zeolites, *J. Org. Chem.*, *67*, 8339 (2002).
117. Sivaguru, J.; Sunoj, R. B.; Wada, T.; Origane, Y.; Inoue, Y.; Ramamurthy, V. Enhanced diastereoselectivity via confinement: Diastereoselective photoisomerization of 2,3-diphenyl-1-benzoylcyclopropane derivatives within zeolites, *J. Org. Chem.*, *69*, 5528 (2004).
118. Zimmerman, H. E.; Flechtner, T. W. Excited-state three-ring bond opening in cyclopropyl ketones. Mechanistic organic photochemistry. LX, *J. Am. Chem. Soc.*, *92*, 6931 (1970).
119. Chong, K. C. W.; Sivaguru, J.; Shichi, T.; Yoshimi, Y.; Ramamurthy, V.; Scheffer, J. R. Use of chirally modified zeolites and crystals in photochemical asymmetric synthesis, *J. Am. Chem. Soc.*, *124*, 2858 (2002).
120. Sivaguru, J.; Jockusch, S.; Turro, N. J.; Ramamurthy, V. Photoisomerization of 2, 3-diphenylcyclopropane-1-carboxylic acid derivatives, *Photochem. Photobiol. Sci.*, *2*, 1101 (2003).
121. Kaanumalle, L. S.; Sivaguru, J.; Arunkumar, N.; Karthikeyan, S.; Ramamurthy, V. Cation-pi interactions as a tool to enhance the power of a chiral auxiliary during asymmetric photoreactions within zeolites, *Chem. Commun.*, 116 (2003).
122. Kaanumalle, L. S.; Sivaguru, J.; Sunoj, R. B.; Lakshminarasimhan, P. H.; Chandrasekhar, J.; Ramamurthy, V. Light-induced geometric isomerization of 1,2-diphenylcyclopropanes included within Y zeolites: Role of cation-guest binding, *J. Org. Chem.*, *67*, 8711 (2002).
123. Shephard, D. S. Nano-clusters, enantioselective catalysis and molecular recognition contrast agents in MCM-41. Part I, *Stud. Surf. Sci. Catal.*, *129*, 789 (2000).
124. Brunel, D.; Lasperas, M. Design of chiral hybrid organic-inorganic mesoporous materials as enantioselective epoxidation and alkylation catalysts, *Nanostruct. Catal.*, 157 (2003).
125. Hutchings, G. J. Enantioselective reactions using modified microporous and mesoporous materials, *Surf. Chem. Catal.*, *34*, 241 (2002).
126. Van de Velde, F.; Arends, I. W. C. E.; Sheldon, R. A. Vanadium-catalyzed enantioselective sulfoxidations: Rational design of biocatalytic and biomimetic systems, *Top. Catal.*, *13*, 259 (2000).
127. Hutchings, G. J. New approaches to rate enhancement in heterogeneous catalysis, *Chem. Commun.*, 301 (1999).
128. Sivaguru, J.; Shichi, T.; Ramamurthy, V. Reactive-state spin-dependent diastereoselective photoisomerization of trans,trans-2,3-diphenylcyclopropane-1- carboxylic acid derivatives included in zeolites, *Org. Lett.*, *4*, 4221 (2002).
129. Sivaguru, J.; Wada, T.; Origane, Y.; Inoue, Y.; Ramamurthy, V. Mechanism of photoisomerization of optically pure trans-2,3-diphenylcyclopropane-1-carboxylic acid derivatives, *Photochem. Photobiol. Sci.*, *4*, 119 (2005).
130. Koodanjeri, S.; Ramamurthy, V. Cyclodextrin mediated enantio and diastereoselective geometric photoisomerization of diphenylcyclopropane and its derivatives, *Tetrahedron Lett.*, *43*, 9229 (2002).
131. Sivasubramanian, K.; Kaanumalle, L. S.; Uppili, S.; Ramamurthy, V. Value of zeolites in asymmetric induction during photocyclization of pyridones, cyclohexadienones and naphthalenones, *Org. Biomol. Chem.*, *5*, 1569 (2007).
132. Lakshminarasimhan, P.; Sunoj, R. B.; Chandrasekhar, J.; Ramamurthy, V. Cation-p interaction controlled selective geometric photoisomerization of diphenylcyclopropane, *J. Am. Chem. Soc.*, *122*, 4815 (2000).
133. Cheung, E.; Chong, K. C. W.; Jayaraman, S.; Ramamurthy, V.; Scheffer, J. R.; Trotter, J. Enantio- and diastereodifferentiating cis,trans-photoisomerization of 2b,3b-diphenylcyclopropane-1a-carboxylic acid derivatives in organized media, *Org. Lett.*, *2*, 2801 (2000).
134. Kaftory, M.; Yagi, M.; Tanaka, K.; Toda, F. Reactions in the solid state. 4. Enantioselective photochemical reactions in crystalline inclusion compounds, *J. Org. Chem.*, *53*, 4391 (1988).
135. Toda, F. Enantiocontrol of photoreactions in the solid state, *Mol. Crys. Liq. Crys.*, *161*, 355 (1988).
136. Toda, F.; Tanaka, K. Enantioselective photoreactions of tropolone alkyl ethers in a crystalline inclusion complex with optically active 1,6-bis(o-chlorophenyl)-1,6-diphenylhexa-2,4-diyne-1,6-diol, *Chem. Commun.*, 1429 (1986).

137. Toda, F.; Tanaka, K.; Yagi, M. Highly selective photoreactions of a-oxoamides and a-tropolone alkyl ethers in crystalline inclusion complexes, *Tetrahedron*, *43*, 1495 (1987).
138. Scheffer, J. R.; Wang, L. Enantioselective photoelectrocyclization of a tropolone derivative in the crystalline state, *J. Phys. Org. Chem.*, *13*, 531 (2000).
139. Ma, L.; Wu, L.-Z.; Zhang, L.-P.; Tung, C.-H. Enantioselectivity of photochemical reactions within polymer microcapsules, *Chin. J. Chem.*, *21*, 96 (2003).
140. Joy, A.; Kaanumalle, L. S.; Ramamurthy, V. Role of cations and confinement in asymmetric photochemistry: Enantio- and diastereo-selective photocyclization of tropolone derivatives within zeolites, *Org. Biomol. Chem.*, *3*, 3045 (2005).
141. Joy, A.; Scheffer, J. R.; Ramamurthy, V. Chirally modified zeolites as reaction media: Photochemistry of an achiral tropolone ether, *Org. Lett.*, *2*, 119 (2000).
142. Kaprinidis, N. A.; Landis, M. S.; Turro, N. J. Supramolecular control of photochemical enantiomeric induction and radical pair recombination in zeolites, *Tetrahedron Lett.*, *38*, 2609 (1997).
143. Edman, J. R. Photorearrangement of benzonorbornadiene, *J. Am. Chem. Soc.*, *91*, 7103 (1969).
144. Hahn, R. C.; Johnson, R. P. Effects of a nitro substituent on di-.pi.-methane rearrangements of benzonorbornadiene and its [3.2.1] homolog, *J. Am. Chem. Soc.*, *99*, 1508 (1977).
145. Joy, A.; Robbins, R. J.; Pitchumani, K.; Ramamurthy, V. Asymmetrically modified zeolite as a medium for enantioselective photoreactions: Reactions from spin forbidden excited states, *Tetrahedron Lett.*, *38*, 8825 (1997).
146. Wada, T.; Shikimi, M.; Inoue, Y.; Lem, G.; Turro, N. J. First photosensitized enantiodifferentiating isomerization by optically active sensitizer immobilized in zeolite supercages, *Chem. Commun.*, *2001*, 1864 (2001).
147. Maeda, H.; Okumura, T.; Yoshimi, Y.; Mizuno, K. Asymmetric induction in an intramolecular [2 + 2] photocycloaddition within chirally modified zeolite supercages, *Tetrahedron: Asymmetry*, *20*, 381 (2009).
148. Benitez, M.; Bringmann, G.; Dreyer, M.; Garcia, H.; Ihmels, H.; Waidelich, M.; Wissel, K. Design of a chiral mesoporous silica and its application as a host for stereoselective di-pi-methane rearrangements, *J. Org. Chem.*, *70*, 2315 (2005).
149. Qiu, H.; Yang, C.; Inoue, Y.; Che, S. Supramolecular photochirogenesis with cyclodextrin—Silica composite. Enantiodifferentiating photocyclodimerization of 2-anthrancenecarboxylate with mesoporous silica wall-capped γ-cyclodextrin, *Org. Lett.*, *11*, 1793 (2009).
150. Fukuhara, G.; Mori, T.; Wada, T.; Inoue, Y. Entropy-controlled supramolecular photochirogenesis: Enantiodifferentiating Z-E photoisomerization of cyclooctene included and sensitized by permethylated 6-O-benzoyl-β-cyclodextrin, *Chem. Commun.*, 4199 (2005).
151. Fukuhara, G.; Mori, T.; Wada, T.; Inoue, Y. Entropy-controlled supramolecular photochirogenesis: Enantiodifferentiating Z-E photoisomerization of cyclooctene included and sensitized by permethylated 6-O-modified β-cyclodextrins, *J. Org. Chem.*, *71*, 8233 (2006).
152. Inoue, Y.; Dong, S. F.; Yamamoto, K.; Tong, L.-H.; Tsuneishi, H.; Hakushi, T.; Tai, A. Inclusion-enhanced optical yield and EIZ ratio in enantiodifferentiating photoisomerization of cyclooctene included and sensitized by p-cyclodextrin monobenzoate, *J. Am. Chem. Soc.*, *113*, 2793 (1995).
153. Lu, R.; Yang, C.; Cao, Y.; Wang, Z.; Wada, T.; Jiao, W.; Mori, T.; Inoue, Y. Supramolecular enantiodifferentiating photoisomerization of cyclooctene with modified β-cyclodextrins: Critical control by a host structure, *Chem. Commun.*, *2008*, 374 (2008).
154. Lu, R.; Yang, C.; Cao, Y.; Tong, L.; Jiao, W.; Wada, T.; Wang, Z.; Mori, T.; Inoue, Y. Enantiodifferentiating photoisomerization of cyclooctene included and sensitized by aroyl-β-cyclodextrins: A critical enantioselectivity control by substituents, *J. Org. Chem.*, *73*, 7695 (2008).
155. Gao, Y.; Inoue, M.; Wada, T.; Inoue, Y. Supramolecular photochirogenesis. 3. Enantiodifferentiating photoisomerization of cyclooctene included and sensitized by 6-O-mono(o-methoxybenzoyl)–cyclodextrin, *J. Incl. Phenom. Macro.*, *50*, 111 (2004).

156. Gao, Y.; Wada, T.; Yang, K.; Kim, K.; Inoue, Y. Supramolecular photochirogenesis in sensitizing chiral nanopore: Enantiodifferentiating photoisomerization of (Z)-cyclooctene included and sensitized by POST-1, *Chirality*, *17*, S19 (2005).
157. Inoue, Y.; Wada, T.; Sugahara, N.; Yamamoto, K.; Kimura, K.; Tong, L.-H.; Gao, X.-M.; Hou, Z.-J.; Liu|, Y. Supramolecular photochirogenesis. 2. Enantiodifferentiating photoisomerization of cyclooctene included and sensitized by 6-O-modified cyclodextrins, *J. Org. Chem.*, *65*, 8041 (2000).
158. Yang, C.; Mori, T.; Wada, T.; Inoue, Y. Supramolecular enantiodifferentiating photoisomerization of (Z,Z)-1,3-cyclooctadiene included and sensitized by naphthalene-modified cyclodextrins, *New J. Chem.*, *31*, 697 (2007).
159. Vizvardi, K.; Toppet, S.; Hoornaert, G. J.; De Keukeleire, D.; Bak, P.; Van der Eycken, E. Intramolecular ortho and meta photocycloadditions of 4-phenoxybut-1-enes substituted in the arene residue with carbomethoxy, carbomethoxymethyl, and 2-carbomethoxyethyl groups, *J. Photochem. Photobiol. A: Chem.*, *133*, 135 (2000).
160. Wender, P. A.; Howbert, J. J. Synthetic studies on arene-olefin cycloadditions: Total synthesis of (.±.)-.alpha.-cedrene, *J. Am. Chem. Soc.*, *103*, 688 (1981).
161. Vizvardi, K.; Desmet, K.; Luyten, I.; Sandra, P.; Hoornaert, G.; Van der Eycken, E. Asymmetric induction in intramolecular meta photocycloaddition: Cyclodextrin-mediated solid-phase photochemistry of various phenoxyalkenes, *Org. Lett.*, *3*, 1173 (2001).
162. Mori, T.; Wada, T.; Inoue, Y. Perfect switching of photoreactivity by acid: Photochemical decarboxylation versus transesterification of mesityl cyclohexanecarboxylate, *Org. Lett.*, *2*, 3401 (2000).
163. Mori, T.; Inoue, Y.; Weiss, R. G. Enhanced photodecarboxylation of an aryl ester in polyethylene films, *Org. Lett.*, *5*, 4661 (2003).
164. Mori, T.; Saito, H.; Inoue, Y. Complete memory of chirality upon photodecarboxylation of mesityl alkanoate to mesitylalkane: Theoretical and experimental evidence for cheletropic decarboxylation via a spiro-lactonic transition state, *Chem. Commun.*, 2302 (2003).
165. Mori, T.; Takamoto, M.; Wada, T.; Inoue, Y. Acid-controlled photoreactions of aryl alkanoates: Competition of transesterification, decarboxylation, Fries-rearrangement and/or transposition, *Photochem. Photobiol. Sci.*, *2*, 1187 (2003).
166. Mori, T.; Weiss, R. G.; Inoue, Y. Mediation of conformationally controlled photodecarboxylations of chiral and cyclic aryl esters by substrate structure, temperature, pressure, and medium constraints, *J. Am. Chem. Soc.*, *126*, 8961 (2004).
167. Tamaki, T.; Kokubu, T. Acceleration of the photodimerization of water-soluble anthracenes included by b and g cyclodextrins, *J. Incl. Phenom. Macro.*, *2*, 815 (1984).
168. Tamaki, T.; Kokubu, T.; Ichimura, K. Regio and stereoselective photodimerization of anthracene derivatives included by cyclodextrins, *Tetrahedron Lett.*, *43*, 1485 (1987).
169. Yang, C.; Nakamura, A.; Fukuhara, G.; Origane, Y.; Mori, T.; Wada, T.; Inoue, Y. Pressure and temperature-controlled enantiodifferentiating [4 + 4]-photocyclodimerization of 2-anthracenecarboxylate mediated by secondary face- and skeleton-modified gamma -cyclodextrins, *J. Org. Chem.*, *71*, 3126 (2006).
170. Ikeda, H.; Nihei, T.; Ueno, A. Template-assisted stereoselective photocyclodimerization of 2-anthracenecarboxylic acid by bispyridinio-appended gamma-cyclodextrin, *J. Org. Chem.*, *70*, 1237 (2005).
171. Nakamura, A.; Inoue, Y. Electrostatic manipulation of enantiodifferentiating photocyclodimerization of 2-anthracenecarboxylate within gamma -cyclodextrin cavity through chemical modification. Inverted product distribution and enhanced enantioselectivity, *J. Am. Chem. Soc.*, *127*, 5338 (2005).
172. Yang, C.; Nishijima, M.; Nakamura, A.; Mori, T.; Wada, T.; Inoue, Y. A remarkable stereoselectivity switching upon solid-state versus solution-phase enantiodifferentiating photocyclodimerization of 2-anthracenecarboxylic acid mediated by native and 3,6-anhydro-gamma -cyclodextrins, *Tetrahedron Lett.*, *48*, 4357 (2007).
173. Yang, C.; Nakamura, A.; Wada, T.; Inoue, Y. Enantiodifferentiating photocyclodimerization of 2-anthracenecarboxylic acid mediated by gamma -cyclodextrins with a flexible or rigid cap, *Org. Lett.*, *8*, 3005 (2006).

174. Yang, C.; Mori, T.; Inoue, Y. Supramolecular enantiodifferentiating photocyclodimerization of 2-anthracenecarboxylate mediated by capped g-cyclodextrins: Critical control of enantioselectivity by cap rigidity, *J. Org. Chem.*, *73*, 5786 (2008).
175. Yang, C.; Ke, C.; Fujita, K.; Yuan, D.-Q.; Mori, T.; Inoue, Y. pH-Controlled supramolecular enantiodifferentiating photocyclodimerization of 2-anthracenecarboxylate with capped γ-cyclodextrins, *Aust. J. Chem.*, *61*, 565 (2008).
176. Yang, C.; Mori, T.; Origane, Y.; Ko, Y. H.; Selvapalam, N.; Kim, K.; Inoue, Y. Highly stereoselective photocyclodimerization of a-cyclodextrin-appended anthracene mediated by g-cyclodextrin and cucurbit[8]uril: A dramatic steric effect operating outside the binding site, *J. Am. Chem. Soc.*, *130*, 8574 (2008).
177. Fukuhara, G.; Mori, T.; Wada, T.; Inoue, Y. The first supramolecular photosensitization of enantiodifferentiating bimolecular reaction: Anti-Markovnikov photoaddition of methanol to 1, 1-diphenylpropene sensitized by modified β-cyclodextrin, *Chem. Commun.*, *2006*, 1712 (2006).
178. Fukuhara, G.; Mori, T.; Inoue, Y. Competitive enantiodifferentiating anti-Markovnikov photoaddition of water and methanol to 1,1-diphenylpropene using a sensitizing cyclodextrin host, *J. Org. Chem.*, *74*, 6714 (2009).
179. Luo, L.; Cheng, S.; Chen, B.; Tung, C.; Wu, L. Stepwise photochemical-chiral delivery in γ-cyclodextrin-directed enantioselective photocyclodimerization of methyl 3-methoxyl-2-naphthoate in aqueous solution, *Langmuir*, *26*, 197 (2010).
180. Festa, C.; Levi-Minzi, N.; Zandomeneghi, M. Photochemistry in biological matrixes: Binding site photoreactivity of ketoprofen in serum albumins and chiral discrimination, *Gazz. Chim. Ital.*, *126*, 599 (1996).
181. Levi-Minzi, N.; Zandomeneghi, M. Photochemistry in biological matrices: Activation of racemic mixtures and interconversion of enantiomers, *J. Am. Chem. Soc.*, *114*, 9300 (1992).
182. Ouchi, A.; Zandomeneghi, G.; Zandomeneghi, M. Complexation with albumins of chiral aromatic substrates and their chemistry in ground and excited states. Catalytic and chirality recognition properties of the protein in the cases of binaphthol, its photoisomers, and ketoprofen, *Chirality*, *14*, 1 (2002).
183. Nishijima, M.; Wada, T.; Mori, T.; Pace, T. C. S.; Bohne, C.; Inoue, Y. Highly enantiomeric supramolecular [4 + 4] photocyclodimerization of 2-anthracenecarboxylate mediated by human serum albumin, *J. Am. Chem. Soc.*, *129*, 3478 (2007).
184. Wada, T.; Nishijima, M.; Fujisawa, T.; Sugahara, N.; Mori, T.; Nakamura, A.; Inoue, Y. Bovine serum albumin-mediated enantiodifferentiating photocyclodimerization of 2-anthracenecarboxylate, *J. Am. Chem. Soc.*, *125*, 7492 (2003).
185. Nishijima, M.; Pace, T. C. S.; Nakamura, A.; Mori, T.; Wada, T.; Bohne, C.; Inoue, Y. Supramolecular photochirogenesis with biomolecules. Mechanistic studies on the enantiodifferentiation for the photocyclodimerization of 2-anthracenecarboxylate mediated by bovine serum albumin, *J. Org. Chem.*, *72*, 2707 (2007).
186. Pace, T.; Nishijima, M.; Wada, T.; Inoue, Y.; Bohne, C. Photophysical studies on the supramolecular photochirogenesis for the photocyclodimerization of 2-anthracenecarboxylate within human serum albumin, *J. Phys. Chem. B*, *113*, 10445 (2009).
187. Kragh-Hansen, U. Molecular aspects of ligand binding to serum albumin, *Pharmacol. Rev.*, *33*, 17 (1981).
188. Peters, T. *All about Albumin: Biochemistry, Genetics, and Medical Applications*; Academic Press: San Diego, CA (1996).
189. Ishida, Y.; Kai, Y.; Kato, S.; Misawa, A.; Amano, S.; Matsuoka, Y.; Saigo, K. Two-component liquid crystals as chiral reaction media: Highly enantioselective photodimerization of an anthracene derivative driven by the ordered microenvironment, *Angew. Chem. Int. Ed.*, *47*, 8241 (2008).
190. Lv, F.-F.; Chen, B.; Wu, L.-Z.; Zhang, L.-P.; Tung, C.-H. Enhanced stereoselectivity in photoelectrocyclization of tropolone ethers via confinement in chiral inductor-modified lyotropic liquid crystals, *Org. Lett.*, *10*, 3473 (2008).

191. Lv, F.; Li, X.; Wu, L.; Tung, C. Photochemical reaction of cyclohexyl phenyl ketone within lyotropic liquid crystals, *Tetrahedron, 64*, 1918 (2008).
192. Xiao, D.; Wada, T.; Inoue, Y. Supramolecular enantiodifferentiating photoisomerization of (Z)-cyclooctene in lyotropic and thermotropic liquid crystals, *Chirality, 21*, 110 (2008).
193. Arumugam, S. Nafion as an efficient reaction medium for diastereoselective photochemical reactions, *Tetrahedron Lett., 49*, 2461 (2008).
194. Arumugam, S.; Kaanumalle, L.; Ramamurthy, V. Alkali ion exchanged nafion as a confining medium for photochemical reactions, *Photochem. Photobiol., 82*, 139 (2006).
195. Breitenlechner, S.; Bach, T. A polymer-bound chiral template for enantioselective photochemical reactions, *Angew. Chem. Int. Ed., 47*, 7957 (2008).
196. Furusawa, T.; Kawano, M.; Fujita, M. The confined cavity of a coordination cage suppresses the photocleavage of alpha -diketones to give cyclization products through kinetically unfavorable pathways, *Angew. Chem. Int. Ed., 46*, 5717 (2007).
197. Yoshizawa, M.; Takeyama, Y.; Okano, T.; Fujita, M. Cavity-directed synthesis within a self-assembled coordination cage: Highly selective [2 + 2] cross-photodimerization of olefins, *J. Am. Chem. Soc., 125*, 3243 (2003).
198. Yoshizawa, M.; Tamura, M.; Fujita, M. Diels-Alder in aqueous molecular hosts: Unusual regioselectivity and efficient catalysis, *Science, 312*, 251 (2006).
199. Nishioka, Y.; Yamaguchi, T.; Kawano, M.; Fujita, M. Asymmetric [2 + 2] olefin cross photoaddition in a self-assembled host with remote chiral auxiliaries, *J. Am. Chem. Soc., 130*, 8160 (2008).
200. Seo, J. S.; Whang, D.; Lee, H.; Jun, S. I.; Oh, J.; Jeon, Y. J.; Kim, K. A homochiral metal-organic porous material for enantioselective separation and catalysis, *Nature, 404*, 982 (2000).
201. Sundaresan, A. K.; Gibb, C. L. D.; Gibb, B. C.; Ramamurthy, V. Chiral photochemistry in a confined space: Torquoselective photoelectrocyclization of pyridones within an achiral hydrophobic capsule, *Tetrahedron, 65*, 7277 (2009).
202. Sundaresan, A. K.; Kaanumalle, L. S.; Gibb, C. L. D.; Gibb, B. C.; Ramamurthy, V. Chiral photochemistry within a confined space: Diastereoselective photorearrangements of a tropolone and a cyclohexadienone included in a synthetic cavitand, *Dalton Trans.*, 4003 (2009).
203. Shirakawa, M.; Fujita, N.; Tani, T.; Kaneko, K.; Shinkai, S. Organogel of an 8-quinolinol platinum (ii) chelate derivative and its efficient phosphorescence emission effected by inhibition of dioxygen quenching, *Chem. Commun., 2005*, 4149 (2005).
204. Natarajan, A.; Mague, J.; Ramamurthy, V. Asymmetric induction during yang cyclization of α-oxoamides: The power of a covalently linked chiral auxiliary is enhanced in the crystalline state, *J. Am. Chem. Soc., 127*, 3568 (2005).
205. Natarajan, A.; Mague, J. T.; Ramamurthy, V. Viability of a covalent chiral auxiliary method to induce asymmetric induction in solid-state photoreactions explored, *Cryst. Growth Des., 5*, 2348 (2005).
206. Xia, W.; Scheffer, J. R.; Botoshansky, M.; Kaftory, M. Photochemistry of 1-isopropylcycloalkyl aryl ketones: Ring size effects, medium effects, and asymmetric induction, *Org. Lett., 7*, 1315 (2005).
207. Patrick, B. O.; Scheffer, J. R.; Scott, C. Preorganization of achiral molecules for asymmetric synthesis through crystallization-induced immobilization in homochiral conformations, *Angew. Chem. Int. Ed., 42*, 3775 (2003).
208. Xia, W.; Scheffer, J.; Patrick, B. Making use of crystallization-induced asymmetric transformations in solid state organic photochemistry: Application to the enantioselective Yang photocyclization of *endo*-bicyclo[2.1.1]hexyl aryl ketones, *CrystEngComm., 7*, 728 (2005).
209. Xia, W.; Yang, C.; Patrick, B. O.; Scheffer, J. R.; Scott, C. Asymmetric synthesis of dihydrofurans via a formal retro-Claisen photorearrangement, *J. Am. Chem. Soc., 127*, 2725 (2005).
210. Chen, S.; Patrick, B. O.; Scheffer, J. R. Enantioselective photochemical synthesis of a simple alkene via the solid state ionic chiral auxiliary approach, *J. Org. Chem., 69*, 2711 (2004).

211. Xia, W.; Yang, C.; Scheffer, J. R.; Patrick, B. O. Engineering acyclic alkyl aryl ketones for enantioselective Norrish/Yang type II photochemistry in the crystalline state, *CrystEngComm.*, *8*, 388 (2006).
212. Koshima, H.; Kawanishi, H.; Nagano, M.; Yu, H.; Shiro, M.; Hosoya, T.; Uekusa, H.; Ohashis, Y. Absolute asymmetric photocyclization of isopropylbenzophenone derivatives using a cocrystal approach involving single-crystal-to-single-crystal transformation, *J. Org. Chem.*, *70*, 4490 (2005).
213. Morimoto, M.; Kobatake, S.; Irie, M. Absolute asymmetric photocyclization in chiral diarylethene co-crystals with octafluoronaphthalene, *Chem. Commun.*, 335 (2008).

7

Enantioselective Photoreactions in Solution

Kerrie A.B. Austin
Technische Universität München

Thorsten Bach
Technische Universität München

7.1 Introduction

While enantioselective reactions can, in the broadest sense, be understood as reactions in which enantiomerically pure compounds are produced, this section will be mostly concerned with reactions in which a new element of chirality is created from achiral starting materials. Auxiliary-induced diastereoselective reactions are therefore not covered by this review. Due to the increasing importance of helically and axially chiral compounds, we have, however, added a section on chirality transfer and chiral memory phenomena. In general, emphasis was put on recently reported work ideally with a synthetic relevance. Previous reviews on the topic have appeared in journals[1] and in books, for example, in Volume 11 of the *Molecular and Supramolecular Photochemistry* series,[2] and the reader is referred to Chapter 61 in the second edition of this handbook[3] as a guideline to older reviews about stereoselective photocycloaddition reactions. Recent reviews on photochemical reactions in total synthesis[4,5] might be useful for those interested in the preparative aspects of photochemistry. In addition, two chapters in this handbook, on photochemistry in confined media (Chapter 11) and on photochirogenesis (Chapter 6), deal with closely related topics. Finally, it should be mentioned that this account deals exclusively with solution-phase photochemistry.

7.2 Asymmetric Induction by Small Molecule Chiral Templates

When prochiral compounds are used as starting materials, a chiral environment is required to induce asymmetry. Chiral templates or complexing agents associate with a substrate via multipoint, noncovalent interactions, and complexation provides a chiral environment for the reaction to occur. If no catalytically active reaction center is present in such a template, the template must be used in stoichiometric or even superstoichiometric

quantities (Section 7.2.1). If, however, the complexation is combined with an energy or electron transfer from or to the template, it is possible to use these templates substoichiometrically (Section 7.2.2).

7.2.1 Stoichiometric Reagents

Several chiral templates that are used in stoichiometric amounts to induce enantioselectivity in photochemical reactions have been reported and are depicted in Scheme 7.1 (**1**–**5**). Each possesses a number of donor and acceptor sites for hydrogen bonding to the appropriate substrates.

The [4 + 4]-photocyclodimerization of anthracene derivatives is a popular target system for the study of template-mediated enantioselective reactions (Scheme 7.2) and will be referred to a number of times during this chapter. When the anthracene core is asymmetrically substituted, four dimeric products are possible (**7**–**10**), two of which are chiral (**7** and **8**). It should be noted that the absolute configurations of dimers **7** and **8** have not been determined in any example discussed in this chapter and therefore the "+" and "–" notation given to these compounds refers only to the order of elution from the HPLC column.

Inoue and coworkers have reported that irradiation of 2-anthracenecarboxylic acid (**6**) in the presence of chiral template **1** afforded chiral dimers "–"-**7** and "–"-**8** in enantiomeric excesses (*ee*) of up to 49% and 43%, respectively.[6,7] NMR studies showed that template **1** binds anthracene **6** through a dual hydrogen-bonding motif incorporating the carboxylic acid and the hydroxymethylpyrrolidine moieties. Coordination of compound **6** to the chiral template leads to the formation of a pair of diastereomeric complexes where either the *re*- or the *si*-face is shielded by the methoxybenzamide moiety, which blocks the approach of the second

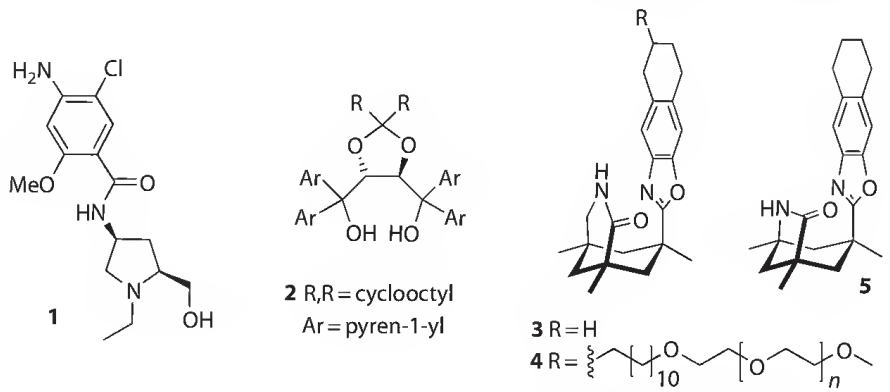

SCHEME 7.1 Structures of chiral templates, **1**–**4**, which are used in stoichiometric amounts to induce enantioselectivity in photochemical reactions.

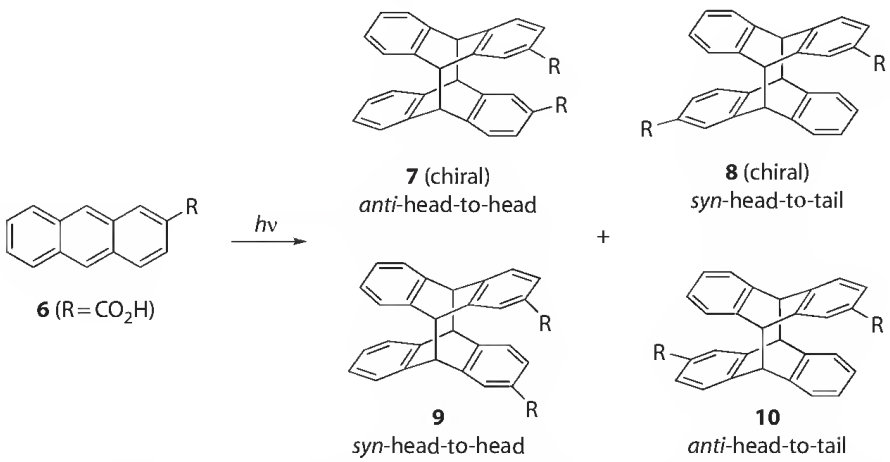

SCHEME 7.2 Intermolecular [2 + 2]-photocyclodimerization of 2-anthracenecarboxylic acid (**6**) to afford chiral dimers **7** and **8**, and achiral dimers **9** and **10**.

anthracene molecule. Circular dichroism was used to prove that while bound to template **1**, anthracene **6** is in a chiral environment. However, further studies indicated that the enantioselectivities observed were not determined solely by the relative amounts of the two diastereomeric complexes in the ground state, but also depended on their relative excited-state lifetimes. Specifically, the *re*-complex, which was determined to have the shorter singlet excited-state lifetime, was found to produce lower *ee* values than the corresponding *si*-complex. This is the first example, in which the combination of the ground- and excited-state properties of a host–guest complex has been invoked to explain the enantioselectivities observed for the reaction.

Functionalized TADDOL derivatives, such as **2** (Scheme 7.1), have also been used as chiral mediators for enantioselective photocycloaddition reactions.[8,9] Enantioselective [3 + 2]-cycloaddition of 3-hydroxyflavone **11** and methyl cinnamate was achieved in the presence of TADDOL **2** affording cycloadduct **13** in 58% yield (Scheme 7.3).[8] The enantioselectivity of the reaction was determined following base-induced rearrangement and reduction of compound **13** and found to be up to 89% *ee*.

On irradiation, oxidopyrylium betaine **12** is generated by excited-state intramolecular proton transfer (ESIPT). Previous studies on racemic material[10] had revealed that a polar solvent such as methanol is required to facilitate this process via double proton transfer. In contrast, the enantioselective variant is conducted in apolar solvents, with compound **2** (Scheme 7.1) having the dual role of imparting chiral information and facilitating ESIPT. Both the aryl substituent (Ar) and the ketyl side chain (R) of compound **2** (Scheme 7.1) were shown to be important for generating enantioselectivity as some substitution patterns resulted in the TADDOL derivatives adopting conformations in which hydrogen bonding to the substrate is no longer possible. It is thought that enantioselectivity is achieved by hydrogen bonding of the electron-rich phenoxide oxygen of betaine **12** to template **2**, resulting in shielding of one of the enantiotopic faces of the substrate. This reaction was successfully applied in the total synthesis of rocaglamide natural products; for example, rocaglaol (**14**) was obtained in three steps from cycloadduct **13** and in 96% *ee* following recrystallization.

Chiral lactam **3** (Scheme 7.1) has been used to induce asymmetry in a variety of photochemically promoted processes including Diels–Alder reactions, [6π]-cyclizations, [4 + 4]-photocycloaddition reactions, intra- and intermolecular [2 + 2]-photocycloaddition reactions, and Norrish–Yang cyclizations.[11] Template **3** possesses a lactam binding site for coordination of amide or lactam substrates and a sterically demanding backbone that shields one of the enantiotopic faces of a bound, prochiral substrate. In order to maximize substrate–template association, the reactions are typically run at low temperature in nonpolar solvents. Due to the bulk of the tetrahydronaphthalene shield, self-association of enantiomerically pure

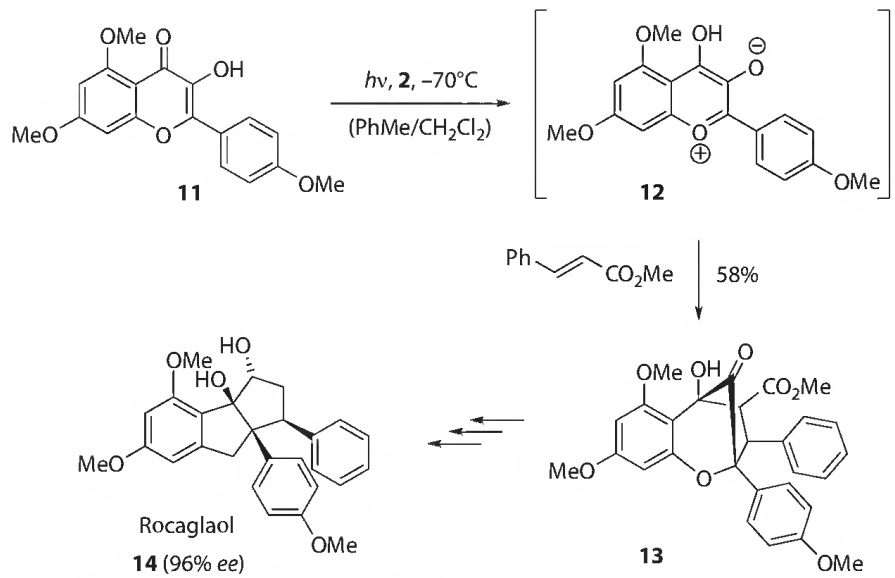

SCHEME 7.3 Enantioselective [3 + 2]-photocycloaddition of photochemically generated oxidopyrylium betaine **12** and methyl cinnamate to give adduct **13**, which was subsequently transformed into rocaglaol (**14**).

template **3** is effectively 0. This allows the use of an excess of template and in most cases the reactions are run in the presence of 2.5 equivalents of compound **3** in order to maximize template–substrate association and minimize substrate self-association. The complexing agent is stable under irradiation at $\lambda \geq 300$ nm and in most cases can be recovered in yields >90% by simple column chromatography. An account of the early successes achieved using this chiral complexing agent was included in the previous edition of this book,[3] so this section will serve only to update the reader of progress that has been made since 2002.

Photochemically generated *o*-quinodimethane **16** was shown to undergo a highly enantioselective Diels–Alder reaction with a number of dienes in the presence of template **3** (Scheme 7.4).[12,13] Enantiomeric excesses of 91%–94% *ee* were obtained for the major diastereomer even when only 1.2 equivalents of the template were used. With increasing template concentrations (up to 2.5 equivalents) selectivities of up to 97% *ee* could be achieved. The simple diastereoselectivity was dependent on the dienophile used with diastereomeric ratios (dr = *endo/exo*) ranging from >95/5 (methyl acrylate) to 25/75 (acrylonitrile).

This level of enantioselectivity is the best that has been achieved to date using template **3**, which can be explained in terms of differences in template-binding affinity of the product relative to the substrate. Titration studies indicated that the product has only weak association with the template and, as a result, the ratio of free template to starting material increases as the reaction progresses. This was supported by the observation that the enantioselectivity improved with increased conversion.

Investigations continue to explore the scope of substrates that can be used in [2 + 2]-photocycloaddition reactions with template **3**. 4-(2′-Aminoethyl)quinolones undergo enantioselective inter- and intramolecular photocycloaddition reactions (70%–92% *ee*) with unsymmetrically 1,1-disubstituted olefins to generate two adjacent quaternary centers.[14,15] This reaction was successfully employed in an enantioselective total synthesis of the indole alkaloid (+)-meloscine (**22**).[16] Intermolecular [2 + 2]-photocycloaddition of the silylenolether derived from methyl pyruvate to quinolone **18** gave, after purification by chiral HPLC, the enantiomerically pure product **19**. Subsequent retro-benzilic acid rearrangement, presumably via intermediate **20**, afforded the tricyclic product **21**, which was further elaborated to the target natural product (**22**) (Scheme 7.5).[17]

Alkenyl-substituted 5,6-dihydro-1*H*-pyridin-2-ones have recently been investigated as substrates for enantioselective intramolecular [2 + 2]-photocycloaddition reactions (Scheme 7.6). Upon irradiation at $\lambda = 254$ nm, and under standard conditions (−60°C to −75°C, nonpolar solvent), these substrates underwent

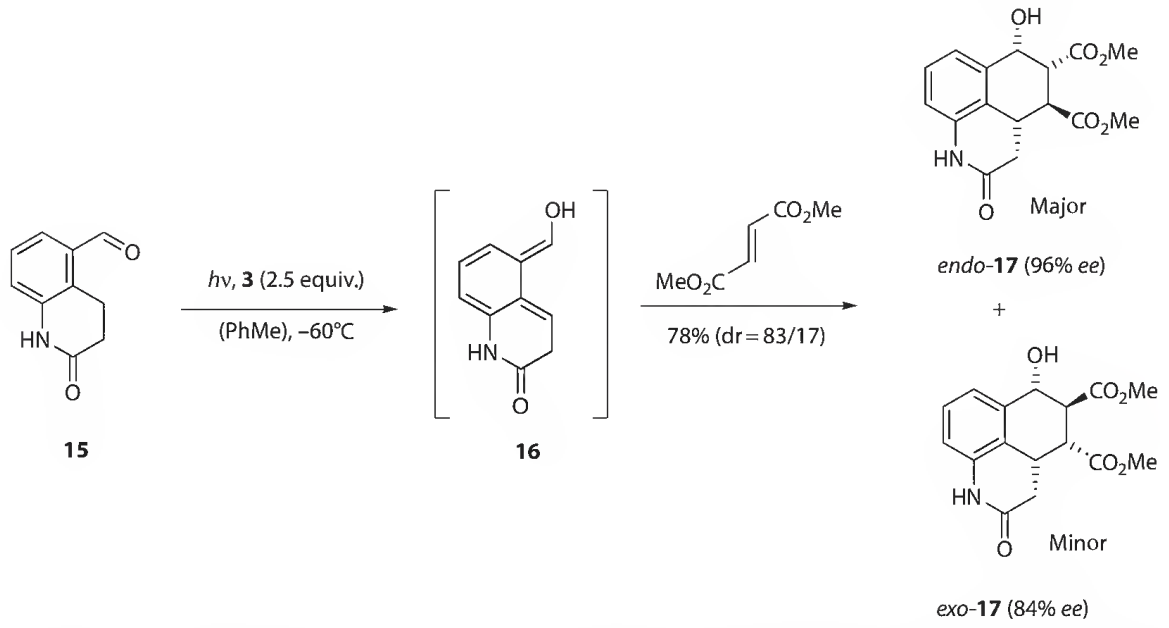

SCHEME 7.4 Enantioselective Diels–Alder reaction of photochemically generated *o*-quinodimethane **16** and dimethylfumarate to afford cycloadducts *endo*- and *exo*-**17** (dr = *endo/exo* = 83/17), in 96% *ee* and 84% *ee*, respectively.

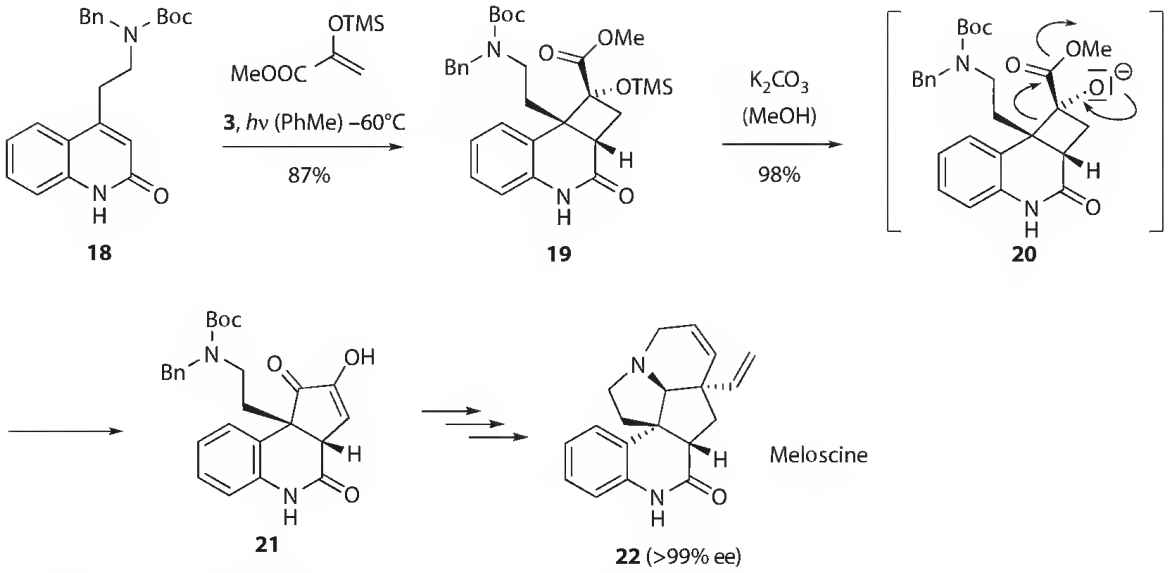

SCHEME 7.5 Total synthesis of the melodinus alkaloid meloscine (**22**), involving an enantioselective [2 + 2]-photocycloaddition of quinolone **18**.

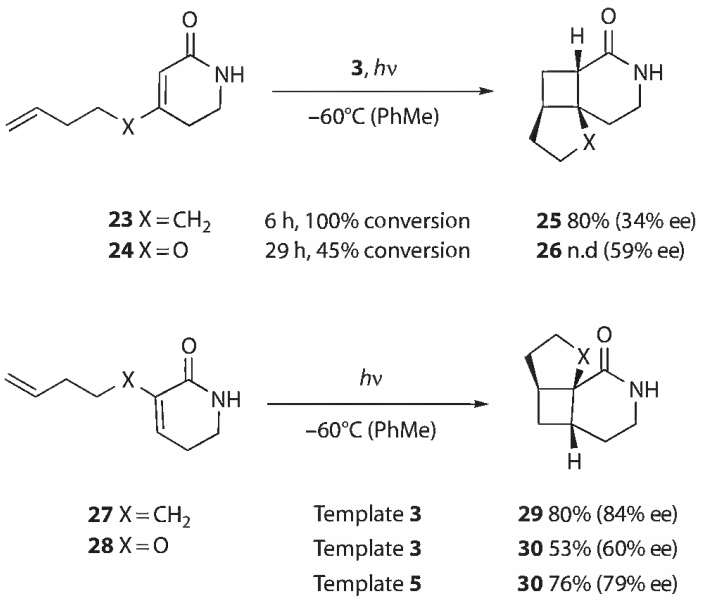

SCHEME 7.6 Enantioselective intramolecular [2 + 2]-photocycloadditions of dihydropyridin-2-ones **23**, **24**, **27**, and **28**.

diastereo- and regioselective [2 + 2]-cycloadditions to afford the corresponding cyclobutane products in moderate to good enantioselectivities (34%–85% *ee*). A large difference in reaction rate and enantioselectivity was observed depending on the nature and position of the tether. Substitution in the 4-position (**23**,**24**) afforded products with disappointingly low enantioselectivity.[18] The reaction of compound **23**, possessing an all carbon tether, was complete within 6 h affording cyclobutane **25** in only 34% *ee*. In contrast, the oxygen-substituted substrate (**24**) showed promising enantioselectivity after 3 h (75% ee) but delivered only 6% conversion. Upon continued irradiation the enantiomeric excess of product **26** decreased, which is thought to be due to decomposition of the complexing agent, and complete conversion was never achieved.

Better results were obtained with the 3-substituted analogues (**27**,**28**).[19] A significant increase in enantioselectivity was observed for compound **27** and improved reaction rates resulted in complete conversion after only 4 h, even for compound **28**, which possesses an oxygen-containing tether. It was

proposed that the differences in reactivity and enantioselectivity exhibited by these 5,6-dihydro-1*H*-pyridin-2-one derivatives are due to a combination of binding affinity, substrate shielding, and conformational aspects in the reaction intermediates.

Modifications to both the shield moiety and the binding site of chiral complexing agent **3** have also been reported. The nor-analogue (**5**, Scheme 7.1), which possesses a γ-lactam rather than a δ-lactam binding site, was prepared and employed in the [2 + 2]-photocycloaddition of 3-substitued 5,6-dihydro-1*H*-pyridin-2-ones (Scheme 7.6).[19] Although there was little difference observed in the enantiomeric excesses obtained for substrates possessing all carbon tethers (compound **29** was obtained in 85% *ee* with template **5** compared to 84% *ee* with template **3**) a significant increase in enantioselectivity was achieved for cycloadditions involving oxygen-tethered substrates such as **28**. Immobilization of template **3** on a polymeric support was investigated as a way to simplify and optimize its recovery and reuse.[20] Methoxypolyethylene glycol (MPEG) bound template (**4**) provided high conversions and enantioselectivity, under the standard irradiation conditions, for the [2 + 2]-photocycloaddition reaction of 4-allyloxyquinolone. Furthermore, the template was easily recovered from the reaction mixture in yields of 97%–99% by precipitation and filtration.

7.2.2 Catalytic Reagents

Enantioselective catalysis in templated photochemistry is possible if the reaction proceeds more rapidly in the bound complex than in the unbound substrate. The photochemical reaction may be accelerated either by energy or electron transfer, but in either case in order for the reaction to be both enantioselective and catalytic direct excitation of the substrate must be completely avoided. Furthermore, the lability of the system must be such that the substrate remains bound while the reaction is taking place but then the product is released to allow the catalyst to bind a new substrate.

To date, only a few distinct catalytic reagents, **31**–**33** (Scheme 7.7), have been reported that have the ability to induce asymmetry in photochemical reactions via hydrogen bonding. Each possesses a combination of a binding motif in a chiral environment and a sensitizer moiety able to accelerate a photochemical reaction by electron or energy transfer.

Catalytic, enantioselective photoinduced cyclization of quinolone **34** was achieved using chiral lactam **31**.[21] Upon irradiation of the host–guest complex, the benzophenone moiety accepts an electron from the bound substrate via photon electron transfer (PET). The benzophenone shield then serves to ensure that intramolecular cyclization of the resultant diradical can only occur from one face of the prochiral substrate. 30 mol% of catalyst afforded product **35** in 64% yield and 70% *ee* (Scheme 7.8).

Chiral template **31** was subsequently investigated as a chiral sensitizer for the intramolecular [2 + 2]-photocycloaddition of quinolones.[22] In this case the benzophenone moiety accelerates the rate of reaction by triplet energy transfer rather than PET. Irradiation of quinolone **36** at λ = 366 nm in the presence of 10 mol% of catalyst **31** afforded compounds **37** and **38** in 39% and 17% *ee*, respectively. The low enantioselectivity was attributed to the relatively low triplet energy and short wavelength absorbance

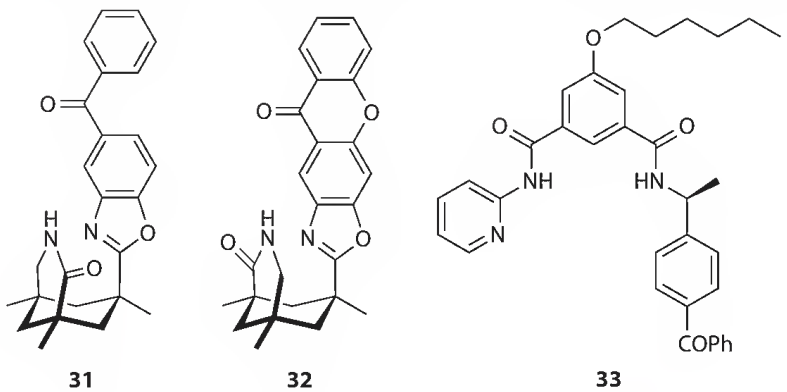

31 **32** **33**

SCHEME 7.7 Structures of catalytic chiral templates, **31**–**33**, employed in enantioselective photochemical reactions.

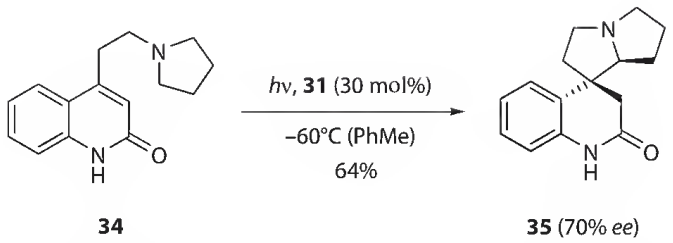

SCHEME 7.8 Enantioselective PET catalysis in the cyclization of quinolone **34** to product **35**.

of the benzophenone moiety. Successful triplet sensitization requires that the triplet energy of the sensitizer be significantly higher than the triplet energy of the substrate to allow rapid energy transfer. In catalyst **32** the benzophenone shield is replaced by a xanthone chromophore, which better fulfills these criteria. Xanthone **32** proved to be a far superior catalyst for the [2 + 2]-cycloaddition of quinolone **36**, affording photoproducts **37** and **38** in up to 90% *ee* with 5 mol% catalyst loading. The enantioselectivity could be improved to 94% by increasing the catalyst loading to 20 mol% (Scheme 7.9).

The proposed catalytic cycle is depicted in Scheme 7.10. Catalyst–substrate complex (**32:36**) formation is achieved via two hydrogen bonds. Irradiation of the complex at λ = 366 nm results in selective

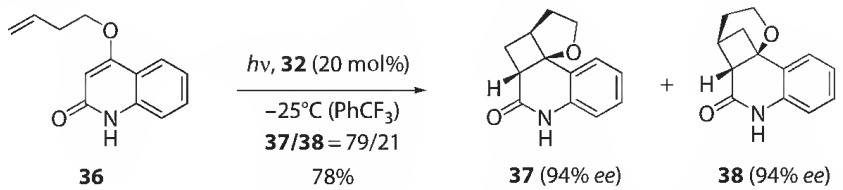

SCHEME 7.9 Catalytic, enantioselective intramolecular [2 + 2]-photocycloaddition of quinolone **36** to afford cycloadducts **37** and **38** in 94% *ee*.

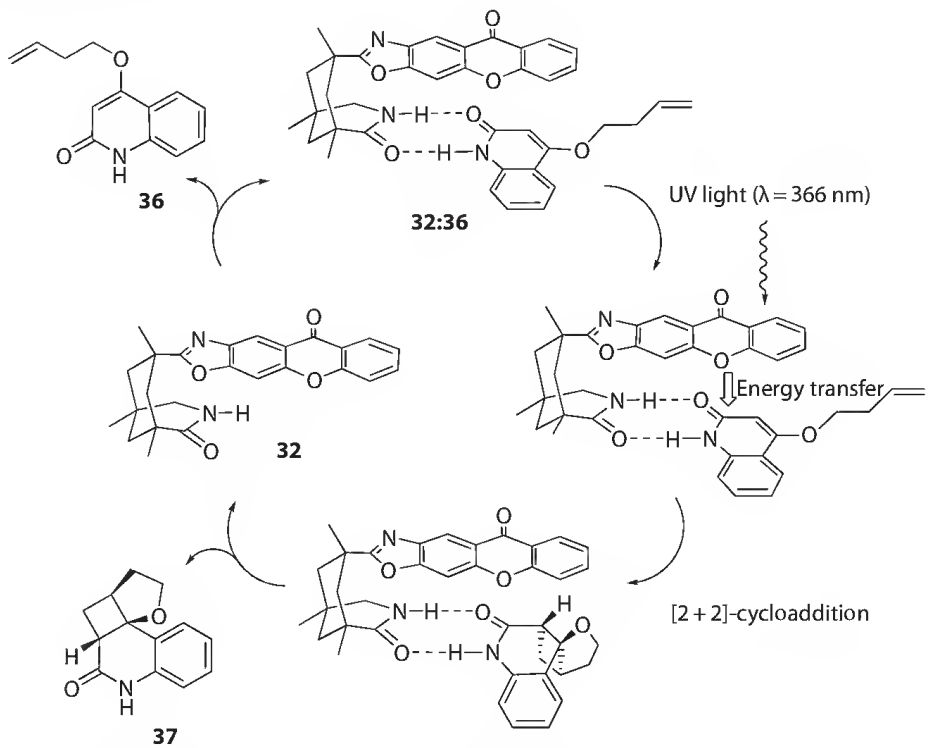

SCHEME 7.10 Proposed catalytic cycle for the enantioselective [2 + 2]-photocycloaddition of quinolone **36** in the presence of chiral catalyst **32**.

excitation of the xanthone chromophore followed by rapid triplet energy transfer from the xanthone to the bound substrate. The excited substrate then undergoes an intramolecular [2 + 2]-cycloaddition, the steric bulk of the xanthone moiety now serving to ensure that cycloaddition only occurs at one face of the bound substrate. The product is, therefore, generated as a single enantiomer and its release from the complex regenerates the catalyst to restart the catalytic cycle.

Template **33** (Scheme 7.7), which also possesses a sensitizing benzophenone moiety, was found to induce asymmetry in substoichiometric amounts in the [2 + 2]-photocycloaddition of quinolone **36**.[23] Irradiation of compound **36** in the presence of 25 mol% of catalyst **33** afforded the enantiomer of **37**, *ent*-**37**, in 19% *ee*. Increasing the catalyst loading did not significantly increase the product *ee* indicating that the low enantioselectivity was not a result of direct excitation of unbound substrate but rather that the face differentiation of the prochiral substrate by the catalyst was not sufficient.

7.3 Asymmetric Induction by Supramolecular Hosts

The distinction between Sections 7.2 and 7.3 may seem a bit arbitrary, but it is justified by the fact that the binding interactions in supramolecular hosts are frequently stronger than in low-molecular-weight templates; however, the orientation of binding is somewhat more difficult to alter and to control. Recent progress includes three major areas: cyclodextrins (Section 7.3.1), self-assembled cavitands (Section 7.3.2), and biological templates (Section 7.3.3).

7.3.1 Cyclodextrins

Cylcodextrins (CDs) are particularly attractive as host molecules because they accept a wide variety of guests with low specificity, are chiral, readily available, and easily modified. Furthermore, their transparency in the UV-vis region means they can be used in photochemical reactions. Nakamura and Inoue observed significant asymmetric induction in the cyclodimerization of 2-anthracenecarboxylate (**6**, R = CO_2^-, Scheme 7.2) in the presence of γ-cyclodextrin.[24] Irradiation of an aqueous solution of anthracene **6** and γ-CD (5 equivalents) at 0°C afforded the *syn*-head-to-tail (*syn*-HT) dimer "+"-**8** in 41% *ee* as the major product (46% yield). γ-Cyclodextrin can accommodate two molecules of compound **6** into its chiral cavity. The relative orientation of these molecules in the ground state complex determines the distribution and selectivity in photoproduct formation. Of the four possible isomers the HT dimers were favored due to electrostatic repulsion of the carboxylate groups (combined yields of dimers **8** and **10** were 85%–90%). In the case of chiral dimer **8** the chirality of the cavity results in one precursor complex being more stable than the other thus one enantiomer is formed preferentially.

Methyl 3-methoxy-2-naphthoate (**39**) was also found to undergo enantioselective photodimerization in the presence of γ-CD. In contrast to the previous reaction, the absence of charged groups resulted in the guest molecules favoring a head-to-head (HH) orientation in the complex. The *anti*-HH cubane-like photodimer **41** was obtained as the major product in 85% yield and 48% *ee* (Scheme 7.11).[25,26] Isolation of the intermediate [4 + 4]-dimer **40** in 39% *ee* revealed that the chirality of cyclobutane **41** is achieved in a stepwise fashion, via an *in situ* increase of the enantioselectivity during the second step of the reaction.

While these results are promising, the inherent chirality of unmodified cyclodextrins has, in most photoreactions, been found to be insufficient to provide significant asymmetric induction.[27,28] A greater

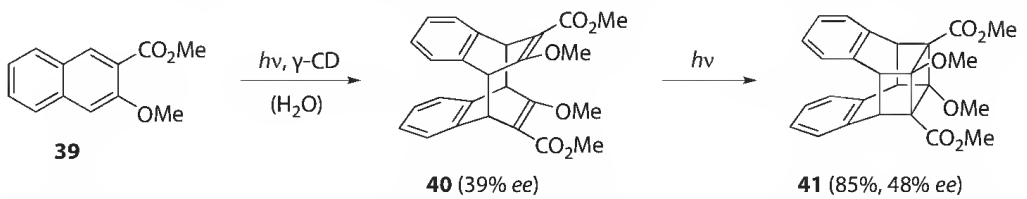

SCHEME 7.11 Stepwise increase in enantioselectivity during the formation of cyclobutane **41** from compound **39** in the presence of γ-cyclodextrin.

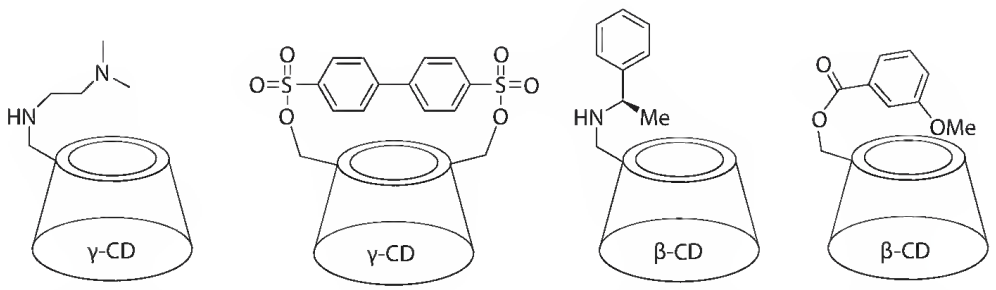

42 Ligand for metal or guest coordination

43 CD "caps"

44 Chiral modification

45 Sensitizer

SCHEME 7.12 Structures of modified cyclodextrins **42–45**.

level of success has been achieved using chemically modified cyclodextrins, several examples of which are depicted in Scheme 7.12 (**42–45**). Each has been rationally designed and represents a particular strategy for achieving an enantiodifferentiating photochemical reaction. Although modifications to the inside of CD have also been reported,[29] CDs **42–45** have all been functionalized at the 6-hydroxy position, which corresponds to the narrow rim of the CD framework.

CDs **42** and **43** have been used to produce enhanced enantioselectivity in the [4 + 4]-photodimerization of anthracenecarboxylate (**6**, R = CO_2^-, Scheme 7.2) by controlling the orientation of the guest molecules in the CD cavity. CDs possessing amino side arms, such as CD **42**, were found to both enhance the enantiomeric excess and induce a dramatic switching in the product selectivity.[30–32]

In the presence of unmodified γ-cyclodextrin, the HH approach is electrostatically unfavored, affording HH dimers **7** and **9** as the minor products and chiral compound "–"-**7** in low *ee* (<5% *ee*). In the presence of modified CD **42** dimers **7** and **9** become the major products, obtained in a combined yield of 74%, and the enantiomeric excess of compound "–"-**7** is dramatically increased to 41% *ee*. This switch in selectivity is the result of stabilization of HH complex by electrostatic interactions. At pH < 5, the diamino cyclodextrins are dicationic and form interactions with the carboxylate anions of the guest molecules.

Enantiodifferentiating catalysis has also been achieved using diamino-CDs similar to CD **42**.[32] Chelation of copper(II) by the side arm resulted in enhanced complexation of compound **6** (R = CO_2^-) in the CD cavity. This not only improved the selectivity of the reaction but also made it possible to use catalytic amounts without significantly decreasing the yield or *ee*. Using only 0.1 equivalents of the metallo-CD, the *anti*-HH dimer "–"-**7** was obtained in 51%–52% yield and 64%–70% *ee*.

Inoue and coworkers synthesized a series of "capped" cyclodextrins, for example, CD **43**, which also demonstrated an ability to influence the orientation of the anthracene **6** in the host–guest complex.[33,34] Modification with either a flexible or a rigid aromatic cap increased the yields of the HH dimers **7** and **9** (33%–41%), relative to native γ-cyclodextrin. This is attributed to compound **6** favoring an orientation in which the anionic carboxylate moieties are directed toward the aqueous environment and away from the hydrophobic cap. More interestingly, CD-**43** was found to produce the opposite enantiomer of the chiral HT dimer, "–"-**8**, relative to both native CD and other capped CDs, and with enhanced enantioselectivity (58% *ee*). The authors proposed that this effect was due to much reduced positional and rotational freedom in the precursor guest–host complex, where one of the carboxylate moieties of compound **6** must protrude through the narrow gap of the biphenyl cap.

Kaliappan and Ramamurthy have used chirally modified CDs, such as CD **44**, to induce low levels of enantioselectivity in photocyclizations of prochiral substrates.[35] For example, irradiation of adamantane **46** in the presence of CD **44** afforded photoproducts **47** and **48** in enantioselectivities of 20% and 9% *ee*, respectively (Scheme 7.13). It was anticipated that the CD cavity would serve to bring the appended chiral substituent and the achiral reactant closer together and thus achieve asymmetric induction. However, although several different enantiomerically pure amines, amino alcohols and amino acids were investigated as chiral attachments the *ee* could not be improved above 20%.

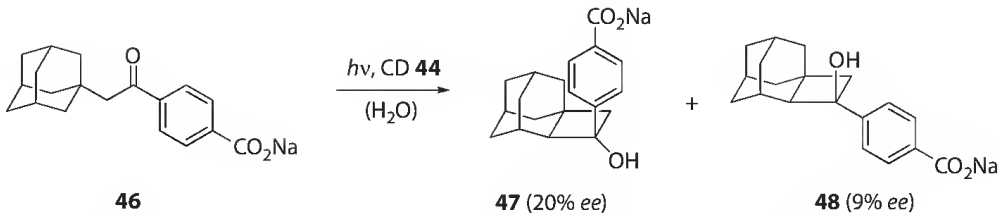

46 **47** (20% *ee*) **48** (9% *ee*)

SCHEME 7.13 Irradiation of adamantane **46** in the presence of modified cyclodextrin **44** generates enantio-enriched photoproducts **47** and **48**.

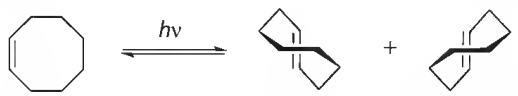

49 (*R*)-(−)-**50** (*S*)-(+)-**50**

SCHEME 7.14 Photoisomerization of achiral (*Z*)-cyclooctene **49** to chiral (*E*)-cyclooctenes **50**.

CD **45** is an example of a sensitizing cyclodextrin host. It possesses a tethered *m*-methoxybenzoyl group, which sensitizes the photoisomerization of (*Z*)-cyclooctene (**49**) within the cavity of the cyclodextrin affording (*E*)-cyclooctene (*R*)-(−)-**50** in 46% *ee* (Scheme 7.14).[36,37] Both the conversion and the enantioselectivity were found to be sensitive to variations in the structure of the sensitizer moiety. The nature and position of the aryl substituent proved critical; while *meta*-methoxy substitution resulted in good asymmetric induction, the corresponding *ortho*- or *para*-substituted CDs afforded only 4%–10% *ee*. Furthermore, exchange of the methoxy group for a proton, methyl or methyl ester substituent also resulted in a dramatic decrease in enantioselectivity (1%–18% *ee*). This indicates that the chromophore not only acts as a sensitizer but also influences the enantiodifferentiation within the cavity by adjusting the position and orientation of the included guest molecule via steric effects.

Permethylation of the cyclodextrin framework was found to have an effect on the enantioselectivity of the reaction.[37] While this modification proved detrimental to the enantioselectivity, it resulted in inversion of the chirality of the product in response to different reaction conditions. This increased sensitivity to environmental variations is attributed to the greater flexibility of the permethylated CD due to the decrease in intramolecular hydrogen bonding.

Cyanonaphthalene-substituted CD was employed as a sensitizing host for the enantiodifferentiating photoaddition of methanol to 1,1-diphenylpropene, affording the methoxy adduct in up to 13% *ee*.[38] In order to enhance complex formation, the reaction was run in aqueous methanol, thus competitive photoaddition of water also occurred to afford the chiral hydroxy adduct, as the minor product, in up to 26% *ee*. In contrast to the other examples covered in this section, in this bimolecular reaction only one of the reagents, diphenylpropene, is included in the cyclodextrin cavity. Irradiation of the host–guest complex generates radical cationic diphenylpropene, via PET to the excited sensitizer moiety of the CD, and subsequent nucleophilic attack by a solvent molecule affords the anti-Markovnikov addition products. The superior enantioselectivity observed for the water adduct suggests that both the complexation and the photoaddition steps contribute to the enantiodifferentiation.

7.3.2 Self-Assembled Supramolecular Hosts

Progress in the area of asymmetric photochemistry in supramolecular hosts has largely been limited by the difficulties associated with the synthesis of novel, chiral supramolecular structures. This limitation can be overcome using self-assembled supramolecular cages or capsules. Fujita and coworkers have demonstrated that fluoranthene (**51**) and maleimide (**52**) undergo enantioselective [2 + 2]-cycloaddition in a chiral self-assembled cage, consisting of six Pd(II) fragments (M) and four pyridine-based bridging ligands (L), to afford cycloadduct **53** in 50% *ee* (Scheme 7.15).[39]

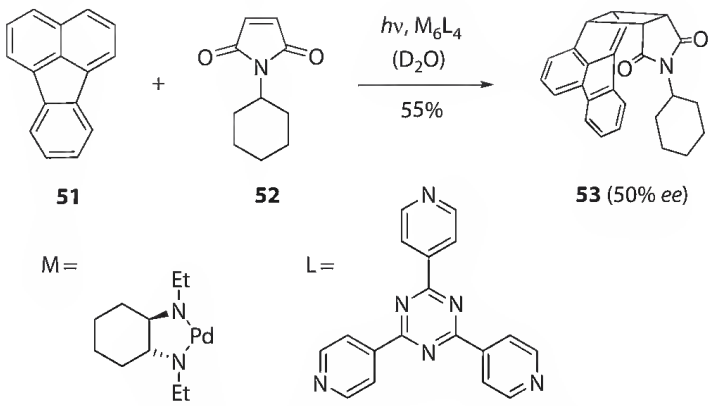

SCHEME 7.15 Enantioselective [2 + 2]-photocycloaddition of fluoranthene (**51**) and maleimide (**52**) in a self-assembled supramolecular host.

Due to the space restriction inside the cavity, the two olefins are incorporated in a pairwise selective manner and in a precise orientation. Therefore, provided the ternary-complex is formed prior to irradiation, no homodimerization is observed, and the reaction occurs in a completely regioselective manner, affording cross-dimer **53** as the sole reaction product (55% yield). The cage also provides a considerable activation effect, allowing the use of otherwise unreactive olefins such as fluoranthene (**51**), which is an inert aromatic compound.

The chiral nature of the cavity is due to the palladium diamine end caps (M). The chirality of the diamino ligand is transferred to palladium, which results in a tilt of the pyridine rings of the coordinated triazine ligands. The magnitude of this tilt, and therefore the level of enantioselectivity, was found to be sensitive to the size of the *N*-substituent. When the ethyl group was replaced with a methyl substituent or a proton, the enantioselectivity decreased to 20% *ee* and 5% *ee*, respectively.

7.3.3 Biological Templates

The chiral environment of biomolecules can be exploited to induce asymmetry in photochemical reactions. Natural supramolecular hosts that have been investigated to date include DNA,[40,41] RNA[41] and proteins, namely, bovine[42,43] and human[44,45] serum albumin. The pioneering work in this area was achieved using RNA and DNA. Inoue and coworkers demonstrated that these molecules act as chiral sensitizing hosts for the photoisomerization of cyclooctene (Scheme 7.14). Irradiation of an aqueous solution of (*Z*)-cyclooctene (**49**) in the presence of calf thymus DNA afforded the (–)-(*E*)-isomer, (*R*)-(–)-**50**, in *ee*s of up to 15%.

The best results have, however, been obtained using the serum albumins. These blood carrier proteins possess several binding pockets, within which enantioselective photochemical reactions can take place. Inoue and coworkers have investigated the [4 + 4]-photocyclodimerization of anthracenecarboxylate (**6**, Scheme 7.2) in the presence of both bovine (BSA) and human serum albumin (HSA).

In the presence of BSA, the photodimerization of anthracene **6** takes place enantioselectively to afford chiral products "+"-**7** and "–"-**8** in *ee*s of up to 41% and 29%, respectively.[42] The regioselectivity of the reaction is switched such that the HH products (**7** and **9**) become favored over the HT products (**8** and **10**) in ratios of up to 4.3:1. The reaction is highly sensitive to the concentration of BSA relative to compound **6**. Not only is the rate of photodimerization reduced by high BSA concentrations but the HH/HT ratio and *ee*s of compounds **7** and **8** are also a function of the BSA concentration. The relationship between concentration and *ee* is complex and the authors propose that this may be due to different binding sites inducing different enantioselectivity. BSA possesses four independent sites at which anthracenecarboxylate can bind. Studies indicated that each site is distinctly different in regard to the chiral environment it provides, the number of molecules it can bind (between one and three), and the binding affinity.[43] As opposed to the

other supramolecular hosts we have discussed, within a particular binding site, the anthracenecarboxylate molecules are not located in close enough proximity to one another to undergo photodimerization. Instead, the reaction involves attack of one molecule of compound **6** that is unbound or mobile within the protein to one bound molecule. This means that the regio- and enantioselectivities are not simply due to the relative orientations of the molecules in the binding site in the ground state but involve a dynamic process.

HSA differs from BSA in only 26 amino acid residues; however, a significant improvement in *ee* was observed when the reaction was conducted in the presence of this protein.[44,45] Under optimum conditions (**6**/HSA = 3 at 5°C), compounds "+"-**7** and "+"-**8** were obtained in *ee*s of 90% and 82%, respectively. Unlike BSA, the regioselectivity of the reaction remained in favor of the HT products (HT/HH = 4–6).

7.4 Asymmetric Photosensitization

In contrast to the previously mentioned organocatalysts (Section 7.2.2), the photosensitizers discussed in this section use weak, short-lived, excited-state interactions to transfer the chirality of the sensitizer to the substrate and thus generate enantiomerically enriched products. This approach is particularly attractive as only catalytic amounts of the chiral source are required. The majority of the work published in this area has used energy transfer type photosensitizers derived from polyalkyl benzene (**54**) or naphthalenepolycarboxylates (**55**),[2] several examples of which are depicted in Scheme 7.16. Although recent efforts have included attempts to develop new types of sensitizers,[46,47] the levels of enantioselectivity obtained with these compounds remains lower than that of the arenepolycarboxylates. Thus, most of the latest improvements have been achieved by manipulating the conditions used for reactions with the existing sensitizers, such as temperature, pressure, and solvent.

The photoisomerization of (*Z*)-cyclooctene (**49**) (Scheme 7.14) is sensitized by optically active polyalkyl benzenepolycarboxylates to afford chiral (*E*)-cyclooctene (**50**). Inoue and coworkers demonstrated that changes in the reaction temperature, solvent,[48,49] or pressure[49,50] not only affect the magnitude of the product *ee* but can also result in inversion of the chirality of the product, such that a single sensitizer can be used to generate either enantiomer of compound **50**. For example, when the reaction is carried out in pentane (–78°C) (*R*)-(–)-**50** is generated in 40% *ee*, while in ether (*S*)-(+)-**50** is formed in 50% *ee*. This result can be improved further by lowering the reaction temperature to afford (*S*)-(+)-**50** in a maximum *ee* of 73% at –110°C.[48] Their investigations concluded that the weak interactions in the diastereomeric exciplex complex are controlled by both enthalpic and entropic factors and that this switching behavior originates from the balance between these factors in the enantiodifferentiation step.

These sensitizers are not limited to use in unimolecular processes but have also been applied in enantioselective bimolecular photoadditions of alcohols to 1,1-diphenyl-1-alkenes. In 2003 an in-depth account was published detailing the effects of varying the sensitizer moiety, chiral auxiliary, nucleophile

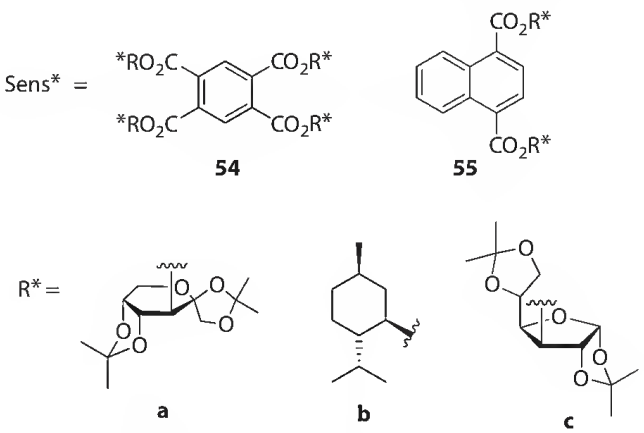

SCHEME 7.16 Examples **54** and **55** of energy transfer photosensitizers.

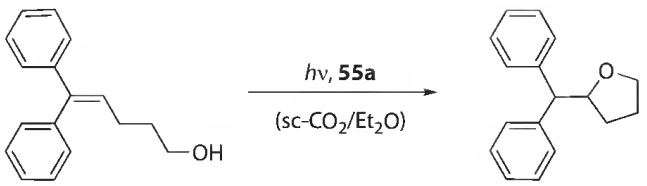

56 **57** (45% *ee*)

SCHEME 7.17 Enatioselective photocyclization of diphenylpentenol **56** to tetrahydrofuran **57**, sensitized by arene **55a**.

(alcohol), solvent, and temperature on the yield and *ee* of photoadduct.[51] In terms of enantioselectivity, the best results were achieved using diisopropylidenefructosyl (**a**, Scheme 7.16) substituted 2,6-naphthalene dicarboxylate as the sensitizer, in combination with a bulky nucleophile (2-propanol). The highest *ee* was obtained when the reaction was carried out at 0°C in diethyl ether, affording the addition product in 58% *ee*, albeit in only 1% yield. While better yields could be obtained using smaller nucleophiles or different solvents, this was accompanied by a decrease in enantioselectivity. Studies conducted in near- and supercritical CO_2 (sc-CO_2) showed that product *ee* increases with increasing pressure.[52,53] This increase was particularly pronounced in the narrow pressure range near the critical density.

In the analogous intramolecular reaction, the enantiodifferentiating photocyclization of 5,5-diphenyl-4-penten-1-ol (**56**) was sensitized by diisopropylidenefructosyl 1,4-naphthalenedicarboxylate (**55a**) to afford tetrahydrofuran **57** as the major product (Scheme 7.17).[54] Enantioselectivities of up to 28% were obtained in low-polarity solvents such as methylcyclohexane, toluene, or diethyl ether. When this reaction was carried out in supercritical CO_2, the *ee*s were comparable to those obtained in conventional solvents; however, the addition of diethyl ether as a cosolvent (entrainer) was found to significantly enhance the enantioselectivity affording compound **57** in up to 45% *ee*. Diethyl ether had previously been shown to improve the enantioselectivity of similar reactions by enhancing the microenvironmental polarity around the sensitizer, thus facilitating electron transfer within the exciplex intermediate.[48,51]

7.5 Asymmetric Induction by Conformational Constraints

The first stereogenic center in a molecule can be created from precursors that carry another element of chirality, that is, a chiral axis or chiral plane, without the need for any external chiral source. While this other element of chirality may not be infinitesimally stable, it may still be sufficient to transport chiral information. Along these lines, some recent developments are summarized in this section. Particular emphasis is given to axial to point chirality transfer (Section 7.5.1) and chiral memory effects (Section 7.5.2).

7.5.1 Axial to Point Chirality Transfer

Carreira and coworkers have exploited the axial chirality of allenes to achieve asymmetric induction in intramolecular [2 + 2]-cycloaddition reactions (Scheme 7.18).[55,56] Enantiomerically pure 1,3-disubstituted allenes, such as **58**, readily undergo allene-enone photocycloadditon reactions, affording the corresponding cycloadducts (**59**) in between 76% and 99% *ee*.

Stereochemical control is derived exclusively from the axial chirality of the allene moiety, which possesses either a tertiary butyl- or trimethylsilyl group. The absolute configuration is established in the initial C–C bond-forming step, with addition of the excited enone to the allene occurring at the face opposite the bulky silyl substituent. Although the allene starting material is optically active the reactions are considered enantioselective as the stereogenic centers in the product are generated at the expense of the axial chirality of the allene. The trimethylsilyl derivatives were developed in order

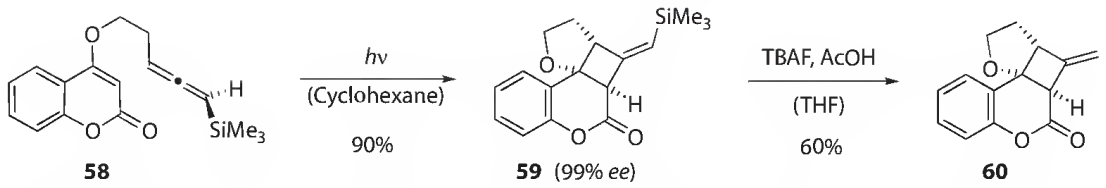

SCHEME 7.18 Intramolecular [2 + 2]-photocycloaddition of allene **58** to generate chiral cyclobutane **59** in 99% *ee*.

to increase the synthetic versatility of this reaction. Following the photocycloaddition, cleavage of the stereocontrolling group from the chiral product can be carried out with TBAF to afford the unsubstituted *exo*-methylene compound **60**.[56]

Atropisomers are axially chiral molecules that arise from restricted rotation around single bonds, as opposed to the multiple bonds of allenes. In molecules of this type, the barrier to rotation is large enough to allow the isolation and characterization of the individual rotamers. Earlier work has revealed that atopisomerism can be used to induce facial diastereoselectivity in a Paternò-Büchi reaction.[57] Recently, it was demonstrated that atropisomeric starting materials undergo enantioselective photochemical reactions in solution by an effective and almost complete axial to point chirality transfer.[58,59] Acrylanilide **61** exists as individual atropisomers (designated *P* and *M*) due to restricted bond rotation around the N–C(aryl) bond (Scheme 7.19). Irradiation of optically pure (+)-**61** resulted in [6π]-photocyclization to afford a mixture of the *cis*-photoproduct **62** and the *trans*-photoproduct **63**, in 99% *ee*. The identical enantiomeric excesses of the diastereomeric products indicate that the stereogenic center at the benzylic position is formed first, in a highly stereoselective ring closure step, while the second stereogenic center is generated with loss of the *ortho t*-butyl substituent in a nonselective proton-transfer step. Irradiation of the optical antipode, (–)-**61**, afforded the opposite enantiomers, *ent*-**62** and *ent*-**63**.

In a subsequent paper, Sivaguru et al. reported that atropisomeric α-oxoamides also undergo enantioselective photocyclization, via a Norrish–Yang mechanism involving axial to point chirality transfer, to afford β-lactam products in 72%–80% *ee*.[59]

For systems that do not exist as separable atropisomers chiral crystallization can be used to generate axial chirality. If a prochiral substrate crystallizes in a chiral space group, enantiomerically pure crystals are generated. If that molecular chirality is maintained even after the crystals are dissolved in a solvent, it can be transferred during a reaction to afford enantiomerically pure products. Sakamoto and coworkers have demonstrated that asymmetric photochemical reactions are possible by exploiting this "frozen chirality."[60,61] *N,N*,-Diethyl-4-coumarin-3-carboxamide has two possible conformations, (*R*)-**64** or (*S*)-**64** (Scheme 7.20). When in solution this molecule is considered prochiral due to rapid interconversion *via* bond rotation. However, compound **64** crystallizes in a chiral space group to afford enantiomerically pure crystals composed of either the (*S*)- or (*R*)-enantiomer. When singularly chiral crystals were dissolved in methanol at –20°C, the molecules retained their chirality and effectively underwent triplet-sensitized intramolecular [2 + 2]-photocycloaddition with alkenes to generate cyclobutane products, for example, **65**, in high enantioselectivity (97%–99% *ee*). The use of benzophenone as a triplet sensitizer was found to be essential as in the singlet-state photoracemization occurs, affording racemic products.

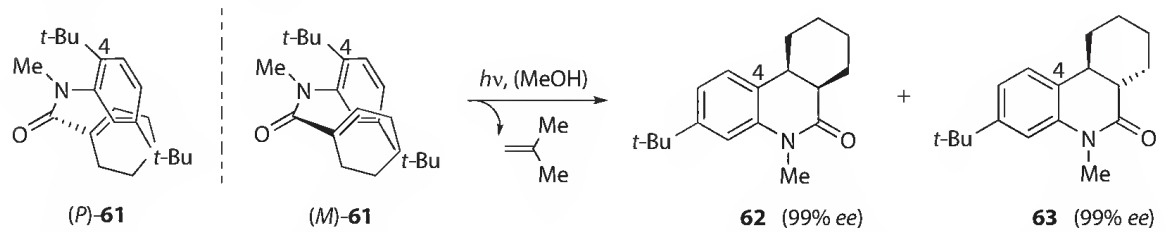

SCHEME 7.19 6π-Photocyclization of molecularly chiral acrylamide **61** to afford chiral photoproducts **62** and **63**.

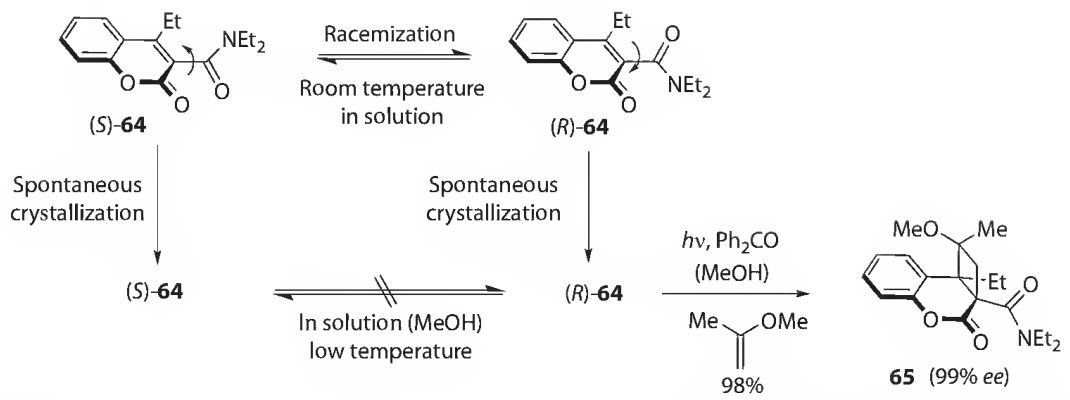

SCHEME 7.20 Generation of singularly chiral crystals of compound **64** by chiral crystallization and [2 + 2]-photocycloaddition of isomer (*R*)-**64** to afford cyclobutane **65** in 99% *ee*.

7.5.2 Chiral Memory Effect[62]

The first example of a chiral memory effect in photochemistry was reported by Giese and coworkers.[63] The Norrish–Yang photocyclization of alanine derivative **66** was shown to occur without racemization, despite proceeding *via* a prochiral diradical intermediate, to afford proline derivate **68**, as the major product, in 40% yield and 92% *ee* (Scheme 7.21). The corresponding *trans*-isomer was obtained as the minor product (7% yield, 88% *ee*). The asymmetric induction was drastically reduced in the absence of a triplet quencher (naphthalene), leading the authors to propose that the lifetime of the triplet diradical is long enough to allow racemization to occur. In contrast, in the singlet state, the activation barrier to cyclization is lower than that of bond rotation, resulting in almost complete memory of chirality. Calculations were later performed, which indicated that a hydrogen bond network in the helical intermediate **67**, involving the N-6, H-9, and O-12 atoms, is the likely reason for this barrier to rotation.[64]

In contrast to the previous example, where formation of a triplet diradical results in almost complete loss of chirality, Griesbeck and coworkers observed high enantiomeric excesses for decarboxylative

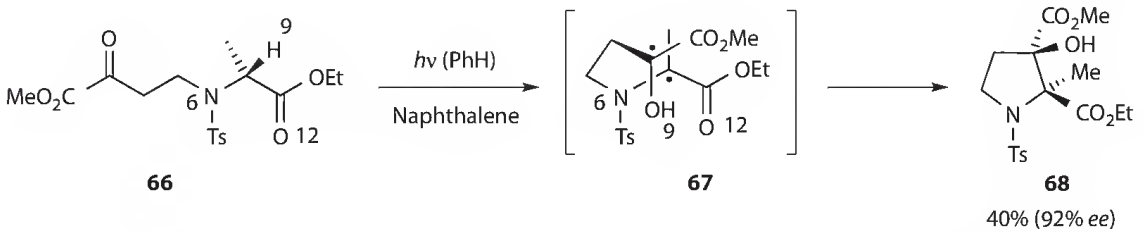

SCHEME 7.21 Norrish–Yang photocyclization of chiral alanine derivative **66** to compound **68** occurs without racemization despite proceeding through prochiral diradical **67**.

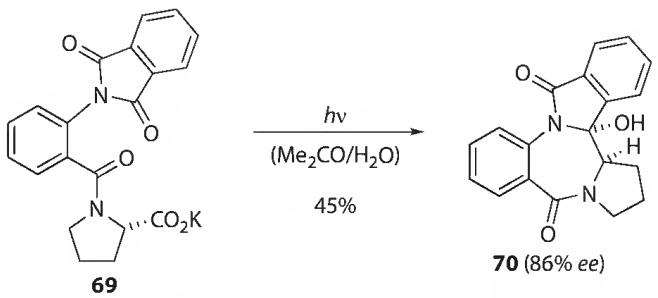

SCHEME 7.22 Decarboxylative photocyclization of proline derivative **69** proceeds via an atropisomeric 1,7-diradical to generate compound **70** in 86% *ee*.

photocyclization reactions involving a triplet 1,7-diradical. Irradiation of proline derivative **69** afforded the pentacyclic product **70** in 86% *ee* with a diastereoselectivity of greater than 98% (Scheme 7.22).[65] In this case, the 1,7-diradical is atropisomeric, with a calculated barrier to rotation of 55 kJ mol^{-1}, resulting in preserved axial chirality that is transferred to the stereogenic centers in the product.

Enantiomerically pure thioimides have been shown to undergo photochemical intramolecular β- or γ-hydrogen abstraction reactions involving a chiral memory effect to afford optically active products. Sakamoto and coworkers generated new stereogenic quaternary carbon centers from the tertiary chiral centers of readily accessible amines and amino acids with almost complete retention of stereochemistry (96%–100% *ee*).[66] This approach was also applied to the synthesis of chiral β-lactams.[67] Irradiation of thioimide **71** afforded a mixture of β-lactams **72** and **73** in 96% and 95% *ee*, respectively (Scheme 7.23). Intramolecular β-hydrogen abstraction by the aryl thiocarbonyl group from the stereogenic center of substrate **71** generates a singlet 1,4-diradical intermediate. Subsequent radical recombination occurs faster than racemization, *via* bond rotation around the radical site, so the products are generated in high enantiomeric excess.

Double memory of chirality (^{2}MOC), in which *two* stereogenic centers retain their chiral information, is known to be possible in the solid state since the reacting centers are held in close proximity and large molecular motions, such as radical rotation, are energetically disfavored. Garcia-Garibay et al. have now proven that ^{2}MOC is also possible in solution (Scheme 7.24).[68] Irradiation of *bis*-(*N*-methylphenylpyrrolidinonyl)-ketone (**74**) in benzene at 25°C resulted in photodecarbonylation with double memory of chirality affording compound **77** possessing two adjacent stereocenters. The reaction occurs *via* the singlet state (**75** → **76**) on a picosecond timescale, thus providing insufficient time for the two radical fragments to rotate and expose the other enantiotopic face before radical recombination takes place.

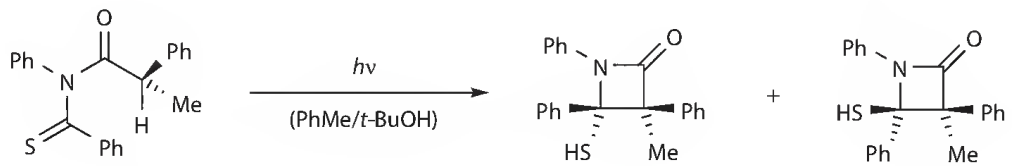

71 (96% *ee*) **72** 50% (96% *ee*) **73** 11% (95% *ee*)

SCHEME 7.23 Enantioselective generation of two new stereogenic quaternary centres in the cyclization of thioimide **71** to β-lactams **72** and **73**.

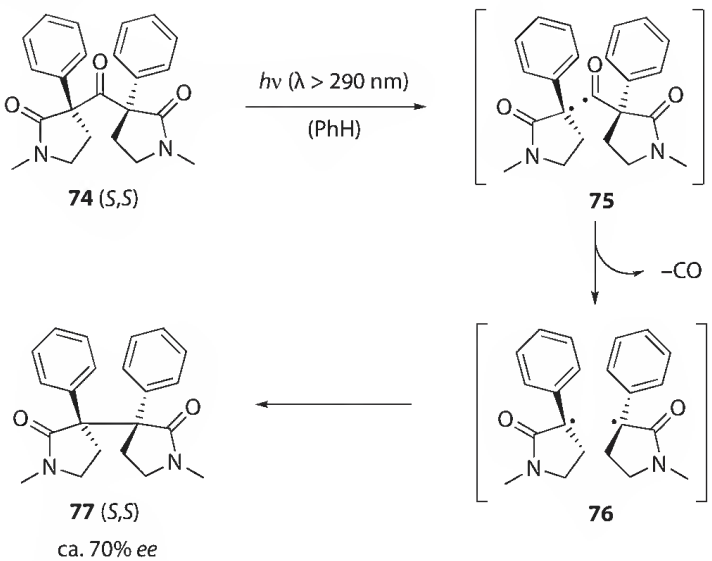

74 (*S,S*) **75** **76** **77** (*S,S*) ca. 70% *ee*

SCHEME 7.24 Double memory of chirality in the photodecarbonylation of ketone **74** to compound **77**.

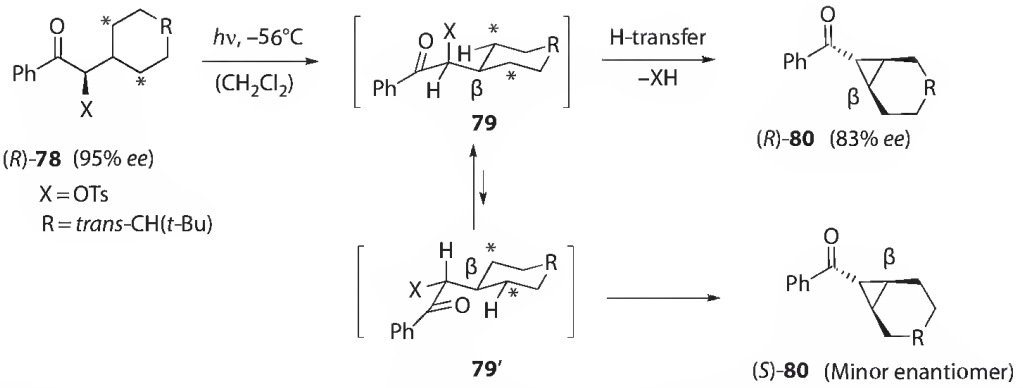

SCHEME 7.25 1,2-Chirality transfer in the cyclization of compound (*R*)-**78** to cyclopropane (*R*)-**80**, via transition state **79**.

One final example of chiral memory is point-to-point chirality transfer, in which one transition state geometry is favored, resulting in transfer of the chiral information from the starting material to the product. Cyclopropane derivatives (e.g., **80**) were generated from chiral phenylalkyl ketones (e.g., **78**) in up to 83% *ee*, *via* a modified Norrish–Yang cyclization involving a 1,2-chirality transfer (Scheme 7.25).[69] Compounds of type **78** adopt a six-membered, chair-like conformation in which the leaving group (X) is either pseudoaxial (**79**) or pseudoequatorial (**79′**). In each transition state, hydrogen transfer can only occur from one of the two diastereotopic methylene groups (*), generating a stereogenic center at the β-position. Subsequent loss of the leaving group generates a 1,3-diradical, which cyclizes to afford the chiral cyclopropane product (**80**). A combination of enthalpic and entropic factors determines which transition state is favored, so the absolute configuration of the major product is not the same for all substrates, despite all the starting materials possessing the (*R*)-configuration.

7.6 Asymmetric Aminocatalysis

Very recently, it has been demonstrated that chiral amine catalysts can be used in conjunction with photochemical processes to achieve new enantioselective reactions.

Córdova et al. performed asymmetric α-oxidations using aminocatalysis and photochemically generated singlet oxygen (Scheme 7.26).[70] They demonstrated that amino acids catalyze the reaction of aldehydes (e.g., **81**) with singlet molecular oxygen to afford a chiral α-hydroperoxide species (e.g., **83**), which can be reduced *in situ* to the corresponding diol (e.g., **84**). L-α-Methyl proline (**82**) was the amino acid found to provide the most effective asymmetric induction, affording the diol products in enantiomeric excesses of between 54% and 66% *ee*.

The reaction is presumed to proceed *via* an enamine pathway. Condensation of the aldehyde with catalyst **82** both activates the aldehyde to electrophilic attack and results in face differentiation of the prochiral starting material due to the directing effects of the proline carboxylic acid group. Singlet oxygen reacts with the resultant enamine *via* an ene-type reaction to generate an iminium ion, which is in equilibrium with aldehyde **83** and thus regenerates the catalyst.

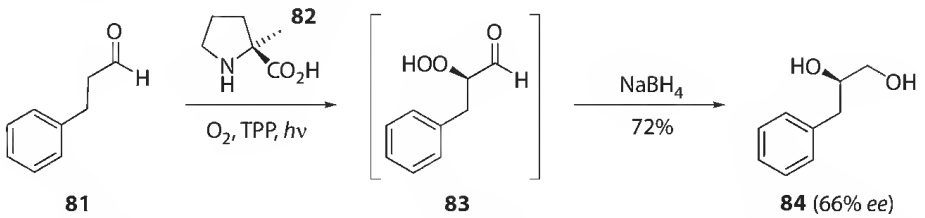

SCHEME 7.26 Enantioselective ene-type reaction of $^1O_2$ and aldehyde **81**, catalyzed by α-methylproline (**82**).

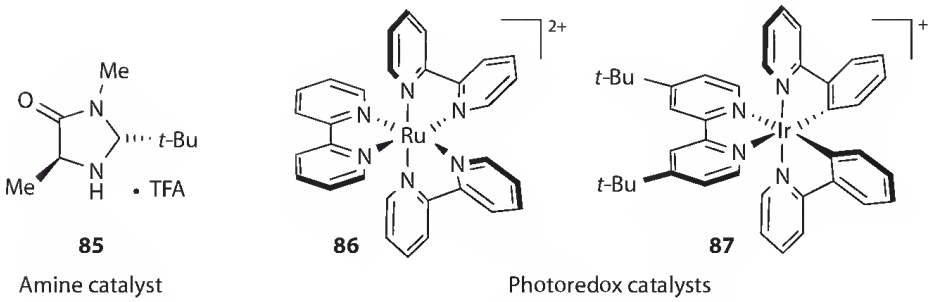

SCHEME 7.27 Structures of the catalysts **85–87** used in photoredox organocatalysis.

Nicewicz and MacMillan have successfully merged the areas of aminocatalysis and photoredox catalysis to achieve an enantioselective α-alkylation of carbonyl compounds.[71,72] The reaction involves the cooperation of two independent catalytic cycles and thus requires a dual catalyst system (Scheme 7.27) consisting of an enantiomerically pure secondary amine (e.g., **85**) and a photoredox catalyst (e.g., **86** or **87**).

Enantioselectivity and activation of the substrate is once again achieved *via* an enamine pathway (Scheme 7.28). *In situ* condensation of aldehyde **88** and imidazolidinone catalyst **85** generates an electron-rich enamine intermediate **89**, which undergoes addition of an electrophilic radical (•Y). Due to the face differentiation provided by the chiral amine catalyst, this addition occurs stereoselectively generating radical intermediate **90** as a single enantiomer. Here, the two catalytic cycles converge. Intermediate **90** is oxidized by single electron transfer (SET) to the excited photoredox catalyst ($*Ru^{2+}$) to afford the corresponding iminium ion **91**, which then undergoes hydrolysis to yield the final product **92** and regenerates the amine catalyst.

Concurrent with the enamine pathway given earlier, a photoredox catalytic cycle takes place involving $[Ru(bpy)_3]^{2+}$ (**86**) a well-established one electron photoredox catalyst. Irradiation of $[Ru(bpy)_3]^{2+}$ results in metal-to-ligand charge transfer, generating the excited-state $*[Ru(bpy)_3]^{2+}$, which possesses enhanced reactivity relative to the ground-state molecule. $*[Ru(bpy)_3]^{2+}$ then acts as an oxidant, removing one electron (SET) from the α-amino radical **90**, generating $[Ru(bpy)_3]^{+}$, which is a powerful reducing agent. A second SET process involving the starting halide (X–Y) and $[Ru(bpy)_3]^{+}$ generates the electron-deficient radical (•Y) required for the alkylation step and regenerates the photoredox catalyst **86**.

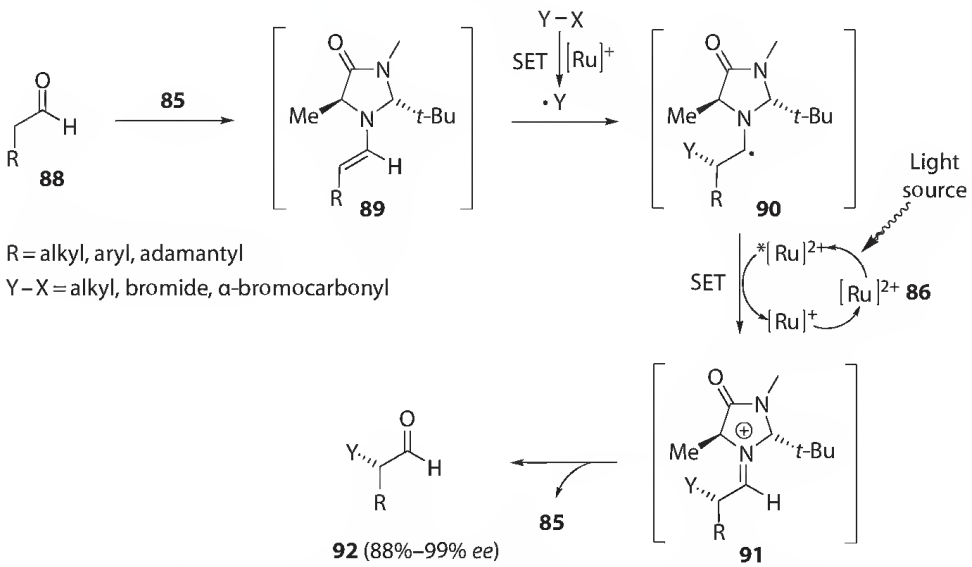

SCHEME 7.28 The enantioselective α-alkylation of carbonyl compounds (e.g., **88**) involves two independent catalytic cycles to generate products **92** in excellent *ee*'s.

Considering that a complex interplay of two independent catalytic processes is required for this reaction to succeed, the yields (63%–93%) and enantiomeric excesses (88%–99% *ee*) achieved are remarkable. The reaction is also operationally simple, no heating or cooling is required, and a 15 W fluorescent light is used as the light source. 20 mol% of the amine catalyst is used while only 0.5 mol% of the photoredox catalyst is required. More recently, MacMillan and coworkers reported that α-fluoroalkylation of aldehydes is also possible using this methodology.[72] α-Trifluoromethyl and α-perfluoroalkyl derivatives of a variety of aldehydes were prepared in yields ranging from 62% to 89% and in 96%–99% *ee*. In this case, the iridium-based catalyst **87** (Scheme 7.27) proved superior and the reaction required cooling to –20°C in order to achieve an asymmetric induction.

References

1. Müller, C. and Bach, T., Chirality control in photochemical reactions: Enantioselective formation of complex photoproducts in solution, *Aust. J. Chem.*, **61**, 557, 2008.
2. Grosch, B. and Bach, T., Template-induced enantioselective photochemical reactions in solution, *Molecular and Supramolecular Photochemistry: Chiral Photochemistry*, Vol. 11, Inoue, Y. and Ramamurthy, V., Eds., Dekker, New York, p. 315, 2004.
3. Grosch, B. and Bach, T., Enantioselective photocycloaddition reactions in solution, *CRC Handbook of Photochemistry and Photobiology*, 2nd edn., Horspool, W. M. and Lenci, F., Eds., CRC Press, Boca Raton, FL, Chapter 61.1, 2004.
4. Hoffmann, N., Photochemical reactions as key steps in organic synthesis, *Chem. Rev.*, **108**, 1052, 2008.
5. Iriondo-Alberdi, J. and Greaney, M. F., Photocycloaddition in natural product synthesis, *Eur. J. Org. Chem.*, 4801, 2007.
6. Mizoguchi, J.-I., Kawanami, Y., Wada, T., Kodama, K., Anzai, K., Yanagi, T., and Inoue, Y., Enantiodifferentiating photocyclodimerization of 2-anthracenecarboxylic acid using a chiral *N*-(2-hydroxymethyl-4-pyrrolidinyl)benzamide template, *Org. Lett.*, **8**, 6051, 2006.
7. Kawanami, Y., Pace, T. C. S., Mizoguchi, J.-I., Yanagi, T., Nishijima, M., Mori, T., Wada, T., Bohne, C., and Inoue, Y., Supramolecular complexation and enantiodifferentiating photocyclodimerization of 2-anthracenecarboxylic acid with 4-aminoprolinol derivatives as chiral hydrogen-bonding templates, *J. Org. Chem.*, **74**, 7908, 2009.
8. Gerard, B., Sangji, S., O'Leary, D. J., and Porco, J. A. Jr., Enantioselective photocycloaddition mediated by chiral Brønsted acids: Asymmetric synthesis of the rocaglamides, *J. Am. Chem. Soc.*, **128**, 7754, 2006.
9. Tanaka, K. and Fujiwara, T., Enantioselective [2 + 2]-photodimerization reactions of coumarins in solution, *Org. Lett.*, **7**, 1501, 2005.
10. Gerard, B., Jones, G. II, and Porco, J. A. Jr., A biomimetic approach to the rocaglamides employing photogeneration of oxidopyryliums derived from 3-hydroxyflavones, *J. Am. Chem. Soc.*, **126**, 13620, 2004.
11. Breitenlechner, S., Selig, P., and Bach, T., Chiral organocatalysis for enantioselective photochemical reactions, *Ernst Schering Foundation Symposium Proceedings: Organocatalysis*, Reetz, M. T., List, B., Jaroch, S., and Weinmann, H., Eds., Springer, Berlin, Germany, p. 255, 2008.
12. Grosch, B., Orlebar, C. N., Herdtweck, E., Massa, W., and Bach, T., Highly enantioselective Diels-Alder reactions of a photochemically generated *o*-quinodimethane with olefins, *Angew. Chem. Int. Ed.*, **42**, 3693, 2003.
13. Grosch, B., Orlebar, C. N., Herdtweck, E., Kaneda, M., Wada, T., Inoue, Y., and Bach, T., Enantioselective [4 + 2]-cycloaddition reaction of a photochemically generated *o*-quinodimethane: Mechanistic details, association studies, and pressure effects, *Chem. Eur. J.*, **10**, 2179, 2004.
14. Brandes, S., Selig, P., and Bach, T., Stereoselective intra- and intermolecular [2 + 2]-photocycloaddition reactions of 4-(2′-aminoethyl)quinolones, *Synlett*, 2588, 2004.

15. Selig, P. and Bach, T., Photochemistry of 4-(2′-aminoethyl)quinolones: Enantioselective synthesis of tetracyclic tetrahydro-1a*H*-pyrido[4′,3′:2,3]-cyclobuta[1,2-*c*]quinoline-2,11(3*H*,8*H*)-diones by intra- and intermolecular [2 + 2]-photocycloaddition reactions in solution, *J. Org. Chem.*, **71**, 5662, 2006.
16. Selig, P. and Bach, T., Enantioselective total synthesis of the *Melodinus* alkaloid (+)-meloscine, *Angew. Chem. Int. Ed.*, **47**, 5082, 2008.
17. Selig, P., Herdtweck, E., and Bach, T., Total synthesis of meloscine by a [2 + 2]-photocycloaddition/ring expansion route, *Chem. Eur. J.*, **15**, 3509, 2009.
18. Albrecht, D., Basler, B., and Bach, T., Preparation and intramolecular [2 + 2]-photocycloaddition of 1,5-dihydropyrrol-2-ones and 5,6-dihydro-1*H*-pyridin-2-ones with C-, N- and O-linked alkenyl side chains at the 4-position, *J. Org. Chem.*, **73**, 2345, 2008.
19. Albrecht, D., Vogt, F., and Bach, T., Diastereo- and enantioselective intramolecular [2 + 2]-photocycloaddition reactions of 3-(ω′-alkenyl)- and 3-(ω′-alkenyloxy)-substituted 5,6-dihydro-1*H*-pyridin-2-ones, *Chem. Eur. J.*, **16**, 4284, 2010.
20. Breitenlechner, S. and Bach, T., A polymer-bound chiral template for enantioselective photochemical reactions in solution, *Angew. Chem. Int. Ed.*, **47**, 7957, 2008.
21. Bauer, A., Westkämper, F., Grimme, S., and Bach, T., Catalytic enantioselective reactions driven by photoinduced electron transfer, *Nature*, **436**, 1139, 2005.
22. Müller, C., Bauer, A., and Bach, T., Light-driven enantioselective organocatalysis, *Angew. Chem. Int. Ed.*, **48**, 6640, 2009.
23. Cauble, D. F., Lynch, V., and Krische, M. J., Studies on the enantioselective catalysis of photochemically promoted transformations: "Sensitizing receptors" as chiral catalysts, *J. Org. Chem.*, **68**, 15, 2003.
24. Nakamura, A. and Inoue, Y., Supramolecular catalysis of the enantiodifferentiating [4 + 4] photocyclodimerization of 2-anthracenecarboxylate by γ-cyclodextrin, *J. Am. Chem. Soc.*, **125**, 966, 2003.
25. Luo, L., Liao, G.-H., Wu, X.-L., Lei, L., Tung, C.-H., and Wu, L.-Z., γ-Cyclodextrin-directed enantioselective photocyclodimerization of methyl 3-methoxyl-2-naphthoate, *J. Org. Chem.*, **74**, 3506, 2009.
26. Luo, L., Cheng, S.-F., Chen, B., Tung, C.-H., and Wu, L.-Z., Stepwise photochemical-chiral delivery in γ-cyclodextrin-directed enantioselective photocyclodimerization of methyl 3-methoxyl-2-naphthoate in aqueous solution, *Langmuir*, **26**, 782, 2010.
27. Furutani, A., Katayama, K., Uesima, Y., Ogura, M., Tobe, Y., Kurosawa, H., Tsutsumi, K., Morimoto, T., and Kakiuchi, K., Asymmetric [2 + 2] photocyloaddition of cycloalkenone-cyclodextrin complexes to ethylene, *Chirality*, **18**, 217, 2006.
28. Mieusset, J.-L., Wagner, G., Su, K.-J., Steurer, M., Pacar, M., Abraham, M., and Brinker, U. H., Supramolecular photochirogenesis with carbenes entrapped in cyclodextrins, *Eur. J. Org. Chem.*, 2009, 5907, 2009.
29. Yang, C., Nakamura, A., Fukuhara, G., Origane, Y., Mori, T., Wada, T., and Inoue, Y., Pressure and temperature-controlled enantiodifferentiating [4 + 4] photocyclodimerization of 2-anthracenecarboxylate mediated by secondary face- and skeleton-modified γ-cyclodextrins, *J. Org. Chem.*, **71**, 3126, 2006.
30. Yang, C., Fukuhara, G., Nakamura, A., Origane, Y., Fujita, K., Yuan, D.-Q., Mori, T., Wada, T., and Inoue, Y., Enantiodifferentiating [4 + 4] photocyclodimerization of 2-anthracenecarboxylate catalyzed by 6^A,6^X-diamino-6^A,6^X-dideoxy-γ-cyclodextrins: Manipulation of product chirality by electrostatic interaction, temperature and solvent in supramolecular photochirogenesis, *J. Photochem. Photobiol. A*, **173**, 375, 2005.
31. Nakamura, A. and Inoue, Y., Electrostatic manipulation of enantiodifferentiating photocyclodimerization of 2-anthracenecarboxylate within γ-cyclodextrin cavity through chemical modification. Inverted product distribution and enhanced enantioselectivity, *J. Am. Chem. Soc.*, **127**, 5338, 2005.

32. Ke, C., Yang, C., Mori, T., Wada, T., Liu, Y., and Inoue, Y., Catalytic enantiodifferentiating photocyclodimerization of 2-anthracenecarboxylic acid mediated by a non-sensitizing chiral metallosupramolecular host, *Angew. Chem. Int. Ed.*, **48**, 6675, 2009.
33. Yang, C., Mori, T., and Inoue, Y., Supramolecular enantiodifferentiating photocyclodimerization of 2-anthracenecarboxylate mediated by capped γ-cyclodextrins: Critical control of enantioselectivity by cap rigidity, *J. Org. Chem.*, **73**, 5786, 2008.
34. Yang, C., Nakamura, A., Wada, T., and Inoue, Y., Enantiodifferentiating photocyclodimerization of 2-anthracenecarboxylic acid mediated by γ-cyclodextrins with a flexible or rigid cap, *Org. Lett.*, **8**, 3005, 2006.
35. Kaliappan, R. and Ramamurthy, V., Chiral photochemistry within natural and functionalized cyclodextrins: Chiral induction in photocyclization products from carbonyl compounds, *J. Photochem. Photobiol. A*, **207**, 144, 2009.
36. Fukuhara, G., Mori, T., Wada, T., and Inoue, Y., Entropy-controlled supramolecular photochirogenesis: Enantiodifferentiating *Z-E* photoisomerization of cyclooctene included and sensitized by permethylated 6-*O*-modified-β-cyclodextrins, *J. Org. Chem.*, **71**, 8233, 2006.
37. Lu, R., Yang, C., Cao, Y., Tong, L., Jiao, W., Wada, T., Wang, Z., Mori, T., and Inoue, Y., Enantiodifferentiating photoisomerization of cyclooctene included and sensitized by aroyl-β-cyclodextrins: A critical enantioselectivity control by substituents, *J. Org. Chem.*, **73**, 7695, 2008.
38. Fukuhara, G., Mori, T., and Inoue, Y., Competitive enantiodifferentiating anti-Markovnikov photoaddition of water and methanol to 1,1-diphenylpropene using a sensitizing cyclodextrin host, *J. Org. Chem.*, **74**, 6714, 2009.
39. Nishioka, Y., Yamaguchi, T., Kawano, M., and Fujita, M., Asymmetric [2 + 2] olefin cross photoaddition in a self-assembled host with remote chiral auxiliaries, *J. Am. Chem. Soc.*, **130**, 8160, 2008.
40. Wada, T., Sugahara, N., Kawano, M., and Inoue, Y., First asymmetric photochemistry with nucleosides and DNA: Enantiodifferentiating *Z-E* photoisomerization of cyclooctene, *Chem. Lett.*, **29**, 1174, 2000.
41. Sugahara, N., Kawano, M., Wada, T., and Inoue, Y., Enantiodifferentiating *Z-E* photoisomerization of cyclooctene sensitized by DNA and RNA, *Nucleic Acids Symp. Ser.*, **44**, 115, 2000.
42. Wada, T., Nishijima, M., Fujisawa, T., Sugahara, N., Mori, T., Nakamura, A., and Inoue, Y., Bovine serum albumin-mediated enantiodifferentiating photocyclodimerization of 2-anthracenecarboxylate, *J. Am. Chem. Soc.*, **125**, 7492, 2003.
43. Nishijima, M., Pace, T. C. S., Nakamura, A., Mori, T., Wada, T., Bohne, C., and Inoue, Y., Supramolecular photochirogenesis with biomolecules. Mechanistic studies on the enantiodifferentiation for the photocyclodimerization of 2-anthracenecarboxylate mediated by bovine serum albumin, *J. Org. Chem.*, **72**, 2707, 2007.
44. Nishijima, M., Wada, T., Mori, T., Pace, T. C. S., Bohne, C., and Inoue, Y., Highly enantiomeric supramolecular [4 + 4] photocyclodimerization of 2-anthracenecarboxylate mediated by human serum albumin, *J. Am. Chem. Soc.*, **129**, 3478, 2007.
45. Pace, T. C. S., Nishijima, M., Wada, T., Inoue, Y., and Bohne, C., Photophysical studies on the supramolecular photochirogenesis for the photocyclodimerization of 2-anthracenecarboxylate within human serum albumin, *J. Phys. Chem. B*, **113**, 10445, 2009.
46. Shi, M. and Inoue, Y., Enantiodifferentiating photoisomerization of (*Z*)-cyclooctene sensitized by chiral C_2-symmetric phosphoramide, *Aust. J. Chem.*, **54**, 113, 2001.
47. Álvaro, M., Formentín, P., García, H., Palomares, E., and Sabater, M. J., Chiral *N*-alkyl-2,4,6-triphenylpyridiniums as enantioselective triplet photosensitizers. Laser flash photolysis and preparative studies, *J. Org. Chem.*, **67**, 5184, 2002.
48. Inoue, Y., Ikeda, H., Kaneda, M., Sumimura, T., Everitt, S. R. L., and Wada, T., Entropy-controlled asymmetric photochemistry: Switching of the product chirality by solvent, *J. Am. Chem. Soc.*, **122**, 406, 2000.

49. Saito, R., Kaneda, M., Wada, T., Katoh, A., and Inoue, Y., First asymmetric photosensitization in supercritical fluid. Exceptionally high pressure/density dependance of optical yield in photosensitized enantiodifferentiating isomerization of cyclooctene, *Chem. Lett.*, **31**, 860, 2002.
50. Kaneda, M., Nakamura, A., Asaoka, S., Ikeda, H., Mori, T., Wada, T., and Inoue, Y., Pressure control of enantiodifferentiating photoisomerization of cyclooctenes sensitized by chiral benzenepolycarboxylates. The origin of discontinuous pressure dependance of the optical yield, *Org. Biomol. Chem.*, **1**, 4435, 2003 and references cited therein.
51. Asaoka, S., Wada, T., and Inoue, Y., Microenvironmental polarity control of electron-transfer photochirogenesis. Enantiodifferentiating polar addition of 1,1-diphenyl-1-alkenes photosensitized by saccharide naphthalenecarboxylates, *J. Am. Chem. Soc.*, **125**, 3008, 2003.
52. Nishiyama, Y., Kaneda, M., Saito, R., Mori, T., Wada, T., and Inoue, Y., Enantiodifferentiating photoaddition of alcohols to 1,1-diphenylpropene in supercritical carbon dioxide: Sudden jump of optical yield at the critical density, *J. Am. Chem. Soc.*, **126**, 6568, 2004.
53. Nishiyama, Y., Kaneda, M., Asaoka, S., Saito, R., Mori, T., Wada, T., and Inoue, Y., Mechanistic study on the enantiodifferentiating anti-Markovnikov photoaddition of alcohols to 1,1-diphenyl-1-alkenes in near-critical and supercritical carbon dioxide, *J. Phys. Chem. A*, **111**, 13432, 2007.
54. Nishiyama, Y., Wada, T., Asaoka, S., Mori, T., McCarty, T. A., Kraut, N. D., Bright, F. V., and Inoue, Y., Entrainer effect on photochirogenesis in near- and supercritical carbon dioxide: Dramatic enhancement of enantioselectivity, *J. Am. Chem. Soc.*, **130**, 7526, 2008.
55. Carreira, E. M., Hastings, C. A., Shepard, M. S., Yerkey, L. A., and Millward, D. B., Asymmetric induction in intramolecular [2 + 2]-photocycloadditions of 1,3-disubstituted allenes with enones and enoates, *J. Am. Chem. Soc.*, **116**, 6622, 1994.
56. Shepard, M. S. and Carreira, E. M., Asymmetric photocycloadditions with an optically active allenylsilane: Trimethylsilyl as a removable stereocontrolling group for the enantioselective synthesis of *exo*-methylenecyclobutanes, *J. Am. Chem. Soc.*, **119**, 2597, 1997.
57. Bach, T., Schröder, J., and Harms, K., Diastereoselective photocycloaddition of an axial chiral enamide, *Tetrahedron Lett.*, **40**, 9003, 1999.
58. Ayitou, A. J.-L. and Sivaguru, J., Light-induced transfer of molecular chirality in solution: Enantiospecific photocyclization of molecularly chiral acrylanilides, *J. Am. Chem. Soc.*, **131**, 5036, 2009.
59. Ayitou, A. J.-L., Jesuraj, J. L., Barooah, N., Ugrinov, A., and Sivaguru, J., Enantiospecific photochemical Norrish/Yang type II reaction of nonbiaryl atropchiral α-oxoamides in solution-Axial to point chirality transfer, *J. Am. Chem. Soc.*, **131**, 11314, 2009.
60. Sakamoto, M., Unosawa, A., Kobaru, S., Saito, A., Mino, T., and Fujita, T., Asymmetric photocycloaddition in solution of a chiral crystallized naphthamide, *Angew. Chem. Int. Ed.*, **44**, 5523, 2005.
61. Sakamoto, M., Kato, M., Aida, Y., Fujita, K., Mino, T., and Fujita, T., Photosensitized 2 + 2 cycloaddition reaction using homochirality generated by spontaneous crystallization, *J. Am. Chem. Soc.*, **130**, 1132, 2008.
62. Zhao, H., Hsu, D. C., and Carlier, P. R., Memory of chirality: An emerging strategy for asymmetric synthesis, *Synthesis*, 1, 1–16, 2005.
63. Giese, B., Wettstein, P., Stähelin, C., Barbosa, F., Neuburger, M., Zehnder, M., and Wessig, P., Memory of chirality in photochemistry, *Angew. Chem. Int. Ed.*, **38**, 2586, 1999.
64. Sinicropi, A., Barbosa, F., Basosi, R., Giese, B., and Olivucci, M., Mechanism of the Norrish–Yang photocyclization reaction of an alanine derivative in the singlet state: Origin of the chiral-memory effect, *Angew. Chem. Int. Ed.*, **44**, 2390, 2005.
65. Griesbeck, A. G., Kramer, W., and Lex, J., Diastereo- and enantioselective synthesis of pyrrolo[1,4] benzodiazepines through decarboxylative photocyclization, *Angew. Chem. Int. Ed.*, **40**, 577, 2001.
66. Sakamoto, M., Kawanishi, H., Mino, T., Kasashima, Y., and Fujita, T., Photochemical asymmetric synthesis of phenyl-bearing quaternary chiral carbons using chiral-memory effect on β-hydrogen abstraction by thiocarbonyl group, *Chem. Commun.*, 4608, 2006.

67. Sakamoto, M., Kawanishi, H., Mino, T., and Fujita, T., Asymmetric synthesis of β-lactams using chiral-memory effect on photochemical γ-hydrogen abstraction by thiocarbonyl group, *Chem. Commun.*, 2132, 2008.
68. Resendiz, M. J. E., Family, F., Fuller, K., Campos, L. M., Khan, S. I., Lebedeva, N. V., Forbes, M. D. E., and Garcia-Garibay, M. A., Radical reactions with double memory of chirality (^{2}MOC) for the enantiospecific synthesis of adjacent quaternary centers in solution: Cleavage and bonding faster than radical rotation, *J. Am. Chem. Soc.*, **131**, 8425, 2009.
69. Muehling, O. and Wessig, P., Stereoselective synthesis of cyclopropanes based on a 1,2-chirality transfer, *Chem. Eur. J.*, **14**, 7951, 2008.
70. Córdova, A., Sundén, H., Engqvist, M., Ibrahem, I., and Casas, J., The direct amino acid-catalyzed asymmetric incorporation of molecular oxygen to organic compounds, *J. Am. Chem. Soc.*, **126**, 8914, 2004.
71. Nicewicz, D. A. and MacMillan, D. W. C., Merging photoredox catalysis with organocatalysis: The direct asymmetric alkylation of aldehydes, *Science*, **322**, 77, 2008.
72. Nagib, D. A., Scott, M. E., and MacMillan, D. W. C., Enantioselective α-trifluoromethylation of aldehydes via photoredox organocatalysis, *J. Am. Chem. Soc.*, **131**, 10875, 2009.

8

Spin-Center Shift Reactions

Pablo Wessig
Universität Potsdam

8.1 Introduction

Ring closure reactions are of fundamental importance in organic chemistry due to the broad occurrence of cyclic structural elements both in natural products and in synthetic drugs. Besides many valuable thermal methods, photochemical ring closure reactions gained increasing importance in recent years. Among the various photochemical cyclization reactions, the *Norrish–Yang* reaction [1] turned out to be particularly versatile.

In 1934, *Norrish* and *Appleyard* observed upon irradiation of aliphatic ketones **1** (R^1 = alkyl, X = C[sp^3]) a cleavage reaction providing ketones **3**, whose alkyl chain was cleaved between the α- and the β-carbon atom with respect to the carbonyl group, and alkenes **4** [2]. Nowadays, this cleavage reaction is named "Norrish-Type-II cleavage." Certainly due to the limited analytical capabilities 75 years ago, it was only *Yang* and *Yang* who recognized 23 years later the formation of cyclobutanes **5** besides the *Norrish-Type-II* cleavage products (**3**,**4**) [3]. This discovery was the basis of a very versatile and valuable ring closure reaction that has therefore been termed "*Norrish–Yang* reaction." Diradicals **5** (in singlet or triplet state) are key intermediates of this reaction and play a central role in the mechanism of the *spin-center shift* reactions discussed in this chapter (Scheme 8.1).

Depending on the linking group X in the reactants **1**, a variety of carbo- and heterocyclic compounds has been prepared by means of the *Norrish–Yang* reaction. Accordingly, cyclopropanes, cyclobutanes (the *Yang* reaction in the narrow sense), azetidines, oxetanes, cyclopentanes, pyrrolidines, tetrahydrofuranes, cyclohexanes, piperidines, quinolines, chromanes, and some macrocyclic compounds were obtained in this way [4]. On one hand, the variety of different cyclic molecules obtained by the *Norrish–Yang* reaction demonstrates the synthetic scope of this reaction. On the other hand, the ring size formed from a certain reactant can hardly be influenced. The basic idea of the *spin-center shift* reactions (in the narrow sense, *vide infra*) is to combine the *Norrish–Yang* reaction with fast processes known from monoradicals, which are accompanied with a shift of the spin center, and, consequently, alter the ring size of the products.

The reactions of radicals could be roughly subdivided into those destroying the radical character and those preserving it. The two most important radical-destroying reactions are the radical recombination

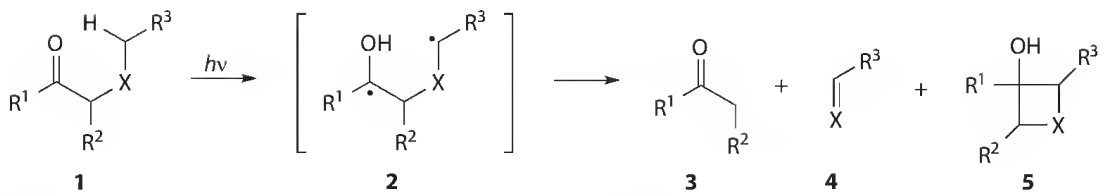

SCHEME 8.1 *Norrish–Yang* reaction and *Norrish-Type-II* cleavage.

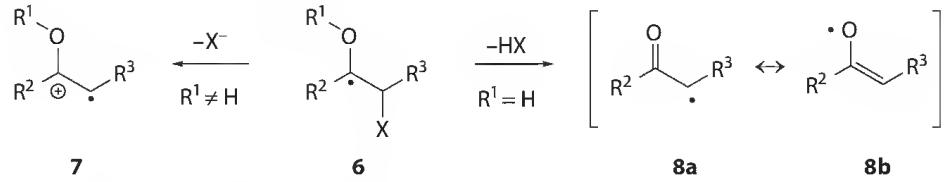

SCHEME 8.2 The *spin-center shift* in the narrow sense.

and the radical disproportionation. Reactions preserving the radical character are rearrangement reactions, addition reactions, and elimination reactions. All of these reactions have in common that the position of the radical center is shifted to another atom in the course of the reaction. Looked at in this way, these reactions could be understood as *spin-center shift* reactions in the broader sense.

Among various types of elimination reactions of radicals, one process is based on the elimination of a leaving group (or the corresponding acid) located on the atom adjacent to the radical center. This process is strongly facilitated if a hydroxy or an alkoxy group is tethered at the radical center. Thus, radicals **6** undergo very rapid elimination either to radical cations **7** or to oxoallyl radicals **8** (sometimes called "enolate radicals") depending on the functional group at the radical center. In both cases, the spin density is shifted to the adjacent atom (Scheme 8.2). We define photochemical reactions involving the *Norrish–Yang* reactions and the reactions summarized in Scheme 8.2 as *spin-center shift* in the narrow sense (SCS-NY) and this is the topic of this chapter [5].

It should be noted that the reactions outlined in Scheme 8.2 play also an important role in some biochemical processes, for example, the deoxygenation of ribonucleotides [6] or the damage of DNA by oxidative stress [7].

8.2 Cyclopropanes

8.2.1 Monocyclic Cyclopropanes

The precondition for the synthesis of cyclopropanes as products of a *Norrish–Yang* reaction is the formation of 1,3-diradicals and consequently a hydrogen abstraction from the β-position with respect to the carbonyl group. The geometrical parameters of the corresponding five-membered transition state, especially the O–H–C bond angle, differ substantially from the ideal parameters reported by *Scheffer* [8]. Therefore, it is not surprising that only few syntheses of cyclopropanes via the *Norrish–Yang* reaction are known [9–11].

This situation was substantially improved by the utilization of the SCS for the synthesis of cyclopropanes [12]. The reactants for the cyclopropane synthesis by SCS-NY are alkyl-aryl ketones **9** bearing a leaving group X at the atom adjacent to the carbonyl carbon atom. Upon irradiation, hydrogen migration from the γ-position to the carbonyl oxygen atom takes place after intersystem crossing (ISC), giving the 1,4-diradical **10**. If the leaving tendency of X is too low (e.g., X = OC(=O)R, Cl), mainly the products of the *Norrish–Yang* reaction and *Norrish-Type-II* cleavage are formed from **10** [13], whereas for X = Br a homolytic C–Br bond cleavage is observed [13b]. In the case of good leaving groups, such as sulfonates and nitrates, a very rapid elimination of acid HX takes place and 1,3-diradicals **11** are obtained, which cyclize to cyclopropanes **12** after repeated ISC to the singlet state (Scheme 8.3).

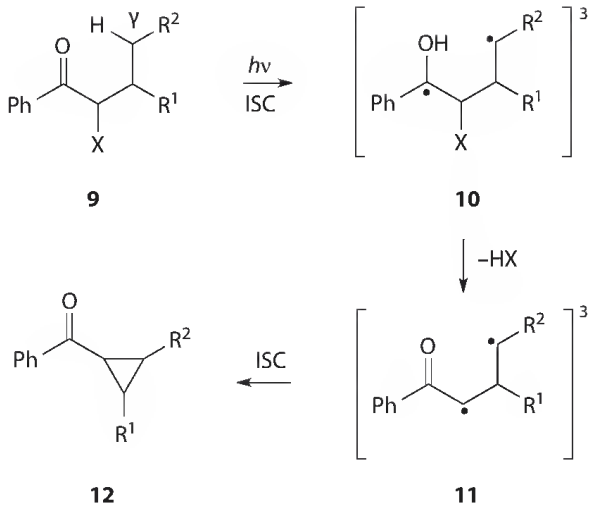

SCHEME 8.3 Formation of cyclopropanes **12** by NY-SCS.

TABLE 8.1 Yields of Cyclopropanes **12a–e**

12	R^1	R^2	X	Yield (%)
a	H	H	OMs	87
b	Me	H	OMs	90
c	H	Ph	OMs	78
d	H	CN	OMs	65
e	H	*c*Pr	OTs	68

Conditions: DCM/NMI (2 equivalents).

A common feature of all preparative SCS applications is the formation of strong acids HX during the irradiation. In the presence of these acids, benzoylcyclopropanes **12** are not stable upon irradiation but undergo rapid ring opening. Consequently, an efficient acid scavenger must be added and it was found that imidazole or *N*-methylimidazole (NMI) is best suited for this purpose. The reaction outlined in Scheme 8.3 is very versatile and tolerates many functional groups. The yields of a selection of cyclopropanes **12** are summarized in Table 8.1.

The formation of compound **12e**, bearing a cyclopropyl group, allows conclusions to be drawn about the lifetimes of diradicals **10** and **11**. It is well known that those cyclopropylcarbinyl radicals undergo a very fast ring opening ($k = 4.0 \times 10^7\,s^{-1}$) and this reaction was often utilized for the determination of radical lifetimes [14]. Consequently, the formation of dicyclopropylketone **12e** in 68% yield and without any indication of an opening of the terminal cyclopropyl ring proves that the sum of the lifetimes of the primarily formed 1,4-diradical **10** and 1,3-diradical **11** is considerably smaller than 25 ns.

8.2.2 Bicyclic Cyclopropanes: 1,2-Chirality Transfer

Extensive quantum chemical calculations on the cyclopropane formation [12b] revealed an interesting peculiarity in the reaction mechanism. Thus, owing to hyperconjugative interaction between the C–X–σ-bond and the semi-filled π-orbital of the excited carbonyl group, the transition states of the initial hydrogen transfer (**9** → **10**) prefer a conformation **TS**^{1} in which the leaving group is arranged pseudoaxially in the cyclohexane-like ring. This phenomenon led to the development of an entirely new stereoselection principle based on a 1,2-chirality transfer [15]. The principle of this approach is portrayed in Scheme 8.4 in simplified terms. If two identical groups R–CH_2 are tethered at the β-position, this atom may be regarded as prochirality center and the positions γ^1 and γ^2 are diastereotopic. On the

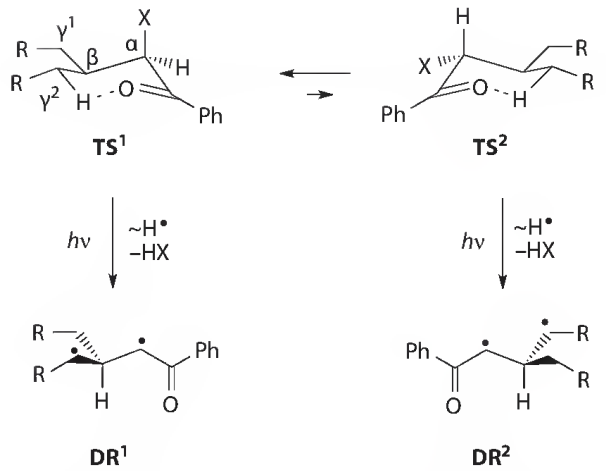

SCHEME 8.4 Principle of the 1,2-chirality transfer in the course of the SCS-NY cyclopropane synthesis.

basis of the preference of **TS¹**, the excited carbonyl group should preferably attack the position γ^2. In the course of the SCS, the chirality center in α-position vanishes, and the chiral information is transferred to the β-carbon atom (1,2-chirality transfer, Scheme 8.4).

This principle was applied to a series of enantiopure ketones *R*-**13**, which have in common that the groups *R* (see Scheme 8.4) are parts of a saturated six-membered ring (Scheme 8.5). The photochemical behavior of these ketones in different solvents and at different temperatures was investigated and the results are summarized in Table 8.2.

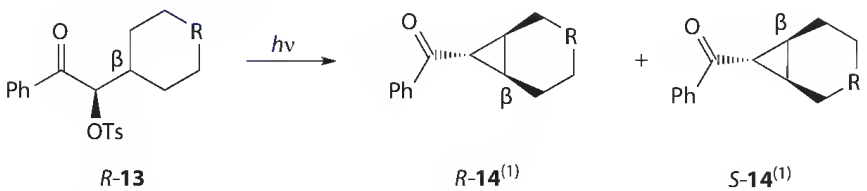

SCHEME 8.5 Photochemical cyclization of ketones *R*-**13**.

TABLE 8.2 Results of Irradiation of Ketones *R*-**13a–d**

Product	R	Solvent	Configuration[a]	*ee* [%] (*CT* [%])[b]
14a	CH(*t*Bu)[c]	DCM	*R*	52 (55)
14a	CH(*t*Bu)[c]	MeOH	*R*	45 (47)
14b	O	DCM	*S*	28 (31)
14b	O	MeOH	*S*	50 (55)
14c	N(Ts)	DCM	*S*	38 (38)
14c	N(Ts)	MeOH	*S*	48 (48)
14d	N(Boc)	DCM	*R*[d]	23 (25)
14d	N(Boc)	MeOH		*rac.*

[a] Configuration at C-β of the preferred enantiomer at 25°C, assigned with VCD spectroscopy. *R*: T_0 lies above 25°C, stereochemical reaction is enthalpy driven; *S*: T_0 lies below 25°C, stereochemical reaction is entropy driven.

[b] Chirality transfer: $CT = (ee[\mathbf{14}]/ee[\mathbf{13}]) * 100$.

[c] The *t*Bu substituent is *trans* arranged with respect to C-β.

[d] A doubtless assignment with VCD spectroscopy was not possible.

The formation of bicyclic ketones **14** proceeds with a significant chirality transfer, in most cases, which depends on the solvent. To verify the postulated stereochemical course depicted in Scheme 8.5, it was necessary to determine the absolute configuration of the preferably formed enantiomer of compounds **14a–d**, which succeeded in most cases by application of vibrational circular dichroism (VCD). By this method, which is based on the comparison of experimental and calculated VCD spectra, it was possible to unambiguously determine the absolute configuration of **14a–d**.

As lowering of the reaction temperature often leads to an increase in stereoselectivity, the temperature dependency of stereoselectivity of the photocyclization of compounds *R*-**13** was investigated. Exemplarily, in Figure 8.1, the relevant Eyring plots for **14b** (ln([*R*-**14b**]/[*S*-**14b**]) = f(1/T)) are shown for irradiation in the solvents dichloromethane (DCM) and methanol (MeOH). Surprisingly, in both solvents, an increasing stereoselectivity with increasing temperature starting from r.t. was found, a behavior, which was previously observed in other photochemical reactions. Photochemically induced reactions with a selectivity reversal at T_0 [ln(A/B) = 0] [16]. The phenomenon appears if the differences of enthalpies of activation $\Delta\Delta H^{\#}$ and entropies of activation $\Delta\Delta S^{\#}$ for the formation of both enantiomers have the same sign. According to Equation 8.1, the selectivity *Se* can be calculated from the difference of free activation energies $\Delta\Delta G^{\#}$, which can be subdivided in an enthalpy and an entropy term. At a certain temperature T_0, expressed by Equation 8.2, these terms may compensate each other and any selectivity vanishes. Upon crossing the temperature T_0, the sign of the selectivity is reversed. The activation parameters $\Delta\Delta H^{\#}$ and $\Delta\Delta S^{\#}$ as well as T_0, obtained from the slopes of the lines in Figure 8.1, are summarized in Table 8.3.

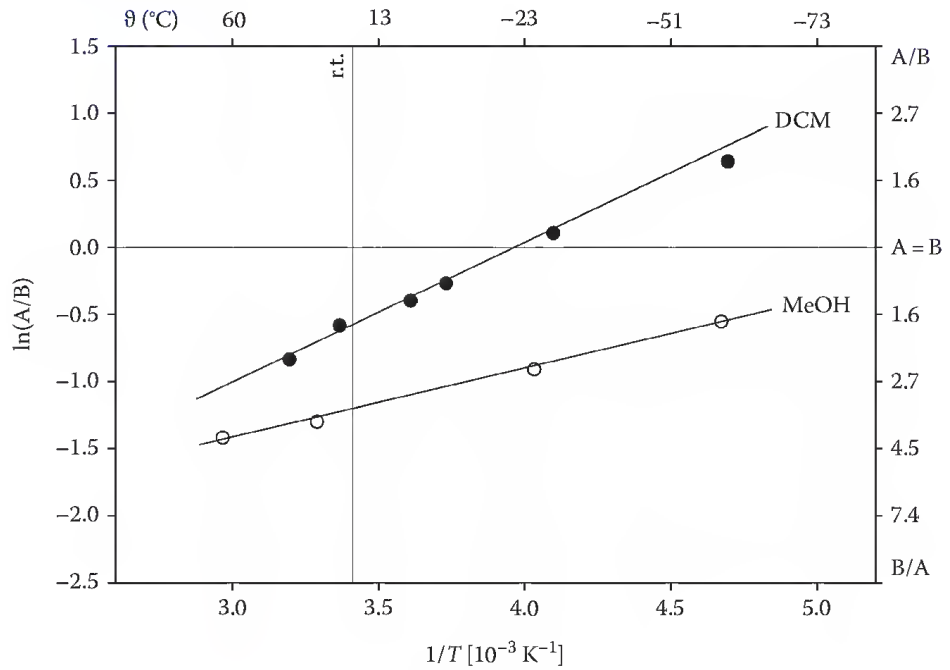

FIGURE 8.1 Temperature dependency of the stereoselective formation of **14b** (A = [*R*-**14b**], B = [*S*-**14b**]).

TABLE 8.3 Activation Parameters for the Formation of **14b**

Solvent	$\Delta\Delta H^{\#}$ (kcal/mol)	$\Delta\Delta S^{\#}$ (cal/mol/K)	T_0 (°C)
DCM	2.0	8.0	−23
MeOH	1.0	5.9	−104

$$Se = \ln\left(\frac{k_A}{k_B}\right) = \frac{-\Delta\Delta G^{\#}}{RT} = -\frac{\Delta\Delta H^{\#}}{RT} + \frac{\Delta\Delta S^{\#}}{R} \tag{8.1}$$

$$T_0 = \frac{\Delta\Delta H^{\#}}{\Delta\Delta S^{\#}} \tag{8.2}$$

8.2.3 Spiro[2.2]pentanes

From investigations on the *Norrish–Yang* reaction, it is well known that the initial intramolecular hydrogen abstraction preferentially takes place at the γ-position of the alkyl side chain [1]. The most established method to prevent a γ-H-shift is to block this position (≠ C(sp³)-H). Furthermore, a *Norrish–Yang* macrocyclization is described for reactants with a cyclopropane moiety located in γ- and δ-position of the side chain [17]. In this case, the significantly higher C–H bond dissociation energy (BDE) of cyclopropane seems to be responsible for the absence of γ-H-abstraction. On the other hand, the cyclopropane formation by SCS-NY (*cf.* preceding section) is characterized by a considerable higher thermodynamic driving force compared with the "normal" *Norrish–Yang* reaction [12]. Therefore, the photochemical behavior of the *cis*-configured 2-mesyloxy cyclopropyl ketone **15** was investigated to find out whether a hydrogen abstraction from the ε-position takes place (Scheme 8.6) [18].

After irradiation (≥300 nm) of **15** in DCM, MeOH, and *t*BuOH, respectively (in the presence of two-equation NMI), no formation of the desired bicyclic ketone **16** could be observed. Instead, the phenyl ketone **17** without leaving group is generated as a consequence of an intermolecular hydrogen shift from the solvent. This is in good agreement with the photochemical behavior of 2-sulfonyloxy phenyl ketones without γ-C(sp³)-H [19]. The question arises which course the reaction will take in the absence of a potential hydrogen donor. Irradiation of **15** in perhalogenated 1,1,2-trichloro-1,2,2-trifluoroethane (R113) leads to a surprising result: the formation of spiro[2.2]pentane **18** as a 1:1 mixture of two diastereomers due to a γ-hydrogen shift.

In contrast to **15**, only one spiro[2.2]pentane isomer is possible in the case of ketone **19**. In fact, complete conversion of **19** on irradiation in R113 and in the presence of NMI (2 equivalents) gave the spiro[2.2] pentane **20** predominantly. In addition, an isomeric methylenecyclobutane **21** resulted (**20**:**21** = 82:18) (Scheme 8.7). By separate irradiation of **20**, it was found that **21** arises from **20**.

The photochemical skeletal rearrangement of **20** to **21** could be explained by a cyclopropane ring opening to 1,3-diradical **22**, which underlies a cyclopropylcarbinyl ring opening ("radical clock") to diradical **23** [14].

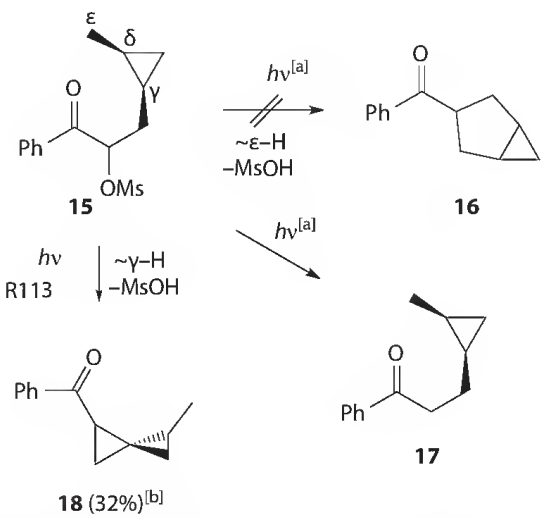

SCHEME 8.6 Photochemical behavior of ketone **15**. ([a]: ≥ 300 nm, solvent: DCM, MeOH, or *t*BuOH. [b]: 1:1 mixture of 2 diastereomers. R113: 1,1,2-trichloro-1,2,2-trifluoro-ethane).

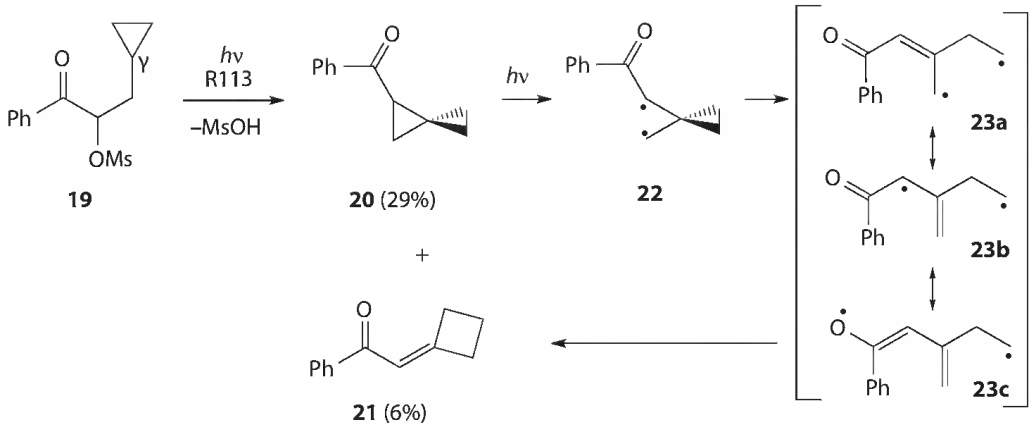

SCHEME 8.7 Photochemical behavior of ketone **19**.

8.3 1-Indanones and Dihydrobenzo[c]furans

The synthesis of cyclopropanes by SCS-NY (Section 8.2) is based on reactants bearing the leaving group within the carbon chain linking the excited carbonyl group and the attacked C–H bond. If the leaving group X is positioned beyond this carbon chain, another mode of SCS is observed. Accordingly, if *o*-alkylaryl-alkyl ketones **24** are irradiated, hydrogen abstraction from the *o*-alkyl residue takes place and 1,4-diradicals **25** are formed (Scheme 8.8). These diradicals may be regarded as triplet form of *o*-quinodimethanes and their lifetimes are considerably longer than that of nonconjugated diradicals [20]. Elimination of acid HX furnishes 1,5-diradicals **26**, which cyclize, after ISC, to 1-indanones **27** [21a]. Owing to the mentioned longer lifetimes, this process tolerates weaker leaving groups X such as phosphates (**24h**) and even carbonates (**24i,j**). Therefore, this system should be suitable for novel photocleavable protective groups [22] for phosphates and alcohols. Indeed, Klán and Wirz demonstrated that 2,5-dimethylphenacylesters [23a–c,e] and carbonates [23d] are excellent protective groups for carboxylic acids, phosphates, sulfonates, alcohols, and phenols. On an application of 2-methyl-phenacylesters as photocleavable linkers in solid phase synthesis was reported as well [24]. The yields of selected 1-indanones **27** are summarized in Table 8.4.

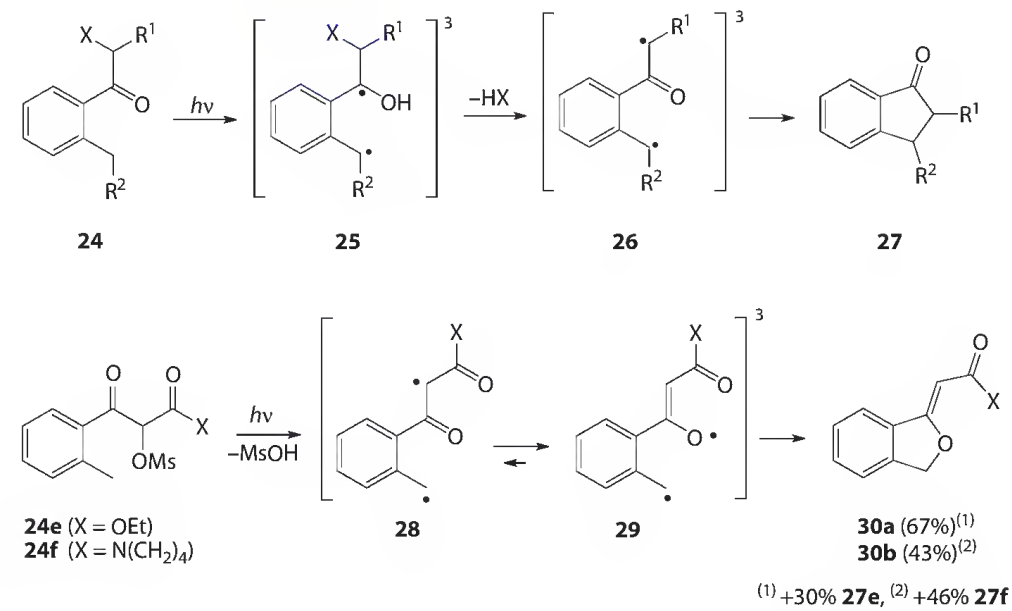

SCHEME 8.8 Photochemical behavior of ketones **24**.

TABLE 8.4 Irradiation of Ketones **24**

24	R^1	R^2	X	Yields (%)	Conditions[a]
a	H	H	OMs	42	C
b	Me	H	OMs	73	C
c	Et	H	OMs	69	B
d	Ph	H	OMs	66	A
e	COOEt	H	OMs	82	D
f	$CON(CH_2)_4$	H	OMs	70	D
g	*i*Pr	H	OMs	46	A
h	Me	H	$OPO(OEt)_2$	62	A
i	Me	H	OCOO*i*Bu	40	A
j	Me	H	OCOOEt	52	A
k	H	Me	OMs	42	C
l	H	COOMe	OMs	77	A
m	H	CN	OMs	58	A

[a] Conditions: A—MeOH/NMI (2 equivalents), B—MeOH, C—DCM/NMI, D—*t*BuOH.

Ketones **24** with an electron withdrawing group at R^1 (**24e,f**) provide 1-indanones **27** only in good yields if *t*BuOH is used as solvent (condition D) whereas in DCM dihydrobenzo[c]furanes **30** are formed as main products. This result could be explained by a shift of the mesomeric equilibrium of oxoallyl radical moiety from carbon centered **28** to oxygen centered **29** (Scheme 8.8, *cf.* Scheme 8.2).

The SCS-NY method for the preparation of 1-indanones was utilized in the total synthesis of pterosines, a class of cyctotoxic natural products occurring in *bracken fern* [21b]. Thus, the fivefold substituted aryl ketones **31**, prepared in 13 steps from 2,6-dimethylphenol, provided upon irradiation in *tert*-butanol 1-indanones **32**. By two additional steps **32a** was converted to Pterosin B (**33**), whereas **32b** provided Pterosin C (**34**, Scheme 8.9).

Klán and coworkers reported on the photochemical synthesis of 1-indanones related to donepezil, an acetylcholinesterase inhibitor used in the treatment of Alzheimer's disease [25].

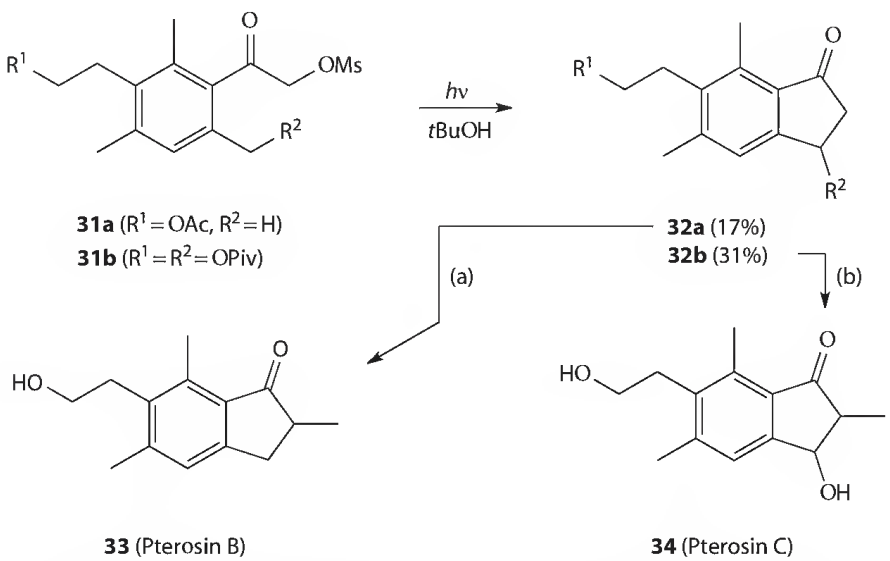

SCHEME 8.9 Total synthesis of Pterosines B and C: (a) 1. K_2CO_3/MeOH, 91%, 2. LDA (two equations)/MeI, 43%. (b) 1. PLE/HEPES, 54%. 2. Three-equation LDA (three equations)/MeI 49%.

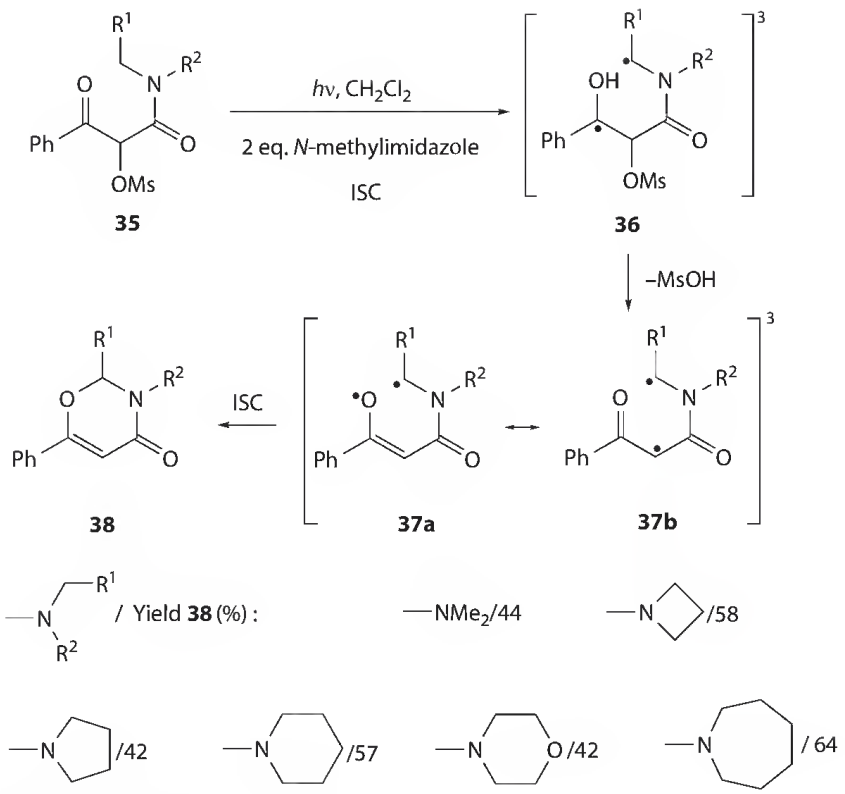

SCHEME 8.10 Preparation of oxazinones **38**.

8.4 Oxazinones

The synthesis of cyclopropanes (Section 8.2) and 1-indanones (Section 8.3) by SCS-NY is based on the carbon-centered mesomer **8a** (see Scheme 8.2) of the oxoallyl radical moiety. In the preceding section, it was shown that this mode of reaction is altered if an electron withdrawing group is directly tethered to the oxoallyl radical moiety (formation of dihydrobenzo[c]furans **30**). This also applies to the photochemical behavior of α-methanesulfonyloxy-β-ketoamides **35**. These compounds are easily accessible by treating of β-ketoamides with hypervalent iodine-(III) reagents [26]. On irradiation, 1,5-diradicals **36** are formed, which are converted into diradicals **37** by elimination of methanesulfonic acid. In contrast to the cyclopropane and 1-indanone synthesis, the enolate radical moiety of diradicals **37** reacts solely as oxygen radicals **37a** to give oxazinones **38** (Scheme 8.10) [27].

References

1. A selection of reviews: (a) P. J. Wagner, *Acc. Chem. Res.* 1971, *4*, 168–177; (b) P. J. Wagner, *Topics Curr. Chem.* 1976, *66*, 1–52; (c) P. J. Wagner, *Acc. Chem. Res.* 1989, *22*, 83–91; (d) P. J. Wagner, B. S. Park, Photoinduced hydrogen atom abstraction by carbonyl compounds, in *Organic Photochemistry*, Vol. 11 (Ed.: A. Padwa), Marcel Dekker, New York, 1991, pp. 227–366; (e) P. J. Wagner, P. Klán, Norrish type II photoelimination of ketones: Cleavage of 1,4-biradicals formed by γ-hydrogen abstraction, in *Organic Photochemistry and Photobiology*, 2nd Edn. (Eds.: W. M. Horspool, F. Lenci), CRC Press, Boca Raton, FL, 2003, pp. 52/1–52/31; (f) T. Hasegawa, Norrish type II processes of ketones: Influence of environment, in *Organic Photochemistry and Photobiology*, 2nd Edn. (Eds.: W. M. Horspool, F. Lenci), CRC Press, Boca Raton, FL, 2003, pp. 55/1–55/14; (g) P. Wessig, Regioselective photochemical synthesis of carbo- and heterocyclic compounds: The Norrish–Yang reaction, in *Organic*

Photochemistry and Photobiology, 2nd Edn. (Eds.: W. M. Horspool, F. Lenci), CRC Press, Boca Raton, FL, 2003, pp. 57/1–57/20; (h) P. J. Wagner, Yang photocyclization: Coupling of biradicals formed by intramolecular hydrogen abstraction, in *Organic Photochemistry and Photobiology*, 2nd Edn. (Eds.: W. M. Horspool, F. Lenci), CRC Press, Boca Raton, FL, 2003, pp. 58/1–58/70; (i) P. J. Wagner, Abstraction of γ-hydrogens by excited carbonyls, in *Molecular and Supramolecular Photochemistry*, Vol. 12 (Eds.: A. G. Griesbeck, J. Mattay), Marcel Dekker, New York, 2005, pp. 11–39.

2. R. G. W. Norrish, M. E. S. Appleyard, *J. Chem. Soc.* 1934, 874–880.
3. N. C. Yang, D.-D. H. Yang, *J. Am. Chem. Soc.* 1958, *80*, 2913–2914.
4. (a) P. Wessig, O. Muehling, Abstraction of (γ ± n)-hydrogens by excited carbonyls, in *Molecular and Supramolecular Photochemistry*, Vol. 12 (Eds.: A. G. Griesbeck, J. Mattay), Marcel Dekker, New York, 2005, pp. 41–87; (b) P. Wessig, Stereoselective photocyclization of ketones (Norrish–Yang reaction), in *Handbook of C-H Transformations*, Vol. 2 (Ed.: G. Dyker), Wiley-VCH, Weinheim, Germany, 2005, pp. 569–579.
5. P. Wessig, O. Muehling, *Eur. J. Org. Chem.* 2007, 2219–2232.
6. (a) H. Eklund, U. Uhlin, M. Farnegardh, D. T. Logan, P. Nordlund, *Prog. Biophys. Mol. Biol.* 2001, *77*, 177–268; (b) S. Licht, J. Stubbe, Mechanistic investigations of ribonucleotide reductases, in *Comprehensive Natural Products Chemistry*, Vol. 5 (Ed.: C. D. Poulter), Elsevier Science, New York, 1999, pp. 163–203; (c) F. Himo, P. E. M. Siegbahn, *Chem. Rev.* 2003, *103*, 2421–2456; (d) H. Zipse, *J. Am. Chem. Soc.* 1995, *117*, 11798–11806.
7. (a) W. K. Pogozelski, T. D. Tullius, *Chem. Rev.* 1998, *98*, 1089–1107; (b) B. Giese, J. Burger, T. W. Kang, C. Kesselheim, T. Wittmer, *J. Am. Chem. Soc.* 1992, *114*, 7322–7324; (c) B. Giese, X. Beyrich-Graf, J. Burger, C. Kesselheim, M. Senn, T. Schäfer, *Angew. Chem.* 1993, *105*, 1850–1852; *Angew. Chem. Int. Ed. Engl.* 1993, *32*, 1742–1743; (d) A. Gugger, R. Batra, P. Rzadek, G. Rist, B. Giese, *J. Am. Chem. Soc.* 1997, *119*, 8740–8741; (e) B. Giese, A. Dussy, E. Meggers, M. Petretta, U. Schwitter, *J. Am. Chem. Soc.* 1997, *119*, 11130–11131; (f) S. Peukert, R. Batra, B. Giese, *Tetrahedron Lett.* 1997, *38*, 3507–3510; (g) B. Giese, X. Beyrich-Graf, P. Erdmann, M. Petretta, U. Schwitter, *Chem. Biol.* 1995, *2*, 367–375.
8. (a) S. Ariel, V. Ramamurthy, J. R. Scheffer, J. Trotter, *J. Am. Chem. Soc.* 1983, *105*, 6959–6960; (b) J. R. Scheffer, C. Scott, Crystal structure-solid state reactivity relationships: Toward a greater understanding of Norrish/Yang type II photochemistry, in *Organic Photochemistry and Photobiology*, 2nd Edn. (Eds.: W. M. Horspool, F. Lenci), CRC Press, Boca Raton, FL, 2003, pp. 54/1–54/25; (c) H. Ihmels, J. R. Scheffer, *Tetrahedron* 1999, *55*, 885–907.
9. (a) W. Weigel, S. Schiller, R. Heck, H.-G. Henning, *Tetrahedron* 1997, *53*, 7855–7866; (b) H. J. Roth, M. H. ElRaie, *Tetrahedron Lett.* 1970, *11*, 2445–2446; (c) H. J. Roth, M. H. ElRaie, *Arch. Pharm.* 1972, *305*, 213–219; (d) H. J. Roth, M. H. ElRaie, T. Schrauth, *Arch. Pharm.* 1974, *307*, 584–595; (e) A. Abdul-Baki, F. Rotter, T. Schrauth, H. J. Roth, *Arch. Pharm.* 1978, *311*, 341–345; (f) A. Padwa, R. Gruber, *J. Am. Chem. Soc.* 1970, *92*, 107–114; (g) H. Haber, H. Buchholz, R. Sukale, H.-G. Henning, *J. Prakt. Chem.* 1985, *327*, 51–62; (h) W. Weigel, P.J. Wagner, *J. Am. Chem. Soc.* 1996, *118*, 12858–12859; (i) M. Yoshioka, S. Miyazoe, T. Hasegawa, *J. Chem. Soc. Perkin Trans. 1* 1993, *22*, 2781–2786; (j) H. E. Zimmermann, J. M. Nuss, A. W. Tantillo, *J. Org. Chem.* 1988, *53*, 3792–3803.
10. (a) E. C. Alexander, R. J. Jackson, Jr., *J. Am. Chem. Soc.* 1974, *96*, 5663–5665; (b) E. C. Alexander, R. J. Jackson, Jr., *J. Am. Chem. Soc.* 1976, *98*, 1609–1610; (c) M. A. Brumfield, W. C. Agosta, *J. Am. Chem. Soc.* 1988, *110*, 6790–6794.
11. A previously reported formation of cyclopropanols (H.-G. Henning, R. Berlinghoff, A. Mahlow, H. Köppel, K. D. Schleinitz, *J. Prakt. Chem.* 1981, *323*, 914–918) seems to be based on a mistake in the interpretation of the spectral data: U. Lindemann, M. Neuburger, M. Neuburger-Zehnder, D. Wulff-Molder, P. Wessig, *J. Chem. Soc. Perkin Trans. 2* 1999, 2029–2036.
12. (a) P. Wessig, O. Muehling, *Angew. Chem.* 2001, *113*, 1099–1101; *Angew. Chem. Int. Ed. Engl.* 2001, *40*, 1064–1065; (b) P. Wessig, O. Muehling, *Helv. Chim. Acta* 2003, *86*, 865–893.

13. (a) L. Ouazzani-Chadi, J.-C. Quirion, Y. Troin, J.-C. Gramain, *Tetrahedron* 1990, *46*, 7751–7762; (b) S. Cho, B. S. Park, *Bull. Korean Chem. Soc.* 2004, *25*, 42–44.
14. M. Newcomb, Kinetics of radical reactions: Radical clocks, in *Radicals in Organic Synthesis*, Vol. 1 (Eds.: P. Renaud, M. P. Sibi), Wiley-VCH, Weinheim, Germany, 2001, pp. 317–336 and references cited therein.
15. (a) P. Wessig, O. Muehling, *Angew. Chem.* 2005, *117*, 6936–6940; *Angew. Chem. Int. Ed. Engl.* 2005, *44*, 6778–6781; (b) O. Muehling, P. Wessig, *Chem. Eur. J.* 2008, *14*, 7951–7960.
16. (a) Y. Inoue, H. Ikeda, M. Kaneda, T. Sumimura, S. R. L. Everitt, T. Wada, *J. Am. Chem. Soc.* 2000, *122*, 406–407 and references cited therein; (b) S. Kohmoto, H. Masu, C. Tatsuno, K. Kishikawa, M. Yamamoto, K. Yamaguchi, *J. Chem. Soc. Perkin Trans. 1* 2000, 4464–4468; (c) O. Benali, M. A. Miranda, R. Tormos, S. Gil, *J. Org. Chem.* 2002, *67*, 7915–7918; (d) W. Adam, V. R. Stegmann, *J. Am. Chem. Soc.* 2002, *124*, 3600–3607 and references cited therein; (e) N. Hoffmann, H. Buschmann, G. Raabe, H.-D. Scharf, *Tetrahedron* 1994, *50*, 11167–11186; (f) M. Abe, T. Kawakami, S. Ohata, K. Nozaki, M. Nojima, *J. Am. Chem. Soc.* 2004, *126*, 2838–2856; (g) X.-M. Hei, Q.-H. Song, X.-B. Li, W.-J. Tang, H.-B. Wang, Q.-X. Guo, *J. Org. Chem.* 2005, *70*, 2522–2527.
17. G. A. Kraus, Y. Wu, *J. Am. Chem. Soc.* 1992, *114*, 8705–8707.
18. O. Muehling, P. Wessig, *Photochem. Photobiol. Sci.* 2006, *5*, 1000–1005.
19. J.-P. Fouassier, D. Burr, *Macromolecules* 1990, *23*, 3615–3619.
20. A. P. Pelliccioli, P. Klán, M. Zabadal, J. Wirz, *J. Am. Chem. Soc.* 2001, *123*, 7931–7932.
21. (a) P. Wessig, C. Glombitza, G. Müller, J. Teubner, *J. Org. Chem.* 2004, *69*, 7582–7591; (b) P. Wessig, J. Teubner, *Synlett* 2006, 1543–1546.
22. Recent Reviews: (a) C. G. Bochet, *J. Chem. Soc. Perkin Trans. 1* 2002, 125–142; (b) A. P. Pelliccioli, J. Wirz, *Photochem. Photobiol. Sci.* 2002, *1*, 441–458.
23. (a) P. Klán, M. Zabadal, D. Heger, *Org. Lett.* 2000, *2*, 1569–1571; (b) M. Zabadal, A. P. Pelliccioli, P. Klán, J. Wirz, *J. Phys. Chem. A* 2001, *105*, 10329–10333; (c) P. Klán, A. P. Pelliccioli, T. Pospisil, J. Wirz, *Photochem. Photobiol. Sci.* 2002, *1*, 920–923; (d) J. Literák, J. Wirz, P. Klán, *Photochem. Photobiol. Sci.* 2005, *4*, 43–46; (e) L. Plístil, T. Solomek, J. Wirz, D. Heger, P. Klán, *J. Org. Chem.* 2006, *71*, 8050–8058.
24. L.-H. Du, S.-J. Zhang, Y.-G. Wang, *Tetrahedron Lett.* 2005, *46*, 3399–3402.
25. T. Pospíšil, A. T. Veetil, L. A. P. Antony, P. Klán, *Photochem. Photobiol. Sci.* 2008, *7*, 625–632.
26. Reviews: (a) G. F. Koser, *Aldrichimica Acta* 2001, *34*, 89–102; (b) R. M. Moriarty, R. K. Vaid, G. F. Koser, *Synlett* 1990, 365–383.
27. P. Wessig, J. Schwarz, U. Lindemann, M. C. Holthausen, *Synthesis* 2001, 1258–1262.

9

Photochemistry in Ecosustainable Syntheses: Recent Advances

Valentina Dichiarante
University of Pavia

and

Service de Bioénergétique Biologie Structurale et Mécanismes

Stefano Protti
University of Pavia

and

Service de Bioénergétique Biologie Structurale et Mécanismes

9.1 Introduction

Nature represents the most significant source of inspiration for researchers, due to the fact that several problems (still unresolved for scientists) have been ingeniously overcome by living organisms, thanks to evolution. A well-known example is represented by plants. Starting from simple materials, such as carbon dioxide, water, and mineral salts, they are able to synthesize a wide range of complex organic molecules, with efficient (and often stereoselective) processes, under mild conditions (room temperature, physiologic pH, and aqueous media). Moreover, the only energy source required is solar light and the only side product is molecular oxygen. What chemists can do is to search inspiration from these ideal laboratories, trying to replicate the same reactions in an artificial way. Although this biomimetic approach has been adopted since early decades of 1900 (see, e.g., Ciamician's research), only in recent years it has been formulated, together with the concept of green chemistry. During the twentieth century, a series of tragic events in the chemical industry, caused partially by both safety shortage and lack of environmental awareness (e.g., Cuyahoga river's fire, Bhopal, and Seveso accidents), impacted deeply on the attitude of public opinion toward chemistry (and sciences in general). These episodes, together with the consciousness of humanity of depending almost exclusively on nonrenewable (and pollutant) energy sources, such as fossils fuels, led to a report from the United Nations World Commission on Environment and Development, published in 1987, and called "our common future" [1]. This is actually considered as the first official proposal of a sustainable development for industry and, in general, for civilization. If the

concepts "green synthesis," "environmental benign," and "sustainable chemistry" are nowadays familiar to chemists and the development of environmental-friendly processes (on both industrial and laboratory scale) is considered as a priority, this is due to the incisive work of few research groups. The formulation of the 12 principles of green chemistry by Anastas and Warner [2] in 1991, then the concept of "atom economy" introduced by Trost [3], and the *E*-factors proposed by Sheldon [4,5] to quantify the greenness of a chemical process give an idea of how fast the mergence of a "green conscience" in chemical sciences was.

In our opinion, a reaction must satisfy four primary conditions, in order to be considered "green":

1. An efficient use of energetic sources
2. A minimization of hazards related both to the use of chemicals and to reaction conditions
3. Minimization of waste
4. Use of renewable resources

Summing up, an ideal eco-friendly process might take place efficiently starting from nontoxic and cheap substrates, in the absence of solvent (or, at least, in water) and without heating. As suggested by natural photosynthesis in plants, synthetic photochemistry could play a significant role in the development of ecosustainable synthetic processes. It is a matter of fact that light is a "chemical principle" (according to the definition proposed by Priestley in 1790 [6], that activates reagents, leading to the desired products without the employ of harsh conditions (high temperature or pressure) or catalysts. Practically, photons are a "safe and clean reagent," because they leave no residues in the reaction mixture, making both workup and purification procedures easier. As mentioned earlier, the synthetically green potentialities of light were described and exalted in the early twentieth century, thanks to the pioneering contributions by Giacomo Ciamician and Emanuele Paternò [7]. Their suggestions were then revisited, a few decades later, by Schönberg [8] and Schenck [9], in their fundamental studies on the photoreactivity of carbonyls and on photo-oxidations, respectively. Notably, most of the reported reactions were carried out under conditions that only now are recognized as "green," including solvent-free conditions or sunlight illumination [6]. In particular, immediately after the Second World War (1947), Schenck developed a pilot plant for the synthesis of antihelmitic ascaridole, based on sunlight exposure of an aerated solution of α-terpinene in a stinging nettle leaves ethanol extract [9]. Although his plant was technically limited by the critical *post bellum* situation in Germany, in our opinion it still represents for photochemistry (and chemistry in general) the way to ecosustainability, because of the use of a renewable solvent (ethanol), nontoxic reagents (e.g., air and chlorophyll, used as natural photosensitizer) and sunlight as energy source. Despite these early promising results, a wide application of photochemistry has never really started, probably due to the fact that several limitations affect the "greenness" of photoreactions. In general, photochemical procedures require the use of dilute conditions (from 5×10^{-3} to 5×10^{-2} M of the limiting substrate), in order to allow light to penetrate into the solution to a significant depth for making molecules absorb and react, resulting in a high environmental (and economical) impact of the procedure. On the other hand, higher concentrations often lead to a lack of selectivity, because of undesired secondary reactions involving both reagents and primary products. Furthermore, since most photoprocesses involve the use of artificial light sources, the electrical supply needed has a strong impact on both the environmental and the economical cost of the reaction, and constitutes the main limitation to the industrial application of photochemical reactions, except when photons are used in substoichiometrical ratio (e.g., photopolymerization or photo-initiated halogenation) [10]. In addition, the energy required by the cooling systems of several artificial light sources (especially high and medium pressure Hg lamps) must be taken into account.

From all these considerations, it appears clear that the concepts of photochemistry and green chemistry do not necessarily complement each other. The still pending question is: "how to employ a green reagent (photons) in green processes?" In order to satisfy the four conditions presented earlier, a detailed analysis of all chemicals involved in the reaction (including reactants, catalysts, solvents, and additional materials for workup and purification procedures) should be carried out and then followed by the minimization of the environmental hazards. Recent works evaluated in parallel photochemical and thermal pathways to some different synthetic targets, finding that both environmental and economical cost of the two alternative

routes are almost comparable [11]. What really matters is the fact that photochemical methods can be optimized more easily, by shifting toward less noxious solvents or, at least, by adopting solvent recycling. It should be noted that the term "synthetic process" includes all the reaction steps, including workup and product purification. From this point of view, large-scale reactions would be desirable, due to the possibility of using more eco-friendly purification methods, such as recrystallization or distillation, rather than column chromatography (that involves large amounts of silica gel or alumina, as stationary phase, and a high volume of eluant). With regard to the reduction of energy supply for artificial lamps, some advances have been reported, based on increased light absorption by the starting substrates. For example, Booker-Milburn has recently proposed a multigram scale flow reactor, in which the solution is driven around a water-cooled immersion well by the means of an high-performance liquid chromatography (HPLC) pump. This facility has been tested on a [2 + 2] cycloaddition between 1-hexyne and maleimide (to give the bicyclic adduct **1**, Scheme 9.1) and on the synthesis of azepine **2** by intramolecular photocyclization (Scheme 9.1). Some hundred grams of both photoproducts were isolated after 24 h of irradiation [12].

In the last years, several photochemical processes have been proposed or, often, rediscovered as green methods. In the following sections, a series of examples of these innovative procedures and optimized technologies for carrying out "green synthetic photochemistry" will be presented. The best way of minimizing the environmental impact of photochemical reactions is to remove the solvent, and Sections 2.1

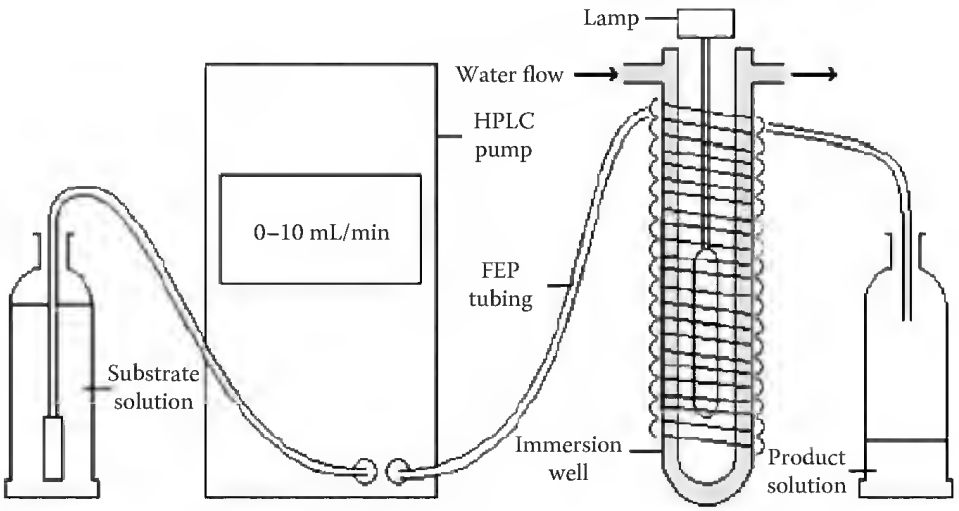

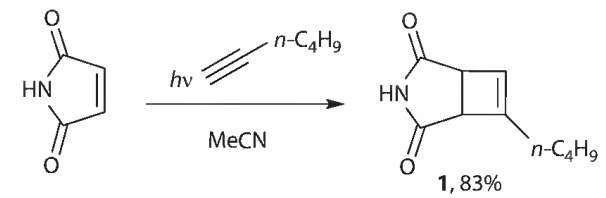

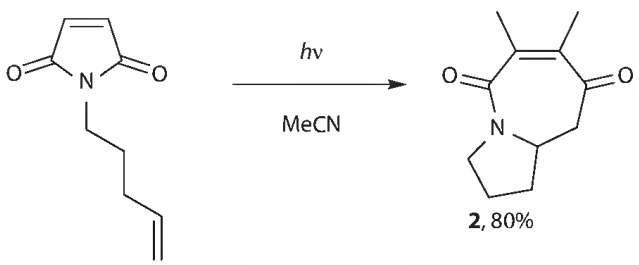

SCHEME 9.1 The continuous flow photoreactor engineered by Booker-Milburn (see Ref. [12]) employed for the synthesis of bicyclic compounds **1** and **2**. (From Hook, B.D.A. et al., *J. Org. Chem.*, 70, 7558, 2005. With permission.)

through 2.3 will be dedicated to this approach. When solvent is necessary for the reaction, more eco-friendly media can be used, as shown in Section 2.4. As far as the energy is concerned, the use of solar light clearly represents the ultimate choice (Section 2.5).

The selected examples have been classified into the previous sections according to what we consider their peculiar feature, even if most of them could be included in different categories.

9.2 Sustainable Methodologies in Photochemistry

9.2.1 Solvent-Free Reactions

As predictable by the use of dilute conditions, the environmental cost of photochemical procedures is mainly due to the solvent. Optimization of solvent free photochemical reactions is still considered a challenge in organic synthesis, and in most cases the preferred route to make ecosustainable chemical processes. Unfortunately, the close dependence existing between the reactivity of photo-generated intermediates and the physical and chemical properties of the solvent, often affects the outcome of such optimization. Nonetheless, several approaches have been developed to overcome the previously mentioned limitations.

When a liquid reactant is involved, it may act as both substrate and solvent. This expedient was first used by Paternò, at the beginning of the twentieth century, studying the photoreactivity of carbonyls in the presence of olefins [7b]. More recently, the photocatalyst 9-phenyl-10-methyl-acrydinium perchlorate (5×10^{-3} M) was dissolved directly into benzyl alcohol, which was then oxidized by molecular oxygen with a quantum yield of 0.35 [13].

Rubiginones are presently investigated as potential drugs for the treatment of AIDS and Alzheimer's diseases. The key step in the synthesis of Rubiginone C_2 (**3**), for example, is the photo-induced one-step desilylation of a protected hydroxyl group, followed by its oxidation to a carbonyl and aromatization. Noteworthy, the reaction takes place under solvent-free conditions and using sunlight as the light source (Scheme 9.2) [14].

In solvent-free reactions, zeolites have been widely used as organic microenvironment, to improve the process selectivity [15] in the photogeneration of several reactive intermediates [16]. The photorearrangement of 3,5-diphenyl-1,2,4-oxadiazole, for example, has been studied in different zeolites, achieving selectively the 1,3,4-oxadiazole isomer (**4**) in 90% yield [17], in contrast with the large number of possible pathways observed in solution (Scheme 9.3).

Photooxidation of alkanes has been investigated by Blatter: irradiation of cyclohexane, loaded into NaY zeolites, with visible (blue or green) light afforded cyclohexanone selectively, with a high consumption of the starting material [18]. In some cases, zeolites are able to force the reaction toward a completely different pathway, with respect to what happens in solution. This is the case for stilbenes,

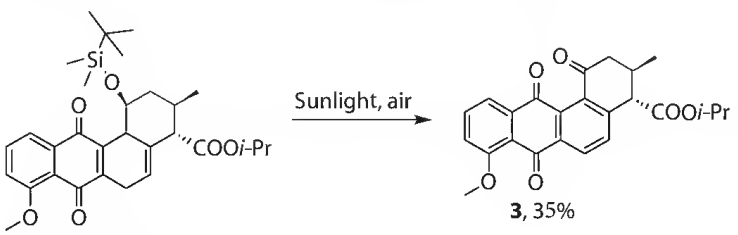

SCHEME 9.2 Synthesis of Rubiginone C_2 **3**.

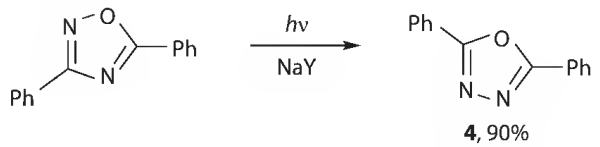

SCHEME 9.3 Photorearrangement of 3,5-diphenyl-1,2,4-oxadiazole in zeolites.

which in Y zeolites are successfully oxidized to the corresponding benzaldehydes, rather than to the endoperoxide products usually observed in dichloromethane solution [19].

9.2.2 Photoreactions in Polymeric Matrix

This approach has been employed mainly in photo-oxidation processes. Photo-oxygenations involving singlet oxygen ($^1\Delta_g$) are appealing reactions in terms of green chemistry, involving only air (or, at least, oxygen) and a dye, as photosensitizer, together with the substrate. Furthermore, the commonly employed dyes absorb significantly in the visible part of the spectrum, allowing the use of sunlight irradiation. Unfortunately, singlet oxygen is a long-lived species only in problematic solvents, such as chloroform or carbon tetrachloride, and at the end of the reaction the dye has to be removed, either by column chromatography or distillation. These limitations have been recently overcome by the use of sensitizers immobilized on a polymeric matrix (by adsorption or covalent bonding), following an approach developed by Griesbeck and coworkers. A photosensitizer formed by *meso*-tetraphenylporphyrin (TPP) or tetratolylporphyrin (TTP), embedded in polystyrene matrix, was applied to the solvent-free oxygenation of sorbic alcohol, to give the corresponding endoperoxyde in high yields [20]. In the same way, less reactive β-pinene (**5**, Scheme 9.4), which is employed as precursor in the industrial synthesis of myrtenol, was converted selectively to hydroperoxide **6** and no side products were observed, even at high conversions, in contrast to the analogous liquid phase reaction. The optimized procedure is extremely simple: immobilization of the dye is carried out by swelling polystyrene particles in a solution of the dye in ethyl acetate, followed by solvent evaporation. The substrate is adsorbed onto the solid phase in the same way, then irradiated in a Petri dish (see Scheme 9.4) and the resulting product is recovered by washing with ethanol. With liquid reagents, loading is carried out directly, without any solvent. It should be underlined that the dye is used only in 0.01% M with respect to the reactant, and as much as 1 g of product can be achieved for every gram of employed polystyrene beads.

Alternatively, beads of tetrastyrylporphyrin (TSP) copolymerized with styrene and divinylbenzene have been employed for the synthesis of several peroxides and endoperoxides (including 1,2,4-dioxazole and hydroperoxides). It should be noted that this sensitizer has a high photooxygenation turnover number (3000) and can be efficiently recycled, without any dye losing or bleaching [21].

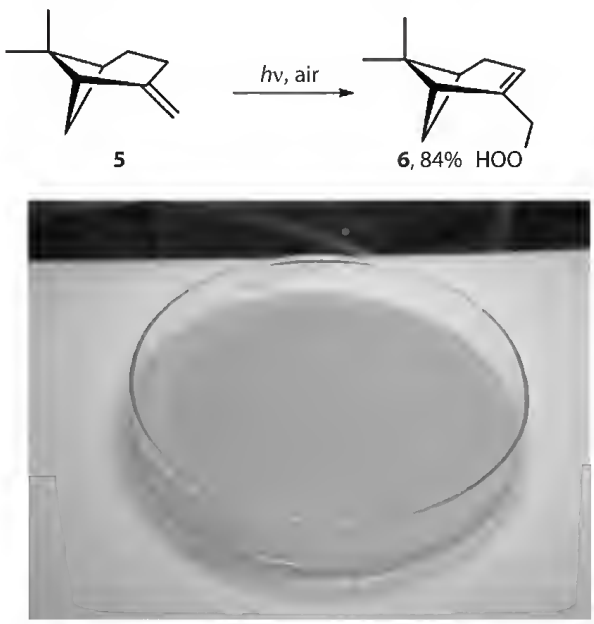

SCHEME 9.4 **(See color insert.)** Photosensitized oxidation of β-pinene **5**. (From Griesbeck, A.G. and Bartoschek, A., *Chem. Commun.*, 1594, 2002. With permission.)

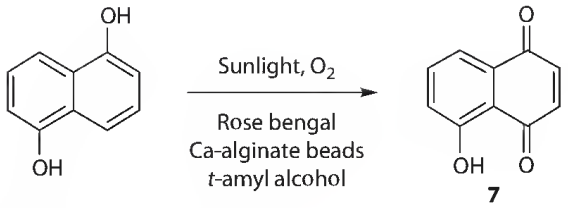

SCHEME 9.5 Photosensitized synthesis of Juglone **7**.

1,5-Dihydroxy-naphthalene was oxidized to pharmacologically active Juglone (**7**), by immobilizing rose bengal on calcium alginate beads. The solvent used to solubilize the reactant and to recover the oxidized product (*tert*-amyl alcohol) was recovered and reused for further cycles (Scheme 9.5) [22].

Maldotti et al. employed iron(III) porphyrins, caged in NAFION membranes, as sensitizers for sunlight-induced allylic oxidation of cycloalkenes to the corresponding alcohols and ketones. Interestingly, the solvent-free process results in a satisfying turnover number (>1000) and efficiency (about 10 times higher than in alcoholic solution) [23]. Scorrano et al. [24] reported the solvent-free benzylic oxidation of aromatics (such as ethyl benzene, cumene, and indane) by a fluorous-tagged decatungstate ($[CF_3(CF_2)_7(CH_2)_3]_3CH_3N)_4W_{10}O_{32}$), embedded on Hyflon membranes.

9.2.3 Solid-State Photoreactions

Since the birth of organic photochemistry, solid state conditions have been largely employed in synthetic processes, as demonstrated by the [2 + 2] dimerization of anthracene and thymoquinone, described by Liebermann and Fritzsche, respectively [6]. Apart from the environmental advantages, photoreactions in crystals often lead to a completely different pathway, with respect to those observed in solution, and sometimes increase selectivity. In a recent example, it was found that head-to-tail arranged crystals of catecholamine **8** underwent efficient photodimerization (dimer **9** in Scheme 9.6a) [25], while an *E*/*Z*

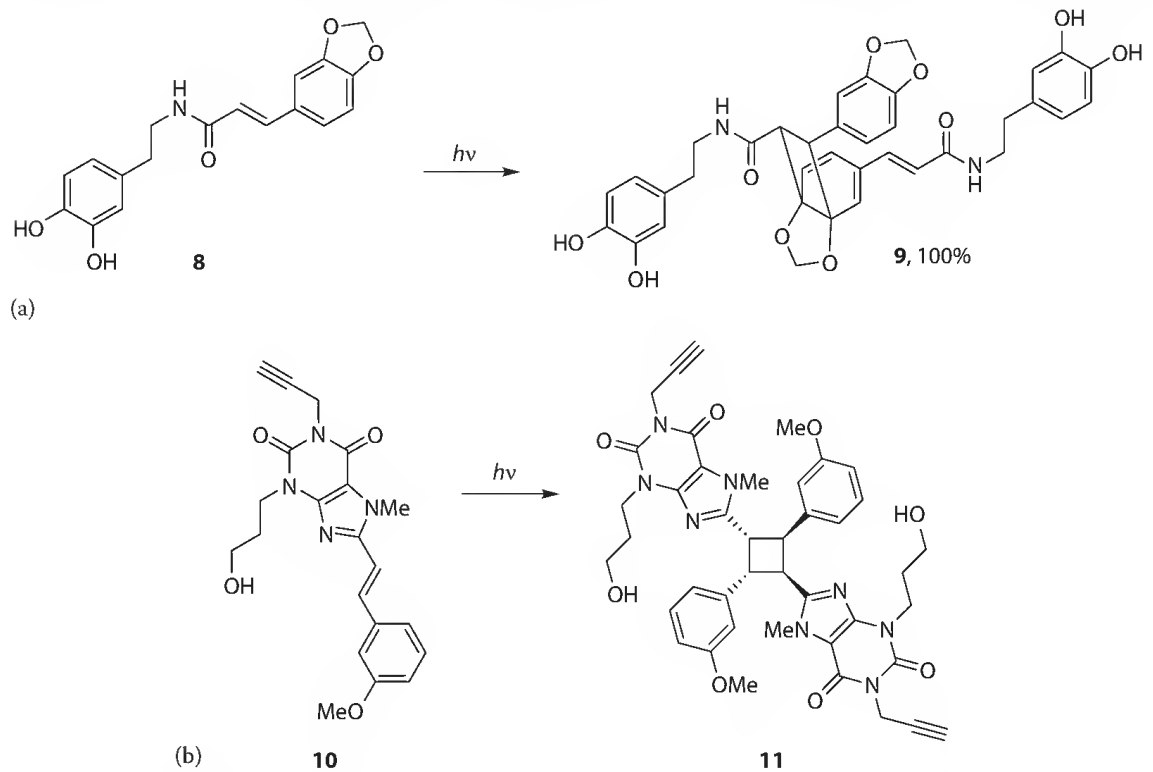

SCHEME 9.6 [2 + 2] photodimerization of (a) catecholamine **8** and of (b) A_{2A} adenosine receptor antagonist **10**.

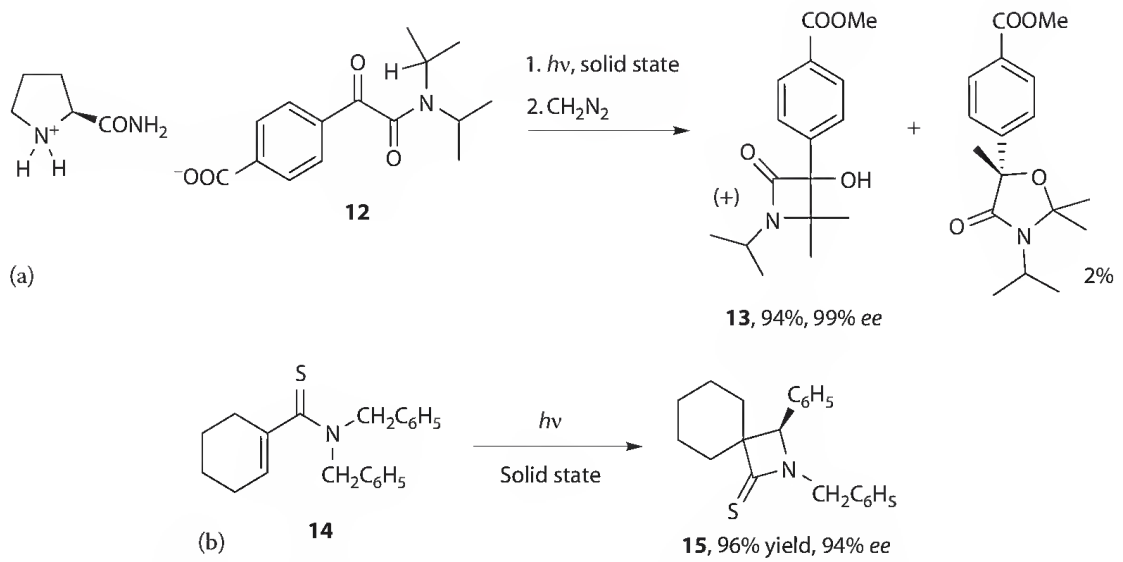

SCHEME 9.7 Solid state, enantioselective route to (a) (+)-lactam **13** and (b) β-thiolactam **15**.

photoisomerization was the only observed path in methanol. An analogous behavior has been reported for 8-styryl-xanthines. In particular, solid state photolysis of molecule **10** (a potent A_{2A} adenosine receptor antagonist, that has been proposed for the treatment of Parkinson's disease) gave selectively the [2 + 2] dimer (**11**), contrary to the isomerization observed in dichloromethane solution (Scheme 9.6b) [26].

The stereochemistry of a reaction can be strongly improved by adopting solid state conditions. For example, lactam (+)-**13** has been easily synthesized through a Norrish-Yang path, by irradiation of an hexane suspension of *N,N*-dialkylglyoxamide chiral salt crystals (**12**) [27]; the desired product was obtained in high yield and with a satisfying enantiomeric excess (99%, Scheme 9.7a). Sometimes, nonchiral molecules are able to adopt a chiral conformation in the crystal lattice, and the resulting molecular environment offers an opportunity for asymmetric induction in the photoreaction. A representative example is the enantioselective synthesis of β-thiolactam **15**, which has been accomplished by irradiation of the relative nonchiral α,β-unsaturated thioamide **14**. The product was formed in excellent yield (96% based on thioamide consumption) and the enantiomeric excess was just slightly affected, when increasing the substrate conversion (Scheme 9.7b) [28].

A smart crystal-to-crystal approach to the decarbonylation of ketones was proposed by Garcia-Garibay and is probably the most significant "green" attempt in the field of solid state photochemistry. In his report, irradiation of finely powdered crystals of 1,3-diphenylacetones, sandwiched between two Pyrex plates, afforded the corresponding 1,2-diphenylethanes in satisfactory yields [29]. Solid state decarbonylation of dicumylketone (**16**), to give dicumene (**17**), has been ingeniously scaled up to 10 g of reactant; in this case, an aqueous suspension of **16** has been irradiated for 19 h, in a flow-reactor made up of a 5 L vessel and a submersible pump, which circulated the suspension through the immersion well (Scheme 9.8) [30]. At the end of the reaction, **17** was easily isolated by filtration through a Whatman cellulose filter.

The same procedure was applied also to six different di-*p*-carboxydiphenyl-2,4-dimethylpentanone ammonium salts (**18**). Decarbonylation occurred in quantitative yield, after only 6 h of irradiation with a Hg medium pressure lamp (Scheme 9.9) [31].

The presence of coordinative bonds (e.g., hydrogen bonds) in the solid state has been exploited in order to enhance stereoselectivity, as demonstrated by MacGillivray [32] in the dimerization of stilbene. For example, assembly of the [resorcinol*(*trans*-1-(4-pyridyl)-2-(4-chlorophenyl)ethylene)$_2$] complex in a head-to-head geometry and subsequent irradiation resulted in a regio-controlled photodimerization, giving the resulting cyclobutane as a single diastereoisomer.

The same strategy has been exploited in the synthesis of *para*-cyclophanes, a class of molecules that find application in material sciences. In this case, cocrystallization of 5-benzyl-resorcinol with 1,4-bis[2-(4-pyridyl)

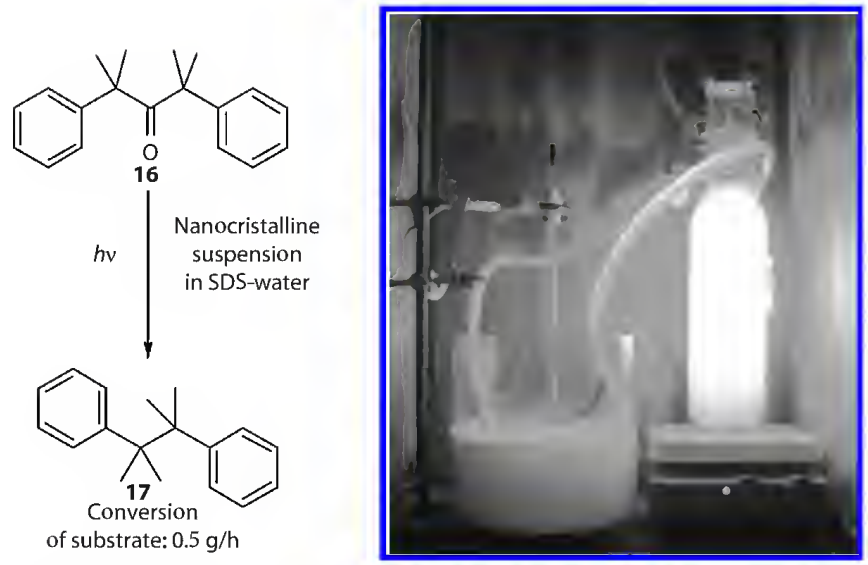

SCHEME 9.8 **(See color insert.)** Solid-state photo-decarbonylation of dicumylketone **16** in a photochemical flow reactor. (From Veerman, M. et al., *Org. Lett.*, 8, 2615, 2006. With permission.)

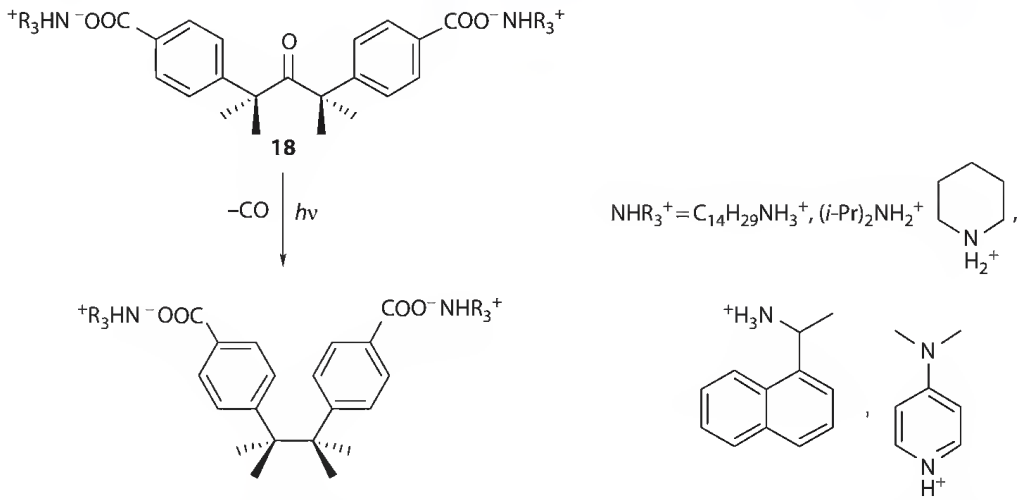

SCHEME 9.9 Solid-state photo-decarbonylation of *p*-carboxydiphenyl-2,4-dimethylpentanone ammonium salts **18**.

ethenyl] benzene (1,4-bpeb) afforded a four-component complex [(Bn-resorcinol)$_2$ · (1,4-bpeb)$_2$], **19** in which the two dienes are already oriented for a double cycloaddition. UV irradiation of the complex afforded the crowded derivative **20**, in a completely stereospecific manner and in 100% yield (Scheme 9.10).

Even supramolecular systems with 3D regularity can be synthesized through solid state photochemical self-assembly. It is the case of 1,2-bis(4-pyridyl)ethylene and benzene 1,2,4,5-tetracarboxylic acid co-crystals (**21**), which dimerized and gave a pure diastereoisomer, in 100% yield. Moreover, when the product was ground with a small amount of dimethylsulfoxide, a nanoporous supramolecular solid with a large channel structure was obtained (**22**, Scheme 9.11) [33].

9.2.4 Photoreactions in Eco-Friendly Solvents

Many photochemical reactions have been discovered and developed when the chronic toxic effects of several organic solvents were unknown or, at least, underestimated. The definition of "green solvent" for a chemical reaction has been recently discussed in two independent works, by Capello [34] and Alfonsi [35].

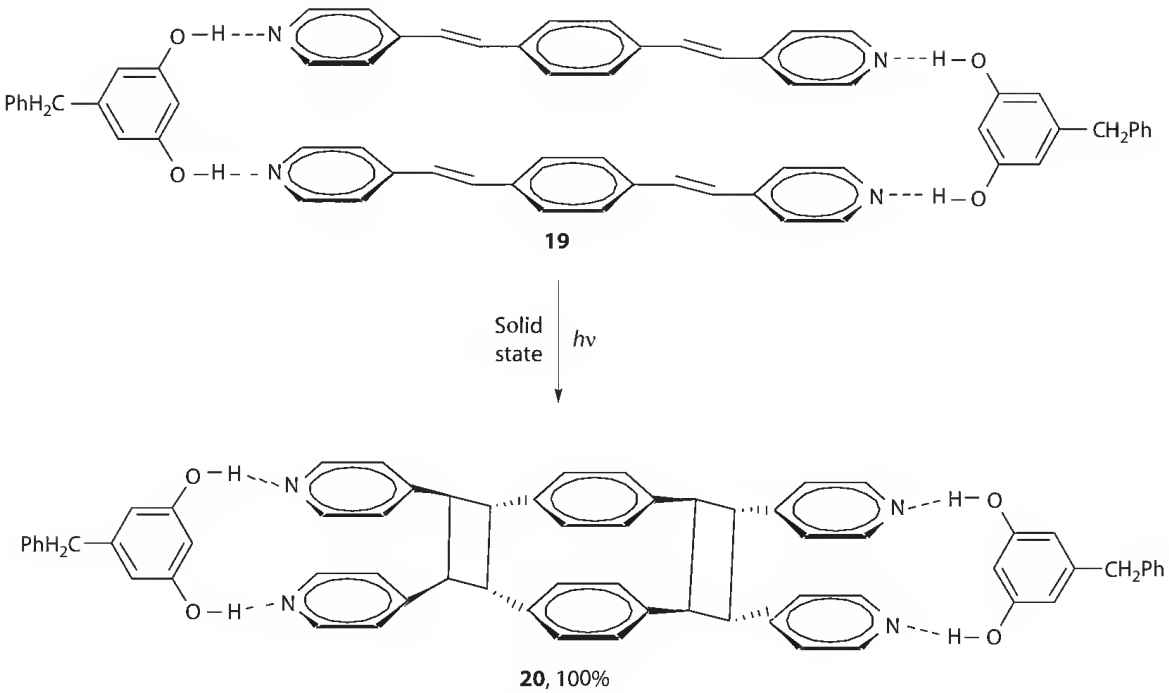

SCHEME 9.10 Double stereospecific [2 + 2] cycloaddition of $[(\text{Bn-resorcinol})_2 \cdot (1,4\text{-bpeb})_2]$ (**19**).

The combined use of green metrics tools (such as EHS or LCA methods) and, of course, a bit of common sense allowed the evaluation of solvents impact on different general areas, such as the safety of workers, of processes and of the environment. This assessment takes into consideration several easily available parameters, such as toxicity, carcinogenicity, flammability, and eco-toxicity. Starting from all these data, a list of undesirable solvents has been established, including high flammable media (such as pentane and diethylether), carcinogenic (as benzene, carbon tetrachloride and chloroform), and highly toxic ones (e.g., *N,N*-dimethylformamide). Since these solvent selection schemes have been developed for thermal reactions, their application to photochemistry suffers from some limitations. Some common replacements, for example, toluene for benzene, cannot be done for photochemical transformations due to reactivity issues. Other problems may derive from low transparency of the reaction medium or its potential sensitization role (as in the case of acetone).

9.2.4.1 Reactions in Water or in Aqueous Mixture

Cheap and nontoxic water is obviously the ideal solvent for green syntheses, although its use is strongly limited by the low solubility of most organic compounds in it. Nevertheless, a few examples of photochemical transformations in water are available in the literature. Among these, the visible light–induced benzylic bromination of methylbenzenes by *N*-bromosuccinimide has been reported; either 40 W bulb irradiation or sunlight can be used for this reaction. Despite the prejudices about workup and purification procedures in water, the previously mentioned method is extremely simple: the starting methylbenzenes (see, e.g., the bromination of benzoic ester **23**, Scheme 9.12) form a layer "on top of the water phase," but as soon as they are brominated, their specific weight increases and the organic phase sinks to the flask bottom. The only by-product formed is succinimide, which is soluble in water and can be smoothly removed (by phase separation or filtration) from the hydrophobic organic product [36].

Another reasonable alternative is the partial substitution of organic solvents with water, according to the rule that, the higher the water percentage in the reaction medium, the lower environmental cost. Photoinduced cyclization of phthalimide derivatives by Griesbeck et al., for example, used a water–acetone mixture as solvent. The mechanism included an initial photoinduced electron transfer, followed by decarboxylation, and led to a wide range of useful synthetic targets, such as pyrrolizidine- and indolizidine-based alkaloids, benzodiazepines, and aristolactams [37]. The process was efficiently scaled up,

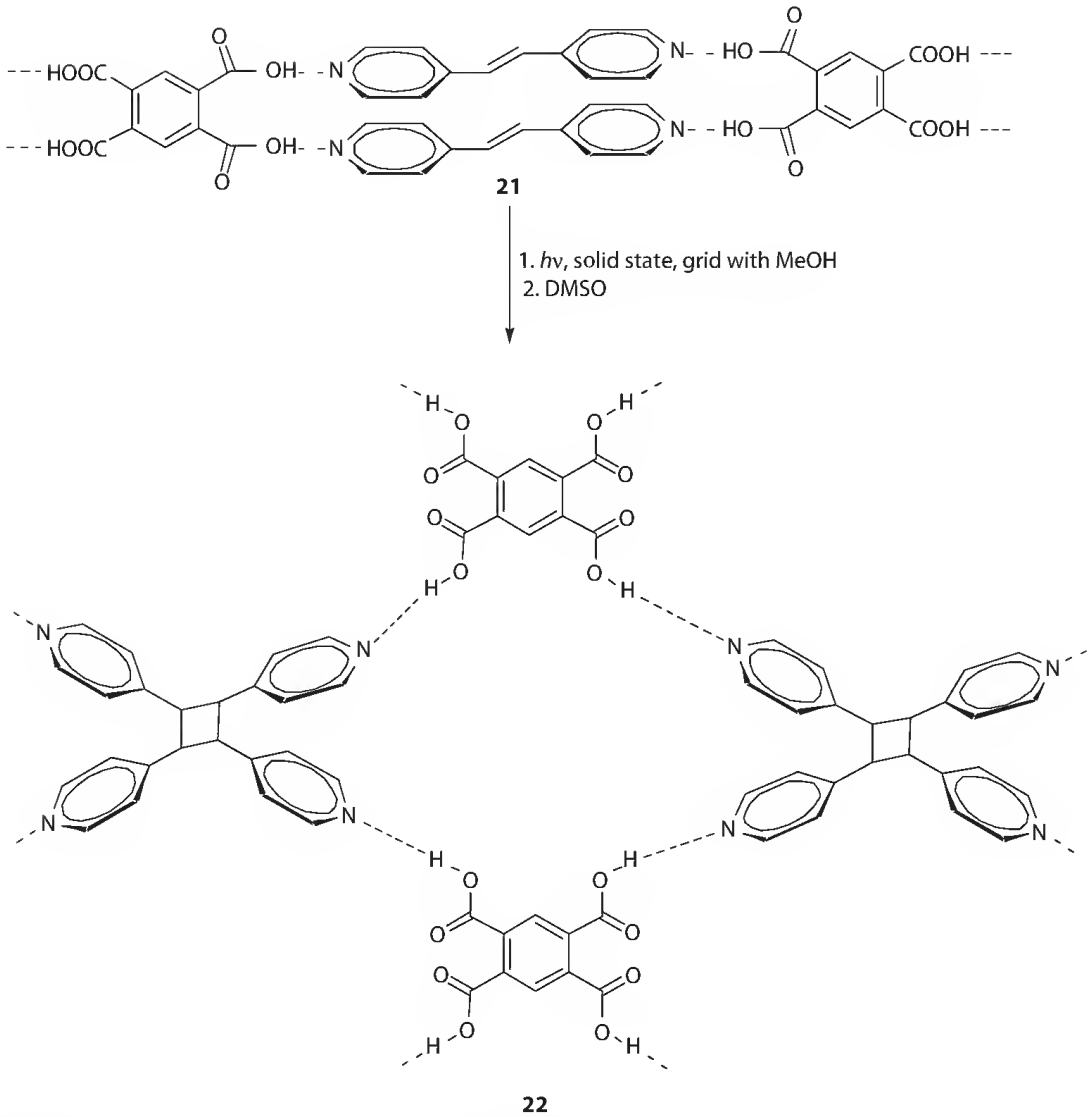

SCHEME 9.11 Synthesis of supramolecular system **22** via diastereomeric dimerization of 1,2-bis(4-pyridyl)ethylene and benzene 1,2,4,5-tetracarboxylic acid co-crystals (**21**).

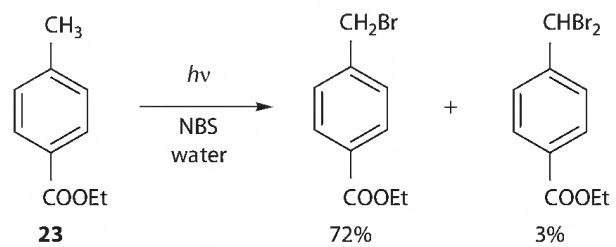

SCHEME 9.12 Visible-light-induced bromination in water.

by means of a photoreactor equipped with a 3 kW XeCl excimer lamp, which is an almost monochromatic (308 nm, Scheme 9.13) and highly efficient light source (the electrical power to light conversion yield is about 10%) [38]. Irradiation of a suspension of potassium carboxylate **24** (Scheme 9.13) in neat water, followed by partial evaporation and filtration of the resulting precipitate, afforded the cyclized derivative **25** in 82% yield; noteworthy, the purity of the isolated product was remarkably higher than the one obtained with traditional photochemical methods [39].

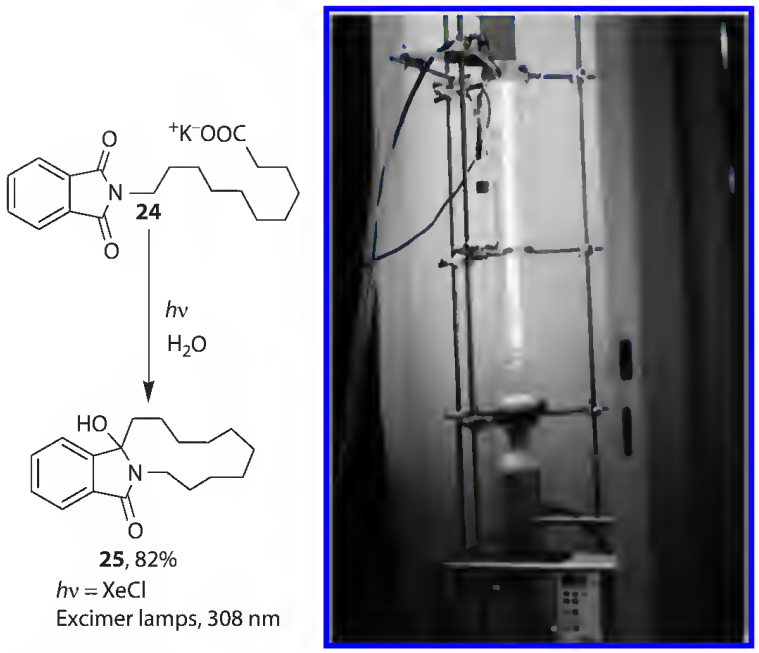

SCHEME 9.13 **(See color insert.)** Photochemical cyclization of potassium carboxylate **24** carried out in a 3 kW XeCl excimer lamp equipped photoreactor. (From Griesbeck, A.G. et al., *Green Chem.*, 1, 205, 1999. With permission.)

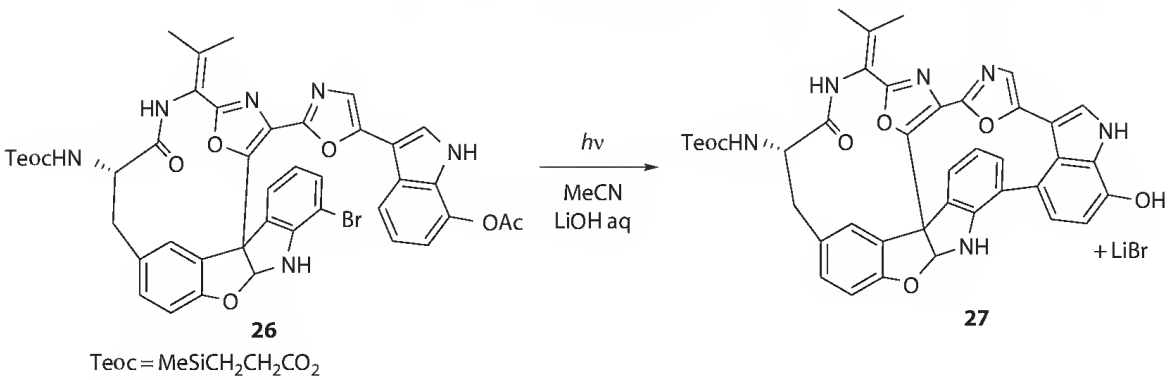

SCHEME 9.14 Synthesis of (–)-diazonamide **27**.

Photoinduced electron transfer (PET) was also involved in arylation processes, such as the successful synthesis of antimycotic (–)-diazonamide (**27**), obtained from bromoarene **26** through irradiation in a LiOH aq/acetonitrile mixture (Scheme 9.14) [40].

In the last years, another metal-free route for the aryl–carbon bond formation has been developed by our research group. Irradiation of electron-rich aromatic halides (chlorides or fluorides) or esters (sulfonates and phosphates) in protic solvents caused heterolytic fragmentation of the aryl–halide or aryl–oxygen bond and gave the corresponding phenyl cations in their triplet state [41]. Trapping of these intermediates by soft nucleophiles (such as alkenes, alkynes, or (hetero)arenes) allowed the synthesis of a wide range of arylated compounds, including allylphenols, biphenyls, and aryl alkynes. As an example, a solution of 4-chlorophenol and 4-penten-1-ol in a 5:1 $MeCN/H_2O$ mixture afforded γ-benzyl tetrahydrofuran **28** in 79% yield, through a tandem C–C and C–O bond formation; furthermore, this reaction was performed up to the gram scale, by using an immersion-well photoreactor, without affecting the process efficiency (84%, Scheme 9.15a) [41]. Triplet phenyl cations react efficiently also with inorganic anions, such as iodide and cyanide. In this way, a photochemical route to benzonitriles was achieved in a water–acetonitrile solution of potassium cyanide, with product yields that vary from moderate to excellent (as shown for the synthesis of **29** in Scheme 9.15b). It should be noted that whereas

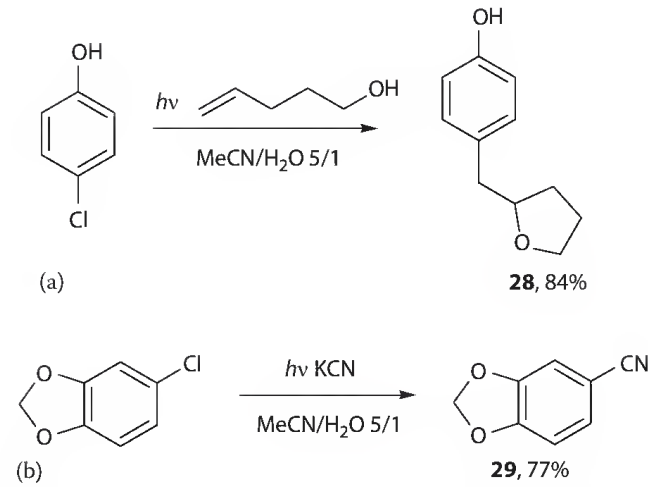

SCHEME 9.15 Synthesis of (a) γ-benzyltetrahydrofurans and (b) benzonitriles via triplet phenyl cation.

benzonitriles are usually accessible through Sandmeyer reaction or Pd-catalyzed cross-couplings, our protocol avoids both the use of transition metal catalysts and the protection of sensitive functional groups (such as phenol or aniline moieties) [41].

Following another strategy, photolysis of pyrene with sodium cyanide in a benzonitrile/water 1:100 emulsion led selectively to 1-cyanopyrene in 83% yield [42].

Regarding alkylations, unsaturated aldehydes were converted to γ-butyrrolactols or lactones in aqueous media, by means of different water-soluble photocatalysts (e.g., disodiumbenzophenone disulfonate [BPSS] or sodium 4-benzoylbenzoate). Irradiation of 2-hexenal in 50% aqueous methanol afforded lactol **30** in good yield and on gram scale (Scheme 9.16a) [43]. Interestingly, 1,4-alkylation took place selectively, in contrast with the competition between 1,4- and 1,2-alkylation observed in the analogous thermal reaction.

The same approach has been recently applied to the solar synthesis of γ-lactones, as well as of monoprotected succinaldehydes; thus, exposure of an isopropanol/water 1:1 solution of maleic acid to moderately concentrated sunlight (by means of SOLFIN facility, see the following text) gave terebic acid (**31**) in 75% yield (Scheme 9.16b) [44].

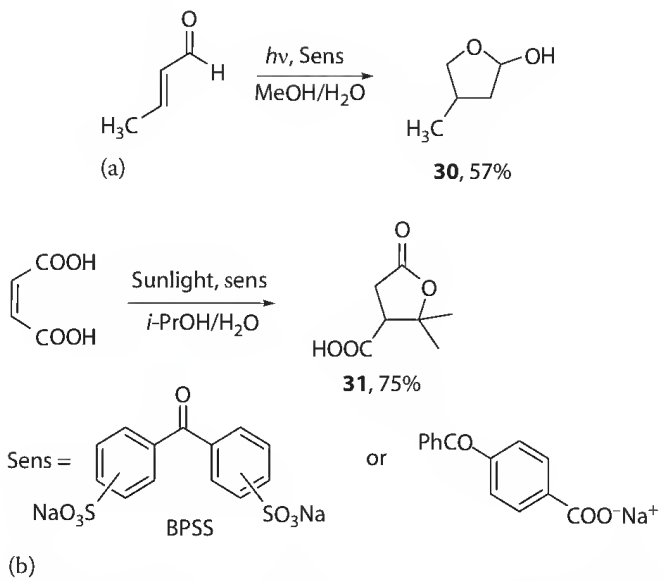

SCHEME 9.16 (a) Photocatalyzed alkylation of 2-hexenal in 50% aqueous methanol; (b) sunlight-induced photocatalyzed route to terebic acid **31**.

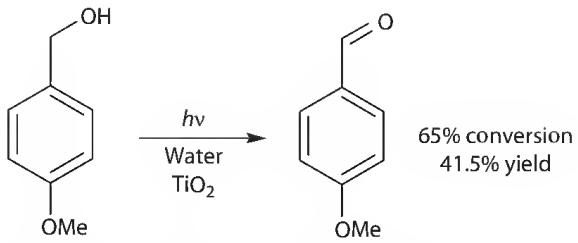

SCHEME 9.17 TiO_2 photocatalyzed oxidation of 4-methoxybenzyl alcohol.

The use of surfactants able to form micelles with hydrophobic cores is a feasible way to overcome the low solubility of organic reactants in water. For example, micelles formed by *N,N*-dimethyl tetradecylamine-*N*-oxide (DTAO) can host iron(III) *meso*-tetrakis(2,6-dichlorophenyl)porphyrin [Fe^{III}(TDCPP)] sensitizer, resulting in a microheterogeneous catalyst for sunlight-induced photooxidations. Under these conditions, epoxidation of cyclooctene was carried out with selectivity higher than 90% [45].

Another alternative medium is represented by aqueous suspensions. Irradiation of benzyl alcohols in a colloidal suspension of TiO_2 proved to be a promising procedure for their selective oxidation to carbonyls, avoiding the use of harmful conditions, such as high temperature or pressure, as well as of noxious oxidants, like chromate or permanganate salts. Palmisano, in particular, reported a home-made TiO_2 photocatalyst for the selective oxidation of *p*-methoxybenzyl alcohol (chosen as a model substrate) to *p*-methoxybenzaldehyde, in water. Although there is a possibility of generating unstable highly oxidizing species, such as hydroxyl radicals, only traces of benzoic acid were detected as a side product. In addition, oxidation yields obtained with the home-prepared titanium dioxide catalyst were always higher than with the commercially available TiO_2 (Scheme 9.17) [46].

9.2.4.2 Reactions in Eco-Friendly Organic Solvents

When water cannot be used as reaction medium, the replacement of an environmentally problematic solvent is possible by using a chemically similar organic medium, with a lower environmental impact. Greener alternatives are represented by *n*-heptane (instead of highly flammable *n*-pentane and more toxic *n*-hexane), ethanol (which is renewable), methanol, and acetone (that are cheap and scarcely toxic). Nevertheless, chemists should remember that the replacement must not affect other important parameters of the reaction, such as its economical cost and efficiency, with the aim of achieving an industrial scale-up of the procedure. Alkoxyamines, for example, are efficient carbon-based radical precursors for polymerization procedures and organic synthesis, and one of them (BlockBuilder **34**, Scheme 9.18) has been produced on large scale by Arkema. Due to its low dissociation temperature (about 30°C), photochemistry was the only tool that allowed a clean synthesis of this product.

The optimized procedure proposed by Guillaneuf et al. involved the photodecomposition of azoderivative **32** and dithiocarbamate **33** in neat ethanol. In contrast to the previously reported photochemical syntheses of alkoxyamines, the latter reagent acted as a catalyst, was added in substoichoimetric amount with respect to the azo-compound, and was finally recovered and reused, lowering production costs [47].

The synthesis of Vitamin D_2 (Calciferol), by irradiation of Ergosterol and following thermal rearrangement, is probably the most important photochemical process that has found industrial application. The multigram preparation of this bioactive compound, which balances the in vivo absorption of calcium and phosphorus, was scaled up to 200 L by Jike et al., through a batch photoreactor. Irradiation of a highly concentrated ethanol solution (1.4 g/L) of Ergosterol led to an excellent yield of Vitamin D_2 thermal precursor (pre-Calciferol, 84% based on consumed Ergosterol). Four of the aforementioned batch photoreactors were connected in series and the resulting flow-system afforded a high conversion of starting Ergosterol (>70%) and a satisfying production of pre-vitamin D2 (62% yield, 62% selectivity) [48].

Acetone proved to be a good solvent for photochemical reactions too. The synthesis of 1-indanone **36** (a precursor of Dopenezil, **37**, used in the treatment of Alzheimer disease), for example, by photolysis

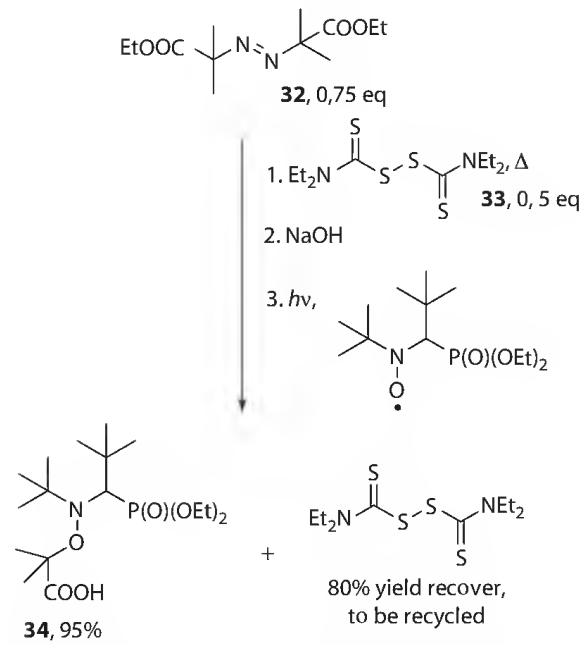

SCHEME 9.18 Synthesis of carbon-based radical precursor for polymerizations BlockBuilder **34**.

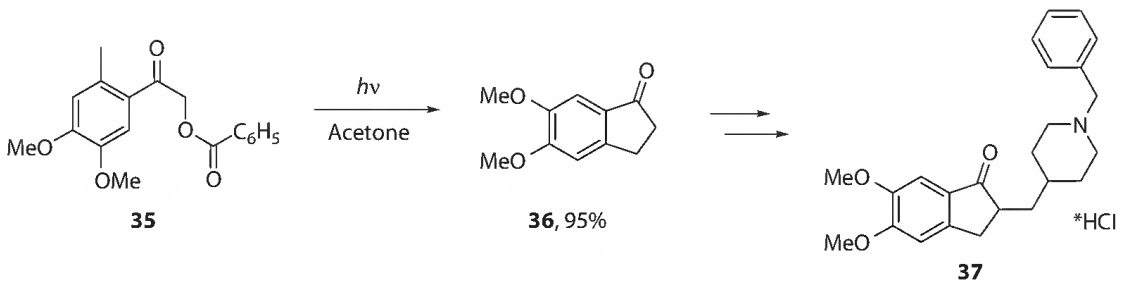

SCHEME 9.19 Photolysis of phenacyl ester **35** as a key step in the synthesis of Dopenezil **37**.

of the corresponding phenacyl ester **35** has been tested in several solvents, of which acetone showed the highest yield (90% yield, Scheme 9.19) [49].

Light-induced hydrolysis of Schiff bases in aqueous acetone was applied to the synthesis of antitumor agent **39**. This approach led to quantitative deprotection of imine **38**, after less than 1 h of UV irradiation; encouraging results were obtained also by exposing the solution directly to sunlight, although with significantly longer exposition times (15 days, Scheme 9.20) [50].

With regard to alcoholic media, photoreduction of imines to the corresponding amines was carried out in 2-propanol, with an excess of triethylamine in order to avoid decomposition of the desired product. Under these conditions, a variety of aldimines were selectively reduced in good yields [51].

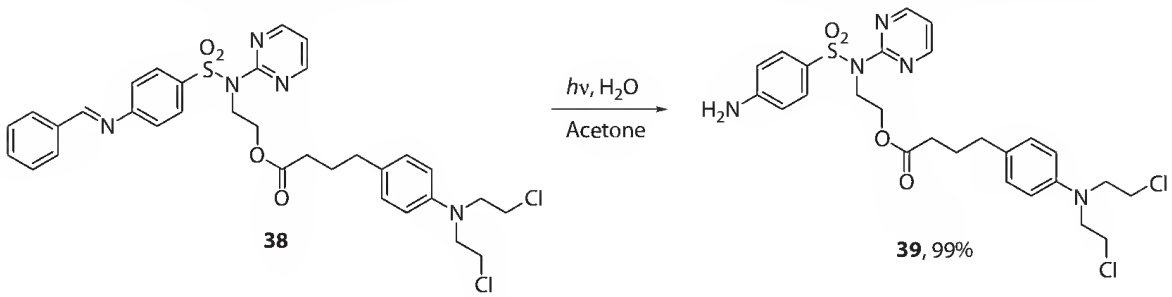

SCHEME 9.20 Photochemical hydrolysis of Schiff bases in aqueous acetone.

Photodehalogenation of aryl chlorides and fluorides, either in neat 2-propanol or in the presence of H_3PO_2, has been developed as a mild alternative to the use of hydrides or of low-valence metals as reductants [52].

9.2.4.3 Reactions in Nonclassical Solvents

Room-temperature ionic liquids (ILs) are low-melting salts, which have recently attracted much interest in the field of green synthesis: their negligible vapor pressure prevents solvent emission and allows their reuse [53]. The main limitation to the use of ionic liquids in photochemistry is the high spectrophotometrical purity needed, which would require particular care during their purification.

The one-pot synthesis of fluoroimidazoles, such as **40**, from the corresponding amino derivatives has been successfully carried out in 1-butyl-3-methylimidazolium tetrafluoroborate ([bmim][BF_4]) and the desired products were isolated in moderate overall yields (about 60%) after 24 h of irradiation. This reaction was carried out at 0°C to prevent photodecomposition of the medium (observed before at higher temperatures) and to maintain its purity at a reasonable grade (Scheme 9.21) [54].

As far as a photoreductive process is concerned, Reynolds et al. [55] reported several amine-mediated reductions of benzophenone moieties in [bmim][BF_4], to selectively give the corresponding benzhydrol. The process was performed three times in the same solvent, without any influence on both product yield and chemoselectivity.

Sometimes, ionic liquids allow an enhanced chemoselectivity, compared to usual solvents. The singlet oxygen–mediated oxidation of phenol in ethylammonium nitrate, for example, was found to give only benzoquinone in nearly 60% yield, whereas the same reaction in water afforded a mixture of quinone and quinhydrone [56].

Among nonclassical solvents, nonflammable and nontoxic supercritical CO_2 has recently attracted much attention, as demonstrated by the singlet oxygen–induced synthesis of ascaridole from α-terpinene: in 140 bar sCO_2, the turnover efficiency of the photocatalyst (5,10,15,20-tetrakis(pentafluorophenyl)porphyrin, TPFPP) is higher than in CCl_4 (16 vs. 7). Moreover, the high solubility of oxygen in this medium allowed the use of a near equimolar concentration of the oxidant with respect to α-terpinene [57].

9.2.5 Sunlight-Induced Syntheses

Solar radiation is the "green" energy source *par excellence*, since it is free, renewable, and it does not produce greenhouse gases. Plants, for example, store sunlight into chemical energy through the photosynthetic process and represent the ideal green laboratory, in which useful biomass (mainly sugars) is produced from nontoxic reagents (carbon dioxide, water, mineral salts) under mild conditions, with oxygen as the only side product.

Unfortunately, the use of solar energy in human-made reactions is affected by several limitations, such as weather conditions, geographic location, and day/night alternance. In addition, only a few organic compounds absorb significantly in the visible region of the spectrum, thus limiting the versatility of the method.

For all these reasons, it is not surprising that sunlight (which, in the dawn of photochemistry, was obviously the only available light source) has been quickly replaced by artificial lamps. The synthetic potential of solar chemistry, however, was again recognized in the 1980s and 1990s, thanks to the works performed in Almería and Cologne by Scharf and coworkers [58].

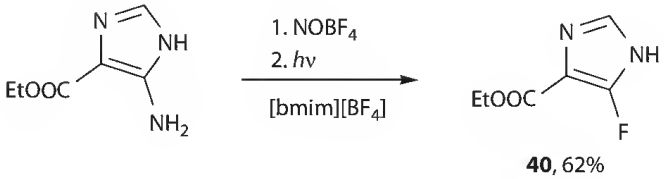

40, 62%

SCHEME 9.21 One-pot synthesis of fluoroimidazoles in [bmim][BF_4].

9.2.5.1 Reactions under Nonconcentrated Sunlight

Despite the low intensity of solar radiation and its dependence on weather conditions, photochemical reactions can often be carried out in reasonable times and good yields, simply by exposing the vessel to natural light on a window ledge. In the following, some representative cases are shown, which constitute only a small fraction of all the photochemical processes that are actually accessible in this way; at least in principle, all the reactions mentioned here could be smoothly scaled up, simply by increasing batch dimensions.

Photopinacolization of aromatic ketones was one of the first photochemical processes observed by Ciamician and Silber, and then investigated for differently substituted benzophenones by Cohen in 1920 [58b]. Recently, a general procedure for the photoreductive coupling of aromatic aldehydes and ketones to 1,2-diols has been reported. Such a protocol represented a valid green alternative to thermal methods, in particular when benzaldehyde was reduced, allowing to reuse the solvent (2-propanol and acetone) three times, without significantly affecting the process efficiency [59].

Photoinduced elimination of a Ph_2S group in *N*-conjugated sulfinimines was adopted for the synthesis of pyrrolo[2,3-d]pyrimidine-2,4-diones such as **41** (Scheme 9.22) [60]. All the desired heterocycles were obtained in closely quantitative yields, after short illumination times (from 40 min to 3.5 h), while the analogous thermal pathway failed, even under harsh conditions (refluxing toluene for 30 h).

Since most organic compounds do not absorb UVA radiation at all, the use of photocatalysts that absorb light instead of the substrates plays a key role in the development of sunlight-mediated syntheses. TiO_2-photocatalyzed functionalization of nitrogen-based protonated heterocycles (such as quinoline, lepidine, and quinoxaline) by formamide (Scheme 9.23, compound **42**) has been reported by Caronna et al. Products were obtained in moderate to excellent yields by exposing the reaction mixtures to sunlight for less than 15 h [61].

In the last years, tetrabutylammonium decatungstate (TABDT) emerged as a versatile photocatalyst for C–H activation of a wide variety of substrates (including aldehydes, cyclic ethers, amides, and alkanes), followed by their addition to electron-poor olefins. Our research group has recently reported scale-up and environmental optimization of these processes: in the reaction reported here, for example, compound **43** was obtained in high selectivity and efficiency, simply by exposing a Pyrex vessel with the reaction mixture on a suntrap (e.g., a window ledge), for a few days. Since the absorbing species is TBADT, UVA-transparent reactants were used in high concentrations (up to 0.5 M), greatly increasing the process efficiency (about 10 g/exposed dm^2, Scheme 9.24) [62].

Visible light irradiation of $[Ru^{II}(bipy)_3]^{2+}$ (λ_{max} = 452 nm) led to a charge-separated intermediate $\left([Ru^{III}(bipy)_3^{\bullet-}]^{2+}\right)$, a powerful photoredox catalyst, that is able to either oxidize or reduce a variety of organic derivatives. As an example, [2 + 2] cycloaddition of acyclic enone **44** with methyl-vinyl ketone

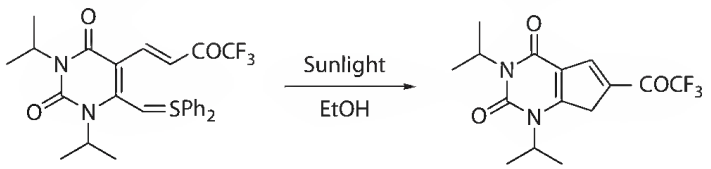

41, 96%

SCHEME 9.22 Photochemical synthesis of pyrrolo[2,3-d]pyrimidine-2,4-diones.

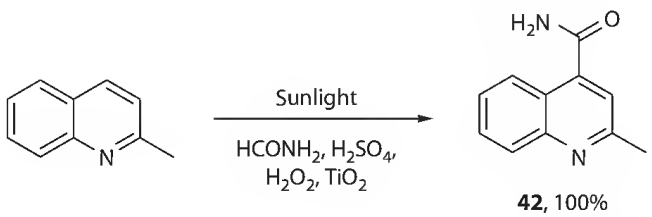

42, 100%

SCHEME 9.23 Photocatalyzed functionalization of 2-methylquinoline by formamide.

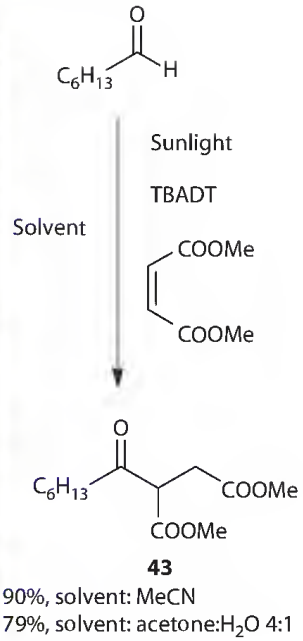

SCHEME 9.24 Sunlight-induced photocatalyzed acylation of electron-poor olefins.

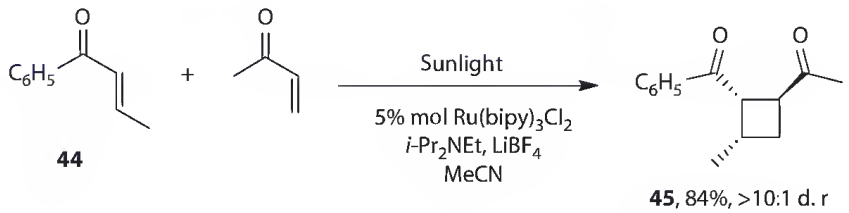

SCHEME 9.25 $[Ru^{II}(bipy)_3]^{2+}$ photocatalyzed synthesis of functionalized cyclobutanes.

was reported, through outdoor illumination, leading to the corresponding cyclobutane derivative (**45**) with an excellent diastereoselectivity (*anti/syn* ratio > 1:10, Scheme 9.25) and in satisfactory yield [63]. Notably, using acyclic bis(enones), intramolecular cyclization took place almost quantitatively but favoring the anti diastereoisomer [64].

The gram-scale triplet-sensitized *E/Z* isomerizations of several molecules including enones and stilbenes have been performed in an ingenious floating solar reactor, to avoid the use of circulating water. Exposition of an ethanol solution of dinitrile **46** and rose bengal to sunlight for only 20 min gave the corresponding *cis*-isomer (**47**) in 71% yield (Scheme 9.26) [65].

9.2.5.2 Reactions under Concentrated Sunlight

In one-sun solar collector reactors (e.g., the pilot plant designed by Schenck, for the synthesis of Ascaridole, see Section 9.1), light was absorbed directly, without being previously concentrated. Due to the low intensity of the radiation, a large exposition area would be necessary to carry out in reasonable times reactions that need short wavelengths (<450 nm) or that are characterized by low quantum yields. During the last decades, more elaborated reactors enabling sunlight concentration were built with a considerable increase of the space–time yield. The SOLFIN (SOLar synthesis of FINe chemicals) and the CPC (Compound Parabolic Collector) facilities, for example, employ moderately concentrated sunlight (concentration factor [CF] = 2–3) for efficient gram-scale syntheses. Both of them consist of coaxial cylindrical mirrors, tilted toward the sun, that collect and concentrate light. The photolyzed solution is placed in the focus line and circulated by means of a centrifugal pump.

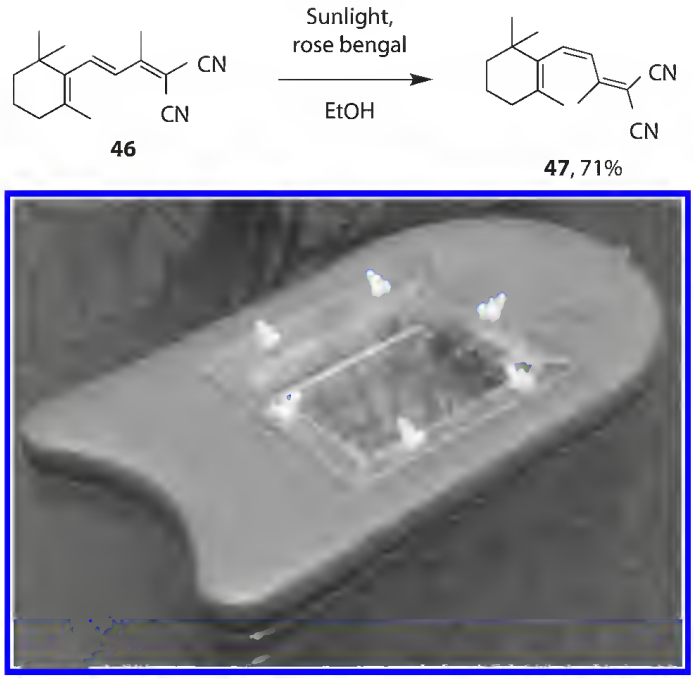

SCHEME 9.26 **(See color insert.)** Sunlight-induced photosensitized *cis–trans* isomerization of dinitrile **46**. (From Zhao, Y.P. et al., *Green Chem.*, 10, 1038, 2008; Zhao, Y.P. et al., *Green Chem.*, 11, 837, 2009. With permission.)

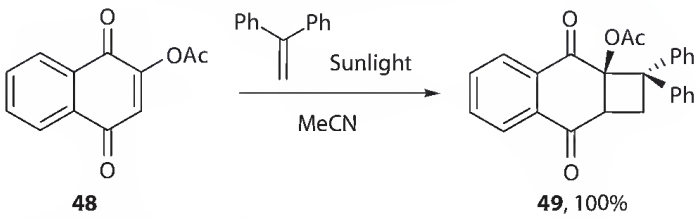

SCHEME 9.27 Sunlight-induced synthesis of tricyclic derivative **49**.

The regio- and stereoselective synthesis of cyclobutane rings, through ($2\pi + 2\pi$) photochemical addition between 2-acetoxy-1,4-naphthoquinone (**48**) and 1,1-diphenylethene (or styrene), was performed by means of a parabolic through collector, both in acetonitrile and in methanol, giving an interesting building block for the synthesis of anthraquinone (**49**, Scheme 9.27) [66].

The cyclization product was obtained in high purity (>99%), simply by removing the solvent *in vacuo* and then recycling it. The quinone concentration could be increased to 6% w/v, without affecting reaction efficiency and selectivity, allowing the successful scale up of the reaction to industrial level.

Photooxidation of naphthols has been deeply investigated by Mattay and Oelgemöller. They achieved the synthesis of pharmaceutically active Juglone (**7**, see also Section 2.2) by illumination of an isopropanol or acetone solution of 1,5-dihydroxynaphtalene, in the presence of Methylene Blue or rose bengal as photosensitizers. The yield of photoxidized product was always higher than 70%, even under cloudy weather conditions. Solid-supported rose bengal was also tested, showing similar yield of Juglone, although the substrate conversion yield was significantly lower [67]. Pioneering experiments on multigram syntheses were performed in Almeria (Spain) by Scharf and coworkers, in the early 1990s, by means of the SOLARIS reactor engineered by G. Schneider (DLR, Cologne, Germany) [9]. That parabolic through collector employed a MAN Helioman module, which is able to track the position of the sun and to simulate the concentration of 20 suns on the absorber tube. The solution was pumped through the recirculating system, until the desired degree of conversion was achieved; the circulating loop had an operating volume between 35 and 70 L. In 1991–1992, several reactions were tested, in order to check the feasibility

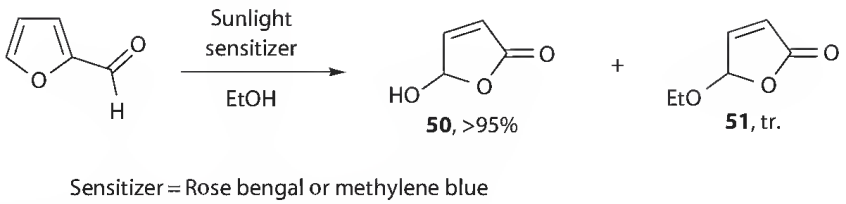

SCHEME 9.28 Singlet-oxygen-mediated oxidation of furfural to 5-ethoxyfuranone (**51**).

of solar photochemistry under these conditions. Singlet oxygen–mediated production of 5-hydroxyfuranone (**50**) from easily available and cheap furfural, in ethanol and in the presence of a photosensitizer gave high yields (>95%) and only traces of 5-ethoxyfuranone (**51,** <3% yield, Scheme 9.28) as by-product.

The SOLARIS plant was dismantled at the end of 1992 and rebuilt in Cologne (Germany). A few years later, the PROPHIS plant (see Scheme 9.29a) was projected by the German Aerospace Center (DRL) in Cologne; this new reactor (concentration factor, CF = 15) supported a reaction volume that varied from 35 to 120 L and was equipped with four parabolic troughs (see Scheme 9.29b).

A set of test reactions were performed with PROPHIS, confirming its synthetic performance [68]. The atom economic synthesis of 2-phenyl-pyridine from acetylene and benzonitrile, in the presence of CpCoCOD as photocatalyst, was particularly efficient when done by solar exposure, while this photocatalyst is not stable under artificial UV light [68]. Among singlet oxygen–mediated oxidations, one of the most industrially relevant is the production of Rose Oxide (**53**) fragrance. The key step is rose bengal sensitized Schenck-ene addition of singlet oxygen to citronellol (**52**), which leads to a mixture of isomeric hydroperoxides (Scheme 9.30). Using PROPHIS, peroxydation of citronellol in 2-propanol

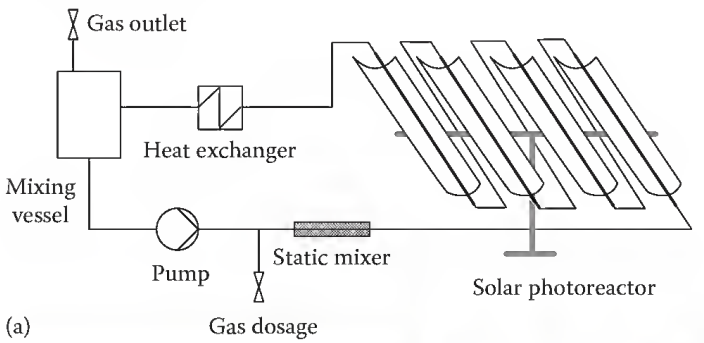

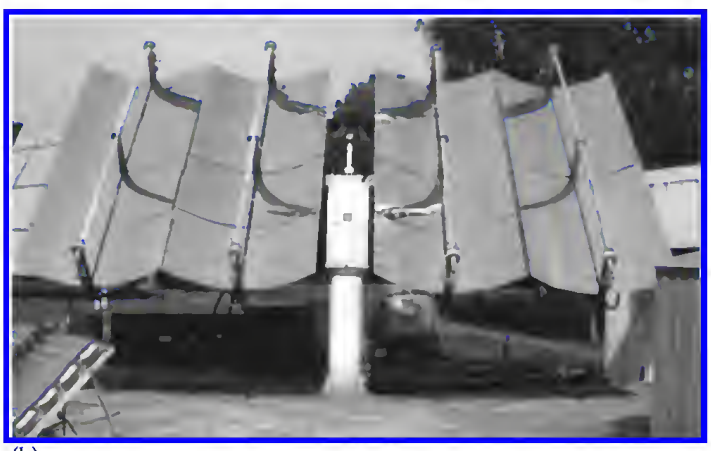

SCHEME 9.29 **(See color insert.)** (a) The PROPHIS plant scheme, projected by German Aerospace center (DLR) in Cologne; (b) an image of the PROPHIS plant equipped by four parabolic troughs as light collector. (From Schiel, C. et al., *J. Green Chem.*, 3, 224, 2001. With permission.)

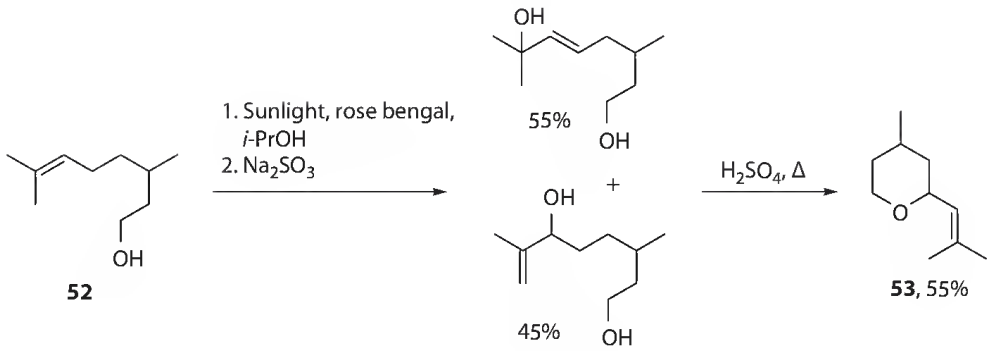

SCHEME 9.30 Photosensitized route to rose oxide (**53**).

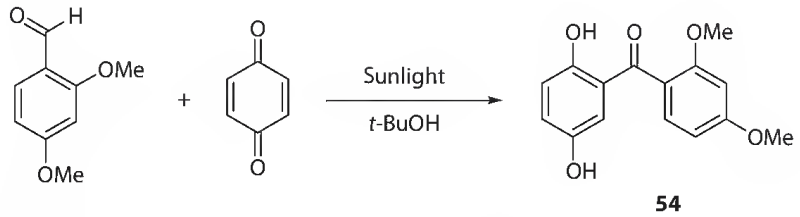

SCHEME 9.31 Sunlight-induced photochemical acylation of quinones.

showed an efficiency close to 1. After reduction by Na_2SO_3 and acid-base catalyzed cyclization, **53** was isolated in 55% yield [69].

The same fragrance was also synthesized in 82% yield by superoxide ion ($O_2^{\cdot-}$)–mediated oxidation; in this case, an aerated acetonitrile solution of citronellol and dehydroabietyl perylene diimide (ABIPER) as photosensitizer was exposed to concentrated sunlight (equivalent to 90–100 suns), by means of a Fix Focus FF 3.5 instrument, with a reflective area of 2.66 m^2 [70].

Radical-based acylation of quinones represents an eco-friendly alternative to Friedel–Crafts processes, in which aldehydes are used as sources of acyl radicals and quinones act both as formyl C–H bond activators and acyl radical acceptors. Since quinones absorb significantly above 300 nm, an alternative process based on concentrated sunlight has been recently proposed: using PROPHIS, naphthoquinone reacted with butanal, in a *tert*-butanol/acetone 3:1 mixture, and afforded the acylated product in high yield (90%, ca. 500 g for 80 L reaction mixture), after 3 days of exposition only. Photochemical acylation of benzoquinone by 2,4-dimethoxybenzaldehyde to give **54** was chosen as a model reaction to compare the use of either concentrated or direct sunlight (Scheme 9.31) and was carried out in three different reactors: PROPHIS loop (CF = 15), CPC (CF = 2–3), and a flat bed reactor (CF = 1). Although CPC does not track the sun (contrary to PROPHIS), it gave the best results in terms of substrate conversion (with an efficiency three times higher than PROPHIS) and it was found to be the less dependent on weather conditions, thanks to the possibility of using both direct and diffuse light [71].

9.3 Perspectives and Conclusions

With the overview of synthetic methods and technologies presented here, we intended to highlight the green potentialities of photochemistry. As shown earlier, recent literature evidences its skill to satisfy green chemistry principles, thanks to the use of solvent-free conditions or aqueous solvents and to the low energy demand (e.g., in sunlight induced reactions). The search for sustainable and scalable photochemical procedures showed some significant advances in the past few years, including the development of new and more efficient flow reactors, solar collectors and micro-reactors, whose applications have been recently reviewed [72,73].

Apart from green synthesis, photochemistry contributes strongly to other fields of sustainable development, such as production of energy by conversion of solar light into electricity [74] or chemical fuels [75]. The development of artificial photosynthetic systems emerged in the last decades as one of the most significant challenges for chemists [76]. Furthermore, photochemistry represents a useful solution to the increasing demand for depollution technologies, mainly through heterogeneous photocatalysts (such as TiO_2) [77].

That being so, we are confident that the evolution of photochemistry, evidenced by the previous selected examples, will greatly contribute to the future progress of green chemistry.

Acknowledgments

We are grateful to Dr. Winfried Leibl, Dr. Joseph H. Hughes (CEA Saclay, France), Prof. Maurizio Fagnoni, and Dr. Davide Ravelli (University of Pavia, Italy) for fruitful discussion. S.P. acknowledges MIUR, Rome (FIRB-Futuro in Ricerca 2008 project RBFR08J78Q) for financial support.

References

1. *Our Common Future*. Oxford University Press, Oxford, U.K., 1987. ISBN 0-19-282080-X; http://www.un-documents.net/wced-ocf.htm
2. Anastas, P. T.; Warner, J. C. Eds. *Green Chemistry: Theory and Practice*. Oxford University Press: Oxford, U.K., 1998.
3. Trost, M. B. *Science* 1991, *254*, 1471–1477.
4. For reviews see: Sheldon, R. A. *Green Chem.* 1997, *9*, 1273–1283.
5. For a recent overview on proposed green metrics see: Lapkin, A.; Constable, D. Eds. *Green Chemistry Metrics*. John Wiley & Sons, Hoboken, NJ, 2008.
6. Roth, H. D. *Angew. Chem. Int. Ed. Eng.* 1989, *28*, 1193–1207.
7. (a) Albini, A.; Dichiarante, V. *Photochem. Photobiol. Sci.* 2009, *8*, 248–254; (b) D'Auria, M. Ed. *Emanuele Paternò, Synthesis in Organic Chemistry by Means of Light*. Società Chimica Italiana, Rome, Italy, 2009.
8. Schönberg, A.; Mustafa, A. *Chem. Rev.* 1947, *40*, 181–200.
9. Esser, P.; Pohlmann, B.; Scharf, H.-D. *Angew. Chem. Int. Ed. Eng.* 1994, *33*, 2009–2023.
10. Pfoertner, K. H. *J. Photochem. Photobiol. A: Chem.* 1990, *51*, 81–86.
11. Protti, S.; Dondi, D.; Fagnoni, M.; Albini, A. *Green Chem.* 2009, *11*, 239–249.
12. Hook, B. D. A.; Dohle, W.; Hirst, P. R.; Pickworth, M.; Berry, M. B.; Booker-Milburn, K. I. *J. Org. Chem.* 2005, *70*, 7558–7564.
13. Ohkubo, K.; Suga, K.; Fukuzumi, S. *Chem. Commun.* 2006, 2018–2020.
14. Carreço, M. C.; Somoza, À.; Ribagorda, M.; Urbano, A. *Chem. Eur. J.* 2007, *13*, 879–890.
15. For a review, see: Tung, C.-H.; Wu, L.-Z.; Zhang, L.-P.; Li, H.-R.; Yi, X.-Y.; Song, K.; Xu, M.; Yuan, Z.-Y.; Guan, J.-Q.; Wang, H.-W.; Ying, Y.-M.; Xu, X.-H. *Pure Appl. Chem.* 2000, *72*, 2289–2298.
16. Garcia, H.; Roth, H. D. *Chem. Rev.* 2007, *102*, 3947–4007.
17. Pace, A.; Buscemi, S.; Vivona, N. *J. Org. Chem.* 2005, *70*, 2322–2324.
18. Sun, H.; Blatter, F.; Frei, H. *J. Am. Chem. Soc.* 1996, *118*, 6873–6879.
19. Li, X.; Ramamurthy, V. *Tetrahedron Lett.* 1996, *357*, 5235–5238.
20. Griesbeck, A. G.; Bartoschek, A. *Chem. Commun.* 2002, 1594–1595.
21. Griesbeck, A. G.; El-Idreesy, T. T.; Bartoschek, A. *Adv. Synth. Catal.* 2004, *346*, 245–251.
22. Santos, D. T.; Albarelli, J. Q.; Joyce, K.; Oelgemöller, M. *J. Chem. Tech. Biotech.* 2009, *84*, 1026–1030.
23. Maldotti, A.; Molinari, A.; Andreotti, L.; Fogagnolo, M.; Amadelli, R. *Chem. Commun.* 1998, 507–508.
24. Carraro, M.; Gardan, M.; Scorrano, G.; Drioli, E.; Fontanova, E.; Bonchio, M. *Chem. Commun.* 2006, 4533–4535.
25. Ito, Y.; Horie, S.; Shindo, Y. *Org. Lett.* 2001, *3*, 2411–2413.

26. Hockemeyer, J.; Burbiel, J. C.; Müller, C. E. *J. Org. Chem.* 2004, *69*, 3308–3318.
27. Scheffer, J. R.; Wang, K. *Synthesis* 2001, 1253–1257.
28. Sakamoto, M.; Takahashi, M.; Kamiya, K.; Yamaguchi, K.; Fujita, T.; Watanabe, S. *J. Am. Chem. Soc.* 1996, *118*, 10664–10665.
29. Resendiz, M. J.; Garcia-Garibay, M. A. *Org. Lett.* 2005, *3*, 371–374.
30. Veerman, M.; Resendiz, M. J. E.; Garcia-Garibay, M. A. *Org. Lett.* 2006, *8*, 2615–2621.
31. Family, F.; Garcia-Garibay, M. A. *J. Org. Chem.* 2009, *74*, 2476–2480.
32. MacGillivray, L. R. *J. Org. Chem.* 2008, *73*, 3311–3317 and references therein.
33. Shan, N.; Jones, W. *Green Chem.* 2003, *5*, 728–730.
34. Capello, C.; Fischer, U.; Hungerbühler, K. *Green Chem.* 2007, *9*, 927–934.
35. Alfonsi, K.; Colberg, J.; Dunn, P. J.; Fevig, T.; Jennings, S.; Johnson, T. A.; Kleine, H. P.; Knight, C.; Nagy, M. A.; Perry, D. A.; Stefaniak, M. *Green Chem.* 2008, *10*, 31–36.
36. Podgoršek, A.; Stavber, S.; Zupan, M.; Iskra, J. *Tetrahedron Lett.* 2006, *47*, 1097–1099.
37. Griesbeck, A. G.; Hoffmann, N.; Warzecha, K.-D. *Acc. Chem. Res.* 2007, *40*, 128–140.
38. Griesbeck, A. G.; Kramer, W.; Oelgemöller, M. *Green Chem.* 1999, *1*, 205–207.
39. Griesbeck, A. G.; Henz, A.; Kramer, K.; Lex, J.; Nerowski, F.; Oelgemöller, M.; Peters, K.; Peters, E.-M. *Helv. Chim. Acta* 1997, *80*, 912–933.
40. Burgett, A. W. G.; Li, Q.; Wei, Q. *Angew. Chem. Int. Ed.* 2003, *42*, 4961–4964.
41. Dichiarante, V.; Fagnoni, M. *Synlett* 2007, *6*, 787–800 and references therein
42. Kitagawa, F.; Murase, M.; Kitamura, N. *J. Org. Chem.* 2002, *67*, 2524–2531.
43. Dondi, D.; Caprioli, I.; Fagnoni, M.; Mella, M.; Albini, A. *Tetrahedron,* 2003, *59*, 947–957.
44. Dondi, D.; Protti, S.; Albini, A.; Mañas Carpio, S.; Fagnoni, M. *Green Chem.* 2009, *10*, 1653–1659.
45. Maldotti, A.; Andreotti, L.; Molinari, A.; Varani, G.; Cerichelli, G.; Chiarini, M. *Green Chem.* 2001, *3*, 42–46.
46. Palmisano, G.; Yurdakal, S.; Augugliaro, V.; Loddo, V.; Palmisano, L. *Adv. Synth. Catal.* 2007, *349*, 964–970; Augugliaro, V.; Kisch, H.; Loddo, V.; Marcì, G.; Palmisano, G.; Palmisano, L.; Yurdakal, S. *Chem. Eur. J.* 2008, *14*, 4640–4646.
47. Guillaneuf, Y.; Couturier, J.-L.; Gigmes, D.; Marque, S. R. A.; Tordo, P.; Bertin, D. *J. Org. Chem.* 2008, *78*, 4728–4731.
48. Jike, L.; Yingbei, M.; Li, D.; Fang, W.; Tianwei, T. *Chem. Res. Tech.* 2007, *30*, 261–264.
49. Pospíl, T.; Veetil, A. T.; Antony, P.; Klán, P. *Photochem. Photobiol. Sci.* 2008, *7*, 625–632.
50. Huang, Z.; Wan, D.; Huang, J. *Chem. Lett.* 2001, 708–709.
51. Ortega, M.; Rodrìguez, M. A.; Campos, P. J. *Tetrahedron* 2005, *61*, 11686–11691.
52. Dichiarante, V.; Fagnoni, M.; Albini, A. *Green Chem.* 2009, *11*, 945–949.
53. Welton, T. *Chem. Rev.* 1999, *99*, 2071–2083.
54. Heredia-Moya, J.; Kirk, K. L. *J. Fluor. Chem.* 2007, *128*, 674–678.
55. Reynolds, J. L.; Erdner, K. R.; Jones, P. B. *Org. Lett.* 2002, *4*, 917–919.
56. Inoue, N.; Ishioka, T.; Harata, A. *Chem. Lett.* 2009, *38*, 358–359.
57. Bourne, R. A.; Han, X.; Chapman, A. O.; Arrowsmith, N. J.; Kawanami, H.; Poliakoff, M.; George, M. W. *Chem. Commun.* 2008, 4457–4459.
58. For recent reviews on solar photochemistry see: (a) Oelgemöller, M.; Jung, C.; Mattay, J. *Pure Appl. Chem.* 2007, *79*, 1939–1947; (b) Protti, S.; Fagnoni, M. *Photochem. Photobiol. Sci.* 2009, *8*, 1599–1616.
59. Li, J.-T.; Yang, J.-H.; Han, J.-F.; Li, T.-S. *Green Chem.* 2003, *5*, 433–435.
60. Matsumoto, N.; Takahashi, M. *Tetrahedron Lett.* 2005, *46*, 5551–5554.
61. Caronna, T.; Gambarotti, C.; Palmisano, L.; Punta, C.; Recupero, F. *Chem. Commun.* 2003, 2350–2351.
62. Protti, S.; Ravelli, D.; Fagnoni, M.; Albini, A. *Chem. Commun.* 2009, 7351–7353.
63. Du, J.; Yoon, T. P. *J. Am. Chem. Soc.* 2009, *131*, 14604–14065.
64. Ischay, M. A.; Anzovino, M. E.; Du, J.; Yoon, T. P. *J. Am. Chem. Soc.* 2008, *130*, 12886–12887.

65. Zhao, Y. P.; Campbell, R. O.; Liu, R. S. H. *Green Chem.* 2008, *10*, 1038–1042; Zhao, Y. P.; Yang, L.-Y.; Liu, R. S. H. *Green Chem.* 2009, *11*, 837–842.
66. Covell, C.; Gilbert, A.; Richter, C. *J. Chem. Res. Synopse* 1998, 316–317.
67. Oelgemöller, M.; Healy, N.; de Oliveira, L.; Jung, C.; Mattay, J. *Green Chem.* 2006, *8*, 831–834.
68. Jung, C.; Funken, K.-H.; Ortner, J. *Photochem. Photobiol. Sci.* 2005, *3*, 409–411.
69. Oelgemöller, M.; Jung, C.; Ortner, J.; Mattay, J.; Zimmermann, E. *Green Chem.* 2005, *7*, 35–38.
70. Dincalp, H.; Içli, S. *J. Photochem. Photobiol. A: Chem.* 2001, *141*, 147–151.
71. Schiel, C.; Oelgemöller, M.; Ortner, J.; Mattay, J. *Green Chem.* 2001, *3*, 224–228.
72. Hessel, V.; Kralisch, D.; Krtschil, U. *Energy Environ. Sci.* 2008, *1*, 467–478.
73. Coyle, E. E.; Oelgemöller, M. *Photochem. Photobiol. Sci.* 2008, *7*, 1313–1322.
74. Balzani, V.; Credi, A.; Venturi, M. *ChemSusChem* 2008, *1*, 26–58; Toyoda, T.; Sano, T.; Nakajima, J.; Doi, S.; Fukumoto, S.; Ito, A.; Tohyama, T.; Yoshida, M.; Kanagawa, T.; Motohiro, T.; Shiga, T.; Higuchi, K.; Tanaka, H.; Takeda, Y.; Fukano, T.; Katoh, N.; Takeichi, A.; Takechi, K.; Shiozawa, M. *J. Photochem. Photobiol. A: Chem.* 2004, *164*, 203–207.
75. Wang, M.; Na, Y.; Gorlov, M.; Sun, L. *Dalton Trans.* 2009, 6458–6467; Grätzel, M. *Chem. Lett.* 2005, *34*, 8–13.
76. Herrero, C.; Lassalle-Kaiser, B.; Leibl, W.; Rutherford, A. W.; Aukauloo, A. *Coord. Chem. Rev.* 2008, *252*, 456–468.
77. See for instance: Maggos, T.; Bartzis, J. G.; Liakou, M.; Gobin, C. *J. Hazard. Mat.* 2007, *146*, 668–673.

10

Solar Photochemistry from the Beginnings of Organic Photochemistry to the Solar Production of Chemicals

Emma E. Coyle
Dublin City University

Michael Oelgemöller
James Cook University

10.1 Introduction

Green chemistry is a multidisciplinary concept that has emerged over the past two decades, commencing in academia and research and development, which has subsequently impacted greatly on the chemical industry.[1,2] The growth of interest in green chemistry has been driven in particular by the increasing desire for sustainable developments and reduction of carbon dioxide emissions. This has led to increasing interest in environmentally friendly technologies and the adoption of green chemistry approaches in both academia and industry.[2–4] The use of light as a "clean reagent" has been reported and indicates that light (in particular, solar light) may provide a green access to chemical reactions.[5] These concepts have been examined in academia over the past century; however, they have only recently come to the fore in mainstream applications.

10.2 Photochemistry and Green Chemistry

In general, synthetic photochemistry has had little impact in industry, although some examples of photochemical processes exist.[6] This low impact is attributed to the high running costs of the commonly used light sources (energy demands and cooling), such as mercury or halogen lamps. Of the electrical

energy supplied, less than half is converted to light energy, resulting in a large quantity of wasted energy. The heat release of conventional lamps additionally causes significant cooling water needs. Another factor that limits the perceived greenness of photochemical processes is the typical reaction conditions. Photochemical reactions, in particular on the large scale, tend to use rather diluted conditions to enable light penetration through the entire reaction mixture.

The potential of photochemistry as a "clean" technology has been discussed by Bochet,[7] who outlines the perceived disadvantages of photochemistry and some approaches to avoid these issues. Albini has discussed the relative merits of photochemistry compared to thermal synthesis using Environmental Assessment Tool for Organic Syntheses[8] (EATOS) models.[9] However, one failing of this model is that it does not include energy demand of the processes, which can be a considerable factor in the overall "greenness" of any process.[10] From the EATOS values obtained, Albini concludes that the major drawback of photochemical methods compared to thermal processes is the concentration of photochemical solutions.

Despite these disadvantages, there are many advantages of photochemistry as a green technology, for example, the use of mild conditions and comparably low temperatures. Photochemical reactions (with the exception of chain reactions) can also be controlled with a "flick of a switch." In addition, many photochemical processes demonstrate good to perfect atom economy, as the transformation is initiated by a photon, rather than an extra reagent.[11] The use of solar light furthermore provides an effective green route to fine chemicals.[12,13]

The concept of photochemistry as a green technology is over 100 years old, as envisaged by Ciamician in the 1900s. At the International Congress of Applied Chemistry in New York in 1912, he presented his remarkable vision of "The Photochemistry of the Future"[14]:

> "On the arid lands there will spring up industrial colonies without smoke and without smokestacks; forests of glass tubes will extend over the plains, and glass buildings will rise everywhere; inside of these will take place the photochemical processes that hitherto have been the guarded secret of the plants, but that will have been mastered by human industry which will know how to make them even more abundant fruit than nature, for nature is not in a hurry and mankind is".

This eloquently foretells a key role for photochemistry in future industrial processes. Therefore, despite the advent of artificial light sources and other leaps in technology, it is not unexpected that mankind turns to the sun as a free energy and light source for solar chemical transformations and true "green" photochemistry.

10.3 Early Solar Studies

Solar chemistry is the earliest form of photochemistry, as photochemical transformations have occurred on earth since before human life came into existence. However, interest in synthetic organic photochemistry did not commence until the eighteenth century, when Joseph Priestly began his investigations into the chemical effects of light, leading to recognition of photosynthesis.[15] Following this work, interest in photochemical transformations slowly increased, until interest peaked in the nineteenth and twentieth centuries. The earliest photochemical processes were all solar in nature, often consisting of jars of solution phase reagents allowed to stand in sunlight for days, weeks, and even months.

Giacomo Ciamician (1857–1922), whose work provides a wealth of information regarding solar chemical transformations, is regarded as the "father of organic photochemistry." Together with Paolo Silber (1851–1932), he identified many types of photochemical reactions, in particular, ketone chemistry such as photoreduction (Scheme 10.1), photopinacolization, intramolecular cycloadditions (e.g., intramolecular [2 + 2] cycloaddition of carvone), and α- and β-cleavage.[16]

Following Ciamician's death in 1922, McPherson stated in his obituary that "anyone visiting the chemical laboratory of the University of Bologna during the early part of the present [twentieth] century, could easily surmise the character of the researches being carried out in that laboratory; for the

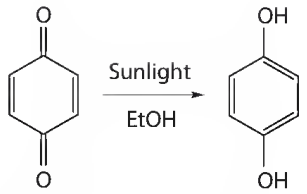

SCHEME 10.1 Photoreduction of 1,4-benzoquinone in ethanol.

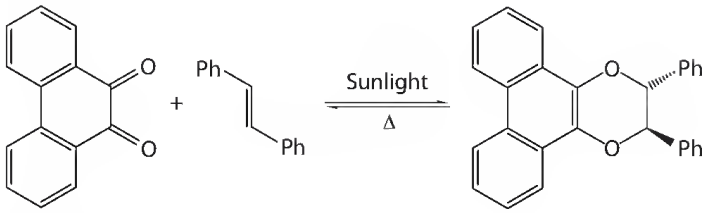

SCHEME 10.2 The Schönberg reaction.

exterior rear of the building was fitted with shelves and on these rested hundreds of bottles and sealed tubes of every description, all exposed to the sun's rays."[17]

Alexander Schönberg (1892–1985) was a German chemist who emigrated to Egypt prior to the Second World War. He is especially credited with the compilation of the first book on preparative organic photochemistry in 1958, which was revised and translated to English in 1968.[18] Over the course of 20 years, he additionally carried out extensive studies of the chemical effect of sunlight. These included the reaction of aldehydes with phenanthraquinoneimine to form 2-hydroxyl-2,3-dihydrophenanthroxazole derivatives, photopolymerization of coumarins and related substances (in aqueous solutions), and photoaddition and photoreduction of aromatic ketones. The Schönberg reaction (also known as the Schönberg–Mustafa reaction) describes the cycloaddition of alkenes to orthoquinones (Scheme 10.2).[19]

10.4 Development of Solar Technology

The earliest photochemical experiments were carried out in glass flasks, which were exposed to natural light without cooling.[15,17] However, there were hazards associated with this practice, in particular, early reports often stated that reaction mixtures were lost in windstorms or other incidents. In addition, the reaction mixtures were often placed in sealed containers, leading to a risk of explosion during exposure, such as gas evolution or evaporation of volatile solvents. Despite these risks, a wealth of solar chemical reactions were investigated under these primitive conditions. With the significant advances in lamp technology in the latter half of the twentieth century, photochemistry moved indoors and became a successful research area.[6]

The "indoor period" of photochemistry continued until the end of the last century, when rising oil prices and awareness of global warming led to a revolution in thought and a reemergence of interest in solar chemistry. To accompany this renewed interest in solar work, new reactors were designed, which could use non-concentrated and concentrated sunlight. Much of the new technology is based on modified reactors for energy production, for example, the parabolic trough-facility for organic photochemical syntheses (PROPHIS) reactor at the German Aerospace Centre (DLR) in Cologne, which is based on reactor design for solar-thermal applications.[20] The compound parabolic collector (CPC) reactor was designed for water treatment processes, but has since been adopted for use in synthetic applications.[21]

10.4.1 Non-Concentrating Reactors

Early photochemical studies simply required that a standard reaction flask be placed outdoors. However, a desire to achieve scale-up or higher conversions in a shorter time has led to the development of more suitable outdoor reactors. More advanced non-concentrating reactors have been developed, such as flatbed

FIGURE 10.1 (See color insert.) Flatbed and tube reactors at the DLR in Cologne.

or tube reactors (Figure 10.1), which can use both direct and diffuse sunlight.[13a] The flatbed reactor type realizes a large surface area with a thin depth.

Other non-concentrating designs include free-falling film reactors, pressurized flat-plate reactors or solar ponds.[21] A novel concept recently reported by Liu is the floating reactor ("lab on a surfboard"), which utilizes the ocean as a "heat sink" for cooling solar chemical transformations.[22] This reactor effectively eliminates both cooling and irradiation costs for the process.

10.4.2 Concentrating Reactors

Reactors for concentrating sunlight were initially developed for solar energy production, such as the line-focus parabolic trough concentrator. This reactor design was easily modified for photochemical work, where the central tube is replaced with a transparent glass (e.g., Pyrex) tube through which the reaction mixture is passed. Many of these parabolic trough reactors are now in use for solar chemical applications and allow laboratory to industrial-scale productions (Figure 10.2).[12,13,21] For small-scale reactions in moderately concentrated sunlight, simple laboratory-scale parabolic trough collectors have been reported. Some of these reactors were constructed from common laboratory equipment, for example, Liebig condensers and simple aluminum mirrors.[13d] More advanced prototypes of laboratory-scale parabolic trough collectors with exchangeable mirrors and tubing, thus accommodating a larger volume of reaction mixture, have also been described.[13c,e–f] These simple parabolic trough reactors require direct sunlight but can theoretically provide the power of 15–18 suns. However, this concentration factor is affected by imperfections in the mirrors and glass tubing, and may be lower than calculated. For industrial-scale reactions, the PROPHIS loop (modified from the SOLARIS loop, previously located at the Platforma Solar de Almeria, PSA[12a]) may be used, through which 35–120 L of reaction mixture may be passed. This reactor represents a line-focusing parabolic trough design, with four troughs of 8 m^2

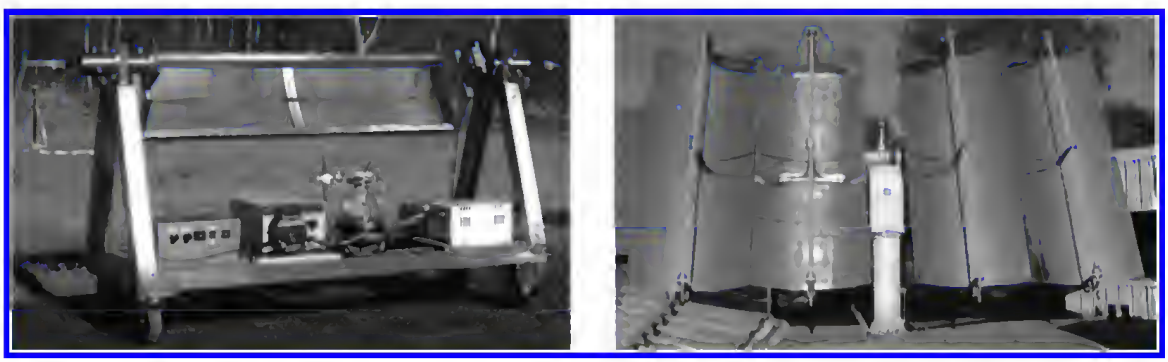

FIGURE 10.2 (See color insert.) Parabolic trough reactor for laboratory-scale experiments and the PROPHIS loop at the DLR in Cologne.

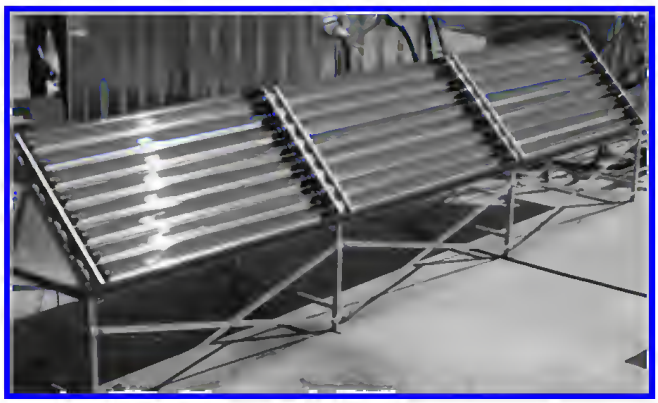

FIGURE 10.3 **(See color insert.)** Compound parabolic collector.

each, equipped with sun tracking systems. The concentrating power is 30–32 suns; however, it is reliant on direct sunlight and cannot be operated in diffuse conditions.[23]

10.4.3 Compound Parabolic Trough Reactors

Compound parabolic trough reactors are a cross between a parabolic trough collector and a non-concentrating reactor, and are capable of utilizing both direct and diffuse sunlight (Figure 10.3).[21] The reflective surface is in an involute shape around a cylindrical tube with a large diameter. As the diameter of the tube is so similar to that of the reflective surface, the concentration factor is considered to be the equivalent of a single sun.

10.4.4 Highly Concentrating Reactors

The use of highly concentrated sunlight for photochemical transformations has been investigated using solar furnaces. The solar furnace at the German Aerospace Centre uses a flat 52 m^2 heliostat and a concentrator composed of 147 spherical mirror facets to focus a highly concentrated beam of sunlight into the laboratory building.[24] Other solar furnaces are located in Golden, Colorado[25] and Odeillo, France.[26] Concentrations of 5,000–20,000 suns may be achieved using these furnaces. The use of highly concentrated sunlight can give higher yields in a shorter amount of time when compared to moderately concentrated light. However, the high costs for installation and the difficult operation of these systems offset the advantages of the high concentration factor.

10.5 Recent Solar Chemical Reactions

Solar applications have become widespread in recent years, within energy production, hydrogen production, and even wastewater treatment.[27] The area of solar chemistry research has also expanded, with investigations into syntheses using both concentrated and non-concentrated sunlight. In particular, the use of new technology has revolutionized solar chemical production, and some studies have suggested that solar plants are viable for industrial-scale production. The solar spectrum provides light in the usable range of 300–700 nm. Therefore, the reactions that may be carried out under solar conditions are limited to those that require light from this region of the spectrum.

10.5.1 Reactions Using Moderately Concentrated Sunlight

Many groups carry out their research using moderately concentrated sunlight, using both small-scale and large-scale apparatus. Campaigns by Scharf at the PSA (SOLARIS) and DLR (PROPHIS) looked at the production of fine chemicals using sunlight.[12] Three reaction types were chosen, based on the

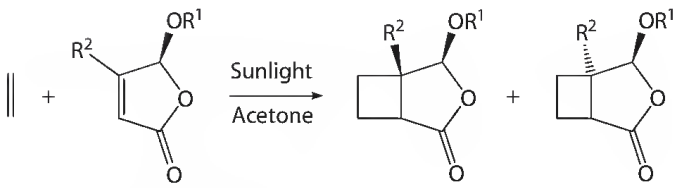

SCHEME 10.3 [2 + 2]-cycloaddition investigated by Scharf.

wavelength of light needed, namely, the Paternò–Büchi reaction (about 400 nm), [2 + 2]-cycloadditions (acetone sensitized, below 330 nm), and dye-sensitized photooxygenations (using rose bengal, 550 nm). These reactions were carried out on the multigram scale (21–45 mol in 30–35 L). This study demonstrated that the [2 + 2]-cycloaddition reaction was feasible under solar conditions, despite the fact that only ca. 4.5% of light from the solar spectrum is ultraviolet (Scheme 10.3).

Heller et al. have reported the synthesis of pyridines via [2 + 2 + 2]-cycloaddition using a cobalt (I) catalyst and concentrated solar light.[28] Several studies were conducted, investigating variation of starting material and reaction solvents. Syntheses in aqueous media and emulsions of water-toluene have proven successful. Using the PROPHIS plant, 2-phenylpyridine was obtained in yields of up to 40% after solar exposure for approximately 4.5–5.5 h (Scheme 10.4).

Oelgemöller et al. have investigated the synthesis of fine chemicals, via photo-Friedel–Crafts acylations and photooxygenations, using the solar facilities at the DLR.[12,29] The photoacylation of 1,4-naphthoquinone with butyraldehyde (Scheme 10.5) was performed on a 500 g (3.2 mol) scale in the PROPHIS loop using three troughs (24 m^2). Although the reaction was run for 3 days, examination of the amount of photons collected showed that almost full conversion was achieved on the first day of irradiation. A final yield of 90% was determined using gas chromatography (GC).

Photooxygenation reactions, namely, ene reaction of citronellol (a photochemical key step in the synthesis of rose oxide, Scheme 10.6a) and [4 + 2]-cycloaddition of 1,5-dihydroxynaphthalene (Scheme 10.6b), were also investigated.[13] Photooxygenation of citronellol was carried out on large scale, using one (32 mol in 40 L) or four (44 mol in 72 L) of the PROPHIS troughs. Complete conversions were achieved within 3 h of illumination. Likewise, photooxygenation of 1,5-dihydroxynaphthalene to juglone was carried out using smaller parabolic trough collectors (1–2 g in 200–250 mL of solvent). Yields of up to 79% were obtained.

Jung and coworkers have summarized the reactions carried out in the PROPHIS loop at the DLR, outlining synthesis of pyridines, photooxygenations, photo-Friedel–Crafts acylations, as well as *trans-cis* isomerization of stilbene.[23]

An interesting study by Dincalp reports the synthesis of rose oxide from citronellol using singlet sensitizers to generate the superoxide anion radical via an electron transfer cascade (rather than the

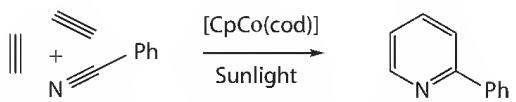

SCHEME 10.4 Synthesis of 2-phenylpyridine via [2 + 2 + 2]-cycloaddition.

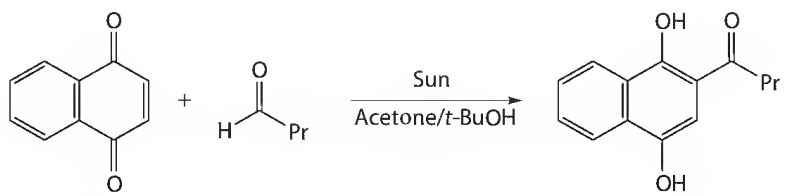

SCHEME 10.5 Photo-Friedel–Crafts acylation of 1,4-naphthoquinone.

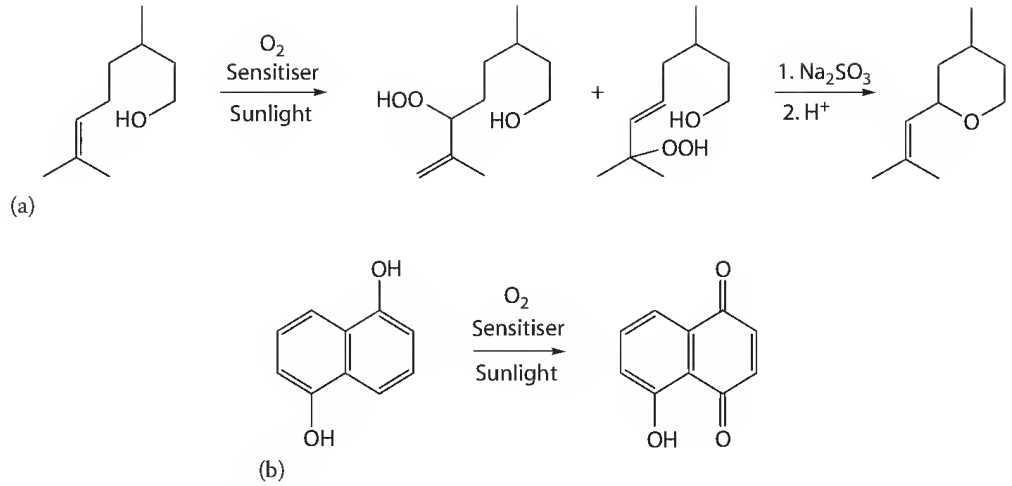

SCHEMES 10.6 Photooxygenation reaction of (a) citronellol and (b) 1,5-dihydroxynaphthalene.

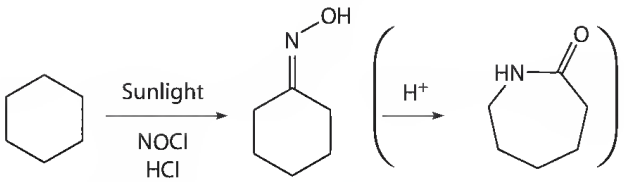

SCHEME 10.7 Synthesis of cyclohexanone oxime and subsequent formation of ε-caprolactam.

commonly encountered singlet oxygen method).[30] This was achieved on a scale of 0.02 mol of starting material in 100 mL acetonitrile, using a fix-focus (FF) 3.5 concentrator, which gives a concentration factor of 90–100 suns. Rose oxide was formed in over 82% yield after just 2 h of illumination. In a related study, α-terpinene was converted mainly into *p*-cymene and ascaridole.[31]

Further reactions using solar concentrators were reported by Cermenati (catalytic reaction using TiO_2) using a parabolic mirror reactor,[32] and Icli (dehydrogenation of abietic acid from both pure acid and pine resin) using a satellite dish of 1 m diameter.[33]

Funken et al. have evaluated the economic viability of solar synthesis of cyclohexanone oxime as an industrial process, which is used in the synthesis of ε-caprolactam (Scheme 10.7).[34] Modeling of a solar industrial plant indicates that energy savings may be achieved on the light source and cooling, as well as reduced carbon dioxide emissions compared to a plant using artificial light sources.

Similarly, Monnerie has reported an economic evaluation of solar synthesis of rose oxide via a photochemical key step, comparing the use of parabolic trough reactors to synthesis using artificial light sources.[35]

10.5.2 Synthesis in Low- to Non-Concentrating Reactors

To date, CPC reactors have primarily been used for water treatment.[21] A synthetic study using a CPC reactor was reported by Caronna, in which thiohelicenes with 5, 7, 9, or 11 rings were synthesized by photo-induced cyclodehydrogenation of the corresponding 1,2-diheteroarylethylenes (Scheme 10.8).[36] In comparison with artificial light sources, the solar study gave the same yield in shorter irradiation times.

Another synthetic study was carried out by Oelgemöller et al. at the DLR in Cologne, where the photo-Friedel–Crafts reaction of 1,4-benzoquinone was investigated (Scheme 10.9).[12a,29b] The reaction was used as a model reaction for comparison of reactors (non-concentrated, concentrated, and PROPHIS), which demonstrated that the use of a non-concentrating reactor gave superior results to those achieved in

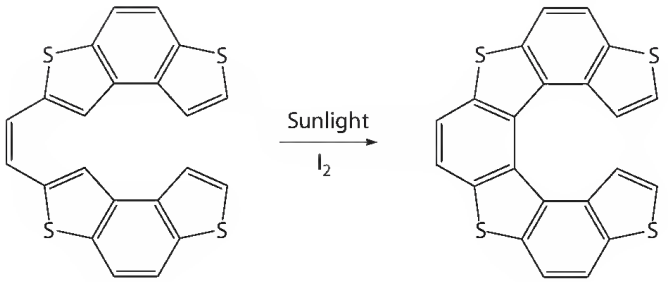

SCHEME 10.8 Synthesis of 7-membered thiohelicene via photo-induced cyclodehydrogenation.

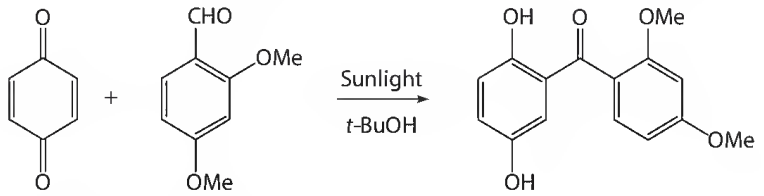

SCHEME 10.9 Photo-Friedel–Crafts acylation of 1,4-benzoquinone.

the PROPHIS loop under cloudy and partially cloudy conditions. The CPC reactor was shown to give greater conversion and product yield under diffuse conditions.

In a similar study, the photooxygenation of (–)-citronellol was used in a reactor comparison study.[12f] Once again, the CPC reactor was found to give the best performance in diffuse conditions.

Covell has reported the [2 + 2]-cycloaddition of styrene to 2-acetoxy-1,4-naphthoquinones (Scheme 10.10) on a 10 g scale in a small-scale CPC reactor (concentration factor of 2).[37] A conversion of >96% was achieved after just 6 h exposure. In addition, the cycloadduct was isolated in high purity by simple evaporation. The by-products from irradiations with artificial light could not be detected in the crude product. Thus, solar photochemistry allowed for a minimum workup procedure.

Solar-driven alkylations have been reported by Fagnoni and coworkers using disodium benzophenondisulfonate (BPSS) as a photocatalyst.[38] Isopropanol and 1,3-dioxolane could be successfully added to electrophilic alkenes and alkynes in the SOLFIN facility at the PSA (concentration factor of ~4). As an example, the reaction of isopropanol with maleic acid furnished terebic acid in an isolated yield of 75% after 14 h of solar exposure (Scheme 10.11).

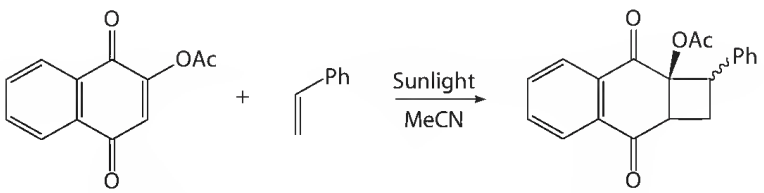

SCHEME 10.10 [2 + 2]-cycloaddition of styrene to 2-acetoxy-1,4-naphthoquinone.

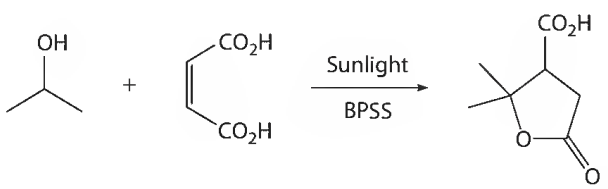

SCHEME 10.11 BPSS-catalyzed addition of isopropanol to maleic acid.

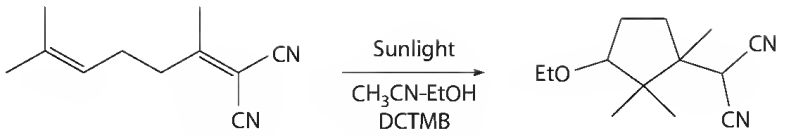

SCHEME 10.12 Photo-induced cyclization of 1,1-dicarbonitrile.

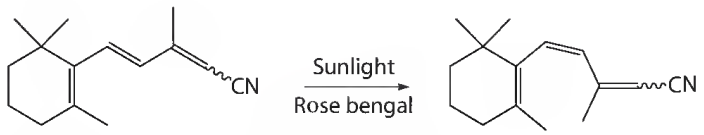

SCHEME 10.13 Rose bengal–sensitized *trans-cis*-isomerization.

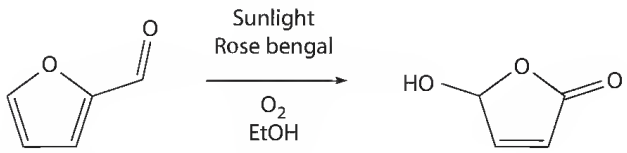

SCHEME 10.14 Photooxygenation of furfural.

The use of a flatbed reactor was reported by Heinemann for the photo-induced cyclization of 1,1-dicarbonitrile using 1,4-dicyano-2,3,5,6-tetramethylbenzene (DCTMB) as an electron acceptor (Scheme 10.12).[39] Comparison with concentrating reactors show that application of a flatbed reactor gives superior results under partially sunny or cloudy conditions.

A recent report by Liu looked at the isomerization of 7-*trans*-isomers of vitamin A to the more hindered *cis*-isomer, using rose bengal as a sensitizer (Scheme 10.13).[22,40] The use of natural water reservoirs as heat sinks for photochemical reactions was demonstrated using a photochemical reactor incorporated into the body of a surfboard or boggie board. Using this reactor, complete conversion was achieved after just 15 min in May sunlight in Hawaii.

Many reactions carried out in non-concentrated sunlight still follow the "flask-in-the-sun" approach.[41,42]

10.5.3 Reactions Using Highly Concentrated Sunlight

Although the solar furnace is primarily used for thermal applications, such as the synthesis of fullerenes (C_{60} and C_{70}) through vaporization of graphite,[25,26,43] there have been some reports of photochemical transformations using this technology.

The synthesis of fine chemicals has been the subject of some studies, such as the solar furnace campaign investigating photooxygenations, [2 + 2]-cycloadditions, and the Paternò–Büchi reaction.[12b] This demonstrated the feasibility of the use of highly concentrated sunlight for synthesis of fine chemicals, such as 5-hydroxyfuranone (Scheme 10.14).

Further success in the synthesis of fine chemicals in highly concentrated sunlight was reported by Funken, who synthesized ε-caprolactam in yields up to 83.5%.[34c]

10.6 Concluding Remarks

Within the area of green chemistry, photochemistry has gone "back to its roots" (and consequently "the roofs") and has reemerged as a successful research discipline. Non-concentrated, direct sunlight is still commonly used to activate solar chemical transformations. With the help of modern solar reactor systems, however, acceleration and scale-up has been achieved. Using this technology, a series of large-scale

syntheses of industrially relevant chemicals has been realized using concentrated and non-concentrated sunlight. The energy demand for operating artificial lamps could be completely annihilated by using natural sunlight as a free and environmental light source. Environmental performance and economical evaluations have additionally shown that solar chemical processes can compete or outperform thermal and lamp-driven processes.[9,35] This, together with the mild conditions and easy reaction control, may make solar photochemistry the *ultimate green chemistry.*

References

1. K. Alfonsi, J. Colberg, P. J. Dunn, T. Fevig, S. Jennings, T. A. Johnson, H. P. Kleine, C. Knight, M. A. Nagy, D. A. Perry, and M. Stefaniak, *Green Chem.*, 2008, **10**, 31–36.
2. P. T. Anastas and J. C. Warner, *Green Chemistry: Theory and Practice*, Oxford University Press, Oxford, U.K., 1998.
3. P. Tundo, P. T. Anastas, D. S. Black, J. Breen, T. Collins, S. Memoli, J. Miyamoto, M. Polyakoff, and W. Tumas, *Pure Appl. Chem.*, 2000, **72**, 1207–1228.
4. M. Lancaster, *Green Chemistry: An Introductory Text*, Royal Society of Chemistry, Cambridge, U.K., 2002.
5. A. Albini and M. Fagnoni, in *Green Chemical Reactions*, eds. P. Tundo and V. Esposito, Springer, Dordrecht, the Netherlands, 2008, pp. 173–189.
6. (a) A. M. Braun, M. T. Maurette, and E. Oliveros, *Photochemical Technology*, Wiley, Chichester, U.K., 1991; (b) K. Gollnick, *Chim. Ind.*, 1982, **63**, 156–166; (c) K. H. Pfoertner, *J. Photochem. Photobiol. A*, 1990, **51**, 81–86.
7. C. L. Ciana and C. G. Bochet, *Chimia*, 2007, **61**, 650–654.
8. M. Eissen and J. O. Metzger, *Chem. Eur. J.*, 2002, **8**, 3580–3585.
9. A. Albini, M. Fagnoni, and M. Mella, *Pure Appl. Chem.*, 2000, **72**, 1321–1326.
10. T. Razzaq and C. O. Kappe, *ChemSusChem*, 2008, **1**, 123–132.
11. S. Protti, D. Dondi, M. Fagnoni, and A. Albini, *Pure Appl. Chem.*, 2007, **79**, 1929–1938.
12. (a) P. Esser, B. Pohlmann, and H. D. Scharf, *Angew. Chem. Int. Ed. Engl.*, 1994, **33**, 2009–2023; (b) B. Pohlmann, H. D. Scharf, U. Jarolimek, and P. Mauermann, *Sol. Energy*, 1997, **61**, 159–168.
13. (a) C. Schiel, M. Oelgemöller, J. Ortner, and J. Mattay, *Green Chem.*, 2001, **3**, 224–228; (b) J. Mattay and M. Oelgemöller, in *CRC Handbook of Organic Photochemistry and Photobiology*, 2nd edn., eds. W. M. Horspool and F. Lenci, CRC Press, Boca Raton, FL, 2004, pp. 88.01–88.45; (c) M. Oelgemöller, C. Jung, J. Ortner, J. Mattay, and E. Zimmermann, *Green Chem.*, 2005, **7**, 35–38; (d) O. Suchard, R. Kane, B. J. Roe, E. Zimmerman, C. Jung, P. A. Waske, J. Mattay, and M. Oelgemöller, *Tetrahedron*, 2006, **62**, 1467–1473; (e) M. Oelgemöller, N. Healy, L. de Oliveira, C. Jung, and J. Mattay, *Green Chem.*, 2006, **8**, 831–834; (f) M. Oelgemöller, C. Jung, and J. Mattay, *Pure Appl. Chem.*, 2007, **79**, 1939–1947.
14. G. Ciamician, *Science*, 1912, **36**, 385–394.
15. (a) H. D. Roth, *Pure Appl. Chem.*, 2001, **73**, 395–403; (b) H. D. Roth, *Angew. Chem. Int. Ed. Engl.*, 1989, **28**, 1193–1207.
16. (a) A. Albini and M. Fagnoni, *ChemSusChem*, 2008, **1**, 63–66; (b) A. Albini and V. Dichiarante, *Photochem. Photobiol. Sci.*, 2009, **8**, 248–254; (c) A. Albini and M. Fagnoni, *Green Chem.*, 2004, **6**, 1–6.
17. W. McPherson, *J. Am. Chem. Soc.*, 1922, **44**, 101–106.
18. (a) A. Schönberg, *Präparative Organische Photochemie*, Springer, Berlin, Germany, 1958; (b) A. Schönberg, G. O. Schenck, and O. A. Neumüller, *Preparative Organic Photochemistry*, Springer, Berlin, Germany, 1968.
19. E. Singer, *Chem. Ber.*, 1987, **120**, I-XIV.
20. K.-H. Funken and M. Becker, *Renew. Energy*, 2001, **24**, 469–474.
21. S. Malato, J. Blanco, A. Vidal, and C. Richter, *Appl. Catal. B*, 2002, **37**, 1–15.
22. Y. P. Zhao, R. O. Campbell, and R. S. H. Liu, *Green Chem.*, 2008, **10**, 1038–1042.
23. C. Jung, K. H. Funken, and J. Ortner, *Photochem. Photobiol. Sci.*, 2005, **4**, 409–411.

24. A. Neumann and U. Groer, *Sol. Energy,* 1996, **58**, 181–190.
25. C. L. Fields, J. R. Pitts, M. J. Hale, C. Bingham, A. Lewandowski, and D. E. King, *J. Phys. Chem.,* 1993, **97**, 8701–8702.
26. G. Flamant, D. Luxembourg, J. F. Robert, and D. Laplaze, *Sol. Energy,* 2004, **77**, 73–80.
27. (a) D. Mills, *Sol. Energy*, 2004, **76**, 19–31; (b) A. Steinfeld, *Sol. Energy*, 2005, **78**, 603–615; (c) D. Bahnemann, *Sol. Energy*, 2004, **77**, 445–459.
28. (a) P. Wagler, B. Heller, J. Ortner, K. H. Funken, and G. Oehme, *Chem. Ing. Tech.*, 1996, **68**, 823–826; (b) G. Oehme, B. Heller, and P. Wagler, *Energy*, 1997, **22**, 327–336; (c) B. Heller, *Nachr. Chem. Tech. Lab.*, 1999, **47**, 9–14; (d) B. Heller, D. Heller, H. Klein, C. Richter, C. Fischer, and G. Oehme, *J. Inf. Recording*, 2000, **25**, 15–23; (e) B. Heller, B. Sundermann, H. Buschmann, H. J. Drexler, J. S. You, U. Holzgrabe, E. Heller, and G. Oehme, *J. Org. Chem.*, 2002, **67**, 4414–4422; (f) B. Heller, B. Sundermann, C. Fischer, J. S. You, W. Q. Chen, H. J. Drexler, P. Knochel, W. Bonrath, and A. Gutnov, *J. Org. Chem.*, 2003, **68**, 9221–9225.
29. (a) J. Zimmerman and P. Anastas, *TCE Today,* 2006, 48–50; (b) C. Schiel, M. Oelgemöller, and J. Mattay, *Synthesis*, 2001, 1275–1279; (c) M. Oelgemöller, C. Schiel, R. Fröhlich, and J. Mattay, *Eur. J. Org. Chem.*, 2002, 2465–2474.
30. H. Dincalp and S. Icli, *J. Photochem. Photobiol. A*, 2001, **141**, 147–151.
31. (a) C. Canan, H. Kolancilar, Ü. Oyman, and S. Icli, *J. Photochem. Photobiol. A. Chem.*, 2002, **153**, 173–184; (b) N. Avcibasi, S. Icli, and A. Gilbert, *Turk. J. Chem.*, 2003, **27**, 1–7.
32. L. Cermenati, C. Richter, and A. Albini, *Chem. Commun.*, 1998, 805–806.
33. S. Icli, A. Bulut, and Y. Gul, *Turk. J. Chem.*, 1992, **16**, 289–292.
34. (a) C. Sattler, F. J. Muller, K. J. Riffelmann, J. Ortner, and K. H. Funken, *J. Phys. IV*, 1999, **9**, 723–727; (b) K. H. Funken, F. J. Muller, J. Ortner, K. J. Riffelmann, and C. Sattler, *Energy*, 1999, **24**, 681–687; (c) K. H. Funken, G. Luedtke, J. Ortner, and K. J. Riffelmann, *J. Inf. Recording*, 2000, **25**, 3–14.
35. N. Monnerie and J. Ortner, *J. Sol. Energy Eng.*, 2001, **123**, 171–174.
36. T. Caronna, M. Catellani, S. Luzzati, L. Malpezzi, S. V. Meille, A. Mele, C. Richter, and R. Sinisi, *Chem. Mater.*, 2001, **13**, 3906–3914.
37. C. Covell, A. Gilbert, and C. Richter, *J. Chem. Res. Synop.*, 1998, 316–317.
38. D. Dondi, S. Protti, A. Albini, S. M. Carpio, and M. Fagnoni, *Green Chem.,* 2009, **11**, 1653–1659.
39. C. Heinemann, X. Xing, K. D. Warzecha, P. Ritterskamp, H. Görner, and M. Demuth, *Pure Appl. Chem.*, 1998, **70**, 2167–2176.
40. Y. Zhao, L. Yang, and R. S. H. Liu, *Green Chem.*, 2009, **11**, 837–842.
41. S. Protti and M. Fagnoni, *Photochem. Photobiol. Sci.*, 2009, **8**, 1499–1516.
42. (a) T. P. Yoon, M. A. Ischay, and J. Du, *Nature Chem.*, 2010, **2**, 527–532; (b) M. A. Ischay, M. E. Anzovino, M. E. Du, and T. P. Yoon, *J. Am. Chem. Soc.*, **130**, 12886–12887.
43. L. P. F. Chibante, A. Thess, J. M. Alford, M. D. Diener, and R. E. Smalley, *J. Phys. Chem.*, 1993, **97**, 8696–8700.

11

Photochemistry in Alternative Media

Tadashi Mori
Osaka University

Yoshihisa Inoue
Osaka University

11.1 Introduction

In this review, we will give a brief overview of recent (year 2000 or later) examples of the photochemical reactions in alternative media. The word "alternative" is rather ambiguous, but we herein deal with any photochemistry that is conducted in organized, but dimensionally not well-defined, media. The photochemistry in well-organized media, such as supramolecular hosts and crystals, will be reviewed in other chapters. The less organized "alternative" media include supercritical fluids, voids in polymer and related films, ionic liquids, liquid crystals, organogels, microemulsions, micelles, vesicles, and passive voids in dendrimers and so on, which have been extensively exploited as unique media for photophysical and photochemical studies.[1] We will focus mostly on the photochemistry in such alternative media with only occasional reference to the photophysics. Because of the diversity and vagueness of the topics, the chapter will not be comprehensive; rather, we will discuss the current status and characteristics of photochemistry in alternative media by illustrating representative examples.

11.2 Photochemistry in Supercritical Fluids

11.2.1 Supercritical CO_2

Dynamically fluctuating supercritical fluids are of special interest for conducting (photo)reactions that are controlled by the diffusion rate of the reactant or intermediate. In particular, supercritical carbon dioxide is desirable not only as a "green" medium but also as a supercritical medium attainable under a relatively mild condition (the critical point at 31°C and 7.38 MPa). It was repeatedly shown that regio- and stereochemical fates of (photo)chemical reactions can be manipulated by changing the medium property,

such as density and dielectric constant, which is readily achieved in supercritical media through alteration of pressure and/or temperature in a narrow range. Supercritical fluids have lower viscosity and higher diffusivity than conventional solvents, and these properties enable reactions to proceed beyond the mass transport limitations often found in traditional multiphase systems. From the practical point of view, the easier retrieval of products simply by reducing the pressure is another clear advantage in synthetic (photo) chemistry. Accordingly, the photochemistry in supercritical fluids has been extensively studied and has been recently reviewed[2]; these (relatively classical) examples will not be repeated in this review.

Since carbon dioxide is totally nonflammable and nontoxic, supercritical CO_2 ($scCO_2$) is one of the best solvents for potentially hazardous oxidation and oxygenation processes. Gaseous oxygen is highly soluble in $scCO_2$, where $^1O_2$ is readily generated and lasts longer (5.1 ms at 14.7 MPa and 41°C), although the lifetime is slightly dependent on the density of $scCO_2$.[3] Consequently, 5,10,15,20-tetrakis(pentafluorophenyl) porphyrin (**1**) has been used as a photosensitizer in $scCO_2$. Perfluorination endows the photosensitizer with reasonable solubility in $scCO_2$ under high pressure. Thus, the efficient singlet oxygenations of α-terpinene (**2**) to ascaridole (**3**) and of 2,3-dimethylbut-2-ene to 3-hydroperoxy-2,3-dimethyl-1-butene were reported to occur in $scCO_2$. These oxygenation processes have been demonstrated to efficiently proceed in a continuous flow system using a tubular sapphire reactor to afford ca. 1 mL of product in 10 min.[4]

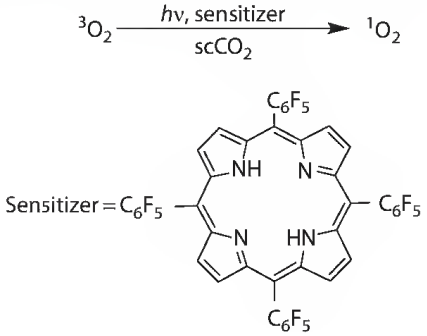

1

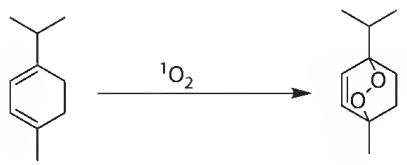

2 **3**

The photoinduced addition of aldehydes to α,β-unsaturated quinones (**4**) and enones (**5**) is an effective method for synthesizing 2-acyl-1,4-hydroquinones (**6**) and 1,4-diketones (**7**). These reactions were also performed in $scCO_2$, instead of benzene. The yields were improved at higher CO_2 pressures or with the addition of 5% *t*-butyl alcohol as cosolvent under the supercritical conditions.[5]

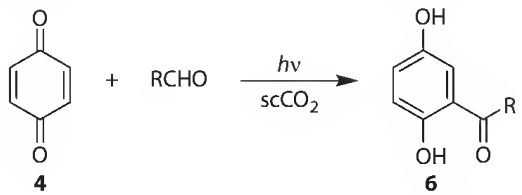

4 **6**

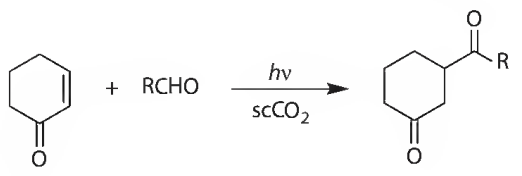

5 **7**

The photolysis of anthracene (**8**) in the presence of appropriate electron and hydrogen donors in $scCO_2$ was reported to give 9,10-dihydro-9-anthracenecarboxylic acid (**9**) in good yields, which is in sharp contrast to the result in the conventional nonpolar aprotic solvents. In this system, $scCO_2$ acts as both reactant and reaction medium. The reaction involves the photo-induced electron transfer from *N,N*-dimethylaniline to anthracene to form a radical anion intermediate, which was trapped by carbon dioxide to produce the reduced aromatic carboxylic acid.[6]

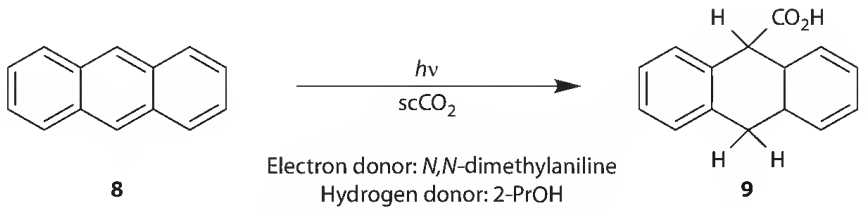

8 **9**

A photoexcitation of 2,4,6-trimethylbenzoyldiphenylphosphine oxide (**10**) in the presence of methyl methacrylate (**13**) was reported to induce free radical polymerization. The rates of propagation in supercritical and liquid CO_2, which were determined by the time-resolved electron paramagnetic resonance studies, were comparable to each other. The rates in much viscous liquid CO_2 were slower than the diffusion-controlled ones and comparable to those in conventional solvents.[7]

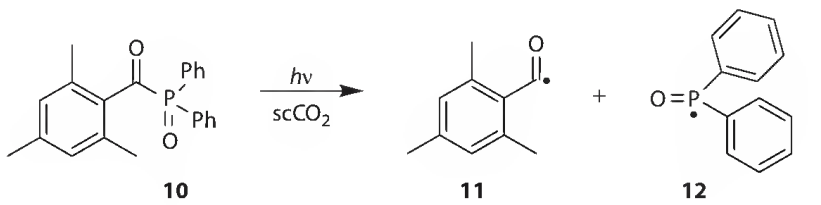

10 **11** **12**

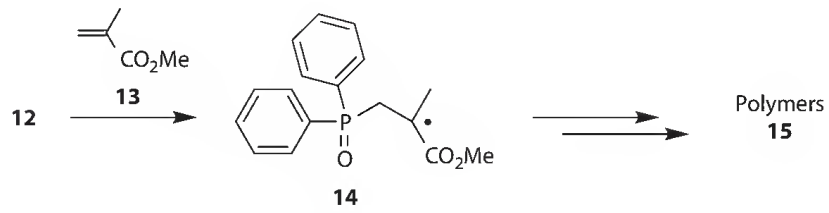

14

The photochemistry of uranyl(VI) tributylphosphate complex in $scCO_2$ was also studied. The result was interpreted as the uranyl(VI) complex was reduced to uranium(V) by photoexcitation in the presence of ethanol, which was followed by the disproportionation to give the uranium(IV).[8] The photocatalytic oxidation of 1-octanol on silanized TiO_2 suspended in aerated $scCO_2$ was also investigated at a various temperatures and pressures. The maximal photocatalytic production was observed at the CO_2 pressure of 10 MPa. These experimental results were explained by differences in mass transfer efficiency of the reactants and products formed on partially desilanized TiO_2 powder in $scCO_2$.[9]

Enantiodifferentiating photoaddition of methanol to 1,1-diphenylpropene (**16**) has been extensively studied using the chiral 1,4-naphthalenedicarboxylate (**17**) as the sensitizer. The enantiomeric excess (ee) of photoadduct (**18**) obtained in the reaction was critically affected by applied pressure and/or temperature. The product's ee was enhanced by increasing alcohol size and pressure, thus affording a best ee of 43% for the photoaddition of 2-propanol in $scCO_2$ at 18 MPa.[10] However, the dependence of ee was discontinuous at the critical density, accompanying a big jump caused most probably by enhanced clustering of the alcohol. Interestingly, such sudden leap in the ee near the critical CO_2 density was observed at any given temperature, but at different pressures.[11] The differential activation volumes, $|\Delta\Delta V^{\ddagger}_{R-S}|$, obtained for the supercritical and particularly the subcritical regions, were

much larger than those obtained with the same photoreaction in conventional solvents, indicating the more selective solvation to one of the diastereomeric exciplexes particularly in the subcritical region. The $\Delta\Delta V^{\ddagger}_{R-S}$ values obtained at the near-critical region (9–10 MPa) were anomalously large, which was attributed to the dynamic nature of $scCO_2$ in the subcritical region, as independently demonstrated physicochemically by the density fluctuation studies. These explanations were also supported by the florescence studies.[12]

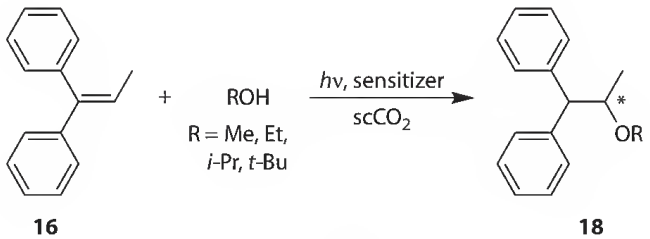

16 18

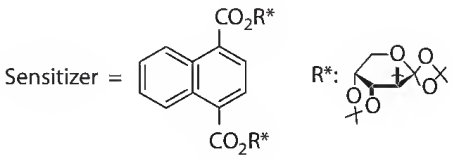

17

The photolysis of 5,5-diphenyl-4-penten-1-ol (**19**) in the presence of the same chiral sensitizer (**17**) was performed in $scCO_2$ to give the intramolecular cyclization product (**20**) in good to modest yields. The ee of product (**20**) was again highly pressure dependent, displaying a dramatic leap from nearly 0 in near-critical CO_2 (8–10 MPa) to the maximum value of 29% in purely $scCO_2$ at 12 MPa. More surprisingly, it was revealed that the dramatic increase of the ee of photoproduct is achieved by simply adding an entrainer such as diethyl ether to $scCO_2$, although the detailed mechanism was not fully elucidated.[13]

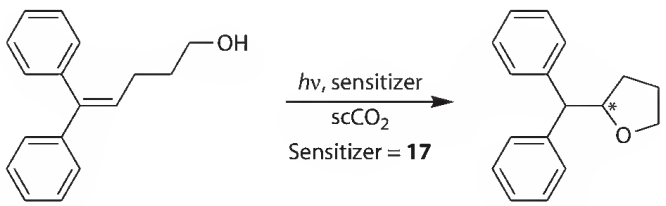

19 20

As another example of the unimolecular reactions, the sensitized enantiodifferentiating photoisomerization of (*Z*)-cyclooctene (**21**) to (*R*)- or (*S*)-(*E*)-cyclooctene (**23**) with chiral benzenepolycarboxylates (such as **22**) was studied in $scCO_2$. A similar jump of the product's enantioselectivity in the near-critical region (8–10 MPa of CO_2) was also observed in this system.[14]

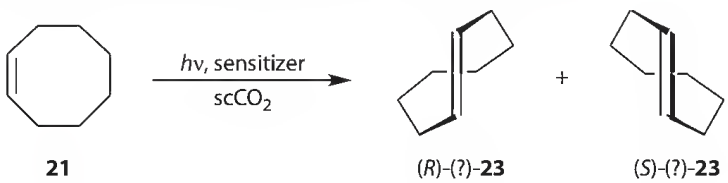

21 (*R*)-(?)-**23** (*S*)-(?)-**23**

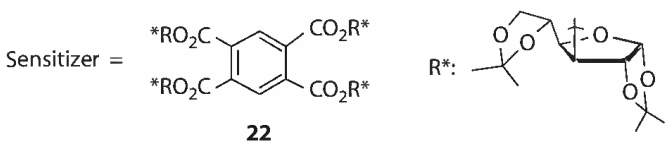

22

11.2.2 Supercritical Rare Gases

The photolysis of iron pentacarbonyl, $Fe(CO)_5$ (**24**), has been widely investigated as a representative compound in organometallic photochemistry, using various techniques such as matrix isolation, flash photolysis, time-resolved infrared spectroscopy, and electron diffraction. Consequently, the addition reactions of the triplet fragments $^3Fe(CO)_4$ and $^3Fe(CO)_3$ (**25–27**) formed upon photolysis of $Fe(CO)_5$ (**24**) in supercritical rare gases (xenon and argon) have been investigated in detail.[15] The photobehavior was compared with that in supercritical methane, as well as in conventional solvents. A theoretical study on these systems revealed that these spin-forbidden reactions are caused by the spin crossover followed by ligand addition via the nonadiabatic transition state.[16] The photochemistry of related molybdenum species, *trans*-$[CpMo(CO)_3]_2$ ($Cp = \eta^5\text{-}C_5H_5$), in $scCO_2$ has been also studied by the time-resolved infrared spectroscopy.[17]

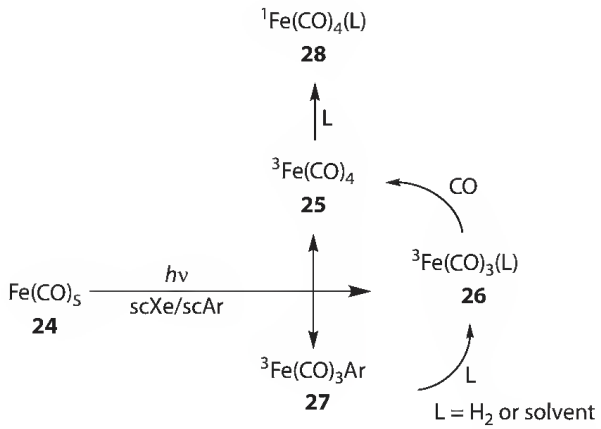

The photolysis of asymmetrically substituted diazene (**29**) in supercritical xenon and CO_2 and compressed krypton was investigated by nanosecond laser flash photolysis.[18] The cage effects on the radical intermediates (**30** and **31**) in different fluids (supercritical CO_2, Xe, and Kr) were examined to disclose the absence of the critical clustering or so-called enhanced cage effect under the near-critical conditions.

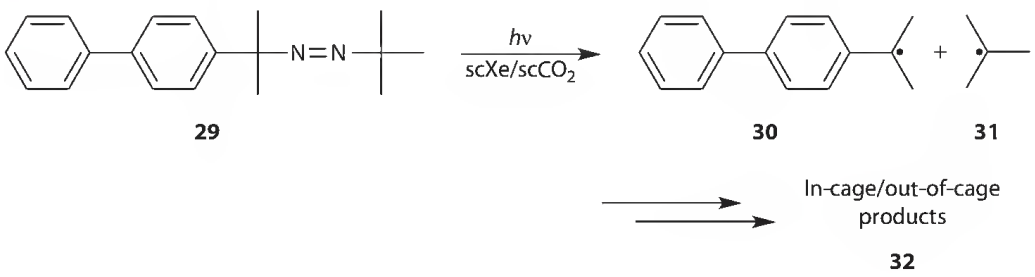

11.2.3 Supercritical Methane, Ethane, and Other Hydrocarbons

Photoreaction of a homogeneous mixture of ethane, carbon monooxide, and rhodium catalyst, $[Rh(CO)(PMe_3)_2Cl]$ (**33**), was reported, and the formation of propionaldehyde was confirmed by mass spectrometry. During the course of photolysis, the catalyst was decomposed to $[Rh(CO)_2(PMe_3)Cl]$ (**34**), and this species was shown to be responsible for the carbonylation of ethane. The photochemical carbonylation of ethane and other hydrocarbons by rhodium catalysts was also reported in $scCO_2$. The similar carbonylation of methane did not proceed in supercritical methane.[19]

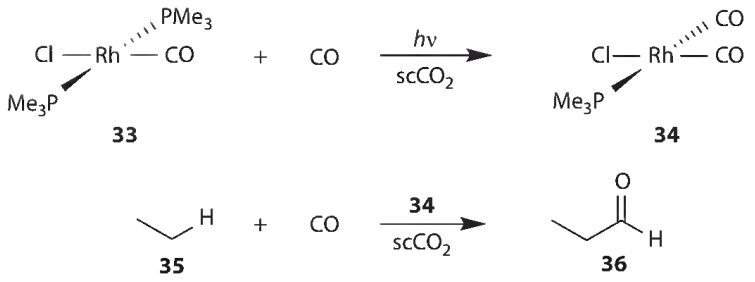

Upon laser irradiation of near-critical benzene at 266 nm, carbon onions were produced in both subcritical (200°C) and supercritical (290°C) benzene, whereas carbon coils were obtained on an alloy catalyst composed of Fe, Cr, and Ni in supercritical benzene. The use of supercritical fluids for preparation of structured carbons is attractive, since the method requires much lower temperature than that used in conventional methods.[20]

11.3 Photochemistry in Polymer and Related Films

11.3.1 Polyethylene and Polypropylene Films

A number of investigations demonstrate that the cavities in polyethylene (PE) films can be subtly "tuned" by temperature and the induced microscopic changes in polymer structure and morphology are valuable for altering or tuning the reactivity and selectivity of a wide variety of photoreactions. The passive voids of PE cavities can be easily modulated by their degree of crystallinities and by unidirectionally stretching the films. The voids can also be templated by incorporating some guest molecules and the template shape is retained for some time even after the removal of the guest template. As such, the passive PE cavities are positively employed for controlling the photochemical reactions, as shown in the following examples.

The selectivity of photo-Fries rearrangements has been widely investigated in isotropic solutions. Accordingly, the photolysis of 1-naphthyl and 2-naphthyl acylates (**37** and **43**) was conducted in unstretched and stretched PE films of different crystallinities and the results were compared with those obtained in isotropic solutions.[21] The influence of variables such as size and position of the aryl groups of the esters, degree of crystallinity, free volume, and unstretched/stretched state of the films has been explored. The void's free volumes were much smaller than the van der Waals volumes of the naphthyl molecules under investigation and the naphthyl esters inside PE cavities acted as templates for the formation of photoproducts. Stretching of the film enhanced the templating effect and strengthened the van der Waals attractions with cavity walls in the case of naphthyl myristates, thus inducing an increase in reaction selectivities in PE films. There was, on the contrary, no direct correlation between the void's free volume of PE films and the selectivity of photoreactions.

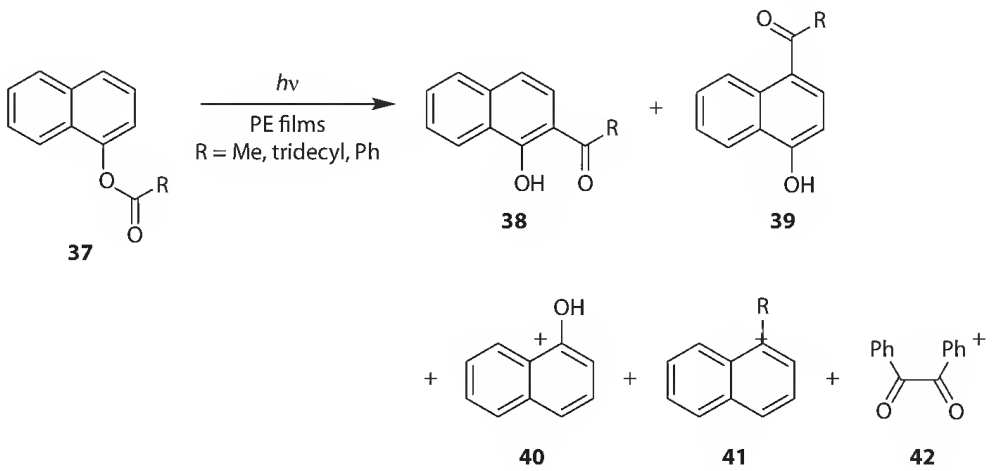

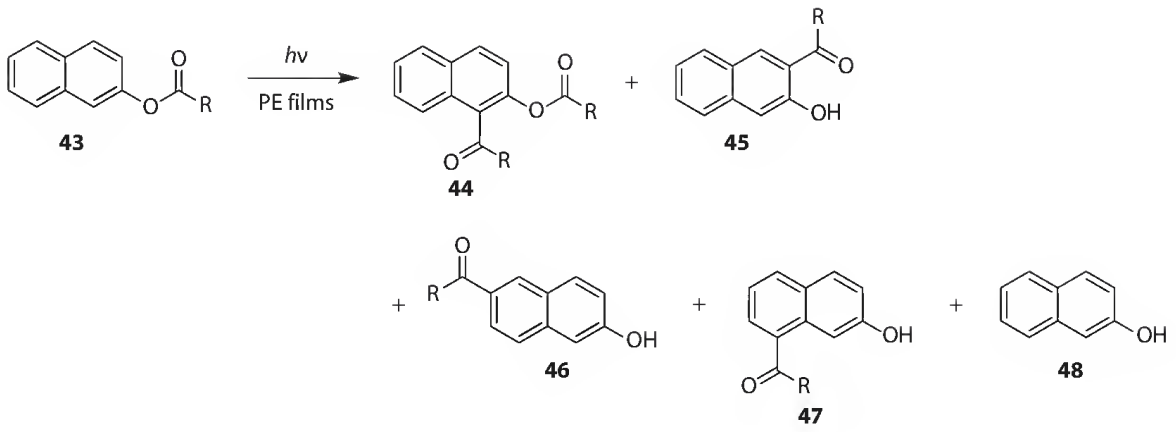

Photo-Fries rearrangements of phenyl phenylacylates (**49**) were investigated in isotropic solutions and in PE films and the results were compared with those obtained for the corresponding naphthyl esters. Unlike the naphthyl esters, the product distribution and the rate of radical recombination were much less sensitive to film stretching or the type of PE employed in the case of phenyl esters. Photoirradiation of 5,6,7,8-tetrahydro-1-naphthyl phenylacetate, which is comparable in size to 1-naphthyl phenylacylates, but electronically equivalent to phenyl phenylacylates, revealed that the electronic properties of the two aryloxy radicals are principally responsible for the differences in the overall rates of recombinations of the intermediate radical pairs.[22]

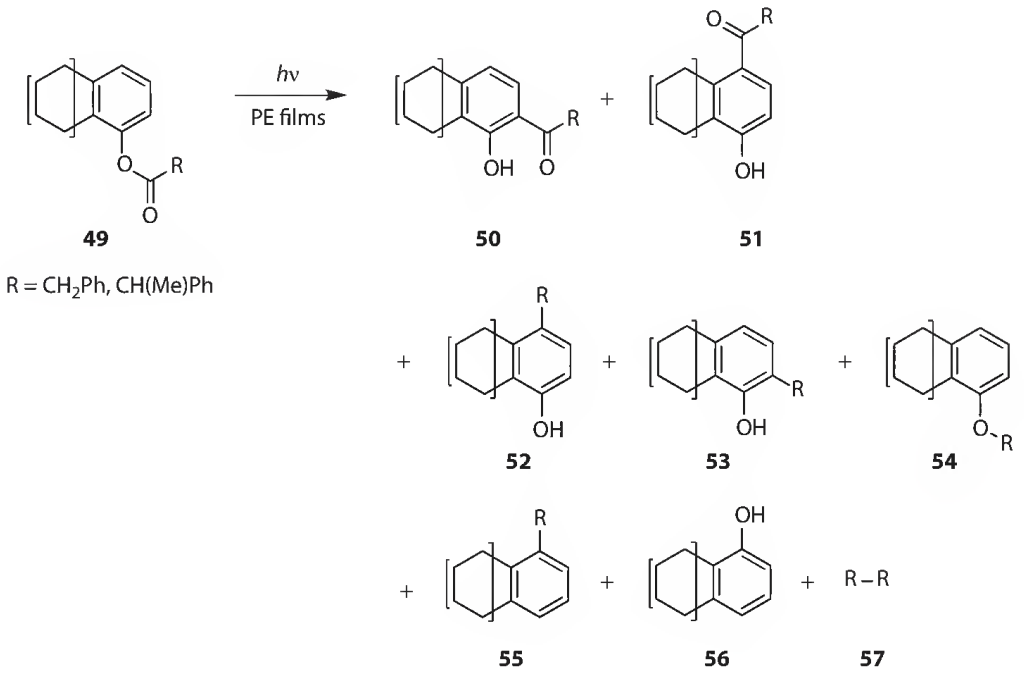

Recombination of prochiral radical pairs derived photochemically from 1-naphthyl (*R*)-2-phenylpropanoate (**58**) in PE films was reported to occur with significant enantioselectivities due to the confining effect in PE cavities. The regioselectivities of photo-Fries (**59** and **60**) and of decarbonylation products (**61**–**63**) obtained upon photolysis of this chiral ester were very different from each other, and the enantioselectivities of the decarbonylation products were heavily dependent on the properties of the PE cavities, such as wall stiffness and mean free volumes.[23]

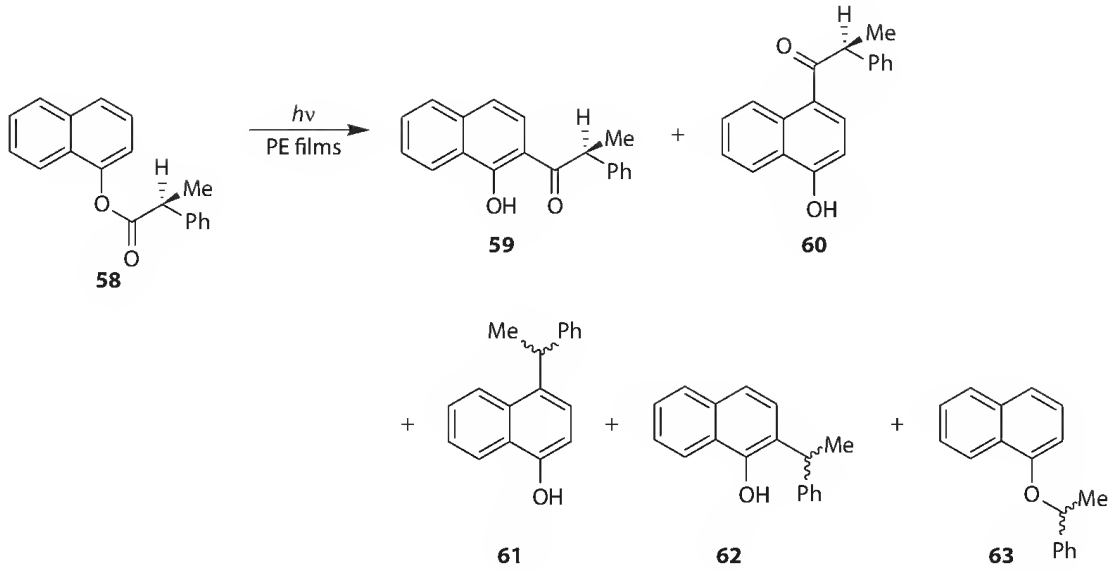

The photochemistry of 1-(4-methylphenyl)-3-phenyl-2-propanone (**64**) has been investigated in PE films of varying crystallinities at different temperatures.[24] The recombination selectivity of the triplet pairs of benzylic radicals derived from the photolysis of ketone **64** has been used as a tool for assessing the nature of the PE cavities and its influence on the motion of the radicals. It was shown that the in-cage recombination is favored at low temperatures and in PE of high crystallinities. These results were interpreted from the structural point of view, by considering the shape, free volume, wall stiffness, and permeability of the reaction cavities, and also from the dynamic point of view, by taking into account of the kinetic competition of the in-cage combination versus cage escape of the radical pairs. Recent examinations by the steady-state and laser-pulse irradiations of dibenzyl ketone derivatives with *p*-methyl or *p*-hexadecyl chain in PE films with 0%, 46%, and 68% crystallinities revealed that the separate components of reaction, affected by the (in-cage) "cage effect" as well as the (out-of-cage) "persistent radical effect," are both responsible for the formation and relative contributions of decarbonylated products (**65–67**).[25]

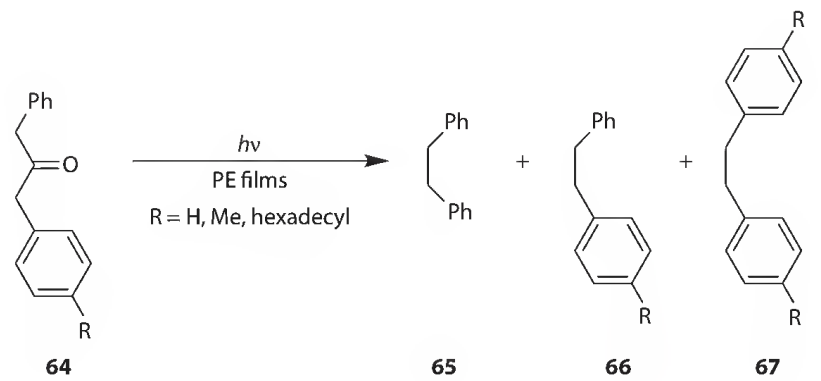

Photo-Claisen rearrangement of benzyl phenyl and benzyl 1-naphthyl ethers (**68**) has been also examined in PE films of different crystallinities. The ratios of the principal rearrangement products, benzyl arylol positional isomers (**69–71**), indicated that the reaction is less selective in the PE films than in the zeolite cavities. The results were explained in terms of the passive walls of the PE cages and the limited free volume of cavities.[26]

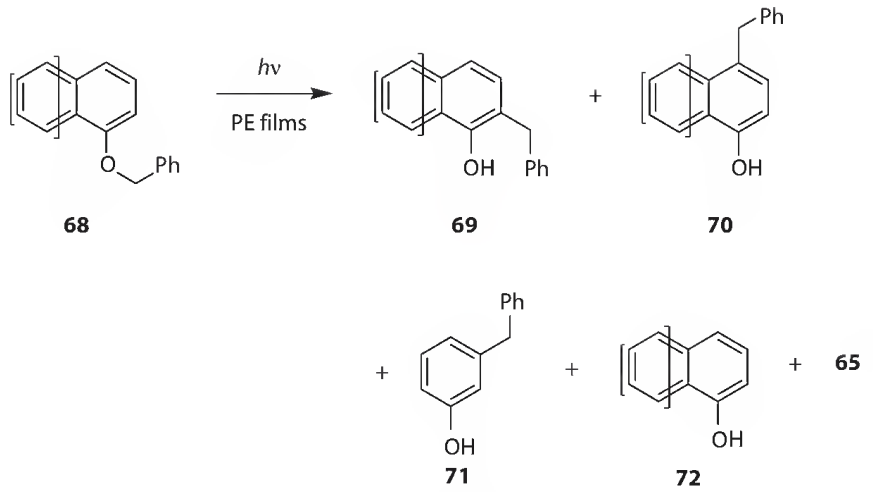

The radical pairs produced directly from the lysis of the first excited singlet state of enantiomerically pure 1-naphthyl (*R*)-1-phenylethyl ether (**73**), or indirectly from the decarbonylation of the aroyl radical formed in the photo-Fries reaction of 1-naphthyl (*R*)-2-phenylpropanoate (**58**), have been shown to (partially) lose their stereochemistry in the PE films, which is in contrast to the photo-Fries rearrangement in PE films, where the stereochemistry is fully preserved.[27] Quite interestingly, these results are better interpreted by assuming that the PE cavities are templated by the guest molecules and the templated shapes are retained to some degree for a period required for decarbonylation. Comparison of the fates of the directly and indirectly formed radical pairs has been employed as a tool for elucidating the nature of the reaction cavities in the polyethylene films and how the combination of the radical pairs is influenced by the initial location within a cavity.

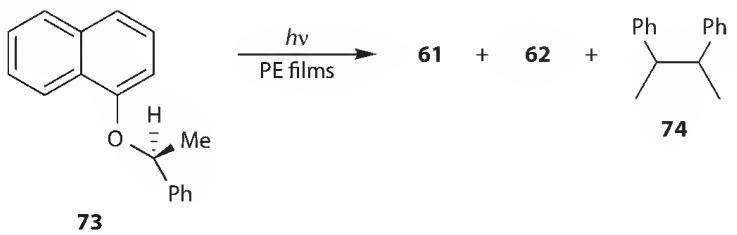

The photodecarboxylation of 2,4,6-trimethylphenyl (*S*)-2-methylbutanoate (**75**) in unstretched high-density polyethylene (HDPE) films afforded (*S*)-1-(2-methylpropyl)-2,4,6-trimethylbenzene (**76**) as the sole detectable product.[28] In other PE films, organic solvents, and cyclodextrin cavities, the cage-escaped products derived from the Fries-type bond scission were concomitantly obtained, but the decarboxylation product was obtained with stereoretention without exception, indicating that the decarboxylation is a completely concerted process.[29] A recent investigation on the photoreaction of *o*-cresyl acylates in PE films confirms that the importance of the shape of substrate and thus the ability to interact with their environment to the stereoselectivity of the photochemical outcomes.[30] These results reveal the importance of the media in controlling the conformation and photoreaction of aryl esters.

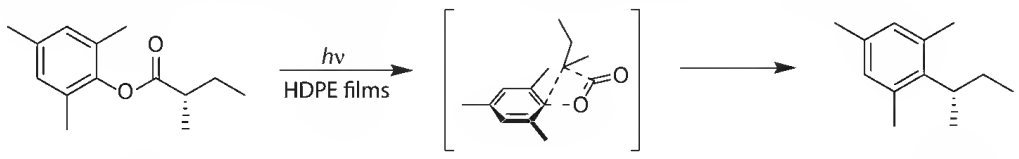

11.3.2 Poly(Vinyl Acetate) Films

The photo-Fries and associated photoreactions of 1-naphthyl acylates (**37**) have been also examined in two types of poly(vinyl acetate) or PVA films above and below their glass transition temperatures.[31] Comparison of the results in PVA films with those in low-viscosity solvents (ethyl acetate and hexane) and low-polarity polymer films (PE and polypropylene) indicated that interactions of the radicals produced in the photolysis of esters with the acetate pendant groups of PVA films, as well as the mode of PVA's chain motions, enormously influence the course of the photo-Fries rearrangements. The distributions of photo-Fries products were reasonably explained by the initial conformation of the guest molecules accommodated in the film cavities.

11.3.3 Nafion Membranes

Methanol-swollen Nafion beads also provide the microenvironment for controlling photochemical reaction pathways. Thus, the product selectivities have been examined in photo-Fries rearrangement of naphthyl esters, Norrish Type I reaction of 1-phenyl-3-*p*-tolyl-propanone, Norrish Type I and Type II reactions of benzoin alkyl ethers, and photodimerization of acenaphthylene and *N*-benzyl maleimide.[32] For example, the photoirradiation of naphthyl benzoate (**37**) in Na^+, Tl^+, and Cs^+ ion exchanged Nafion beads affords single product (2-benzoyl-1-naphthol, **38**), while a pair of rearranged products as well as the cage-escaped products are concomitantly formed in isotropic solvents such as hexane, methanol, and benzene.

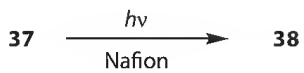

The ion-exchanged Nafion interior was also used to investigate the influence of chiral auxiliaries in photochemical reactions. Thus, the asymmetric photoisomerization of *trans,trans*-2,3-diphenylcyclopropane-1-carboxylic acids, electrocyclization of 2-oxo-1,2-dihydropyridine acetic acids, and oxa-di-π-methane rearrangement of 1,2-dihydronapthalenones have been reported. For example, irradiation of pyridone derivative **77** in Na^+ or Li^+ Nafion yielded the bicyclic products (**78** and **79**) in 13%–21% diastereomeric excess (de), whereas the same reaction in solution afforded only 0%–4% de.[33]

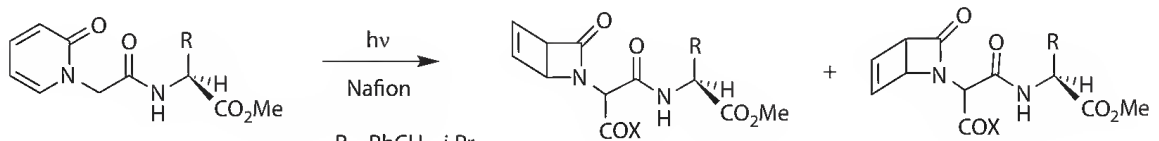

77 **78** **79**

Water- and methanol-swollen Nafion membranes were used as the microenvironment to effectively control the photochemical reaction pathway of stilbazole derivatives (**80**). Azaphenanthrene (**82**) was obtained in high yield upon irradiation of **80** in the membrane, while only the cyclodimerization products (**83** and **84**) were formed in homogeneous solutions.[34]

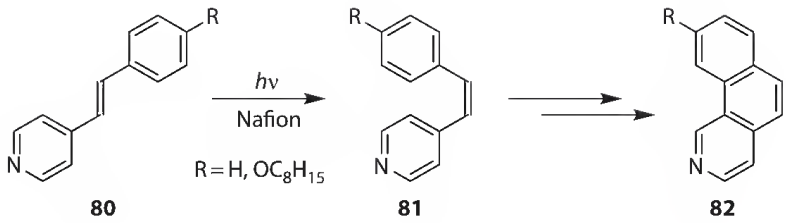

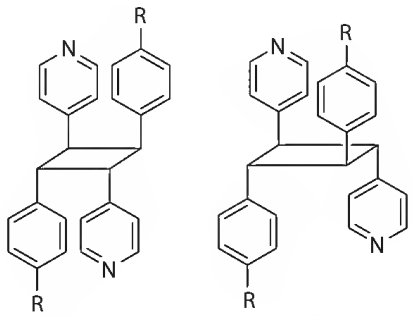

11.4 Photochemistry in Ionic Liquids

The photochemistry in ionic liquids (ILs) has been extensively studied and thus repeatedly reviewed.[35] Therefore, we deal with only the recent development and will not refer to the work cited in the chapter "Photochemistry in Ionic Liquids" of the previous edition of this book.[36] The photochemistry of ILs that contain photoreactive groups will also be disregarded, and we will focus on the systems that use ILs as reaction media for photochemical reactions. Typical room-temperature ILs, such as 1-butyl-3-methylimidazolium tetrafluoroborate (bmim-BF_4) and hexafluorophosphate (bmim-PF_6), are most frequently employed as the media for photoreactions, but the ILs that contain weakly coordinating bis(trifluoromethanesulfonyl)amide moiety, such as 1-butyl- and 1-ethyl-3-methylimidazolium bis(trifluoromethanesulfonyl)amides (bmim-NTf_2 and emim-NTf_2), are also used. The photoreactions can be conducted also in the microemulsions formed by mixing IL with organic solvent and/or aqueous solution. In this section, we will outline the recent examples of photoreactions performed in ILs and in the microemulsions using ILs.

The IL bmim-PF_6 has been employed as a solvent for a series of representative photochemical reactions involving energy transfer, hydrogen transfer, and electron transfer.[37] ILs show unique characteristics such as low oxygen solubility, slow molecular diffusion, elongation of triplet excited state and radical ion lifetimes, and weakening of the donor–acceptor (or charge transfer) interactions. The photoinduced electron transfer of anthraquinone[38] and duroquinone[39] in mixed binary solutions of IL (bmim-PF_6 or bmim-BF_4) and organic solvent has been studied by laser flash photolysis. The absorption of the triplet excited state of the quinone was blueshifted in the IL–acetonitrile mixtures, and the triplet excited state of the quinone abstracted hydrogen from the IL. In a binary mixture of IL and acetonitrile, the rate of electron transfer depended primarily on the concentration of IL at lower fractions of IL. In contrast, at higher fractions of IL, the network structures due to the hydrogen bond and viscosity became dominant and the decay rate constant decreased with increasing fraction of IL. A critical point was observed at a volume fraction of ~0.3 in IL. Photoinduced electron transfer from a series of electron donors to 9,10-dicyanoanthracene has been studied in bmin-PF_6 and omim-PF_6 (1-octyl-3-methylimidazolium hexafluorophosphate).[40] The fluorescence quenching occurred at rates 1–2 orders of magnitude greater than the diffusion limit. This and related theoretical studies revealed that the electron transfer between the excited 9,10-dicyanoanthracene and the donor molecule occurs in the hydrophobic, nonpolar alkyl chain region of the ILs. A detailed study of the photoinduced electron transfer between pyrene

and *N,N*-dimethylaniline was performed recently in four different room-temperature ILs (bmim-BF_4, bmim-PF_6, bmim-NTf_2, and emim-NTf_2), by using the steady-state and time-resolved fluorescence and laser flash photolysis techniques.[41] Because of the slow diffusion in ILs, quenching occurs at a slower rate in ILs than in conventional organic solvents. In sharp contrast to the well-established observation of exciplex fluorescence in conventional media, no exciplex emission was observed in ILs. However, the quenching rate constant, much larger than the diffusion-controlled rate, was explained by the microenvironmental viscosity around the electron donor and acceptor, which is different from the bulk viscosity of the IL. Furthermore, the solvent-mediated electron transfer in a pyridinium IL, *N*-butylpyridinium bis(trifluoromethanesulfonyl)amide, was reported recently.[42] The electron transfer between $Ru(bpy)_3^{2+}$ complex and methyl viologen, coupled with the reduction of the carbonyl group in ILs, was reported.[43] Intramolecular electron transfer was also studied in IL, and the photolysis of 4-(*N*-pyrrolidino)naphthalene-1,8-imide-pyromellitimide was examined in emim-NTf_2.[44]

The photoisomerization of 3,30-diethyloxadicarbocyanine iodide was investigated in bmim-PF_6 and in a binary mixture of the IL and water, by using the steady-state and time-resolved fluorescence spectroscopy. The photoisomerization rate was dramatically retarded in the IL, compared to that in an isotropic solvent of comparable polarity. The activation energy for photoisomerization was also determined in various media.[45] Photoisomerizations of 4′-hydroxyflavylium[46] and 4′,7-dihydroxyflavylium[47] were studied in bmim-PF_6, and their multistate, multifunctional switching properties in a biphasic IL–water mixture were shown to be quite valuable. The photochromic properties of *N*-methyl nitrobenzospiropyran–merocyanine system (**85** and **86**) were studied in ILs containing bis(trifluoromethanesulfonyl) amide anion, and the kinetics and thermodynamics of the process were shown to be sensitive to the nature of the cation.[48] Recently, a variety of ILs containing carboxylate anions were prepared and *N*-substituted photochromic spiropyran derivatives were employed to determine the polarities of these protic or fluorine-containing ILs.[49]

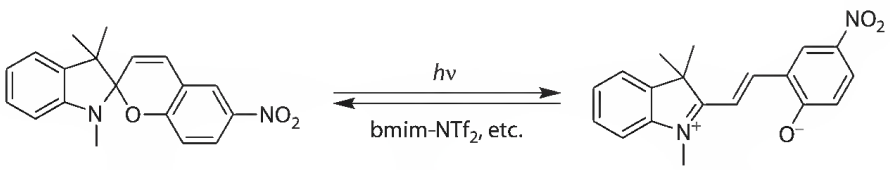

85 **86**

The formation of $^1O_2$ was suggested upon photoirradiation of indigo carmine in bmim-BF_4, and the quantum yield of $^1O_2$ production was estimated to be 0.53.[50] The oxidation of thioanisole photosensitized by methylene blue has recently been studied in a series of anhydrous imidazolium- and pyrrolidinium-containing ILs.[51] It was shown that the ILs can be used as convenient solvents for oxidation of thioanisole, although thioanisole is practically unreactive in conventional aprotic solvents. Upon oxidation of thioanisole by $^1O_2$, a small amount of the corresponding sulfone was formed in pyrrolidinium-based ILs, but the sulfoxide was exclusively produced in imidazolium-based ILs. This was explained as the persulfoxide is converted to a hydroperoxysulfonium ylide intermediate in pyrrolidinium-type ILs (as it occurs in conventional aprotic solvents), while in imidazolium-type ILs hydrogen-bonded persulfoxide is probably formed. The photochemical oxidation of alcohols with molecular oxygen was efficiently performed in high conversion and selectivity in several ILs by using 12-tungstophosphoric acid immobilized in mesoporous MCM-41.[52]

Millimeter-long nanowires of charge transfer silver tetracyanoquinodimethane materials were prepared by the photochemical reduction of tetracyanoquinodimethane in bmim-BF_4 containing benzyl alcohol as a sacrificial electron donor. The nanowires were also prepared in this IL by using the oxidation of water as a counterreaction (at a slower rate), indicating that the ILs may provide a favorable environment for photochemical water splitting. It is to note that the adventitious water as impurity may have affected the photochemical behavior in ILs.[53]

Intra- and intermolecular copper(I)-catalyzed [2 + 2] photocycloaddition reactions of nonconjugated alkenes were recently achieved efficiently in an ammonium salt-based room-temperature ILs such as

trimethyl(butyl)ammonium bis(trifluoromethylsulfonyl)imide (tmba-NTf_2). The IL, tmba-NTf_2, is transparent at the irradiation wavelengths and was quite stable under the irradiation conditions, and was easily recovered and recycled. In contrast, no cycloadduct could be isolated when the same reaction was carried out under the identical irradiation conditions in bmim-NTf_2, which absorbs the UV light to suffer extensive photodecomposition.[54] Intramolecular photocycloaddition of 1,6-diene (**87**) smoothly proceeded in bmim-NTf_2 in yields comparable to those obtained in diethyl ether. Intermolecular [2 + 2] photocycloaddition in tmba-NTf_2 was found to proceed in an even better yield than in conventional organic solvents. Thus, the photoirradiation of bicyclopentadiene and norbornene in IL produced the corresponding dimers in 71% and 90% yield, respectively. The irradiation of cyclopentene derivative (**89**) under the same conditions gave a 8:1 mixture of head-to-tail *cis-anti-cis* cycloadduct (**90**) and its diastereomer in 56% combined yield.

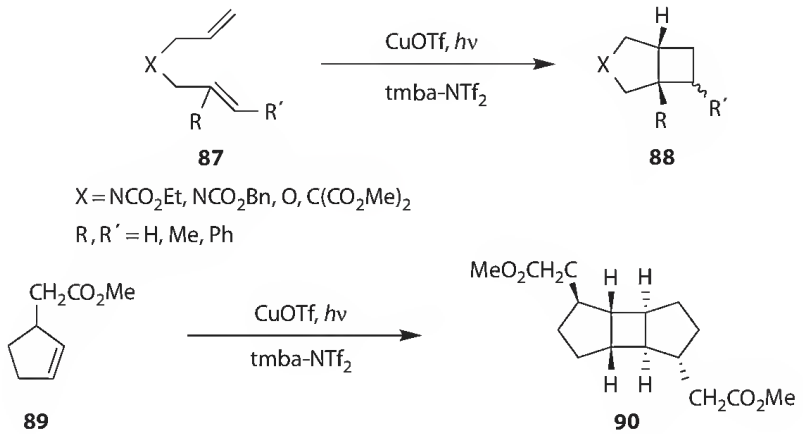

Arenediazonium tetrafluoroborate salts (**91**) underwent the nucleophilic substitution followed by the dediazoniation upon photolysis in bmin-NTf_2 to predominantly give the oxy anion quenching products (**92**) in good yields, together with small amounts of Schiemann reaction product (**93**) and bis(trifluoromethylsulfonyl)imide (**94**).[55] Despite the nonnucleophilic and noncoordinating nature of NTf_2 anion, the nucleophilic attack occurred predominantly at the *O*-atom of NTf_2 anion, while the Schiemann reaction was a minor pathway in this IL. On the contrary, the Schiemann reaction of imidazole derivatives (**96**) was reported to occur efficiently in bmim-BF_4. The use of bmim-BF_4 dramatically improved the yield of the fluorodediazoniation product (**97**). Careful temperature control at 0°C was shown to be essential to minimize the photodecomposition of the IL.[56]

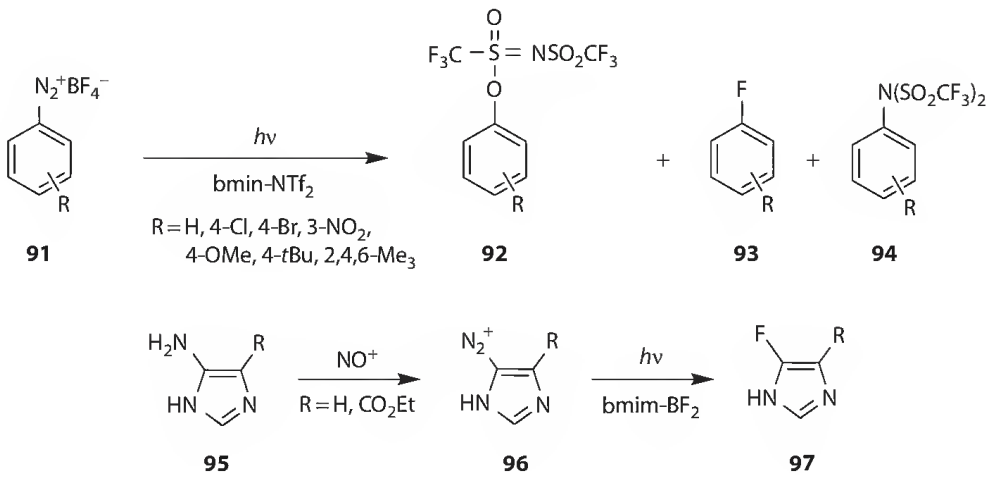

The photochemistry of chiral (salen)aluminum(III) chloride complex (**98**) has been studied in imidazolium ILs (bmim-BF_4 or PF_6). The ILs particularly stabilized the (saren)Al(II) radicaloid species (**99**) generated by the homolysis of the Al–Cl bond. The half-life of this species varied depending on the solvent, indicating that the counteranion of IL played an important role by changing the IL's polarity and viscosity to affect the lifetimes of the singlet excited state of pentacoordinated salen Al(III) and of the Al(II) radicaloid intermediate.[57]

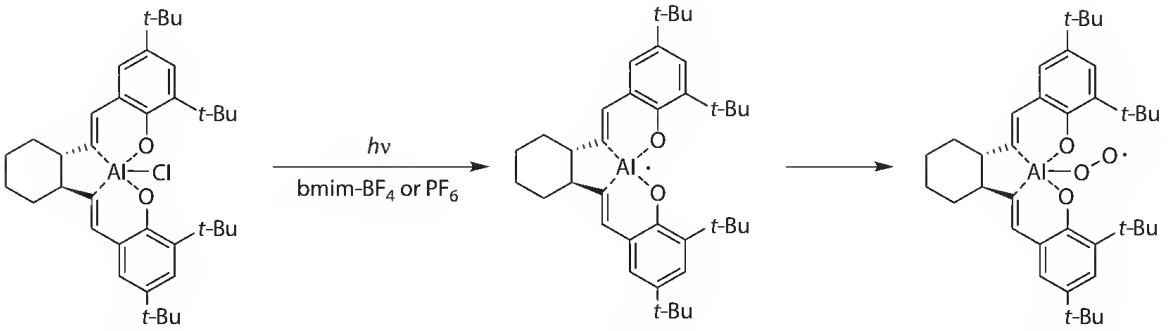

98 **99** **100**

The 1-methylimidazole-containing triplet photosensitizers (**103** and **104**) were designed and synthesized in order to enhance the solubility in room-temperature ILs. The photosensitized isomerization of *trans*- to *cis*-β-ionol (**101** and **102**) was efficiently carried out in bmim-BF_4 and the sensitizer/IL mixture was reusable. These sensitizers remained in the IL layer when the solution was extracted with organic solvent.[58]

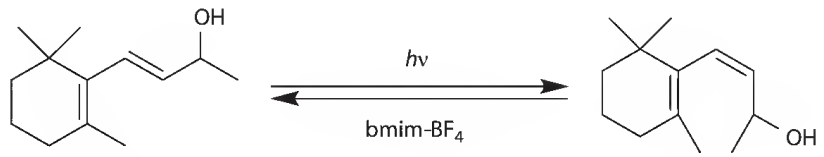

101 **102**

Sensitizers =

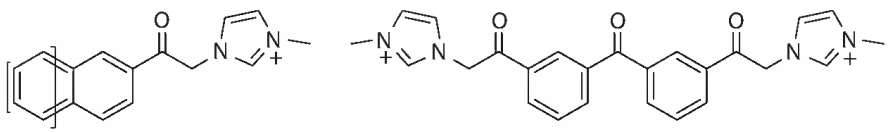

103 **104**

Chiral ILs are particularly attractive in view of their potential ability of chiral recognition and discrimination, which is applicable to asymmetric synthesis and optical resolution. Recently, several chiral ILs (**107**–**110**) have been used as chiral solvents for the enantiodifferentiating photoisomerization of dibenzobicyclo[2.2.2]octatriene diacid (**105**). The enantioselectivities obtained (3%–12%), though modest in an absolute sense, are the highest values reported so far for a unimolecular photochemical reaction performed in chiral IL. The chiral induction was attributed to the ion-pairing interaction of the deprotonated diacid with the IL cation.[59]

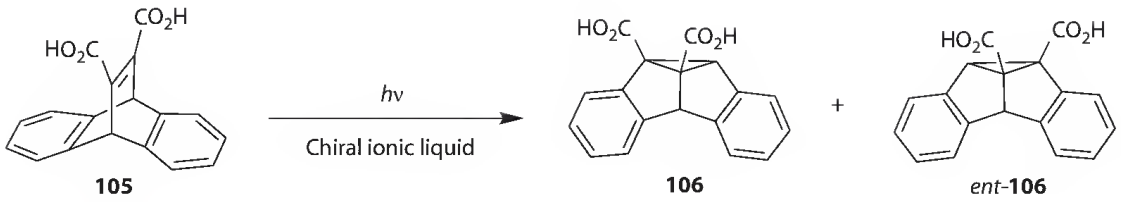

105 **106** *ent*-**106**

Chiral ionic liquids:

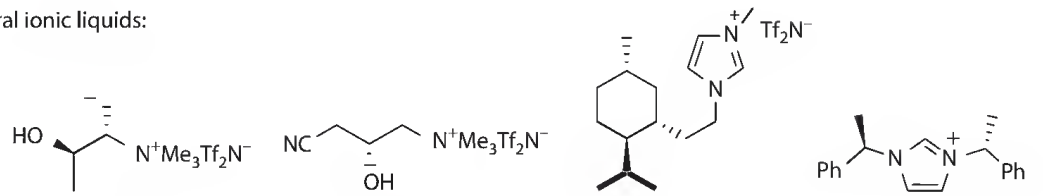

107 **108** **109** **110**

A large magnetic field effect on the photoinduced hydrogen abstraction reaction of benzophenone with thiophenol was reported in the ammonium, pyrrolidinium, and piperidinium ILs.[60] Interestingly, the effect of magnetic field was not straightforward[61]; the yield of escaped benzophenone ketyl radical gradually decreased by applying the magnetic field of up to 2 T, then reached a terrace at 2–10 T, and again decreased at 10–28 T to eventually afford a 25% reduced yield at 28 T, indicating the operation of more than one mechanism for the ketyl radical.

An IL–organic solvent–water ternary system, consisting of 1-tetradecyl-3-methylimidazolium bromide (tmim-Br), *p*-xylene, and water, was employed for the photodimerization of 9-substituted anthracenes (**111**). The ternary system forms hexagonal and lamellar liquid crystals as well as microemulsions. These organized media were effective in solubilizing and preorientating the anthracene derivatives with a polar 9-substituent, and thus enhanced the formation of head-to-head cyclodimer (**112**).[62] Fluorescence resonance energy transfer study from coumarin 480 to rhodamine was also reported in microemulsions comprised of pmim-BF_4 (1-pentyl-3-methylimidazolium tetrafluoroborate) in a mixture of TX-100 and benzene with and without added water.[63]

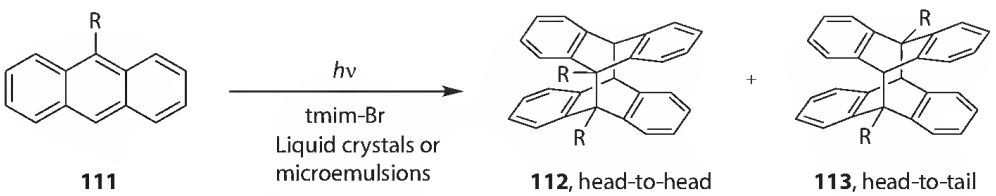

111 **112**, head-to-head **113**, head-to-tail

R = $CH_2N^+Me_3Br^-$, CH_2CO_2Na, CH_2OH,
CO_2H, CHO, COMe, Me

Choosing the proper IL for specific photochemical reaction is encouraged, since the IL used as a solvent is frequently involved in the photoreaction. For instance, the photochemistry of IL investigated by femtosecond pump-probe absorption spectroscopy revealed that, in addition to the generation of solvated electron, di- and trihalide ions are formed upon continuous irradiation of halide-containing ILs (bmim-I or hmim-Cl).[64] It is also to note that the diffusion coefficient of diiodide anion radical in ILs becomes much larger than that in conventional organic solvents, due to the Coulomb interaction between diiodide and IL cation.[65]

11.5 Photochemistry in Microemulsions, Micelles, Vesicles, and Dendrimer Voids

Reverse micelles and water-in-oil microemulsions are microscopic spherical pools of water surrounded by a monolayer of surfactant separating the water pool from the hydrophobic bulk solution. The sensitized photooxidation via the $^1O_2$ has been extensively investigated in such media. Thus, the photooxidation of glycyl-glycine sensitized by water-soluble anthraquinone derivatives was investigated in the micelles and microemulsions of sodium bis(2-ethylhexyl) sulfosuccinate.[66] The formation of semiquinone radicals in the photosensitized oxidation of hydroquinone substrates was also studied in the reverse micelle.[67] The photooxidation of γ,δ-unsaturated ketone was investigated in microemulsion and in homogeneous solution and the results were compared. The photooxidation of homoallylic substrate **114** in acetonitrile or acetone gave tertiary hydroperoxide (**116**) and 3-hydroxy-1,2-dioxane (**117**) as the major products, while dioxane **117** and epoxide (**118**) were obtained in sodium dodecyl sulfate microemulsion, both of which were the secondary products derived from the allylic hydroperoxides (**115** and **116**)[68] Diastereoselectivity of the singlet photooxidation of mesitylol was also examined in microemulsions.[69]

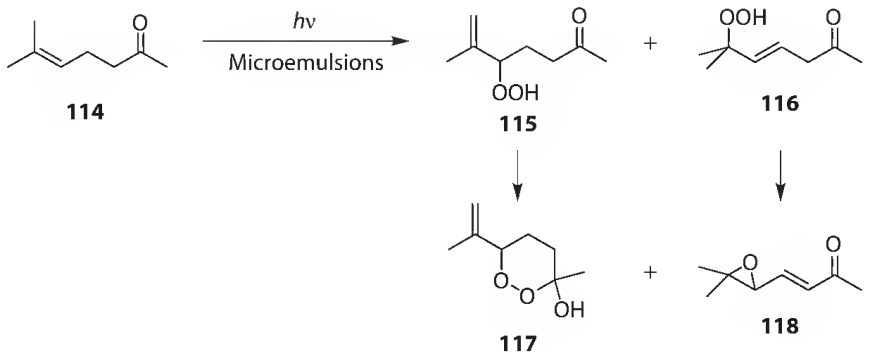

114 **115** **116** **117** **118**

The photosensitized oxidation of several olefins was also investigated in mixed surfactant vesicles. In the photosensitized oxidation of (*E*)-stilbene and (*E,E*)-1,4-diphenyl-1,3-butadiene in vesicles, the corresponding 1,2-dioxetanes were formed in quantitative yields, which is in sharp contrast to the oxidation in homogeneous solution where the [4 + 2] cycloaddition product of singlet oxygen to the diene was the sole product. It is interesting to note that $^1O_2$ generated in the bilayer or the inner water pool of a vesicle is able to diffuse out and enter into the bilayer of another vesicle through the outer aqueous phase and reacts with the target molecules.[70] The singlet oxygenation of α-pinene was also investigated in vesicles.[71] The selectivity of oxygenation in mixed surfactant vesicles was controlled by changing the location of the substrate and sensitizer molecules in the reaction media.[72] The quantum yield of $^1O_2$ upon photosensitization with palladium bacteriopheophorbide, a potential reagent for vascular targeted photodynamic therapy, was almost unity in organic solvents, but only ca. 0.5 in micelles and vesicles, where superoxide and hydroxyl radicals are formed in a minimal quantum yield of 0.1%. Analysis of the photoproducts suggests that the formation of oxygen radicals involves both electron and proton transfer from the pheophorbide at the membrane/water interface to a colliding oxygen molecule, consequently forming superoxide, then hydrogen peroxide, and finally hydroxyl radicals.[73]

The photoisomerization of (*E*)-stilbene (**119**) was studied in microemulsions composed of Triton X-100, 1-pentanol, and water in different ratios. The yield of (*Z*)-stilbene (**120**) increased with the increase of water content or with the decrease of Triton X-100 content, and the oil-in-water structure

was found most suitable for the photoisomerization.[74] (*E*)-1-(4-Methoxyphenyl)propene (anethole, **121**) was employed as a substrate in the study of photochemical behavior in microemulsions, as this substrate undergoes spontaneous emulsification without adding external surfactants.[75] Thus, the photochemical behavior of microemulsions obtained upon dilution of ethanolic solutions of anethole (**121**) with water was compared with that of homogeneous ethanolic solutions of the substrate. The photolysis of **121** afforded the (*Z*)-isomer (**122**) and cyclodimers (**123–125**), along with the oxidation and/or solvolysis products (**126–128**). Significant differences in reactivity were observed in both media, as the yields of isomerization (**122**) and dimerization (**123–125**) were considerably reduced in microemulsions. In contrast to the photoreaction in homogeneous solutions, where the (*Z*)-rich photostationary state (ca. 80%) was reached rapidly, the proportion of (*Z*)-isomer upon irradiation of anethole microemulsions remained below 15%. In the presence of oxygen, the formation of anethole oxide was observed, which further underwent polymerization in the aggregated microemulsion of anethole. The lower photoreactivity of anethole in microemulsions was interpreted in terms of the faster nonradiative decay due to faster internal conversion.

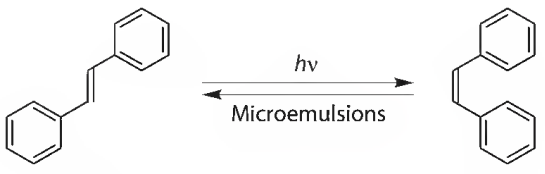

119 **120**

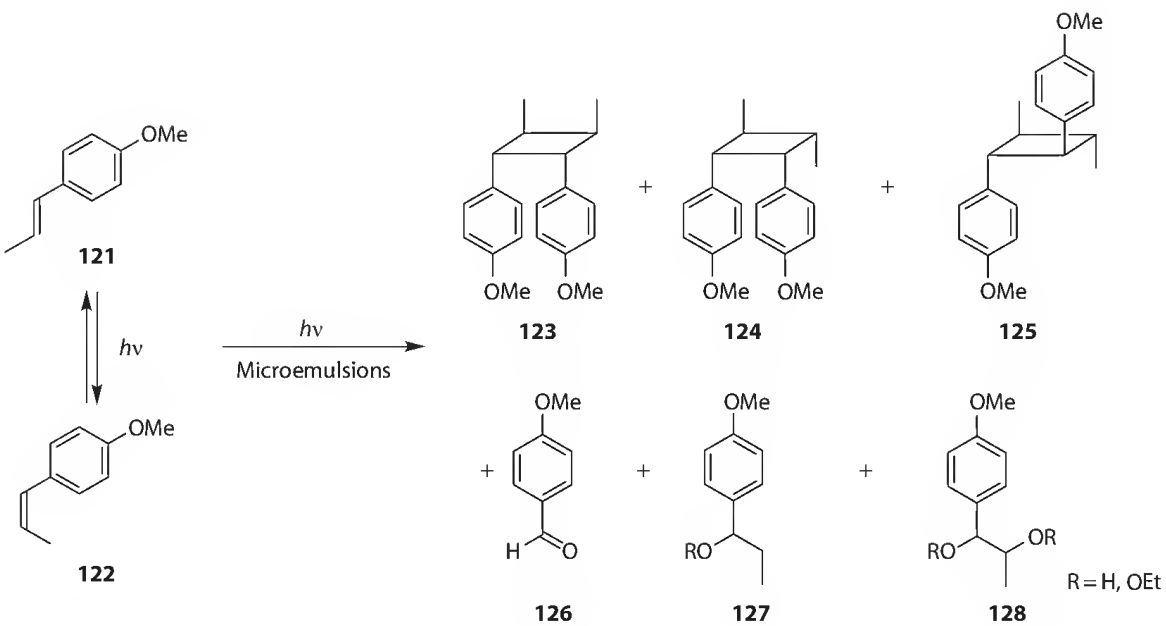

Photosensitizing surfactants (**132** and **136**) have been employed for the polar addition of indene (**129**) and 1,1-diphenylethene (**133**) in oil-in-water emulsion. These photosensitizing surfactants were shown to work more efficiently in microemulsion (in water) than in homogeneous organic solvent.[76] Although the reaction of indene in an oil-in-water emulsion proceeded efficiently to give the corresponding alcohol as a major product, the yield reported was strongly influenced by the size of oil droplet.[77]

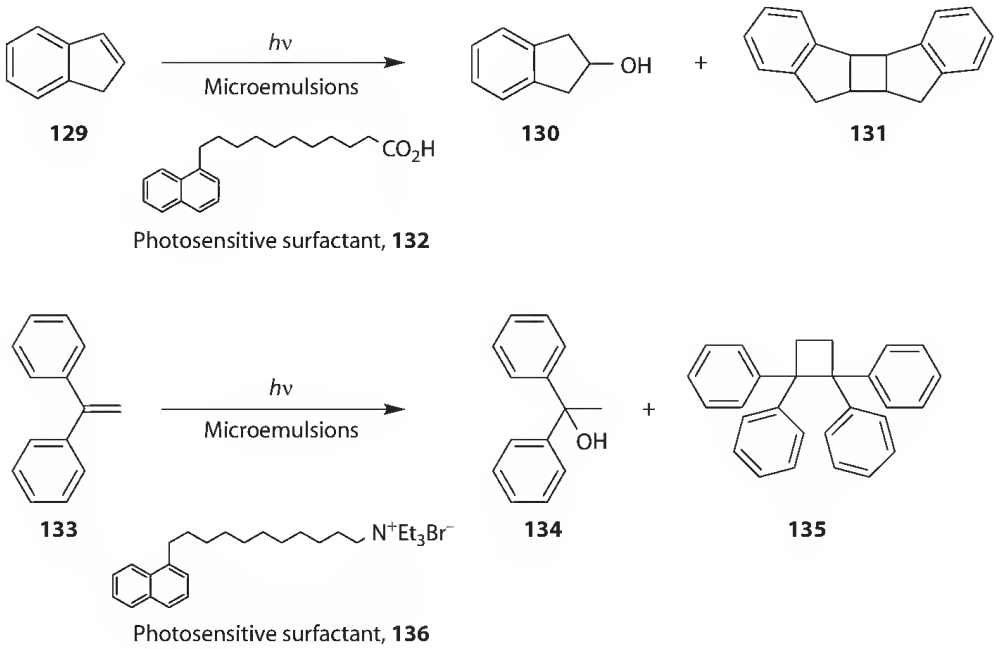

The photocycloaddition of 9-substituted anthracenes (**111**) has been investigated in water-in-oil microemulsions prepared from sodium bis(2-ethylhexyl) sulfosuccinate, dichloromethane, and water. While irradiation of the aforementioned substrates in isotropic media afforded the corresponding head-to-tail photocyclodimer (**113**) as the major product, photoirradiation in the microemulsion almost exclusively yielded the head-to-head dimer (**112**). These observations were interpreted in terms of the preorientation of the substrate molecules at the interface of the water pool in the microemulsions.[78] The reductive photodebromination of polybrominated diphenyl ethers was investigated in nonionic surfactant micelles.[79] Photoinduced electron transfer from zinc tetraphenylporphyrin was studied in nonaqueous microemulsions composed of *n*-heptane, sodium bis(2-ethylhexyl) sulfosuccinate, and ethylene glycol.[80] The thermodynamics and kinetics of photoinduced electron transfer in bacterial photosynthetic reaction centers were also investigated in micelles and vesicles formed from different phospholipids of physiological importance.[81]

Water-soluble poly(alkyl aryl ether) dendrimers (**137**) have been extensively explored for their use as hosts of organic substrates in aqueous media. The photo-Fries reactions of 1-naphthyl benzoate and phenyl ester as well as the α-cleavage reactions of dibenzyl ketones and benzoin alkyl ethers in voids of dendrimers have been examined.[82] The photolysis of 1-phenyl-3-*p*-tolyl-propan-2-one and benzoin ethyl ether as well as the photodimerization of acenaphthylene was investigated in voids of different types of dendrimers.[83] It was demonstrated that the dendrimer can encapsulate the substrate, intermediates, and products in its voids and restricts the mobility of radical intermediates. Comparative studies of the same photoreaction in micellar media demonstrated that dendritic media offers much better constraint than the micelles.

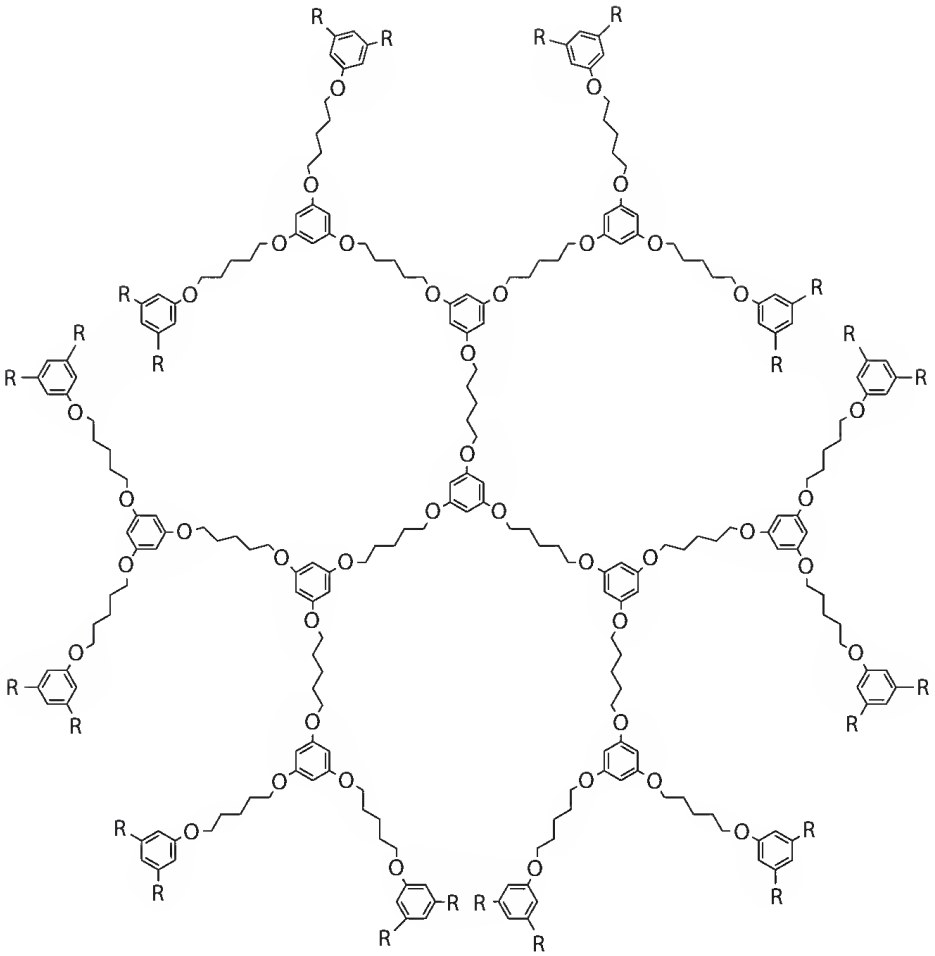

Typical dendrimers for microenvironment: R = OH, CO_2H, CO_2Me

137

11.6 Photochemistry in Liquid Crystals and Organogels

A number of investigations have been carried out to induce the chirality into liquid crystals by means of photochemical procedures and the representative results have recently been reviewed.[84] In this chapter, we focus on the photochemistry of molecules inside the liquid crystals as media, but will not refer to the photochemistry and photophysics of the liquid crystal itself.

The charge separation and recombination processes in a carotenoid–porphyrin–fullerene triad, as a mimic of the photosynthetic reaction center, have been studied in the different phases of two uniaxial liquid crystals.[85] The effects of orientation on the electronic coupling element of the molecular triad in liquid crystal were interpreted by the simulations of the EPR spectra of the carotenoid triplet state, which can be useful in designing a better model system with an optimized charge separation efficiency.

Lyotropic liquid crystals have been used as media for the photochemical inter- and intramolecular hydrogen abstraction of cyclohexyl phenyl ketone (**138**) to afford α-cyclohexylbenzyl alcohol (**139**) and 1-phenyl-6-hepten-1-one (**140**). The efficiency of the photoreaction was much higher in the liquid crystals than in hexane solution. The ratio of intra- and intermolecular products (**140**/**139**) was found to be 30:1 in 1-propanol but less than 3:1 in both lamellar and hexagonal liquid crystals, showing that the intramolecular reaction is greatly hampered in the liquid crystals. Studies on the product distribution

in the absence and presence of electron donors revealed that liquid crystals not only restrict the motion of the substrate and intermediates but also keep the substrate and electron donor together during the photoreaction. A comparison with the same reaction in sodium dodecyl sulfate micelle indicated that the liquid crystal provides a better constraint for the reaction.[86] The chiral induction in **139** obtained upon irradiation with prolinol, ephedrine, and their derivatives added as chiral inductor turned out to be inefficient, affording as low as 4%–5% ee.

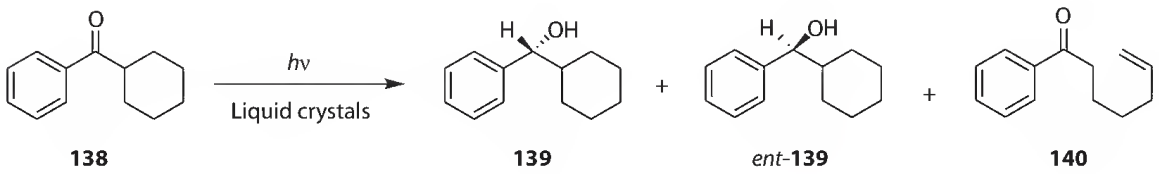

138 **139** *ent*-**139** **140**

Photochemistry of tropolone methyl ether **141** (R = Me) has been examined in lyotropic liquid crystals in the presence of chiral inductor. Anisotropic hexagonal liquid crystals significantly induced the chirality in the photoelectrocyclization of the tropolone methyl ether better than lamellar liquid crystals. Thus, norephedrine was able to give the major product **142** (R = Me) in 40% ee, when the reaction was performed in the hexagonal liquid crystals. The photoreaction of chiral tropolone ether **141** (R = 2-methylbutyl) was also performed in the presence of an additional chiral inductor in liquid crystals. It was shown that norephedorin and prolinol are effective in the hexagonal liquid crystals, both affording **142** in 35% de.[87] The partially rigid environment of liquid crystals was considered to prevent the dissociation of the substrate–inductor complex, enhancing the stereoselectivity of the photoproducts.

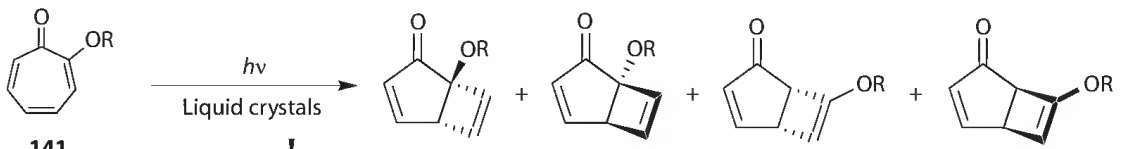

141 **142** *ent*-**142** **143** *ent*-**143**

The photodimerization of 2-anthracenecarboxylic acid (**144**) has been studied in the presence of the amphiphilic amino alcohol (**149**) in the liquid-crystalline medium. The photoreaction was comparatively studied in two smectic and isotropic phases. The two smectic phases were found to show acceptable reactivity to give a mixture of the corresponding dimers (**145**–**148**) in 23%–55% yield upon photoirradiation, while 87% of the starting material was consumed in the isotropic phase under the similar conditions except for the phase and temperature. These and related observations indicated that the liquid-crystalline phases are superior to the crystalline phase in view of reaction probability. Quite interestingly, the regioselectivity (head-to-head versus head-to-tail ratio) of the photodimerization changed dramatically depending on the phase, and the head-to-head dimers were obtained exclusively in both of the smectic phases, demonstrating the peculiar property of liquid crystals as constrained reaction media. The liquid-crystalline media also offer better environments for chiral induction.[88] The photodimerization of 1-anthracenecarboxylic acid (**150**) was also investigated in the liquid-crystalline medium. The reaction proceeded with an excellent regioselectivity to give the head-to-head dimers exclusively. The moderate diastereoselectivity (*anti*/*syn* ratio) of 24% was reported for the dimers **151** and **152**, but the ee of the *anti* head-to-head product **151** was quite unsatisfactory (2% ee).

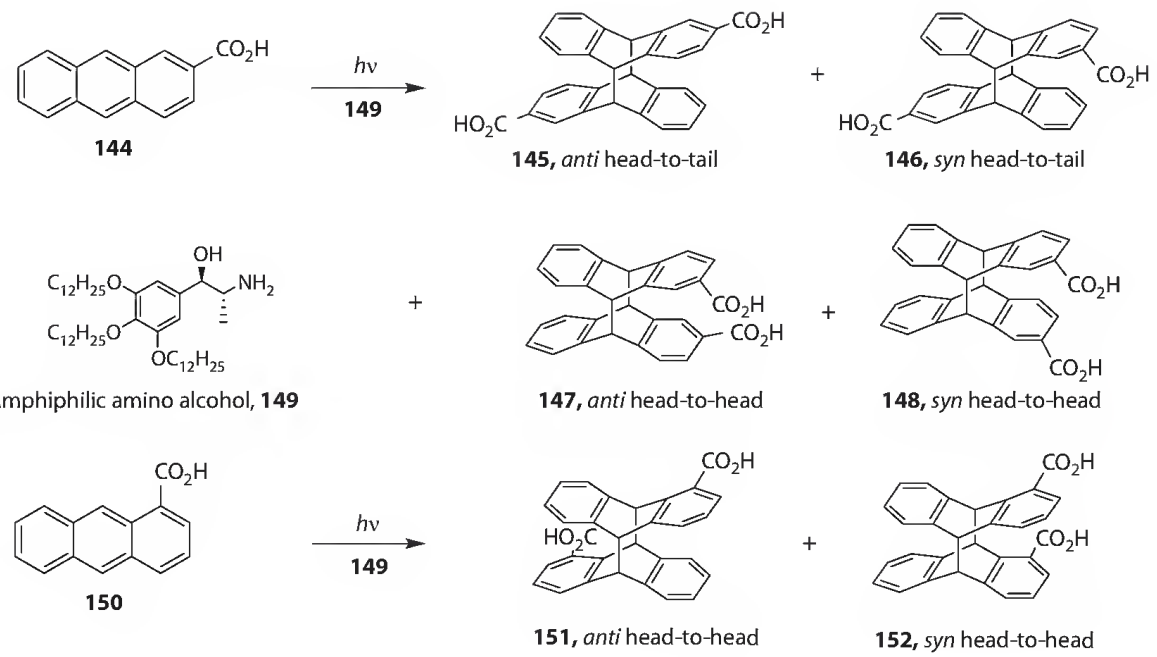

The D-alanine derivative possessing a 3,4,5-tris(*n*-dodecyloxy)benzamide moiety (**153**) was found to be an efficient gelator for nonpolar solvents such as cyclohexane. The photocyclodimerization of 2-anthracenecarboxylic acid (**144**) in the gel matrix was highly stereoselective, exclusively affording the head-to-head photodimers (**147** and **148**). This is in contrast to the results in isotropic media. Unfortunately, the enantioselectivity induced by the chiral gelator was poor (10% ee).[89] The several other gelators containing a 3,4,5-tris(*n*-dodecyloxy)benzoylamide backbone have been developed and their photochemistry was explored.[90]

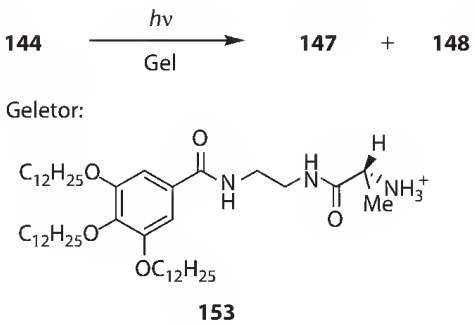

The organogels have been also employed as media for photochromic systems, and the photochromic behavior of a variety of benzopyranindolines was studied in organogels.[91] The lifetime of the colored photomerocyanine with a succinyl ester functionality was found to be increased by a factor of >300 in the organogel derived from 4-*tert*-butyl-1-phenylcyclohexanol.

11.7 Conclusions

In this concise review of the photochemistry in alternative media, we overview the recent exploration of a variety of photoreactions in the nonconventional media.

Supercritical fluids are used as media that provide much efficient diffusion of the reactant and intermediate than in the conventional organic solvents. This usually facilitates the efficiency of bimolecular

reaction, but the most striking features of the supercritical fluids are found in the near-critical region, that is, the transition region from gas phase to supercritical phase. The effect was explained by the specific clustering to the solute of medium molecules in the near-critical region. Although the usefulness of such peculiar phenomena on the control of stereo- and regioselective photoreaction is evident, the detailed mechanism remains to be elucidated.

Polymer films can be employed to provide the passive voids for organic molecules. In contrast to the well-defined, solid cages of zeolites, for example, the passive voids usually restrict the motion and conformational changes of the reactant and intermediate within the voids, as the initial free volume of the cavity tends to be smaller than the species considered. This, of course, affects the reactivity and selectivity of the photoreaction. Therefore, the choice of the proper polymer films, in terms of the free volume, shape, wall stiffness, and permeability of the void modulated by the stretching of the films, may provide the best (or at least better) cavities for the desired photoreactions. It is rather unanticipated and hence emphasized that the cavities are templated or memorized for some period of time, even after releasing the initial substrate, and the secondary reactions within the cavities are shown to be controlled by the templated or memorized shape of the voids.

ILs are distinctive and valuable media for a variety of reactions, as they possess charges and are relatively viscous. The typical room-temperature ILs, such as alkylmethylimidazolium salts, have been employed as media for several photoreactions, but precaution should be excersized to avoid the photodecomposition of the ILs themselves by choosing the irradiation wavelength. The photoinduced electron transfer in ILs has been most extensively studied, as the ionic character as well as the viscosity of the media stabilize the radical ion pairs and alter the rates of electron transfer and recombination processes. The control of other types of photoreactions has been also explored.

Other types of less-defined cavities such as microemulsions, micelles, vesicles, and voids in dendrimers, liquid crystals, and organogels have been also exploited for a range of photochemical reactions. Although none of them becomes an exclusive general approach for controlling photochemical outcomes, the alternative media can be fairly attractive when chosen properly for the specific photoreactions.

References

1. Tung, C.-H., Wu, L.-Z., Zhang, L.-P., Chen, B., Supramolecular systems as microreactors: Control of product selectivity in organic phototransformation, *Acc. Chem. Res.* 36, 39–47 (2003).
2. Brennecke, J. F., Chateauneuf, J. E., Homogeneous organic reactions as mechanistic probes in supercritical fluids, *Chem. Rev.* 99, 433–452 (1999).
3. Worrall, D. R., Abdel-Shafi, A. A., Wilkinson, F., Factors affecting the rate of decay of the first excited singlet state of molecular oxygen $O_2(a^1\Delta_g)$ in supercritical fluid carbon dioxide, *J. Phys. Chem. A* 105, 1270–1276 (2001).
4. Bourne, R. A., Han, X., Chapman, A. O., Arrowsmith, N. J., Kawanami, H., Poliakoff, M., George, M. W., Homogeneous photochemical oxidation via singlet O_2 in supercritical CO_2, *Chem. Commun.* 7, 4457–4459 (2008).
5. Pacut, R., Grimm, M. L., Kraus, G. A., Tankoa, J. M., Photochemistry in supercritical carbon dioxide. The benzophenone-mediated addition of aldehydes to α,β-unsaturated carbonyl compounds, *Tetrahedron Lett.* 42, 1415–1418 (2001).
6. Chateauneuf, J. E., Zhang, J., Foote, J., Brink, J., Perkovic, M. W., Photochemical fixation of supercritical carbon dioxide: The production of a carboxylic acid from a polyaromatic hydrocarbon, *Adv. Environ. Res.* 6, 487–493 (2002).
7. Forbes, M. D. E., Yashiro, H., Initiator addition to methyl methacrylate studied in liquid and supercritical carbon dioxide, *Macromolecules* 40, 1460–1465 (2007).
8. Fazekas, Z., Yamamura, T., Park, Y.-Y., Harada, M., Tomiyasu, H., Photochemistry of uranyl(VI) tributylphosphate in supercritical CO_2: An evidence of photochemical reduction by ethanol, *Chem. Lett.* 29, 30–31 (2000).

9. Hirakawa, T., Whitesell, J. K., Fox, M. A., Effect of temperature and pressure in the photocatalytic oxidation of *n*-octanol on partially desilanized hydrophobic TiO_2 suspended in aerated supercritical CO_2, *J. Phys. Chem. B* 108, 10213–10218 (2004).
10. Nishiyama, Y., Kaneda, M., Saito, R., Mori, T., Wada, T., Inoue, Y., Enantiodifferentiating photoaddition of alcohols to 1,1-diphenylpropene in supercritical carbon dioxide: Sudden jump of optical yield at the critical density, *J. Am. Chem. Soc.* 126, 6568–6569 (2004).
11. Nishiyama, Y., Wada, T., Mori, T., Inoue, Y., Critical control by temperature and pressure of enantiodifferentiating anti-Markovnikov photoaddition of methanol to diphenylpropene in near critical and supercritical carbon dioxide, *Chem. Lett.* 36, 1488–1489 (2007).
12. Nishiyama, Y., Kaneda, M., Asaoka, S., Saito, R., Mori, T., Wada, T., Inoue, Y., Mechanistic study on the enantiodifferentiating anti-Markovnikov photoaddition of alcohols to 1,1-diphenyl-1-alkenes in near-critical and supercritical carbon dioxide, *J. Phys. Chem. A* 111, 13432–13440 (2007).
13. Nishiyama, Y., Wada, T., Asaoka, S., Mori, T., McCarty, T. A., Kraut, N. D., Bright, F. V., Inoue, Y., Entrainer effect on photochirogenesis in near- and supercritical carbon dioxide: Dramatic enhancement of enantioselectivity, *J. Am. Chem. Soc.* 130, 7526–7527 (2008).
14. Saito, R., Kaneda, M., Wada, T., Katoh, A., Inoue, Y., First asymmetric photosensitization in supercritical fluid. Exceptionally high pressure/density dependence of optical yield in photosensitized enantiodifferentiating isomerization of cyclooctene, *Chem. Lett.* 31, 860–861 (2002).
15. Portius, P., Yang, J., Sun, X.-Z., Grills, D. C., Matousek, P., Parker, A. W., Towrie, M., George, M. W., Unraveling the photochemistry of $Fe(CO)_5$ in solution: Observation of $Fe(CO)_3$ and the conversion between $^3Fe(CO)_4$ and $^1Fe(CO)_4$(solvent), *J. Am. Chem. Soc.* 126, 10713–10720 (2004).
16. Besora, M., Carreón-Macedo, J. L., Cowan, A. J., George, M. W., Harvey, J. N., Portius, P., Ronayne, K. L., Sun, Z.-Z., Towrie, M., A combined theoretical and experimental study on the role of spin states in the chemistry of $Fe(CO)_5$ photoproducts, *J. Am. Chem. Soc.* 131, 3583–3592 (2009).
17. Sun, X. Z., Nikiforov, S. M., Dedieu, A., George, M. W., Photochemistry of $[CpMo(CO)_3]_2$ (Cp = η^5-C_5H_5) and $[Cp^*Fe(CO)_2]_2$ (Cp^* =η^5-C_5Me_5) in supercritical CO_2: A fast time-resolved infrared spectroscopic study, *Organometallics* 20, 1515–1520 (2001).
18. Hoijemberg, P. A., Zerbs, J., Japas, M. L., Chesta, C. A., Schroeder, J., Aramendi, P. F., Cage effect in supercritical fluids and compressed gases in the photolysis of an asymmetrically substituted diazene, *J. Phys. Chem. A* 113, 5289–5295 (2009).
19. Bitterwolf, T. E., Kline, D. L., Linehan, J. C., Yonker, C. R., Addleman, R. S., Photochemical carbonylation of ethane under supercritical conditions, *Angew. Chem. Int. Ed.* 40, 2692–2694 (2001).
20. Fukuda, T., Watabe, N., Whitby, R., Maekawa, T., Creation of carbon onions and coils at low temperature in near-critical benzene irradiated with an ultraviolet laser, *Nanotechnology* 18, 415604/1–415604/6 (2007).
21. Gu, W., Hill, A. J., Wang, X., Cui, C., Weiss, R. G., Photorearrangements of five 1- and 2-naphthyl acylates in three unstretched and stretched polyethylene films. Does reaction selectivity correlate with free volumes measured by positron annihilation lifetime spectroscopy? *Macromolecules* 33, 7801–7811 (2000).
22. Gu, W., Weiss, R. G., Photo-Fries rearrangements of phenyl phenylacylates in polyethylene films. Comparison of reactivity and selectivity with 1-naphthyl phenylacylates, *J. Org. Chem.* 66, 1775–1780 (2001).
23. Xu, J., Weiss, R. G., Enantioselectivity of prochiral radical-pair recombinations. Reaction cavity differentiation in polyethylene films, *Org. Lett.* 5, 3077–3080 (2003).
24. Bhattacharjee, U., Chesta, C. A., Weiss, R. G., Temperature-dependent cage effects from triplet radical pairs generated upon irradiation of 1-(4-methylphenyl)-3-phenyl-2-propanone in polyethylene films, *Photochem. Photobiol. Sci.* 3, 287–295 (2004).
25. Chesta, C. A., Mohanty, J., Nau, W. M., Bhattacharjee, U., Weiss, R. G., New insights into the mechanism of triplet radical-pair combinations. The persistent radical effect masks the distinction between in-cage and out-of-cage processes, *J. Am. Chem. Soc.* 129, 5012–5022 (2007).

26. Gu, W., Warrier, M., Schoon, B., Ramamurthy, V., Weiss, R. G., Understanding the influence of active (zeolite) and passive (polyethylene) reaction cages on photo-Claisen rearrangements of aryl benzyl ethers, *Langmuir* 16, 6977–6981 (2000).
27. Xu, J., Weiss, R. G., Combinations of chiral and prochiral singlet radical-pairs in reaction cavities of polyethylene films. Control and analysis of radical tumbling and translation, *Photochem. Photobiol. Sci.* 4, 348–358 (2005).
28. Mori, T., Inoue, Y., Weiss, R. G., Enhanced photodecarboxylation of an aryl ester in polyethylene films, *Org. Lett.* 5, 4661–4664 (2003).
29. Mori, T., Weiss, R. G., Inoue, Y., Mediation of conformationally controlled photodecarboxylations of chiral and cyclic aryl esters by substrate structure, temperature, pressure, and medium constraints, *J. Am. Chem. Soc.* 126, 8961–8975 (2004).
30. Chen, Y.-Z., Weiss, R. G., Photoreactions of substituted *o*-cresyl acylates in cyclohexane and in polyethylene films. The influences of intra- and inter-molecular crowding effects, *Photochem. Photobiol. Sci.* 8, 916–925 (2009).
31. Gu, W., Bi, S., Weiss, R. G., Photo-Fries rearrangements of 1-naphthyl esters in the glassy and melted states of poly(vinyl acetate). Comparisons with reactions in less polar polymers and low-viscosity solvents, *Photochem. Photobiol. Sci.* 1, 52–59 (2002).
32. Arumugam, S., Kaanumalle, L. S., Ramamurthy, V., Alkali ion exchanged Nafion as a confining medium for photochemical reactions, *Photochem. Photobiol.* 82, 139–145 (2006).
33. Arumugam, S., Nafion as an efficient reaction medium for diastereoselective photochemical reactions, *Tetrahedron Lett.* 49, 2461–2465 (2008).
34. Li, X.-H., Wu, L.-Z., Zhang, L.-P., Tung, C.-H., Controlled photocyclization, photodimerization, and photoisomerization of stilbazole salts within Nafion membranes, *Org. Lett.* 4, 1175–1177 (2002).
35. Pagni, R. M., An overview of photochemistry in ionic liquids, in *ACS Symposium Series 856 (Ionic Liquids as Green Solvents)*, 344–356 (2003). Gordon, C. M., Photochemistry in ionic liquids, in *NATO Science Series, II: Mathematics, Physics and Chemistry 92 (Green Industrial Applications of Ionic Liquids), 365–383* (2003). Gordon, C. M., McLean, A. J., Muldoon, M. J., Dunkin, I. R., Photochemistry in ionic liquids, in *ACS Symposium Series 818 (Ionic Liquids)*, 428–443(2002).
36. Pagni, R. M., Gordon, C. M., Photochemistry in ionic liquids, In: *CRC Handbook of Organic Photochemistry and Photobiology* (2nd edn), CRC Press, Boca Raton, FL, pp. 5/1–5/21 (2004).
37. Álvaro, M., Ferrer, B., García, H., Narayana, M., Screening of an ionic liquid as medium for photochemical reactions, *Chem. Phys. Lett.* 362, 435–440 (2002).
38. Zhu, G., Xu, J., Wu, G., Zhu, H., Long, D., Chen, S., Yao, S., Laser photolysis study of anthraquinone in binary mixtures of ionic liquid [bmim][PF_6] and organic solvent, *Int. J. Mol. Sci.* 7, 590–600 (2006).
39. Zhu, G., Wu, G., Sha, M., Long, D., Yao, S., Effects of ionic liquid [bmim][PF_6] on absorption spectra and reaction kinetics of the duroquinone triplet state in acetonitrile, *J. Phys. Chem. A* 112, 3079–3085 (2008).
40. Vieira, R. C., Falvey, D. E., Photoinduced electron-transfer reactions in two room-temperature ionic liquids: 1-Butyl-3-methylimidazolium hexafluorophosphate and 1-octyl-3-methylimidazolium hexafluorophosphate, *J. Phys. Chem. B* 111, 5023–5029 (2007).
41. Paul, A., Samanta, A., Photoinduced electron transfer reaction in room temperature ionic liquids: A combined laser flash photolysis and fluorescence study, *J. Phys. Chem. B* 111, 1957–1962 (2007).
42. Vieira, R. C., Falvey, D. E., Solvent-mediated photoinduced electron transfer in a pyridinium ionic liquid, *J. Am. Chem. Soc.* 130, 1552–1553 (2008).
43. Alvaro, M., Carbonell, E., Ferrer, B., Garcia, H., Herance, J. R., Ionic liquids as a novel medium for photochemical reactions. $Ru(bpy)_3^{2+}$/viologen in imidazolium ionic liquid as a photocatalytic system mimicking the oxido-reductase enzyme, *Photochem. Photobiol.* 82, 185–190 (2006).
44. Lockard, J. V., Wasielewski, M. R., Intramolecular electron transfer within a covalent, fixed-distance donor-acceptor molecule in an ionic liquid, *J. Phys. Chem. B* 111, 11638–11641 (2007).

45. Chakrabarty, D., Chakraborty, A., Hazra, P., Seth, D., Sarkar, N., Dynamics of photoisomerization and rotational relaxation of 3,3′-diethyloxadicarbocyanine iodide in room temperature ionic liquid and binary mixture of ionic liquid and water, *Chem. Phys. Lett.* 397, 216–221 (2004).
46. Fernandez, D., Parola, A. J., Branco, L. C., Afonso, C. A. M., Pina, F., Thermal and photochemical properties of 4′-hydroxyflavylium in water-ionic liquid biphasic systems, *J. Photochem. Photobiol. A: Chem.* 168, 185–189 (2004).
47. Pina, F., Lima, J. C., Parola, A. J., Afonso, C. A. M., Thermal and photochemical properties of 4′,7-dihydroxyflavylium in water-ionic liquid biphasic systems: A write-read-erase molecular switch. *Angew. Chem. Int. Ed.* 43, 1525–1527 (2004).
48. Byrne, R., Fraser, K. J., Izgorodina, E., MacFarlane, D. R., Forsyth, M., Diamond, D., Photo- and solvatochromic properties of nitrobenzospiropyran in ionic liquids containing the $[NTf_2]^-$ anion, *Phys. Chem. Chem. Phys.* 10, 5919–5924 (2008).
49. Wu, Y., Sasaki, T., Kazushi, K., Seo, T., Sakurai, K., Interactions between spiropyrans and room-temperature ionic liquids: Photochromism and solvatochromism, *J. Phys. Chem. B* 112, 7530–7536 (2008).
50. Gandra, N., Frank, A. T., Le Gendre, O., Sawwan, N., Aebisher, D., Liebman, J. F., Houk, K. N., Greer, A., Gao, R., Possible singlet oxygen generation from the photolysis of indigo dyes in methanol, DMSO, water, and ionic liquid, 1-butyl-3-methylimidazolium tetrafluoroborate, *Tetrahedron* 62, 10771–10776 (2006).
51. Baciocchi, E., Chiappe, C., Giacco, T. D., Fasciani, C., Lanzalunga, O., Lapi, A., Melai, B., Reaction of singlet oxygen with thioanisole in ionic liquids: A solvent induced mechanistic dichotomy, *Org. Lett.* 11, 1413–1416 (2009).
52. Shen, H.-Y., Mao, H.-L., Ying, L.-Y., Xia, Q.-H., Photocatalytic selective aerobic oxidation of alcohols to aldehydes and ketones by HPW/MCM-41 in ionic liquids, *J. Mol. Cat. A: Chem.* 276, 73–79 (2007).
53. Zhao, C., Bond, A. M., Photoinduced oxidation of water to oxygen in the ionic liquid $BMIMBF_4$ as the counter reaction in the fabrication of exceptionally long semiconducting silver-tetracyanoquinodimethane nanowires, *J. Am. Chem. Soc.* 131, 4279–4287 (2009).
54. Malik, C. K., Vaultier, M., Ghosh, S., Copper(I)-catalyzed [2 + 2] photocycloaddition of nonconjugated alkenes in room-temperature ionic liquids, *Synthesis* 8, 1247–1250 (2007).
55. Laali, K. K., Okazaki, T., Bunge, S. D., *N*-(Trifluoromethylsulfonyl)aryloxytrifluoromethylsulfoximines [ArO-$SO(CF_3)$:NTf] and *N*-aryltriflimides Ar-$N(Tf)_2$ by thermal and photolytic dediazoniation of $[ArN_2][BF_4]$ in [BMIM]$[Tf_2N]$ ionic liquid: Exploiting the ambident nucleophilic character of a "nonnucleophilic" anion, *J. Org. Chem.* 72, 6758–6762 (2007).
56. Heredia-Moya, J., Kirk, K. L., Photochemical Schiemann reaction in ionic liquids, *J. Fluorine Chem.* 128, 674–678 (2007).
57. Marquis, S., Ferrer, B., Alvaro, M., Garcia, H., Photochemistry of a chiral salen aluminum complex in nonconventional solvents: Use of imidazolium ionic liquids and chiral alcohols, *J. Phys. Chem. A* 111, 6034–6038 (2007).
58. Hubbard, S. C., Jones, P. B., Ionic liquid soluble photosensitizers, *Tetrahedron* 61, 7425–7430 (2005).
59. Ding, J., Desikan, V., Han, X., Xiao, T. L., Ding, R., Jenks, W. S., Armstrong, D. W., Use of chiral ionic liquids as solvents for the enantioselective photoisomerization of dibenzobicyclo[2.2.2]octatrienes, *Org. Lett.* 7, 335–337 (2005).
60. Wakasa, M., The magnetic field effects on photochemical reactions in ionic liquids, *J. Phys. Chem. B* 111, 9434–9436 (2007).
61. Hamasaki, A., Yago, T., Takamasu, T., Kido, G., Wakasa, M., Anomalous magnetic field effects on photochemical reactions in ionic liquid under ultrahigh fields of up to 28 T, *J. Phys. Chem. B* 112, 3375–3379 (2008).
62. Li, X.-W., Zhang, J., Zheng, L.-Q., Chen, B., Wu, L.-Z., Lv, F.-F., Dong, B., Tung, C.-H., Microemulsions of *N*-alkylimidazolium ionic liquid and their performance as microreactors for the photocycloaddition of 9-substituted anthracenes, *Langmuir* 25, 5484–5490 (2009).

63. Adhikari, A., Das, D. K., Sasmal, D. K., Bhattacharyya, K., Ultrafast FRET in a room temperature ionic liquid microemulsion: A femtosecond excitation wavelength dependence study, *J. Phys. Chem. A* 113, 3737–3743 (2009).
64. Brands, H., Chandrasekhar, N., Unterreiner, A. N., Ultrafast dynamics of room temperature ionic liquids after ultraviolet femtosecond excitation, *J. Phys. Chem. B* 111, 4830–4836 (2007).
65. Nishiyama, Y., Terazima, M., Kimura, Y., Charge effect on the diffusion coefficient and the bimolecular reaction rate of diiodide anion radical in room temperature ionic liquids, *J. Phys. Chem. B* 113, 5188–5193 (2009).
66. White, R. C., Tarasov, V. F., Forbes, M. D. E., Photooxidation of diglycine in confined media. Application of the microreactor model for spin-correlated radical pairs in reverse micelles and water-in-oil microemulsions, *Langmuir* 21, 2721–2727 (2005).
67. Akiyama, K., Tero-Kubota, S., One- and two-dimensional EPR studies on the radical pair generated by the photoreduction of 9,10-anthraquinone-1,5-disulfonate in aerosol OT reverse micelles, *J. Phys. Chem. B* 106, 2398–2403 (2002).
68. Griesbeck, A. G., Cho, M., Singlet oxygen addition to homoallylic substrates in solution and microemulsion: Novel secondary reactions, *Tetrahedron Lett.* 50, 121–123 (2009).
69. Nardello, V., Caron, L., Aubry, J.-M., Bouttemy, S., Wirth, T., Saha-Möller, R. C., Adam, W., Reactivity, chemoselectivity, and diastereoselectivity of the oxyfunctionalization of chiral allylic alcohols and derivatives in microemulsions: Comparison of the chemical oxidation by the hydrogen peroxide/sodium molybdate system with the photooxygenation, *J. Am. Chem. Soc.* 126, 10692–10700 (2004).
70. Li, H.-R., Wu, L.-Z., Tung, C.-H., Reactions of singlet oxygen with olefins and sterically hindered amine in mixed surfactant vesicles, *J. Am. Chem. Soc.* 122, 2446–2451 (2000).
71. Li, H.-R., Wu, L.-Z., Tung, C.-H., Controllable selectivity of photosensitized oxidation of olefins included in vesicles, *Tetrahedron* 56, 7437–7442 (2000).
72. Li, H.-R., Wu, L.-Z., Tung, C.-H., Vesicle controlled selectivity in photosensitized oxidation of olefins, *Chem. Commun.* 12, 1085–1086 (2000).
73. Vakrat-Haglili, Y., Weiner, L., Brumfeld, V., Brandis, A., Salomon, Y., McIlroy, B., Wilson, B. C., Pawlak, A., Rozanowska, M., Sarna, T., Scherz, A., The microenvironment effect on the generation of reactive oxygen species by Pd–bacteriopheophorbide, *J. Am. Chem. Soc.* 127, 6487–6497 (2005).
74. Guo, X., Lin, L., Guo, R., The photoisomerization of *trans*-stilbene in triton X-100/*n*-$C_5H_{11}OH/H_2O$ microemulsions, *Colloid. Polym. Sci.* 286, 169–174 (2008).
75. Carteau, D., Brunerie, P., Guillemat, B., Bassani, D. M., Photochemistry in everyday life: The effect of spontaneous emulsification on the photochemistry of *trans*-anethole, *Photochem. Photobiol. Sci.* 6, 423–430 (2007).
76. Yoshimi, Y., Higuchi, M., Itou, T., Hatanaka, M., Photochemical polar addition of 1,1-diphenylethene using photosensitive surfactant in stable oil-in-water emulsion, *Chem. Lett.* 33, 1196–1197 (2004).
77. Yoshimi, Y., Itou, T., Hatanaka, M., Redox-photosensitized reaction of indene using photosensitive surfactant in emulsion: Dependence on oil droplet size and surfactant charge, *Tetrahedron Lett.* 47, 3257–3260 (2006).
78. Wu, D.-Y., Zhang, L.-P., Wu, L.-Z., Wang, B., Tung, C.-H., Water-in-oil microemulsions as microreactors to control the regioselectivity in the photocycloaddition of 9-substituted anthracenes, *Tetrahedron Lett.* 43, 1281–1283 (2002).
79. Li, X., Huang, J., Fang, L., Yu, G., Lin, H., Wang, L., Photodegradation of 2,20,4,40-tetrabromodiphenyl ether in nonionic surfactant solutions, *Chemosphere* 73, 1594–1601 (2008).
80. Costa, S. M. B., López-Cornejo, P., Togashi, D. M., Laia, C. A. T., Photoinduced electron transfer in non-aqueous microemulsions, *J. Photochem. Photobiol. A: Chem.* 142, 151–161 (2001).

81. Milano, F., Dorogi, M., Szebényi, K., Nagy, L., Maróti, P., Váró, G., Giotta, L., Agostiano, A., Trotta, M., Enthalpy/entropy driven activation of the first interquinone electron transfer in bacterial photosynthetic reaction centers embedded in vesicles of physiologically important phospholipids, *Bioelectrochemistry* 70, 18–22 (2007).
82. Kaanumalle, L. S., Nithyanandhan, J., Pattabiraman, M., Jayaraman, N., Ramamurthy, V., Water-soluble dendrimers as photochemical reaction media: Chemical behavior of singlet and triplet radical pairs inside dendritic reaction cavities, *J. Am. Chem. Soc.* 126, 8999–9006 (2004).
83. Kaanumalle, L. S., Ramesh, R., Maddipatla, V. S. N. M., Nithyanandhan, J., Jayaraman, N., Ramamurthy, V., Dendrimers as photochemical reaction media. Photochemical behavior of unimolecular and bimolecular reactions in water-soluble dendrimers, *J. Org. Chem.* 70, 5062–5069 (2005).
84. Tejedor, R. M., Oriol, L., Serrano, J. L., Sierra, T., Chiral photochemical induction in liquid crystals, *J. Mater. Chem.* 18, 2899–2908 (2008).
85. Valentin, M. D., Bisol, A., Agostini, G., Fuhs, M., Liddell, P. A., Moore, A. L., Moore, T. A., Gust, D., Carbonera, D., Photochemistry of artificial photosynthetic reaction centers in liquid crystals probed by multifrequency EPR (9.5 and 95 GHz), *J. Am. Chem. Soc.* 126, 17074–17086 (2004).
86. Lv, F.-F., Li, X.-W., Wu, L.-Z., Tung, C. H., Photochemical reaction of cyclohexyl phenyl ketone within lyotropic liquid crystals, *Tetrahedron* 64, 1918–1923 (2008).
87. Lv, F.-F., Chen, B. Wu, L.-Z., Zhang, L.-P., Tung, C. H., Enhanced stereoselectivity in photoelectrocyclization of tropolone ethers via confinement in chiral inductor-modified lyotropic liquid crystals, *Org. Lett.* 10, 3473–3476 (2008).
88. Ishida, Y., Kai, Y., Kato, S., Misawa, A., Amano, S., Matsuoka, Y., Saigo, K., Two-component liquid crystals as chiral reaction media: Highly enantioselective photodimerization of an anthracene derivative driven by the ordered microenvironment, *Angew. Chem. Int. Ed.* 47, 8241–8245 (2008).
89. Dawn, A., Fujita, N., Haraguchi, S., Sada, K., Shinkai, S., An organogel system can control the stereochemical course of anthracene photodimerization, *Chem. Commun.* 2100–2102 (2009).
90. Dawn, A., Fujita, N., Haraguchi, S., Sada, K., Tamaru, S.-i., Shinkai, S., Studies on a new class of organogelator containing 2-anthracenecarboxylic acid: Influence of gelator and solvent on stereochemistry of the photodimers, *Org. Biomol. Chem.* 7, 4378–4385 (2009).
91. Shumburo, A., Biewer, M. C., Stabilization of an organic photochromic material by incorporation in an organogel, *Chem. Mater.* 14, 3745–3750 (2002).

12

Cryogenic Matrix Photochemistry

Götz Bucher
The University of Glasgow

During the last 50 years, matrix isolation spectroscopy (MI) has contributed much to the development of modern physical organic chemistry. It allows the study of a range of interesting molecules, including a variety of reactive intermediates, some excited states, even ions, in an inert and almost noninteracting environment. In a typical MI experiment, a stable photochemical precursor to the reactive molecule of interest is deposited onto a cold spectroscopic window with a large excess of an inert gas, typically argon or other noble gases, but also nitrogen, methane, or carbon dioxide. The precursor is photolyzed, and the reactive intermediate can be investigated by spectroscopy—typically infrared, UV/Vis, and electron paramagnetic resonance (EPR). The advantages of the technique are obvious: the highly inert, rigid, and cold environment not only prevents intermolecular quenching of the reactive molecule to be studied, it also offers very narrow IR band widths, resulting in very high sensitivity and facile interpretation of spectra. Secondary reactions with other molecules can be investigated by adding these to the inert gas used. Annealing of the matrix after photolysis allows for diffusion and thermal reactions to take place. During the last two decades, advances in computer technology and in the design of quantum chemical software have made it possible to reliably calculate IR, UV/Vis, and EPR spectra of small to mid-sized molecules. Comparing spectroscopic information obtained by experiment with calculated spectra meanwhile is standard practice in MI experiments, and nowadays no matrix isolation study is published without extensive supporting calculations. The technique of MI has been reviewed and described authoritatively.[1,2] This chapter will therefore not deal with technical details of the method, which are summarized elsewhere,[2] nor will it provide a comprehensive review of all literature available. It will leave out studies that mainly focus on thermal generation of reactive species (by flash vacuum pyrolysis [FVP]), and it will not cover photochemical reactions of transition metal complexes. It will instead concentrate on recent studies on the photochemical generation of reactive intermediates, and on the photochemistry of reactive species, from an organic chemist's perspective.

12.1 Photochemical Generation or Photochemistry of Free Radicals

Simple free radicals are relatively difficult to investigate by MI. Any photochemical cleavage of a precursor molecule will automatically result in the formation of two radical centers, which will usually recombine within the rigid cage of the matrix cavity, resulting in poor radical yields. Potential routes around this problem are found in the use of precursor molecules that yield one stable radical upon photolysis, fragment into a radical pair separated by inert spacer molecules, or generate the radical of interest by FVP.

The phenyl radical **1** is one of the most important species in combustion processes. While it can be generated by photolysis of iodobenzene or dibenzoyl peroxide,[3] the FVP of *trans*-azobenzene **2**, followed by trapping of the fragments in solid Ar, provides a cleaner synthesis of **1**. The important reactions of **1** with water and oxygen have recently been investigated.[4,5] Reaction of matrix-isolated **1** with $^3O_2$ yields the phenylperoxy radical **3** in a diffusion-controlled process.[4] Irradiation of **3** with visible light leads to rearrangement of **3** into the 2-oxepinoxy radical **4**, while the phenoxy radical **5** is not formed under the conditions of MI. Extended photolysis of **4** finally yields the ketene radical **6**. If a matrix containing **1** and water is annealed, initially a weak complex **1**/water **7** is formed, which yields a benzene–hydroxyl radical complex **8** upon photochemical excitation.[5]

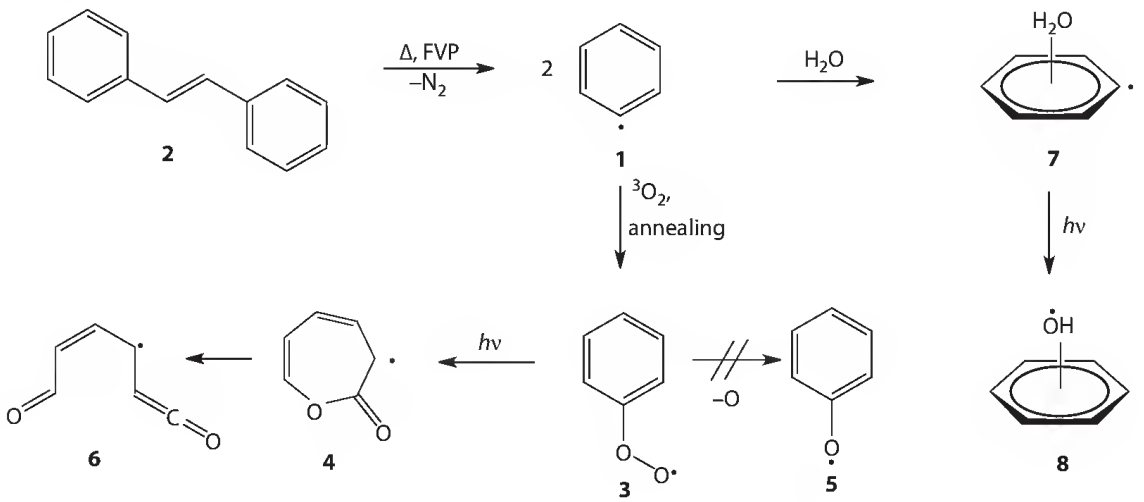

The 2-hydroxyphenoxyl radical **9**, a derivative of **5**, was successfully characterized by photolysis of matrix-isolated 2-nitrophenol **10**.[6] Irradiation of **10** initially leads to 2-hydroxyphenyl nitrite **11**, which subsequently loses NO to yield **9**. The parent phenoxy radical **5** as well as phenyl nitrite (C_6H_5–ONO) had earlier been prepared by irradiation of nitrobenzene.[7]

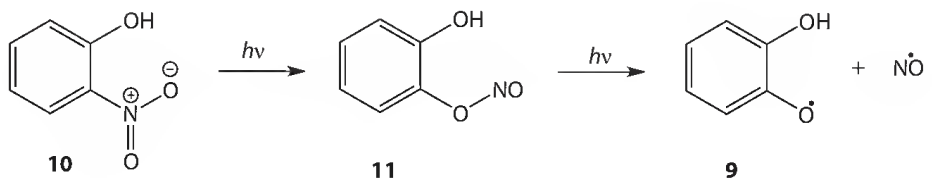

Broadband irradiation of *i*-propyl nitrite $(CH_3)_2CH$–ONO, matrix isolated in Ar, on the other hand, yields at best trace amounts of the isopropoxy radical. Major products include acetone, acetaldehyde, HNO, and nitrosomethane.[8] Closely related to the phenoxy radical are the anilino radical,

Ph-NH, and its derivatives. The 4-methylanilino radical 4-MeC_6H_4NH is formed upon photolysis of matrix-isolated *p*-toluidine.[9]

Oxidation of the matrix-isolated vinyl radical **12** with $^3O_2$ has been reported to yield the vinylperoxy radical **13** in a barrierless reaction.[10] While this finding was not new, the fact that photolysis of **13** results in the formation of a CH_2OH/CO complex **14** clearly came as a surprise. Complex **14** is likely formed by a hydrogen transfer reaction from the $H_2CO–HCO$ radical pair.

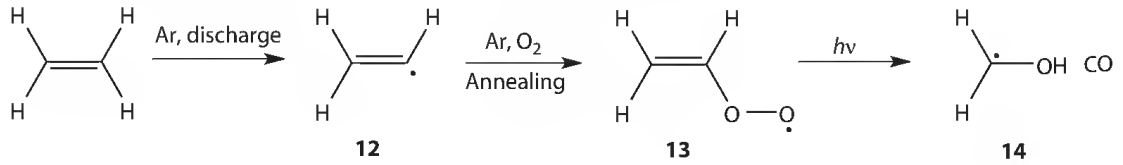

12 **13** **14**

12.2 Diradicals

The characterization of diradicals or electron-deficient species such as carbenes, nitrenes, and silylenes has long been a major application of MI. In recent years, MI has also been employed to characterize aromatic σ,σ-diradicals, like *m*- or *p*-benzyne.

12.2.1 Carbenes

Due to the availability of diazo compounds as convenient precursors, MI is ideally suited for the characterization of free carbenes. A large number of different carbenes has been characterized by MI, and the results have been reviewed.[11,12] Some recent studies deserve mention in this article. In the field of ground-state singlet carbenes, the focus of research has been on carbene rearrangements. Singlet vinylcarbenes represent a very simple class of singlet carbenes. Due to the ease of their rearrangement into allenes or cyclopropenes, there is only very scant information available on these elusive carbenes. If vinylcarbene is stabilized with a chloro substituent as in chlorovinylcarbene **16**, it is sufficiently long lived to be characterized in a nitrogen matrix at $T = 8$ K.[13] Photolysis of the matrix-isolated diazirine **15** initially led to formation of **16**, which upon long-wavelength irradiation (λ = 578 nm) was converted into a mixture of cyclopropene **17** and allene **18**. Even the synthesis of highly strained *anti*-Bredt olefins like the cyclopropene **21**, from diazirine **19** via carbene **20**, was achieved in this study.

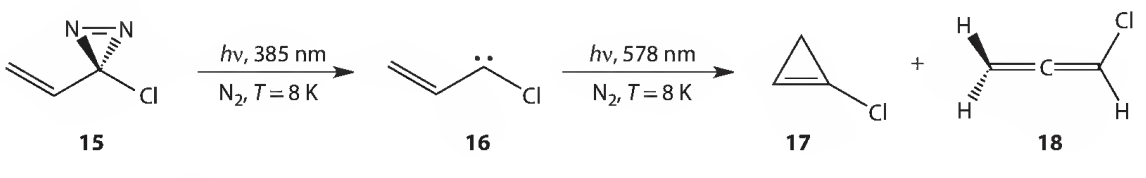

15 **16** **17** **18**

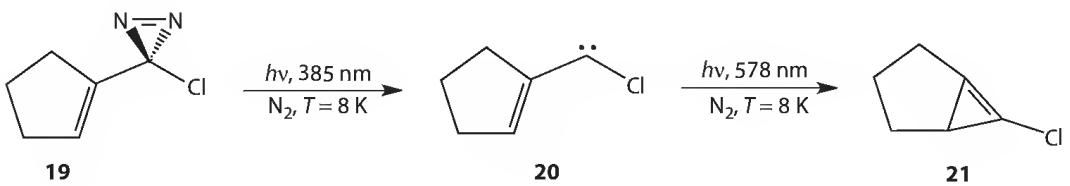

19 **20** **21**

In a similar way, singlet and triplet carbenes derived from heterocycles like benzofuran and benzothiophene undergo complex rearrangements that yield cyclopropenes as well as ring-opened products.[14,15]

Some small-ring carbenes like cyclopropenylidene have been identified as constituents of interstellar matter (IM).[16] Other constituents of IM include linear carbon chains, and carbon chains terminated by nitrile functionalities. In this context, $H–C_n–H$ chains (*n* being an odd number) represent an

important research target. Photolysis of matrix-isolated diazopentadiyne **22** allowed for the successful characterization of H–C_5–H **23**.[17] According to high-level ab initio calculations, **23** is best described as linear ($D_{\infty h}$) triplet diethynylcarbene, and its reaction with oxygen resulted in the formation of carbonyl *O*-oxide **24**, where attack of oxygen occurred at the middle carbon atom.

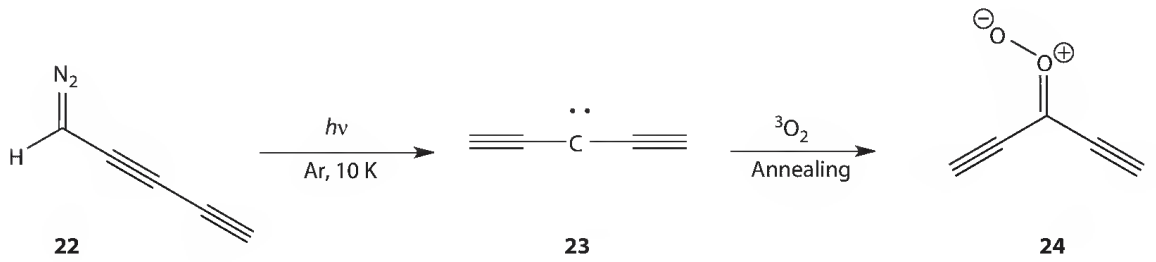

22 **23** **24**

12.2.2 Nitrenes

Nitrenes can be conveniently synthesized by photolysis of organic azides. As these are usually easily accessible, a large body of literature on nitrenes and their rearrangements exists.[18–21] Oxidation of triplet aryl nitrenes with dioxygen is an interesting aspect of aryl nitrene chemistry that has only recently been investigated in detail. In recent work on the matrix photochemistry of 4-azidoaniline **25**, the reactivity of triplet 4-aminophenylnitrene **26** toward $^3O_2$ was explored in depth, using both MI and a variety of computational methods.[22] Photolysis of **25** in Ar doped with 4% oxygen gave triplet nitrene **26**, which upon annealing the matrix to $T = 35$ K yielded a mixture of the rotameric nitroso *O*-oxides **27** and **28**. These could be interconverted by monochromatic irradiation. Long-wavelength ($\lambda > 515$ nm) irradiation of **27**/**28** finally yielded 4-nitroaniline **29**. Importantly, no evidence could be gained for the intermediacy of dioxaziridine **30**, although the formation of such species had been reported before.[23]

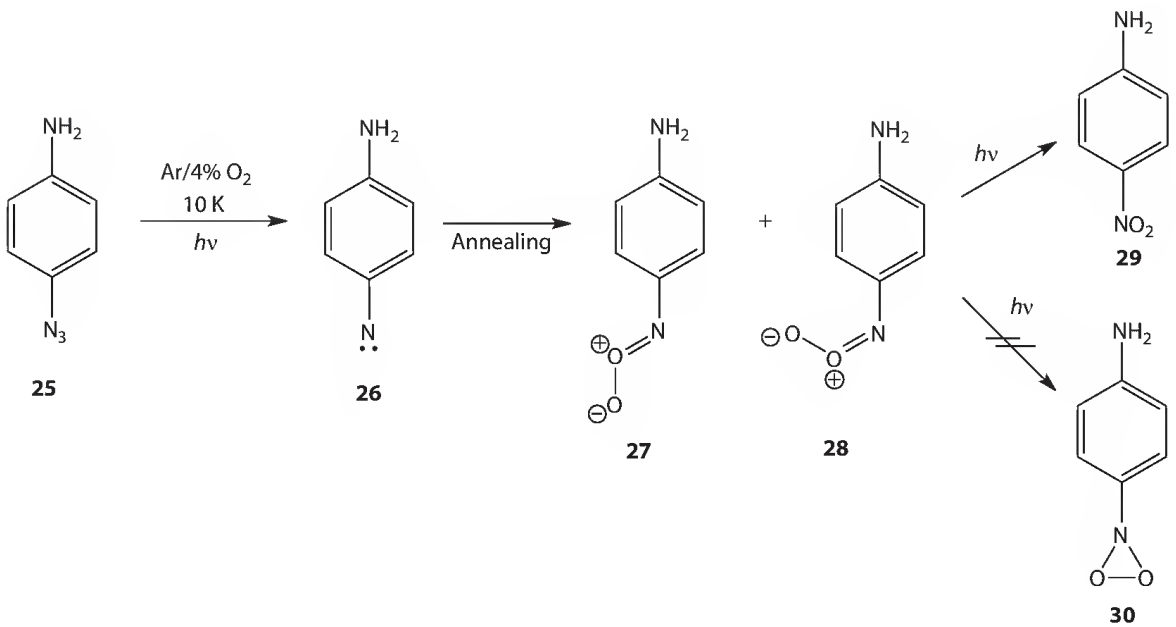

25 **26** **27** **28** **29** **30**

Nitrene oxidation was also studied by MI in another, somewhat more unusual system. Most nitrenes investigated so far contain a nitrene center connected to a carbon atom. In a few cases, the silyl nitrenes had been investigated.[24] Relatively recently, a new class of nitrenes, boryl nitrenes were studied for the first time using MI.[25] Photolysis of *B*-azido-catecholborane **31** in Ar matrix yields a triplet ground-state

nitrene **32**, which does not undergo any further photochemical rearrangements. It can be trapped by CO, yielding a boryl isocyanate, and by triplet oxygen. In the latter reaction, a borylnitroso-*O*-oxide **33** is formed, which is very unstable and is rapidly converted into nitritoborane **34** upon extended photolysis.

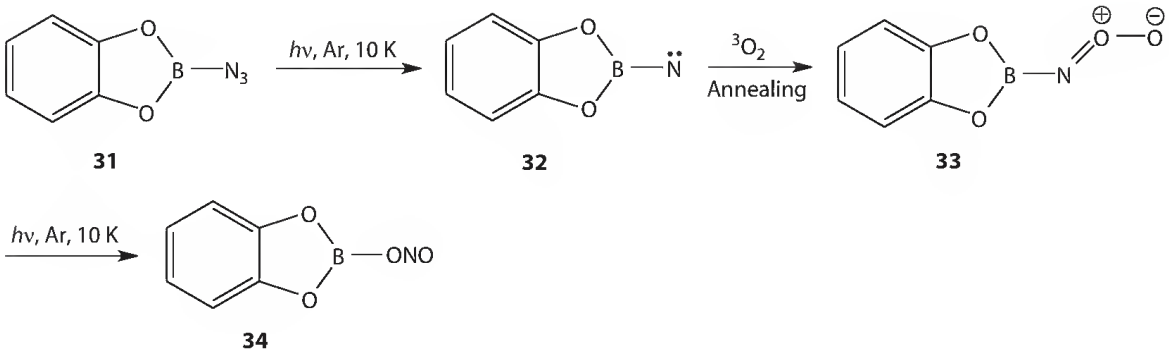

31 **32** **33** **34**

The electronic structure of **32** is related to difluorovinylidene $F_2C{=}C$. The resulting extreme reactivity of **32** allows for facile insertion into the D–D bond of deuterium,[26] and into the C–H bonds of alkanes and even methane.[27] The latter reaction could successfully be worked out into a novel amide synthesis.[27]

A study on the photochemistry of azido-substituted derivatives of pyridine *N*-oxide promised to be particularly interesting, as both the azido function as well as the pyridine *N*-oxide unit[28] are known to be photoreactive. In the case of 4-azidopyridine *N*-oxide **35** solution-phase studies had already shown that the *N*-oxide function was not the primary photoreactive moiety, with 4,4′-azobis(pyridine *N*-oxide) **36** being essentially the only product formed.[29] Under conditions of MI, photolysis of **35** yielded the triplet nitrene **37**.[30] Particularly revealing is a comparison between the EPR zero field splitting (ZFS) parameters of triplet nitrenes **37** and **38** measured in Ar matrix. While **37** showed an unusually low value for $D = 0.62\,cm^{-1}$, the D value of **38** was obtained as $D = 1.05\,cm^{-1}$. This indicates a significant degree of spin delocalization away from the nitrene nitrogen atom in **37**, but not in **38**. Accordingly, the pyridine *N*-oxide moiety significantly stabilizes a nitrene unit if it is in *para*-, but not in *meta*-position relative to the nitrene center. Nitrene **37** is also unusual in that the authors of the study could not obtain evidence for any singlet-nitrene derived chemistry, such as formation of didehydroazepines. Nitrene **38**, on the other hand, readily underwent rearrangement to azacycloheptatetraene *N*-oxides upon prolonged irradiation.[30]

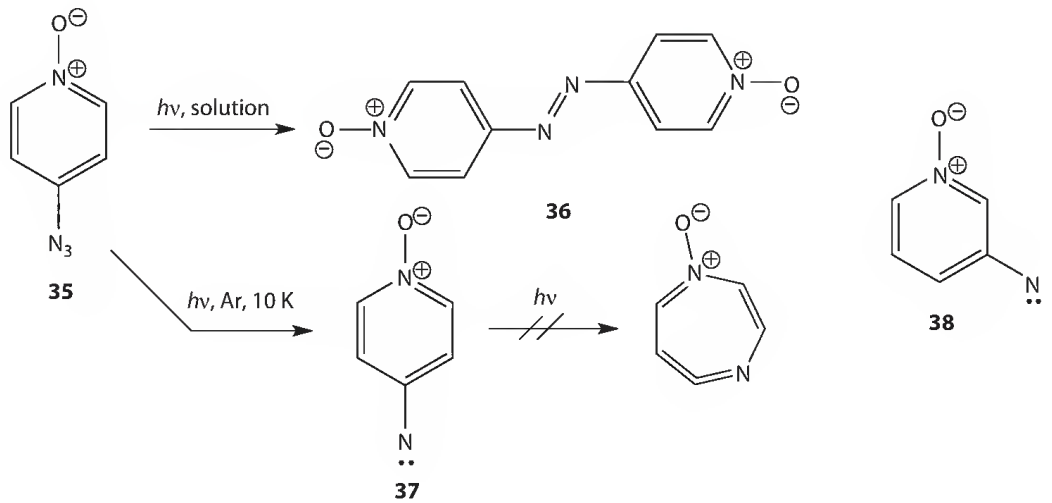

35 **36** **37** **38**

12.2.3 Borylenes

Borylenes—borane-1,1-diyls—represent a class of hypovalent boron compounds that has for a while been known in the form of transition metal complexes.[31] In its free, uncomplexed form phenyl borylene **39** was characterized only recently.[32] Photolysis ($\lambda = 254$ nm) of phenyldiazidoborane **40**, matrix isolated in Ar, led to the exclusive formation of triplet iminoborylnitrene **41**. If the irradiation of **40** was performed in N_2 or Ne matrices, however, borylene **39** could also be identified as product. Irradiation with light of longer wavelength converted it into benzoborirene **42**.[32]

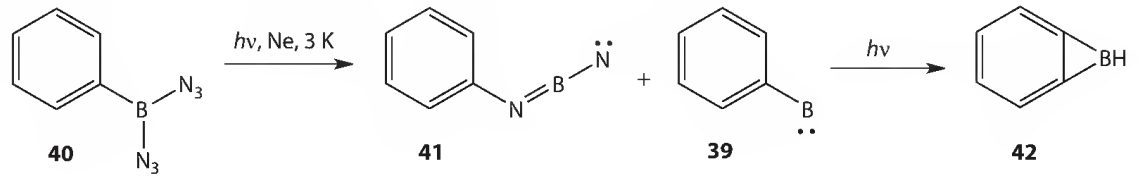

40 **41** **39** **42**

12.2.4 Phosphinidenes

Similar to borylenes, phosphinidenes (compounds of monovalent phosphorus) are mostly known in the form of transition metal complexes.[33] Free triplet mesityl phosphinidene **43** had previously been known from a single low-temperature X-band EPR study.[34] Recent MI work has confirmed the validity of this early EPR study, and has provided the infrared, UV/Vis, and W-band EPR spectra of **43**.[35] Phosphinidene **43** can be generated by photolysis of matrix-isolated phosphirane **44**. Extended photolysis results in intramolecular hydrogen abstraction and the formation of phosphetane **45**. Didehydrophosphepine **46**, on the other hand, is formed in trace amounts at most. It could only tentatively be identified via UV/Vis spectroscopy.

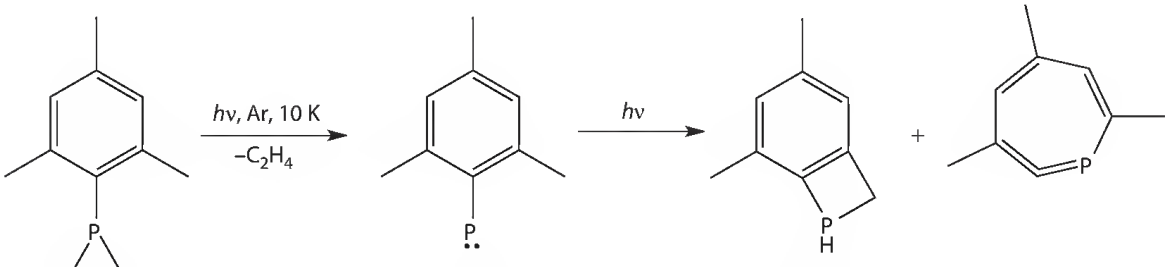

44 **43** **45** **46**

12.2.5 σ,σ-, σ,π-, and π,π-Diradicals

The characterization of 1,2-, 1,3-, and 1,4-diradicals by MI is considerably more difficult than the investigation of 1,1-diradicals such as carbenes and nitrenes. This is due to the fact that convenient photochemical precursors for these species are lacking. Frequently, the problem can be overcome by subjecting thermal precursors like iodo compounds to FVP. As the biradicals involved are photolabile, secondary photolysis experiments following the initial FVP are frequently performed. σ,σ-Diradicals like *o*-, *m*-, and *p*-benzyne and σ,*p*-diradicals like α,3-didehydrotoluene have been generated by thermolysis (*o*-, *m*-benzyne) or photolysis of diiodoarenes or diperoxides,[36,37] and in certain cases by photolysis of quinone diazides.[38] This chemistry has been reviewed.[39] It will only be touched in this review in the context of oligoradicals (discussed later). *m*-Xylylene **47**, a *meta*-quinoid π,π-diradical, has recently been generated by FVP of α,α′-diiodo-*m*-xylene **48**, and characterized by EPR, UV/Vis, and for the first time also by IR spectroscopy.[40] Upon irradiation, it undergoes interesting photochemical rearrangements. Initially, a mixture of the strained bicyclic trienes **49** and **50** is formed, while later in the irradiation, tricyclus **51** is also observed.

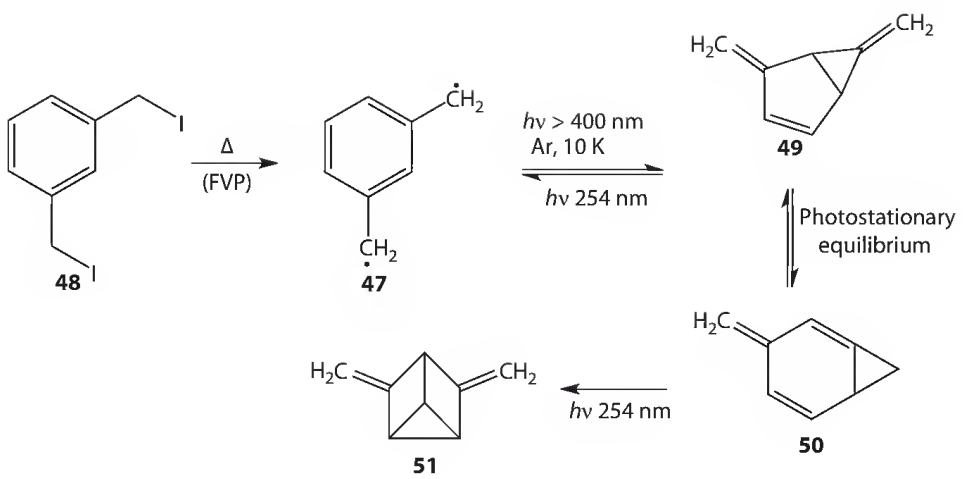

Photolysis of tetrazole **52**, matrix isolated in a nitrogen matrix at $T = 4.6\,K$, resulted in formation of diradical **53**, a triaza-analogue of trimethylenemethane.[41] Being a nondisjoint diradical, **53** is predicted to be a ground-state triplet species, which is confirmed by ESR spectroscopy. IR and UV/Vis spectroscopy confirm this assignment and also rule out the possible formation of the ring-closed isomers **54** and **55**.

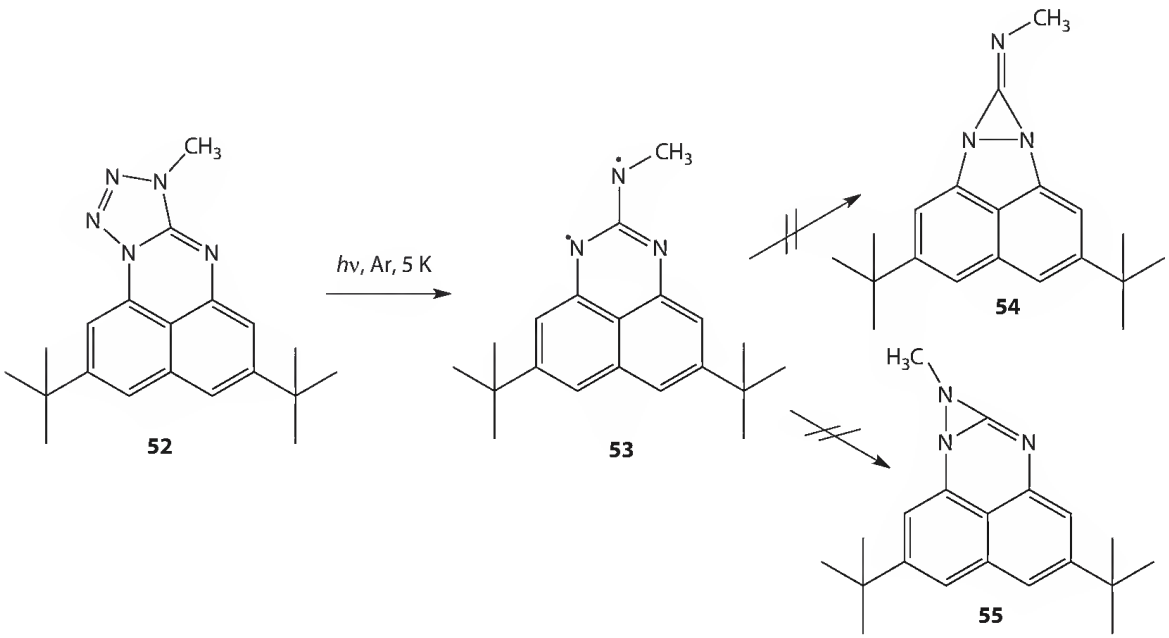

12.3 Tri-, Tetra-, and Oligoradicals

MI has been successfully employed in the characterization of molecules with more than two deficient valencies. Di- and trinitrenes as well as -carbenes can be generated by photolysis of the corresponding bis- or tris-azides or -diazo compounds. This chemistry, which involves molecules with a spin multiplicity of up to tridecet, has been reviewed.[11,42,43] Very challenging, however, still is the characterization of molecules containing both a nitrene or carbene functionality and a free radical center, and of aromatic

σ,σ,σ-, σ,σ,π-, σ,π,π-, or π,π,π-triradicals. A number of nitrene radicals have recently been generated by photolysis of 4-iodo-fluorophenylazides. Cleavage of the carbon–iodine bond and dediazotation results in the formation of the fluorinated *p*-dehydrophenylnitrenes.[44–47] In the case of 4-iodo-2,3,5,6-tetrafluorophenylazide **56**, photolysis in Ar matrix at $T = 4$ K results in formation of 4-dehydro-2,3,5,6-tetrafluorophenylnitrene **57**, a σ,σ,π-type triradical, in its quartet ground state.[44–46] The cleavage of the C–I bond is far less efficient than dediazotation. Hence, photolysis of **56** initially results in formation of the triplet nitrene **58** that later either loses the iodine atom, or undergoes a competing rearrangement to didehydroazepine **59**. The efficiency of the photodeiodination reaction of fluorinated iodophenylnitrenes depends on the number of fluorine atoms present in the molecule—a reduced degree of fluorination results in a lesser yield of nitrene radical.[46] Photolysis of 3-iodo-2,4,5,6-tetrafluorophenylazide **60** in argon or neon matrices, on the other hand, did not allow for a detection of 3-dehydro-2,4,5,6-tetrafluorophenylnitrene **61**. Instead, ring opening of the triplet nitrene **62** (or an isomeric didehydroazepine) to the enallene nitrile **63** was observed exclusively.[47]

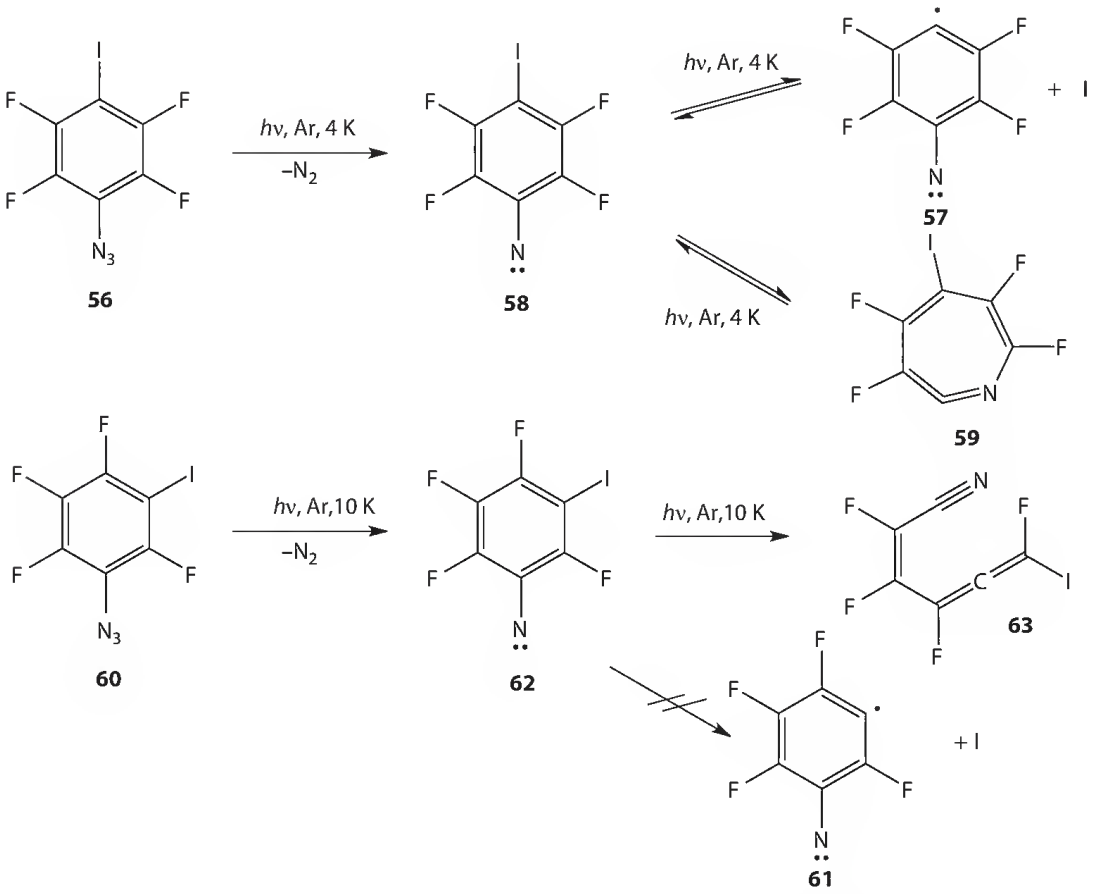

Characterizing triradicals of the σ,σ,σ-type by MI represents a serious challenge, as three single bonds need to be broken in order to achieve this aim. A representative example is 1,2,3-trisdehydrobenzene **64**, which was successfully generated by photolysis of 3-iodophthalic anhydride **65**, isolated in a neon matrix at $T = 3$ K. Excitation of **65** with light of a pulsed XeCl excimer laser ($\lambda = 308$ nm) resulted in competing deiodination or decarboxylation/decarbonylation, leading to 3-dehydrophthalic anhydride **66** or iodobenzyne **67**. Switching the excitation wavelength to $\lambda = 248$ nm (KrF excimer laser) then allowed for the characterization of triradical **64**, which eventually loses another hydrogen atom and undergoes ring opening to hexatriyne **68**.[48] According to high-level ab initio calculations, **64** has a ^{2}A ground state with a short ($r \sim 1.68$ Å) C_1–C_3 distance that resembles a bicylo[3.1.0]hexatrien-6-yl radical **68**.[49]

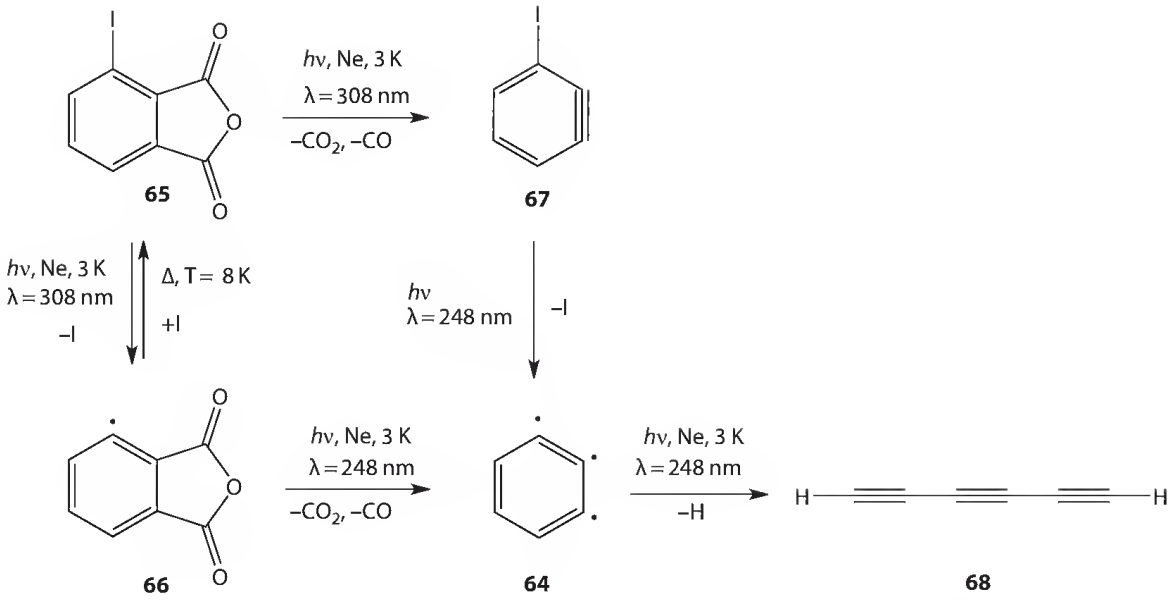

12.4 Photochemical Synthesis of Acenes

With increasing number of annelated rings, linear acenes (naphthalene, anthracene, tetracene, pentacene, etc.) become progressively unstable. Hexacene requires additional bulky substituents to be stable, and heptacene **69** had been unknown until recently, when it was successfully generated by twofold photodecarbonylation of diketone **70**, first in a polymer matrix[50] and then in a cryogenic matrix.[51,52] Remarkably, matrix-isolated samples of **69** undergo charge separation into the radical cation and radical anion of **69** if irradiated with short-wavelength UV light.[51] Similarly, octacene and nonacene could be generated by photolysis of tetraketones in an Ar matrix.[53]

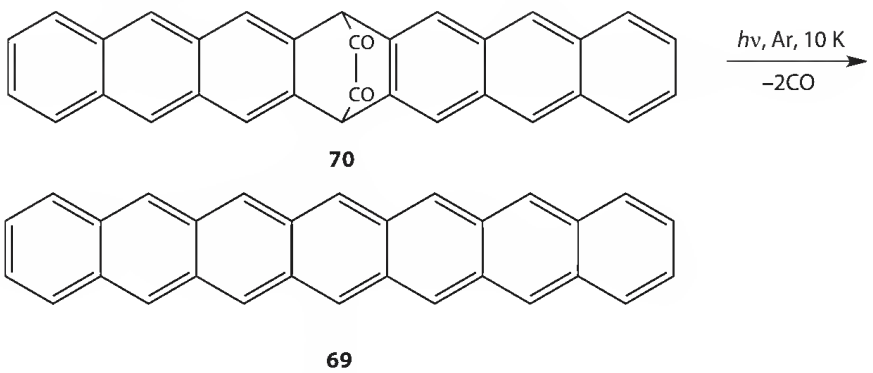

12.5 Photochemistry of Heterocycles

The last five years have seen a number of MI studies published, in which a variety of different heterocyclic molecules were isolated in inert gas matrices and then subjected to photolysis. This section will give a very brief overview about some of these studies. An important question in heterocyclic chemistry frequently is the issue of the existence of various tautomeric forms of a given heterocycle. Narrow-band irradiation of matrix-isolated samples is an ideal way to change the composition of a tautomer mixture by attaining a novel, photostationary equilibrium. For example, the equilibrium of 2-amino-5-methylpyridine **71** and its imino-tautomer **72** normally completely lies on the side of the amine **71**.

UV irradiation of **71** under conditions of MI allows for the formation and characterization of **72**.[54] As a sideproduct, the aminyl radical **73** is also observed.

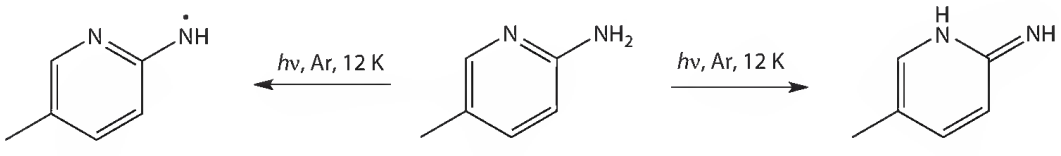

73 **71** **72**

A photochemical conversion of a trithione **74** into a trithiol **75** was observed, when trithiocyanuric acid **74** was UV irradiated under conditions of MI.[55] The product, trimercaptotriazine **75**, is formed in a remarkable triple photochemical proton transfer reaction.

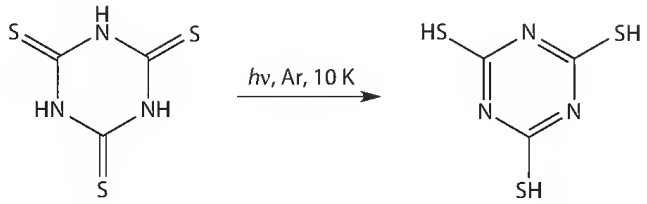

74 **75**

A different type of tautomer interconversion is observed, if *N*-hydroxypyridine-2-thione **76** is photolyzed in inert gas matrices. UV irradiation of **76** results in cleavage of the N–O bond and formation of two conformers of 2-hydroxysulfanylpyridine **77**.[56]

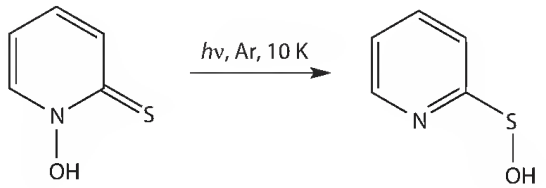

76 **77**

Carbonyl compounds, and to a lesser degree thiocarbonyls, can undergo photochemical α-cleavage (Norrish type I reaction). The two isomers of monothio-α-pyrone **78** and **79** do not constitute an exception to this rule.[57] Photolysis of both **78** and **79**, matrix isolated in Ar, results in the formation of ketene-thioaldehydes like **80** or thioketene-aldehydes such as **81**. Interestingly, **80** is converted into **81** via a photochemical hydrogen shift. As a result, **78** and **79** can be interconverted photochemically.[57]

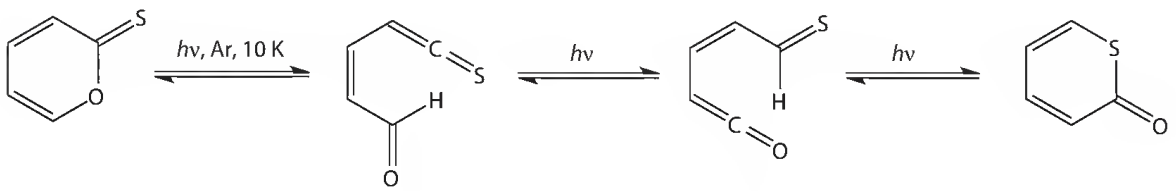

78 **80** **81** **79**

12.6 Photooxidation

The reactions of organic molecules with high-valent metal oxides and oxochlorides play an important role in the repertoire of synthetic organic chemistry. MI can be used to study these reactions, but frequently photoexcitation is required to initiate the oxidation reactions, in which unusual intermediates may be encountered. The photoinitiated reactivity of two oxochlorides, CrO_2Cl_2 (chromyl chloride) and $VOCl_3$, toward a range of organic substrates has recently been investigated in detail. Twin-jet deposition of mixtures of CrO_2Cl_2 and benzene with argon gave no evidence for any significant ground state interaction between the substrates. Irradiation ($\lambda < 590$ nm) of the mixture, however, resulted in oxygen transfer and formation of a complex **82** of 2,4-cyclohexadienone and $CrOCl_2$.[58] Surprisingly, the more stable C_6H_6O isomer phenol was not formed. A mixture of $VOCl_3$ and benzene, on the other hand, proved to be photostable. Similar results were obtained in the reactions of chromyl chloride with methylated derivatives of benzene,[59] and electron-donor[60] as well as electron-acceptor[61] substituted benzenes. In most cases, the reactions led to exclusive formation of cyclohexadienones complexed to a $CrOCl_2$ fragment. In the case of certain organic substrates (e.g., benzonitrile[61]), formation of the phenols was also observed.

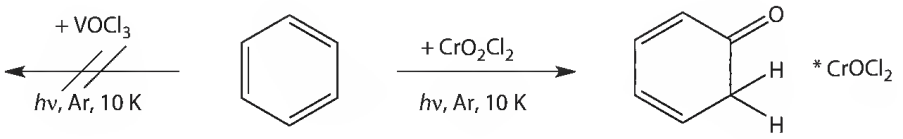

Consistent with the results obtained with arene oxidation, the photochemical reaction of acetonitrile (CH_3CN) with CrO_2Cl_2 or $VOCl_3$ also led to oxygen atom transfer, yielding complexes of acetonitrile *N*-oxide CH_3CNO with $CrOCl_2$ or VCl_3, respectively.[62] Chloroethenes also undergo photoinitiated oxidation with chromyl chloride.[63] In these reactions, an oxygen atom is transferred to the higher substituted carbon atom, and a hydrogen or chlorine atom is shifted to the lesser substituted carbon atom. Oxidation of vinyl chloride thus yields a complex of acetyl chloride with $CrOCl_2$. In contrast, oxidation of bromoethene with chromyl chloride yields the complex of bromoacetaldehyde with $CrOCl_2$.[64] Remarkably, a different regioselectivity is thus observed in the photooxidations of chlorinated and brominated derivatives of ethene. Photochemical reactions between chromyl chloride and organic substrates are not limited to those bearing reactive functional groups. Even pure alkanes such as cyclohexane,[65] cyclopentane, and cyclopropane[66] undergo the reaction. With cyclohexane, oxygen atom transfer to produce cyclohexanol takes place,[65] whereas the photooxidation of cyclopropane results in cleavage of the three-membered ring and formation of a formaldehyde–$CrOCl_2$ complex and ethene.[66]

In contrast to the clean reactions observed with chromyl chloride, the photooxidation of cyclohexene with ozone yielded products indicative of formation of O (^3P).[67] Thermal reaction of ozone and cyclopentadiene, on the other hand, resulted (among others) in the formation of a Criegee intermediate (carbonyl *O*-oxide)—the first time that this type of reactive intermediate had been directly observed as a result of an ozonolysis reaction.[68]

12.7 Conclusion

MI studies have frequently employed photochemical excitation of photolabile precursors (azides, diazo compounds, and diazirines) in order to generate reactive intermediates of interest. This type of research, in which photochemical excitation serves as a tool continues today, as the ever-growing research areas of nitrene and carbene chemistry (among others!) demonstrate. More recently, research efforts have somewhat changed their accentuation, with MI being increasingly utilized to elucidate pathways in little-explored photochemical reactions. This new development is certainly in part due to the rapid development of computational chemistry and of computer technology, which nowadays allows for the

identification of photochemical reaction products by simple comparison of experimental and calculated IR spectra. More than 50 years after its invention,[69–71] MI still is a technique that is employed inventively, yielding results that are published in the topmost scientific journals.[72]

References

1. Almond, M. J., Downs, A. J., *Spectroscopy of Matrix Isolated Species*, John Wiley & Sons, Chichester, U.K., 1989.
2. Bally, T., Matrix isolation, in *Reactive Intermediate Chemistry*, Moss, R. A., Platz, M. S., Jones, M., Jr., Eds., John Wiley & Sons, Hoboken, NJ, 2004.
3. Friderichsen, A. V., Radziszewski, J. G., Nimlos, M. R., Winter, P. R., Dayton, D. C., David, D. E., Ellison, G. B., The infrared spectrum of the matrix-isolated phenyl radical, *J. Am. Chem. Soc.*, 123, 1977, 2000.
4. Mardyukov, A., Sander, W., Matrix isolation and spectroscopic characterization of the phenylperoxy radical and its rearranged products, *Chem. Eur. J.*, 15, 1462, 2009.
5. Mardyukov, A., Sanchez-Garcia, E., Crespo-Otero, R., Sander, W., Interaction and reaction of the phenyl radical with water: A source of OH radicals, *Angew. Chem. Int. Ed.*, 48, 4804, 2009.
6. Nagaya, M., Kudoh, S., Nakata, M., Infrared spectrum of 2-hydroxyphenoxyl radical and photoisomerization between *trans* and *cis* 2-hydroxyphenyl nitrites, *Chem. Phys. Lett.*, 432, 446, 2006.
7. Yang, R., Jin, X., Wang, W., Fan, K., Zhou, M., Infrared spectra of phenyl nitrite and phenoxyl radical-nitric oxide complex in solid argon, *J. Phys. Chem. A*, 109, 4261, 2005.
8. Mátyus, E., Magyarfalvi, G., Tarczay, G., Conformers and photochemistry of propyl nitrites: A matrix isolation study, *J. Phys. Chem. A*, 111, 450, 2007.
9. Akai, N., Yoshida, H., Ohno, K., Aida, M., Photochemistry of *p*-toluidine in a low-temperature argon matrix. Infrared spectrum and geometrical structure of 4-methylanilino radical, *Chem. Phys. Lett.*, 403, 390, 2005.
10. Yang, R., Yu, L., Jin, X., Zhou, M., Carpenter, B. K., Reaction of vinyl radical with oxygen: A matrix isolation infrared spectroscopic and theoretical study, *J. Chem. Phys.*, 122, 014511, 2005.
11. Sander, W., Bucher, G., Wierlacher, S., Carbenes in matrices, *Chem. Rev.*, 93, 1583, 1993.
12. Tomioka, H., Triplet carbenes, in *Reactive Intermediate Chemistry*, Moss, R. A., Platz, M. S., Jones, M., Jr., Eds., John Wiley & Sons, Hoboken, NJ, 2004.
13. Zuev, P. S., Sheridan, R. S., Singlet vinylcarbenes: Spectroscopy and photochemistry, *J. Am. Chem. Soc.*, 126, 12220, 2004.
14. Nikitina, A., Sheridan, R. S., Characterization of a didehydrobenzoxazine intermediate in a novel carbene-to-carbene transformation, *J. Am. Chem. Soc.*, 124, 7670, 2002.
15. Wang, J., Sheridan, R. S., A singlet aryl-CF_3 carbene: 2-benzothienyl(trifluoromethyl)carbene and interconversion with a strained cyclic allene, *Org. Lett.*, 9, 3177, 2007.
16. Thaddeus, P., Vrtilek, J. M., Gottlieb, C. A., Laboratory and astronomical identification of cyclopropenylidene, C_3H_2, *Astrophys. J. Lett.*, 299, L63, 1985.
17. Bowling, N. P., Halter, R. J., Hodges, J. A., Seburg, R. A., Thomas, P. S., Simmons, C. S., Stanton, J. F., McMahon, R. J., Reactive carbon-chain molecules: Synthesis of 1-diazo-2,4-pentadiyne and spectroscopic characterization of triplet pentadiynylidene, *J. Am. Chem. Soc.*, 128, 3291, 2006.
18. Gritsan, N. P., Platz, M. S., Kinetics, spectroscopy, and computational chemistry of arylnitrenes, *Chem. Rev.*, 106, 3844, 2006.
19. Gritsan, N. P., Study of photochemical transformations of organic azides by matrix isolation technique and quantum chemistry, *Russ. Chem. Rev.*, 76, 1139, 2007.
20. Platz, M. S., Nitrenes, in *Reactive Intermediate Chemistry*, Moss, R. A., Platz, M. S., Jones, M., Jr., Eds., John Wiley & Sons, Hoboken, NJ, 2004.
21. Bucher, G., Photochemical reactivity of azides, in *CRC Handbook of Organic Photochemistry and Photobiology*, Horspool, W., Lenci, F., Eds., CRC Press, Boca Raton, FL, 2004.

22. Pritchina, E. A., Gritsan, N. P., Bally, T., Matrix isolation and computational study of the photochemistry of *p*-azidoaniline, *Phys. Chem. Chem. Phys.*, 8, 719, 2006.
23. Harder, T., Wessig, P., Bendig, J., Stösser, R., Photochemical reactions of nitroso oxides at low temperatures: The first experimental evidence for dioxaziridines, *J. Am. Chem. Soc.*, 121, 6580, 1999.
24. Ferrante, R. F., Observation of discrete trimethylsilylnitrene by matrix-isolation spectroscopy, *J. Phys. Chem.*, 94, 3502, 1990.
25. Bettinger, H. F., Bornemann, H., Donor stabilized borylnitrene: A highly reactive BN analogue of vinylidene, *J. Am. Chem. Soc.*, 128, 11128, 2006.
26. Bettinger, H. F., Filthaus, M., Neuhaus, P., Insertion into dihydrogen employing the nitrogen centre of a borylnitrene, *Chem. Commun.*, 2186, 2009.
27. Bettinger, H. F., Filthaus, M., Bornemann, H., Oppel, I. M., Metal-free conversion of methane and cycloalkanes to amines and amides by employing a borylnitrene, *Angew. Chem. Int. Ed.*, 47, 4744, 2008.
28. Albini, A., Alpegiani, M., The photochemistry of the *N*-oxide function, *Chem. Rev.* 84, 43, 1984.
29. Hostetler, K. J., Crabtree, K. N., Poole, J. S., The photochemistry of 4-azidopyridine 1-oxide, *J. Org. Chem.*, 71, 9023, 2006.
30. Crabtree, K. N., Hostetler, K. J., Munsch, T. E., Neuhaus, P., Lahti, P. M., Sander, W., Poole, J. S., Comparative study of the photochemistry of the azidopyridine 1-oxides, *J. Org. Chem.*, 73, 3441, 2008.
31. Braunschweig, H., Dewhurst, R. D., Schneider, A., Electron-precise coordination modes of boron centered ligands, *Chem. Rev.*, 110, 3924, 2010.
32. Bettinger, H. F., Phenylborylene: Direct spectroscopic characterization in inert gas matrices, *J. Am. Chem. Soc.*, 128, 2534, 2006.
33. Aktaş, H., Slootweg, J. C., Lammertsma, K., Nucleophilic phosphinidene complexes: Access and applicability, *Angew. Chem. Int. Ed.*, 49, 2, 2010.
34. Li, X., Weissman, I. S., Lin, T.-S., Gaspar, P. P., Cowley, H. A., Smirnov, H. A., Observation of a triplet phosphinidene by ESR spectroscopy, *J. Am. Chem. Soc.*, 116, 7899, 1994.
35. Bucher, G., Borst, M. L. G., Ehlers, A. W., Lammertsma, K., Ceola, S., Huber, M., Grote, D., Sander, W., Infrared, UV/Vis, and W-band EPR spectroscopic characterization and photochemistry of triplet mesitylphosphinidene, *Angew. Chem. Int. Ed.*, 44, 3289, 2005.
36. Sander, W., Exner, M., Winkler, M., Balster, A., Hjerpe, A., Kraka, E., Cremer, D., Vibrational spectrum of *m*-benzyne: A matrix isolation and computational study, *J. Am. Chem. Soc.*, 124, 13072, 2002.
37. Marquardt, R., Balster, A., Sander, W., Kraka, E., Cremer, D., Radziszewski, J. G., *p*-Benzyne, *Angew. Chem. Int. Ed.*, 37, 955, 1998.
38. Bucher, G., Sander, W., Kraka, E., Cremer, D., 2,4-Didehydrophenol: First IR spectroscopic detection of a *m*-aryne, *Angew. Chem. Int. Ed.*, 31, 1230, 1992.
39. Wenk, H. H., Winkler, M., Sander, W., One century of aryne chemistry, *Angew. Chem. Int. Ed.*, 42, 502, 2003.
40. Neuhaus, P., Grote, D., Sander, W., Matrix isolation, spectroscopic characterization, and photoisomerization of *m*-xylylene, *J. Am. Chem. Soc.*, 130, 2993, 2008.
41. Quast, H., Nüdling, W., Klemm, G., Kirschfeld, A., Neuhaus, P., Sander, W., Hrovat, D. A., Borden, W. T., A perimidine-derived non-kekulé triplet diradical, *J. Org. Chem.*, 73, 4956, 2008.
42. Matsuda, K., Iwamura, H., High-spin organic molecular materials, *Curr. Opin. Solid State Mater. Sci.*, 2, 446, 1997.
43. Iwamura, H., Principles of physical organic chemistry for molecular architecture and functions, *J. Phys. Org. Chem.*, 11, 299, 1998.
44. Wenk, H. H., Sander, W., 2,3,5,6-Tetrafluorophenylnitren-4-yl: A quartet-ground-state nitrene radical, *Angew. Chem. Int. Ed.*, 41, 2742, 2002.
45. Sander, W., Grote, D., Kossmann, S., Neese, F., 2,3,5,6-Tetrafluorophenylnitren-4-yl: Electron paramagnetic resonance spectroscopy of a quartet-ground-state nitreno radical, *J. Am. Chem. Soc.*, 130, 4396, 2008.

46. Grote, D., Sander, W., Photochemistry of fluorinated 4-iodophenylnitrenes: Matrix isolation and spectroscopic characterization of phenylnitrene-4-yls, *J. Org. Chem.*, 74, 7370, 2009.
47. Sander, W., Winkler, M., Cakir, B., Grote, D., Bettinger, H. F., Dehydrophenylnitrenes: Matrix isolation and photochemical rearrangements, *J. Org. Chem.*, 72, 715, 2006.
48. Venkataramani, S., Winkler, M., Sander, W., 1,2,3-Tridehydrobenzene, *Angew. Chem. Int. Ed.*, 44, 6306, 2005.
49. Koziol, L., Winkler, M., Houk, K. N., Venkataramani, S., Sander, W., Krylov, A. I., The 1,2,3-Tridehydrobenzene triradical: ^{2}B or not ^{2}B? The Answer is ^{2}A!, *J. Phys. Chem. A*, 111, 5071, 2007.
50. Mondal, R., Shah, B. K., Neckers, D. C., Photogeneration of heptacene in a polymer matrix, *J. Am. Chem. Soc.*, 128, 9612, 2006.
51. Bettinger, H. F., Mondal, R., Neckers, D. C., Stable photoinduced charge separation in heptacene, *Chem. Commun.*, 5209, 2007.
52. Mondal, R., Tönshoff, C., Khnon, D., Neckers, D. C., Bettinger, H. F., Synthesis, stability, and photochemistry of pentacene, hexacene, and heptacene: A matrix isolation study, *J. Am. Chem. Soc.*, 131, 14281, 2009.
53. Tönshoff, C., Bettinger, H. F., Pushing the limits in acene chemistry: Synthesis of octacene and nonacene, *Angew. Chem. Int. Ed.*, 49, 4125, 2010.
54. Akai, N., Harada, T., Shin-ya, K., Ohno, K., Aida, M., Photoinduced amino-imino tautomerism: An infrared study of 2-amino-5-methylpyridine in a low-temperature argon matrix, *J. Phys. Chem. A*, 110, 6016, 2006.
55. Rostkowska, H., Lapinski, L., Khvorostov, A., Nowak, M. J., UV-induced trithione → trithiol triple proton transfer in trithiocyanuric acid isolated in low-temperature matrixes, *J. Phys. Chem. A*, 109, 2160, 2005.
56. Lapinski, L., Gerega, A., Sobolewski, A. L., Nowak, M. J., Thioperoxy derivative generated by UV-induced transformation of N-hydroxypyridine-2(1*H*)-thione isolated in low-temperature matrixes, *J. Phys. Chem. A*, 112, 238, 2008.
57. Breda, S., Reva, I., Lapinski, L., Cristiano, M. L. S., Frija, L., Fausto, R., Photochemical ring-opening and intramolecular hydrogen shift reactions in sulfur analogues of α-pyrone, *J. Phys. Chem. A*, 110, 6415, 2006.
58. Hoops, M. D., Ault, B. S., Matrix isolation investigation of the photochemical reaction of benzene with $CrCl_2O_2$ and $OVCl_3$, *J. Phys. Chem. A*, 109, 4497, 2005.
59. Hoops, M. D., Ault, B. S., Matrix isolation investigation of the photochemical reaction of methyl-substituted benzenes with $CrCl_2O_2$, *J. Phys. Chem. A*, 110, 892, 2006.
60. Hoops, M. D., Ault, B. S., Matrix isolation investigation of the photochemical reaction of methyl-substituted benzenes with $CrCl_2O_2$, *J. Mol. Struct.*, 888, 277, 2008.
61. Hoops, M. D., Ault, B. S., Matrix isolation investigation of the photochemical reaction of $CrCl_2O_2$ with benzenes substituted with electron withdrawing groups, *Chem. Phys.*, 334, 18, 2007.
62. Goldberg, N., Lubell, S. R., Ault, B. S., Matrix isolation and theoretical study of the photochemical reaction of CH_3CN with $CrCl_2O_2$ and $OVCl_3$, *J. Mol. Struct.*, 740, 125, 2005.
63. Antle, K. A., Ault, B. S., Matrix isolation and theoretical study of the photochemical reaction of $CrCl_2O_2$ with chloroethenes, *J. Phys. Chem. A*, 109, 947, 2005.
64. Lemon, C. E., Goldberg, N., Klein-Riffle, E. T., Kronberg, J. K., Ault, B. S., Matrix isolation and theoretical study of the photochemical reactions of C_2H_3Br and 1,2-$C_2H_2Br_2$ with $CrCl_2O_2$, *Chem. Phys.*, 326, 349, 2006.
65. Hoops, M. D., Ault, B. S., Matrix isolation investigation of the photochemical reaction of cyclohexane and cyclohexene with $CrCl_2O_2$, *J. Mol. Struct.*, 826, 36, 2007.
66. Hoops, M. D., Ault, B. S., Matrix isolation studies of the photochemical and thermal reactions of 3- and 5-membered cyclic hydrocarbons with $CrCl_2O_2$, *J. Phys. Chem. A*, 112, 5368, 2008.

67. Hoops, M. D., Ault, B. S., Matrix isolation study of the photochemical reaction of cyclohexane, cyclohexene and cyclopropane with ozone, *J. Mol. Struct.*, 929, 22, 2009.
68. Hoops, M. D., Ault, B. S., Matrix isolation study of the early intermediates in the ozonolysis of cyclopentene and cyclopentadiene: Observation of two criegee intermediates, *J. Am. Chem. Soc.*, 131, 2853, 2009.
69. Whittle, E., Dows, D. A., Pimentel, G. C., Matrix isolation method for the experimental study of reactive species, *J. Chem. Phys.*, 22, 1943, 1954.
70. Becker, E. D., Pimentel, G. C., Spectroscopic studies of reactive molecules by the matrix isolation method, *J. Chem. Phys.*, 25, 224, 1956.
71. Norman, I., Porter, G., Trapped atoms and radicals in a glass "Cage", *Nature*, 174, 508, 1954.
72. Schreiner, P. R., Reisenauer, H. P., Pickard, F. P., IV, Simmonett, A. C., Allen, W. D., Matyus, E., Csaszar, A. G., Capture of hydroxymethylene and its fast disappearance through tunneling, *Nature*, 453, 906, 2008.

13

Preparative and Mechanistic Semiconductor Photocatalysis

Horst Kisch
Universität Erlangen-Nürnberg

Dariusz Mitoraj
Universität Erlangen-Nürnberg

13.1 Introduction

The chemical conversion and utilization of solar energy is a central topic of general photochemistry. In addition to solar water splitting, the "holy grail" of photochemistry, also cleaning of air and water through aerial photooxidation, fixation of nitrogen and carbon dioxide, and organic syntheses have received considerable attention in research of the last three decades. In general, the most relevant primary reaction steps are the light-induced generation of charges followed by their utilization in electron exchange reactions with substrates. Whereas many systems easily undergo the first step, charge recombination usually prevents the second step, which is essential for the chemical utilization of light energy. The crucial point in the development of an efficient system is therefore how to slow down recombination in favor of electron exchange. Depending on the detailed nature of the system involved, in many cases a sensitizer is necessary to allow utilization visible light, which constitutes about 45% of the solar light arriving at the earth's surface.

An elementary electron transfer reaction $A + D = A^{-\bullet} + D^{+\bullet}$ in principle can be sensitized by both a homogeneous and a heterogeneous photosensitizer. Typical examples for the former are organic compounds or metal complexes having charge-transfer (CT) character. Their basic action can be described

by Equations 13.1 through 13.6 wherein Red and Ox symbolize electron-donating and electron-accepting groups usually connected through a covalently linked molecular bridge. These groups favor the photoinduced charge generation (Equation 13.1) whereas the bridge may be able to slow down the undesired charge recombination converting the chemically valuable redox energy of $A^{\bullet}$ --- $D^{+\bullet}$ into useless heat (Equation 13.2). Only if this reaction is slower than electron exchange with substrates, efficient formation of the usually labile primary intermediates $A^{-\bullet}$ and $D^{+\bullet}$ may occur (Equation 13.3). Their further transformation to the final redox products A_{red} and D_{ox} has to be fast and irreversible (Equations 13.4 and 13.5) in order to avoid back electron transfer (Equation 13.6):

$$\text{Red---Ox} \xrightarrow{h\nu} \text{Red}^{+\bullet} \text{ --- } \text{Ox}^{-\bullet} \tag{13.1}$$

$$\text{Red}^{+\bullet}\text{---Ox}^{-\bullet} \longrightarrow \text{Red---Ox} + h\nu/\Delta T \tag{13.2}$$

$$\text{Red}^{+\bullet}\text{--- Ox}^{-\bullet} + A + D \longrightarrow A^{-\bullet} + D^{+\bullet} + \text{Red---Ox} \tag{13.3}$$

$$A^{-\bullet} \longrightarrow A_{red} \tag{13.4}$$

$$D^{+\bullet} \longrightarrow D_{ox} \tag{13.5}$$

$$A^{-\bullet} + D^{+\bullet} \longrightarrow A + D \tag{13.6}$$

Although a great variety of molecular photosensitizers ranging from simple intramolecular CT compounds to supramolecular systems are known to undergo photoinduced charge generation,[1] only a very few can induce redox reactions with substrates since usually charge recombination and back electron transfer are too efficient.[2] Contrary to this, heterogeneous photosensitizers of semiconductor character enable also the chemically most important electron exchange with substrates. By analogy with the molecular sensitizer discussed earlier, the basic reaction steps may be summarized in a simplified way according to Equations 13.7 through 13.9. Light absorption generates, inter alia, reactive electron–hole pairs trapped at the surface. It is expected that the distance between these redox centers should be larger than in a molecular sensitizer and therefore charge recombination may become slow enough to allow the desired interfacial electron transfer (IFET) between the solid and dissolved substrates. The further reaction steps are described by Equations 13.4 through 13.6.

$$SC \xrightarrow{h\nu} SC(e_r^{-}/h_r^{+}) \tag{13.7}$$

$$SC(e_r^{-}/h_r^{+}) \longrightarrow SC + h\nu/\Delta T \tag{13.8}$$

$$SC(e_r^{-}/h_r^{+}) + A + D \longrightarrow A^{-\bullet} + D^{+\bullet} \tag{13.9}$$

It is noted that no general agreement exists on the definition of the term *photocatalysis*. Generally, it implies that light and a catalyst are necessary to induce or accelerate a chemical transformation[3–13] as also expressed by the IUPAC recommendation, according to which photocatalysis is the "change in the rate of a chemical reaction or its initiation under the action of ultraviolet, visible or infrared radiation in the presence of a substance—the photocatalyst—that absorbs light and is involved in the chemical transformation of the reaction partners."[14] This definition includes *photosensitization*, "a process by which a photochemical alteration occurs in one molecular entity as a result of initial absorption of radiation by another molecular entity called photosensitizer,"[15] but it excludes the photoacceleration of a stoichiometric thermal reaction, irrespective of whether it occurs in homogeneous solution[16] or at

the surface of an illuminated electrode,[17] otherwise any photoreaction would be catalytic. The catalytic nature of a heterogeneous reaction is given when the turnover number, that is, number of molecules reacted divided by the number of active sites, is larger than 1.[18] Is it only one or smaller, it may be called semiconductor-assisted photoreaction, by analogy with homogeneous catalytic reactions.[19,20] However, the number of active sites of a semiconductor photocatalyst powder is usually unknown.* Therefore, in almost all cases the differentiation between a catalytic and *assisted* photoreaction may be impossible. Accordingly, many of the photoreactions conducted in the presence of semiconductor powders and claimed to be "photocatalytic," in reality are semiconductor-assisted photoreactions.[21] Especially if few micromoles of products are produced in the presence of a much larger amount of semiconductor powder and its reusability was not proven.

A further problem of definition arises when not the semiconductor itself but a substrate or a semiconductor–substrate CT complex (vide infra) is the light-absorbing species. We have proposed to use the terms *direct* and *indirect semiconductor photocatalysis*.[22] As well known from thermal heterogeneous catalysis, the pristine surface may be restructured in the very early reaction stages to the catalytically active one having different light absorption properties.

Photoelectrochemistry, the photogeneration of charge and current at semiconductor electrodes in contact with a liquid electrolyte,[23] can be considered as the basis for semiconductor photocatalysis. For a rather large semiconductor single crystal it is generally assumed that the presence of a space-charge region (band-bending) is necessary to explain the charge-separating properties of the semiconductor–liquid interface. For a critical discussion of the basic theories and their underlying assumptions, the reader is referred to review articles.[24–26] Inspired by the early observation of Bard et al., that irradiation of titania powder suspended in a liquid solvent promotes electron-transfer reactions of substrates in solution,[27–30] a great variety of chemical transformations in the presence of semiconductor powders or colloids has been reported.[31–34] Some of these reactions are related to prebiotic chemistry like the TiO_2-[35,36] or CdS-assisted[37] photoreduction of N_2, the generation of amino acids from CH_4, N_2, H_2O in the presence of platinized TiO_2,[38] and the TiO_2- or CdS-induced peptide formation from glycine.[39] The fading of paints[40] and the already technically applied aerial detoxification of water and air[41,42] illustrate important technical and environmental aspects of semiconductor photocatalysis.

Common to all these chemical processes is that well-known products were formed in very low yields and rather identified only spectroscopically than isolated. Although high "quantum yields" were claimed in a few cases, it is mentioned that quantum yields in heterogeneous systems are extremely difficult to obtain due to the problem of varying light reflectance. Furthermore, quantum yields are measured at short irradiation times and therefore do not give information on the synthetic usefulness of the reaction. In general, photocorrosion, the self-destruction of the semiconductor by the light-generated charges, often prevents a long-term reaction, indispensable to obtain the products on a preparative scale. In this chapter we shall therefore focus on the question if semiconductor photocatalysis at all is a useful alternative synthesis method and whether or not it may open novel pathways for chemical synthesis.

13.2 Photocatalysis at Semiconductor Powders

13.2.1 Fundamentals

The use of a metalized semiconductor particle as a kind of "short-circuit" microphotoelectrochemical cell was introduced through the work of Bard et al. on the photo-Kolbe reaction.[43] In this system, a few weight percent of a noble metal, most often platinum, covers the surface of a semiconductor powder like titania. Light absorption generates an electron at platinum and a hole in the valence band of titania constituting cathodic and anodic surface centers. Differences to the macroelectrodes employed in photoelectrochemistry have been discussed.[25,44–47] It is noted that platinization in many but not in all cases is required in

* It was proposed to take the number of molecules present in one monolayer, about 10^{14} per cm^2, as an estimate; Ref. [17].

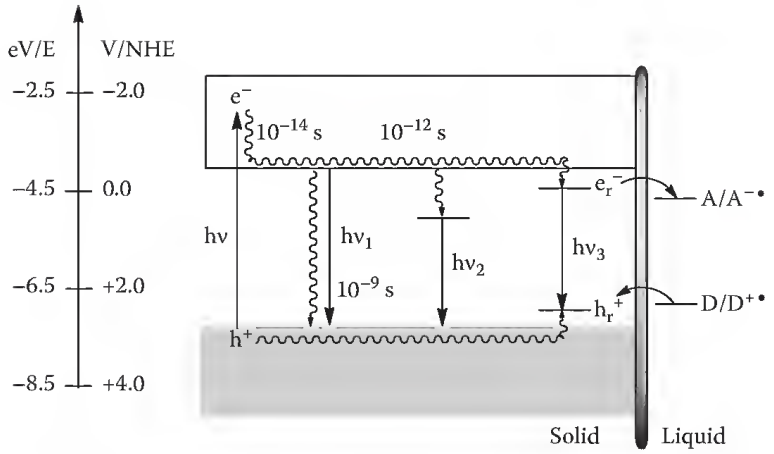

SCHEME 13.1 Primary processes occurring upon photoexcitation of CdS in the presence of an acceptor A and donor D. Conduction (CB) and valence band (VB) have Cd5s and S4p character, respectively. The thick vertical bar symbolizes the solid/liquid interface.

order to obtain acceptable reaction rates. Scheme 13.1 summarizes the early processes occurring in the elementary redox reaction A + D = $A^{-\bullet}$ + $D^{+\bullet}$ photocatalyzed by cadmium sulfide.

The light-generated electron–hole pair, which is initially delocalized throughout the crystal in general, undergoes a fast relaxation to the conduction band edge. From there, radiative and nonradiative charge recombination without ($h\nu_1$) or with intermediate trapping at surface states ($h\nu_2$)* dominates over trapping in the form of reactive electron–hole pairs (e_r^-/h_r^+). Only from the latter electron change with A and D may proceed. For simplicity another, but important primary process, so-called photocorrosion is omitted. It consists of electron exchange with the semiconductor lattice ions inducing a destruction of the photocatalytically active surface (vide infra). The lifetimes indicated in Scheme 13.1 originate from colloidal TiO_2. Rather long is the lifetime of a few microseconds reported for trapped electron–hole pairs.[48] IFET reactions may proceed in the range of picoseconds as illustrated by the values of 18 and 200 ps measured for the IFET from e_r^- to a viologen and from diethyldithiocarbamate to h_r^+, respectively.[49] It is generally assumed that due to the short lifetime of the light-generated charges, only adsorbed substrates can undergo an efficient electron exchange. However, in the case of titania, photocatalyzed aerial oxidation of benzyl alcohol and rhodamine B weakly adsorbed substrates react faster than stronger adsorbed ones.[50–53] It is known that in such type of oxidations the electron-accepting substrate may be located even a few millimeters away from the surface.[54] As mentioned earlier, the primary redox products $A^{-\bullet}$ + $D^{+\bullet}$ are converted in fast secondary reaction steps to A_{red} and D_{ox}, the oxidized and a reduced final product. A corresponding energy diagram is depicted in Scheme 13.2, assuming that the IFET of adsorbed substrates is rate determining. Thus, considering the reactive electrons and holes as types of photogenerated cathodes and anodes, the overall reaction can be viewed as photoelectrolysis.

Since in this basic reaction mechanism light is absorbed by the semiconductor, it may be termed just as semiconductor photocatalysis or more detailed as direct semiconductor photocatalysis. Alternatively, when only the substrate is the light-absorbing component, the mechanism of indirect semiconductor photocatalysis may operate. The two mechanisms are schematically depicted in Scheme 13.3 for titania photocatalysis.

In the direct pathway the electron–hole pair generated by the photon $h\nu_1$ is separated into reactive electrons and holes. The former reduces oxygen to superoxide, which is finally transformed to the strongly oxidizing OH radical. Simultaneously the reactive hole oxidizes water to another OH radical or the donor D to its radical cation, which is converted to stable oxidation products through a multistep reaction cascade including participation of the OH radical. When D is a typical water pollutant

* Surface states are defined as localized energy states, in contrast to energy levels in the conduction and valence band which are delocalized throughout the crystal.

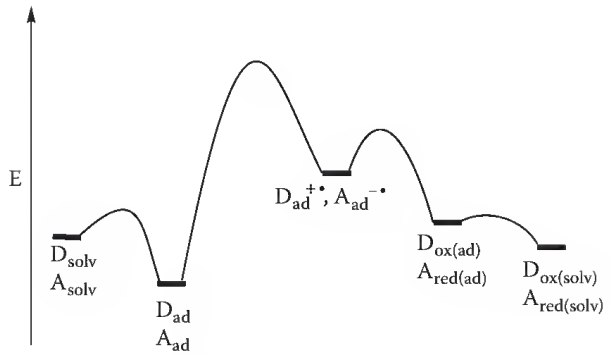

SCHEME 13.2 Energy diagram of the elementary redox reaction $A + D = A_{red} + D_{ox}$.

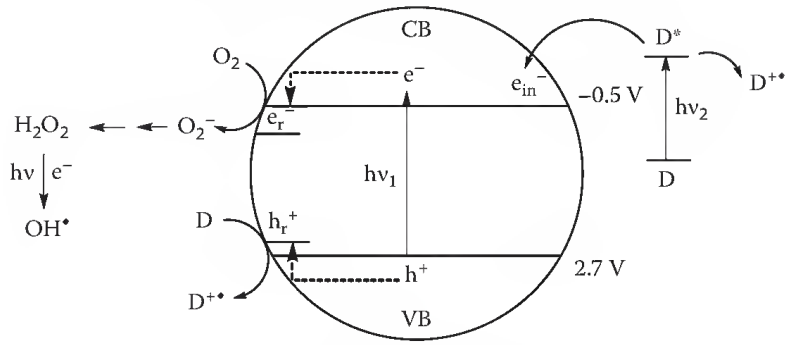

SCHEME 13.3 Direct ($h\nu_1$) and indirect ($h\nu_2$) semiconductor photocatalysis of the aerial oxidation of D. The two horizontal lines designate the upper valence and lower conduction band edges; corresponding redox potentials are referenced vs. NHE and refer to a titania particle in contact with water of pH 7.

like phenol, complete oxidation to carbon dioxide and water is observed. In the indirect pathway light absorption of a photon $h\nu_2$ by D generates the excited state D* followed by electron injection into the conduction band if its redox potential is equal or more negative than the conduction band edge. The resulting e_{in}^- has to perform a fast reduction of oxygen in order to prevent charge recombination with $D^{+\bullet}$. Further conversion to final products proceeds as discussed earlier.

An early example for both mechanisms is the exhaustive dealkylation of methylene blue (MB) and rhodamine B[55,*] photocatalyzed by cadmium sulfide (Scheme 13.4). Dealkylation of MB (**1**) to the

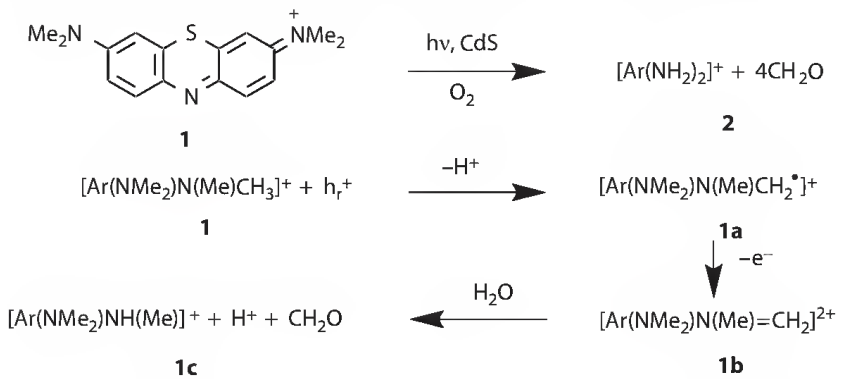

SCHEME 13.4 Overall reaction and key mechanistic steps in the dealkylation of methylene blue photocatalyzed by CdS.

* Here and in the following, the use of the chemical formula indicates that the semiconductor was present as a powder suspension.

diamine **2** occurs only if light is absorbed by CdS and not by MB. In the mechanism proposed for MB, the reactive hole oxidizes the dye to the corresponding radical cation **1a** and a proton whereas the reactive electron reduces oxygen to superoxide. Subsequently the strongly reducing α-amino radical **1a** injects an electron into the conduction band of CdS. Such type of electron injections is well known in photoelectrochemistry (current amplification effect).[56a,*] The produced methyleneiminium salt **1b** in the final step is hydrolyzed to the trimethyl derivative **1c** and formaldehyde. Repeating this typical reaction cycle three times eventually leads to the fully dealkylated product **2**.

Contrary to this, RhB is also dealkylated when only the dye is the light absorbing component. In this case the excited state redox potential of the dye is negative enough to inject an electron into the conduction band affording the radical cation of RhB. The injected electron reduces oxygen and the radical cation again undergoes full dealkylation as discussed for MB. Thus, like in the direct photocatalysis of MB also the indirect photocatalysis affords the same type of reaction product. It is noted that in the latter case the semiconductor plays the role of an electron relay, enabling a fast reduction of oxygen. A similar indirect photocatalysis mechanism may operate also when one of the substrates forms a CT complex with the semiconductor surface leading to a new electronic absorption band. A unique example is the titania-catalyzed photosulfoxidation of *n*-heptane by sulfur dioxide and molecular oxygen affording *n*-heptane sulfonic acid. The reaction proceeds with visible light although all reaction components absorb only in the UV. It was shown that sulfur dioxide forms a CT complex with titania enabling absorption by visible light.[56b]

13.2.2 Thermodynamic Aspects

Scheme 13.5 summarizes the thermodynamic requirements of direct photocatalysis for the case of an n-type semiconductor.[57]

Absorption of light of energy equal or larger than the bandgap E_g induces a splitting of the Fermi level into quasi-Fermi levels of electrons and holes indicated as ${}_nE_F^*$ and ${}_pE_F^*$, respectively. Since redox reactions are connected with reorganization energies (χ), the density of states has a maximum not at the standard potential ($D_{red,ox}$ and $A_{red,ox}$) but at an energy higher (D_{ox} and A_{ox}) and lower (D_{red} and A_{red}) by the amount of χ. Therefore both reductive and oxidative IFET reactions are thermodynamically feasible only when the energies of A_{ox} and D_{red} are equal or below the quasi-Fermi level of electrons and holes, respectively. Whereas standard potentials are usually easy obtainable, this is not true for reorganization energies, which may reach values of up to 1 eV. Thus, a large uncertainty is connected with a precise evaluation of the free energy change of such type of interfacial electron exchange reactions.

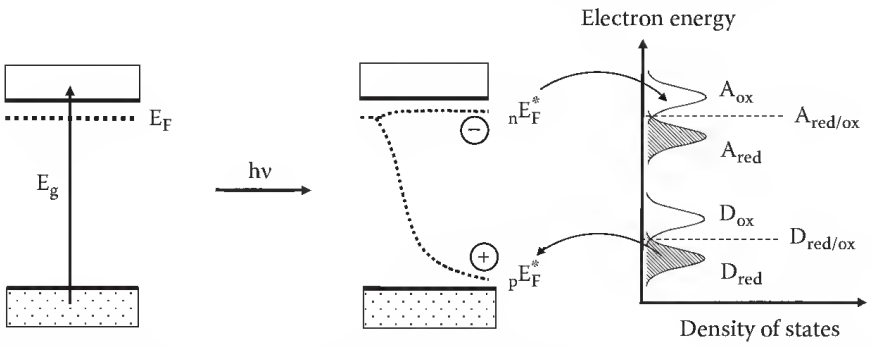

SCHEME 13.5 Thermodynamics of interfacial electron transfer (IFET) between a photoexcited semiconductor solid and dissolved donor and acceptor molecules. Dotted and empty boxes indicate occupied and empty valence and conduction bands, respectively.

* A classical example is also the hole oxidation of ethanol. $CH_3CH_2OH + h^+ = CH_3CHOH + H^+$, $CH_3CHOH = CH_3CHO + H^+ + e^-_{cb}$.

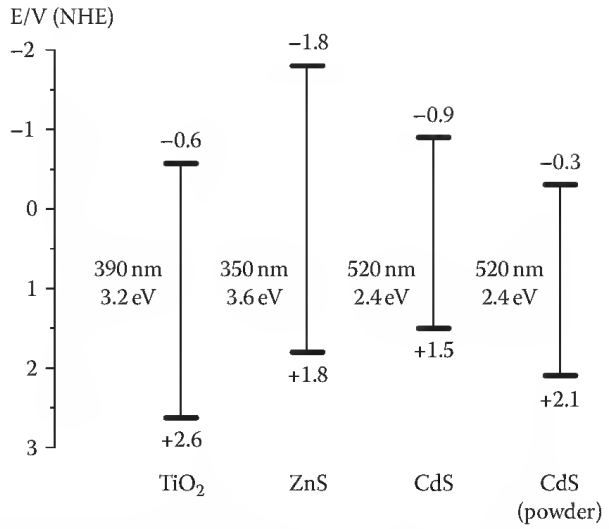

SCHEME 13.6 Bandgaps and band edge positions of some semiconductor single crystals and powder in contact with neutral water. ZnS,[153] CdS,[104] and TiO_2.[212]

The positions of the quasi-Fermi levels can be estimated from the band edges, which are known for the most commonly applied semiconductor powders as summarized in Scheme 13.6. Depending on the amount of doping, they are located a few tenths of an electron Volt below or above the conduction and valence band edge, respectively. It is noted that band edge positions of oxidic and sulfidic semiconductors strongly depend on the presence of impurities and on the solvent they are suspended in. Increasing the pH value of water induces a cathodic shift of the band edges by 0.059 V/pH unit. Similarly, substituting neutral water by, for example, acetonitrile the quasi-Fermi level is shifted by about 1.0 V.[58] In the case of CdS removal of traces of elemental sulfur and cadmium from the surface results in a cathodic shift of 1 V.[59] Adsorption of neutral thiols has no influence, whereas thiolate ions shift the Fermi level by 0.4 V cathodically.[60]

From the earlier discussion it follows that for a given semiconductor photocatalyzed reaction the variation of catalyst preparation, kind of solvent, and adsorption properties of substrates may induce a considerable shift of band positions. The estimation of the driving forces for the two IFET reactions is therefore connected with a large uncertainty. However, in spite of neglecting mutual kinetic barriers, in many cases it rationalizes the observed experimental results. An example is the photooxidation of lactic acid. Whereas platinized TiO_2 catalyzes oxidation to acetaldehyde and carbon dioxide, platinized CdS induces oxidation of only the OH group affording pyruvic acid. This is in accord with the less oxidizing property of h_r^+ since the valence band edge of CdS is located about 0.5 V more cathodic as compared to TiO_2.[61] Another possibility to introduce chemoselectivity is to vary the substrate's reduction potentials but keep the photocatalyst constant. It was reported that introduction of two methoxy groups in the para-positions of benzophenone shifts the reduction potential to the negative of the conduction band edge of highly pure cadmium sulfide and thus prevents the reduction to alcohols by water as observed with other aromatic ketones.[62]

13.2.3 Quantum Yield, Surface Area, Temperature, and Light Intensity

Due to the heterogeneity of the reaction system, kinetic experiments and other standard mechanistic experiments are not as straightforward to conduct and interpret as in homogeneous photochemistry. Especially, quantum yield determinations are ambiguous since it is difficult to correct for the amount of light scattered by the photocatalyst powder in order to obtain the amount of light absorbed. The latter may therefore significantly vary from experiment to experiment depending on the type of photoreactor and on the nature of the suspension. Scattering may lower the effective absorbed light intensity by

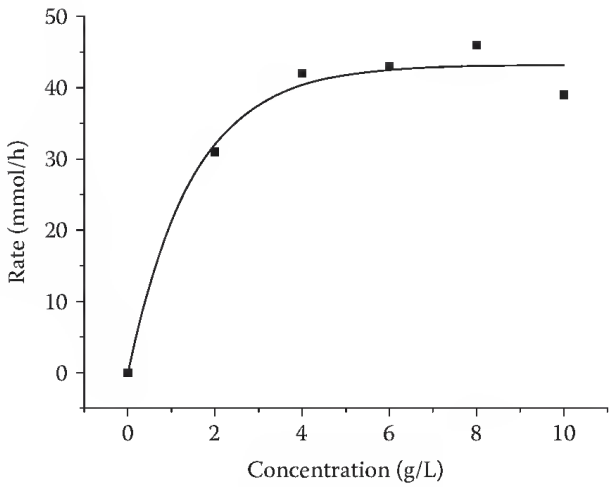

FIGURE 13.1 Reaction rate as function of photocatalyst concentration.

15%–80%.[63] Therefore, all quantum yields reported in the literature are in reality apparent quantum yields and can be compared only qualitatively. Various attempts have been made to overcome these problems[63–65] in order to allow a better comparison. The most important proposal is to calculate a so-called photonic efficiency and relative photonic efficiency by using instead of the absorbed light intensity the incident intensity, that is, intensity of light arriving at the reaction suspension.[64] However, this makes sense only if it is assumed that the fraction of scattered light is the same in every experiment, which is rather unlikely.[66] It seems therefore more practical to compare reaction rates obtained under optimized experimental conditions. This can be easily done by measuring the rate as a function of photocatalyst concentration. A typical example is shown in Figure 13.1 for a photocatalyst powder of specific surface area of $150\,m^2\,g^{-1}$.[67] Reaching a concentration above $4\,g\,L^{-1}$ apparently light absorption is saturated and the reaction rate does not further increase. The resulting optimum rate is a reasonable measure for comparing the efficiencies of various photocatalytic reactions.

The following qualitative discussion of the quantum yield of a reaction photocatalyzed by a semiconductor powder illustrates these problems in more detail.

Assuming that the efficiency of formation of the reactive electron hole pair (η_r), the efficiency of the IFET (η_{ifet}), and the efficiency of product formation from the primary redox products (η_p) are given by the ratio of the rate constants for formation and consumption of the

$$\eta_r = \frac{k_3}{k_1 + k_2 + k_3} \tag{13.10}$$

$$\eta_{ifet} = \frac{k_{6,7}}{k_5 + k_{6,7}} \tag{13.11}$$

$$\eta_p = \frac{k_{9,10}}{k_8 + k_{sb} + k_{9,10}} \tag{13.12}$$

$$A^{-\bullet} + h_r^{+} \rightarrow A \tag{13.13}$$

$$D^{+\bullet} + e_r^{-} \rightarrow D \tag{13.14}$$

$$\text{rate} = \Phi_p I_a = \eta_r \eta_{ifet} \eta_p I_a \tag{13.15}$$

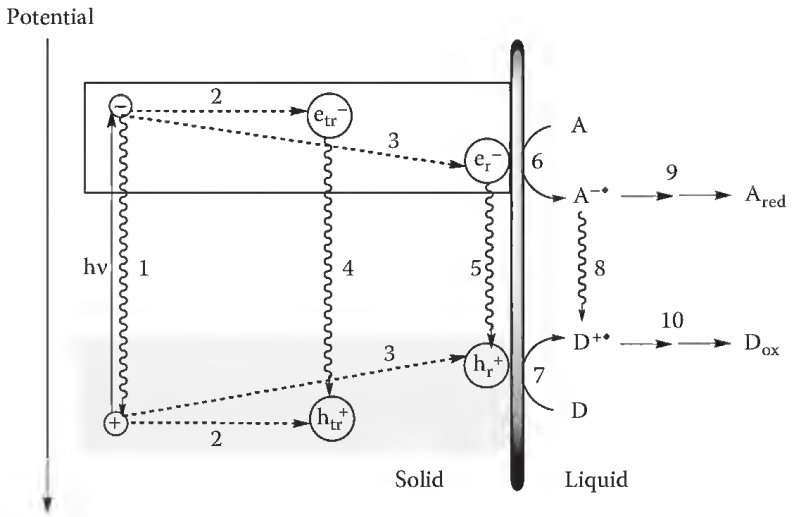

SCHEME 13.7 Schematic description of primary processes occurring during a semiconductor-photocatalyzed redox reaction. For the sake of simplicity photocorrosion is omitted. Light absorption and primary recombination (1); trapping at unreactive (2) or reactive (3) surface sites; secondary recombination (4,5); IFET processes (6,7); primary back electron transfer (8); secondary reactions (9,10).

corresponding intermediate (Equations 13.10 through 13.12, see Scheme 13.7); k_{sb} denotes the rate constant for the secondary back-electron transfer according to Equations 13.13 and 13.14), the rate of reaction is obtained according to Equation 13.15, wherein I_a denotes the intensity of absorbed light. Accordingly, the quantum yield of product formation, Φ_p, can be formulated as the product of $\eta_r \times \eta_{ifet} \times \eta_p$ and it is difficult to prove which term is decisive. The last term may be relatively independent on small changes of the semiconductor properties, whereas the two other terms can change considerably. Rather minor alterations during synthesis of the powder and adsorption of reaction components can strongly affect the photophysical properties of the semiconductor–liquid interface. Furthermore, when the quantum yields for various substrates are compared, it is difficult to relate observed changes to a specific process of the multistep reaction. In most cases, it also unknown if electron–hole pairs observed by emission spectroscopy are identical with the reactive electron–hole pairs involved in the IFET reactions. Emission quenching and reaction inhibition studies offer a simple possibility to decide between these possibilities (see Section 13.3.2).

The dependence of apparent quantum yields on light intensity can be characterized by two limiting cases.[68] At high intensity,* it increases linearly with the square root of the reciprocal intensity. This dependence is typical for homogeneous and heterogeneous photoreactions where recombination of primary products predominates. It has been observed for the TiO_2-catalyzed photooxidation of isopropanol,[68] the TiO_2/Pt-catalyzed photo-Kolbe reaction,[69] and the CdS-catalyzed photoisomerization of *cis*-stilbene.[70] At low light intensity, the quantum yield becomes independent on I_a and the reaction rate increases linearly with the first power of I_a. This is observed when the aforementioned reactions[68,70] are conducted at low light intensities.

From the earlier discussion, it is obvious that Φ_p may differ considerably upon minor changes in photocatalyst preparation and solution composition. Higher light intensities may increase recombination,[71] and photophysical processes like emission are strongly influenced by adsorbed impurities.[72,73] It has been reported that grinding of ZnS powder enhances its photocatalytic activity in the isomerization of olefins[74] through the generation of reactive surface states, probably some kind of sulfur radicals. Once formed, these catalyze the [2 + 2] cycloaddition of phenylvinyl ether even in the absence of further irradiation.[75]

Increasing the temperature may influence the slowest chemical reaction step and adsorption equilibria of substrates and products. Depending on the relation of the two latter steps and on the temperature

* A typical value for a given set-up is $\geq 10^{15}$ photons/s.

range investigated, the measured activation energy, E_a, may be zero and larger or smaller than zero.[76–79] Since these factors depend on the detailed nature of the photocatalyst, minor modifications may induce variations of E_a. Accordingly, values of about 2 and 4 kcal mol^{-1} were reported for two different CdS samples used in the photodimerization of *N*-vinylcarbazole.[80]

The specific surface area of the semiconductor powder may influence the rate of product formation through two opposite effects.[40] One is concerned with the rate of electron–hole recombination, which increases linearly with surface area, and accordingly the reaction rate should decrease. The other is a linear increase of the IFET rate due to increasing concentration of adsorbed substrates per unit volume, which should also increase the product formation rate. It is therefore expected that, depending on the nature of semiconductor and substrates, the reaction rate, or apparent Φ_p, may be constant, increase or decrease with increasing surface area. This is nicely reflected by the CdS/Pt catalyzed photoreduction of water by a mixture of sodium sulfide and sulfite. Highest Φ_p values are observed at small surface areas and are constant up to 2 $m^2\,g^{-1}$. From there a linear decrease to almost zero at a specific surface area of 6 $m^2\,g^{-1}$ takes place. Upon further increase to 100 $m^2\,g^{-1}$ this low quantum yield stays constant.[81] Besides the rate also the chemoselectivity may depend on the surface area, which is usually determined by the particle size.* Especially the possibility whether one or more electrons are transferred from and to substrates may be decided by the particle size as illustrated by the ZnS-catalyzed photooxidation of aqueous ethanol.[82] It was found that only nanometer-sized ZnS induces the formation of the $1h^+$-oxidation product 2,3-butanediol, whereas the $2h^+$-product acetaldehyde is produced by both photocatalysts.

13.2.4 Photocorrosion

Already in 1922, Lenard observed a darkening of the white pigment lithopone, a mixture of zinc sulfide and barium sulfate, upon exposition to sunlight. He assumed that the photocorrosion reaction afforded sulfur and metallic zinc.[83] Later it was shown that the presence of water is necessary for this process.[84] Quantitative investigations revealed the additional formation of hydrogen, zinc sulfate, and zinc hydroxide.[85] The decomposition of photoexcited ZnS into its elements is a consequence of the quasielement electronic configuration "Zn(0)S(0)" of the lowest lying electron–hole pair.[86] Due to the highly covalent Zn–S bond, the effective charges of zinc and sulfur in the ground state can be assumed as +1 and −1, respectively.[86–88] Since valence and conduction band have sulfur 3p and zinc 4s character, respectively,[89,90] the calculated quasielement nature of photoexcited ZnS becomes explainable. Cadmium sulfide behaves very similar and its mechanism of photocorrosion will be briefly discussed.[59] In the absence of air, anodic photocorrosion (Equation 13.16)

$$CdS + 2h^+ \rightarrow Cd^{2+} + S \tag{13.16}$$

affords elemental sulfur and cadmium ions, which are reduced to cadmium metal upon prolonged irradiation (Equation 13.17):

$$Cd^{2+} + 2e^- \rightarrow Cd(0) \tag{13.17}$$

This latter reaction competes with the reduction of lattice metal ions (Equation 13.18).

$$CdS + 2e^- \rightarrow Cd(0) + S^{2-} \tag{13.18}$$

In the case of ZnS or platinized CdS powder, the reduction of water is a further competitive process (Equation 13.19):

$$2H_2O + 2e^- \rightarrow H_2 + 2OH^- \tag{13.19}$$

* Note that only for nonporous materials does the surface area increase with smaller particle size; however, most of the powders employed are very porous.

In the presence of air, at short illumination times the overall reaction is described by Equation 13.20:

$$CdS + 2O_2 \xrightarrow{hv} Cd^{2+} + SO_4^{2-} \tag{13.20}$$

All these photocorrosion processes are of course undesired and it is obvious that their relative importance strongly depends on the presence of surface states, which may facilitate recombination or redox reactions with adsorbed substrates. It is well known from ESR[71,72,91] and emission spectra[92] that most of these metal sulfide powders contain surface states. They are introduced during preparation of the powder as a result of lattice defects,[74,93] trapped holes,[91] surface impurities,[94] and during the catalytic reaction as a consequence of irradiation and substrate adsorption. Different from metal sulfide semiconductors, titanium dioxide is quite photostable.

13.2.5 Photocatalyst Preparation and Characterization

From the results presented in the previous paragraphs of this chapter, it follows that photocatalytic activity and chemoselectivity of a semiconductor photocatalyst should depend on intimate details of preparation. In addition to careful description of the synthetic details, it is important to characterize the obtained powder by bulk and surface elemental analysis, by determination of crystal structure, specific surface area and surface charge, by ESR and electronic absorption and emission spectroscopy, and by photoelectrochemical experiments to prove the semiconducting properties. The latter are of special importance in order to disfavor a general heterogeneous catalysis mechanism, which usually does not involve simultaneous reductive and oxidative interfacial electron transfer steps.[95,96] Their involvement may be demonstrated by the effects of electron and hole scavengers added to the reacting system. In the following, we briefly summarize the most important physical properties of the ZnS and CdS powders employed as photocatalysts in the syntheses of novel organic compounds (vide infra).

13.2.6 Pristine Semiconductor Photocatalysts

Zinc sulfide is easily prepared from sodium sulfide or thiourea and zinc sulfate under an argon atmosphere. Working in the presence of air introduces traces of zinc oxide, which promotes photocorrosion. The resulting porous powder contains 2%–3% water,[97] has a specific surface area in the range of 100–170 $m^2\ g^{-1}$, and consists of 1–10 μm large particles composed of cubic nanocrystals.[98] Elemental analyses of the bulk materials afford the ratio Zn/S = 1.00/0.97, whereas surface analyses reveal values of Zn/S = 1.00/1.35 to 1.00/1.60. This significant excess of surface sulfur is most likely responsible for the pronounced photostability of these samples even when irradiated in an aqueous suspension in absence of any other substrate. Contrary to that, zinc sulfide, which has a surface excess of zinc, immediately suffers photocorrosion.[94] Diffuse reflectance spectroscopy indicates a weak subband gap absorption starting at about 400 nm followed by the steep onset of the band-to-band absorption at 360 nm; in some cases, a weak absorption maximum is observable at 450 nm, most likely due to the presence of surface sulfide species.[94] Accordingly, the emission spectrum of the powder, in addition to the band-gap emission at about 360 nm, contains broad bands around 400 and 490 nm, which originate from recombination of the electron–hole pair scavenged at shallow and deep traps within the band gap.[94,99] Further emissions at 525 and 690 nm are due to traces of zinc oxide. At higher concentrations, ZnO completely inactivates the photocatalyst. Slightly different to the dry powders, the emission spectrum of an aqueous ZnS suspension exhibits in addition to the band-to-band emission only one further band at 430 nm. This self-activated emission[100–102] is generated by excess surface zinc ions (sulfur vacancies) as indicated by its disappearance upon addition of sulfide ions.[103] From the difference to the bandgap energy of 3.6 eV, one can estimate that the corresponding surface state is located about 0.7 eV below the conduction band edge, that is, at a potential of –1.1 V (at pH 7). A value of –1.0 V was reported for colloidal zinc sulfide.[82]

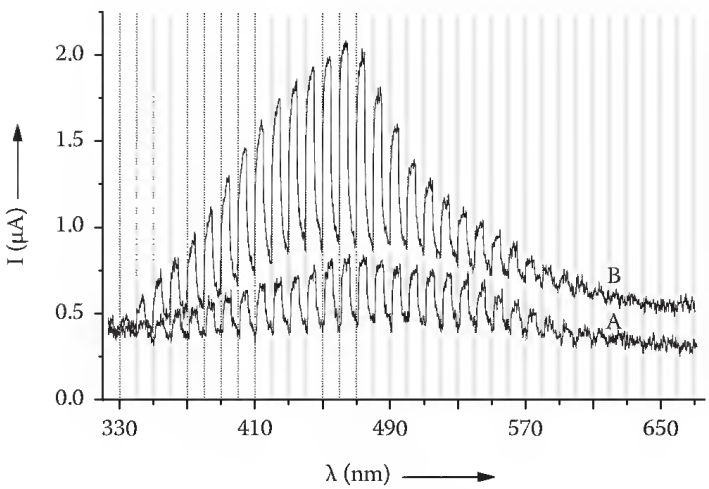

FIGURE 13.2 Photocurrent spectra of a CdS-covered indium tin oxide (ITO) conducting glass electrode (0.5 V vs. Ag/AgCl) as obtained upon chopped irradiation (light and dark phases were 15 s); supporting electrolyte 0.1 M NaOH (A) and 0.1 M NaOH + MeOH (B).

The n-type character of these zinc sulfides is indicated by the observation of an anodic photocurrent upon illumination of a powder-coated electrode.

Cadmium sulfide is prepared from sodium sulfide and an aqueous ammonia solution of cadmium sulfate. Similarly to the self-prepared zinc sulfide, the obtained powder contain 2%–3% water, has specific surface areas of about 160 $m^2\ g^{-1}$, and consists of cubic nanocrystals forming micrometer large aggregates. n-Type semiconductor behavior is indicated by observation of an anodic photocurrent upon irradiating a CdS/ITO powder electrode at wavelengths of 330–650 nm (Figure 13.2).

It is noted that the bandgap absorption of CdS starts at 520 nm. Addition of methanol induces photocurrent amplification with a factor of about 2, irrespective of the energy of excitation. From measurement of the quasi-Fermi potential according to the slurry method,[104,105] the position of the conduction band edge at pH 7 is found to be at −0.4 V (NHE).[106] Values of −0.27 to −0.29 V were reported for other cadmium sulfide powders.[104,105]

13.2.7 Grafted Semiconductor Photocatalysts

In addition to pristine semiconductor powders, also photocatalysts supported onto a carrier may be beneficially employed. The idea is that substrate adsorption at the support may increase adsorption at the semiconductor surface and therefore also the reaction rate. A slight improvement is observable, when mixed oxides of TiO_2/SiO_2 prepared by a sol-gel method are used in the oxidation reactions.[52,53] The genuine photochemical properties of the semiconductor like bandgap and Fermi level are not altered in this case. However, when the semiconductor is not just ground with silica but grafted onto it, that is, chemically bound, bandgap and Fermi level change and the reaction rate is much stronger affected. In the case of CdS grafted by 12 wt% onto silica, the bandgap is enlarged by 0.20 eV (Figure 13.3) and the quasi-Fermi level shifts cathodically from −0.38 V to −0.59 V (at pH 7).[107] In the case of titania grafted by 13 wt% onto silica the bandgap widening is the same but the quasi-Fermi level is shifted anodically from −0.51 to −0.31 V (at pH 7). Contrary to the mechanically prepared mixture the two components are linked together by Cd–O–Si and Ti–O–Si bonds inducing an electronic semiconductor-support interaction (SEMSI effect) and as consequence thereof a considerable change of intrinsic semiconductor properties. The grafted photocatalysts are easily prepared by impregnating silica with cadmium ions or alkoxytitanates followed by precipitation with sodium sulfide or hydrolysis. Whereas the resulting CdS-12/SiO_2 (Figure 13.3) photocatalyst is twelve times more active than pristine CdS, TiO_2-13/SiO_2 is about four times slower than unmodified titania.[107,108] Higher amounts of loading afford less active

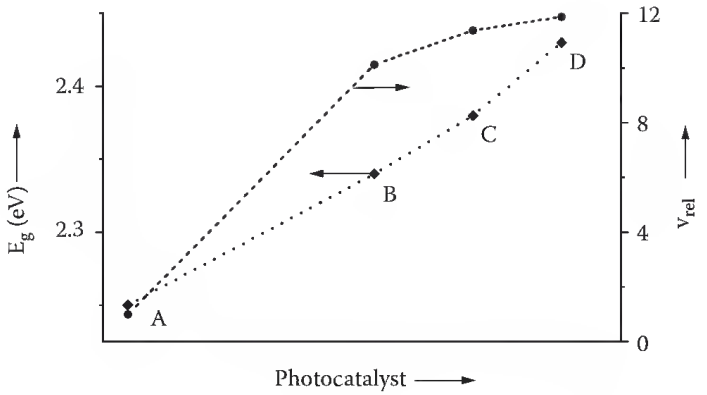

FIGURE 13.3 Decreasing the amount of CdS grafted onto silica increases bandgap and reaction rate. CdS(A, $v_{rel} = 1$), CdS-50/SiO_2(B),CdS-30/SiO_2(C), and CdS-12/SiO_2(D).

photocatalysts (Figure 13.3). The most active CdS-12/SiO_2 exhibits also the largest bandgap widening. This contrary effect of grafted CdS and TiO_2 on the photocatalytic activity agrees with the results of time resolved photocharge measurements on the two grafted photocatalysts embedded in an organic polymer matrix. After laser excitation at 337 nm, a multiexponential decay is observed, which is composed of a fast surface (ns) and slow bulk (μs) component. The decay constant of the fastest process decreases from $11 \times 10^6\ s^{-1}$ for CdS to $2 \times 10^6\ s^{-1}$ for CdS-12/SiO_2, corresponding to lifetimes of 90 and 500 ns.[109] Thus, the SEMSI effect increases the charge-carrier lifetime and therefore the IFET reaction becomes faster. Contrary to that, the lifetime of the light-generated charges in TiO_2-13/SiO_2 is shortened below the detection limit of 40 ns.[108]

Quasi-Fermi levels of the various powder samples are easily obtained by measuring the photovoltage of a semiconductor suspended in aqueous solution of the pH-independent redox system $MV^{2+/+}$ as function of pH value.[105,111] The method is based on the cathodic shift of the Fermi level upon decreasing proton concentration. At the inflection point the quasi-Fermi level and the methylviologen reduction potential are identical. A lower pH_0 value corresponds to a more negative flatband potential.

Whereas the quasi-Fermi level of −0.38 V measured for CdS-50/SiO_2 does not differ from that of unsupported CdS, it is shifted to −0.41 and −0.59 V in the case of CdS-30/SiO_2 and CdS-12/SiO_2, respectively (Figure 13.4). In the same sequence, the relative initial rate[107] increases from 1.0 to 12 (Figure 13.3). Since the 10-fold rate increase exhibited by CdS-50/SiO_2 cannot be caused by a change of the position of the Fermi level, which is the same as for unmodified CdS, it may originate from the anodic shift of

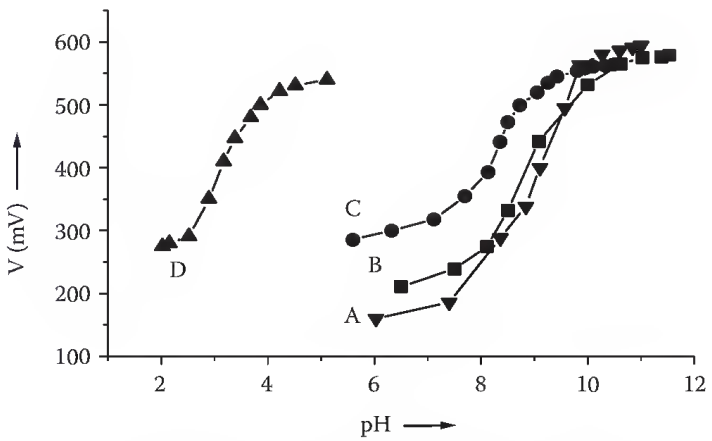

FIGURE 13.4 Dependence of photovoltage (vs. NHE) on pH value of the methylviologen (MV^{2+}) containing electrolyte. CdS (A), CdS-50/SiO_2 (B), CdS-30/SiO_2 (C), and CdS-12/SiO_2 (D).

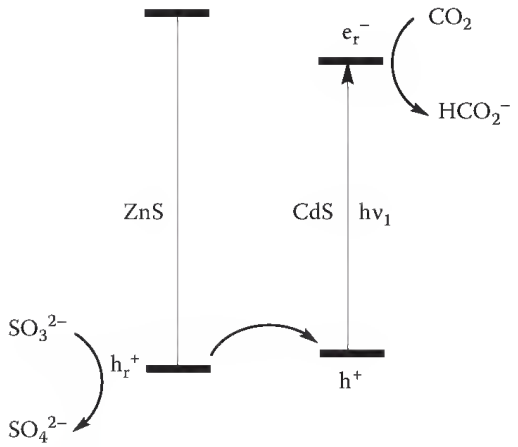

SCHEME 13.8 Schematic description of improved charge separation in CdS-grafted ZnS.

the valence band edge, which should result in an acceleration of the oxidative IFET reaction. Since this energy band has predominantly sulfur character, the shift should increase the binding energy of the sulfur 2*p* electrons. In fact, values of 162.7 and 162.9 eV were measured for CdS and CdS-50/SiO_2, respectively.[107]

A further improvement of photocatalytic activity may be accomplished by replacing the nonconductive silica by a semiconducting support. Grafting CdS onto ZnS affords CdS-17/ZnS having an about 40 times higher visible light activity in the reduction of carbon dioxide to formate than unsupported cadmium sulfide.[110] This can be rationalized by assuming that an interparticle electron transfer from the valence band of zinc sulfide to CdS prevents electron–hole recombination (Scheme 13.8).

13.3 Photocatalysis Type A Reactions

13.3.1 Dealkylation, Cyclization, and Hydroalkylation

Induced by the early work of Bard et al. on the TiO_2-catalyzed photo-Kolbe reaction,[43] many papers appeared thereafter dealing with photocatalytic[112] organic reactions in the presence of colloidal or suspended semiconductor particles.[31] They include *cis–trans* isomerizations,[70,113–117] valence isomerizations,[118,119] substitution and cycloaddition reactions,[75,80,120–123] oxidations,[124,125] and reductions.[126–128] In almost all cases, well-known compounds were formed, which were not isolated but only identified by spectroscopic methods. The nature of products can be rationalized within the mechanistic scheme of semiconductor photocatalysis type A, which means at least one reduced and one oxidized compound are obtained (see Scheme 13.1). In most cases, it is the oxidative part of the reaction wherein the organic substrate is involved. This means that the reactivity of the initially formed radical cation determines the kind of products finally formed. Typical reactions of radical cations are deprotonation, bond cleavage, and electron transfer.[129,130] An early example which illustrates two important mechanistic cases is the exhaustive photodealkylation of methylene blue and rhodamine B[55,131,*] catalyzed by nonplatinized CdS (see Scheme 13.4). This mechanistic case is rather rare since in general light is absorbed by the semiconductor and the radical cation is generated in the oxidative primary step through IFET from the substrate to the reactive hole (h_r^+). In addition to deprotonation via C–H cleavage, radical cations may be transformed to the corresponding radicals also by C–C, C–Si, and other bond cleavages. The *intra-* or *intermolecular* consecutive reactions of these radicals usually determine the chemoselectivity of the overall reaction. Examples for intramolecular reactions are cyclizations of diamino dicarboxylic acids[132,133] and the hydrazone **3**,[134] which both proceed via C–N coupling. The proposed mechanism for

* Here and in the following, the use of the chemical formula indicates that the semiconductor was present as a powder suspension.

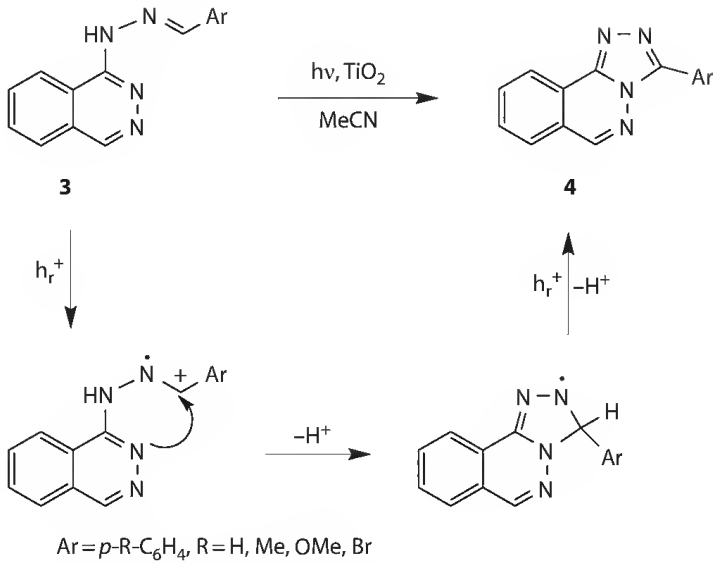

SCHEME 13.9 Cyclization of hydrazone **3**. Deprotonation induced C–N bond formation. Note that two electron–hole pairs are necessary to produce one product molecule **4** ($2e^-/2h^+$ process).

the oxidative part of the latter reaction is summarized in Scheme 13.9, wherein the reductive part, most likely reduction of water, is omitted.

An example for an intermolecular consecutive reaction is the hydroalkylation of olefins.[135,136] TiO_2 photocatalyzes the reaction of benzyltrimethylsilane (**5**) and maleic acid (**6**) to the hydroalkylation product **8** with dibenzyl (**7**) and 1,2-dibenzylsuccinic acid (**9**) as by-products (Scheme 13.10). It is proposed that in the reductive primary step **6** is reduced to the relatively stable radical anion $\mathbf{6}^{-\bullet}$. The oxidatively formed radical cation $\mathbf{5}^{+\bullet}$ undergoes a fast C–Si bond cleavage to Me_3Si^+ and $PhCH_2^\bullet$. Addition of the latter to **6** followed by proton-coupled reduction by $\mathbf{6}^{-\bullet}$ or e_r^- affords **8**. Different from the cyclizations mentioned earlier, only one electron–hole pair is required to obtain one molecule of the product **8** ($1\,e^-/1\,h^+$ process).

The hydrazone cyclization and hydroalkylation reactions are rare examples of semiconductor photocatalysis conducted on a preparative scale, since the products were isolated in milligram amounts and not just identified in solution. As already mentioned in Section 13.2.4, photocorrosion of the semiconductor photocatalyst quite often prevents its use in preparative chemistry. This is very true for colloidal semiconductors; although the pseudo-homogeneous nature of their solutions allows classical mechanistic investigations, until now they were too labile to be used in preparative chemistry.[108,137,138]

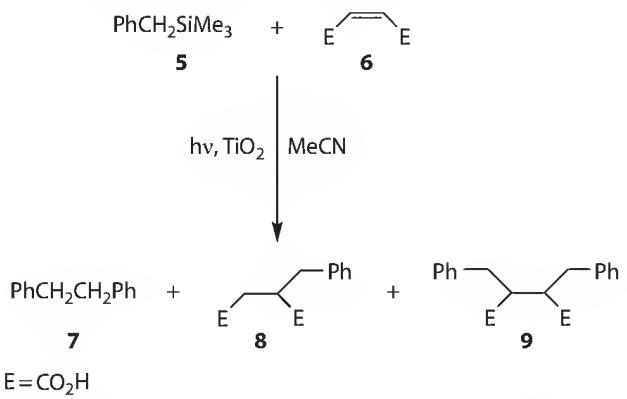

SCHEME 13.10 Hydroalkylation of maleic acid by benzyltrimethylsilane through C–Si bond cleavage of the intermediary radical cation followed by addition of the generated radical to maleic acid and final hydrogen abstraction.

In general, all the reactions mentioned earlier do not lead to novel products nor do they introduce novel aspects to organic synthesis. Different from this, the reactions discussed in the next two chapters produce new compounds on a gram-scale. The major part of them are atom-economic addition reactions, termed semiconductor photocatalysis type B.

13.3.2 Dehydrodimerization of Cyclic Enol or Allyl Ethers and Olefins

Irradiation of an aqueous 2,5-DHF suspension of ZnS (E_{bg} = 3.6 eV, $\lambda \leq 345$ nm) with UV light affords a few liters of hydrogen and gram-amounts of the hitherto unknown dehydrodimer **10** in isolated yields of 60% (Scheme 13.11).[139–141] No reaction is observed in the absence of water and the initially evolved hydrogen gas contains about 90% of D_2 when D_2O is employed. Colloidal zinc sulfide or high-purity single crystals do not catalyze the reaction.[103] The use of platinized CdS (E_{bg} = 4.2 eV, $\lambda \leq 520$ nm) enables a reaction by visible light, but with a poorer yield.[140] Structure and statistical ratio of the three regioisomeric dehydrodimers suggest that the products are formed by dimerization of an intermediate dihydrofuryl radical. Hydrogen and dehydrodimer formation can be rationalized within the scheme for semiconductor photocatalysis type A as depicted in Schemes 13.1 and 13.11. In the reductive reaction step water is reduced to hydrogen (Equation 13.21), whereas in the oxidative part 2,5-DHF is oxidized to the dihydrofuryl radical and a proton (Equation 13.22). According to this, although water is reduced, it should not be consumed, since it is reformed as indicated by the sum of the two equations. In fact, even after production of 2–3 L of hydrogen, no water consumption could be measured. The net reaction can therefore be summarized according to Equation 13.23:

$$2e_r^- + 2H_2O \rightarrow H_2 + 2OH^- \tag{13.21}$$

$$2h_r^+ + 2RH \rightarrow 2R^\bullet + 2H^+ \tag{13.22}$$

$$2RH \xrightarrow[H_2O]{h\nu,\ ZnS} H_2 + R-R \tag{13.23}$$

Further support stems from the observation that the initially observed D_2 content of 90% drops to 40% after evolution of 1 L of hydrogen, whereas the sum of HD and H_2 increased from 10% to 60%.[141] From these results, it is obvious that the formation of D_2 from D_2O in "sacrificial" systems for water reduction is a necessary but not sufficient criterion for "permanent" water cleavage.* This result is of basic importance since in no system for "sacrificial" photochemical hydrogen production the consumption of water was ever proven.

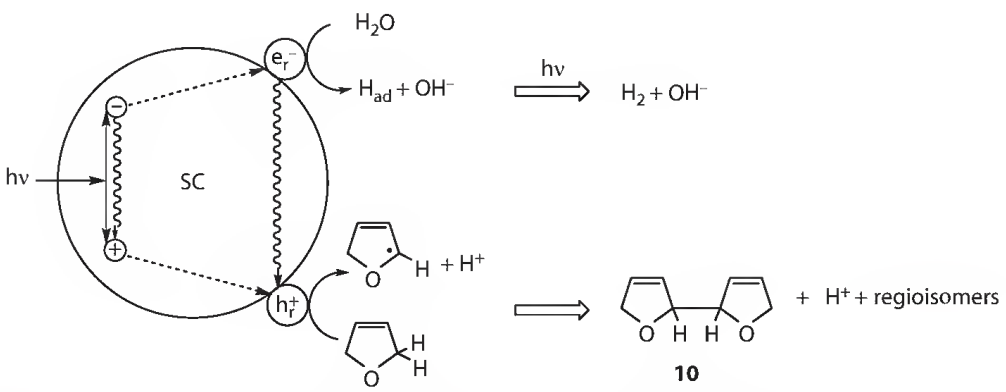

SCHEME 13.11 Semiconductor photocatalyzed dehydrodimerization of 2,5-dihydrofuran. SC = ZnS, Pt/CdS. In the two other product isomers C–C bond formation occurred in the 3,3′- and 3,2′-positions ($2e^-/2h^+$ process).

* An often neglected aspectin many "sacrificial" systems of water splitting.

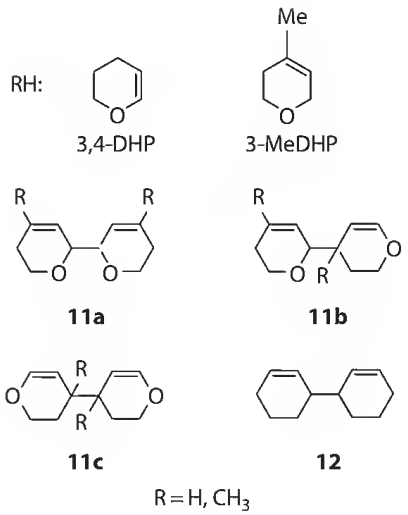

FIGURE 13.5 Structures of dehydrodimers of 3,4-dihydropyran, 3-methyl-2,5-dihydropyran, and cyclohexene.

Since the dehydrodimer **10** was not known before, this reaction is the first example for the preparation of a novel compound through semiconductor photocatalysis. The analogous products **11**, **12** are obtained from 3,4-dihydropyran (3,4-DHP), 3-methyl-2,3-dihydropyran (3-MeDHP), and cyclohexene in isolated yields of 30%–60% (Equation 13.23, Figure 13.5).[94] The saturated ether tetrahydrofuran is also dehydrodimerized while 1,4-dioxane does not react. In situ prepared zinc sulfide, which was independently investigated by Yanagida et al., photocatalyzes the same reactions but exhibits a slightly different chemoselectivity as indicted by the dehydrodimerization of 1,4-dioxane.[142,143]

To unravel the detailed mechanism, substrate adsorption, quenching, inhibition, and kinetic studies were conducted for the ZnS-catalyzed photodehydrodimerization of 2,5-DHF.[97,103] A plot of the amount of 2,5-DHF adsorbed (n_{eq}) against the residual concentration in solution (c_{eq}) exhibits saturation plateaus at $n_{eq(max)}$ of 2.8×10^{-3} and 65×10^{-3} mol g^{-1}. The first plateau is due to formation of a mixed solvent–solute surface monolayer and the second corresponds to multilayer adsorption. Assuming that the formation of the monolayer can be described by competitive adsorption between water and 2,5-DHF, the data can be analyzed according to the Hiemenz model.[144,145] In addition to an adsorption constant of 170 ± 30 L mol^{-1} the average area occupied by 2,5-DHF in the surface-solute monolayer is obtained as 10.2 $Å^2$. The latter value agrees well with 9.1 $Å^2$ as calculated for 2,5-DHF adsorbed edge-on to the ZnS surface.* From the surface density of zinc sites (11.4×10^{-6} mol m^{-2}) of cubic zinc sulfide[146] and the specific surface area (100–170 m^2g^{-1}) of the ZnS employed, one estimates that the surface concentration of 2,5-DHF in the saturated monolayer is in the range of $(1–2) \times 10^{-3}$ mol g^{-1}. This good agreement with the experimental value of 2.8×10^{-3} mol g^{-1} suggests that each zinc site is occupied by a 2,5-DHF molecule. The rather small downfield shift of 1.5 ppm as observed for the C(sp^3) atoms of adsorbed 2,5-DHF by ^{13}C NMR suggest that the oxygen atom does not directly interact with zinc sites but rather indirectly through hydrogen bonding to coordinated water.

To find out if emissive (e_{tr}^-,h_{tr}^+) and reactive (e_r^-,h_r^+) electron–hole pairs are identical or not, emission quenching and reaction inhibition studies were performed.[103] Addition of zinc or cadmium sulfate slightly increases or does not alter the emission intensity of an aqueous ZnS suspension respectively. 2,5-DHF has no significant influence. The two emission bands at 366 and 430 nm correspond to the transitions $h\nu_1$ and $h\nu_2$, respectively. Contrary to emission, the reaction is strongly inhibited when cadmium or zinc salts are added. This indicates that emitting and reacting surface sites are different. A Stern–Volmer plot of the reduced reaction rate as function of the initial inhibitor concentration affords a straight line only, when the concentration of adsorbed ions is employed (Figure 13.6). From the

* Estimated according to 3.8 Å × 2.4 Å.

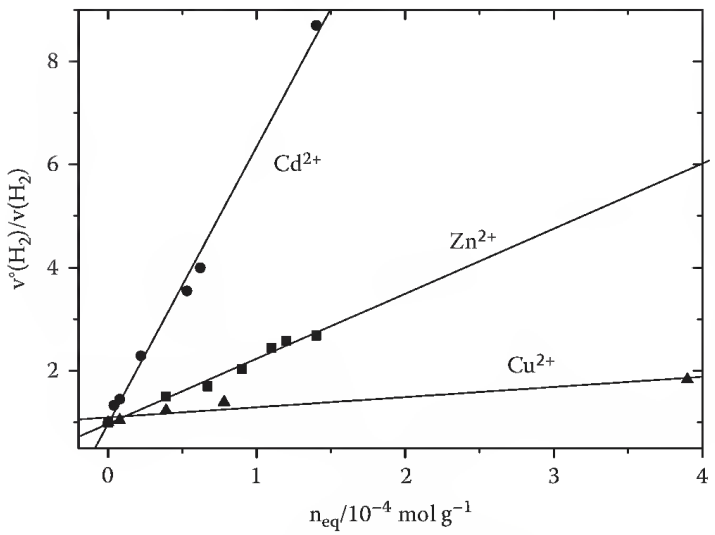

FIGURE 13.6 Stern–Volmer plot of the ZnS-photocatalyzed dehydrodimerization of 2,5-dihydrofuran.

corresponding slopes, Stern–Volmer constants of $13 \times 10^3\,M^{-1}$ and $50 \times 10^3\,M^{-1}$ are calculated for Zn^{2+} and Cd^{2+}, respectively.[24,147,*] Copper(II) ions exert only a very weak inhibition.

Inhibition by Cd^{2+} proceeds via competitive IFET (Equation 13.24), since even at the very low concentration of 3.9×10^{-6} mol g^{-1} formation of elemental cadmium is observable; complete inhibition occurs at 6×10^{-4} mol g^{-1}:

$$2e_r^- + Cd^{2+} \rightarrow Cd \tag{13.24}$$

This differs significantly from the effect of zinc ions in which the expected elemental zinc[101,102] could not be detected, even at the high concentration of 0.8 mol g^{-1}. From this, one can conclude that zinc ions either prevent formation of the reactive electron–hole pair or efficiently promote its radiationless deactivation (Scheme 13.12).

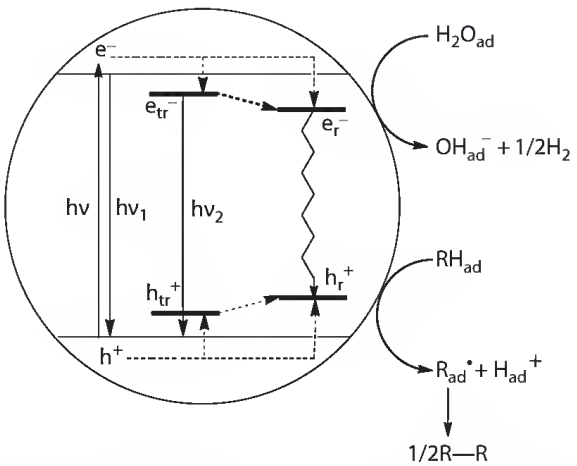

SCHEME 13.12 Simplified mechanistic scheme of the ZnS-photocatalyzed dehydrodimerization. RH = unsaturated ether, olefin.

* Although the lifetime of the reactive electron-hole pair is not known, the reasonable estimate of 10^{-6}–10^{-9} s leads to an electron transfer rate constant between 10^{10} and $10^{13}\,M^{-1}s^{-1}$. In general, electron transfer reactions at the semiconductor-liquid interface are very fast.

From detailed inhibition studies with various metal ions, it follows that Fe^{2+} and Ni^{2+} accelerate the reaction up to a concentration of about 0.7×10^{-3} M, but inhibit the reaction at concentrations above 2×10^{-3} and 6×10^{-3} M, respectively.[97] In the case of Mn^{2+} no maximum is seen, but a plateau starts forming at about 1×10^{-3} M. At a given surface concentration of these ions ($n_{eq} = 3 \times 10^{-5}$ mol g^{-1}), no simple relation is observed with the reduction potentials of the metal ions. However, the reaction rate increases approximately linearly with the exchange current density of hydrogen evolution at the corresponding metal electrode. This strongly suggests that water reduction at the photoexcited ZnS/M_{ad}^{2+}-surface occurs at small metal islands generated by photoreduction.

From these results, the primary events at the ZnS surface can be summarized as schematically depicted in Scheme 13.12. The light generated electron–hole pair has a lifetime of 0.1–20 ns and either recombines through radiative or nonradiative processes or is trapped at emitting (e_{tr}^-,h_{tr}^+) or reacting surface (e_r^-,h_r^+) sites. Whereas the former are detected by their emission at 440 nm, the latter could not be observed directly but their existence is evidenced through the inhibition experiments with the metal ions. The reduction of water most likely is located at surface states generated by zinc metal islands as also postulated for the photooxidation of alcohols at colloidal zinc sulfide.[148] For the formation of the 2,5-dihydrofuryl radical in the oxidative part of the reaction, three pathways may be considered. Firstly, hydrogen abstraction by a surface sulfur radical. Although such radicals have been detected at zinc sulfides,[74,113,149,150] this reaction path is rather unlikely since THF is also dehydrodimerized but does not undergo H-abstraction with sulfur-centered radicals in homogeneous solution.[151] Secondly, a stepwise formation through an initially formed radical cation takes place followed by deprotonation. And thirdly, a concerted process is observed where IFET is coupled to deprotonation, as indicated in Scheme 13.12. Although a final decision between the two latter processes is not possible at present, all experimental evidence is in favor of the concerted pathway.

Although the position of the redox potential of the reactive hole is not known, it can be estimated to be in the range of 1.6–2.0 V by considering that the value of the valence band edge reported for crystals (1.8 V) may be shifted through substrate adsorption as known for other semiconductors.[152–155] From the oxidation potential of 2,5-DHF of 2.6 V, it follows that the oxidation to the radical cation is endergonic by at least 0.6 eV. Accordingly, there is no simple relation between apparent product quantum yield and redox potential when various substrates are compared. On the other hand, a similar estimation for the concerted process (Equation 13.25) reveals that the reaction is exergonic by at least 0.9 eV.[165,*]

$$RH \rightarrow R^{\bullet} + H^+ + e^- \tag{13.25}$$

Since the driving force of this reaction is the difference between the free enthalpy of C–H bond homolysis and the potential of the hydrogen electrode, the former value should be decisive when comparing apparent quantum yields of various substrates. Figure 13.7 displays the relation between quantum yield and calculated bond dissociation energy of the corresponding C–H bond.[103] The expected increase with decreasing bond strength favors the concerted oxidation pathway. The deviation of 3-MeDHP most likely arises from steric hindrance of the radical C–C coupling step by the adjacent methyl group.

Once formed, the dihydrofuryl radicals may undergo a variety of reactions as known from homogeneous chemistry including disproportionation, addition to double bonds, electron transfer, and dimerization. Surprisingly, the latter pathway is followed to about 90% as indicated by the complete material balance.[141] It is therefore likely that C–C coupling occurs between radicals within the water–2,5-DHF surface layer. This is corroborated by the quadratic dependence of the initial rate on the amount of

* Calculated by using $E_0(H^+/H) = -2.40$ V(H_2O)[157] and a bond dissociation energy of 3.22 eV[100]; these were converted to the $\Delta G(H_2O)$ values by subtracting 0.1 eV for the solvent contribution.[157] The same argument was used to explain the photooxidation of alcohols by ZnS[150].

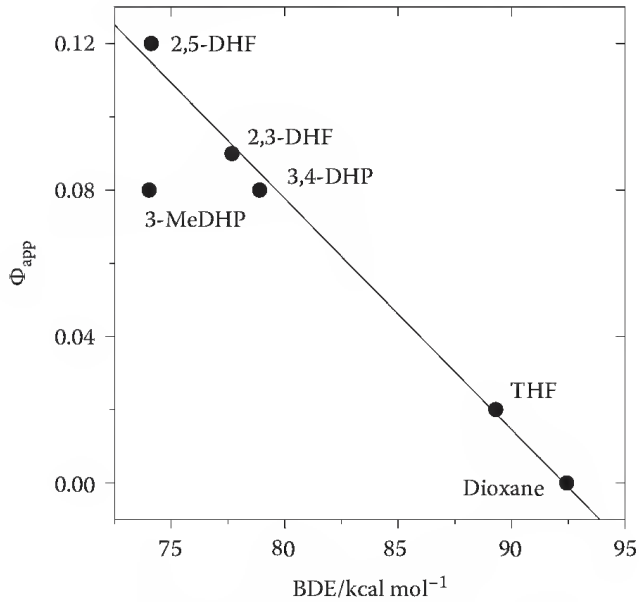

FIGURE 13.7 ZnS-photocatalyzed dehydrodimerization of 2,5-DHF. Dependence of apparent product quantum yield on the calculated bond dissociation energy of the allylic C–H bond.

adsorbed 2,5-DHF. This dependence corresponds to a heterogeneous catalytic dimerization by a modified Langmuir–Hinshelwood mechanism affording easily desorbable products.[157] It further suggests that at early reaction stages the concentration of adsorbed radicals increases linearly with the bulk concentration of 2,5-DHF. The latter relation breaks down as the reaction progresses, since the consumption of 2,5-DHF is faster than its adsorption from solution. Accordingly, the instantaneous rate decreases stronger with time for lower starting concentrations than for higher and finally becomes diffusion controlled.[97] C–C coupling between radicals adsorbed in the water–2,5-DHF surface layer is further supported by competition experiments with THF. Although the unsaturated ether reacts only ten times faster than the saturated one, no THF dehydrodimers or cross-products are detected when THF is present in 10-fold excess over 2,5-DHF. Only at a 500-fold higher concentration the expected products are observed.

In summary, one can conclude that the formation of H_2 and the dehydrodimer occurs via subsequent adsorption of two photons ($2e^-/2h^+$-process). The mutual adsorbed hydrogen atom and dihydrofuryl radical generated by the first photon must have lifetimes long enough to wait for the arrival of the second photon. This requirement is easily fulfilled since at a micrometer-sized ZnS particle the time interval between two successive photon absorptions can be estimated to be in range of 20 ps, much shorter than the lifetime of radicals and radical cations, which are in the range of at least nanoseconds. But the question arises why the C–C homocoupling between two radicals is so highly favored over C–H heterocoupling with an adsorbed hydrogen atom to re-form 2,5-DHF.[141,*] One possibility is that the first electron does not produce an adsorbed hydrogen atom, but is stored at the metallic zinc center and water is subsequently reduced in a two-electron step. Or, the adsorbed hydrogen atom does not undergo coupling to the dihydrofuryl radical because of unknown kinetic barriers. Therefore it seemed worthwhile to replace water by an organic acceptor that could produce a more stable one-electron reduction intermediate, perhaps capable of undergoing the postulated heterocoupling with the one-electron oxidation intermediate. The following chapter illustrates that this concept led to the catalysis of photoaddition reactions, classified as semiconductor photocatalysis type B.

* It is noted that deuterium is not incorporated into unreacted 2,5-DHF and dehydrodimers when D_2O is employed.

13.4 Semiconductor Photocatalysis Type B

13.4.1 Linear Addition of Cyclic Enol/Allyl Ethers and Olefins to 1,2-Diazenes

Upon addition of azobenzene to a running ZnS-catalyzed photodehydrodimerization experiment of 2,5-DHF, hydrogen evolution is completely inhibited in favor of formation of the novel allylhydrazine **13c**, a linear addition product of 2,5-DHF to azobenzene; small amounts of hydrazobenzene (**14**) are formed as a by-product (Scheme 13.13).[137,138] When all the azobenzene is consumed and some excess 2,5-DHF is still present, hydrogen evolution starts again. Replacing ZnS by CdS or silica-supported CdS (CdS/SiO_2),[158] allows to conduct the reaction with visible light; a simple tungsten–halogen lamp can be used instead of the high-pressure mercury lamp. When colloidal CdS[159] is employed in the system 3,4-DHP/1,2-diphenyldiazene/MeOH, no photoaddition but efficient photocorrosion occurs. Scheme 13.13 summarizes the novel allylhydrazines **13a–f** prepared on a gram scale by this simple route employing methanol as the solvent.[137,138] Due to the poor crystallization properties, isolated yields are only in the range of 10%–40% whereas HPLC yields are about twice larger. Structural assignments are based on an x-ray structural analysis of **13b** and on standard spectroscopic data. Dynamic NMR spectra of **13b** reveal that rotation around the N–N bond is hindered; the corresponding free activation enthalpy amounts to 14 kcal mol^{-1}.

From a few examples of limited synthetic utility it is known that the same reaction type may occur in homogeneous solution when either the 1,2-diazene[160–162] or the olefin[163–165] is substituted by electron-withdrawing groups. Some other allylhydrazines have been prepared by more conventional thermal procedures.[166]

The photoaddition exhibits a significant solvent dependence. No reaction occurs in dry *n*-hexane or THF, but upon addition of water or methanol the reaction is as fast as in pure methanol. From the discussion at the end of Section 13.3.2 and the experimental results presented earlier, a simplified reaction scheme can be constructed (Scheme 13.14):

Since the presence of the diazene completely inhibits hydrogen evolution and the reaction proceeds only in protic solvents or in the presence of water, the reductive IFET is formulated as a proton-coupled reduction of the diazene to a hydrazyl radical (Equation 13.26):

$$ArN{=}NAr + e_r^- + H^+ \rightarrow ArN^{\bullet} - N(H)Ar \qquad (13.26)$$

Hydrazyl radicals derived from 1,2 diaryl- and 1,2-dialkyldiazenes have been postulated[167] and identified in homogeneous solution by ESR.[168] The observation that the product **13a**, obtained from

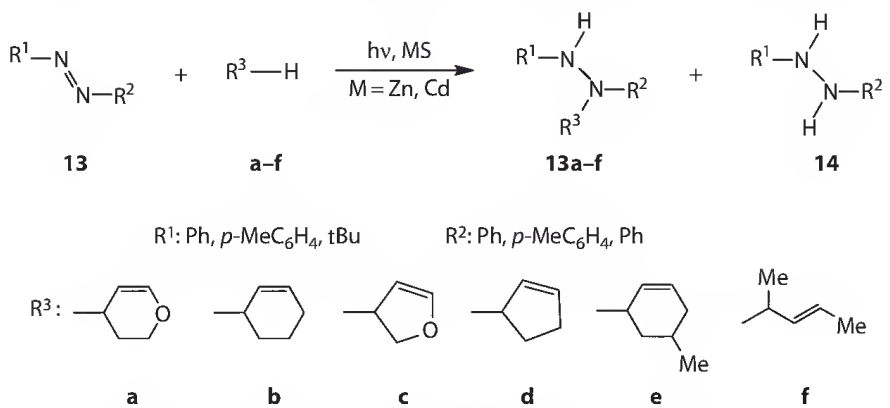

SCHEME 13.13 Synthesis of allyl hydrazines through addition of cyclic allyl/enol ethers and olefins to 1,2-diazenes photocatalyzed by ZnS or CdS suspended in methanol.

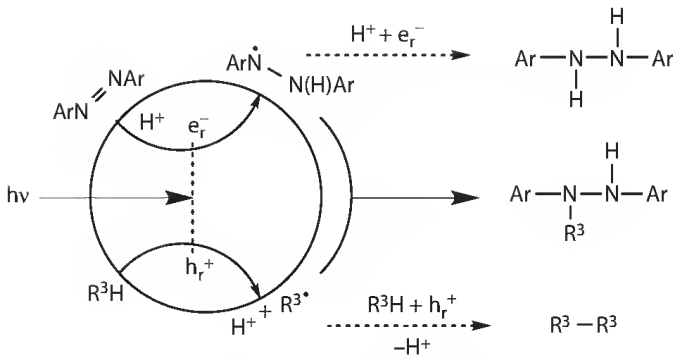

SCHEME 13.14 Simplified mechanistic scheme for the CdS or ZnS photocatalyzed addition of cyclic unsaturated ethers or olefins to 1,2-diazenes (1 e^-/1 h^+ process). See also Scheme 13.13.

1-*tert*-butyl-2-phenyldiazene, consists of only one isomer is in agreement with the expectation that the hydrazyl radical should be more stable when the unpaired electron is localized rather on the PhN than on the *t*BuN group. The oxidative IFET is assumed to proceed as described for the photodehydrodimerization. Heterocoupling of the hydrazyl and allyl radicals affords the allylhydrazine. Thus, formation of the addition product is a $1e^-/1h^+$ process, whereas the by-products are formed via a $2e^-/2h^+$ process, irrespective whether the hydrazobenzene derivative **14** is formed by subsequent reduction or disproportionation of the hydrazyl radical (Equations 13.27 and 13.28). The energetic relations between band positions and redox potentials are summarized in Figure 13.8:

$$2\,\mathrm{ArN(H)-NAr} \rightarrow \mathrm{ArN(H)-N(H)Ar} + \mathrm{ArN=NAr} \tag{13.27}$$

$$\mathrm{ArN(H)-NAr} + e_r^- + \mathrm{H^+} \rightarrow \mathrm{ArN(H)-N(H)Ar} \tag{13.28}$$

Formation of the hydrazobenzene product is strongly favored when platinized zinc or cadmium sulfide is used as the photocatalyst. In both cases the rate decreases considerably and hydrazobenzene becomes the major product. It is known that the presence of platinum favors multielectron processes.[25]

Substrate adsorption studies as conducted with ZnS in aqueous solution were performed also with CdS, CdS/SiO_2, and SiO_2 in methanol, the solvent employed in the photoaddition reaction.[158]

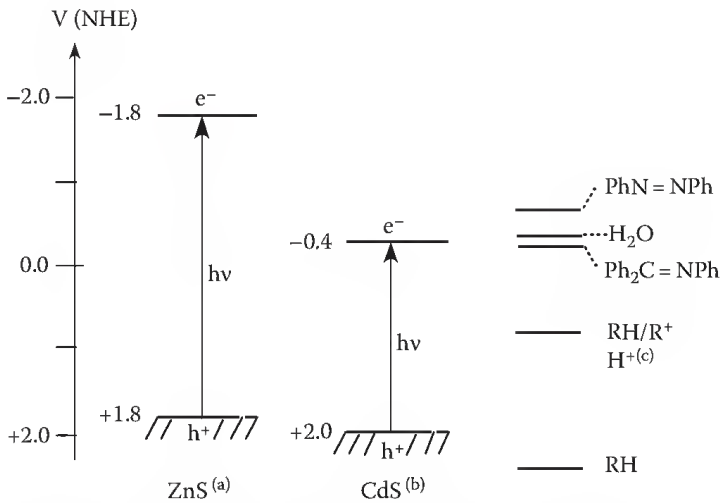

FIGURE 13.8 Metal sulfide band edge and substrate redox potential positions. Single crystal (a), powder (b), RH = 2,5-DHF (c) [166].

From ^{13}C NMR spectra of 2,5-DHF adsorbed from the gas phase onto the dry powders it is concluded that 2,5-DHF is adsorbed parallel to the surface. In the case of CdS/SiO_2 the data resemble those of unmodified SiO_2 and therefore suggest that adsorption of 2,5-DHF occurs primarily at the silica surface. In agreement with this conclusion, SiO_2 and CdS/SiO_2 afford the same adsorption constant of 30 M^{-1}, which is about 50% larger than for pristine CdS (vide infra). From the maximum surface concentration of 0.4×10^{-3} mol g^{-1} found for 2,5-DHF and the maximum number of 1.54×10^{-3} mol g^{-1} calculated for the Cd^{2+} surface in cubic CdS,[169] it is estimated that 2,5-DHF adsorbs at about every fourth Cd^{2+} center, in agreement with a parallel adsorption. However, the presence of also perpendicular adsorption cannot be excluded. Contrary to this, when 2,5-DHF is adsorbed onto ZnS from aqueous suspension, it occupies each Zn^{2+} site in a perpendicular mode and the maximum surface concentration matches the calculated molecular area.[103] This difference can be rationalized by comparing the polarities of the two sulfides with those of 2,5-DHF and the solvents employed. Since the surface polarity parameter E_T^N of CdS (0.68 ± 0.06) is comparable with the value of methanol (E_T^N = 0.762),[170] but is much higher than that of 2,5-DHF (E_T^N = 0.366),[171,*] displacement of $MeOH_{ad}$ by 2,5-DHF should be disfavored. Contrary to that, the highly polar solvent water (E_T^N = 1.0)[170] is displaced almost completely from the less polar ZnS surface (E_T^N = 0.57)[97] by the less polar 2,5-DHF. This explanation is corroborated by the data obtained for 2,5-DHF when it is adsorbed onto CdS from an aqueous solution. In this case, comparison of the maximum surface concentration of 2.1×10^{-3} mol g^{-1} with the calculated maximum number of Cd^{2+} surface sites reveals that about each Cd^{2+} center is occupied by 2,5-DHF. The average area occupied by 2,5-DHF in the surface–solute monolayer is obtained as 7 ± 1 $Å^2$. It matches well with the area of 9 Å calculated for a perpendicular adsorbed molecule. The change to the more polar solvent water enables an almost fivefold higher surface coverage of CdS. For CdS/SiO_2 the maximum surface concentration of 2,5-DHF (1.6×10^{-3} mol g^{-1}) is about the sum of the values for CdS-A (0.4×10^{-3} mol g^{-1}) and SiO_2.

The observation that the adsorption constants of 2,5-DHF onto SiO_2 and CdS/SiO_2 are equal suggests predominant adsorption on the SiO_2 support in the latter case. The better adsorption onto CdS/SiO_2 (K_{ad} = 30 ± 1 M^{-1}) as compared to CdS-A (K_{ad} = 18 ± 2 M^{-1}) is connected with a faster reaction. Since the amount of azobenzene adsorbed is the same for both photocatalysts, it is likely that the higher 2,5-DHF surface concentration induced by SiO_2 increases also the amount of 2,5-dihydrofuryl radicals adsorbed at CdS and therefore accelerates C–N coupling with the PhN–NHPh radicals.

In comparison to 2,5-DHF, the maximum surface concentration $n_{eq(max)}$ for azobenzene of about 10^{-5} mol g^{-1} is two orders of magnitude lower, whereas the adsorption constants are much higher and do not depend on the nature of the adsorbent. Comparison of the σ°-values with the area covered by a flat, unsolvated molecule (52 $Å^2$),[†] reveals that σ° for CdS, CdS/SiO_2, and SiO_2 is 52, 85, and 145 times higher than expected. It is estimated that in the case of CdS only every 220th Cd^{2+} site interacts with an azobenzene molecule. Depending on the adsorbent, only 0.7%–2% of the surface area is covered, which suggests that the more polar methanol (μ = 1.7 D) efficiently competes with the less polar *trans*-azobenzene[‡] ($\mu_{trans} \cong 0$ D) for adsorption sites at the relatively polar CdS surface. Together with the independence of the adsorption constant on the nature of the adsorbent, these results suggest that adsorption occurs through interaction with Brønsted acid sites.[158,172] In this case the independence of the adsorption constant on the adsorbent can be rationalized since according to literature CdS and SiO_2 have similar pK_S values (6.1, 9.0[173] and 6–8,[174] respectively) and the employed photocatalysts CdS or CdS/SiO_2 and SiO_2 have two surface centers of similar pH values.[175]

The considerations outlined earlier are substantiated further by the σ° values as obtained from Hiemenz plots. The area covered by a 2,5-DHF molecule in the saturated surface-solute-monolayer is found to be

---

* From comparison with the dipole moments of THF, 2,5-DHF and furan (1.63, 1.59 and 0.66 D, respectively) one would expect, however, that the E_T^N value of 2,5-DHF should be in the range of 0.164 to 0.27, corresponding to furan and THF, respectively.

† Estimated from a molecular model as 10.8 Å × 4.8 Å.

‡ Since in the dark adsorption experiments light could not be completely excluded, cis-azobenzene was present in about 1%.

50 ± 5, 35 ± 2, and 20 ± 1 Å^2 for CdS–A, SiO_2, and CdS/SiO_2, respectively, and differs not too much from the area of 21 Å^2 as calculated for an unsolvated molecule adsorbed parallel to the surface.* This qualitative agreement with the conclusions drawn from the maximum numbers of metal ion sites as well as the ^{13}C NMR data strongly suggests that 2,5-DHF adsorbs at surface [OH] or [SH] groups via hydrogen bonding.

Apparent quantum yields were measured at 366 nm, the wavelength at which light absorption by the diazene is minimized.[138] In the system, CdS/R^3H/1,2-diphenyldiazene/MeOH Φ_{app} of allylhydrazine formation increases from 0.02 (2,5-DHF) over 0.03 (cyclohexene) and 0.04 (3,4-DHP) to 0.05 (2,3-DHF). As also observed for the ZnS-catalyzed photodehydrodimerization, there is no simple relation with the oxidation potential of the donor, which is 2.6 V for 2,5-DHF and cyclohexene, and 1.9 and 2.0 V for 3,4-DHP and 2,3-DHF, respectively. Although 3,4-DHP as compared to 2,5-DHF is more readily oxidized than 2,5-DHF by 0.7 V, its quantum yield is only twice as large. In contrast to these rather weak effects, lowering of the reduction potential of the diazene causes a strong increase of the *relative* quantum yield† of diazene disappearance. For cyclohexene addition in the series 1,2-bis(*p*-tolyl)diazene, 1,2-diphenyldiazene and 1,2-bis(*p*-chlorophenyl)diazene, E_{red} varies from −0.82 to −0.75 and −0.66 V[176] and Φ_{rel} increases from 0.5 over 1.0 to 5.0, respectively.

Thus, although the *p*-chloro derivative is easily reduced than the *p*-methyl analogue by only 0.16 V, the quantum yield is ten times larger. No photoaddition or reduction is observed in the case of 2,3-diazabicyclo[2.2.1]hept-2-ene. It is known that aliphatic diazenes are much more difficult to reduce than aromatic ones.[177]

The postulated C–N heterocoupling requires diffusion of the two radicals either in the solvent–solute surface layer or in the bulk solution. In both cases one expects that the reaction rate should decrease with increasing solvent viscosity. To achieve the latter, the CdS/SiO_2-catalyzed photoaddition of 2,5-DHF to azobenzene was conducted at pressures ranging from 0.1 to 120 MPa.[159] Both the formation rates of the addition and reduction products **13c** and **14** ($R^1 = R^2 = Ph$) decrease with increasing pressure (Figure 13.9). From a plot of ln(rate) vs. pressure, activation volumes $\Delta V^{\neq}$ are obtained as +17.4 ± 3.4 and +15.8 ± 2.3 cm^3 mol^{-1}, for **13c** and **14**, respectively. However, since with increasing pressure also the dielectric constant increases, the observed effects may originate from the change of this property.[173–181] In order to differentiate between these two possibilities, the rates were measured in a series of alcohols for which viscosity and dielectric constant change in an opposite fashion. Whereas the rates again decrease with

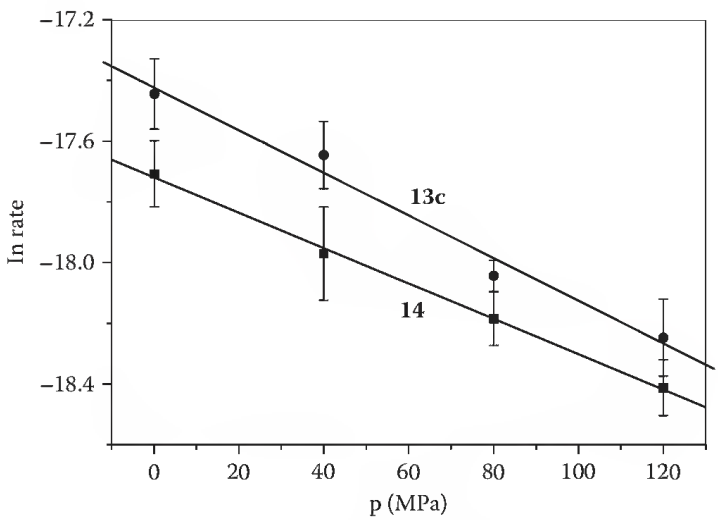

FIGURE 13.9 Dependence of the formation rates of **13c** and **14** on applied pressure.

* Estimated from a molecular model as 4.6 Å × 4.5 Å.

† The apparent quantum yield for 1,2-diphenyldiazene was set to 1.0.

increasing viscosity, they increase when plotted as function of increasing dielectric constant. This indicates that the rate decrease at higher pressure is a viscosity effect.

It is unlikely that the activation volume is connected with substrate adsorption and product desorption[182] or with the interfacial electron transfer steps. Usually interfacial collision rates depend on molecular mass but not on diffusion rates.[183] Therefore, the activation volume measured for the formation of **13c** may stem from the diffusion of the intermediate radicals to each other or from the subsequent C–N coupling step itself. The latter case can be excluded since bond formation between neutral organic species in homogeneous solution in general has a negative activation volume.[184–187] The only exception is radical recombination in the termination step of polymerizations.[188,189] These reactions possess $\Delta V^{\neq}$ values in the range of +13 to +25 $cm^3\ mol^{-1}$, which are composed of the large and positive contribution of diffusion and the small and negative part of radical C–C coupling. Hence, the activation volume found for **13c** most likely originates primarily from diffusion of the intermediate radicals to each other and only to a minor part from C–N coupling and therefore should resemble the activation volume for the viscous flow of methanol. The fact that the latter value of +8 $cm^3\ mol^{-1}$ [188] is significantly smaller suggests that the radicals do not diffuse in the bulk homogeneous solution but in a solvent–solute–surface layer. This should result in a higher viscosity and consequently the activation volume should become more positive. In accordance with this interpretation are also the small activation energies of 2.8 ± 0.3 (**13c**) and 2.5 ± 0.2 kcal mol^{-1} (**14**).

Since the same activation parameters as for **13c** were also found for the formation of the reduction product **14**, the disproportionation pathway (Equation 13.27), which involves radical diffusion, is favored over the secondary reduction step (Equation 13.28). However, the latter may be partly involved as suggested by the slightly smaller pressure effect as compared to **13c**.

The conclusion that changes in solvent viscosity are responsible for the observed pressure and temperature effects is further corroborated by the same dependence of the product ratio **13c**:**14**. Irrespective of whether the viscosity is calculated from the pressure or temperature experiments, a plot of the product ratio vs. viscosity affords two straight lines with slopes identical within experimental error. When the different alcohols were used to change the viscosity, the product ratio also decreased with increasing viscosity.

13.4.2 Linear Addition of Cyclic Enol/Allyl Ethers and Olefins to Imines

According to the proposed mechanism for this novel photoaddition reaction, other substrates capable of forming radicals upon CdS-photoinduced one-electron oxidation or reduction should undergo similar C–C coupling. Replacing the 1,2-diazene by the trisubstituted imine **15** indeed affords the new homoallylamines **16a–g** in isolated yields of 30%–75% (Scheme 13.15).[190]

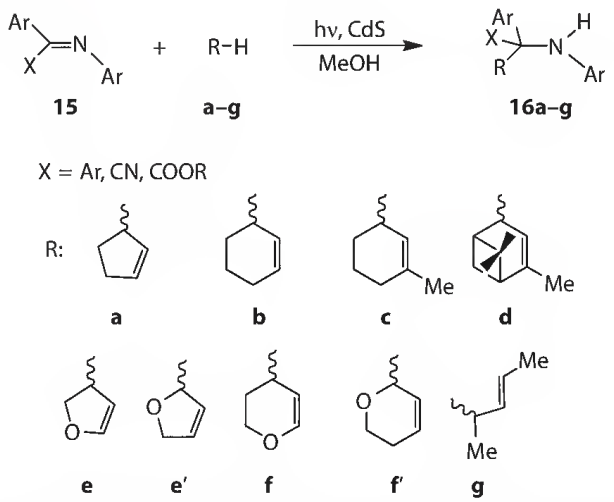

SCHEME 13.15 Synthesis of homoallylamines through addition of cyclic allyl/enol ethers and olefins to trisubstituted imines photocatalyzed by CdS suspended in methanol.

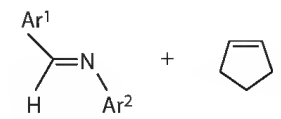

17a–d

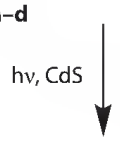

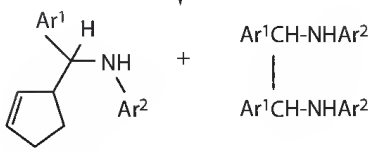

18 **19**

	a	b	c	d
Ar^1	4-ClC_6H_4	2,6-$Cl_2C_6H_3$	4-ClC_6H_4	4-$MeOC_6H_4$
Ar^2	4-ClC_6H_4	C_6H_5	3,5-$Me_2C_6H_3$	4-MeC_6H_4
18[(a)]	60	40	55	80
19[(a)]	20	10	40	—

(a) Isolated yield in %.

SCHEME 13.16 CdS photocatalyzed addition of cyclic allyl/enol ethers and olefins to disubstituted imines photocatalyzed by CdS suspended in methanol. Imine hydrodimers **19** are formed as by-products.

The structure of the new compounds is confirmed by single crystal x-ray analyses of **16a**, **c**, and **d**, and by comparative NMR data in the case of the other products.

When a disubstituted imine (**17a–d**) is employed instead of the trisubstituted one, in addition to the homoallylamine (**18**) also the hydrodimer (**19**) of the imine, that is, the dimer of the postulated α-aminobenzyl radical, is isolated (Schemes 13.16 and 13.17).[191,192] The observation that the hydrodimer is produced only from the disubstituted but not from the trisubstituted imine parallels the electrochemical reduction, which affords hydrodimers from aldimines[193] but not from ketimines.[193,194]

Thus, product formation can be rationalized by assuming that the allylic radical generated in the oxidative IFET, as discussed earlier, undergoes C–C heterocoupling with the α-aminodiphenylmethyl radical produced according to Equation 13.29. When CdS is alkylated through the reaction with 3-bromopropyltrimethoxysilane, the reaction is completely inhibited. However, it occurs again when the imine is substituted by its iminium salt. This indicates that the surface OH and SH groups of pristine cadmium sulfide photocatalyst protonate the imine to render its redox potential more positive.[195]

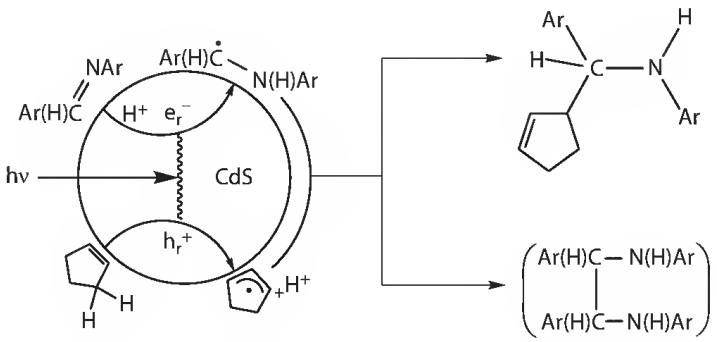

SCHEME 13.17 Simplified mechanistic scheme for the CdS photocatalyzed addition of cyclopentene to imines.

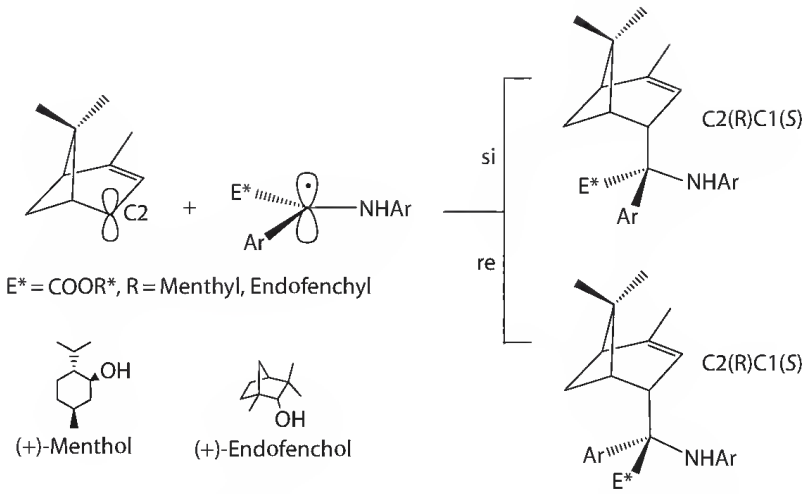

SCHEME 13.18 Diastereoselectivity of C–C coupling. The menthylester affords the C2(R)C1(S), the endofenchylester leads to the C2(R)C1(R) stereoisomer.

In no case, a product arising from C–N heterocoupling could be observed. Thus, different from mutual thermal routes, which usually involve the use of organometallic reagents,[196–198] the reaction is regioselective and much easier to perform.

$$[Ar_2C{=}N(H)Ar]^+ + e_r^- \rightarrow Ar_2C^\bullet - N(H)Ar \tag{13.29}$$

To obtain information on the stereochemistry of the radical C–C coupling, chiral imines were employed in addition reactions with α-pinene (Scheme 13.18). With the menthyliminoester diastereoselective formation of the C2(R)C1(S) isomer occurs, whereas the entdofenchylester leads to the C2(R) C1(S) diastereomer suggesting a stereospecific *si*- and *re*-attack of the aminobenzyl radical at the allyl radical, respectively.

As observed for the adsorption of 2,5-DHF also the imine **17a**, the adsorption isotherm indicates the presence of mono- and multilayer adsorption. From the former a maximum surface concentration of 20×10^{-7} mol g^{-1} can be estimated. Application of the Hiemenz model on the methanol-imine surface monolayer leads to an adsorption constant of $4400 \pm 950\,M^{-1}$ and a σ^0 value of 4000 Å^2. This is far too large as indicated by comparison with 50 Å^2 (14 × 3.5 Å) estimated for a flat unsolvated molecule. This suggests that only 1%–2% of the surface is covered by **17a** in competition with the solvent. The results resemble those obtained for the adsorption of azobenzene. Assuming a size of 8 Å^2 for methanol, one arrives at the conclusion that methanol is present in a 500-fold excess over the imine in the methanol–imine surface monolayer. Therefore it is rational that **17c** does not influence the photocurrent of a CdS electrode whereas methanol induces current doubling.[199] Although these numbers are only rough estimates, they are not unexpected since methanol should adsorb much stronger than **17a** onto the hydrous CdS surface.[200]

Control experiments with **17a** showed that in the absence of olefins hydrodimers were also formed but the reaction rate was decreased by about 90%. Whereas the reductive reaction step can proceed as depicted in Scheme 13.17, the solvent must be involved in the oxidative step since no significant oxidative photocorrosion occurs. Accordingly, irradiation of CdS in a solution of **17a** in different alcohols transforms the imine at different rates and the corresponding addition products **20a–e** and hydrodimers **21a–e** are isolated (Scheme 13.19).

Except for methanol and 2-propanol the products are racemic diastereomeric mixtures isolated in low yields (5%–20%); they are often mixed with the two-electron reduction product *N*-4-chlorobenzyl-4-chloroaniline. The major product in all reactions is the hydrodimer **21**, obtained in yields of 10%

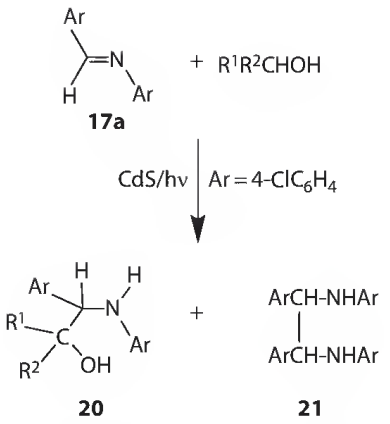

	a	b	c	d	e
R^1	H	Me	Et	Pr	Me
R^2	H	H	H	H	Me
20		5 – 20[a]			
21	10	42	29	28	60

(a) Isolated yield in %.

SCHEME 13.19 CdS-photocatalyzed addition of alcohols to the Schiff base **17a**.

(MeOH), 28% (BuOH), 29% (PrOH), 42% (EtOH), and 60% (*i*PrOH). The structure of **20** indicates that in all cases the α-CH bond of the alcohol is added to the imine in agreement with the preferred formation of α-hydroxyalkyl radicals from oxidation of alcohols.[201,202] In the case of *i*PrOH, involvement of the intermediate hydroxyalkyl radical was corroborated through detection of its disproportionation product acetone. These results show that the solvent can be directly involved in the oxidative step. Formation of hydrodimers in the absence of olefins thus can be explained by the oxidation of alcohols. It is noted that in the presence of olefins, no alcohol addition products could be detected by HPLC analysis, although methanol is present in a 500-fold molar excess.

Increasing the light intensity results in a linear increase of the reaction rate. Above an incident intensity of about 10^{18} quanta s^{-1} a saturation effect is observed. This is in accord with other photoreactions catalyzed by semiconductor powders.[68,70] Noteworthy, the product ratio of 0.9 observed for **18a:19a** is not influenced by changing the light intensity. This suggests that the rates of aminobenzyl radical dimerization and addition to the allyl radical exhibit the same dependence on the concentration of the light-generated electron–hole pairs.[192]

The reaction rate increases approximately linearly on CdS concentration and reaches a plateau at about 3 g L^{-1}. Surprisingly, in the same concentration range the ratio of addition to hydrodimer product (**18a**:**19a**) decreases from 2 to about 1. In the same direction the surface concentration of the intermediate radicals should decrease although the ratio of α-aminobenzyl to cyclopentenyl radical concentration should not change. Therefore the product ratio is expected to stay constant. However, a lower concentration of the radicals increases their lifetime, assuming that they undergo only second-order decay reactions. This effect should favor hydrodimerization, which is a $2e^-/2h^+$ process and therefore requires that a second radical pair is generated during the lifetime of the first one. Furthermore, one can make the plausible assumption that there is still some weak interaction within a reactive electron–hole pair and therefore the distance between the charges in a pair should be smaller than the distance between neighboring pairs. This means that the radical homocoupling most likely requires a longer diffusion path than heterocoupling. Accordingly, a longer radical lifetime should also enable a more efficient diffusion and therefore additionally favor the hydrodimer formation.

Exploring the general applicability of the olefin–imine addition reaction, the N-aryl substituent in the imine **15** (X=CN) was replaced by an N-benzoyl group, which may be easily converted to an amino group. The resulting unsaturated amino acids may be of pharmaceutical relevance.[203,204] Surprisingly, in the presence of CdS- or silica-supported CdS, the addition reactions with cyclopentene and cyclohexene were completely inhibited in favor of a novel thermal transhydrocyanation of the imine component affording novel malononitriles **6** in isolated yields of 40%–50%.[205] However, in the presence of zinc sulfide-supported cadmium sulfide (CdS/ZnS) this dark reaction was completely inhibited in favor of the desired addition products **23** (65%–85% isolated yield). Unexpectedly, both the compounds **23** and **26** were unknown in the literature (Scheme 13.20).

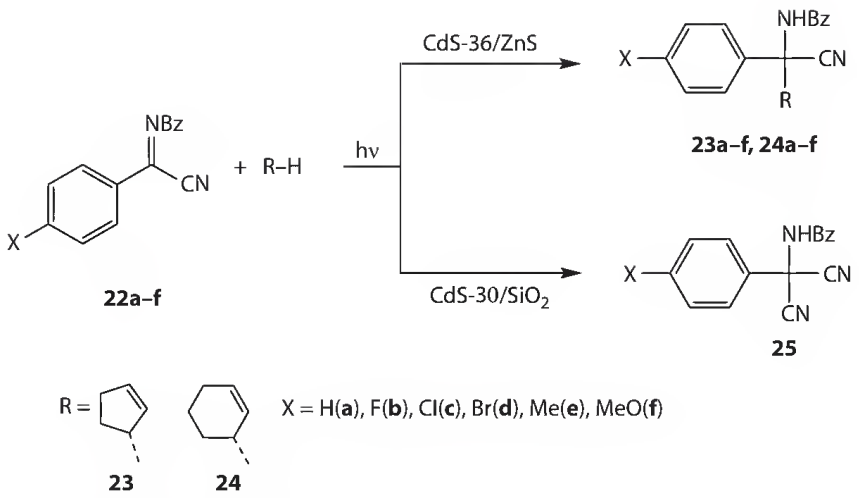

SCHEME 13.20 Support-controlled chemoselectivity in the imine/olefin system.

To obtain information on the lifetime of the photogenerated charges, time resolved photo-electromotive force measurements were performed on various samples embedded in a polymer matrix.[206,207] A fast decay process observed after excitation at $\lambda = 337$ nm in the time range of 0–50 μs is due to surface charge recombination. A positive voltage indicates n-type behavior as observed for all samples containing CdS. Different from this, ZnS possesses p-type character due to the negative voltage, which is still growing in the observed time range. Thus, the supported materials constitute a type of photochemical diode since they consist of the combination n-CdS/p-ZnS. The n/p-character of these aggregates is a significant difference to previously reported "coupled semiconductors" employed in oxidative photodegradation reactions.[208,209] The charge carrier lifetime τ as obtained from the reciprocal decay constant k_1 increases from ~3 μs in CdS to ~4 μs and ~5 μs in CdS-36/ZnS and CdS-13/ZnS containing 36 wt% and 13 wt% of CdS. This slower charge recombination can be rationalized by assuming an interparticle electron transfer at the CdS–ZnS interface as depicted schematically in Scheme 13.21. According to this, the n-CdS/p-ZnS photocatalyst in principle mimics the primary reactions of natural photosystem wherein light absorption by two components, photosystem I and photosystem II, is followed by charge separation and interfacial reduction and oxidation.

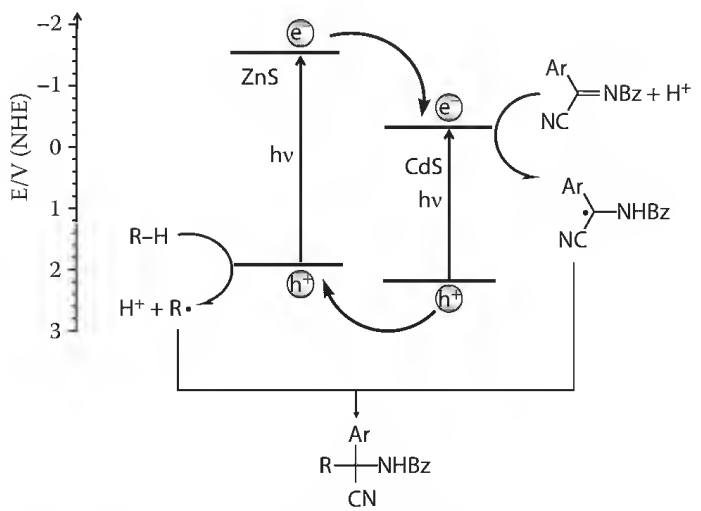

SCHEME 13.21 Photoinduced charge separation facilitated by interparticle charge transfer. The band edge positions for ZnS[212] and CdS[195] refer to aqueous solutions at pH = 7 vs. NHE.

The problems inherent in the understanding of the factors determining the rate of a semiconductor-photocatalyzed reaction are nicely reflected when various *p*-substituted imines are compared. Although one might expect that a higher driving force of imine reduction (Equation 13.29) should increase also the addition rate constant, this is not the case.[210] Thus, whereas the reduction potential of the *p*-chlorophenyl substituted imine **22c** is 150 mV more positive than that of the bromo derivative **22d**, the rate constants to not differ significantly. Accordingly, the reduction potential does not influence the IFET reaction (see Equation 13.11) in a systematic fashion. Assuming then that rather the C–C coupling reaction is the rate-determining factor, the disturbance of the delocalized aromatic system as a function of the *para*-substituent was considered. Assuming that the basic conformational properties of **22a–f** are preserved also in the corresponding benzyl radicals one expects that a larger torsion angle C_{Imin}–N_{Imin}–$C_{Carbonyl}$–C_{Ph} should indicate a lower stability due to a lower degree of electron delocalization. In fact, a steady increase of rate with increasing angle is observed. This can be rationalized by noting that less delocalization implies higher electron localization at the imine carbon atom and therefore a faster C–C coupling, resulting in a larger efficiency of product formation η_p (see Equation 13.12). Only the fluoro derivative **22b** does not follow this correlation, suggesting that radical and imine conformations may be too different.[210]

In order to find out if the dependence of rate on the *para*-substituent of imines **22** may be better described by a parameter reflecting both thermodynamic and kinetic properties, the data were analyzed by application of the Hammett relation (Equation 13.30). In this equation the parameter σ is a constant for a given substituent X in the *p*-XC_6H_4 group of the imine. The value of ρ depends on the specific reaction. Generally, positive ρ-values indicate that enhanced electron-withdrawing properties of the substituents X increase the reaction rate:

$$\log(k_x/k_H) = \rho\sigma \tag{13.30}$$

A corresponding plot of the left term of Equation 13.30 vs. the σ-parameters reveals a linear relationship (Figure 13.10). Once more the fluorophenyl imine **22b** does not follow the general trend, as already observed when considering the imine distortion angle. The positive ρ-values of ρ = 1.18 and ρ = 1.44 for cyclopentene and cyclohexene, respectively, suggest a nucleophilic attack of the allyl radical at the α-aminobenzyl radical.

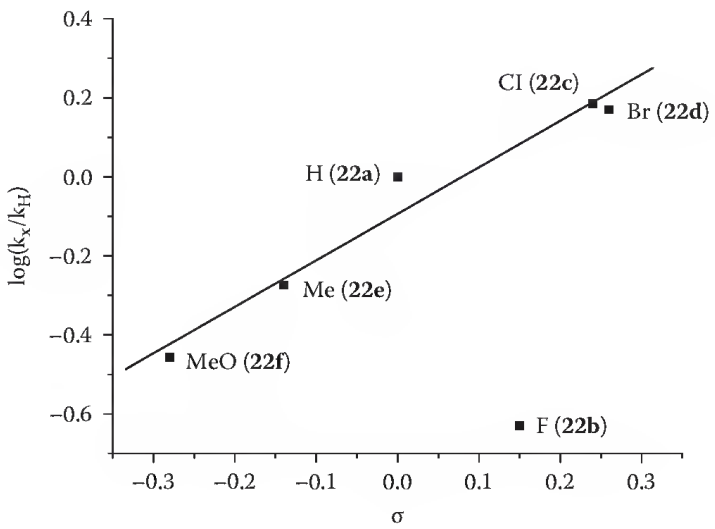

FIGURE 13.10 Hammet plot for the addition of cyclopentene to **22a–f**.

13.5 Summary

The unique charge-separating properties of the semiconductor–liquid interface enable micrometer aggregates of nanoscaled zinc and cadmium sulfide crystallites to act as efficient electron transfer photocatalysts for novel organic syntheses. Grafting of cadmium sulfide onto insulating silica or semiconducting zinc sulfide improves the photocatalytic activity through interparticle electronic interactions. In general reduced and oxidized products are obtained (semiconductor photocatalysis type A), in complete analogy with electrochemical syntheses. An example is the dehydrodimerization of unsaturated ethers in aqueous solution producing stoichiometric amounts of hydrogen. Although the latter is generated by reduction of water, it is not consumed but reformed in a subsequent reaction step as indicated by experiments in D_2O. The observed formation of D_2, therefore, is not a proof for hydrogen production from water as generally assumed in the literature for "sacrificial hydrogen production." In a few cases, the semiconductor photocatalyzes a linear addition reaction between two unsaturated substrates affording one single product (semiconductor photocatalysis type B), a reaction type not known in classical electrochemistry. Typical examples are the addition of olefins or unsaturated ethers to 1,2-diazenes or imines. In both photocatalysis types the semiconductor action is at least bifunctional. It enables a proper assembling of the substrates through adsorption and catalyzes photoinduced interfacial electron transfer to and from substrates. The resulting primary redox products are radicals that may undergo regioselective C–C and C–N coupling to stable products in the case of class B reactions. These reactions are easily conducted and the heterogeneous sensitizer can be conveniently separated from the products by filtration. They are promising examples for a "green chemistry" since they do not produce waste materials and can be driven by solar light. In a formal way, the overall reaction resembles natural photosynthesis, where light absorption also generates reducing and oxidizing centers, which finally induce the synthesis of organic matter through C–C coupling reactions. The *n*-CdS/*p*-ZnS photocatalyst mimics even the primary processes. Like photosystems I and II the two sulfides absorb the light and enable an efficient charge separation followed by interfacial electron transfer. It is expected that this multifunctional nature of the semiconductor powders can be utilized for further novel preparative reactions, especially in the field of chemical solar energy utilization.

References

1. Hahn, U.; Gorka, M.; Vogtle, F.; Vicinelli, V.; Ceroni, P.; Maestri, M.; Balzani, V. *Angew. Chem. Int. Ed.* 2002, *41*, 3595–3598.
2. Moore, T. A.; Gust, D.; Mathis, P.; Mialocq, J. C.; Chachaty, C.; Bensasson, R. V.; Land, E. J.; Doizi, D.; Liddell, P. A. et al. *Nature (London)* 1984, *307*, 630–632.
3. Carassiti, V. *EPA Newsl.* 1984, *21*, 12.
4. Kisch, H.; Hennig, H. *EPA Newsl.* 1983, *19*, 23.
5. Moggi, L.; Juris, A.; Sandrini, M.; Manfrin, M. F. *Res. Chem. Intermed.* 1981, *4*, 171.
6. Plotnikov, J. *Allgemeine Photochemie*; Walter de Gruyter: Berlin, Germany, 1936.
7. Teichner, S. J.; Formenti, M. *Photoelectrochemistry, Photocatalysis and Photoreactors*; M. Schiavello, ed. Reidel Publishing Co.: Dordrecht, the Netherlands, 1985.
8. Albini, A. *J. Chem. Educ.* 1986, *63*, 383–386.
9. Hennig, H.; Rehorek, D.; Archer, R. D. *Coord. Chem. Rev.* 1985, *61*, 1–53.
10. Kutal, C. *Coord. Chem. Rev.* 1985, *64*, 191–206.
11. Salomon, R. G. *Tetrahedron* 1983, *39*, 485–575.
12. Wrighton, M. S.; Ginley, D. S.; Schroeder, M. A.; Morse, D. L. *Pure Appl. Chem.* 1975, *41*, 671–697.
13. Wubbels, G. G. *Acc. Chem. Res.* 1983, *16*, 285–292.
14. Braslavsky, S. E. *Pure Appl. Chem.* 2007, *79*, 293–465.
15. *As defined in Glossary of Terms Used in Photochemistry*, *EPA Newsl.* 1985, *25*, 13.
16. Balzani, V.; Bolletta, F.; Ciano, M.; Maestri, M. *J. Chem. Educ.* 1983, *60*, 447–450.

17. Bard, A. J. *J. Photochem.* 1979, *10*, 59–75.
18. Boudart, M.; Djega-Mariadassou, G. *Kinetics of Heterogeneous Catalytic Reactions*; Princeton University Press: Princeton, NJ, 1984.
19. Basolo, F.; Pearson, R. G. *Mechanism of Inorganic Reactions*; John Wiley & Sons: New York, 1967.
20. Davies, S. G. *Organotransitions Metal Chemistry: Applications to Organic Synthesis*; Pergamon Press: Oxford, U.K., 1982.
21. Childs, L. P.; Ollis, D. F. *J. Catal.* 1980, *66*, 383–390.
22. Macyk, W.; Kisch, H. *Chem. Eur. J.* 2001, *7*, 1862–1867.
23. Gerischer, H. *Physical Chemistry*; M. Eyring, D. Henderson, W. Jots, eds., Academic Press: New York, 1970.
24. Kamat, P. V. *Chem. Rev.* 1993, *93*, 267.
25. Memming, R. *Top. Curr. Chem.* 1988, *143*, 79–112.
26. Tributsch, H. *Photocatalysis*; Serpone, N., Pelizzetti, E., ed., John Wiley & Sons: New York, 1989.
27. Frank, S. N.; Bard, A. J. *J. Phys. Chem.* 1977, *81*, 1484–1488.
28. Frank, S. N.; Bard, A. J. *J. Am. Chem. Soc.* 1977, *99*, 303–304.
29. Frank, S. N.; Bard, A. J. *J. Am. Chem. Soc.* 1977, *99*, 4667–4675.
30. Kraeutler, B.; Bard, A. J. *J. Am. Chem. Soc.* 1977, *99*, 7729–7731.
31. Nozik, A. J.; Memming, R. *J. Phys. Chem.* 1996, *100*, 13061–13078.
32. Fox, M. A. *Top. Curr. Chem.* 1987, *142*, 71–99.
33. Henglein, A. *Top. Curr. Chem.* 1988, *143*, 113–180.
34. Serpone, N.; Pelizzetti, E. *Photocatalysis. Fundamentals and Applications*; John Wiley & Sons: New York, Chichester, Brisbane, Toronto, Singapore, 1989.
35. Schrauzer, G. N.; Guth, T. D. *J. Am. Chem. Soc.* 1977, *99*, 7189–7193.
36. Edwards, J. G.; Davies, J. A.; Boucher, D. L.; Mennad, A. *Angew. Chem.* 1992, *104*, 489–491. (See also *Angew. Chem. Int. Ed. Engl.* 1992, *31*(4), 480–482).
37. Hetterich, W.; Kisch, H. *Chem. Ber.* 1989, *122*, 621–627.
38. Reiche, H.; Dunn, W. W.; Bard, A. J. *J. Phys. Chem.* 1979, *83*, 2248–2251.
39. Onoe, J.; Kawai, T.; Kawai, S. *Chem. Lett.* 1985, 1667–1670.
40. Heller, A.; Degani, Y.; Johnson, D. W., Jr.; Gallagher, P. K. *J. Phys. Chem.* 1987, *91*, 5987–5991.
41. Fujishima, A.; Hashimoto, K.; Watanabe, T. *TiO_2 Photocatalysis. Fundamentals and Applications*; Business Knowledge Consortium Inc.: Tokyo, Japan, 1999.
42. Tryk, D. A.; Fujishima, A.; Honda, K. *Electrochim. Acta* 2000, *45*, 2363–2376.
43. Kraeutler, B.; Bard, A. J. *J. Am. Chem. Soc.* 1978, *100*, 5985–5992.
44. Gerischer, H. *J. Phys. Chem.* 1984, *88*, 6096–6097.
45. Aspnes, D. E.; Heller, A. *J. Phys. Chem.* 1983, *87*, 4919–4929.
46. Bard, A. J. *Science (Washington, DC)* 1980, *207*, 139–144.
47. Hodes, G. *Energy Resources through Photochemistry and Catalysis*; Grätzel, M. ed., Academic Press: New York, 1983.
48. Rothenberger, G.; Moser, J.; Gratzel, M.; Serpone, N.; Sharmaf, D. K. *J. Am. Chem. Soc.* 1985, *107*, 8054–8059.
49. Kamat, P. V.; Ebbesen, T. W.; Dimitrijevic, N. M.; Nozik, A. *J. Chem. Phys. Lett.* 1989, *157*, 384–389.
50. Cunningham, J.; Al-Sayyed, G.; Sedlak, P.; Caffrey, J. *Catal. Today* 1999, *53*, 145–158.
51. Cunningham, J.; Srijaranai, S. *J. Photochem. Photobiol.* 1991, *58*, 361–371.
52. Anderson, C.; Bard, A. J. *J. Phys. Chem. B* 1997, *101*, 2611–2616.
53. Anderson, C.; Bard, A. J. *J. Phys. Chem.* 1995, *99*, 9882–9885.
54. Tatsuma, T.; Tachibana, S.-I.; Fujishima, A. *J. Phys. Chem. B* 2001, *105*, 6987–6992.
55. Watanabe, T.; Takizawa, T.; Honda, K. *J. Phys. Chem.* 1977, *81*, 1845–51.
56. (a) Morrison, S. R.; Freund, T. *J. Chem. Phys.* 1967, *47*, 1543–1552. (b) Parrino, F.; Ramakrishnan, A.; Kisch, H. *Angew. Chem. Int. Ed.* 2008, 7215–7217.
57. Gerischer, H. *Electrochim. Acta* 1990, *35*, 1677–1699.

58. Redmond, G.; Fitzmaurice, D. *J. Phys. Chem.* 1993, *97*, 1426–1430.
59. Meissner, D.; Lauermann, I.; Memming, R.; Kastening, B. *J. Phys. Chem.* 1988, *92*, 3484–3488.
60. Natan, M. J.; Thackeray, J. W.; Wrighton, M. S. *J. Phys. Chem.* 1986, *90*, 4089–4098.
61. Harada, H.; Sakata, T.; Ueda, T. *J. Am. Chem. Soc.* 1985, *107*, 1773–1774.
62. Shiragami, T.; Pac, C.; Yanagida, S. *J. Chem. Soc. Chem. Commun.* 1989, 831–832.
63. Schiavello, M.; Augugliaro, V.; Palmisano, L. *J. Catal.* 1991, *127*, 332–341.
64. Serpone, N.; Terzian, R.; Lawless, D.; Kennepohl, P.; Sauve, G. *J. Photochem. Photobiol.* 1993, *73*, 11–16.
65. Sun, L.; Bolton, J. R. *J. Phys. Chem.* 1996, *100*, 4127–4134.
66. For a critical discussion of this and related basic topics see e.g. Ohtani, B. *Chem. Lett.* 2008, *37*, 217.
67. Zabek, P.; Kisch, H. unpublished.
68. Egerton, T. A.; King, C. J. *J. Oil Colour Chem. Assoc.* 1979, *62*, 386–391.
69. Sato, S. *J. Phys. Chem.* 1983, *87*, 3531–3537.
70. Al-Ekabi, H.; De Mayo, P. *J. Phys. Chem.* 1985, *89*, 5815–5821.
71. Rossetti, R.; Brus, L. *J. Phys. Chem.* 1982, *86*, 4470–4472.
72. Meyer, G. J.; Leung, L. K.; Yu, J. C.; Lisensky, G. C.; Ellis, A. B. *J. Am. Chem. Soc.* 1989, *111*, 5146–5148.
73. Uchihara, T.; Matsumura, M.; Tsubomura, H. *J. Phys. Chem.* 1989, *93*, 3207–3210.
74. Anpo, M.; Matsumoto, A.; Kodama, S. *J. Chem. Soc. Chem. Commun.* 1987, 1038–1039.
75. Draper, A. M.; Ilyas, M.; De Mayo, P.; Ramamurthy, V. *J. Am. Chem. Soc.* 1984, *106*, 6222–6230.
76. Courbon, H.; Herrmann, J. M.; Pichat, P. *J. Catal.* 1985, *95*, 539–545.
77. Hussein, F. H.; Rudham, R. *J. Chem. Soc. Faraday Trans. 1* 1987, *83*, 1631–1639.
78. Pichat, P.; Mozzanega, M. N.; Disdier, J.; Herrmann, J. M. *Nouv. J. Chim.* 1982, *6*, 559–564.
79. Mills, A.; Davies, R. *J. Photochem. Photobiol. A: Chem.* 1995, *85*, 173–178.
80. Al-Ekabi, H.; De Mayo, P. *Tetrahedron* 1986, *42*, 6277–6284.
81. Reber, J. F.; Rusek, M. *J. Phys. Chem.* 1986, *90*, 824–834.
82. Mueller, B. R.; Majoni, S.; Memming, R.; Meissner, D. *J. Phys. Chem. B* 1997, *101*, 2501–2507.
83. Lenard, P. *Ann. Phys. (Berlin, Germany)* 1922, *68*, 553.
84. Weiser, H. B.; Garrison, A. D. *J. Phys. Chem.* 1927, *31*, 1237–1245.
85. Platz, H.; Schenk, P. W. *Angew. Chem.* 1936, *49*, 822–826.
86. Hopfield, J. J. *Phys. Chem. Solids* 1959, *10*, 110–119.
87. Birman, J. L. *Phys. Rev.* 1958, *109*, 810–817.
88. Birman, J. L. *Phys. Rev.* 1959, *115*, 1493–1505.
89. Cardona, M. *Phys. Chem. Solids* 1963, *24*, 1543–1555.
90. Cardona, M.; Harbeke, G. *Phys. Rev.* 1965, *137*, 1467–1476.
91. Yanagida, S.; Ishimaru, Y.; Miyake, Y.; Shiragami, T.; Pac, C.; Hashimoto, K.; Sakata, T. *J. Phys. Chem.* 1989, *93*, 2576–2582.
92. Baral, S.; Fojtik, A.; Weller, H.; Henglein, A. *J. Am. Chem. Soc.* 1986, *108*, 375–378.
93. Kurian, A.; Suryanarayana, C. V. *J. Appl. Electrochem.* 1972, *2*, 223–229.
94. Kuenneth, R.; Twardzik, G.; Emig, G.; Kisch, H. *J. Photochem. Photobiol. A* 1993, *76*, 209–215.
95. Anpo, M.; Moon, S. C.; Chiba, K.; Martra's, G.; Coluccia, S. *Res. Chem. Intermed.* 1993, *19*, 495–519.
96. Anpo, M. *Surface Photochemistry*; John Wiley & Sons: New York, 1996.
97. Hörner, G.; Kisch, H. unpublished results.
98. Hörner, G.; Fernandez, A.; Kisch, H. unpublished results.
99. Marfunin, A. S. *Spectroscopy, Luminescence and Radiation Centers in Minerals*; Springer-Verlag: Berlin, Germany, 1979.
100. Sooklal, K.; Cullum, B. S.; Angel, S. M.; Murphy, C. J. *J. Phys. Chem.* 1996, *100*, 4551–4555.
101. Spanhel, L.; Haase, M.; Weller, H.; Henglein, A. *J. Am. Chem. Soc.* 1987, *109*, 5649–5655.
102. Henglein, A. *Ber. Bunsenges. Phys. Chem.* 1982, *86*, 301–305.
103. Horner, G.; Johne, P.; Kunneth, R.; Twardzik, G.; Roth, H.; Clark, T.; Kisch, H. *Chem. Eur. J.* 1999, *5*, 208–217.
104. White, J. R.; Bard, A. J. *J. Phys. Chem.* 1985, *89*, 1947–1954.

105. Roy, A. M.; De, G. C.; Sasmal, N.; Bhattacharyya, S. S. *Int. J. Hydrogen Energy* 1995, *20*, 627–630.
106. Weiß, H., Fridrich-Alexander-Universität Erlangen-Nürnberg, 1999.
107. Weiss, H.; Fernandez, A.; Kisch, H. *Angew. Chem. Int. Ed.* 2001, *40*, 3825–3827.
108. Gärtner, M.; Dremov, V.; Mueller, P.; Kisch, H. *ChemPhysChem* 2005, *6*, 714–718.
109. Damm, C.; Israel, G.; Weiß, H.; Kisch, H. unpublished.
110. Kisch, H.; Lutz, P. *Photochem. Photobiol. Sci.* 2002, *1*, 240–245.
111. Kisch, H.; Burgeth, G.; Macyk, W. *Adv. Inorg. Chem.* 2004, *56*, 241–259.
112. H. Kisch, *J. Prakt. Chem.* 1994, *336*, 635.
113. Yanagida, S.; Mizumoto, K.; Pac, C. *J. Am. Chem. Soc.* 1986, *108*, 647–654.
114. Anpo, M.; Yabuta, M.; Kodama, S.; Kubokawa, Y. *Bull. Chem. Soc. Jpn.* 1986, *59*, 259–264.
115. Kodama, S.; Nakaya, H.; Anpo, M.; Kubokawa, Y. *Bull. Chem. Soc. Jpn.* 1985, *58*, 3645–3646.
116. Anpo, M.; Sunamoto, M.; Che, M. *J. Phys. Chem.* 1989, *93*, 1187–1189.
117. Kodama, S.; Yagi, S. *J. Phys. Chem.* 1989, *93*, 4556–4561.
118. Ikezawa, H.; Kutal, C. *J. Org. Chem.* 1987, *52*, 3299–3303.
119. Al-Ekabi, H.; De Mayo, P. *J. Phys. Chem.* 1986, *90*, 4075–4080.
120. Maldotti, A.; Amadelli, R.; Bartocci, C.; Carassiti, V. *J. Photochem. Photobiol. A* 1990, *53*, 263–271.
121. Wang, C. M.; Mallouk, T. E. *J. Am. Chem. Soc.* 1990, *112*, 2016–2018.
122. Barber, R. A.; De Mayo, P.; Okada, K. *J. Chem. Soc. Chem. Commun.* 1982, 1073–1074.
123. Ilyas, M.; De Mayo, P. *J. Am. Chem. Soc.* 1985, *107*, 5093–5099.
124. Fox, M. A.; Pettit, T. L. *J. Org. Chem.* 1985, *50*, 5013–5015.
125. Boarini, P.; Carassiti, V.; Maldotti, A.; Amadelli, R. *Langmuir* 1998, *14*, 2080–2085.
126. Joyce-Pruden, C.; Pross, J. K.; Li, Y. *J. Org. Chem.* 1992, *57*, 5087–5091.
127. Mahdavi, F.; Bruton, T. C.; Li, Y. *J. Org. Chem.* 1993, *58*, 744–746.
128. Ohtani, B.; Osaki, H.; Nishimoto, S.; Kagiya, T. *J. Am. Chem. Soc.* 1986, *108*, 308–310.
129. Schmittel, M.; Burghart, A. *Angew. Chem. Int. Ed. Engl.* 1997, *36*, 2551–2589.
130. Linker, T.; Schmittel, M. *Radikale und Radikalionen in der Organischen Synthese*; Wiley-VCH: Weinheim, Germany, 1998.
131. Takizawa, T.; Watanabe, T.; Honda, K. *J. Phys. Chem.* 1978, *82*, 1391–1396.
132. Ohtani, B.; Kusakabe, S.; Nishimoto, S.-I.; Matsumura, M.; Nakato, Y. *Chem. Lett.* 1995, 803–804.
133. Ohtani, B.; Kusakabe, S.; Okada, K.; Tsuru, S.; Izawa, K.; Amino, Y.; Nishimoto, S.-I. *Tetrahedron Lett.* 1995, *36*, 3189–3192.
134. Park, K. H.; Jun, K. *Bull. Korean Chem. Soc.* 1998, *19*, 919–921.
135. Cermenati, L.; Richter, C.; Albini, A. *Chem. Commun.* 1998, 805–806.
136. Cermenati, L.; Mella, M.; Albini, A. *Tetrahedron* 1998, *54*, 2575–2582.
137. Kuenneth, R.; Feldmer, C.; Kisch, H. *Angew. Chem.* 1992, *104*, 1102–1103. (See also *Angew Chem Int Ed Engl*, 1992, *31*(8), 1039–1040).
138. Kuenneth, R.; Feldmer, C.; Knoch, F.; Kisch, H. *Chem. Eur. J.* 1995, *1*, 441–448.
139. Buecheler, J.; Zeug, N.; Kisch, H. *Angew. Chem.* 1982, *94*, 792–793.
140. Hetterich, W.; Kisch, H. *Chem. Ber.* 1988, *121*, 15–20.
141. Zeug, N.; Buecheler, J.; Kisch, H. *J. Am. Chem. Soc.* 1985, *107*, 1459–1465.
142. Yanagida, S.; Azuma, T.; Midori, Y.; Pac, C.; Sakurai, H. *J. Chem. Soc. Perkin Trans.* 1985, *2*, 1487–1493.
143. Yanagida, S.; Kawakami, H.; Midori, Y.; Kizumoto, H.; Pac, C.; Wada, Y. *Bull. Chem. Soc. Jpn.* 1995, *68*, 1811–1823.
144. Adamson, A. W. *Physical Chemistry of Surfaces*; 4th edn.; John Wiley & Sons: New York, 1982.
145. Hiemenz, P. C. *Principles of Colloid and Surface Chemistry*; 2nd edn.; Marcel Dekker: New York, 1986.
146. Zhang, Q.; Xu, Z.; Finch, J. A. *J. Colloid Interface Sci.* 1995, *169*, 414–421.
147. Serpone, N.; Pellizetti, E. *Homogenous and Heterogeneous Photocatalysis*; D. Reidel Publishing Co.: Dordrecht, the Netherlands, 1986.

148. Henglein, A.; Gutierrez, M.; Fischer, C. H. *Ber. Bunsen-Ges. Phys. Chem.* 1984, *88*, 170–175.
149. Kodama, S.; Matsumoto, A.; Kubokawa, Y.; Anpo, M. *Bull. Chem. Soc. Jpn.* 1986, *59*, 3765–3770.
150. Nakaoka, Y.; Nosaka, Y. *Langmuir* 1997, *13*, 708–713.
151. Lunazzi, L.; Placucci, G.; Grossi, L. *Tetrahedron* 1983, *39*, 159–163.
152. Fan, F. R. F.; Leempoel, P.; Bard, A. J. *J. Electrochem. Soc.* 1983, *130*, 1866–1875.
153. Bruening, M.; Moons, E.; Yaron-Marcovich, D.; Cahen, D.; Libman, J.; Shanzer, A. *J. Am. Chem. Soc.* 1994, *116*, 2972–2977.
154. Bruening, M.; Moons, E.; Cahen, D.; Shanzer, A. *J. Phys. Chem.* 1995, *99*, 8368–8373.
155. Bruening, M.; Cohen, R.; Guillemoles, J. F.; Moav, T.; Libman, J.; Shanzer, A.; Cahen, D. *J. Am. Chem. Soc.* 1997, *119*, 5720–5728.
156. Parker, V. D. *J. Am. Chem. Soc.* 1992, *114*, 7458–7462.
157. Wilkinson, F. *Chemical Kinetics and Reaction Mechanism*; Van Nostrand Reinhold Co. Ltd.: Workingman, U.K., 1980.
158. Reinheimer, A.; Van Eldik, R.; Kisch, H. *J. Phys. Chem. B* 2000, *104*, 1014–1024.
159. Fojtik, A.; Weller, H.; Koch, U.; Henglein, A. *Ber. Bunsen-Ges. Phys. Chem.* 1984, *88*, 969–977.
160. Schenck, G. O.; Formanek, H. *Angew. Chem.* 1958, *70*, 505.
161. Cookson, R. C.; Stevens, I. D. R.; Watts, C. T. *Chem. Commun. (London)* 1965, 259–260.
162. Askani, R. *Chem. Ber.* 1965, *98*, 2551–2555.
163. Rosenthal, I.; Elad, D. *Tetrahedron* 1967, *23*, 3193–3204.
164. Ahlgren, G. *J. Org. Chem.* 1973, *38*, 1369–1374.
165. Ninomiya, I.; Naito, T. *Photochemical Synthesis*; Academic Press: New York, 1989.
166. Al-Sader, B. H.; Crawford, R. J. *Can. J. Chem.* 1970, *48*, 2745–2754.
167. Engel, P. S.; Wu, W. X. *J. Am. Chem. Soc.* 1989, *111*, 1830–1835.
168. Lagercrantz, C.; Deinum, J. *Acta Chem. Scand.* 1994, *48*, 670–674.
169. Chan, D.; Perram, J. W.; White, L. R.; Healy, T. W. *J. Chem. Soc. Faraday Trans. 1* 1975, *71*, 1046–1057.
170. Reichardt, C. *Solvents and Solvent Effects in Organic Chemistry*; 2nd edn.; Wiley-VCH: Weinheim, Cambridge, New York, 1988.
171. Lide, D. R.; Raton, H. P. R. *Handbook of Chemistry and Physics*; CRC Press: Boca Raton, FL, 1994.
172. Reinheimer, A.; Fernandez, A.; Kisch, H. *Z. Phys. Chem. (Muenchen)* 1999, *213*, 129–133.
173. Park, S. W.; Huang, C. P. *J. Colloid Interface Sci.* 1987, *117*, 431–441.
174. Bandosz, T. J.; Lin, C.; Ritter, J. A. *J. Colloid Interface Sci.* 1998, *198*, 347–353.
175. Reinheimer, A.; Kisch, H. unpublished.
176. Bard, A. J.; Lund, W. *Encyclopedia of Electrochemistry of the Elements, Organic Section*; Marcel Dekker: New York, 1978.
177. Sustmann, R.; Sauer, R. *J. Chem. Soc. Chem. Commun.* 1985, 1248–1249.
178. Schäfer, K. *Landolt-Börnstein, Zahlenwerte und Funktionen*; Springer: Berlin, Germany, 1969.
179. Srinivasan, K. R.; Kay, R. L. *J. Solution Chem.* 1977, *6*, 357–367.
180. Brazier, D. W.; Freeman, G. R. *Can. J. Chem.* 1969, *47*, 893–899.
181. Gonikberg, M. G. *Chemical Equilibria and Reaction Rates at High Pressure*; Israel Program for Scientific Translations: Jerusalem, Israel, 1963.
182. Miyahara, M.; Iwasaki, S.; Kotera, T.; Kawamura, T.; Okazaki, M. *J. Colloid Interface Sci.* 1995, *170*, 335–339.
183. Andersen, O. S.; Feldberg, S. W. *J. Phys. Chem.* 1996, *100*, 4622–4629.
184. Asano, T.; Le Noble, W. J. *Chem. Rev.* 1978, *78*, 407–489.
185. Van Eldik, R.; Asano, T.; Le Noble, W. J. *Chem. Rev.* 1989, *89*, 549–688.
186. Drljaca, A.; Hubbard, C. D.; Van Eldik, R.; Asano, T.; Basilevsky, M. V.; Le Noble, W. J. *Chem. Rev. (Washington, DC)* 1998, *98*, 2167–2289.
187. Isaacs, N. S. *Liquid Phase High Pressure Chemistry*; John Wiley: Chichester, New York, Brisbane, Toronto, 1981.
188. Nicholson, A. E.; Norrish, R. G. W. *Discussion Faraday Soc.* 1956, *22*, 104–113.

189. Yokawa, M.; Ogo, Y. *Makromol. Chem.* 1976, *177*, 429–436.
190. Keck, H.; Schindler, W.; Knoch, F.; Kisch, H. *Chem.–Eur. J.* 1997, *3*, 1638–1645.
191. Schindler, W.; Knoch, F.; Kisch, H. *Chem. Ber.* 1996, *129*, 925–932.
192. Schindler, W.; Kisch, H. *J. Photochem. Photobiol. A* 1997, *103*, 257–264.
193. Takaki, K.; Tsubaki, Y.; Tanaka, S.; Beppu, F.; Fujiwara, Y. *Chem. Lett.* 1990, 203–204.
194. Thies, H.; Schoenenberger, H.; Bauer, K. H. *Arch. Pharm.* 1960, *293/65*, 67–73.
195. Hopfner, M.; Weiss, H.; Meissner, D.; Heinemann, F. W.; Kisch, H. *Photochem. Photobiol. Sci.* 2002, *1*, 696–703.
196. Jin, S. J.; Araki, S.; Butsugan, Y. *Bull. Chem. Soc. Jpn.* 1993, *66*, 1528–1532.
197. Mauze, B.; Miginiac, M. L. *Bull. Soc. Chim. Fr.* 1973, 1832–1838.
198. Arous-Chtara, R.; Moreau, J. L.; Gaudemar, M. *J. Soc. Chim. Tunis.* 1980, *3*, 1–11.
199. Weiß, H.; Kisch, H. unpublished.
200. Mills, A.; Williams, G. *J. Chem. Soc. Faraday Trans. 1* 1987, *83*, 2647–2661.
201. Feng, L.; Wang, H.; Jin, Z.; Li, Q.; Shi, M. *J. Photochem. Photobiol. A* 1991, *56*, 89–100.
202. Furey, R. L.; Kan, R. O. *Tetrahedron* 1968, *24*, 3085–3093.
203. Kollonitsch, J.; Barash, L.; Kahan, F. M.; Kropp, H. *Nature (London)* 1973, *243*, 346–347.
204. Kollonitsch, J.; Perkins, L. M.; Patchett, A. A.; Doldouras, G. A.; Marburg, S.; Duggan, D. E.; Maycock, A. L.; Aster, S. D. *Nature* 1978, *274*, 906–908.
205. Ballmann, J.; Kasper, S.; Kisch, H. unpublished.
206. Schiller, M.; Muller, F. W.; Damm, C. *J. Photochem. Photobiol. A* 2002, *149*, 227–236.
207. Israel, G.; Muller, F. W.; Damm, C.; Harenburg, J. *J. Inf. Rec.* 1997, *23*, 559–584.
208. Green, K. J.; Rudham, R. *J. Chem. Soc. Faraday Trans.* 1993, *89*, 1867–1870.
209. Kang, M. G.; Han, H.-E.; Kim, K.-J. *J. Photochem. Photobiol. A: Chem.* 1999, *125*, 119–125.
210. Gaertner, M.; Ballmann, J.; Damm, C.; Heinemann, F. W.; Kisch, H. *Photochem. Photobiol. Sci.* 2007, *6*, 159–164.
211. Ward, M. D.; White, J. R.; Bard, A. J. *J. Am. Chem. Soc.* 1983, *105*, 27–31.
212. Tributsch, H.; Bennett, J. C. *J. Chem. Technol. Biotechnol.* 1981, *31*, 565–577.

14

Radical Photochemistry

Uta Wille
The University of Melbourne

14.1 Introduction

During the past four decades, radical chemistry has undergone a dramatic development. From being considered as mostly sluggish in the early times, although some clean and preparatively useful processes were known, nowadays, radical reactions are mechanistically well understood and therefore occupy an unquestionable position in the toolbox of synthetic methodology. The breakthrough from being a mostly useless to a synthetically highly valuable technology was closely linked to the development of easily controllable radical chain processes, which involve a suitable radical precursor (e.g., halides), a mediator (e.g., transition metal hydrides, such as tri-*n*-butyl tin hydride, nBu$_3$SnH), and a radical initiator possessing a labile σ bond, which can undergo facile homolytic fragmentation (e.g., peroxides and azo compounds) [1]. Besides comparatively straightforward reactions, such as radical addition to π systems, specifically domino radical processes consisting of two or more consecutive steps involving both intra- and intermolecular reactions are a powerful method to access complex structural frameworks in only few synthetic steps. Since the generally mild conditions for radical reactions are compatible with a large number of functional groups, time-consuming protection strategies can be minimized. In addition to this, the principles of stereocontrol, which were discovered and developed for ionic chemistry, can also be applied to free radical reactions, which have resulted in the development of highly stereoselective radical processes.

Despite the success of radical chain reactions as synthetic tools, the disadvantage associated with the requirement for toxic heavy metal compounds, such as nBu$_3$SnH, to mediate these transformations has triggered intensive research aimed at the development of less hazardous alternatives. Apart from replacement of nBu$_3$SnH by tin-free hydrides (e.g., cyanoborohydrides [2] or silanes [3]), organoboranes [4,5], and alternative concepts using the persistent radical effect [6], the development of new photochemical methods to generate charged and noncharged free radical species has become an important area of research in radical chemistry, since it offers the opportunity to perform radical reactions without using environmentally problematic reagents [7].

Irradiation of molecules with UV light leads to their electronic excitation. This rearrangement of electrons within the molecule is associated with a change of chemical properties, compared to those in

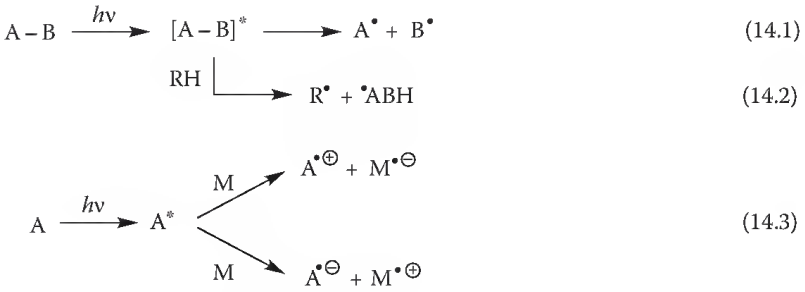

SCHEME 14.1 Chemical reactions following photoexcitation of molecules.

the ground state. As illustrated in Scheme 14.1, depending on the molecular structure and the nature of the atoms in the molecule, irradiation can directly lead to the formation of radicals through homolytic scission (photofragmentation) of a suitably labile bond in the electronically excited molecule (Equation 14.1) or initiate inter- or intramolecular hydrogen atom abstraction (Equation 14.2). Compared with a molecule in its electronic ground state, electronic excitation also leads to significantly increased oxidation and reduction properties. This can be used to generate radical anions or cations from reactants in a subsequent step in a process called photo-induced electron transfer (PET) (Equation 14.3).

PET has become a powerful synthetic method, since the usually harsh conditions associated with similar transformations using ground-state chemistry (e.g., toxic heavy metal oxidants, elevated temperatures, and nonneutral pH requirements) can be largely avoided. Photofragmentation is one of the key processes in the chemistry of the atmosphere. For example, the formation and destruction of the stratospheric ozone layer is largely controlled by photo-induced radical reactions in the gas phase.

"Photosensitization" is another mode of action in light-induced chemical reactions, where the energy of the light absorbed by one molecule is transferred to another reactant. Typically, photosensitizers are used (1) in those cases where the reactant molecules themselves only absorb light at wavelengths that are not readily available and/or (2) to access multiplicity states in the reactant that cannot be accessed through direct photo-induced electronic excitation ("forbidden" transitions).

This chapter will focus on a selection of the most recent developments in condensed-phase synthetic radical photochemistry since the publication of comprehensive reviews, for example, Refs. [8–10]. The chemical reactions presented in this chapter are arranged according to the fundamental photochemical process, for example, PET, photofragmentation, and photo-induced energy transfer. Because of the unique position of polymers in material science, radical polymerizations will be treated separately.

14.2 Photochemically Initiated Radical Polymerizations

One of the most efficient processes for the commercial production of high molecular weight polymers proceeds uses radical chemistry. Specifically the reversible addition–fragmentation chain transfer (RAFT) radical polymerization, which was developed by Rizzardo et al. [11], has become a powerful technique for the synthesis of well-defined polymers with low polydispersity and a functionalized end group, as well as polymers with highly complex architecture. In essence, the RAFT process is a living radical polymerization carried out in the presence of xanthates **1** [12], which operate by establishing an equilibrium between propagating polymer radicals $P_{m,n}$ and dormant chains as shown in Scheme 14.2.

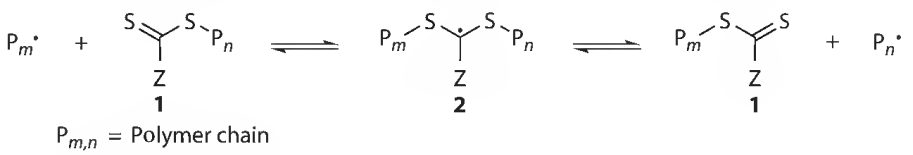

SCHEME 14.2 Mechanism of the RAFT process.

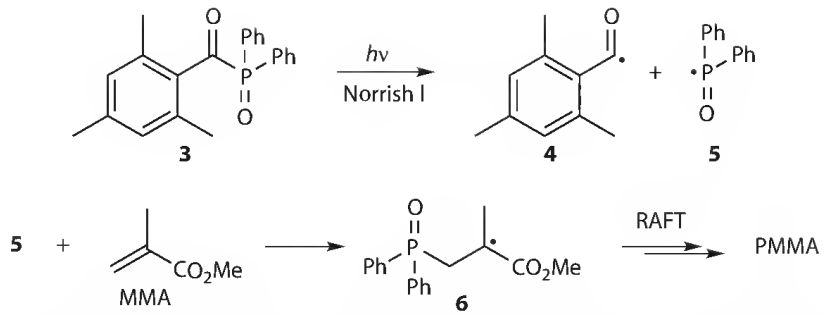

SCHEME 14.3 Photo-induced RAFT polymerization for the synthesis of polymethylmetacrylate (PMMA).

Initiation of the RAFT process has mostly been performed using thermal decomposition of a radical initiator. However, it appears that some RAFT agents have a limited thermal stability, which results in a poor control of the polymerization process. Cai et al. [13] have shown that RAFT polymerization of methyl metacrylate (MMA) under UV-vis irradiation using (2,4,6-trimethylbenzoyl)diphenylphosphine oxide (**3**) as photoinitiator leads to narrow distributed polymethylmetacrylate (PMMA) under ambient conditions (Scheme 14.3). Upon irradiation, initiator **3** undergoes Norrish I cleavage to afford 2,4,6-trimethylbenzoyl (**4**) and diphenylphosphonyl (**5**) radicals. The latter have a higher reactivity toward addition to unsaturated substrates compared to aryoyl radicals [14], and are therefore considered as the initiators of the RAFT polymerization process.

Paczkowski et al. developed a number of sulfur-containing initiators for free radical polymerizations. Sodium 4-phenyl-phenylthiosulfonate (**7**, Scheme 14.4) is water soluble and can be used as a photoinitiator of polymerizations of aqueous monomer solutions or of an emulsion polymerization, for example, styrene in water-Triton-X-100 emulsions [15].

Polymeric photoinitiators have received considerable attention in recent years. These are macromolecular systems, which contain chromophores either as pendants or incorporated into the chain, which upon light absorption can produce radical species that initiate polymerization and cross-linking of mono- and multifunctional monomers and oligomers. A couple of photoactive groups have been explored, for example, polymer-linked thioxanthones **9**, benzil **10**, anthraquinones **11**, and camphorquinone **12** (Scheme 14.5). The initial photochemical step is excitation of the carbonyl group, followed by Norrish I or II type reactions, for example, intramolecular H-transfer. The presence of the polymer chain can in many cases improve the formulation and reduces migration to the film surface, which is of considerable interest for industrial manufacturing of low odor and nontoxic coatings [16].

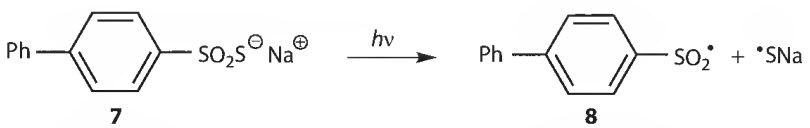

SCHEME 14.4 Water-soluble initiator for photo-induced radical polymerization processes.

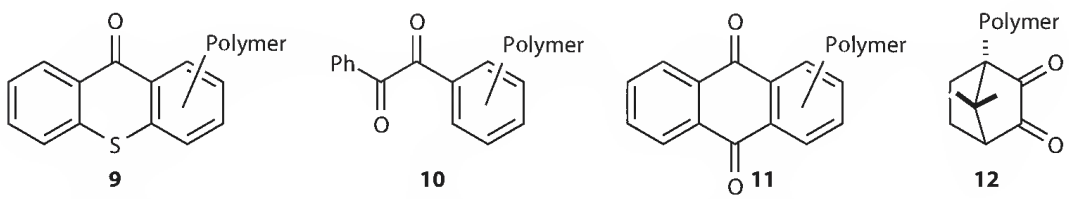

SCHEME 14.5 Polymer-bound photo-initiators for radical polymerization processes.

14.3 Generation of Radicals through Photo-Induced Electron Transfer

Most commonly, PET-induced radical reactions involve an electron transfer sensitizer, which reacts with a substrate in an intermolecular reaction. The resulting substrate radical cation (after oxidative PET) or substrate radical anion (after reductive PET) can be used in subsequent intra- or intermolecular reactions. A recent review on PET sensitization and applications in synthetic organic radical chemistry is given in [17].

14.3.1 Intramolecular Radical Reactions

Using 9,10-dicyanonaphthalene as a mediator for oxidative PET, siloxy cyclopropanes of type **13** can be transformed into β-keto radicals, which can be used in a number of subsequent reactions, for example, through addition to π systems in an intramolecular or intermolecular fashion. In the radical fragmentation/cyclization cascade shown in Scheme 14.6, the initially formed radical cation **14** undergoes opening of the cyclopropyl ring to form a distonic radical cation **15**, which is desilylated by a nucleophile (most commonly the solvent, e.g., acetonitrile). The resulting β-keto radical **16** undergoes a *cis* selective transannular 5-*exo* cyclization to yield the bicyclic ketone **17** after reduction [18].

A radical-cascade access to the skeleton of linear cyclohexano diquinanes, which uses a reductive PET as key step has been reported by Mattay et al. [19] (Scheme 14.7). Electronically excited carbonyl

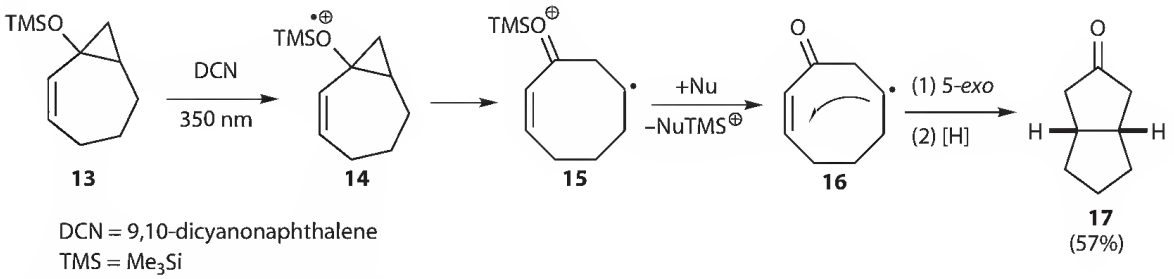

SCHEME 14.6 Photo-induced oxidative ET as initiator of cascade radical processes.

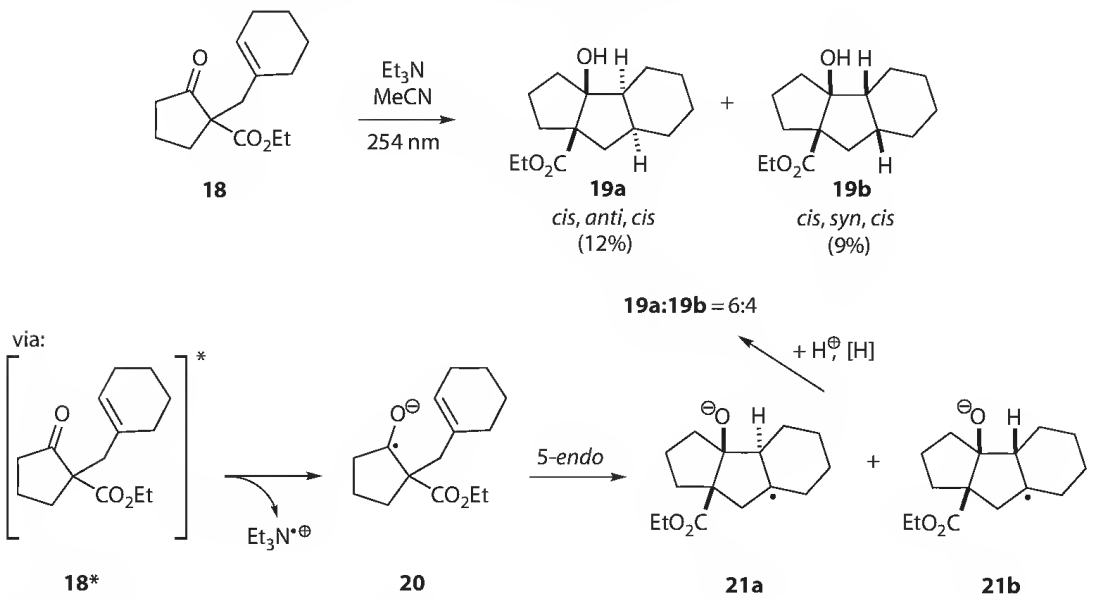

SCHEME 14.7 Radical cyclization cascade induced by reductive ET.

chromophores are strong electron acceptors, which are capable of inducing oxidation of amines. Thus, photoexcitation of the bicyclic carbonyl compound **18** in the presence of triethylamine leads to formation of the tricyclic compounds **19a** and **b**. The reaction involves reduction of the excited state **18*** by triethylamine to yield the distonic ketyl radical anion **20**, which undergoes an unusual 5-*endo* cyclization. Although this radical cyclization is itself not stereoselective (formation of the *anti* arrangement in **21a** is slightly preferred), the subsequent radical reduction of the tricyclic radical intermediates **21a/b** leads selectively to *cis* fusion between the newly formed cyclopentyl and the cyclohexyl ring.

A similar strategy involving reductive PET has been used to synthesize angularly fused cyclopentanoids and analogues tricyclic systems (not shown) [20]. For a recent review on photoreduction of ketones in the presence of amines and synthetic applications of the resulting ketyl radical anions in intramolecular radical cyclizations see Ref. [21].

14.3.2 Intermolecular Radical Reactions

The strong oxidizing power of the electronically excited carbonyl group in aldehydes, ketones, amides, and imides can be used to induce reductive PET through oxidation of a large variety of different functional groups, for example, amines, activated alkenes, thioethers, and carboxylates. This offers interesting opportunities for the synthesis of complex molecular frameworks through pathways involving intermolecular radical reactions between structurally simpler starting materials.

In the previous section, we focused on the synthetic application of ketyl radical anions obtained through reductive PET of the photoexcited carbonyl compound using tertiary amines as electron donor. This process leads to formation of amine radical cations as by-products, which themselves have also considerable synthetic potential. For example, using a carbonyl chromophor, which cannot undergo Norrish I photochemistry (e.g., benzophenones **22**), reduction in the photoexcited state by a tertiary amine, for example, *N*-methylpyrrolidine (**23**), leads to the radical anion/radical cation pair **24/25**. Subsequent intermolecular proton transfer from **25** to the ketyl radical anion **24** results in formation of a secondary α-amino radical **27** (Scheme 14.8).

The nucleophilic α-amino radicals can be trapped by subsequent addition to electron-deficient alkenes. The example illustrated in Scheme 14.9 shows the catalytic role of the photosensitizer in this sequence. Thus, addition of radical **27** to methylacrylate gives radical adduct **28**, which is reduced to the corresponding stabilized anion **29** by the diphenylhydroxymethyl radical **26**, the by-product during formation of the α-amino radical **27**. Proton transfer from **30** to **29** closes the catalytic cycle for the photosensitizer and gives the final product **31** in excellent yield [22].

The photosensitized addition of anilines to alkenes has been applied to the stereoselective synthesis of polycyclic frameworks, for example, **33**, through a tandem radical addition–cyclization sequence

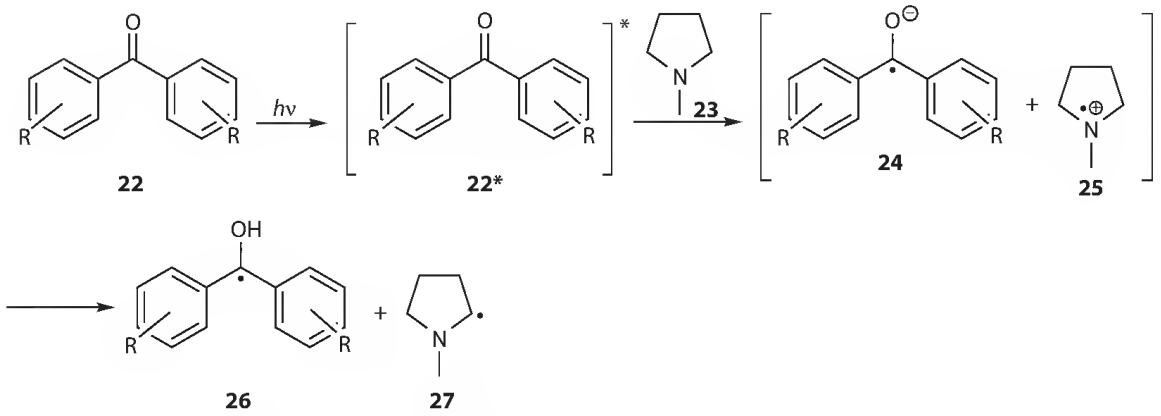

SCHEME 14.8 Generation of α-amino radicals through oxidative PET.

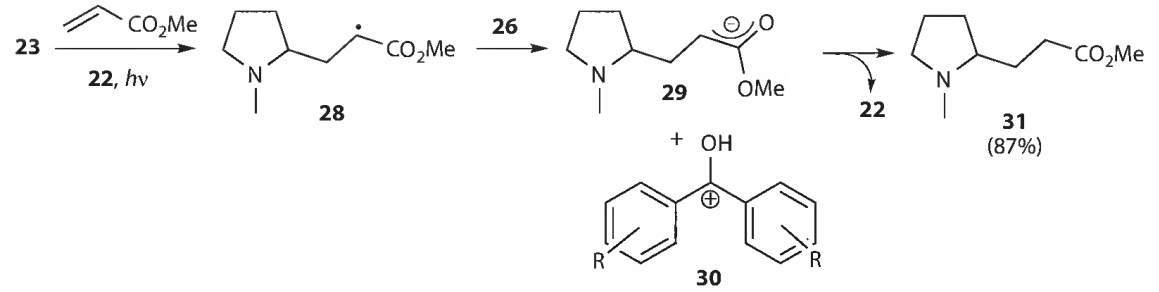

SCHEME 14.9 Radical addition–cyclization cascade using a catalytic photosensitizer.

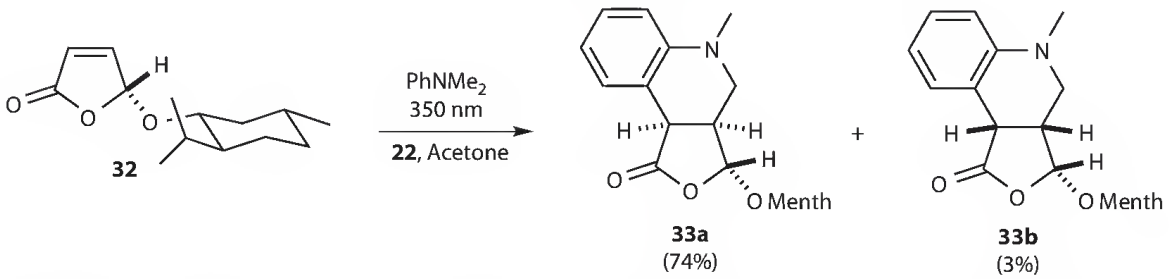

SCHEME 14.10 Diastereoselective radical addition–cyclization cascade using oxidative PET as initial step.

involving an aromatic radical substitution step. The stereochemistry of this cascade is controlled by a menthyl substituent attached to the electron-deficient alkene **32** (Scheme 14.10) [23].

Interestingly, addition of thiocarbonyl compounds to the reaction mixture leads to a significant enhancement of the overall rate, regio- and stereoselectivity of the reaction, in addition to activation of otherwise too unreactive amines (not shown). It has been proposed that persistent radical effects could be the origin of this behavior [24].

Mizuno et al. [25] used a reductive PET to perform regio- and stereoselective photoallylation of electron-deficient alkenes with allylic silanes. Scheme 14.11 illustrates quite well the photosensitized reaction of the dicyanomethylene tetrahydronaphthalene **34** with allyl silane **35**, which gives the allylated compound **36a** as the major product, where the allyl group at C-1 and the alkyl residue at C-2 are *trans*. Phenanthrene was used

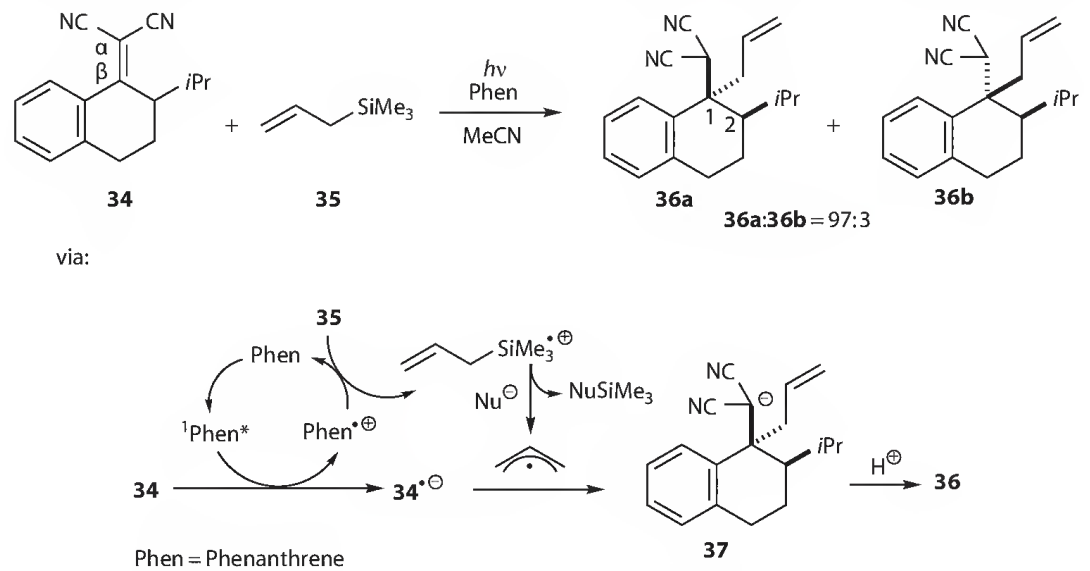

SCHEME 14.11 Regio- and stereoselective photoallylation of electron-deficient alkenes.

as a sensitizer, which in the electronically excited state transfers an electron to the alkene **34**. Regeneration of the photosensitizer occurs through oxidation of allyl silane **35**, which undergoes desilylation under the release of an allyl radical. The latter is trapped by the alkene radical anion $\mathbf{34}^{\bullet-}$ at the benzylic carbon to give anion **37**, followed by protonation. The stereochemistry in the major product can be explained by the fact that attack of the allyl radical occurs from the less hindered site, for example, opposite to the substituent at C-2.

It should be noted that in the case of alkyl substituted 1,1-dicyanoethenes radical recombination occurs selectively at the α-site of the alkene moiety, where the unpaired electron is stabilized by the two adjacent cyano groups (not shown) [25].

PET processes can also be used to generate inorganic radicals (this terminology will be used for radicals that do not contain carbon). Electronic excitation of ceric(IV) ammonium nitrate (CAN) through irradiation at λ = 350 nm results in one-electron reduction of the metal atom with one of the nitrate ligand being the reducing agent (Equation 14.4) [26]. This leads to formation of highly oxidizing nitrate radicals, NO_3^{∞}, which can be trapped by intermolecular reactions. The colorless Ce(III) salt formed as a by-product is (photo)chemically inactive. However, NO_3^{∞} undergoes photochemical decomposition at wavelengths around 650 nm [27].

$$(NH_4)_2Ce(NO_3)_6 \xrightarrow{350\,nm} [(NH_4)_2Ce^{IV}(NO_3)_6]^* \rightarrow NO_3^{\bullet} + (NH_4)_2Ce^{III}(NO_3)_6 \qquad (14.4)$$

In contrast to the majority of radicals described so far, NO_3^{∞} has the unpaired electron located at an O atom [28] and is therefore electrophilic. These have been used for the transformation of alkynes into carbonyl compounds through a highly efficient radical addition/cyclization/fragmentation cascade. Scheme 14.12 shows the reaction of photogenerated NO_3^{∞} with the 10-membered cycloalkyne **38** leading to the *cis* fused bicyclic ketones **39** and **40** [29] and the suggested mechanism based on BHandHLYP/6-311G** calculations of the potential surface [30].

The computed activation barriers (E_a) and reaction energies (ΔE) for each step of the sequence are included in Scheme 14.12 (all values include zero-point vibrational energy correction [zpc]) [30].

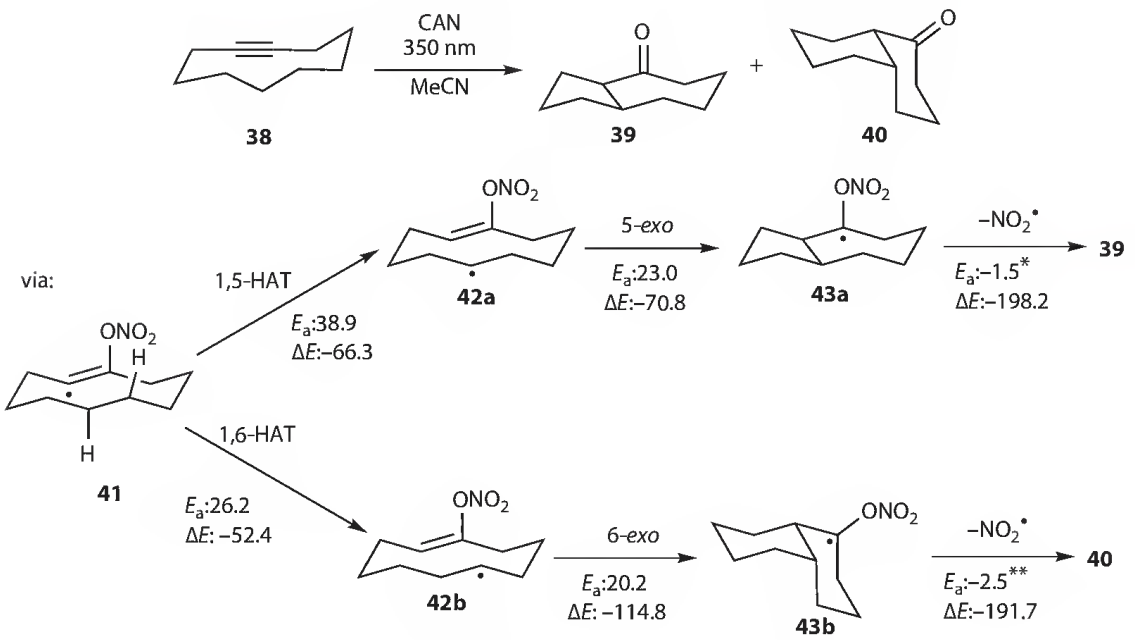

BHandHLYP/6-311G** energies in kJ mol^{-1}, zpc included
*2.3 without zpc; **3.0 without zpc

SCHEME 14.12 $NO_3^{\bullet}$-induced self-terminating radical cyclization cascade of medium-sized cyclolalkynes.

The *E*-configured vinyl radical **41** formed through addition of $NO_3^{\propto}$ to the π system in **38** (this reaction has a low E_a of only few kJ mol^{-1} and is strongly exothermic [31]) undergoes a 1,5- or 1,6-HAT to the secondary radicals **42a/b**, which subsequently cyclize in a *cis* selective 5-*exo* or 6-*exo* fashion, respectively, to the C=C double bond to yield the α-nitrato radicals **43a/b**. The key step in the cyclization cascade is the practically barrierless and highly exothermic β-fragmentation of the O–NO_2 bond in the latter radical intermediates to give the ketones **39** and **40** under the release of nitrogen dioxide, $NO_2^{\propto}$. According to the computations, each individual step in this cascade is not only strongly exothermic, but also associated with a low E_a.

The discovery of this sequence closes a long-existing gap in synthetic radical chemistry. Intermolecular addition of *O*-centered radicals to π systems, specifically to C≡C triple bonds, which offers the unique opportunity to form C–O bonds under mild conditions, have in the past not received much attention. This could originate from the perception that *O*-centered radicals, such as alkoxyl radicals, RO•, or acyloxyl radicals, RC(O)O•, may not react with π systems through intermolecular addition at rates that are competitive to other pathways, for example, allylic hydrogen abstraction or β-fragmentation, respectively. With the inorganic $NO_3^{\propto}$, such complications could apparently be avoided. Thus, with $NO_3^{\propto}$ alkynes can be easily oxidatively functionalized. The mechanism in Scheme 14.12 shows that $NO_3^{\propto}$ can formally be regarded as a synthon for *O*-atoms in solution. Because the released $NO_2^{\propto}$ is too unreactive to initiate a radical chain process under the applied reaction conditions, this sequence is termed a "self-terminating oxidative radical cyclization": the cascade-initiating radical contains the unreactive leaving group, which is released in the final step to terminate the sequence. In contrast to reactions performed under "classical" radical chain conditions and which are nearly always associated with a loss in overall functionality of the molecule, in self-terminating radical cyclizations the net amount of functional groups is unchanged after the reaction.

The initially formed vinyl radical can also be trapped through cyclization onto a carbonyl bond. For example, reaction of electro- or photochemically generated $NO_3^{\propto}$ with 5-cyclodecynone (**44**) leads to the isomeric epoxyketones **45** and **46** (Scheme 14.13) [29].

Since cycloalkyne **44** is not symmetrical, $NO_3^{\propto}$ addition to the C≡C triple bond gives the isomeric nucleophilic vinyl radicals **47** and **50**, which undergo 5-*exo* or 6-*exo* cyclization, respectively, to the less electron-rich carbon end of the carbonyl C=O double bond. The resulting allyloxyl radicals **48** and **51** cyclize in a 3-*exo* fashion to yield the α-oxiranyl radicals **49** and **52**, respectively. In accordance

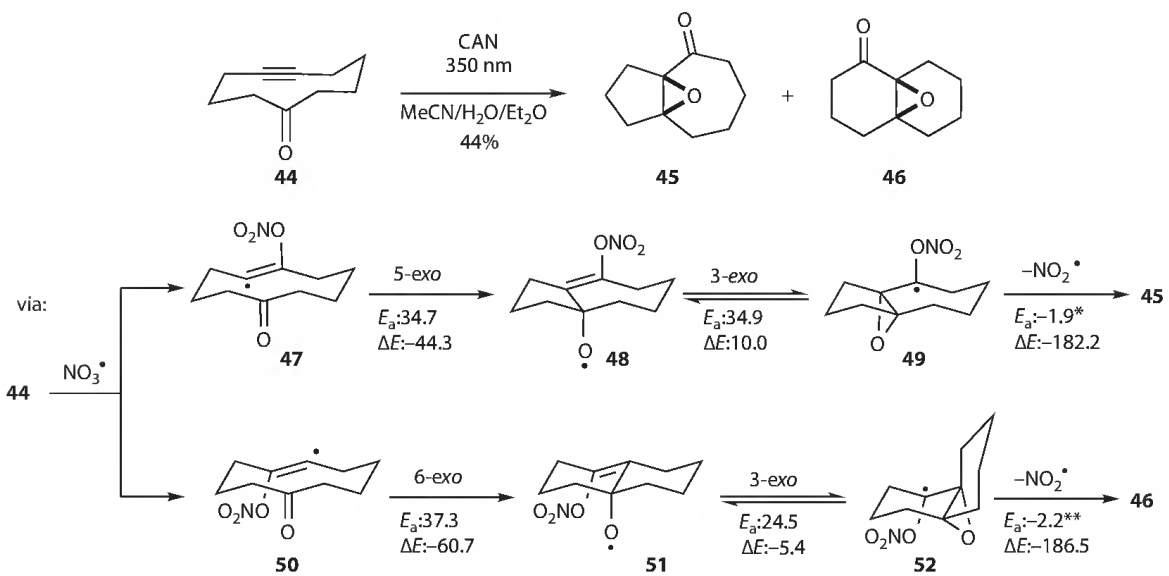

SCHEME 14.13 $NO_3^{\bullet}$-induced self-terminating radical cyclization cascade of medium-sized cyclolalkynones.

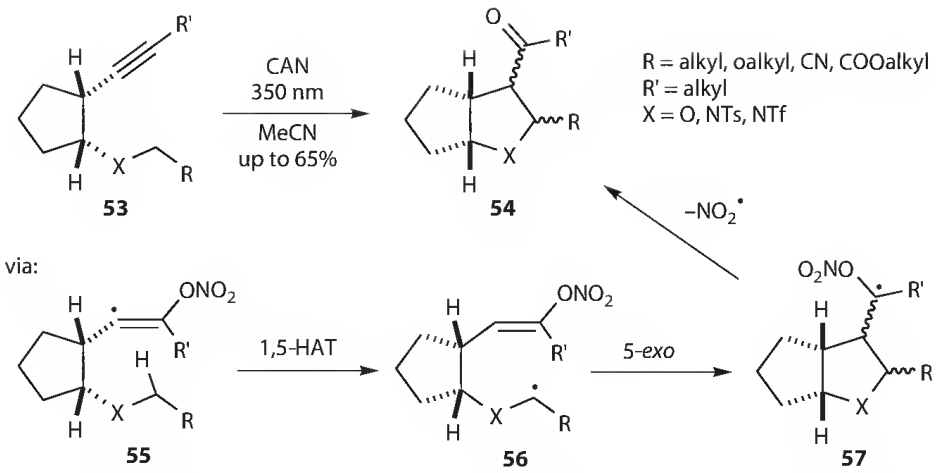

SCHEME 14.14 Diastereoselective formation of anellated tetrahydrofurans and pyrrolidines through an $NO_3^{\bullet}$-induced self-terminating radical cyclization cascade.

with literature [32], the calculations show that this latter step is highly reversible, and the only reason why the reverse ring-opening does not occur in this cascade is the ease by which the radicals **49/52** undergo β-fragmentation to give the respective epoxy ketones **45** and **46** with release of NO_2^{∞}. This self-terminating radical cyclization represents one of the very few examples for the synthetic access to epoxides through a 3-*exo* cyclization of allyloxyl radicals. Interestingly, this sequence can also formally be considered as "retro-Eschenmoser-Ohloff" fragmentation [33].

Self-terminating radical oxygenations are not restricted to cyclic alkynes. Electro- and photochemically generated $NO_3^{\propto}$ can be used for the oxidative cyclization of cycloalkyl-clamped alkynes **53** (Scheme 14.14). This reaction leads to the formation of anellated tetrahydrofurans (**54** with X = O) [34–36] or pyrrolidines (**54** with X = NTs, NTf) [37] possessing four asymmetric centers in good to excellent yields through a cascade consisting of radical addition at the less hindered site of the C≡C triple bond, rate-determining 1,5-HAT [34,36], 5-*exo* cyclization, and terminating β-fragmentation under release of NO_2^{∞}. The diastereoselectivity of this sequence, which is determined in the 5-*exo* cyclization, ranges from moderate to very high and depends on various factors, such as the nature of the heteroatom X and the substituent R.

The role of the cycloalkyl clamp in the starting alkyne **53** is to reduce the conformational degrees of freedom in the intermediate highly reactive vinyl radical **55**, and to achieve a favorable alignment between the SOMO on the π system and the σ-orbital of the respective C–H bond for the 1,5-HAT. The experiments revealed that the self-terminating cyclization cascade worked best using a *cis*-1,2-disubstituted cyclopentyl clamp, however, *trans*-1,2-disubstituted cyclohexyl rings could also be used. With larger ring sizes, both yield and diastereoselectivities were reduced [34–36]. A similar conformational restriction of the intermediate vinyl radical was also obtained using the Thorpe–Ingold effect provided by two geminal ester groups (not shown) [38].

Apart from "typical" radical chemistry, photogenerated $NO_3^{\propto}$ can also be used in ET reactions. Due to the high oxidation power of $NO_3^{\propto}$ (E^0 ($NO_3^{\bullet}/NO_3^{-}$) = 2.3 V vs. NHE [26,39,40]), many organic compounds are principally prone to oxidation by $NO_3^{\propto}$ [26]. With regard to the intrinsic perception that radicals are "damaging" species and contact with environmental radicals should therefore be avoided, it was interesting to realize that NO_3^{∞}, which are the most important oxidants in the nighttime troposphere, can mediate repair of pyrimidine cyclobutane dimers in DNA. The latter are the primary photoproducts formed through UV-light-induced [2 + 2] cycloaddition between two adjacent pyrimidine bases in the same oligonucleotide strand. This damage, if not repaired, can lead to mutations, cell death, and cancer [41]. Scheme 14.15 shows the results of an in vitro study using the *cis,syn* permethylated uracil dimer **58** as simplified model for pyrimidine cyclobutane dimers in DNA, which undergo rapid and efficient cleavage into the respective monomer **59** upon treatment with photogenerated $NO_3^{\propto}$ [42].

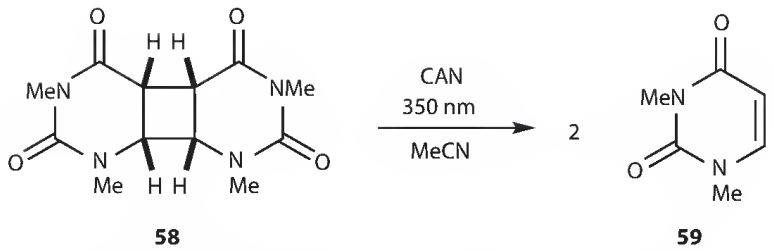

SCHEME 14.15 $NO_3^{\bullet}$-induced oxidative repair of pyrimidine cyclobutane dimers.

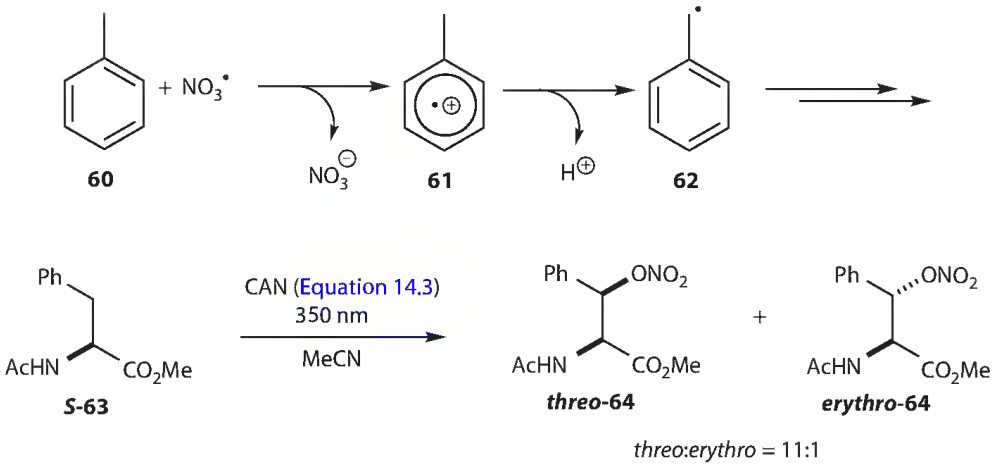

SCHEME 14.16 $NO_3^{\bullet}$-induced oxidative damage of aromatic amino acids.

Reaction of photogenerated $NO_3^{\bullet}$ with electron-rich aromatic compounds of type **60** is a convenient method to oxidatively modify the benzylic position (Scheme 14.16) [26,43]. The reaction is likely to proceed through ET to give radical cation **61**, which loses a proton at the benzylic position to restore the aromatic system. Direct H abstraction from the benzylic position by $NO_3^{\bullet}$ could be excluded, since the intermediate aromatic radical cation **61** could be trapped by additives, such as nitrogen dioxide, $NO_2^{\bullet}$. Thus, treatment of the enantiomerically pure phenylalanine derivative ***S*-63** with $NO_3^{\bullet}$ leads to formation of the diastereomeric β-nitrato esters ***threo/erythro*-64** with a ratio of 11:1 [43]. The reason for the high diastereoselectivity of this reaction, which offers interesting synthetic opportunities, is not yet clear.

It should be noted that reaction of tyrosine with photogenerated $NO_3^{\bullet}$ leads to the formation of 3-nitrotyrosine (not shown), which is a known biomarker for nitrosative stress and has been linked to respiratory tract diseases, such as asthma [43]. With regards to the role of $NO_3^{\bullet}$ in atmospheric chemistry, this reaction may provide a novel and so far unknown, pollution-derived pathway to 3-nitrotyrosine.

14.4 Radical Reactions Induced by Photofragmentation

Generation of radicals through unimolecular fragmentation of a labile bond in a photoexcited molecule offers unique advantages over conventional radical chain conditions, where formation of the target radical species usually involves at least one bimolecular step. In the past years, new photocleavable groups have been designed, which are structurally based on the thiohydroxamate esters **65** developed by the Barton group in 1983 (Scheme 14.17) [44,45]. They all possess a labile N–O bond, which upon cleavage gives initially an *O*-centered radical **67**. Depending on the nature of the substituent R, the latter can either react directly as *O* radical or undergo fragmentation to produce a secondary radical, which then reacts in a subsequent step. Whereas the Barton esters **65** are generally readily accessible from commercially available precursors, their extreme light sensitivity makes handling a tricky task. This difficulty could be overcome with the open-chain thiohydroxamates **68**

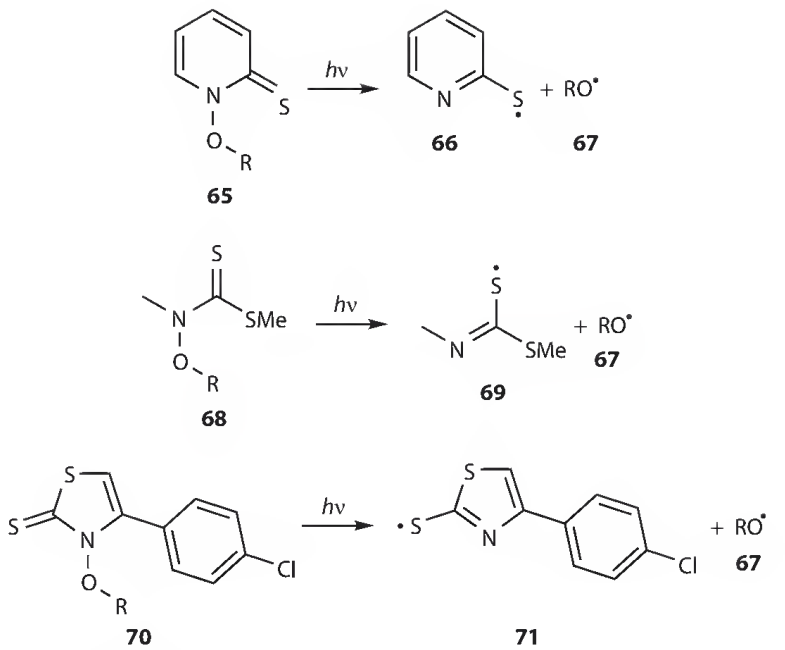

SCHEME 14.17 Photolabile radical precursors.

developed by Kim et al. [46] or Hartung's thiazolthiones **70** [47], respectively, which have a higher stability toward visible light and require UV light to induce fragmentation.

Barton and Kim esters were used to generate a large variety of both inorganic and organic *O*-centered radicals and explored in self-terminating radical cyclizations. Using the reaction with cyclodecyne (**38**) as model system (see Scheme 14.12), hydroxyl (HO•) [48], acyloxyl (RC(O)O•) [49], alkoxycarbonyloxyl (ROC(O)O•) [50], alkoxycarbonylacyloxyl (ROC(O)C(O)O•) [50], carbamoyloxyl ($R_2NC(O)O$•) [50], and alkoxyl radicals (RO•) [51] have been shown to promote the oxidative cyclization to the bicyclic ketones **39** and **40**. Although the organic *O*-centered radicals are known to undergo facile β-fragmentation, under optimized conditions, they could be very efficiently trapped by the alkyne prior to decomposition. In Table 14.1 are shown representative outcomes of these reactions.

It should be noted that with some of these *O*-centered radicals, the terminating β-fragmentation of the O–R bond in the α-oxo radicals of type **43** (see Scheme 14.12, with the NO_2 group being replaced by the respective organic residue) could be energetically challenging. Computational studies suggest that alternative termination pathways may also be active that could involve a radical chain process with the precursor of the respective *O*-centered radical (not shown) [30].

The apparent generality of self-terminating radical cyclizations with regards to different classes of *O*-centered radicals led to the question, whether this sequence could also be applied to other heteroatom-centered radicals, for example, those where the unpaired electron is located on a nitrogen atom. Quite remarkably, only very few examples for radical cascades that are initiated by intermolecular addition of *N*-centered radicals to alkynes have been reported.

Scheme 14.18 shows that reaction of phthalimidyl radicals, Im•, which were generated through photochemical cleavage of the N–Br bond in *N*-bromo phthalimide, with cyclodecyne (**38**) leads to formation of small amounts of unsaturated bicyclic compounds **72** and **73** amongst other products (not shown) [52]. The 10-membered cycloalkyne **38** is a versatile model system for self-terminating radical reactions, since the reaction steps following initial radical addition to the C≡C triple bond are driven by transannular interactions and are therefore highly regioselective. Thus, initial addition of Im• initiates the expected radical translocation sequence consisting of transannular HAT (**74** → **75a/b**), followed by transannular radical cyclization (**75a/b** → **76a/b**). In contrast to the self-terminating radical

TABLE 14.1 Representative Results for the Reaction of Cyclodecyne (38) with Various *O*-Centered Radicals

O–Radical	Conditions	Yield (GC) 39 + 40%	Reference
HO•	Photolysis of 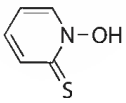	63	[48]
4-$MeOC_6H_4C(O)O$•	Photolysis of 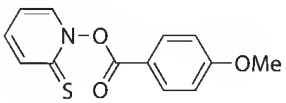	89	[49]
MeOC(O)O•	Photolysis of 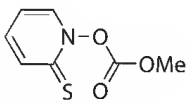	94	[50]
EtOC(O)C(O)O•	Photolysis of 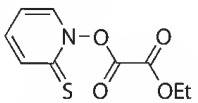	82	[50]
$Et_2NC(O)O$•	Photolysis of 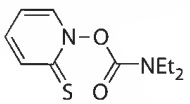	69	[50]
BnO•	Photolysis of 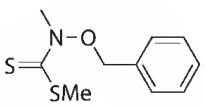	53%	[51]

cyclizations with O-centered radicals presented earlier, however, β-fragmentation in the α-imidyl radical intermediates **76a/b** is not possible, since no stable radical could be released. It is therefore believed that the reaction proceeds through trapping of **76a/b** by bromine atoms, which are formed as by-products during photolysis of *N*-bromophthalimide. The resulting tertiary bromides **77a/b** could subsequently eliminate hydrogen bromide to give the final products **72** and **73**, respectively.

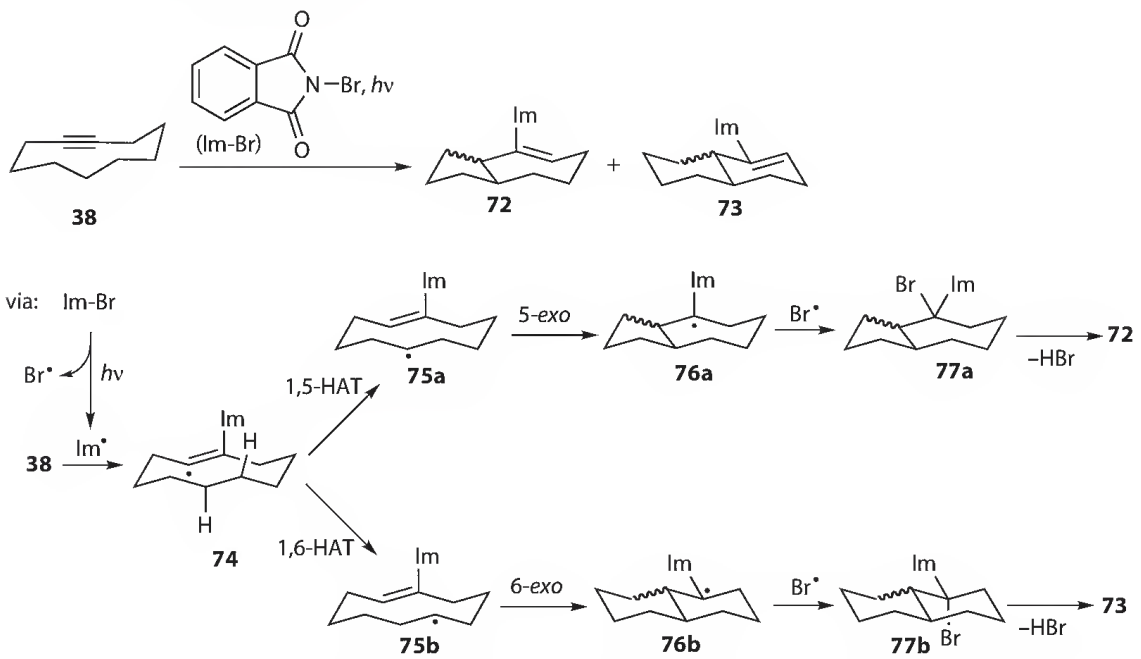

SCHEME 14.18 Self-terminating radical cyclization cascade involving N-centered imidyl radicals.

Self-terminating radical cyclizations have been explored with both aminium and amidyl radicals using the well-established model reaction with cyclodecyne (**38**). The aminium radicals were produced through photolysis of the respective *N*-nitroso or *N*-chloroamines under acidic conditions, whereas the amidyl radicals were obtained from photochemical cleavage of *N*-nitrosoamides. Surprisingly, instead of the expected bicyclic *N*-containing products, ketones **39** and **40** were exclusively formed in these reactions. This finding could be explained by the exemplary mechanism shown for the reaction of the *N*-benzyl acetamidyl radical, AcBnN•, in Scheme 14.19 [53].

N-Radical addition to the C≡C triple bond in cycloalkyne **39** initiates the usual transannular radical translocation/cyclization cascade, which is terminated by β-fragmentation **80** → **81**. The observed bicyclic ketones **39/40** could result from subsequent hydrolysis of the imides **81a/b**. However, experimental findings indicate that the mechanism is more complex. Although the *N*-radicals were equipped with substituents that should form in principle stable radical leaving groups in the terminating β-fragmentation **80** → **81**, namely benzyl or tosyl, no apparent correlation between radical stability and yield of bicyclic

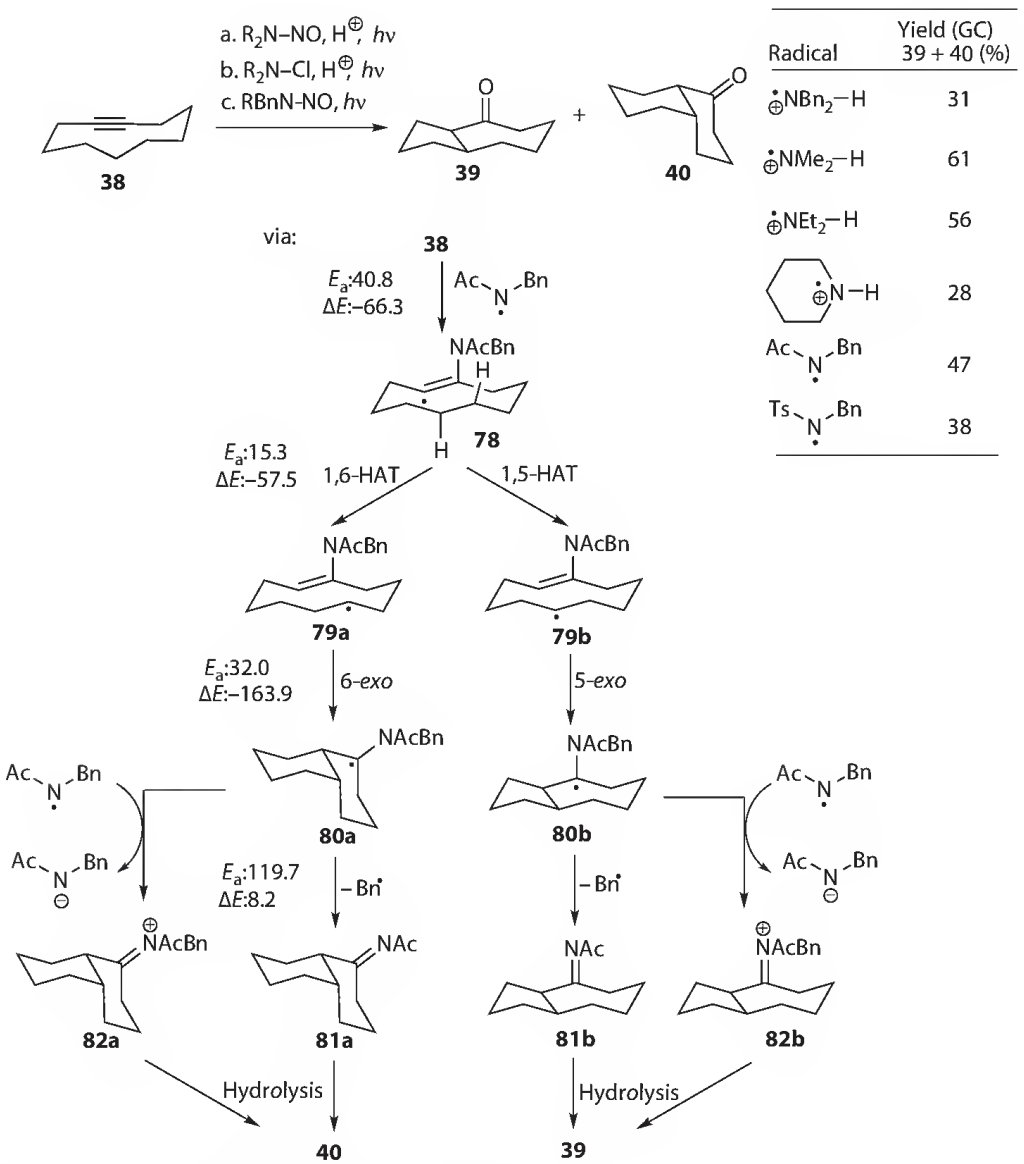

SCHEME 14.19 Self-terminating radical cyclizations involving N-centered aminium and amidyl radicals.

ketones **39/40** was found. It even appeared that N-radicals with primary alkyl substituents, which should not be released as radicals at all, performed significantly better in this cyclization sequence than N-radicals carrying substituents possessing good or excellent radical stabilizing properties (see table in Scheme 14.19).

Mechanistic insights were obtained from extensive computational studies of the potential energy surface of this reaction and the termination step. Selected BHandHLYP/6-311G** data given in Scheme 14.19 for the reaction of AcBnN• show the overall exothermicity of the initial radical addition and the subsequent transannular radical translocation steps. Calculations of the redox properties of α-nitrogen radicals of type **80** and of the various N-centered radicals revealed that the latter are sufficiently strong oxidants to promote oxidation of the α-nitrogen radical to the respective iminium ions **82** (data not shown). Subsequent hydrolysis leads to the ketones **39/40**. Thus, in this sequence, the N-radicals have a dual role, first as initiator of the radical cyclization cascade, and second as terminator of the sequence through a redox process. This is a highly interesting variation of self-terminating radical cyclizations.

Photochemical cleavage of the S–S bond in disulfides has been used to generate thiyl radicals, which can be trapped through addition to alkynes. In the model reaction with cyclodecyne (**38**) the initial radical addition triggers a transannular radical translocation/cyclization, similar to the reaction shown in Scheme 14.12. The products in this sequence are three stereoisomeric bicyclic thiols **83** possessing a decalin [4.4.0] framework, which result from reduction of the intermediate α-thio radical **84** (Scheme 14.20). Products possessing the constitutionally isomeric bicyclo[5.3.0] framework (as observed in the reaction of **38** with O- and N-centered radicals shown earlier, respectively) were not formed [54].

In contrast to self-terminating radical cyclizations with O- and N-centered radicals, respectively, where exclusively *cis*-fused bicyclic systems were obtained (as would be expected for kinetically controlled radical cyclizations), the reaction with S-centered radicals leads also to *trans*-fused products. Mechanistic studies using computational techniques revealed that the difference between the reactions of O- or N-centered radicals, respectively, compared to those involving S-centered radicals is caused by the reversibility (and endothermicity) of the initial S-radical addition to the alkyne C≡C triple bond, which leads to another low-energy conformational isomer of the vinyl radical. The subsequent transannular reaction of the latter occur in a regio- and stereospecific fashion, where formation of the bicyclo[4.4.0] framework is kinetically much more favorable than formation of the isomeric bicyclo[5.3.0] framework [55].

Needless to say, apart from generation of heteroatom-centered radicals, photofragmentation is also a versatile method to generate C-centered radicals in a direct fashion. The xanthate group exploited by Zard et al. [12], which has found important application in the RAFT living polymerization process (see previous paragraphs), has inspired the development of dithiocarbamates as highly efficient precursor for carbamoyl radicals [56]. The example in Scheme 14.21 shows cyclization of a carbamoyl radical **87**, which was obtained through light-driven dissociation of dithiocarbamate **85**, in a *cis*-selective 4-*exo* fashion. The resulting bicyclic radical intermediate **88** initiates a diastereoselective group transfer reaction (the radical **88** is attacking with the less hindered site) with xanthate **85** to give the final bicyclic β-lactam **86**.

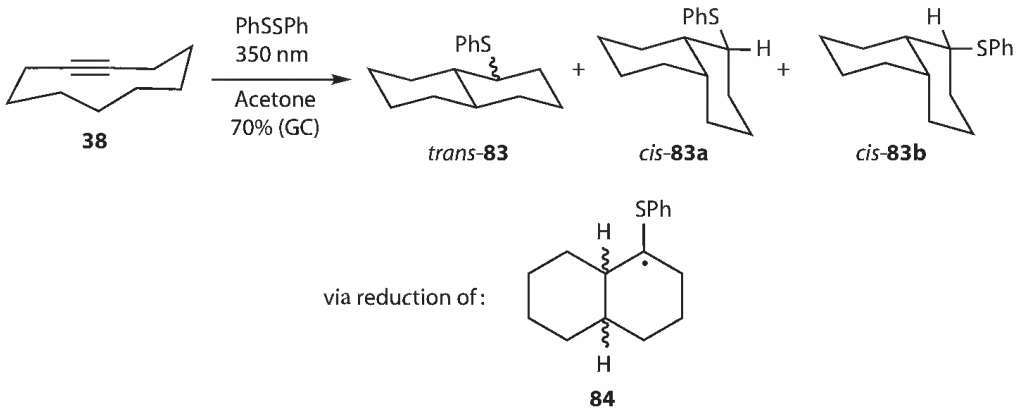

SCHEME 14.20 Self-terminating radical cyclization cascade involving S-centered thiyl radicals.

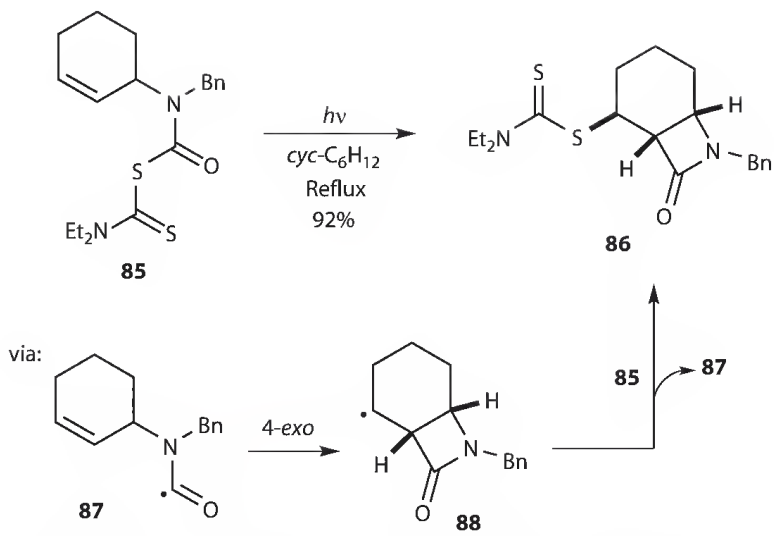

SCHEME 14.21 Diastereoselective cyclization of carbamoyl radicals generated through photolysis of dithiocarbamates.

14.5 Photosensitized Radical Reactions

Energy transfer from a photoexcited donor molecule to an acceptor in the electronic ground state offers highly interesting opportunities for synthetic applications. The most common process is triplet sensitization using carbonyl compound as donor. Excitation, followed by intersystem crossing, leads to the triplet excited state ($^3n\pi^*$ in carbonyl compounds). The triplet character can subsequently be transferred to an acceptor, for example, an alkene, which is photochemically inactive under these conditions. Abe and Hoffmann et al. have used this chemistry to perform stereo- and regioselective radical reactions involving furanone derivatives using acetone as triplet sensitizer (Scheme 14.22) [57].

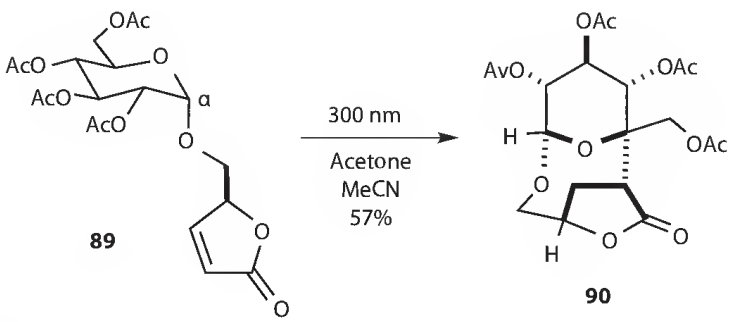

via (simplified system):

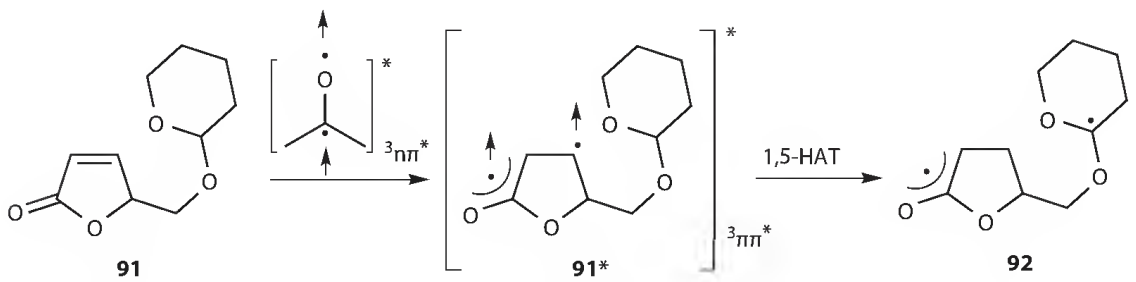

SCHEME 14.22 Triplet-sensitized stereo- and regioselective formation of furanones.

The key step in these reactions is the 1,5-HAT in a triplet biradical of type **91*** obtained by energy transfer, leading to the stabilized the biradical **92**, which undergo an intramolecular radical recombination. When this sequence is applied to the α-glycosyl substituted furanone **89**, radical recombination occurs in a highly stereoselective fashion and leads exclusively to the complex tricyclic compound **90** with a remarkable yield.

References

1. Giese, B. *Radicals in Organic Synthesis: Formation of Carbon-Carbon Bonds.* Organic Chemistry Series, Vol. 5, 1st edn., Pergamon, Oxford, U.K., 1986.
2. Ryu, I.; Uehara, S.; Hirao, H.; Fukuyama, T. *Org. Lett.* 2008, *10*, 1005.
3. Chatgilialoglu, C.; Alberti, A.; Ballestri, M.; Macciantelli, D. *Tetrahedron Lett.* 1996, *37*, 6391.
4. Schaffner, A.-P.; Renaud, P. *Angew. Chem. Int. Ed.* 2003, *42*, 2658.
5. Devin, P.; Fensterbank, L.; Malacria, M. *Tetrahedron Lett.* 1999, *40*, 5511.
6. Studer, A. *Chem. Soc. Rev.* 2004, *33*, 267.
7. Albini, A.; Fagnoni, M.; Mella, M. *Pure Appl. Chem.* 2000, *72*, 1321.
8. Griesbeck, A. G.; Mattay, J. eds. *Synthetic Organic Photochemistry*, Marcel Dekker, New York, 2005.
9. Horspool, W. M.; Lenci, F. eds. *CRC Handbook of Organic Photochemistry and Photobiology*, Vols. 1 and 2, 2nd edn., CRC Press, Boca Raton, FL, 2003.
10. Albini, A.; Fagnoni, M. eds. *Handbook of Synthetic Photochemistry*, Wiley-VCH Verlag, Weinheim, Germany, 2010.
11. Chiefari, J.; Chong, Y. K. B.; Ercole, F.; Krstina, J.; Jeffery, J.; Le, T. P. T.; Mayadunne, R. T. A.; Meijs, G. G.; Moad, C. L.; Moad, G.; Rizzardo, E.; Thang, S. H. *Macromolecules* 1998, *31*, 5559.
12. Taton, D.; Destarac, M.; Zard, S. Z. *Handbook of RAFT Polymerisation* (ed. Barner-Kowollik, C.), Wiley-VCH, Weinheim, Germany, 2008, p. 373.
13. Lu, L.; Zhang, H.; Yang, N.; Cai, Y. *Macromolecules* 2006, *39*, 3770.
14. Sluggett, G. W.; Turro, C.; George, M. W.; Koptyuk, I. V.; Turro, N. J. *J. Am. Chem. Soc.* 1995, *117*, 5148.
15. Paczkowski, J.; Kucybala, Z.; Scigalski, F.; Wrzyszczynski, A. *J. Photochem. Photobiol. A: Chem.* 2003, *159*, 115.
16. Corrales, T.; Catalina, F.; Peinado, C.; Allen, N. S. *J. Photochem. Photobiol. A: Chem.* 2003, *159*, 103.
17. Hoffmann, N. *J. Photochem. Photobiol. C: Photochem. Rev.* 2008, *9*, 43.
18. Rinderhagen, H.; Waske, P. A.; Mattay, J. *Tetrahedron* 2006, *62*, 6589.
19. Tzvetkov, N. T.; Waske, P. A.; Neumann, B.; Stammler, H.-G.; Mattay, J. *Tetrahedron Lett.* 2008, *49*, 1710.
20. Tzvetkov, N. T.; Arndt, T.; Mattay, J. *Tetrahedron* 2007, *63*, 10497–10510.
21. Cossy, J.; Belotti, D. *Tetrahedron* 2006, *62*, 6459.
22. Hoffmann, N.; Betrand, S.; Marinkovic, S.; Pesch, J. *Pure Appl. Chem.* 2006, *78*, 2227.
23. Bertrand, S.; Hoffmann, N.; Humbel, S.; Pete, J. P. *J. Org. Chem.* 2000, *65*, 8690.
24. Harakat, D.; Pesch, J.; Marinkovic, S.; Hoffmann, N. *Org. Biomol. Chem.* 2006, *4*, 1202.
25. Mizuno, K.; Hayamizu, T.; Maeda, H. *Pure Appl. Chem.* 2003, *75*, 1049.
26. Baciocchi, E.; Del Giacco, T.; Murgia, S. M.; Sebastiani, G. V. *J. Chem. Soc., Chem. Commun.* 1987, 1246; and cited literature.
27. Wayne, R.; Barnes, I.; Biggs, P.; Burrows, J.; Canosa-Mas, C.; Hjorth, J.; Le Bras, G.; Moortgat, G.; Perner, D.; Poulet, G.; Restelli, G.; Sidebottom, H. The nitrate radical: Physics, chemistry, and the atmosphere. *Atmos. Environ., Part A.* 1991, *25*, 1.
28. Ishiwata, T.; Fujiwara, I.; Naruge, Y.; Obi, K.; Tanaka, I. *J. Phys. Chem.* 1983, *87*, 1349.
29. Wille, U.; Plath, C. *Liebigs Ann./Recueil* 1997, 111.
30. Wille, U. *J. Phys. Org. Chem.* 2011, *24*, 672–681.
31. Wille, U.; Dreessen, T. *J. Phys. Chem. A* 2006, *110*, 2195.

32. Curran, D. P.; Porter, B. A.; Giese, B. *Stereochemistry of Radical Reactions: Concepts, Guidelines and Synthetic Applications*, Wiley-VCH, Weinheim, Germany, 1996.
33. Felix, D.; Schreiber, J.; Ohloff, G.; Eschenmoser, A. *Helv. Chim. Acta* 1971, *54*, 2896.
34. Wille, U.; Lietzau, L. *Tetrahedron* 1999, *55*, 10119.
35. Lietzau, L.; Wille, U. *Heterocycles* 2001, *55*, 377.
36. Wille, U.; Lietzau, L. *Tetrahedron* 1999, *55*, 11465.
37. Stademann, A.; Wille, U. *Aust. J. Chem*. 2005, *57*, 1055.
38. Li, C. H.; Honours thesis, The University of Melbourne, Australia, 2006. (unpublished).
39. Neta, P.; Huie, R. E. *J. Phys. Chem*. 1986, *90*, 4644.
40. Eberson, L. *Adv. Phys. Org. Chem*. 1981, *18*, 79.
41. Pogozelski, W. K.; Tullius, T. D. *Chem. Rev*. 1998, *98*, 1089.
42. Krüger, O.; Wille, U. *Org. Lett*. 2001, *3*, 1455.
43. Sigmund, D. C. E.; Wille, U. *Chem. Commun*. 2008, 2121.
44. Barton, D. H. R.; Crich, D.; Motherwell, W. B. *J. Chem. Soc., Chem. Commun*. 1983, 939.
45. Barton, D. H. R.; Crich, D.; Motherwell, W. B. *Tetrahedron Lett*. 1983, *24*, 4979.
46. Kim, S.; Lim, C. J.; Song, S. E.; Kang, E. Y. *Synlett* 2001, 688.
47. Hartung, J.; Daniel, K.; Gottwald, T.; Gross, A.; Schneiders, N. *Org. Biomol. Chem*. 2006, *4*, 2313.
48. Wille, U. *Tetrahedron Lett*. 2002, *43*, 1239.
49. Wille, U. *J. Am. Chem. Soc*. 2002, *124*, 14.
50. Jargstorff, C.; Wille, U. *Eur. J. Org. Chem*. 2003, 3173.
51. Sigmund, D.; Schiesser, C. H.; Wille, U. *Synthesis* 2005, 1437.
52. Wille, U.; Krüger, O.; Kirsch, A.; Lüning, U. *Eur. J. Org. Chem*. 1999, 3185.
53. Wille, U.; Heuger, G.; Jargstorff, C. *J. Org. Chem*. 2008, *73*, 1413.
54. Tan, K. J. PhD Thesis, The University of Melbourne, Australia, 2010.
55. Tan, K. J.; White, J. M.; Wille, U. *Eur. J. Org. Chem*. 2010, 4902–4911.
56. Grainger, R. S.; Innocenti, P. *Heteroatom Chem*. 2007, *18*, 568.
57. Jahjah, R.; Gassama, A.; Bulach, V.; Suzuki, C.; Abe, M.; Hoffmann, N.; Martinez, A.; Nuzillard, J.-M. *Chem. Eur. J*. 2010, *16*, 3341.

15

Recent Advances in the Photoinduced Radical Nucleophilic Substitution Reactions

Maria E. Budén
Universidad Nacional de Córdoba

Sandra E. Martín
Universidad Nacional de Córdoba

Roberto A. Rossi
Universidad Nacional de Córdoba

15.1 Introduction

Nucleophilic substitution is feasible through processes that involve electron transfer (ET) steps. In these reactions, a compound bearing an adequate leaving group is substituted at the *ipso* position by a nucleophile. Several reviews have been published on the subject in relation to the mechanism and to the synthetic applications of the process, which has become one of the common methodologies in modern synthesis.[1] In this review, we will describe the most recent advances in photostimulated $S_{RN}1$ reactions. With this aim in mind, we expect to cover recent $S_{RN}1$ substitutions, with an emphasis on the scope of the process in terms of synthetic capability and target applications. The critical review illustrates the mechanistic considerations required for planning synthetic applications and a wide range of synthetic protocols.

The $S_{RN}1$ reaction, which stands for unimolecular radical nucleophilic substitution, is a chain process that involves radicals and radical anions as intermediates. Several nucleophiles can be used for $S_{RN}1$ reactions such as carbanions and heteroatom anions resulting in the formation of new C–C or C-heteroatom bonds in good yields. An exception to this is the reaction of aromatic alkoxides with aromatic substrates. In these cases, C–O bond formation is not observed; instead C–C bond formation is achieved. For example, the unsubstituted phenoxide ions have been reported to react with ArX to afford the *ortho*- (ca. 40%) and *para*- (ca. 20%) C–C coupled products.[1] On the other hand, alkoxide ions afford the *O*-alkylation products with aliphatic substrates with electron withdrawing group (EWG) at the α-carbon.

There is a theoretical study (DFT/B3LYP level) on the reaction of aromatic alkoxide ions with phenyl and 4-nitrobenzyl radicals with the aim of interpreting the factors that control the regiochemical outcome of these reactions. While FMO predicts the experimental regioselectivity of phenyl radicals with good accuracy, it fails in the nitrobenzyl case.[2]

A similar behavior is observed with nitrogen nucleophiles (anions from aromatic amines, pyrrole, diazoles, and triazoles) in reactions with aromatic substrates, no C–N is observed, but C–C bond is formed. On the other hand, with nitrogen nucleophiles N-alkylation products are formed with aliphatic substrates with EWG at the α-carbon.

Anions derived from tin, phosphorus, arsenic, antimony, sulfur, selenium, and tellurium react through the heteroatom to form a new C-heteroatom bond by this mechanism.

15.2 Mechanism

The $S_{RN}1$ mechanism is presented in Scheme 15.1. In the initiation step, the radical anion of the substrate can be formed by an ET from the nucleophile or from a suitable electron source. This radical anion fragments into a radical and the anion of the leaving group. On the other hand, the ET to unsubstituted alkyl halides is proposed to be a dissociative reaction.[3]

The radical can react with the nucleophile to give the radical anion of the substitution product, which by ET to the substrate forms the intermediates needed to continue the propagation cycle. The mechanism has termination steps that depend on the substrate, nucleophile, and experimental conditions.

Inhibition by radical traps has been extensively used to provide mechanistic evidences. The most commonly employed are di-*t*-butylnitroxide or radical anion scavengers such as *p*-dinitrobenzene (*p*-DNB).

Radical probes have also been used in order to assess the formation of radicals along the propagation cycle. Products from ring closure, ring opening, or rearrangement of the radicals were thus taken as evidence of the presence of these intermediates.

The process offers the possibility to afford the substitution of an unreactive nucleophile through *entrainment*[4] conditions. Entrainment is useful when the nucleophile is rather unreactive at initiation, but quite reactive at propagation. Under these conditions the addition of another nucleophile, more reactive at initiation, increases the generation of intermediates and allows the less reactive nucleophile to start its own propagation.

Spontaneous or thermal ET is a possible initiation depending on the relationship between the electron affinity of the substrate and the oxidation potential of the nucleophile; however, few examples are known. Even though photoinduction is a widely used initiation method, there are not many mechanistic studies. These photoinduced ET can conceivably be accomplished in one of the following mechanisms: (1) homolytic cleavage of the C–X bond, (2) ET from the nucleophile to the excited RX (or from the excited nucleophile to the RX), (3) ET from excited charge transfer complex (CTC) of the nucleophile and RX. Depending on the nature of the RX, the nucleophile, and the experimental conditions, any of these mechanisms could probably be considered as an initiation step.

One of the main goals of the $S_{RN}1$ mechanism is the possibility to obtain disubstituted compounds when the reaction is performed with substrates bearing two leaving groups. Few examples are known of trisubstitutions[5] or four consecutive $S_{RN}1$ substitutions.[6,7]

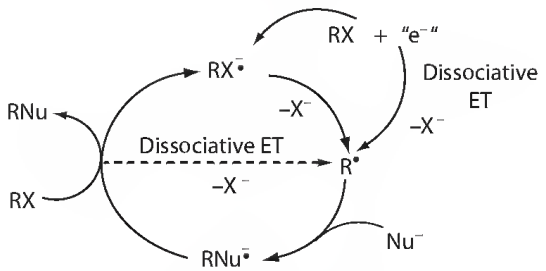

SCHEME 15.1 Representation of the mechanism of the $S_{RN}1$ reaction.

15.3 Aromatic Substrates

15.3.1 Reaction with Carbanions

Aromatic substrates bearing suitable leaving groups can suffer substitution by the $S_{RN}1$ mechanism with a large range of nucleophiles under different reaction conditions. The most widely used nucleophiles are carbanions, such as those derived from ketones, esters, *N,N*-disubstituted amides, etc. The solvents and conditions of choice are usually liquid ammonia or DMSO and irradiation.

When dihalobenzenes react with aliphatic ketone enolate anions, disubstitution products are formed. Under irradiation, as well as under $FeBr_2$ initiation, *o*-iodohalobenzenes **1** (X = Cl, Br, I) react with enolate anions of aromatic ketones, such as acetophenone, propiophenone, and 2-naphthyl methyl ketone in DMSO. For example, the photostimulated reaction of 2-naphthyl methyl ketone ions (2-NaphCOCH_2^-) with **1** forms the radical **2** after C-I bond fragmentation that reacts with the nucleophile to afford the radical anion $\mathbf{3}^{-\bullet}$, in which the odd electron is localized in the ArCO-π moiety (Scheme 15.2). The rate of intermolecular ET to **1** to yield **3** is faster than the intramolecular ET to σ* MO of the C–X bond, giving monosubstitution product **3** with retention of one halogen (Cl: 71%, Br: 86%, I: 65%).[8]

The extent of dehalogenation is discussed in terms of the energetics of the intramolecular ET from the MO ArCO-π* to the σ* MO of the C–X bond in the monosubstituted radical anions $\mathbf{3}^{-\bullet}$ proposed as intermediates.[8]

The photostimulated reaction of a chiral-assisted imide enolate ion **4** with 1-iodonaphthalene provides an example of stereoselective coupling of an aromatic radical with a nucleophile. In this reaction the diasteromeric isomers of the substitution compound are formed (43%–64%) and the selectivity observed is highly dependent on the metal counterion used and its chelation properties (Equation 15.1). All the ions studied (Li^{+1}, Na^{+1}, K^{+1}, Cs^{+1}, Ti^{+4}) are selective; however, the highest stereoselectivity is found with Li^{+1} at low temperature (–78°C) and with Ti^{+4} (d.r. >98%, S/R).[9]

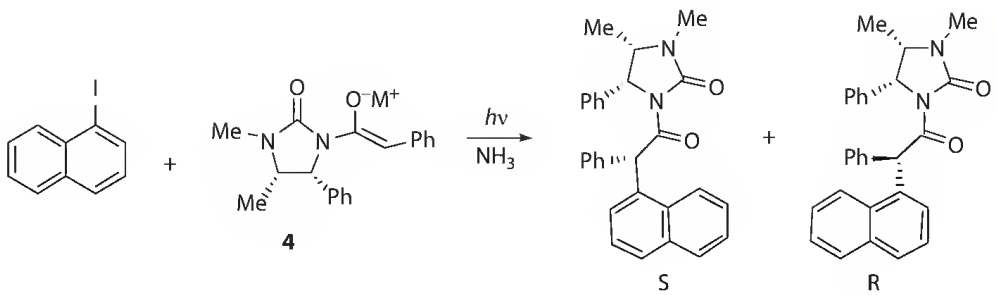

(15.1)

The photostimulated reaction of 4-iodo-1,1,2,2,9,9,10,10-octafluoro[2.2] paracyclophane (**5**) with stabilized carbanions gives good yield of substitution product. For example, the reaction with dimethyl malonate anion affords 85% of the substitution product **6** (Equation 15.2).[10]

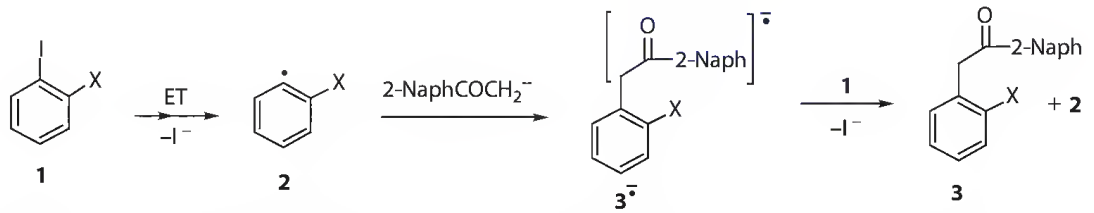

SCHEME 15.2 Mechanism proposed to obtain monosubstitution product from dihalobenzenes **1** and 2-naphthylmethyl ketone enolate anions.

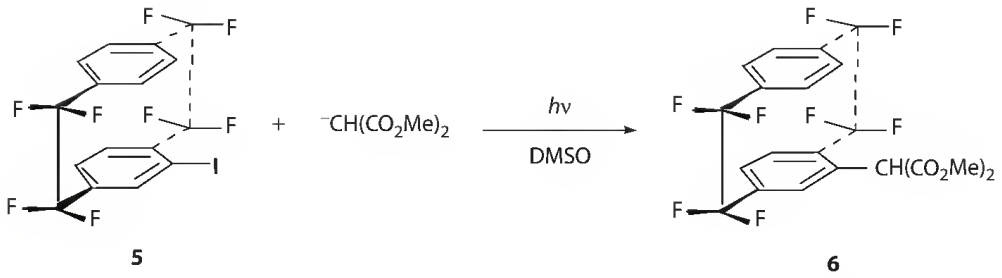

(15.2)

Aryl radicals couple with 2-naphthoxide ions in the position one to form a C–C bond, and the rate of coupling were determined.[11] When the aryl radical has *ortho*-substituents, the amount of reduced product increases. The anion of 9-phenanthrol shows a similar behavior in the photostimulated reaction with PhI, the product 10-phenylphenanthren-9-ol is obtained in 53% yield.[12]

2-Naphthylamide ions react by a photoinduced $S_{RN}1$ process with ArI in liquid ammonia, and 1-aryl-2-napthylamines are formed in 45%–63%.[13] This approach has been used for the synthesis of 10-aryl-9-aminophenanthrene by reaction of the anion of 9-aminophenanthrene with different ArX [(ArX = PhI (100%), 4-$MeOC_6H_4I$ (81%), 4-MeC_6H_4I (75%), 9-bromophenanthrene (93%)].[12]

15.3.2 Reaction with Tin Nucleophiles

Chloroarenes undergo substitution by Me_3Sn^- ions in liquid ammonia under irradiation to afford $ArSnMe_3$ in high yields (88%–100%). On the other hand, ArBr and ArI react by an HME reaction.[14] The reactions of *o*-, *m*-, and *p*-$C_6H_4Cl_2$ with Me_3Sn^- ions furnish products arising from disubstitution in 58%, 90%, and 88% yields, respectively.[5] For the synthesis of Me_3SnAr not only ArCl but also phenols are used as starting substrates through the intermediacy of $(EtO)_2P(O)OAr$ esters. These syntheses proceed in high yields.[15] From 1- and 2-naphthyl diethylphosphate, for instance, 1-naphthyl (93%) and 2-naphthyl (98%) trimethylstannanes were obtained.

The photoinduced reaction of the Me_2Sn^{2-} dianion with ArCl (ArCl = 4-$MeOC_6H_4Cl$, 4-MeC_6H_4Cl, 4-NCC_6H_4Cl, and 1-$ClC_{10}H_7$) gives functionalized Ar_2SnMe_2 in good yields (68%–85%) in liquid ammonia. These stannanes are used in homocoupling reactions in the presence of $Cu(NO_3)_2 \cdot 2.5H_2O$ to prepare almost quantitatively the corresponding biaryls.[16]

15.3.2.1 Cross-Coupling Reaction

The coupling of the tin products obtained from $S_{RN}1$ reactions with an ArI through a Pd-catalyzed process has been developed to obtain polyarylated compounds in a two step-one pot reactions. Thus, from *m*- and *p*-dichlorobenzenes, *m*- and *p*-terphenyls were obtained in 76% and 71% yield, respectively.[17] Following the same process, 1,3,5-triphenylbenzene was obtained in high yields from 1,3,5-$C_6H_3Cl_3$. This has been the first report of a trisubstitution by a cross-coupling reaction catalyzed by Pd.[5]

The fact that ArCl reacts with Me_3Sn^- ions under irradiation to form $ArSnMe_3$ and that the reactivity of ArI in the Pd-catalyzed reaction with stannanes is much greater than that of ArCl, a substrate bearing both leaving groups will react faster by the C–I bond via a chemoselective cross-coupling reaction with a stannane catalyzed by Pd. This will allow the remaining leaving group, chlorine, to react later in another $S_{RN}1$-type reaction to form an organotin intermediate, which can subsequently furnish product by a cross-coupling Pd-catalyzed reaction. This tandem strategy has been used as shown in Equation 15.3. Using this sequential scheme of combined transformations, high yields of other polyaromatic compounds are obtained.[18]

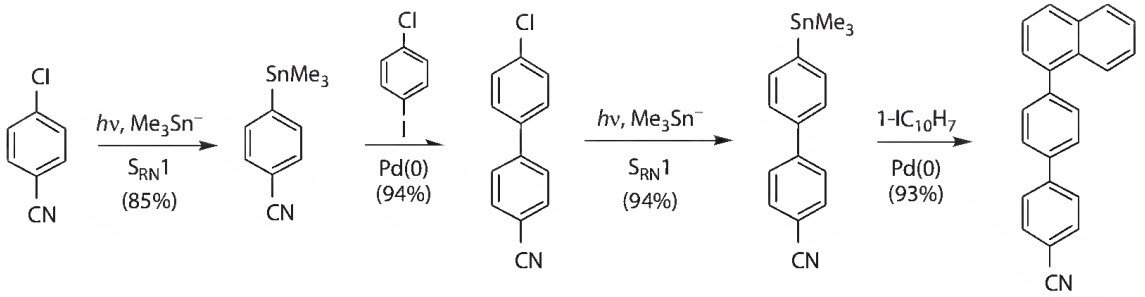

(15.3)

A similar approach based on the different reactivities of ArBr and $ArOP(O)(OEt)_2$ in Pd-catalyzed cross-coupling reactions is applied to the synthesis of asymmetric triaryl compounds in acceptable yields. Mixed biaryl compounds are also obtained in moderate yields through an $S_{RN}1$–Stille sequence.[19]

The synthesis of 6-substituted uracils in a three-step reaction ($S_{RN}1$–Stille–hydrolysis) is accomplished in good yields using commercial 6-chloro-2,4-dimethoxypyrimidine as the starting substrate (Scheme 15.3).[20]

When this novel three-step approach was applied to a one-pot reaction, 6-aryl uracils (1-naphthyl, 4-chlorophenyl, 3-chlorophenyl, 2,3,4,5,6-pentafluorophenyl) were formed and isolated (43%–57%) as pure products. When acid chlorides were the electrophiles (6-benzoyl and 6-(3-chlorobenzoyl), uracils were obtained in 49%–54% of isolated yields.[20]

Methyl 2,5-dichlorobenzoate **7** was studied as a model compound of certain chlorinated herbicides. It was found that **7** reacted with Me_3Sn^- ions in liquid ammonia under irradiation to afford disubstitution product **8** in 99% yield and only trace of product **9** (Equation 15.4). However, in the dark, **7** reacted with Me_3Sn^- ions to give the mono-substitution product **9** in 81% yield.[21,22] The dark reaction is inhibited by di-*tert*-butyl nitroxide, which indicates that **9** is formed by the $S_{RN}1$ mechanism with a spontaneous ET from the nucleophile to **7** to initiate the reaction.

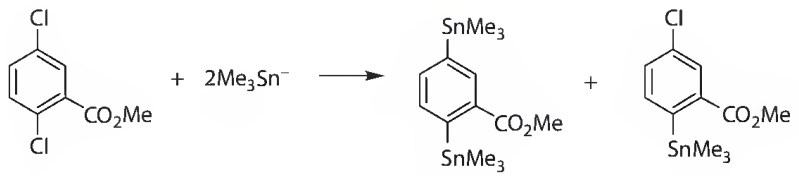

7 **8** **9**

(15.4)

Other chlorinated herbicides were also studied. The stannanes thus synthesized reacted with electrophiles by a Pd-catalyzed reaction, and the products were tested to know their phytotoxicity.[22]

Arylboronic acids are easily available via transmetalation between $ArSnMe_3$ and borane in THF. Consequently, a variety of arylpolyboronic acids is achieved from the stannanes previously synthesized by the $S_{RN}1$ mechanism from ArCl[23] or $ArOP(O)(OEt)_2$[24] in around 80% yields. These arene di- and tri-boronic acids can be used as starting materials for the synthesis of polycyclic aromatic systems via double or triple Suzuki cross-coupling reactions.[23,24]

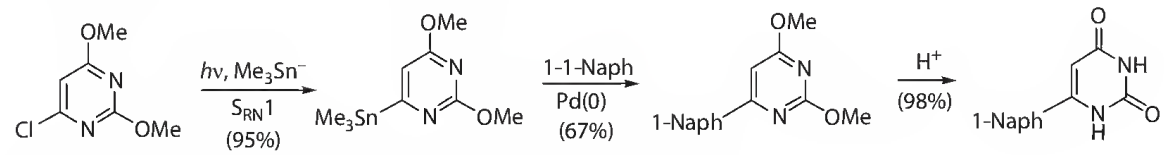

SCHEME 15.3 Tandem reactions to synthesize 6-substituted uracils.

15.3.2.2 Electrophilic Reactions

The exceptional leaving group ability of the trimethylstannyl group in electrophilic aromatic substitutions allows the synthesis of asymmetric diaryl ketones in good yields (40%–78%) through the reaction of trimethylarylstannanes, synthesized by photostimulated $S_{RN}1$ reactions, with acyl chlorides in catalyst-free syntheses in chlorobenzene at 130°C. In addition, these reactions are completely regioselective making possible the synthesis of diarylketones, which are not usually available under Friedel–Crafts reactions. The reaction of stannane **10** with benzoyl chloride, for instance, furnished diarylketone **11** in 78% yield (Equation 15.5).[25]

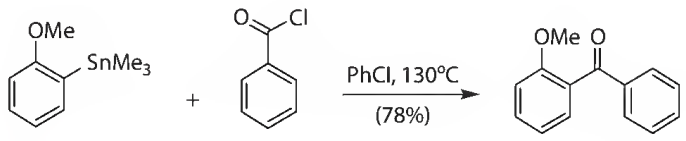

10 **11** (15.5)

These reactions have been used, in a single step, in the synthesis of bi- and triaroylarenes through the reaction of bi- and tristannylarenes with different aroyl halides. Specific di- and triketones are obtained in good to excellent yields (45%–83%).[26]

15.3.3 Reaction with Sulfur Nucleophiles

In general, PhS^- ions react with ArI in liquid ammonia under photostimulation to afford good yields of ArSPh or heteroaryl-SPh (70%–100%).[1a] The reactivity of other sulfur nucleophiles such as thiourea anion[27] and thioacetate anion[28] in photostimulated $S_{RN}1$ reaction has been reported as a one-pot, two-step method for the synthesis of several sulfur-aromatic compounds from moderate to good yields.

These photostimulated reactions with ArX are examples of fragmentation of the radical anion intermediate into a new radical and anion capable of continuing the propagation cycle of the $S_{RN}1$.[29] After the coupling of the aryl radical with urea anion **12** as an example, the radical anion intermediate **13** thus formed fragments into ArS^- and a new carbon-centered radical **14** (Equation 15.6). The deprotonation of the latter afforded a new radical anion intermediate **15** that transfers the odd electron to the ArX to continue the propagation steps (Equation 15.7).

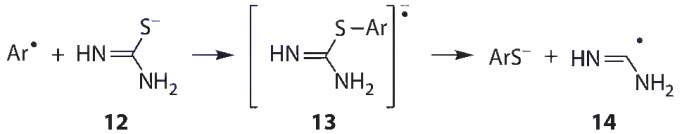

12 **13** **14** (15.6)

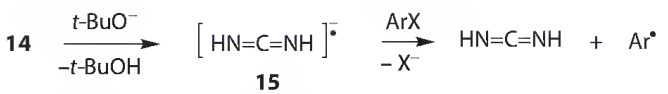

15 (15.7)

The ArS^- ions obtained are quenched with MeI to yield ArSMe in a one-pot procedure, together with Ar_2S in variable yields, from an $S_{RN}1$ between ArS^- ions and aryl radicals. When substrates have EWG, the yields of ArSMe are good (49%–87%).[27]

With the ArS^- ions thus formed a variety of sulfur compounds have been synthesized. By protonation of the reaction products were obtained ArSH (80%), by oxidation ArSSAr (70%), and by reaction with PhI in another $S_{RN}1$ reaction, ArSPh were obtained in 35% yield.[28]

The photostimulated reaction of **12** with **16** (R=Me), and after quenching the reaction with MeI, yielded the substitution product **17** (R=Me) in 97% yield (Equation 15.8).[30]

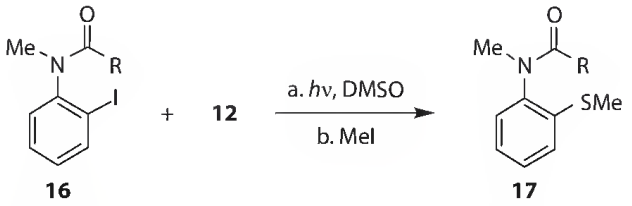

16 17 (15.8)

However, with **16** (R = CH_2Ph) as substrate only the reduction product was observed and it was attributed to a 1,5-hydrogen shift from the benzylic H to the aryl radical intermediate. On the other hand, with the substrate **18**, the product **19** and the rearranged products **20** and **21** were obtained in 10%, 38%, and 25% yield, respectively (Equation 15.9).

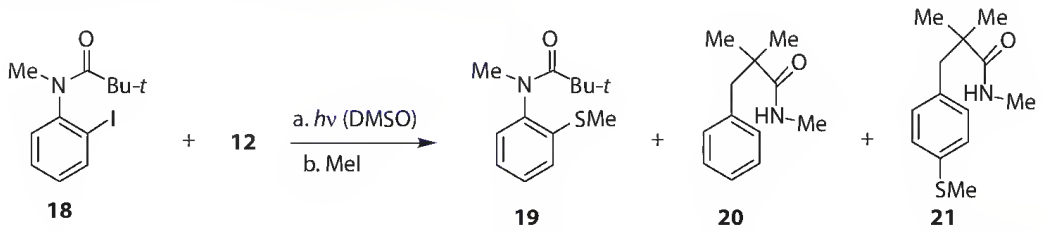

18 19 20 21 (15.9)

The straightforward product **19** is the reaction of the radical **22** with **12** in the sense of Equation 15.8. A competitive reaction is that the radical **22** intermediate, by an 1,6-hydrogen shift, gave the rearranged radical **23** followed by a 1,4-aryl migration through the spiro radical **24**. Coupling reaction of anion **12** to the *para* position of **24**, followed by fragmentation, proton transfer, and ring opening of the spiro intermediate, afforded a thiolate anion. Quenching with MeI finally yielded the product **21** (Equation 15.10).

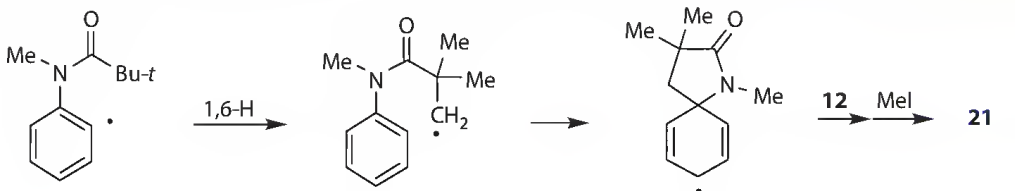

22 23 24 (15.10)

The spiro radical **24** also afforded an amidyl radical by ring opening. This nitrogen-centered radical can be reduced by hydrogen atom abstraction from the medium to give the rearranged amide **20**, the main product of this reaction.[30]

4-Iodo-1,1,2,2,9,9,10,10-octafluoro[2.2]paracyclophane (**5**) undergoes high-yield nucleophilic substitution with PhS^-, 2-$MeC_6H_4S^-$, 3-$MeC_6H_4S^-$ ions by the photoinduced $S_{RN}1$ mechanism, providing ready access to a new group of paracyclophane derivatives in 88%, 70%, and 91% yields, respectively.[10]

15.3.4 Ring Closure Reactions

15.3.4.1 $S_{RN}1$ Reaction Followed by a Polar Reaction

An approach to bring about a ring closure reaction could be developed by using a substrate with an appropriate substituent Z *ortho* to the leaving group, such as **25**, which can react with a nucleophile by the $S_{RN}1$ mechanism to afford product **26**. The ring closure product **27** is achieved by the spontaneous reaction between the Nu group and Z (Equation 15.11).

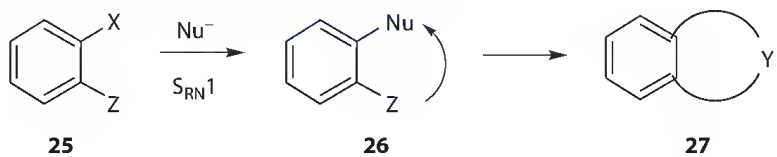

25 26 27 (15.11)

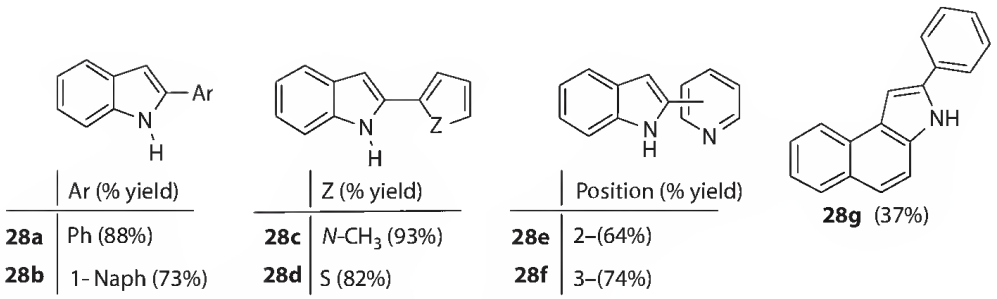

SCHEME 15.4 Synthesis of 2-substituted indoles and 2-phenyl-3*H*-benzo[*e*]indole.

Indoles. An important example is the synthesis of indoles by the photostimulated reaction in liquid ammonia of *o*-iodoaniline with carbanions derived from aliphatic and cyclic ketones to give the substitution product that spontaneously afford substituted indoles.

The photostimulated reactions of *o*-iodoaniline with enolate anions of aromatic ketones yield 2-substituted indoles **28a–f** (Scheme 15.4).[31] Furthermore, the photostimulated reaction of 1-bromo-2-naphthylamine with $PhCOCH_2^-$ anion in DMSO affords 2-phenyl-3*H*-benzo[*e*]indole **28g** (Scheme 15.4).[31b]

The photostimulated reactions of *o*-iodoaniline with enolate anions of cyclic ketones afford the fused indoles in moderate to high yields (Scheme 15.5).[31b] Fused indoles with OMe groups as substituent have been synthesized by the same methodology.[32]

Isoquinolin-1(2H)-ones. The synthesis of 3-substituted isoquinolinones can be performed by the photoinduced $S_{RN}1$ reactions in DMSO of *o*-iodobenzamide with enolate ions of aromatic (acetophenone, 1- and 2-naphthyl methyl ketones, 2-, 3- and 4-acetyl pyridine) and aliphatic ketones (1-adamantyl methyl ketone) in 68%–87% yields.[33] With cyclic ketones the reactions afforded fused isoquinolinones with good yields (Scheme 15.6).

2H-1,2-Benzothiazine 1,1-dioxides. 2-Iodobenzenesulfonamide undergoes photostimulated $S_{RN}1$ reactions in liquid ammonia with enolate ions derived from acetone, pinacolone, 3-methyl-2-butanone, cyclopentanone, cyclohexanone, and cyclooctanone to give fair to good yields of 2*H*-1,2-benzothiazine-1,1-dioxides (Scheme 15.7).[34] On the other hand, ethyl ketone enolate ions such as 3-pentanone and 2-methyl-3-pentanone gave low yields of corresponding benzothiazine and reduction of substrate was the predominated product.

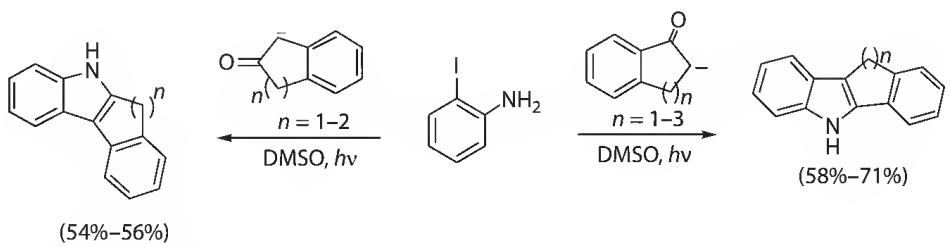

SCHEME 15.5 Synthesis of fused indoles.

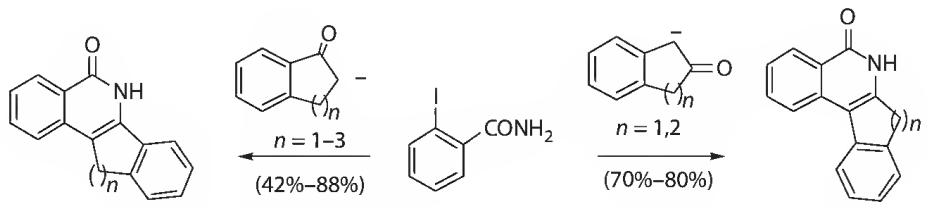

SCHEME 15.6 Synthesis of fused isoquinolinones.

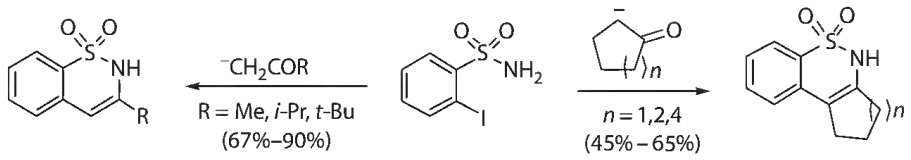

SCHEME 15.7 Synthesis of 2*H*-1,2-benzothiazine 1,1-dioxides.

Other systems. The photostimulated reaction of 1,8-diiodonaphthalene with *p*-methyl-benzenethiolate ions in DMSO yields the substituted cyclized product 10-methylbenzo[*kl*]thioxanthene in moderate yield (Equation 15.12). The mechanism proposed involves an intramolecular radical cyclization after monosubstitution in the propagation cycle of the $S_{RN}1$ process.[35]

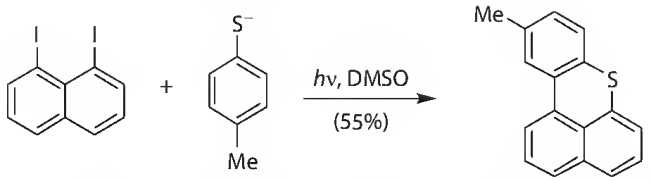

(15.12)

15.3.4.2 5-*Exo* or 6-*Exo* Radical Cyclization Followed by a $S_{RN}1$ Reaction

5-Exo trig ring closure. By this approach, 3-substituted 2,3-dihydro-1-*H*-indoles (**29**, Z = *N*-R) and 2,3-dihydrobenzofurans (**29**, Z = O) are easily reached by the versatile application of a 5-*exo* ring closure process during the propagation cycle in the $S_{RN}1$ reaction (Equation 15.13).[36]

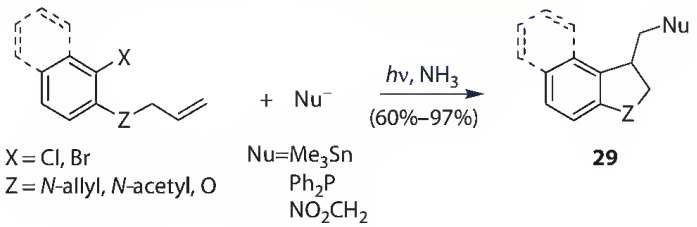

(15.13)

The generation of the aromatic radical, followed by cyclization with a tethered double bond in a 5-*exo* trig fashion afforded a new aliphatic radical that react with nucleophiles by the $S_{RN}1$ mechanism. This radical can be reduced with a hydrogen donor to obtain a reduced cyclized product. The generation and use of a new hydrogen donor, the anion of the dihydro ethyl benzoate reagent derived from nontoxic, reusable, and inexpensive ethyl benzoate was reported for this reaction.[37]

6-Exo trig ring closure. The tandem 6-*exo-trig* cyclization-$S_{RN}1$ reactions with 1-(but-3-enyloxy)-2-halobenzene and 1-(but-3-enyloxy)-2-halo naphthalenes afford 4-substituted chromanes and benzo[*f*] chromanes **30** in good to excellent yields, in same cases together with the open-chain substitution product (**31**) (Equation 15.14).[38] This result agrees with the slower ring closure rate expected for the 6-*exo* cyclization compared with the 5-*exo* process.

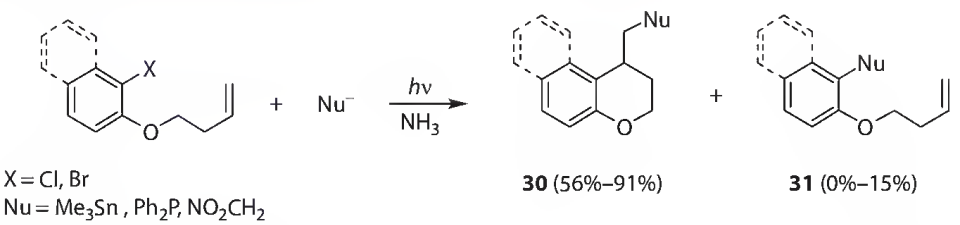

(15.14)

Using the same methodology that *5-exo trig*, the *6-exo* cyclized product was obtained when the anions of substituted dihydro ethyl benzoates anions are used as hydrogen donors to radicals in liquid ammonia and DMSO.[39]

15.3.4.3 Intramolecular $S_{RN}1$ Reactions

When a substrate has both the leaving group and a nucleophilic center in an adequate distance, the intramolecular $S_{RN}1$ reaction could afford the ring closure product. The driving force for the ring closure reaction is the large free energy difference between the distonic radical anion intermediate **33**, formed after the C–X bond fragmentation of the radical dianion intermediate **32**, and a conjugated radical anion **34**, formed after the coupling reaction. This radical finally affords the ring closure product **35** (Equation 15.15).

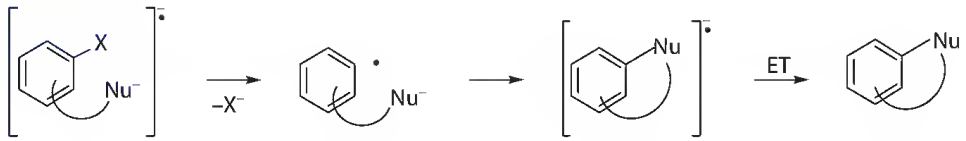

32 **33** **34** **35** (15.15)

1-*Phenyl-indananes and tetralin derivatives.* When ω-(2-bromophenyl)alkyl-2-oxazolines **36** were treated with LDA in THF, the anion **36**⁻ was formed, and under irradiation afforded the ring closure products 1-phenyl-indanes **37a** (n = 1, R = H, 58%), **37b** (n = 1, R = Ph, 57%), and tetralin derivatives **37c** (n = 2, R = Ph, 50%) (Equation 15.16).[40]

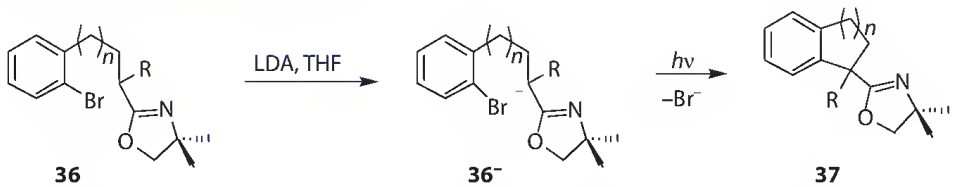

36 **36⁻** **37** (15.16)

The ring closure of anion **38**⁻ occurred via a six-membered ring $S_{RN}1$-type chain affording dihydrophenanthrene derivative **39**. In this strongly basic solution, aromatization of **39** affords the oxazolinophenanthrene derivative **40** in 88% yields. This reaction probably occurs by deprotonation and loss of lithium hydride (Equation 15.17).[41]

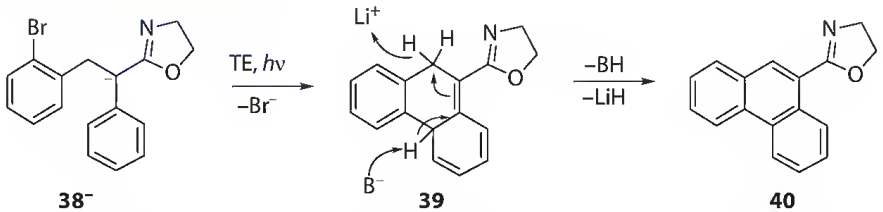

38⁻ **39** **40** (15.17)

Under the same experimental conditions, substrate **41** affords, as major product, benzocycloheptane **42** in 44% yield, in which the oxazoline group has undergone a unique areneotropic (oxazoline) migration to the phenyl ring (Equation 15.18).[41]

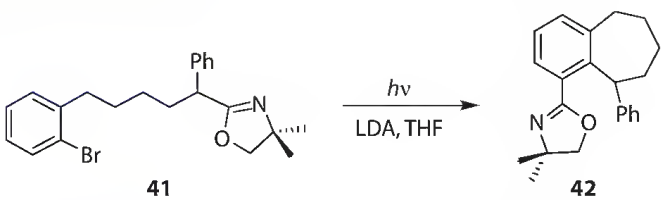

41 **42** (15.18)

Tetracyclic isoquinoline derivative. The substrate **43** that has an oxazolidinone ring reacts with LDA in THF to form the anion, and under laboratory light, a new fused system **44** is formed in 75% yield in a multistage rearrangement (Equation 15.19).[42] Two mechanisms involving an $S_{RN}1$-type process were proposed. EPR spectroscopy and ^{13}C-labeling experiment suggested that both were operative.

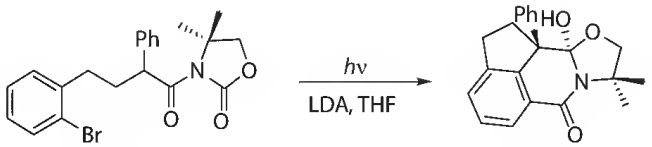

43 **44** (15.19)

Aporphine derivatives. The photostimulated intramolecular *ortho*-arylation reactions of bromoarenes linked with pendant phenoxy containing *N*-substituted tetrahydroisoquinolines as **45** in liquid ammonia afford aporphine alkaloid derivatives **46** (n = 1) via $S_{RN}1$ reactions, exploiting the bidentate behavior of phenoxide ions that allows obtaining the *ortho*-arylation product in very good yields (Equation 15.20).[43]

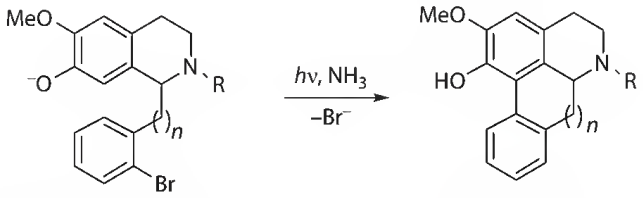

45a, R = CO_2Me, n = 1
45b, R = COMe, n = 1
45c, R = CO_2Me, n = 2

46a (75%)
46b (83%)
46c (40%)

(15.20)

Moreover, tetrahydroisoquinoline precursors that contained EWG groups on nitrogen (i.e., amides, sulfonamides and carbamates) gave cyclized products, whereas precursors with basic nitrogens such as NH failed to afford aporphine skeleton due to a 1,5-hydrogen shift and afforded the aminyl radical. With *N*-Me substitution, aporphine derivative is achieved in low yield (28%) due to an 1,6-hydrogen shift from the *N*-Me group. This strategy was extended for the first time to the synthesis of a homoaporphine alkaloid **46c** (n = 2) from **45c** in 40% yield.

Phenanthridine derivatives. The intramolecular arylation of benzylaryl amide ions with a pendant aryl moiety afforded phenanthridine derivatives in very good yields. When amines **47** were treated with *t*-BuOK in liquid ammonia and irradiated, phenanthridines **49** were obtained. The ring closure products were the dihydrophenanthridines **48**, but they were oxidized in the workup (Equation 15.21). Trispheridine, a natural product, was obtained in very good yield (75%).[44]

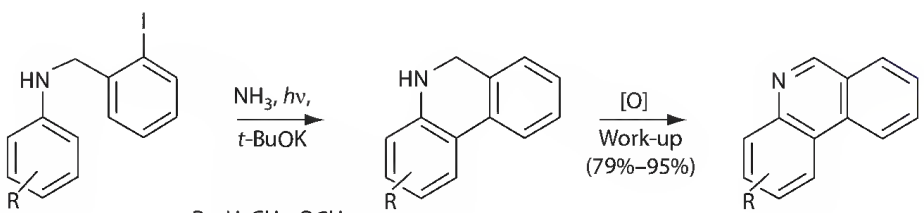

47 R = H, CH_3, OCH_3, Ph, NC_4H_4 **48** **49** (15.21)

Benzophenanthridines **50** (from 2-naphthylamine), **51** (from 1-naphthylamine), and the novel naphthophenanthridine **52** (from 2-anthracyl amine) are obtained by following this strategy (Scheme 15.8).

Carbazoles. The synthesis of a series of substituted 9*H*-carbazoles by the photostimulated $S_{RN}1$ substitution reaction using diarylamines as starting substrate was performed through an intramolecular C–C bond formation.

Good conditions for the ring closure reaction via $S_{RN}1$ processes involve the use of 2 equiv. of *t*-BuOK in liquid ammonia to form the anion **53**$^-$. After irradiation, good yields of 9*H*-carbazole derivatives **54** were obtained (Equation 15.22). Similar results were found when DMSO was used as a solvent.[45]

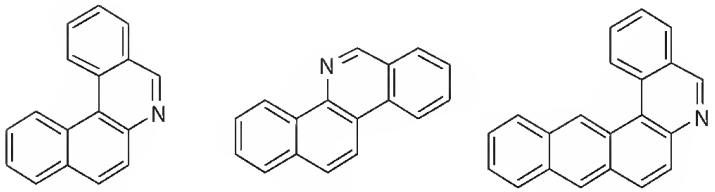

50 (98%) **51** (84%) **52** (72%)

SCHEME 15.8 Synthesis of benzophenanthridines and naphthophenanthridine.

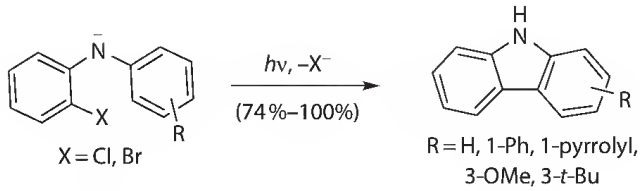

53⁻ **54** (15.22)

With *N*-(2-chlorophenyl)naphthalen-2-amine, *N*-(2-bromophenyl)naphthalen-1-amine and *N*-(2-chlorophenyl) phenanthren-9-amine, the fused carbazoles **55**, **56** and **57** were obtained with good yields (Scheme 15.9).

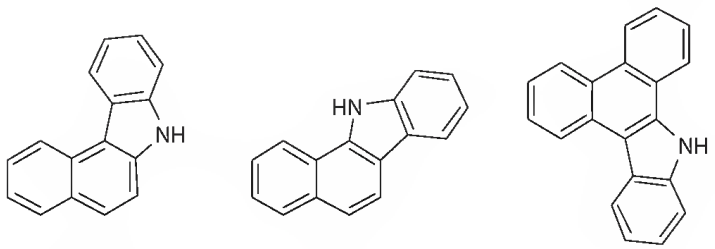

55 (85%) **56** (74%) **57** (95%)

SCHEME 15.9 Synthesis of fused carbazoles.

Furthermore, when $N^4,N^{4'}$-*bis*(2-bromophenyl)biphenyl-4,4′-diamine **58** was treated with 4 equiv. of *t*-BuOK in DMSO and irradiated for 90 min, 3,3′-bi(9*H*-carbazole) **59** was achieved in 67% isolated yield (Equation 15.23).[45]

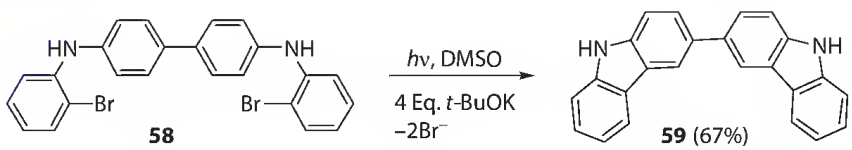

58 **59** (67%) (15.23)

Others fused azaheterocycles. The anion of azaheterocycles, such as pyrrole or imidazole, reacted with ArCl by cathode-induced reactions to give C–C bond formation.[46] When *N*-(2-iodophenyl)-1*H*-pyrrole-2-carboxamide **60** (1 equiv.) was treated with *t*-BuOK (2 equiv.) in liquid ammonia, anion **60**⁻ was formed, and under irradiation the new azaheterocycle 3*H*-pyrrolo[2,3-*c*]quinolin-4(5*H*)-one (**61**) was obtained in 100% yield (Equation 15.24). Product **61** was obtained in 83% yield in DMSO.[47]

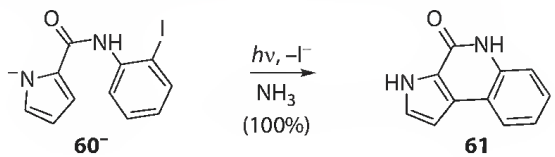

60⁻ **61** (15.24)

Under the same experimental conditions, the anion **62**$^-$ gives 5*H*-indolo[2,3-*c*]quinolin-6(7*H*)-one (**63**) in 94% yield in DMSO (83% yield in liquid ammonia) (Equation 15.25).[47]

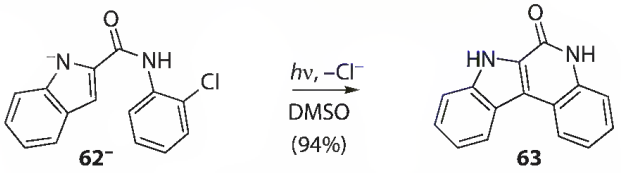

62$^-$ **63** (15.25)

The anions **64**$^-$ (R = H, Me) derived from pyrazole give under irradiation in liquid ammonia the ring closure products **65**, oxidized in the workup to **66**.[47] As the nucleus of pyrazole is quite sensitive to light,[48] it has been suggested that precursors **64** and/or products **65** are partially destroyed by the irradiation. Nevertheless, yields of 54%–56% of fused azaheterocycles **66** (R = H, Me) were obtained (Equation 15.26).

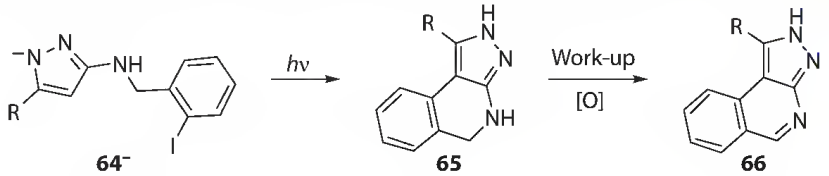

64$^-$ **65** **66** (15.26)

15.3.4.4 Tandem Reactions: $S_{RN}1$ Intermolecular–$S_{RN}1$ Intramolecular

The carbazole **69a** could be formed by double $S_{RN}1$ reactions when 9-aminophenanthrene **67a** reacts with *o*-iodobromobenzene **68a** by a straightforward pathway (Equation 15.27) with 36% yield and the reduced substituted product **70a** (16% yield).[12]

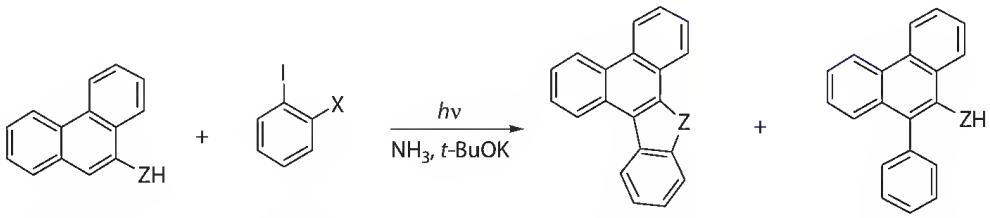

67a, Z=NH
67b, Z=O

68a, X=Br
68b, X=I

69a (36%)
69b (35%)

70a (16%)
70b (26%)

(15.27)

On the other hand, compounds **69b** and **70b** were obtained by reaction of the anion of **67b** with *o*-diiodobenzene **68b** in 35% and 26% yields, respectively (Equation 15.27).

15.4 Other Substrates

15.4.1 Vinyl Halides

Different competitive mechanisms are possible for the nucleophilic substitutions of vinyl halides. The mechanistic route mainly depends on structural features. The vinylic $S_{RN}1$ is not a common route due to strict competition by other polar routes.

For an exclusive vinylic $S_{RN}1$ process to take place, not only the substrate structure but also the nature of the anion constituted an essential factor, in addition to an appropriate combination of both. For instance, unambiguous vinylic $S_{RN}1$ substitutions by carbanions and PhS^- ions are known.[49] A mechanistic study explains the coupling of vinyl radicals with these nucleophiles and the competing H-atom abstraction reactions.[50]

An extension of this work describes more comprehensively the possible competition between ionic and ET routes in nucleophilic vinylic substitution, as well as the reactivity and structure of the vinyl radical intermediate.[51]

Competition from a vinylic S_N1 route was excluded when 2-bromo-3-methylbut-2-ene **71** was the substrate, without vinylic or allylic C–H. Under photostimulation, it gives substitution and reduction products by an $S_{RN}1$ process with $Me_3CCOCH_2^-$ anion (Equation 15.28). Additionally, the same outcome is observed with other anions such as $MeCOCH_2^-$, $PhCOCH_2^-$, $O_2NCH_2^-$ and $(EtO)_2PO^-$.[51]

$$\underset{\mathbf{71}}{Ph_2C{=}C(Br)Ph} \xrightarrow[DMSO]{h\nu,\ Me_3CCOCH_2^-} Ph_2C{=}C(CH_2COCMe_3)Ph + Ph_2C{=}CHPh \qquad (15.28)$$

From the ratios of reduction and substitution products observed in the photostimulated reactions of **71** in DMSO and with the rate of hydrogen abstraction value for radical **71**· in DMSO, the coupling rate constants for radical **71**· with $Me_3CCOCH_2^-$, PhS^-, and $(EtO)_2PO^-$ are 3.9, 1.9, and 0.28 $10^7\ M^{-1}\ s^{-1}$, respectively. All these values are 50-fold lower than the corresponding k_Y values obtained with phenyl radical, which is due to the a stability difference between the two radicals.[51]

Vinyl diethyl phosphate esters (VinDEP) obtained from ketones react under photostimulation with Me_3Sn^- ions in liquid ammonia, affording vinylstannanes via a vinylic $S_{RN}1$ mechanism (Scheme 15.10).[52] The stereochemical results show that these reactions are stereoconvergent.

These vinylic $S_{RN}1$ reactions strongly depend on the structural features of the vinyl phosphate, and only conjugated vinyl phosphates afforded the substitution product by $S_{RN}1$ reactions.

On the other hand, photostimulated reactions of (diethoxyphosphoryl)oxy-1,3-cyclohexadienes with Me_3Sn^- ions in liquid ammonia affords the corresponding trimethylstannylcyclohexadienes in moderate yields.[53] These results represented the first example of vinylic $S_{RN}1$ mechanism without an aryl moiety attached to the vinylic system.

Vinylstannanes can also be obtained in very good yields through the reactions of vinyl chlorides with Me_3Sn^- ions in liquid ammonia by the $S_{RN}1$ mechanism (Equation 15.29).[54] Substrate **72b** reacts in the dark while substrate **72a** needs photostimulation.

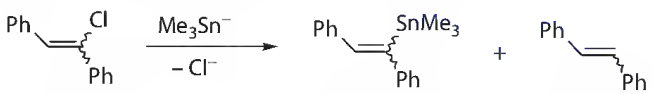

72a (*Z*) **72b** (*E*) **73a** (*Z*, 87%) **73b** (*E*, 92%) **74a** (*Z*) **74b** (*E*) (15.29)

The fact that the reaction affords only one isomer with the same configuration as the starting vinyl chlorides is noteworthy. This indicates an inversion of the vinyl radical intermediate slower than of the coupling reaction with the nucleophile. When the reaction takes place with 1,1-dichloro-1-alkenes, monosubstitution reduced products are formed in an *E*/*Z* mixture and the reaction becomes stereoconvergent. The vinylstannanes obtained are employed in the synthesis of triarylolefins by Pd-catalyzed cross-coupling reactions with several ArI.[54]

3,3-Difluoro-1-iodo-2-phenyl-cyclopropene (**75**) react with thiolate anions RS^- generated in situ from thiol in DMF in laboratory illumination to give the corresponding substitution products **76** (R = Ph, 96%; 4-MeC_6H_4, 90%; *t*-Bu, 50%; 3-$ClC_6H_4CH_2$, 79%) and some amounts of disulfides RSSR (Scheme 15.11).[55]

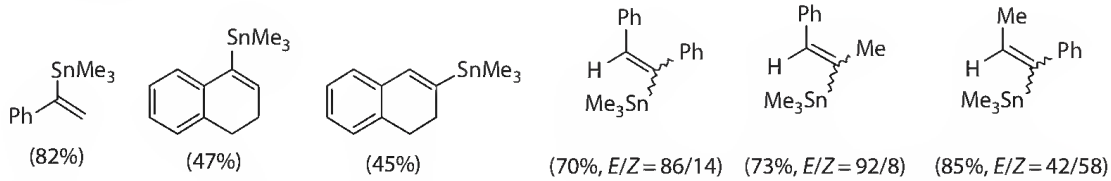

(82%) (47%) (45%) (70%, *E*/*Z* = 86/14) (73%, *E*/*Z* = 92/8) (85%, *E*/*Z* = 42/58)

SCHEME 15.10 Synthesis of vinyl stannanes.

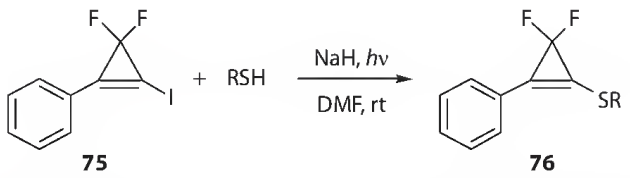

75 **76**

SCHEME 15.11 Reactions of 3,3-difluoro-1-iodo-2-phenyl-cyclopropene **75** with thiolate anions.

15.4.2 Perfluoroalkyl Iodides and Related Compounds

Perfluoroalkyl iodides (R_fI) are able to undergo a variety of nucleophilic substitutions by the $S_{RN}1$ mechanism with different nucleophiles. Some reactions occur in the dark whereas others are accelerated by light. We will only discuss the photostimulated reactions.

The novel compounds Ph_2PR_f ($R_f = C_4F_6$, C_6F_{13}) are synthesized by the $S_{RN}1$ photostimulated reaction of Ph_2P^- ions and R_fI in highly coordinating solvents such as HMPA and DMPU in fairly good yields (68%–85%). The photostimulated reaction of 1,4-diiodoperfluorobutane in HMPA affords the disubstitution product in 55% isolated yield. In tetraglyme, the HME is the main reaction.[56]

It is known that the C–Cl bond in chlorofluorocarbons is usually inert to normal nucleophilic attack, due to the strong EW power of fluorine. However, the thermal reaction of $ArCF_2Cl$ or $ArOCF_2Cl$ with PhO^- and PhS^- ions in DMF or NMP proceeds to give the substitution products in reasonably good yields.[57] The reactivity of $ArOCF_2Cl$ is lower than that of $ArCF_2Cl$. A S_N2 or a $S_{RN}1$ mechanism can be considered for the reaction.

In these conditions, the reaction between $PhSe^-$ ion and $ArCF_2Cl$ requires visible light irradiation to proceed. The reaction of $PhSe^-$ ion with $ArCF_2Cl$ is performed in DMF at 100°C under visible light irradiation affords $ArCF_2SePh$ in 45% yield.[57]

A photostimulated copolymerization reaction between *bis*-phenol A (**77**) and the dichloride **78** has been carried out to form a novel fluoropolymer **79** that has excellent thermal and solubility properties (Equation 15.30). In the model reaction of **77** with **78** in HMPA at 120°C normally reaches 70% conversion after about 12 h, whereas when the reaction was irradiated by a sunlamp, 70% was obtained in less than 3 h. It is proposed that this polymerization reaction occurs via an unprecedented $S_{RN}1$ mechanism.[58]

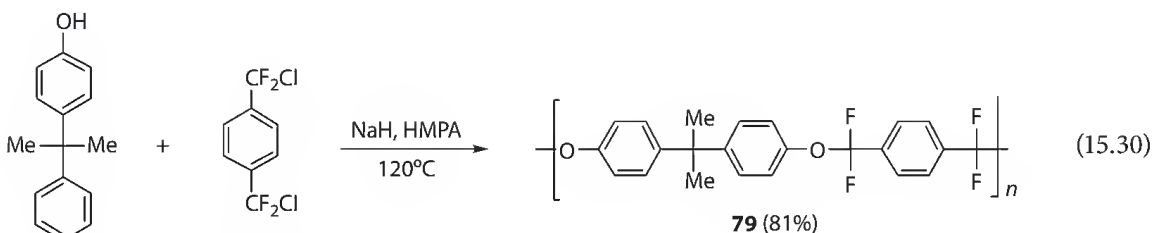

77 **78** **79** (81%) (15.30)

15.4.3 Aliphatic Substrates with EWG at the α-Carbon

These substrates comprise α-substituted nitro alkanes, nitrobenzyl and cumyl derivatives, heterocyclic analogues to benzyl, and other $S_{RN}1$ activated compounds. α-Substituted nitro alkanes are probably the most extensively studied substrates in $S_{RN}1$ reactions at an sp^3 carbon.

The activated benzyl chloride **80** reacts with the nitronate anion derived from 5-(hydroxymethyl)-2,2-dimethyl-5-nitro-1,3-dioxane **81** under $S_{RN}1$ reaction conditions to afford the dinitro compound **82** (Equation 15.31).[59]

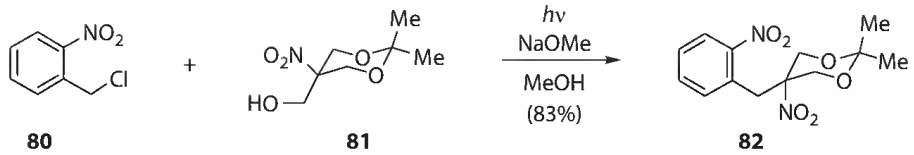

80 81 82 (15.31)

Under the same conditions, 2-fluorobenzyl chloride gives the desired nitro compound in 31% yield. After reduction of both nitro groups of **82**, the cyclization of amino compounds gives 2-spiroindolines nucleus.[59]

Additionally, nitrobenzo[1,3]dioxole **83** has been shown to react with 2-nitropropane anion to give C-alkylation product **84** by an $S_{RN}1$ mechanism (Equation 15.32).[60] The best yields are observed in DMSO as solvent.

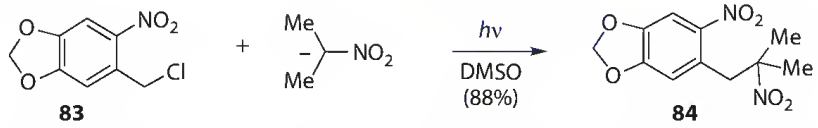

83 84 (15.32)

The reaction was extended to various aliphatic, cyclic, and heterocyclic nitronate anions obtained from commercially available nitroalkanes leading to a new series of nitrobenzo[1,3]dioxole derivatives (13%–69%).[60]

Vanelle, Crozet, and coworkers have reported the $S_{RN}1$ photostimulated reactions of substrate **85** with 2-nitropropyl anion to afford **86** (70% yield) after nitrous acid elimination, and the photostimulated reactions with PhS^-, $PhSO_2^-$, and $(CO_2Et)_2CH^-$ anions to achieve the substitution products **87**–**89** in good yields (80%–85%) (Scheme 15.12).[61]

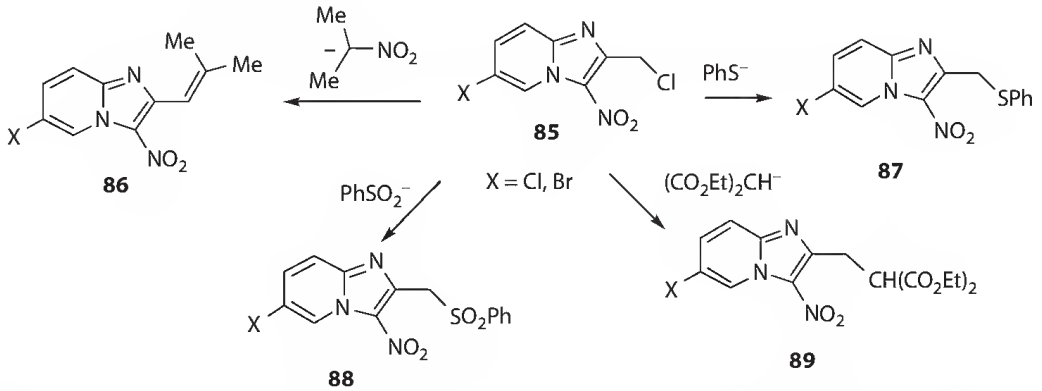

SCHEME 15.12 Reactions of 6-halo-2-(chloromethyl)-3-nitro-2,3-dihydroimidazo[1,2-*a*]pyridine **85** with different nucleophiles.

From the 6-halo-3-nitroimidazo[1,2-*a*]pyridines **89** bearing the diethyl methylmalonate group, new tricyclic pyridinones are synthesized.[62] Further tricyclic pyridinones such as **91** are obtained from **90** as the starting substrate (Equation 15.33).[63] The synthesis involves four steps with a Suzuki-Miyaura cross-coupling reaction and a direct olefination with diethyl ketomalonate as key steps.

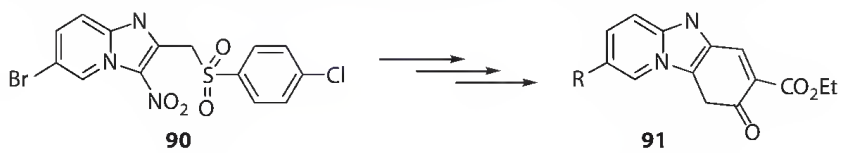

90 91 (15.33)

A series of nitronate and malonate anions reacts only at the chloromethyl group at the 2-position of **92** in DMSO under photostimulation (Scheme 15.13). The reaction with nitroalkane anions gives the ethylenic derivatives resulting from the consecutive C-alkylation and nitrous acid elimination. A $S_{RN}1$ mechanism is confirmed to take place in these reactions and in the reactions with the diethyl malonate anions (Scheme 15.13).[64]

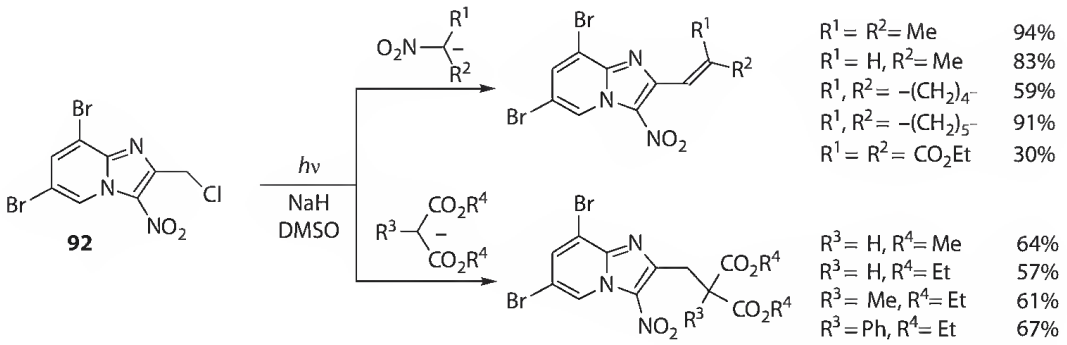

SCHEME 15.13 Reaction of 6,8-dibromo-2-(chloromethyl)-3-nitro-2,3-dihydroimidazo[1,2-*a*]pyridine **92** with different nucleophiles.

On the other hand, when the reaction of **92** is carried out with conventional S-centered anions, it does not follow a free radical chain mechanism exclusively, and a nucleophilic substitution displacement is also operating. Moreover, with PhS^- anion, the main product observed is that from the replacement of bromide atom at the 8-position and chloride atom on the chloromethyl group at 2-position of **92**.[64] In this case, the 8-position reacts only via free radical chain reaction, and the chloromethyl group can follow borderline mechanisms between S_N2 and $S_{RN}1$.

Recently, a $S_{RN}1$ reaction on nonnitrated heterocycle system has been described for the first time.[65] The new 3-bromo-2-(chloromethyl)-4*H*-pyrido[1,2-*a*]pyrimidin-4-one reacts with 2-nitropropane anion under photostimulation to give the ethylenic derivative **93** resulting from the consecutive C-alkylation and nitrous acid elimination (Equation 15.34).

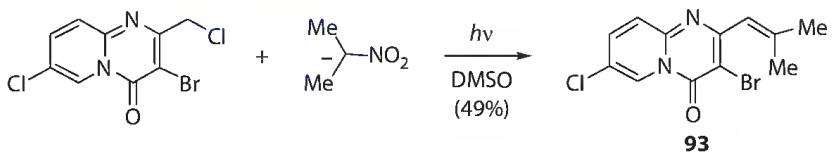

(15.34)

The reaction of **93** with C-centered nucleophiles is through the $S_{RN}1$ mechanism. However, with S-centered nucleophiles, the reaction seems to follow a S_N2 mechanism.[65]

The reaction of 2,3-*bis*(chloromethyl)-1,4-naphthoquinone with 2-nitropropane anions proceeded by two consecutive $S_{RN}1$ reactions leading to a *bis*-C-alkylated product.[66] Extension of this *bis*-$S_{RN}1$ reaction to various nitronate and malonate anions and S-centered anions led to a new class of potentially active benzo[*g*]quinoxaline-5,10-dione derivatives. These compounds are part of a group of bioreductive *bis*-alkylating antitumor agents.

From the 1,4-naphtoquinone **94** obtained by a intermolecular photostimulated $S_{RN}1$ reaction, a new naphtoquinonic alkylating agent **95** is synthesized.[67] The photostimulated reaction of substrate **95** with sodium methoxide in methanol allows the formation of the cyclopentanaphthalenedione **96** by an intramolecular $S_{RN}1$ cyclization (Equation 15.35).

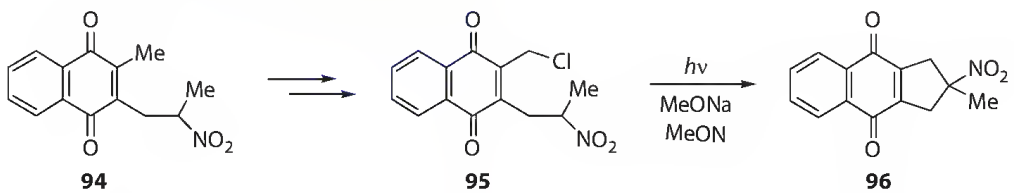

(15.35)

Furthermore, a series of highly functionalized quinones were prepared by the reaction of 2,3-*bis*(chloromethyl)-1,4-dimethoxyanthraquinone with various nitronate anions under ET reaction conditions.[68] The reaction proceeded according to *bis*-$S_{RN}1$ mechanism.

α-Halocarbonyl compounds are the other type of activated aliphatic compounds bearing EWG at the α-carbon employed as substrates for $S_{RN}1$ reactions. For instance, by the reaction of **97** with 2-nitropropyl anion, the ethylenic α,β-unsaturated ketones **98** is obtained via nitrous acid elimination from the C-alkylation intermediate (Equation 15.36). With 2-bromo-1-(4-nitrophenyl)ethanone, ethylenic α,β-unsaturated ketone is obtained in 90% yield.[69]

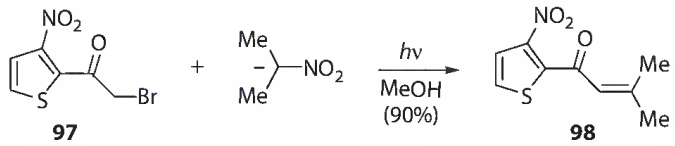

(15.36)

This reaction was extended to cyclic nitronates to synthesize several unknown α,β-unsaturated ketones, which are useful key intermediates bearing the well-known chalcone pharmacophore.

By a simple method, the conversion of aromatic aldehydes to their corresponding phosphates can be achieved.[70] In addition to their biological interest, these esters can be used in further synthetic transformation. Thus, the photostimulated $S_{RN}1$ reaction of phosphate **99** with nitroethylcyclohexene **100** and *t*-BuOK affords the new nitro derivative **101** in 56% isolated yields (Equation 15.37).

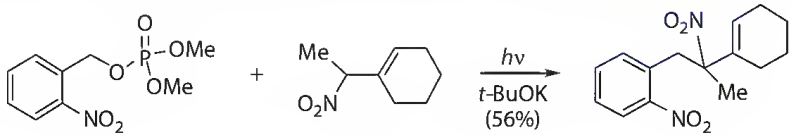

(15.37)

15.4.4 Cycloalkyl, Bridgehead, and Neopentyl and Related Halides

15.4.4.1 Cycloalkyl Halides

2-Haloadamantanes (2-AdX) can be considered halocyclohexanes with an even lower reactivity toward nucleophiles than 1-AdX or the simple halocyclohexanes. In the photostimulated reaction of 2-AdI with carbanions derived from acetophenone (62%), 2-naphthyl methyl ketone (32%), *N*-acetylmorpholine (32%), and anthrone (37%), substitution is achieved. The reaction with $PhCOCH_2^-$ anion induced by $FeBr_2$ affords 88% yield of substitution product. Nitromethane anion is unreactive under irradiation, but in the presence of $Me_3COCH_2^-$ anion as entrainment reagent, 88% yield of substitution is furnished.[71]

Recently, the synthesis of new 1,1-*bis*(trimethylstannyl)cyclopropanes by the $S_{RN}1$ mechanism has been reported.[72] 1,1-Dichlorocyclopropanes react under irradiation with Me_3Sn^- anion in liquid ammonia to give the disubstitution products *bis*-stannylcyclopropanes in good to excellent isolated yield (Scheme 15.14). The starting dichlorocyclopropanes are easily obtained by the addition of dichlorocarbene to alkenes.

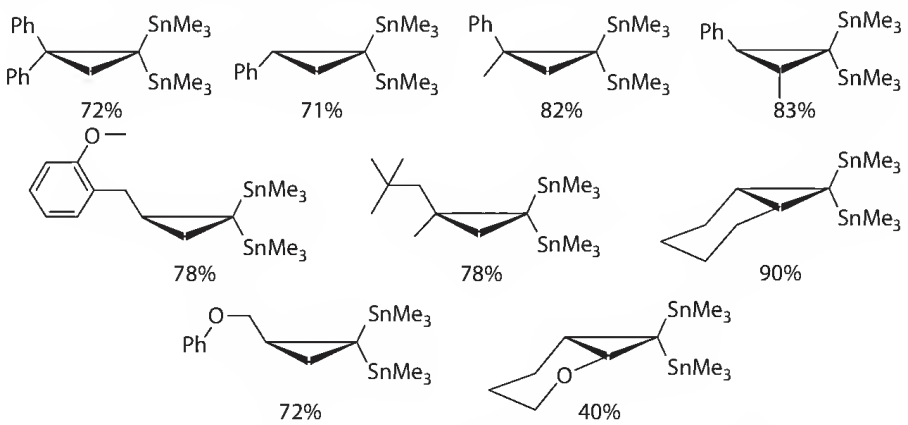

SCHEME 15.14 Synthesis of 1,1-bis(trimethylstannyl)cyclopropanes by the $S_{RN}1$ mechanism.

15.4.4.2 Bridgehead Halides

Bridgehead halides have a high-energy barrier for a polar mechanism owing to strain factors. Many of these halides have been found to react by the $S_{RN}1$ mechanism.

The photostimulated reaction of 1-haloadamantane (1-AdX, X = Br, I) and 2-AdBr with nitromethane anions gives good yields of the substitution product 1-$AdCH_2NO_2$ and 2-$AdCH_2NO_2$, respectively, in the presence of the enolate anions of acetone (entrainment conditions) in liquid ammonia.[73]

1-AdI reacts under photostimulation in DMSO with primary nitroalkane ions in the presence of acetone enolate anion to give the substitution products 1-$AdCHRNO_2$ in very good yields (77%–85%). With secondary nitroalkane ions, the yield of 1-$AdCR_2NO_2$ (R=Me, 17%) is modest.[74]

Furthermore, 1,3-dibromoadamantane reacts under irradiation with $NO_2CH_2^-$ and $Me_3COCH_2^-$ anions (entrainment reagent) to give the disubstitution product in 84% yields.[73] On the other hand, under the same conditions, the reaction of 1,4-dibromoadamantane with $NO_2CH_2^-$ and $MeCOCH_2^-$ anions under irradiation renders the monobromo-substitution products (32%) and the disubstitution product (47%).[73]

Cyanide ions react in a photostimulated reaction (254 nm) with 1,3,5,7-tetrabromoadamantane **102** in DMSO, affording the tetrasubstituted product 1,3,5,7-tetracyanoadamantane **103** in 73% yield by the $S_{RN}1$ mechanism (Equation 15.38).[7]

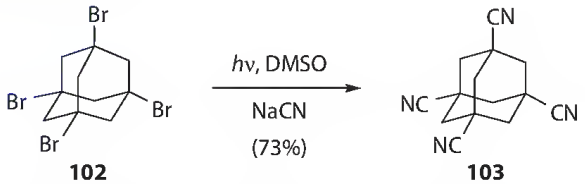

102 **103** (15.38)

The photostimulated reaction of the iodo ketone **104** in DMSO affords the rearranged substitution product **107** (83% yield). The ET to **104** followed by iodine elimination furnishes the bridgehead radical **105**. This radical rearranges quite fast by a 1,5-hydrogen shift to afford the methylene radical **106**, which couples with Ph_2P^- ions to yield the observed substitution product **107** after oxidation (Equation 15.39).[75]

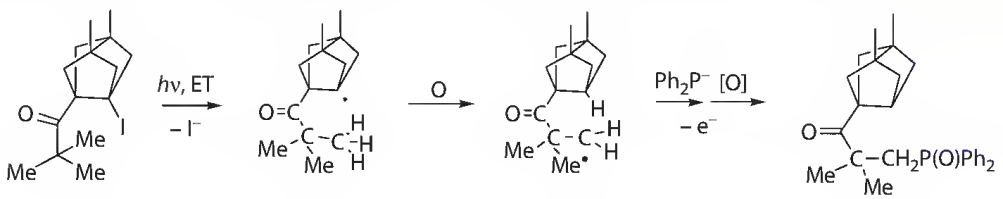

104 **105** **106** **107** (15.39)

The increased reactivity of π-substituted versus unsubstituted alkyl halides in ET-catalyzed nucleophilic substitutions ($S_{RN}1$) has been explained, within the stepwise scheme, by an intramolecular π catalysis or within the dissociative-concerted framework by the study of anionic species in which the π and σ subsystems are separated by aliphatic bridges of different flexibility using DFT functionals.[76] The reductive cleavage of these compounds is controlled by the rigidity of the polycyclic structure, its capability to form an unstrained radical, and by the relative C=O/C–Cl disposition on the bridge. Such control can be exerted by either a concerted-dissociative or a stepwise mechanism with radical anions as intermediates.

15.4.4.3 Neopentyl and Related Halides

Neophyl iodide **108** reacts under irradiation with $PhCOCH_2^-$ anions to afford the straightforward and rearranged substitution compounds **109** (50%) and **110** (16%) in moderate yields (Equation 15.40).[77]

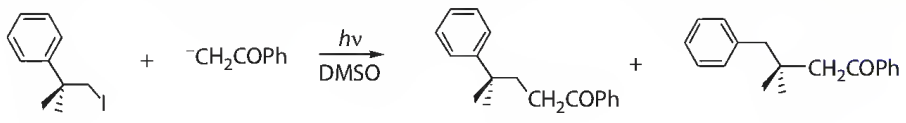

108 **109** **110** (15.40)

Although the overall quantum yields determined for the reactions studied are below unity, the chain lengths ($\Phi_{propagation}$) for the reaction of **108** with $PhCOCH_2^-$ and $NO_2CH_2^-$ anions are 127 and 2, respectively. For the first time, the $\Phi_{propagation}$ for a $S_{RN}1$ process was measured.[77]

Disubstitution at aromatic and aliphatic sites is achieved by the photostimulated reaction of pinacolone and acetophenone ion with 2-(4-halophenyl)-2-methyl-1-chloropropane **111** (Equation 15.41).[78] In DMSO, the main reaction is the $S_{RN}1$ nucleophilic substitution to afford disubstitution **112**, rearranged disubstitution **113**, or reduction at the aliphatic (C_{sp3}-Cl) one. In liquid ammonia, the main reaction is only substitution at the aromatic C-halogen site to yield **114**.

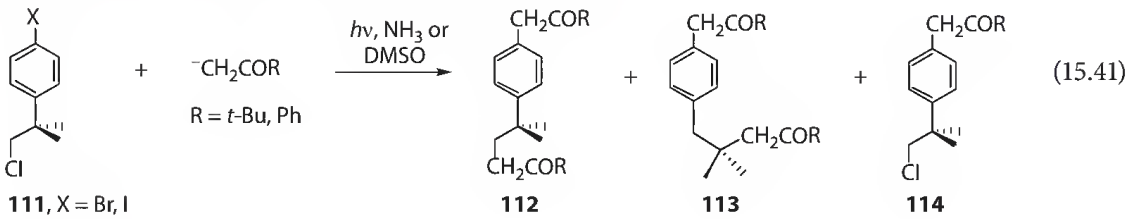

(15.41)

Acknowledgments

This work was supported in part by the Province of Córdoba, the Consejo Nacional de Investigaciones Científicas y Técnicas (CONICET), SECYT, Universidad Nacional de Córdoba, and FONCYT, Argentina. M.E.B. gratefully acknowledges receipt of a fellowship from CONICET.

References

1. (a) Rossi, R. A.; Pierini, A. B.; Peñéñory, A. B. *Chem. Rev.* 2003, *103*, 71–167. (b) Rossi, R. A.; Peñéñory, A. B. The photostimulated $S_{RN}1$ process: Reaction of haloarenes with carbanions. In *CRC Handbook of Organic Photochemistry and Photobiology*, 2nd edn.; Horspool, W. M., Lenel, F., Eds.; CRC Press: Boca Raton, FL, 2004; pp. 47-1–47-28. (c) Rossi, R. A. Photoinduced aromatic nucleophilic substitution reactions. In *Synthetic Organic Photochemistry*, Griesbeck, A. G., Mattay, J., Eds.; Marcel Dekker: New York, 2005; pp. 495–527.
2. Baumgartner, M. T.; Blanco, G. A.; Pierini, A. B. *New J. Chem.* 2008, *32*, 464–471.
3. Savéant, J.-M. *Adv. Phys. Org. Chem.*, Tidwell, T. T., Ed.; Academic Press: New York, 2000, *35*, 117–192 and references cited therein.
4. Braslavsky, S. E. *Pure Appl. Chem.* 2007, *79*, 293–465.
5. Córsico, E. F.; Rossi, R. A. *Synlett* 2000, 227–229.
6. Vanelle, P.; Terme, T.; Crozet, M. P. *Tetrahedron Lett.* 2000, *41*, 6383–6385.
7. Lee, G. S.; Bashara, J. N.; Sabih, G.; Oganesyan, A.; Godjoian, G.; Duong, H. M.; Marinez, E. R.; Gutierrez, C. G. *Org. Lett.* 2004, *6*, 1705–1707.
8. Baumgartner, M. T.; Jiménez, L. B.; Pierini, A. B.; Rossi, R. A. *J. Chem. Soc. Perkin Trans. 2* 2002, 1092–1097.
9. Baumgartner, M. T.; Lotz, G. A.; Palacios, S. M. *Chirality* 2004, *16*, 212–219.
10. Wu, K.; Dolbier, W. R. Jr.; Battiste, M. A.; Zhai, Y. *Mendeleev Commun.* 2006, *16*, 146–147.
11. Tempesti, T. C.; Pierini, A. B.; Baumgartner, M. T. *New J. Chem.* 2009, *33*, 1523–1528.
12. Tempesti, T. C.; Pierini, A. B.; Baumgartner, M. T. *J. Org. Chem.* 2005, *70*, 6508–6511.
13. Pierini, A. B.; Baumgartner, M. T.; Rossi, R. A. *Tetrahedron Lett.* 1987, *28*, 4653–4656.
14. Yammal, C. C.; Podestá, J. C.; Rossi, R. A. *J. Org. Chem.* 1992, *57*, 5720–5725.
15. (a) Chopa, A. B.; Lockhart, M. T.; Dorn, V. B. *Organometallics* 2002, *21*, 1425–1429. (b) Chopa, A. B.; Lockhart, M. T.; Silbestri, G. *Organometallics* 2002, *21*, 5874–5878.
16. Uberman, P. M.; Martín, S. E.; Rossi, R. A. *J. Org. Chem.* 2005, *70*, 9063–9066.
17. Córsico, E. F.; Rossi, R. A. *Synlett* 2000, 230–232.

18. Córsico, E. F.; Rossi, R. A. *J. Org. Chem.* 2002, *67*, 3311–3316.
19. Chopa, A. B.; Silbestri, G. F.; Lockhart, M. T. *J. Organomet. Chem.* 2005, *690*, 3865–3877.
20. Bardagí, J. I.; Rossi, R. A. *J. Org. Chem.* 2008, *73*, 4491–4495.
21. Santiago, A. N.; Basso, S. M.; Montañez, J. P.; Rossi, R. A. *J. Phys. Org. Chem.* 2006, *19*, 829–835.
22. Basso, S. M.; Montañez, J. P.; Santiago, A. N. *Lett. Org. Chem.* 2008, *5*, 633–639.
23. Mandolesi, S. D.; Vaillard, S. E.; Podestá, J. C.; Rossi, R. A. *Organometallics* 2002, *21*, 4886–4888.
24. Fidelibus, P. M.; Silbestri, G. F.; Lockhart, M. T.; Mandolesi, S. D.; Chopa, A. B.; Podestá, J. C. *Appl. Organomet. Chem.* 2007, *21*, 682–688.
25. Silbestri, G. F.; Masson, R. B.; Lockhart, M. T.; Chopa, A. B. *J. Organomet. Chem.* 2006, *691*, 1520–1524.
26. Lo Fiego, M. J.; Badajoz, M. A.; Silbestri, G. F.; Lockhart, M. T.; Chopa, A. B. *J. Org. Chem.* 2008, *73*, 9184–9187.
27. Argüello, J. E.; Schmidt, L. C.; Peñéñory, A. B. *Org. Lett.* 2003, *5*, 4133–4136.
28. Schmidt, L. C.; Rey, V.; Peñéñory, A. B. *Eur. J. Org. Chem.* 2006, 2210–2214.
29. Schmidt, L. C.; Argüello, J. E.; Peñéñory, A. B. *J. Org. Chem.* 2007, *72*, 2936–2944.
30. Rey, V.; Pierini, A. B.; Peñéñory, A. B. *J. Org. Chem.* 2009, *74*, 1223–1230.
31. (a) Baumgartner, M. T.; Nazareno, M. A.; Murguía, M. C.; Pierini, A. B.; Rossi, R. A. *Synthesis* 1999, *64*, 2053–2056. (b) Barolo, S. M.; Lukach, A. E.; Rossi, R. A. *J. Org. Chem.* 2003, *68*, 2807–2811.
32. Barolo, S. M.; Rosales, C.; Guio, J. E. A.; Rossi, R. A. *J. Heterocycl. Chem.* 2006, *43*, 695–699.
33. Guastavino, J. F.; Barolo, S. M.; Rossi, R. A. *Eur. J. Org. Chem.* 2006, *17*, 3898–3902.
34. Layman, W. J.; Greenwood, T. D.; Downey, A. L.; Wolfe, J. F. *J. Org. Chem.* 2005, *70*, 9147–9155.
35. Norris, R. K.; McMahon, J. A. *Arkivoc* 2003, (x), 139–155.
36. Vaillard, S. E.; Postigo, A.; Rossi, R. A. *J. Org. Chem.* 2002, *67*, 8500–8506.
37. Vaillard, S. E.; Postigo, A.; Rossi, R. A. *J. Org. Chem.* 2004, *69*, 2037–2041.
38. Bardagí, J. I.; Vaillard, S. E.; Rossi, R. A. *Arkivoc* 2007, (iv), 73–83.
39. Bardagí, J. I.; Vaillard, S. E.; Rossi, R. A. *Tetrahedron Lett.* 2006, *47*, 3149–3152.
40. Roydhouse, M. D.; Walton, J. C. *Chem. Comm.* 2005, 4453–4455.
41. Marshall, L. J.; Roydhouse, M. D.; Slawin, A. M. Z.; Walton, J. C. *J. Org. Chem.* 2007, *72*, 898–911.
42. Roydhouse, M. D.; Walton, J. C. *Eur. J. Org. Chem.* 2007, 1059–1063.
43 Barolo, S. M.; Teng, X.; Cuny, G. D.; Rossi, R. A. *J. Org. Chem.* 2006, *71*, 8493–8499.
44. (a) Budén, M. E.; Rossi, R. A. *Tetrahedron Lett.* 2007, *48*, 8739–8742. (b) Budén, M. E.; Dorn, V. B.; Gamba, M.; Pierini, A. B.; Rossi, R. A. *J. Org. Chem.* 2010, *76*, 2206–2218.
45. Budén, M. E.; Vaillard, V. A.; Martín, S. E.; Rossi, R. A. *J. Org. Chem.* 2009, *74*, 4490–4498.
46. (a) Chahma, M.; Combellas, C.; Thiébault, A. *Synthesis* 1994, 366–368. (b) Chahma, M.; Combellas, C.; Thiébault, A. *J. Org. Chem.* 1995, *60*, 8015–8022.
47. Vaillard, V. A.; Budén, M. E.; Martín. S. E.; Rossi R. A. *Tetrahedron Lett.* 2009, *50*, 3829–3832.
48. Pavlik, J. W.; Kebede, N. *J. Org. Chem.* 1997, *62*, 8325–8334 and references cited therein.
49. (a) Amatore, C.; Galli, C.; Gentili, P.; Guarnieri, A.; Schottland, E.; Rapporport, Z. *J. Chem. Soc., Perkin Trans. 2* 1995, 2341–2350. (b) Santiago, A. N.; Rossi, R. A.; Lassaga, G.; Rappoport, Z. *J. Org. Chem.* 1996, *61*, 1125–1128. (c) Annunziata, H.; Galli, C.; Gentili, P.; Guarnieri, A.; Beit Yannai, M.; Rappoport, Z. *Eur. J. Org. Chem.* 2002, *67*, 2136–2143.
50. Branchi, B.; Galli, C.; Gentili, P. *Eur. J. Org. Chem.* 2002, 2844–2854.
51. Galli, C.; Rappoport, Z. *Acc. Chem. Res.* 2003, *36*, 580–587.
52. Chopa, A. B.; Dorn, V. B.; Badajoz, M. A.; Lockhart, M. T. *J. Org. Chem.* 2004, *69*, 3801–3805.
53. Dorn, V. B.; Badajoz, M. A.; Lockhart, M. T.; Chopa, A. B.; Pierini, A. B. *J. Organomet. Chem.* 2008, *693*, 2458–2462.
54. Córsico, E. F.; Rossi, R. A. *J. Org. Chem.* 2004, *69*, 6427–6432.
55. Zhou, D. Y.; Dou, H. Y.; Zhao, C. X.; Chen, Q. Y. *J. Fluor. Chem.* 2006, *127*, 740–745.
56. Vaillard, S. E.; Postigo, A.; Rossi, R. A. *Organometallics* 2004, *23*, 3003–3007.
57. Guidotti, J.; Schanen, V.; Tordeux, M.; Wakselman, C. *J. Fluor. Chem.* 2005, *126*, 445–449.

58. Dolbier, W. R.; Rodriguez Garcia, V.; Wu, K.; Angerhofer, A.; Hedhli, L.; Elsheikh, M. *J. Fluor. Chem.* 2008, *129*, 991–993.
59. Sánchez, I.; Sobrino, M.; Pujol, M. D. *Tetrahedron Lett.* 2004, *45*, 1737–1740.
60. Meuche, J.; Rathelot, P.; Crozet, M. P.; Vanelle, P. *Chem. Heterocycl. Comp.* 2003, *39*, 989–997.
61. Crozet, M. D.; Castera, C.; Kaafarani, M.; Crozet, M. P.; Vanelle, P. *Arkivoc* 2003, (x), 273–282.
62. Castera, C.; Crozet, M. D.; Crozet, M. P.; Vanelle, P. *Heterocycles* 2005, *65*, 337–343.
63. Castera-Ducros, C.; Crozet, M. D.; Vanelle, P. *Synthesis* 2006, 2777–2783.
64. Szabo, R.; Crozet, M. D.; Vanelle, P. *Heterocycles* 2008, *75*, 2263–2274.
65. Szabo, R.; Crozet, M. D.; Vanelle, P. *Synlett* 2008, 2836–2840.
66. Remusat, V.; Terme, T.; Gellis, A.; Rathelot, P.; Vanelle, P. *J. Heterocycl. Chem.* 2004, *41*, 221–225.
67. Terme, T.; Beziane, A.; Vanelle, P. *Lett. Org. Chem.* 2005, *2*, 367–370.
68. Beziane, A.; Terme, T.; Vanelle, P. *Molecules* 2005, *10*, 289–294.
69. Curti, C.; Gellis, A.; Vanelle, P. *Molecules* 2007, *12*, 797–804.
70. El Kaim, L.; Gaultier, L.; Grimaud, L.; Dos Santos, A. *Synlett* 2005, 2335–2336.
71. Lukach, A. E.; Rossi, R. A. *J. Org. Chem.* 1999, *64*, 5826–5831.
72. Guastavino, J. F.; Rossi, R. A. *Organometallics* 2009, *28*, 2646–2649.
73. Santiago, A. N.; Toledo, C. A.; Rossi, R. A. *J. Phys. Org. Chem.* 2003, *16*, 413–419.
74. Santiago, A. N.; Basso, S. M.; Toledo, C. A.; Rossi, R. A. *New J. Chem.* 2005, *29*, 875–880.
75. Camps, P.; Lukach, A. E.; Rossi, R. A. *J. Org. Chem.* 2001, *66*, 5366–5373.
76. Uranga, J. G.; Vera, D. M. A.; Santiago, A. N.; Pierini, A. B. *J. Org. Chem.* 2006, *71*, 6596–6599.
77. Argüello, J. E.; Peñéñory, A. B.; Rossi, R. A. *J. Org. Chem.* 2000, *65*, 7175–7182.
78. Pierini, A. B.; Gallego, M. H.; Andrada, K. F. C. *J. Org. Chem.* 2007, *72*, 3089–3092.

16

Photochemistry of Aryl Halides

Luca Pretali
University of Pavia

Angelo Albini
University of Pavia

16.1 Introduction

Aryl halides have an important role in photochemistry since a long time. Historically, studies of the phosphorescence of aromatics and of their halogenated derivatives have been instrumental in defining the modern concept of triplet state, and both the intersystem crossing [1] and the fragmentation of phenyl halides have been long known [2]. In the early years of these studies, attention was given more often to photophysics than to photochemistry. This is because the introduction of electron-withdrawing substituents, such as halogen atoms, in the ring further increases the already high stability of aromatic compounds, both in the ground and excited states. Indeed, many aromatic compounds are quite photostable and the absorption of a photon leads to reemission rather than to reaction, since excitation causes only a partial decrease of the bonding character in the multiple π-electron array of such compounds and the rigid σ-bond skeleton disfavors geometric modifications. Indeed, stability to chemical agents and to irradiation is characteristic of many aryl halides, and this family includes some notoriously persistent environmental pollutants, such as DDT and polychlorobiphenyls. However, photochemistry, albeit often inefficient, is one of the few available paths for the degradation of such compounds and thus this is

an important topic in environmental studies. Furthermore, new discoveries are revealing new reactions and a more various palette of transformations is forming for aryl halides, as a part of the development of the studies on aromatics that form a fast growing field in contemporary photochemistry.

Many reviews on this topic are available in the literature [3–8]. In particular, two excellent accounts by a specialist in the field, Nigel J. Bunce, have been devoted to the most important photochemical reaction of these compounds, dehalogenation, and have been published in the previous editions of this handbook (1995, 2004) [3,4]. Adopting the same pattern, the discussion in this chapter will be grouped in broad mechanistic categories. It has been attempted to review all of the main processes, but certainly not all of the examples that are being published at an increasing pace. Preference has been given to the most recent reports.

16.2 Effect of Halide Substituents on the Photophysical Parameters of Aromatics

Aromatic compounds often exhibit recognizable fluorescence and phosphorescence, as well as transient absorptions upon flashing and have thus always formed a favorite hunting field of photophysics. An important part of these studies involves halogen derivatives that are available through synthetically easy procedures. The effect caused by the introduction of a halide depends first of all on its nature, since, as it is well known, heavy atoms weaken spin exclusion rules. The introduction of a halogen on the ring produces a large effect since the halogen lays directly on the π-system involved in the electronic transition. As a result, the direct generation of T_1 by light absorption becomes more likely (e.g., the $S_0 \rightarrow T_1$ band is visible in the spectrum of *p*-iodotoluene, $\varepsilon \sim 0.5\,mol^{-1}\,cm^{-1}$) [9] and both $S_n \rightarrow T_m$ and $T_1 \rightarrow S_o$ intersystem crossing rates increase. This results in a shortening of the lifetimes of both singlet and triplet states proportionally to the atomic weight [10].

Both fluorescence and phosphorescence are observed, in some cases with further differentiations. As an example, chlorobenzene exhibits a dual phosphorescence in matrix. The two components have been attributed to emission from T_1, a $\pi\pi^*$ state, for the slow one and from T_{11}, a bound, though strongly deformed, $\sigma\pi^*$ state, for the fast one [11,12]. In the case of bromobenzene, the high rate of homolysis further shortens the triplet lifetime and makes emission in a conventional matrix difficult to observe. This is possible, however, in a highly viscous matrix, such as that formed by glycerol or 3-methyloctane [11]. Fluorobenzene is also nonphosphorescent, but a transient T-T spectrum has been detected in solution ($\tau \sim 0.7\,\mu s$ in cyclohexane) [11]. When passing to naphthyl halides or higher aromatics, emission is more intensive. In particular, 1-bromonaphthalene and derivatives are among the few organic compounds for which room temperature phosphorescence is known (see the following). Furthermore, the triplet states of naphthyl halides have been extensively studied by flash photolysis and transient electron paramagnetic resonance (epr) spectroscopy [13,14].

The heavy atom effect on emission is position dependent. As an example, the phosphorescence lifetime for chlorophenanthrenes (in EPA at 77 K) ranges from a maximum of 2.47 s for the 2-substituted derivative to a minimum of 0.32 s for the derivative in 9 (0.197 and 0.0108 for the corresponding bromophenanthrenes, 0.0271 and 0.00173 for the iodophenanthrenes) [15, Chart 16.1].

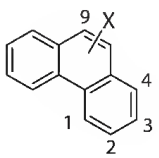

	τ_p, s (1-X)	τ_p, s (2-X)	τ_p, s (3-X)	τ_p, s (4-X)	τ_p, s (9-X)
Cl	—	2.47	1.03	—	0.32
Br	0.0641	0.197	0.0491	0.0260	0.0108
I	—	0.0271	0.00684	—	0.00173

CHART 16.1

TABLE 16.1 Some Photophysical and Photochemical Data on Halonaphthalenes

	τ_P ms, EPA 77K[a]	τ_P s, Solid Adduct Hg Deriv., Room T[a,b]	Rel. Rate Dehalogenat. in MeOH[c]	Same, with 0.1 M LiBr[c]	Same, with 0.08 M LiI[c]
Naphthalene (N)	2700	0.71			
1-Cl-N	370	1.28	0.04	0.02	0.01
1-Br-N	15.8	0.97	0.35	0.13	0.08
1-I-N	2.43	0.54	5.5	3.2	1.9

[a] See Ref. [17].
[b] Solid adducts with trimeric perfluoro-*ortho*-phenylene mercury, room temperature [17].
[c] See Ref. [18].

A synergism between internal and external heavy atom effect has been evidenced both as a shortening of the emission lifetime and as a decrease in reactivity, for example, in adducts with a strong field-perturbating agent such as $TlNO_3$ [16]. In Table 16.1 the phosphorescence lifetimes of naphthalene and its halogenated derivatives in EPA matrix at 77 K are gathered and compared with those from the solid 1 to 2 adducts with a trimeric perfluoro-*ortho*-phenylene mercury derivative [17, see Chart 16.2]. It can be seen that the external effect is more important and reduces the span between the halogen derivatives, which is still appreciable however. The relative rates of dehalogenation [18] are also reported. These increase with the halogen atom weight, since the aryl–X bond is weakened (see Section 16.4), but decrease when the external atom effect shortens the triplet lifetime.

Phosphorescent solid state complexes have important applications, as an example for organic LEDs (OLEDs).

The aforementioned room temperature phosphorescence has found important applications in analytical chemistry. In general, enhanced phosphorescence has been obtained by inhibiting the quenching of triplet states through the use of an organized medium or by rigorously excluding oxygen. Derivatives of 1-bromonaphthalene are a favorite probe for studies on this topic that have been reviewed [19]. Inclusion in cyclodextrins makes phosphorescence well detectable arriving at a lifetime in the microsecond range [16,20]. Cyclodextrin enhancement is preferred in analytical chemistry because of the easy sample preparation (no bubbling in the solution required) and high sensitivity. In cyclodextrins, formation of excimers has been likewise revealed through the typical structureless emission [21,22]. In particular, a 1 to 1 and different 2 to 2 complexes are formed in γ-cyclodextrin under neutral and basic conditions [21]. Ternary complexes involving 1-bromonaphthalene, β-cyclodextrin, and cyclic aliphatic compounds such as cyclohexane, piperidine, and 1-ethylpiperidine are particularly effective in enhancing the emission [23]. This phenomenon has been exploited for the determination of such aliphatic compounds, also in an enantioselective way, based upon the well-known sensitivity of the fluorimetric method [24].

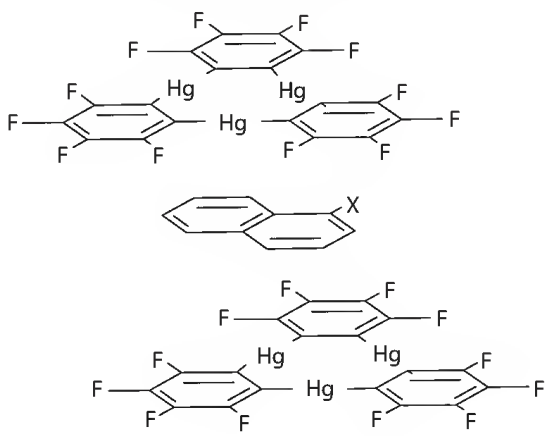

CHART 16.2

As for the bimolecular interactions of excited states, introducing a halogen atom has usually a modest effect on such processes. As an example, fluorobenzene behaves as a normal energy donor and sensitizes the *E/Z* isomerization of 2-butene [25]. Likewise, the process of oxygen sensitization by halobiphenyl or halonaphthalene fits, with regards to rate and efficiency, in the same general frame as halogen-free aromatics in a model based on charge transfer and noncharge transfer paths [26].

16.3 General Scheme of Photoreactivity

In several cases, a fluoro or chloro atom substituted in an aromatic ring behaves as an innocent bystander, introducing no new chemistry. This is certainly the case when a fast reaction not involving the aromatic moiety occurs. An example is the rotation around the double bond in the overcrowded diarylalkene shown hereafter (27, Scheme 16.1). Here, the halide can be used as an inert marker.

In the other cases, when the photochemistry involves the aromatic ring, the reactions may be distinguished into two groups, those that are characteristic of the aromatic ring per se and are affected in some way by the substituent (see Section 16.4) and those involving the aryl–halide bond (see Sections 16.5 to 16.8). The latter group includes first of all unimolecular processes, viz. both homo- (path a) and heterolytic (path b) cleavage, either of which takes place depending on structure and conditions (Scheme 16.2).

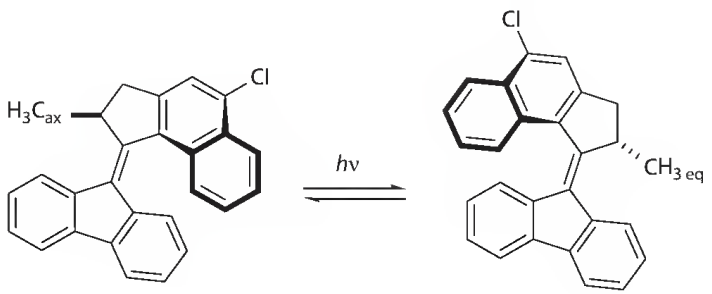

SCHEME 16.1

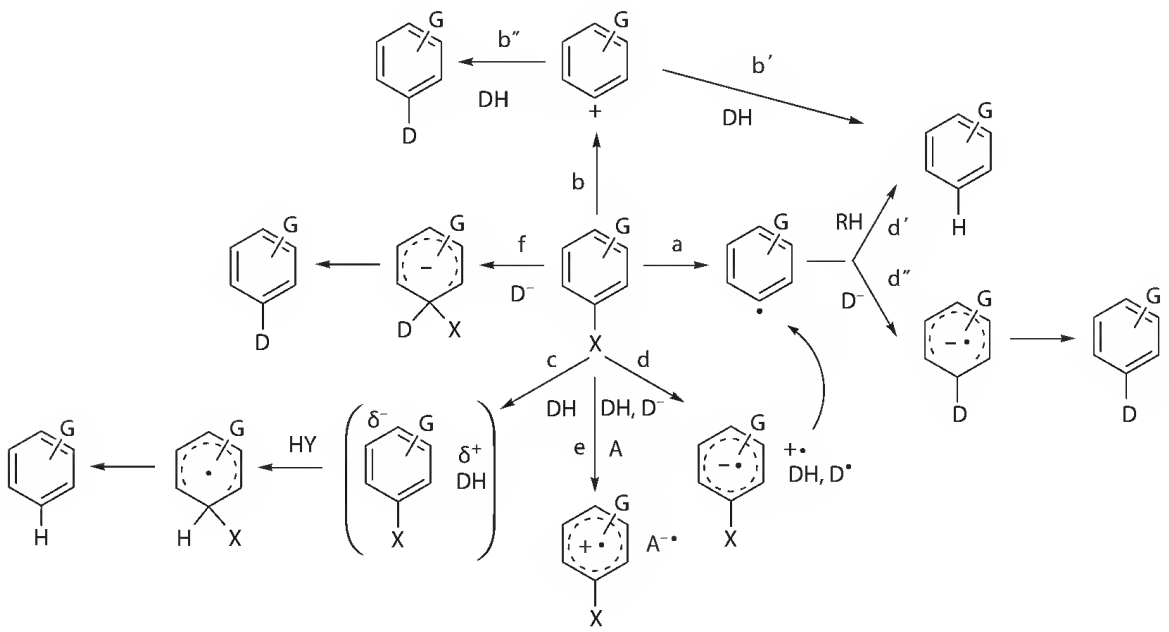

SCHEME 16.2

The first one leads to the phenyl radical and most often to reduction, the latter one to the phenyl cation, the chemical behavior of which depends on the multiplicity and leads either to reduction (b') or to substitution (b", ArS_N1).

Alternatively to the aforementioned processes, a variety of bimolecular reactions may occur. Formation of an exciplex with some donor (path c) followed by trapping by an electrophile HY is another mechanism for reduction. With a better donor, for example, an enolate, or when the halide bears an electron-withdrawing substituent, electron transfer (path d) takes place. This is followed by halide loss from the radical anion leading again to the phenyl radical and eventually to reduction (d'). In this process, as mentioned before, a strong donor (usually an anion) is necessarily present; in a following step, this may combine with the radical and initiate a chain substitution reaction (path d", $ArS_{RN}1$ process). A mirror-like mechanism leading to the radical with reversed roles is also conceivable (path e). Attack to the excited state and substitution via an addition–elimination process, just as in the ground state reactions is another possibility (ArS_N2^*, path f).

16.4 Photochemical Reactions Not Involving the Carbon–Halogen Bond

16.4.1 Rearrangement

Rearrangement and cycloaddition are the typical photochemical reactions of benzene and many of its simple derivatives and generally involve the singlet state. The increased intersystem crossing in aryl halides leads to the expectation that such processes are not favored among these compounds. However, many examples are known, although demonstrating their occurrence is not always trivial. As an example, the isolation and identification of a rearranged product such as benzvalenes is not experimentally simple, since this is a reversible process. Therefore, one may use an indirect indication that witnesses the reversible rearrangement, such as the positional isomerism in polysubstituted benzenes or the trapping by trifluoroethanol of the intermediate prefulvene (a diradical or zwitterion) to give a bicyclo[3.1.0]hexyl trifluoromethyl ether. The formation of such ethers is observed in many simple derivatives, but not, for example, in fluorobenzene, for which, on the other hand, there is little room for a chemical reaction from the singlet, since the sum of quantum yield of fluorescence (0.11) and the quantum yield of intersystem crossing (0.80) is close to 1 [28–30]. Thus, a reversible rearrangement to a bicyclic intermediate does not occur significantly in solution, or at least the equilibrium concentration of the intermediate is quite low [28]. Things may be different in a matrix at low temperature, at least for some derivatives. In fact, some new IR absorptions developing when hexafluorobenzene is irradiated at 193 nm in matrix suggest that rearrangement to perfluorobenzvalene occurs [31]. On the other hand, when irradiated at 254 nm in the vapor phase, hexafluorobenzene and some other heavily fluorinated derivatives give the corresponding Dewar benzene in a good yield [32,33, Scheme 16.3].

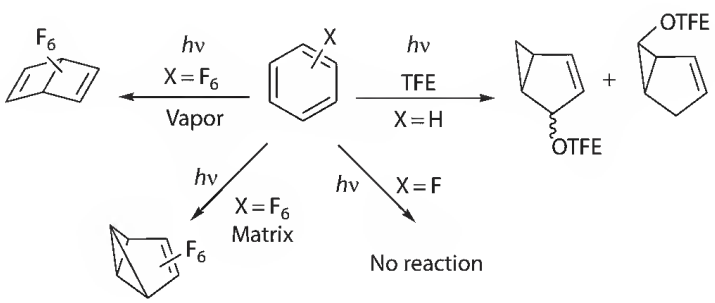

SCHEME 16.3

16.4.2 Cycloaddition and Addition

Probably the most useful photoreaction of aromatics is the photocycloaddition with olefins. In this reaction, fluoro- and chlorobenzene generally conform to the same pattern as the parent molecule. The ionization potential of these compounds only slightly differs (respectively 9.20 and 9.10 eV vs. 2.25 eV for benzene) and the generalizations that have been formulated for the preferred mode of reaction (*meta* cycloaddition when the benzene/olefin IP difference is between 0 and 1.6 eV, *ortho* when this is larger [34]) lead practically to the same predictions. Thus, *meta* cycloaddition is expected with aliphatic alkenes or cyclooctene, *ortho* cycloaddition (followed by a [4 + 2] reaction) for maleic anhydride and maleic and fumaric acid [35]. In fact, the *meta* cycloaddition reaction does take place with both fluoro and chlorobenzene with 1,2-dichloroethene, in the first case giving a 1-to-1 mixture of the two regioisomers, in the latter one a single regioisomer in 50% yield [31,33, Scheme 16.4]. An accompanying process is arylation. With cyclopentene, chlorobenzene mainly gives stereoisomeric phenylchlorocyclopentanes or phenylcyclopentene by dehydrohalogenation of the former compounds. Bromobenzene (and possibly iodobenzene) behave analogously (see further Section 16.5). On the contrary, with fluorobenzene *meta* and *para* cycloadducts are the main products, with a minor contribution of insertion [36, Scheme 16.4]. With this compound a nonselective *meta* addition occurs also with vinyl acetate [37] and a mixture of seven products has been obtained with furan [38]. On the other hand, this is not peculiar of aryl halides, but rather a general limitation of the benzene–olefin cycloaddition, which in fact is synthetically useful in the intramolecular version, when the preferred conformation drives the regioselectivity.

Again hexafluorobenzene behaves differently and undergoes efficient 2 + 2 cycloaddition with alkenes [39], giving products susceptible of synthetically interesting elaboration. With benzene pentafluorobiphenyl is formed and with toluene a mixture of methyltetrafluorobiphenyls [40], perhaps via exciplex rather than via radicals.

With primary and secondary amines chloro and fluorobenzene undergo both addition to give all the possible halo-2,4-cyclohexadienylamines (in some cases the 2,5-cyclohexadienyl derivatives) and substitution to give the anilines, the latter products arising via an addition–elimination path. These reactions appear to arise from the singlet state and the halogen atom decreases the quantum yield of reaction,

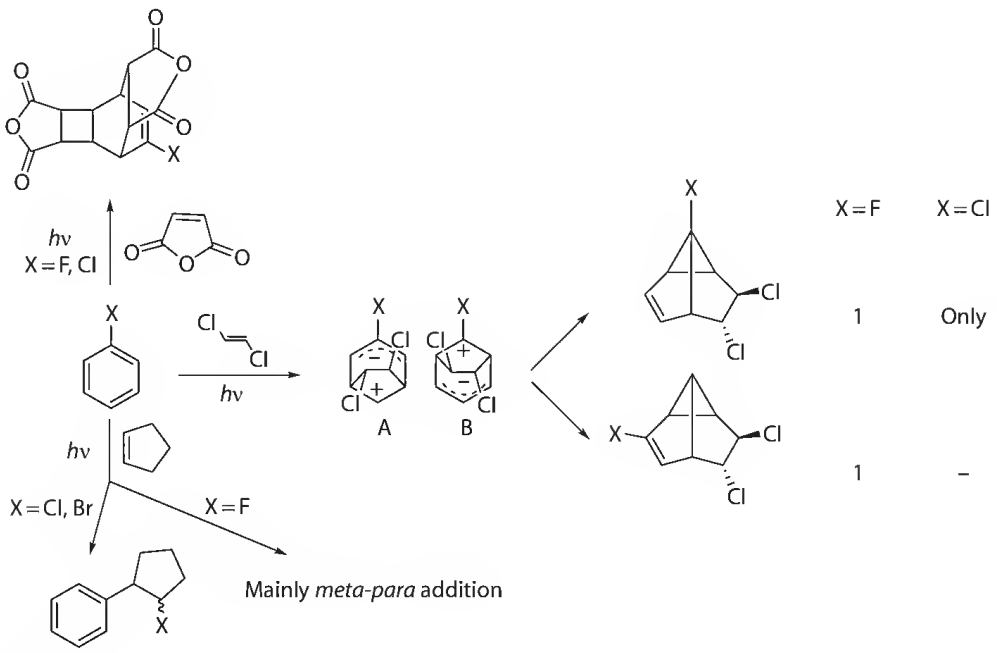

SCHEME 16.4

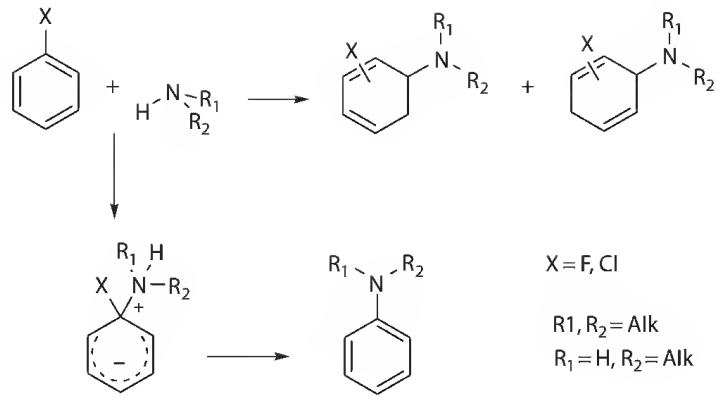

SCHEME 16.5

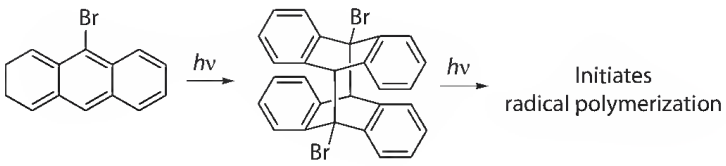

SCHEME 16.6

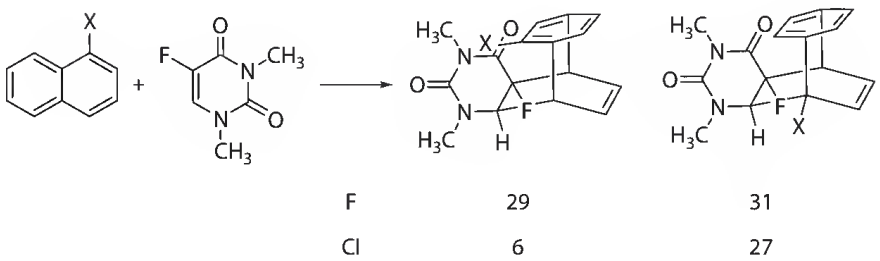

SCHEME 16.7

presumably because it stabilizes an exciplex intermediate, but has little effect on the regioselectivity [41,42, Scheme 16.5]. With tertiary amines α-cyclohexadienylamines are obtained.

With highly condensed aromatics the introduction of halogen atoms does not change the photoreactivity pattern of the hydrocarbon. As an example, the typical 4 + 4 photodimerization in the anthracene series is maintained. Thus, 9-bromoanthracene gives the head-to-tail dimer effectively. The product has proven suitable for the (radical photoinitiated) preparation of vinyl polymers labeled with an aromatic nucleus [43, Scheme 16.6].

Chloro and fluoronaphthalene undergo 4 + 4 cycloaddition with 5-fluorouracil, in the former case predominantly onto the substituted ring, in the latter one in a ca. 1-to-1 proportion between the two regioisomers [44, Scheme 16.7].

16.5 Homolysis

16.5.1 Mechanism

Electronic excitation is a way for activating the aryl–halide bond. The lowest singlet state reactions are geometrically modified with respect to the ground state. Loss of ring planarity leads toward ring rearrangement (see Section 16.4), but hinders labilization of the peripheral aryl–halide σ bond. This seems not to be the case for triplet states, more close to planarity and where both homolytic and heterolytic

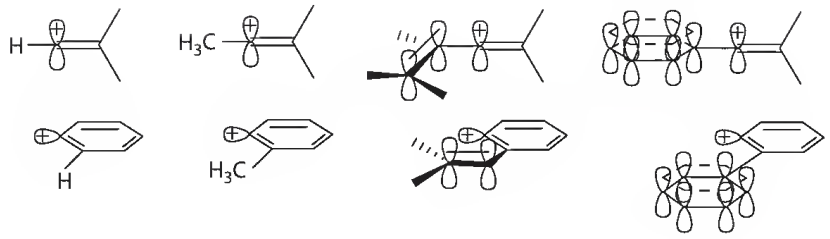

SCHEME 16.8

cleavages are possible. Most investigations identify homolysis in the triplet state as the mechanism for the dehalogenation of simple benzene derivatives. This is in contrast with what is established for vinyl halides that most often undergo heterolytic cleavage. It has been suggested that the difference, somewhat surprising in view of the close similarity of the two moieties and the analogous thermochemistry of the two processes, may reside in the different geometry (linear in the first case, necessarily bent in the latter one). This allows for stabilization by substituents directly on the charged carbon only with the vinyl cation [45, Scheme 16.8]. In the scheme it is indicated how a methyl, a vinyl, and a phenyl group stabilize a vinyl cation through the in plane interaction of orbitals, while this is not possible for the phenyl cation.

However, recent studies have progressively revealed that substituents and conditions may make heterolysis the predominating path also among aryl halides (see Section 16.8).

The C–Cl bond dissociation energy of chlorobenzene, which has been estimated experimentally and through calculations at various levels around 390 kJ/mol, is limitedly affected by introducing substituents on the ring [46]. DFT calculations at the B3LYP/6-31G** level have shown to be an excellent method for the prediction of the BDE in compounds of this type [47]. It results that dissociation from the lowest triplet is only moderately endothermic. Fragmentation from T_1 is favored for bromobenzene (and a fortiori iodobenzene), while is impossible, and is not observed, for the fluoro derivative (see Table 16.2).

16.5.2 Unimolecular Fragmentation in the Gas Phase

Thermochemical considerations establish a sine qua non condition, but are not sufficient for the definition of the mechanism, which at any rate depends on conditions. Many investigations have been devoted to the determination of the detailed path. The problem is the lowest excited states (both singlet and triplet) are of $\pi\pi^*$ type (except for iodides) and thus not directly involved in the fragmentation of the $\sigma_{C\text{-}X}$ bond, as demonstrated in the case of chlorobenzene by multireference CASSF second-order perturbation theory (MSCASPT2) calculations [11].

In the gas phase, the intervention of upper states is possible and appropriate techniques allow to determine the photodissociation dynamics parameters (for a review see [48]). Thus, a study carried out by using femtosecond pump probe spectroscopy (266 nm) combined with time-of-flight spectroscopy has revealed two fast dissociation paths for iodobenzene (lifetime 350 and 700 fs) and less fast paths for bromobenzene (28 ps) and chlorobenzene (1 ns) [49]. A further study on chlorobenzene has demonstrated that the path followed depends on the excitation energy, as experimentally observed and

TABLE 16.2 Triplet Energy and Bond Dissociation Energy for Halobenzenes[a]

	E_T (kJ/mol)	BDE (kJ/mol)
Ph-F	353	519
Ph-Cl	342	ca. 390
Ph-Br	335	331
Ph-I		268

[a] See Ref. [47].

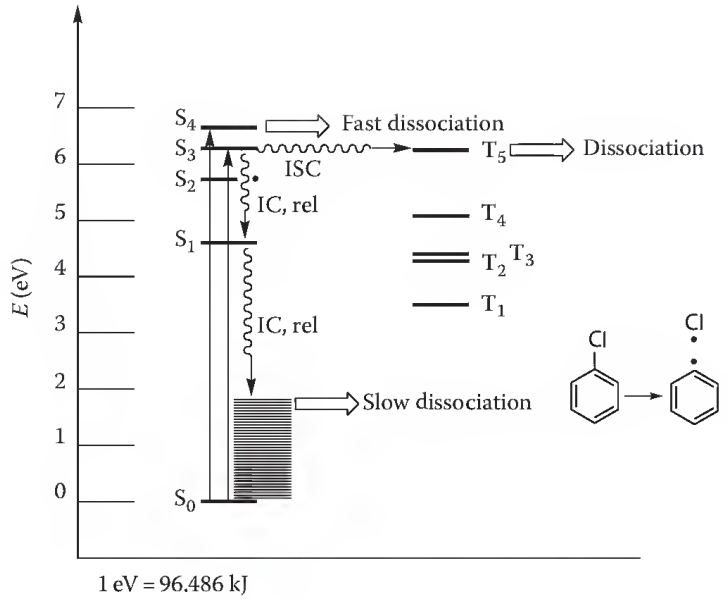

CHART 16.3

computationally rationalized. Irradiation at 193 nm brings up to S_4 (Chart 16.3). Three channels leading to dissociation are accessible in this case, viz. directly from S_4, a $n\sigma^*$ state, via bound S_3 that intersystem crosses to repulsive T_5, also a $n\sigma^*$ state, or through a hot ground state reaction. Only the last path is accessible by irradiation at 266 nm [11, Chart 16.3].

Bromobenzene likewise cleaves via the triplet, S_1 is a bonding $\pi\pi^*$ state that intersystem crosses to a repulsive $n\sigma^*$ triplet (T_4). Iodobenzene has a fast channel directly from S_1, a repulsive $n\sigma^*$ state, and a slow one via bonding S_2 that couples with repulsive triplets. As for fluorobenzene, short wavelength (248, 193, 157 nm) irradiation causes HF elimination, a process that appears to involve the vibrationally excited ground state formed by internal conversion [50].

When more halogens are present, the rate of homolysis can be affected to a large extent (obviously the weakest bond is cleaved when different halides are present). Thus, introducing a single fluorine atom in bromobenzene has little effect on the rate, but two or more drastically reduce the lifetime. The observed behavior has been correlated to the calculated relative location of $\pi\pi^*$ and $\pi\sigma^*$ states [51]. On the contrary, the dissociation of polybromobenzene is slower than that of the monosubstituted derivative, e.g., it decreases by a factor of 15 from bromobenzene to 1,3,5-tribromobenzene [52].

16.5.3 Fragmentation in Solution and in Matrix

In an inert matrix (Ar at 10 K), iodobenzene undergoes homolytic cleavage (see further Section 16.8). In solution, relaxation is faster and fragmentation generally involves the lowest triplet. Bimolecular interactions may affect the unimolecular cleavage rate, however. As an example, the photofragmentation of chlorobenzene in solution is quite efficient (Φ_r ca. 0.5 in cyclohexane) at a low concentration ($<10^{-3}$ M), but much less in concentrated solution, due to the formation of an exciplex that is chemically less reactive than nonassociated T_1 [53, Scheme 16.9] (notice however that in other halides, e.g., in biphenyls, the cleavage is more efficient in the exciplex). During the process a considerable amount of chlorocyclohexane is formed. This results from the photosensitized addition of hydrogen chloride on cyclohexene, in turn arising from the disproportionation of the cyclohexyl radical [54].

In oxygen-equilibrated solution the phenyl radical is trapped by oxygen and the resulting phenylperoxy radical has been likewise detected by flash photolysis [55]. In polar media substitution competes with reduction, as an example, in alcohols, ethers are also formed. It has been suggested that the primary

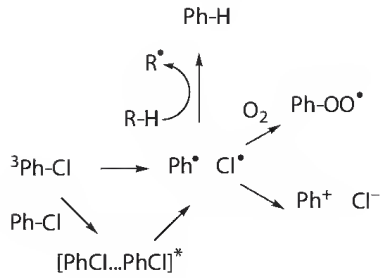

SCHEME 16.9

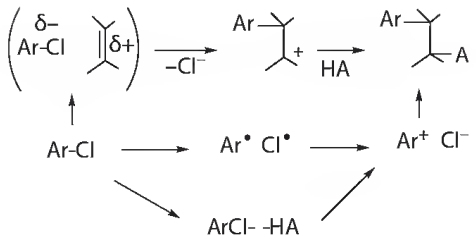

SCHEME 16.10

photoprocess remains homolysis, but electron transfer within the radical pair leads to the phenyl cation and the latter is the intermediate in the solvolysis. This may be true, but under these conditions, adding an alkene leads to the characteristic arylation typical of triplet phenyl cation (see Section 16.8), the occurring of which would be ill reconciled with such a mechanism (that would involve the singlet). Alternative possibilities are that an exciplex with the alkene has a role [56] or that relatively acid solvents drive the system toward the aryl cation (Scheme 16.10).

The reduction/substitution competition and the underlying mechanisms are subject to many variations, however. Notice further that the ratio reduction vs. substitution has been found to depend not only on the medium but also on the temperature [57].

As for polyhalogenated aromatics, the irradiation of a variety of poly(bromo, chloro)benzenes has given a mixture of dehalogenated products, biphenyls, and terphenyls (Scheme 16.11). Some generalizations have been obtained. Thus, in chloro derivatives, a chlorine not flanked by further chlorine atoms is more easily photoactivated than one flanked by one and still more by two of them, while the reaction of polybromoderivatives is less selective. When both Cl and Br are present, bromine is always preferentially lost [58]. It has been noticed that the photoreduction of hexachloro to pentachlorobenzene is accompanied by a considerable increase of the stable carbon isotope ratio [59].

The relatively high aryl–halide bond dissociation energy (see Table 16.2) explains the fact that photohomolysis is not a viable path from higher aromatics, or at least not from the lowest excited states, which are considerably more stabilized than in the benzene series. On the other hand, higher states may intervene. In 9-bromo and 9,10-dibromoanthracene the S_1 state ($\pi\pi^*$) exhibits no photoreactivity either in fluid or in matrix at 80 K, but under the latter conditions fluoresces strongly. As for photoreaction, this occurs only under short-wavelength irradiation and leads to debromination but with a quantum yield that depends on conditions (up to 0.1). The occurring of the reaction in fact requires two conditions, viz.

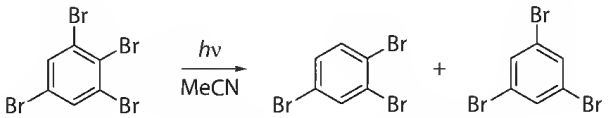

3–7
at 20% conversion

SCHEME 16.11

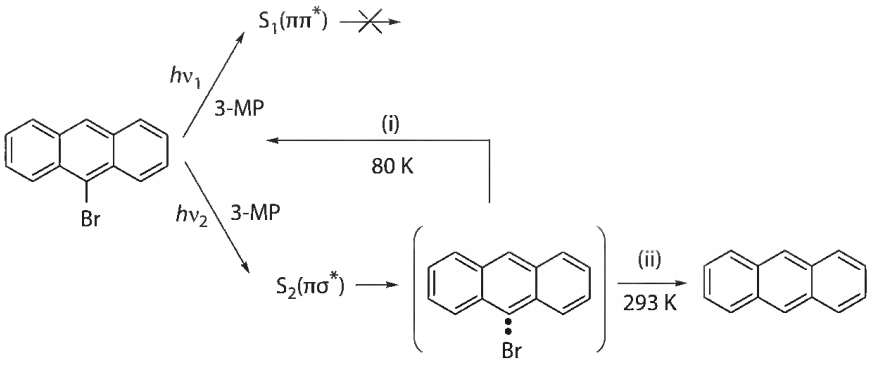

(i) Recombination, high viscosity solvents; (ii) low viscosity solvents

SCHEME 16.12

the intervention of a high-lying state (here C–Br homolysis occurs via the S_2 state of $\pi\sigma^*$ nature) and that the fast recombination of the primarily formed radicals is avoided, the latter process depending on viscosity and temperature [60, Scheme 16.12].

The weakness of the aryl–iodide bond makes deiodination a viable path also for higher aromatics, however. Thus, irradiation of samples of poly(methyl methacrylate) or polystyrene containing iodonaphthalene and iodophenanthrene leads initially to phosphorescence of the iodide, but then a change in the emission shape intervenes and has been attributed to the formation of photoproducts [61].

16.5.4 Assisted Photoreduction

An alternative to the aforementioned unimolecular cleavage is donor-assisted photoreduction. Smooth dehalogenation of chloro and bromoaromatics via an exciplex takes place with aliphatic amines, much more efficiently with secondary (that provide the hydrogen atom) than with tertiary amines [62, Scheme 16.13].

Another example of dehalogenation via exciplex that has been studied in detail involves dichloroanthracene and dienes, which form an exciplex irrespective of the nature of the solvent. Subpicosecond investigation reveals, however, a differentiation in the ensuing course of the reaction. Indeed, the end result is photocycloaddition in apolar media, but reductive dechlorination in polar media. With 2,5-dimethyl-2,4-hexadiene this has been demonstrated to be a kinetically complex phenomenon where the singlet excimer, a terplex and the radical anion are involved. The last intermediate appears to be protonated and then to give the final product, monochloroanthracene, via disproportionation or chloride loss, rather than undergoing initial dechlorination to give the anthracenyl radical [63,64, Scheme 16.14].

Both the exciplex and the terplex appear to dechlorinate with about the same efficiency, whereas the latter intermediate does not react in the analogous reaction with *N*-methylaniline [65]. 1-Bromonaphthalene and some of its derivatives, 9-bromophenanthrene and 2-bromodibenzofuran, are cleanly photoreduced upon irradiation in *iso*-propanol in the presence of bases, the hydroxide ion serving as the electron source [66, Scheme 16.15].

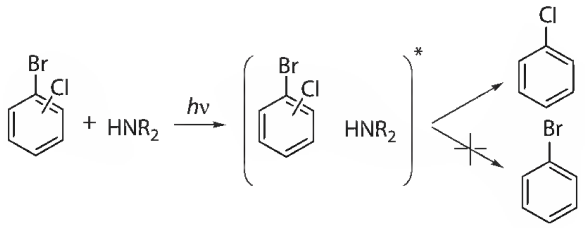

SCHEME 16.13

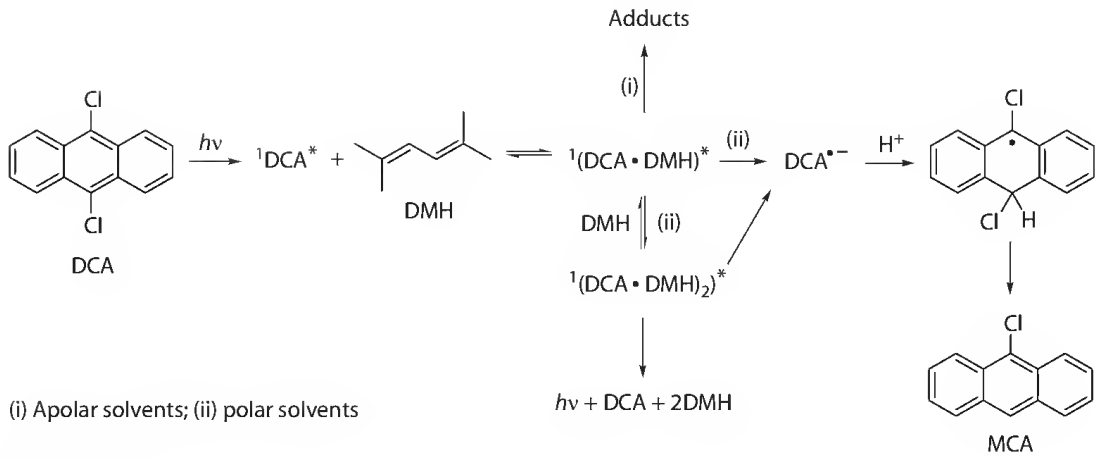

SCHEME 16.14

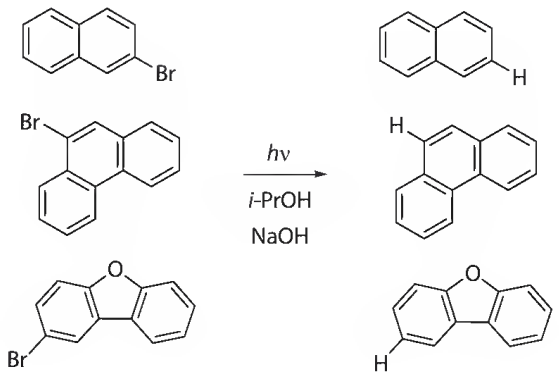

SCHEME 16.15

In the case of 1-chloropyrene, dechlorination occurs also under assistance by cyanide ion [67]. Dehalogenation may be important in laser ablation. In this technique the effect (cavitation) is caused either by local heating and boiling of the liquid or by a photochemical reaction. The latter appears to be the case for polymers doped with iodonaphthalene [61].

16.5.5 Other Reactions

In nonreducing solvents, photochemical activation leads to isomers of the starting halides (Scheme 16.16). Di-, tri-, and tetrachlorobenzene undergo migration of the halogen atom, preferentially to the *meta* position, a reaction that has be rationalized as the result of homolysis and radical recombination at the position with the largest spin. A clean reaction has not been obtained, however, and positional isomerization, reduction, and aryl–aryl coupling all occur to some degree [68,69]. Likewise, chlorobiphenyls in water undergo reductive dechlorination, substitution, and isomerization [70,71].

Furthermore, biphenyls are formed through solvent trapping upon irradiation of aryl halides in neat benzene. Indeed, this is the exclusive process by irradiation of *o*-dichlorobenzene in benzene [68].

16.6 Reactions via the Radical Anion

Electron transfer is a common occurrence in photochemistry and the relatively easy reduction of aryl halides offers another access to phenyl radicals via electron transfer and cleavage of the radical anion. Indeed, this is a topic with most synthetic applications. The chlorobenzene radical anion is extremely

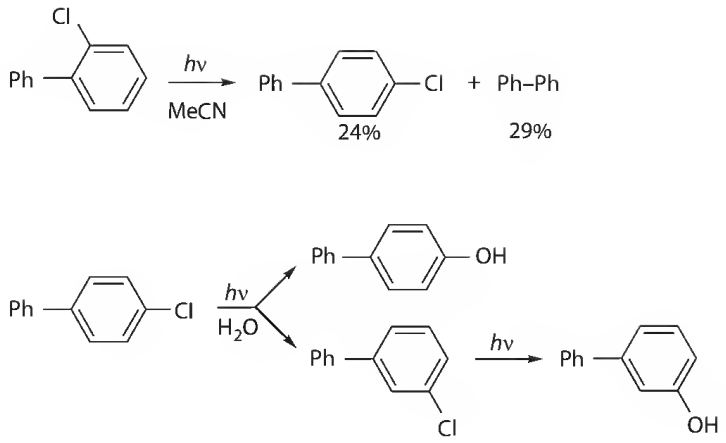

SCHEME 16.16

unstable in the gas phase and under such conditions it seems appropriate to conceive electron transfer and dissociation as synchronous steps [72], although in solution a stepwise mechanism operates [73,74].

16.6.1 Nonchain Processes

A number of inter- and intramolecular cases are known. The intermolecular reactions are exemplified by that of 4-chlorobenzonitrile with 1,1-diphenylethylene, where reductive elimination of the chloro atom produces the 4-cyanophenyl radical that in turn couples with the alkene radical cation [54, Scheme 16.17]. The process is terminated by solvent addition to the carbocation site. Intramolecular cases have likewise been reported. The irradiation of 2′-(chloro or bromo)benzanilide gives, besides photo-Fries rearrangement and cyclization to phenanthridone, reduction and cyclization to the phenylbenzoxazole. The last product, which is more abundant with the bromo derivative in the presence of NaOH, has been attributed to the dehalogenation from the radical anion formed by intramolecular electron transfer (compare Section 16.8) [74,75].

16.6.2 Chain Processes

The situation changes when some additional conditions are fulfilled. These are that the radical forms quite easily (that is the aryl–halide bond is weak) and the nucleophile is so strong that it reacts with aryl radical in the ground state. Under such conditions, a radical chain process sets in (Scheme 16.18). This is the $S_{RN}1$ reaction, typical of aryl iodides (though sometimes observed with different halides) with good donors such as enolates (functioning both as donors in the initiating step and as addends in the chain

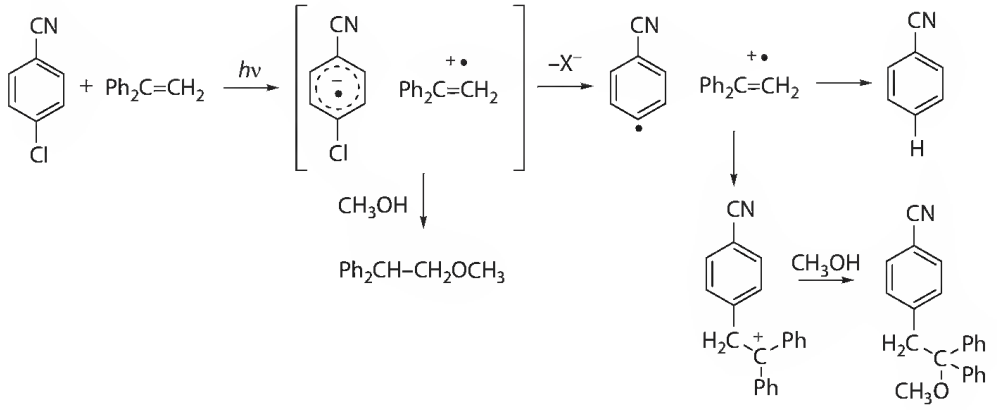

SCHEME 16.17

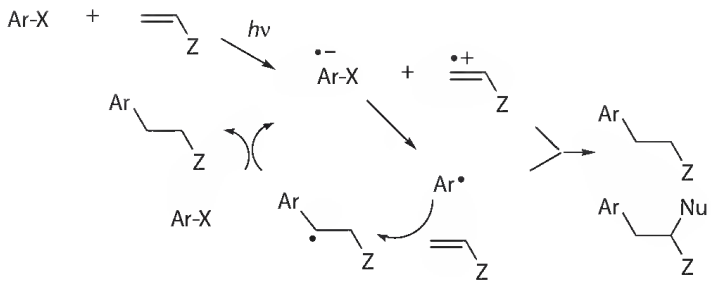

SCHEME 16.18

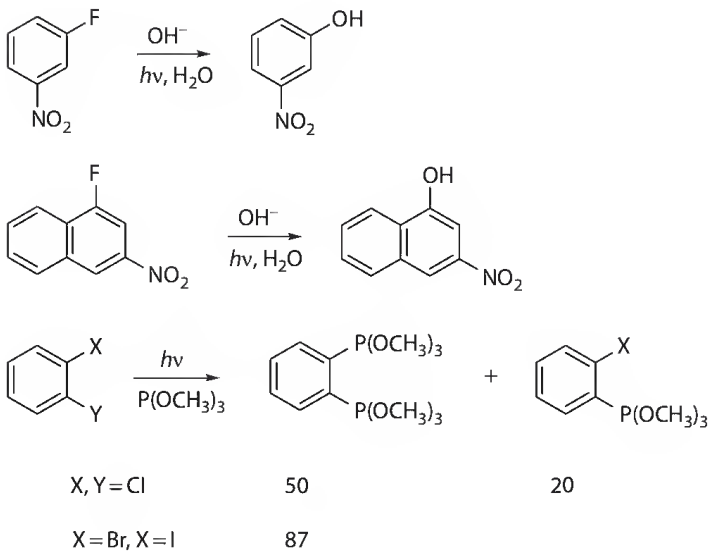

SCHEME 16.19

process). Differently from the previous case, this process, which is discussed in detail elsewhere in this handbook, often occurs with a reaction quantum yield $\Phi r \gg 1$.

16.7 ArS_N2^* Substitution Reactions

ArS_N2^* nucleophilic substitutions have a peculiar role in photochemistry, because the observation by Havinga that such a process is activated by a nitro group in *meta* position has been one of the key observations that initiated the rationalization of molecular photochemistry based on the electronic structure. The reaction follows the same pattern as the thermal ArS_N2 reaction, but the excited state is an electronic isomer of the starting material and the regiochemistry changes (Scheme 16.19). Thus, 3-fluoronitrobenzene is more readily converted to 3-nitrophenol than the isomers in 2 and 4 (though this characteristics does not extends to the chloro and bromo analogues) [76]. With an amine as the nucleophile, nitro group reduction predominates over substitution in the benzene series, but the latter reaction takes over with naphthalenes [77]. The irradiation of 1,2-dichlorobenzene in trimethyl phosphite has been reported to give a mixture of the mono- and di-substituted products [78].

16.8 ArS_N1 Arylation Reactions

The heterolytic cleavage of an aryl–halide bond in the gas phase is energetically unattainable. However, this path is viable for electron-donating substituted aryl halides in polar media (see Table 16.3). In particular, B3LYP calculations evidence that in the solvent-equilibrated triplet state of 4-chloroanisole or

TABLE 16.3 Energetics for the Homolytic and Heterolytic Fragmentation of Some Aryl Halides

From T_1	Ph-Br[a]	$NH_2C_6H_4F$[b]	$NH_2C_6H_4Cl$[b]	$NH_2C_6H_4Br$[b]
ΔE (Ph X$^{\bullet}$)[c]	5	218	98	79
ΔE (Ph$^+$ X$^-$)[c]	490	38	−131	−145

[a] See Ref. [45].
[b] See Ref. [79].
[c] (kJ/mol).

4-chloroaniline the halogen atom tilts out of plane. A further stretch of the bond encounters a moderate barrier and leads to a phenyl cation [79].

The occurring of a heterolytic path has been early suggested in a couple of cases [80], but has been recently more extensively investigated. It appears that this occurs efficiently from electron-donating substituted aryl halides in polar solvents. Also the parent cation has been obtained, though. In an inert matrix at 10 K, high energy irradiation cleaves iodobenzene and gives, among other species, the cation, which has been spectroscopically characterized. Doping the matrix with nitrogen or carbon monoxide produces the phenyldiazonium or benzoyl cation, respectively [81, Scheme 16.20].

Dehalogenation may lead to ring transformation. In particular, 2-chloro and 2-bromophenol eliminate HX and yield a ketocarbene that in turn undergoes a Wolff rearrangement [82, Scheme 16.21]. In the presence of oxygen, trapping of this intermediate gives a carbonyl oxide, detected by flash photolysis [83].

The formation of a small amount of 2-methyl-4,5,6,7-tetrachlorobenzoxazole from the irradiation of pentachlorophenol in acetonitrile has been rationalized through hydrogen chloride loss and solvent addition to the resulting ketocarbene [84, Scheme 16.21].

Apart from such mechanistic studies, the synthetic interest of heterolytic cleavage lies in the triplet state of the phenyl cation. The singlet cation (π^6n^0 localized structure) is completely unselective and reacts at diffusion controlled rate with any nucleophile. Its triplet counterpart is again a strong electrophile, but, as one may expect from its π^5n^1 electronic structure, more similar to a triplet carbene rather than to a localized carbocation [79,85]. This leads to a peculiar preference for reaction with π nucleophiles with respect to n nucleophiles (in fact, the rate of addition is higher by a factor >10^3) [86,87].

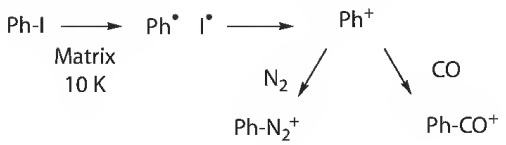

SCHEME 16.20

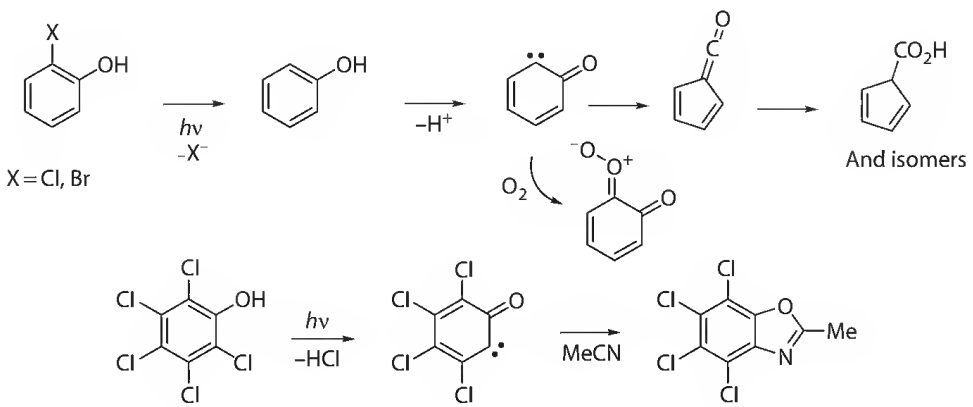

SCHEME 16.21

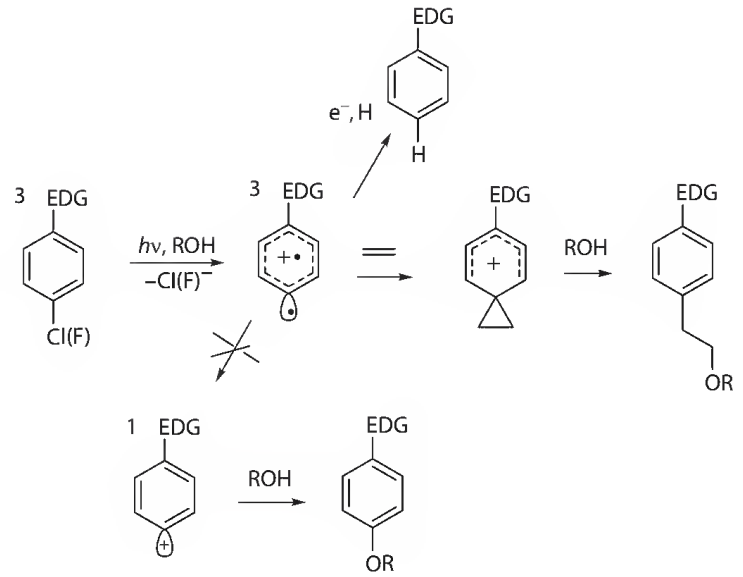

SCHEME 16.22

As mentioned earlier, aryl halides undergo efficient intersystem crossing. Thus, the cation is produced in the synthetically interesting triplet state. In practice, irradiation of the halides (fluorides and chlorides, although the mechanism applies to some bromides too) can be carried out in a polar (and thus usually nucleophilic) solvent, with no risk of competitive trapping of the phenyl cation. ISC to the singlet will occur at the adduct cation level and at this point addition of the nucleophilic solvent or other "typical cationic" reactions take place (Scheme 16.22).

The reaction has a synthetic interest since it allows the formation of an aryl–carbon bond starting from easily available halides. As mentioned, it occurs smoothly with electron-donating substituted fluorides and chlorides, and is thus complementary to both the $S_{RN}1$ process and to the thermal arylations involving transition metal catalysis, which both generally involve bromides and iodides and are favored by electron withdrawing substituents [88]. Attack to alkenes, alkynes, aromatics, and heterocycles is effective. The final product formed depends on the structure of the addend and on conditions. With alkenes, (β-substituted)-alkylbenzenes or allylbenzenes have been obtained. Mixtures can be formed because of the intervening of cationic rearrangements (Wagner–Meerwein type) in the alkyl moiety. The product distribution is simplified, and the synthetic value increased, when the reaction course is directed by the alkene substituents. As an example, phenyl alkenes give styrenes [89,90, see Scheme 16.23].

The biased reaction from the adduct cation may involve a fast cleavage when a good electrofugal group is present, such as a silyl group in the reaction with allyltrimethylsilane that gives an allylbenzene [91, Scheme 16.24] or in the reaction with silylenol ethers for the preparation of α-arylketones [92, Scheme 16.23].

The stabilization of the cationic site may help in directing and simplifying the reaction paths, for example, by making deprotonation from a tertiary carbon predominant over addition of a nucleophile

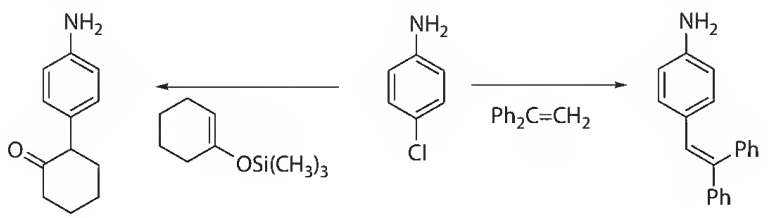

SCHEME 16.23

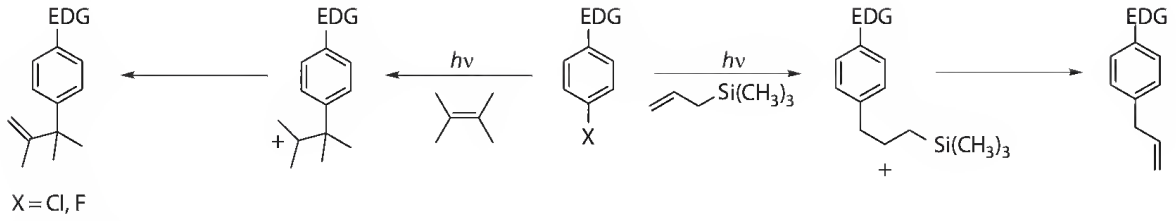

SCHEME 16.24

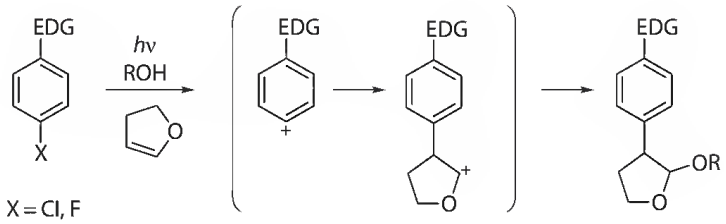

SCHEME 16.25

in the reaction with 2,3-dimethylbutene or by ensuring a sufficient permanence to the cation adduct, so that alcohol addition is effective in the reaction with 2,3-dihydrofuran [93, Scheme 16.25].

Still another possibility for a clean reaction is having the nucleophile in the addend itself. Thus, starting from alkenoic acids the initial attack by the phenyl cation onto the alkene moiety is followed by intramolecular attack by the carboxyl group [94, Scheme 16.26],

Alkynes undergo smooth arylation in a Sonogashira-like process [95, Scheme 16.27]

The arylation is effective with aromatics, giving biphenyls even when sterically hindered [96, Scheme 16.28] and with electron-rich heterocycles, where it occurs selectively on the most nucleophilic position free [97, Scheme 16.28].

When no π nucleophile is present (as a matter of fact one is necessarily present, viz. the aryl halide used as precursor; in fact a certain amount of "self-coupling" products are usually formed), the triplet cation is generally reduced via electron or hydrogen transfer by the solvent, since, as mentioned earlier, it does not add n nucleophiles. This can be considered as a mild method for the reductive dechlorination (and defluorination) in aromatic compounds [98, Scheme 16.29].

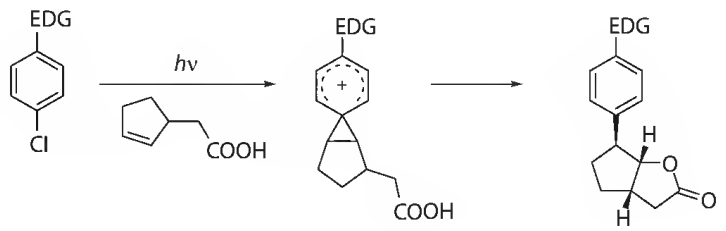

SCHEME 16.26

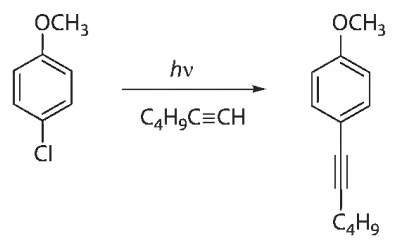

SCHEME 16.27

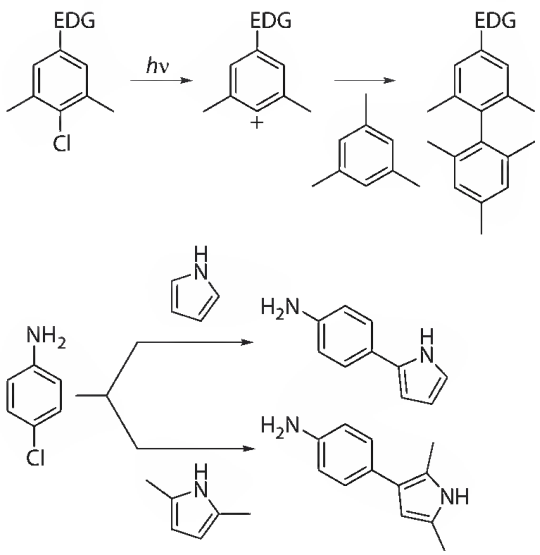

SCHEME 16.28

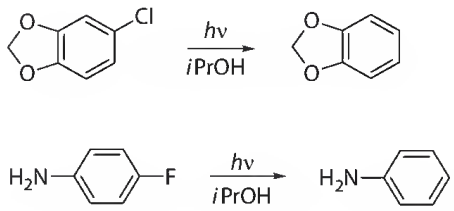

SCHEME 16.29

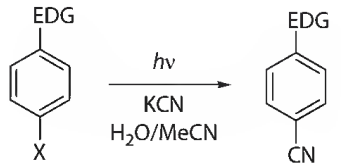

SCHEME 16.30

Charged n nucleophiles add, however. Examples are the irradiation of electron-donating substituted aryl halides in the presence of iodide and cyanide, where a clean substitution results. In the latter case the procedure is a simple and cheap alternative to thermal methods for the preparation of benzonitriles [99, Scheme 16.30].

16.9 Application to Depollution

16.9.1 Direct Irradiation

Halogenated aromatics are important pollutants found in the gas phase, in water, and adsorbed on solid materials, and photochemical reactions may be an important decomposition path. A comparative study of various noncombustion methods has shown that, although it is impossible to establish an efficiency order because different test compounds give different answers, photochemistry certainly is a viable solution for the elimination of PCBs [100]. Studies in water (where a limit is the low solubility) indicate that the main process is solvolysis. Thus, chlorobenzene in deaerated water gives mainly phenol and chloride anion and a low amount of benzene and chlorobiphenyl [101]. Phenol is easily oxidized and thus the process may be thought to be directed toward mineralization.

Under different conditions, however, decomposition cannot always be equated to detoxification. In iced water, as an example, the main processes are reductive dehalogenation and coupling to di- and terphenyls, consistently with a homolytic cleavage and combination [102]. Dehalogenation occurs also in the irradiation of bromobenzene and some dihalo (Cl, Br) benzene in water ice. No phenols are formed, but rather coupling products, halobiphenyls. In these cases, photoproducts are formed that are more toxic and persistent than the starting pollutants.

In polychlorobiphenyls, photodechlorination has been examined as a potential method for the detoxification of marine sediment and found to be rather inefficient (much less, e.g., than radiolysis) [103]. However, the fact that in solution the process in the presence of amines is faster suggest that under optimized conditions this method may give satisfactory results. Indeed, with 2,3,4,5-tetrachlorobiphenyl it was found that a small amount of surfactant have been shown to lead to increased reductive dehalogenation and likewise humic acids at a low concentration to act as an additional hydrogen source, thus favoring degradation [104]. Conversely, liberation of chlorine or bromine from human-made materials, for example, compounds of industrial or agricultural use, may affect the destruction of the ozone layer in the stratosphere.

Dehalogenation, or at least dechlorination, becomes a minor path with higher aromatics, or with a part of them. Thus, photodegradation of chlorinated PAH (that appear to be present in graphite particles) involves processes different from cleavage of the aryl–Cl bond, primarily ring oxidation. The stabilization brought about by the insertion of a chloro atom may thus diminish the photoreactivity, and not increase it as the introduction of a new chemical path would be expected to do. The two effects are balanced, thus 9-chlorophenanthrene and 1-chloropyrene are more photolabile than the corresponding hydrocarbons and the reactivity increases when adding further chlorine atoms, whereas the contrary is true for 7-chlorobenz[*a*]anthracene and 6-chlorobenzo[*a*]pyrene with respect to the corresponding substituted hydrocarbons [105].

Among the many studies of the decomposition of halogenated materials in various environmental locations that have been studied, at least the case of decabromodiphenyl ether, a largely used flame retardant, should be quoted. This compound degrades in some weeks when adsorbed on kaolinite or montmorillonite, but in some months when adsorbed on a carbon-rich sediment. The reaction involves stepwise debromination [106].

Chlorobenzene may be a significant contaminant in gaseous effluents. It has been demonstrated that irradiation by low-pressure mercury lamps in a suitable photochemical reactor leads to the removal of this compound in the range 0.2–2 g/m^3 starting concentration, with an increased efficiency in the presence of moisture [107]. An integrated UV-biofilter system has given excellent results [108].

16.9.2 Photocatalysis

Titania photocatalysis, the technique par excellence in photodepollution, has obviously been applied to the degradation of aryl halides. Chlorobenzene and (polychoro)biphenyls have been investigated extensively [109], and 4-chlorophenol [110] has become the standard material for comparing the efficiency of variously prepared titania sample [111], probably because the oxidation proceeds particularly smoothly (also in view of the adsorption of this polar compound onto the photocatalyst, essential in this heterogeneous technique). In the gas phase, it has been found that humidity decreases the rate of chlorobenzene degradation, because the layer of water prevents the adsorption of the pollutant (contrast with Section 16.8.1). The literature on this topic is quite extensive and ranges from the dependence on conditions [112], to the effect of added reagents, such as hydrogen peroxide [113] and to mechanistic issues [114].

Nanomaterials have proven effective for the reductive dehalogenation of aryl halides. As an example, nanocrystalline ZnS in the presence of triethylamine as sacrificial donor has proved to be effective with the sequential elimination of chlorine from di-, tri-, and tetrachlorobenzene. Nanocrystalline CdS is also quite effective: when using bulk photocatalyst, hexachlorobenzene is only partially reduced to pentachlorobenzene, but with the nanocrystalline material in the same time, a 1–4 mixture of 1,2,3,4-tetrachlorbenzene and 1,2,4,5-tetrachlorobenzene is formed. Defluorination likewise occurs under these conditions [115].

16.10 Conclusions and Outlook

The photochemistry of aryl halides seems to be destined to remain a favored field of investigation. Introducing a halogen on an aromatic ring is experimentally simple and produces a strong effect on the nature of the excited states. Thus, the photochemical and photophysical properties can be manipulated rather easily. It is expected that applications in diverse fields, from analytical methods to OLEDs will be further developed. Although some classes of photoreactions (e.g., cycloaddition) tend to give mixtures, the long established $S_{RN}1$ process and the more recent S_N1 arylations occur selectively under mild conditions. These appear to be useful preparative methods that deserve to be ranged among the general synthetic procedures. Furthermore, aryl halides have convenient properties also in the ground state, which makes them largely used in industry and agriculture and thus, unfortunately, common among pollutants. There again photochemistry has an important role for their degradation in the environment.

Acknowledgment

Miss Carlotta Raviola is thanked for her help in the literature search.

References

1. Lewis, G. N.; Kasha, M. *J. Am. Chem. Soc.* 1944, *66*, 2100.
2. Semenova, O. P.; Tsiknnov, G. S. *Zh. Fiz. Khim.* 1944, *18*, 311.
3. Bunce, N. J. Photochemical C–X bond cleavage in arenes, in *CRC Handbook of Organic Photochemistry and Photobiology*; W. Horspool and P. S. Soon, Eds., CRC Press, Boca Raton, FL, 1995, pp. 1181–1192.
4. Schutt, L.; Bunce, N. J. Photodehalogenation of aryl halides, in *CRC Handbook of Organic Photochemistry and Photobiology*; W. Horspool and F. Lenci, Eds., 2nd edn., CRC Press, Boca Raton, FL, 2004, pp. 38-1–38-18.
5. Sammes, P. G. Photochemistry of the C–X group, in *The Chemistry of the Carbon-Halogen Bond, Part II*; S. Patai, Ed., Wiley, New York, 1973, p. 747.
6. Grimshaw, J.; de Silva, A. P. *Chem. Soc. Rev.* 1981, *10*, 81.
7. Lodder, G.; Cornelisse, J. Recent advances in the photochemistry of the carbon–halogen bond, in *The Chemistry of Functional Groups, Suppl. D2*; S. Patai and Z. Rappoport, Eds., Wiley, New York, 1995, p. 861.
8. Davidson, R. S.; Goodwin, J. W.; Kemp, G. The photochemistry of aryl halides in advances, in *Physical Organic Chemistry*; Vol. 20, Academic Press, London, U.K., 1984, p. 191.
9. Marchetti, A. P.; Kearns, D. R. *J. Am. Chem. Soc.* 1967, *89*, 768.
10. McClure, D. S. *J. Chem. Phys.* 1949, *17*, 905.
11. Liu, Y. J.; Persson, P.; Lunell, S. *J. Chem. Phys.* 2004, *121*, 11000.
12. Takemura, T.; Yamada, Y.; Sugawara, M.; Baba, H. *J. Phys. Chem.* 1986, *90*, 2324.
13. Kawai, A.; Shibuya, K. *J. Photochem. Photobiol. C: Photochem. Rev.* 2006, *7*, 89.
14. Gastilovich, E. A.; Klimenko, V. G.; Serov, S. A.; Nurmukhametov, R. N. *Opt. Spectrosc.* 2009, *106(6)*, 799.
15. Miller, J. C.; Meek, J. S.; Strickler, S. J. *J. Am. Chem. Soc.* 1977, *99*, 8175.
16. Li, L.; Zhao, Y.; Wu, Y.; Tong, A. *Talanta* 1998, *46*, 1147.
17. Elbjeirami, O.; Burress, C. N.; Gabbaï, F. P.; Omary, M. A. *J. Phys. Chem. C* 2007, *111*, 9522.
18. Ruzo, L. O.; Sundstrom, G.; Hutzinger, O.; Safe, S. *Rec. Trav. Chim. Pays-Bas* 1977, *96*, 249.
19. (a) Jin, W. J. Cyclodextrin inclusion complexes: Triplet state and phosphorescence, in *Cyclodextrin Materials Photochemistry, Photophysics and Photobiology*; A. Douhal, Ed., Elsevier, Oxford, U.K., 2006, p. 137. (b) Peng, Y. L.; Wang, Y. T.; Wang, Y.; Jun Jin, W. *J. Photochem. Photobiol. A: Chem.* 2005, *173*, 301.

20. Turro, N. J.; Bolt, J. D.; Kuroda, Y.; Tabushi, I. *Photochem. Photobiol.* 1982, *35*, 69.
21. Hamai, S. *J. Mat. Chem.* 2005, *15*, 2881.
22. Hamai, S. *J. Phys. Chem. B* 1999, *103*, 293.
23. Zhu, Y. X.; Peng, J. H.; Zhang, Y. *Anal. Chim. Acta* 2007, *583*, 364.
24. Garcia-Ruiz, C.; Hu, X. S.; Ariese, F.; Gooijer, C. *Talanta* 2005, *66*, 634.
25. Gray, D.; Al Ali, K.; Phillips, D. *J. Chem. Soc. (A)*, 1971, 2949.
26. Schmidt, R. *J. Phys. Chem. A* 2006, *110*, 5990.
27. Pollard, M. M.; Wesenhagen, P. V.; Pijper, D.; Feringa, B. L. *Org. Biomol. Chem.* 2008, *6*, 1605.
28. Foster, J.; Pincock, A. L.; Pincock, J. A.; Rifai, S.; Thompson, K. A. *Can. J. Chem.* 2000, *78(7)*, 1019.
29. Gonzalez, C. M.; Pincock, J. A. *J. Am. Chem. Soc.* 2004, *126*, 8870.
30. Gonzalez, C. M.; Pincock, J. A. *Can. J. Chem.* 2006, *84*, 10.
31. Laboy, J. L.; Ault, B. S. *Laser Chem.* 1994, *15*, 21.
32. Lemal, D. *Acc. Chem. Res.* 2001, *34*, 662.
33. (a) Gerace, M. J.; Lemal, D. M.; Ertl, H. *J. Am. Chem. Soc.* 1975, *97*, 5584. (b) Camaggi, G.; Gozzo, F. *J. Chem. Soc. C* 1969, 489.
34. Bryce-Smith, D.; Foulger, B.; Forrester, J.; Gilbert, A.; Orger, B. H.; Tyrrell, H. M. *J. Chem. Soc., Perkin Trans 2* 1980, 55.
35. Shaikhrazieva, V. Sh.; Tal'vinskii, E. V.; Tolstikov, G. A. *Zh. Org. Khim.* 1971, *7*, 2225.
36. Gilbert, A.; Heath, P.; Rodwell, P. W. *J. Chem. Soc., Perkin Trans. 1* 1989, 1867.
37. Gilbert, A.; bin Samsudin, W. *J. Chem. Soc., Perkin Trans. 1* 1980, 1118.
38. Garcia, H.; Gilbert, A.; Griffiths, O. *J. Chem. Soc., Perkin Trans. 1* 1994, 247.
39. (a) Lemal, D. M.; Buzby, J. M.; Barefoot, A. C.; Grayston, M. W.; Laganis, E. D. *J. Org. Chem.* 1980, *45*, 3118. (b) Bryce-Smith, D.; Gilbert, A.; Orger, B. H. *J. Chem. Soc., Chem. Commun.* 1969, 800. (c) Bryce-Smith, D.; Gilbert, A.; Orger, B. H.; Twitchett, P. *J. Chem. Soc., Perkin Trans. 1* 1978, 232. (d) Sket, B.; Zupancic, N.; Zupan, M. *J. Chem. Soc., Perkin Trans. 1* 1987, 98. (e) Sket, B.; Zupan, M. *J. Am. Chem. Soc.* 1977, *99*, 3504.
40. Bryce-Smith, D.; Gilbert, A.; Tyrell, H. M. *J. Chem. Soc., Perkin Trans. 1* 1979, 558.
41. Gilbert, A.; Krestonosich, S.; Westover, D. L. *J. Chem. Soc., Perkin Trans. 1* 1981, 295.
42. Gilbert, A.; Krestonosich, S. *J. Chem. Soc., Perkin Trans. 1* 1980, 1393.
43. Roof, A. C.; Tillman, E. S.; Malik, R. E.; Roland, A. M.; Miller, D. J.; Sarry, L. R. *Polymer* 2006, *47*, 3325.
44. Ohkura, K.; Sugaoi, T.; Ishihara, T.; Aizawa, K.; Nishijima, K.; Kuge, Y.; Seki, K. *Heterocycles* 2003, *61*, 377.
45. Galli, C.; Gentili, P.; Guarnieri, A.; Kobayashi, S.; Rappoport, Z. *J. Org. Chem.* 1998, *63*, 9292.
46. Luo, Y. R. *Handbook of Bond Dissociation Energies in Organic Compounds*; Science Press, Beijing, China, 2004.
47. Li, X.-H.; Tang, Z.-X.; Zhang, X.-Z. *J. Struct. Chem.* 2009, *50*, 34.
48. Han, K.-L.; He, G.-Z. *J. Photochem. Photobiol. C: Photochem. Rev.* 2007, *8*, 55.
49. Kadi, M.; Davidsson, J.; Tarnovsky, A. N.; Rasmusson, M.; Akesson, E. *Chem. Phys. Lett.* 2001, *350*, 93.
50. Vàzquez, S. A.; Martìnez-Nùñez, E. *Chem. Phys.* 2008, *349*, 219.
51. Borg, O. A.; Liu, Y.-J.; Persson, P.; Lunell, S.; Karlsson, D.; Kadi, M.; Davidsson, J. *J. Phys. Chem. A* 2006, *110*, 7045.
52. Kadi, M.; Davidsson, J. *Chem. Phys. Lett.* 2003, *378*, 172.
53. Bunce, N. J.; Bergsma, J. P.; Bersma, M. D.; De Graff, W.; Kumar, Y.; Ravanal, L. *J. Org. Chem.* 1980, *45*, 3708.
54. Arnold, D. R.; Wong, P. C. *J. Am. Chem. Soc.* 1977, *99(10)*, 3361.
55. Da Silva, J. P.; Jockush, S.; Turro, N. J. *Photochem. Photobiol. Sci.* 2009, *8*, 210.
56. Lazzaroni, S.; Protti, S.; Fagnoni, M.; Albini, A. *J. Photochem. Photobiol. A: Chem.* 2010, doi:10.1016/j.jphotochem.2010.01.005.

57. Nagaoke, S.; Takemura, T.; Baba, H. *Bull. Chem. Jpn.* 1985, *58*, 2082.
58. Nakada, M.; Miura, C.; Nishiyama, H.; Higashi, F.; Mori, T.; Hirota, M.; Ishii, T. *Bull. Chem. Soc. Jpn.* 1989, *62*, 3122.
59. Zhang, Z.; Yu, G.; Cheng, J.; Wang, X.; Zhang, F.; Zhou, *J. Prog. Nat. Sci.* 2005, *15*, 82.
60. Favaro, G.; di Nunzio, M. R.; Gentili, P. L.; Romani, A.; Becker, R. S. *J. Phys. Chem. A* 2007, *111*, 5948.
61. Andreou, E.; Athanassiou, A.; Fragouli, D.; Anglos, D.; Georgiou, S. *Laser Chem.* 2002, *20*, 1.
62. Bunce, N. J. *J. Org. Chem.* 1982, *47*, 1948.
63. Saltiel, J.; Smothers, W. K.; Schanze, K. S.; Charman, S. A.; Bonneau, R. *Photochem. Photobiol. Sci.* 2009, *8*, 856.
64. Nakayama, T.; Nagahara, T.; Miki, S.; Hamanoue, K. *J. Photochem. Photobiol. A* 2000, *133*, 11.
65. Soloveichik, O. M.; Ivanov, V. I.; Kuz'min, M. G. *Zh. Org. Khim. Eng. Ed.* 1976, *12*, 860.
66. Yoshimi, Y.; Ishise, A.; Oda, H.; Moriguchi, Y.; Kanezaki, H.; Nakaya, Y.; Katsuno, K.; Itou, T.; Inagaki, S.; Morita, T.; Hatanaka, M. *Tetrahedron Lett.* 2008, *49*, 3400.
67. Lemmetyinen, H.; Ovaskainen, R.; Nieminen, K.; Vaskonen, K.; Sychtchikova, I. *J. Chem. Soc., Perkin. Trans. 2*, 1992, 113.
68. Morisaki, K.; Miura Y.; Abe, K.; Hirota, M.; Nakada, M. *Chem. Lett.* 1987, 1589.
69. Hirota, M.; Nakada, M. *Bull. Chem. Soc. Jpn.* 1992, *65*, 2926.
70. Moore, T.; Pagni, R. M. *J. Org. Chem.* 1987, *52*, 770.
71. Orvis, J.; Weiss, J.; Pagni, R. M. *J. Org. Chem.* 1986, *51*, 1851.
72. Beregovaya, I. V.; Shchegoleva, L. N. *Chem. Phys. Lett.* 2001, *348*, 501.
73. Arun Prasad, M.; Sangaranarayanan, M. V. *Tetrahedron Lett.* 2004, *45*, 4741.
74. Mayouf, A. M. *J. Photochem. Photobiol. A: Chem.* 2005, *172*, 258.
75. Rossi, R. A.; Pierini, A. B.; Penényory, A. B. *Chem. Rev.* 2003, *103*, 71.
76. Cornelisse, J.; Havinga, E. *Chem. Rev.* 1975, *75*, 353.
77. Naft Lammers, J. G.; Cornelisse, J. *Isr. J. Chem.* 1977, *16*, 299.
78. Obricki, R.; Griffin, C. E. *Tetrahedron Lett.* 1966, 5049.
79. (a) Freccero, M.; Fagnoni, M.; Albini, A. *J. Am. Chem. Soc.* 2003, *125*, 1382. (b) Dichiarante, V.; Dondi.; Protti, S.; Fagnoni, M.; Albini, A. *J. Am. Chem. Soc.* 2007, *129*, 5605.
80. Yang, N. C.; Huang, A.; Yang, D. H. *J. Am. Chem. Soc.* 1989, *111*, 8060.
81. Winkler, M.; Sander, S. *J. Org. Chem.* 2006, *71*, 6357.
82. Guyon, C.; Boule, P.; Lemaire, J. *Nouv. J. Chim.* 1984, *8*, 685.
83. Grabner, C.; Richard, C.; Koehler, C. *J. Am. Chem. Soc.* 1994, *116*, 11470.
84. Houdhryn, G. H.; Raham, O. A.; Webster, G. R. B. *Can. J. Chem.* 1987, *65*, 2222.
85. Lazzaroni, S.; Dondi, D.; Fagnoni, M.; Albini, A. *J. Org. Chem.* 2008, *73*, 206.
86. Dichiarante, V.; Fagnoni, M.; Albini, A. *J. Org. Chem.* 2008, *73*, 1283.
87. Lazzaroni, S.; Dondi, D.; Fagnoni, M.; Albini, A. *J. Org. Chem.* 2010, *75*, 315.
88. Fagnoni, M.; Albini, A. *Acc. Chem. Res.* 2005, *38*, 713.
89. Mella, M.; Coppo, P.; Guizzardi, B.; Fagnoni, M.; Freccero, M.; Albini, A. *J. Org. Chem.* 2001, *66*, 6344.
90. Guizzardi, B.; Mella, M.; Fagnoni, M.; Freccero, M.; Albini, A. *J. Org. Chem.* 2001, *66*, 6353.
91. Protti, S.; Fagnoni, M.; Albini, A. *Org. Biomol. Chem.* 2005, *3*, 2868.
92. Fraboni, A.; Fagnoni, M.; Albini, A. *J. Org. Chem.* 2003, *68*, 4886.
93. Protti, S.; Dondi, D.; Fagnoni, M.; Albini, A. *Eur. J. Org. Chem.* 2008, *13*, 2240.
94. Protti, S.; Fagnoni, M.; Albini, A. *J. Am. Chem. Soc.* 2006, *128*, 10670.
95. Dichiarante, V.; Fagnoni, M.; Albini, A. *Angew. Chem. Int. Ed.* 2005, *44*, 5675.
96. Protti, S.; Fagnoni, M.; Albini, A. *Angew. Chem. Int. Ed.* 2007, *46*, 6495.
97. Guizzardi, B.; Mella, M.; Fagnoni, M.; Albini, A. *Tetrahedron* 2000, *56*, 9383.
98. Dichiarante, V.; Fagnoni, M.; Albini, A. *Green Chem.* 2009, *11*, 942.
99. Dichiarante, V.; Fagnoni, M.; Albini, A. *Chem. Comm.* 2006, *28*, 3001.
100. Noma, Y.; Sakai, S. *Organohal. Comp.* 2007, *69*, 405/1.

101. Park, H. R.; Yang, I. J.; Kim, M. S. *Bull. Kor. Chem. Soc.* 1998, *19*, 1265.
102. Klàn, P.; Del Favero, D.; Ansorgovà, A.; Klànovà, J.; Holoubek, I. *Environ. Sci. Pollut. Res.* 2001, *8*, 195.
103. Poster, D. L.; Chian, M.; Neta, P.; Huie, R.; Silverman, J.; Al-Sheikhly, M. *Environ. Sci. Technol.* 2003, *37*, 3808.
104. Chu, W.; Chan, K. H.; Kwan, C. Y.; Jafvert, C. T. *Environ. Sci. Technol.* 2005, *39*, 9211.
105. Ahn, M.-Y.; Filley, T. R.; Jafvert, C. T.; Nies, L.; Hua, I.; Bezares-Cruz, J. *Environ. Sci. Technol.* 2006, *40*, 215.
106. Sun, C.; Zhao, D.; Chen, C.; Ma, W.; Zhao, C. *Environ. Sci. Technol.* 2009, *43*, 157.
107. Wang, C.; Xi, J.-Y.; Hu, H.-Y. *J. Air Waste Manag. Assoc.* 2009, *59*, 386.
108. Wang, C.; Xi, J.-Y.; Hu, H.-Y. *Chin. Sci. Bull.* 2008, *53*, 2712.
109. Wang, Y.; Hong, C. S. *Water Res.* 2000, *34*, 2791.
110. Pera-Titus, M.; García-Molina, V.; Baños, M. A.; Giménez, J.; Esplugas, S. *Appl. Catal. B* 2004, *47*, 219.
111. Lettmann, C.; Hildenbrand, K.; Kisch, H.; Macyk, W.; Maier, W. F. *Appl. Catal. B* 2001, *32*, 215.
112. Oncescu, T.; Nitoi, I.; Oancea, P. *J. Adv. Oxid. Technol.* 2008, *11*, 105.
113. Oncescu, T.; Nitoi, I.; Oancea, P.; Mihai, S.; Lucian, C.; Laurentiu, V. *J. Adv. Oxid. Technol.* 2008, *11*, 149.
114. Wahabi, H. S.; Bredow, T.; Aliwi, S. M. *Chem. Phys.* 2008, *353*, 93.
115. Yin, H.; Wada, J.; Kitamura, T.; Yanagida, S. *Environ. Sci. Technol.* 2001, *35*, 227.

17

Photochemistry of Phosphate and Sulfonate Esters

Davide Ravelli
University of Pavia

Maurizio Fagnoni
University of Pavia

17.1 Introduction

Phosphate and especially sulfonate esters (e.g., triflates, mesylates, and tosylates) are extensively used in organic chemistry, mainly under thermal conditions, with the R groups (in compounds **1** and **2** in Schemes 17.1 and 17.2) being the most important moiety. The phosphate or sulfonate esters act as suitable leaving groups having the exclusive role of activating the R groups for the synthesis of the target compound (R–Nu) and are thus eliminated at the end of the reaction (paths a and b). Actually, the capability of sulfonate esters as leaving groups in aliphatic nucleophilic substitution rivals that of the widely used halogen anions. Moreover, an alcoholic function can also act as a leaving group when transformed into a sulfonate ester and, in the last years, vinyl or aryl sulfonates have attracted increasing attention as the electrophilic partner in metal-catalyzed reactions (Scheme 17.2, path b). By means of this approach, Ar–X bonds (X = C, N) have been easily formed by metal-catalyzed activation of the Ar–O bond [1]. However, this is not the same for phosphate esters, which are virtually unused in the synthesis except when activated by a benzyl or a vinyl group and again under metal catalysis (Scheme 17.1, path a) [2].

Contrary to thermal reactions, the photochemical approach involves the activation of these esters by the use of light. More precisely, in phosphate derivatives (e.g., **1**) the irradiation can cause the cleavage of a C–O bond (R–O in Scheme 17.1), whereas in sulfonate esters (e.g., **2**) either a C–O (cleavage *c*) or a S–O bond (cleavage *d*) can be broken (Scheme 17.2).

In most photochemical processes, however, the R group has the role of protecting the particularly significant ester moiety that is liberated upon exposure to light. Accordingly, the R group is eliminated (as a rearranged or functionalized R″ group), thus acting as a photoremovable ester-protecting group [3a]. The photochemical reactions of phosphate esters are devoted to release stable molecules mainly of biological interest via photocleavage of a C–O bond in a starting precursor (known as caged compound;

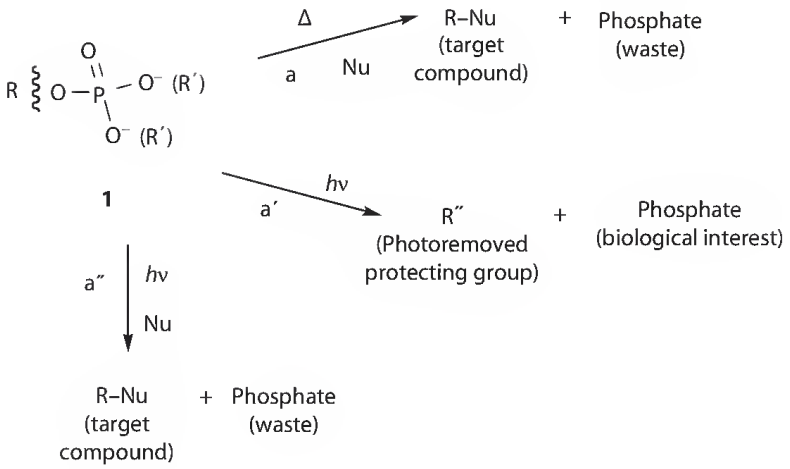

SCHEME 17.1

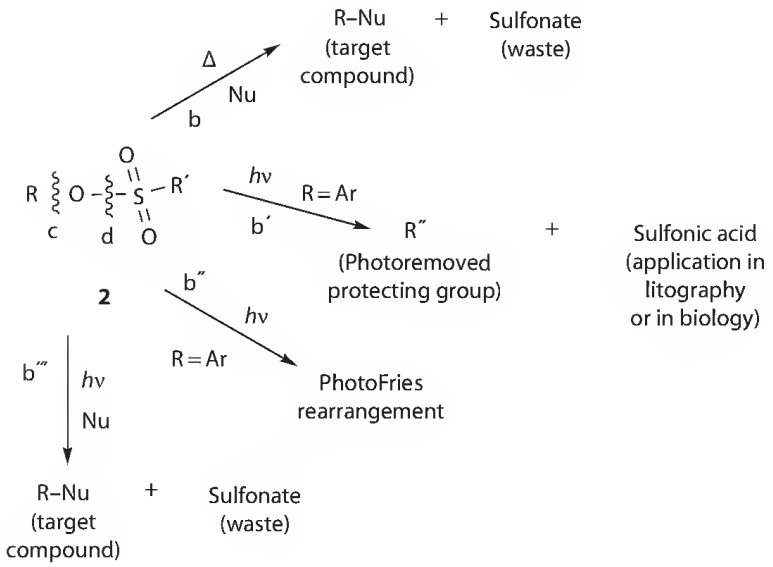

SCHEME 17.2

Scheme 17.1, path a′) [3b]. Alternatively, the sulfonate can be liberated as a free strong sulfonic acid via the photoinduced cleavage of the O–S bond (Scheme 17.2, path b′) in the case of aromatic ester precursors (**2**, R = Ar). These derivatives are commonly called photoacid generators (PAGs) and have found application in photolithography [4] or in biology. The sulfonyl radical formed in the latter process, however, can alternatively react with the other radical species generated from the initial cleavage, leading to photo-Fries rearranged products (Scheme 17.2, path b″). The use of phosphate and sulfonate esters for the synthesis of lead compounds via cleavage of the C–O bond, however, has recently emerged (Scheme 17.1, path a″, Scheme 17.2 path b″), which mainly involves the $S_{RN}1$ reaction of vinyl or aryl phosphates [5] or the S_N1 reaction of aryl phosphates and sulfonates [6]. In rare instances, the cleavage of the R′–S bond has been reported as in the photochemistry of alkyl benzenesulfonates (see Section 3.1).

In conclusion, the aim of this chapter is to review the main paths involved in the photochemistry of phosphate and sulfonate esters, focusing on their application in organic synthesis or in other fields of industrial interest.

17.2 Photochemistry of Phosphate Esters

As stated earlier, the main role of phosphate esters in photochemistry is related to their application as protecting groups. Representative examples dealing exclusively with phosphate ester derivatives, where the C–O bond is cleaved upon direct or sensitized excitation, are discussed here. In the first part, the main classes of photoprotecting groups that liberate the (substituted) phosphates upon UV light irradiation are listed. Many phosphates have a biological functionality (e.g., ATP), that can be released in solution starting from biologically inactive phosphates referred to as "caged molecules" (e.g., caged ATP). These compounds are of fundamental importance in biochemistry, since the delivery of active molecules to living cells is feasible having recourse to an exposure to light. Scheme 17.3 illustrates the main phosphate protecting groups, including the (nitro)benzyl phosphate esters (a), the benzoin esters (b), the (*p*-substituted)phenacyl (c), and methylcoumaryl phosphates (d).

17.2.1 (Nitro)benzyl Phosphates

o-Nitrobenzyl compounds are the most widely known protecting groups for the phosphate function [2,7,8]. The mild deprotection step (no harsh chemical treatment is needed for removal) is well suited with biological conditions and has no remarkable effects on intracellular processes. Accordingly, the *o*-nitrobenzyl compounds are in many cases photoactivable derivatives of biologically significant molecules. Although the photochemistry of these compounds is well known, no exhaustive information about the reaction mechanism is available so far. The first step is thought to be the light-induced tautomerization of the *o*-nitrobenzyl phosphate moiety (as in **3**, Scheme 17.4) to the quinonoid *aci*-nitro tautomer (**4**). As a result, the phosphate and the corresponding nitroso aromatic are formed, probably via the intermediacy of a hemiacetal (**5**).

Some drawbacks in the use of these derivatives have to be stressed, however, including the slow release of the active species, as well as the highly absorbing and reactive side products (e.g., the nitrosoaromatic) formed. Nevertheless, some caged compounds based on *o*-nitrobenzyl esters are commercially supplied as molecular probes [9].

Selected recent new applications are presented here. The first deals with the caged D-erythro-sphingosine 1-phosphate (**6**), which was introduced in cultured cells. UV illumination of this molecule led

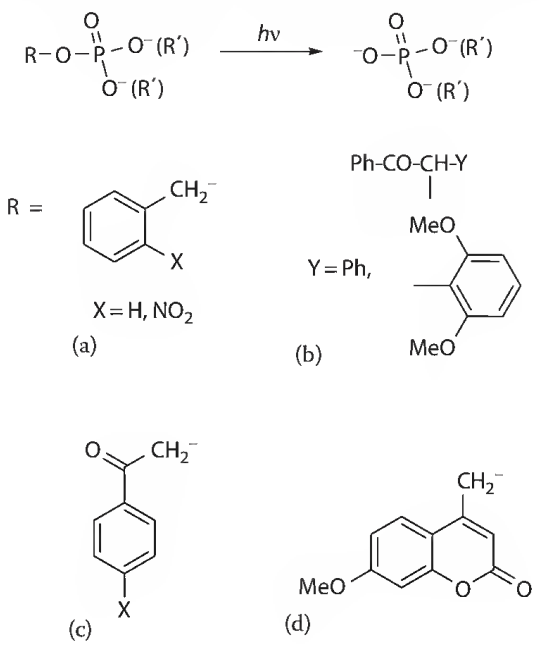

SCHEME 17.3

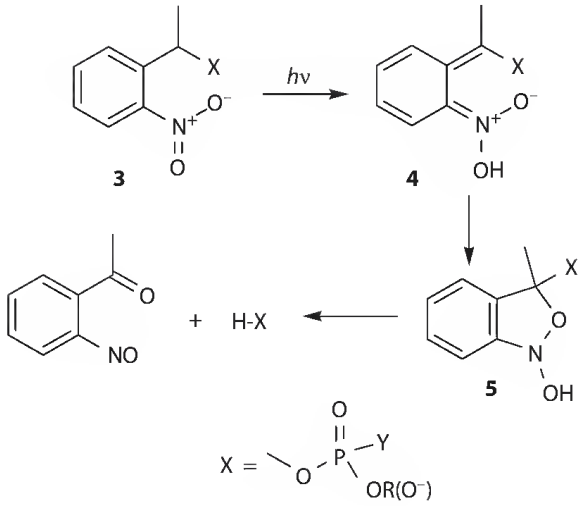

SCHEME 17.4

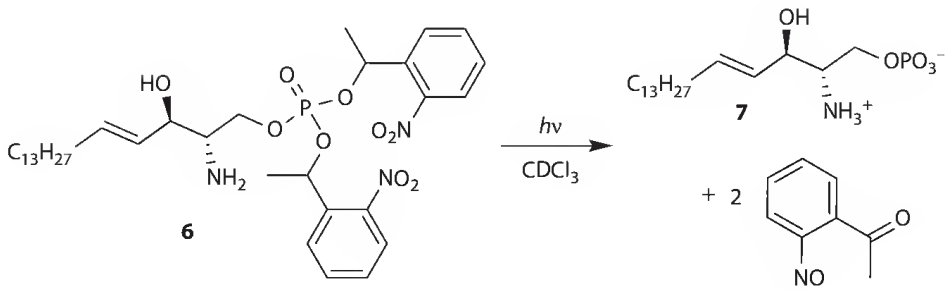

SCHEME 17.5

to the liberation of D-erythro-sphingosine 1-phosphate (**7**) along with two molecules of *o*-nitrosoacetophenone (Scheme 17.5) [10]. This was considered an elegant way to stimulate the DNA synthesis by the enhancement of the intracellular level of **7**.

The release of oligonucleotides from the corresponding caged derivatives is of obvious importance and not trivial since these molecules have to penetrate the lipid membranes of the eukaryotic cells. These derivatives may find application in designing new types of antisense oligonucleotides or investigating the nucleic acid interactions with proteins and other compounds. As an example, the *o*-nitroveratryl moiety was linked to thymidine dinucleotides and thus used as a photolabile protecting group. The presence of two methoxy groups in the aromatic ring markedly increased the absorbance at longer wavelength and 365 nm irradiation was adopted in this case [11].

The phosphate esters of adenine nucleotide analogues (e.g., caged ATP) are likewise widely studied compounds [12] both from the mechanistic point of view [13] and as a means to detect molecular interactions in biological systems. As an example, the interaction between ATP photoreleased from its inactive P^3-[1-(*o*-nitrophenyl)]ethyl ester and bovine intestinal alkaline phosphatase has been studied by reaction-induced infrared difference spectroscopy [14]. This allowed the study of the molecular interactions between the nucleotide and the enzyme in the same cuvette with no interference by the other biological compounds present. Phosphate-related compounds, viz., the phenylphosphonamidate (**8**, Scheme 17.6), can likewise act as precursors of biological compounds [15].

In this case, an *o*-nitrobenzyl photolabile moiety functioned as a linker between a spermine molecule and a solid phase consisting of polyethylene oxide beads. The polyamine used allowed capture of DNA by formation of a complex via strong electrostatic interactions. Such a complex was then completely released using light (365 nm) under very mild conditions (no need for high temperature or acidic/basic

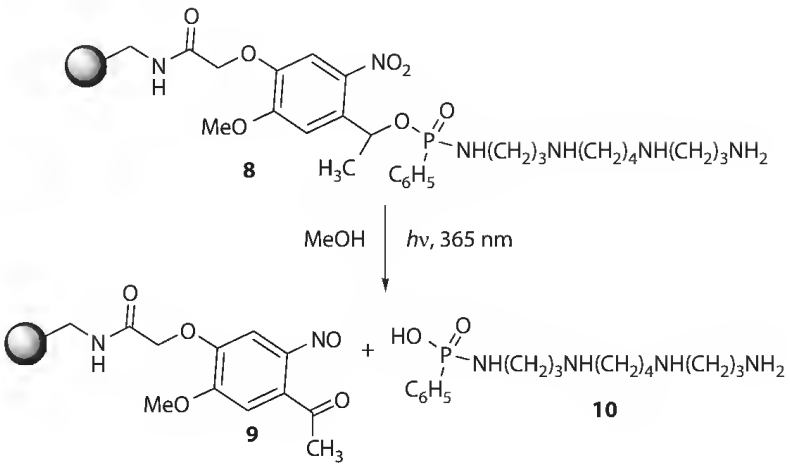

SCHEME 17.6

conditions) [15]. The spermine derivative **10** was completely soluble in the reaction medium contrary to the insoluble supported nitrosoaromatic by-product **9**. The thus obtained controlled release of nucleic acid is of marked importance in several gene transfer applications.

Very recently, a quantitative liberation of inorganic phosphate from α-carboxy-4-nitrobenzyl phosphate caused by an initial photorelease of carbon dioxide has been reported [16].

Benzyl phosphates lacking the *o*-nitro group (as **11**, Scheme 17.7) were found to be likewise smoothly photocleaved, forming various benzyl cation-derived products depending on the reaction medium along with negligible amounts of the corresponding bibenzyls (Scheme 17.7) [7,17–19]. The reaction mechanism changes dramatically from the *o*-nitro analogues since a heterolytic cleavage of the C–OP bond from the ester singlet state is envisaged [7,17–19]. Thus, benzyl ethers **14** and amides **13** (formed from a Ritter reaction between a benzylic cation and MeCN) were obtained in a good yield by using methanol (or butanol) and aqueous acetonitrile, respectively, as the reaction media. Noteworthy, the reaction can lead to C–C bond formation as in the case of the synthesis of benzylated derivative **12** by irradiation of **11** in benzene. Moreover, among the cases examined, the most efficient and clean photofragmentations were those of naphthylmethyl phosphates.

A new class of photolabile *N*-alkyl-4-picolinium phosphate esters has been recently introduced by Falvey and coworkers [20]. The reaction was sensitized by suitable pyrromethene or coumarin-based laser dyes via a photoinduced electron transfer (PET) process. Tungsten lamp (λ > 400 nm, 300 W) irradiation of an acetonitrile solution of phosphate **15**, the sensitizer, and the radical scavenger 1,4-cyclohexadiene caused the reduction of **15** to radical **16**. Quantitative phosphate release then took place with the concomitant formation of the picoline salt **17**, as illustrated in Scheme 17.8 [20].

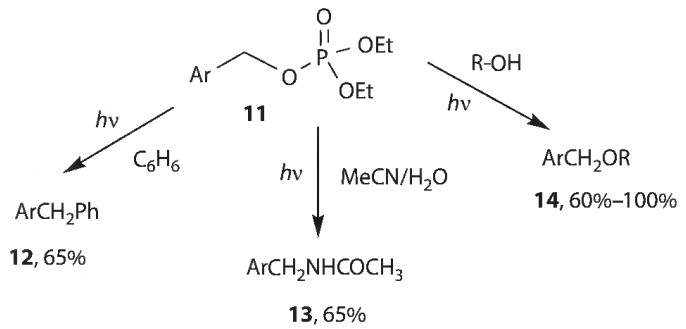

SCHEME 17.7

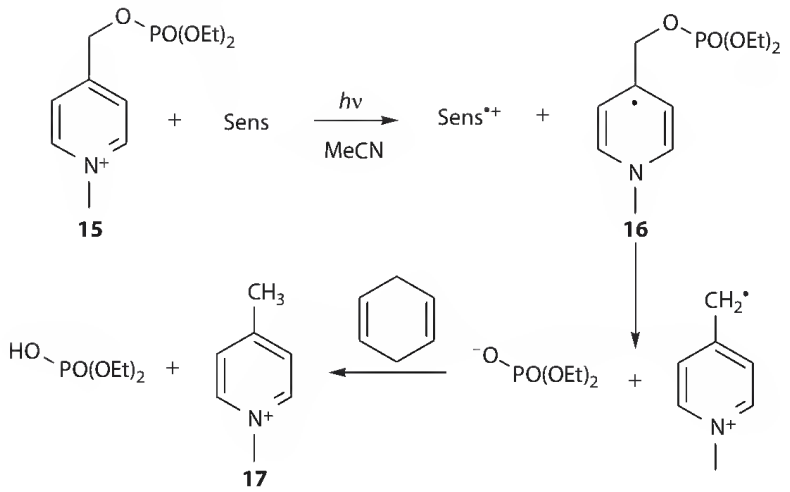

SCHEME 17.8

17.2.2 Benzoin Phosphates

The product distribution obtained in the photolysis of benzoin phosphates depends on the solvent used. Accordingly, irradiation of benzoin ester **18** in MeCN led to the diradical intermediate **19** by a cyclization step; formation of benzofuran **20** besides diethyl phosphoric acid release ensued [17]. On the contrary, in protic media such as aqueous acetonitrile or fluorinated alcohols, a different path was followed where a heterolytic cleavage of the C–O bond took place liberating a phosphate anion with the concomitant formation of triplet cation **21** (Scheme 17.9) [21]. ISC and solvent addition (water in this case) completed the sequence. Interestingly, formation of benzoin **22** or related products was a very minor side reaction in acetonitrile. The mechanism has been recently confirmed by a combined femtosecond transient absorption and nanosecond time-resolved resonance Raman study [22]. This photoreaction thus provides an entry to alpha-keto carbocations (e.g., **21**), an intermediate so far unexploited in organic chemistry.

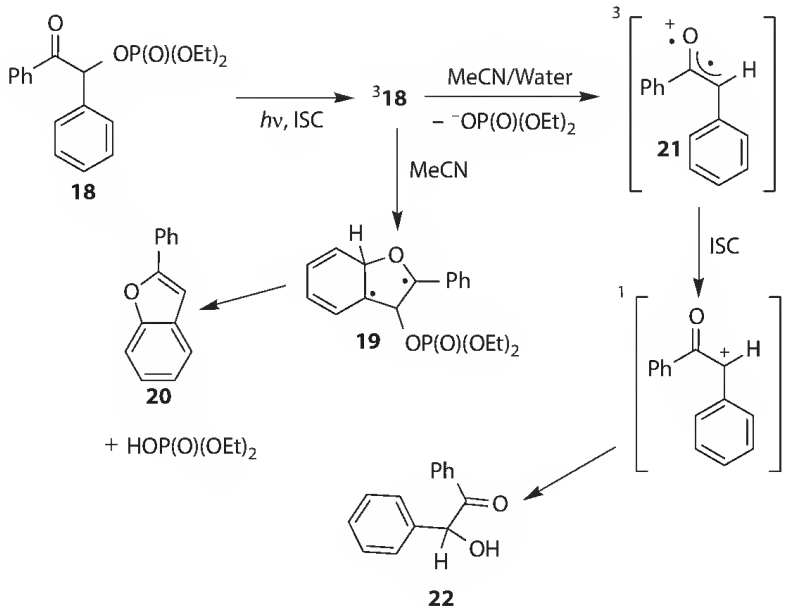

SCHEME 17.9

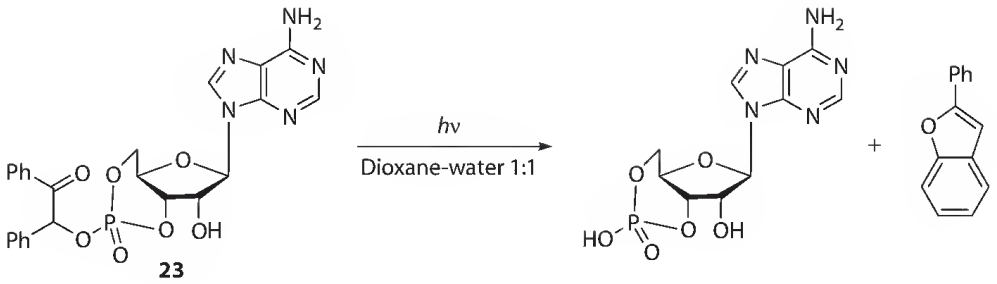

SCHEME 17.10

The type and the position of substituents on the phenyl rings markedly affect the quantum yield of phosphate release. In fact the presence of two methoxy groups in position 3′ and 5′, or 2′ and 3′ induced a fast photocleavage, whereas when in position 2′ and 5′ made the benzoin photostable [23].

Benzoin phosphate esters were exploited as phototriggers for the photorelease of biologically active molecules, such as cAMP as illustrated in Scheme 17.10, where irradiation of desyl "caged" cAMP (**23**) in an aqueous dioxane mixture liberated cAMP, along with phenylbenzofuran, which is biochemically benign [24].

17.2.3 Phenacyl Phosphates

Phenacyl derivatives (e.g., **24**) were later introduced to improve the performance of benzoin derivatives by removing the phenyl moiety from the α position and thus eliminating the stereogenic center present (Scheme 17.11) [25]. The mechanism of phosphate release strongly depends on the substituents present on the aromatic ring (usually in *para*-position with respect to the carbonyl group). With unsubstituted

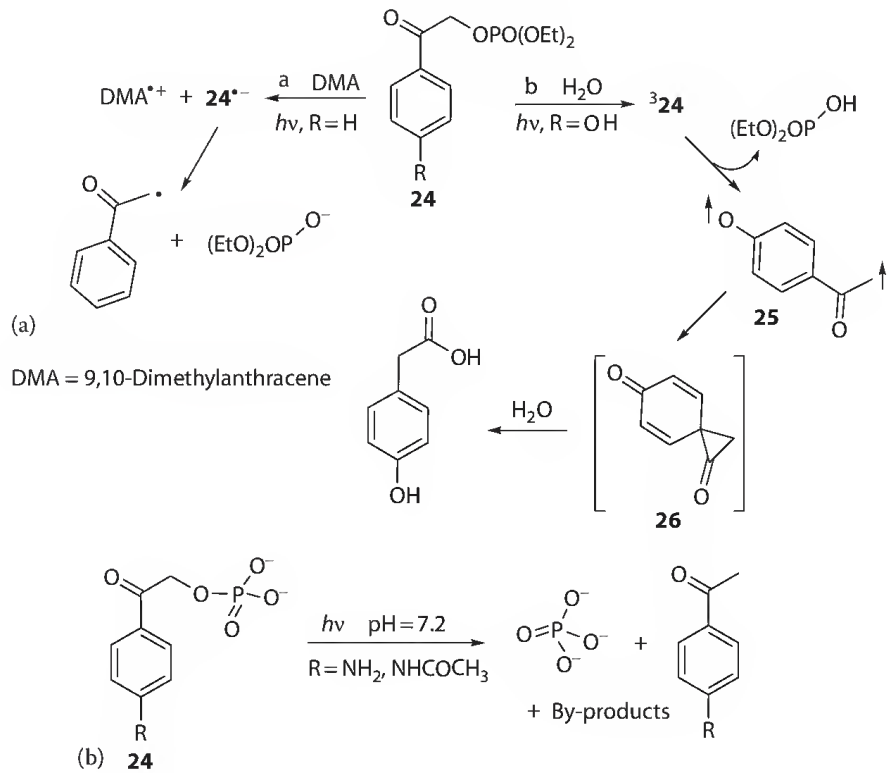

SCHEME 17.11

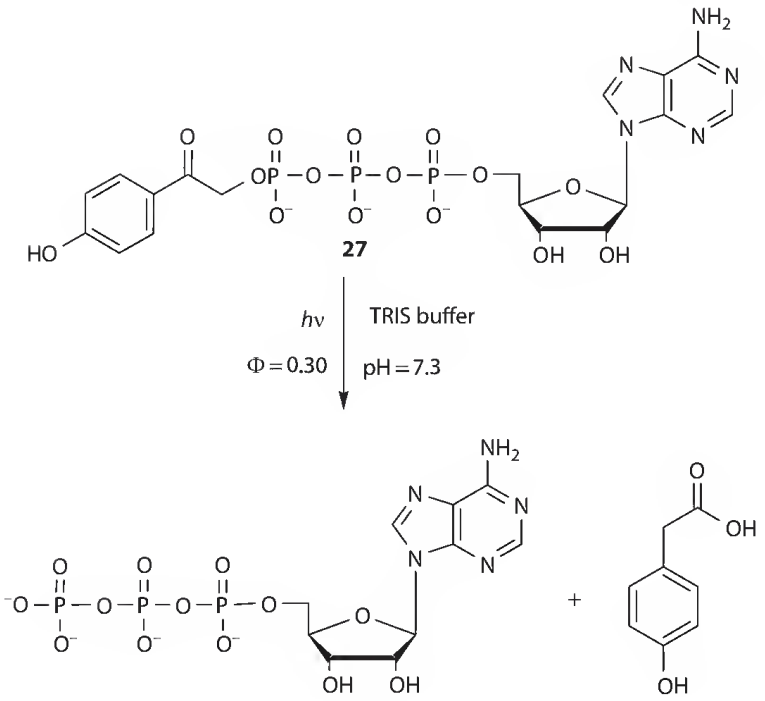

SCHEME 17.12

phenacyl phosphates the liberation of phosphate anion can be induced by a PET process sensitized by 9,10-dimethylanthracene (DMA) as the reductant (Scheme 17.11, path a) [26]. The resulting radical anion **24**$^{\bullet-}$ cleaved, forming the phosphate anion and a phenacyl radical.

An interesting result was found in the photoreactions (λ = 300 nm) in a Tris buffer (pH = 7.2) of phenacyl phosphates having electron-donating groups. In fact, an amino group strongly decreased the photoreactivity of the ester, whereas the reaction quantum yield of acetamido and carbamoyl derivatives was quite high (Φ = 0.34–0.38, Scheme 17.11, part b) [27]. Unfortunately the reaction was not clean since several phenacyl deriving by-products were formed along with acetophenone and phosphate anion (Scheme 17.11, part b). A more clear-cut reaction took place when substituting a methoxy group for the carbamoyl group, since only two products (acetophenone and a rearranged product, namely *p*-methoxyphenylacetic acid) were detected [28].

Moreover, when the phosphate was substituted with a *p*-hydroxyphenacyl group, the aqueous solubility was dramatically enhanced and, apart from the phosphate group, *p*-hydroxyphenylacetic acid was the exclusive photoproduct (Scheme 17.11a). Several investigations have been carried out with the attempt of clarifying the mechanism of this photo-Favorskii process [29]. The reaction sequence is initiated by ^{3}**24** and the phosphate release is concomitant with a water-assisted deprotonation to give the triplet biradical **25**. The spirodienedione intermediate **26** is then formed and hydrolyzed to the phenylacetic acid in aqueous medium [29b]. Apart from the mechanistic importance, the *p*-hydroxyphenacyl group was useful for the liberation of biochemical probes. As an example, ATP was photoreleased from *p*-hydroxyphenacyl-caged ATP (**27**) with a quantum efficiency of 0.30 via the triplet state (Scheme 17.12) [27].

17.2.4 Coumarylmethyl Phosphates

Coumaryl derivatives have been recently introduced as innovative photolabile precursors [17,30], since their UV absorption spectrum has an enhanced redshift with respect to both phenacyl esters and benzoin derivatives. Moreover, coumarylmethyl esters are among the fastest-reacting caged compounds.

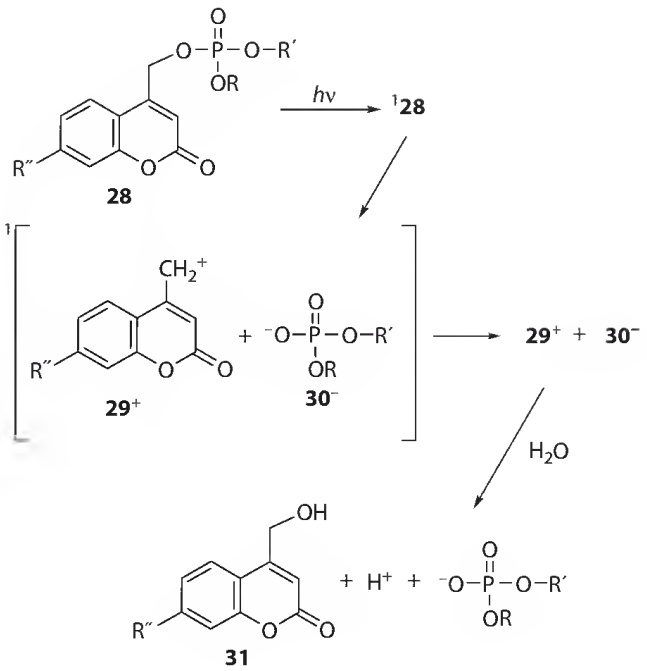

SCHEME 17.13

The cleavage takes place as described in Scheme 17.13, where phosphate **28** is initially excited to the singlet state (^{1}**28**), causing a marked weakening of the C–O ester bond that causes a solvent-assisted photoheterolysis to a singlet ion pair ^{1}[**29**$^+$ + **30**$^-$]. Water trapping by **29**$^+$ forms (coumarin-4-yl)methyl alcohol **31** and liberates an equivalent of phosphoric acid [31].

As for the above, various caged compounds containing the coumarylmethyl moiety have been synthesized. As an example, caged cytidine 5′-diphosphate **32** that contains the photolabile (7-diethylaminocoumarin-4-yl)methyl moiety was prepared (Scheme 17.14) [32]. The release of cytidine 5′-diphosphate (**33**) was used to study the *Escherichia coli* ribonucleotide reductase (RNR) and took place smoothly upon irradiation at wavelengths between 365 and 436 nm (where the RNR is actually transparent). The quantum yield of disappearance of **32** and the rate constant of the formation of **33** have been measured and found to be 0.029 and $2 \times 10^8\,s^{-1}$, respectively [32].

Tailor-made coumarin derivatives have been obtained by varying the substituents on the aromatic ring. As an example, the presence of a bromo substituent in a hydroxycoumarin has the effect of accelerating the ISC of the molecule and at the same time amplifies the acidity of the phenolic OH group [33]. The negative charge of the phenolate group thus imparted a better hydrophilicity to the system increasing its water solubility. Caged cyclic nucleotides with an extinction coefficient >14.000 in the 375 nm region have been devised accordingly [33].

As noted earlier, the phosphate moiety is liberated as a free acid. Since the diethyl phosphate monoacid has a pK_a value of 0.71 [34], coumarylmethyl esters can be viewed as "caged protons," suitable to induce a rapid pH jump in solution when photocleaved. This phenomenon can also have a biological effect, as protons have an active role in cellular signal transduction. Since nitrobenzyl derivatives can have a distinct disadvantage of forming reactive *o*-nitrosocarbonyl by-products, (6,7-dimethoxycoumarin-4-yl)methyl (DMCM) diethyl phosphate as well as [7-(dimethylamino) coumarin-4-yl]methyl (DMACM) diethyl phosphate have recently been tested as valid alternatives [34]. As for the DMACM phosphate, it showed a high extinction coefficient (ε = 16,100 at 386 nm), a release quantum yield of 0.36 and it was used for the study of proton migration along the membrane surface.

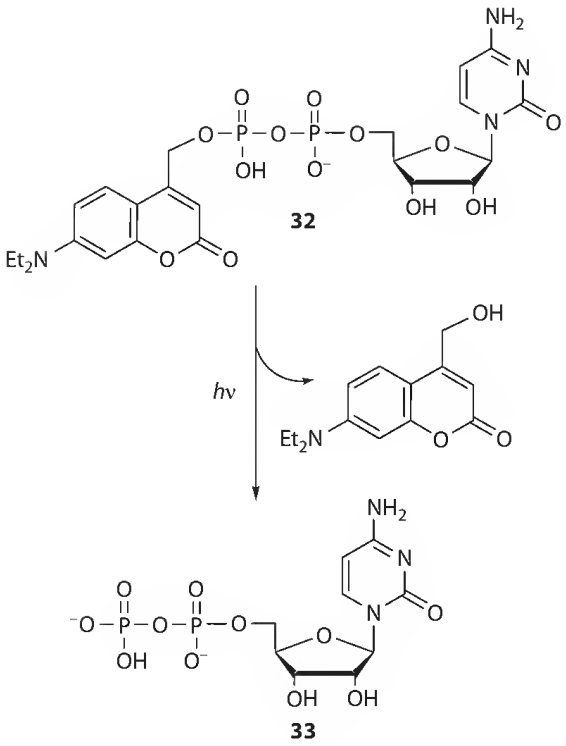

SCHEME 17.14

17.2.5 Aryl Phosphates

Aryl phosphate esters (contrary to the corresponding sulfonates) are not actually used for arylation reactions via the commonly used metal-mediated coupling methodologies [1]. On the contrary, the Ar–OP bond is more labile when irradiated with UV light and this process could have interesting and yet unexploited applications in organic synthesis. The photochemistry of aryl phosphates has been known for 50 years, when Havinga et al. discovered that the photohydrolysis of *m*-nitrodiethylphosphorylbenzene was accelerated by light [35] and this reaction actually opened the path to photonucleophilic aromatic substitutions [36,37]. Depending on the reaction conditions, the predominant cleavage of the P–O (in neat water, Scheme 17.15, path a) or the C–O bond (in alkaline aqueous medium, path b) has been reported [37,38]. *m*-Nitro substituted phosphates were the most reactive isomers among the substrates considered and this laid the basis of a milestone in the photochemistry of aromatics, viz., the so-called "*meta*-effect." Despite the importance of such a discovery, however, only a handful of photosubstitution reactions involving aryl phosphates are known [36].

Contrary to Havinga's experiments on aryl phosphates substituted with an electron-withdrawing group, electron-rich aryl phosphates displayed a different intriguing chemistry. Thus, irradiation in polar solvents (e.g., 2,2,2-trifluoroethanol (TFE) or aqueous acetonitrile) of *N*,*N*-dimethylamino (e.g., **34a**) or

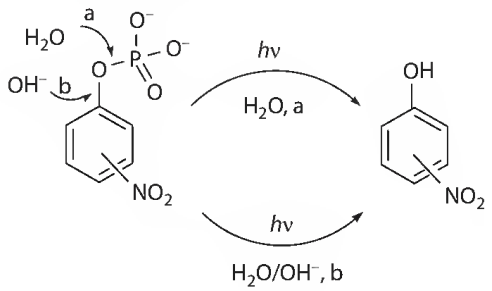

SCHEME 17.15

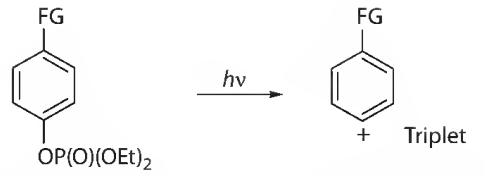

SCHEME 17.16

methoxy-substituted (e.g., **34b**) aryl diethyl phosphates induced heterolysis of the aryl–oxygen bond forming the corresponding aryl cations (**35a**$^+$ and **35b**$^+$, Scheme 17.16) [39]. The importance of this process resides in the fact that the formation of the last species is a rare occurrence thermally, requiring the solvolysis of precursors with limited availability, such as substituted phenyl triflates or (trifluoromethanesulfonyl)oxydienynes [40]. Apart from these disadvantages, under these conditions a rather unselective strong electrophile such as a singlet phenyl cation is formed. Contrary to thermal reactions, the photochemical generation of aryl cations allows their formation in the triplet state, a rather reactive but selective strong electrophile [41]. Accordingly, a new strategy based on ArS_N1 reactions is thus emerging and involves the chemoselective addition of triplet phenyl cations onto suitable carbon nucleophiles to give Ar–C bonds under mild conditions [6,42,43]. Noteworthy, no concurrent cleavage of the O–P bond takes place.

Schemes 17.17 and 17.18 illustrate some examples regarding the reaction of selected nucleophiles with the 4-*N*,*N*-dimethylaminophenyl and 4-methoxyphenyl triplet cations, respectively.

Cation **35a**$^+$ smoothly reacted with cyanide ion in MeCN/H_2O 3:1 forming 4-*N*,*N*-dimethylaminobenzonitrile in 70% yield (Scheme 17.17, path a) [44]. Noteworthy, the large amount of water present in the solvent mixture did not interfere with the reaction (no phenols were formed), but actually favored both the photoheterolytic step and the dissolution of the cyanide salt (KCN). This straightforward synthesis of benzonitriles was thus possible by substituting light for the metal catalyst required for activating the Ar–O bond. Terminal alkenoic acids (e.g., 5-pentenoic acid) were suitable for the construction of oxygen containing five-membered rings, an important structural motif present in many

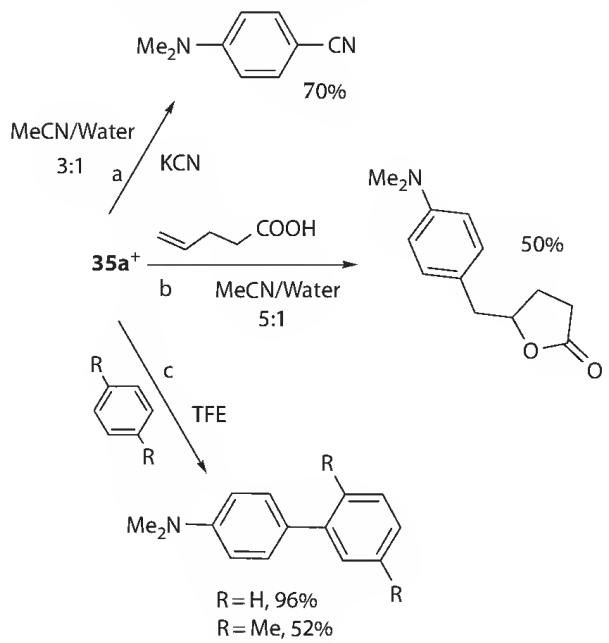

SCHEME 17.17

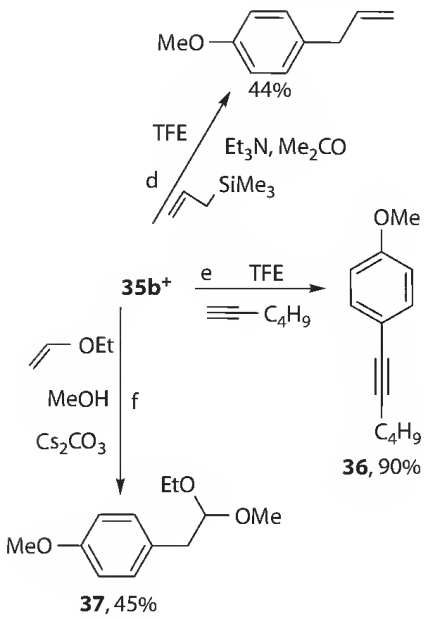

SCHEME 17.18

biologically active natural compounds (path b) [45]. Thus, the electrophilic addition of the phenyl cation onto alkenoic acids occurred efficiently and was followed by an intramolecular attack by the carboxylic group, resulting in the formation of a benzyl substituted γ-lactone (path b) [45]. This one-step procedure mimics the well-known iodo-lactonization reaction and has little precedent under Pd-catalyzed conditions. Electrophilic aromatic substitution-like reactions were also feasible. Accordingly, both benzene [39] or methyl-substituted aromatics (e.g., xylene) [46] could be arylated affording the biaryl derivatives via an Ar–Ar bond formation in 96% and 52% yield, respectively (path c).

Scheme 17.18 illustrates the versatile chemistry of 4-methoxyphenyl cation (**35b**$^+$). Allyltrimethylsilane is one of the most studied nucleophiles, since allyl aromatics can be formed in one step by this route. In this case, TFE must be used as the solvent along with triethylamine as the base. Acetone sensitization (0.9 M) was also needed to increase the reaction efficiency (path d) [39]. A metal-free protocol for the mild alkynylation of aromatic compounds again involves the reaction of cation **35b**$^+$ with terminal alkynes. When 1-hexyne was used, aryl alkyne **36** was formed in 90% yield in TFE (path e). In this case, trapping of **35b**$^+$ by an alkyne resulted in the generation of a vinylenebenzenium ion, which gave **36** after a complete chemoselective deprotonation step [47]. A photochemical multicomponent reaction is a rare occurrence, but irradiation of **34b** in a methanolic solution of ethyl vinyl ether afforded acetal **37** in 45% yield via a three-component reaction (path f) [48].

As evidenced in Schemes 17.17 and 17.18, the arylation was particularly effective when the phosphate group was placed in the *para*-position with respect to the activating group (whether NMe_2 or OMe). Nevertheless, the isomeric *ortho*- and *meta*-methoxyphenyl phosphates likewise underwent the photoheterolysis of the Ar–O bond [49]. In the latter case, however, the triplet phenyl cation formed easily underwent an ISC process to the more stable singlet cation and the subsequent solvolysis reaction became more competitive [41,49].

Scheme 17.19 illustrates this quite interesting new "*meta*-effect" in photochemistry, which, contrary to Havinga's reaction, does not involve the multiplicity of the excited state but that of the intermediate formed upon photolysis [49]. Thus, irradiation of phosphate **38** in TFE in the presence of benzene led to the expected arylation product **39** in 34% yield. The high stabilization of the triplet cation formed, however, allowed ISC to give the singlet cation that gave the trifluoroethylether **40** in 25% yield by solvent addition.

A different approach for the phosphate group release in aryl phosphates relies on the $S_{RN}1$ reaction. This is a well-known process that mainly allows the formation of new C–C bonds by photostimulation

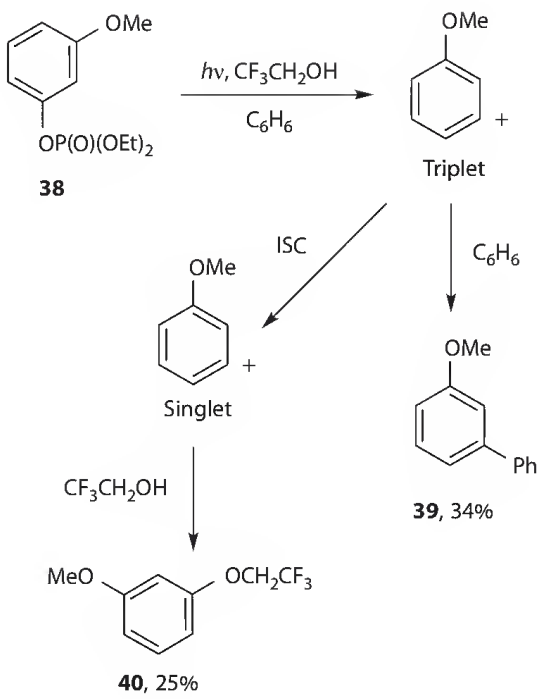

SCHEME 17.19

of a mixture containing an aryl-X (or vinyl-X) derivative (mostly X = I, Br) in the presence of a strong nucleophile (mainly an enolate anion) [5,43]. The phosphate ester can act as the leaving group of the reaction, though this is seldom used [5]. Most of the reported examples deal with the use of tin anions (Me_3SnNa or Ph_3SnNa) as electron donors for the formation of new interesting C–Sn bonds. Accordingly, various arylstannanes were accessible starting from aryl diethyl phosphate esters [50–54]. Methoxy group substituents present in the aryl esters were tolerated easily in the reaction, whereas if a halogen (I, Br, Cl) was also present, this resulted in substitution along with the phosphate ester group [51].

As an example, Scheme 17.20 illustrates the synthesis of 2,7-bis(trimethylstannyl)naphthalene (**43**) from the corresponding alcohol **41**. 2,7-Dihydroxynaphthalene (**41**) was first transformed in the

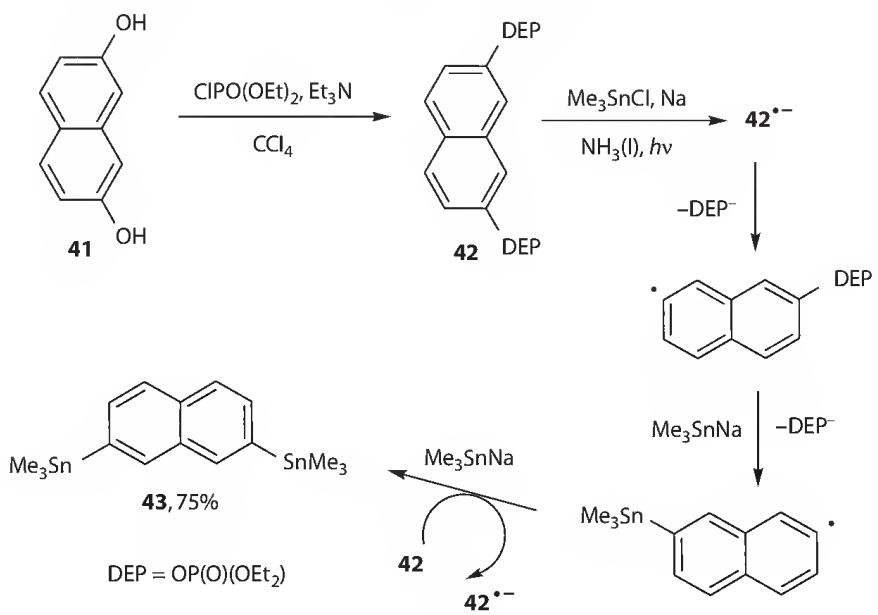

SCHEME 17.20

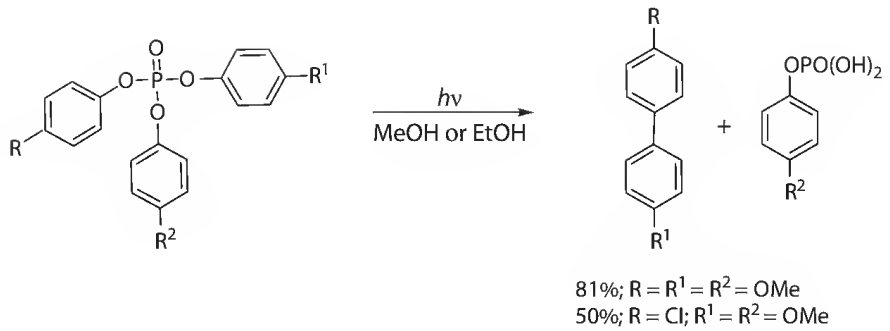

SCHEME 17.21

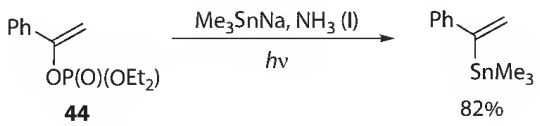

SCHEME 17.22

diester **42**, which underwent an $ArS_{RN}1$ process. Stannane **43** was then isolated by two consecutive substitutions of the phosphate ester by a tin nucleophile [54].

If the phosphate ester is substituted with more than one aryl group, a different photochemistry results [55,56]. Biaryl or triarylphosphates may seem unusual starting materials for the synthesis of biphenyls. Nevertheless, the photolysis of triaryl esters in alcoholic solvent formed a biaryl derivative with the concomitant elimination of a monoaryl phosphate [55]. The reaction, one of the rare examples of metal-free formation of an Ar–Ar bond, was satisfactory and clean only when at least two aryls bore a methoxy group as depicted in Scheme 17.21.

Moreover, the amount of biphenyl formed could be increased by adding water to the reaction mixture [55c]. Alkylbiaryl phosphates can be likewise employed [55b]; the formation of biphenyls is similar to that reported for triarylphosphates and involves an intramolecular excimer, generated from the singlet state of the starting ester. On the contrary, a cationic migration of the aryl group to a neighboring olefinic moiety was postulated when irradiating alken-1-yl aryl methyl phosphates, where a mixture of arylalkanones and aryl alkenyls was usually formed [56].

17.2.6 Vinyl Phosphates

In rare instances the $S_{RN}1$ reaction can also be applied to vinyl phosphate esters (e.g., vinyl diethyl phosphates) obtained from the corresponding ketones under thermodynamic- or kinetic-controlled enolization. New tin–carbon bonds were formed under photostimulation of a liquid ammonia solution of triorganostannyl anions (e.g., sodium trimethylstannide) and the vinyl phosphate. The reaction is of significant interest, since vinyl stannanes are useful intermediates in metal-catalyzed reactions. Unfortunately, this regioselective substitution reaction seemed to apply only to conjugated vinyl phosphates such as **44** (Scheme 17.22) [57] or (diethoxyphosphoryl)oxy-1,3-cyclohexadienes [58].

17.3 Photochemistry of Sulfonate Esters

As mentioned in Section 17.1, sulfonate esters can be both used as photoremovable protecting groups (e.g., of a hydroxy group) and as PAGs, where a sulfonic acid is liberated in the process. The photochemistry of these esters varies according to the type of sulfonates investigated. It is only recently that aryl esters have been employed in organic synthesis for metal-free formation of Ar–C bonds. The photolysis of alkyl (mainly benzyl) or phenyl sulfonate esters [43] will be briefly described here.

17.3.1 Aliphatic Sulfonates

Alkyl arenesulfonates of general formula Ar–SO_2–OAlkyl can undergo a photochemical cleavage either of the Ar–S or the S–OAlkyl bond depending on the reaction conditions, as summarized in Scheme 17.23.

Izawa and Kuromiya reported that, in the irradiation of methyl benzenesulfonate in methanol (Ar = Ph, Alk = Me in Scheme 17.23), three products were detected, viz., benzene (34%), biphenyl (10%), and anisole (traces) with a $\Phi = 0.07$ [59]. The authors postulated a scission of the Ar–S bond (Scheme 17.23, path a) from the excited singlet state of the starting sulfonate. The formation of the Ar· accounted for the formation of benzene (via hydrogen abstraction) and biphenyl (via radical coupling). The small amount of anisole arose from the radical coupling between an alkoxy and an aryl radical via the a → a′ → a″′ sequence. Homolytic fragmentation of the S–OAlk bond was excluded (Scheme 17.23, path b) since no aryl radical could be formed in such a case because the sulfur dioxide loss from $ArSO_2^{\bullet}$ was estimated to be largely endothermic and, moreover, no sulfonic anhydride derivatives, such as $ArSO_2$–SO_2Ar, were detected.

A similar behavior was reported in the photolysis of several alkyl arenesulfonates in different solvents where the corresponding aliphatic alcohols (Alk–OH) were isolated in good yields [60]. Accordingly, the cleavage of the Ar–S bond was followed by SO_2 elimination from $Alk-OSO_2^{\bullet}$ (path a′) ensued by hydrogen abstraction from the reaction medium (path a″). The presence of a base caused a more efficient and cleaner reaction [60]. On the other hand, in benzene, biphenyls arising from aryl radical addition onto the solvent were also detected.

The leaving group capability of sulfonate esters under photolytic conditions has been employed in the photodeprotection of the alcoholic groups (protected as tosylate esters) in carbohydrates. A dated example deals with the photodeprotection at room temperature of the tosyl group of methyl 6-*O*-tosyl-α-D-glucopyranoside in a methanolic solution of a base, such as sodium methoxide. After 5 h irradiation the parent methyl-α-D-glucopyranoside was recovered in 90% yield [61]. Further studies demonstrated that the first step of the reaction involves an electron transfer process between the sulfonate ester and the base forming the radical anion of the ester (Scheme 17.23, path c); the following cleavage of the S–OAlk bond liberates the alkoxyde anion, which, upon protonation, releases the desired sugar (paths d and e). As expected, the process was accentuated by increasing the electron-donating property of the base. Aliphatic amines such as DABCO, Et_3N, and *i*-Pr_2NEt_2 could be used since the ΔG_{et} between the singlet excited state of the protected sugar and the amine was apparently exoergonic (by ca. 23 kcal/mol) [62]. The mechanism was confirmed by laser flash photolysis studies, which detected both the DABCO

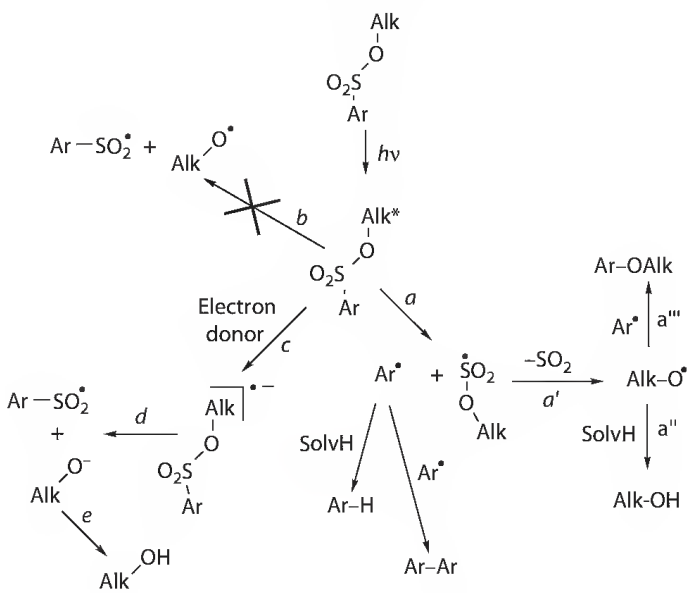

SCHEME 17.23

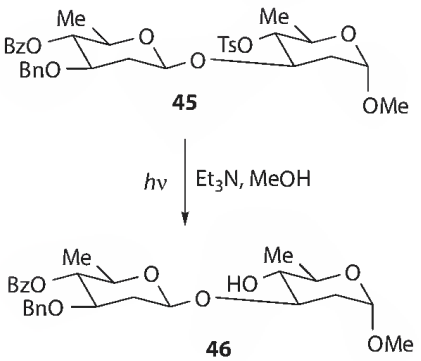

SCHEME 17.24

radical cation and the *p*-tolylsulfonyl radical [62]. Hydroxide anion can also be used as the base, however, as seen in the quantitative detosylation of 1,2:3,4-di-*O*-isopropylidene-6-*O*-(*p*-tolylsulfonyl)-α-D-galactopyranose when irradiated in methanol in the presence of excess NaOH (2.5 equiv.) [62]. An elegant application of this photodeprotection procedure was reported in the synthesis of mithramycin analogues starting from compound **45**, which has three orthogonal OH protecting groups (Scheme 17.24) [63]. The tosyl group was selectively removed to afford **46,** by irradiation of a methanolic solution of **45** (triethylamine as the electron donor) eliminating the need for acidic or basic conditions, which could have removed the other OH protecting groups. Prolonged irradiation, however, caused a partial loss of the benzyl group (Bn) [63].

In some cases, the liberation of the sulfonic group takes place as the secondary step of a photoreaction, as in the benzoin derivative **47** (Scheme 17.25) [64]. In this case, the reaction was initiated by a C–C homolysis of the **47** triplet state, yielding a benzoyl and an α-hydroxy-α-sulfonyloxymethylbenzyl radical. The latter radical rearranged to the phenacyl radical **48** with the concomitant liberation of methanesulfonic acid. Heterolytic cleavages were ruled out by the positive radical-trapping experiments. Actually, sulfonate **47** acted as a photoacid radical generator (PARG), which was able to initiate both a radical polymerization and a polycondensation simultaneously. As an example, derivatives such as **47** were useful as initiators in photocuring processes [65].

17.3.1.1 (Nitro)benzyl Sulfonates

Both *ortho*- and *para*-nitrobenzyl sulfonates (or sulfates) have been largely applied as PAGs [66–68] in chemically amplified deep UV (248 nm) photoresists [4,69,70]. Contrary to other PAGs (e.g., triphenylsulfonium salts), these derivatives have the advantage of being less polar and, accordingly, do not tend to phase separate when present in polymer matrices [69]. Unfortunately, the quantum yields of decomposition of these esters were not high enough, in fact never exceeding 0.16 [69]. The mechanism of acid release in nitrobenzyl sulfonates depends on the position of the nitro group on the aromatic ring (*ortho*- or *para*-). In the former case, the mechanism is common for other *o*-nitrobenzyl derivatives and involves

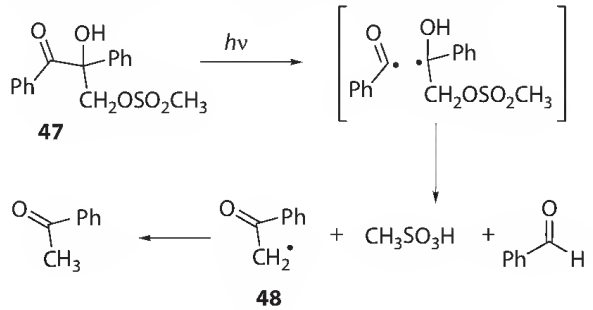

SCHEME 17.25

a photoenolization step followed by formation of the *o*-nitrosoaromatic derivative and liberation of the sulfonic acid (see Scheme 17.4, X = R–SO_3) [70].

These PAGs were also used in rapid biomedical release applications [71] or to study the effect of a fast pH decrease on protein conformational changes, as well as to investigate protein folding driven by protonation of carboxylate side chains. Unfortunately, in the previous case the *o*-nitrosobenzaldehyde formed during the process could be oxidized under the photolytic conditions and the carboxylic acid thus formed could interfere with the FTIR measurement used to follow this phenomenon. Since the changes to the resulting IR absorbance of the PAG should be as minimal as possible after irradiation, a sulfate (e.g., the 1-(*o*-nitrophenyl)ethyl sulfate, $\Phi = 0.47$) was therefore employed as a new caged proton [72]. The large pH jump obtained with this system was able to induce a partial unfolding of metmyoglobin [72].

Unlike *o*-nitrobenzyl esters, the corresponding *p*-nitro derivatives do not dissociate upon photolysis since they do not contain a benzylic carbon–hydrogen bond *ortho*- to the nitro group. Nevertheless, photoinduced monoelectronic reduction of *p*-nitrobenzyl esters causes the release of the sulfonate group from the intermediate radical anion. The process can take place inter- or intramolecularly as depicted in Scheme 17.26. In the first case (Scheme 17.26, part a), compound **49** functioned as a photoactivable surfactant since a hexadecyl sulfonate group was photoreleased by means of a PET reaction with 2-ethyl-9,10-dimethoxyanthracene (**50**) [73]. The process was investigated for the photoinduced interfacial adhesive forces modification induced by the surfactant in photosensitive imaging systems [73].

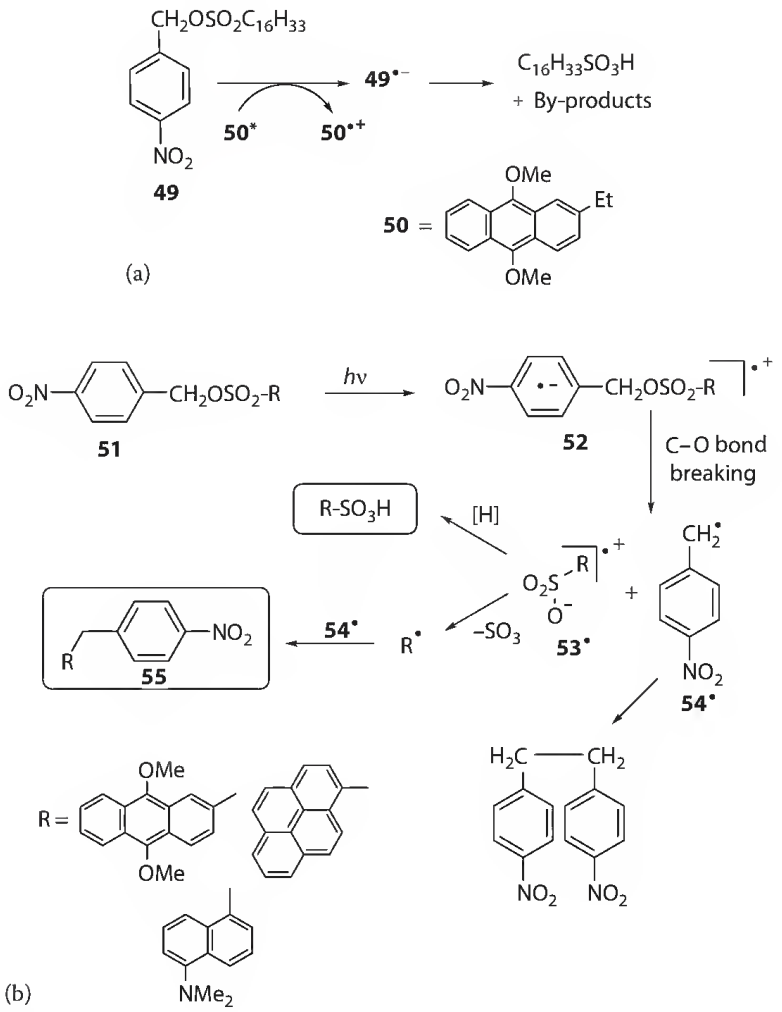

SCHEME 17.26

Intramolecular electron transfer processes, however, can be induced by tethering an appropriate donor moiety to the *p*-nitrobenzyl sulfonate group [74]. As a result, a C–O cleavage takes place (from **52**, see Scheme 17.26, part b) if it is competitive with the deactivation of the lowest singlet excited state of the aromatic sulfonyl moiety in **51**. Apart from the rate of the intramolecular electron transfer process, the factors that affect the photocleavage rate are the feasibility of C–O bond scission and the stability of the benzyl-type radical formed **54**• [74a,b]. The first donor investigated was 9,10-dimethoxyanthracene in *p*-nitrobenzyl 9,10-dimethoxyanthracene-2-sulfonate [74a,b]. The photocleavage led to radical **54**• (that in turn dimerized) and to the sulfonate radical **53**•. The latter radical either formed the corresponding sulfonic acid or lost sulfur trioxide, thus generating a phenyl radical that, in the event, coupled with **54**• to give the diarylmethane **55**.

In the effort to design more efficient PAGs, *p*-nitrobenzyl sulfonate esters linked to donors having a lower oxidation potential than 9,10-dimethoxyanthracene were next tested [74c]. Accordingly, it was found that upon irradiation, *p*-nitrobenzyl 5-dimethylaminonaphthalene-1-sulfonate and *p*-nitrobenzyl pyrene-l-sulfonate dissociated more efficiently ($\Phi = 0.16–0.20$) with respect to the previous anthracene-based sulfonate studied.

Benzoin 4-substituted benzenesulfonates were likewise used as PARGs. Thus, the crosslinking of a film of 3-acryloxypropyl trimethoxysilane containing 1% of the sulfonate smoothly took place upon UV irradiation. The photocuring process induced a concomitant polymerization of the acrylate units and a polycondensation of the trimethoxysilane groups, as demonstrated by FT-IR and Raman spectroscopy analyses [75].

In Section 2.4 the photoreactivity of coumarylmethyl phosphate derivatives was described. Similar (coumarin-4-yl)methyl sulfonates (and sulfates) have been devised for the photogeneration of a strong acid in solution (e.g., methanesulfonic acid). The cleavage also occurred by photosolvolysis of the $RCH_2–OSO_2X$ bond (see again Section 2.4) [76]. Sulfonates have been demonstrated to be better leaving groups than phosphates and this was rationalized mainly by the different pK_a values of the acids released. The pK_a value for methansulfonic acid (–1.54) is lower than that of diethyl phosphoric acid (0.71) and the sulfonate derivatives exhibit a higher photoreactivity, accordingly. As a result, the quantum yield of release of (7-methoxycoumarin-4-yl)methyl sulfonate ($\Phi = 0.08$) was measured and found to be roughly twice as much of the corresponding diethyl phosphate ($\Phi = 0.037$) [76]. Substituting a *N,N*-dimethylamino group for a methoxy group in the coumarin ring gave a highly photosensitive compound with both a high extinction coefficient (17,100 at 388 nm) and a high photoacid generation quantum yield (0.79) [34].

17.3.2 Aryl Sulfonates

Aryl sulfonates, whether $Ar'–SO_2–O–Ar$ or $Alkyl–SO_2–O–Ar$, generally lose the sulfonyl group when exposed to UV light with a mechanism that may change according to the ester structure. Thus, aryl sulfonates (similarly to aryl phosphates, Section 2.5) can be interesting triplet phenyl cation precursors, provided that the aromatic ring bears an electron-rich substituent (again a OMe or a NMe_2 group) [39]. The efficiency of formation of these cations depends mainly on the sulfonate used, since the photo-Fries process can compete in some cases (see the following). As an example, aryl tosylates were found unsuitable for the phenyl cation chemistry since no arylation occurred starting from 4-dimethylaminophenyl tosylate and low arylation yields were obtained from 4-methoxyphenyl tosylate [39]. On the contrary, aryl-substituted mesylates and triflates were successfully used, as shown in Schemes 17.27 and 17.28. 4-Methoxyphenyl mesylates and triflates gave the corresponding 4-methoxyphenyl cation that was used in some arylation reactions, such as those forming estragole **56** (quantitative yield, Scheme 17.27, path a) [39], aryl alkynes (**57** and **58**, path b) [47], and a benzyl lactone (**59**, path c) [45].

4-Dimethylaminophenyl cation was only photochemically generated with the use of mesylate **60**, since the corresponding triflate led almost exclusively to the photodeprotection of the triflate group [39]. Typical arylation reactions are shown in Scheme 17.28 and involve the synthesis of

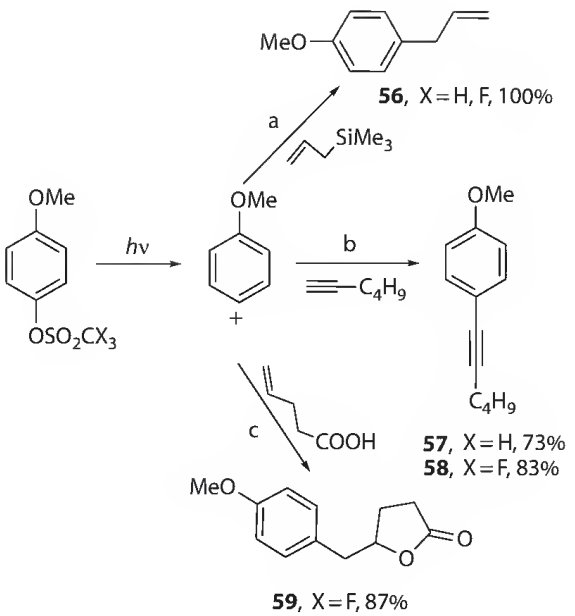

SCHEME 17.27

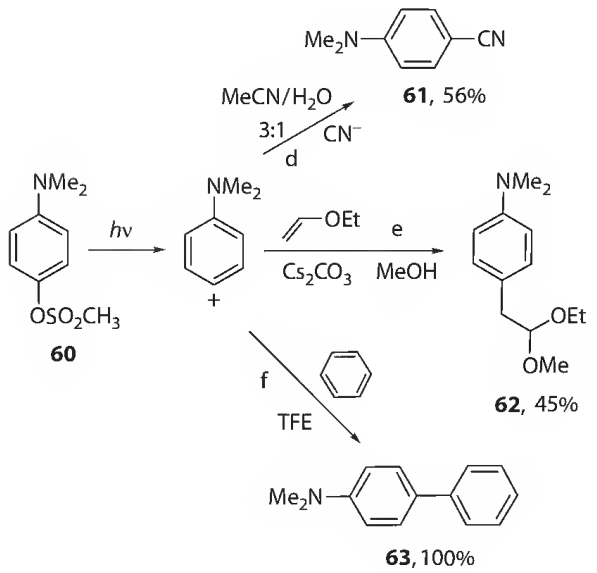

SCHEME 17.28

4-*N*,*N*-dimethylaminobenzonitrile (**61**, 56% yield, path d) [44], β-aryl acetal (e.g., **62**, 45% yield, path e) [48], and 4-*N*,*N*-dimethylaminobiphenyl (**63**, 100% yield, path f) [39].

Recently, an optimization of the arylation process by using the environmental indexes of the EATOS method has been reported [77]. It was demonstrated that substitution of TFE with an acetonitrile–water mixture as the reaction medium markedly improves the eco-sustainability of the arylation process. Interestingly, the synthesis of biaryl **65** starting from mesylate **64** was found to be more environmentally benign if compared to other thermal or photochemical alternatives (Scheme 17.29) [77]. Notably, in this case the solvent was found to be the main contributor to the environmental impact.

An intramolecular formation of Ar–Ar bonds mimicking the phenyl cation chemistry was reported about 20 years ago. Thus, the triflate ester of the commercial pesticide 5-chloro-2-(2,4-dichlorophenoxy)

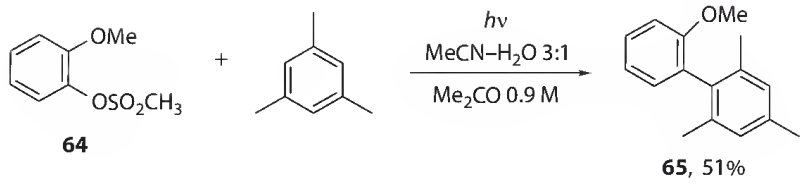

SCHEME 17.29

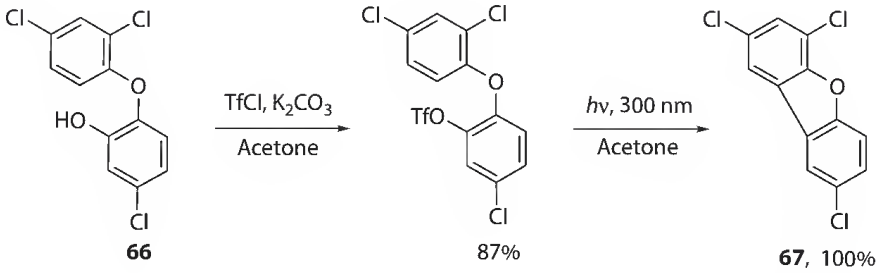

SCHEME 17.30

phenol (Irgasan DP300, **66**), when irradiated at 300 nm in acetone, gave 2,4,8-trichlorodibenzofuran (**67**) quantitatively. A triplet sensitized photolytic cyclization via triflate anion loss was invoked in this case (Scheme 17.30) [78].

Aryl sulfonates substituted with strong electron-withdrawing groups, such as fluorine, showed a peculiar chemistry when irradiated in neat aromatics (e.g., benzene or other various alkyl substituted benzenes). Thus, photolysis of a benzene solution of a pentafluorophenyl perfluoro- or a polyfluoroalkanesulfonate afforded the corresponding pentafluorobiphenyls in high yields [79]. The authors postulated an initial photoinduced electron transfer between the electron-deficient arene and the (alkyl) benzene. The mechanism is shown in Scheme 17.31 for the photoreaction between pentafluorophenyl triflate (**68**) and toluene (**69**). A radical ion couple was initially formed and then fragmentation of the radical anion generated a pentafluorophenyl radical that added to **69**$^{\bullet+}$. Both *ortho*- and *para*-isomers of pentafluorophenyl toluene were thus formed with a poor regioselectivity but with a high mass balance (86%) [79]. Since neither benzylpentafluorobenzenes nor bibenzyls were obtained in this reaction, a proton transfer within the radical ion pair was ruled out due to the low basicity of **68**$^{\bullet-}$.

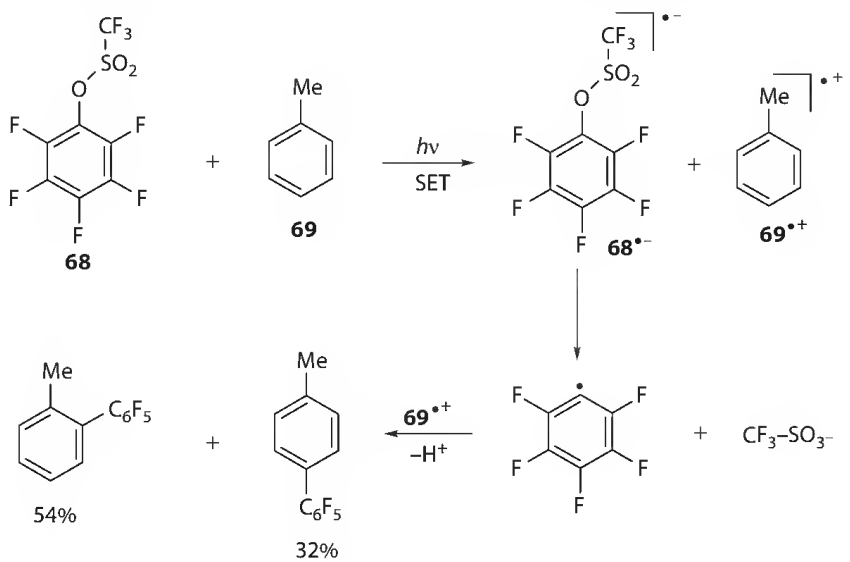

SCHEME 17.31

17.3.2.1 Photo-Fries and Related Reactions

Originally, the photo-Fries reaction of sulfur-containing compounds was described by Havinga and coworkers. They evidenced that UV exposure of phenyl (or α-naphthyl) *p*-toluenesulfonates as well as phenyl methanesulfonate formed a mixture of rearranged *o*- and *p*-hydroxyphenyl sulfones, along with variable amounts of phenol [80]. The reaction is initiated by a photoinduced homolytic S–O scission with a radical pair formation (Scheme 17.32). The phenoxy radical thus formed can lead to phenol (by hydrogen abstraction) or, in alternative, recombination with the sulfonyl radical may give the two sulfone isomers via cyclohexadienone intermediates [81]. The product distribution was strictly dependent on the solvent used; being benzene the medium, the *ortho*-isomer was preferentially formed as shown in Scheme 17.32 for the case of phenyl benzenesulfonate (**70**) [81]. Interestingly, in alcoholic media the *para*-isomer was by far the main product.

A more clear-cut reaction was found if a complexing agent such as a β-cyclodextrin was either present in solution or formed a solid complex with the sulfonate ester [82]. In the former case, the irradiation of a β-cyclodextrin/water 1:5 solution of **70** led to the two photo-Fries adducts with no phenol formation. Noteworthy, in the photoreaction of the solid complex, a regioselective reaction took place, the *ortho*-rearranged derivative being the exclusive product [82].

The photo-Fries approach can be a mild, Lewis-acid-free, useful tool for the formation of Ar–S bond in heteroaromatic derivatives such as carbazoles. Accordingly, the photolysis in methanol of the mesylate ester of 9*H*-carbazol-2-ol (**71**) gave 1-(methylsulfonyl)-9*H*-carbazol-2-ol (**72**), 3-(methylsulfonyl)-9*H*-carbazol-2-ol (**73**) along with some hydroxycarbazole (**74**) in a ratio 6:2:1 (Scheme 17.33, part a). Moreover, the product distribution was not affected by changing the polarity of the medium [83].

8-Quinolinyl benzenesulfonates such as **75** likewise underwent homolytic cleavage of the S–O bond when photolyzed at 300–330 nm [84a]. The reaction was quite clean and both 8-quinolinol and benzenesulfonic acid were formed with negligible formation of by-products (Scheme 17.33, part b). The reaction involved the excited triplet state of **75** as confirmed by the high efficiency found in the benzophenone-sensitized photocleavage of this sulfonate. Also in this case, a radical couple was initially formed (see Scheme 17.32) and when a small amount of Et_3N was present in solution, its hydrogen transfer ability avoided the radical recombination, thus largely increasing the quantum yield of the reaction (up to 7–8 fold) [84a]. This protocol was then applied in the field of photocleavable biotin linkers that allowed the isolation of specific receptors by a photoinduced separation of the avidin matrix (as the avidin–biotin

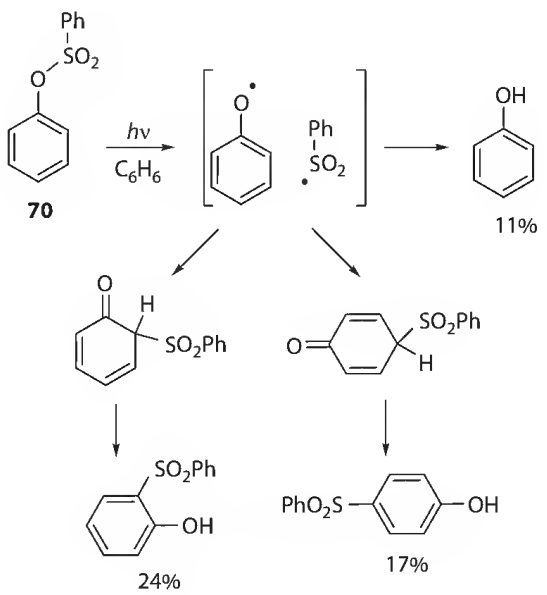

SCHEME 17.32

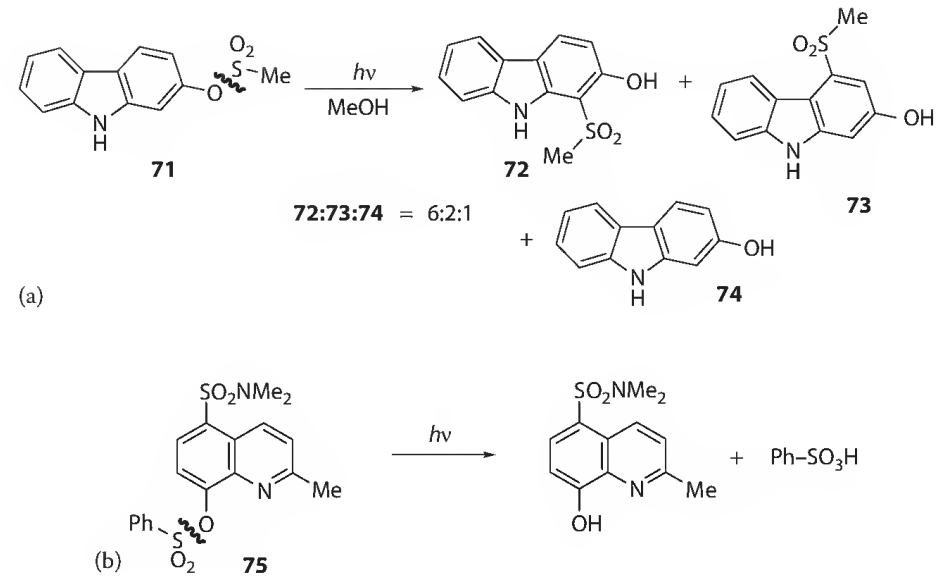

SCHEME 17.33

complex) from the originally linked ligand–receptor complexes [84b]. The advantage of this approach is due to the mild conditions used, since the process took place without the need for any aggressive reagents.

Non-Fries pathways in aryl sulfonate photochemistry have led to acid generation, an interesting phenomenon widely used in microlithography [4]. These sulfonates (e.g., tris(methanesulfonyloxy)benzene) [85] were easily prepared, were soluble in a wide range of solvents (nonionic in character), and showed an UV absorption suitable for deep-UV exposure. Recently, Scaiano et al. [86] investigated the photochemical behavior of some phenyl sulfonates and the results are resumed in Scheme 17.34 (R = methyl, benzyl, tolyl).

Both H_2SO_3 and H_2SO_4 were released in solution as confirmed by ion chromatography analysis. These acids arose from the ensuing reactions of the radical pair that escaped from the solvent cage (Scheme 17.34). The scenario in Scheme 17.34 was further supported both by detection of the phenoxyl radical by laser flash photolysis experiments and by the presence of a large amount of non-Fries rearrangement products, that mainly accounted for the overall mass balance.

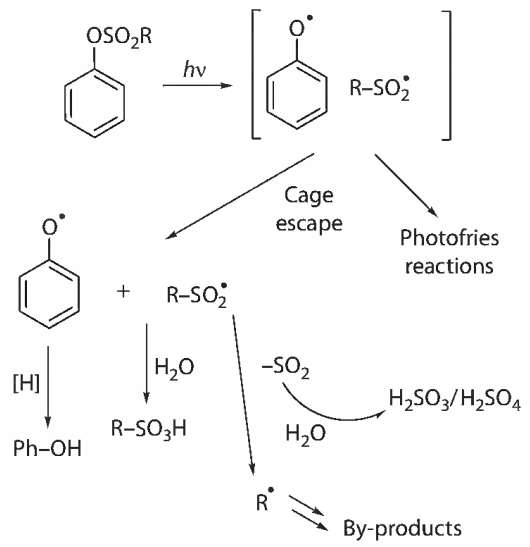

SCHEME 17.34

17.4 Conclusion

This chapter offers an overview of the different paths involved in the photochemistry of both phosphate and sulfonate esters. In some cases, despite the different ester moiety, the photochemistry of these compound shares a common mechanism as in the case of *o*-nitrobenzyl and coumarylmethyl derivatives. Nevertheless, phosphate and sulfonate esters have found application in different fields as inactive compounds that release the molecule of interest under very mild and selective conditions upon light exposure. Thus, phosphates were mainly used in biology (as "caged" compounds) because of the role of the released phosphate derivatives in living systems (e.g., ATP) [3b]. On the other hand, sulfonate esters have found a widespread application in material science, for example, in the field of photolithography as PAGs. The use of these esters in organic synthesis, however, is so far limited in scope. In fact an unsatisfactory effort has been devoted to this topic despite the promising application to the chemistry of phenyl cations, the virtually unexplored photoreactions of bi- and triaryl phosphates, the photo-Fries reaction of aryl sulfonates, and the $ArS_{RN}1$ process of aryl phosphates. Moreover, interesting photogenerated intermediates such as benzyl and alpha-keto carbocations deserve more attention for the formation of C–C or other C–X bonds.

References

1. Ackermann, L. Ed., *Modern Arylation Methods*; Wiley-VCH Verlag GmbH & Co: Weinheim, Germany, 2009.
2. Protti, S.; Fagnoni, M. *Chem. Commun.* 2008, 3611.
3. (a) Givens, R. S.; Conrad II, P. G.; Yousef, A. L.; Lee, J.-I. Photoremovable protecting groups. In *CRC Handbook of Organic Photochemistry and Photobiology*; Horspool, W.; Lenci, F. Eds., 2nd edn.; CRC Press: Boca Raton, FL, 2004, pp. 69/1–69/46. (b) Goeldner, M.; Givens, R. Eds., *Dynamic Studies in Biology*; Wiley-VCH Verlag: Weinheim, Germany, 2005.
4. Moon, S.-Y.; Kim, J.-M. *J. Photochem. Photobiol. C* 2007, *8*, 157.
5. Rossi, R. A.; Pierini, A. B.; Santiago, A. N. Aromatic Substitution by the $S_{RN}1$ Reaction. In *Organic Reactions*; Paquette, L. A.; Bittman, R., Eds.; Wiley: New York, 1999, Vol. 54, p. 1.
6. (a) Fagnoni, M. *Lett. Org. Chem.* 2006, 3, 253. (b) Dichiarante, V.; Fagnoni, M. *Synlett* 2008, 787. (c) Penenory, A. B.; Argüello, J. E. Aromatic and Heteroaromatic Substitution by $S_{RN}1$ and S_N1 Reactions. In *Handbook of Synthetic Photochemistry*; Albini, A.; Fagnoni, M. Eds.; Wiley-VCH: Weinheim, Germany, 2010, pp. 319–351.
7. Givens, R. S.; Kueper III, L. W. *Chem. Rev.* 1993, *93*, 55.
8. Pelliccioli, A. P.; Wirz, J. *Photochem. Photobiol. Sci.* 2002, *1*, 441.
9. Ellis-Davies, G. C. R. *Nat. Methods* 2007, *4*, 619.
10. Qiao, L.; Kozikowski, A. P.; Olivera, A.; Spiegel, S. *Bioorg. Med. Chem. Lett.* 1998, *8*, 711.
11. Abramova, T. V.; Leonetti, J. P.; Vlassov, V. V.; Lebleu, B. *Russ. J. Bioorg. Chem.* 2000, *26*, 174.
12. Walker, J. W.; Reid, G. P.; McCray, J. A.; Trentham, D. R. *J. Am. Chem. Soc.* 1988, *110*, 7170.
13. Corrie, J. E. T.; Gilbert, B. C.; Munasinghe, V. R. N.; Whitwood, A. C. *J. Chem. Soc., Perkin Trans. 2* 2000, 2483.
14. Zhang, L.; Buchet, R.; Azzar, G. *Biochem. Biophys. Res. Commun.* 2005, *328*, 591.
15. Kim, M. S.; Diamond, S. L. *Bioorg. Med. Chem. Lett.* 2006, *16*, 5572.
16. Corrie, J. E. T.; Munasinghe, V. R. N.; Rudbeck, M.; Barth, A. *Photochem. Photobiol.* 2009, *85*, 1089.
17. Givens, R. S.; Matuszewski, B. *J. Am. Chem. Soc.* 1984, *106*, 6860.
18. Givens, R. S.; Matuszewski, B.; Athey, P. S.; Stoner, M. R. *J. Am. Chem. Soc.* 1990, *110*, 6016.
19. DeCosta, D. P.; Howell, N.; Pincock, A. L.; Pincock, J. A.; Rifai, S. *J. Org. Chem.* 2000, *65*, 4698.
20. Sundararajan, C.; Falvey, D. E. *J. Am. Chem. Soc.* 2005, *127*, 8000.
21. Rajesh, C. S.; Givens, R. S.; Wirz, J. *J. Am. Chem. Soc.* 2000, *122*, 611.
22. Ma, C.; Du, Y.; Kwok, W. M.; Phillips, D. L. *Chem. Eur. J.* 2007, *13*, 2290.

23. Pirrung, M. C.; Shuey, S. W. *J. Org. Chem.* 1994, *59*, 3890.
24. Givens, R. S.; Athey, P. S.; Kueper III, L. W.; Matuszewski, B.; Xue, J.-Y. *J. Am. Chem. Soc.* 1992, *114*, 8708.
25. Givens, R. S.; Lee, J.-I. *J. Photoscience* 2003, *10*, 37.
26. Banerjee, A.; Lee, K.; Falvey, D. E. *Tetrahedron*, 1999, *55*, 12699.
27. Park, C.-H.; Givens, R. S. *J. Am. Chem. Soc.* 1997, *119*, 2453.
28. Givens, R. S.; Athey, P. S.; Matuszewski, B.; Kueper III, L. W.; Xue, J.-Y.; Fister, T. *J. Am. Chem. Soc.* 1993, *115*, 6001.
29. (a) Conrad II, P. G.; Givens, R. S.; Hellrung, B.; Rajesh, C. S.; Ramseier, M.; Wirz, J. *J. Am. Chem. Soc.* 2000, *122*, 9346. (b) Givens, R. S.; Heger, D.; Hellrung, B.; Kamdzhilov, Y.; Mac, M.; Conrad II, P. G.; Cope, E.; Lee, J. I.; Mata-Segreda, J. F.; Schowen, R. L.; Wirz, J. *J. Am. Chem. Soc.* 2008, *130*, 3307.
30. Furuta, T.; Torigai, H.; Sugimoto, M.; Iwamura, M. *J. Org. Chem.* 1995, *60*, 3953.
31. Schmidt, R.; Geissler, D.; Hagen, V.; Bendig, J. *J. Phys. Chem. A* 2007, *111*, 5768.
32. Schönleber, R. O.; Bendig, J.; Hagen, V.; Giese, B. *Bioorg. Med. Chem.* 2002, *10*, 97.
33. Furuta, T.; Takeuchi, H.; Isozaki, M.; Takahashi, Y.; Kanehara, M.; Sugimoto, M.; Watanabe, T.; Noguchi, K.; Dore, T. M.; Kurahashi, T.; Iwamura, M.; Tsien, R. Y. *ChemBioChem* 2004, *5*, 1119.
34. Geissler, D.; Antonenko, Y. N.; Schmidt, R.; Keller, S.; Krylova, O. O.; Wiesner, B.; Bendig, J.; Pohl, P.; Hagen, V. *Angew. Chem. Int. Ed.* 2005, *44*, 1195.
35. Havinga, E.; De Jongh, R. O.; Dorst, W. *Recl. Trav. Chim. Pays-Bas* 1956, *75*, 378.
36. Fagnoni, M; Albini, A. Molecular and supramolecular photochemistry. In *Organic Photochemistry and Photophysics*; Ramamurthy, V.; Schanze, K. Eds.; Dekker: New York, 2006, p. 131.
37. Karapire, C.; Icli, S. Photochemical Aromatic Substitution. In *CRC Handbook of Organic Photochemistry and Photobiology*; Horspool, W. H.; Lenci, F., Eds.; 2nd edn. CRC Press: Boca Raton, FL, 2004, pp. 37/1–37/14.
38. (a) De Jongh, R. O.; Havinga, E. *Recl. Trav. Chim. Pays-Bas* 1968, *87*, 1318. (b) De Jongh, R. O.; Havinga, E. *Recl. Trav. Chim. Pays-Bas* 1968, *87*, 1327.
39. De Carolis, M.; Protti, S.; Fagnoni, M.; Albini, A. *Angew. Chem. Int. Ed.* 2005, *44*, 1232.
40. Guizzardi, B.; Mella, M.; Fagnoni, M.; Freccero, M.; Albini, A. *J. Org. Chem.* 2001, *66*, 6353 and reference therein.
41. Lazzaroni, S.; Dondi, D.; Fagnoni, M.; Albini, A. *J. Org. Chem.* 2008, *73*, 206.
42. Fagnoni, M.; Albini, A. *Acc. Chem. Res.* 2005, *38*, 713.
43. Dichiarante, V.; Fagnoni, M.; Albini, A. Photochemical arylation reactions. In *Modern Arylation Methods*; Ackermann, L. Ed.; Wiley-VCH Verlag GmbH & Co: Weinheim, Germany, 2009, pp. 513–535.
44. Dichiarante, V.; Fagnoni, M.; Albini, A. *Chem. Commun.* 2006, 3001.
45. Protti, S.; Fagnoni, M.; Albini, A. *J. Am. Chem. Soc.* 2006, *128*, 10670.
46. Dichiarante, V.; Fagnoni, M.; Albini, A. *Angew. Chem. Int. Ed.* 2007, *46*, 6495.
47. Protti, S.; Fagnoni, M.; Albini, A. *Angew. Chem. Int. Ed.* 2005, *44*, 5675.
48. Lazzaroni, S.; Protti, S.; Fagnoni, M.; Albini, A. *Org. Lett.* 2009, *11*, 349.
49. Dichiarante, V.; Dondi, D.; Protti, S.; Fagnoni, M.; Albini, A. *J. Am. Chem. Soc.* 2007, *129*, 5605. Correction: 11662.
50. Chopa, A. B.; Lockhart, M. T.; Silbestri, G. *Organometallics* 2000, *19*, 2249.
51. Chopa, A. B.; Lockhart, M. T.; Dorn, V. B. *Organometallics* 2002, *21*, 1425.
52. Chopa, A. B.; Lockhart, M. T.; Silbestri, G. *Organometallics* 2002, *21*, 5874.
53. Chopa, A. B.; Silbestri, G.; Lockhart, M. T. *J. Organomet. Chem.* 2005, *690*, 3865.
54. Fidelibus, P. M.; Silbestri, G. F.; Lockhart, M. T.; Mandolesi, S. D.; Chopa, A. B.; Podestà, J. C. *Appl. Organometal. Chem.* 2007, *21*, 682.
55. (a) Finnegan, R. A.; Matson, J. A. *J. Am. Chem. Soc.* 1972, *94*, 4780. (b) Shi, M.; Yamamoto, K.; Okamo, Y.; Takamuku, S. *Phosphorous, Sulfur.* 1991, *60*, 1. (c) Okamoto, Y.; Tatsuno, T.; Takamuku, S. *Heteroatom Chem.* 1996, *4*, 257.

56. Nakamura, M.; Okamoto, Y.; Takamuku, S. *Chem. Commun.* 1996, 209.
57. Chopa, A. B.; Dorn, V. B.; Badajoz, M. A.; Lockhart, M. T. *J. Org. Chem.* 2004, *69*, 3801.
58. Dorn, V. B.; Badajoz, M. A.; Lockhart, M. T.; Chopa, A. B.; Pierini, A. B. *J. Organomet. Chem.* 2008, *693*, 2458.
59. Izawa, Y.; Kuromiya, N. *Bull. Chem. Soc. Jpn.* 1975, *48*, 3197.
60. Pete, J.-P.; Portella, C. *Bull. Soc. Chim. Fr.* 1980, II-275.
61. Zen, S.; Tashima, S.; Koto, S. *Bull. Chem. Soc. Jpn.* 1968, *41*, 3025.
62. Masnovi, J.; Koholic, D. J.; Berki, R. J.; Binkley, R. W. *J. Am. Chem. Soc.* 1987, *109*, 2851.
63. Binkley, R. W.; Koholic, D. J. *J. Org. Chem.* 1989, *54*, 3577.
64. Gaur, H. A.; Groenenboom, C. J.; Hageman, H. J.; Hakvoort, G. T. M.; Oosterhoff, P.; Overeem, T.; Polman, R. J.; Van der Werf, S. *Makromol. Chem.* 1984, *185*, 1795.
65. Aoki, S.; Oba, T.; Hara, Y. UV-curable organopolysiloxane compositions. JP Patent 4033960, February 05, 1992.
66. Houlihan, F. M.; Shugard, A.; Gooden, R.; Reichmanis, E. *Macromolecules* 1988, *21*, 2001.
67. Neenan, T. X.; Houlihan, F. M.; Reichmanis, E.; Kometani, J. M.; Bachman, B. J.; Thompson, L. F. *Macromolecules* 1990, *23*, 145.
68. Houlihan, F. M.; Neenan, T. X.; Reichmanis, E.; Kometani, J. M.; Chin, T. *Chem. Mater.* 1991, *3*, 462.
69. Shirai, M.; Tsunooka, M. *Bull. Chem. Soc. Jpn.* 1998, *71*, 2483.
70. Houlihan, F. M.; Nalamasu, O.; Kometani, J. M.; Reichmanis, E. *J. Imaging Sci. Technol.*, 1997, *41*, 35.
71. Kim, M. S.; Diamond, S. L. *Bioorg. Med. Chem. Lett.* 2006, *16*, 4007.
72. Barth, A.; Corrie, J. E. *Biophys. J.* 2002, *83*, 2864.
73. Busman, S. C.; Trend, J. E. *J. Imaging Technol.* 1985, *11*, 191.
74. (a) Yamaoka, T.; Adachi, H.; Matsumoto, K.; Watanabe, H. *J. Chem. Soc. Perkin Trans. 2* 1990, 1709. (b) Naitoh, K.; Yoneyama, K.; Yamaoka, T. *J. Phys. Chem.* 1992, *96*, 238. (c) Naitoh, K.; Yamaoka, T. *J. Chem. Soc. Perkin Trans. 2* 1992, 663.
75. Inoue, H.; Matsukawa, K.; Tanaka, Y.; Nishioka, N. *J. Photopol. Sci. Technol.* 1999, *12*, 129.
76. Schade, B.; Hagen, V.; Schmidt, R.; Herbrich, R.; Krause, E.; Eckardt, T.; Bendig, J. *J. Org. Chem.* 1999, *64*, 9109.
77. Protti, S.; Dondi, D.; Fagnoni, M.; Albini, A. *Green Chem.* 2009, *11*, 239.
78. Chang, Y.-S.; Jang, J.-S.; Deinzer, M. L. *Tetrahedron* 1990, *46*, 4161.
79. Chen, Q.-Y.; Li, Z.-T. *J. Org. Chem.* 1993, *58*, 2599.
80. Stratenus, J. L.; Havinga, E. *Recl. Trav. Chim. Pays-Bas* 1966, *85*, 434.
81. Ogata, Y.; Takagi, K.; Yamada, S. *J. Chem. Soc. Perkin Trans. 2* 1977, 1629.
82. Pitchumani, K.; Durai Manickam, M. C.; Srinivasan, C. *Indian J. Chem.* 1993, *32B*, 1074.
83. Crevatín, L. K.; Bonesi, S. M.; Erra-Balsells, R. *Helv. Chim. Acta* 2006, *89*, 1147.
84. (a) Kageyama, Y.; Ohshima, R.; Sakurama, K.; Fujiwara, Y.; Tanimoto, Y.; Yamada, Y.; Aoki, S. *Chem. Pharm. Bull.* 2009, *57*, 1257. (b) Aoki, S.; Matsuo, N.; Hanaya, K.; Yamada, Y.; Kageyama, Y. *Bioorg. Med. Chem.* 2009, *17*, 3405.
85. Schlegel, L.; Ueno, T.; Shiraishi, H.; Hayashi, N.; Iwayanagi, T. *Chem. Mater.* 1990, *2*, 299.
86. Andraos, J.; Barclay, G. G.; Medeiros, D. R.; Baldovi, M. V.; Scaiano, J. C.; Sinta, R. *Chem. Mater.* 1998, *10*, 1694.

18

Stabilized Carbocations Generated by Photoheterolysis

Hans-Werner Abraham
Humboldt-Universität zu Berlin

18.1 Introduction

Carbocations play important roles as intermediates in organic chemistry. Stable and metastable ions are formed in acidic media [1] and since the lifetime of these intermediate species is often very short, time-resolved spectroscopy on the order of fs–ns is used to detect them. For this purpose, carbocations must be generated by laser impulses or lamp flashes of shorter duration than the time resolution of the spectroscopic equipment. A common method of photochemical carbocation generation is heterolytic bond fission of C–X bonds, whereby X is an electron-withdrawing group with proper nucleofuge properties [2]. Heterolytic photocleavage is favored in solvents of high polarity and with compounds yielding cations with low pK_R^+ values and having leaving groups X^- with low pK_a values for the conjugate acid. While the photoreaction may start from either the excited singlet or triplet state, singlet states are most often involved. The pathways of the photoreactions differentiate between adiabatic or diabatic bond fissions. The diabatic photoreaction is the dominant process, but in some cases, indications of the generation of excited carbenium ions were found [3,4]. In general, the efficiency of the photoheterolysis is high, resulting in high quantum yields [2].

Often heterolytic bond fission must compete with the homolytic bond fission, resulting in the generation of radicals that undergo reactions different from those of ions. The radicals generated by homolytic cleavage may react together by electron transfer, resulting in the same ionic species as obtained by direct heterolysis of the bond. The competition between both reaction pathways can be controlled by the solvent and the structure of the compound containing the fissable C–X bond. The lifetime of the carbocation depends strongly on the ability of the positive charge to delocalize within the cationic moiety.

The term "stabilized carbocation" is a matter of definition. The primary focus of this chapter will be on carbocations with lifetimes longer than μs detectable by conventional flash photolysis or even generated using stationary lamps and steady state spectroscopy.

The electrophilic reactivity of carbocations is high. Protic solvents react with a cation in the order methanol>ethanol>water≫trifluoroethanol (TFE)≫1,1,1,3,3,3-hexafluoroisopropyl alcohol (HFIP) [2].

Carbocations are pseudo acids according to Equation 18.1 with a corresponding equilibrium constant K_R.

$$R^+ + H_2O \underset{k_H}{\overset{k_W}{\rightleftharpoons}} ROH + H^+ \quad K_R = \frac{k_W}{k_H} = \frac{[ROH][H^+]}{[R^+]} \tag{18.1}$$

A single linear free energy correlation (log $k_W = f(pK_R)$) does not exist, but the data separate into families of structurally related ions. The reactivity follows the order 9-unsubstituted-9-xanthylium ion>phenyltropylium>diarylmethyl≈9-arylxanthylium>triarylmethyl≈9-aryl-9-fluorenyl [2].

Like protic solvents, added nucleophiles such as oxyanions, thiolates, amines, and azides react with carbocations. Fast kinetics data were obtained using laser flash photolysis [1]. Ritchie proposed that the data could be satisfied by Equation 18.2:

$$\log(k/k_0) = N_+ \tag{18.2}$$

with

k and k_0 as rate constants for the combination of a carbocation and a reference nucleophile, respectively
N_+ is a parameter dependent on the nucleophile and the reaction conditions [5]

This chapter, however, will not deal with the reactivity of carbenium ions as related to nucleophiles, but will focus on reversible photoheterolysis, which can be repeated several times. Because of the strongly different properties of the carbocations and their corresponding photoprecursors, applications such as photoswitches will also be considered. The generation of selected carbocations, their physical properties, their reactivities, and, if known, their applications will be included in the discussion.

18.2 Di- and Triarylmethyl Cations

Di- and triarylmethyl cations can be generated from their respective precursor acetates and *p*-cyanophenyl ethers by photoheterolysis in aqueous and alcoholic solvents (Scheme 18.1) [6–8]. Arylmethyl cations are less stable cations that are commonly encountered as reactive intermediates. For example, the lifetime of the triphenylmethyl cation in aqueous acetonitrile solution is only 4 μs [9]. The substituted arylmethyl cations have lifetimes ranging from 0.1 s for the tri-(4-MeOPh)methyl cation to 30 ns for the di-(4-methylphenyl)methyl cation. The formation of radicals competes with the generation of cations, and the presence of water in the solution counteracts the radical formation. Cation formation was not observed in dichloromethane solution. The formation of the cations in the ground state was complete after the 20 ns laser pulse. As expected, diarylmethyl cations are more reactive than triarylmethyl cations.

Steenken and colleagues [10] have extensively studied the photolytic bond fission of substituted diphenylmethyl halides in acetonitrile solution. Both diarylmethyl radicals and cations were obtained by laser flash photolysis at 248 nm. The two transient species can be easily differentiated by their UV-Vis spectra.

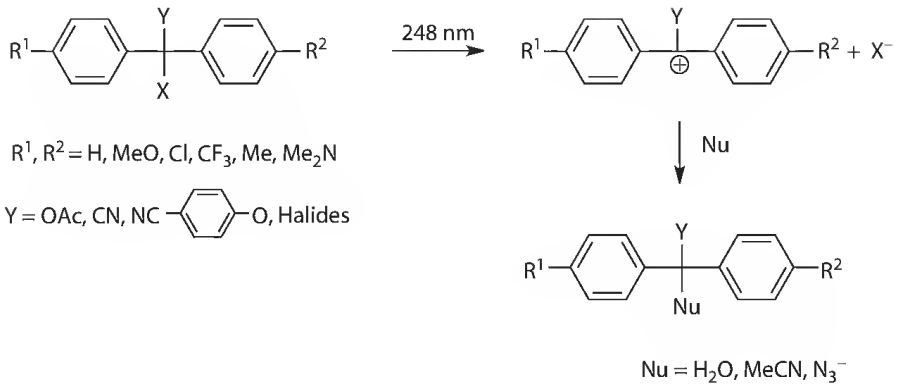

SCHEME 18.1 Generation and following reactions of arylmethyl cations.

While the radicals absorb in the region around 300 nm, the cations exhibit absorption bands around 450 nm. The radical $(4\text{-ClPh})_2CH^{\bullet}$ disappears in a second-order fashion, but the diphenylmethyl cation with substituents such as CF_3, Cl, F, and H decay by first-order kinetics. However, the decay of stabilized cations such as $(4\text{-MeOPh})_2CH^+$ involves ion recombination and, therefore, second-order kinetics were observed. Photolysis of benzhydryl chloride including scavenger experiments of the products is shown in Scheme 18.2 [10]. The reaction of the cation with the solvent is reversible; therefore, by addition of water, the carbinol is the main product. Water reacts exclusively with the cation generated by the back reaction of the acetonitrile adduct. The ion combination was shown to progress by a diffusion controlled process.

The observed heterolysis: homolysis ratios correlate with the pK_a values of the acids HX and not with the electron affinity of X. Whereas the quantum yields for homolysis (0.2–0.4) are independent of the nature of the substituent on the phenyl groups, those for heterolysis increase with increasing electron donor strength from ≤ 0.07 for CF_3 to 0.3 for OMe.

It is noteworthy that bond fission also occurs in the triplet state whereby the ratio of heterolysis to homolysis differs from that observed in the singlet state. Cations were formed exclusively in the ground state.

A consideration of the thermochemical aspects of bond cleavage makes the role of the solvent impressively clear: whereas photohomolysis (248 nm) in the gas phase is exothermic, photoheterolysis is not possible [10]. The degree to which heterolysis occurs as compared to homolysis depends on the extent of solvation of the incipient ions in the process of bond rupture. Because the solvation of ions requires a reorientation of the solvent molecules within ps, the heterolytic break must occur in the same time domain.

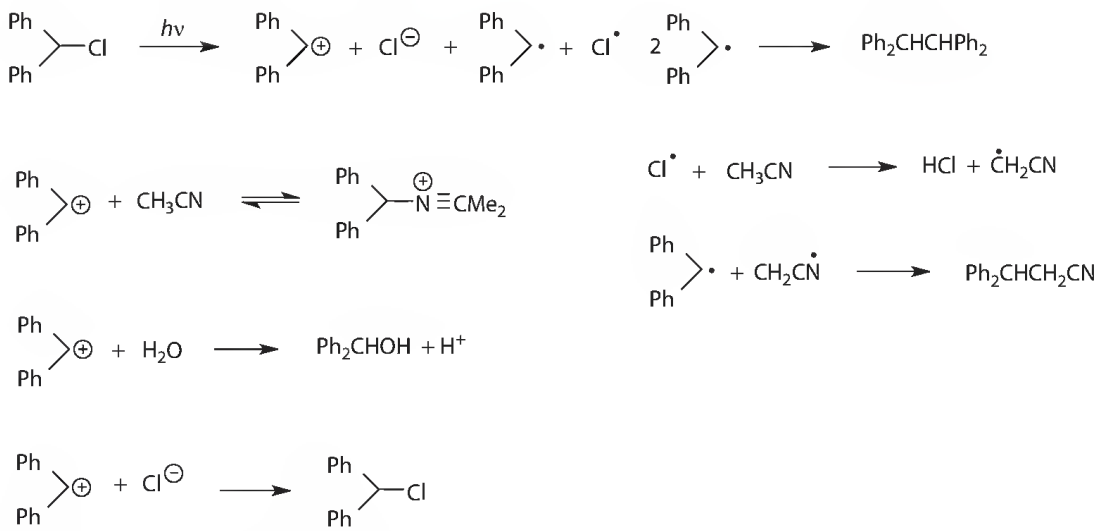

SCHEME 18.2 Formation and decay of diphenyl cations and radicals.

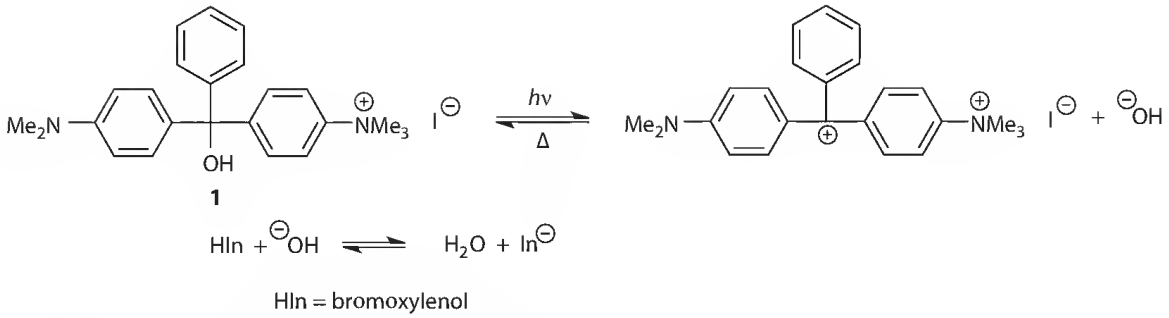

SCHEME 18.3 Deprotonation of an indicator by photogenerated hydroxyl ions.

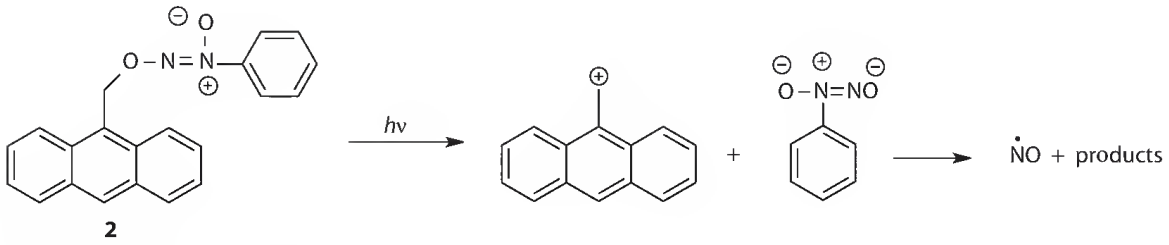

SCHEME 18.4 Photocaged nitric oxide.

Solvation of charged species would also be necessary to enable homolytic bond breakage, followed by electron transfer between the radicals. Therefore, based on the identity of the products, direct heterolysis and the electron transfer pathway cannot be distinguished.

18.2.1 Caged Hydroxyl Ions and Nitric Oxide

Like halides, triarylmethyl alcohols are also able to produce the corresponding cation whereby a strong base OH^- is released, thus causing a pH increase [11–13].

The stability of the cation controls the rate of recombination. Therefore, the lifetime of the hydroxide ion generated by photoheterolysis of trityl alcohol is too short to be of practical use [11]. Improved results were obtained in studies using Malachite green, and the increased pH value was maintained for seconds [12].

The photolysis of the ammonium salt **1** (Scheme 18.3) in aqueous solution at pre-pulse pH = 10.9 resulted in the heterolytic cleavage of the carbinol with a rate constant greater than $10^8 s^{-1}$ [13]. The multiphasic decay of the transient absorbance at 633 nm was associated with recombination reactions of the carbocation with hydroxide from the solution, but the source of the heterogeneity extending from the nanosecond timescale to the tens of seconds is not clear. The hydroxide ions photogenerated at neutral pH were shown to deprotonate the pH indicator bromoxylenol, as reflected in the rise of the absorbance at 633 nm.

An irreversible C–O bond break occurs upon photolysis (390 nm) of compound **2** (Scheme 18.4).

The reaction can be used to liberate nitric oxide by light [14]. Both NO and the carbocation are expected to inhibit or encourage the proliferation of tumors depending on the dose. It has also been shown that the carbocation generated by photolysis of **2** is scavenged by guanosine.

18.3 Fluorenyl, Dibenzosuberenyl, and Xanthyl Cations

The introduction of a bridge between the phenyl groups of diphenylmethanol should result in the generation of more planar cations by photoheterolysis. However, the lifetime of the resulting cations is not increased compared with the corresponding diarylmethyl radicals. On the contrary, the fluoren-9-yl cation is extremely short lived.

18.3.1 Fluoren-9-yl Cation

Electronically excited 9-fluorenol **3** (Scheme 18.5) undergoes homo- and heterolytic cleavage of the C–O bond [15–19]. The bond-breaking process is strongly influenced by the solvent. As for the arylmethyl cations (see previous paragraphs), the solvation of the incipient ions must be very rapid so that the ionic path is already preformed by the solvent; accordingly the solvent must play an active part in the early stages of the cleavage process [20].

Indeed, the rate of decay of the excited state of 9-fluorenol in THF was quenched by addition of HFIP with a rate constant of $\sim 2 \times 10^9\ M^{-1}\ s^{-1}$. Probably, this is caused by a chemical reaction in which the excited state acts as a Brönsted base; water, at levels of 1.2%–2.0%, reduces the singlet lifetime from 160 ps in neat MeCN to 50–60 ps [20]. In all solvents (except for HFIP, TFE, and water) the 9-fluorenyl radical is formed from the excited singlet state. The first half life of the radical is in the range 0.5–1 μs. In HFIP, TFE, and H_2O, the transient absorption spectrum peaks at 515 nm and differs from that in other solvents. The absorption spectrum can be assigned to the 9-fluorenyl cation whose lifetime in HFIP is 30 ms and 1 ns in TFE. The fluorenyl cation **4** was also observed in water, as detected by a strong transient at 515 nm with a lifetime of only 15 ps. In water solutions, the only photoreaction is heterolysis. In contrast, in methanol both homolysis and heterolysis can occur.

In H_2O at very early times after the laser flash, the absorption maximum of the cation band lies at <450 nm. The redshift of the band to 515 nm is attributed to the solvation of the initial "naked" cation or to the contact ion pair (see Scheme 18.5).

In accord with Scheme 18.5, 9-fluorenol is photostable in aqueous solution.

The solvent has a large influence on both the ionization and dissociation, but affects each parameter differently. Ion pair formation, the first step, strongly depends on the ability of the solvent to function as an electron acceptor or a donor as reflected in the Kosower Z-value or the Reichardt E_T solvent parameters. The dissociation of the contact ion pair depends on the ability of the solvent to lower the strong attraction between the ions leading to free solvated ions. For this function of the solvent, the dielectric constant is important. With respect to the first step, the proton transfer properties of the solvent may drive the C–O bond cleavage into the heterolytic direction as symbolized in Scheme 18.5. In contrast to hydration, proton transfer is sufficiently rapid to contribute in the transient state of the dissociation [20].

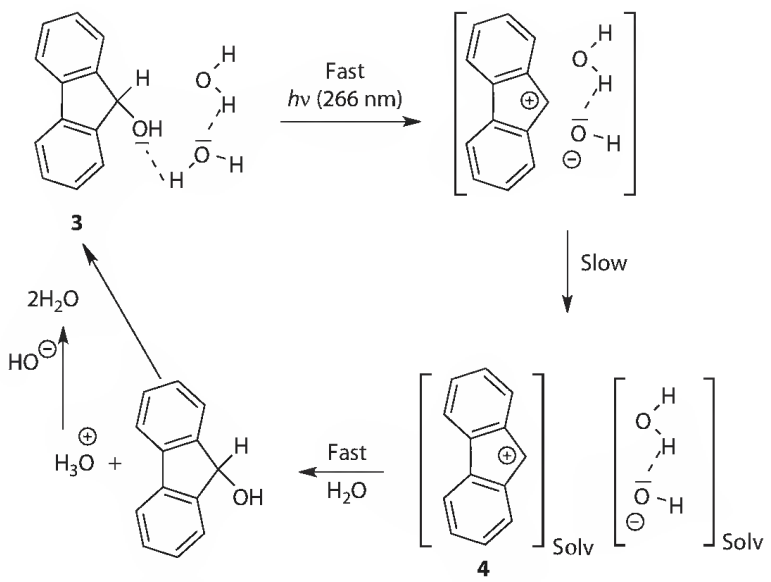

SCHEME 18.5 Kinetic scheme of the 9-fluorenol photolysis.

18.3.2 9-Arylfluoren-9-yl Cations

9-Aryl-9-fluorenol undergoes a very efficient photoheterolysis in TFE and H_2O/MeCN 4:1 solutions. Quantum yields are on the order of 0.5–0.8, and are relatively insensitive to the nature of the substituent in the 9-aryl group [21]. In contrast, triphenylmethanol undergoes an inefficient photolysis under the same conditions (248 nm excitation wavelength).

The lifetimes of the 9-aryl-fluoren-9-yl cations are much longer than that of the unsubstituted fluoren-9-yl cation. The rate constants of the exponential decay of 9-aryl-fluoren-9-yl cations range from 2×10^2 to $1 \times 10^5 s^{-1}$ in TFE and 2×10^5 to $5 \times 10^7 s^{-1}$ in H_2O/MeCN. The 9-aryl substituent significantly retards the reactivity of the fluoren-9-yl cations. Kinetic stabilization by the aryl substituent may be attributed to both resonance and steric effects. Compared with other benzylic-type cations, the general trend is observed that the more inherently stable the cation, the smaller the effect of an additional phenyl substituent. Because the fluoren-9-yl cation is inherently unstable, substituents in the 9-aryl-group have a significant effect despite the fact that the phenyl ring is twisted out of the plane by probably more than 30°. The greater polar interaction observed for *p*-substituents may be a compensation for the smaller resonance interaction between the substituted phenyl group and the positive charge in the 9-position caused by the twisting of the aryl ring [21].

18.3.3 9-Acyl-Fluoren-9-yl Cations

Fluoren-9-yl cations are not only stabilized by aryl groups but also by electron deficient substituents such as carbonyl and thiocarbonyl groups [22,23]. The lifetime of **6** is about 1 ms in HFIP.

Absolute rate constants for the reactions of cations **6** with methanol in HFIP solution reveal that the thiocarbonyl-substituted cation reacts slower than the cation substituted with an ester group (Scheme 18.6). According to the transient absorption spectrum of **6**, stabilization is supported by the open resonance structures rather than by a cyclic oxyranyl cation.

18.3.4 Intermediates of Photopinacol Rearrangement

Fluoren-9-yl cations are also intermediates of the photochemical pinacol rearrangement [24,25].

The cation **10** primarily generated by photoheterolysis was detected by transient absorption spectra showing absorption bands at 505 and 700 nm. The transient observed at 350 nm may be associated with the ketyl radical **9** yielding the byproduct fluorenone (Scheme 18.7).

The fluorenol **11** (Scheme 18.8) was photolyzed in order to explore the possibility of hydride transfer within the cation [26].

However, it was demonstrated that such hydride migration does not occur. The lifetime of the transient cation **12** is within 14 μs in TFE, a significant increase in lifetime as compared with the parent fluoren-9-yl cation. In this case, steric crowding also contributes to the enhanced lifetime. Cation **12**

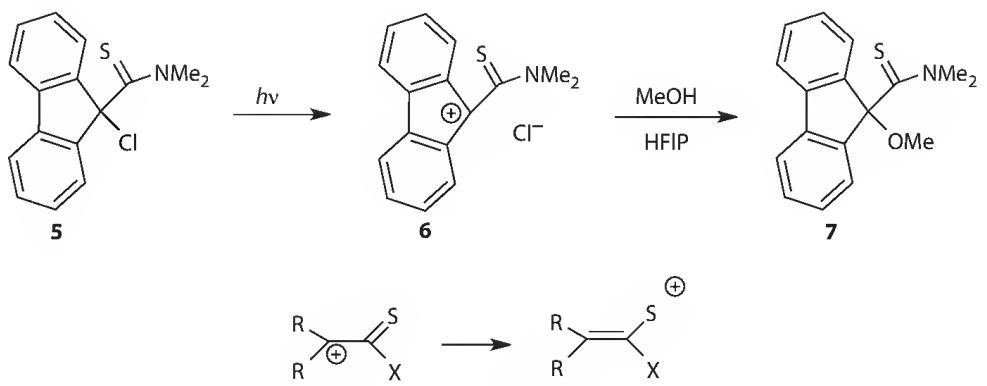

SCHEME 18.6 Photosolvolysis of acyl-substituted chlorofluorene.

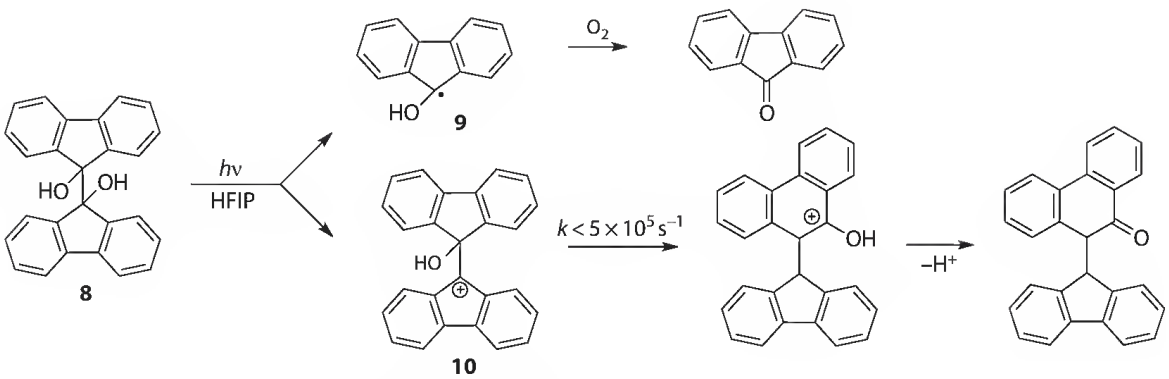

SCHEME 18.7 Photopinacol rearrangement in HFIP.

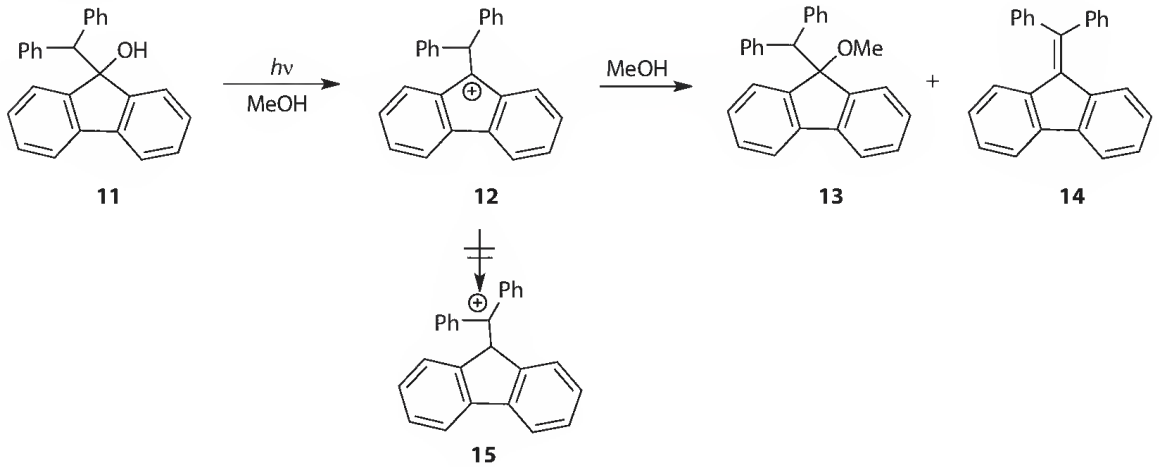

SCHEME 18.8 Photoreaction of the fluorenol **11**.

reacts efficiently with nucleophiles such as Br^-, MeOH, EtOH, i-PrOH, and H_2O with bimolecular quenching rate constants from 9.5×10^8 (Br^-) to $5.9 \times 10^3\ M^{-1}\ s^{-1}$ (i-PrOH).

18.3.5 Dibenzosuberenol

The expansion of the π-system of the fluorenol **3** leads to the 5H-dibenzo[a,d]cyclohepten-5-ol **16** (Scheme 18.9). In laser flash experiments, the formation of the cation **17** was detected by its transient absorption spectrum [27].

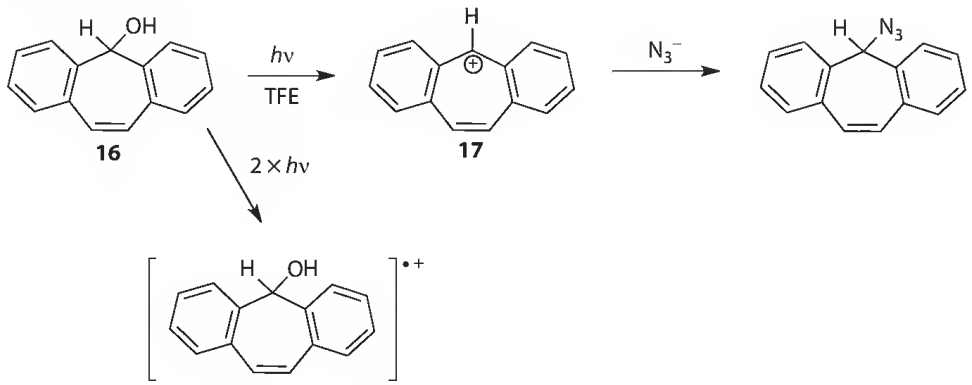

SCHEME 18.9 Processes observed by laser flash photolysis of the alcohol **16** in TFE.

The intermediate cation **17** has a lifetime >100 μs in TFE solution, much longer than that of the cation **4**. Azide anions quench the cation with a quenching constant $1.1 \times 10^9\ s^{-1}$. Although there may be some adiabatic formation of **17**, the majority of cations were diabatically formed. The formation of radical cations was observed at high laser doses via photoejection of electrons.

18.3.6 Xanthenol

Photoexcited 9-phenyl-9-xanthenol **18** undergoes heterolysis with a quantum yield of 0.6 in water/MeCN 4:1 [7]. The parent xanthen-9-yl cation is formed with a quantum yield 0.8.

Relative yields of cation **19** and radical **20** (Scheme 18.10) strongly depend on the solvent (Table 18.1) [28]. The cation is directly formed in the ground state. In contrast, besides the diabatic pathway, about 1% adiabatic, water-catalyzed formation of the excited cation in water/methanol solution was reported [28]. The 9-phenyl-xanthen-9-yl cation **19** (Scheme 18.10) decays in water/MeCN 4:1 with a first-order rate constant of $23\ s^{-1}$. In water/acetonitrile 1:1, a complex decay of **19** was observed suggesting that the recombination of **19** with HO^- competes with its reaction with water (Scheme 18.10) [28].

Due to the high stability of **19** as reflected by its long lifetime in water/MeCN 4:1, the reactions of nucleophiles such as water with **19** are relatively slow ($k_{solvent} = 2.3 \times 10^4\ s^{-1}$). Interestingly, the rate constants of photoexcited **19*** are much higher than those of the ground state **19**. Double laser experiments

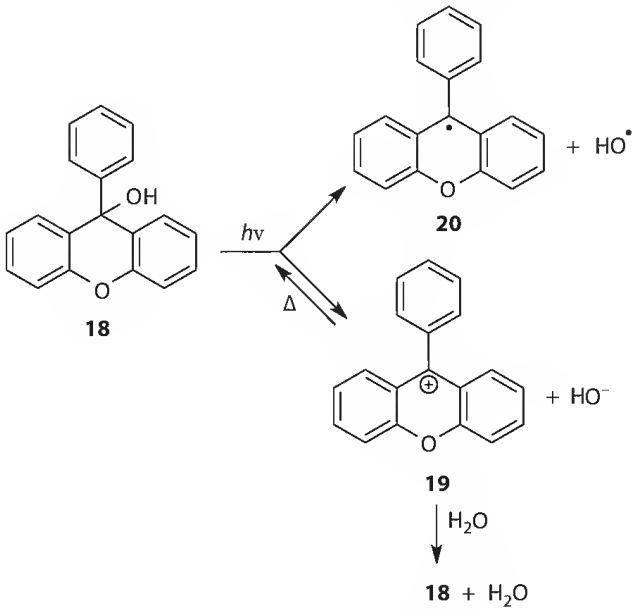

SCHEME 18.10 Photoheterolysis and -homolysis of the alcohol **18**.

TABLE 18.1 Relative Yields of Cation **19** and Radical **20** in the Course of 248 nm Laser Flash Photolysis in Various Solvents

	Relative Yield	
Solvent	19	20
H_2O/MeCN 1:1	0.5	<0.1
H_2O/MeOH 1:1	1.0	—
MeOH	0.2	0.5
MeCN	<0.05	1.0
n-Heptane	—	1.0

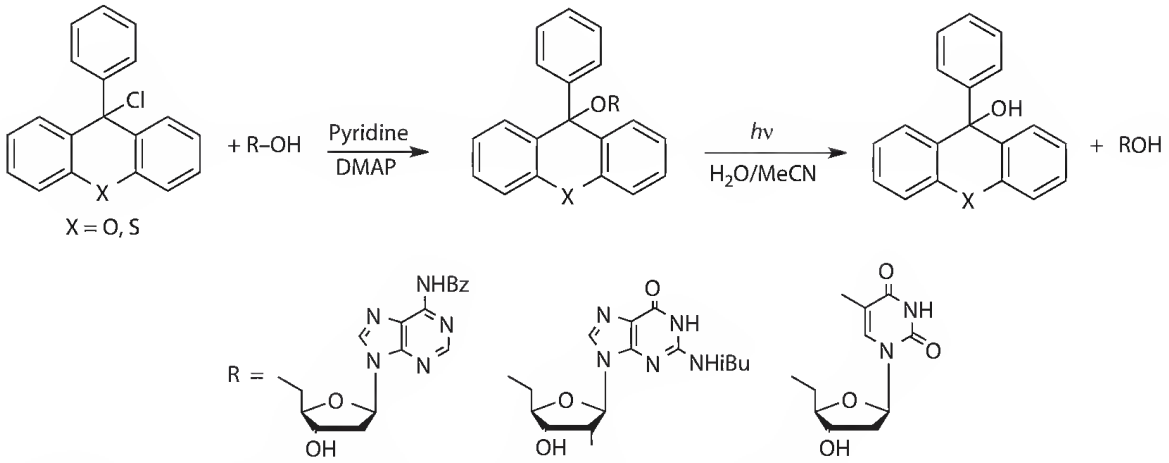

SCHEME 18.11 Pixyl and *S*-pixyl groups as photocleavable protecting groups.

provided evidence for the chemical quenching of the singlet state of **19** [28]. The rate constants of **19*** with water and MeOH in acetonitrile solution are 3.3×10^7 and $9.7 \times 10^7\ M^{-1}\ s^{-1}$, respectively.

18.3.7 Photocleavable Protecting Groups

The 9-phenylxanthyl (pixyl) and 9-phenylthioxanthyl (*S*-pixyl) moiety can be used for protecting groups of nucleosides that are cleavable under neutral conditions by light (Scheme 18.11) [29,30].

18.4 Acridinium Ions

18.4.1 Photoheterolysis of Acridanes

9-Phenyl-9-hydroxy-9,10-dihydroacridine (9-phenyl-9-hydroxyacridane) **21** undergoes efficient photoheterolysis in various alcohols with quantum yields ranging from 0.4 (i-PrOH) to 0.8 (EtOH) [31]. The rate constants of photoheterolysis were calculated to be $>10^9\ s^{-1}$.

The formation of the acridinium ion **22** (Scheme 18.12) occurs diabatically from the excited singlet state. Although the recovery of the acridane by the nucleophilic attack of the alcohol used was not demonstrated, it was shown that the cation completely disappeared in the presence of propanol with a solvolysis constant $7 \times 10^{-3}\ s^{-1}$.

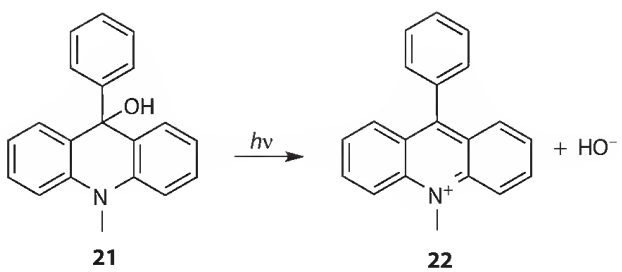

$$\mathbf{22} + H_2O \rightleftharpoons \mathbf{21} + H^+ \qquad (18.3)$$

$$K_{R^+} = \frac{[H^+]\,[\mathbf{21}]}{[\mathbf{22}]} \qquad pK_{R^+} = 11.03$$

SCHEME 18.12 Photoheterolysis of the acridane **21** and the pseudo base equilibrium.

The formation of hydroxide ions by photoheterolysis of **21** in MeCN/water (3:1) has been observed indirectly by the increase of the pH value to about 12 during the photolysis [12]. A pH value above 11 was maintained for more than 10 h, and illustrates an example of photocaged hydroxyl ions. The lifetime of the acridinium ion is exceptionally long and supports the high stability of the acridinium ion under solvolytic conditions.

If a completely reversible photoheterolysis and thermal recovery of the acridane occurs, a photochromic system can be developed. Acridanes are colorless compounds with absorption bands around 320 and 280 nm, but the acridinium compounds absorb light from 430 to 550 nm, depending on the 9-aryl substituent on the acridinium ion.

The acridanes are pseudo bases according to Equation 18.3. Kinetic data obtained by stopped flow spectrometry [32] showed that substituents at the 9-position reduced the rate of hydroxide ion attack at C-9. The C-9 substituent of **22** influences the stability of the acridinium ion in aqueous solution mainly via unfavorable *peri* interactions between the aryl group and the C-1 and C-8 protons. For 9-aryl substituents, possible contributions from resonance interaction must also be considered. However, this interaction must be quite small because ΔpK_R^+ between the 9-phenyl and the 9-(4-dimethylaminophenyl) acridinium ions is only 0.5; the stabilization by the dimethylamino group is only 0.7 kcal mol^{-1} [32]. The angles between the planes of the aryl substituent and the acridinium plane are more than 40°, and account for this minor effect on stabilization. On the other hand, the electronic absorption spectra of the 9-(4-dimethylaminophenyl) acridinium ion shows pronounced bathochromic shifts relative to the 9-phenylacridinium ion. Strong electron donating aryl groups change the nature of the first excited singlet state [33]. While the long-wavelength absorption of 9-phenylacridinium ion is determined by the locally excited state in the acridinium moiety, the long-wavelength absorption of 9-(4-dimethylaminophenyl) acridinium ion is attributed to a delocalized charge-transfer state. Charge shift species arising from the intramolecular electron transfer have been identified through observation of redshifted fluorescence emission bands and the appearance of radical and radical cation transients [34]. The data reveal that there is a significant electron coupling between the acridinium moiety and the aryl group.

Figures 18.1 [35] and 18.2 [36] demonstrate the uniform photoreaction observed upon irradiation of two acridane derivatives having aryl substituents of different electron donor strengths (Scheme 18.13).

The thermal recovery of acridane **23** after irradiation obeys a first-order kinetics with a rate constant $8.3 \times 10^{-4}\ s^{-1}$ (lifetime of the acridinium ion **24** = 20 min). UV-Vis absorption spectra recorded at different time after irradiation show the same isosbestic points as observed in the photoreaction

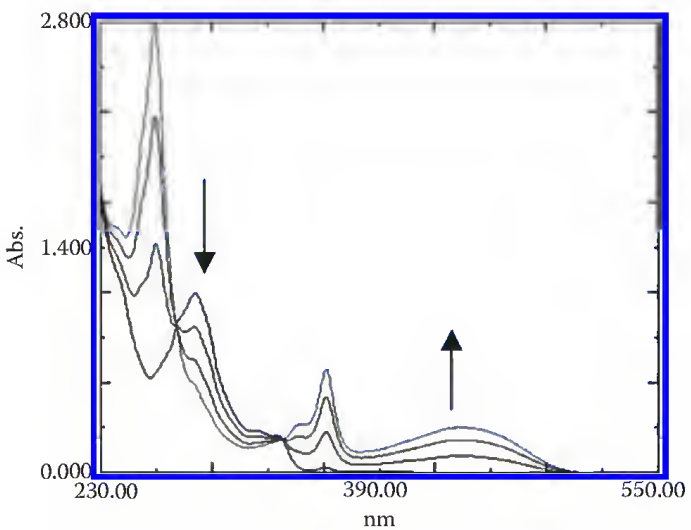

FIGURE 18.1 UV-Vis spectra recorded after consecutive irradiation of acridane **23** (0, 1, 3, 11 min, 313 nm) in EtOH/MeCN (5:1) solution.

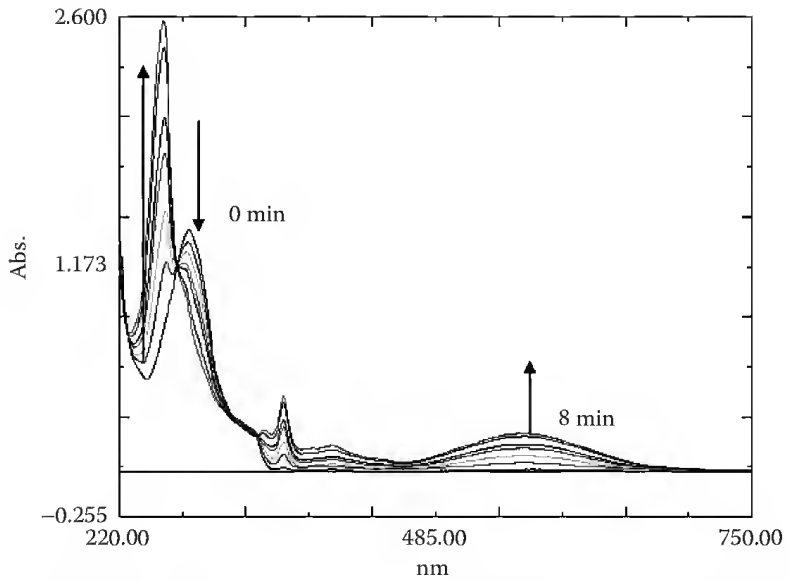

FIGURE 18.2 UV-Vis spectra recorded after consecutive irradiation of acridane **25** (20 s ... 8 min, 313 nm) in acetonitrile solution.

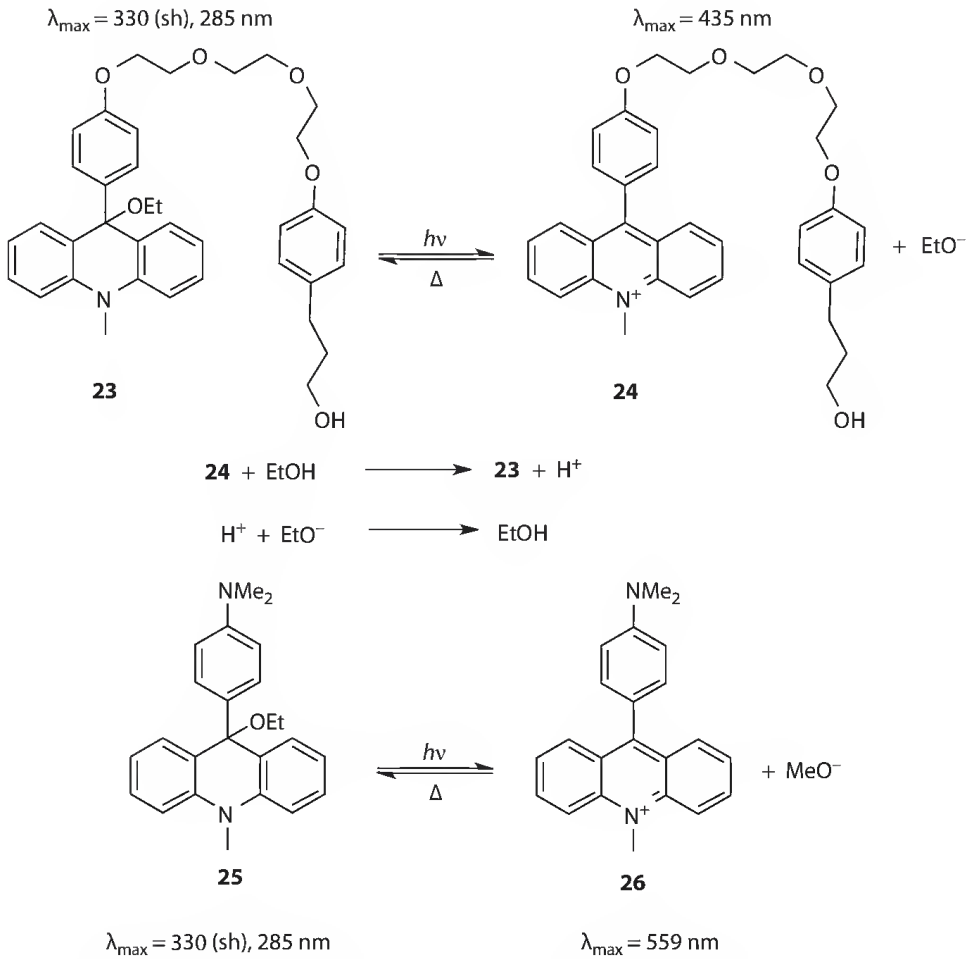

SCHEME 18.13 Photoheterolysis of compound **23** and **25** and thermal back reaction of the acridinium ions.

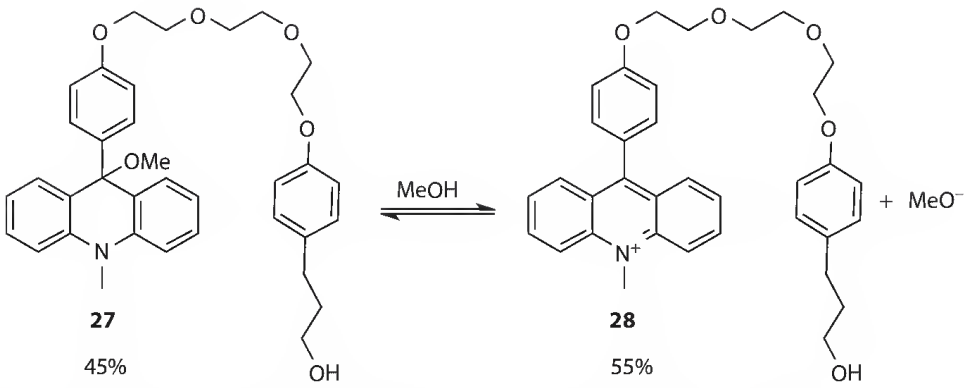

SCHEME 18.14 Equilibrium between acridane and acridinium ion in methanol solution.

revealing the presence of only two species: the acridinium ion **24** and the acridane **23**. According to the pseudo-first-order kinetics the acridinium ion reacts with the alcoholic solvent, assisted by the ethoxide ion that scavenges the proton (Scheme 18.13). The photoreaction using conventional lamps must compete with the thermal back reaction. Therefore, the maximum turnover depends on the light intensity.

Irradiation of acridane **25** was performed in acetonitrile solution. The lifetime of the acridinium methoxide in this aprotic solvent is more than 10 h, and the complete recovery of the acridanes was not observed. However, both in air-saturated acetonitrile and in argon-purged solutions only the characteristic absorption bands of the acridinium ions were observed. There were no indications that radicals had been formed via homolytic bond fission. Accordingly, quantum yields of photoheterolysis were determined in acetonitrile solution. For example, the quantum yield of photoheterolysis of the acridane **23** is 0.5 [35].

Because of the reversibility of the acridane/acridinium system in solvents containing at least 5% alcohol, the photochromic system can also represent a molecular photoswitch. The properties of acridanes and acridinium alkoxides are markedly different with regard to their shape, their basicity, and their electronic properties. The photoheterolysis transforms an electron donor into an electron acceptor, and this switching can be used to design photoswitchable rotaxanes as will be discussed in the following.

Acridanes possessing 9-aryl substituents with electron donor character are stable in EtOH and PrOH, but are ionogenic compounds in methanol solution (Scheme 18.14). Therefore, applications of photoheterolysis are restricted to solvents containing EtOH or PrOH.

18.4.2 Acridanes on Gold Nanoparticles

Esterification of **27** with liponic acid leads to **29** (Scheme 18.15), which is able to bind onto gold surfaces. Gold nanoparticles (GNPs) protected by dodecanthiol can be loaded with **29** by the exchange method [37]. Photoheterolysis of **30** in acetonitrile/MeOH is observed, but a complete recovery of acridane **30** by the thermal attack of the methoxide ion on the acridinium ion on the GNPs could not be observed.

18.4.3 Acridane Photoswitch for Switchable Rotaxanes

Rotaxanes are mechanically coupled molecules consisting of a wheel and an extended molecular axle, and these two parts are freely movable relative to each other. These nanostructures are promising candidates for the development of molecular machines [38,39]. The position of the wheel is governed by the interaction between the so-called recognition stations present in both the wheel and the axle. If at least two stations are present within the axle, the dynamics of the ring translation along the axle depends on the presence of identical or different stations. Degenerate rotaxanes contain two identical stations and

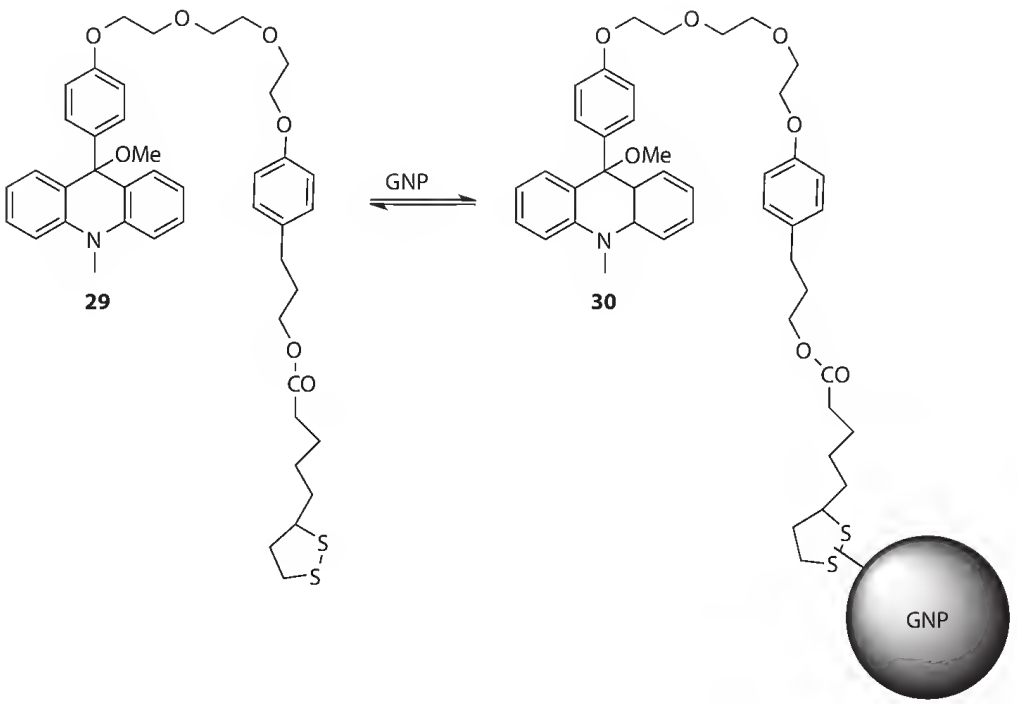

SCHEME 18.15 Immobilized acridane **30**.

the wheel shuttles between them by Brownian motion. The activation energy of this shuttle movement depends on both the chemical structure of the axle and the distance between the two stations [40]. If the energy of the interaction between the two different stations and the wheel is sufficiently large, the wheel will exclusively reside on the station that supplies the highest energy gain for the wheel–axle interaction. In switchable rotaxanes, the energy of interaction for the recognition station and the wheel is drastically weakened by an external stimulus. Accordingly, the interaction with the second, unchanged station is favored and the ring moves to this station and the so-called co-conformation is completely rearranged by Brownian motion. Solvents, chemicals, electrons, and photons are able to act as stimuli. Using light is advantageous because no side products of the switching process are evolved and because light action is addressable. The reset can take place either photochemically or thermally.

Photoresponsive rotaxanes based on the photoheterolysis of an acridane unit, which is at the same time a bulky end group, has been developed (Scheme 18.16) [35,36]. The tetracationic wheel cyclobis(paraquat-4,4′-bisphenylene (**CBQT**$^{4+}$) is a strong electron acceptor. Accordingly, recognition stations within the axle should be the electron donors. Besides charge-transfer π-stacking, edge-to-face interactions and C–H–O hydrogen bonds also contribute to the interaction between the wheel and the axle stations. In rotaxanes **31** and **33**, the acridane stations and the evasive stations B must compete for the interaction with the wheel. Although the aryl groups present at the 9-position of the acridane of **31** and the station B are very similar, the wheel exclusively resides on station A because an additional edge-to-face interaction is only possible with the acridane station. The position of the wheel can easily be determined by ^{1}H-NMR, ^{13}C-NMR, and two-dimensional NMR spectroscopy such as ROESY. The acridane units in the rotaxanes undergo photoheterolysis resulting in the acridinium rotaxanes **32** and **34** (Scheme 18.16). The formation of the acridinium moiety is evidenced by transient UV-Vis absorption spectra. Due to the generation of a positive charge, the tetracationic wheel is repelled and moves to the evasive station B, driven by Brownian motion. Because of the inner filter effect of the absorption by the wheel and the low-lying charge-transfer state formed by the interaction between the acridane station and the wheel, the quantum yield of photoheterolysis is drastically reduced to ≤0.1 for **31** and ≤0.05 for **33**. This process is a general disadvantage of systems based on charge–transfer interaction. The lifetime of

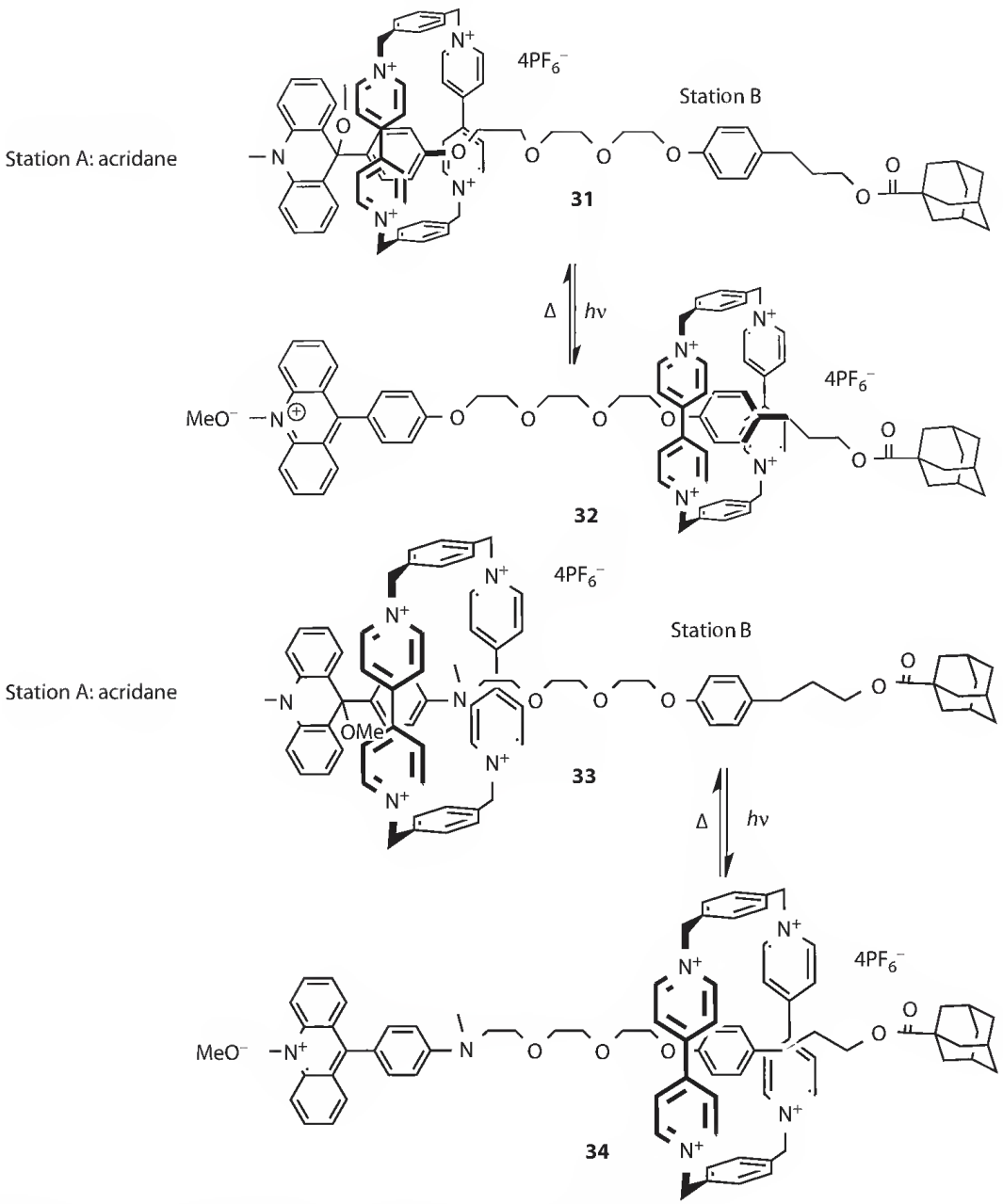

SCHEME 18.16 Two photoswitchable rotaxanes based on photoheterolysis.

the acridinium state of the rotaxanes depends strongly on the solvent used, ranging from about 100 s in neat methanol to several hours in acetonitrile with 10%–20% ethanol. In every case, there is enough time for ring movement. Owing to the reaction of the acridinium moiety with the alcohol assisted by the methoxide, the acridane is recovered and the wheel moves back to station A. This cycle can be repeated without fading of the system.

The drawback of reduced efficiency of photoheterolysis caused by the charge-transfer state is circumvented in rotaxanes with two acridane stations such as in **35** (Scheme 18.17). Because only one of the two acridane stations can be occupied by the wheel, the free acridane station is exclusively excited to give the acridinium station. Now, the type of movement is changed. In rotaxanes such as **31**/**32** only one of the two stations is always occupied, and thus, the wheel does not move. In the degenerate rotaxane **35**, the wheel

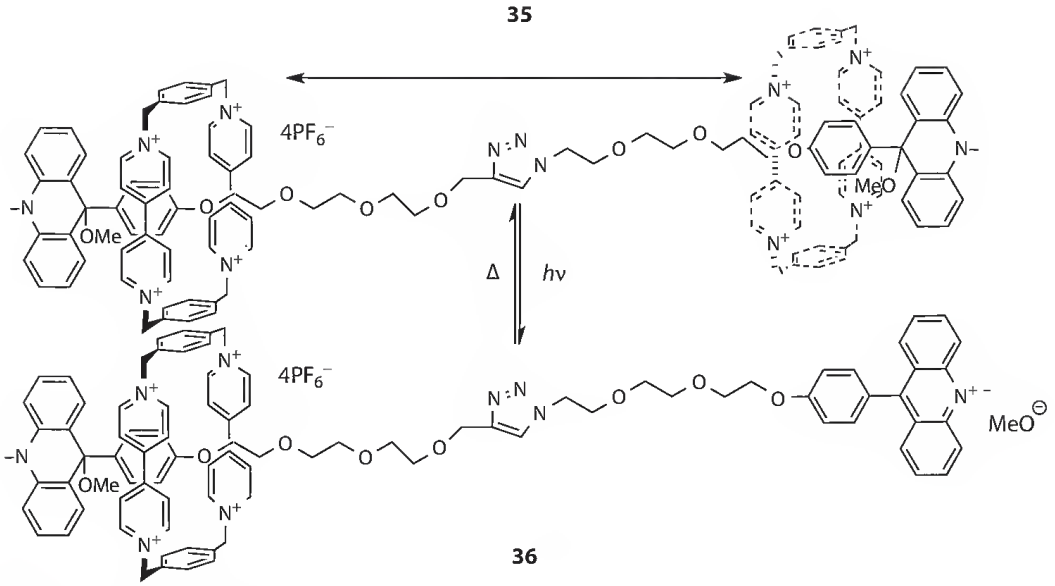

SCHEME 18.17 A rotaxane with two acridane units.

translates from one acridane station to the other. By photoheterolysis of only one of the two acridane stations, the wheel will remain at the unchanged station, thereby stopping the wheel movement [41].

It is noteworthy that the interaction of the wheel with the acridane units in rotaxanes **31**, **33**, and **35** protects the acridane moiety from solvolysis. In contrast to compounds **23** and **25** (Scheme 18.13), the acridinium rotaxanes react in diluted solutions of protic solvents to give the corresponding acridane rotaxanes [35,36]. This behavior is attributed to the energy gained by the interaction between the wheel and axle.

18.4.4 Photoswitchable Hosts with Acridane Subunits

The change of electronic properties and of the molecular shape by switching from acridanes to acridinium ions can also be used to switch the complexation properties of hosts such as calixarenes [42–44] and crowns [45].

The change in shape between the acridane and acridinium moieties results in the respective opening and closing of the inner cavity of calixarenes (Scheme 18.18) [42].

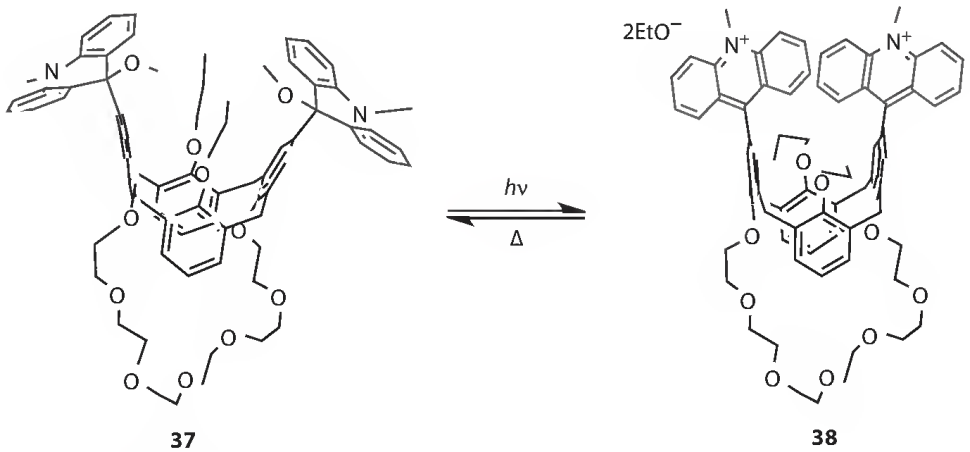

SCHEME 18.18 Blocking of the cavity of a calixarene by photoheterolysis.

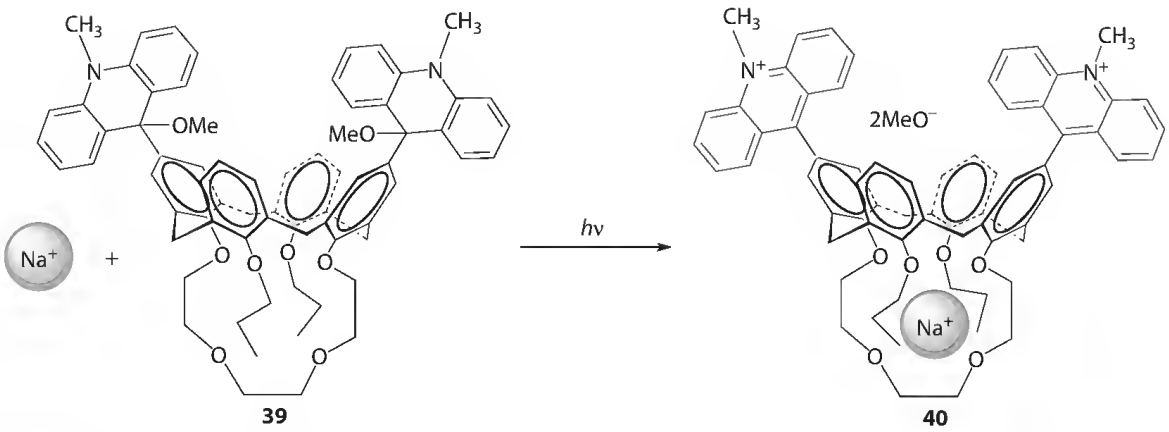

SCHEME 18.19 Uptake of Na^+ ions induced by photoheterolysis of acridane calixarene **39** in acetonitrile solution.

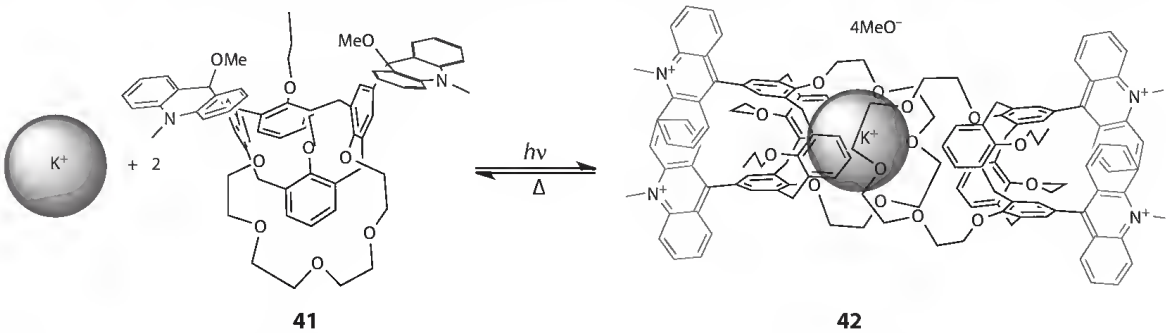

SCHEME 18.20 Uptake of K-ions induced by photoheterolysis of calixarene **41** in acetonitrile/EtOH 4:1 solution.

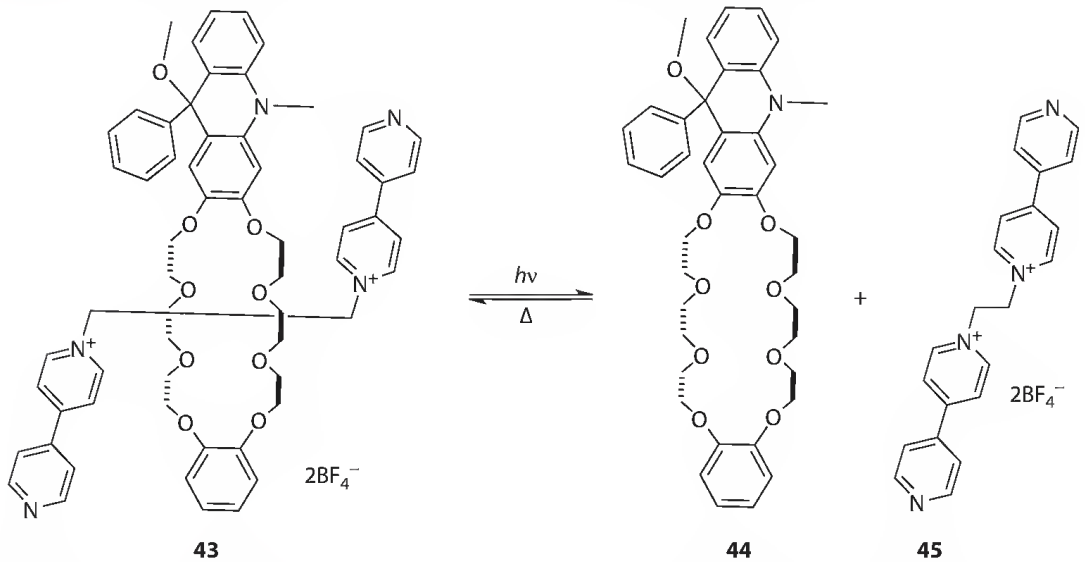

SCHEME 18.21 Decomplexation of the pseudorotaxane **43** by photoheterolysis of the acridane host in acetonitrile solution.

Acridane and acridinium ions, respectively, at the wide rim of calix[4]arenes influence the complexation properties of the glycol chain at the narrow rim, as illustrated in Scheme 18.19 [43]. Against all expectations, the acridinium-substituted calixarene **40** binds Na-ions more strongly than the corresponding acridane-substituted host. This process also holds true for calixarenes **41** and **42** (Scheme 18.20).

In contrast to **41**, the complexation of K^+ by **42** occurs in acetonitrile containing 20% ethanol. The latter solvent is necessary to support the thermal back reaction, thus making the system reversible. The complexation of different alkali ions by acridane- and acridinium-substituted calixarenes such as **41** and **42** has been studied by isothermal calorimetry. According to the results obtained for **42**, two host molecules are needed for complexation of one K-ion (Scheme 18.20) [44].

Furthermore, the complexation behavior of the crown **44** is changed by transformation into the acridane-substituted host [45]. The pseudorotaxane **43** is dethreaded by photoheterolysis in acetonitrile solution (Scheme 18.21). The slow recovery of the rotaxane can be followed by NMR spectroscopy.

18.5 Aryltropylium Ions

18.5.1 7-Methoxy-Aryl Cycloheptatriene as Precursors of Aryl Tropylium Ions

Aryltropylium salts such as **46–48** (Scheme 18.22) are converted into aryl-methoxy-cycloheptatrienes by reaction with methanol, resulting in three isomers (Scheme 18.22).

Cycloheptatrienes **49–51** contain the leaving group methoxide and the aryl substituent, which stabilizes the tropylium ion. Nevertheless, all tropylium ions react nearly quantitatively with methanol without the support of a base [46]. Laser flash photolysis of mixtures of the three isomers of **49–51** resulted in the formation of the corresponding aryltropylium methoxides both in methanol and acetonitrile solution. The transient UV-Vis absorption spectra corresponded to the absorption spectra recorded with stable tropylium salts. Simultaneously with the transient absorption, a photocurrent was formed, indicating the generation of ionic species. The quantum yield is 0.1 for the formation of **48** in MeOH solution. At constant absorbed dose, the transient absorption of **48** is much weaker in MeCN than in MeOH,

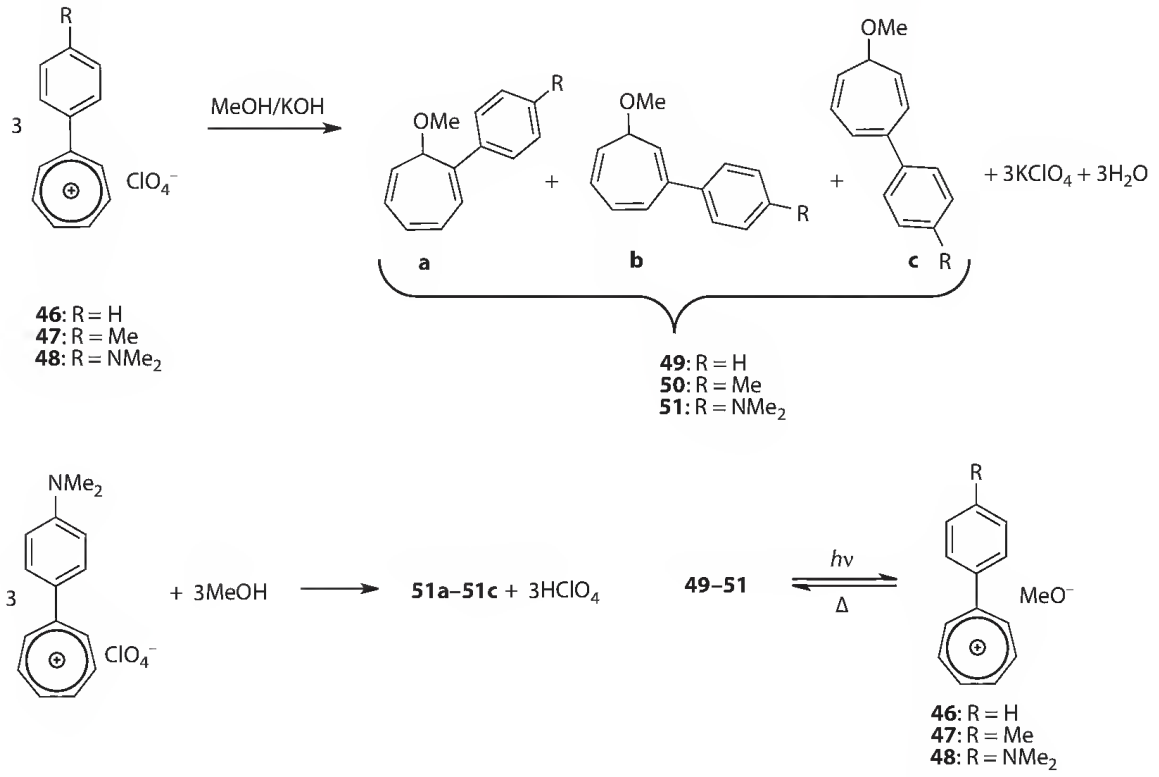

SCHEME 18.22 Formation of isomeric aryl-methoxy-cycloheptatrienes **49–51** and their photolysis.

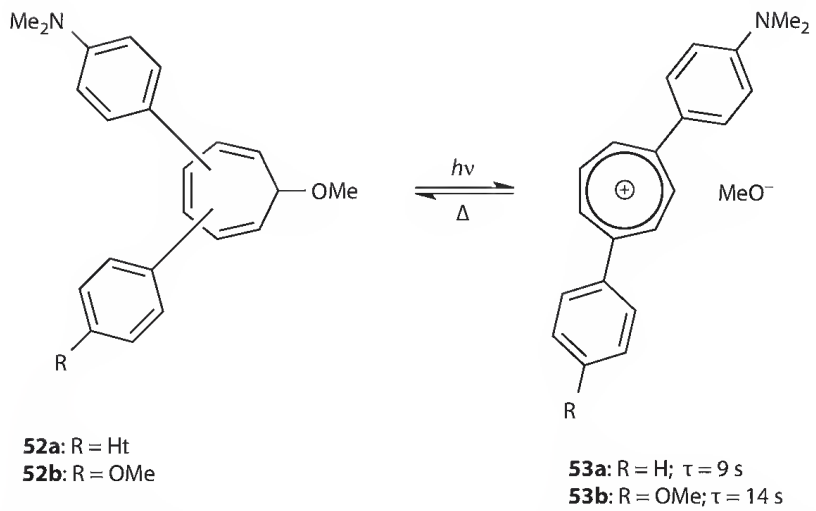

52a: R = Ht
52b: R = OMe

53a: R = H; τ = 9 s
53b: R = OMe; τ = 14 s

SCHEME 18.23 Photoheterolysis of isomeric 7-methoxy-diaryl-cycloheptatrienes in methanol solution.

indicating different ion yields in the two solvents. Additional transient absorptions by radicals were not observed. The lifetimes of the transient aryltropylium methoxides are in accord with the electron donating power of the aryl substituent (**46**: 190 µs, **47**: 270 µs and **48**: 3 s). The lifetimes can be elongated further by introduction of a second aryl group into the seven-membered ring (see Scheme 18.23) [47].

The aryltropylium methoxide **48** generated by laser flash photolysis of the isolated isomer **51c** disappeared by second-order kinetics because the direct combination of the ions takes place. In contrast, using a solution of **48** in MeOH without the addition of a base, the disappearance followed first-order kinetics exactly. In this case, the tropylium ion reacts with the solvent, because the methoxide ion is scavenged by protons formed in the reaction of **48** with methanol (see Scheme 18.22).

The switch cycle with **51c** can be repeated several times. However, irradiation of **51c** with 10 laser flashes (5.7×10^{-5} E l^{-1} $flash^{-1}$, flash duration 20 ns) reduces the intensity of the transient optical absorption due to the presence of **48** by a factor of 2. It is worth noting that 17 flashes (1×10^{-4} E l^{-1} $flash^{-1}$) reduce the intensity of the transient absorption of the tropylium ion **53b** to 50% [47]. Diaryl-substituted 7-methoxycycloheptatrienes allow an increased number of cycles.

The observed fading of tropylium ion generation is attributed to the competing hydrogen shift that shifts the methoxy group from the sp^3-C to sp^2-C, thus inhibiting the photoheterolysis.

The photochemistry of arylcycloheptatrienes is determined by a sigmatropic hydrogen shift and electrocyclization [48]. Therefore, it is astonishing that photoheterolysis is able to compete with these pericyclic reactions. The photochemistry of compound **51c** has been studied in more detail [49]. Steady-state irradiation of **51c** with light of 365 nm in acetonitrile solution resulted in the formation of the isomeric compound **51d** (Scheme 18.24). Isosbestic points observed with UV-Vis spectra recorded after consecutive irradiation revealed a uniform reaction. The formation of tropylium ions could not been observed with steady-state methods. However, neither could a uniform reaction be observed in methanol solution, indicating the occurrence of a second reaction, which is attributed to photoheterolysis followed by thermal reactions leading to various isomers from **51c**. The quantum yield of tropylium ion formation depends on the hydrogen bond capacity of the solvent ($\Phi_{MeOH} > \Phi_{ethyleneglycol} > \Phi_{EtOH} > \Phi_{i\text{-}PrOH}$).

Transient absorption spectra measured with methanol and acetonitrile solutions of **51c** using the pump-supercontinuum-probe technique [50] allowed the examination of reaction events during the time period immediately after the absorption of the 150 fs laser pulse [51]. Factor analysis of the spectra in the range 340–650 nm pointed only to two major components, which can be assigned to the excited singlet state of **51c** and to processes of two-photon absorption and relaxation of highly excited states. The lifetime of the first excited state is 440 ± 44 ps. This value corresponds to the rate of the formation of

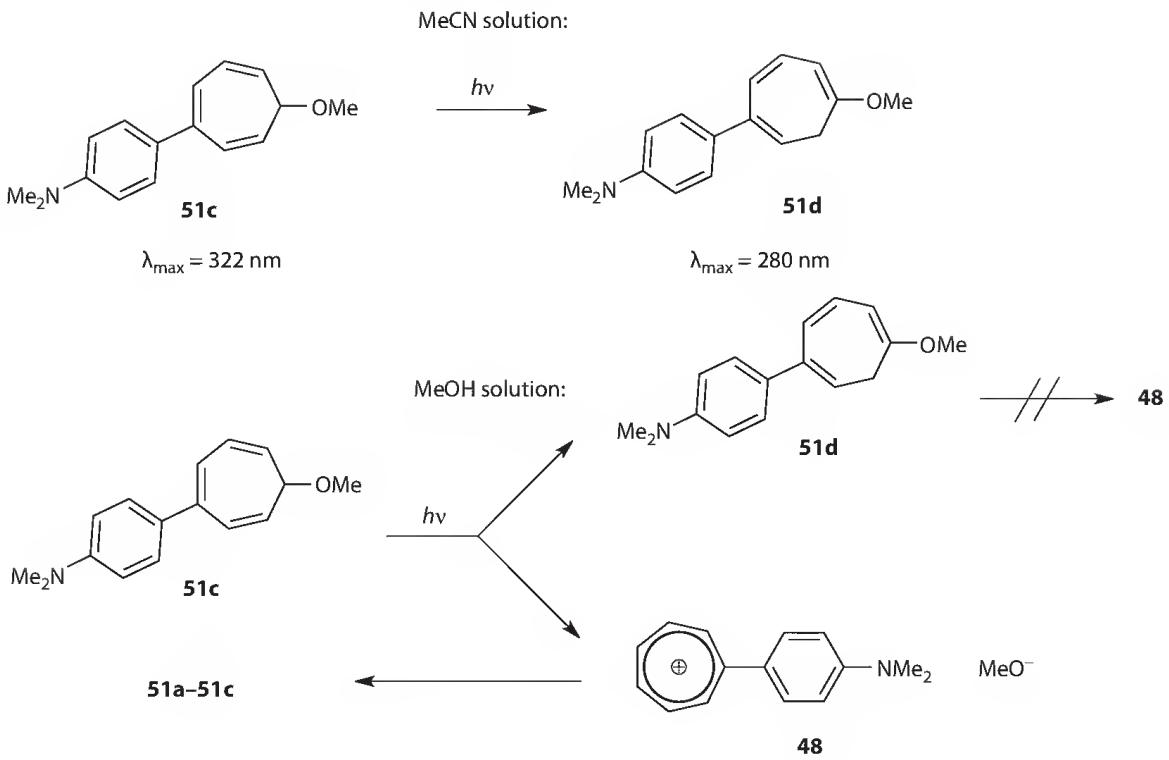

SCHEME 18.24 Photochemistry of compound **51c**.

the tropylium ion **48** (see Figure 18.3). The assignment of the component with the 440 ps lifetime to the first excited state was confirmed by fluorescence decay measurements ($\tau = 480 \pm 50$ ps).

The formation of **48** by photoexcitation of **51c** in acetonitrile was not observed.

18.5.2 Rotaxanes with the Cycloheptatriene Switch

Like the acridane switch, arylcycloheptatrienes with the methoxide leaving group convert an electron donor into an electron acceptor; the boat-like structure of the cycloheptatriene is transformed into the planar seven-membered ring of the tropylium ion and the color changes from colorless to blue (in the case of **51c**) [52]. Accordingly, photoswitchable rotaxanes were designed with **CBQT**$^{4+}$ as the wheel and with axles containing the cycloheptatriene switch in the center. Two examples are shown in Schemes 18.25 [53] and 18.26 [54].

Rotaxanes **54** and **56** also are based on charge transfer interactions between the cycloheptatriene stations and the tetracationic wheel. Therefore, the quantum yield of photoheterolysis of the 7-methoxy-diaryl-cycloheptatrienes is diminished to about 0.01 due to the higher rate of non-radiative decay of the excited state of the rotaxanes resulting from the existence of low-lying charge-transfer states. On the other hand, the hydrogen shifts as photoreactions competing with heterolysis are quenched in the rotaxanes, allowing more switching cycles of rotaxanes compared with the corresponding free molecular axle molecules. The lifetime of the rotaxane **55** is 15 s, a value significantly higher than that of **48**. Certainly, the lifetime is long enough to allow wheel movement from one station to another [55].

18.6 Retinyl Cation

Retinol is one of the chromophores of rhodopsin, and *trans-cis*-isomerization and heterolytic bond cleavage play important roles [1]. The quantum yield of photoheterolysis of **58a** (Scheme 18.27) was estimated as 0.1 and that of **58b** as 0.5 in methanol [56].

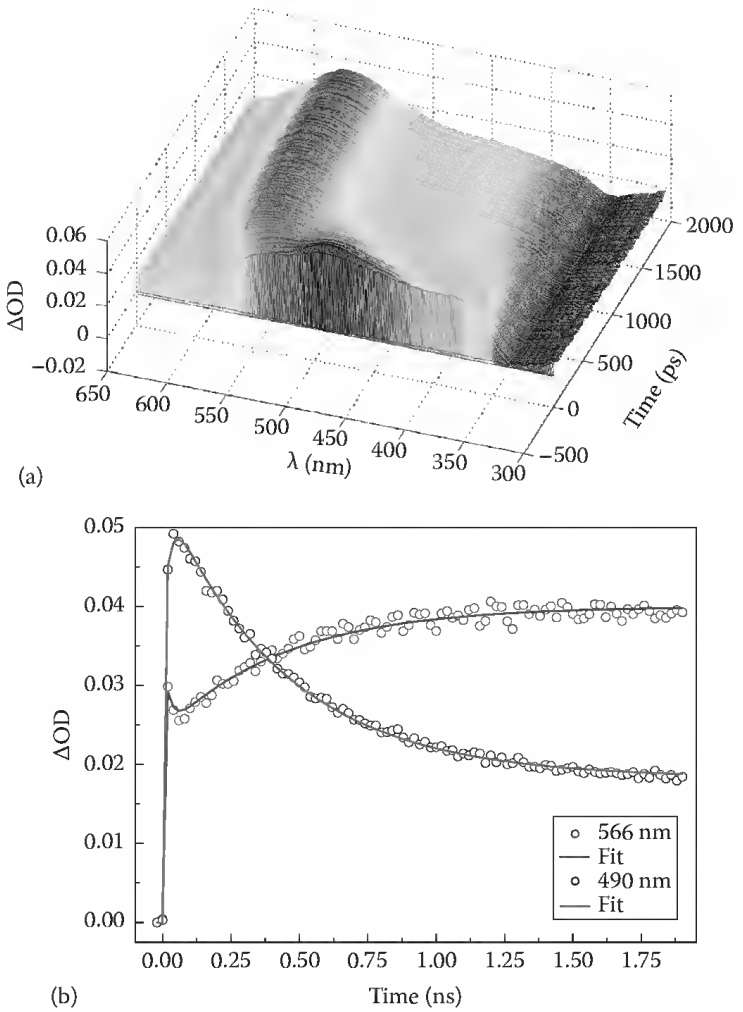

FIGURE 18.3 (a) **(See color insert.)** Three-dimensional representation of transient absorption spectra of **51c** in methanol recorded after excitation at 260 nm. (b) The transient absorption decays of **51c** in methanol measured after excitation at 260 nm—green line decay of the first excited state (490 nm); red line formation of **48** (566 nm).

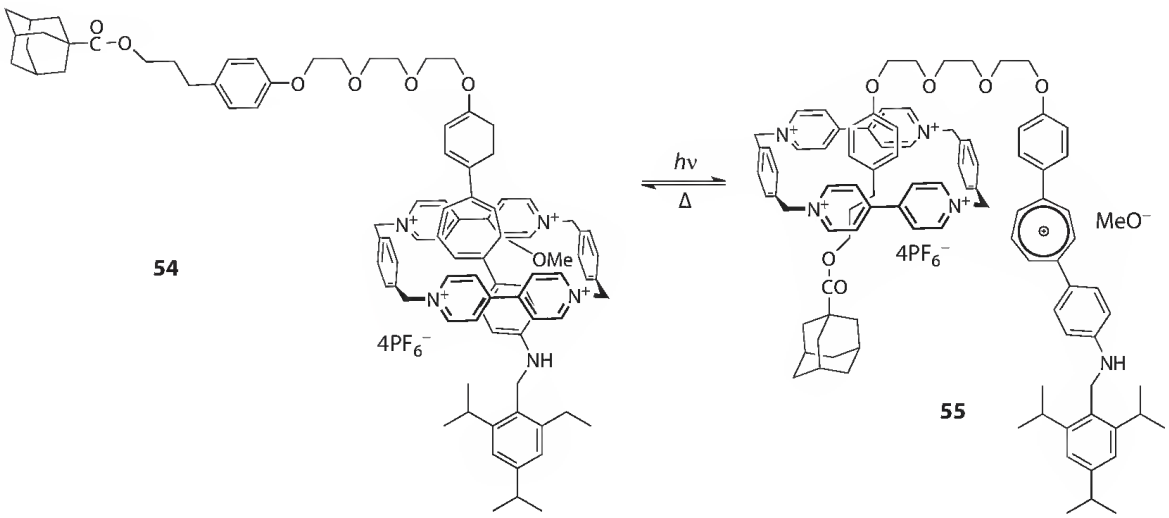

SCHEME 18.25 Switching the position of the wheel.

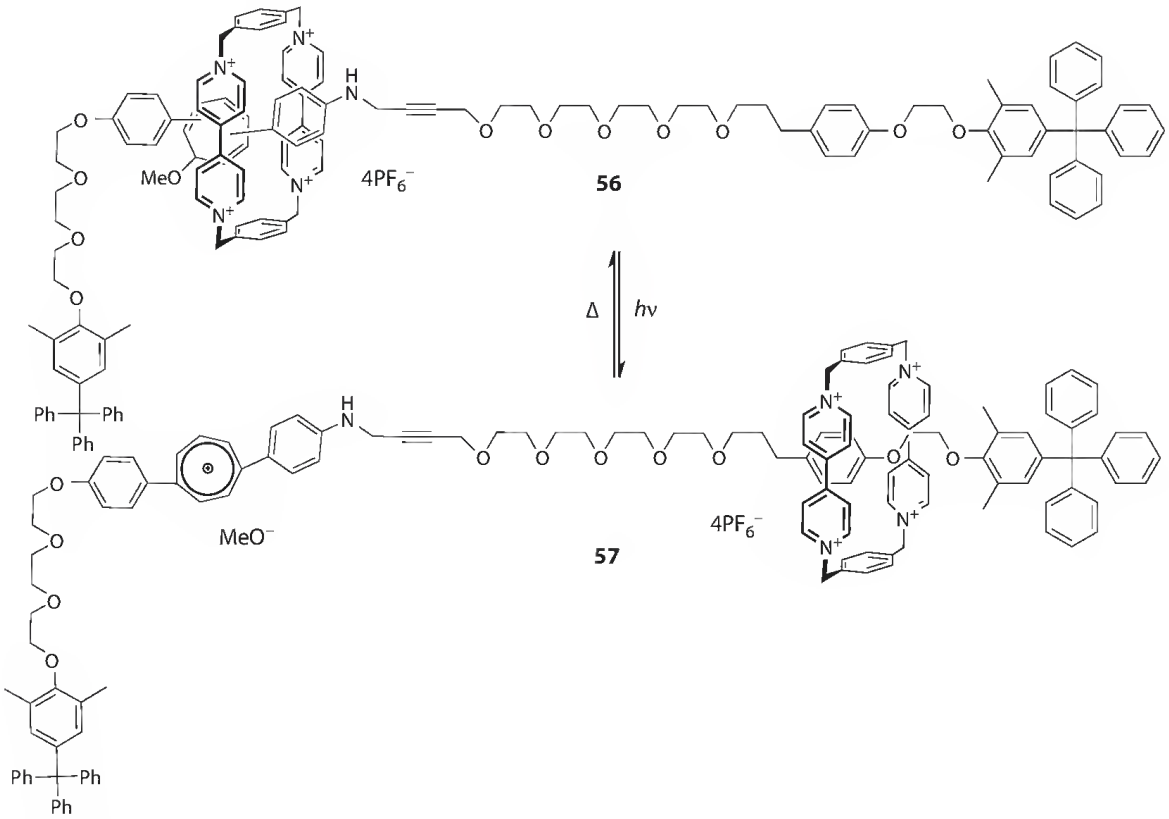

SCHEME 18.26 Photoswitchable rotaxane **56**.

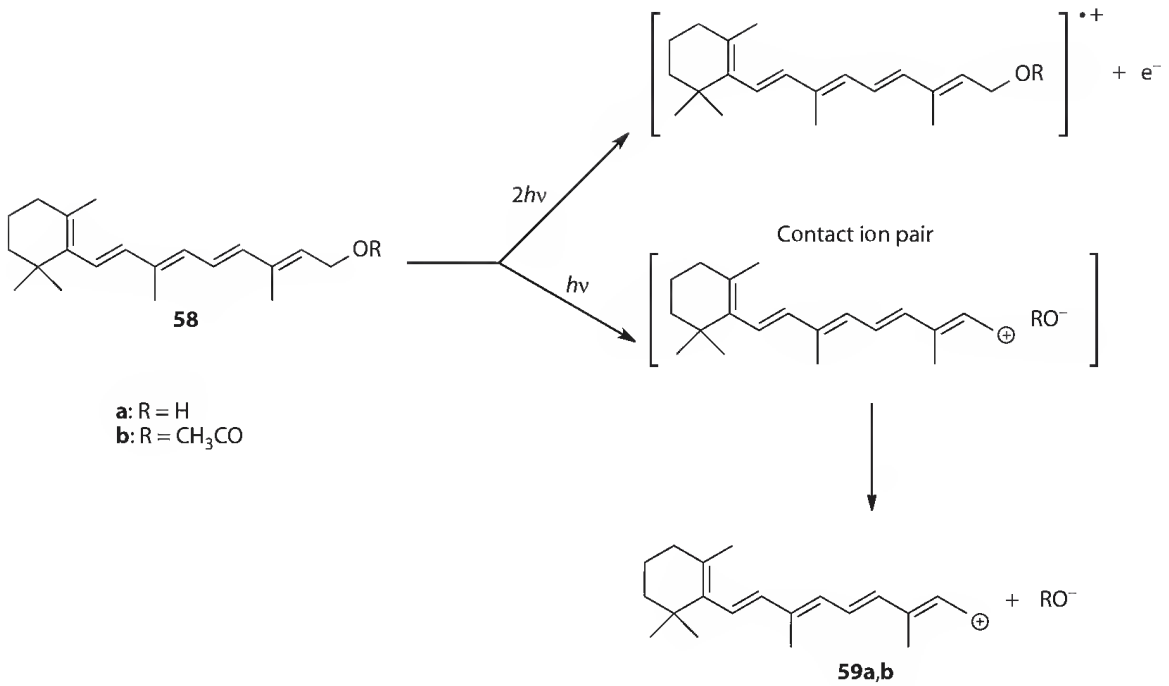

SCHEME 18.27 Generation of the retinyl cation by photoheterolysis.

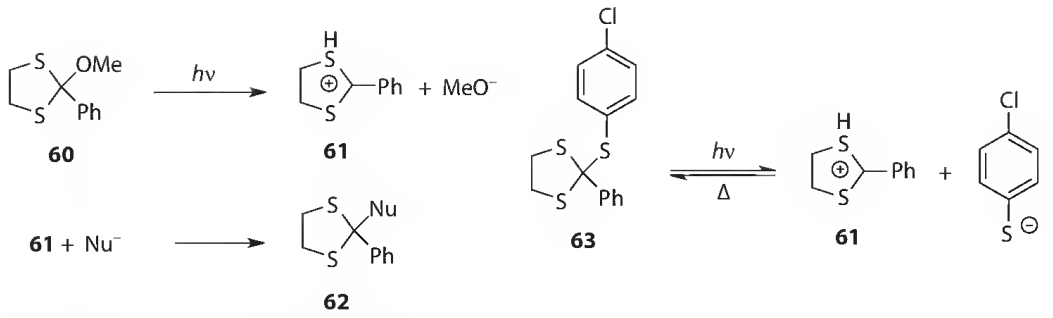

SCHEME 18.28 Photoheterolysis of 1,3-dithiolanes.

The lifetime of the cation is 20 µs in methanol [57]. The transient absorption of the retinyl cation peaking at 600 nm is blueshifted in viscous solvents such as 1-decanol in the time range of 1 ns [58]. Thus, it was concluded that the primarily heterolysis product was the contact ion pair. The heterolysis process is monophotonic. In contrast, the formation of the radical cation in methanol is a two-quantum process.

18.7 Dithio Carbocations

Sulfur atoms adjacent to positively charged carbon centers strongly stabilize the cations, thus shifting the lifetime into the second range (Scheme 18.28).

Transient UV spectra peaking at 342 nm in water/EtOH (1:1) were recorded in time intervals on the order of milliseconds. Time-dependent absorbance changes follow a pseudo-first-order decay with a rate constant of 0.56 s^{-1} [59]. The leaving group thiolate of **63** is a better nucleophile than water. Accordingly, in aqueous solution second-order kinetics were observed, indicating the ion combination in this case.

18.8 Concluding Remarks

The field of photolytic generation of carbocations has been developed over the last four decades, with the reactivity of carbocations with nucleophiles being the main focus of research. However, some examples of reversible heterolysis have been presented in the last decade. Reversible dissociation of suitable precursors results in very stable cations with lifetimes on the order of seconds to minutes. Such carbocations together with their precursors represent photoswitches. The following switchable properties are of interest:

1. Because the leaving groups mainly are strong bases, the pH of solutions is increased for a limited time, and the pH increase can be localized by laser flashes. This pH jump may be applicable for base-catalyzed polymerization or for base-catalyzed reactions. Up to now, studies with caged alkoxide bases have not been performed.
2. The switch from an electron donor to an electron acceptor has been used to govern the co-conformation of rotaxanes and the complexation properties of host molecules. However, further developments of applications are expected.
3. Because photoheterolysis results in the formation of two solvated ions, the conductivity of solutions can be switched. No applications of this effect are yet known.
4. Just the precursors of most stable carbocations are photochromic systems, and their colors are tunable by substituents. The lifetimes of the colored species are tunable by the solvents used for heterolysis.
5. At present, there have been no studies of photoheterolysis in polymers.

References

1. Das, P. K. Transient carbocations and carbanions generated by laser flash photolysis and pulse radiolysis. *Chem. Rev.* 1993, 93, 119–144.
2. McClelland, R. A. Flash photolysis generation and reactivities of carbenium ions and nitrenium ions. *Tetrahedron*, 1996, 52, 6823–6858.
3. Wan, P.; Yates, K.; Boyd, M. K. Adiabatic photodehydroxylation of 9-phenylxanthen-9- ol. Observation of carbocation fluorescence in neutral aqueous solution. *J. Org. Chem.* 1985, 50, 2881–2886.
4. Boyd, M. K.; Lai, H. Y.; Yates, K. J. Water quenching behavior of excited 9-xanthylium cations in aqueous sulfuric acid solutions. *J. Am. Chem. Soc.* 1991, 113, 7294–7300.
5. Ritchie, C. D. Cation-anion combination reactions. 26. A review. *Can J. Chem.* 1986, 64, 2239–2250.
6. McClelland, R. A.; Kanagasabapathy, V. M.; Steenken, S. Nanosecond laser flash photolytic generation and lifetimes in solvolytic media of diarylmethyl and p-methoxyphenethyl cations. *J. Am. Chem. Soc.* 1988, 110, 6913–6914.
7. McClelland, R. A.; Banait, N.; Steenken, S. Electrophilic reactions of xanthylium carbocations produced by flash photolysis of 9-xanthenols. *J. Am. Chem. Soc.* 1989, 111, 2929–2935.
8. McClelland, R. A.; Kanagasabapathy, V. M.; Narinder, S. B.; Steenken, S. Flash photolysis generation of triarylmethyl and diarylmethyl cations in aqueous solutions. *J. Am. Chem. Soc.* 1989, 111, 3966–3972.
9. McClelland, R. A.; Banait, N.; Steenken, S. Electrophilic reactivity of the triphenylmethyl carbocation in aqueous solutions. *J. Am. Chem. Soc.* 1986, 108, 7023–7027.
10. Bartl, J.; Steenken, S.; Mayr, H.; McClelland, R. A. Photo-heterolysis and -homolysis of substituted diphenylmethyl halides, acetates and phenyl ethers in acetonitrile: Characterization of diphenylmethyl cations and radicals generated by 248 nm laser flash photolysis. *J. Am. Chem. Soc.* 1990, 112, 6918–6928.
11. Irie, M. Light-induced reversible pH change. *J. Am. Chem. Soc.* 1983, 105, 2078–2079.
12. Ackman, A. J.; Frechet, J. M. J. The generation of hydroxide and methoxide ions by photo-irradiation: Use of aromatization to stabilize ionic photo-products from acridine derivatives. *Chem. Commun.* 1996, 605–606.
13. Abbruzzetti, S.; Carcelli, M.; Pelagatti, P.; Rogolino, D.; Viappiani, C. Photoinduced alkaline pH-jump on the nanosecond time scale. *Chem. Phys. Lett.* 2001, 344, 387–394.
14. Vittorino, E.; Cicciarella, E.; Sortino, S. A "Dual Function" photocage releasing nitric oxide and an anthrylmethyl cation with a single wavelength light. *Chem. Eur. J.* 2009, 15, 6802–6806.
15. Wan, P.; Krogh, E. J. Evidence for the generation of aromatic cationic systems in the excited state. Photochemical solvolysis of fluoren-9-01. *Chem. Soc. Chem. Commun.* 1985, 1207–1208.
16. Wan, P.; Krogh, E. J. Contrasting photosolvolytic reactivities of 9-fluorenol vs. 5-suberenol derivatives. Enhanced rate of formation of cyclically conjugated four π carbocations in the excited state. *J. Am. Chem. Soc.* 1989, 111, 4887–4895.
17. Gaillard, E.; Fox, M. A.; Wan, P. A kinetic study of the photosolvolysis of 9-fluorenol. *J. Am. Chem. Soc.* 1989, 111, 2180–2186.
18. Blazek, A.; Pungente, M.; Krogh, E.; Wan, P. Photosolvolysis of 9-fluorenol derivatives in aqueous solution—Exploratory studies of reactivity of photogenerated 9-fluorenyl cations. *J. Photochem. Photobiol. A* 1992, 64, 315–327.
19. Fischer, M.; Shi, Y. J.; Zhao, B. P.; Snieckus, V.; Wan, P. Contrasting behaviour in the photosolvolysis of 1- and 2-hydroxy-9-fluorenols in aqueous solution. *Can. J. Chem.* 1999, 77, 868–874.
20. Gurzadyan, G. G.; Steenken, S. Solvent_dependent C–OH homolysis and heterolysis in electronically excited 9-fluorenol: The life and solvation time if the 9-fluorenyl cation in water. *Chem. Eur. J.* 2001, 7, 1808–1815.
21. Cozens, L. F.; Mathivanan, N.; McClelland, R. A.; Steenken, S. Reactivities of 9-arylfluoren-9-yl and 1-(4-dimethylaminophenyl)ethyl cations in water and trifluoroethanol studies by laser flash photolysis. *J. Chem. Soc. Perkin Trans. 2* 1992, 2083–2090.

22. Lew, C. S. Q.; Wrong, D. F.; Johnston, L. J.; Bertone, M.; Hopkinson, A. C.; Lee-Ruff, E. Characterization and reactivity of the [N,N-dimethyl(thioformamidyl)]-9-fluorenyl cation. *J. Org. Chem.* 1996, 61, 6805–6808.
23. Johnston, L. J.; Kwond, P.; Shelemay, A.; Lee-Ruff, E. Electron-deficient carbocations. Direct observation of α-carbonyl methyl cations by laser flash photolysis. *J. Am. Chem. Soc.* 1993, 115, 1664–1669.
24. Hoang, M.; Gadosy, T.; Ghazi, H.; Hou, D.-F.; Hopkinson, A. C.; Johnston, L. J.; Lee-Ruff, E. Photochemical pinacol rearrangement. *J. Org. Chem.* 1998, 63, 7168–7171.
25. Mladenova, G.; Singh, G.; Acton, A.; Chen, L.; Rinco, O.; Johnston, L. J.; Lee-Ruff, E. Photochemical pinacol rearrangements of unsymmetrical diols. *J. Org. Chem.* 2003, 69, 2017–2023.
26. Mladenova, G.; Chen, L.; Rodriquez, C. F.; Stu, K. W. M.; Johnston, L. J.; Hopkinson, A. C.; Lee-Ruff, E. Studies of 9-fluorenyl carbocations. Intramolecular hydride migration in a substituted 9-fluorenyl carbocation. *J. Org. Chem.* 2001, 66, 1109–1114.
27. Johnston, L. J.; Lobaugh, J.; Wintgens, V. Laser flash photolysis studies of dibenzosuberenyl cations and radical cations. *J. Phys. Chem.* 1989, 93, 7370–7374.
28. Minto, R. E.; Das, P. K. A laser flash photolysis study of photodehydroxylation phenomena of 9-phenylxanthen-9-ol and photobehavior of related intermediates. Enhanced electrophilicity of 9-phenylxanthenium cation singlet. *J. Am. Chem. Soc.* 1989, 111, 8858–8866.
29. Misetic, A.; Boyd, M. K. The pixyl (Px) group: A novel photocleavable protecting group for primary alkohols. *Tetrahedron Lett.* 1998, 39, 1653–1656.
30. Coleman, M. P.; Boyd, M. K. The *S*-pixyl group: An efficient photocleavable protecting group for the 5′ hydroxy function of deoxyribonucleosides. *Tetrahedron Lett.* 1999, 40, 7911–7915.
31. Grigor'eva, T. M.; Ivanov, V. L.; Kuz'min, M. G. Photodissociation of derivatives of N-methyl-9-phenylacridan. *Zh. Org. Khim.* 1981, 17, 423–428.
32. Bunting, J. W.; Chew, V. S. F.; Abhyankar, S. B.; Goda, Y. Pseudo base formation from 9-substituted 10-methylacridinium cations in aqueous solution. *Can. J. Chem.* 1984, 62, 351–354.
33. Jonker, S. A.; Ariese, F.; Verhoeven, J. W. Cation complexation with functionalized 9-arylacridinium ions: Possible applications in the development of cation-selective optical probes. *Recl. Trav. Chim. Pays-Bas* 1989, 108, 109–115.
34. Jones II, G.; Farahat, M. S.; Greenfield, S. R.; Gosztola, D. J.; Wasielewski, M. R. Ultrafast photoinduced charge-shift reactions in electron donor-acceptor 9-arylacridinium ions. *Chem. Phys. Lett.* 1994, 229, 40–46.
35. Abraham, W.; Buck, K.; Orda-Zgadzaj, M.; Schmidt-Schäffer, S.; Grummt, U.-W. Novel photoswitchable rotaxanes. *Chem. Commun.* 2007, 3094–3096.
36. Abraham, W.; Wlosnewski, A.; Buck, K.; Jacob, S. Photoswitchable rotaxanes using the photolysis of alkoxyacridanes. *Org. Biomol. Chem.* 2009, 7, 142–154.
37. Duo, S.; Jacob, S.; Abraham, W. Photoswitchable rotaxanes on gold nanoparticles, *Org. Biomol. Chem.* 2011, 9, 3549–3559.
38. Stoddart, J. F. Molecular machines. *Acc. Chem. Res.* 2001, 34, 410–411.
39. Balzani, V.; Venturi, M.; Credi, A. *Molecular Devices and Machines*, Wiley-VCH, Weinheim, Germany, 2003.
40. Kay, E. R.; Leigh, D. A.; Zerbetto, F. Synthetic molecular motors and mechanical machines. *Angew. Chem. Int. Ed. Engl.* 2007, 46, 72–191.
41. Vetter, A.; Abraham, W. Controlling Ring Translation of Rotaxanes, *Org. Biomol. Chem.* 2010, 8, 4166–4681.
42. Grubert, L.; Abraham, W. Photoswitchable calix[4]arenes bearing dihydroacridine substituents at the upper rim. *Tetrahedron* 2007, 63, 10778–10787.
43. Grubert, L.; Hennig, H.; Abraham, W. Photo, proton and metal ion responsive wide-rim acridane substituted calix[4]arenes. *Tetrahedron* 2009, 65, 5936–5944.

44. Grubert, L.; Hennig, H.; Grummt, U.-W.; Abraham, W. Photoswitchable ionophores based on 1,3-alternate calix[4]arenes bearing acridane units at the wide rim and bridged at the narrow rim by glycol chains. *Tetrahedron* 2009, 65, 8402–8406.
45. Orda-Zgadzaj, M.; Abraham, W. Pseudorotaxanes and rotaxanes from macrocyclic rings incorporating acridinone, 9-phenylacridinium and 9-phenyl-9-methoxy-acridane moieties. *Tetrahedron* 2008, 64, 2669–2676.
46. Pischel, U.; Abraham, W.; Schnabel, W.; Müller, U. The photogeneration of aryltropylium ions: A potential photo-switch for supramolecular assemblies based on donor-acceptor interaction. *Chem. Commun.* 1997, 1383–1384.
47. Pischel, U.; Abraham; W. 1998, unpublished results.
48. Abraham, W.; Kharlanov, V. 2003. Photochemistry of cycloheptatrienes and their related tropylium ions. In *Handbook of Photochemistry and Photobiology, Vol. 2: Organic Photochemistry*, ed. H. S. Nalwa, pp. 299–333. American Sci. Pub., Los Angeles, CA.
49. Kharlanov, V. A.; Abraham, W.; Pischel, U. Theoretical and spectroscopic studies of the photochemistry of 3-(4-dimethylaminophenyl)-7-methoxy-cyclohepta-1,3,5-triene. *J. Photochem. Photobiol. A: Chemistry* 2004, 162, 213–223.
50. Ernsting, N. P.; Kovalenko, S. A.; Senyushkina, T.; Saam, J.; Farztdinov, V. Wave-packet-assisted decomposition of femtosecond transient ultraviolet-visible absorption spectra: Application to excited-state intramolecular proton transfer in solution. *J. Phys. Chem. A* 2001, 105, 3443–3453.
51. Tokarczyk, B.; Wirz, J.; Abraham, W. 2004, unpublished results.
52. Abraham, W.; Grubert, L.; Schmidt-Schäffer, S.; Buck, K. Pseudorotaxanes and rotaxanes incorporating diarylcycloheptatriene stations. *Eur. J. Org. Chem.* 2005, 374–386.
53. Abraham, W.; Grubert, L.; Grummt, U.-W.; Buck, K. A photoswitchable rotaxane with a folded molecular thread. *Chem. Eur. J.* 2004, 10, 3562–3568.
54. Schmidt-Schäffer, S.; Grubert, L.; Grummt, U.-W.; Buck, K.; Abraham, W. A photoswitchable rotaxane with an unfolded molecular thread. *Eur. J. Org. Chem.* 2006, 378–398.
55. Balzani, V.; Gómez-López, M.; Stoddart, J. F. Molecular machines. *Acc. Chem. Res.* 1998, 31, 405–414.
56. Rosenfeld, T.; Alchalal, A.; Ottolenghi, M. 1976. Intersystem crossing, ionic dissociation and cis-trans isomerization mechanisms in the photolysis of retinal and related molecules. In *Excited States of Biological Molecules*, ed. J. B. Birks, p. 540. New York: Wiley.
57. Pienta, N. J.; Kessler, R. J. Pentaenyl cations from the photolysis of retinal acetate. Solvent effects on the leaving group ability and relative nucleophilicities: An unequivocal and quantitative demonstration of the importance of hydrogen bonding. *J. Am. Chem. Soc.* 1992, 114, 2419–2428.
58. Gurzadyan, G. G.; Reynisson, J.; Steenken, S. Photoionization *versus* photoheterolysis of all-*trans*-retinol. The effects of solvent and laser radiation intensity. *Phys. Chem. Chem. Phys.* 2007, 9, 288–298.
59. Okuyama, T.; Haga, N.; Takane, S.-Y.; Ueno, K.; Fueno, T. Flash photolytic generation of a dithio carbocation from 1,3-dithiolane derivatives and its reaction with nucleophiles. *Bull. Chem. Soc. Jpn.* 1991, 64, 2751–2756.

19

Intermolecular Photochemical Hydrogen Abstraction: Synthetic Applications in Relation to Carbon–Carbon Bond Formation

Niall W.A. Geraghty
National University of Ireland Galway

Mary Treasa Lohan
National University of Ireland Galway

19.1 Introduction

19.1.1 Overview

The formation of carbon–carbon bonds is the key process in the synthesis of the vast majority of organic molecules, and, understandably, an enormous range of methods for carrying it out is currently available. As a result of developments in synthetic methodology over the last 20–30 years, many of these now involve C-radicals [1]. Although such methods are synthetically very valuable, their use is problematic as the generation of the C-radicals generally involves the use of tin compounds, peroxides, or azo compounds, all of which are undesirable in terms of clean/green chemistry and of the concept of sustainability in general. This chapter explores the synthetic utility of photochemical intermolecular H-abstraction as an alternative method of generating C-radicals for use in C–C bond formation (Scheme 19.1). This process is one of a number of related photochemical processes that tend to be grouped together under the general heading of "photocatalytic methods." The synthetic potential of these methods has been recognized in a recent comprehensive review [2], although they have been largely ignored in an otherwise

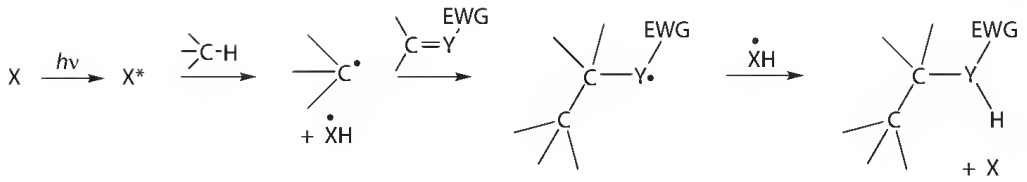

SCHEME 19.1

thorough description of the role of C–H transformations in organic synthesis [3]. The particular focus of this chapter is on systems in which C-radical formation involves intermolecular H-atom abstraction from a C–H bond; intramolecular H-abstraction processes are only considered when they are relevant to a discussion of related intermolecular reactions. Photoreactions that involve a single electron transfer (SET) have also been excluded; details of such processes, which include the generation of α-aminoalkyl radicals, are available elsewhere [2]. Photochemical C-radical forming reactions involving peroxides, tin compounds, or γ-radiation make up a third group that are not dealt with in this chapter.

The reactions considered fall into two different classes. In one of these the radical generation process involves the intervention of what is here called a photomediator, X, which until recently was most often an aromatic ketone (Scheme 19.1). The terms "photoinitiator" and "photocatalyst" have also been used to describe the role played by this agent, but as there is rarely evidence for a chain mechanism and as most reactions of this type involve quantities of X that are well in excess of what could reasonably be called "catalytic," the term "photomediator" is preferred*. Once generated, these C-radicals are indistinguishable from those generated in any other way, for example, using peroxides. They are in general nucleophilic in character and if generated in the presence of a molecule containing an electron-deficient multiple bond that includes at least one C-atom, conjugate addition will lead to the formation of a C–C bond [4]. In reactions in the second class, no specific photomediator is added and instead it is the unsaturated substrate that, following excitation, abstracts a H-atom from the donor molecule. The term "direct" is used in this review to describe reactions of this second class.

In addition to avoiding the use of undesirable reagents, the method has a number of other advantages. It is atom efficient in the usual sense that all of the atoms in the reactant molecules end up in the product. The nature of the reaction allows molecules such as cycloalkanes and cyclic ethers, which are not functionalized in the normal sense and are most commonly encountered as solvents, to participate as H-donors. It also opens up different reaction pathways for molecules, such as in the case of a secondary alcohol, which reacts through its methine hydrogen rather than in the usual way through its hydroxyl group. In many cases, the photomediator is effective in significantly substoichiometric quantities [5,6] relative to the amount of the unsaturated reactant and so its involvement does not materially affect the atom efficiency of the process. An interesting property of the reaction system is that it can be driven by solar radiation [7], as two of the most widely used photomediators, benzophenone [8] and the polyoxometallate tetrabutylammonium decatungstate (TBADT) [9], absorb at approximately 350 nm, a wavelength that is available in the sunlight reaching the surface of the earth.

The approach also has its disadvantages such as the requirement that the H-donor is present in large excess, and thus must be removed from the product mixture. This effectively restricts the reaction to readily available H-donors of relatively low molecular mass, which can be recovered by distillation after the reaction is complete. The fact that the photomediators are not selective in terms of H-abstraction also precludes the use of large molecules with many different types of C–H bond. In some cases an efficient reaction requires the use of approximately stoichiometric quantities of the photomediator, partly because some, or indeed most of it, is rendered inactive as a result of ketyl radical recombination (Scheme 19.2). This again adds to the experimental difficulties associated with the isolation of the product. The problem of removing the photomediator and a desire to enhance the reaction system from the clean/green chemistry

* For a discussion of the use of these terms, see: Ref. [2, p. 2726].

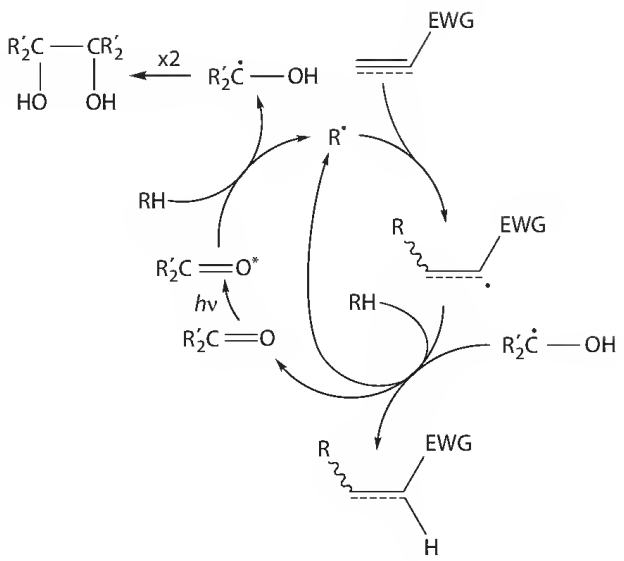

SCHEME 19.2

perspective have led to an interest in the use of supported photomediators, which can be removed by simple filtration after the reaction and recycled [8]. The introduction of TBADT, a photomediator that can be used in essentially catalytic quantities and that is effective with greatly reduced amounts of the H-donor [6], is a further indication that these problems can be, at least partially, ameliorated.

Aromatic ketones are widely used as photomediators and the mechanism by which they function (Scheme 19.2) provides an insight into the issues that are generically important for all classes of photomediators and facilitates a discussion of the factors relating to the behavior of the H-donor, photomediator, and unsaturated system. In addition, it underlines the fact that when most inefficient, the process requires at least one photon of light to complete the reaction cycle. However there is the possibility that the back H-transfer to the radical precursor of the product may involve a molecule of H-donor, RH, rather than the ketyl radical or its equivalent, and that as a result the process can assume the character of a chain reaction. The amount of photomediator required to achieve an efficient reaction is system dependent, suggesting that the contribution of a chain reaction to product formation also depends on the particular molecules involved. Although the possibility of developing reaction systems that are based on a chain mechanism is attractive, the evidence suggests that at best the chains involved are relatively short. The mechanism also emphasizes that if the back transfer of the H-atom is slow then recombination of the ketyl radicals can occur, leading to a removal of the aromatic ketone from the reaction cycle. The degree to which this process is a problem depends on the reaction system involved and the fact that it is not an option for photomediators such as TBADT is one of the major differences between aromatic ketones and such polyoxometallates, the two most widely used classes of photomediator.

19.1.2 Hydrogen Donors

Ketones, and in particular aromatic ketones such as benzophenone, are the most widely used photomediators. The similarity in the behavior of such ketones, in their (n,π*) excited state, and that of alkoxy radicals was first pointed out over 40 years ago [10] and still remains the basis for rationalizing the photochemistry of ketones in that particular excited state. Although there is evidence to suggest that H-abstraction from relatively weak C–H bonds (bond dissociation energies (BDEs) < 92 kcal mol^{-1}) by the sterically hindered *t*-butoxy radical is entropy controlled [11], the general implication of the Evans–Polanyi relationship is that the rate constants for H-abstraction are expected to increase with decreasing BDE. This suggests that a consideration of BDEs [12] would be a reasonable way to identify suitable H-donors for photochemical H-abstraction (Table 19.1, Column 1), and that there should be a

TABLE 19.1 Correlation between Reactivity of H-Donors and Bond Dissociation Energy (BDE)

H-Donors That Produce Nucleophilic C-Radicals				H-Donors That Produce Non-Nucleophilic C-Radicals		Systems That Are Unsuitable as H-Donors due to Large C–H BDE	
H-Donor	BDE[a]	H-Donor	BDE[a]	H-Donor	BDE[a]	H-Donor	BDE[a]
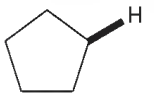	400.0	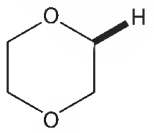	401.7	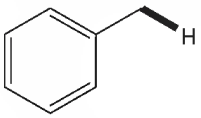	375.5	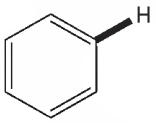	472.2
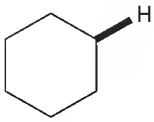	416.3	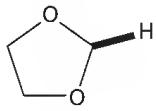	381.2	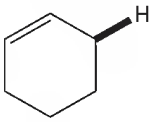	341.5		464.8
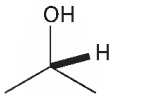	390.5	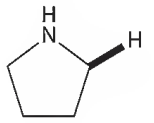	377.0	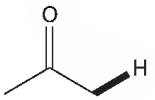	401.7	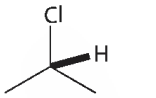	423.1
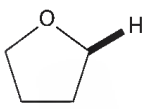	391.6	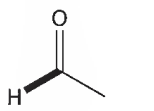	374.0				544.8

[a] kJ mol^{-1}; values taken from Ref. [12].

correlation between the regioselectivity of the process and the strength of the various C–H bonds in a molecule. There are however many C–H systems with relatively small BDEs that do not participate in C–C bond formation with electron-deficient alkenes following H-abstraction (Table 19.1, Column 2). The radicals in these cases have, as a result of resonance, low-energy SOMOs, which will not interact with the alkene LUMO, and are thus non-nucleophilic. Interestingly, resonance is also the reason why the abstraction of an aldehydic hydrogen occurs so readily (Table 19.1, Column 1) and why the acyl radicals thus formed are nucleophilic (Figure 19.1). For many molecules, the size of the BDE of their C–H bonds precludes H-abstraction on thermodynamic grounds (Table 19.1, Column 3). In addition to resonance and the general BDE order, primary C–H > secondary C–H > tertiary C–H, which reflects the induction and hyperconjugation determined stability of the C-radicals resulting from the dissociation, a number of other factors have been implicated in the C–H bond dissociation process. The rate of H-abstraction from C–H bonds α to O-atoms (Table 19.1, Column 1), for example, is subject to a stereoelectronic effect [13–16]. A high rate is associated with a small dihedral angle, θ, between the p-type lone pair of electrons on the O-atom and the dissociating C–H bond (Figure 19.2). A similar effect has

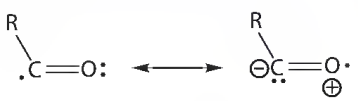

FIGURE 19.1

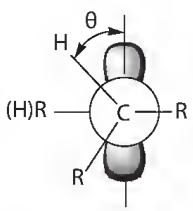

FIGURE 19.2

been observed for amines [17], with those for which the α-C–H and the lone pair of the N-atom have an eclipsing relationship again being the most reactive. A strain-enhanced hyperconjugation effect, involving the cyclobutane ring, has been invoked in an attempt to rationalize the surprisingly low BDE of the α-keto methylene hydrogens in pinonaldehyde [18].

The photomediated reaction of alcohols with alkynes [19] provides a good example of what can be expected from photomediated H-abstraction in terms of reactivity and regioselectivity (Table 19.2). The highly regiospecific abstraction of the methine hydrogen in 1,2-propanediol and 1,2-butanediol is an example of the well-established preference for the formation of a tertiary rather than a secondary radical. The difference between the BDEs of the α-C–H bonds of 1-propanol and 2-propanol, 399.5 and 390.5 kJ mol^{-1} [20], respectively, contributes to the observed regiochemical preference. The essentially exclusive formation of a product derived from the formal cleavage of the methine C–H bond may also be in part due to the fact that a large excess of the alcohol is involved, as is usual in this type of reaction [21], resulting in the conversion of any secondary radicals to the corresponding, and more thermodynamically stable, tertiary radicals. Although the methine C–H in 2-pentanol still enjoys a BDE advantage relative to the other C–H bonds, this is now balanced by the statistical effect of the increased number of C–H bonds and the formation of a complex mixture of addition products ensues. Overall, synthetically useful photochemical H-abstractions involve H-donors of the general types discussed earlier (Table 19.1, Column 1), which for reasons of reactivity and/or symmetry contain effectively only one reactive C–H bond. In practice, and as discussed earlier, the requirement for a large excess of the H-donor generally restricts the process to H-donors of relatively high volatility, which can be removed by distillation once the reaction is complete.

19.1.3 Photomediators

In terms of synthetic applications, benzophenone is the most extensively used photomediator and in many ways is a model of how a good photomediator should behave. It has absorption bands at approximately 350 nm, a wavelength where most of the reactants and products that might be involved in the process are almost transparent and so there is little competition for the incident light. The formation of its triplet state occurs with $\Phi \sim 1$, the (n,π^*) configuration being the lowest in energy. This has a relatively long lifetime (0.71 ms [22]) and involves a significant localization of spin density on the O-atom that gives it the alkoxy radical character, which is essential in terms of H-abstraction. Ketones for which the lowest triplet state is of the (π,π^*) type do not have alkoxy radical character and so do not function as photomediators [23]. The benzophenone ketyl radical, the product of the H-abstraction process, is very stable for electronic and steric reasons and does not interact with either the unsaturated reactant or the product; it does however complete the reaction by back transferring the abstracted H-atom to the product radical (Scheme 19.2). Dimerization of the ketyl radical becomes competitive if this back transfer is slow (Scheme 19.2); as outlined earlier, this removes the photomediator from the reaction loop, necessitating the use of larger amounts in order to secure complete reaction, and thus adding to the problems associated with product isolation. The effectiveness of a photomediator can also be reduced if it undergoes a unimolecular reaction. Thus although the reactivity of decafluorobenzophenone in terms of H-abstraction from alkanes and alcohols is 10–40 times greater than that of benzophenone [24], an effect attributed to enhanced spin localization on the carbonyl oxygen [25], its attractiveness is reduced by a propensity to undergo a disproportionation reaction forming decafluorobenzhydrol in polar solvents [26]. In general however, the effect of substituents on the rate of H-abstraction has been shown to be relatively slight, with a single order of magnitude covering the reactivities of a range of typical aromatic ketones [27]. Thus, for example, acetophenone, and benzophenone have almost identical reactivities.

All these photomediators suffer, however, from the disadvantage that chromatography is required to remove them from the product mixture, an issue that becomes more problematic as the amount of photomediator required to promote the reaction increases. Although less desirable from the photophysical and photochemical perspectives, the use of acetone as photomediator, and often as cosolvent, obviates this problem. The availability of a range of water-soluble derivatives of benzophenone [28], such as the sulfonic

TABLE 19.2 Photomediated Addition of Alcohols to Alkynes

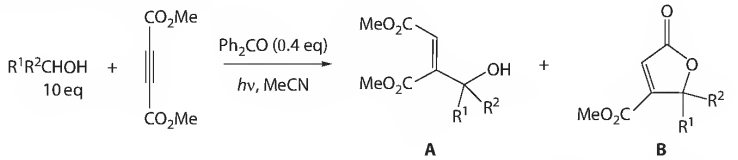

A B

R^1R^2CHOH	Reaction Time (min)	Isolated Yield of A (%)	Isolated Yield of B (%)
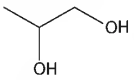	35	61 R^1 = Me; R^2 = CH_2OH	18 R^1 = Me; R^2 = CH_2OH
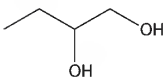	50	60 R^1 = Et; R^2 = CH_2OH	0 R^1 = Et; R^2 = CH_2OH
	45	37 R^1 = R^2 = Me	31 R^1 = R^2 = Me
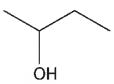	70	40 R^1 = Me; R^2 = Et	0 R^1 = Me; R^2 = Et
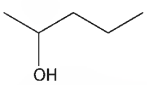	80	Complex mixture of products (IR: 1723 cm^{-1})	

Source: Data from Geraghty, N. W. A. and Hernon, E. M., *Tetrahedron Lett.*, 50, 570, 2009.

acid sodium salt (**1**) [29] or the commercially available quaternary ammonium salt (**2**) [30], enhances the methodology from the green chemistry perspective. In addition such photomediators can be separated from the reaction product without the need for chromatography. A number of inorganic ions, particularly the decatungstate anion, $W_{10}O_{32}^{4-}$, in the form of the acetonitrile soluble TBADT, have also found use as photomediators [31,32]. TBADT is similar to benzophenone in that it absorbs at approximately 350 nm, but significantly it is reported to be effective in catalytic amounts in systems where a stoichiometric quantity of benzophenone is required, all of which is converted to a variety of by-products in the course of the reaction [33]; in addition their use involves a simpler product isolation procedure than is the case with aromatic ketones. The efficiency of the decatungstate anion, in comparison to that of aromatic ketones, has been attributed to the relative rates of back H-transfer to the radical precursor of the product. The immobilization of photomediators on solid supports offers to these reactions the same advantages that have encouraged the development of supported reagents and catalysts for a wide variety of synthetic applications: ease of removal of the reagent, facilitating its reuse, and the purification of the reaction product. In this context, supported photomediators based on silica, or a Merrifield resin, have been successfully used to promote the reaction of cycloalkanes [8] and secondary alcohols [19] with alkynes. The green credentials of photochemical H-abstraction are further enhanced by the fact that these supported photomediators, and indeed soluble photomediators such as benzophenone and TBADT as well, function under solar conditions [7], the molar spectral direct solar irradiance at sea level being typically 0.8 mol m^{-2} s^{-1} nm^{-1} at 350 nm [34].

19.1.4 Unsaturated Systems

The addition of a nucleophilic C-radical to an unsaturated system containing at least one C-atom results in the formation of a C–C bond (Scheme 19.1). The reaction is thus effectively a Michael reaction and is most successful with alkenes and alkynes activated by the presence of one or more of the usual electron-withdrawing groups (EWGs): –C(O)R, $-CO_2R$, C(O)H, $C(O)NH_2$, $-SO_2R$, CN, CO_2H, etc. On the other hand, the electronically neutral styrene appears to be unreactive, as the photomediated addition of standard H-donors such as 2-propanol, THF, 2-alkyl-1,3-dioxolanes, aldehydes or cyclohexane, to this alkene has not been reported. Phenylacetylene is more reactive and 1-methyl-1,3-dioxolane [16] and THF [35] have been successfully added to this alkyne (Scheme 19.3).* This limitation on the type of unsaturated component that can be used also applies to thermally generated C-radicals, as the few reported examples of the addition of such radicals to alkenes and alkynes without EWGs involve extreme conditions: sealed tube reactions in a microwave at 200° [36], high temperatures [37], supercritical alcohols at 350° [38], high temperatures and pressures [39], or high temperatures and peroxides [40]. The thiol-catalyzed addition

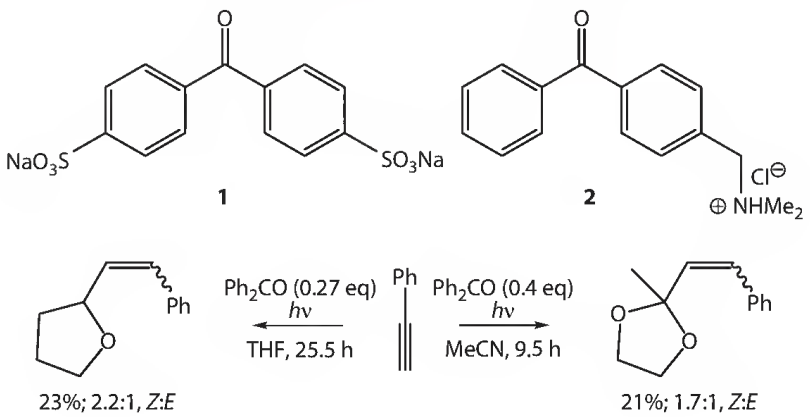

SCHEME 19.3

* The amount of photomediator used is a key parameter for these and similar reactions. As in almost all cases the H-donor is used in large excess, a sense of the amount of photomediator used is best conveyed in terms of the number of equivalents used relative to the unsaturated system. This method of reporting has been adopted consistently in this review.

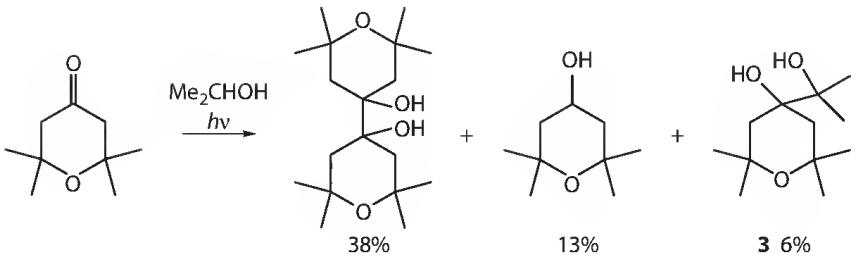

SCHEME 19.4

of acyl radicals, generated from aldehydes using *t*-butoxy radicals derived from di-*t*-butyl hyponitrite, to enol acetates, vinyl ethers, etc., is a rare example of a reaction involving electron-rich alkenes [41].

In view of the nucleophilic character of C-radicals, they would be expected to react with the electrophilic carbon of a C=N bond and in accordance with this expectation a range of C–C bond forming reactions involving the interaction of photochemically produced C-radicals with imine and oxime bonds have been reported (see the following). On the other hand, examples of the addition of C-radicals to carbonyl bonds are extremely rare and there does not appear to be any that involve C-radicals produced by photochemical H-abstraction. Although the isolation from photochemical reactions of products such as (**3**) (Scheme 19.4), formally the result of the addition of an α-hydroxyalkyl radical to a carbonyl group, is common, these actually result from the recombination of two α-hydroxyalkyl radicals [42]. The relative reactivity of C=C, C=N, and C=O bonds in relation to radical addition can be attributed to the strengths of the π-bonds [43], an estimate of which is given by the difference between the average bond energies of the respective single and double bonds: C=C, 270 kJ mol^{-1}; C=N, 295 kJ mol^{-1}; and C=O, 373 kJ mol^{-1} [44].

19.2 Photochemical Addition Reactions of Cycloalkanes

The photomediated reaction of a cycloalkane with an electron-deficient unsaturated system is of importance as it is one of the relatively few methods of resolving a classic problem of synthetic organic chemistry, the functionalization of an unactivated C–H bond. The first examples of the photochemical addition of a cycloalkane to an unsaturated system were independently reported within 6 months of each other in 1969 [45,46]. Synthetically, they were not encouraging (Scheme 19.5). A photomediator was not used in either case, the reactions presumably involving the abstraction of a hydrogen from cyclohexane by an electronically excited substrate molecule, an ynoate in each case. Recombination within the solvent cage or the addition of the C-radical to another unsaturated molecule accounts for the formation of the observed products. The formation of 3-cyclohexylcyclopentanone in 22% yield on irradiation of a solution of cyclopenten-2-one in cyclohexane is the result of a similar process [47]. The only other example of this type of

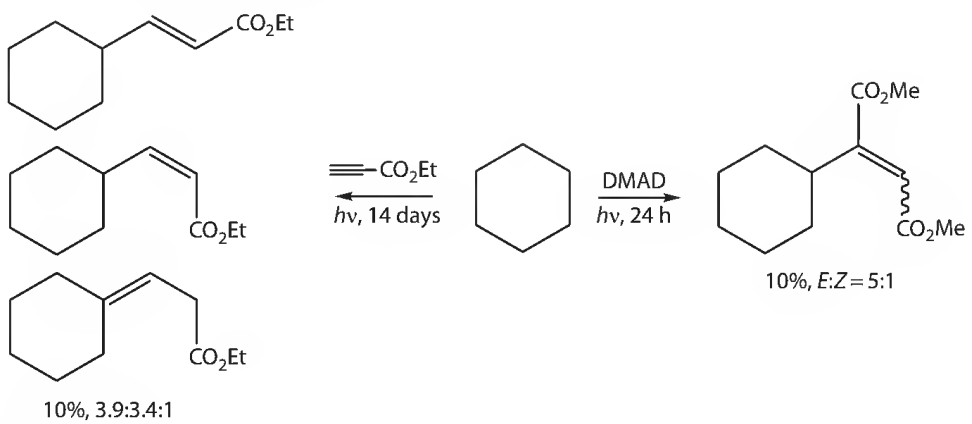

SCHEME 19.5

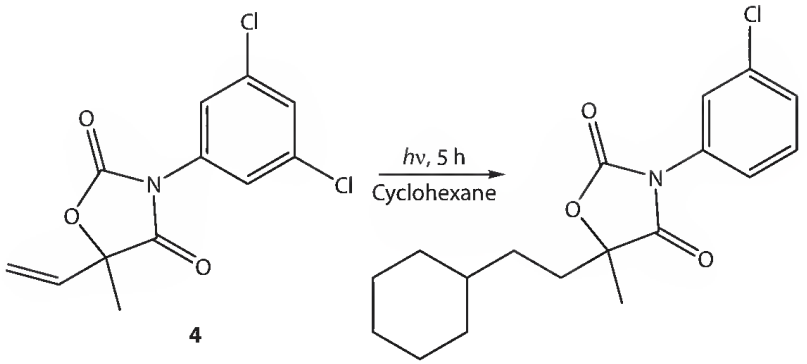

SCHEME 19.6

reaction is more recent and involves the herbicide vinclozolin (**4**), which on irradiation in cyclohexane produces a monochloro cyclohexyl adduct (Scheme 19.6) [48]. Although the precise origin of the cyclohexyl radicals is unclear, the reaction is notable as it is the only example of the addition of a photochemically generated cycloalkyl radical to an alkene that does not have an EWG as a substituent.

The first example of the deliberate use of a photomediator to generate cycloalkyl radicals for subsequent reaction relates to the benzophenone mediated photoreaction of hexafluorobenzene with cyclohexane (Scheme 19.7) [49]; benzpinacol was produced as a by-product. Interestingly, cyclopentane performed poorly in this reaction, giving instead larger amounts of benzpinacol, and also bicyclopentyl. Cycloheptane and a number of *n*-alkanes failed to react. The use of xanthone to promote the addition of cyclohexane, or an alcohol, to an unsaturated thiolactone is another early example of the use of an aromatic ketone as a photomediator (Scheme 19.8) [50]. In the last decade a number of systematic studies have helped to define the synthetic scope of the process in terms of substrate, photomediator, and general reaction conditions (Table 19.3). In many of the reactions reported, dimerization of the photomediator-derived ketyl radical,

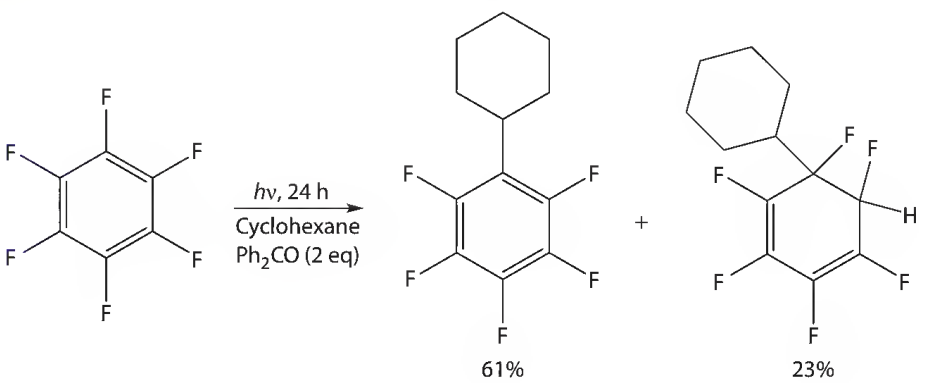

SCHEME 19.7

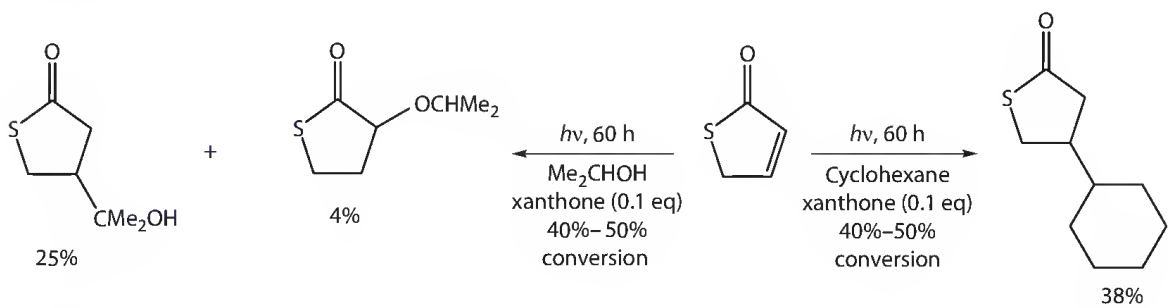

SCHEME 19.8

TABLE 19.3 Photomediated Addition of Cycloalkanes to Unsaturated Systems

Entry	Unsaturated System	H-Donor	PM[a] (eq[b])	Time (h)	Product	Yield (%)	Ref.
1	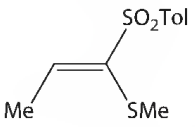	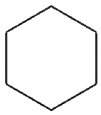	Ph_2CO (1)	15	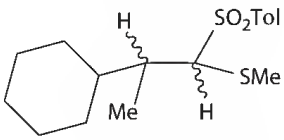	89	51
2	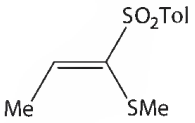	Adamantane	Ph_2CO (0.1)	18	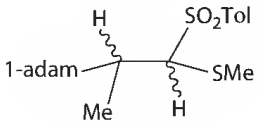	90	51
3	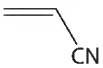	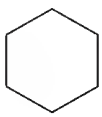	Xanthone (1)	15	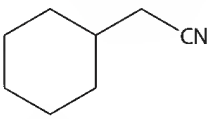	35	52
4	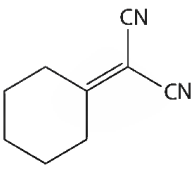		Ph_2CO (1)	40	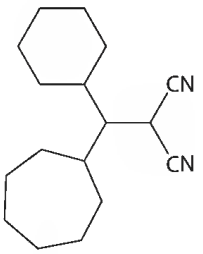	80	52
5	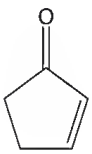	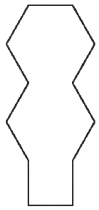	Ph_2CO (1)	15	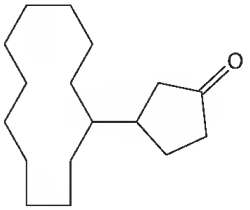	48	33
6			Ph_2CO (1)	2.5	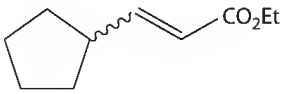	70	53
7	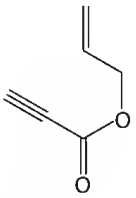		Ph_2CO (0.14)	4.5	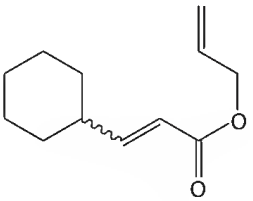	52	5
8	DMAD	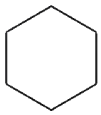	Ph_2CO (0.14)	13.5	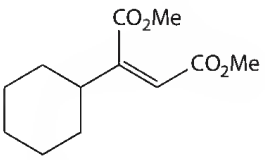	31	5
9			Ph_2CO (0.14)	3	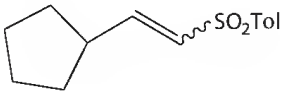	56	5
10	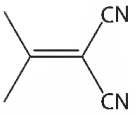	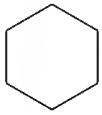	TBADT (0.02)	3	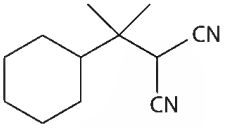	66	56

[a] Photomediator.

[b] Relative to the unsaturated substrate.

forming a pinacol, is competitive with back transfer of a H-atom to the product forming radical. This has led to a need to use up to 1 eq of photomediator in order to ensure complete reaction of the unsaturated substrate and to consequential problems in terms of product isolation. The use of the silica- and Merrifield resin-supported photomediators, (**5**) and (**6**), respectively, facilitates product purification and opens up the potential for facile recovery and recycling of the photomediator [8]. Ketyl radical dimerization, and thus removal of the photomediator from the reaction cycle, should also be less of a problem with these supported photomediators if the surface coverage is kept low. In terms of the photomediator, alkynes appear to be more attractive as substrates in that as little as 0.14 eq of benzophenone can be used without adversely affecting either the yield or the rate of the reaction [5]. Interestingly the rate of the reaction, but not the yield, drops dramatically if the amount of photomediator is reduced below this level. This difference between the behavior of alkenes and alkynes as substrates may relate to the relative reactivity of the respective alkyl and alkenyl radical intermediates in terms of H-transfer. No overall pattern emerges in terms of the relative reactivity of the cycloalkanes. Thus although cyclopentane is the most reactive in terms of the alkynes [5], it is much less reactive than cyclohexane in terms of reaction with hexafluorobenzene [49], and whereas DMAD does not react with cycloalkanes larger than the cyclohexane [6], 2-cyclopentenone reacts readily with dodecane (Table 19.3, Entry 5) [33].

The use of TBADT as a photomediator has also been reported [54], with direct H-abstraction again being the key step in the generation of C-radicals from H-donors such as cycloalkanes [55]. The synthetic potential of this photomediator is considerable in the context, again, of reactions involving electron-deficient alkenes (Table 19.3, Entry 10) [9,56], with the fact that it is effective in catalytic quantities being particularly attractive [33]. The difference between TBADT and aromatic ketones in terms of the rate of the final back H-transfer to the radical precursor of the product, the factor that is believed to be responsible for the activity of the former [31], provides the opportunity of controlling the synthetic outcome of a reaction through an appropriate choice of photomediator (Scheme 19.9) [52,56]. A careful examination of the alkylation of monoalkylcyclohexanes indicates that these reactions deliver a modest level of regio- and stereoselectivity, with similar product distributions being obtained with both benzophenone and TBADT (Scheme 19.10) [31]. The observed selectivity is attributed to steric factors.

Although the addition of thermally generated carbon radicals to C=N bonds is currently an active area of research [57], there appears to be only one report of the addition to C=N bonds of cycloalkyl radicals, which have been generated by photomediated H-transfer. This involves an exploration of the use of polytungstates, including TBADT, in the functionalization of a series of hydrocarbons using methyl cyanoformate (Scheme 19.11) [58]. The data obtained confirm that the key step is a H-atom transfer involving an electronically excited decatungstate ion (Scheme 19.12). This is followed by the establishment of a radical chain in which the key intermediate is the iminyl radical (**8**). If the reaction is conducted at room temperature, competitive breakdown of this radical to form a nitrile is minimal (1%–2%); at 90° this becomes the predominant process. In addition to underlining the potential of polyoxotungstates as photomediators, this work provides a rare example of the functionalization of an acyclic hydrocarbon and illustrates how non-nucleophilic allylic and benzylic radicals undergo recombination rather than addition to an unsaturated bond.

19.3 Photomediated Addition Reactions of Cyclic Ethers

The photomediated α-alkylation and α-alkenylation of cyclic ethers constitute further examples of the use of this synthetic methodology for the functionalization of an unactivated system more usually viewed as a solvent than as a substrate. The α-alkoxyalkyl radicals resulting from H-abstraction would be expected to be more reactive than the corresponding cycloalkyl radicals due to the stereoelectronic effect involving the p-type lone pair of electrons on the O-atom [13–16]; this is reflected in the existence of a resonance form in which the α-carbon is carbanionic (Figure 19.3). The first systematic study of reactions of this type described the addition of THF, and other cyclic ethers, to diethyl maleate and fumarate

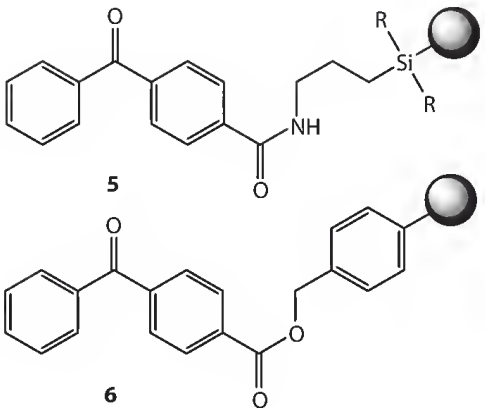

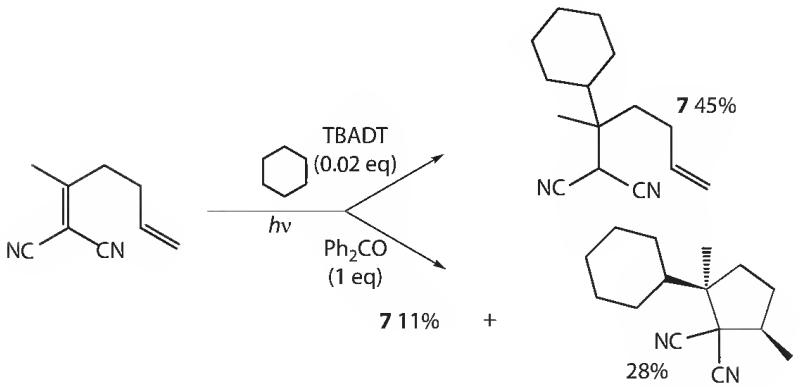

SCHEME 19.9

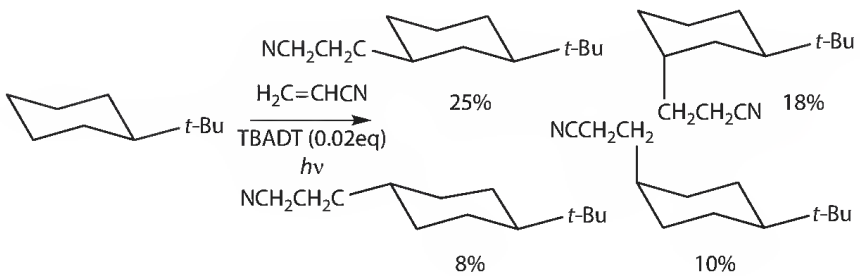

SCHEME 19.10

(Scheme 19.13) [59], and the formation of pinacols and cyclic ether dimers as by-products. Interestingly however the solar chemistry potential of the process was recognized and indeed product yields obtained using sunlight for a range of cyclic ethers were higher than those obtained using a high-pressure mercury vapor lamp. Although the greater nucleophilic character of the C-radicals produced from THF, relative to cycloalkyl radicals, may play a role in accounting for their reaction with the relatively electron-rich terminal alkene, 1-heptene, the fact that reaction occurs at the less sterically hindered alkene carbon, rather than at the most electrophilic, suggests that steric factors may be decisive, as is so often the case in the reactions being considered here. Other examples of this behavior even include the direct addition of diethyl ether to the terminal alkene unit in (**9**) (Scheme 19.14) [60], a process that presumably involves the unsaturated lactone acting as the photomediator, but in what may be another example of the importance of steric effects in these reactions, does not result in radical addition to its alkene bond. In the context of the reaction between DMAD, and either THF or oxetane [61], the involvement of a ketone–ether exciplex and of a ether–alkyne charge-transfer complex have been suggested for the ketone-photomediated and direct reactions, respectively. The possibility that the direct addition of THF to an enone involves a SET

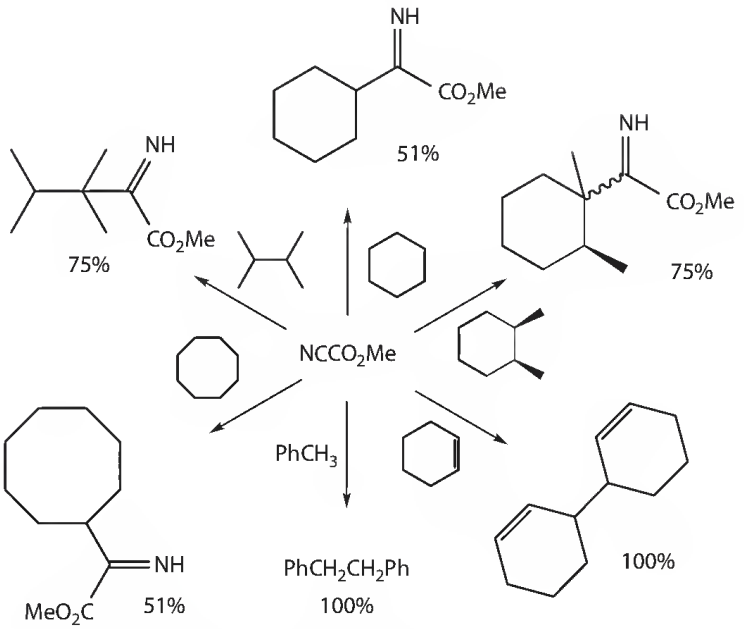

Condition: *hν* > 280 nm (pyrex), MeCN, 0.006 eq polyoxotungstate, rt, yields based on a methyl cyanoformate conversion of approximately 15%

SCHEME 19.11

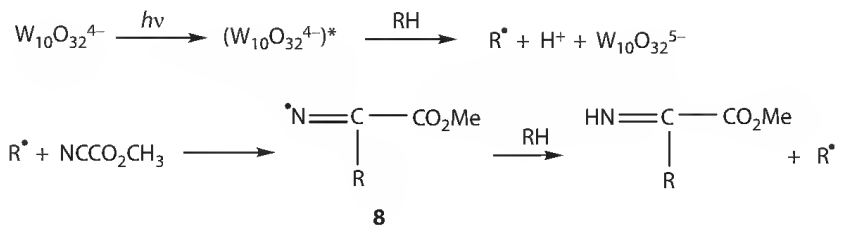

SCHEME 19.12

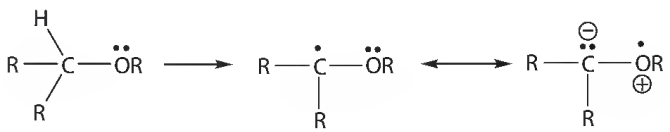

FIGURE 19.3

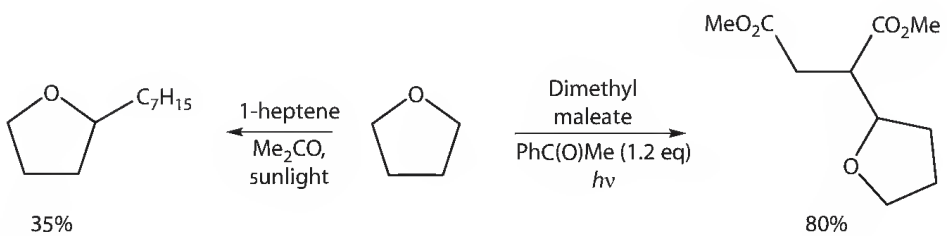

SCHEME 19.13

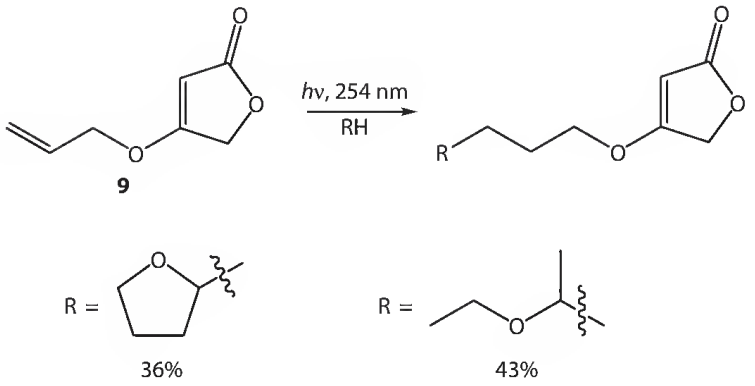

SCHEME 19.14

mechanism was, however, considered improbable on the basis of the high oxidation potentials of aliphatic ethers in relation to the expected electron affinities of the excited states of the enones [62].

Most of the synthetically interesting examples of the photochemical addition of ethers to carbon–carbon multiple bonds involve cyclic ethers, and electron-deficient alkenes and alkynes (Table 19.4). Many of these reactions (Table 19.4, Entries 3–6) involve direct irradiation. The formation of a regioisomeric mixture on addition of THF to the 1,3-dimethyluracil (**10**) (Table 19.4, Entry 3) is not unprecedented (cf. Scheme 19.8) and is best understood in terms of competitive H-abstraction by the carbonyl group and the β-carbon of the enone [64]. A high degree of stereoselectivity is observed in those reactions where face selectivity is an issue. Thus although the addition of THF to the norcodeinone (**11**) (Table 19.4, Entry 4) generates a mixture of diastereomers as a result of the generation of a new stereogenic center on the THF ring, the product is stereochemically pure at what was the β-carbon of the enone [62]. In the same way, the addition of a THF derived α-alkoxyalkyl radical to the 1,3-dioxin-4-one (**12**) (Table 19.4, Entry 5) occurs stereoselectively on its more exposed face [65]. In terms of the unsaturated system (**12**), the radical's behavior was found to be similar to that observed for a diene in an Diels–Alder reaction or an alkene in a photochemical [2 + 2] cycloaddition, rather than that of a nucleophile in a cuprate addition.

Fluorinated alkenes, or alkenes with a trifluoromethyl substituent, are electron-deficient and react readily with the nucleophilic α-alkoxyalkyl radicals derived from cyclic ethers. If a photochemical approach is employed to generate the radicals, a photomediator is not in general essential (Table 19.4, Entry 6) [66] as irradiation of the fluorinated alkene results in the generation of a triplet state, which because of its biradical character is capable of abstracting an α-H-atom from the ether [67]. In the usual way however, acetone has also been employed as a photomediator in some reactions involving fluorinated alkenes. An order of reactivity has been established for the reaction with fluorinated alkenes of the α-alkoxyalkyl radicals derived from cyclic ethers using γ-radiation: oxolane > oxepane > oxane ≈ dioxane [68]. This order is identical to that observed previously by others and rationalized on the basis of a stereoelectronic effect involving the oxygen's p-type lone pair of electrons (Section 19.2) [15].

The diastereoselective addition of the α-alkoxyalkyl radical from THF to the chiral 4-methyleneoxazolidin-5-one (**13**) (Table 19.4, Entry 7) forms the basis of a method for the preparation of chiral homoserine derivatives [69]. The ability of the polytungstate TBADT to act as a photocatalyst is again evident in terms of the addition of ethers to electron-poor alkenes (Table 19.4, Entry 8) [9]. α-Alkoxyalkyl radicals have also been generated using hydroxyl radicals derived photochemically from *N*-hydroxy-2-pyridinethione (**14**) (Scheme 19.15) [71]. The radicals generated in this way add to vinyl sulfone, with the resulting α-sulfonylalkyl radical abstracting a H-atom from a solvent molecule, or undergoing recombination with the thio radical, which is also formed on homolysis of (**14**).

In principle, the addition of an ether to a C=N bond can occur in two ways: a process in which the key step is H-atom transfer, or one that involves a SET. Many involve the latter and thus fall outside the scope of this review. Thus, for example, following a consideration of both mechanisms, it was

TABLE 19.4 Photomediated Addition of Cyclic Ethers to Unsaturated Systems

Entry	Unsaturated System	Ether	PM[a] (eq[b])	Time (h)	Product	Yield (%)	Ref.
1	DMAD	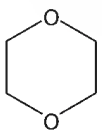	Acetone cosolvent	15	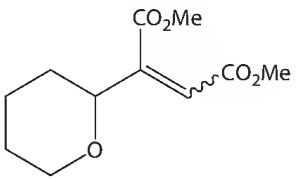	36	63
2		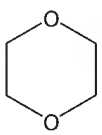	PhC(O)Me (4.9)	—	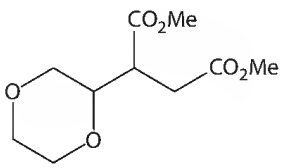	73	59
3	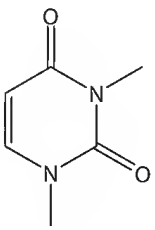 **10**		Direct	15	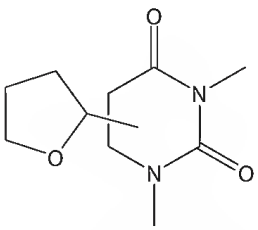 2-THF:3-THF, 1:1	80	64
4	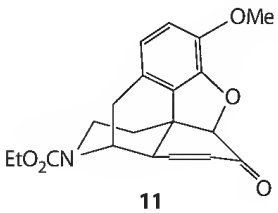 **11**		Direct	40	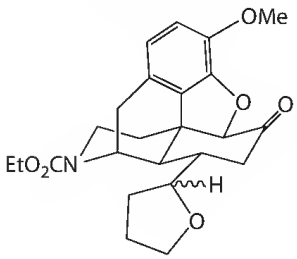	—	62
5	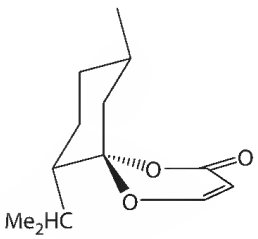 **12**		Direct	120	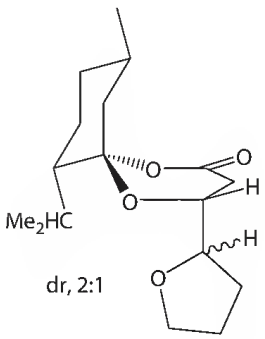 dr, 2:1	63	65
6	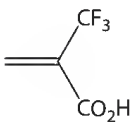		Direct	20	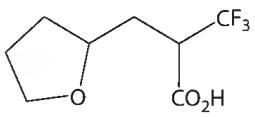	85	66

(*continued*)

TABLE 19.4 (continued) Photomediated Addition of Cyclic Ethers to Unsaturated Systems

Entry	Unsaturated System	Ether	PM[a] (eq[b])	Time (h)	Product	Yield (%)	Ref.
7	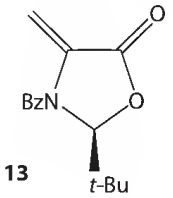 **13**		Ph_2CO (1)	1	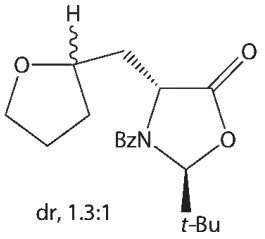 dr, 1.3:1	55	69
8	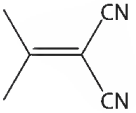		TBADT (0.02)	20	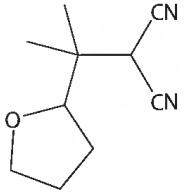	75	9
9	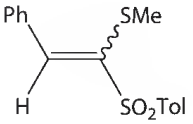	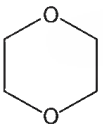	Ph_2CO (1)	2.5	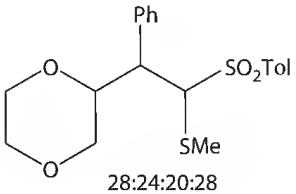 28:24:20:28	80	70

[a] Photomediator.
[b] Relative to the unsaturated substrate.

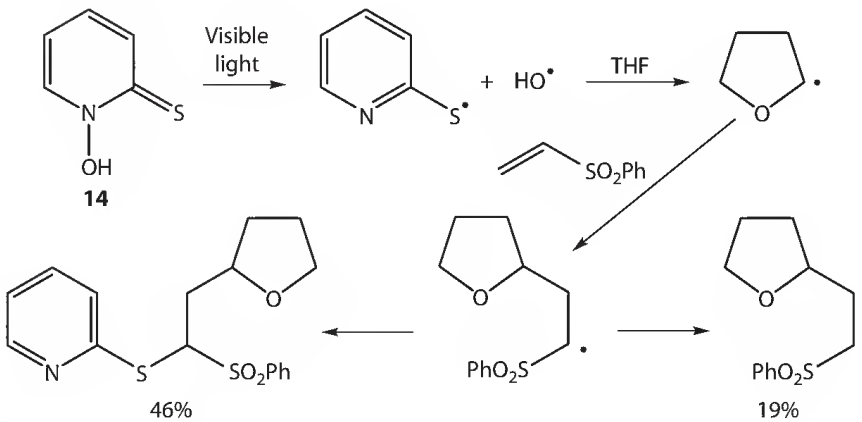

SCHEME 19.15

concluded that the addition of THF to iminium salts occurs via a SET pathway [72]. The addition of THF to *N*-phenylimines also occurs by the same route [73]. There are however a number of examples of the addition of photochemically generated α-alkoxyalkyl radicals to C=N bonds that involve a H-atom transfer. The addition of cyclic and acyclic ethers, and uniquely of cyclic (Scheme 19.16) and acyclic thioethers, to pyrimidin-2(1*H*)-ones is believed, for example, to involve H-abstraction by the imino group nitrogen of the pyrimidone in its triplet state [74]. The reaction is thus a formal 1,4-addition to a 1-azadiene. A more conventional example of the photoaddition of an ether to a C=N bond is provided by the acetone-mediated reaction of 1,4-dioxane with the pyrimido[4,5-*d*]pyridazine (**15**) (Scheme 19.17) [75]. Interestingly, the product appears to have been obtained as a single diastereomer.

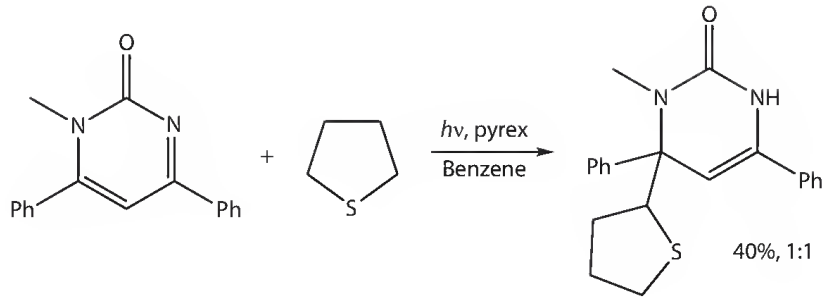

SCHEME 19.16

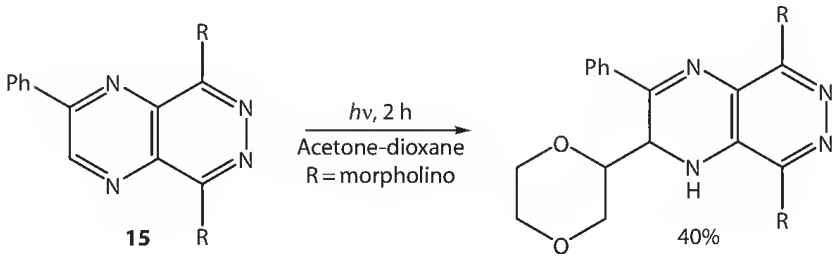

SCHEME 19.17

19.4 Photomediated Addition Reactions of 1,3-Dioxolanes and Related Systems

The 1,3-dioxanyl radical, which is readily accessible through photochemical H-abstraction, is synthetically equivalent to an acyl anion (Scheme 19.18). As the 1,3-dioxolane precursor is readily available from the corresponding aldehyde, and as the H-abstraction occurs under neutral conditions, this method of generating an acyl anion equivalent has found application in multistep syntheses. The stereoelectronic assistance that is available from at least one of the oxygen lone pairs of electrons [13–15] ensures that in terms of H-abstraction, a 1,3-dioxolane is particularly reactive at its 2-position, and that the addition of the resulting 1,3-dioxan-2-yl radical to electron-deficient unsaturated systems is an efficient process. This is particularly true of 2-methyl-1,3-dioxolane whose regiospecific and essentially quantitative reaction with DMAD, for example, is complete in 15 min (Scheme 19.19) [16]. The first reported example of this type of reaction involves the acetone-, acetophenone-, or benzophenone-mediated addition of 1,3-dioxolane and 1,3,5-trioxane to diethyl maleate, and, interestingly, to terminal alkenes (Table 19.5, Entries 1–3) [76]. Dioxolane or trioxane dimers, and photomediator-alkene adducts were obtained as by-products and once again the yields reported for reactions carried out in sunlight were higher than those

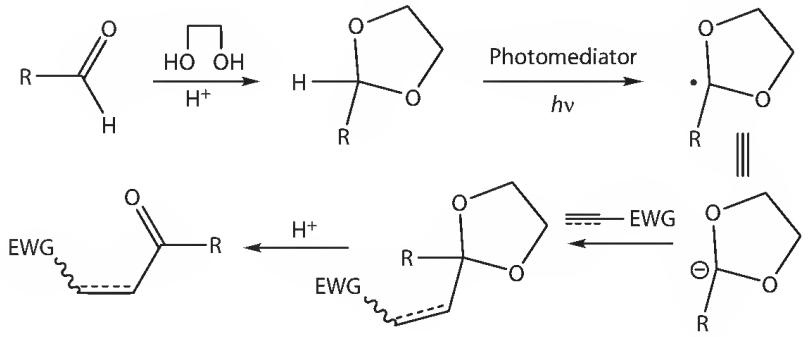

SCHEME 19.18

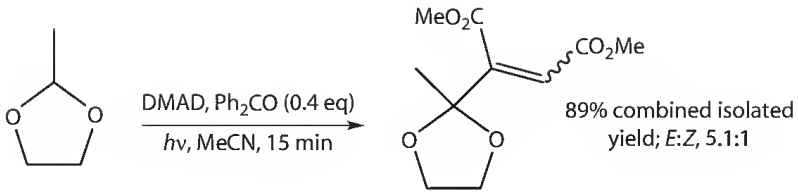

SCHEME 19.19

carried out using a mercury vapor lamp. The regioselectivity of the reactions involving terminal alkenes again suggests that steric rather than electronic factors are product determining. The same regioselectivity is observed in the addition of 1,3-dioxolane to the alkene units in the furanoses (**16**) and (**17**) (Scheme 19.20), the reaction of the latter being stereoselective as well [77]. Its photoaddition to enoses with endocyclic double bonds also occurs regiospecifically and with a high degree of stereoselectivity [78].

Although the reaction is not completely regioselective, the addition of photochemically generated dioxanyl radicals to fluorinated alkenes occurs readily (Table 19.5, Entry 4) [79]. The regioselectivity of the addition of methylated dioxolanes to perfluoroalkenes has been the considered in detail [79], and reaction at both the 2- and the 4-position is also a feature of the addition of 1,3-dioxolane to 2,2-difluorovinyl carbamate (Table 19.5, Entry 5) [80]. On the other hand, the reaction of 1,3-dioxolane, and even of 2-isopropyl-1,3-dioxolane, with a wide range of mono- and di-substituted alkynes is entirely regioselective. The reaction occurs remarkably rapidly and in high yield, the result in the case of the 2-alkylated dioxolanes of a particularly favorable stereoelectronic effect involving the 2-CH bond and the p-type lone pairs of electrons of both O-atoms (Table 19.5, Entry 6, 7) [16]. Regioselectivity is not a problem either in the decatungstate-catalyzed reaction of 1,3-dioxolane with α,β-unsaturated nitriles; very low concentrations of TBADT are again sufficient to promote the alkylation process (Table 19.5, Entry 8) [9].

1,3-Dioxolanes readily undergo a photomediated addition reaction with simple cyclic and acyclic enones [29,81,82], which is synthetically valuable as it provides ready access to monoprotected 1,4-dicarbonyl compounds. If 1,3-dioxolane itself is used, a monoprotected 1,4-ketoaldehyde is obtained (Scheme 19.21) [29]; as subsequent hydrolysis would give a 1,4-ketoaldehyde, the process overall results in the β-formylation of the enone. The reactions can be carried out in neat dioxolane using benzophenone as photomediator, or in water/MeCN/dioxolane mixtures using the water-soluble benzophenone disodium disulfonate. The photochemistry of the initially formed 4-oxobutanal acetals can also be exploited with open-chain systems undergoing a Yang cyclization affording hydroxycyclobutanols, aryl derivatives a Norrish Type II cleavage, and cyclic ketones a Norrish Type I cleavage (Scheme 19.22) [81]. If a 2-alkyl-1,3-dioxolane is used, hydrolysis of the product would give a 1,4-diketone, the reaction constituting a formal β-acylation of the enone (Scheme 19.21) [82]. In the context of this particular application, the thermal generation of dioxanyl radicals using initiators such as AIBN or benzoyl peroxide led to significantly poorer results. A high degree of stereoselectivity is observed in the addition of 2-substituted 1,3-dioxolanes to carbohydrate enones (Scheme 19.23), although surprisingly the steroidal enones, 1-cholesten-3-one and 1-cholesten-3-one, fail to react [83,84]. It is worth noting that although these enones are equally unreactive in terms of the addition of alcohols, the photomediated addition of aldehydes occurs in modest yield (Section 19.5). The photomediated reaction of 1,3-dioxolane to the electronically related 3-nitro-2-enopyanosides also produces adducts but with varying levels of stereoselectivity [85].

There is also an increasing number of applications that demonstrate the potential for stereochemical control in the addition of photochemically generated 1,3-dioxolany radicals to unsaturated systems in general. The addition of these radicals to (*E*)-fumaryl-bis(oxazolidines), for example, occurs with a de of between 88.9% and 98.9% (Scheme 19.24) [86], and the photoadduct resulting from the addition of 1,3-dioxolane to the chiral 4-methyleneozazolidin-5-ones (**13**) (Scheme 19.24) [69] is formed with a de of >98%. The addition of dioxolane to chiral cyclic and acyclic α-(arylsulfinyl)enones is

TABLE 19.5 Photomediated Addition of 1,3-Dioxolanes, etc., to Unsaturated Systems

Entry	Unsaturated System	Dioxolane	PM[a] (eq[b])	Time (h)	Product	Yield (%)	Ref.
1		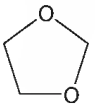	PhC(O) Me (3.3)	6	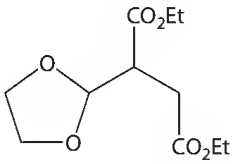	90	76
2		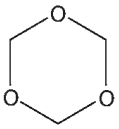	Acetone cosolvent	6	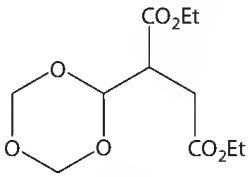	27	76
3	1-Heptene	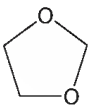	Acetone cosolvent	72	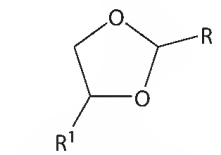 a: R = 1-heptyl, R^1 = H b: R = H, R^1 = 1-heptyl	a, 28 b, 5	76
4	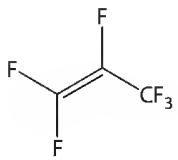	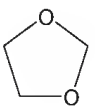	Direct	2	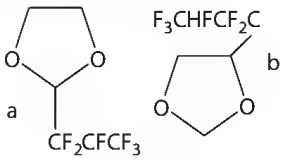 11.4:1	92	79
5	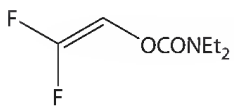	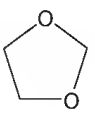	Direct	7	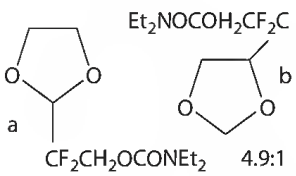 4.9:1	86	80
6	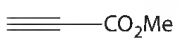	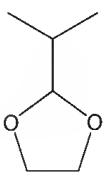	Ph_2CO (0.4)	0.25	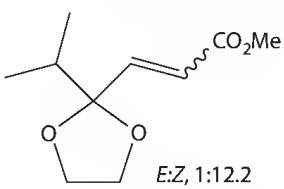 *E*:*Z*, 1:12.2	75	16
7	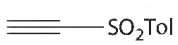	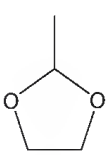	Ph_2CO (0.4)	0.25	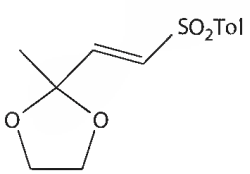	60	16
8	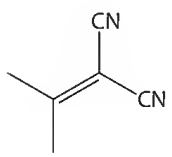	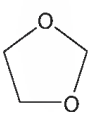	TBADT (0.02)	—	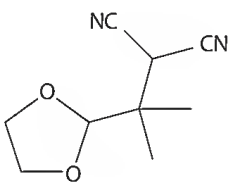	50	9

[a] Photomediator.

[b] Relative to the unsaturated substrate.

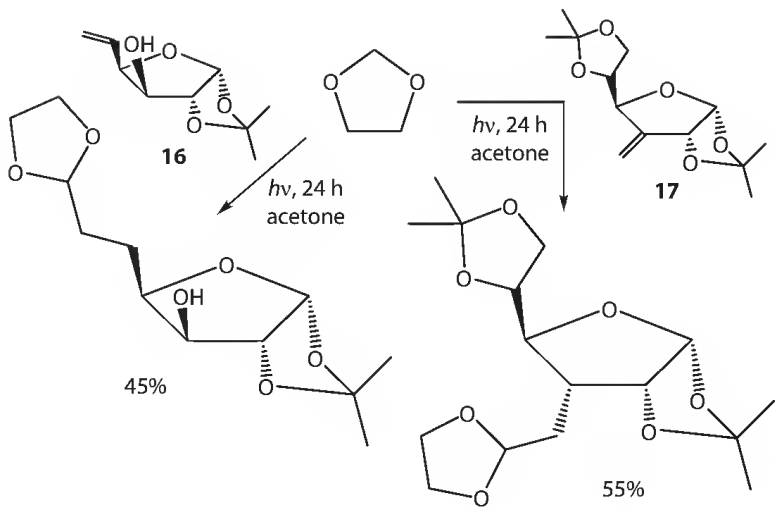

SCHEME 19.20

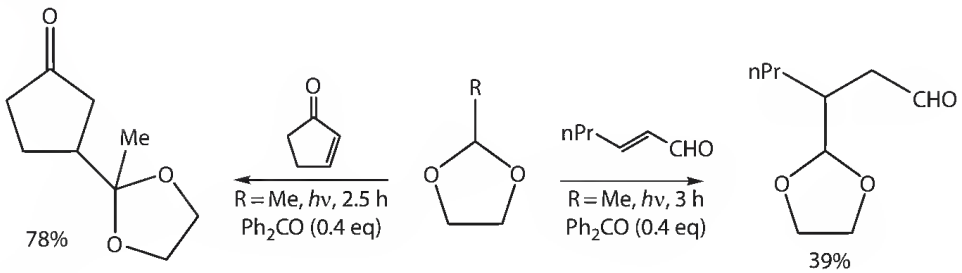

SCHEME 19.21

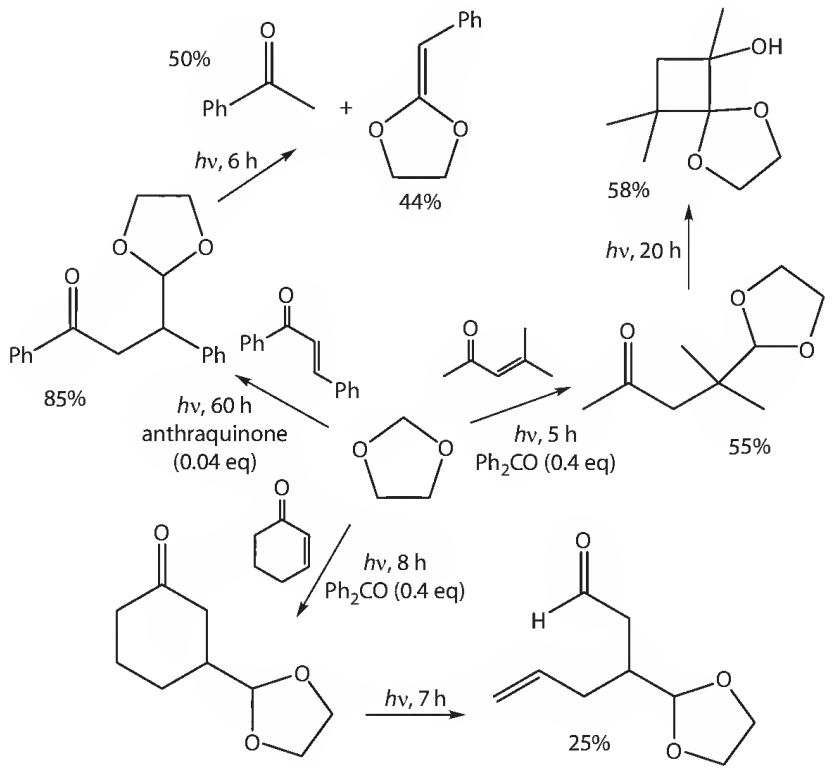

SCHEME 19.22

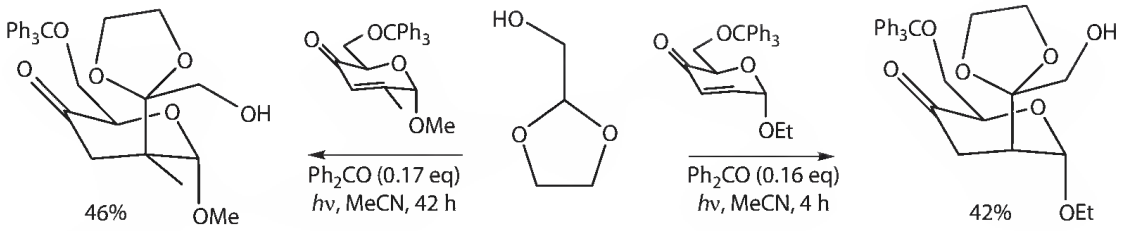

SCHEME 19.23

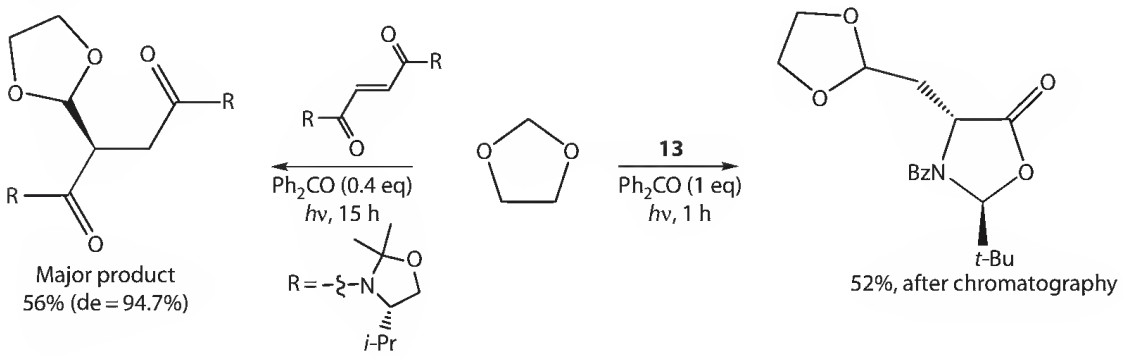

SCHEME 19.24

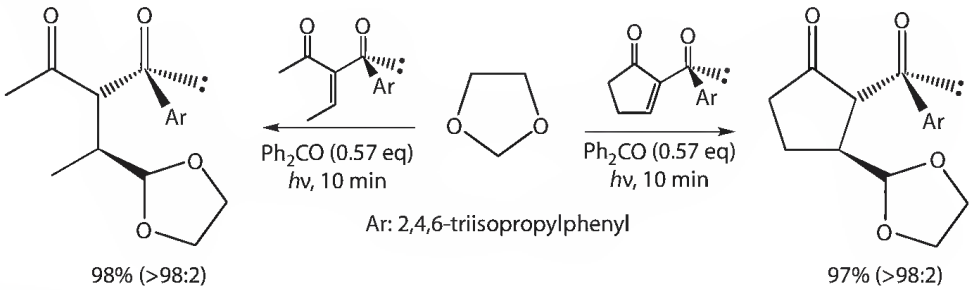

SCHEME 19.25

a further example of the stereochemical potential of these photomediated reactions (Scheme 19.25) [87]. The 1,3-asymmetric induction achieved in these reactions is due to a face selectivity that is the result of a steric interaction between the bulky arylsulfinyl groups and the incoming radical. The sulfinyl group can be removed and thus the reaction sequence constitutes a method of synthesizing chiral 3-substituted 1-cyclopentanones and 4-substituted 2 pentanones.

Cyclization procedures based on the intramolecular additions of 1,3-dioxanyl and related radicals have been reported with stereoselectivity again being a feature of the reactions in many cases. Thus the irradiation of a benzene solution of the 1,3-dithiane (**18**), containing benzophenone, gave the cyclized product (**19**) (Scheme 19.26) [88]. A detailed analysis of this photocyclization indicated that although the corresponding 1,3-dithiolane was equally reactive, the corresponding 1,3-oxathiane and 1,3-dioxolane were significantly less so. The presence of an EWG on the alkene was essential and the reaction failed with tethered alkynes; attempts to produce seven-membered rings also failed. Chiral acetals, such as (**20**), produced separable mixtures of diastereomers. A similar photomediated cyclization of the dioxecinones (**21**) gives the doubly spiro products (**22**) (Scheme 19.27) [65]; cyclization of chiral dioxecinones related to (**12**) occurs with very low levels of diastereoselectivity. Synthetic studies related to the synthesis of (–)-tetrodotoxin have included the development of a tandem radical addition–cyclization of procedure based on alkynyl ketoxime ethers (Scheme 19.28) [89]. Radical addition to the alkyne

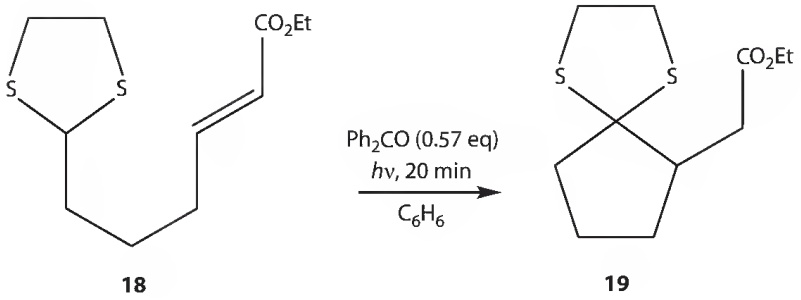

18 19

SCHEME 19.26

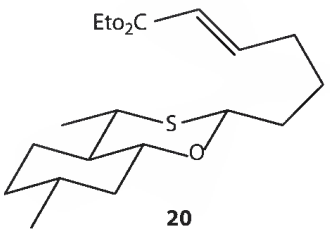

20

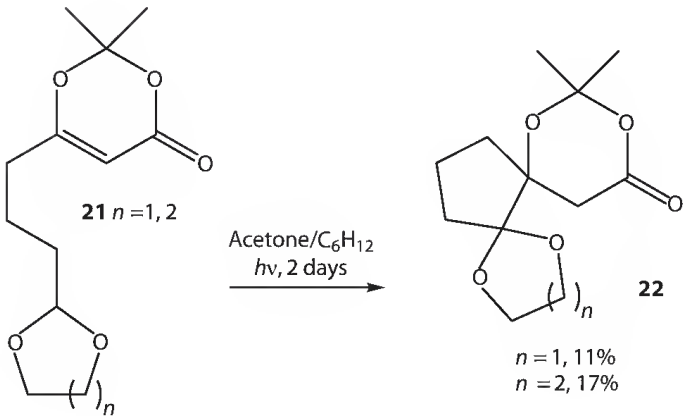

SCHEME 19.27

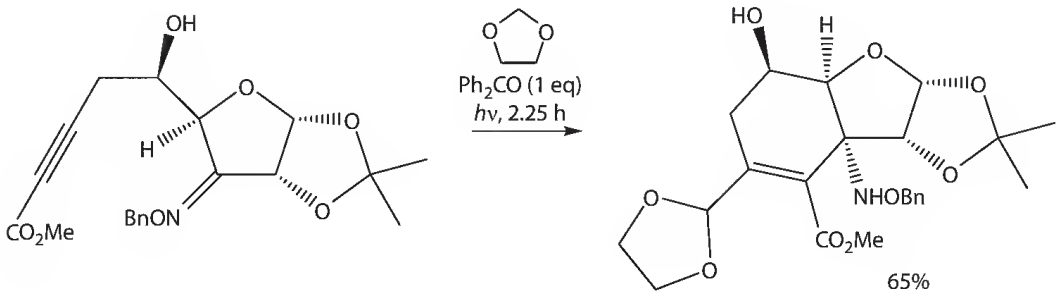

SCHEME 19.28

generates an alkenyl radical that adds to the C=N of the oxime ether to give a cyclized product. It was found that the regioselectivity of the radical addition to the alkyne was dependent on the alkyne substituent and the radical involved, creating the possibility of controlling whether cyclization resulted in the formation of a six- or a five-membered ring. 1,3-Dioxanyl radicals, produced by photomediated H-abstraction, gave selectively the former.

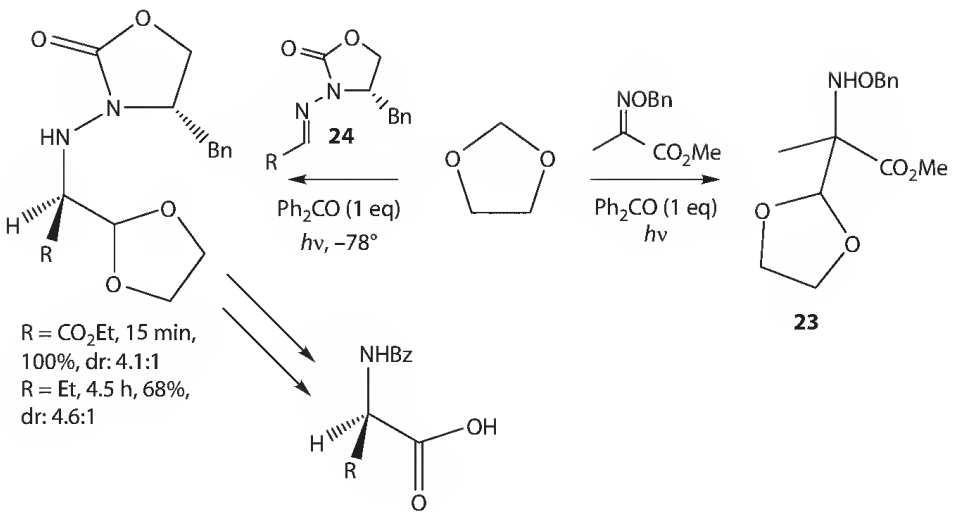

SCHEME 19.29

Relatively few examples of the addition of dioxanyl radicals to C=N bonds have been reported. Their intermolecular addition to ketoxime ethers leads to the formation of α,α-disubstituted amino acid derivatives (**23**) (Scheme 19.29), a reaction that, with appropriate substrates, occurs with complete diastereoselectivity [90]. Photoaddition to *N*-acyl aldohydrazones derived from 3-amino-4-benzyl-1,3-oxazolan-2-one (**24**) (Scheme 19.29) proceed with reasonable diastereoselectivity, particularly in the presence of $InCl_3$, and so the approach constitutes a method for the preparation of enantiomerically pure α-amino acids [91].

The photomediated addition of 1,3-dioxolanes has been used as the key step in a number of synthetic methodologies and target syntheses. The addition of 1,3-dioxolane to α-cyanovinylsulfones, for example, occurs in good to excellent yield and the 3-cyano-3-sulfonylpropanal acetals thus formed can be converted to 3,4-disubstituted pyrroles [92]. The first step in the total synthesis of the pancreatic lipase inhibitor, (–)-tetrahydrolipstatin (**25**) involves the acetophenone-mediated addition of 2-undecyl-1,3-dioxolane to the exocyclic double bond of diketene (Scheme 19.30) [93]. Similarly, the highly diastereoselective addition of 1,3-dioxolane to the unsaturated γ-lactone (**26**) is a key step in the synthesis of a bis-tetrahydrofuranyl ligand for a HIV protease inhibitor (**27**) (Scheme 19.31) [94].

19.5 Photomediated Addition Reactions of Aldehydes and Related Systems

The photoacylation of an alkene can be achieved, as indicated in the previous section, by the photomediated addition of 1,3-dioxolane, or 2-alkylated-1,3-dioxolanes, and the subsequent hydrolysis of the dioxolane ring. The photoacylation of an alkene can also be carried out by the direct addition of an aldehyde. Apart from its scientific value, this process is of enormous historical importance for organic photochemistry as the photoacylation of quinones, a classic example of the type of reaction being considered here, was discovered by Klinger in 1888 [95] and was thus one of the very first organic photochemical reactions to be identified and studied. The importance of photoacylation as it applies to simple alkenes is similar, as this process was first described in one of Kharasch's seminal papers on radical chemistry, which appeared in the 1940s [96]. This report related to the photochemical and peroxide-promoted addition of aldehydes to terminal alkenes, with the best results being obtained in reactions involving long-chain aldehydes and long-chain alkenes (Table 19.6, Entry 1). Combinations involving styrene or butenal underwent

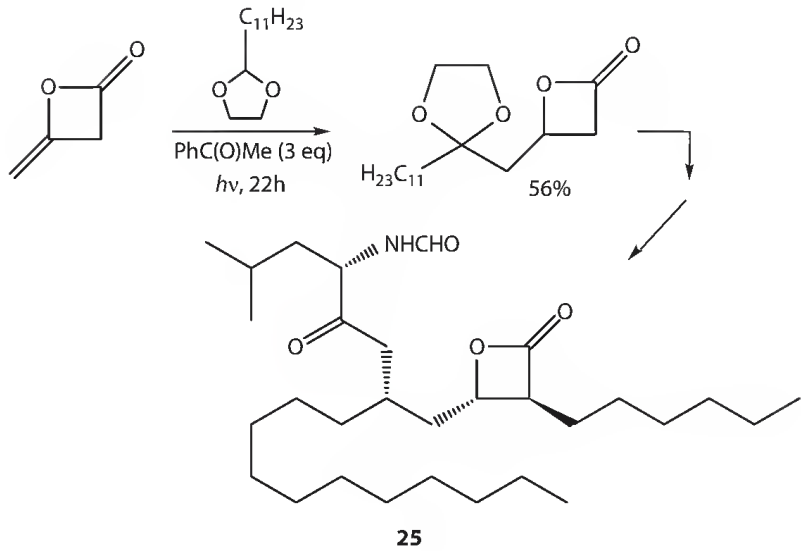

SCHEME 19.30

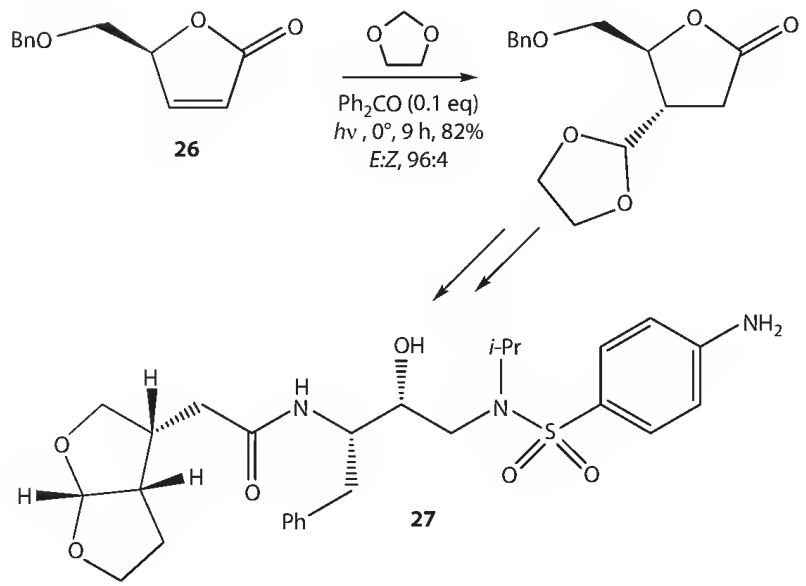

SCHEME 19.31

polymerization exclusively, and cyclohexene gave very poor yields of adducts. It was also noted that reactions that were initiated photochemically gave less complex mixtures than those obtained from reactions involving acyl peroxides. Another early contribution in this area reported that irradiation of a mixture of propionaldehyde and cyclohexene resulted in the competitive formation of a photoacylation product and an unsaturated alcohol produced by the recombination of cyclohexenyl and ketyl radicals (Table 19.6, Entry 2) [97].

There are very few reports relating to the photochemical addition of aldehydes to alkynes, the earliest of which again features an unactivated system (Scheme 19.32) [98]. Although the reaction produces small amounts of a variety of radical recombination products, it is worth noting that (**28**), (**29**), and (**30**), the products of the photoacylation of 1-hexyne and subsequently of the enone thus formed, are obtained in a combined yield of 80%. Early results with electron-deficient fluoroalkenes were disappointing from

TABLE 19.6 Photomediated Addition of Aldehydes, etc., to Unsaturated Systems

Entry	Unsaturated System	Aldehyde	PM[a] (eq[b])	Time (h)	Product	Yield (%)	Ref.
1	1-Octene	Heptanal	Direct	23	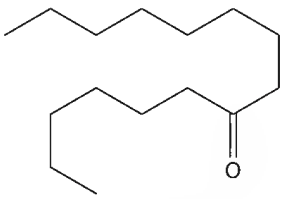	90	96
2	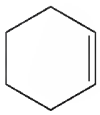	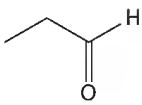	Direct	24	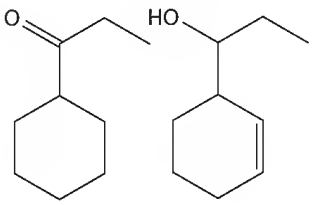	—	97
3	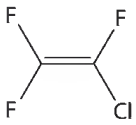	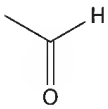	Direct	—	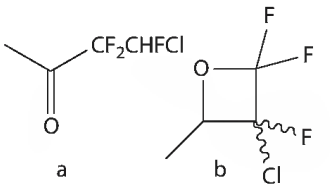	a:10 b:2.4	99
4	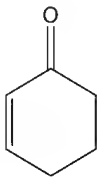	PhCHO	Ph_2CO (–)	—	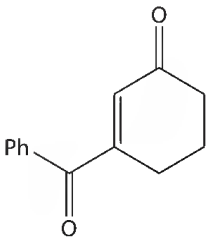	69	102
5	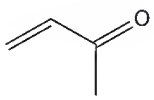	Heptanal	TBADT (0.002 eq)	24	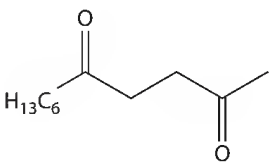	60	6
6		PhCHO	TBADT (0.02 eq)	0.5	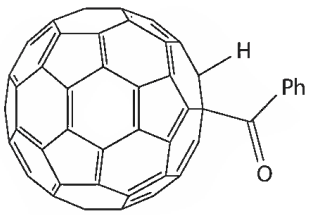	35	104
7	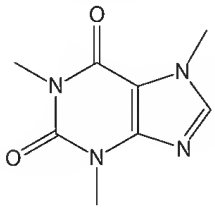	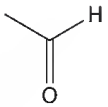	Direct	7	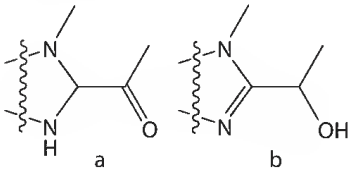	a:20 b:15	108

(*continued*)

TABLE 19.6 (continued) Photomediated Addition of Aldehydes, etc., to Unsaturated Systems

Entry	Unsaturated System	Aldehyde	PM[a] (eq[b])	Time (h)	Product	Yield (%)	Ref.
8	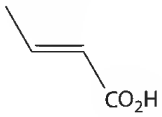	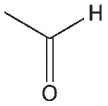	Ph_2CO (0.1)	24	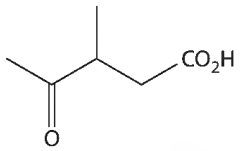	60	109
9		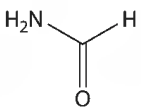	Ph_2CO (18)	3	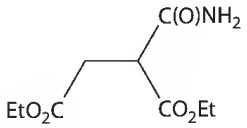	82	117
10	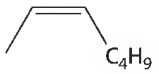	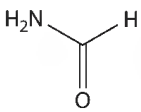	Acetone cosolvent	44	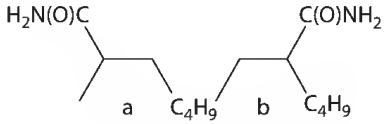	a:34 b:17	119

[a] Photomediator.
[b] Relative to the unsaturated substrate.

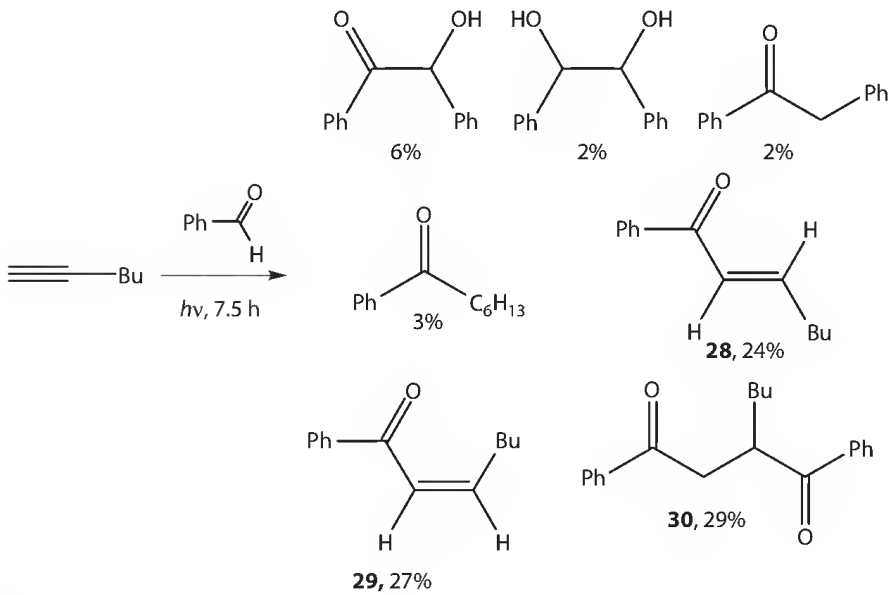

SCHEME 19.32

the synthetic perspective as gas-phase reactions involving acetaldehyde gave not only the ketone resulting from photoacylation, but in some cases the oxetane formed by the [2 + 2] cycloaddition of the aldehyde and the alkene as well (Table 19.6, Entry 3) [99]. The direct photoaddition of pentanal to diethyl maleate, with a quantum yield of about 200, has been achieved using a Nd-YAG pulsed laser as a light source [100]. It is proposed that the key H-abstraction step involves an interaction between ground-state and excited-state aldehyde molecules, a process that must be common to all direct photoacylation reactions. It is suggested that the very large quantum yield is due to the operation of a chain reaction based on a product forming back H-transfer, which involves a molecule of ground-state aldehyde rather than a ketyl radical. The development of a classic tandem intermolecular photoacylation–cyclization procedure with the dienoate (**31**) (Scheme 19.33) provided a basis for comparing a number of different C-radical generation methods [101]. Both photochemical methods were superior to the use of benzoyl

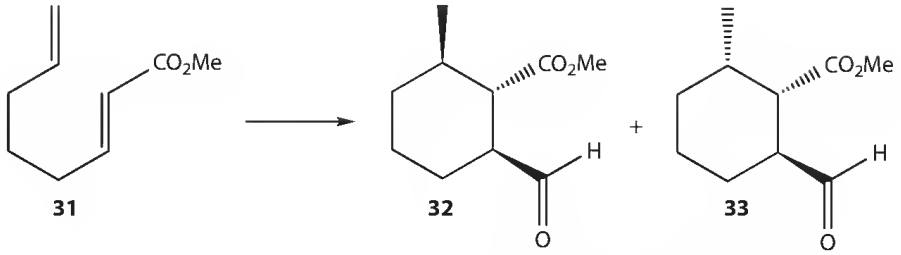

Initiator (0.1 eq)	°C	t (h)	% Cyclized Products	(33):(32)
$(BzO)_2$, Δ	95	16	15	1:1.36
p-$BzC_6H_4CO_3t$-Bu, *hν*	4	9	57	1:1.35
Ph_2CO, *hν*	4	5	30	1:1.34

SCHEME 19.33

peroxide; the lower yield obtained with benzophenone, relative to that obtained with the perester, was ascribed to quenching effects that reduce the former's efficiency.

The photomediated addition of aldehydes to enones has been shown to be a general reaction of aliphatic and aromatic aldehydes (Table 19.6, Entry 4) [102], with the addition to carbohydrate enones demonstrating the same, presumably steric driven, stereoselectivity as is observed in the addition of 1,3-dioxanyl radicals (Scheme 19.23) [83,84]. Steric control of stereoselectivity is also a feature of the addition of acyl radicals to 4-cholesten-3-one; the success of this reaction is in contrast to the fact that alcohols and dioxolanes fail to react [84]. The decatungstate TBADT has been shown to possess significant advantages as a photomediator in this area, compared to benzophenone [6]. In catalytic quantities (2 mol%), it effectively promotes the reaction of equimolar mixtures of aliphatic aldehydes and electron-deficient alkenes (Table 19.6, Entry 5). This result is not only important in the context of photomediated intermolecular H-abstraction, but also in terms of almost all thermal and photochemical methods that involve the generation and intermolecular trapping of C-radicals, as the use of a very large excess of the H-donor is a standard feature of such reactions [103]. The fact that the method is photochemical in nature also allows the use of low temperatures to suppress the decarbonylation process, which is competitive with acylation for α-substituted aldehydes (Scheme 19.34) [6]. The photoacylation of [60]-fullerene has also been achieved using TBADT as a photomediator (Table 19.6, Entry 6) [104]. It is believed that the reaction proceeds in the usual way through the addition to the fullerene of acyl radicals generated by H-abstraction from the aldehyde. As in the previous example, a low reaction temperature is used to suppress the decarbonylation of the acyl radicals and

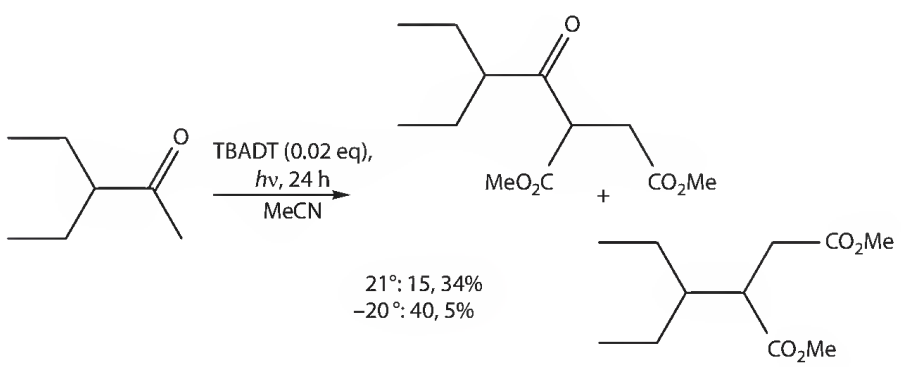

SCHEME 19.34

the consequent formation of alkylfullerenes. This photomediated approach provides access to a wide variety of new C_{60}-based materials.

The photochemical addition of aldehydes to quinones, sometimes referred to as a photo-Friedel–Crafts reaction, has been the topic of systematic research from both synthetic and mechanistic perspectives since it was first discovered in 1888 [95]. The reaction has however been the subject of a thorough and comprehensive review in a previous volume of this work [105] and so will not be considered here. The direct reaction follows the predictable route: H-abstraction from the aldehyde by a triplet state quinone, followed by in cage recombination of the radicals thus formed. Reports that have appeared since the 2004 review provide an indication of the scope of this reaction. One of these focuses on the photoacylation of 2-methyl- and 2-methoxy-1,4-naphthoquinone by direct irradiation (Scheme 19.35) [106]. This process has synthetic value as it results in the formation of a 2,3-disubstituted 1,4-naphthoquinone, a starting point for the synthesis of a range of biologically active quinonoids, which includes antimalarials, antibiotics, and pesticides. Thus the irradiation of a benzene solution of 2-methyl-1,4-naphthoquinone containing an excess of an aldehyde results in the formation of an acylated product (Scheme 19.35), occasionally accompanied by a triketone, which is the result of in-cage radical recombination at the tertiary position. In addition to the acylated quinone, photoacylation of 2-methoxy-1,4-naphthoquinone can also lead to the formation of the corresponding hydroquinone, which is relatively stable in solution but rapidly oxidizes to the quinone in the solid state. A subsequent communication reported an improved procedure for converting 1,4-naphthoquinones to the corresponding 2-acylhydroquinones [107]. This involves the expedient of combining UV lamps with $\lambda_{max} = 300 \pm 25$ nm with pyrex reaction vessels in an annular reactor. Due of the spectral characteristics of the reactant and product, this results in efficient light absorption by naphthoquinone, with little competition from the product hydroquinone.

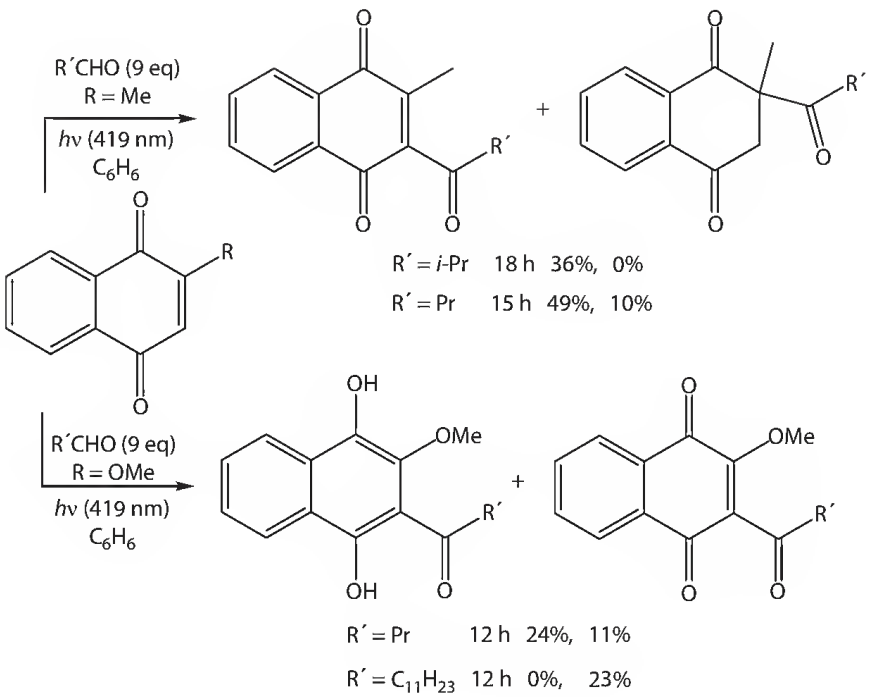

SCHEME 19.35

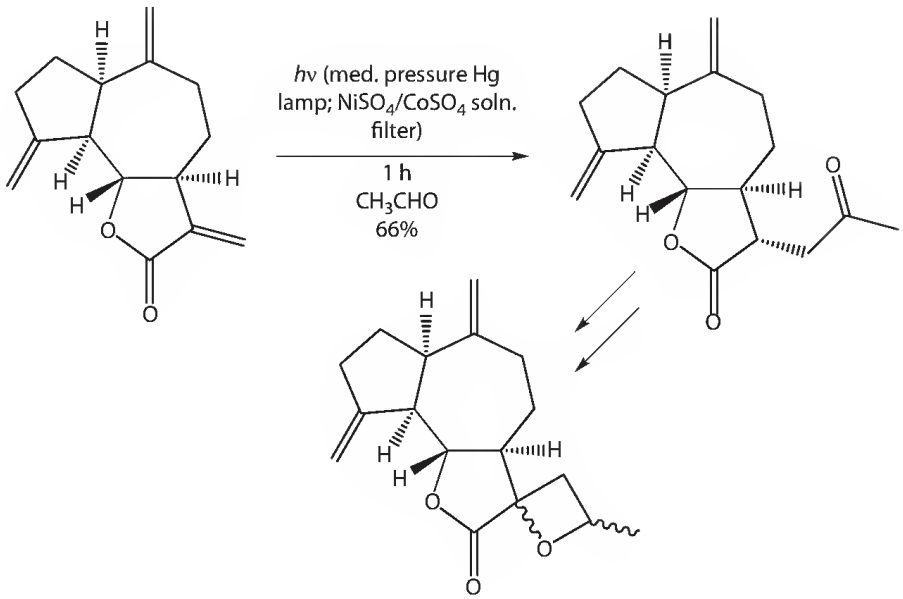

SCHEME 19.36

There appears to be only one example of the photoaddition of an aldehyde to a C=N bond: the direct addition of ethanal, propanal, and butanal gives 8-acyl-8,9-dihydrocaffeines and 8-(α-hydroxyalkyl) caffeines as the major products (Table 19.6, Entry 7) [108], together with smaller amounts of 8,8′-(8-acyl-8,9-dihydrocaffeine) dimers, and 8-acylcaffeines.

A number of synthetic procedures have been developed in which the photoacylation of an alkene plays a key role. Thus the photomediated addition of an aldehyde to α,β-unsaturated esters and acids has been used to produce 4-oxoalkanoic esters and acids in a single step (Table 19.6, Entry 8) [109]. These are synthetically useful building blocks, normally produced from acetoacetates and chloroacetates in a three-step process. A partial synthetic route to sesquiterpene lactones containing an oxetane ring, a structural unit associated with a wide range of biological activity, has been developed in which a key step is the photoaddition of an aldehyde to an α-methylene-γ-lactone (Scheme 19.36) [110]. The development of this synthetic method involved a detailed exploration of the scope and mechanism of the photoacylation process [111,112]. Results were obtained that appeared to suggest that the presence of molecular oxygen promoted the reaction, an effect that was attributed to enhanced intersystem crossing for the aldehyde in the excited singlet state. Overall the picture presented is rather puzzling and it may be worth noting that in the most recent report of the use of the method, no mention is made of a need for molecular oxygen [110]. Ketene dithioacetal *S*,*S*-dioxides have been shown to be synthetically versatile components in photoacylation reactions. Thus the adducts obtained from the addition of aromatic aldehydes to (**34**), in the presence or absence of benzophenone, can be used in the synthesis of indanones (Scheme 19.37) [113]. Efficient 1,2-asymmetric induction is possible if the photoacylation involves 3-hydroxy-1-(methylthio)-1-(*p*-tolylsulfonyl)-1-alkenes or the corresponding acetates [114], an example being the benzophenone-promoted addition of propanal to (**35**), followed by treatment with Raney nickel, that gave the sulfone (**36**) as an 83:17 mixture of diastereomers (Scheme 19.38). Finally, an intramolecular photoacylation involving the 3-(3-formylpropyl)furan-2(5*H*)-one (**37**) (Scheme 19.39) provides a nice example of how varying the photochemical conditions can control the outcome of a reaction [115]. In the presence of benzophenone, the photochemically active species is the benzophenone triplet, which abstracts a H-atom from the aldehyde forming an acyl radical that adds to the enone giving a single bicyclic adduct, (**38**). In the absence of benzophenone, the photochemically active species

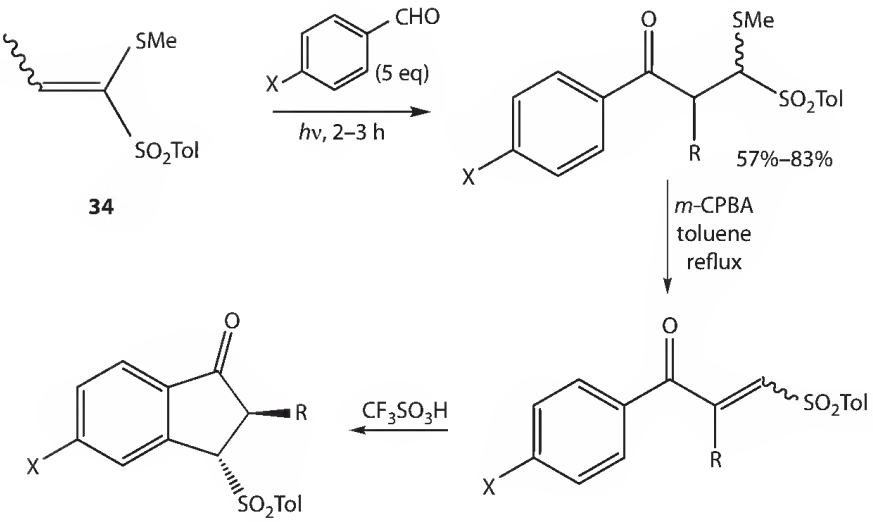

SCHEME 19.37

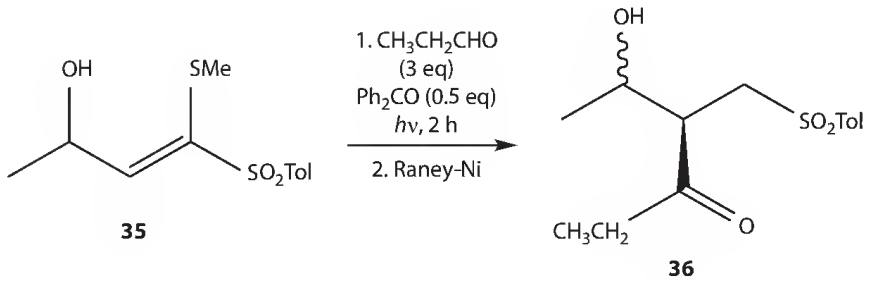

SCHEME 19.38

is the furanone triplet, which produces an acyl radical by intramolecular H-abstraction. This acyl radical cyclizes to give the spirobicyclic lactones, (**39**) and (**40**).

Photoamidation with formamide is also a general reaction of alkenes, occurring not only for electron-deficient alkenes (Table 19.6, Entry 9) [116,117], but also for unactivated terminal, nonterminal, and cyclic alkenes. Reactions with terminal alkenes occur almost regiospecifically in an anti-Markovnikov sense [118], whereas those with nonterminal alkenes give mixtures (Table 19.6, Entry 10) [119]. The yield obtained in these reactions using solar radiation was in many cases better than that obtained using pyrex-filtered high-pressure mercury lamps [117,119]. The photoamidation of norbornene, directly or in the presence of acetone, gives the *exo* addition product stereoselectively [120]. The acetone- or benzophenone-photomediated amidation of unactivated alkynes has also been reported [121], with surprisingly the major product obtained with a terminal alkyne such as 1-hexyne being (**41**), a 2:2 adduct for which an *E* stereochemistry is assumed. Internal alkynes give preferentially a 1:2 adduct, for example (**42**) in the case of 4-octyne. In terms of synthetic applications with more complex molecules, the stereoselective photomediated α-addition of formamide to the galactal (**43**) is a key step in the synthesis of a daucic acid ester with a D-*xylo* configuration (**44**) (Scheme 19.40) [122]. The synthesis of alkyl-substituted azetidine-2,4-diones has been achieved by the photocyclization of α,β-unsaturated *N*-formyl-*N*-methyl amides (Scheme 19.41) [123]. The reaction is believed to proceed via the 1,4-biradical formed through intramolecular H-abstraction by the electronically excited enone unit.

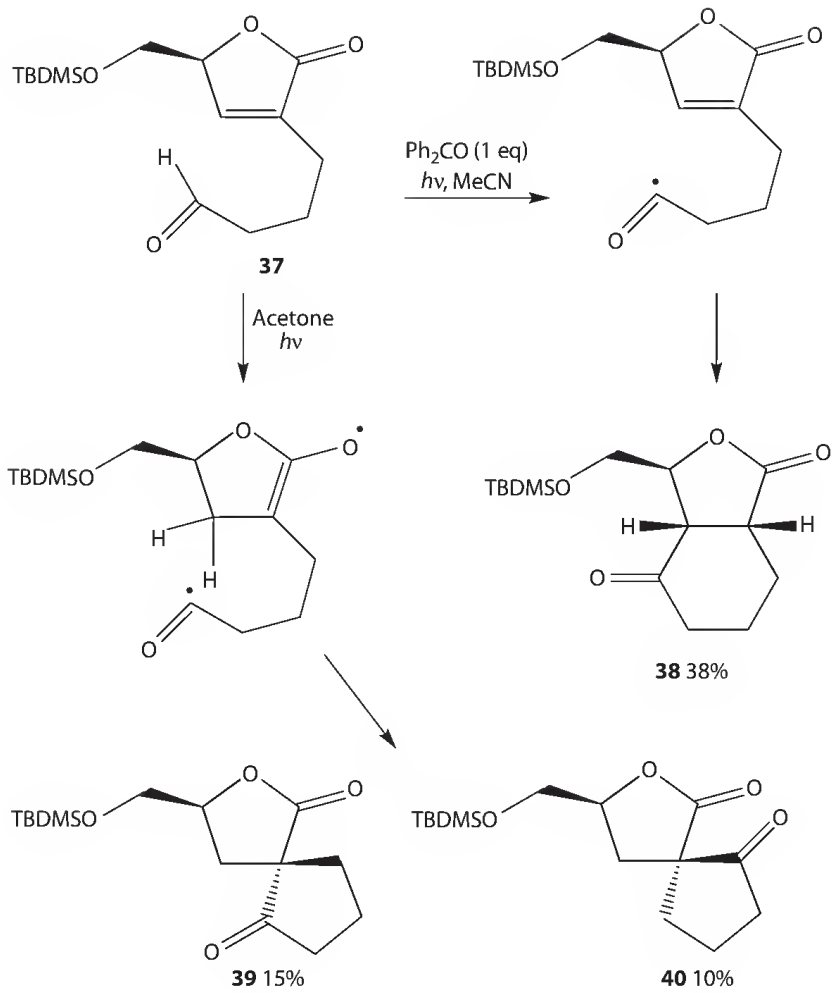

SCHEME 19.39

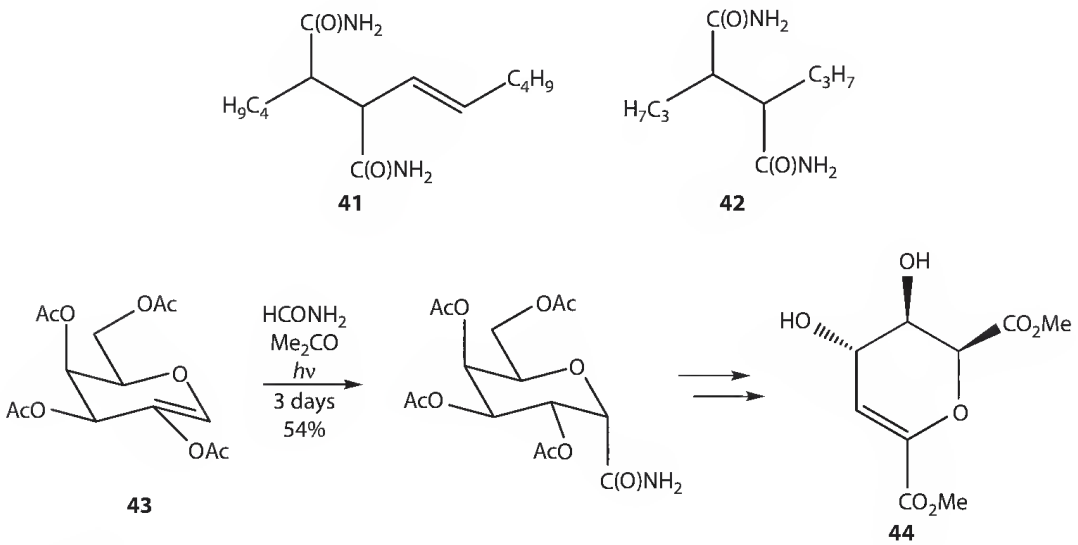

SCHEME 19.40

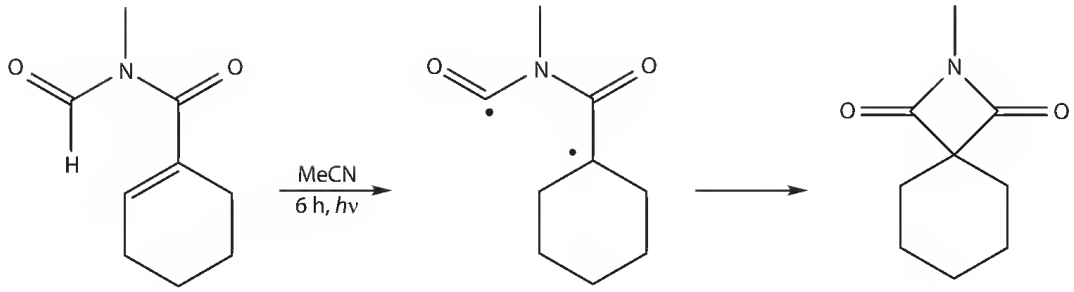

SCHEME 19.41

19.6 Photomediated Addition Reactions of Alcohols

The photochemical addition of secondary and primary alcohols to unsaturated systems extends the synthetic utility of the alcohol functional group in that it opens a reactivity channel, based on the nucleophilic character of the α-hydroxyalkyl radical, which is quite distinct from that which involves the nucleophilic oxygen. The p-type nonbonding electron pair, which is implicated in the weakness of the α-CH bond, is also responsible for the nucleophilic character of the α-hydroxyalkyl radical, a property that is apparent from a consideration of its resonance forms (Figure 19.4). The greater reactivity of secondary alcohols and the failure of benzyl alcohols to react can be attributed to inductive and resonance effects, respectively, in the α-hydroxyalkyl radicals derived from them. The first reported example of the photochemically induced addition of an alcohol to an alkene involved unactivated terminal alkenes under direct conditions and gave telomeric by-products (Table 19.7, Entry 1) [124]. Schenk's synthesis of terebic acid (**45**) (Scheme 19.42) [125] a few years later demonstrated that the photomediated addition of alcohols had synthetic potential. Another early example involved the irradiation of a solution of pregnadienolone acetate in cyclohexanol giving an addition product, together with the product of a reduction reaction (Table 19.7, Entry 2) [126], a process that has been found to be competitive with addition in other systems as well [127]. Interestingly, the reaction extends to alkenes, which, at least formally, are electron rich (Table 19.7, Entry 4) [129], and in terms of the alcohol component to diols in a reaction that is stereoselective (Table 19.7, Entry 5) [130]. The central role played by photochemical H-abstraction in these processes has been confirmed by a mechanistic study of the benzophenone-mediated addition of methanol to carbohydrate enones [131].

As is the case with all the other H-donors discussed in this review, the photomediated and direct addition of alcohols to the strongly electrophilic double bond in fluoroalkenes have both been extensively used in the synthesis of fluorinated molecules (Table 19.7, Entry 7) [80,132–137]. The addition of secondary alcohols to maleimide has been described (Table 19.7, Entry 8) [138], with this report being among those that note the lower reactivity of primary alcohols [19] and the effective failure of benzyl alcohols to react at all [124]. The psoralens (furocourmarins) give rise to a number of photobiological effects that are due to their photochemical reactions with the pyrimidine bases in DNA that usually involve the formation of [2 + 2] adducts. There are indications that the photocarcenogenicity of the psoralens may also be due to reactions involving the purine bases and model studies suggest that an alcohol photoaddition may be involved. Thus the reaction of the coumarin (**46**), a psoralen model, with adenosine leads to the formation of the adduct (**47**) (Scheme 19.43) [139]. Interestingly, other studies

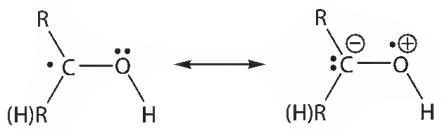

FIGURE 19.4

TABLE 19.7 Photomediated Addition of Alcohols, etc., to Unsaturated Systems

Entry	Unsaturated System	ROH	PM[a] (eq[b])	Time (h)	Product	Yield (%)	Ref.
1	1-Octene		Direct	96	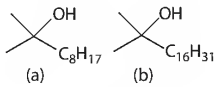 (a) (b)	a:38 b:24	124
2	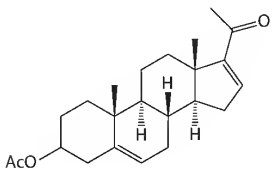	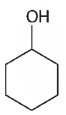	Direct or Ph_2CO	1	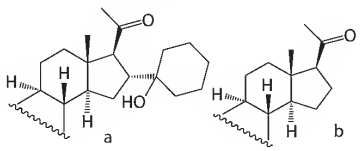 a b	a:25 b:40	126
3	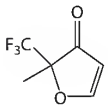		Direct	18	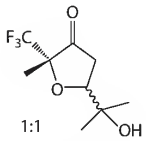 1:1	68	128
4	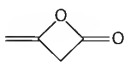		Acetone 3.5 eq	24	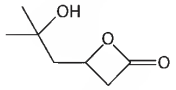	63	129
5	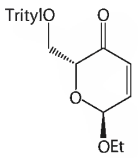		Ph_2CO (0.17 eq)	5	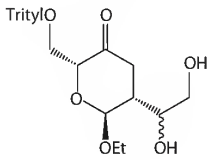	72	130

(*continued*)

TABLE 19.7 (continued) Photomediated Addition of Alcohols, etc., to Unsaturated Systems

Entry	Unsaturated System	ROH	PM[a] (eq[b])	Time (h)	Product	Yield (%)	Ref.
6	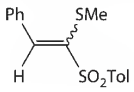	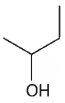	Ph_2CO (1)	3	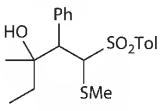 16:19:28:37	92	70
7	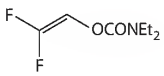		Direct	31	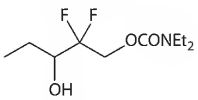	81	80
8	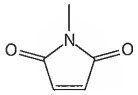		Direct	1	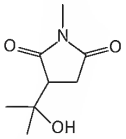	70	138
9			TBADT (0.02 eq)	15	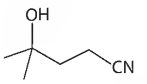	72	9
10	DMAD	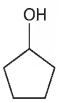	Ph_2CO (0.4 eq)	0.25	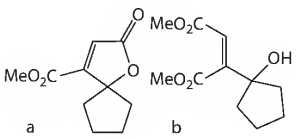 a b	a:31 b:28	19

[a] Photomediator.
[b] Relative to the unsaturated substrate.

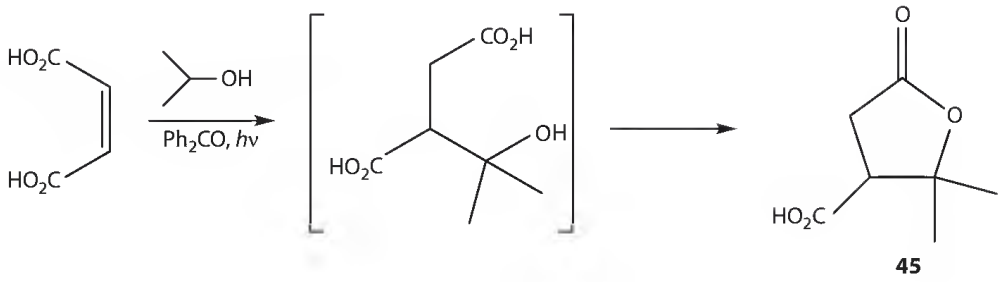

SCHEME 19.42

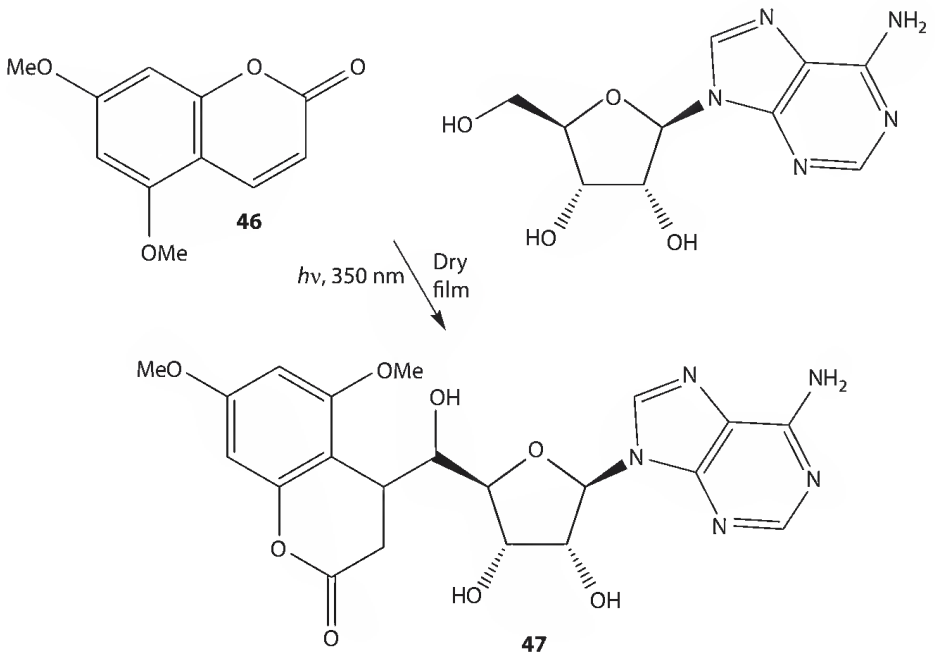

SCHEME 19.43

suggest that a photoreaction involving H-abstraction from the furan ring in adenosine may occur competitively [140]. The irradiation of pyridazine (**48**) (Scheme 19.44) in the presence of a large excess of an alcohol led to the formation of addition products, which on heating dehydrated and re-aromatized [141]. The reaction of (**48**) with benzyl alcohol gave (**49**), a product produced, it is suggested, by a reverse-aldol-type reaction involving an intermediate presumably formed by a H-abstraction-radical recombination sequence (Scheme 19.44). It is worth noting that the potential of TBADT as a photomediator in catalytic quantities has also been demonstrated in terms of the generation of α-hydroxyalkyl radicals (Table 19.7, Entry 9) [9].

The first reported example of the photoaddition of an alcohol to an alkyne involved the direct irradiation of a solution of ethyl propiolate in ethanol or 2-propanol (Scheme 19.45) [45]; the lactone (**50**) results from the cyclization of the initially formed *Z*-adduct. Other work, also based on a direct irradiation approach, has indicated that 2-propanol reacts with unactivated monosubstituted alkynes, but not with phenylacetylene, or disubstituted alkynes where the substituents are not activating [142,143]. In contrast, the photoaddition of 2-propanol to phenyl-*t*-butylacetylene, albeit in low yield has been reported [144]. The use of a photomediator dramatically increases the rate and overall yield of reactions involving acetylenes (Table 19.7, Entry 10) [19] and this approach has been applied to a wide range of alkyne/alcohol combinations, which in the case of the latter includes secondary and primary alcohols, and diols

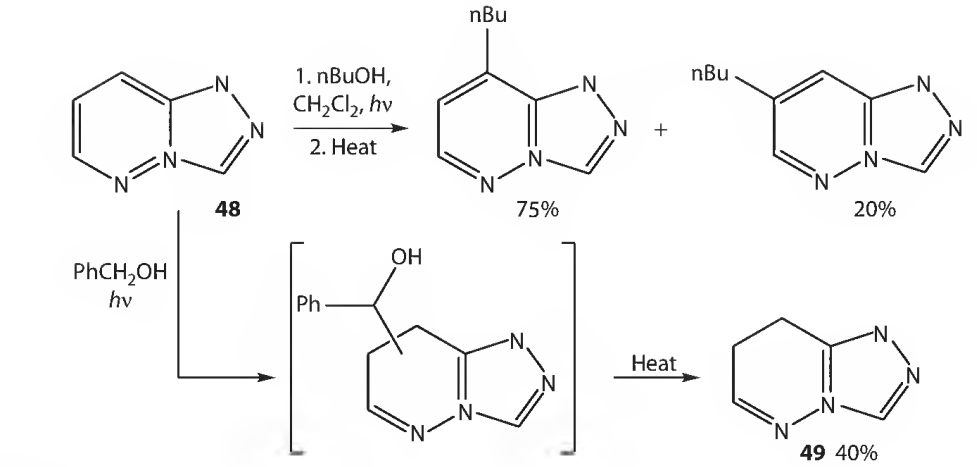

SCHEME 19.44

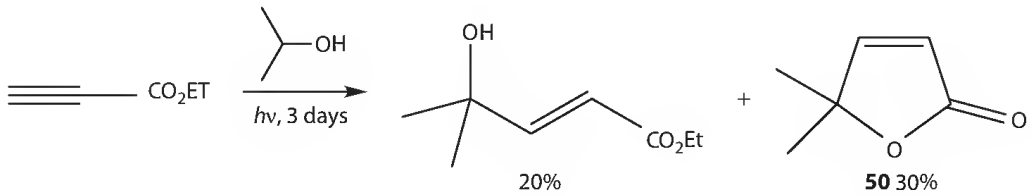

SCHEME 19.45

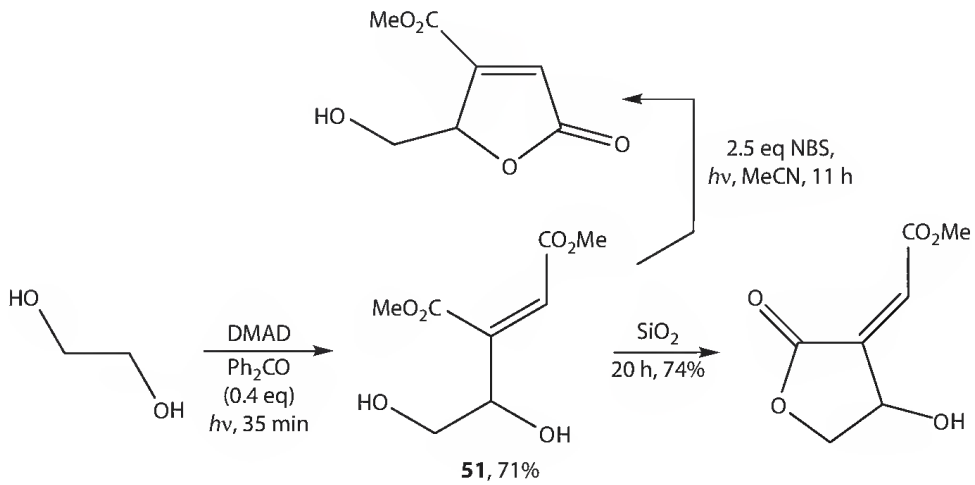

SCHEME 19.46

(Scheme 19.46). The formation in these reactions of a γ-butenolide, a common structural unit in many natural products, through the spontaneous cyclization of the initially formed cis-3-(hydroxyalkyl) propenoate, is of particular synthetic importance. The synthetically less interesting trans-isomer can be converted to the butenolide using NBS, and in the case of (**51**), which is formed stereoselectively from ethylene glycol, the regiochemistry of the cyclization process can be controlled (Scheme 19.46). The effectiveness of supported photomediators particularly those based on silica, which can be removed from the reaction product by simple filtration and are recyclable, further enhances the synthetic potential of this photoaddition reaction [19].

Primary and secondary alcohols have been added, under both direct and photomediated conditions, to a variety of *N*-heterocyclic systems, in what constitutes their addition to an imine bond (Scheme 19.47)

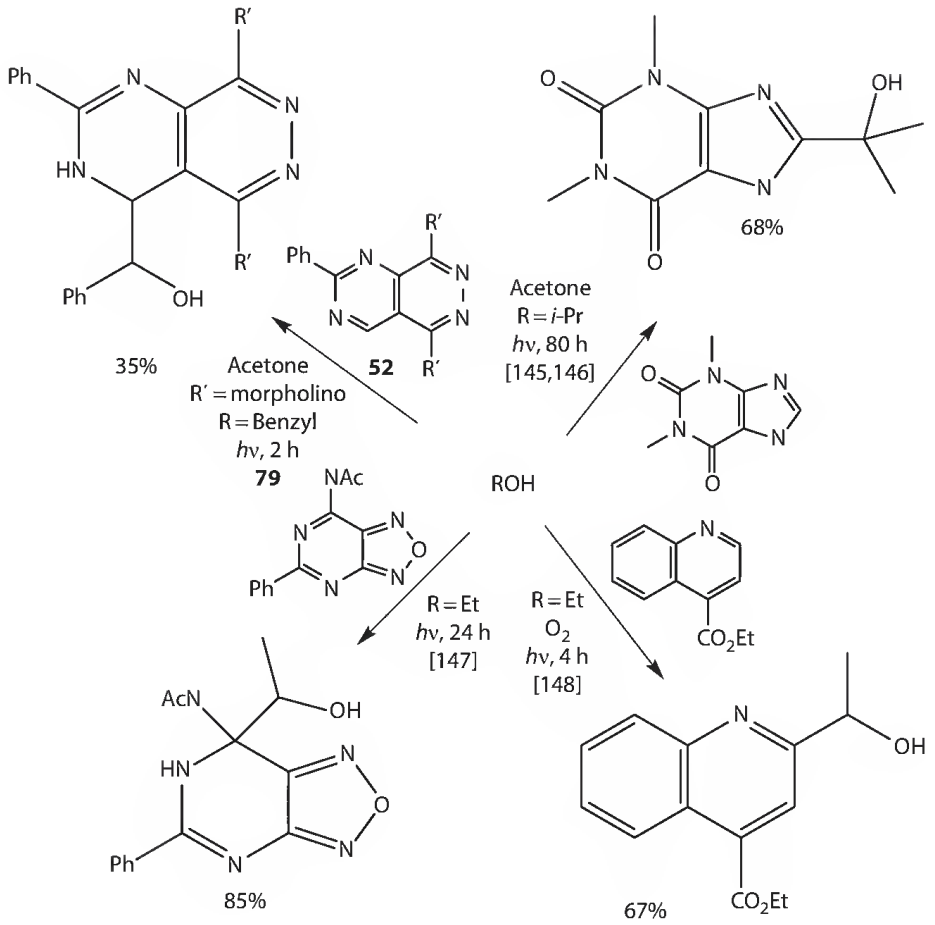

SCHEME 19.47

[75,145–148]. Under direct conditions the reaction involves H-abstraction by the electronically excited heterocyclic system, followed by recombination at the α-position. The photomediated variation involves the normal H-abstraction by the photomediator to give an α-hydroxyalkyl radical, which then adds to the heterocyclic system. The apparently photomediated addition of benzyl alcohol to (**52**) (Scheme 19.47) [75] is best understood in terms of H-abstraction by the excited heterocyclic system, rather than the nominal photomediator, followed by radical recombination. Depending on the details of the reaction system involved, this may involve either photosensitization or selective excitation of the heterocyclic system. In general, both electronic and stereochemical factors seem to be important in determining the regiochemical outcome of these reactions of *N*-heterocyclic systems.

In common with many of the reactions already discussed, the photoaddition of alcohols to unsaturated systems can occur with varying levels of stereoselectivity. Thus the addition of α-hydroxyalkyl radicals to chiral α-(triisopropylphenyl)sulfinyl enones occurs with the same high levels of diastereoselectivity that were obtained for the addition of dioxanyl radicals (Scheme 19.25) [87]. In a similar fashion the addition of benzophenone produced α-hydroxyalkyl radicals to (*E*)-γ-hydroxy-α,β-unsaturated esters occurred with high *anti*-selectivity, giving selectively the lactone (**53**) (Scheme 19.48) [149] on cyclization. Radical addition to the acetates of these α,β-unsaturated esters, and the corresponding sulfones, also proceeds with high stereoselectivity, the (*E*)- and (*Z*)-sulfones giving products of opposite stereochemistry. The addition of α-hydroxyalkyl radicals to 3-hydroxy-1-(methylthio)-1-(*p*-tolylsulfonyl)-1-alkenes, again reflecting the outcome of analogous photoacylation reactions (Scheme 19.38) [114], results in high 1,2-asymmetric induction [150,151]. As (**35**) and analogous alkenes are readily available in chiral form, the method can be used for enantioselective

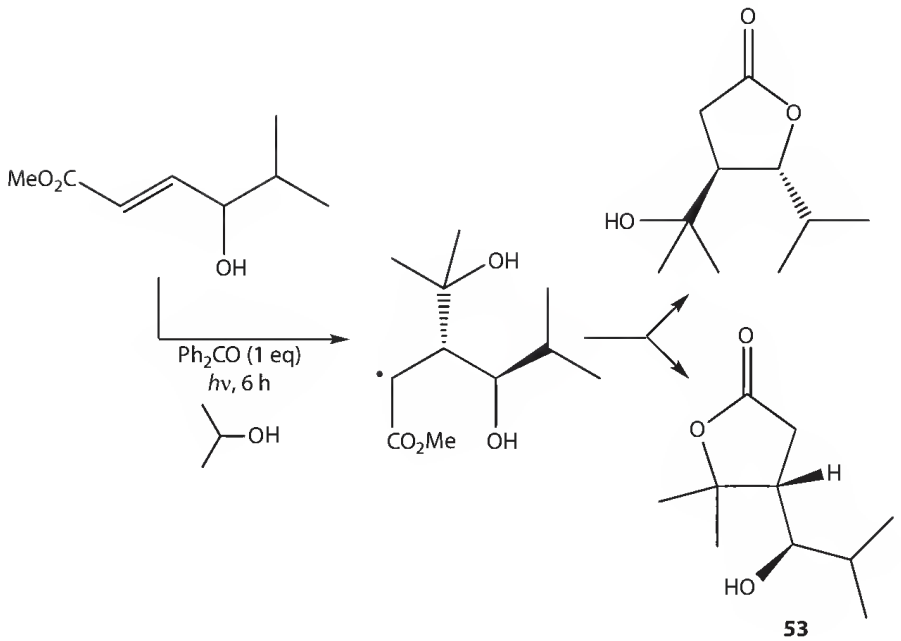

SCHEME 19.48

syntheses. Chiral induction has also been observed in the photomediated addition of alcohols to the mono- and dimenthyl esters of maleic and fumaric acids [152].

Reactions involving the photomediated abstraction of an α-H from an alcohol and the addition of the resulting radical to an unsaturated bond have been used in target synthesis and as subunits in methodologies designed to achieve specific synthetic goals. The photochemical conjugate addition of 2-propanol to carbohydrate derived enones forms part of a procedure that produces cyclohexanes and cyclopentanes from carbohydrates [153] (Scheme 19.49). The approach is based on the earlier work of Fraser-Reid [131,154] and involves using a pendant alkene to trap the intermediate α-keto radical before back H-transfer can occur. The acetophenone-photomediated stereoselective addition of 2-propanol to (*S*)-5-hydroxymethylfuran-2(5*H*)-one gave a *trans* 4,5-disubstituted lactone (**54**), which was used to prepare 3′-*C*-branched 2′,3′-dideoxynucleosides (Scheme 19.50) [155]. In terms of total synthesis, the lactone (**54**), prepared in this case by direct irradiation in up to 94% yield on a multigram scale, has been converted into (**55**) an intermediate in the synthesis of the pyrethrin insecticide, *cis*-chrysanthemic acid (**56**) (Scheme 19.50) [156]. The photoinduced addition of an alcohol to an imine bond has been used to produce an intermediate in the synthesis of the immunosuppressant (+)-myriocin (Scheme 19.51) [90]. Finally, returning to the material that was the subject of one of the earliest publications in this area [125], the asymmetric synthesis of terebic acid has now been carried out using the highly diastereoselective addition of photochemically produced α-hydroxyalkyl radicals to (*R*)-(−)-menthyloxy-2[5*H*]-furanone (Scheme 19.52) [157].

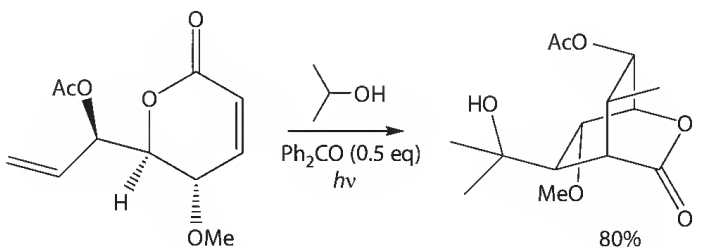

SCHEME 19.49

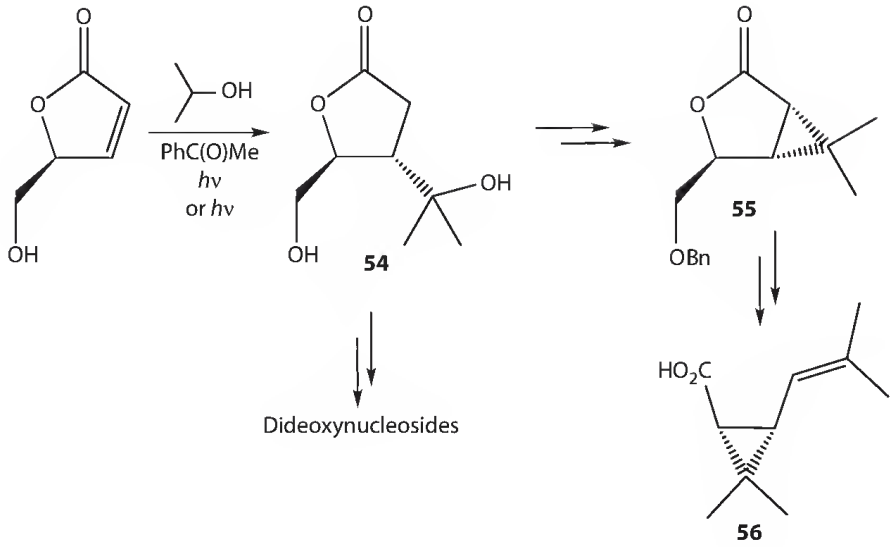

SCHEME 19.50

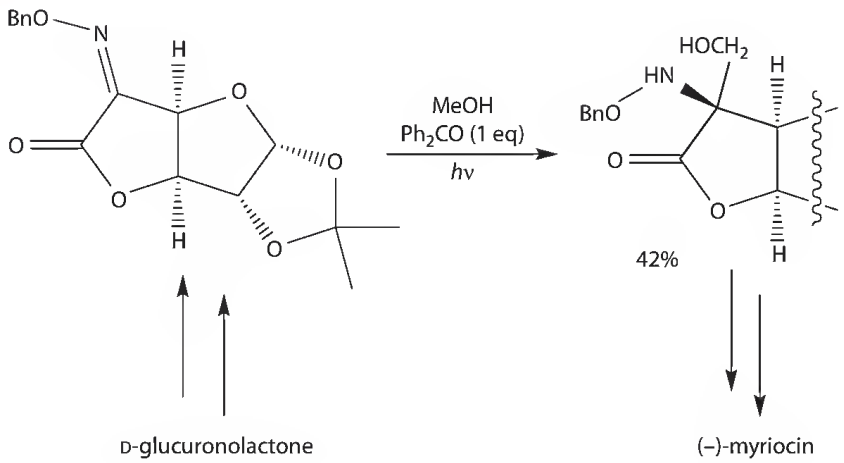

SCHEME 19.51

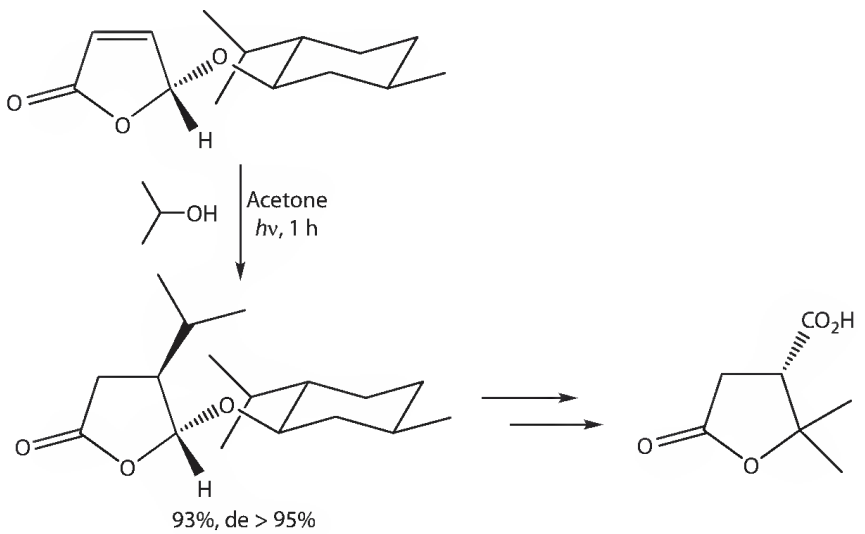

SCHEME 19.52

19.7 Conclusion

The generation of nucleophilic C-radicals by the intermolecular photomediated abstraction of H-atoms from a donor molecule with a weak C–H bond has considerable synthetic potential. The *in situ* addition of these radicals to unsaturated systems, containing at least one C-atom is, for example, an attractive method of forming C–C bonds, not least because it avoids the use of problematic tin and azo compounds, and peroxides. Other attractions of the approach include the fact that it allows unactivated molecules, such as cyclic ethers and cycloalkanes, to be used as reactants, and further that it opens up reaction pathways for molecules, such as secondary alcohols, which complement their normal mode of reaction. Similarly, direct photoacylation using aldehydes, or indirect using 1,3-dioxolanes, constitutes a synthetically valuable method of introducing a key functional group under mild, neutral conditions. In many cases reactions involving photochemically generated C-radicals occur with high levels of sterically controlled stereoselectivity.

It does have weaknesses, among them the need for a large excess of H-donor, which effectively restricts the methodology to donors that are sufficiently volatile to be removed by distillation following the reaction; the use of small, simple H-donors is also essential because of the lack of selectivity in terms of H-abstraction. The problems associated with the removal of the photomediator also make this approach to C–C bond formation less appealing. In the recent past however there have been developments that have addressed many of these issues. Thus the introduction of TBADT as a photomediator, which is effective in catalytic quantities and, at least in some cases, with approximately equimolar amounts of the unsaturated system and the H-donor, together with the development of supported and water-soluble photomediators, have enhanced the attractiveness of the approach, particularly from the clean/green chemistry perspective. A recent publication [158] touches on many of these issues and focuses on what is an ever interesting, and by no means the least important, aspect of these reactions, the fact that they can be driven by solar radiation.

References

1. A. Gansäuer. Ed., *Radicals in Synthesis I: Methods and Mechanisms, Topics in current chemistry*, Vol. 263, Springer-Verlag, Berlin, Germany, 2006; (b) A. Gansäuer. Ed., *Radicals in Synthesis II: Complex Molecules, Topics in current chemistry*, Vol. 264, Springer-Verlag, Berlin, Germany, 2006.
2. M. Fagnoni, D. Dondi, D. Ravelli, and A. Albini, *Chem. Rev.*, 2007, **107**, 2725–2756.
3. G. Dyker. Ed., *Handbook of C–H Transformations*, Wiley-VCH, Weinheim, Germany, 2005.
4. G. S. C. Srikanth and S. L. Castle, *Tetrahedron*, 2005, **61**, 10377–10441.
5. R. A. Doohan, J. J. Hannan, and N. W. A. Geraghty, *Org. Biomol. Chem.*, 2006, **4**, 942–952.
6. S. Esposti, D. Dondi, M. Fagnoni, and A. Albini, *Angew. Chem. Int. Ed.*, 2007, **46**, 2531–2534.
7. M. Oelgemöller, N. Healy, L. de Oliveira, C. Jung, and J. Mattay, *Green Chem.*, 2006, **8**, 831–834, and references therein.
8. R. A. Doohan and N. W. A. Geraghty, *Green Chem.* 2005, **7**, 91–96.
9. D. Dondi, M. Fagnoni, and A. Albini, *Chem. Eur. J.*, 2006, **12**, 4153–4163.
10. A. Padwa, *Tetrahedron Lett.*, 1964, **5**, 3465–3469.
11. M. Finn, R. Friedline, N. K. Suleman, C. J. Wohl, and J. M. Tanko, *J. Am. Chem. Soc.*, 2004, **126**, 7578–7584.
12. Y.-R. Luo, *Comprehensive Handbook of Chemical Bond Energies*, CRC Press, Boca Raton, FL, 2007.
13. V. Malatesta and K. U. Ingold, *J. Am. Chem. Soc.*, 1981, **103**, 609–614.
14. A. L. J. Beckwith and C. J. Easton, *J. Am. Chem. Soc.*, 1981, **103**, 615–619.
15. V. Malatesta and J. C. Scaiano, *J. Org. Chem.*, 1982, **47**, 1455–1459.
16. N. W. A. Geraghty and A. Lally, *Chem. Commun.*, 2006, 4300–4302.
17. D. Griller, J. A. Howard, P. R. Marriott, and J. C. Scaiano, *J. Am. Chem. Soc.*, 1981, **103**, 619–623.
18. L. Vereecken and J. Peeters, *Phys. Chem. Chem. Phys.*, 2002, **4**, 467–472.

19. N. W. A. Geraghty and E. M. Hernon, *Tetrahedron Lett.*, 2009, **50**, 570–573.
20. E. T. Denoosv and V. E. Tumanov, *Russ. Chem. Rev.*, 2005, **74**, 825–858.
21. K. Yamada, M. Nakano, M. Maekawa, T. Akindele, and K. Tomioka, *Org.* 2008, **10**, 3805–3808.
22. C. A. Parker and T. A. Joyce, *Chem. Commun.*, 1968, 749–750.
23. M. B. Rubin, *CRC Handbook of Organic Photochemistry and Photobiology*, Eds. W. M. Horspool and P.-S. Song, CRC Press, Boca Raton, FL, 1994, pp. 430–436.
24. L. C. T. Shoute and J. P. Mittal, *J. Phys. Chem.*, 1993, **97**, 8630–8637.
25. R. Anandhi and S. Umapathy, *J. Raman Spectrosc.*, 2000, **31**, 331–338.
26. N. Filipescu, J. P. Pinion, and F. L. Minn, *Chem. Commun.*, 1970, 1413.
27. P. J. Wagner, R. J. Truman, and J. C. Scaiano, *J. Am. Chem. Soc.*, 1985, **107**, 7093–7097.
28. P. Green, W. A. Green, A. Harriman, M.-C. Richoux, and P. Neta, *J. Chem. Soc., Faraday Trans. 1*, 1988, **84**, 2109–2127.
29. D. Dondi, I. Caprioli, M. Fagnoni, M. Mella, and A. Albini, *Tetrahedron*, 2003, **59**, 947–958.
30. D. J. Lougnot and J. P. Fouassier, *J. Polym. Sci., A: Polym. Chem.*, 1988, **26**, 1021–1033.
31. D. Dondi, D. Ravelli, M. Fagnoni, M. Mella, A. Molinari, A. Maldotti, and A. Albini, *Chem. Eur. J.*, 2009, **15**, 7949–7957.
32. M. D. Tzirakis and M. Orfanopoulos, *J. Am. Chem. Soc.*, 2009, **131**, 4063–4069.
33. D. Dondi, A. M. Cardarelli, M. Fagnoni, and A. Albini, *Tetrahedron*, 2006, **62**, 5527–5535.
34. M. Oelgemöller, C. Jung, and J. Mattay, *Pure Appl. Chem.*, 2007, **79**, 1939–1947.
35. N. W. A. Geraghty and D. J. Forkan, unpublished results.
36. Y. Zhang and C.-J. Li, *Tetrahedron Lett.*, 2004, **45**, 7581–7584.
37. K. K. Thoen, J. C. Thoen, and F. M. Uckun, *Tetrahedron Lett.*, 2000, **41**, 4019–4024.
38. T. Kamitanaka, T. Hikida, S. Hayashi, N. Kishida, T. Matsuda, and T. Harada, *Tetrahedron Lett.*, 2007, **48**, 8460–8463.
39. J. O. Metzger and M. Blumenstein, *Chem. Ber.*, 1993, **126**, 2493–2500.
40. T. A. Ryabinina, D. E. Kruglov, E. V. Pastushenko, and A. B. Terent'ev, *Zh. Org. Khim.*, 1992, **28**, 786–790.
41. H.-S. Dang and B. P. Roberts, *J. Chem. Soc., Perkin. Trans. 1*, 1998, 67–75.
42. N. Nemeroff, M. M. Jouillié, and G. Preti, *J. Org. Chem.*, 1978, **43**, 331–334.
43. J. Fossey, D. Lefort, and J. Sorba, *Free Radicals in Organic Chemistry*, Wiley, Chichester, U.K., 1995, p. 147.
44. M. B. Smith and J. March, *March's Advanced Organic Chemistry*, 5th edn., Wiley, New York, 2001, p. 24.
45. G. Büchi and S. H. Feairheller, *J. Org. Chem.*, 1969, **34**, 609–612.
46. E. Grovenstein, T. C. Campbell, and T. Shibata, *J. Org. Chem.*, 1969, **34**, 2418–2428.
47. S. Wolff, W. L. Schreiber, A. B. Smith, and W. C. Agosta, *J. Am. Chem. Soc.*, 1972, **94**, 7797–7806.
48. W. Schwack, F. Walker, and B. Bourgeois, *J. Agric. Food Chem.*, 1995, **43**, 3088–3092.
49. M. Zupan, B. Sket, and B. Pahor, *J. Org. Chem.*, 1978, **43**, 2297–2299.
50. E. Anklam and P. Margaretha, *Helv. Chim. Acta*, 1984, **67**, 2198–2205.
51. A. M. González-Cameno, M. Mella, M. Fagnoni, and A. Albini, *J. Org. Chem.*, 2000, **65**, 297–303.
52. A. M. Cardarelli, M. Fagnoni, M. Mella, and A. Albini, *J. Org. Chem.*, 2001, **66**, 7320–7327.
53. N. W. A. Geraghty and J. J. Hannan, *Tetrahedron Lett.*, 2001, **42**, 3211–3213.
54. C. L. Hill, *Synlett*, 1995, 127–132.
55. C. Tanielian, R. Seghrouchni, and C. C. Schweiter, *J. Phys. Chem. A*, 2003, **107**, 1102–1111.
56. D. Dondi, M. Fagnoni, A. Molinari, A. Maldotti, and A. Albini, *Chem. Eur. J.*, 2004, **10**, 142–148.
57. K. Yamada, Y. Yamamoto, M. Maekawa, and K. Tomioka, *J. Org. Chem.*, 2004, **69**, 1531–1534.
58. Z. Zheng and C. L. Hill, *Chem. Commun.*, 1998, **6**, 2467–2468.
59. I. Rosenthal and D. Elad, *Tetrahedron*, 1967, **23**, 3193–3204.
60. M. Kemmler, E. Herdtweck, and T. Bach, *Eur. J. Org. Chem.*, 2004, 4582–4595.
61. G. Ahlgren, *J. Org. Chem.*, 1973, **38**, 1369–1374.

62. A. G. Schultz, D. M. Graves, N. J. Green, R. R. Jacobson, and D. M. Nowak, *J. Am. Chem. Soc.*, 1994, **116**, 10450–10462.
63. P. Singh, *J. Org. Chem.*, 1972, **37**, 836–841.
64. M. D. Shetlar, *Chem. Commun.*, 1975, 653–654.
65. H. Graalfs, R. Fröhlich, C. Wolff, and J. Mattay, *Eur. J. Org. Chem.*, 1999, 1057–1073.
66. N. Reineke, N. A. Zaidi, M. Mitra, D. O'Hagan, A. S. Batsanov, J. A. K. Howard, and D. Y. Naumov, *J. Chem. Soc., Perkin Trans. 1*, 1995, 147–150.
67. O. Paleta, V. Církva, and J. Kvícala, *J. Fluorine Chem.*, 1996, **80**, 125–134.
68. R. D. Chambers and B. Grievson, *J. Chem. Soc., Perkin. Trans. 1*, 1985, 2215–2218.
69. S. G. Pyne and K. Schafer, *Tetrahedron*, 1998, **54**, 5709–5720.
70. K. Ogura, A. Yanagisawa, T. Fujino, and K. Takahashi, *Tetrahedron Lett.*, 1988, **29**, 5387–5390.
71. J. Boivin, E. Crepon, and S. Z. Zard, *Tetrahedron Lett.*, 1990, **31**, 6869–6872.
72. P. S. Mariano, J. Stavinoha, and E. Bay, *Tetrahedron*, 1981, **37**, 3385–3396.
73. A. Ishida, D. Sugita, Y. Itoh, and S. Takamuku, *J. Am. Chem. Soc.*, 1995, **117**, 11687–11694.
74. T. Nishio and Y. Omote, *J. Chem. Soc., Perkin Trans. 1*, 1988, 957–960.
75. A. Miyake, Y. Oka, and S. Yurugi, *Chem. Pharm. Bull.*, 1975, **23**, 1500–1504.
76. I. Rosenthal and D. Elad, *J. Org. Chem.*, 1968, **33**, 805–811.
77. J. S. Jewell and W. A. Szarek, *Tetrahedron Lett.*, 1969, **10**, 43–46.
78. K. Matsuura, K. Nishiyama, K. Yamada, Y. Araki, and Y. Ishido, *Bull. Chem. Soc. Jpn.*, 1973, **46**, 2538–2542.
79. V. Církva and O. Paleta, *J. Fluorine Chem.*, 1999, **94**, 141–156.
80. T. Okano, A. Nakajima, and S. Eguchi, *Synlett*, 2001, 1449–1451.
81. C. Manfrotto, M. Mella, M. Freccero, M. Fagnoni, and A. Albini, *J. Org. Chem.*, 1999, **64**, 5024–5028.
82. R. Mosca, M. Fagnoni, M. Mella, and A. Albini, *Tetrahedron*, 2001, **57**, 10319–10328.
83. B. Fraser-Reid, D. R. Hicks, D. L. Walker, D. E. Iley, M. B. Yunker, S. Y.-K. Tam, R. C. Anderson, and J. Saunders, *Tetrahedron Lett.*, 1975, **16**, 297–300.
84. B. Fraser-Reid, R. C. Anderson, D. R. Hicks, and D. L. Walker, *Can. J. Chem.*, 1977, **55**, 3986–3995.
85. T. Sakakibara, A. Takaide, and A. Seta, *Carbohydr. Res.*, 1992, **226**, 271–278.
86. G. Campari, M. Fagnoni, M. Mella, and A. Albini, *Tetrahedron: Asymmetry*, 2000, **11**, 1891–1906.
87. N. Mase, Y. Watanabe, and T. Toru, *Bull. Chem. Soc. Jpn.*, 1998, **71**, 2957–2965.
88. A. Nishida, N. Kawahara, M. Nishida, and O. Yonemitsu, *Tetrahedron*, 1996, **52**, 9713–9734.
89. M. Fernández-González and R. Alonso, *J. Org. Chem.*, 2006, **71**, 6767–6775.
90. S. Torrente and R. Alonso, *Org. Lett.*, 2001, **3**, 1985–1987.
91. M. Fernández and R. Alonso, *Org. Lett.*, 2003, **5**, 2461–2464.
92. M. Inomata, H. Suhara, H. Kinoshita, and H. Kotake, *Chem. Lett.*, 1988, **17**, 813–816.
93. P. J. Parsons and J. K. Cowell, *Synlett*, 2000, 107–109.
94. A. K. Ghosh, S. Leshchenko, and M. Noetzel, *J. Org. Chem.*, 2004, **69**, 7822–7829.
95. H. Klinger, *Justus Liebigs Ann. Chem.*, 1888, **249**, 137–146.
96. M. S. Kharasch, W. H. Urry, and B. M. Kuderna, *J. Org. Chem.*, 1949, **14**, 248–253.
97. P. de Mayo, J. B. Stothers, and W. Templeton, *Can. J. Chem.*, 1961, **39**, 488–497.
98. J. S. Bradshaw, R. D. Knudsen, and W. W. Parish, *J. Chem. Soc., Chem. Commun.*, 1972, 1321–1322.
99. E. R. Bissell and D. B. Fields, *J. Org. Chem.*, 1964, **29**, 249–252.
100. R. Stringat, G. Fabre, R. Fellous, and P. Paquet, *Tetrahedron Lett.*, 1992, **33**, 4303–4306.
101. P. Gottschalk and D. C. Neckers, *J. Org. Chem.*, 1985, **50**, 3498–3502.
102. G. A. Kraus and P. Liu, *Tetrahedron Lett.*, 1994, **35**, 7723–7726.
103. K. Yamada, M. Maekawa, Y. Yamamoto, M. Nakano, T. Akindele, and K. Tomioka, *Tetrahedron Lett.*, 2009, **50**, 6040–6043.
104. M. D. Tzirakis and M. Orfanopoulos, *J. Am. Chem. Soc.*, 2009, **131**, 4063–4069.
105. M. Oelgemöller and J. Mattay, In *CRC Handbook of Organic Photochemistry and Photobiology*, 2nd edn., Eds. W. M. Horspool and F. Lenci, CRC Press, Boca Raton, FL, 2004, **88**, 1–45.

106. P. A. Waske, J. Mattay, and M. Oelgemöller, *Tetrahedron Lett.*, 2006, **47**, 1329–1332.
107. F. Friedrichs, B. Murphy, D. Nayrat, T. Ahner, M. Funke, M. Ryan, J. Lex, J. Mattay, and M. Oelgemöller, *Synlett*, 2008, 3137–3140.
108. A. Erndt, M. Fiedorowicz, A. Kostuch, and A. Para, *Justus Liebigs Ann. Chem.*, 1993, 1043–1046.
109. H. Cerfontain and P. C. M. van Noort, *Synthesis*, 1980, 490–492.
110. F. A. Macias, V. M. Vinolo, F. R. Fronczek, G. M. Massanet, and J. M. G. Molinillo, *Tetrahedron*, 2006, **62**, 7747–7755.
111. F. A. Macías, J. M. G. Molinillo, I. G. Collado, G. M. Massanet, and F. Rodríguez-Luis, *Tetrahedron Lett.*, 1990, **31**, 3063–3066.
112. F. A. Macías, J. M. G. Molinillo, G. M. Massanet, and F. Rodríguez-Luis, *Tetrahedron*, 1992, **48**, 3345–3352.
113. K. Ogura, T. Arai, A. Kayano, and M. Akazome, *Tetrahedron Lett.*, 1998, **39**, 9051–9054.
114. K. Ogura, T. Arai, A. Kayano, and M. Akazome, *Tetrahedron Lett.*, 1999, **40**, 2537–2540.
115. D. Brown, M. G. B. Drew, and J. Mann, *J. Chem. Soc., Perkin. Trans. 1*, 1997, 3651–3656.
116. D. Elad, *Proc. Chem. Soc.*, 1962, 225.
117. D. Elad and J. Rokach, *J. Org. Chem.*, 1966, **31**, 4210–4215.
118. D. Elad and J. Rokach, *J. Org. Chem.*, 1964, **29**, 1855–1859.
119. D. Elad and J. Rokach, *J. Org. Chem.*, 1965, **30**, 3361–3364.
120. D. Elad and J. Rokach, *J. Chem. Soc.*, 1965, 800–802.
121. D. Elad and G. Friedman, *J. Chem. Soc. C*, 1970, 893–896.
122. F. W. Lichtenthaler, K. Nakamura, and J. Klotz, *Angew. Chem. Int. Ed.*, 2003, **42**, 5838–5843.
123. K. Maruyama, T. Ishitoku, and Y. Kubo, *J. Org. Chem.*, 1981, **46**, 27–34.
124. W. H. Urry, F. W. Stacey, E. S. Huyser, and O. O. Juveland, *J. Am. Chem. Soc.*, 1954, **76**, 450–455.
125. G. O. Schenck, G. Koltzenburg, and H. Grossmann, *Angew. Chem.*, 1957, **69**, 177–178.
126. P. Bladon and I. A. Williams, *J. Chem. Soc. C*, 1967, 2032–2037.
127. C. Semisch and P. Margaretha, *J. Fluorine Chem.*, 1986, **34**, 105–116.
128. R.-C. Gebel and P. Margaretha, *Chem. Ber.*, 1990, **123**, 855–858.
129. T. Kato, M. Sato, Y. Kitagawa, and R. Sato, *Chem. Pharm. Bull.*, 1981, **29**, 1624–1628.
130. B. Fraser-Reid and D. L. Walker, *Can. J. Chem.*, 1980, **58**, 2694–2702.
131. Z. Benko, B. Fraser-Reid, P. S. Maraino, and A. L. J. Beckwith, *J. Org. Chem.*, 1988, **53**, 2066–2072.
132. V. Dedek and I. Hemer, *Collect. Czech. Chem. Commun.*, 1985, **50**, 2743–2752.
133. R. N. Haszeldine, R. Rowland, R. P. Sheppard, and A. E. Tipping, *J. Fluorine Chem.*, 1985, **28**, 291–302.
134. O. Paleta, Z. Budková, J. Kvícala, and H.-J. Timpe, *Tetrahedron Lett.*, 1991, **32**, 251–254.
135. V. Církva, R. Polák, and O. Paleta, *J. Fluorine Chem.*, 1996, **80**, 135–144.
136. O. Paleta, V. Církva, Z. Budková, and S. Böhm, *J. Fluorine Chem.*, 1997, **86**, 155–172.
137. V. Církva, S. Böhm, and O. Paleta, *J. Fluorine Chem.*, 2000, **102**, 159–168.
138. M. A. S. Al-Amoudi and J. M. Vernon, *J. Chem. Soc., Perkin. Trans. 2*, 1999, 2667–2670.
139. S. C. Shim, H. K. Shim, and T. H. Cho, *Chem. Lett.*, 1986, 19–22.
140. L. Voituriez and J. Cadet, *Photochem. Photobiol.*, 1999, **70**, 152–158.
141. D. H. Brown and J. S. Bradshaw, *J. Org. Chem.*, 1980, **45**, 2320–2324.
142. L. M. Kostochka, E. P. Serebyakov, and V. F. Kucherov, *Zh. Org. Khim.*, 1973, **9**, 1611–1617.
143. E. P. Serebyakov, L. M. Kostochka, and V. F. Kucherov, *Zh. Org. Khim.*, 1973, **9**, 1617–1623.
144. H. E. Zimmerman and J. A. Pincock, *J. Am. Chem. Soc.*, 1973, **95**, 3246–3250.
145. A. Erndt, A. Kostuch, A. Para, and M. Fiedorowicz, *Monatsh. Chem.*, 1984, **115**, 383–390.
146. D. H. Murgida, P. F. Aramendia, and R. Erra-Balsells, *Photochem. Photobiol.*, 1998, **67**, 487–494.
147. E. C. Taylor, Y. Maki, and B. E. Evans, *J. Am. Chem. Soc.*, 1969, **91**, 5181–5182.
148. I. Ono and N. Hata, *Bull. Chem. Soc. Jpn.*, 1987, **60**, 2891–2897.
149. K. Ogura, A. Kayano, and M. Akazome, *Bull. Chem. Soc. Jpn.*, 1997, **70**, 3091–3101.
150. K. Ogura, A. Kayano, N. Sumitani, M. Akazome, and M. Fujita, *J. Org. Chem.*, 1995, **60**, 1106–1107.

151. A. Kayano, M. Akazome, M. Fujita, and K. Ogura, *Tetrahedron*, 1997, **53**, 12101–12114.
152. R. Vassen, J. Runsink, and H.-D. Scharf, *Chem. Ber.*, 1986, **119**, 3492–3497.
153. A. M. Gómez, S. Mantecón, S. Valverde, and J. C. López, *J. Org. Chem.*, 1997, **62**, 6612–6614.
154. U. E. Udodong and B. Fraser-Reid, *J. Org. Chem.*, 1989, **54**, 2103–2112.
155. J. Wengel, K. Oestergaard, and A. Hager, *Nucleos. Nucleot.*, 1996, **15**, 1361–1368.
156. J. Mann and A. Weymouth-Wilson, *Carbohydr. Res.*, 1991, **216**, 511–515.
157. N. Hoffmann, *Tetrahedron: Asymmetry*, 1994, **5**, 879–886.
158. D. Dondi, S. Protti, A. Albini, S. M. Carpio, and M. Fagnoni, *Green. Chem.*, 2009, **11**, 1653–1659.

20

Inter- and Intramolecular Photocycloaddition of Aromatic Compounds

Hajime Maeda
Kanazawa University

Kazuhiko Mizuno
Osaka Prefecture University

20.1 Introduction

Photocycloaddition of alkenes to aromatic rings is an important method for chemical conversion and construction of polycyclic compounds. In comparison with photocycloaddition of two alkenes and that of enone with alkenes, mild and chemoselective excitation by light is possible because aromatic rings often have absorption bands in longer wavelengths. In addition, most of them proceed via structurally controlled exciplexes consisting of aromatic rings with alkenes.[1] Therefore, highly selective photocycloaddition can be designed by control of structure and reactivity of substrates and exciplexes, although there are several modes in photocycloaddition of aromatic rings with alkenes, these are [2 + 2], [3 + 2], [4 + 2], [4 + 4], and so on.

The reaction modes are summarized in Scheme 20.1. Photoreaction of benzene and its derivatives proceeds [2 + 2] (*ortho*) and [3 + 2] (*meta*) modes. Arenes and alkenes having either electron-releasing or electron-withdrawing substituents favor the *ortho* addition, whereas relatively simple arenes and alkenes undergo *meta* addition.[2–5] The [4 + 2] (*para*) mode is a rare case. Photocycloaddition to fused aromatic rings occurs onto the positions that have highly double bond character. Namely, 1,2-, 9,10-, 4,5-, and 5,6-positions of naphthalene, phenanthrene, pyrene, and chrysene tend to undergo [2 + 2] photocycloaddition, respectively. Crossed photocycloaddition of alkenes to anthracene hardly proceeds, because [4 + 4] photodimerization of anthracene is a fast and efficient process.

Photocycloaddition of unsaturated bonds such as alkenes, alkynes, and cyclopropanes to aromatic rings is reviewed in this chapter. Since several excellent reviews have been published,[6–11] and previous version of this handbook[12] also treated this topics, recent advances in this field after 2004 will be surveyed.

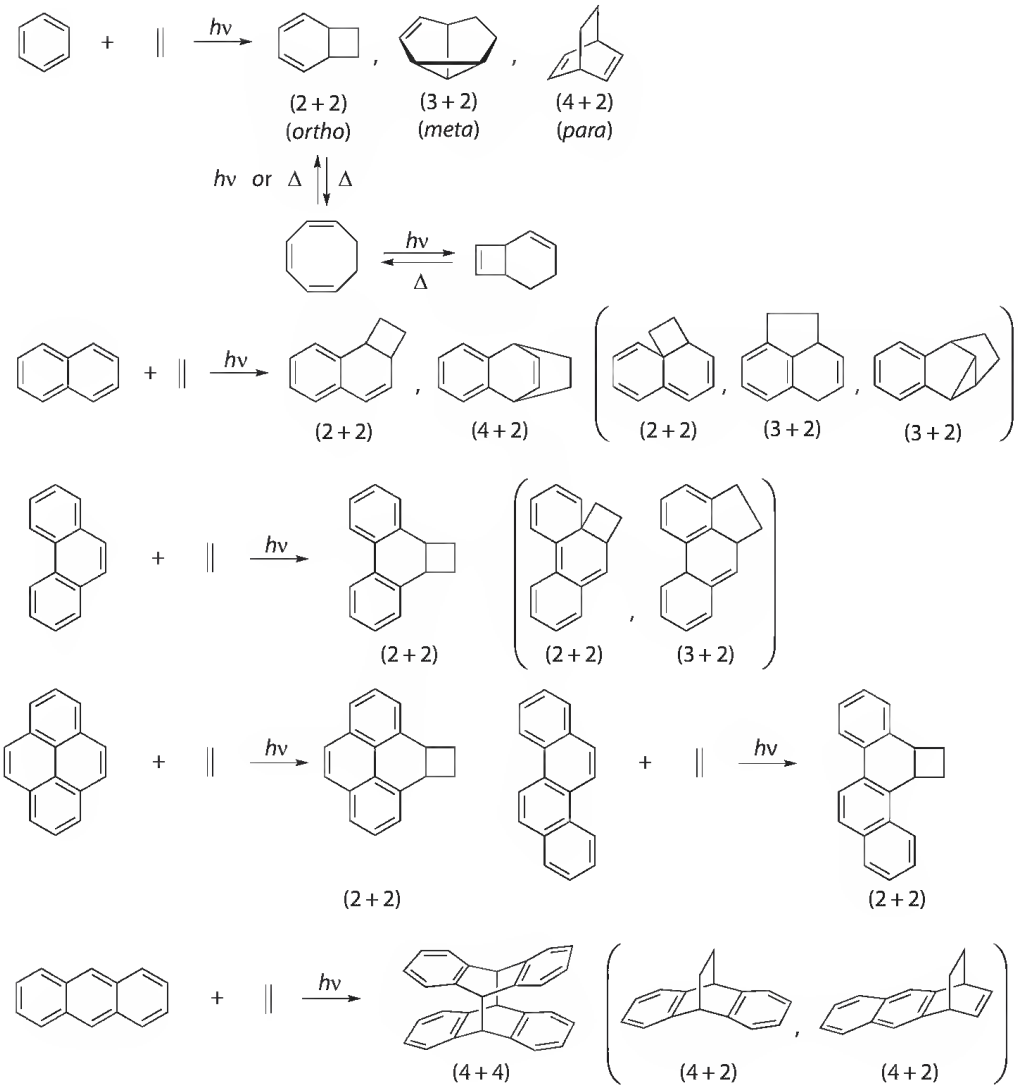

SCHEME 20.1

20.2 Photocycloaddition of Alkenes to Benzene Derivatives

From a pioneering work by Wender in 1981, that is, synthesis of (±)-α-cedrene from compound **1** (Scheme 20.2),[13] intramolecular *meta*-photocycloaddition between benzene ring and alkenes has been utilized as a key step for the construction of various natural products. Since exhaustive reviews have been published,[11,14] only recent two examples will be introduced in this section.

Mulzer et al. reported total synthesis of sesquiterpenoids named penifulvins A, B, and C, insecticides with a dioxafenestrane, by means of *meta*-photocycloaddition of enantiomerically pure silphinenes **2a–c**

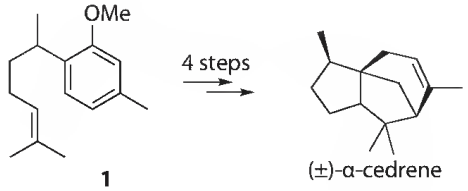

SCHEME 20.2

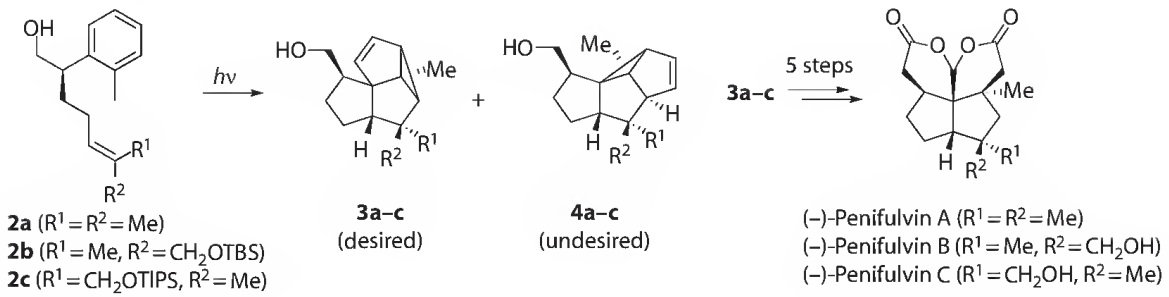

SCHEME 20.3

as a key step (Scheme 20.3).[15,16] The intramolecular *meta*-photocycloaddition of **2a** gave regioisomers **3a** and **4a** in 55:45 ratio. Intramolecular *meta*-photocycloaddition of **2b–c** gave not only **3b–c** and **4b–c** but also epimers at stereogenic centers attaching substituents R^1 and R^2. The all regioisomers could be separated by flash column chromatography. From the isolated desired isomers **3a–c**, synthesis of enantiomerically pure penifulvins A, B, and C is accomplished.

Chen et al. reported core skeleton of lancifodilactone F, one of the triterpenoid isolated from the Chinese herb *Schisandra*, could be constructed via intramolecular *meta*-photocycloaddition (Scheme 20.4).[17] Photoreaction of racemic **5** produced photocycloadducts **6** and **7** in a 1:1.2 ratio. Since separation of **6** and **7** failed, the mixture was converted to allylic alcohols **8** and **9** by acid hydrolysis after epoxidation. Compounds **8** and **9** could be separated by silica gel column chromatography. A five-step synthesis from **9** afforded compound **10** (racemic), which has a 5,6,7-tricyclic skeleton of lancifodilactone F.

As can be seen in the aforementioned reactions, the intramolecular *meta*-photocycloaddition gives products involving 1,3-addition-2,4-closure, 1,3-addition-2,6-closure, and 2,6-addition-1,3-closure, whose ratio can be controlled by electronic and steric nature of the aromatic rings, alkenes, and tethers (Scheme 20.5).[10]

Jenkins et al. reported that photoreaction of diastereomerically pure compound **11**, which has alkyl and hydroxy groups at appropriate positions, gave only 2,6-addition-1,3-closure product **12** as a single diastereomer although there are two possibilities of face selectivity (Scheme 20.6).[18] Sugimura found that asymmetric synthesis of photocycloadducts can be achieved in photoreaction of enantiomerically pure **13** (2*R*, 4*R*) to give **14** and **15** in 40% and 15% yields, respectively.[19,20] This photoreaction is highly stereocontrolled with the initial addition at the *Si*-face of the vinyl moiety.

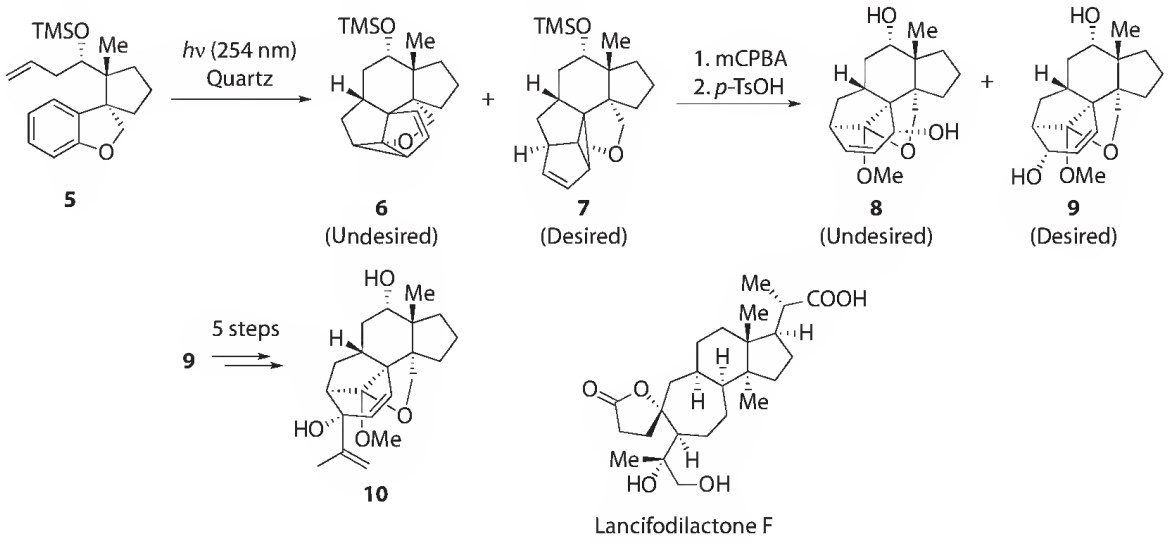

SCHEME 20.4

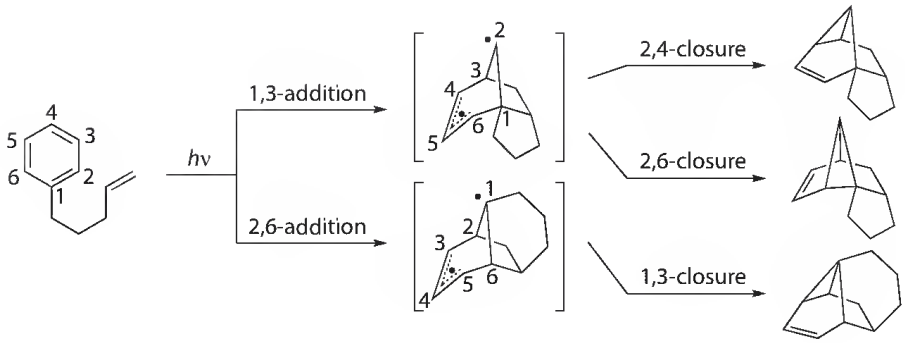

SCHEME 20.5

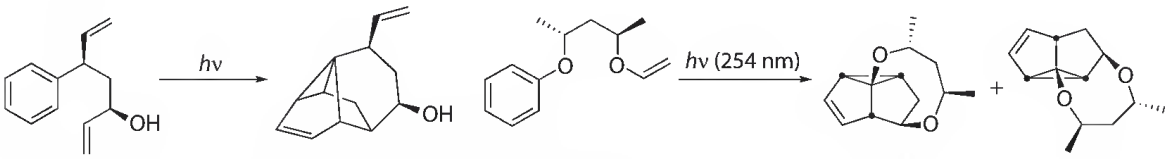

SCHEME 20.6

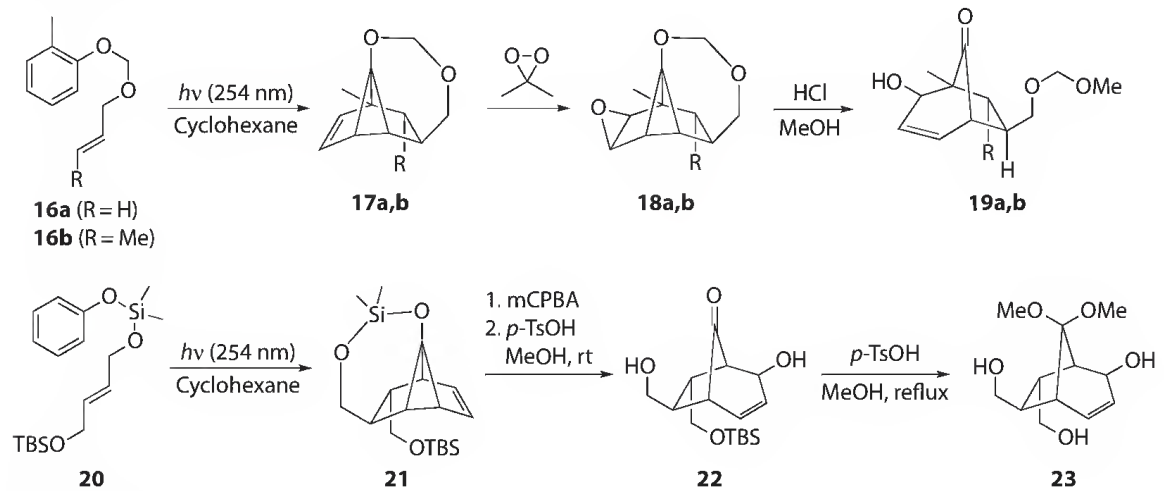

SCHEME 20.7

The use of temporary tethers in the *meta*-photocycloaddition was investigated by Penkett et al. in 2004.[21] Photoreaction of compounds **16a–b** tethered by methylene acetal proceeds regioselectively to give **17a–b** (Scheme 20.7). Epoxidation of **17a–b** followed by treatment with acids gave open-chained allyl alcohols **19a–b**. Disiloxane-tethered compound **20** also undergo regioselective photocycloaddition to give **23** via **21** and **22**. Silyl tethers are known to be also used in control of photodimerization of styrene and stilbene derivatives.[22–24]

Penkett also reported that when methoxy-substituted benzaldehyde diallyl acetal **24** was irradiated, novel double [3 + 2] photocycloadduct **26** was obtained stereoselectively with the formation of angular triquinanes **27** and **28** (Scheme 20.8).[25] When **24** was irradiated to the point of its total consumption, linear triquinane **25** could be detected. From the results of control experiments including the photoreaction of a deuterium-labeled compound, linear triquinane **25** produces **26**, while **27** photoisomerizes to **28**. The fact that photoirradiation of **25** also gave **28** can be explained by photoisomerization between **25** and **27** via a biradical **29**.

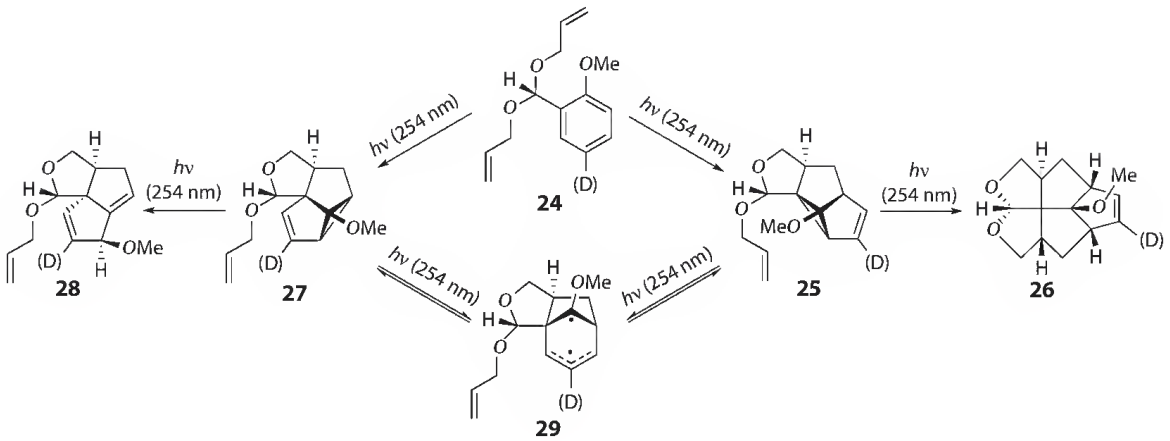

SCHEME 20.8

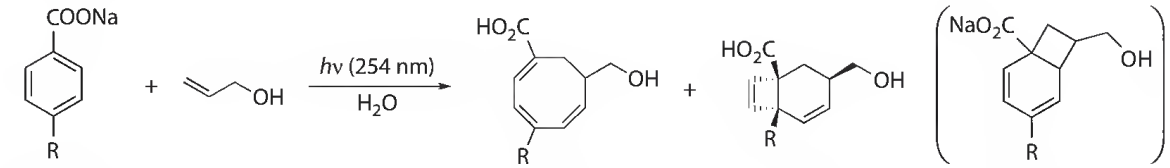

30a (R = H)
30b (R = Me)
30c (R = OMe)

SCHEME 20.9

Yoshimi and Hatanaka reported that sodium salts of *para*-substituted benzoic acids **30a–c** undergo photocycloaddition when it was irradiated in H_2O in the presence of allyl alcohol **31** to give cyclooctatriene derivatives **32a–c** and bicyclooctadienes **33a–b** (Scheme 20.9).[26] From the structure of products and the fact that the photoirradiation of the isolated **32b** gave **33b** and *p*-methylbenzoic acid, they concluded that **32** should be produced via [2 + 2] (*ortho*) photocycloadduct **34** but it is reversible, and that **33** produces by the photochemical ring closure of **32.**

Oshima et al. reported when 1,1-diphenylethene **35** was photoirradiated in the presence of methyl-substituted 1,4-benzoquinones **36a–d**, the products, **37** and **38** further reacted intramolecularly to give [2 + 2] (*ortho*) photocycloadducts **39** and **40** reversibly (Scheme 20.10).[27]

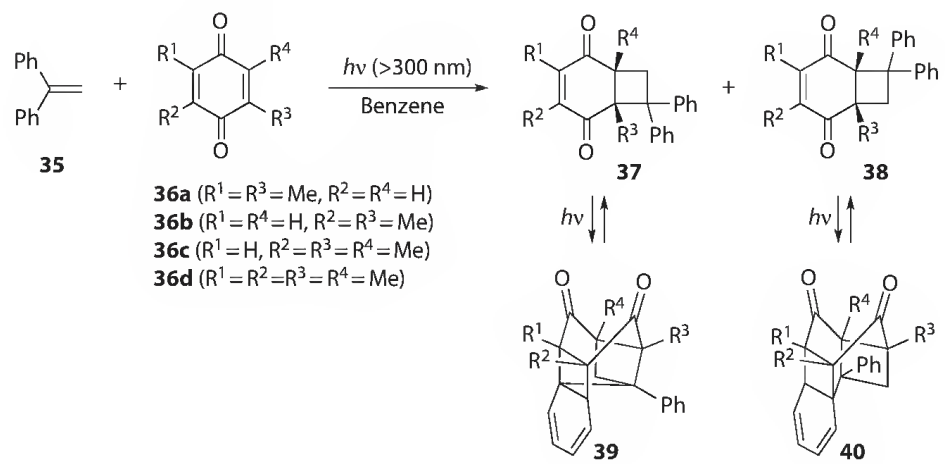

36a ($R^1 = R^3 = Me$, $R^2 = R^4 = H$)
36b ($R^1 = R^4 = H$, $R^2 = R^3 = Me$)
36c ($R^1 = H$, $R^2 = R^3 = R^4 = Me$)
36d ($R^1 = R^2 = R^3 = R^4 = Me$)

SCHEME 20.10

20.3 Photocycloaddition of Alkenes to Naphthalene Derivatives and Related Arenes

Most of photocycloaddition of alkenes to naphthalene derivatives proceeds at 1,2-position of the naphthalene ring. Kubo et al. has been disclosed unusual [3 + 2] photocycloaddition of alkenes to 1,8-position in 1992.[28,29] In this section, recent advances in this field are surveyed.

Mizuno et al. have disclosed that the photoirradiation of benzene and acetonitrile solutions containing 2-(2-alkenyloxymethyl)naphthalene-1-carbonitriles **41a–c** afforded photocycloadducts at 1,2-position (**42a–c**) and 2,4-position (**43a–c**) of the naphthalene ring via singlet exciplexes **44** and **45** (Scheme 20.11).[30,31] The compound **42** was predominantly obtained at the initial stage of the reaction, but prolonged irradiation afforded the [3 + 2] photocycloadduct **43** as a major product, because photocycloreversion from **42** to **41** takes place, but that from **43** to **41** does not occur. This reversibility is supported by the UV absorption spectra of **41–43**. Under the irradiation conditions using high-pressure mercury lamp and Pyrex filter (>280 nm), **41** and **42** competitively absorb UV light, but **43** does not absorb incident light. Similar photoreaction of the related compounds **47a–b** afforded pentacyclic compounds **48a–b** stereoselectively in 74% and 85% yields, respectively.

Photoreaction of compounds **49a–c**, which are connected two chromophores by an ether linkage, proceeded in a similar manner (Scheme 20.12). Namely, at the initial stage of the photoreaction, **50a–c** was predominantly produced, but prolonged irradiation led to an accumulation of **51a–c**. In such a reaction system in which both a fast reversible process and a slow irreversible process coexist, the microflow system is appropriate for the selective formation of the initial product.[32,33] Under the batch conditions without stirring, the primary product is produced only near the surface of vessel at the initial stage of the photoreaction, then a secondary reaction proceeds faster than the diffusion of the primary product that has been already accumulated near the surface. On the other hand, in the flow system, selective

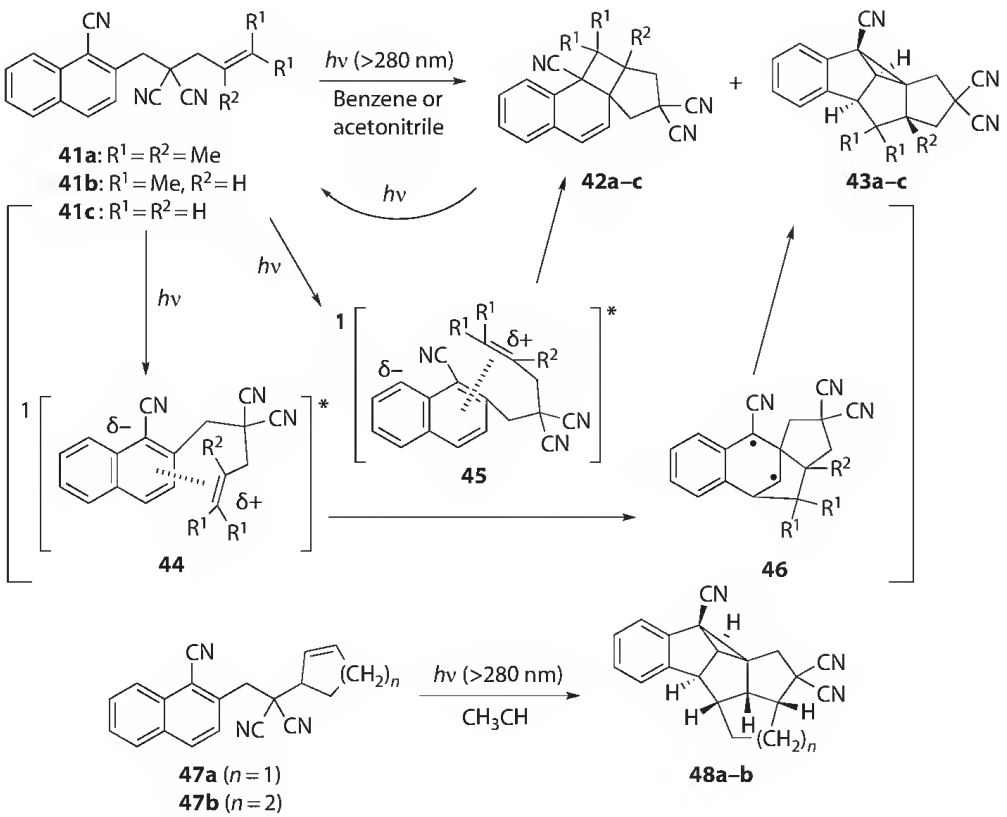

SCHEME 20.11

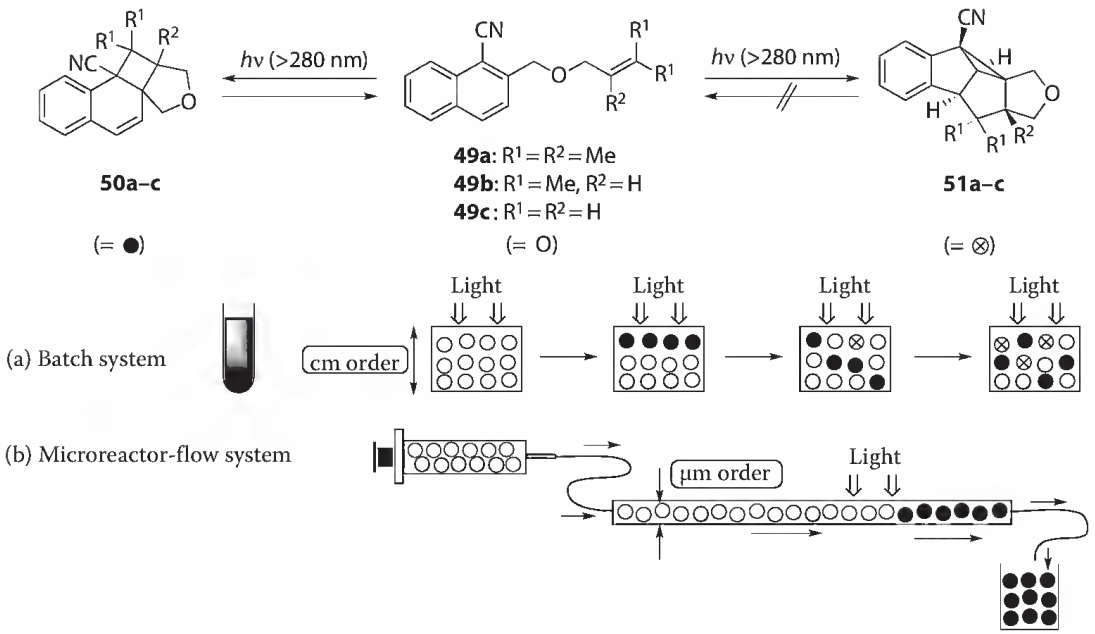

SCHEME 20.12

formation of primary product can be achieved by the quick outflow of the primary product from the reaction system.

Asymmetric induction in the intramolecular [2 + 2] photocycloaddition of **49b** by its incorporation in chirally modified zeolites has been observed (Scheme 20.13).[34] Photoirradiation of **49b**, included in NaY zeolites along with phenylalaninol **52**, gives **50b** with a maximum 15% ee. The degree of enantioselectivity was found to depend on the Si/Al ratio, the nature of cations in the zeolites, the structure of chiral inductors, and the molar ratio of substrate and chiral inductors.

A novel intramolecular [4 + 2] photocycloaddition between naphthalene and alkene was developed by Banerji et al. (Scheme 20.14).[35] When 2-methyl-2-ethenyl naphthalene-4-chromanone **53** in methanol or ethanol in the presence of H_2O was irradiated, alcohol-incorporated [4 + 2] photocycloadducts **55a–b** were produced in both 20% yields.

Intermolecular photocycloaddition of uracil derivatives to naphthalene and its derivatives was developed by Seki et al. UV irradiation of 6-chloro-1,3-dimethyuracil **57** with naphthalene **56** in nonpolar

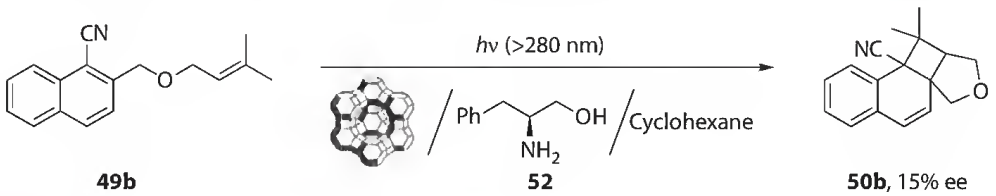

49b **52** **50b**, 15% ee

SCHEME 20.13

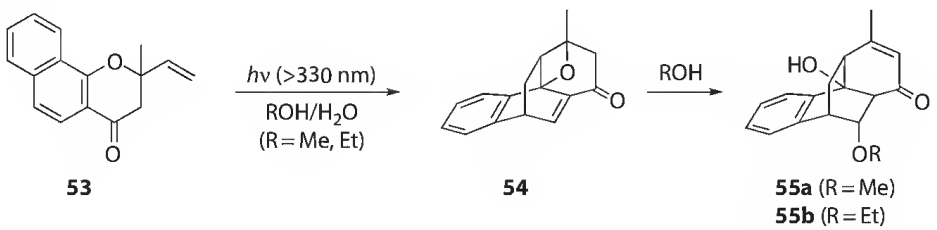

53 **54** **55a** (R = Me)
55b (R = Et)

SCHEME 20.14

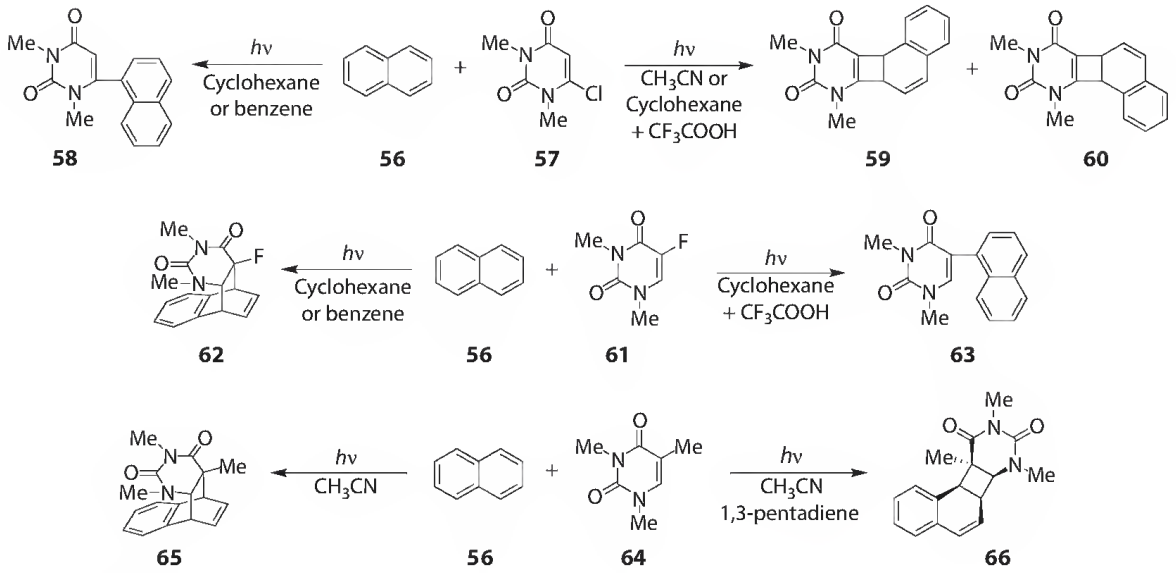

SCHEME 20.15

solvents such as cyclohexane and benzene gave substitution product **58**, while photoreaction in acetonitrile or cyclohexane in the presence of trifluoroacetic acid gave 1,2-cycloadducts including cyclobutene ring **59** and **60** (Scheme 20.15).[36] In contrast, 5-fluoro derivative **61** reacts with naphthalene to give [4 + 2] cycloadduct **62**, whereas substitution product **63** was obtained in the presence of acid.[37,38] In the photoreaction of 5-methyl derivative **64**, [4 + 2] photocycloadduct **65** was produced, but in the presence of 1,3-pentadiene as a triplet quencher, [2 + 2] photocycloadduct **66** was obtained.[39,40] Photoreactions of 6-chloro derivative **57** with phenanthrene and pyrene were also investigated by them, which afforded [2 + 2] photocycloadducts at 9,10-position of phenanthrene and 4,5-position of pyrene.[41]

Novel photocycloaddition of *N*-methyl-2,3-naphthalenedicarboximide **67** was observed by Qing-Jian in 2007 (Scheme 20.16).[42] When **67** was irradiated with excess amount of phenylacetylene **68**, hexacyclic adduct **69** was obtained in 68% yield. Structure of **69** was confirmed by x-ray crystallographic analysis, which contains three molecules of **68**.

Fujita et al. reported that confined cavities consisted from tri(4-pyridyl)triazine and Pd-TMEDA complex **70** is suitable media for [4 + 2] thermal (Diels–Alder) and [2 + 2] photocycloaddition reactions (Scheme 20.17).[43,44] Suspending pyrene and *N*-cyclohexylmaleimide into **70** in aqueous solution forms ternary complex **71** in 81% yield. The aqueous solution was irradiated to give a complex **72** including cross-photocycloadduct indicating *syn* stereochemistry quantitatively. Efficient *syn*-selective and regioselective [2 + 2] photocycloaddition is also observed in fluoranthene-included complex **73**.

Helix structure of cholesteric phase influences stereochemistry of [2 + 2] photocycloaddition. Maeda and Mizuno et al. reported that photocycloaddition of cholesteryl cinnamate **76** with methyl 9-phenanthrenecarboxylate **75** under neat conditions at 150°C–170°C produced a 14% diastereomeric excess of **77** (Scheme 20.18).[45]

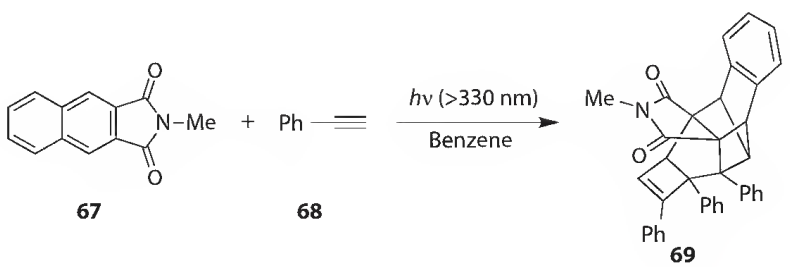

SCHEME 20.16

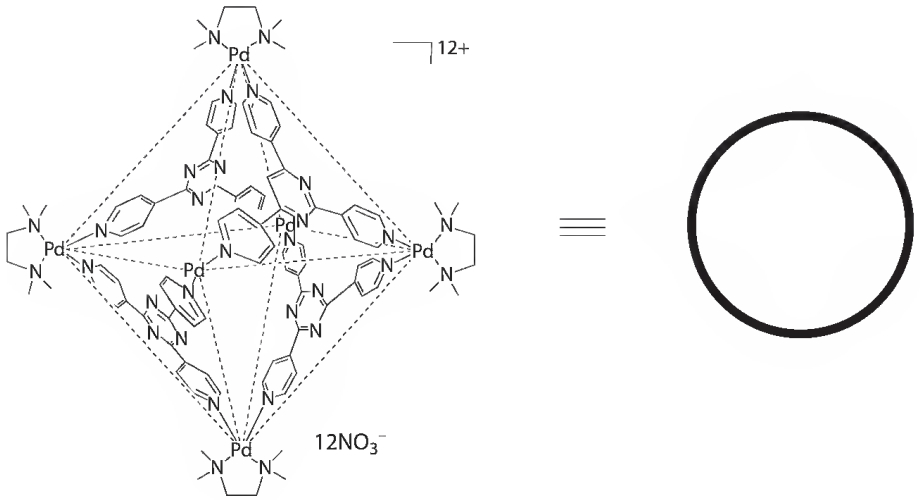

70

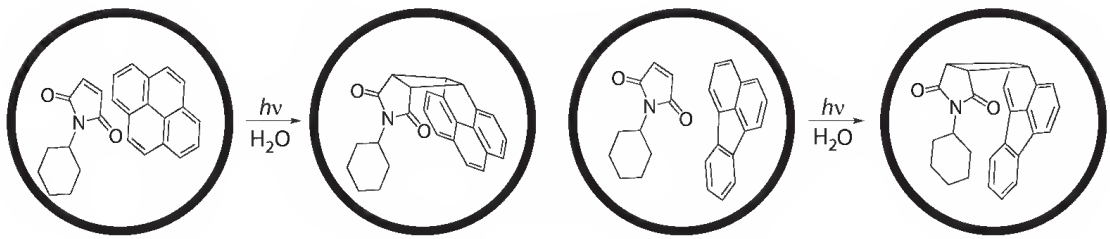

71 **72** **73** **74**

SCHEME 20.17

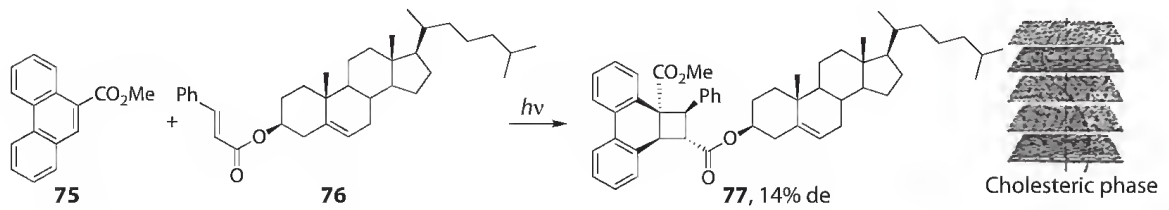

75 **76** **77**, 14% de

SCHEME 20.18

20.4 Photodimerization of Anthracene Derivatives and Related Compounds

Anthracene and its derivatives are susceptible for photodimerization at their 9,10-position. For 9-substituted anthracene **78**, there are both possibilities upon photoirradiation to produce head-to-tail dimer **79** and head-to-head dimer **80** (Scheme 20.19). Intramolecular photodimerization of tethered two anthracenes **81** and photochemical and thermal cleavage of **82** are often utilized for photoswitching devices. There are excellent reviews treating this photoreaction,[11,46–51] so only recent development is introduced.

Molecules tethering two naphthyl rings are less susceptible for photodimerization than anthracene analogues. Tung et al. reported photoreaction of **83** is very inert in homogeneous solutions, but photoreaction of **83** within supercages of NaY zeolite proceeds smoothly (Scheme 20.20).[52] Tung also reported cucurbit[8]uril **86** can encapsulate **83** to make a stable 1:1 inclusion complex **84** in aqueous solution. Intramolecular photocycloaddition of **84** in aqueous solution proceeds with remarkable selectivity and efficiency.[53] Tung et al. also clarified that nanosized particles of modified silica with 3-ammoniumpropyl

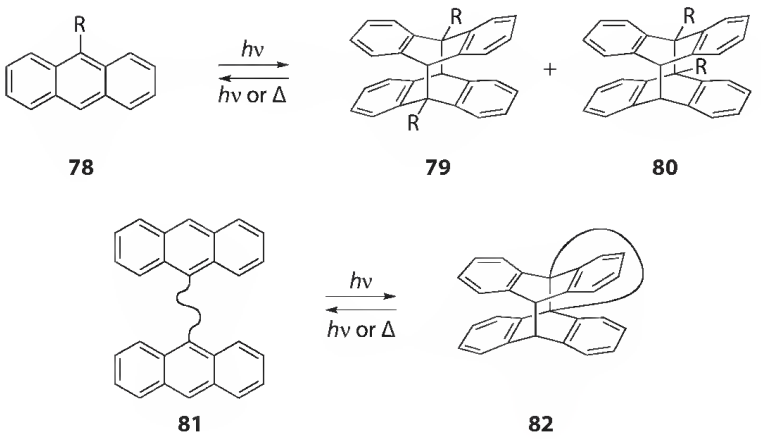

SCHEME 20.19

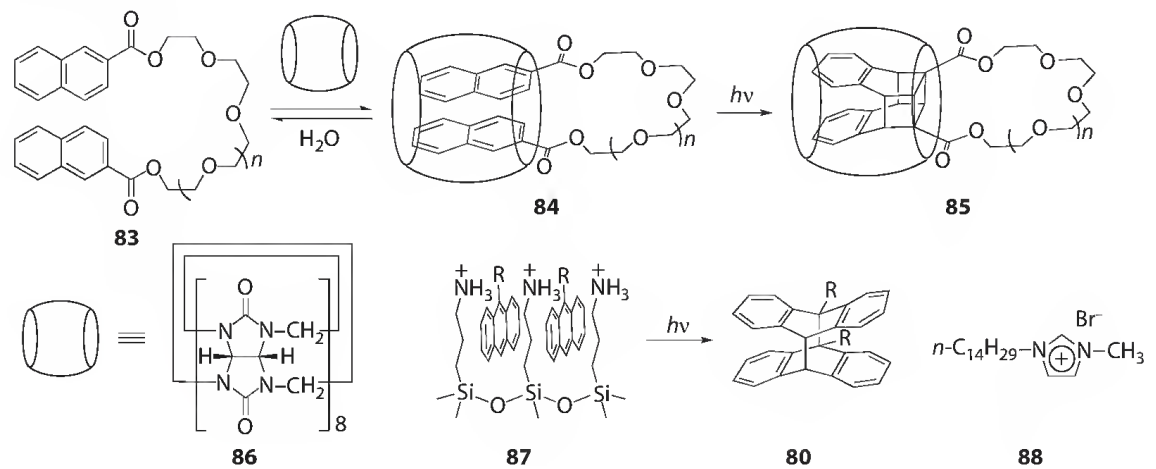

SCHEME 20.20

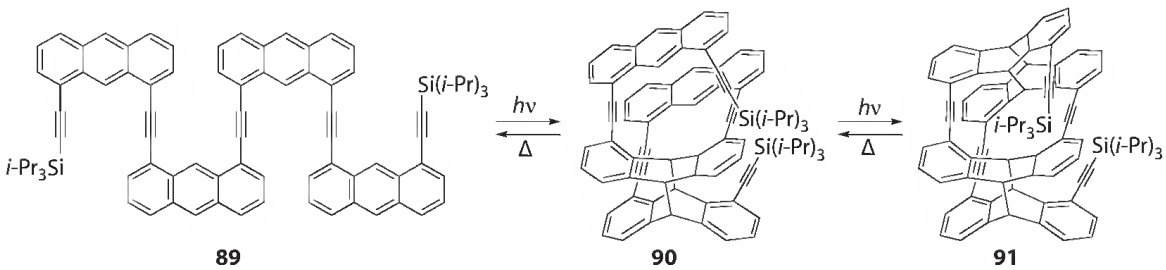

SCHEME 20.21

residue **87**[54] and microemulsions of *N*-alkylimidazolium ionic liquid **88** [55] are effective for the regioselective photodimerization of 9-substituted anthracenes.

Intramolecular [4 + 4] photocycloaddition of **89** gave **90** and then **91** (Scheme 20.21).[56] This is called "molecular folding screen," which can be unfolded by thermal cycloreversion.

Since [4 + 4] photodimerization of anthracene is an efficient and fast process, intramolecular photocycloaddition of anthracene and another chromophore competes with intermolecular photodimerization. However, Meier et al. recently investigated substituent effects of a benzene ring of **92** on selectivity between intra- and intermolecular photocycloaddition in detail (Scheme 20.22).[57] They concluded that methoxy groups on benzene ring of **92** made the photoreaction to unimolecular process to give **93** selectively, since high electron density of the benzene ring causes electron transfer from benzene ring to S_1 of anthracene moiety.

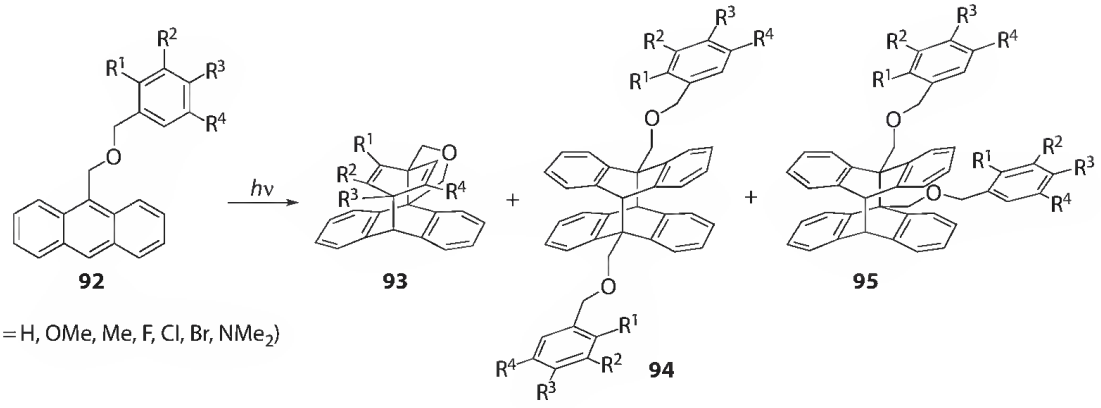

SCHEME 20.22

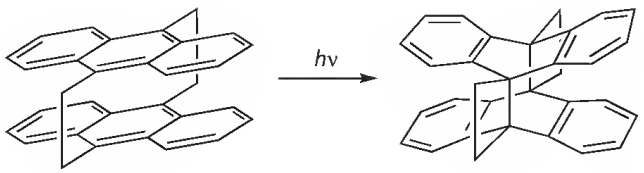

SCHEME 20.23

Studies of the photodimerization in crystalline state have also progressed. Trzop and Turowska-Tryk monitored structural change of the photoreaction of anthracenophane **96** in crystal in detail using x-ray diffraction in 2008 (Scheme 20.23).[58] The cell volume increased by 0.8% until the reaction was 40% complete, and afterward decreased by 1.6% during the remainder of the photoreaction. The distance between reacting carbon atoms was constant until 20% photoreaction progress, then decreased, and stabilized from 40% photoreaction progress. This phenomenon was explained by interplay between stress resulting from the presence of product molecules and the rigidity of reactant molecules.

Since pentacene is a powerful candidate for p-type organic semiconductor, its synthesis and crystal structure has attracted much attention. However, pentacene and its derivatives easily suffer oxygenation and photodimerization. Fallis et al. investigated regiochemistry of photodimerization of 2,9-diethynylpentacene **98** and its crystal packing in detail (Scheme 20.24).[59]

2-Alkoxy-1-naphthamide **100** is potentially chiral because bond rotation between the naphthalene ring and the C=O(NR^{1}R^2) group corresponds to enantiomerization of **100** (Scheme 20.25).[60] However, in solution, it racemizes easily. Sakamoto et al. found that recrystallization of **100** in hexane/chloroform mixed solvent gave crystals in a chiral space group, $P2_12_12_1$, it reveals that each single crystal was chiral and composed of one enantiomer. The half-life of the enantiomerization was 11.8 min when the crystals were dissolved in THF at 15°C, and the lifetime was lengthened with lowered temperature and

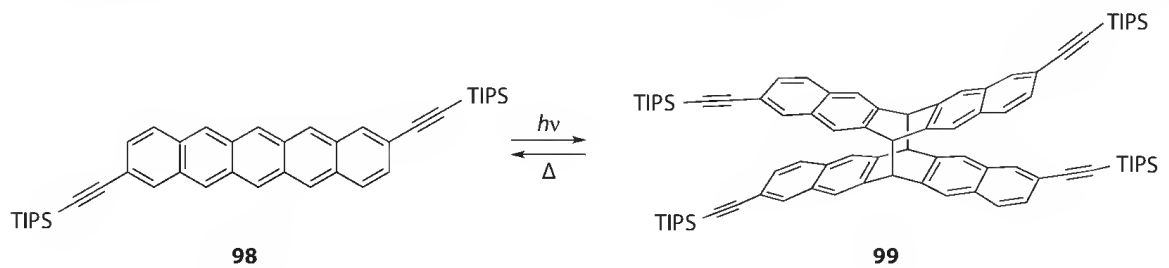

SCHEME 20.24

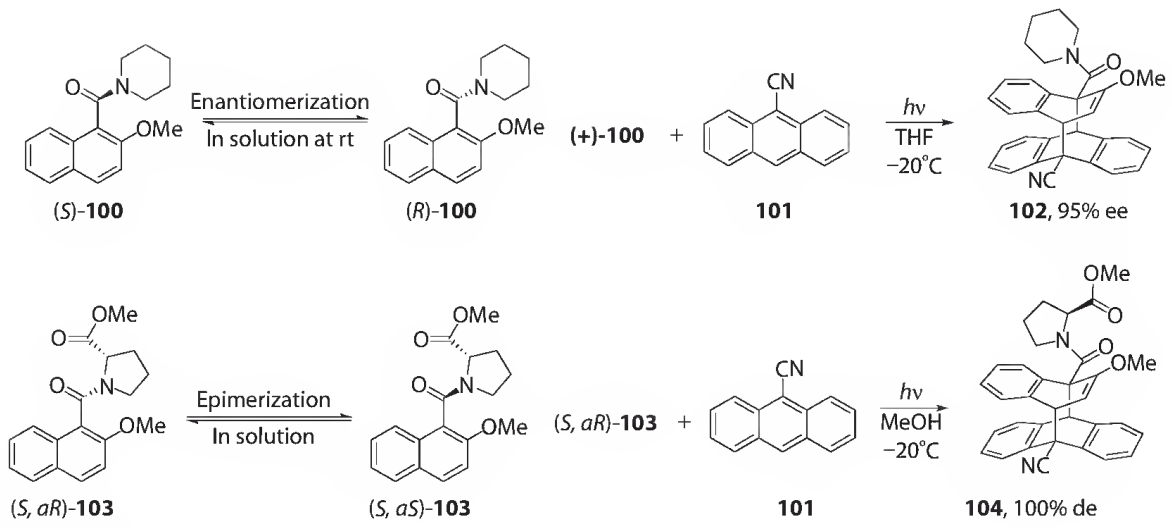

SCHEME 20.25

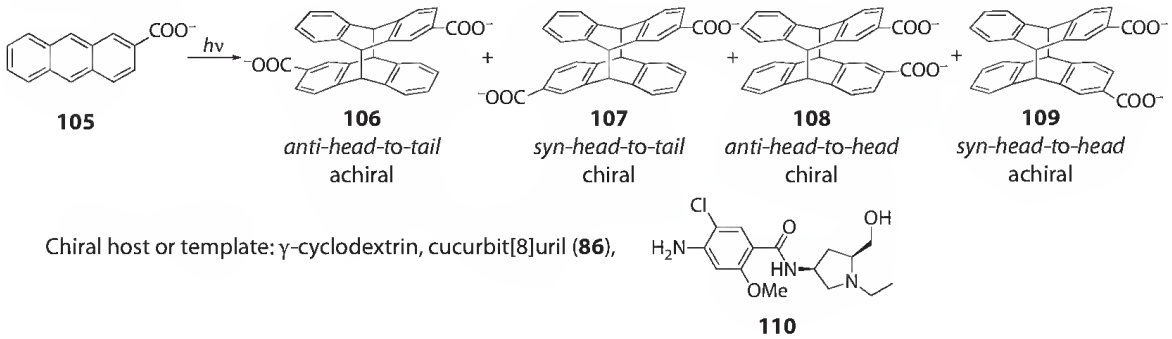

SCHEME 20.26

addition of MeOH. Asymmetric photocycloaddition of **100** with 9-cyanoanthracene **101** was achieved when some chiral crystals of **(+)-100** were allowed to react with **101** under photoirradiation to give **102** in 95% ee. Naphthamide derived from L-proline **103** exists as a mixture of diastereomers in (*S*, *aR*)-form and (*S*, *aS*)-form.[61] Compound **103** also crystallized in a chiral space group $P2_1$ and formed the (*S*,*aR*)-conformation in the crystals. Photoreaction of the crystal with **101** diastereoselectively gave **104.**

Nakamura and Inoue reported that 2-anthracenecarboxylic acid **105** makes a stable 1:2 inclusion complex with γ-cyclodextrin (Scheme 20.26). Photodimerization of **105** included in γ-cyclodextrin gave photodimers **106–109.** The ee of chiral *syn*-head-to-tail dimer **106** was 41% at 0°C irradiation.[62] Yields and ee of chiral *anti*-head-to-head dimer **107** increased by using 2-(dimethylamino)ethylamino-substituted γ-cyclodextrin.[63] γ-Cyclodextrins capped by arenesulfonyl groups could control orientation and ee of dimer **106**.[64] 2-Antracenecarbonyl-substituted α-cyclodextrin[65] and human serum albumin[66] made the ee of **106** and **107** more than 90%. A chiral template **110** provides a novel hydrogen-bonding and shielding motif for enantioselectivity.[67,68]

20.5 Photocycloaddition of Heteroaromatic Compounds with Unsaturated Compounds

In this section, recent advances in photocycloaddition of heteroaromatic compounds with unsaturated bonds will be introduced.

West et al. reported that photoreaction of **111** having substituted pyran-2-one and furan gave **113** via thermal decarboxylation of intramolecular photocycloadduct **112** (Scheme 20.27).[69,70] Compound

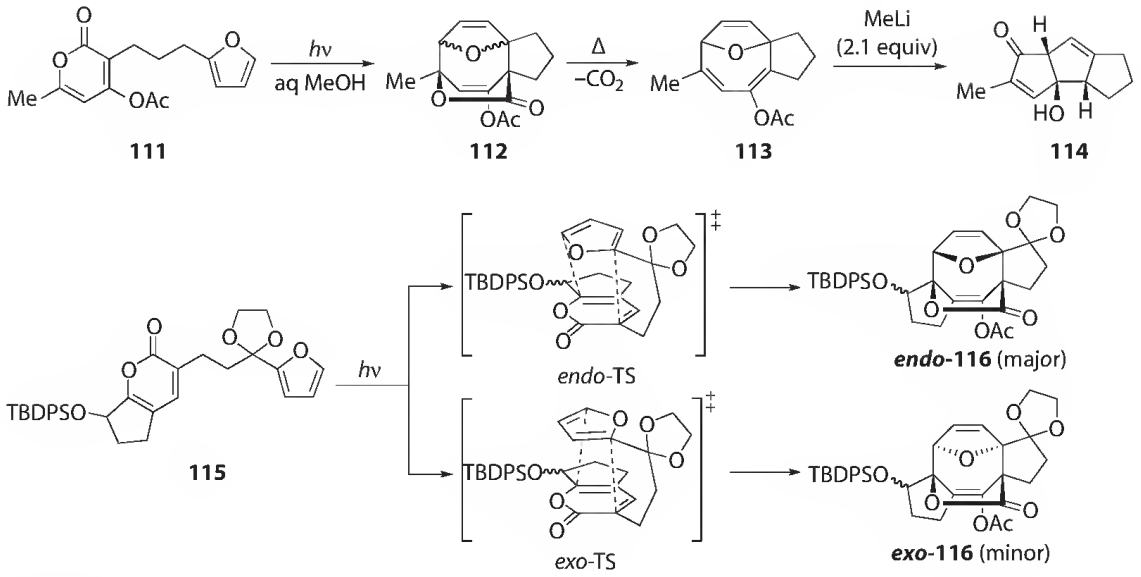

SCHEME 20.27

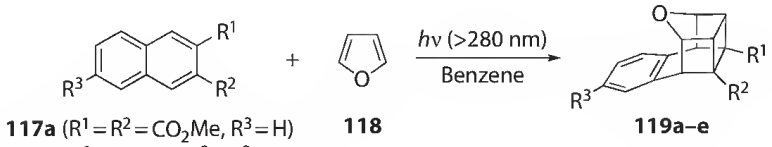

SCHEME 20.28

113 reacted with MeLi to furnish triquinane compound **114** via β-elimination, 1,5-hydrogen shift, and transannular aldolization. Diastereoselectivity of the initial [4 + 4] photodimerization was investigated in the photoreaction of **115**.[71] *Endo*-selectivity of the **116** was obtained via *endo*-TS, and the diastereoselectivity depends on the solvent used.

Mizuno et al. reported that photocycloaddition of furan **118** to naphthalene derivatives **117a–e** afforded caged products **119a–e** in high yields when the naphthalene derivatives have electron-withdrawing groups at 2- or 2,3-position (Scheme 20.28).[72] For the formation of caged products **119**, dipole moments of each substrate were important.

Garcia-Garibay reported photoreaction of ketone **120** having thiophene and *S,S*-dioxothiophene (Scheme 20.29).[73] Rather than the expected photodecarbonylation to give **121**, UV-vis irradiation of **120** led to the intramolecular [2 + 2] photocycloadduct **122** in quantitative yield both in solution and crystalline solid state.

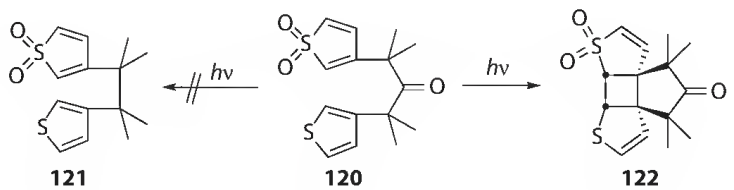

SCHEME 20.29

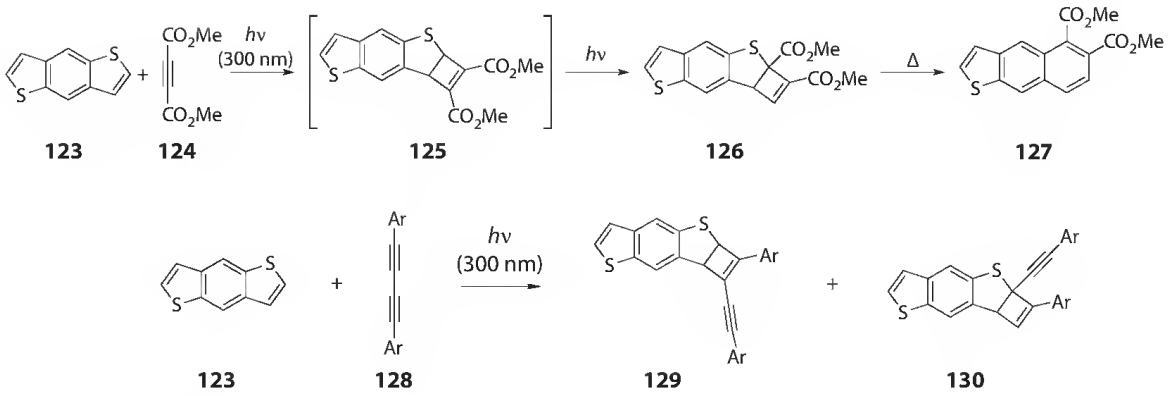

SCHEME 20.30

Photochemical [2 + 2] cycloaddition of alkynes and butadiynes to benzo[1,2-*b*:4,5-*b*′]dithiophene **123** was investigated by Neckers et al. (Scheme 20.30).[74] Irradiation of **123** and **124** for 16 h gave a rearranged product **126** in 16% yield. Photoreaction of **123** with diarylbutadiyne **128** gave cyclobutene compounds **129** and **130**.

As for pyridine derivatives, Sakamoto et al. has already reported photocycloaddition of 2-cyano-3-alkoxypyridine derivatives **131** with methacrylonitrile **132** as an electron-poor alkene, in 1996, to give bicyclic azetine **133**, 3-acetyl-4-amino-1,5-dicyano-2,5-dimethylcyclohexa-1,3-diene **134**, and rearranged pyridine derivative **135** (Scheme 20.31).[75] They confirmed that **134** is produced by hydrolysis of **133**. The compound **133** might be formed via [2 + 2] photocycloadduct **136** at 2,3-position of **131**

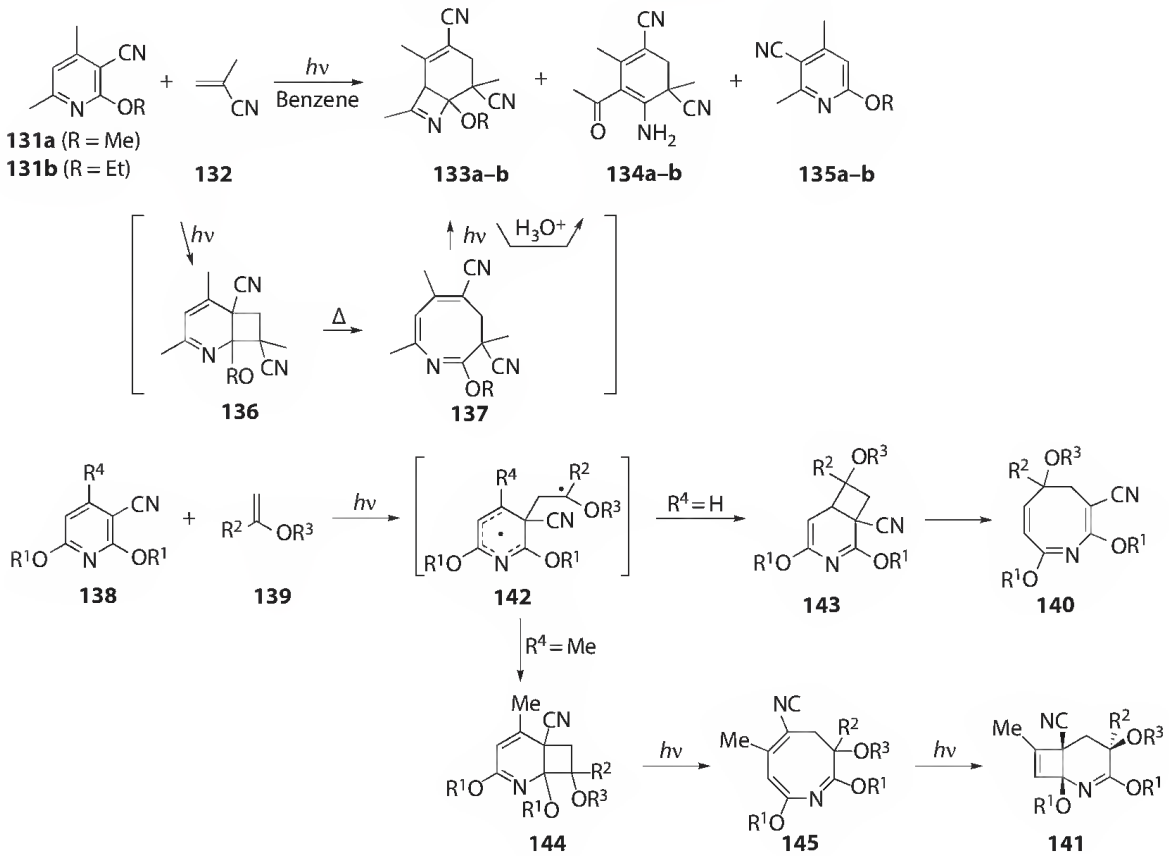

SCHEME 20.31

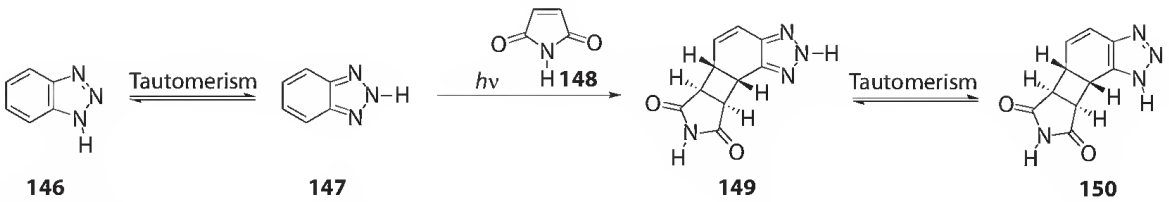

SCHEME 20.32

and azacyclooctatriene derivative **137**. They reported that photoreaction of **138** with vinyl ethers **139**, which are electron-rich alkenes, gave azacyclooctatriene derivative **140** (when R^4 = H) and 2-azabicyclo[4.2.0]octa-2,7-diene **141** (When R^4 = Me).[76] These products are produced from [2 + 2] photocycloadducts **143** and **144**, respectively. PM3 calculation showed that $\Delta\Delta E$ value between lower SOMO of the excited state of **138** and HOMO of **139** is smaller than the value between higher SOMO of the excited state of **138** and LUMO of **139**. Coefficient at the C-3 position of **138** is bigger than those at other positions in lower SOMO of the excited state of **138**. So they proposed a mechanism that both **143** and **144** may be produced from biradical **142**, which will be formed by C-3 attack of **139** to the excited state of **138**.

Booker-Milburn reported that photoirradiation of benzotriazole **146** with a variety of maleimide derivatives leads to regio- and stereoselective formation of [2 + 2] photocycloadduct **150** (Scheme 20.32). They explained this high selectivity by tautomerization from 1*H*-benzotriazole **146** to 2*H*-benzotriazole **147** and high double bond character of the reactive position of **147**.[77] Novak and Kovac demonstrated the correlation of the double bond character of **147** with complete regioselectivity in this photoreaction by UV photoelectron spectroscopy and *ab initio* calculation in 2009.[78]

Acridizinium ion **151** has an isoelectronic structure with anthracene (Scheme 20.33). Since **151** undergoes [4 + 4] photodimerization to give **152** and its regioisomers, and thermal cycloreversion of **152** recovers **151**, the reactions can be used for photochromic systems.[79] Tbt-substituted 9-silaanthracene **153** is a stable crystalline compound synthesized by Tokitoh et al.[80] When degassed benzene-d_6 solution of **153** in a sealed Pyrex tube was irradiated with light of λ = 300–500 nm at room temperature, the orange color of **153** disappeared and a new species, 9,10-dewar-9-silaanthracene **154** was formed exclusively. The compound **154** can be detected by ^{1}H, ^{13}C, ^{29}Si NMR, and UV-vis spectroscopy, but could not be isolated as a stable compound and undergo gradual thermal tautomerization into **153** even at −80°C in hexane. Conversion of **153** to its dimer **155** can be achieved by 110°C for 15 days in benzene-d_6 solution (42% yield) or 180°C for 1 h in the solid state (58% yield). Dimer **155** is a stable compound and no cycloreversion to **153** was observed in 1,2-dichlorobenzene-d_4 solution even at 200°C.

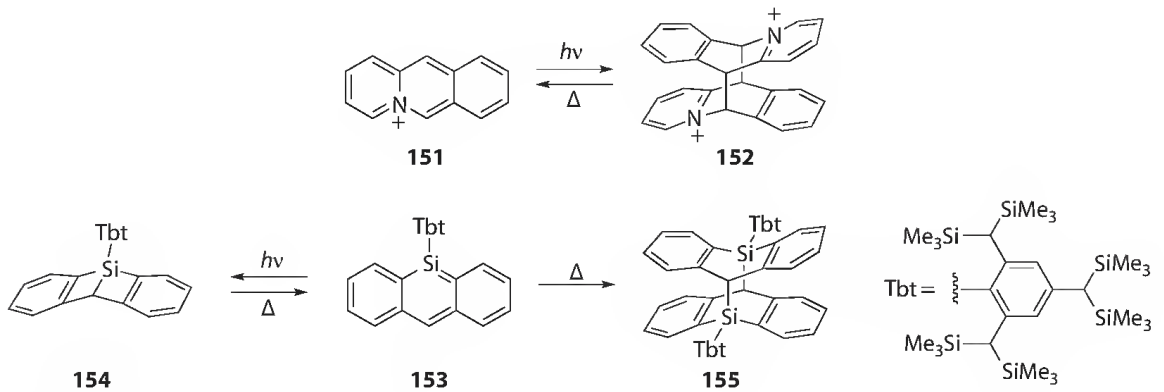

SCHEME 20.33

20.6 Photocycloaddition and Photoalkylation of Aromatic Rings with Cyclopropanes

Cyclopropanes, whose bonding and antibonding σ-orbitals are banana shaped, are expected to behave chemically like unsaturated compounds. However, only a few reports have appeared describing photoreactions between aromatic compounds and cyclopropanes. In 1986, Mizuno et al. reported (4 + 3) photocycloaddition of 9,10-dicyanoanthracene **156** with 1,2-diphenylcyclopropane **157** in degassed acetonitrile (Scheme 20.34).[81,82] 1-Amino-2-phenylcyclopropanes[83] and methylenecyclopropanes[84] also react with **156** in a similar manner to give [4 + 3] photocycloadducts.

A novel [3 + 2] photocycloaddition between cyclopropane derivatives with aromatic rings was developed by Mizuno.[85] 9-Cyanophenanthrene **160** reacts with 1,2-dianisylcyclopropane **161** to give [3 + 2] photocycloadduct **162** in a stereoselective manner (Scheme 20.35). From the *cis*-stereochemistry of **162**, structures of by-products **163–165**, substituent effect of 1,2-diarylcyclopropane, and control experiments, they proposed a reaction mechanism involving stepwise C–C bond coupling via singlet exciplexes **166**, **167** and biradicals **168**, **169**.

Photoreaction of a naphthalene derivative **117e** with methoxy-substituted 1,2-diarylcyclopropanes led to the formation of photoalkylated product **171** with excellent regioselectivity (Scheme 20.36).[86,87]

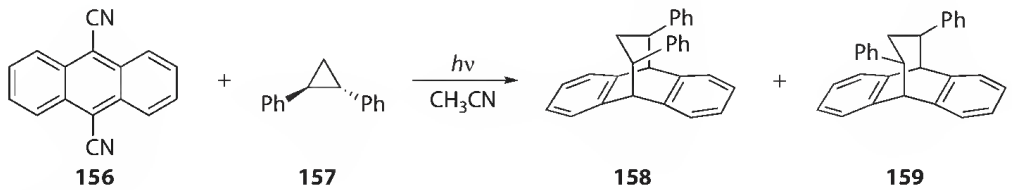

156 **157** **158** **159**

SCHEME 20.34

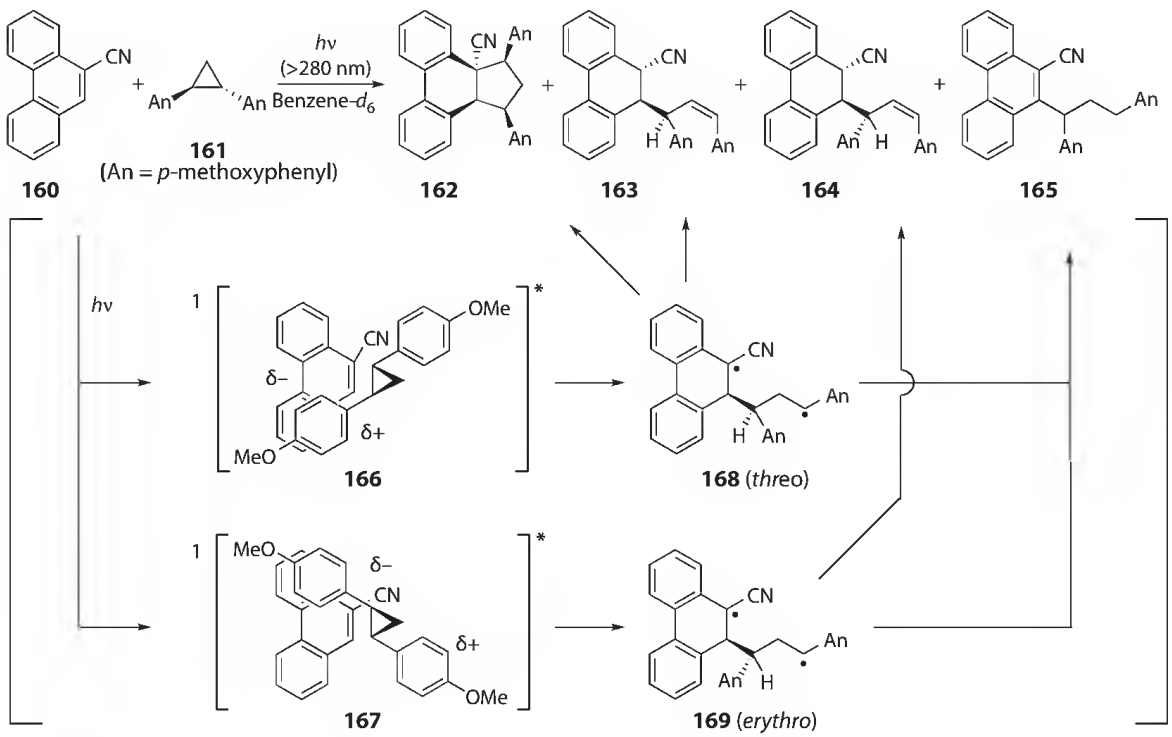

160 **161** (An = *p*-methoxyphenyl) **162** **163** **164** **165**

166 **168** (*threo*) **167** **169** (*erythro*)

SCHEME 20.35

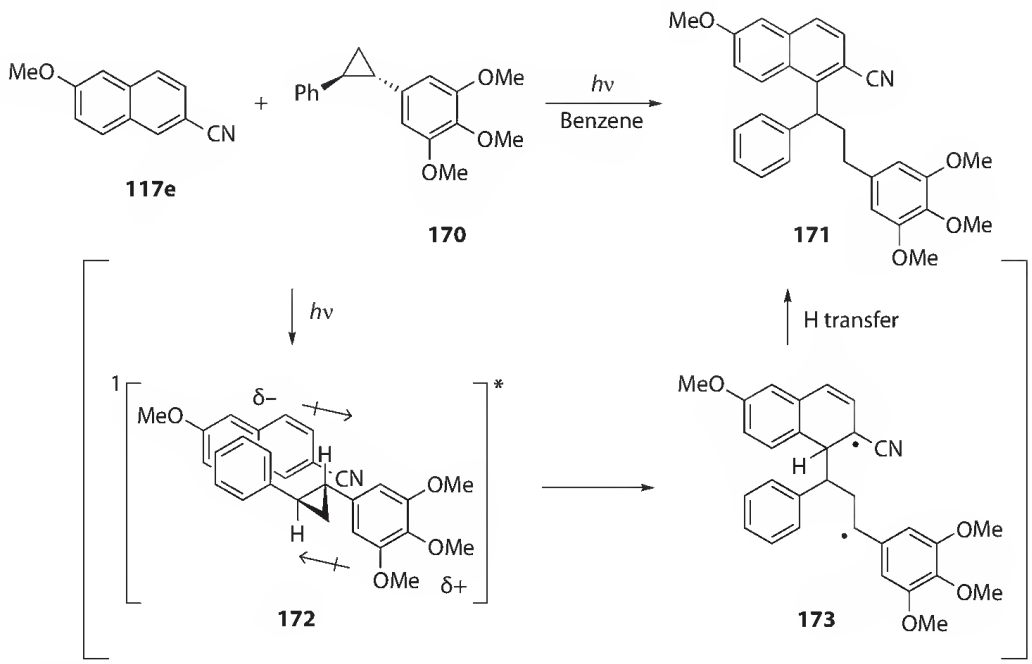

SCHEME 20.36

As also seen in the photoreaction of **160**, singlet exciplex **172** and biradical **173** are postulated as intermediates of the photoreaction. The secondary C–C bond formation, which can be seen in the reaction of **160**, did not occur but intramolecular hydrogen transfer took place to give **171**.

References

1. Caldwell, R. A. and Creed, D., Exciplex intermediates in [2 + 2] photocycloadditions, *Acc. Chem. Res.*, 13, 45–50, 1980.
2. Gilbert, A. and Yianni, P., Regio- and stereo-selectivities of the *ortho* and *meta* photocycloaddition reactions of ethylenes to benzene and its simple derivatives, *Tetrahedron*, 37, 3275–3283, 1981.
3. Mattay, J., Selectivity and charge transfer in photoreactions of arenes with olefins 1. Substitution versus cycloaddition, *Tetrahedron*, 41, 2393–2404, 1985.
4. Mattay, J., Selectivity and charge transfer in photoreactions of arenes with olefins 2. Mode of cycloaddition, *Tetrahedron*, 41, 2405–2417, 1985.
5. Al-Qaradawi, S., Gilbert, A., and Jones, D. T., Factors influencing the reaction-mode selectivity and regiochemistry of intermolecular photocycloaddition reactions of ethenes to polysubstituted benzenes, *Recl. Trav. Chim. Pays-Bas*, 114, 485–491, 1995.
6. Gilbert, A., Photoaddition and photocyclization processes of aromatic compounds, in *Synthetic Organic Photochemistry*, Horspool, W. M. Ed., Plenum Press, New York and London, 1984, pp. 1–60.
7. McCullough, J. J., Photoadditions of aromatic compounds, *Chem. Rev.*, 87, 811–860, 1987.
8. Müller, F. and Mattay, J., Photocycloadditions: Control by energy and electron transfer, *Chem. Rev.*, 93, 99–117, 1993.
9. De Keukeleire, D. and He, S.-L., Photochemical strategies for the construction of polycyclic molecules, *Chem. Rev.*, 93, 359–380, 1993.
10. Cornelisse, J., The meta photocycloaddition of arenes to alkenes, *Chem. Rev.*, 93, 615–669, 1993.
11. Mizuno, K., Maeda, H., Sugimoto, A., and Chiyonobu, K., Photocycloaddition and photoaddition reactions of aromatic compounds, in *Molecular and Supramolecular Photochemistry Vol. 8: Understanding and Manipulating Excited-State Processes*, Ramamurthy, V. and Schanze, K. S. Eds., Marcel Dekker, Inc., New York, 2001, pp. 127–241.

12. Horspool, W. M. and Lenci, F. Eds., *CRC Handbook of Photochemistry and Photobiology*, Vol. 2, CRC Press, Boca Raton, FL, 2004.
13. Wender, P. A. and Howbert, J. J., Synthetic studies on arene-olefin cycloadditions: Total synthesis of (±)-α-cedrene, *J. Am. Chem. Soc.*, 103, 688–690, 1981.
14. Chappell, D. and Russell, A. T., From α-cedrene to crinipellin B and onward: 25 years of the alkene-arene *meta*-photocycloaddition reaction in natural product synthesis, *Org. Biomol. Chem.*, 4, 4409–4430, 2006.
15. Gaich, T. and Mulzer, J., Total synthesis of (−)-penifulvin A, an insecticide with a dioxafenestrane skeleton, *J. Am. Chem. Soc.*, 131, 452–453, 2009.
16. Gaich, T. and Mulzer, J., From silohinenes to penifulvins: A biomimetic approach to penifulvins B and C, *Org. Lett.*, 12, 272–275, 2010.
17. Wang, Q. and Chen, C., An approach to the core skeleton of lancifodilactone F, *Org. Lett.*, 10, 1223–1226, 2008.
18. Morales, R. C., Lopez-Mosquera, A., Roper, N., Jenkins, P. R., Fawcett, J., and García, M. D., Diastereocontrol in the intramolecular *meta*-photocycloaddition of arenes and olefins, *Photochem. Photobiol. Sci.*, 5, 649–652, 2006.
19. Hagiya, K., Yamasaki, A., Okuyama, T., and Sugimura, T., Asymmetric *meta*-arene-alkene photocycloaddition controlled by a 2,4-pentanediol tether, *Tetrahedron: Asymmetry*, 15, 1409–1417, 2004.
20. Sugimura, T., Yamasaki, A., and Okuyama, T., Stereocontrolled intramolecular *meta*-arene-alkene photocycloaddition reactions using chiral tethers: Efficiency of the tether derived from 2,4-pentanediol, *Tetrahedron: Asymmetry*, 16, 675–683, 2005.
21. Penkett, C. S., Byrne, P. W., Teobald, B. J., Rola, B., Ozanne, A., and Hitchcock, P. B., The use of temporary tethers in the *meta* photocycloaddition reaction, *Tetrahedron*, 60, 2771–2784, 2004.
22. Maeda, H., Yagi, H., and Mizuno, K., Intramolecular ($2\pi + 2\pi$) photocycloaddition of styrenes tethered by siloxanes, *Chem. Lett.*, 33, 388–389, 2004.
23. Maeda, H., Nishimura, K., Mizuno, K., Yamaji, M., Oshima, J., and Tobita, S., Synthesis and photochemical properties of stilbenophanestethered by silyl chains. Control of ($2\pi + 2\pi$) photocycloaddition, cis-trans photoisomerization, and photocyclization, *J. Org. Chem.*, 70, 9693–9701, 2005.
24. Fleming, S. A., Parent, A. A., Parent, E. E., Pincock, J. A., and Renault, L., Mechanistic analysis of the photocycloaddition of silyl-tethered alkenes, *J. Org. Chem.*, 72, 9464–9470, 2007.
25. Penkett, C. S., Woolford, J. A., Day, I. J., and Coles, M. P., The double [3 + 2] photocycloaddition reaction, *J. Am. Chem. Soc.*, 132, 4–5, 2010.
26. Itou, T., Yoshimi, Y., Kamiya, K., Takedani, H., Morita, T., and Hatanaka, M., Formation of cyclooctatriene and bicyclooctadiene through regioselective intermolecular (2 + 2) photocycloaddition of benzoic acids to allyl alcohol in water, *J. Photochem. Photobiol. A Chem.*, 202, 235–239, 2009.
27. Asahara, H., Mochizuki, E., and Oshima, T., Conformational analysis in the reversible intramolecular [2 + 2] photocycloaddition of diphenylbicyclo[4.2.0]oct-3-ene-2,5-diones, *Tetrahedron Lett.*, 47, 7881–7884, 2006.
28. Kubo, Y., Inoue, T., and Sakai, H., A novel 1,8-photoaddition of dimethyl 1,4-naphthalenedicarboxylate to alkenes, *J. Am. Chem. Soc.*, 114, 7660–7663, 1992.
29. Kubo, Y., Kiuchi, K., and Inamura, I., Photochemical reactions of 1,2-dicyanonaphthalene with alkenes and dienes, *Bull. Chem. Soc. Jpn.*, 72, 1101–1108, 1999.
30. Mukae, H., Maeda, H., and Mizuno, K., One-step synthesis of benzotetra- and benzopentacyclic compounds through intramolecular [2 + 3] photocycloaddition of alkenes to naphthalene, *Angew. Chem. Int. Ed.*, 45, 6558–6560, 2006.
31. Mattay, J., Photochemistry of arenes—Reloaded, *Angew. Chem. Int. Ed.*, 46, 663–665, 2007.
32. Maeda, H., Mukae, H., and Mizuno, K., Enhanced efficiency and regioselectivity of intramolecular ($2\pi + 2\pi$) photocycloaddition of 1-cyanonaphthalene derivative using microreactors, *Chem. Lett.*, 34, 66–67, 2005.

33. Mukae, H., Maeda, H., Nashihara, S., and Mizuno, K., Intramolecular photocycloaddition of 2-(2-alkenyloxymethyl)-naphthalene-1-carbonitriles using glass-made microreactors, *Bull. Chem. Soc. Jpn.*, 80, 1157–1161, 2007.
34. Maeda, H., Okumura, T., Yoshimi, Y., and Mizuno, K., Asymmetric induction in an intramolecular [2 + 2] photocycloaddition within chirally modified zeolite supercages, *Tetrahedron: Asymmetry*, 20, 381–384, 2009.
35. Kalena, G. P., Pradhan, P., Puranik, V. S., and Banerji, A., A novel intramolecular arene-alkene photocycloaddition in 2-alkenyl naphtha-4-chromanones—A short route to functionalised multicyclic systems, *Tetrahedron Lett.*, 44, 2011–2013, 2003.
36. Ohkura, K., Uchiyama, S., Aizawa, K., Nishijima, K., and Seki, K., Photochemical synthesis of naphthocyclobutapyrimidines *via* 1,2-cycloaddition of 6-chloro-1,3-dimethyluracil with naphthalenes, *Heterocycles*, 57, 1403–1408, 2002.
37. Ohkura, K., Sugaoi, T., Sakushima, A., Nishijima, K., Kuge, Y., and Seki, K., Thermodynamically controlled photocycloaddition of 5-fluoro-1,3-dimethyluracil to naphthalenes, *Heterocycles*, 58, 595–600, 2002.
38. Ohkura, K., Sugaoi, T., Ishihara, T., Aizawa, K., Nishijima, K., Kuge, Y., and Seki, K., Facile synthesis of 4a-fluoro-5,10-ethenobenzo[*f*]quinazolines through 1,4-photocycloaddition of 5-fluoro-1,3-dimethyluracil with substituted naphthalenes, *Heterocycles*, 61, 377–389, 2003.
39. Ohkura, K., Ishihara, T., Takahashi, H., Takechi, H., and Seki, K., Direct C–C bond formation between thymine derivatives and naphthalene through [2 + 2]-photocycloaddition, *Heterocycles*, 66, 143–146, 2005.
40. Ohkura, K., Sugaoi, T., Takahashi, M., and Seki, K., Diastereodifferentiating [4 + 2]-photocycloaddition of tegafur with naphthalene, *Heterocycles*, 72, 691–695, 2007.
41. Ohkura, K., Uchiyama, S., Sato, M., Diakur, J. M., and Seki, K., Acid-catalyzed photocycloaddition of 6-chloro-1,3-dimethyluracil to polycyclic aromatic hydrocarbons, *Heterocycles*, 59, 459–464, 2003.
42. Liu, Q.-J., Novel photocycloaddition reactions of *N*-methyl-2,3-naphthalenedicarboximide with phenylacetylene, *Chin. J. Chem.*, 25, 1076–1077, 2007.
43. Yoshizawa, M., Takeyama, Y., Okano, T., and Fujita, M., Cavity-directed synthesis within a self-assembled coordination cage: Highly selective [2 + 2] cross-photodimerization of olefins, *J. Am. Chem. Soc.*, 125, 3243–3247, 2003.
44. Nishioka, Y., Yamaguchi, T., Yoshizawa, M., and Fujita, M., Unusual [2 + 4] and [2 + 2] cycloadditions of arenes in the confined cavity of self-assembled cages, *J. Am. Chem. Soc.*, 129, 7000–7001, 2007.
45. Maeda, H., Horiuchi, A., Koshio, N., and Mizuno, K., Diastereoselectivity in ($2\pi + 2\pi$) photocycloaddition of cholesteryl cinnamate to methyl 9-phenanthrenecarboxylate: Control of the stereoselectivity in liquid crystalline phase, *Chem. Lett.*, 33, 966–967, 2004.
46. Burnelle, L., Lahiri, J., and Detrano, R., On the photodimerization of anthracene and its mesosubstituted derivatives, *Tetrahedron*, 24, 3517–3531, 1968.
47. Bouas-Laurent, H., Castellan, A., and Desvergne, J.-P., From anthracene photodimerization to jaw photochromic materials and photocrowns, *Pure Appl. Chem.*, 52, 2633–2648, 1980.
48. Becker, H.-D., On the relationship between molecular geometry and excited state reactivity. Adiabatic photoreactions involving anthracenes, *Pure Appl. Chem.*, 54, 1589–1604, 1982.
49. Becker, H.-D., Unimolecular photochemistry of anthracenes, *Chem. Rev.*, 93, 145–172, 1993.
50. Bouas-Laurent, H., Castellan, A., Devergne, J.-P., and Lapouyade, R., Photodimerization of anthracenes in fluid solution: Structural aspects, *Chem. Soc. Rev.*, 29, 43–55, 2000.
51. Bouas-Laurent, H., Castellan, A., Devergne, J.-P., and Lapouyade, R., Photodimerization of anthracenes in fluid solutions: (Part 2) mechanistic aspects of the photocycloaddition and of the photochemical and thermal cleavage, *Chem. Soc. Rev.*, 30, 248–263, 2001.
52. Tung, C.-H., Wu, L.-Z., Zhang, L.-P., and Chen, B., Supramolecular systems as microreactors: Control of product selectivity in organic phototransformation, *Acc. Chem. Res.*, 36, 39–47, 2003.

53. Wu, X.-L., Luo, L., Lei, L., Liao, G.-H., Wu, L.-Z., and Tung, C.-H., Highly efficient cucurbit[8] uril-templated intramolecular photocycloaddition of 2-naphthalene-labeled poly(ethylene glycol) in aqueous solution, *J. Org. Chem.*, 73, 491–494, 2008.
54. Wu, D.-Y., Chen, B., Fu, X.-G., Wu, L.-Z., Zhang, L.-P., and Tung, C.-H., Nanosized particles of organically modified silica as microreactors to enhance the regioselectivity in the photocycloaddition of 9-substituted anthracenes, *Org. Lett.*, 5, 1075–1077, 2003.
55. Li, X.-W., Zhang, J., Zheng, L.-Q., Chen, B., Wu, L.-Z., Lv, F.-F., Dong, B., and Tung, C.-H., Microemulsions of *N*-alkylimidazolium ionic liquid and their performance as microreactors for the photocycloaddition of 9-substituted anthracenes, *Langmuir*, 25, 5484–5490, 2009.
56. Toyota, S., Kuga, M., Takatsu, A., Goichi, M., and Iwanaga, T., Molecular folding screen: Folding and unfolding of 1,8-anthrylene-ethynylene oligomers by photochemical cycloaddition and thermal cycloreversion, *Chem. Commun.*, 1323–1325, 2008.
57. Cao, D., Gao, C., Dobis, S., and Meier, H., Competition between inter- and intramolecular photocycloaddition reactions of 9-substituted anthracenes, *Synthesis*, 13, 1995–2001, 2007.
58. Trzop, E. and Turowska-Tryk, I., Monitoring structural transformations in crystals. 12. Course of an intramolecular [4 + 4] photocycloaddition in a crystal, *Acta Cryst. Sec. B*, B64, 375–382, 2008.
59. Bénard, C. P., Geng, Z., Heuft, M. A., VanCrey, K., and Fallis, A. G., Double Diels–Alder strategies to soluble 2,9- and 2,9,6,13-tetraethynylpentacenes, photolytic [4 + 4] cycloadditions, and pentacene crystal packing, *J. Org. Chem.*, 72, 7229–7236, 2007.
60. Sakamoto, M., Unosawa, A., Kobaru, S., Saito, A., Mino, T., and Fujita, T., Asymmetric photocycloaddition in solution of a chiral crystallized naphthamide, *Angew. Chem. Int. Ed.*, 44, 5523–5526, 2005.
61. Sakamoto, M., Unosawa, A., Kobaru, S., Hasegawa, Y., Mino, T., Kasashima, Y., and Fujita, T., Diastereoselective photocycloaddition using memory effect of molecular chirality controlled by crystallization, *Chem. Commun.*, 1632–1634, 2007.
62. Nakamura, A. and Inoue, Y., Supramolecular catalysis of the enantiodifferentiating [4 + 4] photocyclodimerization of 2-anthracenecarboxylate by γ-cyclodextrin, *J. Am. Chem. Soc.*, 125, 966–972, 2003.
63. Nakamura, A. and Inoue, Y., Electrostatic manipulation of enantiodifferentiating photocyclodimerization of 2-anthracenecarboxylate within γ-cyclodextrin cavity through chemical modification. Inverted product distribution and enhanced enantioselectivity, *J. Am. Chem. Soc.*, 127, 5338–5339, 2005.
64. Yang, C., Nakamura, A., Wada, T., and Inoue, Y., Enantiodifferentiating photocyclodimerization of 2-anthracenecarboxylic acid mediated by γ-cyclodextrins with a flexible or rigid cap, *Org. Lett.*, 8, 3005–3008, 2006.
65. Yang, C., Mori, T., Origane, Y., Ko, Y. H., Selvapalam, N., Kim, K., and Inoue, Y., Highly stereoselective photocyclodimerization of α-cyclodextrin-appended anthracene mediated by γ-cyclodextrin and cucurbit[8]uril: A dramatic steric effect operating outside the binding site, *J. Am. Chem. Soc.*, 130, 8574–8575, 2008.
66. Nishijima, M., Wada, T., Mori, T., Pace, T. C. S., Bohne, C., and Inoue, Y., Highly enantiomeric supramolecular [4 + 4] photocyclodimerization of 2-anthracenecarboxylate mediated by human serum albumin, *J. Am. Chem. Soc.*, 129, 3478–3479, 2007.
67. Mizoguchi, J., Kawanami, Y., Wada, T., Kodama, K., Anzai, K., Yanagi, T., and Inoue, Y., Enantiodifferentiating photocyclodimerization of 2-anthracenecarboxylic acid using a chiral *N*-(2-hydroxymethyl-4-pyrrolidinyl)benzamide template, *Org. Lett.*, 8, 6051–6054, 2006.
68. Kawanami, Y., Pace, T. C. S., Mizoguchi, J., Yanagi, T., Nishijima, M., Mori, T., Wada, T., Bohne, C., and Inoue, Y., Supramolecular complexation and enantiodifferentiating photocyclodimerization of 2-anthracenecarboxylic acid with 4-aminoprolinol derivatives as chiral hydrogen-bonding templates, *J. Org. Chem.*, 74, 7908–7921, 2009.
69. Li, L., McDonald, R., and West, F. G., Concise route to triquinanes from pyran-2-ones, *Org. Lett.*, 10, 3733–3736, 2008.

70. Li, L., Chase, C. E., and West, F. G., Cyclooctatrienes from pyran-2-ones *via* a tandem [4 + 4]-photocycloaddition/decarboxylation process, *Chem. Commun.*, 4025–4027, 2008.
71. Song, D., McDonald, R., and West, F. G., Diastereoselective [4 + 4]-photocycloaddition reactions of pyran-2-ones: Rapid access to functionalized 5-8-5 skeletons, *Org. Lett.*, 8, 4075–4078, 2006.
72. Mizuno, K., Tachibana, Y., Konishi, G., Chiyonobu, K., and Maeda, H., Formation of caged compounds in the photocycloaddition of furan to 2-, 2,3-, and 2,6-substituted naphthalenes via dipole-dipole interaction, *J. Chin. Chem. Soc.*, 53, 75–78, 2006.
73. Resendiz, M. J. E., Taing, J., Khan, S. I., and Garcia-Garibay, M. A., Unexpected solid-state photochemistry of an α-thiophenyl-α′-thiophenyl-*S*,*S*-dioxo-substituted ketone, *J. Org. Chem.*, 73, 638–643, 2008.
74. Wex, B., Kaafarani, B. R., Oliver, A. G., Bauer, J. A. K., and Neckers, D. C., Photoaddition reactions of acetylene and butadiyne derivatives to benzodithiophene, *J. Org. Chem.*, 68, 8258–8260, 2003.
75. Sakamoto, M., Sano, T., Takahashi, M., Yamaguchi, K., Fujita, T., and Watanabe, S., Photochemistry of heteroaromatics—A novel photocycloaddition of 2-alkoxy-3-cyanopyridines with metacrylonitrile, *Chem. Commun.*, 1349–1350, 1996.
76. Sakamoto, M., Sano, T., Fujita, S., Ando, M., Yamaguchi, K., Mino, T., and Fujita, T., Regioselective photocycloaddition of pyridine derivatives to electron-rich alkenes, *J. Org. Chem.*, 68, 1447–1450, 2003.
77. Booker-Milburn, K. I., Wood, P. M., Dainty, R. F., Urquhart, M. W., White, A. J., Lyon, H. J., and Charmant, J. P. H., Photochemistry of benzotriazole: An unprecedented tautomer-selective intermolecular [2 + 2] photocycloaddition, *Org. Lett.*, 4, 1487–1489, 2002.
78. Novak, I., Abu-Izneid, T., Kovac, B., and Klasinc, L., Electronic structure and stability of benzotriazoles, *J. Phys. Chem. A*, 113, 9751–9756, 2009.
79. Ihmels, H. and Luo, J., The reversible [4 + 4] photocycloaddition of acridizinium derivatives, *J. Photochem. Photobiol. A: Chem.*, 200, 3–9, 2008.
80. Shinohara, A., Takeda, N., and Tokitoh, N., Photochemical and thermal reactions of a kinetically stabilized 9-silaanthracene: The first spectroscopic observation of a 9,10-dewar-9-silaanthracene isomer, *J. Am. Chem. Soc.*, 125, 10804–10805, 2003.
81. Ichinose, N., Mizuno, K., Hiromoto, Z., and Otsuji, Y., ($2\sigma + 4\pi$) Photocycloaddition of 1,2-diarylcyclopropanes to 9,10-dicyanoanthracene via geminate radical ion pair, *Tetrahedron Lett.*, 27, 5619–5620, 1986.
82. Mizuno, K., Ichinose, N., and Otsuji, Y., Photochemistry of 9,10-dicyanoanthracene-1,2-diarylcyclopropane systems. Photocycloaddition and photoisomerization, *J. Org. Chem.*, 57, 1855–1860, 1992.
83. Wang, Y., Luttrull, D. K., Dinnocenzo, J. P., Goodman, J. L., Farid, S., and Gould, I. R., Associative return electron transfer. A bond-coupled electron transfer in the photoreactions of cyclopropylamines, *Photochem. Photobiol. Sci.*, 2, 1169–1176, 2003.
84. Ikeda, H., Nomura, T., Akiyama, K., Oshima, M., Roth, H. D., Tero-Kubota, S., and Miyashi, T., Divergent oxidative rearrangements in solution and in a zeolite: Distal vs. proximal bond cleavage of methylenecyclopropanes, *J. Am. Chem. Soc.*, 127, 14497–14504, 2005.
85. Maeda, H., Miyata, Y., and Mizuno, K., A novel photoreaction of 1,2-diarylcyclopropanes with 9-cyanophenanthrene: The formation of (3 + 2) photocycloadducts, *Tetrahedron Lett.*, 43, 1481–1486, 2002.
86. Maeda, H., Matsukawa, N., Shirai, K., and Mizuno, K., Photoalkylation of 2,3-dicyanonaphthalene by methoxy-substituted 1,2-diarylcyclopropanes, *Tetrahedron Lett.*, 46, 3057–3060, 2005.
87. Maeda, H., Matsuda, S., and Mizuno, K., Regioselective photoalkylation of 2-cyano-6-methoxynaphthalene by methoxy-substituted 1,2-diarylcyclopropanes, *J. Photochem. Photobiol. A: Chem.*, 206, 129–133, 2009.

21

Di-π-Methane Rearrangement

Howard E. Zimmerman
University of Wisconsin

21.1 Introduction

The di-π-methane rearrangement consists, as its name implies, of a photochemical reaction of a reactant with two π moieties bonded to a single carbon, this is generally sp^3-hybridized and hence a "methane" atom. The reaction is one of the most common, most versatile, and best understood of photochemical transformations.

21.2 Discovery and Mechanism

The beginnings go back to the photolysis of barrelene, which leads to semibullvalene in an intriguing process [1]. This is shown mechanistically in Equation 21.1. Barrelene, of course, has more than two π groups bonded to each bridgehead carbon and thus uses only pair set of these. This reaction proceeds via the triplet with an acetone sensitizer.

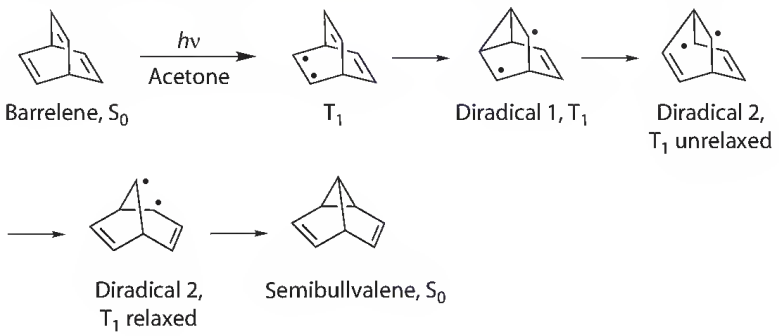

(21.1)

Probably the first di-π-methane examples [2,3] are depicted in Equations 21.2 and 21.3. But these "Type-A" and "Type-B" rearrangements involve excitation of the enone moiety to an n-π* triplet state rather than the more common π-π* excitation; and we will arbitrarily not include these in our present discussion. Nevertheless, these rearrangements, involving a pair of π groups bonding to an sp^3-hydridized carbon led us to look for generality of the reaction. Another early example of the di-π-methane rearrangement is illustrated in Equation 21.4 [4]. In contrast to the Barrelene example, this acyclic di-π-methane reactant, the Mariano diene, utilizes the singlet excited state (i.e., S_1). Again due to symmetry there is only one available mode of ring opening of the cyclopropyldicarbinyl diradical species. However, in the case of the unsymmetrical diene in Equation 21.5 there are two a priori ways, a and b, for cyclopropyldicarbinyl ring opening [5]. The cyclopropyldicarbinyl diradical species selects only one of these (i.e., b). The reaction regioselectivity results from the demand for maintenance of benzhydryl odd-electron delocalization; thus the benzhydryl odd-electron is not used by the cyclopropyldicarbinyl diradical. This was an early example of regioselectivity. One of two examples by Griffin and coworkers [6] is shown in Equation 21.6. Although no mechanisms were advanced at the time, we can see that the usual di-π-methane mechanism suffices to lead to the observed photoproducts using the mechanism we write in Equation 21.6.

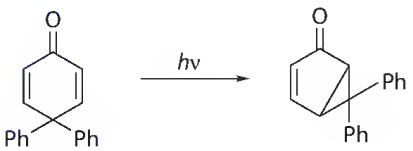

(21.2)

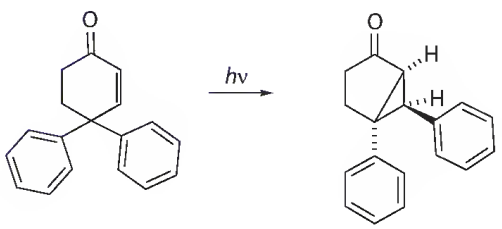

(21.3)

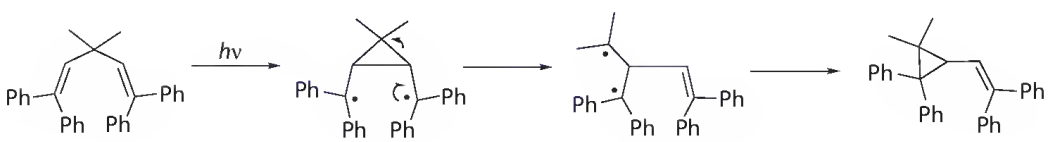

(21.4)

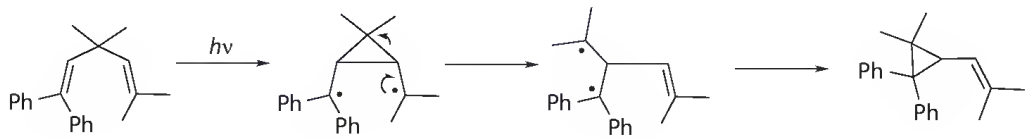

(21.5)

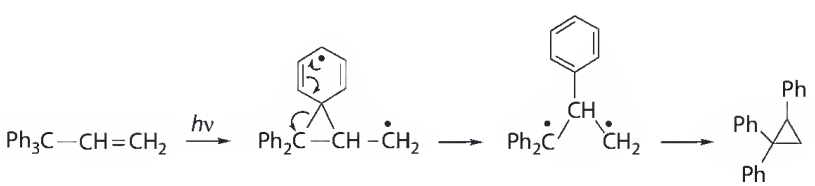

(21.6)

However, we cannot assume that all 1,4-di-π-methane systems proceed via the general mechanism we have suggested. One example [7] is seen in Equation 21.7 where a central hydrogen migrates to the terminus of a diphenylvinyl group in a sigma plus pi rearrangement. Lacking central alkyl substitution, the molecule does not undergo a di-π-methane rearrangement. Of course we cannot extrapolate this result to all 1,4-di-π systems. For example, one reaction (see Equation 21.8) studied by Griffin [6b] may follow the 1,4-di-π-methane mechanism or, instead, as in Equation 21.7, may proceed via the σH + π route. Deuterium labeling is needed to determine which mechanism is followed.

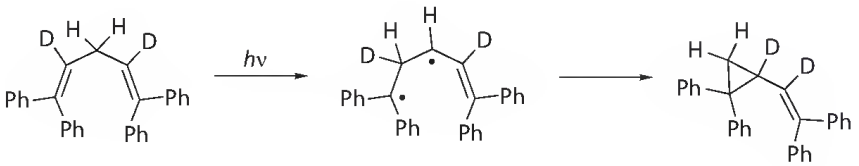

(21.7)

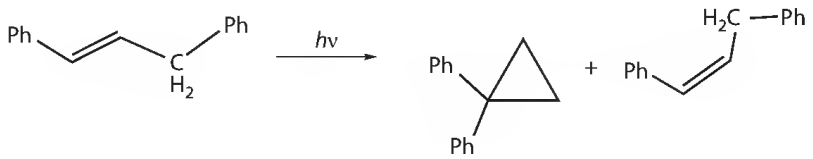

(21.8)

21.3 Regioselectivity in the Di-π-Methane Rearrangement

In pursuing the regiochemistry of the di-π-methane rearrangement further, we looked at the case of a Mariano-type reactant, however, with *p*-cyano substitution on one-half of the molecule [8]. Scheme 21.1 shows the two alternative pathways, **a** and **b**, leading to two possible vinylcyclopropanes. The experimentally observed product arises from pathway **a** when the aryl group is *p*-cyanophenyl and from pathway **b** when the aryl group is anisyl. In the former the odd-electron density delocalized into the cyano group is preserved. It is seen that this route avoids a 1,3-diradical species in which the cyano group no longer interacts with the odd-electron density.

Scheme 21.2 presents some further examples [9] of regioselectivity. In the case where there is a terminal methylene (i.e., X = H), path **a** uses electron density that is originally heavily diffused throughout the benzhydryl moiety, while path **b** utilizes density that is largely concentrated at the methylene group.

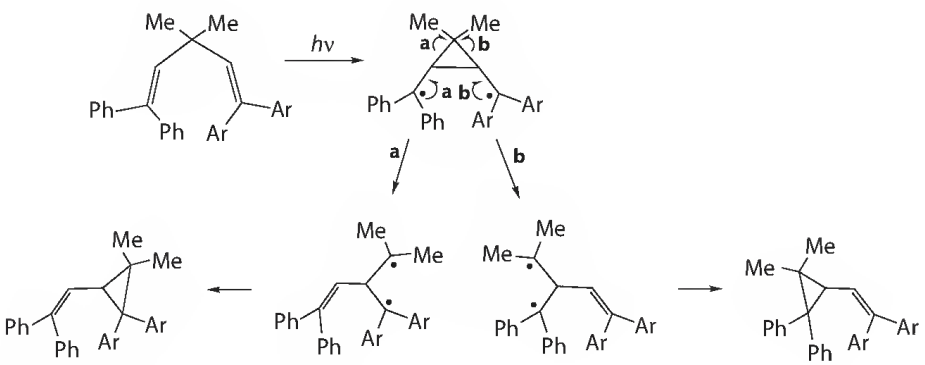

SCHEME 21.1 Regioselectivity with *p*-cyano substitution.

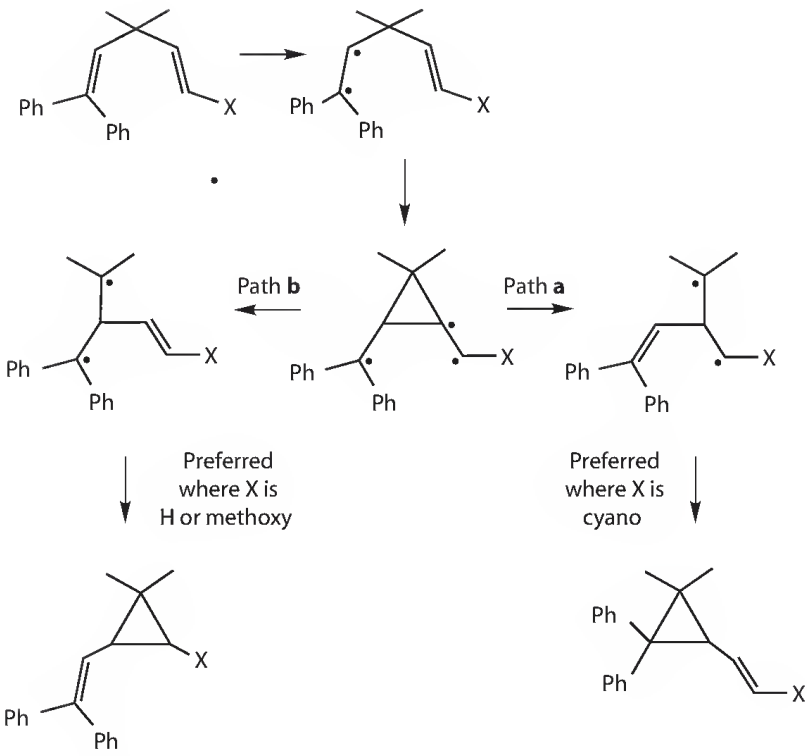

SCHEME 21.2 Further examples of regioselectivity.

In path **a** the electron density in the benzhydryl group thus is largely lost as is the energy of benzhydryl delocalization. Hence path **b** is preferred. Where X is cyano or methoxy prediction is more difficult. However, cyano groups are particularly efficient in delocalizing electron density and thus it is not surprising that path **a** is now preferred. In the methoxy case the same factors as for X = H dominate resulting in preference for path **b**.

21.4 Reality of Diradical Intermediates in the Di-π-Methane Rearrangements

One may consider whether the diradical species written in the aforementioned mechanisms are actual intermediates, are merely points on the reaction hypersurface, or if the mechanisms involve instead a sigma plus pi process as suggested by Woodward and Hoffmann [10] as an alternative. In the case of barrelenes, there is evidence on this point, demonstrating that the triplet diradicals proposed earlier are indeed involved. Thus the azo-bridged precursor, on triplet sensitization, affords the same ratio of two dimethyl naphthosemibullvalenes as obtained from the dimethyl naphthobarrelene itself (Scheme 21.3) [11]. Two independent approaches to the same species will give the same partition of products only if that species is of appreciable lifetime and thermally equilibrated as observed here. Hence, it is clear that the photochemistry of the naphthobarrelene itself proceeds via the same triplet (i.e., T_1) 1,3-diradical **3**. This species must then be an energy minimum. With xanthone T_2 becomes involved.

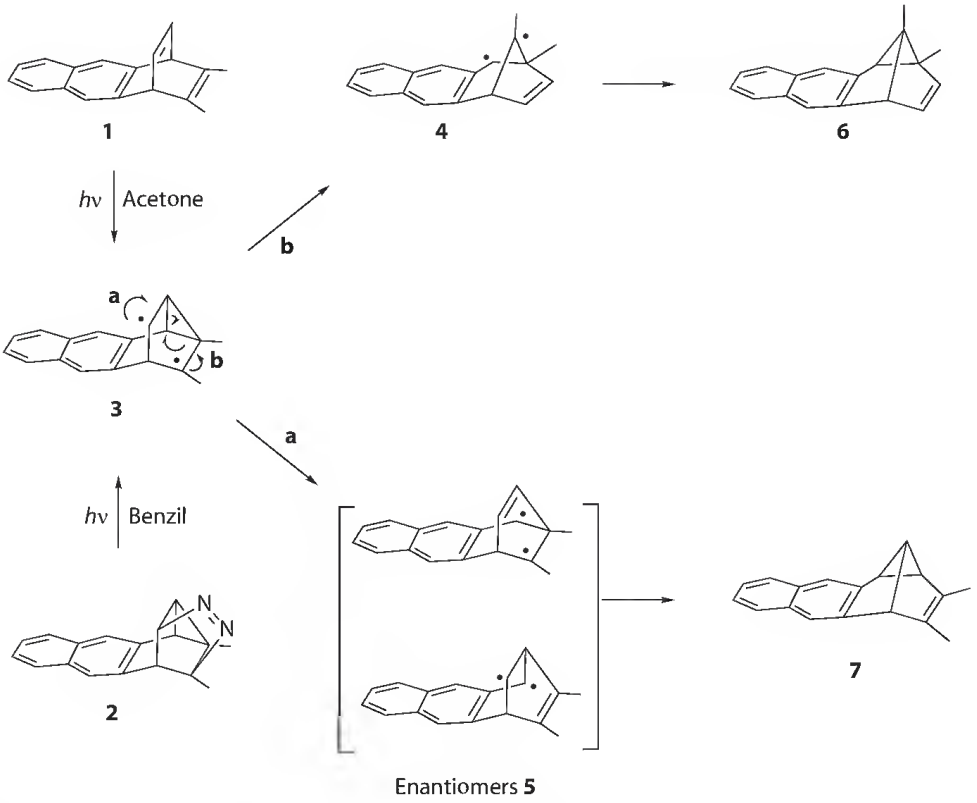

SCHEME 21.3 Evidence for a common triplet 1,3-diradical (**4** or **5**).

21.5 Reaction Stereochemistry

In the di-π-methane rearrangement, there are several sites where stereochemistry is involved. One is at carbon-5 (the carbon ending as part of the product cyclopropyl ring; Scheme 21.4). In Equations 21.9 and 21.10, it is seen that with *cis*-styryl the phenyl becomes *cis* on the three-ring, while a *trans* phenyl becomes *trans*. In Equations 21.11 and 21.12 we note the experimental observation of inversion of configuration at C-5, the methane carbon. In inspecting the basis set of p and hybrid orbitals involved in the rearrangement, as drawn in Scheme 21.5, we see an overlapping sequence of localized orbitals 1-2-3-4-5 in the reactant with orbital 3 being at the "methane" carbon. As the reaction begins, orbitals 2 and 4 begin to overlap and also 5 and 6 and 1 and 3 to give a cyclic array of 1-2-4-5-6-3-1. Inspection of this cycle shows a single plus-minus overlap (i.e., between 5 and 6) and thus a Möbius array [12]. The bonding between orbitals 1 and 3 is disrotatory in closing a three-ring and involves inversion of configuration at the methane carbon (here 3). Also, the substituent R_2, which is *trans* to the vinyl group at 4–5 in the reactant, becomes *trans* to vinyl in the photoproduct.

We count 6 electrons in the cyclic array (i.e., 4 electrons in the two reactant π bonds and 2 in the 3–6 σ bond). With 6 electrons in the Möbius cycle, the reaction is excited state "allowed." Finally, the original stereochemistry of the vinyl group is maintained despite the original p bond between orbitals 4 and 5 being replaced by one resulting from orbitals 5 and 6. If a conrotatory stereochemistry were to be followed the reaction would be forbidden and a reaction course in any case not experimentally observed.

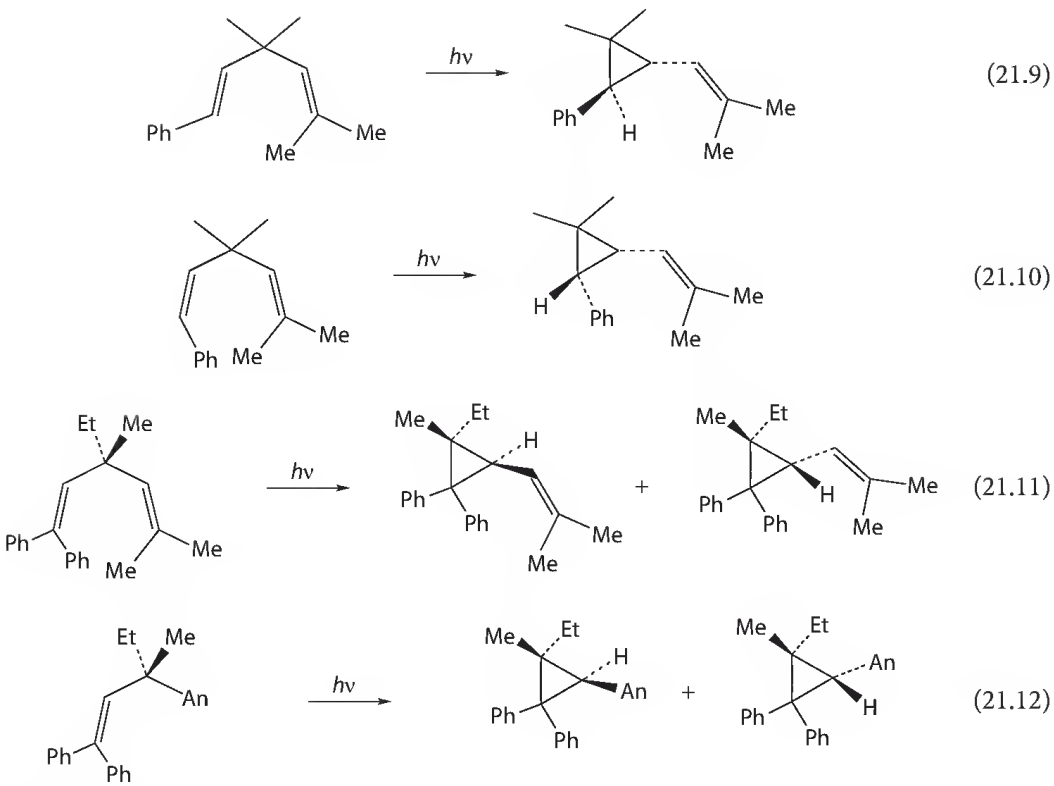

SCHEME 21.4 Stereochemistry.

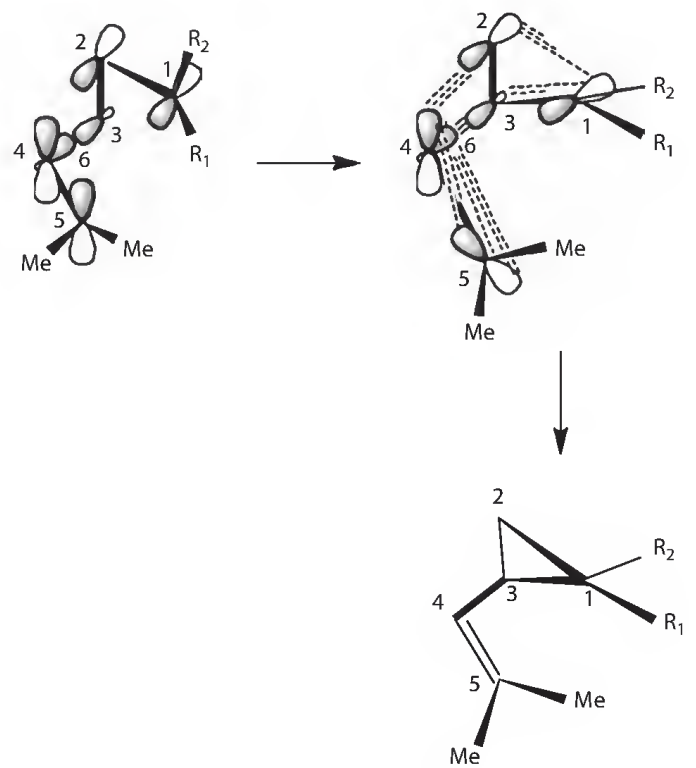

SCHEME 21.5 Basis orbital view giving rise to inversion at C-3.

21.6 Multiplicity Dependence of Regioselectivity

One interesting case is the reaction of 1,1,3,3-tetraphenyl-5,5-dicarbomethoxy-1,4-pentadiene in Scheme 21.6. A direct irradiation proceeding via S_1 results in scission of bond ***a*** while a sensitized irradiation involving T_1 leads to fission of bond ***b*** [13].

Another example of multiplicity dependence [16] is outlined in Scheme 21.7. Here direct irradiation affords three products, including one arising from phenyl–vinyl bridging and two from vinyl–vinyl bonding. Unzipping of the cyclopropyldicarbinyl diradical after vinyl–vinyl bonding leads 3:1 to the isomer with cyano on the three-membered ring. This is reversed in the triplet.

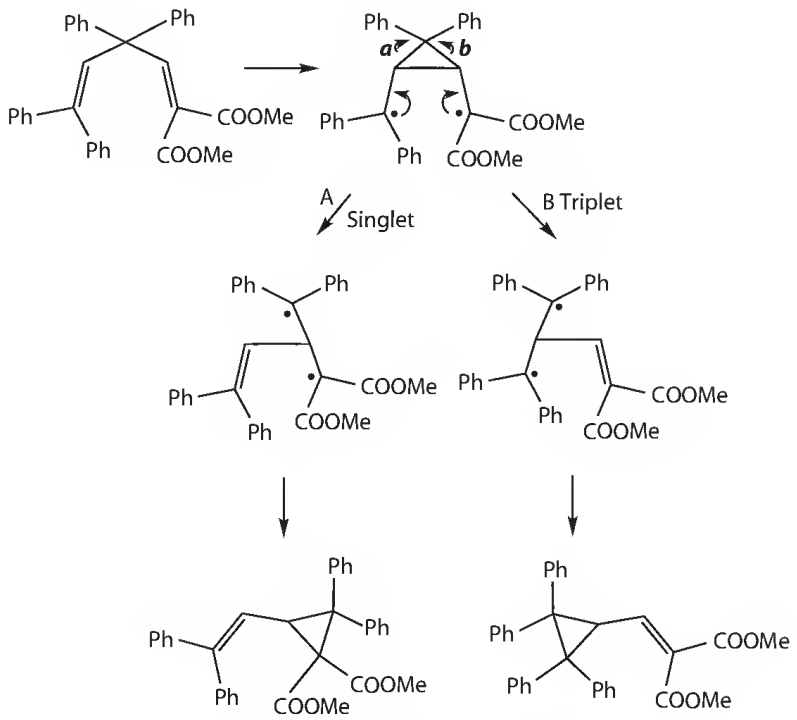

SCHEME 21.6 Multiplicity dependence of a di-π-methane rearrangement.

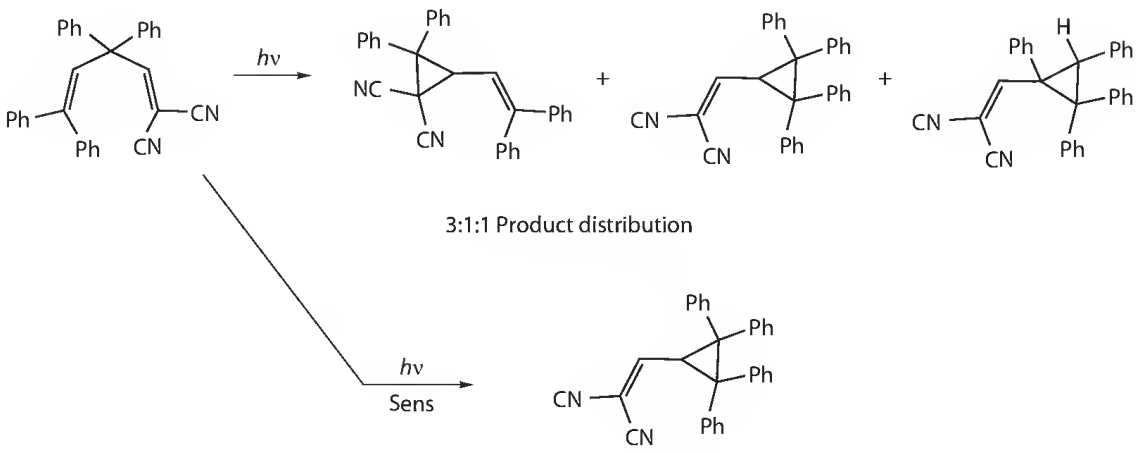

SCHEME 21.7 A further example: regiochemistry versus multiplicity.

21.7 Detailed Reactivity of Intermediate Diradicals in the Barrelene to Semibullvalene Rearrangement

We need to begin by recognizing that the behavior of electronically excited states, and thus photochemistry, is subject to two forms of control. As noted throughout our early reports, excited states follow low-energy pathways and avoid energy barriers. Additionally for singlets, where nearby conical intersections or avoided crossings present themselves, a pathway to the ground state surface results. Similarly for triplets, intersystem crossing (ISC) may lead to the ground state surface. In both singlet and triplet cases conversion to S_0 may lead back to ground state reactant or to ground state product depending on the location of the S_0 species when formed. The former is most likely when conversion to S_0 occurs prior to encountering a ground state barrier and the latter is most likely when conversion to S_0 occurs after encountering a ground state barrier and when the geometry is close to that of the product.

In the di-π-methane rearrangement the two intermediate species—diradical 1 and diradical 2—are particularly subject to consideration. Scheme 21.3 has noted evidence for intervention of diradical 1 in the reaction of benzobarrelenes. We now turn to Scheme 21.8 where the diradicals arising from barrelene, benzobarrelene, and 2,3-naphthobarrelene are generated from azo precursors [14]. We note that loss of nitrogen in the ground state by warming leads to reversion to the corresponding barrelene. While this may be envisioned, at one extreme, as a concerted reverse electrocyclic [3σ 6 electron] Hückel process, it may similarly be pictured at the other extreme as proceeding by loss of nitrogen to afford the diradical 1. It has been noted in our earlier work that there are possible all gradations between these alternatives. This process affords ground state (S_0) barrelene. If the S_0 diradical is truly involved, we would still anticipate formation of the barrelenes. This reversion of the 1,4-diradical on the S_0 surface indicates a ground state barrier between this diradical and photoproduct. The corresponding triplets, obtained by sensitization, lead nicely to the corresponding semibullvalenes rather than the Grob 1,4(2,3) fragmentation (Scheme 21.9).

Further, the triplet diradicals 1 and 2 were determined computationally to be energy minima [11,16,17] and close to degenerate with the S_0 ground state surface. With the knowledge (vide supra) that the S_0 species with the geometry of diradical 1 undergoes reversion to the reactant barrelene, it is clear by default that intersystem crossing to ground state must occur later once diradical 2 is formed [11]. Computation of the spin–orbit coupling at these the two stages of reaction, affording diradical 1 and diradical 2, reveals that the SOC for diradical 2 is much larger.

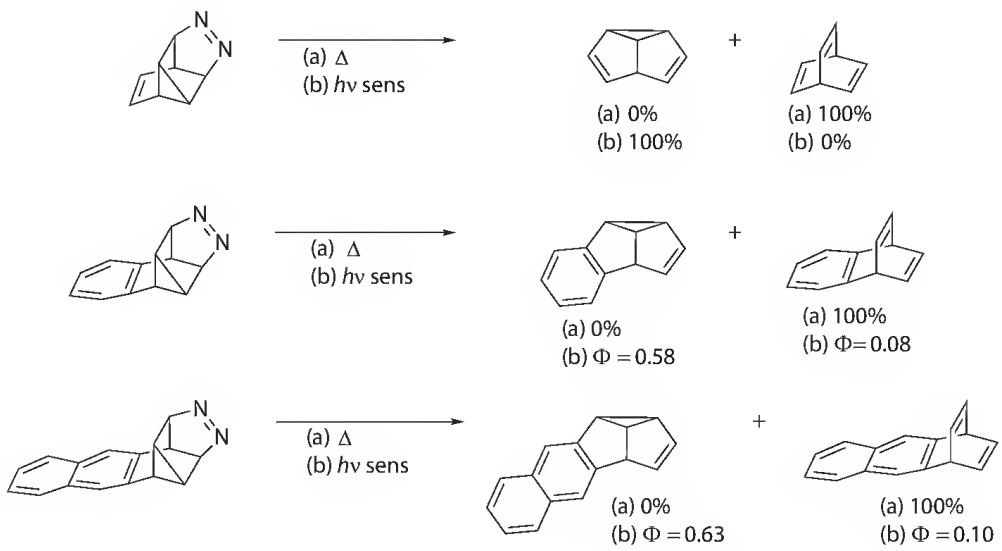

SCHEME 21.8 Generation and behavior of diradical 1.

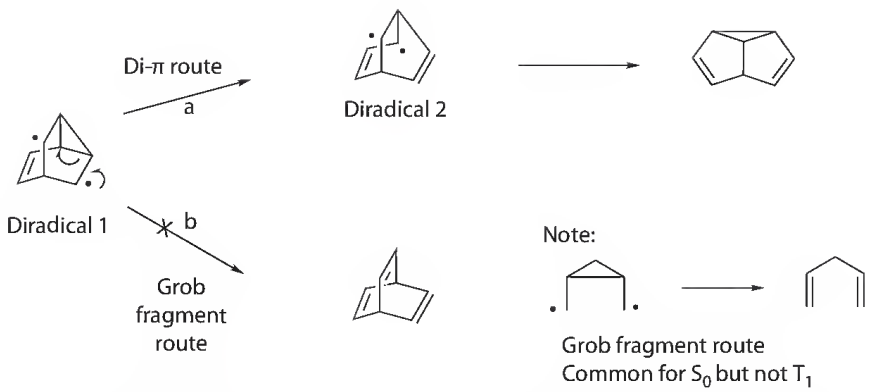

SCHEME 21.9 Triplet Diradical 1 giving di-π-methane behavior and not Grob 1,4(2,3) fragmentation.

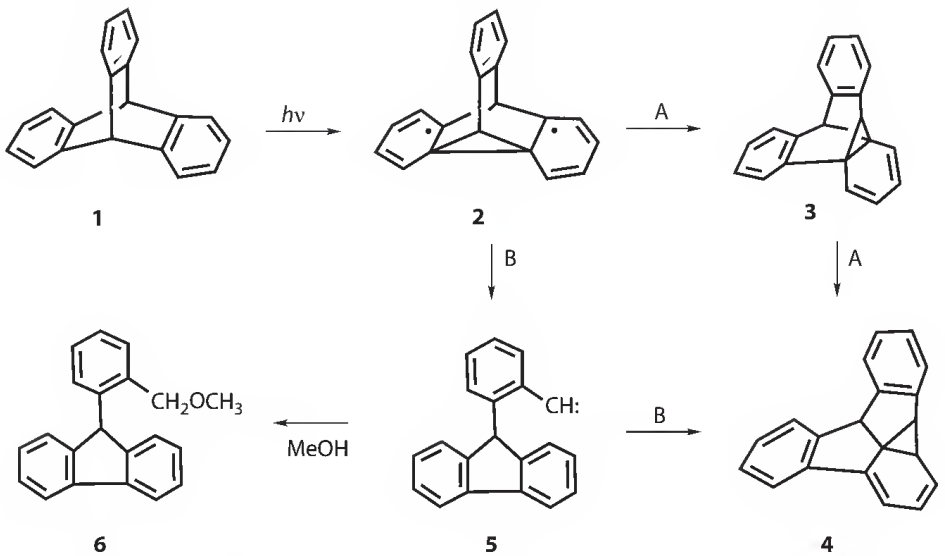

SCHEME 21.10 The unusual pathway for the photolysis of triptycene.

A further finding with regard to the three systems in Scheme 21.8 was that all the T_1 diradicals 1 are subject to a Jahn–Teller distortion in which one of the π bonds is stretched. The triplet computations on diradicals 1 and 2 were done at the CASSCF(6,6)/6-31G* level.

A particularly interesting reaction (Scheme 21.10) involves the photolysis of triptycene **1**. This had been reported by Turro and Friedman [18] as giving photoproduct **4** and not the anticipated di-π-methane product **3**. It was suggested that, once formed, **3** undergoes a sigmatropic rearrangement to **4**. Note Mechanism A in Scheme 21.10. However, in a series of thorough studies, Iwamura [19] has shown that a different route is followed, namely Mechanism B in Scheme 21.10. This proceeds via the carbene **5**, which can be trapped by methanol to afford the benzylic methyl ether **6**. In a control experiment, Iwamura [19] showed that photolysis of **4** in methanol does not lead to trapping of the carbene. And thus the benzylic methyl ether is not formed from photoproduct **4**. In the absence of methanol, photoproduct **4** results. The reaction mechanism is seen to involve benzo–benzo bridging to afford diradical **2**, which can extrude the bridgehead carbon leading to carbene **5**. The divalent carbene carbon then attacks one benzo ring to form photoproduct **4**.

21.8 Aryl-Vinyl Di-π-Methane Rearrangements

One simple typical example involves phenyl–vinyl bridging [14–20] and is illustrated in Scheme 21.11 along with the reaction mechanism; this is the same mechanism we have postulated for the reaction of Griffin and shown in Equation 21.6. Thus in Scheme 21.11 the lower energy chromophore

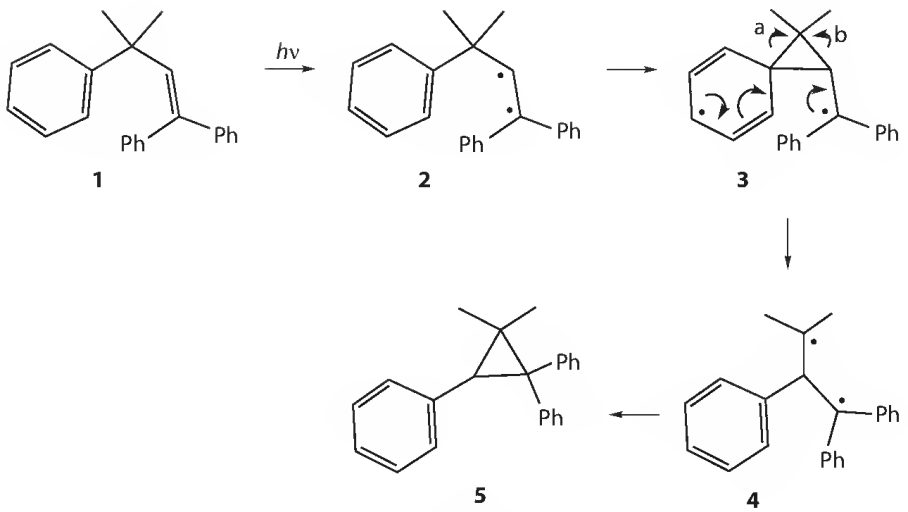

SCHEME 21.11 The phenyl–vinyl di-π-methane rearrangement.

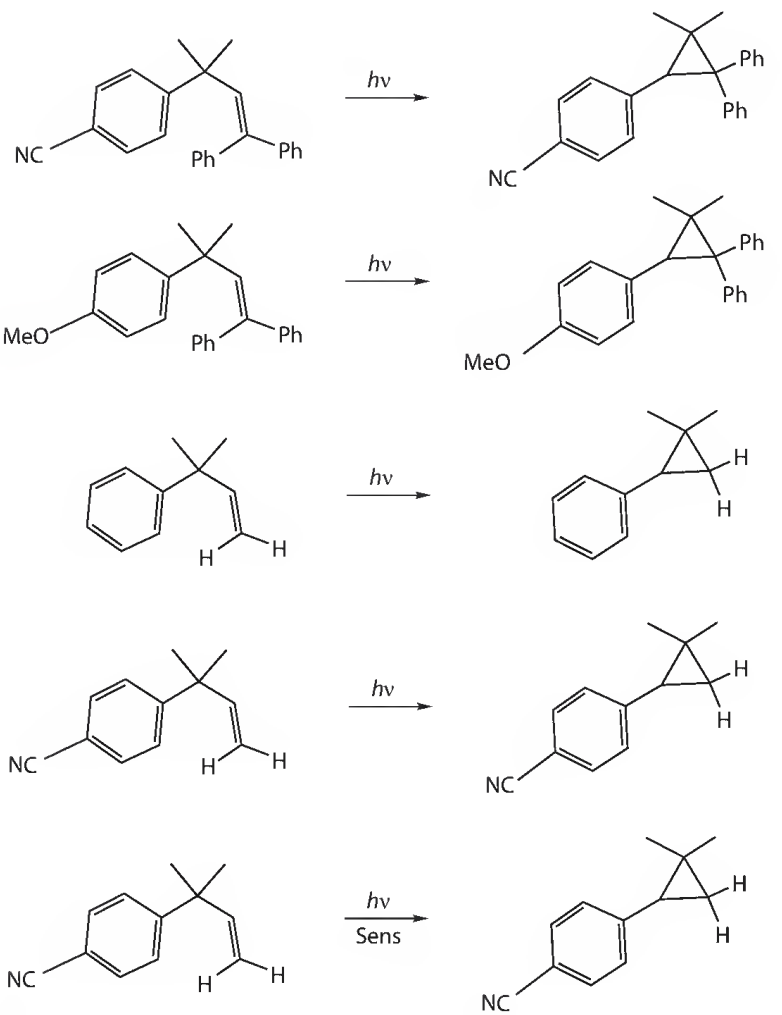

SCHEME 21.12 Further examples.

is the diphenylvinyl group that is excited with formation of species **2**. Phenyl–vinyl bridging leads to singlet diradical **3** with loss of benzenoid aromaticity. In comparing electron redistributions a and b in this diradical, process a is seen to restore benzenoid aromaticity and retains benzhydryl delocalization while process b does not restore benzenoid aromaticity and loses the delocalization of the benzyhydryl moiety. Scheme 21.12 provides further examples.

21.9 Triplet Reactivity

Although the generalization has been drawn that cyclic di-π-methane reactants such as barrelene react via triplets while acyclics react via singlets, the source of this reasoning needs to be recognized. Thus the competing process for triplets of free-rotor energy dissipation is inhibited for the cyclic π systems and for severely hindered acyclic systems where double bond rotation is impossible or difficult. Additionally, it needs to be recognized that where the quantum yield for the triplet process is finite, extended irradiation can be synthetically successful as long as competing processes do not do more than effect *cis-trans* interconversion. Note also the examples in Scheme 21.12.

Indeed, there are examples of acyclic di-π-methane rearrangements proceeding via the triplet with appreciable efficiency. Thus, although the reactant in Equation 21.18 is acyclic, we note that excitation will primarily affect the diphenylethylene moiety and not the less conjugated vinyl. Thus free rotation will be slower. Most interestingly, there is a temperature effect in which the quantum yield is increased fivefold (27°C–73°C) [9].

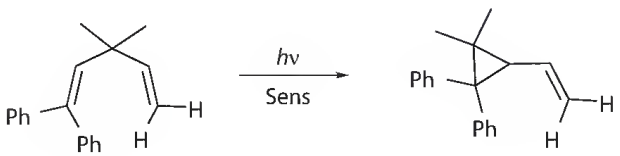

(21.18)

Temperature	Quantum
27	0.011
73	0.058

Another example [21] is that of *p*-cyanophenylbutene (Equation 21.19), which, on acetone sensitization, rearranges with a quantum yield of 0.71. The *meta*-isomer has a quantum yield of 0.25.

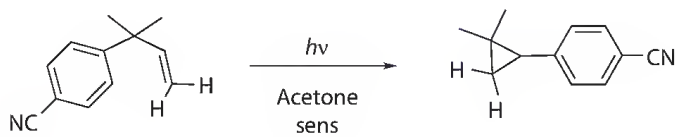

(21.19)

It seems that the potential free-rotor C=CH_2 is a high-energy portion of the molecule and with its excitation being inaccessible, energy dissipation by the free-rotor effect is lost. A further example is seen in the tetraphenyl example [21] in Equation 21.20. The triplet quantum yield is 0.42, which is remarkably high. Electronic factors have been considered. However in this case steric factors are involved. A potential free-rotor, namely the Me_2C=C group is substituted on the methane carbon, and that carbon bears three large substituents—phenyl, phenyl, and diphenylvinyl. Thus the free-rotor is gauche to two of these and is sterically hindered. Additionally, the dimethyl vinyl is a high-energy chromophore. The reaction in Equation 21.21 [16] has a quantum yield of 0.79, which is even more remarkable and there seems to be incursion of an electronic factor as well as the steric factor just mentioned.

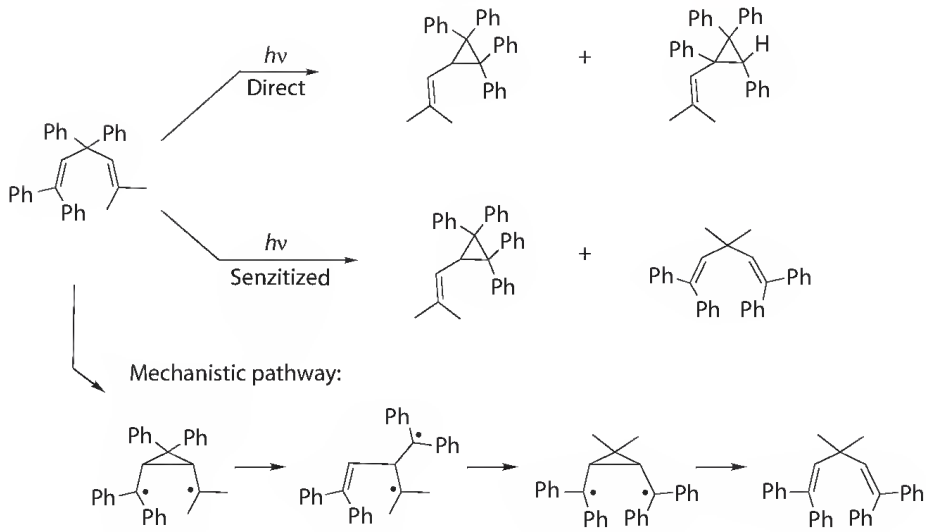

SCHEME 21.13 Phenyl migration from the singlet and also diene rearrangement from the triplet.

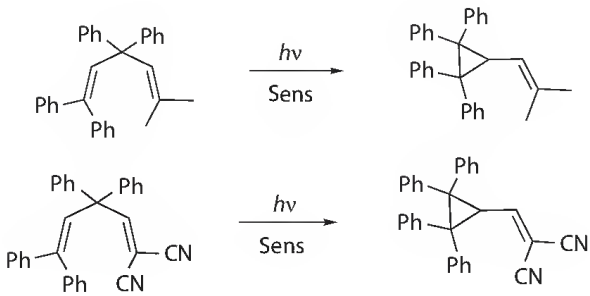

(21.20)

(21.21)

An additional point of interest is that the direct irradiation of the reactant in Equation 21.20 differs in additionally having product deriving from phenyl migration (Scheme 21.13). Further, the triplet leads additionally to the rearranged di-π-methane diene as depicted in Scheme 21.13.

21.10 Reaction Rates

Considerable information can be obtained from reaction rates in the di-π-methane rearrangements. In principle, one should correlate mechanistic reactivity with reaction rates rather than quantum yields. We now consider the three examples in Equation 21.22.

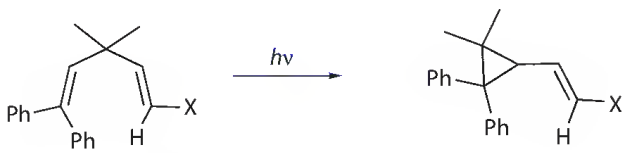

(21.22)

Compound 1 X = H
Compound 2 X = CN
Compound 3 X = MeO

For these three reactions the regiochemistry, the quantum efficiency, the multiplicity, and the excited state reaction rates were studied. We discuss the direct, singlet processes first. The room temperature quantum yields were φ (**1**, parent) = 0.011, φ (**2t**, *trans* CN Diene) = 0.36 and φ (**2c**, *cis* CN Diene) = 0.20,

φ (**3t**, *trans* MeO Diene) = 051, φ (**3c**, *cis* MeO Diene) = 0.050. However, it has long been recognized that inherent reactivity is signified by reaction rates and not quantum yields. The latter give only the reaction rates relative to all rates including decay.

Single-photon counting reaction rates for the singlets were k_r (**1**, parent) = 4.7×10^8 s^{-1}, k_r (**2t**, *trans*) = 1.5×10^{10} s^{-1}, k_r (**2c**, *cis*) = 8.0×10^9 s^{-1}, and k_r (**3t**, *trans*) = 1.8×10^9 s^{-1} [9]. It is seen that the cyano di-π-methane dienes are the most reactive, the methoxy dienes next, and the parent hydrocarbon the least.

On sensitization, the cyano and methoxy dienes gave only *cis–trans* isomerization. However, in the case of the parent diene **1** an exciting result was encountered. The parent diene did give the same photoproduct as obtained on direct irradiation (note Equation 21.22) and with the same quantum efficiency, φ = 0.011, as in the direct irradiation. While one might be tempted to conclude from this that both direct and sensitized reactions proceed via the same, triplet excited state, this is not the case as seen in the differences in temperature dependence. In an increase in temperature from 27°C to 73°C, the quantum efficiency in the direct irradiation was unchanged while in the sensitized reaction the efficiency increased from φ = 0.011 to φ = 0.058, a fivefold increase. One might attribute this to a temperature dependence of sensitization efficiency except that it has been demonstrated that energy transfer has unit efficiency.

Thus with direct irradiation showing no temperature dependence and the sensitized, T1, reaction exhibiting the fivefold effect, it is clear that the direct irradiation is a singlet process, that is, S_1.

Of course, the temperature dependence of the T1 reaction signifies that there is an energy barrier for reaction while the lack of one for S1 shows that this process has none. But proceeding further, we note that the temperature dependence of the triplet di-π-methane rearrangement leads to a 7.5 kcal/mole Arrhenius activation energy. This requires the assumption that the rate of radiationless decay of the triplet is temperature independent; otherwise a still higher activation energy results.

Most interesting are the results of Lewis [22] who found the singlet reaction of 1,3-diphenyl-3,3-dimethylpropene **1** (note Equation 21.23) to be temperature dependent with an activation energy of 1.9 kcal/mole; and with varying substitution at the methane carbon similar values were obtained. In these cases the triplet did not exhibit temperature dependence.

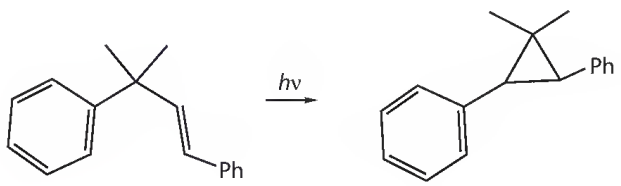

(21.23)

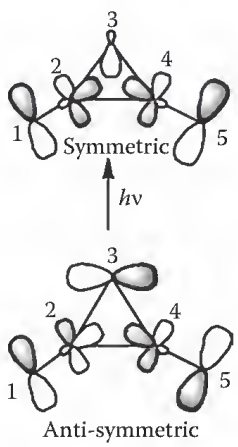

FIGURE 21.1 Excitation of the cyclopropyldicarbinyl diradical moiety.

Some items are particularly relevant [9]. One item is computational. Initially the π bonds are at carbons 1–2 and 4–5 and excitation is largely there. Thus for the diphenylvinyl type di-π-methane rearrangements, it is not surprising that computations reveal the vertical (i.e., initial) excitation is largely located in the diphenylvinyl moiety. What is especially interesting is that after π-π bridging excitation is found to reside in the cyclopropyldicarbinyl group. This, perhaps, is not that surprising since the cyclopropyldicarbinyl diradical moiety (note Figure 21.1), in the limit without delocalization with the orbitals in the cyclopropyl group, would have a pair unconjugated p-orbitals and complete degeneracy of HOMO–LUMO. Additionally, it is seen that the ground state S_0 is antibonding between atoms 2 and 4; but S_1 is bonding between these centers. Herein lies the basis for vinyl–vinyl or phenyl–vinyl π-π bonding in the di-π-methane rearrangement.

21.11 Conclusion

The di-π-methane rearrangement can be seen to be particularly general and subject to mechanistic understanding. The reaction is successful with a broad variation structurally and with singlet and triplet multiplicity. Patterns of behavior are seen experimentally and follow computational exploration.

References

1. (a) Zimmerman, H. E.; Grunewald, G. L., The chemistry of barrelene. III. A unique photoisomerization to semibullvalene, *J. Am. Chem. Soc.*, 1966, *88*, 183–184; (b) Zimmerman, H. E., Mechanistic organic photochemistry, *Angew. Chem.*, 1969, *81*, 45–55. *Angew. Chem. Int. Ed. Engl.*, 1969, *8*, 1–11.
2. Zimmerman, H. E.; Schuster, D. I., Mechanistic organic photochemistry. IV. Photochemical rearrangements of 4,4-diphenylcyclohexadienone, *J. Am. Chem. Soc.*, 1962, *84*, 4527–4540.
3. Zimmerman, H. E.; Wilson, J. W., Mechanistic and exploratory organic photochemistry, IX. Phenyl migration in the irradiation of 4,4-diphenylcyclohexenone, *J. Am. Chem. Soc.*, 1964, *86*, 4036–4042.
4. Zimmerman, H. E.; Mariano, P. S., The di-π-methane rearrangement. Interaction of electronically excited vinyl chromophores, *J. Am. Chem. Soc.*, 1969, *91*, 1718–1727.
5. Zimmerman, H. E.; Pratt, A. C., Organic photochemistry. LIII. Directionality of the di-π-methane rearrangement and alkyl migration in a unique singlet vinylcyclopropane transformation, *J. Am. Chem. Soc.*, 1970, *92*, 1407–1409.
6. (a) Griffin, G. W.; Marcantonio, A. F.; Kristinsson, H.; Petterson, R. C.; Irving, C. S., Photocyclization of propenes to cyclopropanes: Novel phenyl and hydrogen migrations in π,π* systems, *Tetrahedron Lett.*, 1965, *34*, 2951–2958; (b) Giffin, G. W.; Covell, J.; Petterson, R. C.; Dodson, R. M.; Klose, G., Photoisomerization of cyclopropane derivatives. Photointerconversion of propenes and cyclopropanes, *J. Am. Chem. Soc.*, 1965, *87*, 1410–1411.
7. (a) Zimmerman, H. E.; Pincock, J. A., Sigma plus pi rearrangements of di-π-methane systems. Central substitution and di-π-methane reactivity. Mechanistic and exploratory organic photochemistry, LXXVI, *J. Am. Chem. Soc.*, 1973, *95*, 2957–2963; (b) Zimmerman, H. E.; Pincock, J. A., An unexpected sigma plus pi rearrangement of a di-π-methane reactant. Inhibition of the di-π-methane rearrangement. Mechanistic and exploratory organic photochemistry. LXX, *J. Am. Chem. Soc.*, 1972, *94*, 6208–6209.
8. (a) Zimmerman, H. E.; Cotter, B. R., Substituent effects and the di-π-methane rearrangement. Mechanistic and exploratory organic photochemistry, *J. Am. Chem. Soc.*, 1974, *96*, 7445–7453; (b) Zimmerman, H. E.; Welter, T. R., Control of regioselectivity and excited state singlet reaction rates by substitution in the di-π-methane rearrangement. Mechanistic and exploratory organic photochemistry, *J. Am. Chem. Soc.*, 1978, *100*, 4131–4145.

9. Zimmerman, H. E.; Klun, R. T., The di-π-methane rearrangement of systems with simple vinyl moieties. Mechanistic and exploratory organic photochemistry, *Tetrahedron*, 1978, *43*, 1775–1803.
10. Woodward, R. B.; Hoffmann, R., The conservation of orbital symmetry, *Angew. Chem. Int. Ed. Engl.*, 1969, *8(11)*, 781–932.
11. Zimmerman, H. E.; Kutateladze, A. G.; Maekawa, Y.; Mangette J. E., Excited state reactivity as a function of diradical structure: Evidence for two triplet cyclopropyldicarbinyl diradical intermediates with differing reactivity, *J. Am. Chem. Soc.*, 1994, *116*, 9795–9796.
12. (a) Zimmerman, H. E., On molecular orbital correlation diagrams, the occurrence of möbius systems in cyclization reactions, and factors controlling ground and excited state reactions. I, *J. Am. Chem. Soc.*, 1966, *88*, 1564–1565; (b) Zimmerman, H. E., On molecular orbital correlation diagrams, möbius systems, and factors controlling ground and excited state reactions. II, *J. Am. Chem. Soc.*, 1966, *88*, 1566–1567.
13. Zimmerman, H. E.; Factor, R. E., Di-π-methane hypersurfaces and reactivity; multiplicity and regioselectivity; relationship between the di-π-methane and bicycle rearrangements, *Tetrahedron*, 1981, *37, Supplement 1*, 125–141.
14. Zimmerman, H. E.; Swafford, R. L., Reactivity of aryl vinyl di-π-methane systems. Mechanistic and exploratory organic photochemistry. 1, *J. Org. Chem.*, 1984, *49*, 3069–3083. (CNPh C=CH_2) and MeOPh C–CH_2).
15. Zimmerman, H. E.; Boettcher, R. J.; Buehler, N. E.; Keck, G. E.; Steinmetz, M. G., Independent generation of cyclopropyldicarbinyl diradical species of the di-π-methane rearrangement. Excited singlet, triplet and ground state hypersurfaces of barrelene photochemistry, *J. Am. Chem. Soc.*, 1976, *98*, 7680–7689.
16. Zimmerman, H. E.; Armesto, D.; Amezua, M. G.; Gannett, T. P.; Johnson, R. P., Unusual organic photochemistry effected by cyano and methoxy substitution. Exploratory and mechanistic organic photochemistry, *J. Am. Chem. Soc.*, 1979, *101*, 6367–6383.
17. Zimmerman, H. E.; Sulzbach, H. M.; Tollefson, M. B., Experimental and theoretical exploration of the detailed mechanism of the rearrangement of barrelenes to semibullvalenes: Diradical intermediates and transition states, *J. Am. Chem. Soc.*, 1993, *115*, 6548–6556.
18. Turro, N. J.; Tobin, M.; Friedman, L.; Hamilton, J. B., Photochemistry of triptycene, *J. Am. Chem. Soc.*, 1969, *91*, 516.
19. (a) Iwamura, H. and Yoshimura, K., Trapping of the carbene intermediates in the photolysis of triptycenes, *J. Am. Chem. Soc.*, 1974, *96*, 2652–4654; (b) Iwamura, H., The carbene mechanism for photoisomerization of triptycene, *Chem. Lett.*, 1974, 5–8; (c) Iwamura, H., Excite state reactions of triptycenes. IV. Photolytic one step synthesis and stereochemistry of 1,4-dimethyl-9-arylfluorenes, *Chem. Lett.*, 1974, 1205–1208; (d) Iwamura, M.; Mori, E.; Koike, A.; Kitagawa, T.; Koga, N.; Iwamura, H., Photochemistry of 9-benzyloxytriptycenes, *Chem. Lett.*, 1992, 2051–2054.
20. Zimmerman, H. E.; Steinmetz, M. G.; Kreil. C. L., The aryl vinyl methane version of the di-π-methane rearrangement. Mechanistic and exploratory organic photochemistry, *J. Am. Chem. Soc.*, 1978, *100*, 4146–4162. (CNPh, MeOPh, H.)
21. (a) Zimmerman, H. E.; Boettcher, R. J.; Braig, W., Accentuation of di-π-methane reactivity by central carbon substitution. Mechanistic and exploratory organic photochemistry. LXXV, *J. Am. Chem. Soc.*, 1973, *95*, 2155–2163; (b) Armesto, D.; Ortiz, M. J.; Agarrabeitia, A. R.; Martin-Fontecha, M.; El-Boulifi, N.; Duran-Sampedro, G.; Enma, D., Remarkable observations on triplet-sensitized reactions. The di-π-methane rearrangement of acyclic 1,4-dienes in the triplet excited state, *Org. Lett.*, 2009, *11*, 4148–4151.
22. (a) Lewis, F. D.; Zuo, X.; Kalgutkar, R. S.; Miranda, M. A.; Font-Sanchis, E.; Perez-Prieto, J., The di-π-methane reaction of 3,3-dimethyl-1,3-diphenylpropene revisited: Dynamics and barriers for competitive singlet state reactions, *J. Am. Chem. Soc.*, 2000, *122*, 8571–8572; (b) Lewis, F. D.; Zuo, X.; Kalgutkar, R. S.; Wagner-Brennan, J. M.; Miranda, M. A.; Font-Sanchis, E.; Perez-Prieto, J., Temperature-dependent photochemistry of 1,3-diphenylpropenes. The di-π-methane reaction revisited, *J. Am. Chem. Soc.*, 2001, *123*, 11883–11889.

22

Oxa-Di-π-Methane Rearrangement of β,γ-Unsaturated Ketones

V. Jayathirtha Rao
Indian Institute of Chemical Technology

and

National Institute of Pharmaceutical Education and Research

Kolupula Srinivas
National Institute of Pharmaceutical Education and Research

22.1 Introduction to ODPM Rearrangement

Carbonyl compounds played an important role and became part of the leading research domain of organic photochemistry. Particularly, β,γ-unsaturated carbonyl compounds have attracted more attention. These β,γ-unsaturated carbonyls exhibit a variety of photochemical processes like (a) acyl migration, (b) oxa-di-π-methane (ODPM) rearrangement, (c) decarbonylation, (d) epimerization, (e) cycloaddition, (f) Norrish type I and type II processes, (g) *cis–trans* (*E–Z*) isomerization, and (h) reduction. Among the various photochemical processes of β,γ-unsaturated carbonyls, the ODPM rearrangement has attracted the attention of various researchers. This is because photochemical ODPM rearrangement provides high yields of products having synthetic exploitation, good photochemical quantum yields, making complex molecules in a very simple way, maintaining excellent selectivity, understanding the role of various excited states (involving multiplicity), and also understanding the role and link between carbonyl and olefin chromophores within the molecule to predict the reactivity.

22.2 Historical Perspective

The photochemical rearrangement of β,γ-unsaturated carbonyl compounds involving 1,2-acylmigration coupled with cyclization leading to the formation of three-membered ring is termed as "oxa-di-π-methane (ODPM)" rearrangement. The photochemical ODPM rearrangement is analogous to the "di-π-methane"

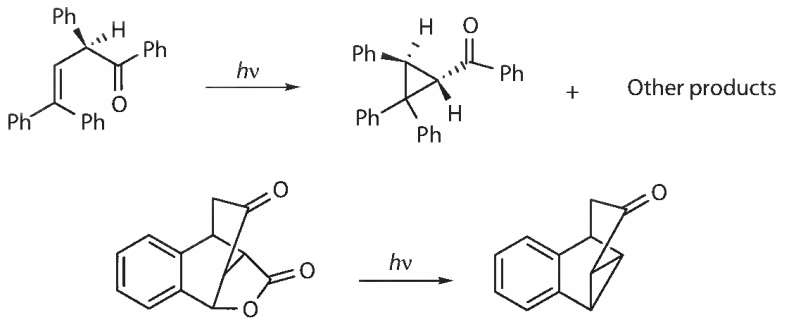

SCHEME 22.1 First example of ODPM rearrangement.

rearrangement (see the other chapter) reported earlier. The first example of an ODPM rearrangement[1] was reported in 1966 for β,γ-unsaturated ketone (Scheme 22.1) and it went largely unnoticed.

The first mechanistic pathway was suggested by Swenton[2] and later Givens[3] explained the mechanism for the photochemistry of butyrolactone (Scheme 22.1) derivative as analogous to di-π-methane (DPM) rearrangement. Immediately Dauben[4] came up with a description for the photoreaction as "oxa-di-π-methane (ODPM)" rearrangement. Since then several researchers got involved in this ODPM rearrangement research domain and this resulted in a large number of publications in this area. The preference to conduct ODPM rearrangement with β,γ-unsaturated carbonyls is increasing, because of its very good chemical yields, photochemical quantum yields, and observed selectivity, which encouraged many researchers to work in this area of research. The ODPM rearrangement reaction has been successfully applied for the synthesis of many complex natural products and other intermediates, which are otherwise difficult to obtain by other means. Interestingly, the ODPM rearrangement originates from triplet excited manifold and this became an advantage to conduct photoreaction under triplet-sensitized conditions with higher yields. Several reviews[5–23] have appeared on this subject of ODPM and DPM rearrangement during the last three to four decades. In this chapter, we discuss a brief introduction, mechanistic aspects, various examples, scope and limitations, representative experimental procedures, and targeted structures. Selectivity and stereochemical aspects are highlighted wherever appropriate and necessary. This is a short review highlighting the basic fundamental aspects of ODPM rearrangement to enthuse new researchers into this research domain. For more details, the reader may consult various review articles and book chapters available in the literature.[5–23]

22.3 Reactive Excited State

ODPM rearrangement reaction is found to be originating from triplet excited state in almost all the compounds studied. Several model compounds[24–26] (Scheme 22.2) displayed that ODPM rearrangement can be conducted by direct excitation or more conveniently by triplet-sensitized conditions. Under direct excitation conditions the substrate undergoes intersystem crossing in the singlet excited state, leading to formation of triplet excited state and then the ODPM rearrangement follows (Scheme 22.2). Under triplet sensitization conditions, the triplet excited state of sensitizer transfers energy to substrate molecule (triplet–triplet energy transfer) and then the ODPM rearrangement is observed (Scheme 22.2). The direct excitation experiments may be ambiguous with respect to involvement of excited singlet or triplet state responsible for the observed ODPM rearrangement. Detailed investigations on a set of model compounds [25,27,28] (Scheme 22.3) informed that indeed the ODPM rearrangement originates from the triplet excited state. It is well documented that $\pi\pi^*$ triplet is responsible for ODPM rearrangement based on low-temperature phosphorescence measurements and theoretical and mechanistic studies.

A recent report by Diego Armesto[29] clearly pointed out the important role of "energy of triplet sensitizer" on the ODPM rearrangement reactivity of β,γ-unsaturated carbonyls (Scheme 22.4). Among the sensitizers employed, the thioxanthone (E_T = 63 kcal/mol) is found to be effective for the observed

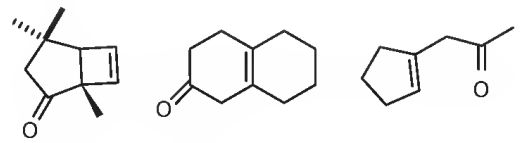

Direct excitation pathway

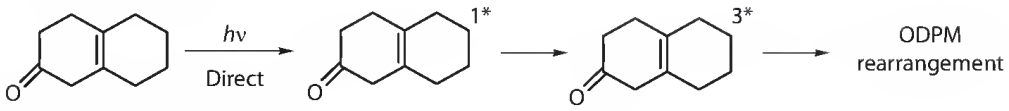

Triplet sensitization pathway

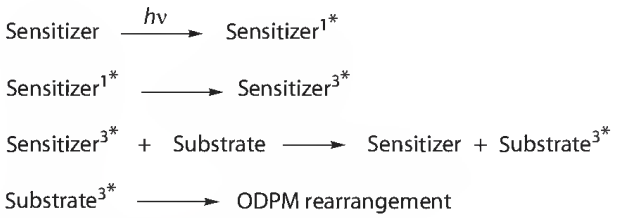

SCHEME 22.2 Model compounds of ODPM rearrangement.

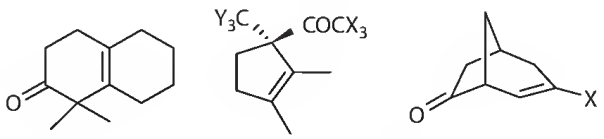

SCHEME 22.3 Model compounds defining "triplet" as reactive state.

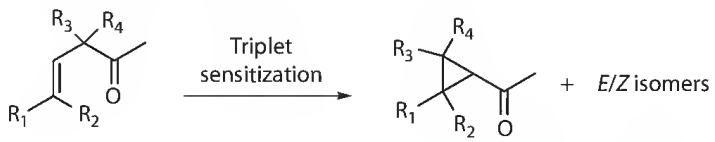

$R_1 = Ph$; $R_2 = H$; $R_3 = R_4 = Me$
$R_1 = Ph$; $R_2 = H$; $R_3 = R_4 = -(CH_2)-_4$
$R_1 = R_2 = Ph$; $R_3 = R_4 = Me$
$R_1 = R_2 = CN$; $R_3 = R_4 = Me$
$R_1 = Me_2C = CH-$; $R_2 = H$; $R_3 = R_4 = Me$

Sensitizers:
Acetophenone ($E_T = 74$ kcal/mol)
3-Methoxyacetophenone ($E_T = 71$ kcal/mol)
Thiaxanthone ($E_T = 63$ kcal/mol)
4-Phenylbenzophenone ($E_T = 61$ kcal/mol)
Chrysene ($E_T = 57$ kcal/mol)

SCHEME 22.4 Role of sensitizer in ODPM rearrangement.

ODPM rearrangement reactivity (Scheme 22.4). The authors[29] have used mainly free rotor effect (*E/Z* isomerism) and also 1,3-acyl migration as dominating photochemical pathways for the compounds shown in Scheme 22.4.

These observations definitely point out to verify the ODPM rearrangement activity for the β,γ-unsaturated carbonyls[30–32] earlier reported to be not active compounds (Scheme 22.5). Triplet sensitizer energy–dependent ODPM rearrangement is reported for quinuclidinone (azabicyclo-β,γ-unsaturated ketone), where the authors[33] have successfully conducted ODPM rearrangement using triplet sensitizer acetophenone, but not with acetone as triplet sensitizer (Scheme 22.6). The efficiency of ODPM rearrangement is found to be increased (compared to solution-phase photolysis) upon confinement of

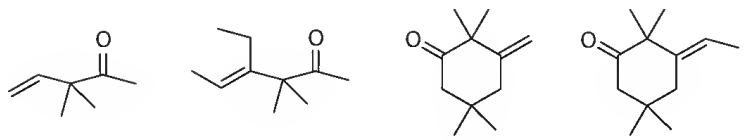

SCHEME 22.5 β,γ-Unsaturated ketones not active toward ODPM rearrangement.

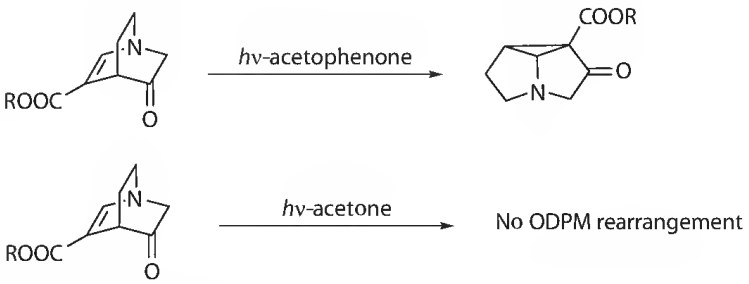

SCHEME 22.6 Role of sensitizer in ODPM rearrangement.

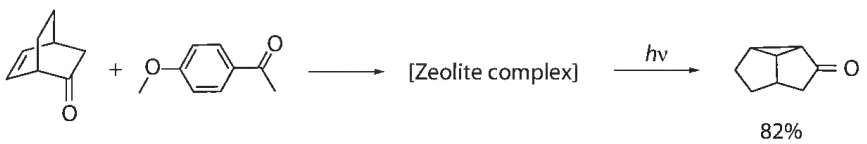

SCHEME 22.7 Improvement in reactivity of ODPM rearrangement upon confinement.

substrate and triplet sensitizer (Scheme 22.7) in a zeolite.[34] Considering the data given earlier, the reactive excited state involved in these β,γ-unsaturated ketones leading to ODPM rearrangement is a triplet excited state of ππ* origin. Further, it was observed that a sensitizer with suitable triplet energy is also another condition to conduct the ODPM rearrangement efficiently.

22.4 Theoretical Aspects

The majority of experimental results reveal that direct irradiation on β,γ-enones yields mainly the [1,3]-acyl shift product where as triplet sensitization yields the ODPM product.[24,35] A possible explanation for the divergent behavior of β,γ-unsaturated ketone singlet and triplets has been proposed by various groups. Schuster et al.[36] suggested that different spin density distributions in the excited singlet and triplet states lead to differing initial bonding interactions and ultimately to different products and implicitly it is assumed that both excited singlet and triplets were nπ* excited states. Later, Houk and coworkers[37] explained based on the differences in the electronic configurations of the excited states and by considering the concept of probable bonding charges in the excited state can be predicted based on the bond order differences between the ground state and the excited state. However, the selectivity of singlet and triplet states yielding [1,3]-acyl and ODPM products is not universal. In few instances, the ODPM rearrangement is formed on direct photolysis of certain β,γ-enones, while the [1,3]-acyl photoproduct has been observed on triplet sensitization.[25,26,38,39] Although the existence of intersystem crossing (ISC) is assumed to be an integral part of these mechanisms for the triplet-sensitized reactions, Schaffner and coworkers[40] admit that it is known neither by which mechanism the T_1 and T_2 species return to S_0 nor whether energy transfer or chemical scavenging (or both) are involved in the quenching of these excited states. Pertaining to mechanism based on theoretical calculations, the literature is very limited.[41–44] Robb and coworkers explored the excited state reaction pathways and decay mechanisms for the simplest model β,γ-enone, but-3-enal using quantum chemical computations at multiconfiguration self-consistent field (MC-SCF).[41] The authors have proposed that the ODPM reaction path involves

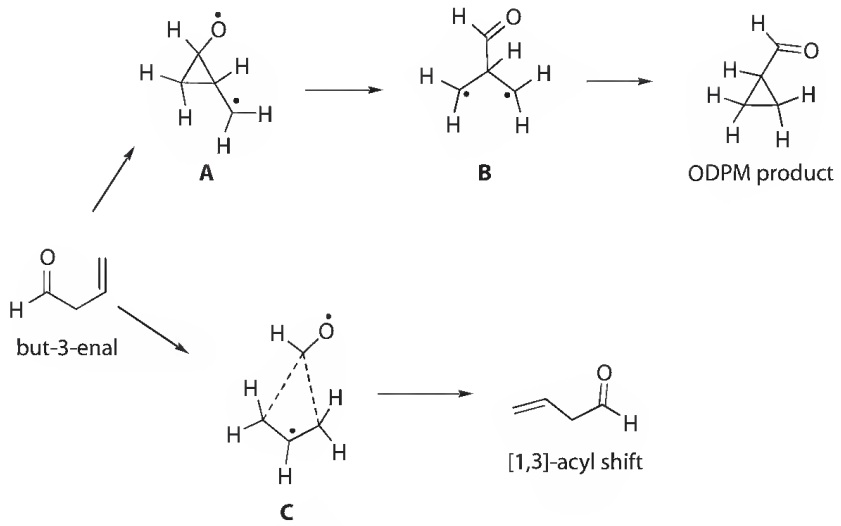

FIGURE 22.1 Biradical and concerted mechanism proposed based on MCSCF computations.

two biradical intermediates **A** and **B**, with **A** being the primary photoproduct and **B** being a short-lived 1,3-biradical that rapidly produces the final three-membered ring product (Figure 22.1). This occurs as intermediates in a three-step process. The reaction profile shows that the accessibility of the decay region for the ODPM reaction is controlled by an excited state barrier. The $^3(\pi\pi^*)$ surface is the lowest energy excited state surface at all geometries before the conical intersection region, and it is usually assumed that the majority of ODPM product is formed from this surface on triplet sensitization. In the model system studied by authors, the barrier to $^1(n\pi^*)$ fragmentation is about 2 kcal/mol lower than the $^1(n\pi^*)$ ODPM reaction barrier, such that the dissociation–recombination reaction can compete effectively with the ODPM reaction. However, this competition will be sensitive to perturbations introduced by substituent effects.[41]

The authors have concluded that the $^3(\pi\pi^*)$ ODPM rearrangement and the $^3(\pi\pi^*)$ [1,3]-acyl shift reaction both correspond to mechanisms involving ISC at a crossing region (**A** and **C**, respectively), although the difference in barrier heights is only 2 kcal/mol in favor of the ODPM reaction (Figure 22.1). Further, the transition state leading to dissociation on the $^1(n\pi^*)$ surface lies 2 kcal/mol below the transition state for the ODPM path. This is consistent with the fact that on direct photolysis acyclic enones give exclusively the [1,3]-acyl shift product via dissociation and recombination. However, in other cases both steric and dynamic effects could change the order of these barriers such that both the ODPM reaction and the stereospecific [1,3]-acyl shift reaction could also occur on direct photolysis.[41]

Robb and coworkers have proposed that the mechanism of triplet reactions is a stepwise process with the formation of the biradicaloid intermediate **A** where the stereochemistry of the reactant can be lost, but this decay can be quite efficient.[41] On the other hand, singlet ODPM reaction will be essentially concerted since decay via the S_1/S_0 conical intersection will occur within one vibrational period and leads to the S_0 intermediate, which will immediately rearrange. The lack of selectivity of direct versus sensitized irradiation, the sensitivity of the reaction outcome to substituents, and the degree of stereospecificity are therefore related to the character of these decay regions.[41]

22.5 Mechanistic Details

There are at least three types of mechanisms discussed in order to explain the ODPM rearrangement. The first mechanism (Scheme 22.8) is radicaloid in nature: involves a Norrish type I cleavage leading to the formation of acyl and allyl radical and recombination of these radicaloid species to the ODPM rearrangement product in two ways.

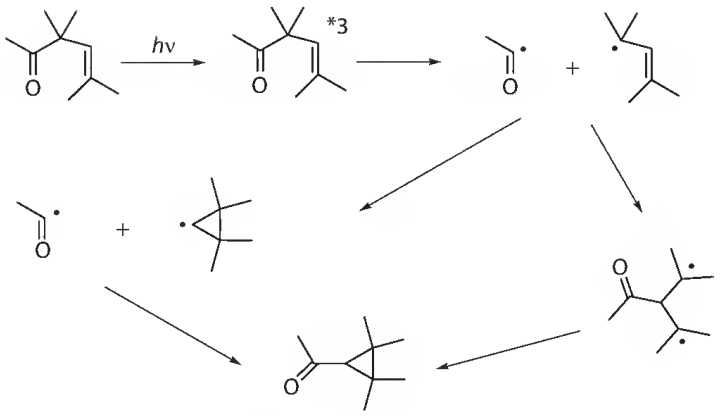

SCHEME 22.8 Radicaloid mechanism for ODPM rearrangement.

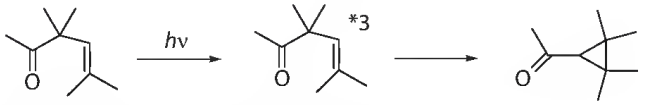

SCHEME 22.9 Concerted mechanism for ODPM rearrangement.

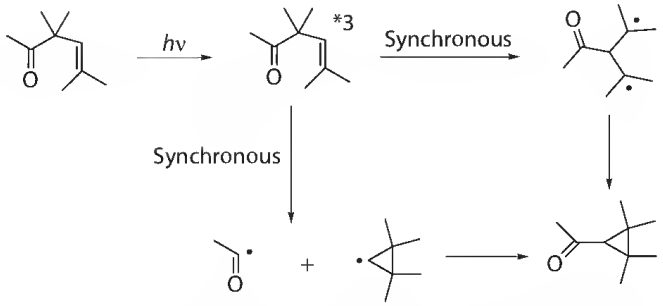

SCHEME 22.10 Radicaloid and concerted mixed mechanism for ODPM rearrangement.

The second mechanism is a concerted (Scheme 22.9) rearrangement involving symmetry-allowed processes. The third mechanism (Scheme 22.10) is a mixed mechanism involving one concerted process leading to radicals and followed by radical combination to give ODPM rearrangement products. These different mechanistic routes were applied in order to explain selectivity phenomena within the ODPM rearrangement. Interestingly, Armesto[16] and his group introduced photochemical electron transfer type mechanism involving radical-ion intermediates in DPM and aza-di-π-methane (ADPM) rearrangement reactions. Many reports suggest that radicaloid intermediates are very much involved in these ODPM rearrangement reactions.[45–47] A concerted mechanism is proposed to explain the results of high degree of specificity observed in a set of bicyclic substrate compounds shown in Scheme 22.11. Support for the mixed mechanism came from the example shown in Scheme 22.12. These mechanisms are still a matter of debate and create enough curiosity to continue creative and innovative research in order to understand the ODPM rearrangement. Interesting questions are, why β,γ-unsaturated ketone upon excitation largely prefers ODPM rearrangement pathway, even though several other pathways are available that in general dominate the photochemistry of ketones? Also how the excitation energy is localized within the molecule and utilized to cleave (mode selective) a particular chemical bond? One study[48] reported that ODPM rearrangement is also possible from the singlet excited state, but this is a matter of debate.

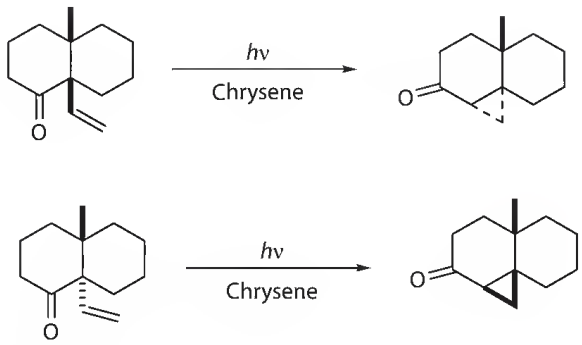

SCHEME 22.11 ODPM rearrangement with high degree of specificity.

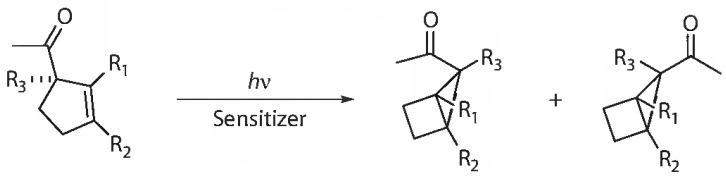

SCHEME 22.12 Example for mixed mechanism of ODPM rearrangement.

22.6 Selectivity, Scope, and Limitations

Liao and coworkers[49] prepared bicyclo[2,2,2]octene derivatives (Scheme 22.13) with an aim to understand the intramolecular competition between ODPM, ADPM, and DPM rearrangements. Some of these substrates prepared by Liao displayed remarkable chemoselectivity toward ODPM rearrangement (Scheme 22.14), whereas only a few examples exist with high chemoselective ODPM rearrangement.[50,51] The ODPM rearrangement reaction in these substrates is found to be dependent on the energy of triplet sensitizer, and acetophenone is found to be very effective. The observed selectivity is attributed to the stability of diradicals involved in ODPM rearrangement reaction.

The oximes **2a–2d** and exocyclicmethylene compounds **3a–3d** (Scheme 22.13) did not display ODPM rearrangement activity under triplet sensitization conditions and this may be due to free rotor effect leading to *E/Z* isomerization. The diastereo- and enantioselectivities in ODPM rearrangement reactions are reported by Ramamurthy and coworkers[34,52–54] by confining the substrates in zeolite environment and also attaching chiral molecules to substrates. The preference of reactivity results from orientation of substrate and the proximity of the chiral attachment within the tight cage or rigid host molecule. Scheme 22.15 illustrates a few examples. The enhancement in the ODPM reaction is noticed when the substrates are confined to zeolites and also sensitized by triplet sensitizers (Scheme 22.16). Triplet sensitization is found to be very efficient within the zeolitic cages and this happens to improve the rearrangement product compared to solution-phase photolysis.[34]

In another study, the ODPM rearrangement product found to exhibit polymorphism as determined by the x-ray diffraction data[55] (Scheme 22.17).

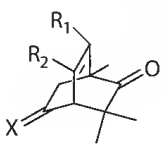

1a = X = O; R_1 = COOEt; R_2 = H
1b = X = O; R_1 = COOMe; R_2 = COOMe
1c = X = O; R_1 = Ph; R_2 = H
1d = X = O; R_1 = Ph; R_2 = Ph

2a = X = NOH; R_1 = COOEt; R_2 = H
2b = X = NOH; R_1 = COOMe; R_2 = COOMe
2c = X = NOH; R_1 = Ph; R_2 = H
2d = X = NOH; R_1 = Ph; R_2 = Ph

3a = X = CH_2; R_1 = COOEt; R_2 = H
3b = X = CH_2; R_1 = COOMe; R_2 = COOMe
3c = X = CH_2; R_1 = Ph; R_2 = H
3d = X = CH_2; R_1 = Ph; R_2 = Ph

SCHEME 22.13 Chemoselectivity in ODPM rearrangement.

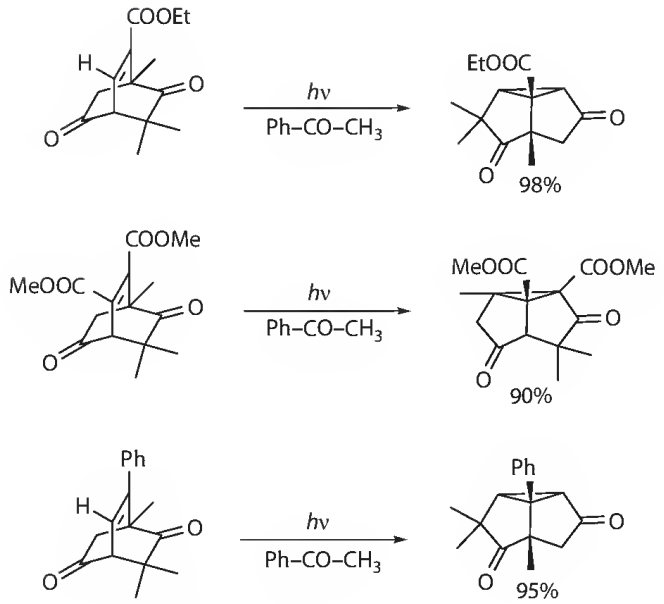

SCHEME 22.14 Regioselectivity in ODPM rearrangement.

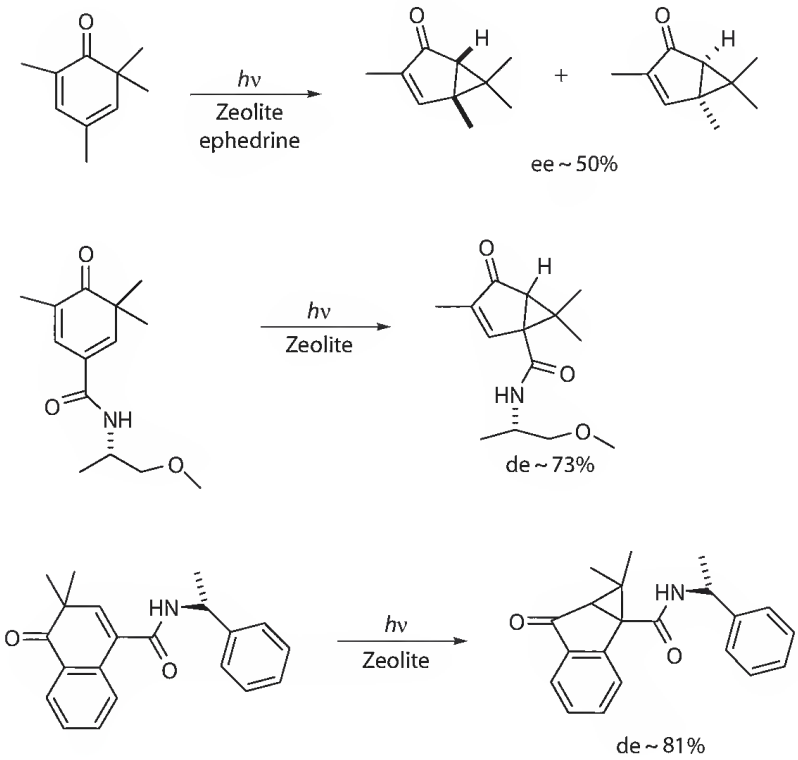

SCHEME 22.15 Enantio- and diastereoselectivity in ODPM rearrangement.

Schaffner et al.[56–58] studied the photochemistry of cyclic β,γ-unsaturated aldehydes (Scheme 22.18) and found that they underwent mainly decarbonylation reaction, although they can display ODPM rearrangement.

Another study by Dürr et al.[59] indicated that β,γ-unsaturated aldehydes (Scheme 22.19) exhibited decarbonylation and electrocyclization reactions and not ODPM rearrangement. Nevertheless, Schafner et al.[60] reported the first ODPM rearrangement reaction in β,γ-unsaturated (steroid-type) aldehyde (Scheme 22.20), along with decarbonylation and 1,3-acyl migration products.

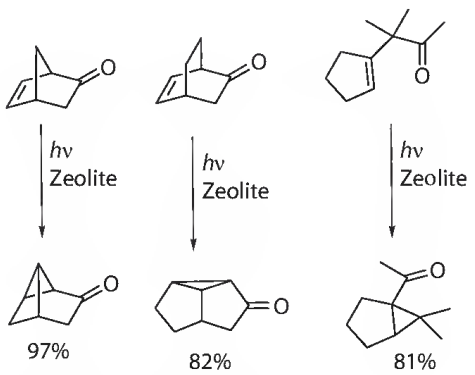

SCHEME 22.16 ODPM rearrangement in a caged environment.

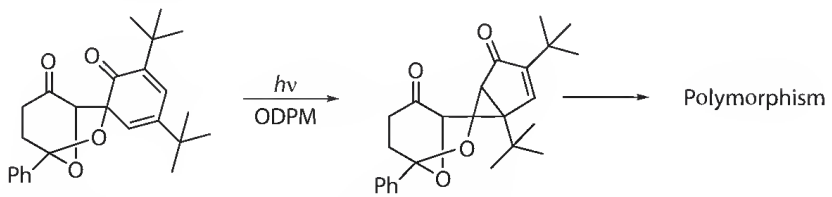

SCHEME 22.17 Polymorphism in ODPM rearrangement product.

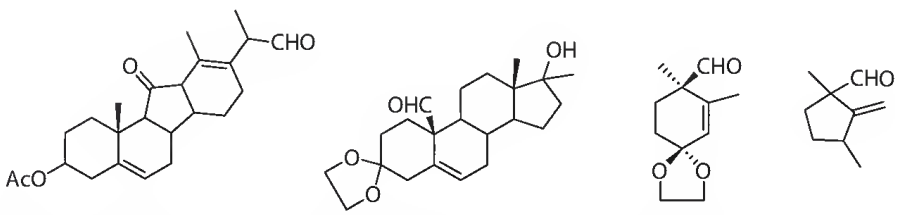

SCHEME 22.18 Compounds active in decarbonylation over ODPM rearrangement.

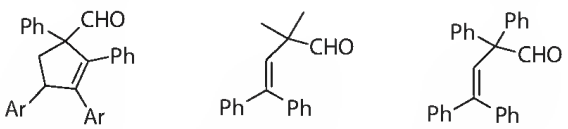

SCHEME 22.19 Compounds active in decarbonylation and electrocyclization over ODPM rearrangement.

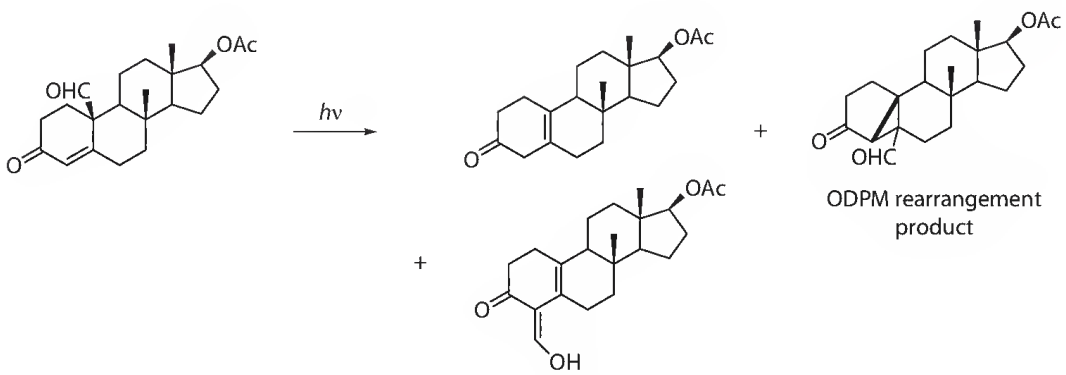

SCHEME 22.20 First example of ODPM rearrangement in β,γ-unsaturated aldehydes.

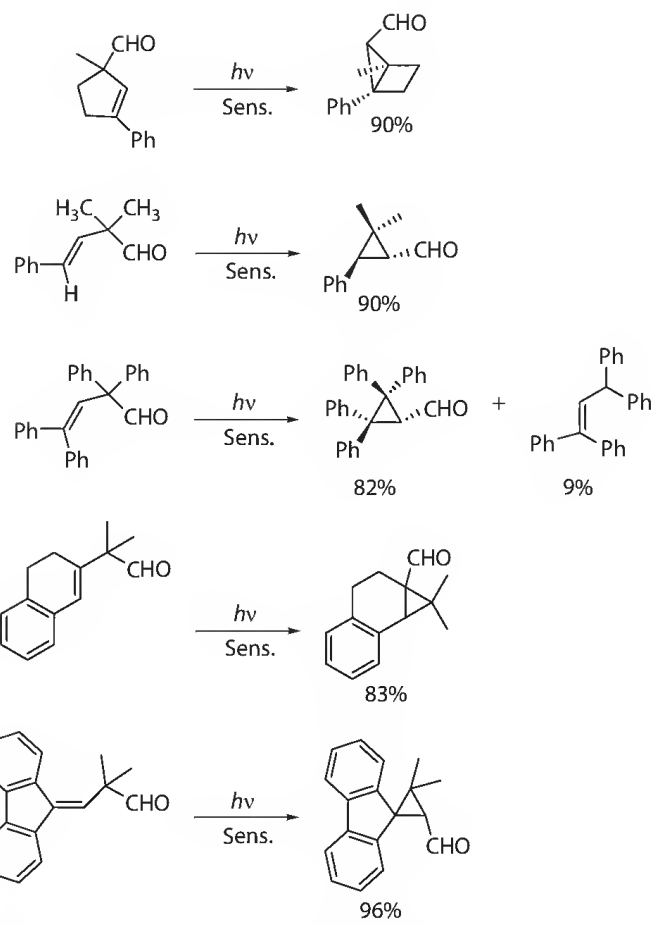

SCHEME 22.21 Selected examples of ODPM rearrangement in β,γ-unsaturated aldehydes.

Later, Zimmerman also reported triplet reactivity of β,γ-unsaturated aldehyde showing ODPM rearrangement.[61] Many people considered that these β,γ-unsaturated aldehydes are not good substrates for ODPM rearrangement, because of other competing photoreactions. Then Armesto group carried out many photochemical studies on β,γ-unsaturated aldehydes to prove that suitably designed and/or selected β,γ-unsaturated aldehydes can undergo efficient ODPM rearrangement with good selectivity and high efficiency. Some of the examples given in Scheme 22.21 indicate the efforts by Armesto group.[62]

These results from Armesto group changed the earlier notion and proved that β,γ-unsaturated aldehydes can readily undergo ODPM rearrangement. The rationale given for the observed ODPM rearrangement activity in β,γ-unsaturated aldehydes is the selective population of triplet $\pi\pi^*$ state. The singlet and triplet $n\pi^*$ excited states may be responsible for decarbonylation reactions. The reactive state ordering and relative energy levels of singlet and triplet of $n\pi^*$ and singlet and triplet of $\pi\pi^*$ excited states in a given molecule may be directing the photoreactivity.

Cyclopentylmethyl ketones undergo ODPM rearrangement and as well as 1,3-acyl shift (Scheme 22.22) in solution phase.[27,63,64] Gas phase photolysis of these cyclopentylmethyl ketones also produced products corresponding to ODPM rearrangement and 1,3-acyl shift. These studies indicate that there is a scope for conducting ODPM rearrangement in gas phase also to follow the mechanistic aspects.

van der Anton and Cerfontain[65] utilized several acyclic β,γ-unsaturated ketones to study ODPM rearrangement (Scheme 22.23). All these acyclic analogues primarily displayed *E/Z* (*cis-trans*) isomerization upon direct excitation or triplet sensitization. But, there were products related with ODPM rearrangement in small quantities. Further studies by Koppes and Cerfontain[66] on several β,γ-unsaturated ketones (Scheme 22.24) revealed interesting information. Cerfontain and coworkers[65,66] studies revealed

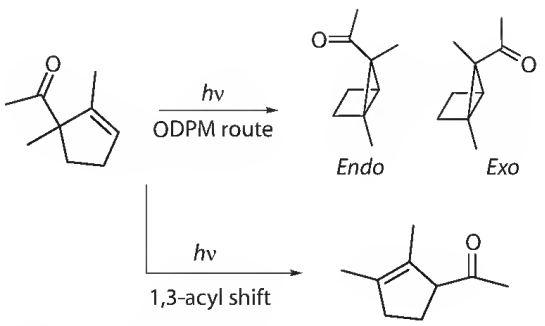

SCHEME 22.22 ODPM rearrangement in gas phase.

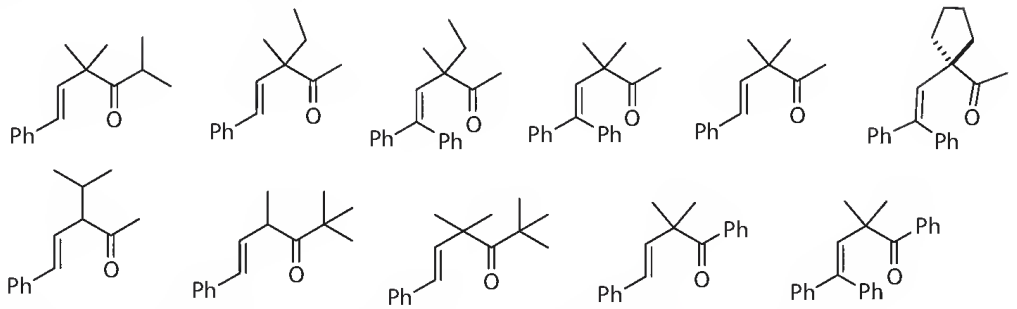

SCHEME 22.23 β,γ-Unsaturated ketones that do not exhibit ODPM rearrangement.

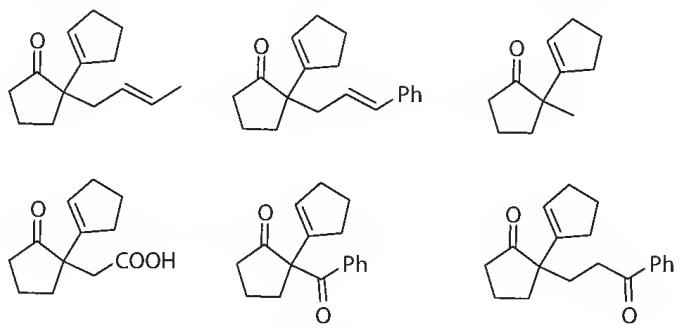

SCHEME 22.24 Extra groups that reduce the ODPM activity.

that selective sensitization opened the way for ODPM rearrangement products, but direct photolysis provided mainly *E/Z* (*cis–trans*) isomerization with inefficient 1,3-acyl shift product. The substrates (Schemes 22.23 and 22.24) having γ,δ-double bond and also benzoyl group did not exert any influence on the photoreactivity. They have introduced a new hypothesis that charge-transfer interaction within the molecule enhances the internal conversion and this phenomenon reduces the ODPM activity.

Liao and coworkers[67] prepared various bicyclo[2.2.2]octadieneones to study their photochemical properties (Scheme 22.25) and these compounds are well-suited substrates for DPM and ODPM rearrangements. Direct excitation of **1**a–e (Scheme 22.25) in benzene, methanol, and acetonitrile gave only benzene derivative with extrusion of dimethylketene (Scheme 22.25). Interestingly, **1**f upon direct excitation provided benzene derivative (extrusion of dimethylketene) as a major product together with small amounts of rearranged products—tricyclic compounds (Scheme 22.25).

Compound **1**a upon acetone or acetophenone sensitization gave only benzene derivative as the main product (Scheme 22.25) and **1**b–c are unreactive. Compounds **1**d–f upon acetone sensitization gave small amounts of rearranged tricyclic products along with benzene derivative. Acetophenone was found to be an efficient sensitizer in producing higher amounts of rearranged tricyclic products (Scheme 22.25). The rearranged tricyclic products are the result of DPM rearrangement and there were no products related

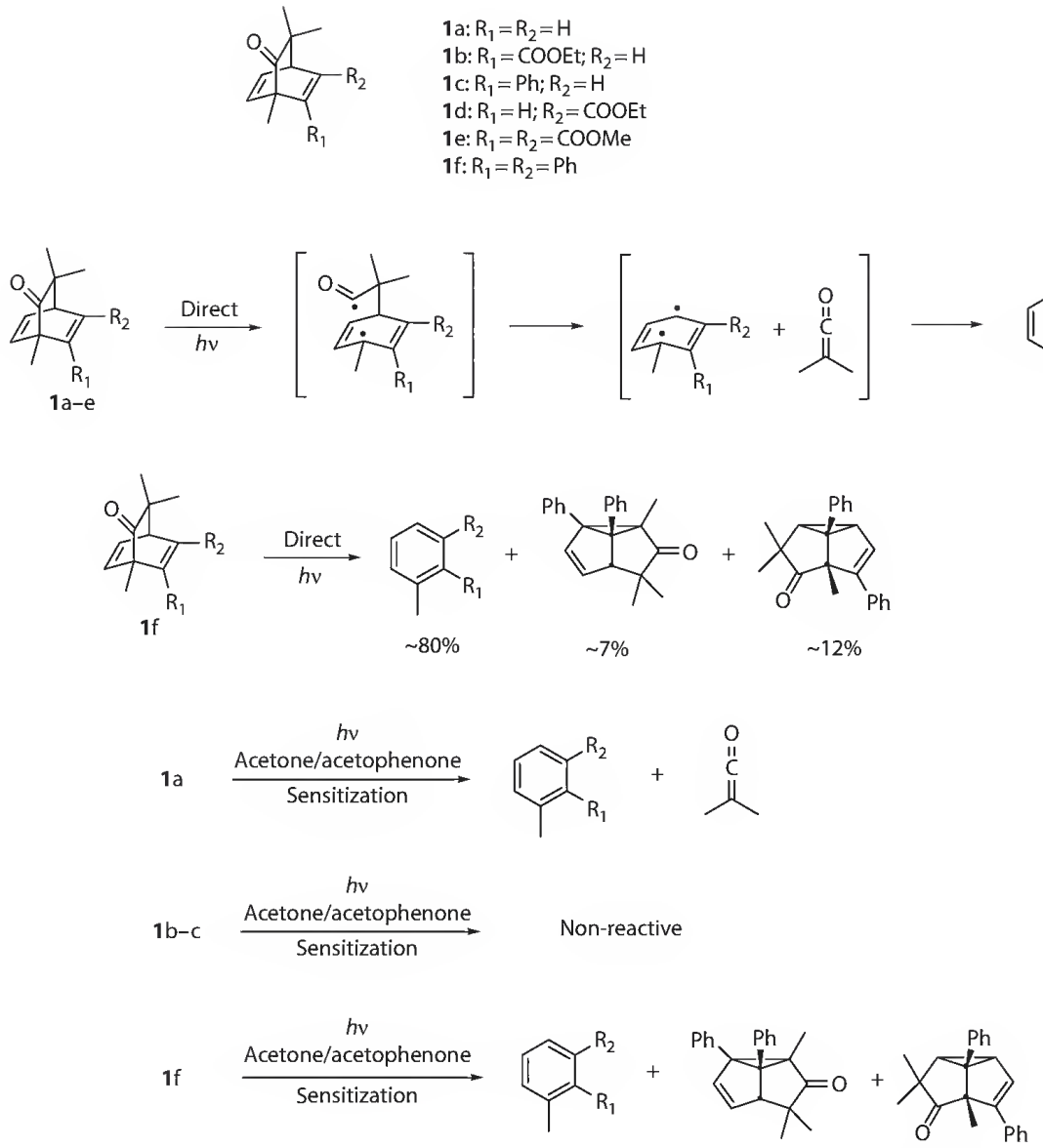

SCHEME 22.25 Photochemistry of bicyclo[2.2.2]octadienones by direct and sensitized excitation.

with ODPM rearrangement. The authors provided extensive mechanistic considerations for the photochemical transformations studied. DPM rearrangement products and regioselectivities observed were believed to be due to stabilized diradical intermediates. These studies clearly indicate that there is a large scope to understand in detail the mechanistic aspects explaining product formation with selectivity.

22.7 Synthetic Potential

Banwell and coworkers[68–70] reported the enantiomerically pure (–)-hirsutene (linear triquinanes) involving chemoenzymatic, Diels–Alder, and ODPM rearrangement reactions as key steps (Scheme 22.26) in their synthesis. The same key steps were utilized in the synthesis of (–)-compliatic acid and (+)-hirsutic acid.

Liao and coworkers[71] reported the synthesis of (±)-magellanine (Scheme 22.27) using masked *o*-benzoquinone Diels–Alder protocol, via a triquinane intermediate involving ODPM rearrangement, intramolecular cyclization, selective oxidative cleavage, and double reductive amination as key steps.

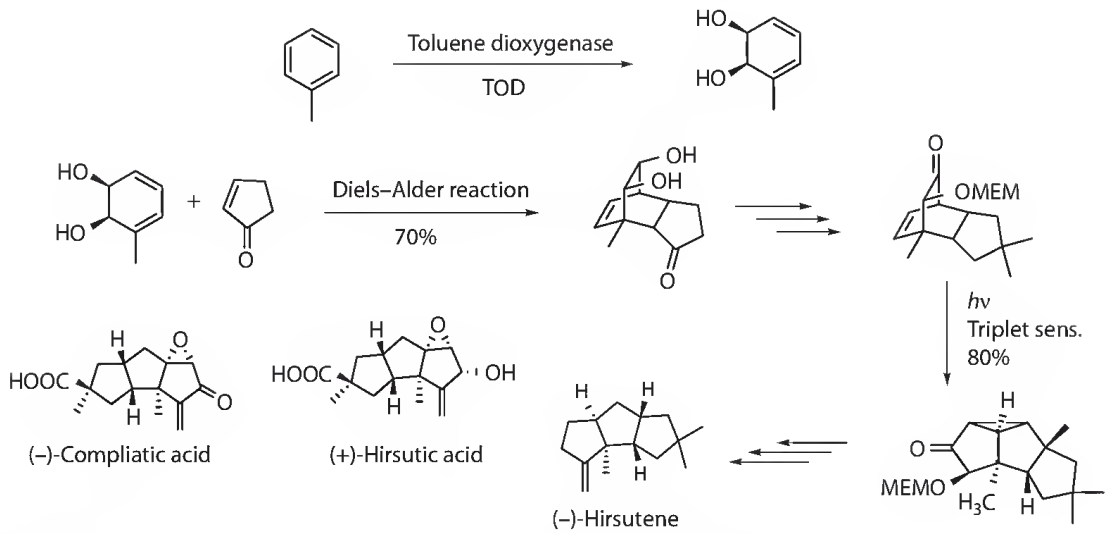

SCHEME 22.26 Enantiomeric synthesis of (–)-hirsutene involving the ODPM route.

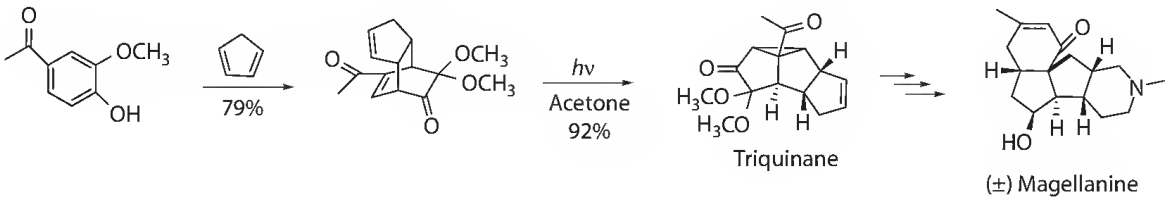

SCHEME 22.27 Synthesis of (±)-magellanine via ODPM rearrangement.

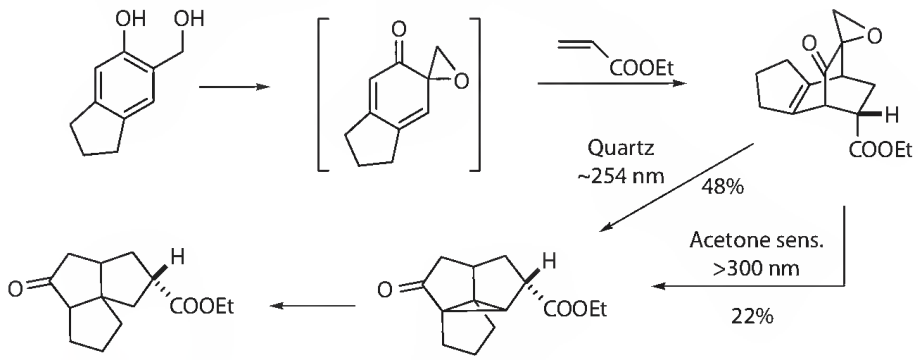

SCHEME 22.28 Synthesis of triquinane derivatives via ODPM protocol.

Bicyclo[2.2.2]octenones photochemistry served a lot in the synthesis of tricyclopentanoid compounds. Initially the ODPM rearrangement protocol was set by Demuth and Schafner[15] and later it was Singh[18] who conducted extensive studies. Diels–Alder reaction was utilized by Singh et al.[72] to make extensive compounds of bicyclo[2.2.2]octenones and subjected them to ODPM rearrangement to make several triquinanes. These cycloadducts synthesized selectively underwent acetone-sensitized ODPM rearrangement, but did not undergo [2+2] cycloaddition reaction and not even 1,3-acyl migration sometimes. The bicyclo[2.2.2]octenone prepared from indanol derivative (Scheme 22.28) was photolyzed, under quartz envelope (254 nm) and also under acetone-sensitized conditions to get angular triquinane derivative.[73] Singh and coworkers have reported synthesis of bicyclo octenone and used them for ODPM rearrangement to complete the synthesis of several moieties and the same is described in the following.

(±)-Hirsutene was synthesized from a very simple starting material—salicyl alcohol via ODPM rearrangement. Salicyl alcohol was converted in to a tricyclic intermediate possessing β,γ-unsaturated ketone

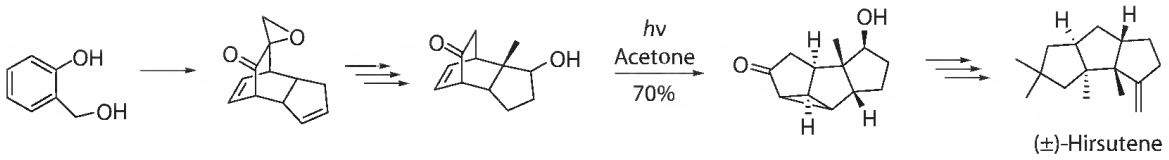

SCHEME 22.29 Synthesis of (±)-hirsutene through ODPM rearrangement.

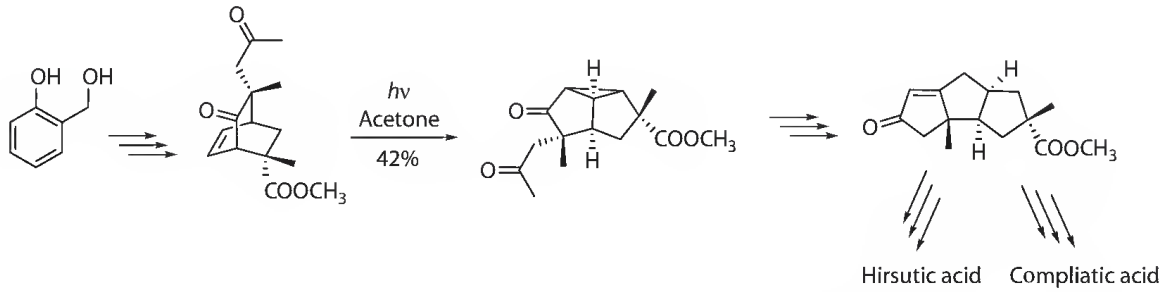

SCHEME 22.30 Synthesis of hirsutic acid and compliatic acid via ODPM route.

system (Scheme 22.29). Then it was photolyzed in acetone solvent to get tricyclopentanoid skeleton, which was readily converted into hirsutene.

Bicyclo[2.2.2]octenone derivatives have been synthesized and utilized in making (±)-hirsutic acid and compliatic acid via ODPM rearrangement (Scheme 22.30).[74,75]

Scheme 22.31 explains the synthesis of tetraquinanes using indanol and also hydroxyl methyl tetrahydro naphthol as starting materials involving ODPM rearrangement reaction.[76]

Liao and coworkers[77] developed a method to make bicycloctenone suitable for undergoing ODPM rearrangement and further leading to the natural product synthesis. They have used masked *o*-benzoquinone cycloaddition protocol to generate precursors to ODPM rearrangement (Scheme 22.32). These intermediates have a lot of potential in leading to several interesting molecules of interest.

Armesto group reported ODPM rearrangement in β,γ-unsaturated aldehydes (Scheme 22.33)[62] where the products became significant as a possible intermediates leading to the synthesis of chrysanthemic acid (a pyrethroid) and its derivatives.

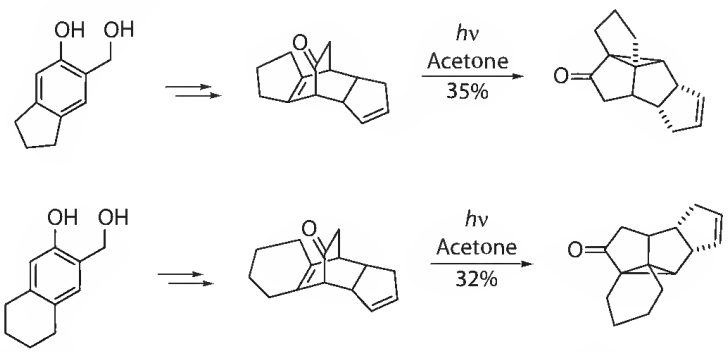

SCHEME 22.31 Synthesis of tetraquinane derivatives via ODPM rearrangement.

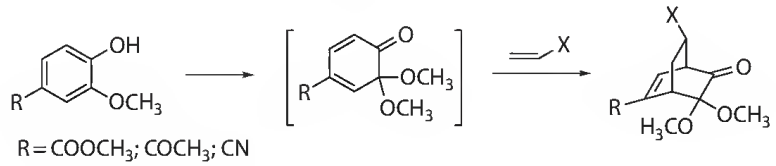

SCHEME 22.32 Synthesis of precursors to ODPM rearrangement.

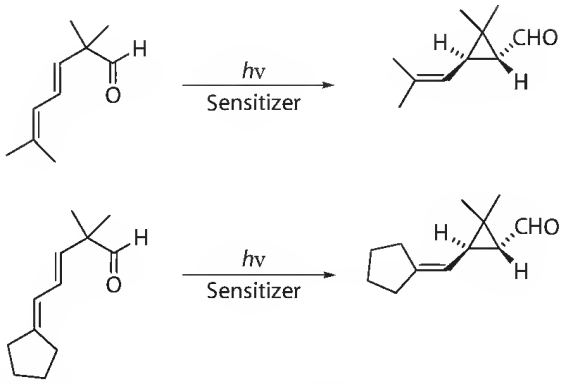

SCHEME 22.33 Synthesis of pyrethroid derivatives via ODPM route.

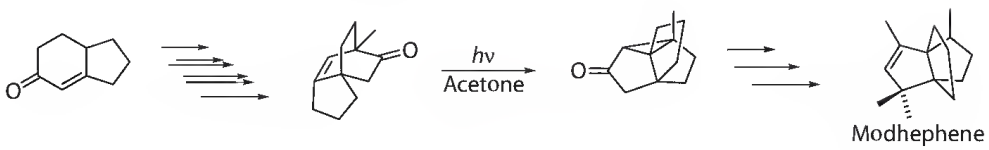

SCHEME 22.34 Synthesis of modhephene via ODPM rearrangement.

The propellane-type terpene *modhephene* is another example of a complex natural product. The synthesis of modhephene involves first making of bicyclic-octenone derivative and followed by ODPM rearrangement. The resulting ODPM product served as key intermediate and was successfully converted to modhephene (Scheme 22.34).[78,79]

Uyehara et al.[80] provided angularly annulated triquinanes by adopting ODPM route (Scheme 22.35). Indeed bicyclo[2.2.2]octenone derivative served as a precursor to ODPM rearrangement. Formation of third cyclopentane ring, after ODPM rearrangement, is an interesting aspect of the synthesis of angular triquinane.

A [4+2] cycloaddition, involving cyclohexadieneone, methodology developed to make precursors to ODPM rearrangement[81] and these precursors yielded tetracyclic products (Scheme 22.36). Other strained, ring enlarged, and benzannulated analogues were also introduced by this procedure (Scheme 22.36). The yields of ODPM route are found to be very good in these conversions.

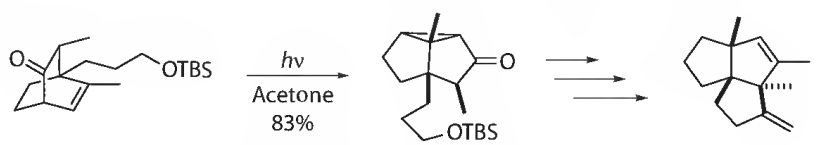

SCHEME 22.35 Synthesis of angular triquinane derivative via ODPM rearrangement.

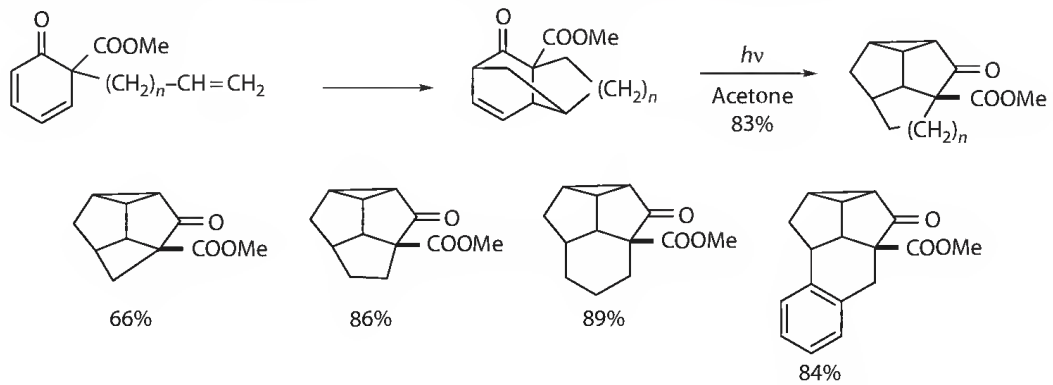

SCHEME 22.36 Synthesis of tetracyclic and benzannulated analogues via ODPM protocol.

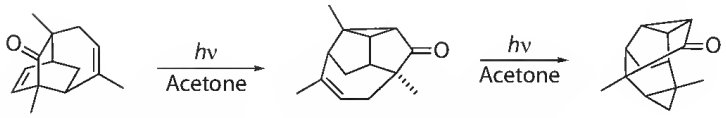

SCHEME 22.37 Synthesis of bridged diquinanes through ODPM route.

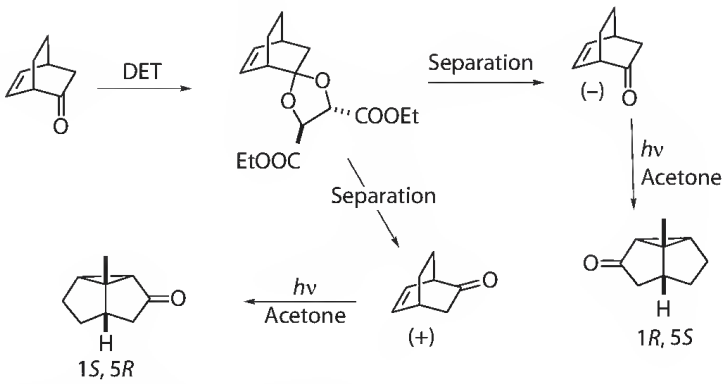

SCHEME 22.38 ODPM rearrangement in enantiomers.

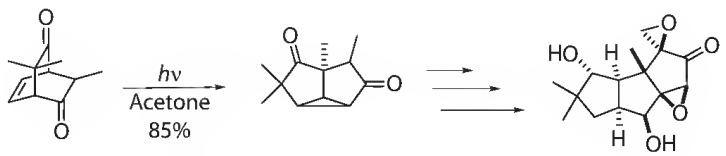

SCHEME 22.39 Synthesis of (–)-coriolin via ODPM rearrangement.

Another study, intramolecularly bridged bicyclo[2.2.2]octenone (the precursor to ODPM route), upon triplet sensitization leads to formation of bridged diquinanes[82] (Scheme 22.37). An interesting photochemical reaction was also informed from the ODPM rearrangement product (Scheme 22.37).

The ultimate challenge for an efficient synthetic pathway to complex chiral target molecules is the generation of enantiomerically pure products either by use of enantiomerically pure starting materials or by application of asymmetric induction using prochiral substrates. The bicyclo[2.2.2]octenone is available in an enantiomerically pure form by a simple resolution procedure[83] from the racemic mixture involving the acetal diastereoisomers formed with tartaric acid (Scheme 22.38). Irradiation of the separated parent compound enantiomers under triplet sensitization conditions leads to diquinane in high enantiomeric purity. Another approach to enantiomerically pure ODPM substrates is described for bicyclo[2.2.1]heptenone.[84]

This concept has been applied for the synthesis of the structurally complex and highly oxy-functionalized triquinane (–)-coriolin (Scheme 22.39).[50] Two carbonyl groups, both in the right position for 1,2-acyl shift, were present in the trimethyl functionalized bicyclo[2.2.2]octenone. The expected regioisomeric tricyclicdione was formed with high selectivity (Scheme 22.39). Subsequent chemical transformations provided the desired natural product coriolin.

22.8 Representative Experimental Procedures

22.8.1 Synthesis of Tricyclo[3.3.0.0.0]octane-3-One[83]

A solution of 10 g of the β,γ-unsaturated bicyclic ketone (Scheme 22.40) in 1000 mL of acetone was purged with argon and irradiated in a water-cooled quartz vessel placed in a Rayonet RPR-208 photochemical reactor equipped with RUL ~ 3000 lamps (λ ~ 300 nm). Irradiation was continued for 72 h and

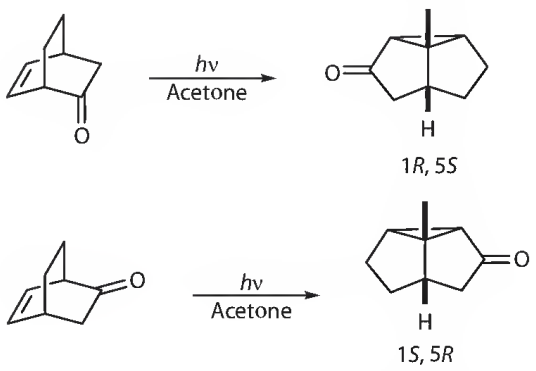

SCHEME 22.40 Synthesis of tricyclo[3.3.0.0.0]octane-3-one through ODPM route.

the reaction was monitored by TLC. After 72 h of irradiation, the conversion was ~98% and the only detectable compound was the ODPM rearrangement product, tricyclo[3.3.0.0]octane-3-one (Scheme 22.40). The solvent was distilled off and the residue was chromatographed over silica gel using a benzene/ether solvent mixture. The product, which was eluted (8.6 g), was further distilled under vacuum (50°C/1 mm) to get the pure ODPM rearrangement product (tricyclic ketone) in 81% yield with 99.5% purity. The quantum efficiency determined was found to be $\phi = 1.0$.

22.8.2 Synthesis of 4,4,9,9-Tetramethyltetracyclo[6.4.0.0.0] dodecane-7,12-Dione[85]

A solution of 1.25 g of 8,8,9,9-tetramethyl-1,3,4,6,7,8-hexahydro-1,4-ethanonaphthalene-2,5-dione (a δ-oxo-β,γ-unsaturated ketone; Scheme 22.41) in 300 mL cyclohexane was degassed by bubbling nitrogen through the solution and was irradiated for 3 h in Rayonet photochemical reactor ($\lambda \sim 300$ nm). The reaction was monitored by TLC and only one product was detectable. Evaporation of the solvent and recrystallization of the crude photolysate afforded the ODPM rearrangement product in 78% yield. The quantum yield of the reaction was determined as $\phi = 0.67$. Solvents like acetonitrile, benzene, or acetone and sensitizers like acetone or xanthone, respectively, can be employed for this reaction without altering the yield of the ODPM rearrangement product.

22.8.3 Synthesis Fluorenylcyclopropane Derivative[62]

A solution of 3-(9*H*-fluoren-9-ylidene)-2,2-dimethylpropanal (400 mg, 1.6 mmol) and *m*-methoxyacetophenone (10 g, 66 mmol) in dry dichloromethane (420 mL) was purged for 1 h with argon and irradiated for 2 h with a Pyrex filter and a 400 W medium-pressure Hg arc lamp. After completion of the irradiation, the solvent was removed under reduced pressure, and the products were separated by flash chromatography using hexane/Et_2O (9:1) as eluent on silica gel gave 385 mg (96%) of cyclopropyl aldehyde as colorless oil (Scheme 22.42).

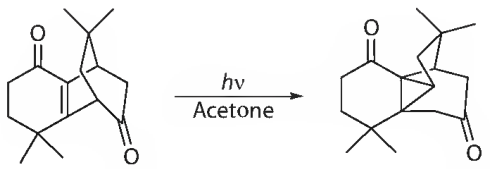

SCHEME 22.41 Synthesis of 4,4,9,9-tetramethyl tetracyclo [6.4.0.0.0] dodecane-7,12-dione via ODPM route.

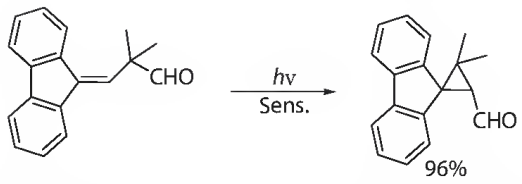

SCHEME 22.42 Synthesis of cyclopropenyl fluorenyl derivative through ODPM route.

22.9 Target Molecules for ODPM Rearrangement Studies

There are several molecules mentioned as target molecules for the possible study of ODPM rearrangement. The future will definitely have many applications toward the ODPM activity. The small molecules will be more interesting to study, because of the recent findings on the nature and energy of the triplet sensitizer–dependent ODPM activity.

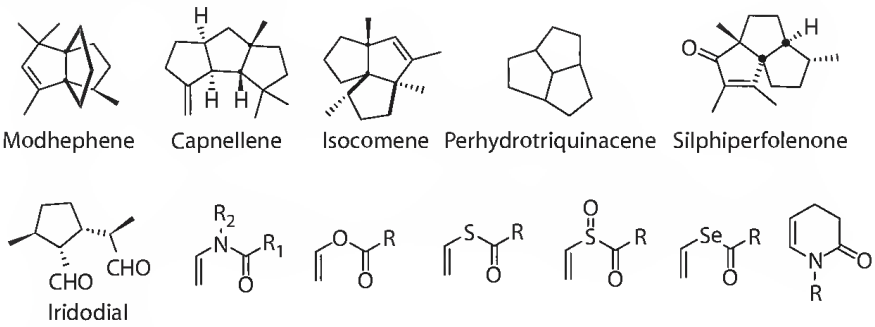

Acknowledgments

V. Jayathirtha Rao thanks DST, New Delhi, for financial support and Director, IICT, for encouragement. K. Srinivas thanks Project Director, NIPER-Hyderabad, for encouragement. The authors thank Dr. K. Bhanuprakash, IICT, for fruitful discussions.

References

1. Tenny, P.L.; Boykins, D.; Lutz, R.E. Novel photocyclization of a highly phenylated β,γ-unsaturated ketone to a conjugated cyclopropyl ketone. An oxa-di-π-methane rearrangement. *J. Am. Chem. Soc.* 1966, 88, 1835–1836.
2. Swenton, J.S. Photochemistry of organic compounds. II, Carbonyl compounds. *J. Chem. Educ.* 1969, 46, 217.
3. Givens, R.S.; Oettle, F.W. Photorearrangement of γ-butyrolactone: Generation of intermediates in photochemical reactions. *J. Chem. Soc. Chem. Commun.* 1969, 1164–1165.
4. Dauben, W.G.; Kellog, M.S.; Seeman, J.I.; Spitzer, W.A. Photochemical rearrangement of an acyclic β, γ-unsaturated ketone to a conjugated cyclopropyl ketone. An oxa-di–π-methane rearrangement. *J. Am. Chem. Soc.* 1970, 92, 1786–1787.
5. Houk, K.N. The photochemistry and spectroscopy of β,γ-unsaturated carbonyl compounds. *Chem. Rev.* 1976, 76, 1–74.
6. Schuster, D.I. Photochemical rearrangements of enones. In: *Rearrangements in Ground and Excited States*, de Mayo P. Ed., Academic Press: New York, 1980, Vol. 3, pp. 167–279.
7. Hixson, S.S.; Mariano, P.S.; Zimmerman, H.E. The di-π-methane and oxa-di-π-methane rearrangements. *Chem. Rev.* 1973, 73, 531–551.
8. Zimmerman, H.E. The di-π-methane rearrangement. *Org. Photochem.* 1991, 11, 1–36.

9. Zimmerman, H.E.; Armesto, D. Synthetic aspects of the di-π-methane rearrangement. *Chem. Rev.* 1996, 96, 3065–3112.
10. Demuth, M. Synthesis of natural products based on photochemical key transformations. *Pure Appl. Chem.* 1986, 58, 1233–1238.
11. Demuth, M. The Oxa-di-π-methane rearrangement. In: *Organic Photochemistry*, Padwa, A., Ed., Marcel Dekker: New York, 1991, Vol. 11, pp. 37–109.
12. Demuth, M. Oxa-di-π-methane photoisomerizations. In: *Comprehensive Organic Synthesis*, Trost B.M.; Fleming I.; Paquette L.A. Eds., Pergamon Press: Oxford, U.K., 1991, Vol. 5, pp. 215–237.
13. Mehta, G.; Srikrishna, A. Synthesis of polyquinane natural products: An update. *Chem. Rev.* 1997, 97, 671–720.
14. Singh, V.; Thomas, B. Recent developments in general methodologies for the synthesis of linear triquinanes. *Tetrahedron* 1998, 54, 3647–3692.
15. Demuth, M.; Schaffner, K. Tricyclo[3.3.0.$0^{2,8}$]octan-3-ones: Photochemically prepared building blocks for enantiospecific total syntheses of cyclopentanoid natural products. *Angew. Chem. Int. Ed. Engl.* 1982, 21, 820–836.
16. Armesto, D.; Ortiz, M.J.; Agarrabeitia, A.R. Recent advances in di-π-methane process. Novel reactions of 1,4-unsaturated compounds by triplet sensitization and photoelectron transfer. *J. Photoscience* 2003, 10, 9–20.
17. Dauben, W.G.; Lodder, G.; Ipakstchi, J. Photochemistry of β,γ-unsaturated ketones. *Top. Curr. Chem.* 1975, 54, 73–114.
18. Singh, V. Spiroepoxycyclohexa-2,4-dieneones in organic synthesis. *Acc. Chem. Res.* 1999, 32, 324–333.
19. Singh, V. Photochemical rearrangements in β,γ-unsaturated enones: The oxa-di-π-methane rearrangement. In: *CRC Handbook of Photochemistry and Photobiology*, 2nd Edn. Horspool W.M.; Lenci F. Eds., CRC Press: Boca Raton, FL, 2004, pp. 78-1–78-34.
20. Armesto, D.; Ortiz, M.J.; Agarrabeitia, A.R. New results on the triplet reactivity of β,γ-unsaturated carbonyl compounds. In: *CRC Handbook of Photochemistry and Photobiology*, 2nd Edn. Horspool W.M.; Lenci F. Eds., CRC Press: Boca Raton, FL, 2004, pp. 77-1–77-11.
21. Schaffner, K.; Demuth, M. Photochemically generated building blocks. I. The tricyclooctanone approach to polyquinane syntheses. Part I: The underlying photochemistry. In: *Modern Synthetic Methods*, Scheffold, R., Ed., Springer Verlag, Berlin, Germany, 1986, Vol. 4, p. 61.
22. Rao, V.J.; Griesbeck, A.G. Oxa-di-π-methane rearrangements. In: *Synthetic Organic Photochemistry*. Griesbeck, A.G.; Mattay, J. Eds., Marcel Dekker: New York, 2005, pp. 189–210.
23. Hoffman, N. Photochemical reactions as key steps in organic synthesis. *Chem. Rev.* 2008, 108, 1052–1103.
24. Buchi, G.; Burgess, E.M. Photochemical reactions. IX. Isomerization of eucarvone. *J. Am. Chem. Soc.* 1960, 82, 4333–4337.
25. Engel, P.S.; Schexnayder, M.A.; Ziffer, H.; Seeman, J.I. Effect of α-methyl groups on the photochemistry of 3,4,5,6,7,8-hexahydronaphthalen-2(1H)-one. *J. Am. Chem. Soc.* 1974, 96, 924–925.
26. Engel, P.S.; Schexnayder, M.A. Systematic structural modifications in the photochemistry by β,γ.-unsaturated ketones. I. Cyclic olefins. *J. Am. Chem. Soc.* 1975, 97, 145–153.
27. Baggiolini, E.; Schaffner, K.; Jegger, O. Acetyl migrations in a photoexcited β,γ-unsaturated methyl ketone: 1,3-shift in the excited singlet state and 1,2-shift in the triplet state. *J. Chem. Soc. Chem. Commun.* 1969, 1103–1104.
28. Givens, R.S.; Chae, W.K. Photorearrangements of bicyclo[3.2.1]oct-2-en-7-ones. A substituent effect study. Mechanistic studies in photochemistry.19. *J. Am. Chem. Soc.* 1978, 100, 6278–6280.
29. Armesto, D.; Ortiz, M.J.; Agarrabeitia, A.R.; El-Boulifi, N. The effects of triplet sensitizers' energies on the photoreactivity of b,g-unsaturated methyl ketones. *Angew. Chem. Int. Ed. Engl.* 2005, 44, 7739–7741.
30. Schexnayder, M.; Engel, P.S. Systematic structural modifications in the photochemistry of β,γ-unsaturated ketones II. Acyclic olefins and acetylenes. *J. Am. Chem. Soc.* 1975, 97, 4825–4836.

31. (a) Hannock, K.G.; Grider, R.O. The photochemistry of 3-alkylidenecyclohexanones. The role of olefin geometrical isomerization in the triplet state reactivity of β, γ-unsaturated ketones. *J. Am. Chem. Soc.* 1974, 96, 1158–1168; (b) Hannock, K.G.; Grider, R.O. Photochemistry of 3-methylene-2,2,5,5-tetramethycyclohexanone. *Tetrahedron Lett.* 1971, 12, 4281–4284; (c) Hannock, K.G.; Grider, R.O. Free rotor effect in β, γ-unsaturated ketone photochemistry. The diverging singlet and triplet reaction of 3-ethylidene-2,2,5,5-tetramethylcyclohexanone. *Tetrahedron Lett.* 1972, 13, 1367–1370.
32. Schexnayder, M.; Engel, P.S. Triplet sensitization of 2-norbornenone and other β, γ-unsaturated ketones. *Tetrahedron Lett.* 1975, 16, 1153–1156.
33. McClure, C.K.; Keissling, A.J.; Link, J.S. Oxa-di-π-methane photochemical rearrangement of quinuclidinones. Synthesis of pyrrolizinones. *Org. Lett.* 2003, 5, 3811–3813.
34. Pitchumani, K.; Warrier, M.; Kaanumalle, L.S.; Ramamurthy, V. Triplet photochemistry within zeolites through heavy atom effect, sensitization and light atom effect. *Tetrahedron* 2003, 59, 5763–5772.
35. Schuster, D.I.; Axelrod, M.; Auerbach, J. The photochemical isomerization and fragmentation of dehydronorcamphor. *Tetrahedron Lett.* 1963, 4, 1911–1916.
36. Schuster, D.I.; Underwood, G.R.; Knudsen, T.P. Photochemistry of ketones in solution. XXX. Application of simple theoretical methods to the solution of chemical problems. V. Divergent behavior of singlet and triplet excited states of β,γ-unsaturated ketones. Explanation based on spin distribution. *J. Am. Chem. Soc.* 1971, 93, 4304–4306.
37. Houk, K.N.; Northington, D.J.; Duke, R.E. Molecular orbital model for the photochemistry of β,γ-unsaturated ketones. *J. Am. Chem. Soc.* 1972, 94, 6233–6235.
38. Schuster, D.I.; Sussman, D.H. The nature of the reactive excited states in the photochemical buchi rearrangement of bicyclo[3.2.0]hex-6-en-2-ones. *Tetrahedron Lett.* 1970, 11, 1661–1664.
39. Engel, P.S.; Schexnayder, M.A. Effect of ring size on the photochemical behaviour of β, γ-unsaturated ketones. *J. Am. Chem. Soc.* 1972, 94, 9252–9254.
40. Reimann, B.; Sadler, D.E.; Schaffner, K.J. Gas-phase photochemistry of a β,γ-unsaturated ketone. Concerted and radical mechanisms of the 1,3-acetyl shift in 1,2-dimethylcyclopent-2-enyl methyl ketone. *J. Am. Chem. Soc.* 1986, 108, 5527–5530.
41. Wilsey, S.; Bearpark, M.J.; Bernardi, F.; Olivucci, M.; Robb, M.A. Mechanism of the oxa-di-π-methane and [1,3]-acyl sigmatropic rearrangements of β,γ-enones: A theoretical study. *J. Am. Chem. Soc.* 1996, 118, 176–184.
42. Wilsey, S.; Houk, K.N. H/allyl and alkyl/allyl conical intersections: Ubiquitous control elements in photochemical sigmatropic shifts. *J. Am. Chem. Soc.* 2000, 122, 2651–2652.
43. Wilsey, S. A computational study of the factors controlling triplet-state reactivity in 1,4-pentadiene. *J. Org. Chem.* 2000, 65, 7878–7888.
44. Frutos, L.M.; Sancho, U.; Castano, O. Intramolecular triplet-triplet energy transfer in oxa- and aza-di-π-methane photosensitized systems. *J. Phys. Chem. A* 2005, 109, 2993–2995.
45. Domb, S.; Schaffner, K. Photochemical reactions. Part 58. On the mechanism of the rearrangement of the triplet-excited α,β-unsaturated δ-diketone 3,7-dioxo-4,4-dimethyl-17β-acetoxy-Δ^5-androstene. *Helv. Chim. Acta.* 1970, 53, 677–684.
46. Daubern, W.G.; Lodder, G.; Robbins, J.D. The 'methane carbon' stereochemistry of the acyclic oxa-di-π-methane photorearrangement. *J. Am. Chem. Soc.* 1976, 98, 3030–3031.
47. Dauben, W.G.; Lodder, G.; Robbins, J.D. The "methane carbon" stereochemistry of the acyclic oxa-di-π-methane photorearrangement. Evidence for a stepwise rearrangement mechanism. *Nouv. J. Chim.* 1977, 1, 243–254.
48. Eckersley, T.; Parker, S.D.; Rogers, N.A.J. Photochemistry of 1-methoxybicyclo [2.2.2]-oct-5-en-one: A singlet oxa-di-π-methane rearrangement. *Tetrahedron Lett.* 1976, 17, 4393–4394.
49. Yang, M.-S.; Lu, S.-S.; Rao, C.P.; Tsai, Y.-F.; Liao, C.-C. Photochemistry of bicyclo[2.2.2]oct-7-ene-2,5-diones and the corresponding 5-hydroxyimino and 5-methylene derivatives. *J. Org. Chem.* 2003, 68, 6543–6553.

50. Dermuth, M.; Ritterskamp, P.; Weigt, E.; Schaffner, K. Total synthesis of (-)-coriolin. *J. Am. Chem. Soc.* 1986, 108, 4149–4154.
51. Yates, P.; Burnell, D.J.; Freer, V.J.; Sawyer, J.F. Synthesis of cedranoid sesquiterpenes. III. Functionalization at carbon 4. *Can. J. Chem.* 1987, 65, 69–77.
52. Singarapu, J.; Natarajan, A.; Shailaja, K.J.; Upplili, S.; Joy, A.; Ramamurthy, V. Asymmetric photoreactions within zeolites: Role of confinement and alkali metal ions. *Acc. Chem. Res.* 2003, 36, 509–521.
53. Uppili, S.; Ramamurthy, V. Enhanced enantio- and diastereoselectivities via confinement: Photorearrangements of 2,4-cyclohexadienones included in zeolites. *Org. Lett.* 2002, 4, 87–90.
54. Sundaresan, A.K.; Kaanumalle, L.S.; Gibb, C.L.D.; Gibb, B.C.; Ramamurthy, V. Chiral photochemistry with in a confined space: Diastereoselective photorearrangements of a tropolone and cyclohexadieneone included in a synthetic cavitand. *Dalton Trans.* 2009, 4003–4011.
55. Kumar, V.S.S.; Sheela, K.C.; Nair, V.; Rath, N.P. Concomitant polymorphism in a spirobicyclic dienone. *Crystal Growth and Design* 2004, 4, 1245–1247.
56. Baggiolini, von E.; Berscheid, H.G.; Bozzato, G.; Cavalieri, E.; Schaffner, K.; Jeger, O. Die photofragmentierung von O-acetyljervin. *Helv. Chim. Acta*, 1971, 54, 429–449.
57. Hill, J.; Iriarte, J.; Schaffner, K.; Jeger, O. UV-bestrahlung von gesättigten und β,γ-ungesättigten, homoallylisch konjugierten steroidaldehyden. *Helv. Chim. Acta* 1966, 49, 292–311.
58. Baggiolini, E.; Hamlow, H.P.; Schaffner, K. Photochemical reactions. LIX. On the mechanism of the photodecarbonylation of β,γ-unsaturated aldehydes. *J. Am. Chem. Soc.* 1970, 92, 4906–4921.
59. Dürr, H.; Herbst, P.; Heitkämper, P.; Leismann, H. Photochemie β,γ-unsättigter aldehyde. Mechanismus der photofragmentierung phenylsubstituierter cyclopentanecarbaldehyde. *Chem. Ber.* 1974, 107, 1835–1855.
60. Pfenninger, E.; Poel, D.E.; Berse, C.; Wehrli, H.; Schaffner, K.; Jeger, O. Zur photochemie von α,β-ungesättigten γ-aldehydoketonen. I. Die UV.-bestrahlung von 3,19-dioxo-17β-acetoxy-Δ^4-andostren. *Helv. Chim. Acta* 1968, 51, 772–803.
61. Zimmeman, H.E.; Casel, J.M. Unusual rearrangements in di-π-methane systems: Mechanistic and exploratory organic photochemistry. *J. Org. Chem.* 1989, 54, 3800–3816.
62. Armesto, D.; Ortiz, M.J.; Romano, S.; Agarrabeitia, A.R.; Gallego, M.G.; Ramos, A. Unexpected oxa-di-π-methane rearrangement of β,γ-unsaturated aldehydes. *J. Org. Chem.* 1996, 61, 1459–1466.
63. Gonzenbach, H.-U.; Tegmo-Larsson, T.-M.; Grosclaude, J.-P.; Schaffner, K. The photochemistry of 2-cyclopentenyl methyl ketones. *Helv. Chim. Acta*. 1977, 60, 1091–1123.
64. Schaffner, K. 1-acyl-2-cyclopentenes and 5-acylbicyclo[2.1.0]pentanes: Photochemical and thermal isomerizations. *Tetrahedron* 1976, 32, 641–653.
65. van der Weerdt, A.J.A.; Cerfontain, H. Photochemistry of acyclic β,γ -unsaturated ketones. The effect of substituents at the α -C and the carbonyl group on the occurrence of oxa-di-π -methane rearrangement. *Rec. Trav. Chim. Pays-Bas* 1977, 96, 247–248.
66. Koppes, M.J.C.M.; Cerfontain, H. Photochemistry of β,γ -enones. 9. Mechanistic photochemical studies on the 1,3-acyl shift and oxa-di-π -methane rearrangement of two β,γ and γ,δdienones. *Rec. Trav. Chim. Pays-Bas* 1985, 104, 272–276.
67. Chang, S.-Y.; Huang, S.-L.; Villarante, N.R.; Liao, C.-C. Photochemical reactions of 1,3,3,-trimethylbicyclo[2.2.2]octa-5,7-dien-2-ones. *Eur. J. Org. Chem.* 2006, 4648–4657.
68. Banwell, M.G.; Austin, K.A.B.; Willis, A.C. Chemoenzymatic total synthesis of the linear triquinane-type natural products (+)-hirsutic acid and (−) complicatic acid from toluene. *Tetrahedron* 2007, 63, 6388–6403.
69. Banwell, M.G.; Edwards, A.J.; Harfoot, G.J.; Jolliffe, K.A. A chemoenzymatic synthesis of (−)-hirsutene from toluene. *J. Chem. Soc. Perkin Trans. I* 2002, 2439–2441.
70. Banwell, M.G.; Edwards, A.J.; Harfoot, G.J.; Jolliffe, K.A. A chemoenzymatic synthesis of the linear triquinane (−)-hirsutene and identification of possible precursors to the naturally occurring (+)-enantiomer. *Tetrahedron* 2004, 60, 535–547.

71. Yen, C.-F.; Liao, C.-C. Concise and efficient total synthesis of Lycopodium alkaloid magellanine. *Angew. Chem. Int. Ed. Engl.* 2002, 41, 4090–4093.
72. Singh, V.K.; Deota, P.T.; Bedekar, A.V. Studies in the synthesis of polycyclopentanoids: Synthesis, oxa-di-πmethane rearrangement of annulated bicyclo[2.2.2]octenones and cyclopropane ring cleavage of tetracyclo[6.3.0.0.0]undecanones. *J. Chem. Soc. Perkin Trans. 1* 1992, 903–912.
73. Singh, V.; Lahiri, S. $\pi^{4s} + \pi^{2s}$ cycloaddition between electron deficient π-systems and photoreaction of β,γ-enones: A novel stereoselective entry into angular triquinanes. *Tetrahedron Lett.* 2003, 44, 4239–4242.
74. Singh, V.; Vedantham, P.; Sahu, P.K. Reactive species from aromatics and oxa-di-π-methane rearrangement: A stereoselective synthesis of (±)-hirsutene from salicyl alcohol. *Tetrahedron* 2004, 60, 8161–8169.
75. Singh, V.; Tosh, D.K.; Mobin, S.M. Synthesis of embellished bicyclo[2.2.2]octenones and a sigmatropic 1,2-acyl shift in an excited state: A novel and stereoselective route to (±)-hirsutic acid C and complicatic acid. *Tetrahedron Lett.* 2004, 45, 1729–1732.
76. Singh, V.; Singh, R.B.; Mobin, S.M. Cycloaddition of annulated cyclohexa-2,4-dienones and novel reduction of halogen at bridgehead: An expedient route to tetracyclo[$6.5.2.0^{2,7}.0^{9,13}$]-pentadec-2(7),11-dien-14-one and framework of conindiogenol and conindiogenome. *Tetrahedron* 2009, 65, 7969–7974.
77. Chang, C.-P.; Chen, C.-H.; Chuang, G.J.; Liao, C.-C. Cyclopropane ring-opening of tricycle[3.3.30.02,8]octane-3-ones: A quick access to bicyclo[3.2.1]Octanones from 2-methoxyphenols. *Tetrahedron Lett.* 2009, 50, 3414–3417.
78. Mehta, G.; Subrahmanyam, D. A total synthesis of (±)-modhephene. *J. Chem. Soc. Chem. Commun.* 1985, 768–769.
79. Mehta, G.; Subrahmanyam, D. Photochemical oxa-di-π–methane rearrangement approach to [3.3.3]propellanes. Total synthesis of sesquiterpene hydrocarbon (±)-modhephene. *J. Chem. Soc. Perkin Trans. 1* 1991, 395–401.
80. Uyehara, T.; Murayama, T.; Sakai, K.; Onda, K.; Ueno, M.; Sato, T. Rearrangement approaches to cyclic skeletons. XIII. Total synthesis of triquinane sesquiterpenes, (±)-modhephene, and (±)-isocomene, on the basis of formal substitution at both bridgeheads of a bicyclo[2.2.2]oct-5-en-2-one. *Bull. Chem. Soc. Jpn.* 1998, 71, 231–242.
81. Schultz, A.G.; Lavieri, F.P.; Snead, T.E. 2,4-Cyclohexadien-1-ones in organic synthesis. Intramolecular Diels-Alder reactivity and the oxa-di-π-methane photorearrangement of Diels-Alder adducts. *J. Org. Chem.* 1985, 50, 3086–3091.
82. Hayakawa, K.; Schmid, H.; Frater, G. Photochemie von tricyclischen β,γ–γ,δ-ungesättigten Ketonen. 50. Mitteilung über photoreaktionen. *Helv. Chim. Acta.* 1977, 60, 561–567.
83. Oren, J.; Schleifer, L.; Shmueli, U.; Fuchs, B. Photochemistry of homoconjugated ketones: 2-(carbomethoxy)spiro[5.5]undeca-1, 3-dien-7-one. *Tetrahedron Lett.* 1984, 25, 981–984.
84. Corey, E.J.; Guzman-Perez, A.; Loh, T.P. Demonstration of the synthetic power of oxazaborolidine-catalyzed enantioselective Diels-Alder reactions by very efficient routes to cassiol and gibberellic acid. *J. Am. Chem. Soc.* 1994, 116, 3611–3612.
85. Kilger, R.; Korner, W.; Maragretha, P. Photochemistry of 8,8,9,9-tetramethyl-1,3,4,6,7,8-hexahydro-1,4-ethanonaphthalene-2,5-dione, a δ-oxo-β,γ-unsaturated ketone. *Helv. Chim. Acta.* 1984, 67, 1493–1495.

23

Photochemical Bergman Cyclization and Related Photoreactions of Enediynes

Igor V. Alabugin
Florida State University

Wang-Yong Yang
Florida State University

Runa Pal
Florida State University

23.1 Cycloaromatization Reactions: Introduction

Naturally occurring enediyne antibiotics[1] are often hailed as the most potent family of anticancer agents discovered to date.[2] These molecules were developed by microorganisms as the most powerful chemical warfare targeting cellular DNA with astounding efficiency. The key step in the chemical mechanism responsible for this activity is the transformation of the enediyne moiety to a reactive *p*-didehydrobenzene diradical (*p*-benzyne). This step, the simplest version of which is given in Scheme 23.1, is a cycloaromatization reaction called the Bergman cyclization.[3] The simultaneous formation of two radical centers is important because it results in the abstraction of two hydrogen atoms (one from each strand of a double-stranded (ds) DNA), which, after a sequence of reactions, ultimately leads to ds DNA cleavage.[4]

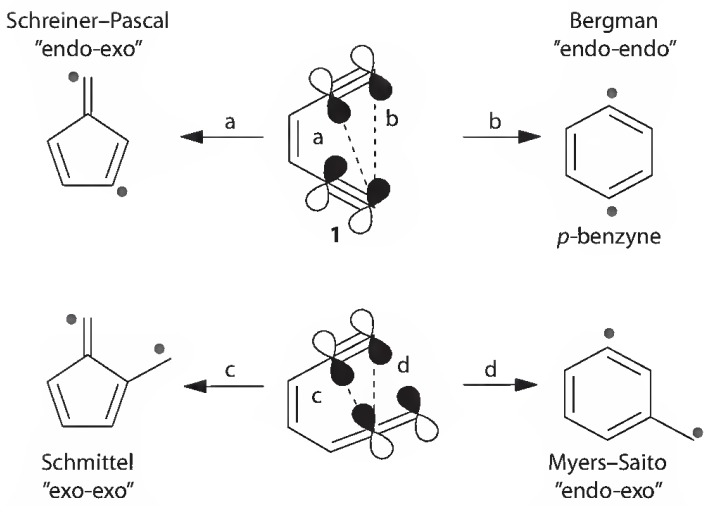

SCHEME 23.1 The four cyclizations of (*Z*)-hex-3-ene-1,5-diyne (a, b) and (*Z*)-hept-3,5,6-triene-1-yne (c, d). (From Alabugin, I.V. et al., *Adv. Phys. Org. Chem.*, 42, 1, 2007. With permission.)

While cycloaromatization reactions came to the forefront of active research after the discovery of the remarkable biological activity of natural enediynes, these processes present unique challenges from the fundamental perspective as well. A characteristic feature of cycloaromatization reactions is that one σ-bond is formed in the cyclization step at the expense of two in-plane π-bonds. When the two π-bonds are transformed into a σ-bond and a pair of radical centers, the process leads to a net loss of one chemical bond and, thus, should be strongly disfavored thermodynamically. However, the overall energy penalty for this seemingly unfavorable process is lower than that in the analogous cyclizations of alkenes.[5] For example, ΔH for the cycloaromatization process of the parent enediyne **1** into a *p*-benzyne diradical[3b] (the Bergman cyclization, Scheme 23.1) is only 8–9 kcal/mol.[6] Such a low value is explained by the stabilization of the product provided by the aromatic system created at the expense of the out-of-plane π-orbitals of the parent system. Developing aromatic stabilization in the conjugated out-of-plane system plays an important role in deepening the potential energy well for the diradical product to the extent where this species can be trapped by external reactions.

Scheme 23.1 summarizes the possible cyclizations involving the prototype enediyne (*Z*)-hex-3-ene-1,5-diyne (the Bergman and Schreiner–Pascal cyclizations) and the prototype eneyneallene (*Z*)-hept-3,5,6-triene-1-yne (the Schmittel and Myers–Saito cyclizations). In all of these processes, diradical species and new bonds are formed at the expense of the in-plane π-orbitals in the presence of an orthogonal π-system. However, the properties of the newly formed cyclic conjugated systems and the thermodynamic driving force for these reactions are quite different. In the ground state, an aromatic system is formed only in the Bergman and Myers–Saito cyclizations, and thus, in a sense, only these two processes are true cycloaromatization reactions. The Schreiner–Pascal[7] and Schmittel[8] cyclizations do not have the beneficial effect of the formation of an aromatic system. Consequently, these reactions are much more endothermic than the Bergman and the Myers–Saito cyclizations in the ground state. However, the situation can be changed by addition of electrons, as illustrated by the significantly more efficient reductive C1–C5 cyclizations of enediynes where, unlike the fulvene product of the thermal closure, the anionic product possesses some of the aromatic character of cyclopentadienyl anion.[9]

This chapter will be selective in coverage since a number of reviews are already available on various aspects of the enediyne chemistry and biochemical applications of cycloaromatization reactions. For example, Rawat and Zaleski[10] discussed geometric and electronic control of thermal Bergman cyclizations, while Basak and coworkers[11] described the use of enediynyl ligands in chelation-controlled Bergman cyclizations. König and coworkers[12] provided a review of electronic effects in the Bergman cyclization. Alabugin and Breiner dissected the relative importance of the two π-systems at different

stages of cycloaromatization processes.[13] Schreiner scrutinized computational approaches to studies of cycloaromatization reactions.[14] The early development of photochemical Bergman cyclization has been reviewed by Jones and Russell.[15] Basak and coworkers[16] compared different approaches to selective activation of enediyne prodrugs including photo- and pH-activation. These comprehensive reviews give us an opportunity to be selective in the choice of material and focus on the newer findings, while limiting ourselves to only those examples that illustrate the key trends in the cyclization efficiency.

23.2 Photochemical Reactions of Enediynes

23.2.1 Impetus for the Development of Photochemical Bergman Cyclizations

Despite their highly elaborate architecture and high activity, natural enediynes do not differentiate between healthy cells and cancer cells and, thus, are extremely toxic. Such lack of selectivity toward cancer cells is the greatest problem that prevents enediyne antibiotics from achieving their full potential as anticancer drugs. Numerous attempts to achieve higher spatial and temporal control over reactivity have produced a lot of research into the synthesis of analogues of the naturally occurring enediynes.[17,18] This includes attempts to tune the reactivity of designed enediynes through either strain[19–21] or electronic[22,23] effects, and most recently, to conjugate natural enediynes with monoclonal antibodies.[24] The challenge is that these compounds have to be relatively stable to allow handling at ambient temperatures but need to become activated at body temperature for attack upon DNA. Unless a special triggering event is used to convert a prodrug to its active form, there is only a narrow temperature/time window where reactivity and stability are balanced for thermally activated enediynes.

All of the aforementioned points explain why the ever-increasing efforts have concentrated on selective activation of enediynes by light.[25–32] The use of tissue-penetrating light allows for efficient spatial and temporal control over prodrug activation because light can be delivered directly at the tumor at the right time when it contains high concentration of the drug. This advantage is illustrated by the emergence of photodynamic therapy (PDT) as a powerful and convenient alternative to traditional cancer therapy methods.

23.2.2 Experimental Studies of Photochemical Bergman Cyclization

Although Bergman himself found that no photochemical cyclization is observed during irradiation of the parent enediyne,[3] a photochemical transformation that can be classified as a photo-Bergman reaction was reported as early as 1968 by Campbell and Eglinton (Scheme 23.2).[33] The substituted naphthalene structures of the products were assigned on the basis of mass-spectral analysis and their conversion to naphthalene upon hydrogenolysis. The yields for the cyclic products were low, most likely due to the lack of suitable H-donor in these experiments.

Since the early examples were discouraging, it took about 25 years and the discovery of anticancer enediyne antibiotics for the idea of photochemical triggering of the Bergman cyclization to reemerge as the focus of active scientific pursuit. The first attempt to use enediynes for photochemical DNA cleavage

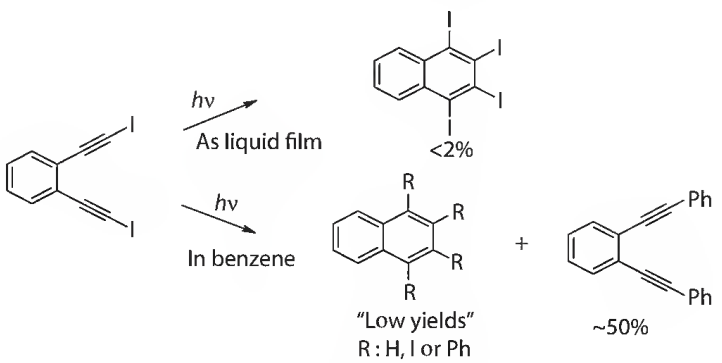

SCHEME 23.2 First report of photochemical Bergman cyclization.

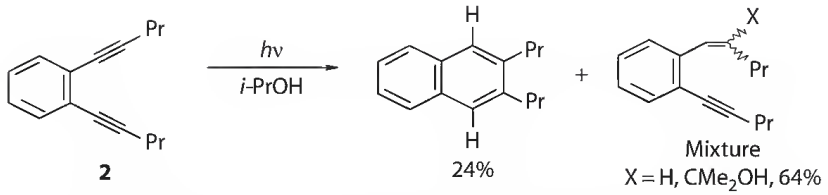

SCHEME 23.3 Photochemical Bergman cyclization of aromatic enediynes. (From Evenzahav, A. et al., *J. Am. Chem. Soc.*, 120, 1835, 1998. With permission.)

was reported by Kagan et al. in 1993.[25] However, irradiation of 1,6-diphenyl-3-hexene-1,5-diyne in THF did not yield any of the expected product of the Bergman cyclization, *o*-terphenyl. Instead, the enediyne underwent *cis–trans* bond isomerization along with formation of a minor amount of polymer product. This disappointing result notwithstanding, the authors found that the same enediyne causes extensive single-stranded (ss) DNA photocleavage in supercoiled pBR322 DNA. The origin of the photodamage still remains unclear until a recent report disclosed that efficient DNA cleavage can be achieved by monoalkynes incapable of the Bergman cyclization.[34]

In 1994, Turro et al. reported that the photochemical Bergman cyclization becomes more efficient once the central bond isomerization is prevented through incorporation of this bond into a ring (Scheme 23.3).[26] Although photochemical alkyne reduction remained a major reaction pathway and the yield of the cyclized product was rather low (24% in isopropanol), the result was conceptually very important and encouraged a number of subsequent studies.

Evenzahav and Turro,[26b] also reported that the photo-Bergman cyclization can proceed when the terminal propyl groups in enediyne **2** are replaced by phenyl groups (Scheme 23.4, top). Literature data for the photochemical reactivity of this specific molecule are mixed. More recent reports suggest that, despite the high (~75%) conversion, the yield of the naphthalene products is low (<10%,[35] ~1%[36]). Interestingly, Ramkumar et al. reported formation of fulvene products from the same enediyne under oxidative electron transfer conditions (Scheme 23.4, bottom).[31f,37]

In 2000, Jones et al. found that several cycloalkene diynes **3** with the analogous 1,6-diphenyl substitution underwent the photochemical Bergman cyclization in slightly higher yields but the respective cyclopentene diyne was not reactive at all (Scheme 23.5, top).[27] A monophenyl substituted cyclohexenediyne **3b** gives even lower yield (<10%) of the cyclized product than the diphenyl-substituted cyclohexene diyne **3a**. Interestingly, when the enediyne part is coupled with a moderately bulky group attached at the *meta*-position through an alkyne linker in **3c**, the photochemical Bergman cyclization becomes quite efficient (44%). No explanation of such different reactivity has been provided so far.

Poor photoreactivity of cyclopentene diynes was also reported by Kaneko et al.[28] (Scheme 23.5, bottom) who found that only dimethyl substituted enediyne **4d** was reactive even under harsh irradiation conditions (254 nm). None of the substrates was reactive under Pyrex-filtered light. The latter result is

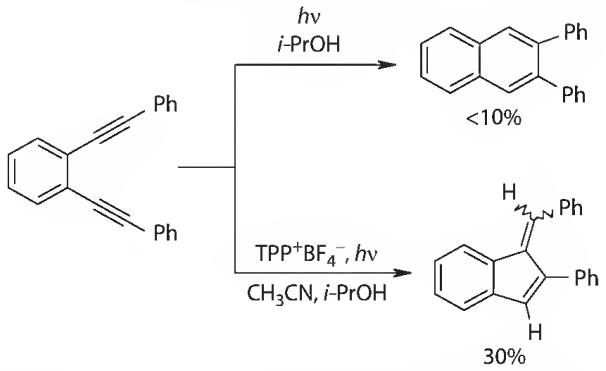

SCHEME 23.4 Photochemical transformations of 1,2-bis(2-phenylethynyl)benzene. (From Evenzahav, A. et al., *J. Am. Chem. Soc.*, 120, 1835, 1998. With permission.)

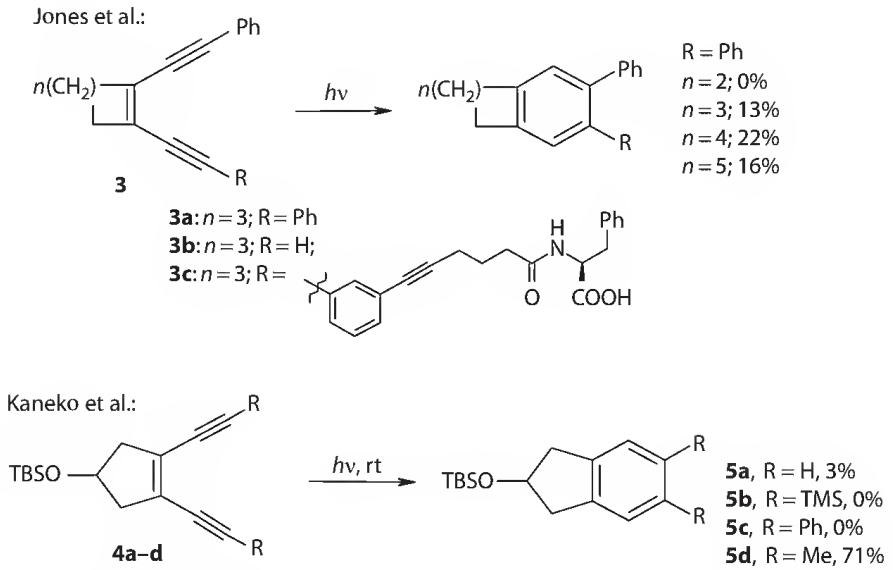

SCHEME 23.5 Photoreactivity of cycloalkene diynes. (From Kaneko, T. et al., *Angew. Chem. Int. Ed. Engl.*, 38, 1267, 1999. With permission.)

not surprising because enediynes without terminal aryl substituents do not absorb above 280–310 nm. No explanation for the remarkable effect of the two methyl substituents has been offered to date.

A very interesting observation by Spence and coworkers[35] is that 1-ethynyl-2-phenylethynylbenzene requires shorter irradiation times and affords higher yields of the photo-Bergman cyclization product than 1,2-bis(2-phenylethynyl)benzene (Scheme 23.6). This is an opposite trend in comparison to that for compounds **3a** and **3b** in Scheme 23.5.

When the acetylenic termini are included in a 10-membered ring as in cyclodec-3-ene-1,5-diyne, the formation of *p*-benzyne intermediate proceeds in high yield (Scheme 23.7).[28] However, the rate of

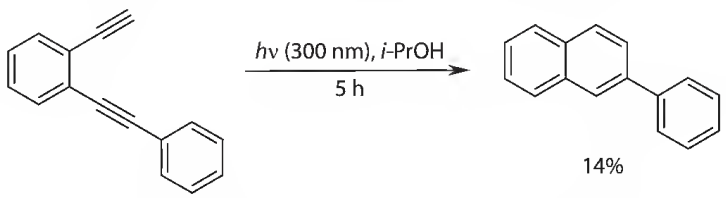

SCHEME 23.6 Photoreactivity of 1-ethynyl-2-phenylethynylbenzene. (From Spence, J.D. et al., *Tetrahedron Lett.*, 48, 725, 2007. With permission.)

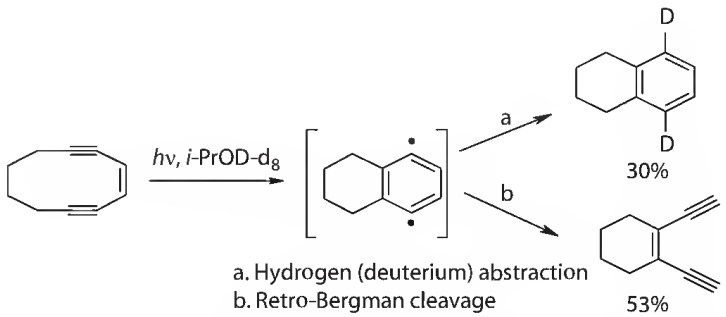

SCHEME 23.7 Competition between photo-Bergman cyclization and retro-Bergman cleavage in the photochemistry of cyclodec-3-ene-1,5-diyne. (From Kaneko, T. et al., *Angew. Chem. Int. Ed. Engl.*, 38, 1267, 1999. With permission.)

hydrogen abstraction by the intermediate 1,4-diradical is apparently slower than the rate of the retro-Bergman opening leading to the formation of 1,2-ethynylcyclohexene. The overall transformation can be considered as a strain-driven photo-Cope rearrangement. This result suggests that the ratio of products is likely to depend on the nature and concentration of the hydrogen donor. Indeed, although the hydrogen donor concentration effects were not studied, the product ratio was found to differ from solvent to solvent.

The aforementioned results are consistent with observations of Funk et al.[29] who found that strained, cyclic enediynes annealed to a polycyclic aromatic core undergo especially facile photochemical Bergman cyclization while related terminal acetylenic compounds such as 4,5-diethynylpyrene are unreactive. Obviously, the retro-Bergman cleavage in this case is possible only in the direction of the starting material and no isomerization is expected, unlike the case of cyclodecenediyne. However, the fact that the cyclization in Scheme 23.8 proceeds more slowly with less than 30 equivalents of 1,4-cyclohexadiene (1,4-CHD) suggests that the cyclization is reversible and that the retro-Bergman ring cleavage may provide a more efficient pathway for diradical deactivation than hydrogen abstraction. This notion is further confirmed by the contrasting reactivity of two naphthalene-fused enediynes—only the formation of a more thermodynamically stable phenanthrene cycle is observed.

Peterson et al. reported the photochemical reactivity of imidazole-fused cyclic enediynes.[38] Irradiation of degassed enediyne solutions with 450 W low-pressure Hg lamp with a quartz filter gave benzimidazole derivatives in yields that were dependent on the nature of solvent and the substituents at the alkyne termini (Scheme 23.9). The cycloaromatized product was obtained in the highest yields (26%–64%) for R = Ph, with the best yield obtained using THF as solvent. Yields for the two alkyl substituted enediynes (R = Me and Bu) depend very strongly on the solvent. The relatively low yields for R = Me contrast the 75% reported for an analogous enediyne with a benzene core (Scheme 23.5, bottom). The cyclic enediyne yielded 45% of cycloaromatized product upon irradiation, even though related 11-membered ring enediynes were shown to be thermally unreactive.[39]

Russell and coworkers reported thermal and photochemical cyclizations of cyclic pyrimidine enediynol and enediynone (Scheme 23.10).[30] Again, the cyclic structure favors the cyclization and irradiation of the alcohol and provides 83% of the cyclized product. On the other hand, irradiation of the corresponding ketone leads to a complex mixture with only 10% of cyclized products. No solvent or hydrogen donor concentration effects were studied.

Branda and coworkers provided another example of a cyclic enediyne that undergoes a photochemical reaction different from a photo-Bergman ring closure.[40] This group reported the elegant design of a cyclic photochromic enediyne that undergoes hexatriene electrocyclization when activated with 365 nm light. The cyclized compound can be reopened with >525 nm light. Interestingly, photochemical

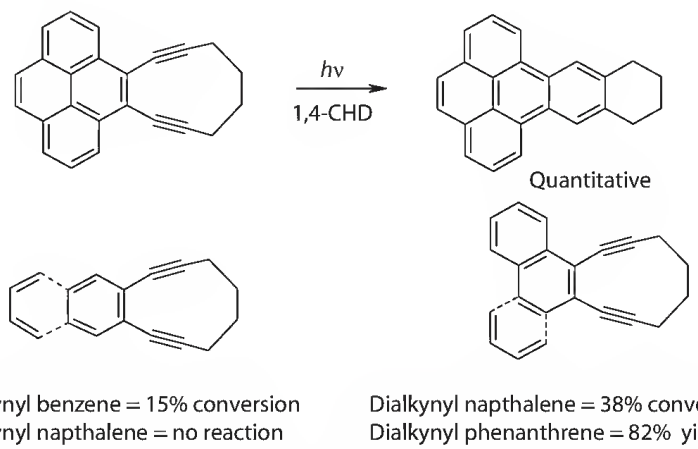

SCHEME 23.8 Photoreactivity of cyclic enediynes with polyaromatic core. (From Funk, R.L. et al., *J. Am. Chem. Soc.*, 118, 3291, 1996. With permission.)

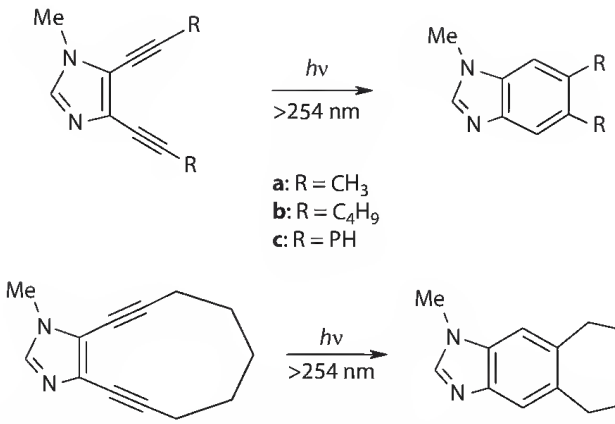

Solvent	a (%)	b (%)	c (%)
THF	6	31	64
i-PrOH	Trace	24	58
Hexane	7	22	47
Cyclohexane	6	16	51
CH_3CN	6	Trace	46
n-Hexane/ 1,4-CHD	6	15	44
CH_2Cl_2	Trace	Trace	40
t-Butanol	Trace	Trace	26

45% in hexane
45% in *i*-PrOH

SCHEME 23.9 Photochemical reactivity of imidazole-fused cyclic enediynes. (From Zhao, Z. et al., *Tetrahedron Lett.*, 46, 1373, 2005. With permission.)

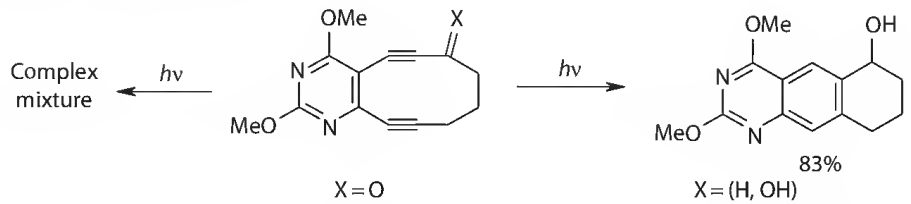

SCHEME 23.10 Photochemical reactivity of pyrimidine-fused cyclic enediynes. (From Choy, N. et al., *Org. Lett.*, 2, 3761, 2000. With permission.)

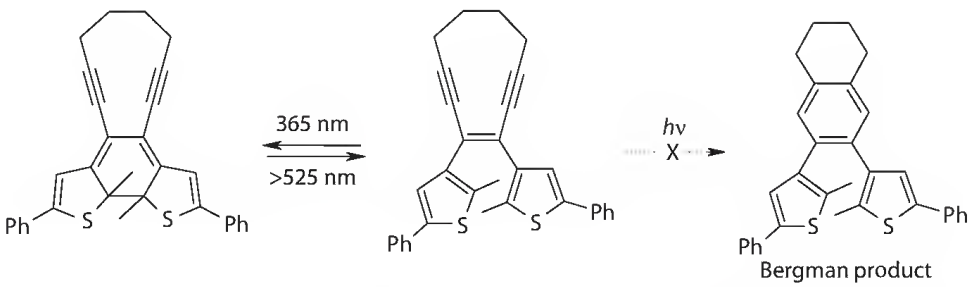

SCHEME 23.11 Competition of photo-Bergman ring closure with hexatriene electrocyclization in photochromic enediynes. (From Sud, D. et al., *Angew. Chem. Int. Ed.*, 46, 8017, 2007. With permission.)

Bergman cyclization was not observed (Scheme 23.11) suggesting that the electrocyclic ring closure is much faster.

The complex effect of the chromophore nature on the enediyne reactivity was further illustrated by Alabugin and Kovalenko, who found that an increase in the electron acceptor ability of the chromophore[9] changes the direction of the cyclization path. When tetrafluoropyridyl (TFP) groups were attached to the enediyne moiety (Scheme 23.12, top)[9a], cyclization proceeded with the formation of indenes instead of the naphthalene products of the Bergman cyclization. When the core chromophore is changed to pyrazine (Scheme 23.12, bottom), interaction of enediyne moiety with 1,4-cyclohexadiene proceeds to a cycloadduct.[41] The latter change in reactivity is attributed to the particularly fast formation of an electrophilic triplet state, which attacks the π-bond of 1,4-CHD.

The radical-anionic C_1–C_5 cyclization of enediynes represents a new type of cycloaromatization reaction—the "cyclorearomatization" process driven by rearomatization in the vicinity of the transition state (TS).[9b] Experimental work unambiguously established photoinduced electron transfer (PET) as

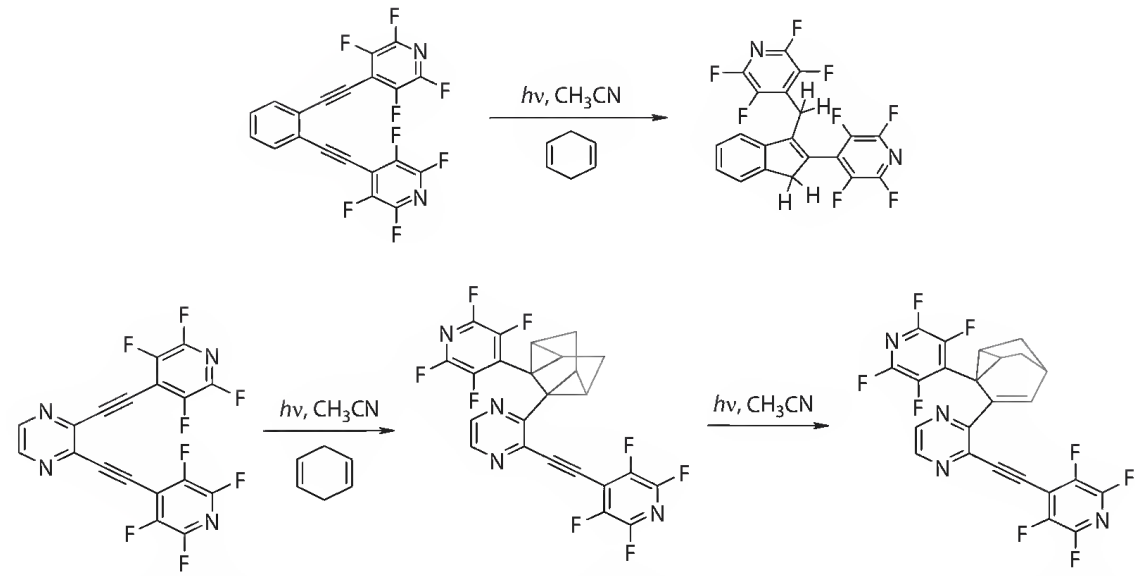

SCHEME 23.12 New photochemical reactions of enediynes promoted by variations at the core and terminus of the enediyne moiety. (From Alabugin, I.V. et. al., *J. Am. Chem. Soc.*, 124, 9052, 2002. With permission.)

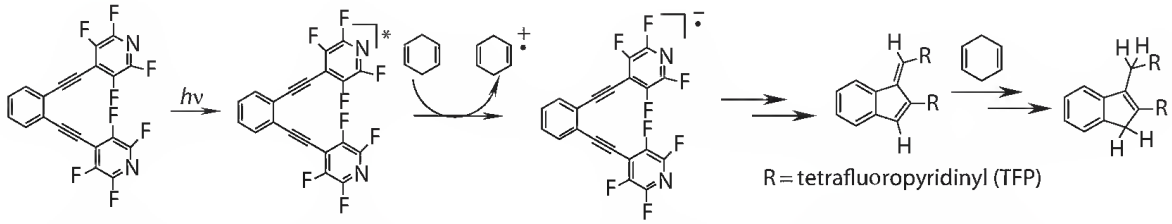

SCHEME 23.13 Photochemically induced reductive **C1–C5** cyclization of enediynes. (From Alabugin, I.V. et al., *J. Am. Chem. Soc.*, 124, 9052, 2002. With permission.)

the triggering event for the C1–C5 cascade and the intermediacy of the second PET step in the indene-forming cascade. Unlike the stable benzene product of the Bergman cycloaromatization, the fulvene intermediate of C1–C5 cyclization (prepared independently through Bu_3Sn radical mediated 5-exo-cyclization of enediynes)[42,43] is capable of further photoreduction to indenes with abstraction of two additional hydrogen atoms from the environment (Scheme 23.13). Due to this feature, C_1–C_5 cyclizations are interesting from the medicinal perspective, because incorporation of four rather than two hydrogen atoms from the environment as the result of the cycloaromatization cascade increases the DNA-damaging potential of the enediyne "warheads."[9a] Indeed, TFP-enediynes equipped with DNA-recognition elements have been shown to be capable of inducing 100–1000 times more ds DNA cleavage than expected from a combination of random coincident ss cleavages.[44]

An interesting example of a five-membered ring formation related to the photo-Bergman cyclization has been reported by the Matzger group.[45] Photochemical activation of bis-(phenylethynyl) sulfide in hexane in the presence of 1,4-CHD produced 3,4-diphenyl-thiophene through the presumed intermediacy of the 2,5-didehydrothiophene diradical (Scheme 23.14). The thermal version

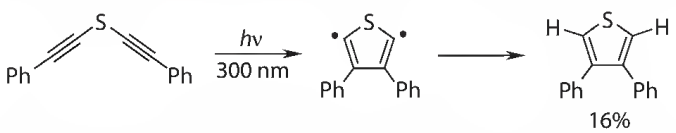

SCHEME 23.14 Photochemical transformation of bis-(phenylethynyl) sulfide in 3,4-diphenyl-thiophene. (From Lewis, K.D. et al., *Org. Lett.*, 5, 2195, 2003. With permission.)

of this process is also known and constitutes the first example of a cycloaromatization reaction exploiting the aromaticity of a heterocyclic ring.

23.2.2.1 Summary of Experimental Trends

The experimental evidence indicates that incorporating an enediyne in a strained ring favors the photochemical Bergman cyclization. However, the same evidence also shows that the cyclic structure makes the cyclization step reversible through the retro-Bergman cleavage. As a consequence, the diradical may undergo many cyclization/ring opening (Bergman/retro-Bergman) cycles before it actually abstracts a hydrogen atom from a hydrogen donor. Unfortunately, no photochemical quantum yields for the photochemical Bergman cyclization of a cyclic enediyne have been determined and the role of the retro-Bergman deactivation pathway remains unexplored.

Unlike the cyclic structure, the terminal Ph substitution is not consistently efficient. For example, it fails to promote the photochemical Bergman cyclization of cyclopentenediynes and is only moderately effective in the other cases (Scheme 23.5). Also, it is not clear why the introduction of a *meta* substituent into a terminal aryl group on the enediyne has such a large positive effect.

The effect of methyl substitution at the acetylene terminus on the cyclization efficiency is mixed as well. However, with just a limited number of known examples, there is not enough data to understand the reasons for this inconsistency, especially because the analogous propyl substitution in benzannelated enediynes does not lead to an efficient cyclization[38] whereas butyl substitution in an imidazole-fused enediyne favors the cyclization more than methyl substitution. More detailed studies are required.

To complicate the matter even further, electronic excitation enables additional reaction pathways different from the Bergman cyclization such as *cis–trans* isomerization, photoreduction, C1–C5 cyclization, and photocycloadditions. Since some of these reactions are not cycloaromatization processes, we need to discuss briefly the relevant photochemistry of bis-alkynes and related enynes.

23.2.3 Relation between Photo-Bergman Cyclization and Other Photochemical Reactions of Alkynes: Photo-Bergman Cyclization as Interrupted [2 + 2] Cycloaddition

Changes in the in-plane π-orbitals during the Bergman ring closure are analogous to the first step of an asynchronous [2 + 2] cycloaddition (Figure 23.1). The main difference is that the cyclobutene formation, which is the usual escape route for the 1,4-diradical intermediate, is impossible due the geometric restrictions imposed by the cyclic framework. Additional stabilization of the intermediate by its aromatic out-of-plane π-system further facilitates formation of this species. An alternative regioselectivity of the σ-bond formation would lead to the formation of a similar 1,4-diradical but in a five-membered

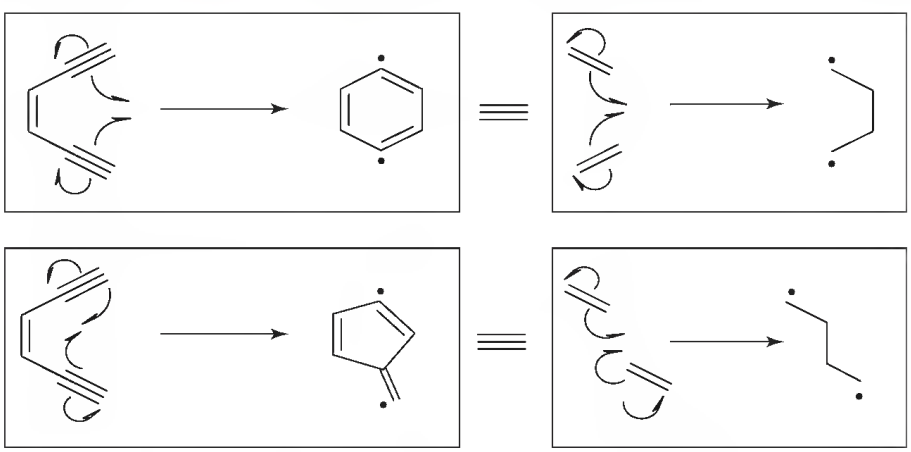

FIGURE 23.1 Comparison of Bergman and C1–C5 cyclizations with interrupted [2 + 2] cycloadditions.

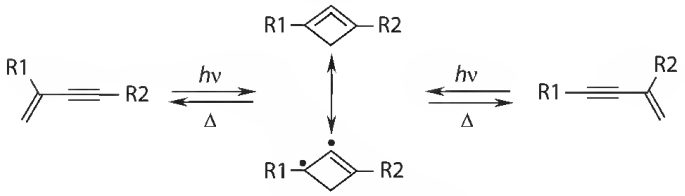

SCHEME 23.15 Photorearangement of enynes. (From Zheng, M. et al., *J. Am. Chem. Soc.*, 115, 12167, 1993. With permission.)

ring, which is not stabilized by aromaticity in the ground state but possesses aromaticity in some of the excited states.[46]

In accord with this analysis, even when no aromatic system is formed, photochemical processes topologically similar to the photo-Bergman cyclization are still possible. A remarkable example is provided by the photorearangement of acyclic conjugated enynes reported by Johnson and coworkers[47] (Scheme 23.15). This transformation is consistent with enyne photocyclization to highly strained 1,2-cyclobutadienes through singlet excited state formation and subsequent thermal ring opening. The overall photoinduced equilibrium bears striking topological resemblance to the Bergman cyclization coupled with the retro-Bergman ring opening (Scheme 23.7).

A classic example of a photochemical process that follows Figure 23.1 and does not provide an aromatic product is the photochemical cyclization of diethynylmethanes, discovered by Zimmerman and Pincock[48] around the time that Bergman reported enediyne cyclization. The reaction (Scheme 23.16) can proceed upon direct excitation of a nonconjugated 1,4-diyne in isopropyl alcohol or upon triplet sensitization by acetophenone or xanthone. A moderately high quantum yield (0.25) upon sensitization with acetophenone indicates a relatively efficient triplet reaction.

A similar photocyclization of a conjugated triaryl "Y-enyne" has been reported by Kaafarani and Neckers (Scheme 23.17).[49] Unlike the previous example, the cyclization proceeds at a pendant aromatic ring. A related nonphotochemical reductive cyclization involves both triple bonds and leads to the formation of a five-membered ring.[50]

Schmittel et al. illustrated the potentially broader scope of photochemical cycloaromatization reactions in their report of triplet photochemical reactions of enyne-carbodiimides and enyne-ketenimines (Scheme 23.18).[51] Photolysis of degassed solutions of substituted enyne-carbodiimides led to the formation of indoloquinolines. When the enyne-carbodiimides are substituted by an electron-withdrawing group either at the alkyne or at the carbodiimide termini, direct irradiation at 300 nm or longer wavelengths proceeds as an efficient (>90%) and highly regioselective 5-*exo*-dig closure. The cyclization is suggested to take place via triplet heterobenzofulvene biradical intermediates. The photochemical cyclization in toluene and *n*-hexane could be completely suppressed in the presence of 1,4-diphenyl-1,3-butadiene, a triplet quencher with E_T = 42 kcal/mol. The photocyclization of enyne-ketenimines under the same reaction conditions resulted in slightly lower yields due to formation of a polymeric material.

The above data illustrate the multichannel nature of alkyne/enediyne photoreactivity and reiterate the importance of a basic understanding of the factors controlling the nature of excitation in the enediyne system. A robust theoretical model that incorporates the disjointed experimental data in a coherent and logical framework is crucial for explaining the aforementioned experimental observations

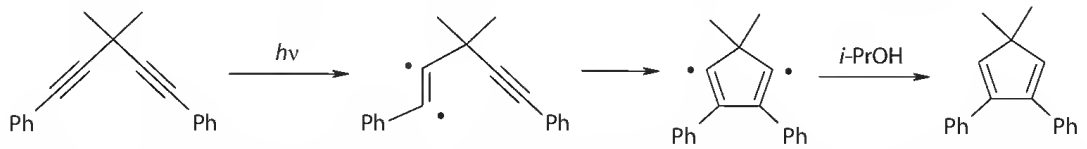

SCHEME 23.16 Photochemical cyclization yielding a nonaromatic five-membered ring. (From Zimmerman, H.E. et al., *J. Am. Chem. Soc.*, 95, 3246, 1973. With permission.)

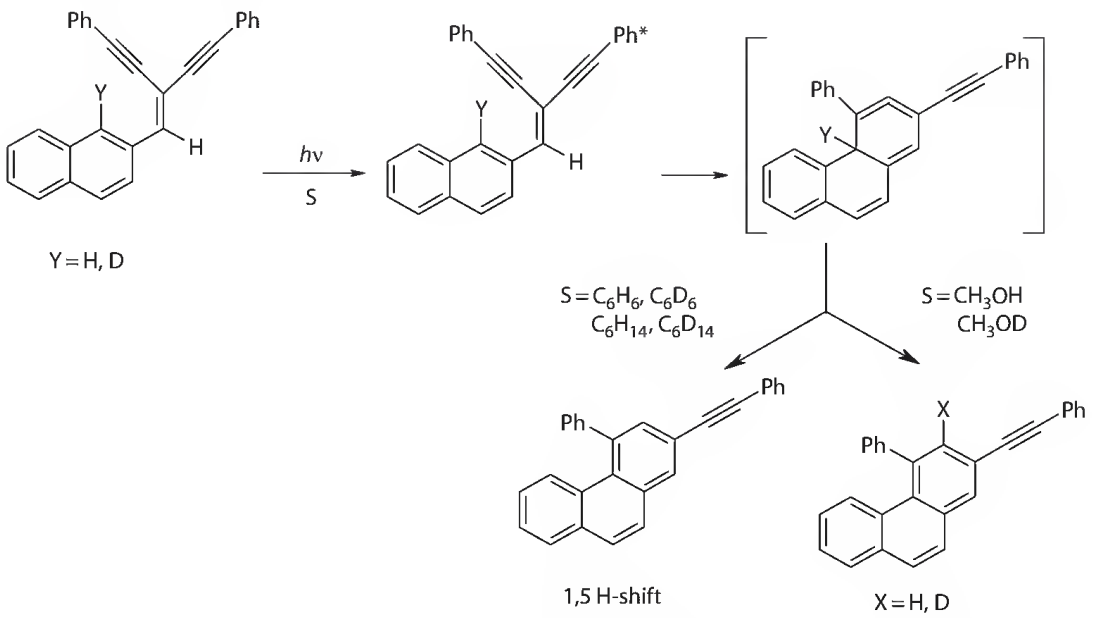

SCHEME 23.17 Photocyclization of a conjugated "Y-enyne." (From Kaafarani, B.R. et al., *Tetrahedron Lett.*, 42, 4099, 2001. With permission.)

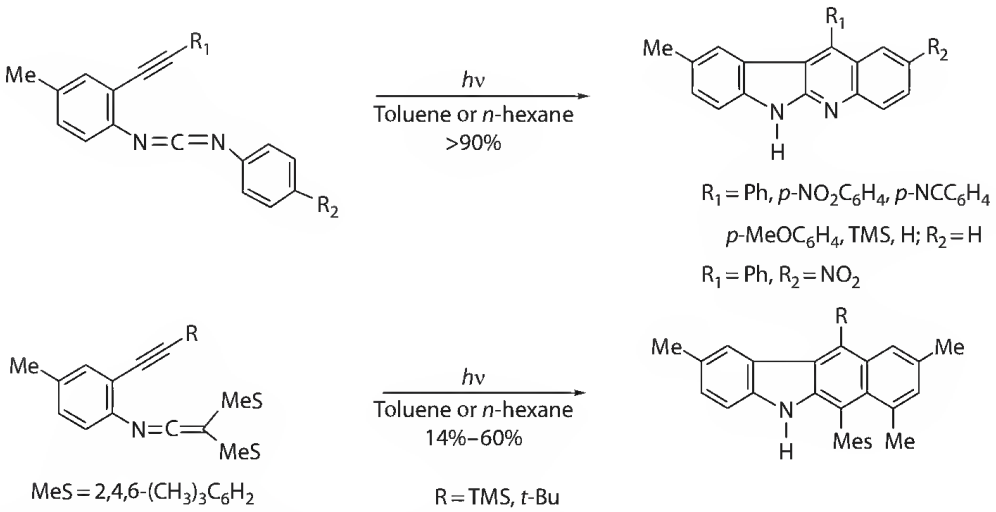

SCHEME 23.18 Photocyclizations of enyne-carbodiimides and enyne-ketenimines. (From Schmittel, M. et al., *Angew. Chem. Int. Ed.*, 39, 2152, 2000. With permission.)

and guiding the future development of this field. The following section provides such a framework by discussing electronic changes that accompany the cycloaromatization process and how these changes are related to photochemical activation.

23.3 MO Analysis of Cycloaromatization Reactions

The relative contributions of the two orthogonal π-systems, which are important for the understanding of electronic factors in the thermal Bergman cyclization, become even more relevant in the photochemical processes. Not only can the substituent effects on the cyclization originate from the two sources (in-plane and out-of-plane MOs) but the two orbital arrays may also be directly involved in the excitation processes, potentially providing different electronically excited states, each with unique

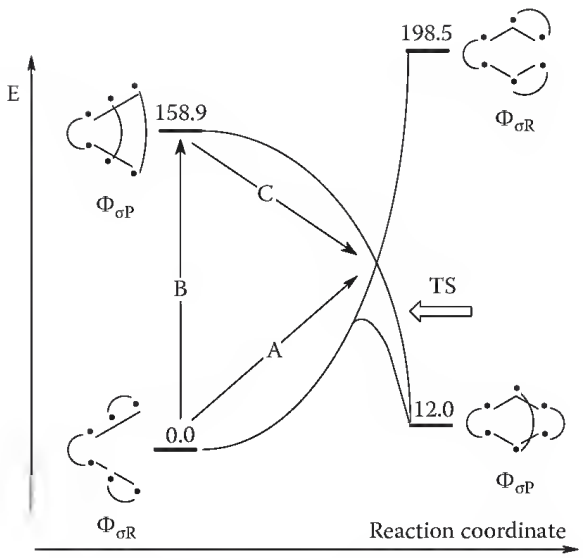

FIGURE 23.2 VB curve crossing diagram showing the crossing between the valence bond configurations involving in-plane bonds and orbitals in the reactant and product of the Bergman cyclization, $\Phi_{\sigma R}$ and $\Phi_{\sigma P}$.[52] Actual surface after mixing is shown as the continuous curve connecting $\Phi_{\sigma R}$ of enediyne with $\Phi_{\sigma P}$ of *p*-benzyne. Energies are in kcal/mol relative to the ground state of the parent enediyne at the σ-l-VB-DFT level. A—thermal Bergman cyclization, B + C—photochemical route to the same TS. (From Galbraith, J.M. et al., *Chem. Eur. J.*, 6, 1446, 2000. With permission.)

reactivity. Communication between the two orthogonal π-systems can lead to an interconversion of different excited states and drive chemical reactivity in directions that are difficult to achieve in a purely thermal process.[9b] As a result, the relative roles of the two π-arrays becomes crucial and warrant the detailed analysis provided in this section.

Galbraith et al.[52] utilized VB theory to gain insight into the structural and electronic nature of the transition state and the role of the σ- and π-frameworks in thermal Bergman cyclization. The dominant VB configuration of the enediyne reactant, $\Phi_{\sigma R}$, plays only a minor role in the *p*-benzyne diradical, while the dominant VB configuration in the biradical product, $\Phi_{\sigma P}$, is insignificant in the starting material (Figure 23.2). The avoided crossing of the energy curves corresponding to these two VB configurations (or electronic states corresponding to these configurations) corresponds to the transition state. This analysis is useful for the design of the photochemical Bergman cyclization because it clearly illustrates that both the position and the energy of the TS depend on the ground and excited state energy surfaces. A particularly relevant corollary of this analysis is that the state crossing (the TS) can be reached starting either with the ground state or from a suitable excited state and that, in the latter case, the cyclization should be much more energetically favorable.

The main challenge in achieving the aforementioned transformation efficiently is in finding a way to reach the correct excited state surface selectively and in directing the distribution of excitation energy in a productive way through appropriate molecular design. Since both π-systems are involved in the cycloaromatization process, clear dissection of their respective roles is important for the analysis of reactivity. Alabugin and Manoharan illustrated how these challenges can be tackled via the analysis of MO correlation diagrams.[53,9b] In this analysis, monitoring the cyclization process at the level of individual MOs enables detailed understanding of electronic reorganization along the reaction coordinate (Scheme 23.19). The most important changes at the TS stage are the dramatic increase in the energy of HOMO-1 and the decrease in the energy of LUMO + 1, which occur due to the transformation of the enediyne in-plane π- and π*-orbitals (bonding and antibonding, respectively) into the nonbonding MOs (radical centers) of the diradical (Scheme 23.19, left). Destabilization of the HOMO-1 is the greatest energy penalty for the enediyne to reach the Bergman cyclization TS. This effect is partially offset by a

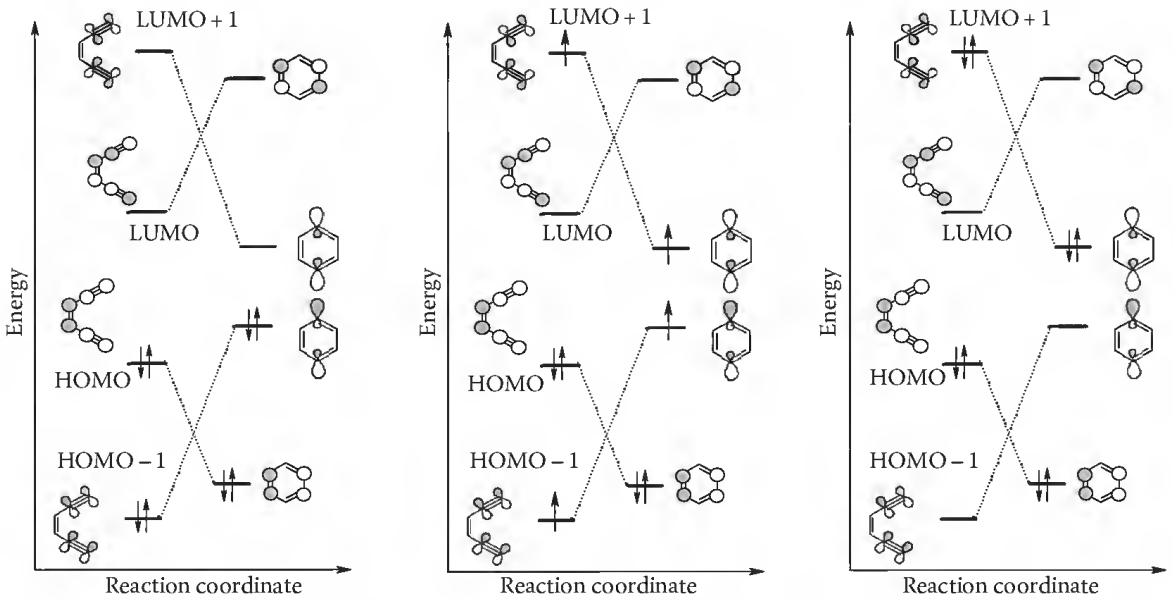

SCHEME 23.19 Left: Partial MO diagram that illustrates the frontier MO (FMO) changes in the process of thermal Bergman cycloaromatization. Center: Analogous changes for a hypothetical photochemical Bergman cyclization promoted by excitation, which involved the *in-plane* FMOs. This reaction should be more favorable than the ground state Bergman cyclization. Right: Even more potentially favorable adiabatic photochemical Bergman cyclization from a higher excited state. (From Poluokhtine, A. et al., *J. Org. Chem.*, 71, 7417, 2006. With permission.)

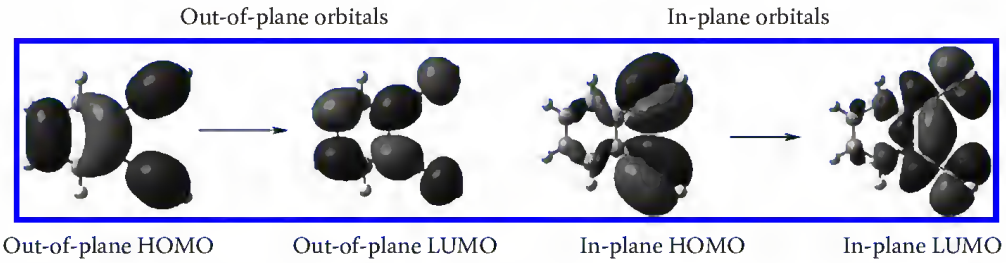

FIGURE 23.3 The key molecular orbitals of *o*-diethynylbenzene.

σ-bond forming interaction that stabilizes HOMO-2 (not shown, the in-phase combination of the in-plane enediyne π-orbitals). Developing aromatic stabilization of the out-of-plane π-system lags behind the aforementioned changes but becomes progressively more and more important as the reaction coordinate approaches the *p*-benzyne product.[54]

The key MOs of the parent benzannelated enediyne, *o*-diethynylbenzene, are shown in Figure 23.3. They are analogous to the MOs of the parent enediyne and, thus, the main points of the aforementioned analysis are applicable to benzannelated enediynes as well.

23.3.1 MO Analysis of Photochemical Bergman Cyclization

23.3.1.1 Allowed Photo-Bergman Cyclizations

The MO correlation diagram illustrates that the thermal Bergman cyclization is a symmetry-allowed process (Scheme 23.19, left) because the antisymmetric combination of the nonbonding (radical) orbitals is lowered in energy relative to the symmetric combination by through-bond (TB) interaction between the two radical centers.[55]

An adiabatic photochemical Bergman cyclization should also be a symmetry-allowed process as long as it involves excitation of the in-plane orbitals (Scheme 23.19, center and right). Moreover, inspection of

the in-plane orbitals suggests that promotion of an electron from the highest occupied in-plane orbital, which is antibonding between the end atoms of the enediyne system, to the lowest unoccupied in-plane orbital, which is bonding between the same atoms, should greatly facilitate the cyclization. These in-plane MOs correspond to HOMO-1 and LUMO + 1 in the parent enediyne.

However, excitation of the "frontier" in-plane orbitals does not correspond to the lowest energy excited state in simple enedynes* and, according to the Kasha's rules,[56] is unlikely to manifest itself directly in the observed photochemical reactivity. Does it mean that the photo-Bergman cyclization is destined to be an inefficient process? In the next section, we will discuss how this limitation can be overcome.

23.3.1.2 Orbital Crossings in "Forbidden" Photo-Bergman Cyclizations

The photo-Bergman cyclization from the lowest excited state corresponding, in the first approximation to a HOMO–LUMO transition between the out-of-plane MOs, can be formally classified as a symmetry-forbidden process because electronic states of the reactant and the product are different. As the result, the reaction has to suffer from an additional energy penalty needed to reach the orbital crossing that interconverts the two states (Figure 23.4). In this scenario, the crossing point should control the energy to the transition state for the photochemical Bergman cyclization.

Two points are especially important in this analysis. First, unlike the usual ground state reactions where the additional energy penalty due to the "forbiddeness" is substantial as the result of the large energy difference between the crossing states (the ground state and an excited state), this penalty is not prohibitive for the crossing between the two excited states because the energy difference between the

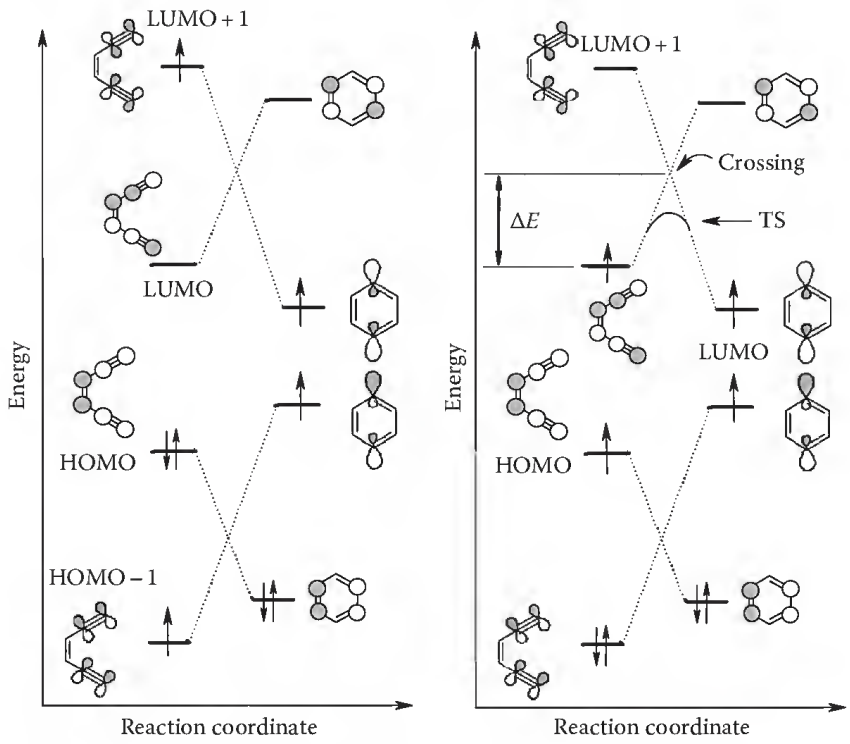

FIGURE 23.4 Comparison of FMO correlation diagrams for two adiabatic photochemical Bergman cyclizations. *Left*: Excitation involves the in-plane MOs and the cyclization is allowed. *Right*: The excitation involves the out-of-plane MOs and the process has an additional penalty ΔE imposed by the MO crossing between the lowest excited states of reactant and the product (an analogous crossing and analogous energy penalty would be observed for a diabatic photocyclization, which forms the ground state of the product).

* The difference in the excitation energy of the *out-of-plane* and *in-plane* orbitals is expected to be close in magnitude to the difference between the energy of $\pi \rightarrow \pi^*$ absorptions in hexatriene and ethylene.

two excited states is usually smaller than the difference between the ground and excited states. Second, the TS energy depends on both the out-of-plane (initially populated) MO and the in-plane (populated after crossing) MO and the overall reaction barrier can be controlled through a rather interesting interplay of electronic effects, which include both of the two orthogonal π-arrays. In short, the TS energy for this class of photochemical Bergman cyclizations can be decreased by either destabilizing the out-of-plane MO (usually the LUMO) or by stabilizing the in-plane MO (LUMO + 1, Figure 23.4).

An additional consideration is that electronic coupling between the crossing states will result in an avoided crossing, which lowers the observed barrier. Such coupling would depend on the efficiency of interaction between the two initially orthogonal π-arrays and would be facilitated through deviations from planarity, which lowers the initial symmetry.[9]

The general MO analysis discussed earlier explains why no photochemical cyclization has been observed during irradiation of the enediyne **1** at the room temperature[7] and why such side reactions as *cis–trans* isomerization[25] and photoreduction[26] are observed instead in related compounds. In those cases, the lowest excited state does not involve the in-plane orbitals directly involved in the cyclization. Instead, the lowest excited state involves transitions with participation of only the out-of-plane π-orbitals that mostly correspond to the enediyne HOMO and LUMO.

This general analysis agrees well with UDFT and MCSCF calculations of the photochemical Bergman cyclization of enediynes by Clark et al.[57] who computed the three lowest singlet and triplet vertical excited states of the parent enediyne, *cis*-hex-1,5-diyne-3-ene as well as several of the respective potential energy surfaces for its Bergman cyclization. Despite the high exothermicity (–42 kcal/mol at the CASMP2 level), Bergman cyclization along the a ^{3}B path was found to be unfavorable due to the competition with *cis–trans* isomerization at the central bond and H-abstraction at the terminal alkyne carbons. Singlet photoexcitation to an alkyne-localized excited π-π* state was more efficient in promoting an in-plane geometric distortion leading to the Bergman diradical.

In summary, for the successful design of the photochemical Bergman cyclization one needs to decrease the energy of the in-plane absorption. It is not clear at this point whether such decrease can be sufficiently large to achieve the allowed photo-Bergman cyclizations described in the previous sections. However, even if the "in-plane" excited state remains higher in energy than the "out-of-plane" excited state, the "in-plane" state energy lowering will result in a parallel lowering of the crossing between the two states and, as discussed earlier, decrease in the activation barrier for the cyclization. As the result, even forbidden photo-Bergman cyclizations should still be facilitated by the "in-plane excited state" stabilization.

One can see that control of photo-Bergman cyclizations requires a detailed understanding of the nature of photochemical excitation.[58] Generally, this task is not a trivial undertaking, especially when considering the highly delocalized and multiconfigurational nature of the excited states. However, analysis of molecular orbitals involved in the excitation reveals several promising approaches that not only rationalize the available experimental data from the multiple literature sources but also suggest new ideas that can be tested experimentally. In order to understand the logic of these approaches, it is illustrative to consider the energy gap between the LUMO and LUMO + 1 of the enediyne moiety. If the gap is decreased, the excitation energy should decrease as well and, at some point, it may become possible to deliver the excitation to the in-plane MO manifold. Several ways to decrease this gap are discussed in the following.

23.3.2 Factors Controlling Photo-Bergman Cyclizations

23.3.2.1 Strain

The first way to decrease the gap is to include the enediyne moiety in a strained cycle where the terminal enediyne carbons are brought closer.[20] This change should destabilize the HOMO-1 where the interaction between the end orbitals is antibonding and stabilize the LUMO + 1 where the π*-orbitals overlap constructively as shown in Figure 23.5.

This model offers an interesting attenuation of the concept of strain control in enediyne reactivity by Nicolaou et al.[19] who had argued that the increase of strain promotes the Bergman cyclization by the

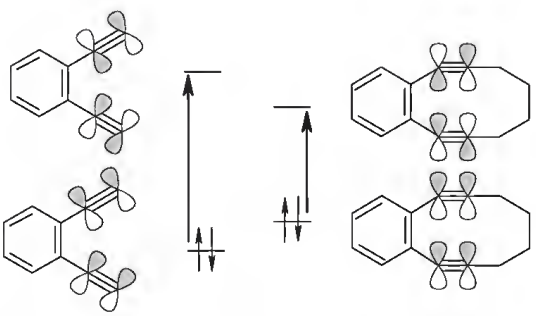

FIGURE 23.5 Comparison of the in-plane FMO gap between the in acyclic (left) and cyclic (right) enediynes. Incorporation of the enediyne moiety into a cyclic structure simultaneously increases the energy of the HOMO-1 and lowers the energy of the LUMO + 1. In this example, the central part of the enediyne moiety is included into a benzene ring to prevent the retro-Bergman opening into an acyclic product. (From Alabugin, I.V. et al., *J. Phys. Chem. A*, 107, 3363, 2003. With permission.)

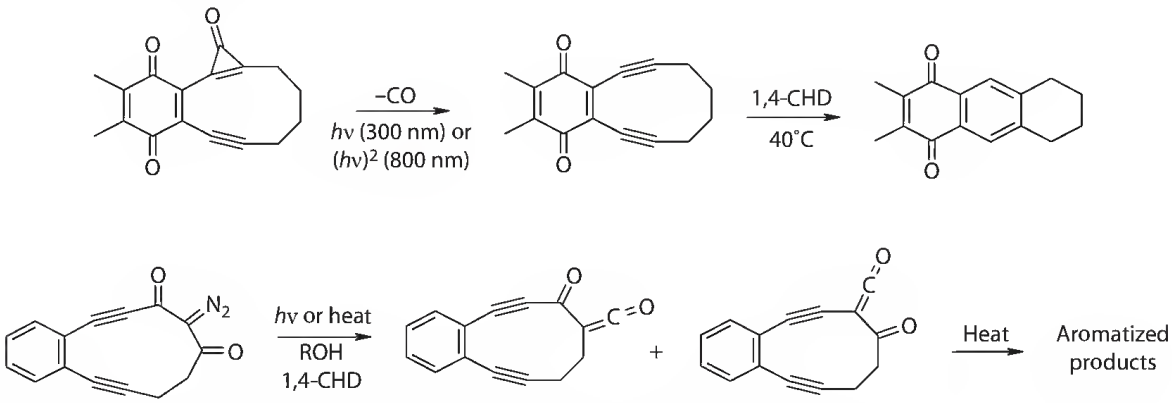

SCHEME 23.20 Synthesis of reactive enediynes via photochemical ring contraction. (From Karpov, G.V. et al., *J. Am. Chem. Soc.*, 129, 3792, 2007. With permission.)

ground state destabilization.* The aforementioned MO analysis agrees well with this rationale but also points out to the importance of excited state stabilization in strained cyclic enediynes. The ground state destabilization and the excited state stabilization together should facitate the photochemical Bergman cyclization in a synergistic manner. This expectation is fully confirmed by the available experimental findings (Schemes 23.7 through 23.10) of efficient photo-Bergman cyclizations in strained cyclic enediynes.

Popik and coauthors described photochemical ring contraction via the photo-Wolff rearrangement or CO extrusion from a cyclopropenone moiety that generates strained and thermally reactive enediynes (Scheme 23.20). Extrusion of CO proceeds efficiently and also can be promoted via low-energy two-photon absorption approach (the first report of two-photon-induced generation of reactive enediynes). In all of the reported examples, the following Bergman cyclization proceeds via thermal activation. It would be interesting to design systems in which the cycloaromatization step also proceeds photochemically via excitation of the initially formed ring contraction product.[59]

23.3.2.2 Electronic Effects

Alternatively, the in-plane excitation energy can be lowered when the in-plane π-orbitals are incorporated in a more extended conjugated system. Several ways can be used to achieve this goal. For example, one

* Schreiner analyzed the Bergman cyclization of cyclic enediynes systematically using DFT analysis and found that the differences in reactivity are not solely based on strain effect. In particular, since alkyl substituents stabilize acetylenic bonds to a greater extend than olefinic bonds, alkyl substituents stabilize the starting material, thus increasing the activation barrier and the endothermicity. See Ref [20e].

can use conjugation from the acetylene end of the enediyne system by introduction of an appropriately oriented aryl and heteroaryl substituents at the terminal alkyne atoms. Extending the "in-plane" conjugation from the core is more difficult since one has to rely on either hyperconjugation or homoconjugation.

23.3.2.2.1 Conjugation at the Alkyne Termini

A potential problem with the enediyne activation through terminal aryl substitution is that the aryl group can be in conjugation with either the in-plane or out-of plane part of the acetylenic π-system depending on the relative orientation of the aromatic system. If the aromatic ring is in the plane of the enediyne moiety, than the aromatic π-orbitals are out-of-plane and do not conjugate with the in-plane orbitals responsible for the cyclization. Only when the aromatic ring is rotated out of the enediyne plane can the aromatic π-orbitals overlap with the in-plane π-orbitals of the enediyne system as illustrated in Figure 23.6.

This model rationalizes a number of experimental results discussed in the previous sections. In particular, it explains the contrasting reactivity of 1,6-diphenyl substituted enediynes discussed earlier. Table 23.1 illustrates that the results for the enediynes where the phenyl groups remain in the enediyne

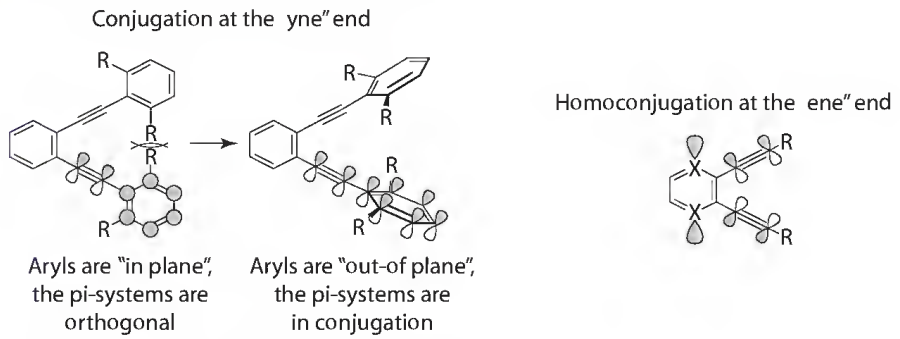

FIGURE 23.6 Two conjugation modes for the in-plane π-system of enediyne moiety and effect of orientation of the aromatic ring on the conjugation with the enediyne system.

TABLE 23.1 Comparison of Computed Geometries of 1,6-Diphenyl Substituted Enediynes with the Experimental Efficiency of Their Photochemical Bergman Cyclization

Enediyne	H…H Distance (Å)[a]	HC_3C_4H Dihedral Angle (Degrees)[a]	Yield of the Photo-Bergman Product (%)
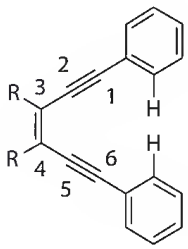 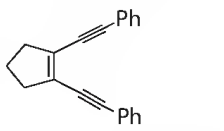	3.00	0.1	0[30]
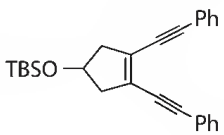	2.95	0.1	0[28]
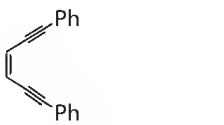	2.58	0.0	0[25]
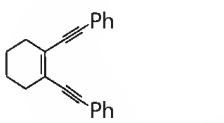	2.31	6.1	13[30]

[a] Complete AM1 geometry optimization starting from the flat geometry.

plane (rows 1–3 where the H–H distances are more than 2.5 Å) contrast the results for the row 4 where the terminal aryl groups are rotated out of the enediyne plane and conjugate with the in-plane orbitals of the enediyne moiety. The photo-Bergman cyclization was observed experimentally only in the last case.

Presumably, this effect can be amplified through introduction of larger substituents at the ortho positions of the terminal aryl/hetaryl groups. Steric repulsion between such substituents may force the aromatic rings out of the enediyne plane and enable their conjugation with the reacting in-plane system. The effect should be even more pronounced with polycyclic aromatics attached to the acetylenic ends. However, one has to be careful in avoiding those polycyclic moieties that may have their own photochemical reactivity and those *ortho* substituents that are so large that they destabilize the product due to steric crowding.[60]

Potentially, *meta*-substitution may have a similar effect on the orientation of the terminal aryl groups. Note that introduction of a *meta*-substituent increased the cyclization yield from 13% to 44% in Scheme 23.5.[27] It is not clear, at this time, whether this increase results from the rotation of the terminal aryl group or from a manifestation of the photochemical "*meta*-effect."[61]

23.3.2.2.2 Homoconjugation

The only way to influence electronic properties of the *in-plane* π-system from the "ene" end is to involve homoconjugation.[62] Although homoconjugation is expected to be weaker than direct interactions, it provides an additional way to control the symmetry of the highest in-plane orbital, which can be useful for increasing the efficiency of two-photon excitation. The two-photon activation (TPA) of antitumor drugs is an especially useful for biological applications because it provides extremely mild conditions for the drug activation with photons of very low (near IR) energy and allows for photon delivery through the therapeutic window of tissues.[63] Additionally, the quadratic dependence of the two-photon absorption on the light intensity minimizes photo damage to the healthy tissue because it confines the affected part to the focus point of the laser, assuring excellent three-dimensional spatial control over the localization of the therapy.

Figure 23.7 provides an example of how homoconjugation can be used to control photophysical properties of the enediyne moiety. Introduction of two nitrogen atoms in the 1,4-positions of the aromatic ring adds another high-energy MO to the manifold of occupied in-plane orbitals. This orbital can be qualitatively described as a combination of the nitrogen lone pairs, which is symmetric relative to the plane of symmetry that bisects the enediyne moiety. Since this orbital is positioned between the frontier in-plane MOs of 1,2-diethynylbenzene, its presence decreases the gap between in-plane occupied and unoccupied orbitals. Different symmetry of this MO and potential electron transfer from the core to the alkyne termini associated with the excitation may be interesting in fine-tuning TPA of enediyne chromophores (vide infra).[64]

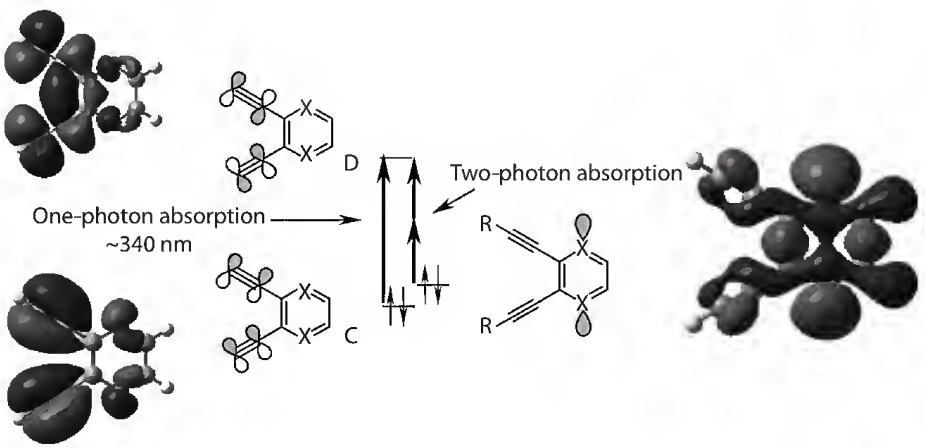

FIGURE 23.7 The key in-plane molecular orbitals of *o*-diethynylpyrazine.

23.3.2.2.3 Combining In-Plane and Out-of-Plane Effects in "Forbidden" Radical-Anionic Bergman and C1–C5 Cyclizations

Because the breaking π-bonds and the developing radical centers are orthogonal to the out-of-plane π-system and because the aromatic system develops mostly after the system proceeds through the transition state, the activation barrier for thermal cycloaromatization reactions is relatively insensitive to effects in the out-of-plane π-system. This provides a challenge for substituent control of such reactions, which often has to rely on indirect thermodynamic contributions to the reaction barrier as described by the Marcus theory.[65]

As we discussed in the previous sections, communication of different electronic states plays an important role in the photochemical Bergman cyclization. Interestingly, the "forbidden" character of these cyclizations provides a way for the π and σ electrons to "communicate" with each other. As the result, even remote substituents can influence the cyclization. This phenomenon was investigated recently for photoinduced cyclizations of enediynes that proceed through a reductive single electron transfer to enediyne from a suitable donor.[7a]

In both the Bergman cyclization and the C_1–C_5 cyclization, a σ-bond is formed at the expense of the same two in-plane π-bonds in either an endo-endo (Bergman) or an endo-exo (C_1–C_5) fashion. Both cyclizations of the parent enediyne should be forbidden in the excited state corresponding to the HOMO–LUMO excitation and both reactions have to go through a state crossing in the vicinity of the cyclization transition states. This crossing is a direct result of the bond-forming interaction that transforms the in-plane π-orbitals into a σ-bond and a pair of nonbonding MOs (two radical centers). In the reactant, both HOMO and LUMO correspond to out-of-plane orbitals yet both of the frontier MOs are localized at in-plane orbitals in the product.

In the radical-anionic version, the activation barrier for both C_1–C_6 and C_1–C_5 cyclizations of enediyne radical-anions can also be described as the avoided crossing between the out-of-plane and in-plane MOs (or electronic states that correspond to population of these MOs). One-electron reduction populates the out-of-plane LUMO (now the SOMO) of the enediyne moiety. At the TS (the crossing), the electron is "transferred" between the orthogonal π-systems to the new (in-plane) SOMO. Such a switch in MO populations should proceed through a crossing between electronic configurations with either an out-of-plane or an in-plane singly occupied MO (SOMO) along the reaction path (Figure 23.8).

This model successfully explains the acceleration of cyclization of radical-anions of benzannelated enediynes, the enhanced sensitivity of these cyclizations to π-conjugative effects of remote substituents and the fact that this selectivity is inverse compared to that of the Bergman cyclization.

The effect on the cycloaromatization potential energy surfaces of the parent enediyne is illustrated in Figure 23.9. Both directions of the ring closure become more favorable upon one-electron reduction. The cyclization barrier drops more significantly for the C1–C5 cyclization but the Bergman cyclization is still predicted to be kinetically favored. Interestingly, the latter is also predicted to be strongly exothermic (as opposed to the endothermic cyclization of the neutral enediyne).

Even more remarkable is how dramatic is the effect of one-electron reduction in benzannelated enediynes (Figure 23.10). Now the C1–C5 closure carries no thermodynamical penalty and becomes an essentially thermoneutral process with a relatively low barrier.

The large effect of benzannelation was shown to be due to the loss of aromaticity in the preexisting benzene ring of the benzannelated starting material upon its one-electron reduction. MO crossing moves the extra electron into the sigma framework where it does not interfere with the aromaticity. As the result, aromaticity of the preexisting ring A is restored in the TS (Figure 23.11). This rearomatization process is intimately connected with aromatization in the newly formed cycle B, overall providing a much stronger driving force for the radical-anionic cyclizations in benzannelated substrates.

Another interesting feature of these reactions is that they are predicted to be much more sensitive to the effects of remote substituents than the thermal Bergman cyclization of their neutral counterparts. In agreement with the experimental results of Russell and coworkers,[22c,67] the influence of *para*-substituents

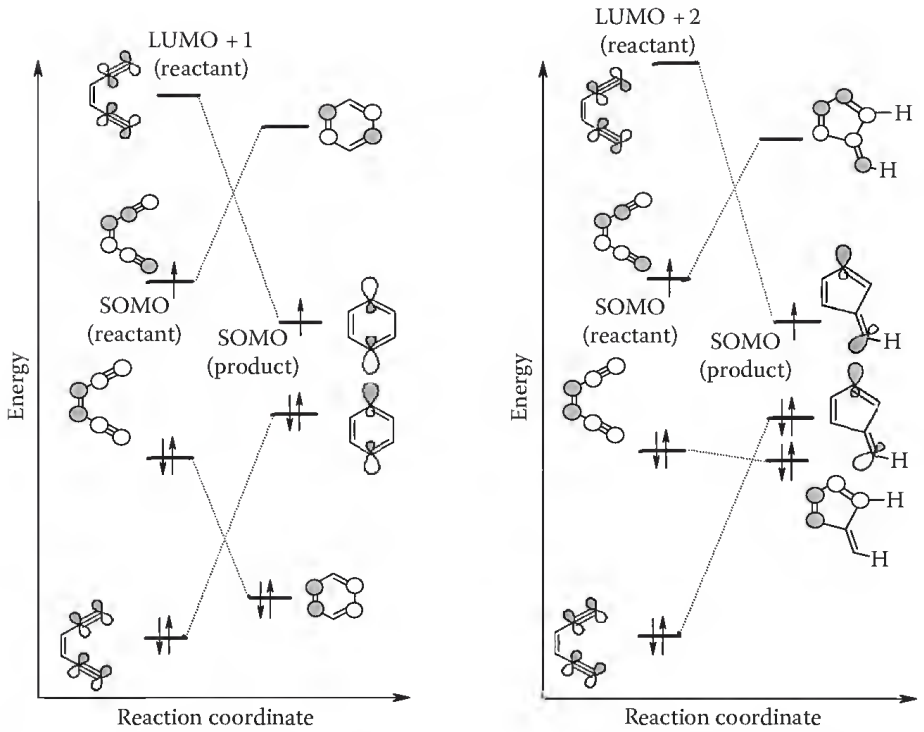

FIGURE 23.8 Crossings of in-plane and out-of-plane frontier MOs in radical-anionic Bergman and C1–C5 cyclizations (crossings for photochemical, dianionic, and radical-cationic cyclizations involve the same MOs but differ in the number of electrons). (From Alabugin, I.V. et al., *J. Am. Chem. Soc.*, 125, 14014, 2003 and reference therein. With permission.)

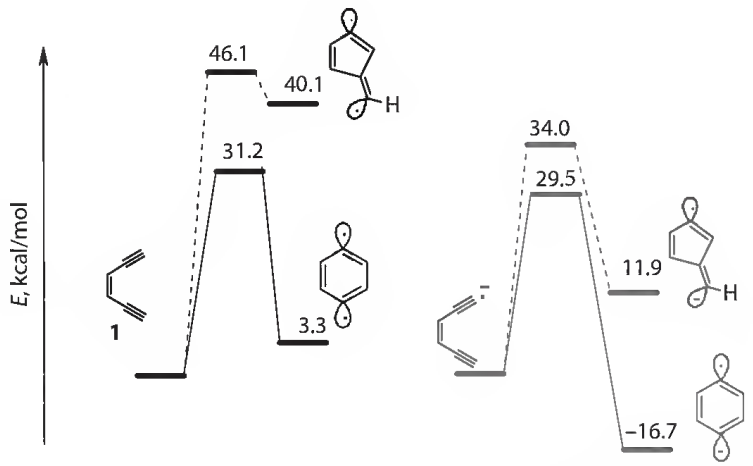

FIGURE 23.9 The reaction energy profiles for thermal (on the left) and radical-anionic (on the right) C1–C6 and C1–C5 cyclizations of parent enediyne **1** computed at the B3LYP/6–31G** level. (From Alabugin, I.V. et al., *J. Am. Chem. Soc.*, 125, 14014, 2003 and reference therein. With permission.)

on the thermal Bergman cyclization is small. The activation energies for the neutral substituents lie within a range of only 0.6 kcal/mol. On the other hand, effect of the same substituents on the activation energies of radical-anionic cyclizations is dramatic as illustrated by ~20 kcal/mol variation in the activation barriers in Figure 23.12.

The generality of these findings is enforced by the fact that reductive electron transfer can be accomplished in a variety of ways. For example, Whitlock et al.[68] showed that the cyclization of enediynes

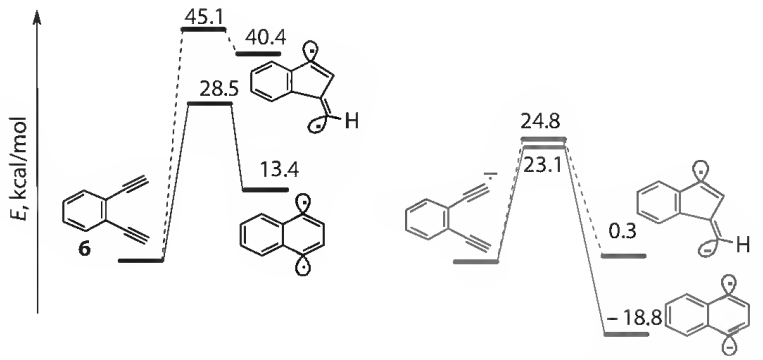

FIGURE 23.10 The reaction energy profiles for thermal (on the left) and radical-anionic (on the right) C1–C6 and C1–C5 cyclizations of benzannelated enediyne **6** computed at the B3LYP/6–31G** level. (From Alabugin, I.V. et al., *J. Am. Chem. Soc.*, 125, 4495, 2003. With permission.)

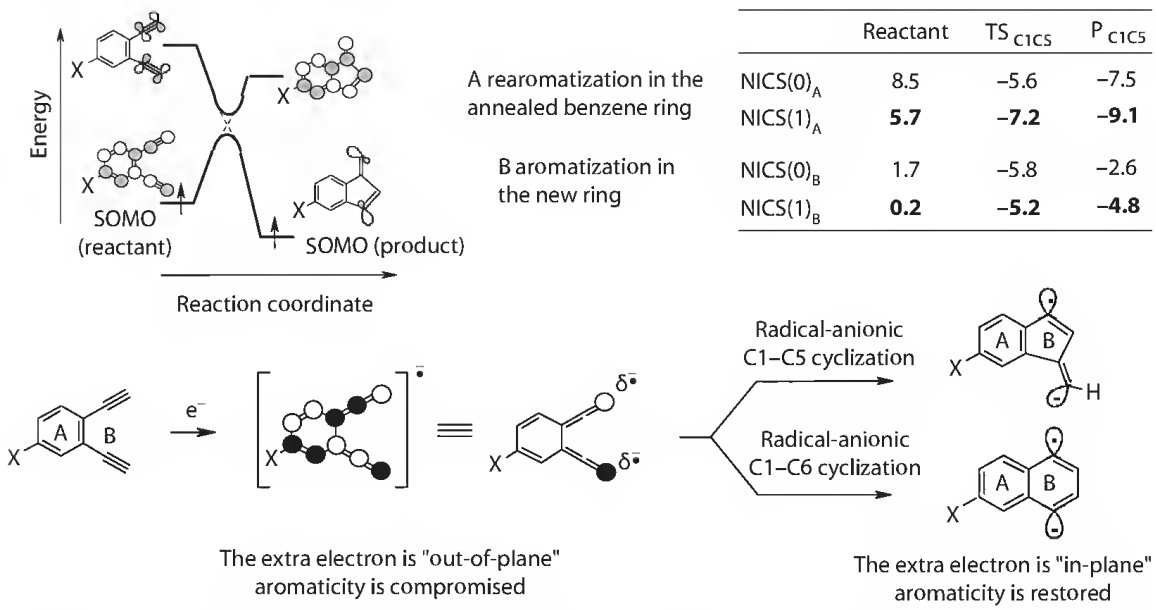

FIGURE 23.11 The interplay of rearomatization and cycloaromatization in the radical-anionic C1–C5 cyclizations of 1,2-diethynylbenzene. Nucleus-independent chemical shift (NICS) values are computed at the B3LYP/6–31G** level. Positive NICS[66] values for enediyne radical-anion, which indicate antiaromaticity of the reactant, are changed to negative NICS values in the TS and the products of both C1–C5 and C1–C6 cyclizations. (From Alabugin, I.V. et al., *J. Am. Chem. Soc.*, 125, 14014, 2003 and reference therein. With permission.)

(Scheme 23.21) by lithium naphthalenide is dianionic and provides substituted fulvenes. The cyclization may proceed at either the radical-anionic or the dianion stage.

The dianionic cyclizations can also produce heterocycles. Tamao and coworkers reported that reduction of bis(phenylethynyl)dialkylsilanes with lithium naphthalenide leads to the formation of a cyclized product via endo-endo ring closure.[69] An analogous dianionic endo-endo cyclization of cyclic 1,2-bis(silylethynyl)benzene opens access to 1,4-dilithio-2,3-disilylnaphthalenes (Scheme 23.22).[70]

Along the similar lines, Wenthold applied the radical-anionic activation to the Cope rearrangement,[71] which can be considered a more saturated analog of the Bergman cyclization.[5] He found the reaction to have an inverted potential energy surface where the open-shell intermediate is more stable than the corresponding diene. Consequently, one-electron reduction of 2,5-dicyano-1,5-hexadiene resulted in spontaneous cyclization under the experimental conditions. This finding directly supports the concept described in Figure 23.2 and Figure 23.8.

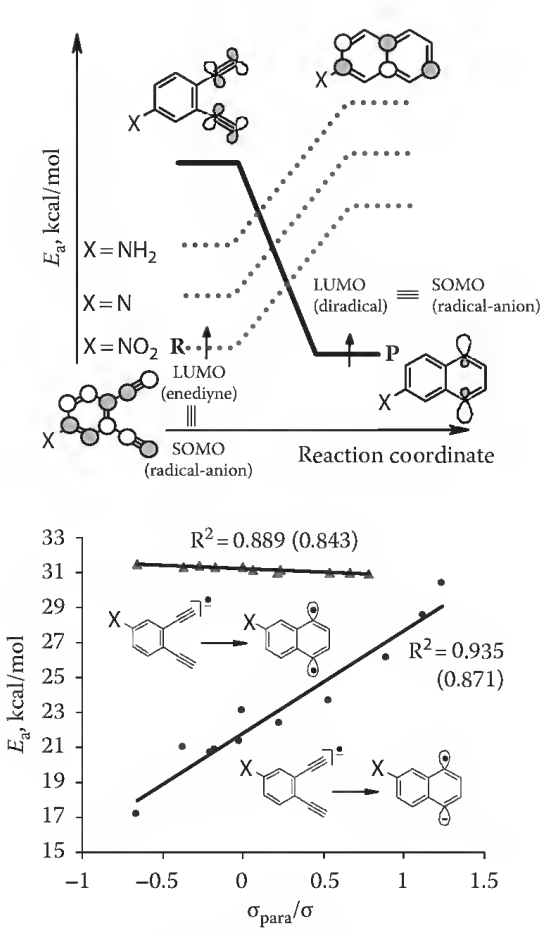

FIGURE 23.12 *Top*: The crossings of in-plane and out-of-plane frontier MOs in the radical-anionic Bergman cyclizations. *Bottom*: Correlation of UB3LYP(UBLYP)/6–31G** barriers for the radical anionic Bergman of substituted benzannelated enediynes with Hammett constants of remote substituents (σ(–) constants were used when available (X=NO_2, CHO, CN, F, Cl, OMe). Substituent effects on the C1–C5 cyclizations (not shown) follow an analogous trend. (Reprinted from Alabugin, I.V. et al., *J. Am. Chem. Soc.*, 125, 4495, 2003. With permission.)

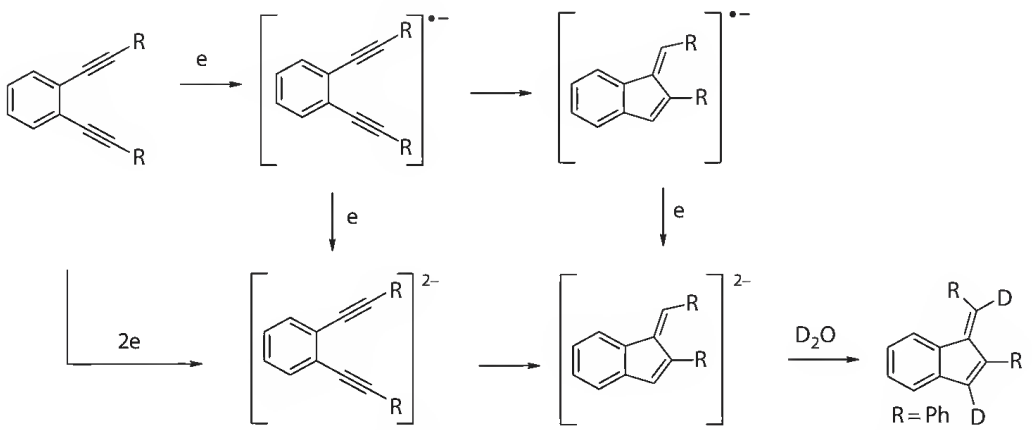

SCHEME 23.21 Dianionic cyclization of enediynes promoted by lithium naphthalenide reduction.

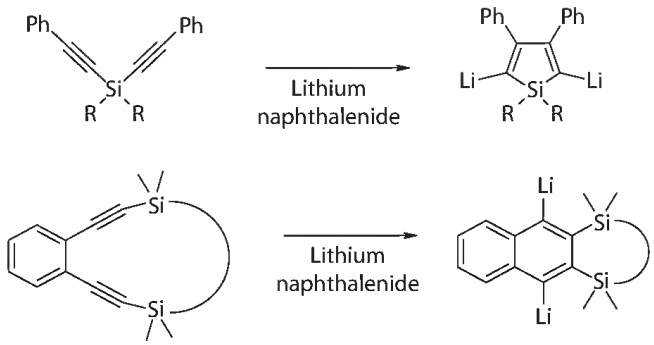

SCHEME 23.22 Endo-endo reductive cyclization of diethynylsilanes and cyclic 1,2-bis(silylethynyl)benzenes. (From Tamao, K. et al., *J. Am. Chem. Soc.*, 116, 11715, 1994. With permission.)

23.4 Other Electronic Perturbations in the Enediyne Moiety

At this point, it is not clear how electronic effects known to be important for the thermal Bergman cyclization[9b,10,11,22a–f,72,73] change their behavior in the photochemical version of this process. Based on the MO crossing model, the effects of *para*-substituents in the central ring of benzannelated enediynes may be even greater than such effects in thermal cyclization. Moreover, the substantial yield increase upon introduction of a *meta*-substituent in a terminal aryl group (Scheme 23.5) suggests the possibility of new electronic effects that are selectively applicable for the photochemical process, such as the photochemical *meta*-effect (also known as the *ortho,meta*-effect).[61] If the *meta*-effect is substantial, the effect of *ortho*-substituents is likely to be significant too and should reveal itself not only through sterics[64,74] but through an electronic interaction.

23.5 Control of Photo-Bergman Cyclization through Additional Excited States

23.5.1 Excited States Involving Coordinated Metal Ions

The work of Zaleski et al. combined the strain effects discussed earlier with unique electronic and structural features introduced by enediyne-metal coordination. New photochemical transitions derived from spatial overlap between the metal dσ or dπ molecular orbitals and enediyne orbitals can lead to the development of new strategies for the initiation of Bergman cyclization with lower energy photons. In particular, vanadium (V) metalloenediyne compounds (Scheme 23.23) exhibited strong ligand-to-metal charge transfer (LMCT) transitions in the near-IR region because of low redox potentials of the high valent vanadium center and the easily oxidizable metal-binding motif.[32a,75] These LMCT transitions were used to photothermally activate the metalloenediyne toward Bergman cyclization upon 785 nm laser excitation, despite the compound's relative inertness to photo-Bergman reactivity upon electronic

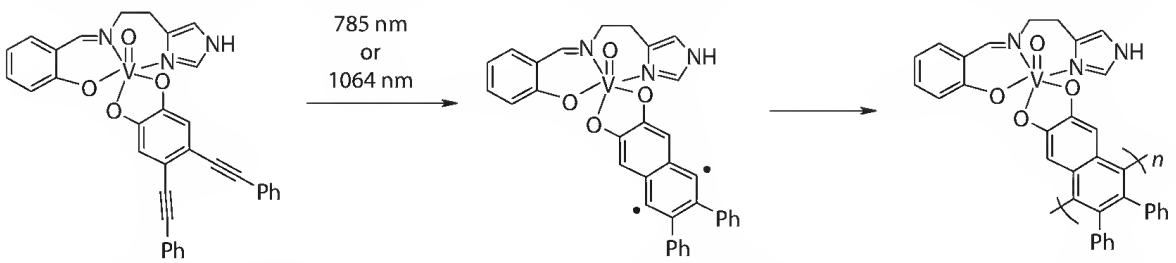

SCHEME 23.23 Photothermal cyclization of vanadium (V) metalloenediyne in the solid state. (From Kraft, B.J. et al., *Inorg. Chem.*, 42, 1663, 2003. With permission.)

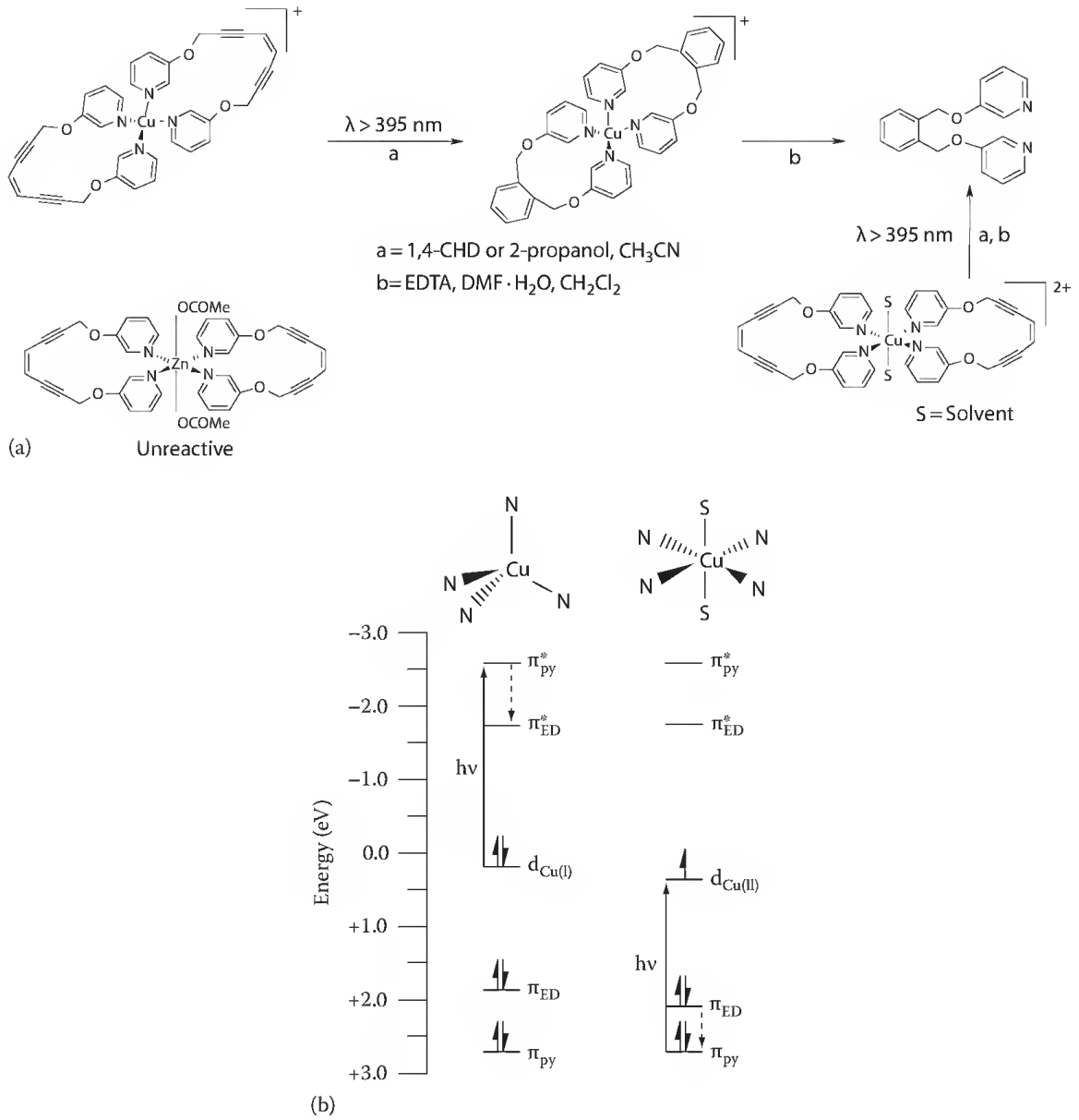

SCHEME 23.24 (a) Photo-Bergman cyclization of copper metalloenediynes via metal–ligand charge transfer complex. (b) Relative energies of copper and ligand MOs proposed to be involved in the photoelectronic Bergman cyclization of Cu(I) and Cu(II)-metalloenediynes. (Reprinted from Kraft, B.J. et al., *Inorg. Chem.*, 42, 1663, 2003. With permission.)

excitation in the ultraviolet spectral region. Formation of black, sparingly soluble products with vibrational characteristics of poly(*p*-phenylene) together with the detection of high-molecular-weight species (MW up to 274,000 Da) suggests photopolymerization as the major process.

Photo-Bergman cyclization can also be promoted by charge transfer from metals to ligands (MLCT). Zaleski et al.[76] suggested that MLCT from the metal dπ orbital to the empty π* orbital of the pyridine ring is responsible for the Bergman cyclization of the enediyne Cu(I) complexes in Scheme 23.24. Neither the uncomplexed ligand nor the analogous Zn complex was photochemically reactive. In the case of Cu(II) complex, the charge transfer from π-orbital of the pyridine to *d*-orbital of the metal results in a partial π-hole in the pyridine ring, which is transferred, to some extent, onto the enediyne unit. Thus, the photoreaction may involve an enediyne-centered state, despite initial population of the formal Cu-pyridine CT manifold.

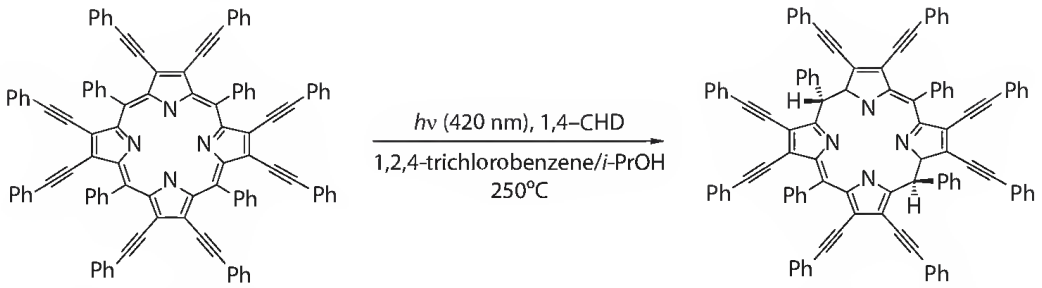

SCHEME 23.25 Reduction of the porphyrin backbone during photolysis of tetraphenyl octakis (phenylethynyl) porphyrine. (From Chandra, T. et al., *Inorg. Chem.*, 42, 5158, 2003. With permission.)

A more detailed analysis with time-dependent density functional theory (TD-DFT) indicated that chelation to Cu(I) or Cu(II) creates several low-energy (<3.0 eV) charge transfer excited states. The multiconfigurational nature of the charge transfer excited states indicates the electronic similarities between the excited MLCT or LMCT configuration and the cyclization transition state electronic structure, which drives the Bergman cyclization of metalloenediynes. In agreement with the experimental data, the Zn(II) complex does not exhibit low-energy charge transfer states because of the poor energetic overlap between the Zn(II) d-orbitals and the pyridine orbitals, resulting in *cis–trans* photoisomerization.

Zaleski and coworkers also prepared an interesting family of enediynes based on the porphyrine core.[77] These porphyrinic enediynes (Scheme 23.25) show systematic red shifts in their electronic spectra as a function of the number of conjugated alkyne units (~13 nm/alkyne), which indicates participation of the enediyne units in the electronic excited states. Photochemical activation of the free base of tetraphenyl octakis(phenylethynyl) porphyrine derivative only led to the reduction of the porphyrin backbone via H-atom addition at the opposing *meso*-positions, suggesting significant activation barriers for the photo-Berman cyclization.

A very interesting set of observations that correlated thermal and photochemical reactivity of porphyrine-based enediynes was reported recently by Zaleski and coworkers.[78] Unlike the previous example, electronic excitation of the porphyrine chromophore is capable of activating the acyclic enediyne unit toward cycloaromatization (albeit the reduction products have been formed as well). The cyclization efficiency depends, however, on the excitation wavelengths (35% vs. 15% vs. 6% of the photoproduct for the $\lambda \geq 395$ nm (Soret), ≥ 515 nm and ≥ 590 nm (Q-band) excitation, respectively). The initially formed cyclic product is trapped via radical addition to the adjacent *meso*-phenyl rings and subsequent rearomatization with the formation of final picenoporphyrin products (Scheme 23.26).

Barriers for the Bergman cyclization step in the excited state depend on the steric bulk of the substituents R at the alkyne termini. For R=H, the corresponding photoproduct is formed in up to 35% yield

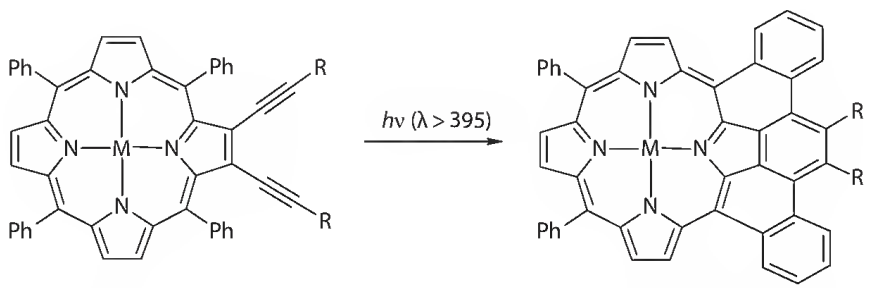

SCHEME 23.26 Formation of picenoporphyrins from dialkynylporphyrinic enediynes. (From Nath, M. et al., *J. Am. Chem. Soc.*, 127, 478, 2005. With permission.)

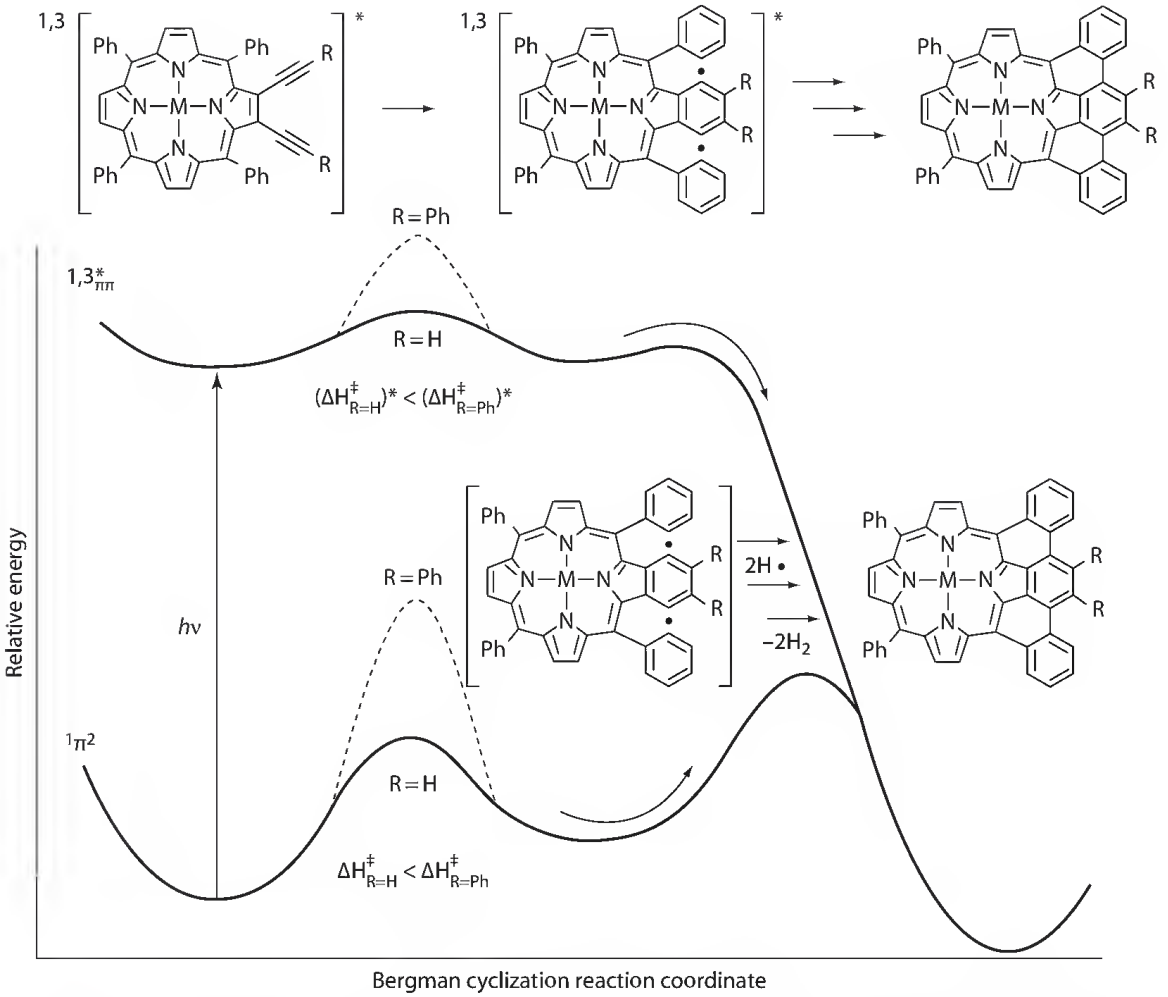

SCHEME 23.27 Suggested reaction energy profiles for ground- and excited-state Bergman cyclization of porphyrin-based enediynes. (Reprinted from Nath, M. et al., *J. Am. Chem. Soc.*, 127, 478, 2005. With permission.)

even at ~10°C whereas irradiation of the diphenyl substituted enediyne produced only small amounts (5%–8%) of picenoporphyrin even at 125°C. Because no thermal Bergman cyclization has been observed at 125°C with R = Ph, this result suggests that the excited state cyclization barrier is still lower than the ground state barrier. Based on the comparison of thermal and photochemical reactivity for the two enediynes, the authors suggested qualitative potential energy surfaces summarized in Scheme 23.27. The presence of substantial activation barriers in the excited state hypersurface is consistent with the theoretical analysis of formally forbidden photo-Bergman cyclizations presented in Section 23.3.1.2.

An interesting variation where the photo-Bergman cyclization is inhibited by metal complexation as described by O'Connor et al.[79] (Scheme 23.28). In contrast to the parent benzannelated cyclic enediyne, its ruthenium complex did not produce any cyclized product upon photoactivation. The reluctance of this compound to be involved in photochemical cycloaromatization is tentatively attributed to decreased aromaticity in the incipient 1,4-diradical, potentially providing an interesting corollary to the results summarized in Scheme 23.8.

23.5.2 Intramolecular Electron Transfer

Schmittel and coauthors described a novel concept for activation of enediynes for DNA cleavage based on intramolecular electron transfer between a donor and an acceptor attached at the opposite enediyne termini.[32b] There is evidence that the mode of action may involve a biscumulenic

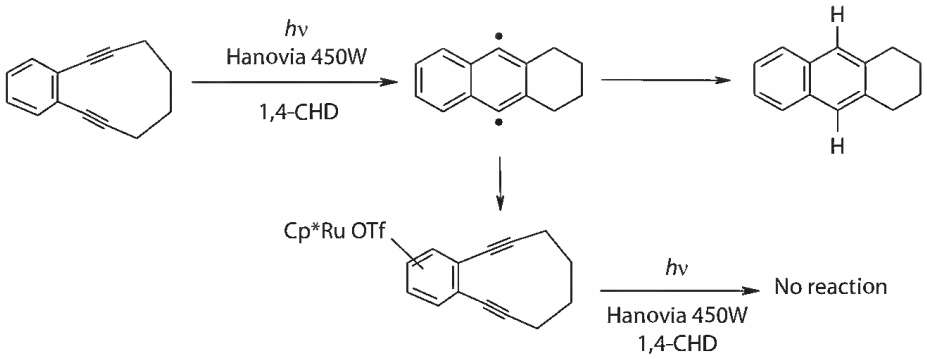

SCHEME 23.28 Inhibition of photo-Bergman cyclization upon Ru complexation.

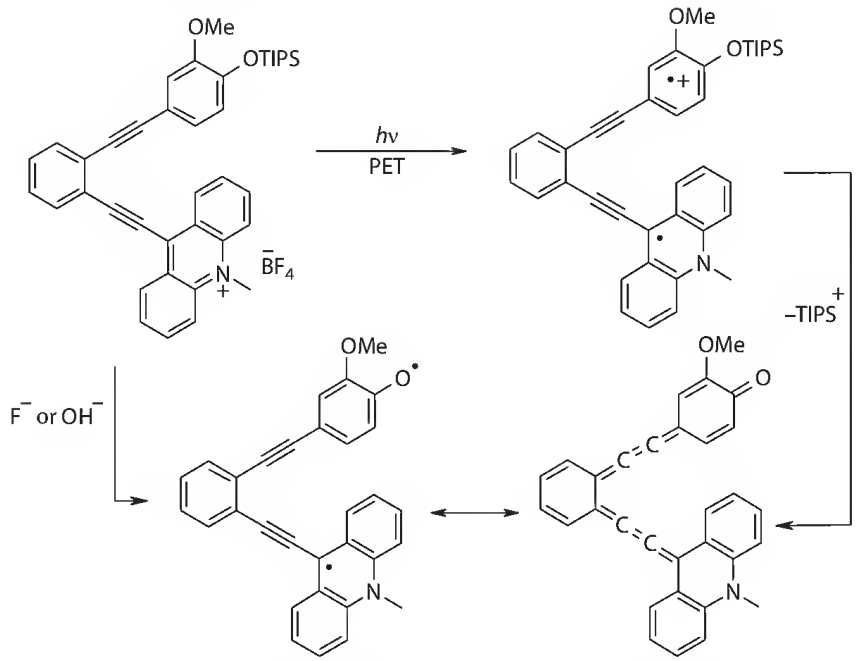

SCHEME 23.29 Activation of enediynes through photoinduced intramolecular electron transfer. (From Schmittel, M. et al., *Chem. Comm.*, 7, 646, 2003. With permission.)

intermediate (Scheme 23.29). Although the exact fate of this intermediate is still speculative, the available experimental data suggest that this intermediate is capable of inducing efficient DNA cleavage (vide infra).

23.6 H-Abstraction Ability of Diradicals Produced in Thermal and Photochemical Bergman Cyclizations

A common theme in photochemical Bergman cyclizations discussed in the previous sections is the relatively low efficiency of *p*-benzyne trapping through H-abstraction. Very often, a large excess of the H-donor is needed to achieve high yields of cycloaromatized products.

In general, *p*-benzyne diradicals are known to be less reactive in H-abstraction reactions than the phenyl radical due to coupling between the two radical centers. The nonbonding electrons in diradicals can interact by either direct coupling through space (TS) or by indirect coupling through antibonding (σ^*) bridge orbitals (through bond (TB) coupling). In the ground state *p*-benzyne species, TB coupling

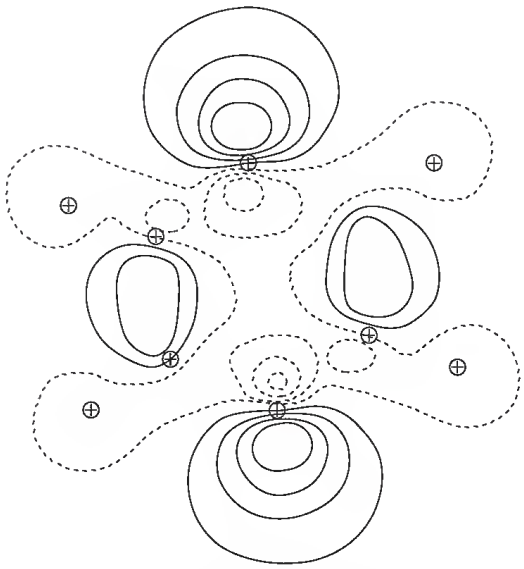

FIGURE 23.13 Singly occupied MO (SOMO) for *p*-benzyne radical anion. (From Alabugin, I.V. et al., *J. Am. Chem. Soc.*, 125, 14014, 2003 and reference therein. With permission.)

of the two σ radicals through σ* bridge orbitals is the main conduit for the electronic interaction.[55] This interaction, which is absent in monoradicals and triplet *p*-benzynes,[80] provides an additional 3–5 kcal/mol of stabilization energy to *p*-benzyne-type diradicals. Since this stabilizing energy is lost with the first H-atom abstraction, the ground state *p*-benzyne diradicals are less reactive and more selective than simple phenyl radicals.

Interestingly, the magnitude of coupling between the nonbonding electrons increases dramatically in the radical-anionic cycloaromatization reactions.[9b] In brief, this increase can be attributed to the fact that the LUMO of the diradicals, which is populated by the one-electron reduction, corresponds to a symmetric combination of the two nonbonding orbitals. This effect and the more spatially diffuse anionic orbitals allow for an increased direct through-space interaction of the two radical-anionic centers in *p*-benzyne (Figure 23.13).

The markedly increased coupling of non-bonding orbitals in σ,σ-radical-anions may be of general importance not only for radical-anionic reactions,[81] but also for their photochemical analogues where the same MO is populated by excitation instead of reduction. Consequently, an adiabatic photochemical Bergman cyclization in the singlet state should lead to the *p*-benzyne intermediate having significant bonding character between the "radical" orbitals. This interaction can contribute to the relative inefficiency of H-abstraction by the photochemically produced *p*-benzynes, provided that such a diradical is converted into the ground state *p*-benzyne sufficiently slowly.

23.7 Photophysical Properties of Enediynes

Common photophysical considerations, such as excited state lifetimes, excitation energies, geometries of excited states, excited state potential energy surfaces, availability of relevant conical intersections, efficiency of intersystem crossing, molar absorptivities, and two-photon absorption cross section, are important for the development of photochemical reactions of enediynes. Detailed photophysical studies of these molecules are still rare. An exception to this rule is provided by a recent systematic analysis of photophysical properties of a family benzannelated enediynes.[64] Although this study concentrated on the two-photon excitation of these compounds, it provided useful basic photophysical information, which is summarized in Table 23.2.

All enediynes in Figure 23.14 showed two major absorption peaks, corresponding to the S1 and S2 excited states, respectively. According to TD-DFT analysis, in most compounds, the first excited state

TABLE 23.2 Selected Photophysical Parameters for Enediynes from Figure 23.14

	Absorption			Emission		
Compound	S1 λ_{peak}	λ_{max} (nm)	ε (λ_{max})	λ_{max} (nm)	τ_{fl} (ns)	Quantum Yield
7	310	273	66,000	360	1.5	0.52
8	300	278	50,500	370	1.8	0.63
9	360	272	55,300	460	5.3	0.9
10	350	320	23,300	—	—	—
11	315	278	86,700	370	3.9	0.49
12	320	286	70,300	380	2.1	0.83
13	325	281	89,200	380	2.1	0.81
14	315	313	36,200	380	0.46, 0.20	0.07
15	305	303	49,300	440	5.5, 0.47	0.011

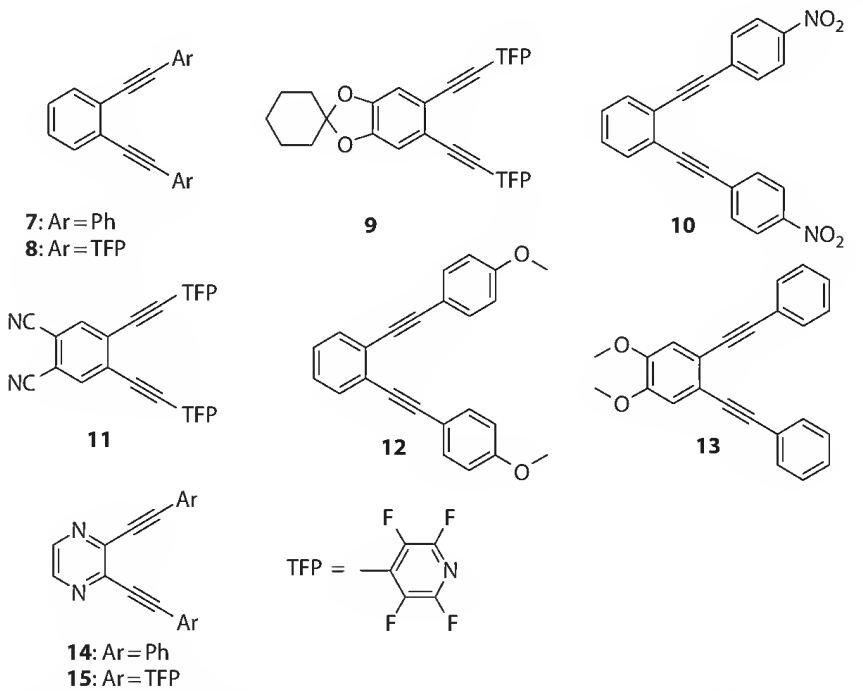

FIGURE 23.14 Structures of aromatic and heteroaromatic enediynes used to investigate electronic effects at photophysical properties of the enediyne moiety. (From Kauffman, J.F. et al., *J. Phys. Chem. A*, 110, 241, 2006. With permission.)

has B symmetry with energies in the 300–360 nm range. This absorption is redshifted related to that of *o*-diethynylbenzene and nonbenzenoid enediynes, which absorb below 280 nm.[82] The S1 energies are sensitive to the presence of donor and acceptor substituents and the lowest energy absorption peak for all the compounds except the two pyrazines corresponds to the first excited state of B symmetry. For pyrazines only, the lowest observed OPA (one-photon-absorption) state has A symmetry and corresponds to the excitation to the third excited state calculated by TD-DFT method. Since all the molecules have axial rather than central symmetry, both transitions conserving and changing symmetry are dipole allowed in the linear optical response.

The two-photon excited fluorescence (TPEF) spectra of these enediynes are identical to their one-proton emission spectra, indicating that the same excited state is ultimately populated. However, the TPEF is allowed only via two-photon absorption by the S2 (or higher) state of the enediynes. In perfect agreement with the experiment, the B states disappear from the picture in the two-photon computed excited states.

TABLE 23.3 Two-Photon Excited Fluorescence (TPEF) of Enediynes

Compound	Excitation λ (nm)	$\lambda_{ex}/2$ (nm)	Relative Quantum Yield	Ratio of TPA Cross Sections, $\frac{\delta_n^{TPA}}{\delta_3^{TPA}}$
7	542	271	0.58	0.55
8	553	277	0.70	0.37
9	542	271	1.0	1
10	458	229	—	—
11	553	277	0.54	0.26
12	565	283	0.92	0.46
13	565	283	0.90	0.39
14	504	252	0.082	1.34
15	514	257	—	—

All TPA states have the same A symmetry as the ground state, mimicking selection rules for centrosymmetric molecules. However, unlike the centrosymmetric case, the state with the largest TPA cross section is also active (and even dominant) in the OPA spectrum. This observation can be rationalized by recalling that typically strong TPA activities are observed in the substituted chromophores in the direction of intramolecular charge transfer, which would correspond to the symmetry axis in this case. The summary for TPEF of enediynes is shown in Table 23.3. TPA cross sections in benzannelated enediynes are sensitive to substitutions at both the core and the periphery of the enediyne chromophore: introduction of donor substituents at the core and strongly acceptor substituents at the periphery increase the TPA cross section.

23.8 DNA Cleavage by Photochemically Activated Enediynes

Reactive species generated from enediynes upon photochemical excitation can potentially target multiple cellular targets. Because protein damage by enediynes has been discussed in detail earlier,[15] this section will concentrate on reactivity of photoactivated enediynes toward DNA.

Comparison of reactivity of different enediynes toward DNA is complicated by significant variations in experimental conditions such as enediyne concentration, irradiation time, light intensity, irradiation wavelengths, as well as potential differences in the nature of chemical steps involved in the mechanism of DNA damage. Enediyne-based DNA photocleavers may operate not only through a photochemical Bergman reaction but also via photoactivation of thermal Bergman cyclization via photolytic activation of enediyne prodrugs, photothermal Bergman cyclization where excitation followed by radiationless decay provides thermal energy for the cyclization, C1–C5 cyclization, photoinduced electron transfer, direct H-transfer to an excited state of the reactant, as well as nucleobase alkylation. To further complicate the comparison, the efficiency of DNA cleavage depends not only on the efficiency of the radical-generating step but also from such factors as solubility in water, binding mode (e.g., intercalation vs. groove binding) and overall affinity to DNA, involvement of electron transfer in quenching of excited states and in the propagation of damage by hole- or exciton-hopping, the intermediacy of diffusing oxygen species etc. As the result, some of the illustrative data shown in Table 23.4 may reflect a complex combination of factors.

Interestingly, hybrid antitumor antibiotic dynemicine A (20 μM) induces considerable DNA cleavage when activated by visible (<580 nm) light.[83] This process is suggested to proceed through photoreduction of the antibiotic quinone core, followed by a thermal Bergman cyclization. Natural enediynes esperamicin and neocarzinostatin were also reported to cause DNA cleavage upon photochemical activation.[90] About 13% of ds DNA cleavage by 1 μM esperamicin A_1 has been observed after 15 min of 254 nm irradiation. The exact chemical mechanism of these photochemical processes is still unknown

TABLE 23.4 Comparison of DNA Cleavage by Photochemically Activated Enediynes

Structure	Condition	DNA Cleavage	Chemical Mechanism	Ref.
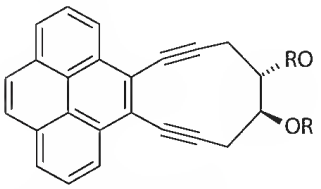 R = $OC(O)(CH_2)_3N^+HMe_2Cl^-$	>290 nm, pH 8, 15–60 min	20 μM: ss	Photo-Bergman cyclization	29
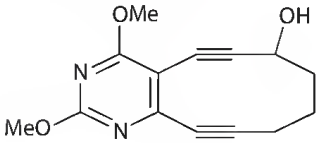		40 μM: ss 4000 μM: signs of ds	Photo-Bergman cyclization	30
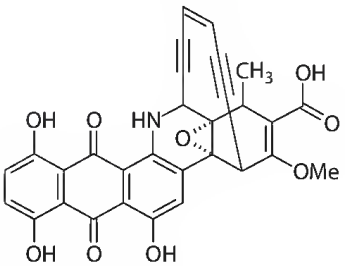 Dynemicin A	580 nm, pH 7.5, 30 min	20 μM: ss/ds	Photoactivation of thermal Bergman cyclization	83
Esperamicin	254 nm, pH 7.5, 15 min	1 μM: ss (41.4%), ds (13.0%) T, C preferential cleavage	Possibly photo-Bergman cyclization	90
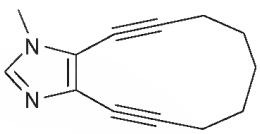	254 nm, pH 7.5, 15 min	100 μM: ss/ds T, C, G preferential cleavage	Unknown	90
Neocarzinostatin	>290 nm, 60 min	15 μM: ss (43%)	Photo-Bergman cyclization	38
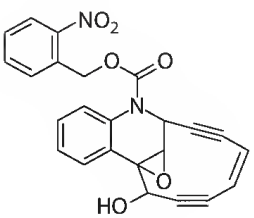	>300 nm, pH 6, 7, 15 min	210 μM: ss/ds	Photo-activation of thermal Bergman cyclization	31a
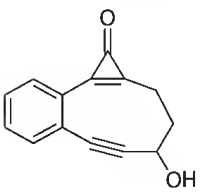		1 mM: ss (45%), ds (>5%) 5 mM: ss (67%), ds (10%)	Activation of prodrug via photolysis → thermal Bergman cyclization	19e

(*continued*)

TABLE 23.4 (continued) Comparison of DNA Cleavage by Photochemically Activated Enediynes

Structure	Condition	DNA Cleavage	Chemical Mechanism	Ref.
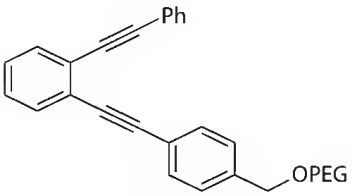	pH 8.5, 3 h	1 μM: ss (24%) ds (?)	Photo-Bergman cyclization	93
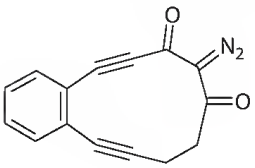	351.1 nm, 8 min	<500 μM: ss >500 μM: ss/ds	Photo-activation of thermal Bergman cyclization	19e
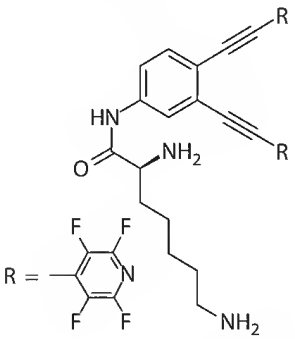	>310 nm, pH 6, 7, 8, 10 min	15 μM: pH 6: ss (68%), ds (15%), pH 7: ss (45%), ds (3%), pH 8: ss (23%), ds (0%)	Combination of C1–C5 cyclization, photoinduced electron transfer (PET), nucleobase alkylation, and generation of reactive oxygen species	34
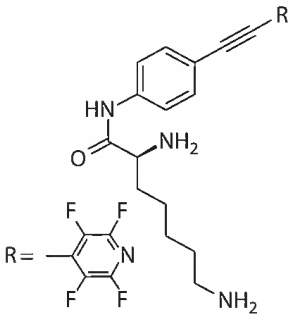	>310 nm, pH 6, 7, 8, 10 min	15 μM: pH 5.5: ss (65%), ds (32%), pH 7: ss (34%), ds (6%), pH 8: ss (14%), ds (0%)	PET, H-abstraction, nucleobase alkylation,	34
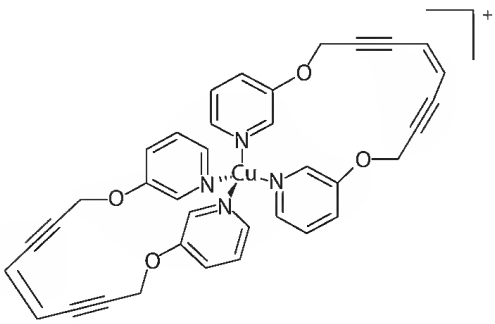	≥395 nm, pH 7.6, 8 h	12.5 μM: ss 50–500 μM: ss (80%–60%), ds (20%–40%)	Metal–ligand charge-transfer-promoted photo-Bergman cyclization	75
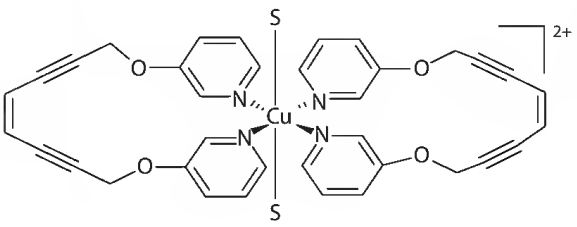	≥395 nm, pH 7.6, 8 h	10–25 μM: ss 50–500 μM: ss (60%–50%), ds (40%–50%) C-4′ H-atom abstraction	Metal–ligand charge-transfer-promoted photo-Bergman cyclization	75

TABLE 23.4 (continued) Comparison of DNA Cleavage by Photochemically Activated Enediynes

Structure	Condition	DNA Cleavage	Chemical Mechanism	Ref.
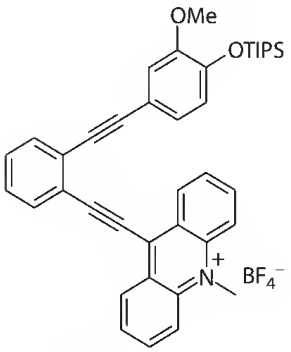	419 nm, pH 8	66 M: 0.5–1 h: ss 2–4 h: ss/ds	Formation of a biscumulenic intermediate by photoinduced electron transfer (PET)	31b
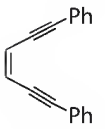 *E-Z* isomers	350 nm, pH 7.4	200 μM: ss 44% (Z), 57% (E) in O_2 18% (Z), 32% (E) in Ar	Formation of photosensitized reactive oxygen species and photodynamic reactions (?)	25

although spin-trapping experiments support radical species formation. Esperamicin shows the same base selectivity for the photochemical DNA cleavage and the usual, thiol-activated thermal pathway. In contrast, light-activated neocazinostatin attacks G-bases that are rarely damaged by the thiol-activated neocarzinostatin, suggesting that the involved chemistry is different for the photochemical DNA cleavage by this natural enediyne.

De novo designed enediynes can induce photochemical DNA cleavage as well. Whereas the ss cleavage is rather common, efficient ds cleavage remains a difficult goal to accomplish. This is an important problem because the ds DNA cleavage is much more difficult to repair and more important therapeutically than ss DNA cleavage.[84]

Representative examples are summarized in Table 23.4. A water-soluble dialkynylpyrene reported by Funk et al.[29] provided some ds DNA cleavage at 20 μM enediyne concentration after only 15 min of irradiation. Pyrimidine alcohol (Scheme 23.10) yields significant DNA ss cleavage at 40 μM and signs of ds cleavage at 4000 μM under irradiation with 313 nm light.[30] A recent report of Zaleski et al. showed that copper complexes of bis(pyridine) enediynes lead to a mixture of ds and ss cleavage with complete consumption of the supercoiled plasmid DNA after 8 h irradiation at concentrations of enediynes in the range of 50–500 μM.[80] At the lower concentrations, only ss cleavage is observed. Schmittel et al. reported[32b] that the mixture of ds and ss DNA cleavage was observed at the rather high (1 mM) enediyne concentration after 4 h of 419 nm irradiation.

These results do not suggest the relative inefficiency of the photo-Bergman cyclization in comparison to the thermal Bergman cyclization because most literature examples of DNA cleavages promoted by thermal activation of enediynes are ss cleavages as well. This lack of efficiency is not surprising because the two radical centers of a *p*-benzyne diradical should target the opposite DNA strands with 100% efficiency for the ds cleavage to occur. In practice, one of the radical centers is often quenched by reaction with the environment or by abstraction of hydrogen atoms from an already damaged strand ("silent damage"). Even the most efficient of natural enediynes, calicheamicin γ1 only leads to 1:2–1:3 ds:ss cleavage ratios.[85] Although these numbers still compare favorably with bleomycin-mediated DNA cleavage (1:6–1:20),[86–88] there is clearly room for improvement.

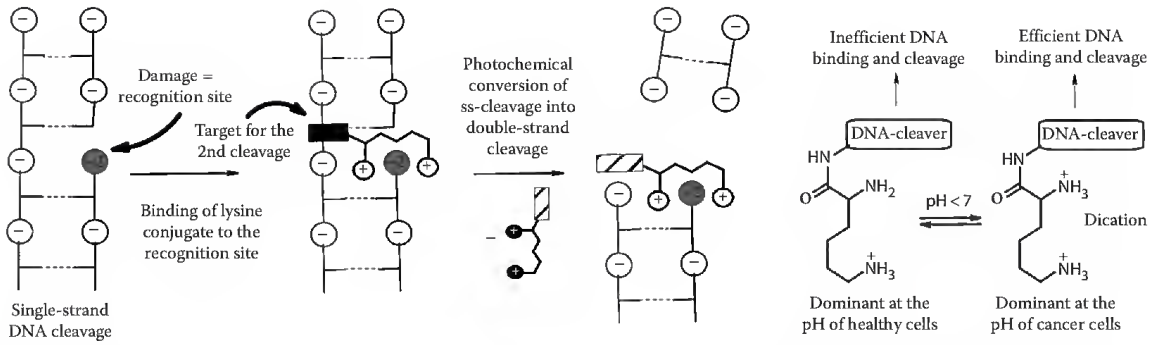

FIGURE 23.15 *Left*: Photochemical conversion of ss DNA cleavage into more therapeutically important ds DNA cleavage through lysine-phosphate monoester recognition of the initial damage site. *Right*: Design of pH-dependent DNA cleavers based on different stages of protonation of the lysine side chain.

Designing a more powerful DNA-damaging warhead capable of a larger number of hydrogen abstractions provides a promising approach toward increasing the ds cleavage efficiency. In accord with these expectations, TFP-enediynes provide significant amounts of ds DNA cleavage at relatively low concentrations (<10 μM). This efficiency stems from the fact that this reaction (C1–C5 cyclization) leads to the formal abstraction of four H-atoms (compared to only two H-abstractions in the Bergman cyclization). Not only is the increase in the net number of DNA-damaging events likely to result in the efficient abstraction of H-atoms and protons from the ribose backbone but these compounds can also damage DNA through a synergistic combination of oxidative damage (initiated via photoinduced electron transfer from DNA) and nucleobase alkylation.

The intrinsically high efficiency of ds cleavage by bis-TFP-enediynes can be improved even further by combining the light-activated part with functional groups capable of binding selectively to the site of an initial ss cleavage and transforming the easily repairable ss DNA damage into much more therapeutically important ds DNA damage (Figure 23.15, left).[89] Equally interesting is that this class of DNA binders displays pH dependency, which makes it suitable for selective targeting of cancer cells (Figure 23.15, right).

The pH-switching behavior of lysine–enediyne conjugates results in a dramatic increase in reactivity at the lower pH of hypoxic tumor cells. Remarkably, the change in reactivity occurs at a relatively narrow and predefined pH point (~pH 6). Molecular hybrids that combine lysine and TFP-substituted DNA photocleavers provide the DNA cleavage ratios of up to the 1:2 ds:ss at pH 5.5 at concentrations and irradiation times where almost no ds cleavage is observed at the pH of healthy cells (Figure 23.16).

Moreover, recent findings of efficient DNA cleavage by monoalkynes incapable of the Bergman or C_1–C_5 cyclizations[34,92] and involvement of PET in the DNA damage by phenyl- substituted enediynes expected to undergo the photo-Bergman cyclization[92] suggest that chemical mechanisms assumed in previous studies should be revisited.

Binding to DNA is also important for the efficiency of DNA cleavage. For example, bis-TFP-enediyne/lysine conjugates damage DNA through a complex mechanism that involves PET. Because this damage can be decreased by addition of chemical agents that can trap (Figure 23.17a). Other alternative photochemical pathways different from the photo-Bergman cyclization are also plausible as illustrated in Figure 23.18.

Interestingly, DNA cleavage with a related monoalkyne (Figure 23.17b) is less sensitive to the effects of the aforementioned additives, especially at the lower pH, suggesting that tight binding and efficient DNA cleavage without the involvement of diffusing species. The differences between the two DNA cleavers may be a consequence of their DNA-binding modes because the enediyne is an intercalator while the monoacetylene is a major groove binder according to a spectroscopic evidence.

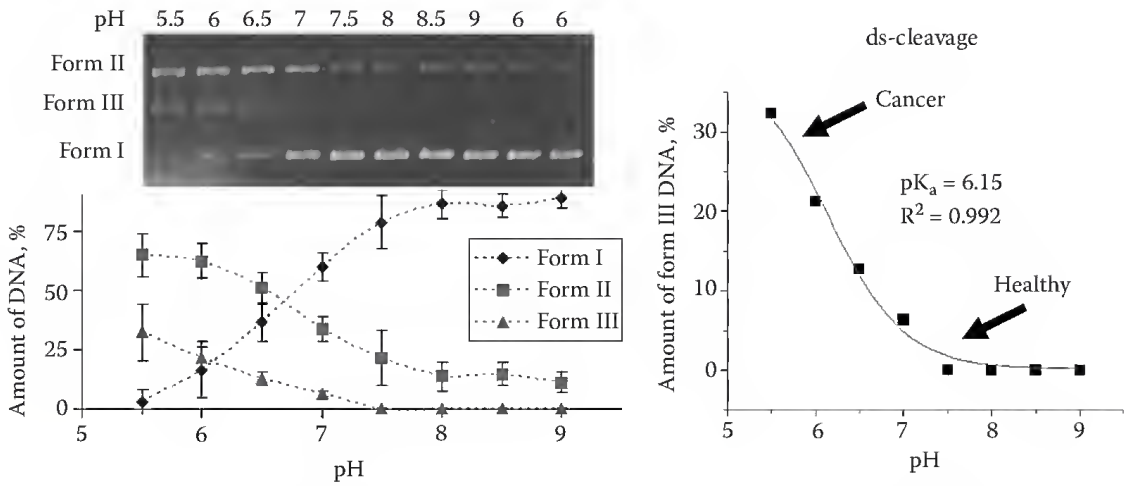

FIGURE 23.16 *Left*: Plasmid relaxation assays with TFP-acetylene-lysine conjugate (shown as entry 10 in Table 23.4, 15 μM) and pBR 322 plasmid DNA (30 μM/bp) in 20 mM phosphate buffer after 3 min of irradiation. Form I = intact supercoiled DNA, Form II = relaxed form (ss cleavage), Form III = linear form (ds cleavage). Lanes 1–8: from pH 5.5 to pH 9, lane 9: no compound + UV, lane 10: compound + no UV. Cleavage data were quantified through densitometry. Reported values represent the average of four experiments. *Right*: Dependence of the efficiency of ds cleavage from pH and its fit to the Henderson-Hasselbalch equation. (Reprinted from Yang, W.-Y. et al., *J. Am. Chem. Soc.*, 131, 11458, 2009. With permission.)

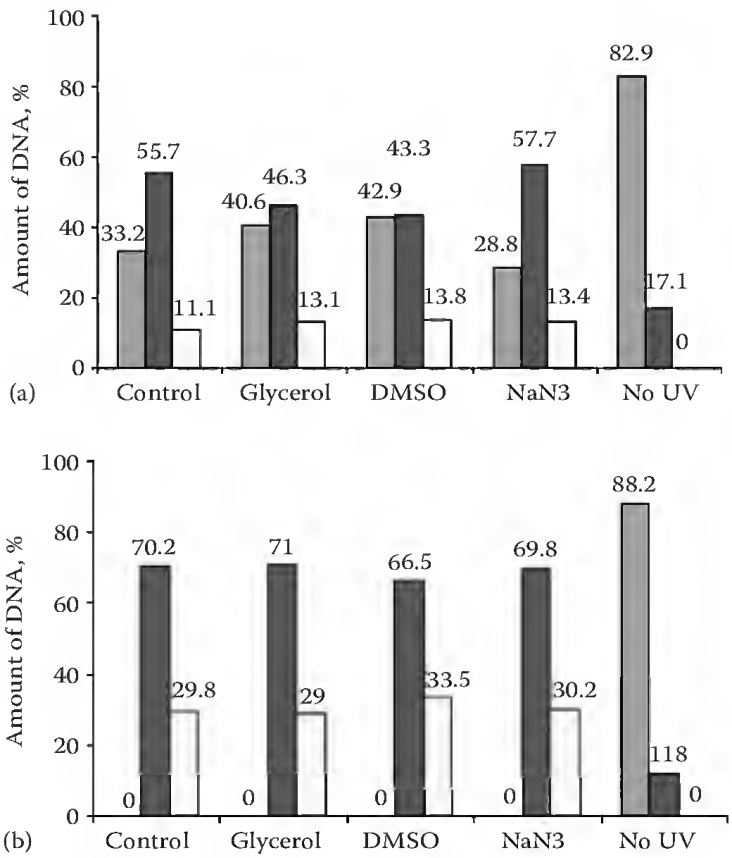

FIGURE 23.17 Effect of hydroxyl radical/singlet oxygen scavengers upon the efficiency of DNA cleavage by amino acid/enediyne (a) and amino acid/acetylene (b) conjugates at pH 6 after 5 min irradiation. Color coding: light blue, supercoiled DNA; dark purple, relaxed DNA (=ss cleavage); light yellow, linear DNA (=ds cleavage.) (From Yang, W.-Y. et al., *J. Am. Chem. Soc.*, 131, 11458, 2009. With permission.)

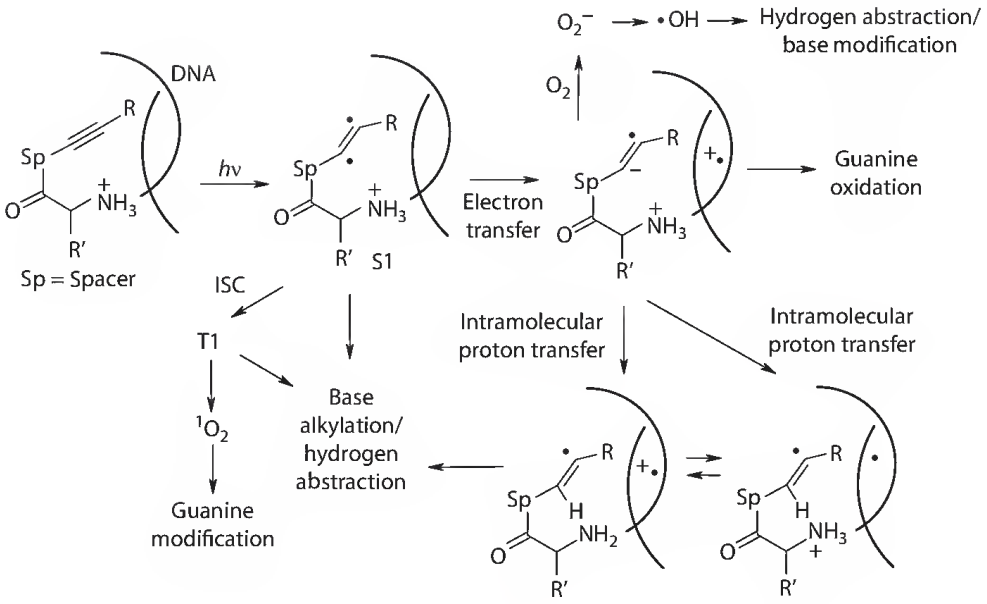

FIGURE 23.18 Summary of possible mechanistic alternatives for the observed DNA cleavage by amino acid/acetylene conjugates. (From Yang, W.-Y. et al., *J. Am. Chem. Soc.*, 131, 11458, 2009. With permission.)

Remarkably, the TFP-acetylene-lysine conjugates can destroy more than 90% of LNCap cancer cells in one treatment as concentrations as low as 10 nM. It is encouraging that, at these concentrations, toxicity without light is negligible. Similar increases in reactivity upon activation with light were observed in parallel experiments with UMRC3, UMRC6, and 786-O cancer cell lines.[34]

23.9 Conclusion

The fast-growing body of research expanded our knowledge of photochemical reactions of enediynes and demonstrated the vast potential of these molecules as tools for efficient DNA modification and design of light-activated drugs.

Although it is clear now that efficient photochemical cycloaromatization reactions are possible, further research is needed to fully elucidate the electronic factors that control these processes. A robust theoretical model that incorporates the experimental data in a coherent and logical framework is needed for guiding the future development of this field.

The presence of the two orthogonal π-systems in alkynes is especially important for the understanding and control of photochemical cycloaromatization reactions where the two systems play complementary important roles. General understanding of the key photophysical processes and barriers on the excited state surfaces is still insufficient. Excited states that involve the in-plane MOs are likely to play the key role in the control of photochemical reactivity. Two-photon excitation of enediynes should be possible via inclusion of additional frontier MOs of different symmetry or excitation to a higher energy excited state.

From a practical perspective, it is important to increase the efficiency of ds DNA cleavage and develop a deeper understanding of the molecular details of DNA-enediyne binding and chemical mechanisms of DNA damage. From a synthetic perspective, it would be very interesting to harness the bond-forming potential of these processes in the design of efficient cascade sequences that open access to new conjugated materials.[17c,45b,93]

Acknowledgment

We are grateful to the National Science Foundation (CHE-0848686) for partial support of this research.

References

1. Nicolaou, K. C.; Smith, A. L.; Yue, E. W., Chemistry and biology of natural and designed enediynes, *Proc. Natl. Acad. Sci. USA* 1993, *90*, 5881.
2. Galm, U.; Hager, M. H.; Lanen, S. G. V.; Ju, J.; Thorson, J. S.; Shen, B., Antitumor antibiotics: Bleomycin, enediynes, and mitomycin, *Chem. Rev.* 2005, *105*, 739.
3. (a) Jones, R. R.; Bergman, R. G., *p*-Benzyne. Generation as an intermediate in a thermal isomerization reaction and trapping evidence for the 1,4-benzenediyl structure, *J. Am. Chem. Soc.* 1972, *94*, 660. (b) Bergman, R. G., Reactive 1,4-dehydroaromatics, *Acc. Chem. Res.* 1973, *6*, 25.
4. Pogozelski, W. K.; Tullius, T. D., Oxidative strand scission of nucleic acids: Routes initiated by hydrogen abstraction from the sugar moiety, *Chem. Rev.* 1998, *98*, 1089.
5. Navarro-Vazquez, A.; Prall, M.; Schreiner, P. R., Cope reaction families: To be or not to be a biradical, *Org. Lett.* 2004, *6*, 2981.
6. Roth, W. R.; Hopf, H.; Horn, C., Energy well of diradicals, V. 1,3,5-cyclohexatriene-1,4-diyl and 2,4-cyclohexadiene-1,4-diyl, *Chem. Ber.* 1994, *127*, 1765. Wenthold, P. G.; Squires, R. R., Biradical thermochemistry from collision-induced dissociation threshold energy measurements. Absolute heats of formation of *ortho*-, *meta*-, and *para*-benzyne, *J. Am. Chem. Soc.* 1994, *116*, 6401. Davico, G. E.; Bierbaum, V. M.; De Puy, C. H.; Ellison, G. B.; Squires, R. R., The C–H bond energy of benzene, *J. Am. Chem. Soc.* 1995, *117*, 2590.
7. (a) Prall, M.; Wittkopp, A.; Schreiner, P. A., Can fulvenes form from enediynes? A systematic high-level computational study on parent and benzannelated enediyne and enyne–allene cyclizations, *J. Phys. Chem. A* 2001, *105*, 9265. (b) Vavilala, C.; Byrne, N.; Kraml, C. M.; Ho, D. M.; Pascal, R. A., Thermal C^1–C^5 Diradical cyclization of enediynes, *J. Am. Chem. Soc.* 2008, *130*, 13549.
8. Engels, B.; Lennartz, C.; Hanrath, M.; Schmittel, M.; Strittmatter, M., Regioselectivity of diradical cyclizations of enyne-allenes: Influence of substituents on the switch from the Myers-Saito to the novel C2–C6 cyclization, *Angew. Chem.* 1998, *37*, 1960. Schmittel, M.; Kiau, S.; Siebert, T.; Strittmatter, M., Thermal and electron transfer induced reactions of enediynes and enyne-allenes. 6. Steric effects in enyne-allene thermolyses: Switch from the Myers-Saito reaction to the C2–C6 cyclization and DNA strand cleavage, *Tertrahedron Lett.* 1996, *37*, 7691. Schmittel, M.; Keller, M.; Kiau, S.; Strittmatter, M., Thermal and electron-transfer-induced reactions of enediynes and enyne-allenes. Part 8. A surprising switch from the Myers-Saito cyclization to a novel biradical cyclization in enyne-allenes: Formal diels-alder and ene reactions with high synthetic potential, *Chem. Eur. J.* 1997, *3*, 807. Schmittel, M.; Strittmer, M.; Kiau, S., Switching from the Myers reaction to a new thermal cyclization mode in enyne-allenes, *Tetrahedron Lett.* 1995, *36*, 4975.
9. (a) Alabugin, I. V.; Kovalenko, S. V., C1–C5 Photochemical cyclization of enediynes, *J. Am. Chem. Soc.* 2002, *124*, 9052. (b) Alabugin I. V.; Manoharan, M., Radical-anionic cyclizations of enediynes: Remarkable effects of benzannelation and remote substituents on cyclorearomatization reactions, *J. Am. Chem. Soc.* 2003, *125*, 4495.
10. Rawat, D. S.; Zaleski, J. M., Geometric and electronic control of thermal Bergman cyclization, *Synlett.* 2004, *35*, 393.
11. Basak, A.; Mandal, S.; Bag, S. S., Chelation-controlled Bergman cyclization: Synthesis and reactivity of enediynyl ligands, *Chem. Rev.* 2003, *103*, 4077.
12. Klein, M.; Walenzyk, T.; König, B., Electronic effects on the Bergman cyclisation of enediynes. A review, *Collect. Czech. Chem. Commun.* 2004, *69*, 945.
13. Alabugin, I. V.; Breiner, B.; Manoharan, M., Cycloaromatization reactions: The testing ground for theory and experiment, *Adv. Phys. Org. Chem.* 2007, *42*, 1.
14. Schreiner, P. R.; Navarro-Vazquez, A.; Prall, M., Computational studies on the cyclizations of enediynes, enyne-allenes, and related polyunsaturated systems, *Acc. Chem. Res.* 2005, *38*, 29.
15. Jones, G. B.; Russell, K. C., The photo-Bergman cycloaromatization of enediynes, *CRC Handbook of Organic Photochemistry and Photobiology*, 2nd edn.; CRC Press: Boca Raton, FL, 2004; pp. 29/1–29/21.

16. Kar, M.; Basak, A., Design, synthesis, and biological activity of unnatural enediynes and related analogues equipped with pH-dependent or phototirggering devices. *Chem. Rev.* 2007, *107*, 2861.
17. (a) Nicolaou, K. C.; Smith, A. L., Molecular design, chemical synthesis, and biological action of enediynes, *Acc. Chem. Res.* 1992, *25*, 497. (b) Grissom, J. W.; Gunawardena, G. U.; Klingberg, D.; Huang, D., The chemistry of enediynes, enyne allenes and related compounds, *Tetrahedron* 1996, *52*, 6453. (c) Wang, K. K., Cascade radical cyclizations via biradicals generated from enediynes, enyne-allenes, and enyne-ketenes, *Chem. Rev.* 1996, *96*, 207.
18. Nicolaou, K. C.; Pitsinos, E. N.; Theodorakis, E. A.; Saimato, H.; Wrasidlo, W., Synthetic calicheamicin mimics with novel initiation mechanisms: DNA cleavage, cytotoxicity, and apoptosis, *Chem. Biol.* 1994, *1*, 57.
19. For experimental work on the strain effects in Bergman cyclization see: (a) Nicolaou, K. C.; Zuccarello, G.; Ogawa, Y.; Schweiger, E. J.; Kumazawa, T., Cyclic conjugated enediynes related to calicheamicins and esperamicins: Calculations, synthesis, and properties, *J. Am. Chem. Soc.* 1988, *110*, 4866. (b) Nicolaou, K. C.; Zuccarello, G.; Riemer, C.; Estevez, V. A.; Dai, W.-M., Design, synthesis, and study of simple monocyclic conjugated enediynes. The 10-membered ring enediyne moiety of the enediyne anticancer antibiotics, *J. Am. Chem. Soc.* 1992, *114*, 7360. (c) IIda, K.; Hirama, M., Synthesis and characterization of nine-membered cyclic enediynes. Models of C-1027 and kedarcidin chromophore: Equilibration with a *p*-benzyne diradical and kinetic stabilization, *J. Am. Chem. Soc.* 1995, *117*, 8875. (d) Magnus, P.; Carter, P.; Elliott, J.; Lewis, R.; Harling, J.; Pitterna, T.; Bauta, W. E.; Fortt, S., Release of strain in the transition state: Synthetic and mechanistic studies on the antitumor antibiotics esperamicin A1 and calicheamicin γ_1 synthesis of 2-ketobicyclo [7.3.1.] enediyne and 13-ketocyclo [7.3.1] enediyne cores mediated by η^2 dicobalt hexacarbonyl alkyne complexes. Cycloaromatization rate studies, *J. Am. Chem. Soc.* 1992, *114*, 2544. (e) Plourde, G. W.; Warner, P. M.; Parrish, D. A.; Jones, G. B., Halo-enediynes: Probing the electronic and stereoelectronic contributions to the Bergman cycloaromatization, *J. Org. Chem.* 2002, *67*, 5369.
20. Selected theoretical analyses: (a) Snyder, J. P., The cyclization of calichemicin-esperamicin analogs: A predictive biradicaloid transition state, *J. Am. Chem. Soc.* 1989, *111*, 7630. (b) Snyder, J. P.; Tipsword, G. E., Proposal for blending classical and diradical mechanisms in antitumor antibiotics: Dynemicin A, *J. Am. Chem. Soc.* 1990, *112*, 4040. (c) Snyder, J. P., Monocyclic enediyne collapse to 1,4-diyl biradicals: A pathway under strain control, *J. Am. Chem. Soc.* 1990, *112*, 5367. (d) Kraka, E.; Cremer, D., Effect of 1,6-distance on the activation barrier: CCSD(T) investigation of the Bergman cyclization of enediyne. Relative stability of *o*-, *m*-, and *p*-didehydrobenzene, *J. Am. Chem. Soc.* 1994, *116*, 4929. (e) Schreiner, P. R., Monocyclic enediynes: Relationships between ring sizes, alkyne carbon distances, cyclization barriers, and hydrogen abstraction reactions. Singlet–triplet separations of methyl-substituted *p*-benzyne, *J. Am. Chem. Soc.* 1998, *120*, 4184.
21. Warner, B. P.; Millar, S. P.; Broene, R. D.; Buchwald, S. L., Control of strain through ligand-metal coordination, *Science* 1995, *269*, 814. Bhattacharyya, S.; Pink, M.; Baik, M.; Zaleski, J. M., A unique approach to metal-induced Bergman cyclization: Long-range enediyne activation by ligand-to-metal charge transfer, *Angew. Chem. Int. Ed.* 2005, *44*, 592. Bhattacharyya, S.; Dye, D. F.; Pink, M.; Zaleski, J. M., A geometric switching approach toward thermal activation of metalloenediynes, *Chem. Commun.* 2005, *14*, 5295. For a review on metal- coordinated enediynes, see: Ref. [10].
22. (a) Schmittel, M.; Kiau, S., Polar effects in the transition state of the Bergman cyclization, *Chem. Lett.* 1995, 953. (b) Mayer, M.E.; Greiner, B., Synthesis and reactivity of a p-methoxyphenyl-substituted enediyne. A case of electronic influence on the rate of the Bergman cycloaromatization, *Liebiqs Ann. Chem.* 1992, *23*, 855. (c) Kim, C.-S.; Russell, K. C., Rapid Bergman cyclization of 1,2-diethynylheteroarenes, *J. Org. Chem.* 1998, *63*, 8229. (d) Jones, G. B.; Plourde, G. W., Electronic control of the Bergman cycloaromatization: Synthesis and chemistry of chloroenediynes, *Org. Lett.* 2000, *2*, 1757. (e) Hoffner, J.; Schottelius, J.; Feichtinger, D.; Chen, P., Chemistry of the 2,5-didehydropyridine diradical: Computational, kinetic, and trapping studies toward drug design, *J. Am. Chem. Soc.*

1998, *120,* 376. (f) Choy, N.; Kim, C.-S.; Ballestero, C.; Argitas, L., Diez, C.; Lichtenberg, F.; Shapiro, J.; Russell, K. C., Linear free energy relationships in the Bergman cyclization of 4-substituted-1,2-diethynylbenzenes, *Tetrahedron Lett.* 2000, *41*, 6955.

23. Nath, M.; Huffman, J. C.; Zaleski, J. M., Accelerated Bergman cyclization of porphyrinic enediynes, *Chem. Comm.* 2003, 858 and references therein.
24. For representative recent references, see: Knoll, K.; Wrasidlo, W.; Scherberich, J. E.; Gaedicke, G.; Fischer, P., Targeted therapy of experimental renal cell carcinoma with a novel conjugate of monoclonal antibody 138H11 and calicheamicin θ^{I}1., *Cancer Research* 2000, *60*, 6089. Nabhan, C.; Tallman, M. S., Early phase I/II trials with gemtuzumab ozogamicin (Mylotarg (R)) in acute myeloid leukemia, *Clin. Lymphoma* 2002, *2*, S19–S23.
25. Kagan, J.; Wang, X.; Chen, X.; Lau, K. Y.; Batac, I. V.; Tuveson, R. W.; Hudson. J. B., DNA cleavage, antiviral and cytotoxic reactions photosensitized by simple enediyne compounds, *J. Photochem. Photobiol. B: Biol.* 1993, *21*, 1352.
26. (a) Turro, N. J.; Evenzahav, A.; Nicolaou, K. C., Photochemical analog of the Bergman cycloaromatization reaction, *Tetrahedron Lett.* 1994, *35*, 8089. (b) Evenzahav, A.; Turro, N., Photochemical rearrangement of enediynes: Is a "Photo-Bergman" cyclization a possibility? *J. Am. Chem. Soc.* 1998, *120,* 1835.
27. Jones, G. B.; Wright, J. M.; Plourde, II, G.; Purohit, A. D.; Wyatt, J. K.; Hynd, G.; Fouad, F., Synthesis and photochemical activity of designed enediynes, *J. Am. Chem. Soc.* 2000, *122*, 9872.
28. Kaneko, T.; Takanashi, M.; Hirama, M., Photochemical cycloaromatization of non-benzenoid enediynes, *Angew. Chem. Int. Ed. Engl.* 1999, *38*, 1267.
29. Funk, R. L.; Young, E. R. R.; Williams, R. M.; Flanagan, M. F.; Cecil, T. L., Photochemical cycloaromatization reactions of ortho-dialkynylarenes: A new class of DNA photocleaving agents, *J. Am. Chem. Soc.* 1996, *118,* 3291.
30. Choy, N.; Blanco, B.; Wen, J.; Krishan, A.; Russell, K. C., Photochemical and thermal Bergman cyclization of a pyrimidine enediynol and enediynone, *Org. Lett.* 2000, *2,* 3761.
31. Reports of indirect, photochemically triggered, but thermal Bergman cycloaromatizations: (a) Wender, P. A.; Zercher, C. K.; Beckham, S.; Haubold, E.-M., A photochemically triggered DNA-cleaving agent—Synthesis, mechanistic and DNA cleavage studies on a new analog of the antitumor antibiotic dynemicin, *J. Org. Chem.* 1993, *58*, 5867. Wender, P. A.; Beckham, S.; O'Leary, J. G., A 2nd-generation photochemically activatable dynemicin analog—A concise synthesis and DNA cleavage studies, *Synthesis* 1994, 1278. (b) Nicolaou, K. C.; Dai, W. M.; Wendeborn, S. V.; Smith, A. L.; Torisawa, Y.; Maligres, P.; Hwang, C. K., Enediyne compounds equipped with acid-sensitive, base-sensitive and photo-sensitive triggering devices—Chemical simulation of the dynemicin a reaction cascade, *Angew. Chem., Int. Ed. Engl.* 1991, *30*, 1032. (c) Nakatani, K.; Isoe, S.; Maekawa, S.; Saito, I., Photoinduced DNA cleavage by designed molecules with conjugated ene-yne-ketene functionalities, *Tetrahedron Lett.* 1994, *35*, 605. Nakatani, K.; Maekawa, S.; Tanabe, K.; Saito, I., Alpha-diazo ketones as photochemical DNA cleavers—A mimic for the radical generating-system of neocarzinostatin chromophore, *J. Am. Chem. Soc.* 1995, *117,* 10635. (d) Basak, A.; Moh'd Bdour, H.; Shain, J. S.; Mandal, S.; Rudra, K. R.; Nag, S., DNA-cleavage studies on N-substituted monocyclic enediynes: Enhancement of potency by incorporation of intercalating or electron poor aromatic ring and subsequent design of a novel phototriggerable acyclic enediyne, *Bioorg. Med. Chem. Lett.* 2000, *10,* 1321. (e) Konig, B.; Schofield, E.; Bubenitschek, P.; Jones, P. G., Synthesis and photoinduced *cis-trans* isomerization of diaryl enediyne chromophores, *J. Org. Chem.* 1994, *59,* 7142. (f) Ramkumar, D.; Kalpana, M.; Varghese, B.; Sankararaman, S.; Jagadeesh, M. N.; Chandrasekhar, J., Cyclization of enediyne radical cations through chemical, photochemical, and electrochemical oxidation: The role of symmetry, *J. Org. Chem.* 1996, *61,* 2247. (g) Poloukhtine, A.; Popik, V. V., Highly efficient photochemical generation of a triple bond: Synthesis, properties, and photodecarbonylation of cyclopropenones, *J. Org. Chem.* 2003, *68,* 7833.

32. (a) Benites, P. J.; Holmberg, R. C.; Rawat, D. S.; Kraft, B. J.; Klein, L. J.; Peters, D. G.; Thorp, H. H.; Zaleski, J. M., Metal-ligand charge-transfer-promoted photoelectronic Bergman cyclization of copper metalloenediynes: Photochemical DNA cleavage via C-4′ H-atom abstraction, *J. Am. Chem. Soc.* 2003, *125*, 6434. (b) Schmittel, M.; Viola, G.; Dall'Acqua, F.; Morbach, G., A novel concept to activate enediynes for DNA cleavage, *Chem. Comm.* 2003, *7*, 646.
33. Campbell, I. D.; Eglinton, G., A novel photochemical cyclisation of *o*- bisiodoethynylbenzene to substituted napthalenes, *J. Chem. Soc.(C)* 1968, *16*, 2120.
34. (a) Yang, W.-Y.; Breiner, B.; Kovalenko, S. V.; Ben, C.; Singh, M.; LeGrand, S. N.; Sang, Q.-X. A.; Strouse, G. F.; Copland, J. A.; Alabugin, I. V., C-lysine conjugates: pH-controlled light-activated reagents for efficient double-stranded DNA cleave with implications for cancer therapy, *J. Am. Chem. Soc.* 2009, *131*, 11458. (b) Yang, W.-Y.; Marrone, S. A.; Minors, N.; Zorio, D. A. R.; Alabugin, I. V., Fine-tuning alkyne cycloadditions: Insights into photochemistry responsible for the double-strand DNA cleavage via structural perturbations in diaryl alkyne conjugates, *Beilstein J. Org. Chem.* 2011, *7*, 813.
35. Spence, J. D.; Hargrove, A. E.; Crampton, H. L.; Thomas, D. W., Porphyrenediynes: Synthesis and cyclization of *meso*-enediynylporphyrins, *Tetrahedron Lett.* 2007, *48*, 725.
36. Lewis, K. D.; Matzger, A. J., Bergman cyclization of sterically hindered substrates and observation of phenyl-shifted products, *J. Am. Chem. Soc.* 2005, *127*, 9968.
37. For a follow-up mechanistic study, see: Schmittel, M.; Kiau, S., Thermal and electron-transfer induced reactions of enediynes and enyne-allenes. Part 9. Electron-transfer versus acid catalysis in enediyne cyclizations, *Liebigs. Ann. Recueil* 1997, *7*, 1391.
38. Zhao, Z.; Peacock, J. G.; Gubler, D. A.; Peterson, M. A., Photoinduced Bergman cycloaromatization of imidazole-fused enediynes, *Tetrahedron Lett.* 2005, *46*, 1373.
39. Wandel, H.; Wiest, O., Enediynes in 11-membered rings. Synthesis, structure, and reactivity of highly strained but unusually stable macrocycles, *J. Org. Chem.* 2002, *67*, 388.
40. Sud, D.; Wigglesworth, T. J.; Branda, N. R., Creating a reactive enediyne by using visible light: Photocontrol of the Bergman cyclization, *Angew. Chem. Int. Ed.* 2007, *46*, 8017.
41. Zeidan, T.; Clark, R. J.; Kovalenko, S. V.; Ghiviriga, I.; Alabugin I. V., Triplet acetylenes as synthetic equivalents of 1,2-dicarbenes. II. New supramolecular scaffolds from photochemical cycloaddition of diarylacetylenes to 1,4-cyclohexadienes, *Chem. Eur. J.* 2005, *11*, 4953. Zeidan, T.; Kovalenko, S. V.; Manoharan, M.; Clark, R. J.; Ghiviriga, I.; Alabugin, I. V., Triplet acetylenes as synthetic equivalents of 1,2-dicarbenes. Phantom n,π^* state controls reactivity in triplet photocycloaddition, *J. Am. Chem. Soc.* 2005, *127*, 4270.
42. Kovalenko, S. V.; Peabody, S.; Manoharan, M.; Clark, R. J.; Alabugin, I. V., 5-Exo-dig radical cyclization of enediynes: The first synthesis of tin-substituted benzofulvenes, *Org. Lett.* 2004, *6*, 2457.
43. Peabody, S.; Breiner, B.; Kovalenko, S. V.; Patil, S.; Alabugin, I. V., Synthesis of selectively deuterated fulvenes and indenes from enediynes, *Org. Biomol. Chem.* 2005, *3*, 218.
44. Kovalenko, S. V.; Alabugin, I. V., Lysine-enediyne conjugates as photochemically triggered DNA double-strand cleavage agents, *Chem. Comm.* 2005, 1444.
45. (a) Lewis, K. D.; Wenzler, D. L.; Matzger, A. J., Photochemistry of diethynyl sulfides: A cycloaromatization for the formation of five-membered rings, *Org. Lett.* 2003, *5*, 2195. Related Thermal Cycloaromatization: (b) Lewis, K. D.; Rowe, M. P.; Matzger, A. J., Ethynyl sulfides as participants in cascade cycloaromatizations, *Tetrahedron* 2004, *60*, 7191. Theoretical analysis: (c) Kawatkar, S.P.; Schreiner, P. R., Cycloaromatization of 1,4-pentadiynes: A viable possibility? *Org. Lett.* 2002, *4*, 3643. (d) Alabugin, I.V.; Manoharan, M., Thermodynamic and strain effects in the competition between 5-exo-dig and 6-endo-dig cyclizations of vinyl and aryl radicals, *J. Am. Chem. Soc.* 2005, *127*, 12583.
46. Möllerstedt, H.; Piqueras, M. C.; Crespo, R.; Ottosson, H., Fulvenes, fulvalenes, and azulene: Are they aromatic chameleons? *J. Am. Chem. Soc.* 2004, *126*, 13938.

47. Zheng, M.; DiRico, K. J.; Kirchhoff, M. M.; Phillips, K. M.; Cuff, L. M.; Johnson, R. P., Photorearrangements of acyclic conjugated enynes: A photochemical analog of the Bergman rearrangement, *J. Am. Chem. Soc.* 1993, *115*, 12167.
48. Zimmerman, H. E.; Pincock, J. A., Photochemistry of mono- and diacetylenic systems. Exploratory and mechanistic organic photochemistry. LXXVII, *J. Am. Chem. Soc.* 1973, *95*, 3246.
49. Kaafarani, B. R.; Neckers, D. C., Photocyclization of a conjugated triaryl "Y-enyne," *Tetrahedron Lett.* 2001, *42*, 4099.
50. Eshdat, L.; Berger, H.; Hopf, H.; Rabinovitz, M., Anionic cyclization of a cross-conjugated enediyne, *J. Am. Chem. Soc.* 2002, *124*, 3822. Treitel, N.; Eshdat, L.; Sheradsky, T.; Donovan, P. M.; Tykwinski, R. R.; Scott, L. T.; Hopf, H.; Rabinovitz, M., Reductive Bergman-type cyclizations of cross-conjugated enediynes to fulvene and fulvalene anions: The role of the substituent, *J. Am. Chem. Soc.* 2006, *128*, 4703.
51. Schmittel, M.; Rodríguez, D.; Steffen, J. P., A highly efficient triplet analogue of a thermal biradical cyclization—The photochemical C^2–C^6 cyclization of enyne-heteroallenes, *Angew. Chem. Int. Ed.* 2000, *39*, 2152.
52. Galbraith, J. M.; Schreiner, P. R.; Harris, N. R.; Wei, W.; Wittkopp, A.; Shaik, S., A valence bond study of the Bergman cyclization: Geometric features, resonance energy, and nucleus-independent chemical shift (NICS) values, *Chem. Eur. J.* 2000, *6*, 1446.
53. Alabugin, I. V.; Manoharan, M., Reactant destabilization in the Bergman cyclization and rational design of light- and pH-activated enediynes, *J. Phys. Chem. A* 2003, *107*, 3363.
54. Haberhauer, G.; Gleiter, R., Transannular ring closure of 10-membered cyclic diynes: Model calculations, *J. Am. Chem. Soc.* 1999, *121*, 4664.
55. (a) Hoffmann, R.; Imamura, A.; Hehre, W. J., Benzynes, dehydroconjugated molecules, and the interaction of orbitals separated by a number of intervening sigma bonds, *J. Am. Chem. Soc.* 1968, *90*, 1499. (b) Hoffmann, R., Interaction of orbitals through space and through bonds, *Acc. Chem. Res.* 1971, *4*, 1. (c) Gleiter, R.; Schafer, W., Interactions between nonconjugated π-systems, *Acc. Chem. Res.* 1990, *23*, 369. (d) Paddon-Row, M. N., Some aspects of orbital interactions through bonds: Physical and chemical consequences, *Acc. Chem. Res.* 1982, *15*, 245. (e) Brodskaya, E. I.; Ratovskii, G. V.; Voronkov, M. G., Orbital interactions through space and through σ -bonds, *Usp. Khim.* 1993, *62*, 975.
56. Kasha, M., Characterization of electronic transitions in complex molecules, *Discuss. Faraday Soc.* 1950, *9*, 14.
57. Clark, A. E.; Davidson, E. R.; Zaleski, J. M., UDFT and MCSCF descriptions of the photochemical Bergman cyclization of enediynes, *J. Am. Chem. Soc.* 2001, *123*, 2650.
58. For a general way to predict the most likely direction of photochemical reactivity from the energy distribution in the Franck-Condon excited states, see: (a) Zimmerman, H.E.; Alabugin, I.V., Excited state energy distribution and redistribution and chemical reactivity; Mechanistic and exploratory organic photochemistry, *J. Am. Chem. Soc.* 2000, *122*, 952. (b) Zimmerman, H.E.; Alabugin, I.V., Energy distribution and redistribution and chemical reactivity. The generalized delta overlap-density method for ground state and electron transfer reactions: A new quantitative counterpart of electron-pushing, *J. Am. Chem. Soc.* 2001, *123*, 2265.
59. Karpov, G. V.; Popik, V. V., Triggering of the Bergman cyclization by photochemical ring contraction. Facile cycloaromatization of benzannulated cyclodeca-3,7-diene-1,5-diynes, *J. Am. Chem. Soc.* 2007, *129*, 3792. Poluokhtine, A.; Popik, V. V., Two-photon photochemical generation of reactive enediyne, *J. Org. Chem.* 2006, *71*, 7417. Pandithavidana, D. R.; Poloukhtine, A.; Popik, V. V., Photochemical generation and reversible cycloaromatization of a nine-membered ring cyclic enediyne, *J. Am. Chem. Soc.* 2009, *131*, 351. Polukhtine. A.; Karpov, G.; Popik. V. V., Towards photoswitchable enediyne antibiotics: Single and two-photon triggering of Bergman cyclization, *Curr. Top. Med. Chem.* 2008, *8*, 460. Karpov, G.; Kuzmin, A.; Popik, V. V., Enhancement of the reactivity of photochemically generated enediynes via keto-enol tautomerization, *J. Am. Chem. Soc.* 2008, *130*, 11771.

60. Korovina, N.; Gherman, B. F.; Spence, J. D., Synthesis and photoreactivity of 1,2-bis(naphthalene-1-ylethynyl)benzene: A combined experimental and computational investigation, *Abstracts of Papers, 238th ACS National Meeting*, Washington, DC, 2009. Chang, M. L.; Spence, J. D. Syntheses and reactivity of (Naphthalen-2-yl)ethynyl and (Phenanthren-9-yl)ethynyl arenediynes, *Abstracts of Papers, 237th ACS National Meeting*, Salt Lake City, UT, 2009.
61. Zimmerman, H. E., The meta effect in organic photochemistry: Mechanistic and exploratory organic photochemistry, *J. Am. Chem. Soc.* 1995, *117*, 8988.
62. Alabugin, I.V.; Manoharan, M.; Zeidan, T. A., Homoanomeric effects in saturated heterocycles, *J. Am. Chem. Soc.* 2003, *125*, 14014 and reference therein.
63. Fisher, W. G.; Partridge, W. P.; Dees, C.; Wachter, E., A simultaneous two-photon activation of type-I photodynamic therapy agents, *Photochem. Photobiol.* 1997, *66*, 141.
64. Kauffman, J. F.; Turner, J. M.; Alabugin, I. V.; Breiner, B.; Kovalenko, S. V.; Badaeva, E. A.; Masunov, A.; Tretiak, S., Two photon excitation of substituted enediynes, *J. Phys. Chem. A* 2006, *110*, 241.
65. Alabugin, I. V.; Manoharan, M.; Breiner, B.; Lewis, F. D., Control of kinetics and thermodynamics of [1,5]-shifts by aromaticity: A view through the prism of marcus theory, *J. Am. Chem. Soc.* 2003, *125*, 9329.
66. Schleyer, P. V. R.; Manoharan, M.; Wang, Z.-X.; Kiran, B.; Jiao, H.; Puchta, R.; van Eikema Hommes, N. J. R., Dissected nucleus-independent chemical shift analysis of π-aromaticity and antiaromaticity, *Org. Lett.* 2001, *3*, 2465. Schleyer, P. V. R.; Jiao, H.; Hommes, N. J. R. V. E.; Malkin, V. G.; Malkina, O. L., An evaluation of the aromaticity of inorganic rings: Refined evidence from magnetic properties, *J. Am. Chem. Soc.* 1997, *119*, 12669. Schleyer, P. V. R.; Maerker, C.; Dransfeld, A.; Jiao, H.; Hommes, N. J. R. V. E., Nucleus-independent chemical shifts: A simple and efficient aromaticity probe, *J. Am. Chem. Soc.* 1996, *118*, 6317. For the seminal paper on using NICS for open shell species, see: Gogonea, V.; Schleyer, P. V. R.; Schreiner, P. R., Consequences of triplet aromaticity in 4 nπ - electron annulenes: Calculation of magnetic shieldings for open-shell species, *Angew Chem., Int. Ed. Engl.* 1998, *37*, 1945.
67. Choy, N.; Russell, K. C., Synthesis and cyclization of novel lumazine—Enediyne chimeras, *Heterocycles* 1999, *51*, 13. Kim, C.-S.; Russell, K. C., Solvent dependent Bergman cyclization of 2,3-diethynylquinoxaline, *Tetrahedron Lett.* 1999, *40*, 3835. Kim, C.-S.; Diez, C.; Russell, K. C., Tautomer-dependent Bergman cyclization of novel uracil-enediyne chimeras, *Chem. Eur. J.* 2000, *6*, 1555.
68. Whitlock, H. W. Jr.; Sandvick, P. E.; Overman, L. E.; Reichardt, P. B., Chemical behavior of *o*-Bis(phenylethynyl)benzene toward some electrophilic and nucleophilic reagents, *J. Org. Chem.* 1969, *34*, 879.
69. Tamao, K.; Yamaguchi, S.; Shiro, M., Oligosiloles: First synthesis based on a novel endo-endo mode intramolecular reductive cyclization of diethynylsilanes, *J. Am. Chem. Soc.* 1994, *116*, 11715.
70. Yamaguchi, S.; Miyasato, M.; Tamao, K., Endo-endo mode intramolecular reductive cyclization of cyclic 1,2-bis(silylethynyl)benzenes, *Chem. Lett.* 2003, *32*, 1104.
71. Wenthold, P. G., A Computational study of the electron affinities of substituted cope rearrangement transition states, *J. Chem. Soc., Perkin Trans.* 1999, *2*, 2357. Hammad, L. A.; Wenthold, P. G., An electron-catalyzed cope cyclization. The structure of the 2,5-dicyano-1,5-hexadiene radical anion in the gas phase, *J. Am. Chem. Soc.* 2003, *125*, 10796.
72. (a) Maier, M. E.; Greiner, B., Synthesis and reactivity of a *p*-methoxyphenyl-substituted enediyne. A case of electronic influence on the rate of the Bergman cycloaromatization, *Lieb. Ann. Chem.* 1992, 855. (b) Jones, G. B.; Warner, P. M., Electronic control of the Bergman cyclization: The remarkable role of vinyl substitution, *J. Am. Chem. Soc.* 2001, *123*, 2134. (c) König, B.; Pitsch, W.; Klein, M.; Vasold, R.; Prall, M.; Schreiner, P. R., Carbonyl- and carboxyl-substituted enediynes: Synthesis, computations, and thermal reactivity, *J. Org. Chem.* 2001, *66*, 1742. (d) Prall, M.; Wittkopp, A.; Fokin, A. A.; Schreiner, P. R., Substituent effects on the Bergman cyclization of (*Z*)-1,5-hexadiyne-3-enes: A systematic computational study, *J. Comput. Chem.* 2001, *22*, 1605.

73. (a) Nagata, R.; Yamanaka, H.; Okazaki, E.; Saito, I., Biradical formation from acyclic conjugated eneyne-allene system related to neocarzinostatin and esperamicin-calichemicin, *Tetrahedron Lett.* 1989, *30*, 4995. (b) Myers, A. G, Kuo, E. Y.; Finney, N. S., Thermal generation of α,3-dehydrotoluene from (*Z*)-1,2,4-heptatrien-6-yne, *J. Am. Chem. Soc.* 1989, *111*, 8057. (c) Nagata, R.; Yamanaka, H.; Murahashi, E.; Saito, I., DNA cleavage by acyclic enyne-allene systems related to neocarzinostatin and esperamicin-calicheamicin, *Tetrahedron Lett.* 1990, *31*, 2907. (d) Myers, A. G.; Dragovich, P. S.; Kuo, E. Y., Studies on the thermal generation and reactivity of a class of (σ,π)-1,4-biradicals, *J. Am. Chem. Soc.* 1992, *114*, 9369.
74. Zeidan, T.; Kovalenko, S. V.; Manoharan, M.; Alabugin, I. V., Ortho effect in the Bergman cyclization: Interception of *p*-Benzyne intermediate by intramolecular hydrogen abstraction, *J. Org. Chem.* 2006, *71*, 962. Alabugin, I. V.; Manoharan, M.; Kovalenko, S.V., Tuning rate of the Bergman cyclization of benzannelated enediynes with *Ortho* substituents, *Org. Lett.* 2002, *4*, 1119. Baroudi, A.; Mauldin, J.; Alabugin, I. V., Conformationally gated fragmentations and rearrangements promoted by interception of the Bergman cyclization through intramolecular H-abstraction: A possible mechanism of auto-resistance to natural enediyne antibiotics? *J. Am. Chem. Soc.* 2010, *132*, 967.
75. Kraft, B. J.; Coalter, N. L.; Nath, M.; Clark, A. E.; Siedle, A. R.; Huffman, J. C.; Zaleski, J. M., Photothermally induced Bergman cyclization of metalloenediynes via near-infrared ligand-to-metal charge-transfer excitation, *Inorg. Chem.* 2003, *42*, 1663.
76. Benites, P. J.; Holmberg, R. C.; Rawat, D. S.; Kraft, B. J.; Klein, L. J.; Peters, D. G.; Thorp, H. H.; Zaleski, J. M., Metal-ligand charge-transfer-promoted photoelectronic bergman cyclization of copper metalloenediynes: Photochemical DNA cleavage via C-4' H-atom abstraction, *J. Am. Chem. Soc.* 2003, *125*, 6434.
77. Chandra, T.; Kraft, B. J.; Huffman, J. C.; Zaleski, J. M., Synthesis and structural characterization of porphyrinic enediynes: Geometric and electronic effects on thermal and photochemical reactivity, *Inorg. Chem.* 2003, *42*, 5158.
78. Nath, M.; Pink, M.; Zaleski, J. M., Controlling both ground- and excited-state thermal barriers to Bergman cyclization with alkyne termini substitution, *J. Am. Chem. Soc.* 2005, *127*, 478.
79. (a) O'Connor, J. M.; Lee, L. I.; Gantzel, P.; Rheingold, A. L.; Lam, K.-C., Inhibition and acceleration of the Bergman cycloaromatization reaction by the pentamethylcyclopentadienyl ruthenium cation, *J. Am. Chem. Soc.* 2000, *122*, 12057. (b) For Fe and Ru-mediated reactivity, see O'Connor, J. M.; Friese, S. J.; Rodgers, B. L., A transition-metal-catalyzed enediyne cycloaromatization, *J. Am. Chem. Soc.* 2005, *127*, 16342.
80. Kraka, E.; Cremer, D., Computer design of anticancer drugs. A new enediyne warhead, *J. Am. Chem. Soc.* 2000, *122*, 8245.
81. For the representative examples of benzyne radical-anions, see: Wenthold, P. G.; Hu, J.; Squires, R. R., *o*-, *m*-, and *p*-benzyne negative ions in the gas phase: Synthesis, authentication, and thermochemistry, *J. Am. Chem. Soc.* 1996, *118*, 11865. Reed, D. R.; Hare, M.; Kass, S. R., Formation of gas-phase dianions and distonic ions as a general method for the synthesis of protected reactive intermediates. Energetics of 2,3- and 2,6-dehydronaphthalene, *J. Am. Chem. Soc.* 2000, *122*, 10689.
82. Behr, O. M.; Eglington, G.; Galbraith, A.R.; Raphael, R. A., Macrocyclic acetylenic compounds. II. 1,2:7,8-dibenzocyclododeca-1,7-diene-3,5,9,11-tetrayne, *J. Chem. Soc.* 1960, 3614.
83. Shiraki, T.; Sugiura, Y., Visible light induced DNA cleavage by the hybrid antitumor antibiotic dynemicin A, *Biochemistry*, 1990, *29*, 9795.
84. Weaver, D. T., Regulation and repair of double-strand DNA breaks. *Crit. Rev. Eukaryot Gene Exp.* 1996, *6*, 345.
85. The ds/ss ratio is 1:2 for plasmid DNA and 1:3 for cellular DNA: Elmroth, K.; Nygren, J.; Martensson, S.; Ismail, I. H.; Hammarsten, O., Cleavage of cellular DNA by calicheamicin γ_1, *DNA Repair* 2003, *2*, 363.

86. About 10% of the DNA strand breaks induced by bleomycin are double-strand breaks: Charles, K.; Povirk, L. F., Action of bleomycin on structural mimics of intermediates in DNA double-strand cleavage, *Chem. Res. Toxicol.* 1998, *11*, 1580. Povirk, L. F.; Wubker, W.; Kohnlein, W.; Hutchinson, F., DNA double-strand breaks and alkali-labile bonds produced by bleomycin, *Nucleic Acids Res.* 1977, *4*, 3573–3580.
87. (a) Lloyd, R. S.; Haidle, C. W.; Hewitt, R. R., Bleomycin induced alkaline-labile and direct strand breakage of PM2 DNA, *Cancer Res.* 1978, *38*, 3191. (b) Harsch, A.; Marzilli, L. A.; Bunt, R. C.; Stubbe, J.; Vouros, P., Accurate and rapid modeling of iron-bleomycin-induced DNA damage using tethered duplex oligonucleotides and electrospray ionization ion trap mass spectrometric analysis, *Nucleic Acids Res.* 2000, *28*, 1978. (c) Stubbe, J.; Kozarich, J. W., Mechanisms of bleomycin-induced DNA degradation, *Chem. Rev.* 1987, *87*, 1107. Burger, R. M., Cleavage of nucleic acids by bleomycin, *Chem. Rev.* 1998, *98*, 1153. (d) Hecht, S. M., Bleomycin: New perspectives on the mechanism of action, *J. Nat. Prod.* 2000, *63*, 158.
88. Standke, K. H. C.; Brunnert, H., Estimation of affinity constants for the binding of model peptides to DNA by equilibrium dialysis, *Nucleic Acids Res.* 1975, *2*, 1839. Ahmad, J.; Ashok, B. T.; Ali, R., Detection of oxidative DNA damage by a monoclonal antibody: Role of lysyl residues in antigen binding, *Immun. Lett.* 1998, *62*, 87. Tyler, J. K.; Allen, K. E.; Everett, R, D., Mutation of a single lysine residue severely impairs the DNA recognition and regulatory functions of the VZV gene 62 transactivator protein, *Nucl. Acids Res.* 1994, *22*, 270.
89. Breiner, B.; Schlatterer, J. C.; Kovalenko, S. V.; Greenbaum, N. L.; Alabugin, I. V., DNA Damage-site recognition by lysine conjugates. *Proc. Natl. Acad. Sci.* 2007, *104*, 13016.
90. Uesawa, Y.; Sugiura, Y., Light-induced DNA cleavage by esperamicin and neocarzinostatin, *Biochem. Biophys. Res. Commun.* 1989, *164*, 903.
91. Falcone, D.; Li, J.; Kale, A.; Jones, G. B., Photoactivated enediynes as targeted antitumoral agents: Efficient routes to antibody and gold nanoparticle conjugates, *Bioorg. Med. Chem. Lett.* 2008, *18*, 934.
92. Breiner, B.; Schlatterer, J. C.; Kovalenko, S. V.; Greenvaum, N. L.; Alabugin, I. V., Protected ^{32}P-labels in deoxyribonucleotides: Investigation of sequence selectivity of DNA photocleavage by enediyne-, fulvene-, and acetylene-lysine conjugates, *Angew. Chem. Int.* 2007, *45*, 3666.
93. Bowles, D. M.; Palmer, G. J.; Landis, C. A.; Scott, J. L.; Anthony, J. E., The Bergman reaction as a synthetic tool: Advantages and restrictions, *Tetrahedron* 2001, *57*, 3753. Alabugin, I. V.; Gilmore, K.; Patil, S.; Manoharan, M.; Kovalenko, S. V.; Clark, R. J.; Ghiviriga, I., Radical cascade transformations of tris(*o*-aryleneethynylenes) into substituted benzo[a]indeno[2,1-c]fluorenes, *J. Am. Chem. Soc.* 2008, *130*, 11535. Matzger, A.; Vollhardt, P., From phenylenes to acenes: Flash vacuum pyrolytic isomerization of angular [3]phenylene to benzo[ghi]fluoranthene, *Chem. Commun.* 1997, 1415. Lin, C.-F.; Wu, M.-J., Synthesis, double cycloaromatization, and DNA-cleaving activities of (*Z*,*Z*)-11-sulfonylundeca-3,7-diene-1,5,9-triyne System, *J. Org. Chem.* 1997, *62*, 4546. Han, X.; Zhang, Y.; Wang, K. K., Synthesis of diindeno-fused 4*H*-cyclopenta[*def*]phenanthren-4-ones and related compounds via benzannulated enediynyl propargylic alcohols, *J. Org. Chem.* 2005, *70*, 2406.

24

Scope and Limitations of Hula-Twist Mechanism of Photoisomerization

Robert S.H. Liu
University of Hawaii

Yao-Peng Zhao
University of Hawaii

Lan-Ying Yang
University of Hawaii

24.1 Introduction

Ever since the introduction of the torsional potential curves for the excited states of ethylene [1], it became commonly accepted that the mechanism of photoisomerization of substituted ethylenes is torsional relaxation [2], that is, turning over one-half of the molecule around the formal double bond (also known as one-bond-flip [OBF]) [3]. This appears to be logical because the excited state bond order of the formal double bond is considerably reduced in both the excited singlet and triplet states [1]. However, in the 1970s, the observation of facile isomerization of polyene chromophores in confined media raised the question whether the volume demanding torsional relaxation mechanism can indeed take place within the observed picosecond or subpicosecond timescale [4]. Therefore, several less volume-demanding mechanisms for photoisomerization were proposed.

First proposed was the bicycle-pedal (BP) mechanism of photoisomerization [5] where two alternating double bonds in a conjugated system isomerize simultaneously (Figure 24.1). The only in-and-out-of-plane motion involved in this transformation is turning over of the two middle CH units while the remaining portions of the molecule remained in place. The stereochemical consequence is one-photon-two-bond isomerization. Very few examples of such two-bond isomerization have since been observed, limited to the energy downhill transformation of a di-*cis* moiety to a di-*trans* moiety (see more discussion in the following). This is in agreement with theoretical calculations showing that such processes in the excited singlet state are activated [6].

Subsequently the hula-twist (HT) mechanism of isomerization was proposed [3] in which two adjacent single and double bonds in a conjugated system rotate simultaneously (Figure 24.1). In effect, only one CH unit rotates in-and-out of the plane of the molecule while the remaining portions of the molecule

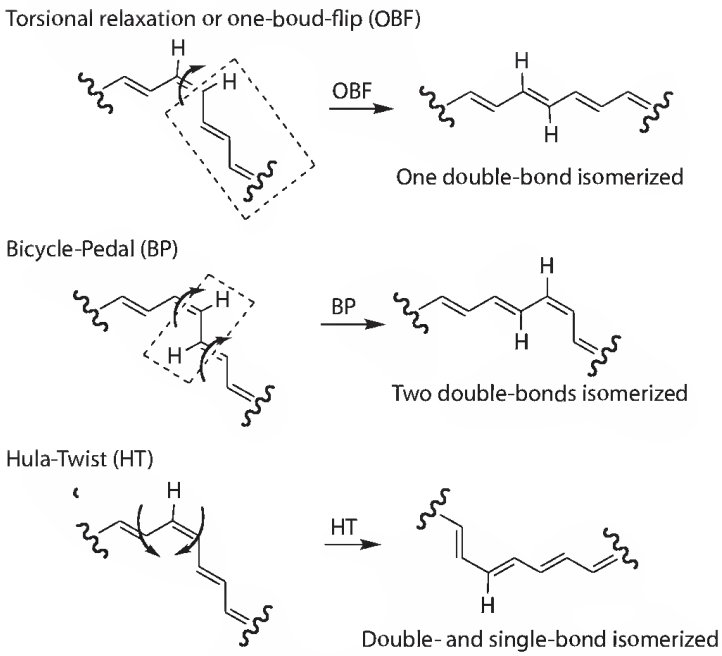

FIGURE 24.1 Three possible mechanisms of photoisomerization. *Top*: torsional relaxation where one-half of the molecule flips around the formal double bond (or one-bond-flip, OBF). *Middle*: the bicycle-pedal (BP) process that results in isomerization at two formal double bonds. *Bottom*: the hula-twist (HT) that results in configurational isomerization at one double bond and conformational isomerization at an adjacent single bond.

remain largely in-plane (or sliding in the plane of the molecule). Thus, it is also not volume demanding. And, the stereochemical consequence is simultaneous configurational isomerization of one double bond and conformational isomerization of the adjacent single bond. Calculations [6,7] have since shown that such processes are indeed energetically downhill from the Franck–Condon excited singlet species of the polyenes (described in detail later). Not surprisingly, many photochemical examples of simultaneous isomerization of double bond and single bond isomerization are now known (see the following). In this chapter, we wish to discuss the scope and limitation of photoisomerization by this mechanism.

24.2 Examples of Hula-Twist Photoisomerization

24.2.1 Early Examples

The first example of photoisomerization yielding a primary photoproduct that involved simultaneous double-bond and single-bond isomerization was that of pro-vitamin D, **1**, in EPA glass reported by Fuss and coworkers [8]:

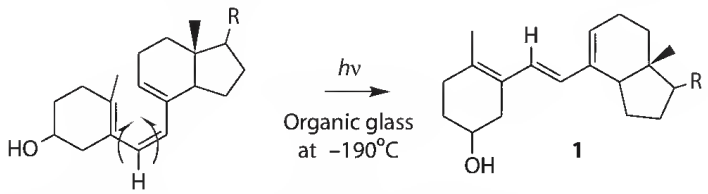

Starting from the strained triene (obtained from ring opening of the corresponding cyclohexadiene isomer), the stable *trans* isomer **1** was obtained with an obvious simultaneous *s-cis* to *s-trans* conversion. Similarly, the more stable triene derivative was found to yield an unstable *trans* photoproduct.

This and other early examples of conformational changes of polyenes under UV irradiation were reviewed in our previous contribution [9]. This chapter will emphasize recent examples, the medium effects on the isomerization process, and clarification on perceived controversy on the HT mechanism.

It was known for some time that the medium exerts a strong effect on efficiency of photoisomerization. For example, Fischer [10] showed that the efficiencies of photoisomerization of stilbene were highly dependent on viscosity of the medium. In the case of the *trans* isomer, efficiencies of *trans* to *cis* isomerization dropped significantly upon an increase of solvent viscosity eventually becoming zero (only fluorescence was observed) when the solvent turned into a rigid organic glass. However, the drop of efficiency of isomerization of the *cis* isomer was less dramatic and reaction still persisted in organic glasses with efficiency less than one-third of that at room temperature [11]. Fisher [12] and, independently, Alfimov [13] were able to take advantage of this observation and produce unstable conformer of the *trans* isomer during low-temperature irradiation of a series of diarylethylenes.

24.2.2 More Recent Examples

The pioneering work of Fuss shed light on ways to design new systems and experimental conditions for detecting more examples of HT. The strategy was outlined in two papers [9b,c]. Many experimental examples have since appeared in the literature. These examples can be categorized in the following manner.

First, we should point out that to study HT isomerization, very often a strategically located substituent must be introduced. For example, for stilbenes, *o,o′*-disubstituted compounds, **2**, are quite suitable for producing the high-energy HT products; however, the corresponding *p,p′*-disubstituted compounds, **3**, are not (producing products indistinguishable from that of the OBF process [14]).

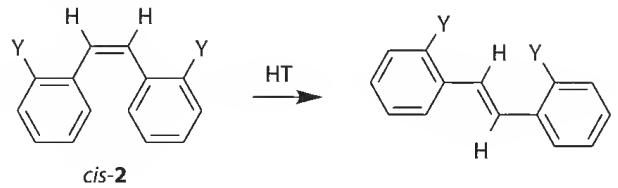

cis-**2**

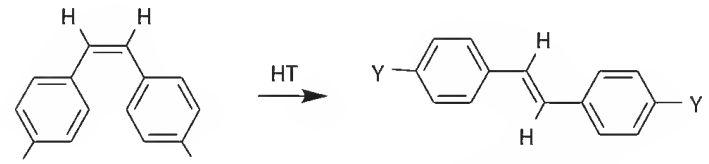

cis-**3**

Simple styrene derivatives: Styryl compounds are the simplest systems that exhibit HT photoisomerization that can be readily detected by low-temperature UV spectroscopy. A simple example is compound **4** that was converted to a blueshifted product during low-temperature irradiation in EPA glass [14]. Upon slight warming, the product reverted back to the starting material. These transformations were also detected in argon matrix at liquid helium temperature, [15] where the recording of the infrared spectrum of the metastable photoproduct was possible.

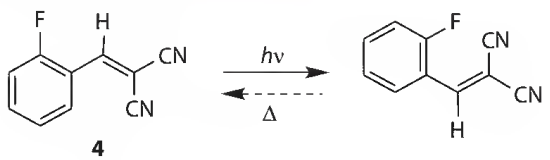

4

Similar two-way interconversions were observed for more delocalized colored systems, **5–7** [16]. However, the shifts of absorption maxima were generally small, making the systems not particularly useful as new photochromic systems.

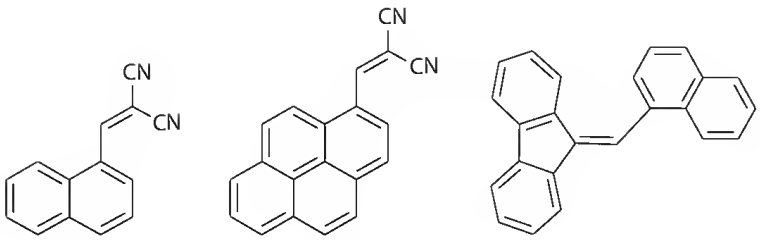

5 **6** **7**

Stilbene derivatives: Low-temperature photoisomerization studies of a series of substituted stilbenes or 1,2-diarylethylenes were reported. The result of *cis-o,o′*-diphenylstilbene in *n*-propanol glass at 78 K (*cis*-**8**) [17] is typical of observations made for this group of compounds (Figure 24.2): an unstable isomerized photoproduct was formed, which rearranged to the stable conformer under mild heating.

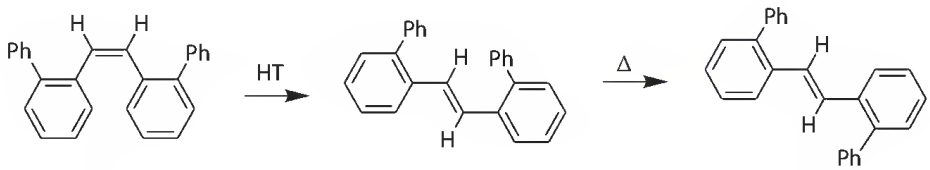

cis-**8** *trans*-**8**

Additionally, studies were carried out on conformationally restricted analog **9** [11], the corresponding seven- and five-ring compounds [18], and more delocalized systems **10** and **11** [18,19].

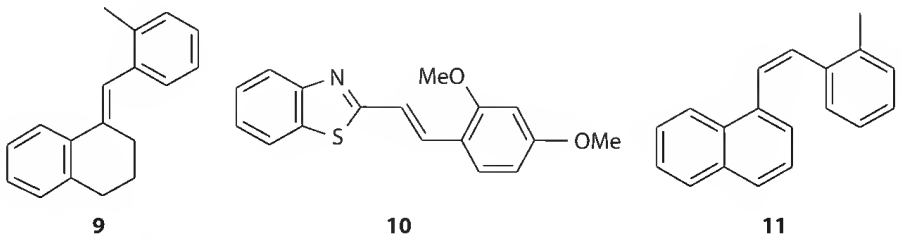

9 **10** **11**

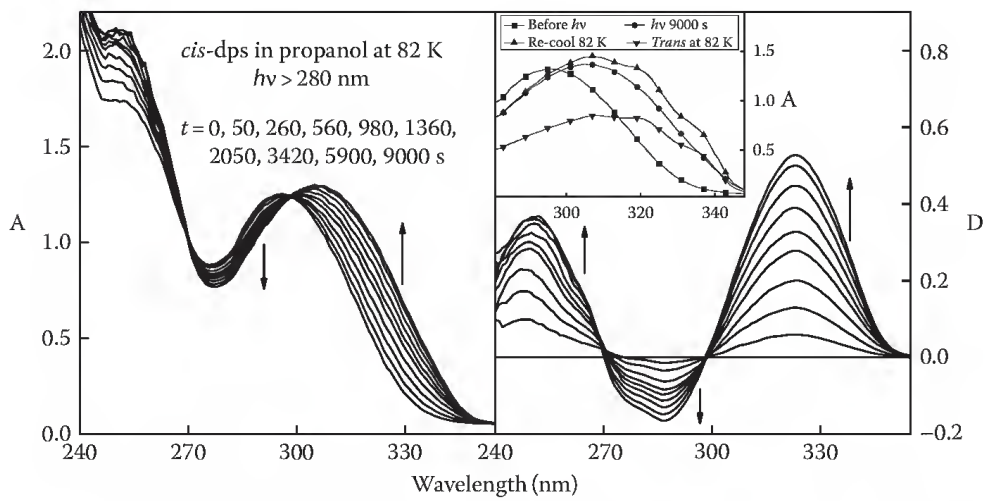

FIGURE 24.2 Low-temperature photoisomerization of *o,o′*-diphenylstilbene, *cis*-**8**, in *n*-propanol glass. *Left*: UV absorption spectra during progressive irradiation (>280 nm) to 9000 s. *Right*: difference absorption spectra ($t - t_0$) from spectra in left. *Insert*: final irradiated spectra (squares) and after warming to 200 K (circles) and recooled to 82 K (triangles up) showing transformation to the stable *trans*.

Diene derivatives: In addition to an earlier report of conformational interconversion during low-temperature irradiation of 1,3-butadiene [20], similar changes were also reported for substituted butadienes, **12**, in argon matrix [21]. More recently the study was extended to 1,1-diphenyl-1,3-butadiene, **13**, in organic glasses [22].

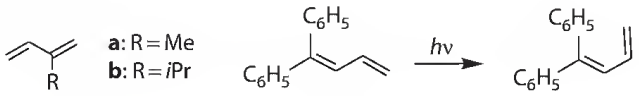

12 **13**

More revealing were the observations made with isomers of 1,4-diphenyl-1,3-butadiene and its derivatives [23]. Thus, irradiation of *cis*-**14a** in EPA glass was found to yield a thermally unstable conformer of the *trans,trans* isomer (Figure 24.3). The observation was inconsistent with OBF isomerization (giving the stable *trans,trans* isomer). Since a separate study with that of the parent *cis*-**14b** had ruled out HT-isomerization at carbon-2 (i.e., within limit of detection of ~5%), the observed result of *cis*-**14a** was only consistent with HT-1.

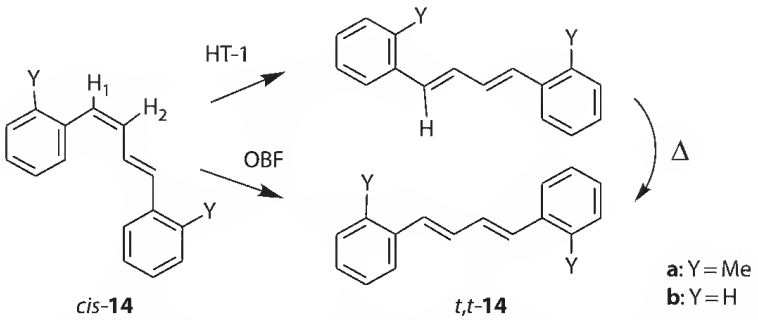

cis-**14** *t,t*-**14**

Low-temperature photoisomerization of *cis*-1,4-dimethyl-1,4-diphenylbutadiene was initially taken as an example of HT around a methyl group [24]. However, following the demonstration of the importance of local melting effect in low-temperature photochemical studies [17], it became clear that the result was also consistent with OBF photoisomerization in locally softened glasses (see more discussion on glass effect in the following).

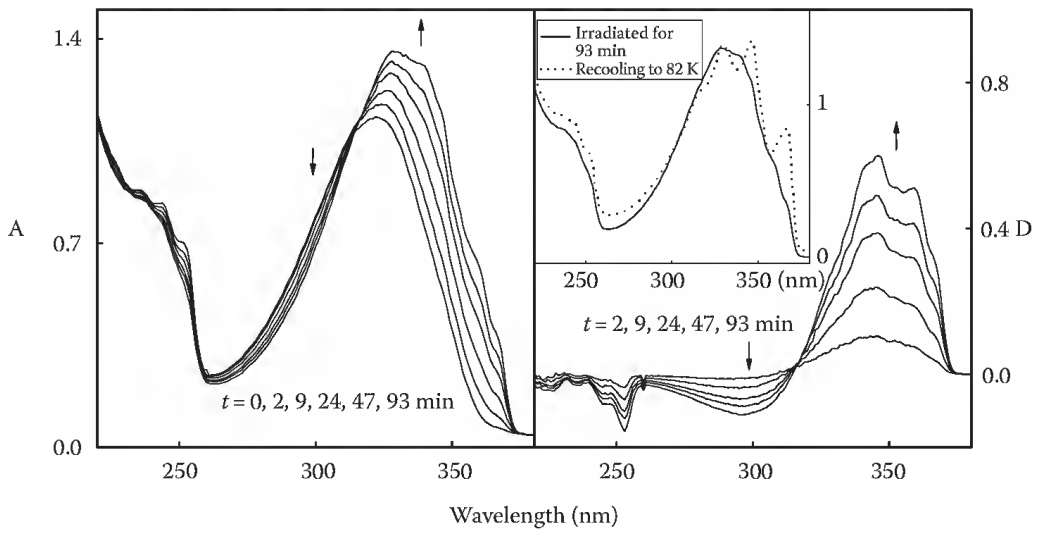

FIGURE 24.3 Low-temperature (80 K) photoisomerization of *o,o′*-dimethyl-DPB, *cis*-**14a**, in EM (1:1 mixture of ethanol and methanol). *Left*: progressive changes of UV absorption spectra during 93 m of irradiation (>310 nm). *Right*: difference absorption spectra from left. *Insert*: Final irradiated spectra (broad structureless solid line) and after warming and recooling to 80 K (dotted line), identical to the structured band of the stable *trans,trans* isomer.

Trienes and longer polyenes: The only conclusive result on low-temperature photochemical studies of trienes was those of pro-vitamin D as described earlier [8]. *cis*-Isomers (1-*cis* or 3-*cis*) of 1,6-diphenyl-1,3,5-hexatriene were found to be stable under UV irradiation in organic glasses [25]. Photoisomerization of 2,5-dimethyl-1,3,5-hexatriene (**15a**) in argon matrix was reported [26]. However, because of the lack of conformational preference of the starting *cis* isomer, the observed result was not clear-cut as far as mechanism of reaction was concerned. Photoisomerization of the parent hexatriene (**15b**) was also studied under the condition of vapor deposition of the *cis* isomer. The results were not interpreted in terms of mechanism of photoisomerization [27].

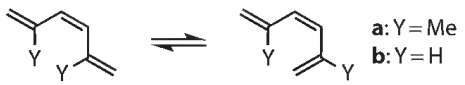

15

Photochemical conformational reorganization (all-*trans* to 2-s-*cis*) of 1,3,5,7-octatetraene in *n*-octane crystals was reported in an early but elegant study [28].

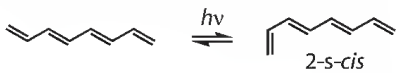

Low-temperature photoisomerization of the hindered 11-*cis*-retinal (**16**) in EPA glass was reported [29]. The observed photochemical transformation followed by thermal rearrangements was consistent with HT-11 or HT-12 photoisomerization. (The results are different from those obtained in solution: giving the all-*trans* and 11,13-di*cis* isomers) [30]. Interestingly, as earlier reported, low-temperature irradiation of all-*trans*-retinal [31] was also consistent with multiple HT isomerizations yielding a highly blueshifted unstable conformer.

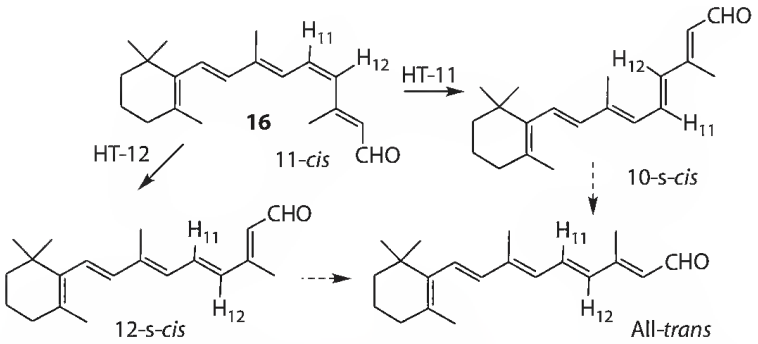

Nitrogen-containing compounds: Earlier we mentioned that the styryl derivatives yielded a slightly blueshifted photoproduct when irradiated in low-temperature glassy media. However, for several nitrogen-containing compounds we found more extensive changes in UV absorption. One such example is the pyrrole derivative **17** [32]. The results are shown in Figure 24.4. The compound did not undergo detectable changes when irradiated into the longest absorption band (>360 nm). However, upon irradiation with shorter wavelength light (> 310 nm), there was a dramatic lowering of the absorption intensity of the longest wavelength band. This photochemical transformation was found to be reversible, that is, irradiating at even shorter wavelength (>250 nm) resulting in partial regain of the intensity of the longest wavelength band.

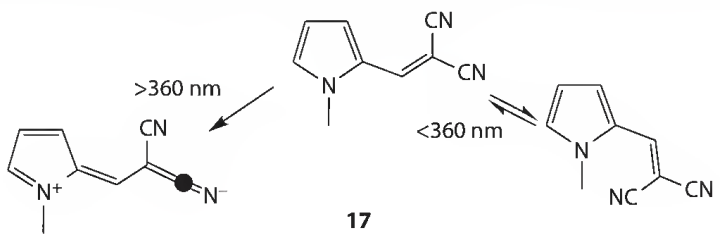

17

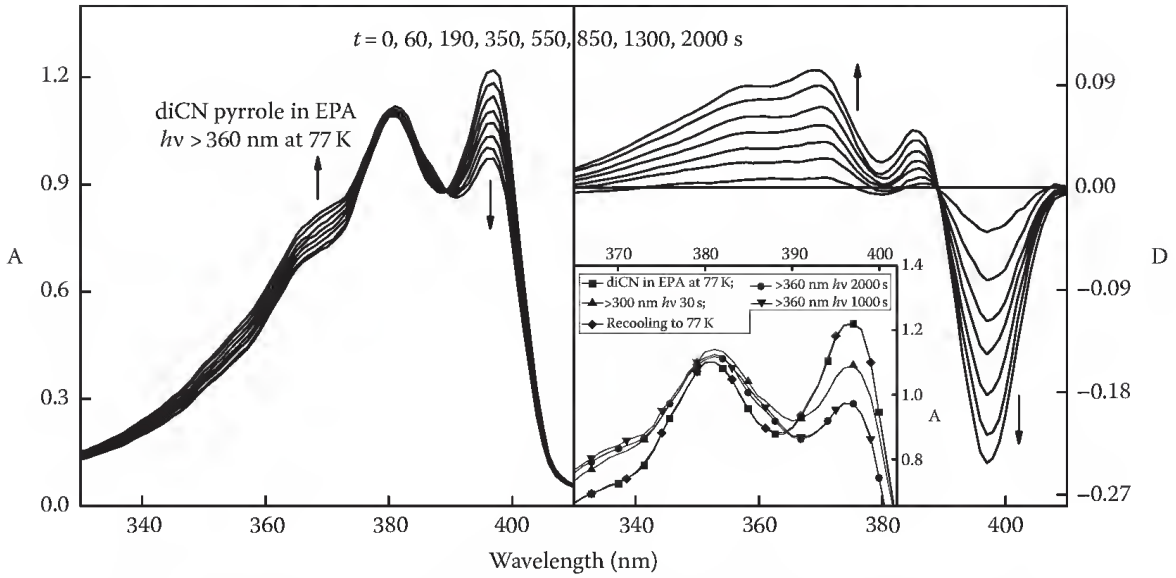

FIGURE 24.4 Wavelength-dependent, low-temperature photochemical reaction of push-and-pull dicyano compound **17**. *Left*: low-temperature (77 K) irradiation in EPA with light >360 nm (no change when irradiated with light >390 nm). *Right*: difference absorption spectra. *Insert*: absorption band before (squares) and after 2000 s of irradiation (circles), additional 30 s of irradiation with >300 nm light (triangles, up), followed by 1000 s irradiation of >360 nm light (triangles, down), demonstrating reversibility of the photoisomerization. Final line: after warming and recooling to 77 K (diamonds), identical to the initial line.

The N-atom in the 5-ring in **17** is nicely situated to interact with the remote electron-withdrawing groups in a charge-transfer manner. Hence, the compound is similar to those reported to exhibit TICT phenomenon [33]. We, therefore, believe that the long wavelength absorption was due to light excitation into the photochemically inactive charge-transfer band. Only when exciting into the higher energy π,π^* band, the normal HT isomerization was observed. However, the change of absorption bands was amplified by the difference in intensity of the charge-transfer bands with the highly twisted HT-product exhibiting a much weaker band of this type.

Similar behavior was detected in low-temperature photoisomerization of compound **18** [32]. However, the photoinactive long-wavelength band was completely in the visible region, making it and related compounds interesting candidates for photochromic studies. For the more delocalized diarylethylene derivative **19**, no wavelength-dependent photoisomerization was detected [32]. Apparently, the absence of strongly electron-withdrawing groups has ruled out the possibility of having a low-lying charge-transfer band. However, unstable photoproduct was produced for the *cis* isomer of **19**, similar to the diarylethylenes described earlier.

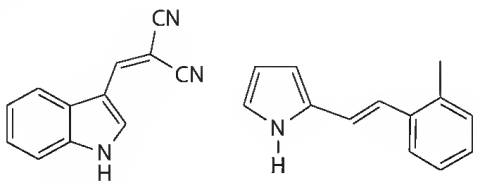

18 **19**

24.3 Complications in HT Photoisomerization Studies

HT is an ultrafast process directly originating from the Franck–Condon species of the excited singlet, kinetically competing against other fast decay processes. Therefore, production of the photoproducts is controlled by kinetic factors. On the other hand, in the triplet processes, such as in triplet-sensitized

reactions, photoproducts reflect the thermodynamic stability of equilibrated species in the excited state such as relaxed triplets (i.e., no HT is expected in triplet sensitized isomerizations). For a recent paper on triplet sensitized isomerization see Ref. [34]. Most of the reported successful studies on HT took advantage of the formation of thermodynamically unstable products, which however, could be detected only under conditions when trapping of such products was possible.

24.3.1 Detection Limitations

UV absorption spectroscopy is a convenient method for detecting formation of unstable (usually highly twisted hence blueshifted) conformer. The method will not be effective when there is no significant difference in relative stability of the reactant and the photoproduct (i.e., the latter present in an equilibrated mixture). Hence, for the following two isomers of naphthalene-substituted styryl derivatives, only the α-substituted isomer (**5**) will give a twisted, hence more readily detectable product while the β-isomer (**20**) will give a perturbed equilibrated mixture making its detection by UV a difficult proposition.

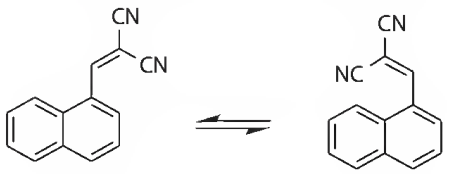

5

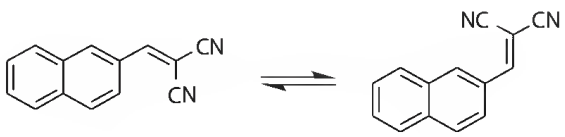

20

Also, the distinctly different absorption spectra of the unstable photoproduct(s) from that of the stable product were easily detected only in rigid organic glasses (often with vibrational structures). There were indications that in solution, even at low temperatures, such fine structures are no longer present (due to solvent broadening). This finding discouraged us from attempting ultrafast time-resolved UV absorption studies to detect the twisted HT product(s) [42].

Attempts were made to introduce the method difference FT-IR to detect formation of new photoproduct during irradiation of **1** in an organic glass, a technique successfully used in studies of primary photoproducts of the biopigments rhodopsin and bacteriorhodopsin [35]. Indeed, a unique IR spectrum was recorded. However, the assignment to the twisted conformer was ambiguous because the simulated IR spectra of the energy-minimized conformers do not match well with those observed for the proposed high-energy conformer nor for the starting stable conformer [36].

24.3.2 Glass Effects

While organic glasses have proven to be useful media for trapping metastable primary photoproducts, it was known for some time that such purportedly rigid media could easily soften under intense UV irradiation. Thus, Porter and coworkers [37] reported in their authoritative spectroscopic studies of trapped free radicals: "The excess energy .... in photolysis of ethyl iodide using radiation of 2537 Å, will amount to over 50 kcal/mole, and since a temperature rise of only 10°C is sufficient to produce noticeable softening of the glasses ..., each quantum absorbed by ethyl iodide should result in a viscosity-lowering of several hundred molecules of the solvent sufficient to enable the radicals to diffuse apart. Heat will rapidly be conducted away and the glass will again become rigid ..." Such local softening of the glassy medium is likely to have a more profound effect on stability of the high-energy conformer(s) produced by HT photoisomerization,

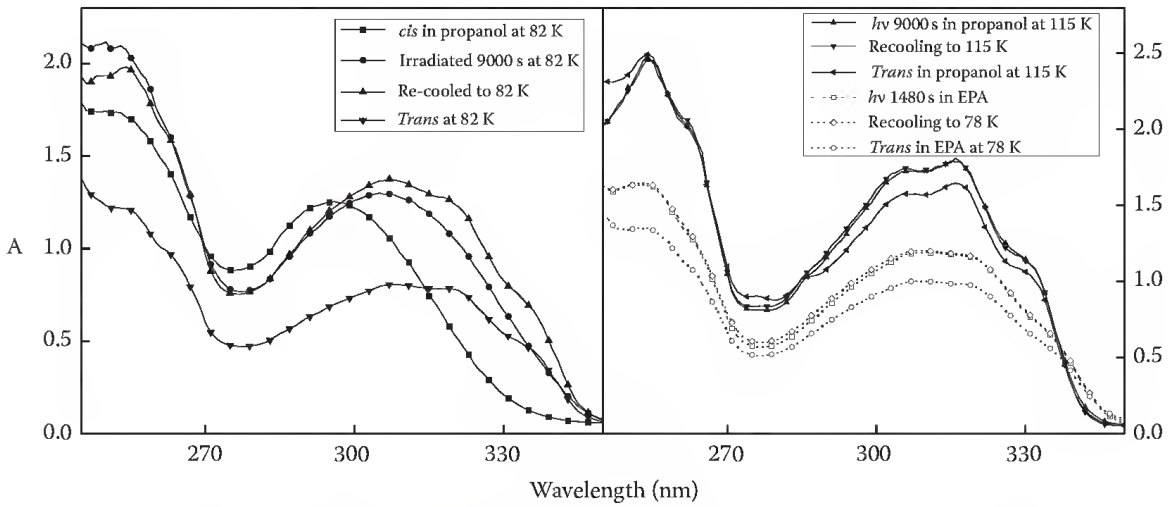

FIGURE 24.5 Glass effect on low-temperature photoisomerization of compound *cis*-**8**. *Left*: before and after irradiated spectra (at 82 K in *n*-propanol) from Figure 24.2 (*left*) superimposed with that after warming to 200 K and recooling to 82 K (triangles, up) and that of authentic sample of the stable *trans*. *Right*: similar irradiation carried out in EPA at 78 K and no significant changes after warming to 200 K and recooling to 78 K. Similar irradiation in *n*-propanol at 115 K also showed no significant changes detected after warming to 200 K and recooling to 78 K.

which disappears through unimolecular conformational reorganization (taking place rapidly at ~50 K) [28] rather than bimolecular radical–radical recombination in Porter's case. We have demonstrated that indeed such glass-softening effect could take place if the glassy medium was not carefully chosen.

This is exemplified by the case of *cis-o,o′*-diphenylstilbene (**8a**) in EPA glass at liquid nitrogen temperature [17] (Figure 24.5). For the redshifted photoproduct, warming did not cause a change in the UV absorption spectrum, an observation normally associated with formation of stable product conformation (in disagreement with HT photoisomerization). However, EPA is a softer glass with setting temperature (~95 K) lower than that of *n*-propanol (~120 K) in which successful trapping of the high-energy conformer was already described (Figure 24.2).

Hence, in EPA, the excess heat from the absorbed photon can easily soften the glass molecules surrounding the substrate allowing the primary photoproduct to undergo thermal rearrangement to the stable conformer. Only in glasses of higher setting temperature (i.e., *n*-propanol), the dissipated excess thermal energy was not sufficient to soften the glasses, hence the photoproduct was successfully trapped. We further carried out irradiation of **8a** in *n*-propanol at a higher temperature (115 K). The result observed (Figure 24.5) was essentially the same as that in EPA at 82 K. Hence, at 115 K, even in *n*-propanol glass the unstable HT product could not be trapped.

This glass effect has since been demonstrated in other systems such as 1,1′-dimethylstilbene [32] and α,α′-dimethyl-1,4-diphenyl-1,3-butadiene (**14a**) [17]. It should be pointed out that soft hydrocarbon glasses such as *iso*-hexane or 3-methylpentane are particularly sensitive to the excess thermal energy effect. In the case of *iso*-pentane, it is doubtful that it can ever be used as rigid glass for any photoisomerization study at liquid nitrogen temperatures. In fact, Porter et al. specifically commented on the fact that in their hands *iso*-pentane remained fluid at such temperatures [37].

24.3.3 Regioselectivity

In the case of 1,4-diphenyl-1,3-butadiene, we reported exclusive detection of the HT-1 process at the expense of the HT-2 process [23]. In reality, when UV spectroscopy was used for detection of the primary photoproduct(s), it was unlikely that any minor product (say that from HT-2) could be detected if it were formed in less than one tenth of the primary photoproduct (that from HT-1). In the case of the parent 1,3-butadiene, we suspect HT-2 is a very minor process relative to HT-1. Its detection was

facilitated by the fact that the major HT-1 process did not give a new product when there was no stereochemical label at C-1. However, with a simple label at this position, OBF would lead to a product identical to that from HT-1.

Neither would there be detectable changes from HT-1 (at the α-carbon) of cinnamonitrile that is different from OBF. However, in the case of ethyl cinnamate, **22**, HT-1 is detectable [38] giving a conformationally rearranged ester group in the product.

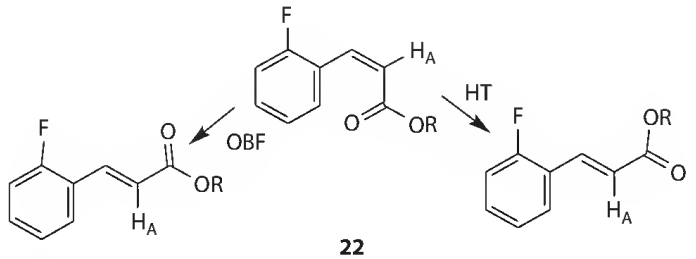

22

24.3.4 Alternative Mechanism, Examples of BP Photoisomerization

There are several cases in the literature where photoisomerization of crystalline polyenes resulted in two-bond isomerization in a manner consistent with bicycle-pedal (BP) process, that is, simultaneous isomerization of two double bonds. The first example was crystals of the *cis,cis*-muconate salt (**22**), rearranging directly to its *trans,trans* isomer [39]. Subsequently, other related examples later appeared in the literature: *cis,cis*-1,4-diphenyl-1,3-butadiene (**23**) crystals [40] and 1-*cis*,5-*cis*-1,6-diphenyl-1,3,5-hexatriene (**24**) crystals directly to the corresponding all-*trans* isomer [25].

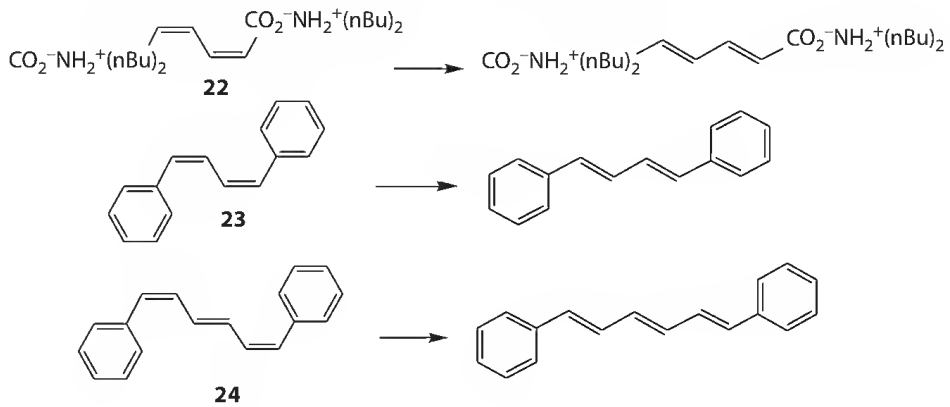

It should be noted that the environment in a crystal cavity is very different from that in a glassy medium. For those di-*cis* isomers mentioned earlier, they all contain immobilized large head and tail making OBF or HT process not possible. On the other head, the connecting middle diene moiety faces a relatively large intermolecular empty space that allows an energetically downhill (*cis,cis* to *trans,trans*) BP motion [39b]. The locally available empty space around the 11-*cis*-retinyl chromophore when coupled with the long tethers linked to the chromophore even allows a OBF process for photoisomerization of the visual chromophore [40b].

24.4 HT versus OBF

Liu and coworkers held the notion that OBF process is a preferred process for compounds isomerizing in unconfined environments such as in solution or in the vapor phase while HT is a preferred process in confined environment such as rigid organic glasses [9]. Fuss held a different and interesting view that

HT is the preferred process under all conditions of photoisomerization. Failure to detect HT product(s) under unconfined conditions was merely due to difficulties in accumulating the unstable conformer for detection [41]. It appears that a pulsed experiment with a specially designed system will be able to resolve this issue if a reliable spectroscopic method capable of distinguishing between conformational isomers can be devised. (A picosecond time-resolved study at room temperature was abandoned after demonstrating the close similarity of UV absorption characteristics of conformational isomers at elevated temperatures [43].)

However, if one considers that the deviation of the experimental data obtained in high solvent viscosity from the calculated Kramer equation for excited state lifetime of stilbene [43] is due to participation of HT process [44] that was not considered in the calculation, then one would reach the following conclusion. For solvents of low viscosity, the OBF process dominates, while for solvents of high viscosity the HT begins to play an increasing role, a conclusion that is a compromise between the views held by Liu and Fuss.

There are several papers in the literature questioning the necessity of invoking the HT process. Unfortunately, in these papers, either systems incapable of distinguishing between OBF and HT isomerization [40a,45] or the questionable *iso*-pentane glassy medium (see previous paragraphs) were used [45,46]. Thus, the results obtained were indeed those expected from OBF.

24.5 Theoretical Studies

Several theoretical papers confirming HT being an ultrafast or a low-energy pathway of decay for an excited polyene are available in the literature. Seltzer first showed by MNDO calculations [6] that both the OBF and HT photoisomerization of a model retinyl Schiff base did not require activation energy while isomerization by BP was activated. Higher order calculations showed that HT was indeed a low-energy decay pathway for excited hexatriene [47], octatetraene [48], and stilbene [49]. And, more recently decay pathways of butadiene [7b] and hexatriene [50] were shown to proceed via HT followed by pyramidalization of the HT carbon. The latter change nicely accounted for the well-known 1,5-H-migration process while not affecting the predicted stereochemical consequence of HT.

24.6 Conclusion

Hula-twist was first proposed as a volume-conserving photoisomerization reaction mechanism to account for the ultrafast rate of reaction of the retinyl chromophore confined in the binding cavity. Subsequent crystallographic evidence revealed that the retinal chromophore is not in close contact throughout the binding site. In fact, there are ample empty intramolecular empty spaces for the chromophore to execute the traditional OBF process. Nevertheless, the proposed simultaneous single-and-double-bond isomerization of HT has since been successfully detected in many examples of substrates trapped in the more closely interacting organic glassy media with products consistent with the expected stereochemical consequences (especially after removal of art effects such as softening of surrounding glasses). Whether HT is a general reaction mechanism for all isomerizations, including reactions under fluid solutions, remains to be established. There are also documented but limited number of examples of two double-bond BP isomerizations.

Acknowledgment

The work was partially supported by a grant from the National Science Foundation (CHE-0132250). We thank contributions by early workers in this research group: G. Krishnamoorthy, S. Schieffer, S. Shevyakov, A. E. Asato, and C. Hirata.

References

1. Mullikan, R. S. and Roothaan, C. C. I. (1947) *Chem. Rev.*, **41**, 219–231.
2. See, e.g.: Saltiel, J., Agostino, J. D., Megarity, E. D., Metts, D., Neuberger, K. R., Wrighton, M., and Zafiriou, O. C. (1973) *Org. Photochem.*, **3**, 1–113; and for a more detailed review on *cis,trans* photoisomerization see: Dugave, C. and Demange, L. (2005) *Chem. Rev.*, **103**, 2475–2532.
3. (a) Liu, R. S. H. and Asato, A. E. (1985) *Proc. Natl. Acad. Sci. USA*, **82**, 259–263; (b) Liu, R. S. H. and Browne, D. (1986) *Acc. Chem. Res.*, **19**, 42–48.
4. (a) Busch, G. D., Applebury, M. L., Lamola, A. A., and Rentzepis, P. (1972) *Proc. Natl. Acad. Sci. USA*, **69**, 2802–2806; (b) Wang, Q., Schoenlein, R. W., Peteanu, L. A., Mathies, R. A., and Shank, C. V. (1994) *Science*, **266**, 422–424.
5. Warshel, A. (1976) *Nature (London)*, **260**, 679–683.
6. Seltzer, S. (1987) *J. Am. Chem. Soc.*, **109**, 1627–1631.
7. (a) Fuss, W., Lochbrunner, S., Muller, A. M., Schkarki, T., Schmid, W. E., and Trushin, S. A. (1988) *Chem. Phys.*, **116**, 2034–2048; (b) Wilsey, S. and Houk, K. N. (2002) *Photochem. Photobiol.*, **76**, 616–621.
8. Muller, A. M., Lochbrunner, S., Schmid, W. E, and Fuss, W. (1998) *Angew. Chem. Int. Ed.*, **37**, 505–507.
9. (a) Liu, R. S. H. and Hammond, G. S. (2004) *Handbook of Photochemistry and Photobiology*, Vol. 26, 2nd edn., Eds. Horspool, W. M. and Lenci, F., CRC Press, Boca Raton, FL, pp. 1–11. (b) Liu, R. S. H. and Hammond, G. S. (2000) *Proc. Natl. Acad. Sci. USA*, **97**, 11153–11158; (c) Liu, R. S. H. and Hammond, G. S. (2001) *Chem. Euro. J.*, **7**, 4536–4544.
10. Malkin, S. and Fisher, E. (1964) *J. Phys. Chem.*, **68**, 1153–1163.
11. Imamoto, Y., Kuroda, T., Kataoka, M., Shevyakov, S., Krishnamoorthy, G., and Liu, R. S. H. (2003) *Angew. Chem. Int. Ed.*, **42**, 3630–3633.
12. Castel, N. and Fisher, E. (1985) *J. Mol. Struct.*, **127**, 159–166.
13. Alfimov, M. V., Razumov, V. F., Rachinsky, A. G., Listvan, V. N., and Scheck, Yu. B. (1983) *Chem. Phys. Lett.*, **101**, 593–597.
14. Krishnamoorthy, G., Asato, A. E., and Liu, R. S. H. (2003) *Chem. Commun.*, 2170–2171.
15. Nakane, N., Nicolaides, A., Tomioka, H., Asato, A. E., and Liu, R. S. H. (2006) *J. Mol. Phys.*, **104**, 1009–1015.
16. Unpublished results of C. Hirata and R. S. H. Liu.
17. Zhao, Y.-P., Yang, L.-Y., and Liu, R. S. H. (2009) *Chem. Asian J.*, **4**, 754–759.
18. Yang, L.-Y., Harigai, M., Imamoto, Y., Kataoka, M., Ho, T.-I., Andioukhina, E., Federova, O., and Liu, R. S. H. (2006) *Photochem. Photobiol. Sci.*, **5**, 874–882.
19. Yang, L.-Y. and Liu, R. S. H. (2007) *Photochem. Photobiol.*, **84**, 1436–1440.
20. Squillacote, M. E., Sheridan, R. S., Chapman, O., and Anet, F. A. L. (1975) *J. Am. Chem. Soc.*, **101**, 3657–3659.
21. (a) Squillacote, M. E., Semple, T. C., and Mui, P. W. (1985) *J. Am. Chem. Soc.* **107**, 6842–6846; (b) Squillacote, M. E. and Semple, T. C. (1990) *J. Am. Chem. Soc.*, **112**, 5546–5551.
22. Krishnamoorthy, G., Schieffer, S., Shevyakov, S., Asato, A. E., Wong, K., Head, J., and Liu, R. S. H. (2004) *Res. Chem. Intermed.*, **30**, 397–405.
23. Yang, L.-Y., Liu, R. S. H., Bowman, K. J., Wendt, N. L., and Liu, J. (2005) *J. Am. Chem. Soc.*, **127**, 2404–2405.
24. Yang, L.-Y., Liu, R. S. H., Wendt, N. L., and Liu, J. (2005) *J. Am. Chem. Soc.*, **127**, 9378–9379.
25. Sonoda, Y., Kawanishi, Y., Tsuzuki, S., and Goto, M. (2005) *J. Org. Chem.*, **70**, 9755–9763.
26. Brouwer, A. M. and Jacobs, H. J. C. (1995) *Recl. Trav. Chim. Pay-Bas*, **114**, 449–456.
27. Furukawa, Y., Takeuchi, H., Harada, I., and Tasumi, M. (1983) *J. Mol. Struct.*, **100**, 341–350.
28. Ackerman, J. R. and Kohler, B. (1984) *J. Chem. Phys.*, **80**, 45–50.
29. Yang, L.-Y. and Liu, R. S. H. (2006) *J. Ch. Chem. Soc.*, **53**, 1219–1224.

30. Ganapathy, S. and Liu, R. S. H. (1992) *Photochem. Photobiol.*, **56**, 959–964.
31. (a) Jurkowitz, L. (1959) *Nature*, **184**, 614–617; (b) Loeb, J. N., Brown, P. K., Wald, G. *ibid*, 617–620; (c) Wald, G. *ibid*, 620–624.
32. Unpublished results of Y.-P. Zhao and R. S. H. Liu.
33. Rettig, W. (1986) *Angew. Chem. Int. Ed.*, **25**, 971–988.
34. Zhao, Y.-P., Campbell, R. O., Liu, R. S. H. (2008) *Green Chem.*, **10**, 1038–1041.
35. Kandori, H. (2000) *Biochim. Biophys. Acta*, **1460**, 177–191.
36. Liu, R. S. H., Yang, L.-Y., Zhao, Y.-P., Kawanabe, A., and Kandori, H. In: *Supramolecular Photochemistry*, 2nd edn., Eds. V. Ramamurthy and Y. Inoue, in press.
37. Norman, I. and Porter, G. (1955) *Proc. Roy. Soc. London A*, **230**, 399–414.
38. Schieffer, S., Pescatore, J., Ulsh, R., and Liu, R. S. H. (2004) *Chem. Commun.*, 2680–2681.
39. (a) Odani, T., Matsumoto, A., Sada, K., and Miyata, M. (2001) *Chem. Commun.*, 2004–2005; (b) Furukawa, D., Kobatake, S., and Matsumoto, A. (2008) *Chem. Commun.*, 55–57.
40. (a) Saltiel, J., Krishna, T. S. R., Turek, A. M., and Clark, R. J. (2006) *Chem. Commun.*, 1506–1508; (b) Liu, R. S. H., Yang, L.-Y., and Liu, J. (2007) *Photochem. Photobiol.*, **83**, 2–10.
41. Ruiz, D. S., Cembrau, A., Garavelli, M., Olivucci, M., and Fuss, W. (2002) *Photochem. Photobiol.*, **76**, 622–633.
42. Unpublished results of Zhao, Y.-P., Liu, R. S. H., Luk, C., and Platz, M.
43. See e.g.: Waldeck, D. H. (1990) *Chem. Rev.*, **91**, 415–436.
44. Liu, R. S. H. (2002) *Photogr. Sci. Photochem.*, **20**, 81–87.
45. Saltiel, J., Krishna, T. S. R., and Turek, A. M. (2005) *J. Am. Chem. Soc.*, **127**, 6938–6939.
46. Saltiel, J., Bremwer, M. A., Laohhasurayotin, S., and Krishna, T. S. R. (2008) *Angew. Chem. Int. Ed.*, **47**, 1237–1240.
47. Olivucci, M., Bernardi, F., Celani, P., Rayazos, I., and Robb, M. A. (1994) *J. Am. Chem. Soc.*, **116**, 1077–1085.
48. Garavelli, M., Celani, P., Yamamoto, N., Bernardi, F., Robb, M. A., and Olivucci, M. (1996) *J. Am. Chem. Soc.*, **118**, 11656–11657.
49. Levine, B. G., Ko, C., Quenneville, J., and Martinez, T. (2006) *J. Mol. Phys.*, **104**, 1053–1060.
50. Norton, J. E. and Houk, K. N. (2006) *J. Mol. Phys.*, **104**, 993–1008.

25

Fulgimides

Karola Rück-Braun
Technische Universität Berlin

Kerstin Mayer
Technische Universität Berlin

Andreas Hebert
Technische Universität Berlin

Fabian Michalik
Technische Universität Berlin

Fulgimides and their parent fulgides constitute a class of thermally irreversible photochromic compounds. Their derivatives are interesting building blocks for both material and life sciences, for example, for the switching of functions and the development of novel devices. The early work on fulgides in particular was directed toward memory devices, and they are still considered to be promising candidates for photon-controlled memory media. Fulgides and their derivatives as well as their applications have been the subject of various comprehensive reviews covering the literature up to 2004.[1–4] In this chapter, we will discuss structure–property relationships observed over the years for furyl-, thienyl-, oxazolyl-, pyrryl-, 2-indolyl-, and 3-indolylfulgides and their fulgimide derivatives. The preferred notations furylfulgide, pyrrylfulgide, etc., will be used in this chapter. However, for a search of the published literature, the reader should also refer to the notations furyl fulgide, pyrryl fulgide, etc. Research toward applications in nanotechnology and biosensor technology is also covered, as well as synthetic methods for the preparation of fulgimides and recent advances in the preparation of their parent fulgides.

25.1 Fulgimides and Their Parent Fulgides: Structure–Property Relationships

Photochromic heterocyclic fulgides and fulgimides exist in three isomeric states: two open forms (*Z*- and *E*-form) and a closed *C*-form. Upon illumination with UV light besides other radiationless processes, three transformations occur: *Z*-to-*E* and *E*-to-*Z* isomerization and the *E*-to-*C* electrocyclization reaction.[1–4] With *Z*/*E* isomerization, the light-yellow *Z*- and *E*-forms are reversibly converted into each other. Upon UV-light irradiation the *E*-form undergoes the conrotatory electrocyclic ring-closure reaction (coloring) furnishing the ring-closed, colored *C*-form. The reverse *C*-to-*E* ring-opening process (bleaching) is observed upon illumination with visible light. These two processes (coloring and

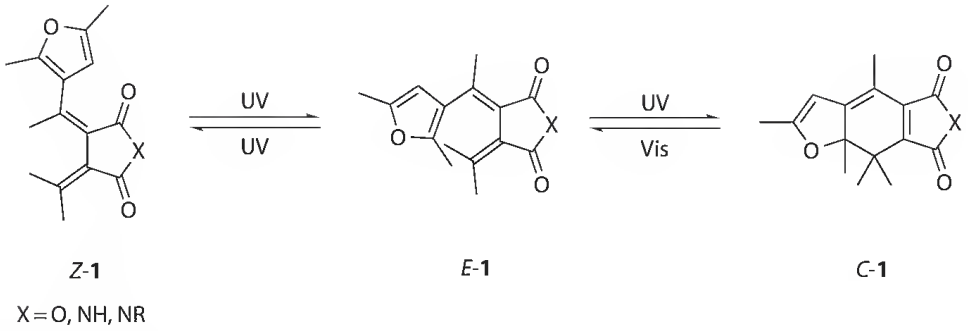

FIGURE 25.1 Photochemical isomerization of furylfulgides and furylfulgimides.

bleaching) are furnishing thermally stable isomeric states and are responsible for photochromism. Thus, the photochromic reaction is based on two reversible photon-induced concerted transformations of a hexatriene (*E*-form)—cyclohexadiene (*C*-form) system, in which both forms are thermodynamically stable (Figure 25.1).

Depending upon the heteroaromatic ring system it is often solely the *Z*-forms that are obtained via the common synthetic routes (e.g., furyl- and thienylfulgides).[1–4] However, the *Z*-forms have more or less been neglected within the photochromic systems. The *E*-to-*Z* and *Z*-to-*E* isomerizations complicate the photochromism of fulgides and fulgimides and are considered to be energy-wasting processes.

During the research period covered in this review, through to the beginning of 2010, there has been a focus on five main classes of heteroaromatic fulgides and fulgimides: thienyl- (**2**), pyrryl- (**3**), oxazolyl- (**4**), 3-indolyl- (**5**), and 2-indolyl derivatives (**6**). In slight contrast to this, Matsushima reported a comparative study of 14 heteroaromatic fulgides back in 1988.[5] In these studies, 3-indolylfulgide (**5**), oxazolylfulgide (**4**), and the related thiazolyl fulgide showed very low thermal degradabilities, and 3-indolylfulgide (**5**) also showed low photochemical fatigues as compared to furyl-, thienyl-, and pyrryl derivatives. In these early days, a low photoresponsiveness for coloration was observed for 3-indolylfulgides since the quantum yield of **5** under UV irradiation was significantly lower compared to furylfulgide **1** (**5**: below 0.1; **1**: 0.20).[5] Nevertheless, during the last decade especially 2-indolylfulgimides, as well as Yokoyamas 3-indolylfulgimides, have been intensively studied (Figure 25.2).

Generally, the *E*- and *Z*-forms of these heteroaromatic fulgides display similar optical properties. Whereas the ring-opened *Z*- and *E*-forms are nonplanar (see e.g., 3-indolylfulgide **5**), the ring-closed *C*-forms are almost planar, and as a consequence of their extended planar π-electron systems, a strong and broad absorption band in the visible wavelength range is observed. The absorption maxima

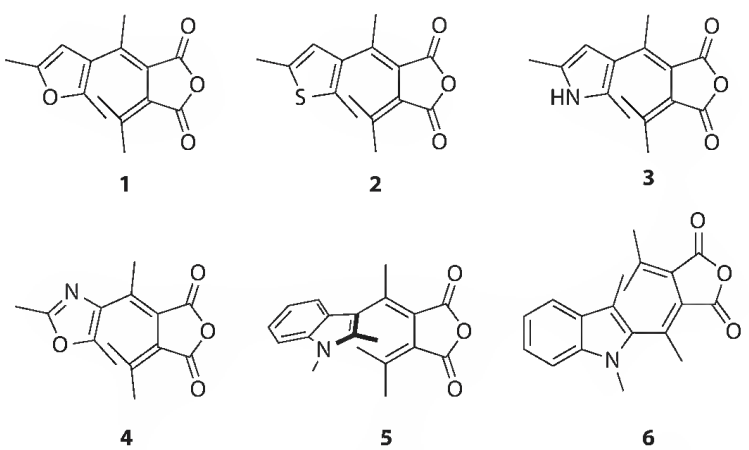

FIGURE 25.2 The five main classes of heteroaromatic fulgides (represented as *E*-isomers).

of the colored *C*-forms tend to redshift with the electron-donating ability of the heterocyclic groups: furyl < thienyl < *N*-methyl-pyrryl.[5] In general, heteroaromatic fulgides and their derivatives show a good separation of the absorption spectra of the photochromic *E*- and *C*-forms.

Heller reported that the quantum yield for the *E*-to-*C* isomerization process (coloring) of furylfulgide **1** is independent of the reaction temperature and the irradiation wavelength, whereas for the *C*-to-*E* isomerization process (bleaching/decoloration) a strong dependence on both parameters was observed.[6,7] A wavelength dependence of the *C*-to-*E* quantum yield for 3-indolylfulgides[8,9] was also detected, and a series of theoretical papers report on the Arrhenius-type temperature dependence of the photochemical *C*-to-*E* isomerization.[10]

In the beginning, fulgides, which had a 2,5-dimethylfuryl moiety, were intensively examined on route to thermally irreversible photochromic compounds. Nowadays they are milestones in the research history of fulgides. In 1981 Heller reported the parent furylfulgide **1**,[11,12] which contains the necessary methyl groups on the heterocyclic moiety to prevent the thermal ring-opening of the *C*-form by a disrotatory pathway. This was due to steric repulsion between the methyl groups in the ring-closed *C*-form.[3,11–13] Some general trends within the substitution pattern of heteroaromatic fulgides and fulgimides can be described as follows:

In the furyl-, thienyl-, and 3-indolylfulgide series, bulky substituents R^1 (e.g., R^1 = *i*-Pr, *n*-Pr) at the methylene carbon next to the heteroaromatic ring increase the ring-closing *E*-to-*C* (coloring) quantum yield upon UV-light irradiation, while simultaneously decreasing the *E*-to-*Z* isomerization quantum yield (see structures **A** and **B**). With an isopropyl or *tert*-butyl group the *E*-to-*Z* isomerization can be completely suppressed.[3] 2-Indolylfulgides **6**,[14–17] in which R^1 is a hydrogen atom, are photochromic, in contrast to the related 3-indolylfulgides[3] and the five-membered heteroaromatic fulgides with R^1 = H, which are not photochromic. For example, the *E*-form of 3-indolylfulgide **5** upon irradiation at 365 nm only undergoes *E*-to-*Z* isomerization.[18] Another general trend already studied in the early days of research is observed upon replacement of an isopropylidene group (R^2) by an adamantylidene group (R^2).[19] The bulky adamantylidene substituent is found to increase the ring-opening *C*-to-*E* (bleaching) quantum yield upon irradiation with visible light (Figure 25.3).

When fulgides were still a new topic, most research efforts focused on useful fulgides and fulgimides for rewriteable memory media. Accordingly the following properties amongst others were considered to be of major importance: (a) fatigue resistance, (b) nondestructive readout ability, and (c) thermal stability of the photochromic *C*- and *E*-forms. For example, early studies by Matsushima observed that an *N*-benzylfulgimide showed poor photochemical fatigue resistance in comparison to the parent furylfulgide **1** when undergoing repeated bleaching–coloration cycles in toluene upon irradiation with UV light. However, the thermal storage stability of the *C*-form of the fulgimide in toluene–ethanol solution at room temperature was significantly improved in comparison to the parent fulgide.[20,21] Most important for fatigue resistivity is the elimination of oxygen from the photochromic system and to avoid benzyl and allyl substituents.

In comparison to furyl-, thienyl-, and pyrryl derivatives, other heterocyclic systems, especially 3-indolyl- and oxazolylfulgides, show excellent fatigue resistance during repeated bleaching–coloration

R^1 = *i*-Pr, *n*-Pr, *t*-Bu, CF_3
R^2 = isopropylidene, adamantylidene
Y = O, S
X = O, NH, NR

FIGURE 25.3 Substitution pattern of furyl-, thienyl-, and 3-indolylfulgides and furylfulgimides.

cycles, for example, in PMMA films containing 15–20 wt% of fulgide. 3-Indolyl derivatives also possess low medium dependence compared to the five-membered heterocyclic systems.[5,22] The dilemma that was already observed in early days is the fact that highly resistant photochromic compounds generally offered only a low photoresponsiveness for coloration upon UV irradiation.[5]

In the following sections, the development of thermally stable and photochemically fatigue-resistant heteroaromatic fulgides and fulgimides is highlighted for the particular classes of heteroaromatic ring systems listed earlier. Selected data dealing with specific substitution patterns are discussed in these specialized sections.

Nowadays, fulgimides replace fulgides to reduce solvolytic degradations without affecting the photochromic performance.[1–4] The imide functionality was used for attachment to the side chain of polymers but also to incorporate the photochromic unit into the main chain of polymers. Linkers were introduced via the imide group for coupling of the molecule to proteins. Fluorescence dyes and other chromophores were also attached via the imide functionality to the photochromic unit. Specific compounds and applications are discussed in the following sections.

25.1.1 Thienyl-, Pyrryl-, and Oxazolylfulgides and –Fulgimides

Upon introduction of an electron-donating substituent to the thienyl ring of thienylfulgides and their derivatives, a bathochromic shift of the absorption maximum was observed with an increase of the molar absorption coefficient (ε_{max}) being detected for the *C*-form. At the same time it was noted that the *C*-to-*E* (bleaching) quantum yield decreased.[23] Port observed that thienylfulgide **2** in PS can be colored and bleached at all temperatures between 300 and 10 K.[23] The molecular structures of a series of thienylfulgimides **7–14** with linkers attached to the imide functionality are shown in Figure 25.4. The photochromic properties of these compounds have been reported by Effenberger (**7**),[24] Rück-Braun (**8**,**9**),[25] Krayushkin (**10**,**11**),[26] Fox (**12**,**13**),[27] and Köse (**14**).[28]

More recently there was a detailed study of pyrrylfulgides by Fan.[4] During studies using nanosecond laser flash photolysis they found that the *E*-to-*C* cyclization reactions of pyrrylfulgides occur from the π-π* excited singlet state. Furthermore, from their results they were able to conclude that the π-π* excited triplet state was also involved.[29–31] Matsushima (**15**,**16**),[5,32,33] Chen (**17**,**18**),[34,35] and Yao[36] reported the photochromic properties of some pyrrylfulgimides (Figure 25.5).

Oxazolylfulgides and their derivatives are known to be fairly thermally and photochemically stable. This is explained by the higher oxidation potentials of the oxazole ring.[37] A selection of oxazolylfulgides and fulgimides (**19–22**)[38,39] from the literature is shown in Figure 25.6.

More recently, the photochromic properties of cationic oxazolylfulgimides **23–27** were examined in neutral aqueous solution.[21,33] In addition to this, the photochromic properties of the neutral precursors

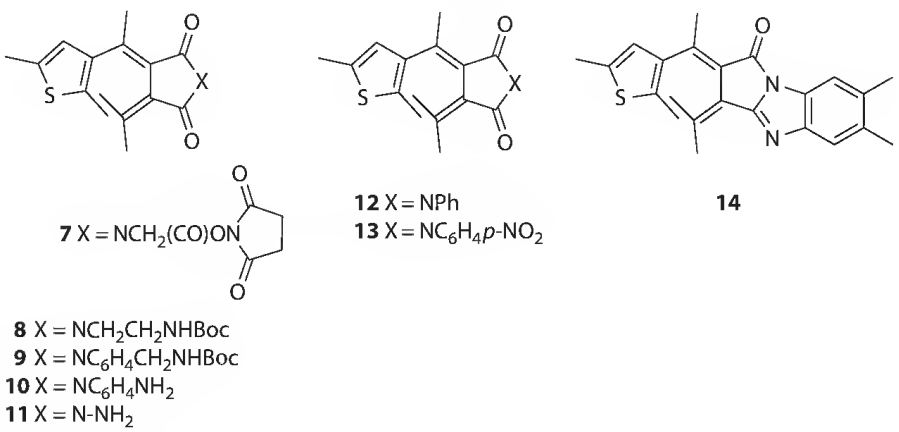

FIGURE 25.4 Molecular structures of a series of thienylfulgimides.

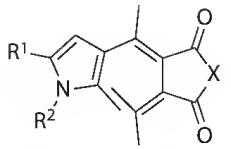

15 R^1 = Me, R^2 = Ph, X = O
16 R^1 = Me, R^2 = Ph, X = NH
17 R^1 = Ph, R^2 = Me, X = O
18 R^1 = Ph, R^2 = C_6H_4OMe, X = O

FIGURE 25.5 Molecular structures of a series of pyrrylfulgides and pyrrylfulgimides.

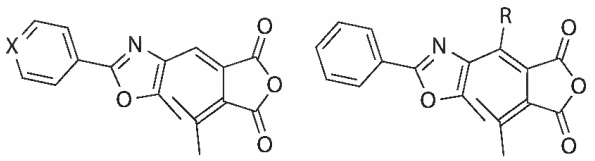

19 X = CH
20 X = N

21 R = Me
22 R = $C_{17}H_{35}$

FIGURE 25.6 Molecular structures of a series of oxazolylfulgides.

(**23**,**25**) were compared with their allylated cationic derivatives (**24**,**26**,**27**), which were measured in methanol. The introduction of the cationic electron-withdrawing substituent at the phenyl ring, attached to the oxazole ring, led to large shifts of the electronic transitions and to significant changes in the photochromic response rates. Similar effects and trends were observed upon allylation of a dimethylamino group in the *para*-position of a phenyl ring at the imide nitrogen. From the results obtained, Matsushima concluded that the majority of the photochromic phenomena known from organic media and solvents are also observed in aqueous or hydroxylic media.[21] Not long ago the use of dibenzyl fulgenate derivative of the parent oxazolylfulgide in rewritable films was reported.[33] The colored *C*-form of this fulgenate led to a hypsochromic shift of the absorption maximum to 405 nm and to a larger absorption coefficient when compared to the *C*-form of the parent oxazolylfulgide. This fulgide derivative was applied in the development of simple full-color rewritable films, in combination with other fulgide derivatives (Figure 25.7).

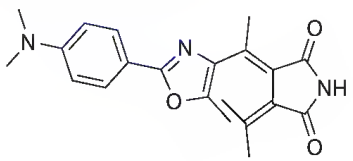

23

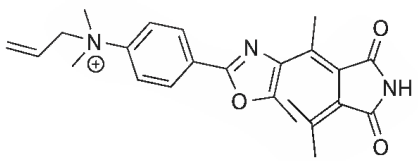

24

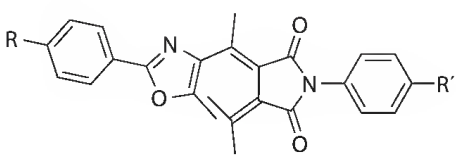

25 R = R′ = NMe_2
26 R = NMe_2, R′ = $N^+Me_2CH_2CH{=}CH_2$
27 R = R′ = $N^+Me_2CH_2CH{=}CH_2$

FIGURE 25.7 Molecular structures of a series of oxazolylfulgimides.

25.1.2 3-Indolylfulgides and 3-Fulgimides

Analogous to furylfulgides, bulky alkyl substitutents (R^1) at the methylene group besides the indole ring increased the coloring quantum yield, whereas a bulky alkylidene groups (R^2) increased the bleaching quantum yield, see structure **B**. However, if R^1 and R^2 are both sterically demanding the coloring quantum yield decreased and only an increase of the bleaching quantum yield was observed.[19] For a related study of the consequences of miscellaneous alkyl substituents in position R^1 on a 3-indolylfulgimide were determined.[40] (Figure 25.8).

In early days already electronic and steric effects of substituents on the indole ring were investigated.[3,41,42] Electron-donating substituents (MeS, MeO, Me_2N) in the 5-position of the indole ring redshifted the absorption maxima of the colored *C*-forms, but also decreased the quantum yields of the photoreactions.[22,41] The colored form of 5-dimethylamino-substituted indolylfulgide was found to be highly resistant toward photobleaching.[22] However, a methoxy group in the 6-position of the indole ring resulted in a higher molar absorption coefficient.[43] For two methoxy groups on the indole ring in 5- and 6-position both effects were observed.[43] Replacement of the methyl by an ethyl group in 2-position (R‴) also redshifted the absorption maxima of the colored *C*-form but also lowered the molar ratio of the colored form in the photostationary state upon UV irradiation (examples for molar ratios: **5** R‴ = Me, *E*/*Z*/*C* 35/9/56;[19] **32**: R‴ = Et, *E*/*Z*/*C* 39/31/30[19]; and **30**: R′ = NMe_2, *E*+*Z*/*C* 3/97[22]) (Figure 25.9).

During the studies with 5-dimethylaminoindolylfulgide **30** a new type of nondestructive readout methodology, using an acid–base equilibrium was discovered. The *C*-form of **30a** showed absorption at 780 nm and it did not bleach upon irradiation with visible light.[22,41] However, upon treatment with trichloroacetic acid, a mixture of the parent fulgide *C*-**30a** and its protonated species *C*-**30b** formed an equilibrating system.[44] The protonated species *C*-**30b** had no absorption at 780 nm and underwent ring-opening upon irradiation with 554 nm light to a protonated *E*-form *E*-**30b**. This equilibrium mixture is regarded to be an ideal nondestructive readout system, using 403 nm light for writing, 554 nm light for erasing, and 780 nm light for readout.[3,45] The phenomena were also observed in different PMMA films (Figure 25.10).[9,46]

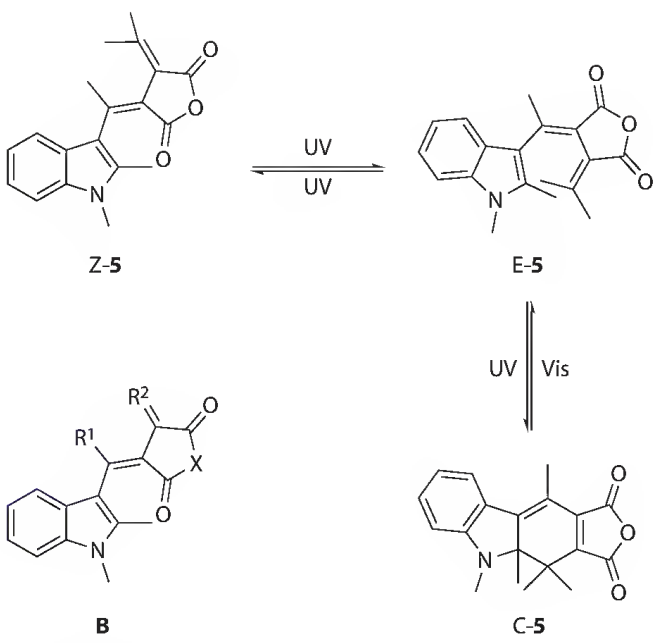

FIGURE 25.8 Photochromism of 3-indolylfulgides and 3-indolylfulgimides.

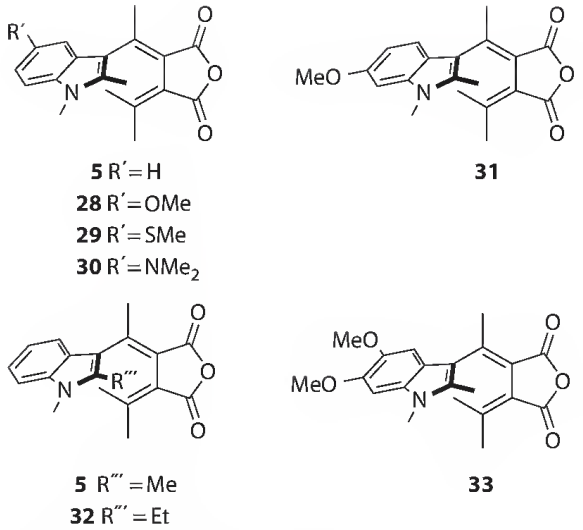

5 R′ = H
28 R′ = OMe
29 R′ = SMe
30 R′ = NMe_2

31

5 R‴ = Me
32 R‴ = Et

33

FIGURE 25.9 Substitution pattern of a series of 3-indolylfulgides.

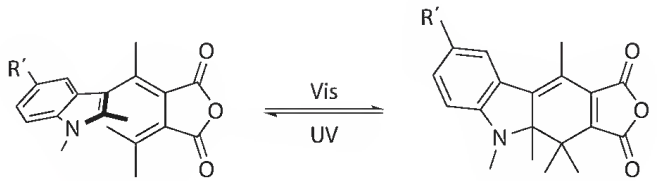

E-**30a** R′ = NMe_2
E-**30b** R′ = $^{+}NHMe_2$

C-**30a** R′ = NMe_2
C-**30b** R′ = $^{+}NHMe_2$

FIGURE 25.10 Molecular structures of the *E*- and *C*-isomers of 5-dimethylaminoindolylfulgide **30** and its protonated forms.

A selection of 3-indolylfulgides (**34**,**35**) with additional modifications on the indole ring is presented in Figure 25.11.[33,47]

Electronic effects of substitutents on indole nitrogen were also investigated (Me, Et[19] and H, Ts[41]) by Yokoyama (see structures **C** and **D**). The photochromic properties of indolylfulgide **32** observed upon replacement of the methyl group by an ethyl group were reported to be almost the same as observed for **5**, however, an increase of the molar ratio of the *C*-form in the photostationary state upon UV-light irradiation was observed (see structure **D**: R^3 = Me, *E*/*Z*/*C* = 35/9/56, R^3 = Et, *E*/*Z*/*C* = 22/10/67).[19] The electron-withdrawing group (R^3 = Ts) shortened the absorption maximum of the colored form, suppressed thermal *E*-*Z* isomerization, and enlarged the quantum yield of the photochromic reactions.[41] More recently Russian researchers also reported on the use of *N*-aryl substituted indolylfulgides (Figure 25.12).[48]

A CF_3 group placed on the methylene group next to the indole ring (R^1 = CF_3) increased the ring-opening (bleaching) quantum yield significantly.[49] The absorption maximum of the open form was shifted

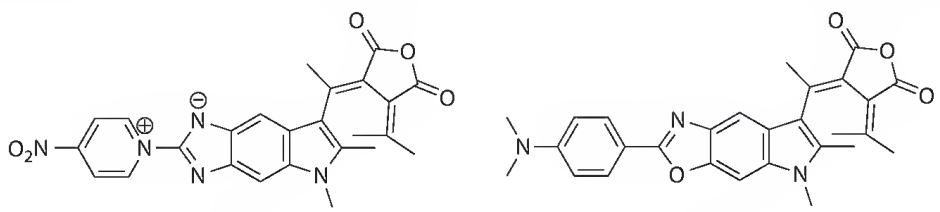

34

35

FIGURE 25.11 3-Indolylfulgides **34**, **35**: Modifications of the substitution pattern of the indole ring.

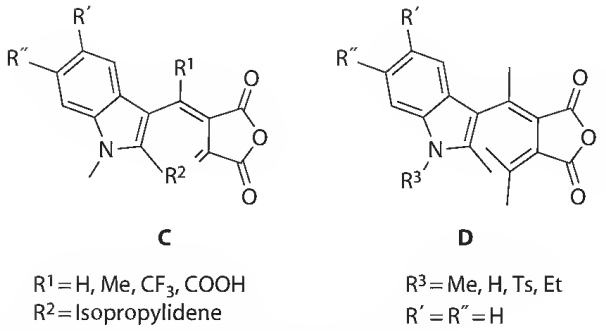

FIGURE 25.12 Substitution pattern of a series of 3-indolylfulgides.

toward longer wavelengths, whereas the absorption maximum of the closed form was observed at slightly shorter wavelengths.[49] Similar trends were observed by Lees within a series of fluorinated indolylfulgide ($R^1 = C_2F_5$ or a C_3F_7) derivatives, either containing the adamantylidene or the isopropylidene moiety.[50–57]

Lees intensively studied the thermal stability of fluorinated indolylfulgides and related fulgimides. A CF_3 group increased the thermal stability of the closed form, decreased the thermal stability of the open form, and increased the photochemical repeatability. Recently the fluorinated substituents at the methylene group next to the indole ring were replaced by a carboxylic acid residue. This modification led to water solubility and according to Lees resulted in the most robust 3-indolylfulgide and derivatives published in the literature.[56]

The thermal stabilities of the colored *C*-forms of 3-indolylfulgides and their derivatives were investigated, for instance by thermal degradation studies of the colored *C*-forms in PMMA films in the dark at 323 or 353 K. Excellent stabilities for indolylfulgides were detected in comparison to the fairly good stability of thienylfulgides, and only poor stabilities of furyl- and pyrrylfulgide compounds.[5] The parent indolylfulgide **5** was also trapped as a model compound in various media at different pH values as well as in a sol-gel matrix.[58]

A series of chiral derivatives was prepared and investigated from indolylfulgides with variable substituents R^1, for example, (R)-binaphthol-condensed indolylfulgides.[59–63] However, this topic has been extensively reviewed in the past, and therefore is not covered in this chapter.[64,65]

However, most importantly, for derivative **36** (R^1 = *n* – Pr) compared to **37** (R^1 = *i* – Pr) a 10-fold increase in fluorescence intensity was detected. Upon excitation with 470 nm light or 320 nm light, the *C*-form of the *n*-propyl-substituted indolylfulgide **36** fluoresced at 610 nm (Figure 25.13).[66]

Russian authors in 2008 reported on the fluorescence characteristics of a series of 1-aryl-5-methoxy-indolylfulgides **38–40** observed in toluene at 293 K. Excitation of indolylfulgide **40** at 380 nm and 640 nm led to emission at 800 nm.[48] This is remarkable, because earlier the colorless *Z/E*-forms and the colored *C*-forms of furyl-, thienyl-, and indolylfulgides[66] were only found to emit fluorescence at low temperature (Figure 25.14).

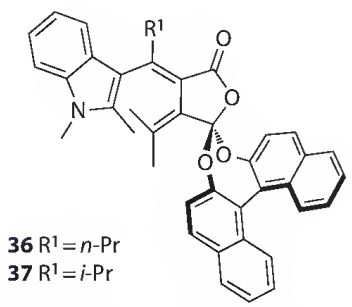

FIGURE 25.13 Chiral derivatives of 3-indolylfulgides: (R)-binaphthol-condensed indolylfulgides **36**, **37**.

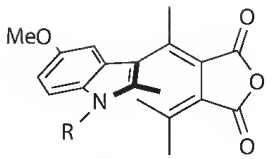

38 R = Ph
39 R = 4-$MeOC_6H_4$
40 R = 4-$Me_2NC_6H_4$

FIGURE 25.14 Molecular structures of a series of 1-aryl-5-methoxy-indolylfulgides.

25.1.3 2-Indolylfulgides and 2-Fulgimides

There are many interesting spectroscopic and photochromic properties of 2-indolylfulgides and their derivatives.[16,17,67–78] The most significant for the *C*-form of 2-indolylfulgides is that the absorption maximum is observed at a longer wavelength, in addition to emitting fluorescence at 678 nm when irradiated with visible light of 580 nm. Thus, illumination of the ring-closed *C*-form with visible light leads to the electrocyclic ring-opening to the *E*-form, fluorescence of the *C*-form, and radiationless processes. The quantum yield for the *E*-to-*C* ring-closure (coloring) process was compared to other heteroaromatic fulgides and was found to be the same as that of the analogously substituted furylfulgide and thienylfulgides but higher than the quantum yields of 3-indolylfulgides.[78] It was observed for 2-indolylfulgides and their derivatives that the quantum yield of the *C*-to-*E* ring-opening (bleaching) process is strongly dependent on the polarity of the solvents. In polar solvents the quantum yield decreased. The low quantum yields observed were explained by the existence of strong interactions between a charge-separated state of the excited molecules with polar solvents leading to an increase of the activation energy for the ring-opening pathway (Figure 25.15).

Analogously to the earlier studies on 3-indolylfulgides and derivatives, the influence of the substitution pattern at the indolylmethylene moiety of 2-indolylfulgides was investigated, as well as the effects of substituents at the 5-position on the indole ring (see structure **F**) and at the indole nitrogen atom.

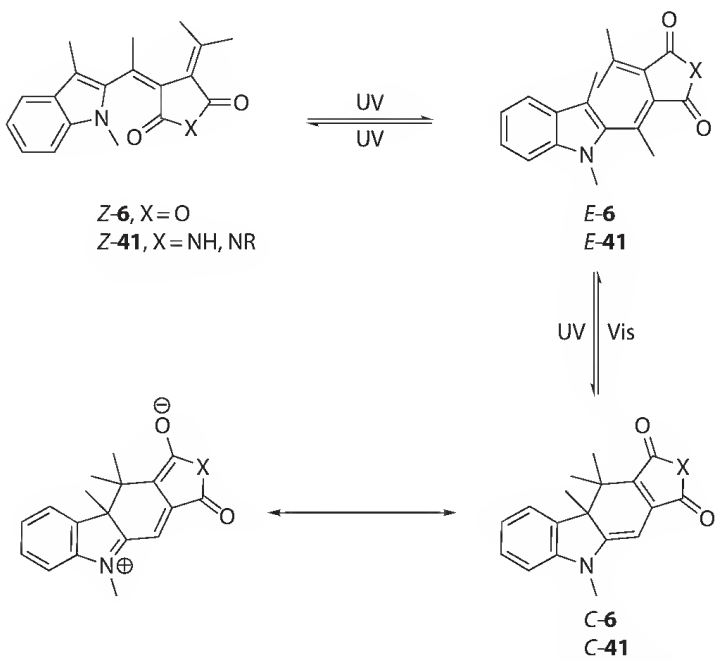

Z-**6**, X = O
Z-**41**, X = NH, NR

E-**6**
E-**41**

C-**6**
C-**41**

FIGURE 25.15 Photochemical isomerization of 2-indolylfulgides and 2-indolylfulgimides.

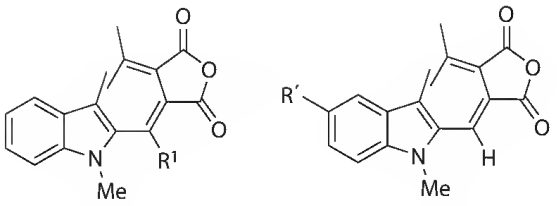

FIGURE 25.16 Substitution pattern of 2-indolylfulgides.

In comparison to the nonsubstituted parent fulgide **6**, a methyl group in position R^1 increased the *E*-to-*C* (coloring) quantum yield, however, concurrently the fluorescence quantum yield decreased (see structure **E**). Similar to the effects observed in the 3-indolylfulgide series an isopropyl substituent in position R^1 almost completely prevented the *E*-to-*Z* isomerization. Nevertheless, a methyl or an isopropyl group also decreased the fatigue resistance of 2-indolylfulgides.[71] Photochemical decomposition of 2-indolyl- as well as 3-indolyl-fulgides[49] and derivatives is considered to be complicated and medium dependent.[71] However, Yokoyama and Rentzepis concluded from their independent experiments that hydrogen atom abstraction from the alkyl group in position R^1 by the neighboring carbonyl oxygen of the fulgide/fulgimide moiety in the excited state might be a serious side reaction, responsible for the low fatigue resistance observed during repeated coloration/bleaching cycles, especially in the presence of an electron-rich isopropyl residue (Figure 25.16).

Electron-donating substituents in 5-position of the indole ring (see structure **F**) resulted in a bathochromic shift of the absorption maxima of the *C*- and the *E*-form, yet the substituents investigated (R′ = OMe, Me, H, Cl, F) were found not to affect the fatigue resistance. However, upon placement of a methoxy group in 5-position a dramatic decrease of the *C*-to-*E* (bleaching) quantum yield was observed. Obviously, the *C*-form is stabilized by resonance effects between an electron-donating substitutent in 5-position and the imide moiety. A related resonance stabilization has previously been observed in the 3-indolyl series, however, between the 5-substituent and the indole nitrogen but only with a dimethylamino group.[9,44]

For the synthesis of a series of *N*-substituted fluorescing 2-indolyfulgimides from the parent fulgides, Rentzepis reported a Lewis acid and hexamethyldisilazane-promoted one-pot reaction.[17] The photophysical characteristics of the fulgimides were found to be similar to the values of the parent fulgides. Again the quantum yield for the *E*-to-*C* ring-closure process was found to be solvent dependent, and when switching from a nonpolar solvent (hexane) to a polar solvent the quantum yield increased by a factor of 2.

25.2 Synthetic Methods for the Preparation of Fulgides and Fulgimides

To date, the syntheses of fulgides have generally been achieved via Stobbe condensation of ketones **G**.[1–4] However, a key step of an alternative route toward fulgides with a sterically demanding *tert*-butyl group in position R^1 is the palladium(II)-mediated carbonylation of 2-butyne-1,4-diols.[79–81] For the Stobbe condensation with the diethylisopropylidenesuccinate **H**, lithium enolates were most commonly used.[1–4] These were obtained by treatment of the former succinate ester with lithium diisopropylamide. However, sodium hydride was also successfully used as a base in a number of papers[71] and potassium *tert*-butoxide in *tert*-butanol was also found to be a good alternative.[18,82]

Nevertheless, the synthesis of heteroaromatic halfesters **I** from electron-rich aromatic ketone precursors did not always proceed smoothly and then cerium enolates were successfully applied instead.[22] In certain cases, the formation of lactone intermediates was reported, which were hydrolyzed to the

half-esters, for example by treatment with sodium hydride in DMF,[52] or with potassium *tert*-butoxide/*tert*-butanol.[82] More recently, yields were also improved by the application of potassium hexamethyldisilazide followed by treatment with potassium *tert*-butoxide/*tert*-butanol.[83]

By saponification of the half-esters **I** with potassium hydroxide in refluxing ethanol, the diacid **J** is obtained. For the subsequent dehydration to the fulgides **K** acetylchloride,[16,71] and acetic anhydride[52] were used in most published procedures. However, dicyclohexylcarbodiimide[71,84] or a water-soluble carbodiimide[83] was also successfully applied as dehydration reagents, in addition to 1-trifluoroacetylimidazole[41] or carbonyldiimidazole.[26]

By aminolysis of the fulgides **K** (anhydride ring opening), an isomeric mixture of the corresponding *N*-substituted succinamic acids **L** is obtained.[16,25,52,56,71,83] In this transformation, the reactivity of electron-poor anilines was enhanced by metallation with sodium hydride NaH or lithium diisopropylamide (LDA).[55]

For the dehydration to the fulgimide **M**, either acetyl chloride or acetic anhydride under thermal conditions was previously used in analogy to the fulgide formations.[55,56] More recently, microwave-assisted one-pot syntheses proved to be superior in comparison to thermal methods, because side reactions are being reduced.[85,86] Rentzepis and others used zinc chloride and hexamethyldisilazane to promote a one-pot procedure of the ring-opening of a fulgide with amines to the succinamic acids **L** and subsequent ring-closure to the fulgimides **M**.[17,83] The synthesis of fulgimides has also been achieved by base-catalyzed cyclization of the methyl esters[87] or the phenacyl ester[25] of the succinamic acids (Figure 25.17).

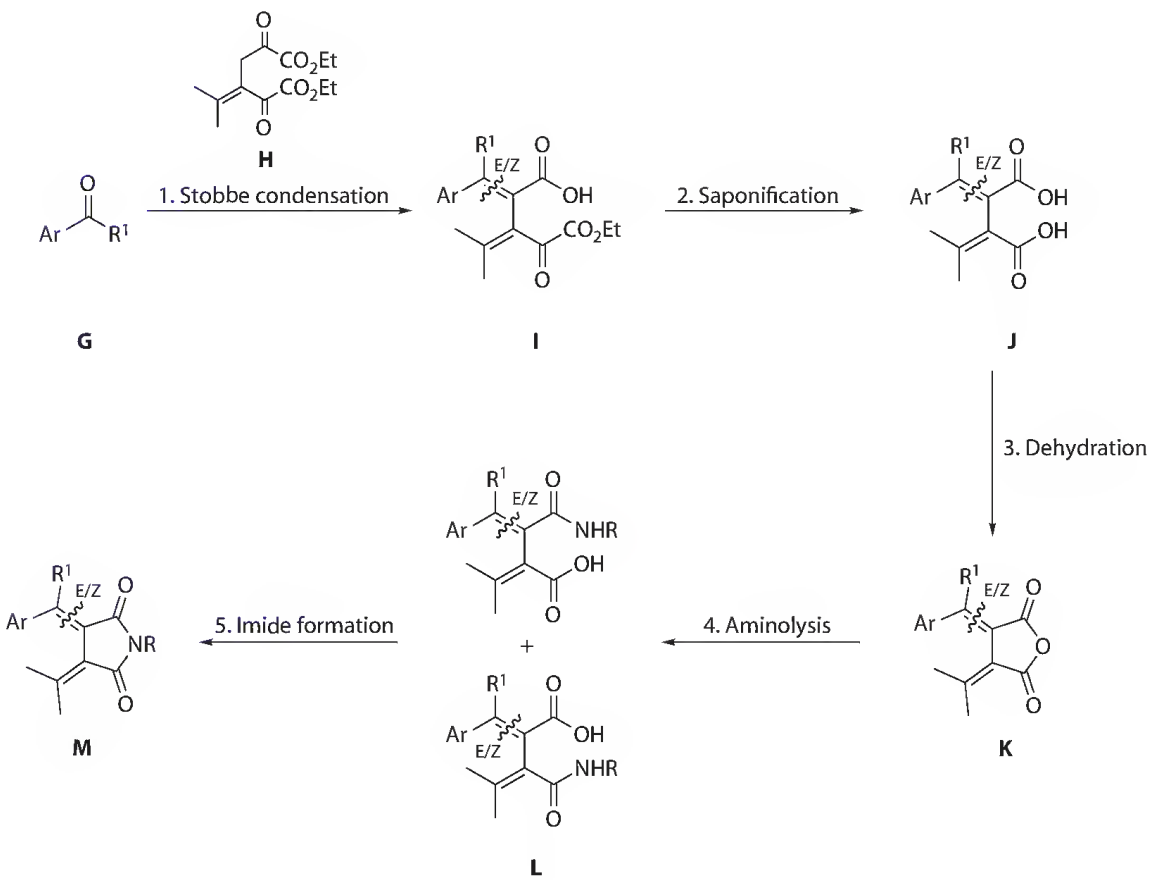

FIGURE 25.17 General synthetic routes to fulgides and fulgimides.

25.3 Photophysical Studies of the Photochromic Mechanisms

The photophysical studies dealing with fulgides and their derivatives have been very well covered in recent review articles.[4] Following this, the ultrafast dynamics of photochromic fulgides and fulgimides were completely evaluated and characterized, for example, by Braun and Zinth,[88–94] as well as by other research groups.[95] Therefore this work is not covered in this chapter.

25.4 Fulgides and Fulgimides for Optical Recording Media

From the beginning, fulgide research was directed toward application in memory devices. This topic was extensively covered in previously published reviews.[1–4] Over the years it became obvious that most of the heteroaromatic fulgides underwent extensive photooxidative degradations upon preparation and handling of the spin-coated polymer films in air.[5,32,37,39] It has been shown that the degradation could be substantially suppressed and the thermal stabilities slightly improved by sealing the films with an adhesive to keep them airtight.[38,96] In early studies conducted by Matsushima, furyl-, thienyl-, thiazolyl-, and oxazolylfulgides along with a furylfulgimide were investigated.[38] In 2005, Matsushima reported on the use of pyrrolylfulgides as cyan dyes in polymer films[32] and in 2009 he reported on the application of oxazolylfulgenates as yellow dyes in full-color rewritable films.[33] PMMA was doped with a pyrrolylfulgide and was used for holographic recording.[35] A pyrrolylfulgide in combination with an oxazolylfulgide was also used in dual-wavelength optical memory for parallel recording.[34,36] Multilevel recording of a photochromic *N*-benzyl indolylfulgide was also investigated.[97] For studies where the molecule was incorporated in hydroxylic solid films water-soluble cationic oxazolylfulgimides have been prepared and examined.[21] The cationic derivatives were prepared from the parent fulgimide by allylation using allyl bromide. The fulgimide derivatives were chosen because of their higher stability toward solvolytic degradation in hydroxylic media. A series of novel thienylfulgimides for the development of recording media was also reported more recently by Krayushkin.[26,98]

Within a series of papers, Rentzepis put forward 2-indoylfulgimides and derivatives for optical storage devices.[68] Photochromic cross-linked copolymers were derived from methyl methacrylate monomer and the fulgimide monomer **42**,[70] and more recently copolymers containing azobenzene and fulgimide units, for example, **43**, were also investigated (Figure 25.18).[99,100]

Rentzepis developed an energy transfer dyad **44** consisting of a 2-indolylfulgimide and covalently attached strongly fluorescing oxazine dyes.[67,74,76] The dyes ideally performed in a PMMA disk resulting in an erasable, rewritable molecular optical storage medium with nondestructive read-out. For data storage, the polar *C*-form of the photochromic unit was ring-opened with 530 nm light. Read-out was achieved by measuring the fluorescence of the oxazine dye upon irradiation at the 650 nm absorption maximum. This fluorescence was only observed in the presence of the nonpolar ring-opened *E*-form of the photochromic unit.[74] The data stored were stable between 223 and 323 K. Furthermore, more than 10^4 write/read/erase cycles could be performed with only a minor loss in information (Figure 25.19).[67]

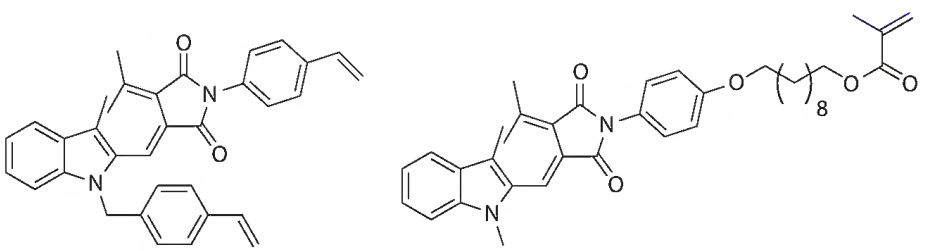

42 **43**

FIGURE 25.18 Monomers **42**, **43** for the synthesis of polymers for optical recording media.

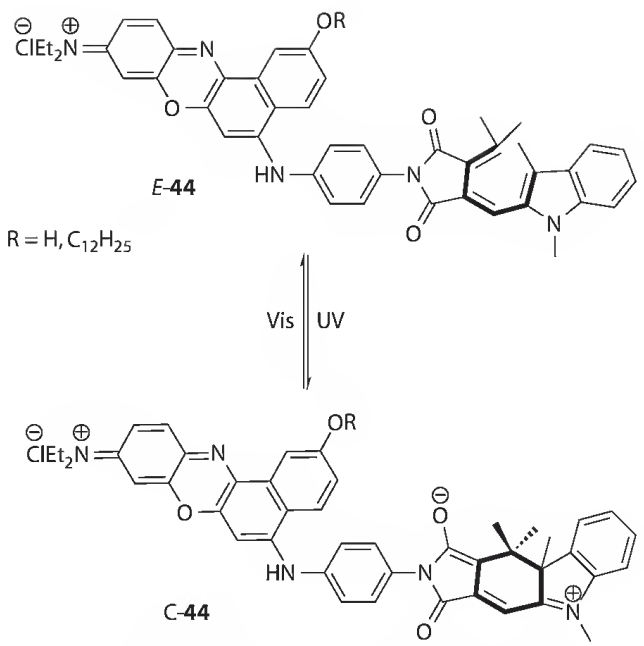

FIGURE 25.19 Energy transfer dyad **44** consisting of a 2-indolylfulgimide and a covalently attached strongly fluorescing oxazine dye.

25.5 Fulgimide Architectures for Molecular Electronics

Novel technologies in opto- and bioelectronics have produced a strong interest in new functional modules. For example, photoswitchable organic molecules are of interest for using light as input and output signal between connected chromophores within a logic gate. However, for nano- and optoelectronic devices, immobilization of system modules on metals and semiconductors is essential for future applications. Recent results in these areas directed toward the design of functional modules containing fulgimides are covered in this section.

25.5.1 Photoswitchable Energy Transfer Systems

Port et al. investigated a photoswitchable donor-switch-acceptor energy transfer system **45** (triad) containing a photochromic fulgimide as the switching unit, an anthracene donor group, and a coumarin acceptor group.[101,102] The intramolecular energy transfer was found to depend upon the isomeric configuration of the photochromic fulgimide, thus, by photoinduced ring-closure and ring-opening of the fulgimide switching unit, the intramolecular energy transfer was switched on and off (Figure 25.20).

A covalently linked 2-indolylfulgimide was applied in order to control the generation of a porphyrin excited state[103] on route to a molecular triad consisting of a porphyrin linked to two photochromic compounds, a 2-indolylfulgimide and a dithienylethene.[104] Upon excitation of the isomeric form

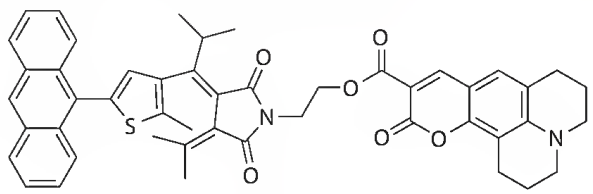

45

FIGURE 25.20 Photoswitchable energy transfer triad **45** containing a fulgimide, an anthracene donor group, and a coumarin acceptor group.

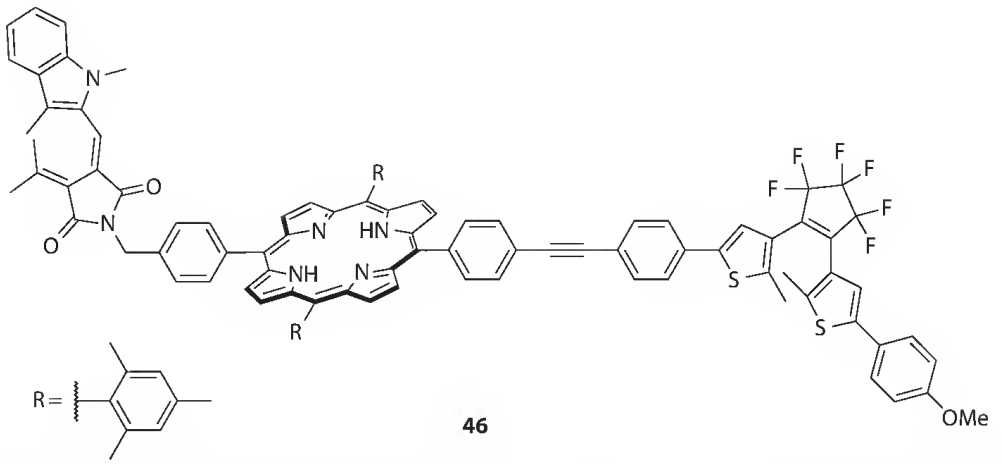

FIGURE 25.21 Energy transfer triad **46** consisting of a porphyrin linked to two photochromic compounds: a 2-indolylfulgimide and a dithienylethene.

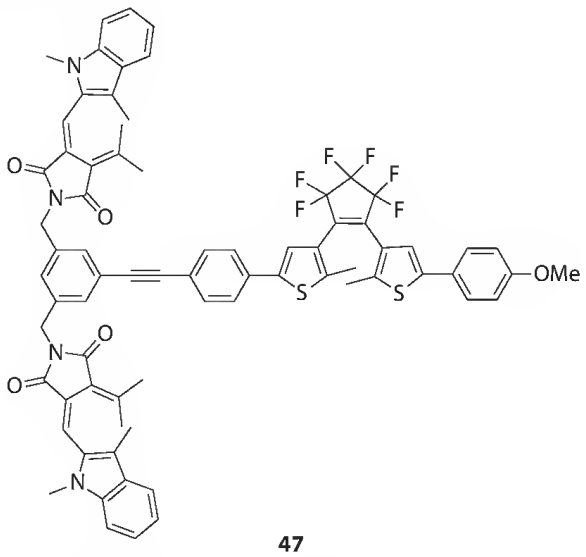

FIGURE 25.22 Photoswitchable compound **47** performing logic functions.

of compound **46** containing both photochromic units in their visible light absorbing forms (fulgimide: *C*-form, diarylethene: closed-form; structure not shown) at 470 nm a two-step singlet energy transfer was observed, first to the porphyrin unit within the dyad and then to the dithienylethene (Figure 25.21).

However, upon ring-opening of the dithienylethene using visible light, the second step was eliminated. The excitation of the fulgimide then resides on the porphyrin and fluorescence of the porphyrin was observed. Four isomeric states of the molecule with different light absorption and singlet energy-transfer properties were characterized.[103,104] Other concepts toward molecules performing logic functions have also been reported based on the principle of using light as inputs and outputs in combination with photochromic compounds that interact photochemically and photophysically with chromophores attached to their molecular skeleton via appropriate linker strategies, for example, compound **47** (Figure 25.22).[105]

25.5.2 Photoswitch-Linker-Conjugates for SAMs on Metal and Semiconductor Surfaces

Chromophore containing self-assembled monolayers (SAMs) on metal or semiconductor surfaces are promising research fields toward the development of materials with novel optical and electronical

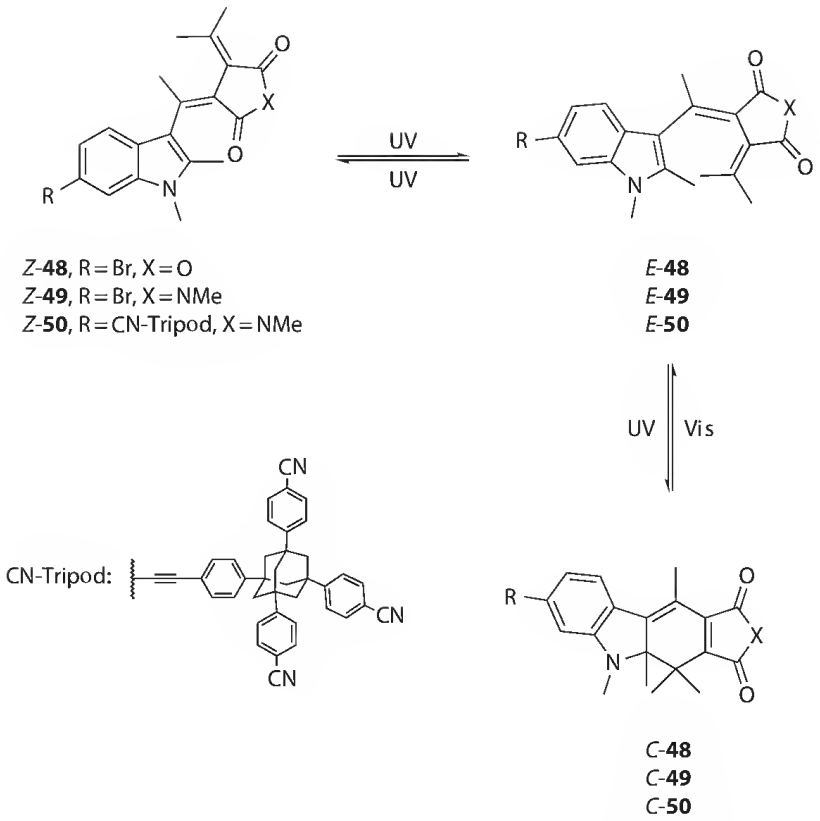

FIGURE 25.23 Photochromism of a fulgimide-linker-conjugate **50**, and molecular structures of the fulgide and fulgimide precursors **48**, **49**.

properties. However, π-aggregation between chromophores of dye-containing SAMs is a known problem that can dramatically change the chromophore properties. Linkers with a tetrahedral shape have been developed to control the chromophore to surface distance and also to minimize the lateral interaction among chromophores within the SAM. More recently, this concept was applied to photoswitchable chromophores.[106,107] In the fulgimide series the preparation of an indolylfulgimide adamantane linker conjugate with nitrile anchoring groups was reported.[83] To maintain the attachment of fluorescence dyes to the imide functionality of fulgimides, the 6-position on the indole ring was chosen for the attachment of the tripodal linker system with an adamantane core. Furthermore, the 6-position seemed to be ideal in light of the previously observed effects upon placement of an electron-donating substituent in 5-position, for example, the decrease of the quantum yield of the photoreactions.[22,41] The indolylfulgimide linker conjugate **50** was synthesized from the 6-bromo-substituted indolylfulgimide **49** and an ethynylene linker precursor by Sonogashira cross-coupling.[83] For conjugate **50**, a satisfying molar absorption coefficient was detected in analogy to 3-indolylfulgimides with a methoxy group in 6-position. The molar ratios for the *C*-form in the photostationary states of **49**, **50** were comparable to Yokoyama's compounds **5** and **30** (Figure 25.23).[22,41]

References

1. Yokoyama, Y.; Kose, M. 2004. Fulgides and related systems. In *CRC Handbook of Organic Photochemistry and Photobiology*, eds. W. M. Horspool and F. Lenci, Chapter 86. Boca Raton, FL: CRC Press LLC.
2. Yokoyama, Y.; Kose, M. 2004. Reversible control of properties of materials by thermally irreversible photochromism. *J. Photochem. Photobiol. A Chem.* 166: 9–18.
3. Yokoyama, Y. 2000. Fulgides for memories and switches. *Chem. Rev.* 100: 1717–1739.

4. Fan, M.-G.; Yu, L.; Zhao, W. 1999. Fulgide family compounds: Synthesis, photochromism and applications. In *Organic Photochromic and Thermochromic Compounds, Volume 1: Main Photochromic Families*, eds. J. C. Crano and R. J. Guglielmetti, Chapter 4. New York: Plenum Press.
5. Kaneko, A.; Tomoda, A.; Ishizuka, M. et al. 1988. Photochemical fatigue resistances and thermal stabilities of heterocyclic fulgides in PMMA Film. *Bull. Chem. Soc. Jpn.* 61: 3569–3573.
6. Heller, H. G. 1986. New fatigue-resistant organic photochromic materials. *Spec. Publ. R. Soc. Chem. Fine Chem. Electron. Ind.* 60: 120–135.
7. Glaze, A. P.; Heller, H. G; Whittall, J. 1992. Photochromic heterocyclic fulgides. Part 7.1 (E)-Adamantylidene-[1-(2,5-dimethyl-3-furyl)ethylidenel]succinic anhydride and derivatives: Model photochromic compounds for optical recording media. *Chem. Soc. Perkin Trans. 2* 591–594.
8. Lenoble, C.; Becker, R.S. 1986. Photophysics, photochemistry, and kinetics of photochromic fulgides. *J. Phys. Chem.* 90: 2651–2654.
9. Matsui, F.; Taniguchi, H.; Yokoyama, Y. et al. 1994. Application of photochromic 5-dimethylaminoindolylfulgide to photon-mode erasable optical memory media with non-destructive readout ability based on wavelength dependence of bleaching quantum yield. *Chem. Lett.* 10: 1869–1872.
10. Rappon, M.; Syvitski, R. T. 1996. Kinetics of photobleaching of aberchrome 540 in various solvents: Solvent effects. *J. Photochem. Photobiol., A* 94: 243–247.
11. Heller, H. G.; Oliver, S. 1981. Photochromic heterocyclic fulgides. Part 1. Rearrangement reactions of (E)-α-3-furylethylidene(isopropylidene)succinic anhydride. *J. Chem. Soc. Perkin Trans. 1* 197–201.
12. Darcy, P. J.; Heller, H. G.; Strydom, P. J. et al. 1981. Photochromic heterocyclic fulgides. Part 2. Electrocyclic reactions of (E)-α-2,5-dimethyl-3-furylethylidene(alkyl-substituted methylene)succinic anhydrides. *J. Chem. Soc. Perkin Trans. 1* 202–205.
13. Heller, H. G.; Megit, R. M. 1974. Overcrowded molecules. IX. Fatigue-free photochromic systems involving (E)-2-isopropylidene-3-(mesitylmethylene)succinic anhydride and N-phenylimide. *J. Chem. Soc. Perkin Trans. 1* 923–927.
14. Grishin, I. Y.; Przhiyalgovskaya, N. M.; Chunaev, Y. M. et al. 1989. Photochromic fulgides based on 1-methyl-2-formylindole. *Khimiya Geterotsiklicheskikh Soedinenii* 7: 907–710.
15. Grishin, I. Y.; Chunaev, Y. M.; Przhiyalgovskaya, N. M. et al. 1992. Fulgides based on 1,3-dimethyl-2-formylindole and 1,3-dimethyl-2-acetylindole. *Khimiya Geterotsiklicheskikh Soedinenii* 3: 422–423.
16. Liang, Y.; Dvornikov, A.; Rentzepis, P. 1998. Fluorescent photochromic fulgides. *Res. Chem. Intermed.* 24: 905–914.
17. Liang, Y.; Dvornikov, A.; Rentzepis, P. 1999. Synthesis of novel photochromic fluorescing 2-indolylfulgimides. *Tetrahedron Lett.* 40: 8067–8069.
18. Li, Y.-Z.; Wang, H.-Z.; Zhu, H.-S. et al. 1991. Synthesis and photochromism of 3-indolylfulgides. *Chin. J. Chem.* 9: 258–261.
19. Uchida, S.; Yamada, S.; Yokoyama, Y. et al. 1995. Steric effects of substituents on the photochromism of indolylfulgides. *Bull. Chem. Soc. Jpn.* 68: 1677–1682.
20. Tomoda, A.; Tsuboi, H.; Kaneko, A. et al. 1993. Photochromic performance of N-benzylimide derivative of fulgide. *Nippon Kagaku Kaishi* 2: 209–212.
21. Kohno, Y.; Tamura, Y.; Matsushima, R. 2009. Photochromic properties of cationic oxazolylfulgimides in hydroxylic media. *J. Photochem. Photobiol. A Chem.* 203: 161–165.
22. Yokoyama, Y.; Tanaka, T.; Yamana, T. et al. 1991. Synthesis and photochromic behavior of 5-substituted indolylfulgides. *Chem. Lett.* 7: 1125–1128.
23. Ulrich, K.; Port, H.; Baeuerle, P. 1989. Photochromic thiophenefulgide absorption spectra and kinetics of photochemical isomerizations. *Chem. Phys. Lett.* 155: 437–442.
24. Willner, I.; Rubin, S.; Wonner, J. et al. 1992. Photoswitchable binding of substrates to proteins: Photoregulated binding of α-D-mannopyranose to concanavalin A modified by a thiophenefulgide dye. *J. Am. Chem. Soc.* 114: 3150–3151.

25. Otto, B.; Rück-Braun, K. 2003. Synthesis and UV/Vis properties of amino-functionalized fulgimides. *Eur. J. Org. Chem.* 13: 2409–2417.
26. Krayushkin, M.; Barachevski, V.; Irie, M. 2007. Synthesis of thienyl-containing photochromes (dithienylethenes, fulgides, fulgimides, and spirocompounds). *Heteroat. Chem.* 18: 557–567.
27. Fox, M.-A.; Hurst, J. R. 1984. Electrochemically induced pericyclic reactions—A radical anionic cyclization. *J. Am. Chem. Soc.* 106: 7626–7627.
28. Köse, M.; Orhan, E. 2009. Comparison of photochromic properties and thermal stabilities of fulgide, fulgimide, and benzimidazole [1,2-a]pyrrolidine-2-one derivates. *Turk. J. Chem.* 33: 579–588.
29. Zhao, W.; Ming, Y.; Zhu, Z. et al. 1992. Mechanism of a photochromic reaction of (*E*)-α-(1,2,4,5-tetramethyl-3-pyrryl)ethylidene(isopropylidene)succinic anhydride. *J. Photochem. Photobiol. A* 63: 235–240.
30. Yu, L.; Ming, Y.; Zhang, X. et al. 1993. Nanosecond laser photolysis studies of photochromic processes in pyrryl fulgides. *J. Photochem. Photobiol. A* 74: 37–41.
31. Yu, L.; Ming, Y.; Fan, M. 1993. Studies on the photochromic mechanism of 1,2-dimethyl-5-phenyl-3-pyrryl succinic anhydride. *Res. Chem. Intermed.* 19: 829–838.
32. Matsushima, R.; Ito, Y.; Yamashi, K. et al. 2005. Photochromic cyan dyes of fulgide derivates in polymer film. *Chem. Lett.* 34: 574–575.
33. Kohno, Y.; Tamura, Y.; Matsushima, R. 2009. Simple full-color rewritable film with photochromic fulgide derivates. *J. Photochem. Photobiol. A* 201: 98–101.
34. Chen, Y.; Xiao, J.; Yao, B. et al. 2006. Dual-wavelength photochromic fulgides for parallel recording memory. *Opt. Mater.* 28: 1068–1071.
35. Chen, Y.; Wang, C.; Fan, M. et al. 2004. Photochromic fulgide for holographic recording. *Opt. Mater.* 26: 75–77.
36. Lei, M.; Yao, B.; Chen, Y. 2003. Experimental investigation of parallel optical data storage using pyrrylfulgide photochromic material. *Chin. Sci. Bull.* 48: 1548–1550.
37. Matsushima, R.; Morikane, H.; Kohno, Y. 2003. Oxazolylfulgides as yellow photochromic dyes. *Chem. Lett.* 32: 302–303.
38. Matsushima, R.; Nishiyama, M.; Doi, M. 2001. Improvements in the fatigue resistances of photochromic compounds. *J. Photochem. Photobiol. A* 139: 63–69.
39. Suzuki, H.; Tomoda, A.; Ishizuka, M. et al. 1989. Photochromism of 4-oxazolyl fulgides. *Bull. Chem. Soc. Jpn.* 62: 3968–3971.
40. Okuyama, T.; Yokoyama, Y.; Yokoyama, Y. 2001. Control of the Association of Indolylfulgimide with Bis(acylamino)pyridine by Photochromism. *Bull. Chem. Soc. Jpn.* 74: 2181–2187.
41. Uchida, S.; Yokoyama, Y.; Kiji, J. et al. 1995. Electronic effects of substituents on indole nitrogen on the photochromic properties of indolylfulgides. *Bull. Chem. Soc. Jpn.* 68: 2961–2967.
42. Yokoyama, Y. 1996. Chemistry of organic photochromism. Chemistry of fulgides and related compounds. *Kikan Kagaku Sosetsu.* 28: 110–128.
43. Yokoyama, Y.; Sagisaka, T.; Mizuno, Y. et al. 1996. Role of the methoxy substituent on the photochromic indolylfulgides. Absorption maximum vs. molar absorption coefficient of the colored form. *Chem. Lett.* 8: 587–588.
44. Yokoyama, Y.; Yamane, T.; Kurita, Y. 1991. Photochromism of a protonated 5-dimethylaminoindolylfulgide: A model of a non-destructive readout for a photon mode optical memory. *J. Chem. Commun.* 24: 1722–1724.
45. Yokoyama, Y.; Kurita, Y. 1992. Photochromic fulgides applicable to optical information storage. Discovery of new nondestructive readout method. *Nippon Kagaku Kaishi* 10: 998–1006.
46. Yokoyama, Y.; Kurita, Y. 1994. Photochromism of fulgides and related compounds. *Mol. Cryst. Liq. Cryst.* 246: 87–94.
47. Abe, J.; Nemoto, N.; Nagase, Y. et al. 1997. Novel concept for non-destructive readout method for photochromic rewritable memory devices. *Chem. Phys. Lett.* 276: 450–454.

48. Balenko, S.; Rybalkin, V.; Makarova, N. et al. 2008. Synthesis, structures, and photochromic properties of N-aryl-3-indolylfulgides. *Russ. Chem. Bull. Int. Ed.* 57: 1435–1443.
49. Yokoyama, Y.; Takahashi, K. 1996. Trifluoromethyl-substituted photochromic indolylfulgide. A remarkably durable fulgide towards photochemicals and thermal treatments. *Chem. Lett.* 12: 1037–1038.
50. Wolak, M.; Gillespie, N.; Thomas, C. et al. 2001. Optical properties of photochromic fluorinated indolylfulgides. *J. Photochem. Photobiol. A* 144: 83–91.
51. Wolak, M.; Gillespie, N.; Thomas, C. et al. 2002. Optical and thermal properties of photochromic fluorinated adamantylidene indolylfulgides. *J. Photochem. Photobiol. A* 147: 39–44.
52. Thomas, C.; Wolak, M.; Birge, R. et al. 2001. Improved synthesis of indolyl fulgides. *J. Org. Chem.* 66: 1914–1918.
53. Wolak, M.; Sullivan, J.; Thomas, C. et al. 2001. Thermolysis of a fluorinated indolylfulgide features a novel 1.5-indolyl shift. *J. Org. Chem.* 66: 4739–4741.
54. Wolak, M.; Gillespie, N.; Birge, R. et al. 2003. Thermolysis of fluorinated cycloalkylidene fulgides yields a new class of photochromic compounds. *Chem. Commun.* 8: 992–993.
55. Wolak, M.; Thomas, C.; Gillespie, N. et al. 2003. Tuning the optical properties of fluorinated indolylfulgimides. *J. Org. Chem.* 68: 319–326.
56. Chen, X.; Islamowa, N. I.; Garcia, S. P. et al. 2009. Synthesis and optical properties of aqueous soluble indolylfulgimides. *J. Org. Chem.* 74: 6777–6783.
57. Islamowa, N.; Chen, X.; DiGirolamo, J. et al. 2008. Thermal stability and photochromic properties of a fluorinated indolylfulgimide in a protic and aprotic solvent. *J. Photochem. Photobiol. A* 199: 85–91.
58. Biteau, J.; Chaput, F.; Yokoyama, Y. et al. 1998. Photochromism of an indolylfulgide trapped in a hybrid sol-gel matrix. *Chem. Lett.* 4: 359–360.
59. Yokoyama, Y.; Uchida, S.; Yokoyama, Y. et al. 1996. Diastereoselective photochromism of an (R)-binaphthol-condensed indolylfulgide. *J. Am. Chem. Soc.* 118: 3100–3107.
60. Ankai, E.; Sakakibara, K.; Uchida, S. et al. 2001. Theoretical CD spectrum evaluation of the indolylfulgide molecules by using semi-empirical molecular orbital calculations. *Bull. Chem. Soc. Jpn.* 74: 1101–1108.
61. Sagisaka, T.; Yokoyama, Y. 2000. Reversible control of the pitch of cholesteric liquid crystals by photochromism of chiral fulgide derivates. *Bull. Chem. Soc. Jpn.* 73: 191–196.
62. Yokoyama, Y.; Shimizu, Y.; Uchida, S. et al. 1995. Optical resolution of a thermally irreversible photochromic indolylfulgide. *J. Chem. Soc. Chem. Commun.* 7: 785–786.
63. Yokoyama, Y.; Sagisaka, T. 1997. Reversible control of pitch of induced cholesteric liquid crystal by optically active photochromic fulgide derivates. *Chem. Lett.* 8: 687–688.
64. Yokoyama, Y.; Uchida, S.; Yokoyama, Y. et al. 1998. Chiral photochromic compounds and control of functions. *Enantiomer* 3: 123–132.
65. Yokoyama, Y. 2004. Seasoning materials chemistry by using a well-matured organic concept. *Chem. Eur. J.* 10: 4388–4394.
66. Inada, T.; Uchida, S.; Yokoyama, Y. 1997. Perfect on/off switching of emission of fluorescence by photochromic reaction of a binaphthol-condensed fulgide derivate. *Chem. Lett.* 4: 321–322.
67. Dvornikov, A.; Liang, Y.; Rentzepis, P. 2005. Dependence of the fluorescence of a composite photochromic molecule on structure and viscosity. *J. Mater. Chem.* 15: 1072–1078.
68. Liang, Y.; Dvornikov, A.; Rentzepis, P. 2003. New near infrared-sensitive photochromic fluorescing molecules. *J. Mater. Chem.* 13: 286–290.
69. Liang, Y.; Dvornikov, A.; Rentzepis, P. 2000. Synthesis and photochemistry of photochromic fluorescing indol-2-ylfulgimides. *J. Mater. Chem.* 10: 2477–2482.
70. Liang, Y.; Dvornikov, A.; Rentzepis, P. 2000. Photochromic cross-linked copolymer containing thermally stable fluorescing 2-indolylfulgimide. *Chem. Commun.* 17: 1641–1642.

71. Liang, Y.; Dvornikov, A.; Rentzepis, P. 2001. Photochemistry of photochromic 2-indolylfulgides with substituents at the 1-position of the indolylmethylene moiety. *J. Photochem. Photobiol. A* 146: 83–93.
72. Dvornikov, A.; Walker, E.; Rentzepis, P. 2009. Two-photon three-dimensional optical storage memory. *J. Phys. Chem. A* 113: 13633–13644.
73. Liang, Y.; Dvornikov, A.; Rentzepis, P. 2002. Synthesis and properties of photochromic fluorescing 2-indolyl fulgide and fulgimide copolymers. *Macromolecules* 35: 9377–9382.
74. Liang, Y.; Dvornikov, A.; Rentzepis, P. 2003. Nonvolatile read-out molecular memory. *PNAS* 100: 8109–8112.
75. Berns, M. W.; Krasieva, T.; Sun, C.-H. et al. 2004. A polarity dependent fluorescence "switch" in live cells. *J. Photochem. Photobiol. B* 75: 51–56.
76. Dvornikov, A.; Liang, Y.; Cruse, C. et al. 2004. Spectroscopy and kinetics of a molecular memory with nondestructive readout for use in 2D and 3D storage systems. *J. Phys. Chem. B* 108: 8652–8658.
77. Dvornikov, A.; Liang, Y.; Rentzepis, P. 2004. Ultra-high-density non-destructive readout, rewritable molecular memory. *Res. Chem. Intermed.* 30: 545–561.
78. Liang, Y.; Dvornikov, A.; Rentzepis, P. 1999. Solvent and ring substitution effect on the photochromic behavior of fluorescent 2-indolylfulgide derivates. *J. Photochem. Photobiol. A* 125: 79–84.
79. Yokoyama, Y.; Sagisaka, T.; Yamaguchi, Y. et al. 2000. Highly diastereoselective photochromic cyclization of a bisthienylfulgide. *Chem. Lett.* 3: 220–221.
80. Kiji, J.; Okano, T.; Takemoto, A. 2000. A convenient and general synthetic method for photochromic fulgides by palladium-catalyzed carbonylation of 2-butyne-1,4-diols. *Mol. Cryst. Liq. Cryst.* 344: 235–240.
81. Kiji, J.; Kondou, Y.; Asahara, M. et al. 2003. Palladium-catalyzed carbonylation of 2-butyne-1,4-diol derivatives: Formation of fulgide or lactone. *J. Mol. Catal. A: Chem.* 197: 127–132.
82. Ulrich, K.; Port, H.; Wolf, H. C. et al. 1991. Photochromic thiophenefulgides. Photokinetics of two isopropyl derivatives. *Chem. Phys.* 154: 311–322.
83. Zarwell, S.; Dietrich, S.; Schulz, C. et al. 2009. Preparation of an indolylfulgimide-adamantane linker conjugate with nitrile anchoring groups through palladium-catalyzed transformations. *Eur. J. Org. Chem.* 13: 2088–2095.
84. Effenberger, F.; Wonner, J. 1992. Darstellung und photochemie eines (anthrylvinyl)thiophenfulgids. *Chem. Ber.* 125: 2583–2590.
85. Lee, W.-W. W.; Gan, L.-M.; Loh, T.-P. 2007. Microwave-assisted synthesis of photochromic fulgimides. *J. Photochem. Photobiol. A* 185: 106–109.
86. Li, X.; Li, C.; Pang, S. et al. 2010. Convenient, microwave-assisted, one-pot synthesis of photochromic fulgimides bearing reactive groups. *Synth. Commun.* 40: 157–166.
87. Cabrera, I.; Dittrich, A.; Ringsdorf, H. 1991. Thermally irreversible photochromic liquid crystal polymers. *Angew. Chem. Int. Ed. Engl.* 30: 76–78.
88. Draxler, S.; Brust, T.; Malkmus, S. et al. 2008. Ultrafast reaction dynamics of the complete photo cycle of an indolylfulgimide studied by absorption, fluorescence and vibrational spectroscopy. *J. Mol. Liq.* 141: 130–136.
89. Brust, T.; Draxler, S.; Malkmus, S. et al. 2008. Ultrafast dynamics and temperature effects on the quantum efficiency of the ring-opening reaction of a photochromic indolylfulgide. *J. Mol. Liq.* 141: 137–139.
90. Koller, F.; Schreier, W.; Schrader, T. et al. 2008. Ultrafast ring-closure reaction of photochromic indolylfulgimides studied with UV-pump—IR-probe spectroscopy. *J. Phys. Chem. A* 112: 210–214.
91. Heinz, B.; Malkmus, S.; Laimgruber, S. et al. 2007. Comparing a photoinduced pericyclic ring opening and closure: Differences in the excited state pathway. *J. Am. Chem. Soc.* 129: 8577–8584.
92. Brust, T.; Draxler, S.; Eicher, J. et al. 2010. Increasing the efficiency of the ring-opening reaction of photochromic indolylfulgides by optical pre-excitation. *Chem. Phys. Lett.* 489: 175–180.

93. Koller, F.; Schreier, W.; Schrader, T. et al. 2006. Ultrafast structural dynamics of photochromic indolylfulgimides studied by vibrational spectroscopy and DFT calculations. *J. Phys. Chem. A* 110: 12769–12776.
94. Malkmus, S.; Koller, F.; Heinz, B. et al. 2006. Ultrafast ring opening reaction of a photochromic indolyl-fulgimide. *Chem. Phys. Lett.* 417: 266–271.
95. Renth, F.; Foca, M.; Petter, A. 2006. Ultrafast transient absorption spectroscopy of the photo-induced *Z-E* isomerization of a photochromic furylfulgide. *Chem. Phys. Lett.* 428: 62–67.
96. Matsushima, R.; Hayashi, T.; Nishiyama, M. 2000. Remarkable improvements in the photochromic reversibilities of fulgides in solid films. *Mol. Cryst. Liq. Cryst.* 344: 241–246.
97. Sun, X.; Park, S.; Shin, D. et al. 2007. Multi-level recording of photochromic indolylfulgide. *Opt. Mater.* 30: 652–656.
98. Barachevsky, V. A.; Strokach, Y.; Puankov, Y. et al. 2007. Thermally irreversible organic photochromic compounds for optical memory. *J. Phys. Org. Chem.* 20: 1007–1020.
99. Saravanan, C.; Senthil, S.; Kannan, P. 2008. Click chemistry-assisted triazole-substituted azobenzene and fulgimide units in the pendant-based copoly(decyloxymethacrylate)s for dual-mode optical switches. *J. Polym. Sci. A Polym. Chem.* 46: 7843–7860.
100. Saravanan, C.; Kannan, P. 2009. Dual-mode optical switching property of copolymers containing pendant nitro and cyano substituted azobenzenes and fulgimide units. *Polym. Degrad. Stab.* 94: 1001–1012.
101. Walz, J.; Ulrich, K.; Port, H. et al. 1993. Fulgides as switches for intramolecular energy transfer. *Chem. Phys. Lett.* 213: 321–324.
102. Ramsteiner, I. B.; Hartschuh, A.; Port, H. 2001. Relaxation pathway and fs dynamics in a photoswitchable intramolecular D→A energy transfer system. *Chem. Phys. Lett.* 343: 83–90.
103. Straight, S.; Terazono, Y.; Kodis, G. et al. 2006. Photoswitchable sensitization of porphyrin excited states. *Aust. J. Chem.* 59: 170–174.
104. Straight, S.; Liddell, P.; Terazono, Y. et al. 2007. All-photonic molecular XOR and NOR logic gates based on photochemical control of fluorescence in a fulgimide-porphyrin-dithienylethene triad. *Adv. Funct. Mater.* 17: 777–785.
105. Andreasson, J.; Straight, S.; Moore, T. et al. 2008. Molecular all-photonic encoder-decoder. *J. Am. Chem. Soc.* 130: 11122–11128.
106. Zarwell, S.; Rück-Braun, K. 2008. Synthesis of an azobenzene-linker-conjugate with tetrahedral shape. *Tetrahedron Lett.* 49: 4020–4025.
107. Wagner, S.; Leyssner, F.; Kördel, C. et al. 2009. Reversible photoisomerization of an azobenzene-functionalized self-assembled monolayer probed by sum-frequency generation vibrational spectroscopy. *Phys. Chem. Chem. Phys.* 11: 6242–6248.

26

Photoenolization and Its Applications

Petr Klán
Masaryk University

Jakob Wirz
Universität Basel

Anna D. Gudmundsdottir
University of Cincinnati

26.1 Introduction

Photoenolization reactions have been comprehensively reviewed in 1976 by Sammes (Sammes 1976) and, to some extent, in several more recent reviews and book chapters (Klan and Wirz 2009; Mehta and Kotha 2001; Michalak and Gebicki 1993; Sankaranarayanan et al. 2009; Segura and Martin 1999; Wagner and Klan 2003; Weedon 1990; Yoshioka and Saito 2001). The available kinetic and thermodynamic parameters of keto-enol equilibria in aqueous solution have recently been summarized (Wirz 2010). The present chapter attempts to recapitulate the main features of this remarkable phototransformation focusing on advances made with *o*-alkyl aromatic ketones in the past 20 years. The related photoenolization reactions of nonaromatic ketones and esters are not covered.

In 1961, Yang and Rivas demonstrated that the quinonoid dienol intermediates formed by irradiation of 2-methylbenzophenone were sufficiently long lived to allow for chemical trapping (Yang and Rivas 1961). Mechanistic studies of this reaction by flash photolysis initially led to conflicting results due to the strong overlap of transient absorptions observed in the region of 300–500 nm. The mechanism summarized in Scheme 26.1 for 2-methylacetophenone was put forth in 1977 (Haag et al. 1977; Small and Scaiano 1977). It was consistent with the evidence then available from both flash photolysis and chemical trapping studies and has stood the test of time. It also serves, *mutatis mutandis*, as a blueprint for the reactions of related 2-alkylphenacyl compounds.

The equilibrium between the *syn*- and *anti*-conformers in the ground-state matters, because the rotational barrier increases upon n,π* excitation, and only the excited *syn*-conformers can abstract the γ-hydrogen atom. Thus, the excited singlet state of the *anti*-conformer undergoes exclusive intersystem crossing (ISC) to the triplet state within a few picoseconds, whereas ISC of the *syn*-conformer competes with photoenolization yielding the (*Z*)-dienol in the ground state through a conical intersection (Klan and Wirz 2009). The excited triplet ketones undergo adiabatic H-atom transfer to yield the triplet enol ^{3}**E** (also called triplet biradical). Quenching studies indicated two kinetically independent excited state precursors of ^{3}**E**, with lifetimes of on the order of 1 and 10 ns, which were attributed to the

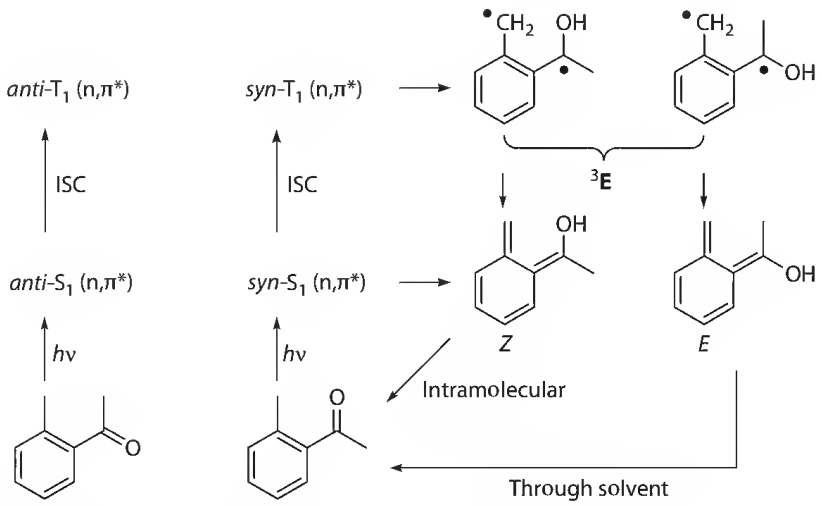

SCHEME 26.1 Mechanism of the photoenolization of 2-methylacetophenone.

syn- and *anti*-conformers of the triplet ketone, respectively (Haag et al. 1977). When the triplet pathway is completely suppressed using high concentrations of a triplet quencher such as piperylene, only the (*Z*)-dienol is formed via the excited singlet state of the *syn*-conformer. The structure of the triplet enol ^{3}E has not been established. Least-motion H-transfer from the *syn*-triplet ketone would lead to a *syn*-conformer of ^{3}E that, upon ISC to the ground state, should yield the (*Z*)-dienol. From the fact that both the (*Z*)- and the (*E*)-dienol are formed via ^{3}E, we must conclude that either the ketyl group is rotated out of plane in the relaxed geometry of ^{3}E or that two near-planar *syn*- and *anti*-conformers of ^{3}E are rapidly equilibrated prior to ISC, as shown in Scheme 26.1.

The short-lived ground-state (*Z*)-dienols (*o*-xylylenols or α-hydroxy-*o*-xylylenes) revert to the starting 2-alkylphenyl ketone via 1,5-sigmatropic hydrogen transfer. Their lifetimes are strongly solvent dependent. Those of the (*Z*)-dienol formed from 2-methylacetophenone range from <20 ns in cyclohexane to 160 μs in hexamethylphosphoramide (HMPA), a strong hydrogen-bond acceptor solvent (Haag et al. 1977). Hydrogen bonding of the hydroxyl group thus strongly retards intramolecular back transfer. In contrast, reketonization of the (*E*)-dienols requires intermolecular proton transfer that may occur either by protonation of the methylene group by a general acid or by proton transfer from the enol to the solvent or to a general base, followed by carbon protonation of the dienol anion. The resulting long lifetime of the (*E*)-isomers in dry solvents allows for thermal conrotatory ring closure to give benzocyclobutenols, or they can be trapped by diverse dienophiles such as alkenes, alkynes, or carbonyl compounds in a stereospecific [4 + 2] (Diels–Alder) cycloaddition reaction (Scheme 26.2). Endoperoxides are formed mostly by spin-allowed trapping of the triplet enol ^{3}E by triplet oxygen (see Section 26.4); they may also be formed when the ground-state dienols encounter singlet oxygen that was generated by oxygen quenching of the triplet ketones or of the triplet enol ^{3}E (Redmond and Scaiano 1989).

Irradiation of 2-alkylphenacyl compounds in alcohols deuterated on oxygen or in D_2O may lead to isotopic exchange at the alkyl group via the dienols (Scheme 26.2). This will always be the case with (*E*)-dienols, which reketonize by protonation through the solvent. However, ionization of (*Z*)-dienols, which are weak acids ($pK_a \approx 8$), will generally be slower than intramolecular 1,5-H transfer; the lifetime of the (*Z*)-dienol formed from 2-methylacetophenone is 1 μs in neutral water (Haag et al. 1977). Therefore, isotopic exchange via the (*Z*)-dienols will occur only in the presence of sufficient amounts of acid, base, or buffer to promote isotopic exchange with the solvent. A remarkable finding reported by Gebicky and coworkers (Gebicki et al. 1992; Marcinek et al. 1992) is that radiolytic ionization 2-methylacetophenone in cryogenic matrices yields the corresponding dienol radical cations as the thermodynamically stable tautomers.

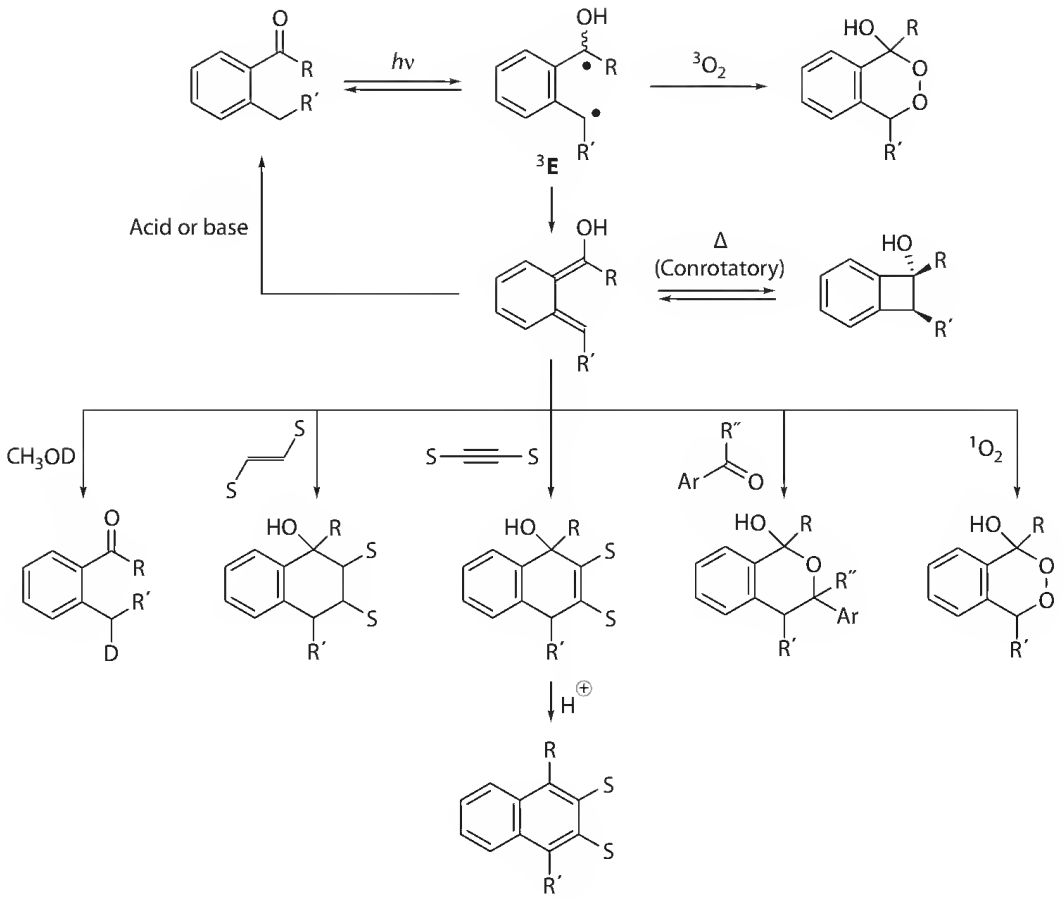

SCHEME 26.2 Reactions of the photoenols.

Hydrogen abstraction by excited ketones is not restricted to the γ-position; preference for γ-abstraction is mostly of entropic origin. δ-Hydrogen abstraction competes when it is energetically preferred or when γ-hydrogens are absent (Wagner and Klan 2003; Wagner et al. 1990, 1995). The intrinsic preference for γ- over δ-hydrogen abstraction has been estimated as 20:1 (Wagner et al. 1972). Even ε-hydrogen abstraction has been observed in special circumstances (Carless and Fekarurhobo 1984; Meador and Wagner 1985; Wirz 1974; Zhou and Wagner 1989). Cyclization of the resulting 1,5- and 1,6-biradical intermediates yields five- and six-membered rings, respectively.

The involvement of H-atom tunneling in photoenolization has been investigated by several research groups. The kinetics for photoenolization have been studied extensively in *o*-methylbenzophenone and *o*-methylacetophenone (Das et al. 1979; Findlay and Tchir 1976; Garcia-Garibay et al. 1996; Haag et al. 1977; Ito et al. 1980; Scaiano 1980; Tseng 1976; Wagner and Chen 1976; Wagner et al. 1992), but the kinetics are complicated by conformational flexibility. More recent work has, however, focused on studying H-atom tunneling in molecules such as *o*-methylanthrone (**1**, **2**) and *o*-methyltetralone (**3**) derivatives (Gamarnik et al. 1998; Garcia-Garibay et al. 1994, 1995; Gritsan et al. 1991; Johnson et al. 1996; Johnson and Garcia-Garibay 1999). These compounds are rigid and require only a small conformational change to make photoenolization possible. In methylcyclohexane, the lowest energy triplet ketone in *o*-methylanthrone has a n,π* configuration and it undergoes photoenolization even at cryogenic temperatures. Since the Arrhenius plot obtained for the triplet ketone abstracting a D-atom from deuterated *o*-methyl group was nonlinear and large isotope effects were observed, the authors concluded that the triplet ketone undergoes a temperature-independent D-atom tunneling between 18 and 30 K with rate of $2 \times 10^3\ s^{-1}$ (Garcia-Garibay et al. 1995).

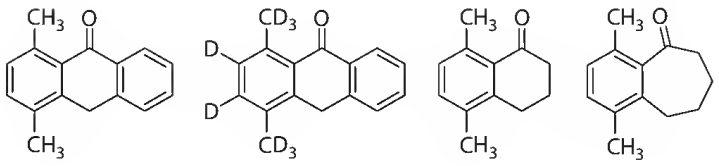

1 2 3 4

In comparison, the lowest triplet ketone in *o*-methylanthrone has a π,π^* configuration in 2,2,2-trifluoroethanol and its phosphorescence lifetime showed a large isotope effect (Gamarnik et al. 1998), indicating that the π,π^* triplet ketone also undergoes H-atom tunneling at low temperature. Furthermore, by measuring the secondary α isotope effect for *o*-methylanthrone, Garcia-Garibay and coworkers were able to determine that the width of the transition state barrier affects the rate of H-atom tunneling (Campos et al. 2005). Johnson et al. determined that the different sublevels of the triplet ketone in *o*-methyltetralone react with different tunneling rates (Johnson and Garcia-Garibay 1999).

Johnson et al. studied photoenolization in 6,9-dimethylbenzosuberone (**4**) at cryogenic temperatures and found that the rates of H- and D-transfer from the *o*-methyl group were nearly the same (Johnson et al. 2001). The authors theorized that the rate-limiting step for photoenolization in 6,9-dimethylbenzosuberone is given by isotope-independent skeletal motions, or, in other words, vibrationally assisted tunneling.

Several theoretical calculations have been done to further verify that H-atom tunneling is involved in the photoenolization of *o*-methylanthrones and *o*-methyltetralones (Moreno and Lluch 2007; Smedarchina et al. 1994) as well as in some more flexible systems (Arnaut et al. 1984; Barroso et al. 2010; Rao and Chandra 1996; Sengupta and Chandra 1994).

26.2 Cyclization Reactions

When the *o*-alkyl (benzylic) position bears a substituent, four xylylenol isomers are possible (Scheme 26.3). Wagner and coworkers suggested that the geometry of the lowest triplet enol ^{3}E determines which xylylenol isomers are formed (Sobczak and Wagner 1998; Wagner et al. 1998). This assumed that the triplet state lifetime is sufficiently long to allow structural equilibration, the twisted ends of the system rotate in both directions when collapsing to the ground state, and the population of (*Z*,*Z*)- and (*E*,*Z*)-isomers is suppressed when the R/R' substituents are large.

Not only 2,6-dialkylphenyl ketones (Sammes 1976) (e.g., **5**, (Wagner et al. 1991)), but also simple *o*-alkylphenyl ketones can form (*E*)-cyclobutenols efficiently upon irradiation (Scheme 26.4). Wagner and coworkers have shown that the acetophenone derivatives **6** give the benzocyclobutenols **7** nearly

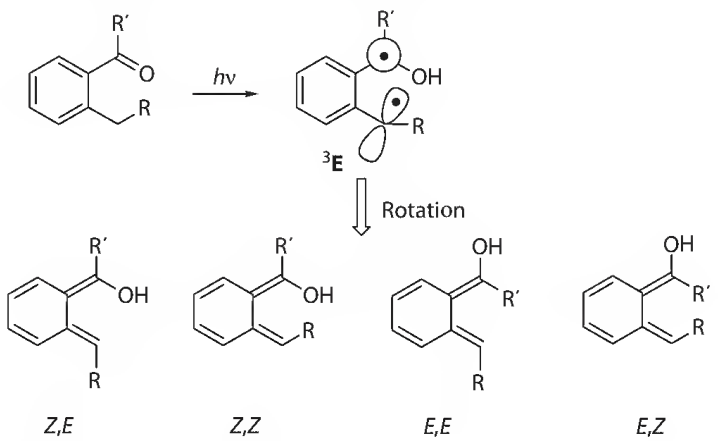

SCHEME 26.3 Formation of the xylylenol stereoisomers.

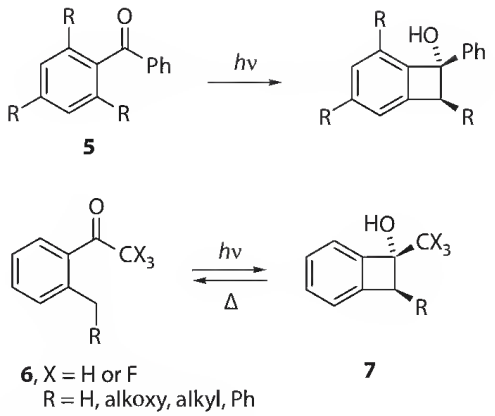

SCHEME 26.4 Formation of (*E*)-cyclobutenols.

exclusively when irradiated at >290 nm (Wagner et al. 1991, 1998). A single diastereomer with the (*E*)-configuration was formed in all cases. Heating at 80°C quantitatively converted **7** into the starting acetophenones, which invalidates the GC analyses used in some previous studies (the (*Z*)-isomers are thermally stable (Arnold et al. 1974b)).

There has been some controversy whether cyclobutenols are formed from the photoenol intermediates or directly from the triplet biradicals ^{3}**E**. The high-yield production of previously undetected (*E*)-cyclobutenols, the diastereoselectivity of cyclobutenol cyclization, and trapping experiments were sufficient evidence for Wagner and coworkers to be convinced that only conrotatory cyclization of (*E*)-enols leads to cyclobutenols (Scheme 26.5, path (a)) (Wagner et al. 1991, 1998). In contrast, Ito and collaborators proposed in the 1980s (Ito et al. 1980, 1981) and later asserted (Ito et al. 1998) that excitation of 2,4,6-triisopropylbenzophenone leads to a "direct" cyclization of the triplet biradical (after ISC) both in solution and the solid state (Scheme 26.5, path (b)).

In addition, Ito and coworkers recently investigated the photocyclization of the 2,4,6-triethylbenzophenone derivatives **8** both in the solid state and in solution (Scheme 26.6) (Ito et al. 2009). The authors conclude that cyclobutenol is formed via conrotatory cyclization of the (*E*)-enol in solution, while "direct cyclization" of the photoenol intermediates is said to be important in the solid state and in sterically hindered ketones. The formation of the indanol (**9**) and (*Z*)-cyclobutenol ((*Z*)-**10**) derivatives were attributed to the topochemical (least motion) principle.

In our view, there is no unequivocal evidence for a distinction between paths (a) and (b) in these reactions (see Scheme 26.5). Adiabatic cyclization of ^{3}**E** to form the cyclobutenol triplet can be ruled out on energetic grounds. Thus, ISC must occur in the triplet biradicals, $^3\mathbf{E} \rightarrow {}^1\mathbf{E}$, as is assumed by Ito and coworkers.

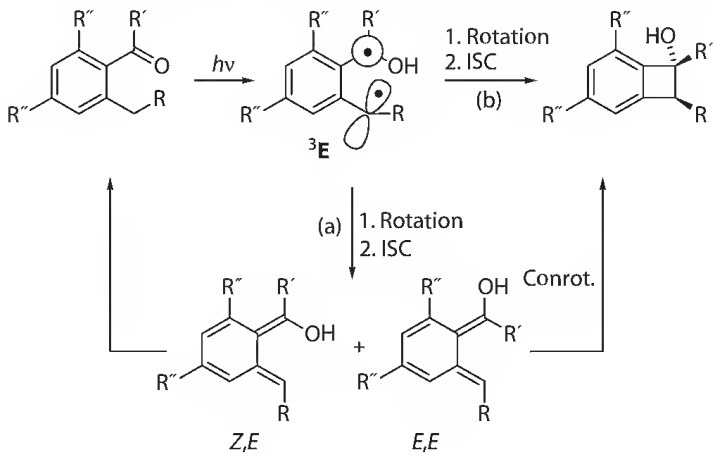

SCHEME 26.5 Formation of (*E*)-cyclobutenols from the triplet biradical.

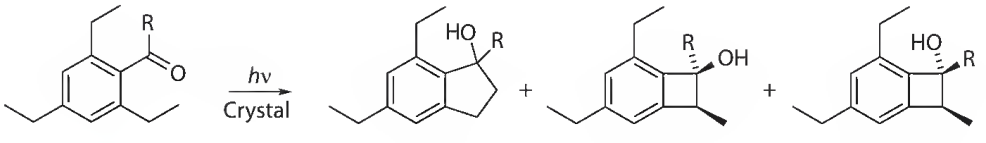

8	9	(*Z*)-**10**	(*E*)-**10**
R = 4-*tert*-butylphenyl:	68%	26%	6%
R = 3-4-dichlorophenyl:	0%	18%	69%

SCHEME 26.6 Photocyclization in the crystalline state.

The nascent singlet biradical ^{1}**E** is in fact nothing but the ground-state (*E*,*E*)-enol **E**, if, presumably, in a somewhat distorted geometry. The claim that "the singlet biradical [^{1}**E**] can spontaneously lead to the cyclobutenol without any activation energy" (Ito et al. 1980) is debatable.

Cyclobutenols can be utilized in organic synthesis (Mehta and Kotha 2001). These strained compounds are not very stable; they are sensitive toward acids and bases, which possess limitations for many practical applications. Their thermal conrotatory ring opening leads to the corresponding *o*-xylylenes (*o*-quinodimethanes) that can undergo various cycloaddition reactions (Segura and Martin 1999); cyclobutenols can also be converted into heterocyclic aromatic compounds by reaction with electrophiles (Fitzgerald et al. 1992, 1994a,b), undergo a thermal interconversion of the diastereomers (Kawata et al. 2000) or other transformations (Iida et al. 1999, 2000; Takahashi et al. 1996).

In the past two decades, several examples of the photochemical preparation of cyclobutenols for synthetic purposes were reported. Stereoselective photocyclization of 2-(methoxymethyl)benzophenones (**11**) was shown to give cyclobutenols in >90% yields, which served as precursors for the synthesis of lignans via additional hydrogenation and cycloaddition steps (Scheme 26.7) (Coll et al. 1992).

An interesting twofold photoenolization reaction in *o*- (**12a**) and *p*-dicarbonyl-substituted benzenes (**12b**) leading to the formation of the benzocyclobutenol derivatives **13** (e.g., [*anti*-**13a**]/[*syn*-**13a**] = 1.7 and 1 for R = Ph and benzyl, respectively) was reported by Moorthy and Samanta (Scheme 26.8) (Moorthy and Samanta 2007). The products were obtained in high chemical yields (40%–91%) and were sufficiently stable to be purified by column chromatography. The cyclization was regioselective; the hydrogen was always abstracted from the methyl group in *para* position to the second carbonyl group. Interestingly, only such sterically congested (permethylated) diketones gave bis-benzocyclobutenols. The authors implied that the steric hindrance between the methyl group and the OH group of the photoenol promotes cyclization. In addition, the tandem photoenolization/Diels–Alder cycloaddition reaction (see also later in the text) of **14** was shown to give the adduct **15** in high yields.

2-Alkylphenyl-1,3-dicarbonyl compounds (Yoshioka et al. 1990, 1991) and 3-hydroxy/3-acetoxy-1-alkylphenyl ketones (Yoshioka et al. 1993, 1997) also undergo cyclization to benzocyclobutenols via a photoenolization step. The course of the reaction of **16** was found to depend on the bulkiness of the ester group (Scheme 26.9) (Saito et al. 1998).

Interestingly, several cyclobutenol derivatives have been reported to form in high yields by solid state irradiation of benzaldehyde derivatives (Moorthy et al. 2001a,b; Sarkar et al. 2000). For example, Moorthy et al. reported that the benzaldehyde **17** forms cyclobutenol selectively in the solid state, whereas the benzaldehyde derivatives **18** yield a mixture of the cyclobutenol isomers **19a** and **19b** in

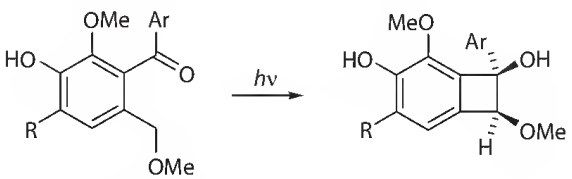

11, R = H, OMe; Ar = (di)methoxyphenyl

SCHEME 26.7 Stereoselective photocyclization of 2-(methoxymethyl)benzophenones.

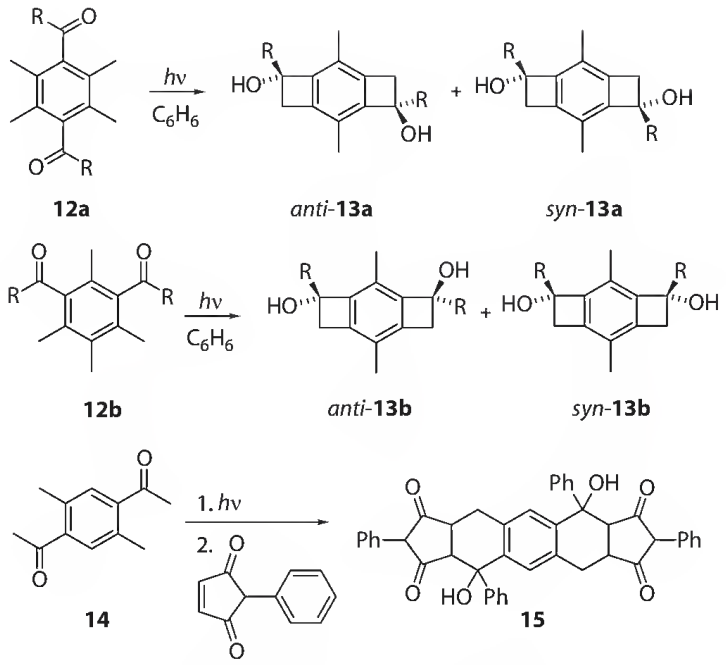

SCHEME 26.8 Photoenolization reaction of *o*- and *p*-dicarbonyl-substituted benzenes.

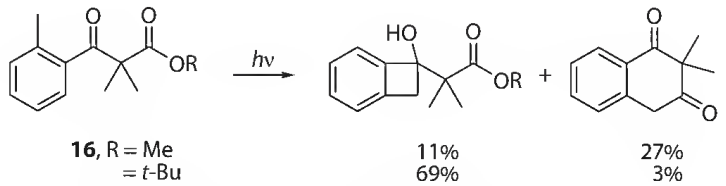

SCHEME 26.9 Reactions of 2-alkylphenyl-1,3-dicarbonyl compounds.

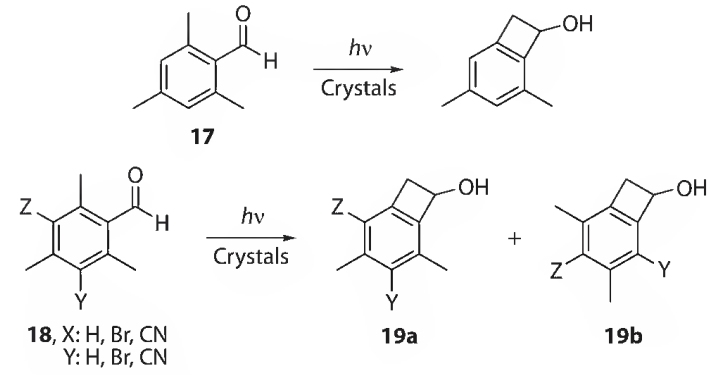

SCHEME 26.10 Reactions of substituted benzaldehydes.

high (82%–100%) yields (Scheme 26.10) (Moorthy et al. 2001b). Furthermore, Moorthy and coworkers were able to use crystal engineering to observe dicyclobutenols from solid state irradiation of iso- and terephthaladehyde (Moorthy et al. 2003). Generally, formation of cyclobutenols in the crystalline phase results in better yields than that in solution. The benzaldehyde derivatives **20** display solid state photochromism and do not form cyclobutenols (Scheme 26.11) (Moorthy et al. 2001b). More specifically, when crystals of **20** are exposed to light, they turn deep red, and the color persists anywhere from seconds to hours. The authors concluded that the red color was due to formation of (*E*)-photoenols, which do not cyclize to form cyclobutenols, but rather decay by reforming the starting material. The authors

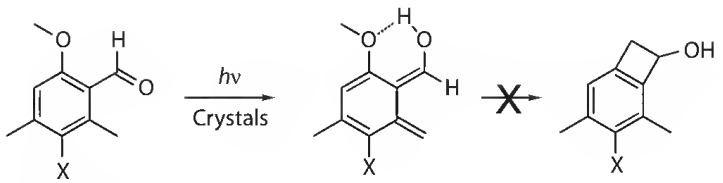

20, X: Br, CN

SCHEME 26.11 Solid-state photochromism of **20**.

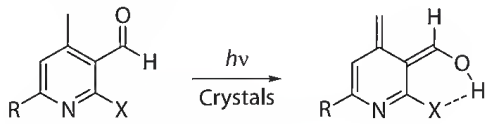

21, X: Cl, OMe

SCHEME 26.12 Intramolecular H-atom bonding in substituted pyridine-3-carboxaldehydes.

theorized that (*E*)-photoenols stabilized by intramolecular H-atom bonding (Scheme 26.11) are more stable than the corresponding cyclobutenols, therefore, no cyclization was observed. They supported their theory by AM1 calculations, which indicated that the benzaldehyde derivatives (**20**), exhibiting solid state photochromism, formed (*E*)-photoenols that are more stable than the corresponding cyclobutenols. Formation of cyclobutanols in the solid state is not limited to benzaldehyde derivatives. Mal et al. demonstrated that pyridine-3-carboxaldehydes derivatives such as **21**, which have their (*E*)-photoenols stabilized either by intramolecular H-atom bonding or electron-donating substituents, did not yield cyclobutenols in the solid state but exhibited photochromism (Scheme 26.12) (Mal et al. 2003). It supported an assumption that the solid state photochromism is due to long-lived (*E*)-photoenols that are prohibited from undergoing electrocyclic ring closure to form cyclobutenols. In addition, Ito et al. reported that solid state photolysis of some triisopropylbenzophenone derivatives yields cyclobutanols (Ito et al. 1998), whereas solid state irradiation of triethylbenzophenone derivatives results in formation of indanols, presumably via an intramolecular δ-H-atom abstraction (Ito et al. 2009).

26.3 Trapping of Ground-State Oxygen

Oxidation products are frequently observed when photoenolization reactions are carried out in aerated solution and in some cases cyclic peroxides have been isolated (Arnold et al. 1974a; Henderson and Ullman 1965; Yates et al. 1968). Several mechanisms have been considered: (i) trapping of the dienols by ground-state oxygen ($^3O_2$), (ii) trapping of the dienols by singlet oxygen ($^1O_2$) that was generated by oxygen quenching of the triplet ketones or the triplet enol ^{3}**E** (Redmond and Scaiano 1989), and (iii) trapping of ^{3}**E** by $^3O_2$. Reactions (ii) and (iii) are spin-allowed [4 + 2] Diels–Alder-type additions and may be close to diffusion controlled (Haag et al. 1977; Redmond and Scaiano 1989), whereas reaction (i) is inhibited by a spin barrier and is much slower. The rate constant for the reaction of the (*E*)-dienol of 2-methylacetophenone with oxygen is 2×10^5 M^{-1} s^{-1} (Lutz et al. 1973).

Sammes and coworkers (Arnold et al. 1974a) have isolated the peroxide **22** (Scheme 26.13). In this case, only the (*Z*)-dienol can be formed, which has a submicrosecond lifetime (Haag et al. 1977) under

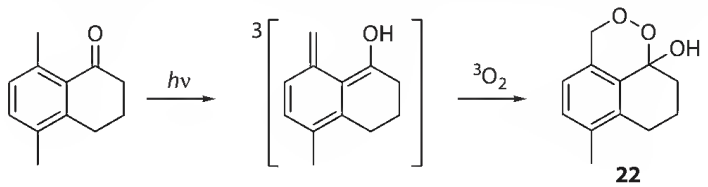

22

SCHEME 26.13 Trapping of the dienols by ground-state oxygen.

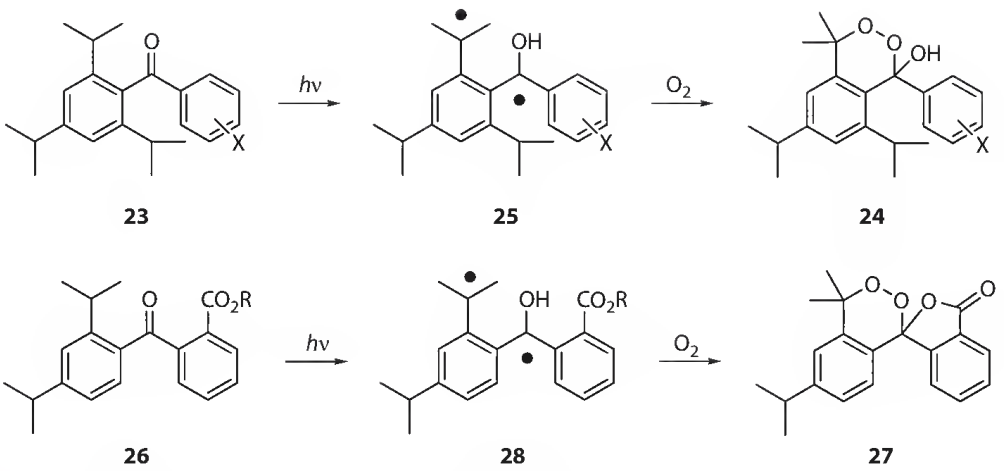

SCHEME 26.14 Trapping of the biradicals **25** and **28** with oxygen.

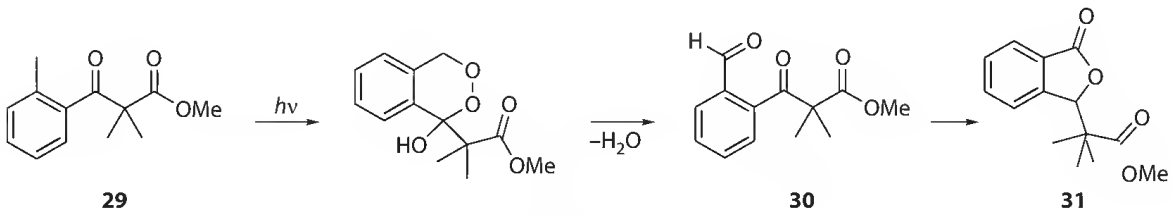

SCHEME 26.15 Rearrangement of a cyclic peroxide intermediate.

the experimental conditions used by Sammes. Hence, reactions (i) and (ii) can be ruled out and the peroxide formation must be attributed to path (iii), trapping of the triplet enol ^{3}E by $^3O_2$, as was originally suggested by Sammes.

Furthermore, Ito et al. showed that irradiation of solid **23** turns the crystal blue. When the irradiated crystals are dissolved in air-saturated solvents, a small amount of the cyclic peroxide **24** is formed (Ito et al. 1998). Ito et al. hypothesized that **24** was formed by trapping of the biradical **25** with oxygen (Scheme 26.14). Similarly, Pika and coworkers demonstrated that irradiation of **26** in air- and oxygen-saturated solutions resulted in **27** by trapping of **28** with oxygen, followed by intramolecular lactonization (Pika et al. 2003). Furthermore, irradiation of **26** in thin films permitted the same reaction.

Most cyclic peroxides are not stable and rearrange to form various carbonyl products. For example, the irradiation of the diketone **29** (Scheme 26.15) yields a peroxide intermediate, which dehydrates into the tricarbonyl product **30** to give the isobenzofuranone derivative **31** (Saito et al. 1998; Yoshioka et al. 1995).

Similarly, irradiation of **32** in oxygen-saturated solutions leads to the peroxide **33**, which dehydrates to form **34** (Scheme 26.16) (Konosonoks et al. 2005). Additionally, irradiation of **34** results in intramolecular H-atom abstraction to form **35**, which lactonizes to **36**. The photooxidiation of **29** and **32** is similar to that reported by Pfau et al. who studied photooxidization of *o*-methylbenzophenone (Pfau et al. 1983).

26.4 Cycloaddition Reactions

Ground-state *o*-xylylenes that live long enough can undergo the Diels–Alder cycloaddition with alkenes, alkynes, carbonyl compounds, or other substrates. They can be produced by thermolysis of the corresponding benzocyclobutenes (Segura and Martin 1999) or photochemically (Sammes 1976; Weedon 1990). Before 1990, the stereoselective cycloadditions of *o*-xylylenes with alkenes was introduced in the synthesis of chiral tetralines (e.g., Arnold et al. 1973; Macdonald and Durst 1986; Quinkert et al. 1981, 1982). In the past two decades, many examples demonstrated that this reaction is practical to synthesize

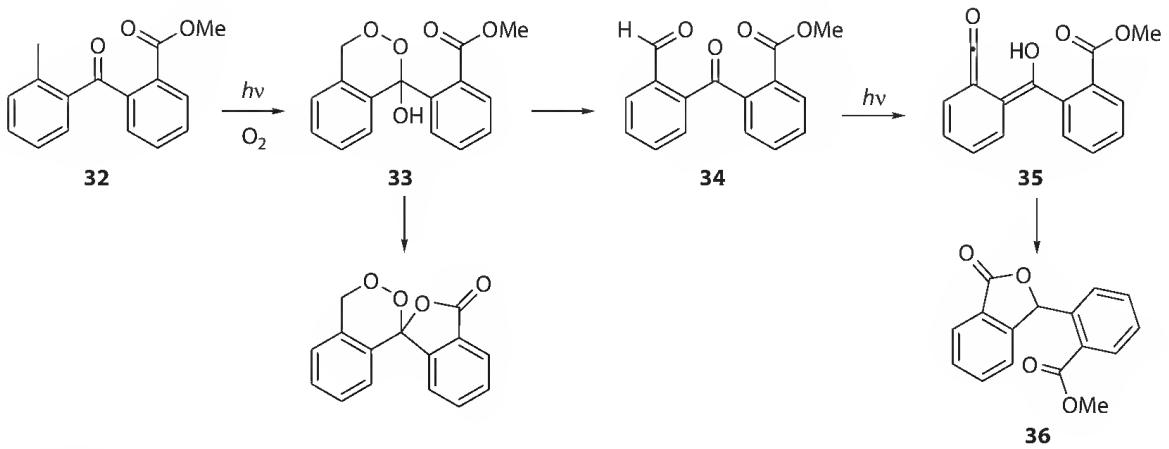

SCHEME 26.16 Photooxidiation of **32**.

tetrahydronaphthalene derivatives. Charlton and coworkers published a series of accounts of the asymmetric Diels–Alder reactions of photochemically formed *o*-xylylenols with various acrylate, fumarate, or lactate esters (Charlton and Koh 1990, 1992; Charlton and Maddaford 1993; Charlton et al. 1989a,b, 1990, 1993). For example, the fumarate **37** was found to react with the photoenol **38**, generated from the aldehyde **39** with very high diastereoselectivity (>90% de) (Scheme 26.17) (Charlton et al. 1990). The product **40**, obtained from **41** in four subsequent steps, is an analogue of podophyllotoxin, known by its strong mitotic activity. In a similar fashion, Kraus and coworkers also demonstrated usefulness of the tandem photoenolization/Diels–Alder cycloaddition reactions in the synthesis of biologically active compounds, such as podophyllotoxin (Kraus and Wu 1992), an anthraquinone derivative G-2N (Kraus and Zhao 1995, 1996), pleurotin (Kraus and Chen 1991a; Kraus et al. 1993), or 4-deoxyaklavinone (Kraus and Chen 1991b).

It was also shown that a methyl lactate derivative adds to the *o*-xylylenol **42** to produce preferentially an unexpected *exo* product (**43**) in 77% yield (Scheme 26.18; only one enantiomer shown). The calculations revealed that the stereoselectivity is related to the hydrogen bonding between the hydroxy group of the enol and the ester (**44**) carbonyl group (Charlton and Maddaford 1993). Narasaka and coworkers showed that phenylboronic acid **45** can be used as a template to trap a short-lived *o*-xylylenol photochemically formed from 2-tolualdehyde (**46**) and methyl 4-hydroxy-2-butenoate (**47**) to allow formation

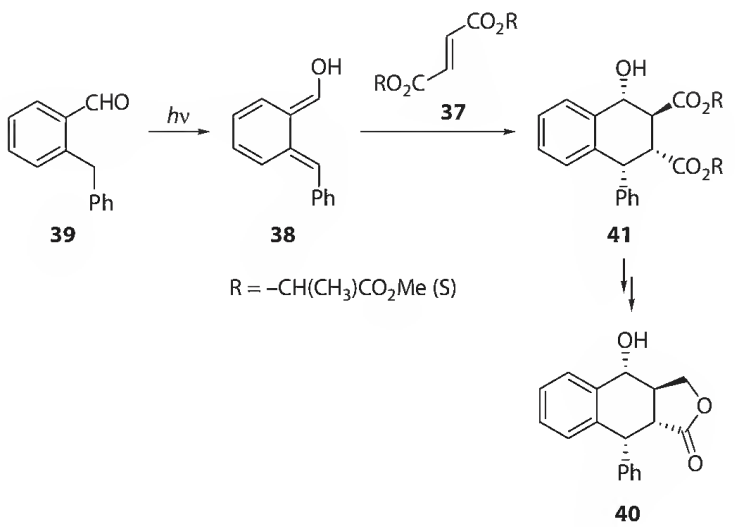

SCHEME 26.17 Diels–Alder reactions of photochemically formed *o*-xylylenols.

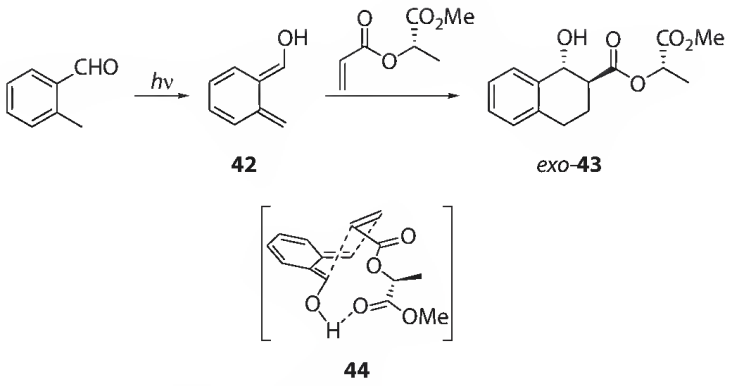

SCHEME 26.18 Addition of an olefin to the *o*-xylylenol.

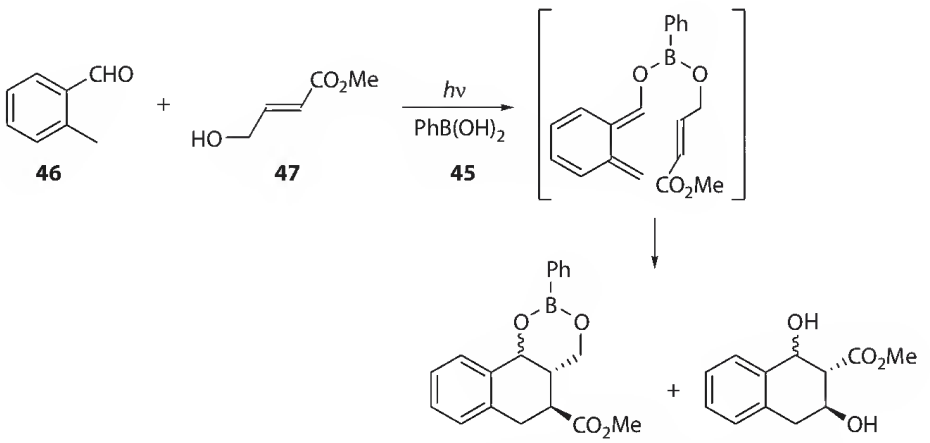

SCHEME 26.19 Addition of an olefin to the *o*-xylylenol in the presence of phenylboronic acid.

of the Diels–Alders products (Scheme 26.19) (Shimada et al. 1993). Some other derivatives of 2-alkylbenzaldehydes, such as 2-formylbenzamines (Kessar et al. 1993) or *o*-formylbenzyltrialkylstannanes (Sano et al. 1999), were also reported to produce tetrahydronaphthalen-1-ol cycloaddition products when irradiated in the presence of various dienophiles.

The total synthesis of hamigerans, naturally occurring cytotoxic substances, was accomplished by the Diels–Alder reaction of photochemically generated photoenols from substituted benzaldehydes (Nicolaou et al. 2001a,b, 2004; Nicolaou and Gray 2004). In one example, both (*E*)- and (*Z*)-isomers of **48** were photochemically converted to the corresponding *o*-xylylenols that subsequently underwent intramolecular cycloaddition to give the tetralines **49** in 78%–91% yields (Scheme 26.20) (Nicolaou et al. 2004). Irradiation of (*E*)-**48** led to *syn*- and *anti*-**49** in a concentration ratio of 25:1, whereas irradiation of (*Z*)-**48** gave a reverse ratio (1:3). These results were found to depend on the photostationary state concentrations of the isomers of **48**, which interconvert via *E*–*Z* photoisomerization. The authors concluded that only a single diastereomer is formed in both cycloaddition reactions because the repulsion between the methyl and hydroxymethyl groups is minimized when they are *anti* to one another in the transition state (represented by the intermediate **50**).

Diels–Alder trapping of *o*-xylylenols was successfully utilized to synthesize some other oligocyclic compounds. Bicyclic aldehydes **51** (Connolly and Durst 1997), a bicyclic oxyquinoline-5-aldehyde **52** (Grosch et al. 2003, 2004), 2-methylbenzaldehyde (**53**) (Tsuno and Sugiyama 1991, 1992, 1994) (Scheme 26.21), and the diketones **54** and **55** (Ilhan et al. 2006) (Scheme 26.22) were reported to form the corresponding photoenols upon irradiation and subsequently the cycloaddition products (the chemical yields are shown in the schemes). In addition, two interesting recent applications can be found in the literature. Production of photoenol from 2-methylbenzophenone attached to a monolayer-protected gold cluster

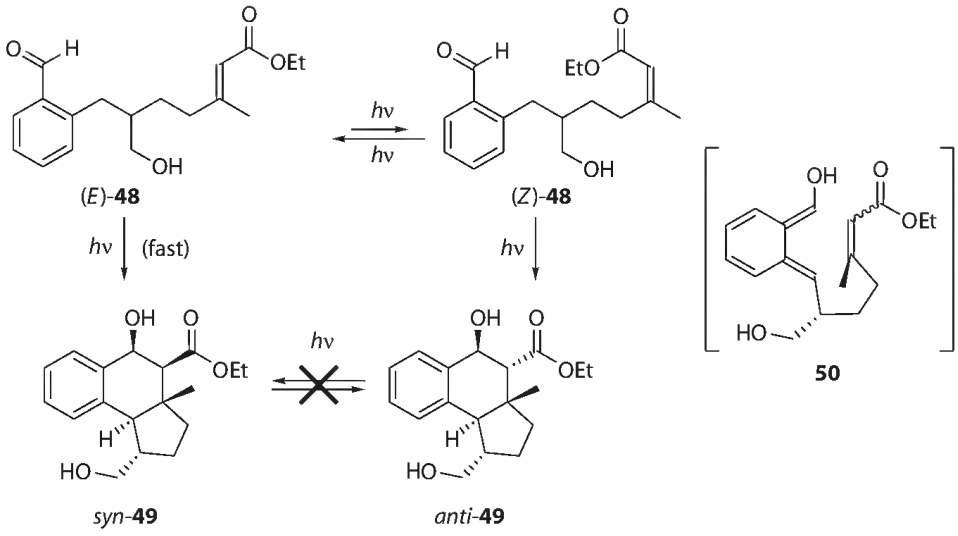

SCHEME 26.20 Synthesis of hamigerans using a photoenolization step.

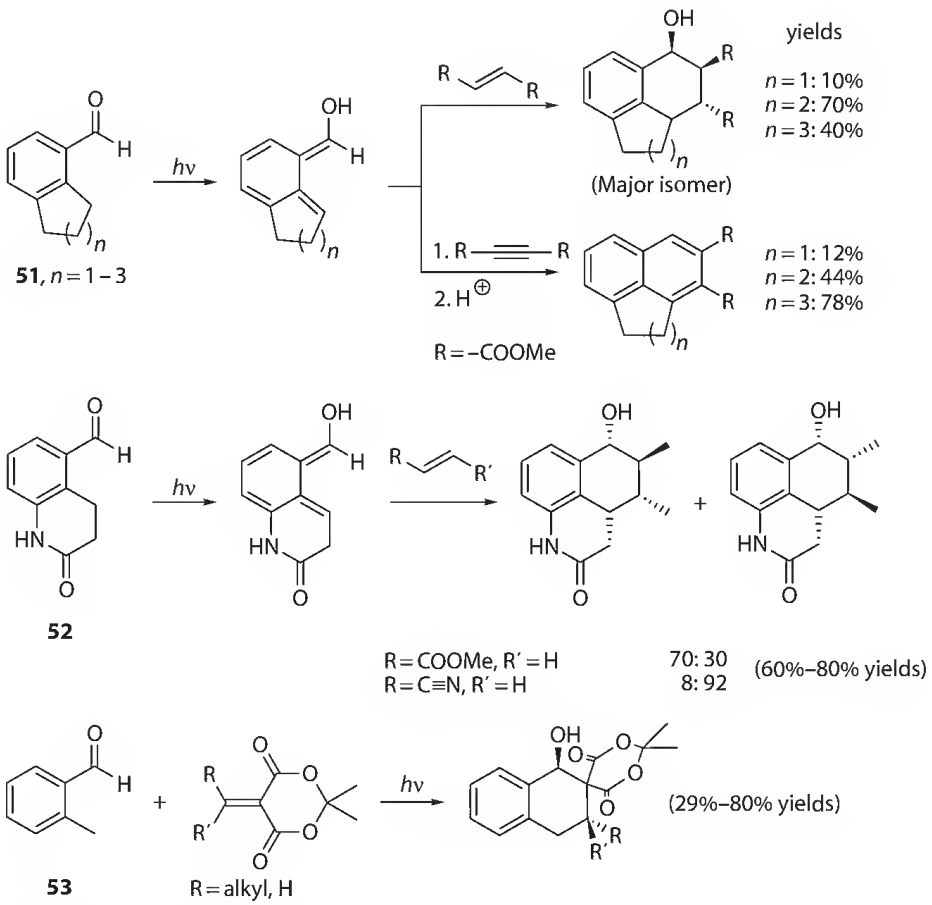

SCHEME 26.21 Diels–Alder trapping of *o*-xylylenols.

and the subsequent Diels–Alder reaction with alkene or alkyne dienes was described by Workentin and coworkers (Kell et al. 2003). Nishimura and coworkers reported trapping of *o*-xylylenols, photochemically formed from various aromatic aldehydes and ketones, by [60]fullerene (Nakamura et al. 2002). Meador and coworkers have recently used Diels–Alder trapping of (*E*)-photoenols as an alternate route to form photocured polymers (Meador et al. 2007; Tyson et al. 2005).

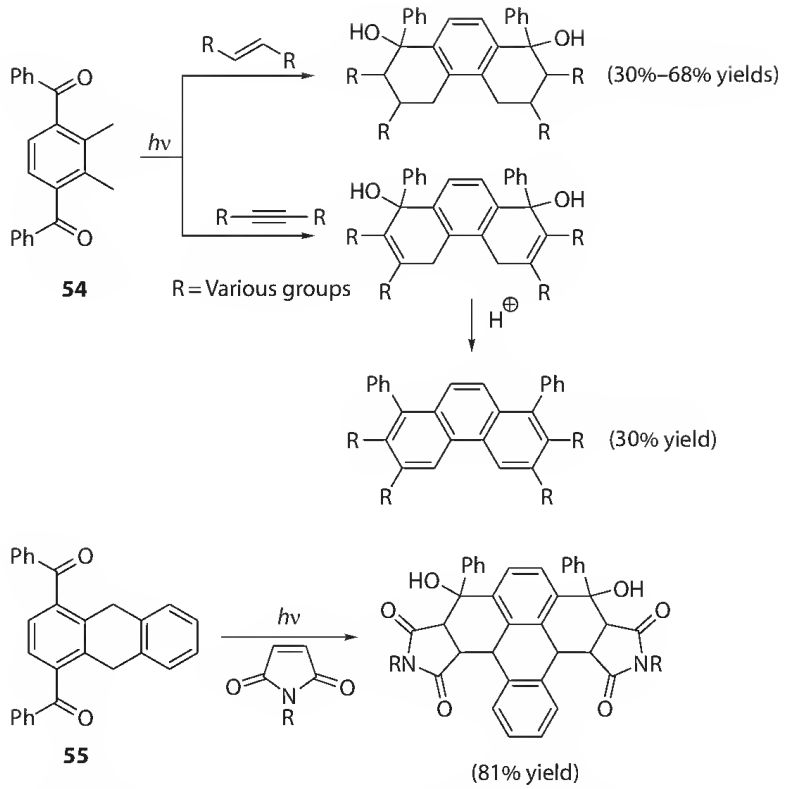

SCHEME 26.22 Diels–Alder trapping of *o*-xylylenols formed from aromatic diketones.

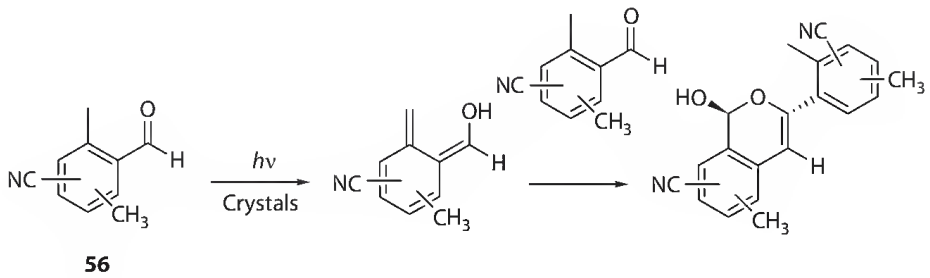

SCHEME 26.23 Diels–Alder trapping of *o*-xylylenols formed from benzaldehydes.

Moorthy et al. demonstrated that solid state irradiation of several benzaldehyde derivatives (**56**, Scheme 26.23) results in formation of hemiacetals in excellent yields (88%–100%) (Moorthy et al. 2004). The authors speculated that these hemiacetals are formed via (*E*)-photoenols undergoing the Diels–Alder cycloaddition with its precursor. They also proposed that intermolecular H-atom abstraction by the triplet ketone might by responsible for formation of the hemiacetals.

26.5 Other Addition Reactions

In the absence of trapping agents, *o*-xylylenols dimerize to form the hemiacetal products (Findlay and Tchir 1974). Durst and coworkers showed that irradiation of the 2-methylbenzoyl cyanide **57** (Connors and Durst 1992) or its derivatives (Connors et al. 1996) results in the formation of the dimers **58** (80% yield for R = H) (Scheme 26.24). These products can be converted to substituted naphthols or isoquinolones by reactions with various nucleophiles.

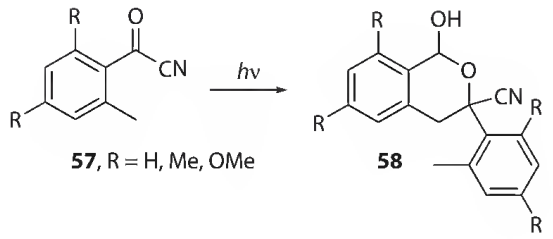

57, R = H, Me, OMe **58**

SCHEME 26.24 Dimerization of *o*-xylylenols.

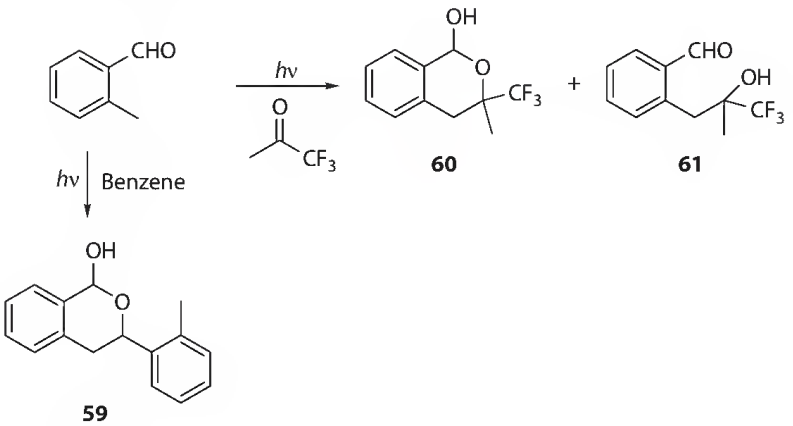

60 **61**

59

SCHEME 26.25 Photoreactions of 2-methylbenzaldehyde.

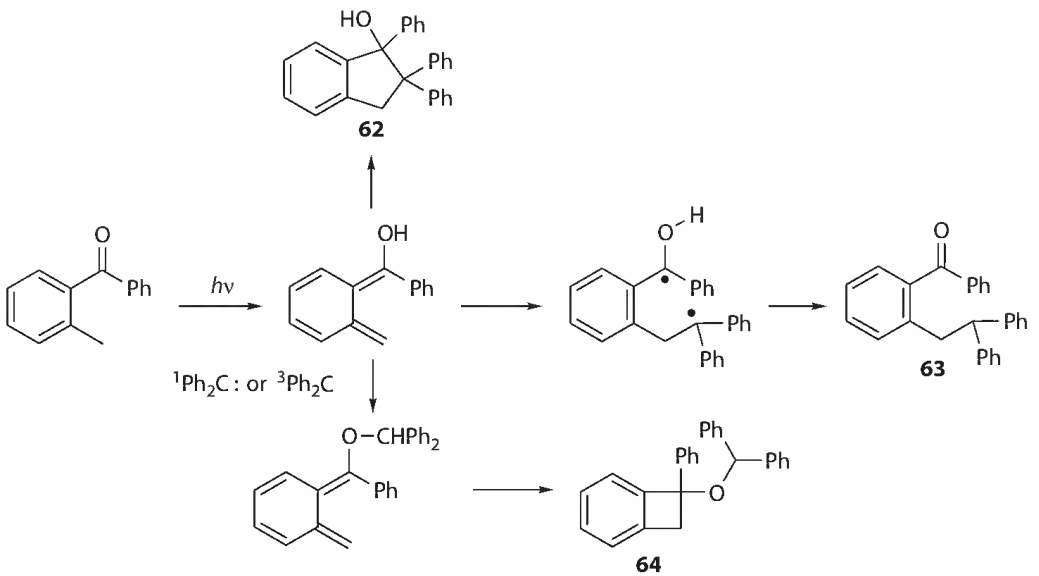

62 **63** **64**

SCHEME 26.26 Trapping of diphenylcarbene by *o*-xylylenol.

Griesbeck and Stadtmüller reported that while irradiation of 2-methylbenzaldehyde in benzene gives **59**, a mixture of the hemiacetal **60** and its open form **61** (the combined yield was 91%) is formed in the presence of 1,1,1-trifluoroacetone (Scheme 26.25) (Griesbeck and Stadtmüller 1993).

It was also reported that short-lived diphenylcarbene ($\tau \sim 1\,\mu s$), generated photochemically from diphenyldiazomethane, can be trapped by a longer lived photoenol of 2-methylbenzophenone under laser-jet conditions (Scheme 26.26) (Wilson et al. 1987, 1992). All three products (**62–64**) are the trapping adducts; the diphenylmethyl ether **64** could also be a coupling product of benzocyclobutenol with the carbene. The course of reactions was suggested to depend on the diphenylcarbene multiplicity.

26.6 Photodienols to Release Nucleophiles

When leaving groups are present in an appropriate position, the photoenol intermediates can undergo elimination reactions. The leaving groups on the α-carbon of 2-methylphenacyl compounds are released efficiently and in high yields (up to 96%) to form the indanone derivatives **65** in non-nucleophilic solvents (Scheme 26.27). The acetophenone derivatives substituted on the *o*-methyl group **66** can be produced in the presence of a nucleophile (such as methanol). This reaction, introduced by Bergmark (phenacyl chlorides and bromides) (Bergmark 1978; Bergmark et al. 1985), was later shown to be applicable in the field of photoremovable protecting groups (Pelliccioli and Wirz 2002). Klán, Wirz, and coworkers demonstrated that the 2,5-dimethylphenacyl (DMP) group can be used to protect carboxylic acids (Klan et al. 2000; Ruzicka et al. 2002; Zabadal et al. 2001), phosphates, sulfonates (Klan et al. 2002), alcohols (as carbonates) (Literak et al. 2005), as well as amines (as carbamates) (Kammari et al. 2007). It was established that only moderately good leaving groups can be released within the photoenol lifetime. Investigations by laser flash photolysis indicated that irradiation produces all expected intermediates, the short-lived triplet enol ^{3}E, and two longer lived photoenols assigned to (*Z*)- and (*E*)-xylylenols in the ground state (see also Scheme 26.3) (Klan et al. 2002; Literak et al. 2005; Zabadal et al. 2001). The (*E*)-xylylenols were found to have sufficient lifetime to release carboxylates, while the (*Z*)-xylylenols recovered the starting ketone. In contrast, the chloride anion, an excellent leaving group, was found to be released also from the (*Z*)-xylylenol (Pelliccioli et al. 2001). Constrained ketones, such as 1-oxoindan-2-yl or 1,3-dioxoindan-2-yl moieties, which are either nonreactive (see Section 26.1) or form only short-lived (*Z*)-xylylenols, cannot be used as photoremovable protecting groups (Literak et al. 2008).

To overcome the problem that the DMP chromophore cannot serve as a photoremovable group for alcohols or amines, which are relatively poor leaving groups, they were attached through carbonate (Literak et al. 2005) or carbamate (Kammari et al. 2007) linkers, respectively, possessing similar leaving group ability to that of a carboxylate. For example, the galactopyranosyl carbonate **67** was found to release the corresponding alcohol **68** in >70% chemical yields (Scheme 26.28) (Literak et al. 2005). Other authors also reported photochemical applications of the *o*-methylphenacyl group. Wang and coworkers used this moiety in polymer-supported synthesis (Du et al. 2005), and Park and Lee showed that this group can be part of new photoresponsive polymers (Park and Lee 2008).

When the acetyl or benzoyl group is attached to the α-position of *o*-methylacetophenone, the photoreaction results in efficient decarboxylation (Scheme 26.29) (Sobczak and Wagner 2002). The authors proposed that an intramolecular proton transfer step is essential for the reaction.

In a different way, Wirz (Pelliccioli and Wirz 2002) and later Banerjee and their coworkers (Atemnkeng et al. 2003) proposed a new photoremovable protecting group based on the 1-[2-(2-hydroxyalkyl) phenyl]ethanone moiety **69** (Scheme 26.30). Here the leaving group is attached in the β-position of

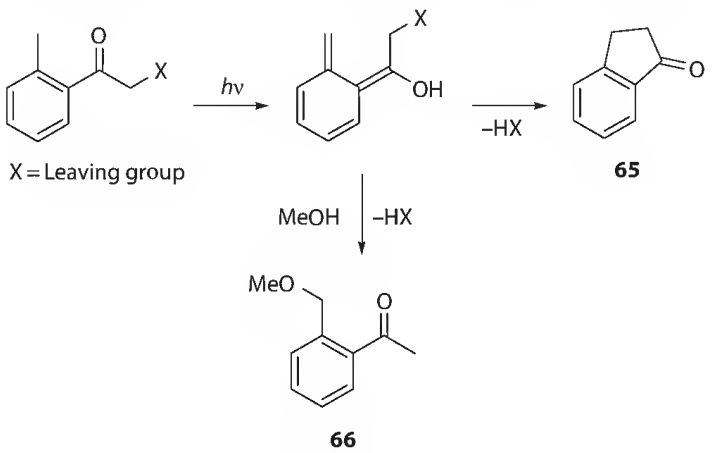

SCHEME 26.27 2-Methylphenacyl compounds as photoremovable protecting groups.

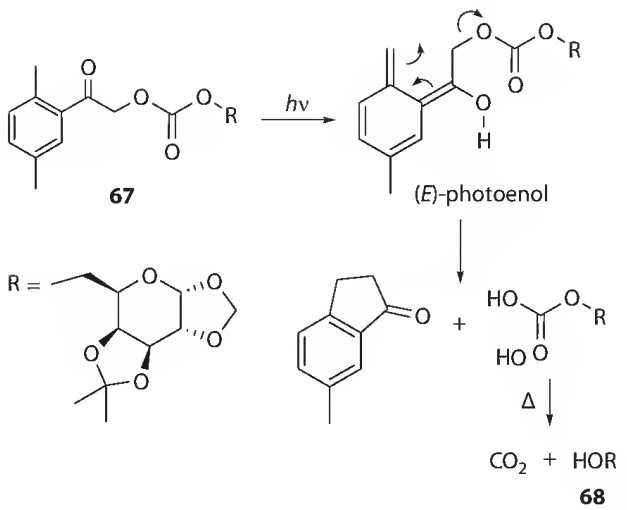

SCHEME 26.28 Release of alcohols using a carbonate linker.

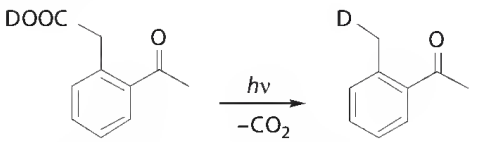

SCHEME 26.29 Decarboxylation of substituted phenylacetic acid.

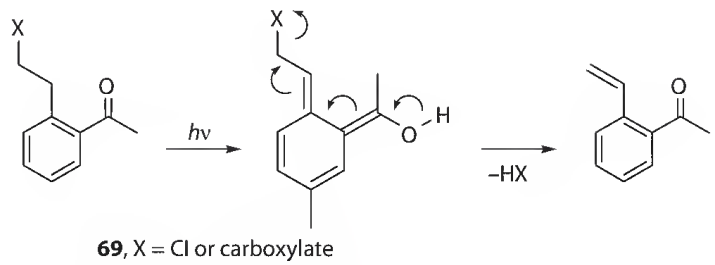

SCHEME 26.30 1-[2-(2-Hydroxyalkyl)phenyl]ethanone moieties as photoremovable protecting groups.

o-ethylacetophenone. This relatively inefficient photoreaction was shown to release the carboxylic acid in 70%–85% isolated yields (Atemnkeng et al. 2003).

The same mechanism operates in 5-(ethylen-2-yl)-1,4-naphthoquinone, a photoremovable protecting group that absorbs up to 405 nm and provides fast and efficient release of bromide or diethyl phosphate ($\Phi = 0.7$ in aqueous solution) (Kamdzhilov and Wirz 2007). The blue photoenol is formed in the ground state within 2 ps of excitation and with a quantum yield of unity (Chiang et al. 1997).

Photoenols can also be used for elimination reactions via intramolecular lactonization. More specifically, elimination can be initiated by intramolecular lactonization of the hydroxyl group of an (*E*)-photoenol. For example, Pika et al. showed that irradiation of **70** gives the corresponding (*Z*)- and (*E*)-photoenols, and that the (*E*)-photoenol undergoes intramolecular lactonization to release an alcohol (Scheme 26.31) (Pika et al. 2003). The elimination or release of the alcohol takes place in various solvents as well as in thin films. This reaction is not quenched by molecular oxygen because the peroxide formed by trapping the biradical **71** with oxygen undergoes intramolecular lactonization to release the alcohol moiety.

In comparison, Konosonoks et al. found that irradiation of **72** in aprotic solvents did not yield any products (Scheme 26.32) (Konosonoks et al. 2005). Transient spectroscopy showed that the photoenols formed were considerably shorter lived than the photoenol obtained from **70** (Scheme 26.31). Thus, the

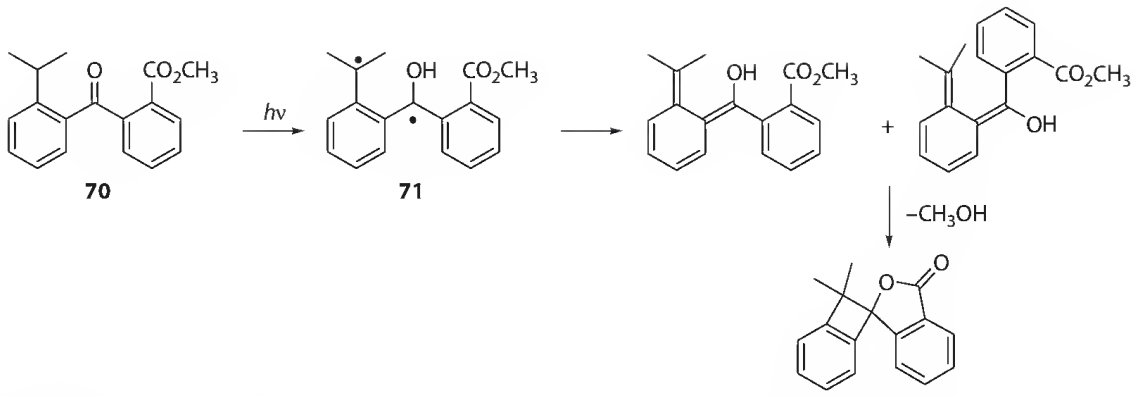

SCHEME 26.31 Elimination reactions via intramolecular lactonization of an (*E*)-photoenol.

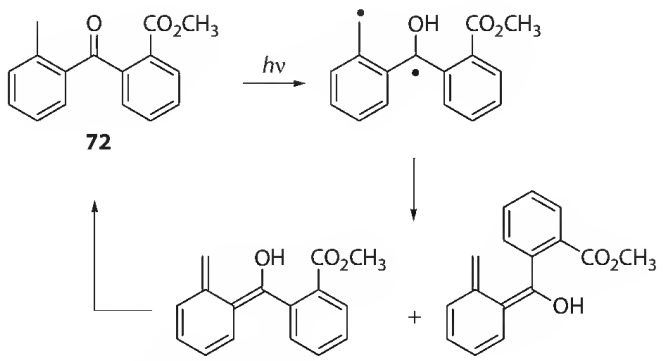

SCHEME 26.32 Nonproductive photochemistry of **72**.

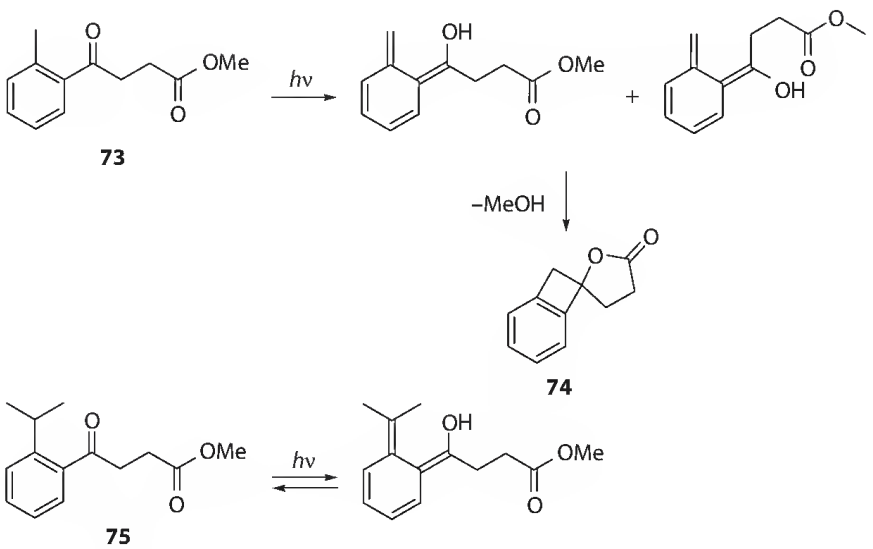

SCHEME 26.33 (*E*)-Photoenol lactonization to release an alcohol.

authors concluded that intramolecular lactonization was not efficient enough to compete with the reketonization of the (*E*)-photoenol from **72**.

Similarly, the ketone **73** forms (*E*)- and (*Z*)-photoenols upon exposure to light, while only the (*E*)-photoenol undergoes lactonization to release an alcohol to form **74** (Scheme 26.33) (Muthukrishnan et al. 2010). However, irradiation of **75** does not lead to any photoproducts because it only forms a

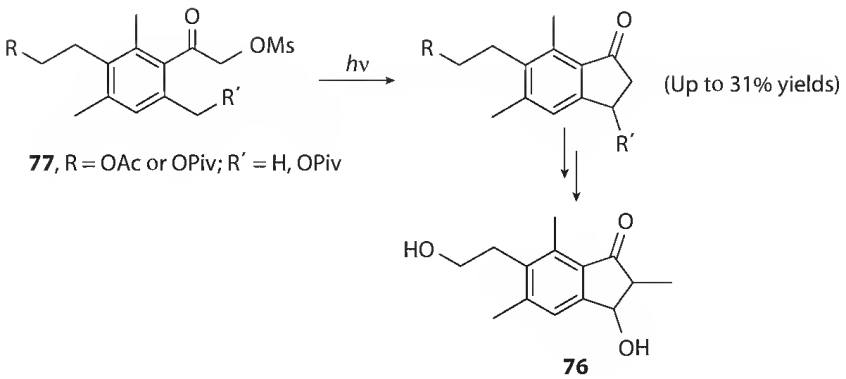

SCHEME 26.34 Photochemical closure reactions of **77**.

(*Z*)-photoenol that decays back to the starting material. Intramolecular pseudo H-atom bonding and rotation barrier prevent **75** from ISC to form the (*E*)-photoenol. The major difference between the benzophenone **70** and the butyrophenone **73** is flexibility of an alkyl chain in **73**. This presumably allows the (*E*)-photoenol formed from **73** to release its alcohol moiety faster than **70**.

Various synthetically interesting functionalized indan-1-ones have been produced using photoenolization reaction that involves the release of the leaving group from the α-position of an *o*-methylacetophenone derivative. Berkessel and collaborators used this reaction to study the cyclization of 4′-benzophenone-substituted nucleoside derivatives as models for ribonucleotide reductases (Lehmann et al. 2000). Wessig and coworkers used this concept for the preparation of various 1-indanone derivatives (Wessig et al. 2004), and for the total synthesis of two sesquiterpene indane derivatives, pterosine B or C (e.g., **76**, Scheme 26.34), in which the key step is the photochemical closure reaction of **77** (Wessig and Teubner 2006). Klán and coworkers showed that irradiation of a 4,5-dimethoxyphenacyl derivative can lead to an indanone precursor for the synthesis of donepezil, a centrally acting reversible acetylcholinesterase inhibitor used to treat Alzheimer's disease (Pospisil et al. 2008). Interestingly, Park and Ryu have recently reported that irradiation of 2,4,6-trialkylphenacyl benzoates yields the corresponding benzocyclobutenols in addition to the corresponding indanones and benzoic acid (Park and Ryu 2010).

Irradiation of 2-(alkoxymethyl)-5-methyl-α-chloroacetophenones (**78**) was reported by Klán and coworkers to be very sensitive to traces of water in the solvent (Scheme 26.35) (Plistil et al. 2006). While

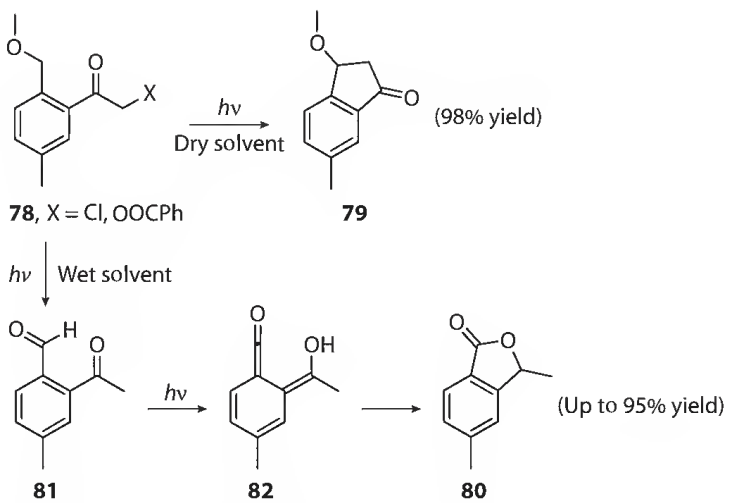

SCHEME 26.35 Photochemistry of 2-(alkoxymethyl)-5-methyl-α-chloroacetophenones.

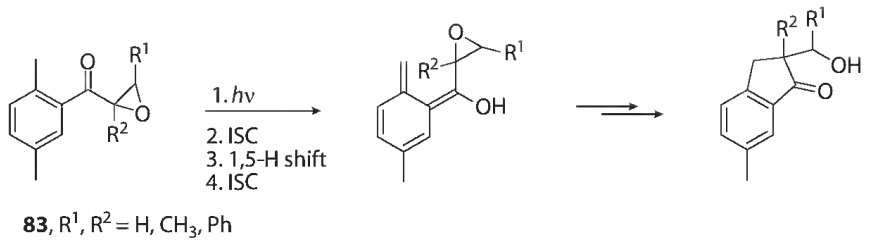

SCHEME 26.36 Photochemistry of 2,5-dimethylbenzoyl oxiranes.

3-methoxy-6-methylindan-1-one (**79**) was formed in dry, non-nucleophilic solvents, the isobenzofuran-1(3*H*)-one **80** was isolated as a major photoproduct in the presence of trace amounts of water. It was explained that photoenols produced by irradiation of **78** add water as a nucleophile to form 2-acetyl-4-methylbenzaldehyde (**81**), which is further converted to **82** through a second, singlet state photoenolization process.

Klán and coworkers recently reported that irradiation of the 2,5-dimethylbenzoyl oxiranes **83** results in a relatively efficient (Φ = 11–25) and high-yielding (~70%) formation of β-hydroxy functionalized indanones that structurally resemble biologically active pterosines (Scheme 26.36). Laser flash photolysis experiments and quantum-chemical calculations provided solid evidence that the indanone photoproducts are formed via a photoenolization mechanism (Solomek et al. 2010).

References

Arnaut, L. G., Formosinho, S. J., and Da Silva, A. M. 1984. Structure-efficiency relationships in hydrogen photoabstraction reactions by ketones: Thermal activation versus nuclear tunnelling. *J. Photochem.* 27: 185–203.

Arnold, B. J., Mellows, S. M., and Sammes, P. G. 1973. Photochemical reactions. 1. New route to tetradehydropodo-phyllotoxin, taiwanin E, and related compounds. *J. Chem. Soc. Perkin Trans. 1* 1973: 1266–1270.

Arnold, B. J., Mellows, S. M., Sammes, P. G., and Wallace, T. W. 1974a. Photochemical reactions. 2. Cycloaddition reactions with photoenols from 2-methylbenzaldehyde and related systems. *J. Chem. Soc. Perkin Trans. 1* 1974: 401–409.

Arnold, B. J., Sammes, P. G., and Wallace, T. W. 1974b. Photochemical reactions. 4. Thermal generation of photoenols and their derivatives from disubstituted 1,2-dihydrobenzocyclobutenes. *J. Chem. Soc. Perkin Trans. 1* 1974: 415–420.

Atemnkeng, W. N., Louisiana, L. D., Yong, P. K., Vottero, B., and Banerjee, A. 2003. 1–2-(2-Hydroxyalkyl)phenyl ethanone: A new photoremovable protecting group for carboxylic acids. *Org. Lett.* 5: 4469–4471.

Barroso, M., Arnaut, L. G., and Formosinho, S. J. 2010. Tunnelling corrections in hydrogen abstractions by excited-state ketones. *J. Phys. Org. Chem.* 23: 702–710.

Bergmark, W. R. 1978. Photolysis of α-chloro-*o*-methylacetophenones. *J. Chem. Soc. Chem. Commun.* 1978: 61–62.

Bergmark, W. R., Barnes, C., Clark, J., Paparian, S., and Marynowski, S. 1985. Photoenolization with α-chloro substituents. *J. Org. Chem.* 50: 5612–5615.

Campos, L. M., Warrier, M. V., Peterfy, K., Houk, K. N., and Garcia-Garibay, M. A. 2005. Secondary alpha isotope effects on deuterium tunneling in triplet *o*-methylanthrones: Extraordinary sensitivity to barrier width. *J. Am. Chem. Soc.* 127: 10178–10179.

Carless, H. A. J. and Fekarurhobo, G. K. 1984. Photochemical ε-hydrogen abstraction as a route to tetrahydropyran-3-ols. *Tetrahedron Lett.* 25: 5943–5946.

Charlton, J. L. and Koh, K. 1990. Asymmetric and stereoselective cycloaddition of the acrylate and fumarate of (R)-methyl mandelate to α-hydroxy-*o*-quinodimethane. *Synlett* 1990: 333–334.

Charlton, J. L. and Koh, K. 1992. Asymmetric synthesis of (-)-neopodophyllotoxin. *J. Org. Chem.* 57: 1514–1516.

Charlton, J. L., Koh, K., and Plourde, G. L. 1989a. Thermal generation of α-hydroxy-*o*-quinodimethane and reaction with the fumarate, maleate and acrylate of S-methyl lactate. *Tetrahedron Lett.* 30: 3279–3282.

Charlton, J. L. and Maddaford, S. 1993. The mechanism of stereoselectivity in the cycloaddition reactions of α-hydroxy-*o*-quinodimethanes with the fumarate of methyl lactate and mandelate. *Can. J. Chem. Rev. Can. Chim.* 71: 827–833.

Charlton, J. L., Maddaford, S., Koh, K., Boulet, S., and Saunders, M. H. 1993. An asymmetric Diels-Alder cycloaddition to α-hydroxy-α-phenyl-*o*-quinodimethane. *Tetrahedron Asymm.* 4: 645–648.

Charlton, J. L., Plourde, G. L., Koh, K., and Secco, A. S. 1989b. Diels-Alder addition of the fumarate and acrylate of S-methyl lactate to α-hydroxy *o*-quinodimethanes. *Can. J. Chem. Rev. Can. Chim.* 67: 574–579.

Charlton, J. L., Plourde, G. L., Koh, K., and Secco, A. S. 1990. Asymmetric synthesis of podophyllotoxin analogs. *Can. J. Chem. Rev. Can. Chim.* 68: 2022–2027.

Chiang, Y., Kresge, A. J., Hellrung, B., Schunemann, P., and Wirz, J. 1997. Flash photolysis of 5-methyl-1,4-naphthoquinone in aqueous solution: Kinetics and mechanism of photoenolization and of enol trapping. *Helv. Chim. Acta* 80: 1106–1121.

Coll, G., Costa, A., Deya, P. M., Flexas, F., Rotger, C., and Saa, J. M. 1992. Stereoselective photocyclization of some phenolic, highly congested benzophenones and benzaldehydes. Use of *cis*-2-arylbenzocyclobutenol methyl ethers for the synthesis of lignans. *J. Org. Chem.* 57: 6222–6231.

Connolly, T. J. and Durst, T. 1997. Photochemically generated bicyclic *o*-quinodimethanes: Photoenolization of bicyclic aldehydes and ketones. *Tetrahedron* 53: 15969–15982.

Connors, R. and Durst, T. 1992. Acyl cyanides as carbonyl heterodienophiles. *Tetrahedron Lett.* 33: 7277–7280.

Connors, R., Tran, E., and Durst, T. 1996. Acyl cyanides as carbonyl heterodienophiles: Application to the synthesis of naphthols, isoquinolones, and isocoumarins. *Can. J. Chem. Rev. Can. Chim.* 74: 221–226.

Das, P. K., Encinas, M. V., Small, R. D., and Scaiano, J. C. 1979. Photoenolization of *o*-alkyl-substituted carbonyl compounds. Use of electron transfer processes to characterize transient intermediates. *J. Am. Chem. Soc.* 101: 6965–6970.

Du, L. H., Zhang, S. H., and Wang, Y. G. 2005. Phenacyl esters as a new photocleavable linker in liquid-phase chemistry. *Tetrahedron Lett.* 46: 3399–3402.

Findlay, D. M. and Tchir, M. F. 1974. Photochemistry of *o*-tolualdehyde: Photoenolization and photobenzoin condensation. *J. Chem. Soc., Chem. Commun.* 1974: 514–515.

Findlay, D. M. and Tchir, M. F. 1976. Photoenolization of *o*-alkyl-substituted acetophenones: Evidence for enol triplet-state. *J. Chem. Soc. Faraday Trans. I* 72: 1096–1100.

Fitzgerald, J. J., Drysdale, N. E., and Olofson, R. A. 1992. A rapid, convergent, and regioselective synthesis of anthracenes. *J. Org. Chem.* 57: 7122–7126.

Fitzgerald, J. J., Michael, F. E., and Olofson, R. A. 1994a. Reaction of benzocyclobutenoxides with nitriles: Synthesis of hypecumine and other 3-substituted isoquinolines. *Tetrahedron Lett.* 35: 9191–9194.

Fitzgerald, J. J., Pagano, A. R., Sakoda, V. M., and Olofson, R. A. 1994b. Reaction of benzocyclobutenoxides with aldehydes: Synthesis of peshawarine and other 3,4-dihydroisocoumarins. *J. Org. Chem.* 59: 4117–4121.

Gamarnik, A., Johnson, B. A., and Garcia-Garibay, M. A. 1998. Effect of solvents on the photoenolization of omicron-methylanthrone at low temperatures. Evidence for H-atom tunneling from nonequilibrating triplets. *J. Phys. Chem. A* 102: 5491–5498.

Garcia-Garibay, M. A., Gamarnik, A., Bise, R., Pang, L., and Jenks, W. S. 1995. Primary isotope effects on excited-state hydrogen-atom-transfer reactions: Activated and tunneling mechanisms in an *o*-methylanthrone. *J. Am. Chem. Soc.* 117: 10264–10275.

Garcia-Garibay, M. A., Gamarnik, A., Pang, L., and Jenks, W. S. 1994. Excited-state intramolecular hydrogen-atom-transfer at ultralow temperatures: Evidence for tunneling and activated mechanisms in 1,4-dimethylanthrone. *J. Am. Chem. Soc.* 116: 12095–12096.

Garcia-Garibay, M. A., Jenks, W. S., and Pang, L. 1996. Heterogeneous hydrogen and deuterium transfer in the excited state of 2-methylbenzophenone in ether-pentane-alcohol glasses at 77 K. *J. Photochem. Photobiol. A: Chem.* 96: 51–55.

Gebicki, J., Marcinek, A., Michalak, J., Rogowski, J., Bally, T., and Tang, W. L. 1992. Spontaneous hydrogen-atom transfer upon ionization: Characterization of enol radical cations. *J. Mol. Struct.* 275: 249–255.

Griesbeck, A. G. and Stadtmüller, S. 1993. Omega-hydroxy-*o*-quinodimethane: Trapping with trifluoroacetone and photocyclization. *Chem. Ber. Recl.* 126: 2149–2150.

Gritsan, N. P., Khmelinski, I. V., and Usov, O. M. 1991. Experimental and theoretical study of photoenolization mechanism for 1-methylanthraquinone. *J. Am. Chem. Soc.* 113: 9615–9620.

Grosch, B., Orlebar, C. N., Herdtweck, E., Kaneda, M., Wada, T., Inoue, Y., and Bach, T. 2004. Enantioselective [4 + 2]-cycloaddition reaction of a photochemically generated *o*-quinodimethane: Mechanistic details, association studies, and pressure effects. *Chem. Eur. J.* 10: 2179–2189.

Grosch, B., Orlebar, C. N., Herdtweck, E., Massa, W., and Bach, T. 2003. Highly enantioselective Diels-Alder reaction of a photochemically generated *o*-quinodimethane with olefins. *Angew. Chem. Int. Ed.* 42: 3693–3696.

Haag, R., Wirz, J., and Wagner, P. J. 1977. The photoenolization of 2-methylacetophenone and related compounds. *Helv. Chim. Acta* 60: 2595–2607.

Henderson, W. A. and Ullman, E. F. 1965. Photochemistry of 2-benzyl and 2-benzhydryl-3-benzoylchromon. *J. Am. Chem. Soc.* 87: 5424–5433.

Iida, K., Komada, K., Saito, M., and Yoshioka, M. 1999. Mechanistic study on thermal isomerization of 1-methylbenzocyclobutenol to 2-methylacetophenone. *J. Org. Chem.* 64: 7407–7411.

Iida, K., Saito, M., and Yoshioka, M. 2000. Stereospecific thermal isomerization of 2,2-dimethylbenzocyclobutenols to 2-isopropenylphenyl alcohols. *J. Org. Chem.* 65: 4909–4912.

Ilhan, F., Tyson, D. S., and Meador, M. A. 2006. Phenacenes from Diels-Alder trapping of photogenerated *o*-xylylenols: Phenanthrenes and benzo[e]pyrene bisimide. *Org. Lett.* 8: 577–580.

Ito, Y., Nishimura, H., Matsuura, T., and Hayashi, H. 1981. Effect of ring substituents on the lifetime of biradicals photogenerated from 2,4,6-tri-isopropylbenzophenones. *J. Chem. Soc. Chem. Commun.* 1981: 1187–1188.

Ito, Y., Takahashi, H., Hasegawa, J. Y., and Turro, N. J. 2009. Photocyclization of 2,4,6-triethylbenzophenones in the solid state. *Tetrahedron* 65: 677–689.

Ito, Y., Umehara, Y., Hijiya, T., Yamada, Y., and Matsuura, T. 1980. Photoinduced reactions. 121. Sterically promoted benzocyclobutenol formation from 2,4,6-triisopropylbenzophenone photolysis. *J. Am. Chem. Soc.* 102: 5917–5919.

Ito, Y., Yasui, S., Yamauchi, J., Ohba, S., and Kano, G. 1998. Solid-state photocyclization of 2,4,6-triisopropyl-4 '-(methoxycarbonyl)benzophenone. Evidence for a narrow reaction cavity and a photoenol diradical intermediate. *J. Phys. Chem. A* 102: 5415–5420.

Johnson, B. A., Gamarnik, A., and Garcia-Garibay, M. A. 1996. Deuterium tunneling in triplet 5,8-dimethyl-1-tetralone by phosphorescence detection between 80 and 15 K. *J. Phys. Chem.* 100: 4697–4700.

Johnson, B. A. and Garcia-Garibay, M. A. 1999. Rate acceleration below 20 K in the H-atom tunneling of triplet *o*-methyltetralones. *J. Am. Chem. Soc.* 121: 8114–8115.

Johnson, B. A., Hu, Y. F., Houk, K. N., and Garcia-Garibay, M. A. 2001. Vibrationally assisted tunneling in a hydrogen atom transfer reaction. *J. Am. Chem. Soc.* 123: 6941–6942.

Kamdzhilov, Y. and Wirz, J. 2007. Synthesis and reaction mechanism of a photoremovable protecting group based on 1,4-naphthoquinone. *Photochem. Photobiol. Sci.* 6: 865–872.

Kammari, L., Plistil, L., Wirz, J., and Klan, P. 2007. 2,5-Dimethylphenacyl carbamate: A photoremovable protecting group for amines and amino acids. *Photochem. Photobiol. Sci.* 6: 50–56.

Kawata, E., Saito, M., and Yoshioka, M. 2000. Thermal reaction of diastereomeric benzocyclobutenols. Evidence for reversible opening of 1,2-dihydrobenzocyclobutenols to hydroxy-*o*-xylylenes. *J. Chem. Soc. Perkin Trans. 1* 2000: 1015–1019.

Kell, A. J., Montcalm, C. C., and Workentin, M. S. 2003. Photogeneration of a diene template for surface Diels-Alder reactions: Photoenolization of an *o*-methyl-benzophenone-modified Au cluster. *Can. J. Chem. Rev. Can. Chim.* 81: 484–494.

Kessar, S. V., Mankotia, A. K. S., and Agnihotri, K. R. 1993. Intramolecular photoreactions of 2-formyl-benzamides and 2-formylbenzylamines. *J. Chem. Soc., Chem. Commun.* 1993: 598–599.

Klan, P., Pelliccioli, A. P., Pospisil, T., and Wirz, J. 2002. 2,5-Dimethylphenacyl esters: A photoremovable protecting group for phosphates and sulfonic acids. *Photochem. Photobiol. Sci.* 1: 920–923.

Klan, P. and Wirz, J. 2009. *Photochemistry of Organic Compounds: From Concepts to Practice: Postgraduate Chemistry Series*. Wiley, Chichester, U.K.

Klan, P., Zabadal, M., and Heger, D. 2000. 2,5-Dimethylphenacyl as a new photoreleasable protecting group for carboxylic acids. *Org. Lett.* 2: 1569–1571.

Konosonoks, A., Wright, P. J., Tsao, M. L., Pika, J., Novak, K., Mandel, S. M., Bauer, J. A. K., Bohne, C., and Gudmundsdottir, A. D. 2005. Photoenolization of 2-(2-methylbenzoyl)benzoic acid, methyl ester: Effect of *E*-photoenol lifetime on the photochemistry. *J. Org. Chem.* 70: 2763–2770.

Kraus, G. A. and Chen, L. 1991a. The development of a direct synthetic route to pleurotin. *Synlett* 1991: 89–90.

Kraus, G. A. and Chen, L. 1991b. Photoenolization reactions in organic synthesis: A direct synthesis of 4-deoxyaklavinone. *Synlett* 1991: 51–52.

Kraus, G. A., Chen, L., and Jacobson, R. A. 1993. Synthesis and evaluation of a pleurotin analog. *Synth. Commun.* 23: 2041–2049.

Kraus, G. A. and Wu, Y. S. 1992. Hydrogen-atom abstraction reactions in organic synthesis: A formal total synthesis of racemic podophyllotoxin. *J. Org. Chem.* 57: 2922–2925.

Kraus, G. A. and Zhao, G. 1995. Direct synthesis of the dimethyl ether of benzo[a] naphthacenequinone G-2N. *Synlett* 1995: 541–542.

Kraus, G. A. and Zhao, G. H. 1996. Direct synthesis of G-2N. *J. Org. Chem.* 61: 2770–2773.

Lehmann, T. E., Muller, G., and Berkessel, A. 2000. Photochemistry of 4 '-benzophenone-substituted nucleoside derivatives as models for ribonucleotide reductases: Competing generation of 3 '-radicals and photoenols. *J. Org. Chem.* 65: 2508–2516.

Literak, J., Hroudna, L., and Klan, P. 2008. 1-Oxoindan-2-yl and 1,3-dioxoindan-2-yl esters as photoremovable protecting groups. *J. Photochem. Photobiol. A Chem.* 194: 59–66.

Literak, J., Wirz, J., and Klan, P. 2005. 2,5-Dimethylphenacyl carbonates: A photoremovable protecting group for alcohols and phenols. *Photochem. Photobiol. Sci.* 4: 43–46.

Lutz, H., Breheret, E., and Lindqvis, L. 1973. Photoenolization of *o*-methyl-substituted acetophenones: Solvent effects on triplet-state reactivity. *J. Chem. Soc. Faraday Trans. I* 69: 2096–2102.

Macdonald, D. I. and Durst, T. 1986. A highly stereoselective Diels-Alder based synthesis of (+/−)-podophyllotoxin. *J. Org. Chem.* 51: 4749–4750.

Mal, P., Lourderaj, U., Parveen, Venugopalan, P., Moorthy, J. N., and Sathyamurthy, N. 2003. Conformational control and photoenolization of pyridine-3-carboxaldehydes in the solid state: Stabilization of photoenols via hydrogen bonding and electronic control. *J. Org. Chem.* 68: 3446–3453.

Marcinek, A., Michalak, J., Rogowski, J., Tang, W. L., Bally, T., and Gebicki, J. 1992. Enolization in radical cations of *o*-methylacetophenone and related species under cryogenic conditions. *J. Chem. Soc. Perkin Trans. 2* 1992: 1353–1357.

Meador, M. A., Meador, M. A., Tyson, D. S., and Ilhan, F. 2007. Use of diels-alder cyclopolymerizations in the photocuring of polymers. *High Perform. Polym.* 19: 665–683.

Meador, M. A. and Wagner, P. J. 1985. Photocyclization of α-(*o*-benzyloxyphenyl)acetophenone: Triplet state ε-hydrogen abstraction. *J. Org. Chem.* 50: 419–420.

Mehta, G. and Kotha, S. 2001. Recent chemistry of benzocyclobutenes. *Tetrahedron* 57: 625–659.

Michalak, J. and Gebicki, J. 1993. Fotoenolizacja *ortho*-alkilopodstawionych ketonow i aldehydow arylowych. *Wiadom. Chem.* 47: 407–418.

Moorthy, J. N., Mal, P., Natarajan, R., and Venugopalan, P. 2001a. Efficient photocyclization of *o*-alkylbenzaldehydes in the solid state: Direct observation of (*E*)-xylylenols en route to benzocyclobutenols. *J. Org. Chem.* 66: 7013–7019.

Moorthy, J. N., Mal, P., Natarajan, R., and Venugopalan, P. 2001b. Solid-state photochromism and photoreactivity of *o*- and *p*-anisaldehydes. Remarkable stabilization of o-xylylenols. *Org. Lett.* 3: 1579–1582.

Moorthy, J. N., Mal, P., Singhal, N., Venkatakrishnan, P., Malik, R., and Venugopalan, P. 2004. Highly diastereoselective tandem photoenolization-hetero-Diels-Alder cycloaddition reactions of *o*-tolualdehydes in the solid state. *J. Org. Chem.* 69: 8459–8466.

Moorthy, J. N. and Samanta, S. 2007. Photochemistry of dicarbonyl-substituted benzenes: Influence of steric and electronic factors in the cyclization and Diels-Alder trapping reactions of photoenols. *Arkivoc*: viii, 324–340.

Moorthy, J. N., Venkatakrishnan, P., Mal, P., and Venugopalan, P. 2003. Solid-state diphotocyclization of iso- and terephthalaldehydes via dihalogen substitution. *J. Org. Chem.* 68: 327–330.

Moreno, M. and Lluch, J. M. 2007. Secondary kinetic isotope effect on the photoenolization of triplet *o*-methylanthrones. A microcanonical transition state theory calculation. *J. Phys. Chem. A* 111: 10090–10097.

Muthukrishnan, S., Sankaranarayanan, J., Pace, T. C. S., Konosonoks, A., DeMichiei, M. E., Meese, M. J., Bohne, C., and Gudmundsdottir, A. 2010. The effect of alkyl substituents on photorelease from butyrophenone derivatives. *J. Org. Chem.* 75: 1393–1401.

Nakamura, Y., O-kawa, K., Minami, S., Ogawa, T., Tobita, S., and Nishimura, J. 2002. Photochemical synthesis, conformational analysis, and transformation of [60]fullerene-*o*-quinodimethane adducts bearing a hydroxy group. *J. Org. Chem.* 67: 1247–1252.

Nicolaou, K. C. and Gray, D. L. F. 2004. Total synthesis of hybocarpone and analogues thereof. A facile dimerization of naphthazarins to pentacyclic systems. *J. Am. Chem. Soc.* 126: 607–612.

Nicolaou, K. C., Gray, D., and Tae, J. S. 2001a. Total synthesis of hamigerans: Part 1. Development of synthetic technology for the construction of benzannulated polycyclic systems by the intramolecular trapping of photogenerated hydroxy-*o*-quinodimethanes and synthesis of key building blocks. *Angew. Chem. Int. Ed.* 40: 3675–3678.

Nicolaou, K. C., Gray, D., and Tae, J. S. 2001b. Total synthesis of hamigerans: Part 2. Implementation of the intramolecular Diels-Alder trapping of photochemically generated hydroxy-*o*-quinodimethanes; Strategy and completion of the synthesis. *Angew. Chem. Int. Ed.* 40: 3679–3683.

Nicolaou, K. C., Gray, D. L. F., and Tae, J. S. 2004. Total synthesis of hamigerans and analogues thereof. Photochemical generation and Diels-Alder trapping of hydroxy-*o*-quinodimethanes. *J. Am. Chem. Soc.* 126: 613–627.

Park, B. S. and Lee, H. M. 2008. New photosensitive polymer containing *o*-methylphenacyl photocage. *Bull. Korean Chem. Soc.* 29: 2054–2056.

Park, B. S. and Ryu, H. J. 2010. Unique solvent effect on photochemistry of ortho-alkylphenacyl benzoates. *Tetrahedron Lett.* 51: 1512–1516.

Pelliccioli, A. P., Klan, P., Zabadal, M., and Wirz, J. 2001. Photorelease of HCl from *o*-methylphenacyl chloride proceeds through the *Z*-xylylenol. *J. Am. Chem. Soc.* 123: 7931–7932.

Pelliccioli, A. P. and Wirz, J. 2002. Photoremovable protecting groups: Reaction mechanisms and applications. *Photochem. Photobiol. Sci.* 1: 441–458.

Pfau, M., Molnar, J., and Heindel, N. D. 1983. Photoenolization. 11. Photooxidation of *omicron*-methylbenzophenones. *Bull. Soc. Chim. Fr.* (5–6): 164–169.

Pika, J., Konosonoks, A., Robinson, R. M., Singh, P. N. D., and Gudmundsdottir, A. D. 2003. Photoenolization as a means to release alcohols. *J. Org. Chem.* 68: 1964–1972.

Plistil, L., Solomek, T., Wirz, J., Heger, D., and Klan, P. 2006. Photochemistry of 2-alkoxymethyl-5-methylphenacyl chloride and benzoate. *J. Org. Chem.* 71: 8050–8058.

Pospisil, T., Veetil, A. T., Lovely Angel, P. A., and Klan, P. 2008. Photochemical synthesis of substituted indan-1-ones related to donepezil. *Photochem. Photobiol. Sci.* 7: 625–632.

Quinkert, G., Schwartz, U., Stark, H., Weber, W. D., Adam, F., Baier, H., Frank, G., and Durner, G. 1982. Asymmetric total synthesis of 19-nor-steroids via a photochemical key reaction: Enantiomerically pure target compounds. *Liebigs Ann. Chem.* 1982: 1999–2040.

Quinkert, G., Weber, W. D., Schwartz, U., Stark, H., Baier, H., and Durner, G. 1981. Highly selective total synthesis of 19-nor-steroids via a photochemical key reaction: Racemic target compounds. *Liebigs Ann. Chem.* 1981: 2335–2371.

Rao, V. S. and Chandra, A. K. 1996. Photochemical intramolecular γ-hydrogen abstraction in a ketone and an alkene and the role of tunneling of hydrogen. *J. Photochem. Photobiol. A: Chem.* 101: 189–196.

Redmond, R. W. and Scaiano, J. C. 1989. Photoenol biradicals as singlet-oxygen sensitizers. *J. Phys. Chem.* 93: 5347–5349.

Ruzicka, R., Zabadal, M., and Klan, P. 2002. Photolysis of phenacyl esters in a two-phase system. *Synth. Commun.* 32: 2581–2590.

Saito, M., Kamei, Y., Kuribara, K., Yoshioka, M., and Hasegawa, T. 1998. Solvent dependent photochemical reactions of 3-(2-alkylphenyl)-2,2-dimethyl-3-oxopropanoates and their related compounds. *J. Org. Chem.* 63: 9013–9018.

Sammes, P. G. 1976. Photoenolisation. *Tetrahedron* 32: 405.

Sankaranarayanan, J., Muthukrishnan, S., and Gudmundsdottir, A. D. 2009. Photoremovable protecting groups based on photoenolization. *Adv. Phys. Org. Chem.* 43: 39–77.

Sano, H., Asanuma, D., and Kosugi, M. 1999. Photochemical reaction of *o*-formylbenzyltrialkylstannanes for the generation of α-oxy-*o*-quinodimethane. *Chem. Commun.* 1999: 1559–1560.

Sarkar, T. K., Ghosh, S. K., Moorthy, J. N., Fang, J. M., Nandy, S. K., Sathyamurthy, N., and Chakraborty, D. 2000. Photochromism and photoreactivity of 2,6-dichloro-4-methyl-3-pyridinecarboxaldehyde in the solid state. *Tetrahedron Lett.* 41: 6909–6913.

Scaiano, J. C. 1980. Temperature dependence of the photochemistry of *o*-methylacetophenone: A laser flash-photolysis study. *Chem. Phys. Lett.* 73: 319–322.

Segura, J. L. and Martin, N. 1999. *o*-Quinodimethanes: Efficient intermediates in organic synthesis. *Chem. Rev.* 99: 3199–3246.

Sengupta, D. and Chandra, A. K. 1994. Role of tunneling of hydrogen in photoenolization of a ketone. *Int. J. Quantum Chem.* 52: 1317–1328.

Shimada, S., Osoda, K., and Narasaka, K. 1993. Boron compound as a trapping reagent of α-hydroxy *o*-quinodimethanes in the Diels-Alder reaction. *Bull. Chem. Soc. Jpn.* 66: 1254–1257.

Small, R. D. and Scaiano, J. C. 1977. Role of biradical intermediates in the photochemistry of *o*-methylacetophenone. *J. Am. Chem. Soc.* 99: 7713–7714.

Smedarchina, Z., Enchev, V., and Lavtchieva, L. 1994. Theoretical study of intramolecular proton-transfer in solution: Application to the photoenolization of 5,8-dimethyl-1-tetralone. *J. Phys. Chem.* 98: 4218–4229.

Sobczak, M. and Wagner, P. J. 1998. The photochemistry of *o*-benzylbenzophenone: A pericyclic cornucopia. *Tetrahedron Lett.* 39: 2523–2526.

Sobczak, M. and Wagner, P. J. 2002. Light-induced decarboxylation of (*o*-acylphenyl)acetic acids. *Org. Lett.* 4: 379–382.

Solomek, T., Stacko, P., Veetil, A. T., Pospisil, T., and Klan, P. 2010. Photoenolization-induced oxirane ring opening in 2,5-dimethylbenzoyl oxiranes to form pharmaceutically promising indanone derivatives. *J. Org. Chem.* 75: 7300–7309.

Takahashi, Y., Miyamoto, K., Sakai, K., Ikeda, H., Miyashi, T., Ito, Y., and Tabohashi, K. 1996. Electrocycloreversion of benzocyclobutenols promoted by photoinduced electron transfer. *Tetrahedron Lett.* 37: 5547–5550.

Tseng, S. U. E. F. 1976. Elimination reactions induced by photoenolization of *o*-alkylbenzophenones. *J. Am. Chem. Soc.* 98: 541–544.

Tsuno, T. and Sugiyama, K. 1991. Diels-Alder reaction of photoenol of 2-methylbenzaldehyde with 5-alkylidene-1,3-dioxane-4,6-dione derivatives. *Heterocycles* 32: 1989–2004.

Tsuno, T. and Sugiyama, K. 1992. Photochemistry of *o*-methyl-substituted aromatic ketone with 5-isobutylidene-1,3-dioxane-4,6-dione derivatives. *Tetrahedron Lett.* 33: 2829–2832.

Tsuno, T. and Sugiyama, K. 1994. Addition-reaction of photoenols from *o*-methyl-substituted aromatic ketones with 5-alkylidene-1,3-dioxane-4,6-dione derivatives. *Heterocycles* 38: 859–876.

Tyson, D. S., Ilhan, F., Meador, M. A. B., Smith, D. D., Scheiman, D. A., and Meador, M. A. 2005. Diels-Alder trapping of photochemically generated o-quinodimethane intermediates: An alternative route to photocured polymer film development. *Macromolecules* 38: 3638–3646.

Wagner, P. J. and Chen, C. P. 1976. Rotation-controlled excited-state reaction: Photoenolization of *o*-alkylphenyl ketones. *J. Am. Chem. Soc.* 98: 239–240.

Wagner, P. J., Giri, B. P., Frerking, H. W., and DeFrancesco, J. 1992. Spacer-independent intramolecular triplet energy-transfer in diketones. *J. Am. Chem. Soc.* 114: 8326–8327.

Wagner, P. J., Kelso, P. A., Kemppainen, A. E., and Zepp, R. G. 1972. Type II photoprocesses of phenyl ketones. Competitive δ-hydrogen abstraction and the geometry of intramolecular hydrogen atom transfers. *J. Am. Chem. Soc.* 94: 7500–7506.

Wagner, P. J. and Klan, P. 2003. Norrish type II photoelimination of ketones: Cleavage of 1,4-biradicals formed by α-hydrogen abstraction (Chapter 52). In *CRC Handbook of Organic Photochemistry and Photobiology*. W. M. Horspool and F. Lenci, eds., CRC Press LLC, Boca Raton, FL, pp. 1–31.

Wagner, P. J., Meador, M. A., and Park, B. S. 1990. The photocyclization of *o*-alkoxyphenyl ketones. *J. Am. Chem. Soc.* 112: 5199–5211.

Wagner, P. J., Park, B. S., Sobczak, M., Frey, J., and Rappoport, Z. 1995. Photocyclization of 2,4,6,2′,4′,6′-hexaalkylbenzils. *J. Am. Chem. Soc.* 117: 7619–7629.

Wagner, P. J., Sobczak, M., and Park, B. S. 1998. Stereoselectivity in *o*-alkylphenyl ketone photochemistry: How many *o*-xylylenes can one ketone form? *J. Am. Chem. Soc.* 120: 2488–2489.

Wagner, P. J., Subrahmanyam, D., and Park, B. S. 1991. Mechanism for the photocyclization of *o*-alkyl ketones to cyclobutenols. *J. Am. Chem. Soc.* 113: 709–710.

Weedon, A. C. 1990. Photochemical reactions involving enols. In *The Chemistry of Enols*. Z. Rappoport, ed., Wiley, New York, pp. 591–638.

Wessig, P., Glombitza, C., Muller, G., and Teubner, J. 2004. Photochemical preparation of highly functionalized 1-indanones. *J. Org. Chem.* 69: 7582–7591.

Wessig, P. and Teubner, J. 2006. Total synthesis of pterosines B and C via a photochemical key step. *Synlett* 2006: 1543–1546.

Wilson, R. M., Hannemann, K., Heineman, W. R., and Kirchhoff, J. R. 1987. Laser-jet delayed trapping: Electron-transfer trapping of the photoenol from 2-methylbenzophenone. *J. Am. Chem. Soc.* 109: 4743–4745.

Wilson, R. M., Schnapp, K. A., and Patterson, W. S. 1992. High-intensity, argon ion laser-jet photochemistry. Reactions between transient species: The addition of diphenylcarbene to the photoenol of 2-methylbenzophenone. *J. Am. Chem. Soc.* 114: 10987–10989.

Wirz, J. 1974. Primary photophysical and photochemical processes in the photoreduction of a naphthoquinone methide: 2-Phenylnaphtho[l, 8-bc]furan-5-one. *Helv. Chim. Acta* 57: 1283–1301.

Wirz, J. 2010. Kinetic studies of keto–enol and other tautomeric equilibria by flash photolysis. *Adv. Phys. Org. Chem.* 44: 325–356.

Yang, N. C. and Rivas, C. 1961. A new photochemical primary process, the photochemical enolization of *o*-substituted benzophenones. *J. Am. Chem. Soc.* 83: 2213.

Yates, P., Mackay, A. C., and Garneau, F. X. 1968. Photooxidation of 1-methylanthraquinone and *o*-methylacetophenone. *Tetrahedron Lett.* 9: 5389–5392.

Yoshioka, M., Arai, M., Nishizawa, K., and Hasegawa, T. 1990. Photochemical reaction of *o*-alkylphenyl 1,3-diketones: A new method for the preparation of benzocyclobutenones. *J. Chem. Soc. Chem. Commun.* 1990: 374–375.

Yoshioka, M., Iida, K., Kawata, E., Maeda, K., Kumakura, S., and Hasegawa, T. 1997. Preparation of isopropylidenebenzocyclobutenes via the photochemical cyclization of 1-(o-alkylaryl)-3-hydroxy-2,2-dimethyl-alkan-1-ones. *J. Org. Chem.* 62: 2655–2657.

Yoshioka, M., Miyazoe, S., and Hasegawa, T. 1993. Photochemical reaction of 3-hydroxy-1-(*o*-methylaryl) alkan-1-ones: Formation of cyclopropane-1,2-diols and benzocyclobutenols through β-hydrogen and γ-hydrogen abstractions. *J. Chem. Soc. Perkin Trans. 1* 1993: 2781–2786.

Yoshioka, M., Nishizawa, K., Arai, M., and Hasegawa, T. 1991. Photochemical reaction of 1-(*o*-methylphenyl)-2,2-dimethyl 1,3-diketones. *J. Chem. Soc. Perkin Trans. 1* 1991: 541–547.

Yoshioka, M., Nishizawa, K., Suzuki, J., Iwata, Y., Kumakura, S., and Hasegawa, T. 1995. Photochemical reaction of 1-(*o*-methylaryl)-2,2-dimethyl 1,3-diketones in the presence of oxygen. *J. Chem. Soc. Perkin Trans. 1* 1995: 3097–3101.

Yoshioka, M. and Saito, M. 2001. Chemistry of benzocyclobutenols. *J. Synth. Org. Chem. Jpn.* 59: 689–696.

Zabadal, M., Pelliccioli, A. P., Klan, P., and Wirz, J. 2001. 2,5-Dimethylphenacyl esters: A photoremovable protecting group for carboxylic acids. *J. Phys. Chem. A* 105: 10329–10333.

Zhou, B. and Wagner, P. J. 1989. Long-range triplet hydrogen abstraction. Photochemical formation of 2-tetralols from beta-arylpropiophenones. *J. Am. Chem. Soc.* 111: 6796–6799.

27

Paternò–Büchi Reaction

Maurizio D'Auria
Università della Basilicata

27.1 Introduction

The Paternò–Büchi reaction is one of the most ancient reactions in organic photochemistry (Scheme 27.1). Paternò and Chieffi reported obtaining oxetanes from the photocycloaddition of ketones to olefins in 1909, but this reaction was recognized as an important synthetic reaction only after the work of Büchi [1,2].

After these pioneering works, several reviews cover the enormous number of papers published in this field [3–13]. The synthesis of oxetanes can have a great importance in the development of compounds with relevant biological properties: oxetane ring is present in the scaffold of Taxol® (**1**), an important drug used in the treatment of ovarian cancer [14]; merrilactone A (**2**), a sesquiterpene dilactone with neurotrophic activity [15]; and several antiviral oxetanes, such as **3**, **4**, and **5**, have been described in the literature (Scheme 27.2) [16–18].

27.2 The Reaction

The Paternò–Büchi reaction is a photocycloaddition reaction of a n,π* carbonyl compound to an alkene in the ground state from either the S_1 or the T_1 state. Frontier orbitals approach can be used to explain the formation of oxetanes. We can observe HSOMO–LUMO interaction in which the half-occupied π* carbonyl orbital interacts with the unoccupied π* molecular orbital of an electron-deficient alkene in a parallel configuration and a C,O-biradical is formed. When the LSOMO–HOMO interaction, in which the half-occupied n orbital of the carbonyl O atom interacts with the π-orbital of an electron-rich alkene in a perpendicular conformation, is prevalent, a C,C-biradical is formed [19–22]. The majority of Paternò–Büchi reactions occur from the carbonyl triplet state, which is accessed by an intersystem crossing. Intermediate 1,4-biradicals derived from carbonyl triplets were studied spectroscopically [23–26] and they were trapped by radical quenchers [27–30]. In the reaction between 1,4-dioxene and benzaldehyde, theoretical calculations showed that the only transition able to give the observed transient absorption is that from LSOMO to LUMO (549 nm) and that it is a π→π* transition; the same result was obtained for the reaction between furan and benzaldehyde [12].

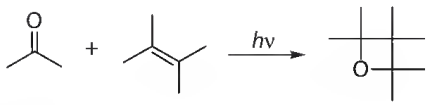

SCHEME 27.1 Paternò–Büchi reaction.

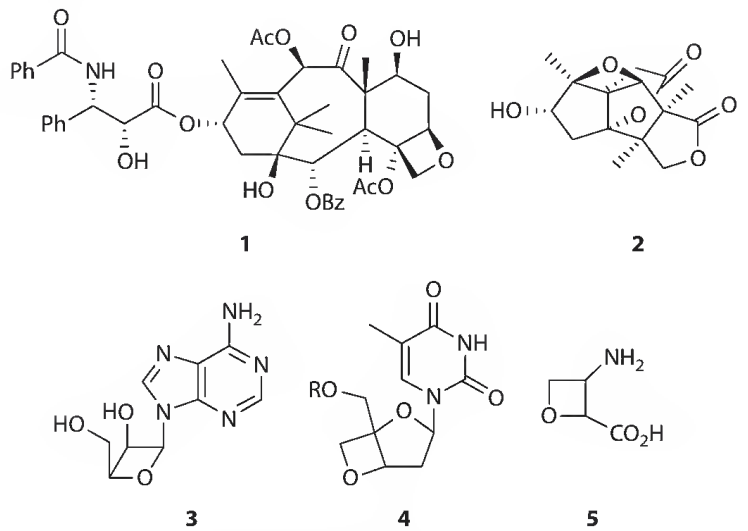

SCHEME 27.2 Naturally occurring or biologically active compounds bearing an oxetane ring.

An approach where the regioselectivity of the reaction was explained considering the hard-soft acids and bases theory has been published and it gave results in agreement with the experimental results [31]. On the other hand, the regiochemistry of the Paternò–Büchi reaction has been explained using an approach considering that atoms arrange themselves so that the obtained molecule reaches the minimum electrophilicity [32].

A theoretical study of the Paternò–Büchi reaction showed that there are two conical intersection points located near the C–C and C–O bonded biradical regions of the ground state. These two conical intersections support a mechanism where the decay from the excited state is accompanied by a geometric rotation of the terminal group, in the case of C–O attack, and by an orbital rotation at the oxygen center, in the case of C–C attack. Furthermore, for C–O attack, the triplet surface must cross the singlet to reach a diradicaloid minimum. For C–C attack, the triplet biradical minimum is located at the same geometry as the conical intersection between the two singlet states, and the efficiency of the intersystem crossing will be determined by the nature of the spin–orbit coupling. Thus, for the triplet, the reaction path can be predicted by the most stable biradical rule [33]. A conformational analysis of the biradicals also appeared [34,35].

A CAS SCF geometry optimization in TZV basis set of the intermediate biradicals showed that the diradical region corresponding to the C–C attack lies about 10 kcal mol^{-1} lower in energy than the C–O region [36,37]. We have to note that this result is not in agreement with reported experimental results.

The formation of exciplex is used to explain the reaction behavior of simple alkene. However, evidence of monoelectron transfer processes is reported for electron-rich alkenes [38].

The reaction is quite general. 5-Substituted adamantan-2-ones gave the corresponding cycloadducts via the n,π* excited singlet state, giving a regiospecific reaction without stereoselectivity (the best result was 59:41 in favor of the *anti* isomer) [39–42]. When methyleneadamantane reacted with acetone, the Paternò–Büchi adduct was obtained in only 5% yield [39]. The reaction of biacetyl with benzvalene gave the corresponding adduct, while benzophenone gave as the only product benzene [43]. Ethyl phenylglyoxylate reacted with homobenzvalene to give the corresponding adduct in 70% yield with high stereoselectivity (Scheme 27.3) [44].

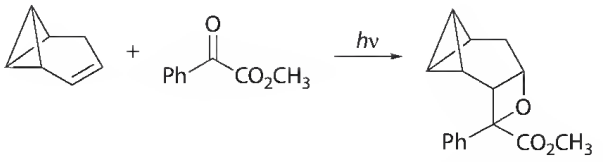

SCHEME 27.3 Paternò–Büchi reaction of homobenzvalene with methyl phenylglyoxylate.

A stereoselective behavior has been described in the reaction between benzophenone and cyclooctene. Whereas at −95°C the *cis* adduct was formed in a very high *cis* diastereoselectiviy from *cis*-cyclooctene, both diastereoisomers were generated at −20°C. At higher temperatures, the *trans* adduct dominated. The more strained *trans*-cyclooctene gave over a broad temperature range (−80 to +60°C) nearly exclusively the *trans* adduct [45,46]. This behavior can be understood considering that triplet ketone can attack the double bond to give two biradical intermediates: the authors suggested that temperature-dependent conformational changes of the biradical compete with the cyclization to the oxetane and the retro cleavage to the *cis*-cyclooctene. The increasing of *trans*-oxetane with the temperature can be due to the activation barrier between two conformers of the biradical intermediate [46].

1-Acetylisatin reacted with styrene and furan derivatives to give stereoselectively the *endo* adduct [47,48]. The reaction of quinones with stilbene derivatives has been described [49,50]. In this case, a charge-transfer absorption band was observed at 480 nm. Time-resolved (ps) absorption spectrum showed an absorption at 480 nm (chloranil anion radical) and a broad band around 760 nm. After 50 ps a transient absorption typical for triplet chloranil at 510 nm was observed. The reaction occurs through selective excitation at 480 nm. Quinones react with diarylacetylene giving a product deriving from the ring opening of a transient oxetene. Time-resolved (ps) absorption spectrum is in agreement with an electron transfer mechanism [51]. In the reaction between 2-chloro-5-methoxybenzoquinone with arylacetylenes, CIDNP experiments are in agreement with a mechanism involving the attack of the triplet quinone on the acetylene to give a biradical intermediate [52]. The same behavior has been observed in the reaction between quinone and quadricyclane and norbornadiene [53,54]. A Paternò–Büchi adduct was found also in the reaction between quinones and acenaphthylene [55].

A reaction between benzophenone and a paracyclophane derivative **6** has been described (Scheme 27.4) [56]. An intramolecular Paternò–Büchi reaction on a paracyclophane derivative **7** has been reported giving the corresponding adduct in quantitative yield (Scheme 27.4) [57].

The Paternò–Büchi reaction can also be applied to other unsaturated systems other than an alkene, such as dienes [4], allenes [58], acetylenes [59], and ketenimines [58]. In the reaction of tetramethylallene with aromatic ketones the main products often resulted from bis-addition of the carbonyl compounds to give dioxaspiroheptanes [60,61]. In the reaction of 1,1-dimethylallene with aliphatic aldehydes, only

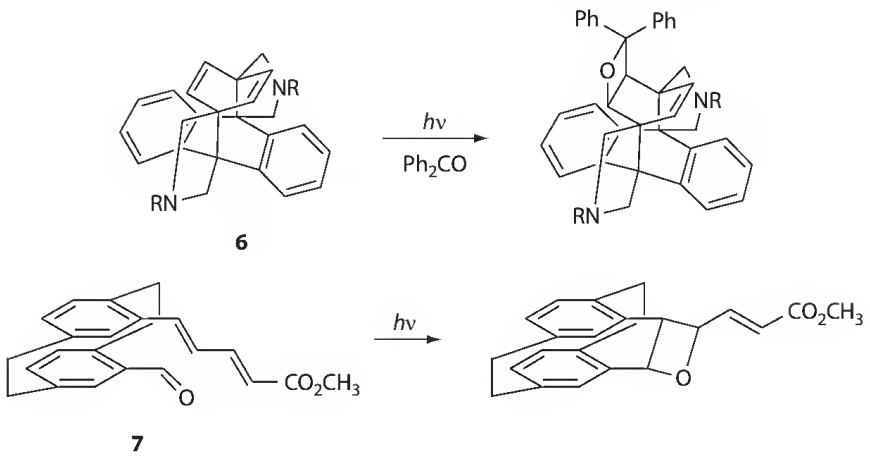

SCHEME 27.4 Paternò–Büchi reaction on paracyclophane derivatives.

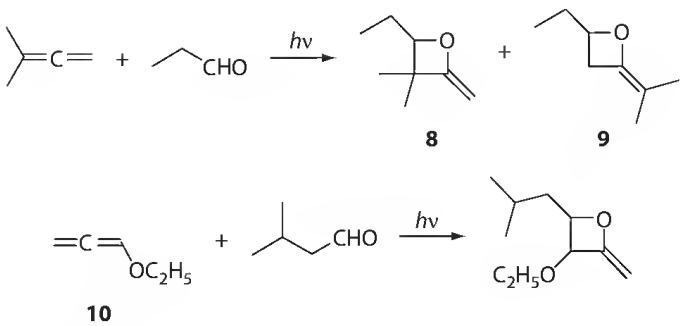

SCHEME 27.5 Paternò–Büchi reactions on allenes.

the monoaddiction products **8** and **9** were obtained, with a low regioselectivity (2:1) (Scheme 27.5) [62]. A higher regioselectivity was obtained using the allene **10** (Scheme 27.5).

27.3 Reactions of Carbonyl Compounds with Enolethers and Enolthioethers

The first oxetane deriving from ethyl vinyl ether and benzophenone was described by Paternò [63]. The reaction between acetone and ethyl vinyl ether in the presence of ultrasounds gave a different mixture of regioisomers than that obtained without the use of the ultrasounds [43].

Substituted pyruvates reacted with 1,3-dioxol **11** to give the *endo* isomer **12** (Scheme 27.6) [64–66]. The observed stereochemical behavior was explained on the basis of the analysis of the conformations of the biradical intermediate [67].

Unsubstituted cyclopropyl enol ethers gave the corresponding oxetane rings. On the other hand, substitution on the cyclopropyl ring induced the formation of oxepanes derived from cyclopropyl ring opening at the level of the biradical intermediate [68]. The enol ether **13** reacts with benzaldehyde giving, after acid hydrolysis, the oxetane **14** with a good diastereoselectivity (Scheme 27.7) [69].

1,2,3-Indanetrione reacts with 2,3-diphenyl-1,4-dioxene to give the oxetane on the carbonyl in 2 position [70]. When 2,3-dimethyl-2-butene is used, a complex mixture of products is obtained [56]. The irradiation of 2,3-dihydrofuran with benzophenone in benzene gave adduct **15** (Scheme 27.8) [71]

By using acetone the adducts were obtained in 52% yield in a 200:1 isomeric ratio [72]. The reaction of 5,5-dimethyl-2,3-dihydrofuran with both aromatic and aliphatic aldehydes gave the corresponding adducts with high *endo* selectivity [73]. When acetaldehyde was used, the adduct was obtained in

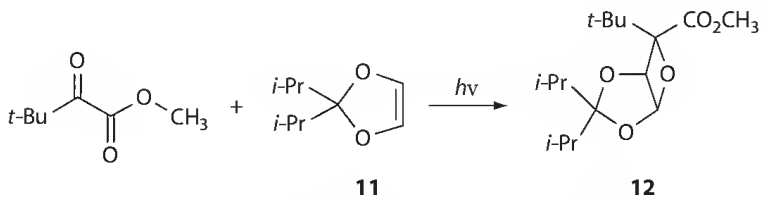

SCHEME 27.6 The reaction of a 1,3-dioxol derivative with a substituted pyruvates.

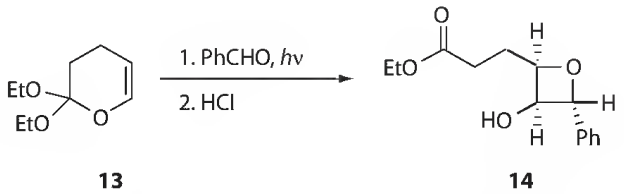

SCHEME 27.7 The reaction of the enol ether **13** with benzaldehyde followed by acid hydrolysis.

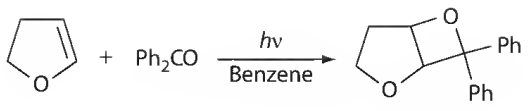

15

SCHEME 27.8 Paternò–Büchi reaction of 2,3-dihydrofuran with benzophenone.

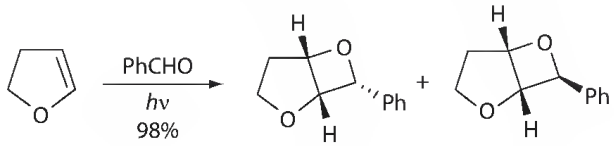

SCHEME 27.9 Paternò–Büchi reaction of 2,3-dihydrofuran with benzaldehyde.

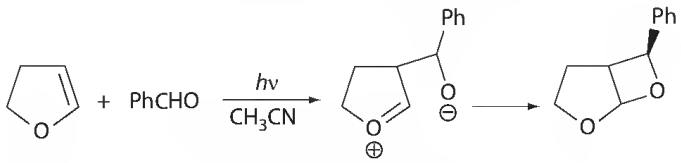

SCHEME 27.10 Electron transfer in the reaction between 2,3-dihydrofuran and benzaldehyde in polar solvents.

63% yield as a mixture of stereoisomers. The selectivity depended on 2,3-dihydrofuran concentration: this behavior was in agreement with a switch from a triplet mechanism to a singlet mechanism at higher concentration [74–77]. When benzaldehyde was used as carbonyl compounds the adducts were obtained with an overall yield of 98% as a >98:2 regioisomeric mixture. The major isomer is 88:12 *endo/exo* mixture. The reaction showed a good regio- and stereoselectivity (Scheme 27.9) [77–80]. This stereoselectivity was partially lost when benzaldehyde reacts with 2-methyl-2,3-dihydrofuran [78,81].

A change of regioselectivity was observed when the reaction with benzaldehyde was performed in high polar solvent in agreement with an electron transfer mechanism (Scheme 27.10) [74,75].

This reaction is the first example where a spin controlled selectivity is observed [76,82]. In singlet photoreactions, stereoselectivity is often controlled by the optimal geometries for radical–radical combinations, whereas in triplet photoreactions the geometries most favorable for ISC are considered to be of similar relevance. The singlet biradicals should be too short lived to enable rotation about the endocyclic C–O or C–C bonds and therefore, conformation memory effects on the stereochemistry are expected. The geometries in the triplet state can be quite different from the former ones due to differences of the spin–orbit coupling (SOC) values. The lifetimes of many triplet biradical intermediates are definitely high enough to enable bond rotations and the formation of the thermodynamically favored product can be expected because the radical–radical combination step should no longer be influenced by the approach geometry, that is, "memory effects" should be erased due to the relatively long lifetimes. After transition from the triplet to the singlet potential energy surface, immediate product formation is expected. Thus, the ISC is expected to proceed in a concerted fashion with the formation of a new bond or the cleavage of the primarily formed single bond. As a consequence, the stereoselectivity of the Paternò–Büchi reaction is the result of a combination of several rate constants for cyclization versus cleavage reactions.

The biradicals are the direct consequence of the precursor spin and their lifetimes are connected with the mode of spin inversion processes and the mechanism, which leads to the formation of closed-shell products. Benzaldehyde reacts in its triplet state. This way, a triplet biradical is formed as an intermediate. For the formation of the products, intersystem crossing into the singlet manifold is necessary. The most important factor influencing an intersystem crossing for flexible triplet biradicals is spin–orbit coupling. The angle between *p* orbitals at the radical centers is approximately 90° for maximum spin orbit coupling. For the pronounced *endo* selectivity in the reaction between aromatic aldehydes and

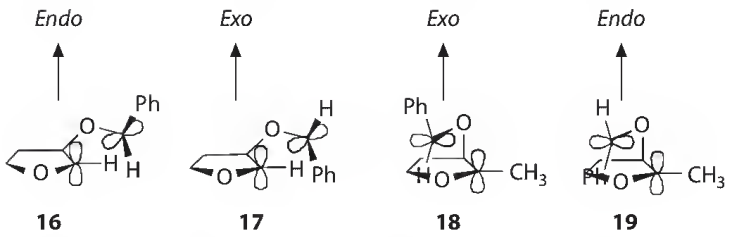

SCHEME 27.11 Possible conformations of the 1,4-biradical from the reaction of 2,3-dihydrofuran with benzaldehyde.

2,3-dihydrofuran, we can consider the two biradical conformers **16** and **17** to be responsible, with the alkyloxy substituent localized in a pseudoequatorial position and **16** being more populated because of fewer steric interactions (Scheme 27.11). When a methyl group is present, the increasing *gauche* interactions with the β-alkyloxy substituent lead to a certain concentration of **18** and **19**, again with **18** being preferred because of fewer steric interactions.

Another approach has been used in order to explain regio- and stereochemistry [83]. In fact, theoretical calculations showed that the biradical **20** is more stable than **21** for 1.49 kcal mol^{-1} (Figure 27.1).

Furthermore, the HSOMO is mainly localized on the aromatic ring and it is extended until the radical carbon. The LSOMO is mainly localized on the dihydrofuran ring. The coupling between the radical carbons in these two orbitals is possible (the atomic orbitals involved can superimpose themselves) only if the *endo* isomer is formed (Figure 27.2) [83].

α- and β-naphthaldehydes, on the contrary, gave high *exo* selectivity. The reaction occurs also in the presence of triplet quenchers, while fluorescence quenching in the presence of dihydrofuran was observed: in this case, singlet excited states are responsible for the high *exo* selectivity [77,84]. Why? The explanation is simple. In this case, the coefficients on the HSOMO and LSOMO allowed the coupling of the radical carbons only if the *exo* isomer is obtained [85].

The stereoselectivity of the reaction between ethanal and 2,3-dihydrofuran was found to depend on the viscosity of the solvent (higher viscosity induces a higher *endo* stereoselectivity) and significant temperature dependence: at room temperature, the *exo* adduct was formed with low selectivity, predominantly through the singlet channel. This selectivity increases with decreasing temperature and reaches an inversion point at −17°C. At this point, the triplet reactivity gains sufficient influence to increase the *endo* selectivity [86].

When 2,3-dihydrofuran derivatives react with α,β-unsaturated carbonyl compounds, 2 + 2 cycloaddition between the olefins occurs [87]. Benzaldehyde reacts with L-ascorbic acid giving a mixture of regioisomeric compounds with *exo* stereoselectivity [50].

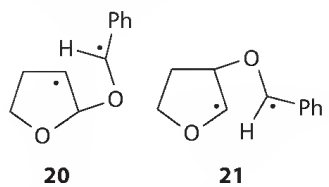

FIGURE 27.1 Possible biradical intermediates in the reaction of 2,3-dihydrofuran with benzaldehyde.

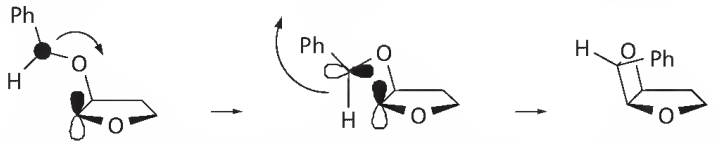

FIGURE 27.2 Ring closure reaction in the formation of the *endo* isomer of the adduct between 2,3-dihydrofuran and benzaldehyde.

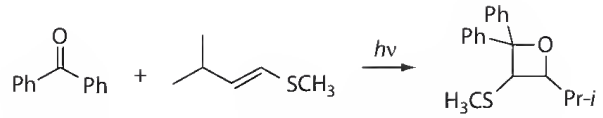

SCHEME 27.12 Paternò–Büchi reaction of benzophenone with alkenyl sulphides.

The reaction of benzophenone with alkenyl sulphide showed a high regioselectivity (Scheme 27.12) [88]. A similar regioselectivity was obtained when ethyl vinyl ether was used as an alkene with benzaldehyde and benzophenone [89].

27.4 Reactions with Enol Esters, Enol Silyl Ethers, and Enamines

27.4.1 Enol Acetates

High regio- and stereoselectivity (*syn* addition) was observed in the reaction of pentafluorobenzaldehyde with enol acetates [90]. The reaction between a 2,3-thiophenone derivative and vinyl acetate gave the corresponding adduct on a ketonic function in low yields [55].

27.4.2 Silyl Enol Ethers

The reaction between a trimethylsilyl derivative of cinnamyl alcohol and benzaldehyde gave the *trans* oxetane with high stereoselectivity (Scheme 27.13) [91].

3-(Silyloxy)oxetanes **24** were successfully prepared from silyl enol ethers **23** containing carbon–chlorine, carbon–silicon, or carbon–sulfur bonds (Scheme 27.14) [92,93]. Also ether and ester groups are compatible with the reaction. The presence of alkene moiety is also compatible. When a β-alkyl substituted silyl enol ether is used, *trans*-oxetanes are obtained. This result does not depend on the (*E*)- or (*Z*)-nature of the alkene. The products were obtained with high simple diastereoselectivity (ds 74%–95%) [94].

In the triplet biradical, free rotation leads to highly preferred, sterically least congested conformation. The further reaction pathway of this species includes ISC and an assumed selection step (cleavage versus ring closure) at the singlet 1,4-diradical level, which accounts for the high simple diastereoselectivity at C-2/C-3.

The oxetanes **24** can be converted into the corresponding diols **25** by using hydrogenolysis under Pd catalyst (Scheme 27.15). Acid-sensitive substrates can be protected using $Pd(OH)_2$ as a catalyst as reported in the reaction of the acetal **26** (Scheme 27.15) [95]. Also $LiAlH_4$ can be used in order to induce the cleavage of the oxetane ring [96].

The presence of a stereogenic center in the β-alkyl group (as in **28**) induced a facial diastereoselectivity with high diastereoisomeric ratios in some cases (Scheme 27.16) [97].

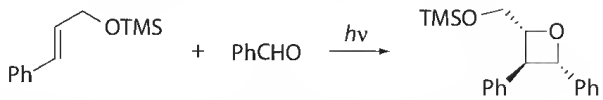

SCHEME 27.13 Paternò–Büchi reaction of silyl ether of cinnamyl alcohol.

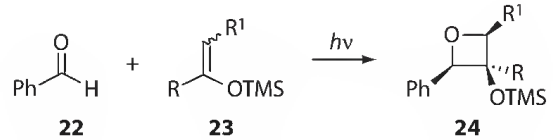

SCHEME 27.14 Paternò–Büchi reaction between enol silyl ethers and benzaldehyde.

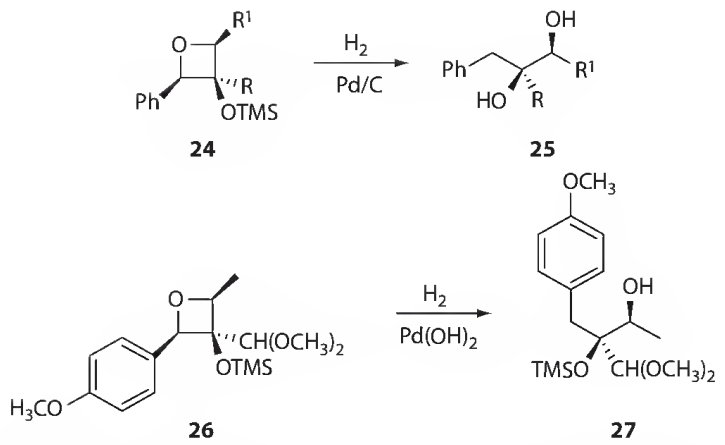

SCHEME 27.15 Synthetic modifications of the oxetane ring obtained from enol silyl ethers.

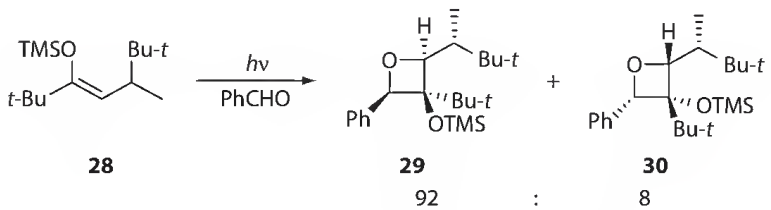

SCHEME 27.16 Paternò–Büchi reaction of enol silyl ethers with β-alkyl substituents.

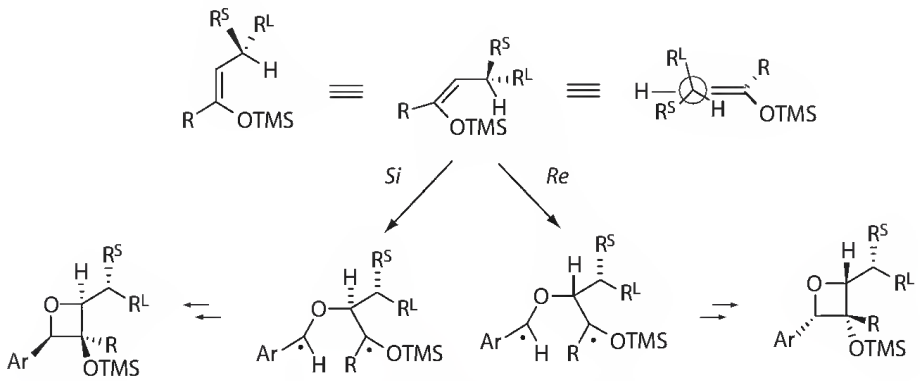

FIGURE 27.3 Diastereoselectivity in chiral enol silyl ethers' reaction with benzaldehyde.

The diastereoselectivity is probably due to the presence of a conformational preference represented in the Figure 27.3. This conformation allows the *Si* attack [96].

In this case a fluoride-promoted cleavage procedure can be used to open the oxetane ring [97]. When the chiral center is in α position low facial diastereoselectivity was observed [98]. The best results were obtained by using both the silyl enol ether **31**, which gave the adducts **32** and **33** with a 67/33 d.r. and the compound **34**, giving the adducts **35** and **36** in 15/85 d.r. (Scheme 27.17) [98].

The possible synthetic utility of the oxetanes, when in the side chain a removable protecting group is present, has been studied. The possible intramolecular nucleophilic attack on the oxetane ring gave some interesting products [99].

Oxetanes were obtained in low yields in the reaction of 1,2-diketones with trimethylsilyl ketene acetals [100]. Oxetanes can be obtained as a by-product in the reaction of ketene silyl acetals with aromatic carbonyl compounds: in some cases it represents the main product [101]. Cyclic ketene silyl acetals **37**

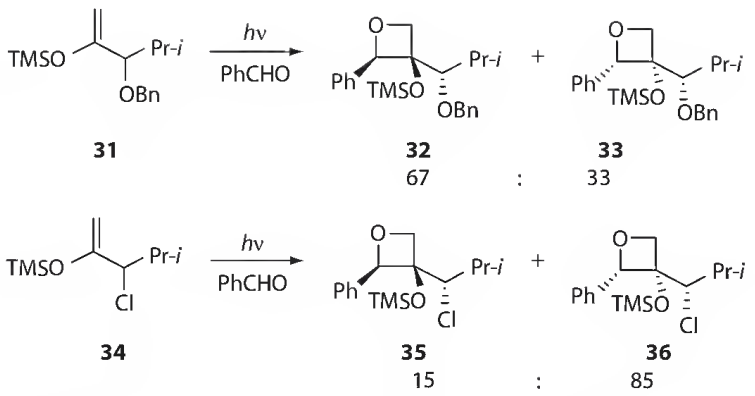

SCHEME 27.17 Stereoselectivity in the Paternò–Büchi reaction of enol silyl ethers.

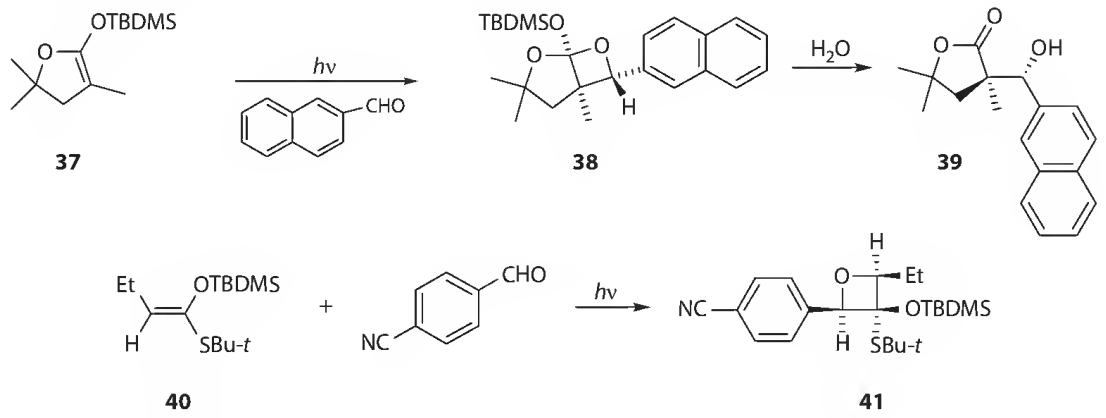

SCHEME 27.18 Paternò–Büchi reaction of silyl ketene acetals.

reacts with 2-naphthaldehyde to give the corresponding adduct **38**, determined via NMR analysis, while the treatment of the reaction mixture with water gave the aldol-type product **39** with high stereoselectivity (Scheme 27.19). The oxetane was obtained with *anti* stereochemistry [57,102]. The effect of both the solvent and the nature of the silyl group has been examined [52]. Good results were obtained silyl O,S-ketene acetals were used [45]. In particular when the *E* isomer **40** was used only the *trans,trans*-isomer **41** was obtained (Scheme 27.18).

The stereochemical behavior was explained considering the capability of the sulfur atom to coordinate the oxygen atom of the carbonyl compound [45]. The same regio-and stereoselectivity was observed when silyl O,Se-ketene acetals were used [46].

27.4.3 Enamines

N-Acyl enamines **42** and **45** gave the corresponding adducts with high regio- and stereoselectivity (Scheme 27.19) [103–106]. The thermodynamically more stable isomer is obtained [107].

The use of chiral enamines did not give high diastereoselectivity, with the exception of the enamine **47**, which gave the corresponding adduct with 62% *de* (Scheme 27.20) [108,109].

N-Formyl protected oxetanes can be converted into the corresponding *syn*-1,2-amino alcohols through treatment with $LiAlH_4$ [110]. Alternatively, the treatment of **50** with TFA gave the oxazolidinone **51**, which can be converted into the corresponding *anti*-1,2-amino alcohol **52** (Scheme 27.21) [104,110].

This approach has been used in the synthesis of both (±)-oxetin [111] and (+)-preussin [112,113].

We have also reactions on alkenes bearing both electron-donating groups (nitrogen atoms) and electron-withdrawing groups. 2-Morpholinopropenenitrile gave in the reaction with naphthalene-1,4-dicarboxylic

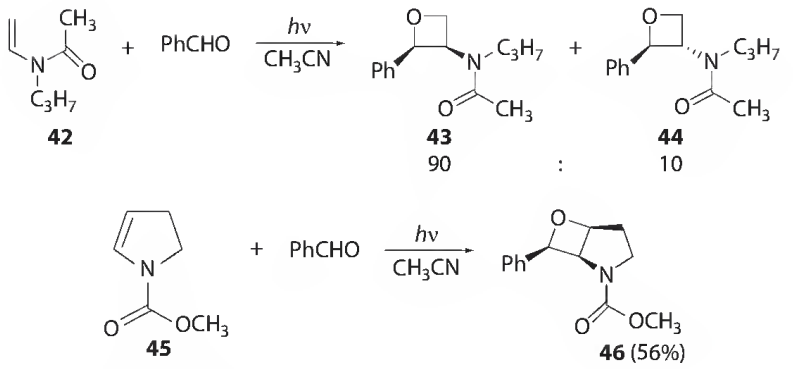

SCHEME 27.19 Paternò–Büchi reaction on enamines.

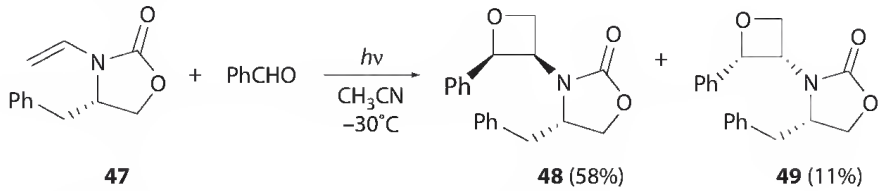

SCHEME 27.20 Stereoselectivity in the reaction of chiral enamines.

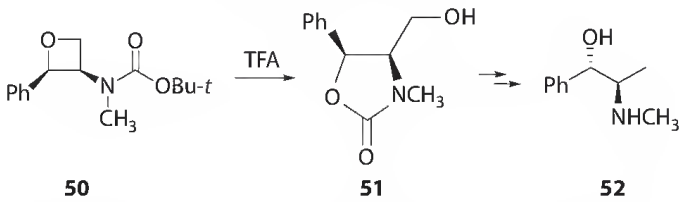

SCHEME 27.21 Synthetic modifications of the oxetan ring obtained from enamines.

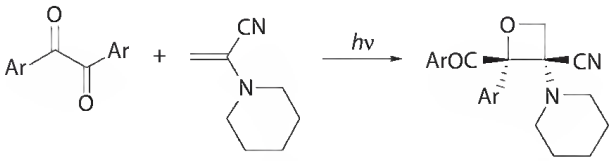

SCHEME 27.22 The reaction of benzyl with a 2-aminopropenenitrile derivative.

acid in very low yields a product deriving from a Paternò–Büchi reaction [114]. The same result was obtained when benzil was used as substrate, while, when methyl phenylglyoxylate was used as carbonyl compound, the corresponding adduct was isolated in good yields [115].

Benzyl reacted with 2-aminopropenenitrile derivative to give the corresponding adduct in variable yields (Scheme 27.22) [116]. The reaction shows a good stereoselectivity. When unsymmetrical benzyl derivatives are used, both the isomers were obtained.

27.5 Reactions with Heterocyclic Compounds

27.5.1 Furan

Schenck reported that the irradiation of benzophenone in furan gave the corresponding adduct in 94% yield (Scheme 27.23) [117]. The structure was confirmed by Gagnaire et al. [118].

Two years later furan and 2-methylfuran were found to react with propanal and benzaldehyde [119–125]. The *exo* stereochemistry at C–6 on the dioxabicyclo[3.2.0]heptene skeleton has been

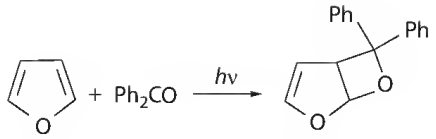

SCHEME 27.23 Paternò–Büchi reaction of furan with benzophenone.

assigned [126]. Good regioselectivity was observed using silyl and stannyl furan derivatives: the reaction in this case occurred on the less hindered side of the molecule [127]. 2-Silyloxyfuran gave a 1:1 mixture of regioisomeric products when it reacted with aliphatic carbonyl compounds or with benzaldehyde. On the contrary, the regioisomer obtained on the most hindered side of the molecule was obtained when benzophenone was used as a ketone. The same result was obtained using acetone in a reaction when a low concentration of furan was used. In all the cases, an *exo* selectivity was observed [128]. On the contrary, 2-furylmethanol and the corresponding silyl ether gave low regioselectivity [128,129].

The high *exo* stereoselectivity of the reaction has been extensively studied: the formation of the product occurs on a triplet 1,4-biradical, which must be converted into the singlet biradical to give the product. In order to explain the pronounced *exo* stereoselectivity, a secondary orbital effect can be postulated: an interaction between the rather flexible α-oxy radical center and the allyloxy ring localized radical in **53** likely plays a major role (Scheme 27.24) [130,131].

The regioisomeric biradical intermediates **A** and **B** resulting from the head-to-head and head-to-tail addition, respectively, have been examined (Figure 27.4) [83]. The biradical **A** is more stable than **B** by 16.5 kcal mol^{-1}. The biradical **A** exists as two conformers and we considered only that conformer able to give the ring closure.

The HSOMO is mainly localized on the benzaldehyde fragment of the biradical while the LSOMO is mainly localized on the furanoid part of the molecule. The coupling between the radical carbons in these two orbitals, considering that the atomic orbitals involved can superimpose themselves, can give only the *exo* isomer, in agreement with the experimental results (Figure 27.5).

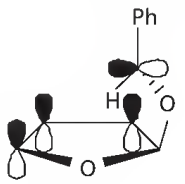

53

SCHEME 27.24 The 1,4-biradical intermediate in the reaction between furan and benzaldehyde.

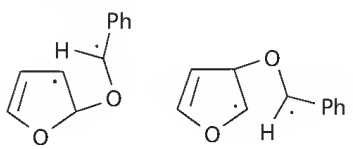

A **B**

FIGURE 27.4 Possible biradical intermediates in the reaction of furan with benzaldehyde.

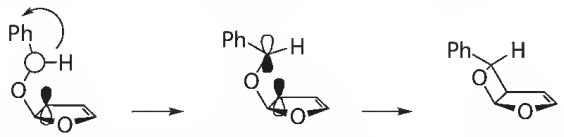

FIGURE 27.5 Ring closure reaction in the formation of the *exo* isomer of the adduct between furan and benzaldehyde.

When the reaction was carried out in benzene, dimers can be obtained [71,132–134]. Furan reacts with chloral to give unexpectedly the corresponding 2-furyl carbinols [135]. Furthermore, 2-cyanofuran did not react, while 2-furfural diacetate and furfural ethylene acetal showed low reactivity [135].

The cycloaddition reaction can be performed on esters. In this case, the adducts can be obtained in a few cases. In most of the examples, they underwent a cycloreversion reaction to give the ring opening products [136]. More recently, this result has been questioned and a 95:5 mixture of stereoisomeric adducts was identified as the product [131].

Coupling products can be obtained carrying out the reaction between an amide and furan: also in this case the cycloadduct cannot be isolated, but the subsequent decomposition products can be isolated [137]. Furan quenches the fluorescence of the substrate, while a small new emission at 500 nm appears, in agreement with a mechanism involving a reaction in the excited singlet state via the formation of an exciplex.

Schenck reported also the reaction of some aromatic carbonyl compounds (benzophenone, benzaldehyde) with benzofuran (Scheme 27.25); he showed that when high triplet energy compounds were used, dimers of benzofuran were obtained, while oxetanes were the products of the reaction when low triplet energy carbonyls were used [138]. As in the case of furan, he obtained only one product showing that the reaction has a high regioselectivity. Reinvestigation of the reaction of benzofuran with acetophenone or propiophenone showed that, also in this case, oxetanes were obtained [139].

The irradiation of **54** in the presence of benzaldehyde in benzene gave the corresponding adduct **55** in good yields (Scheme 27.26) [140]. It is interesting to note that the reaction allowed the formation of the *endo* isomer. The reaction between benzo[*b*]furan and benzaldehyde gave an adduct whose stereochemistry has not been described [138].

Oxetanes can be converted into the corresponding 3-furylcarbinol through reaction with TsOH [125]. The formation of a protonated oxetane is in agreement with the high negative entropy of the activation [141]. If the irradiation was performed in the presence of an acid, 3-furylcarbinol can be obtained in a one-step procedure in better yields [142]. This procedure has been used in the synthesis of perillaketone, a naturally occurring 3-substituted furan [142]. On the contrary, Lewis acids catalyzed a different behavior: the treatment with $BF_3 \cdot Et_2O$ gave only 3-substituted furan in THF and 89% of 2-substituted furan in acetonitrile [141].

The oxetane derivatives can be treated also with $KMnO_4$ and the resulting *cis* diol was treated with acetone in the presence of an acid. This procedure allows the synthesis of a carbohydrate derivative [143]. The same epimerization reaction occurs on the *trans* diol obtained through treatment of the oxetane with MCPBA [143]. The possible chemical modifications on the cycloadduct deriving from the reaction between an aldehyde and furan were extensively studied by Schreiber [144]. Hydrolytic ring opening, reductions, hetero Diels–Alder, the reaction with MCPBA, and hydroboration–oxidation were the

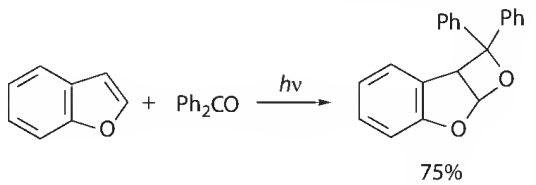

SCHEME 27.25 Paternò–Büchi reaction of benzofuran with benzophenone.

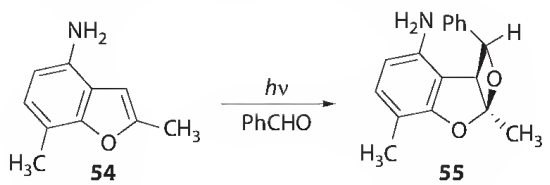

SCHEME 27.26 Paternò–Büchi reaction of a benzofuran derivative with benzaldehyde.

object of this work. The reaction with MCPBA was used by Schreiber and coworkers in the synthesis of asteltoxin [145,146], and in that of avenaciolide, an antifungal metabolite [147]. The reaction of tributylstannylfuran with butyl glyoxylate [127] was used in the synthesis of a ginkgolide B-kadsurenone hybrid of two inhibitors of a platelet-activating factor.

Furthermore, the cycloadduct obtained from the reaction between furan and an aldehyde can be treated with an excess of Schlosser's base (BuLi, *t*-BuOK) to give the corresponding anion, which can react with carbonyl compounds or alkyl halides [148].

A possible further application of the Paternò–Büchi reaction between carbonyl compounds and furan could be related to the use of the oxetane ring. The most important target in this field was oxetanocin (**3**), a nucleoside isolated from *Bacillus megaterium* NK 84-0218 showing anti-HIV activity. An approach to the synthesis of this compound has been reported [149]. Oxetanocin was obtained carrying out the reaction between 2-methylfuran and benzoyloxyacetaldehyde [150].

The reaction of glyoxylates with furan can be performed also using chiral glyoxylate. In particular, the use of *R*-(–)-menthol, 2-octanol, and 2,2-dimethyl-3-butanol as chiral auxiliaries gave the corresponding oxetanes in high yields. These compounds can be converted into the corresponding 3-substituted furans. The furans showed low enantiomeric excess (Scheme 27.27) [151]. On the basis of the experimental data the configuration of the oxetane was 1*R*, 5*S*, 6*S*.

The use of chiral phenylglyoxylate gave better results. The use of chiral alcohols gave diastereoisomeric excess in the range of 4%–80% (Scheme 27.28) [152–155].

The authors also observed an important variability of the diastereoisomeric excess in function of the temperature, with the presence of an inversion temperature. These results were explained assuming that the diastereoselection is produced on two levels: (1) the preferred formation of the diastereoisomeric 1,4-biradical intermediate **56** and (2) the preferred retrocleavage of the energetically unfavored diastereoisomeric intermediate **57** to the starting materials [156]. The diastereoisomeric excess in the high-temperature region ($T > T_{inv}$) is dominantly controlled by steric effects of the chiral auxiliaries, whereas in the low-temperature region ($T < T_{inv}$), the nature of the olefin has a dominating influence. When the reaction is carried out on 2-methylfuran, a 2:1 regioisomeric mixture was obtained with a very high diastereoisomeric excess [157].

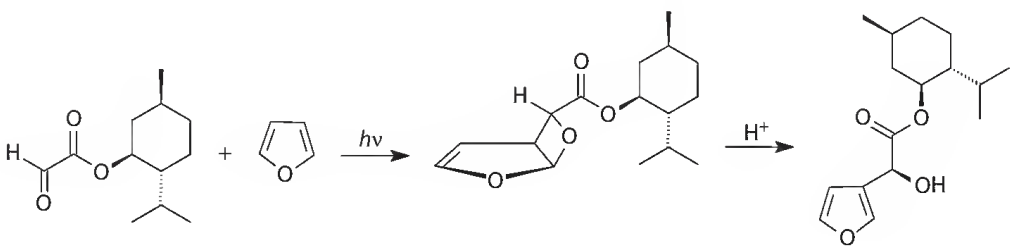

SCHEME 27.27 The reaction of chiral-substituted glyoxylates with furan.

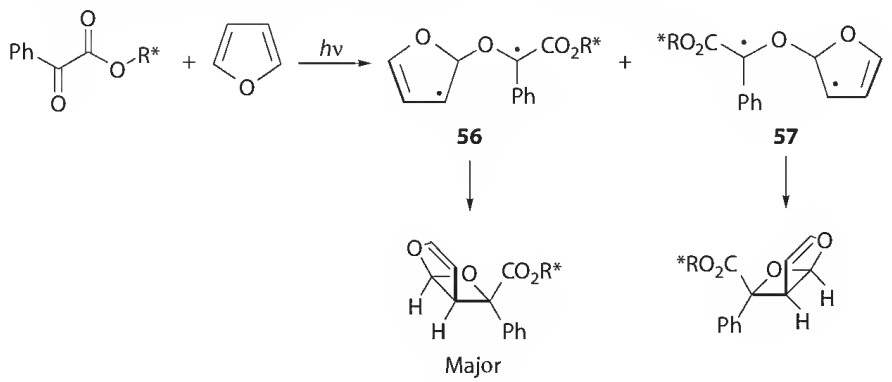

SCHEME 27.28 The reaction of chiral-substituted phenylglyoxylates with furan.

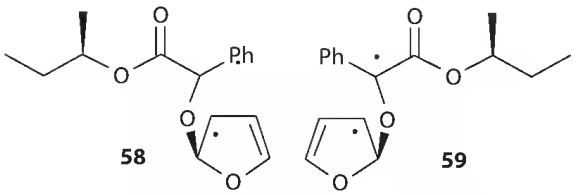

FIGURE 27.6 Radical intermediates in the reaction of chiral phenylglyoxylates with furan.

The best results in order to justify the observed stereoselectivity can be obtained considering the energy of the triplet biradical intermediates in the reaction of some phenylglyoxylate derivatives with furan [155]. Calculations on these biradical intermediates showed that **58** (the precursor of the observed product) was more stable than **59** by 0.73 kcal mol^{-1} (Figure 27.6).

To improve diastereoselectivity, the reaction was carried out in an organized medium. In another study the chiral phenylglyoxylate esters were used in the presence of different zeolites [158]. NaY was the best solid support for this reaction. The origin of this behavior can be explained considering the possible effect of the confinement on the reaction. In the Paternò–Büchi reaction on furan derivatives the biradical intermediate **60** can assume two possible conformations [26,83]. One of these has the radical carbons in almost *anti* conformation, while the other one is almost a *syn* conformation (Scheme 27.29).

The *syn* conformation is in a steric situation where the following cyclization, after the intersystem crossing from the triplet to the singlet state, is a favored process. In the *anti* conformation the most favored process is the retrocleavage to the starting material. The *syn* conformations take up a smaller volume than the *anti* one. The preferential formation of a stereoisomer in the reaction within a zeolite can be explained: the *SS-syn* conformer is obtained preferentially, while the *RS* conformer is obtained preferentially in *anti* conformation. The latter conformer has to rotate along the C–O bond to give one able to cyclize. Zeolites can act as agents able to reduce the conformational mobility of the intermediates, inhibiting the rotation of this conformer and, then, favoring the formation of the product deriving from the *SS* biradical intermediate.

The reaction of furan with acyl cyanides yields the corresponding oxetanes but both diastereoisomeric *endo*- and *exo*-oxetanes are formed. When chiral acyl cyanides are used, low asymmetric induction is observed [159]. Furan reacts also with chiral ketones. In this case, an α-cleavage reaction before the 2 + 2 cycloaddition modifies the expected products (Scheme 27.30). When (–)-menthone was used as a substrate, a chiral product was obtained as 2:1 diastereoisomeric mixture where the most abundant product has 1*R*, 3*R* configuration [160]. When the reaction was performed on the ketonic group of a protected carbohydrate, a complex reaction mixture was obtained [160,161].

Attempts to obtain stereoselective Paternò–Büchi reactions were performed carrying out the reaction between 3,4-dimethylfuran and *R*-isopropylidene glyceraldehyde. The coupling products were obtained with an overall yield of 35% as a 1.2:1 mixture of diastereoisomers. Furthermore, the compound **61** was obtained with 54% ee (Scheme 27.31) [162,163].

This behavior suggests the operation of a mechanism that is insensitive to the substitution pattern of chiral aldehydes. Reaction between an excited aldehyde (singlet or triplet state) and furan proceeds with initial carbon–oxygen bond formation to produce either of the two biradical species. The stereocenter adjacent to the carbonyl is now in a 1,4-relationship to the newly formed stereocenter at the acetal carbon and is expected to exert little influence as a stereocontrol device [162]. The extensive racemization

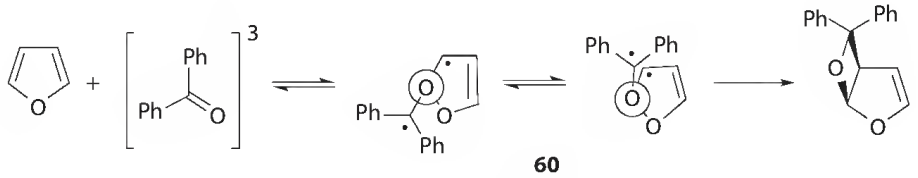

SCHEME 27.29 Possible conformations in the Paternò–Büchi reaction of benzophenone with furan.

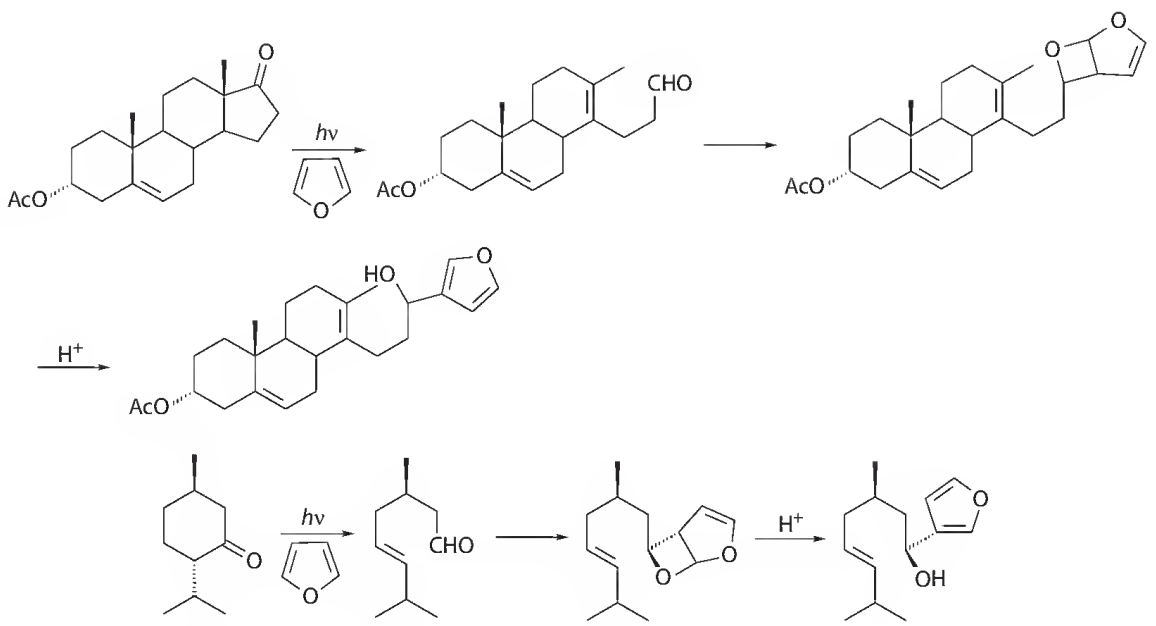

SCHEME 27.30 Paternò–Büchi reaction between dialkyl ketones and furan.

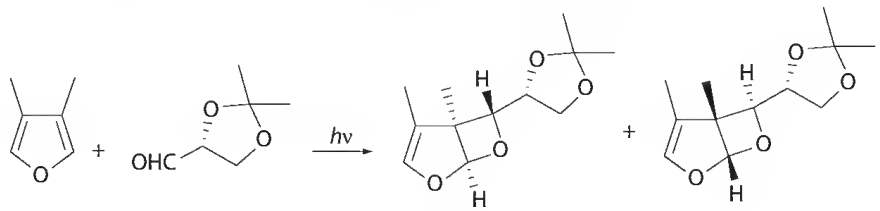

61

SCHEME 27.31 Paternò–Büchi reaction of *R*-isopropylidene glyceraldehyde with furan.

observed probably reflects the photolability of the aldehydes toward racemization under the conditions of the reaction [163]. Nevertheless, compound **61** can be used in a chiral synthesis of the bicyclic part of asteltoxin confirming the assigned absolute configuration [163]. If the chiral center is near the reaction site the diastereoselectivity increases. Benzoin reacted with furan to give the corresponding adduct in acceptable yield (56%) and *de* > 98% (Scheme 27.32) [164].

The observed stereoselectivity was explained considering the relative stability of the biradical intermediates. When chiral ketones were used as substrates the Norrish type II reaction is the only observed reaction. In order to avoid Norrish type II reaction a substrate without γ-hydrogen was used [165].

In 1990 Griesbeck found that the reaction of benzaldehyde with homoallylic alcohols did not show diastereoselectivity [77]. Ten years later, Adam showed that allylic alcohols reacted with benzophenone to give the corresponding adducts with high regio- and diastereoselectivity (Scheme 27.33) [166–169].

The diastereoselectivity dropped drastically in presence of protic methanol and totally disappeared for the corresponding silyl ethers. These data are in agreement with the presence of a hydroxyl directing

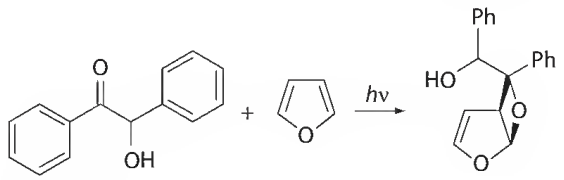

SCHEME 27.32 Paternò–Büchi reaction of benzoin with furan.

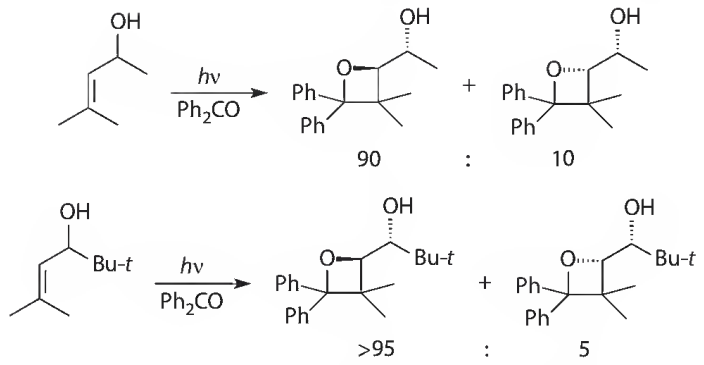

SCHEME 27.33 Paternò–Büchi reaction of allylic alcohols with benzophenone.

effect in the Paternò–Büchi reaction. *Threo* stereoisomer can be favored through the formation of a hydrogen bond between triplet excited benzophenone and the substrate in the exciplex, while the formation of the *erythro* stereoisomer would be less favored due to allylic strain.

The formation of a hydrogen bond to direct the Paternò–Büchi reaction has been considered by other researchers. Diastereoselective cycloaddition has been obtained using chiral enamide [170,171], or in the reaction of allylic alcohols with naphthalene rings [172]. When unsymmetrical carbonyl partners such as acetophenone or benzaldehyde were used, high diastereoselectivity was observed to give the corresponding *cis* isomer. The regioselectivity was high with acetophenone but lower with benzaldehyde [167].

Cis diastereoselectivity can be explained by using the Griesbeck rule on the possible triplet biradicals formed in the reaction. Steric interactions are minimized when the biradical assumes the optimal conformation and this conformation accounts for the formation of the observed stereoisomer [169].

When chiral allylic alcohols were used as substrates in the reaction *cis* diastereoisomers were formed. Furthermore, also in this case, a pronounced *threo* diastereoselectivity was observed, in agreement with a less pronounced hydroxy directing effect when acetophenone and benzaldehyde were used [167,169]. Chiral allyl ether gave the corresponding adduct with high diastereoselectivity [106].

The reaction of 2,3-dihydrofuran-3-ol derivatives (a particular type of allylic alcohol) with benzophenone gave the corresponding adducts showing that in methanol a *trans* relationship between the oxetane ring and the hydroxyl group was obtained, while, in benzene the *cis* isomer prevailed. The Eyring plot showed that the *trans* isomer increased with a not linear behavior decreasing the temperature [173].

The reaction of allylic alcohols with carbonyl compounds was tested also on a particular type of allylic alcohol such as 2-furylmethanol derivatives. The presence of large substituents on the carbon bearing the alcoholic function allows a high regioselectivity (Scheme 27.34) [174].

When 5-methyl-2-furyl derivatives were used as substrates, a different regioselectivity was observed. Compound **62** gave a 1:1 mixture of regioisomers, when irradiated in the presence of benzophenone, and a single regioisomer in the presence of benzaldehyde (Scheme 27.35) [175]. In agreement with the results obtained with 2-furyl derivatives, the products deriving from the attack on the side bearing the alcoholic function were obtained as a single diastereoisomer, while those deriving from the attack on the side bearing the methyl group were obtained as a mixture of diastereoisomers.

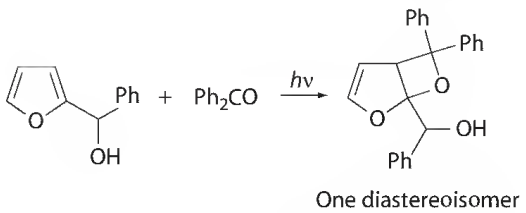

SCHEME 27.34 Paternò–Büchi reaction on 2-furylmethanol derivatives.

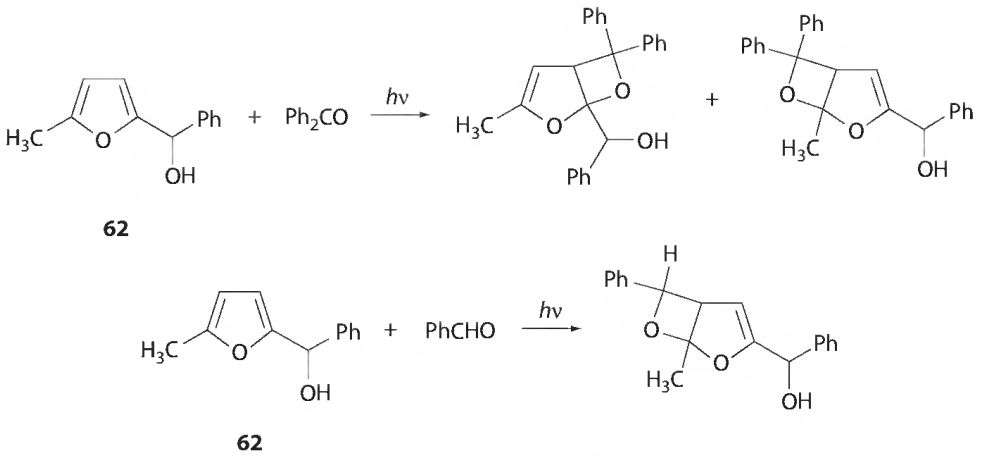

SCHEME 27.35 Paternò–Büchi reaction on 5-methyl-2-furylmethanol derivatives.

The reaction of 2-furylmethanol derivatives with aliphatic aldehydes and ketones gave the corresponding adducts with high regioselectivity (on the most hindered side of the substrate) but no diastereoselectivity [176]. The regioselectivity of the reaction was explained on the basis of the relative stability of the biradical intermediates. Theoretical study (density functional theory [DFT]) showed that the biradical obtained on the most hindered side of the molecule was more stable than the other one [175].

The observed diastereoselectivity in the reaction with aromatic carbonyl compounds clearly shows that it increases in relation to the nature of the substituents on the carbon bearing the alcoholic function as described by Adam. However, while Adam considers the allylic strain with a methyl group as the driving force for the diastereoselectivity, in this case, the methyl group is not present.

In order to have more data to explain the observed stereoselectivity, the photochemical behavior of tertiary 2-furylcarbinols was studied [177]. The photochemical reaction of 1-methyl-1-phenyl-1-(2-furyl)methanol with benzaldehyde gave a mixture of two regioisomeric product. The regioisomer on the most hindered side of the molecule was obtained in low yield but it showed a complete diastereoisomeric control. On the contrary, the main product was a mixture of four diastereoisomeric products (Scheme 27.36). The reaction of the same compound with benzophenone gave only the product

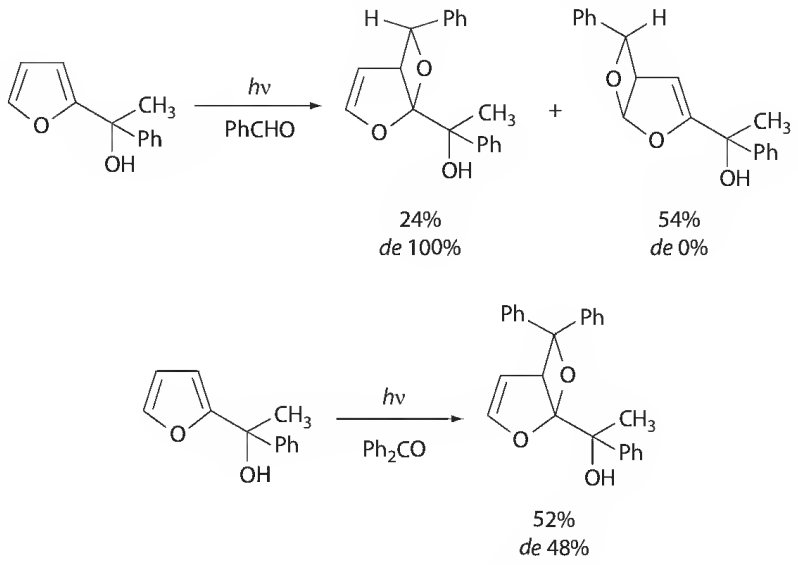

SCHEME 27.36 Paternò–Büchi reaction on tertiary 2-furylcarbinols.

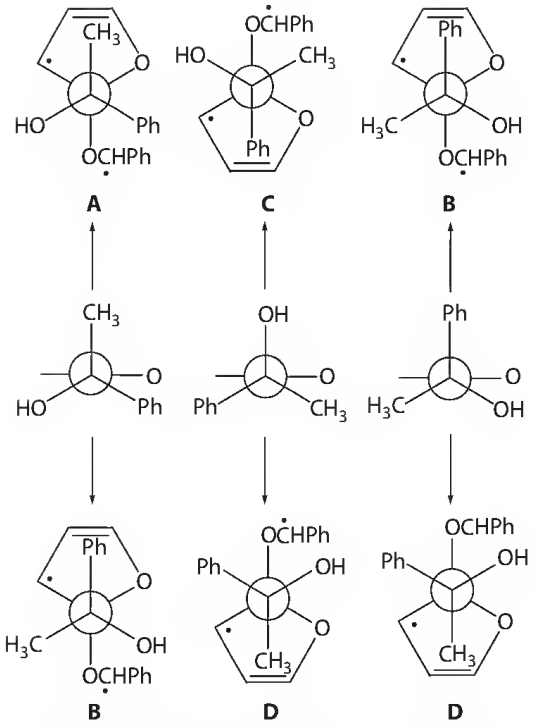

FIGURE 27.7 Possible conformations of the biradical intermediate from the reaction of 1-methyl-1-phenyl-1-(2-furyl) methanol with benzaldehyde.

deriving from the attack on the most hindered side of molecule. This compound was obtained with 48% diastereoisomeric excess.

The regioselectivity was explained, as described earlier, considering the relative stability of the biradical intermediates. In this case, in the reaction of the 1-methyl-1-phenyl-1-(2-furyl)methanol with benzaldehyde the biradical obtained on the less hindered side of the substrate was more stable than the other one by 18.03 kJ mol^{-1}. The same behavior was not observed using cyclic 2-furyl methanol derivatives [178].

On the basis of these results, an explanation of the stereochemical behavior was attempted [177]. 1-methyl-1-phenyl-1-(2-furyl)methanol showed three conformations. All three conformers were in the range of 1.97 kJ mol^{-1} and they did not show a preference. The directing effect exerted by the hydroxyl group is due to the formation of a hydrogen bond between the hydroxyl group and the oxygen of the excited carbonyl compound, or it is due to the formation of a complex. This type of interaction could favor the formation of a preferential conformation in the biradical intermediate where the hydroxyl group and the oxygen of the carbonyl compound are near. These conformations could have different energies for different diastereoisomeric biradicals, giving an explanation of the observed behavior. The aforementioned hypothesis requires that the biradical intermediates have a very short life enabling them to equilibrate to the most stable one. In the case of 1-methyl-1-phenyl-1-(2-furyl)methanol, if the hydroxyl group drives the attack of the oxygen of the carbonyl group, the conformations of the biradical intermediate represented in Figure 27.7 were obtained. **B** and **D** are the preferential conformation: calculations on these conformations showed that there is a difference of 13.26 kJ mol^{-1} between the energies of these two conformations. This difference can account for the observed complete diastereoselectivity of the reaction. In the reaction of the same substrate with benzophenone the corresponding conformers **B** and **D** show a energy difference of 7.79 kJ mol^{-1}: this difference is in agreement with the observed diastereoselectivity.

The same approach can be used to justify the stereochemical behavior of the reaction of allylic alcohols with benzophenone [179]. The irradiation of (*R*)-**63** in the presence of benzophenone gave (1*S*,5*S*,1′*R*)-**64** (Scheme 27.37) [180]. The stereochemical behavior was explained considering the same approach described earlier.

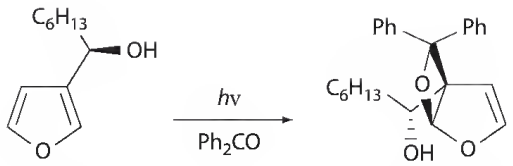

(*R*)-**63** (1*S*, 5*S*,1′*R*)-**64**

SCHEME 27.37 Paternò–Büchi reaction on 3-furylmethanol derivatives.

27.5.2 Other Pentaatomic Heterocycles

The reactivity of pentaatomic aromatic heterocycles different from furan toward carbonyl compounds to give the corresponding oxetanes has been the object of other review articles [181]. These compounds show lower reactivity than furan. The reason of this behavior is not clear. It could be related to the different aromaticity of these compounds in comparison with that of furan, or could be due to the quenching properties of the heterocycles.

Thiophene does not react with benzophenone. It reacts only when irradiated in the presence of BF_3 [182]. In this reaction, BF_3 is able to catalyze the ring opening of the oxetane. On the contrary, dimethylthiophenes react with benzophenone to give the corresponding cycloadduct with high regioselectivity [122,183–185]. On the contrary, 2,3-dimethyl- and 2,3,5-trimethylthiophene do not react.

Pyrrole, such as thiophene, does not react with benzophenone to give the corresponding oxetane. However, pyrrole reacts with aliphatic aldehydes and ketones to the corresponding 3-pyrryl carbinols [186]. Pyrrole can give the corresponding oxetane when irradiated in the presence of benzophenone only when an electron-attracting group such as benzoyl is bounded to the nitrogen atom [187,188].

Selenophene does not react with benzophenone [122]. On the contrary, 2-methylselenophene gives the corresponding cycloadduct. Also in this case the reaction occurs on the most hindered side of the molecule [189].

Imidazole, *N*-methylimidazole, and 1,2-dimethylimidazole react with aliphatic aldehydes and ketones to give the corresponding 4-imidazolyl carbinols in good yields [186,190]. 1,2-Dimethylimidazole reacts with benzophenone giving in low yield a reaction on the methyl in 2 position [191,192]. Some other imidazole derivatives showed the same behavior [191–193].

2,4-Dimethylthiazole gives the corresponding oxetane when irradiated in the presence of benzophenone [192].

Aliphatic and aromatic carbonyl compounds react with oxazole derivatives with good to high *exo* diastereoselectivity, but low facial stereoselctiviy. This reaction can be used in the synthesis of *erythro*-α-amino β-hydroxy carboxylic acid derivatives [194–198].

Indole does not react with benzophenone under irradiation condition. On the contrary, a benzoyl derivative reacts with it, giving the corresponding oxetane [199]. The same reaction has been described on *N*-acetyl derivative of 7-azaindole. Although the reaction represents a method able to obtain a new class of compound, the low yields of the product (4%) prevent a synthetic use of this reaction [200].

The results reported earlier represent all the available data on the Paternò–Büchi reaction on pentaatomic heterocycles different from furan. We can see that there are very few data: in particular, (1) most of the unsubstituted compounds tested did not react and (2) only few substituted derivatives showed a significative reactivity toward excited carbonyl compounds.

This behavior can be due to different reasons. First, the different aromaticity of the compounds could play an important role in order to define the reactivity of the compounds. Furan is the lowest aromatic pentaatomic heterocyclic compound known, while the other compounds show higher aromaticity. However, this type of explanation cannot justify why thiophene does not react while simple dimethylthienyl derivatives react and why some dimethylthienyl derivatives react while some others do not show any reactivity.

Stern–Volmer analysis of the quenching of benzophenone photoreduction showed that N-substituted pyrroles and selenophenes need an electron transfer mechanism [201].

27.5.3 Pyrimidines

The (6-4) photoproduct is an adduct of two pyrimidines that occupy adjacent sites on the same DNA strand. It is the second major lesion induced in DNA by UV radiation. Although statistically four times less frequent than CPD lesion, (6-4) photoproducts are believed to be severely mutagenic. Its formation is believed to occur via an initial Paternò–Büchi type cycloaddition to form an oxetane intermediate. Subsequent C4–O bond cleavage gave the observed (6-4) photoproducts. This is one of the major mutagenic classes of DNA photoproduct and is involved in the etiology of skin cancer. The oxetane **65** was prepared in a triplet reaction and both electron donor and acceptor substituents were found to be able to photosensitize the splitting reaction (Scheme 27.38) [202–205]. Only one regioisomer (**65**) was observed. The other regioisomer **66** was rarely observed [206].

The regiochemistry of the reaction depends on the temperature. At −38°C the regioisomer **65** dominates (61:39). On the other hand, at 70°C the regioisomeric behavior of the reaction is inverted [207,208]. A nonlinear Eyring plot was obtained showing a change of the selectivity-determining step. This behavior can be explained assuming two different cases: the situation where the conformational changes of the triplet intermediates are slower than ISC at low temperature and the case where the conformational changes exceed the ISC process [207]. When the conformational interchange is faster than the ISC process, the population of high potential energy conformations decreases, while the population of a lower potential energy conformer increases. The substituents on benzophenone modify the regiochemistry of the reaction: When *p*-methoxybenzophenone is used on 1,3-dimethyluracil, the isomer **65** is obtained (**65/66** > 95:5), while, using *p*-cyanobenzophenone, a 32:68 **65/66** ratio was observed [208,209]. The photochemical efficiency correlates with the energy gap between SOMO of benzophenone derivatives and the HOMO of the base. A small energy gap implies a strong interaction, and then a higher efficiency of the reaction. Recently, a theoretical approach to this reaction has been performed [210]. The authors considered the biradical intermediates **67** and **68** (Figure 27.8). They found that **68** is more stable than **67**, and that the formation of **67** is faster than **68**. Then, **66** can be considered as a thermodynamic product, while **65** a kinetic one.

A weak solvent effect was observed on the regioselectivity of the reaction [211]. The oxetane was obtained also in the reaction between benzophenone and benzophenone-derived drugs and thymidine [206,212]. An enantioselectivity factor for triplet deactivation was found using enantiopure ketoprofen. The enantioselective quenching of the chiral ketoprofen triplet state by thymidine can be associated with the formation of C–O bond, the first step of oxetane formation [81]. An intramolecular reaction

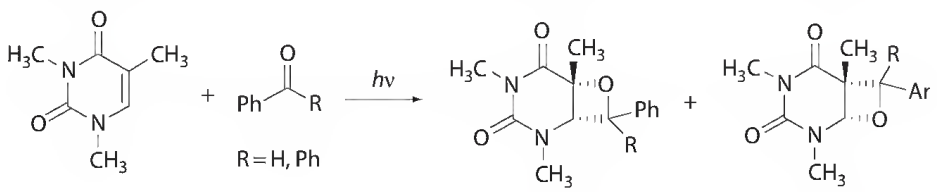

SCHEME 27.38 Paternò–Büchi reaction of a pyrimidine derivative.

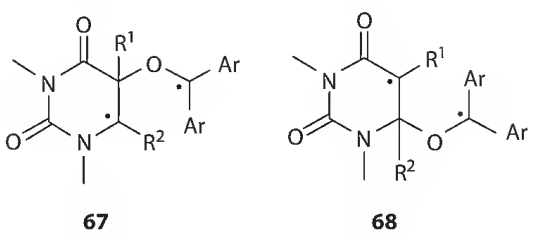

FIGURE 27.8 Biradical intermediate in the reaction of dimethyluracil.

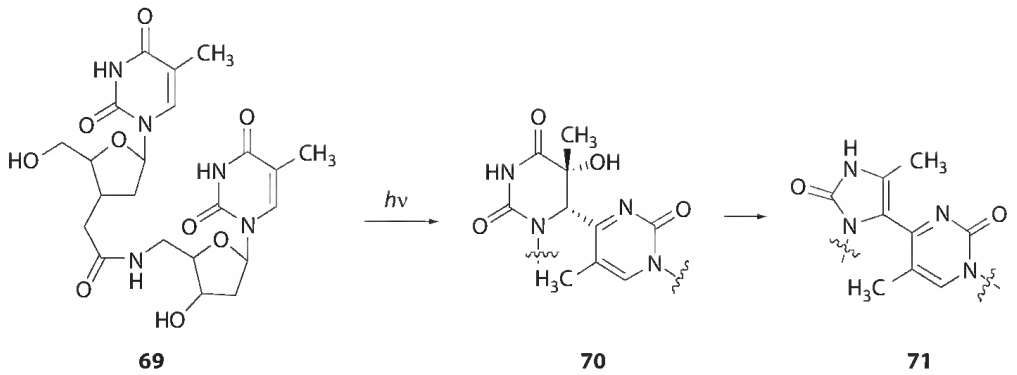

SCHEME 27.39 Intramolecular photochemical reaction between two pyrimidine units.

between thymidine esterified by ketoprofen has been described [213]. The irradiation of **69** gave **71** deriving from the (6–4) photoadduct **70** (Scheme 27.39) [214].

A reaction between 5-fluoro-1,3-dimethyluracil with 1,5-dimethoxynaphthalene has been reported [215]. The reaction gave product where an aromatic ring of naphthalene is broken. The presence of the intermediate cycloadduct has been proposed.

27.6 Intramolecular Reactions

2,7,9-Trimethylenetricyclo[4.3.0.$0^{3,8}$]nonane **72** can be obtained in a synthetic procedure involving an intramolecular Paternò–Büchi reaction of **73** to give **74** (Scheme 27.40) [216].

The same synthetic scheme was used in the synthesis of 2,7,9-trimethylenetricyclo[4.3.0.$0^{3,8}$]non-4-ene [217]. Some stelladiones such as tricyclo[3.3.0.$0^{3,7}$]octane-2,4-dione **75** or tricyclo[3.3.0.$0^{3,7}$]-octane-2,6-dione **76**, were obtained using the same synthetic strategy (Scheme 27.40) [218]. This type of intramolecular reaction was used also in the synthesis of diquinanes and triquinanes (Scheme 27.41) [219–221].

The synthesis of 1,13-herbertenediol **77** was performed using the same approach (Scheme 27.42) [222]. Intramolecular stereoselective Paternò–Büchi reactions were observed also in the reaction of some derivatives of *R*-(+)-sclareolide [223]. A synthesis of the scaffold of merrilactone A involved also an intramolecular 2 + 2 cycloaddition to give the adduct **78** (Scheme 27.42) [224].

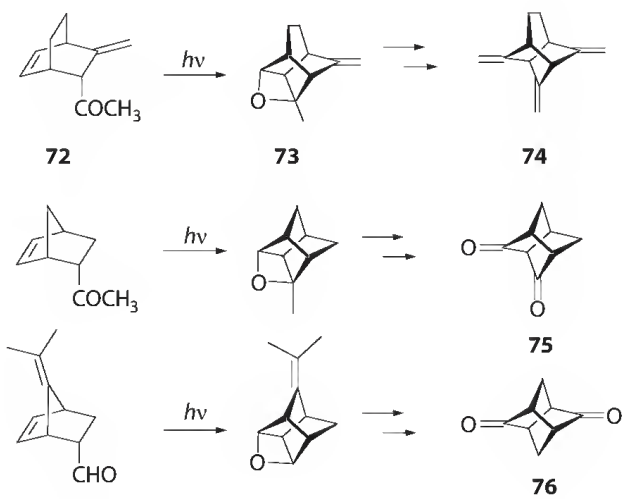

SCHEME 27.40 Paternò–Büchi reaction in the synthesis of tricyclononane scaffolds.

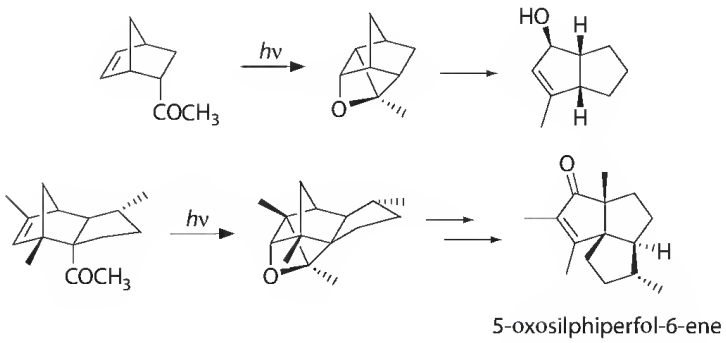

SCHEME 27.41 Synthesis of diquinanes and triquinanes.

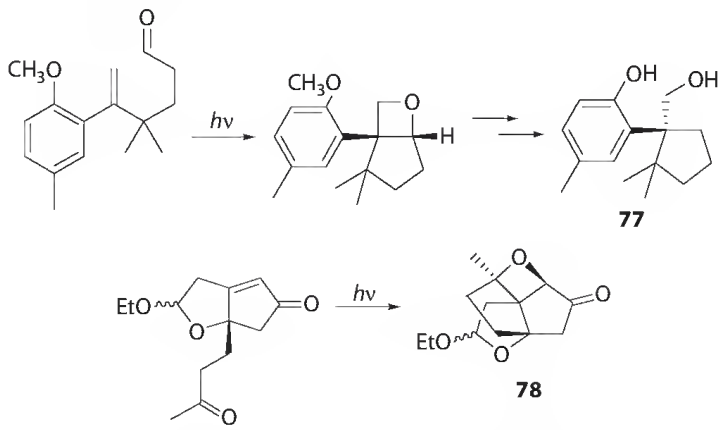

SCHEME 27.42 Synthesis of 1,13-herbertenediol (77) and of merrilactone scaffold.

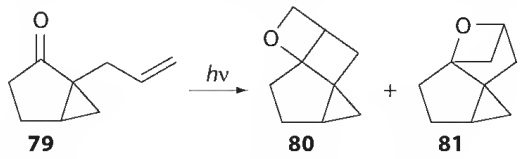

SCHEME 27.43 Paternò–Büchi reaction on allylcyclopentanone derivatives.

On the other hand, an attempt to obtain tromboxane analogs using an intramoelcular reaction of a carbonyl group with an enol ether, failed [225]. An intramolecular reaction on allyl cyclopentanone derivatives has been reported [44,226,227]. In this case both *straight* **80** and *crossed* **81** oxetanes can be obtained (Scheme 27.43). Using 2-allylcyclopentanone nearly equal amounts of these isomers were obtained: the use of the more rigid starting material **79** allowed the preferential formation the *straight* isomer.

An intramolecular cycloaddition reaction was found in the reaction of **82** to give **83** (Scheme 27.44) [228].

The reaction of **84** gave in quantitative yield the oxetane **85** that can be converted into **86** via fluoride desilylation (Scheme 27.45) [229].

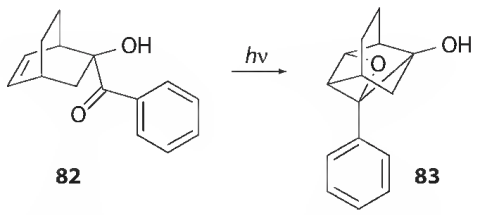

SCHEME 27.44 Intramolecular Paternò–Büchi reaction on a bycyclo[2.2.2]octane derivative.

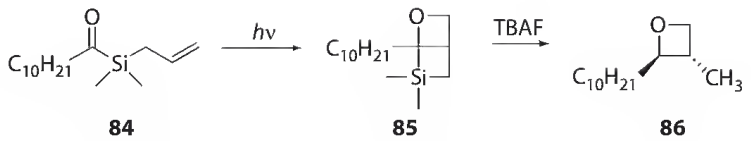

84 **85** **86**

SCHEME 27.45 Intramolecular Paternò–Büchi reaction on allyl silyl derivative.

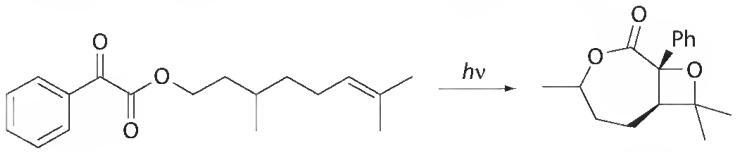

87 **88**

SCHEME 27.46 Intramolecular Paternò–Büchi reaction on a phenylglyoxylate derivative.

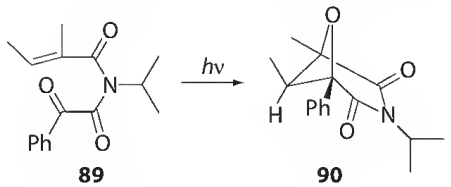

89 **90**

SCHEME 27.47 Stereoselective intramolecular Paternò–Büchi reaction on an amide derivative.

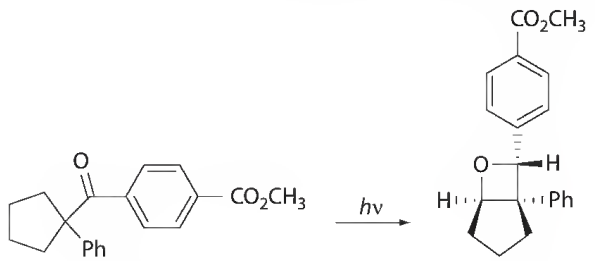

91 **92**

SCHEME 27.48 Norrish-type I and Paternò–Büchi reaction on the ketone **91**.

Some years ago, Scharf and coworkers studied the Paternò–Büchi reaction between electron-rich alkenes and chiral phenyl glyoxylates [156,230]. Neckers studied the reaction of ethyl phenylglyoxylates with several alkenes showing that it gave the cycloaddition reaction only when electron-rich alkenes were used. Monosubstituted alkenes gave Norrish type II reaction and the same behavior was observed reducing the electron richness of the alkenes [231]. Methyl 2-thienylglyoxylate showed a transient absorption at 390 nm and a broad band around 600 nm assigned to the triplet state and this compound reacts with 2,3-dimethyl-2-butene to give the corresponding adduct [232]. When alkenyl phenylglyoxylates were used as substrates, Norrish type II is the main reaction in most of the cases, with the exception, for example, of compound **87** able to give the adduct **88** (Scheme 27.46) [233,234].

N-Isopropyl-*N*-tigloylbenzoylformamides gave an intramolecular cycloaddition reaction in high yields (50%–99%) to give the *syn* adduct (*syn/anti* = 2.1) [235,236]. The compound **89**, irradiated in solid state showed a different behavior: the crystals of **89** are in a chiral group, so **89** gave **90** with a *syn/anti* = 6.7 and *syn*-**90** was obtained with a high ee value (>99%) (Scheme 27.47) [236].

When the ketone **91** was irradiated in the solid state, a Norrish type I reaction occurred, giving an alkene and a carbonyl compounds, able to give the corresponding adduct **92** (Scheme 27.48). The reaction occurs with high stereoselectivity, and, when performed on a chiral salt gave the product with ee in the range 42%–52% [53].

References

1. Paternò, E. In *Synthesis in Organic Chemistry by Means of Light*, D'Auria, M., Ed.; Società Chimica Italiana: Rome, Italy, 2009; pp. 85–105.
2. Büchi, G.; Inman, C. G.; Lipinsky, E. S. *J. Am. Chem. Soc.* 1954, *76*, 4327–4331.
3. Arnold, D. R. *Adv. Photochem.* 1968, *6*, 301–423.
4. Jones, G. *Org. Photochem.* 1981, *5*, 1–122.
5. Carless, H. A. J. In *Synthetic Organic Photochemistry*, Horspool, W. M., Ed.; Plenum: New York, 1984, pp. 425–487.
6. Porco, J. A.; Schreiber, S. L. In *Comprehensive Organic Synthesis*, Trost, B. M.; Fleming, I.; Paquette, L. A., Eds.; Plenum: New York, 1991; Vol. 5, pp. 151–192.
7. Griesbeck, A. G. In *Handbook of Photochemistry and Photobiology*, Horspool, W. A.; Song, P.-S., Eds.; CRC Press: Boca Raton, FL, 1994; pp. 522–535, 550–559.
8. Bach, T. *Synthesis* 1998, 683–703.
9. D'Auria, M.; Emanuele, L.; Racioppi, R.; Romaniello, G. *Curr. Org. Chem.* 2003, *7*, 1443–1459.
10. D'Auria, M. In *Targets in Heterocyclic Systems, Chemistry and Properties*, Attanasi, O. A.; Spinelli, D., Eds.; Italian Society of Chemistry: Rome, Italy, 2003; Vol. 7, pp. 157–173.
11. D'Auria, M.; Emanuele, L.; Racioppi, R. In *Advances in Photochemistry,* Neckers, D. C.; Jenks, W. S.; Wolff, T., Eds.; John Wiley & Sons: Hoboken, NJ, 2005; Vol. 28, pp. 81–127.
12. D'Auria, M.; Emanuele, L.; Racioppi, R. In *Photochemistry Research Progress*, Sanchez, A.; Gutierrez, S. J., Eds.; Nova Science Publishers Inc.: Hauppage, NY, 2008; pp. 373–438.
13. D'Auria, M.; Racioppi, R. *Curr. Org. Chem.* 2009, *13*, 939–954.
14. Kingston, D. G. I. *Pharmacol. Ther.* 1991, *52*, 1–34.
15. Huang, J.; Yokoyama, R.; Yang, C.; Fukuyama, Y. *Tetrahedron Lett.* 2000, *41*, 6111–6114.
16. Wang, Y.; Fleet, G. W. J.; Storer, R.; Myers, P. L.; Wallis, C. J.; Doherty, O.; Watkin, D. J.; Vogt, K.; Witty, D. R.; Wilson, F. X.; Peach, J. M. *Tetrahedron Asymm.* 1990, *1*, 527–530.
17. Yang, C. O.; Kurz, W.; Eugui, E. M.; Mc Roberts, M. J.; Verheyden, J. P. H.; Kurz, L. J.; Walker, K. A. M. *Tetrahedron Lett.* 1992, *33*, 41–44.
18. Kawahata, Y.; Takatsuto, S.; Ikekawa, N.; Murata, M.; Omura, S. *Chem. Pharm. Bull.* 1986, *34*, 3102–3110.
19. Kopecký, J. *Organic Photochemistry,* VCH: New York, 1992, p. 126.
20. Turro, N. J.; Dalton, J. C.; Dawes, K.; Farrington, G.; Hautala, R.; Morton, D.; Niemczyk, M.; Schore, N. *Acc. Chem. Res.* 1972, *5*, 92–101.
21. Turro, N. J.; Farrington, G. L. *J. Am. Chem. Soc.* 1980, *102*, 6051–6055.
22. Turro, N. J.; Farrington, G. L. *J. Am. Chem. Soc.* 1980, *102*, 6056–6063.
23. Freilich, S. C.; Peters, K. S. *J. Am. Chem. Soc.* 1981, *103*, 6255–6257.
24. Caldwell, R. A.; Majima, T.; Pac, C. *J. Am. Chem. Soc.* 1982, *104*, 629–630.
25. Freilich, S. C.; Peters, K. S. *J. Am. Chem. Soc.* 1985, *107*, 3819–3822.
26. Abe, M.; Kawakami, T.; Ohata, S.; Nozaki, K.; Nojima, M. *J. Am. Chem. Soc.* 2004, *126*, 2838–2846.
27. Wilson, R. M.; Wunderly, S. W.; Walsh, T. F.; Musser, A. K.; Outcalt, R.; Geiser, F.; Gee, S. K.; Brabender, W.; Yerino, L., Jr.; Conrad, T. T.; Tharp, G. A. *J. Am. Chem. Soc.* 1982, *104*, 4429–4446.
28. Adam, W.; Kliem, U.; Lucchini, V. *Tetrahedron Lett.* 1986, *27*, 2953–2956.
29. Adam, W.; Kliem, U.; Mosandl, T.; Peters, E.-M.; Peters, K.; von Schnering, H. G. *J. Org. Chem.* 1988, *53*, 4986–4992.
30. Adam, W.; Kliem, U.; Lucchini, V. *Liebigs Ann.* 1988, 869–875.
31. Pinter, B.; De Proft, F.; Veszprémi, T.; Geerlings, P. *J. Chem. Sci.* 2005, *117*, 561–571.
32. Noorizadeh, S. *J. Phys. Org. Chem.* 2007, *20*, 514–524.
33. Palmer, I. J.; Ragazos, I. N.; Bernardi, F.; Olivucci, M.; Robb, M. A. *J. Am. Chem. Soc.* 1994, *116*, 2121–2132.
34. Kutateladze, A. G. *J. Am. Chem. Soc.* 2001, *123*, 9279–9282.

35. Kutateladze, A. G.; McHale, W. A., Jr. *Arkivoc* 2005, *4*, 88–101.
36. Minaev, B. F.; Ågren, H. *J. Mol. Struct. (Theochem)* 1998, *434*, 193–206.
37. Minaev, B. F.; Ågren, H. *EPA Newslett.* 1999, *65*, 7–38.
38. Mattay, *J. Angew. Chem., Int. Ed. Engl.* 1987, *26*, 825–845.
39. Chung, W.-S.; Turro, N. J.; Srivastava, S.; Li, H.; le Noble, W. J. *J. Am. Chem. Soc.* 1988, *110*, 7882–7883.
40. Chung, W.-S.; Turro, N. J.; Srivastava, S.; le Noble, W. J. *J. Org. Chem.* 1991, *56*, 5020–5025.
41. Chung, W.-S.; Wang, N.-J.; Liu, Y.-D.; Leu, Y.-J.; Chiang, M. Y. *J. Chem. Soc. Perkin Trans. 2* 1995, 307–313.
42. Chung, W.-S.; Liu, Y.-D.; Wang, N.-J. *J. Chem. Soc. Perkin Trans. 2* 1995, 581–586.
43. Gáplovský, A.; Donovalová, J.; Toma, S.; Kubinec, R. *Ultrasonics Sonochem.* 1997, *4*, 109–115.
44. Kossanyi, J.; Jost, P.; Furth, B.; Daccord, G.; Chaquin, P. *J. Chem. Res. Synop.* 1980, 368.
45. Abe, M.; Fujimoto, K.; Nojima, M. *J. Am. Chem. Soc.* 2000, *122*, 4005–4010.
46. Abe, M.; Tachibana, K.; Fujimoto, K.; Nojima, M. *Synthesis* 2001, 1243–1247.
47. Xue, J.; Zhang, Y; Wu, T.; Fun, H.-K.; Xu, J.-H. *J. Chem. Soc. Perkin Trans. 1* 2001, 183–191.
48. Zhang, Y.; Xue, J.; Gao, Y.; Fun, H.-K.; Xu, J.-H. *J. Chem. Soc. Perkin Trans. 1* 2002, 345–353.
49. Bosch, E.; Hubig, S. M.; Kochi, J. K. *J. Am. Chem. Soc.* 1998, *120*, 386–395.
50. Thopate, S. R.; Kulkarni, M. G.; Puranik, V. G. *Angew. Chem. Int. Ed. Engl.* 1998, *37*, 1110–1112.
51. Christl, M.; Braun, M. *Liebigs Ann./Recueil* 1997, 1135–1141.
52. Abe, M.; Shirodai, Y.; Nojima, M. *J. Chem. Soc. Perkin Trans. 1* 1998, 3253–3260.
53. Kang, T.; Scheffer, J. R. *Org. Lett.* 2001, *3*, 3361–3364.
54. Adam, W.; Stegmann, V. R. *J. Am. Chem. Soc.* 2002, *124*, 3600–3607.
55. Kollenz, G.; Terpetschnig, E.; Sterk, H.; Peters, K.; Peters, E.-M. *Tetrahedron* 1999, *55*, 2973–2984.
56. Silva, M. T.; Braz-Filho, R.; Netto-Ferreira, J. C. *J. Braz. Chem. Soc.* 2000, *11*, 479–485.
57. Abe, M.; Ikeda, M.; Shirodai, Y.; Nojima, M. *Tetrahedron Lett.* 1996, *37*, 5901–5904.
58. Horspool, W.; Armesto, D. *Organic Photochemistry: A Comprehensive Treatment*, Prentice Hall, London, U.K., 1992.
59. Büchi, G.; Kofron, J. T.; Koller, E.; Rosenthal, D. *J. Am. Chem. Soc.* 1956, *78*, 876–877.
60. Arnold, D.; Glick, A. *J. Chem. Soc. Chem. Commun.* 1966, 813–814.
61. Gotthardt, J. K.; Steinmetz, R.; Hammond, G. S. *J. Org. Chem.* 1968, *33*, 2774–2780.
62. Howell, A. R.; Fan, R.; Truong, A. *Tetrahedron Lett.* 1996, *37*, 8651–8654.
63. Paternò, E.; Chieffi, G. *Gazz. Chim. Ital.* 1910, *40*(II), 321–331.
64. Mattay, J.; Buchkremer, K. *Helv. Chim. Acta* 1988, *71*, 981–987.
65. Mattay, J.; Buchkremer, K. *Heterocycles* 1988, *27*, 2153–2166.
66. Buhr, S.; Griesbeck, A. G.; Lex, J.; Mattay, J.; Schröer, *J. Tetrahedron Lett.* 1996, *37*, 1195–1196.
67. Abe, M.; Taniguchi, K.; Hayashi, T. *Arkivoc* 2007, *8*, 58–65.
68. Gan, C. Y.; Lambert, J. N. *J. Chem. Soc. Perkin Trans. 1* 1998, 2363–2372.
69. Park, S.-K.; Lee, S.-J.; Baek, K.; Yu, C.-M. *Bull. Korean Chem. Soc.* 1998, *19*, 35–36.
70. Netto-Ferreira, J. C.; Silva, M. T.; Puget, F. P. *J. Photochem. Photobiol. A* 1998, *119*, 165–170.
71. Ogata, M.; Watanabe, H.; Kano, H. *Tetrahedron Lett.* 1967, 533–537.
72. Carless, H. A.; Haywood, D. J. *J. Chem. Soc., Chem. Commun.* 1980, 1067–1068.
73. Bondock, S.; Griesbeck, A. G. *Int. J. Photoenergy* 2005, *7*, 23–25.
74. Griesbeck, A. G.; Fiege, M.; Bondock, S.; Gudipati, M. S. *Org. Lett.* 2000, *2*, 3623–3625.
75. Griesbeck, A. G. *J. Photoscience* 2003, *10*, 49–60.
76. Griesbeck, A. G. *Synlett* 2003, 451–472.
77. Griesbeck, A. G.; Abe, M.; Bondock, S. *Acc. Chem. Res.* 2004, *37*, 919–928.
78. Griesbeck, A. G.; Stadtmüller, S. *J. Am. Chem. Soc.* 1990, *112*, 1281–1283.
79. Griesbeck, A. G.; Stadtmüller, S. *J. Am. Chem. Soc.* 1991, *113*, 6923–6928.
80. Griesbeck, A. G.; Stadtmüller, S. *Chem. Ber.* 1990, *123*, 357–362.
81. Lhiaubet-Vallet, V.; Encinas, S.; Miranda, M. A. *J. Am. Chem. Soc.* 2005, *127*, 12774–12775.
82. Abe, M. *J. Chin. Chem. Soc.* 2008, *55*, 479–486.

83. D'Auria, M.; Emanuele. L.; Racioppi, R. *Lett. Org. Chem.* 2006, *3*, 244–246.
84. Griesbeck, A. G.; Mauder, H.; Peters, K.; Peters, E.-M.; von Schnering, H. G. *Chem. Ber.* 1991, *124*, 407–410.
85. D'Auria, M.; Racioppi, R. *Eur. J. Org. Chem.* 2010, *2010*, 3831–3836.
86. Griesbeck, A. G.; Bondock, S.; Gudipati, M. S. *Angew. Chem. Int. Ed.* 2001, *40*, 4684–4687.
87. Smith, A. B., III.; Sulikowski, G. A.; Sulikowski, M. M.; Fujimoto, K. *J. Am. Chem. Soc.* 1992, *114*, 2567–2576.
88. Khan, N.; Morris, T. H.; Smith, E. H.; Walsh, R. *J. Chem. Soc. Perkin Trans. 1* 1991, 865–870.
89. Schroeter, S. H.; Orlando, C. M. *J. Org. Chem.* 1969, *34*, 1181–1187.
90. Vasudeva, S.; Brock, C. P.; Watt, D. S.; Morita, H. *J. Org. Chem.* 1994, *59*, 4677–4679.
91. Fleming, S. A.; Gao, J. J. *Tetrahedron Lett.* 1997, *38*, 5407–5410.
92. Bach, T.; Kather, K. *Tetrahedron* 1994, *50*, 12319–12328.
93. Bach, T. *Tetrahedron Lett.* 1991, *32*, 7037–7038.
94. Bach, T. *Liebigs Ann.* 1995, 855–865.
95. Bach, T. *Liebigs Ann.* 1995, 1045–1053.
96. Bach, T.; Jödicke, K.; Kather, K.; Fröhlich, R. *J. Am. Chem. Soc.* 1997, *119*, 2437–2445.
97. Bach, T.; Jödicke, K.; Kather, K.; Hecht, *J. Angew. Chem. Int. Ed. Engl.* 1995, *34*, 2271–2273.
98. Bach, T.; Jödicke, K.; Wibbeling, B. *Tetrahedron* 1996, *52*, 10861–10878.
99. Bach, T.; Kather, K.; Krämer, O. *J. Org. Chem.* 1998, *63*, 1910–1918.
100. Cho, D. W.; Lee, H.-Y.; Oh, S. W.; Choi, J. H.; Park, H. J.; Mariano, P. S.; Yoon, U. C. *J. Org. Chem.* 2008, *73*, 4539–4547.
101. Yoon, U. C.; Kim, M. J.; Moon, J. J.; Oh, S. W.; Kim, H. J.; Mariano, P. S. *Bull. Korean Chem. Soc.* 2002, *23*, 1218–1228.
102. Abe, M.; Ikeda, M.; Nojima, M. *J. Chem. Soc. Perkin Trans. 1* 1998, 3261–3266.
103. Bach, T. *Angew. Chem. Int. Ed. Engl.* 1996, *35*, 884–886.
104. Bach, T.; Schröder, J. *J. Org. Chem.* 1999, *64*, 1265–1273.
105. Bach, T.; Bergmann, H.; Brummerhop, H.; Lewis, W.; Harms, K. *Chem. Eur. J.* 2001, *7*, 4512–4521.
106. Bach, T. *Liebigs Ann./Recueil* 1997, 1627–1634.
107. Bach, T.; Schröder, *J. Synthesis* 2001, 1117–1124.
108. Bach, T.; Schröder, J.; Brandl, T.; Hecht, J.; Harms, K. *Tetrahedron* 1998, *54*, 4507–4520.
109. Bach, T. *Synlett* 2000, 1699–1707.
110. Bach, T.; Schröder, *J. Tetrahedron Lett.* 1997, *38*, 3707–3710.
111. Bach, T.; Schröder, *J. Liebigs Ann./Recueil* 1997, 2265–2267.
112. Bach, T.; Brummerhop, H. *Angew. Chem. Int. Ed.* 1998, *3*, 3400–3402.
113. Bach, T.; Brummerhop, H.; Harms, K. *Chem. Eur. J.* 2000, *6*, 3838–3848.
114. Kugelberg, A.; Döpp, D.; Görner, H. *J. Inf. Recording* 2000, *25*, 187–194.
115. van Wolven, C.; Döpp, D.; Fischer, M. A. *J. Inf. Recording* 2000, *25*, 209–214.
116. Döpp, D.; Fischer, M.-A. *Recl. Trav. Chim. Pays-Bas* 1995, *114*, 498–503.
117. Schenck, G. O.; Hartman, W.; Steinmetz, R. *Chem. Ber.* 1963, *96*, 498–508.
118. Gagnaire, D.; Payo-Subiza, E. *Bull. Soc. Chim. Fr.* 1963, 2623–2631.
119. Toki, S.; Shima, K.; Sakurai, H. *Bull Chem. Soc. Jpn* 1965, *38*, 760–762.
120. Nakano, T.; Rivas, C.; Perez, C. *J. Chem. Soc. Perkin Trans. 1* 1973, 2322–2327.
121. Rivas, C.; Payo, E. *J. Org. Chem.* 1967, *32*, 2918–2920.
122. Rivas, C.; Bolivar, R. A.; Cucarella, M. *J. Heterocyclic Chem.* 1982, *19*, 529–535.
123. Shima, K.; Sakurai, H. *Bull. Chem. Soc. Jpn.* 1966, *39*, 1806–1808.
124. Toki, S.; Sakurai, H. *Bull. Soc. Chim. Jpn.* 1967, *40*, 2885–2889.
125. Zamojski, A.; Koźluk, T. *J. Org. Chem.* 1977, *42*, 1089–1090.
126. Whipple, E. B.; Evanega, G. R. *Tetrahedron* 1968, *24*, 1299–1310.
127. Schreiber, S. L.; Desmaele, D.; Porco, J. A. *Tetrahedron Lett.* 1988, *29*, 6689–6693.
128. Abe, M.; Torii, E.; Nojima, M. *J. Org. Chem.* 2000, *65*, 3426–3431.

129. Carless, H. A. J.; Halfhide, A. F. *J. Chem. Soc. Perkin Trans. 1* 1992, 1081–1082.
130. Griesbeck, A. G.; Mauder, H.; Stadtmüller, S. *Acc. Chem. Res.* 1994, *27*, 70–76.
131. Griesbeck, A. G.; Buhr, S.; Fiege, M.; Schmickler, H.; Lex, J. *J. Org. Chem.* 1998, *63*, 3847–3854.
132. Leitich, *J. Tetrahedron Lett.* 1967, 1937–1939.
133. Evanega, G. R.; Whipple, E. B. *Tetrahedron Lett.* 1967, 2163–2168.
134. Toki, S.; Sakurai, H. *Tetrahedron Lett.* 1967, 4119–4122.
135. Sekretar, S.; Rudā, J.; Štibranyi, L. *Coll. Czech. Chem. Commun.* 1984, *49*, 71–77.
136. Cantrell, T. S.; Allen, A.; Ziffer, H. *J. Org. Chem.* 1989, *54*, 140–145.
137. Kubo, Y.; Suto, M.; Tojo, S.; Araki, T. *J. Chem. Soc. Perkin Trans. 1* 1986, 771–779.
138. Krauch, C. H.; Metzner, W.; Schenck, G. O. *Chem. Ber.* 1966, *99*, 1723–1731.
139. Farid, S.; Hartman, S. E.; DeBoer C. D. *J. Am. Chem. Soc.* 1975, *97*, 808–812.
140. Capozzo, M.; D'Auria, M.; Emanuele, L.; Racioppi, R. *J. Photochem. Photobiol., A: Chem.* 2007, *185*, 38–43.
141. Jarosz, S.; Zamojski, A. *J. Org. Chem.* 1979, *44*, 3720–3723.
142. Kitamura, T.; Kawakami, Y.; Imagawa, T.; Kawanisi, M. *Synth. Commun.* 1977, *7*, 521–528.
143. Kozluk, T.; Zamojski, A. *Tetrahedron*, 1983, *39*, 805–810.
144. Schreiber, S. L.; Hoveyda, A. H.; Wu, H.-J. *J. Am. Chem. Soc.* 1983, *105*, 660–661.
145. Schreiber, S. L.; Satake, K. *J. Am. Chem. Soc.* 1983, *105*, 6723–6724.
146. Schreiber, S. L.; Satake, K. *J. Am. Chem. Soc.* 1984, *106*, 4186–4188.
147. Schreiber, S. L.; Hoveyda, A. H. *J. Am. Chem. Soc.* 1984, *106*, 7200–7202.
148. Schreiber, S. L.; Porco, J. A. *J. Org. Chem.* 1989, *54*, 4721–4723.
149. Hambalek, R.; Just, G. *Tetrahedron Lett.* 1990, *31*, 4693–4696.
150. Hambalek, R.; Just. G. *Tetrahedron Lett.* 1990, *31*, 5445–5448.
151. Jarosz, S.; Zamojski, A. *Tetrahedron* 1982, *38*, 1447–1451.
152. Pelzer, R.; Jütten, P.; Scharf, H.-D. *Chem. Ber.* 1989, *122*, 487–491.
153. Pelzer, R.; Scharf, H.-D.; Buschmann, H.; Runsink, *J. Chem. Ber.* 1989, *122*, 1187–1192.
154. Hu, S.; Neckers, D. C. *J. Chem. Soc. Perkin Trans. 2*, 1999, 1771–1778.
155. D'Auria, M.; Emanuele, L.; Racioppi, R. *Photochem. Photobiol. Sci.* 2003, *2*, 904–913.
156. Buschmann, H.; Scharf, H.-D.; Hoffmann, N.; Plath, M. W.; Runsink, J. *J. Am. Chem. Soc.* 1989, *111*, 5367–5373.
157. Buschmann, H.; Scharf, H.-D.; Hoffmann, N.; Esser, P. *Angew. Chem., Int. Ed. Engl.* 1991, *30*, 477–515.
158. D'Auria, M.; Emanuele, L.; Racioppi, R. *Lett. Org. Chem.* 2008, *5*, 249–256.
159. Žagar, C.; Scharf, H.-D. *Chem. Ber.* 1991, *124*, 967–969.
160. Jarosz, S.; Zamojski, A. *Tetrahedron* 1982, *38*, 1453–1456.
161. Tronchet, J. M. J.; Baehler, B. *J. Carbohydrates Nucleosides Nucleotides* 1974, *1*, 449–459.
162. Schreiber, S. L. *Science* 1985, *227*, 857–863.
163. Schreiber, S. L.; Satake K. *Tetrahedron Lett.* 1986, *27*, 2575–2578.
164. D'Auria, M.; Emanuele, L.; Racioppi, R. *Tetrahedron Lett.* 2004, *45*, 3877–3880.
165. D'Auria, M.; Emanuele, L.; Pace, V.; Racioppi, R. *Lett. Org. Chem.* 2006, *3*, 350–355.
166. Adam, W.; Peters, K.; Peters, E. M.; Stegmann, V. R. *J. Am. Chem. Soc.* 2000, *122*, 2958–2959.
167. Adam, W.; Stegmann, V. R. *Synthesis* 2001, 1203–1214.
168. Adam, W.; Prein, M. *Angew. Chem., Int. Ed. Engl.* 1996, *35*, 477–494.
169. Griesbeck, A. G.; Bondock, S. *J. Am. Chem. Soc.* 2001, *123*, 6191–6192.
170. Bach, T.; Schröder, J.; Harms, K. *Tetrahedron Lett.* 1999, *40*, 9003–9004.
171. Bach, T.; Bergmann, H.; Harms, K. *J. Am Chem. Soc.* 1999, *121*, 10650–10651.
172. Yokohama, A.; Mizuno, K. *Org. Lett.* 2000, *2*, 3457–3459.
173. Abe, M.; Terazawa, M.; Nozaki, K.; Masuyama, A.; Hayashi, T. *Tetrahedron Lett.* 2006, *47*, 2527–2530.
174. D'Auria, M.; Racioppi, R.; Romaniello, G. *Eur. J. Org. Chem.* 2000, 3265–3272.
175. D'Auria, M.; Racioppi, R. *Arkivoc* 2000, *1*, 133–140.

176. D'Auria, M.; Emanuele, L.; Poggi, G.; Racioppi, R.; Romaniello, G. *Tetrahedron* 2002, *58*, 5045–5051.
177. D'Auria, M.; Emanuele, L.; Racioppi, R. *Photochem. Photobiol. Sci.* 2004, *3*, 927–932.
178. Yabuno, Y.; Hiraga, Y.; Abe, M. *Chem. Lett.* 2008, *37*, 822–823.
179. D'Auria, M.; Emanuele, L.; Racioppi, R. *Lett. Org. Chem.* 2005, *2*, 132–135.
180. D'Auria, M.; Emanuele, L.; Racioppi, R.; Valente, A. *Photochem. Photobiol. Sci.* 2008, *7*, 98–103.
181. Rivas, C.; Vargas, F. In *CRC Handbook of Organic Photochemistry and Photobiology*, Horspool W. M.; Song P.-S., Eds.; CRC Press: Boca Raton, FL, 1995, p. 536.
182. Vargas, F.; Rivas, C.; Navarro, M.; Alvarado, Y. *J. Photochem. Photobiol., A: Chem.* 1996, *93*, 169–171.
183. Rivas, C.; Velez, M.; Crescente, O. *J. Chem. Soc., Chem. Commun.* 1970, 1474.
184. Rivas, C.; Bolivar, R. A. *J. Heterocyclic Chem.* 1973, *10*, 967–971.
185. Rivas, C.; Pacheco, D.; Vargas, F.; Ascanio J. *J. Heterocyclic Chem.* 1981, *18*, 1065–1067.
186. Jones, G.; Gilow, H. M.; Low, J. *J. Org. Chem.* 1979, *44*, 2949–2951.
187. Rivas, C.; Velez, M.; Cucarella, M.; Bolivar, R. A.; Flores, S. E. *Acta Cient. Venezolana* 1971, *22*, 145–146.
188. Rivas, C.; Bolivar, R. A. *J. Heterocyclic Chem.* 1976, *13*, 1037–1040.
189. Rivas, C.; Pacheco, D.; Vargas, F. *Acta Sud Am. Quim.* 1982, *2*, 1–3.
190. Matsuura, T.; Banba, A.; Ogura, K. *Tetrahedron* 1971, *27*, 1211–1219.
191. Nakano, T.; Rivas, C.; Perez, C.; Larrauri, J. M. *J. Heterocyclic Chem.* 1976, *13*, 173–174.
192. Nakano, T.; Rodriguez, W.; de Roche, S. Z.; Larrauri, J. M.; Rivas, C.; Perez, C. *J. Heterocyclic Chem.* 1980, *17*, 1777–1780.
193. Ito, Y.; Ji-Ben, M.; Suzuki, S.; Kusunaga, Y.; Matsuura, T.; Fukuyama, K. *Tetrahedron Lett.* 1985, *26*, 2093–2096.
194. Griesbeck, A. G.; Fiege, M.; Lex, *J. Chem. Commun.* 2000, 589–590.
195. Griesbeck, A. G.; Bondock, S.; Lex, J. *J. Org. Chem.* 2003, *68*, 9899–9906.
196. Griesbeck, A. G.; Bondock, S.; Lex. *J. Org. Biomol. Chem.* 2004, *2*, 1113–1115.
197. Bondock, S.; Griesbeck, A. G. *Monatsh. Chem.* 2006, *137*, 765–777.
198. Griesbeck, A. G.; Bondock, S. *Aust. J. Chem.* 2008, *61*, 573–580.
199. Julian, D. R.; Tringham, G. D. *J. Chem. Soc., Chem. Commun.* 1973, 13.
200. Nakano, T.; Santana, M. *J. Heterocyclic Chem.* 1976, *13*, 585–587.
201. Vargas, F.; Rivas, C. *Int. J. Photoenergy* 2000, *2*, 97–101.
202. von Wilucki, I.; Matthaus, H.; Krauch, C. H. *Photochem. Photobiol.* 1967, *6*, 497–500.
203. Prakash, G.; Falvey, D. E. *J. Am. Chem. Soc.* 1995, *117*, 11375–11376.
204. Joseph, A.; Prakash, G.; Falvey, D. E. *J. Am. Chem. Soc.* 2000, *122*, 11219–11225.
205. Lhiaubet-Vallet, V.; Belmadoui, N.; Climent, M. J.; Miranda, M. A. *J. Phys. Chem. B* 2007, *111*, 8277–8282.
206. Nakatani, K.; Yoshida, T.; Saito, I. *J. Am. Chem. Soc.* 2002, *124*, 2118–2119.
207. Hei, X.-M.; Song, Q.-H.; Li, X.-B.; Tang, W.-J.; Wang, H.-B.; Guo, Q.-X. *J. Org. Chem.* 2005, *70*, 2522–2527.
208. Song, Q.-H.; Wang, H.-B.; Li, X.-B.; Hei, X.-M.; Guo, Q.-X.; Yu, S.-Q. *J. Photochem. Photobiol. A* 2006, *183*, 198–204.
209. Song, Q.-H.; Zhai, B.-C.; Hei, X.-M.; Guo, Q.-X. *Eur. J. Org. Chem.* 2006, 1790–1800.
210. Kong, F.-F.; Zhai, B.-C.; Song, Q.-H. *Photochem. Photobiol. Sci.* 2008, *7*, 1332–1336.
211. Zhai, B.-C.; Luo, S.-W.; Kong, F.-F.; Song, Q.-H. *J. Photochem. Photobiol. A* 2007, *187*, 406–409.
212. Encinas, S.; Belmadoui, N.; Climent, M. J.; Gil, S.; Miranda, M. A. *Chem. Res. Toxicol.* 2004, *17*, 857–862.
213. Belmadoui, N.; Encinas, S.; Climent, M. J.; Gil, S.; Miranda, M. A. *Chem. Eur. J.* 2006, *12*, 553–561.
214. Thomas, M.; Guillaume, D.; Fourrey, J.-L.; Clivio, P. *J. Am. Chem. Soc.* 2002, *124*, 2400–2401.
215. Seki, K.-I.; Aizawa, K.; Sugaoi, T.; Kimura, M.; Ohkura, K. *Chem. Lett.* 2008, *37*, 872–873.
216. Gleiter, R.; Herb, T.; Borzyk, O.; Hyla-Kryspin, I. *Liebigs Ann.* 1995, 357–364.
217. Herb, T.; Gleiter, R. *Angew. Chem. Int. Ed. Engl.* 1996, *35*, 2368–2369.

218. Gleiter, R.; Gaa, B.; Sigwart, C.; Lange, H.; Borzyk, O.; Rominger, F.; Irngartinger, H.; Oeser, T. *Eur. J. Org. Chem.* 1998, 171–176.
219. Rawal, V. H.; Dufour, C. *J. Am. Chem. Soc.* 1994, *116*, 2613–2614.
220. Dvorak, C. A.; Dufour, C.; Iwasa, S.; Rawal, V. H. *J. Org. Chem.* 1998, *63*, 5302–5303.
221. Reddy, T. J.; Rawal, V. H. *Org. Lett.* 2000, *2*, 2711–2712.
222. Boxall, R. J.; Ferris, L.; Grainger, R. S. *Synlett* 2004, 2379–2381.
223. de la Torre, M.; Garca, I.; Sierra, M. A. *J. Org. Chem.* 2003, *68*, 6611–6618.
224. Iriondo-Alberdi, J.; Perea-Buceta, J.; Greaney, M. F. *Org. Lett.* 2005, *7*, 3969–3971.
225. Carless, H. A. J.; Fekarurhobo, G. K. *J. Chem. Soc. Chem. Commun.* 1984, 667–668.
226. Furth, B.; Daccord, G.; Kossanyi, *J. Tetrahedron Lett.* 1975, *48*, 4259–4262.
227. Kirschberg, T.; Mattay, J. *J. Org. Chem.* 1996, *61*, 8885–8896.
228. Gescheidt, G.; Neshchadin, D.; Rist, G.; Borer, A.; Dietliker, K.; Misteli, K. *Phys. Chem. Chem. Phys.* 2003, *5*,1071–1077.
229. Hammaecher, C.; Portella, C. *Chem. Commun.* 2008, 5833–5835.
230. Buschmann, H.; Scharf, H.-D.; Hoffmann, N.; Esser, P. *Angew. Chem. Int. Ed. Engl.* 1991, *103*, 477–515.
231. Hu, S.; Neckers, D. C. *J. Org. Chem.* 1997, *62*, 564–567.
232. Kaneko, Y.; Hu, S.; Neckers, D. C. *J. Photochem. Photobiol. A* 1998, *114*, 173–179.
233. Hu, S.; Neckers, D. C. *J. Org. Chem.* 1997, *62*, 6820–6826.
234. Rochat, S.; Minardi, C.; de Saint Laumer, J.-Y.; Herrmann, A. *Helv. Chim. Acta* 2000, *83*, 1645–1671.
235. Sakamoto, M.; Aoyama, H.; Omota, Y. *J. Chem. Soc. Perkin 1* 1986, 1759–1762.
236. Sakamoto, M.; Takahashi, M.; Fujita, T.; Watanabe, S.; Nishio, T.; Iida, I.; Aoyama, H. *J. Org. Chem.* 1997, *62*, 6298–6308.

28

Quinone Photochemistry

Helmut Görner
Max-Planck-Institute for Bioinorganic Chemistry

28.1 Introduction

Quinones are ubiquitous in biological systems and cofactors in the photosynthetic reaction centers where the initial products are radical ion pairs. The photochemistry of quinones has been intensively investigated and reviewed earlier (Bruce 1974). Thereafter, advances and new applications were presented (Maruyama and Osuka 1988). The scope of the quinone photochemistry covers a broad range from being a key molecule in a computational model of photocatalytic water splitting (Sobolewski and Domcke 2008) to the material on bioinspired electron transfer (ET) systems (Fukuzumi 2006) as well as the natural and artificial photosynthetic energy conversion (Barber 2009). The application of quinone cycloaddition is widespread, extending from the beginning of photochemistry to modern applications and has been updated in several contributions (Creed 1994, Maruyama and Kubo 1994, Gilbert 2004, Oelgemöller and Mattay 2004). Attention has been focused on the production of fine chemicals with quinones and sunlight (Oelgemöller et al. 2007). A further review deals with the role of quinones in toxicology (Bolton et al. 2000). The literature concerning quinones in both synthetic photochemistry and photosynthetic reaction centers is numerous and only a few selected papers could be cited here.

This chapter aims at a deeper insight into the quinone photochemistry in organic solvents. Another approach refers to the specific role of water in these photoprocesses. An adequate description of the field would greatly exceed the allocated space. This chapter is therefore limited to a presentation of the 2009 state-of-the-art mechanistic aspects; it focuses on quinones mainly from a reactivity point of view and does not deal too much with photosynthetic topics. Nevertheless, some earlier studies are highlighted and the references may allow the reader to find an entry into the wider literature. A major goal is a systematic presentation and better understanding of the fundamental framework of reactions. In order to gain an insight into the details of the molecular structure versus function relationship, the effects of specific additives on the intermediates and reactivities of a series of 1,4-benzoquinones (BQ),

1,4-naphthoquinones (NQ), and 9,10-anthraquinones (AQ) are presented in a compact form. The presentation refers to *p*-quinones in solvents at room temperature, whereas *o*-quinones and low temperatures are mostly omitted or indicated where considered.

28.2 Photoreduction

The photoreduction of BQ, NQ, AQ, and their derivatives is rather efficient and follows a common mechanism. The quantum yields of formation of dihydroquinones (QH_2) in the presence of a donor (DH_2) are up to unity. In particular, anthraquinol, the corresponding QH_2, is formed for AQ in mixtures of benzene and 2-propanol with $\Phi = 0.9–1$ (Wilkinson 1962, Schulte-Frohlinde and von Sonntag 1965). Most organic solvents react with excited quinones and these processes can be analyzed clearer using an inert solvent and an alcohol or amine. 2-Propanol and triethylamine (TEA) were chosen here as two model donors owing to a high reactivity and virtually no absorption at 254–313 nm for the latter. Some quantum yields are compiled in Table 28.1. For comparison, $\Phi^{TEA} = 0.4$ for both BQ and duroquinone (Me_4BQ), but 0.05 for ubiquinone-0: 2,3(OMe)$_2$5MeBQ (UQ_0) (Görner 2003a). Generally, the quantum yield of decomposition in the absence of a donor is small or moderate, for example, 0.002–0.05 for BQ, NQ, or AQ (Görner 2003b). Examples of the photoinduced spectral changes are shown in Figure 28.1 for BQ and Me_4BQ. A minimum of reaction steps is shown in Scheme 28.1.

TABLE 28.1 Quantum Yield Φ^D of Reduction Using 2-Propanol, TEA, Ascorbic Acid, and Φ^{H_2O} of Substrate Decomposition[a]

Compound	Φ^{2P}	Φ^{TEA}	Φ^{AscH} [b]	Φ^{H_2O} [b]
BQ	0.8	0.4	>0.3	0.5
Me_2BQ	0.7	0.5	0.6	0.7
Me_3BQ	0.04	0.3	0.3	0.1
Me_4BQ	0.02	0.4	0.1	0.1
Cl_2BQ	0.8	0.8		1.3
Cl_4BQ	0.1			0.1
NQ	0.7	0.45	0.1	0.15
AQ	0.9		0.03	0.02

[a] In deoxygenated acetonitrile (Görner 2003a,b, 2004a,b).

[b] In deoxygenated acetonitrile–water 1:1.

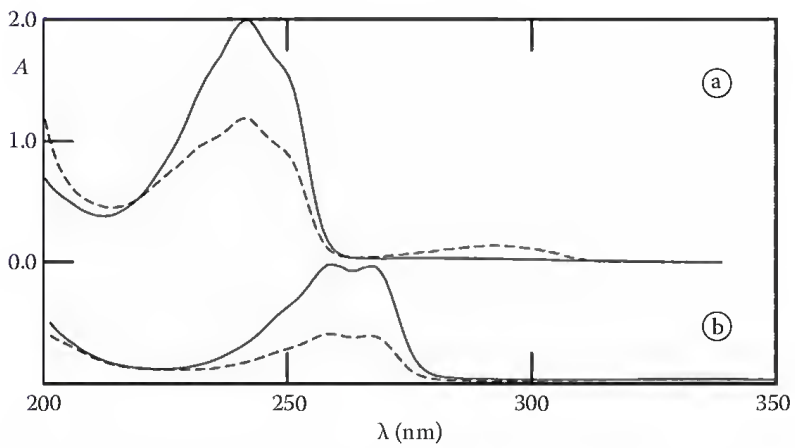

FIGURE 28.1 Absorption spectra in argon-saturated acetonitrile: 2-propanol of (a) BQ (9:1) and (b) Me_4BQ (1:1) prior to (full) and after irradiation at 254 nm (broken), cf. Görner (2003a).

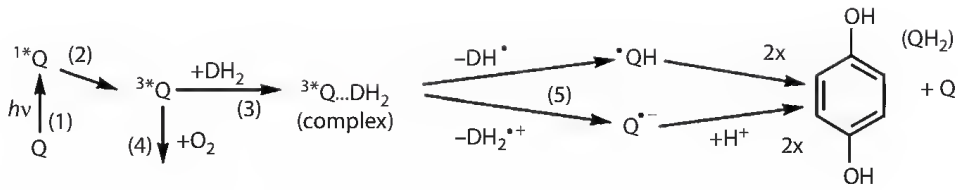

SCHEME 28.1 Photoreduction in the presence of donors via H-abstraction and ET.

Excitation of the ground state leads to the first excited singlet state (^{1*}Q), step (1), which is characterized by its electronic energy and by different vibrational states. Decay of ^{1*}Q leads to the lowest triplet state (^{3*}Q), step (2). The molecule also can fluoresce or revert radiationlessly to Q through internal conversion. Irradiation in the presence of DH_2-type additives then generates long-lived semiquinone radicals, reaction (3), and finally a relatively stable dihydroquinone, step (5). In competition, triplet quenching by oxygen (4) occurs, and some consequences are discussed in Chapter 9. The radical anion ($Q^{\bullet-}$) and the conjugated semiquinone radical ($^{\bullet}$QH) are rather unique (cf. Rosokha et al. 2009) and the earlier literature of short-lived radicals has been reviewed (Khudyakov and Kuzmin 1975, Das and Venkataraman 2005). For all three types, BQs, NQs, or AQs, optimized conditions can be chosen, where Φ^{Donor} is close to unity. This likewise implies a quantum yield of intersystem crossing (Φ_{isc}) of close to unity. Two semiquinone radicals are formed by one photon, whereby one radical is due to H-atom transfer from the alcohol and one from the donor radical. Alternatively, ET from an amine to ^{3*}Q takes place; for details see Chapters 4, 5, and 7. Nevertheless, several changes, for example, substitution with electron-donating groups, can lower the reduction significantly, for example, for $(OMe)_2$BQ where $\Phi^{2P} = 0.01$ and $\Phi^{TEA} = 0.05$ (Görner 2003a).

28.3 Excited Singlet State and Ground State Reactions

The absorption spectrum of BQ has a maximum at 240 nm (Figure 28.1a) with a molar absorption coefficient of 2×10^4 M^{-1} cm^{-1} and extends to the visible with $\varepsilon_{440} = 200\,M^{-1}\,cm^{-1}$. Those of BQ derivatives are redshifted (see Figure 28.1b) for Me_4BQ. For NQ the values are $\varepsilon_{250} = 2 \times 10^4$ and $\varepsilon_{330} = 3 \times 10^3$ M^{-1} cm^{-1}; for AQ $\varepsilon_{250} = 5 \times 10^4$ and $\varepsilon_{400} = 90\,M^{-1}\,cm^{-1}$. Substitution of AQ has relatively large effects and various AQs serve as dyestuffs (McKellar 1971). Concerning ground state interactions, a few papers should briefly be mentioned. In some cases, for example, xanthene dyes and quinones, complexation has been reported, the association constants are 20–1500 M^{-1} (Gutiérrez and García 1998). Chlorin pigments show hypsochromism, when complexed with BQs (Mennenga et al. 2006). A thermal reduction of quinones by OH^- or MeO^- can take place (Fukuzumi and Yorisue 1991). Another thermal quinone reduction is known (Pandey 1982, Isaacs and van Eldik 1997) in the presence of ascorbic acid (vitamin C: AscH).

The excited singlet state of most quinones is extremely short lived. Population of the lowest triplet state of parent BQ occurs within 20 ps, as concluded from hydrogen abstraction in a time-resolved Raman scattering study (Rossetti and Brus 1986). This is in excellent agreement with data for BQ in acetonitrile (Yuasa et al. 2004). The fast ET from a singlet excited pigment to a quinone is the subject of various studies (see Chapter 11). For BQs and NQs, the ^{3*}Q state (rather than ^{1*}Q) is the first spectroscopically and kinetically accessible species. One exception is constituted by hydroxyAQs (Diaz 1990), where the ISC step is longer than a few picoseconds. HydroxyAQs therefore exhibit fluorescence, but the quantum yields (Φ_f) are generally smaller than 0.01 (Table 28.2). AlkylaminoAQs belong to another class of quinones showing fluorescence. AminoAQs have a fluorescence maximum in the 500–600 nm range, small or moderate Φ_f, and a fluorescence lifetime (τ_f) of 0.2–5 ns (Müller et al. 2006); some properties are compiled in Table 28.3. For purpurin in acetonitrile $\Phi_f = 0.08$ and $\tau_f = 2$ ns (Del Giacco et al. 2003). The fluorescence of quinizarin is quenched by a series of amines (Kumbhakar et al. 2004). Intramolecular charge transfer (CT) can occur through hydrogen bonding. For 2-aminoAQ the major deactivation

TABLE 28.2 Quantum Yields of Fluorescence, ISC, and Singlet Molecular Oxygen of HydroxyAQs[a]

Compound	Common Name	Φ_f	Φ_{isc}	Φ_Δ	S_Δ
AQ			0.9	0.70 (0.62)[b]	0.8
1-OHAQ	ErythroxyAQ	0.001	≥0.17	≤0.25	1
2-OHAQ		0.00001	0.72	0.68	0.9
1,2-$(OH)_2$AQ	Alizarin	0.004	0.16	0.03 (0.03)[b]	0.2
1,4-$(OH)_2$AQ	Quinizarin	0.1	0.3	0.08	0.27
1,8-$(OH)_2$AQ	Chrysazin	0.017	0.7	0.7 (0.69)[b]	0.96
2,6-$(OH)_2$AQ	Anthraflavin	0.00001	0.75	0.34	0.45
1,8-$(OH)_2$-3-CH_2OHAQ	Aloe Emodin[c]			0.54	
1,6-$(OH)_2$-2-MeAQ	Soranjidiol[d]			0.47	
1,2,4-$(OH)_3$AQ	Purpurin[e]	0.005	0.05	0.47	

[a] In acetonitrile (Gollnick et al. 1992).
[b] Gutiérrez et al. (1997).
[c] Vath et al. (2002).
[d] In chloroform (Núñez Montoya et al. 2005).
[e] In chloroform (Comini et al. 2007).

TABLE 28.3 Fluorescence Lifetime and Quantum Yields of AminoAQs[a]

Compound	Solvent	λ_f (nm)	τ_f (ns)	Φ_f	Φ_{isc}
1-NH_2AQ	Cyclohexane	543	1.75	0.066	
	Toluene	566	1.7	0.047	0.097
	Acetonitrile	590	0.94	0.022	
2-NH_2AQ	Toluene	532	5.0	0.19	0.40
1-NHMeAQ	Cyclohexane	563	0.4	0.01	0.04[b](0.19)[c]
	Acetonitrile	617	0.2	0.0026	
1-NMe_2AQ	Toluene	600	<0.001	<0.001	<0.001
2-NMe_2AQ	Toluene	568	11	0.33	0.08
1,4-$(NH_2)_2$AQ	Acetonitrile	617		0.02	

[a] Dahiya et al. (2005, 2006a,b).
[b] In toluene (Borst et al. 1992).
[c] For 2-NHMeAQ in toluene.

occurs radiationlessly through hydrogen bonding, that is, via intramolecular CT (Morimoto et al. 2001). A hard-soft anionic character in the excited singlet state has been suggested (Umadevi et al. 2008). Nevertheless, most quinone reactions start from the ^{3*}Q state.

28.4 Triplet State Reactions of BQs and NQs

The T-T absorption spectra of BQ or NQ have a major band at 300–320 nm and a minor one at 400–500 nm. Φ_{isc} of various quinones is high (0.5–1), based on photoacoustic calorimetry (Serpa and Arnaut 2000). This, however, does not hold for BQs with electron-donating groups including ubiquinones (Land et al. 1971). For UQ_{30}, Φ_{isc} = 0.04–0.09 (Bensasson et al. 1972, Amouyal et al. 1974). For comparison, Φ_{isc} = 0.15 for 2,5-$(OMe)_2$BQ. The triplet energy (E_T) of BQ is 220 kJ mol^{-1} and the one-electron reduction potential (*vs.* SCE) E^0 = −0.52 and 0.08 V in acetonitrile and water, respectively. Examples for significant effects of structure on E_T and E^0 are compiled in Table 28.4, for example, E^0 = 0 for Cl_4BQ in acetonitrile.

TABLE 28.4 One-Electron Reduction Potential and Triplet Energy of Quinones[a]

Compound	E_T (kJ mol^{-1})	E^0 (V)[b]	E^0 (V) H_2O[c]
BQ	220	−0.52	0.08
Me_2BQ	220	−0.61	−0.07
Me_4BQ	218	−0.84	−0.26
Cl_4BQ	261	−0.01	0.65
NQ	225	−0.71	−0.14
MeNQ	225	−0.80	−0.24
AQ	261	−0.95	−0.45

[a] In acetonitrile (Goez and Frisch 1995).
[b] Vs. SCE.
[c] In water (Roginsky et al. 1999).

The triplet lifetime of quinones (τ_T) in oxygen-free nonaqueous solution is up to the millisecond time range. However, for many BQs or NQs at room temperature, τ_T is as short as a few microseconds. In a typical experiment, when time-resolved UV-vis spectroscopy with 248 or 308 nm pulses is applied, τ_T = 5–10 µs, for example, for BQ in acetonitrile? (Serpa and Arnaut 2000, Görner 2006a). The triplet state of quinones is quenched by oxygen, the rate constant ($k_4^{O_2}$) of quenching is (0.3–3) × 10^9 M^{-1} s^{-1}, and some values are listed in Table 28.5. For UQ_{30} in benzene $k_4^{O_2} = 1.5 \times 10^9 M^{-1}s^{-1}$ (Bensasson et al. 1972). The major step of triplet quenching by oxygen is formation of singlet molecular oxygen. The quantum yield (Φ_Δ) of its formation is relatively large (see Chapter 9). Φ_Δ can be considered as a minimum of Φ_{isc}. Note that the triplet can undergo a specific quenching process by ground state quinone, the so called self-quenching reaction (see Chapter 7). This shortens τ_T markedly and can lead to radicals as intermediates and eventually to additional photoproducts. Thus, one can expect a limiting τ_T and no secondary products only at a low enough quinone concentration.

Secondary intermediates can be produced by reaction of the triplet with the solvent or other donors. The rate constant of triplet quenching by TEA and 2-propanol, reaction (3), depends essentially on the conditions, for example, the one-electron potentials in the case of ET. For BQ in acetonitrile k^{2P} = 9 × 10^7 M^{-1} s^{-1} and k^{TEA} = 1 × 10^{10} M^{-1} s^{-1} and for other quinones the rate constants are smaller. Some effects of substitution on k^{Donor} can be seen in Table 28.5. For 2-OMeBQ in acetonitrile k^{EtOH} = 1 × 10^7 M^{-1} s^{-1} and for Me_4BQ k^{EtOH} is as low as (2–3) × 10^4 M^{-1} s^{-1} (Scheerer and Grätzel 1977), that is, methoxyBQs and

TABLE 28.5 Rate Constants for Quenching of Triplet Quinones (10^9 M^{-1} s^{-1}) by Oxygen, TEA, 2-Propanol, Ascorbic Acid, NaTyr, and DMSO[a]

Compound	$k_4^{O_2}$	k^{TEA}	k^{2P} ×10^{-3}	k^{AscH}	k^{NaTyr}	k^{DMSO}
BQ	0.5	10	90	(9)[b]		2.7
Me_2BQ	1.4	12 [2][c]	35	9 (5)	3	2
Me_4BQ	1.8	6 [2]	0.05	3.4 (1)	2	<0.01
Cl_2NQ	1.2		18			
Cl_4BQ	1.1	6 [3]	0.1			2
$(OMe)_2BQ$	1.5	6 [3]	0.1			
NQ	0.3			(4)		5
AQ			2	4 (3.5)	1.4	2

[a] In acetonitrile or 1:1 with water (Görner, 2003a,b, 2004a,b, 2006a,b, 2007a), DMSO: dimethyl sulfoxide.
[b] In parentheses: 90% water.
[c] In brackets: benzene.

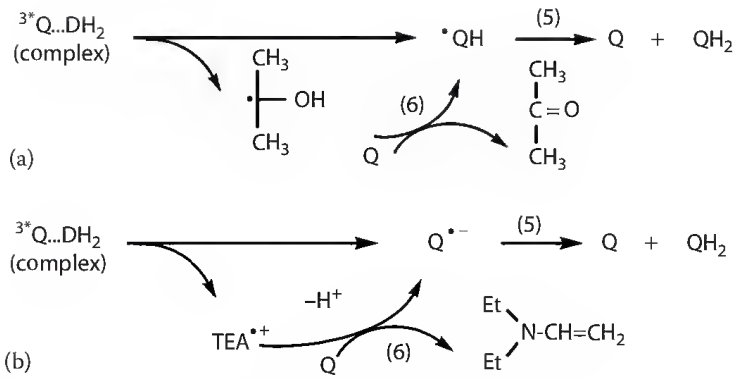

SCHEME 28.2 Photoreduction in the presence of (a) 2-propanol and (b) TEA.

Me_4BQ have a much lower reactivity than parent BQ. Photoinduced H-transfer occurs from alcohols and many other solvents. Alternatively, ET reactions from amines to $^{3*}Q$ take place. These reductions were observed for a series of quinones in benzene or acetonitrile as examples of quasi-inert solvents of low and large polarity, respectively.

The products derived from oxidation of 2-propanol and TEA are acetone and diethylvinylamine (see Scheme 28.2a and b). The intermediates are donor and semiquinone radicals of which the latter react by self-termination/combination in Q and the QH_2 (step (5)). Photoinduced ET in benzene leads to $^{\bullet}QH$ rather than $Q^{\bullet-}$. In organic solvents, no equilibrium is established between these radicals. Reaction (6) accounts for the second reduction step, the intermediates, which are virtually nonobservable by UV spectroscopy, are propyl and α-aminoethyl radicals, respectively. The absorption of the short-lived triplet state is overlapped with that of the semiquinone radical (see examples in Figure 28.2). The photoconversion to QH_2 products of several BQs, but not of NQ or AQ, is relatively clean, when a modified ascorbic acid serves as electron donor in 1,2-dimethoxyethane (Kulkarni and Kate 2000); for the quinone/ascorbate system, see Chapter 8.

Mono- and diphenylBQs play a special role since the photoreactions in nonpolar and polar solvents lead to cyclobutane-type dimers and 2-hydroxydibenzofurans, respectively; the photoinduced key step is H-transfer and/or ET from the selected donor molecule to the sensitizer triplet state (Hageman and

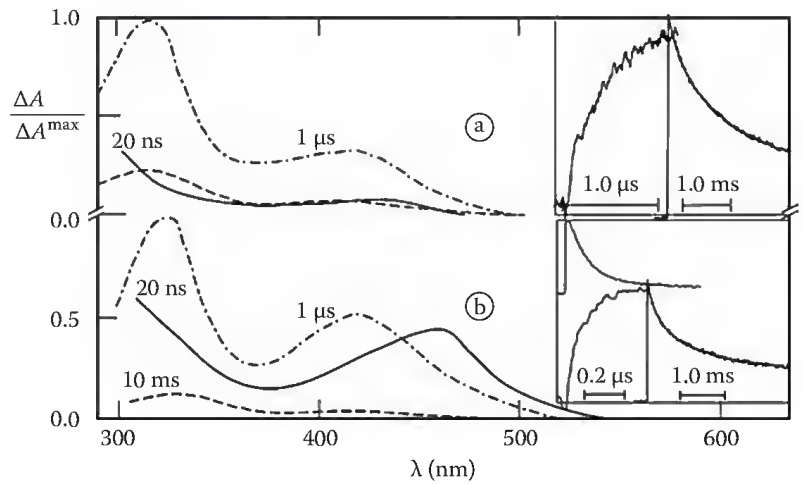

FIGURE 28.2 Transient absorption spectra of (a) BQ and (b) Me_4BQ in argon-saturated acetonitrile (1–2 mM TEA) at 20 ns, 1 μs, and 10 ms after the 308 nm pulse; insets: kinetics at 410 nm, cf. Görner (2003a).

Verhoeven 1997). Photocyclization of 2,5-Cl_2-3,6-bis(dialkylamino)BQ is wavelength dependent (Shi et al. 2007). Depending on the conditions, for example, solvent polarity, the mechanism can be directed to different product distributions. The singlet ion pair of chloranil (Cl_4BQ) and aromatic donors is formed within 5 ps (Hubig et al. 1997). Quinones function as sensitizers for preparative photolysis and especially Cl_4BQ has been frequently employed in this role (Gschwind and Haselbach 1979, Bergmark and Jones 1997, Jones et al. 1997, Baciocchi et al. 1998, Bosch et al. 1998, Hubig and Kochi 1999, Del Giacco et al. 2001, Fukuzumi et al. 2001, Latour et al. 2005, Krongauz and Kim 2006, Murakami et al. 2008). The formation of enrofloxacin, levofloxacin, and ofloxacin with Cl_4BQ is rapid and sensitive (Ulu 2009). Dimers result from semiquinone radicals, for example, for methoxyBQs (Marquardt et al. 1992, Béarnais-Barbry et al. 2001). Some related topics with BQs have been discussed (Kuzmin et al. 1979, Levin et al. 1996, Goez and Eckert 2006). The semiquinone radical can also be formed in biomimetic materials based on SiO_2 and indole (Christoforidis et al. 2008).

The triplet state properties of NQs in organic solvents have been studied by several groups (Gan and Whitten 1993, Amada et al. 1996, Mac and Wirz 2002). The triplet state of parent NQ is short lived and the T-T absorption is overlapped with that of the long-lived semiquinone radical. The addition of substituents lowers the intermolecular reactivity for most of the NQ derivatives, but does not drastically change the overall behavior in nonaqueous solution. The photoproduct of 2,3-Cl_2NQ in the presence of furan is 2-Cl-3-furanylNQ and Φ is up to 0.12 (Yamaji et al. 1999). The photoreaction between Cl_2NQ and *N,N′*-diphenylthiourea involves an electron donor acceptor adduct as intermediate (Datta and Mukherjee 2004). Formation of singlet molecular oxygen is efficient for NQs (see Φ_Δ in Table 28.6). Φ_Δ = 0.6–0.7 for juglone and plumbagin in acetonitrile. For lapachol: 2-hydroxy-3-(3-methyl-2-butene-1-yl)NQ, Chart 28.1, however, where Φ_Δ in CCl_4 is nearly zero, an efficient singlet reaction takes place; this is similar for vitamin K_1 and plumbagin (Chapter 10). The reactivity and photosensitizing properties of the triplet state of α- and β-lapachone have been characterized (Ci et al. 1989, Netto-Ferreira et al. 2008, 2009). ET from TEA to triplet NQ within 1 μs and the radical decay within 0.2 ms is shown in Figure 28.3a. For MeNQ in acetonitrile $k^{TEA} = 2 \times 10^{10}$ M^{-1} s^{-1} (Swartz et al. 2008). The triplet states of mono- and dimethylNQs were studied at low temperatures (Shimokage et al. 1997), and the phosphorescence lifetime of 2-OMeNQ in (m) ethanol at 77 K is 4 ms (Aaron and Winefordner 1972). Similar lifetimes have been found for Cl_2NQ

TABLE 28.6 Quantum Yields of Formation of Singlet Molecular Oxygen and Superoxide Ion for Quinones[a,b]

Compound	Common Name	Φ_Δ			Φ_{O_2}
		CCl_4	MeCN	H_2O[b]	
BQ				0.14	0.29
MeBQ				0.11	0.06
Me_4BQ	Duroquinone			0.8	
NQ		0.6	0.6	0.27	0.06
MeNQ	Menadione	0.7			
Cl_2NQ		0.6	0.6		
BrNQ		0.7	0.7		
OMeNQ		0.7	0.8		
2-OHNQ	Lawsone				0.003
5-OHNQ	Juglone	0.1	0.7	0.14	0.005
2-Me-5-OHNQ	Plumbagin	0.1	0.6	(0.2)[c]	
Sulfonate-AQ				0.41	0.04

[a] Görner (2005a).
[b] In water (Alegría et al. 1999).
[c] For 5,8-$(OH)_2$-NQ.

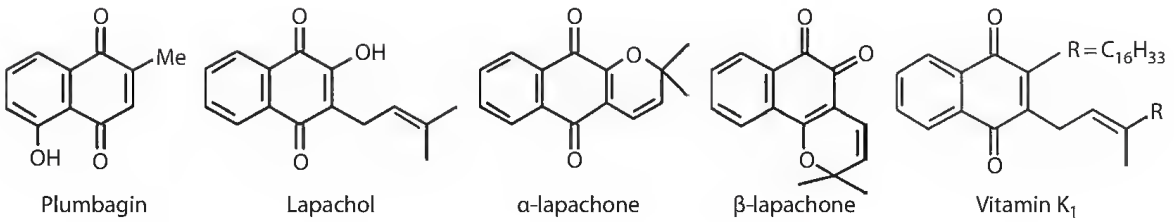

CHART 28.1 Structures of specific NQs.

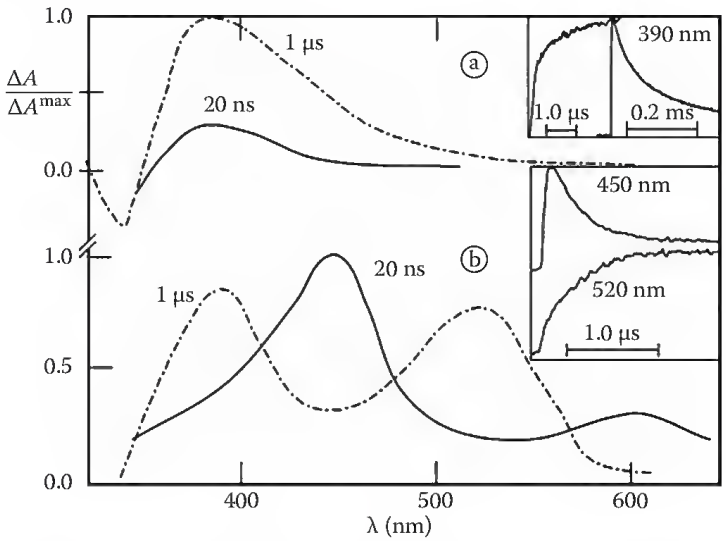

FIGURE 28.3 Transient absorption spectra of (a) NQ and (b) Me_2AQ in argon-saturated acetonitrile plus 2 mM TEA at 20 ns and 1 μs after the 308 nm pulse; insets: kinetics as indicated, cf. Görner (2003b, 2004a).

and vitamin K_1 and somewhat shorter ones for NQ and BrNQ (Amada et al. 1995). The Paterno–Büchi reaction between NQ and anetholes in polar solvents involves ET (Eckert and Goez 1994). The photoacylation of 2-R-NQs gives access to biologically active NQs (Friedrichs et al. 2008).

28.5 Photoreactions of AQs

The triplet state properties and subsequent radical reactions of AQs are in principle the same as for BQs and NQs. ET and H-transfer to triplet AQ were studied by CIDEP and flash photolysis (Yoshihara et al. 2000, 2001). An example of ET from TEA is shown in Figure 28.3b for Me_2AQ, where, in contrast to AQ, the T-T and radical absorption spectra are well-enough separated (Görner 2003c). AQs provide a wide application potential due to the large variety in substitution pattern (Hamanoue et al. 1992). One class contains hydroxy groups, another alkylamino, and a third nitro groups. Marked effects of substitution on Φ can be seen from the data compiled in Tables 28.2 and 28.3. For alizarin, a naturally occurring hydroxyAQ, $\Phi_\Delta = 0.03$. For 1,5-$(OH)_2$AQ in acetonitrile $\Phi_\Delta < 0.01$, whereas $\Phi_\Delta = 0.5$ for 1,8-$(OH)_2$-4,5-$(MeO)_2$AQ in benzene (Davies et al. 1972a). Aloe emodin, due to a substantial Φ_{isc}, exhibits phototoxicity (Vath et al. 2002). The ratio $S_\Delta = \Phi_\Delta/\Phi_{isc}$ is close to 1 for AQ and depends significantly on substitution. Introduction of amino groups causes CT effects, which lowers Φ_{isc} significantly (Table 28.2); a certain part of the excitation energy dissipates as internal conversion.

For 1,4-diazabicyclo[2.2.2]octane (DABCO) as specific amine, virtually no QH_2 product can be observed, whereas the k^{DABCO} values are high and similar to those with TEA. The reason is efficient electron back transfer, thereby restoring both the amine and the quinone. For ClAQ $\Phi^{TEA} = 0.9$ (Hamanoue et al. 1985). For 1,8-$(OH)_2$AQ in acetonitrile $k^{Anilin} = (2–19) \times 10^9\ M^{-1}\ s^{-1}$ for triplet quenching by anilines (Pan et al. 2007). Triplet quenching reactions by dimethyl sulfide are also rather efficient, $k^S = (2–3) \times 10^{10}\ M^{-1}\ s^{-1}$ for BQs,

NQ, and AQ in acetonitrile and roughly 5–10 times smaller for DMSO (Görner 2006a). A photoinduced methylene/AQ shuttle results in two-electron oxidation of a tertiary amine (Gun et al. 1991). The ET from TEA to triplet AQ was examined by Fourier-transform (FT) EPR spectroscopy (Beckert and Fessenden 1996, Kausche et al. 1996). Interactions between AQ and aromatic amines were also studied in micellar media (Chowdhury and Basu 2006). For MeAQ, H-transfer occurs from the methyl group to the carbonyl oxygen (Nakayama et al. 1999).

Some new photoreactions use skillfully substituted AQs (Brinson et al. 2005, Mitchell et al. 2005, Hou and Wan 2008). For example, a novel excited-state intramolecular reaction of 2-(hydroxymethyl)AQ in aqueous solution has been presented (Lukeman et al. 2002). A simple and smart oxygen sensor was developed based on the intrazeolite reactions of R-AQs (McGilvray et al. 2006). Biradical intermediates have been proposed to account for the photoproducts of 1-alkoxyAQs (Smart et al. 1997). Triplet formation for aminoAQs is not efficient, in contrast to diaminoAQs (Borst et al. 1992, Reszka et al. 1992). The properties of polymers containing in-chain quinone moieties have been outlined (Hodge and Gautrot 2009); their application potential, however, is limited by the rather low solubility.

The major photoprocess of nitroAQs is the conversion to 1-aminoAQs, and the full conversion requires six reduction equivalents (El'tsov et al. 1977, Studzinskii et al. 1978). An example is shown in Figure 28.4. The first step is population of the triplet state, which has τ_T of ca. 20 ns for 2-methyl-1-nitroAQ. H-transfer from the alcohol generates nitroAQ-derived radicals that combine bimolecularly in nitroAQ and nitrosoAQ (Gruen and Görner 2008, Görner and Gruen 2010). The reactions are summarized by step (a) in Scheme 28.3. The same radical can be produced by ET from an amine. Further ET steps occur, whereby 1-aminohydroxylAQ is formed (step b). The quantum yield of complete reduction is up to 0.2. In 1-phenylethanol, acetophenone, which acts as a sensitizer, was found as trace impurity. Various sensitizer-donor couples with ketones and alcohols or amines can likewise be used to achieve efficient conversion. For 1-nitroAQs, however, the carbonyl groups function in steps (c) and (d) as H-atom acceptor sites. The further reduction by prolonged irradiation, shown in the inset of Figure 28.4 as secondary band around 390 nm, yields the dihydro-1-aminoAQ, step (e). Admission of oxygen yields back the 1-aminoAQ, this being a common reaction of quinones.

Larger quinones partly follow a photochemical pattern analogous to that of AQ (Davies et al. 1972b, Harada et al. 2005). For 9,10-phenanthrenequinone (Taguchi et al. 2007) two close-lying triplet states were proposed (Silva and Nicodem 2008); self-quenching in acetonitrile is efficient, $k = 7 \times 10^8$ M^{-1} s^{-1} (Yamaji et al. 2002). The rate constant of triplet quenching by 9,10-phenanthrenequinone in

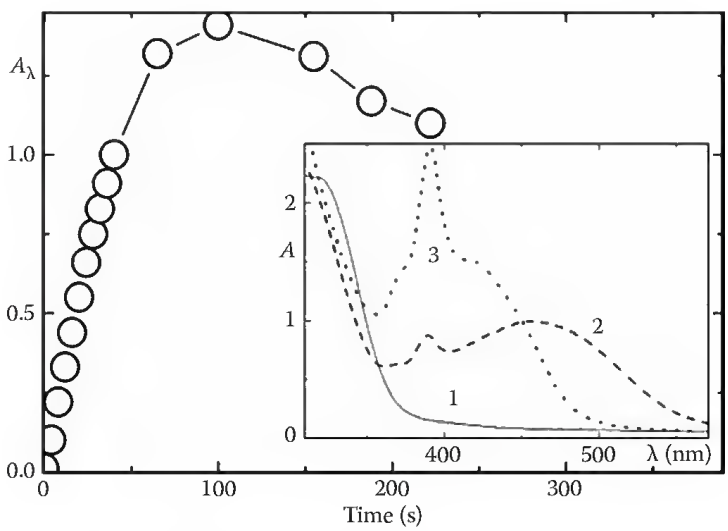

FIGURE 28.4 Absorption changes at 470 nm *vs.* time of irradiation at 313 nm for 2-methyl-1-nitroAQ in argon-saturated acetonitrile in the presence of 1 M 1-phenylethanol; insets: spectra at 0, 240, and 400 s, 1–3, respectively, cf. Gruen and Görner (2008).

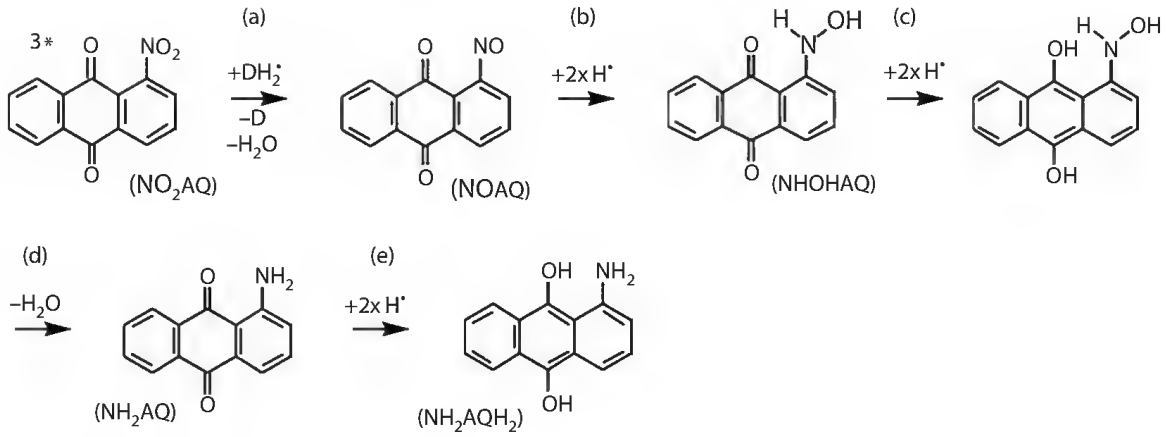

SCHEME 28.3 Photoreduction of 1-nitroAQ.

acetonitrile is $k^Q = 4 \times 10^8$ M^{-1} s^{-1} (Nicodem et al. 2005). For 6,11-dihydroxynaphthacene-5,12-dione in acetonitrile $\Phi_f = 0.4$; an exciplex has been detected upon interaction with aromatic hydrocarbons (Rath and Mukherjee 1997, Rath et al. 2001). For 5,12-naphthacenequinone in CCl_4, self-quenching occurs with a rate constant of 4×10^7 M^{-1} s^{-1} (Yamaji et al. 2002). For 6-phenyloxy-5,12-naphthacenequinone the *trans*→ana photoreaction takes place within 15 ns via a triplet biradical, whereas the reverse photoreaction occurs via the excited singlet state (Born et al. 2007). Photochemical H-abstraction by pyrene-4,5-dione has been studied (de Lucas et al. 2009). CT properties and solvent dependence have been found for a quaterthiophene-AQ dyad (Wan et al. 2008).

A different pattern results for violanthrone (V) and 16,17-R_2Vs (Seybold and Wagenblast 1989), the reduction of which was recently studied (Gruen and Görner 2009, 2010). Due to the absence of an accessible triplet state, sensitizers, such as acetone, acetophenone, or benzophenone, were employed. The photoproducts of Vs are the fluorescing dihydroviolanthrones (VH_2s), which undergo back-oxidation to Vs on admission of oxygen. This quinone reconstitution is common for NQs and AQ (see Chapter 9). An example of the photopromoted conversion is shown in Figure 28.5. Formation of VH_2 is effected by the presence of an alcohol or TEA. The intermediacy of the semiquinone radical (VH•, Scheme 28.4a) is indicated by the formation of VH_2 within 1 ms. The back-reaction on admission of oxygen via the VH• radical is shown in Scheme 28.4b.

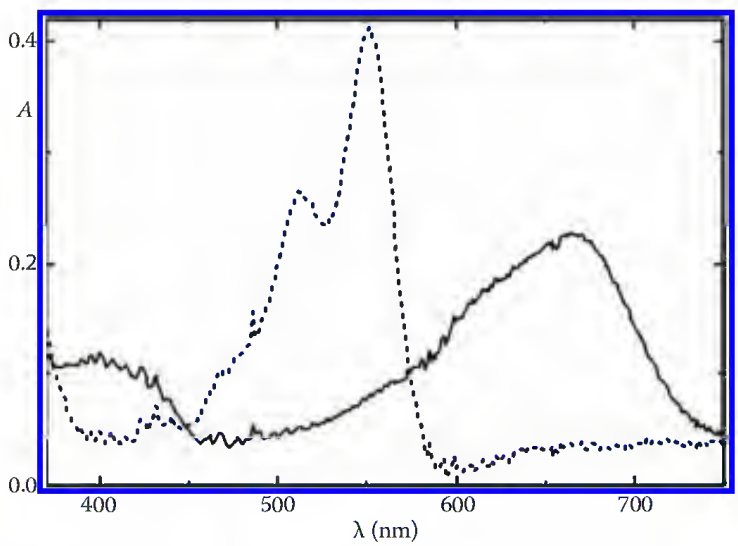

FIGURE 28.5 Absorption spectra of 16,17-dihydroxyviolanthrone in argon-saturated glycerol triacetate in the presence of 10 mM acetophenone prior to (full) and after irradiation at 313 nm (broken), cf. Gruen and Görner (2009).

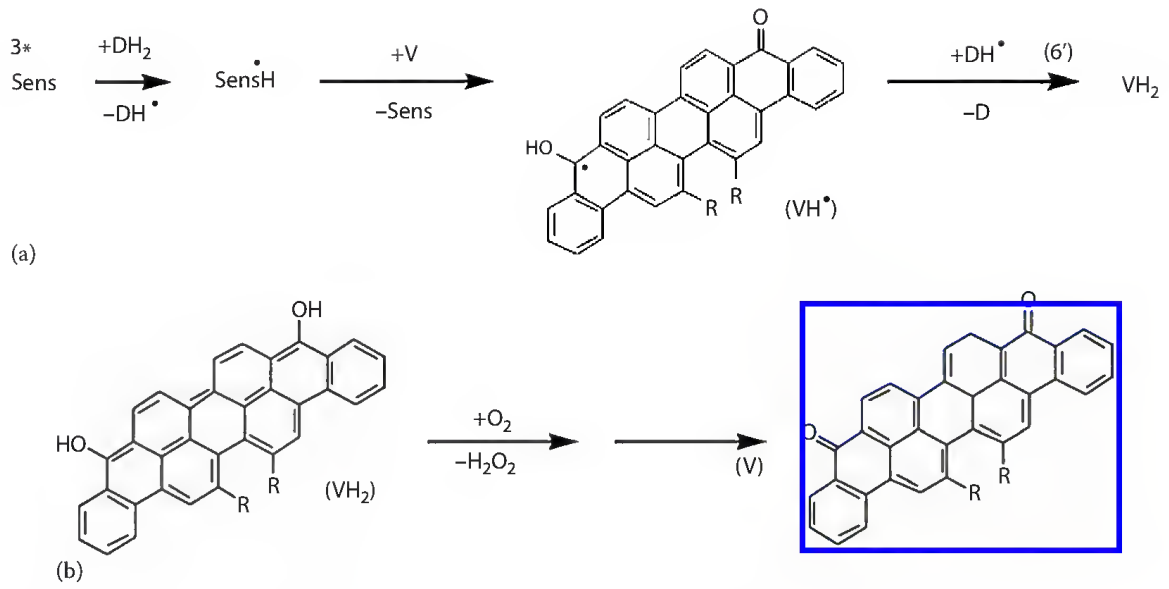

SCHEME 28.4 (a) Photoreduction of violanthrones and (b) oxidation of dihydroviolanthrones.

28.6 Properties of Semiquinone Radicals

Various reactions of free radicals in aqueous solution with quinones have been investigated. The literature concerning the properties of radicals derived from quinones is numerous and only a few papers can be cited here (Roginsky et al. 1998, Yashiro et al. 2005, Folkes et al. 2007). Some new data concerns *p*-quinones (Land et al. 2001, 2003). The reduction potentials and equilibria of various one-electron couples, for example, quinones and oxygen, were determined by pulse radiolysis (Meisel and Czapski 1975). Fortunately, the topic has been reviewed (Wardman 1989). The radical anion and its conjugate acid of most quinones have different maxima (λ_R) and molar absorption coefficients; some values are listed in Table 28.7. The inflection point is located at pK_a. While pK_a of BQs, NQs and AQs is at 4–5, that of riboflavin is much larger (8.3; Steenken and Neta 2003).

$Q^{\bullet-}$ of AQ has a second peak at 480 nm in contrast to $^{\bullet}QH$. Such a two-*vs.*-one peak behavior of the conjugate radicals is not known for BQs and NQs. For the reaction of semiquinone radicals of 2,5-di-*tert*-butylBQ in acetonitrile with oxygen the rate constant is small, $k = 2 \times 10^5\ M^{-1}\ s^{-1}$ (Valgimigli et al. 2008). A molecular-level understanding of the reactivity differences for radical anions of juglone and plumbagin was approached by electrochemical methods (Hernández-Muñoz et al. 2009). The fluorescence of the radical anion of BQ in methyltetrahydrofuran at 77 K has $\Phi_f = 0.003$ and a lifetime $\tau_f = 63$ ns (Cook et al. 1997). The 1,2,4-trihydroxybenzenes (benzenetriols: $(HO)_3C_6R_3$) react with BQs to BQH_2s and 2-hydroxybenzoquinones (BQOHs) (Schuchmann et al. 1998). This has major consequences on the photoproduct pattern (see Chapter 7).

TABLE 28.7 Radial Maximum and Absorption Coefficient of Quinones[a]

		Semiquinone Radical		Radical Anion	
Compound	pK_a	λ_R (nm)	ε ($10^3\ M^{-1}\ cm^{-1}$)	λ_R (nm)	ε ($10^3\ M^{-1}\ cm^{-1}$)
BQ	4.0	404	5.0	430	6.1
Me_4BQ	5.0	420	4.4	445	7.4
NQ	4.1	370	7.1	390	12.5
MeNQ	4.5	370	9.5	390	12.0
Vitamin K_1	4.7	380	9.9	400	10.2
AQ	5.3	375	7.8	480	7.3

[a] Neta (1988) and Steenken and Neta (2003).

28.7 Effects of Water on the Quinone Photoprocesses

The photoreactivity of certain quinones, Me_4BQ for example, is quite similar in the absence and presence of water. A different situation holds for the photoprocesses of more reactive BQs, which give rise to 2-hydroxyBQs as additional products in water (Fukuzumi and Yorisue 1991). $(HO)_3C_6H_3$s are pH-dependent intermediates (von Sonntag et al. 2004). Φ^{H_2O} of substrate decomposition is large for BQs (Table 28.1) and the major part is due to formation of 2-hydroxyBQs. The values at pH 7 show some scatter, from $\Phi^{H_2O} = 0.35$ (Kurien and Robins 1970) to 0.5 (Görner 2003b). The presence of air/oxygen has only a small effect. The effect of water dominates since Φ^{H_2O} with and without 50% acetonitrile are very similar. For BQ in both water and heavy water $\tau_T = 0.2\,\mu s$ (Yuasa et al. 2008). The pH dependence of the transient conductivity of BQ (Figure 28.6) reveals a large positive signal after a few microseconds at pH 5–8 and then the decay due to neutralization. In the basic range, a photoinduced proton is removed by reaction with OH^- from bulk solution, resulting in a negative signal after a few microseconds, which is followed by partial decay.

The role of hydroxyl radicals in the photochemistry of BQs and NQs has been discussed (Ronfard-Haret et al. 1980). Some authors gave evidence against this (Shirai et al. 1975, von Sonntag et al. 2004) and others (Beck and Brus 1982, Ononye and Bolton 1986, Parker et al. 1992) favored it. Evidence has also been given against the formation of free hydroxyl radicals in the photochemical oxidation of water by MeBQ (Pochon et al. 2002). For Me_2BQ $\Phi^{H_2O} = 0.5$, the amount of hydroxyquinone is ca. 60% (Mazellier and Bolte 1996). The mechanism of dilute BQs does not involve free radicals at all, except at a later stage (Scheme 28.5a) where R = H, Me, or Cl. In particular, no OH radical is involved in the absence of a donor as long as self-quenching is avoided. Based on transient spectroscopy and conductivity, it could be demonstrated that the proposed pathway is initiated via nucleophilic addition of water to the lowest triplet state, reaction (7). The photohydrate (HI_{aq}) is converted to $(HO)_3C_6H_3$, step (8), which, in turn, generates hydroxyquinone in a thermal exchange reaction (9).

A more extended mechanism of photoreduction of parent BQ, methylBQs and chloroBQs in aqueous solution is compiled in Scheme 28.6. An important step is self-quenching, that is, reaction (11) of a quinone molecule in the triplet state with one in the ground state. A complex of such an excited BQ and a ground state BQ has been proposed, the equilibrium constant is $5500\,M^{-1}$ (von Sonntag et al. 2004). As a consequence of reactions (11) and (12), a radical ion pair can be formed. The radical cation then reacts with water in the 2-hydroxyquinone radical, which, in turn, reacts with Q in hydroxyquinone and QH_2. The hydroxyphotoproduct is spectroscopically accessible, the anion has $\varepsilon_{500} = 2 \times 10^3\,M^{-1}\,cm^{-1}$ and $pK_a = 4.2$. The formation of a $(HO)_3C_6R_3$ intermediate has independently been published for 2,6-Cl_2BQ, where $\Phi^{H_2O} = 1.5$, the amount of hydroxyquinone is ca. 40% and QO^- is observable with $\varepsilon_{524} = 2.5 \times 10^3\,M^{-1}\,cm^{-1}$ (Lente and Espenson 2004). Mono-, di-, and trichloroBQs were recently studied (Görner and von Sonntag 2008) and examples

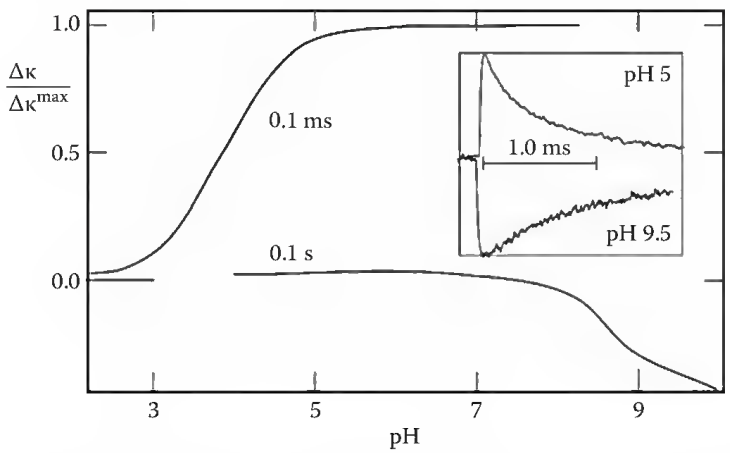

FIGURE 28.6 pH dependence of the transient conductivity signal of BQ in argon-saturated aqueous solution at two times; insets: decay of the conductivity signals at pH 5 and 9.5, cf. Görner (2003b).

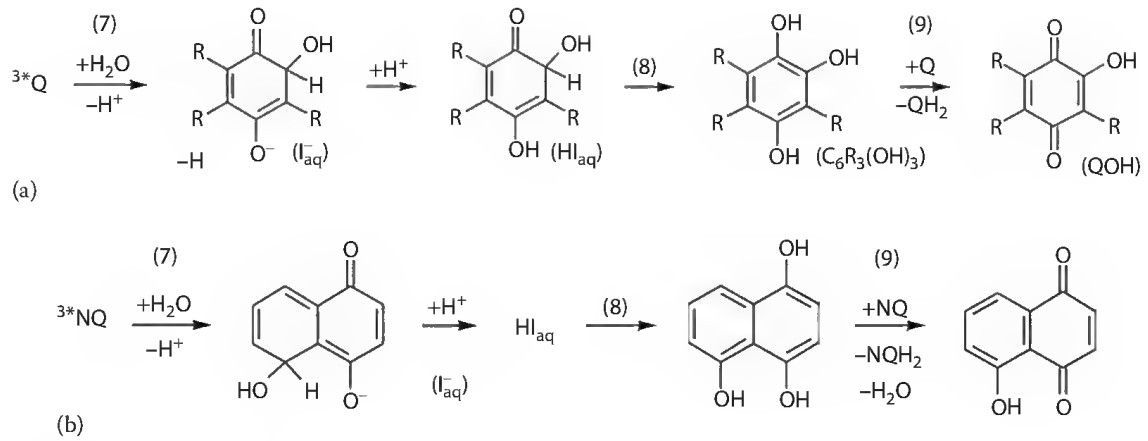

SCHEME 28.5 Photoprocesses of (a) BQs and (b) NQ in water.

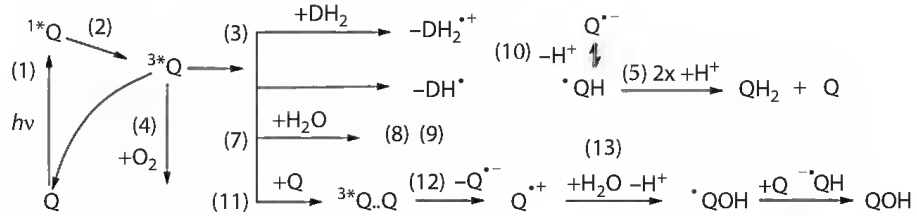

SCHEME 28.6 Photoreactions of BQ in water.

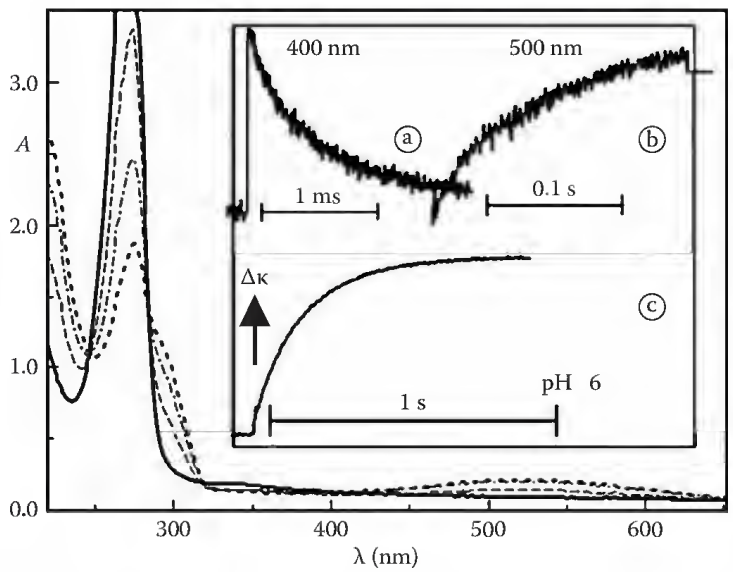

FIGURE 28.7 Absorption spectra of Cl_2BQ in acetonitrile–water (1:10) at pH 7–8 prior to (full) and after irradiation (broken, 10 s interval) at 254 nm; insets: (a) decay of the hydrate and formation of QO^- when registered by (b) absorption and (c) conductivity, cf. Görner and von Sonntag (2008).

of the spectra and kinetics including a transient conductivity signal are shown in Figure 28.7. For ClBQ and Cl_3BQ $\Phi^{H_2O} = 0.3 - 0.4$, respectively. BQ in aqueous acid can be photohydrated (Ramseier et al. 2003). The Marcus inversion region of ET between excited quinones and amines has been studied in micellar media (Satpati et al. 2008).

Analogously, the photoprocesses of dilute aqueous NQ solutions do not involve free radicals (Brahmia and Richard 2005). The mechanism is shown in Scheme 28.5b. Trihydroxynaphthalene ($(HO)_3C_{10}H_5$)

is the pH-dependent intermediate and juglone the additional photoproduct in water, the contribution changes from $\Phi^{H_2O} = 0.03$ at pH 7 to 0.8 at pH 2.4 (Brahmia and Richard 2003). The increase of Φ^{H_2O} on going to the acidic pH has also been found for MeNQ (Görner 2005a). The rate constant of triplet self-quenching is $k_{11} = 4 \times 10^9\ M^{-1}\ s^{-1}$ (Loeff et al. 1991); that is, it is difficult to avoid formation of the radical pair (see the corresponding case, steps (11)–(13) in Scheme 28.6). The photolysis of vitamin K_3 has been examined (Chen et al. 1999). The rate constant for H-transfer from lysozyme to triplet NQ is $k^{Lys} = 2.4 \times 10^{10}\ M^{-1}\ s^{-1}$ (Zhang et al. 2008). Menadione (2-MeNQ) is a frequently utilized sensitizer for the initiation of strand breaks in DNA and polynucleotides; an easily overlooked secondary process is cross-linking (Melvin et al. 1996, Bergeron et al. 2007). NQs were employed for the analysis of the interaction with bases and DNA components (Bose et al. 2008, 2009). Evidence was given by FT infrared spectroscopy for an intramolecular H-transfer in NQ as well as ubiquinone and plastoquinone (Burie et al. 1995). For 5-MeNQ, photoenolization and enol trapping takes place (Chiang et al. 1997).

AQs in aqueous solution are the subject of intensive photochemical investigations (Goez 1990, Goez and Sartorius 2003, Forbes et al. 2006, Roth 2006). Photohydrates are formed and the product pattern, for example, mono- and di-hydroxyAQs, is different, when water is present; $\Phi^{H_2O} = 0.08$ for HOAQ (Broadbent and Newton 1972, Broadbent et al. 1975). The involvement of hydroxyl radicals in the photochemistry of AQs has been discussed (Clark and Stonehill 1972, Moore et al. 1986) and later disregarded (Loeff et al. 1983, 1984). The rate constant for deprotonation of the semiquinone radical of sulfonated AQ in acetonitrile/2-propanol increases with the water content (Wakisaka et al. 1987). A 1,5-disulfonatedAQ/TEA couple was used to examine two-photon ionization with 308 nm pulses; one photon produces the radical anion via ET and the second ejects a hydrated electron (Goez and Zubarev 1999).

ET occurs from thymine or amino acids to triplet excited AQs (Geimer et al. 1997, Geimer and Beckert 1998, Tarábek et al. 2006). For α-glycine as amino acid, decarboxylation was observed by FT-EPR (Lü et al. 2001). A thymine dimer can be oxidatively cleaved by ET to excited AQ (Sheng et al. 2004). Under certain conditions, photoamination of AQ takes place (Tajima et al. 2009). The photochemistry of NQs in cyclodextrins (Takamori et al. 2001) and of AQs in liposomes (Moribe et al. 2008) has been studied by time-resolved EPR spectroscopy. AQs efficiently function as sensitizers of polynucleotides and their components (Bose et al. 2008, 2009) as well as for the initiation of damage in DNA (Armitage et al. 1994, Schuster 2000). The photoreduction of parent AQ is also efficient in hydrogels that are swollen with water and 2-propanol (Foyle et al. 1992).

28.8 Effects of Quenchers

Several aspects of the ET process from amino acids to triplet quinones have been studied. For *N*-acetyltyrosine (NaTyr), some rate constant values are listed in Table 28.5. While the rate constant of triplet quenching by phenylalanine, tyrosine, and tryptophan is close to the diffusion-controlled limit, those of aliphatic amino acids are several orders of magnitude smaller; no reaction can take place for quencher concentrations in the mM range and their Φ_d are therefore negligible. A decarboxylation has been revealed in a FT-EPR study after ET from α-amino acids to triplet AQs (Tarábek et al. 2007). A tyrosyl radical and semiquinone charge pair was detected upon ET in photosystem II at low temperatures (Zhang et al. 2004).

The ET reactions from ascorbic acid to $^{3*}Q$ of a series of quinones were observed under oxygen-free conditions; H-abstraction was proposed in water-free solution (Bisby and Parker 1995), but this is unlikely, especially in water. The deprotonated ascorbate and the acid are in equilibrium with $pK_a = 4.15$. Therefore, without buffer Asc^- and AscH are present at lower and higher concentration, respectively. $\Phi^{AcsH} = 0.1–0.6$ for methylBQs but relatively small for AQ (Table 28.1). The reactivity k^{AscH} is sufficiently large for AscH and most quinones (Table 28.5). The photoinduced mechanism involves semiquinone radicals and leads to the hydroquinones (steps (3) plus (5), Scheme 28.7). For comparison, Φ^{DABCO} is lower than 0.03, that is, ET from DABCO does not yield much QH_2 in contrast to ascorbic acid. AscH is unique in the respect that a reduction step of the semiquinone radical, analogous to step (6), does not occur. Instead, the radicals

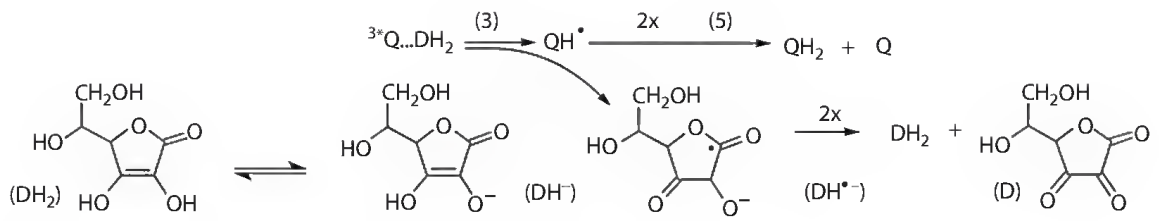

SCHEME 28.7 Oxidation of ascorbic acid via triplet quinines.

recombine to deoxyascorbate and AscH. Interestingly, k^{TEA} of triplet quinones is much lower in neutral than strongly basic solution (Scaiano and Neta 1980), in contrast to EDTA, which has no significant pH effect. Formate functions as efficient H-donor, but the rate constant is lower than the diffusion-controlled reaction, for example, $k^{For} = 2 \times 10^7\ M^{-1}\ s^{-1}$ for AQ (Loeff et al. 1991).

ET from dimethyl sulfide and DMSO to ^{3}*Q is rather efficient for chloroBQs and AQ (Görner 2006a). Methides are also quenched by DMSO (Swartz et al. 2008). The oxidation of DMSO has been used in the analysis of the photoprocesses of Cl_2BQ (Lente and Espenson 2004). The photoreactions with DMSO were not unambiguous. It had been argued that DMSO is not a physical quencher and plays a certain role in the generation of hydroxylation intermediate (Pochon et al. 2002). However, the proposed intermediacy of a kind of krypto radical, that is, OH radicals complexed to the semiquinone radical (Gan et al. 2008), has been ruled out since *tert*-butanol has no effect on the BQ/DMPO-spin-trap system upon irradiation. This is in contrast to the well-known scavenging behavior against hydroxyl radicals, excluding that the precursor is formed via •OH attack (von Sonntag et al. 2004). The mechanism of the photoreactions of MeBQ has recently been modified (Gan et al. 2008) and is open to further discussion. The AQ-sensitized photoconversion of oxygen in hydrogen peroxide is quenched by DMSO (Garg et al. 2007).

28.9 Triplet State Reactions Involving Singlet Oxygen or $O_2^{\bullet-}$ Radicals

Triplet quenching by oxygen is less efficient for BQs in aqueous solution than in organic solvents, but significant for most quinones. The rate constant of reaction of singlet molecular oxygen with BQ is much smaller, for example, $k = 4.6 \times 10^6\ M^{-1}\ s^{-1}$ in acetonitrile (Gutiérrez 2008) and the data of Φ_Δ (Alegría et al. 1997, 1999, 2002) have been reviewed (Redmond and Gamlin 1999). For juglone, $\Phi_\Delta = 0.14$, but Φ_Δ <0.01 for lawsone; some values are listed in Table 28.6. The admission of oxygen reverts QH_2 back to NQs or AQs.

The photooxidation of 5-OH-1-naphthol to juglone has frequently been studied (Brahmia and Richard 2005, Oelgemöller et al. 2007). Juglone serves as a valuable building block for the synthesis of biologically active quinoids. The photoinduced key step is reaction (a) of the substrate with singlet molecular oxygen, in which the latter is produced via energy transfer from a triplet sensitizer. The product is formed after rearrangement (b) and release of water. AQ is one photoproduct of anthracene in air-saturated aqueous solution; no external sensitizer is required, but an endoperoxide is also the intermediate, similar to reactions a and b in Scheme 28.8 (Alegría et al. 2004). Singlet oxygen and radical reactions were examined in various systems, for example, by diaminoAQ-photosensitized oxidation of human

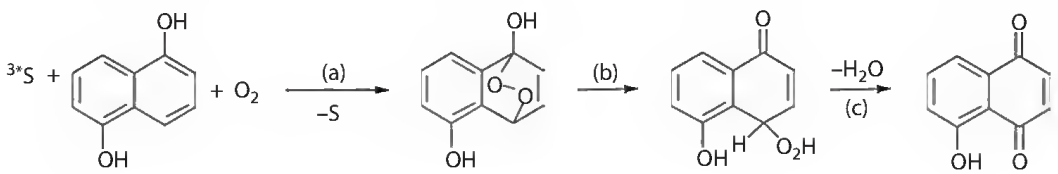

SCHEME 28.8 Photoreactions of TQ.

leukemic cells (Reszka et al. 1988, 1992). In water, the role of the superoxide ion $O_2^{\bullet-}$ and the hydroperoxyl radical $HO_2^{\bullet}$, the conjugate acid with $pK_a = 4.8$, is to be considered (von Sonntag 1987, 2006, Cabelli 1997, Bobrowski et al. 2007).

Self-quenching of a triplet state (11) (see Scheme 28.6) and the subsequent reaction of the radical anion with oxygen can lead to formation of $O_2^{\bullet-}$. This is in competition to the formation of singlet molecular oxygen, which may also play a role in aqueous solution. The yield of $O_2^{\bullet-}$ can be strongly enhanced by ET from a donor. Alternatively, H-transfer can be employed (Wilkinson 1962). The hydroperoxyl radical can easily be converted into hydrogen peroxide, thereby consuming oxygen. The reactions become more complex, when appropriate donors are present. Photoinduced oxygen uptake was studied for BQs, NQs, and AQs using several donors, including aromatic amino acids. The reactivities of some donors in acetonitrile–water (1:1) are similar to those in Table 28.6 without water. Examples of the weak (Me_4BQ) and strong (BrNQ) oxygen uptake as a function of the time are shown in Figure 28.8.

The mechanism in the presence of formate, ascorbic acid, alcohols, and amines is summarized in Scheme 28.9 (Görner 2004b, 2006b, 2007a,b). The reaction is initiated by triplet quenching (3), oxygen then reacts with the semiquinone radical (forward step in equilibrium (14)), and eventually, the hydroperoxyl radical terminates to hydrogen peroxide (15). Large differences in the constant K_{14} are known for BQ *vs.* AQ or NQ, the equilibrium lies on the BQ side, but in the cases of NQ and AQs on the $HO_2^{\bullet}$ side. If Φ_{isc} is close to unity, the quantum yield of oxygen uptake (Φ_{-O_2}) can approach 0.5–0.9 (Table 28.8). With ascorbic acid (Roginsky et al. 1999, Roginsky and Barsukova 2000), each hydroperoxyl radical is

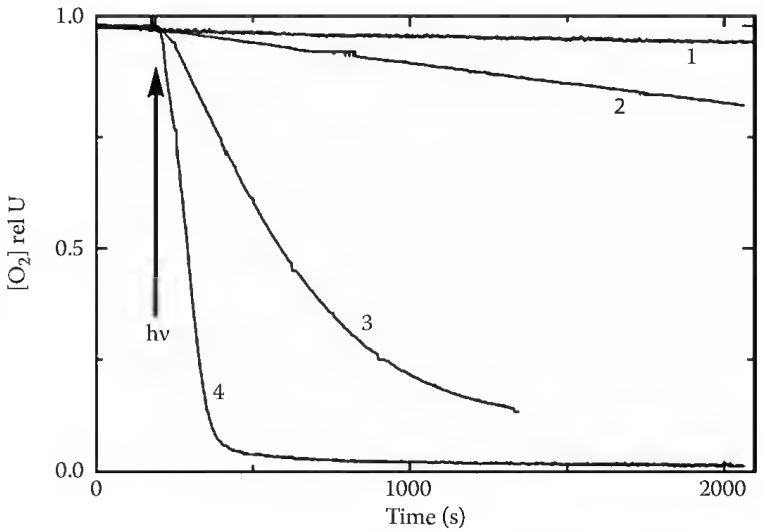

FIGURE 28.8 Plots of the O_2 concentration *vs.* time for irradiation at 313 nm in air-saturated acetonitrile: water in the presence of 2-propanol: for Me_4BQ (1:1) and 2-propanol (0.1 M: 1, 5 M: 2) and for BrNQ (1:10) and 2-propanol (0.1 M: 3, 5 M: 4), cf. Görner (2007b).

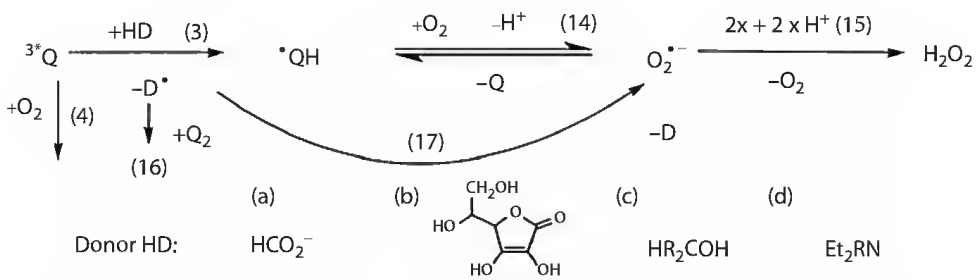

SCHEME 28.9 Photoprocesses in the presence of oxygen of quinones and (a) formate, (b) ascorbate, (c) alcohols and (d) amines.

TABLE 28.8 Quantum Yield of Oxygen Consumption for Quinones in the Presence of Donors[a]

Compound	Formate	AscH	2-Propanol	EDTA[b]
	Conc. 0.3 M	0.01 M	7 M	0.03 M
BQ	<0.01	0.04	0.02	0.01
Me_4BQ		0.15	0.1	0.08
NQ	0.6	0.25	0.8	
AQ	0.08	0.6	0.6	0.5

[a] In air-saturated acetonitrile–water, 1:10 (Görner 2007b).
[b] Ethylenediaminetetraacetate.

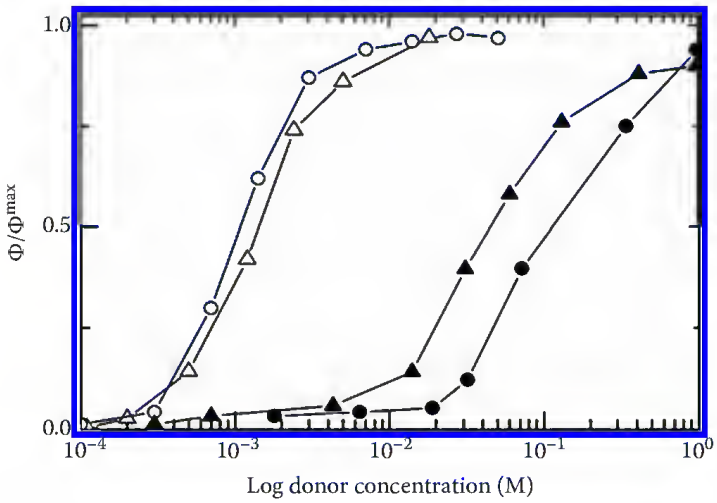

FIGURE 28.9 Semilogarithmic plots of Φ_{-O_2} as a function of the formide (▲), ascorbic acid (o), EDTA (△), and 2-propanol (●) concentrations for NQ in air-saturated acetonitrile: water (1:10), cf. Görner (2007b).

converted to hydrogen peroxide, in contrast to other donors. Plots of Φ_{-O_2} as a function of the log of the donor concentration are shown in Figure 28.9. Differences in the rate constants are the main reason for the shift of the curves. The role of singlet oxygen versus radical peroxidation in the photooxidation of human blood plasma has been analyzed (Barclay et al. 2003). AQ is the major photoproduct of anthracene in air-saturated aqueous solution (Sigman et al. 1991).

28.10 Effects of Side Groups

Most quinones so far presented do not have side chains. One exception refers to the ubiquinone moiety and another to plastoquinones or lapachol. Vitamin K_1 contains a isoprenoid chain and, in contrast to other quinones without an olefinic chain, intramolecular H-atom and/or CT processes from the isoprenoid group take place. The photoreactivity of vitamin K compounds has been examined (Hangarter et al. 2003, Swartz et al. 2008) and the mechanism of vitamin K_1 is shown in Scheme 28.10a. The products have been characterized as *E* and *Z* tautomers of 1,2-quinone methide (1,2-QM) and two 1,3-quinone methide diradicals (1,3-QM) as intermediates. The rate constant of quenching of 1,3-QM in acetonitrile is $5 \times 10^8\ M^{-1}\ s^{-1}$. The mechanism for lapachol is very similar (Görner 2004a, Scheme 28.10b). Intramolecular H-transfer from the side chain to the NQ moiety has also been found for 5-ethylene-2-ylNQ, a product is a 5-vinylNQ (Balakrishnan and Umapathy 1999).

Other quinones with side chains are 2-Me-5-isopropylBQ: thymoquinone (TQ), the 2,5-dibromo derivative (Br_2TQ), and 2-*tert*-butylBQ. Intramolecular proton/H-transfer successfully competes with

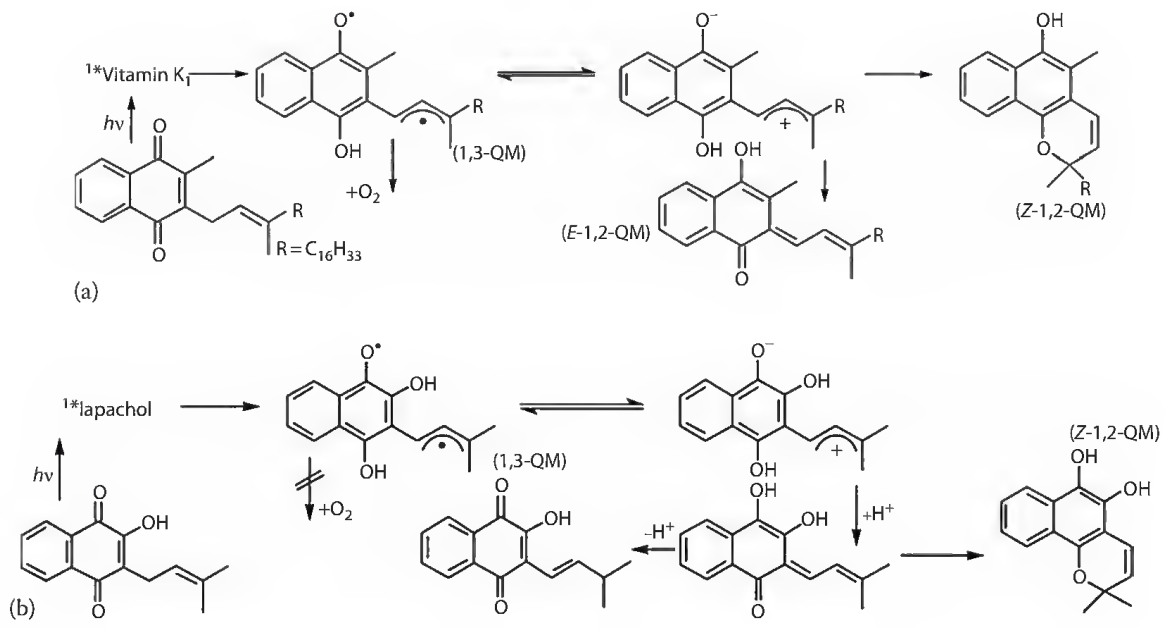

SCHEME 28.10 Photoprocesses of (a) vitamin K_1 and (b) lapachol.

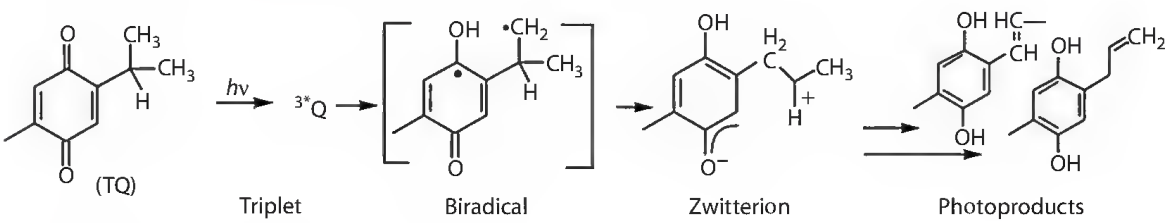

SCHEME 28.11 Photoprocesses of thymoquinone.

intermolecular photoprocesses. Φ of photodecomposition of the three BQs is large in neat acetonitrile and other solvents even in the presence of oxygen. The mechanism is shown in Scheme 28.11. The first short-lived transient of Br_2TQ with a lifetime of 0.02–0.1 μs is assigned to the triplet state (see Figure 28.10). This is in contrast to 2-*tert*-butylBQ, where no intermediate could be detected under comparable conditions, and to TQ, where a different mechanism operates. The effects of solvent polarity and other

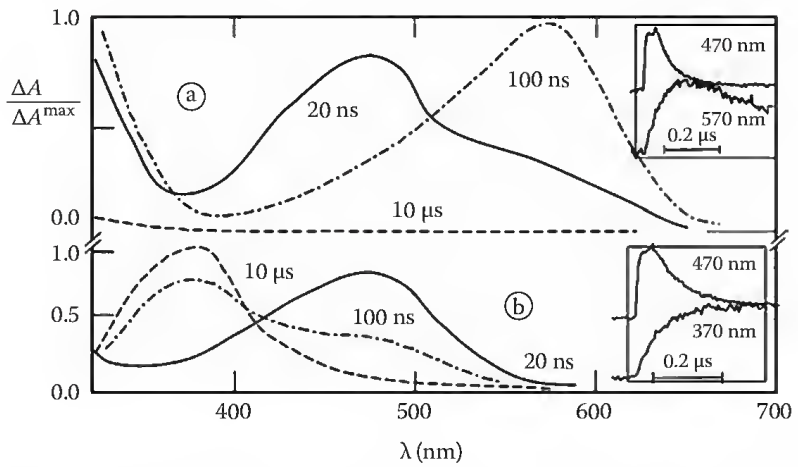

FIGURE 28.10 Transient absorption spectra of Br_2TQ in argon-saturated acetonitrile (a) dry and (b) plus 1 M water at 20 ns, 0.1 μs, and 10 μs after the 308 nm pulse; insets: kinetics as indicated, cf. Görner (2005b).

specific properties of intramolecular H-transfer with TQ and Br_2TQ were described. Φ_Δ = 0.2–0.3 for Br_2TQ in CCl_4 and acetonitrile but nearly zero for TQ (Görner 2004c, 2005b). The triplet state of Br_2TQ converts into a zwitterion, which is formed after intramolecular H-transfer from the side chain. Further conversion into hydroquinones, not involving free radicals, is proposed. For Cl_2BQs, which are 3,6-substituted by aliphatic amino acids, biradical zwitterions and intramolecular trapping of an excited CT state have been suggested (Jones and Qian 1998). Drastic differences in lifetimes of the charge-separated state were found for a formanilideAQ versus the ferrocene-attached AQ (Okamoto et al. 2005). A reaction mechanism of a photoremovable protecting group based on NQ has been proposed (Kamdzhilov and Wirz 2007).

28.11 Biological Aspects

The role of quinones in photosynthetic reaction centers has been addressed by various groups (Antolovich et al. 1991, Johnson et al. 1993, Kurreck et al. 1995, Macpherson et al. 1995, Fajer et al. 1996, Murtinho et al. 2000, Springer et al. 2003, Osyczka et al. 2006, Barbafina et al. 2008) but is only briefly touched upon here. Especially the cascade reactions of excited pigments, for example, porphyrins, linked to quinones were investigated. Modeling of the ET in photosynthetic systems over a long range is based on rigidly bridged donor–acceptor, for example, porphyrin–quinone pairs, the topic has been reviewed (Verhoeven 2006). Alternative electron donors are ruthenium salts (Borgström et al. 2003, Benniston et al. 2005). Hydrogen bonding to quinones (Biczók et al. 1994) was found in virtually all bacterial reaction centers. The remarkably high efficiency of photosynthesis is based on light harvesting by the (bacterio)chlorophyll antenna system. The energy is transferred to the reaction center from where electrons are passed to noncovalently attached quinones. The redox properties are of great importance when mimicking the primary photochemistry of pigment/quinone-type reaction centers. The quinoid end groups of a carotenoid, in contrast to phenolic groups, were found to be fully integrated into the conjugation system (Marian et al. 2009).

One model system consists of zinc *meso*-tetrakis(sulfonatophenyl) porphyrin and UQ_0; it undergoes ET in both the triplet and the excited singlet state. Quenching of excited porphyrins by BQs has been analyzed via optoacoustic spectroscopy (Malkin et al. 1994, Yeow and Braslavsky 2002, Andres et al. 2006). Accelerating effects of ammonium cations on the ET of triplet porphyrin to BQ or NQ have been reported (Okamoto et al. 2004). Other systems contain chlorins, for example, Zn-chlorin-6. Scheme 28.12 shows the reactions involved in fast ET from a singlet excited chlorin to a quinone (Mennenga et al. 2006). The quinone quenches the first excited chlorin state (^{1}*P) and the lowest triplet state (^{3}*P) by formation of the correlated radical pairs: $^1(P^{\bullet+}..Q^{\bullet-})$ and $^3(P^{\bullet+}..Q^{\bullet-})$, where the former is only involved at high BQ concentrations. A direct ET from the ^{3}*P state to a quinone can be observed by transient absorption spectroscopy, whereby the rate constant for the triplet decay and the appearance of the radical cation $P^{\bullet+}$ should be the same. Some photoprocesses of other

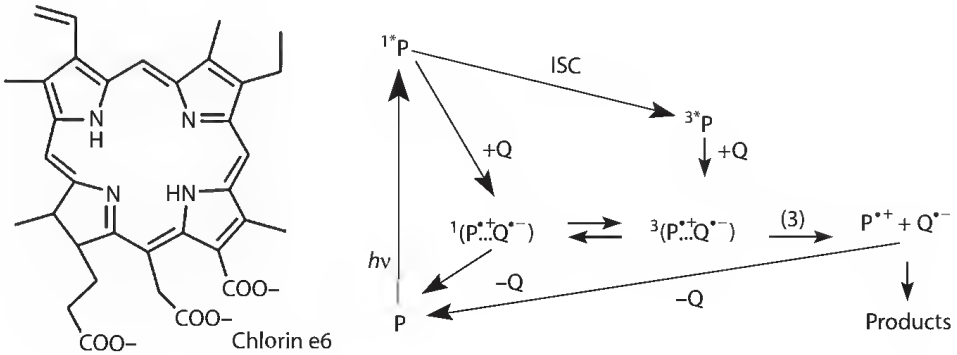

SCHEME 28.12 Photoprocesses of chlorines.

tetrapyrroles and related chromophores with quinones in solution have been examined in great detail. These investigations have revealed a broad variation of interactions and reactivities.

Much effort has been made to mimic the function of reaction centers in peptide models (Singh et al. 2007). De novo design of quinoproteins is possible (Li et al. 2006). Incorporation of metallochlorins into de novo synthesized proteins provides the possibility to study the photochemical reaction of monomeric chlorins, and upon addition of an electron acceptor, to mimic biological ET proteins found in photosynthesis and respiration. Intramolecular photochemical ET takes place for stabilized charge separation in linked porphyrin–quinone molecules (McIntosh et al. 1983). The low-temperature EPR spectroscopy of quinones and radical pairs in photosynthesis has been improved (Burghaus et al. 1993), reviewed (Lubitz et al. 2002), and updated (Sinnecker et al. 2006). The role of reaction centers containing BQs, NQs, or AQs in the place of ubiquinone has been examined (Woodbury et al. 1986). An identification of FT infrared bands is due to internal water molecules around the quinone binding sites in the reaction center from *Rhodobacter spaeroides* (Iwata et al. 2009). Several updates concerning photosynthesis are available (Gust et al. 2005, Arellano et al. 2007, Renger and Renger 2008, Barber 2009).

References

Aaron, J.J., Winefordner, D.J. 1972. Phosphorescence study of excited triplet state properties of some K vitamins and their analytical usefulness. *Anal. Chem.* 44: 2122–2127.

Alegría, A.E., Ferrer, A., Santiago, G., Sepúlveda, E., Flores, W. 1999. Photochemistry of water-soluble quinones. Production of the hydroxyl radical, singlet oxygen and the superoxide ion. *J. Photochem. Photobiol. A: Chem.* 127: 57–65.

Alegría, A.E., Ferrer, A., Sepúlveda, E. 1997. Photochemistry of water-soluble quinones. Production of a water-derived spin adduct. *Photochem. Photobiol.* 66: 436–442.

Alegría, A.E., Rivera, L., Cordones, E., Castro, V., Sanchez-Cruz, P. 2002. Role of membrane charge and semiquinone structure on oxygen consumption rates. *J. Chem. Soc. Perkin Trans. 2* 11: 1823–1828.

Alegría, A.E., Sanchez-Cruz, P., Rivas, L. 2004. Alkaline-earth cations enhance *ortho*-quinone-catalyzed ascorbate oxidation. *Free Rad. Biol. Med.* 37: 1631–1639.

Amada, I., Yamaji, M., Sase, M., Shizuka, H. 1995. Laser flash photolysis studies on hydrogen atom abstraction from phenol by triplet naphthoquinones in acetonitrile. *J. Chem. Soc. Faraday Trans.* 91: 2751–2759.

Amada, I., Yamaji, M., Tsunoda, S., Shizuka, H. 1996. Laser photolysis studies of electron transfer between triplet naphthoquinones and amines. *J. Photochem. Photobiol. A: Chem.* 95: 27–32.

Amouyal, E., Bensasson, R., Land, E.J. 1974. Triplet states of ubiquinone analogs studied by ultraviolet and electron nanosecond irradiation. *Photochem. Photobiol.* 20: 415–422.

Andres, G.O., Martinez-Junza, V., Crovetto, L., Braslavsky, S.E. 2006. Photoinduced electron transfer from tetrasulfonated porphyrin to benzoquinone revisited. The structural volume-normalized entropy change correlates with Marcus reorganization energy. *J. Phys. Chem. A* 110: 10185–10190.

Antolovich, M., Keyte, P.J., Oliver, A.M. et al. 1991. Modeling long-range photosynthetic electron transfer in rigidly bridged porphyrin-quinone systems. *J. Phys. Chem.* 95: 1933–1941.

Arellano, J.B., Yousef, Y.A., Melø, T.B., Mohamad, S.B.B., Cogdell, R.J., Naqvi, K.R. 2007. Formation and geminate quenching of singlet oxygen in purple bacterial reaction center. *J. Photochem. Photobiol. B: Biol.* 87: 105–112.

Armitage, B., Yu, C., Devadoss, C., Schuster, G.B. 1994. Cationic anthraquinone derivatives as catalytic DNA photonucleases: Mechanisms for DNA damage and quinone recycling. *J. Am. Chem. Soc.* 116: 9847–9859.

Baciocchi, E., Del Giacco, T., Elisei, F., Lanzalunga, O. 1998. Homolytic vs heterolytic C-H bond cleavage in alkylaromatic radical cations. Formation of diarylmethyl cation in the photoinduced electron transfer reaction of bis(4-methoxyphenyl)methane sensitized by chloranil. *J. Am. Chem. Soc.* 120: 11800–11801.

Balakrishnan, G., Umapathy, S. 1999. Photogenerated radical intermediates of vitamin K_1: A time-resolved resonance Raman study. *J. Mol. Struct.* 475: 5–11.

Barbafina, A., Elisei, F., Latterini, L., Milano, F., Agostiano, A., Trotta, M. 2008. Photophysical properties of quinones and their interaction with the photosynthetic reaction centre. *Photochem. Photobiol. Sci.* 7: 973–978.

Barber, J. 2009. Photosynthetic energy conversion: Natural and artificial. *Chem. Soc. Rev.* 38: 185–196.

Barclay, L.R.C., Basque, M.C., Stephenson, V.C., Vinqvist, M.R. 2003. Photooxidations initiated or sensitized by biological molecules: Singlet oxygen versus radical peroxidation in micelles and human blood plasma. *Photochem. Photobiol.* 78: 248–255.

Béarnais-Barbry, S., Bonneau, R., Castellan, A. 2001. Photochemistry of methoxyhydroquinone and methoxy-*p*-benzoquinone in solution related to the photoyellowing of the lignocellulosics. *Photochem. Photobiol.* 74: 542–548.

Beck, S.M., Brus, L.E. 1982. Transient Raman scattering study of the initial semiquinone radical kinetics following photolysis of aqueous benzoquinone and hydroquinone. *J. Am. Chem. Soc.* 104: 4789–4792.

Beckert, D., Fessenden, R.W. 1996. Time-resolved ESR study of spin exchange processes in the photoreduction of 9,10-anthraquinone-1,5-disulfonate. *J. Phys. Chem.* 100: 1622–1629.

Benniston, A.C., Chapman, G.M., Harriman, A., Rostron, S.A. 2005. Reversible luminescence switching in a ruthenium(II) Bis(2,2′,6′,2′-terpyridine)-benzoquinone dyad. *Inorg. Chem.* 44: 4029–4036.

Bensasson, R., Chachaty, C., Land, E.J., Salet, C. 1972. Nanosecond irradiation studies of biological molecules - I. Coenzyme Q6 (ubiquinone-30). *Photochem. Photobiol.* 16: 27–37.

Bergeron, F., Klarskov, K., Huting, D.J., Wagner, J.R. 2007. Near-UV photolysis of 2-methyl-1,4-naphthoquinone–DNA duplexes: Characterization of reversible and stable interstrand cross-links between quinone and adenine moieties. *Chem. Res. Toxicol.* 20: 745–756.

Bergmark, W., Jones, G. 1997. Photoinduced sequential electron-transfer reactions of chloranil. *J. Photochem. Photobiol. A: Chem.* 109: 119–124.

Biczók, L., Linschitz, H., Walter, R.I. 1994. Reduction of triplet tetraphenyl-prophyrin dication by aryl amines and hydroquinones: Kinetics and primary radical yields. *Res. Chem. Intermed.* 20: 939–951.

Bisby, R.H., Parker, A.W. 1995. Reactions of excited triplet duroquinone with α-tocopherol and ascorbate: A nanosecond laser flash photolysis and time-resolved resonance Raman investigation. *J. Am. Chem. Soc.* 117: 5664–5670.

Bobrowski, M., Liwo, A., Hirao, K. 2007. Theoretical study of the energetics of the reactions of triplet dioxygen with hydroquinone, semiquinone, and their protonated forms: Relation to the mechanism of superoxide generation in the respiratory chain. *J. Phys. Chem. B* 111: 3543–3549.

Bolton, J.L., Trush, M.A., Penning, T.M., Dryhurst, G., Monks, T.J. 2000. Role of quinones in toxicology. *Chem. Res. Toxicol.* 13: 135–160.

Borgström, M., Johansson, O., Lomoth, R. et al. 2003. Electron donor-acceptor dyads and triads based on tris(bipyridine)ruthenium(II) and benzoquinone: Synthesis, characterization, and photoinduced electron transfer reactions. *Inorg. Chem.* 42: 5173–5184.

Born, R., Fischer, W., Heger, D., Tokarczyk, B., Wirz, J. 2007. Photochromism of phenoxynaphthacenequinones: Diabatic or adiabatic phenyl group transfer? *Photochem. Photobiol. Sci.* 6: 552–559.

Borst, H.-U., Kelemen, J., Fabian, J., Nepraš, M., Kramer, H.E.A. 1992. Triplet formation in aminoanthraquinones and its importance for the catalytic fading of dye mixtures. *J. Photochem. Photobiol. A: Chem.* 69: 97–107.

Bosch, E., Hubig, S.M., Kochi, J.K. 1998. Paterno-Büchi coupling of (diaryl)acetylenes and quinone via photoinduced electron transfer. *J. Am. Chem. Soc.* 120: 386–395.

Bose, A., Chowdhury, S.D., Basu, S. 2009. Role of sugar in controlling reaction pattern: A comparative study with adenine and 2′-deoxyadenosine. *J. Photochem. Photobiol. A: Chem.* 201: 197–202.

Bose, A., Dey, D., Basu, S. 2008. Interactions of guanine and guanosine hydrates with quinones: A laser flash photolysis and magnetic field effect study. *J. Phys. Chem. A* 112: 4914–4920.

Brahmia, O., Richard, C. 2003. Phototransformation of 1,4-naphthoquinone in aqueous solution. *Photochem. Photobiol. Sci.* 2: 1038–1043.

Brahmia, O., Richard, C. 2005. Photochemical transformation of 1-naphthol in aerated aqueous solution. *Photochem. Photobiol. Sci.* 4: 454–458.

Brinson, R.G., Hubbard, S.C., Zuidema, D.R., Jones, P.B. 2005. Two new anthraquinone photoreactions. *J. Photochem. Photobiol A: Chem.* 175: 118–128.

Broadbent, A.D., Matheson, H.B., Newton, R.P. 1975. Photolysis of aqueous solutions of 9,10-anthraquinone-2-sulfonate. Part II. Dependence of rates of hydroxylation on reaction conditions. *Can. J. Chem.* 53: 826–829.

Broadbent, A.D., Newton, R.P. 1972. Photolysis of aqueous solutions of 9,10-anthraquinone-2-sulfonate. Part I. Dependence of product yields on reaction conditions. *Can. J. Chem.* 50: 381–387.

Bruce, J.M. 1974. Photochemistry of quinones. In *The Chemistry of the Quinoid Compounds*, ed. S. Patei, pp. 465–538, New York: Wiley.

Burghaus, O., Plato, M., Rohrer, M., Möbius, K., MacMillan, F., Lubitz, W. 1993. 3-mm High-field EPR on semiquinone radical anions $Q^{\bullet -}$ related to photosynthesis and on the primary donor $P^{\bullet +}$ and acceptor $Q_A^{\bullet -}$ in reaction centers of *Rhodobacter sphaeroides* R-26. *J. Phys. Chem.* 97: 7639–7647.

Burie, J.-R., Boussac, A., Boullais, C., Berger, G., Mattioli, T., Mioskowski, C., Nabedryk, E., Breton, J. 1995. FTIR spectroscopy of UV-generated quinone radicals: Evidence for an intramolecular hydrogen atom transfer in ubiquinone, naphthoquinone, and plastoquinone. *J. Phys. Chem.* 99: 4059–4070.

Cabelli, D.E. 1997. The reactions of HO_2/O_2^- radicals in aqueous solution. In *Peroxyl Radicals*, ed. Z.B. Alfassi, pp. 407–437, Chichester, U.K.: Wiley.

Chen, J.F., Ge, X.W., Chu, G.S., Zhang, Z.C., Zhang, M.W., Yao, S.D., Lin, N.Y. 1999. Nanosecond laser photolysis studies of vitamin K_3 in aqueous solution. *Radiat. Phys. Chem.* 55: 35–39.

Chiang, Y., Kresge, A.J., Hellrung, B., Schünemann, P., Wirz, J. 1997. Flash photolysis of 5-methyl-1,4-naphthoquinone in aqueous solution: Kinetics and mechanism of photoenolization and of enol trapping. *Helv. Chim. Acta* 80: 1106–1121.

Chowdhury, A., Basu, S. 2006. Interactions between 9,10-anthraquinone and aromatic amines in homogeneous and micellar media: A laser flash photolysis and magnetic field effect study. *J. Lumin.* 121: 113–122.

Christoforidis, K.C., Louloudi, M., Rutherford, A.W., Deligiannakis, Y. 2008. Semiquinone in molecularly imprinted hybrid amino acid–SiO_2 biomimetic materials. An experimental and theoretical study. *J. Phys. Chem. C* 112: 12841–12852.

Ci, X., da Silva, R.S., Nicodem, D., Whitten, D.G. 1989. Electron and hydrogen atom transfer mechanisms for the photoreduction of *o*-quinones. Visible light induced photoreactions of β-lapachone with amines, alcohols, and amino alcohols. *J. Am. Chem. Soc.* 111: 1337–1343.

Clark, K.P., Stonehill, H.I. 1972. Photochemistry and radiation chemistry of anthraquinone-2-sodium-sulphonate in aqueous solution, part 1. Photochemical kinetics in aerobic solution. *J. Chem. Soc. Faraday Trans.1* 68: 577–589.

Comini, L.R., Núñez Montoya, S.C., Sarmiento, M., Cabrera, J.L., Argüello, G.A. 2007. Characterizing some photophysical, photochemical and photobiological properties of photosensitizing anthraquinones. *J. Photochem. Photobiol. A: Chem.* 188: 185–191.

Cook, A.R., Curtiss, L.A., Miller, J.R. 1997. Fluorescence of the 1,4-benzoquinone radical anion. *J. Am. Chem. Soc.* 119: 5729–5734.

Creed, D. 1994. 1,4-Quinone cycloaddition reactions with alkenes, alkynes, and related compounds. In *CRC Handbook of Organic Photochemistry and Photobiology*, eds. W.M. Horspool and P.-S. Song, pp. 737–747, Boca Raton, FL: CRC Press.

Dahiya, P., Kumbhakar, M., Maity, D.K., Mukherjee, T., Mittal, J.P., Tripathi, A.B.R., Chattopadhyay, N., Pal, H. 2005. Photophysical properties of 2-amino-9,10-anthraquinone: Evidence for structural changes in the molecule with solvent polarity. *Photochem. Photobiol. Sci.* 4: 100–105.

Dahiya, P., Kumbhakar, M., Maity, D.K., Mukherjee, T., Tripathi, A.B.R., Chattopadhyay, N., Pal, H. 2006b. Solvent polarity and intramolecular hydrogen bonding effects on the photophysical properties of 1-amino-9,10-anthraquinone dye. *J. Photochem. Photobiol. A: Chem.* 81: 338–347.

Dahiya, P., Kumbhakar, M., Mukherjee, T., Pal, H. 2006a. Effects of the amino and hydroxy substituents on the photophysical properties of 1,4-disubstituted-9,10-anthraquinone dyes. *J. Mol. Struct.* 798: 40–48.

Das, R., Venkataraman, B. 2005. Hydrogen abstraction from solvents by the triplet state of *p*-benzoquinone: A time-resolved electron paramagnetic resonance and laser flash photolysis study. *Res. Chem. Intermed.* 31: 167–192.

Datta, K., Mukherjee, A.K. 2004. Study of a reaction between 2,3-dichloro-1,4-naphthoquinone and *N,N'*-diphenyl thiourea involving an EDA adduct as intermediate. *Spectrochim. Acta* A 60: 1641–1647.

Davies, A.K., Ford, R., Gee, G.A., McKellar, J.F., Phillips, G.O. 1972b. Primary photochemical processes of two phototendering vat dyes. *J. Chem. Soc. Chem. Commun.* 1972: 873–874.

Davies, A.K., Ford, R., McKellar, J.F., Phillips, G.O. 1972a. Participation of an upper excited n-π^* triplet state in the photoreduction of 1-dimethylaminoanthraquinone. *J. Chem. Soc. Perkin Trans. 2* 923–925.

de Lucas, N.C., Elias, M.M., Firme, C.A., Corrêa, R.J., Garden, S.J., Netto-Ferreira, J.C., Nicodem, D.E. 2009. A combined laser flash photolysis, density functional theory and atoms in molecules study of the photochemical hydrogen abstraction by pyrene-4,5-dione. *J. Photochem. Photobiol. A: Chem.* 201: 1–7.

Del Giacco, T., Baciocchi, E., Lanzalunga, O., Elisei, F. 2001. Competitive decay pathways of the radical ions formed by photoinduced electron transfer between quinones and 4,4'-dimethoxydiphenylmethane in acetonitrile. *Chem. Eur. J.* 7: 3005–3013.

Del Giacco, T., Latterini, L., Elisei, F. 2003. Photophysical and photochemical properties of 1,2,4-trihydroxy-9,10-anthraquinone adsorbed on inorganic oxides. *Photochem. Photobiol. Sci.* 2: 681–687.

Diaz, A.N. 1990. Absorption and emission spectroscopy and photochemistry of 1,10-anthraquinone derivatives: A review. *J. Photochem. Photobiol. A: Chem.* 53: 141–167.

Eckert, G., Goez, M. 1994. Photoinduced electron-transfer reactions of aryl olefins. 1. Investigation of the Paterno-Büchi reaction between quinones and anetholes in polar solvents. *J. Am. Chem. Soc.* 116: 11999–12009.

El'tsov, A.V., Studzinskii, O.P., Levental, Y.K., Florinskaya, M.V. 1977. Photolysis of nitroanthraquinones in alcohols. *Z. Org. Khimii* 13: 1061–1067, *J. Org. Chem.* 13: 975–980.

Fajer, J., Barkigia, K.M., Melamed, D. et al. 1996. Molecular structures of porphyrin-quinone models for electron transfer. *J. Phys. Chem.* 100: 14236–14239.

Folkes, L.K., Christlieb, M., Madej, E., Stratford, M.R.L., Wardman, P. 2007. Oxidative metabolism of combretastatin A-1 produces quinone intermediates with the potential to bind to nucleophiles and to enhance oxidative stress via free radicals. *Chem. Res. Toxicol.* 20: 1885–1894.

Forbes, M.D.E., Tarasov, V.F., White, R.C. 2006. Photo-oxidation of diglycine in confined media: Relaxation of longitudinal magnetization in spin correlated radical pairs. *Spectrochim. Acta A* 63: 776–783.

Foyle, V.P., Takahashi, Y., Guillet, J.E. 1992. Photoproducts in 2-hydroxyethyl methacrylate hydrogels swollen with water and 2-propanol. *J. Polym. Sci. A* 30: 257–269.

Friedrichs, F., Murphy, B., Nayrat, D. et al. 2008. An improved procedure for the photoacylation of 1,4-naphthoquinones with aliphatic aldehydes. *Synlett.* 20: 3137–3140.

Fukuzumi, S. 2006. Bioinspired electron-transfer systems and applications. *Bull. Chem. Soc. Jpn.* 79: 177–195.

Fukuzumi, S., Mori, H., Imahori, H., Suenobu, T., Araki, Y., Ito, O., Kadish, K.M. 2001. Scandium ion-promoted photoinduced electron-transfer oxidation of fullerenes and derivatives by *p*-chloranil and *p*-benzoquinone. *J. Am. Chem. Soc.* 123: 12458–12465.

Fukuzumi, S., Yorisue, T. 1991. Quinone/hydroxide ion induced oxygenation of *p*-benzoquinone to rhodizonate dianion ($C_6O_6^{2-}$) accompanied by one-electron reduction to semiquinone radical anion. *J. Am. Chem. Soc.* 113: 7764–7765.

Gan, D., Jia, M., Vaughan, P.P., Falvey, D.E., Blough, N.V. 2008. Aqueous photochemistry of methylbenzoquinone. *J. Phys. Chem. A* 112: 2803–2812.

Gan, H., Whitten, D.G. 1993. A sterically controlled recyclable system: Reversible photoredox reactions between anthraquinone and hindered tertiary amines. *J. Am. Chem. Soc.* 115: 8031–8037.

Garg, S., Rose, A.L., Waite, T.D. 2007. Production of reactive oxygen species on photolysis of dilute aqueous quinone solutions. *Photochem. Photobiol.* 83: 904–913.

Geimer, J., Beckert, D. 1998. Study of radical pairs generated by photoreduction of anthraquinone-2, 6-disulfonic acid with thymine by Fourier transform electron paramagnetic resonance. *Chem. Phys. Lett.* 288: 449–458.

Geimer, J., Brede, O., Beckert, D. 1997. Fourier transform EPR study of N-centered pyrimidine radicals in the nanosecond time-scale. *Chem. Phys. Lett.* 276: 411–417.

Gilbert, A. 2004. 1,4-Quinone cycloaddition reactions with alkenes, alkynes, and related compounds. In *CRC Handbook of Organic Photochemistry and Photobiology*, eds. W.M. Horspool and F. Lenci, 2nd edn., pp. 87, 1–12, Boca Raton, FL: CRC Press.

Goez, M. 1990. Flash CIDNP investigation of a cyclic photoreaction. *Chem. Phys.* 147: 143–154.

Goez, M., Eckert, G. 2006. Olefin isomerization via radical-ion pairs in triplet states studied by chemically induced dynamic nuclear polarization (CIDNP). *Helv. Chim. Acta* 89: 2183–2199.

Goez, M., Frisch, I. 1995. Photocycloadditions of quinones with quadricyclane and norbornadiene. A mechanistic study. *J. Am. Chem. Soc.* 117: 10486–10502.

Goez, M., Sartorius, I. 2003. CIDNP determination of the rate of in-cage deprotonation of the triethylamine radical cation. *J. Phys. Chem. A* 107: 8539–8546.

Goez, M., Zubarev, V. 1999. Two-photon ionization of 1,5-anthraquinonedisulfonate via photoinduced electron transfer. *J. Phys. Chem. A* 103: 9605–9613.

Gollnick, K., Held, S., Mártire, D.O., Braslavsky, S.E. 1992. Hydroxyanthraquinones as sensitizers of singlet oxygen reactions: Quantum yields of triplet formation and singlet oxygen generation in acetonitrile, *J. Photochem. Photobiol. A: Chem.* 69: 155–165.

Görner, H. 2003a. Photoreduction of *p*-benzoquinones: Effects of alcohols and amines on the intermediates and reactivities in solution. *Photochem. Photobiol.* 78: 440–448.

Görner, H. 2003b. Photoprocesses of *p*-benzoquinones in aqueous solution. *J. Phys. Chem. A* 107: 11587–11595.

Görner, H. 2003c. Photoreduction of 9,10-anthraquinone derivatives: Transient spectroscopy and effects of alcohols and amines on reactivity in solution. *Photochem. Photobiol.* 77: 171–179.

Görner, H. 2004a. Photoprocesses of *p*-naphthoquinones and vitamin K_1: Effects of alcohols and amines on the reactivity in solution. *Photochem. Photobiol. Sci.* 3: 71–78.

Görner, H. 2004b. Photoreactions of *p*-benzo-, *p*-naphtho- and *p*-anthraquinones with ascorbic acid. *Photochem. Photobiol. Sci.* 3: 933–938.

Görner, H. 2004c. Photoreactions of 2-methyl-5-isopropyl-1,4-benzoquinone. *J. Photochem. Photobiol. A: Chem.* 165: 215–222.

Görner, H. 2005a. Photoreactions of 1,4-naphthoquinones: Effects of substituents and water on the intermediates and reactivity. *Photochem. Photobiol.* 81: 376–383.

Görner, H. 2005b. Photoreactions of 2,5-dibromo-3-methyl-6-isopropyl-1,4-benzoquinone. *J. Photochem. Photobiol. A: Chem.* 175: 138–145.

Görner, H. 2006a. Photoreactions of *p*-quinones with dimethyl sulfide and dimethyl sulfoxide in aqueous acetonitrile. *Photochem. Photobiol.* 82: 71–77.

Görner, H. 2006b. Photoinduced oxygen uptake for 9,10-anthraquinone in air-saturated aqueous acetonitrile in the presence of formate, alcohols, ascorbic acid or amines. *Photochem. Photobiol. Sci.* 5: 1052–1058.

Görner, H. 2007a. Electron transfer from aromatic amino acids to triplet quinones. *J. Photochem. Photobiol. B: Biol.* 88: 83–89.

Görner, H. 2007b. Oxygen uptake upon photolysis of 1,4-benzoquinones and 1,4-naphthoquinones in air-saturated aqueous solution in the presence of formate, amines, ascorbic acid and alcohols. *J. Phys. Chem. A* 111: 2814–2819.

Görner, H., Gruen, H. 2010. Direct and ketone-sensitized photoconversion of 1-nitro-9,10-anthraquinone to 1-amino-9,10-anthraquinone mediated by donor radicals. *Chem. Phys.* 368: 20–27.

Görner, H., von Sonntag, C. 2008. Photoprocesses of chloro-substituted *p*-benzoquinones. *J. Phys. Chem. A* 112: 10257–10263.

Gruen, H., Görner, H. 2008. Photoreduction of 2-methyl-1-nitro-9,10-anthraquinone in the presence of 1-phenylethanol. *Photochem. Photobiol. Sci.* 7: 1344–1352.

Gruen, H., Görner, H. 2009. Reduction of the polynuclear quinonoid dyes 16,17-dihydroxy- and dimethoxyviolanthrone with photogenerated radicals. *Photochem. Photobiol. Sci.* 8: 1164–1171.

Gruen, H., Görner, H. 2010. Properties of 16,17-disubstituted dihydroviolanthrones formed by reaction of violanthrones with photogenerated radicals. *Photochem. Photobiol. Sci.* 9: 1088–1093.

Gschwind, R., Haselbach, E. 1979. Laserflash-photolysis of the *p*-chloranil/naphthalene system: Characterization of the naphthalene radical cation in a fluid medium. *Helv. Chim. Acta* 62: 941–955.

Gun, H., Zhao, X., Whitten, D.G. 1991. Amine photoredox reactions: A photoinduced methylene shuttle initiated via two-electron oxidation of a tertiary amine by anthraquinone. *J. Am. Chem. Soc.* 113: 9409–9411.

Gust, D., Moore, T.A., Moore, A.L. 2005. Mimicking bacterial photosynthesis. In *Artificial Photosynthesis*, eds. A.F. Collings and C. Critchley, pp. 187–210, Weinheim, Germany: Wiley-VCH.

Gutiérrez, M.I. 2008. Solvent effect on the physical quenching of singlet molecular oxygen by *p*-quinones. *Photochem. Photobiol. Sci.* 7: 480–484.

Gutiérrez, I., Bertolotti, S.G., Biasutti, M.A., Soltermann, A.T., García, N.A. 1997. Quinones and hydroxyquinones as generators and quenchers of singlet molecular oxygen. *Can. J. Chem.* 75: 423–428.

Gutiérrez, M.I., García, N.A. 1998. Dark and photoinduced interactions between xanthene dyes and quinones. *Dyes Pigm.* 38: 195–209.

Hageman, H.J., Verhoeven, J.W. 1997. Photoreactions of some monoaryl- and diaryl-*p*-benzoquinones in solution. Dependence of dimerizations, cyclizations and rearrangements on the substituents and solvents. *J. Photochem. Photobiol. A: Chem.* 103: 75–83.

Hamanoue, K., Nakayama, T., Asada, S., Ibuki, K. 1992. Electron transfer from ground-state triethylamine to the second and lowest excited triplet states of haloanthraquinones (1-chloro, 2-chloro, 1,5-dichloro, 1,8-dichloro and 1,8-dibromo compounds) in acetonitrile at room temperature studied by picosecond and nanosecond laser spectroscopy. *J. Phys. Chem.* 96: 3736–3741.

Hamanoue, K., Yokoyama, K., Kajiwara, Y., Kimoto, M., Nakayama, T., Teranishi, H. 1985. The absorption kinetics of photoreduction of anthraquinone and 1-chloroanthraquinone by triethylamine in toluene and ethanol. *Chem. Phys. Lett.* 113: 207–212.

Hangarter, M.-A., Hörmann, A., Kamdzhilov, Y., Wirz, J. 2003. Primary photoreactions of phylloquinone (vitamin K_1) and plastoquinone-1 in solution. *Photochem. Photobiol. Sci.* 2: 524–535.

Harada, Y., Watanabe, S., Suzuki, T., Ichimura, T. 2005. Photochemical reaction dynamics of 9,10-phenanthrene-quinone and 1,2-naphthoquinone with hydrogen donors in solution. *J. Photochem. Photobiol. A: Chem.* 170: 161–167.

Hernández-Muñoz, L.S., Gómez, M., González, F.J., González, I., Frontana, C. 2009. Towards a molecular-level understanding of the reactivity differences for radical anions of juglone and plumbagin: An electrochemical and spectroelectrochemical approach. *Org. Biomol. Chem.* 7: 1896–1903.

Hodge, P., Gautrot, J.E. 2009. Polymers containing in-chain quinone moieties: Synthesis and properties. *Polym. Int.* 58: 261–266.

Hou, Y., Wan, P. 2008. Formal intramolecular photoredox chemistry of anthraquinones in aqueous solution: Photodeprotection for alcohols, aldehydes and ketones. *Photochem. Photobiol. Sci.* 7: 588–596.

Hubig, S.M., Bockman, T.M., Kochi, J.K. 1997. Identification of photoexcited singlet quinones and their ultrafast electron-transfer vs intersystem-crossing rates. *J. Am. Chem. Soc.* 119: 2926–2935.

Hubig, S.M., Kochi, J.K. 1999. Electron-transfer mechanisms with photoactivated quinones. The encounter complex versus the Rehm-Weller paradigm. *J. Am. Chem. Soc.* 121: 1688–1694.

Isaacs, N.S., van Eldik, R. 1997. A mechanistic study of the reduction of quinones by ascorbic acid. *J. Chem. Soc. Perkin Trans. 2* 1465–1467.

Iwata, T., Paddock, M.L., Okamura, M.Y., Kandori, H. 2009. Identification of FTIR bands due to internal water molecules around the quinone binding sites in the reaction center from *Rhodobacter spaeroides*. *Biochem.* 48: 1220–1229.

Johnson, D.G., Niemczyk, M.P., Minsek, D.W., Wiederrecht, G.P., Svec, W.A., Gaines III, G.L., Wasielewski, M.R. 1993. Photochemical electron transfer in chlorophyll-porphyrin-quinone triads: The role of the porphyrin-bridging molecule. *J. Am. Chem. Soc.* 115: 5692–5701.

Jones, G., Mouli, N., Haney, W.A., Bergmark, W.R. 1997. Photoreduction of chloranil by benzhydrol and related compounds. Hydrogen atom abstraction vs sequential electron-proton transfer via quinone triplet radical ion-pairs. *J. Am. Chem. Soc.* 119: 8788–8794.

Jones, G., Qian, X. 1998. Photochemistry of quinone-bridged amino acids. Intramolecular trapping of an excited charge-transfer state. *J. Phys. Chem. A* 102: 2555–2560.

Kamdzhilov, Y., Wirz, J. 2007. Synthesis and reaction mechanism of a photoremovable protecting group based on 1,4-naphthoquinone. *Photochem. Photobiol. Sci.* 6: 865–872.

Kausche, T., Säuberlich, J., Trobitzsch, E., Beckert, D., Dinse, K.P. 1996. Photoreduction of 9,10-anthraquinone by triethylamine: A Fourier-transform EPR study. *Chem. Phys.* 208: 375–390.

Khudyakov, I.V., Kuzmin, V.A. 1975. Short-lived phenoxyl and semiquinone radicals. *Russ. Chem. Rew.* 44: 801–815.

Krongauz, V.V., Kim, H.Y. 2006. Competitive consecutive electron transfer in determination of ionization potentials: Ketene derivatives. *J. Phys. Chem. A* 110: 13808–13815.

Kulkarni, M.G., Kate, S.D. 2000. Chemistry of L-ascorbic acid. Part 3. Photoreduction of quinones with 5,6-*O*-isopropylidene-L-ascorbic acid. *J. Chem. Soc. Perkin Trans. 1* 4242–4244.

Kumbhakar, M., Nath, S., Rath, C., Mukherjee, T., Pal, H. 2004. Electron transfer interaction of dihydroxyquinones with amine quenchers: Dependence of the quenching kinetics on the aliphatic and aromatic nature of the amine donors. *Photochem. Photobiol.* 79: 1–10.

Kurien, K.C., Robins, P.A. 1970. Photolysis of aqueous solutions of *p*-benzoquinone: A spectrophotometric investigation. *J. Chem. Soc. B* 855–859.

Kurreck, H., Aguirre, S., Dieks, H. et al. 1995. Mimicking primary processes in photosynthesis-covalently linked porphyrin quinones. *Radiat. Phys. Chem.* 45: 853–865.

Kuzmin, V.A., Darmanyan, A.P., Levin, P.P. 1979. Laser photolysis study of the spectral-kinetic characteristics of short-lived triplet exciplexes and the mechanism of atomic hydrogen transfer in the course of 2,6-diphenyl-1,4-benzoquinone triplet quenching with aromatic amines. *Chem. Phys. Lett.* 63: 509–514.

Land, E.J., Ramsden, C.A., Riley, P.A. 2001. Pulse radiolysis studies of *ortho*-quinone chemistry relevant to melanogenesis. *J. Photochem. Photobiol. B: Biol.* 64: 123–135.

Land, E.J., Ramsden, C.A., Riley, P.A. 2003. Tyrosinase autoactivation and the chemistry of *ortho*-quinone amines. *Acc. Chem. Res.* 36: 300–308.

Land, E.J., Simic, M., Swallow, A.J. 1971. Optical absorption spectrum of half-reduced ubiquinone. *Biochim. Biophys. Acta* 226: 239–240.

Latour, V., Pigot, T., Simon, M., Cardy, H., Lacombe, S. 2005. Photooxidation of di-n-butylsulfide by various electron transfer sensitizers in oxygenated acetonitrile. *Photochem. Photobiol. Sci.* 4: 221–229.

Lente, G., Espenson, J.H. 2004. Photoreduction of 2,6-dichloroquinone in aqueous solution. Use of a diode array spectrophotometer concurrently to drive and detect a photochemical reaction. *J. Photochem. Photobiol. A Chem.* 163: 249–258.

Levin, P.P., Costa, S.M.B., Ferreira, L.F.V. 1996. Pore size effect on kinetics of photoinduced electron transfer in the quinone-amine system on the silica surface studied by diffuse-reflectance laser flash photolysis. *J. Phys. Chem.* 100: 15171–15179.

Li, W.-W., Hellwig, P., Ritter, M., Haehnel, W. 2006. De novo design, synthesis, and characterization of quinoproteins. *Chem. Eur. J.* 12: 7236–7245.

Loeff, I., Goldstein, S., Treinin, A., Linschitz, H. 1991. Reaction of formate ion with triplets of anthraquinone-2-sulfonate, 1,4-naphthoquinone, benzophenone-4-carboxylate, and benzophenone-4-sulfonate. *J. Phys. Chem.* 95: 4423–4430.

Loeff, I., Treinin, A., Linschitz, H. 1983. The photochemistry of 9,10-anthraquinone-2-sulfonate in solution. 1. Intermediates and mechanism. *J. Phys. Chem.* 87: 2536–2544.

Loeff, I., Treinin, A., Linschitz, H. 1984. The photochemistry of 9,10-anthraquinone-2-sulfonate in solution. 2. Effects of inorganic anions: Quenching vs. radical formation at moderate and high anion concentrations. *J. Phys. Chem.* 88: 4931–4937.

Lü, J.-M., Wu, L.M., Geimer, J., Beckert, D. 2001. Time resolved FT EPR study of the decarboxylation following photo-induced electron transfer between α-amino acids and anthraquinone-2,6-disulfonic acid in aqueous solution. *Phys. Chem. Chem. Phys.* 3: 2053–2058.

Lubitz, W., Lendzian, F., Bittl, R. 2002. Radicals, radical pairs and triplet states in photosynthesis. *Acc. Chem. Res.* 35: 313–320.

Lukeman, M., Xu, M., Wan, P. 2002. Excited state intramolecular redox reaction of 2-(hydroxymethyl)-anthraquinone in aqueous solution. *J. Chem. Soc. Chem. Commun.* 136–137.

Mac, M., Wirz, J. 2002. Salt effects on the reactions of radical ion pairs formed by electron transfer quenching of triplet 2-methyl-1,4-naphthoquinone by amines. Optical flash photolysis and step-scan FTIR investigations. *Photochem. Photobiol. Sci.* 1: 24–29.

Macpherson, A.N., Liddell, P.A., Lin, S., Noss, L., Seely, G.R., DeGraziano, J.M., Moore, A.L., Moore, T.A., Gust, D. 1995. Ultrafast photoinduced electron transfer in rigid porphyrin-quinone dyads. *J. Am. Chem. Soc.* 117: 7202–7212.

Malkin, S., Churio, M.S., Shochat, S., Braslavsky, S.E. 1994. Photochemical energy storage and volume changes in the microsecond time range in bacterial photosynthesis—A laser induced optoacoustic study. *J. Photochem. Photobiol. B: Biol.* 23: 79–85.

Marian, C.M., Kock, S.C., Hundsdörfer, C. et al. 2009. Spectroscopic properties of phenolic and quinoid carotenoids: A combined theoretical and experimental study. *Photochem. Photobiol. Sci.* 8: 270–278.

Marquardt, R., Grandjean, S., Bonneau, R. 1992. Competition between intersystem crossing and intramolecular electron transfer in substituted benzoquinones. *J. Photochem. Photobiol. A: Chem.* 69: 143–153.

Maruyama, K., Kubo, Y. 1994, Photochemical hydrogen abstraction of quinones. In *CRC Handbook of Organic Photochemistry and Photobiology*, eds. W. M. Horspool and P.-S. Song, pp. 748–756, Boca Raton, FL: CRC Press.

Maruyama, K., Osuka, A. 1988. Recent advances in the photochemistry of quinones. In *The Chemistry of the Quinoid Compounds*, eds. S. Patei and Z. Rappoport, Vol. 2, pp. 757–875, New York: Wiley.

Mazellier, P., Bolte, M. 1996. Photochemical behaviour of 2,6-dimethylbenzoquinone in the absence and in the presence of iron(III). *J. Photochem. Photobiol. A: Chem.* 98: 141–147.

McGilvray, K.L., Chrétien, M.N., Lukeman, M., Scaiano, J.C. 2006. A simple and smart oxygen sensor based on the intrazeolite reactions of a substituted anthraquinone, *J. Chem. Soc. Chem. Commun.* 4401–4403.

McIntosh, A.R., Siemiarczuk, A., Bolton, J.R., Stillman, M.J., Ho, T.-F., Weedon, A.C. 1983. Intramolecular photochemical electron transfer. 1. EPR and optical absorption evidence for stabilized charge separation in linked porphyrin-quinone molecules. *J. Am. Chem. Soc.* 105: 7215–7223.

McKellar, J.F. 1971. Phototendering of the antraquinone VAT dyes. A review. *Rad. Res. Rev.* 3: 141–165.

Meisel, D., Czapski, G. 1975. One-electron transfer equilibria and redox potentials of radicals studied by pulse radiolysis. *J. Phys. Chem.* 79: 1503–1509.

Melvin, T., Bothe, E., Schulte-Frohlinde, D. 1996. The reaction of triplet 2-methyl-1,4-naphthoquinone (menadione) with DNA and polynucleotides. *Photochem. Photobiol.* 64: 769–776.

Mennenga, A., Gärtner, W., Lubitz, W., Görner, H. 2006. Effects of noncovalently bound quinones on the ground and triplet states of zinc chlorins in solution and bound to *de novo* synthesized peptides. *Phys. Chem. Chem. Phys.* 8: 5444–5453.

Mitchell, D., Lukeman, M., Lehnherr, D., Wan, P. 2005. Formal intramolecular photoredox chemistry of meta-substituted benzophenones. *Org. Lett.* 7: 3387–3389.

Moore, J.N., Phillips, D., Nakashima, N., Yoshihara, K. 1986. Photochemistry of 9,10-anthraquinone-2, 6-disulphonate. *J. Chem. Soc. Faraday Trans. 2* 82: 745–761.

Moribe, S., Ikoma, T., Akiyama, K., Tero-Kubota, S. 2008. Time-resolved EPR study on photoreduction of sodium anthraquinone-2-sulfate in liposomes. *Chem. Phys. Lett.* 457: 66–68.

Morimoto, A., Yatsuhashi, T., Shimada, T., Biczók, L., Tryk, D.A., Inoue, H. 2001. Radiationless deactivation of an intramolecular charge transfer excited state through hydrogen bonding: Effect of molecular structure and hard-soft anionic character in the excited state. *J. Phys. Chem. A* 105: 10488–10496.

Müller, C., Schroeder, J., Troe, J. 2006. Intramolecular hydrogen bonding in 1,8-dihydroxyanthraquinone, 1-aminoanthraquinone, and 9-hydroxyphenalenone studied by picosecond time-resolved fluorescence spectroscopy in a supersonic jet. *J. Phys. Chem. B* 110: 19820–19832.

Murakami, M., Ohkubo, K., Mandal, P., Ganguly, T., Fukuzumi, S. 2008. Does bimolecular charge recombination in highly exergonic electron transfer afford the triplet excited state or the ground state of a photosensitizer? *J. Phys. Chem. A* 112: 635–642.

Murtinho, D., Pineiro, M., Pereira, M.M., dA Rocha Gonsalves, A.M., Arnaut, L.G., da Graça Miguel, M., Burrows, H.D. 2000. Novel porphyrins and a chlorin as efficient singlet oxygen photosensitizers for photooxidation of naphthols or phenols to quinones. *J. Chem. Soc. Perkin Trans. 2* 2441–2447.

Nakayama, T., Torii, Y., Nagahara, T., Miki, S., Hamanoue, K. 1999. Photophysics and photochemistry of planar alkylanthraquinones (the 1-methyl and 1,4-dimethyl compounds) studied by subpicosecond and nanosecond laser photolysis as well as steady-state photolysis. *J. Phys. Chem. A* 103: 1696–1703.

Neta, P. 1988. Radiation chemistry of quinonoid compounds. In *The Chemistry of the Quinoid Compounds*, eds. S. Patei and Z. Rappoport, Vol. 2, pp. 879–899, New York: Wiley.

Netto-Ferreira, J.C., Lhiaubet-Vallet, V., Bernardes, B.O., Ferreira, A.B.B., Miranda, M.A. 2008. Characterization, reactivity and photosensitizing properties of the triplet excited state of α-lapachone. *Phys. Chem. Chem. Phys.* 10: 6645–6652.

Netto-Ferreira, C.J., Lhiaubet-Vallet, V., Bernardes, B., Ferreira, A.B.B., Miranda, M.A. 2009. Photosensitizing properties of triplet β-lapachones in acetonitrile solution. *Photochem. Photobiol.* 85: 153–159.

Nicodem, D.E., Silva, R.S., Togashi, D.M. 2005. Solvent effects on the quenching of the equilibrating n,π* and π,π,* triplet states of 9,10-phenanthrenequinone by 2-propanol. *J. Photochem. Photobiol. A: Chem.* 175: 154–158.

Núñez Montoya, S.C., Comini, L.R., Sarmiento, M. et al. 2005. Natural anthraquinones probed as type I and type II photosensitizers: Singlet oxygen and superoxide anion production. *J. Photochem. Photobiol. B: Biol.* 78: 77–83.

Oelgemöller, M., Jung, C., Mattay, J. 2007. Green photochemistry: Production of fine chemicals with sunlight. *Pure Appl. Chem.* 79: 1939–1947.

Oelgemöller, M., Mattay, J. 2004. The photochemical Friedel-Crafts acylation of quinones: From the beginning of photochemistry to modern solar chemical applications. In *CRC Handbook of Organic Photochemistry and Photobiology*, eds. W.M. Horspool and F. Lenci, 2nd edn., pp. 88, 1–45. Boca Raton, FL: CRC Press.

Okamoto, K., Hasobe, T., Tkachenko, N.V., Lemmetyinen, H., Kamat, P.V., Fukuzumi, S. 2005. Drastic difference in lifetimes of the charge-separated state of the formanilide-anthraquinone dyad versus the ferrocene-formanilide-anthraquinone triad and their photoelectrochemical properties of the composite films with fullerene clusters. *J. Phys. Chem. A* 107: 4662–4670.

Okamoto, K., Ohkubo, K., Kadish, K.M., Fukuzumi, S. 2004. Remarkable accelerating effects of ammonium cations on electron-transfer reactions of quinones by hydrogen bonding with semiquinone radical anions. *J. Phys. Chem. A* 108: 10405–10413.

Ononye, A.I., Bolton, J.R. 1986. Mechanism of the photochemistry of *p*-benzoquinone in aqueous solutions. 2. Optical flash photolysis studies. *J. Phys. Chem.* 90: 6270–6274.

Osyczka, A., Zhang, H., Mathé, C., Rich, P.R., Moser, C.C., Dutton, P.L. 2006. Role of the PEWY glutamate in hydroquinone-quinone oxidation-reduction catalysis in the Q_0 site of cytochrome bc_1. *Biochem.* 45: 10492–10503.

Pan, Y., Gao, Y., Yan, L., Pan, H., Chen, J., Yu, S. 2007. Reactivity of aromatic amines with triplet 1,8-dihydroxyanthraquinone: A laser flash photolysis study. *Spectrochim. Acta A* 66: 63–67.

Pandey, N.K. 1982. Spectrophotometric and titrimetric determinations of ascorbic acid. *Anal. Chem.* 54: 793–796.

Parker, A.W., Hester, R.E., Phillips, D., Umapathy, S. 1992. Time-resolved resonance Raman spectroscopic investigation of the photochemistry of ubiquinone. *J. Chem. Soc. Faraday Trans.* 88: 2649–2653.

Pochon, A., Vaughan, P.P., Gan, D., Vath, P., Blough, N.V., Falvey, D.E. 2002. Photochemical oxidation of water by 2-methyl-1,4-benzoquinone: Evidence against the formation of free hydroxyl radical. *J. Phys. Chem. A* 106: 2889–2894.

Ramseier, M., Senn, P., Wirz, J. 2003. Photohydration of benzophenone in aqueous acid. *J. Phys. Chem. A* 107: 3305–3315.

Rath, M.C., Mukherjee, T. 1997. Photophysics of 6,11-dihydroxynaphthacene-5,12-dione in different organic solvents. *J. Chem. Soc. Faraday Trans.* 93: 3331–3336.

Rath, M.C., Pal, H., Mukherjee, T. 2001. Excited singlet (S_1) state interactions of 6,11-dihydroxy-5, 12-naphthacenequinone with aromatic hydrocarbons. *J. Phys. Chem. A* 105: 7945–7956.

Redmond, R.W., Gamlin, N.J. 1999. A compilation of singlet oxygen yields from biologically relevant molecules. *Photochem. Photobiol.* 70: 391–475.

Renger, G., Renger, T. 2008. Photosystem II: The machinery of photosynthetic water splitting. *Photosynth. Res.* 98: 53–80.

Reszka, K.J., Bilski, P., Chignell, C.F., Hartley, J.A., Khan, N., Souhami, R.L., Mendonca, A.J., Lown, J.W. 1992. Photosensitization by anticancer agents 11. Mechanisms of photosensitization of human leukemic cells by diaminoanthraquinones: Singlet oxygen and radical reactions. *J. Photochem. Photobiol. B: Biol.* 15: 317–335.

Reszka, K., Kolodziejczyk, P., Tsoungas, P.G., Lown, J.W. 1988. Photosensitization by antitumor agents. 6. Production of superoxide radical and hydrogen peroxide during illumination of diaminoanthracenediones in the presence of NADH in aqueous solutions: An EPR study. *Photochem. Photobiol.* 47: 625–633.

Roginsky, V.A., Barsukova, T. 2000. Kinetics of oxidation of hydroquinones by molecular oxygen. Effect of superoxide dismutase. *J. Chem. Soc. Perkin Trans. 2* 1575–1582.

Roginsky, V.A., Barsukova, T.K., Stegmann, H. 1999. Kinetics of redox interaction between substituted quinones and ascorbate under aerobic conditions. *Chem.-Biol. Interact.* 121: 177–197.

Roginsky, V.A., Pisarenko, L.M., Bors, W., Michel, C., Saran, M. 1998. Comparative pulse radiolysis studies of alkyl- and methoxy-substituted semiquinones formed from quinones and hydroquinones. *J. Chem. Soc. Faraday Trans.* 94: 1835–1840.

Ronfard-Haret, J.-C., Bensasson, R.V., Amouyal, E. 1980. Assignment of transient species observed on laser flash photolysis of *p*-benzoquinone and methylated *p*-benzoquinones in aqueous solution. *J. Chem. Soc. Faraday Trans. I* 76: 2432–2436.

Rosokha, S.V., Lu, J., Rosokha, T.Y., Kochi, J.K. 2009. Counter-ion modulation of long-distance π-bonding of the open-shell *p*-benzoquinone anions. *Phys. Chem. Chem. Phys.* 11: 324–332.

Rossetti, R., Brus, L. E. 1986. Picosecond time resolved Raman scattering study of hydrogen abstraction by triplet excited benzoquinone. *J. Am. Chem. Soc.* 108: 4718–4720.

Roth, H.D. 2006. Nuclear-spin polarization in electron-transfer reactions of amines. *Helv. Chim. Acta* 89: 2847–2860.

Satpati, A.K., Kumbhakar, M., Nath, S., Pal, H. 2008. Photoinduced electron transfer between quinones and amines in micellar media: Tuning the Marcus inversion region. *J. Photochem. Photobiol. A: Chem.* 200: 270–276.

Scaiano, J.C., Neta, P. 1980. Effect of pH on the behavior of duroquinone triplets. *J. Am. Chem. Soc.* 102: 1608–1611.

Scheerer, R., Grätzel, M. 1977. Laser photolysis studies of duroquinone triplet state electron transfer reactions. *J. Am. Chem. Soc.* 99: 865–871.

Schuchmann, M.N., Bothe, E., von Sonntag, J., von Sonntag, C. 1998. Reaction of OH radicals with benzoquinone in aqueous solutions. A pulse radiolysis study. *J. Chem. Soc. Perkin Trans.* 2: 791–796.

Schulte-Frohlinde, D., von Sonntag, C. 1965. Zur Photoreduktion von Chinonen in Lösung. *Z. Phys. Chem. N. F.* 44: 314–327.

Schuster, G.B. 2000. Long-range charge transfer in DNA: Transient structural distortions control the distance dependence. *Acc. Chem. Res.* 33: 253–260.

Serpa, C., Arnaut, L.G. 2000. Does molecular size matter in photoinduced electron transfer reactions? *J. Phys. Chem. A* 104: 11075–11086.

Seybold, G., Wagenblast, G. 1989. New perylene and violanthrone dyestuffs for fluorescent collectors. *Dyes Pigm.* 11: 303–317.

Sheng, Z., Pan, Y., Yan, L., Hei, X., Guo, Z., Dai, J., Song, Q., Yu, S. 2004. Steady-state and laser flash photolysis studies on the oxidative splitting of cyclobutane thymine dimer by triplet 9,10-anthraquinone-2-sulfonate. *J. Photochem. Photobiol. A: Chem.* 161: 99–104.

Shi, M., Yang, W.-G., Wu, S. 2007. Wavelength-dependent photolyses of 2,5-dichloro-3,6-bis(dialkylamino)-[1,4] benzoquinone. *J. Photochem. Photobiol. A: Chem.* 185: 140–143.

Shimokage, T., Ikoma, T., Akiyama, K., Tero-Kubota, S., Yamaji, M., Shizuka, H. 1997. Substituent and matrix effects on the excited triplet states of 1,4-naphthoquinones. *J. Phys. Chem. A* 101: 9253–9256.

Shirai, M., Awatsuji, T., Tanaka, M. 1975. Photolysis of *p*-benzoquinone in aqueous solution. Possibility of a polar mechanism in the primary process. *Bull. Chem. Soc. Jpn.* 48: 1329–1330.

Sigman, M.E., Zingg, S.P., Pagni, R.M., Burns, J.H. 1991. Photochemistry of anthracene in water. *Tetrahedron Lett.* 32: 5737–5740.

Silva, R.S., Nicodem, D.E. 2008. Deuterium isotope effects on the photoreduction of 9,10-phenanthrenequinone and benzophenone by 2-propanol. *J. Photochem. Photobiol. A: Chem.* 194: 76–80.

Singh, N.J., Lee, H.M., Suh, S.B. et al. 2007. *De novo* design approach based on nanorecognition toward development of functional molecules/materials and nanosensors/nanodevices. *Pure Appl. Chem.* 79: 1057–1075.

Sinnecker, S., Flores, M., Lubitz, W. 2006. Protein–cofactor interactions in bacterial reaction centers from *Rhodobacter sphaeroides* R-26: Effect of hydrogen bonding on the electronic and geometric structure of the primary quinone. A density functional theory study. *Phys. Chem. Chem. Phys.* 8: 5659–5670.

Smart, R.P., Peelen, T.J., Blankespoor, R.L., Ward, D.L. 1997. Short-lived 1,5-biradicals formed from triplet 1-alkoxy- and 1-(benzyloxy)-9,10-anthraquinones. *J. Am. Chem. Soc.* 119: 461–465.

Sobolewski, A.L., Domcke, W. 2008. Computational model of photocatalytic water splitting. *J. Phys. Chem. A* 112: 7311–7313.

Springer, J., Kodis, G., de la Garza, L., Moore, A.L., Moore, T.A., Gust, D. 2003. Stepwise sequential and parallel photoinduced charge separation in a porphyrin-triquinone tetrad. *J. Phys. Chem. A* 107: 3567–3575.

Steenken, S., Neta, P. 2003. Transient phenoxyl radicals: Formation and properties in aqueous solutions. In *The Chemistry of Phenols*, ed. Z. Rappoport, pp. 1107–1152, New York: Wiley.

Studzinskii, O.P., Levental, Y.K., Eltsov, A.V. 1978. Photochemical reduction of nitroanthraquinones in alcohols. *Z. Org. Khimii* 14: 2150–2161, *J. Org. Chem.* 14: 1991–2000.

Swartz, A.M., Patton, V., Heppleston, M.J., Barra, M. 2008. On the photoreactivity of vitamin K compounds. *Int. J. Chem. Kin.* 40: 839–844.

Taguchi, K., Fujii, S., Yamano, S. et al. 2007. An approach to evaluate two-electron reduction of 9,10-phenanthraquinone and redox activity of the hydroquinone associated with oxidative stress. *Free Rad. Biol. Med.* 43: 789–799.

Tajima, M., Katoh, K., Matsunaga, K., Inoue, H. 2009. Photoamination of 1-hydroxyanthraquinone in a water-actonitrile mixed solvent. *J. Phys. Org. Chem.* 22: 313–320.

Takamori, D., Aoki, T., Yashiro, H., Murai, H. 2001. Time-resolved ESR study on the photochemistry of naphthoquinones included in cyclodextrins. *J. Phys. Chem. A* 105: 6001–6007.

Tarábek, P., Bonifačic, M., Beckert, D. 2006. Time-resolved FT EPR and optical spectroscopy study on photooxidation of aliphatic α-amino acids in aqueous solutions; electron transfer from amino vs carboxylate functional group. *J. Phys. Chem. A* 110: 7293–7302.

Tarábek, P., Bonifačic, M., Beckert, D. 2007. Oxidation of cyclic dipeptides by photoinduced H-atom abstraction. A laser flash FT EPR and optical spectroscopy study. *J. Phys. Chem. A* 111: 4958–4964.

Ulu, S.T. 2009. Rapid and sensitive spectrofluorimetric determination of enrofloxacin, levofloxacin and ofloxacin with 2,3,5,6-tetrachloro-*p*-benzoquinone. *Spectrochim. Acta A* 72: 1038–1042.

Umadevi, M., Vanelle, P., Terme, T., Rajkumar, B.J.M., Ramakrishnan, V. 2008. Spectral investigations of solvatochromism and preferential solvation on 1,4-dihydroxy-2,3-dimethyl-9,10-anthraquinone. *J. Fluoresc.* 18: 1139–1149.

Valgimigli, L., Amorati, R., Fumo, M.G., DiLabio, G.A., Pedulli, G.F., Ingold, K.U., Pratt, D.A. 2008. The unusual reaction of semiquinone radicals with molecular oxygen. *J. Org. Chem.* 73: 1830–1841.

Vath, P., Wamer, W.G., Falvey, D.E. 2002. Photochemistry and phototoxicity of aloe emodin. *Photochem. Photobiol.* 75: 346–352.

Verhoeven, J.W. 2006. On the role of spin correlation in the formation, decay, and detection of long-lived, intramolecular charge-transfer states. *J. Photochem. Photobiol. C: Photochem. Rev.* 7: 40–60.

von Sonntag, C. 1987. In *The Chemical Basis of Radiation Biology*, London, U.K.: Taylor & Francis.

von Sonntag, C. 2006. *Free-Radical-Induced DNA Damage and Its Repair, a Chemical Perspective*, Berlin, Germany: Springer.

von Sonntag, J., Mvula, E., Hildenbrand, K., von Sonntag, C. 2004. Photohydroxylation of 1,4-benzoquinone in aqueous solution revisited. *Chem. Eur. J.* 10: 440–451.

Wakisaka, A., Ebbesen, T.W., Sakuragi, H., Tokumaru, K. 1987. Effect of water concentration on photoreduction of anthraquinone-2-sulfonate by 2-propanol in aqueous acetonitrile solution. *J. Phys. Chem.* 91: 6547–6551.

Wan, J.D., Ferreira, A., Xia, W., Chow, C.H., Takechi, K., Kamat, P.V., Jones II, G., Vullev, V.I. 2008. Solvent dependence of the charge-transfer properties of a quaterthiophene-anthraquinone dyad. *J. Photochem. Photobiol. A: Chem.* 197: 364–374.

Wardman, P. 1989. Reduction potentials of one-electron couples involving free radicals in aqueous solution. *J. Chem. Phys. Ref. Data* 18: 1637–1655.

Wilkinson, F. 1962. Transfer of triplet state energy and the chemistry of excited states. *J. Phys. Chem.* 66: 2569–2573.

Woodbury, N.W., Parson, W.W., Gunner, M.R., Princec, R.C., Dutton, L.P. 1986. Radical-pair energetics and decay mechanisms in reaction centers containing anthraquinones, naphthoquinones or benzoquinones in place of ubiquinone. *Biochim. Biophys. Acta* 851: 6–22.

Yamaji, M., Itoh, T., Tobita, S. 2002. Photochemical properties of the triplet π, π^* state, anion and ketyl radicals of 5,12-naphthacenequinone in solution studied by laser flash photolysis: Electron transfer and phenolic H-atom transfer. *Photochem. Photobiol. Sci.* 1: 869–876.

Yamaji, M., Kurumi, M., Kimura, H., Shizuka, H. 1999. Hydration effects on the triplet exciplex between 2,3-dihalo-1,4-naphthoquinone and furan studied by steady-state and laser flash photolyses. *Phys. Chem. Chem. Phys.* 1: 1859–1865.

Yashiro, H., White, R.C., Yurkovskaya, A.V., Forbes, M.D.E. 2005. Methionine radical cation: Structural studies as a function of pH using X- and Q-band time-resolved electron paramagnetic resonance spectroscopy. *J. Phys. Chem. A* 109: 5855–5864.

Yeow, E.K.L., Braslavsky, S.E. 2002. Quenching of zinc tetraphenylporphine by oxygen and by 1,4-benzoquinone in nitrile solvents: An optoacoustic spectroscopy study. *Phys. Chem. Chem. Phys.* 4: 239–247.

Yoshihara, T., Yamaji, M., Itoh, T., Nishimura, J., Shizuka, H., Tobita, S. 2001. Photochemistry of 1,4-anthraquinone studied by steady-state and laser-flash photolysis. *J. Photochem. Photobiol. A: Chem.* 140: 7–13.

Yoshihara, T., Yamaji, M., Itoh, T., Shizuka, H., Shimokage, T., Tero-Kubota, S. 2000. Hydrogen atom transfer and electron transfer reactions in the triplet π,π^* state of 1,4-anthraquinone studied by CIDEP techniques and laser flash photolysis. *Phys. Chem. Chem. Phys.* 2: 993–1000.

Yuasa, J., Ohkubo, K., Guldi, D.M., Fukuzumi, S. 2004. Drastic changes in the lifetime and electron transfer and energy transfer reactivity of the triplet excited state of *p*-benzoquinone by complex formation with scandium ion salts. *Phys. Chem. A* 108: 8333–8340.

Yuasa, J., Yamada, S., Fukuzumi, S. 2008. One-step versus stepwise mechanism in protonated amino acid-promoted electron-transfer reduction of a quinone by electron donors and two-electron reduction by a dihydronicotinamide adenine dinucleotide analogue. Interplay between electron transfer and hydrogen bonding. *J. Am. Chem. Soc.* 130: 5808–5820.

Zhang, C.X., Boussac, A., Rutherford, A.W. 2004. Low-temperature electron transfer in photosystem II: A tyrosyl radical and semiquinone charge pair. *Biochemistry* 43: 13787–13795.

Zhang, Z., Hao, S., Zhu, H., Wang, W. 2008. Photoreactions of 1,4-naphthoquinone with lysozyme studied by laser flash photolysis and steady-state analysis. *J. Photochem. Photobiol. B: Biol.* 92: 77–82.

29

Photodecarboxylation of Arylacetic Acids

Matthew Lukeman
Acadia University

29.1 Introduction

Photodecarboxylation (PDC) is an important fundamental photoreaction that has significance in many areas of chemistry. PDC is responsible for the *in vivo* decomposition of many pharmaceuticals, including several nonsteroidal anti-inflammatory drugs (NSAIDS).[1–3] PDC reactions have found application in organic synthesis, particularly in the production of "disciplined radicals" by PDC of Barton esters[4–6] and in the photodecarboxylative addition reactions of Griesbeck and Oelgemöller.[7–10] The photodegradation of many organic compounds can be carried out through photocatalytic PDC reactions such as the photo-Kolbe reaction,[11,12] and similar reactions can be used to initiate polymerization reactions.[13]

Several reviews are available that provide excellent coverage of various aspects of PDC chemistry.[14–17] The focus of the present chapter is on the PDC of phenylacetic acids, since recent applications of this class of reactions have brought them into the spotlight.

29.2 PDC of Electron-Rich Arylacetic Acids

The photochemistry of phenylacetic acid (**1**) has been studied by Meiggs and Miller,[18] who observed the production of bibenzyl (**3**) and polyacid following irradiation in methanol. Both products are consistent with initial homolysis to give the benzyl radical (**2**) (Equation 29.1). The authors observed a transient absorption (λ_{max} = 302 and 314 nm) that they attribute to **2**. The observation of this transient and later deuterium incorporation studies both support a homolytic mechanism for the reaction of **1**.[19]

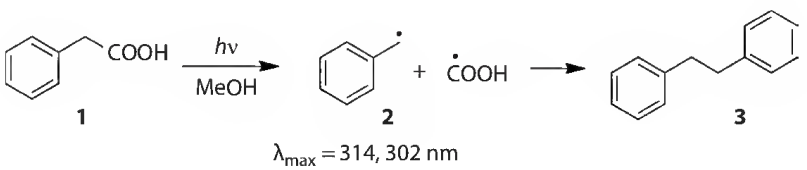

(29.3)

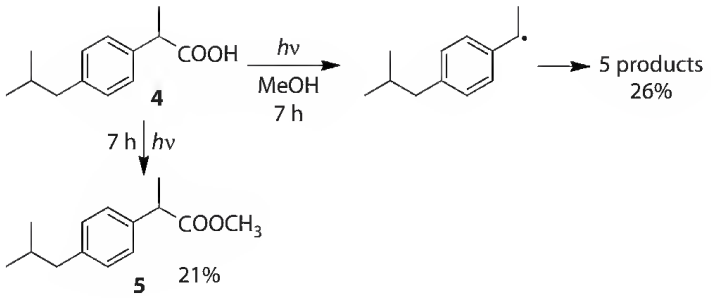

SCHEME 29.1

The quantum yield for production of CO_2 on irradiation of **1** is only 0.037, indicating that the homolytic reaction is relatively inefficient. The phenylacetate ion ($\mathbf{1}^-$) undergoes PDC in water with similarly low efficiency, although via a different mechanism: photoejection of an electron gives the phenylacetyl radical, which then loses CO_2 to give the benzyl radical (**2**)[20]. In methanol (but not in water), toluene was formed as the major product, and is consistent with formation of the benzyl anion, indicating that a solvent-dependent heterolytic pathway might potentially be competitive.

Addition of alkyl groups to phenylacetic acid does not significantly modulate its photochemical behavior. For example, ibuprofen (**4**), a widely used NSAID, is an alkylated derivative of **1**. Irradiation of **4** in methanol has been observed to give six products, five of which are expected photoproducts resulting from homolytic decarboxylation to give the benzyl radical (Scheme 29.1).[21] The origin of the sixth product (**5**) accounting for nearly half of the product mixture is not known, but is not an obvious product arising from either the benzyl radical or anion. Although a PDC quantum yield was not reported, the long irradiation times required to achieve ~50% decomposition (7 h) suggest an inefficient reaction.

Reaction pathways analogous to those for **1** and **4** were observed for 1-naphthylacetic acids. Radical derived products were observed on irradiation of 1-naphthylacetic acid in ethanolic or in aqueous solution,[22,23] and signals corresponding to the 1-naphthylmethyl radical (λ 330 nm) and solvated electron (λ = 700 nm) were observed by laser flash photolysis (LFP).[23] These results point to a mechanism in which the primary photochemical step is photoejection of an electron to the solvent, followed by decarboxylation to give the naphthylmethyl radical.

Electron-rich NSAIDS naproxen and carprofen are aryl acetic acids, and exhibit photochemistry similar to **1**.[24–27] Both initially photoionize, producing solvated electrons, and subsequently decarboxylate to give radical intermediates. PDC proceeds with very low efficiency ($\Phi \sim 0.01$), both when they are in their acid and carboxylate forms. Radical PDC pathways, either involving direct homolysis or involving initial photoionization, have come to typify the photochemistry of electron-rich arylacetic acids.

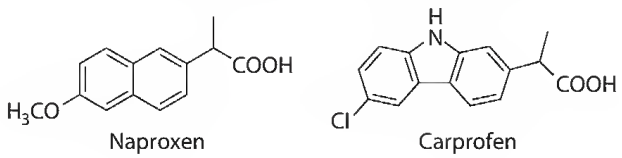

29.3 PDC of Electron-Poor Arylacetic Acids

29.3.1 Trifluoromethylphenylacetic and Mandelic Acids

Burns and Lukeman have recently investigated the photochemistry of a variety of phenylacetic and mandelic acids substituted with trifluoromethyl substituents, and found that they undergo PDC efficiently in aqueous solution (pH 7 or higher), to give substituted toluene products consistent with initial formation of carbanion intermediates.[28] A total of eight examples (**6–13**), comprising *ortho*, *meta*, *para*, and di-substituted derivates, all underwent the reaction efficiently, with relative efficiencies apparently

governed by the "*meta* effect" ($\Phi_m > \Phi_o > \Phi_p$). The derivatives were much less reactive at lower pH values, indicating that the reaction proceeds from the carboxylate rather than the acid form. Sensitization and quenching studies support reactivity occurring from the singlet state.

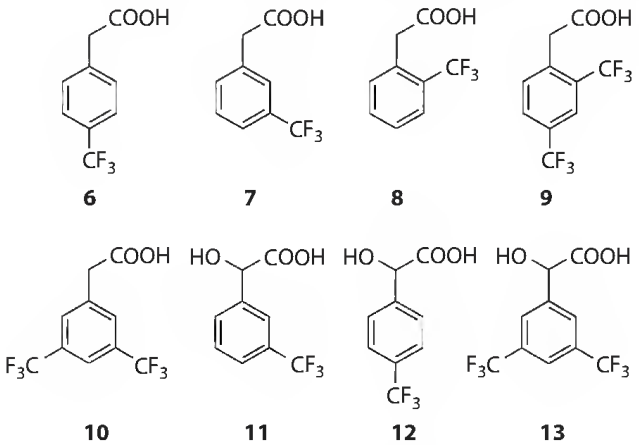

The efficient PDC of **6–13** to produce products consistent with ionic intermediates is very different behavior from that of electron-rich arylacetic acids. The carbanion intermediates produced following PDC of these derivatives can result either from direct heterolysis from the excited state, or homolysis followed by a rapid electron transfer.

29.3.2 Nitrophenylacetic Acids

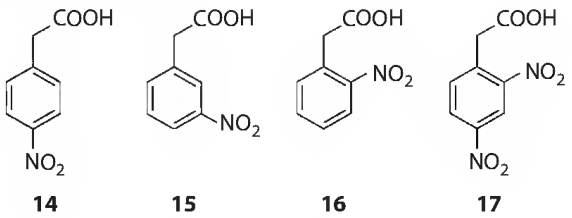

The photochemistry of the carboxylates of nitrophenylacetic acids **14–17** in aqueous solution was investigated by Margerum and Petrusis, and all derivatives were found to undergo PDC.[29,30] Very high quantum yields ($\Phi \sim 0.6$) were observed for the *meta* and *para* derivatives **14** and **15**, although the efficiencies of the *ortho* isomers **16** and **17** were much more modest ($\Phi \sim 0.04$). The only products observed following irradiation of **15–17** were the corresponding nitrotoluenes, which are consistent with the formation of carbanion intermediates. Irradiation of *para*-nitrophenylacetate (**14**) gave rise to carbanion **18**, which persisted with a lifetime of close to 1 min, and was easily detectable by conventional UV-Vis spectroscopy (λ_{max} = 355 nm). This strongly resonance-stabilized carbanion decayed to give two products: reaction with water gave *p*-nitrotoluene as a minor product (3%) while the major product was bibenzyl **19**, a product known to result from carbanion **18** (Equation 29.2). Craig and Atherton later studied the chemistry of carbanion **18** in greater detail using LFP, and provided rate constants for formation of the two reaction products.[31]

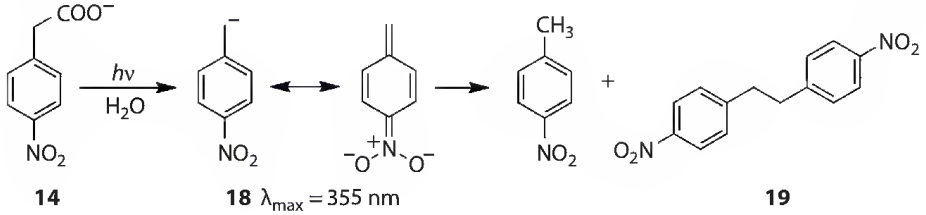

(29.2)

Wan and coworkers later showed that the ability of the nitro group to facilitate heterolytic PDC is actually enhanced on moving from the nitrophenyl to the nitrobiphenyl chromophore, despite the greater distance between the activating nitro group and the reaction center.[32] Nitrobiphenylacetic acid **20** undergoes PDC with unity quantum yield to give the corresponding nitrobiphenyltoluene via carbanion **21** (Equation 29.3).

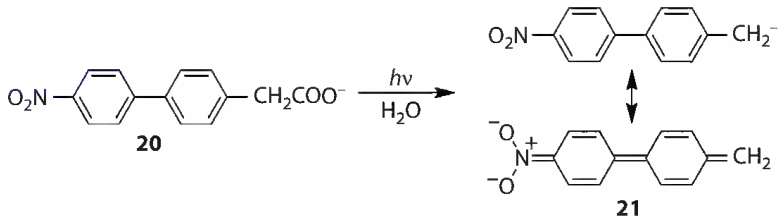

(29.3)

The α-carboxy-2-nitrobenzyl (CNB) photoremovable protecting group (PPG) is a water-soluble derivative of the popular *ortho*-nitrobenzyl PPG, and has been used to enact the photorelease of bioactive molecules in aqueous solution.[33,34] Prior to a recent report by Corrie and coworkers,[35] it had always been assumed that the photochemistry of CNB is the same as for related *o*-nitrobenzyl systems and that the benzylic carboxylate is retained throughout the reaction. However, given the structural similarity between CNB and *o*-nitrophenylacetate **16**, it would have been reasonable to expect PDC to be a competing side reaction. Indeed, Corrie et al. determined that PDC does play a role in the photochemistry of the CNB group when they were able to directly observe the generation of CO_2 on photolysis of CNB-caged glycine (via carbamate linkage) and phosphate.[35] In subsequent work, Hagen et al. have detected products arising from PDC of CNB caged peptides using HPLC, but found that the extent to which PDC reduces the photorelease efficiency is strongly dependent on the nature of the peptide and the buffer system used.[36]

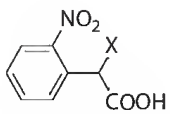

CNB caging group

29.3.3 Keto-Substituted Phenylacetic Acids

The photochemistry of ketoaromatics has been intensely studied for more than 100 years, effectively beginning when Ciamician observed the photoreduction of benzophenone in isopropanol when he exposed such solutions to sunlight on the rooftop of the Bologna laboratories.[37] The photochemistry of ketoaromatics is typified by radical formation via homolytic processes as hydrogen abstraction and Norrish type I and II reactions. As we shall see, the photochemistry of keto-substituted phenylacetic acids is distinctly different; radical chemistry is almost entirely avoided and heterolytic PDC to give ionic intermediates predominates.

Wan and coworkers investigated the photochemistry of 3- and 4-acetylphenylacetic acids **22** and **23** in aqueous solution, and found both to undergo efficient PDC at pH 7 (Φ = 0.6 and 0.22 for **22** and **23**, respectively).[38] The transients detected by LFP and the products observed were consistent with a mechanism involving heterolytic PDC to give carbanion intermediates. Both derivatives react from the triplet state of the carboxylate form, although reaction was still observed for **22** at pH values lower than 3, suggesting an additional acid-catalyzed pathway.

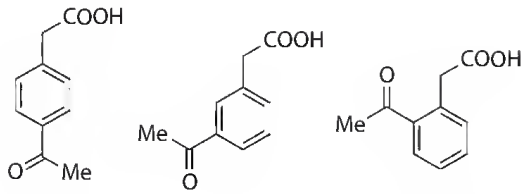

22 **23** **24**

The photochemistry of the *ortho* derivative **24** in benzene was examined by Sobczak and Wagner, who also found that decarboxylation took place efficiently in this solvent to give a single isolable product—2-methylacetophenone.[39] In this same solvent, no reactivity is observed from **22** and **23**, indicating a unique reaction mechanism only available to the *ortho* isomer. Indeed, later work by Ding et al. indicates that the likely mechanism in the PDC of **24** involves an initial intramolecular proton transfer from the carboxylic acid to the carbonyl oxygen—a reaction that is geometrically forbidden in the *meta* and *para* cases.[40] This proton transfer would generate a protonated carbonyl group, a suggestion that is in line with the acid-catalyzed route proposed by Wan for **22**.[38]

Less work has been carried out with the corresponding formylphenylacetic acids, however, the results from a recent report by Kresge and co-workers suggest that similar chemistry takes place, at least for the *para* derivative.[41]

29.3.3.1 Ketoprofen and Related Derivatives

Ketoprofen (**25**) is an NSAID whose photochemistry has received much more attention than the other NSAIDs, partially because the ionic chemistry it displays is very unusual for a benzophenone derivative. Costanza first reported that ketoprofen undergoes PDC in neutral aqueous solution with a quantum yield of 0.75.[42] When irradiated in de-aerated solution, the only product was 3-ethylbenzophenone (**26**), as would be expected from a heterolytic mechanism involving a carbanion intermediate (Equation 29.4). In aerated solution, **26** was still the major product, however three additional oxidation products were obtained, suggesting that the reactive intermediate responsible for the reaction is sufficiently long lived to react appreciably with dissolved oxygen. Bosca et al. proposed a mesolytic mechanism whereby the carboxylate of ketoprofen undergoes photoejection of an electron and PDC to generate a benzylic radical and a solvated electron.[43] The oxidation products are proposed to result from capture of the radical by oxygen, while **26** would arise from carbanion **27** formed by recombination of the benzylic radical and the solvated electron. Martinez and Scaiano were able to detect both solvated electrons and carbanion **27** on LFP of ketoprofen in neutral aqueous solution.[44] Laser power dependence studies showed that the solvated electron was formed as a result of a biphotonic process, and would therefore not contribute to the observed photochemistry under steady-state photolysis conditions that employ much less intense light sources. Also, the generation of the carbanion is prompt, having formed within the time window of the laser pulse. They propose an alternative mechanism in which **27** is formed directly from the ketoprofen carboxylate, either from a singlet or very short-lived triplet state. Additional mechanistic details have been provided by the work of Monti et al.,[45,46] and while their work is mostly consistent with the overall mechanism presented by Martinez and Scaiano (PDC within 10 ns, followed by slower protonation); consensus has yet to be reached regarding the multiplicity of the reaction. Using picosecond LFP, Monti et al. have observed a subnanosecond transient with spectral features reminiscent of the ketoprofen triplet state and whose decay rate matches the rate of appearance of the carbanion signal.[45] Cosa and Scaiano have instead offered convincing evidence of a singlet pathway[47]; they observed both the triplet state of ketoprofen and carbanion **27** simultaneously on LFP of **25** in water–acetonitrile mixtures, thus ruling out a product–precursor relationship between the two, at least in acetonitrile–water mixtures. Computational studies carried out by Erikkson and coworkers suggest that it is feasible for the ketoprofen carboxylate to undergo PDC from either the singlet or triplet manifold.[48] Suzuki et al. proposed

that the intermediate formed via the prompt decarboxylation of ketoprofen is in fact a triplet carbanion (with biradical character), which undergoes protonation at the oxygen to form a neutral biradical, which then converts to **26** on the microsecond timescale.[49] Phillips and co-workers investigated the photochemistry of ketoprofen using time-resolved resonance Raman spectroscopy and similarly conclude that the transient formed following the prompt PDC is a triplet carbanion, based on its sensitivity to oxygen.[50] However, the ionic reactions that ketoprofen-derived carbanions undergo (S_N2, E1cb, *vide infra*) are inconsistent with triplet biradical character.

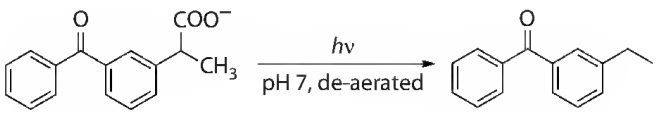

25 **26** $\Phi = 0.75$ (29.4)

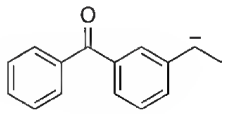

27

Scaiano and co-workers have extensively investigated the chemistry of carbanions obtained on PDC of ketoprofen analogues, beginning with derivatives **28–30** that have varying degrees of alkylation of the benzylic carbon.[51] Each of **28–30** was found to undergo PDC with high quantum yield, similar to that of **25**. The degree of substitution was found to have a dramatic effect on the rate at which the carbanions generated by the PDC reaction were protonated by water: the primary benzylic carbanion obtained on PDC of **28** was protonated with a rate constant of $2.7 \times 10^7\ s^{-1}$ whereas the tertiary benzylic carbanion obtained on PDC of **29** reacted a full order of magnitude more slowly. This result runs contrary to expectations based on carbanion stability, since alkyl groups are electron donating and should increase the charge localized on the benzylic site, thus making them more reactive. The reactivity reversal has been rationalized as being the result of entropic rather than enthalpic factors, that the steric hindrance imposed by the additional alkyl groups is responsible for the slowing of the rate of protonation.

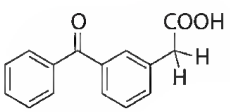

28

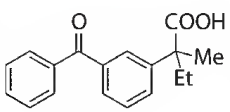

29

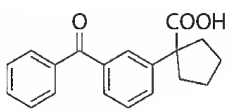

30

Scaiano et al. also investigated ketoprofen derivatives substituted with benzylic haloalkyl groups (**31–42**) with chain lengths of 4 or 5 carbons.[52,53] The idea behind this series was that the carbanions produced on PDC of these derivatives would have additional reaction pathways available to them other than protonation by solvent. The expected reactions from these carbanions were intramolecular S_N2 substitutions to produce cyclic alkanes, and E2 eliminations to produce alkenes. When irradiated in an aqueous solvent, protonation was the dominant reaction for all derivatives, and S_N2 or E2 processes were not able to effectively compete. However, when the solvent was changed to dry DMSO, the major products obtained in all cases were the cyclized products expected from the S_N2 reaction, with no elimination products detected. LFP of **31–42** in dry DMSO enabled characterization of the intermediate carbanions and determination of the S_N2 rate constants in this solvent. The dependency of the rate constants on the leaving group followed expected trends, with $k_{Cl} < k_{Br} < k_I$. Cyclization to give five-membered rings was found to be around two orders of magnitude faster than the analogous reaction to produce six-membered rings.

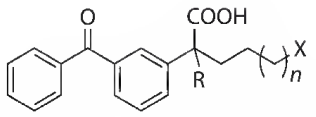

31 R = H, *n* = 2, X = Cl
32 R = H, *n* = 2, X = Br
33 R = H, *n* = 2, X = I
34 R = CH_3, *n* = 2, X = Cl
35 R = CH_3, *n* = 2, X = Br
36 R = CH_3, *n* = 2, X = I
37 R = H, *n* = 3, X = Cl
38 R = H, *n* = 3, X = Br
39 R = H, *n* = 3, X = I
40 R = CH_3, *n* = 3, X = Cl
41 R = CH_3, *n* = 3, X = Br
42 R = CH_3, *n* = 3, X = I

Interest in the mechanistic details of the PDC of ketoprofen has spurred a number of groups to examine the photochemistry of derivatives closely related to ketoprofen, but with modified chromophores. Wan and Xu studied 3- and 4-benzoylphenylacetic acids (**28** and **43**) and found both to undergo reactions similar to ketoprofen itself—heterolytic PDC to give benzoyltoluenes consistent with initial formation of carbanion intermediates.[54,55] Transients were detected on LFP of **28** and **43** that were conclusively assigned to the carbanion intermediates. Wan and coworkers also prepared and studied the photochemistry of **44** and **45**, which are derivatives of ketoprofen in which an additional phenyl ring was placed between the activating carbonyl group and the acetic acid functionality.[54] Both of these derivatives also underwent efficient PDC to only the corresponding benzoylphenyltoluenes (Φ = 0.73 and 0.30 for **44** and **45**, respectively). A heterolytic mechanism involving carbanion intermediates was proposed for both derivatives, and absorptions attributable to the expected carbanion intermediates were detected by nanosecond LFP. However, several interesting mechanistic details were uncovered during the study of **44** and **45**. Firstly, both derivatives show enhanced PDC at low pH values, suggesting that there may exist an acid-catalyzed mechanism of PDC for these derivatives. Secondly, **44** and **45** show large solvent deuterium isotope effects (4.3 and 2.3, respectively), indicating that a proton transfer from the solvent (or at least formation of significantly strong hydrogen bonds) to the substrate occurs during the primary photochemical step. For *para* derivative **45**, such an interaction can be easily envisioned since PDC could occur simultaneously with proton (deuteron) transfer from the solvent to the carbonyl oxygen to directly generate the neutral enol (Equation 29.5), bypassing the carbanion/enolate altogether.

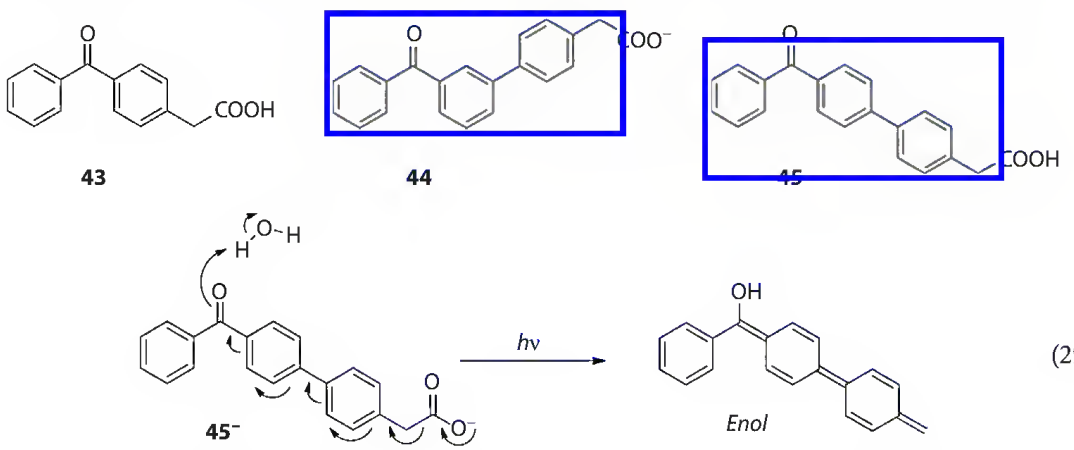

(29.5)

Blake et al. investigated the photochemistry of the conjugate bases of 2-, 3-, and 4-xanthoneacetic acids **46**–**48** in aqueous solution (pH 7.4), and found very efficient PDC for **46** and **48** (Φ ~ 0.65), whereas **47** was photoinert.[56] The stark contrast in the PDC efficiency of the positional isomers was attributed to the "*meta* effect," since the two reactive isomers have the electron-withdrawing keto group positioned *meta* to the reaction center. The methyl xanthone products observed on PDC of **46** and **48** are consistent with a carbanion intermediate and heterolytic PDC, although no transients attributable to these carbanions

were detected by LFP.[56,57] Quenching and fluorescence results provided strong evidence that the reaction proceeds exclusively from the S1 state, behavior that is unusual for aromatic ketones.

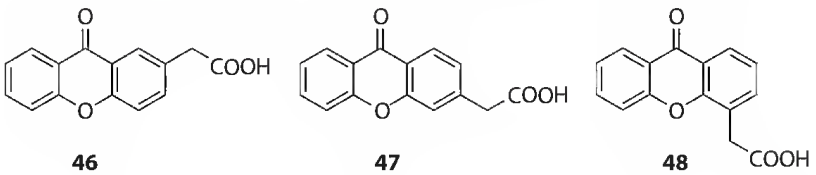

A new class of PPGs (**49**) has been developed by Lukeman and Scaiano that rely on PDC as the primary photochemical step.[58] These PPGs consist of ketoprofen as the core structure, with a leaving group (X) attached to β to the benzylic carbon. PDC of the conjugate base of the "ketoprofenate" PPG **49** (which is the major prototropic form at physiological pH) gives a benzylic carbanion (**50**) that subsequently ejects the leaving group as an anion via an E1cb-type mechanism (Equation 29.6). Several leaving groups were successfully released in this way, including halides, carboxylates, and methoxide. For most leaving groups, protonation of the intermediate cation was unable to compete with the elimination, and the alkene product (**51**) was the only one observed. Using the known protonation rate constants of 3-benzoylbenzyl carbanions in water, a minimum elimination rate constant of 10^8 s^{-1} was estimated for the elimination of good leaving groups. In the case of methoxide release, protonation was able to effectively compete with elimination, and the elimination product **51** was found to comprise only 20% of the product mixture. The intermediate carbanion was detected using LFP for this example, and a rate constant for elimination of methoxide was determined to be 5.1×10^6 s^{-1}, which is more than six orders of magnitude faster than for release of the same leaving group from the *o*-nitrobenzyl PPG in the same solvent.[59] The ketoprofenate PPG shows several advantages over the *o*-nitrobenzyl group including very fast release kinetics (subnanosecond for most leaving groups), high quantum yield ($\Phi > 0.7$), good water solubility, and the production of relatively noninterfering products.

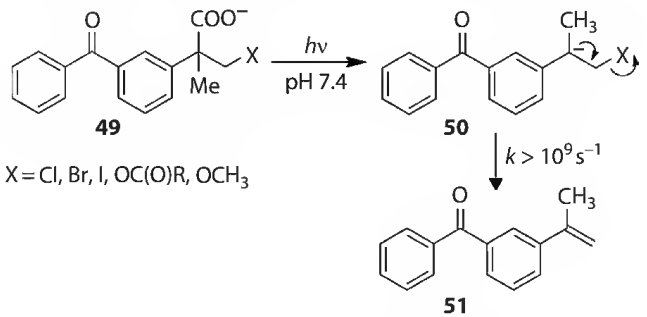

(29.6)

Subsequent to the initial report of the photochemistry of the ketoprofenate PPG, Blake et al. reported the development of a second-generation carbanion-mediated PPG based on the known PDC reaction of xanthone acetic acid.[57] These "xanthonate" PPGs (**52**) are believed to operate via a mechanism entirely analogous to that of **49**, and release of carboxylic acids and amines (via the carbamate) has been demonstrated. The xanthonate PPGs appear to retain all of the advantages of the ketoprofenate PPGs, but have a much higher molar absorptivity in the UVA region. In addition, the vinylxanthone photoproduct that is formed on photolysis of **52** shows strong fluorescence emission, which can be used as a "reporter" allowing quantification of the decaying reaction.

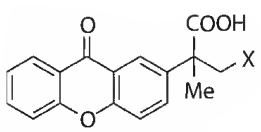

52 X = OAc, OC(O)NHPh

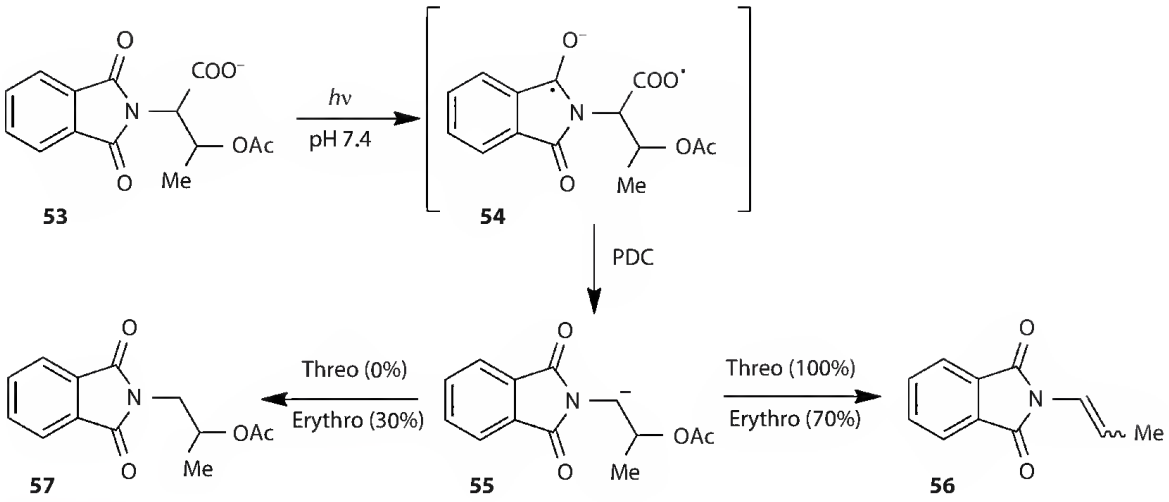

SCHEME 29.2

A related PPG for carboxylic acids that involves PDC in the photorelease mechanism has been developed by Soldevilla and Greisbeck.[60] PPG **53** contains the phthalimide chromophore, which is a good electron acceptor for photoinduced electron transfer (PET) reactions. The proposed mechanism is shown in Scheme 29.2: irradiation of **53** prompts an intramolecular PET from the carboxylate to the phthalimide to generate biradical **54**, which can then undergo PDC (Scheme 29.2) to give carbanion **55**. E1cB elimination of acetate from **55** leads to release of the caged substrate and production of alkene **56**. Based on analogy to the known photochemistry of the phthalimide chromophore and on sensitization studies, the authors support a triplet-mediated mechanism. The eventual photorelease yields are strongly linked to the PPG stereochemistry; the *threo* and *erythro* diastereomers of **53** show markedly different product distributions. The *threo* form shows essentially only elimination products (**56**) on irradiation, whereas the *erythro* form shows up to 30% of **57**, which would arise as the result of simple protonation, and is indicative of a slower elimination reaction.

29.4 Conclusions and Outlook

Great strides have been made over the past two decades in our understanding of the mechanisms of PDC reactions. In general, arylacetic acids that possess electron-withdrawing groups, such as the trifluoromethyl, nitro, and keto groups, undergo PDC with high efficiency to give carbanion intermediates and the associated ion-derived products. Arylacetic acids lacking such groups will generally undergo PDC inefficiently to give radical-derived products. Because heterolytic PDC reactions often proceed cleanly and efficiently, efforts have been made to make use of the carbanion intermediates generated. They have been successfully employed in S_N2 substitution (alkylation) reactions, although their use as nucleophiles in synthetic applications is so far limited in scope. Perhaps more promising, the PDC reactions of arylacetic acids that produce carbanions have been exploited in the design of a new class of PPGs with superior attributes. There is little doubt that PDC reactions will continue to be a source of interest for both those interested in the development of new applications (such as PPGs) and those interested in improving our understanding of the underlying mechanisms.

References

1. Lhiaubet-Vallet, V.; Miranda, M. A. 2006. Drug-biomolecule interactions in the excited states. *Pure Appl. Chem.* 78: 2277–2286.
2. Boscá, F.; Marín, M. L.; Miranda, M. A. 2001. Photoreactivity of the nonsteroidal anti-inflammatory 2-arylpropionic acids with photosensitizing side effects. *Photochem. Photobiol.* 74: 637–655.

3. Boscá, F.; Marín, M. L.; Miranda, M. A. 2004. Photodecarboxylation of acids and lactones: Antiinflammatory drugs. In *CRC Handbook of Organic Photochemistry and Photobiology*, 2nd edn., eds. W. Horspool, and F. Lenci, Chapter 64. Boca Raton, FL: CRC Press.
4. Barton, D. H. R.; Crich, D.; Motherwell, W. B. 1983. New and improved methods for the radical decarboxylation of acids. *J. Chem. Soc. Chem. Commun.* 939–941.
5. Barton, D. H. R.; Blundell, P.; Jaszberenyi, J. C. 1991. Quantum yields in the photochemically induced radical chemistry of acyl derivatives of thiohydroxamic acids. *J. Am. Chem. Soc.* 113: 6937–6942.
6. Dalko, P. I. 2004. The photochemistry of Barton esters. In *CRC Handbook of Organic Photochemistry and Photobiology*, 2nd edn., eds. W. Horspool, and F. Lenci, Chapter 67. Boca Raton, FL: CRC Press.
7. Hatoum, F.; Gallagher, S.; Baragwanath, L.; Lex, J.; Oelgemöller, M. 2009. Photodecarboxylative benzylations of phthalimides. *Tet. Lett.* 50: 6335–6338.
8. Oelgemöller, M.; Cygon, P.; Lex, J.; Griesbeck, A.G. 2003. The photodecarboxylative addition of carboxylates to phthalimides: Scope and limitations. *Heterocycles.* 59: 669–684.
9. Griesbeck, A. G.; Oelgemöller, M. 2000. Decarboxylative photoadditions of heteroatom-substituted carboxylates to phthalimides. *Synlett.* 71–72.
10. Griesbeck, A. G.; Oelgemöller, M. 1999. Photodecarboxylative addition of carboxylates and α-keto carboxylates to phthalimides. *Synlett.* 492–494.
11. Tamimi, M.; Qourzal, S.; Assabbane, A.; Chovelon, J. M.; Ferronato, C.; Ait-Ichou, Y. 2006. Photocatalytic degradation of pesticide methomyl: Determination of the reaction pathway and identification of intermediate products. *Photochem. Photobiol. Sci.* 5: 477–482.
12. Minabe, T.; Tryk, D. A.; Sawunyama, P.; Kikuchi, Y.; Hashimoto, K.; Fujishima, A. 2000. TiO_2-mediated photodegradation of liquid and solid organic compounds. *J. Photochem. Photobiol. A: Chem.* 137: 53–62.
13. Yang, D.; Ni, X. Y.; Chen, W. K.; Weng, Z. 2008. The observation of photo-Kolbe reaction as a novel pathway to initiate photocatalytic polymerization over oxide semiconductor nanoparticles. *J. Photochem. Photobiol. A: Chem.* 195: 323–329.
14. Budac, D.; Wan, P. 1992. Photodecarboxylation: Mechanism and synthetic utility. *J. Photochem. Photobiol. A: Chem.* 67: 135–166.
15. Wan, P.; Budac, D. 1995. Photodecarboxylation of acids and lactones. In *CRC Handbook of Organic Photochemistry*, 1st edn., eds. W. M. Horspool and P.-S. Song, pp. 384–392. Boca Raton, FL: CRC Press.
16. Pitchumani, K.; Madhavan, D. 2004. Induced diastereoselectivity in photodecarboxylation reactions. In *CRC Handbook of Organic Photochemistry and Photobiology*, 2nd edn., eds. W. Horspool, and F. Lenci, Chapter 65. Boca Raton, FL: CRC Press.
17. Pincock, J. A. 2004. The photochemistry of esters of carboxylic acids. In *CRC Handbook of Organic Photochemistry and Photobiology*, 2nd edn., eds. W. Horspool, and F. Lenci, Chapter 66. Boca Raton, FL: CRC Press.
18. Meiggs, T. O.; Miller, S. I. 1972. Photolysis of phenylacetic acid and methyl phenylacetate in methanol. *J. Am. Chem. Soc.* 94: 1989–1996.
19. Epling, G. A; Lopes, A. 1977. Fragmentation pathways in the photolysis of phenylacetic acid. *J. Am. Chem. Soc.* 99: 2700–2704.
20. Meiggs, T. O.; Grossweiner, L. I.; Miller, S. I. 1972. Extinction coefficient and recombination rate of benzyl radicals. I. photolysis of sodium phenylacetate. *J. Am. Chem. Soc.* 94: 7981–7986.
21. Castell, J. V.; Gomez-L, M. J.; Miranda, M. A.; Morera, I. M. 1987. Photolytic degradation of ibuprofen. Toxicity of the isolated photoproducts on fibroblasts and erythrocytes. *Photochem. Photobiol.* 46: 991–996.
22. Watkins, D. A. M. 1969. The effect of ultra-violet light on 1-naphthalene-acetic acid. *Phytochemistry* 8: 979–983.
23. Steenken, S.; Warren, C. J.; Gilbert, B. C. 1990. Generation of radical-cations from naphthalene and some derivatives, both by photoionization and reaction with SO_4^-: Formation and reactions studied by laser flash photolysis. *J. Chem. Soc. Perkin. Trans. 2.* 335–342.

24. Moore, D. E.; Chappuis, P. P. 1988. A comparative study of the photochemistry of the non-steroidal anti-inflammatory drugs, naproxen, benoxaprofen and indomethacin. *Photochem. Photobiol.* 47: 173–180.
25. Bosca, F.; Miranda, M. A.; Vaño, L.; Vargas, F. 1990. New photodegradation pathways for naproxen, a phototoxic nonsteroidal anti-inflammatory drug. *J. Photochem. Photobiol. A: Chem.* 54: 131–134.
26. Castell, J. V.; Gomez-Lechon, M. J.; Grassa, C.; Martinez, L. A.; Miranda, M. A.; Tarrega, P. 1993. Involvement of drug derived peroxides in the phototoxicity of naproxen and tiaprofenic acid. *Photochem. Photobiol.* 57: 486–490.
27. Bosca, F.; Encinas, S.; Heelis, P.; Miranda, M. A. 1997. Photophysical and photochemical characterization of a photosensitizing drug: A combined steady state photolysis and laser flash photolysis study on carprofen. *Chem. Res. Toxicol.* 10: 820–827.
28. Burns, M. D.; Lukeman, M. 2010. Efficient photodecarboxylation of trifluoromethyl-substituted phenylacetic and mandelic acids. *Photochem. Photobiol.* 86: 821–826.
29. Margerum, J. D. 1965. Transient photodecarboxylation intermediates. *J. Am. Chem. Soc.* 87: 3772–3773.
30. Margerum, J. D.; Petrusis, C. T. 1969. The photodecarboxylation of nitrophenylacetate ions. *J. Am. Chem. Soc.* 91: 2467–2472.
31. Craig, B. B.; Atherton, S. J. 1988. Kinetic and spectral properties of the photogenerated *p*-nitrobenzyl carbanion in aqueous media. *J. Chem. Soc. Perkin Trans. II.* 1929–1935.
32. Morrison, J.; Osthoff, H.; Wan, P. 2002. Enhanced reactivity of the nitrobiphenyl chromophore. *Photochem. Photobiol. Sci.* 1: 22–23.
33. Walker, J. W.; McCray, J. A.; Hess, G. P. 1986. Photolabile protecting groups for an acetylcholine-receptor ligand-synthesis and photochemistry of a new class of ortho-nitrobenzyl derivatives and their effects on receptor function. *Biochemistry.* 25: 1799–1805.
34. Milburn, T.; Matsubara, N.; Billington, A. P.; Udgaonkar, J. B.; Walker, J. W.; Carpenter, B. K.; Webb, W. W.; Marque, J.; Denk, W.; McCray, J. A.; Hess, G. P. 1989. Synthesis, photochemistry, and biological activity of a caged photolabile acetylcholine receptor ligand. *Biochemistry.* 28: 49–55.
35. Corrie, J. E. T.; Munasinghe, V. R. N.; Trentham, D. R.; Barth, A. 2008. Studies of decarboxylation in photolysis of a-carboxy-2-nitrobenzyl (CNB) caged compounds. *Photochem. Photobiol. Sci.* 7: 84–97.
36. Kotzur, N.; Briand, B.; Beyermann, M.; Hagen, V. 2009. Competition between cleavage and decarboxylation in photolysis of α-carboxy-2-nitrobenzyl protected cysteine derivatives. *Chem. Comm.* 3255–3257.
37. Ciamician, G.; Silber, P. 1900. Chemische lichtwirkungen. *Ber. Dtsch. Chem. Ges.* 33: 2911–2913.
38. Huck, L. A.; Xu, M.; Forest, K.; Wan, P. 2004. Efficient photodecarboxylation of 3- and 4-acetylphenylacetic acids in aqueous solution. *Can. J. Chem.* 82: 1760–1768.
39. Sobczak, M.; Wagner, P. J. 2002. Light-Induced decarboxylation of (*o*-acylphenyl)acetic acids. *Org. Lett.* 4: 379–382.
40. Ding, L.; Chen, X. B.; Fang, W. H. 2009. Ultrafast asynchronous concerted excited-state intramolecular proton transfer and photodecarboxylation of o-acetylphenylacetic acid explored by combined CASPT2 and CASSCF studies. *Org. Lett.* 11: 1495–1498.
41. Chiang, Y.; Kolmakov, K.; Kresge, A. J. 2008. Ketonization of the unusually acidic elongated enol generated by flash photolytic decarboxylation of *p*-formylphenylacetic acid in aqueous solution. *Can. J. Chem.* 86: 101–104.
42. Costanzo, L. L.; De Guidi, G.; Condorelli, G.; Cambria, A.; Fama, M. 1989. Molecular mechanism of drug photosensitization—II. Photohemolysis sensitized by ketoprofen. *Photochem. Photobiol.* 50: 359–365.
43. Bosca, F.; Miranda, M. A.; Carganico, G.; Mauleón, D. 1994. Photochemical and photobiological properties of ketoprofen associated with the benzophenone chromophore. *Photochem. Photobiol.* 60: 96–101.

44. Martinez, L. J.; Scaiano, J. C. 1997. Transient intermediates in the laser flash photolysis of ketoprofen in aqueous solutions: Unusual photochemistry for the benzophenone chromophore. *J. Am. Chem. Soc.* 119: 11066–11070.
45. Monti, S.; Sortino, S.; De Guidu, G.; Marconi, G. 1997. Photochemistry of 2-(3-benzoylphenyl)propionic acid (ketoprofen) part 1. A picosecond and nanosecond time resolved study in aqueous solution. *J. Chem. Soc., Faraday Trans.* 93: 2269–2275.
46. Borsarelli, C. D.; Braslavsky, S. E.; Sortino, S.; Marconi, G.; Monti, S. 2000. Photodecarboxylation of ketoprofen in aqueous solution. A time resolved laser-induced optoacoustic study. *Photochem. Photobiol.* 72: 163–171.
47. Cosa, G.; Martínez, L.; Scaiano, J. C. 1999. Influence of solvent polarity and base concentration on the photochemistry of ketoprofen: Independent singlet and triplet pathways. *Phys. Chem. Chem. Phys.* 1: 3533–3537.
48. Musa, K. A. K.; Matxain, J. M.; Erikkson, J. A. 2007. The mechanism of photoinduced decomposition of ketoprofen. *J. Med. Chem.* 50: 1735–1743.
49. Suzuki, T.; Okita, T.; Osanai, Y.; Ichimure, T. 2008. Reaction dynamics of excited 2-(3-benzoylphenyl)propionic acid (ketoprofen) with histidine. *J. Phys. Chem. B.* 112: 15212–15216.
50. Chuang, Y. P.; Xue, J.; Du, Y.; Li, M.; An, H.-Y.; Phillips, D. L. 2009. Time-resolved resonance Raman and density functional theory investigation of the photochemistry of (S)-ketoprofen. *J. Phys. Chem. B.* 113: 10530–10539.
51. Cosa, G.; Llauger, L.; Scaiano, J. C.; Miranda, M. A. 2002. Absolute rate constants for water protonation of 1-(3-benzoylphenyl)alkyl carbanions. *Org. Lett.* 4: 3083–3085.
52. Llauger, L.; Miranda, M. A.; Cosa, G. Scaiano, J. C. 2004. Comparative study of the reactivities of substituted 3-(benzoylphenyl)benzyl carbanions in water and DMSO. *J. Org. Chem.* 69: 7066–7071.
53. Llauger, L.; Cosa, G.; Scaiano, J. C. 2002. First determination of absolute rate constants for the reaction of aroyl-substituted benzyl carbanions in water and DMSO. *J. Am. Chem. Soc.* 124: 15308–15312.
54. Xu. M.; Wan, P. 2000. Efficient photodecarboxylation of aroyl-substituted phenylacetic acids in aqueous solution: A general photochemical reaction. *Chem. Commun.* 2147–2148.
55. Xu, M.; Lukeman, M.; Wan, P. 2009. Photodecarboxylation of benzoyl-substituted biphenylacetic acids and photo-retro-aldol reaction of related compounds in aqueous solution. Acid and base catalysis of reaction. *J. Photochem. Photobiol. A: Chem.* 204: 52–62.
56. Blake, J. A.; Gagnon, E.; Lukeman, M.; Scaiano, J. C. 2006. Photodecarboxylation of xanthone acetic acids: C–C bond heterolysis from the singlet excited state. *Org. Lett.* 8: 1057–1060.
57. Blake, J. A.; Lukeman, M.; Scaiano, J. C. 2009. Photolabile protecting groups based on the singlet state photodecarboxylation of xanthone acetic acid. *J. Am. Chem. Soc.* 131: 4127–4135.
58. Lukeman, M.; Scaiano, J. C. 2005. Carbanion-mediated photocages: Rapid and efficient photorelease with aqueous compatibility. *J. Am. Chem. Soc.* 127: 7698–7699.
59. Il'ichev, Y. V.; Schwörer, M. A.; Wirz, J. 2004. Photochemical reaction mechanisms of 2-nitrobenzyl compounds: methyl ethers and caged ATP. *J. Am. Chem. Soc.* 126: 4581–595.
60. Soldevilla, A.; Griesbeck, A. G. 2006. Chiral photocages based on phthalimide photochemistry. *J. Am. Chem. Soc.* 128: 16472–16473.

30

Photooxygenation, [2+2] and [4+2]

Maria Rosaria Iesce
University of Naples "Federico II"

Flavio Cermola
University of Naples "Federico II"

30.1 Introduction

The great synthetic potential of peroxides accounts for the wide interest of scientific community to the photooxygenation reaction that represents one of the most versatile and simple procedures to prepare a variety of peroxides. Generally the reaction is carried out in the presence of a sensitizer whose role is important to determine the type of mechanism. The use of a sensitizer such as a dye whose energy of excited triplet state can be transferred to the ground state oxygen produces singlet oxygen (Type II photooxygenation) [1]. This species adds to unsaturated substrates by [4+2] or [2+2] or ene-mode leading to endoperoxides or dioxetanes or allylic hydroperoxides, respectively (Scheme 30.1) [2–4].

Singlet oxygen is a highly reactive electrophilic species, but it is possible to control the order and timing of such reactions. Chemoselectivity is dictated by structural features. Thus, the [4+2]-cycloaddition is favorite with s-*cis*-dienes but competes with [2+2]-cycloaddition particularly in the presence of heteroatom substituents, which have a pronounced activation effect on dioxetane formation, or with the ene-reaction in the presence of allylic hydrogens. The electrophilic character of singlet oxygen (it prefers to react with electron-rich bonds) [5], steric interactions (in spite of the small dimensions, singlet oxygen attacks the less hindered side) [6], or favorable structural features (the correct alignment of the allylic hydrogen to the olefinic plane promotes ene-addition) [4] are other determinant factors. Singlet oxygen can also react with sulfur, selenium, phosphorous, and nitrogen compounds or undergo physical quenching [7,8].

The high potential of singlet oxygen together with the mild reaction conditions accounts for the high number of publications on this topic, in some cases exclusively dedicated [9,10]. No book nor publication on peroxides ignores singlet oxygen oxygenation [11,12].

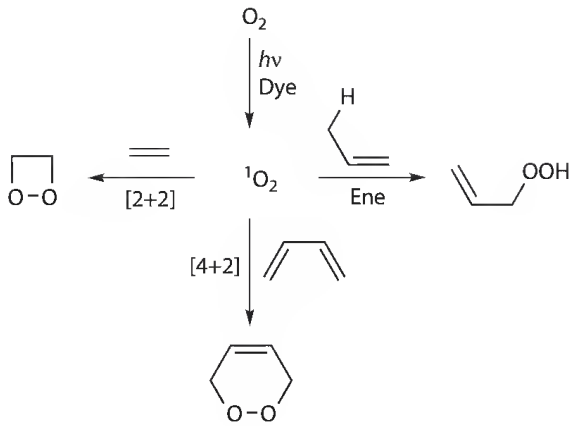

SCHEME 30.1 Reaction modes of singlet oxygen.

In this Chapter, we focus on the [4+2] and [2+2] photooxygenations that involve singlet oxygen. The chapter is concentrated to evidence the high potential of these reactions and recent interesting applications in the field of stereoselective reactions.

30.2 Experimental Procedure for Type II Photooxygenation

The classical conditions to carry out oxygenation with singlet oxygen require halogenated or deuterated solvents, low temperatures, continuous flow of oxygen, halogenated lamps and dyes as methylene blue (MB), rose bengal (RB), or tetraphenylporphyrin (TPP) [13], and recently fullerene derivatives [14]. The use of halogen lamps prevents the possibility of the peroxide decomposition, which may occur with UV lamps, and with the latter the use of filters is necessary. Due to the high number of the dye sensitizers available, the reaction can be carried out in a variety of organic solvents, from apolar to polar, from water to ionic liquids [15]. Photooxidation has also been performed using supercritical carbon dioxide ($scCO_2$) as medium and a perfluorinated analogue of TPP, 5,10,15,20-tetrakis(pentafluorophenyl)porphyrin (TPFPP), as sensitizer [16]. This procedure requires an appropriate apparatus but offers a number of advantages since $scCO_2$ is fully oxidized and hence nonflammable and nontoxic, completely miscible with gaseous O_2 and has lower viscosity and higher diffusivity than more conventional solvents. The use of fluorinated surfactants and co-solvents enlarges the applicability of the system to polar sensitizer and substrates [17].

Homogeneous conditions generally used in these oxygenations have some disadvantages with respect to the removal of the solvent or the separation of the sensitizer from the reaction mixture. Promising results have been obtained by carrying out the oxygenation under solvent-free conditions [18] or using heterogeneous media as zeolites [19], micelles and vesicles [20], by immobilization of sensitizers (commercially available polystyrene-bound RB, polyethylene glycol-supported tetraarylporphyrin [18], silica gel-linked [60]fullerene [21] or nafion-supported catalyst [22], or by using heterogeneous sensitizers as photoexcited porous silicon (PSi) nanostructures [23]. During recent years, investigation has also been directed to perform singlet oxygenation in miniaturized processes by means of nano- [24] and microreactors [25,26].

30.3 [4+2]-Cycloaddition

[4+2]-Cycloaddition of singlet oxygen to unsaturated systems is generally described as concerted, even if nonsynchronous [27], [4π+2π]-cycloaddition [28]. Conjugated systems from acyclic to cyclic, from aromatic to heteroaromatic compounds are the appropriate substrates for this reaction.

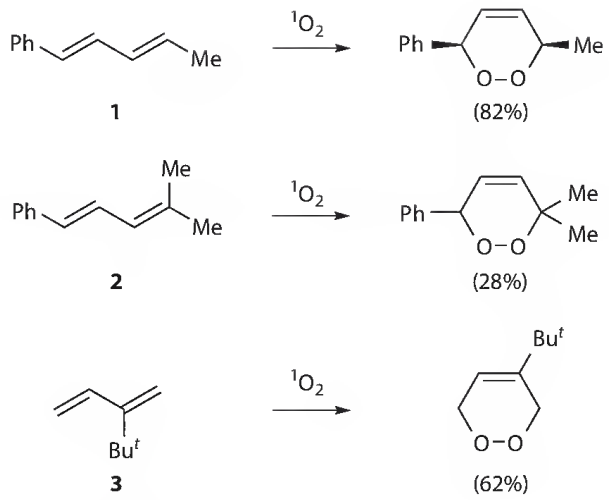

SCHEME 30.2 Singlet oxygen cycloaddition to acyclic dienes **1–3**.

30.3.1 Substrates

30.3.1.1 Acyclic and Carbocyclic Conjugated Systems

30.3.1.1.1 Acyclic Dienes

Oxygenation of conjugated dienes occurs preferentially via a 1,4-cycloaddition to form an endoperoxide, but it is complicated by the possibility that all the three pathways of singlet oxygen can occur [3,4]. Apolar solvents may favor this mode [29], but the chemoselectivity in acyclic dienes mainly depends on the amount of s-*cis*-conformer in the equilibrium necessary for a concerted [4+2]-addition. Even the presence of a little of the s-*cis*-conformer can give rise to an appreciable amount of endoperoxide due to the very low activation energies of this reaction mode. The decreasing yield of 1,4-adducts from **1** to **2** [30] can be easily explained on the basis of steric factors that play a role in the s-*cis*/s-*trans* conformational isomerism (Scheme 30.2). A *cis*-1-substituent increases the strain energy of the *cis*-conformation required for the 1,4-cycloaddition so that this reaction mode becomes difficult and other oxygenations, [2+2] or ene-addition, take place. On the contrary, a bulky substituent at 2-position as in **3** makes the *trans*-conformation less stable and, hence, favors the 1,4-addition [30]. Attempts have been made to rationalize the stereocontrolling factors in the oxygenation of acyclic dienes with scarce results due to the flexibility of these substrates and hence to the role of conformational features [6].

30.3.1.1.2 Vinyl Compounds

Substrates having one endocyclic C–C double bond (even in carbo- or heteroaromatic rings) and one conjugated exocyclic C–C double bond undergo [4+2]-cycloaddition, even in the presence of allylic hydrogens [31,32] or alkoxy groups [33].

In the oxygenation of vinylcycloalkenes **4**, the ratio [4+2] vs. ene-products changes with ring size, due to the influence of this factor on the alignment of allylic hydrogens [31] (Scheme 30.3).

The photooxygenation of a vinylbenzene derivative, such as **5**, leads to dihydrobenzo-1,2-dioxin in the primary step, which is followed by rapid oxygenation of the cyclohexadiene chromophore to give diendoperoxides as **6** and **7** (Scheme 30.4) [32].

The oxygenation of vinylnaphthalenes *trans*- and *cis*-**8** occurs with retention of stereochemistry [33]. The lower yield of the endoperoxide *cis*-**9** than that of *trans*-**9** would be due to the steric interaction between the two methoxy groups, which makes the [4+2]-cycloaddition more difficult and, therefore, makes the [2+2] reaction on the electron-rich double bond competitive (Scheme 30.5).

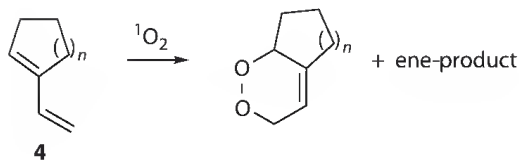

4

n	[4+2]	ene
1	16	84
2	77	23
3	22	78
4	50	50
5	47	53
6	67	33

SCHEME 30.3 [4 + 2]-Cycloaddition vs. ene-reaction of dienes **4**.

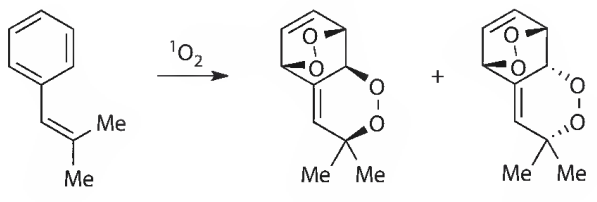

5 **6** **7**

(51%)
(**6**:**7** = 68:32)

SCHEME 30.4 Photooxygenation of vinylbenzene **5**.

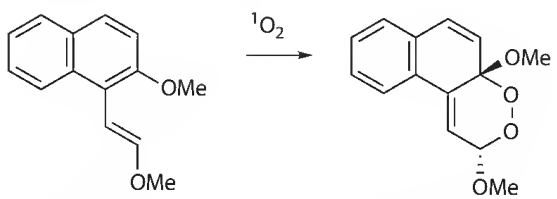

trans-**8** *trans*-**9**

(98%)

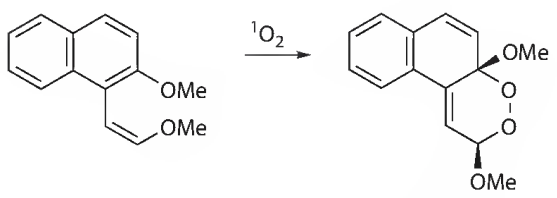

cis-**8** *cis*-**9**

(46%)

(and 40% of a product from [2+2]-cycloaddition)

SCHEME 30.5 Photooxygenation of vinylnaphthalenes **8**.

30.3.1.1.3 Cyclic Dienes and Polyenes

Endoperoxidation is the preferred process with cyclic dienes, and simple five-, six-, seven-, and eight-membered ring aliphatic dienes lead, by photooxygenation, to the corresponding endoperoxides that, except for that of cyclopentadiene, are quite stable (Scheme 30.6).

The oxygenation of cyclopentadiene **10** has been experimented in a falling-film microstructured reactor (Scheme 30.7) [25]. The unstable endoperoxide **11** is formed in the reactor, kept at 10°C, and reduced

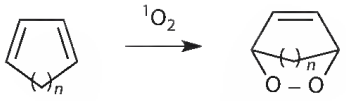

n	Yield (%)	References
1	86	[34]
2	21	[35]
3	29	[36]
4	53	[37]

SCHEME 30.6 Oxygenation of cyclic dienes.

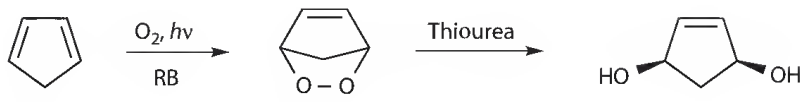

10 **11** **12**

(20% from **10**)

SCHEME 30.7 Photooxygenation of cyclopentadiene (**10**) in falling-film microreactor.

immediately after leaving it by passing the effluent into a solution of thiourea in methanol at 10°C. The diol **12** has been obtained in 20% yield for the non-optimized process [25]. The procedure evidences the feasibility of this reaction type on a safe preparative scale. Indeed, the system ensures that the quantity of the potentially explosive endoperoxide intermediate is always kept at a safe level and the volume of aerated solvent in the system at any time is in the region of microliters.

For 1,3-cyclopentadiene derivatives, the 1,4-cycloadduct is still the only product independently from the alkylation or arylation at positions 1–4 [6]. For higher homologues, the chemoselectivity can change depending on the substitution. Thus, oxygenation of cyclohexadiene **13** affords a mixture of *syn/anti*-endoperoxides **14** and ene-products in 65% and 35%, respectively while 1,4-disubstituted α-terpinene **15** gives endoperoxide ascaridol **16** almost quantitatively [38] (Scheme 30.8).

α-Terpinene is widely used as $^1O_2$ trap in model oxygenation reactions due to its easy reactivity with singlet oxygen. Hence, oxygenation of this compound to ascaridol has been recently investigated using $scCO_2$ as solvent and TPFPP as sensitizer [16,17]. Experiments have also been performed in a continuous reactor [39]. Under these conditions, the reaction is rapid (of the orders of few minutes) and quantitative. The reactor operates with unchanged efficiency over 8 h, and the result represents a 3000-fold scale-up of the batch reaction. Oxygenation has also been performed in a microreactor using [60]fullerene as sensitizer [26]. This device has been designed to host, within the microchannels network, the photosensitizer [60]fullerene that has been immobilized on polystyrene beads or silica gel microparticles. Nearly quantitative conversion has been achieved in about 50 s, but a partial photodegradation of the ascaridole (30%–50% yield) has been observed [26].

The stereoselectivity of the cycloaddition can be influenced by steric factors and depends on the substitution and the ring type. The presence of the encumbered $OSi(Me)_2Bu^t$ substituent induces the selective formation of the *anti*-isomer **17**, and this peroxide has been usefully employed for the synthesis of natural chiral compounds (Scheme 30.9) [40]. The photooxygenation of cycloheptadiene **18** leads to the diastereomeric mixture of peroxides *syn/anti*-**19** in *ca* 5:1 molar ratio (Scheme 30.9) since conformational requirements to better allocate the silyl group direct singlet oxygen to the less hindered β-face [41]. The major isomer has been used as precursor of deoxy-hexoses and -heptoses.

1,3,5-cycloheptatrienes undergo valence tautomerization and may exist as the tropilidenes **20** or the norcaradiene valence isomers **21** (Scheme 30.10). Consequently, the photooxygenation can lead to the

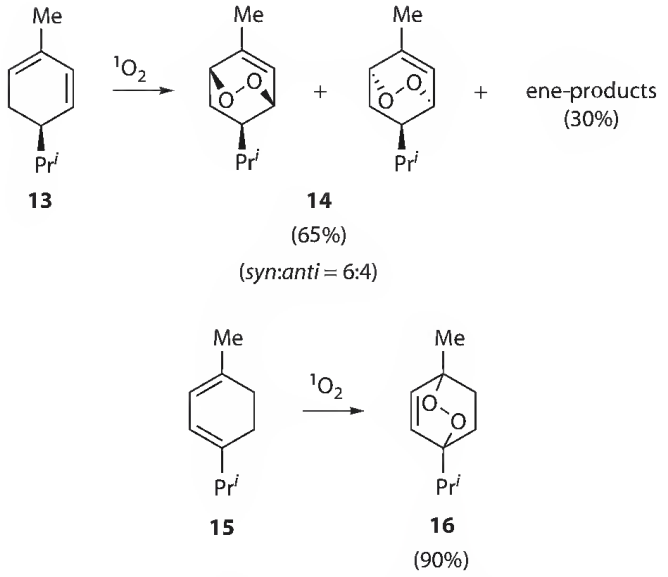

SCHEME 30.8 [4 + 2]-Cycloaddition vs. ene-reaction of cyclic dienes **13** and **15**.

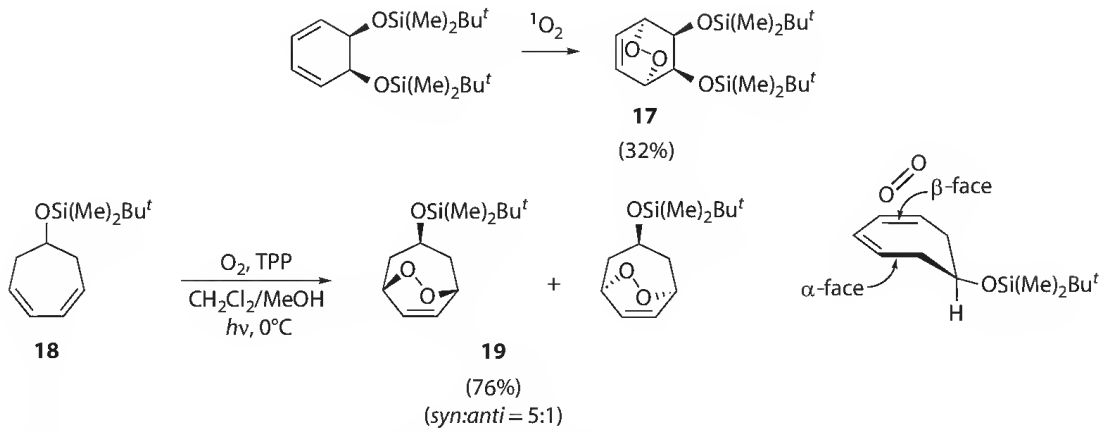

SCHEME 30.9 Stereoselectivity of the photooxygenation of cyclic dienes.

bicyclic endoperoxides **22** and/or tricyclic derivatives **23** and this depends on the steric and electronic nature of the substituents. The tropilidene endoperoxide **22** is the main or the only one formed when R^1 = H [42] or with electron-rich substituent as OMe, respectively (Scheme 30.10) [43]. The norcaradiene endoperoxide **23** is favored with bulky groups as alkyl or aromatic groups [44] and, especially, with π-electron acceptor substituents as CO_2Me or CHO [43].

Fused bis-cycloheptatriene **24** gives the stable norcaradiene peroxide **25** and by further addition of singlet oxygen the *syn*-bis(norcaradiene) bis(endoperoxide) **26** (Scheme 30.11) [45].

Oxygenation of asymmetric cycloheptatrienes affords complex mixtures of endoperoxides depending on the location and type of the substituent. Thus, compounds **27** and **29** give the peroxides **28** [46] and **30** [47] while benzotropone **31** affords the peroxide **32** (Scheme 30.12) [48]. Peroxide **30** shows an unusual behavior since it produces singlet oxygen and the parent tropone **29** upon thermolysis and, hence, represents one of the rare non-benzenoid systems generating singlet oxygen [47]. The development of general and flexible synthetic routes to tropone (cyclohepta-2,4,6-trien-1-one) and tropolone (2-hydroxycyclohepta-2,4,6-trien-1-one) derivatives is of continuous

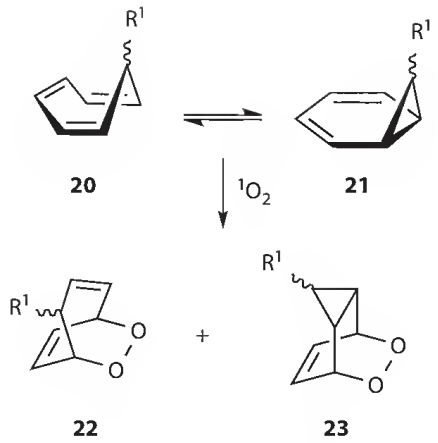

R^1	22	23
H	92	8
CO_2Me	—	100
CHO	—	100
Ph	14	86
OMe	100	—

SCHEME 30.10 Photooxygenation of cycloheptatrienes **20**.

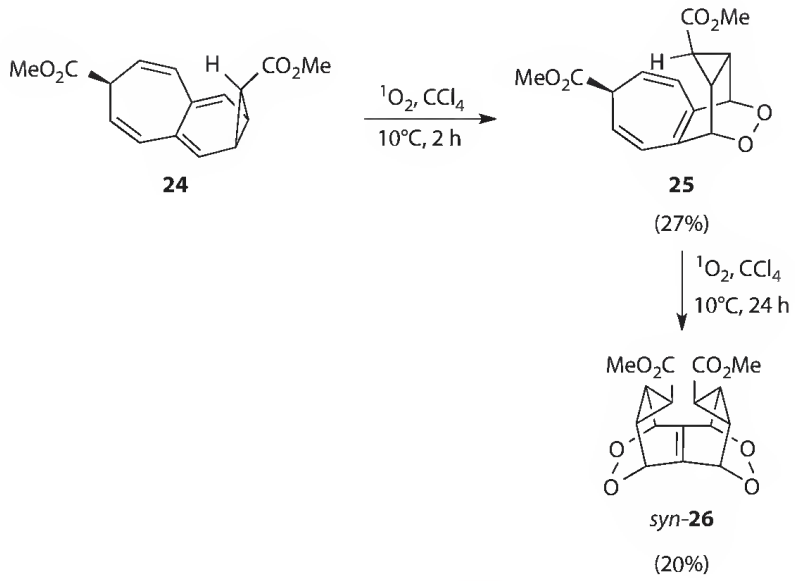

SCHEME 30.11 Photooxygenation of fused bis-cycloheptatriene **24**.

interest since they represent the structural key elements in a wide range of natural products, many of which display interesting biological activity [46–48].

As found for the cycloheptatriene system, cycloocta-1,3,5-triene affords a mixture of both the relatively stable bicyclic and tricyclic endoperoxides **33** and **34** (Scheme 30.13) [49].

Cyclooctatetraene **35a** reacts with singlet oxygen to give the endoperoxide 7,8-dioxabicyclo[4.2.2] deca-2,4,9-triene **36a** in 26% yield (Scheme 30.14) [50]. Substituted derivatives **35b,c** give the endoperoxides with the substituents located at the vinylic position **36b,c** and at the bridgehead position **37b** (Scheme 30.14) [50].

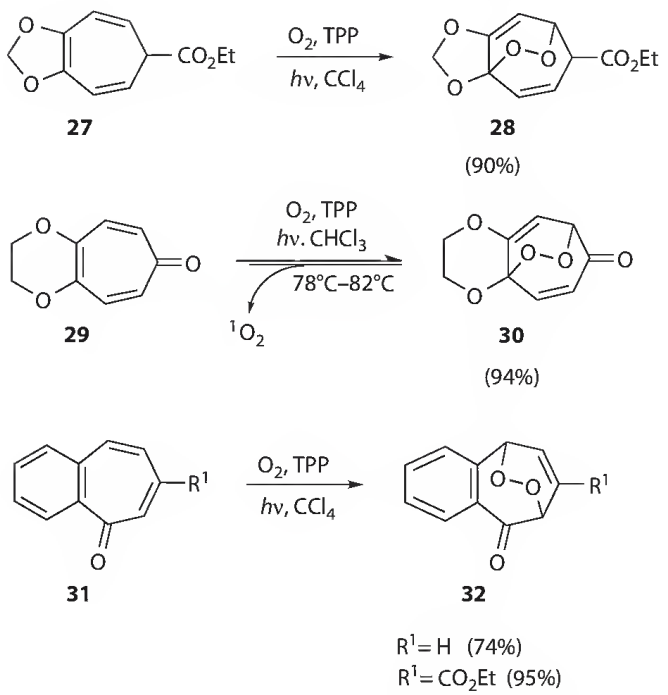

SCHEME 30.12 Photooxygenation of symmetric and asymmetric cycloheptatrienes.

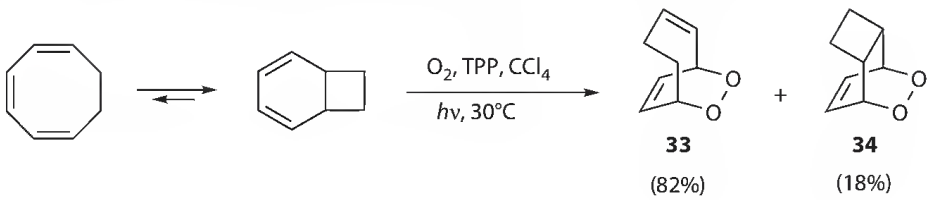

SCHEME 30.13 Photooxygenation of 1,3,5-cyclooctatriene.

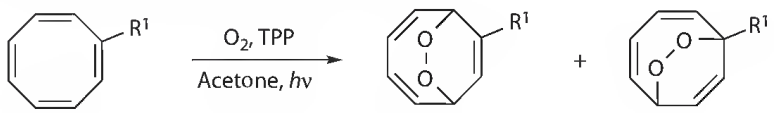

a; R^1 = H — 26%
b; R^1 = OMe — 10%
c; R^1 = Ph — 33%
37 — 8%

SCHEME 30.14 Photooxygenation of cyclooctatetraenes **35**.

30.3.1.1.4 Aromatic Compounds

The capability of aromatic compounds to react with singlet oxygen enhances when the number of condensed rings is increased [51]. Benzene derivatives react only if electron-donating substituents are present [52] or when the benzene moiety is incorporated into strained metacyclophanes [53,54]. The reaction of compound **38** proceeds in high yields in various solvents, even in the absence of sensitizer, affording the endoperoxide **39** (Scheme 30.15) [53].

Analogously, singlet oxygen adds to electron-rich naphthalenes. Derivatives with electron-donating substituents at 1- and 4-position lead to the 1,4-endoperoxides. The regioselectivity can be modified by both electronic and steric effects. 5,8-Endoperoxides have been observed when at least one additional

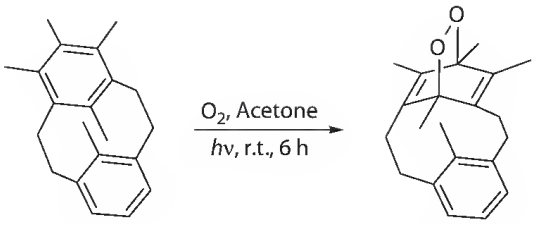

38 **39** (72%)

SCHEME 30.15 Photooxygenation of metacyclophane **38**.

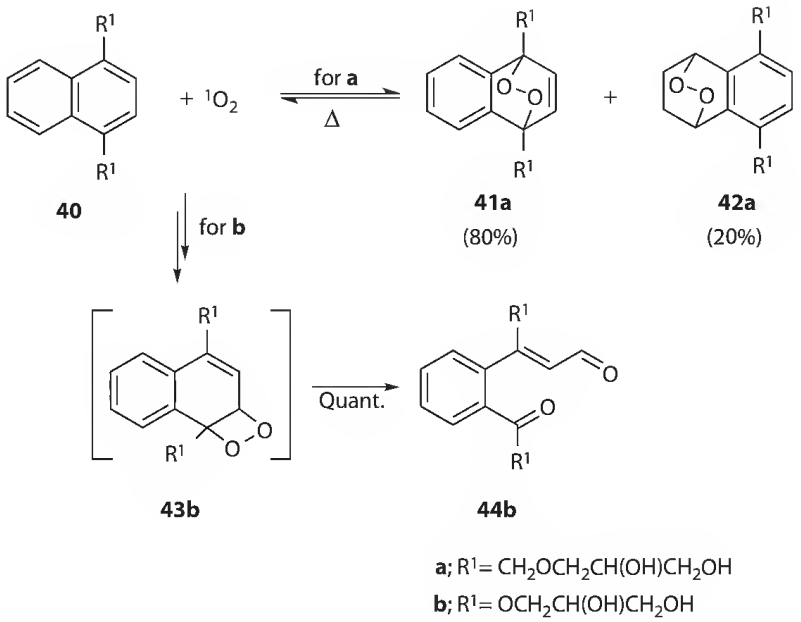

40 **41a** (80%) **42a** (20%)

43b **44b**

a; $R^1 = CH_2OCH_2CH(OH)CH_2OH$
b; $R^1 = OCH_2CH(OH)CH_2OH$

SCHEME 30.16 Photooxygenation of 1,4-disubstituted naphthalenes **40**.

methyl group is placed on the 6,7 [55] or 8 position [6], or when bulky groups are present in 1,4-positions. Naphthalene **40a** reacts with singlet oxygen in water and/or methanol, giving both 1,4- and 5,8-endoperoxide **41a** and **42a**, even if the latter as minor product (Scheme 30.16) [56]. When an oxygen linker separates the alkyl chain from the aromatic core as in compound **40b**, the aldehyde ester **44b** is found probably via the typical C–C/O–O fragmentation of a preliminarily formed dioxetane, such as **43b** (Scheme 30.16) [57].

The extent and purpose of π-facial selectivity can be controlled in the reaction of chiral naphthalenes **45** by electronic factors [6]. In particular, *syn*-selectivity is highly favored by attractive interactions between a hydroxy group, even in the homobenzylic position, and the incoming $^1O_2$, while crowded substituents or electrostatic repulsions as those caused by a methoxycarbonyl group or a halogen favor the *anti*-attack (Scheme 30.17).

Oxidation of anthracene or higher acenes occurs even in the absence of a dye, since the same substrates act as sensitizers in singlet oxygenation [51]. These compounds react mainly at the meso-positions of the aromatic nucleus but electron-donating groups have a strong directing effect when placed at the 1- and 4-positions [28,51]. Due to the high reactivity toward singlet oxygen, suitably substituted anthracene derivatives are used as $^1O_2$ traps, even in biological systems [58]. Currently, acene derivatives are receiving high attention since they are useful in organic electronics for preparing organic field-effect transistor films [59]. Synthetic studies are therefore conducted on various pentacene derivatives to acquire more information on this compound type. Pentacene derivatives **47** and **49** have been prepared

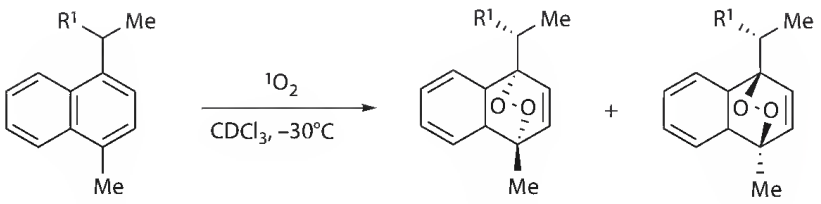

45 *syn*-**46** *anti*-**46**

(≥95%)

R^1	*syn*-**46**/*anti*-**46**
OH	85:15
OMe	66:34
CH_2OH	90:10
CO_2Me	22:78
t-Bu	34:66

SCHEME 30.17 Stereoselectivity of the photooxygenation of chiral naphthalenes **45**.

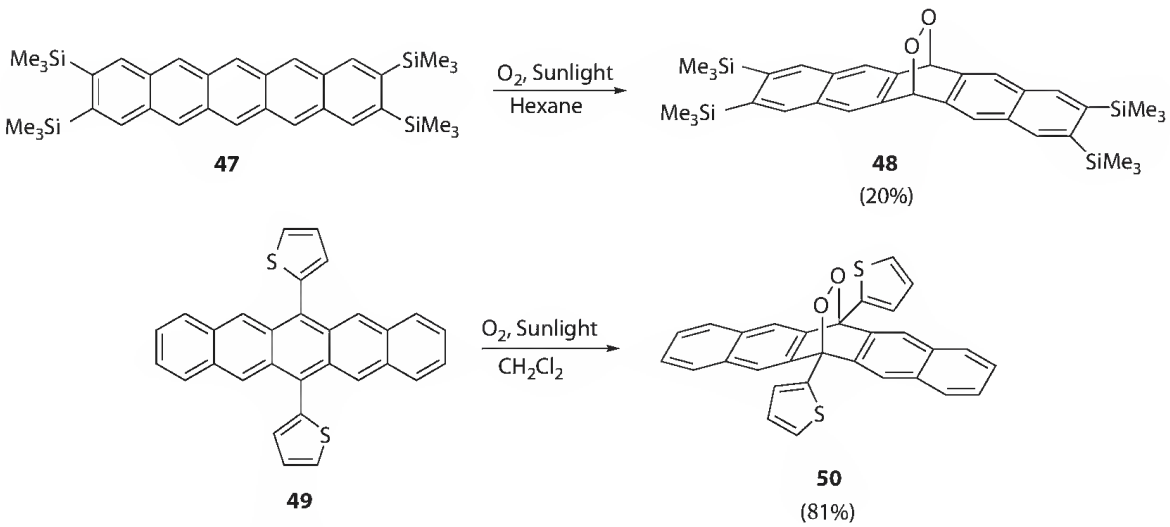

47 **48** (20%)

49 **50** (81%)

SCHEME 30.18 Photooxygenation of pentacenes **47** and **49**.

and investigated for their electronic properties as well as for their photoaddition reactions with oxygen. In both cases, the corresponding peroxides **48** [60] and **50** [61] are formed by simple exposure to sunlight (Scheme 30.18).

The thermal stability of the endoperoxides of aromatic compounds enhances going from the only spectroscopically detectable endoperoxides of benzene derivatives to those from acenes, which are stable enough to be stored for several days [51]. A peculiar property of these endoperoxides is that they can revert thermally to the aromatic molecule and oxygen. Naphthalene or anthracene peroxides generally produce singlet oxygen, so that they are currently used to generate singlet oxygen by means of an alternative route to photosensitization [13]. This behavior of naphthalene endoperoxides is of particular interest, especially for mechanistic studies in biological systems. Water-soluble derivatives known as NDP [62] and DHPN [63,64] are widely used in the biological media to generate singlet oxygen free from other reactive oxygen species at the physiological temperature (Scheme 30.19).

Interestingly, for 1-naphthol derivatives **51**, the [4+2]-cycloaddition of singlet oxygen is followed by a breakdown of the endoperoxide intermediate leading to 1,4-naphthoquinones **52** (Scheme 30.20).

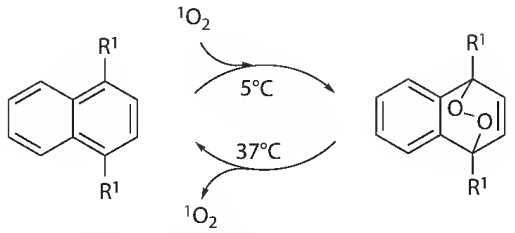

NDP; $R^1 = CH_2CH_2COO^-Na^+$
DHPN; $R^1 = CH_2CH_2CONHCH_2CH(OH)CH_2OH$

SCHEME 30.19 Reversible oxygenation of water-soluble naphthalene derivatives.

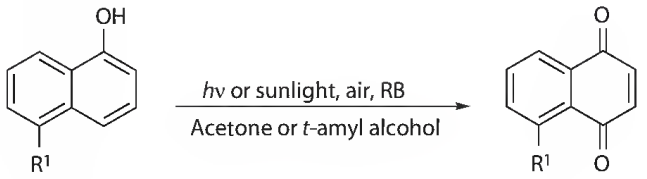

51 **52**

(53%–90%)

R^1 = H, OH, OAc, NHCO–R′
R′ = Me, Et, CycloPr, Bu^t, C_6H_5, *p*-ClC_6H_4, *p*-MeC_6H_4

SCHEME 30.20 Photooxygenation of 1,4-naphthols **51**.

The reaction has been investigated under non-concentrated and concentrated sunlight [65–67]. In particular, oxygenation of **51** (R^1 = OH) gives **52** (R^1 = OH) known as juglone, a versatile building block for the synthesis of bioactive quinoid compounds. The solar-chemical synthesis with medium concentrated sunlight operates efficiently and affords juglone in moderate to good yields up to 79% on multiple gram-scales [67].

In addition to the substituent effects, the extent of reversion of acene peroxides to the parent compounds and singlet oxygen depends on the number of condensed rings and decreases from anthracene to higher acenes. Thus, compound **54** reverts slowly to **53** and oxygen by heating above 100°C (Scheme 30.21) [68]. The thermal stability of these and similar compounds together with the diverse colored forms of the endoperoxides and parent compounds are useful properties in the field of organic photochromism [69]. The retrocycloaddition in fact can be induced photochemically. Representative is heterocoerdianthrone endoperoxide **56** (HECDPO) (Scheme 30.21). It is formed from an air-saturated solution of heterocoerdianthrone **55** (HECD) in methylene chloride that has been irradiated by sunlight with a 420–480 nm band-pass filter and stored in the dark [70]. The oxidation of heterocoerdianthrone is reversible, and the system can be used as a reversible actinometer with oxygen addition in the visible and reversion in the UV range (248–334 nm region) [70]. Between 253 and 302 nm, the reaction efficiency does not depend on irradiation wavelength.

30.3.1.2 Heterocyclic Compounds

Pentatomic aromatic heterocycles react with singlet oxygen, generally via [4+2]-cycloaddition leading to unstable endoperoxides [71]. As expected on the basis of higher aromaticity than pyrroles or furans, thiophenes undergo hardly addition of singlet oxygen [72]. Isoxazoles, 1,2,5-oxadiazoles and 1,3,4-oxadiazoles are apparently inert under dye-sensitized photooxygenation [73] as well as nitrogen-containing six-membered heterocycles [71]. Endoperoxides of heterocycles are generally highly thermally unstable and can afford characteristic rearranged products.

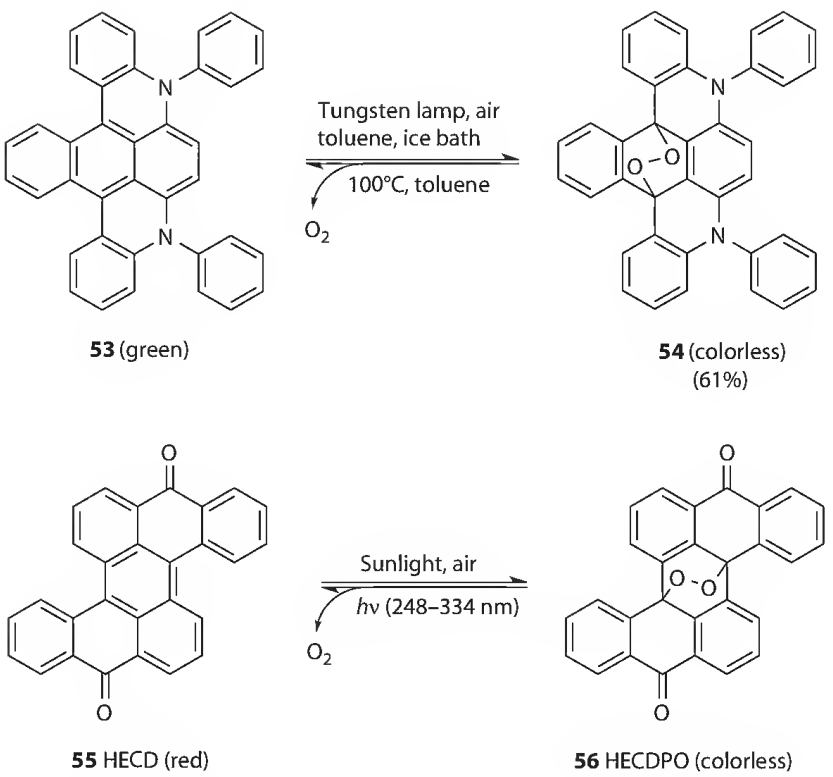

SCHEME 30.21 Reversible oxygenation of acenes **53** and **55**.

In the series of furans, the thermal stability of the related endoperoxides, as well as the type of rearranged products, is rigorously related to the nature of the α,α- substituents, and follows the order Me (0°C)>Ph>H>OMe (−80°C) when these substituents are in α-positions [71,74]. Epoxides, diepoxides, enol esters, enediones, ketoesters, epoxyfuranones, furanones are only some of the products obtainable from the photooxygenation of furans depending on substituents, solvents, and concentration [71,74]. Investigation has evidenced that straight correlations exist between the electronic effects of the functional groups and the type of the observed rearrangement products so that the fate of the endoperoxide is predictable. More complex is the photooxygenation of pyrroles, imidazoles, and other heterocycles since they exhibit low chemoselectivity, giving generally mixtures of products deriving from [4+2]- and [2+2]-cycloaddition or hydroperoxides [19,71,75]. Anyhow, these heterocylic systems continue to be extensively studied because they are involved in photobiosynthesis and other biological processes (see, e.g., the special issue of Photochemistry and Photobiology-2006 [10]).

Oxazoles are highly reactive toward singlet oxygen [19,71,76]. In particular, endoperoxides of aryl- or alkyl-substituted oxazoles are highly unstable, converting almost quantitatively to triamides **58** [76] (Scheme 30.22). Since the imide group is an activated leaving group, this reaction represents a means of generating a masked carboxyl function. Indeed, the oxygenation of aryl and/or alkyl oxazoles **57** has been employed in diverse synthetic applications [76]. Remarkably, 5-alkoxyoxazoles **59** afford 3*H*-1,2,4-dioxazoles **60** either in homogeneous medium [77] or under solvent-free conditions by using sensitizer/polymer system (PP-S-DVB) [78] (Scheme 30.22).

Condensed derivatives as benzofurans or indoles undergo mainly [2+2]-cycloaddition, the latter also give hydroperoxides [71]. The large resonance energies of the benzene ring are dominant to such an extent that [4+2]-cycloadditions are not possible. Recently, it has been reported that 4,7-dimethylbenzofurazan (**61**) adds singlet oxygen to give the corresponding 4,7-endoperoxide **62** [79]. The latter decomposes back to the parent compound and singlet oxygen at room temperature (Scheme 30.23).

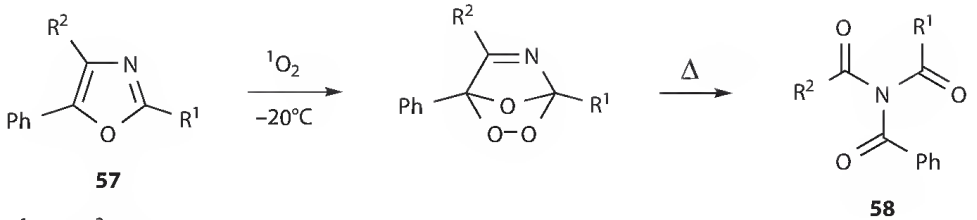

57

58

R^1= Ph, R^2= CH_2R

R^1= CH_2R, R^2= Ph

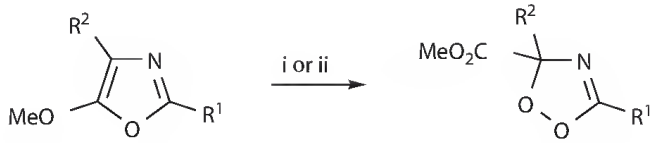

59 **60**

i [77]; O_2, *hv*, MB, $CHCl_3$, DABCO, (73%–97%)

ii [78]; O_2, *hv*, PP-S-DVB, (44%–90%)

SCHEME 30.22 Photooxygenation of oxazoles **57** and **59**.

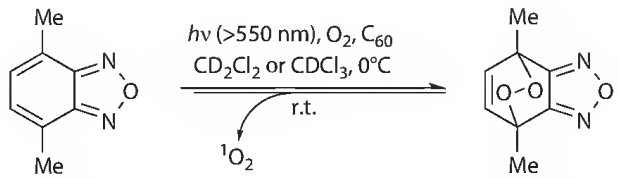

61 **62** (93%)

SCHEME 30.23 Reversible oxygenation of benzofurazan **61**.

30.3.2 Synthetic Applications

Photooxygenation of [4+2] type is a powerful synthetic tool to introduce, simultaneously, oxygenated *syn*-1,4-functionalizations in 1,3-diene systems. The endoperoxide can undergo a variety of transformations, which can either or not involve the cleavage of the O–O bond and, often, can be performed *in situ* and at low temperature overcoming the thermal instability problem of the peroxide intermediate. Selective transformations include reductions to unsaturated (with thiourea, sodium tetrahydroborate) or saturated (with PtO_2, Ni, Pd/C) diols or to dioxanes (with diimide), rearrangements to hydroxyl carbonyl compounds (with base as NEt_3 or metal catalysis) or to epoxy carbonyl compounds (by metal catalysis) or to bis-epoxides (by metal catalysis, by thermolysis), acid-mediated heterolysis [3,19,80–82]. Here just a brief description of some recent applications to evidence the synthetic potential of this reaction starting mainly from dioxines, endoperoxides of tropone derivatives, aromatic compounds, and furans is presented.

30.3.2.1 Endoperoxides of Acyclic and Carbocyclic Conjugated Systems

The possibility to control stereoselectively, the endoperoxide formation, and the reduction of O–O bond with thiourea has been successfully employed in the stereospecific synthesis of diverse polyhydroxylated compounds, as the bis-homoinositol **63** [83] (Scheme 30.24), or aminocyclitols [84]. Highly oxygenated cyclohexane derivatives (cyclitols) occur widely in nature and usually possess interesting biological activities [85].

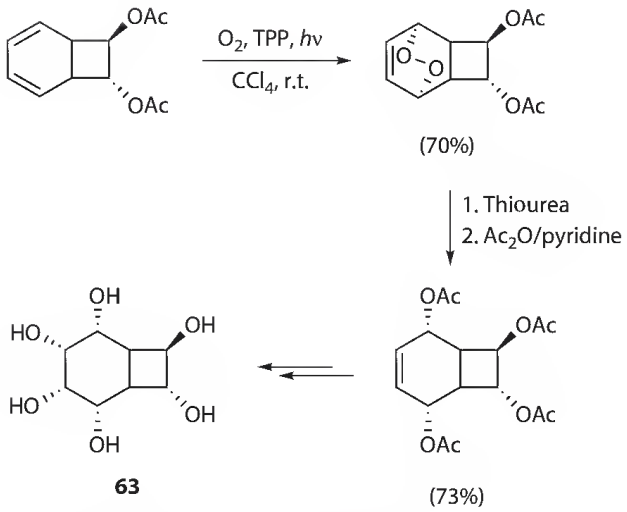

SCHEME 30.24 Synthesis of a precursor of bis-homoinositol **63**.

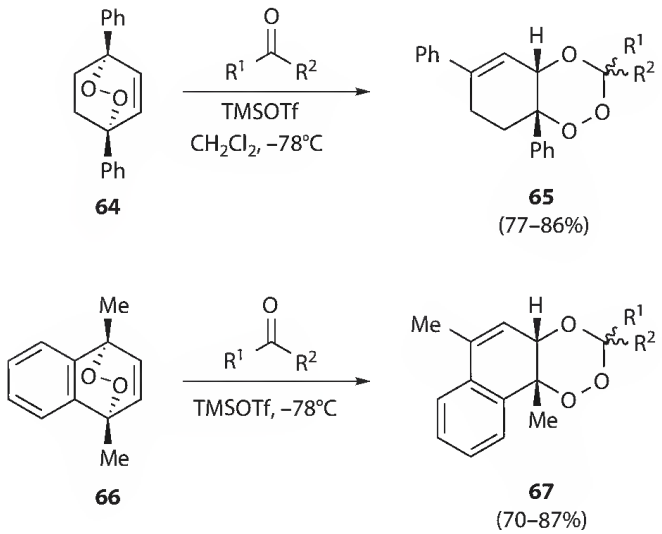

SCHEME 30.25 Synthesis of 1,2,4-trioxanes **65** and **67** via acid-catalyzed reaction of cyclic peroxides **64** and **66** with carbonyl compounds.

Acid-catalyzed reaction of bridged 1,2-dioxines, e.g., **64**, with carbonyl compounds leads to 5,6-*cis* fused 1,2,4-trioxanes **65** in high yields (Scheme 30.25) [86]. The acid usually employed is trimethylsilyl trifluoromethanesulfonate (TMSOTf). This reaction also occurs with 1,4-dimethylnaphthalene endoperoxide **66** [86], even intramolecularly [87]. Synthetic cyclic peroxides as trioxanes are receiving high attention since many derivatives show significant promise as antimalarial drugs because of their artemisinin-like activity [88].

An interesting application of the acid-catalyzed ring opening of endoperoxides is depicted in Scheme 30.26. In the presence of TMSOTf, the peroxides **68** react with allyltrimethylsilane to give the *cis*-configured endoperoxides **69** via the attack of the allylsilane on the carbocation derived from heterolytic cleavage of the endoperoxide bridge [89]. The reaction proceeds with a high degree of diastereoselectivity due to the bulky $-CH_2SiMe_3$ substituent that adopts an equatorial position in a product-like transition state.

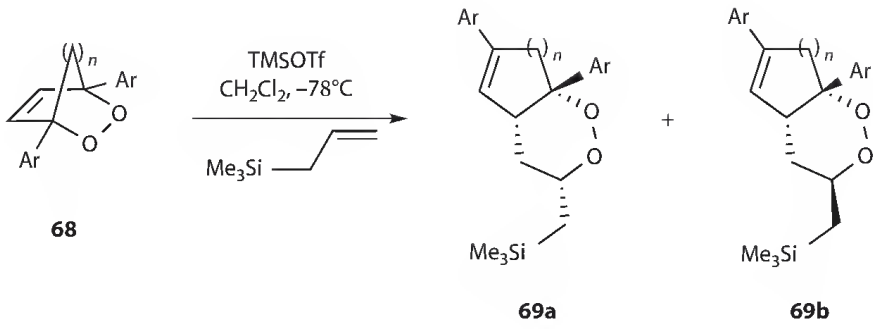

Ar	*n*	Yield (%)	**69a/b**
Ph	1	54	1:0
p-F-C_6H_4	1	60	1:0.8
Ph	2	10	1:0
p-F-C_6H_4	2	48	1:0

SCHEME 30.26 Synthesis of peroxides **69** via acid-catalyzed reaction of bicyclic peroxides **68** with allylsilane.

Peroxides undergo a base-catalyzed rearrangement to *cis*-γ-hydroxyenones, known as the Kornblum-DeLamare rearrangement [3,80–82]. This treatment has been performed using a cinchona-alkaloid catalyst (deMeQDAc) on diverse peroxides of 1,3-dienes leading to enantioenriched γ-hydroxyenones [90]. Thus, hydroxyenone **71** has been prepared from the diene **70** by a two-step sequence involving TPP-sensitized photooxygenation and chiral base-catalyzed desymmetrization of the resulting endoperoxide (Scheme 30.27).

Application of base treatment to the endoperoxide **28** represents a novel method for stipitatic acid isomer **72** (Scheme 30.28) [46]. Interestingly, treatment with CoTPP gives the other isomer **74**, probably via the ring opening of the initially formed bis-epoxide **73** [46].

In 1,2-dioxines **75**, the transformation to enones **76** may be difficult to control due to the inherent instability of these compounds. Enones can convert to 1,4-diketones **77**, under excessively basic conditions [91] or undergo dehydration to generate furans **78** in the presence of acid (Scheme 30.29) [92].

Some nucleophiles have been shown to be weakly basic to rearrange the 1,2-dioxine and then undergo proton exchange with the hydroxyl enone allowing for one-pot ring-opening/nucleophilic addition. Malonate is sufficiently mild to promote rearrangements of substituted naphtho- and phenanthro-1,2-dioxines **79** and **81** to the transient *cis*-γ-hydroxyenone species with no further rearrangement (Scheme 30.30) [93]. Hence, malonate as nucleophile readily adds to the double bond of the *cis*-γ-hydroxyenones in a highly diastereoselective fashion, which yield highly substituted *cis*-fused bis-lactones **80** and **82** through an intramolecular domino cyclization.

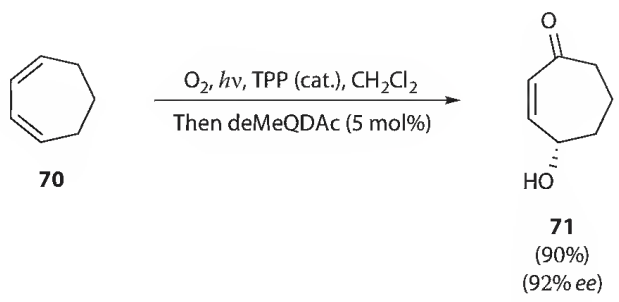

SCHEME 30.27 Enantioselective synthesis of γ-hydroxy enone **71**.

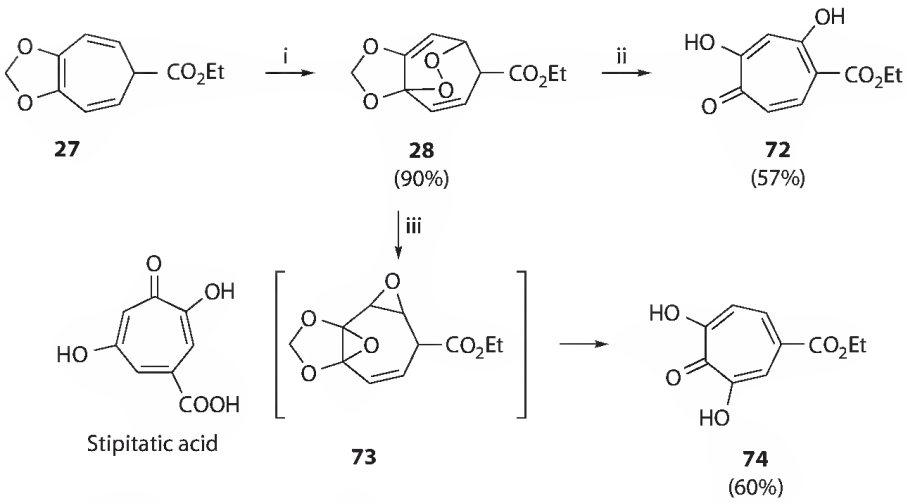

i; TPP, O_2, *hν*, CCl_4, r.t. ii; NEt_3, $CHCl_3$, −10°C iii; CoTPP, CH_2Cl_2, 0°C

SCHEME 30.28 Synthesis of stipitatic acid isomers **72** and **74**.

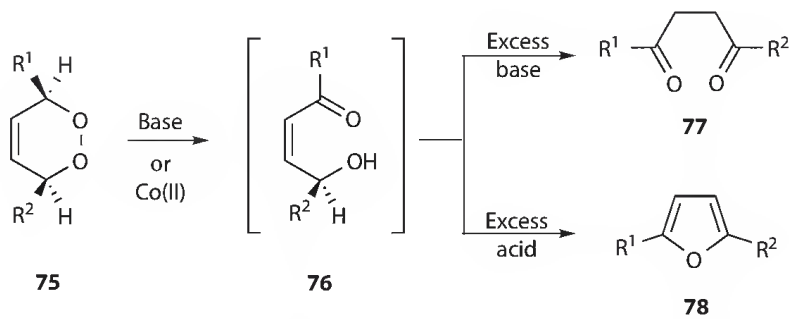

SCHEME 30.29 Transformations of γ-hydroxy enones **76** under stressed basic or acid conditions.

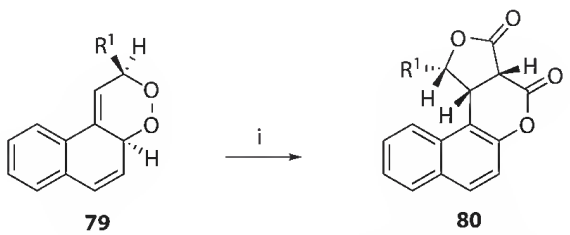

R^1 = Me (76%), cyclohexyl (79%), Ph (84%), *p*-$MeOC_6H_4$ (87%)

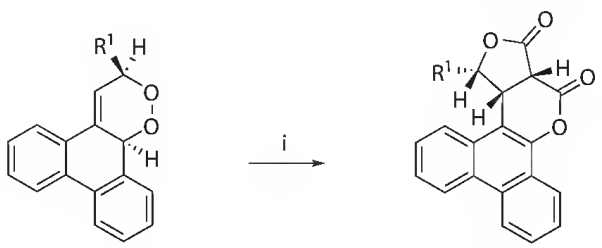

i; Diethyl malonate, NaOEt, THF, r.t. R^1 = Me (65%), Ph (67%)

SCHEME 30.30 Bis-lactones **80** and **82** by reaction of 1,2-dioxines **79** and **81** with diethyl malonate.

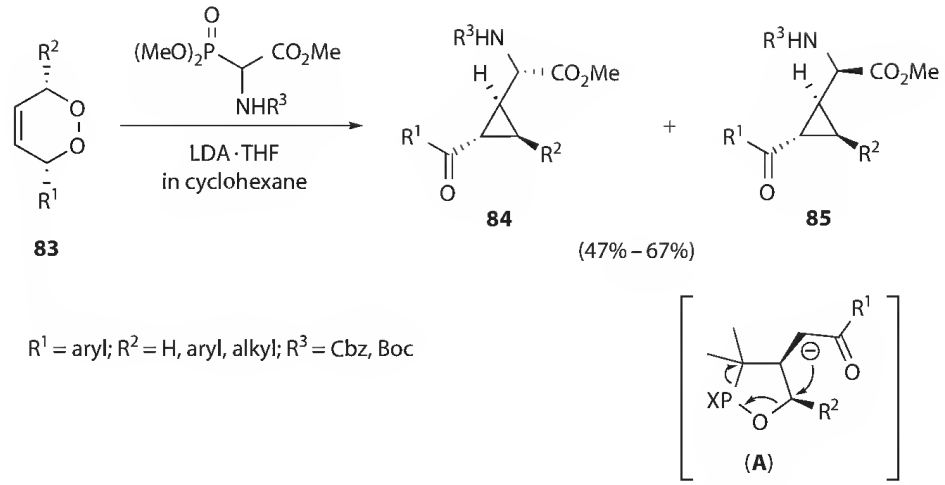

SCHEME 30.31 Synthesis of cyclopropane derivatives **84** and **85** by reaction of 1,2-dioxines **83** with phosphonates.

Removal of the acidic proton adjacent to the O–O linkage by a stabilized phosphorous ylide acting as base is the key step for the synthesis of cylopropane derivatives from dioxines [94]. The *cis*-γ-hydroxyenone undergoes Michael addition and concomitant P–O bond formation with the phosphorus ylide giving an oxaphospholane intermediate (**A**) ultimately leading to a cyclopropane (Scheme 30.31). This reaction has been applied to dioxines **83** using stabilized phosphonate nucleophiles and has afforded β-cyclopropyl amino acids **84** and **85** in good yields [95].

Transition metals as Fe(II), Ru(II), Co(II) catalyze rearrangement to *cis*-γ-hydroxyenones by homolytic cleavage of the peroxide bond [81]. In addition to the dehydration to furans and/or rearrangement to 1,4-diketones, metal catalysis can induce the formation of 1,4-diols and bis-epoxides, often yielding mixtures of products [81]. Optimized conditions using $FeSO_4$ have been pointed out and have led to the synthesis of 2,3-di- and 2,3,4-trisubstituted furans **88** and **89** starting from 1,2-dioxines **87**. The latter have been generated by Diels–Alder reaction of the enyne-RCM (ring-closing metathesis) adducts with singlet oxygen (Scheme 30.32) [96].

Intramolecular insertion of a carbenoid into a peroxide linkage of dioxines **90** generates bicyclic compounds **91** via a rhodium (II) catalyzed cyclization (Scheme 30.33) [97]. Insertion into the olefin moiety gives tricyclic peroxides **92**.

An intermolecular cyclopropanation with diazomethane has been performed on endoperoxides **93** using palladium acetate as catalyst (Scheme 30.34) [98]. The unsaturated endoperoxides in the [2.2.1] series are attacked by the carbene from the *exo* face while the analogs with larger bridges are preferentially attacked from the face *syn* to the peroxo bridge, affording **94** and **95**, respectively. Only in the case of the benzannelated [2.2.2] system **96** does the attack occur exclusively from the face proximal to the benzene ring leading to **97** (Scheme 30.34).

Diimide is able to reduce the double C=C bond preserving the peroxide linkage and this reaction constitutes the most important breakthrough in the synthesis and characterization of stable saturated endoperoxides [99]. Many peroxides previously postulated as intermediates in the singlet oxygenation of cyclic dienes have thus been rendered stable enough for further exploration of chemical, physical, and spectroscopic properties [82]. Transformations of endoperoxides that preserve the peroxide linkage are limited since the presence of the olefin inherently makes any proton adjacent the peroxide linkage acidic, resulting in compounds highly sensitive to acidic and basic media and metal-based reagents may induce fragmentation of the peroxide bond. In addition, in a bicyclic framework, the weak peroxide bond (–36 kcal mol^{-1}) is compounded by the additional strain brought on by the double bond in the bicyclic framework. The peroxide linkage of 1,2-dioxines exhibits stability to epoxidation with

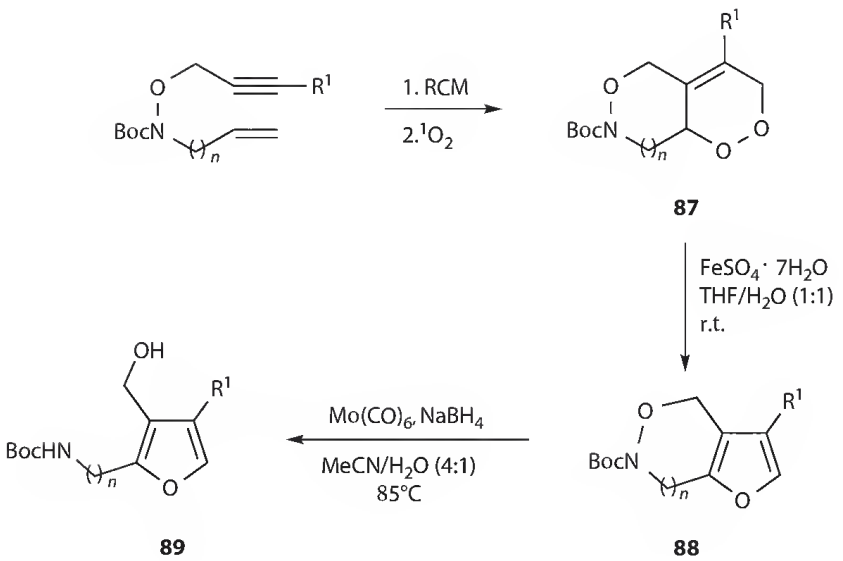

R^1	n	Yield (%)	
		88	**89**
H	2	98	87
H	3	88	67
CH_2OTBS	1	31	98
CH_2OTBS	2	61	65

SCHEME 30.32 Controlled synthesis of substituted furans **88** and **89** from 1,2-dioxines **87**.

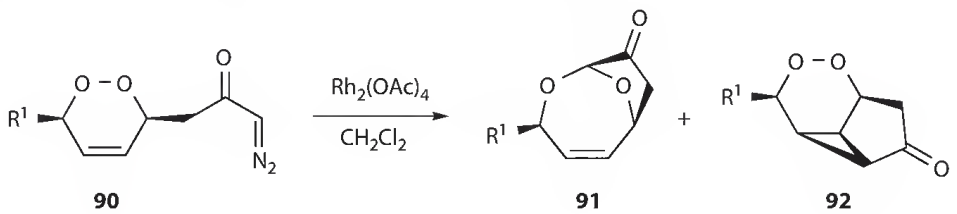

R^1	Yield (%)	
	91	**92**
Me	41	14
Ph	62	11
H	32	–

SCHEME 30.33 Rhodium-catalyzed cyclization of dioxines **90**.

m-chloroperbenzoic acid [100], dihydroxylation with osmium tetroxide [101], inverse-Diels–Alder reaction with dimethyl 1,2,4,5-tetrazine-3,6-dicarboxylate [102], and bromination [103].

30.3.2.2 Furan Endoperoxides

Although endoperoxides are formed from heterocyclic dienes containing nitrogen or sulfur, this section will deal only with those of furans since (1) furans are the most studied and used among the heterocyclic compounds due to the widespread occurrence of this functionality both in biologically important substrates and pharmaceuticals [104], (2) the high reactivity toward singlet oxygen overcomes even that of

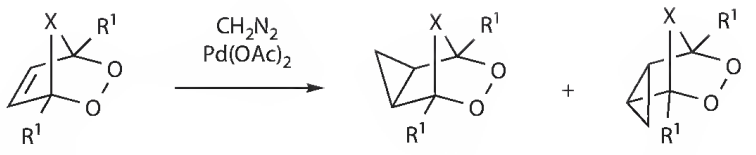

93 **94** **95**

(57%–85%)

X = O, R^1 = Me; X = CH_2, $(CH_2)_2$, $(CH_2)_3$, $(CH_2)_4$, CH = $CHCH_2$, R^1 = H

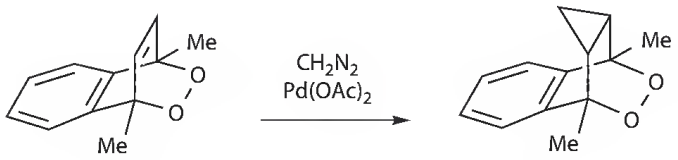

96 **97**

(92%)

SCHEME 30.34 Palladium-catalyzed cyclopropanation of endoperoxides **93** and **96.**

tri- and tetrasubstituted olefins in side chains [105] and, hence, (3) diverse derivatives are used as probes for the presence of this species even in aqueous media [106], (4) this system has a prominent role as key architectural feature in organic synthesis for natural products [107,108].

In particular, we focus on two general applications of the photooxygenation of furans for the preparation of 4-hydroxybutenolides and enediones, compounds of great synthetic interest. A large number of these derivatives have been incorporated into the framework of more complex molecules and have been obtained by the action of singlet-oxygen-mediated reaction sequences [104,107,108].

Butenolides are obtained by oxygenation of α- and α,α'-unsubstituted furans through a Kornblum-DeLamare rearrangement of the related endoperoxides, which is favored by a basic solvent as acetone [109] or water or ionic liquids [15], or MeOH. Using this solvent, butenolides have been directly formed in the self-sensitized photooxygenation of 3,4-dialkoxyfurans [110]. In particular, irradiation of derivative **98** possessing photodegradable groups affords ascorbic acid **99** in a one-pot reaction in 74% (Scheme 30.35).

The regiospecific generation of the carbonyl function may be achieved using a hindered base (which promotes hydrogen abstraction from the sterically most accessible bridgehead in the furan endoperoxide) [111] or, better, starting from 2-trimethylsilylfurans [112]. The Katsamura protocol has been employed as key step in a wide number of complex syntheses [19,104,107,108]. A fascinating application is in the construction of the tricyclic bis(spiroketal) core of prunolides, a family of cytotoxic natural products (Scheme 30.36) [113]. Photosensitized oxidation of both the (*Z*) and (*E*)-bis(2-trimethylsylilfuran) **100** followed by *in situ* dehydration of the intermediate bis(γ-hydroxy butenolide) **101** and spirocyclization provides the same 2:1 mixture of the *trans*- and *cis*-**102**.

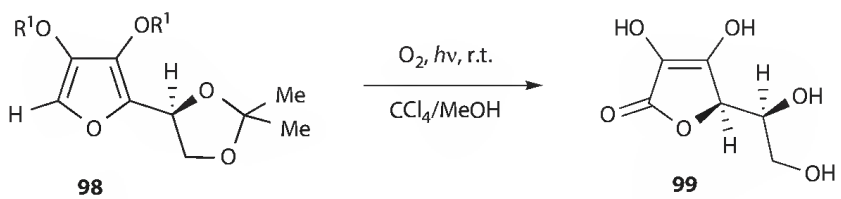

98 **99**

(74%)

R^1 = *p*-MeO-$C_6H_4CH_2$

SCHEME 30.35 Synthesis of L-ascorbic acid **99.**

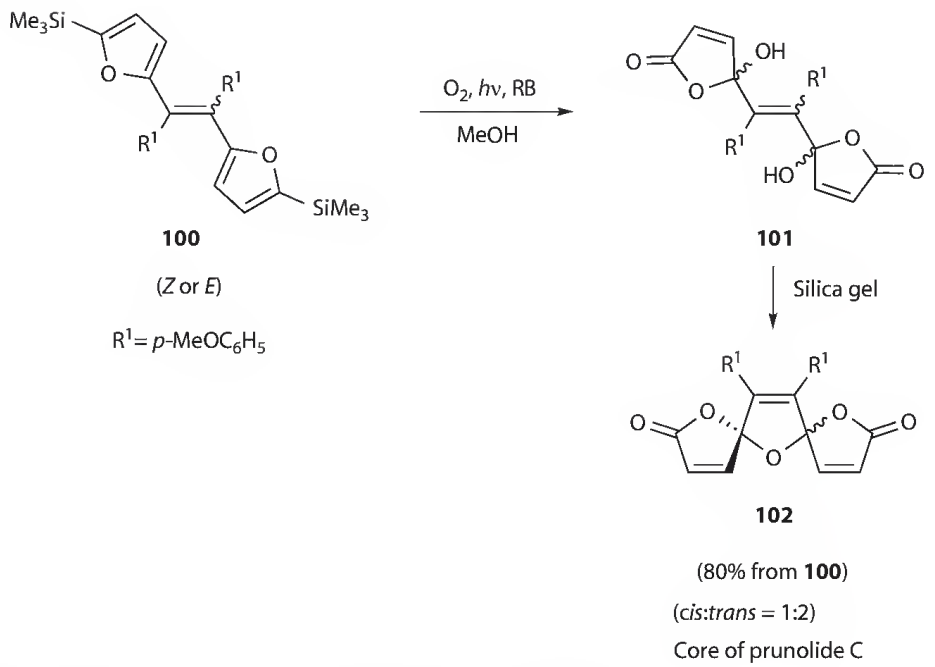

SCHEME 30.36 Synthesis of the bis-spiroketals **102** via butenolides **101**.

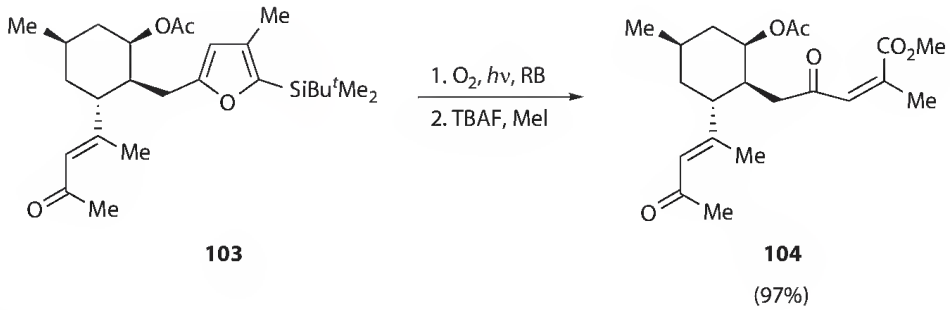

SCHEME 30.37 Synthesis of norzoanthamine precursor **104**.

Oxidation of furan **103** followed by treatment with tetrabutylammonium fluoride (TBAF) and iodomethane affords the methyl ester **104** that is a crucial product in the 41-steps total synthesis of the alkaloid norzoanthamine (Scheme 30.37) [114].

Cis-1,4-enediones are prepared by low temperature treatment of furan endoperoxides with reductants such as triphenylphosphine or dialkyl sulfides [71]. They generally form almost quantitatively and hence are used without isolation as, e.g., in the synthesis of the spirocyclic *C*-nucleoside **107** (Scheme 30.38) [115]. Compound **107** has been obtained by NEt_3 addition to the crude intermediate enedione **106** in 50% yield (from furan **105**).

The use of an acid catalyst has allowed to obtain 3-keto-tetrahydrofurans, such as **109**, from 2-(β-hydroxyalkyl) furans such as **108** in one-pot synthetic operation (Scheme 30.39) [116].

Oxidation of the enantiomerically pure furan **110** followed by *in situ* treatment with Me_2S gives pyranone **111** that is the key product for the ring **A** in the total synthesis of (+)-ambruticin S (Scheme 30.40) [117].

To overcome the thermal instability of furan endoperoxides, and hence working at low temperatures, a convenient alternative to the use of endoperoxides is to carry out the reduction on the methanol-trapping products which are more stable at room temperature and hence, more manageable than the related endoperoxides. These derivatives (e.g., compound **113** in Scheme 30.41) are simply

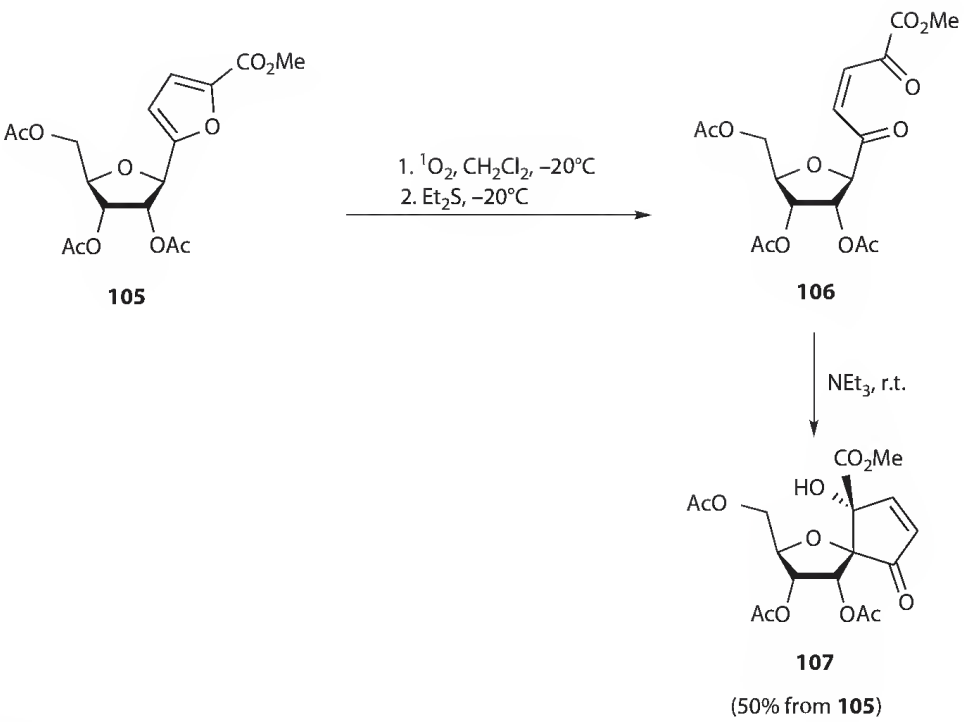

SCHEME 30.38 Synthesis of spirocyclic nucleoside **107**.

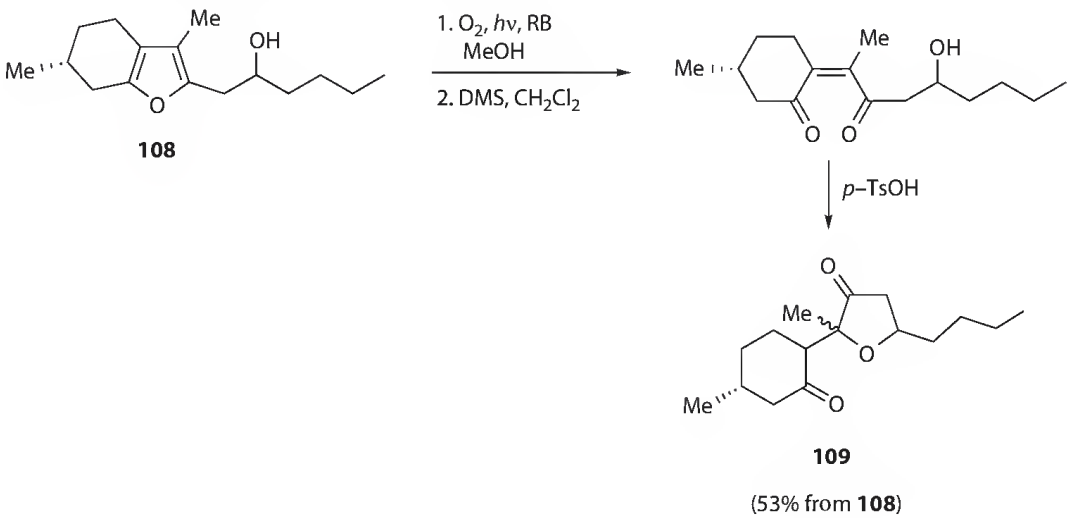

SCHEME 30.39 Synthesis of 3-keto-tetrahydrofuran **109**.

prepared by oxygenating furans in methanol and are reduced by alkyl sulfide generally *in situ*. This approach starting from furan **112** and the base-catalyzed cyclization of enediones using Hünig's base have been used to construct the 4-hydroxycyclopentenone core in a series of litseaverticillols [105]. The authors exploit the chemo- and regioselectivity of the reaction of singlet oxygen with the [4+2]-cycloaddition occurring at a much faster rate than the subsequent ene-mode to obtain the first (derivatives **A** and **C**, via *a* in Scheme 30.41) and second generation (derivatives **D**, **F**, **G** from **A** via *b* in Scheme 30.41) of these compounds.

The *cis*-relationship of the two carbonyl groups in enedione **115** has allowed to carry out a cyclization to a pyridazine *C*-nucleoside **116** in a one-pot three-steps synthesis starting from furan **114** (Scheme 30.42) [118].

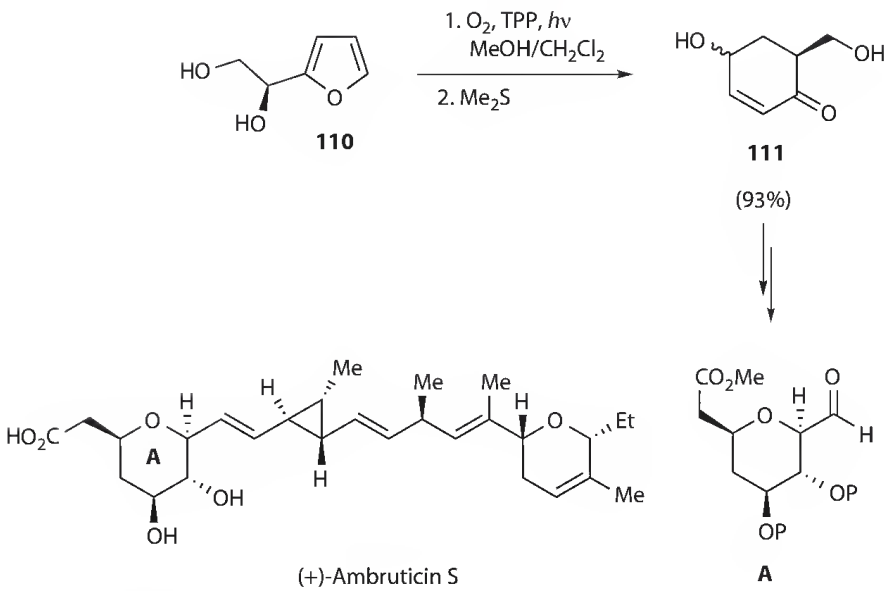

SCHEME 30.40 Synthesis of pyranone **111**.

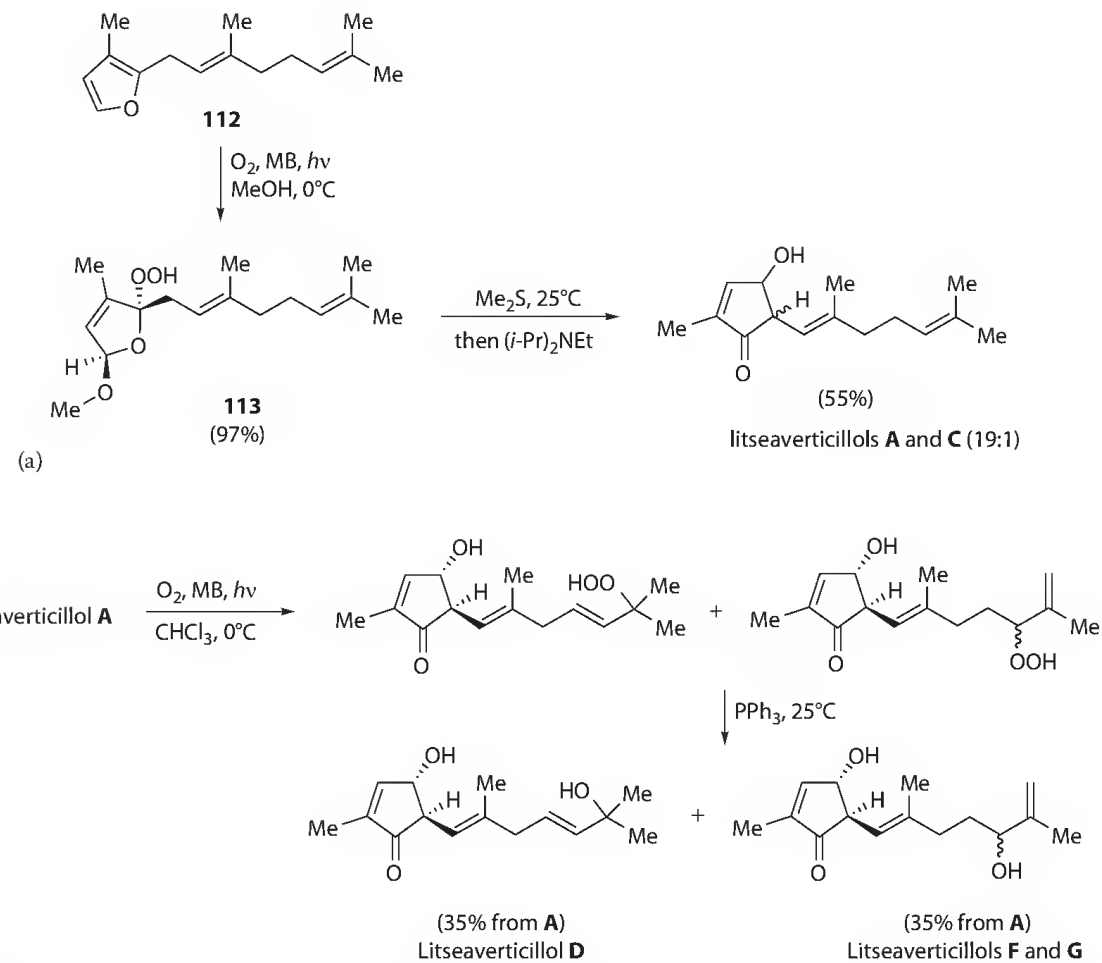

SCHEME 30.41 Synthetic pathways for compounds **A**, **C**, **D**, **F**, and **G**.

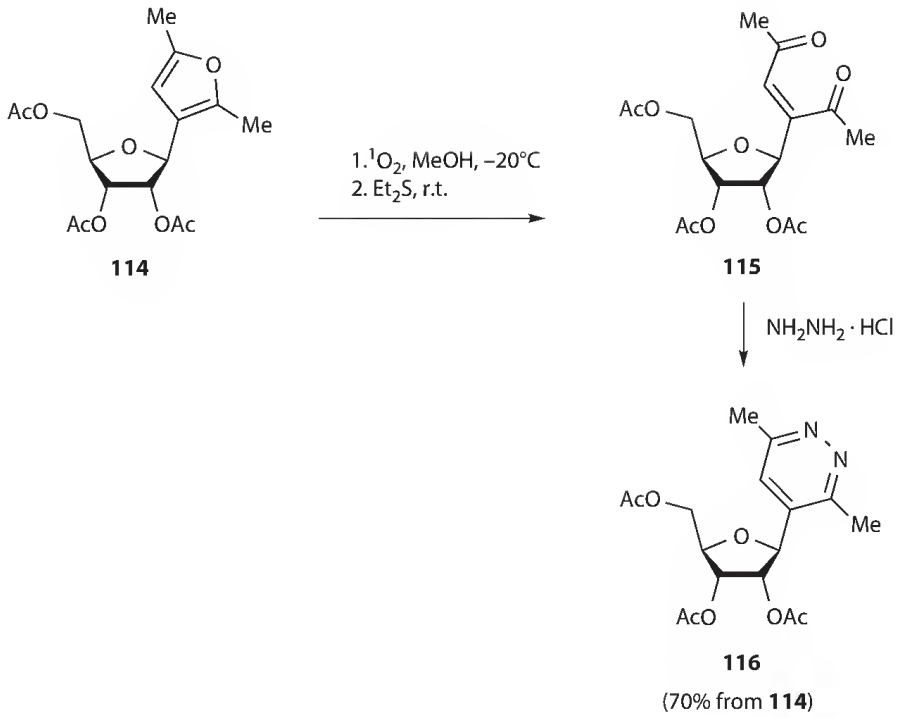

SCHEME 30.42 Synthesis of the pyridazine *C*-nucleoside **116**.

30.4 [2+2]-Cycloaddition

Two research groups synthesized independently for the first time 1,2-dioxetanes by photooxygenation of electron-rich alkenes, namely the *trans*- and *cis*- 3,4-diethoxyderivatives [119] and tetramethoxy-1,2-dioxetane [120]. Since then the photooxygenation of electron rich alkenes such as vinyl ethers, ketene acetals, enamines, vinyl sulfides as well as of olefins without allylic hydrogens or with inaccessible allylic hydrogens (on bridgeheads) is a general route for 1,2-dioxetanes [121,122]. [2+2]-Cycloaddition is generally the route in the photooxygenation of condensed aromatic compounds as indenes, benzofurans, indoles, sometime it occurs in pyrroles [71] and in partially saturated heterocycles [8]. In many cases dioxetanes are thermally unstable and their formation has been postulated on the basis of the characteristic cleavage products, frequently accompanied with emission of light. Synthesis and isolation are the major difficulties encountered with these peroxides, and photochemical methods represent a valid alternative to thermal approaches [121,122].

The most accredited mechanism for dioxetane mode involves polar species as open zwitterions [123]. Experimental evidences have been provided by solvent effects [124] and trapping reactions with alcohols and aldehydes [123].

30.4.1 Chemoselectivity and Diasteroselectivity

Chemoselectivity in favor of dioxetane-mode is observed by increasing solvent polarity [124] or in the presence of heteroatom substituents. The mesomeric effect of heteroatoms is evident in the oxygenation of 5,6-dihydro-1,4-oxathiin **117a** [125] and 1,4-dithiin **117b** [126] (Scheme 30.43). Despite the presence of allylic hydrogens and sulfide moiety, the sole reaction products are dicarbonyl compounds **119** deriving from the corresponding dioxetanes **118** through the classical fragmentation of this peroxide class [125,126].

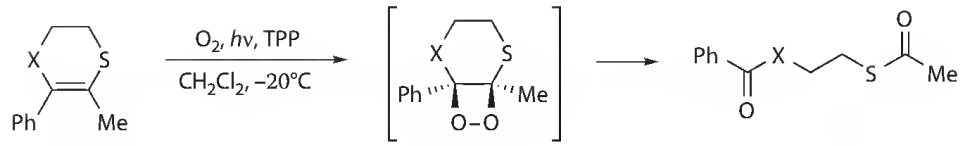

117 **118** **119**

a; X = O
b; X = S

SCHEME 30.43 Photooxygenation of 1,4-oxathiin **117a** and 1,4-dithiin **117b**.

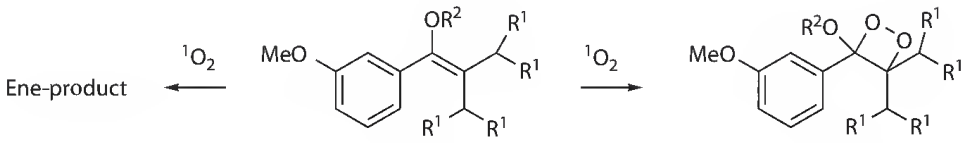

120 **121**

R^1	R^1	R^2	Reaction Temperature (°C)	
			25	–78
			121:ene	**121**:ene
-CH_2-CH_2-		Me	22:78	67:33
Me	Me	Me	29:71	95:5
Me	Me	Et	80:20	99:1
Me	Me	*i*-Pr	98:2	100:0
Me	Me	*t*-Bu	100:0	100:0

SCHEME 30.44 [2 + 2]-Cycloaddition vs. ene-reaction of olefins **120** at different temperatures.

Dioxetane mode is also favored at low temperature as demonstrated in the oxygenation of olefins **120** (Scheme 30.44) [127]. The formation of dioxetanes **121** increases on lowering the temperature from 25 to –78°C. As shown in Scheme 30.44, the ratio 1,2-addition/ene-reaction is also increased by increasing the bulkiness of the alkoxy group due to unfavorable steric factors that make the appropriate alignment of allylic hydrogens difficult to give the ene-reaction [127].

Optically active oxazolidinones have been successfully used as sterically controlling chiral auxiliaries [128,129]. Thus, the photooxygenation of oxazolidinone-substituted enecarbamates **122** leads to diastereomerically pure dioxetanes **123** (Scheme 30.45). The selectivity is independent from the size of the alkyl group at the C4 of the oxazolidinone but does depend on whether this stereogenic center is *R* or *S* configured [128]. For example, oxazolidinone with an *R* configuration at the C4 favors the 1'*S*/2'*S* dioxetane **123**. Alternatively the oxazolidinone with an *S* configuration at the C4 favors the 1'*R*/2'*R* dioxetane [128]. The chirality at the phenethyl group (C3') does not influence the π-selectivity. Temperature, solvent and alkene geometry are instead important factors [129]. As shown in Scheme 30.45, the diastereofacial control followed by appropriate reagents can be used to obtain synthetically useful, enantiomerically pure hydroxylated products [128].

Diastereoselectivity can also be controlled by electronic effects as hydrogen bonding [130]. The hydroxyl-directed stereocontrol has been observed in the photooxygenation of adamantylidene-substituted chiral allylic alcohol **124** that gives *threo*-dioxetane **125** with high stereoselectivity (Scheme 30.46) [130]. The use of CD_3OD/CCl_4 as solvent causes a drop in diastereoselectivity from >95:5 in $CDCl_3$ to 89:11. This is due to the loss of the above mentioned hydrogen bonding between the substrate and $^1O_2$. Instead,

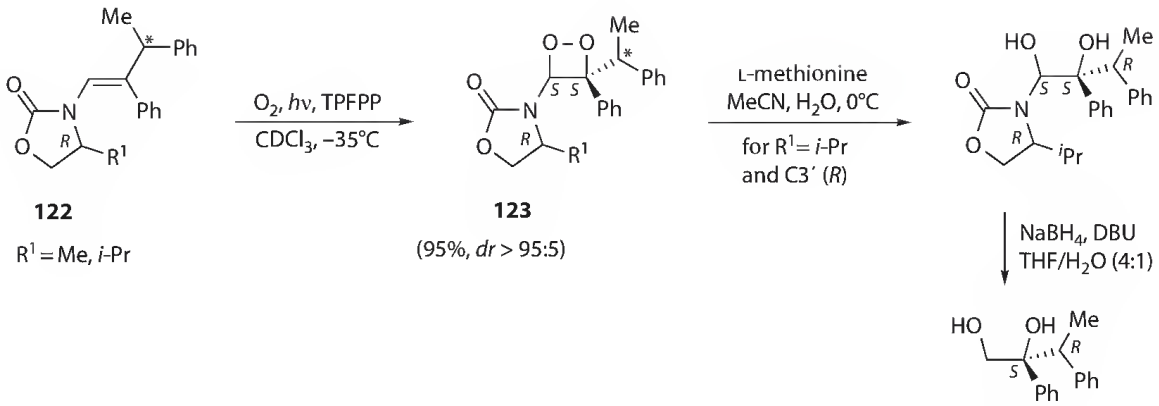

122

R^1 = Me, *i*-Pr

123

(95%, *dr* > 95:5)

SCHEME 30.45 Diastereoselective dioxetane formation in the photooxygenation of enecarbamates **122**.

124

threo-**125**

erythro-**125**

Solvent	*threo*/*eritro*	Yield (%)
$CDCl_3$	>95:5	47
CD_3OD/CCl_4	89:11	95

SCHEME 30.46 Diastereoselective dioxetane formation in the photooxygenation of chiral allylic alcohol **124**.

intermolecular hydrogen bonding occurs with the solvent methanol. The polar solvent increases the dioxetane yield from 47% (in $CDCl_3$) to 95%.

30.4.2 Chemiluminescent Properties

Bis(adamantylidene)dioxetane **127a** (Scheme 30.47) is the most thermally stable among hitherto known dioxetanes [131] and a single adamantylidene group has been proven to exert a strong stabilizing effect [132]. Really, steric hindrance between geminal substituents of a dioxetane (3,3-steric interaction) appears to especially stabilize the peroxidic ring [127]. Dioxetanes with annelated six-membered rings are less stable than their five- or seven-membered analogues [133]. The steric interaction of a bulky *tert*-butyl group at the 5-position with two methyls at the 4-position can improve the thermal persistency of the peroxide ring in five- [134] and six-annulated dioxetanes [133]. Conversely, the presence of an easily oxidized substituent, which has a low oxidation potential [135,126], or of a heteroatom as sulfur [72] at the double bond considerably decreases the thermal stability of the peroxidic intermediate. Indeed, sulfur-substituted dioxetanes are much more thermally unstable than the O-analogues and have been detected by spectroscopic means at very low temperature, if at all [125,126,136]. Some representative stable dioxetanes prepared by photooxygenation of alkenes are drawn in Scheme 30.47.

There is a high interest to know the structural features that endow the thermal stability of dioxetanes since this property makes the molecule easy to handle and, if accompanied with high chemiluminescence [142], usable as enzyme labels in bioanalytical clinical applications [143,144].

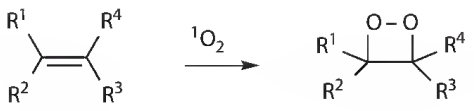

126 **127**

Entry	R^1	R^2	R^3	R^4	Yield (%)	Reference
A					66	[131]
B	OMe	3-$MeOC_6H_4$			90	[127]
C			3-$TBDMSOC_6H_4$	OMe	76	[137]
D			OMe	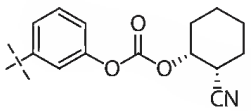	100	[138]
E	TBDMSO 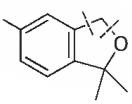		*i*-Pr	*i*-Pr	89	[139]
F	*t*-Bu	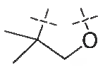		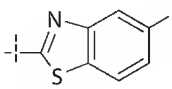 OTBDMS	88	[140]
G	3-$MeOC_6H_4$	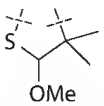 OMe		*t*-Bu	85	[141]

SCHEME 30.47 Photooxygenation of olefins **126.**

Dioxetanes have the unique property to decompose thermally to electronically excited carbonyl products with consequent emission of blue light (λ_{max} 400–430 nm) (e.g., **127a** in Scheme 30.48) [145]. Thus, functionalized adamantylideneadamantane-1,2-dioxetanes have been described as labels for thermochemiluminescent immunoassays [146].

Particularly in the last years, more effective are CIEEL-active dioxetanes that decompose in a manner quite distinct from rather simple dioxetanes [142]. A CIEEL-dioxetane generally contains an adamantyl group to provide stability and a fluorgenic electron-donor substituent, mostly a protected phenolic substituent. On demand, the stable dioxetane can be transformed into an unstable dioxetane that bears a phenolate ion and decomposes spontaneously to emit light by CIEEL mechanism (CIEEL = chemically initiated electron exchange luminescence). This has been explained through an intramolecular electron

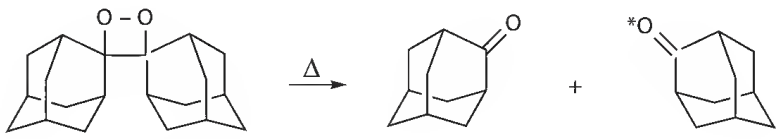

127a

SCHEME 30.48 Thermal decomposition of dioxetane **127a.**

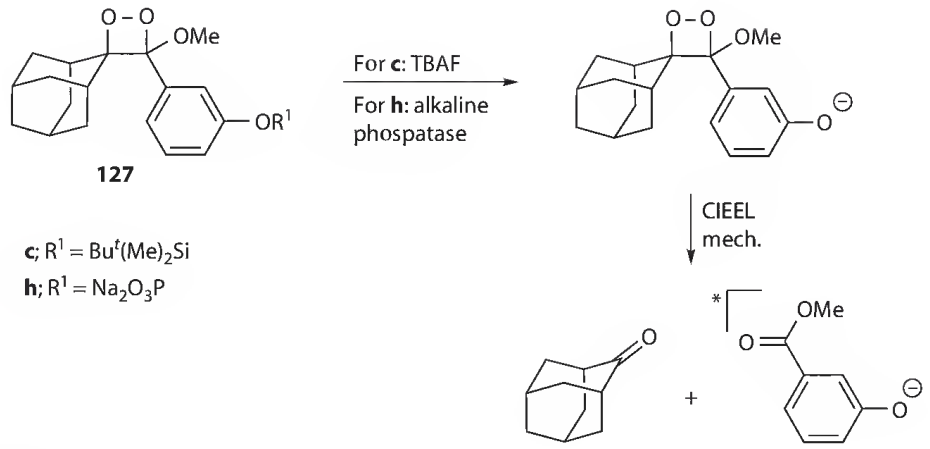

SCHEME 30.49 CIEEL decomposition of dioxetane **127**.

transfer that occurs from the aryloxy to the O–O bond and generates an intermediate, which produces the excited singlet product. Scheme 30.49 reports some examples of CIEEL-dioxetanes for which the phenolic hydroxy group is protected as *t*-butyldimethylsilyl ether and phosphate [147,148]. These dioxetanes are thermally stable and can be triggered as desired by deprotection, chemically or enzymatically.

Compound **127h** ($R^1 = Na_2O_3P$) is the commercially available AMPPD (or PPD®) and is used for biochemical and clinical applications [146]. The advantages of the use of luminescent labels if compared with that of radioactive isotopes are that they are safer, faster, and more sensitive (two or three orders of magnitude more sensitive than scintillation counting).

30.4.3 Synthetic Applications

The [2+2]-cycloaddition of singlet oxygen to alkenes is generally followed by thermal decomposition of the dioxetane intermediate to carbonyl fragments so that it can represent an alternative to ozonolysis, although limited to electron-rich olefins due to the competition of the other reaction modes (ene and [4+2]-addition). This behavior has been exploited for the synthesis of 11-oxaestrogens starting from some estrogens with vinylanisole structure, such as **128** (Scheme 30.50) [149]. Oxygenation of this compound leads to **129** via vinyl moiety oxidative cleavage.

The oxygenation of 5-dialkylamino-4-pyrrolin-3-ones **130** gives highly functionalized ureas **132** by cleavage of the initially formed [2+2] cycloadducts **131** (Scheme 30.51) [150].

The photooxidative double bond cleavage can be usefully adopted for the construction of large heterocyclic rings containing carbonyl groups. Thus, oxygenation of the enamine **133** is a convenient route to compound **134** in the synthesis of protopine-type alkaloids (Scheme 30.52) [151].

The oxidative ring-opening to keto-amide **136**, followed by *in situ* treatment with aqueous $NaHCO_3$, is the key step to convert the indole **135** to quinoline **137** in the synthesis of the quinine alkaloid camptothecin (Scheme 30.53) [152].

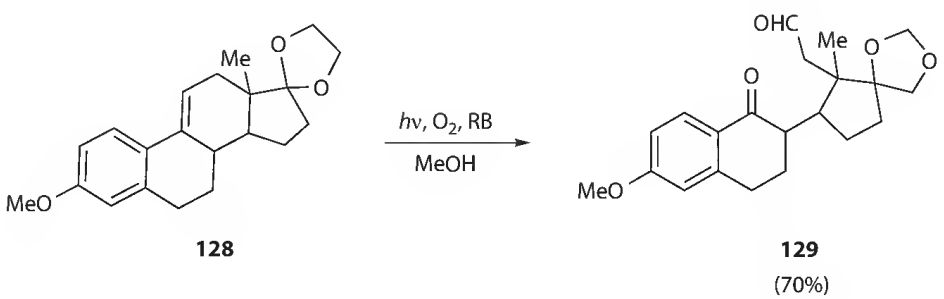

SCHEME 30.50 Synthesis of 11-oxaestrogen **129**.

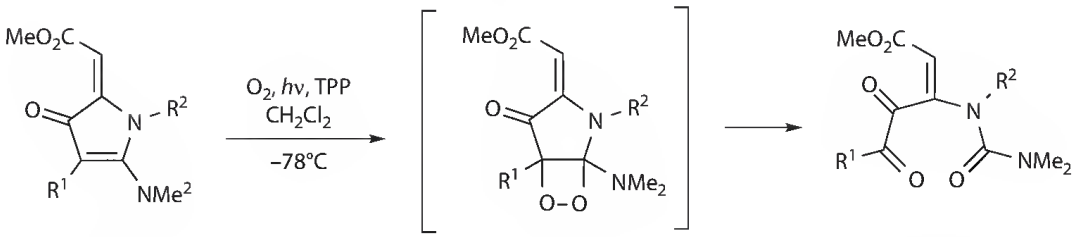

SCHEME 30.51 Synthesis of functionalized ureas **132**.

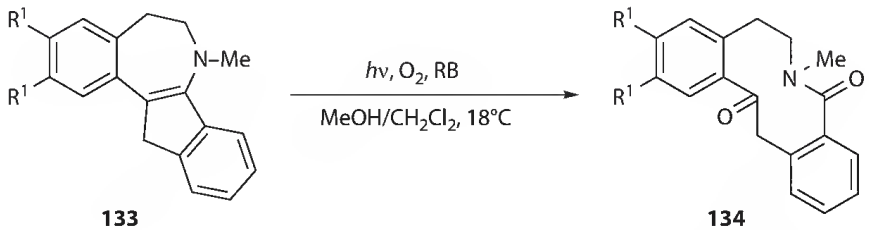

SCHEME 30.52 Synthesis of protopine-type compounds **134**.

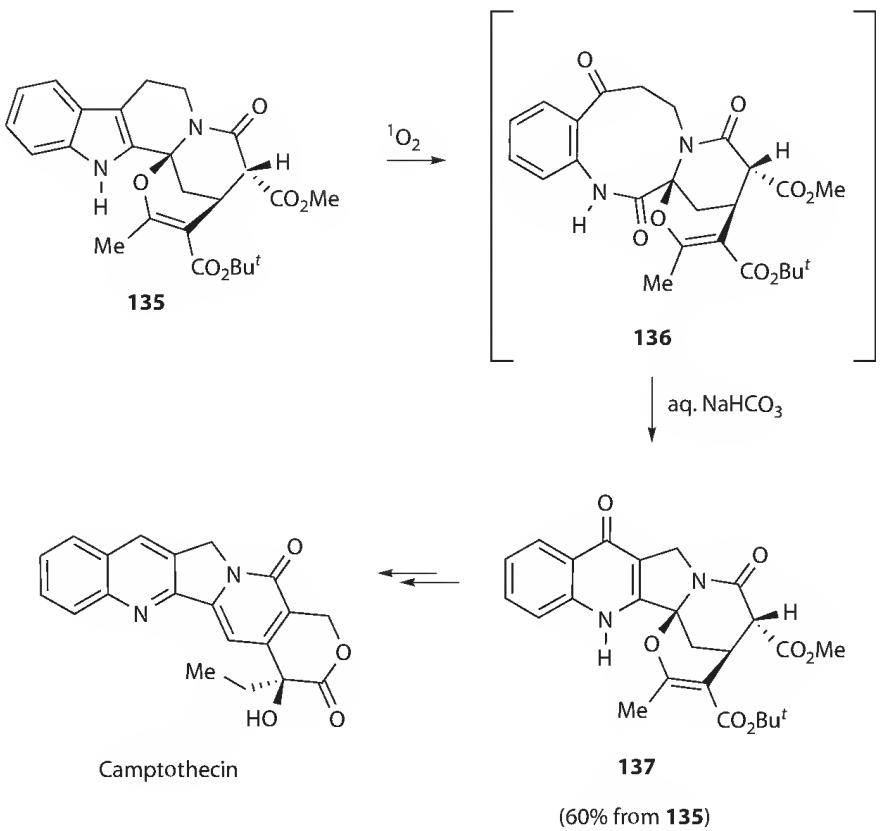

SCHEME 30.53 Synthesis of camptothecin precursor **137**.

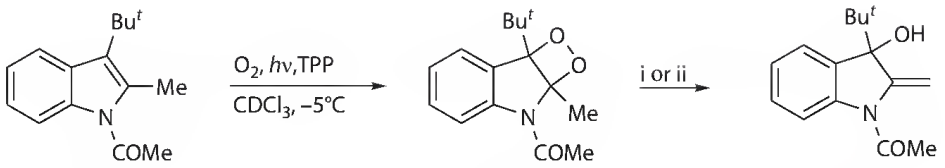

138 **139** **140**

i: $(MeO)_3P$
ii: Me_2S

(i; 64% from **138**)
(ii; 51% from **138**)

SCHEME 30.54 Synthesis of the allylic alcohol **140**.

With careful control of the temperature or with stable dioxetanes, reduction to 1,2-diols can be obtained by treatment with reductants as lithium aluminum hydride [3,121,122]. Epoxides are instead formed by treatment with phosphines or sulfides [3,121,122], often followed by rearrangement or ring contraction. Thus, a peculiar open product, the allylic alcohol **140**, has been obtained by treatment of dioxetane **139** with $P(OMe)_3$ or Me_2S (Scheme 30.54) [153].

Labile undetected epoxides formed by an intramolecular nucleophilic attack of sulfur to the O–O bond have been proposed to explain the formation of sulfoxides, e.g., **144** (Scheme 30.55), instead of the expected dicarbonyl compounds in the oxygenation of some oxathiins and dithiins substituted with electron-withdrawing groups at the double bond [125,126]. It has been suggested that in the dioxetane, e.g., **142**, the increased electron demand by the O–O bond favors the intramolecular nucleophilic attack of the ring sulfur, leading to the final product **144** via the sulfoxide epoxide **143** (Scheme 30.55) [126].

One of the most interesting and useful applications of dioxetanes is in the synthesis of 1,2,4-trioxanes. This is due to the capacity of some alkoxy-substituted dioxetanes to undergo heterolytic C–O bond cleavage to zwitterionic intermediates, which can be trapped inter- or intramolecularly by carbonyl compounds [123,154]. This behavior has been exploited for the total synthesis of the antimalarial (+) artemisinin [155] and related analogs [156]. In particular, the Posner reaction is based on the generation of 1,2-dioxetanes, e.g., **146**, through low-temperature photooxygenation of electron-rich vinyl ethers, e.g., **145**, and *in situ* acid-induced intramolecular coupling with carbonyl groups to give peroxides **147** (Scheme 30.56) [154]. The reaction allows the introduction of a variety of substituents at positions 3,4,5′,7,9, and 10 of the tricyclic molecular core.

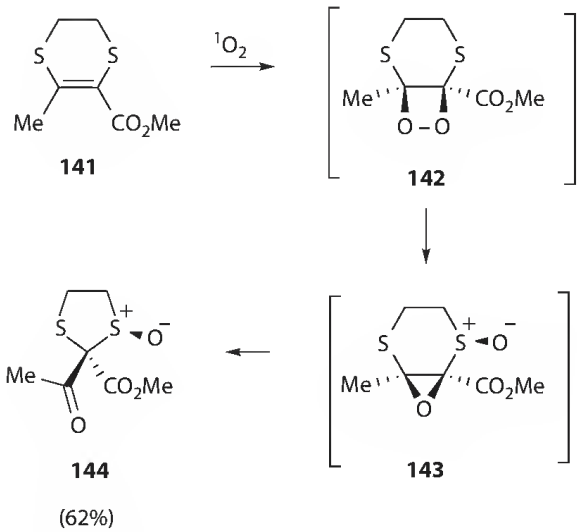

141 **142** **143** **144**

(62%)

SCHEME 30.55 Synthesis of sulfoxide **144**.

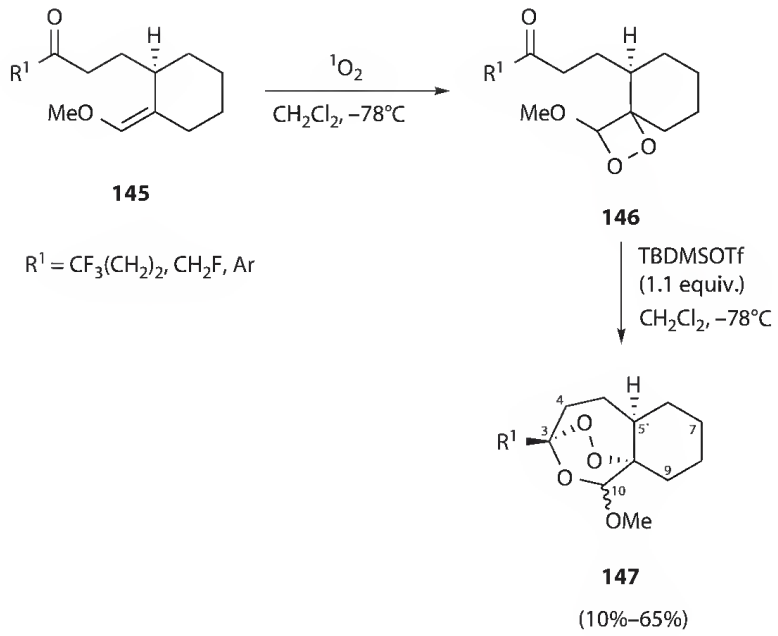

SCHEME 30.56 Synthesis of 1,2,4-trioxanes **147**.

30.5 Conclusion

As shown in this chapter, photooxygenation of unsaturated compounds continues to receive high attention from scientists. After the 1970s–1980s, dedicated to mechanistic investigation on singlet oxygenation and to exploring the scope of the reaction, in recent years efforts have been directed to the stereochemical aspects and to the exploitation of stereoselective (in many cases, also stereospecific) applications in order to improve the use of this procedure for the synthesis of natural bioactive compounds and/or their analogues [157]. Moreover, post photo-oxidation modification reactions containing cyclic peroxide functionalities while maintaining the peroxide linkage intact are becoming relatively common.

In the last decade, a newly relevant challenge is in adapting photooxygenation processes for large-scale production. Hence, an emerging area of interest is in research of new technologies to be applied to these reactions, and has been stimulated by developments in microreactor design [158] and use of more specific light sources, as light-emitting diodes (LEDs) [26,159]. Due to the short holdup in the microstructures, the hazard of highly exothermic and explosive reactions is considerably reduced. Solar photooxygenations with medium concentrated sunlight are also investigated [160]. This increasing interest is due to the growing demand for environmentally friendly technologies, and photochemical approaches are regarded as clean routes. Dye-sensitized photooxygenation, in addition, uses oxygen as oxidant with a complete atom economy, leading to products that generally present both atoms of oxygen, and hence represents one of the most efficient and cleanest oxidation processes.

References

1. Foote, C. S. 1991. Definition of type I and type II photosensitized oxidation. *Photochem. Photobiol.* 54: 659.
2. Frimer, A. A. 1985. *Singlet Oxygen*, CRC Press: Boca Raton, FL.
3. Iesce, M. R. 2005. Photooxygenation of [4+2] and [2+2] type. In *Synthetic Organic Photochemistry*, Griesbeck, A. G., Mattay, J., Eds., Marcel Dekker: New York, Vol. 12, pp. 299–363.
4. Clennan, E. L. 2005. Photo-oxygenation of the ene-type. In *Synthetic Organic Photochemistry*, Griesbeck, A. G., Mattay, J., Eds., Marcel Dekker: New York, Vol. 12, pp. 365–390.

5. Paquette, L. A., Liotta, D. C., Baker, A. D. 1976. Frontier molecular orbital basis for the structurally dependent regiospecific reactions of singlet ($^1\Delta_g$) oxygen with polyolefins. *Tetrahedron Lett.* 2681–2684.
6. Adam, W., Prein, M. 1996. π-Facial diastereoselectivity in the [4+2]-cycloaddition of singlet oxygen as a mechanistic probe. *Acc. Chem. Res.* 29: 275–283.
7. Akasaka, T., Ando, W. 1992. Peroxides from photosensitized oxidation of heteroatom compounds. In *Organic Peroxides*, Ando, W., Ed., Wiley: Chichester, U.K., pp. 599–659.
8. Iesce, M. R., Cermola, F., Rubino, M. 2007. Photooxygenation of non-aromatic heterocycles. *Curr. Org. Chem.* 11: 1053–1075.
9. Greer, A. (Guest editor) 2006. Organic chemistry of singlet oxygen. *Tetrahedron* 62(46): 10603–10776.
10. Ogilby, P. E. (Guest editor). 2006. Singlet oxygen. *Photochem. Photobiol.* 82: 1133–1390.
11. Berkessel, A. (Ed.). 2009. *Peroxides. Science of Synthesis*, Georg Thieme Verlag: Stuttgart, Vol. 38, pp. 469–524.
12. Ando, W. (Ed.). 1992. *Organic Peroxides*, Wiley: Chichester, U.K.
13. Foote, C. S., Clennan, E. L. 1995. Properties and reactions of singlet oxygen. In *Active Oxygen in Chemistry*, Foote, C. S., Valentine, J. S., Greenberg, A., Liebman, J. F., Eds., Chapman & Hall: London, U.K., pp. 105–140.
14. Takaguchi, Y., Yanagimoto, Y., Fujima, S., Tsuboi, S. 2004. Photooxygenation of olefins, phenol, and sulfide using fullerodendrimer as catalyst. *Chem. Lett.* 33: 1142–1143.
15. Astarita, A., Cermola, F., DellaGreca, M., Iesce, M. R., Previtera, L., Rubino, M. 2009. Photooxygenation of furans in water and ionic liquid solutions. *Green Chem.* 11: 2030–2033.
16. Bourne, R. A., Han, X., Chapman, A. O., Arrowsmith, N. J., Kawanami, H., Poliakoff, M., George, M. W. 2008. Homogeneous photochemical oxidation via singlet O_2 in supercritical CO_2. *Chem. Commun.* 4457–4459.
17. Han, X., Bourne, R. A., Poliakoff, M., George, M. W. 2009. Strategies for cleaner oxidations using photochemically generated singlet oxygen in supercritical carbon dioxide. *Green Chem.* 11: 1787–1792.
18. Griesbeck A. G., El-Idreesy, T. T., Bartoschek, A. 2004. Photooxygenation in polystyrene beads with covalently and non-covalently bound tetraarylporphyrin sensitizers. *Adv. Synth. Catal.* 346: 245–251.
19. Clennan, E. L., Pace, A. 2005. Advances in singlet oxygen chemistry. *Tetrahedron* 61: 6665–6691.
20. Li, H.-R., Wu, L.-Z., Tung, C.-H. 2000. Reactions of singlet oxygen with olefins and sterically hindered amine in mixed surfactant vesicles. *J. Am. Chem. Soc.* 122: 2446–2451.
21. Hino, T., Anzai, T., Kuramoto, N. 2006. Visible-light induced solvent-free photooxygenations of organic substrates by using [60]fullerene-linked silica gels as heterogeneous catalysts and as solid-phase reaction fields. *Tetrahedron Lett.* 47: 1429–1432.
22. Zhang, D., Wu, L.-Z., Yang, Q.-Z., Li, X.-H., Zhang, L.-P., Tung, C.-H. 2003. Versatile photosensitization system for $^1O_2$-mediated oxidation of alkenes based on nafion-supported platinum(II) terpyridyl acetylide complex. *Org. Lett.* 5: 3221–3224.
23. Loponov, K., Goller, B., Moskalenko, A., Kovalev, D., Lapkin, A. 2010. Efficiency of porous silicon photosensitizer in the singlet oxygen-mediated oxidation of organic compounds. *J. Photochem. Photobiol. A: Chem.* 211: 74–77.
24. Wootton, R. C. R., Fortt, R., de Mello, A. J. 2002. A microfabricated nanoreactor for safe, continuous generation and use of singlet oxygen. *Org. Proc. Res. Dev.* 6: 187–189.
25. Jahnisch, K., Dingerdissen, U. 2005. Photochemical generation and [4+2]-cycloaddition of singlet oxygen in a falling-film microreactor. *Chem. Eng. Technol.* 28: 426–427.
26. Carofiglio, T., Donnola, P., Maggini, M., Rossetto, M., Rossi, E. 2008. Fullerene-promoted singlet-oxygen photochemical oxygenations in glass-polymer microstructured reactors. *Adv. Synth. Catal.* 350: 2815–2822.
27. Sevin, F., McKee, M. L. 2001. Reaction of 1,3-cyclohexadiene with singlet oxygen. A theoretical study. *J. Am. Chem. Soc.* 123: 4591–4600.

28. Aubry, J.-M., Pierlot, C., Rigaudy, J., Schmidt, R. 2003. Reversible binding of oxygen to aromatic compounds. *Acc. Chem. Res.* 36: 668–675.
29. Griesbeck, A. G., Fiege, M., Gudipati, M. S., Wagner, R. 1998. Photooxygenation of 2,4-dimethyl-1,3-pentadiene: Solvent dependence of the chemical (ene reaction and [4+2]-cycloaddition) and physical quenching of singlet oxygen. *Eur. J. Org. Chem.* 1998: 2833–2838.
30. Matsumoto, M., Dobashi, S., Kuroda, K., Kondo, K. 1985. Sensitized photo-oxygenation of acyclic conjugated dienes. *Tetrahedron* 41: 2147–2154.
31. Herz, W., Juo, R.-R. 1985. Photooxygenation of 1-vinylcycloalkenes. The competition between "ene" reaction and cycloaddition of singlet oxygen. *J. Org. Chem.* 50: 618–627.
32. Matsumoto, M., Dobashi, S., Kuroda, K. 1977. Sensitized photooxygenation of β,β-dimethylstyrenes; synthesis of (±)-crotepoxide. *Tetrahedron Lett.* 3361–3364.
33. Matsumoto, M., Kuroda, K., Suzuki, Y. 1981. The 1,4-addition of singlet oxygen to 2,6-dimethoxy-1-(2-methoxyethenyl)benzene and 2-methoxy-1-(2-methoxyethenyl)naphthalene. The 1,4-endoperoxides as equivalents of 6-oxo-2,4-cyclohexadienylidenacetates. *Tetrahedron Lett.* 22: 3253–3256.
34. Schenck, G. O., Dunlop, D. E. 1956. Photosynthesis of cyclopentadiene endoperoxide at −100°C and hydrogenation of endo peroxides with thiourea. Application of sodium vapor lamps in preparative photochemistry. *Angew. Chem.* 68: 248–249.
35. Schenck, G. O. 1952. Problems in photochemical synthesis. *Angew. Chem.* 64: 12–23.
36. Cope, A. C., Liss, T. A., Wood, G. W. 1957. Proximity effects. X. *cis*-1,4-Cycloheptanediol from solvolysis of cycloheptene oxide. *J. Am. Chem. Soc.* 79: 6287–6292.
37. Horinaka, A., Nakashima, R., Yoshikawa, M., Matsuura, T. 1975. Photoinduced reactions. LXXXVI. Photosensitized oxygenation of unconjugated cyclic dienes. *Bull. Chem. Soc. Jpn.* 48: 2095–2098.
38. Matusch, R., Schmidt, G. 1988. Competition of endoperoxide and hydroperoxide formation in the reaction of singlet oxygen with cyclic, conjugated dienes. *Angew. Chem. Int. Ed. Engl.* 27: 717–718.
39. Bourne, R. A., Han, X., Poliakoff, M., George, M. W. 2009. Cleaner continuous photo-oxidation using singlet oxygen in supercritical carbon dioxide. *Angew. Chem. Int. Ed.* 48: 5322–5325.
40. Carless, H. A. J., Billinge, J. R., Oak, O. Z. 1989. Photochemical routes from arenes to inositol intermediates: The photooxidation of substituted cis-cyclohexa-3,5-diene-1,2-diols. *Tetrahedron Lett.* 30: 3113–3116.
41. Johnson, C. R., Golebiowski, A., Steensma, D. H., Scialdone, M. A. 1993. Enantio- and diastereoselective transformations of cycloheptatriene to sugars and related products. *J. Org. Chem.* 58: 7185–7194.
42. Adam, W., Balci, M. 1979. Photooxygenation of 1,3,5-cycloheptatriene: Isolation and characterization of endoperoxides. *J. Am. Chem. Soc.* 101: 7537–7541.
43. Adam, W., Balci, M., Pietrzak, B. 1979. Reaction of 7-substituted cycloheptatrienes with singlet oxygen and 4-phenyl-1,2,4-triazoline-3,5-dione. *J. Am. Chem. Soc.* 101: 6285–6291.
44. Adam, W., Rebollo, H. 1982. Singlet oxygenation of 7-aryl- and 7-alkyl-1,3,5-cycloheptatrienes. Substituent effects on the product distribution of tropylidene- and norcaradiene-derived endoperoxides. *Tetrahedron Lett.* 23: 4907–4910.
45. Saracoglu, N., Menzek, A., Sayan, S., Salzner, U., Balci, M. 1999. Pyramidalized double bonds containing endoperoxide linkages: Photooxygenation of dimethyl *cis*-3,8-dihydroheptalene-3,8-dicarboxylate. *J. Org. Chem.* 64: 6670–6676.
46. Dastan, A., Saracoglu, N., Balci, M. 2001. A new method for the synthesis of stipitatic acid isomers: Photooxygenation of ethyl 6*H*-cyclohepta[d][1,3]dioxole-6-carboxylate. *Eur. J. Org. Chem.* 18: 3519–3522.
47. Daştan, A., Balci, M. 2006. Chemistry of dioxine-annelated cycloheptatriene endoperoxides and their conversion into tropolone derivatives: An unusual non-benzenoid singlet oxygen source. *Tetrahedron* 62: 4003–4010.

48. Gueney, M., Dastan, A., Balci, M. 2005. Chemistry of the benzotropone endoperoxides and their conversion into tropolone derivatives: Unusual endoperoxide rearrangements. *Helv. Chim. Acta* 88: 830–838.
49. Adam, W., Erden, I. 1979. Singlet oxygenation of cycloocta-1,3,5-triene: Formation of (4.2.2)- and (2.2.2.)-cycloadducts. *Tetrahedron Lett.* 30: 2781–2784.
50. Adam, W., Klug, G., Peters, E.-M., Peters, K., von Schnering, H. G. 1985. Synthesis of endoperoxides derived from cyclooctatetraenes via singlet oxygenation. *Tetrahedron* 41: 2045–2056.
51. Bloodworth, A. J., Eggelte, H. J. 1985. Endoperoxides. In *Singlet Oxygen*, Frimer, A. A., Ed., CRC Press: Boca Raton, FL, Vol. 2, pp. 193–203.
52. Van den Heuvel, C. J. M., Hofland, A., Steinberg, H., De Boer, T. J. 1980. The photooxidation of hexamethylbenzene and pentamethylbenzene by singlet oxygen. *Recl. Trav. Chim. Pays-Bas* 99: 275–278.
53. Sawada, T., Mimura, K., Thiemann, T., Yamato, T., Tashiro, M., Mataka, S. 1998. Stable endoperoxide of 4,5,6,8,16-pentamethyl[2.2]metacyclophane; structural analysis and deoxygenation. *J. Chem. Soc., Perkin Trans. 1: Org. Biomol. Chem.* 1369–1371.
54. Paudel, A., Shimizu, T., Yamato, T. 2008. Synthesis and photoreactions of polymethyl substituted [2.2]metacyclophanes. *J. Chem. Res.* 11: 650–654.
55. Van den Heuvel, C. J. M., Steinberg, H., de Boer, T. J. 1980. The photooxidation of mono- and dimethylnaphthalenes by singlet oxygen. *Recl. Trav. Chim. Pays-Bas* 99: 109–113.
56. Pierlot, C., Aubry, J.-M. 1997. First evidence of the formation of 5,8-endoperoxide from the oxidation of 1,4-disubstituted naphthalene by singlet oxygen. *J. Chem. Soc. Chem. Commun.* 2289–2290.
57. Pierlot, C., Poprawski, J., Marko, J., Aubry, J.-M. 2000. Effects of oxygenated substituents on the [4+2]-cycloaddition of singlet oxygen in the photooxygenation of water-soluble naphthyl ethers. *Tetrahedron Lett.* 41: 5063–5067.
58. Martinez, G. R., Garcia, F., Catalani, L. H., Cadet, J., Oliveira, M. C. B., Ronsein, G. E., Miyamoto, S., Medeiros, M. H. G., Di Mascio, P. 2006. Synthesis of a hydrophilic and non-ionic anthracene derivative, the *N,N'*-di-(2,3-dihydroxypropyl)-9,10-anthracenedipropanamide as a chemical trap for singlet molecular oxygen detection in biological systems. *Tetrahedron* 62: 10762–10770.
59. Reese, C., Roberts, M., Ling, M.-M., Bao, Z. 2004. Organic thin film transistors. *Mater. Today* 7: 20–27.
60. Chan, S. H., Lee, H. K., Wang, Y. M., Fu, N. Y., Chen, X. M., Cai, Z. W., Wong, H. N. C. 2005. A soluble pentacene: Synthesis, EPR and electrochemical studies of 2,3,9,10-tetrakis(trimethylsilyl) pentacene. *Chem. Commun.* 66–68.
61. Ono, K., Totani, H., Hiei, T., Yoshino, A., Saito, K., Educhi, K., Tomura, M., Nishida, J., Yamashita, Y. 2007. Photooxidation and reproduction of pentacene derivatives substituted by aromatic groups. *Tetrahedron* 63: 9699–9704.
62. Aubry, J. M. 1985. Search for singlet oxygen in the decomposition of hydrogen peroxide by mineral compounds in aqueous solutions. *J. Am. Chem. Soc.* 107: 5844–5849.
63. Martinez, G. R., Ravanat, J.-L., Medeiros, M. H. G., Cadet, J., Di Mascio, P. 2000. Synthesis of a naphthalene endoperoxide as a source of ^{18}O-labeled singlet oxygen for mechanistic studies. *J. Am. Chem. Soc.* 122: 10212–10213.
64. Klotz, L.-O., Pellieux, C., Briviba, K., Pierlot, C., Aubry, J. M., Sies, H. 1999. Mitogen-activated protein kinase (p38-, JNK-, ERK-) activation pattern induced by extracellular and intracellular singlet oxygen and UVA. *Eur. J. Biochem.* 260: 917–922.
65. Suchard, O., Kane, R., Roe, B. J., Zimmermann, E., Jung, C., Waske, P. A., Mattay, J., Oelgemoller, M. 2006. Photooxygenations of 1-naphthols: An environmentally friendly access to 1,4-naphthoquinones. *Tetrahedron* 62: 1467–1473.
66. Haggiage, E., Coyle, E. E., Joyce, K., Oelgemöller, M. 2009. Green photochemistry: Solar-chemical synthesis of 5-amido-1,4-naphthoquinones. *Green Chem.* 11: 318–321.
67. Oelgemoller, M., Healy, N., de Oliveira, L., Jung, C., Mattay, J. 2006. Green photochemistry: Solar-chemical synthesis of Juglone with medium concentrated sunlight. *Green Chem.* 8: 831–834.

68. Goma, D., Nagashima, I., Tachikawa, T., Shiroishi, H., Kaneko, M., Tokita, S. 2001. Reaction of 5,8-diphenyl-5,8-dihydroanthra[1,9-*bc*:4,10-*b'c'*]diquinoline or its endoperoxide with trifluoroacetic acid. *J. Photopolym. Sci. Technol.* 14: 239–244.
69. Bouas-Laurent, H., Durr, H. 2001. Organic photochromism. *Pure Appl. Chem.* 73: 639–665.
70. Schmidt, R., Brauer, H.-D. 1984. Self-sensitized photo-oxidation of aromatic compounds and photocycloreversion of endoperoxides: Applications in chemical actinometry. *J. Photochem.* 25: 489–499.
71. Iesce, M. R., Cermola, F. Temussi, F. 2005. Photooxygenation of heterocyclic compounds. *Curr. Org. Chem.* 9: 109–139.
72. Ando, W., Takata, T. 1985. Photooxidation of sulfur compounds. In *Singlet Oxygen*, Frimer, A. A., Ed., CRC Press: Boca Raton, FL, Vol. 3, pp. 95–117.
73. Gollnick, K., Koegler, S. 1988. [4+2]-Cycloaddition of singlet oxygen to oxazoles. Formation of oxazole endoperoxides. *Tetrahedron Lett.* 29: 1003–1006.
74. Gollnick, K., Griesbeck, A. 1985. Singlet oxygen photooxygenation of furans. Isolation and reactions of [4+2]-cycloaddition products (unsaturated sec.-ozonides). *Tetrahedron* 41: 2057–2068.
75. Kang, P., Foote, C. S. 2002. Photosensitized oxidation of ^{13}C,^{15}N-labeled imidazole derivatives. *J. Am. Chem. Soc.* 124: 9629–9638.
76. Wasserman, H. H., Gambale, R. J., Pulwer, M. J. 1981. Activated carboxylates from the photooxygenation of oxazoles. Application to the synthesis of recifeiolide, curvularin, and other macrolides. *Tetrahedron* 37: 4059–4067.
77. Graziano, M. L., Iesce, M. R., Carotenuto, A., Scarpati, R. 1977. 3*H*-1,2,4-Dioxazoles from 1,3-oxazoles. *Synthesis* 572–573.
78. Griesbeck, A. G., El-Idreesy, T. T. 2005. Solvent-free photooxygenation of 5-methoxyoxazoles in polystyrene nanocontainers doped with tetrastyrylporphyrine and protoporphyrine-IX. *Photochem. Photobiol. Sci.* 4: 205–209.
79. Takabatake, T., Miyazawa, T., Hasegawa, M., Foote, C. S. 2001. Reaction of 4,7-dimethylbenzofurazan with singlet oxygen. *Tetrahedron Lett.* 42: 987–989.
80. Dussault, P. 1995. Reactions of hydroperoxides and peroxides. In *Active Oxygen in Chemistry*, Foote, C. S., Valentine, J. S., Greenberg, A., Liebman, J. F., Eds., Chapman & Hall: London, U.K., pp. 141–203.
81. Clennan, E. L., Foote, C. S. 1992. Endoperoxides. In *Organic Peroxides*, Ando, W., Ed., Wiley: London, U.K., pp. 255–318.
82. Balci, M. 1981. Bicyclic endoperoxides and synthetic applications. *Chem. Rev.* 81: 91–108.
83. Kara, Y., Balci, M. 2003. A new and stereospecific synthesis of an inositol analogue: Bis-homoinositol. *Tetrahedron* 59: 2063–2066.
84. Kelebekli, L., Celik, M., Sahin, E., Kara, Y., Balci, M. 2006. Stereospecific synthesis of a new class of aminocyclitol with the conduramine D-2 configuration. *Tetrahedron Lett.* 47: 7031–7035.
85. Gueltekin, M. S., Celik, M., Balci, M. 2004. Cyclitols. Conduritols and related compounds. *Curr. Org. Chem.* 8: 1159–1186.
86. Jefford, C. W., Boukouvalas, J., Kohmoto, S. 1984. Reactions of cyclic peroxides with aldehydes and ketones catalysed by trimethylsilyl trifluoromethanesulphonate. An efficient synthesis of 1,2,4-trioxanes. *J. Chem. Soc., Chem. Commun.* 523–524.
87. Jefford, C. W., Favarger, F., Ferro, S., Chambaz, D., Bringhen, A., Bernardinelli, G., Boukouvalas, J. 1986. The formation of bridged bicyclic 1,2,4-trioxanes by intramolecular capture of β-hydroperoxy cations. *Helv. Chim. Acta* 69: 1778–1786.
88. Jefford, C. W. 2007. New developments in synthetic peroxidic drugs as artemisinin mimics. *Drug Discov. Today* 12: 487–495.
89. O'Neill, P. M., Rawe, S. L., Storr, R. C., Ward, S. A., Posner, G. H. 2005. Lewis acid catalysed rearrangements of unsaturated bicyclic [2.2.*n*] endoperoxides in the presence of vinyl silanes; access to novel Fenozan BO-7 analogues. *Tetrahedron Lett.* 46: 3029–3032.
90. Staben, S. T., Linghu, X., Toste, F. D. 2006. Enantioselective synthesis of γ-hydroxyenones by chiral base-catalyzed Kornblum DeLamare rearrangement. *J. Am. Chem. Soc.* 128: 12658–12659.

91. Sengul, M. E., Ceylan, Z., Balci, M. 1997. Unusual triethylamine catalyzed rearrangement of bicyclic endoperoxides derived from substituted cycloheptatrienes. *Tetrahedron* 53: 10401–10408.
92. Sammond, D. M., Sammakia, T. 1996. A mild synthesis of substituted furans from γ-hydroxy-α,β-unsaturated ketones. *Tetrahedron Lett.* 37: 6065–6068.
93. Greatrex, B., Jevric, M., Kimber, M. C., Krivickas, S. J., Taylor, D. K., Tiekink, E. R. T. 2003. A novel bis-lactonisation of naphtho- and phenanthro-1,2-dioxines with malonate nucleophiles. *Synthesis* 668–672.
94. Avery, T. D., Taylor, D. K., Tiekink, E. R. T. 2000. A new route to diastereomerically pure cyclopropanes utilizing stabilized phosphorus ylides and γ-hydroxy enones derived from 1,2-dioxines: Mechanistic investigations and scope of reaction. *J. Org. Chem.* 65: 5531–5546.
95. Avery, T. D., Greatrex, B. W., Pedersen, D. S., Taylor, D. K., Tiekink, E. R. T. 2008. A concise route to β-cyclopropyl amino acids utilizing 1,2-dioxines and stabilized phosphonate nucleophiles. *J. Org. Chem.* 73: 2633–2640.
96. Yang, Y.-K., Choi, J.-H., Tae, J. 2005. Synthesis of 2,3-di- and 2,3,4-trisubstituted furans from 1,2-dioxines generated by an enyne-RCM/Diels–Alder reaction sequence. *J. Org. Chem.* 70: 6995–6998.
97. Zvarec, O., Avery, T. D., Taylor, D. K. 2010. Carbenoid insertion into the peroxide bond vs the olefin bond of cyclic peroxides. *J. Org. Chem.* 75: 450–454.
98. Emerzian, M. A., Davenport, W., Song, J., Li, J., Erden, I. 2009. Palladium-catalyzed cyclopropanation of unsaturated endoperoxides. A new peroxide-preserving reaction. *Adv. Synth. Catal.* 351: 999–1004.
99. Adam, W., Eggelte, H. J. 1977. Cyclic peroxides. 57. Prostanoid endoperoxide model compounds: 2,3-dioxabicyclo[2.2.1]heptane via selective diimide reduction. *J. Org. Chem.* 42: 3987–3988.
100. Macreadie, I. G., Avery, T. D., Robinson, T. V., Macreadie, P., Barraclough, M., Taylor, D. K., Tiekink, E. R. T. 2008. Design of 1,2-dioxines with anti-*Candida* activity: Aromatic substituted 1,2-dioxines. *Tetrahedron* 64: 1225–1232.
101. Valente, P., Avery, T. D., Taylor, D. K., Tiekink, E. R. T. 2009. Synthesis and chemistry of 2,3-dioxabicyclo[2.2.2]octane-5,6-diols. *J. Org. Chem.* 74: 274–282.
102. Oezer, G., Saracoglu, N., Balci, M. 2003. Synthesis and chemistry of unusual bicyclic endoperoxides containing the pyridazine ring. *J. Org. Chem.* 68: 7009–7015.
103. Cantekin, S., Baran, A., Caliskan, R., Balci, M. 2009. Synthesis of bromo-conduritol-B and bromo-conduritol-C as glycosidase inhibitors. *Carbohydr. Res.* 344: 426–431.
104. Keay, B. A., Hopkins, J. M., Dibble, P. W. 2008. Furans and their benzo derivatives: Applications. In *Comprehensive Heterocyclic Chemistry III*, Katritzky, A. R. Ed., Elsevier: Oxford, U.K., pp. 571–621.
105. Vassilikogiannakis, G., Stratakis, M. 2003. Biomimetic total synthesis of litseaverticillols A, C, D, F and G: Singlet-oxygen-initiated cascades. *Angew. Chem. Int. Ed.* 42: 5465–5468.
106. Halladja, S., Ter Halle, A., Aguer, J.-P., Boulkamh, A., Richard, C. 2007. Inhibition of humic substances mediated photooxygenation of furfuryl alcohol by 2,4,6-trimethylphenol. Evidence for reactivity of the phenol with humic triplet excited states. *Environ. Sci. Technol.* 41: 6066–6073.
107. Montagnon, T., Tofi, M., Vassilikogiannakis, G. 2008. Using singlet oxygen to synthesize polyoxygenated natural products from furans. *Acc. Chem. Res.* 41: 1001–1011.
108. Merino, P., Tejero, T., Delso, J. I., Matute, R. 2007. Furan oxidations in organic synthesis: Recent advances and applications. *Curr. Org. Chem.* 11: 1076–1091.
109. Graziano, M. L., Iesce, M. R. 1985. Photosensitized oxidation of furans; XI. A simple general method for the synthesis of 3-, 4-, or 3,4-functionalized 5-hydroxyfuran-2(5*H*)-ones (4-hydroxy-2-butenolides). *Synthesis* 1151–1153.
110. Hakimelahi, G. H., Jain, M. L., Ly, T. W., Chen, I.-C., Ethiraj, K. S., Hwu, J. R., Moshfegh, A. A. 2001. Self-sensitized photooxygenation of 3,4-dialkoxyfurans to vitamin C or its derivatives. *J. Org. Chem.* 66: 7067–7071.
111. Kernan, M. R., Faulkner, D. J. 1988. Regioselective oxidation of 3-alkylfurans to 3-alkyl-4-hydroxybutenolides. *J. Org. Chem.* 53: 2773–2776.

112. Katsumura, S., Hori, K., Fujiwara, S., Isoe, S. 1985. Regiospecific synthesis of γ-hydroxybutenolide. Photosensitized oxygenation of substituted 2-trimethylsilylfuran. *Tetrahedron Lett.* 26: 4625–4628.
113. Sofikiti, N., Tofi, M., Montagnon, T., Vassilikogiannakis, G., Stratakis, M. 2005. Synthesis of the spirocyclic core of the prunolides using a singlet oxygen-mediated cascade sequence. *Org. Lett.* 7: 2357–2359.
114. Miyashita, M., Sasaki, M., Hattori, I., Sakai, M., Tanino, K. 2004. Total synthesis of norzoanthamine. *Science* 305: 495–499.
115. Astarita, A., Cermola, F., Iesce, M. R., Previtera, L. 2008. Dye-sensitized photooxygenation of sugar furans: Novel bis-epoxide and spirocyclic C-nucleosides. *Tetrahedron* 64: 6744–6748.
116. Tofi, M., Koltsida, K., Vassilikogiannakis, G. 2009. Singlet-oxygen-mediated one-pot synthesis of 3-keto-tetrahydrofurans from 2-(β-hydroxyalkyl) furans. *Org. Lett.* 11: 313–316.
117. Berberich, S. M., Cherney, R. J., Colucci, J., Courillon, C., Geraci, L. S., Kirkland, T. A., Marx, M. A., Schneider, M. F., Martin, S. F. 2003. Total synthesis of (+)-ambruticin S. *Tetrahedron* 59: 6819–6832.
118. Cermola, F., Iesce, M. R., Buonerba, G. 2005. Dye-sensitized photooxygenation of furanosyl furans: Synthesis of a new pyridazine C-nucleoside. *J. Org. Chem.* 70: 6503–6505.
119. Bartlett, P. D., Schaap, A. P. 1970. Stereospecific formation of 1,2-dioxetanes from *cis*- and *trans*-diethoxyethylenes by singlet oxygen. *J. Am. Chem. Soc.* 92: 3223–3225.
120. Mazur, S., Foote, C.S. 1970. Chemistry of singlet oxygen. IX. Stable dioxetane from photooxygenation of tetramethoxyethylene. *J. Am. Chem. Soc.* 92: 3225–3226.
121. Saha-Moller, C. R., Adam, W. 1996. Four-membered rings with two oxygen atoms. In *Comprehensive Heterocyclic Chemistry II*, Padwa, A. Ed., Pergamon: New York, Vol. 1B, pp. 1041–1082.
122. Baumstark, A. L. 1985. The 1,2-dioxetane ring system: Preparation, thermolysis and insertion reactions. In *Singlet Oxygen*, Frimer, A. A., Ed., CRC Press: Boca Raton, FL, Vol. 2, pp. 1–35.
123. Jefford, C. W. 1993. The photooxygenation of olefins and the role of zwitterionic peroxides. *Chem. Soc. Rev.* 22: 59–66.
124. Greer, A., Vassilikogiannakis, G., Lee, K.-C., Koffas, T. S., Nahm, K., Foote, C. S. 2000. Reaction of singlet oxygen with *trans*-4-propenylanisole. Formation of [2+2] products with added acid. *J. Org. Chem.* 65: 6876–6878.
125. Cermola, F., Iesce, M. R. 2002. Substituent and solvent effects on the photosensitized oxygenation of 5,6-dihydro-1,4-oxathiins. Intramolecular oxygen transfer vs. normal cleavage of the dioxetane intermediates. *J. Org. Chem.* 67: 4937–4944.
126. Cermola, F., Guaragna, A., Iesce, M. R., Palumbo, G., Purcaro, R., Rubino, M., Tuzi, A. 2007. New insight in the reaction of singlet oxygen with sulfur-containing cyclic alkenes: Dye-sensitized photooxygenation of 1,4-dithiins. *J. Org. Chem.* 72: 10075–10080.
127. Watanabe, N., Suganuma, H., Kobayashi, H., Mutoh, H., Katao, Y., Matsumoto, M. 1999. Synthesis of 3-alkoxy-3-aryl-4,4-diisopropyl-1,2-dioxetanes and their base-induced chemiluminescence. *Tetrahedron* 55: 4287–4298.
128. Adam, W., Bosio, S. G., Turro, N. J. 2002. Highly diastereoselective dioxetane formation in the photooxygenation of enecarbamates with an oxazolidinone chiral auxiliary: Steric control in the [2+2]-cycloaddition of singlet oxygen through conformational alignment. *J. Am. Chem. Soc.* 124: 8814–8815.
129. Solomon, M. R., Sivaguru, J., Jockusch, S., Adam, W., Turro, N. J. 2010. Decoding stereocontrol during the photooxygenation of oxazolidinone-functionalized enecarbamates. *Org. Lett.* 12: 2142–2145.
130. Adam, W., Saha-Moller, C. R., Schambony, S. B., Schmid, K. S., Wirth, T. 1999. Stereocontrolled photooxygenations—A valuable synthetic tool. *Photochem. Photobiol.* 70: 476–483.
131. Schuster, G. B., Turro, N. J., Steinmetzer, H.-C., Schaap, A. P., Faler, G., Adam, W., Liu, J. C. 1975. Adamantylideneadamantane-1,2-dioxetane. An investigation on chemiluminescence and decomposition kinetics of an unusually stable 1,2-dioxetane. *J. Am. Chem. Soc.* 97: 7110–7118.
132. Adam, W., Encarnacion, L. A. A., Zinner, K. 1983. Thermal stability of spiro[adamantane-[1,2]dioxetanes]. *Chem. Ber.* 116: 839–846.

133. Matsumoto, M., Murayama, J., Nishiyama, M., Mizoguchi, Y., Sakuma, T., Watanabe, N. 2002. Synthesis of 1-(3-tert-butyldimethylsiloxy)phenyl-5,5-dimethyl-2,7,8-trioxabicyclo[4.2.0]octanes: New dioxetanes giving high chemiexcitation yields in thermolysis and in fluoride-induced CIEEL-decay. *Tetrahedron Lett.* 43: 1523–1527.
134. Matsumoto, M., Watanabe, N., Kasuga, N. C., Hamada, F., Tadokoro, K. 1997. Synthesis of 5-alkyl-1-aryl-4,4-dimethyl-2,6,7-trioxabicyclo[3.2.0]heptanes as a chemiluminescent substrate with remarkable thermal stability. *Tetrahedron Lett.* 38: 2863–2866.
135. Schaap, A. P., Gagnon, S. D., Zaklika, K. A. 1982. Substituent effects on the decomposition of 1,2-dioxetanes: A Hammett correlation for substituted 1,6-diaryl-2,5,7,8-tetraoxabicyclo[4.2.0] octanes. *Tetrahedron Lett.* 23: 2943–2946.
136. Gollnick, K., Knutzen-Mies, K. 1991. Dye-sensitized photooxygenation of 2,3-dihydrothiophenes: Formation of stable 1,2-dioxetanes from 4,5-dialkyl-substituted derivatives. *J. Org. Chem.* 56: 4027–4031.
137. Bastos, E. L., Ciscato, L. F., Monteiro L., Weiss, D., Beckert, R., Baader, W. J. 2006. Comparison of convenient alternative synthetic approaches to 4-[(3-tert-butyldimethylsilyloxy)phenyl]-4-methoxyspiro[1,2-dioxetane-3,2′-adamantane]. *Synthesis* 1781–1786.
138. Sawa, M., Imaeda, Y., Hiratake, J., Fujii, R., Umeshita, R., Watanabe, M., Kondo, H., Oda, J. 1998. Toward the antibody-catalyzed chemiluminescence. Design and synthesis of hapten. *Bioorg. Med. Chem. Lett.* 8: 647–652.
139. Matsumoto, M., Watanabe, N., Shiono, T., Suganuma, H., Matsubara, J. 1997. Chemiluminescence of spiro[1,2-dioxetane-3,1′-dihydroisobenzofuran]s, spiro[1,2-dioxetane-3,1′-isochroman]s and a spiro[1,2-dioxetane-3,1′-(2-benzoxepane)]. *Tetrahedron Lett.* 38: 5825–5828.
140. Watanabe, N., Nagamatsu, K., Mizuno, T., Matsumoto, M. 2005. Bicyclic dioxetanes bearing an inden-2-yl or a benzo[b]thiazol-2-yl moiety as a CIEEL-active chemiluminescent substrate emitting red light. *Luminescence* 20: 63–72.
141. Watanabe, N., Kikuchi, M., Maniwa, Y., Ijuin, H. K., Matsumoto, M. 2010. Synthesis of sulfanyl-, and sulfonyl-substituted bicyclic dioxetanes and their base-induced chemiluminescence. *J. Org. Chem.* 75: 879–884.
142. Matsumoto, M. 2004. Advanced chemistry of dioxetane-based chemiluminescent substrates originating from bioluminescence. *J. Photochem. Photobiol. C: Photochem. Rev.* 5: 27–53.
143. Mayer, A., Neuenhofer, S. 1994. Luminescent labels. *Angew. Chem. Int. Ed. Engl.* 33: 1044–1072.
144. Beck, S., Koster, H. 1990. Applications of dioxetane chemiluminescent probes to molecular biology. *Anal. Chem.* 62: 2258–2270.
145. Wilson, T. 1985. Mechanism of peroxide chemiluminescence. In *Singlet Oxygen*, Frimer, A. A., Ed., CRC Press: Bocan Raton, FL, Vol. 2, pp. 37–65.
146. Hummelen, J. C., Luider, T. M., Wynberg, H. 1986. Stable 1,2-dioxetanes as labels for thermochemiluminescent immunoassays. In *Bioluminescence and Chemiluminescence Methods, Part B—Methods in Enzymology*, DeLuca, M., McElroy, W. D., Eds., Vol. 133, Academic: London, U.K., pp. 531–557.
147. Schaap, A. P., Chen, T.-S., Handley, R. S., DeSilva, R., Giri, B. P. 1987. Chemical and enzymatic triggering of 1,2-dioxetanes. 2: Fluoride-induced chemiluminescence from *tert*-butyldimethylsilyloxy-substituted dioxetanes. *Tetrahedron Lett.* 28: 1155–1158.
148. Adam, W., Bronstein, I., Edwards, B., Engel, T., Reinhardt, D., Schneider, F. W., Trofimov, A. V., Vasil'ev, R. F. 1996. Electron exchange luminescence of spiroadamantane-substituted dioxetanes triggered by alkaline phosphatase. Kinetics and elucidation of pH effects. *J. Am. Chem. Soc.* 118: 10400–10407.
149. Planas, A., Sala, N., Bonet, J. 1989. Synthesis of 11-oxaestrogens via dye-sensitized photo-oxygenation of a 9,11-didehydroestrone derivative. *Helv. Chim. Acta* 72: 725–730.
150. Erden, I., Ozer, G., Hoarau, C., Cao, W., Song, J., Gartner, C., Baumgardt, I., Butenschon, H. 2008. Photooxygenation of 5-dialkylamino-4-pyrrolin-3-ones. Synthesis of highly functionalized ureas, 2-oxazolidinones, and 2-oxazolinones. *J. Org. Chem.* 73: 6943–6945.

151. Orito, K., Kurokawa, Y., Itoh, M. 1980. On the synthetic approach to the protopine alkaloids. *Tetrahedron* 36: 617–621.
152. Ihara, M., Noguchi, K., Ohsawa, T., Fukumoto, K. 1985. Conversion of indoles into quinolines through the N-1-C-2 fission by singlet oxygen as a model experiment of biomimitic synthesis of quinine alkaloids. *Tetrahedron* 41: 2109–2114.
153. Zhang, X., Foote, C. S., Khan, S. I. 1993. Reactions of *N*-acylated indoles with singlet oxygen. *J. Org. Chem.* 58: 47–51.
154. Posner, G. H., Cumming, J. N., Woo, S.-H., Ploypradith, P., Xie, S., Shapiro, T. A. 1998. Orally active antimalarial 3-substituted trioxanes: New synthetic methodology and biological evaluation. *J. Med. Chem.* 41: 940–951.
155. Zhou, W.-S., Xu, X.-X. 1994. Total synthesis of the antimalarial sesquiterpene peroxide qinghaosu and yingzhaosu. *Acc. Chem. Res.* 27: 211–216.
156. Butler, A. R., Wu, Y.-L. 1992. Artemisinin (qinghaosu): A new type of antimalarial drug. *Chem. Soc. Rev.* 85–90.
157. Margaros, I., Montagnon, T., Tofi, M., Pavlakos, E., Vassilikogiannakis, G. 2006. The power of singlet oxygen chemistry in biomimetic syntheses. *Tetrahedron* 62: 5308–5317.
158. Coyle, E. E., Oelgemoller, M. 2008. Micro-photochemistry: Photochemistry in microstructure reactors. The new photochemistry of the future? *Photochem. Photobiol. Sci.* 7: 1313–1322.
159. Meyer, S., Tietze, D., Rau, S., Schafer, B., Kreisel, G. 2007. Photosensitized oxidation of citronellol in microreactors. *J. Photochem. Photobiol. A: Chem.* 186: 248–253.
160. Oelgemoller, M., Jung, C., Ortner, J., Mattay, J., Zimmermann, E. 2005. Green photochemistry: Solar photooxygenations with medium concentrated sunlight. *Green Chem.* 7: 35–38.

31

Singlet Oxygen-Mediated Allylic Oxidation

Mariza N. Alberti
University of Crete

Michael Orfanopoulos
University of Crete

31.1 Introduction

The chemistry of singlet molecular oxygen ($^1O_2$)[1] has attracted continuous and remarkable attention for its synthetic,[2] mechanistic, environmental,[3] as well as therapeutic applications.[4] In 1931, Kautsky first demonstrated the importance of a "reactive oxygen molecule" in dye-sensitized photooxidation reactions.[5] However, Kautsky's pioneering work and careful reasoning were largely ignored for many years. Later on, Foote and Wexler[6a] provided new experimental evidence for the involvement of $^1O_2$ as the reactive intermediate in photochemical processes in solution.[6] This breakthrough brought $^1O_2$ into the mainstream of chemical research. The reaction of $^1O_2$ with C=C bonds can be classified into three fundamental categories: (1) conjugated dienes react preferably by [4 + 2] cycloaddition to yield endoperoxides;[7] (2) electron-rich alkenes, without allylic hydrogen atoms of proper orientation, react by [2 + 2] cycloaddition to form 1,2-dioxetanes[7c,8] and (3) inactivated alkenes bearing allylic hydrogen atoms react via the so-called ene or Schenck[9] reaction yielding allylic hydroperoxides. The latter reaction type has arguably drawn the most extensive experimental as well as theoretical attention.[10] Notably, this reaction has been applied toward the synthesis of several natural products[11] as well as 1,2,4-trioxanes.[12] Moreover, the allylic hydroperoxides that have been obtained from this reaction can be further transformed to useful target molecules such as allylic or epoxy alcohols and enones.

31.2 Mechanistic Studies

The mechanistic aspects of the title reaction were for many years the subject of considerable discussion and arguments; the main question was whether the reaction is concerted[13] (via a cyclic six-membered transition state **1**, Scheme 31.1) or involves intermediates. The reported stepwise pathway has invoked an open biradical/dipolar **2**,[14] a dioxetane **3**,[15] a perepoxide **4**,[16] or an exciplex **5**[17] intermediate. The lack

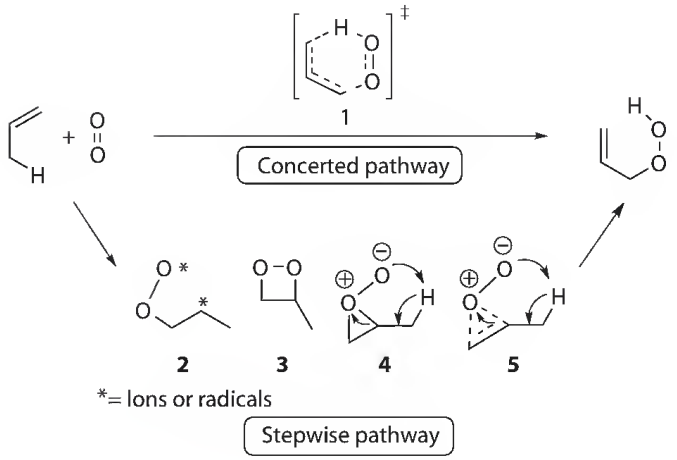

SCHEME 31.1 Proposed mechanisms for the $^1O_2$-mediated ene reaction.

of Markovnikov-type directing effects,[1a,6a] specific trapping experiments,[18] the results of intra/intermolecular kinetic isotope effects (KIEs) (Section 31.2.2), as well as the observed selectivities (Section 31.3) provide strong evidence for the intermediacy of a perepoxide in the $^1O_2$-mediated allylic oxidation. Ultimately, recent theoretical and experimental results (which will be described in Sections 31.2.1 and 31.2.3, respectively) provide important implications for the precise mechanism of the title reaction.

31.2.1 Theoretical and Computational Methods

Theoretical and computational methods have been widely used in order to either elucidate reaction mechanisms or provide useful mechanistic details. However, in the case of $^1O_2$-mediated reactions, these mechanistic tools have encountered complicated as well as challenging problems.[19]

Early and recent theoretical calculations concerning the mechanism of $^1O_2$ ene reaction are notably contradictory. In the mid-1970s, according to semiempirical MINDO/3 calculations, the addition of $^1O_2$ to propene appears to be non-concerted involving the formation of *cis*- and *trans*-methylperoxirane as intermediates.[20] In 1980, Harding and Goddard predicted (using a combination of *ab initio* calculation and thermochemical methods) that the title reaction proceeds via a favorable biradical intermediate; the perepoxide is 40 kJ/mol higher in energy.[21] One year later, Yamaguchi et al. reported that perepoxides are too high in energy to qualify as viable intermediates (as are zwitterions) in $^1O_2$-mediated allylic oxidations of weakly polar alkenes.[22] In the early 1990s, calculations have shown that both concerted and stepwise pathways (involving strained perepoxide-type intermediates), exist on PM3 semiempirical potential-energy surfaces for the addition of $^1O_2$.[23] In the mid-1990s, *ab initio* molecular orbital studies supported a concerted mechanism (involving a non-radical transition state with a perepoxide-like conformation) for the ene reactions of allylic olefins and enol ethers bearing allylic hydrogen atoms.[24] In 2001, the $^1O_2$ addition to 1,3-cyclohexadiene was calculated to occur in a concerted fashion without any intermediates along the reaction coordinate.[25]

Among the more notable contributions toward understanding the mechanism of the title reaction is the collaborative effort by the Singleton, Houk, and Foote groups.[26] In particular, they proposed (mainly based on high level *ab initio* calculations) that the $^1O_2$ ene reaction with simple alkenes proceeds via two transition states without an intervening intermediate. In this "*two-step no intermediate*" mechanism, the symmetrical addition of $^1O_2$ is rate limiting on a potential-energy surface that bifurcates at a valley-ridge inflection (VRI) point[27] into two isomeric products. It is worth mentioning that the second transition structure (with the elusive perepoxide-like structure) lays near the VRI point. Later on, Maranzana et al. investigated the "gas-phase" mechanism of the $^1O_2$ ene reaction with propene[28a] and (*E*)-2-methyl-but-2-enal.[28b] The main result of these studies is that a stepwise pathway, passing through a polar biradical intermediate, is sharply favored. In 2008, B3LYP/6-31G* and CASMP2 calculations

have been employed in order to study the title reaction with *trans*-cyclooctene or tetramethylethylene.[29] In the case of *trans*-cyclooctene (which imposes a substantial strain in the transition state for hydrogen abstraction), these methods predict that the reaction involves a perepoxide intermediate. On the other hand, for tetramethylethylene (in accordance with previously reported calculations)[26] the $^1O_2$ ene reaction takes place through a *two-step no-intermediate* mechanism. Importantly, Sheppard and Acevedo (using novel three-dimensional potentials of mean force calculations coupled to QM/MM simulations) reported that the $^1O_2$ addition to tetramethylethylene proceeds though a stepwise mechanism with a perepoxide intermediate.[30] Furthermore, this computational study provides, for the first time, insight into the effect of solvent on the $^1O_2$-mediated allylic oxidation.

31.2.2 Kinetic Isotope Effects

Over the last 40 years, several KIE measurements for the $^1O_2$-mediated allylic oxidation have been reported. In the early 1970s, no significant intermolecular KIE was found for *cis*- or *trans*-1,2-dimethylstilbene.[31] Later on, low intermolecular KIE was also measured in the case of tetramethylethylene (**6**-d_0 versus **6**-d_{12} and **6**-d_0 versus *gem*-**6**-d_6, Scheme 31.2).[16b,32] The first detailed as well as revealing mechanistic study, by means of intramolecular KIEs on the title reaction, was reported by Stephenson et al.[16b,33] In particular, three types of isotope competition, namely, *cis*, *trans*, and *geminal*, were identified; these types of isotope competition were measured by using *cis*-**6**-d_6, *trans*-**6**-d_6, and *gem*-**6**-d_6 deuterated tetramethylethylenes (TMEs) as the substrates, respectively (Scheme 31.2). It is important to underline the fact that the product isotope effect was found to exhibit a stereochemical dependence; an isotope effect was only observed when the competing isotopes were *cis* to one another (as in *trans*-**6**-d_6 and *gem*-**6**-d_6). At this point, it can be concluded that the small intermolecular, in combination with the substantial intramolecular KIEs in TMEs, provide strong evidence for an intermediate in the $^1O_2$ ene reaction with structural requirements to the perepoxide.

Similar results were observed in the case of *cis*-disubstituted[34] and trisubstituted[35] alkenes. On the other hand, for the highly unreactive *trans*-butene-d_3, an intramolecular KIE of $k_H/k_D = 1.25$ was observed;[34b] this KIE was much larger than that measured with *cis*-**6**-d_6 ($k_H/k_D = 1.04–1.09$, Scheme 31.2). The $^1O_2$-addition to *trans*-butene-d_3 was suggested to proceed through the reversible formation of a perepoxide intermediate.[34b] In the late 1990s, the $^1O_2$ ene reaction of 2,5-dimethyl-2,4-hexadiene-d_6 was examined.[36] Particularly, a substantial primary isotope effect of $k_H/k_D = 1.58$ was measured. In a similar manner with the case of *trans*-butene-d_3, this isotope effect was rationalized in terms of partial reversion of the perepoxide intermediate to the starting materials.

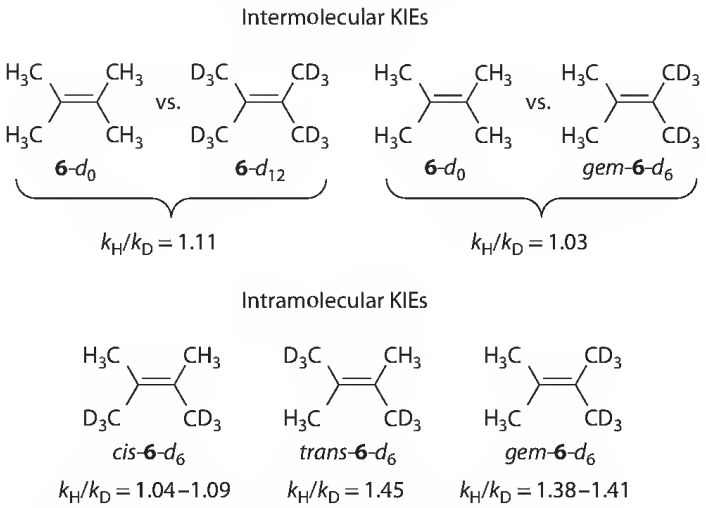

SCHEME 31.2 Inter/intramolecular KIEs on the $^1O_2$ ene reaction of TMEs.

31.2.3 Recent Experimental Developments: The Use of Hypersensitive Probes

Despite the great amount of studies reported over the last decades (Sections 31.2.1 and 31.2.2), there is no consensus about the precise mechanism of the $^1O_2$-mediated allylic oxidation. The aim of a recent experimental study was to investigate the possible involvement of an open biradical/dipolar intermediate in the title reaction.[37] For this purpose, informative alkenes that bear mono- and disubstituted cyclopropyl groups as mechanistic probes were assayed.

It is instructive to note that several very fast radical rearrangements based on cyclopropylcarbinyl radical ring openings have been applied in various mechanistic studies. In the early 1990s, Newcomb et al. reported that 2,2-diphenylcyclopropylcarbinyl radical (**7**, Scheme 31.3) rearranges exceedingly fast (to the homoallyl radical **8**) with an experimental rate constant of 5×10^{11} s^{-1} at room temperature.[38] Later on, the same research group designed a second-generation hypersensitive probe **9**, which is presented in Scheme 31.3.[39] This probe is capable of distinguishing between radical and carbocation intermediates. It is obvious that a phenyl group will stabilize an incipient radical center more strongly than does an alkoxy group, whereas the reverse is true for an incipient carbocation.

The photooxidations of alkenes *E*-**12**, *Z*-**12** and *E*/*Z*-**15** (Scheme 31.4) were run in several aprotic as well as protic solvents. In all cases, the only detected, isolated, and fully characterized products (after their reduction with PPh_3) were allylic alcohols **13**, **14**, **16**, and **17**. Notably, these alcohols bear an intact cyclopropyl ring. Even when the reaction solvent was MeOH, no rearranged products were detected. Importantly, the reaction mechanism seems to be independent of solvent polarity. At this point, it is worth mentioning that if a biradical intermediate (having a lifetime greater than 10^{-11}–10^{-12} s)[38,40]

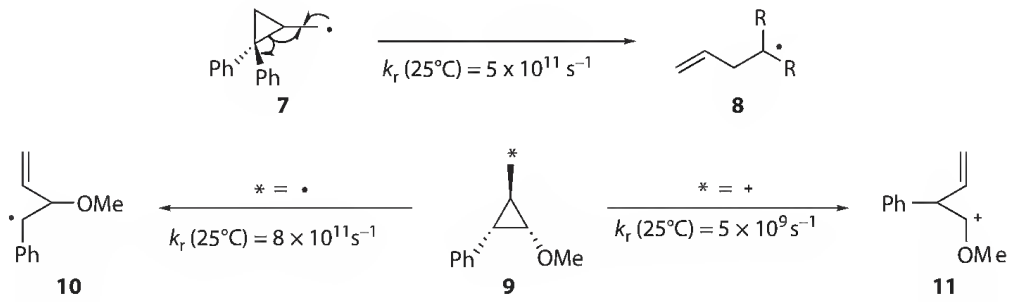

SCHEME 31.3 Radical/cationic rearrangements based on cyclopropylcarbinyl radical/cation ring openings.

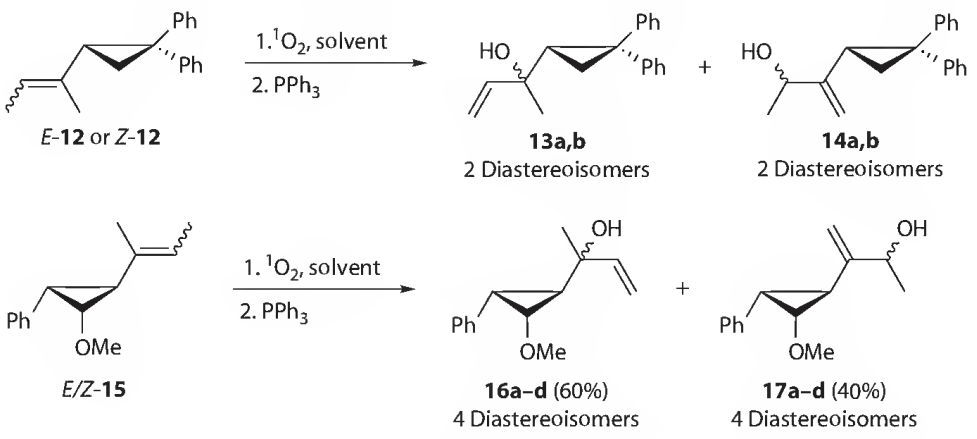

SCHEME 31.4 $^1O_2$ addition to alkenes *E*-**12**, *Z*-**12** and *E*/*Z*-**15**.

had been formed during the $^1O_2$ ene reaction, the rearranged oxygenated products should have been detected. Taking into account the findings reported in Section 31.2, it is difficult to propose a biradical or dipolar mechanism for the title reaction. On the other hand, these findings in combination with the results reported in the Sections 31.2.1 and 31.2.2 support the formation of a perepoxide as the reaction intermediate.

31.3 Studies on Selectivity

31.3.1 Regioselectivity

The study on site selectivity of $^1O_2$-mediated allylic oxidation has proven to be a powerful mechanistic tool in order to determine the trajectory of the enophile attack. Two excellent reviews have extensively covered this issue.[41] Several noteworthy empirical rules (such as the "*cis* effect," the *anti* "*cis* effect," the large group nonbonding effect and the "*gem* effect") have been proposed in order to allow the *a priori* determination of the regioselectivity in the $^1O_2$ addition to a variety of alkenes. Moreover, some interesting solvent and electronic effects on the regioselectivity have provided valuable information regarding the reaction mechanism.

31.3.1.1 "*cis* Effect"

In the $^1O_2$ addition to acyclic or cyclic trisubstituted alkenes[42] as well as enol ethers,[43] the more substituted side of the double bond has been found to be the more reactive (Scheme 31.5). Several models have been proposed in order to explain the so-called "*cis* effect" selectivity. The majority of these models is consistent with the existence of an interaction between the incoming $^1O_2$ and two allylic hydrogen atoms, which highly stabilizes the transition state TS_1, versus TS_2, of perepoxide formation (Scheme 31.5). Particularly, in the late 1970s, Frimer and Bartlett et al. suggested that the formation of the C–O bond requires a closer approach to the alkene carbons compared to the C–H bond cleavage; a transition state, which is less hindered, is energetically preferred.[44] In 1980, Stephenson reported that an interaction between the LUMO orbital of the oxygen and the HOMO orbital of the alkene stabilizes the transition state for the formation of perepoxide intermediate.[45] In the same year, Schulte-Elte and Rautenstrauch proposed that for a cycloalkene there is a correlation between the orientation of the allylic hydrogen atoms in the ground state and their reactivity; the allylic hydrogen atoms at the axial

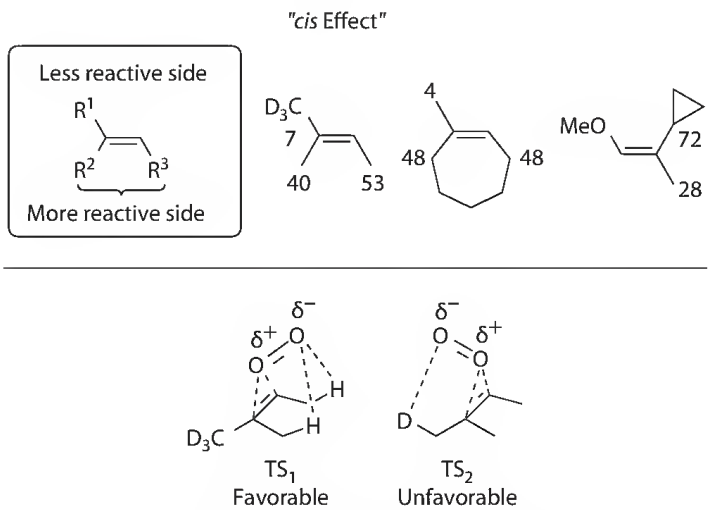

SCHEME 31.5 "*cis* Effect" selectivity. In the representative substrates, numerical values indicate percentage of double bond formation in the ene adducts.

position are more reactive.[42c] In 1981, Houk et al. (using STO-EG semiempirical calculations) postulated that the lower the rotational barrier of a specific alkyl group at the double bond, the higher the reactivity of this group toward hydrogen abstraction by $^1O_2$.[46] However, this postulate was later on challenged by experimental results which showed that rotational barriers do not always predict the reactivity of the allylic hydrogens during the ene abstraction step.[47] Finally, Hurst et al. (based on measurements of the activation parameters $\Delta H^{\ddagger}$ and $\Delta S^{\ddagger}$ in the $^1O_2$ ene reaction with a variety of alkenes) reported that there is a type a hydrogen bonding interaction in the rate-limiting step of the formation of the perepoxide intermediate.[48]

31.3.1.2 *anti "cis* Effect"

In trisubstituted alkenes with highly crowded *cis* alkyl groups, the "*cis* effect" selectivity could not apply. In contrast, it has been found that in these cases there is a strong preference for hydrogen abstraction on the less substituted side of the double bond (Scheme 31.6).[49] Accordingly, this selectivity has been defined as the *anti* "*cis* effect." Examination of the possible transition states that lead to the ene products has provided reasonable mechanistic explanation for the observed selectivity. For instance, in TS_3 (that leads to the minor ene product), the nonbonding interactions between the incoming oxygen and the large *t*-Bu group are stronger than those in TS_4 where these interactions are diminished (Scheme 31.6).

31.3.1.3 Large Group Nonbonding Effect

The $^1O_2$ addition to *cis/trans* alkenes[41a,50] as well as *geminal* dimethyl/diethyl trisubstituted alkenes[41a,51] shows a general preference for hydrogen abstraction from the side of the large alkyl group of the double bond (Scheme 31.7). This selectivity has been rationalized by examining the possible transition states that lead to the formation of the ene adducts. In the case of a *cis* alkene, TS_6 is expected to have lower energy than TS_5 (Scheme 31.7); in TS_6, the repulsive 1,3-nonbonding interactions between the oxygen atom and the large group are smaller than those in TS_5. For a *geminal* dimethyl/diethyl trisubstituted alkene, TS_7 is also expected to be higher in energy than TS_8 (Scheme 31.7); in the latter transition state, the nonbonding interactions involving the large group and the oxygen atom are smaller than those of TS_7.

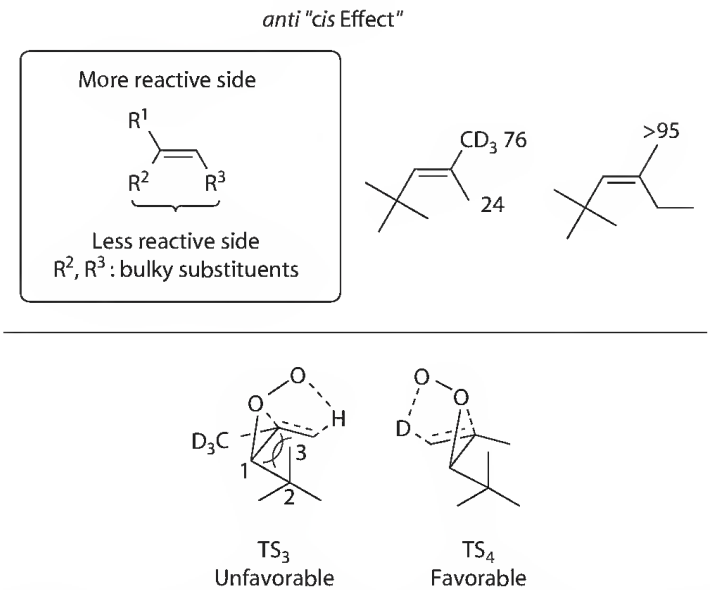

SCHEME 31.6 *anti "cis* Effect" selectivity. In the representative substrates, numerical values indicate percentage of double bond formation in the ene adducts.

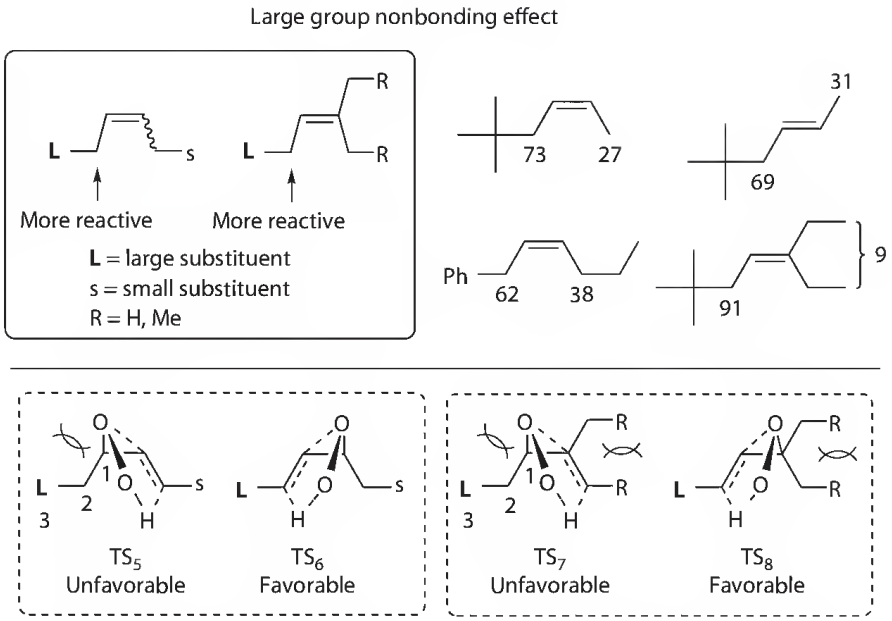

SCHEME 31.7 Large group nonbonding effect selectivity. In the representative substrates, numerical values indicate percentage of double bond formation in the ene adducts.

31.3.1.4 *Geminal* Selectivity

In similar independent studies, Clennan and Orfanopoulos and their coworkers have reported that the $^1O_2$ ene reaction of alkenes (which bear a large substituent either at the allylic,[52] or at the vinylic[52c] position) and substituted cycloalkenes[53] occurs regioselectively by hydrogen abstraction in the alkyl group *geminal* to the large double-bond substituent. This selectivity has been defined as the "*gem* effect." Some general examples are depicted in Scheme 31.8. The observed *geminal* selectivities have been mainly rationalized by the energy difference of isomeric transition states in the product

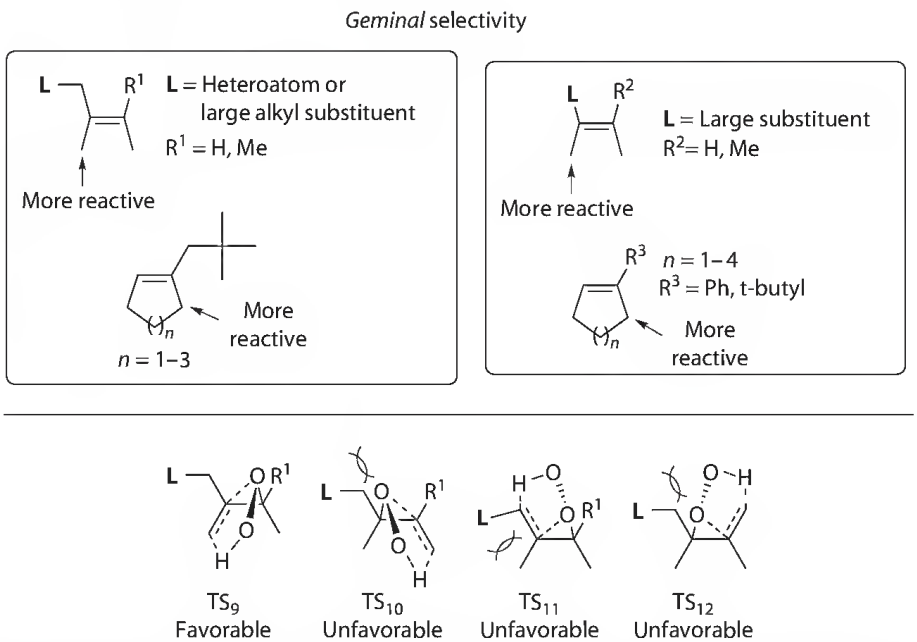

SCHEME 31.8 *Geminal* selectivity on the $^1O_2$ ene reaction of alkenes bearing a large substituent either at the allylic or at the vinylic position.

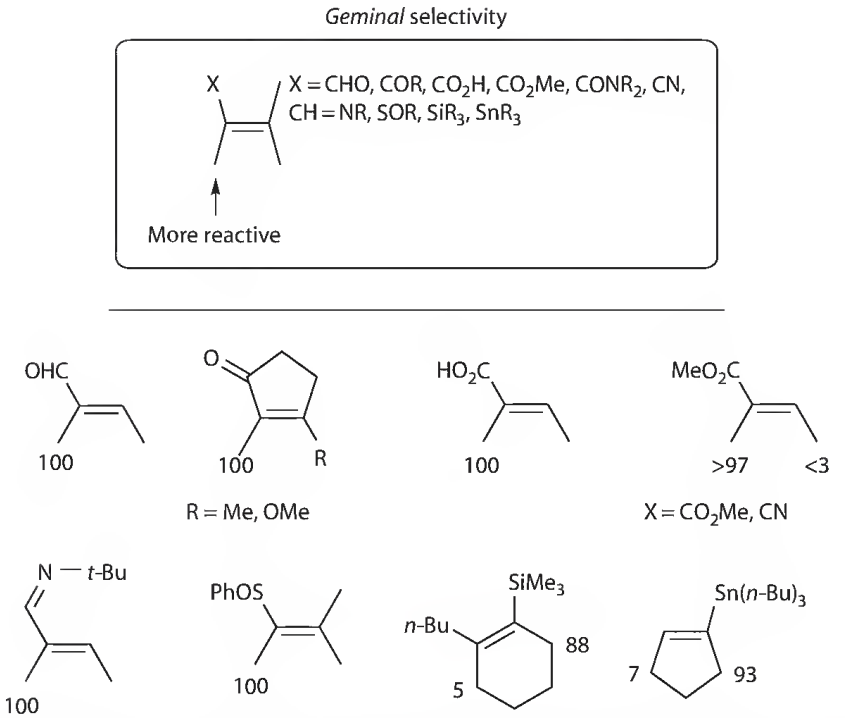

SCHEME 31.9 *Geminal* selectivity on the $^1O_2$ ene reaction of alkenes bearing an electron withdrawing group at the α position. In the representative substrates, numerical values indicate percentage of double bond formation in the ene adducts.

determining step. These energy differences arise from the repulsive nonbonding interactions of the incoming oxygen with the large substituent. In particular, TS_9 has lower energy than TS_{10} and TS_{12}, due to the relief of 1,3-repulsions; TS_9 leads to the formation of the major ene adduct (Scheme 31.8). On the other hand, TS_{10} and TS_{12} are unfavorable due to the presence of 1,3-nonbonding interactions between the oxygen atom and the L group; these transition states lead to the formation of minor ene products. It is worth mentioning that, in the case of TS_{11}, two *geminal* substituents (L and Me) adopt a *cis* conformation in the newly forming double bond. This pathway is highly unfavorable and thus no product is detected.

The *geminal* site selectivity is also observed for alkenes which bear an electron withdrawing group (such as an aldehyde,[54] a ketone,[55] a carboxylic acid,[56] an ester,[57] an amide,[58] a cyano,[54a] an iminyl,[59] a sulfinyl,[60] a silyl,[61] or a stannyl[62] group) at the α position. Some representative examples are outlined in Scheme 31.9. For the aforementioned alkenes, there are two competing factors that affect the site selectivity in the $^1O_2$-mediated allylic oxidation: (1) the driving force to form the new double bond in conjugation with the functionality in the ene product and (2) the 1,3-nonbonding interactions between the oxygen atom and the electron withdrawing group, which favor again the conjugated product.

31.3.1.5 Solvent and Electronic Effects

Previously reported studies have shown that the site selectivity as well as the rate of the $^1O_2$ ene reaction of alkenes is almost independent on the solvent polarity.[63] However, later work has shown that a change on the solvent polarity causes a small but significant variation in the distribution of the ene adducts (using either non-functionalized[64] or functionalized[65] alkenes as starting materials).

At this point, it is worth mentioning that in the addition of $^1O_2$ to α,β-unsaturated ester **18** (Scheme 31.10),[65a] the efficiency of a hydrogen abstraction from the methyl group, which is *geminal* to the ester group (forming **19**), decreases substantially as the solvent polarity increases. In particular, the

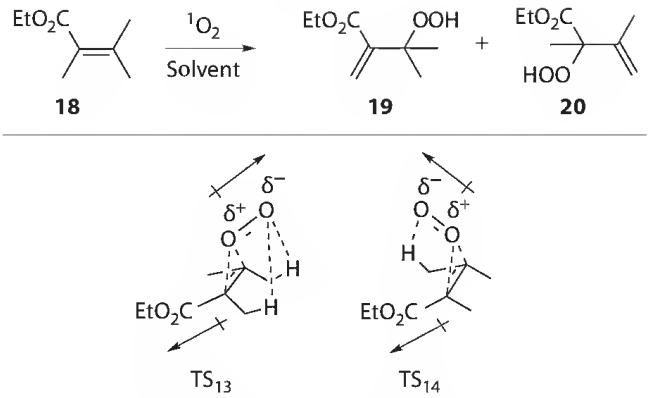

SCHEME 31.10 Solvent effect on the site selectivity in the $^1O_2$ ene reaction of α,β-unsaturated ester **18**.

ratio of ene products **19/20** decreases by a factor of 5 in going from carbon tetrachloride to the more polar solvent dimethyl sulfoxide. This solvent effect has been rationalized by examining the possible transition states that lead to the formation of perepoxide intermediate (Scheme 31.10). In TS_{14}, the pendant oxygen atom is oriented *syn* with respect to the ester group and the net dipole moment is expected to be larger than in TS_{13}; in the latter transition state, the pendant oxygen atom is placed *anti* to the ester group. Ultimately, TS_{14} (which is more polar than TS_{13}) is better stabilized by polar solvents than TS_{13}.

In the late 1990s, the regioselectivity in the photooxidation of β,β-dimethylstyrene [**21** (R = H), Scheme 31.11] with $^1O_2$ was examined.[66] Specifically, the major ene product was derived from the preferential hydrogen abstraction from the methyl *syn* to the phenyl group. In addition, it was found that the magnitude of this selectivity depends on the solvent polarity. For instance, the ratio of *syn/anti* ene products (**22/23**, R = H) increases by a factor of 3.4 on going from carbon tetrachloride to methanol. In accordance with previously reported studies, this selectivity has been rationalized by examining the possible transition states that lead to the formation of perepoxide intermediate. In particular, $^1O_2$ prefers to form the transition state on the more crowed side (TS_{15}, Scheme 31.11); there are positive interactions between the incoming electrophile and the phenyl ring. In TS_{15}, the benzylic carbon of the double bond has significant cationic character and it is stabilized by the phenyl group through resonance. The partially negative charge, which is developing into the pendant oxygen atom during

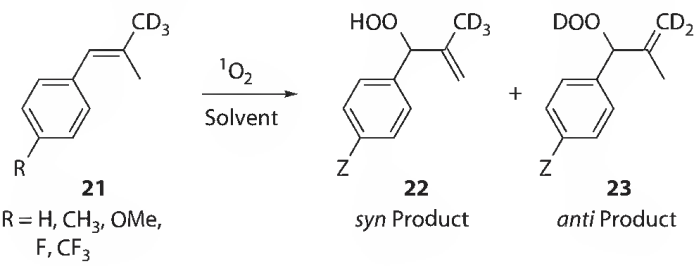

SCHEME 31.11 Solvent and electronic effects on the site selectivity in the $^1O_2$ ene reaction of alkenes **21**.

the formation of the perepoxide, is stabilized by the partially positive charge on the phenyl ring. Therefore, the overall effect stabilizes better the *syn* transition state TS_{15} than the *anti* TS_{16} where this effect is absent.

In the light of the above-mentioned *syn* selectivity, electronic and solvent effects of the addition of $^1O_2$ to labeled isobutenylarenes have been also studied.[67] Concerning the electronic effect, it was found that the site selectivity depends on the electronic nature of the aryl substituents.[67a] Electron withdrawing substituents, such as $-CF_3$ or -F, increase the reactivity of the allylic hydrogen atoms in the *syn* methyl group. In contrast, electron donating substituents, such as -OMe, significantly increase the reactivity of the allylic hydrogen atoms in the *anti* methyl group. Similarly, the transition states presented in Scheme 31.11 were again used in order to rationalize these results. For instance, electron-withdrawing substituents decrease the electron density of the phenyl group, thus the stabilizing interaction of the partially negative charged oxygen to the arene is more efficient. A similar argument may be applied in the case of electron-donating substituents. Concerning the solvent effect, it has been found that there is a similar trend for the site selectivity as that observed in the case of β,β-dimethylstyrene.[67b]

31.3.2 Diastereoselectivity

In the late 1990s, Prein and Adam categorized the factors that govern the π-facial selectivity of the $^1O_2$-mediated allylic oxidation.[68] These factors are (1) steric, when nonbonding repulsion between substrate and $^1O_2$ makes the one π face of the double bond less accessible than the other; (2) stereoelectronic, when one face of the double bond displays a higher π electron density due to some features of the substrate's geometry (e.g., orbital distortion); (3) electronic, related to hydrogen bonding and electrostatic attractions/repulsions between a substituent of the substrate and the enophile; and (4) conformational, which deals with the proper alignment of substrate's allylic hydrogen atoms. Concerning this concept, some case studies in the diastereoselectivity of the $^1O_2$ addition to either acyclic or cyclic alkenes will be presented.

31.3.2.1 Acyclic Alkenes

31.3.2.1.1 Alkenes Bearing Chiral Auxiliaries

There is no doubt that $^1O_2$ (a linear two-atomic molecule) cannot itself transmit steric effects. Thus, diastereoselection in $^1O_2$-mediated reactions may only arise through substrate control. Examination of the $^1O_2$ addition to alkenes bearing chiral auxiliaries might open up promising prospects in the preparation of optically active building blocks for asymmetric synthesis. The majority of attempts reported so far has concentrated on the incorporation of an α,β-unsaturated carboxylic acid unit into a chiral environment, though with only low or moderate diastereoselectivity.[58,68,69] Three of the most satisfying examples concerning the diastereoselectivity of the $^1O_2$ addition to optically active tiglic acid derivatives **24** and **26** are outlined in Scheme 31.12.[70] In the early 2000s, Adam et al. reported a high chiral-auxiliary-controlled diastereoselectivity in the $^1O_2$ addition to oxazolidine-substituted alkenes **28** (Scheme 31.12).[71] It is worth mentioning that the observed diastereoselectivity was attributed to electronic attraction through hydrogen bonding between the negatively charged pendant oxygen and the NH group of the urea functionality. This hydrogen bonding directivity will be presented in detail in the following section.

31.3.2.1.2 Alkenes Bearing Adjacent Stereogenic Centers

Over the last 40 years, a variety of allylic substituents has been tested for their directing properties in the $^1O_2$-addition to chiral acyclic alkenes.[68] The substituents can be classified into two classes with respect to their tendency to direct the $^1O_2$ attack either with *erythro* or *threo* diastereoselectivity.

It is generally conceded that chiral alkenes bearing on the asymmetric-adjacent carbon atom other than the hydroxyl or amino functionality afford preferentially *erythro* allylic hydroperoxides.[72,73]

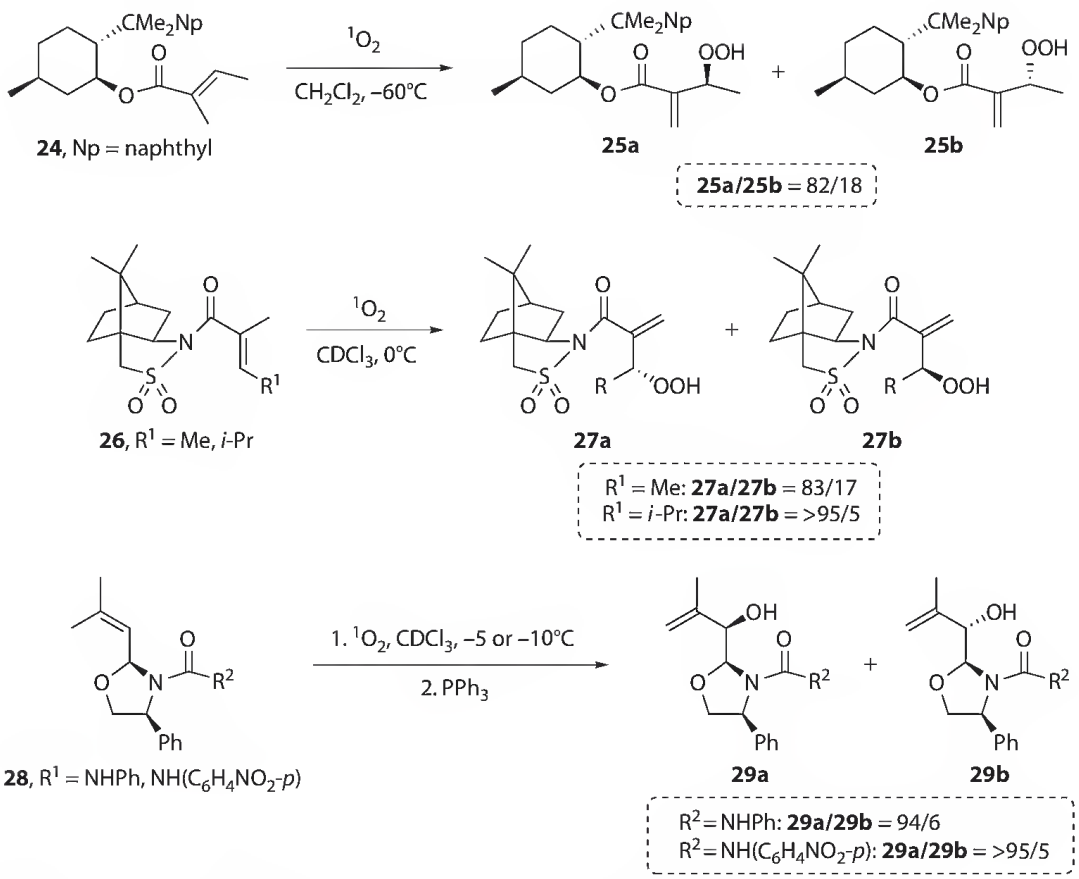

SCHEME 31.12 Diastereoselection in the chiral–auxiliary–controlled $^1O_2$ ene reaction.

Some typical examples are listed in Table 31.1 (entries 1–9). This high diastereoselectivity is explained in terms of the reversible formation of perepoxide-like diastereomeric exciplexes E_1 and E_2 (Scheme 31.13). Notably, the preferable conformational arrangement in these exciplexes is fixed by 1,3-allylic strain.[74] For chiral alkenes without functional groups containing heteroatom at the stereogenic center (X = *t*-Bu or Ph), the observed *erythro* selectivity is attributed to the operating steric repulsion between the X substituent and the incoming oxygen in the *threo*-configurated exciplex E_2. In the case of chiral alkenes, which bear an electron-accepting substituent on the stereogenic center (X = NHBoc, $NBoc_2$, Cl, Br, SO_2Ph, COOH or COOEt), the electrostatic repulsion between the X substituent and the incoming oxygen in the *threo*-configurated exciplex E_2 appears to be primarily responsible for the high preference of the *erythro* ene product.

On the other hand, Adam et al. have examined the diastereoselectivity of the $^1O_2$-mediated allylic oxidation with chiral allylic alcohols[75] or amines[72b,76] and found a high *threo* selectivity in nonpolar solvents (Table 31.1, entries 10 and 12). When the reaction solvent is methanol-d_4, a substantial drop in *threo* selectivity is observed in both cases (Table 31.1, entries 11 and 13). Moreover, an important increase of *erythro* selectivity has been achieved either by protection of the allylic hydroxyl or by acylation of the amino group (for the latter, see the entries 3 and 4 in Table 31.1). The requirement of a substituent in the *cis* position relative to the hydroxyalkyl group in order to induce 1,3-allylic strain was also demonstrated; this strain proved to be essential for the observation of a high *threo* selectivity.[75] The proposed mechanistic rationalization, for the aforementioned results, is based on the development of a hydrogen bond (in the *threo*-configurated exciplex E_2, Scheme 31.13) between the partially negatively charged $^1O_2$ and the hydroxyl or amino group.[72b,75,76] This type of stabilizing electronic interaction is ineffective in the *erythro*-configurated exciplex E_1 (Scheme 31.13) due to the presence of unfavorable 1,3-allylic strain.

TABLE 31.1 *Threo/Erythro* Diastereoselectivity in the $^1O_2$ ene Reaction of Chiral Alkenes **30**

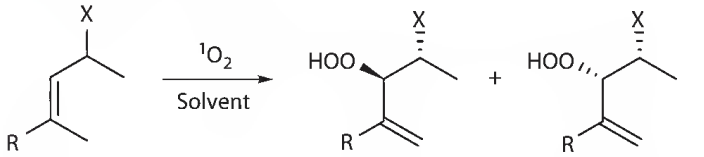

30 **31a**, *threo* **31b**, *erythro*

Entry	X	R	Solvent	**31a**	**31b**
1	Ph	Me	CCl_4	19	81
2	*t*-Bu	Me	CCl_4	29	71
3	NHBoc	Me	CCl_4	24	76
4	$NBoc_2$	Me	CCl_4	5	95
5	Cl	Me	$CDCl_3$	15	85
6	Br	Me	$CDCl_3$	11	89
7	SO_2Ph	Me	CCl_4	<5	>95
8	COOH	H	CCl_4	21	79
9	COOEt	H	CCl_4	22	78
10	OH	H or Me	CCl_4	93	7
11	OH	Me	CD_3OD	73	27
12	NH_2	Me	CCl_4	>95	<5
13	NH_2	Me	CD_3OD	85	15

Sources: Reprinted with permission from *J. Am. Chem. Soc.*, 1995, 117, 3976–3982; *J. Am. Chem. Soc.*, 1996, 118, 1899–1905. Copyright 2010 American Chemical Society.

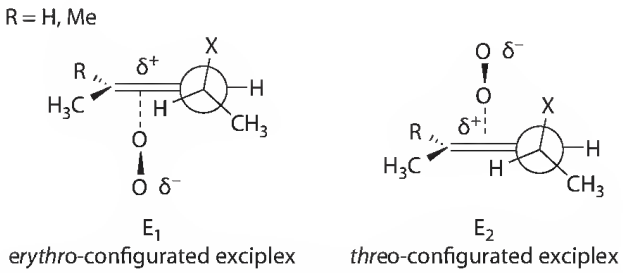

SCHEME 31.13 Newman projections views of possible exciplexes for the $^1O_2$ ene reaction of alkenes bearing adjacent stereogenic centers.

Additional studies revealed that 1,2-allylic strain (caused by a *geminal* substituent near the stereogenic center) does not play a crucial role in the hydroxyl group directed $^1O_2$ ene reaction.[77] It was also reported that electron-poor allylic alcohols react with $^1O_2$ in a *threo*-selective manner, regardless of whether the hydroxyl functionality is free or masked by alkyl or silyl groups.[78] This diastereoselectivity was attributed to stereoelectronic effects. Soon after, it was shown that a hydroxyl group at a stereogenic center in homoallylic position is incapable of controlling the stereochemical outcome in photooxidations.[79] In the same year, Dussault and Schultz examined the $^1O_2$ additions to chiral 2-alkenols and found that the diastereoselectivity of hydroxyl-directed oxidations decreased by the presence of an ester (adjacent to the stereogenic center) or an hydroxyl/alkyloxy group (in the 2 position relative to the stereogenic center). This decrease has been rationalized considering the development of a competitive intramolecular hydrogen bond and steric effects.[80]

31.3.2.2 Cyclic Alkenes

31.3.2.2.1 Monocyclic and Bicyclic Hydrocarbons

The factors that may influence the diastereoselectivity for monocyclic hydrocarbons, such as monoterpenes, predominantly are steric and conformational. Noteworthy, the photooxidations of monoterpenes (having only carbon substituents) exhibit relatively low overall *syn/anti* selectivities;[81] there is no special steric preference for $^1O_2$ attack from either side of the double bond in these substrates. Nevertheless, the ground state conformation of monoterpenes (specifically the availability of abstractable allylic hydrogen atoms) has a significant impact on the diastereoselectivity.

In accordance with monocyclic hydrocarbons, the diastereoselectivity in the photooxidation of steroids,[82] as well as [2.2.1], [3.1.1] and [4.1.0] rigid bicyclic compounds[83] is governed by steric and conformational factors. In the majority of these reactions, high π-facial selectivities have been observed. Concerning the $^1O_2$ addition to [2.2.1], [3.1.1] and [4.1.0] bicyclic hydrocarbons, some representative examples are outlined in Scheme 31.14. In particular, the $^1O_2$ addition to 2-methylnorborn-2-ene (**32**, R^1 = H) favorably takes place on the sterically less congested π face forming the *exo* ene product **33a** (R^1 = H).[84] As can be seen in Scheme 31.14, addition to norbornene derivative **32** (R^1 = H), with two methyl groups at the methylene bridge, inverted the stereochemical outcome; the *endo* ene adduct **33b** (R^1 = Me) is the major detectable product.[84] Moreover, the $^1O_2$ attack to α-pinene (**34**) occurs diastereoselectively *anti* to the methylene bridge.[85] In 1976, Paquette et al. investigated the photooxidations of several cyclopropanated cyclohexenes **36**.[86] For these [4.1.0] bicyclic systems, the attack of $^1O_2$ occurs diastereoselectively. Depending on the overall substitution pattern, **37a** or **37b** ene adducts are formed exclusively.

31.3.2.2.2 Cyclic Hydrocarbons Bearing Heteroatom Substituents

The diastereoselectivity of $^1O_2$ attack on cyclic substrates, which contain an additional functional group, is determined by combined effects. In these cases, it clearly appears that apart from steric or conformational factors, also electronic or stereoelectronic features come into play. For instance, the

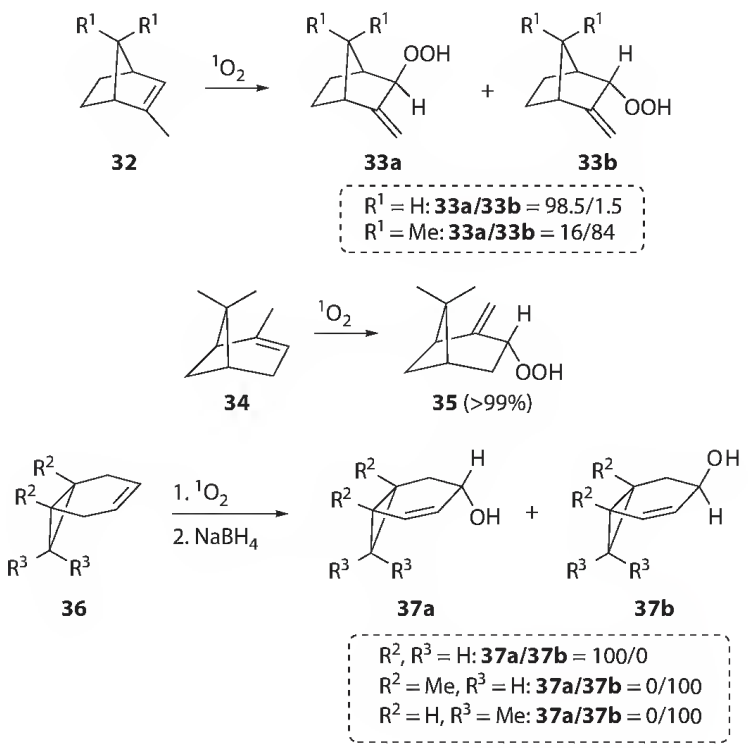

SCHEME 31.14 Diastereoselection in the $^1O_2$ ene reaction of selected [2.2.1], [3.1.1] and [4.1.0] bicyclic alkenes.

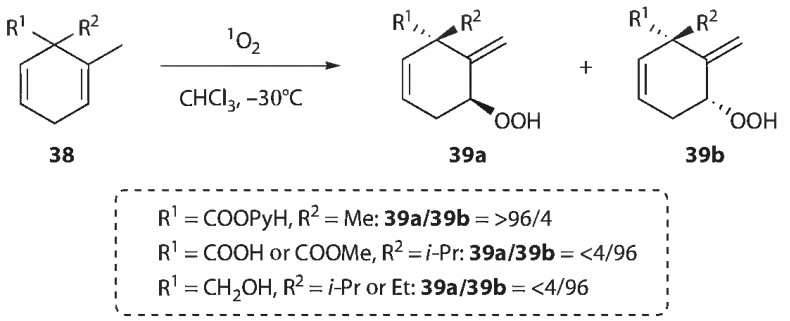

SCHEME 31.15 Diastereoselection in the $^1O_2$ ene reaction of cyclohexadienes **38**.

diastereoselectivity of substituted 7-isopropylidenenorbornene was found to be sensitive to the electronic interactions between the incoming enophile and electron-donating/withdrawing substituents on these substrates.[87] Notably, Linker and Fröhlich observed high diastereoselectivities in the photooxidation of cyclohexadienes **38** to afford hydroperoxides **39a,b** (Scheme 31.15).[88] These selectivities have been rationalized in terms of a combination of electronic and steric interactions. Similar interactions also determine the diastereoselectivity of the photooxidations of α-cyclogeranyl derivatives.[89]

31.3.3 Stereoselectivity

The first detailed stereochemical investigation of the $^1O_2$-mediated allylic oxidation was reported in 1980.[90] Recently, the stereochemistry of this reaction was reinvestigated by a more informative substrate. In this study, the addition of $^1O_2$ to (*S,S*)-*cis*-1,4-diphenyl-2-butene-1,4-d_2 (**40**, Scheme 31.16) has been examined.[91] It is worth mentioning that this alkene has three distinctive characteristics: (1) chirality at the two reactive allylic carbons, (2) different substituents at both allylic carbons, and (3) a C_2 symmetry axis resulting such that the two faces of the double bond are equivalent.

The sensitized oxidations of **40** were run in $CHCl_3$, $(CH_3)_2CO$, CH_3CN, and MeOH. In all cases, the allylic hydroperoxides **41a** and **41b** (Scheme 31.16) were obtained in high yield. The mechanistic possibilities, considering the approach of $^1O_2$ from only one of the two equivalent faces of the double bond, are presented in Scheme 31.16. In particular, approach of $^1O_2$ from the top face will abstract hydrogen and will form a new *S* stereogenic center (at the allylic hydroperoxide **41a**). On the other hand, abstraction of deuterium will form a new *R* stereogenic center (at the allylic hydroperoxide **41b**). The ratio of

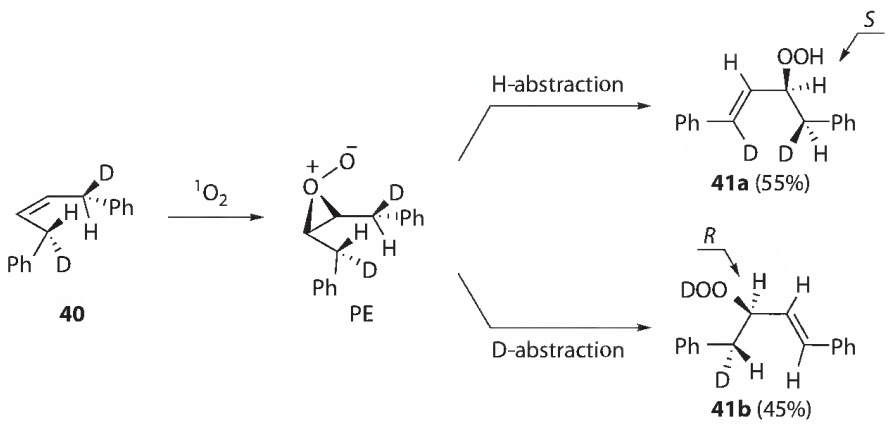

SCHEME 31.16 Stereoselection in the $^1O_2$ ene reaction of chiral alkene **40**. (Reprinted with permission Alberti, M.N., Vassilikogiannakis, G., and Orfanopoulos, M., Stereochemistry of the singlet oxygenation of simple alkenes: A stereospecific transformation, *Org. Lett.*, 10, 3997–4000, 2008. Copyright 2010 American Chemical Society.)

products **41a**:**41b** (which is proportional to the primary isotope effect) was determined by the ^{1}H NMR integration of their vinylic signals. A primary isotope effect $k_H/k_D = 1.20 \pm 0.05$ was found when $CHCl_3$, $(CH_3)_2CO$, CH_3CN, and MeOH were used as the reaction solvents. The diastereomeric ratio *S/R* of **41** was measured by the ^{1}H NMR integration of the diastereotopic benzylic protons of **41a** and **41b**. In $CHCl_3$, the chirality of the new stereogenic centers *S/R* was found to be 1.23 ± 0.05. Identical diastereomeric ratios were measured when $(CH_3)_2CO$, CH_3CN, and MeOH were used as the reaction solvents. Herein, it is important to emphasize the correspondence of the isotopic k_H/k_D ratio of 1.20 with the diastereomeric *S/R* ratio of 1.23.

The aforementioned findings are best rationalized by involving the formation of a perepoxide (PE, Scheme 31.16) as an intermediate. H atom abstraction from PE and subsequent C–O bond formation leads to the formation of the new *S* stereogenic center with deuterium remaining in the product double bond. In a similar manner, D atom abstraction from PE leads to the formation of the new *R* stereogenic center with hydrogen remaining in the product double bond. These results confirm that the $^1O_2$-mediated allylic oxidation of simple olefins is a highly stereospecific suprafacial process, independent of solvent polarity. Last but not least, the observation of an isotope effect, which matched exactly the diastereomeric ratio, makes it difficult to argue that the title reaction proceeds through an open biradical or dipolar intermediate.

31.4 Photooxidation in Confined Media

A great deal of attention has been devoted in recent years to influence the selectivity in photochemical reactions. The use of molecular microreactors seems to be a promising method to pursue this issue.[92] Molecular microreactors refer to heterogeneous, organized, and constrained systems that provide cavities and/or surfaces to accommodate the substrate molecules and allow photochemical reactions to occur. Generally speaking, the interactions of the substrate with these media may direct the photochemical reaction to the desired product(s). Considering the $^1O_2$-mediated allylic oxidation, the dye-supported Y-type zeolites have been extensively used as media, mainly by the research teams of Ramamurthy,[93] Clennan,[94] and Stratakis.[95] It is instructive to note that the study of the title reaction using alternative molecular microreactors, such as pentasil zeolites,[96] Nafion-Na^+ membranes,[97] surfactant vesicles,[98] polystyrene beads,[99] mesoporous silica SBA-15,[100] octa acid capsules,[101] and IRA-resin,[102] has also received considerable attention in recent years.

Acknowledgment

The Foundation for Education and European Culture is acknowledged for providing a 1 year fellowship to M.N.A. We are also thankful to Dr. M. D. Tzirakis for helpful discussions.

References

1. (a) Kearns, D. R. 1971. Physical and chemical properties of singlet molecular oxygen. *Chem. Rev.* 71: 395–427. (b) Schweitzer, C. and Schmidt, R. 2003. Physical mechanisms of generation and deactivation of singlet oxygen. *Chem. Rev.* 103: 1685–1757.
2. (a) Wasserman, H. H. and Ives, J. L. 1981. Singlet oxygen in organic synthesis. *Tetrahedron* 37: 1825–1852. (b) Hoffmann, N. 2008. Photochemical reactions as key steps in organic synthesis. *Chem. Rev.* 108: 1052–1103. (c) Montagnon, T., Tofi, M., and Vassilikogiannakis, G. 2008. Using singlet oxygen to synthesize polyoxygenated natural products from furans. *Acc. Chem. Res.* 41: 1001–1011.
3. (a) Abdou, M. S. A. and Holdcroft, S. 1993. Mechanisms of photodegradation of poly(3-alkylthiophenes) in solution. *Macromolecules* 26: 2954–2962. (b) Scurlock, R. D., Wang, B., Ogilby, P. R., Sheats, J. R., and Clough, R. L. 1995. Singlet oxygen as a reactive intermediate in the photodegradation of an electroluminescent polymer. *J. Am. Chem. Soc.* 117: 10194–10202.

4. (a) Dougherty, T. J., Gomer, C. J., Henderson, B. W. et al. 2003. Photodynamic therapy. *J. Natl. Cancer Inst.* 90: 889–905. (b) Dolmans, D. E., Fukumura, D., and Jain, R. K. 2003. Photodynamic therapy for cancer. *Nature Rev. Cancer* 3: 380–387.
5. Kautsky, H. and De Bruijn, H. 1931. Die aufklärung der photoluminescenztilgung fluorescierender systeme durch Sauerstoff: Die bildung aktiver, diffusionsfähiger Sauerstoffmoleküle durch sensibilisierung. *Naturwissenschaften* 19: 1043.
6. (a) Foote, C. S. and Wexler, S. 1964. Singlet oxygen. A probable intermediate in photosensitized autooxidations. *J. Am. Chem. Soc.* 86: 3880–3881. (b) For an account of Foote's work, see: Greer, A. 2006. Christopher Foote's discovery of the role of singlet oxygen [$^1O_2$ ($^1\Delta_g$)] in photosensitized oxidation reactions. *Acc. Chem. Res.* 39: 797–804.
7. (a) Adam, W. and Prein, M. 1996. π-Facial diastereoselectivity in the [4+2] cycloaddition of singlet oxygen as a mechanistic probe. *Acc. Chem. Res.* 29: 275–283. (b) Adam, W., Bosio, S., Bartoschek, A., and Griesbeck, A. G. 2004. Photooxygenation of 1,3-dienes. In *Handbook of Organic Photochemistry and Photobiology*, eds. W. M. Horspool and F. Lenci, pp. 25/1–25/19. (c) Iesce, M. R. 2005. Photooxygenation of the [4+2] and [2+2] type. In *Synthetic Organic Photochemistry,* ed. A. G. Griesbeck and J. Mattay, pp. 299–363. Marcel Dekker: New York.
8. Baumstark, A. L. and Rodriguez, A. 1995. Photochemical methods for the synthesis of 1,2-dioxetanes. In *Handbook of Organic Photochemistry and Photobiology*, eds. W. M. Horspool and P.-S. Song, pp. 335–345. CRC Press: Boca Raton, FL.
9. Schenck, G. O., Eggert, H., and Denk, W. 1953. *Liebigs Ann. Chem.* 584: 177–198.
10. (a) Alberti, M. N. and Orfanopoulos, M. 2010. Recent mechanistic insights in the singlet oxygen ene reaction. *Synlett.* 7: 999–1026. (b) Alberti, M. N. and Orfanopoulos, M. 2010. Unraveling the mechanism of the singlet oxygen ene reaction: Recent computational and experimental approaches. *Chem. Eur. J.* 16: 9414–9421.
11. For selected examples, see: (a) Paquette, L. A., Tae, J., Arrington, M. P., and Sadoun, A. H. 2000. Enantioselective double Michael addition/cyclization with an oxygen-centered nucleophile as the first step in a concise synthesis of natural (+)-asteriscanolide. *J. Am. Chem. Soc.* 122: 2742–2748. (b) Vassilikogiannakis, G. and Stratakis, M. 2003. Biomimetic total synthesis of litseaverticillols A, C, D, F, and G: Singlet-oxygen-initiated cascades. *Angew. Chem. Int. Ed.* 42: 5465–5468.
12. For selected examples, see: (a) Griesbeck, A. G., El-Idreesy, T. T., Fiege, M., and Brun, R. 2002. Synthesis of antimalarial 1,2,4-trioxanes via photooxygenation of a chiral allylic alcohol. *Org. Lett.* 4: 4193–4195. (b) Griesbeck, A. G., Blunk, D., El-Idreesy, T. T., and Raabe, A. 2007. Bicyclic peroxides and perorthoesters with 1,2,4-trioxane structures. *Angew. Chem. Int. Ed.* 46: 8883–8886. (c) Sabbani, S., La Pensée, L., Bacsa, J., Hedenström, E., and O'Neill, P. M. 2009. Diastereoselective Schenck ene reaction of singlet oxygen with chiral allylic alcohols; access to enantiomerically enriched 1,2,4-trioxanes. *Tetrahedron* 65: 8531–8537.
13. (a) Nickon, A. and Bagli, J. F. 1961. Reactivity and geometry in allylic systems. I. Stereochemistry of photosensitized oxygenation of monoölefins. *J. Am. Chem. Soc.* 83: 1498–1508. (b) Gollnick, K. and Schenck, G. O. 1964. Mechanism and stereoselectivity of photosensitized oxygen transfer reactions. *Pure Appl. Chem.* 9: 507–525. (c) Foote, C. S. 1968. Photosensitized oxygenations and the role of singlet oxygen. *Acc. Chem. Res.* 1: 104–110. (d) Gorman, A. A. 1981. Singlet molecular oxygen. *Chem. Soc. Rev.* 10: 205–231.
14. (a) Harding, L. B. and Goddard, W. A. 1978. Mechanistic implications of the stereochemistry of singlet oxygen-olefin reactions. *Tetrahedron Lett.* 19: 747–750. (b) Jefford, C. W. 1993. The photooxygenation of olefins and the role of zwitterionic peroxides. *Chem. Soc. Rev.* 22: 59–66.
15. Kearns, D. R. 1969. Selection rules for singlet-oxygen reactions. Concerted addition reactions. *J. Am. Chem. Soc.* 91: 6554–6563.
16. (a) For the first report concerning the intermediacy of the perepoxide, see: Sharp, P. L. 1960. *Abstracts of Papers*, 138th Nat. Meet. Am. Chem. Soc., Washington, DC, p. 79. (b) Stephenson, L. M., Grdina, M. B., and Orfanopoulos, M. 1980. Mechanism of the ene reaction between singlet oxygen and olefins. *Acc. Chem. Res.* 13: 419–425.

17. (a) Gorman, A. A., Gould, I. R., and Hamblett, I. 1982. Time-resolved study of the solvent and temperature dependence of singlet oxygen ($^1\Delta_g$) reactivity toward enol ethers: Reactivity parameters typical of rapid reversible exciplex formation. *J. Am. Chem. Soc.* 104: 7098–7104. (b) Gorman, A. A., Hamblett, I., Lambert, C., Spencer, B., and Standen, M. C. 1988. Identification of both preequilibrium and diffusion limits for reaction of singlet oxygen, $O_2(^1\Delta_g)$, with both physical and chemical quenchers: Variable-temperature, time-resolved infrared luminescence studies. *J. Am. Chem. Soc.* 110: 8053–8059.
18. For selected examples, see: (a) Poon, T. H. W., Pringle, K., and Foote, C. S. 1995. Reaction of cyclooctenes with singlet oxygen. Trapping of a perepoxide intermediate. *J. Am. Chem. Soc.* 117: 7611–7618. (b) Clennan, E. L., Chen, M.-F., and Xu, G. 1996. New potent trapping agents for the peroxidic intermediates formed in the reactions of singlet oxygen. *Tetrahedron Lett.* 37: 2911–2914.
19. Paterson, M. J., Christiansen, O., Jensen, F., and Ogilby, P. R. 2006. Overview of theoretical and computational methods applied to the oxygen-organic molecule photosystem. *Photochem. Photobiol.* 82: 1136–1160.
20. Dewar, M. J. S. and Thiel, W. 1975. Ground states of molecules. XXX. MINDO/3 study of reactions of singlet ($^1\Delta_g$) oxygen with carbon-carbon double bonds. *J. Am. Chem. Soc.* 97: 3978–3986.
21. Harding, L. B. and Goddard, W. A. 1980. The mechanism of the ene reaction of singlet oxygen with olefins. *J. Am. Chem. Soc.* 102: 439–449.
22. Yamaguchi, K., Yabushita, S., Fueno, T., and Houk K. N. 1981. On the mechanism of photooxygenation reactions. Computational evidence against the diradical mechanism of singlet oxygen ene reactions. *J. Am. Chem. Soc.* 103: 5043–5046.
23. Davies, A. G. and Schiesser, C. H. 1991. A PM3 study of the reactions of propene with singlet oxygen and other enophiles. *Tetrahedron* 47: 1707–1726.
24. Yoshioka, Y., Yamada, S., Kawakami, T., Nishino, M., Yamaguchi, K., and Saito, I. 1996. Ab initio molecular orbital studies of singlet oxygen reactions of olefins, enol ethers and enamines. *Bull. Chem. Soc. Jpn.* 69: 2683–2699.
25. Sevin, F. and McKee, M. L. 2001. Reactions of 1,3-cyclohexadiene with singlet oxygen. A theoretical study. *J. Am. Chem. Soc.* 123: 4591–4600.
26. (a) Leach, A. G. and Houk, K. N. 2002. Diels–Alder and ene reactions of singlet oxygen, nitroso compounds and triazolinediones: Transition states and mechanisms from contemporary theory. *Chem. Commun.* 12: 1243–1255. (b) Singleton, D. A., Hang, C., Szymanski, M. J. et al. 2003. Mechanism of ene reactions of singlet oxygen. A two-step no-intermediate mechanism. *J. Am. Chem. Soc.* 125: 1319–1328.
27. For the concept of the VRI point, see: (a) Valtazanos, P. and Ruedenberg, K. 1986. Bifurcations and transition-states. *Theor. Chim. Acta* 69: 281–307. (b) Valtazanos, P., Elbert, S. T., and Ruedenberg, K. 1986. Ring opening of cyclopropylidenes to allenes: Reactions with bifurcating transition regions, free internal motions, steric hindrances, and long-range dipolar interactions. *J. Am. Chem. Soc.* 108: 3147–3149.
28. (a) Maranzana, A., Ghigo, G., and Tonachini, G. 2003. The $^1\Delta_g$ dioxygen ene reaction with propene: A density functional and multireference perturbation theory mechanistic study. *Chem. Eur. J.* 9: 2616–2626. (b) Maranzana, A., Canepa, C., Ghigo, G., and Tonachini, G. 2005. Theoretical study on the reactivity and regioselectivity of the ene reaction of $^1\Delta_g$ O_2 with α,β-unsaturated carbonyl compounds. *Eur. J. Org. Chem.* 3643–3649.
29. Leach, A. G., Houk, K. N., and Foote, C. S. 2008. Theoretical prediction of a perepoxide intermediate for the reaction of singlet oxygen with *trans*-cyclooctene contrasts with the two-step no-intermediate ene reaction for acyclic alkenes. *J. Org. Chem.* 73: 8511–8519.
30. Sheppard, A. N. and Acevedo, O. 2009. Multidimensional exploration of valley-ridge inflection points on potential-energy surfaces. *J. Am. Chem. Soc.* 131: 2530–2540.
31. Kopecky, K. R. and Van de Sande, J. H. 1972. Deuterium isotope effects in the oxidation of 2,3-dimethyl-2-butene via the bromohydroperoxide, by singlet oxygen and by triphenyl phosphite ozonide. *Can. J. Chem.* 50: 4034–4049.

32. Gollnick, K., Hartmann, H., and Paur, H. 1981. Oxygen and oxyradicals. In *Chemistry and Biology*, eds. M. A. J. Rodgers and E. L. Powers, pp. 379–395. Academic Press: New York.
33. Grdina, M. B., Orfanopoulos, M., and Stephenson, L. M. 1979. Stereochemical dependence of isotope effects in the singlet oxygen-olefin reaction. *J. Am. Chem. Soc.* 101: 3111–3112.
34. (a) Orfanopoulos M. and Foote, C. S. 1988. Intermediate in the ene reaction of singlet oxygen with 1,4-diphenyl-*cis*-2-butene and 2-butene. *J. Am. Chem. Soc.* 110: 6583–6584. (b) Orfanopoulos, M., Smonou, I., and Foote, C. S. 1990. Intermediates in the ene reactions of singlet oxygen and *N*-phenyl-1,2,4-triazoline-3,5-dione with olefins. *J. Am. Chem. Soc.* 112: 3607–3614.
35. Stratakis, M., Orfanopoulos, M., Chen, J., and Foote, C. S. 1996. Reaction profile of the photooxygenation of trisubstituted alkenes. *Tetrahedron Lett.* 37: 4105–4108.
36. Vassilikogiannakis, G., Stratakis, M., and Orfanopoulos, M. 1998. Primary and secondary isotope effects in the photooxidation of 2,5-dimethyl-2,4-hexadiene. Elucidation of the reaction energy profile. *J. Org. Chem.* 63: 6390–6393.
37. Alberti, M. N. and Orfanopoulos, M. N. 2008. The cyclopropyl group as a hypersensitive probe in the singlet oxygen ene reaction mechanism. *Org. Lett.* 10: 2465–2468.
38. Newcomb, M., Johnson, C. C., Manek, M. B., and Varick, T. R. 1992. Picosecond radical kinetics. Ring openings of phenyl substituted cyclopropylcarbinyl radicals. *J. Am. Chem. Soc.* 114: 10915–10921.
39. (a) Newcomb, M. and Chestney, D. L. 1994. A hypersensitive mechanistic probe for distinguishing between radical and carbocation intermediates. *J. Am. Chem. Soc.* 116: 9753–9754. (b) Le Tadic-Biadatti, M.-H. and Newcomb, M. 1996. Picosecond radical kinetics. Rate constants for ring openings of (2-alkoxy-3-phenylcyclopropyl)methyl radicals. *J. Chem. Soc., Perkin Trans.* 2: 1467–1473.
40. For clocking secondary and tertiary cyclopropyl rearrangements, see: (a) Engel, P. S., He, S.-L., Banks, J. T., Ingold, K. U., and Lusztyk, J. 1997. Clocking tertiary cyclopropylcarbinyl radical rearrangements. *J. Org. Chem.* 62: 1210–1214. (b) Choi, S.-Y., Toy, P. H., and Newcomb, M. 1998. Picosecond radical kinetics. Fast ring openings of secondary and tertiary *trans*-2-phenylcyclopropylcarbinyl radicals. *J. Org. Chem.* 63: 8609–8613.
41. (a) Stratakis, M. and Orfanopoulos, M. 2000. Regioselectivity in the ene reaction of singlet oxygen with alkenes. *Tetrahedron* 56: 1595–1615. (b) Clennan, E. L. 2000. New mechanistic and synthetic aspects of singlet oxygen chemistry. *Tetrahedron* 56: 9151–9179.
42. (a) Schulte-Elte, K. H., Muller, B. L., and Rautenstrauch, V. 1978. Preference for syn ene additions of $^1O_2$ to trisubstituted, acyclic olefins. *Helv. Chim. Acta* 61: 2777–2783. (b) Orfanopoulos, M., Grdina, M. B., and Stephenson, L. M. 1979. Site specificity in the singlet oxygen-trisubstituted olefin reaction. *J. Am. Chem. Soc.* 101: 275–276. (c) Schulte-Elte, K. H. and Rautenstrauch, V. 1980. Preference for the syn ene additions of $^1O_2$ to 1-methylcycloalkenes. Correlation with ground-state geometry. *J. Am. Chem. Soc.* 102: 1738–1740.
43. (a) Rousseau, G., Le Perchec, P., and Conia, J.M. 1977. Stereochemical course in the addition of singlet oxygen to vinylcyclopropane derivatives. *Tetrahedron Lett.* 18: 2517–2520. (b) Lerdal, D. and Foote, C. S. 1978. Chemistry of singlet oxygen. XXVII. Directing effect of methoxy group in additions to methoxystyrenes. *Tetrahedron Lett.* 19: 3227–3230.
44. (a) Frimer, A. A., Bartlett, P. D., Boschung, A. F., and Jewett, J. D. 1977. Reaction of singlet oxygen with 4-methyl-2,3-dihydro-γ-pyrans. *J. Am. Chem. Soc.* 99: 7977–7986. (b) Bartlett, G. P. and Frimer, A. A. 1978. The reaction of singlet oxygen with 1-methoxycyclohexene. *Heterocycles* 11: 419–425.
45. Stephenson, L. M. 1980. The mechanism of the singlet oxygen ene reaction. *Tetrahedron Lett.* 21: 1005–1008.
46. Houk, K. N., Williams, J. C., Mitchell, P. A., and Yamaguchi, K. 1981. Conformational control of reactivity and regioselectivity in singlet oxygen ene reactions: Relationship to the rotational barriers of acyclic alkylethylenes. *J. Am. Chem. Soc.* 103: 949–951.
47. Orfanopoulos, M., Stratakis, M., Elemes, Y., and Jensen, F. 1991. Do rotational barriers dictate the regioselectivity in the ene reactions of singlet oxygen and triazolinedione with alkenes? *J. Am. Chem. Soc.* 113: 3180–3181.

48. (a) Hurst, J. R., McDonald, J. D., and Schuster, G. B. 1982. Lifetime of singlet oxygen in solution directly determined by laser spectroscopy. *J. Am. Chem. Soc.* 104: 2065–2067. (b) Hurst, J. R., Wilson, S. L., and Schuster, G. B. 1985. The ene reaction of singlet oxygen: Kinetic and product evidence in support of a perepoxide intermediate. *Tetrahedron* 41: 2191–2197.
49. Stratakis, M. and Orfanopoulos, M. 1995. Anti "cis effect" selectivity in the reaction of singlet oxygen with trisubstituted alkenes. *Tetrahedron Lett.* 36: 4291–4294.
50. Orfanopoulos, M., Stratakis, M., and Elemes, Y. 1989. Regioselective reaction of singlet oxygen with *cis*-alkenes. *Tetrahedron Lett.* 30: 4875–4878.
51. (a) Hélesbeux, J.-J., Guilet, D., Séraphin, D., Duval, O., Richomme, P., and Bruneton, J. 2000. *ortho*-Prenylphenol photooxygenation as a straightforward access to *ortho*-(2-hydroxy-3-methylbut-3-enyl)phenols. *Tetrahedron Lett.* 41: 4559–4562. (b) Hélesbeux, J.-J., Duval, O., Guilet, D., Séraphin, D., Rondeau, D., and Richomme, P. 2003. Regioselectivity in the ene reaction of singlet oxygen with *ortho*-prenylphenol derivatives. *Tetrahedron* 59: 5091–5104.
52. (a) Clennan, E. L. and Chen, X. 1988. Geminal selectivity in singlet oxygen reactions. *J. Org. Chem.* 53: 3124–3125. (b) Clennan, E. L., Chen, X., and Koola, J. J. 1990. Steric and electronic effects on the conformations and singlet oxygen ene regiochemistries of substituted tetramethylethylenes. The origin of the geminal effect. *J. Am. Chem. Soc.* 112: 5193–5199. (c) Orfanopoulos, M., Stratakis, M., and Elemes, Y. 1990. Geminal selectivity of singlet oxygen ene reactions. The nonbonding large group effect. *J. Am. Chem. Soc.* 112: 6417–6419.
53. Stratakis, M. and Orfanopoulos, M. 1993. Regioselective formation of cyclic and allylic hydroperoxides. *Synth. Commun.* 23: 425–430.
54. Adam, W., Gatalani, L. H., and Griesbeck, A. 1986. Diastereoselective ene reaction in the photooxygenation of the silyl cyanohydrins of α,β-unsaturated aldehydes: Necessity for a common symmetrical intermediate of the perepoxide type. *J. Org. Chem.* 51: 5494–5496.
55. (a) Ensley, H. E., Carr, R. V. C., Martin, R. S., and Pierce, T. E. 1980. Reaction of singlet oxygen with α,β-unsaturated ketones and lactones. *J. Am. Chem. Soc.* 102: 2836–2838. (b) Kwon, B.-M., Kanner, R. C., and Foote, C. S. 1989. Reaction of singlet oxygen with 2-cyclopenten-1-ones. *Tetrahedron Lett.* 30: 903–906.
56. Adam, W. and Griesbeck, A. 1985. Synthesis of the first α-methylene-β-peroxylactone: Regiospecific ene reaction of $^1O_2$ with α,β-unsaturated carboxylic acids. *Angew. Chem. Int. Ed. Engl.* 24: 1070–1071.
57. Orfanopoulos, M. and Foote, C. S. 1985. Regioselective reaction of singlet oxygen with α,β-unsaturated esters. *Tetrahedron Lett.* 26: 5991–5994.
58. Adam, W. and Griesbeck, A. 1986. Regioselective synthesis of 2-hydroperoxy-2-methylene-butanoic acid derivatives via photooxygenation of tiglic acid derivatives. *Synthesis* 1050–1052.
59. (a) Akasaka, T., Takeuchi, K., and Ando, W. 1987. Reaction of singlet oxygen with α,β-unsaturated aldimines. *Tetrahedron Lett.* 28: 6633–6636. (b) Akasaka, T., Misawa, Y., Goto, M., and Ando, W. 1989. Reaction of singlet oxygen with α,β-unsaturated aldimines: Novel formation of 3-amino-4-methylene-1,2-dioxolanes. *Heterocycles* 28: 445–451.
60. Akasaka, T., Misawa, Y., Goto, M., and Ando, W. 1989. Singlet oxygen and triazolinedione additions to α,β-unsaturated sulfoxides. *Tetrahedron* 45: 6657–6666.
61. (a) Fristad, W. E., Bailey, T. R., Paquette, L. A., Gleiter, R., and Böhm, M. C. 1979. Regiospecific photosensitized oxygenation of vinylsilanes. A method for converting saturated ketones to 1,2-transposed allylic alcohols. Possible role of silicon in directing the regioselectivity of epoxysilane cleavage reactions. *J. Am. Chem. Soc.* 101: 4420–4423. (b) Fristad, W. E., Bailey, T. R., and Paquette, L. A. 1980. Silanes in organic synthesis. 9. Enesilylation as a method for 1,2-carbonyl migration within ketones and for conversion to 1,2-transposed allylic alcohols. *J. Org. Chem.* 45: 3028–3037. (c) Adam, W. and Richter, M. 1992. Highly regio- and diastereoselective synthesis of epoxy alcohols directly from vinyl silanes by photo-oxygenation and titanium-catalyzed oxygen transfer. *Tetrahedron Lett.* 33: 3461–3464. (d) Adam, W. and Richter, M. J. 1994. Regioselectivity of the singlet oxygen ene reaction (Schenck reaction) with vinylsilanes. *J. Org. Chem.* 59: 3335–3340.

62. Adam, W. and Klug, P. 1993. Photooxygenation of vinylstannanes: Tin-substituted allylic hydroperoxides through the regio- and diastereoselective ene reaction with singlet oxygen. *J. Org. Chem.* 58: 3416–3420.
63. (a) Foote, C. S. and Denny, R. W. 1971. Chemistry of singlet oxygen. XIII. Solvent effects on the reaction with olefins. *J. Am. Chem. Soc.* 93: 5168–5171. (b) Gollnick, K. and Griesbeck, A. 1984. Solvent dependence of singlet oxygen/substrate interactions in the ene-reactions, (4+2) and (2+2)-cycloaddition reactions. *Tetrahedron Lett.* 25: 725–728. (c) Griesbeck, A. G., Adam, W., Bartoschek, A., and El-Idreesy, T. T. 2003. Photooxygenation of allylic alcohols: Kinetic comparison of unfunctionalized alkenes with prenol-type allylic alcohols, ethers and acetates. *Photochem. Photobiol. Sci.* 2: 877–881.
64. (a) Manring, L. E. and Foote, C. S. 1983. Chemistry of singlet oxygen. 44. Mechanism of photooxidation of 2,5-dimethylhexa-2,4-diene and 2-methyl-2-pentene. *J. Am. Chem. Soc.* 105: 4710–4717. (b) Rautenstrauch, V., Thommen, W., and Schulte-Elte, K. H. 1986. Singlet-oxygen ene reactions of (*E*)-4-propyl[1,1,1–$^2H_3$]oct-4-ene. *Helv. Chim. Acta* 69: 1638–1643.
65. (a) Orfanopoulos, M. and Stratakis, M. 1991. Solvent effects on the side selectivity of singlet oxygen with α,β-unsaturated esters. New evidence for a perepoxide intermediate. *Tetrahedron Lett.* 32: 7321–7324. (b) Stratakis, M., Orfanopoulos, M., and Foote, C. S. 1996. Solvent effects in the stereoselectivity of the ene reaction of singlet oxygen with allylic alcohols. *Tetrahedron Lett.* 37: 7159–7162. (c) Vassilikogiannakis, G., Stratakis, M., Orfanopoulos, M., and Foote, C. S. 1999. Stereochemistry in the ene reactions of singlet oxygen and triazolinediones with allylic alcohols. A mechanistic comparison. *J. Org. Chem.* 64: 4130–4139. (d) Stensaas, K. L., Payne, J. A., Ivancic, A. N., and Bajaj, A. 2002. Novel solvent hydrogen-bonding effects in the singlet oxygen ene reaction: A comparison of α,β-unsaturated esters and acids. *Tetrahedron Lett.* 43: 25–27. (e) Stensaas, K. L., Bajaj, A., and Al-Turk, A. 2005. Novel regiochemistry in the aqueous singlet oxygen ene reactions of carboxylic acid salts: A comparison of substrate structure. *Tetrahedron Lett.* 46: 715–718.
66. Stratakis, M., Orfanopoulos, M., and Foote, C. S. 1998. Reactions of singlet oxygen and *N*-methyltriazolinediones with β,β-dimethylstyrene. Exceptional *syn* selectivity in the ene products. *J. Org. Chem.* 63: 1315–1318.
67. (a) Alberti, M. N., Vougioukalakis, G. C., and Orfanopoulos, M. 2003. Electronic effects in the regioselectivity of the singlet oxygen and 4-methyl-1,2,4-triazoline-3,5-dione ene reactions with isobutenylarenes. *Tetrahedron Lett.* 44: 903–905. (b) Alberti, M. N. and Orfanopoulos, M. 2006. Stereoelectronic and solvent effects on the allylic oxyfunctionalization of alkenes with singlet oxygen. *Tetrahedron* 62: 10660–10675.
68. Prein, M. and Adam, W. 1996. The Schenck ene reaction: Diastereoselective oxyfunctionalization with singlet oxygen in synthetic applications. *Angew. Chem. Int. Ed. Engl.* 35: 477–494.
69. (a) Adam, A., Wirth, T., Pastor, A., and Peters, K. 1998. Dramatic diastereoselectivity differences in the asymmetric ene reactions of triazolinediones and singlet oxygen with chiral 2,2-dimethyloxazolidine derivatives of tiglic acid. *Eur. J. Org. Chem.* 4: 501–506. (b) Adam, W., Bosio, S. G., Degen, H. G., Krebs, O., Stalke, D., and Schumaster, D. 2002. A comparative study on the diastereofacial control in the [4+2] cycloaddition of sorbates and the ene reaction of tiglates with singlet oxygen and PTAD by a variety of chiral auxiliaries. *Eur. J. Org. Chem.* 3944–3953. (c) Pastor, A., Adam, W., Wirth, T., and Tóth, G. 2005. Diastereoselective reactions of the tiglic acid functionality mediated by oxazoline chiral auxiliaries: A mechanistic comparison of DMD and *m*-CPBA epoxidations versus singlet oxygen and PTAD ene reactions. *Eur. J. Org. Chem.* 3075–3084.
70. (a) Dussault, P. H., Woller, K. R., and Hillier, M. C. 1994. Stereoselective dioxygenation of enoates. *Tetrahedron* 50: 8929–8940. (b) Adam, W., Degen, H.-G., Krebs, O., and Saha-Möller, C. R. 2002. Efficient π-facial control in the ene reaction of nitrosoarene, triazolinedione, and singlet oxygen with tiglic amides of the bornane-derived sultam as chiral auxiliary: An economical synthesis of enantiomerically pure nitrogen- and oxygen-functionalized acrylic acid derivatives. *J. Am. Chem. Soc.* 124: 12938–12939.

71. (a) Adam, W., Peters, K., Peters, E. M., and Schambony, S. B. 2000. Diastereoselective and regioselective singlet-oxygen ene reaction of oxazolidine-substituted alkenes: Control through hydrogen bonding mediated by the urea functionality of chiral auxiliaries. *J. Am. Chem. Soc.* 122: 7610–7611. (b) Adam, W., Peters, K., Peters, E. M., and Schambony, S. B. 2001. Efficient control of the diastereoselectivity and regioselectivity in the singlet-oxygen ene reaction of chiral oxazolidine-substituted alkenes by a remote urea NH functionality: Comparison with dimethyldioxirane and *m*-chloroperbenzoic acid epoxidations. *J. Am. Chem. Soc.* 123: 7228–7232.
72. (a) Kropf, H. and Reichwaldt, R. 1987. Photooxygenation of phenyl-substituted propenes, but-2-enes and pent-2-enes: Reactivity, regioselectivity and stereoselectivity. *J. Chem. Res.* XX: 412–413. (b) Brünker, H.-G. and Adam, W. 1995. Diastereoselective and regioselective singlet oxygen ene oxyfunctionalization (Schenck reaction): Photooxygenation of allylic amines and their acyl derivatives. *J. Am. Chem. Soc.* 117: 3976–3982.
73. Adam, W., Brünker, H.-G., Kumar, A. S., Peters, E.-M., Peters, K., Schneider, U., and von Schnering, H. G. 1996. Diastereoselective singlet oxygen ene reaction (Schenck reaction) and diastereoselective epoxidations of heteroatom-substituted acyclic chiral olefins: A mechanistic comparison. *J. Am. Chem. Soc.* 118: 1899–1905.
74. Hoffmann, R. W. 1989. Allylic 1,3-strain as a controlling factor in stereoselective transformations. *Chem. Rev.* 89: 1841–1860.
75. (a) Adam, W. and Nestler, B. 1992. Photooxygenation of chiral allylic alcohols: Hydroxyl-directed regio- and diastereoselective ene reaction of singlet oxygen. *J. Am. Chem. Soc.* 114: 6549–6550. (b) Adam, W. and Nestler, B. 1993. Hydroxyl-directed regio- and diastereoselective ene reaction of singlet oxygen with chiral allylic alcohols. *J. Am. Chem. Soc.* 115: 5041–5049.
76. Adam, W. and Brünker, H.-G. 1993. Diastereoselective and regioselective photooxygenation of a chiral allylic amine and its acyl derivatives: Stereochemical evidence for a steering effect by the amino group in the ene reaction of singlet oxygen. *J. Am. Chem. Soc.* 115: 3008–3009.
77. Adam, W. and Nestler, B. 1993. (*Z*)-Methyl-3-penten-2-ol as stereochemical probe 1,2 *versus* 1,3 allylic strain in the photooxygenation epoxidation of chiral allylic alcohols. *Tetrahedron Lett.* 34: 611–614.
78. Adam, W., Renze, J., and Wirth, T. 1998. Stereoelectronic control of the diastereoselectivity in the photooxygenation (Schenck ene reaction) of an electron-poor allylic alcohol and its ethers. *J. Org. Chem.* 63: 226–227.
79. Adam, W., Saha-Möller, C. R., Schambony, S. B., Schmid, K. S., and Wirth, T. 1999. Stereocontrolled photooxygenations—A valuable synthetic tool. *Photochem. Photobiol.* 70: 476–483.
80. Dussault, P. H. and Schultz, J. A. 1999. Diastereoselective addition of singlet oxygen to highly functionalized *Z*-allylic alcohols: Effect of neighboring functional groups. *J. Org. Chem.* 64: 8419–8422.
81. For selected examples, see: (a) Schenck, G. O. 1952. Probleme präparativer Photochemie. *Angew. Chem.* 64: 12–23. (b) Schulte-Elte, K. H., Gadola, M., and Müller, B. L. 1971. Farbstoffsensibilisierte photooxygenierung von (-)-*cis*-Pulegol und (+)-Pulegon zur addition von O_2 ($^1\Delta_g$) an Doppelbindungen mit allylständiger hydroxyl- oder carbonyl-gruppe. *Helv. Chim. Acta* 54: 1870–1880.
82. For selected examples, see: (a) Nickon, A. and Mendelson, W. L. 1965. Reactivity and geometry in allylic systems. VI. Stereospecific conversion of allylic alcohols to α,β-epoxy ketones by photosensitized oxygenation. *J. Am. Chem. Soc.* 87: 3921–3928. (b) Marshall, J. A. and Hochstetler, A. R. 1966. Oxygenation of 1,10-dimethyl-1(9)-octalin. *J. Org. Chem.* 31: 1020–1025. (c) Nickon, A., DiGiorgio, J. B., and Daniels, P. J. L. 1973. Chemical evidence for transition-state geometry in reaction of monoolefins with singlet oxygen. *J. Org. Chem.* 38: 533–539.
83. For selected examples, see: (a) Gollnick, K. and Schade, G. 1966. Studien in der Caranreihe. VI. Photosensibilisierte O_2-übertragung auf (-)-*cis*-Δ^2-Caren, (-)-*trans*-Δ^4-Caren, (+)-$\Delta^{4(10)}$-Caren und (+)-Δ^4-Caren. Darstellung des (+)-*trans*-Carans. *Tetrahedron Lett.* 7: 2335–2341. (b) Jefford, C. W. and Rimbault, C. G. 1978. Reaction of singlet oxygen with 2-methylnorbornadiene and 2-methylidenenorbornene. Evaluation of electronic and steric effects on the course of hydroperoxidation.

J. Org. Chem. 43: 1908–1912. (c) Jefford, C. W. and Rimbault, C. G. 1978. Reaction of singlet oxygen with norbornenyl ethers. Characterization of dioxetanes and evidence for zwitterionic peroxide precursors. *J. Am. Chem. Soc.* 100: 6437–6445.

84. Jefford, C. W. and Boschung, A. F. 1974. Reaction of singlet oxygen with 2-methylnorborn-2-ene, 2-methylidenenorbornane, and their 7,7-dimethyl derivatives. The transition state geometry for hydroperoxidation. *Helv. Chim. Acta* 57: 2242–2257.
85. Schenck, G. O., Eggert, H., and Denk, W. 1953. Photochemische reaktionen. 3. Uber die bildung von hydroperoxyden bei photosensibilisierten reaktionen von O_2 mit geeigneten akzeptoren, insbesondere mit α-Pinen und β-Pinen. *Justus Liebigs Ann. Chem.* 584: 177–198.
86. Paquette, L. A., Liao, C. C., Liotta, D. C., and Fristad, W. E. 1976. Reversal of stereospecificity during allylic hydroperoxidation of 3-norcarene and bicyclo[4.2.0]oct-3-ene derivatives arising from structurally enforced quenching of singlet oxygen by the hydrazide functionality. *J. Am. Chem. Soc.* 98: 6412–6413.
87. (a) Okada, K. and Mukai, T. 1978. Stereoselective addition of singlet oxygen to 7-isopropylidenenorbornene derivatives. Possibility of π-orbital distortion in the homoconjugated system. *J. Am. Chem. Soc.* 100: 6509–6510. (b) Paquette, L. A., Hertel, L. W., Gleiter, R., and Böhm, M. 1978. Electronic control of stereoselectivity. 1. Singlet oxygen and related electrophilic additions to aryl-substituted 7-isopropylidenebenzonorbornene. *J. Am. Chem. Soc.* 100: 6510–6512. (c) Paquette, L. A., Hertel, L. W., Gleiter, R., Böhm, M. C., Beno, M. A., and Christoph, G. G. 1981. Electronic control of stereoselectivity. 8. The stereochemical course of electrophilic additions to aryl-substituted 9-isopropylidenebenzonorbornenes. *J. Am. Chem. Soc.* 103: 7106–7121.
88. (a) Linker, T. and Fröhlich, L. 1994. Regio- and diastereoselective photooxygenation of chiral 2,5-cyclohexadiene-1-carboxylic acids. *Angew. Chem. Int. Ed. Engl.* 33: 1971–1972. (b) Linker, T. and Fröhlich, L. 1995. Substituent effects in the highly regioselective and diastereoselective ene reaction of singlet oxygen with chiral cyclohexadienes. *J. Am. Chem. Soc.* 117: 2694–2697.
89. Tsangarakis, C., Zaravinos, I.-P., and Stratakis, M. 2005. Highly regioselective and diastereoselective photooxygenation of α-cyclogeranyl derivatives. *Synlett* 1857–1860.
90. Orfanopoulos, M. and Stephenson, L. M. 1980. Stereochemistry of the singlet oxygen olefin-ene reaction. *J. Am. Chem. Soc.* 102: 1417–1418. For the first study concerning the stereochemistry of the $^1O_2$ ene reaction, see: Stephenson, L. M., McClure, D. E., and Sysak, P. K. 1973. Stereochemistry of the singlet oxygen ene reaction with olefins. *J. Am. Chem. Soc.* 95: 7888–7889.
91. Alberti, M. N., Vassilikogiannakis, G., and Orfanopoulos, M. 2008. Stereochemistry of the singlet oxygenation of simple alkenes: A stereospecific transformation. *Org. Lett.* 10: 3997–4000.
92. (a) Maldotti, A., Molinari, A., and Amadelli, R. 2002. Photocatalysis with organized systems for the oxofunctionalization of hydrocarbons by O_2. *Chem. Rev.* 102: 3811–3836. (b) Tung, C.-H., Wu, L.-Z., Zhang, L.-P., and Chen, B. 2003. Supramolecular systems as microreactors: Control of product selectivity in organic phototransformation. *Acc. Chem. Res.* 36: 39–47.
93. For selected examples, see: (a) Li, X. and Ramamurthy, V. 1996. Selective oxidation of olefins within organic dye cation-exchanged zeolites. *J. Am. Chem. Soc.* 118: 10666–10667. (b) Robbins, R. J. and Ramamurthy, V. 1997. Generation and reactivity of singlet oxygen within zeolites: Remarkable control of hydroperoxidation of alkenes. *Chem. Commun.* 1071–1072. (c) Ramamurthy, V., Lakshminarasimhan, P., Grey, C. P., and Johnston, L. J. 1998. Energy transfer, proton transfer and electron transfer reactions within zeolites. *Chem. Commun.* 2411–2424. (d) Ramamurthy, V., Shailaja, J., Kaanumalle, L. S., Sunojb, R. B., and Chandrasekharb, J. 2003. Controlling chemistry with cations: Photochemistry within zeolites. *Chem. Commun.* 1987–1999.
94. For selected examples, see: (a) Clennan, E. L. and Sram, J. P. 2000. Photochemical reactions in the interior of a zeolite. Part 5: The origin of the zeolite induced regioselectivity in the singlet oxygen ene reaction. *Tetrahedron* 56: 6945–6950. (b) Clennan, E. L., Sram, J. P., Pace, A., Vincer, K., and White, S. 2002. Intrazeolite photooxidations of electron-poor alkenes. *J. Org. Chem.* 67: 3975–3978. (c) Pace, A. and Clennan, E. L. 2002. A new experimental protocol for intrazeolite photooxidations.

The first product-based estimate of an upper limit for the intrazeolite singlet oxygen lifetime. *J. Am. Chem. Soc.* 124: 11236–11237. (d) Pace, A., Pierro, P., Buscemi, S., Vivona, N., and Clennan, E. L. 2007. Photooxidations of alkenes in fluorinated constrained media: Fluoro-organically modified NaY as improved reactors for singlet oxygen "ene" reactions. *J. Org. Chem.* 72: 2644–2646.

95. For selected examples, see: (a) Stratakis, M. and Froudakis, G. 2000. Site specificity in the photooxidation of some trisubstituted alkenes in thionin-supported zeolite Na-Y. On the role of the alkali metal cation. *Org. Lett.* 2: 1369–1372. (b) Stratakis, M., Nencka, R., Rabalakos, C., Adam, W., and Krebs, O. 2002. Thionin-sensitized intrazeolite photooxygenation of trisubstituted alkenes: Substituent effects on the regioselectivity as probed through isotopic labeling. *J. Org. Chem.* 67: 8758–8763. (c) Stratakis, M., Rabalakos, C., Mpourmpakis, G., and Froudakis, G. E. 2003. Ene hydroperoxidation of isobutenylarenes within dye-exchanged zeolite Na-Y: Control of the site selectivity by cation-arene interactions. *J. Org. Chem.* 68: 2839–2843. (d) Stratakis, M., Kalaitzakis, D., Stavroulakis, D., Kosmas, G., and Tsangarakis, C. 2003. Remarkable change of the diastereoselection in the dye-sensitized ene hydroperoxidation of chiral alkenes by zeolite confinement. *Org. Lett.* 5: 3471–3474.
96. (a) Tung, C.-H., Wang, H., and Ying, Y.-M. 1998. Photosensitized oxidation of alkenes absorbed on pentasil zeolites. *J. Am. Chem. Soc.* 120: 5179–5186. (b) Chen, Y.-Z., Wu, L.-Z., Zhang, L.-P., and Tung, C.-H. 2005. Confined space-controlled hydroperoxidation of trisubstituted alkenes adsorbed on pentasil zeolites. *J. Org. Chem.* 70: 4676–4681.
97. (a) Tung, C.-H. and Guan, J.-Q. 1998. Remarkable product selectivity in photosensitized oxidation of alkenes within Nafion membranes. *J. Am. Chem. Soc.* 120: 11874–11879. (b) Maldotti, A., Andreotti, L., Molinari, A., Borisov, S., and Vasil'ev, V. 2001. Photoinitiated catalysis in Nafion membranes containing palladium(II) *meso*-tetrakis(*N*-methyl-4-pyridyl)porphyrin and iron(III) *meso*-tetrakis-(2,6-dichlorophenyl)porphyrin for O_2-mediated oxidations of alkenes. *Chem. Eur. J.* 7: 3564–3571. (c) Li, X.-H., Wu, L.-Z., Zhang, L.-P., Tung, C.-H., and Che, C.-M. 2001. Luminescence and photocatalytic properties of a platinum(II)–quaterpyridine complex incorporated in Nafion membrane. *Chem. Commun.* 2280–2281. (d) Zhang, D., Wu, L.-Z., Yang, Q.-Z., Li, X.-H., Zhang, L.-P., and Tung, C.-H. 2003. Versatile photosensitization system for $^1O_2$-mediated oxidation of alkenes based on Nafion-supported platinum(II) terpyridyl acetylide complex. *Org. Lett.* 5: 3221–3224.
98. (a) Li, H.-R., Wu, L.-Z., and Tung, C.-H. 2000. Vesicle controlled selectivity in photosensitized oxidation of olefins. *Chem. Commun.* 1085–1086. (b) Li, H.-R., Wu, L.-Z., and Tung, C.-H. 2000. Controllable selectivity of photosensitized oxidation of olefins included in vesicles. *Tetrahedron* 56: 7437–7442.
99. (a) Griesbeck, A. G. and Bartoschek, A. 2002. Sustainable photochemistry: Solvent-free singlet oxygen-photooxygenation of organic substrates embedded in porphyrin-loaded polystyrene beads. *Chem. Commun.* 1594–1595. (b) Griesbeck, A. G., El-Idreesy, T. T., and Bartoschek, A. 2004. Photooxygenation in polystyrene beads with covalently and non-covalently bound tetraarylporphyrin sensitizers. *Adv. Synth. Catal.* 346: 245–251. (c) Griesbeck, A. G., Bartoschek, A., Neudörfl, L., and Miara, C. 2006. Stereoselectivity in ene reactions with $^1O_2$: Matrix effects in polymer supports, photo-oxygenation of organic salts and asymmetric synthesis. *Photochem. Photobiol.* 82: 1233–1240.
100. Feng, K., Zhang, R.-Y., Wu, L.-Z. et al. 2006. Photooxidation of olefins under oxygen in platinum(II) complex-loaded mesoporous molecular sieves. *J. Am. Chem. Soc.* 128: 14685–14690.
101. Natarajan, A., Kaanumalle, L. S., Jockusch, S. et al. 2007. Controlling photoreactions with restricted spaces and weak intermolecular forces: Exquisite selectivity during oxidation of olefins by singlet oxygen. *J. Am. Chem. Soc.* 128: 4132–4133.
102. Feng, K., Wu, L.-Z., Zhang, L.-P., and Tung, C.-H. 2007. IRA-200 resin-supported platinum(II) complex for photooxidation of olefins. *Tetrahedron* 63: 4907–4911.

32

Photooxygenations of Sulfur Compounds

Edward L. Clennan
University of Wyoming

32.1 Introduction

Molecular oxygen (O_2) was independently discovered by Joseph Priestly and Carl Wilhelm Scheele in the late eighteenth century [1]. It can react at sulfur and with nearly every other element under a variety of conditions to produce oxides [2]. The first photooxygenations (photochemically initiated incorporation of oxygen into molecules) were reported as early as 1867 [3], well before the electronic character of oxygen was understood. It was not until 1924 that G. N. Lewis attributed the paramagnetism of oxygen to a structure with unpaired electrons [4,5]. This discovery was rapidly followed in 1928 by R. S. Mulliken's suggestion that the electronic configuration of oxygen, $[(\sigma_{1s})^2(\sigma^*_{1s})^2(\sigma_{2s})^2(\sigma^*_{2s})^2(\sigma_{2p})^2(\pi_{2p})^4(\pi^*_{2p})^2]$, leads to three states in order of increasing energy, $^3\Sigma_g^-$, $^1\Delta_g$, and $^1\Sigma_g^+$ since the π^*_{2p} orbital is only half filled [6,7]. Finally, it was not until the early 1930s that Kautsky and coworkers [8,9] reported that the metastable $^1\Delta_g$ state of oxygen was involved in many of these photooxygenations. It is now well appreciated that photooxygenations can involve both the ground-state triplet, $^3\Sigma_g^-$, and the metastable $^1\Delta_g$ oxygen. On the other hand, the higher energy $^1\Sigma_g^+$ state at 37 kcal/mol above the $^3\Sigma_g^-$ ground state is vibrationally and quantitatively deactivated to the lower energy $^1\Delta_g$ state (22.5 kcal/mol) and does not have a sufficient lifetime to chemically react with organic substrates [10].

Photooxygenations of sulfur compounds have been most often conducted using photosensitization. This technique employs sensitizers such as Rose Bengal, methylene blue, tetraphenylporphine, protoporphyrin IX dimethyl ester, 2,4,6-triphenylpyrylium tetrafluoroborate, and N-methylquinolinium tetrafluoroborate (Figure 32.1) that absorb in the visible where competitive absorption by substrate does not occur [11]. These sensitizers can induce photooxygenation of sulfur compounds by either Type I or Type II processes [12]. These two reaction types differ in the order in which the substrate and oxygen appear on the reaction surface and in the identity of the reactive intermediate produced by interaction with the sensitizer. In the Type I reaction, the substrate is activated by either electron transfer or hydrogen transfer to the sensitizer and then subsequently

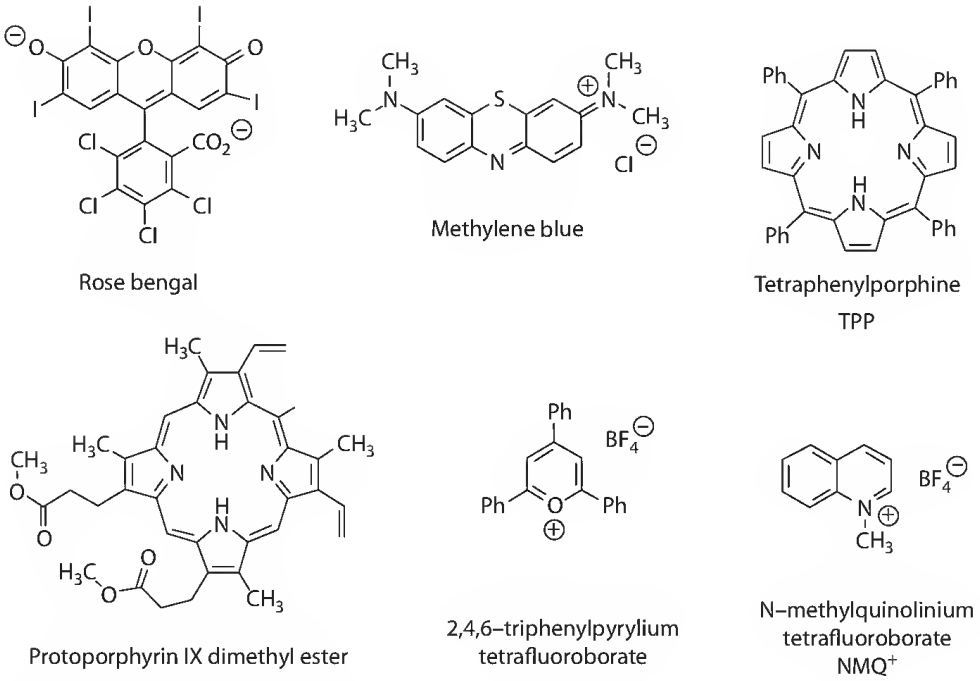

FIGURE 32.1 Photooxygenation sensitizers.

reacts with oxygen. In the Type II reaction, oxygen is initially activated by energy transfer from the sensitizer to form singlet oxygen, which then reacts with the substrate.

32.2 Type II Sulfur Photooxygenations

32.2.1 Sulfides

Type II photooxygenations of dialkyl sulfides were first reported by Schenck and Krausch in 1962 as a new synthetic method for the formation of sulfoxides [13]. The reaction has subsequently proven to be generally applicable to a wide range of sulfides including dialkyl- [14,15], aryl alkyl- [16], and cyclic sulfides [17,18] as shown in Figure 32.2. For example, photooxygenation of 2-methylthiirane, **4**, in methylene chloride which produces no major product at room temperature nevertheless reacts to give the *cis*- and *trans*-sulfoxides at –20°C along with a small amount of polymeric material [17]. These products, however, polymerized upon warming the reaction mixture to room temperature. This report is consistent with earlier work of Ando and coworkers [19,20], who reported polymerizations of these sensitive small-ring sulfoxides. These workers also reported that addition of dimethyl sulfoxide allowed isolation of the sulfoxide at room temperature and resulted in concomitant formation of dimethyl sulfone. A temperature effect was also observed during photooxygenation of pentamethylsulfide, **3** [18]. In this case, the sulfoxide is the exclusive product of the reaction at room temperature but approximately 30% of the sulfone was also observed at –80°C.

Small amounts of by-products are also formed in the reactions of **1**–**4** and in the reactions of many sulfides with singlet oxygen. For example, photooxygenation of di-*n*-butyl sulfide, **1**, to 98% conversion with 2.6×10^{-4} M Rose Bengal produces approximately 7% of dibutyl disulfide in addition to the sulfoxide (87%) and sulfone (6%) [14]. Photooxygenation of thioanisole, **2**, in methanol produces the sulfoxide as the major product (85%) along with minor amounts of the sulfone (5%), diphenyl disulfide (1%), methyl benzenesulfenate (4%), and benzene sulfinate (3%) [16]. In some unusual cases, cleavage products become major components of the reaction mixtures. (Figure 32.3) For example, the combined yield of the anticipated sulfoxide and sulfone in the photooxygenations of 9-ethylthiofluorenone, **5** [21], and

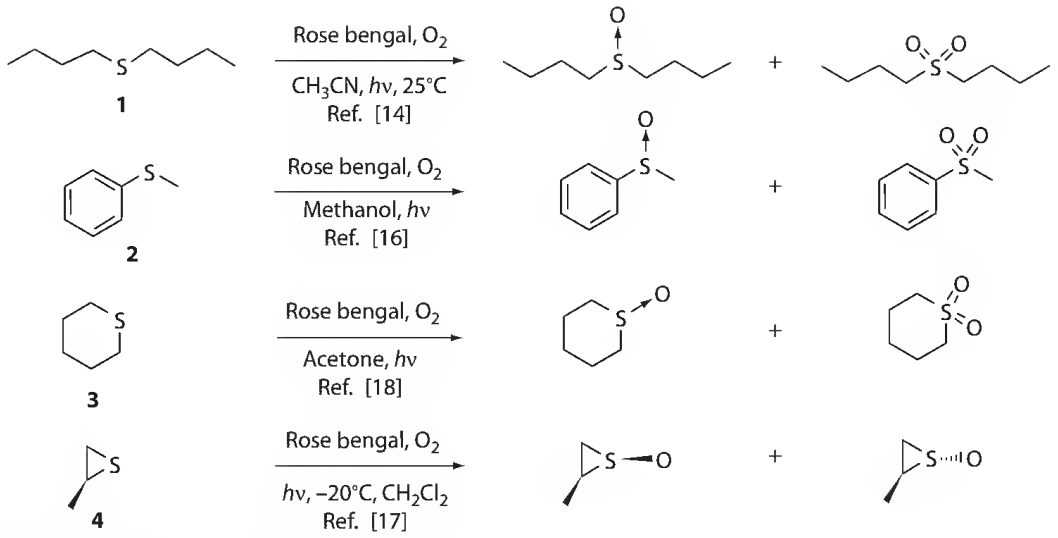

FIGURE 32.2 Sulfide photooxygenation products.

dibenzyl sulfide, **6** [22], are less than 50% and the reaction mixtures are dominated by carbon–sulfur bond cleavage products. (Figure 32.3) There are also sulfides that do not react or react extremely slowly with singlet oxygen. These appear to fall into three categories; (1) sulfides that are sterically shielded; (2) sulfides that are electronically deactivated; and (3) sulfides that have appended reactive functional groups that preferentially react with singlet oxygen. Diphenyl sulfide and di-*tert*-butyl sulfide both deactivate singlet oxygen at rates more than 400–500 times slower than diethyl sulfide, and the sulfoxides are only formed upon extended irradiations [23]. This can be attributed to a steric effect in di-*tert*-butyl sulfide, however, Albini and coworkers [23] have pointed out that the low reactivity of diphenyl—in comparison to diethyl sulfide—must be due in part to electronic effects. The HOMO on diethyl sulfide is localized for the most part on sulfur while in the C_2 symmetric diphenyl sulfide [24], it is significantly delocalized onto the phenyl rings reducing reactivity at sulfur [25]. The HOMO on thiophenes in general are more delocalized and in thiophene itself is completely localized on the π-system [25] and as a consequence, *cis*- or *trans*-3-styrylthiophenes, **7**, do not react with singlet oxygen even after 10 h of irradiation [26]. On the other hand, reactions of singlet oxygen with more highly substituted thiophenes, such as 2,5-dimethylthiophene [27], do occur but prefer [4 + 2] cycloadditions to form thioozonides rather than reaction at sulfur. The less substituted *trans*-2-styrylthiophene, **8**, also reacts, but in this case primarily by the thiophene ring functioning as part of a diene acceptor in a [4 + 2] cycloaddition rather than to form the thioozonide [28]. The electronic deactivation of vinyl sulfides also preclude sulfoxide formation and [2 + 2] cycloadditions are often observed (e.g., **9**) [29–32]. Thioanisole, **2**, reacts readily with singlet oxygen but the more reactive tetrasubstituted double bond in **10** competitively inhibits this reaction and allylic hydroperoxides are the observed products [33,34].

32.2.2 Mechanism of Sulfoxide Formation

The current understanding of the mechanism of sulfoxide formation is depicted in Figure 32.4 [35–39]. Two important features of this mechanism are (1) the presence of two intermediates on the reaction surface on the way to the sulfoxide product, the persulfoxide, **PS**, and the S-hydroperoxy sulfonium ylide, **SY**; and (2) the decomposition of the **PS** via a physical quenching step, k_q [40]. Evidence for the existence of the intermediates was obtained by detailed kinetic studies of reaction mixtures containing diphenyl sulfoxide, Ph_2SO, and diphenyl sulfide, Ph_2S [41]. Neither Ph_2SO nor Ph_2S reacts appreciably with singlet oxygen; however, under these co-photooxygenation conditions, they are readily converted to diphenyl

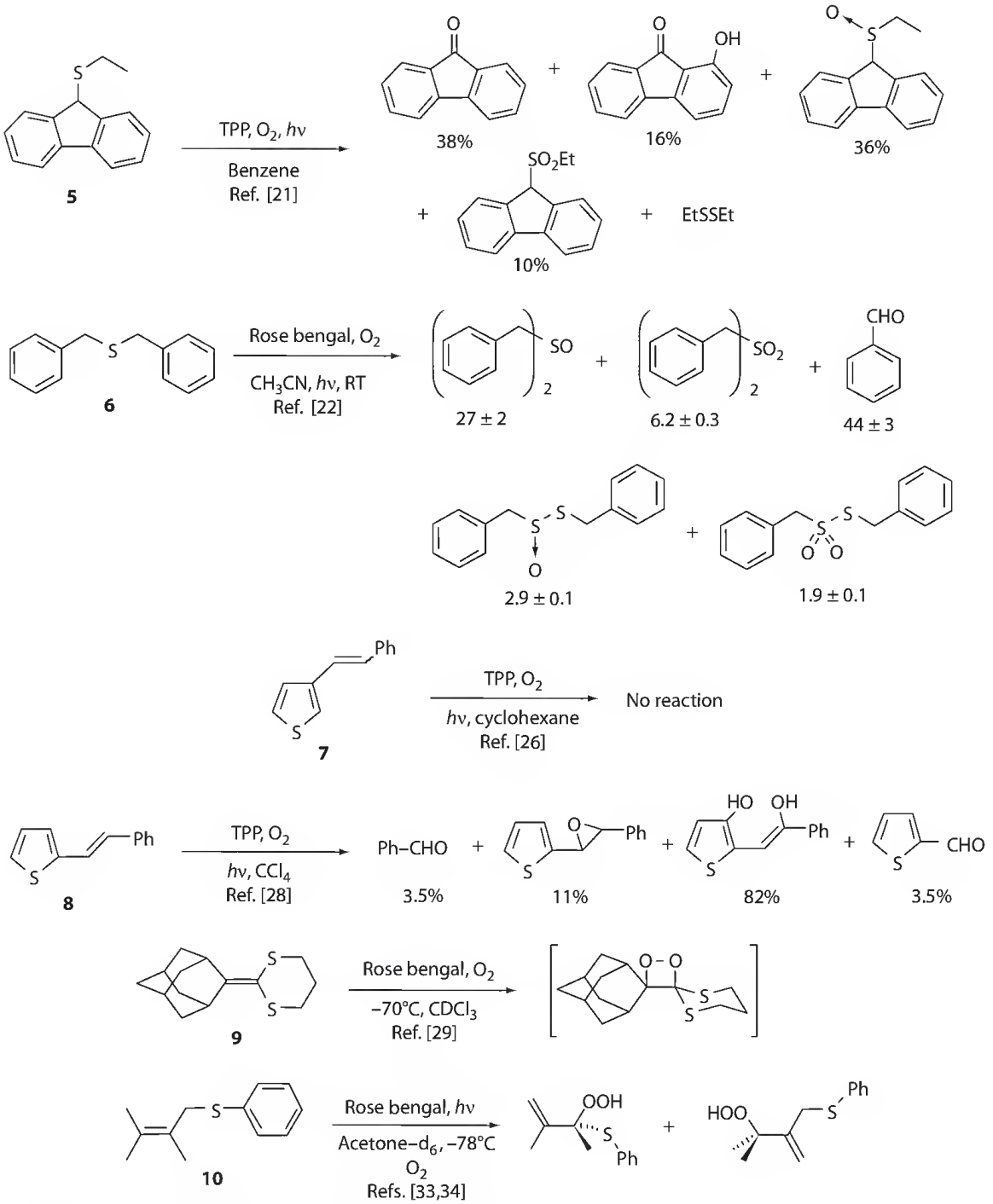

FIGURE 32.3 Sulfides that do not produce sulfoxides as major products.

sulfone, Ph_2SO_2, and Ph_2SO, respectively. Plots of [sulfoxide]/[Ph_2SO_2] and [sulfoxide]/[Ph_2SO] versus 1/[Ph_2SO] and 1/[Ph_2S], respectively, are linear as predicted by equations 1 and 2 (Figure 32.4) that were derived by steady-state treatment of both the **PS** and **SY** intermediates in this mechanistic scheme [18]. Furthermore, as predicted by this mechanism, the slopes of these plots are independent of the sulfide concentration in the Ph_2SO but not the Ph_2S trapping experiments. The physical quenching step, k_q, is readily detected by comparing the rate constant for disappearance of singlet oxygen, k_T, to the rate constant for sulfoxide formation, $k_r = 2k_T[k_X/(k_X + k_q)]$ [42]. When physical quenching is unimportant

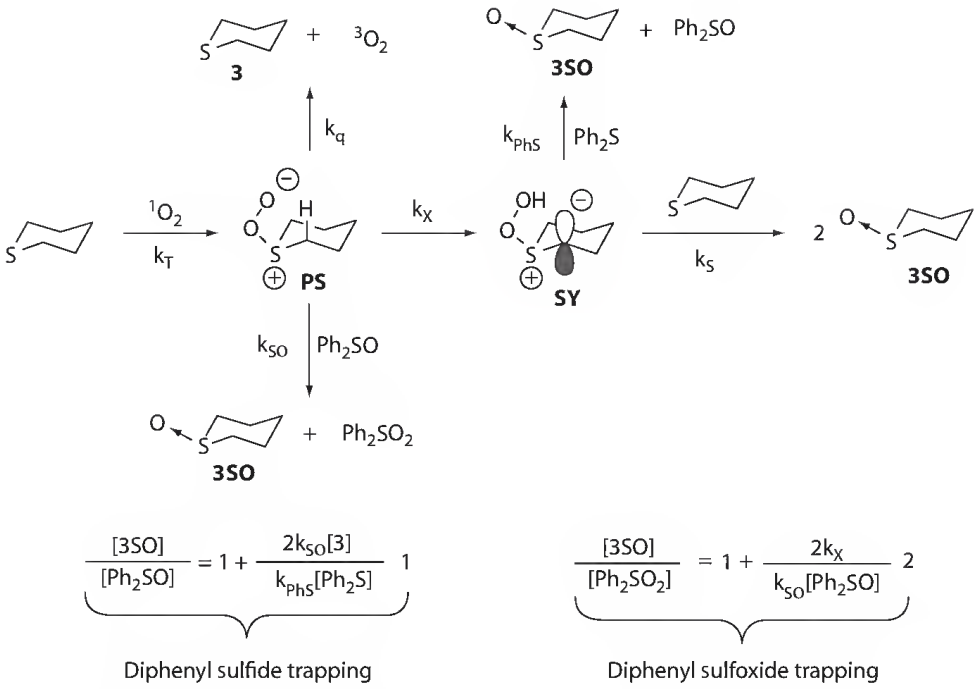

FIGURE 32.4 Mechanism of sulfoxide formation.

($k_q = 0$), the chemical rate constant for sulfoxide formation, k_r, should be equal to $2k_T$ since disappearance of one singlet oxygen produces two sulfoxide molecules. Experimentally, it has been shown for many sulfides that physical quenching, k_q, dominates the interactions with singlet oxygen. For example, in the reaction of diethyl sulfide, 95% of the singlet oxygen is deactivated to form triplet oxygen and only 5% is incorporated into product. Addition of Ph_2S to sulfide, photooxygenation reactions does not improve the efficiencies of the reactions since k_{PhS} does not compete with k_q. On the other hand, addition of Ph_2SO does improve the efficiency by converting **PS** to the sulfoxide, k_{SO}, before it has a chance to decompose by the physical quenching channel, k_q.

The chemistry and properties of the persulfoxide intermediate, **PS**, are well established. However, whether or not it has been isolated is a matter of debate. Its direct observation has been claimed in an infrared spectroscopy experiment by irradiation at 13 K into an oxygen sulfide charge-transfer band [43]. The presence of the two required nonequivalent oxygen atoms was confirmed by observing a splitting in the assigned S–O stretch when ^{16}O–^{18}O was used in the experiment. Jensen, however, has questioned this assignment pointing out the poor agreement with the MP2/6-31G* derived vibrational frequencies [44]. Other sulfur bis-oxides would also be expected to have nonequivalent oxygens, and one such species, the thiadioxirane, (**TD** in Figure 32.5), has calculated vibrational frequencies much closer to the experimentally observed values.

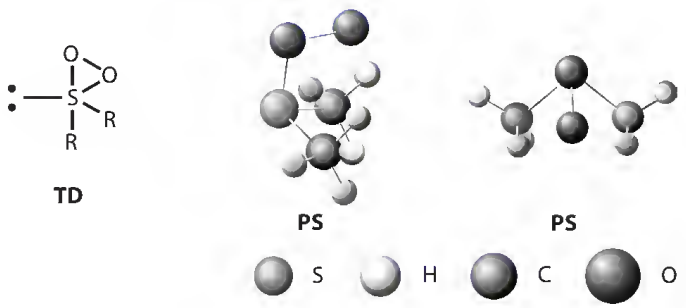

FIGURE 32.5 The thiadioxirane, **TD**, and two perspectives of the MP2/6-31G* minimized dimethyl persulfoxide.

A minimum energy structure corresponding to the **PS** has been located with several different computational models [45–47]. Two different views of the MP2/6-31G* minimized dimethyl persulfoxide are shown in Figure 32.5. The **PS** has C_S symmetry with a nearly tetrahedral-like geometry with a >C–S–C angle of 99.71°, and >C–S–O angles of 100.39°. The O–O bond length is 1.43Å and S–O bond length is 1.65Å but shortens to 1.59Å at the MP2/6-311+G(2df) level of theory. The most striking structural feature is the fact that the O–O bond bisects the C–S–C angle despite the close approach (2.10Å) to a hydrogen atom on each methyl group. The transition state for formation of the persulfoxide involving donation of the sulfur lone pair into the empty π_g orbital on singlet oxygen has also been located with both the MP2/6-31G(d) and MP2/6-311+G(2df) computational models. This transition state bears a remarkable similarity to the persulfoxide, suggesting a small barrier for dissociation [46].

The Mulliken charges on the **PS** indicate a sulfonium-like sulfur and build up of negative charge on both oxygens. The nucleophilic character of the pendant oxygen is supported experimentally by a Hammett reaction constant of 0.252 in the trapping of dimethyl persulfoxide with substituted diaryl sulfoxides [48]. Sulfoxides are not the only molecules that can accept an oxygen from a persulfoxide. Electrophilic trapping agents such as phosphites [49], sulfenate esters [50], sulfinate esters [51], and sulfinamides [51] can also remove an oxygen from the **PS**. An interesting example of the nucleophilic reaction of a **PS** was observed during the photooxygenation of [1-(ethylthio)-1-methylethoxy]trimethylsilane, **11** [52] (Figure 32.6). In this reaction, the pendant oxygen in the **PS** attacks at the silicon to give a six-membered ring intermediate that decomposes by a methyl migration to give a silicate product, **12**. The formation of the six-membered ring intermediate was detected by observing increasing amounts of the sulfoxide, **13**, with increasing concentrations of **11**. The silicate **12**, on the other hand, does not react with sulfide, **11**.

In Figure 32.4, the **PS** is also shown (k_X) abstracting a α-hydrogen to produce the S-hydroperoxy sulfonium ylide, **SY**. Several groups [53–58] have suggested this ylide as an intermediate and it has been located as a viable species using a variety of different computational models [49,59–61]. Dimethyl S-hydroperoxysufonium ylide exists in several conformations but the most stable is the rotomer in which the peroxy hydrogen is located 3.15 Å above the CH_2 group [46]. This is the ideal geometry for the subsequent reaction that involves attack of the starting material on the peroxy linkage, delivery of the hydroperoxy hydrogen back to the α-carbon, and formation of two sulfoxide products. At the MP2/6-311+G(2df) level of theory, dimethyl S-hydroperoxysulfonium ylide has a short 1.62 Å CH_2–S bond indicative of substantial double bond character and a long 1.85 Å S–O bond similar to that found in sulfuranes. G2-extrapolated CCSD(T)/6-311+G(2df) energies place the **SY** 6 kcal/mol lower in energy than the **PS**.

A transition state has been located for interconversion of dimethyl persulfoxide to dimethylhydroperoxysulfonium ylide with the CCSD(T)/6-31G(d) computational model. It is 6 kcal/mol above the **PS** and is characterized by S–O and C–H bond lengths of 2.02 Å and 1.44 Å, respectively. A thiadioxirane, **TD**, (Figure 32.5) has also been located computationally [46]. However, the barrier for its formation from

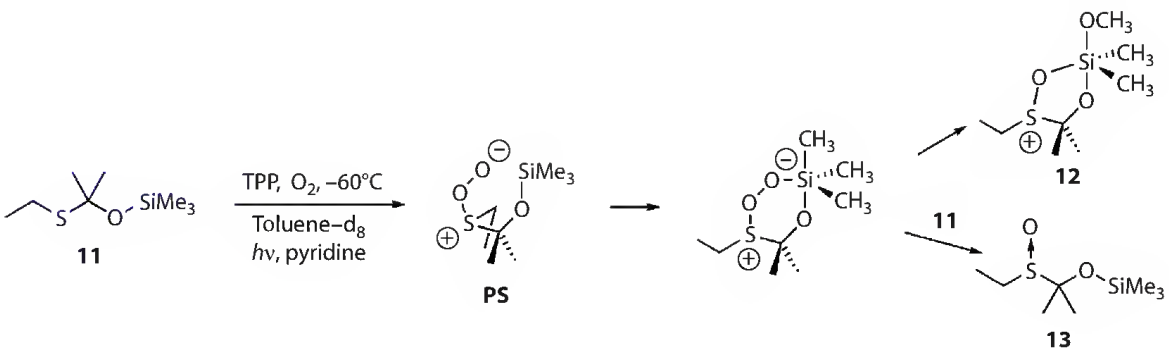

FIGURE 32.6 Trapping of a persulfoxide by silicate formation.

the **PS** is considerably larger than the barrier for formation of **SY** and it is not likely to be an important intermediate on the reaction path to the sulfoxide.

Experimental evidence for the interconversion of the **PS** and **SY** is also compelling. For example, photooxygenations of 1,3-dithianes **14** and **15**, occur with substantial isotope effects at C_2 to give a sulfoxide as the exclusive product [62]. (Figure 32.7) In addition, the isolation of an unusual dimer during photooxygenation of 1,3-dithiane **16** is most easily rationalized by invoking an intramolecular electron transfer in the hydroperoxysulfonium ion intermediate to give a captodatively stabilized radical, **17**. Formation of 1,2-dithiolane, **18**, and a 1,2-dithiolane-oxide, **19**, provide supporting evidence for this mechanism. A smaller, yet substantial isotope effect, in the photooxygenation of 2,2,6,6-tetradeuterio-1,4-dithiane, **20**, provides evidence for the generality of **SY** formation even in simple sulfides with less acidic α-hydrogens [63]. (Figure 32.7) An independent confirmation of **SY** formation was also provided by photooxygenation of β-chloroethyl ethyl sulfide, **21**, that formed an elimination product by β-elimination in a hydroperoxysulfonium ion intermediate [64].

Persulfoxide will also undergo several other reactions not depicted in Figure 32.4. For example, persulfoxides are susceptible to attack by nucleophiles at the sulfonium ion center. Dialkyl sulfides are in general too sterically bulky to function as nucleophiles in this reaction. An exception to this generalization, however, occurs in the photooxygenation of thietane, **22** [65]. (Figure 32.8) Thietane **22** and a

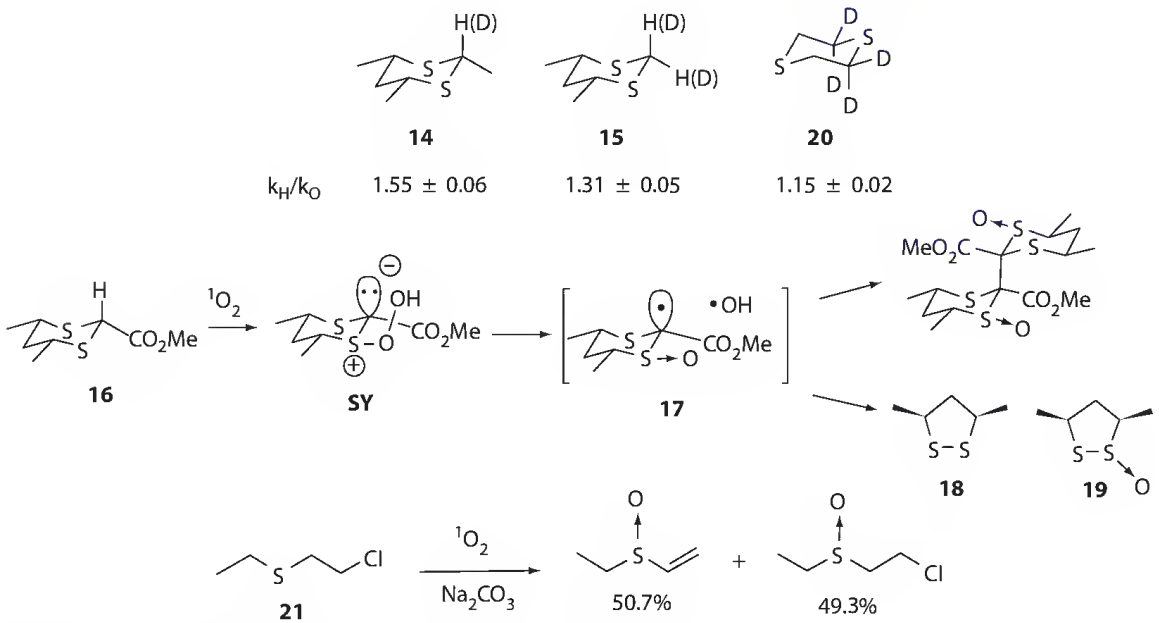

FIGURE 32.7 Evidence for S-Hydroperoxysulfonium ylide formation.

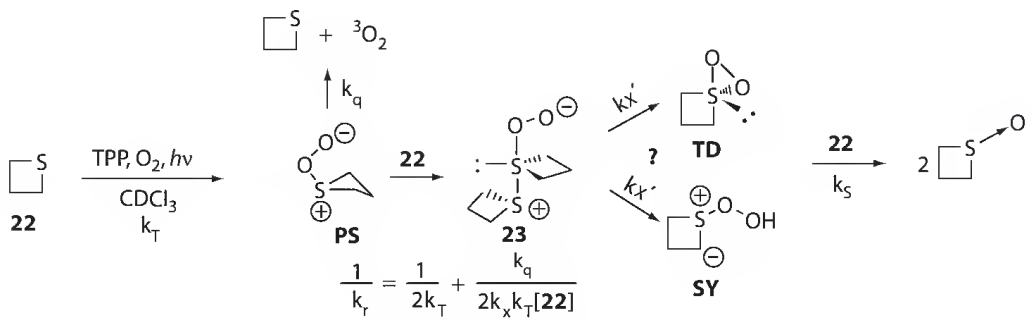

FIGURE 32.8 Mechanism of photooxygenation of thietane.

typical sulfide such as diethyl sulfide quench the emission of singlet oxygen at approximately the same rate, $(3.13 \pm 0.22) \times 10^7\ M^{-1}s^{-1}$ and $(3.04 \pm 0.52) \times 10^7\ M^{-1}s^{-1}$, respectively, suggesting that in both cases the initial interaction with singlet oxygen leads to a **PS**. However, under conditions where all the singlet oxygen is captured, the extent of product formation is dependent upon the thietane concentration but independent of diethyl sulfide concentration. This observation can easily be accommodated by suggesting that thietane attacks the **PS** to form a sulfurane intermediate, **23**, and competes with chemically unproductive physical quenching, k_q. The straight line observed when plotting the inverse of the chemical rate constant of product formation, $1/k_r$, versus the inverse of the sulfide concentration, 1/[22], is consistent with this mechanism. The intercept/slope ratio in this plot, k_X/k_q, reveals that addition of **22** to the **PS** is six times faster than decomposition of the persulfoxide via the physical quenching route, k_q. The unusual behavior of **22** in comparison to other sulfides is a result of the smaller C–S–C angle of 78°, compared to the MP2/6-31G(d) C–S–C angle in dimethyl sulfide of 98.6°, which allows for unencumbered approach to the sulfonium-like sulfur in the **PS**. The identity of an electrophilic intermediate trapped in this reaction has not been conclusively identified (vide infra); however, a hydroperoxy sulfonium ylide, **SY**, or thiadioxirane, **TD** are likely candidates.

Oxygen nucleophiles can also attack at the sulfonium center in the **PS**. For example, the attack of a hydroxyl group at the sulfonium sulfur of a **PS** is responsible for the formations of unusual oxidative elimination products during the photooxygenations of a series of γ-hydroxyalkyl aryl sulfides, **24** [66,67]. (Figure 32.9) The addition of the hydroxyl group to the sulfonium sulfur generates diastereomeric sulfuranes that decompose by intramolecular hydrogen abstraction to form a novel hydrated sulfone that looses water to form the unusual elimination products. (Figure 32.9) When ^{17}O labeled starting material, **24**-^{17}O, was used, the label quantitatively migrated to the sulfur consistent with this mechanism. In addition, the ^{17}O was only found in the alkenes and not in the sulfoxide or sulfone **25** formed by the normal sulfide photooxygenation mechanism shown in Figure 32.4.

Persulfoxides can also function as hydrogen bond acceptors [68]. Additions of as little as 1.5% methanol to benzene has the effect of increasing the rate of photooxygenation of diethyl sulfide by a factor of 10 [69]. This is consistent with hydrogen bonding competitively inhibiting the decomposition of diethyl persulfoxide via the physical quenching reaction channel, k_q. (Figure 32.4) In their 1983 seminal paper discussing the mechanism of sulfide photooxygenation, Foote and coworkers reported that only a single intermediate was necessary to fit the kinetic data in methanol [40]. In that paper they speculated that

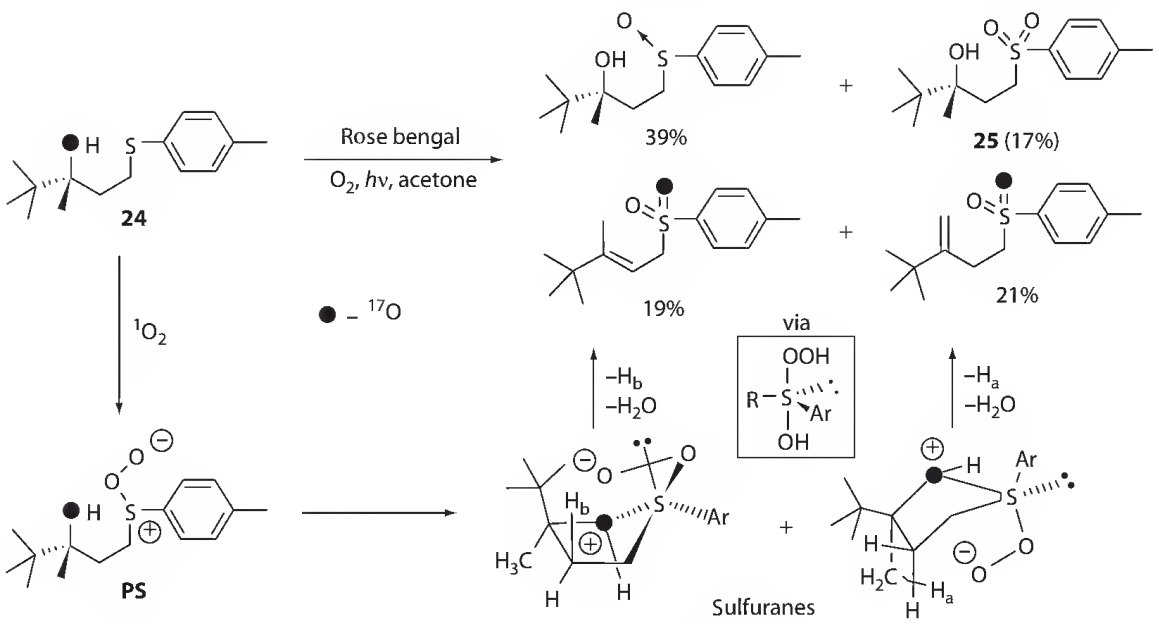

FIGURE 32.9 Addition of an oxygen nucleophile to a persulfoxide.

this result was either consistent with hydrogen bonding to the pendant oxygen of the **PS** or nucleophilic addition to form a sulfurane intermediate. In support of the hydrogen bonding hypothesis, Albini and coworkers have subsequently shown that the rate constants for photooxygenation of diethyl sulfide are linearly correlated to the acid strengths of additives in the reaction [68]. Sulfurane formation, however, certainly occurs as demonstrated by the intramolecular addition shown in Figure 32.9. However, sulfurane formation cannot be responsible for the increased efficiency in the reaction and it is not the kinetically important intermediate formed in protic nucleophilic solvents. This can be deduced by examining the kinetic results depicted in Figure 32.10 from the study of a series of sulfides connected to a hydroxy group with variable length alkyl tethers [70]. The ratio of the physical quenching and chemical reaction rate constants, k_q/k_r, is the smallest for the sulfide that can form a five-membered ring sulfurane (circled value in Figure 32.10). This is consistent with a considerable amount of evidence that five-membered ring bidentate ligands can provide more stabilization to hypervalent species, including sulfuranes, than can ligands that form other ring sizes [71]. However, despite the favorable intramolecular entropic effect and the enthalpic effect of forming a five-membered ring, physical quenching still dominates the reactivity by more than a factor of 30, suggesting that another factor (hydrogen bonding) is responsible for the complete inhibition of physical quenching in protic solvents.

32.2.3 Mechanism of Sulfone Formation

In a large number of sulfide photooxygenations, the sulfoxide product is accompanied by formation of a small amount of sulfone. It is unlikely that the sulfones are formed directly by reactions of sulfoxides with singlet oxygen. Sawaki and Ogata [48] have reported that diphenyl sulfoxide reacts approximately 50 times slower than dimethyl sulfide with singlet oxygen. Trapping the **PS** intermediate by adventitious sulfoxide (k_{SO} in Figure 32.4), however, is a viable pathway to form sulfones. (Figure 32.4)

Careful examination of the photooxygenation of di-n-butyl sulfide in benzene to very low conversions followed by extrapolation back to time zero reveals a sulfone/sulfoxide ratio of approximately ½ [72]. This suggests that trapping, k_{SO} in Figure 32.4, cannot be the only mechanism for sulfone formation. Oxygen-18 tracer studies indicate that both oxygens in the "early formed" sulfone product come from the same oxygen molecule. This data suggest that a thiadioxirane, **TD**, (Figure 32.5) is a potential precursor. However, a detailed theoretical study of the thiadioxirane was unable to locate a path to sulfone [73]. Instead a mechanism involving the hydroperoxy sulfonium ylide, **SY**, is currently thought to

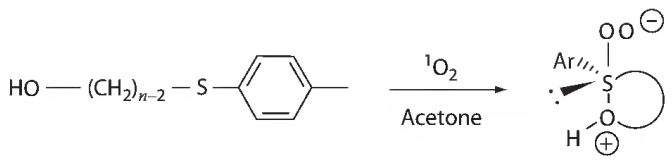

Ring size n	k_T ($M^{-1}s^{-1}$)	k_r ($M^{-1}s^{-1}$)	k_q ($M^{-1}s^{-1}$)	k_q/k_r
4	$(1.5 \pm 0.1) \times 10^6$	$(4.2 \pm 0.3) \times 10^4$	1.46×10^6	34.8
5	$(2.3 \pm 0.2) \times 10^6$	$(7.1 \pm 0.3) \times 10^4$	2.22×10^6	31.3
6	$(2.7 \pm 0.1) \times 10^6$	$(4.1 \pm 0.2) \times 10^4$	2.66×10^6	64.9
7	$(2.9 \pm 0.1) \times 10^6$	$(1.5 \pm 0.1) \times 10^4$	2.88×10^6	192.0
8	$(2.2 \pm 0.1) \times 10^6$	$(0.61 \pm 0.2) \times 10^4$	2.19×10^6	359.0

FIGURE 32.10 Kinetic behavior of hydroxy tethered sulfides.

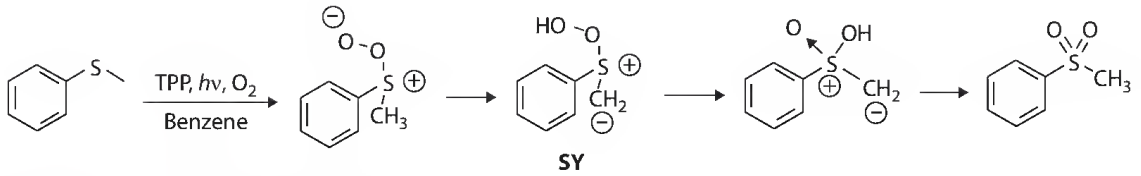

FIGURE 32.11 A mechanism for sulfone formation.

be responsible for sulfone formation in the early part of photooxygenation reactions [61] (Figure 32.11). This mechanism is supported by observation of hydrogen–deuterium exchange during sulfone formation and a kinetic isotope effect, k_H/k_D, of 2–4 in a variety of different solvents [61]. Theoretical calculations (RHF-PM3) also suggest that this pathway is energetically accessible.

32.2.4 Mechanism of Cleavage Product Formation

The cleavage of carbon–sulfur bonds during photooxygenations of organic sulfides was first reported by Corey and Ouannes in 1976 [54]. Two different mechanisms to account for the cleavage reactions have been proposed, as shown in Figure 32.12. In both mechanisms, an α-hydroperoxy sulfide, **HY**, is a key intermediate. In one mechanism, the reaction occurs via the persulfoxide, **PS** (pathway **a** in Figure 32.12) [74], and in the second mechanism the persulfoxide is bypassed completely (pathway **b** in Figure 32.12) [22] and the α-hydroperoxy sulfide is instead formed via a radical pair, **A**. The α-hydroperoxy sulfide, **HY**, can then either decompose by bimolecular reduction with the sulfide (pathway **d** in Figure 32.12) or in a unimolecular process (pathway **c** in Figure 32.12). The electronic character of the sulfide dictates the choice of the intramolecular pathway **c** or intermolecular pathway **d** [74]. For example, the electron-withdrawing group in $EtSCH_2CO_2Et$ destabilizes the three-member oxothiiranium ion and directs the reaction along the intermolecular pathway, **d**. On the other hand, the electron-donating –SEt group in $EtSCH_2SEt$ promotes the intramolecular process and thiosulfinate product, EtS(O)SEt rather than EtSSEt is formed exclusively.

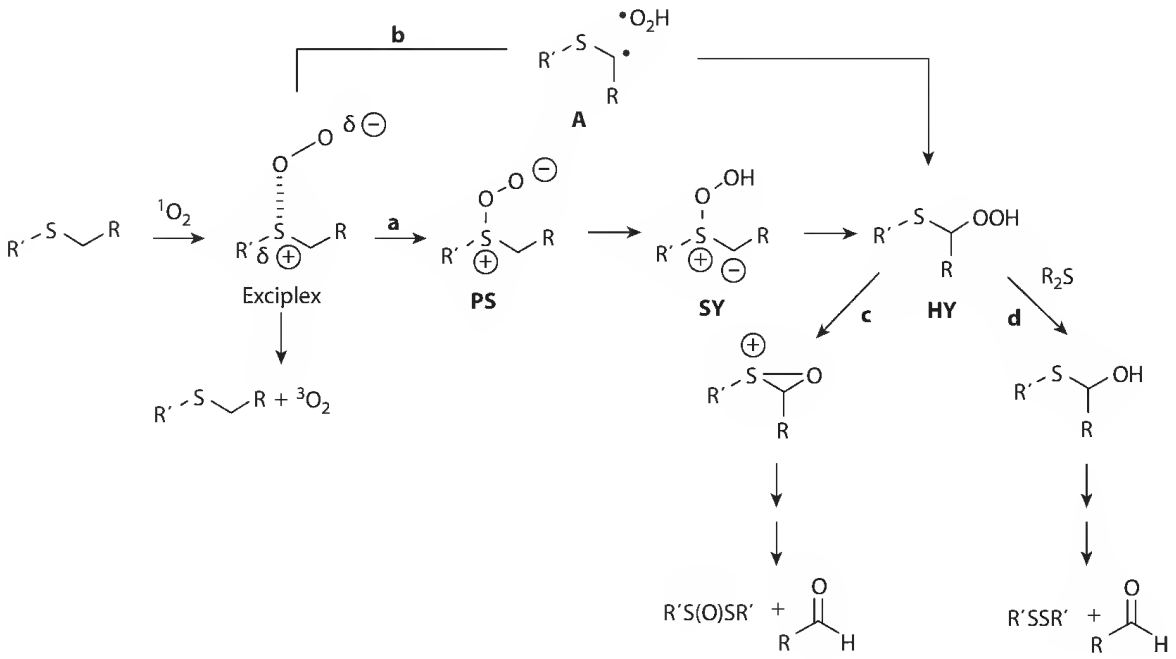

FIGURE 32.12 Mechanism of carbon–sulfur bond cleavage.

32.2.5 Disulfides, Sulfenate Esters, and Sulfenamides

Photooxygenations of sulfenic acid derivatives have not received the same level of investigative interest as dialkyl sulfides. In general, the reactivity with singlet oxygen decreases in the order sulfides > disulfides > trisulfides. (Table 32.1) Furthermore, as the electronegativity of the atom attached to sulfur increases, the rate constants for removal of singlet oxygen from solution decrease. (i.e., dialkyl sulfides > sulfenamides > sulfenate esters) Steric effects play a dominate role in determination of the rate constants for reaction of singlet oxygen with dialkyl sulfides and sufenamides. On the other hand, steric bulk of the substitutents do not control the reactivity of disulfides, and di-*tert*-butyl disulfide actually deactivates singlet oxygen more than four times more efficiently than diethyl disulfide.

Disulfides **26** and **27** (Figure 32.13) react with singlet oxygen to give both thiosulfinates, RS(O)SR, and thiosulfonates, $RS(O)_2R$ [75–78]. Disulfide **26** has the small methyl group appended and disulfide **27** has a constrained $-CH_2SSCH_2-$ dihedral angle allowing unfettered close approach of singlet oxygen to the disulfide linkage to form a persulfoxide, **PS**, intermediate. Formation of the **PS** in the reaction with **27** also replaces a destabilizing electron lone-pair–lone-pair interaction with a less destabilizing bonding-pair–lone-pair electronic interaction. However, many disulfides only physically deactivate singlet oxygen without giving any product [79]. A plot of log k_T versus IP_{eV} for these disulfides is linear (Figure 32.14) consistent with a charge-transfer mechanism for deactivation of singlet oxygen. The deviation of both disulfides **26** and **27** from the linear regression line reflects both deactivation of singlet oxygen by chemical reaction and by decomposition of the persulfoxide to disulfide and triplet oxygen.

The remarkable solvent effect observed during photooxygenation of **27** is a general phenomenon for disulfides and is potentially synthetically useful [80]. The mechanism of this process is not completely understood. However, an oxygen isotopic tracer study has revealed that the two oxygens in the sulfonate product are from the same oxygen molecule [81]. This result differentiates disulfides from every other sulfenic acid derivative and implicates a unique photooxygenation mechanism. It is tempting to suggest that the reaction proceeds by insertion of singlet oxygen into the sulfur–sulfur bond, perhaps via the persulfinate intermediate, to give a dithioperoxide, RSOOSR, that would be expected to decompose to a sulfenate acid radical, RSO•, that would be expected to dimerize to give the thiosulfonate product.

TABLE 32.1 Rate Constants for Deactivation of Singlet Oxygen

	k_T ($M^{-1}s^{-1}$) × 10^{-7}		k_T ($M^{-1}s^{-1}$) × 10^{-7}
Et_2S	1.71	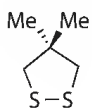	14.4
	1.48	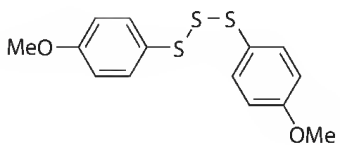	<0.0009
MeSSMe	0.0426	$PhSNHCH_3$	34
EtSSEt	0.0073	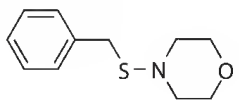	0.128
tBuSStBu	0.0334	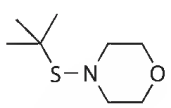	0.00404
	0.0014	PhSOEt	0.0558

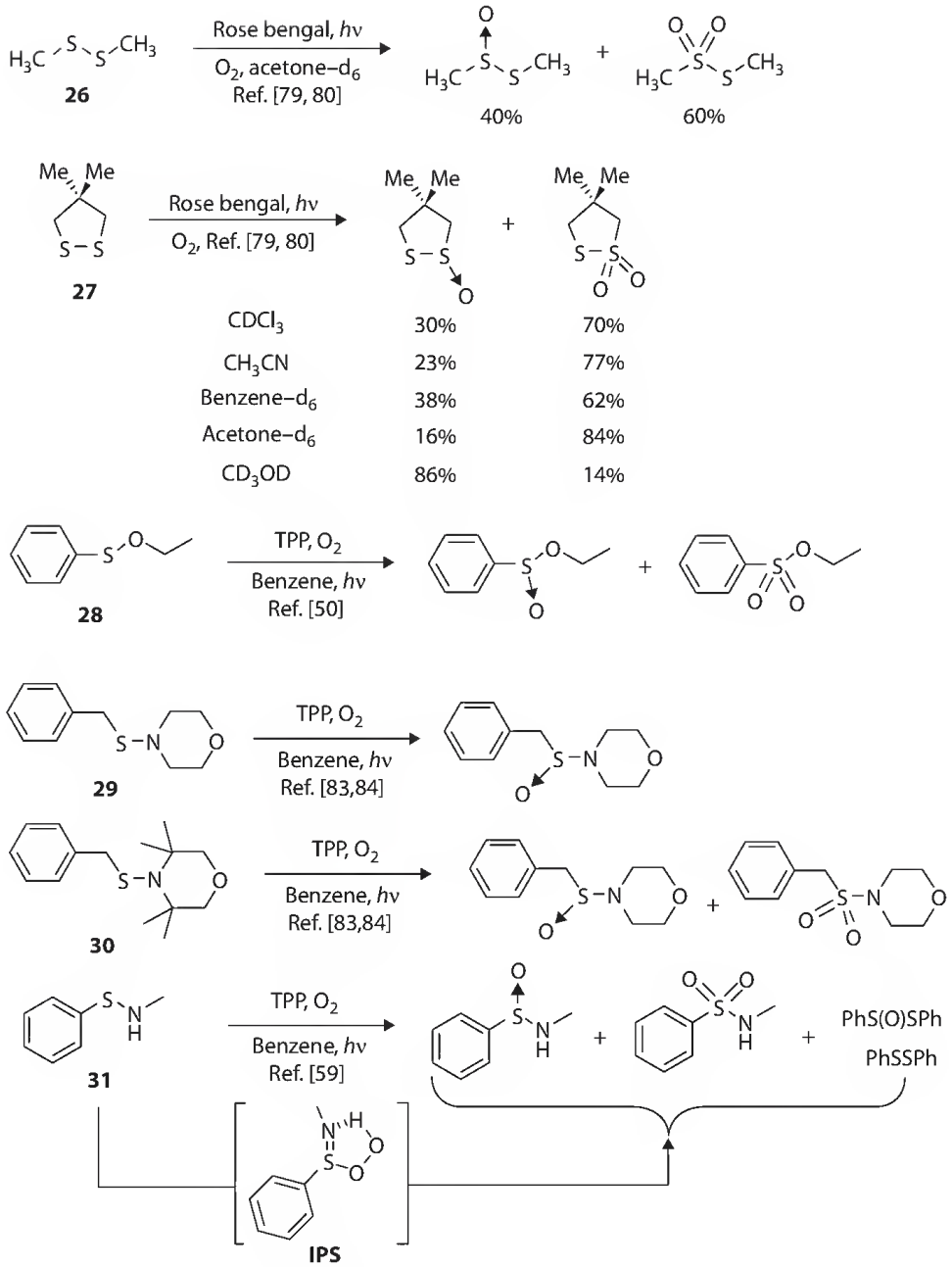

FIGURE 32.13 Sulfenic acid derivative photooxygenation products.

Akasaka and Ando have reported that triazolinediones insert into the sulfur–sulfur bond of disulfides to give the nitrogen analogue of the dithioperoxide [82].

Ethyl phenylsulfenate ester, **28**, reacts with singlet oxygen to give both the sulfinate and sulfonate ester product [50]. At low conversions, the sulfinate ester was the exclusive product consistent with it, acting as the precursor of the sulfonate ester. A careful kinetic study of this reaction reveals that it is 100% efficient and that only one intermediate is kinetically required on the reaction surface. The lack of physical quenching is in stark contrast to the reactions of sulfides in which deactivation of singlet oxygen to form triplet oxygen is often the dominant process. Sulfenamides, **29** and **30**, are in many ways intermediate in reactivity between dialkyl sulfides and sulfenate esters [83,84]. Like sulfides, they react via two intermediates, but **29**, like sulfenate esters, does not physically deactivate singlet oxygen

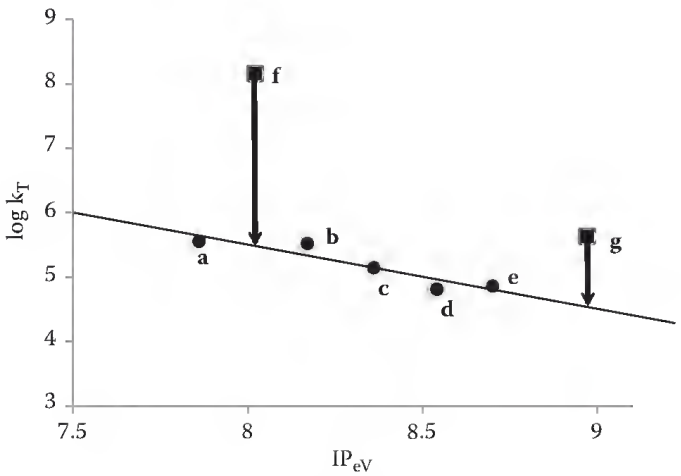

FIGURE 32.14 Log (k_T) versus photoelectron spectroscopy ionization potentials of disulfides. **a**-di-(1-adamantyl) disulfide; **b**-di-*tert*-butyl disulfide; **c**-1,2-dithiacyclohexane; **d**-di-*iso*-propyl disulfide; **e**-diethyl disulfide; **f-27**; **g-26**.

and it chemically reacts with high efficiency. However, *tert*-Butyl 4-morpholinyl sulfide does physically quench singlet oxygen in 45%–55% of its encounters.

The reactions of singlet oxygen with N-monosubstituted sulfenamides, such as **31**, are far more complicated than reactions of N,N′-disubstituted sulfenamides and give poor mass balances [59]. Co-photooxygenations of **31** with norbornene led to the formation of norbornene oxide. Epoxidation was not observed if norbornene was added after completion of the photooxygenation except in the presence of N-*tert*-butylphenyl sulfenamide (PhSNH-*t*-butyl) [59]. This suggests the intriguing possibility that an iminopersulfinic acid (**IPS** in Figure 32.13) is formed in the reaction. Indeed, computational studies with the MP2/6-31G* model were successful in locating an iminopersulfinic acid and established that its minimum energy conformation has an internal hydrogen bond reminiscent of the structures of peracids.

32.2.6 Organometallic Sulfides

Metal-bound thiolate photooxygenations have only been investigated for approximately 15 years. They are of interest to bioinorganic chemists because of numerous reports of oxidative damage to sulfur-rich metalloenzymes. Convincing evidence that this damage occurs in several metalloenzymes by oxidation at sulfur in S-bound cysteine has been reported [85]. Studies of the reactions of singlet oxygen with transition metal thiolates are complicated by reactivity with triplet oxygen that can result in formation of polymetallic complexes [86]. Nevertheless, reactions of singlet oxygen with several organometallic thiolates with sterically shielded sulfurs and/or rigid ligands that stabilize the systems from unwanted side reactions have been examined [86–92] (Figure 32.15). Both persulfoxide and thiadioxirane intermediates have been suggested in these reactions [86]. However, trapping of the persulfoxide with phosphite in the photooxygenation of the Co(III) thiolato complex shown in Figure 32.15 was unsuccessful [93]. It is clear that much work needs to be done to establish the mechanisms of these interesting reactions.

32.2.7 Sulfide Photooxygenations in Heterogeneous Media

Sulfide photooxygenations have been conducted in both micelles [94] and on clay surfaces [95]. However, the most detailed work has been in sensitizer doped zeolite-Y [96]. Zeolites are crystalline porous inorganic solids with long-range order that are better known as molecular sieves. Zeolite-Y is a aluminosilicate characterized by a network of silicon and aluminum tetrahedra with a typical unit cell composition of $M_{56}(AlO_2)_{56}(SiO_2)_{136}\cdot 253(H_2O)$. Zeolite-Y (Figure 32.16) has local T_d symmetry with four

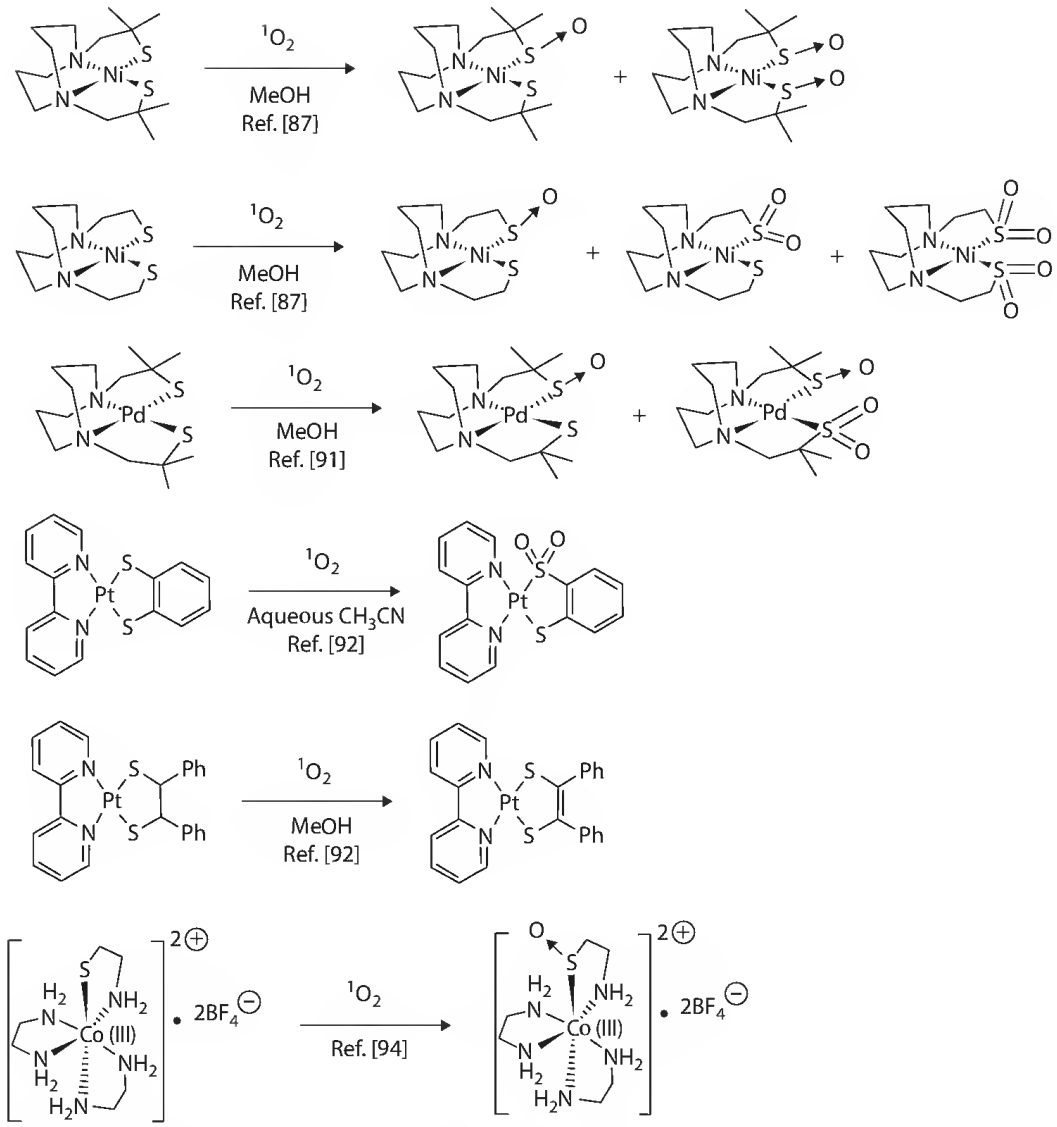

FIGURE 32.15 Photooxygenations of organometallic thiolates.

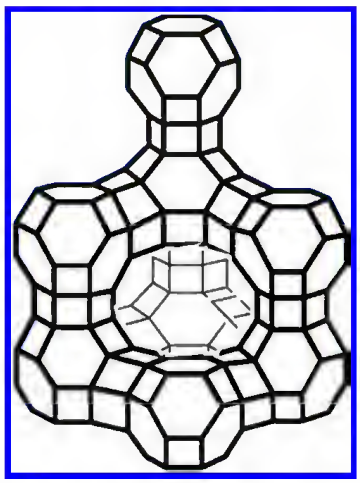

FIGURE 32.16 Convential stick drawing of zeolite-Y with oxygen bridges represented by lines between the vertices.

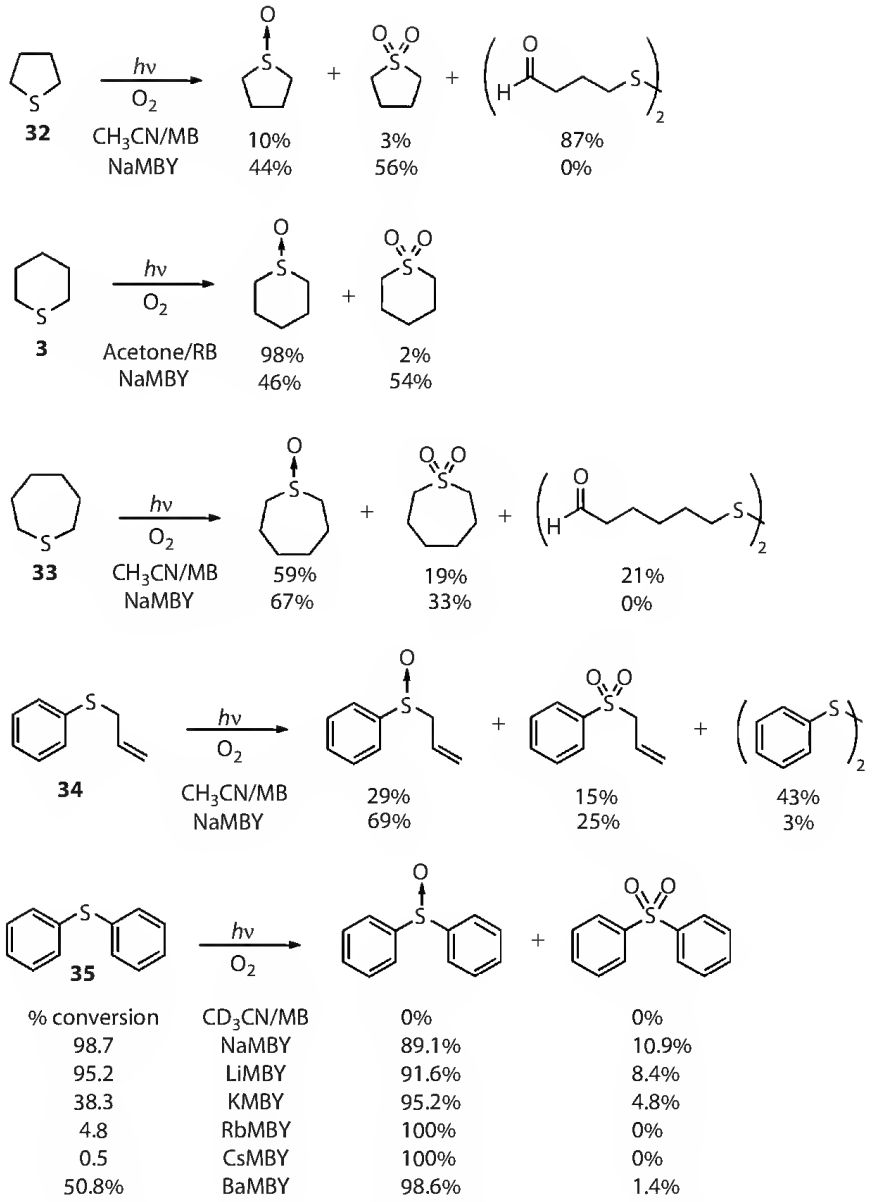

FIGURE 32.17 A comparison of solution and intrazeolite photooxygenations of sulfides.

tetrahedrally disposed 7.4 Å diameter windows surrounding a larger 13Å supercage. The metal ions, M, are needed to provide electrical neutrality and balance the charge on the framework aluminum atoms and their identity determines the void volume of a supercage that is available for substrate intercalation. These cations can also be exchanged in order to modify the electrostatic potential experienced by substrates within the supercage.

The intrazeolite photooxygenations shown in Figure 32.17 were conducted by irradiations of hexane slurries of zeolite-Y doped with both methylene blue (Figure 32.1) and the sulfide substrates [97,98]. The loading level of methylene blue was on average one molecule per every 100 supercages and the loading level of the sulfide was much higher at approximately 1 molecule per supercage. These reactions occur in the interior of the zeolite and involve singlet oxygen since product formation was quenched by addition of 2,3-dimethyl-2-butene, which can migrate into the zeolite, but not by addition of β-carotene, which is size excluded.

Intrazeolite sulfide photooxygenations are very efficient and 100% conversions to products, even with substrates that are unreactive in solution (e.g., **35**), are often observed within 60 min or less. In addition,

the carbon–sulfur bond cleavage reactions, which can dominate many sulfide photooxygenations, are nearly completely suppressed (e.g., **32**, **33**, and **34** in Figure 32.17) in the zeolite. In order to rationalize the remarkable influence of the zeolite environment, a metal complexed persulfoxide has been invoked as the key intermediate. The importance of the metal is especially evident in the reaction of diphenyl sulfide, **35**, (Figure 32.17), which does not react in solution but reacts nearly quantitatively in methylene blue doped sodium Y. The precipitous drop in % conversion of **35** (Figure 32.17) as the sodium is replaced with cations that generate decreasing electrostatic fields is also consistent with stabilization of the persulfoxide by metal complexation. Finally, a dramatic increase in the rate of sulfide photooxygenation in substrates containing a tethered olefinic linkage in the zeolite in comparison to solution is best explained by suppression of physical quenching (k_q in Figure 32.4) by this complexation [99].

32.3 Type I Sulfur Photooxygenations

The vast majority of Type I sulfide photooxygenations occur by sensitized formation of sulfur radical cations. A noteworthy exception to this was recently reported by Shiraishi et al. [100], who reported the photooxygenations of a series of dialkyl sulfides within amphiphilic dendrimers consisting of a benzophenone core, a nonpolar interior, and a polar dendron exterior surface. They suggested that the triplet-excited benzophenone core undergoes energy transfer to give triplet sulfide that reacts with ground state triplet oxygen. These reactions gave exclusively sulfoxide products with no trace of either sulfones or carbon–sulfur cleavage products. The product uniformity along with the lack of substantial quenching by DABCO was used as evidence for the triplet energy-transfer reaction mechanism. No detail on the identity of intermediates or mechanism of oxygen transfer was given.

In 1977, Foote and coworkers [101] reported that 9,10-dicyanoanthracene, **DCA**, (Figure 32.18) sensitized photooxygenation of diphenyl sulfide, **35**, gave diphenyl sulfoxide while diethyl sulfide reacted under the same conditions to give both the sulfoxide and sulfone. Neither reaction was quenched by the potent singlet oxygen quencher, β-carotene. These workers suggested that **DCA** was acting as an electron shuttle removing an electron from the sulfide and donating it to oxygen. The efficiency of the reaction is governed by the competition between return electron transfer (RET in Figure 32.18) and trapping of the DCA radical anion with oxygen to give superoxide. The sulfoxides and sulfones were subsequently formed in a reaction between the superoxide and sulfide radical cation. (Figure 32.18)

Foote and coworkers never suggested a structure for the initial adduct formed in the reactions between superoxide and the sulfides; however, several authors have assumed that it is a persulfoxide [102,103]. However, this view changed in 2003 when Baciocchi and coworkers [104] reported that diphenyl sulfoxide does not trap an intermediate in electron-transfer-initiated photooxygenations. (Figure 32.19) On the other hand, they reported that the intermediate formed in the reaction between thianthrene, **TA**, radical cation, and KO_2 is capable of oxidizing diphenyl sulfide [105]. These results led to the suggestion that a thiadioxirane rather than a persulfoxide is the key intermediate in sulfide radical cation-mediated photooxygenations [106] (Figure 32.19).

The key feature of the **DCA** (Figure 32.18) and **NMQ**$^+$ (Figure 32.19) catalyzed Type I photooxygenations is the ability of the reduced sensitizers (**DCA**• and **NMQ**•) to transfer an electron to triplet oxygen

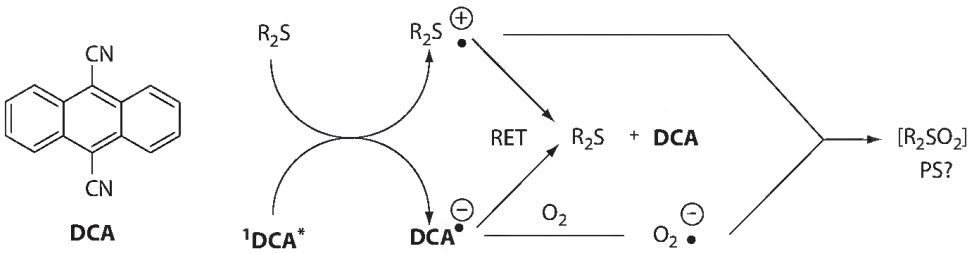

FIGURE 32.18 Mechanism of 9,10-dicyanoanthracene photooxygenations of sulfides.

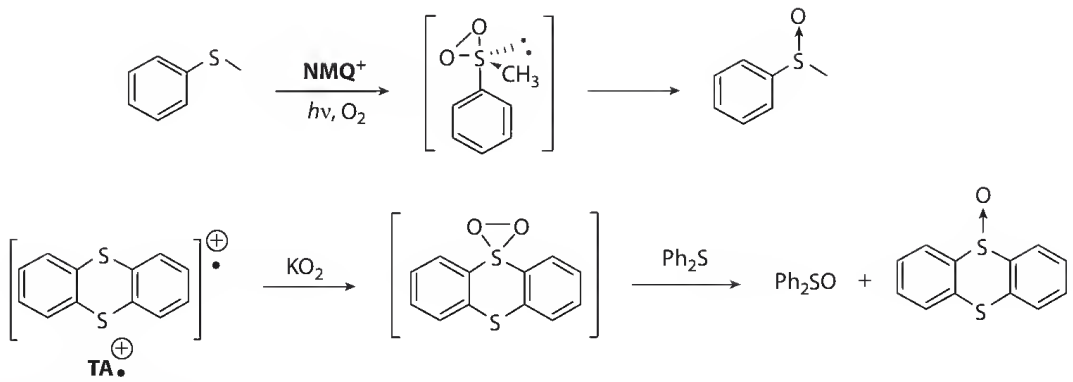

FIGURE 32.19 Sulfide photooxygenations involving thiadioxirane intermediates.

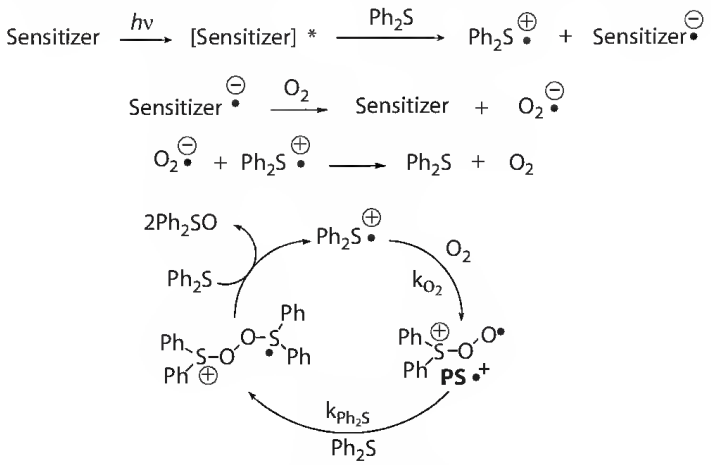

FIGURE 32.20 A chain mechanism for a type I sulfide photooxygenation.

to generate superoxide $\mathbf{O_2}$•. On the other hand, 2,4,6-triarylpyrylium tetrafluoroborates (Figure 32.1) catalyze sulfide Type I photooxygenations despite the fact that the pyrylium radicals are thermodynamically incapable of reducing oxygen. In order to rationalize these non-superoxide photooxygenations, Che [107] and Memarian [108] have both suggested mechanisms initiated by direct reaction of the sulfide radical cation with oxygen to give a persulfoxide radical cation, $\mathbf{PS^+}$•. (Figure 32.20) However, this reaction is not observed on the pulse radiolysis time scale [109,110] and a detailed computational study by Huang and Rauk [111] was unable to locate a bound structure corresponding to $\mathbf{PS^+}$•. Instead, they located a loose ion-dipole complex between oxygen and dimethyl sulfide radical cation bound by 3.2 kcal/mol, with a sulfur–oxygen distance only slightly shorter than the sum of the van der Waals radii.

In 2006, Albini and coworkers pointed out that unproductive electron transfers between superoxide and sulfur radical cations are substantially more exothermic than reactions to form thiadioxiranes [112]. Consequently, they rejected the Baciocchi thiadioxirane mechanism [104] and instead suggested the chain reaction depicted in Figure 32.20. They circumvent the problem with the instability of $\mathbf{PS^+}$• by suggesting its rapid trapping by the sulfide substrate to give an unusual dithioperoxide radical cation, Ph_2S^+-OOS•$(Ph)_2$. However, in 2008, Clennan and Liao [113] reported that the mechanism shown in Figure 32.20 is not general and that the function of electron-transfer sensitizers can be more complex than simply fulfilling a role as an electron shuttle.

Acknowledgment

The author thanks the National Science Foundation for the generous support of his research.

References

1. Gilbert, D. L. In *Oxygen and Living Processes. An Interdisciplinary Approach*; Gilbert, D. L., Ed.; Springer-Verlag: New York, 1981, pp. 1–43.
2. Gilbert, D. L. In *Oxygen and Living Processes. An Interdisciplinary Approach*; Gilbert, D. L., Ed.; Springer-Verlag: New York, 1981, pp. 73–101.
3. *Singlet Molecular Oxygen*; Schaap, A. P., Ed.; Dowden, Hutchinson & Ross Inc.: Stroudsburg, PA, 1976; Vol. 5.
4. Lewis, G. N. *Chem. Rev.* 1924, *1*, 231–248.
5. Lewis, G. N. *J. Am. Chem. Soc.* 1924, *46*, 2027–2032.
6. Mulliken, R. S. *Nature* 1928, *122*, 505.
7. Mulliken, R. S. *Rev. Mod. Phys.* 1932, *4*, 54–56.
8. Kautsky, H.; De Bruijn, H. *Naturwiss.* 1931, *19*, 1043.
9. Kautsky, H.; de Brujin, H.; Neuwirth, R.; Baumeister, W. *Chem. Ber.* 1933, *66*, 1588–1600.
10. Schmidt, R. *Photochem. Photobiol.* 2006, *82*, 1161–1177.
11. Foote, C. S.; Clennan, E. L. In *Active Oxygen in Chemistry*; Foote, C. S., Valentine, J. S., Greenberg, A., Liebman, J. F., Eds.; Blackie Academic & Professional: New York, 1995; Vol. 2, pp. 105–140.
12. Foote, C. S. *Photochem. Photobiol.* 1991, *54*, 659.
13. Schenck, G. O.; Krauch, C. H. *Angew. Chem.* 1962, *74*, 510.
14. Latour, V.; Pigot, T.; Simon, M.; Cardy, H.; Lacombe, S. *Photochem. & Photobiol. Sci.* 2005, *4*, 221–229.
15. Cauzzo, G.; Gennari, G.; Da Re, F.; Curci, R. *Gazz. Chim. Ital.* 1979, *109*, 541–544.
16. Bonesi, S. M.; Fagnoni, M.; Albini, A. *J. Org. Chem.* 2004, *69*, 928–935.
17. Jensen, F.; Foote, C. S. *J. Am. Chem. Soc.* 1987, *109*, 1478–1485.
18. Clennan, E. L.; Wang, D.-X.; Yang, K.; Hodgson, D. J.; Oki, A. R. *J. Am. Chem. Soc.* 1992, *114*, 3021–3027.
19. Akasaka, T.; Kako, M.; Sonobe, H.; Ando, W. *J. Am. Chem. Soc.* 1988, *110*, 494–496.
20. Ando, W.; Sonobe, H.; Akasaka, T. *Tetrahedron Lett.* 1986, *27*, 4473–4476.
21. Ando, W.; Nagashima, T.; Saito, K.; Kohmoto, S. *J. Chem. Soc. Chem. Commun.* 1979, 154–156.
22. Baciocchi, E.; Del Giacco, T.; Lanzalunga, O.; Lapim, A. *J. Org. Chem.* 2007, *72*, 9582–9589.
23. Bonesi, S. M.; Fagnoni, M.; Monti, S.; Albini, A. *Photochem. & Photobiology* 2004, *3*, 489–493.
24. Naumov, V. A.; Tafipol'skii, M. A.; Naumov, A. V. *Russ. J. General Chem.* 2007, *77*, 1268–1274.
25. Clennan, E. L. Calculations at the B3LYP/6–31G(d) level of theory. unpublished results.
26. Song, K.; Wu, L.-Z.; Yang, C.-H.; Tung, C.-H. *Tetrahedron Lett.* 2000, *41*, 1951–1954.
27. Gollnick, K.; Griesbeck, A. G. *Tetrahedron Lett.* 1984, *25*, 4921–4924.
28. Song, K.; Peng, M. L.; Xu, M.; Wu, L. Z.; Zhang, L. P.; Tung, C. H. *Tetrahedron Lett.* 2002, *43*, 6633–6636.
29. Adam, W.; Arias, L. A.; Scheutzow, D. *Tetrahedron Lett.* 1982, *23*, 2835–2836.
30. Adam, W.; Kumar, A. S.; Saha-Möller, C. R. *Tetrahedron Lett.* 1995, *36*, 7853–7854.
31. Stensaas, K. L.; McCarty, B. V.; Touchette, N. M.; Brock, J. B. *Tetrahedron* 2006, *62*, 10683–10687.
32. Cermola, F.; Guaragna, A.; Iesce, M. R.; Palumbo, G.; Purcaro, R.; Rubino, M.; Tuzi, A. *J. Org. Chem.* 2007, *72*, 10075–10080.
33. Clennan, E. L.; Chen, X. *J. Am. Chem. Soc.* 1989, *111*, 5787–5792.
34. Clennan, E. L.; Chen, X. *J. Am. Chem. Soc.* 1989, *111*, 8212–8218.
35. Ando, W. *Sulfur Reports* 1981, *1*, 147–213.
36. Ando, W.; Takata, T. In *Singlet* O_2. Reaction Modes and Products. Part 2; Frimer, A. A., Ed.; CRC Press, Inc.: Boca Raton, FL, 1985; Vol. 3, pp. 1–117.
37. Clennan, E. L. In *Advances in Oxygenated Processes*; Baumstark, A. L., Ed.; JAI Press: Greenwich, CT, 1995; Vol. 4, pp. 49–80.
38. Clennan, E. L.; Pace, A. *Tetrahedron* 2005, *61*, 6665–6691.

39. Iesce, M. R.; Cermola, F.; Rubino, M. *Curr. Org. Chem.* 2007, *11*, 1053–1075.
40. Liang, J.-J.; Gu, C.-L.; Kacher, M. L.; Foote, C. S. *J. Am. Chem. Soc.* 1983, *105*, 4717–4721.
41. Gu, C.; Foote, C. S.; Kacher, M. L. *J. Am. Chem. Soc.* 1981, *103*, 5949–5951.
42. Clennan, E. L.; Greer, A. *Tetrahedron Lett.* 1996, *37*, 6093–6096.
43. Akasaka, T.; Yabe, A.; Ando, W. *J. Am. Chem. Soc.* 1987, *109*, 8085–8087.
44. Jensen, F. In *Advances in Oxygenated Processes*; Baumstark, A. L., Ed.; JAI Press: Greenwich, CT, 1995; Vol. 4, pp 1–48.
45. Jensen, F.; Foote, C. S. *J. Am. Chem. Soc.* 1988, *110*, 2368–2375.
46. Jensen, F.; Greer, A.; Clennan, E. L. *J. Am. Chem. Soc.* 1998, *120*, 4439–4449.
47. McKee, M. L. *J. Am. Chem. Soc.* 1998, *120*, 3963–3969.
48. Sawaki, Y.; Ogata, Y. *J. Am. Chem. Soc.* 1981, *103*, 5947–5948.
49. Nahm, K.; Foote, C. S. *J. Am. Chem. Soc.* 1989, *111*, 1909–1910.
50. Clennan, E. L.; Chen, M.-F. *J. Org. Chem.* 1995, *60*, 6444–6447.
51. Clennan, E. L.; Stensaas, K. L.; Rupert, S. D. *Heteroatom Chem.* 1998, *9*, 51–56.
52. Clennan, E. L.; Dillon, D. L. *Tetrahedron Lett.* 1998, *39*, 6827–6830.
53. Akasaka, T.; Sakurai, A.; Ando, W. *J. Am. Chem. Soc.* 1991, *113*, 2696–2701.
54. Corey, E. J.; Ouannes, C. *Tetrahedron Lett.* 1976, 4263–4266.
55. Takata, T.; Hoshino, K.; Takeuchi, E.; Tamura, Y.; Ando, W. *Tetrahedron Lett.* 1984, *25*, 4767–4770.
56. Takata, T.; Huang, L.; Ando, W. *Chem. Lett.* 1985, 1705–1708.
57. Takata, T.; Ishibashi, K.; Ando, W. *Tetrahedron Lett.* 1985, *26*, 4609–4612.
58. Takata, T.; Tamura, Y.; Ando, W. *Tetrahedron* 1985, *41*, 2133–2137.
59. Clennan, E. L.; Chen, M.-F.; Greer, A.; Jensen, F. *J. Org. Chem.* 1998, *63*, 3397–3402.
60. Greer, A.; Chen, M.-F.; Jensen, F.; Clennan, E. L. *J. Am. Chem. Soc.* 1997, *119*, 4380–4387.
61. Ishiguro, K.; Hayashi, M.; Sawaki, Y. *J. Am. Chem. Soc.* 1996, *118*, 7265–7271.
62. Toutchkine, A.; Clennan, E. L. *J. Org. Chem.* 1999, *64*, 5620–5625.
63. Clennan, E. L.; Pan, G.-l. *J. Org. Chem.* 2003, *68*, 5174–5179.
64. Toutchkine, A.; Clennan, E. L. *Tetrahedron Lett.* 1999, *40*, 6519–6522.
65. Clennan, E. L.; Dobrowolski, P.; Greer, A. *J. Am. Chem. Soc.* 1995, *117*, 9800–9803.
66. Clennan, E. L.; Yang, K. *J. Am. Chem. Soc.* 1990, *112*, 4044–4046.
67. Clennan, E. L.; Yang, K. *J. Org. Chem.* 1992, *57*, 4477–4487.
68. Bonesi, S. M.; Albini, A. *J. Org. Chem.* 2000, *65*, 4532–4536.
69. Clennan, E. L.; Greer, A. *J. Org. Chem.* 1996, *61*, 4793–4797.
70. Clennan, E. L.; Yang, K.; Chen, X. *J. Org. Chem.* 1991, *56*, 5251–5252.
71. Hayes, R. A.; Martin, J. C. In *Organic Sulfur Chemistry. Theoretical and Experimental Advances*; Bernardi, F., Csizmadia, I. G., Mangini, A., Eds.; Elsevier: Amsterdam, the Netherlands, 1985; Vol. 19, pp. 408–483.
72. Watanabe, Y.; Kuriki, N.; Ishiguro, K.; Sawaki, Y. *J. Am. Chem. Soc.* 1991, *113*, 2677–2682.
73. Jensen, F. *J. Org. Chem.* 1992, *57*, 6478–6487.
74. Toutchkine, A.; Clennan, E. L. *J. Am. Chem. Soc.* 2000, *122*, 1834–1835.
75. Barltrop, J. A.; Hayes, P. M.; Calvin, M. *J. Am. Chem. Soc.* 1954, *76*, 4348–4367.
76. Murray, R. W.; Jindal, S. L. *J. Org. Chem.* 1972, *37*, 3516–3520.
77. Murray, R. W.; Jindal, S. L. *Photochem. Photobiol.* 1972, *16*, 147–151.
78. Murray, R. W.; Smetana, R. D.; Block, E. *Tetrahedron Lett.* 1971, 299–302.
79. Clennan, E. L.; Wang, D.; Clifton, C.; Chen, M.-F. *J. Am. Chem. Soc.* 1997, *119*, 9081–9082.
80. Clennan, E. L.; Wang, D.; Zhang, H.; Clifton, C. H. *Tetrahedron Lett.* 1994, *35*, 4723–4726.
81. Clennan, E. L.; Zhang, H. *J. Org. Chem.* 1994, *59*, 7952–7954.
82. Akasaka, T.; Ando, W. In *Organic Peroxides*; Ando, W., Ed.; John Wiley & Sons: Chichester, West Sussex, England, 1992, pp. 599–659.
83. Clennan, E. L.; Zhang, H. *J. Am. Chem. Soc.* 1994, *116*, 809–810.
84. Clennan, E. L.; Zhang, H. *J. Am. Chem. Soc.* 1995, *117*, 4218–4227.

85. Henderson, R. K.; Bouwman, E.; Spek, A. L.; Reedijk, *J. Inorg. Chem.* 1997, *36*, 4616–4617.
86. Grapperhaus, C. A.; Darensbourg, M. Y. *Acc. Chem. Res.* 1998, *31*, 451–459.
87. Galvez, C.; Ho, D. G.; Azod, A.; Selke, M. *J. Am. Chem. Soc.* 2001, *123*, 3381–3382.
88. Hernandez, B.; Wang, Y. J.; Zhang, D.; Selke, M. *Chem. Commun.* 2006, 997–999.
89. Grapperhaus, C. A.; Darensbourg, M. Y.; Sumner, L. W.; Russell, D. H. *J. Am. Chem. Soc.* 1996, *118*, 1791–1792.
90. Grapperhaus, C. A.; Maguire, M. J.; Tuntulani, T.; Darensbourg, M. Y. *Inorg. Chem.* 1997, *36*, 1860–1866.
91. Connick, W. B.; Gray, H. B. *J. Am. Chem. Soc.* 1997, *119*, 11620–11627.
92. Zhang, Y.; Ley, K. D.; Schanze, K. S. *Inorg. Chem.* 1996, *35*, 7102–7110.
93. Zhang, D.; Hernandez, B.; Selke, M. *J. Sulfur Chem.* 2008, *29*, 377–388.
94. Hovey, M. C. *J. Am. Chem. Soc.* 1982, *104*, 4196–4202.
95. Fujita, S.; Sato, H.; Kakegawa, N.; Yamagishi, A. *J. Phys. Chem. B* 2006, *110*, 2533–2540.
96. Clennan, E. L. In *Adv. Phys. Org. Chem.*; Academic Press, Ltd: London, U.K., 2008, pp. 225–269.
97. Clennan, E. L.; Zhou, W.; Chan, *J. J. Org. Chem.* 2002, *67*, 9368–9378.
98. Zhou, W.; Clennan, E. L. *J. Am. Chem. Soc.* 1999, *121*, 2915–2916.
99. Zhou, W.; Clennan, E. L. *Org. Lett.* 2000, *2*, 437–440.
100. Shiraishi, Y.; Koisumi, H.; Hirai, T. *J. Phys. Chem. B* 2005, *109*, 8580–8586.
101. Eriksen, J.; Foote, C. S.; Parker, T. L. *J. Am. Chem. Soc.* 1977, *99*, 6455–6456.
102. Akasaka, T.; Ando, W. *Tetrahedron Lett.* 1985, *26*, 5049–5052.
103. Baciocchi, E.; Crescenzi, C.; Lanzalunga, O. *Tetrahedron* 1997, *53*, 4469–4478.
104. Baciocchi, E.; Del Giacco, T.; Elisei, F.; Gerini, M. F.; Guerra, M.; Lapi, A.; Liberali, P. *J. Am. Chem. Soc.* 2003, *125*, 16444–16454.
105. Ando, W.; Kabe, Y.; Kobayashi, S.; Takyu, C.; Yamagishi, A.; Inaba, H. *J. Am. Chem. Soc.* 1980, *102*, 4526–4528.
106. See also; Che, Y.; Ma, W.; Ren, Y.; Chen, C.; Zhang, X.; Zhao, J.; Zang, L. *J. Phys. Chem. B* 2005, *109*, 8270–8276.
107. Che, Y.; Ma, W.; Ji, H.; Zhao, J.; Zang, L. *J. Phys. Chem. B* 2006, *110*, 2942–2948.
108. Memarian, H. R.; Mohammadpoor-Baltork, I.; Bahrami, K. *Bull. Korean Chem. Soc.* 2006, *27*, 106–110.
109. Schäfer, K.; Bonifacic, M.; Bahnemann, D.; Asmus, K.-D. *J. Phys. Chem.* 1978, *82*, 2777–2780.
110. Schöneich, C.; Aced, A.; Asmus, K.-D. *J. Am. Chem. Soc.* 1993, *115*, 11376–11383.
111. Huang, M. L.; Rauk, A. *J. Phys. Chem. A* 2004, *108*, 6222–6230.
112. Bonesi, S. M.; Manet, I.; Freccero, M.; Fagnoni, M.; Albini, A. *Chem. Eur. J.* 2006, *12*, 4844–4857.
113. Clennan, E. L.; Liao, C. *J. Am. Chem. Soc.* 2008, *130*, 4057–4068.

33

Porphycenes: Spectroscopy, Photophysics, and Tautomerism

Jacek Waluk
Polish Academy of Sciences

33.1 Introduction

Synthesis of porphycene, first reported in 1986,[1] opened up a new area of interdisciplinary research, devoted to constitutional isomers of porphyrin. Four pyrrole rings and four methine units can be reshuffled in many different ways. Seven "nitrogen in" structural isomers of porphyrin that preserve an N_4 coordination site are possible.[2] Of those, four have been obtained until now—all, except porphycene, in the form of alkylated derivatives.[3–7] In addition, another isomer, labeled "inverted"[8] or "confused"[9] porphyrin, has also been synthesized. The structures and names of these compounds are presented in Figure 33.1.

Owing to their crucial role in such processes as photosynthesis, electron and oxygen transport, and detoxification, porphyrins have justly been dubbed "pigments of life." [10] Their biological importance stems from spectral, photophysical, and redox properties, combined with complexing abilities. An obvious question, therefore, regards these properties in the structural isomers. It turns out that while the basic patterns are often quite similar, quantitative characteristics can make the isomers even more attractive than the parent compound. This is especially true for porphycenes, which remain by far the most investigated class of porphyrin isomers, with ca. 300 different derivatives described in the literature. Various potential applications of porphycenes have been suggested. These include information storage,[11] catalysis,[12] and use of porphycenes as molecular conductors[13] and transistors.[14] Liquid crystalline materials based on porphycenes have been reported.[15] It was also possible to modify proteins by replacing the native heme by an artificial one, based on iron[16] or cobalt[17] porphycenes.

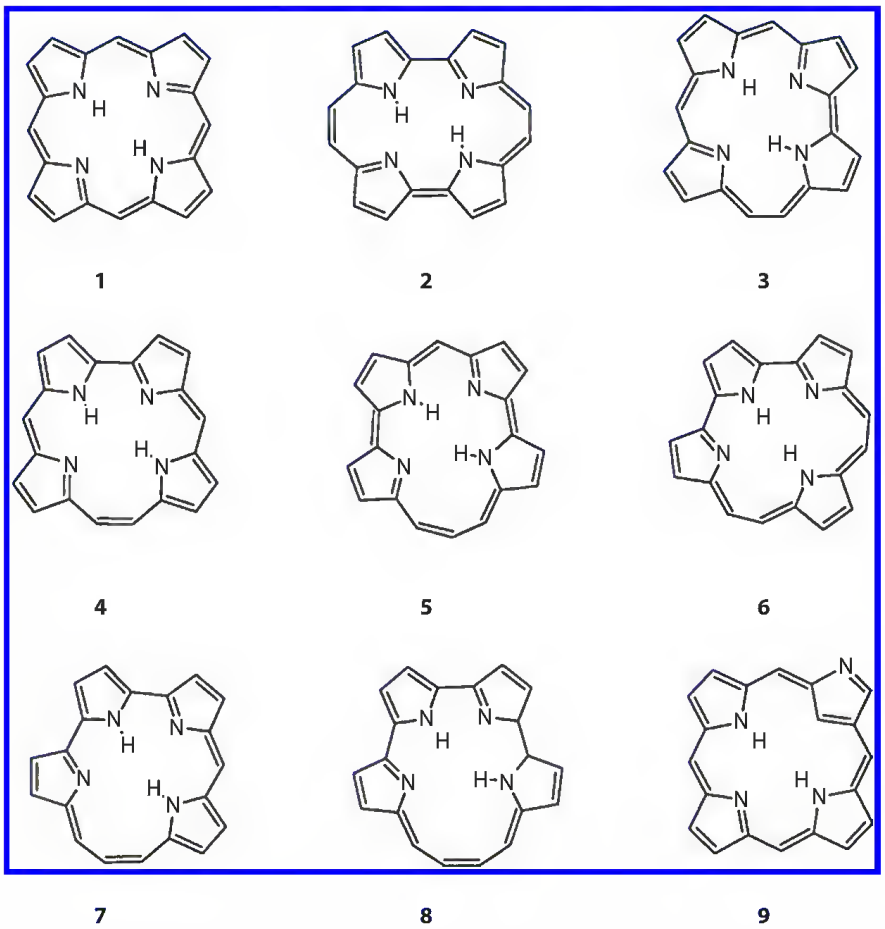

FIGURE 33.1 Porphyrin (**1**) and its constitutional isomers: porphycene (**2**), hemiporphycene (**3**), corrphycene (**4**), isoporphycene (**5**), inverted ("confused") porphyrin (**9**). Molecules **6**–**8** have not yet been synthesized.

A particularly important field where porphycenes are likely to replace porphyrins is photodynamic therapy, destruction of malignant tissue by reactive oxygen species, produced after light absorption by a photosensitizer.[18] Some porphycenes have been found to be much more effective as phototherapeutic agents than Photofrin®, a drug based on a mixture of porphyrin derivatives.[19]

With regard to fundamental research, porphycenes became role models for investigating intramolecular cooperative hydrogen transfer.[20–39] The two inner hydrogen atoms can migrate between four nitrogen atoms which form the inner cavity. The same process has been studied earlier for porphyrins, but the mechanisms are very different for the two isomers. The intramolecular NH···N hydrogen bonds in porphycenes are very strong compared to those in porphyrin. Actually, DFT calculations predict that free base porphycene is lower in energy by about 1.5 kcal mol^{-1} than porphyrin.[40] This is due to the nearly rectangular shape of the cavity in porphycene, enabling short and linear hydrogen bonds. On the other hand, the same property leads to weaker metal-complexing propensity of porphycenes as compared with porphyrins, which have larger and square cavity.

The intramolecular exchange of two hydrogens in porphyrins and porphycenes leads to a chemically equivalent structure (Figure 33.2). The symmetrical double minimum character can be perturbed by appropriate substitution. This provides excellent models for studying tunneling, as it is very sensitive to the shape and symmetry of the potential energy governing the proton/hydrogen transfer. Moreover, studies of porphycenes in the regime of isolated molecule (supersonic jets, helium nanodroplets) provide evidence of coherent double proton tunneling as well as of the multidimensional character of the hydrogen transfer path; the latter is manifested by the coupling between vibrations, involving protons

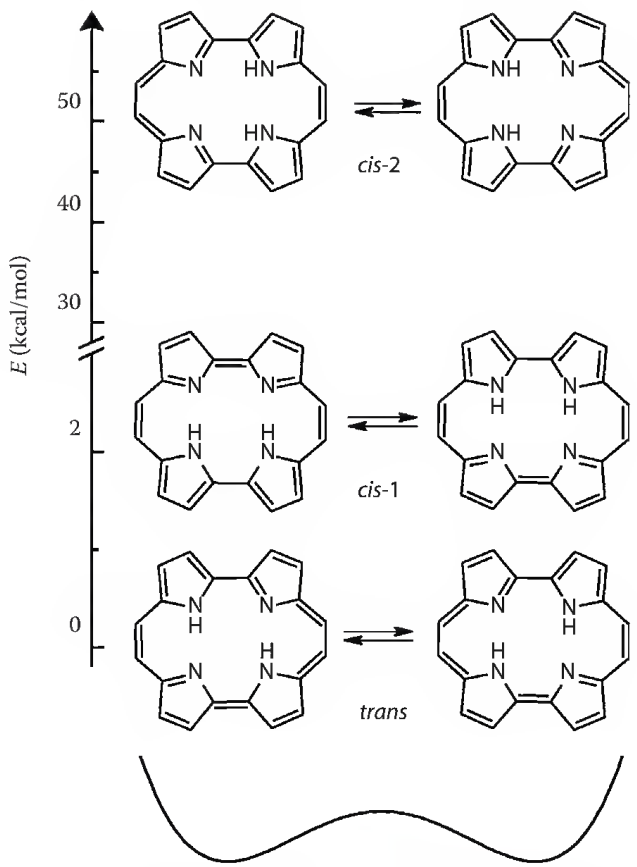

FIGURE 33.2 Possible tautomeric forms of porphycene and their relative energies predicted by calculations. The symmetric double minimum potential character indicated schematically at the bottom.

and heavy atoms. In turn, the fact that two hydrogen bonds are present makes it possible to study cooperativity effects, both in the hydrogen bonds and in tautomerization. Finally, for studies in condensed phase, it is important that the hydrogen transfer occur in the cavity located inside a molecule and well shielded from the environment, which minimizes the influence of the latter.

In this work, we start by presenting the basic features of electronic absorption of porphycenes and the origin of differences with respect to porphyrins. We, then, review the photophysical properties of variously substituted porphycenes (see Figure 33.3 for numbering) and discuss a recently proposed model, which explains large differences in emissive properties in different alkyl derivatives.[41] This model involves intramolecular hydrogen exchange, the primary subject of this paper, discussed further in detail for both the excited and the ground electronic states of porphycenes.

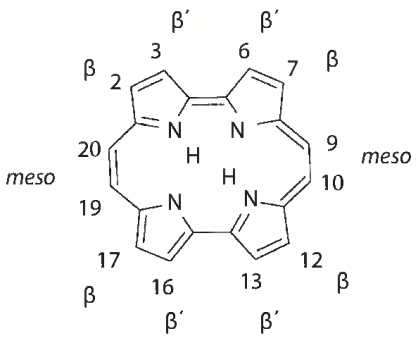

FIGURE 33.3 Atom numbering and symbols indicating the positions of substitution for porphycene.

33.2 Electronic Spectra

The electronic absorption spectra of porphyrins are quite complex and substituent dependent. Different patterns are observed in the region of the low-energy transitions, comprising the so-called Q bands. They correspond to a single, doubly degenerate electronic transition in high-symmetry (D_{4h}) porphyrins. When the symmetry is lowered, the degeneracy is lifted, and two electronic transitions, Q_x and Q_y, are observed. The *x* and *y* indices indicate the transition moment directions. In free-base porphyrin, which has D_{2h} symmetry, *x* corresponds to the direction along the NH···HN bonds and *y* to the in-plane direction perpendicular to it. The intensity of Q bands is usually much lower than that of the Soret bands, observed in the blue part of the visible range (Figure 33.4). Moreover, the 0–0 transition of the lowest energy band is often quite weak, and followed by rich vibronic structure.

The absorption spectra of porphycenes are significantly different from those of the porphyrins (Figure 33.4). Even though the basic pattern, Q transitions followed by stronger Soret bands, is preserved, their intensities are now quite similar. In parent porphycene, the ratio of the absorption coefficient of the maximum of the first Q band to that of the Soret band maximum is about 0.37. This is due to much stronger absorption of porphycenes in the low-energy range, about an order of magnitude larger in porphycenes than in porphyrins. Contrary to the behavior of porphyrins, the absorption intensity of porphycenes is not strongly affected by solvent or substitution. Moreover, the 0–0 transitions are quite strong, and their intensity not much sensitive to substitution or environment.

These differences in absorption patterns can be readily explained using a four orbital model, developed for porphyrins by Gouterman[42] and extended by Michl,[43] as a "perimeter model" in order to interpret the absorption and magnetic circular dichroism (MCD) spectra of 4N+2 π electrons aromatic compounds. The properties of four lowest ππ* electronic states may be described by taking into account four singly excited configurations involving single electron promotions from the two highest occupied π orbitals (HOMO) into the two lowest unoccupied ones (LUMO). Configuration interaction leads to four electronic transitions of which the intensities depend on the relative energy splittings in the pairs of LUMO and HOMO. In Michl's terminology, the situation where the splittings are equal or similar (ΔHOMO ≈ ΔLUMO) corresponds to the so-called "soft chromophores," whereas molecules characterized by ΔHOMO > ΔLUMO or ΔHOMO < ΔLUMO are labeled "hard chromophores" (positively hard or negatively hard, respectively).

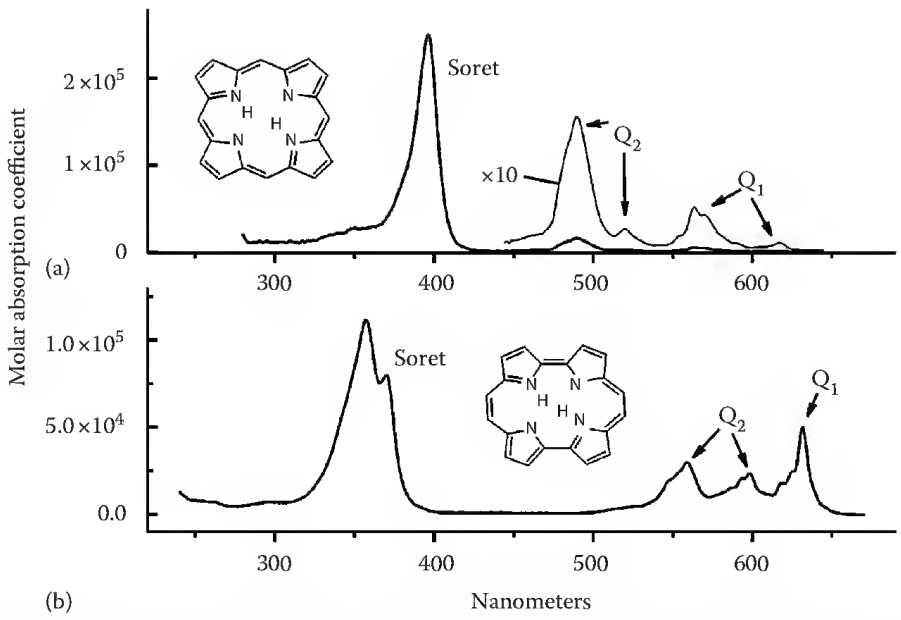

FIGURE 33.4 Electronic absorption spectra of porphyrin in toluene (a) and porphycene in *n*-hexane (b) at 293 K. The positions of Q and Soret bands are indicated.

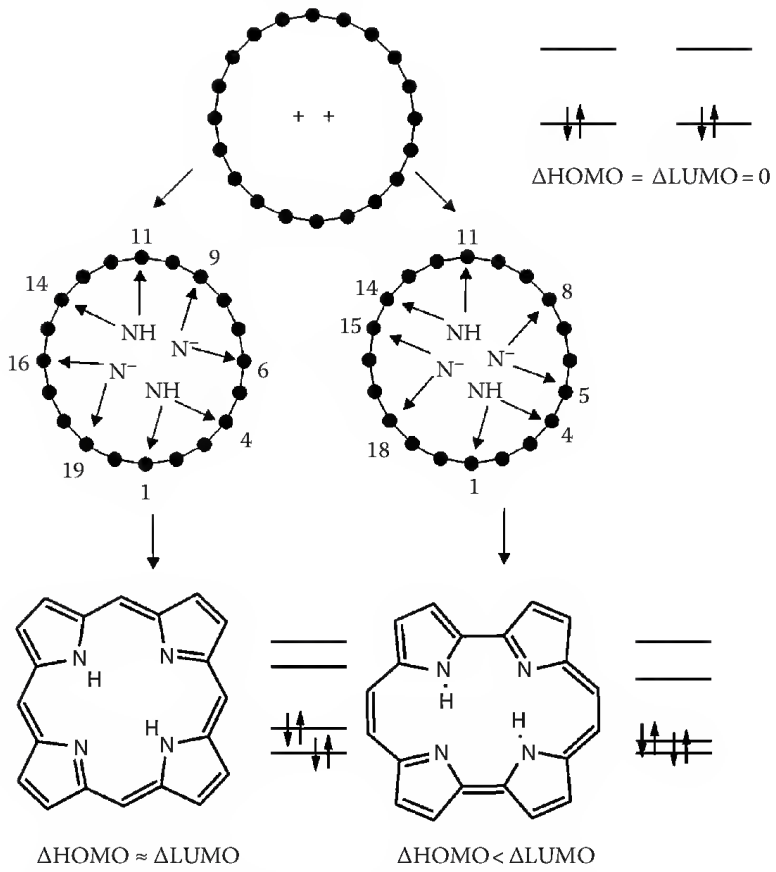

FIGURE 33.5 Derivation of porphyrin and porphycene from a 4N+2 electron $C_{20}H_{20}^{++}$ ideal perimeter and the resulting orbital splitting patterns.

The splitting pattern is quite easy to predict: it can be done by inspecting the nodal properties of the orbitals of the parent 4N+2 π electrons [n]-membered perimeter. For porphyrin and its isomers, this perimeter corresponds to $C_{20}H_{20}^{++}$, containing 18 electrons. Formation of a molecule from an ideal perimeter is treated by introducing two NH and two N^- bridges (Figure 33.5). This lifts the degeneracy of HOMO and LUMO pairs. Due to different topology of the two isomers, ΔHOMO ≈ ΔLUMO for porphyrin, whereas for porphycene, ΔHOMO << ΔLUMO. The former is thus a soft chromophore, while the latter is a negatively hard chromophore. It has been demonstrated that the intensity of Q transitions relative to the Soret ones should grow with the increasing difference in the HOMO and LUMO splittings. Different absorption patterns of porphyrins and porphycenes can then be understood.

Differences between soft and hard chromophores are even more spectacular when probed by MCD spectroscopy. For the two lowest electronic transitions, the sign of Faraday *B* terms, which characterize the MCD spectra, is determined by the sign of ΔHOMO - ΔLUMO. For soft chromophores, such as porphyrins, it is, therefore, very sensitive even to minor structural perturbations, for example, substitution or change in the tautomeric equilibrium involving the inner protons. For hard chromophores, however, this is not the case. Since in porphycenes ΔHOMO << ΔLUMO, a –,+ sequence of *B* terms is predicted. This sequence is not expected to change for differently substituted porphycenes. Indeed, the same pattern of MCD spectra has been observed for all porphycenes studied so far, including free bases, dianions, dications, and metal complexes. As an example, Figure 33.6 shows the absorption and MCD spectra of porphycene and three differently substituted derivatives.

According to the perimeter model, porphycene is the strongest hard chromophore of all the porphyrin isomers. Corrphycene should be a soft chromophore, whereas hemiporphycene, a hard one. The absorption and MCD characteristics of the latter are expected to resemble those of porphycene, whereas

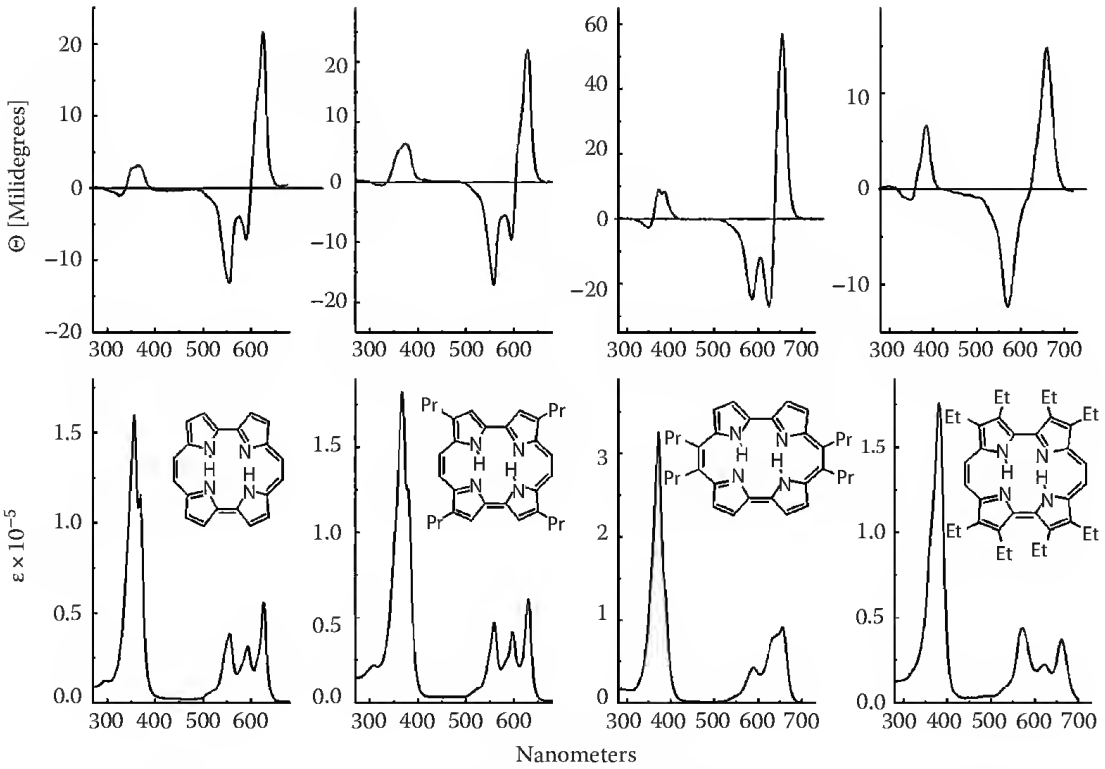

FIGURE 33.6 Bottom, absorption, top, MCD spectra recorded in acetonitrile at 293 K. From left to right: parent porphycene, 2,7,12,17-tetra-*n*-propylporphycene, 9,10,19,20-tetra-*n*-propylporphycene, and 2,3,6,7,12,13,16,17-octaethylylporphycene.

those of the former should be similar to the spectral properties of porphyrin. This was first predicted theoretically[2] and confirmed experimentally a decade later for corrphycene[44] and hemiporphycene,[45] when both compounds became available.

33.3 Photophysics

The photophysical properties of metalloporphycenes or free base porphycenes substituted by heavy atoms are similar to the properties of porphyrin analogues. Fluorescence is weak, and the dominant channel of S_1 deactivation is the intersystem crossing to the triplet state.[46–48] Usually, singlet oxygen formation is very efficient and its yield is close to that of triplet formation. The differences between porphyrins and porphycenes are more pronounced for free bases not containing heavy atoms. Fluorescence quantum yields of free base porphyrins are usually a few percent, whereas the lifetime is about 10 ns. The dominant depopulation channel of the lowest excited singlet state is the intersystem crossing to the triplet manifold. In free base porphycenes, fluorescence quantum yield and lifetime depend strongly on the position of substitution. In the parent, unsubstituted porphycene, quantum yields of fluorescence and intersystem crossing are similar, about 40%; this implies that about 20% of the molecules decay via internal conversion to the ground state. Very similar photophysical parameters are observed for porphycenes substituted by alkyl groups in the β positions (2,7,12,17, cf. Figure 33.3); substitution by phenyl leads to about two-fold decrease in fluorescence intensity.[47] Octuple alkyl substitution in the β and β′ positions (2,3,6,7,12,13,16,17) leads to the decrease of fluorescence intensity and lifetimes by a factor of 20–50. Even more drastic effects are observed for *meso*-substituted tetraalkylporphycenes: in liquid, nonviscous solutions fluorescence intensity and lifetime are several hundred times lower than those of the parent compound. The dominant radiationless process is the S_1–S_0 internal conversion. An important observation is that for weakly emitting *meso*-tetraalkylporphycenes and octaethylporphycenes the emission characteristics are strongly viscosity dependent. In rigid

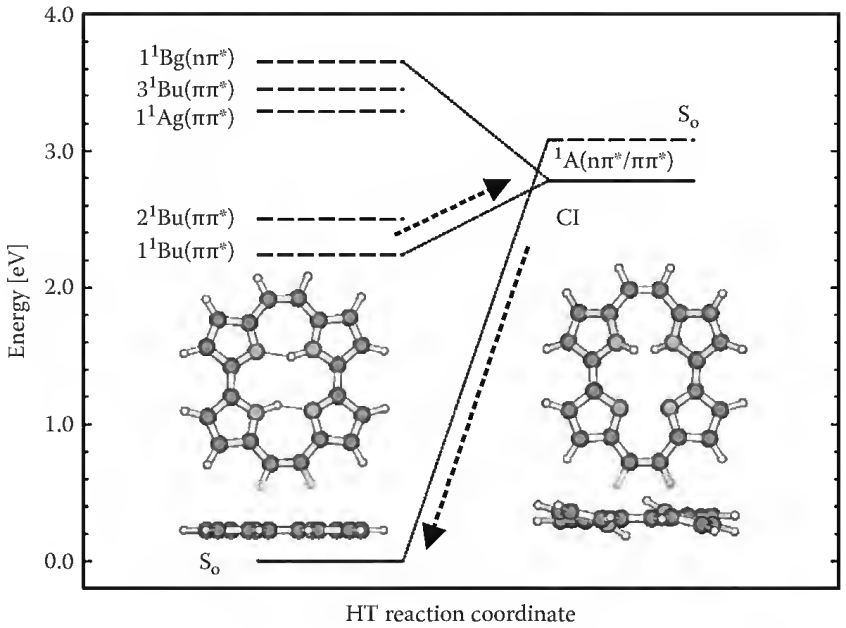

FIGURE 33.7 Correlation of electronic states in *trans* and *cis*-2 tautomeric forms of porphycene, resulting in the appearance of conical intersection (CI). The dashed arrows indicate the excited state radiationless deactivation pathway along the hydrogen transfer coordinate. (Adapted from Sobolewski, A., Gil, M., Dobkowski, J., and Waluk, J., *J. Phys. Chem. A* 113, 7714–7716, 2009. Copyright 2009 American Chemical Society.)

environments such as polymer films, both fluorescence yield and decay time increase, approaching the values observed for low-temperature glassy solvents. This finding, combined with ab initio calculations, has led to the suggestion that the origin of the radiationless process responsible for deactivation is the conical intersection along the hydrogen transfer path corresponding to *trans–cis*-2 conversion (Figure 33.7).[41] Interestingly the *cis*-2 tautomeric structure, with protons localized on the pyrroles linked to the same ethylene bridge lies much higher in energy than the other, *cis*-1 form, with protons on the same bipyrrole unit (see Figure 33.2). The calculations showed that the lowest energy structure of the *cis*-2 tautomer corresponds to an open-shell configuration. The closed-shell configuration is slightly higher in energy. The latter has to be correlated with the ground state of the *trans* tautomer while analyzing the *trans–cis*-2 reaction, whereas the former should be correlated with the excited *trans* structure. As a consequence, conical intersection should exist along the hydrogen transfer path. The open-shell *cis*-2 structure is strongly distorted from planarity, by twisting of the two protonated pyrrole units. Therefore, the *trans–cis*-2 tautomerization involves not only proton translocation, but also twisting, a large amplitude motion. This explains the experimentally observed decrease in the rate of radiationless depopulation while increasing the viscosity of the environment. The activation barrier values were predicted by calculations to decrease for a series of differently substituted porphycenes in the order: (i) the parent, unsubstituted compound; (ii) 9,19-dimethylporphycene; (iii) 2,3,6,7,12,13,16,17-octamethylporphycene; (iv) 9,10,19,20-tetramethyl porphycene. These predictions perfectly match the experimentally observed changes in the radiationless depopulation rates. It remains to be seen whether this model can be generalized to include other derivatives, for example, 2,7,12,17-tetraphenyl- or 2,7,12,17-tetrakis(*p*-substituted phenyl)-3,6,13,16-tetraazaporphycenes. For the latter, S_1–S_0 internal conversion values exceeding 90% have been reported.[47]

33.4 Tautomerism

While comparing free base porphycenes with their porphyrin analogues, one should take into account different sizes and symmetries of the inner cavity: a slightly distorted rectangle in the former, the square in the latter (Figure 33.1). This difference significantly influences the intramolecular hydrogen bond

parameters. The smaller NH···N distances (2.63 vs. 2.89 Å) and larger angles (152° vs. 116°) leave no doubt that the hydrogen bonds in porphycene should be much stronger. Moreover, the energy difference between the dominant *trans* tautomers and *cis* tautomers is also much smaller: B3LYP/TZ2P calculations predict for porphyrin the *cis–trans* energy difference of 8.3 kcal mol^{-1},[49] whereas for porphycene the *cis*-1 –*trans* separation is much lower, 2.4 kcal mol^{-1}.[50] On the other hand, the other, *cis*-2 tautomer of porphycene lies very high in energy. However, as discussed earlier, it should not be neglected, due to its possible role in the radiationless deactivation of the excited state.

33.4.1 Condensed Phase Studies

33.4.1.1 Ground State Tautomerization in Polycrystalline Porphycenes

Ground state tautomerization in porphyrin, involving two chemically identical *trans* tautomers as the substrate and the product, has been intensely studied for years, mostly by NMR techniques. It is now recognized that the reaction proceeds in a stepwise fashion (Figure 33.8).[51] First, the molecule is thermally activated to a level from which *trans*→cis tunneling can occur. Subsequently, the *cis* structure undergoes a second hydrogen transfer, which leads either to the other *trans* tautomeric form or back to the substrate. The *cis* structure of porphyrin has never been experimentally detected.

Comparison of ^{15}N-CPMAS-NMR spectra of ^{15}N-enriched crystalline porphycene and porphyrin[20] revealed that the ground state tautomerization is much faster in the former. For porphyrin, lowering of temperature results in broadening of a narrow, single line observed at 356 K. For sufficiently low temperatures (<250 K), two lines are observed, corresponding to N and NH nitrogens. Line shape simulations allowed estimating the rate constant of the double hydrogen exchange: it drops from a value larger than 30,000 s^{-1} at 356 K to 500 s^{-1} at 244 K. For porphycene, such approach was not possible. Upon temperature decrease, a single line does not reveal broadening. Instead, it becomes split into four narrow lines. This was interpreted as indication of very rapid hydrogen exchange on the NMR time-scale. The process is not slowed even at temperatures as low as 107 K. The origin of four lines may be alternatively explained by the following: (i) the existence of two different molecules in the crystal lattice, of which each has access to two proton transfer systems; and (ii) the presence of only one molecule, but with access to four tautomeric species. One should note that the crystal field removes the degeneracy of two *trans-trans* or *cis-cis* minima. Further studies of crystalline porphycene using ^{15}N and ^{2}H NMR spectroscopy and longitudinal relaxometry allowed estimating the tautomerization rate.[37] Quite surprisingly, it was found to increase dramatically—from a microsecond to a nanosecond range—at lower temperatures, below 255 K. A phase transition was suggested to occur at that temperature. Low temperature studies revealed the presence of two inequivalent molecules in

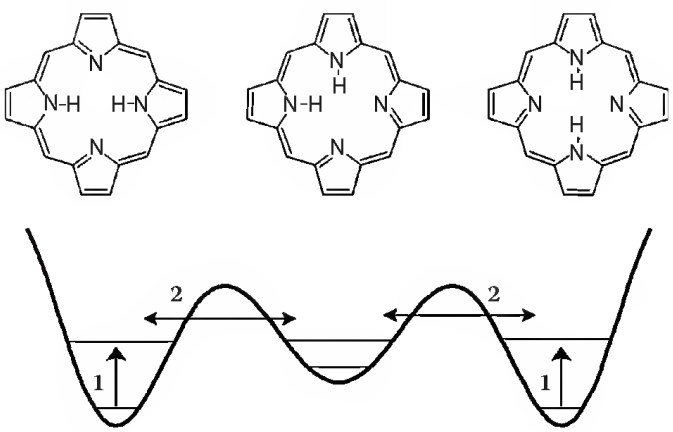

FIGURE 33.8 Stepwise mechanism of double hydrogen transfer in porphyrin: **1**, thermal activation, **2**, tunneling.

a unit cell, each with access to two *trans* tautomeric states. The Arrhenius plots in the low temperature range were typical for tunneling. It was postulated that tautomerization occurs in a concerted fashion at high temperatures and as a step-wise process at low temperatures, due to lowering in energy of one of the *cis* intermediates.

Rapid ground state tautomerization in the solid state was also demonstrated for three porphycene derivatives: 2,3,6,7,12,13,16,17-octaethyl-, 9,10,19,20-tetrapropyl-, and 2,7,12,17-tetrapropylporphycene by variable temperature ^{13}C- and ^{15}N-CPMAS NMR measurements.[52]

33.4.1.2 Ground and Excited State Tautomerism in Solutions, Glasses, Polymers, and Rare Gas Matrices

An indication that the ground state hydrogen exchange in porphycene cannot be frozen even at liquid helium temperature was the failure to photo-orient this molecule by irradiation of rare gas matrices with polarized light. Such procedure, successfully performed for porphyrin at temperatures below 80 K,[53] requires that the ground state tautomers do not interconvert on the time scale of the experiment. This is not the case for porphycene, as was confirmed later on, by low temperature studies of 9-acetoxy-2,7,12,17-tetra-*n*-propyl derivative.[25] In this molecule, the two *trans* tautomers are no longer equivalent, but their ground state energies are very similar. Both *trans* tautomeric forms were observed even at cryogenic temperatures, with their ratio remaining practically constant between 20 and 100 K. Most important, this ratio was not changed upon selective excitation of only one form, which was transformed to the other in the excited state. These results proved that ground state interconversion occurs, most probably by tunneling.

A clear demonstration that tautomerization occurs in the lowest excited electronic state of porphycene was provided by fluorescence anisotropy studies.[21,22] The value of fluorescence anisotropy measured for excitation into S_1 was much lower than the "normal" value of 0.40, expected for collinear arrangement of absorption and emission transition moments. On the other hand, the value obtained while exciting into S_2 was much higher than expected, since the calculations predict that the S_0–S_1 and S_0–S_2 transition moments are orthogonal (Figure 33.9). Such unusual behavior could be explained by assuming rapid *trans-trans* tautomerization in S_1. In the "fast" reaction regime, when the exchange occurs in a time shorter than the S_1 lifetime, the value of the fluorescence anisotropy obtained upon S_1 excitation of the chromophore embedded in a rigid matrix is determined by the angle formed between the transition moments of two chemically equivalent, but spatially differently oriented species (Figure 33.10).[33,36] By now, the same value of 0.12 ± 0.01, corresponding to the angle of 75° has been obtained independently using three different techniques: (i) stationary emission anisotropy measurements[36]; (ii) anisotropy of transient absorption[39]; and (iii) single molecule spectroscopy of porphycene and its derivatives.[26,54] This value is in excellent agreement with 76°, the value predicted by TDDFT B3LYP/6-31G(d,p) calculations. Using fluorescence anisotropy measurements, it was also possible to determine transition moment directions for the higher excited singlet electronic states.[22] It has to be noted that, because of the low (C_{2h}) symmetry of porphycene, the electronic $\pi\pi^*$ transitions can be polarized along any direction in the molecular plane, and therefore the determination of transition moments by other techniques, such as standard linear dichroism, would be difficult and less accurate. Finally, the depolarization of fluorescence proved that the *trans* tautomers are dominant, both in S_0 and S_1. No depolarization should be expected for *cis-cis* conversion, whereas for a *cis–trans* reaction, the anisotropy values should be higher than observed.

Stationary measurements of the emission anisotropy performed for several alkyl-substituted porphycenes provided the first evidence of a strong dependence of the tautomerization rate on the NH···N distance, that is, the hydrogen bond strength.[22] In glassy propanol matrices at 113 K, fluorescence was found to be depolarized for parent porphycene and two tetra-*n*-propyl derivatives substituted at β and *meso* positions. In contrast, no depolarization was observed for 2,3,6,7,12,13,16,17-octaethyl derivative (Figure 33.9). The X-ray data for the latter show the largest NH···N distance compared to the other three (2.80 vs. 2.63, 2.62, and 2.53 Å). Also, large differences in the proton chemical shifts (0.65 vs. 3.15, 3.15, and 6.82) indicate a weaker hydrogen bond in the octaethyl derivative.

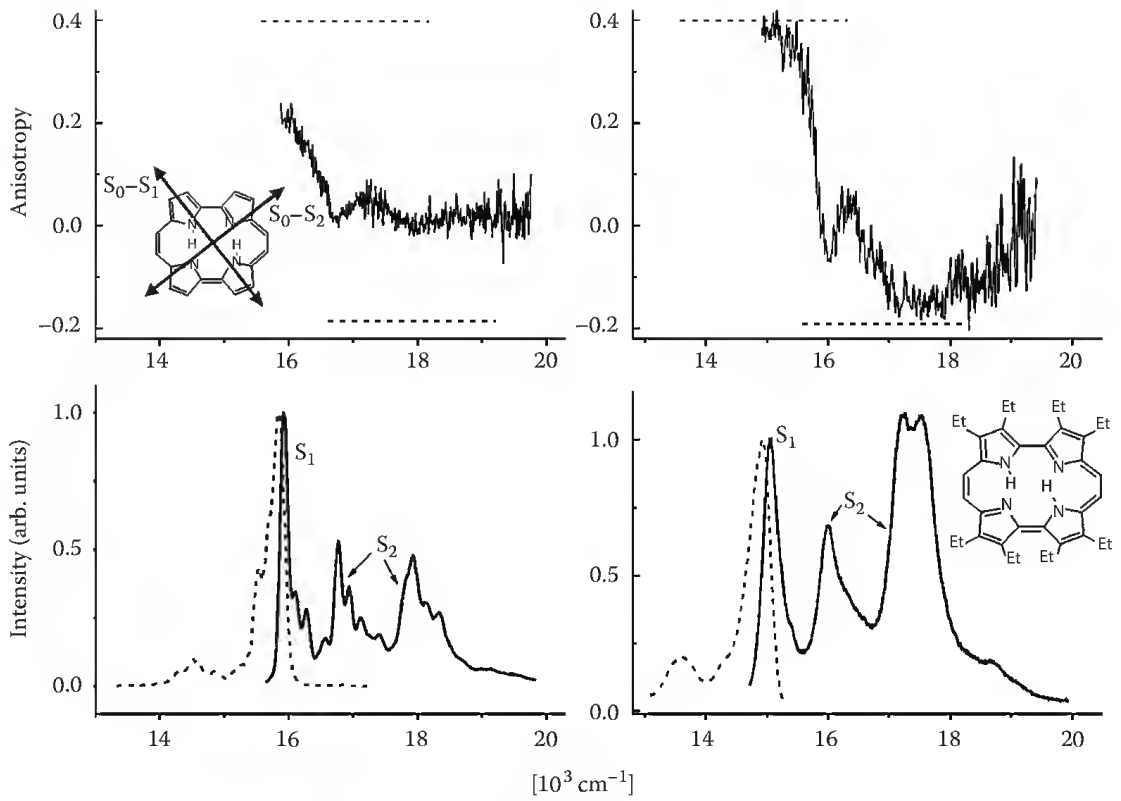

FIGURE 33.9 Bottom, fluorescence and fluorescence excitation spectra; top, anisotropy of fluorescence excitation for porphycene and 2,3,6,7,12,13,16,17-octaethyl-porphycene in *n*-propanol glass at 113 K. The inset shows the calculated transition moment directions for the transitions into the first and second lowest excited singlet states. The horizontal dashed lines represent the anisotropy values expected for orthogonal S_0–S_1 and S_0–S_2 transition moments in the absence of phenomena leading to depolarization.

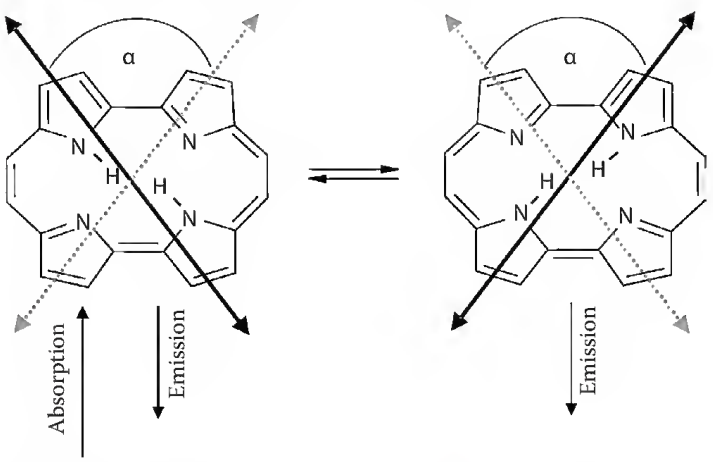

FIGURE 33.10 S_0–S_1 transition moment directions in the initially excited *trans* tautomer (left) and in the tautomerization product. α is the angle between the transition moments in the two forms.

A procedure that enabled determining the excited state tautomerization rate from the analysis of fluorescence anisotropy values, measured either in stationary or time-resolved modes, was developed and applied to the parent porphycene.[36] The Arrhenius plot yielded a surprisingly low value of the activation barrier, 0.55 ± 0.05 kcal mol^{-1}. To explain this result, a mechanism of thermally activated double hydrogen tunneling was proposed. The apparent activation barrier corresponds to 181 cm^{-1}, the frequency of a

vibration that simultaneously shortens the NH···N distance in both intramolecular hydrogen bonds. In this way, a barrier for concerted *trans-trans* tautomerization becomes lower. This hypothesis was subsequently confirmed by measurements of mode-selective tunneling splittings, discussed below.

Further development of methodology based on using polarized light to determine tautomerization rates resulted in the formula which links the kinetic profiles of the anisotropy of transient absorption with the hydrogen exchange rates in both the ground and lowest excited singlet states. Depending on the choice of pumping and probing wavelengths, it is possible to separately determine the rates in S_0 and S_1. This was achieved at 293 K for parent porphycene and four alkyl derivatives using polarized pump-probe spectroscopy with tunable femtosecond laser pulses.[39] The results demonstrated a huge dependence of the rate on the hydrogen bond strength, expressed in terms of NH···N distances or proton chemical shifts. The tautomerization rates differ by about four orders of magnitude between the derivatives with the strongest (*meso*-substituted) and the weakest (octaethyl) hydrogen bond (Figure 33.11). In the former, the reaction proceeds in S_0 in < 100 fs, whereas in the latter it takes >100 ps. For parent porphycene dissolved in ethylene glycol, tautomerization at 293 K occurs in 1.7 ± 0.1 ps and 14 ± 2 ps in S_0 and S_1, respectively. In general, for all the porphycenes measured so far, the S_1 rate is about an order of magnitude lower

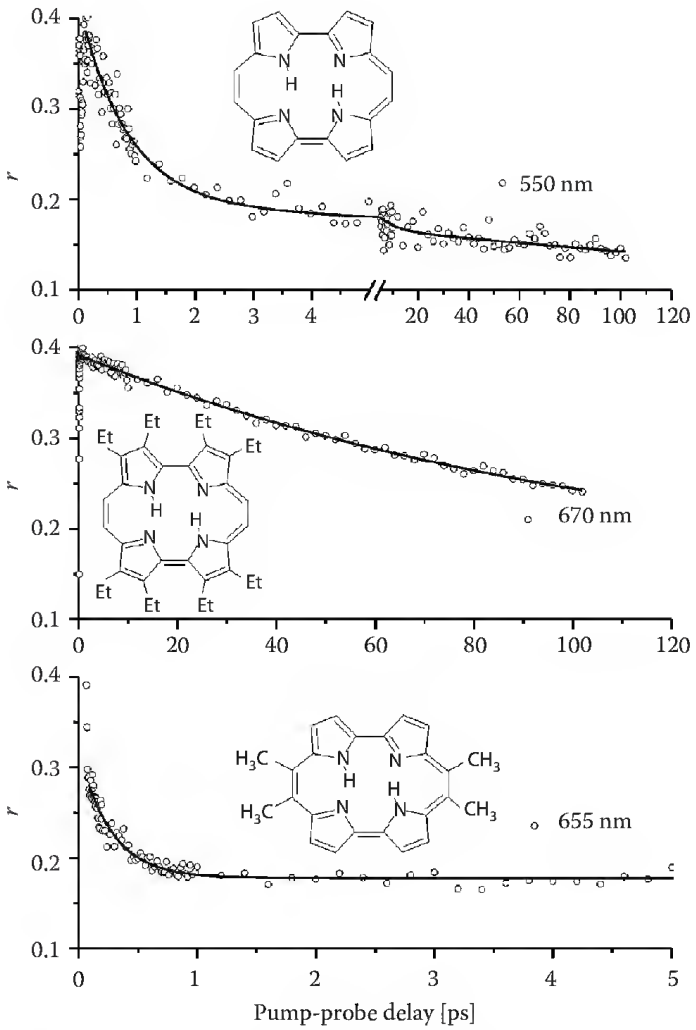

FIGURE 33.11 Decay profiles of anisotropy measured at 293 K for ethylene glycol solutions using femtosecond pump-probe spectroscopy. Top to bottom: porphycene, 2,3,6,7,12,13,16,17-octaethyl-porphycene, and 9,10,19,20-tetramethyl-porphycene. Very different decay times reflect different tautomerization rates. Pump and probe wavelength indicated for each compound ($\lambda_{pump} = \lambda_{probe}$).

than in S_0, due probably to an increase in the NH···N separation upon excitation; such behavior has been predicted by calculations. The H/D isotope effects were determined for both ground and excited states. The values of 4.3 ± 0.3 and 8.0 ± 0.5 were obtained for parent porphycene. For 2,7,12,17-tetra-*tert*-butyl derivative, the isotope effects are 5.0 ± 0.4 and 7.7 ± 0.4 for S_0 and S_1, respectively.[39]

Using the same pump-probe methodology, it was possible to determine the rates of the intermolecular exchange of the inner protons in porphycene for deuterons, by dissolving the porphycenes in deuterated ethanol and butanol-1.[34] The rates of the first and second proton/deuteron exchange turned out to be the same and about 17 orders of magnitude slower than that of intramolecular tautomerization. This provided another proof of exceptionally strong intramolecular hydrogen bonds in porphycene.

Tautomerization in the parent porphycene has also been studied in the lowest triplet state in a wide temperature range using time-resolved EPR and electron spin echo techniques.[55] It was concluded that porphycene has a *trans* configuration in both S_0 and T_1. The NH tautomerism was suggested to occur in T_1 at 100 K with the lower and upper limits of the rates of 9×10^6 and 7×10^8 s^{-1}, respectively. The value of the tautomerization rate in S_1 at this temperature, determined from stationary fluorescence anisotropy[36] is 2×10^7 s^{-1}, and thus fits well into the range estimated for the reaction in the triplet state.

In summary, the results obtained from condensed phase studies allowed determining the *trans-trans* conversion rates in both S_0 and S_1 electronic states. Several findings suggest an important role of tunneling and its possible sensitivity to the mode of vibrational excitation. These issues have been studied in detail by measurements of porphycenes isolated in molecular beams and helium nanodroplets, discussed in the next section. The problem that remains to be explained is the large difference obtained for the values of exchange rates at 293 K using different methods for porphycenes in different environments. The values obtained for polycrystalline porphycene using NMR techniques are several orders of magnitude lower than those provided by polarized spectroscopy studies in liquids and polymeric films. It is interesting to note that the low temperature data provided by the two techniques agree with each other. Another question that awaits a definitive answer is that of concerted versus stepwise mechanism. The *cis* tautomer has not been detected for parent porphycene, but it may exist as a very short-lived species, difficult to pinpoint experimentally. Careful studies of the temperature dependence of kinetic isotope effects may help in solving this issue.

33.4.2 Coherent Double Hydrogen Tunneling in Isolated Porphycenes

In the condensed phase, the tautomerization in porphycene can be described as a rate process. On the other hand, in an isolated molecule the wave function is delocalized. Coherent double hydrogen transfer tunneling is manifested by line splittings (Figure 33.12), of which the value is the function of the effective barrier height and its shape, as well as of the mass and the distance the tunneling particle has to travel.

Fluorescence excitation spectrum recorded for free base porphyrin isolated in a supersonic jet consists of single lines.[56] In contrast, the spectra of parent porphycene for which the tautomerization barrier is lower than in porphyrin, show doublets, separated by 4.4 cm^{-1} (Figure 33.12).[23] Single line pattern is recovered when one or both internal protons are replaced by deuterons, indicating that the splitting is due to hydrogen tunneling. The doublet structure is also not observed for complexes with water or alcohol, which suggests that the double minimum potential is no longer symmetrical, which leads to localization of inner hydrogens.

On the basis of a constant value of the splitting across all vibronic bands and the red shift observed in the fluorescence excitation spectra of singly and doubly deuterated chromophores, which indicates a weaker hydrogen bonding in S_1 compared to S_0, the observed separation of lines by 4.4 cm^{-1} was attributed to the tunneling splitting in the ground state vibrationless level, from which the transitions observed in the fluorescence excitation spectrum originate. In consequence, the splitting in S_1 should be lower than 0.1 cm^{-1}, the resolution of the jet spectrometer. These results were confirmed, first by recording the dispersed fluorescence from jet-isolated porphycene and then, with much better spectral resolution, by measuring fluorescence spectra for porphycene embedded in helium

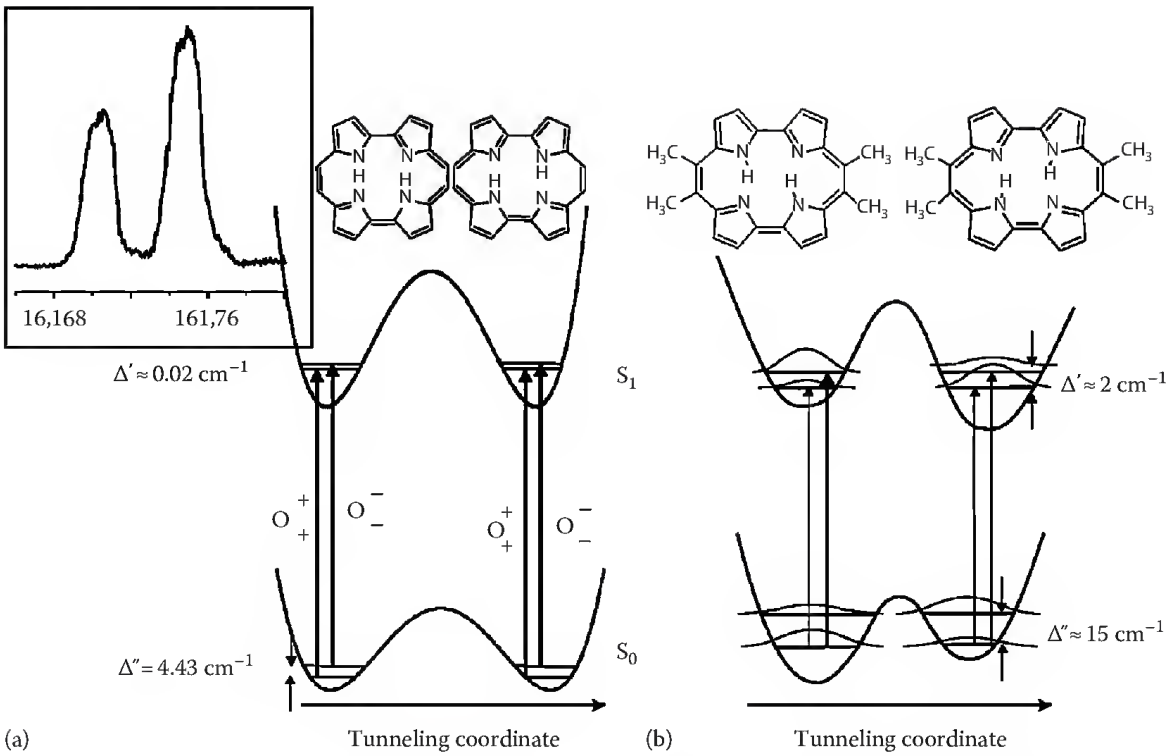

FIGURE 33.12 Double minimum potential energy curves for ground and excited state tautomerization in porphycene (a) and 9,10,19,20-tetramethylporphycene (b). The inset shows the doublet splitting observed in the fluorescence excitation spectrum for the 0–0 transition of porphycene isolated in a supersonic jet.

nanodroplets.[38] In the latter experimental regime, the temperature of 0.37 K ensures that the upper tunneling level of the ground state molecule is not accessible. Under such conditions, only one of the lines of the doublet is observed. On the other hand, a doublet was observed for singly deuterated porphycene, its components separated by 0.58 cm^{-1}. This value corresponds to ground state tunneling splitting reduced by single H→D substitution. Replacement of the second hydrogen results in further reduction of the splitting, so that it could not be resolved. The helium droplet experiments established that the ground state splitting in parent porphycene is 4.43 cm^{-1}, whereas the splitting in S_1 amounts to about 0.02 cm^{-1}.

Measurements of the emission spectra of porphycene in helium droplets allowed determining the values of tunneling splittings for various ground state vibrational levels. Since each vibronic line in the fluorescence originates from the same tunneling doublet in S_1, of which the components are nearly degenerate, the observed energy differences between the doublet components correspond to the ground state splittings for each particular vibration, or that of the vibrationless level. The splittings have been found to be very much different for different vibrations. Some modes reveal splittings of about 4.4 cm^{-1}, the value obtained for the S_0 vibrationless level. They can be, therefore, labeled "neutral" with respect to their influence on the effective tautomerization barrier. The most interesting ones are (i) a 182 cm^{-1} mode revealing a much larger splitting, 12 cm^{-1}; practically the same value is observed for combinations of this vibration with two "neutral" modes; (ii) a 145 cm^{-1} mode, for which the splitting is too small to be resolved. Thus, for the 182 cm^{-1} mode the reaction barrier is smaller than that for the vibrationless level, whereas it becomes larger for the 145 cm^{-1} vibration. In other words, the former mode promotes and the latter hinders the reaction. These vibrations can be readily assigned. The promoting mode corresponds to a vibration in which both NH···N distances change in phase. This leads to simultaneous strengthening of both intramolecular hydrogen bonds. It is the same vibration that was postulated to activate the excited state tautomerization observed in S_1 in condensed environments.[36] The hindering mode involves

FIGURE 33.13 The forms of two low frequency modes of porphycene, of which one hinders, the other accelerates tautomerization (a and b, respectively). Calculated using B3LYP/6-31G(d,p).

out-of-phase rocking motion of the two bipyrrole units (Figure 33.13). The splitting patterns observed for these two modes strongly suggest a concerted character of hydrogen transfer.

Tunneling splittings have also been observed for jet-isolated *meso*-substituted tetramethyl and tetra-*n*-propyl-substituted porphycenes.[28] Since this pattern of substitution leads to an increase in hydrogen bond strength, larger splittings than in the parent compound could be expected. This is indeed the case (Figure 33.12). From the analysis of fluorescence and fluorescence excitation spectra, the values of about 15 and 2 cm^{-1} were obtained for S_0 and S_1, respectively. Moreover, the potential was found not to be symmetric, with the ordering of energy minima reversed upon excitation. The origin of this effect was attributed to the coupling of hydrogen motion with the rotation of alkyl substituents, an effect previously detected for methyl-substituted tropolone[57] and hydroxyphenalenone.[58]

The experiments for *meso*-substituted porphycenes revealed the presence of two different forms. One of them disappeared in the colder part of the jet, away from the nozzle. It was assigned to the *cis*-1 tautomeric form, of which the calculated energy is only less than 1 kcal mol^{-1} higher than that of the dominant *trans* tautomer. The presence of two tautomeric forms has also been revealed for condensed phases by observing biexponential fluorescence decays. Interestingly, the values of tunneling splittings, deduced from supersonic jet spectra, are very similar for both forms. A more detailed analysis of mode-specific tunneling is difficult, because fluorescence disappears at very low excitation energy excess. The onset of efficient radiationless deactivation is in line with condensed phase studies discussed earlier, which demonstrated that this channel becomes most efficient in low-viscosity media. Supersonic jets represent exactly such an environment.

33.4.3 Tautomerization in Single Molecules of Porphycenes

Polarized spectroscopy studies of porphycene demonstrated that, owing to its tautomeric properties, porphycene is a special chromophore. The self-exchange of the inner hydrogen atoms results in the rotation of the S_0–S_1 transition moment by a large angle, exceeding 70° (Figure 33.10). This effect has been exploited to detect tautomerization in single molecules of porphycene embedded in polymeric matrices.[26,54] On the time scale of the experiment (seconds), the molecule is a "dual emitter," composed of two nearly orthogonal dipoles. For such a case, the spatial pattern of fluorescence intensity should be different from that of a "normal" molecule, considered as a single emitting dipole. Indeed, using the azimuthal polarization mode of the exciting laser beam, it was possible to observe a pattern which cannot correspond to a single dipole: a nearly perfect ring (Figure 33.14). This pattern could be reproduced by simulations, which assumed two equally emitting dipoles. An angle of 72° ± 3° provided the best fit, in excellent agreement with the value first obtained from fluorescence anisotropy studies of bulk porphycene in polymer films,[36] and then reproduced by femtosecond transient absorption spectroscopy.[39]

In some single molecule emitters, a different pattern was observed, consisting of double lobes (molecule B, Figure 33.14). Two explanations of such behavior are possible: (i) freezing of tautomerization by the

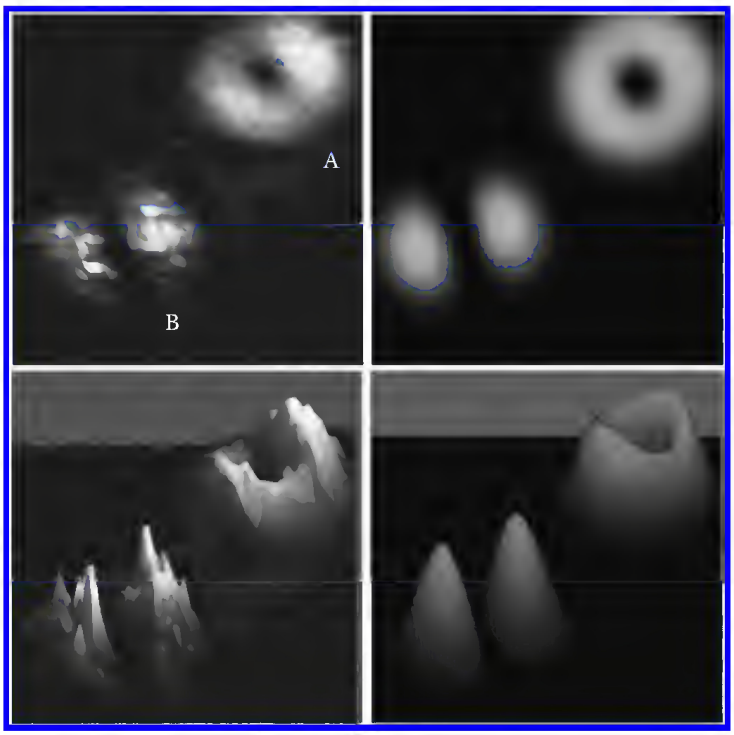

FIGURE 33.14 Left, spatial distribution of fluorescence intensity from two single molecules of porphycene embedded in poly(methyl methacrylate) at 293 K. Right, simulation of the distribution. (Adapted from Piwoński, H., Stupperich, C., Hartschuh, A., Sepioł, J., Meixner, A., and Waluk, J., *J. Am. Chem. Soc.*, 127, 5302–5303, 2005. Copyright 2005 American Chemical Society.)

environment or (ii) orientation of molecular plane perpendicular to the sample surface. The issue was resolved by comparing spatial patterns of the emission obtained for the same single molecule by using azimuthally and radially polarized laser beams.[54] Besides parent porphycene, three derivatives have been studied. The dual dipole character of the emission was confirmed, proving that tautomerization does occur and that different spatial patterns originate from different orientation in polymeric matrices. In fact, it was

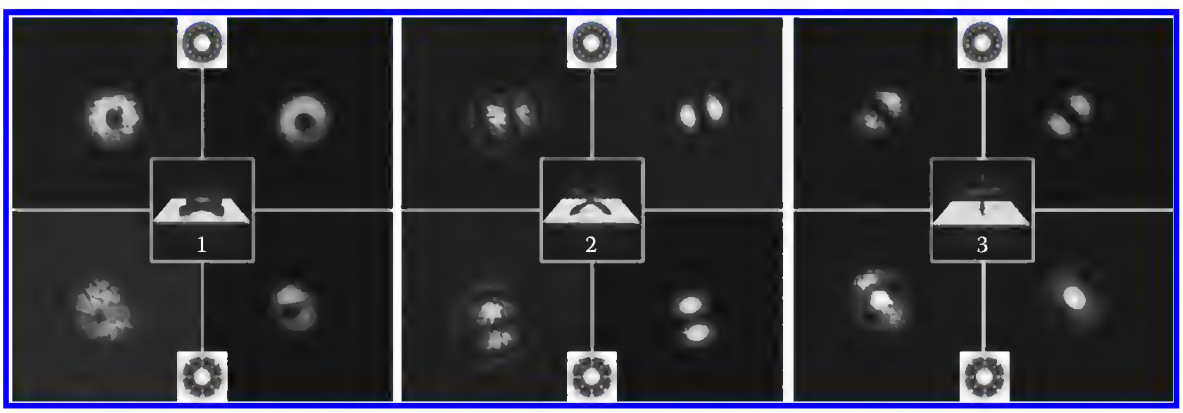

FIGURE 33.15 Fluorescence images of three differently oriented single molecules of 2,7,12,17-tetra-*tert*-butylporphycene in poly(methyl methacrylate) at 293 K. The insets show the directions of S_0–S_1 transition moments with respect to the sample support plane. Top, azimuthal; bottom, radial polarization of the exciting 632.8 nm laser beam. Left, experimental; right, simulated patterns. (Adapted from Piwoński, H., Hartschuh, A., Urbańska, N., Pietraszkiewicz, M., Sepioł, J., Meixner, A., and Waluk, J., *J. Phys. Chem. C*, 113, 11514–11519, 2009. Copyright 2009 American Chemical Society.)

not only possible to distinguish between the molecules lying flat on the sample surface but also those perpendicular to it. For the latter case, use of two different polarization modes allowed separating molecules with both dipoles forming approximately the same angle with the surface from those with one dipole parallel and the other, approximately perpendicular to it (Figure 33.15). Once again, tautomerization in porphycenes served as a tool for spectroscopy, this time enabling exact molecular orientation.

33.5 Summary and Outlook

Structural, spectral, and photophysical characteristics of porphycenes make them equally attractive for fundamental research and applications. With regard to the latter, the results described in this work provide a basis for custom-designing porphycene-related chromophores for a specific purpose. For instance, the finding that the fluorescence intensity of *meso* derivatives is strongly viscosity dependent suggests their use as local microviscosity probes. Probing the interior of a cell is a challenging perspective, especially because the same porphycene chromophore could be, in principle, used not only as a viscosity reporter, but also as a phototherapeutic and/or photodiagnostic agents. The effectiveness of porphycenes in phototherapy has been convincingly demonstrated for numerous derivatives.[18,59] The main obstacle to general applications lies in difficult and costly synthesis, but progress is being reported.[60–62]

Studies of tautomerization in porphycenes are closely linked to the investigations of hydrogen bond. In this respect, porphycenes are unique for several reasons. First, using "mild" alkyl substituents, one is able to manipulate the dimensions of the inner cavity, and thus the strength of intramolecular hydrogen bonds. This enables systematic studies of double hydrogen transfer rates as a function of hydrogen bond properties expressed in terms of such parameters as distances, angles, or chemical shifts. These studies have brought spectacular results. Changing the N-N separation by 0.27 Å, from 2.80 Å in 2,3,6,7,12,13,16,17-octaethylporphycene to 2.53 Å in 9,10,19,20-tetramethylporphycene results in more than three orders of magnitude increase in the tautomerization rates, both in the ground and lowest excited electronic states. Such behavior is strongly suggestive of tunneling, a phenomenon whose occurrence is not easy to prove in condensed phase studies. On the other hand, coherent double hydrogen tunneling has now been demonstrated in the isolated molecule regime for parent porphycene and two *meso* alkyl-substituted derivatives. Moreover, these studies have revealed the mode-selective character of tunneling by showing that the values of tunneling splitting are strongly vibration dependent.

Of particular value is the possibility to study the same phenomenon in the same molecule in two completely different regimes. A challenging problem is to interpret the tunneling splitting data, obtained for isolated molecules, along with the rates determined from condensed phase studies. In a simple 1D picture, the residence time of a particle oscillating between two wells is given by h/Δ, where Δ is the tunneling splitting. Assuming $\Delta = 4.4\,cm^{-1}$, the value obtained for porphycene yields the residence time of 7.6 ps, of the same order as the lifetime of 1.7 ps obtained for porphycene in solution at 293 K. For $\Delta = 12\,cm^{-1}$, the value observed for the $181\,cm^{-1}$ mode, the residence time decreases to 2.8 ps. There is no doubt that tautomerization in porphycenes is a multidimensional phenomenon, and therefore, the process may be crucially dependent on the mode of vibrational excitation. This opens up a field for designing experiments that could result in laser control of the reaction. It should be noted that the techniques for monitoring the process in the condensed phase are based on pump-probe polarized spectroscopy, and the reaction kinetics is directly related to the measured temporal anisotropy profile. This is in contrast to an alternative technique, NMR relaxometry, which relies on the assumed values of hydrogen bond distances and angles. We also note that the tautomerization rate in porphycene is larger than the rate of vibrational cooling. This provides an opportunity to study hydrogen transfer rates in a nonequilibrated system.

The data accumulated so far strongly suggest that the tautomerization occurs in a concerted fashion. This is in line with cooperative coupling of the two intramolecular hydrogen bonds, demonstrated by NMR[30] and theoretical[31] studies of geometric H/D isotope effects. However, the movement of the two inner hydrogens need not necessarily be synchronous. The exact description of the transfer is a

challenge for both experiment and theory. For the latter, it should be kept in mind that tunneling cannot be neglected, even when considering the system at room temperature.

Another challenge for the theory is to properly characterize the tautomerization path, both for the ground and electronically excited states. So far, the theory succeeded in predicting very different energy values for the stationary and transition states in porphyrin and porphycene. These results allowed explaining different tautomerization mechanisms in the two isomers.[36] The concerted mechanism of double hydrogen transfer in porphycene results from the fact that the energy required for the *trans-trans* conversion (most probably, with tunneling involved) is lower than the *cis–trans* energy difference. In the case of porphyrin, it is more favorable to first populate the *cis* tautomer, from which the second hydrogen transfer can occur.

The methodologies developed for studying the self-exchange processes are relatively simple and can be extended to all processes that lead to a change of transition moment directions. They are also not limited to electronic absorption/emission measurements, but can be applied in other areas, such as IR spectroscopy.

Finally, porphycenes turned out to be good chromophores for single molecule spectroscopy experiments. This fact, combined with their spectroscopic, photophysical, and phototherapeutic properties, makes this class of molecules very promising for future biology and medicine-related studies.

Acknowledgments

I am indebted to many colleagues who contributed to the results presented in this work: Michał Gil, Hubert Piwoński, Natalia Urbańska, Alexander Vdovin, Piotr Fita, Czesław Radzewicz, Oksana Pietraszkiewicz, Marek Pietraszkiewicz, Jerzy Sepioł, Alfred Meixner, Alkwin Slenczka, Bernhard Dick, Achim Hartschuh, Clemens Stupperich, Jacek Dobkowski, Paweł Borowicz. Grażyna Orzanowska, Sylwester Gawinkowski, Andrzej Mordziński, Alexander Starukhin, Alexander Kyrychenko. I am especially grateful to Emanuel Vogel and Josef Michl, who stimulated my interest in porphycenes. This work was partially supported by the grant N20414132/3545 from the Polish Ministry of Science and Higher Education.

References

1. Vogel, E., Köcher, M., Schmickler, H., and Lex, J., Porphycene—a novel porphin isomer, *Angew. Chem. Int. Ed. Engl.* 25, 257–259, 1986.
2. Waluk, J. and Michl, J., The perimeter model and magnetic circular dichroism of porphyrin analogues, *J. Org. Chem.* 56, 2729–2735, 1991.
3. Aukauloo, M. A. and Guilard, R., The "Etioporphycerin": Synthesis and characterization of a new porphyrin isomer, *New J. Chem.* 18, 1205–1207, 1994.
4. Sessler, J. L., Brucker, E. A., Weghorn, S. J., Kisters, M., Schafer, M., Lex, J., and Vogel, E., Corrphycene—a new porphyrin isomer, *Angew. Chem. Int. Ed. Engl.* 33, 2308–2312, 1994.
5. Callot, H. J., Metz, B., and Tschamber, T., A novel porphyrin isomer: hemiporphycene. Formation and single-crystal X-ray diffraction structure determination of a hemiporphycene nickel complex, *New J. Chem.* 19, 155–159, 1995.
6. Vogel, E., Bröring, M., Weghorn, S. J., Scholz, P., Deponte, R., Lex, J., Schmickler, H., Schaffner, K., Braslavsky, S. E., Müller, M., Pörting, S., Fowler, C. J., and Sessler, J. L., Octaethylhemiporphycene: Synthesis, molecular structure, and photophysics, *Angew. Chem. Int. Ed. Engl.* 36, 1651–1654, 1997.
7. (a) Vogel, E., Bröring, M., Erben, C., Demuth, R., Lex, J., Nendel, M., and Houk, K. N., Palladium complexes of the new porphyrin isomers (Z)- and (E)- isoporphycene - Pd^{II}-induced cyclization of tetrapyrrolealdehydes, *Angew. Chem. Int. Ed. Engl.* 36, 353–357, 1997; (b) Vogel, E., Scholz, P., Demuth, R., Erben, C., Broring, M., Schmickler, H., Lex, J., Hohlneicher, G., Bremm, D., and Wu, Y. D., Isoporphycene: The fourth constitutional isomer of porphyrin with an N_4 core - Occurrence of E/Z isomerism, *Angew. Chem. Int. Ed.* 38, 2919–2923, 1999.
8. Chmielewski, P. J., Latos-Grażynski, L., Rachlewicz, K., and Glowiak, T., Tetra-*p*-tolylporphyrin with an inverted pyrrole ring: a novel isomer of porphyrin, *Angew. Chem. Int. Ed. Engl.* 33, 779–781, 1994.

9. Furuta, H., Asano, T., and Ogawa, T., "N-confused porphyrin": A new isomer of tetraphenylporphyrin, *J. Am. Chem. Soc.* 116, 767–768, 1994.
10. Battersby, A. R., Fookes, C. J. R., Matcham, G. W. J., and McDonald, E., Biosynthesis of the pigments of life: Formation of the macrocycle, *Nature* (*London*) 285, 17–21, 1980.
11. (a) Ogiso, A., Inoue, S., Tsukahara, H., Nishimoto, T., Misawa, T., and Koike, T., Optical recording medium and porphycene compound, European Patent 1180765B1, 2005, US Patent 6627288B1, 2003; (b) Kondou, T. and Nagataki, Y., Porphycene compound and optical information recording medium made by using it, Patent abstracts of Japan, JP2002114923, 2002.
12. (a) Lo, W. C., Che, C. M., Cheng, K. F., and Mak, T. C. W., Catalytic and asymmetric cyclopropanation of styrenes catalysed by ruthenium porphyrin and porphycene complexes, *Chem. Commun.*, 1205–1206, 1997; (b) Hayashi, T., Okazaki, K., Urakawa, N., Shimakoshi, H., Sessler, J. L., Vogel, E., and Hisaeda, Y., Cobaltporphycenes as catalysts. The oxidation of vinyl ethers via the formation and dissociation of cobalt-carbon bonds, *Organometallics* 20, 3074–3078, 2001.
13. (a) Barbe, J. M., Richard, P., Aukauloo, M. A., Lecomte, C., Petit, P., and Guilard, R., Electrocrystallization and X-ray structure of a new porphycene-based material, $Ni(IMPc)_{2.5}(BF_4)_2$ $C_{10}H_7Cl$, *J. Chem. Soc. Chem. Commun.*, 2757–2758, 1994; (b) Miller, D. C., Bollinger, J. C., Hoffman, B. M., and Ibers, J. A., Structural, magnetic, and charge-transport properties of a new one-dimensional molecular conductor, $Ni(tprpc)I_{1.67}$ (tprpc=2,7,12,17-tetrapropylporphycenato), *Inorg. Chem.* 33, 3354–3357, 1994.
14. Che, C. M., Xiang, H. F., Chui, S. S. Y., Xu, Z. X., Roy, V. A. L., Yan, J. J., Fu, W. F., Lai, P. T., and Williams, I. D., A high-performance organic field-effect transistor based on platinum(II) porphyrin: Peripheral substituents on porphyrin ligand significantly affect film structure and charge mobility, *Chem. Asian J.* 3, 1092–1103, 2008.
15. Stępień, M., Donnio, B., and Sessler, J. L., Discotic liquid-crystalline materials based on porphycenes: A mesogenic metalloporphycene-tetracyanoquinodimethane (TCNQ) adduct, *Chem. Eur. J.* 13, 6853–6863, 2007.
16. (a) Hayashi, T., Dejima, H., Matsuo, T., Sato, H., Murata, D., and Hisaeda, Y., Blue myoglobin reconstituted with an iron porphycene shows extremely high oxygen affinity, *J. Am. Chem. Soc.* 124, 11226–11227, 2002; (b) Matsuo, T., Dejima, H., Hirota, S., Murata, D., Sato, H., Ikegami, T., Hori, H., Hisaeda, Y., and Hayashi, T., Ligand binding properties of myoglobin reconstituted with iron porphycene: Unusual O_2 binding selectivity against CO binding, *J. Am. Chem. Soc.* 126, 16007–16017, 2004; (c) Hayashi, T., Murata, D., Makino, M., Sugimoto, H., Matsuo, T., Sato, H., Shiro, Y., and Hisaeda, Y., Crystal structure and peroxidase activity of myoglobin reconstituted with iron porphycene, *Inorg. Chem.* 45, 10530–10536, 2006; (d) Matsuo, T., Ikegami, T., Sato, H., Hisaeda, Y., and Hayashi, T., Ligand binding properties of two kinds of reconstituted myoglobins with iron porphycene having propionates: Effect of β-pyrrolic position of two propionate side chains in porphycene framework, *J. Inorg. Biochem.* 100, 1265–1271, 2006; (e) Matsuo, T., Murata, D., Hisaeda, Y., Hori, H., and Hayashi, T., Porphyrinoid chemistry in hemoprotein matrix: Detection and reactivities of iron(IV)-oxo species of porphycene incorporated into horseradish peroxidase, *J. Am. Chem. Soc.* 129, 12906–12907, 2007; (f) Matsuo, T., Ito, K., Nakashima, Y., Hisaeda, Y., and Hayashi, T., Effect of peripheral trifluoromethyl groups in artificial iron porphycene cofactor on ligand binding properties of myoglobin, *J. Inorg. Biochem.* 102, 166–173, 2008.
17. Matsuo, T., Tsuruta, T., Maehara, K., Sato, H., Hisaeda, Y., and Hayashi, T., Preparation and O_2 binding study of myoglobin having a cobalt porphycene, *Inorg. Chem.* 44, 9391–9396, 2005.
18. Stockert, J. C., Cañete, M., Juarranz, A., Villanueva, A., Horobin, R. W., Borrell, J., Teixidó, J., and Nonell, S., Porphycenes: Facts and prospects in photodynamic therapy of cancer, *Curr. Med. Chem.* 14, 997–1026, 2007.
19. Richert, C., Wessels, J. M., Müller, M., Kisters, M., Benninghaus, T., and Goetz, A. E., Photodynamic antitumor agents: ß-methoxyethyl groups give access to functionalized porphycenes and enhance cellular uptake and activity, *J. Med. Chem.* 37, 2797–2807, 1994.

20. Wehrle, B., Limbach, H. H., Kocher, M., Ermer, O., and Vogel, E., ^{15}N-CPMAS-NMR study of the problem of NH tautomerism in crystalline porphine and porphycene, *Angew. Chem. Int. Ed. Engl.* 26, 934–936, 1987.
21. Waluk, J., Müller, M., Swiderek, P., Köcher, M., Vogel, E., Hohlneicher, G., and Michl, J., Electronic states of porphycenes, *J. Am. Chem. Soc.* 113, 5511–5527, 1991.
22. Waluk, J. and Vogel, E., Distance dependence of excited-state double proton transfer in porphycenes studied by fluorescence polarization, *J. Phys. Chem.* 98, 4530–4535, 1994.
23. Sepioł, J., Stepanenko, Y., Vdovin, A., Mordziński, A., Vogel, E., and Waluk, J., Proton tunnelling in porphycene seeded in a supersonic jet, *Chem. Phys. Lett.* 296, 549–556, 1998.
24. Langer, U., Hoelger, C., Wehrle, B., Latanowicz, L., Vogel, E., and Limbach, H. H., ^{15}N NMR study of proton localization and proton transfer thermodynamics and kinetics in polycrystalline porphycene, *J. Phys. Org. Chem.* 13, 23–34, 2000.
25. Gil, M., Jasny, J., Vogel, E., and Waluk, J., Ground and excited state tautomerization in 9-acetoxy-2,7,12,17-tetra-*n*-propylporphycene, *Chem. Phys. Lett.* 323, 534, 2000.
26. Piwoński, H., Stupperich, C., Hartschuh, A., Sepioł, J., Meixner, A., and Waluk, J., Imaging of tautomerism in a single molecule, *J. Am. Chem. Soc.* 127, 5302–5303, 2005.
27. Walewski, L., Krachtus, D., Fischer, S., Smith, J. C., Bala, P., and Lesyng, B., SCC-DFTB energy barriers for single and double proton transfer processes in the model molecular systems malonaldehyde and porphycene, *Int. J. Quantum Chem.* 106, 636–640, 2006.
28. Vdovin, A., Sepioł, J., Urbańska, N., Pietraszkiewicz, M., Mordziński, A., and Waluk, J., Evidence for two forms, double hydrogen tunneling, and proximity of excited states in bridge-substituted porphycenes: Supersonic jet studies, *J. Am. Chem. Soc.* 128, 2577–2586, 2006.
29. Waluk, J., Ground- and excited-state tautomerism in porphycenes, *Acc. Chem. Res.* 39, 945–952, 2006.
30. Pietrzak, M., Shibl, M. F., Bröring, M., Kühn, O., and Limbach, H. H., ^{1}H/^{2}H NMR studies of geometric H/D isotope effects on the coupled hydrogen bonds in porphycene derivatives, *J. Am. Chem. Soc.* 129, 296–304, 2007.
31. Shibl, M. F., Pietrzak, M., Limbach, H. H., and Kühn, O., Geometric H/D isotope effects and cooperativity of the hydrogen bonds in porphycene, *ChemPhysChem* 8, 315–321, 2007.
32. Smedarchina, Z., Shibl, M. F., Kühn, O., and Fernández-Ramoz, A., The tautomerization dynamics of porphycene and its isotopomers - Concerted versus stepwise mechanisms, *Chem. Phys. Lett.* 426, 314–321, 2007.
33. Waluk, J., Tautomerization in porphycenes, in *Hydrogen-Transfer Reactions*, Hynes, J. T., Klinman, J. P., Limbach, H. H., andSchowen, R. L. (eds.), Wiley-VCH, Weinheim, Germany, 2007, pp. 245–271.
34. Fita, P., Urbańska, N., Radzewicz, C., and Waluk, J., Unusually slow intermolecular proton-deuteron exchange in porphycene, *Z. Phys. Chem.* (*Munich*) 222, 1165–1173, 2008.
35. Smedarchina, Z., Siebrand, W., Fernandez-Ramos, A., and Meana-Paneda, R., Mechanisms of double proton transfer. Theory and applications, *Z. Phys. Chem. Int. J. Res. Phys. Chem. Chem. Phys.* 222, 1291–1309, 2008.
36. Gil, M. and Waluk, J., Vibrational gating of double hydrogen tunneling in porphycene, *J. Am. Chem. Soc.* 129, 1335–1341, 2007.
37. Lopez del Amo, J., Langer, U., Torres, V., Pietrzak, M., Buntkowsky, G., Vieth, H. M., Shibl, M. F., Kühn, O., Bröring, M., and Limbach, H. H., Isotope and phase effects on the proton tautomerism in polycrystalline porphycene revealed by NMR, *J. Phys. Chem. A* 113, 2193–2206, 2009.
38. Vdovin, A., Waluk, J., Dick, B., and Slenczka, A., Mode-selective promotion and isotope effects of concerted double-hydrogen tunneling in porphycene embedded in superfluid helium nanodroplets, *ChemPhysChem* 10, 761–765, 2009.
39. Fita, P., Urbańska, N., Radzewicz, C., and Waluk, J., Ground and excited state tautomerization rates in porphycenes, *Chem. Eur. J.* 15, 4851–4856, 2009.
40. Wu, Y. D., Chan, K. W. K., Yip, C. P., Vogel, E., Plattner, D. A., and Houk, K. N., Porphyrin isomers: Geometry, tautomerism, geometrical isomerism, and stability, *J. Org. Chem.* 62, 9240–9250, 1997.

41. Sobolewski, A., Gil, M., Dobkowski, J., and Waluk, J., On the origin of radiationless transitions in porphycenes, *J. Phys. Chem. A* 113, 7714–7716, 2009.
42. Gouterman, M., Spectra of porphyrins, *J. Mol. Spectrosc.* 6, 138–163, 1961.
43. Michl, J., Magnetic circular dichrosim of aromatic molecules, *Tetrahedron* 40, 3845–3934, 1984.
44. Gorski, A., Vogel, E., Sessler, J. L., and Waluk, J., Magnetic circular dichroism of octaethylcorrphycene and its doubly protonated and deprotonated forms, *J. Phys. Chem. A* 106, 8139–8145, 2002.
45. Gorski, A., Vogel, E., Sessler, J. L., and Waluk, J., Magnetic circular dichroism of neutral and ionic forms of octaethylhemiporphycene, *Chem. Phys.* 282, 37–49, 2002.
46. Berman, A., Michaeli, A., Feitelson, J., Bowman, M. K., Norris, J. R., Levanon, H., Vogel, E., and Koch, P., Photophysics and photoinduced-electron-transfer reactions of zinc and free-base octaethylporphycene, *J. Phys. Chem.* 96, 3041–3047, 1992.
47. Rubio, N., Prat, F., Bou, N., Borrell, J. I., Teixidó, J., Villanueva, A., Juarranz, A., Cañete, M., Stockert, J. C., and Nonell, S., A comparison between the photophysical and photosensitising properties of tetraphenyl porphycenes and porphyrins, *New J. Chem.* 29, 378–384, 2005.
48. Shimakoshi, H., Baba, T., Iseki, Y., Aritome, I., Endo, A., Adachi, C., and Hisaeda, Y., Photophysical and photosensitizing properties of brominated porphycenes, *Chem. Commun.*, 2882–2884, 2008.
49. Baker, J., Kozlowski, P. M., Jarzecki, A. A., and Pulay, P., The inner-hydrogen migration in free base porphyrin, *Theor. Chem. Acc.* 97, 59–66, 1997.
50. Kozlowski, P. M., Zgierski, M. Z., and Baker, J., The inner-hydrogen migration and ground-state structure of porphycene, *J. Chem. Phys.* 109, 5905–5913, 1998.
51. (a) Schlabach, M., Wehrle, B., Rumpel, H., Braun, J., Scherer, G., and Limbach, H. H., NMR and NIR studies of the tautomerism of 5,10,15,20-tetraphenylporphyrin, including kinetic HH/HD/DD isotope and solid state effects, *Ber. Bunsen-Ges. Phys. Chem.* 96, 821–833, 1992; (b) Braun, J., Schlabach, M., Wehrle, B., Köcher, M., Vogel, E., and Limbach, H. H., NMR study of the tautomerism of porphyrin including the kinetic HH/HD/DD isotope effects in the liquid and the solid state, *J. Am. Chem. Soc.* 116, 6593–6604, 1994; (c) Braun, J., Limbach, H. H., Williams, P. G., Morimoto, H., and Wemmer, D. E., Observation of kinetic tritium isotope effects by dynamic NMR. The tautomerism of porphyrin, *J. Am. Chem. Soc.* 118, 7231–7232, 1996.
52. Frydman, B., Fernandez, C. O., and Vogel, E., Variable-temperature solid-state ^{13}C- and ^{15}N-CPMAS NMR analyses of alkyl-substituted porphycenes, *J. Org. Chem.* 63, 9385–9391, 1998.
53. (a) Radziszewski, J. G., Waluk, J., Nepraš, M., and Michl, J., Fourier transform fluorescence and phosphorescence of porphine in rare gas matrices, *J. Phys. Chem.* 95, 1963–1969, 1991; (b) Radziszewski, J., Waluk, J., and Michl, J., FT visible absorption spectroscopy of porphine in noble gas matrices, *J. Mol. Spectrosc.* 140, 373–389, 1990; (c) Radziszewski, J. G., Waluk, J., and Michl, J., Site-population conserving and site-population altering photo-orientation of matrix-isolated free-base porphine by double proton transfer: IR dichroism and vibrational symmetry assignments, *Chem. Phys.* 136, 165–180, 1989.
54. Piwoński, H., Hartschuh, A., Urbańska, N., Pietraszkiewicz, M., Sepioł, J., Meixner, A., and Waluk, J., Polarized spectroscopy studies of single molecules of porphycenes: tautomerism and orientation, *J. Phys. Chem. C* 113, 11514–11519, 2009.
55. (a) Kay, C. W. M., Elger, G., and Möbius, K., The photoexcited triplet state of free-base porphycene: a time-resolved EPR and electron spin echo investigation, *Phys. Chem. Chem. Phys.* 1, 3999–4002, 1999; (b) Kay, C. W. M., Gromadecki, U., Törring, J. T., and Weber, S., An investigation of the structure of free-base porphycene by time-resolved electron nuclear double resonance and density functional theory on the photoexcited triplet state, *Mol. Phys.* 99, 1413–1420, 2001; (c) Kay, C. W. M. and Möbius, K., A time-resolved electron paramagnetic resonance study of the photoexcited triplet state of free-base porphycene, *Mol. Phys.* 95, 1013, 1998.
56. Even, U. and Jortner, J., Isolated ultracold porphyrins in supersonic expansions. III. Free base porphine, *J. Chem. Phys.* 77, 4391–4399, 1982.

57. Nishi, K., Sekiya, H., Kawakami, H., Mori, A., and Nishimura, Y., Tunneling in jet-cooled 5-methyltropolone and 5-methyltropolone–OD. Coupling between internal rotation of methyl group and proton transfer, *J. Chem. Phys.* 111, 3961–3969, 1999.
58. (a) Busch, J. H. and De la Vega, J. R., Coupling between the rotation of the methyl group and the proton exchange in 5-methyl-9-hydroxyphenalen-1-one, *J. Am. Chem. Soc.* 108, 3984–3987, 1986; (b) Nishi, K., Sekiya, H., Mochida, T., Sugawara, T., and Nishimura, Y., Coupling between the internal rotation of the methyl group and proton/deuteron transfer in jet-cooled 5-methyl-9-hydroxyphenalenone(OH) and 5-methyl-9-hydroxy-phenalenone(OD): Tunneling rate dependence of coupling potential, *J. Chem. Phys.* 112, 5002–5011, 2000.
59. Arnbjerg, J., Jiménez-Banzo, A., Paterson, M., Nonell, S., Borrell, J., Christiansen, O., and Ogilby, P. R., Two-photon absorption in tetraphenylporphycenes: are porphycenes better candidates than porphyrins for providing optimal optical properties for two-photon photodynamic therapy? *J. Am. Chem. Soc.* 129, 5188–5199, 2007.
60. Sánchez-Garcia, D. and Sessler, J. L., Porphycenes: Synthesis and derivatives, *Chem. Soc. Rev.* 37, 215–232, 2008.
61. Urbańska, N., Pietraszkiewicz, M., and Waluk, J., Efficient synthesis of porphycene, *J. Porphyrins Phthalocyanines* 11, 596–600, 2007.
62. Anju, K. S., Ramakrishnan, S., Thomas, A. P., Suresh, E., and Srinivasan, A., 9,10,19,20-Tetraarylporphycenes, *Org. Lett.* 10, 5545–5548, 2008.

34

Photochemical Transformations Involving Porphyrins and Phthalocyanines

Natalia N. Sergeeva
Trinity College Dublin

Mathias O. Senge
Trinity College Dublin

34.1 Introduction

Photochemistry of the porphyrins and their relatives has been largely inspired by photosynthetic processes in nature. As a result of this, most current studies generally utilize the chemistry of magnesium and zinc porphyrin analogues. Especially, magnesium tetrapyrrole chelates, that is, magnesium porphyrins and phthalocyanines, have found wide interest. This is primarily related to the biological relevance of magnesium porphyrins in nature, notably in photosynthesis and electron transfer (ET), and thus, we will focus on this aspect in this review. Outside these areas, not many "true" photochemical studies have been performed with magnesium tetrapyrroles.

Although porphyrins and especially phthalocyanines are stable compounds, both will undergo photooxidative degradation or photoexcited ET reactions. An additional problem of magnesium complexes is their low stability in aqueous solution, as they are prone to demetallation. As a result of this, many photochemical studies targeted at modeling the natural situation use the more stable zinc complexes. Zinc derivatives exhibit photochemical properties similar to the natural magnesium derivatives while being more stable and easier to synthesize (Li et al. 1997). Secondly, the propensity of zinc to act as an acceptor atom is used in many supramolecular approaches and/or for the modulation of chromophore properties *via* axial ligand binding. Thus, due to their biological relevance, technical importance, and good stability, substituted zinc tetrapyrroles have found significant use as industrial pigments and ET components, for photochemical transformations, and in photobiotechnology. Likewise, industrial attention has been given to the stable copper derivatives and copper tetrapyrroles have found industrial uses for oil desulfurization, as photoconducting agents in photocopiers, deodorants, germicides, optical computer disks, semiconductor devices, photovoltaic cells, optical and electrochemical sensing, and as molecular electronic materials.

However, even in this area, the body of the available literature is overwhelming and we will only use selected examples to highlight the state of the art of this field. A description of syntheses, methodology, or ET reactions with the various associated model systems is outside the purview of this work and the present work aims to give a broad overview and highlights selected examples in this area.

34.2 Basic Photochemistry of Porphyrins and Phthalocyanines

34.2.1 General Concepts and Theoretical Background

Tetrapyrroles are heteroaromatic macrocycles, where the aromatic character of the tetrapyrrole moiety, the central metal, and the reactivity of the functional groups in the side chains govern their chemistry. The tetrapyrrole ligands coordinate almost any known metal with the core nitrogen atoms. Together with the conformational flexibility of the macrocycle and the variability of its side chains, this accounts for their unique role in photosynthesis, medicine, biochemistry, and other applications (Senge 1992a,b, Kadish et al. 2000a,b, 2003).

Porphyrins and phthalocyanines **1–3** are well-known representatives of the tetrapyrrole class of heteroaromatic compounds and they are closely related. Tetraazaporphyrin (or porphyrazine) **2** is the first member of the phthalocyanine class. In phthalocyanines, the carbon atoms of the methine bridges (positions: 5, 10, 15, and 20 in **1**) are replaced by four nitrogen atoms and the parent structure of a phthalocyanine is structure **3**, formally a tetrabenzotetraazaporphyrin.

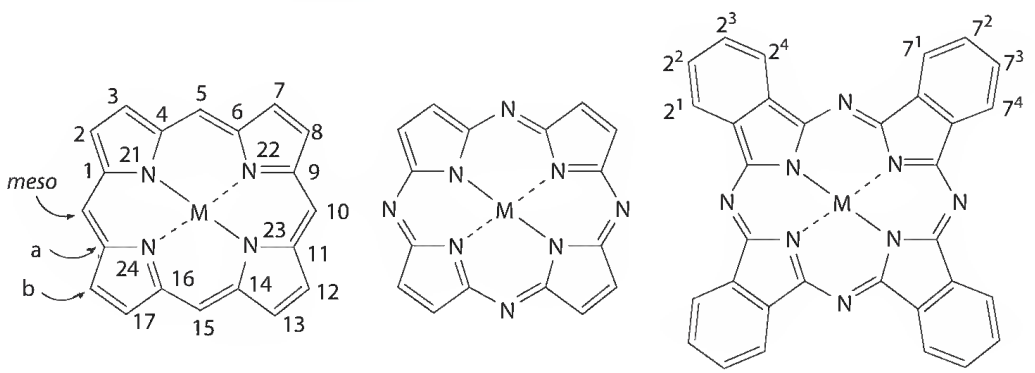

1 **2** **3**

M: 2H or Metal

Tetrapyrroles contain an extended π-conjugated system, which is responsible for their use in many applications ranging from technical (pigments, catalysts, photoconductors) to medicinal (photodynamic therapy) uses. The electronic absorption spectra are controlled by the aromatic 18

π-electron system and typically consist of two main bands. In phthalocyanines, the Q band around 660–680 nm is the most intense one and is accompanied by a weaker Soret band near 340 nm (Nyokong and Isago 2004). In porphyrins, the situation is reversed with an intense Soret band around 380–410 nm and weaker Q bands in the 550–650 nm region. The position and intensity of the absorption bands are affected by the central metal, axial ligands, solvation, substituents and their regiochemical arrangement, and aggregation. The theoretical background has been widely reviewed and established in pioneering works by Gouterman and Stillman (Gouterman 1978, Mack and Stillman 2003). The spectral characteristics strongly depend on the substituent pattern. By now almost all possible combinations of electron donating, electron withdrawing or sterically demanding groups have been prepared. Tetrapyrroles behave like most other organic chromophores. The absorption of light results in the rapid formation of the lowest excited singlet state *via* promotion of an electron from the highest occupied molecular orbital (HOMO) to the lowest unoccupied molecular orbital (LUMO). The excited state can then either relax to the ground state *via* radiative (fluorescence) or nonradiative processes (internal conversion of vibrational relaxation). Another possibility is intersystem crossing to form a triplet state, which again can relax either *via* radiative (phosphorescence) or nonradiative processes. In our context, both types of excited states can take part in photochemical reactions and, in the presence of donor or acceptor units, energy or ET between the chromophores can compete with these processes (Gust and Moore 2000). In addition, metalloporphyrins and phthalocyanines may form ions upon illumination. These are either anion or π-cation radicals and can undergo further photochemical reactions (Senge and Sergeeva 2006, Sergeeva and Senge 2008). Numerous reviews have been published in this area, the most comprehensive ones being by Wasielewski (1992) and by Gust et al. (2001). Recent studies have addressed questions of regiochemistry, theoretical calculations, solubility, and the influence of sterically demanding or heteroatom containing substituents (Flamigni 2007, Lo et al. 2007, Takagi et al. 2006).

34.2.2 Photophysics of Metallated Tetrapyrroles

The basic photochemical behavior of magnesium tetrapyrroles is similar to that of other metallo tetrapyrroles. Magnesium porphyrins (Fajer et al. 1970, Smalley et al. 1983, Slota and Dyrda 2003) and phthalocyanines (Bobrovskii and Kholmogorov 1973, Kim 1986, van Willigen and Ebersole 1987, Ough et al. 1991) may form cation radicals and ions via the triplet state upon illumination. For (phthalocyaninato) magnesium, both photochemical oxidations and reductions have been shown to occur. In the presence of carbon tetrabromide as an irreversible electron acceptor, the mechanism proceeds via the radical cation (Stiel et al. 1994). The suggested mechanism for the photochemical oxidation is through the lowest lying triplet state of the phthalocyanine and is thought to be similar to that of porphyrins such as (2,3,7,8,12,13,17,18-octaethylporphyrinato) magnesium and (5,10,15,20-tetraphenylporphyrinato) magnesium.

Copper ions are known to be excited state quenchers with the partially filled d orbitals. Copper(II) ions are capable of fluorescence quenching through electron or energy transfer. Furthermore, Cu(II), with its d^9 valence electron configuration, is paramagnetic. These special features have a strong influence on the subsequently discussed photochemical tetrapyrrole transformations. Copper(II) porphyrins are interesting complexes from both a theoretical and experimental point of view. The unpaired electron in the $d_x2\text{-}_y2$ orbital couples with the normal porphyrin (π, π^*) excited states to form the singdoublet [$^2S(\pi, \pi^*)$], tripdoublet [$^2T(\pi, \pi^*)$], and quartet [$^4T(\pi, \pi^*)$] states (Kim et al. 1984). These complexes do not exhibit the typical fluorescence of closed-shell metalloporphyrins, but rather show moderately strong phosphorescence from the tripdoublet-quartet manifold (Smith and Gouterman 1968, Eastwood and Gouterman 1969, Gouterman et al. 1970, van Dijk et al. 1981, Bohandy and Kim 1983). The relaxation processes in excited copper porphyrins (CuP) have been extensively studied by picosecond transient absorption spectroscopy (Hilinski et al. 1984, Serpone et al. 1984, Kruglik et al. 1995). It was found that photoexcitation of a CuP in the $^2S_0 \rightarrow {}^2S_n$ channel was followed by an extremely fast (1 ps) intersystem crossing to the

excited $^2T_1$ state, thus suppressing porphyrin fluorescence. The equilibrium formation between the $^2T_1$ and $^4T_1$ states proceeds within hundreds of picoseconds. The splitting between the excited $^2T_1$ and $^4T_1$ states for different Cu-porphyrins varies, depending on the porphyrin macrocycle structure.

Similar to metalloporphyrins, the central metal in metallophthalocyanines has a significant effect on the nature and the lifetime of the excited states. An interesting feature of metallophthalocyanines is their ability to participate in stacked assemblies with others or with metalloporphyrins. Investigations of these assemblies have shown that metallophthalocyanines with transition metals often display an excited-state relaxation pathway associated with the interactions of the macrocyclic π-system and d-orbitals of the central metal. Although H_2Pc and Zn(II)Pc are both strongly fluorescent probes in room-temperature emission experiments, neither fluorescence nor phosphorescence was observed for Cu(II)Pc. Implicit in the fluorescence silence is an ultrafast deactivation of the initially excited state of this paramagnetic compound with a d_9-metal center. A similar mechanism has been proposed for the analogous CuP, which showed, however, activation of moderately strong and long-lived phosphorescence as a result of thermally equilibrated triplet-doublet/triplet-quartet states (Sergeeva and Senge 2010). Due to the comparable nature of the porphyrin and phthalocyanine macrocycles and binding of the transition-metal center (i.e., Cu-N), it is likely that a similar ultrafast deactivation pattern governs the photophysics of copper phthalocyanine (CuPc).

Many spectroscopic studies provide details on magnetic interactions and spin dynamics of states with different multiplicities, such as doublets, triplets, and charge-transfer states. The communication between theses states strongly depends on the temperature and the solvent, and the spectroscopic studies established the existence of radical species deduced through ps optical experiments and the corresponding theoretical calculations.

34.3 Photosynthesis

The natural photosynthetic process is a rather complex biochemical system that primarily relies on the light absorption by organic chromophores, followed by generation of reduction equivalents and ATP. The main photosynthetic pigments are chlorophylls or bacteriochlorophylls that have very strong absorption bands in the visible region of the spectrum. Together with accessory pigments (carotenoids and open-chain tetrapyrroles), the various photosynthetic pigments complement each other in absorbing sunlight. Photosynthetic bacteria mostly contain bacteriochlorophylls with absorption maxima shifted toward the bathochromic region compared to the chlorin-based pigments.

In its simplest form photosynthesis can be described as the absorption of light through pigments arranged in a light-harvesting complex. These antenna systems permit an organism to increase greatly the absorption cross section for light and the use of light harvesting complexes with different pigments allows for a more efficient process through absorption of more photons and a more efficient use of the whole visible spectrum. The antenna pigments funnel the excitation energy through exciton transfer to a closely coupled pair of (b)chl molecules in the photochemical reaction center (Figure 34.1). The reaction center is an integral membrane pigment-protein that carries out light-driven ET reactions. The excited (bacterio) chlorophyll molecule transfers an electron to a nearby acceptor molecule, thereby creating a charge-separated state consisting of the oxidized chlorophyll and the reduced acceptor.

After the initial ET event, a series of ET reactions takes place that eventually stabilizes the stored energy in reduction equivalents and ATP. Higher plants have two different reaction center complexes that work together in sequence, with the reduced acceptors of one photoreaction (photosystem II) serving as the electron donor for photosystem I. Here, the ultimate electron donor is water, liberating molecular oxygen, and the final electron acceptor is carbon dioxide, which is reduced to carbohydrates. More simple and evolutionary older types of photosynthetic organisms contain only a single photosystem, either similar to photosystem II or photosystem I (Raghavendra 1998, Kadish et al. 2000a,b, van Grondelle and Novoderezhkin 2006). A simplified scheme of the complex photosynthetic apparatus is shown in an adaptation of the Z-scheme in Figure 34.2. The Z-scheme illustrates the two light-dependent reactions in photosynthetic systems of higher plants and exemplifies that two photosystems function in sequence to convert solar energy into chemical energy.

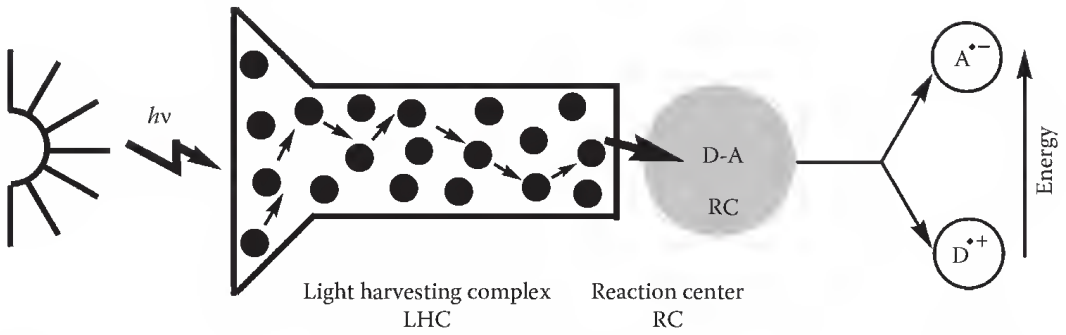

FIGURE 34.1 Cartoon scheme of a photosynthetic system (RC = reaction center, DA = donor–acceptor complex, LHC = light harvesting complex).

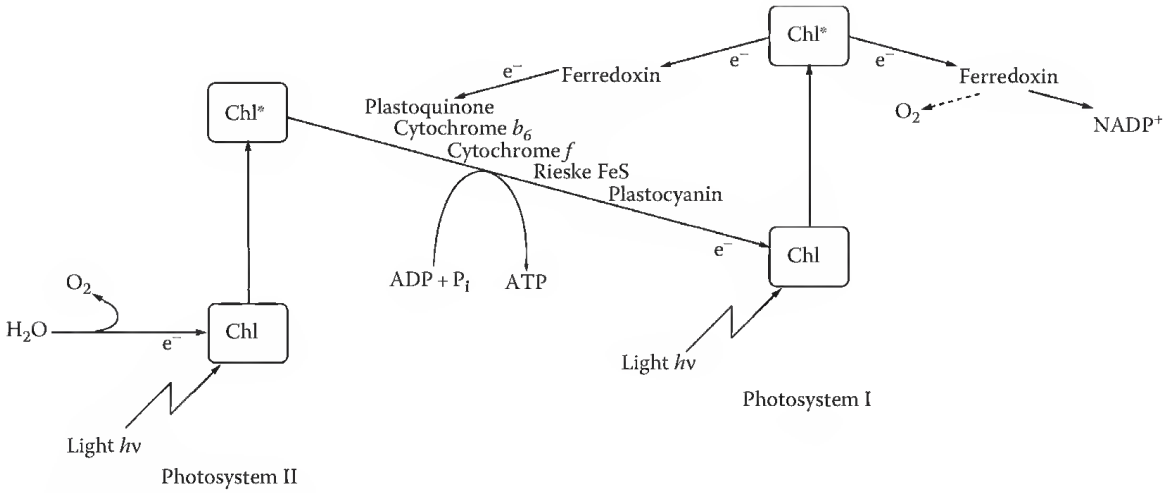

FIGURE 34.2 Simplified Z-scheme of the photosynthetic apparatus in higher plants.

In chemical terms the photoinduced electron transfer (PET) results in transfer of an electron across the photosynthetic membrane in a complex sequence that involves several donor–acceptor molecules. Finally, a quinone acceptor is reduced to a semiquinone and subsequently to a hydroquinone. This process is accompanied by the uptake of two protons from the cytoplasma. The hydroquinone then migrates to a cytochrome *bc* complex, a proton pump, where the hydroquinone is reoxidized and a proton gradient is established via transmembrane proton translocation. Finally, an ATP synthase utilizes the proton gradient to generate chemical energy. Due to the function of tetrapyrrole-based pigments as electron donors and quinones as electron acceptors most biomimetic systems utilize donor–acceptor constructs to model the natural photosynthetic process (Figure 34.3). Variation of the components (donor, bridge, linking group, acceptor),

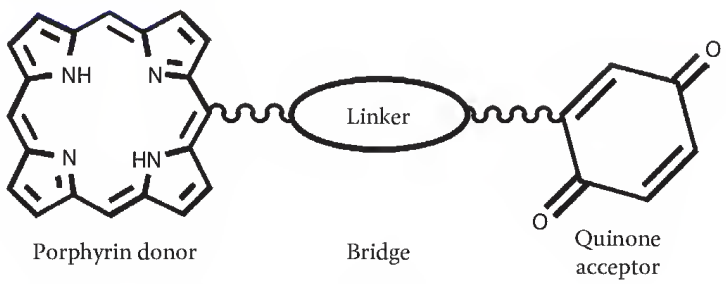

FIGURE 34.3 Schematic view of a biomimetic ET compound.

their spatial relationship, solvents, and environmental factors then serves to modulate and optimize the physicochemical properties. Several thousand systems of this general type have been prepared and used for investigation of the PET and numerous reviews have been published in this area (Wasielewski 1992, Gust and Moore 2000). Most of the available literature on ET studies in donor–acceptor compounds focuses on porphyrins. Phthalocyanine building blocks have been used more rarely, a result of their low solubility and the lack of appropriate synthetic methodologies to selectively introduce functional groups or for the synthesis of unsymmetrically substituted derivatives. However, this situation is rapidly changing with the renewed interest in solar energy conversion systems. An overview of the various synthetic and structural principles to model the components of the photosynthetic apparatus has been given in the relevant chapter on zinc(II) porphyrins (Senge and Sergeeva 2006).

34.3.1 Chlorophylls and Related Pigments

Chlorophylls (chl) and bacteriochlorophylls (bchl) are the ubiquitous pigments of photosynthetic organisms and the predominant class of magnesium tetrapyrroles in nature. As such they share common structural principles and functions. They are either involved in light harvesting (exciton transfer) as antenna pigments or charge separation (ET) as reaction center pigments. The best-known pigment is chl *a* **4**, which occurs in all organisms with oxygenic photosynthesis. In higher plants it is accompanied in a 3:1 ratio by chl *b* **6**, where the 7-methyl group has been oxidized to a formyl group. Both compounds typically consist of the tetrapyrrole moiety and a C-20 terpenoid alcohol, phytol. Most compounds are magnesium chelates, but the free base of chl *a*, pheo *a* **5**, is also active in ET. Chl *a* and *b* can be obtained easily from plants or algae and their synthetic chemistry has mainly targeted total syntheses and medicinal application in photodynamic therapy (PDT) (Scheer 1991, Senge 1992b).

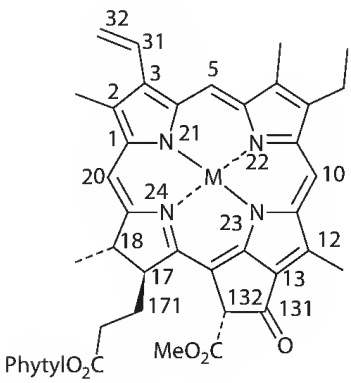

4 M = Mg, chl *a*
5 M = 2H, pheo *a*

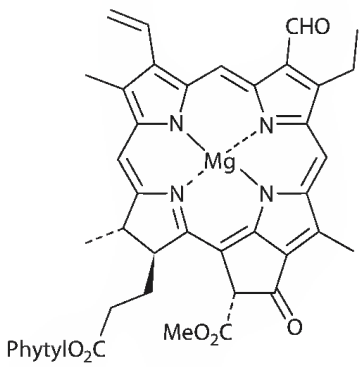

6 chl *b*

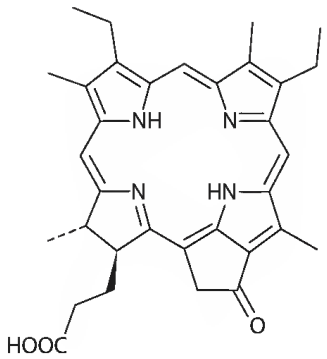

7 Phytochlorin

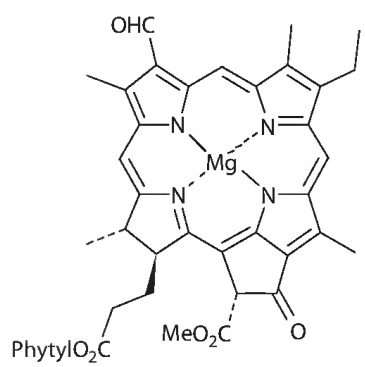

8 chl *d*

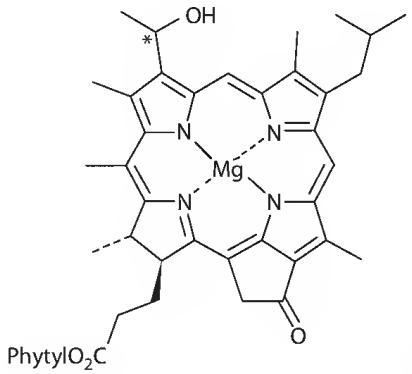

9 bchl *c*

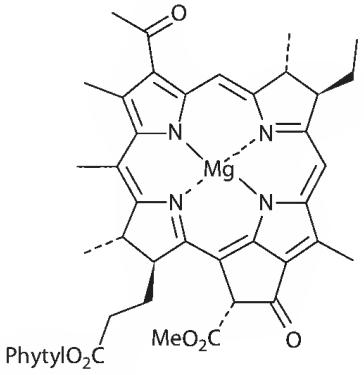

10 bchl *a*

However, many other similar photosynthetic pigments occur in nature (Scheer 1991, Senge 1992a,b, Senge and Richter 2006, Sergeeva and Senge 2008). All share either a phytochlorin **7** or a 7,8-dihydrophytochlorin framework and more than 100 related pigments have been isolated (Senge et al. 2006). For example, these compounds include chl *d* **8** from Rhodophytes, the bchls *c* **9**, *d*, and *e* (which are chlorins **12** and show significant variability in their peripheral groups) from Chlorobiaceae and Chloroflexaceae, and bchl a **10** and *b* (true bacteriochlorins **13**) found in Rhodospirillales. Other natural pigments are chl *c* and bchl *g*, and many of these are esterified with different isoprenoid alcohols. Chemically related chlorins have also been found in many oxidoreductases, marine sponges, tunicates, and in *Bonella viridis*. The deep-sea dragon fish *Malacosteus niger* utilizes a chl derivative as a visual pigment (Douglas et al. 1998). These compounds are derived from chl and then processed by the plant or animal.

Photosynthetic organisms that utilize chls or bchls containing metals other than Mg were unknown for a long time (Hiraishi and Shimada 2001). Past years have seen increasing evidence that both Mg and Zn chlorophylls do exist in nature. By now it has been satisfactorily demonstrated that a purple pigment occurring in a group of obligatory aerobic bacteria is in fact a zinc-chelated-bchl (Zn-bchl) (Wakao et al. 1996, 1999, Hiraishi et al. 1998). The natural occurrence of Zn-bchl *a* has been proven for a limited group of aerobic acidophilic proteobacteria, including species of the genus *Acidiphilium*. The major photopigment in *Acidiphilium* was first identified tentatively as Mg-bchl *a* on the basis of preliminary spectral analyses (Wakao et al. 1993, Kishimoto et al. 1995). However, more detailed studies revealed that all previously known species of *Acidiphilium* contained Zn-BChl *a* as the major photopigment and showed *Acidiphilium* to be a photosynthetic organism (Wakao et al. 1996, Hiraishi et al. 1998).

The naturally occurring Zn-bchl *a* and Mg-bchl *a* show large structural similarities and have very similar physicochemical characteristics (Scheer and Hartwich 1995). Likewise, Zn-chl *a* exhibits features similar to Mg-chl *a* with regard to redox potential and absorption maxima in organic solvents. The light-harvesting efficiency of Zn-chl *a* and Mg-chl *a* are very similar, although the fluorescence quantum yield of the former is lower than the latter. Compared to other chlorophyll-type pigments, Zn-bchl *a* is much more stable toward acid. For example, the rate of pheophytinization for Zn-bchl *a* is 10^6-fold slower than for Mg-bchl *a* (Kobayashi et al. 1998). In fact, it is difficult to fully demetallate Zn-bchl *a* to bacteriopheophytin (BPhe) by treatment with 1N HCl, which is commonly used for pheophytinization of Mg-bchl and Mg-chl. Due to the chemical stability of Zn-(b)chl *a* and their photo- and electrochemical similarities with Mg-(b)chl *a*, Zn-(b)chls are an alternative pigment for photosynthetic studies. Thus, it is not surprising that they have been used along with magnesium porphyrins in studies on artificial photosynthetic systems (Wasielewski and Niemczyk 1984, Osuka et al. 1993a,b).

34.3.2 Light-Harvesting Complexes and Reaction Center Models

The propensity of metal tetrapyrroles for aggregation has been widely used to mimic natural antenna systems of photosynthesis. The best studied system is the chlorosome, where bacteriochlorophylls self-organize *without* the use of a protein scaffold. Depending on the light conditions these require constructing arrays with as many chromophores as possible. Thus, many studies on the self-assembly of bacteriochlorophyll model compounds or dendritic/polymeric approaches have been performed (Haycock et al. 2000, Ikeda et al. 2001). Current studies focus on large aggregates and chirality effects (Balaban et al. 2003). A typical example involves perylene monoimide donors that have been used to construct antenna models in which up to 8 perylene units where covalently bound to a zinc(II) porphyrin (Tomizaki et al. 2002). Osuka and coworkers' windmill porphyrins also present excellent antenna complex building blocks (*vide infra*) (Nakano et al. 2001). In addition, several "porphyrin wheel" antenna complexes were prepared by template-assisted synthesis (Yu and Lindsey 2001, Tomizaki et al. 2003) or self-aggregation (Kuramochi et al. 2004). Intramolecular cyclization of porphyrin dodecamers to a porphyrin wheel has also been achieved (Peng et al. 2004).

Classic examples for structural models of the photosynthetic reaction center are the cofacial bisporphyrins or bischlorins (Kalisch et al. 1998), which model the structural arrangement of the

special pair in the reaction center (Pascard et al. 1993, Brettar et al. 2001, Fletcher and Therien 2002). Zinc(II) bisporphyrins with various other geometrical arrangements, for example, skewed (Shultz et al. 1999), have been prepared as well, including those bearing C_{60} acceptor groups (Liddell et al. 2004). The important two-tetrapyrrole-unit found in the special pair has by now been realized in a multitude of different geometrical arrangements. Depending on the porphyrin-porphyrin or porphyrin-acceptor linkage meso–meso, meso–β (Senge et al. 2004), and β–β (Deng et al. 2000) linked systems have been prepared. Similar arrangements are also possible using noncovalent self-assembly. Noncovalent binding of substrates at the zinc(II) center can be used to control the PET in such systems (Yagi et al. 2003)

Today, most reaction center models carry suitable antenna pigments and acceptor groups and in effect are photosystem models. A typical example for a state of the art system that incorporates many aspects of a photosystem consisted of a boron dipyrrin covalently linked to a zinc(II) porphyrin, which carried a suitably modified C_{60} derivative as axial ligand. Selective excitation of the boron dipyrrin as antenna pigment resulted in energy transfer to a zinc(II) porphyrin followed by ET to the C_{60} acceptor (D'Souza et al. 2004a). These and other photoactive complexes will be discussed in more detail later in the section on ET systems.

34.4 Electron Transfer Systems and Photochemical Reactions

34.4.1 Introduction

Studies on photoinduced energy and ET in supramolecular assemblies have witnessed a rapid growth in the past decade. Most of these studies focused on the mechanistic details of light-induced chemical processes. Researchers attempt to generate systems with ultra fast charge transfer and charge recombination applicable as light-induced switches or with long lived charge-separated states to mimic the photosynthesis or for solar energy conversion (Iseki and Inoue 1994). The development of novel photochemically active systems has focused on polychromophoric, dendritic, supramolecular systems, and novel materials. These endeavors have produced an expanding body of information on porphyrin/phthalocyanine dyads, their design, and energy, exciton, and charge transfer properties. Incorporation of these systems into larger architectures now offers the possibility for applications in molecular photonics, electronics, solar energy conversion, nanomaterials, and quantum optics.

Most ET studies are aimed at the synthesis and investigation of donor–acceptor complexes that mimic the natural processes. Typically, this involves the construction of systems consisting of donor(s), a covalent or noncovalent bridging unit, and acceptor(s) (Figure 34.4). In an ideal situation, all requirements of the natural system would be modeled. These include (1) unidirectional ET → redox gradient in subunits; (2) rigid linker groups that do not play a role in ET → no heteroatoms, conjugated systems, etc.; (3) defined overall geometry with correct relative orientation of the subunits → for example, special pair model with cofacial orientation of the macrocycles → use of coupling reactions that give products with defined geometry; and (4) modeling the protein environment → scaffold, electronic, and steric effects/reconstituted pigment-protein systems.

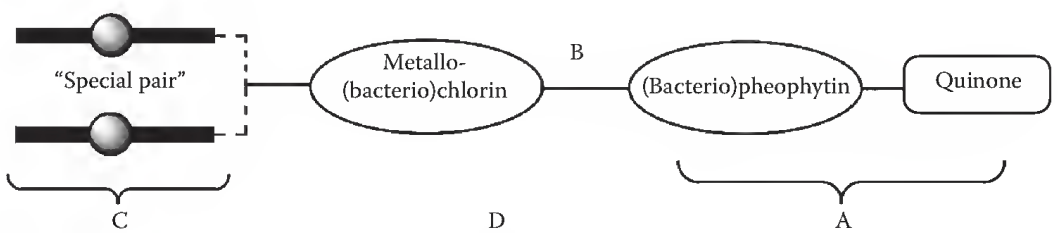

FIGURE 34.4 Synthetic model of a natural photosynthetic system.

34.4.2 Donor–Acceptor Electron Transfer Compounds

Most of the available literature on ET studies in donor–acceptor compounds focuses on porphyrins. Phthalocyanine building blocks have been used less often, a result of their low solubility and (until recently) the lack of appropriate synthetic methodologies to selectively introduce functional groups or for the synthesis of unsymmetrically substituted derivatives.

The simplest covalently linked systems consist of porphyrin linked to electron acceptor or donor moiety with appropriate redox properties as outlined in Figure 34.3. Most of these studies have employed free base, zinc and magnesium tetrapyrroles because the first excited singlet state is relatively long-lived, so that ET can compete with other decay pathways. Additionally, these pigments have relatively high fluorescence quantum yields. These tetrapyrroles are typically linked to electron acceptors such as quinones, perylenes (Yang et al. 2001a,b, Fukuzumi et al. 2005), fullerenes (El-Khouly et al. 2005, D'Souza et al. 2005), acetylenic fragments (**11,12**), aromatic spacers (Li et al. 1997, Youngblood et al. 2002, Mitzel et al. 2003, Chandra et al. 2003), and other tetrapyrroles (e.g., boxes and arrays).

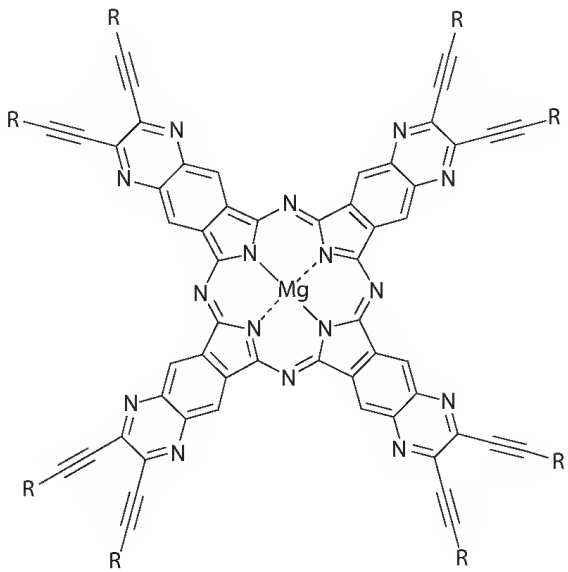

11

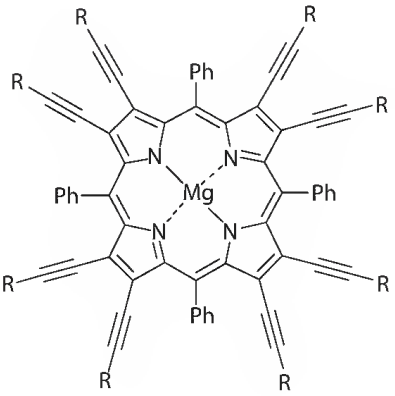

12

Biomimetic systems composed of porphyrins and quinones have been studied extensively with regard to their ET and charge transfer properties. Porphyrin-quinone (PQ) model systems in which the quinone is fused directly to the porphyrin periphery therefore have a special relevance for the fundamental understanding of rapid biological ET reactions as they are related to photosynthesis and solar energy conversion. In many cases, the magnitude of the reduction potentials of quinones covalently linked to porphyrins suggests light-induced radical-pair generation. However, use of quinones as acceptors decreases the energy that can be stored in the photoinduced radical pair, thus diminishing the likelihood of a mechanism via radical-pair generation (Connolly 1982). Many artificial systems with wide range of functionalized quinine units have been synthesized and extensively studied (Gust and Moore 2000). Here, we will only highlight selected recent works.

A series of "black" (tris- and tetra-β-quinonoporphyrinato)zinc(II) chelates was prepared via thermolysis of a tetra-β-sulfolenoporphyrin in the presence of excess benzoquinone followed by oxidation with dicyanodichlorobenzoquinone in up to 86% yield. Surprisingly, the absorption spectra of these tetrapyrroles represent broad and intense electronic transitions covering the whole range of visible wavelengths region (Banala et al. 2009).

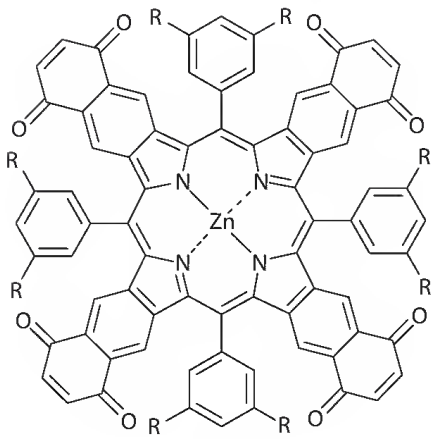

13 R: *t*-Bu

While most studies utilized quinones as acceptor compounds, these studies almost exclusively used *p*-quinones. Nevertheless, the isomeric, but synthetically less accessible porphyrin-*o*-quinones are much better electron acceptors (Giangiacomo and Dutton 1989). This results in a higher ΔG_{ET} and thus in a higher efficiency of the ET and several *o*-quinone containing zinc(II) porphyrin dyads (e.g., **14–16**), triads, and tetrads have been prepared by us (Speck et al. 1997, 2000, Senge et al. 2003). In order to achieve a variation of ΔG_{ET}, the general strategy in ET studies generally involves the synthesis of different models via chemical modification of the porphyrin donor or the quinone acceptor. However, this also leads to changes in a number of other variables such as distance, solvent term, and electronic matrix element resulting in altered ET rates. Here, the utilization of porphyrin-*o*-quinones as ET systems offers an attractive alternative. With them, a facile and simple variation of ΔG_{ET} can be achieved by using the in situ formed semiquinones for metal chelatization (Figure 34.5) (Speck et al. 2002). Some of the sterically hindered parent free base systems (e.g., free base of **6**) can undergo photochemical degradation reactions. However, such side reactions were not observed with the zinc(II) complexes (Speck et al. 1997, 2000).

Although the importance of these compounds as structurally simple models with large electronic donor–acceptor coupling has long been recognized, only few examples of magnesium containing systems have been reported so far. For mechanistic studies, it is essential to have acceptor moieties other than quinones with systematically variable reduction potentials so that the energy of P^+-A^- falls between the energies of the excited singlet and triplet states and beyond. CuP and CuPc play a very important

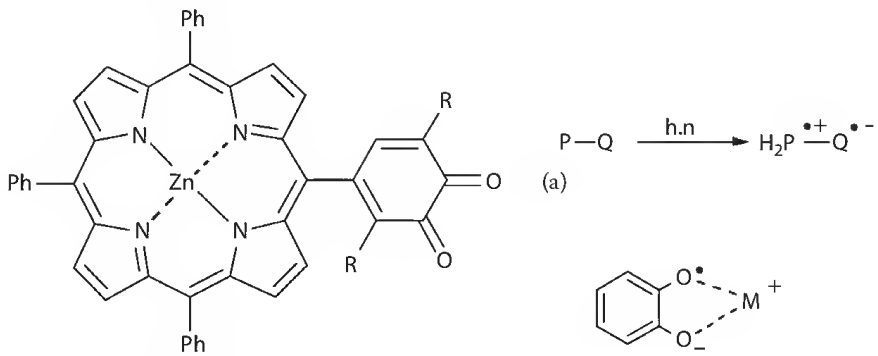

14 R: Me
15 R: H
1616 R: *t*-Bu

FIGURE 34.5 Porphyrin-*o*-quinone systems.

role in the ET processes. One example for alternatives to PQ model systems are the copper picryl porphyrins **17** (Maiya and Krishnan 1985). Here, the interaction between the porphyrin and trinitroaryl group is relatively stronger than in PQ systems (Yamada et al. 1983).

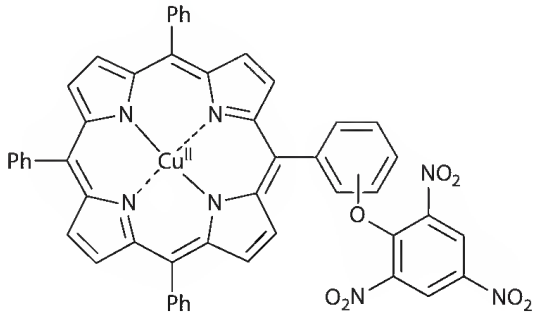

17

Novel systems of zinc porphyrin containing fluorescent dyes attached to the surface of bacteriophage MS2 enabled energy transfer and sensitization of the porphyrin at previously unavailable wavelengths and participated in the photocatalytic reduction reactions at multiple excitation wavelengths (Stephanopoulos et al. 2009).

Viologen (4,4′-bipyridyl) derivatives are attractive electron-accepting units for tetrapyrrole-containing dyads and more complex donor–acceptor systems as they can be easily reduced, conveniently linked to other molecules via *N*-alkylation of precursors, and can be used to vary the solubility in polar solvents by virtue of their charged nature. Based on the fact that the viologen radical monocation absorbs in the visible region they can be used as convenient charge separation indicators. As a result, a number of magnesium porphyrins (Szulbinski 1995, Zakrzewski and Giannotti 1995) and phthalocyanine (Harriman et al. 1981, Ohtani et al. 1984) –viologen systems have been studied. Typically, excitation of a porphyrin-viologen dyad **18** leads to the porphyrin first excited singlet state, which can than induce photoelectron transfer to the viologen or undergo intersystem crossing to yield the porphyrin triplet state. As viologen is easily reduced, the porphyrin triplet state may also act as an electron donor in these systems.

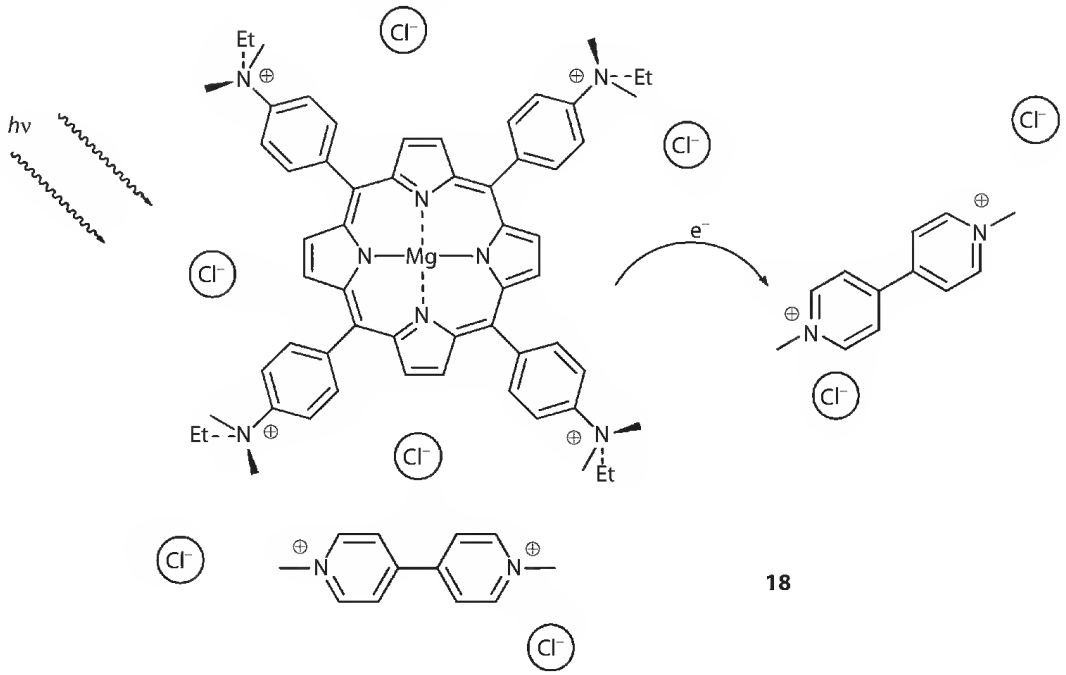

18

A different strategy involves using a transition metal center linked to an organic chromophore. This greatly expands the number of electron/energy transfer reactions that can take place within the assembly compared to pure organic or inorganic–organometallic systems. Covalently linking metal complexes to porphyrins yields a cornucopia of candidates for photosynthesis-related studies. Again, only a few examples of photoinduced processes based on magnesium phthalocyanine (Kobyshev et al. 1963) and porphyrins (Monnereau et al. 2005, Gabrielsson et al. 2006) have been reported so far (e.g., compounds **19** and **20**).

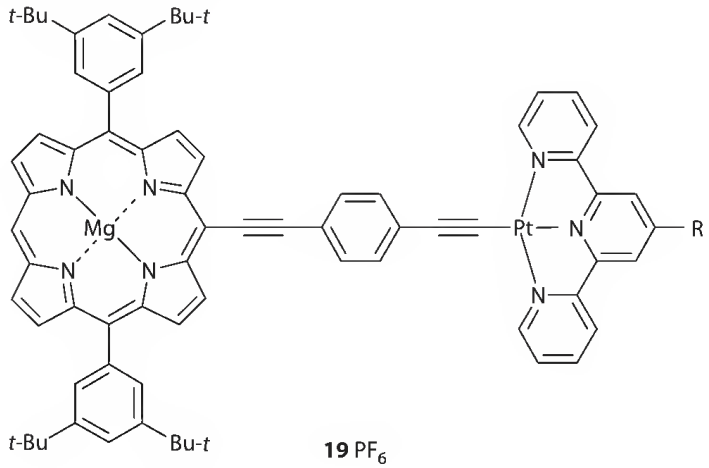

19 PF_6

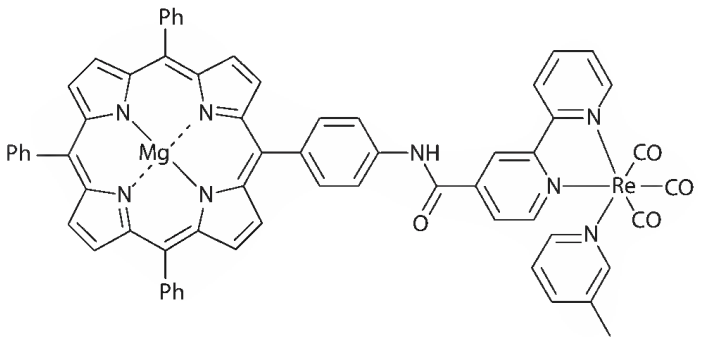

20 PF_6

For example, in 1963, the photochemistry of magnesium phthalocyanine with coordinated uranium cations was studied in pyridine and ethanol and indicated the occurrence of PET to the uranium complex (Kobyshev et al. 1963). A rapid PET (2–20 ps) followed by an ultra fast charge recombination was shown for various zinc and magnesium porphyrins linked to a platinum terpyridine acetylide complex (Monnereau et al. 2005). The results indicated the electronic interactions between the porphyrin subunit and the platinum complex, and underscored the potential of the linking *p*-phenylene bisacetylene bridge to mediate a rapid ET over a long donor–acceptor distance.

Complexes of rhenium(bipyridine)(tricarbonyl)(picoline) units linked covalently to magnesium tetraphenylporphyrins via an amide bond between the bipyridine and one phenyl substituent of the porphyrin **20** exhibited no signs of electronic interaction between the $Re(CO)_3(bpy)$ units and the metalloporphyrin units in their ground states. However, emission spectroscopy revealed a solvent-dependent quenching of porphyrin emission upon irradiation into the long-wavelength absorption bands localized on the porphyrin. The presence of the charge-separated state involving ET from Mg(II)TPP to Re(bpy) was shown by time-resolved IR spectroscopy (Gabrielsson et al. 2006).

The system is reversible in the absence of an added electron donor but undergoes irreversible reaction at the reduced rhenium bipyridine center in the presence of added triethylamine. The observation of

reaction at the rhenium site upon excitation in the absorption band of the metalloporphyrin site is compatible with an ultra fast back ET provided that the triethylamine coordinated to the magnesium prior to absorption and that the ET from the metalloporphyrin to the bipyridine was followed rapidly by irreversible ET from the triethylamine to the metalloporphyrin. The experiments graphically demonstrated the benefits of the incorporation of carbonyl ligands at the electron acceptor as they allowed a tracking of the sequence of charge separation and back ET via time-resolved IR data (Gabrielsson et al. 2006).

Applications of fullerenes in PET studies derive from the fact that back ET is inhibited in donor–acceptor systems incorporating [60]fullerene (C_{60}). Fullerenes can accept up to 6 electrons and exhibit small reorganization energies while the photoinduced charge separation is accelerated and charge recombination is slowed. The effect of the introduction of C_{60} as an electron acceptor into tetrapyrrole molecules should enhance our knowledge of the dependence of PET dynamics on molecular topology. Thus, relatively long-lived charge-separated states are obtained without a special environment such as an apoprotein (Imahori et al. 2002a). Several self-assembled donor–acceptor systems containing fullerenes as three-dimensional (3-D) electron acceptors and porphyrins as electron donors have been described. A recent system consisting of a ferrocene, two porphyrins, and one C_{60} unit exhibited a life-time of 1.6 s (!), comparable to bacterial photosynthetic reactions centers. The quantum yields for charge separation in complex biomimetic systems can reach unity. Recent advances in their synthetic methodologies allow the functionalization of fullerenes and linking them to other pigments.

Fullerenes [mostly C_{60} but also C_{70} (Kesti et al. 2003)] have been incorporated into multicomponent systems with step-wise charge separation (Bell et al. 2002, Imahori et al. 2002a,b, 2004, Kesti et al. 2003, Imahori 2004, Imahori and Fukuzumi 2004) and used as core groups for dendrimers with zinc(II) porphyrin donors (Camps et al. 1999). Already, C_{60} has also been linked to chlorins and phytochlorin derivatives (Helaja et al. 1999, Fukuzumi et al. 2001) and carotenoid-porphyrin-C_{60} systems are under investigation (Kodis et al. 2004). Many of these systems utilize a pyrrolidine linkage, but bislactone (Montforts et al. 2003), or Diels-Alder derived cyclohexene-linked systems (Fukuzumi et al. 2001, Bell et al. 2002) have also found wide applications. Currently, nanostructured systems are emerging (Yamaguchi et al. 2003) and new attention has been focused on combining the utility of fullerene acceptor groups with rotaxane systems (Watanabe et al. 2003, Schuster et al. 2004, Li et al. 2004a,b). Zinc(II) porphyrins have been used in many systems for complexation studies (Guldi et al. 2001) and to modulate the ET properties by using axial coordination effects (D'Souza et al. 2001, 2002a,b) or to construct self-assembled donor–acceptor systems (D'Souza et al. 2002a, 2003, 2004b).

For example, pyridinofullerenes were used as axial ligands for Zn(II)TPP or Zn(II)OEP and the formation of the noncovalent porphyrin-fullerene dyads was indicated by fluorescence quenching of Zn(II)TPP (Wilson et al. 2004). This PET is an exergonic process (D'Souza et al. 1999). PET in nonpolar media was reported for porphyrin tripod fullerene systems synthesized via "click" chemistry (Takai et al. 2010). Likewise, a photoactive [2]catenane containing zinc(II)-porphyrin (ZnP) and/or [60]fullerene (C_{60}) as appended groups also prepared via "click" chemistry was described as well (Megiatto et al. 2010). For a related triad (C_{60} + 2Zn(II) porphyrins), it was shown that the main quenching pathway involved charge separation from the excited singlet state Zn(II)TPP to the C_{60} unit in noncoordinating solvents and from the triplet excited state of Zn(II)TPP in coordinating solvents (El-Khouly et al. 2003). Porphyrin-fullerene dyads with an azobenzene linker were synthesized, and the photophysicochemical properties were investigated using steady-state and time-resolved spectroscopic methods (Schuster et al. 2007). Photosynthetic models containing dendritic C_{60}-H_2P-$(ZnP)_3$ conjugates were analyzed in relation to the primary events in photosynthesis, that is, light harvesting, unidirectional energy transfer, charge transfer, and charge-shift reactions (Schlundt et al. 2009). Similar approaches have been used with zinc(II) phthalocyanines (Guldi et al. 2002). Some of the characteristics of fullerene containing systems, for example, recombination to the triplet state, were also observed with specifically designed triads without a fullerene unit (Gould et al. 2004).

In line with the general development in the field noncovalently and covalently linked Mg porphyrin-fullerene, dyads have been synthesized and investigated spectroscopically (El-Khouly et al. 2005,

D'Souza et al. 2005). For example, a covalently linked magnesium porphyrin-fullerene (MgP-C_{60}) dyad with a flexible ethylene dioxide bridge (El-Khouly et al. 2005) was compared to a self-assembled noncovalently linked dyad (MgP...C_{60}Im, **21**). In the latter, axial coordination of an imidazole (Im)-functionalized fullerene (D'Souza et al. 2005) to the magnesium porphyrin was used for bonding. Significant increases in the lifetime of the charge-separated states were observed upon coordinating nitrogenous axial ligands to the latter.

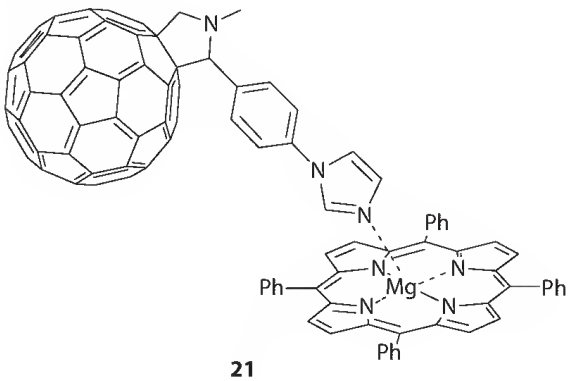

21

Likewise, different types of noncovalently and covalently linked CuPc-fullerene dyads have been prepared (Nierengarten et al. 2000, El-Khouly et al. 2002, Li et al. 2004b). An example is a series of fulleropyrrolidinophthalocyanines containing free base, Zn, and Cu used as electron-donating building blocks in fullerene dyes of type **22** (Guldi et al. 2004). These experiments support the view that the $C_{60}/C_{60}^{\bullet-}$ couple exhibits the strongest electron affinity, while the different $Pc/Pc^{\bullet+}$ couples play the role of electron donors.

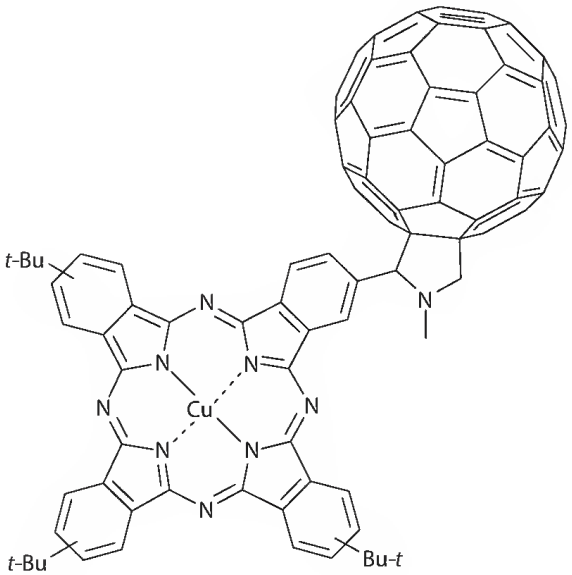

22

Further investigations showed that the donor ability increases in the following order: CuPc < H_2Pc < ZnPc. In other words, starting from the free base (H_2Pc), addition of either Cu (CuPc) or Zn (ZnPc) increases or decreases the electron density on the phthalocyanine, respectively. Similarly, the energy for the radical ion pair $CuPc^{\bullet-}$–$C_{60}^{\bullet+}$ formed in a PET reaction (*vide infra*), decreases in the following order: (1.40 eV) > H_2Pc-C_{60} (1.36 eV) > ZnPc-C_{60} (1.23 eV).

Many other building blocks have been developed for use in photochemically active compounds. Perylene units have attracted attention as energy transfer donors, as they increase the light-harvesting efficiency in the green spectral region (where porphyrins are relatively transparent). Classic cases of magnesium porphyrins are **23** and **25.** They represent a family of closely related bichromophoric systems with properties designed to utilize PET strategies (Yang et al. 2001a,b, Fukuzumi et al. 2005). A typical example for zinc tetrapyrroles is **23** (Prathapan et al. 2001) but larger arrays including some with phthalocyanine units have been described as well and perylene units have been used as bridging units in D-B-A systems (Hayes et al. 2000, You and Würthner 2004).

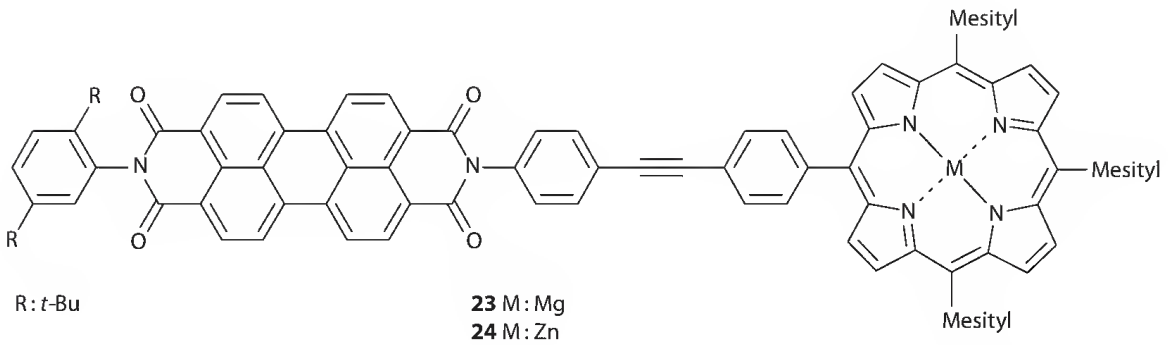

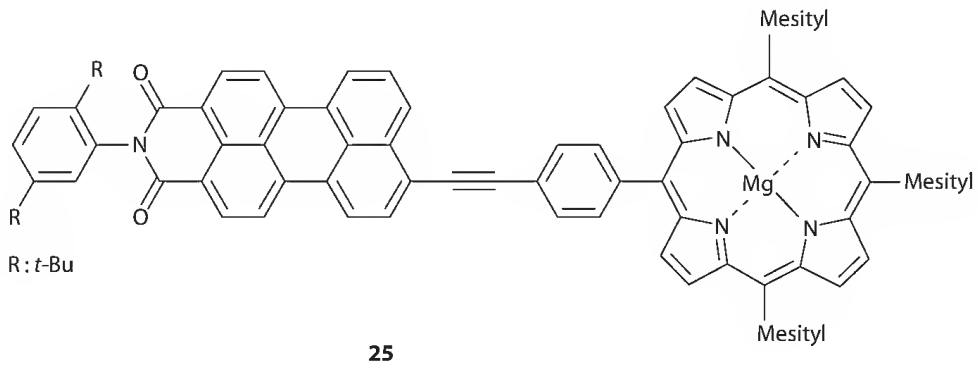

25

34.4.3 Heteroligand Systems

The PET between metalloporphyrins and free bases in dimeric, trimeric, and oligomeric porphyrin systems has been studied extensively. Depending on the choice of the donor and acceptor unit, ET from either singlet or triplet states may be observed. ET studies in systems based on heterodimers with covalent or electrostatic bonds are of particular interest as it relates directly to the natural photosynthetic process.

For systems such as the magnesium free base porphyrin heterodimer **26**, electron paramagnetic resonance (EPR) spectroscopy is an essential analytical tool that provides information not available from optical studies. It provides details on the magnetic interactions and spin dynamics of states with different multiplicities, such as doublets, triplets, and charge-transfer states. The communication between these states strongly depends on the temperature and the solvent, and the EPR results established the existence of the radical species deduced in ps optical experiments and the corresponding theoretical calculations (Zaleski et al. 1993, Levanon et al. 1993, Zhang et al. 1995).

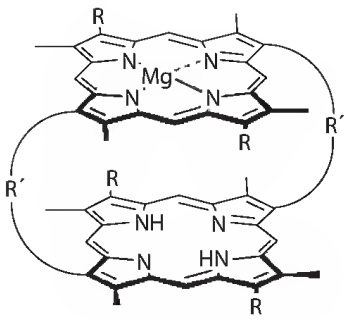

26

R: n-C_8H_{17}, R′ = $CH_2CON(n\text{-}Bu)CH_2CH_2$

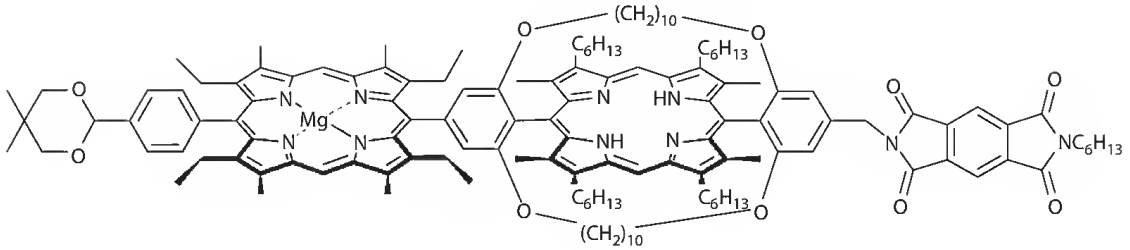

27

A series of conformationally restricted magnesium free base hybrid arrays bridged linearly via aryl-spacers to form di- (**27**) or trimeric porphyrins was used to study the intramolecular ET reactions from the singlet excited state of the remote doubly strapped free base porphyrin to the pyromellitimide acceptor by time-resolved ps fluorescence and transient absorption spectroscopy (Osuka et al. 1993b, 1994a,b). The ET was more effective in magnesium-porphyrin bridged models than in the related zinc-porphyrin bridged ones, indicating that the past reliance on the use of zinc-based biomimetic models is not always sufficient. Remarkably, the ET rates over two porphyrins were almost similar to those for the ET over one porphyrin independent of the bridging metalloporphyrin. Compound **28** is an example of multichromophoric systems that are now more frequently used to study the intramolecular electronic communications between chromophore subunits (Li et al. 1997, Youngblood et al. 2002).

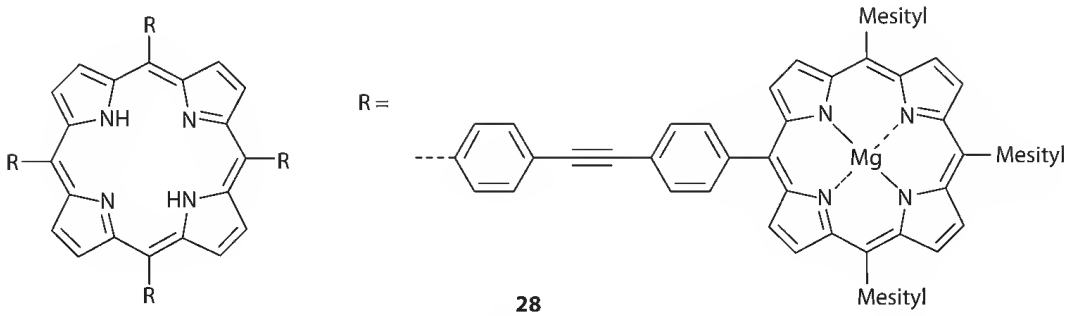

28

Another example involving dimeric systems linked through noncovalent bonds used (5,10,15,20-tetrakis(4-sulfonatophenyl)porphyrinato)zinc(II) and (5,10,15,20-tetrakis(4-*N,N,N*-trimethylanilinium)

porphyrinato)magnesium(II) with complementary charge results in dimerization in solution. Continuous wave time-resolved EPR spectroscopy demonstrated that intramolecular electron and/or energy transfer in electrostatically bound metalloporphyrin dimers can be controlled via simple metal and substituent effects. Although the metal constituents were identical in these two dimers, the peripheral charged substituents governed the fate of the ET, whereas the energy transfer is controlled via the metal substituents (Murov et al. 1993, Berg et al. 1996).

ET from CuP to its free base partner was observed in the CuP-H_2P hybrid dimer **29** (Asano-Someda et al. 1994). Clearly, the advantage of a hybrid system is that the energy donor and an acceptor are distinct. The lowest excited singlet and triplet states of the free base porphyrin monomer are lower than those of the CuP. Based on T–T transient absorption spectra, the triplet yield of the free base porphyrin was found to be increased in the hybrid dimer compared to a monomeric free base porphyrin. Time-resolved ESR showed that the intermolecular energy transfer occurs between the triplets. The lowest excited triplet state of the CuP-H_2P dimer is generated both by energy transfer processes from the triplet manifolds in the CuP moiety and by intersystem crossing from the lowest excited singlet state of the free base moiety. As a result of the paramagnetic perturbation, intersystem crossing in CuP is remarkably accelerated and seems to prevent singlet–singlet energy transfer to another porphyrin moiety.

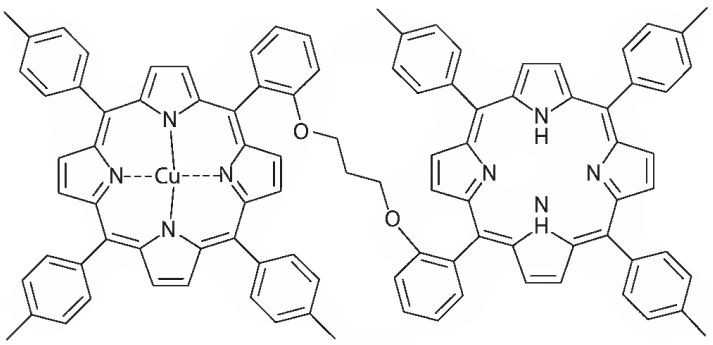

29

Electrostatically linked dimers can easily be produced by a coupling of two monomers with oppositely charged substituents in the liquid phase. An example of such systems has been illustrated by Tran-Thi et al. (1992), where Zn-porphyrin units were linked with Cu-phthalocyanines. Drastic changes in the ground-state absorption of the electrostatically linked dimer compared to the corresponding monomers indicate a strong interaction between the two chromophores. According to femto- and nano-second absorption spectroscopy, very efficient intersystem conversion takes place in the excited ZnP-CuPc, leading to the final 'triplet' state. In contrast, excitation of a ZnP-AlPc dimer led to an ET from the porphyrin to the phthalocyanine moiety. The different behavior in ET can be explained by the peculiar properties of the paramagnetic CuPc.

For systems such as the copper–copper dibenzofuran-bridged cofacial bisporphyrins **30** and **31**, EPR spectroscopy has been shown to be an essential analytical tool that provides information not available from optical studies. It also complements crystallographic studies by probing intramolecular metal–metal arrangements in frozen solution (Chang et al. 2002).

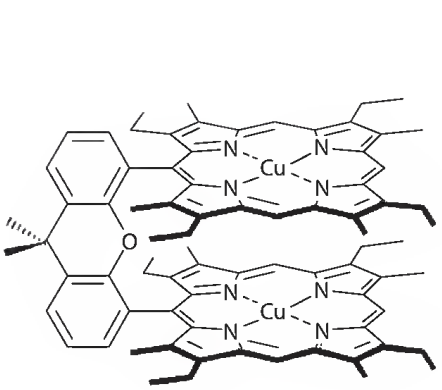

30

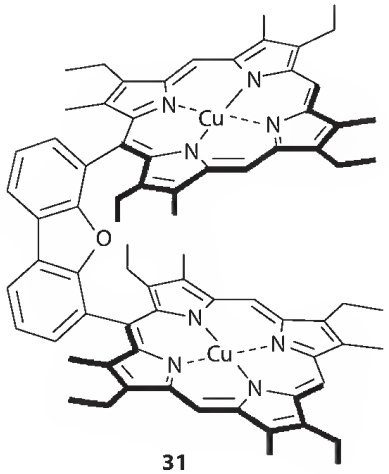

31

Mixed cyclization of porphyrin containing phthalonitrile compounds with an europium(III) half-sandwich phthalocyanine complex in the presence of 1,8-diazabicyclo[5.4.0]undec-7-ene (DBU) gave a series of porphyrin-appended europium(III)bis(phthalocyaninato)complexes. These mixed tetrapyrrole triads and tetrad were spectroscopically characterized with steady-state and transient spectroscopic methods. The porphyrin fluorescence was effectively quenched by the double-decker unit through an intramolecular PET process. Both the PET and recombination of the charge-separated state depended on the number and position of the porphyrin units attached to phthalocyanines (Bian et al. 2007).

Many systems were prepared and detailed photophysical analyses were carried out for zinc tetrapyrrole systems (Senge and Sergeeva 2006). Other examples for hybrid systems are slipped-cofacial dimers consisting of directly linked zinc porphyrin–zinc phthalocyanine units (Ito et al. 2006).

34.5 Photochemical Reactions

34.5.1 Porphyrins

Photoinduced metallation of porphyrin was reported first in the 1970s (Bluestein and Sugihara 1973). Various porphyrins, geoporphyrins, and Cu(II) 1,3-diketonates underwent a quantitative conversion into Cu(II) porphyrins in a short period of time (depending on the light intensity) upon light irradiation (~400 nm). Dark experiments required several hours or days to achieve a comparable conversion. Since the photochemical reaction occurred upon irradiation by light (~400 nm) in the Soret band, the formation of a porphyrin-excited form may be assumed.

Another example for photochemical transformations involved the copper(II) porphyrins **32** and **33**. These compounds were shown to undergo an unusual self-sensitized photo-oxygenation reaction (Jiao et al. 2006). While stable in the dark under inert gas, they were rapidly transformed into oxygenated adducts upon exposure to both light and air. Compound **33** was less stable and its major photooxygenation product was the α,β-unsaturated ketone **34** (52%). In contrast, the cofacial bis-porphyrin **35** was isolated from the reaction of **32** in the presence of DBU in good yield (60%) and its structure was confirmed by x-ray analysis

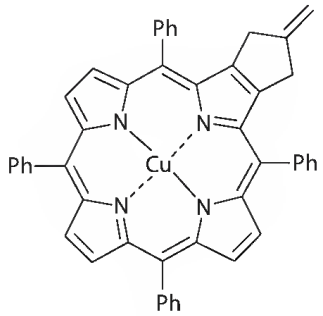

32

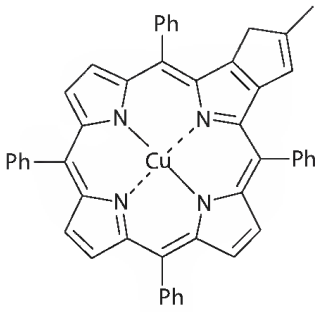

33

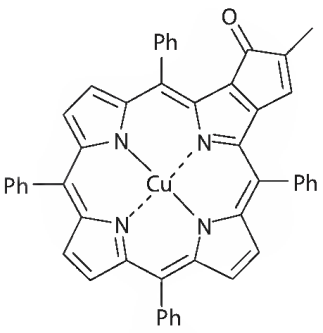

34

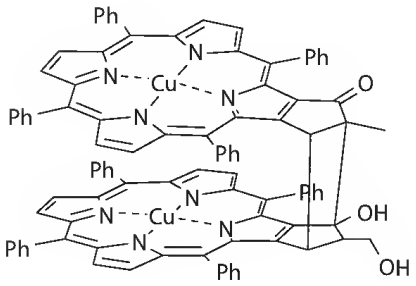

35

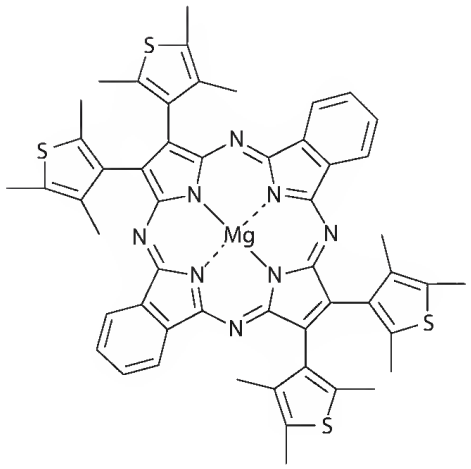

36

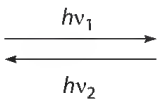

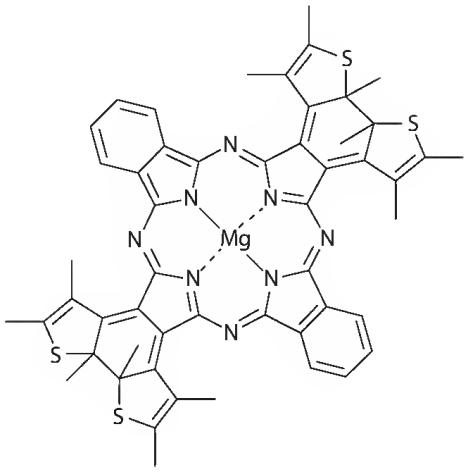

37

One of the few true photochemical reactions described for Mg(II) phthalocyanines involved a wavelength dependent photocyclization of **36**–**37**. Together with the back reaction, this system was developed as a photochromic readout system (Luo et al. 2007). A related example involving molecular motion used a "scissor"-like porphyrin dyad with flexible ferrocene-azabenzene-linkers where light-induced change in conformation of the host molecule forced a noncovalently bound guest to change its conformation as well (Muraok et al. 2006).

34.5.2 Photoinduced Ring-Opening Reactions

The photochemistry of chlorophylls is one of the oldest photochemical topics involving tetrapyrroles. The formation of long-lived excited states of chlorophyll and its function as energy-storage and catalytic material in photosensitization reactions has been postulated for some time on the basis of indirect evidence. For example, in the 1930s, Rabinowitch and Weiss performed spectrophotoelectrochemical studies on the reversible oxidation and reduction of chl (Rabinowitch and Weiss 1936, 1937). An ethyl chlorophyllide solution was reversibly oxidized by $FeCl_3$ to a yellow, unstable intermediate from which the green solution was regenerated by reduction with $FeCl_2$. The oxidation was greatly favored by illumination and the equilibrium was shifted by light toward the yellow form. The nature of the reversible reaction with Fe^{3+} was considered to be an oxidation in which Fe^{3+} was reduced to Fe^{2+} and chlorophyll was oxidized to a chl cation or a dehydrochlorophyll species.

About a decade later, Calvin and coworkers reported photochemical reactions of simple chlorins and either oxygen or various *ortho/para* quinones that led to the corresponding porphyrins and unidentified products. Based on kinetic experiments, they proposed a mechanism for the photochemical oxidation of 5,10,15,20-tetraphenylchlorin (H_2TPC) and β-naphthoquinone involving the triplet state of the chlorin molecule as an intermediate (Calvin and Dorough 1948). The production of P^+ and P^- ions from the first excited triplet state **(T)** of Mg(II)OEP **(P)** predominantly involves triplet-triplet annihilation. Evidence indicated that the reaction of T with ground-state P is not a significant source of ions. On the other hand the two triplets initially can combine to form an excited charge-transfer complex. Less extensive experiments were carried out with Mg(II)TPC due to its instability. However, the data obtained confirmed the existence of a phosphorescence state (Huennekens and Calvin 1949a). The photooxidation rates for the magnesium chlorins were significantly lower (~8 times) than for the corresponding zinc complexes.

The magnesium and zinc complexes of TPC can also be photooxidized using quinones as hydrogen acceptors. More detailed studies showed that the reaction between quinones and Zn(II)TPC resulted in the formation of Zn(II)TPP (Huennekens and Calvin 1949a). Subsequent work showed that Mg(II) TPC and Zn(II)TPC can be photooxidized by molecular oxygen and *o/p*-quinones. Oxygen is reduced to hydrogen peroxide with a concomitant reduction of quinones to hydroquinones. However, oxygen differs from quinones, as the primary formation of oxidation to porphyrins here is followed by secondary reactions. This second reaction involves H_2O_2 that can react either directly or as an initiator of Haber-Weiss processes and resulted in the formation of unidentified products (Huennekens and Calvin 1949b) similar to those obtained by "bleaching" of chlorophyll in the presence of oxygen (Rabinowitch and Weiss 1936, 1937).

Subsequent work in this area clarified some aspects of the photooxidation of magnesium porphyrins. Barrett found no alteration in the spectral and chromatographic properties of nonfluorescent protoporphyrin complexes of Fe, Ni, Co, Cu, and Ag upon irradiation (Barrett 1967). However, irradiation of (protoporphyrinato dimethyl ester)magnesium(II) **38** in various organic solvents resulted in rapid photooxygenation to green-brown products that did not contain magnesium. Moreover, spectroscopic data indicated an interruption of the aromatic ring system, showed no fluorescence and the appearance of a strong band at 1680 cm^{-1} (CCl_4) in the IR spectrum of the newly formed compound. This green pigment was very photolabile and quickly decomposed to yield 15,16-hydrobiliverdin **39**. Magnesium porphyrins without vinyl side chains were photooxidized to similar green compounds with the band at 1680 cm^{-1}, confirming no oxidation of the vinyl group. The UV/vis spectra of these green products were similar to those of the phlorins obtained by photoreduction of uro-, copro- and hematoporphyrins (Mauzerall 1962). Thus, photooxidation of magnesium protoporphyrins resulted in the formation of 15,16-hydrobiliverdins upon ring cleavage. This is in contrast to the enzymatic breakdown of heme that proceeds through biochemical transformations *via* biliverdin **40** toward the phycobilins (Beale and Cornejo 1991a–c).

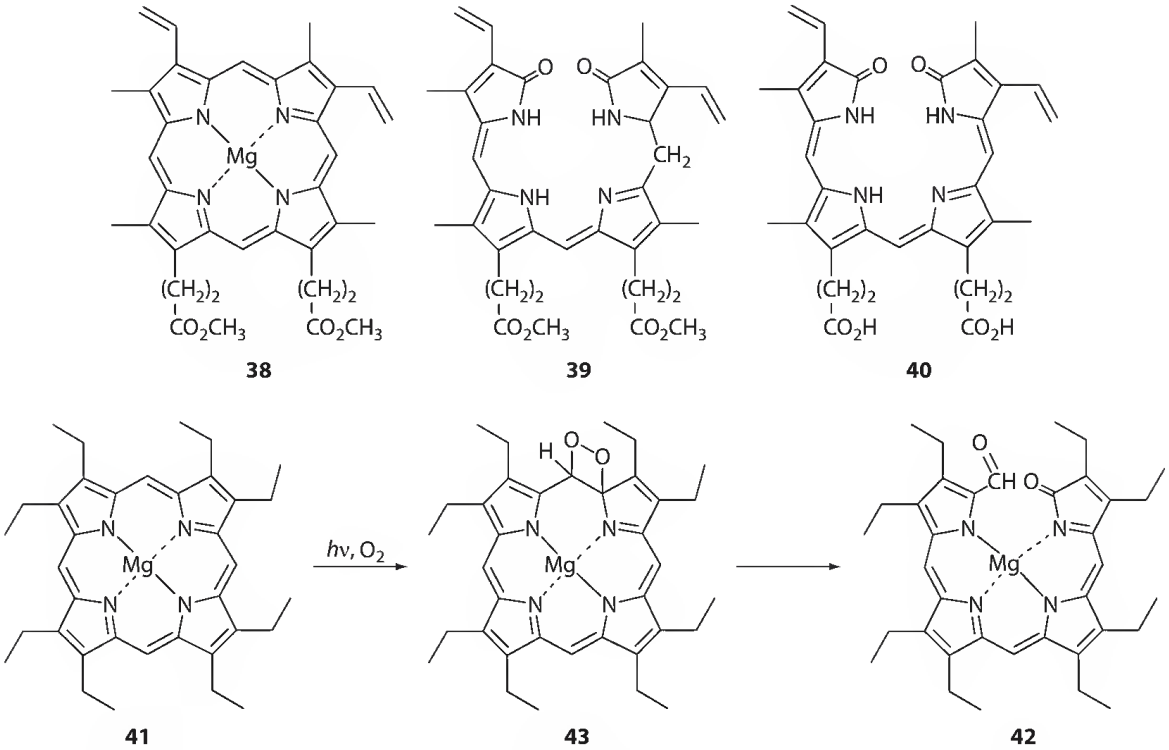

SCHEME 34.1 Photochemical ring-opening reactions of Mg(II)OEP.

The reaction of porphyrin ligands with molecular oxygen is related to catabolic processes of naturally occurring porphyrins and drugs and is of great medical relevance. Various metalloporphyrins, particularly the chlorophylls present in photosynthetic organisms, can be rapidly destroyed by light and oxygen. In fact, without the presence of photoprotective pigments such as carotenes, no natural chlorophyll-based photosynthetic system would be stable. Initial studies on the photooxygenation of Mg(II) OEP (**41**) (Fuhrhop and Mauzerall 1971, Fuhrhop 1974, Fuhrhop et al. 1974), Mg(II)TPP (Matsuura et al. 1980, Smith et al. 1980), and Mg(II)protoporphyrin and Mg(II)(tetrabenzoporphyrin) (Goedheer 1967, Goedheer and Siero 1967) were reported in the 1970s and 1980s.

For example, exposure of Mg(II)OEP to visible light in the presence of air in benzene solution, resulted in the quantitative conversion of the porphyrin into a chromophore with an intense absorption band above 800 nm. This reaction proceeded uniformly and no intermediates with lifetimes of more than 10s were observed. The primary product was an open-chain magnesium formylbiliverdin complex **42** that can be easily demetallated to the formylbiliverdin. A similar photooxidation pathway was found for Mg(II)TPP. It reacted readily with molecular oxygen to yield the corresponding 15,16-dihydrobiliverdin similar to the one shown for Mg(II)OEP in Scheme 34.1. Further studies have proposed that the photooxygenation of metallo-*meso*-tetrasubstituted porphyrins proceeds *via* a one-molecule mechanism involving only one oxygen molecule. Most likely, the first intermediates formed upon photooxygenation are short-lived peroxides. Such compounds are very instable and a possible dioxetane structure is shown in formula **43**.

34.5.3 Reactions of Chlorophyll

The most obvious chemical reaction involving chlorophyll is the chlorophyll breakdown in fall during senescence. This process involves annually more than 10^9 tons of chlorophyll and despite its obvious prominence in the natural beauty of the fall season remained unknown until about 25 years ago (Hendry et al. 1987). Different groups have shown that the central step is a ring-opening reaction at the 5-position (Iturraspe et al. 1995, Gossauer and Engel 1996, Kräutler and Matile 1999).

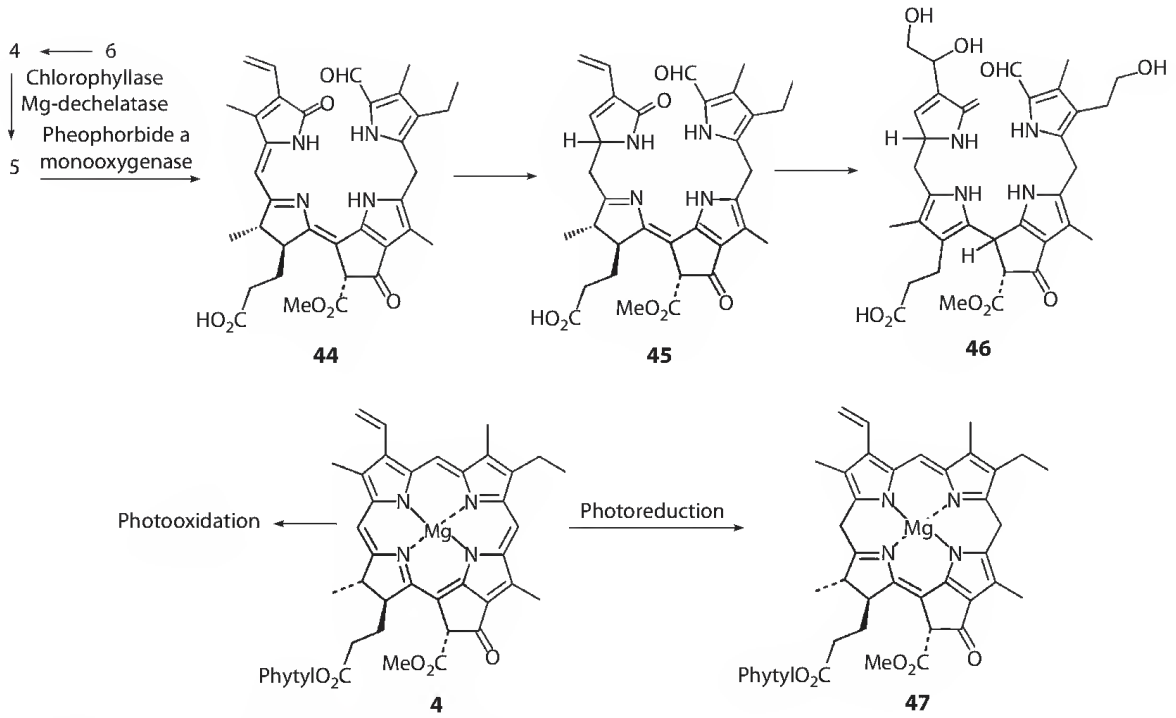

SCHEME 34.2 Photochemical reactions of chlorophyll.

This is in contrast to the situation encountered for heme, which is oxidatively cleaved at the 20-position. As shown in Scheme 34.2, the crucial steps during chl degradation are the conversion of chl *a* into pheophorbide *a* **5**, followed by enzymatic transformation into the bilinone **44**. During this step, the macrocycle undergoes oxidative C5 ring-opening, incorporates 2 oxygen atoms (the CHO one from O_2), and is saturated at the 10-position. This reaction is catalyzed by a monooxygenase and the red compound **44** is further converted to the still fluorescing compound **45**, and finally into the nonfluorescing derivative **46** along with some changes in the side chains directed to increase the hydrophilicity of the breakdown products. Chl *b* **6** is first converted into chl *a* **4** and then subjected to the same reactions. Note that this is an enzymatic process not a simple photochemical reaction and should not be confused with the photooxidative ring-opening reactions.

A second reaction involves the classic chlorin to porphyrin conversion. Any chlorin that has hydrogen atoms at the sp^3-hybridized centers of the reduced ring can be oxidized to the respective porphyrin. Oxidation may be achieved by various oxidants including oxygen (Inhoffen 1968). Likewise, reductions to hydroporphyrins and other reactions of the macrocycle are possible. However, most of these are of interest only for the specialist. The best known reaction is probably the Krasnovskii photoreduction to **47** (Scheer and Katz 1974).

Similar to porphyrins chls undergo photooxygenation (Hynninen 1991, Gurinovich and Tsvirko 2001). Chls are potent photosensitizers and will produce singlet oxygen in the presence of air or triplet oxygen (Inhoffen 1968). Thus, chls can undergo self-destruction. The chemistry of this photooxygenation is heavily involved and differs somewhat for individual types of (b)chls (Inhoffen 1968, Troxler et al. 1980, Llewellyn et al. 1990a,b, Iturraspe et al. 1995). While being partially responsible for the low stability of chls in solution (Peled et al. 2000) and for unwanted side reactions in food stuff (Min and Boff 2002), the same reaction also offers potential for future applications. Chl and derivatives thereof may be used as photosensitizers to affect desired chemical transformations and they have been utilized for applications in PDT (Nyman and Hynninen 2004).

As lipophilic pigments, where the (b)chls are embedded in natural systems in apoproteins, photosynthesis in general is a transmembrane process. Thus, PET reactions in lipid membranes have been investigated

extensively. Many reports have been published on photo-initiated (i.e., the photo-initiated species acts as a catalysts to mediate thermodynamically favored reactions) and photo-driven (i.e., some of the light energy is converted into the products) processes (Tunuli and Fendler 1981). Typical examples are Mg(II)OEP (2,3,7,8,12,13,17,18-octaethylporphyrin) sensitized ET reactions across lipid bilayer membranes (Ilani et al. 1989). The reaction mechanism involves a reduction of photoexcited Mg(II)OEP at the reducing (ascorbate) side of the bilayer with the charge carrier most likely being a neutral protonated Mg(II)OEP anion. Thus, the magnesium porphyrin participated as a sensitizer and a transmembrane redox mediator.

A well-studied system is an Mg-substituted horseradish peroxidase. This system can form stable porphyrin π-cation radicals in the presence of oxidants (Kuwahara et al. 1982, Deguchi et al. 1985) and photooxidation and photoreduction occur through direct reaction of the excited-state porphyrins with oxidants and reductants, respectively. In general, porphyrins appear to be photooxidized both via ET and $^1O_2$ mechanisms. Thus, photoirradiation of the Mg-substituted horseradish peroxidase under aerobic conditions results in two simultaneously occurring reactions. A porphyrin π-cation radical is generated through ET from excited porphyrin to O_2 and a so-called the 448 nm compound via a singlet oxygen mechanism. A species with an absorption band at 448 nm was first formed upon irradiation and was then converted in the dark to a final product with a band at 489 nm, probably via an isomerization reaction.

34.6 Photoinduced Electron Transfer in Applied Photochemistry

Tetrapyrroles have found applications in the different areas of current research targeting highly interesting topics of organic and medicinal chemistry, material, and nanoscience. They have shown to be effective photocatalysts for aquatic wastes and organic pollutants degradation in green chemistry. On the other hand, they can also be used as efficient stabilizing agents for polymers and dyes.

The search for alternative energy sources is one of the most important aims of the present century that has found renewed attention after a lack of interest for several decades. Solar energy conversion, electrophotography, hydrogen production, and photocatalysis are the most popular topics involving tetrapyrroles. Photoenergy conversion systems have been designed using donor–acceptor molecules, polymers, and carbon nanotubes. The mechanism of PET is extensively studied and a variety of the artificial systems applying PET are examined for use as molecular devices. Here we will highlight the future potential of these materials as molecular devices in emerging areas of nanoscience, especially in the utilization as prospective (photo)catalysts in areas of green chemistry and hydrogen production, and in solar energy as photovoltaic cells and junctions.

34.6.1 Nanomaterials: Molecular Electronic Devices

The discovery of charge transfer across donor–acceptor systems opened an effective way to improve the photooptical response of organic materials. Here, the development and use of organic ultrathin monolayers as potential models for optoelectronic devices and catalysts in solid photochemistry has attracted great attention. Some studies focused on the fabrication of CuPc and CuP thin films using photoinduced deposition methodologies (Yamanouchi and Saji 1996, Hoshino et al. 1996, Bearinger et al. 2008) and investigated their optical (Yamada et al. 1995), optical memory and photoswitching (Liu et al. 1994), and xerographic properties (Xu et al. 2002).

Many memory and switching phenomena in organic solid films have been described as prototypical candidates for molecular electronic devices and photogeneration in these organic superlattices under an applied electric field may play a fundamental role. Some work has been reported on PET and back ET (charge recombination) of hetero-Langmuir-Blodgett films with phthalocyanines as a sensitizer. For example, a transient electric current was observed upon the selective photoexcitation of CuPc and the

resulting charge-separated state in the device survived for a few minutes. Applying electric biases and/or lowering temperatures caused the charge-separated state to last much longer (Naito and Miura 1993).

Disk-shaped like monomers can form rod-like aggregates (discotic mesophase materials) and they exhibit long-range order, large electrical anisotropies. The high interest in these materials stems from their promise as organic electronic devices requiring high charge mobility and dense integration (e.g., organic field effect transistors, organic light-emitting diodes, and photovoltaic cells).

Tetrapyrroles, especially with flexible hydrocarbon chains, exhibit a remarkable feature to form discotic mesophase architectures. An example are the octa-substituted phthalocyanines **48–50** with and without polymerizable styryl side chains: $CuPc(OC_2H_4OCH{=}CHPh)_8$ (**49**) with styryl groups at the termini on the side chains, or with one alkoxy group removed $CuPc(OC_2H_4CH{=}CHPh)_8$ (**50**) (Drager et al. 2001) and $CuPc(OCH_2)_2OBz)_8$ (**49**). The latter compound **49** formed highly coherent rodlike aggregates in Langmuir-Blodgett films with excellent control of rod orientation (Smolenyak et al. 1999, Zangmeister et al. 2001). Irradiation of the styryl π–π^* absorbance bands with $\lambda \sim 254$ nm for horizontally transferred LB films of **48** and **50** resulted in a stabilization of their rodlike aggregates, through formation of cyclobutane links between adjacent side chains (through common [2 + 2] cycloaddition (Donley et al. 2003). Polymerized thin films have shown a long-range order that was confirmed by atomic force microscopy and x-ray reflectometry. The differences in the orientation of individual Pc's, between films of **48** and **49**, were determined by transmission and reflectance. Higher dark photoconductivities and electrical anisotropies were observed in films of **48** after annealing and polymerization, compared with those found for films of **49**.

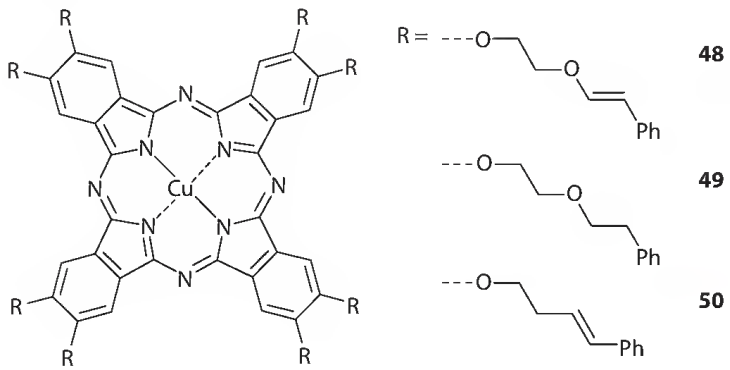

Several studies were aimed at the fabrication of molecular-based photoelectrodes and special attention has been given to the efficient uptake of visible light and conversion into output of the photosystems. Typical examples are the construction, determination of photoelectric characteristics, and an evaluation of the photoelectrodes (Meshitsuka and Tamaru 1977, Ichikawa et al. 1994). For example, photoelectrode devices constructed from CuPc as a p-type semiconductor in combination with *N,N′*-diphenylglyoxaline-3,4,9,10-perylenetetracarboxylic acid bisbenzimidazole as n-type semiconductor in the water phase were investigated in terms of kinetics. Each film of the p/n bilayer presents a photoanode, where the photoinduced oxidation of thiol occurs. The holes originate on account of the photophysical events in the p/n interior, involving the charge separation of excitons at the p/n interface (Abe et al. 2008).

Gas-sensitive electrodes can be fabricated by use of CuPc incorporation into a polypyrrole backbone. The photoresponse in electrochemical mode increases due to the presence of phthalocyanine in the films and enhanced sensitivity toward nitrogen gas as compared to pure polypyrrole film was observed (Radhakrishnan and Deshpande 2001).

Molecular conductance junctions (Nitzan and Ratner 2003) are another important utilization of phthalocyanines. Here, a molecule or a small cluster of molecules conduct electrical current between two electrodes. CuPc has been used in silicon-based molecular nanotechnology to integrate molecular electronic function with silicon surfaces (Hersan et al. 2000). The knowledge about the mechanisms of

charge transfer and the role of the outer phenyl ring is important to understand the interaction with the surrounding substrate when the CuPs molecule is bound to the surface *via* its central copper atom (Abramczyk et al. 2006). One example is the intercalation of CuPc pyridinium complex and iron phthalocyanine into two-layered titanates from $Na_2Ti_3O_7$ to study the microstructure control (Kaito et al. 2002).

34.6.2 Solar Energy

The current targets in solar energy conversion are reaching 10% conversion efficiency. This is within reach and has caused an intensive development of organic and hybrid thin film photovoltaics (third generation solar cells). Substantial improvements have been made resulting in new device concepts and improved understanding of energy conversion processes. Films of tetrapyrrole semiconductors are promising candidates for stable and low cost electrode materials that can be used for solar energy conversion. Various CuPcs have been investigated as thin-film electrodes in photoelectrochemical cells (Osada and Mizumoto 1986, Yanagi et al. 1993). Most likely, due to their stability, this field will be dominated by phthalocyanine derivatives although porphyrin systems are continuously advancing (Yamashita et al. 1989).

Zinc porphyrin dimers have been incorporated into solar cells to improve their light harvesting efficiency to yield enhanced performance. Such materials have potential in next generation solar energy conversion systems as 3-D light harvesting arrays (Mozer et al. 2009). Photochemical solar cells constructed from organized assemblies of single-walled carbon nanotubes and a protonated porphyrin on nanostructured SnO_2 electrodes are photoactive and absorbed in the entire visible region (Hasobe et al. 2006). Organic–inorganic hybrid cells also demonstrated enhanced performance through use of nanoporous Si as *n*-type and CuPc (Levitsky et al. 2004).

Other studies reported the construction and analysis of photovoltaic cells fabricated with CuPc and TiO_2 (Arbour et al. 1990, Grätzel and Halmann 1990, Ding et al. 2005, Doherty et al. 2007) or ZnS (Zhang et al. 2005) nanoparticles. The dye-sensitized TiO_2 solar cell showed conversion efficiencies of 7%–10% under standard solar conditions. These high efficiencies are associated with ultrafast charge transfer from the dye to TiO_2, the high internal surface area of the TiO_2 films, the broad absorption of the dye, and the efficient separation of opposite charges between the domains. Recently, some attention has been given to composites of metal phthalocyanines and carbon nanotubes due to their high quantum efficiency facilitated by charge transfer between them and the complementary properties of the composites. These are regarded as promising candidates for the fabrication of donor–acceptor heterojunction diodes and photovoltaic devices. An example of such constructions has been reported recently for a CuPc with long dodecyl chains covalently attached to modified multiwalled carbon nanotubes (Wang et al. 2005).

34.6.3 Hydrogen Production

Photochemical processes capable of the evolution of molecular hydrogen are one of the most important areas of current research. Considerable interest has followed after Fujishima and Honda reported the photoelectrochemical water splitting using a UV-responsive TiO_2 electrode (Fujishima and Honda 1972). At present, dihydrogen (H_2) energy is attracting significant attention as a "clean energy" source with water photolysis being one of the most promising procedures to produce H_2. Some of the strategies are based on the development of the an efficient solid/water interface to achieve the (photo)chemical energy conversion under solar irradiation.

A number of photosensitization reactions have been described that offer potential use in chemical applications or are of fundamental interest. One of the oldest photochemical reactions that involves tetrapyrrole photosensitizers is the photoreduction of methyl viologen (MV). Being *p*-type of semiconductors, CuPcs can be used to construct *p/n* type of organic bilayers as photoelectrodes and used in water phase (Abe and Nagai 2007). Copper tetrapyrroles can be used in aqueous solution to reduce MV from MV^{2+} to $MV^{\bullet+}$ that is capable of decomposing water in the presence of a catalyst. Three-component

system [chromophore/donor/MV] for hydrogen production was analyzed using CuPc as a chromophore (Yarnaguchi et al. 1986). However, sulfonated phthalocyanines compared unfavorably to metalloporphyrins (Harrimana and Reichoux 1980). Some studies were carried out on the photodynamics of these systems for future applications (Ichikawa et al. 1995). In addition, studies on the photoexcitation of zinc porphyrin-viologen systems showed their potential use in hydrogen production (Petersson et al. 2009).

Another approach used hydrogenase active side models and metalloporphyrins. Visible-light-driven hydrogen generation was observed from noncovalent assembly of a pyridyl-functionalized hydrogenase active-site model complex and zinc tetraphenylporphyrin (Li et al. 2008a). Others examples included two kinds of light-sensitive, electro- and enzyme-active electrodes modified with zinc porphyrins, hydrogenase, and viologen triad multilayers. Here, the first zinc porphyrin or viologen layer was covalently immobilized on the substrate surfaces followed by hydrogenase and polyviologen layers or electrostatically adsorbed positively charged porphyrin (Liu et al. 2008).

34.6.4 Dye Industry

Improvements in the lightfastness of disperse dyes is a major goal in dye industry. The relationship between chemical structure and lightfastness of dispersed dyes and complete determination of the reaction mechanisms that characterize the photofading of disperse dyes on polyamide and PET substrates is of great interest. Many studies have been focused on investigating the light-induced reduction, photooxidation by singlet oxygen, and wavelength-dependent of photo-reduction in various organic solvents, to name a few.

Himeno et al. (2000) reported that reductive fading of monoazo disperse dyes combined with vinylsulfonyl CuPc on nylon or polyester substrates was decreased compared to the rate of reductive fading of disperse dyes without the CuPc dye. Singlet oxygen generated by the photosensitization of CuPc dyes suppressed the reductive fading of disperse dyes. Nylon had a greater tendency to give light-induced reduction and oxidation of disperse dyes than polyester, depending upon the properties of the adsorbed dye. Some investigations were carried out purely on CuPc dyes. Examples are the photosensitized oxidation of CuPc reactive dye on cellulose under different conditions (Okada et al. 1990a,b, Okada 1992) and additives (Hihara et al. 2001), and photochemical reduction of tetrasodium salt of copper tetrasulphonatophthalocyanines with amines (Kaneko et al. 1995, 1996).

Dyes are utilized in polymer materials to enhance their color-changing properties. However, these additives can affect considerably the polymer stability toward degradation. Interestingly, CuPc can play the role of a polymer stabilizer against degradation as well as in some cases to be its trigger. The interaction mechanism of dyes can occur via two pathways (Bamford and Dewar 1949, Allen 1994, Sánchez et al. 2004). In one pathway, after the light absorption in oxygen containing media, the dye produces chemical species such as singlet oxygen and superoxide anions. These reactive species then accelerate polymer degradation. In the other pathway, the dye reaches excited singlet (S_1, S_2) and triplet (T_1, T_2) states. The energy absorbed is then transferred to the chemical groups in the polymeric chain via intermolecular energy transference.

For example, CuPc incorporated into polycarbonate resulted in accelerated degradation under UV radiation. As a strong sensitizer, CuPc very likely enhances the formation of reactive species in polycarbonate. Excited states of CuPc may increase the formation of free radicals, which is the beginning for the sequential photooxidation processes leading to the degradation of a polycarbonate. Alternatively, photodegradation of polycarbonate triggered by CuPc may proceed via ET sensitization (Saron et al. 2006). In contrast, a three-component system involving hindered piperidine (known to be effective photostabilizers for some polymers), antioxidant, and CuPc have shown synergistic effects. Interestingly, CuPc alone offered little photoprotection and some enhanced photoprotection was observed for antioxidant-CuPc. These results indicate that CuPc and a hindered piperidine exhibit a highly favorable interaction for photostabilization (Allen and Parkinson 1983). Finally, CuPc dyes can also be used as heterogeneous sensitizers to induce the photopolymerization of trimethylolpropane triacrylate (Rosche et al. 1997).

34.7 Green Chemistry of Tetrapyrrole-Based Dyes: Photodegradation, Stabilization, and Photocatalysis

High levels of environmental contamination have been associated with dye wastewater contents from textile dyeing and finishing industry. Various types of synthetic dyes are used in textile industry including azo, anthraquinone, triarylmethane, and phthalocyanines designed to be highly robust. Moreover, due to the complexity and variety of the dyes used for different purposes, as well as their nonbiodegradability, it is rather difficult to find unique treatment methods that would result in effective degradation of all types of dyes. Azo dyes are the largest class of commercially used colorants, while phthalocyanines are mainly utilized as blue and green dyes. CuPcs (**51–54**, **56** are examples of the commercially used CuPc dyes) are the most important derivatives of the phthalocyanine pigment class (Gordon and Gregory 1983). Their commercial success is based on three features: beautiful bright blue to green shades and strength, remarkable chemical stability, and excellent fastness to light. Due to their low tendency to migrate in materials, CuPc are used in inks and printing, coatings, some plastics, textile, and leather. However, environmentally, these advantages as robust and efficient colorants decrease the efficiency of convenient treatment technologies. Additional contamination associates with metals such as copper released during the process from the metallized dyes.

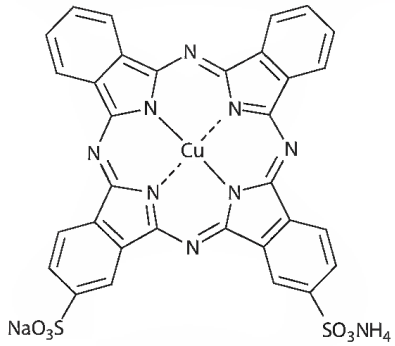

C.I. Direct blue 199
51

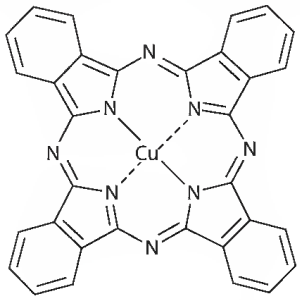

Phthalocyanine blue BN
52

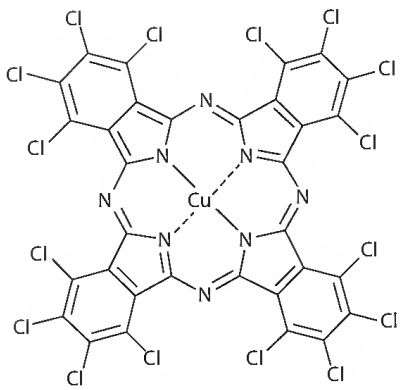

Phthalocyanine green G
53

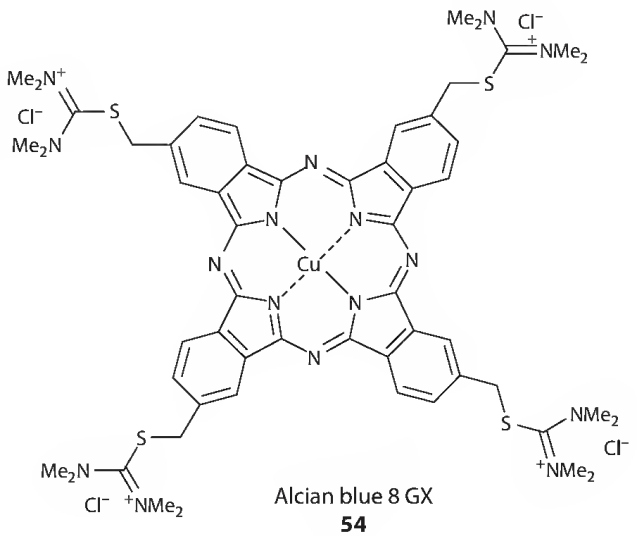

Alcian blue 8 GX
54

34.7.1 Tetrapyrrole-Based Photocatalysts

Tetrapyrroles are suitable candidates for use in (photo)catalysis, an advanced oxidation process that is used to eliminate organic pollution. The oxidation rates depend strongly on the oxidation potential of the central metal, and thus zinc(II) derivatives typically take up a central position. Some selected

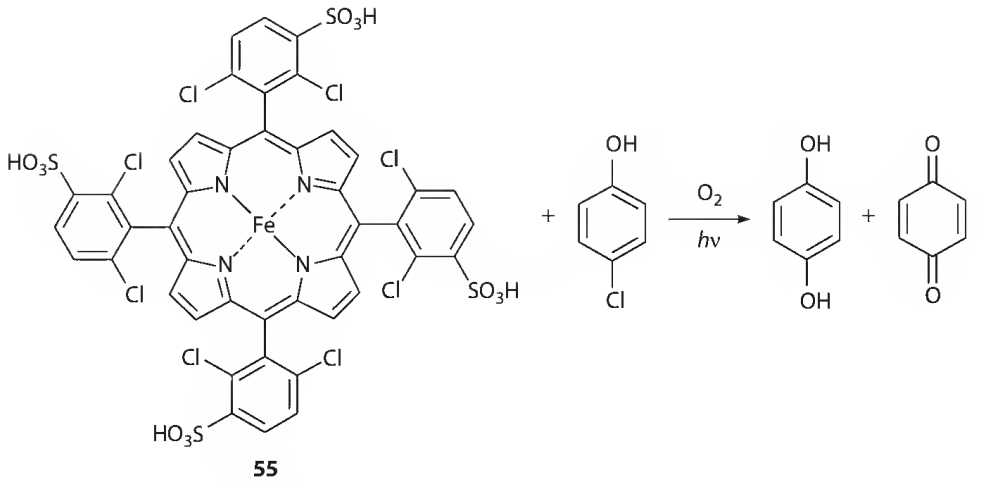

55

SCHEME 34.3 Photooxidation of phenols.

examples for the use of zinc(II) tetrapyrroles as photosensitizers are the oxidation of isopropyl alcohol (Uchida et al. 1977) or water (Gerasimov et al. 1991), the photochemical dediazoniation of arene diazonium salts with a zinc(II) phthalocyanine derivative (Becker et al. 1986), the photocatalytic decomposition of CCl_4 (Khairutdinov et al. 1982), trichlorophenol (Kasuga et al. 2000), amino acids (Zhang and Xu 1994, Spikes et al. 1995), and of atrazine (Héquet et al. 2000). Likewise reactions with hydroquinone (Fan and Bard 1979), cellulose (Thomas and Allen 2002), and the photocatalytic destruction of organic matter in effluents from paper industry (Machado et al. 2003) were studied and a variety of antimony porphyrin–based photocatalysts were prepared and analyzed (Shiragami et al. 2005).

Phenol photooxidation can also be performed by an iron porphyrin in the presence of oxygen. The main photooxidation product was *p*-benzoquinone (33%, λ_{max} 245 nm), although some *p*-hydroquinone (6%, λ_{max} 288 nm) was also observed (Silva et al. 2004). This is similar to reports for the degradation of phenols in the presence of phthalocyanines and other photosensitizers (Scheme 34.3).

5,10,15,20-Tetrakis(2,6-dichloro-3-chlorosulfophenyl)porphyrin and its Sn and Zn complexes were also successfully used in the photodegradation of 4-chlorophenol and 2,6-dimethylphenol (Monteiro et al. 2005). Likewise, silica microspheres functionalized with 5-(4-allyloxy)phenyl-10,15,20-tri(2, 6-dichlorophenyl)porphyrin were used to oxidize 1,5-dihydroxynaphthalene under visible light irradiation in aerated aqueous solution (Cai et al. 2009). Visible light photocatalysis using SiO_2 immobilized water-soluble and -insoluble tin porphyrins degraded 4-chlorophenol and Acid Orange 7 in water. Interestingly, the visible light activity of the porphyrin photocatalyst was enhanced by increasing the loading of insoluble tin porphyrin (Kim et al. 2008).

Photocatalysts prepared in situ by CuPc immobilization on Al and encapsulated inside zeolite-X showed a remarkable affinity toward CN^-. Here, photooxidation is based on transferring electrons from the zeolite to cyanide ions in solution (Mohamed and Mohamed 2008). Mesoporous catalysts prepared from 3-aminopropyltrimethoxysilane and (hexadecafluorophthalocyaninato)copper(II), followed by cocondensation of tetraethylorthosilicate around a micelle formed by *n*-dodecylamine demonstrated efficacy for photodegradation of organochloride compounds, industrial dyes, and pesticides with unproblematic recuperation from the reaction medium (DeOliveira et al. 2008).

34.7.2 Titanium Dioxide–Based Tetrapyrrole Photocatalysts

Titanium dioxide (TiO_2)–based photocatalysts are being used in photocatalytic technologies for the degradation of organic compounds in water. In the past decades, focus of interest has been on the development of economically and environmentally friendly catalytic systems with enhanced activity of TiO_2-based catalysts for use in the oxidative degradation of various organic pollutants. Several studies have been also

carried out to investigate the influence of different semiconductor types such as Al_2O_3 or WO_3 and phthalocyanine complexes on the photoacticity. For example, it was found that the photocatalytic activity of the phthalocyanine complexes, supported on TiO_2 or WO_3 was much higher compared to dielectric Al_2O_3.

Thus, TiO_2 is one of the most popular materials to be used as a photocatalyst for air treatment and degradation of organic pollutants in water. Having a large band gap (3.2 eV with $\lambda \leq 385$ nm), TiO_2 can consume only about 5% (with energy above 3.0 eV, $\lambda \leq 410$ nm) of solar light reaching the earth surface. Thus, to increase the efficiency of solar energy utilization through TiO_2, it is often doped with transition metal ions or organic dyes to shift the photoresponse of the catalyst into the visible region. In view of its low cost and feasibility, dye sensitization is considered to be an effective method to modify the photochemical properties of TiO_2 particles. Mechanistically, the photosensitization of TiO_2 proceeds via initial excitation of the dye. A PET from excited dye to TiO_2 and the surface reaction of TiO_2 conductive band electron were suggested as the key processes.

Systematic investigations demonstrated the existence of an optimum photoreactivity depending on the amount of impregnated porphyrin. It was shown that TiO_2 impregnated with Cu-based sensitizers is beneficial for the photoactivation of TiO_2, and CuPs (Mele et al. 2003, 2005, Wang et al. 2007) and CuPcs have shown to improve the photocatalytical activities of these photocatalysts.

Comparative studies showed that TiO_2 samples doped with CuP and FeP are more photoactive than simple TiO_2 (anatase), whereas samples including MnP showed less photoreactivity (Mele et al. 2007a). Free base porphyrins have shown slightly higher photoactivity than TiO_2, suggesting that the porphyrin macrocycle is photocatalytic as well. However, samples impregnated with CuP exhibited the highest photoactivity. These results, related to the photodegradation of 4-nitrophenol (4-NP) in an aqueous heterogeneous environment, suggest that the Cu(II)-Cu(I) photocatalytic redox cycle plays the main role in the process.

Similar results were shown for a series of TiO_2-CuPc's systems where different Cu(II)Pc (TiO_2-CuPc) were examined for their photocatalytic degradation of 4-NP (Mele et al. 2002). The high photocatalytic activity was explained by an ET from the conduction band of the excited Pc to the conduction band of a semiconductor. Recent studies have shown that the photocatalytic activity of polycrystalline TiO_2 samples impregnated with rare-earth-metal diphthalocyanines in the 4-NP photocatalytic degradation show better photoactivity for the complexes of lanthanide metals, such as Nd, Sm, and Ho (Mele et al. 2007b). Improved photocatalytic activity was observed in the decomposition rates of 4-NP for TiO_2-lanthanide diphthalocyanines over those impregnated with Cu(II)Ps.

Plastic is widely used all over the world and its waste, the so-called "white pollution," has been recognized as one of the central environmental problems. Heterogeneous photocatalytic oxidation can occur under moderate conditions, such as room temperature, atmospheric pressure, and molecular oxygen as the only oxidant. Recently, studies of the solid phase photodegradation of TiO_2-embedded plastic upon irradiating the composite film for 300 h under air have shown reduction of its average molecular weight by two-thirds and weight by 27% (Cho and Choi 2001). Comparative studies have been carried out on polystyrene incorporated in (TiO_2/CuPc) and TiO_2 alone. Faster photocatalytic degradation of polystyrene was observed in polystyrene-TiO_2/CuPc than in polystyrene-TiO_2. During photocatalytic degradation, activation of polystyrene by the reactive oxygen species attacking neighboring polymer chains leads to chain cleavage and production of new reactive radicals. The higher charge separation efficiency of TiO_2/CuPc photocatalyst results in more effective generation of reactive oxygen species both on surface and inside thin film; polystyrene undergoes faster and more complete mineralization over TiO_2/CuPc than over TiO_2 photocatalyst (Shang et al. 2003).

Another serious environmental problem is caused by azo dyes from textile industry. Here, methyl orange is often selected as a reliable model to investigate decolorization and decomposition of azo dyes using photocatalysts. Photo-stable copper 2,9,16,23-tetracarboxyl phthalocyanine (CuTcPc) doped with amorphous TiO_2 (am-TiO_2) hybride photocatalyst exhibits excellent photocatalytic activity toward methyl orange under visible irradiation ($\lambda > 550$ nm) (Chen et al. 2005). In contrast, no photobleaching of methyl orange was observed with bare am-TiO_2 at $\lambda > 550$ nm. Degradation of acid chrome blue K was achieved with TiO_2-based photocatalysts containing carboxy and nitroporphyrins. Here, the photoexcited sensitizer had remarkable effects on the photodegradation of the dye under natural sunlight (Li et al. 2008b).

34.7.3 Photodegradation of CuP and CuPc Dyes

Although porphyrins and especially phthalocyanines are stable compounds, both will undergo photooxidative degradation or photoexcited ET reactions. The phthalocyanine systems are very stable even in advanced catalytic processes such as photocatalytic oxidation. Photoelectrocatalytic oxidation attracts considerable attention as a way to increase the photocatalytic efficiency in degradation of organic pollutants and studies have been carried on to apply this methodology for decolorization of Pc systems.

For example, the decolorization of commercially relevant reactive CuPc-dyes—for example, the *Remazol Turquoise Dyes* family—was studied in aqueous solutions under different conditions. For example, *Remazol Turquoise Blue 15* (**56**) was investigated by direct cathodic reduction on platinum electrode and photoelectrocatalytic oxidation on Ti/TiO_2 as nanostructured semiconductor thin-film electrodes with higher efficiency for combined processes of photoelectrocatalytic oxidation and electrochemical reduction (Osugi et al. 2006).

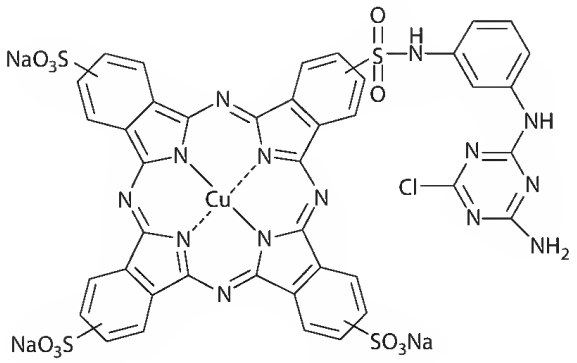

Remazol turquoise blue 15
56

Some studies on photostable CuPc sulfonates sodium salts were carried out under UV ($\lambda > 320$ nm) or visible light ($\lambda > 450$ nm) in the presence of a TiO_2 semiconductor in an aqueous medium. They underwent photobleaching in the presence of TiO_2. The spectral analysis showed that the dye photobleaching led to complete destruction of the phthalocyanine ring. In addition, the stability of the dye toward visible light was greatly affected by the physical properties of TiO_2 semiconductors, and the dye photostability could be improved through addition of electron sacrificers such as 4-chlorophenol (Sun et al. 2005).

Another example of photodegradation catalyzed by TiO_2 is illustrated for the CuPc dye **54** (*Alcian Blue 8 GX*) (Caliman et al. 2007). This dye is one of the so-called "biological stains," such as *Eosin Y, Auramine O, Hematoxylin,* or *Rose Bengal,* etc., which are widely used in biomedical research laboratories and for diagnostic purposes. Some of them are known to be toxic or mutagenic to humans and animals, highly resistant to microorganisms such that biological wastewater treatment processes are very inefficient in treating of these dyes. Decolorization and mineralization of phthalocyanine dye **51** (*C.I. Direct Blue 199*) has been studied using an advanced oxidation process. Decolorization was found to be more difficult than that of an azo dye (*C.I. Acid Black 1*) under the same operating conditions (Shu and Chang 2005).

34.8 Photomedicine

34.8.1 Photodynamic Therapy and Singlet Oxygen Production

The interaction of tetrapyrrole derivatives with oxygen under the influence of light, and their photostability, has been a matter of great interest due to its medicinal relevance. PDT presents the only one clearly established medicinal application of porphyrins and relies on the selective accumulation

of a tetrapyrrole photosensitizer in target tissue where it can be activated with light to produce toxic singlet oxygen resulting in, for example, tumor necrosis. Typically, two different photosensitization processes are discussed. Type I reactions include charge transfer, whereas the type II pathway involves transfer of excitation energy from porphyrin to triplet oxygen. Several porphyrin-based compounds have been approved for medicinal applications and others are in Phase-2 trials (Spikes and Bommer 1991, Dougherty et al. 1998, Kessel and Dougherty 1999, Bonnett 2000, Wiehe et al. 2005, O'Connor et al. 2009). Amongst these tetrapyrroles, chlorophyll derivatives are currently under active investigation and show some promise (Nyman and Hynninen 2004). The use of chlorophyll derivatives in technical applications is still in the early developmental stage.

Although many different derivatives are under investigation the majority of compounds are free base derivatives. The situation is different for zinc(II) phthalocyanines. A classic study on zinc(II)phthalocyanine of type **3** showed that it is an efficient photosensitizer for singlet oxygen with a quantum yield of *ca* 0.4 (Valduga et al. 1988). The efficiency of the photosensitization reaction strongly depends on the macrocycle conformation and substituent pattern (Weitman et al. 2001). Thus, the quantum yield for singlet oxygen generation for tetrasulfonated zinc(II) phthalocyanines (0.7) is almost three times that of the zinc(II) naphthalocyanines (0.25) (Spikes et al. 1995). Phthalocyanine derivatives exhibit some photophysical advantages compared to porphyrins: increased Q-band absorption coefficient, red-shifted absorption bands resulting in deeper light tissue penetration (Ochsner 1996), high triplet quantum yields, long triplet lifetimes and high singlet oxygen, and fluorescence yields (Rosenthal 1993). For specific substituents pattern, this can result in improved photodynamic activities compared to commercial photosensitizers (Ochsner 1996, Ball et al. 1998).

A few current examples are shown in the following and include unsymmetrically substituted derivatives **57** (Kudrevich et al. 1997), the cationic derivative **58** (Fernández et al. 1997), the neutral derivative **59** (Ball et al. 1998), and the classic anionic derivative **60** (Griffiths et al. 1994, 1997). "(Tetrabenzoporphyrinato)zinc(II)," an intermediate structure between that of porphyrins and phthalocyanines, has also been investigated in this respect. However, its quantum yield for singlet oxygen generation in liposomes (0.023) is much lower than that of Photofrin (0.19) (Gross et al. 1993). Other examples are zinc, palladium, copper and free base porphyrin complexes of 5-(4-(trimethylammonium) phenyl)-10,15,20-tris(2,4,6-trimethoxyphenyl)porphyrin iodide (Milanesio et al. 2008) or compounds with photocleavable linkers as photodynamic prodrug systems (Jiang and Dolphin 2008, Bakar et al. 2009). Note that zinc derivatives are not necessarily the best metal derivatives of phthalocyanines for use in PDT (Canti et al. 1992). Taking aspects like tissue clearance and target-specific localization into account, porphyrin derivatives will most likely carry the field in this application. In addition, many of these systems are under scrutiny for their antibacterial action (Segalla et al. 2002).

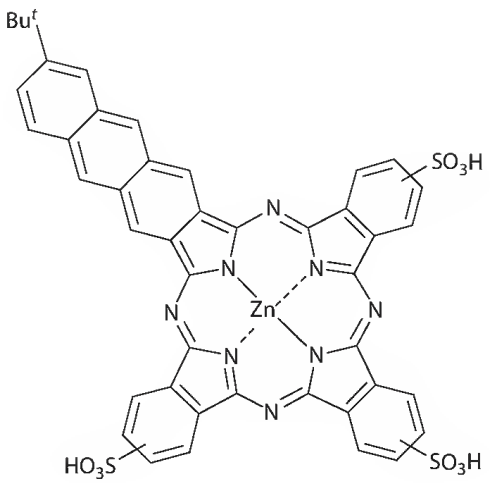

57

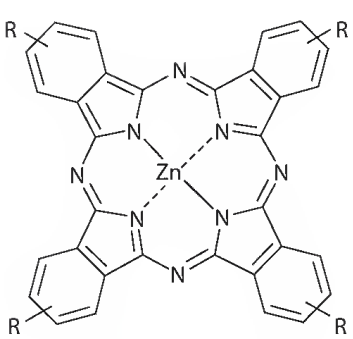

58 R = $C(CH_3)_2CH_2N^+$

59 R = $SO_2N(C_8H_{17})_2$

60 R = SO_3^-

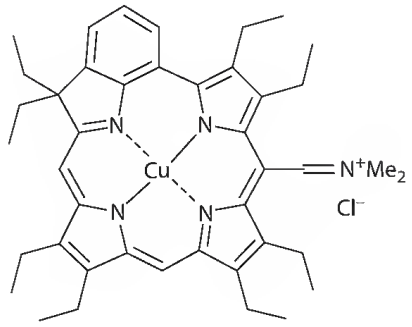

61

A series of meso-substituted tetracationic porphyrins have been synthesized and the role of amphiphilicity and zinc insertion in PDT efficacy (such as fluorescence and singlet oxygen quantum yields, uptake by vesicles, mitochondria and HeLa cells, dark and phototoxicity in HeLa cells) were studied (Pavani et al. 2009). Some studies have been carried out to investigate copper tetrapyrroles with regard to singlet oxygen production for use in PDT. For example, the iminium salt of octaethylbenzochlorin copper complex **61** was tested for its tumoricidal effects on the AY-27 N-[4-(5-nitro-2-furyl)-2-thiazolyl] formamide tumor line and was found to be an effective photosensitizer in vivo in combination with noncoherent light sources. Skin photosensitization was found to be minimal when drug-injected mice were illuminated in a solar simulator (Selman et al. 1993). As expected, the photodynamic ability of this complex required the presence of molecular oxygen in order to generate reactive species upon light activation (Hampton et al. 1993, Cavaleiro et al. 2001).

Sometimes, the efficacy of one-photon PDT is limited by hypoxia, which can prevent the production of the cytotoxic singlet oxygen species, leading to tumor resistance for PDT. To solve this problem, two-photon excitation of the photosensitizer can be employed. Excitation of the CuPc triplet state leads to an upper excited triplet state with distinct photochemical properties, which could inflict biological damage independently from the presence of molecular oxygen (Fournier et al. 2004). The potential of a two-photon excitation process was investigated on Jurkat cells incubated with CuPc tetrasulfonate (Mir et al. 2008). Significant advances can be expected from this line of research.

Tetrapyrroles have also found wide use in DNA binding and intercalation studies (Meunier 1992) and type II photosensitized reactions (Foote 1991) offer an intriguing possibility for site-specific photoinduced oxidation of DNA. Most studies were performed with free base porphyrins (Caminos and Durantini 2008) but a recent example is the use of a tetraruthenated zinc(II) porphyrin (Adam et al. 1997) for the specific photooxidation of 2-deoxyguanosine bases to form 8-oxo-2-deoxyguanosines (Araki et al. 2000).

Other studies showed that copper-based tetrapyrroles can exhibit photonucleolytic activity and may be used for the DNA cleavage. Many copper complexes have been shown to exhibit nuclease activity in the presence of external cooxidants (Hegg and Burstyn 1996, Itoh et al. 1997, Borah et al. 1998, Baudoin et al. 1998, Dhar and Chakravarty 2003, Melvin et al. 2000). Only few reports are available where copper-(II) complexes promote DNA cleavage on their own (Reddy et al. 2004, Verma et al. 2004). For example, hexaporphyrin dyads were synthesized from *n*-butyl stannonic acid and 5-(4-carboxyphenyl)-10,15,20-tritolylporphyrin ($H_2TTP\text{-}CO_2H$) followed by copper insertion as artificial nucleases (Chandrasekhar et al. 2005) The Cu-hexaporphyrin **62** showed high nuclease activity toward DNA supercoils. Interestingly, DNA cleavage did not occur in the presence of the free base hexaporphyrin alone and a monomeric CuP complex also failed to cleave it. Considerable inhibition of DNA cleavage in the presence of singlet oxygen quencher NaN_3 suggests the involvement of reactive oxygen species for cleavage.

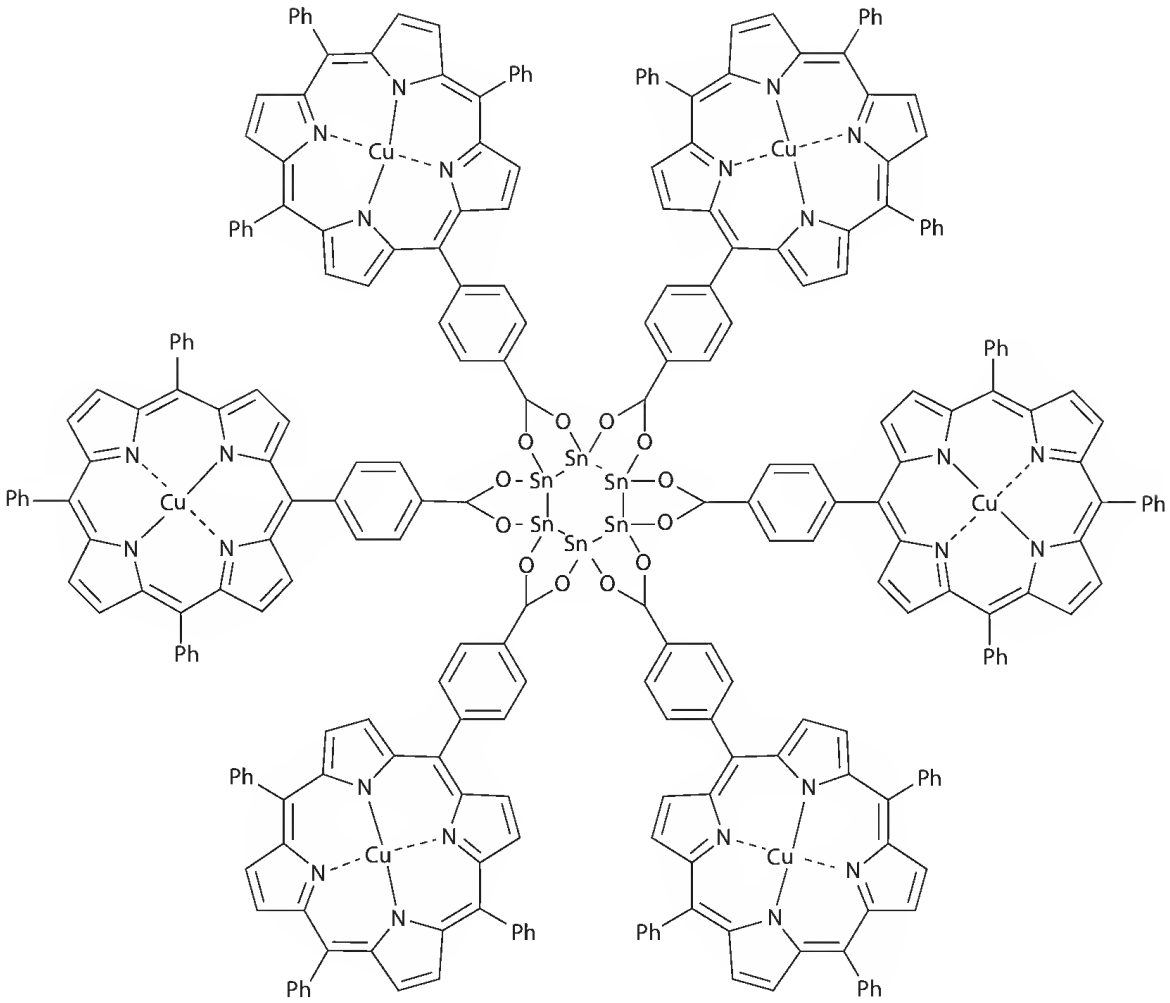

62

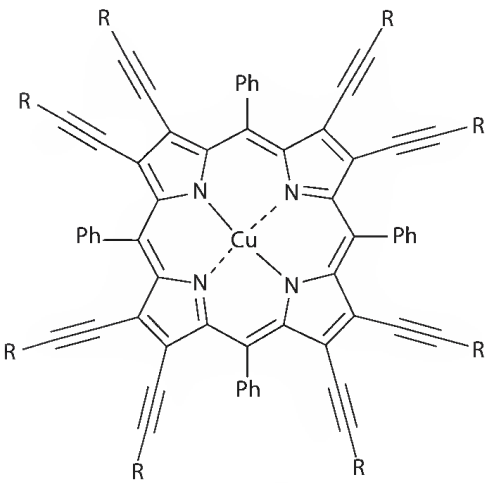

R: Ph, $SiMe_3$

63

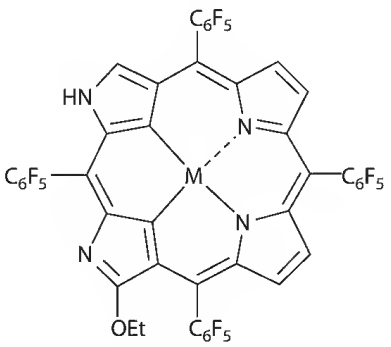

64 M: 2H

65 M: Cu(III)

Another example of potentially useful biomolecules is presented by the porphyrin **63** (Chandra et al. 2003) units. Enediynes (Lee et al. 1987, Golik et al. 1987) themselves are known to undergo rearrangements to form diradicals upon photoactivation leading to H-abstraction from DNA and cell death (Smith and Nicolaou 1996). It is interesting to note that "doubly N-confused" copper porphyrins have also been synthesized and investigated in terms of their singlet oxygen production. The free base "doubly *N*-confused" porphyrin complex **64** exhibits a low fluorescence quantum yield of 9.1×10^{-3}, which is completely suppressed in the Cu(III)P complex **65**. However, a high singlet oxygen quantum yield ($\varphi\Delta = 0.66$) was observed for the Cu(III). These results were explained in terms of enhanced intersystem crossing rates, induced by a heavy atom effect, rather than a redox quenching involving the metal ions in an unusually high oxidation state. The "confused porphyrins" are photochemically stable in oxygen-free solution but are bleached more or less rapidly by photogenerated singlet oxygen in the absence of other quenchers (Engelmann et al. 2004).

Phthalocyanines act as photosensitizers for the production of singlet oxygen in a similar manner to the porphyrins. Besides their catalytic properties, as discussed earlier, TiO_2 can be used to kill bacteria under UV irradiation. For instance, *Lactobacillus acidophilus*, *Saccharomyces cerevisiae*, and *Escherichia coli* can be completely sterilized when incubated with platinum-loaded TiO_2. TiO_2 photocatalysis is known to generate various active oxygen species, such as hydroxyl radicals and peroxide, and superoxide radical anions under UV irradiation. These properties can be used to develop disinfection materials and self-disinfecting thin films particularly attractive in places such as hospitals or for emergency medicine in disaster zones. Dye-sensitized TiO_2 films prepared with CuPc as sensitizers have shown bactericidal activities. For example, such films can kill *E. coli* DH5α bacteria under visible light irradiation ($\lambda > 420$ nm) and the bactericidal activity is related to the adsorption amount of the dye on film (Yu et al. 2003).

Dyes can also be attached to polymers soluble in water or/and in polar solvents, or to the insoluble polymer supports for recovery from the reaction medium for further reuse. CuPc can be easily functionalized for preparation of polymer hybrid thin films (Choe et al. 2004). For example, CuPc was linked to an amino group of *Amberlite IRA-93* and is strongly fluorescent in the solid state and in N,N-dimethyllformaide (DMF) suspension. Singlet oxygen quantum yields were determined in suspension by monitoring the photooxidation of diphenylisobenzofuran. Fluorescence and singlet oxygen production are environmentally depended on dye aggregation (Bourdelande et al. 1997). The degree of aggregation plays an important role in the photochemical mechanisms of photooxidation. Singlet oxygen production in these systems is expected to be different for monomers (Abramczyk et al. 2004).

Currently, photodynamic antimicrobial treatment is gaining more interest. Although photosensitizing agents and light have been used for medical purposes for a very long time, only little information is available about the exact mechanism of protein disulfide isomerase (PDI) for bacteria. Some studies have been carried on gram-negative bacteria involved in chronic infections such as cystic fibrosis and also one of the common causes of hospital-acquired infections. Recent examples are studies of the phototoxic effects of the (acridyl)bis(arginyl)porphyrin on the sensitivity of *Pseudomonas aeruginosa* (Steenkeste et al. 2010). The photodynamic inactivation efficiency of *E. coli* was investigated in bacteria treated with 5,10,15-tris[4-(3-N,N,N-trimethylammoniumpropoxy)phenyl]-20-(4-trifluoromethylphenyl)porphyrin iodide. Here, photosensitization activity of the porphyrin such as damage of plasmid and genomic DNA was compared with other porphyrin-based active tetracationic sensitizers (Caminos et al. 2008).

Acknowledgments

Writing of this article was made possible by generous funding from Science Foundation Ireland (SFI P.I. 09/IN.1/B2650) and the Health Research Board (translational research award 2007 TRA/2007/11).

References

Abe, T., Miyakushi, S., Nagai, K. et al. 2008. Study of the factors affecting the photoelectrode characteristics of a perylene/phthalocyanine bilayer working in the water phase. *Phys. Chem. Chem. Phys.* 10: 1562.

Abe, T. and Nagai, K. 2007. Novel photofunctions of bilayer composed of p-type phthalocyanine and n-type organic semiconductor as photoelectrodes in the water phase. *Org. Electron.* 8: 262.

Abramczyk, H., Brożek-Płuska, B., Kurczewski, K. et al. 2006. Femtosecond transient absorption, Raman, and electrochemistry studies of tetrasulfonated copper phthalocyanine in water solutions. *J. Phys. Chem. A* 110: 8627.

Abramczyk, H., Szymczyk, I., Waliszewska, G. et al. 2004. Photoinduced redox processes in phthalocyanine derivatives by resonance Raman spectroscopy. *J. Phys. Chem. A* 108: 264.

Adam, W., Saha-Möller, C. R., and Schönberger, A. 1997. Type I and Type II photosensitized oxidative modification of 2′-deoxyguanosine (dGuo) by triplet-excited ketones generated thermally from the 1,2-dioxetane HTMD. *J. Am. Chem. Soc.* 119: 719.

Allen, N. S. 1994. Photofading and light stability of dyed and pigmented polymers. *Polym. Degrad. Stab.* 44: 357.

Allen, N. S. and Parkinson, A. 1983. Interaction between colored pigments and hindered piperidine/antioxidant combinations in the photostabilization of polypropylene. *Polym. Degrad. Stab.* 5: 189.

Araki, K., Silva, C. A., Toma, H. E. et al. 2000. Zinc tetraruthenated porphyrin binding and photoinduced oxidation of calf-thymus DNA. *J. Inorg. Biochem.* 78: 269.

Arbour, C., Sharma, D. K., and Langford, C. H. 1990. Picosecond flash spectroscopy of TiO_2 colloids with adsorbed dyes. *J. Phys. Chem.* 94: 331.

Asano-Someda, M., Ichino, T., and Kaizu, Y. 1994. A time-resolved ESR study on triplet-triplet energy transfer processes in a copper(II)-free-base porphyrin dimmer. *Coord. Chem. Rev.* 132: 243.

Bakar, M. B., Oelgemöller, M., and Senge, M. O. 2009. Lead structures for applications in photodynamic therapy 2. Synthetic studies for photo-triggered release systems of bioconjugate porphyrin photosensitizers. *Tetrahedron* 65: 7064.

Balaban, T. S., Bhise, A. D., Fischer, M. et al. 2003. Controlling chirality and optical properties of artificial antenna systems with self-assembling porphyrins. *Angew. Chem. Int. Ed.* 42: 2140.

Ball, D. J., Wood, S. R., Vernon, D. I. et al. 1998. The characterisation of three substituted zinc phthalocyanines of differing charge for use in photodynamic therapy. A comparative study of their aggregation and photosensitising ability in relation to mTHPC and polyhaematoporphyrin. *J. Photochem. Photobiol. B: Biol.* 45: 28.

Bamford, C. H. and Dewar, M. J. S. 1949. Photosensitization by vat dyes. *Nature* 153: 214.

Banala, S., Ruehl, T., Wurst, K. et al. 2009. "Blackening" porphyrins by conjugation with quinones. *Angew. Chem. Int. Ed.* 48: 599.

Barrett, J. 1967. Photooxidation of magnesium porphyrins and formation of protobiliviolin. *Nature* 215: 733.

Baudoin, O., Fichou, M. P. T., Vigneron, J. P. et al. 1998. Efficient copper (II)-mediated nuclease activity of ortho-quinacridines. *J. Chem. Soc., Chem. Commun.* 21: 2349.

Beale, S. I. and Cornejo, J. 1991a. Biosynthesis of phycobilins. 3(Z)-phycoerythrobilin and 3(Z)-phycocyanobilin are intermediates in the formation of 3(E)-phycocyanobilin from biliverdin IX alpha. *J. Biol. Chem.* 266: 22333.

Beale, S. I. and Cornejo, J. 1991b. Biosynthesis of phycobilins. 15,16-Dihydrobiliverdin IX alpha is a partially reduced intermediate in the formation of phycobilins from biliverdin IX alpha. *J. Biol. Chem.* 266: 22341.

Beale, S. I. and Cornejo, J. 1991c. Biosynthesis of phycobilins. Ferredoxin-mediated reduction of biliverdin catalyzed by extracts of Cyanidium caldarium. *J. Biol. Chem.* 266: 22328.

Bearinger, J. P., Stone, G., Christian, A. T. et al. 2008. Porphyrin-based photocatalytic lithography. *Langmuir* 24: 5179.

Becker, H. G. O., Krueger, R., and Schuetz, R. 1986. Photochemical dediazoniation of arene diazonium salts sensitized by zinc phthalocyanine tetra(sulfomorpholide). *J. Prakt. Chem.* 328: 729.

Bell, T. D. M., Ghiggino, K. P., Jolliffe, K. A. et al. 2002. Photoinduced energy and electron transfer in a giant zinc porphyrin-bridge-C_{60} system. *J. Phys. Chem. A* 106: 10079.

Berg, A., Rachamim, M., Galili, T. et al. 1996. Effect of peripheral substitution on electron and energy transfer in electrostatically bonded zinc-magnesium porphyrin dimers. *J. Phys. Chem.* 100: 8791.

Bian, Y., Chen, X., Wang, D. et al. 2007. Porphyrin-appended europium(III) bis(phthalocyaninato) complexes: Synthesis, characterization, and photophysical properties. *Chem. Eur. J.* 13: 4169.

Bluestein, A. and Sugihara, J. M. 1973. Tartrate complex of yttrium(III). *J. Inorg. Nucl. Chem.* 35: 1050.

Bobrovskii, A. P. and Kholmogorov, V. E. 1973. Single-electron photoreduction of magnesium phthalocyanine by piperidine. *Russ. J. Phys. Chem.* 47: 983.

Bohandy, J. and Kim, B. F. 1983. Anomalous temperature-dependent phosphorescence of copper porphine in anthracene. *J. Chem. Phys.* 78: 4331.

Bonnett, R. 2000. *Chemical Aspects of Photodynamic Therapy*. Gordon and Breach Sci. Publ., Amsterdam, the Netherlands.

Borah, S., Melvin, M. S., Lindquist, N. et al. 1998. Copper-mediated nuclease activity of a tambjamine alkaloid. *J. Am. Chem. Soc.* 120: 4557.

Bourdelande, J. L., Karzazi, M., Dicelio, L. E. et al. 1997. Phthalocyanines bound to insoluble polystyrene. Synthesis and properties as energy-transfer photosensitizers. *J. Photochem. Photobiol. A: Chem.* 108: 273.

Brettar, J., Gisselbrecht, J.-P., Gross, M. et al. 2001. Tweezers hosts for intercalation of Lewis base guests: Tuning physico-chemical properties of cofacial porphyrin dimers. *Chem. Commun.* 8: 733.

Cai, J. H., Huang, J. W., Zhao, P. et al. 2009. Silica microspheres functionalized with porphyrin as a reusable and efficient catalyst for the photooxidation of 1,5-dihydroxynaphthalene in aerated aqueous solution. *J. Photochem. Photobiol. A: Chem.* 207: 236.

Caliman, A. F., Cojocaru, C., Antoniadis, A. et al. 2007. Optimized photocatalytic degradation of Alcian Blue 8 GX in the presence of TiO_2 suspensions. *J. Hazard. Mater. B* 144: 265.

Calvin, M. and Dorough, G. D. 1948. The possibility of a triplet state intermediate in the photo-oxidation of a chlorine. *J. Am. Chem. Soc.* 70: 699.

Caminos, D. A. and Durantini, E. N. 2008. Interaction and photodynamic activity of cationic porphyrin derivatives bearing different patterns of charge distribution with GMP and DNA. *J. Photochem. Photobiol. A: Chem.* 198: 274.

Caminos, D. A., Spesia, M. B., Pons, P. et al. 2008. Mechanisms of *Escherichia coli* photodynamic inactivation by an amphiphilic tricationic porphyrin and 5,10,15,20-tetra(4-N,N,N-trimethylammoniumphenyl) porphyrin. *Photochem. Photobiol. Sci.* 7: 1071.

Camps, X., Dietel, E., Hirsch, A. et al. 1999. Globular dendrimers involving a C_{60} core and a tetraphenyl porphyrin function. *Chem. Eur. J.* 5: 2362.

Canti, G., Lattuada, D., Cubeddu, R. et al. 1992. Comparative studies of photoactivated sulfonated phthalocyanines ZnS4Pc and alS2Pc in tumor bearing mice. *Med. Biol. Environ.* 20: 165.

Cavaleiro, J. A. S., Görner, H., and Lacerda, P. S. S. 2001. Singlet oxygen formation and photostability of meso-tetraarylporphyrin derivatives and their copper complexes. *J. Photochem. Photobiol. A: Chem.* 144: 131.

Chandra, T., Kraft, B. J., Huffman, J. C. et al. 2003. Synthesis and structural characterization of porphyrinic enediynes: Geometric and electronic effects on thermal and photochemical reactivity. *Inorg. Chem.* 42: 5158.

Chandrasekhar, V., Nagendran, S., Azhakar, R. et al. 2005. A lipophilic hexaporphyrin assembly supported on a stannoxane core. *J. Am. Chem. Soc.* 127: 2410.

Chang, C. J., Baker, E. A., Pistorio, B. J. et al. 2002. Structural, spectroscopic, and reactivity comparison of xanthene- and dibenzofuran-bridged cofacial bisporphyrins. *Inorg. Chem.* 41: 3102.

Chen, F., Deng, Z., Li, X. et al. 2005. Visible light detoxification by 2,9,16,23-tetracarboxyl phthalocyanine copper modified amorphous titania. *Chem. Phys. Lett.* 415: 85.

Cho, S. and Choi, W. 2001. Solid-phase photocatalytic degradation of PVC-TiO_2 polymer composites. *J. Photochem. Photobiol. A: Chem.* 143: 221.

Choe, Y., Kim, T., and Kim, W. 2004. Dispersion of functional tetraphenylporphyrin-ligated metal into ultra-thin flexible acrylate films. 1. Preparation of thin films. *Coll. Surf. B* 38: 155.

Connolly, J. S. 1982. The role of porphyrins and chlorophylls in artificial photosynthesis. In *Photochemical Conversion and Storage of Solar Energy-1982*, (ed.) J. Rabani, pp. 175–204, Part A, The Weizmann Science Press of Israel, Jerusalem, Israel.

D'Souza, F., Deviprasad, G. R., El-Khouly, M. E. et al. 2001. Probing the donor-acceptor proximity on the physicochemical properties of porphyrin-fullerene dyads: "Tail-on" and "tail-off" binding approach. *J. Am. Chem. Soc.* 123: 5277.

D'Souza, F., Deviprasad, G. R., Rahman, M. S. et al. 1999. Self-assembled porphyrin-C_{60} and porphycene-C_{60} complexes via metal axial coordination. *Inorg. Chem.* 38: 2157.

D'Souza, F., Deviprasad, G. R., Zandler, M. E. et al. 2002b. Electronic interactions and photoinduced electron transfer in covalently linked porphyrin-C_{60}(pyridine) dyads and supramolecular triads formed by self-assembling the dyads and zinc porphyrin. *J. Phys. Chem. B* 106: 4952.

D'Souza, F., Deviprasad, G. R., Zandler, M. E. et al. 2003. Photoinduced electron transfer in "two-point" bound supramolecular triads composed of N,N-dimethylaminophenyl-fullerene-pyridine coordinated to zinc porphyrin. *J. Phys. Chem. A* 107: 4801.

D'Souza, F., El-Khouly, M. E., Gadde, S. et al. 2005. Self-assembled via axial coordination magnesium porphyrin-imidazole appended fullerene dyad: Spectroscopic, electrochemical, computational, and photochemical studies. *J. Phys. Chem. B* 109: 10107.

D'Souza, F., Gadde, S., Zandler, M. E. et al. 2002a. Studies on covalently linked porphyrin-C_{60} dyads: Stabilization of charge-separated states by axial coordination. *J. Phys. Chem. A* 106: 12393.

D'Souza, F., Smith, P. M., Gadde, S. et al. 2004b. Supramolecular triads formed by axial coordination of fullerene to covalently linked zinc porphyrin-ferrocene(s): Design, syntheses, electrochemistry, and photochemistry. *J. Phys. Chem. B* 108: 11333.

D'Souza, F., Smith, P. M., Zandler, M. E. et al. 2004a. Energy transfer followed by electron transfer in a supramolecular triad composed of boron dipyrrin, zinc porphyrin, and fullerene: A model for the photosynthetic antenna-reaction center complex. *J. Am. Chem. Soc.* 126: 7898.

Deguchi, J., Tamura, M., and Yamazaki, I. 1985. Photooxidation of porphyrin in Mg-substituted horseradish peroxidase. *J. Biol. Chem.* 260: 15542.

Deng, Y., Chang, C. K., and Nocera, D. G. 2000. Facile synthesis of β-derivatized porphyrins—Structural characterization of a β-β-bis-porphyrin. *Angew. Chem. Int. Ed.* 39: 1066.

DeOliveira, E., Neri, C. R., Ribeiro, A. O. et al. 2008. Hexagonal mesoporous silica modified with copper phthalocyanine as a photocatalyst for pesticide 2,4-dichlorophenoxiacetic acid degradation. *J. Colloid Interface Sci.* 323: 98.

Dhar, S. and Chakravarty, A. R. 2003. Efficient visible light induced nuclease activity of a ternary mono-1,10-phenanthroline copper(II) complex containing 2-(methylthio)ethylsalicylaldimine. *Inorg. Chem.* 42: 2483.

Ding, H., Zhang, X., Ram, M. K. et al. 2005. Ultrathin films of tetrasulfonated copper phthalocyanine-capped titanium dioxide nanoparticles: Fabrication, characterization, and photovoltaic effect. *J. Colloid Interface Sci.* 290: 166.

Doherty III, W. J., Friedlein, R., and Salaneck, W. R. 2007. Layer-by-layer deposition of copper phthalocyanine from aqueous solution: Molecular orientation, ordering parameters, and electronic structure. *J. Phys. Chem. C* 111: 2724.

Donley, C. L., Xia, W., Minch, B. A. et al. 2003. Thin films of polymerized rodlike phthalocyanine aggregates. *Langmuir* 19: 6512.

Dougherty, T. J., Gomer, C. J., Henderson, B. W. et al. 1998. Photodynamic therapy. *J. Natl. Cancer Inst.* 90: 889.

Douglas, R. H., Partridge, J. C., Dulai, K. et al. 1998. Dragon fish see using chlorophyll. *Nature* 393: 423.

Drager, A. S., Zangmeister, R. A. P., and Armstrong, N. R. 2001. One-dimensional polymers of octasubstituted phthalocyanines. *J. Am. Chem. Soc.* 123: 3595.

Eastwood, D. and Gouterman, M. 1969. Porphyrins. XII. Luminescence of copper complexes at liquid nitrogen temperature. *J. Mol. Spectrosc.* 30: 437.

El-Khouly, M. E., Araki, Y., Fujitsuka, M. et al. 2002. Photoinduced electron transfer between metal octaethylporphyrins and fullerenes (C_{60}/C_{70}) studied by laser flash photolysis: Electron-mediating and hole-shifting cycles. *Phys. Chem. Chem. Phys.* 4: 3322.

El-Khouly, M. E., Araki, Y., Ito, O. et al. 2005. Spectral, electrochemical, and photophysical studies of a magnesium porphyrin-fullerene dyad. *Phys. Chem. Chem. Phys.* 7: 3163.

El-Khouly, M. E., Gadde, S., Deviprasad, G. R. et al. 2003. Self-assembled supramolecular triad composed of fulleropyrrolidine bearing two pyridine moieties axially coordinated to two zinc porphyrins. *J. Porphyrins Phthalocyanines* 7: 1.

Engelmann, F. M., Mayer, I., Araki, K. et al. 2004. Photochemistry of doubly N-confused porphyrin bonded to non-conventional high oxidation state Ag(III) and Cu(III) ions. *J. Photochem. Photobiol. A: Chem.* 163: 403.

Fajer, J., Borg, D. C., Forman, A. et al. 1970. π-Cation radicals and dications of metalloporphyrins. *J. Am. Chem. Soc.* 92: 3451.

Fan, F. R. F. and Bard, A. J. 1979. Spectral sensitization of the heterogeneous photocatalytic oxidation of hydroquinone in aqueous solutions at phthalocyanine-coated titanium dioxide powders. *J. Am. Chem. Soc.* 101: 6139.

Fernández, D. A., Awruch, J., and Dicelio, L. E. 1997. Synthesis and photophysical properties of a new cationic water-soluble Zn phthalocyanine. *J. Photochem. Photobiol. Part B: Biol.* 41: 227.

Flamigni, L. 2007. Photoinduced processes in interlocked structures containing porphyrins. *J. Photochem. Photobiol. C: Photochem. Rev.* 8: 191.

Fletcher, J. T. and Therien, M. J. 2002. Strongly coupled porphyrin arrays featuring both π-cofacial and linear-π-conjugative interactions. *Inorg. Chem.* 41: 331.

Foote, C. S. 1991. Definition of type I and type II photosensitized oxidation. *Photochem. Photobiol.* 54: 659.

Fournier, M., Pépin, C., Houde, D. R. et al. 2004. Ultrafast studies of the excited-state dynamics of copper and nickel phthalocyanine tetrasulfonates: Potential sensitizers for the two-photon photodynamic therapy of tumors. *Photochem. Photobiol. Sci.* 3: 120.

Fuhrhop, J. H. 1974. Reactivity of the porphyrin ligands. *Angew. Chem. Int. Ed. Engl.* 86: 363.

Fuhrhop, J. H. and Mauzerall, D. 1971. Photooxygenation of magnesium octaethylporphin. *Photochem. Photobiol.* 13: 453.

Fuhrhop, J. H., Wasser, P. K. W., and Subramanian, J. 1974. Formylbiliverdins and their metal complexes. *Liebig. Ann. Chem.* 1450.

Fujishima, A. and Honda, K. 1972. Electrochemical photolysis of water at a semiconductor electrode. *Nature* 238: 37.

Fukuzumi, S., Ohkubo, K., Imahori, H. et al. 2001. Photochemical and electrochemical properties of zinc chlorin-C_{60} dyad as compared to corresponding free-base chlorin-C_{60}, free-base porphyrin-C_{60}, and zinc porphyrin-C_{60} dyads. *J. Am. Chem. Soc.* 123: 10676.

Fukuzumi, S., Ohkubo, K., Ortiz, J. et al. 2005. Formation of a long-lived charge-separated state of a zinc phthalocyanine-perylenediimide dyad by complexation with magnesium ion. *J. Chem. Soc., Chem. Commun.* 30: 3814.

Gabrielsson, A., Hartl, F., Zhang, H. et al. 2006. Ultrafast charge separation in a photoreactive rhenium-appended porphyrin assembly monitored by picosecond transient infrared spectroscopy. *J. Am. Chem. Soc.* 128: 4253.

Gerasimov, O. V., Limar, S. V., and Parmon, V. N. 1991. Water photooxidation sensitized by zinc(II) meso-tetrakis(N-methyl-4-pyridyl)porphine. *J. Photochem. Photobiol. A: Chem.* 56: 275.

Giangiacomo, K. M. and Dutton, P. L. 1989. In photosynthetic reaction centers, the free energy difference for electron transfer between quinones bound at the primary and secondary quinone-binding sites governs the observed secondary site specificity. *Proc. Natl. Acad. Sci. USA* 86: 2658.

Goedheer, J. C. 1967. Magnesium tetrabenzoporphyrin. II. Redox and photochemical properties in organic solvents and aqueous medium. *Photochem. Photobiol.* 6: 521.

Goedheer, J. C. and Siero, J. P. J. 1967. Magnesium tetrabenzoporphyrin. I. Absorption and fluorescence in organic solution and aqueous medium. *Photochem. Photobiol.* 6: 509.

Golik, J., Dubay, G., Groenewold, G. et al. 1987. Esperamicins, a novel class of potent antitumor antibiotics. 3. Structures of esperamicins A1, A2, and A1b. *J. Am. Chem. Soc.* 109: 3462.

Gordon, P.F. and Gregory, P. 1983. *Organic Chemistry in Colour*, Springer-Verlag, New York.

Gossauer, A. and Engel, N. 1996. Chlorophyll catabolism—Structures, mechanisms, conversions. *J. Photochem. Photobiol. B: Biol.* 32: 141.

Gould, S. L., Kodis, G., Palacios, R. E. et al. 2004. Artificial photosynthetic reaction centers with porphyrins as primary electron acceptors. *J. Phys. Chem. B* 108: 10566.

Gouterman, M. 1978. Optical spectra and electronic structure of porphyrins and related rings. In *The Porphyrins*, (ed.) D. Dolphin, Vol. 3, Academic Press, New York.

Gouterman, M., Mathies, R. A., Smith, B. E. et al. 1970. Porphyrins. XIX. Tripdoublet and quartet luminescence in copper and vanadyl complexes. *J. Chem. Phys.* 52: 3795.

Grätzel, M. and Halmann, M. 1990. Photosensitized oxidation of bromide to bromine with phthalic acid derivatives in aqueous-solutions. *Sol. Energ. Mater.* 20: 177.

Griffiths, J., Cruse-Sawyer, J., Wood, S. R. et al. 1994. On the photodynamic therapy action spectrum of zinc phthalocyanine tetrasulphonic acid in vivo. *J. Photochem. Photobiol. B: Biol.* 24: 195.

Griffiths, J., Schofield, J., Wainwright, M. et al. 1997. Some observations on the synthesis of polysubstituted zinc phthalocyanine sensitizers for photodynamic therapy. *Dyes Pigments* 33: 65.

Gross, E., Ehrenberg, B., and Johnson, F. M. 1993. Singlet oxygen generation by porphyrins and the kinetics of 9,10-dimethylanthracene photosensitization in liposomes. *Photochem. Photobiol.* 57: 808.

Guldi, D. M., Luo, C., Schwartz, A. et al. 2001. Self-organisation in photoactive fullerene porphyrin based donor-acceptor ensembles. *Chem. Commun.* 12: 1066.

Guldi, D. M., Ramey, J., Martínez-Díaz, M. V. et al. 2002. Reversible zinc phthalocyanine fullerene ensembles. *Chem. Commun.* 23: 2774.

Guldi, D. M., Zilbermann, I., Gouloumis, A. et al. 2004. Metallophthalocyanines: Versatile electron-donating building blocks for fullerene dyads. *J. Phys. Chem. B* 108: 18485.

Gurinovich, V. V. and Tsvirko, M. P. 2001. Quantum efficiency of photooxidation of porphyrins by halomethanes in solutions. *J. Appl. Spectrosc.* 68: 110.

Gust, D. and Moore, T. A. 2000. Intermolecular photoinduced electron-transfer reactions of porphyrins. In *The Porphyrin Handbook*, (eds.) K. M. Kadish, K. M. Smith, and R. Guilard, Vol. 8, pp. 153–190, Academic Press, San Diego, CA.

Gust, D., Moore, T. A., and Moore, A. L. 2001. Mimicking photosynthetic solar energy transduction. *Acc. Chem. Res.* 34: 40.

Hampton, J. A., Skalkos, D., and Taylor, P. M. 1993. Iminium salt of copper benzochlorin (CDS1), a novel photosensitizer for photodynamic therapy: Mechanism of cell killing. *Photochem. Photobiol.* 58: 100.

Harriman, A., Poter, G., and Richoux, M. C. 1981. Photoreduction of methyl viologen sensitized by the excited singlet state of a magnesium phthalocyanine. *J. Chem. Soc. Faraday Trans.* 77: 1175.

Harrimana, A. and Reichoux, M. C. 1980. Attempted photoproduction of hydrogen using sulphophthalocyanines as chromophores for three-component systems. *J. Chem. Soc. Faraday Trans.* 76: 1618.

Hasobe, T., Fukuzumi, S., and Kamat, P. V. 2006. Organized assemblies of single wall carbon nanotubes and porphyrin for photochemical solar cells: Charge injection from excited porphyrin into single-walled carbon nanotubes. *J. Phys. Chem. B* 110: 25477.

Haycock, R. A., Yartsev, A., Michelsen, U. et al. 2000. Self-assembly of pentameric porphyrin light-harvesting antennae complexes. *Angew. Chem. Int. Ed.* 39: 3616.

Hayes, R. T., Wasielewski, M. R., and Gosztola, D. 2000. Ultrafast photoswitched charge transmission through the bridge molecule in a donor-bridge-acceptor system. *J. Am. Chem. Soc.* 122: 5563.

Hegg, E. L. and Burstyn, J. N. 1996. Copper(II) macrocycles cleave single-stranded and double-stranded DNA under both aerobic and anaerobic conditions. *Inorg. Chem.* 35: 7474.

Helaja, H., Tauber, A. Y., Abel, Y. et al. 1999. Chlorophylls. IX. The first phytochlorin-fullerene dyads: Synthesis and conformational studies. *J. Chem. Soc. Perkin Trans. 1* 16: 2403.

Hendry, G. A., Houghton, J. D., and Brown, S. B. 1987. The degradation of chlorophyll—A biological enigma. *New Phytol.* 107: 255.

Héquet, V., Le Cloirec, P., Gonzalez, C. et al. 2000. Photocatalytic degradation of atrazine by porphyrin and phthalocyanine complexes. *Chemosphere* 41: 379.

Hersan, M. C., Guighges, N. P., and Lyding, J. W. 2000. Silicon-based molecular nanotechnology. *Nanotechnology* 11: 70.

Hihara, T., Okada, Y., and Morita, Z. 2001. Photofading, photosensitization and the effect of aggregation on the fading of triphenodioxazine and copper phthalocyanine dyes on cellulosic film. *Dyes Pigments* 50: 185.

Hilinski, E. F., Straub, K. D., and Rentzepis, P. M. 1984. Solvent effects on the relaxation mechanism of copper(II) protoporphyrin. *Chem. Phys. Lett.* 111: 333.

Himeno, K., Okada, Y., and Morita, Z. 2000. Photofading of monoazo disperse dyes on polyester and polyamide substrates. *Dyes Pigments* 45: 109.

Hiraishi, A., Nagashima, K. V. P., Matsuura, K. et al. 1998. Phylogeny and photosynthetic features of *Thiobacillus acidophilus* and related acidophilic bacteria: Its transfer to the genus *Acidiphilium* as *Acidiphilium acidophilum* comb. nov. *Int. J. Syst. Bacteriol.* 48: 1389.

Hiraishi, A. and Shimada, K. 2001. Aerobic anoxygenic photosynthetic bacteria with zinc-bacteriochlorophyll. *J. Gen. Appl. Microbiol.* 47: 161.

Hoshino, K., Kurasako, K., Inayama, T. et al. 1996. Formation of organic pigment films using photocatalytic reactions of tris(2,2′-bipyridine)ruthenium(II). Mechanistic study on negative patterned film formation. *J. Electroanal. Chem.* 406: 175.

Huennekens, F. M. and Calvin, M. 1949a. Photochemical studies of the porphyrins. II. The photo-oxidation of chlorins by various quinones. *J. Am. Chem. Soc.* 71: 4024.

Huennekens, F. M. and Calvin, M. 1949b. Photochemical studies of the porphyrins. III. The photo-oxidation of chlorins by oxygen. *J. Am. Chem. Soc.* 71: 4031.

Hynninen, P. H. 1991. Chemistry of chlorophylls: Modifications. In *Chlorophylls*, (ed.) H. Scheer, pp. 145–209, CRC Press, Boca Raton, FL.

Ichikawa, M., Fukumura, H., and Masuhara, H. 1994. Picosecond regular reflection spectroscopic study on ultrafast photoinduced heat generation in copper phthalocyanine solid. *J. Phys. Chem.* 98: 12211.

Ichikawa, M., Fukumura, H., and Masuhara, H. 1995. Ultrafast electron-transfer and recombination processes in copper phthalocyanine solid/water interface as revealed by picosecond regular reflection spectroscopy. *J. Phys. Chem.* 99: 12072.

Ikeda, C., Tanaka, Y., Fujihara, T. et al. 2001. Self-assembly of a porphyrin array via the molecular recognition approach: Synthesis and properties of a cyclic zinc(II) porphyrin trimer based on coordination and hydrogen bonding. *Inorg. Chem.* 40: 3395.

Ilani, A., Woodle, M., and Mauzerall, D. 1989. Photoinduced electron transfer across lipid bilayers containing magnesium octaethylporphyrin. *Photochem. Photobiol.* 49: 673.

Imahori, H. 2004. Porphyrin-fullerene linked systems as artificial photosynthetic mimics. *Org. Biomol. Chem.* 2: 1425.

Imahori, H. and Fukuzumi, S. 2004. Porphyrin- and fullerene-based molecular photovoltaic devices. *Adv. Funct. Mater.* 14: 525.

Imahori, H., Sekiguchi, Y., Kashiwagi, Y. et al. 2004. Long-lived charge-separated state generated in a ferrocene-meso, meso-linked porphyrin trimer-fullerene pentad with a high quantum yield. *Chem. Eur. J.* 10: 3184.

Imahori, H., Tamaki, K., Araki, Y. et al. 2002a. Linkage dependent charge separation and charge recombination in porphyrin-pyromellitimide-fullerene triads. *J. Phys. Chem. A* 106: 2803.

Imahori, H., Tamaki, K., Araki, Y. et al. 2002b. Stepwise charge separation and charge recombination in ferrocene-meso, meso-linked porphyrin dimer-fullerene triad. *J. Am. Chem. Soc.* 124: 5165.

Inhoffen, H. H. 1968. Chlorophyll and porphyrin chemistry. *Pure Appl. Chem.* 17: 443.

Iseki, Y. and Inoue, S. 1994. Photoswitchable complexation of metalloporphyrins. *J. Chem. Soc., Chem. Commun.* 22: 2577.

Ito, F., Ishibashi, Y., Khan, S. R. et al. 2006. Photoinduced electron transfer and excitation energy transfer in directly linked zinc porphyrin/zinc phthalocyanine composite. *J. Phys. Chem. A* 110: 12734.

Itoh, T., Hisada, H., Sumiya, T. et al. 1997. Hydrolytic cleavage of DNA by a novel copper(II) complex with cis,cis-1,3,5-triaminocyclohexane. *J. Chem. Soc., Chem. Commun.* 677.

Iturraspe, J., Moyano, N., and Frydman, B. 1995. A new 5-formylbilinone as the major chlorophyll a catabolite in tree senescent leaves. *J. Org. Chem.* 60: 6664.

Jiang, M. Y. and Dolphin, D. 2008. Site-specific prodrug release using visible light. *J. Am. Chem. Soc.* 130: 4236.

Jiao, L., Courtney, B. H., Fronczek, F. R. et al. 2006. β,β′-Linked cofacial bis-porphyrins. *Tetrahedron Lett.* 47: 501.

Kadish, K. M., Smith, K. M., and Guilard, R. 2000a. *The Porphyrin Handbook*, Academic Press, San Diego, CA.

Kadish, K. M., Smith, K. M., and Guilard, R. 2000b. *The Porphyrin Handbook*, Vol. 13, Academic Press, San Diego, CA.

Kadish, K. M., Smith, K. M., and Guilard, R. 2003. *The Porphyrin Handbook*, Academic Press, San Diego, CA.

Kaito, R., Miyamoto, N., Kuroda, K. et al. 2002. Intercalation of cationic phthalocyanines into layered titanates and control of the microstructures. *J. Mater. Chem.* 12: 3463.

Kalisch, W. W., Senge, M. O., and Ruhlandt-Senge, K. 1998. Synthesis and crystal structures of cofacial bisoctaethylchlorins as structural models for the special pair. *Photochem. Photobiol.* 67: 312.

Kaneko, Y., Arai, T., and Sakuragi, H. 1996. Effect of excitation wavelength on photoreduction of metal-free and copper(II) 1,4,8,11,15,18,22,25-octabutoxyphthalocyanines with triethanolamine. *J. Photochem. Photobiol. A: Chem.* 97: 155.

Kaneko, Y., Nishimura, Y., Arai, T. et al. 1995. UV light and red light chemistry of metallophthalocyanine: Wavelength-dependent photochemical reduction of tetrasodium salts of Zn(II) and Cu(II) tetrasulfonatophthalocyanines with amines. *J. Photochem. Photobiol. A: Chem.* 89: 37.

Kasuga, K., Fujita, A., Miyazako, T. et al. 2000. Photocatalytic decomposition of trichlorophenol by zinc(II) phthalocyanine derivatives in aerated organic solvents. *Inorg. Chem. Commun.* 3: 634.

Kessel, D. and Dougherty, T. J. 1999. Agents used in photodynamic therapy. *Rev. Contemp. Pharmacother.* 10: 19.

Kesti, T., Tkachenko, N., Yamada, H. et al. 2003. C_{70} vs. C_{60} in zinc porphyrin-fullerene dyads: Prolonged charge separation and ultrafast energy transfer from the second excited singlet state of porphyrin. *Photochem. Photobiol. Sci.* 2: 251.

Khairutdinov, R. F., Brikenshtein, E. K., and Strekova, L. N. 1982. Photochemical reactions of zinc and magnesium porphyrins in a glassy matrix containing donor and acceptor particles. *Izv. Akad. Nauk SSSR, Ser. Khim.* 7: 1504; *Chem. Abstr.* 97: 136553t (1982).

Kim, D. 1986. Effect of solvent on some excited state processes of magnesium and zinc phthalocyanines. *Bull. Korean Chem. Soc.* 7: 416.

Kim, D., Holten, D., and Gouterman, M. 1984. Evidence from picosecond transient absorption and kinetic studies of charge-transfer states in copper(II) porphyrins. *J. Am. Chem. Soc.* 106: 2793.

Kim, W., Park, J., Jo, H. et al. 2008. Visible light photocatalysts based on homogeneous and heterogenized tin porphyrins. *J. Phys. Chem. C* 112: 491.

Kishimoto, N., Fukaya, F., Inagaki, K. et al. 1995. Distribution of bacteriochlorophyll a among aerobic and acidophilic bacteria and light-enhanced CO_2-incorporation in *Acidiphilium rubrum*. *FEMS Microbiol. Ecol.* 16: 291.

Kobayashi, M., Yamamura, M., Akiyama, M. et al. 1998. Acid resistance of Zn-bacteriochlorophyll a from an acidophilic bacterium *Acidiphilium rubrum*. *Anal. Sci.* 14: 1149.

Kobyshev, G. I., Lyalin, G. N., and Terenin, A. N. 1963. Photoreactions of Mg phthalocyanine with a coordinated uranium cation. *Dokl. Akad. Nauk SSSR* 153: 865; *Chem. Abstr.* 60: 14357e.

Kodis, G., Liddell, P. A., Moore, A. L. et al. 2004. Synthesis and photochemistry of a carotene-porphyrin-fullerene model photosynthetic reaction center. *J. Phys. Org. Chem.* 17: 724.

Kräutler, B. and Matile, P. 1999. Solving the riddle of chlorophyll breakdown. *Acc. Chem. Res.* 32: 35.

Kruglik, S. G., Apanasevich, P. A., Chirvony, V. S. et al. 1995. Resonance Raman, CARS, and picosecond absorption spectroscopy of copper porphyrins: The evidence for the exciplex formation with oxygen-containing solvent molecules. *J. Phys. Chem.* 99: 2978.

Kudrevich, S., Brasseur, N., La Madeleine, C. et al. 1997. Syntheses and photodynamic activities of novel trisulfonated zinc phthalocyanine derivatives. *J. Med. Chem.* 40: 3897.

Kuramochi, Y., Satake, A., and Kobuke, Y. 2004. Light-harvesting macroring accommodating a tetrapodal ligand based on complementary and cooperative coordinations. *J. Am. Chem. Soc.* 126: 8668.

Kuwahara, Y., Tamura, M., and Yamazaki, I. 1982. The reactivity of Mg-substituted horseradish peroxidases. *J. Biol. Chem.* 257: 11517.

Lee, M. D., Dunne, T. S., Chang, C. C. et al. 1987. Calichemicins, a novel family of antitumor antibiotics. 2. Chemistry and structure of calichemicin γ1I. *J. Am. Chem. Soc.* 109: 3466.

Levanon, H., Regev, A., Galili, T. et al. 1993. Photoelectron transfer between a magnesium-free-base porphyrin heterodimer and duroquinone. Selective excitation and time-resolved EPR studies. *J. Phys. Chem.* 97: 13198.

Levitsky, I. A., Euler, W. B., Tokranova, N. et al. 2004. Hybrid solar cells based on porous Si and copper phthalocyanine derivatives. *Appl. Phys. Lett.* 85: 6245.

Li, K., Bracher, P. J., Guldi, D. M. et al. 2004a. [60]Fullerene-stoppered porphyrinorotaxanes: Pronounced elongation of charge-separated-state lifetimes. *J. Am. Chem. Soc.* 126: 9156.

Li, D., Dong, W., Sun, S. et al. 2008b. Photocatalytic degradation of acid chrome blue K with porphyrin-sensitized TiO_2 under visible light. *J. Phys. Chem. C* 112: 14878.

Li, F., Gentemann, S., Kalsbeck, W. A. et al. 1997. Effects of central metal ion (Mg, Zn) and solvent on singlet excited-state energy flow in porphyrin-based nanostructures. *J. Mater. Chem.* 7: 1245.

Li, K., Schuster, D. I., Guldi, D. M. et al. 2004b. Convergent synthesis and photophysics of [60]fullerene/porphyrin-based rotaxanes. *J. Am. Chem. Soc.* 126: 3388.

Li, X., Wang, M., Zhang, S. et al. 2008a. Noncovalent assembly of a metalloporphyrin and an iron hydrogenase active-site model: photo-induced electron transfer and hydrogen generation. *J. Phys. Chem. B* 112: 8198.

Liddell, P. A., Kodis, G., de la Garza, L. et al. 2004. Benzene-templated model systems for photosynthetic antenna-reaction center function. *J. Phys. Chem. B* 108: 10256.

Liu, S., Fujihira, M., and Saji, T. 1994. Formation of an organic thin film by photochemical isomerization of a surfactant with a spiropyran moiety. *J. Chem. Soc., Chem. Commun.* 1855.

Liu, A. R., Wang, X., Nakamura, C. et al. 2008. Assembly and characterization of zinc porphyrin-hydrogenase-(poly)viologen triads on substrate surfaces. *J. Phys. Chem. C* 112: 1582.

Llewellyn, C. A., Mantoura, R. F. C., and Brereton, R. G. 1990a. Products of chlorophyll photodegradation-1. Detection and separation. *Photochem. Photobiol.* 52: 1037.

Llewellyn, C. A., Mantoura, R. F. C., and Brereton, R. G. 1990b. Products of chlorophyll photodegradation-2. Structural identification. *Photochem. Photobiol.* 52: 1043.

Lo, P. C., Leng, X., and Ng, D. K. P. 2007. Hetero-arrays of porphyrins and phthalocyanines. *Coord. Chem. Rev.* 251: 2334.

Luo, Q., Tian, H., Chen, B. et al. 2007. Effective non-destructive readout of photochromic bisthienylethene-phthalocyanine hybrid. *Dyes Pigments* 73: 118.

Machado, A. E. H., de Miranda, J. A., de Freitas, R. F. et al. 2003. Destruction of the organic matter present in effluent from a cellulose and paper industry using photocatalysis. *J. Photochem. Photobiol. A: Chem.* 155: 231.

Mack, J. and Stillman, M. J. 2003. Electronic structure of metal phthalocyanine and porphyrin complexes from analysis of the UV-visible absorption and magnetic circular dichroism spectra and molecular orbital calculations. In *The Porphyrin Handbook*, (eds.) K. M. Kadish, K. M. Smith, and R. Guilard, Vol. 16, pp. 43–116, Academic Press, San Diego, CA.

Maiya, G. B. and Krishnan, V. 1985. Intramolecular electron transfer in donor-acceptor systems. Porphyrins bearing trinitroaryl acceptor group. *J. Phys. Chem.* 89: 5225.

Matsuura, T., Inoue, K., Ranade, C. R. et al. 1980. Photooxygenation of magnesium meso-tetraphenylporphyrin. *Photochem. Photobiol.* 31: 23.

Mauzerall, D. 1962. The photoreduction of porphyrins: Structure of the products. *J. Am. Chem. Soc.* 84: 2437.

Megiatto, J. D., Schuster, D. I., Abwandner, S. et al. 2010. [2]Catenanes decorated with porphyrin and [60]fullerene groups: design, convergent synthesis, and photoinduced processes. *J. Am. Chem. Soc.* 132: 3847.

Mele, G., Ciccarella, G., Vasapollo, G. et al. 2002. Photocatalytic degradation of 4-nitrophenol in aqueous suspension by using polycrystalline TiO_2 samples impregnated with Cu(II)-phthalocyanine. *Appl. Catal. B* 38: 309.

Mele, G., Del Sole, R., Vasapollo, G. et al. 2003. Photocatalytic degradation of 4-nitrophenol in aqueous suspension by using polycrystalline TiO_2 impregnated with functionalized Cu(II)-porphyrin or Cu(II)-phthalocyanine. *J. Catalysis* 217: 334.

Mele, G., Del Sole, R., Vasapollo, G. et al. 2005. 4-Nitrophenol photodegradation TRMC, XPS, and EPR characterizations of polycrystalline TiO_2 porphyrin impregnated powders and their catalytic activity for 4-nitrophenol photodegradation in aqueous suspension. *J. Phys. Chem. B* 109: 12347.

Mele, G., Del Sole, R., Vasapollo, G. et al. 2007a. TiO_2-based photocatalysts impregnated with metalloporphyrins employed for degradation of 4-nitrophenol in aqueous solutions: Role of metal and macrocycle. *Res. Chem. Intermed.* 33: 433.

Mele, G., García-López, E., Palmisano, L. et al. 2007b. Photocatalytic degradation of 4-nitrophenol in aqueous suspension by using polycrystalline TiO_2 impregnated with lanthanide double-decker phthalocyanine complexes. *J. Phys. Chem. C* 111: 6581.

Melvin, M. S., Tomlinson, J. T., Saluta, G. R. et al. 2000. Double-strand DNA cleavage by copper prodigiosin. *J. Am. Chem. Soc.* 122: 6333.

Meshitsuka, S. and Tamaru, K. 1977. Spectral distributions of photo-electrochemical reactions over metal phthalocyanine electrodes. *J. Soc. Chem., Faraday Trans. 1* 73: 760.

Meunier, B. 1992. Metalloporphyrins as versatile catalysts for oxidation reactions and oxidative DNA cleavage. *Chem. Rev.* 92: 1411.

Milanesio, M. E., Alvarez, M. G., Bertolotti, S. G. et al. 2008. Photophysical characterization and photodynamic activity of metallo 5-(4-(trimethylammonium)phenyl)-10,15,20-tris(2,4,6-trimethoxyphenyl)porphyrin in homogeneous and biomimetic media. *Photochem. Photobiol. Sci.* 7: 963.

Min, D. B. and Boff, J. M. 2002. Chemistry and reaction of singlet oxygen in foods. *Compr. Rev. Food Sci. Food Saf.* 1: 58.

Mir, Y., van Lier, J. E., Paquette, B. et al. 2008. Oxygen dependence of two-photon activation of zinc and copper phthalocyanine tetrasulfonate in Jurkat cells. *Photochem. Photobiol.* 84: 1182.

Mitzel, F., FitzGerald, S., Beeby, A. et al. 2003. Acetylenic quinoxalinoporphyrazines as photosensitizers for photodynamic therapy. *Chem. Eur. J.* 9: 1233.

Mohamed, R. M. and Mohamed, M. M. 2008. Copper(II) phthalocyanines immobilized on alumina and encapsulated inside zeolite-X and their applications in photocatalytic degradation of cyanide: A comparative study. *Appl. Catalysis A: Gen.* 340: 16.

Monnereau, C., Gomez, J., Blart, E. et al. 2005. Photoinduced electron transfer in platinum(II) terpyridinyl acetylide complexes connected to a porphyrin unit. *Inorg. Chem.* 44: 4806.

Monteiro, C. J. P., Pereira, M. M., Azenha, M. E. et al. 2005. A comparative study of water soluble 5,10,15,20-tetrakis(2,6-dichloro-3-sulfophenyl)porphyrin and its metal complexes as efficient sensitizers for photodegradation of phenols. *Photochem. Photobiol. Sci.* 4: 617.

Montforts, F. P., Vlassiouk, I., Smirnov, S. et al. 2003. Long-lived photoinduced charge transfer state of synthetically affable porphyrin-fullerene dyads. *J. Porphyrins Phthalocyanines* 7: 651.

Mozer, A. J., Griffith, M. J., Tsekouras, G. et al. 2009. Zn-Zn porphyrin dimer-sensitized solar cells: Toward 3-D light harvesting. *J. Am. Chem. Soc.* 131: 15621.

Muraok, T., Kinbara1, K., and Aida, T. 2006. Mechanical twisting of a guest by a photoresponsive host. *Nature* 440: 512.

Murov, S., Carmichael, I., and Hug, G. 1993. *Handbook of Photochemistry*, Marcel Dekker Inc., New York.

Naito, K. and Miura, A. 1993. Photogenerated charge storage in hetero-Langmuir-Blodgett films. *J. Am. Chem. Soc.* 115: 5185.

Nakano, A., Osuka, A., Yamazaki, T. et al. 2001. Modified windmill porphyrin arrays: Coupled light-harvesting and charge separation, conformational relaxation in the S1 state, and S2–S2 energy transfer. *Chem. Eur. J.* 7: 3134.

Nierengarten, J. F., Eckert, J. F., Felder, D. et al. 2000. Synthesis and electronic properties of donor-linked fullerenes towards photochemical molecular devices. *Carbon* 38: 1587.

Nitzan, A. and Ratner, M. A. 2003. Electron transport in molecular wire junctions. *Science* 300: 1384.

Nyman, E. S. and Hynninen, P. H. 2004. Research advances in the use of tetrapyrrolic photosensitizers for photodynamic therapy. *J. Photochem. Photobiol. B: Biol.* 73: 1.

Nyokong, T. and Isago, H. 2004. The renaissance in optical spectroscopy of phthalocyanines and other tetraazaporphyrins. *J. Porphyrins Phthalocyanines* 8: 1083.

Ochsner, M. 1996. Light scattering of human skin: A comparison between zinc (II)-phthalocyanine and photofrin II. *J. Photochem. Photobiol. B: Biol.* 32: 3.

O'Connor, A. E., Gallagher, W. M., and Byrne, A. T. 2009. Porphyrin and nonporphyrin photosensitizers in oncology: Preclinical and clinical advances in photodynamic therapy. *Photochem. Photobiol.* 85: 1053.

Ohtani, H., Kobayashi, T., Ono, T. et al. 1984. Nanosecond spectroscopy on the mechanism of the reduction of methylviologen sensitized by metallophthalocyanine. *J. Phys. Chem.* 88: 4431.

Okada, Y. 1992. Oxidative and reductive fading of monochlorotriazinyl reactive dyes on cellulose under wet conditions. *Dyes Pigments* 19: 203.

Okada, Y., Hirose, M., and Kato, T. 1990a. Photofading of vinylsulfonyl reactive dyes on cellulose under wet conditions. *Dyes Pigments* 14: 113.

Okada, Y., Hirose, M., and Kato, T. 1990b. Fading of vinylsulfonyl reactive dyes on cellulose in admixture under wet conditions. *Dyes Pigments* 14: 265.

Osada, Y. and Mizumoto, A. 1986. Preparation and electrical-properties of polymeric copper phthalocyanine thin-films by plasma polymerization. *J. Appl. Phys.* 59: 1776.

Osugi, M. E., Umbuzeiro, G. A., De Castro, F. J. V. et al. 2006. Photoelectrocatalytic oxidation of remazol turquoise blue and toxicological assessment of its oxidation products. *J. Hazard. Mater. B* 137: 871.

Osuka, A., Kobayashi, F., Maruyama, K. et al. 1993a. Geometry- and solvent-polarity-dependent photoinduced electron transfer in conformationally restricted magnesium-free-base hybrid diporphyrins. *Chem. Phys. Lett.* 201: 223.

Osuka, A., Marumo, S., Maruyama, K. et al. 1994b. Picosecond excited-state dynamics of fixed-distance triads consisting of metalloporphyrin, doubly strapped metal-free porphyrin, and pyromellitimide. *Chem. Phys. Lett.* 225: 140.

Osuka, A., Marumo, S., Taniguchi, S. et al. 1994a. Electron transfer over two porphyrins in linear porphyrin arrays. *Chem. Phys. Lett.* 230: 144.

Osuka, A., Nakajima, S., Maruyama, K. et al. 1993b. 1,2-Phenylene-bridged diporphyrin linked with porphyrin monomer and pyromellitimide as a model for a photosynthetic reaction center: Synthesis and photoinduced charge separation. *J. Am. Chem. Soc.* 115: 4577.

Ough, E., Gasyna, Z., and Stillman, M. J. 1991. Photochemical, electrochemical, and chemical formation of the π-cation-radical species of magnesium phthalocyanine. Analysis of the absorption and MCD spectra of [MgPc(-1)].bul.+. *Inorg. Chem.* 30: 2301.

Pascard, C., Guilhem, J., Chardon-Noblat, S. et al. 1993. Molecular structure of an oblique bis-zinc porphyrin 1,10-phenanthroline. Model of a fragment of the photosynthetic reaction center. *New J. Chem.* 17: 331.

Pavani, C., Uchoa, A. F., Oliveira, C. S. et al. 2009. Effect of zinc insertion and hydrophobicity on the membrane interactions and PDT activity of porphyrin photosensitizers. *Photochem. Photobiol. Sci.* 8: 233.

Peled, A., Dror, Y., Baal-Zedaka, I. et al. 2000. Photobleaching and photodeposition in a chlorophyll based solution. *Syn. Metals* 115: 167.

Peng, X., Aratani, N., Takagi, A. et al. 2004. A dodecameric porphyrin wheel. *J. Am. Chem. Soc.* 126: 4468.

Petersson, J., Eklund, M., Davidsson, J. et al. 2009. Variation of excitation energy influences the product distribution of a two-step electron transfer: S2 vs. S1 electron transfer in a Zn(II) porphyrin-viologen complex. *J. Am. Chem. Soc.* 131: 7940.

Prathapan, S., Yang, S. I., Seth, J. et al. 2001. Synthesis and excited-state photodynamics of perylene-porphyrin dyads. 1. Parallel energy and charge transfer via a diphenylethyne linker. *J. Phys. Chem. B* 105: 8237.

Rabinowitch, E. and Weiss, J. 1936. Reversible oxidation and reduction of chlorophyll. *Nature* 138: 1098.

Rabinowitch, E. and Weiss, J. 1937. Reversible oxidation of chlorophyll. *Proc. Roy. Soc. (London) A1* 62: 251.

Radhakrishnan, S. and Deshpande, S. D. 2001. Electrical properties of conducting polypyrrole films functionalized with phthalocyanine. *Mater. Lett.* 48: 144.

Raghavendra, A. S. 1998. *Photosynthesis*, Cambridge University Press, Cambridge, U.K.

Reddy, P. A. N., Nethaji, M., and Chakravarthy, A. R. 2004. Hydrolytic cleavage of DNA by ternary amino acid Schiff base copper(II) complexes having planar heterocyclic ligands. *Eur. J. Inorg. Chem.* 7: 1440.

Rosche, K., Decker, C., Israel, G. et al. 1997. Pigment polymer layers sensitizers for the photopolymerization of trimethylolpropane triacrylate. *Eur. Polym. J.* 33: 849.

Rosenthal, I. 1993. Phthalocyanines as photodynamic sensitizers. *Photochem. Photobiol.* 53: 859.

Sánchez, E. I., Calderón, M., and Gutiérrez, M. I. 2004. Synthesis of a new polymer containing Rose Bengal. *Polym. Bull.* 51: 271.

Saron, C., Zulli, F., Giordano, M. et al. 2006. Influence of copper-phthalocyanine on the photodegradation of polycarbonate. *Polym. Degrad. Stab.* 91: 3301.

Scheer, H. 1991. Structure and occurrence of chlorophylls. In *Chlorophylls*, (ed.) H. Scheer, pp. 3–30, CRC Press, Boca Raton, FL.

Scheer, H. and Hartwich, G. 1995. Bacterial reaction centers with modified tetrapyrrole chromatophores. In *Anoxygenic Photosynthetic Bacteria*, (eds.) R. E. Blankenship, M. T. Madigan, and C. E. Bauer, pp. 649–663, Kluwer Academic Publishers, Dordrecht, the Netherlands.

Scheer, H. and Katz, J. J. 1974. Structure of the Krasnovskii photoreduction product of chlorophyll a. *Proc. Natl. Acad. Sci. USA* 71: 1626.

Schlundt, S., Kuzmanich, G., Spaenig, F. et al. 2009. Dendritic porphyrin-fullerene conjugates: Efficient light-harvesting and charge-transfer events. *Chem. Eur. J.* 15: 12223.

Schuster, D. I., Li, K., and Guldi, D. M. 2004. Novel porphyrin-fullerene assemblies: From rotaxanes to catenanes. *Org. Lett.* 6: 1919.

Schuster, D. I., Li, K., Guldi, D. M. et al. 2007. Azobenzene-linked porphyrin-fullerene dyads. *J. Am. Chem. Soc.* 129: 15973.

Segalla, A., Borsarelli, C. D., Braslavsky, S. E. et al. 2002. Photophysical, photochemical and antibacterial photosensitizing properties of a novel octacationic Zn(II)-phthalocyanine. *Photochem. Photobiol. Sci.* 1: 641.

Selman, S. H., Hampton, J. A., Morgan, A. R. et al. 1993. Copper benzochlorin, a novel photosensitizer for photodynamic therapy: Effects on a transplantable urothelial tumor. *Photochem. Photobiol.* 57: 681.

Senge, M. O. 1992a. Structure and biosynthesis of bacteriochlorophylls. *Chem. Unserer Zeit* 26: 86.

Senge, M. O. 1992b. The conformational flexibility of tetrapyrroles—Current model studies and photobiological relevance. *J. Photochem. Photobiol. B: Biol.* 16: 3.

Senge, M. O., Hatscher, S., Ökten, Z. et al. 2003. Synthetic potential and limitations of *o*-quinones as acceptor groups in electron transfer compounds. *Tetrahedron Lett.* 44: 4463.

Senge, M. O. and Richter, J. 2006. Adding color to green chemistry? An overview of the fundamentals and potential of chlorophylls. In *Biorefineries-Industrial Processes and Products*, (eds). B. Kamm, P. R. Gruber, and M. Kamm, pp. 325–343, Vol. 2, Wiley-VCH, Weinheim, Germany.

Senge, M. O., Rößler, B., von Gersdorff, J. et al. 2004. The meso-β-linkage as structural motif in porphyrin-based donor-acceptor compounds. *Tetrahedron Lett.* 45: 3363.

Senge, M. O. and Sergeeva, N. N. 2006. Photochemical transformations involving zinc porphyrins and phthalocyanines. In *The Chemistry of Organozinc Compounds*, (eds.) Z. Rappoport and I. Marek, pp. 395–419, Wiley, Chichester, U.K.

Senge, M. O., Wiehe, A., and Ryppa, C. 2006. Synthesis, reactivity and structure of chlorophylls. In *Chlorophylls and Bacteriochlorophylls*, (eds.) B. Grimm, R. J. Porra, W. Rüdiger, and H. Scheer, pp. 27–37, Springer, Dordrecht, the Netherlands.

Sergeeva, N. N. and Senge, M. O. 2008. Photochemical transformations involving magnesium porphyrins and phthalocyanines. In *The Chemistry of Organomagnesium Compounds*, (eds.) Z. Rappoport and I. Marek, pp. 189–218, Wiley, Chichester, U.K.

Sergeeva, N. N. and Senge, M. O. 2010. Photochemical transformations involving copper porphyrins and phthalocyanines. In *The Chemistry of Organocopper Compounds*, (eds.) Z. Rappoport and I. Marek, pp. 217–245, Wiley, Chichester, U.K.

Serpone, N., Ledon, H., and Netzel, T. 1984. Excited-state spectra and lifetimes for oxomethoxomolybdenum(V) tetraphenylporphine: a comparison of d1 and d9 metalloporphyrin photophysics. *Inorg. Chem.* 23: 454.

Shang, J., Chai, M., and Zhu, Y. 2003. Photocatalytic degradation of polystyrene plastic under fluorescent light. *Environ. Sci. Technol.* 37: 4494.

Shiragami, T., Matsumoto, J., Inoue, H. et al. 2005. Antimony porphyrin complexes as visible-light driven photocatalysts. *J. Photochem. Photobiol. C: Photochem. Rev.* 6: 227.

Shu, H. Y. and Chang, M. C. 2005. Decolorization and mineralization of a phthalocyanine dye C.I. Direct Blue 199 using UV/H_2O_2 process. *J. Hazard. Mater. B* 125: 96.

Shultz, D. A., Lee, H., Kumar, K. et al. 1999. Cross-conjugated bis(porphyrin)s: Synthesis, electrochemical behavior, mixed valency, and biradical dication formation. *J. Org. Chem.* 64: 9124.

Silva, E., Pereira, M. M., Burrows, H. D. et al. 2004. Photooxidation of 4-chlorophenol sensitised by iron *meso*-tetrakis(2,6-dichloro-3-sulfophenyl)porphyrin in aqueous solution. *Photochem. Photobiol. Sci.* 3: 200.

Slota, R. and Dyrda, G. 2003. UV photostability of metal phthalocyanines in organic solvents. *Inorg. Chem.* 42: 5743.

Smalley, J. F., Feldberg, S. W., and Brunschwlg, B. S. 1983. Mechanism of porphyrin ion production from the triplet state of magnesium octaethylporphyrin. *J. Phys. Chem.* 87: 1757.

Smith, K. M., Brown, S. B., Troxler, S. B. et al. 1980. Mechanism of photooxygenation of meso-tetraphenylporphyrin metal complexes. *Tetrahedron Lett.* 21: 2763.

Smith, B. E. and Gouterman, M. 1968. Quartet luminescence from copper porphyrins. *Chem. Phys. Lett.* 2: 517.

Smith, A. L. and Nicolaou, K. C. 1996. The enediyne antibiotics. *J. Med. Chem.* 39: 2103.

Smolenyak, P., Peterson, R., Nebesny, K. et al. 1999. Highly ordered thin films of octasubstituted phthalocyanines. *J. Am. Chem. Soc.* 121: 8628.

Speck, M., Kurreck, H., and Senge, M. O. 2000. Porphyrin-*o*-quinones as model systems for electron transfer and catecholase reactions. *Eur. J. Org. Chem.* 2000: 2303.

Speck, M., Niethammer, D., and Senge, M. O. 2002. Isomeric porphyrin phenanthrenequinones: Synthesis, NMR spectroscopy, electrochemical properties, and in situ EPR/ENDOR studies of the *o*-semiquinone anion radicals. *J. Chem. Soc. Perkin Trans. 2*: 455.

Speck, M., Senge, M. O., Schäfer, A. et al. 1997. Novel oxidation reactions of sterically demanding 3,6-di-*tert*-butyl porphyrin-*o*-quinones to mucconic anhydride derivatives. *Bioorg. Med. Chem. Lett.* 7: 2589.

Spikes, J. D. and Bommer, J. C. 1991. Chlorophyll and related pigments as photosensitizers in biology and medicine. In *Chlorophylls*, (ed.) H. Scheer, pp. 1181–1204, CRC Press, Boca Raton, FL.

Spikes, J. D., van Lier, J. E., and Bommer, J. C. 1995. A comparison of the photoproperties of zinc phthalocyanine and zinc naphthalocyanine tetrasulfonates: Model sensitizers for the photodynamic therapy of tumors. *J. Photochem. Photobiol. A: Chem.* 91: 193.

Steenkeste, K., Tfibel, F., Perree-Fauvet, M. et al. 2010. Tracking the photosensitizing antibacterial activity of mono(acridyl)bis(arginyl)porphyrin (mabap) by time-resolved spectroscopy. *J. Phys. Chem. A* 114: 3334.

Stephanopoulos, N., Carrico, Z. M., and Francis, M. B. 2009. Nanoscale integration of sensitizing chromophores and porphyrins with bacteriophage ms2. *Angew. Chem. Int. Ed.* 48: 9498.

Stiel, H., Teuchner, K., Paul, A. et al. 1994. Two-photon excitation of alkyl-substituted magnesium phthalocyanine: radical formation via higher excited states. *J. Photochem. Photobiol. A: Chem.* 80: 289.

Sun, A., Zhang, G., and Xu, Y. 2005. Photobleaching of metal phthalocyanine sulfonates under UV and visible light irradiation over TiO_2 semiconductor. *Mater. Lett.* 59: 4016.

Szulbinski, W. S. 1995. A spectroelectrochemical and photochemical investigation of photoinduced electron transfer reaction between Mg(II) porphyrin and viologen. *Inorg. Chim. Acta* 228: 243.

Takagi, S., Eguchi, M., Tryk, D. A., and Inoue, H. 2006. Porphyrin photochemistry in inorganic/organic hybrid materials: Clays, layered semiconductors, nanotubes, and mesoporous materials. *J. Photochem. Photobiol. C: Photochem. Rev.* 7: 104.

Takai, A., Chkounda, M., Eggenspiller, A. et al. 2010. Efficient photoinduced electron transfer in a porphyrin tripod-fullerene supramolecular complex via π–π interactions in nonpolar media. *J. Am. Chem. Soc.* 132: 4477.

Thomas, J. L. and Allen, N. S. 2002. The degradation of dyed cotton fabrics by the sensitized production of singlet oxygen via an aqueous soluble phthalocyanine dye. *Dyes Pigments* 53: 195.

Tomizaki, K., Loewe, R. S., Kirmaier, C. et al. 2002. Synthesis and photophysical properties of light-harvesting arrays comprised of a porphyrin bearing multiple perylene-monoimide accessory pigments. *J. Org. Chem.* 67: 6519.

Tomizaki, K., Yu, L., Wei, L. et al. 2003. Synthesis of cyclic hexameric porphyrin arrays. Anchors for surface immobilization and columnar self-assembly. *J. Org. Chem.* 68: 8199.

Tran-Thi, T. H., Lipskier, J. F., Houde, D. et al. 1992. Subpicosecond excitation of strongly coupled porphyrin-phthalocyanine mixed dimmers. *J. Chem. Soc., Faraday Trans.* 88: 2129.

Troxler, R. F., Smith, K. M., and Brown, S. B. 1980. Mechanism of photooxidation of bacteriochlorophyll-C derivatives. *Tetrahedron Lett.* 21: 491.

Tunuli, S. and Fendler, J. H. 1981. Aspects of artificial photosynthesis. Photosensitized electron transfer across bilayers, charge separation, and hydrogen production in anionic surfactant vesicles. *J. Am. Chem. Soc.* 103: 2507.

Uchida, K., Soma, M., Onishi, T. et al. 1977. The effect of phthalocyanines added to zinc oxide on the photocatalytic oxidation of isopropyl alcohol. *Z. Phys. Chem.* 106: 317.

Valduga, G., Nonell, S., Reddi, E. et al. 1988. The production of singlet molecular oxygen by zinc(II) phthalocyanine in ethanol and in unilamellar vesicles. Chemical quenching and phosphorescence studies. *Photochem. Photobiol.* 48: 1.

van Dijk, N., Noort, M., and van der Waals, J. H. 1981. Zeeman spectroscopy of the $^4E_u \rightarrow {}^2B_{1g}$ phosphorescence of copper porphine in an n-alkane single crystal. II. The intensity problem. *Mol. Phys.* 44: 913.

van Grondelle, R. and Novoderezhkin, V. I. 2006. Energy transfer in photosynthesis: Experimental insights and quantitative models. *Phys. Chem. Chem. Phys.* 8: 793.

van Willigen, H. and Ebersole, M. H. 1987. ESR and ENDOR study of the photooxidation of magnesium and zinc tetrakis(4-sulfonatophenyl)porphyrins. *J. Am. Chem. Soc.* 109: 2299.

Verma, S., Srivatsan, S. G., and Madhavaiah, C. 2004. Copper containing nuclease mimics: Synthetic models and biochemical applications. *Nucleic Acids Mol. Biol.* 13: 129.

Wakao, N., Hiraishi, A., Shimada, K. et al. 1999. Discovery, characteristics and distribution of zinc-BChl in aerobic acidophilic bacteria including *Acidiphilium* species and other related acidophilic bacteria. In *The Phototrophic Prokaryotes*, (ed.) G. A. Peschek, pp. 745–753, Kluwer Academic/Plenum Publishers, New York.

Wakao, N., Shiba, T., Hiraishi, A. et al. 1993. Distribution of bacteriochlorophyll a in species of the genus Acidiphilium. *Curr. Microbiol.* 27: 277.

Wakao, N., Yokoi, N., Isoyama, N. et al. 1996. Discovery of natural photosynthesis using Zn-containing bacteriochlorophyll in an aerobic bacterium *Acidiphilium rubrum*. *Plant Cell Physiol.* 37: 889.

Wang, Y., Chen, H. Z., Li, H. Y. et al. 2005. Fabrication of carbon nanotubes/copper phthalocyanine composites with improved compatibility. *Mater. Sci. Eng. B* 117: 296.

Wang, C., Li, J., Mele, G. et al. 2007. Efficient degradation of 4-nitrophenol by using functionalized porphyrin-TiO_2 photocatalysts under visible irradiation. *Appl. Catal. B* 76: 218.

Wasielewski, M. R. 1992. Photoinduced electron transfer in supramolecular systems for artificial photosynthesis. *Chem. Rev.* 92: 435.

Wasielewski, M. R. and Niemczyk, M. P. 1984. Photoinduced electron transfer in *meso*-triphenyltriptycenylporphyrinquinones. *J. Am. Chem. Soc.* 106: 5043.

Watanabe, N., Kihara, N., Furusho, Y. et al. 2003. Photoinduced intrarotaxane electron transfer between zinc porphyrin and [60]fullerene in benzonitrile. *Angew. Chem. Int. Ed.* 42: 681.

Weitman, H., Schatz, S., Gottlieb, H. E. et al. 2001. Spectroscopic probing of the acid-base properties and photosensitization of a fluorinated phthalocyanine in organic solutions and liposomes. *Photochem. Photobiol.* 73: 473.

Wiehe, A., Shaker, Y. M., Brandt, J. C. et al. 2005. Lead structures for applications in photodynamic therapy. Part 1: Synthesis and variation of *m*-THPC (Temoporfin) related amphiphilic A_2BC-type porphyrins. *Tetrahedron* 61: 5535.

Wilson, S. R., MacMahon, S., Tat, F. T. et al. 2004. A new fullerene complexation ligand: N-pyridylfulleropyrrolidine. *J. Org. Chem.* 69: 4602.

Xu, M. S., Xu, J. B., Wang, M., and Que, D. L. 2002. Optical and xerographic properties of phthalocyanine co-deposited composite film and ultrathin multilayered structure. *J. Appl. Phys.* 91: 748.

Yagi, S., Ezoe, M., Yonekura, I. et al. 2003. Diarylurea-linked zinc porphyrin dimer as a dual-mode artificial receptor: Supramolecular control of complexation-facilitated photoinduced electron transfer. *J. Am. Chem. Soc.* 125: 4068.

Yamada, S., Kuwata, K., Yonemura, H. et al. 1995. Second-order nonlinear optical properties of amphiphilic porphyrins in Langmuir-Blodgett monolayer assemblies. *J. Photochem. Photobiol. A: Chem.* 87: 115.

Yamada, S., Sata, T., Kano, K. et al. 1983. Fluorescence quenching of 5,10,15,20-tetra(p-tolyl)porphine and its zinc complex by quinones. Charge-transfer interaction and transient effect. *Photochem. Photobiol.* 37: 257.

Yamaguchi, T., Ishii, N., Tashiro, K. et al. 2003. Supramolecular peapods composed of a metalloporphyrin nanotube and fullerenes. *J. Am. Chem. Soc.* 125: 13934.

Yamanouchi, H. and Saji, T. 1996. Formation of organic pigment films by photochemical reduction of surfactants containing an azobenzene group. *Chem. Lett.* 7: 531.

Yamashita, K., Harima, Y., and Matsubayashi, T. 1989. Conductance control of porphyrin solids by molecular design and doping. *J. Phys. Chem.* 93: 5311.

Yanagi, H., Tsukatani, K., Yamaguchi, H. et al. 1993. Semiconducting behavior of substituted tetra-azaporphyrin thin-films in photoelectrochemical cells. *J. Electrochem. Soc.* 140: 1942.

Yang, S. I., Lammi, R. K., Prathapan, S. et al. 2001b. Synthesis and excited-state photodynamics of perylene-porphyrin dyads Part 3. Effects of perylene, linker, and connectivity on ultrafast energy transfer. *J. Mater. Chem.* 11: 2420.

Yang, S. I. S., Prathapan, M. A., Miller, J. et al. 2001a. Synthesis and excited-state photodynamics in perylene-porphyrin dyads 2. Effects of porphyrin metalation state on the energy-transfer, charge-transfer, and deactivation channels. *J. Phys. Chem. B* 105: 8249.

Yarnaguchi, H., Fujiwara, R., and Kusuda, K. 1986. Water-soluble substituted polystyrene with pendant tetrametal 2,9,16,23-phthalocyaninetetracarboxylate metal complexes, sensitizing the reduction of 1,1′-dimethyl-4,4′-bipyridinium dichloride. *Chem. Rapid Commun.* 7: 225.

You, C. C. and Würthner, F. 2004. Porphyrin-perylene bisimide dyads and triads: Synthesis and optical and coordination properties. *Org. Lett.* 6: 2401.

Youngblood, W. J., Gryko, D. T., Lammi, R. K. et al. 2002. Glaser-mediated synthesis and photophysical characterization of diphenylbutadiyne-linked porphyrin dyads. *J. Org. Chem.* 67: 2111.

Yu, L. and Lindsey, J. S. 2001. Rational syntheses of cyclic hexameric porphyrin arrays for studies of self-assembling light-harvesting systems. *J. Org. Chem.* 66: 7402.

Yu, J. C., Xie, Y., Tang, H. Y. et al. 2003. Visible light-assisted bactericidal effect of metalphthalocyanine-sensitized titanium dioxide films. *J. Photochem. Photobiol. A: Chem.* 156: 235.

Zakrzewski, J. and Giannotti, C. 1995. Photoreduction of metallophthalocyanines and phthalocyanine-sensitized photoreduction of methylviologen in the presence of azaferrocene. *Inorg. Chim. Acta* 232: 63.

Zaleski, J. M., Wu, W., Chang, C. K. et al. 1993. Dynamic solvent effects in inverted region electron transfer. *Chem. Phys.* 176: 483.

Zangmeister, R. A. P., Smolenyak, P. E., Drager, A. S. et al. 2001. Transfer of rodlike aggregate phthalocyanines to hydrophobized gold and silicon surfaces: Effect of phenyl-terminated surface modifiers on thin film transfer efficiency and molecular orientation. *Langmuir* 17: 7071.

Zhang, B., Mu, J., and Wang, D. 2005. Self-assembly and surface photovoltage response of ZnS nanoparticulate films sensitized by tetrasulfonated copper phthalocyanine. *J. Dispers. Sci. Tech.* 26: 521.

Zhang, H., Schmidt, E., Wu, W. et al. 1995. Picosecond time-resolved resonance Raman spectroscopy of the charge separated state of Mg-free base diporphyrins. *Chem. Phys. Lett.* 234: 133.

Zhang, X. F. and Xu, H. J. 1994. Mechanism of photosensitized oxidation of tyrosine by gallium or zinc phthalocyanine in homogeneous and aqueous micellar media. *J. Photochem. Photobiol. B: Biol.* 24: 109.

35

Photochemical Routes for Metal Nanoparticle Synthesis

Katherine L. McGilvray
University of Ottawa

J.C. Scaiano
University of Ottawa

35.1 Introduction

The synthesis of metal nanomaterials has received considerable attention in the past few decades owing to the enhancement of chemical, catalytic, and optical properties of the metal upon approaching dimensions on the order of the Bohr radius.[1] Several photochemical routes have been established for the synthesis of colloidal nanoparticles, where selection of reducing agent, stabilizing agents, and irradiation conditions all play a role in particle yield. This chapter will review different photochemical methodologies for particle generation as well as highlight their applications.

One major application of metal nanoparticles is their use as a sensor through exploitation of their enhanced optical properties, and this enhancement is characteristic of noble metals. Noble metal nanoparticles in particular possess strong collective oscillations of surface electrons in the conduction band, whose resonating frequency absorbs strongly in the visible spectrum. These characteristic special features are referred to as a metal's surface plasmon resonance band (SPB).[2] The frequency of oscillations is a function of the metal, particle size, shape, and interparticle distance, as well as the temperature, dielectric constant,

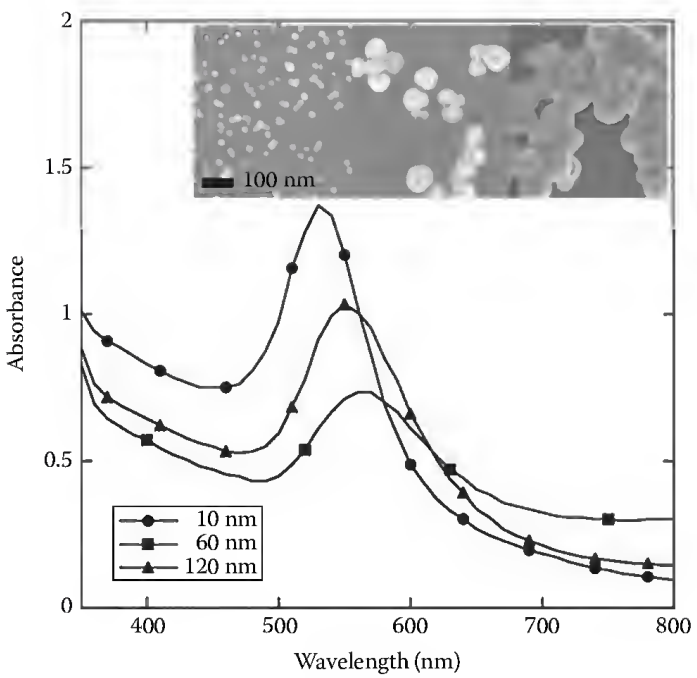

FIGURE 35.1 UV-Vis absorbance of gold nanoparticles of variable diameter displaying their SPBs, along with their corresponding SEM image in the inset.

and viscosity of the medium. As particle size increases or as interparticle distance decreases, the resonance energy decreases and results in a redshift of absorbance maximum (Figure 35.1).

Gustav Mie investigated the photophysics of metal colloids in depth, where the sizes of spherical particles could be deduced from the position of a translational dipole.[3] Additionally, oblong, prismatic, or elongated particles could be characterized by a longitudinal plasmon dipole where the position of the resonance dipole corresponds to oscillations of electrons along the major axis and depends on their aspect ratio.

35.2 Particle Growth

As the optical, electric, and catalytic properties are principally dependent on particle size and shape, great focus has been executed to determine mechanisms for particle growth and to establish optimal methods for the synthesis of small and monodisperse colloidal metal particles. Nanoparticles can be formed by a top-down approach via laser ablation[4] or other destructive high-energy techniques, as well as the more common bottom-up wet chemical approach via self-assembly. In the latter case, metal ions are reduced to their atomic state at which nucleation of clusters can ensue.[2,5] Nucleation occurs when a thermodynamically unstable saturated solution possesses a positive free energy change, where this change represents the driving force for the formation of a new volume and free energy relating to its surface. Above a critical radius, the free energy of this volume diminishes, allowing atoms to stabilize through agglomeration. Nucleation can continue via collisions and lead to particle growth until thermodynamic stability is attained by adsorption of ligands or solvent molecules. Slower nucleation can also ensue in an autocatalytic growth mechanism, in which metal ions are reduced on the surface of growing clusters. Both mechanisms are outlined in Scheme 35.1.

Small particles grow quickly due to their high surface energy, which decreases with growth until a narrowed and homogeneous population of particles is produced. Herein, nucleation and growth are well separated; and small, monodisperse, crystalline particles are prepared.[6] Particle growth also occurs via molecular addition where nuclei deposit on the surfaces of growing clusters followed by coalescence.[2] Size broadening, also referred to as Oswald ripening, can occur where larger particles

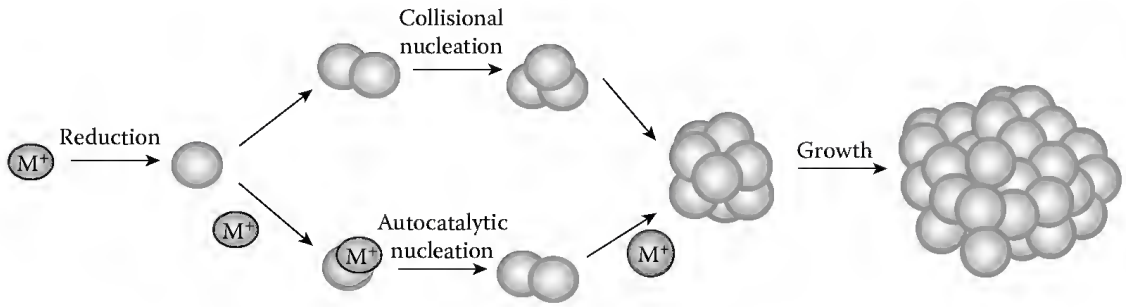

SCHEME 35.1 Nucleation pathways toward nanoparticle growth.

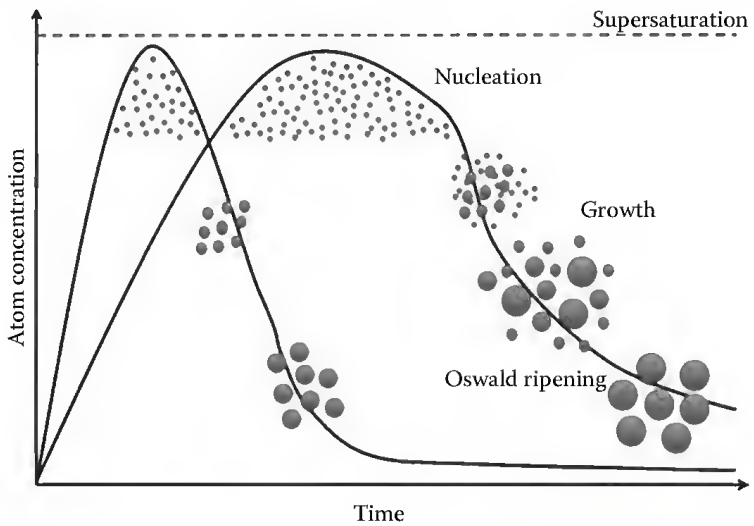

SCHEME 35.2 Particle growth pathways. (Redrawn from a web source: http://www.icmm.csic.es/gsc/sol.htm.)

continue to grow while smaller ones dissolve and the critical nuclei radius increases thus resulting in polydisperse or ultimately larger particles (Scheme 35.2).[2,5]

As surface energy decreases with particle growth, remaining metal ions are reduced to generate new nuclei, resulting in an overlap of nucleation and growth processes at the same time. This results in the formation of polydisperse and polycrystalline, multi-twinned particles with a tendency to coalesce. Control of particle growth can be attained with surface stabilization; achieved through ligand attachment of self-assembled monolayers, polymer, dendrimer, surfactant, oligonucleotides, amino acids, and other small biomolecules, films, glass, or other solid supports.[7,8] Essentially, the more the stabilizer present during the synthetic steps, the smaller the resulting particle.

35.3 Photochemical Preparation of Nanoparticles

Photochemical methods to generating nanoparticles offer several advantages over traditional thermal methods. These include cleaner synthesis with fewer byproducts, lower temperatures, often less overall energy to drive the reaction, as well as spatiotemporal control over reduction rates and sites. Additionally, nanomaterials can benefit from reduction in a variety of different media, including aqueous and organic environments, polymers, micelles, films, semiconductor surfaces, and biological systems.

There are several ways to reduce metal ions to atomic metals, and many ways to achieve this goal using photochemistry. From a wet chemical perspective, nanoparticles can be synthesized from a metal salt and a reducing agent. Several photochemical pathways exist for reduction of a metal from an excited state.

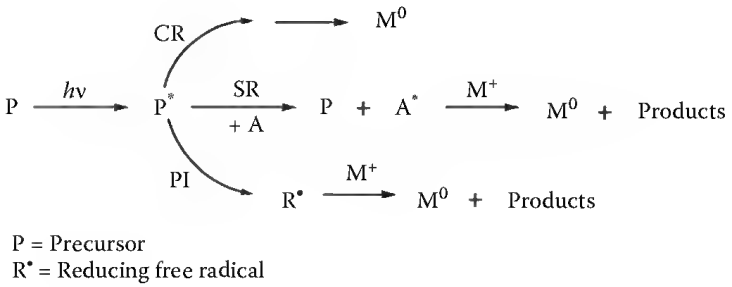

SCHEME 35.3 Photochemical pathways for reductions of metal salts. Photoinduced CR, SR, and PI reduction.

In some cases, the light-driven chemistry can be the result of excitation and reduction of a chromophore at the metal salt complex itself, as illustrated in the complex reduction (CR) pathway of Scheme 35.3. This was the case for the formation of copper nanoparticles (CuNP) from the 254 nm photolysis of $Cu(acac)_2$ in ethanol or polyvinylpyrrolidone (PVP),[9] or the formation of gold nanoparticle (AuNP) from photolysis of (*p*-tosyl)$CH_2NCAuCl$ or Au(CO)Cl, where the latter reduction was attributed to π-acceptance ability of the ligands toward photochemical reactivity.[10] In another approach, a photochemical polythiol process was devised by Warren et al. by using the strong reduction potentials of metal thiolates complexes to form bismuth, copper, lead, and antimony nanoparticles upon photolysis.[11] Nanoparticles can also be prepared via a sensitized reduction (SR) approach, where an excited state of one reagent transfers energy to an acceptor molecule (which then acts as a reducing agent), through proposed energy transfer for electron transfer mechanisms. Highlights of this approach will be addressed later in this chapter.

Additionally, nanoparticles can be formed from the photolysis of photoinitiators (PIs), outlined in the PI pathway in Scheme 35.3. This chapter deals largely with this case, where we present a series of strategies and methods for photochemical synthesis of metal nanoparticles mediated by reductive free radicals derived from PIs. PIs are molecules that tend to have high absorbance in the 250–450 nm range, whose excited states form reactive intermediates such as free radicals. PIs can be described in two categories: those formed by intramolecular bond cleavage (PI_1) through a unimolecular reaction, and those undergoing intermolecular hydrogen abstraction (PI_2) following bimolecular kinetics. Beyond well-established examples, there are numerous literature reports where metal reduction can be traced back to radical-mediated processes. This is something that we illustrate in some of our examples; however, no attempt has been made to be exhaustive and without a doubt, other such examples could be identified in the literature.

In designing a photochemical method using radical-mediated PIs, one must select a reducing intermediate based on energetics and thus reduction potential, stability, excited state lifetime, reactivity, and solubility. Additionally, the photochemistry required to create these reactive species is also worth considering. Utilizing chromophores with large extinction coefficients at the wavelength of absorption, while avoiding any screening by other absorbers such as metal salts or stabilizers, is paramount to efficient nanoparticle production. PI-mediated particle synthesis can be separated into two strategies based on reducing radical generation; a photorelease mechanism via homolytic cleavage (PI_1) as well as a hydrogen abstraction mechanism (PI_2), as described in the following sections.

35.4 Part I: PI_1—Photoinduced Nanoparticle Synthesis via Unimolecular Cleavage

Photochemical generation of metal nanoparticles can occur through intramolecular bond cleavage to photorelease a reducing agent, normally a free radical. The concentration of reducing agent can be finely tuned along with the rate of its delivery for optimal spatial-temporal control of nanoparticle synthesis. This photochemical control illustrates a major advantage over traditional thermal methods, since the

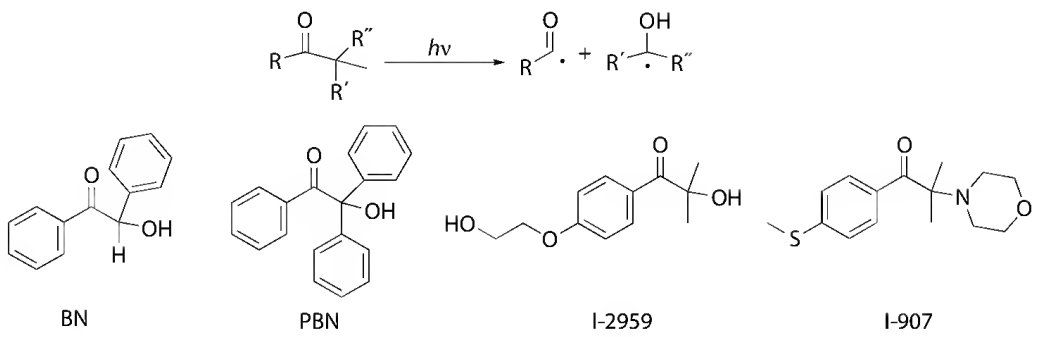

SCHEME 35.4 PI_1 pathway. Intramolecular bond cleavage.

rate of reduction can separate nucleation and growth phenomena throughout nanoparticle growth and thus facilitate the preparation of small and monodisperse nanomaterials.

Significant work with photoreleasing reducing agents has succeeded with a series of benzoins, whose photodissociation is described in Scheme 35.4. Norrish-I α-cleavage generates a benzoyl radical and a ketyl radical, or an α-amino alkyl radical in the case of I-907.[12] The quantum yield for Norrish Type I photodissociation for various α-hydroxy ketones is approximately 0.3 with a excited triplet state lifetime below 100 ns.[13] The short triplet lifetime is a key requirement for successful nanoparticle synthesis, for the excited-state species can escape both quenching from metal salts and oxygen on this timescale.

35.4.1 Nanoparticle Synthesis Mediated by Photorelease of Ketyl Radicals

Initial investigations into applications of PI_1 type photoinitiators toward nanoparticle synthesis relied on unimolecular bond cleavage to yield ketyl radicals. These were reported by Itakura et al. using BN, where UVB photolysis generated the benzoyl and the phenyl hydroxymethyl radical in deaerated ethanol solutions in the presence of metal salts with PVP as a stabilizer to yield uniform nanoparticles within 30 min.[14] Silver nanoparticles (AgNP) were prepared as well from BN with $AgClO_4$ and PVP, where an increase in the ratio of BN:Ag^+ from 1:1 to 10:1 resulted in a decrease in particle size from 17 to 7 nm. They attributed the decrease in size to the stabilization by electron injection by radicals and strong surface repulsion forces. In the same report, CuNP were prepared from $Cu(ClO_4)_2$ at a 5:1 PI: Cu^{2+} concentration ratio to afford 3 nm CuNP. The ketyl radical reduces the cupric state to Cu(I) by a one-electron reduction, where further reduction can take place with another ketyl radical or slow disproportionation of the cuprous species. AuNP were also prepared in the study by a parallel fashion with BN, yet an increase in the ketone resulted in an increase in gold particle size as well as size distribution. The authors proposed the difference with gold occurring at the initial stage of nucleation with chlorine ions, where additional radicals would lead to additional growth. The mechanism for AuNP formation follows a similar series of reduction and disproportionation events outlined in Scheme 35.5, as the unstable Au(II) oxidation state disproportionates instantaneously followed by slow subsequent disproportionation of Au(I) or further reduction in the presence of another radical.

$$AuCl_4^- \xrightarrow{h\nu} AuCl_4^{-*}$$

$$Au^{III}Cl_4^{-*} + RC\dot{O}HR' \longrightarrow Au^{II}Cl_3^- + ROR' + HCl$$

$$2Au^{II}Cl_3^- \longrightarrow Au^{I}Cl_2 + Au^{III}Cl_4^-$$

$$2AuCl_2^- \longrightarrow Au^{II}Cl_3^- + Au^0 + Cl^-$$

$$n\text{Au} \longrightarrow \text{AuNP}$$

SCHEME 35.5 Reduction steps to gold nanoparticles.

Interestingly, in the absence of BN, significant formation of AuNP occurred as a result of the photochemical (reducing) properties of PVP, whereas minimal growth occurred for silver and negligible reduction occurred with copper. The mechanism for photoreduction from PVP remains unclear but has been observed in numerous cases. Bimetallic reductions were also pursued in this study for the combination of Ag/Cu alloys, as well as Ag/Au composites. Further investigations were performed by Esumi et al. to determine nanoparticle properties from BN photoreduction using dendrimers for stabilization.[15] Poly(amidoamine) (PAMAM) and poly(propyleneimine) (PPI) dendrimers of G3–G5 generations were used in the preparation of gold and Ag/Au composites. They found that a greater dendrimer concentration from a larger generation could decrease the size of AuNP down to 9.1 nm for PAMAM G5, and 6.2 nm for PPI G4. The absence of BN neglected to form nanomaterials, yet an increase in BN continued to result in an increase in particle size. The PPI dendrimer nanocomposites formed as a result of BN photolysis remained to be alloy in composition at various PPI:metal molar ratios and different dendrimer generations.

Further work on BN came from Kotenani et al. who identified the α-hydroxybenzyl radical as the reducing agent over that of the benzoyl radical through transient studies in the preparation of AgNP in PVP.[16] No AgNP were prepared upon 355 nm laser flash photolysis (LFP) of benzil in the absence of a hydrogen donor. Additional work was carried out by Marin et al. using BN as a PI for the synthesis of AuNP upon continuous wave (CW) 365 nm photolysis in deaerated aqueous solutions stabilized with various surfactants.[17] While different surfactants were evaluated for optimal particle yield, it was found that a positively charged surfactant such as cetyl trimethyl ammonium chloride (CTAC) offered better stability as evidenced by a narrow and blueshifted SPB in comparison with negatively charged surfactants such as sodium dodecyl sulfate (SDS) at equivalent concentrations above the critical micelle concentrations. In addition to reduction from BN photolysis, they investigated the formation of AuNP in the nanosecond timescale and measured electron transfer rates via LFP studies of α-phenyl benzoin (PBN). Excitation of the chromophore at 355 nm resulted in α-cleavage from the lowest lying excited triplet state to yield the benzoyl radical as well as the benzophenone ketyl radical (BPK). The quenching of BPK monitored at 540 nm in deaerated acetonitrile/dimethyl sulfoxide in the presence of increasing amounts of $AuCl_4^-$ led to a rate constant for electron transfer of $k_{ET} = 9.9 \times 10^8\ M^{-1}\ s^{-1}$. When identical studies were performed with AuCl, a rate constant of $k_{ET} = 2.5 \times 10^8\ M^{-1}\ s^{-1}$ was obtained.[17] The highly favorable processes occurred at a slower rate likely due to solvation differences between the two salts over differences in redox potentials. Despite different environments and monitoring species at different wavelengths, these values agree with previous investigations, where $k_{ET} = 7.2 \times 10^8\ M^{-1}\ s^{-1}$ was obtained from quenching of the α-hydroxy benzyl radical of BN by $AgClO_4$ monitored at 310 nm in deaerated ethanol.[16] In addition to transient studies performed by Marin et al.,[17] steady-state growth of AuNP from reduction via PBN with different salts was investigated. Under CW UVA photolysis, it was observed that the reduction commenced sooner for AuCl with the absence of an induction period, compared to the Au^{3+} salt. Interestingly, both methods produced AuNP in 25 min yet the rate of reduction was greater for Au^{3+} than for Au^+ after the induction period. Furthermore, average AuNP sizes were 7.8 and 17.1 nm prepared from AuCl and $AuCl_4^-$, respectively, highlighting the relationship between shorter nucleation periods and smaller nanoparticles. When PBN was present in a stoichiometric excess of Au^+, the same minimal induction period of less than a minute was observed but with a parallel growth rate similar to reduction with $AuCl_4^-$. Thus, the appearance of the SPB using Au(III) can only commence once a critical concentration of Au(I) is attained.

Table 35.1 summarizes a number of examples where unimolecular PIs have been used for the synthesis of metal nanoparticles. The table is not exhaustive and emphasizes examples from our own laboratory.

Another successful photoreleasing reducing agent has been 1-[4-(2-hydroxyethoxy)phenyl]-2-hydroxy-2-methyl-1-propane-1-one, or under the name of Irgacure-2959™ (I-2959) as a commercial PI from Ciba Specialty Chemicals (Figures 35.3 and 35.4). The lowest lying triplet state of the α-hydroxy ketone has a short lifetime of 11 ns, and the molecule dissociates to yield a benzoyl radical and the 2-hydroxy-2-propyl radical.[13]

AuNP synthesis has been thoroughly studied using benzoins I-2959, BN and PBN as PIs in deaerated CTAC solutions, and a comparative growth experiment at equimolar 1.0 mM BN revealed the formation

TABLE 35.1 PI_1 for Generation of Metal Nanoparticles

Metal	Reducing Agent	Stabilizer Added	Atmosphere	Irradiation Conditions	*hv* Time	Particle Size (nm)	Particle Shape	References
Ag	BN	PVP	N_2	UVB	30 min	5.4	Spherical	[14]
Cu	BN	PVP	N_2	UVB	30 min	2.8	Spherical	[14]
Au	BN	PVP	N_2	UVB	30 min	7.8–17	Spherical	[14]
Ag/Cu	BN	PVP	N_2	UVB	30 min	3–5	Spherical	[14]
Au	BN	PAMAM G3 or G5	N_2	UV	70 min	9.1–67	Spherical	[15]
Au	BN	PPI G2 or G4	N_2	UV	70 min	6.2–14	Spherical	[15]
Au/Ag	BN	PPI G2, G3, or G4	N_2	UV	10 min	2.7–15	Spherical	[15]
Au	BN	CTAC	N_2	350 nm	10 min	n.a.	Spherical	[17]
Ag	BN	PVP	N_2	365 nm	30 min	n.a.	Spherical	[16]
Ag	Benzaldehyde	PVP	N_2	365 nm	30 min	n.a.	Spherical	[16]
Ag	Benzyl	PVP	N_2	365 nm	30 min	n.a.	Spherical	[16]
Au	I-2959	None	Air	350 nm	30 min	8–10	Spherical	[18]
Au	I-2959	None	N_2	350 nm	30 min	8–10	Spherical	[17]
Au	I-2959	None	O_2	350 nm	30 min	50–100	Spheres and prisms	[17]
Au	I-2959	CTAC	N_2	350 nm	30 min	7	Spherical	[17]
Au	I-2959	BSA, PEG-SH	Air	300 nm	2 h	4–50	Spherical	[19]
Au	I-2959	PNIPAAm, MPEG-SH, biotin	Air	350 nm	10 min	90–100	Spherical	[20]
Ag	I-2959	Cyclohexylamine	Air, N_2	350 nm	6 min	3.4	Spherical	[21]
Ag	I-2959	Citrate	Air	350 nm	5 min	3	Spherical	[22]
Ag	I-2959	Citrate, Ag seed	Air	405 nm	26 h	25	Spherical	[22]
Ag	I-2959	Citrate, Ag seed	Air	455 nm	2 h	60	Dodecahedra	[22]
Ag	I-2959	Citrate, Ag seed	Air	505 nm	7 h	50–300	Platelets	[22]
Ag	I-2959	Citrate, Ag seed	Air	627 nm	144 h	200+	Platelets	[22]
Ag	I-2959	Citrate, Ag seed	Air	720 nm	76 h	2:1, 50–75 length	Rods	[22]
Au/Ag	I-2959	SDS	Ar	350 nm	7 min	7.4	Spherical alloy	[23]
Au/Ag	I-2959	CTAC	Ar	350 nm	8 min	12.7	Spherical core/shell	[23]
Cu	I-2959	CTAB	Ar	350 nm	30 min	8–18	Spherical	[24]
Au	α-Phenyl BN	CTAC	N_2	350 nm	15 min	n.a.	Spherical	[17]
Cu	I-907	CTAC	Ar	350 nm	60 min	30	Spherical	[24]
Au	Carbazole	PMMA or PVAc	n.a.	364, 515 nm	20 min	19	Spherical	[25]

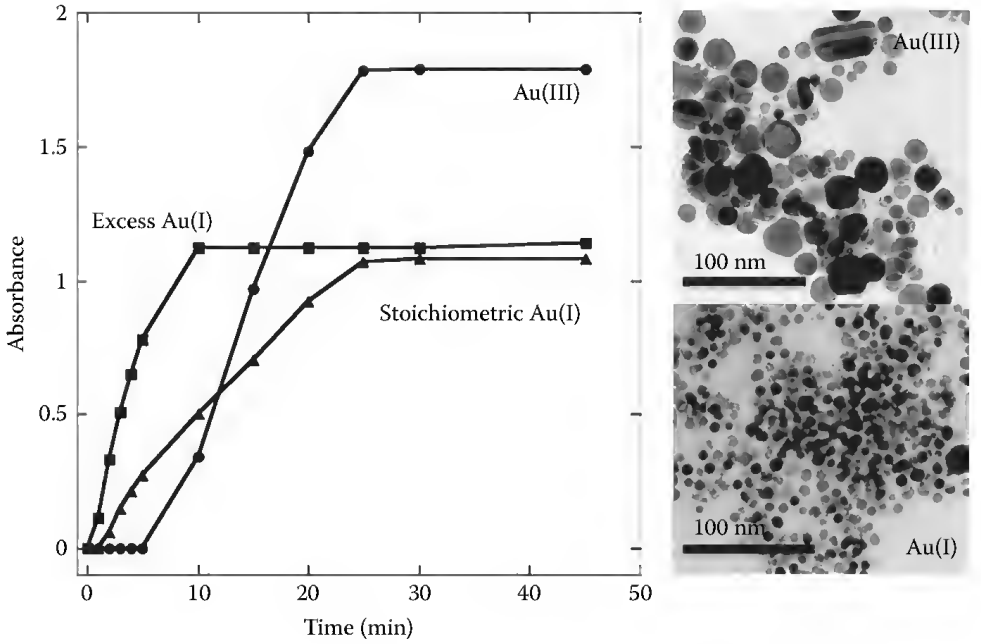

FIGURE 35.2 Formation of AuNP with PBN from Au(I) and Au(III) in deaerated 66 mM CTAC.

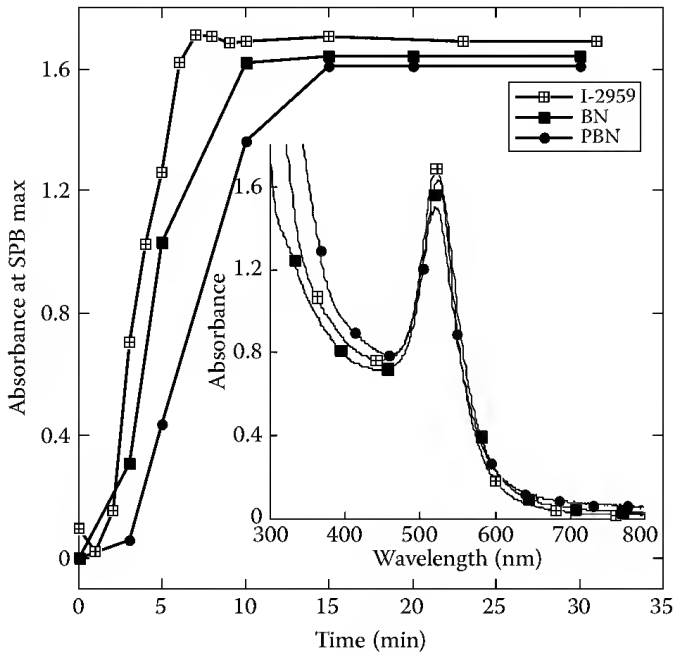

FIGURE 35.3 UV-Vis absorbance of AuNP derived from deaerated solutions of BNs I-2959, BN, and PBN in CTAC solutions after 30 min UVA.

of similar SPB within minutes with I-2959 yielding AuNP faster than BN and PBN. In a micellar solution, the trend is likely attributed to the transients with a greater dipole moment being located closer to the micellar Stern layer and therefore more readily accessible for reduction of aqueous species.[17]

The hydroxyethoxyl functional group of I-2959 facilitates water solubility, and the rapid photocleavage allows for ideal photoreduction in an aqueous environment. McGilvray et al. determined favorable growth conditions for AuNP in aqueous, ambient conditions by optimizing a number of factors through photochemical control.[17,18] Such variables included reagent concentrations, irradiation intensities, and

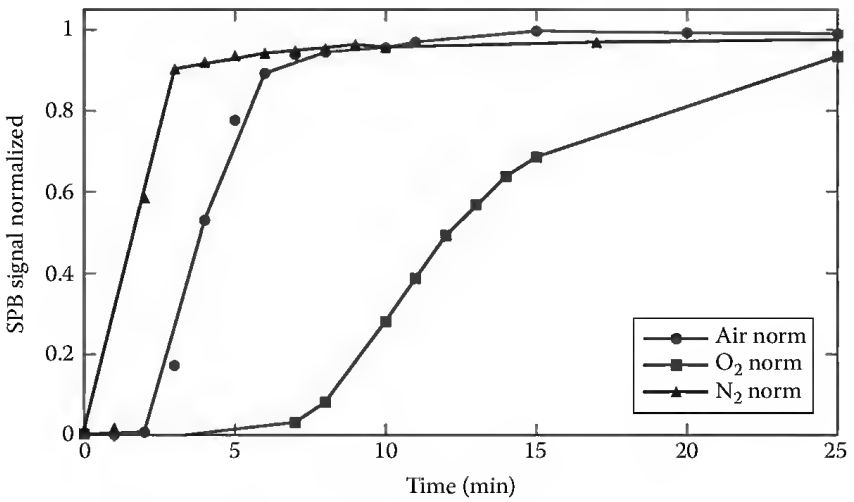

FIGURE 35.4 Normalized growth of I-2959-generated AuNP over time under different O_2 environments; the lines are simply visual aids.

irradiation time. Synthesizing stable nanoparticles involves working in an excess of stabilizer relative to the concentration of metal salt, and an optimal ratio of 3:1 PI:Au^{3+} (i.e., reflecting the stoichiometry) has been quite effective with I-2959.[18,26] At lower I-2959 concentrations, slow growth was observed with the yield of larger, unstable anisotropic gold prisms and micron-sized plates similar to those in Figure 35.5A. With more I-2959, reduction occurs rapidly to yield small AuNP, but in the absence of substantial stabilizer, AuNP agglomerated and typically precipitated within a few hours. These findings define a comfortable window at which nanoparticle synthesis can occur at just the right rate and concentration. The presence of oxygen in ambient aqueous solutions was found to be beneficial as this liberated the need for any additional stabilizer.[17,18] Oxygen is known to quench the excited triplet state of many ketones and react with free radicals.[12,27]

The growth of AuNP over time is presented in Figure 35.4. Working with an excess of I-2959 allowed for a portion of the photocleaved radicals to be sacrificially consumed by oxidative addition. Ketyl radicals reacted quickly at near diffusion control rates to reduce the aurous salt; building up a threshold concentration of Au^0 during nucleation represented by an induction period prior to the appearance of an SPB. Nanoparticles formed within 5 min after which growth was arrested by photogenerated stabilizers. Particularly, benzoyl radicals underwent oxidation to yield 4-hydroxyethoxy benzoic acid (4-HEBA), as confirmed by GCMS.[17] The photoproduct serves as a stabilizer of surface Au^+ charges through physisorption of the carboxylate moiety in a similar function as trisodium citrate and accounts for the negative charge of the electronic double layer on the particle surface detected by zeta potential measurements.

At higher oxygen concentration, a longer induction period and a slower rate of growth were observed. Larger, prismatic particles were obtained owing to the overlap of nucleation and growth phenomena. Alternatively, in the absence of oxygen and any additional stabilizer, AuNP grew rapidly with a short induction period, yet coalesced into larger aggregates.

Conditions to yield small, monodisperse AuNP have also been optimized by controlling irradiation intensity and the wavelength of the light source.[17,18] Higher irradiance under ambient conditions allowed for fast nucleation from a high concentration of ketyl radicals under CW UVA to yield 8–10 nm particles as depicted in Figure 35.5D. Irradiation with UVB or UVC light where the PI absorbs strongly resulted in much greater α-cleavage. Nanoparticle synthesis was more rapid, yet the higher concentration of acid produced led to NP aggregation. The homogeneity of the irradiation source also affected the yield of nanoparticles, such that the more uniform the irradiation from the light source, the more uniform the nucleation for monodisperse particles.

Silver nanoparticles have also been formed using I-2959. Maretti et al. have succeeded in generating AgNP using PIs to reduce the monovalent salts along with a strategic selection of stabilizers to minimize

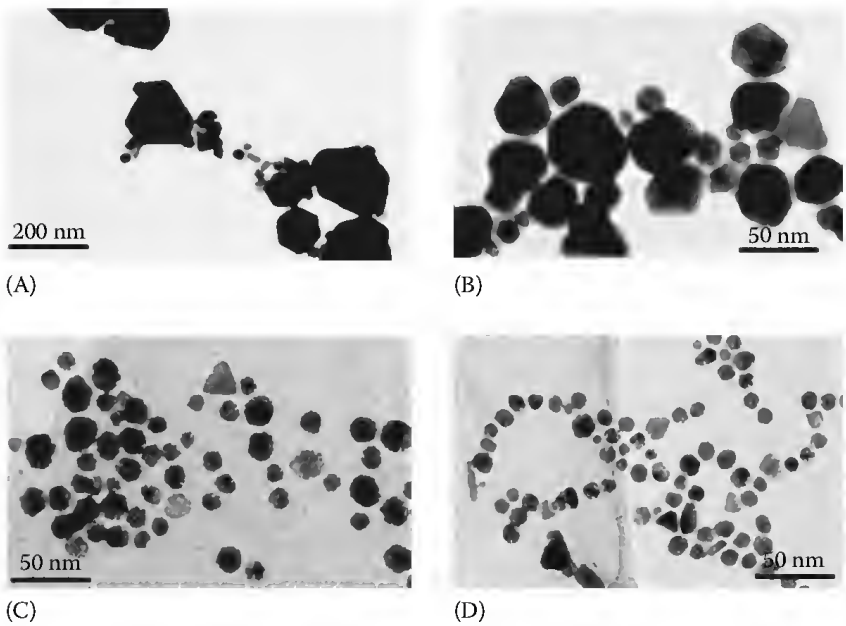

FIGURE 35.5 TEM images of gold nanoparticles prepared with I-2959 under different irradiation conditions. (A) Vis light (3% UVA), (B) 7 W/m^2 UVA, (C) 40 W/m^2 UVA, and (D) 40 W/m^2 UVA.

the facile oxidation of silver nanoparticles.[21] Particles grown under aqueous conditions in the absence of stabilizers agglomerated quickly as indicated by the broadening and redshifting of the SPB. Silver nanoparticles have also been synthesized with I-2959 in aqueous, deaerated sodium citrate solution at room temperature and the carboxylate groups of the citrate functioned to stabilize the spherical particles with an average size of ~3 nm.[22] Alternatively, when AgNP were prepared from an organic silver salt $AgCF_3COO$ in an organic medium such as toluene or tetrahydrofuran and stabilized in the presence of various amines, the resulting spherical nanoparticles were found to be approximately 3.4 nm and showed fluorescence due to Ag_2 (vide infra).[21,26]

CuNP have also been prepared using I-2959 as a benzoin PI.[24] The synthesis of stable CuNP has been possible by photolysis in a deaerated, aqueous environment to prevent oxidation and agglomeration. Optimal conditions for synthesis of small, stable CuNP were established by studying different copper precursor salts. $CuSO_4$, $Cu(NO_3)_2$, and $CuCl_2$ were observed to give varying results, whereby growth of CuNP from $CuCl_2$ occurred significantly faster to generate a greater yield relative to the other precursors. CuNP from $CuSO_4$ produced monodisperse, 7 nm particles, whereas reduction of $Cu(NO_3)_2$ was sluggish to generate a smaller yield of larger particles. $CuCl_2$ generated a mixture of small 5 nm particles along with larger aggregates and prisms around 100 nm. The reduction with $CuCl_2$ was further investigated, where the rapid, autocatalytic growth was attributed to chlorine ligands (Figures 35.6 and 35.7).[24]

Moreover, a variety of particle morphologies were produced upon varying the surfactant and the surfactant counter anion. It was established that CuNP synthesis with Cl^- counterion surfactants CTAC, TMACl or TPAC or TBAC generated plasmon absorbances of varying widths and maxima with a single plasmon, while the identical Br^- counterion surfactant synthesis generally led to the appearance of a secondary SPB characteristic of anisotropic particle formation. Furthermore, by analyzing the effects of the different surfactants on stabilization, it was found that the more hindered the interaction of the nitrogen of the ammonium salt with the metallic surface, the greater the polydispersity and greater deviation from spherical morphology. These studies indicate that while the anion is likely to govern the nucleation rate, particularly for catalysis by Cl^-, the adsorption of organic stabilizer on specific facets of the copper nanocrystal can determine the final shape.

The PI I-2959 has also been used to generate bimetallic nanoparticles, particularly, silver/gold systems.[23,28,29] Bimetallic nanoparticles can possess increased catalytic activity relative to monometallic

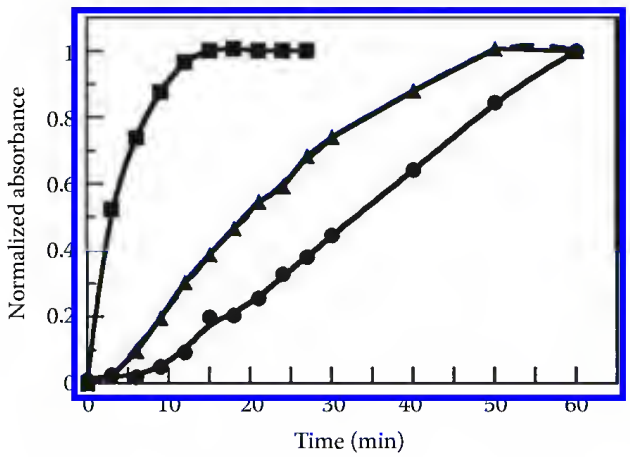

FIGURE 35.6 Absorbance changes at the plasmon band maximum as a function of irradiation time for deaerated aqueous solutions containing 0.66 mM $CuSO_4$ (▲), $CuCl_2$ (■), or $Cu(NO_3)_2$ (●) and 1.3 mM I-2959.

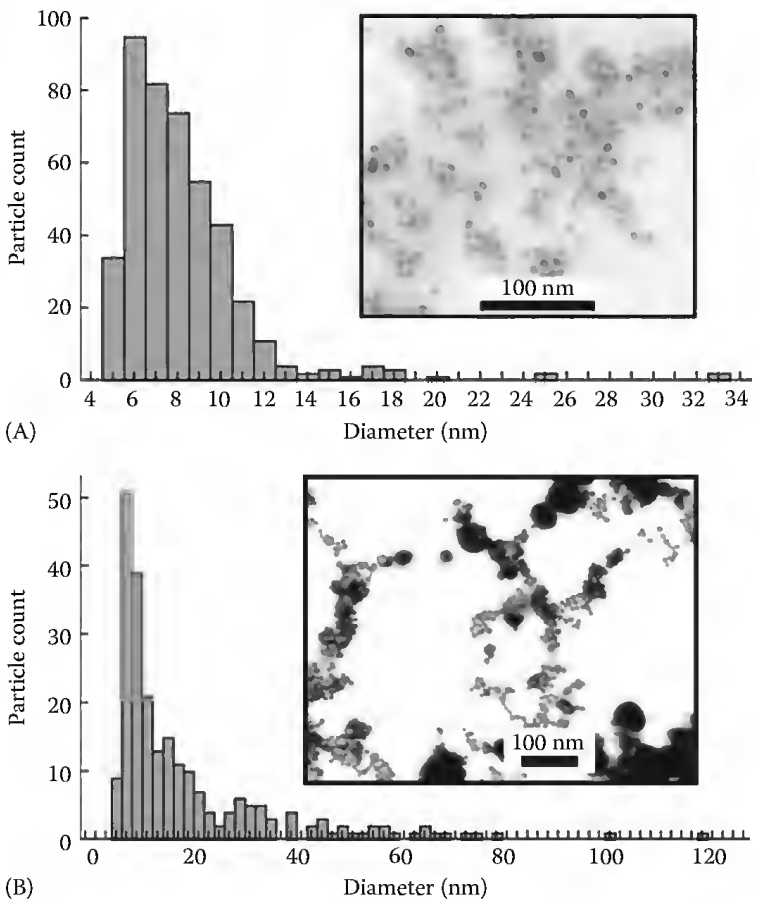

FIGURE 35.7 Size distribution histograms and SEM images (inset) for CuNP obtained from $CuSO_4$ (A) and $CuCl_2$ (B). (Adapted from Pacioni, N.L. et al., *Photochem. Photobiol. Sci.*, 9, 766, 2009.)

particles, and both gold/silver alloys and core/shell AgNP/AuNP have been prepared. Alloy nanoparticles were prepared with the $HAuCl_4$, $AgNO_3$, I-2959, and SDS micelles during UVA photolysis. When the ratio of starting material salts was varied to observe changes in alloy composition, clear changes in the SPB of the resulting colloids were observed. As the ratio of Au:Ag was increased, a single, broad SPB characteristic of alloys redshifted from 400 nm toward the absorbance of gold at 520 nm, as depicted in

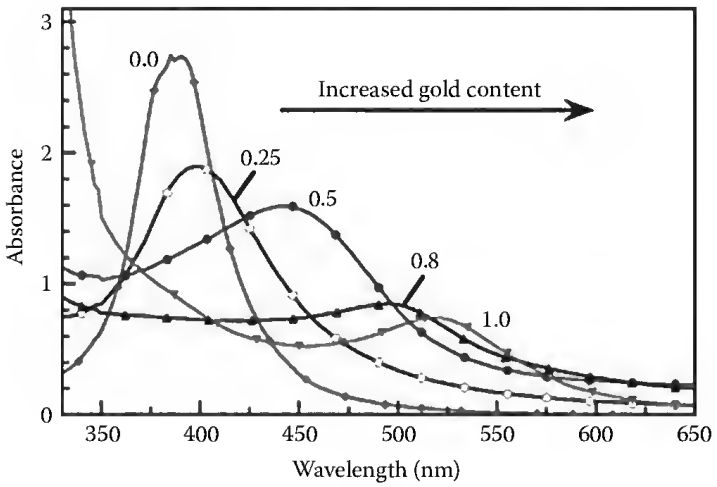

FIGURE 35.8 UV-vis absorption spectra of Au-Ag alloy nanoparticles with increasing gold molar fraction X_{Au} shown in the numbers. In all cases the total cation concentration was 0.2 mM. (Adapted from Gonzalez, C.M., and Scaiano, J.C., *J. Phys. Chem. C*, 113, 11861, 2009.)

Figure 35.8. Stable Ag/Au alloy NPs were prepared at a 20:80 composition with an average size of 7.4 nm spherical particles. High-resolution transmission electron microscopy (TEM) further revealed lattice defects indicative of stacking faults. Time-resolved steady-state kinetic studies indicated that the gold salt was reduced first following generation of the characteristic SPB, followed by a reduction of $AgNO_3$ and concomitant blueshifting of the translational plasmon band.[23]

Further, bilayer Ag/Au core/shell NPs were constructed by simple deviations in the order of addition or reagents throughout the synthesis. In this case, $HAuCl_4$ was first combined with CTAC, followed by the addition of I-2959, finalized by the addition of $AgNO_3$ following immediate irradiation. The temporal isolation of $AuCl_4^-$ from Ag^+ and I-2959 by the micellar interface facilitated the initial sole reduction of AuNP followed by the formation of a silver shell. One of the primary characteristics of identifying bilayer nanoparticles is the presence of two maxima with the SPB for Au blueshifted relative to its characteristic monometallic plasmon.[29] In Figure 35.9, the peak representing the Ag SPB

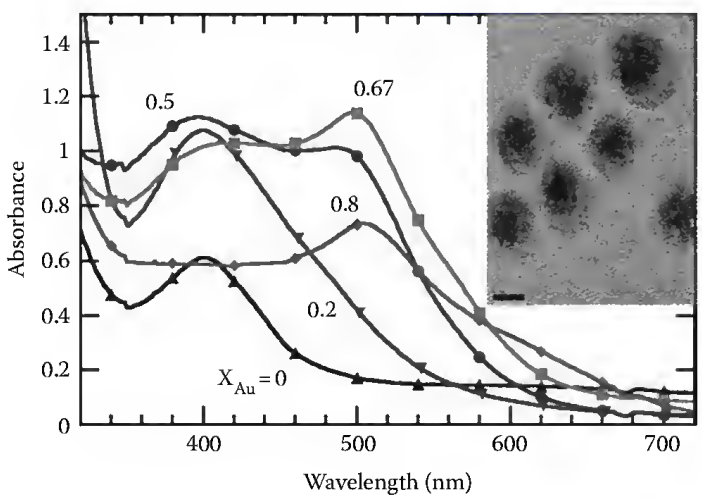

FIGURE 35.9 UV-Vis spectra of self-assembled Au–Ag core–shell nanoparticles with varying gold:silver ratio for a 0.2 mM solution (total metal ions) containing CTAC and I-2959 irradiated for 6–8 min. The inset shows the core–shell structure as seen in a TEM image: the size bar is 5 nm. (Adapted from Gonzalez, C.M. and Scaiano, J.C., *J. Phys. Chem. C*, 113, 11861, 2009.)

remained at a similar wavelength. In contrast, when separate solutions of prepared AuNP and AgNP were combined, their absorption maxima remained at their characteristic wavelengths.[23]

35.4.2 Nanoparticle Synthesis Mediated by Photorelease of α-Aminoalkyl Radicals

Along the lines of photorelease from triplet ketones, another PI I-907, or 2-methyl-1-[4-(methylthio) phenyl]-2-(morpholinyl)phenyl-1-butanone, undergoes α-cleavage under UVA photolysis to generate a benzoyl radical and an α-aminoalkyl radical with strong reducing properties.[30] CuNP were also prepared by in deaerated acetonitrile from copper acetate ($Cu(OAc)_2$) using CTAC as stabilizer to afford 30 nm CuNP after 60 min irradiation.[24] CuNP were also prepared with thiophene or cyclohexylamine as stabilizer with reduction complete in half of the time. Trioctylphosphine oxide (TOPO) was also tested for stabilization, yet the resulting particles seemed larger and more polydisperse, judging from the broader SPB.

35.4.3 Two-Color, Two-Laser AuNP Synthesis

Sakamoto et al. devised a method for the generation of AuNP in polymer films by a two-color, two-laser method[25] that has been proposed to involve H atoms. In a poly(methylmethacrylate) (PMMA) or ply(vinyl acetate) (PVAc) matrix, carbazole was illuminated by 368.8 nm laser to generate the lowest lying singlet state, which decays to the lowest lying triplet upon intersystem crossing. Alternatively, when 368.8 and 514.5 nm lasers photolyze the sample simultaneously, carbazole is excited to a higher singlet state where N–H bond cleavage to generate the carbazyl radical and the hydrogen radical was suggested. Surprisingly, the presence of oxygen did not play a role in quenching the reaction. The resulting hydrogen radical possesses strong reducing properties and generates AuNP only at the fine intersection of the two laser beams, allowing for precise localization of nanoparticle generation. TEM analysis revealed the formation of spherical AuNP of approximately 19 nm. The two-laser technique also allowed for writing and patterning, with linewidths as thin as 4–5 μm.

The application of type 1 PIs has stretched beyond the accustomed generation of polymers and plastics, and into new domains for nanomaterials synthesis. UV absorption, short triplet lifetimes, and n,π* reactivity allow for easy generation of reducing species for colloidal nanoparticle synthesis.

35.5 Part II: Photosensitized Generation of Metal Nanoparticles via Ketone Photoreduction

Photoinduced hydrogen atom abstraction by ketones is one of the most important reactions in organic photochemistry,[12,31] where the excited triplet ketone will abstract hydrogen from a donor to yield two radicals or a biradical. Aryl ketones are a common photochemical sensitizer owing to their low-lying n,π* state and thus high reactivity for hydrogen abstraction (Scheme 35.6).[12]

The rate of hydrogen abstraction is dependent on the electronic configuration of the ketone, where ketones with n,π* character have been reported to be more than 100 times faster than carbonyls with π,π* character.[12,32] Additionally, the rate of reactivity also depends on the donor, where primary and

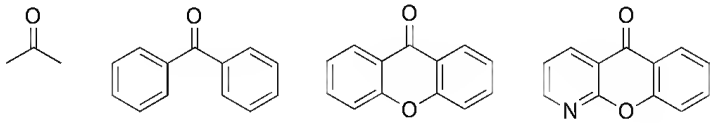

SCHEME 35.6 Schematic structures of BP, XAN, and 1-axaxanthone (AZX).

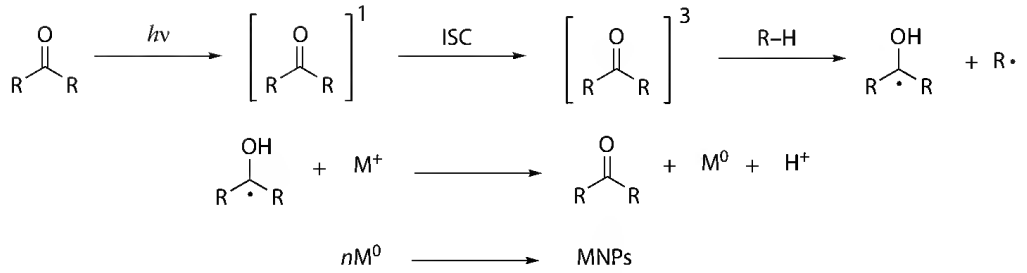

SCHEME 35.7 PI_2 pathway via intermolecular hydrogen atom transfer.

secondary alcohols, ethers, and alkyl benzenes induce faster reactivity with n,π* character over π,π* dominant ketones, yet phenolic hydrogen donors induce faster hydrogen transfer with π,π* carbonyls.[33] Hydrogen abstraction results in the formation of two radicals, which can undergo photoaddition, dimerization, further hydrogen abstraction, or chemical reduction in the case of ketyl radicals in the presence of many metal salts. Ketyl radicals can reduce metal ions to metal atoms in the same manner as described in Section 35.4. Scheme 35.7 illustrates the process for M^+, where only one electron is needed.

There has been abundant research into generating ketyl radical species via hydrogen abstraction from triplet ketones.[17,31,34–37] The lifetime of the reducing radical or its precursor can dictate the efficiency of the reaction. Notably, it has been widely observed that metal salts can quench the excited-state triplets of many carbonyls with rates approaching diffusion control (vide infra). With this hindrance in mind, one way to maximize photochemical nanoparticle generation has been to prepare the materials in the presence of stabilizers such as polymers, dendrimers, or micelles, as they can compartmentalize the excited-state triplet species and enhance radical-pair generation via hydrogen abstraction,[38] yet the supramolecular structures also function to minimize quenching. As a proof of concept, nanoparticle synthesis in the absence of micelles using benzophenone (BP) in acetonitrile remains a challenge as a low yield of metal nanoparticle aggregates was obtained for experiments with silver or gold. A review of commonly used sensitizers for nanoparticle synthesis will be presented.

35.5.1 Acetone

Many reports exist for the photochemical generation of nanoparticles and nanorods using acetone.[36,39–44] In many cases, particle formation requires 254 nm light and irradiation times on the order of several hours. Significant progress has been put forth by Dong et al. in the use of acetone to produce colloidal AuNP using a variety of different hydrogen donors, stabilizers, and photon energies.[43,44] Solar irradiation of an Au(III)–sodium citrate solution produced 9–12 nm particles. Nanoparticles of approximately 7.5 nm in diameter were prepared by photolysis of an Au(III)–sodium dodecyl sulfonate–acetone system, yet substitution with sodium dodecylbenzene sulfonate yielded smaller, 6.7 nm particles with a narrower size distribution. Further, 3–5 nm particles have been prepared by 300 nm photolysis and subsequently used as seeds for further photochemical growth of 10–66 nm particles in an Au(III)–poly(ethylene glycol) (PEG)–acetone solution. Bimetallic Au/Ag core/shell particles were also synthesized utilizing the photochemical seeding technique where 3 nm AuNP seeds were added to a PEG–acetone–$AgNO_3$ solution. Finally, gold nanorods were prepared from an Au(III)–dimethylformamide–CTAC–acetone system to yield monodisperse rods with high aspect ratios greater than 10:1. Other syntheses of nanorods from acetone have been reported, many of which require the addition of $AgNO_3$ for directed growth.[40–42] Interestingly, none of the reports mentioned here addressed deaeration during synthesis. With triplet lifetimes around 1–4 μs in aqueous systems, significant quenching by oxygen or other metal species were likely contributors to the required long irradiation times. Working with aryl or biaryl ketones, on the other hand, employs chromophores with absorption shifted to lower energies in the UV region, and thus shorter necessary irradiation times as well as shorter triplet lifetimes. An example of such a chromophore is BP.

35.5.2 Benzophenone

BP has been a widely used sensitizer for the generation of colloidal nanoparticles.[34,45–48] In one example, Eustis et al. prepared colloidal AgNP from photolysis of BP with 265 nm 100 fs pulses and CW light in the presence of $AgNO_3$ and cetyl trimethyl ammonium bromide (CTAB) as a stabilizer.[46] They investigated the growth mechanism and observed a competition between formation and ablation at irradiation times over 2 h, as well as aggregation once BP had been consumed. They also established BP as the limiting reagent in their system. Increasing the laser power or the irradiation time resulted in sharper SPB peaks as ablation processes dominate at the higher intensities and photodecomposition could displace the capping material and lead to aggregation. In another report, Esumi et al. prepared AgNP by tethering BP to the surface of SiO_2 nanoparticles in the presence of isopropyl alcohol.[48] Positioning the reducing agent on an inert support minimized the formation of light absorbing transients produced from primary photochemical reactions of isopropyl alcohol and BP and thus minimized the degree of post irradiation particle degradation allotted to ketone transient recombination.[39] CuNP were prepared by Kapoor et al. using $CuSO_4$, BP, and PVP as a stabilizer in the presence of CW 253.7 nm light.[49] LFP studies of this system revealed that the BP triplet transferred its energy to PVP without hydrogen abstraction. As the BP ketyl radical was not detected in the 470–600 nm region, this implied that the excited PVP was responsible for the reduction. Photolysis of PVP in the presence of $CuSO_4$ alone, however, did not yield nanoparticles. This preparation yielded polydisperse particles as small as 15 ± 4 nm. In later studies, the author succeeded in preparing 10–40 nm CuNP from BP with gelatin as a hydrogen donor.[50] AgNP have also been prepared using BP from $AgClO_4$ in 2-propanol/acetonitrile and SDS as a stabilizer.[51] The rate constants for BP triplet quenching were measured as 4.3×10^{10} M^{-1} s^{-1}, and 4.3×10^{9} M^{-1} s^{-1} for quenching of the BPK by Ag^+.

While micelles can segregate photochemical reactions from quenching events, their cage-like function can also enhance geminal recombination of radical pairs and thus decrease micellar escape of reducing radicals to yield nanoparticles.[52] This challenge can be overcome by working in the presence of a magnetic field. Since geminal recombination of these reactive triplet transients requires a spin-flip, lifting the degeneracy of the triplet states in the magnetic field significantly reduces probability for recombination and hence promotes micellar exit, which is not affected by magnetic fields, and subsequent nanoparticle synthesis. With this knowledge in mind, Scaiano et al. prepared AgNP via 320 nm photolysis of BP with $AgNO_3$ via hydrogen abstraction from 1,4-cyclohexadiene (1,4-CHD) in 0.1 M SDS, where 1,4-CHD was strategically used as a strong hydrogen donor (Figure 35.10).[34] The yield of

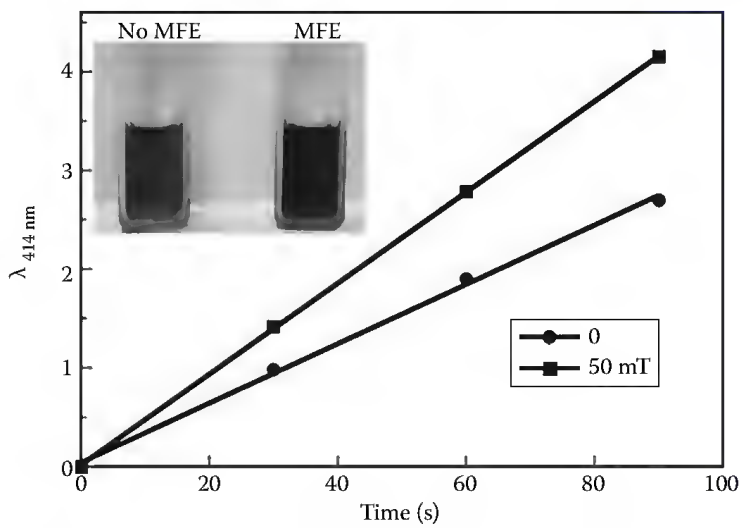

FIGURE 35.10 Formation of silver nanoparticles during UV irradiation in the absence (●) and presence (■) of a 50 mT magnetic field (BP 0.005 M, SDS 0.1 M, Ag^+ = 0.01 M, and 0.04 M 1,4-CHD). The inset shows AgNP photographs in the presence and absence of an applied magnetic field. (Adapted from Scaiano, J.C. et al., *J. Phys. Chem. B*, 110, 12856, 2006.)

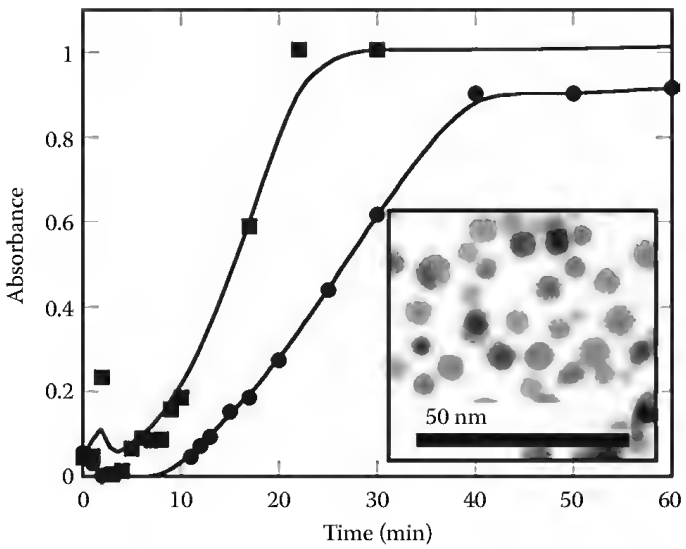

FIGURE 35.11 Growth of AuNP over time incorporating BP (●) or BP and 1,4-CHD (■) in CTAC. The TEM image in the inset illustrates the particles obtained in the absence of 1,4-CHD. (Adapted from Marin, M.L. et al., *J. Am. Chem. Soc.*, 130, 16572, 2008.)

nanoparticles was seen to increase up to 67% upon application of a magnetic field and saturated at around 100 mT. An increase in the size of spherical particles from 4 to 8 nm was also observed, along with an increase in the rate of their formation by 30%.

BP has also been used as a sensitizer for the generation of AuNP. BP was photolyzed in an aqueous system in the presence of CTAC and $HAuCl_4$ to yield 7 nm particles with good monodispersity (Figure 35.11).[17]

Under these conditions, the surfactant behaves as a mild hydrogen donor, whereby the methylene hydrogens have been known to be abstracted at rates approaching $3 \times 10^6\ M^{-1}\ s^{-1}$.[34] Varying the R groups of the ketyl radical will modify the energy levels required for carbonyl excitation and consequently determine the reactivity of the excited state. To illustrate the diversity in chromophore selection, xanthone (XAN) was also tested for nanoparticle synthesis.

35.5.3 Xanthones

In aqueous media, xanthones is known to have a low-lying $^3\pi,\pi^*$ state and thus has poor reactivity toward hydrogen abstraction.[37,53] AuNP were generated from XAN slowly and with very low yield as indicated by the redshifted and low-lying SPB absorbance for the produced colloid. Alternatively, when a pyridine ring is substituted into the framework, the excited triplet state of 1-azaxanthone has a low-lying $^3n,\pi^*$ state and is higher in energy than that of BP.[37] Owing to this, the generation of AuNP from the 1-azaxanthone system provides the fastest generation (<1 min vs. ~10 min for BP) as well as blueshifted SPB of 511 nm, and smallest particle size in comparative studies. A TEM image of AuNP prepared from AZX in CTAC is provided in Figure 35.12.

These structural differences highlight the ability to control the size and efficiency of nanoparticle generation by selection of a ketyl radical precursor with high hydrogen abstraction reactivity. In the presence of 1,4-CHD, even XAN reaches high SPB absorbances. As a strategy, those ketones with low-lying $^3n,\pi^*$ states perform best.[17] Note that the ketone plays a catalytic role, since it is reformed following electron transfer to the metal ion. A summary of bimolecular reactions is shown in Table 35.2; as in the case of Table 35.1, it emphasizes work from our laboratory (Scheme 35.8).

Control experiments were also conducted in the presence of the diene yet the absence of a ketone, which revealed the formation of AuNP after some 20 min with a higher absorption intensity and greater

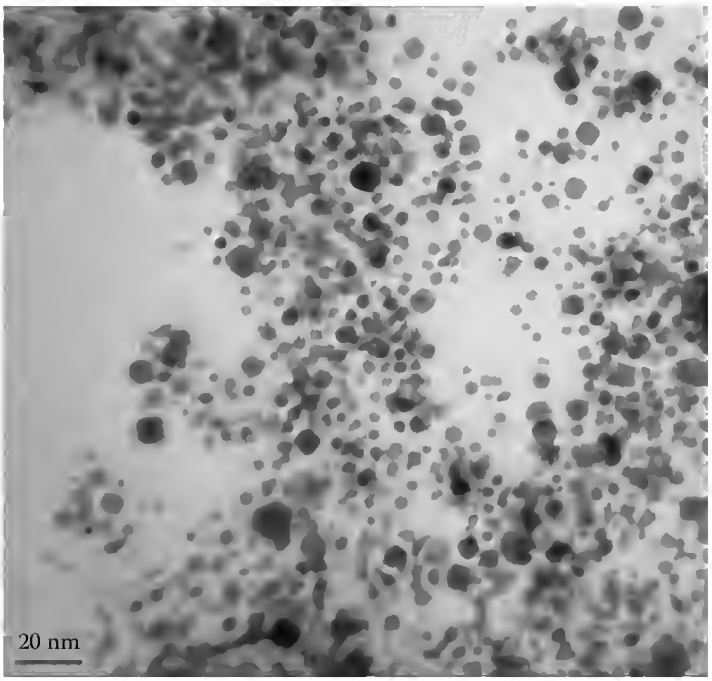

FIGURE 35.12 TEM image of AuNP prepared from 0.33 mM $HAuCl_4$ and 1.0 mM 1-azaxanthone in deareated 17 mM CTAC following 30 minutes UVA photolysis. Scale bar represents 20 nm.

redshift. This would suggest that the formation of the cyclohexadienyl radical could also play a role in the reduction of metal salts. As many of these ketone triplets or their ketyl radicals can be quenched by molecular oxygen, these studies were performed with deaerated samples. Nevertheless, when hydrogen abstraction synthesis was performed under air, a similar relative reactivity among the three chromophores was still observed with longer induction periods.

35.5.4 Polymers

Various polymers have been utilized in metal nanoparticle synthesis with the function of macromolecular stabilization of small particles, where careful selection of polymer, its molecular weight, and additives offer control over particle size and shape in solution and in thin films. Interestingly, various polymers can also partake in photochemical reduction owing to the presence of a ketone and undergo hydrogen atom transfer between sensitizer and donor to form the reducing ketyl radical. AgNP were produced in the presence of PVP under 254 nm photolysis, where Huang et al. acknowledged that a higher %wt PVP resulted in both a greater yield and smaller nanoparticles.[63] Platinum and AuNP have also been produced in deaerated aqueous/ethanol polymer solutions containing PVP.[55,56] Average particle sizes were reported to be 2–2.5 nm for platinum nanoparticle (PtNP) and 10.6 nm for AuNP, where the growth mechanisms were investigated using extended x-ray absorption fine structure (EXAFS). Nanoparticles have also been prepared in poly(vinyl alcohol) (PVA) solutions where the polymer performs as a hydrogen donor for BP, where the ketyl radical of BP in the D_1 excited state is generated by two-photon LFP to generate AuNP in films,[47] or by hydrogen abstraction with a known sensitizer such as BP for the formation of Au/Cu bimetallic nanoparticles.[54] An interesting report by Korchev et al. revealed their development of Cu, Ag, and AuNP in polymer films utilizing a sulfonated poly(ether ether ketone) (SPEEK)/PVA system.[57] Herein, the BP moiety of the SPEEK polymer abstracted hydrogen from PVA to yield two ketyl radicals and subsequently reduce metal salts in the presence of 350 nm light. PVA has been known to initiate a thermal reduction of metal salts over long time periods (days) as well as a slower photochemical reduction in the absence of sensitizer,

TABLE 35.2 Nanoparticle Photosynthesis Using Bimolecular Reactions

Metal	Reducing Agent	Stabilizer Added	Atmosphere	Irradiation Conditions	CW *hv* Time	Particle Size (nm)	Particle Shape	References
Au	Acetone	Citrate	Air	Solar	70 min	9–12	Spherical	[43]
Au	Acetone	Sodium dodecylsulfonate	Air	UV	n.a.	7.5	Spherical	[43]
Au	Acetone	Sodium dodecylbenzene	Air	UV	n.a.	6.7	Spherical	[43]
Au	Acetone	PEG	n.a.	300 nm	n.a.	5	Spherical	[43]
Au	Acetone	AuNP seed, PEG	n.a.	300 nm	n.a.	10–66	Spherical	[43]
Au/Ag	Acetone	AuNP seed, PEG, $AgNO_3$	n.a.	n.a.	n.a.	4.7–6.6	Sphere/dodecahedra	[43]
Au	Acetone	DMF/CTAC	n.a.	n.a.	4 h	10:1	Nanorod	[43]
Au	Acetone	Cyclohexane, CTAB, $AgNO_3$	Air	254 nm	30 h	4:1 rod	Nanorod	[40]
Au	Acetone	Cyclohexane, TDAB, $AgNO_3$	Air	8 W 254 nm	7–88 h	25–40 2:1–8:1	Nanorod	[41]
Au	Acetone	Cyclohexane, CTAB, $AgNO_3$	n.a.	254, 300 nm	1–20 h	2–90	Spherical, rods	[42]
Ag	BP	CTAB, 2-propanol	n.a.	100 fs 266 nm	60 min	5–20	Spherical	[46]
Ag	BP	CTAB, 2-propanol	n.a.	CW 254 nm	45 min	10	Spherical	[46]
Ag	BP	BP@SiO_2, 2-propanol	Ar	254 nm, 365 nm	30 min	10–12	Spherical	[48]
Cu	BP	PVP	N_2	254 nm	20 min	15	Spherical	[49]
Cu	BP	Gelatin	N_2	254 nm	8 min	10–15	Spherical	[50]
Cu	BP	Carboxymethyl cellulose	N_2	254 nm	8 min	30–40	Spherical	[50]
Ag	BP	2-Propanol, SDS	n.a.	365 nm	30 min	n.a.	n.a.	[51]
Ag	BP	SDS, 1,4-CHD	N_2	320 nm, magnetic field	30 s	4–8	Spherical	[34]
Au	BP	PVA, formic acid	n.a.	355 nm, 532 nm	n.a.	2.5–4	Spherical	[47]

Au	4-Methoxy BP	PVA, formic acid	n.a.	355 nm, 532 nm	n.a.	n.a.	n.a.	[47]
Au/Cu	BP	PVA, formic acid	Ar	365 nm	9 h	2–8	Spherical	[54]
Au	BP	CTAC, 1,4-CHD	N_2	350 nm	30 min	12.8	Spherical	[17]
Au	BP	CTAC	N_2	350 nm	30 min	7.0	Spherical	[17]
	BP	1,4-CHD	N_2	350 nm	30 min	n.a.	Spherical	[17]
Au	XAN	CTAC, 1,4-CHD	N_2	350 nm	30 min	12–20	Spherical	[17]
Au	XAN	CTAC	N_2	350 nm	30 min	n.a.	Spherical	[17]
Au	XAN	1,4-CHD	N_2	350 nm	30 min	n.a.	Spherical	[17]
Au	1-Azaxanthone	CTAC, 1,4-CHD	N_2	350 nm	30 min	3–10	Spherical	[17]
Au	1-Azaxanthone	CTAC	N_2	350 nm	30 min	n.a.	Spherical	[17]
Au	1-Azaxanthone	1,4-CHD	N_2	350 nm	30 min	n.a.	Spherical	[17]
Ag	PVP	Ethanol	N_2	300 nm	60 min	80–100	Spherical	[14]
Au	PVP	Ethanol	N_2	300 nm	30 min	6.9	Spherical	[14]
Pt	PVP	1:1 H_2O:ethanol	N_2	254 nm	10–120 min	2.0–2.5	Spherical	[55]
Au	PVA	1:1 H_2O:ethanol	N_2	254 nm	5 h	11–93	Spherical, dodecahedra	[56]
Cu	SPEEK	PVA	N_2	350 nm	13 min	5–40	Spherical	[57]
Ag	SPEEK	PVA	N_2	350 nm	60 s	6	Spherical	[57]
Au	SPEEK	PVA	N_2	350 nm	20 min	3	Spherical	[57]
Ag	Methoxy PEG	None	N_2	254 nm	10 min	7–15	Spherical	[58]
Ag	Methoxy PEG	None	N_2	254 nm	25 min	50–60	Spherical	[58]
Au	Methoxy PEG	None	N_2	254 nm	10–25 min	15–80	Spherical	[59]
Au/Ag	Methoxy PEG	None	N_2	254 nm	9 min	50–200	Spherical	[60]
Au	Acetic acid	Collagen	Yes	254 nm	1 h	37–101	Spheres, large prisms	[61]
Au	H_2O_2	None	O_2	350 nm	30 min	10–120	Spheres, large prisms	[62]

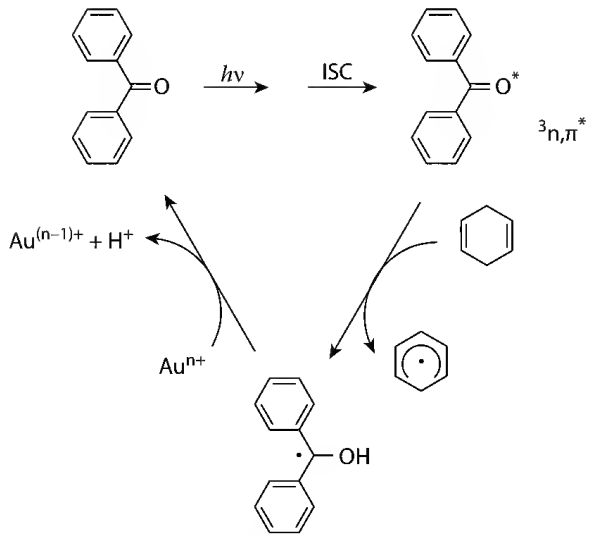

SCHEME 35.8 Hydrogen abstraction from 1,4-CHD, illustrated for BP and followed by electron transfer to the metal ion. Note that the ketone is reformed at the end of the process.

yet kinetics of systems incorporating SPEEK/PVA were considerably faster. AgNP of 6 nm diameter were generated from $AgClO_4$ in as little as 30 s, and it was observed that lower concentrations (18 μM) of the metal salt formed AgNP at faster rates than at higher concentrations (90 μM). At higher salt concentrations, more protons are produced as photoproducts, which can quench the SPEEK ketyl radical and thus inhibit reduction. CuNP were prepared from $CuSO_4$ under identical deaerated conditions to yield a broader sized distribution of 5–40 nm particles. The authors attributed the primary reduction of Cu(II) to Cu(I) to the ketyl radical with the formation of a CuOH complex absorbing at 460 nm, where no further reduction ensued if illumination was stopped. Additionally, when $CuSO_4$ was injected into a pre-irradiated solution of SPEEK/PVA in the dark, only a peak at 460 nm was produced. They interpret the final reduction as occurring via disproportionation of the cupric ion in acidic media to form Cu(0) leading to nucleation and growth, adding that the reduction of Cu^+ to Cu(0) is further catalyzed in the presence of CuNP. AuNP were also prepared in an identical system, and investigated the kinetics of the induction period prior to SPB generation, and attributed it to the initial reduction and disproportionation to $AuCl_2^-$ with an absorbance at 246 nm but screened by the competitive absorption of SPEEK. Au^+ eventually yields Au(0) and nucleate to form nanoparticles.

Another approach to the photochemical generation of nanoparticles using polymers has been through the 254 nm photolysis of methoxy polyethylene glycol in water to generate the highly reactive primary alcohol radical to form silver, gold, or Au/Ag bimetallic particles.[58,60]

35.5.5 Nanoparticle Generation from Inorganic Free Radicals

AuNP have also been prepared by an alternative photochemical method free from inorganic free radicals and thus reducing contaminants (Scheme 35.9). In a recent publication, the photochemistry of $HAuCl_4$ has been utilized to generate spherical and anisotropic gold nanomaterials.[62] Upon absorption

$$\begin{aligned} Cl^{\bullet} + HOOH &\longrightarrow HCl + HOO^{\bullet} \\ HOO^{\bullet} + Au^{3+} &\longrightarrow Au^{+} + O_2 + H^{+} \\ HOO^{\bullet} + Au^{+} &\longrightarrow Au^{0} + O_2 + H^{+} \\ n\mathrm{Au} &\longrightarrow \mathrm{AuNP} \end{aligned}$$

SCHEME 35.9 Proposed mechanism for AuNP generation from H_2O_2.

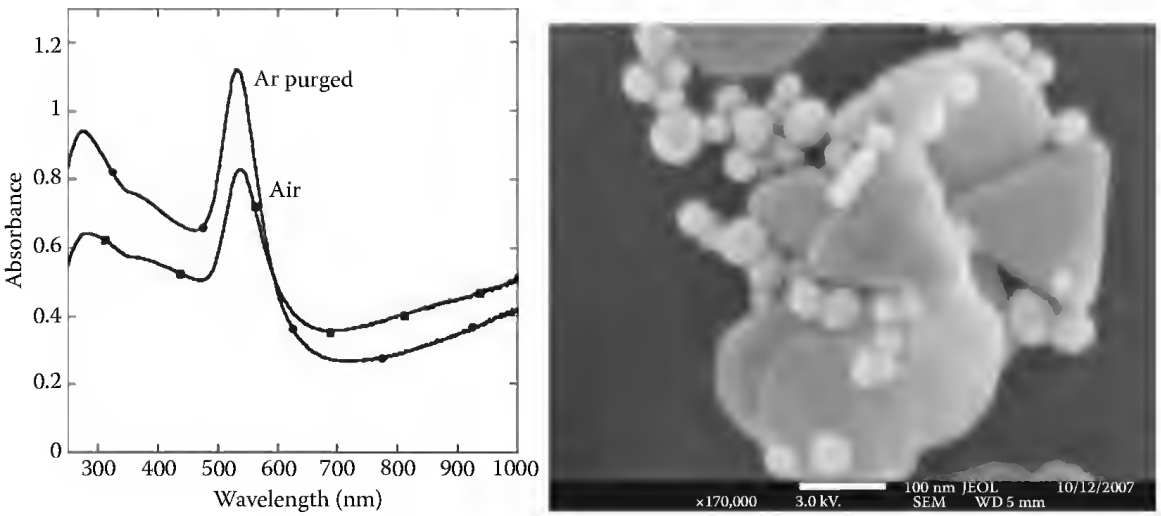

FIGURE 35.13 UV-vis absorbance of AuNP generated from UVA photolysis of $HAucl_4$ and H_2O_2, and corresponding SEM image of AuNP prepared under aerated conditions.

of UV light, the excited state of the salt, $AuCl_4^{-*}$, dissociates homolytically under aqueous conditions to generate $AuCl_3^-$ and liberate $Cl^•$.

The chlorine atom, in turn, is a powerful hydrogen abstractor and reacts with hydrogen peroxide to yield HCl and the hydroperoxyl radical, $HOO^•$ under aerated or deaerated conditions. This free radical can operate as a one-electron reducing agent to form AuNP. Representative data are shown in Figure 35.13.

Under deaerated conditions, nanoparticle formation occurs quickly to yield a strong SPB absorbance. An air or argon atmosphere yields similar absorbance spectra. If, however, an aqueous stabilizer is added to the synthesis such as 4-HEBA, platelet formation is significantly suppressed.

35.5.6 Direct Photoreduction by Excited-State Species

One approach for photochemical preparation of AgNP utilized the reduction potential of excited-state species of pyrene or L-crown-pyrene created from 350 nm laser excitation of methanolic solutions to reduce $AgClO_4$.[65] With fluorescence lifetimes of 296 and 51 ns for pyrene and L-crown-pyrene, respectively, the addition of $AgClO_4$ resulted in singlet quenching with rate constants of 4.7×10^9 M^{-1} s^{-1} and 3.7×10^9 M^{-1} s^{-1}, respectively. The reduction path from the pyrene moiety was attributed to electron transfer from the excited singlet state owing to a large ΔE_{ST} = 28.9 kcal mol^{-1} and energetically favorable emf values. The generation of colloidal silver was evident from SPB at 405 and 425 nm for pyrene and L-crown-pyrene, respectively. The absorption intensity for L-crown-pyrene was redshifted and more than twice as large as that for pyrene at equimolar pyrene moiety concentrations, indicating larger particles and a greater particle yield due to enhanced Ag^0 stabilization in the crown ether cavity. In the absence of additional stabilizer, the colloids were found to decompose overnight. Other reports by Gratzel et al. have identified similar Ag^0–chromophore–azo-crown ether complexes from photosensitized reduction of a cyanine dye in the presence of lipids, vesicles, and micelles, and attributed the stability of the reduced species to the segregating function of the stabilizer.[66]

In a report from Sudeep et al., thionene was photolyzed with visible light to generate transients capable of forming AgNP in the 2–20 nm range.[67] Steady-state photolysis with a 530 nm cutoff filter or using a 532 nm laser source generated triplet thionene. Triplet thionene could either react with a donor through electron transfer or undergo self-quenching with the ground-state species to yield semithionene. LFP studies indicated little triplet quenching upon addition of $AgNO_3$, and that the reductive semithionene was proven to be generated from self-quenching at micromolar concentrations, followed by electron transfer to form the

reduced semithionene. The electron transfer process is solvent dependent, where Ag^+ is effectively reduced in 1:1 toluene:ethanol, yet no AgNP evolved when the photolysis was performed in aqueous media.

Another photochemical synthesis of metal nanoparticles was developed from singlet oxygen-mediated photooxidation of amphiphilic dendrimers to generate reductive radicals upon photocleavage.[68] Oligo (*p*-phenylenevinylene) core branches and oligo(ethylene oxide) terminal chains were oxidized at the olefin center to generate the oxygen biradical, which photodegraded to yield the reductive α-hydroxymethyl radical as well as the aryl aldehyde product; 20 nm AuNP was prepared from the radical-induced reduction and was stabilized by the dendrimer or photodegraded dendrimer fragments.

35.6 Applications

35.6.1 Fluorescent Nanoparticles

In a recent publication, Maretti et al. reported the ability to construct fluorescent silver clusters following Ag^+ photoreduction with I-2959.[21] AgNP were prepared from UVA photolysis of I-2959 and silver trifluoroacetate in the presence of cyclohexylamine or hexadecylamine as stabilizing agents in toluene or tetrahydrofuran. Small Ag_2 silver clusters were stabilized on the surface of the larger 3 nm AgNP and displayed strong fluorescence centered at 550 nm (Figure 35.14). The silver clusters show absorption and emission properties that did not overlap with the small SPB for AgNP at 390 nm. The emission has molecular-type properties with a characteristic mirror-image resemblance between absorption and emission, relatively long fluorescence lifetimes, simple monoexponential decay, and static quenching by nitroxides. These silver fluorescent nanoparticles (AgFNP) are stable for months, prepared under deaerated, yet stored under ambient conditions and lighting. AgFNP could be transferred to other solvents such as tetrahydrofuran (THF) with preservation of the fluorescent properties. AgFNP synthesized in THF displayed a narrower size distribution. The fluorescence was attributed to the Ag_2 silver clusters on the surface of the larger AgNP. Control experiments have been performed to rule out fluorescence from I-2959 photoproducts, residual amines complexing with silver salts, or from starting materials. The fluorescence quantum yield of the Ag_2 clusters was measured to be 0.11–0.15 depending on the solvent and the stabilizing amine. Fluorescence lifetimes were also measured for the AgFNP, and their decays (>98%) were found to be monoexponential with a lifetime of 2.6 ± 0.1 ns. These values agreed well with reported lifetimes of Ag_2 clusters in encapsulated or inert gas phase environments. The trifluoroacetate anion was critical to the synthesis of fluorescent AgNP, and ^{19}F NMR studies confirmed the presence of surface

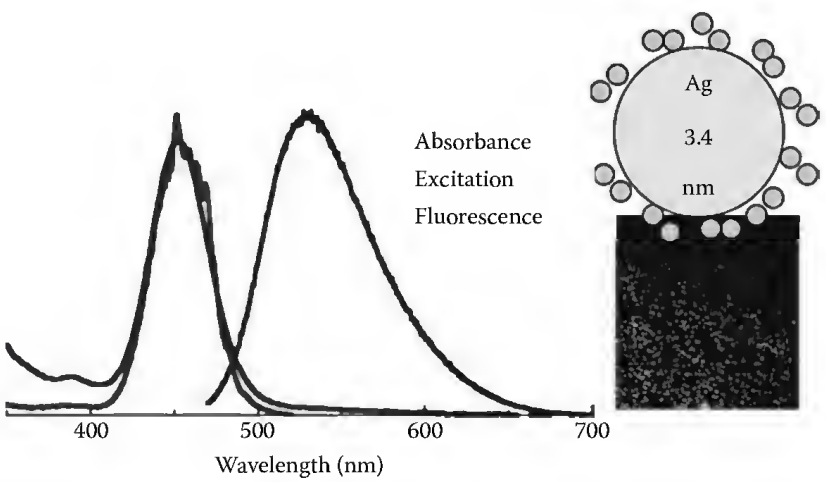

FIGURE 35.14 Spectroscopy of fluorescent AgNP; fluorescence of Ag clusters on AgNP surface and schematic representation of the aggregates responsible for the fluorescence emission.

trifluoroacetate. The stability of the particle fluorescence was also found to depend on the ammonium ion, where larger ions are paramount to the particle and cluster stability.

TEM studies on AgFNP showed a particle size to be 3.4 ± 0.7 nm when prepared in THF and transferred to toluene for TEM analysis. Fluorescence microscopy studies were performed to localize the fluorescence in an environment most similar to solution conditions, optimized in a thin polystyrene film containing hexadecylamine AgFNP, where it was verified that emission arose from discrete particles and that Ag_2 fluorescent clusters must reside on the AgNP.

The clusters exhibit simple monoexponential decay characteristic more of smaller molecules than the complex, multiexponential decay of metal particles such as quantum dots. Other reports have also detected fluorescence of NP in the 2–3 nm range and attributed it to Ag_2 clusters.[69] These clusters still possess their emissive properties upon aggregation, yet the sharpness of their absorption and emission profiles are compromised. The generation of AgFNP in organic media has numerous possible applications for polymer, lithographic, and conductive material applications.

35.6.2 Photochemical Control over Particle Morphology

In a separate report, Stamplecoskie et al. have recently devised a method for synthesizing AgNP with tailored morphology.[22] Aqueous AgNP were prepared from equimolar I-2959 and $AgNO_3$ with UVA irradiation in the presence of excess sodium citrate as a stabilizer to afford spherical nanoparticles 3.3 ± 0.4 nm in diameter. When colloidal solutions were subsequently exposed to light-emitting diodes (LEDs) with intense irradiation, anisotropic nanoparticles with different geometries were realized, depending on the irradiation wavelength. Essentially, excitation of the local plasmon reduced the intensity of the translation SPB of silver seeds at 395 nm and induces the growth of another SPB at a wavelength of lower energy than the excitation wavelength. Upon illumination with a 405 nm LED, the SPB of the AgNP solution shifted from 395 to 416 nm with a corresponding increase in size of spherical particles from 3 to 25 nm for as long as 2 h of irradiation (Scheme 35.10). This illustrated a strategic method for tuning the size of spherical AgNP photochemically and emerges as one of the simplest and cleanest methods for producing monodisperse nanoparticles, while other photochemical methods necessitate the presence of citrate, L-arginine, and PVP with long irradiation times for resultant polydisperse particles and variable morphology.

The architecture of AgNP could also be tuned by excitation at different wavelengths. Irradiation at 455 nm light, for instance, generated larger dodecahedra nanoparticles via the light-induced agglomeration of multi-twinned seeds to form lower energy surfaces. Analysis of the changes in absorption spectroscopy revealed a decrease in the dipole transient SPB at 395 nm and growth of a new peak at 495 nm and a broad shoulder appearing around 650 nm. Further, irradiation between 505 and 627 nm led to the generation of nanoprisms where the aspect ratio increased with irradiation wavelength. The appearance of truncated triangular or hexagonal prisms also appeared to be less prominent with lower irradiation energy. A similar decrease in the intensity of the translational SPB was followed by the appearance of a longitudinal SPB at a wavelength of lower energy relative to the excitation source. When 720 nm LEDs are used, the translational surface plasmon is excited, resulting in a variety of nanorods of different aspect

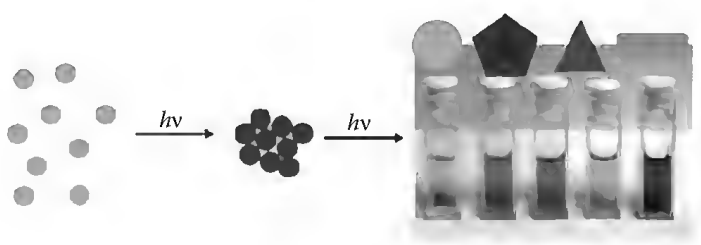

SCHEME 35.10 Generation of AgNP with differing morphology from LED-seeded growth. (From Stamplecoskie, K.G. and Scaiano, J.C., *J. Am. Chem. Soc.*, 132, 1825, 2010.)

ratios. The mechanism has been theorized to be dependent on the excitation of surface electrons where the corresponding electromagnetic field is generated, which induces agglomeration followed by growth along the direction of the excited dipole. Generally, the resulting absorption is redshifted relative to the LED source, and the morphologies tend to be a single species of anisotropic species when one sharp SPB peak emerges, or a mixture of shapes when translational and longitudinal SPBs are apparent with significant scattering. In terms of time required to prepare the different morphologies, synthesis can be complete in as little as 2 h for dodecahedra, yet 7 h or more for conversion to plates. Since nanoparticle growth and agglomeration are dependent on excitation of the SPB, it is reasonable that nanoparticle synthesis utilizing an LED source with longer wavelengths requires longer irradiation times since the absorbance intensity is significantly lower. To verify the aggregation/coalescence mechanism for this photochemical approach, it was observed that different morphologies were only successfully prepared using a CW light source, and that no change in the spherical seed AgNP occurred when a pulsed lamp such as a YAG-pumped OPO at 410 nm with a 10 ns laser pulse was used.

A secondary approach to photochemical control over particle morphology has been applied to AuNP adapting a photochemical seeding technique. Several reports have been recently presented on the optimization monodispersity of nanoparticle size by way of seeding.[6–8,70,71] This method physically and temporally separates the nucleation and growth stages of nanoparticle formation by placing preformed nanoparticles (or seeds) in the presence of additional metal salt and a mild reducing agent. In the case of AuNP, mild reducing agents such as ascorbic acid or hydroxylamine hydrochloride are too weak to reduce the aurous salt, yet strong enough to induce surface-catalyzed reduction for the metal salt physisorbed to the nanoparticle. One challenge in this approach is to limit the degree of growth of new nanoparticles formed, otherwise known as secondary nucleation, where nanoparticle surfaces can catalyze the reduction of gold salts to atoms, yet the atoms nucleate independently to generate new small nanoparticles. Work by Gearheart et al. advanced seeded growth of spherical particles as well as extending growth into nanorods with the use of CTAB, acetone, and $AgNO_3$ and careful control of growth solution and seed concentrations.[70] While seeding of the photochemically generated nanoparticles can be executed thermally using mild reducing agents, we have recently been able to carry out photochemical seeding (Figure 35.15). While ketyl radicals have a high reduction potential, minimizing the concentration and performing subsequent seeding has allowed for optimal growth conditions. A similar approach has been developed using H_2O_2 as a mild reducing agent. With this photochemical subsequent seed-mediated growth method, gold nanoparticles were synthesized using the I-2959 method[18], and employed as seeds for addition to a growth solution $HAuCl_4$ and photochemical reducing agent and irradiated through CW UVA photolysis. The resulting enlarged seeds were used again as seeds for

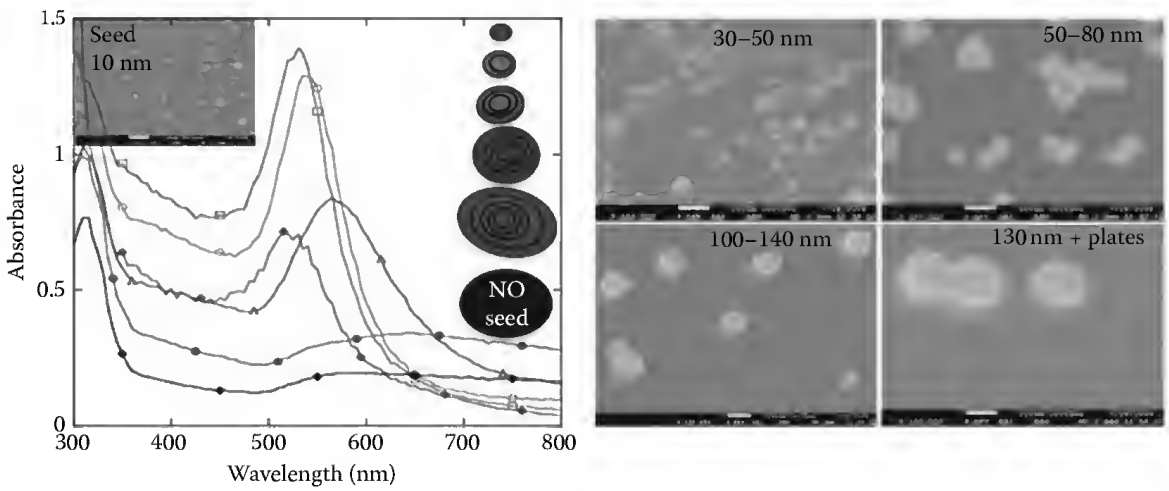

FIGURE 35.15 Sequential photoinduced seeding of AuNP using H_2O_2 and $HAuCl_4$.

further subsequent photochemical seeding. Spherical seeds with great monodispersity were produced up to ~120 nm. Upon further successive seeding, anisotropic particles and platelets took shape, presumably owing to the lower surface energies of larger particles. Control experiments in the absence of seeds resulted in slow growth of platelets and large prisms of micrometer length, thus confirming that controlled growth of spheres is a result of catalytic growth at the particle surface. Controlled photochemical seeded growth was also carried out using H_2O_2 as a reducing agent in the growth solution with I-2959 generated AuNP. In these experiments, the concentration of H_2O_2 was also kept approximately equimolar with the aurous salt concentration. Greater yields of nanoparticles were formed using H_2O_2. While these larger (>20 nm) nanoparticles offer little use for catalytic reaction, many applications can harness into the strong surface plasmon absorption from larger particles, in such cases as imaging and drug delivery.

35.6.3 Functionalization of Metal Nanoparticles for Biological Applications

Recent studies by Narain et al. have revealed bioconjugated Steptavidin to AuNP with a photochemical approach.[19,20] Here, AuNP were prepared via photolysis of I-2959 in the presence of $HAuCl_4$, methoxy-poly(ethylene glycol) thiol (MPEG-SH), poly(*N*-isopropylacrylamide) (PNIPAAm), and a specific glycopolymer containing biotin under 350 nm light. Exposure to streptavidin resulted in a bathochromic shift in the SPB solution, indicative of selective binding of the functionalized AuNP. Subsequently, the authors also succeeded in stabilizing AuNP with bovine serum albumin as well as PEG-SH, where these biocompatible shells can allow stabilization and further functionalization for drug delivery applications.

35.6.4 Photo-Patterning of Metal Nanoparticles

Photochemical synthesis of nanomaterials has also been extended into lithographic deposition with spatiotemporal control over feature size and shape. Notable efforts have been put forth by Sakamoto et al. in the generation of various metal features patterned in polymer matrices.[25,47] In particular, two-photon production of AuNP in PMMA and PVAc films has yielded 3D patterns such as grids and writing of Chinese characters with feature sizes in the nanoscale. Seeding growth has also been employed in the growth of preassembled nanostructures.[7]

35.7 Conclusions

Photochemical synthesis of metal nanoparticles offers some of the advantages that are common to photochemistry, such as relatively mild conditions along with spatial and temporal control. The reaction intermediates responsible are frequently (even if not always) reducing free radicals, such as ketyl and α-aminoalkyl radicals; a key to utilizing these efficiently involves avoiding precursor quenching, usually of an excited triplet state.[17,26] Standard approaches to achieve this include (a) selection of short-lived excited state (a few nanoseconds) to minimize quenching by precursor metal ions and oxygen; (b) "segregation," such as the use of micelles, polymers, and dendrimers to minimize exposure of excited states to metal ions; (c) addition of good hydrogen donors that compete favorably with metal ion quenching; and (d) presence of stabilizing agents, some photogenerated as in the case of I-2959, to enhance the stability and monodispersity of the yielded particles. Furthermore, photochemistry of the metal salt itself can also be critical to nanoparticle synthesis, particularly where absorption by the metal complex can generate an excited-state complex capable of reduction itself such as the case for Cu(acac) or enhancement of reactivity due to cleavage of Cl atoms for $HAuCl_4$.

Photochemical approaches can also be use to control shape and size, either by seeding growth methods of by LED exposure.[22] The absence of multiple step syntheses or a complex pot of stabilizing agents and additives offers several advantages to these clean photochemical modification techniques. Other possible strategies may involve taking advantage of intense plasmon fields in the vicinity of the particle, an emerging field in nanoparticle research.[72]

Glossary

AgNP	Silver nanoparticle
AuNP	Gold nanoparticle
AZX	1-Axaxanthone
BN	Benzoin
BP	Benzophenone
BPK	Benzophenone ketyl radical
BSA	Bovine serum albumin
1,4-CHD	1,4-Cyclohexadiene
CTAB	Cetyl trimethyl ammonium bromide
CTAC	Cetyl trimethyl ammonium chloride
CuNP	Copper nanoparticle
CW	Continuous wave
ΔE_{ST}	Singlet-triplet energy gap
EXAFS	Extended x-ray absorption fine structure
4-HEBA	4-Hydroxyethoxy benzoic acid
I-2959	1-[4-(2-Hydroxyethoxy)phenyl]-2-hydroxy-2-methyl-1-propane-1-one, or Irgacure-2959
I-907	2-Metyl-1-[4 = (methylthio)phenyl]-2-(morpholinyl)phenyl-1-butanone, or Irgacure-907
LED	Light-emitting diode
LFP	Laser flash photolysis
MPEG-SH	Methoxy-poly(ethylene glycol) thiol
PBN	α-Phenyl benzoin
PEG	Poly(ethylene glycol)
PMMA	Poly(methylmethacrylate)
PNIPAAm	Poly(*N*-isopropylacrylamide)
PtNP	Platinum nanoparticle
PVA	Poly(vinyl alcohol)
PVAc	Ply(vinyl acetate)
SDS	Sodium dodecyl sulfate
SPB	Surface plasmon resonance band
SPEEK	Sulfonated poly(ether ether ketone)
TBAC	tetrabutylammonium chloride
TDAB	tetradecylammonium bromide
THF	tetrahydrofuran
TMACL	tetramethylammonium chloride
TPAC	tetrapropylammonium chloride
XAN	Xanthone

References

1. M.-C. Daniel, Arstruc, D., Gold nanoparticles: Assembly, supramolecular chemistry, quantum-size-related properties, and applications toward biology, catalysis and nanotechnology, *Chem. Rev.*, 2004, 104, 293–346; G. A. Ozin, Arsenault, A. C., *Nanochemistry: A Chemical Approach to Nanomaterials*, Royal Society of Chemistry, London, U.K., 2005.
2. C. Burda, Chen, X., Narayanan, R., El-Sayed, M. A., Chemistry and properties of nanocrystals of different shapes, *Chem. Rev.*, 2005, 105, 1025–1102.
3. G. Mie, Beitrage zur optik truber medien, speziell kolloidaler metallosungen, *Ann. Phys.*, 1908, 330, 377–445.

4. A. V. Kabashin, Meunier, M., Laser ablation-based synthesis of functionalized colloidal nanomaterials in biocompatible solutions, *J. Photochem. Photobiol. A*, 2006, 182, 330–334; M. F. Becker, Brock, J. R., Cai, H., Henneke, D. E., Keto, J. W., Lee, J., Nichols, W. T., Glicksman, H. D., Metal nanoparticles generated by laser ablation, *Nanostruct. Mater.*, 1998, 10, 853–863.
5. S. Eustis, El-Sayed, M. A., Why gold nanoparticles are more precious than pretty gold: Noble metal surface plasmon resonance and its enhancement of the radiative and nonradiative properties of nanocrystals of different shapes, *Chem. Soc. Rev.*, 2006, 35, 209–217.
6. A. R. Tao, Habas, S., Yang, P. D. Shape control of colloidal metal nanocrystals, *Small*, 2008, 4, 310–325.
7. S. Meltzer, Resch, R., Koel, B. E., Thompson, M. E., Madhukar, A., Requicha, A. A. G., Will, P., Fabrication of nanostructures by hydroxylamine seeding of gold nanoparticle templates, *Langmuir*, 2001, 17, 1713–1718.
8. Q. H. Zeng, Jiang, X. C., Yu, A. B., Lu, G. Q., Growth mechanisms of silver nanoparticles: A molecular dynamics study, *Nanotechnology*, 2007, 18, 035708.
9. G. G. Condorelli, Costanzo, L. L., Fragala, I. L., Giuffrida, S., Ventimiglia, G., A single photochemical route for the formation of both copper nanoparticles and patterned nanostructured films, *J. Mater. Chem.*, 2003, 13, 2409–2411; S. Giuffrida, Costanzo, L. L., Ventimiglia, G., Bongiorno, C., Photochemical synthesis of copper nanoparticles incorporated in poly(vinyl pyrrolidone), *J. Nanopart. Res.*, 2008, 10, 1183–1192.
10. O. Elbeijirami, Omary, M. A., Photochemistry of neutral isonitrile gold(I) complexes: Modulation of photoreactivity by aurophilicity and π-acceptance ability, *J. Am. Chem. Soc.*, 2007, 129, 11384–11393.
11. S. C. Warren, Jackson, A. C., Cater-Cyker, Z. D., DiSalvo, F. J., Wiesner, U., Nanoparticle synthesis via the photochemical polythiol process, *J. Am. Chem. Soc.*, 2007, 129, 10072–10073.
12. N. J. Turro, Ramamurthy, V., Scaiano, J. C., *Modern Molecular Photochemistry of Organic Molecules*, University Science Publishers, New York, 2010.
13. S. Jockusch, Landis, M. S., Freiermuth, B., Turro, N. J., Photochemistry and photophysics of α-hydroxy ketones, *Macromolecules*, 2001, 34, 1619–1626.
14. T. Itakura, Torigoe, K., Esumi, K., Preparation and characterization of ultrafine metal particles in ethanol by UV irradiation using a photoinitiator, *Langmuir*, 1995, 11, 4129–4134.
15. K. Esumi, Matsumoto, T., Seto, Y., Yoshimura, T., Preparation of gold-, gold/silver-dendrimer nanocomposites in the presence of benzoin in ethanol by UV irradiation, *J. Colloid Interface Sci.*, 2005, 284, 199–203.
16. N. Kometani, Kohara, Y., Yonezawa, Y., Preparation of colloidal silver nanoparticles using benzoin as a photoinitiator, *Colloids Surf. A Physicochem. Eng. Asp.*, 2008, 313–314, 43–46.
17. M. L. Marin, McGilvray, K. L., Scaiano, J. C., Photochemical strategies for the synthesis of gold nanoparticles from Au(III) and Au(I) using photoinduced free radical generation, *J. Am. Chem. Soc.*, 2008, 130, 16572–16585.
18. K. L. McGilvray, Decan, M. R., Wang, D., Scaiano, J. C., Facile photochemical synthesis of unprotected aqueous gold nanoparticles, *J. Am. Chem. Soc.*, 2006, 128, 15980–15981.
19. A. Housni, Ahmed, M., Liu, S., Narain, R., Monodisperse protein stabilized gold nanoparticles via a photochemical process, *J. Phys. Chem. C*, 2008, 112, 12282–12290.
20. R. Narain, Housni, A., Gody, G., Boullanger, P., Charreyre, M.-T., Delair, T., Preparation of biotinylated glyconanoparticles via a photochemical process and study of their bioconjugation to streptavidin, *Langmuir*, 2007, 23, 12835–12841.
21. L. Maretti, Billone, P. S., Liu, Y., Scaiano, J. C., Facile photochemical synthesis and characterization of highly fluorescent silver nanoparticles, *J. Am. Chem. Soc.*, 2009, 131, 13972–13980.
22. K. G. Stamplecoskie, Scaiano, J. C., Light emitting diode irradiation can control the morphology and optical properties of silver nanoparticles, *J. Am. Chem. Soc.*, 2010, 132, 1825–1827.
23. C. M. Gonzalez, Scaiano, J. C., Photochemical strategies for the facile synthesis of gold–silver alloy and core–shell bimetallic nanoparticles, *J. Phys. Chem. C*, 2009, 113, 11861–11867.

24. N. L. Pacioni, Pardoe, A., McGilvray, K. L., Chretien, M. N., Scaiano, J. C., Synthesis of copper nanoparticles mediated by photogenerated free radicals: Catalytic role of chloride anions, *Photochem. Photobiol. Sci.*, 2009, 9, 766–774.
25. M. Sakamoto, Tachikawa, T., Fujistuka, M., Majima, T., Two-laser-guided three-dimensional microfabrication and processing in a flexible matrix, *Adv. Mater.*, 2008, 20, 3427–3432.
26. J. C. Scaiano, Billone, P., Gonzalez, C. M., Maretti, L., Marin, M. L., McGilvray, K. L., Yuan, N., Photochemical routes to silver and gold nanoparticles, *Pure Appl. Chem.*, 2009, 81, 635–647.
27. B. Maillard, Ingold, K. U., Scaiano, J. C., Rate constants for the reactions of free radicals with oxygen in solution, *J. Am. Chem. Soc.*, 1983, 105, 5095–5099.
28. S. Link, Burda, C., Wang, Z. L., El-Sayed, M. A., Electron dynamics in gold and gold–silver alloy nanoparticles: The influence of a nonequilibrium electron distribution and the size dependence of the electron–phonon relaxation, *J. Chem. Phys.*, 1999, 111, 1255–1264; M. Treguer, de Cointet, C., Remita, H., Khatouri, J., Mostafavi, M., Amblard, J., Belloni, J., de Keyzer, R., Dose rate effects on radiolytic synthesis of gold–silver bimetallic clusters in solution, *J. Phys. Chem. B*, 1998, 102, 4310–4321.
29. S. Link, Wang, Z. L., El-Sayed, M. A., Alloy formation of gold–silver nanoparticles and the dependence of the plasmon absorption on their composition, *J. Phys. Chem. B*, 1999, 103, 3529–3533.
30. J. C. Scaiano, Photochemical and free radical processes in benzil-amine systems. Electron donor properties of α-aminoalkyl radicals, *J. Phys. Chem.*, 1981, 85, 2851–2855.
31. J. C. Scaiano, Intermolecular photoreductions of ketones, *J. Photochem.*, 1973/1974, 2, 81.
32. P. J. Wagner, Truman, R. J., Scaiano, J. C., Substituent effects on hydrogen abstraction by phenyl ketone triplets, *J. Am. Chem. Soc.*, 1985, 107, 7093–7097.
33. P. K. Das, Encinas, M. V., Steenken, S., Scaiano, J. C., Reaction of *tert*-butoxy radicals with phenols. Comparison with the reactions of carbonyl triplets, *J. Am. Chem. Soc.*, 1981, 103, 4162–4166.
34. J. C. Scaiano, Aliaga, C., Maguire, S., Wong, D., Magnetic field control of photoinduced silver nanoparticle formation, *J. Phys. Chem. B*, 2006, 110, 12856–12859.
35. S. Eustis, El-Sayed, M. A., Molecular mechanism of the photochemical generation of gold nanoparticles in ethylene glycol: Support for the disproportionation mechanism, *J. Photochem. Photobiol. B*, 2006, 110, 14014–14019.
36. E. Gachard, Remita, H., Khatouri, J., Keita, B., Nadjo, L., Belloni, J., Radiation-induced and chemical formation of gold clusters, *New J. Chem.*, 1998, 22, 1257–1265.
37. L. J. Martinez, Scaiano, J. C., The photochemistry of 1-azaxanthone in aqueous solutions and in micellar environments, *J. Phys. Chem. A*, 1999, 103, 203–208; J. C. Scaiano, Weldon, D., Pliva, C. N., Martínez, L. J., Photochemistry and photophysics of 1-azaxanthone in organic solvents, *J. Phys. Chem. A*, 1998, 102, 6898–6903.
38. J. C. Scaiano, Does intersystem crossing in triplet biradicals generate singlets with conformational memory? *Tetrahedron*, 1982, 38, 819–824.
39. Y. Yonezawa, Sato, T., Kuroda, S., Photochemical formation of colloidal silver: Peptizing action of acetone ketyl radical, *J. Chem. Soc. Faraday Trans.*, 1991, 87, 1905–1910.
40. F. Kim, Song, J. H., Yang, P., Photochemical synthesis of gold nanorods, *J. Am. Chem. Soc.*, 2002, 124, 14316–14317.
41. T. Placido, Comparelli, R., Giannici, F., Cozzoli, P. D., Capatani, G., Striccoli, M., Agostano, A., Curri, M. L., Photochemical synthesis of water-soluble gold nanorods: The role of silver in assisting anisotropic growth, *Chem. Mater.*, 2009, 21, 4192–4202.
42. O. R. Miranda, Ahmadi, T. S., Effects of intensity and energy of CW UV light on the growth of gold nanorods, *J. Phys. Chem. B*, 2005, 109, 15724–15734.
43. S.-A. Dong, Zhou, S.-P., Photochemical synthesis of colloidal gold nanoparticles, *Mater Sci. Eng. B*, 2007, 140, 153–159.
44. S. Dong, Tang, C., Zhou, H., Zhao, H., Photochemical synthesis of gold nanoparticles by the sunlight radiation using a seeding approach, *Gold Bull.*, 2004, 37, 187–195.

45. S. Kapoor, Preparation, characterization, and surface modification of silver particles, *Langmuir*, 1998, 14, 1021–1025.
46. S. Eustis, Krylova, G., Eremenko, A., Smirnova, N., Schill, A., El-Sayed, M., Growth and fragmentation of silver nanoparticles in their synthesis with fs laser and CW light by photo-sensitization with benzophenone, *Photochem. Photobiol. Sci.*, 2005, 4, 154–159.
47. M. Sakamoto, Tachikawa, T., Fujistuka, M., Majima, T., Two-color two-laser fabrication of gold nanoparticles in PVA film, *Chem. Phys. Lett.*, 2006, 420, 90–94.
48. S. Eustis, Krylova, G., Smirnova, N., Eremenko, A., Tabor, C., Huang, W., El-Sayed, M. A., Using silica films and powders modified with benzophenone to photoreduce silver nanoparticles, *J. Photochem. Photobiol. A*, 2006, 181, 385–393.
49. S. Kapoor, Mukherjee, T., Photochemical formation of copper nanoparticles in poly(*N*-vinylpyrrolidone), *Chem. Phys. Lett.*, 2003, 370, 83–87.
50. S. Kapoor, Palit, D. K., Mukherjee, T., Preparation, characterization and surface modification of Cu metal nanoparticles, *Chem. Phys. Lett.*, 2002, 355, 383–387.
51. N. Kometani, Doi, H., Asami, K., Yonezawa, Y., Laser flash photolysis study of the photochemical formation of colloidal Ag nanoparticles in the presence of benzophenone, *Phys. Chem. Chem. Phys.*, 2002, 4, 5142–5147.
52. J. C. Scaiano, Abuin, E. B., Stewart, L. C., Photochemistry of benzophenone in micelles. Formation and decay of radical pairs, *J. Am. Chem. Soc.*, 1982, 104, 5673–5679.
53. J. C. Scaiano, Solvent effects in the photochemistry of xanthone, *J. Am. Chem. Soc.*, 1980, 102, 7747–7753; N. Mohtat, Cozens, F. L., Scaiano, J. C., Multistage exit of excited xanthone from micelles, *J. Phys. Chem. B*, 1998, 102, 7557–7562.
54. M. Sakamoto, Tachikawa, T., Fujistuka, M., Majima, T., Photochemical formation of Au/Cu bimetallic nanoparticles with different shapes and sizes in a poly(vinyl alcohol) film, *Adv. Funct. Mater.*, 2007, 17, 857–862.
55. M. Harada, Einaga, H., Formation mechanism of Pt particles by photoreduction of Pt ions in polymer solutions, *Langmuir*, 2006, 22, 2371–2377.
56. M. Harada, Einaga, H., In situ EXAFS studies of Au particle formation by photoreduction in polymer solutions, *Langmuir*, 2007, 23, 6536–6543.
57. A. S. Korchev, Bozack, M. J., Slaten, B. L., Mills, G., Polymer-initiated photogeneration of silver nanoparticles in SPEEK/PVA films: Direct metal photopatterning, *J. Am. Chem. Soc.*, 2003, 126, 10–11.
58. K. Mallick, Witcomb, M. J., Scurrell, M. S., Polymer stabilized silver nanoparticles: A photochemical synthesis route, *J. Mater. Sci.*, 2004, 4459–4463.
59. K. Mallick, Witcomb, M. J., Scurrell, M. S., Polymer-stabilized colloidal gold: A convenient method for the synthesis of nanoparticles by a UV-irradiation approach, *Appl. Phys. A*, 2005, 80, 395–398.
60. K. Mallick, Witcomb, M. J., Scurrell, M. S., Self assembly of the metal nanoparticles: Formation of the highly oriented, core–shell type, bimetallic gold–silver film, *J. Nanopart. Res.*, 2007, 9, 323–330.
61. G. Wei, Wang, L., Sun, L., Song, Y., Sun, Y., Guo, C., Yang, T., Li, Z., Type I collagen-mediated synthesis and assembly of UV-photoreduced gold nanoparticles and their application in surface-enhanced Raman scattering, *J. Phys. Chem. C*, 2007, 111, 1976–1982.
62. K. L. McGilvray, Granger, J., Correia, M., Banks, J. T., Scaiano, J. C., Opportunistic use of tetrachloroaurate photolysis in the generation of reductive species for the production of gold nanostructures, *Phys. Chem. Chem. Phys.*, 2011, 13, 11914–11918.
63. H. H. Huang, Ni, X. P., Loy, G. L., Chew, C. H., Tan, K. L., Loh, F. C., Deng, J. F., Xu, G. Q., Photochemical formation of silver nanoparticles in poly(*N*-vinylpyrrolidone), *Langmuir*, 1996, 12, 909–912.
64. Unpublished results from the author's laboratory at the University of Ottawa, Canada.
65. T.-C. Jao, Beddard, G. S., Tundo, P., Fendler, J. H., Stabilization of colloidal silver produced by pyrene-sensitized photoreduction of silver ions in methanol, *J. Phys. Chem.*, 1981, 85, 1963–1966.

66. K. Monserrat, Gratzel, M., Tundo, P., Light-induced charge injection in functional crown ether vesicles, *J. Am. Chem. Soc.*, 1980, 102, 5527–5529.
67. P. K. Sudeep, Kamat, P. V., Photosensitized growth of silver nanoparticles under visible light irradiation: A mechanistic investigation, *Chem. Mater.*, 2005, 17, 5404–5410.
68. D. W. Chang, Dai, L., Photo-induced formation and self-assembling of gold nanoparticles in aqueous solution of amphiphilic dendrimers with oligo(*p*-phenylenevinylene) core branches and oligo(ethylene oxide) terminal chains, *Nanotechnology*, 2007, 18, 365605.
69. S. Fedrigo, Harbich, W., Buttet, J., Optical response of Ag_2, Ag_3, Ag_4 and Au_3 in argon matrices, *J. Chem. Phys.*, 1993, 99, 5712–5717; T. Vosch, Antoku, Y., Hsiang, J. C., Richards, C. I., Gonzalez, J. I., Dickson, R. M., Strongly emissive individual DNA-encapsulated Ag nanoclusters as single-molecule fluorophores, *PNAS*, 2007, 104, 12616–12621; J. Zheng, Dickson, R. M., Individual water-soluble dendrimer-encapsulated silver nanodot fluorescence, *J. Am. Chem. Soc.*, 2002, 124, 13982–13983.
70. N. R. Jana, Gearheart, L., Murphy, C. J., Seeding growth for size control of 5–40 nm diameter gold nanoparticles, *Langmuir*, 2001, 17, 6782–6786.
71. K. R. Brown, Walter, D. G., Natan, M. J., Seeding of colloidal Au nanoparticle solutions. 2. Improved control of particle size and shape, *Chem. Mater.*, 2000, 12, 306–313.
72. P. Anger, Bharadwaj, P., Novotny, L., Enhancement and quenching of single-molecule fluorescence, *Phys. Rev. Lett.*, 2006, 96, 4; P. Bharadwaj, Novotny, L., Spectral dependence of single molecule fluorescence enhancement, *Opt. Express*, 2007, 15, 14266–14274; B. Deutsch, Hillenbrand, R., Novotny, L., Visualizing the optical interaction tensor of a gold nanoparticle pair, *Nano Lett.*, 2010, 10, 652–656.

36

Photocatalytic Water Splitting

Junwang Tang
University College London

Alexander J. Cowan
Imperial College London

36.1 Introduction

The global annual energy consumption is predicted to rise from 13.5 TW/year (2001) to 27 TW/year by 2050 and triple by the end of the century.[1,2] This massive increase in demand is driven by both the predicted rapid economic growth in the developing world and an overall increase in the global population. Currently, the vast majority of energy is obtained through the combustion of fossil fuels with nuclear, hydroelectric, biomass, and renewable energy (solar, wind, wave, and tide), contributing a combined total of less than 15% of the required demand.[3] The limited fossil fuel reserves, coupled to acute environmental concerns related to their utilization, is the driving force behind the development of renewable and clean energy resource. Solar energy represents the most abundant energy source on the planet, with 100,000 TW/year of energy reaching the earth's surface.[3] The ability to capture this energy efficiently and store it in the form of a chemical fuel, allowing for its later use in dark periods, is a key goal for researchers. Development of this technology would offer access to a clean renewable source of fuels and would remove our dependence on fossil fuels.

The light-driven production of hydrogen and oxygen from water utilizing a photocatalytic material has been widely investigated due to its ability to provide a chemical fuel, H_2, from widely available, low-cost resources (sunlight and water). The water-splitting photocatalytic material can be considered to be a mimic of the light reaction center in natural photosynthesis (Figure 36.1). In natural photosynthesis, the oxidation of water by PSII leads to the formation of O_2 and production of reducing equivalents, which are further used in the Calvin cycle in the reduction of CO_2. Here, our artificial systems are also designed to oxidize the water, in a light-driven process, to produce O_2; however, in this case, the goal is also to drive the reduction of protons to produce H_2 (Equation 36.1).

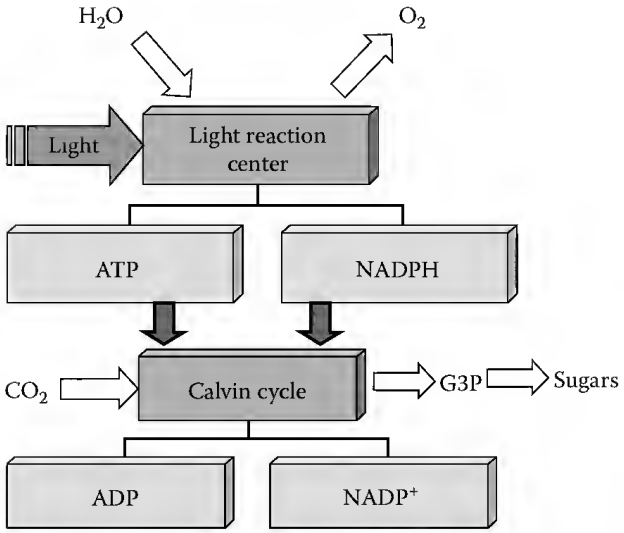

FIGURE 36.1 Schematic diagram of natural photosynthesis.

$$2H_2O + 4H^+ \rightarrow O_2 + 4H^+$$
$$2H^+ + 2e^- \rightarrow H_2 \qquad (36.1)$$

The use of hydrogen, either directly in combustion or in a fuel cell, leads to the release of energy and the formation of water, making this benign cycle a potentially carbon free way to power our lives using solar energy. The photocatalytic splitting of water over semiconductor materials was first demonstrated over 30 years ago by Fujishima and Honda.[4] Their work utilizing a robust, cheap inorganic semiconductor, TiO_2, as a photoanode illustrated the great potential of this technology. However, TiO_2 is only responsive to UV light, which consists of only a very small portion of the solar spectrum (ca. 4%), leading to a very low-energy conversion efficiency. Since this pioneering report, extensive studies have been carried out with the aim of developing materials that can efficiently absorb solar radiation and utilize the energy in the water-splitting reaction. It has been estimated that a minimum 10% solar energy to hydrogen fuel conversion efficiency is required for the commercialization of this technology.[5] While several materials have been found to be active toward visible light, to date no single material has been able to deliver the required efficiency over a sustained period at an acceptable cost.

In this review focusing on water splitting over inorganic semiconductor photocatalysts, we first describe the principles in water splitting over inorganic photocatalysts and then we consider several categories of representative materials. Next, some important factors influencing water-splitting efficiency will be listed. Finally, we consider mechanistic work that is being carried out to guide the design of future materials. This is a very widely studied and fast moving field. A number of excellent review articles have been published in recent years.[6–11] Therefore, due to the limited space available, we have concentrated on looking at a limited number of materials, and we have not considered in detail the use of photocatalytic materials as photoanodes in the photoassisted electrolysis of water.

36.2 Fundamentals of Water Splitting on Semiconductor Photocatalysts

If an incident photon has an energy that is in excess of the semiconductors bands gap, the region extending from the top of the filled valence band (VB) to the bottom of the vacant conduction band (CB), then absorption of the photon and formation of an electron, hole pair can occur, Figure 36.2. If these charge carriers are able to reach the material's surface, then the VB holes and CB electrons can act as oxidizing and reducing species, respectively.

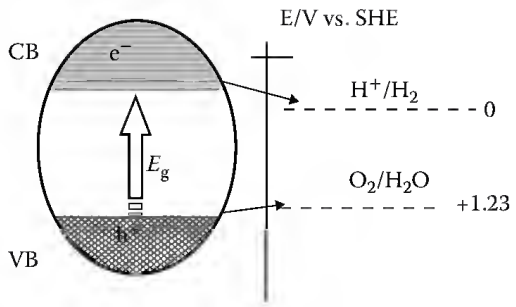

FIGURE 36.2 Idealized energetic diagram of a semiconductor photocatalyst for photochemical water splitting. VB refers to the valence band and CB the conduction band.

For hydrogen production to occur during water splitting, the electrons in the VB are required to have a potential that is more negative than the redox potential of H^+/H_2 (0 V vs. standard hydrogen electrode (SHE)). While for water oxidation and oxygen production to occur, a hole potential that is more positive than the redox potential of O_2/H_2O (+1.23 vs. SHE) is needed. On this basis, a minimum theoretical band gap energy of 1.23 eV is required. In reality, the minimum practical energy required to drive water splitting is much higher due to energy losses associated with the overpotentials required for hydrogen and oxygen production and driving force for charge carrier transportation. It has been commonly predicted that a practical minimum bang gap energy of 1.6 eV (775 nm) is required. Therefore, development of a photocatalyst with activity from the UV through to visible wavelengths (~750 nm) with a VB and CB that straddle the water-splitting potentials is a key goal in obtaining optimum solar to hydrogen fuel efficiency. The band levels of some simple semiconductors have been measured and are shown in Figure 36.3.[6]

These energetic requirements make knowledge of the band gap and position an essential condition when considering semiconductor materials for photocatalytic water splitting. Band gaps of materials are commonly measured by UV–visible absorption spectroscopy. The position of the CB edge is measured using several photoelectrochemical and spectroscopic measurements. On the other hand, the CB edge of an oxide can also be obtained by calculation. This is based upon the Mulliken electronegativities of the constituent atoms. It has been found to be a relatively simple and useful technique.[12–14] The Mulliken electronegativities of atoms are based upon physical measurements and are often described as

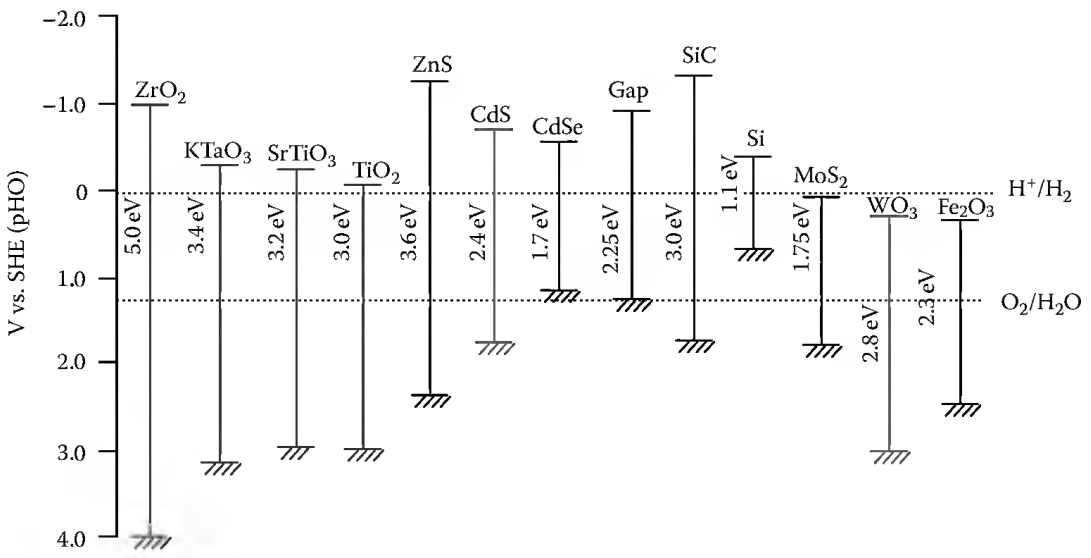

FIGURE 36.3 Band positions of selected semiconductor materials. (Reproduced from Kudo, A. and Miseki, Y., *Chem. Soc. Rev.*, 38, 253, 2009. With permission.)

the absolute electronegativity, in a sense being electrochemical potential of the electron in the neutral atom. The CB position of a semiconductor at the point of zero charge can be expressed empirically by Equation 36.2:

$$E_{CB} = X - 0.5E_g \tag{36.2}$$

where

E_{CB} is the CB edge potential relative to vacuum

X is the electronegativity of the semiconductor, which is the geometric mean of the Mulliken electronegativity of the constituent atoms

E_g is the band gap energy of the semiconductor

The process of water splitting by semiconductor photocatalysts is often considered as encompassing three steps: (1) charge carrier (electron/hole) generation following absorption of a photon of suitable energy, (2) charge carrier separation and transportation, and (3) chemical reaction between surface species and the charge carriers. Photocatalytic water splitting is therefore a complicated combination of photophysical and photochemical processes. There have been numerous examples within the literature of semiconductor materials that are able to evolve both hydrogen or oxygen from water in the presence of a suitable charge carrier scavenger (e.g., to observe H_2 production a hole scavenger is employed), but that are unable to produce both oxygen and hydrogen simultaneously through photochemical water splitting. This demonstrates that although the correct positioning and energy of the band gap is a prerequisite, it is not the sole factor in determining water-splitting activity. Other factors such as kinetic competition, through charge carrier recombination, which may occur at a greater rate than the required surface reductive and oxidative chemistry, can be the dominant factor in determining materials reactivity toward the water-splitting reaction and following a overview of UV and visible active materials, kinetic studies will be examined in Section 36.4.

36.3 Material Development

To date, there are approximately 200 different materials that have been developed for either overall water splitting (hydrogen and oxygen production) or for hydrogen or oxygen production alone (utilizing the relevant scavengers) under UV and visible light irradiation. These materials can be grouped into three main categories, transition metal oxide photocatalysts, main group metal oxide photocatalyst, and others including sulfides and nitrides. In the following sections, we have attempted to provide an overview of key materials that are either active under UV or visible irradiation in each of these categories. Where a material is described as having water-splitting activity, it refers to the production of H_2 and O_2 in a 2:1 ratio from water. If it is described as being active for H_2 or O_2 production, then chemical scavengers will have been employed to scavenge either holes or electrons. Hole scavengers commonly include methanol (MeOH), Na_2S, and Na_2SO_3; and these are used to selectively produce hydrogen. Electron scavengers commonly include Ag^+, $S_2O_8^{2-}$, and $Ce(SO_4)_2$; and these are used to selectively produce oxygen. Reported H_2 and O_2 production rates can be misleading as indicators of material activity as these will depend heavily on conditions such as light source and reactor design. Where possible, we have attempted to report quantum yield for a particular wavelength of light [QY = (number of reacted charge carriers/incident photons) × 100].

36.3.1 UV Active Semiconductors

36.3.1.1 Transition Metal Oxides

It is over three decades since Fujishima and Honda first demonstrated photoassisted electrolysis of water for O_2 production on a TiO_2 anode under an external bias in a three electrode system, where a Pt counter electrode was used to generate H_2.[4] This stimulated extensive research interest in solar hydrogen

generation over metal oxide semiconductors. A key advantage of a number of the metal oxides, such as TiO_2, is their high stability under a range of conditions; unfortunately, this is often associated with a large band gap leading to photocatalytic activity under UV light only. UV-active metal oxides normally have a VB composed of filled O 2p orbitals and CB, which is composed of empty d orbitals for transition metal oxides or s, p orbitals for main group metal oxides. In the following section, a number of UV-driven transition metal oxide photocatalysts are reviewed.

TiO_2 has continued to be widely studied as a UV-active water-splitting material. Various studies have been carried out since that have confirmed the initially reported activity of TiO_2 and these have identified O_2 and H_2 as the products formed during water splitting.[5,15] In place of an externally applied electrical bias, a pH difference between two compartments of a cell can be used to promote electron transportation from a TiO_2 photoanode to a Pt cathode.[16] Subsequent studies on powdered TiO_2 catalysts have examined the photoactivity of TiO_2 in the absence of any applied bias, and it has been reported that TiO_2 can split preabsorbed water vapor.[17] Grätzel et al.[18] reported that UV irradiation of colloidal TiO_2 loaded with both Pt and RuO_2 lead to the formation of both H_2 and O_2, though O_2 was believed to be bound to the catalyst surface preventing its observation for an initial period. Mills and Porter[19] also investigated the addition of a Pt catalyst to the TiO_2 surface and reported that H_2 production but no O_2 production was observed, presumably due to photoabsorption of the O_2 produced. In 1985, Yamaguti and Sato[20] found loaded both Rh and NaOH onto TiO_2 and reported a greatly enhanced activity for photochemical splitting of water vapor (QY = 29%). Since these initial reports, there have been a range of other transition metal oxides developed that are active under UV illumination and Table 36.1 shows a brief summary of their activities.

From Table 36.1, it can be seen that the oxides of groups IV (Ti, Zr), V (Nb, Ta), and VI (Mo, W) have been heavily researched for their photocatalytic ability. From group IV, particular attention has been paid to $SrTiO_3$ except TiO_2, a perovskite structured material. In the presence of a NiO cocatalyst, $SrTiO_3$ has been reported to be active for both O_2 and H_2 production under UV illumination (H_2: 40 μmol/h, O_2: 19 μmol/h).[22–27] In these studies, the NiO cocatalyst was prepared by H_2 reduction and subsequent O_2 oxidation of NiO to form a Ni/NiO double layer structure. RhO_x has also been reported to be an active cocatalyst for water splitting on $SrTiO_3$.[71]

Other important titanates that have been studied include, $La_2Ti_2O_7$, a layered structure consisting of four TiO_6 unit slabs separated by La^{3+} ions layers. $La_2Ti_2O_7$ has demonstrated stoichiometric oxygen and hydrogen production from photocatalytic water splitting with a high QY (up to 12%) when used with a NiO cocatalyst.[28] The doping of $La_2Ti_2O_7$/NiO with BaO and the addition of NaOH to the catalyst suspension leads to an even greater enhancement in the water-splitting ability and a QY of ~50% (UV region), the second highest QY for a UV-water-splitting photocatalyst in the absence of scavengers, has been reported.[72] The closely related layered perovskite materials, $M_2La_2Ti_3O_{10}$ (M = alkaline metal) also have reported high activities for water splitting following UV excitation.[30,31]

ZrO_2 with a rutile structure has a very large band gap of 5.0–5.7 eV.[70,73] Unlike most binary metal oxides, it has been shown to be active for water splitting without a cocatalyst under UV irradiation. The rate of water splitting can be optimized by the addition of alkali carbonates to the water and $NaHCO_3$ treatment has been found to give the highest efficiency.[70] In contrast to a number of other metal oxides, the addition of cocatalysts such as Pt, Cu, Au, or RuO_2 to the ZrO_2 surface actually leads to a decrease in photocatalytic water splitting, suggesting a large energetic barrier between the cocatalyst and semiconductor material as a result of the large band gap and position of the CB and VB.

In group V, a number of tantalates and niobates have shown high levels of activity for photocatalytic water splitting, these include $MTaO_3$ (M = alkaline metal),[38–40] MTa_2O_6,[42] $M_2Ta_2O_7$,[43–46] and $M_2Nb_2O_7$ (M = earth alkaline metal).[44–46,48] While these materials are suitable for both H_2 and O_2 production, their large band gap limits there potential use as a practical solar hydrogen material. Most of these materials are characterized by a perovskite-type structure (ABO_3), which allows for the preparation of a wide range of derivative photocatalysts by means of incorporating suitable metals into A and/or B sites. $NaTaO_3$ when loaded with a NiO cocatalyst exhibits a particularly high QY (20% at 270 nm)

TABLE 36.1 UV Active Transition Metal Oxide Photocatalysts

Photocatalyst	Experimental Conditions	Cocatalyst	H_2 Evolution (μmol/h)	O_2 Evolution (μmol/h)	QY (%)	References
TiO_2	500 W Hg, water vapor	Rh	449	Stoich	29	[20]
TiO_2 (rutile)	360 W Hg, water vapor	None	0.4	0.2		[17]
Nb_2O_5:TiO_2	450 W Xe, pure water	Pt and RuO_2	200	100		[21]
$SrTiO_3$	450 W Hg, NaOH solution	NiO	40	19		[22–27]
La_2TiO_5	450 W Hg, pure water	NiO	442	Stoich		[28]
$La_2Ti_3O_9$	450 W Hg, pure water	NiO	386	Stoich		[28]
$La_2Ti_2O_7$	450 W Hg, pure water	NiO	441	Stoich	12 (360 nm)	[28]
Ba:$La_2Ti_2O_7$	450 W Hg, NaOH solution	NiO	5,000	Stoich	50	[28]
$Sr_3Ti_2O_7$	400 W Hg, pure water	NiO	144	72		[29]
$Rb_2La_2Ti_3O_{10}$	450 W Hg, RbOH solution	NiO	869	430	5 (330 nm)	[30]
$K_2La_2Ti_3O_{10}$	450 W Hg, KOH solution	NiO	2,186	1,131		[30,31]
$Cs_2La_2Ti_3O_{10}$	450 W Hg, pure water	NiO	700	340		[30]
$BaTi_4O_9$	400 W Xe, pure water	RuO_2	33	16		[32,33]
$Na_2Ti_3O_7$	300 W Xe, MeOH solution	Pt	19			[34]
$K_2Ti_2O_5$	300 W Xe, MeOH solution	Pt	35			[34]
$K_2Ti_4O_9$	300 W Xe, MeOH solution	Pt	5			[34]
$Cs_2Ti_2O_5$	400 W Hg, MeOH solution	None	500			[35]
H^+–$Cs_2Ti_2O_5$	400 W Hg, MeOH solution	None	852			[35]
$Cs_2Ti_5O_{11}$	400 W Hg, MeOH solution	None	90			[35]
SiO_2–$K_2Ti_4O_9$	400 W Hg, MeOH solution	None	560			[36]
Ta_2O_5	400 W Hg, pure water	NiO	1,150	530		[37,38]
$LiTaO_3$	400 W Hg, pure water	NiO	430	220		[39,40]
$NaTaO_3$	400 W Hg, pure water	NiO	2,180	1,100	20 (270 nm)	[39,40]
$KTaO_3$	400 W Hg, pure water	NiO	6	2		[38,40]
La:$NaTaO_3$	400 W Hg, pure water	NiO	19,800	9,700	56 (270 nm)	[41,42]
Ti:$KTaO_3$	500 W Xe, pure water	NiO	100	30		[43]
$SrTa_2O_6$	400 W Hg, pure water	NiO	960	490	7 (270 nm)	[44]
$BaTa_2O_6$	400 W Hg, pure water	NiO	629	303		[44]
$CaTa_2O_6$	400 W Hg, pure water	NiO	72	32		[44]
$Ca_2Ta_2O_7$	450 W Hg, pure water	NiO	170	83		[45]
$Sr_2Ta_2O_7$	450 W Hg, pure water	NiO	1,000	480	12 (270 nm)	[46–48]
$K_2Sr_{1.5}Ta_3O_{10}$	400 W Hg, pure water	RuO_2	100	39.4	2 (252 nm)	[49]
$KBa_2Ta_3O_{10}$	400 W Hg, pure water	NiO	170		8 (<350 nm)	[50]
La_3TaO_7	400 W Hg, pure water	NiO	164	80		[51,52]
$LaTaO_4$	400 W Hg, pure water	NiO	116	52		[53]
$BaZn_{1/3}Ta_{2/3}O_3$	400 W Hg, MeOH solution	Pt	195			[54]

TABLE 36.1 (continued) UV Active Transition Metal Oxide Photocatalysts

Photocatalyst	Experimental Conditions	Cocatalyst	H_2 Evolution (μmol/h)	O_2 Evolution (μmol/h)	QY (%)	References
$BaZn_{1/3}Nb_{2/3}O_3$	400 W Hg, MeOH solution	Pt	708			[54]
$Ca_2Nb_2O_7$	450 W Hg, pure water	NiO	101		7 (<228 nm)	[50]
$Sr_2Nb_2O_7$	450 W Hg, pure water	NiO	217	97		[46,48,50]
$Ba_5Nb_4O_{15}$	400 W Hg, pure water	NiO	2,366	1,139	7 (270 nm)	[55]
$K_4Nb_6O_{17}$	450 W Hg, pure water	NiO	1,837	850	5 (330 nm)	[56,57]
$Rb_4Nb_6O_{17}$	450 W Hg, pure water	NiO	936	451	10 (330 nm)	[38]
H^+–$KCa_2Nb_3O_{10}$	400 W Hg, MeOH solution for H_2 and Ag^+ solution for O_2	Pt	19,000	8		[58]
H^+–$RbCa_2Nb_3O_{10}$	400 W Hg, MeOH solution for H_2 and Ag^+ solution for O_2	Pt	17,000	16		[58]
H^+–$KSr_2Nb_3O_{10}$	400 W Hg, MeOH solution for H_2 and Ag^+ solution for O_2	Pt	43,000	30		[58]
Bi_2AlNbO_7	400 W Hg, MeOH solution for H_2 and Ag^+ solution for O_2		710	25		[59]
$PbWO_4$	200 W Hg–Xe pure water	RuO_2	24	12		[60,61]
Ag_2WO_4	300 W Xe, MeOH solution for H_2 and Ag^+ solution for O_2	Pt	6	8		[62]
$AgInW_2O_8$	400 W Hg, MeOH solution for H_2 and Ag^+ solution for O_2	Pt	100	266		[13]
$AgBiW_2O_8$	300 W Xe, MeOH solution for H_2 and Ag^+ solution for O_2	Pt	12	7		[62]
$RbTaWO_6$	400 W Hg, RbOH solution	NiO	69.7	34.5		[63]
$BaCeO_3$	400 W Hg, pure water	RuO_2	59	26		[64]
Ca_2NiWO_6	300 W Xe, MeOH solution for H_2 and Ag^+ solution for O_2	Pt	4.12	0.38		[65]
$Na_2W_4O_{13}$	300 W Xe, MeOH solution for H_2 and Ag^+ solution for O_2	Pt	21	9		[66]
$Bi_2W_2O_9$	400 W Hg, MeOH solution for H_2 and Ag^+ solution for O_2	Pt	18	281		[64,67]
$PbMoO_4$	300 W Xe, MeOH solution for H_2 and Ag^+ solution for O_2	Pt	1.9	12.8		[68]
Sr:CeO_2	400 W Hg, pure water	RuO_2	110	55		[69]
ZrO_2	400 W Hg, $NaHCO_3$ solution	None	309	167		[70]

Where available, QY should be used as a measure of material activity for photochemical water splitting. An O_2 evolution rate of "Stoich" refers to a reported stoichiometric production of H_2:O_2 but with no directly reported rate of O_2 evolution. Pt cocatalyst was used for hydrogen evolution with the relevant electron donors and NiO or RuO_2 cocatalysts for complete water splitting. It is same in the following tables unless stated otherwise.

for water splitting.[39,40] Doping of this material ($NaTaO_3$/NiO) with 2 mol% La was believed to cause reduction in the particle size of the catalyst, enhancing the materials surface area. The increase in photocatalyst surface area along with a nanostructuring effect, that was believed to spatially separate the sites of water oxidation and hydrogen evolution, was attributed to be the cause of a massive increase in the QY for water splitting. The QY of 56% is the current record for the UV-driven photocatalytic splitting of water in the absence of any scavengers.[41,42]

An interesting layered material is $M_4Nb_6O_{17}$ (M = alkaline metal), which is active for water splitting under UV irradiation.[38,54,55] It has been suggested that H_2 production occurs on one interlayer while O_2 production occurs in the other interlayer. This is a key advantage of this material as it facilitates H_2 and O_2 separation, preventing recombination, which is a key issue with photochemical water splitting using a photocatalyst suspension.[72] These materials have shown activity for water splitting even in the absence of a cocatalyst. It has been reported that an enhanced activity for H_2 production can be achieved by ion exchange of protons with a suitable hole scavenger.[74]

$BaNi_{1/3}M_{2/3}O_3$ (M = Nb, Ta) and $BaZn_{1/3}M_{2/3}O_3$ (M = Nb, Ta)[52] are derivatives of tantalates and niobates with a ABO_3 perovskite structure. These compounds show the same lattice parameters due to the same ionic radius of Nb^{5+} and Ta^{5+}. Raman spectra and photocatalytic measurement were used to correlate material activity with the phonon modes inside these materials. Some phonon modes in the bending branch of the Raman spectra of the Ta-containing photocatalysts show an obvious redshift in their frequency, compared with those of Nb-containing photocatalysts. The Ta-containing materials have a lower activity for H_2 production compared to the Nb-containing materials even though the latter samples have a smaller surface area and larger band gap. The authors suggested that these phonon modes play an important role in the control of migration of the charge carriers inside the photocatalyst and this dominates photocatalytic activity. The ability of these ABO_3 perovskites to accommodate a range of different transition metal dopants has led to a high level of interest into these materials with the aim of tuning dopants to not just enhance UV-light-driven efficiency but also extend activity into the visible region.

Tungstates and molybdates have also displayed UV-driven photocatalytic activity. It has been demonstrated that these materials require an appropriate sacrificial electron or hole scavenger to observed the generation of O_2 or H_2, respectively. For example, $AgInW_2O_8$ has been reported to be active for H_2 production in an aqueous MeOH solution and O_2 production in silver nitrate solution under UV illumination.[62] However, in the absence of chemical scavengers, H_2 is produced without O_2 evolution on NiO-loaded $AgInW_2O_8$ under UV light. This result would suggest that O_2 formation is occurring but that it is absorbed on the photocatalyst surface, which greatly limits the materials efficiency.[62]

36.3.1.2 Main Group Metal Oxides

Metal oxides containing the elements of groups XIII and XIV, such as In, Sn, Sb, Ga, and Ge, have been reported to be active for water splitting when loaded with a suitable cocatalyst (e.g., RuO_2) under UV light (Table 36.2). MIn_2O_4 (M = Ca, Sr, and Ba),[79,80] containing distorted InO_6 octahedra, shows H_2 and O_2 production from pure water when a cocatalyst (RuO_2) is added to the material through an impregnation method. Among these structures, $CaIn_2O_4$ has the highest demonstrated activity for water splitting under UV light. Materials of the type $MSnO_3$ (M = Ca, Sr, and Ba) have also demonstrated O_2 and H_2 production from pure water when a RuO_2 cocatalyst is deposited on the semiconductor sutface.[75–77] RuO_2 loaded $SrSnO_3$ shows the highest level of activity for photochemical water splitting among these tin oxides, which has been attributed to the suitable positioning of the conduction and VB edges and to the high mobility of the photogenerated charge carriers caused by the proper distortion of SnO_6 connection in $SrSnO_3$. The influence of $SrSnO_3$ morphology on H_2 and O_2 production yields in the presence of sacrificial charge carrier scavengers was investigated further. A nanorod morphology that was obtained by hydrothermal synthesis was found to be the most active with a 10-fold increase in photocatalytic activity when compared to standard particles prepared by high-temperature solid-state reaction with a similar surface area and optical density.[77] $M_2Sb_2O_7$ (M = Ca, Sr) containing corner-shared octahedral

TABLE 36.2 UV Active Main Group Metal Oxide Photocatalysts

Photocatalyst	Experimental Conditions	Cocatalyst	H_2 Evolution (μmol/h)	O_2 Evolution (μmol/h)	QY (%)	References
$CaSnO_3$	400 W Hg, pure water	RuO_2	46	23		[75]
$SrSnO_3$	400 W Hg, pure water	RuO_2	227.2	113.5		[75,76]
$SrSnO_3$	400 W Hg, MeOH solution for H_2 and Ag^+ solution for O_2	Pt	8,200	2,500		[77]
Sr_2SnO_4	300 W Xe, pure water	RuO_2	5	2.5		[78]
$CaIn_2O_4$	200 W Xe, pure water	RuO_2	21	10		[79,80]
$SrIn_2O_4$	200 W Xe, pure water	RuO_2	7	3.5		[79,80]
$SrIn_2O_4$	300 W Xe, pure water	RuO_2	7	3		[79,80]
$Sr_2Sb_2O_7$	300 W Xe, pure water	RuO_2	8	3		[81]
Ga_2O_3	450 W Hg, pure water	NiO	46	23		[82]
$Zn:Ga_2O_3$	450 W Hg, pure water	NiO	4,100	2,200		[83]
Zn_2GeO_4	300 W Xe, pure water	RuO_2	22	10		[84]

Where available, QY should be used as a measure of material activity for photochemical water splitting.

SbO_6 units are known to be active photocatalysts for the overall splitting of water when loaded with RuO_2 and these materials have displayed near-stoichiometric H_2 and O_2 yields.[81] Ga_2O_3 has also shown some activity for water splitting under UV illumination when loaded with a NiO cocatalyst,[82] and this can be greatly enhanced through doping with 1% Zn, which leads to an eightfold increase in water-splitting activity.[83]

36.3.1.3 Other Compounds

A number of sulfides and nitrides have reported photocatalytic water-splitting ability under UV illumination in which the VB is primarily composed of S 3p or N 2p orbitals, Table 36.3. ZnS has a band gap of 3.66 eV limiting its activity to UV light, despite this it has been extensively investigated for photocatalytic hydrogen production.[85–87] Yanagida et al. first reported the evolution of hydrogen over ZnS under illumination of a 125 W Hg lamp in the presence of tetrahydrofuran or an alcohol hole scavenger. To confirm that photocatalytic hydrogen evolution was occurring from water experiments in the presence of D_2O were carried out leading to the evolution of D_2.[87] Reber and Meier.[86] systematically investigated the photochemistry of ZnS examining a range of factors including electron donors, pH, and temperature, which lead to a record QY of 90% following 313 nm excitation of ZnS coated with Pt in a solution of Na_2S, H_3PO_3, and NaOH.[85,86] $CuInS_2$ and $CuIn_5S_8$ have also shown activity for UV-driven hydrogen production from water in the presence of a sulfite electron donor.[88] However, in

TABLE 36.3 UV Active Nonoxide Photocatalysts

Photocatalyst	Experimental Conditions	Cocatalyst	H_2 Evolution (μmol/h)	O_2 Evolution (μmol/h)	QY (%)	References
ZnS	200 W Hg, Na_2S, H_3PO_3, NaOH solution	None	13,000		90 (313 nm)	[85,86]
$CuInS_2$	400 W Xe, Na_2SO_3 solution	None	0.3			[88]
$CuIn_5S_8$	400 W Xe, Na_2SO_3 solution	None	1.8			[88]
Ag:CdS	900 W Xe, Na_2S, Na_2SO_3 solution	Pt	11,440		25 (450 nm)	[89]
Ge_3N_4	450 W Hg, pure water	RuO_2	1,400	700	9 (300 nm)	[90–93]
GaN	450 W Hg, H_2SO_4 solution	$Rh_{2-x}Cr_xO_3$	19	9.5	0.7 (300 nm)	[94]
Mg:GaN	450 W Hg, pure water	RuO_2	730	290		[95]

Where available, QY should be used as a measure of material activity for photochemical water splitting.

common with all of the sulfide materials reported here photochemical corrosion has proved to be a major obstacle, with sulfide oxidation to sulfates and sulfur occurring in the absence of suitable sacrificial electron donors.

Domen et al. recently developed a new family of UV-active nitride photocatalysts.[90–95] The VB of these photocatalysts is composed primarily of N 2p orbitals, instead of O 2p orbitals as in metal oxides, resulting in a narrowing of the band gap. When loaded with a RuO_2 cocatalyst Ge_3N_4 is an active photocatalysts for water splitting under UV irradiation. Ge_3N_4 is also the first reported nonoxide photocatalyst for the complete splitting of water in the absence of a chemical scavenger, and a QY of 9% at 300 nm has been reported.[90–93] GaN, the widely used material in blue light emitting diodes (LEDs), also displays water-splitting activity under UV illumination when modified with an $Rh_{2-x}Cr_xO_3$ cocatalyst.[94]

36.3.2 Visible Light–Driven Photocatalysts

In the following section, a review of materials suitable for visible light–driven photocatalytic water splitting is carried out. In order to achieve visible light absorption, a number of groups have examined using of anion- or cation-doped materials. In these materials, a dopant level is introduced into the band gap, for example, between the VB (mainly O 2p) and the CB (transition metal 3d) of a metal oxide. The function of the dopant is to lead to the formation of either a new VB (anion doping, such as N, C, and P) or CB (cation doping, such as Cr and Ni).

36.3.2.1 Metal Oxides

WO_3 has been widely studied for its known ability to act as a photocatalyst for water oxidation under visible light irradiation in the presence of an electron acceptor, such as Ag^+. However, the position of the CB of WO_3 makes H_2 production energetically unfavorable (Figure 36.2).[96] Numerous groups have attempted to modify tungsten oxide to enable both H_2 and O_2 evolution. Theoretical calculations predicted that a series of tungsten oxide–based photocatalysts including $AgInW_2O_8$, $AgBiW_2O_8$, Ag_2WO_4 would have a raised CB compared to WO_3 allowing for both H_2 and O_2 production. Experimental photocatalytic water studies have since confirmed these theoretical studies with these materials demonstrating activity for both O_2 and H_2 production (Table 36.4).[13,62,63]

There has been considerable interest in the modification of $SrTiO_3$. This material has shown activity for water splitting under UV light and research has concentrated on extending the absorption profile of this material into the visible region with the hope of producing a cheap, robust visible-light active-water-splitting photocatalyst. Cr–Sb codoped $SrTiO_3$ with a Pt cocatalyst has been used to produce H_2 under visible light irradiation in a solution containing methanol as an electron donor.[97] Doping of $SrTiO_3$ with solely Cr has also been shown to enhance H_2 evolution under visible irradiation, provided that the Cr occupies Sr sites in the $SrTiO_3$ structure, if Cr replaces Ti sites, then it retards photocatalytic ability, demonstrating that the site of doping is a crucial factor influencing material performance.[99] Rh-doped $SrTiO_3$ has also been studied and under visible irradiation photocatalytic H_2 production has been reported when a Pt cocatalyst and a methanol hole scavenger are used.[101] In these studies, doping of $SrTiO_3$ with Rh and Cr has not led to effective visible light water oxidation catalysts with reported O_2 production rates being very limited even in the presence of sacrificial electron donors such as Ag^+. Solid solutions of $AgNbO_3$–$SrTiO_3$ have been shown to photocatalytically split water to produce oxygen under visible light in the presence of an electron scavenger, though this material does not appear to have any H_2 evolution acitivity.[102]

Kudo et al. have reported that monoclinic $BiVO_4$ is a very active water oxidation photocatalyst under visible irradiation with a QY for O_2 production of 9% at 450 nm.[117–119] The photocatalytic activity of $BiVO_4$ has been found to be strongly influenced by the material preparation route, with precipitation method producing more active photocatalyst than the other reaction syntheses regardless of the low surface area of the catalyst.[119] The lower efficiency of the materials prepared by high-temperature solid synthetic routes has been proposed to be due to an increase in the defect concentration in this material

TABLE 36.4 Visible Light Active Transition Metal Oxide Photocatalysts

Photocatalyst	Experimental Conditions	Cocatalyst	H_2 Evolution (μmol/h)	O_2 Evolution (μmol/h)	QY (%)	References
Cr–Sb:TiO_2	>420 nm, Ag^+ solution			32		[97]
Rh–Sb:TiO_2	>420 nm, Ag^+ solution			17		[98]
$(Sr_{0.95}Cr_{0.05})TiO_3$	>420 nm, MeOH solution	Pt	21		0.86 (H_2, 420 nm)	[99]
$Sr(Ti_{0.95}Cr_{0.05})O_3$	>420 nm, MeOH solution	Pt	0.2			[99]
Cr–Sb:$SrTiO_3$	>420 nm, MeOH solution for H_2 and Ag^+ solution for O_2	Pt	78	0.9		[97]
Cr–Ta:$SrTiO_3$	>420 nm, MeOH solution	Pt	70			[100]
Rh:$SrTiO_3$	>420 nm, MeOH solution	Pt	117			[101]
$(AgNbO_3)_{(1-x)}$ $(SrTiO_3)_{(x)}$	>420 nm, Ag^+ solution			162	16.4 (O_2, 420 nm)	[102]
$In_3CrTi_2O_{10}$	>420 nm, MeOH solution	Pt	0.3			[103]
$In_6NiTi_6O_{22}$	>420 nm, MeOH solution	Pt	0.2			[103]
$In_{12}NiCr_2Ti_{10}O_{42}$	>420 nm, MeOH solution	Pt	8.2			[103]
Rh:$CaTiO_3$	>420 nm, MeOH solution	Pt	8.5			[104]
Cr/Fe:$La_2Ti_2O_7$	>420 nm, MeOH solution	Pt	10			[105,106]
$SnNb_2O_6$	>420 nm, MeOH solution for H_2 and Ag^+ solution for O_2	Pt	14	63		[107,108]
$AgNbO_3$	>420 nm, MeOH solution for H_2 and Ag^+ solution for O_2		8	37		[109]
$InMO_4$ (M = Nb, Ta)	>420 nm, pure water	NiO	4	None		[110]
WO_3	>420 nm, Ag^+ solution			65		[96]
Bi_2WO_6	>420 nm, Ag^+ solution			3		[67,111]
$AgInW_2O_8$	>420 nm, Ag^+ solution			4		[63]
Bi_2MoO_6	>420 nm, Ag^+ solution			55		[112]
Cr:$PbMoO_4$	>420 nm, Ag^+ solution			72		[113]
$Zn_3V_2O_8$	>420 nm, MeOH solution for H_2 and Ag^+ solution for O_2	Pt	None	10.2		[114]
$Mg_3V_2O_8$	>420 nm, MeOH solution for H_2 and Ag^+ solution for O_2	Pt	None	3.6		[114]
$Na_{0.5}Bi_{1.5}VMoO_8$	>420 nm, Ag^+ solution			74		[115]
$AgVO_4$	>420 nm, Ag^+ solution			17		[116]
$BiVO_4$	>420 nm, Ag^+ solution			421	9 (O_2, 450 nm)	[117–119]
Bi $Mo_{0.02}V_{0.98}O_4$	>420 nm, Ag^+ solution			370	31 (O_2, 420 nm)	[120]
$InVO_4$	>420 nm, pure water	NiO	5	None		[121]
$AgLi_{1/3}Sn_{2/3}O_2$	>420 nm, Ag^+ solution			53		[122]
$BaCr_2O_4$	>420 nm, MeOH solution for H_2 and $Ce(SO_4)_2$ solution for O_2	Pt	100	8		[123]
$In_{0.9}Ni_{0.1}TaO_4$	>400 nm, pure water	NiO	16.6	8.3	0.66 (402 nm)	[124]

Where available, QY should be used as a measure of material activity for photochemical water splitting.

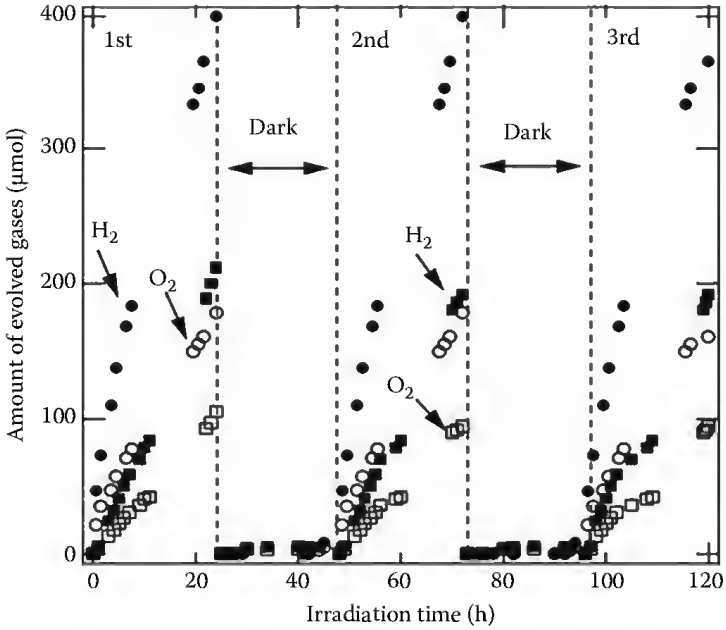

FIGURE 36.4 Water splitting on Ni-doped $InTaO_4$ under visible light irradiation. (Reproduced from Zou, Z.G. et al., *Nature*, 414, 625, 2001. With permission.)

as a result of the high temperatures employed. Ye et al.[120] have investigated the effect of doping $BiVO_4$ with Mo, which led to the reporting of a very high QY for O_2 production (31%) at 420 nm.

The group of Ye has also investigated many photocatalysts containing Cr or V including $In_6NiTi_6O_{22}$, $In_3CrTi_2O_{10}$, and $In_{12}NiCr_2Ti_{10}O_{42}$.[103] These materials all have a similar monoclinic crystal system and the same space group $P2_1/a$, which allowed the authors to clarify the effects of transition metal cations (Ni and/or Cr) with partially filled 3d orbitals on the photocatalytic properties of the system. Even though the band gap energies of the three systems are very similar, they showed significantly different photocatalytic H_2 evolution rates. The much higher activity of $In_{12}NiCr_2Ti_{10}O_{42}$ for H_2 evolution was attributed to continuous CB and VB, formed by the hybridization of split Ni 3d and Cr 3d orbitals with Ti 3d and O 2p orbitals, which would be expected to be beneficial for charge carrier transportation, suggesting the importance of charge carrier mobility in these systems.

All of the materials described earlier have reported activity for H_2 and/or O_2 production under visible light, only in the presence of an appropriate sacrificial reagents. To date, the only metal oxide (other than solid solution) with reported visible light activity for water splitting in the absence of scavenger species is Ni-doped $InTaO_4$, which was reported by Zou et al.[124] When an RuO_2 or NiO cocatalyst is employed on the Ni-doped $InTaO_4$, H_2 and O_2 are produced with a ratio of 2:1 from pure water under visible irradiation with a QY of 0.66% at 402 nm (Figure 36.4). The photoactivity of undoped NiO–$InTaO_4$ has been investigated and found to be less active. It is suggested that Ni^{2+} ions displace In^{3+} causing a contraction of the lattice and that the partially filled Ni d orbitals reduce the band gap of the material leading to visible light absorption (<480 nm).

36.3.2.2 Metal Sulfides and Nitrides

Both sulfides and nitrides have great potential as visible light photocatalysts for the production of solar H_2 and the representative materials are listed in Table 36.5. Among them, sulphides application has been limited due to photocorrosion that hampers the materials stability. In an attempt to improve resistance to photocorrosion, electron donors such as S^{2-} and SO_3^{2-} are often added into the water solution. Among the sulfides, CdS is the most extensively investigated material due to its narrow band gap and ideal bands positions for both O_2 and H_2 evolution (CB at −0.87 V and VB 1.5 V vs. SHE) (Figure 36.3).[89,125,126]

TABLE 36.5 Visible Light Active Metal Sulfide and Nitride Photocatalysts

Photocatalyst	Experimental Conditions	Cocatalyst	H_2 Evolution (μmol/h)	O_2 Evolution (μmol/h)	QY (%)	References
Ta_3N_5	>420 nm, MeOH solution for H_2 and Ag^+ solution for O_2	Pt	10	420	10 (O_2, 420 nm)	[127,128]
TaON	>420 nm, MeOH solution for H_2 and Ag^+ solution for O_2	Pt	9	660	34 (O_2, 420–500 nm)	[129]
$MTaO_2N$ (M = Ca, Sr, Ba)	420 nm, MeOH solution for H_2 and Ag^+ solution for O_2	Pt	15	0		[130]
$Y_2Ta_2O_5N_2$	420 nm, MeOH solution for H_2 and Ag^+ solution for O_2	Pt–Ru	250	140		[131]
$CaNbO_2N$	420 nm, MeOH solution for H_2 and Ag^+ solution for O_2	Pt	2	46		[132]
$Ga_{0.88}N_{0.88} \cdot Zn_{0} \cdot _{12}O_{0.12}$	>420 nm, H_2SO_4 solution	$Rh_{2-x}Cr_xO_3$	800	400	5.9 (420 nm)	[133–135]
$Zn1 \cdot _{44}GeN_{2.08}O_{0.38}$	>420 nm, pure water	RuO_2	14	7		[136]
$AgGaS_2$	>420 nm, Na_2S, K_2SO_3 solution	Rh	1,340		25 (H_2, 440 nm)	[137]
$AgIn_5S_8$	>420 nm, Na_2S, K_2SO_3 solution	Pt	60		5.3 (H_2 410 nm)	[138]
$ZnIn_2S_4$	>420 nm, Na_2S, K_2SO_3 solution	Pt	77			[139]
Cu:ZnS	>420 nm, K_2SO_3 solution	None	450		H_2: 3.7 (420 nm)	[140]
Ni:ZnS	>420 nm, Na_2S, K_2SO_3 solution	None	280			[141]
CdS–ZnS	>420 nm, Na_2S, Na_2SO_3 solution	None	250			[142]
$AgInZn_7S_9$	>420 nm, Na_2S, K_2SO_3 solution	Pt	940		20 (H_2, 420 nm)	[143]
$Cu_{0.25}Ag_{0.25}In_{0} \cdot _5ZnS_2$	>420 nm, Na_2S, K_2SO_3 solution	Ru	2,300		7.4 (H_2, 520 nm)	[144]
$Cu_{0.09}In_{0.09}Zn_{1.82}S_2$	>420 nm, Na_2S, K_2SO_3 solution	Pt	1,200		12.5 (H_2, 420 nm)	[145]
CdS	>390 nm, $NaSO_3$ solution	Pt	40		35 (H_2, 430 nm)	[89,125,126]
CdS	>420 nm, Na_2S, Na_2SO_3 solution	Pt–PdS	8,770		93 (H_2 420 nm)	[146]

Where available, QY should be used as a measure of material activity for photochemical water splitting.

Both Mills et al.[19] and Darwent[147,148] investigated CdS for water splitting using Ethylenediaminetetraacetic acid (EDTA) as an electron donor. Under visible light irradiation, Pt coating of CdS was found to improve H_2 evolution rates from aqueous EDTA by a factor of 10. A very high activity for H_2 evolution was reported on Pt–CdS in $NaSO_3$ aqueous solution (QY = 35%, 430 nm). Very recently, Li et al. improved the activity of CdS for H_2 production in Na_2S and Na_2SO_3 solution by co-functionizing CdS with Pt and PdS leading to a QY of 93% at 420 nm.[146] Grätzel et al. have also reported that co-functionized CdS with Pt and RuO_2 is an effective water-splitting photocatalyst under visible irradiation and, furthermore, that the RuO_2 on the CdS surface mediates photocorrosion.[149] A number

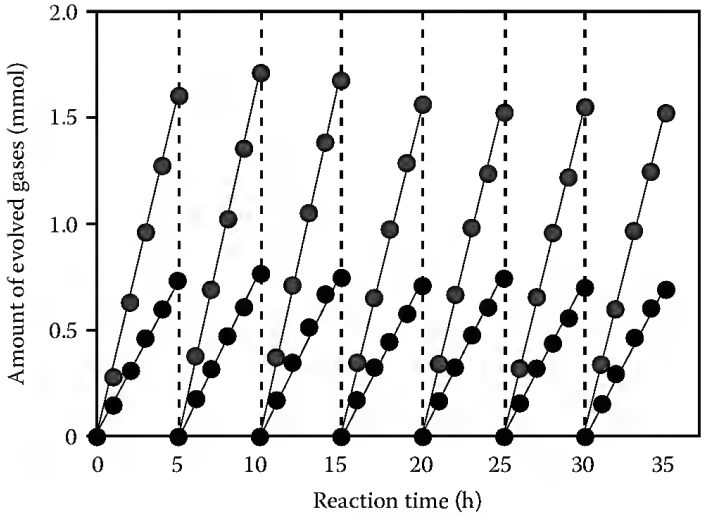

FIGURE 36.5 Water splitting on solid solution of GaN–ZnO under visible light irradiation. (Reproduced from Maeda, K. et al., *Nature*, 440, 295, 2006. With permission.)

of different strategies have been employed to overcome the photocorrosion of CdS including encapsulation of CdS nanoparticles,[150,151] forming composites of CdS with materials such as TiO_2[152,153] and ZnS,[126] and doping of CdS by noble metals and transition metals[154,155]; however, photocorrosion still remains a significant problem with CdS photocatalysts.

Domen et al. have developed a family of nitrides/oxynitrides visible light–driven photocatalyst.[127–132] The oxynitrides can be prepared by nitrodizing metal oxides using ammonia. TaON has a band gap of 2.5 eV and has been found to be active for O_2 evolution (QY = 34%, 420–500 nm) in the presence of a sacrificial electron acceptor ($AgNO_3$(aq)) and separately for H_2 production when used with a Pt cocatalyst in an La_2O_3 buffered methanol/water solution.[129] Tantalum nitride (Ta_3N_5) also has reported activity for both H_2 and O_2 evolution in the presence of sacrificial electron/hole scavengers, though the QY for O_2 production (10%, 420 nm) is significantly lower than that of TaON.[127,128] It should be noted that the nitrides/oxynitrides reported earlier need an La-containing material such as La_2O_3 or $La(NO_3)_3$ to be added to the aqueous solution to buffer the pH for to maintain continuous O_2 production.

Solid solutions of nitride-oxide mixes such as GaN–ZnO and $ZnGeN_2$–ZnO have been found to be active photocatalysts under visible light irradiation.[133–136] $Ga_{0.88}N_{0.88}\cdot Zn_{0.12}O_{0.12}$ coated with a cocatalyst is able to photocatalytically split water with a high QY under visible illumination (QY = 5.9%, 420 nm), Figure 36.5.[133–135] In order to obtain this record high QY, it is essential that a $Rh_{2-x}Cr_xO_3$ cocatalyst with a particle size of 10–30 nm is deposited on the $Ga_{0.88}N_{0.88}\cdot Zn_{0.12}O_{0.12}$ surface and that the pH is adjusted to 4.5 with H_2SO_4. In the absence of the cocatalyst, negligible water-splitting activity is observed. It has been proposed that the $Rh_{2-x}Cr_xO_3$ sites promote H_2 production and inhibit potential O_2 photoreduction.

36.3.2.3 Other Materials

In the previous sections, we have reviewed a large number of materials that are active for only H_2 or O_2 production, but very few that are able to photocatalytically split water to produce H_2 and O_2 simultaneously. Recently, Z-scheme systems have been employed to combine two semiconductor materials, one for H_2 production, one for oxygen production together to make a complete system for water splitting, Figure 36.6. The Z-scheme methodology has been applied to several different material combinations including Pt/$SrTiO_3$–Pt/WO_3 and Pt/$SrTiO_3$–$BiVO_4$.[156,157] Of particular interest is the Z-scheme of Pt/TaON–Pt/WO_3 with an iodine couple electron mediator, which has obtained a QY of 0.4% under 420 nm irradiation and maintains this even after 100 h of use.[158]

A recent exciting report has demonstrated photocatalytic hydrogen production under visible illumination using carbon nitride, a metal free catalyst. While the reported activity for hydrogen production

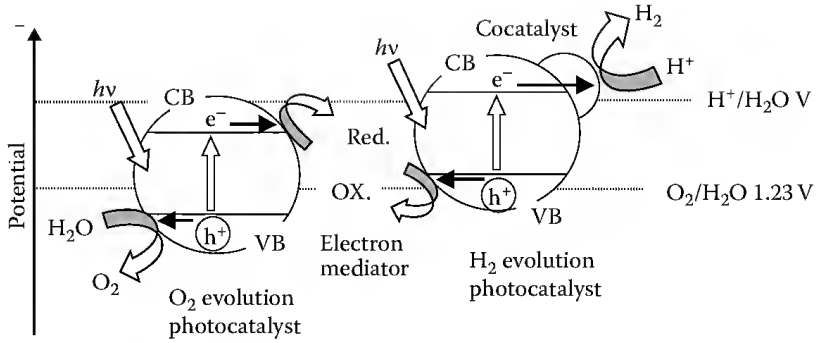

FIGURE 36.6 Z-scheme diagram employing two photocatalysts. (Reproduced from Kudo, A. and Miseki, Y., *Chem. Soc. Rev.*, 38, 253, 2009.)

in the presence of an electron scavenger was very low, this research is very promising due to its utilization of a polymeric organic semiconductor that is both thermally and chemically stable under water-splitting conditions, which is based on cheap and commonly available materials.[159] The authors did achieve an enhancement in hydrogen evolution by the use of a Pt cocatalyst and O_2 evolution was also observed when a RuO_2 cocatalyst was employed on the carbon nitride in a solution containing an appropriate sacrificial reagent; however, the QY reported for H_2 production remained relatively low (~0.1%, 420–460 nm).

36.3.3 Key Factors in Determining Photocatalyst Activity

36.3.3.1 Photocatalyst Surface Area

It might be expected that an increase in the catalyst surface area would be advantageous due to an increased number of active surface reaction sites. While this phenomenon is commonly observed in thermal heterogeneous catalysis, the influence of surface area on water-splitting photocatalysis is less well understood. In the photocatalysis systems discussed earlier, the surface catalysis is only one of the three steps outlined in Section 36.2, and the photocatalyst particle size can have a significant effect on the initial charge carrier separation and on the rate of electron–hole recombination. For example, in studies on $NaNbO_3$ samples prepared by different methods an increase in the surface area from 1.7 m^2/g (solid-state reaction) to 38 m^2/g (polymerized complex method) enhanced the O_2 evaluation rates threefold from 42 to 137 μmol/h and the H_2 evolution rate sixfold from 1100 to 7200 μmol/h.[160] This in contrast is not the case for the activity of $BiVO_4$ for O_2 production. Kudo et al. reported that crystalline $BiVO_4$ samples (49–490 nm) prepared either through precipitation and hydrothermal approaches had similar optical absorptions at wavelengths less than 520 nm, yet the smaller particles displayed much lower activities for O_2 evolution.[119] In another report, hydrothermally synthesized $La_2Ti_2O_7$ with a large surface area of 54 m^2/g exhibited a high activity for H_2 production (72 μmol/h), while material prepared by solid-state reaction with a surface are of 1 m^2/g showed a very low level of photocatalytic activity (<1 μmol/h).[161]

36.3.3.2 Choice of Cocatalyst

The choice of cocatalyst has been shown to be very important in determining the activity of a system for photochemical water splitting with materials such as NiO, RuO_2, Pt, and $Rh_{2-x}Cr_xO_3$ being employed. Numerous examples of the role of cocatalysts are listed earlier. From Table 36.1, it can be seen that NiO has been very widely employed to realize stoichiometric hydrogen and oxygen production from water.[22] The role of cocatalysts is particularly evident on the two most active materials for the photocatalytic splitting of water under visible light. With the NiO/Ni shell/core structure being key in the activity of $In_{0.9}Ni_{0.1}TaO_4$,[124] while $Ga_{0.88}N_{0.88}{\cdot}Zn_{0.12}O_{0.12}$ does not show any activity for water splitting in the absence

of $Rh_{2-x}Cr_xO_3$.[134] Currently, the exact mechanisms of enhancement of activity of most cocatalysts are not known, which complicates the choice of the appropriate material.

36.3.3.3 Other Factors

The morphology and crystal structure of the photocatalyst are also very important factors influencing the performance of photocatalysts for water splitting. Ye et al. found that $SrSnO_3$ prepared by two different methods, by solid reaction or hydrothermal routes, show significantly different levels of activity.[75,76] $SrSnO_3$ synthesized by a solid-state reaction consisted of sphere-like particles while hydrothermal synthesis produced nanorod-structured materials. It was found that both materials had a similar surface area and optical absorption but the nanorod morphology lead to a greater than 10-fold increase in photocatalytic ability for H_2 and O_2 production from water. In Section 36.3.1.1, the effect of La doping of $NaTaO_3$ was reviewed where the presence of the dopant led to a nanostructuring effect that was proposed to be a key factor in a large enhancement in photocatalytic activity.[41,42] $LiTaO_3$ and $KTaO_3$ have also been investigated for water splitting, here the effect of alkali metal ion on material structure and activity has been investigated. These materials have similar perovskite-like structure and are composed of corner-shared TaO_6 octahedra; it was found that as the bond angle of Ta–O–Ta approaches 180° upon changing the alkali metal from $LiTaO_3$ to $KTaO_3$. This was reported to enhance electron–hole migration through the crystal ($LiTaO_3 < NaTaO_3 < KTaO_3$), which had an effect on the materials photocatalytic activity.[38–40]

36.4 Mechanism of Photocatalytic Water Splitting

It has been estimated that a 10% solar energy to hydrogen fuel conversion efficiency is required to make solar hydrogen production from water economically viable.[5] Currently, there are no reported economically feasible materials that are able to deliver this required efficiency for prolonged periods of use. Fundamental mechanistic research can greatly aid the design of new materials with enhanced photocatalytic activities. Despite this, there have been only a limited number of studies that have addressed the fundamental mechanisms occurring during photocatalytic water splitting.

36.4.1 Transient Spectroscopy of Charge Carriers

In addition to extending the absorption profile of photocatalysts to harvest a greater portion of the solar spectrum, a key goal is to enhance the utilization of the charge carriers formed. Measuring charge recombination processes and the rate of charge carrier reactions to produce photoproducts in candidate photocatalysts is therefore a powerful tool to aid the evaluation of potential materials. Transient absorption spectroscopy (TAS) has been used to monitor the charge carriers following initial UV laser excitation of TiO_2 colloids and nanocrystalline (nc-) TiO_2 films. Following UV excitation initial trapping of the photoholes and photoelectrons has been reported to occur within 200 fs, with further electron relaxation occurring within 500 ps.[162] Several groups have identified the transient absorption spectra of the trapped photoelectrons and holes in nc-TiO_2, with the hole having an absorption maximum of ~450 nm, while photoelectrons have been reported an absorption that increases with wavelength, with trapped electrons having a maxima from ~800 nm upward.[163–165]

Following initial electron–hole trapping, recombination has been reported to occur at a range of different rates, with up to 90% of charge carriers recombining within 10 ns in one report using a high UV laser intensity.[166] Several TAS studies have since demonstrated that the rate of recombination is strongly dependent upon the UV excitation intensity, and under light intensities that are more comparable to solar radiation intensities, power law type decays that have significant electron–hole concentrations beyond the microsecond timescales have been observed.[162,165,167] This fast (sub-ms) electron–hole recombination has been found to be the key factor in determining the lack of water-splitting activity of nc-TiO_2 in the absence of a cocatalyst or chemical scavenger.[165] Experiments in the presence of Ag^+ prevent electron–hole recombination allowing for the rate of hole reaction with water to produce O_2,

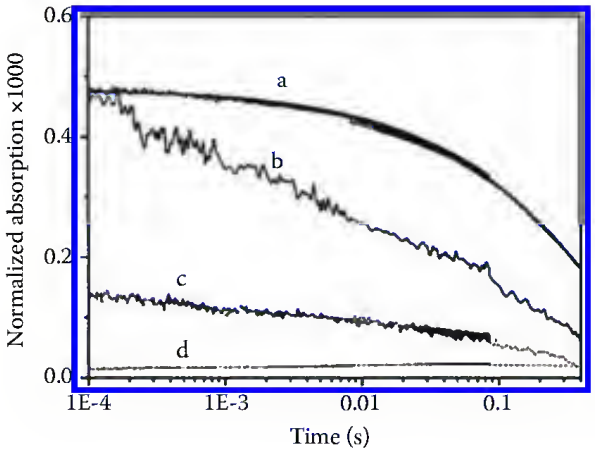

FIGURE 36.7 Kinetics of holes (traces a and b) and electrons (traces c and d) in TiO_2 film with Ag^+ (traces a and d) and Pt (traces b and c) as the electron scavengers after band gap excitation with laser wavelength of 335 nm. (Reproduced from Tang, J.W. et al., *J. Am. Chem. Soc.*, 130, 13885, 2008. With permission.)

to be observed [trace (d) Figure 36.7].[165] This reaction has found to be very slow with an averaged hole lifetime of ~0.2 s at neutral pHs. The observed rate of decay of the holes on nc-TiO_2 is composed of several components as water oxidation is a multihole process. The yield of QY oxygen versus number of photons absorbed per TiO_2 particle has been examined, and it has been observed that the yield peaks at ~4 photons per TiO_2 particle suggesting that the production of one oxygen molecule requires four holes in artificial water-splitting systems, which although is an expected requirement for water oxidation this was the first experimental observation of four hole chemistry in artificial water-splitting systems.[165] Based on a range of TAS studies,[165,166,168] a summary diagram has been produced to illustrate key reaction timescales during nc-TiO_2 water splitting, Figure 36.8.

Transient measurements have also been used to study several other materials closely related to nc-TiO_2. The electron dynamics of TiO_2 codoped with both Sb and Cr have been examined. These materials show visible light activity for oxygen evolution in the presence of Ag^+. It was observed experimentally that the oxygen yield was optimized when the TiO_2 was doped with a Cr:Sb ratio of between 1 and 2, which was found to be due to an increased electron lifetime at this Cr:Sb ratio, leading to a decrease in electron–hole recombination.[169] The electron–hole dynamics on a range of materials including TiO_2 hybrids and doped TiO_2 samples has been examined by the group of Majima et al.,[170] although these studies primarily concentrate on the oxidation of organic materials they do provide important insights into electron–hole dynamics that are directly applicable to the study of water splitting.

The effect of La doping on electron lifetimes in $NaTaO_3$ has also been examined.[171] In previous sections, the large increase in photocatalytic water-splitting activity of $NaTaO_3$ upon La has been discussed in relation to changes in the catalysts nanomorphology. Transient measurements have also revealed

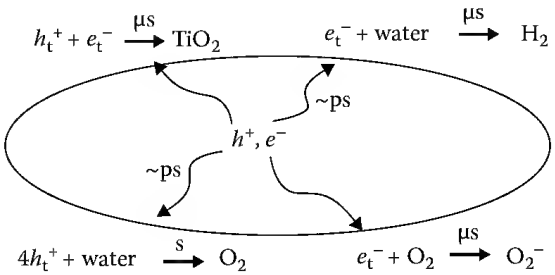

FIGURE 36.8 Timescales of processes occurring on nc-TiO_2 following UV excitation. (Reproduced from Tang, J.W. et al., *J. Am. Chem. Soc.*, 130, 13885, 2008. With permission.)

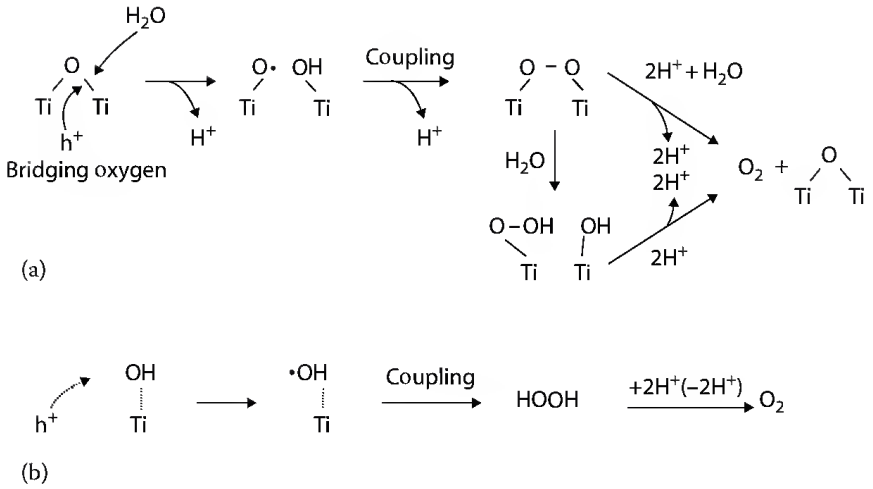

FIGURE 36.9 Proposed mechanisms of water photooxidation on TiO_2 materials at pH < 12. (a) Nucleophilic attack mechanism of Nakato et al.[179] and (b) Ti-OH oxidation pathway.[177] (Adapted from Wilson, R.H., *J. Electrochem. Soc.*, 127, 228, 1980.)

that the La doping greatly reduces electron–hole recombination. In the absence of an La dopant, electron decay occurs within 1 ms when the sample is under a vacuum, while addition of 2% La leads to an electron signal at times beyond 1 s. Addition of a NiO cocatalyst lead to electron transfer from $NaTaO_3$ to NiO within 1 μs and further studies in the presence of water vapor provided evidence for H_2 formation on the milliseconds timescale. Interesting TAS experiments have also been carried out on several materials including Fe_2O_3[172] and a TiO_2/dye/IrO_2 hybrid that are for use in photoelectrochemical cells,[173] though in this review materials that require the application of an electrical bias are not being considered.

36.4.2 Reaction Pathway

Several groups have examined the surface mechanism of photocatalytic water splitting on TiO_2. Experiments have employed a range of techniques including using electrochemical methods,[174] electron paramagnetic resonance (EPR) spectroscopy,[175,176] photoluminescence,[177,178] and Fourier transform infrared spectroscopy (FTIR) spectroscopy.[179] Nakato et al. have used attenuated total reflectance (ATR), FTIR spectroscopy, and photoluminescence measurements at range of pHs. At pH < 12, they have reported that initial nucleophilic attack of a water molecule to a surface-trapped hole at oxygen bridging sites leads to the formation of TiOOH and TiOOTi, which have been reported to be primary intermediates of the oxygen photoevolution reaction, Figure 36.9a.[178–180] This is in contrast with a previously proposed mechanism where the initial step in water oxidation on TiO_2 at pH < 12 is the oxidation of a surface Ti-OH group leading to the formation of OH radicals that could then couple to form H_2O_2, which is readily decomposed in a further two hole oxidation to form O_2, Figure 36.9b.[174,177,181]

36.5 Conclusions

It has been over 30 years since the initial reports of photoassisted electrochemical water splitting on TiO_2. Since then progress has been made toward the development of materials and systems that are able to photocatalytically evolve both O_2 and H_2 under solar illumination, without the need for an additional electrical bias. Despite this to date, no material has reached the required 10% solar to hydrogen fuel conversion efficiency to make this an economical process. The current "state-of-the-art" materials for the complete photocatalytic splitting of water (both O_2 and H_2 evolution) include, under (a) UV light include NiO-modified La/$NaTaO_3$ (QY = 56%, 270 nm), and NiO-Ba/$La_2Ti_2aO_7$ (QY = 50%, 0.01 M NaOH, wavelength unknown) and (b) under visible light; $Rh_{2-x}Cr_xO_3/Ga_{0.88}N_{0.88}{\cdot}Zn_{0.12}O_{0.12}$ (QY = 5.9%, 420 nm,

H_2SO_4 solution), NiO-$In_{0.9}Ni_{0.1}TaO_4$ (QY = 0.66%, 400 nm), and the Z-scheme system of Pt/$SrTiO_3$:Cr, Ta–Pt/WO_3 (QY = 1%, 420 nm, IO_3^-/I^- electrolyte). While CdS is a very effective photocatalyst for H_2 production in the presence of a suitable electron donor, problems persist with its stability due to photocorrosion of the catalysts that has greater limited its application in photocatalytic water splitting.

Several key factors have been identified in the research reported, such as the choice of cocatalyst, nanomorphology, etc. Although these are known to be important in enhancing material efficiency the exact mechanisms occurring during photocatalysis are often not well understood, highlighting the need for fundamental mechanistic research to enhance our understanding of the factors controlling photocatalyst activity.

Acknowledgments

We are grateful to Prof. James Durrant, Prof. David Klug in Chemistry, Imperial College London and Prof. Jinhua Ye, National Institute for Materials Science, Japan for their useful suggestions on water-splitting research.

References

1. M. I. Hoffert, K. Caldeira, A. K. Jain et al., *Nature*, 1998, **395**, 881–884.
2. N. S. Lewis and D. G. Nocera, *Proceedings of the National Academy of Sciences of the United States of America*, 2006, **103**, 15729–15735.
3. J. Barber, *Chemical Society Reviews*, 2009, **38**, 185–196.
4. A. Fujishima and K. Honda, *Nature*, 1972, **238**, 37–38.
5. A. J. Bard and M. A. Fox, *Accounts of Chemical Research*, 1995, **28**, 141–145.
6. A. Kudo and Y. Miseki, *Chemical Society Reviews*, 2009, **38**, 253–278.
7. F. E. Osterloh, *Chemistry of Materials*, 2008, **20**, 35–54.
8. K. Maeda and K. Domen, *Journal of Physical Chemistry C*, 2007, **111**, 7851–7861.
9. A. Hagfeldt and M. Gratzel, *Chemical Reviews*, 1995, **95**, 49–68.
10. A. J. Nozik, *Annual Review of Physical Chemistry*, 1978, **29**, 189–222.
11. H. Arakawa and K. Sayama, *Catalysis Surveys from Japan*, 2000, **4**, 75–80.
12. M. A. Butler, *Journal of Applied Physics*, 1977, **48**, 1914–1920.
13. J. W. Tang, Z. G. Zou, and J. H. Ye, *Journal of Physical Chemistry B*, 2003, **107**, 14265–14269.
14. J. W. Tang, Z. G. Zou, and J. H. Ye, *Journal of Physical Chemistry C*, 2007, **111**, 12779–12785.
15. M. S. Wrighton, D. S. Ginley, P. T. Wolczanski et al., *Proceedings of the National Academy of Sciences of the United States of America*, 1975, **72**, 1518–1522.
16. E. Selli, G. L. Chiarello, E. Quartarone et al., *Chemical Communications*, 2007, 5022–5024.
17. G. N. Schrauzer and T. D. Guth, *Journal of the American Chemical Society*, 1977, **99**, 7189–7193.
18. D. Duonghong, E. Borgarello, and M. Gratzel, *Journal of the American Chemical Society*, 1981, **103**, 4685–4690.
19. A. Mills and G. Porter, *Journal of the Chemical Society—Faraday Transactions I*, 1982, **78**, 3659–3669.
20. K. Yamaguti and S. Sato, *Journal of the Chemical Society—Faraday Transactions I*, 1985, **81**, 1237–1246.
21. J. Kiwi, E. Borgarello, E. Pelizzetti, M. Visca, and M. Gratzel, *Angewandte Chemie International Edition in English*, 1980, **19**, 646–648.
22. K. Domen, S. Naito, M. Soma, T. Onishi, and K. Tamaru, *Journal of the Chemical Society—Chemical Communications*, 1980, 543–544.
23. K. Domen, S. Naito, T. Onishi, and K. Tamaru, *Journal of Physical Chemistry*, 1982, **86**, 3657–3661.
24. K. Domen, S. Naito, T. Onishi, and K. Tamaru, *Chemical Physics Letters*, 1982, **92**, 433–434.
25. K. Domen, A. Kudo, T. Onishi, N. Kosugi, and H. Kuroda, *Journal of Physical Chemistry*, 1986, **90**, 292–295.

26. K. Domen, A. Kudo, and T. Onishi, *Journal of Catalysis*, 1986, **102**, 92–98.
27. A. Kudo, A. Tanaka, K. Domen, and T. Onishi, *Journal of Catalysis*, 1988, **111**, 296–301.
28. J. Kim, D. W. Hwang, H. G. Kim et al., *Topics in Catalysis*, 2005, **35**, 295–303.
29. H. Jeong, T. Kim, D. Kim, and K. Kim, *International Journal of Hydrogen Energy*, 2006, **31**, 1142–1146.
30. T. Takata, Y. Furumi, K. Shinohara et al., *Chemistry of Materials*, 1997, **9**, 1063–1064.
31. S. Ikeda, M. Hara, J. N. Kondo et al., *Chemistry of Materials*, 1998, **10**, 72–77.
32. S. Ogura, K. Sato, and Y. Inoue, *Physical Chemistry Chemical Physics*, 2000, **2**, 2449–2454.
33. Y. Inoue, T. Niiyama, Y. Asai, and K. Sato, *Journal of the Chemical Society—Chemical Communications*, 1992, 579–580.
34. M. Shibata, A. Kudo, A. Tanaka et al., *Chemistry Letters*, 1987, 1017–1018.
35. A. Kudo and T. Kondo, *Journal of Materials Chemistry*, 1997, **7**, 777–780.
36. M. Machida, X. W. Ma, H. Taniguchi, J. Yabunaka, and T. Kijima, *Journal of Molecular Catalysis A—Chemical*, 2000, **155**, 131–142.
37. K. Sayama and H. Arakawa, *Journal of Photochemistry and Photobiology A—Chemistry*, 1994, **77**, 243–247.
38. K. Sayama, H. Arakawa, and K. Domen, *Catalysis Today*, 1996, **28**, 175–182.
39. H. Kato and A. Kudo, *Chemical Physics Letters*, 1998, **295**, 487–492.
40. H. Kato and A. Kudo, *Journal of Physical Chemistry B*, 2001, **105**, 4285–4292.
41. A. Kudo and H. Kato, *Chemical Physics Letters*, 2000, **331**, 373–377.
42. H. Kato, K. Asakura, and A. Kudo, *Journal of the American Chemical Society*, 2003, **125**, 3082–3089.
43. C. Mitsui, H. Nishiguchi, K. Fukamachi, T. Ishihara, and Y. Takita, *Chemistry Letters*, 1999, 1327–1328.
44. H. Kato and A. Kudo, *Chemistry Letters*, 1999, 1207–1208.
45. S. Ikeda, M. Fubuki, Y. K. Takahara, and M. Matsumura, *Applied Catalysis A—General*, 2006, **300**, 186–190.
46. A. Kudo, H. Kato, and S. Nakagawa, *Journal of Physical Chemistry B*, 2000, **104**, 571–575.
47. H. Kato and A. Kudo, *Journal of Photochemistry and Photobiology A—Chemistry*, 2001, **145**, 129–133.
48. M. Yoshino and M. Kakihana, *Chemistry of Materials*, 2002, **14**, 3369–3376.
49. W. F. Yao and J. H. Ye, *Chemical Physics Letters*, 2007, **435**, 96–99.
50. H. G. Kim, D. W. Hwang, J. Kim, Y. G. Kim, and J. S. Lee, *Chemical Communications*, 1999, 1077–1078.
51. R. Abe, M. Higashi, K. Sayama, Y. Abe, and H. Sugihara, *Journal of Physical Chemistry B*, 2006, **110**, 2219–2226.
52. M. Wiegel, M. H. J. Emond, E. R. Stobbe, and G. Blasse, *Journal of Physics and Chemistry of Solids*, 1994, **55**, 773–778.
53. M. Machida, S. Murakami, T. Kijima, S. Matsushima, and M. Arai, *Journal of Physical Chemistry B*, 2001, **105**, 3289–3294.
54. J. Yin, Z. G. Zou, and J. H. Ye, *Journal of Physical Chemistry B*, 2004, **108**, 8888–8893.
55. Y. Miseki, H. Kato, and A. Kudo, *Chemistry Letters*, 2006, **35**, 1052–1053.
56. A. Iwase, H. Kato, and A. Kudo, *Catalysis Letters*, 2006, **108**, 6–9.
57. K. Domen, A. Kudo, A. Shinozaki et al., *Journal of the Chemical Society—Chemical Communications*, 1986, 356–357.
58. K. Domen, J. N. Kondo, M. Hara, and T. Takata, *Bulletin of the Chemical Society of Japan*, 2000, **73**, 1307–1331.
59. Z. G. Zou, J. H. Ye, and H. Arakawa, *Chemistry of Materials*, 2001, **13**, 1765–1769.
60. N. Saito, H. Kadowaki, H. Kobayashi et al., *Chemistry Letters*, 2004, **33**, 1452–1453.
61. H. Kadowaki, N. Saito, H. Nishiyama et al., *Journal of Physical Chemistry C*, 2007, **111**, 439–444.
62. J. W. Tang and J. H. Ye, *Journal of Materials Chemistry*, 2005, **15**, 4246–4251.
63. S. Ikeda, T. Itani, K. Nango, and M. Matsumura, *Catalysis Letters*, 2004, **98**, 229–233.
64. Y. P. Yuan, J. Zheng, X. L. Zhang et al., *Solid State Ionics*, 2008, **178**, 1711–1713.

65. D. F. Li, J. Zheng, and Z. G. Zou, *Journal of Physics and Chemistry of Solids*, 2006, **67**, 801–806.
66. A. Kudo and H. Kato, *Chemistry Letters*, 1997, **26**, 421–422.
67. A. Kudo and S. Hijii, *Chemistry Letters*, 1999, **28**, 1103–1104.
68. A. Kudo, M. Steinberg, A. J. Bard et al., *Catalysis Letters*, 1990, **5**, 61–66.
69. H. Kadowaki, N. Saito, H. Nishiyama, and Y. Inoue, *Chemistry Letters*, 2007, **36**, 440–441.
70. K. Sayama and H. Arakawa, *Journal of Physical Chemistry*, 1993, **97**, 531–533.
71. J. M. Lehn, J. P. Sauvage, and R. Ziessel, *Nouveau Journal De Chimie—New Journal of Chemistry*, 1980, **4**, 623–627.
72. A. Kudo, K. Sayama, A. Tanaka et al., *Journal of Catalysis*, 1989, **120**, 337–352.
73. S. M. Chang and R. A. Doong, *Journal of Physical Chemistry B*, 2004, **108**, 18098–18103.
74. K. Domen, A. Kudo, M. Shibata et al., *Journal of the Chemical Society—Chemical Communications*, 1986, 1706–1707.
75. W. F. Zhang, J. W. Tang, and J. H. Ye, *Journal of Materials Research*, 2007, **22**, 1859–1871.
76. W. F. Zhang, J. W. Tang, and J. H. Ye, *Chemical Physics Letters*, 2006, **418**, 174–178.
77. D. Chen and J. H. Ye, *Chemistry of Materials*, 2007, **19**, 4585–4591.
78. J. Sato, N. Saito, H. Nishiyama, and Y. Inoue, *Journal of Physical Chemistry B*, 2001, **105**, 6061–6063.
79. J. Sato, H. Kobayashi, N. Saito, H. Nishiyama, and Y. Inoue, *Journal of Photochemistry and Photobiology A—Chemistry*, 2003, **158**, 139–144.
80. J. Sato, H. Kobayashi, and Y. Inoue, *Journal of Physical Chemistry B*, 2003, **107**, 7970–7975.
81. J. Sato, N. Saito, H. Nishiyama, and Y. Inoue, *Journal of Photochemistry and Photobiology A—Chemistry*, 2002, **148**, 85–89.
82. T. Yanagida, Y. Sakata, and H. Imamura, *Chemistry Letters*, 2004, **33**, 726–727.
83. Y. Sakata, Y. Matsuda, T. Yanagida et al., *Catalysis Letters*, 2008, **125**, 22–26.
84. J. Sato, H. Kobayashi, K. Ikarashi et al., *Journal of Physical Chemistry B*, 2004, **108**, 4369–4375.
85. M. Wu, W. Z. Gu, W. Z. Li et al., *Science and Technology in Catalysis 1994*, 1995, **92**, 257–262.
86. J. F. Reber and K. Meier, *Journal of Physical Chemistry*, 1984, **88**, 5903–5913.
87. S. Yanagida, T. Azuma, and H. Sakurai, *Chemistry Letters*, 1982, 1069–1070.
88. K. Kobayakawa, A. Teranishi, T. Tsurumaki, Y. Sato, and A. Fujishima, *Electrochimica Acta*, 1992, **37**, 465–467.
89. J. F. Reber and M. Rusek, *Journal of Physical Chemistry*, 1986, **90**, 824–834.
90. J. Sato, N. Saito, Y. Yamada et al., *Journal of the American Chemical Society*, 2005, **127**, 4150–4151.
91. Y. G. Lee, T. Watanabe, T. Takata et al., *Journal of Physical Chemistry B*, 2006, **110**, 17563–17569.
92. K. Maeda, N. Saito, D. L. Lu, Y. Inoue, and K. Domen, *Journal of Physical Chemistry C*, 2007, **111**, 4749–4755.
93. K. Maeda, N. Saito, Y. Inoue, and K. Domen, *Chemistry of Materials*, 2007, **19**, 4092–4097.
94. K. Maeda, K. Teramura, N. Saito, Y. Inoue, and K. Domen, *Bulletin of the Chemical Society of Japan*, 2007, **80**, 1004–1010.
95. N. Arai, N. Saito, H. Nishiyama et al., *Chemistry Letters*, 2006, **35**, 796–797.
96. N. Serpone and E. Pelizzetti, *Photocatalysis*, Wiley, New York, 1989.
97. H. Kato and A. Kudo, *Journal of Physical Chemistry B*, 2002, **106**, 5029–5034.
98. R. Niishiro, R. Konta, H. Kato et al., *Journal of Physical Chemistry C*, 2007, **111**, 17420–17426.
99. D. F. Wang, J. H. Ye, T. Kako, and T. Kimura, *Journal of Physical Chemistry B*, 2006, **110**, 15824–15830.
100. T. Ishii, H. Kato, and A. Kudo, *Journal of Photochemistry and Photobiology A—Chemistry*, 2004, **163**, 181–186.
101. R. Konta, T. Ishii, H. Kato, and A. Kudo, *Journal of Physical Chemistry B*, 2004, **108**, 8992–8995.
102. D. F. Wang, T. Kako, and J. H. Ye, *Journal of Physical Chemistry C*, 2009, **113**, 3785–3792.
103. D. F. Wang, J. H. Ye, H. Kitazawa, and T. Kimura, *Journal of Physical Chemistry C*, 2007, **111**, 12848–12854.
104. S. Nishimoto, M. Matsuda, and M. Miyake, *Chemistry Letters*, 2006, **35**, 308–309.
105. D. W. Hwang, H. G. Kim, J. S. Jang et al., *Catalysis Today*, 2004, **93–95**, 845–850.

106. D. W. Hwang, H. G. Kirn, J. S. Lee et al., *Journal of Physical Chemistry B*, 2005, **109**, 2093–2102.
107. Y. Hosogi, K. Tanabe, H. Kato, H. Kobayashi, and A. Kudo, *Chemistry Letters*, 2004, **33**, 28–29.
108. Y. Hosogi, Y. Shimodaira, H. Kato, H. Kobayashi, and A. Kudo, *Chemistry of Materials*, 2008, **20**, 1299–1307.
109. H. Kato, H. Kobayashi, and A. Kudo, *Journal of Physical Chemistry B*, 2002, **106**, 12441–12447.
110. Z. G. Zou, J. H. Ye, and H. Arakawa, *Chemical Physics Letters*, 2000, **332**, 271–277.
111. J. W. Tang, Z. G. Zou, and J. H. Ye, *Catalysis Letters*, 2004, **92**, 53–56.
112. Y. Shimodaira, H. Kato, H. Kobayashi, and A. Kudo, *Journal of Physical Chemistry B*, 2006, **110**, 17790–17797.
113. Y. Shimodaira, H. Kato, H. Kobayashi, and A. Kudo, *Bulletin of the Chemical Society of Japan*, 2007, **80**, 885–893.
114. D. F. Wang, J. W. Tang, Z. G. Zou, and J. H. Ye, *Chemistry of Materials*, 2005, **17**, 5177–5182.
115. W. F. Yao and J. H. Ye, *Chemical Physics Letters*, 2008, **450**, 370–374.
116. R. Konta, H. Kato, H. Kobayashi, and A. Kudo, *Physical Chemistry Chemical Physics*, 2003, **5**, 3061–3065.
117. A. Kudo, K. Ueda, H. Kato, and I. Mikami, *Catalysis Letters*, 1998, **53**, 229–230.
118. A. Kudo, K. Omori, and H. Kato, *Journal of the American Chemical Society*, 1999, **121**, 11459–11467.
119. J. Q. Yu and A. Kudo, *Advanced Functional Materials*, 2006, **16**, 2163–2169.
120. W. Yao, H. Iwai, and J. Ye, *Dalton Transactions*, 2008, 1426–1430.
121. J. H. Ye, Z. G. Zou, M. Oshikiri et al., *Chemical Physics Letters*, 2002, **356**, 221–226.
122. Y. Hosogi, H. Kato, and A. Kudo, *Journal of Materials Chemistry*, 2008, **18**, 647–653.
123. D. F. Wang, Z. G. Zou, and J. H. Ye, *Chemical Physics Letters*, 2003, **373**, 191–196.
124. Z. G. Zou, J. H. Ye, K. Sayama, and H. Arakawa, *Nature*, 2001, **414**, 625–627.
125. M. Matsumura, Y. Saho, and H. Tsubomura, *Journal of Physical Chemistry*, 1983, **87**, 3807–3808.
126. C. J. Xing, Y. J. Zhang, W. Yan, and L. J. Guo, *International Journal of Hydrogen Energy*, 2006, **31**, 2018–2024.
127. M. Hara, G. Hitoki, T. Takata et al., *Catalysis Today*, 2003, **78**, 555–560.
128. T. Takata, G. Hitoki, J. N. Kondo et al., *Research on Chemical Intermediates*, 2007, **33**, 13–25.
129. M. Hara, J. Nunoshige, T. Takata, J. N. Kondo, and K. Domen, *Chemical Communications*, 2003, 3000–3001.
130. D. Yamasita, T. Takata, M. Hara, J. N. Kondo, and K. Domen, *Solid State Ionics*, 2004, **172**, 591–595.
131. M. Y. Liu, W. S. You, Z. B. Lei et al., *Chemical Communications*, 2004, 2192–2193.
132. G. Hitoki, T. Takata, J. N. Kondo et al., *Electrochemistry*, 2002, **70**, 463–465.
133. K. Maeda, T. Takata, M. Hara et al., *Journal of the American Chemical Society*, 2005, **127**, 8286–8287.
134. K. Maeda, K. Teramura, D. L. Lu et al., *Nature*, 2006, **440**, 295–295.
135. K. Maeda, K. Teramura, and K. Domen, *Journal of Catalysis*, 2008, **254**, 198–204.
136. Y. Lee, H. Terashima, Y. Shimodaira et al., *Journal of Physical Chemistry C*, 2007, **111**, 1042–1048.
137. A. Kudo, *International Journal of Hydrogen Energy*, 2006, **31**, 197–202.
138. D. Chen and J. H. Ye, *Journal of Physics and Chemistry of Solids*, 2007, **68**, 2317–2320.
139. Z. B. Lei, W. S. You, M. Y. Liu et al., *Chemical Communications*, 2003, 2142–2143.
140. A. Kudo and M. Sekizawa, *Catalysis Letters*, 1999, **58**, 241–243.
141. A. Kudo and M. Sekizawa, *Chemical Communications*, 2000, 1371–1372.
142. N. Kakuta, K. H. Park, M. F. Finlayson et al., *Journal of Physical Chemistry*, 1985, **89**, 732–734.
143. I. Tsuji, H. Kato, H. Kobayashi, and A. Kudo, *Journal of the American Chemical Society*, 2004, **126**, 13406–13413.
144. I. Tsuji, H. Kato, and A. Kudo, *Chemistry of Materials*, 2006, **18**, 1969–1975.
145. I. Tsuji, H. Kato, H. Kobayashi, and A. Kudo, *Journal of Physical Chemistry B*, 2005, **109**, 7323–7329.
146. H. Yan, J. Yang, G. Ma et al., *Journal of Catalysis*, 2009, **266**, 165–168.
147. J. R. Darwent, *Journal of the Chemical Society—Faraday Transactions I*, 1981, **77**, 1703–1709.

148. J. R. Darwent and G. Porter, *Journal of the Chemical Society—Chemical Communications*, 1981, 145–146.
149. K. Kalyanasundaram, E. Borgarello, D. Duonghong, and M. Gratzel, *Angewandte Chemie International Edition in English*, 1981, **20**, 987–988.
150. H. C. Youn, S. Baral, and J. H. Fendler, *Journal of Physical Chemistry*, 1988, **92**, 6320–6327.
151. T. Hirai, S. Shiojiri, and I. Komasawa, *Journal of Chemical Engineering of Japan*, 1994, **27**, 590–597.
152. H. Fujii, M. Ohtaki, K. Eguchi, and H. Arai, *Journal of Molecular Catalysis A—Chemical*, 1998, **129**, 61–68.
153. J. Sabate, S. Cerveramarch, R. Simarro, and J. Gimenez, *International Journal of Hydrogen Energy*, 1990, **15**, 115–124.
154. M. Sathish, B. Viswanathan, and R. P. Viswanath, *International Journal of Hydrogen Energy*, 2006, **31**, 891–898.
155. I. B. Rufus, B. Viswanathan, V. Ramakrishnan, and J. C. Kuriacose, *Journal of Photochemistry and Photobiology A—Chemistry*, 1995, **91**, 63–66.
156. K. Sayama, K. Mukasa, R. Abe, Y. Abe, and H. Arakawa, *Chemical Communications*, 2001, 2416–2417.
157. H. Kato, M. Hori, R. Konta, Y. Shimodaira, and A. Kudo, *Chemistry Letters*, 2004, **33**, 1348–1349.
158. R. Abe, T. Takata, H. Sugihara, and K. Domen, *Chemical Communications*, 2005, 3829–3831.
159. X. C. Wang, K. Maeda, A. Thomas et al., *Nature Materials*, 2009, **8**, 76–80.
160. G. Q. Li, T. Kako, D. F. Wang, Z. G. Zou, and J. H. Ye, *Journal of Physics and Chemistry of Solids*, 2008, **69**, 2487–2491.
161. H. Song, T. Peng, P. Cai, H. Yi, and C. Yan, *Catalysis Letters*, 2007, **113**, 54–58.
162. Y. Tamaki, A. Furube, M. Murai et al., *Physical Chemistry Chemical Physics*, 2007, **9**, 1453–1460.
163. T. Yoshihara, R. Katoh, A. Furube et al., *Journal of Physical Chemistry B*, 2004, **108**, 3817–3823.
164. D. Bahnemann, A. Henglein, J. Lilie, and L. Spanhel, *Journal of Physical Chemistry*, 1984, **88**, 709–711.
165. J. W. Tang, J. R. Durrant, and D. R. Klug, *Journal of the American Chemical Society*, 2008, **130**, 13885–13891.
166. N. Serpone, D. Lawless, R. Khairutdinov, and E. Pelizzetti, *Journal of Physical Chemistry*, 1995, **99**, 16655–16661.
167. M. Murai, Y. Tamaki, A. Furube, K. Hara, and R. Katoh, *Catalysis Today*, 2007, **120**, 214–219.
168. A. Yamakata, T. Ishibashi, and H. Onishi, *Journal of Physical Chemistry B*, 2001, **105**, 7258–7262.
169. T. Ikeda, T. Nomoto, K. Eda et al., *Journal of Physical Chemistry C*, 2008, **112**, 1167–1173.
170. T. Tachikawa, M. Fujitsuka, and T. Majima, *Journal of Physical Chemistry C*, 2007, **111**, 5259–5275.
171. A. Yamakata, T. Ishibashi, H. Kato, A. Kudo, and H. Onishi, *Journal of Physical Chemistry B*, 2003, **107**, 14383–14387.
172. A. G. Joly, J. R. Williams, S. A. Chambers et al., *Journal of Applied Physics*, 2006, **99**, 053521.
173. W. J. Younpblood, S. H. A. Lee, Y. Kobayashi et al., *Journal of the American Chemical Society*, 2009, **131**, 926–927.
174. R. H. Wilson, *Journal of the Electrochemical Society*, 1980, **127**, 228–234.
175. R. F. Howe and M. Gratzel, *Journal of Physical Chemistry*, 1987, **91**, 3906–3909.
176. R. F. Howe and M. Gratzel, *Journal of Physical Chemistry*, 1985, **89**, 4495–4499.
177. P. Salvador and C. Gutierrez, *Journal of Physical Chemistry*, 1984, **88**, 3696–3698.
178. R. Nakamura, T. Okamura, N. Ohashi, A. Imanishi, and Y. Nakato, *Journal of the American Chemical Society*, 2005, **127**, 12975–12983.
179. R. Nakamura and Y. Nakato, *Journal of the American Chemical Society*, 2004, **126**, 1290–1298.
180. A. Imanishi, T. Okamura, N. Ohashi, R. Nakamura, and Y. Nakato, *Journal of the American Chemical Society*, 2007, **129**, 11569–11578.
181. A. J. Bard and L. R. Faulkner, *Electrochemical Methods Fundamentals and Applications*, Wiley, New York, 2001.

37

Overview of the Development of Integrated Photocatalytic Adsorbents (IPCAs) for Water Treatment Using Titanium Dioxide (TiO_2) and Activated Carbon

David Keane
Dublin City University

Kieran Nolan
Dublin City University

Anne Morrissey
Dublin City University

Michael Oelgemöller
James Cook University

Shaik Basha
Council of Scientific and Industrial Research

John Tobin
Dublin City University

37.1 Introduction

Scientific studies using titanium dioxide photocatalysis to purify water began almost four decades ago and since then research effort has diversified into several different approaches. One of the newest methods is combining titanium dioxide and an adsorbent material to create integrated photocatalytic adsorbents (IPCAs). This chapter surveys and critically reviews studies involving IPCAs synthesized using titanium dioxide and activated carbon (AC). A brief introduction and history of photocatalysis is included and the technical, environmental, and economic advantages of IPCAs are outlined.

The approaches used to create IPCAs are categorized according to AC type and the differing preparation methods are summarized. Various mathematical kinetic models developed for the IPCA systems are described. The research needs for photocatalytic water treatment are also explored and it is concluded that demonstration of the effectiveness of IPCAs in treating actual water and wastewater samples in pilot plant scale reactors is the next stage required in the development of this technology.

37.1.1 Photocatalysts

In recent times, considerable attention has been focused on the safety and efficiency of water treatment technology [1,2]. The reasons for this include increasing concerns about hazardous organic pollutants (HOPs) such as endocrine-disrupting chemicals (EDCs), active pharmaceutical ingredients (APIs), and pesticides found in drinking water and the surrounding environment [3–7]. In addition, conventional water treatment processes such as ozonization and chlorination create disinfection by-products (DBP) such as bromate and trihalomethanes, respectively, which are potentially toxic [1,8–10]. In order to avoid such problems, attention is now being focused on advanced oxidative processes (AOP) including photodegradation. Photodegradation is defined by the International Union of Pure and Applied Chemistry (IUPAC) as "the photochemical transformation of a molecule into lower molecular weight fragments, usually in an oxidation process" [11]. This process is usually too slow and inefficient to be useful in water treatment and requires the addition of a photocatalyst. These catalysts are activated by light and the resulting photocatalytic reactions are defined by IUPAC as "catalytic reaction involving light absorption by a catalyst or by a substrate" [11]. Several types of photocatalysts are available, but most scientific effort has been concentrated on titanium dioxide due to its high photocatalytic activity, chemical stability, nontoxic nature, and relatively low price [12].

When titanium oxides are irradiated with light that exceeds their band gap energy, electrons are promoted from the valence band to the conduction band. The resulting electrons are highly reactive and have a very large reduction potential. The promotion of these electrons creates electron "holes" in the valence band and these have a highly reactive oxidation potential [13]. These "electron–hole pairs" are responsible for the photocatalytic properties of titanium oxides and can degrade organic pollutants on the catalysts surface either directly or indirectly in a water solution by creating hydroxide and superoxide radicals [14].

The original research on the photocatalytic properties of TiO_2 focused on solar energy conversion using an electrochemical photocell with TiO_2 and platinum electrodes [12]. Under illumination with near-UV light, photoelectrolysis occurred resulting in the splitting of water into hydrogen and oxygen. The hydrogen yield from this experiment was too low to be of practical use although there are continuing developments in this field [15]. In the late 1970s, the ability of TiO_2 to oxidize organic matter was applied to cyanide degradation and this led to a substantial increase in research interest in the environmental applications of photocatalysts [16]. This research focused on air purification especially the photodegradation of volatile organic carbons (VOCs) and nitrogen oxides (NO_x), water pollutants, and microorganisms [14]. Photocatalysts have since been commercialized in several consumer and industrial products, especially self cleaning surfaces—due to the photocatalytic properties of TiO_2—and air cleaning equipment/surfaces [13].

The first study of IPCAs to degrade water pollutants was conducted in 1996 [17] and the number of published studies using IPCAs has grown steadily since then (Figure 37.1). The term IPCA was coined much later in 2005 [18]. Photocatalysts have not yet been commercially deployed in large-scale water treatment, although research and development is ongoing [19] worldwide.

37.1.2 Activated Carbon

AC is "a porous carbon material, a char which has been subjected to reaction with gases, sometimes with the addition of chemicals, e.g., $ZnCl_2$, before, during or after carbonization in order to increase its adsorptive properties." [20]. In this review, AC is categorized based on its physical form as the diverse physical

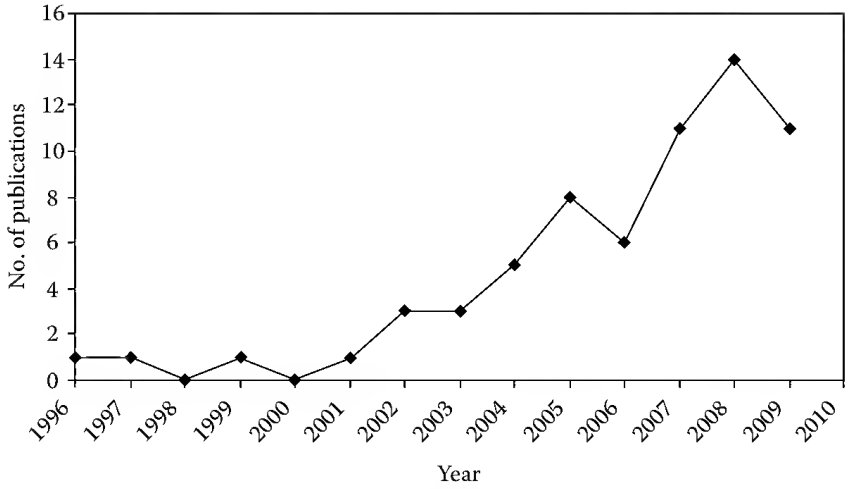

FIGURE 37.1 Number of surveyed AC/TiO_2 IPCA (degrading water pollutants) studies published per year 1996–2009.

and chemical properties of AC such as iodine number, N_2 adsorption, density, mesopore, and micropore volume are not detailed in the majority of articles cited. The most popular forms of AC are powdered activated carbon (PAC) and granular activated carbon (GAC). Other forms such as extruded activated carbon (EAC) and activated carbon cloths (ACC)/activated carbon filters (ACF) are also available but are not widely used in water treatment. GAC is most commonly used in water treatment due to its relatively large size, which makes it easy to handle and form filter beds, unlike PAC, which due to its small grain size becomes easily suspended in solution and thus must be filtered or coagulated out of the solution.

The porosity of AC is the most important factor affecting its adsorption ability. More porous carbons have higher adsorption capacity, which is usually described using Brunauer, Emmett, and Teller (BET) surface area. Generally, 1 g of AC will have a surface area of between 500 and 2000 m^2, which is determined by N_2 gas adsorption or a simple liquid adsorption, calculated using Langmuir isotherm for monolayer adsorption or BET isotherm for multilayer adsorption [21]. The porosity of AC can be further classified into micropores (widths smaller than 2 nm), mesopores (widths between 2 and 50 nm), and macropores (widths larger than 50 nm) [21]. Mesopores are often expressed as a methylene blue (MB) number as it is assumed that a large molecule such as MB cannot penetrate the micropores. Micropores are usually expressed as iodine number as the iodine atom can penetrate into the micropores. By comparing the iodine and MB numbers of an AC, it is possible to determine the relative microporosity to mesoporosity ratio. The point of zero charge of an AC is the pH at which the AC has no charge. At a pH below this, the carbon is positively charged and above this it is negatively charged. This property will greatly influence the adsorption of HOPs onto the carbon surface and is an important consideration when selecting an AC for creating IPCAs as changes in pH will greatly influence adsorption [22] and the photodegradation rate [23,24].

37.2 Integrated Photocatalytic Adsorbents

The chemical inertness of titanium oxides is both an advantage and disadvantage: the inertness prevents toxicity and ensures longevity of the catalyst, but it severely limits the adsorption potential of the catalyst, which is negligible in most cases [24–26], although this varies with substrate and pH [23]. This is significant as the electron–hole pairs are only effective if the target chemical is near or on the catalyst surface as the absence of a suitable electron acceptor (e.g., a pollutant) will cause a dramatic decrease in photocatalytic reactions due to charge–carrier recombination [14]. Hydroxide and superoxide radicals recombine easily and therefore are only effective near the catalyst surface.

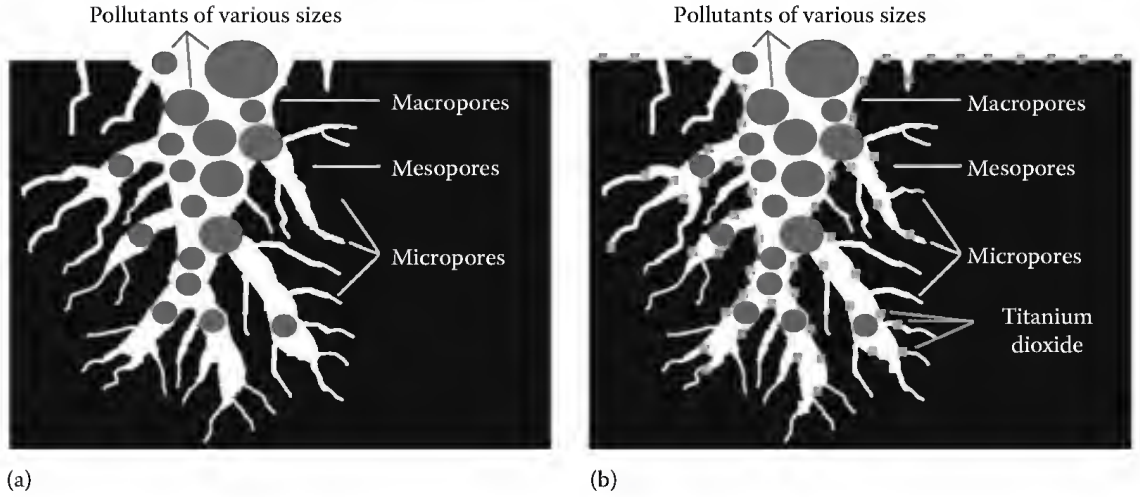

FIGURE 37.2 (a) Unmodified AC. (b) AC modified with TiO_2.

By combining the adsorption potential of ACs (Figure 37.2a) with the photocatalytic properties of titanium dioxide, it is possible to create an IPCA (Figure 37.2b) with improved photocatalytic potential. IPCAs may consist of either AC coated with TiO_2 or TiO_2 coated with a carbonaceous material that has been heat treated to form an AC. Several studies (Tables 37.1 and 37.2) have reported synergistic effects between mixtures as opposed to composites of TiO_2 and AC [27–33]. Other adsorbent types have been used to create IPCAs including zeolites [18,34–39], alumina silicates [40–45], and carbon nanotubes (CNTs) [46–53].

Composites of TiO_2 and CNTs are unusual as they can be considered doped TiO_2 as well as an IPCA. The CNT acts as an adsorbent providing all the associated benefits (adsorption capacity, substrate concentration) as AC [47]. The conductive properties of CNTs allow electrons that have been promoted to the valence band by the photocatalysis process to be transferred away from the TiO_2 surface. This reduces electron–hole pair recombination, and by prolonging the electron holes on the TiO_2 surface increases the likelihood of a photodegradation reaction and therefore a corresponding increase in the photodegradation rate [47,52]. CNTs are also claimed to increase the adsorption spectrum of TiO_2 in the visible spectrum allowing photodegradation using visible light [49]. The progress and challenges of CNT IPCAs have been reviewed elsewhere [132].

37.2.1 Photocatalyst Choice

TiO_2 occurs in several phases or polymorphs which are different arrangements of the TiO_2 molecules crystal structure, the three polymorphic forms of notes are anatase, rutile, and brookite [133–135]. Rutile is the most thermodynamically stable phase, whereas anatase and brookite are metastable and are readily transformed to rutile when heated. The phase change from anatase to rutile has been reported to occur in different temperature ranges from 600°C to 1100°C, depending on the preparation conditions, particle size, and the presence of impurities [135,136]. The most photoactive form of TiO_2 is the anatase phase and it has been widely studied due to its technological importance in various applications. The rutile phase has lower photoactivity although it has a high refractive index that is useful for optical devices [137]. The basic difference between anatase and rutile is the symmetry about oxygen atoms as well as differences in the polarization of the oxygen ions [77,138,139].

Pure anatase TiO_2 is the most popular photocatalyst for preparing IPCAs (Tables 37.1 and 37.2). Anatase TiO_2 can be prepared using a sol-gel method with low calcination temperatures or can be bought commercially in powdered form. After pure anatase, IPCAs composed of a mixture of anatase and rutile TiO_2 are the most numerous. Studies that use high calcination temperature for preparing

TABLE 37.1 IPCA Wet Preparation Methods

Preparation Method	Adsorbent	Photocatalyst	Substrate (Initial Concentration)	Irradiation Source	References
Sol-gel method used to prepare TiO_2 and magnetic particles solution. Impregnated using refluxing and ultrasonification	Magnetic AC: (PAC containing magnetic magnetite particles)	Anatase TiO_2	X-3B (50 mg L^{-1})	250 mL breaker irradiated with UV: 200 W UV, Visible: halogen 500 W lamp	[54]
As given previously	Magnetic AC (PAC)	Anatase TiO_2	Phenol (100 mg L^{-1})	Cylindrical stainless steel photoreactor with a 20 W UV lamp (365 nm) covered by a quartz glass sleeve	[55]
Preparation methods as given previously with the exception that some of the samples were calcinated at 350°C or 450°C in a N_2 atmosphere for 2 h	Magnetic AC (PAC)	Anatase TiO_2	Phenol (100 mg L^{-1})	Photoreactor consisting of a glass beaker covered in silver paper with an 8 W UV lamp (365 nm)	[56]
Separate sol-gel methods were used to prepare TiO_2 and magnetic ferrite particles. The ferrite and TiO_2 particles were then applied to the AC using ultrasonification	Magnetic ferrite AC (PAC)	Anatase and rutile (P25 as reference)	MO (20 mg L^{-1})	500 mL cylindrical glass reactor with a UV lamp (365 nm) and circulating water jacket. Aeration of 0.6 L min^{-1} was used	[57]
Sol-gel method was used to prepare a TiO_2 solution. Impregnation used ultrasonification and dip coating onto glass plates	PAC coated on a glass plate	Anatase TiO_2 (P25 as reference)	4-Chlorophenol (100 mg L^{-1})	Cylindrical silica reactor with 200 W UV lamp (365 nm, 9 mW cm^{-2})	[58]
TiO_2 was synthesized using a sol-gel method and a "dip coating method" and sonification for impregnation	GAC	Anatase TiO_2	Phenol (10 mg L^{-1})	Electrodeless discharge lamp (EDL) excited by microwave irradiation (254–579 nm, output not stated)	[59]
As given previously	PAC	Anatase TiO_2	Rhodamine B (RhB) (30 mg L^{-1})	50 mL solution irradiated in a microwave with a microwave-electrodeless discharge mercury lamp (MW-EDML) output not stated	[60]
TiO_2 prepared using a sol-gel method. Impregnation using heating and stirring, followed by calcination	GAC	Anatase TiO_2 (P25 as reference)	MO (50 mg L^{-1})	500 mL cylindrical glass reactor inside equipped with an UV lamp (365 nm, output not stated) with aeration	[61]
Sol-gel method used to prepare TiO_2. Impregnation using ultrasonification followed by heat treatment	GAC	Anatase and rutile TiO_2	MO (5×10^{-3} mol L^{-1} and 3, 6, 7, 12, 15×10^{-3} mol L^{-1})	280 mL photoreactor with 10–40 W UV lamp (135 mW cm^{-2}, λ: 320–400 nm, peak: 365 nm) and aeration (56 mL min^{-1})	[62]
Sol-gel method was used to prepare TiO_2. Impregnation using ultrasonification followed by calcination	GAC	Anatase/rutile TiO_2, % ratios 1:0 and 35:65	MB (20 mg L^{-1})	As given previously	[63]

(*continued*)

TABLE 37.1 (continued) IPCA Wet Preparation Methods

Preparation Method	Adsorbent	Photocatalyst	Substrate (Initial Concentration)	Irradiation Source	References
Sol-gel method was used to prepare TiO_2. Impregnation using stirring followed by calcination	GAC	Anatase and rutile TiO_2	MO (1×10^{-3} mol L^{-3})	Pyrex reaction cell equipped with an air-aerated stopcock, 40 W UV lamp, fixed in the middle of the quartz cell	[64]
As given previously	GAC	Anatase to rutile TiO_2 in the ratio of 2.3	Rhodamine B (RhB) (1, 2.5, 5, 8, and 10 mmol L^{-1})	UV light intensity in 250 mL Pyrex photoreactor: 0, 15, 25, 40, and 60 mW cm^{-2} with aeration (56 mL s^{-1})	[65]
As given previously	GAC	Anatase and/or rutile phase	*Escherichia coli* (*E. coli*, NCIMB 8277)	IPCA was suspended in sterilized water using ultrasonication and stirred. Irradiation using a black light fluorescent lamp	[66]
Sol-gel method using a rotary evaporator was used to prepare the IPCA	GAC	TiO_2 (phase not stated)	Microcystin-LR (cyanobacteria endotoxin) (50 mg L^{-1})	Cylindrical continuous flow fluidized bed reactor with a 4 W black light lamp (370 nm, 0.6 mW cm^{-2})	[67]
As given previously	GAC	Anatase TiO_2	Microcystin-LR (200 mg L^{-1})	1 L glass cylinder with a water jacket for cooling. Irradiation was provided by a 4 W black light lamp (370 nm, 0.6 mW cm^{-2})	[68]
Commercial TiO_2 was loaded onto an ACF using an epoxy resin followed by calcination	ACF	P25 (30 nm)	Paper mill effluent	350 mL cylindrical photoreactor with water-cooling jacket, 500 W high-pressure Hg lamp (365 nm), and aeration	[69]
As given previously	ACF	Degussa P25 (30 nm)	b-Cyclodextrin ($(C_2H_{10}O_5)_7$) (200 mg L^{-1})	As given previously	[70]
As given previously	ACF	P25 (30 nm)	MB (85 mg L^{-1})	As given previously	[71]
Sol-gel method was used to prepare a TiO_2 solution and ultrasonification was used for impregnation	PAC	Anatase TiO_2	Phenol (100 mg L^{-1})	500 mL photoreactor with 20 W UV lamp (peak 365 nm)	[72]
Sol-gel method was used to prepare TiO_2 solution. Impregnation involved mixing followed by heat treatment	PAC, powdered silica, mordenite	TiO_2 (phase not stated most likely anatase)	Propyzamide (7.8 mg L^{-1})	Pyrex reaction cell with a 400 W Xe lamp and UV cutoff filter ($\lambda > 300$ nm, 135 mW cm^{-2})	[17]
As given previously	PAC	TiO_2 (phase not stated most likely anatase)	Dichloromethane, trichloromethane, tetrachloromethane (1.0 mmol dm^{-3})	Reaction cell with l0 W fluorescent black lamp (300–430 nm, peak of 352 nm, 1.8 mW cm^{-2})	[73]

Sol-gel method used to apply TiO_2 to the surface of Poly(Vinyl Butyral) (PVB) followed by heat treatment	PVB carbonized to form an AC	Anatase and rutile TiO_2 in the ratio of 1–0.3	Phenol (0.05 g L^{-1})	Degradation experiments were carried out under illumination from six UV lamps with 20 W power	[74]
Carbon precursor applied to P25. The composite was then dehydrated and carbonized at 600°C	Cellulose/TiO_2 microsphere composites	P25 (20 nm)	Acetaldehyde (2000 mg L^{-1})	Cell containing 3 cm^3 reactant illuminated with two 4 W black lights λ: 300–400 nm)	[75]
As given previously	ACF	Anatase and rutile TiO_2	MB (concentration not stated)	Not stated (looks at reuse of an IPCA)	[76]
Sol-gel method used to prepare TiO_2. Impregnated onto the AC cloth by dip coating followed by calcination	ACC	Anatase and rutile TiO_2	MB (2.94×10^{-4} mol L^{-1})	"UV irradiation"	[77]
Sol-gel method was used to prepare the pure TiO_2 and impregnate the AC. The solutions were then dried and calcinated at different temperatures	PAC	Anatase and rutile TiO_2 (P25 as reference)	Chromotrope 2R (10–80 mg L^{-1})	Low-pressure Hg-vapor lamp (λ max: 253.7 nm, 3 W radiant flux)	[78]
Coating of commercial TiO_2 with a carbon-based precursor. The mixture was then carbonized at 700°C	Carbon-coated TiO_2	Anatase TiO_2 (traces of rutile)	MB (2.94×10^{-4} mol L^{-1}) and heavy oil	10 W m^{-2} UV irradiation from a "black light" for MB and 16.4 W m^{-2} UV irradiation for the heavy oil	[79]
The IPCAs were prepared by several methods, mechanofusion using a theta composer, and boiling impregnation (boiling dry a solution of TiO_2 and AC)	PACs and GACs prepared by different activation methods	P25	MB, Procion red MX-B5 (reactive red 2)	4 W low-pressure Hg UV lamp (approx 0.37 mW cm^{-2} for batch studies and 2 mW cm^{-2} for column studies)	[22]
TiO_2 solution	ACF	Anatase TiO_2	MO and acid fuchsine (120 mg L^{-1})	250 mL cylindrical photoreactor and water-cooled quartz jacket with 500 W high-pressure Hg lamp (365 nm, 12.5 mW cm^{-2}) and aeration	[80]
The WO_3–TiO_2 photocatalyst was prepared by a sol-gel method. Impregnation involved stirring and calcination	GAC	WO_3–TiO_2 (anatase TiO_2)	Congo Red (10–50 mg L^{-1} with H_2O_2 addition)	2.5 L "fluidized bed photoreactor" with 500 W high-pressure Hg-vapor lamp and aeration (0.2 m^3 h^{-1})	[81]
P25 was added to an epoxy resin solution and drip coated onto an ACF and then calcinated	ACF	P25	MB (85 mg L^{-1})	350 mL cylindrical photoreactor with a water-cooled quartz jacket and 500 W high-pressure Hg lamp (365 nm)	[82]
Various quantities of commercial TiO_2 and AC were mixed in an aqueous solution and stirred for 1 h before filtration	AC (form not stated)	P25	Phenol, salicylic acid, 4-aminophenol, or *p*-nitrophenol (100 mg L^{-1})	250 mL photoreactor(s) with air sparging (100 mL min^{-1}) and irradiated with a "UV lamp." Natural sunlight was also used (no further information given)	[83,84]

(*continued*)

TABLE 37.1 (continued) IPCA Wet Preparation Methods

Preparation Method	Adsorbent	Photocatalyst	Substrate (Initial Concentration)	Irradiation Source	References
Sol-gel methods were used to prepare a TiO_2 solution and impregnation used stirring, followed by calcination	PAC	Anatase and Rutile TiO_2 (depending on calcination temperature)	Phenol (50 mg L^{-1})	Six UV lamps were used to irradiate the solution from the top	[85]
Sol-gel method was used to prepare the IPCA. Impregnation involved stirring and was followed by calcination	PAC	Anatase TiO_2 (P25 as reference)	Phenol, MO, and Cr(VI)	Cylindrical quartz photoreactor (with water-cooling jacket) with an 8 W UV lamp (365 nm) position	[86]
Commercial TiO_2 powder was carbon coated by mixing with polyvinyl alcohol in different mass ratios. The resulting IPCA was then calcinated	Carbon-coated anatase powders	Anatase TiO_2	MB (3.2×10^{-5} mol dm^{-3})	PMR with direct-contact membrane distillation and Hg UV lamp (355 nm, 146.1 W m^{-2} at irradiation plate)	[87]
The Fe was added to the ACF by dip coating. The Fe-ACF was then added to a solution of TiO_2 precursor and stirred followed by vaporization and calcination at 700°C	Fe-ACF	Mixture of anatase and rutile TiO_2	MB (1.0×10^{-5} mol L^{-1})	UV lamp above the solution (20 W, 365 nm)	[88]
LPD used to apply TiO_2 to the ACF. The ACF was then dried and annealed at high temperature	ACF	Anatase TiO_2	AOII (200 mg L^{-1})	Photoreactor consisting of quartz reactor irradiated by a 15 W germicidal lamp (90% output at 253.7 nm). The IPCA was used as the photoanode, Pt wire used as the counter electrode	[89]
A sol-gel method was used to prepare carbon-coated TiO_2. The resulting solution was dried, pulverized, and calcinated	Carbon-coated TiO_2	Anatase and rutile TiO_2	MB (1.6×10^{-5} M)	UV light bulb (0.5 mW cm^{-2}, 364 nm) and visible light from an incandescent light bulb (13.6 mW cm^{-2}). LEDs used to provide lighting for NO degradation	[90]
Electrophoretic deposition was used to apply a suspension of P25 and AC to a conductive glass plate electrode. The electrodes were then placed in an oven and heated in air at 450°C for 30 min	PAC	P25	Orange-II (OG-II) (50 mg L^{-1})	Glass reactor with direct illumination by a low-pressure mercury vapor UV lamp (75 mW cm^{-2}, λ: 365 nm)	[91]
Commercial TiO_2 was carbon coated by exposing it to ethanol vapors for 1 h in temperature ranging from 150°C to 400°C	Carbon-coated TiO_2	Tytanpol A11 (Police, Poland) and P25 (Degussa, Germany)	Phenol (100 mg L^{-1})	Artificial solar light was provided by using a 100 W lamp (354 W m^{-2} visible, 0.09 W m^{-1} UV) and UV light was provided by six, 20 W UV lamps (100 W m^{-2} visible, 154 W m^{-2} UV)	[92]

A sol-gel method was used to prepare TiO_2/ACF composite. The gel was then dried and then calcinated	ACF	Anatase and rutile TiO_2	Toluene (20 mg L^{-1})	Solution was irritated with a 500 W high-pressure mercury lamp (380 nm)	[93]
A sol-gel method was used to prepare F-doped TiO_2. Impregnation used ultrasonification	PAC	F-doped anatase TiO_2 (brookite traces)	Phenol (25 mg L^{-1})	Silica photoreactor with 250 W halogen lamp with a light filter cutting the light <400 nm (11.3 mW cm^{-2})	[94]
Commercial TiO_2 was impregnated on the ACF by stirring and then sonification. The resulting IPCA was then calcinated	ACF	Anatase TiO_2	MB (100 mg L^{-1})	Lamp fitted along reaction cell and the ACF was fixed horizontally along the reaction cell (no information on power output or lamp type)	[95]
Commercial TiO_2 was impregnated onto the PAC using sonification. N-doped IPCA was prepared by adding saturated urea to the TiO_2 suspension and then following the procedure outlined earlier	PAC	Anatase TiO_2	Soman, VX, and Yperite (concentration not stated)	Photoreactor consisting of a closed quartz tube flushed with air (50 cm^3 min^{-1}), 125 W high-pressure black-bulb lamp (λ: 365 nm, 3.0 W UVA, λ: 315–400 nm)	[96]
Commercial TiO_2 powder was coated with poly(vinyl alcohol) and then carbonized. The powder was then adhered onto organic adhesive tape or a film using an organic binder	Carbon-coated TiO_2	Anatase TiO_2 (ST-01)	MB (2.94×10^{-5} mol L^{-1})	3 × 20 W UV light bulbs were placed 200 mm from the IPCA tape or film	[97]
Commercial TiO_2 was applied to the GAC using ultrasonification. Commercial TiO_2 was added to a chitosan solution and cast into beads by a "phase-inversion technique"	GAC	Anatase TiO_2	*Salmonella choleraesuis* subsp. ATCC 14028 (10^8 cfu mL^{-1})	1 L batch photoreactor with 20 W high-pressure mercury lamp (320–400 nm)	[98]
Sol-gel method was used to prepare the entire IPCA followed by heat treatment at 200°C in air	GAC	Anatase TiO_2, rutile and brookite traces	Color (organics absorption at 254 nm)	Adsorption was carried out separately. UV regeneration using six 18 W UVA or UVC lamps and/or ultrasonic bath	[99]
Sol-gel method used to prepare TiO_2 solution. Varying amounts of GAC were added to this solution, which underwent hydrothermal treatment at 180°C for 8 h. Calcination at 600°C for 2 h was the final step in IPCA calcination	GAC	Anatase TiO_2	MO (50 mg L^{-1})	500 mL cylindrical glass reactor using a central UV lamp (365 nm, 300 W) containing a 250 mL solution	[100]

(*continued*)

TABLE 37.1 (continued) IPCA Wet Preparation Methods

Preparation Method	Adsorbent	Photocatalyst	Substrate (Initial Concentration)	Irradiation Source	References
Sol-gel processes were used to prepare separate solutions of $ZnFe_2O_4$ and TiO_2. The latter solution was added dropwise to the $ZnFe_2O_4$. GAC was then added to the combined solution and shaken for 12 h and dried. The samples were then calcined at 500°C for 2 h	GAC	Anatase TiO_2 doped with $ZnFe_2O_4$	Acid dye—brillred-RH (not stated)	"Recycle fluidized bed reactor" with 150 W visible light source	[101]
CdS P25 was prepared by a sol-gel and a precipitation method. These catalysts were applied to ACFs using an adhesive and dip coating	ACFs	CdS doped P25	MB (50 mg L^{-1})	75 mm × 50 mm pieces of the IPCA were put into 100 mL flasks and exposed to natural sunlight for 5 h	[102]
Sol-gel method used to prepare the doped TiO_2. This solution was added dropwise to the ACF. Followed by calcination at 600°C–800°C in N_2	ACF	Fe(III) and Ho(III) doped TiO_2	MO (120 mg L^{-1})	250 mL cylindrical vessel with a water-cooled quartz jacket with a 500 W high-pressure Hg (365 nm). Aeration was used	[103]
Sol-gel method used to prepare Fe(0)-doped TiO_2. ACF was dip coated using this solution and calcined at 200°C for 2 h	ACF	Fe(0) TiO_2 (phase not stated)	2,4-Dichlorophenol (10–100 mg L^{-1})	Cylindrical quartz tube 30 cm × 3 cm (height × diameter) with a 20 W germicidal low-pressure Hg lamp (λ: 254 nm, 92 W cm^{-2} at 365 nm)	[104]
The IPCAs were obtained by mixing P25 and AC at different proportions in water and stirred for 3 h followed by filtering and drying	PAC	P25	Pentafluorobenzoic acid (100–600 mg L^{-1})	*Heber* immersion type photoreactor with either a 16 W low-pressure Hg lamp (λ: 253.7 nm, photon flux: 2.54×10^{-5} Einstein L^{-1} s^{-1}) or 8 W medium pressure Hg lamp (λ: 365 nm, photon flux: 2.08×10^{-6} Einstein L^{-1} s^{-1}). Aeration 8.1 mL s^{-1}	[105]
A commercial solution of amorphous TiO_2 was applied to either a plain PET film or a PET film with GAC adhered to it using a silicon binder. The GAC film was sprayed with the TiO_2 and dried a total of five times	GAC	Anatase TiO_2	2,4-Dinitrophenol (1–250 mg L^{-1})	Batch-recirculation flow system with 6 W black light blue fluorescent lamp (λ: 300–400 nm)	[106]
As given previously	As given previously	As given previously	2,4-Dinitrophenol (5–80 mmol m^{-3})	As given previously	[107]

Sol-gel method used to prepare a TiO_2 solution. The ACF was impregnated with TiO_2 by immersing it in this solution for 1 h followed by calcination at 500°C in an Ar atmosphere	ACF	Anatase TiO_2	Phenol, MO (80 and 120 mg L^{-1}, respectively)	Quartz reactor with Hg UV lamp (300 W, 365 nm)	[108]
P25 was added to an acetone and epoxy solution and stirred vigorously. Prewashed GAC was added to this solution. The suspension was filtered, washed, and dried. Followed by calcination at 500°C for 2 h in an N_2 atmosphere. These processes were repeated once to yield the final IPCA	GAC	P25	Rhodamine B (5×10^{-3} mol L^{-1})	Photodegradation experiments used a Pyrex reaction cell aerated at 0.6 L min^{-1}. A UV lamp was fixed in the middle of the quartz cell (light intensity varied between 50 and 200 W)	[109]
Catalyst I: TiO_2 deposited on cellulose fibers. Catalyst II: A composite of a layer of cellulose fibers with deposited TiO_2, a layer of carbon fibers and a layer of cellulose fibers. Both catalysts were rinsed for 12 h by deionized water	Commercial photocatalyst fibers from Ahlstrom (France)	Commercial TiO_2 (type not stated)	Basic red 46 (10 and 25 mg L^{-1})	Polytetrafluoroethylene (PTFE)-coated flat plate photoreactor inclined at 30° with two 15 W UV lamps (emission λ: 365 nm) or two visible light lamps. Natural sunlight was also used (180–190 W m^{-2})	[110]
Sol-gel method used to prepare TiO_2. ACF was then added to this solution and stirred vigorously for 1 h. IPCA was then dried and calcined at 900°C for 2 h in an N_2 atmosphere	ACF	TiO_2 (type not stated)	MO (80 mg L^{-1})	200 mL pulsed discharge reactor with aeration (oxygen flow rate of 96 L h^{-1}). UV light generated by the pulse discharges irradiated a suspended ACF IPCA	[111]
Sol-gel method was used to prepared Fe-doped TiO_2 using $Fe(NO_3)_3$ and tetrabutyl orthotitanate. Ultrasonic impregnation was used to apply the doped TiO_2 to the AC. The dried IPCA was calcined at 250°C in air and then 500°C in N_2	GAC	Fe-TiO_2 (anatase and rutile TiO_2)	Wastewater (from a "dye factory," municipal wastewater was also used)	Continuous flow 6.3 L stainless steel cylindrical photoreactor with two UV lamps mounted in the center. Aeration (56 mL s^{-1}) was used	[112]
Boiling impregnation was used to apply commercial TiO_2 to the adsorbent. These were then heat treated at 550°C	GAC, glass beads, zeolite, brick, quartz	P25	Propoxur (4.78×10^{-4} M)	1 L double-jacked vessel with a quartz cover. UV irradiation was provided by three 10 W low-pressure Hg lamps (peak λ: 254 nm) above the reactor	[113]
V-doped titania (VTO) was prepared using a sol-gel method. Ultrasonic impregnation was used to apply the VTO to PAC. This IPCA was then applied using dip coating to a glass plate	PAC	VTO	X-3B (50 mg L^{-1})	Cylindrical silica batch photoreactor system with 250 W halogen lamp (light filter cutting off < 400 nm) and vertical aeration with IPCA placed on the bottom of the reactor	[114]

(*continued*)

TABLE 37.1 (continued) IPCA Wet Preparation Methods

Preparation Method	Adsorbent	Photocatalyst	Substrate (Initial Concentration)	Irradiation Source	References
Solution of P25 was applied to the AC and carbon foam by mixing in a rotary evaporator followed by drying. Carbon form prepared by acid modification of coal tar pitch followed by heat treatment at 600°C in N_2 and then stream activation at 800°C for 1 h	"Carbon foams" & GAC	P25	Phenol (100 mg L^{-1})	400 mL photoreactor with 125 W high-pressure Hg lamp vertically suspended in a cylindrical quartz cooling jacket	[115]
A sol-gel method was used to prepare N-doped TiO_2. PAC was then added to this solution and stirred followed by filtration to remove the IPCA, which was calcined at 400°C in N_2	PAC	Anatase TiO_2 with traces of brookite	Bisphenol—A (36 mg L^{-1})	250 mL solar simulator equipped with a 150 W Xe arc lamp (light intensity: 1000 W m^{-2}, UV/Vis intensity approx 6.5%/40%). Additional light filters used to control certain wavelengths	[116]
Chitosan/ACF composite films were prepared by adding the ACF to a chitosan and pore-forming agent solution. A separate sol-gel TiO_2 solution was prepared and applied to the chitosan/ACF using dip coating	Chitosan/ACF	TiO_2 (phase not stated)	2,4-Dichlorophenol (1–50 mg L^{-1})	On-site regeneration: irritation with 20 W UV light (λ: 254 nm). Off-site regeneration: IPCA was dipped in distilled water in a shallow tank reactor under the same light source. Fenton reagent was also investigated for regeneration	[117]
Prepared by a one-step carbonization (at 450°C under vacuum) of a self-assembled matrix consisting of titanium tetra-isopropoxide and a triblock copolymer	Form not stated	C-doped Anatase TiO_2	MB (10 mg L^{-1})	25 mL quartz photochemical reactor with 150 W Xe lamp (180 mW cm^{-2}) with UV-cut off filter (<400 nm)	[118]
Ultrasonication used to apply P25 to GAC followed by oven drying, filtering, and washing	GAC	P25	Indomethacin (0.1–1.5 mmol L^{-1})	1 L photoreactor and water-cooled immersion well with 125 W medium pressure Hg lamp	[119]

TABLE 37.2 IPCA Dry Preparation Methods

Preparation Method	Adsorbent	Photocatalyst	Substrate	Irradiation Source	References
AP-MOCVD (atmospheric pressure-metal organic chemical vapor deposition) used to prepare the IPCA	PAC	Anatase TiO_2	MO (100 mg L^{-1})	1.5 L cylindrical glass photoreactor, with a central UV lamp (356 nm, 1.2 mW cm^{-2})	[120]
MOCVD was used to apply TiO_2 to a commercial AC to create an IPCA	PAC	Anatase TiO_2	MO (100 mg L^{-1})	1.5 L cylindrical glass photoreactor, with a UV lamp (356 nm, 1.2 mW cm^{-2}) in the center	[121]
As given previously	PAC	Anatase TiO_2	MO (100 mg L^{-1})	1 L cylindrical glass photoreactor with a 300 W high-pressure mercury lamp (356 nm). Aeration was used (1.2 m^3 h^{-1})	[122]
MOCVD—using tetrabutyl orthotitanate and N_2—was used to apply TiO_2 onto pretreated PAC	PAC	Anatase TiO_2	MO (100 mg L^{-1})	1.5 L photoreactor with UV lamp (365 nm, 1.2 W cm^{-2})	[123]
$TiCl_4$ was deposited onto ACFs using MAD, a form of CVD to create an IPCA	ACF	Anatase/ rutile TiO_2	MB (2.498 mmol L^{-1})	Pyrex reaction cell (80 mm diameter × 95 mm height) with 24 W low-pressure mercury lamp (254 nm)	[124]
As given previously	ACF	Anatase TiO_2	MB (10–16 × 10^{-4} mol L^{-1})	Two pieces of the IPCA were placed on a reaction cell described above and aeration was used (90 mL min^{-1})	[125]
TiO_2 was applied to AC using CVD. Ag was applied to the TiO_2-AC composite using the same method	PAC	Anatase TiO_2 doped with Ag	MO (200 mg L^{-1})	1 L cylindrical photoreactor with UV lamp (356 nm, 1.2 mW cm^{-2})	[126]
TiO_2 was applied to AC using MOCVD. A sol-gel method was also used to prepare a TiO_2 and AC was added using stirring. IPCA was then calcinated at 873 K	PAC	Anatase TiO_2	MO (100 mg L^{-1})	1 L cylindrical glass reactor, with a 300 W high-pressure Hg lamp and aeration (1.2 m^3 h^{-1})	[127]
CVD was used to apply TiO_2 precursors to the support materials using various conditions for each adsorbent	EAC, silica gel, g-Al_2O_3	Anatase TiO_2	Phenol (400 mg L^{-1})	Photoreactor with 8 W UV fluorescent tube (356 nm). Oxygen was bubbled through the system	[128]

(*continued*)

TABLE 37.2 (continued) IPCA Dry Preparation Methods

Preparation Method	Adsorbent	Photocatalyst	Substrate	Irradiation Source	References
TiO_2 was applied to AC using MOCVD. Another IPCA was prepared using a sol-gel method and stirring for impregnation. This IPCA was then calcinated at 873 K	PAC	Anatase TiO_2	MO (100 mg L^{-1})	1 L cylindrical glass reactor, with a 300 W high-pressure mercury lamp and aeration (1.2 m^3 h^{-1})	[127]
Different preparation methods used CVD, direct air-hydrolysis (DAH) and high-temperature impregnation (HTI)	GAC	Anatase TiO_2	MB (10–250 mg L^{-1})	Irradiation apparatus not stated	[129]
CVD was used to prepare the IPCAs. The composites were dried and then calcined at 150°C	Four types of PAC: unoxidized, oxidized by HNO_3, H_2SO_4, or H_2SO_4, and H_2O_2	Anatase TiO_2	3-Chlorophenol (40 mg L^{-1})	Photoreactor with 100 W Hg lamp (λ: 365 nm, 7 mW cm^{-2} of 365 nm) and 50 mL min^{-1} aeration	[130]
APCVD was then used to apply TiO_2 precursor to the ACF, which was followed by calcination	ACF	Anatase TiO_2	Phenol (50 mg L^{-1})	Cylindrical shallow vessel photoreactor irradiated with a 20 W low-pressure mercury lamp (254 nm)	[131]

IPCAs create mixed-phase photocatalysts comprising a mixture of rutile and anatase, for instance, 30%:70% rutile:anatase [77,124]. These mixtures are an inevitable consequence of using a calcination step to prepare IPCAs as the anatase phase is converted to the rutile phase by high temperatures. These studies usually investigate a range of temperatures (e.g., 700°C–900°C) to create different IPCAs in order to determine which temperature produces the most photoactive IPCA [77]. Higher calcination temperatures cause more anatase to be converted to the rutile phase. However, increasing calcination temperature will also cause the TiO_2 particles to become larger and it has been suggested [77] that the larger TiO_2 particles will not block the pores of the AC thus increasing the adsorption capacity of the IPCA. It has been noted that certain adsorbents (ACFs) [124] can protect the anatase phase thus allowing the use of high calcination temperatures without causing a phase change.

The next most popular is P25, a photocatalyst manufactured commercially by the Evonik Industries (formerly the Degussa Corporation) and sold under the trade mark AEROXIDE® P25. P25 is a mixture of anatase and rutile in the range of 70%–90% anatase and is manufactured by flame synthesis. P25 has an average particle diameter of 35–40 nm (anatase), 85–95 nm (rutile) as determined by x-ray diffraction (XRD) and transmission electron microscopy (TEM) analysis and a specific surface area of 44–50 m^2 g^{-1} [140]. There is disagreement in the literature about the precise composition of P25, it has been cited as 92% anatase, 8% rutile [42], 75% anatase, 25% rutile [48], and 80% anatase, 20% rutile [53]. The anatase and rutile phases exist separately in powdered form and while the anatase phase is more photoactive, the mixture of the two phases is synergetic and allows P25 to have better activity than anatase and rutile separately [141]. The wide availability of P25 means that it is used both as photocatalyst in IPCAs but also as a reference photocatalyst to compare IPCA performance [142]. Five authors in the surveyed literature [17,67,73,111,117] did not state the TiO_2 phase that they were using.

37.2.2 Doping/TiO_2 Modification

Doping has been used to improve the photocatalytic performance of TiO_2. The purpose of doping is to apply a transition metal (V, Cr, Mo, Fe), lanthanide metal (La, Eu, Nd, Ce), or nonmetal atom (C, N, O) to the TiO_2 either to alter its band gap [143], serve as an electron scavenger [112] (thus preventing recombination of the electron–hole pairs) or to act as an adsorbent [144] in its own right. Chemical vapor deposition (CVD) has been used to add Ag to an IPCA in order to overcome its lower photocatalytic performance compared to TiO_2 slurry [126]. Six IPCAs using different Ti:Ag ratios and deposition times were prepared and compared to an IPCA using P25 as the photocatalyst. The performance of the doped IPCAs increased with the Ti:Ag ratio and deposition time and with the exception of the IPCA with the highest deposition time and Ti:Ag ratio, all of the doped IPCAs had higher photodegradation ability for methyl orange (MO) than the P25 IPCA. Doping has also been attempted with the adsorbent used in the IPCA albeit with limited success. A laboratory-prepared ACF doped with Fe by immersion in ferric nitrate solutions was then added to a tetrabutyl orthotitanate solution in order to apply TiO_2 to the IPCA [88]. However, the resulting IPCAs possessed similar photodegradation ability as the undoped TiO_2 ACF.

$ZnFe_2O_4$ has been applied to TiO_2, which was then coated onto GAC [101]. The absorption spectrum of this IPCA increased significantly in visible wavelengths (400–800 nm) and the reaction rate constant in ideal photodegradation conditions was increased by 79% for degrading brillred-RH compared to the unmodified GAC. However, due to the lack of an undoped TiO_2 control, it is unclear if this photocatalyst has any advantages over unmodified TiO_2. P25 modified with CdS was prepared using separate sol-gel and precipitation methods [102]. The modified P25 was applied to an ACF and used to degrade MB with sunlight as the irradiation source. The apparent reaction rate constants of the doped IPCA prepared using the precipitation methods and sol-gel methods were 70% and 21% higher, respectively, than the unmodified P25 IPCA. Another approach used co-doping of anatase TiO_2 with Fe(III) and Ho(III) followed by application to an ACF [103]. It was noted that the doping could "restrain the forming of crack[s] in TiO_2 films" on the surface of the ACF, although the mechanism remains unknown. Fe(0) was applied to TiO_2 and then impregnated onto an ACF [104]. The doped IPCA degraded approximately 20% more 2,4-dichlorophenol than the IPCA using unmodified P25. The improved photodegradation performance was attributed to the superior dechlorination ability of Fe(0) combined with the synergist properties of the TiO_2 ACF IPCA.

Another study [112] utilized a Fe-doped TiO_2 to prepare an ACF IPCA that was used to degrade dye wastewater. COD removal was approximately 50% higher than the unmodified TiO_2, while color removal was comparable. The improvement in performance was attributed to trapping of photogenerated electrons in the conduction band of Fe^{3+}, which decreased electron–hole pair recombination in the TiO_2, although no direct evidence of this was provided. V-doped TiO_2 has been used to degrade X-3B (Reactive Brilliant Red dye) under visible light [114]. The doped IPCA, V-doped TiO_2, and P25 degraded 89%, 60%, and 7% of the X-3B, respectively. The diffuse reflection spectra of the V-doped TiO_2 showed enhanced adsorption of visible light (380–800 nm) compared to the unmodified TiO_2 causing its enhanced performance. The V-doped TiO_2 also displayed enhanced hydrophilicity, which was attributed to photogenerated holes diffusing to the surface and reacting with the surface oxygen lattice leading to the dissociative adsorption of water at those defective sites.

TiO_2 has been doped with C and then surrounded by AC [118]. Anatase TiO_2 grains were prepared in a copolymer that was then heat treated to form an AC. The anatase grains become doped with C during the carbonization process and develop enhanced visible light adsorption. Under visible light illumination, MB was effectively degraded in less than 1 h.

The choice of substrate for degradation is an important consideration in measuring doping performance. At visible wavelengths, photoadsorption of visible light by MB can induce a reaction in TiO_2 that causes photodegradation of the MB [145]. This is a separate effect to conventional doping

allowing the TiO_2 to photodegrade under visible light and has led to the recommendation that "transparent substrates" be used for determining photocatalytic activity of visible light photocatalysis in the 540–680 nm range [145].

37.2.3 Activated Carbon Type

IPCAs can be made with a wide variety of ACs and these carbons exist in a multitude of physical forms. PAC is the adsorbent most widely used in the literature for synthesis of IPCAs (Tables 37.1 and 37.2), followed by GAC and ACFs. The other major group of adsorbents is carbon-coated TiO_2 that appears to be in the form of PACs. Some studies used AC and other adsorbents in order to provide a comparison between adsorbents [17,113,128]. Other studies used specialist adsorbents such as proprietary photocatalyst fibers [110] and carbon foams [115] for preparing IPCA.

AC provides a synergistic effect by creating a common interface between both the AC and the TiO_2 particle phases [29]. The synergism results due to enhanced adsorption of the target pollutant onto the AC phase followed closely by a transfer through an interphase to the TiO_2 phase, giving a complete photodegradation process.

The abundance of literature describing the use of PAC is most likely due to its ease of use and preparation compared to GAC and EAC especially given that the latter is prepared by compressing PAC and a binder. IPCAs have also been prepared using AC created in the laboratory from a diverse set of precursors including wood [29,30], coconut shell [67,68], Jordanian olive stone [129], pyrolyzed sewage sludge [27], and coal tar pitch [115]. In theory, any natural organic material can be converted to AC, although economic considerations limit the number of viable feedstocks for commercial production [146]. The flexibility of source materials for AC production will allow IPCAs to be prepared from a multitude of raw materials and industrial wastes permitting sustainable production.

37.3 Methods of Preparation

IPCAs preparation methods can be broadly divided into "*dry*" and "*wet*" methods. Dry methods use a physical and/or gaseous/vapor process, whereas wet processes use an aqueous phase in applying the TiO_2 to the adsorbent. Wet processes including sol-gel, boiling impregnation, liquid phase deposition (LPD), and electrophoretic deposition constitute the majority of methods used to prepare IPCAs (Tables 37.1 and 37.2). However, there is an increasing number of papers on dry methods for preparing IPCAs and further developments in combining dry powders such as PAC and powdered TiO_2, which may be used to create IPCAs [147,148]. Proponents of dry methods cite as advantages the absence of waste streams and avoidance of several of the preparation steps needed for sol-gel methods such as saturation, aging, and drying [126,149]. In spite of these claimed advantages, wet methods are much more common in the literature. Wet methods are generally more accessible because complex, specialist, and proprietary equipment is not a prerequisite for their use [101].

37.3.1 Wet

Wet methods comprise more than three-quarters of the methods surveyed in the literature and nearly 90% of wet methods involve sol-gel processes with only two studies using a non sol-gel wet method. Other wet methods such as spray pyrolysis that is used to prepare metal oxide thin films [143] would be suitable for photocatalytic applications, however, there are to date no studies reporting their use for IPCA preparation.

37.3.1.1 Sol-Gel

Sol-gel methods are used to prepare either the virgin TiO_2 or the complete IPCA. Although these methods are generally categorized as sol-gel, there is considerable variation relating to precursor and adsorbent choice and the method of impregnation.

While the majority of IPCAs are prepared by applying TiO_2 to AC, a smaller subset of IPCA preparation methods apply either the TiO_2 to a carbonaceous material or vice versa, which is then converted to AC. For instance, hydroxypropyl cellulose has been applied to commercial TiO_2 powder (ST-01) and then activated at 700°C in N_2 and the resulting IPCA was used to decolorize MB [79]. The IPCA with the highest carbon content was the least effective at decolorizing MB when the IPCA was not presaturated before illumination. However, when the IPCAs were presaturated, the reverse was true.

Tetrabutyl orthotitanate was used to precipitate TiO_2 onto the surface of poly(vinyl butyral), which was then carbonized and used to degrade phenol [74]. The best performing IPCA removed >95% of the phenol in solution after 5 h of illumination compared to greater than 12 h for P25. A one-step sol-gel method was used to prepare IPCAs consisting of P25 and cellulose microspheres, which were then carbonized [42]. The IPCA was twice as effective at degrading acetaldehyde as plain TiO_2 of the same particle size. Poly(vinyl alcohol) and commercial TiO_2 (ST-01) combined in different ratios and then carbonized and the resulting IPCAs were then immobilized onto a thin film or tape using an organic binder [97]. A plain TiO_2 control was not included to provide a benchmark to the IPCAs photocatalytic performance. Repeated photodegradation cycles demonstrated that these IPCAs could be reused for a minimum of six cycles although photocatalytic performance decreased with each cycle.

The second category of sol-gel studies used a sol-gel process to prepare the TiO_2 used in the impregnation process. Sol-gel TiO_2 prepared using tetrabutyl orthotitanate dissolved in absolute ethanol was applied using dip coating to a GAC [59]. The resulting IPCAs had twice—in terms of reaction rate constants—the photodegradation ability of P25. Another study used the same solution but containing diethanolamine dissolved in the ethanol. GAC was added to this solution and the gel-coated GAC was heat treated in air at 250°C and the temperature was then raised from 300°C to 800°C in a nitrogen atmosphere [64]. All of the resulting IPCAs had considerably higher photodegradation ability than unmodified TiO_2 slurry. Tetrabutyl orthotitanate dissolved in ethanol has been used as a precursor solution to prepare nano-sized TiO_2 particles. A mixture of water and nitric acid was added to prepare the TiO_2 solution followed by the addition of GAC. After gelation of the solution, the IPCA was heat treated in air at 200°C [99]. The resulting IPCA exhibited similar adsorption ability as the unmodified GAC, and using a separate regeneration step, its adsorption ability could be returned to almost original levels.

Low-temperature methods have been used to prepare IPCAs and these methods are reported to be superior to high-temperature preparation methods as the surface area of the TiO_2 particles is not decreased as a result of heat treatment [55,72,119]. Preparation involves a sol-gel method to prepare TiO_2 but uses ultrasonification to mix the TiO_2 and PAC solution followed by drying with a rotary evaporator. Another low-temperature preparation method stirred different proportions of commercial TiO_2 powder (P25) and AC in an aqueous solution for an hour followed by filtration and drying [83]. The resulting IPCA had improved photodegradation ability in both natural sunlight (six times higher apparent first-order rate constants) and UV light (two-thirds higher) compared to virgin TiO_2.

37.3.1.2 Other Wet Methods

Wet chemical impregnation techniques are of interest due to their straightforward protocols, low temperature, and energy costs. Boiling impregnation was used to apply TiO_2 to GAC [22]. The method involves mixing TiO_2 and AC and repeatedly boiling dry the solution to create an IPCA. The resulting IPCA degraded 80% and 90% of MB initial concentrations of 10 and 20 mg L^{-1}, respectively, and it was regenerated twice. This method was also used to apply a solution of P25 (sonicated beforehand) to a series of inert and adsorbent supports including GAC and zeolite [113]. The coated supports were then calcined and used to degrade propoxur. The GAC-based IPCA removed almost four times more propoxur than P25. When the adsorption capacity of the IPCA was taken into account, its mineralization and oxidation performance was approximately equivalent to P25.

The LPD method is a simple and easily-controlled process for fabricating thin films coating on ACF and does not require special equipment [89]. It consists of submerging a pretreated ACF into a solution of TiO_2 precursor for several hours followed by drying and annealing for 180 min at 350°C in an N_2

atmosphere. The resulting IPCA demonstrated much higher photodegradation (49.1%) of acid orange II (AOII) compared to virgin TiO_2 (10.7%). In the same study, electro-photocatalysis was used parallel to conventional UV photocatalysis. The IPCA was used as an anode and an electric current was passed through it to decrease electron–hole recombination and this achieved a degradation rate approximately 10% greater than conventional UV photocatalysis [89].

Electrophoretic deposition—a form of electroplating—has been used to apply a suspension of commercial P25 [in a 5% (v/v) 2-propanol] and PAC to iridium glass plates [91], which function as the cathode in the process. The resulting nanocomposite electrodes prepared using a range of different synthesis suspensions were sintered (heat treated) in air. The IPCA present on the surface of the electrodes was three times more effective at decolorizing Orange-II dye (30% reduction of Orange-II compared to a 10% reduction in the TiO_2 control after 200 min of UV irradiation). The study did not use a photolysis control or total organic carbon (TOC) to monitor degradation but measured the production of H_2O_2 (a key reactive oxygen species) and determined that it was 50% higher in the IPCA compared to virgin TiO_2.

37.3.2 Dry

Dry methods constitute less than a quarter of the methods used in the literature, with CVD and its variants comprising the majority of these methods.

37.3.2.1 Chemical Vapor Deposition

CVD involves creating a vapor using an inert carrier gas (typically N_2) and a chemical precursor(s) that is to be applied to a substrate, typically AC. CVD can be categorized according to the pressure or the physical characteristics of the vapor used for deposition. Atmospheric pressure (AP) CVD [126,128,130] and metal organic chemical vapor deposition (MOCVD) [120,121] have been used to prepare IPCAs. Although not explicitly mentioned in every study, all CVD methods appear to have been used at AP. The distinguishing feature of MOCVD is that it uses a metallic or metalloid precursor for deposition onto the substrate. Given that all CVD methods use a carrier gas containing titanium, then all CVD methods may be categorized as MOCVD. Low-pressure MOCVD [150] was used to prepare supported anatase TiO_2 on the surface of silica gel. The photocatalytic activity of the supported TiO_2 was nearly half of that of the powder photocatalyst (P25). Coated anatase thin films generated using MOCVD have been applied onto a window glass substrate, which resulted in the larger surface area for photocatalytic dissociation of benzene [151]. CVD has been used to create an EAC-based IPCA as well as IPCAs using silica gel and γ-Al_2O_3 [128]. The silica gel had the highest photodegradation ability of the IPCAs, in degrading phenol and this is attributed to its greater surface area. An initial increase in phenol concentration was attributed to the release of phenol from the EAC-based IPCA and no TiO_2 slurry was included as a control. These factors limit the usefulness of this study in comparing AC to other adsorbents.

Molecular adsorption–deposition (MAD) has been used to apply a TiO_2 precursor ($TiCl_4$) to ACFs [124]. The method consists of heating the ACF under vacuum followed by adsorption of $TiCl_4$ vapor and saturated water vapor at room temperature. The system was then heated to 90°C and evacuated, followed by calcination. As this method creates a vapor that is deposited on a substrate, it could also be considered lower pressure chemical vapor deposition (LPCVD).

37.3.2.2 Mechanofusion: Theta Composer

A dry mechanical process used a Theta Composer® to apply P25 to PAC [22]. The Theta Composer® is a proprietary elliptical rotor-type powder mixer that uses a rotating vessel and rotor to create high shear forces that bind the particles together. Resulting IPCAs exhibited MB decolorizing potential comparable to IPCAs prepared by boiling impregnation. The most important consideration for IPCAs prepared using this method was the process used to activate the AC as the ACs prepared by acid washing were ineffective compared to AC activated by steam. The increasing number of dry methods and equipment

available to prepare composite powders have been reviewed [148]. It is likely that other mechanofusion methods and equipment such as magnetic assisted impaction coating (MAIC), hybridizer, and rotating fluidized bed coater (RFBC) will be adopted for IPCA preparation in the future [147].

37.4 Substrate for Photodegradation

IPCAs have been used principally to photodegrade a variety of organic contaminates, typically hazardous substances such as phenol, chlorophenol, azo dyes, and dichloromethane (Figure 37.3).

However, only three studies in the literature surveyed involved an actual characterized wastewater sample. For wastewater from a paper mill, the best performing ACF-based IPCAs removed 15 mg L^{-1} more COD and color removal was 50% faster as compared to P25 [69]. The IPCA showed minimal loss of photocatalysis ability after several cycles. A similar study used an Fe-doped, ACF-based IPCA [112]. The Fe-doped IPCA could reduce COD by a third more than the IPCA containing nondoped TiO_2 and was twice as effective as unmodified TiO_2. The same pattern was repeated for color removal although the differences in the color removal rate were much smaller with the Fe-doped IPCA removing almost 100% of the color compared to 80% for bare TiO_2. Regeneration using UV light allowed it to maintain a 50% removal rate for COD under pilot plant conditions. The IPCA was also used to reduce the COD of effluent from a municipal sewage plant demonstrating the longevity of the IPCA in typical operating conditions. This study is one of only two in the surveyed IPCA literature to use an IPCA on municipal wastewater; however no other information was provided on the characteristics of the wastewater other than the COD that the IPCA removed. This makes assessing the overall effectiveness of this IPCA—as a polishing treatment of municipal wastewater—impossible. An IPCA based on a GAC designed for wastewater treatment was used to remove color compounds (absorbance at 254 nm, with molecular weights of 400–10,000 Da) for a municipal sewage treatment plant [99]. The initial color removal declined from 90% to 50% after 10 adsorption cycles, and using separate regeneration steps, the color removal could be returned to approximately original levels. Because the comparison for the regeneration step was undertaken only once, there is no indication of the long-term lifespan of the IPCA.

GAC IPCAs prepared using a sol-gel method with 3%–63% TiO_2 loading have been used to sterilize microorganisms [66]. The best performing IPCA (47% TiO_2) sterilized the sample in 175 min compared to a 70% reduction in viable *E. coli* numbers in 250 min for 100% TiO_2 slurry. Another IPCA prepared by a sol-gel method was used to degrade 50 and 200 mg L^{-1} of microcystin-LR (cyanobacteria endotoxin) [67,68].

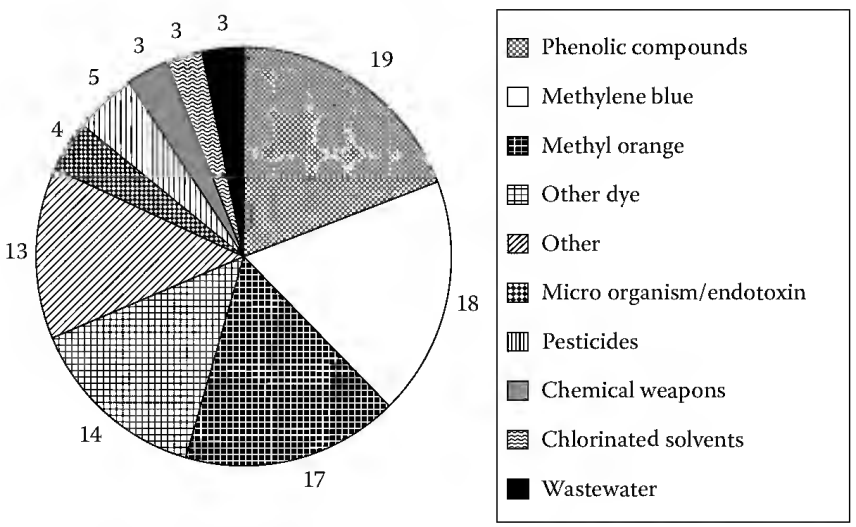

FIGURE 37.3 Number of substrates used for photodegradation in the surveyed literature (some studies use more than one).

The removal of microcystin-LR was accomplished in 15 min under UV illumination compared to a 60% reduction in 60 min without illumination. No TiO_2 slurry control was included, so it is unclear if this IPCA has enhanced photodegradation properties compared to virgin TiO_2.

A mixture of P25 and AC—prepared by pyrolysis (activation) of sewage sludge—was used to reduce ionic mercury Hg(II) to elemental mercury Hg(0) [27]. Hg(0) is less soluble in water than Hg(II) and thus has a higher affinity for AC. Under UV illumination, this system was able to remove a third more mercury than the AC on its own. Recovery from the AC of 40%–65% of the adsorbed Hg(0) was possible using separate chemical processing.

Generally, studies of dyes as target compounds use decoloration to measure degradation [22,59,64,124], while studies using HOPs measure the degradation of the target compound [34,73]. TOC and/or dissolved organic carbon (DOC) or CO_2 released during photodegradation can also be used to measure the mineralization of the compound [152]. If the target substrate is a simple compound or is well characterized, then investigation of intermediate formation yields additional information on IPCA efficiency. For instance, MO photodegradation creates phenol as an intermediate product. Comparing sol-gel with CVD IPCA, both are equally efficient in degrading MO; however, the CVD IPCA was more effective at degrading the intermediate product (phenol) and consequently the mineralization rate measured by TOC was approximately 100% higher [127].

Artificial aeration has been incorporated into some experimental designs [61,62,65,81,122,125,127,128]. Aeration may improve photodegradation by ensuring that there is sufficient O_2 that can be reduced to the superoxide radical $O_2^{\bullet-}$ that speeds up degradation [23]. However, it remains unclear if O_2 addition improved performance in all cases. IPCAs have also been used to degrade gaseous or volatile pollutants such as formaldehyde [153], methanol [154], ethylene [155], and BTEX (benzene, toluene, ethylbenzene, and xylenes) compounds [156]. This application of IPCAs has been commercialized for air cleaners [16] and remains the only current practical demonstration of the technology.

37.5 Mathematical Models

Heterogeneous photocatalysis is a complicated process, involving several factors and possible synergies. Photocatalysis reactions proceed at the surface of the semiconductor and are the result of several steps: production of electron–hole pairs by irradiation of TiO_2 with photons; formation of highly reactive hydroxyl radicals ($OH^{\bullet}$); reaction between the photogenerated hydroxyl radicals with the pollutant. In the case of immobilized catalyst, the coupling between mass transfer from the liquid phase to the catalyst surface, adsorption of the pollutant, and an "intrinsic" reaction has to be taken into account in the modeling of the photocatalytic reactor. Generally, adsorption occurs at the surface of the catalyst particles with very low microporous volume. Assuming that the surface adsorption rate for physical adsorption is rapid enough to be considered instantaneous relative to transfer across the fluid film around the particle, the flux density (N_f) of pollutant at the catalyst surface is given by

$$N_f = -K_f(C - C_e) = -K_s(q_e - q), \tag{37.1}$$

where

C is the pollutant concentration in the fluid bulk phase

C_e is its concentration at the surface of the catalyst in equilibrium with the adsorbed phase

K_f is the fluid film mass transfer coefficient

Similarly, the flux density can be expressed with a mass transfer coefficient K_s based on the solid phase with q the adsorbed-phase concentration and q_e the adsorbed-phase concentration in equilibrium with the bulk fluid phase.

According to Ollis [157,158], the "intrinsic" reaction rate may be expressed as a first-order expression of the amount of pollutant adsorbed:

$$r = kq = (\alpha I)q = (\alpha^* I_r)q, \tag{37.2}$$

with k being the rate constant (s^{-1}) depending of the production of hydroxyl radicals $OH^\bullet$, which is assumed to be directly proportional to local UV irradiations, I, and the α coefficient is related to the semiconductor activity. The coefficient α* can be defined by considering the system geometry involved and the irradiation at the external surface of the reactor, I_r.

In order to represent the dynamic behavior of any reaction system, the species balances have to be considered for both liquid and solid phases [159]. By considering the total volume of liquid present in the system (V_T), the reactor volume (V_r), and the equivalent surface of catalyst per unit of reactor (S_{cat}), the material balance equations are given by

$$\frac{dC}{dt} = -\frac{V_r}{V_T} S_{cat} K_S (q_e - q), \tag{37.3}$$

$$\frac{dq}{dt} = K_S (q_e - q) - (\alpha^* I_r)q. \tag{37.4}$$

Solution of the aforementioned (Equations 37.3 and 37.4) system of differential equations provides the concentration profiles as a function of the time. Dark adsorption experiments correspond to the special cases of an irradiation I_r equal to 0. First-order kinetics have been successfully used to model the photocatalytic degradation of various organic molecules [160–166]:

$$r = -\frac{dC}{dt} = k_{app} C, \tag{37.5}$$

where k_{app} is the apparent first-order rate constant (with the same restriction of $C = C_0$ at $t = 0$, with C_0 being the initial content in the bulk solution after adsorption and t the reaction time). The kinetic behavior in which k_{app} is affected by the initial organic content is commonly described in terms of a modified Langmuir–Hinshelwood (L–H) model. This has been successfully used in heterogeneous photocatalytic degradation to determine the relationship between the apparent first-order rate constant and the initial content of the organic substrate [167,168], and is commonly expressed as Equation 37.6:

$$r = -\frac{dC}{dt} = \frac{k_r K_S C}{1 + K_S C_0} = k_{app} C, \tag{37.6}$$

$$\frac{1}{k_{app}} = \frac{1}{k_r K_S} + \frac{C_0}{k_r}, \tag{37.7}$$

where

C_0 is the initial organic content
k_r is the reaction rate constant
K_S is the adsorption rate constant

The reaction rate is dependent on the light intensity and adsorption performance of the catalyst. In certain cases [76], the light intensity affected both constants (k_r and K_S) in the L–H model.

The Elovich rate equation is widely used to describe heterogeneous photocatalysis [169–171]. It is empirical in nature and given as follows:

$$r = \frac{dq_t}{dt} = \alpha_E \exp\left(-\beta_E q_t\right), \tag{37.8}$$

where

r (or dq_t/dt) is the photocatalytic rate (in units of mg g^{-1} min^{-1})
α_E is the initial rate (mg g^{-1} min^{-1}) when q_t approaches zero (at irradiation time t = 0)
β_E is related to the extent of surface coverage for photocatalytic activity of pollutant degradation

Integrating Equation 37.8 with the condition ($q_t = 0$ at t = 0) and subsequently linearizing the integrated equation results in

$$q_t = \frac{1}{\beta_E}\ln(t_0) + \frac{1}{\beta_E}\ln\left(t + t_0\right), \tag{37.9}$$

where t_0 is equal to $1/\alpha_E\beta_E$. If $\alpha_E\beta_E\, t \gg 1$, then Equation 37.10 can further be simplified as

$$q_t = \frac{1}{\beta_E}\ln\left(\alpha_E\beta_E\right) + \frac{1}{\beta_E}\ln(t). \tag{37.10}$$

A plot of q_t versus ln(t) yields the apparent Elovich rate constants, α_E and β_E, from the intercept and the slope of the linearity equation.

37.6 Regeneration

The ability of IPCAs to be regenerated with UV light is a primary consideration if practical applications of IPCAs are to be demonstrated. Repeated adsorption/degradation tests have been conducted on a limited number of IPCAs using 3 [22,69], 4 [103,108], 5 [56,119], 6 [54,55,72,106], 7 [104], or 15 [112] regeneration/degradation cycles. Fifteen adsorption/degradation cycles using MB led to a reduction of the MB removal rate from 100% to 92% with a 7% TiO_2 loss [76]. The photodegradation ability decreased with each cycle to varying degrees. This is attributed to the blocking of micropores and the inability of the UV light to enter these pores to trigger photodegradation. Another consideration is that the presence of UV light may enhance/inhibit π–π interactions and thus adsorption of certain organic compounds (MB, procion red MX-5B) on the carbon surface and this may be responsible for some of the reported degradation of IPCAs [172].

For regenerating IPCAs, several processes have been investigated either as an alternative to or supplement to UV light. A hybrid ultrasound (from an ultrasonic bath) and UV system was used to regenerate an IPCA used to remove color compounds from treated wastewater [99]. Regeneration using UV light alone required 16 h, UV light and hydrogen peroxide required 3 h, but regeneration using UV and ultrasound required only 30 min and achieved the highest regeneration standard levels. This study did not consider the effect of ultrasound on the stability of the AC. Separate research using ultrasound to regenerate GAC [173] has shown that the percentage of particles smaller than what could be considered GAC (<2.5 mm) increased from 0% to 4.6% after 1 h of sonication. While it was noted that this is smaller than the loss of GAC in thermal reactivation of approximately 10%, it is a disadvantage of ultrasonic regeneration. This is especially relevant to IPCAs as ultrasonication may not only affect particle size but also loosen the deposited TiO_2 on the IPCA surface. Another study compared the efficiency of regenerating

a coated chitosan ACF IPCA using UV light with regeneration using Fenton reagent [117]. In six subsequent adsorption/regeneration cycles, the removal rate of the UV-regenerated and Fenton-regenerated IPCAs remained above 82% and 86%, respectively, while the removal rate of the nonregenerated IPCA declined from 91% initially to 51% after six cycles. Although the Fenton reagent performed marginally better, UV regeneration was recommended in order to avoid the "very violent oxidants [Fenton reagent] that may affect the structure of [the] composite membrane."

Ultrasonification is an alternative to UV light for creating positive electron holes in an IPCA. In ultrasonification studies, 90 g L^{-1} of IPCA degraded 1 mol L^{-1} of phenol in 180 min, while 1.5 g L^{-1} IPCA degraded 0.6 mol L^{-1} of phenol in 540 min [174]. Increasing catalyst loadings markedly increased phenol degradation rates and it was noted that this would not be possible using photocatalysis due to light penetration problems. However, the effect of ultrasonification on the stability of the IPCA was not investigated.

37.7 IPCAs and Photocatalytic Reactor Design

Conventional photocatalysis test systems typically use either a suspension of TiO_2 [24,25,175] or an immobilized layer [19,176,177] of unmodified TiO_2. In order to treat wastewaters effectively, the TiO_2 must be kept under constant illumination. This represents a major drawback when one considers the lengthy reaction times for pollutant photodegradation and mineralization. Under illumination from a 125 W Hg lamp, up to 28 h were required for complete mineralization of a 47 mg L^{-1} solution of gemfibrozil with 0.4 g L^{-1} of photocatalyst [178] although mineralization times for gemfibrozil in a membrane photoreactor (with 1.0 g L^{-1} photocatalysts) can be as short as 150 min for greater than 97% mineralization [25]. In contrast, an IPCA can concentrate the pollutant in a smaller area improving efficiency by increasing substrate contact time with the photocatalyst [179], which is important when the pollutant concentration is very low. Moreover a photocatalysis system using a suspension of TiO_2 (or a PAC-based IPCA) requires that the suspension be removed from the water after the photocatalysis step is finished. In a water treatment plant, this may be done via filtration or coagulation limiting the possibility of recovery of the catalyst and increasing the cost of treatment. This problem can be overcome by using a GAC-, EAC-, or ACF-based IPCA that can be readily filtered from the water or used in a fixed or fluidized bed arrangement obviating the need for separation.

An alternative approach is the use of photocatalytic membrane reactors (PMRs), which filter out the TiO_2 after the photocatalysis step [180]. While PMRs remove the TiO_2 suspension and allow its reuse, they do not overcome the low adsorption and constant illumination problems of TiO_2 suspensions. Systems that use immobilized thin films of unmodified TiO_2 have higher photodegradation efficiencies [181]—most likely due to a reduction in the extinction coefficient—and do not have the removal problems of suspensions of TiO_2. However they are limited by their low surface to volume ratio and therefore require large capacities although the use of microstructured reactors is being investigated to overcome these problems [182,183].

Magnetic separation represents an innovative solution to liquid–catalyst separation. It involves applying TiO_2 to an inert silica or AC support that had been impregnated with magnetic magnetite particles [54,55,57,184]. The resulting composites are used in photocatalytic reactors where a magnetic field is used to both stir and recover the catalyst.

The cost of a typical detoxification system is broadly divided into nonrecurring capital costs and recurring operation and maintenance (O and M) costs. While capital costs can be reduced by designing more efficient systems, O and M costs depend on factors including the type and concentration of the pollutant, the degradation rate constants, the desired level of treatment, IPCA dose, and regeneration [185]. In terms of economies of scale for intermediate and large reactors designs, the costs of photocatalysis were comparable to those of AC systems [185]. The process economics between photocatalytic systems and AC adsorption was evaluated using a reference integrated water treatment process for the removal of polychlorobiphenyls (PCBs) [157].

IPCAs generally have reaction rates higher than unmodified or virgin TiO_2 (Section 37.3) and the use of IPCAs with larger particles sizes allows the use of IPCAs in fluidized bed type reactors which are simpler and do not require active filtration thus reducing reactor costs. In the future, low-cost manufacture of IPCAs will significantly reduce the cost of photocatalytic water treatment, especially if they have been modified (doped) to work better with natural sunlight.

37.8 Conclusion

In conclusion, the recent literature shows that IPCAs have considerable potential as the basis of an efficient water treatment process for the degradation of hazardous organics, including microorganisms. Almost 100 studies describing "proof of concept" IPCAs have been published in the last 14 years. By combining an adsorbent with titanium dioxide it is possible to create a composite that has both high adsorption capacity and photocatalytic activity [72]. These confer several notable process advantages over virgin TiO_2:

1. IPCAs remove pollutants from the water with or without UV light, while systems based on only TiO_2 require constant irradiation to continue functioning. Moreover, if the IPCA is to be regenerated using sunlight, this allows water treatment process to continue at night.
2. The adsorbent also immobilizes the pollutant near the TiO_2 surface, allowing photodegradation of both pollutants that do not bind to the catalyst surface and intermediate degradation products [17,96,104,113,117].
3. By employing AC with different chemical properties (porosity, point of zero charge, etc.), it is possible to tailor the adsorption properties of IPCAs for different applications [22].

At this point, demonstration of the effectiveness of IPCAs in treating actual water and wastewater samples under typical operating conditions is required. On the theoretical front, given that most batch laboratory-scale IPCA studies with HOPs have been empirical, a mechanistic model that can elucidate the kinetics between different working processes (i.e., adsorption, diffusion, and photocatalysis) within IPCA system is yet to be fully developed. Finally, pilot plant and larger scale reactor design studies are needed to confirm the economic viability of IPCA water/wastewater treatment.

Acknowledgments

This work was supported by funding from the STRIVE program from the Environmental Protection Agency (EPA) Ireland and technical assistance from ENVA environmental. SB thanks the Irish Research Council for Science, Engineering and Technology (IRCSET) for financial support in the form of IRCSET EMPOWER postdoctoral fellowship and Central Salt & Marine Chemicals Research Institute (CSMCRI) for grant of Study/Earned leave.

References

1. Hrudey, S. E., *Water Res.*, 2009, **43**, 2057–2092.
2. Choi, H., Stathatos, E. and Dionysiou, D. D., *Desalination*, 2007, **202**, 199–206.
3. Gültekin, I. and Ince, N. H., *J. Environ. Manage.*, 2007, **85**, 816–832.
4. Mills, L. J. and Chichester, C., *Sci. Total Environ.*, 2005, **343**, 1–34.
5. Mompelat, S., Le Bot, B., and Thomas, O., *Environ. Int.*, 2009, **35**, 803–814.
6. Khetan, S. K. and Collins, T. J., *Chem. Rev.*, 2007, **107**, 2319–2364.
7. von Gunten, U. and Hoigne, J., *Environ. Sci. Technol.*, 1994, **28**, 1234.
8. Nieuwenhuijsen, M. J., Toledano, M. B., Eaton, N. E., Fawell, J., and Elliott, P., *Occup. Environ. Med.*, 2000, **57**, 73–85.
9. Hamidin, N., Yu, Q. J., and Connell, D. W., *Water Res.*, 2008, **42**, 3263–3274.

10. Boorman, G. A., Dellarco, V., and Dunnick, J. K., *Environ. Health Perspect.*, 1999, **107**, 207–217.
11. Verhoeven, J. W., *Pure Appl. Chem.*, 1996, **68**, 2223–2286.
12. Fujishima, A., Rao, T. N., and Tryk, D. A., *J. Photochem. Photobiol. C*, 2000, **1**, 1–21.
13. Anpo, M., *Pure Appl. Chem.*, 2000, **72**, 1265–1270.
14. Hoffmann, M. R., Martin, S. T., Choi, W., and Bahnemann, D. W., *Chem. Rev.*, 1995, **95**, 69–96.
15. Ni, M., Leung, M. K. H., Leung, D. Y. C., and Sumathy, K., *Renew. Sustain. Energ. Rev.*, 2007, **11**, 401–425.
16. Fujishima, A. and Zhang, X., *C. R. Chim.*, 2006, **9**, 750–760.
17. Torimoto, T., Ito, S., Kuwabata, S., and Yoneyama, H., *Environ. Sci. Technol.*, 1996, **30**, 1275–1281.
18. Haque, F., Vaisman, E., Langford, C. H., and Kantzas, A., *J. Photochem. Photobiol. A*, 2005, **169**, 21–27.
19. Blanco, J., Malato, S., Fernández-Ibañez, P., Alarcón, D., Gernjak, W., and Maldonado, M. I., *Renew. Sustain. Energ. Rev.*, 2009, **13**, 1437–1445.
20. Fitzer, E., Kochling, K.-H., Boehm, H. P., and Marsh, H., *Pure Appl. Chem.*, 1995, **67**, 473–506.
21. Rouquerol, J., Avnir, D., and Fairbridge, C. W., *Pure Appl. Chem.*, 1994, **66**, 1739–1758.
22. Khan, A. Y. *Titanium Dioxide Coated Activated Carbon: A Regenerative Technology for Water Recovery*, PhD thesis, Master of Engineering, University of Florida, Gainesville, FL, 2002.
23. Zhang, X., Wu, F., Wu, X., Chen, P., and Deng, N., *J. Hazard. Mater.*, 2008, **157**, 300–307.
24. Zhang, Y., Zhou, J. L., and Ning, B., *Water Res.*, 2007, **41**, 19–26.
25. Molinari, R., Caruso, A., Argurio, P., and Poerio, T., *J. Membr. Sci.*, 2008, **319**, 54–63.
26. Hu, L., Flanders, P. M., Miller, P. L., and Strathmann, T. J., *Water Res.*, 2007, **41**, 2612–2626.
27. Zhang, F., Nriagu, J. O., and Itoh, H., *J. Photochem. Photobiol. A*, 2004, **167**, 223–228.
28. Qourzal, S., Assabbane, A., and Ait-Ichou, Y., *J. Photochem. Photobiol. A*, 2004, **163**, 317–321.
29. Cordero, T., Duchamp, C., Chovelon, J., Ferronato, C., and Matos, J., *J. Photochem. Photobiol. A*, 2007, **191**, 122–131.
30. Cordero, T., Chovelon, J., Duchamp, C., Ferronato, C., and Matos, J., *Appl. Catal. B*, 2007, **73**, 227–235.
31. Matos, J., Laine, J., and Herrmann, J., *Appl. Catal. B*, 1998, **18**, 281–291.
32. Matos, J., Laine, J., Herrmann, J.-M., Uzcategui, D., and Brito, J. L., *Appl. Catal. B*, 2007, **70**, 461–469.
33. Areerachakul, N., Vigneswaran, S., Ngo, H., and Kandasamy, J., *Korean J. Chem. Eng.*, 2008, **25**, 663–669.
34. Yoneyama, H. and Torimoto, T., *Catal. Today*, 2000, **58**, 133–140.
35. Vaisman, E., Kabir, M., Kantzas, A., and Langford, C., *J. Appl. Electrochem.*, 2005, **35**, 675–681.
36. Kabir, M. F., Vaisman, E., Langford, C. H., and Kantzas, A., *Chem. Eng. J.*, 2006, **118**, 207–212.
37. Wang, C., Lee, C., Lyu, M., and Juang, L., *Dyes Pigm.*, 2008, **76**, 817–824.
38. Shankar, M. V., Anandan, S., Venkatachalam, N., Arabindoo, B., and Murugesan, V., *Chemosphere*, 2006, **63**, 1014–1021.
39. Huang, M., Xu, C., Wu, Z., Huang, Y., Lin, J., and Wu, J., *Dyes Pigm.*, 2008, **77**, 327–334.
40. Maekawa, K., Chiyoda, O., Ohshiro, S., Okada, S., Anpo, M., and Yamashita, H., *C. R. Chim.*, 2006, **9**, 817–821.
41. Yamashita, H., Maekawa, K., Nakao, H., and Anpo, M., *Appl. Surf. Sci.*, 2004, **237**, 393–397.
42. Yamashita, H., Kawasaki, S., Yuan, S., Maekawa, K., Anpo, M., and Matsumura, M., *Catal. Today*, 2007, **126**, 375–381.
43. Ménesi, J., Körösi, L., Bazsó, É., Zöllmer, V., Richardt, A., and Dékány, I., *Chemosphere*, 2008, **70**, 538–542.
44. Ding, Z., Zhu, H. Y., Greenfield, P. F., and Lu, G. Q., *J. Colloid Interface Sci.*, 2001, **238**, 267–272.
45. Kun, R., Mogyorósi, K., and Dékány, I., *Appl. Clay Sci.*, 2006, **32**, 99–110.
46. Zhu, Z. P., Huang, K. L., and Zhou, Y., *Trans. Nonferr. Metal. Soc. China*, 2007, **17**, 1117–1121.
47. Gao, Y., Liu, H., and Ma, M., *React. Kinet. Catal. Lett.*, 2007, **90**, 11–18.
48. Xia, X., Jia, Z., Yu, Y., Liang, Y., Wang, Z., and Ma, L., *Carbon*, 2007, **45**, 717–721.

49. Wang, H., Wang, H., Jiang, W., and Li, Z., *Water Res.*, 2009, **43**, 204–210.
50. Wu, H., Wang, Q., Yao, Y., Qian, C., Zhang, X., and Wei, X., *J. Phys. Chem. C*, 2008, **112**, 16779–16783.
51. Lee, S. H. *Photocatalytic Nanocomposites Based on TiO_2 and Carbon Nanotubes*, PhD thesis, University of Florida, Gainesville, FL, 2004.
52. Yao, Y., Li, G., Ciston, S., Lueptow, R. M., and Gray, K. A., *Environ. Sci. Technol.*, 2008, **42**, 4952–4957.
53. Yu, Y., Yu, J. C., and Chan, C., *Appl. Catal. B*, 2005, **61**, 1–11.
54. Ao, Y., Xu, J., Fu, D., and Yuan, C., *J. Alloy Comp.*, 2009, **471**, 33–38.
55. Ao, Y., Xu, J., Fu, D., Shen, X., and Yuan, C., *Sep. Purif. Technol.*, 2008, **61**, 436–441.
56. Ao, Y., Xu, J., Fu, D., and Yuan, C., *Carbon*, 2008, **46**, 596–603.
57. Wang, S. and Zhou, S., *Appl. Surf. Sci.*, 2010, **256**, 6191–6198.
58. Ao, Y., Xu, J., Fu, D., Shen, X., and Yuan, C., *Appl. Surf. Sci.*, 2008, **254**, 4001–4006.
59. Liu, Y., Yang, S., Hong, J., and Sun, C., *J. Hazard. Mater.*, 2007, **142**, 208–215.
60. He, Z., Yang, S., Ju, Y., and Sun, C., *J. Environ. Sci.*, 2009, **21**, 268–272.
61. Wang, X., Hu, Z., Chen, Y., Zhao, G., Liu, Y., and Wen, Z., *Appl. Surf. Sci.*, 2009, **255**, 3953–3958.
62. Li, Y., Li, X., Li, J., and Yin, J., *Catal. Commun.*, 2005, **6**, 650–655.
63. Li, Y., Zhang, S., Yu, Q., and Yin, W., *Appl. Surf. Sci.*, 2007, **253**, 9254–9258.
64. Li, Y., Li, X., Li, J., and Yin, J., *Water Res.*, 2006, **40**, 1119–1126.
65. Li, Y., Sun, S., Ma, M., Ouyang, Y., and Yan, W., *Chem. Eng. J.*, 2008, **142**, 147–155.
66. Li, Y., Ma, M., Wang, X., and Wang, X., *J. Environ. Sci.*, 2008, **20**, 1527–1533.
67. Lee, D., Kim, S., Cho, I., Kim, S., and Kim, S., *Sep. Purif. Technol.*, 2004, **34**, 59–66.
68. Lee, D., Kim, S., Kim, S., Chung, I., and Kim, S., *Chem. Eng. J.*, 2004, **102**, 93–98.
69. Yuan, R., Guan, R., Liu, P., and Zheng, J., *Colloids Surf. A Physicochem. Eng. Asp.*, 2007, **293**, 80–86.
70. Yuan, R., Guan, R., and Zheng, J., *Scr. Mater.*, 2005, **52**, 1329–1334.
71. Yuan, R., Guan, R., Shen, W., and Zheng, J., *J. Colloid Interface Sci.*, 2005, **282**, 87–91.
72. Ao, Y., Xu, J., Fu, D., Shen, X., and Yuan, C., *Colloids Surf. A Physicochem. Eng. Asp.*, 2008, **312**, 125–130.
73. Torimoto, T., Okawa, Y., Takeda, N., and Yoneyama, H., *J. Photochem. Photobiol. A*, 1997, **103**, 153–157.
74. Tryba, B., Morawski, A. W., and Inagaki, M., *Appl. Catal. B*, 2003, **46**, 203–208.
75. Nagaoka, S., Hamasaki, Y., and Ishihara, S., *J. Mol. Catal. A Chem.*, 2002, **177**, 255–263.
76. Fu, P., Luan, Y., and Dai, X., *Trans. Nonferr. Metal. Soc. China*, 2006, **16**, 965–969.
77. Xu, D., Huang, Z., Kang, F., Inagaki, M., and Ko, T.-H., *Catal. Today*, 2008, **139**, 64–68.
78. Wang, W., Silva, C. G., and Faria, J. L., *Appl. Catal. B*, 2007, **70**, 470–478.
79. Tsumura, T., Kojitani, N., Umemura, H., Toyoda, M., and Inagaki, M., *Appl. Surf. Sci.*, 2002, **196**, 429–436.
80. Shi, J., Zheng, J., Wu, P., and Ji, X., *Catal. Commun.*, 2008, **9**, 1846–1850.
81. Sun, J., Wang, Y., Sun, R., and Dong, S., *Mater. Chem. Phys.*, 2009, **115**, 303–308.
82. Yuan, R., Zheng, J., Guan, R., and Zhao, Y., *Colloids Surf. A Physicochem. Eng. Asp.*, 2005, **254**, 131–136.
83. Araña, J., Doña-Rodríguez, J. M., and Tello Rendón, E., *Appl. Catal. B*, 2003, **44**, 161–172.
84. Araña, J., Doña-Rodríguez, J. M., and Tello Rendón, E., *Appl. Catal. B*, 2003, **44**, 153–160.
85. Tryba, B., Morawski, A. W., and Inagaki, M., *Appl. Catal. B*, 2003, **41**, 427–433.
86. Liu, S. X., Chen, X. Y., and Chen, X., *J. Hazard. Mater.*, 2007, **143**, 257–263.
87. Mozia, S., Toyoda, M., Inagaki, M., Tryba, B., and Morawski, A. W., *J. Hazard. Mater.*, 2007, **140**, 369–375.
88. Oh, W., Zhang, F., Chen, M., Lee, Y., and Ko, W., *J. Ind. Eng. Chem.*, 2009, **15**, 190–195.
89. Hou, Y., Qu, J., Zhao, X., Lei, P., Wan, D., and Huang, C. P., *Sci. Total Environ.*, 2009, **407**, 2431–2439.
90. Treschev, S. Y., Chou, P., Tseng, Y., Wang, J., Perevedentseva, E. V., and Cheng, C., *Appl. Catal. B*, 2008, **79**, 8–16.
91. Peralta-Hernández, J. M., Manríquez, J., and Meas-Vong, Y., *J. Hazard. Mater.*, 2007, **147**, 588–593.
92. Janus, M., Inagaki, M., Tryba, B., Toyoda, M., and Morawski, A. W., *Appl. Catal. B*, 2006, **63**, 272–276.
93. Liu, J., Yang, R., and Li, S., *J. Environ. Sci.*, 2006, **18**, 979–982.
94. Xu, J., Ao, Y., Fu, D., and Yuan, C., *J. Phys. Chem. Solid.*, 2008, **69**, 2366–2370.
95. Jia, B., Duan, L., Ma, C., and Wang, C., *Chin. J. Chem.*, 2007, **25**, 553–557.

96. Cojocaru, B., Neatu, S., and Pârvulescu, V. I., *ChemSusChem*, 2009, **2**, 427–436.
97. Inagaki, M., Nonaka, M., Kojin, F., Tsumura, T., and Toyoda, M., *Environ. Toxicol.*, 2006, **27**, 521–528.
98. Kim, T. Y., Lee, Y., Park, K., Kim, S. J., and Cho, S. Y., *Res. Chem. Intermed.*, 2005, **31**, 343–358.
99. Zhu, B. and Zou, L., *J. Environ. Manage.*, 2009, **90**, 3217–3225.
100. Wang, X., Liu, Y., Hu, Z., Chen, Y., Liu, W., and Zhao, G., *J. Hazard. Mater.*, 2009, **169**, 1061–1067.
101. Wang, R., Fan, K., and Chang, J., *J. Taiwan Inst. Chem. Eng.*, 2009, **40**, 533–540.
102. Zhao, W., Bai, Z., Ren, A., Guo, B., and Wu, C., *Appl. Surf. Sci.*, 2010, **256**, 3493–3498.
103. Shi, J., *Chem. Eng. J.*, 2009, **151**, 241–246.
104. Liu, L., Chen, F., and Yang, F., *Sep. Purif. Technol.*, 2009, **70**, 173–178.
105. Ravichandran, L., Selvam, K., and Swaminathan, M., *J. Mol. Catal. A Chem.*, 2010, **317**, 89–96.
106. Cao, X., Oda, Y., and Shiraishi, F., *Chem. Eng. J.*, 2010, **156**, 98–105.
107. Cao, X. and Shiraishi, F., *Chem. Eng. J.*, 2010, **160**, 651–659.
108. Yao, S., Li, J., and Shi, Z., *Particuology*, 2010, **8**, 272–278.
109. Zhang, W., Li, Y., Wang, C., and Wang, P., *Desalination*, 2011, **266**, 40–45.
110. Mounir, B., Pons, M. N., Zahraa, O., Yaacoubi, A., and Benhammou, A., *J. Hazard. Mater.*, 2007, **148**, 513–520.
111. Zhang, Y., Xiong, X., and Han, Y., *Chem. Eng. J.*, 2010, **162**, 1045–1049.
112. Li, Y., Chen, J., Liu, J., Ma, M., Chen, W., and Li, L., *J. Environ. Sci.*, 2010, **22**, 1290–1296.
113. Lu, M., Chen, J., and Chang, K., *Chemosphere*, 1999, **38**, 617–627.
114. Xu, J., Ao, Y., Chen, M., Fu, D., and Yuan, C., *Thin Solid Films*, 2010, **518**, 4170–4174.
115. Velasco, L. F., Tsyntsarski, B., and Petrova, B., *J. Hazard. Mater.*, **184**, 843–848.
116. Yap, P., Lim, T., Lim, M., and Srinivasan, M., *Catal. Today*, 2010, **151**, 8–13.
117. Liu, L. F., Zhang, P. H., and Yang, F. L., *Sep. Purif. Technol.*, 2010, **70**, 354–361.
118. Lee, Y., Chang, K., Hu, C., and Lin, K., *J. Mater. Chem.*, 2010, **20**, 5682–5688.
119. Basha, S., Keane, D., Morrissey, A., Nolan, K., Oelgemöller, M., and Tobin, J., *Ind. Eng. Chem. Res.*, 2010, Article ASAP.
120. Zhang, X., Zhou, M., and Lei, L., *Carbon*, 2005, **43**, 1700–1708.
121. Zhang, X., Zhou, M., and Lei, L., *Carbon*, 2006, **44**, 325–333.
122. Zhang, X., Zhou, M., and Lei, L., *Mater. Res. Bull.*, 2005, **40**, 1899–1904.
123. Zhang, X. and Lei, L., *Chin. Sci. Bull.*, 2007, **52**, 3339–3345.
124. Fu, P., Luan, Y., and Dai, X., *J. Mol. Catal. A Chem.*, 2004, **221**, 81–88.
125. Fu, P., Luan, Y., and Dai, X., *China Particuology*, 2004, **2**, 76–80.
126. Zhang, X., Zhou, M., and Lei, L., *Mater. Chem. Phys.*, 2005, **91**, 73–79.
127. Zhang, X. and Lei, L., *J. Hazard. Mater.*, 2008, **153**, 827–833.
128. Ding, Z., Hu, X., Yue, P. L., Lu, G. Q., and Greenfield, P. F., *Catal. Today*, 2001, **68**, 173–182.
129. El-Sheikh, A. H., Newman, A. P., Al-Daffaee, H., Phull, S., Cresswell, N., and York, S., *Surf. Coat. Technol.*, 2004, **187**, 284–292.
130. El-Sheikh, A. H., Al-Degs, Y. S., Newman, A. P., and Lynch, D. E., *Sep. Purif. Technol.*, 2007, **54**, 117–123.
131. Yang, H., Liu, L., Yang, F., and Yu, J., *J. Zheejiang Univ. Sci.*, 2008, **9**, 981–987.
132. Woan, K., Pyrgiotakis, G., and Sigmund, W., *Adv. Mater.*, 2009, **21**, 2233–2239.
133. Wang, C., Deng, Z., and Li, Y., *Inorg. Chem.*, 2001, **40**, 5210–5214.
134. Mo, S. and Ching, W. Y., *Phys. Rev. B*, 1995, **51**, 13023–13032.
135. Ovenstone, J. and Yanagisawa, K., *Chem. Mater.*, 1999, **11**, 2770–2774.
136. Djaoued, Y., Brüning, R., Bersani, D., Lottici, P. P., and Badilescu, S., *Mater. Lett.*, 2004, **58**, 2618–2622.
137. Yamabi, S. and Imai, H., *Chem. Mater.*, 2002, **14**, 609–614.
138. Kumar, P. M., Badrinarayanan, S., and Sastry, M., *Thin Solid Films*, 2000, **358**, 122–130.
139. Smith, S. J., Stevens, R., and Liu, S., *Am. Mineral.*, 2009, **94**, 236–243.
140. Balázs, N., Mogyorósi, K., and Srankó, D. F., *Appl. Catal. B*, 2008, **84**, 356–362.
141. Ohno, T., Sarukawa, K., Tokieda, K., and Matsumura, M., *J. Catal.*, 2001, **203**, 82–86.

142. Mills, A. and Le Hunte, S., *J. Photochem. Photobiol. A*, 1997, **108**, 1–35.
143. Begum, N. and Farveez Ahmed, H., *Bull. Mater. Sci.*, 2008, **31**, 43–48.
144. Xu, J., Ao, Y., Fu, D., and Yuan, C., *J. Colloid Interface Sci.*, 2008, **328**, 447–451.
145. Yan, X., Ohno, T., Nishijima, K., Abe, R., and Ohtani, B., *Chem. Phys. Lett.*, 2006, **429**, 606–610.
146. Marsh, H. and Rodríguez-Reinoso, F. 2006. *Introduction to the Scope of the Text. Activated Carbon.* Oxford, U.K.: Elsevier Science Ltd., pp. 1–12.
147. Pfeffer, R., Dave, R. N., Wei, D., and Ramlakhan, M., *Powder Technol.*, 2001, **117**, 40–67.
148. Yang, J., Sliva, A., Banerjee, A., Dave, R. N., and Pfeffer, R., *Powder Technol.*, 2005, **158**, 21–33.
149. Wu, C., Nguyen, J., and Cai, M., *J. Eng. Mater. Technol.*, 2003, **125**, 163–169.
150. Ding, Z., Hu, X., Lu, G. Q., Yue, P., and Greenfield, P. F., *Langmuir*, 2000, **16**, 6216–6222.
151. Byun, D., Jin, Y., Kim, B., Kee Lee, J., and Park, D., *J. Hazard. Mater.*, 2000, **73**, 199–206.
152. Eggins, B. R., Palmer, F. L., and Byrne, J. A., *Water Res.*, 1997, **31**, 1223–1226.
153. Mo, D. and Ye, D., *Surf. Coat. Technol.*, 2009, **203**, 1154–1160.
154. Tao, Y., Wu, C., and Mazyck, D. W., *Chemosphere*, 2006, **65**, 35–42.
155. Ye, S., Tian, Q., Song, X., and Luo, S., *J. Photochem. Photobiol. A*, 2009, **208**, 27–35.
156. Jo, W. and Yang, C., *Sep. Purif. Technol*, 2009, **66**, 438–442.
157. Ollis, D. F., *J. Phys. Chem. B*, 2005, **109**, 2439–2444.
158. Mills, A., Wang, J., and Ollis, D. F., *J. Phys. Chem. B*, 2006, **110**, 14386–14390.
159. Serrano, B., Salaices, M., Ortiz, A., and de Lasa, H. I., *Chem. Eng. Sci.*, 2007, **62**, 5160–5166.
160. Matos, J., Laine, J., and Herrmann, J.-M., *J. Catal.*, 2001, **200**, 10–20.
161. Kaneco, S., Katsumata, H., Suzuki, T., and Ohta, K., *Chem. Eng. J.*, 2006, **125**, 59–66.
162. Chen, D. and Ray, A. K., *Appl. Catal. B*, 1999, **23**, 143–157.
163. Peiró, A. M., Ayllón, J. A., Peral, J., and Doménech, X., *Appl. Catal. B*, 2001, **30**, 359–373.
164. Theurich, J., Lindner, M., and Bahnemann, D. W., *Langmuir*, 1996, **12**, 6368–6376.
165. Rideh, L., Wehrer, A., Ronze, D., and Zoulalian, A., *Catal. Today*, 1999, **48**, 357–362.
166. Hügül, M., Erçağ, E., and Apak, R., *J. Environ. Sci. Health A Tox. Hazard. Subst. Environ. Eng.*, 2002, **37**, 365–383.
167. Tennakone, K., Tilakaratne, C. T. K., and Kottegoda, I. R. M., *Water Res.*, 1997, **31**, 1909–1912.
168. Meng, Y. B., Huang, X., and Shi, H. C. *In: Proceedings of the First Joint China/Japan Chemical Engineering Symposium*, Beijing, China, 2000, pp. 201–202.
169. Önal, Y., *J. Hazard. Mater.*, 2006, **137**, 1719–1728.
170. Chang, C., Chang, C., Chen, K., Tsai, W., Shie, J., and Chen, Y., *J. Colloid Interface Sci.*, 2004, **277**, 29–34.
171. Teng, H. and Hsieh, C., *Ind. Eng. Chem. Res.*, 1999, **38**, 292–297.
172. Khan, A. Y. and Mazyck, D. W., *Carbon*, 2006, **44**, 182–184.
173. Lim, J. and Okada, M., *Ultrason. Sonochem.*, 2005, **12**, 277–282.
174. Kubo, M., Fukuda, H., Chua, X. J., and Yonemoto, T., *Ind. Eng. Chem. Res.*, 2007, **46**, 699–704.
175. Karpova, T., Preis, S., Kallas, J., and Torres, A., *Environ. Chem. Lett.*, 2007, **5**, 219–224.
176. Byrne, J. A., Eggins, B. R., Brown, N. M. D., McKinney, B., and Rouse, M., *Appl. Catal. B*, 1998, **17**, 25–36.
177. Guillard, C., Debayle, D., Gagnaire, A., Jaffrezic, H., and Herrmann, J., *Mater. Res. Bull.*, 2004, **39**, 1445–1458.
178. Yurdakal, S., Loddo, V., Augugliaro, V., Berber, H., Palmisano, G., and Palmisano, L., *Catal. Today*, 2007, **129**, 9–15.
179. Augugliaro, V., Litter, M., Palmisano, L., and Soria, J., *J. Photochem. Photobiol. C*, 2006, **7**, 127–144.
180. Mozia, S., Tomaszewska, M., and Morawski, A. W., *Catal. Today*, 2007, **129**, 3–8.
181. Ochuma, I. J., Osibo, O. O., and Fishwick, R. P., *Catal. Today*, 2007, **128**, 100–107.
182. Coyle, E. E. and Michael, O., *Photochem. Photobiol. Sci.*, 2008, **7**, 1313–1322.
183. Matsushita, Y., Ichimura, T., and Ohba, N., *Pure Appl. Chem.*, 2007, **79**, 1959–1968.
184. Kostedt, W. L., Drwiega, J., and Mazyck, D. W., *Environ. Sci. Technol.*, 2005, **39**, 8052–8056.
185. Mukherjee, P. S. and Ray, A. K., *Chem. Eng. Technol.*, 1999, **22**, 253–260.

38

Molecular Logic Based on Optical Signaling

Uwe Pischel
Universidad de Huelva

Joakim Andréasson
Chalmers University of Technology

38.1 Introduction: From Switches to Basic Logic Operations

Logic has many implications in everyday life. Especially in our modern society, which is driven by information technology, logic plays a fundamental part in the focus of computing. The concept of logic, commonly based on binary numbers, that is, 0 and 1, is universal. Thus, any type of signal, which is processed by a physical system in a bistable manner, could be imagined for this purpose. This generalization opened the doors for molecular systems as subnanometric building blocks for logic devices. In the context of the pressing need to increase the density of functional units per electronic circuit and, thus, to obtain more powerful computing devices, the miniaturization of building blocks (the so-called bottom-up approach) has found increased attention in recent years [1]. On the other hand, conventional lithographic techniques (top-down approach), which are currently used for microchip fabrication, have physical limits of spatial resolution.

The basic idea to use molecular components for electronics is classically resumed in Aviram's famous "Gedankenexperiment" [2]. Some years later, further ideas were formulated for the specific application of molecules for "memory, logic, and amplification" [3]. The first molecular logic gate was reported by the group of de Silva [4]. They used fluorescence switching through modulation of photoinduced electron transfer (PET) as mechanistic basis for their molecular design. As a point of fact, optical outputs (changes in absorbance, transmission, and fluorescence) are probably the most popular choice for basic molecular logic gates and their combinations in more complex circuits (*vide infra*). In this chapter, we will therefore mainly focus on molecular logic devices based on optical signaling with either only optical outputs or all-photonic devices, that is, optical inputs *and* outputs.

Generally, and if thermodynamically favorable, the excited state emission of a fluorophore linked to *one* PET-active electron-donating receptor (e.g., an amine) via an electronically isolating spacer is quenched when the receptor is not occupied (left state in Scheme 38.1) [5]. This is, for example, true for compound **1**

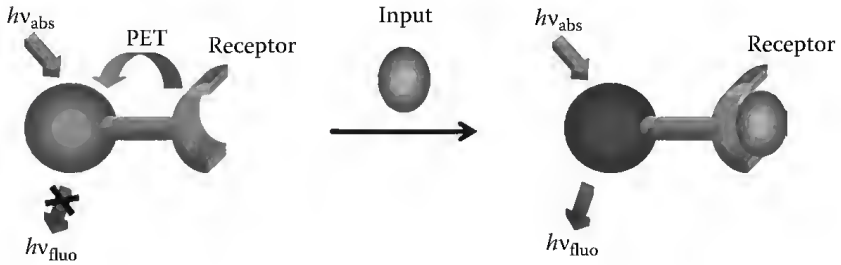

SCHEME 38.1 Fluorescence switching based on PET.

(shown in Scheme 38.2) [6]. Hence, for the absence of a chemical input (binary 0), the signal output of the system is a binary 0, which is the logic synonym for the *off* state. This situation changes for addition of an input (binary 1), upon which the properties of the receptor change in such a way that PET is now thermodynamically less favorable or even totally blocked (right state in Scheme 38.1). In our example of an amine receptor (e.g., in compound **1**), its electron-donating properties are drastically decreased by protonation with acid and concomitant formation of an ammonium ion. This is accompanied by the enhancement of the fluorophore emission intensity, which corresponds in logic terms to a binary 1 for the output (*on* state). In total, the system behaves like an IDENTITY gate: high-fluorescence output is only observed for high chemical input concentration. This effect can be harnessed for the realization of a two-input logic AND operation. For this purpose, *two* receptors of the kind described earlier are combined with a fluorophore (i.e., an anthracene

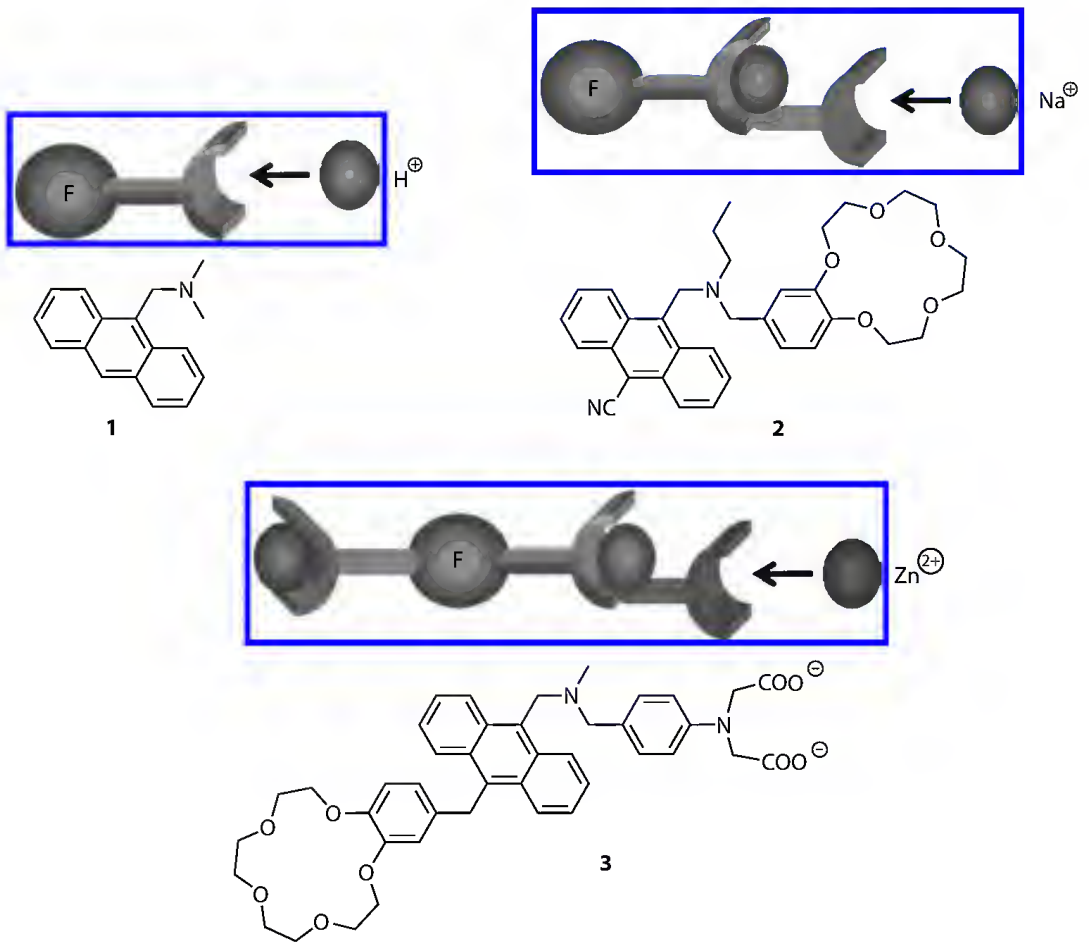

SCHEME 38.2 **(See color insert.)** Family of fluorescent PET switches with one receptor (IDENTITY gate, **1**), two receptors (two-input AND gate, **2**), and three receptors (three-input AND gate, **3**).

derivative). Now, both receptors have to be occupied to switch *off* PET-induced quenching effectively. In the concrete example of the first reported molecular logic gate **2** (Scheme 38.2), an amine and a benzo-15-crown-5 were used as electron-donating receptors, which can be blocked by addition of H^+ and Na^+ ions as chemical inputs, respectively. Indeed, high fluorescence (λ_{obs} = 446 nm) is only observed for the simultaneous presence of both inputs, which translates into the function of a two-input logic AND gate [4].

The complexity level of input-induced fluorescence switching via PET can be extended beyond one-input IDENTITY and two-input AND gates by adding a third receptor. This yields a three-input AND operation, for which the de Silva group reported recently a molecular example [7]. The design (compound **3**; Scheme 38.2) relied again on the anthracene fluorophore, this time linked to an amine (for H^+ as input), a benzo-15-crown-5 (for Na^+ ions as input), and an iminodiacetate-type receptor (for Zn^{2+} ions as input). As required for a three-input AND gate, the highest fluorescence of the system is detected for the simultaneous occupation of all receptors with their respective inputs (enhancement factor of ca. 20 with respect to absence of inputs). Noteworthy, an important issue for the successful implementation of these and other two- and three-input AND gates is the avoidance of chemical cross talk between the inputs.

The functions of the aforementioned AND gates are not influenced by the order of input application. The counterpart to this behavior is described as priority AND (PAND) gate, which distinguishes between the sequential orders of input applications. These gates are as well described in terms of sequential logic. An interesting example of a three-input PAND gate, which serves as molecular keypad lock, was described by the Shanzer group and will be discussed later in this chapter [8]. Two-input PAND gates have been also demonstrated, like triad **4** (Scheme 38.3), recently described by the groups of Andréasson and Gust. The triad integrates a porphyrin derivative (P) as fluorescent output unit, which is linked to two photochromes [a fulgimide (FG) and a dithienylethene (DTE)] [9]. The photochromes are converted between their open

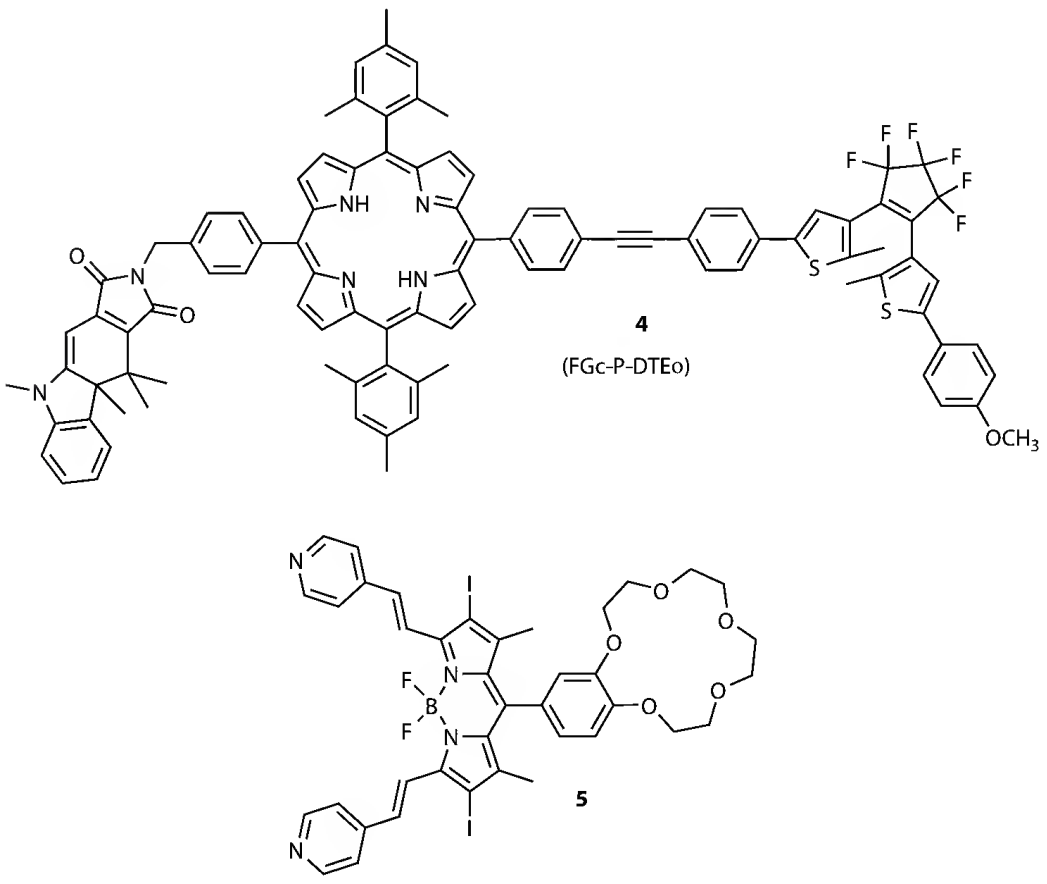

SCHEME 38.3 All-photonic two-input PAND gate **4** and chemically driven (H^+ and Na^+) AND gate **5** with singlet oxygen output.

and closed forms by light of different wavelengths as optical inputs. Selecting FGo-P-DTEo as starting state, the fluorescent FGc-P-DTEo form is observed for UV light irradiation (λ = 366 nm) followed by application of red light (λ > 580 nm). Reversal of the input order produces the nonfluorescent FGc-P-DTEc form. The FGc-P-DTEo form has the highest fluorescence because FGc acts as energy transfer sensitizer of P, while DTEo is an inefficient energy transfer quencher of P. On the other hand, DTEc is a strong energy transfer quencher of P fluorescence. Irradiation with broadband green light enables resetting to the initial state. The molecular setup delivers the fluorescence signal only for application of both irradiation wavelengths (AND) and under the condition that a certain sequential order is maintained (priority). Noteworthy, this example is also a nice demonstration of an all-photonic logic device.

For molecular logic to become a real alternative to silicon circuitry, higher degrees of complexity need to be achieved. In order to combine various logic gates in a comprehensive logic circuit, physical integration through gate-to-gate wiring, that is concatenation, is a common approach in conventional electronics. While electrons need wires to allow gate-to-gate communication, molecular logic gates with all-photonic operation (i.e., optical inputs and outputs) may use photophysical processes like emission/reabsorption [10,11] or resonance energy transfer [12]. On the downside, disadvantages like the multidirectional nature of emitted light or limitations for the maximum number of concatenated elements due to often downhill energy transfer have to be taken into account. However, unlike all-photonic devices, many molecular logic gates are addressed with chemical inputs and produce optical outputs (e.g., fluorescence). This input/output inhomogeneity constitutes a major problem for concatenation. On the other hand, the molecular world offers strategies to bypass physical integration. For example, a unimolecular platform can perform complex logic operations by *functional integration*, without the need to provide a molecular mimic for each required gate (*vide infra*). Also reconfiguration is easily achieved with molecules, because simple changes of observation parameters (e.g., emission wavelengths) may already be sufficient to obtain a different logic operation (*vide infra*). Confessedly, promising progress has been made in the development of programmable logic arrays in conventional electronics. However, in many other cases, wiring between electronic logic gates would have to be simply destroyed in order to achieve reconfiguration.

Besides the future objective of molecular data processing, molecular logic has also important implications in much less distant contexts. The aforementioned three-input AND gate **3** is interesting for multianalyte chemosensing [7]. A rather complex analytical situation of three analytes, with each of them either present or not (eight possible combinations), is translated into a simple answer signal: high (all inputs present) or low fluorescence (for two or less inputs). A different type of application of two-input AND logic was recently discussed by the Akkaya group [13]. Instead of reading the fluorescence as output signal of the gate, they presented a system (**5**) that is set for singlet oxygen production (see structure in Scheme 38.3). For this purpose, a BODIPY chromophore was modified with two types of receptors, pyridine as H^+ acceptor and benzo-15-crown-5 as Na^+ ion acceptor. The pyridines are linked to the chromophore with conjugative ethylene spacers. Thus, pyridine protonation leads to the modulation of internal charge transfer (ICT) properties of the BODIPY derivative, which is accompanied by a redshift of the long wavelength absorption band of the dye. The excitation wavelength of 660 nm coincides with the shifted band. Na^+ ion complexation, on the other hand, leads to blocking of PET, similar to the observations made for the systems **2** and **3** (*vide supra*). Hence, protonation *and* Na^+ ion addition result in excited triplet state activation of the dye and consequently singlet oxygen formation in the framework of a logic AND operation. This may have very interesting applications for photodynamic therapy. Noteworthy, lower pH and high Na^+ ion concentrations coincide with the differentiation characteristics of cancerous tissues in comparison with healthy cells.

38.2 Molecular Mimics for Basic Logic Gates: A Brief Overview

Before we discuss more complex molecular logic circuits, the most basic logic gates will be briefly overviewed in this section. While numerous examples could be cited for each specific logic gate type, we will concentrate herein on a few selected examples (**6–15** in Scheme 38.4). The interested reader is further referred to a series of excellent and comprehensive reviews on the topic [14–18].

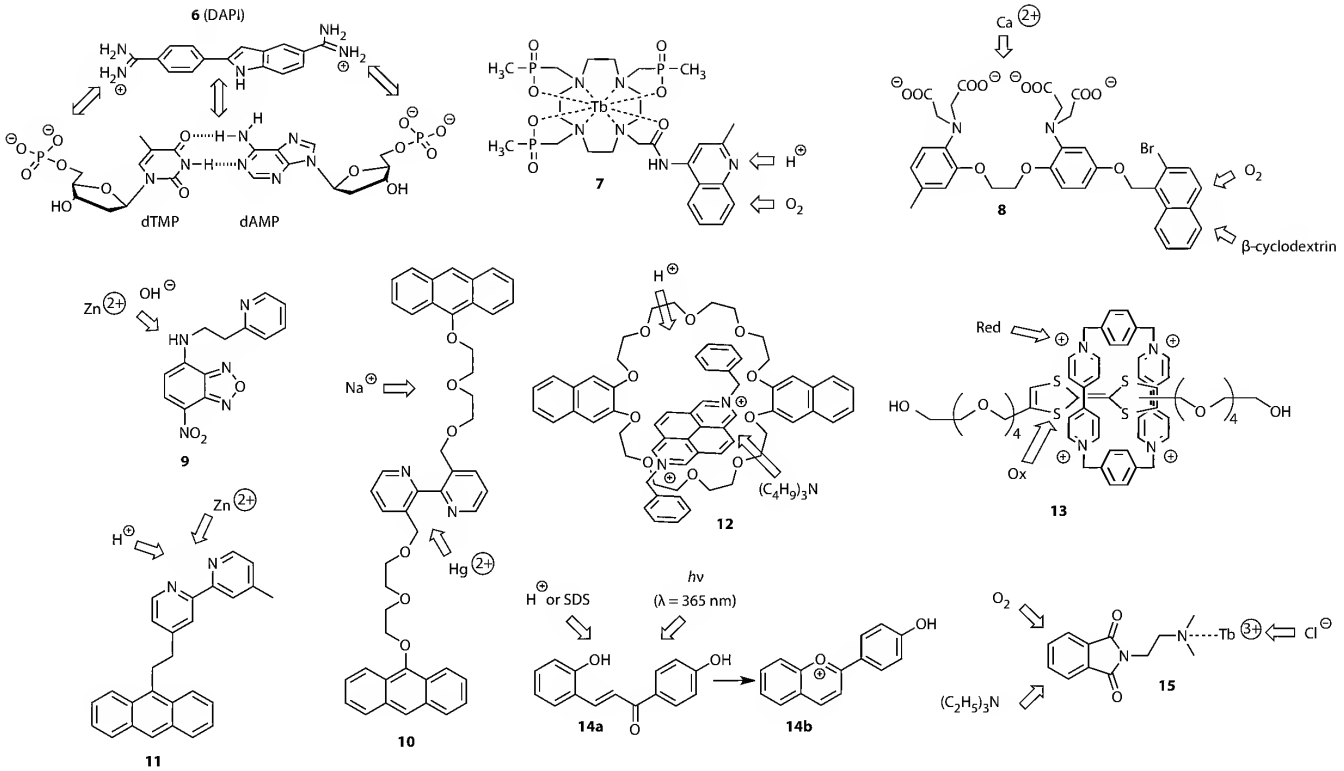

SCHEME 38.4 Examples for basic molecular logic gates and their respective inputs: **6**—NAND, **7**—two-input INH, **8**—three-input INH, **9**—IMP, **10**—OR, **11**—NOR, **12**—XOR, **13**—XNOR, **14a/14b**—EnOR, **15**—EnNOR.

38.2.1 AND–NAND

The AND gate, which was discussed earlier in more detail, has in the NAND its complementary logic gate. That means that the output of an AND gate is simply reversed to yield a NAND. In conventional electronics, the NAND gate is of special importance because it is a universal gate. Every other logic function can be expressed by the combination of various NAND gates. This prime position the NAND gate shares with the NOR gate (*vide infra*).

Akkaya and coworkers provided an example for molecular NAND logic based on hydrogen-bonding interactions between the well-known fluorescent DNA intercalator dye **6** [4′,6-diamidino-2-phenylindole (DAPI)] and the monophosphates of deoxyadenosine (dAMP) and deoxythymidine (dTMP) [19]. In presence of dAMP, a blueshift of the dye emission is observed, while addition of dTMP leaves the DAPI fluorescence virtually unaltered with respect to the absence of inputs. For these situations, an isoemissive point at 455 nm was observed. On the other hand, the formation of a ternary complex between DAPI and the two nucleotides with complementary hydrogen-bonding patterns yields a significant blueshift of the emission spectrum and additionally a drop of the fluorescence intensity (more than twofold decrease at 455 nm). This is in agreement with NAND logic behavior, which yields high output signals (binary 1) for all input combinations, except in the presence of both inputs, that is, dAMP and dTMP in this case.

38.2.2 Inhibit (INH)–Implication (IMP)

The first two-input molecular INH gate was described by Gunnlaugsson et al. [20,21]. The intricate photophysical behavior of a Tb^{3+}-cyclen complex (**7**) with an appended quinoline antenna was interpreted for this purpose. In brief, the antenna acts as efficient energy transfer sensitizer of long-lived Tb^{3+} luminescence (τ_{lum} = 0.98 ms), when it is in the protonated state and when oxygen is excluded from the solution. In all other situations, the luminescence is lower by a factor of ca. 25–50, depending on the specific input combination. It is well known that the energy level of the excited triplet state of the antenna chromophore is of crucial importance in the energy transfer process. The absence of oxygen is required in order to avoid the quenching of the antenna excited triplet state, which may be populated by back energy transfer from the lanthanide.

The first three-input version of an INH gate (**8**) was described by de Silva et al. [22]. Again, a long-lived excited state emission was used as optical output information, this time in the form of 2-bromonaphthalene phosphorescence (τ_{phos} = 0.14 ms). A PET-active bis(iminodiacetate) receptor for Ca^{2+} as input was integrated in the dyad, while the quenching of the naphthalene excited triplet state by oxygen and the prevention of bimolecular triplet–triplet annihilation in the supramolecular host–guest complex with β-cyclodextrin constitute the mechanistic basis for the other two inputs. Only in the absence of oxygen, which still could quench the excited triplet state of the host–guest complexed 2-bromonaphthalene moiety, the presence of Ca^{2+} ions (blocking of PET quenching by the receptor), and complexation with β-cyclodextrin, a high output signal is observed. This is reminiscent of a three-input INH logic gate. Interestingly, the required INVERTER gate (for the oxygen input) and the AND gate are functionally integrated in a single molecular entity. This molecular system mimics the functions of two wired logic gates without the need of their physical implementation. Hence, the realized INH gate is a simple case of functional integration with a single molecular platform.

The complementary logic gate of an INH is the IMP. The IMP gate corresponds to an OR gate with one of the inputs being inverted. For this logic function, rather few examples have been published up to date [23,24]. Samanta and coworkers reported system **9**, which integrates the 4-amino-7-nitrobenzoxa[1,3]diazole (ANBD) fluorophore and a pyridine receptor for *d*-block metal ions like Zn^{2+} [23]. The fluorescence properties of ANBD are governed by the ICT character of the emissive excited state. While at neutral pH, the fluorophore shows an intense emission at 558 nm, deprotonation of the amino NH at basic pH yields almost complete fluorescence quenching. On the other hand, addition of $Zn(ClO_4)_2$ has no influence on the high

ANBD fluorescence at neutral pH and at basic pH it restores the intense ICT emission. Defining OH^- and Zn^{2+} ions as inputs, the only combination for which a low-output fluorescence is observed is basic pH in absence of Zn^{2+}. Thus, the system operates according to the function of an IMP gate.

38.2.3 OR–NOR

The flexibility of PET-induced fluorescence switching in terms of logic operations was also demonstrated for the logic OR gate. The de Silva group developed a series of dyads, which recognize earth alkali metal ions such as Ca^{2+} or Mg^{2+}. Upon coordination of either metal ion, PET is blocked and the integrated fluorophore (e.g., anthracene) shows an unselective switching-*on* of fluorescence [25]. Hence, addition of either cation or their simultaneous presence yields a high emission output, in accordance with OR logic.

In 2000, the groups of Tucker and Desvergne reported a very interesting variation of a photoactive molecular logic gate, which produces a photochromic reaction as output [26]. The idea is based on the triad **10** with a central bipyridine (bpy) moiety, which contains on each pyridine ring an oligoether sidearm with a terminal anthracene unit. Intrinsically, the molecule is present in its extended conformation, thereby avoiding electronic repulsions between lone pairs of bpy nitrogens and also between oxygen lone pairs of the sidearms. In this situation, the two anthracene moieties are distant from each other and their photoinduced intramolecular [4 + 4] cycloaddition proceeds with a moderate quantum yield of $\Phi_r = 0.23$ for triad **10**. However, metal complexation can improve this situation by exerting a template effect. Hg^{2+} ions bind to bpy, while Na^+ ions stabilize a pseudo crown ether arrangement of the sidearms. For both situations, a triad conformation with the anthracene units in close proximity results. The simultaneous presence of both inputs has the same effect. As a result, the [4 + 4] cycloadduct is formed with considerably higher photoreaction quantum yields (e.g., $\Phi_r = 0.37–0.43$, depending on the metal ion input) in the presence of one or both metal ions. Hence, an OR logic operation is achieved with metal ion inputs and the efficiency of a photoreaction as output.

The NOR logic gate is realized by reversal of the output of an OR gate through serial wiring with an INVERTER gate. The group of de Silva has described system **11**, which enabled the successful functional integration of the two required gates in one molecule [22]. Their starting point was the notion that the INVERTER function corresponds to input-induced fluorescence quenching, while the OR gate is implemented by the nonselective interaction of inputs with the molecular logic system. Hence, nonselective fluorescence quenching by the inputs is a possible photophysical scenario for a molecular logic NOR operation. Compound **11**, as an example for the realization of this straightforward interpretation of photophysical phenomena in terms of molecular logic, is composed of anthracene as fluorophore and a bpy unit linked via an electronically isolating ethylene spacer. Thus, the system fulfills the basic conditions for observing fluorescence quenching via PET. The bpy unit is a weak electron donor in its free state, but turns into a strong electron acceptor upon protonation with acid or complexation with Zn^{2+} ions as chemical inputs. This induces strong fluorescence quenching (>85%) for the presence of either input or both inputs as required for the NOR gate operation.

38.2.4 Exclusive OR (XOR)–Exclusive NOR (XNOR)

The realization of an XOR gate is not trivial, because the highest output signal is observed for the presence of either input, while their simultaneous presence yields again a low signal as also observed for the absence of inputs. Acid–base neutralization is an elegant way of canceling two antagonistic inputs. If a system is encountered, which yields a high signal for the presence of either acid or base, then an XOR gate can be realized in a rather straightforward manner. This has been explored by Credi, Balzani, and Stoddart who reported the first molecular XOR gate [27]. A supramolecular assembly in form of the [2]pseudorotaxane **12** was used. As macrocyclic ring an electron-rich and intrinsically fluorescent 2,3-dinaphtho-30-crown-10 was chosen. The formation of a charge transfer (CT) complex with an electron-poor diazapyrenium dication thread leads to supramolecular recognition and concomitant quenching of the

naphthalene fluorescence (λ_f = 343 nm). However, dethreading can reverse this quenching and restore the naphthalene fluorescence. As inputs, H^+ (trifluoromethanesulfonic acid) and tri-*n*-butylamine were applied, which compete with the thread or the ring for the complexation of the other component, respectively. Thus, addition of either input disassembles the [2]pseudorotaxane and restores the naphthalene fluorescence. On the other hand, absence of inputs or their simultaneous presence (acid–base neutralization) leaves the supramolecular assembly intact, which results in CT-induced fluorescence quenching. Noteworthy, recently a logically reversible XOR was also reported by the groups of Pischel and Pérez-Inestrosa [28].

An example for an Exclusive NOR (XNOR) gate (complementary gate of XOR) was realized with the [2] pseudorotaxane **13** [29]. Here the roles of electron donor and acceptor were exchanged: an electron-rich thread in the form of a tetrathiafulvalene derivative with oligoether sidearms and the electron-accepting tetracationic cyclophane cyclobis(paraquat-*p*-phenylene) as ring. The supramolecular interaction is mainly defined by CT between these components, which results in a typical strongly redshifted absorption band at λ_{max} ca. 830 nm. The disassembly of the complex causes the disappearance of this optical signal, which constitutes the output of the system. The inputs were defined as positive (+0.5 V) and negative (−0.3 V) potentials, which yield electrochemical oxidation of the thread and reduction of the ring, respectively. For reasons of consistency, the negative potential input signal requires negative logic convention (low signal: binary 1; high signal: binary 0). Both electrochemical processes cause a weakening of the CT interactions and therefore lead to the dissociation of the complex, that is, the CT absorption vanishes. The simultaneous oxidation and reduction (application of both potentials) in the same pseudorotaxane is unlikely. However, the global state of the bulk system remains unchanged for this input situation, that is, the same as in the absence of electrochemical inputs [14].

38.2.5 Enabled OR (EnOR)–Enabled NOR (EnNOR)

An EnOR gate is essentially a two-input OR gate, which has to be enabled in presence of a third input. Such operation requires that the output of an OR gate is fed together with the enabling input into an AND gate. A molecular example for this type of logic was reported by the groups of Pina and Balzani [30]. They used the chalcone/flavylium system **14a/b** and defined irradiation with 365 nm light, addition of H^+, and addition of SDS (sodium dodecyl sulfate) surfactant as inputs. The output was read as absorption change at 450 nm, which corresponds to the yellow-colored flavylium ion **14b**. The chalcone **14a** is transformed to the flavylium ion by irradiation *and* protonation. Protonation is either achieved at a bulk pH ≤ 1 (H^+ as input 1) or by presence of SDS surfactant (input 2), which works as H^+ concentrator in the microenvironment of **14a** and thereby facilitates the stabilization of **14b** even at relatively high bulk pH. Thus, the inputs 1 and 2 serve for the OR gate. The irradiation at 365 nm (input 3) plays the role of the enabling input, because the conversion between **14a** and **14b** is a photodriven process.

An example for a molecular enabled NOR (EnNOR) gate, that is, the complementary device of an EnOR gate, has been published by Pischel and coworkers [31]. They used an amino-substituted phthalimide as antenna for Tb^{3+} luminescence sensitization via energy transfer (**15**). The combination of triethylamine as electron donor and oxygen as antenna triplet quencher yielded the NOR operation, which was only enabled in presence of anions, such as chloride, which protect the lanthanide from quenching by water traces. As a result, long-lived Tb^{3+} luminescence (τ_{lum} = 1.6 ms) was observed for the absence of triethylamine and oxygen and presence of chloride. All other combinations led to much lower luminescence outputs, which is compatible with an EnNOR gate.

38.3 Advanced Molecular Logic Circuits

Functional integration is a frequently adopted approach in molecular logic and used to bypass the need for concatenation of individual logic gates in the realization of advanced molecular logic devices [32]. Instructive examples are the encoder/decoder functions (*vide supra*) where the electronic circuitries

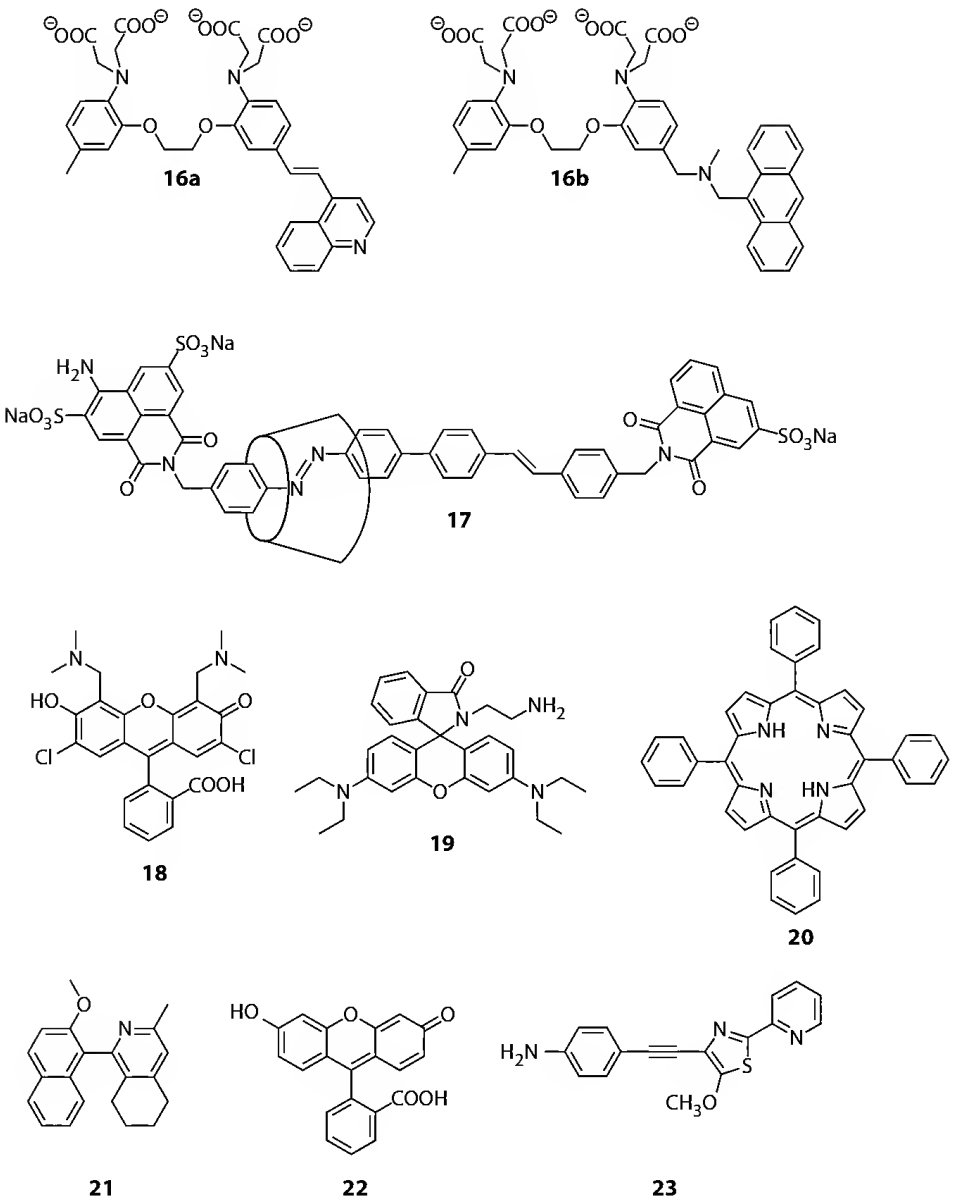

SCHEME 38.5 Examples for advanced molecular logic devices for arithmetic processing: HA (**16a/16b**,**17**, **18/19**), HS (**20**,**21**), moleculator (**22**), password-protected HA/HS (**23**).

consist of four and six individual logic gates, respectively, wired together. Hence, walking in the footsteps of silicon-based devices, it would take four and six separate concatenated molecular gates to accomplish these functions by physical integration. Instead, by using functional integration, the entire functions of both the encoder and the decoder are now loaded onto one and the same molecular species.

In the following sections, it will be described how the functions of a large selection of advanced logic devices have been mimicked by molecular counterparts (see structures **16–30** in Schemes 38.5 and 38.6). In the vast majority of these examples, functional integration has been used, although clever attempts based on concatenation have been described as well [10–12,33].

38.3.1 Half-Adders

The function performed by a half-adder (HA) is the addition of two binary digits. In the 10-based world, the arithmetic operations are the well-known 0 + 0 = 0, 0 + 1 = 1, 1 + 0 = 1, and 1 + 1 = 2. Translated into

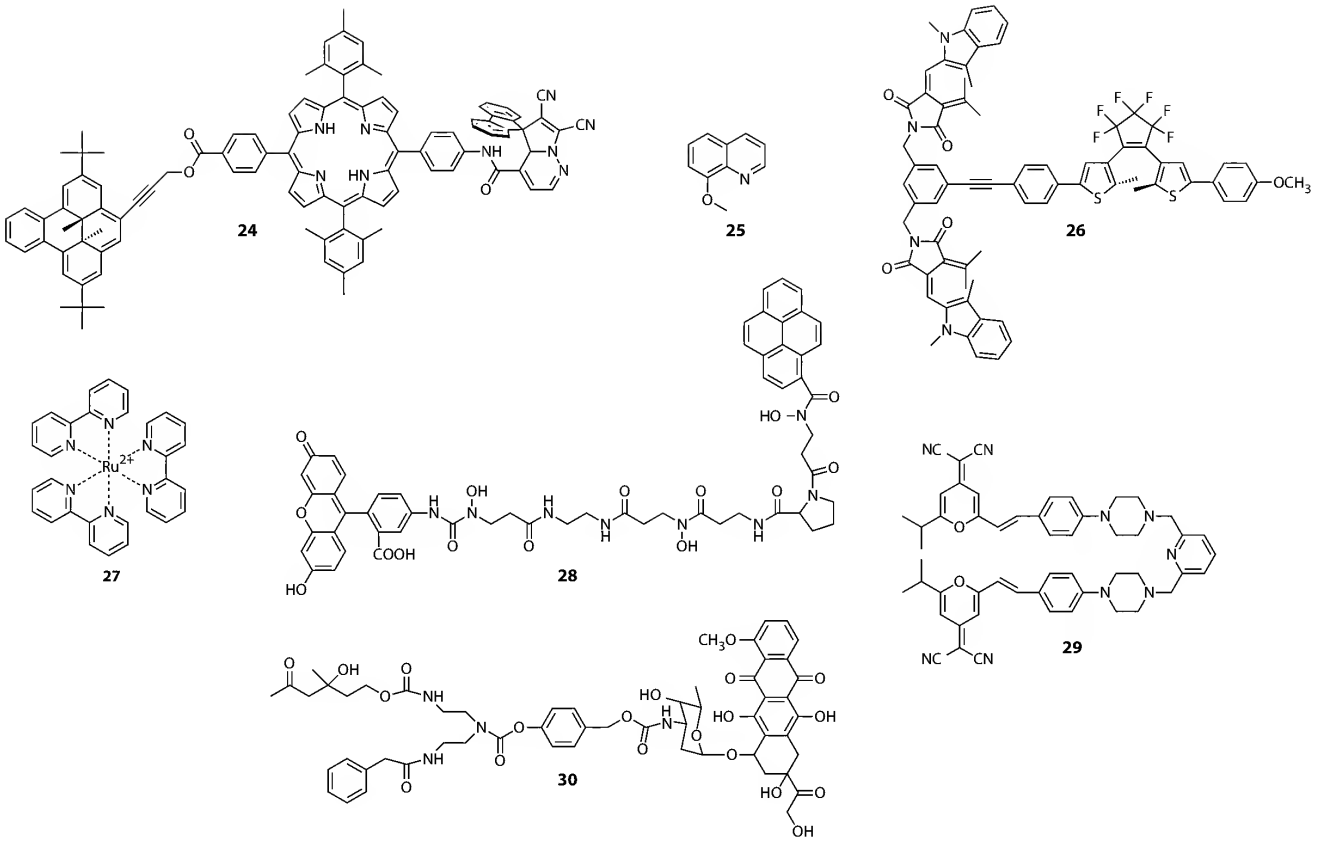

SCHEME 38.6 Examples for a molecular 2:1 MUX/1:2 DEMUX (**24**,**25**), a molecular 4:2 encoder/2:4 decoder (**26**,**27**), molecular keypad locks and memory devices (**28**,**29**), and an OR-gate activated prodrug (**30**).

binary numbers, the corresponding operations are 0 + 0 = 00, 0 + 1 = 01, 1 + 0 = 01, and 1 + 1 = 10. Upon closer inspection, it is seen that the least significant bit (the sum bit) is described by the output of an XOR gate, having the two bits to be added as inputs, whereas the carry bit follows the output of an AND gate. Hence, the HA can be realized by the combined action of an XOR and an AND gate with shared input signals. It is worth pointing out that the two gates are run in parallel through output reconfiguration, that is, concatenation is not needed.

The first molecular half-adder was reported in 2000 by de Silva et al. [34]. Here, a "cocktail" approach was used, where two separate molecules perform the XOR and the AND gate functions, respectively, in response to the addition of Ca^{2+} and H^+ (input signals). The push–pull ICT chromophore **16a** used for the XOR gate displays redshifted absorption upon addition of H^+, whereas Ca^{2+} results in a corresponding blueshift. In the presence of both H^+ and Ca^{2+}, the opposing spectral shifts cancel each other, leaving the absorption spectrum virtually unchanged. Monitoring the transmittance at the maximum of the original absorption spectrum yields the outputs required for an XOR gate. The AND gate **16b** consists of an anthracene fluorescent reporter, covalently attached to H^+ and Ca^{2+} recognizing units. Both these units quench the fluorescence from anthracene by PET in the absence of their respective cation, so that the fluorescence is only switched *on* in the presence of both H^+ and Ca^{2+}. These are the prerequisites for the AND gate.

A more recent example of a HA based on the supramolecular [2]rotaxane **17** equipped with two photoisomerizable units (azobenzene and stilbene) and two stopper chromophores (fluorescent naphthalimide derivatives) was reported by Tian and coworkers [35]. This molecular construct has the advantage of being operated in an all-photonic mode, that is, light is used for both input stimulations and readout of the optical outputs. The azobenzene and the stilbene can be independently photoisomerized, with all four isomeric states (EE, EZ, ZE, and ZZ) being accessible. The α-cyclodextrin macrocycle traversing the photoswitchable subunit is positioned at different positions depending on the isomerization state, which in turn affects the absorption and the emission properties of the rotaxane. By a judicious choice of input and output signals, the system describes the function of an all-photonic HA. The downside with this study is that the function of the XOR gate requires the output signal to be read at different wavelengths, depending on the input combination.

Although the major body of the molecular HA systems reported so far is demonstrated in bulk solution, approaches have been made to take the first steps toward fully miniaturized systems. One such example was recently presented by Park and coworkers, where a microfluidic device was used as the platform for the solutions of the information processing molecules [36]. The underlying chemistry is based on conventional acid–base switching of the emission of two fluorophores (fluorescein and rhodamine B derivatives). The fluorescein derivative **18** displays emission only at neutral pH, whereas the rhodamine B derivative **19** fluoresces exclusively in acidic environment. With a basic solution as the initial state, the XOR and the AND gates were realized by monitoring the emission of the fluorescein and rhodamine derivatives, respectively, using H^+ as degenerate input signals.

38.3.2 Half-Subtractors

Subtraction of binary digits is performed by a half-subtractor (HS). In the binary notation, the arithmetic operations performed are 0 − 0 = 00, 1 − 0 = 01, 0 − 1 = 11, and 1 − 1 = 00. Hence, the scheme of an HS is realized by representing the least significant bit (difference bit) by the output of an XOR gate, whereas the corresponding borrow bit follows the INHIBIT gate truth table. The first molecular HS was described by Langford and Yan, using the pH-sensitive emission and absorption properties of tetraphenylporphyrin (**20**, $TPPH_2$) [37,38]. Upon acidification, **20** is doubly protonated to form $TPPH_4^{2+}$, whereas addition of base results in the corresponding deprotonation to form TPP^{2-}. The Sôret-band absorption of **20** experiences a significant redshift upon both protonation and deprotonation, whereas the Q-band emission is blueshifted upon deprotonation. Monitoring the transmittance and the emission intensity at strategically chosen wavelengths and using acid and base, as inputs, the behavior of

both the XOR and the INHIBIT gate is properly described. It is worth noting that the XOR gate function, as in many other molecular XOR gates (*vide supra*), relies on acid–base neutralization.

Pischel and Heller recently reported another example of a molecular HS [24]. They utilized the electron-donating and the basic properties of a tertiary amine (diisopropyl-3-pentylamine [DiPPA]) together with acid (trifluoroacetic acid [TFA]) to switch the fluorescence emission of the pyridine-substituted naphthalene **21**. The fluorescence from the locally excited (LE) state (λ_{max} = 353 nm) is quenched by intermolecular electron transfer upon addition of DiPPA. Addition of TFA protonates the pyridine moiety, and the LE state is quenched by formation of a fluorescent ICT state, displaying emission centered at around 470 nm. By monitoring the emission intensities at the aforementioned wavelengths after application of the different input combinations, the function of an HS was described. Again, acid–base neutralization accounted for the (**1,1**) input situation.

38.3.3 Moleculators

Following de Silva's demonstration of the first molecular HA, there have been a plethora of examples for HA and HS molecules [39]. Despite the clever molecular design behind these constructs, until 2005 none of these molecules were potent enough to perform *both* addition and subtraction. A bit surprisingly, it was the off-shelf compound fluorescein (**22**) that, in the hands of Shanzer's group, proved to fulfill the prerequisites for both HA and HS performance [40]. A year later, the same group incorporated also a third input to the HA and the HS schemes to make fluorescein function as a full-adder and a full-subtractor, adding and subtracting three binary digits, and the term *moleculator* was coined [41].

Compound **22** exists in four ionization states (cation, neutral, monoanion, and dianion), which can be easily interconverted by pH changes. Each of these four states displays a characteristic absorption spectrum. Hence, acid/base proved useful as inputs, and absorbance values at carefully selected wavelengths were chosen as output signals. With the initial state in the charge neutral form and OH^- as degenerate input signals, the monoanion and the dianion were formed, respectively, upon application of one or both input signals. For the HA, monitoring the absorbance at 447 nm gave the XOR gate response, whereas the 501 nm absorbance gave the corresponding AND gate. The same initial situation was used in operation of the HS, although the system had to be reconfigured with respect to the input set, as the HS was operated using OH^- and H^+ as stimuli. This, unfortunately, prevents the system from performing addition and subtraction simultaneously.

Since Shanzer's pioneering paper, there have been many other reported HA + HS moleculators. Some of them have been equipped with various "add-on" functions to make the overall performance even more sophisticated. An interesting example of such a device is the multiswitchable 2-(4-aminophenylethynyl)-5-methoxy-2-(2-pyridyl)thiazole (**23**) fluorophore described by Yan and coworkers [42]. This molecular device is capable of authorizing the use of its HA or HS function by the correct entry of four-digit codes (represented by chemical and photonic inputs). Furthermore, the output signals (sums or differences) may be chemically encrypted.

The numerical calculations performed by the HA and HS play a key role in the machinery of today's processors. There are, however, many other logic operations that must be executed in data processing, such as transmission and compression. These are based on multiplexing/demultiplexing and encoding/decoding of data streams (Section 38.3.4).

38.3.4 Multiplexers/Demultiplexers and Encoders/Decoders

A multiplexer (MUX) is receiving information from several data lines. The information in the data lines is then combined into a common transmission line in the multiplexing process, that is, the MUX is combining two or more input signals into a single output signal for transmission to a receiver. The state of the selector input *Sel* is determining which of the incoming input signals will be transmitted to the common output line at any given time. After multiplexing, the data is again disentangled in the corresponding demultiplexer (DEMUX) by the use of an address input *Ad*.

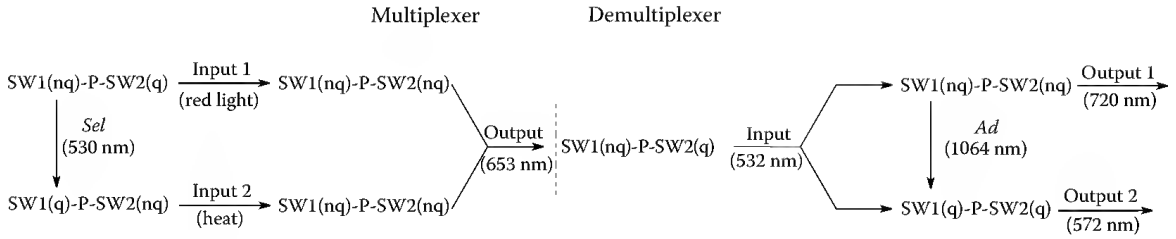

SCHEME 38.7 All-photonic switching schemes for the 2:1 MUX and 1:2 DEMUX based on triad **24**.

The first molecular MUX representation was reported by the groups of Andréasson and Gust in 2007 using triad **24** consisting of two photochromic switches (a dihydroindolizine SW1 and a dihydropyrene SW2) and a fluorescent porphyrin (P) as reporter [43]. Both photochromic switches exist in two forms: one form that quenches the fluorescence from the porphyrin (denoted q), and one that does not (denoted nq). The prerequisite for the porphyrin to display strong emission is therefore that both switches must be in the non-quenching form, nq. As shown in Scheme 38.7, the initial state for the MUX is SW1(nq)-P-SW2(q), that is, the fluorescence is quenched by SW2. Application of *Sel* (530 nm light) isomerizes the triad to SW1(q)-P-SW2(nq), where SW1 is the sole quencher. Heating the sample will induce the isomerization SW1(q) → SW1(nq), whereas exposure to red light isomerizes SW2(q) to SW2(nq). Thus, using red light as input 1 and heat as input 2 makes it possible to switch the fluorescence output to the *on* state using input 1 or input 2, respectively, depending on if *Sel* is applied or not, and the function of a MUX is properly described.

The same triad **24** can be operated as a DEMUX, where the setup is reconfigured to use IR light as *Ad* and green light as data input, respectively, whereas the absorbance and emission intensities at selected wavelengths are read as outputs (see Scheme 38.7) [44]. As presented, the DEMUX cannot function in concert with the MUX, due to the input/output inhomogeneity.

Credi and coworkers used 8-methoxyquinoline (**25**) in their interpretation of a MUX/DEMUX system [45]. Compound **25** and its protonated form **25**H^+ can be excited with a high degree of selectivity and the fluorescence of both species may be read at a common wavelength. At the same time, after excitation at the isosbestic point, the emission of **25** and **25**H^+ may also be monitored selectively. These spectral properties form the functional basis for the MUX and the DEMUX, respectively. This is yet another example of simplicity-guided approaches toward molecular logic, as a simple unimolecular species driven by H^+ and light is performing the advanced MUX/DEMUX operations. Another example of a molecular DEMUX, based on acidochromic switching of an isoquinoline *N*-oxide system, was reported by the group of Pérez-Inestrosa [46].

A device very similar to the MUX/DEMUX is the encoder/decoder combination. An encoder converts data from one form to another, whereas the information is reverted to the original form in the decoder. This process is frequently used in the compression of data for transmission or storage. One example is the 4:2 encoder/2:4 decoder. This encoder is converting 0, 1, 2, or 3 in 10-base to the binary notation, whereas the corresponding decoder is reversing the operation. Hence, the encoder is processing four inputs into two outputs, whereas the decoder has two inputs and four outputs. The electronic circuit equivalents for an encoder and a decoder are shown in Scheme 38.8. The first molecule designed to perform these operations was the photochromic triad **26**, which incorporates FG and DTE photochromes and which was reported by the groups of Andréasson and Gust [47]. With the use of a light source in the visible and three wavelengths in the UV, the triad may be selectively isomerized to all four isomeric states. Monitoring the absorbance at two wavelengths in the visible region as outputs, the function of the encoder was mimicked. When used as a decoder, two wavelengths in the UV were used as inputs, whereas four separate spectral features constituted the set of outputs. Due to the all-photonic nature of both the encoder and the decoder, the device is operated without any buildup of chemical waste, and applications in rigid or semi-rigid media may be foreseen, because the need for molecular diffusion of chemical inputs is eliminated.

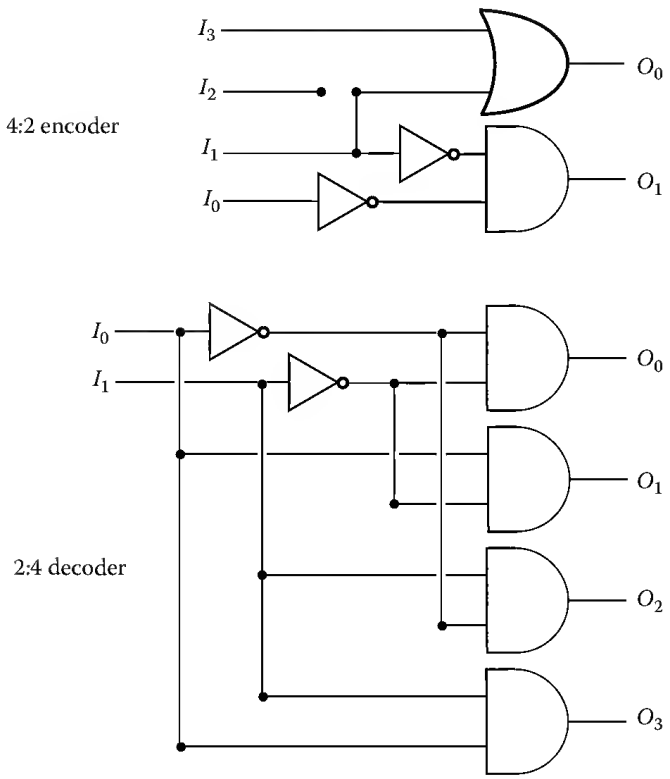

SCHEME 38.8 Electronic representations of a 4:2 encoder and a 2:4 decoder.

Balzani and coworkers recently harnessed the electrochemical and optical properties of the well-characterized ruthenium complex $[Ru(bpy)_3]^{2+}$ (**27**) to mimic the encoder/decoder function [48]. The functional basis is the different spectral properties displayed by the three oxidation states and the excited state of **27**: $[Ru(bpy)_3]^{2+}$, $[Ru(bpy)_3]^{3+}$, $[Ru(bpy)_3]^{+}$, and $^*[Ru(bpy)_3]^{2+}$. By a careful choice of conditions for electrochemical oxidations/reductions and photoexcitation of **27**, a delicate balance between these four forms was achieved, and thus, the function of both the encoder and decoder was described.

38.4 Molecular Logic with Memory Effect: Sequential Logic Devices

The logic devices described so far have an output that is only dependent on the present inputs. These devices are referred to as combinational logic devices. If instead the output depends on the input history, that is, if the device is remembering also the preceding input application and the respectively generated output, then the device is capable of performing so-called sequential logic operations. In other words, a memory effect applies.

The first molecular approach to sequential logic was the keypad lock described by Shanzer and coworkers [8]. The system used is the Fe^{3+} complex of a fluorescein-linker-pyrene dyad **28**. For the keypad lock function, the emission at 525 nm is monitored upon UV excitation and used as the output signal. The UV light used for readout excitation is mainly being absorbed by pyrene, and the emission at 525 nm is ascribed to the energy-transfer-sensitized fluorescence from the fluorescein dianion. Initially, **28** is set to the Fe^{3+}-complexed form, with fluorescein in the monoanionic state. Hence, before strong emission at 525 nm is to be observed, the monoanion must be deprotonated by the addition of base to form the dianion, and Fe^{3+} must be removed by ethylenediaminetetraacetic acid (EDTA) to suppress Fe^{3+}-induced fluorescence quenching (electron transfer). Due to the fact that the rate of Fe^{3+} extraction is significantly enhanced in acidic media compared to a basic solution, the kinetically favored sequence to

reach the fluorescent form is the addition of EDTA followed by base. If the three input signals are represented by EDTA, base, and UV excitation, the fluorescent output at 525 nm is only switched *on* when the inputs are applied in the aforementioned order. In this system, the sequence dependence is governed by a kinetically controlled process. This may be less desirable, as the output has to be read within a certain time limit. Else, the system response is not unique for a specific input order, and the sequential logic behavior is lost.

The sequential logic system (**29**) reported by Tian and coworkers is another construct where the underlying mechanism is kinetically controlled [49]. The molecular platform has multiple N-containing binding sites, where one site binds Cu^{2+} and another shows preference for Hg^{2+}. Hg^{2+} coordination results in increased emission intensity, whereas Cu^{2+} efficiently quenches the emission. The binding events are competitive, but the equilibration kinetics occurs on a timescale of several hours, why the first added cation will overrule the effect of the second, given that the readout is done before the system is approaching equilibrium. Hence, the fluorescence output will increase upon the addition of Hg^{2+} followed by Cu^{2+}, but decrease upon Cu^{2+} followed by Hg^{2+}.

Interestingly, molecular Set–Reset memory devices have also been realized recently. For example, the Willner group reported a Set–Reset latch based on a photo-electroswitch in the form of a DTE-type photochrome immobilized on a gold electrode, which can be addressed by light and electrochemical inputs [50].

38.5 Molecular Logic for Bioinspired Applications

In 15 years, molecular logic has developed from single logic gate performance to the mimicry of the most common logic operations of both combinational and sequential type. Nevertheless, the silicon-based predecessors are much ahead, and one can only speculate when and how molecular logic will catch up. Hence, going behind the silicon-based devices may not lead to the soonest real world applications, and it is now being realized that there may be areas of more direct use. Of particular interest are fields with which semiconductor materials are not compatible. Biological systems, for example, the human body, are examples where the logic response from molecules may be used to trigger the activation of drugs, etc. For example, the action of the new-generation cancer drugs is adequately described by AND logic. Here, tumor-specific receptors are being used to guide the inactive drug conjugate to cancer cells. The subsequent activation of the conjugate, that is, the release of the cytotoxic substance, is being dramatically accelerated by intracellular components, for example, enzymes, with high concentrations in tumor cells. Thus, both tumor-specific receptors and high concentrations of the activating component (inputs) are used to switch *on* the output (high cytotoxicity). Another example is system **5**, which is described as AND-logic-activated singlet oxygen generator (*vide supra*) [13].

There are several "proof-of-principle" studies that explicitly describe biological applications of molecular logic. It is worth pointing out that biomolecules themselves have been also implemented as platforms for logic operations, in what could be referred to as "biomolecular logic" [51]. This approach will not be described here, but instead the focus will be on organic molecules that may affect biological functions according to logic input schemes.

A recent example is the OR-logic controlled prodrug activation described by Shabat and coworkers [52]. A prodrug is administered in the body in the inactive form, and has thus a low initial level of toxicity. It is then being metabolized into its active form, typically by an enzyme with a high local concentration in the region of the body to be targeted by the drug. In the OR-logic interpretation by Shabat, the drug was covalently attached to a central diethylenetriamine together with two separate enzymatic substrates (a phenylacetamide unit and a retro-aldol retro-Michael substrate) to constitute the prodrug **30**. The cleavage of the drug from the two substrates, that is, the activation of the prodrug, is independently triggered by penicillin G amidase or antibody 38C2. Using the Boolean logic language to describe this protocol, the two enzymes serve as inputs, whereas the corresponding output is defined as high toxicity of the liberated drug.

In another study, reported by Stoddart, Zink, and coworkers, an AND-activated drug delivery system is envisioned [53]. Here, the drug is initially encapsulated in the pores of silica nanoparticles. The surface of the nanoparticles is covered by pH-switchable pseudorotaxanes consisting of cucurbit [6] uril rings threaded onto polyammonium stalks forming a lid over the nanopores, thereby preventing the encapsulated drug from being delivered. In addition, the walls of the nanopores are covered with azobenzene nanoimpeller units. Irradiation with 448 nm light triggers a dynamic wagging motion, impelling the encapsulated drug toward the opening of the nanopores. In order to effectuate drug release, irradiation and proper adjustment of pH conditions must be applied, which is compatible with AND logic. Application of only one input leaves the drug immersed in the pores of the silica nanoparticles.

Medical diagnostics is another area where molecular logic may be applicable. An illustrative example of this is the aforementioned three-input AND gate **3** to probe the presence of three different clinically relevant ionic species (H^+, Na^+ ions, and Zn^{2+} ions), rather than undertake three separate tests to monitor the presence of each of them [7]. Another example of such multiparameter analytics is a method devised by Walt and Konry [54]. In concrete, their system was designed for the detection of different combinations of bacterial DNA and proinflammatory cytokines (e.g., IL-8 protein) by implementation of AND and INHIBIT logic. The motivation for such a logically controlled diagnosis device is that bacterial infections are often accompanied by secretion of specific cytokins. Monoclonal antibody (mAb)-functionalized microspheres form the platform of the device. The mAb-conjugated microspheres were used to capture the IL-8 protein, and the subsequent binding of a capture-probe DNA-sequence to the protein via biotin/avidin chemistry opens up the possibility for sequence specific binding of the bacterial target gene. The bacterial target gene is complementary to a Cy3-labelled oligonucleotide, so that the Cy3 emission is only observed from the microspheres if both the protein and the bacterial DNA are present. In the absence of the target DNA, a Cy5-labelled oligonucleotide binds to the capture probe DNA, and Cy5 emission is instead observed. Hence, the Cy3 and Cy5 emission outputs describe AND logic and INHIBIT logic behavior, respectively, with respect to the IL-8 and bacterial DNA inputs.

38.6 Conclusions

The few herein discussed examples for basic and advanced molecular logic devices serve to demonstrate the importance of photophysical and photochemical engineering for the realization of such functions.* They also illustrate the enormous bandwidth of design possibilities based on a handful of excited state processes such as PET, ICT, energy transfer, and photoisomerizations (e.g., photochromic reactions). The implementation of approaches like functional integration and reconfiguration has helped to reach reasonable levels of complexity realized with unimolecular entities, such as the functions of adders/subtractors, MUXs/DEMUXs, encoders/decoders, or sequential logic. However, for the future objective of molecular computing, much work is waiting ahead, including the organization of molecular logic arrays on surfaces and gate-to-gate communication (i.e., concatenation) within these assemblies. In this context, the all-photonic operation of molecular logic devices seems a very promising approach.

On the other hand, molecular logic is expected to have impact in many other application fields that are at more immediate reach. As briefly highlighted with a few representative examples in Section 38.5, the concept of logic is of high interest for bioinspired applications such as drug delivery and prodrug activation. Here and in other areas, surely further innovative approaches will be reported in the near future.*

* The herein discussed works cover reports until December 2009.

References

1. Ball, P. *Nature* 2000, *406*, 118–120.
2. Aviram, A. and Ratner, M. A. *Chem. Phys. Lett.* 1974, *29*, 277–283.
3. Aviram, A. *J. Am. Chem. Soc.* 1988, *110*, 5687–5692.
4. de Silva, A. P., Gunaratne, H. Q. N., and McCoy, C. P. *Nature* 1993, *364*, 42–44.
5. de Silva, A. P., Gunaratne, H. Q. N., Gunnlaugsson, T., Huxley, A. J. M., McCoy, C. P., Rademacher, J. T., and Rice, T. E. *Chem. Rev.* 1997, *97*, 1515–1566.
6. Beeson, J. C., Huston, M. E., Pollard, D. A., Venkatachalam, T. K., and Czarnik, A. W. *J. Fluorescence* 1993, *3*, 65–68.
7. Magri, D. C., Brown, G. J., McClean, G. D., and de Silva, A. P. *J. Am. Chem. Soc.* 2006, *128*, 4950–4951.
8. Margulies, D., Felder, C. E., Melman, G., and Shanzer, A. *J. Am. Chem. Soc.* 2007, *129*, 347–354.
9. Andréasson, J., Straight, S. D., Moore, T. A., Moore, A. L., and Gust, D. *Chem. Eur. J.* 2009, *15*, 3936–3939.
10. Raymo, F. M. and Giordani, S. *Org. Lett.* 2001, *3*, 1833–1836.
11. Raymo, F. M. and Giordani, S. *J. Am. Chem. Soc.* 2002, *124*, 2004–2007.
12. Remacle, F., Speiser, S., and Levine, R. D. *J. Phys. Chem. B* 2001, *105*, 5589–5591.
13. Ozlem, S. and Akkaya, E. U. *J. Am. Chem. Soc.* 2009, *131*, 48–49.
14. Raymo, F. M. *Adv. Mater.* 2002, *14*, 401–414.
15. Balzani, V., Credi, A., and Venturi, M. *ChemPhysChem* 2003, *4*, 49–59.
16. de Silva, A. P. and McClenaghan, N. D. *Chem. Eur. J.* 2004, *10*, 574–586.
17. de Silva, A. P. and Uchiyama, S. *Nat. Nanotechnol.* 2007, *2*, 399–410.
18. Szaciłowski, K. *Chem. Rev.* 2008, *108*, 3481–3548.
19. Baytekin, H. T. and Akkaya, E. U. *Org. Lett.* 2000, *2*, 1725–1727.
20. Gunnlaugsson, T., Mac Dónaill, D. A., and Parker, D. *Chem. Commun.* 2000, 93–94.
21. Gunnlaugsson, T., Mac Dónaill, D. A., and Parker, D. *J. Am. Chem. Soc.* 2001, *123*, 12866–12876.
22. de Silva, A. P., Dixon, I. M., Gunaratne, H. Q. N., Gunnlaugsson, T., Maxwell, P. R. S., and Rice, T. E. *J. Am. Chem. Soc.* 1999, *121*, 1393–1394.
23. Sarkar, M., Banthia, S., Patil, A., Ansari, M. B., and Samanta, A. *New J. Chem.* 2006, *30*, 1557–1560.
24. Pischel, U. and Heller, B. *New J. Chem.* 2008, *32*, 395–400.
25. de Silva, A. P., Gunaratne, H. Q. N., and Maguire, G. E. M. *J. Chem. Soc., Chem. Commun.* 1994, 1213–1214.
26. McSkimming, G., Tucker, J. H. R., Bouas-Laurent, H., and Desvergne, J.-P. *Angew. Chem. Int. Ed.* 2000, *39*, 2167–2169.
27. Credi, A., Balzani, V., Langford, S. J., and Stoddart, J. F. *J. Am. Chem. Soc.* 1997, *119*, 2679–2681.
28. Remón, P., Ferreira, R., Montenegro, J.-M., Suau, R., Pérez-Inestrosa, E., and Pischel, U. *ChemPhysChem* 2009, *10*, 2004–2007.
29. Asakawa, M., Ashton, P. R., Balzani, V., Credi, A., Mattersteig, G., Matthews, O. A., Montalti, M., Spencer, N., Stoddart, J. F., and Venturi, M. *Chem. Eur. J.* 1997, *3*, 1992–1996.
30. Roque, A., Pina, F., Alves, S., Ballardini, R., Maestri, M., and Balzani, V. *J. Mater. Chem.* 1999, *9*, 2265–2269.
31. de Sousa, M., de Castro, B., Abad, S., Miranda, M. A., and Pischel, U. *Chem. Commun.* 2006, 2051–2053.
32. Andréasson, J. and Pischel, U. *Chem. Soc. Rev.* 2010, *39*, 174–188.
33. Raymo, F. M. and Giordani, S. *Proc. Natl. Acad. Sci. USA* 2002, *99*, 4941–4944.
34. de Silva, A. P. and McClenaghan, N. D. *J. Am. Chem. Soc.* 2000, *122*, 3965–3966.
35. Qu, D.-H., Wang, Q.-C., and Tian, H. *Angew. Chem. Int. Ed.* 2005, *44*, 5296–5299.
36. Kou, S., Lee, H. N., van Noort, D., Swamy K. M. K., Kim, S. H., Soh, J. H., Lee, K.-M., Nam, S.-W., Yoon, J., and Park, S. *Angew. Chem. Int. Ed.* 2008, *47*, 872–876.
37. Langford, S. J. and Yann, T. *J. Am. Chem. Soc.* 2003, *125*, 11198–11199.
38. Langford, S. J. and Yann, T. *J. Am. Chem. Soc.* 2003, *125*, 14951.

39. Pischel, U. *Angew. Chem. Int. Ed.* 2007, *46*, 4026–4040.
40. Margulies, D., Melman, G., and Shanzer, A. *Nat. Mater.* 2005, *4*, 768–771.
41. Margulies, D., Melman, G., and Shanzer, A. *J. Am. Chem. Soc.* 2006, *128*, 4865–4871.
42. Sun, W., Zhou, C., Xu, C.-H., Fang, C.-J., Zhang, C., Li, Z.-X., and Yan, C.-H. *Chem. Eur. J.* 2008, *14*, 6342–6351.
43. Andréasson, J., Straight, S. D., Bandyopadhyay, S., Mitchell, R. H., Moore, T. A., Moore, A. L., and Gust, D. *Angew. Chem. Int. Ed.* 2007, *46*, 958–961.
44. Andréasson, J., Straight, S. D., Bandyopadhyay, S., Mitchell, R. H., Moore, T. A., Moore, A. L., and Gust, D. *J. Phys. Chem. C* 2007, *111*, 14274–14278.
45. Amelia, M., Baroncini, M., and Credi, A. *Angew. Chem. Int. Ed.* 2008, *47*, 6240–6243.
46. Pérez-Inestrosa, E., Montenegro, J.-M., Collado, D., and Suau, R. *Chem. Commun.* 2008, 1085–1087.
47. Andréasson, J., Straight, S. D., Moore, T. A., Moore, A. L., and Gust, D. *J. Am. Chem. Soc.* 2008, *130*, 11122–11128.
48. Ceroni, P., Bergamini, G., and Balzani, V. *Angew. Chem. Int. Ed.* 2009, *48*, 8516–8518.
49. Guo, Z., Zhu, W., Shen, L., and Tian, H. *Angew. Chem. Int. Ed.* 2007, *46*, 5549–5553.
50. Baron, R., Onopriyenko, A., Katz, E., Lioubashevski, O., Willner, I., Wang, S., and Tian, H. *Chem. Commun.* 2006, 2147–2149.
51. Benenson, Y. *Mol. BioSyst.* 2009, *5*, 675–685.
52. Amir, R. J., Popkov, M., Lerner, R. A., Barbas III, C. F., and Shabat, D. *Angew. Chem. Int. Ed.* 2005, *44*, 4378–4381.
53. Angelos, S., Yang, Y.-W., Khashab, N. M., Stoddart, J. F., and Zink, J. I. *J. Am. Chem. Soc.* 2009, *131*, 11344–11346.
54. Konry, T. and Walt, D. R. *J. Am. Chem. Soc.* 2009, *131*, 13232–13233.

39

Application of Photophysics to the Study of Supramolecular Dynamics

Tamara C.S. Pace
University of Victoria

Cornelia Bohne
University of Victoria

39.1 Introduction

Supramolecular systems are assemblies of two or more individual molecular components, held together through noncovalent forces. These intermolecular interactions can include hydrogen bonds, electrostatic interactions, π-stacking, and the hydrophobic effect.[1-5] In general, intermolecular interactions are weaker than covalent bonds and thus reversible. Such reversibility is an important feature of supramolecular systems, contributing to the functions that can be obtained, and dictating that dynamics play a crucial role in defining the characteristics of the system.

The characterization of a molecular system is based on structural studies and the determination of the thermodynamics of the system. Almost all molecules are stable, and dynamics are therefore only important in the context of reactivity. Because of the inherent reversibility of supramolecular systems, knowledge of kinetic aspects, as well as the structural and thermodynamic characteristics, is needed. Thermodynamic and structural studies provide information on the equilibrium state of the system: stoichiometry and organization of the complex, as well as complex stability. Study of the system's dynamics reveals information on how fast a complex is formed and how long it exists. Thermodynamic information can be inferred from dynamic studies, but no information on the kinetics of a system can be obtained from thermodynamic or structural studies.

The dynamics of a system can be determined using real-time kinetic techniques to measure absolute rate constants, or by relative rate measurements. In real-time kinetic measurements, the concentration of the species of interest is measured as a function of time and rate constants can be obtained from the

fit of the kinetic data to rate laws derived for the system. Measuring relative rates requires comparison to a standard system for which rate constants are known, and for which the same reaction mechanism is assumed. The relative importance of different intermolecular interactions in supramolecular systems are not understood well enough to determine appropriate standard reactions, and thus relative rate measurements have limited application. Instead kinetic measurements need to be carried out using real-time techniques.

The time scale for the association and dissociation processes involving the various components of a supramolecular system is influenced by the size and complexity of the system. The fastest time scale on which encounter between two molecules completely separated in solution can occur is limited by the rate of diffusion. When reactant concentrations are 0.1 M or less in aqueous solution at 25°C ($k_{dif} = 7.4 \times 10^9\ M^{-1}\ s^{-1}$)[6] the association reaction will be slower than 1 ns. Supramolecular systems range in size from 1 to 100 nm, and the size of the supramolecular system determines the fastest reaction that can be expected. The diffusion of a small molecule, such as glucose, in aqueous solution at 25°C takes 3 ns for 1 nm and 30 μs for 100 nm, indicating that dynamics in small supramolecular systems are expected to occur in the nanosecond to microsecond time range.[7,8] Dissociation of a molecular component from the supramolecular system is a unimolecular process. Rate constants for unimolecular processes are $10^{12}\ s^{-1}$ or lower. In supramolecular systems, complete dissociation normally occurs in nanoseconds or slower, while internal processes, such as relocation or solvation changes, occur on faster time scales.[9–12] The fast processes related to the association/dissociation dynamics necessitate kinetic techniques that cover nanosecond and slower time scales for dynamics studies with supramolecular systems.

Most commonly, real-time kinetic measurements are carried out using methods that involve perturbation of a system, though a few methods do not have this requirement. Subsequent to a perturbation that is faster than the relaxation of the system to a new equilibrium the relaxation kinetics are measured, from which the rate constants for the relevant processes can be obtained. There are a number of ways in which a system can be perturbed, including creation of a new chemical species (excited state) or changes in temperature, pressure, or concentration. Advantages and disadvantages of these techniques have been previously reviewed.[13] Photophysical methods are inherently applicable to kinetic studies in the nanosecond to microsecond time range and are therefore ideal for the study of supramolecular dynamics.

This chapter provides the conceptual framework on how photophysics can be applied to the determination of dynamics in supramolecular systems. Selected techniques, that is, stopped-flow, fluorescence correlation spectroscopy (FCS), time-resolved fluorescence, and transient absorption, will be included to highlight how kinetic information can be obtained for binding of small guests with representative host systems, that is, micelles, bile salt aggregates, and cyclodextrins (CDs). This chapter focuses on association and dissociation processes in supramolecular systems, occurring on time scales faster than seconds, and does not focus on internal mobility within the system. Examples were chosen to illustrate the concepts and are not intended to provide a comprehensive review.

39.2 Host Systems

39.2.1 Micelles

Micelles are self-assemblies of surfactant molecules (Figure 39.1). Usually the surfactant consists of a hydrophobic chain with an ionic or polar head group. Micelles are formed when the surfactant concentration exceeds a critical micelle concentration (cmc). Guest molecules can be solubilized in the hydrophobic interior of the micelle. Micelles are themselves quite dynamic, with exchange of individual monomers between the micelle and the aqueous phase occurring in microseconds, while the whole assembly has a lifetime of milliseconds.[14] However, on the time scales relevant to guest binding events micelles can generally be viewed as a static host system.

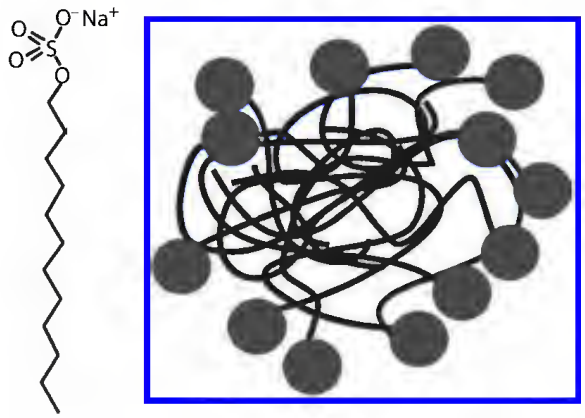

FIGURE 39.1 Structure of sodium dodecyl sulfate (SDS), a typical surfactant, and a cartoon representation of a micelle.

39.2.2 Bile Salt Aggregates

Bile salts are amphiphilic molecules, with a relatively hydrophobic convex face, and a more hydrophilic concave face (Figure 39.2). Bile salt aggregates form in aqueous solution and, as opposed to micelles, the size of the bile salt aggregate increases continuously with concentration (Figure 39.2).[15–17] The most widely used structural model for the aggregates suggests that small primary aggregates are formed at low concentrations, which provide a hydrophobic binding site for guest molecules.[18,19] At higher concentrations, further aggregation leads to the formation of secondary aggregates, which provide a relatively more hydrophilic binding site.[18,19]

39.2.3 Cyclodextrins

Cyclodextrins (CDs) are oligosaccharides consisting of various numbers of glucose units (6, 7, or 8 for α-, β-, and γ-CD) with a relatively rigid, hydrophobic internal cavity in which guests can bind (Figure 39.3).[20,21] The formation of 1:1 host–guest complexes is common, but higher order complexes, such as 1:2 and 2:2 complexes, can be formed with some guests. The efficiency of complex formation is determined by the hydrophobicity of the guest, as well as steric constraints concerning the fit of the guest in the CD cavity.[22,23]

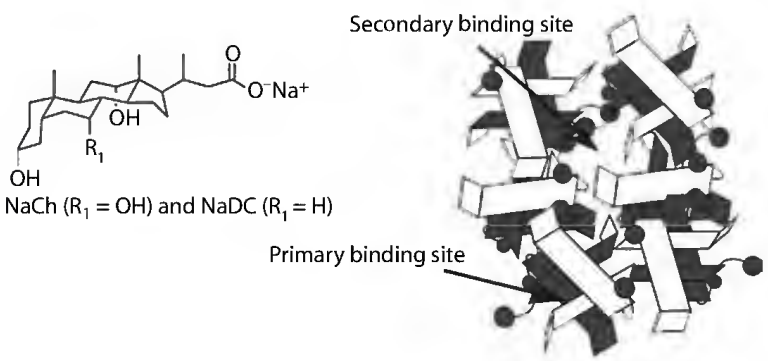

FIGURE 39.2 Structure of bile salts sodium cholate (NaCh) and sodium deoxycholate (NaDC) and a cartoon representation of a bile salt aggregate with a primary and secondary binding site.

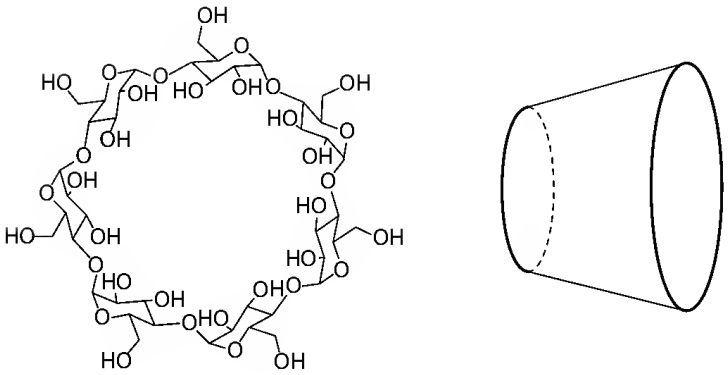

FIGURE 39.3 Structure of β-CD and a cartoon representation of a CD.

39.3 Photophysical Techniques for the Study of Supramolecular Dynamics

Photophysical methods can be used either as an analytical tool to monitor the concentration of reactants or products by absorption or emission spectroscopy (e.g., stopped-flow), or to create a perturbation in the system where dynamics of the excited state reveal kinetic information (e.g., laser flash photolysis).

39.3.1 Photophysics as an Analytical Method

When photophysics are used to monitor systems, kinetic measurements are made using continuous irradiation of the sample. For these techniques, the lifetime of the excited state is not relevant to the experiment. Fluorescence is a much more sensitive technique than absorption. Fluorescence is an absolute measurement where light intensity is detected, whereas absorption is a relative measurement where changes in light intensity are detected. For this reason, when a choice between the two techniques is available, fluorescence is generally preferable.

39.3.1.1 Stopped-Flow

Stopped-flow experiments use a concentration jump to examine kinetic processes. Two separate solutions are driven through a mixing chamber where they are thoroughly mixed before flow is stopped abruptly in an observation cell, and further changes in the system are monitored. Mixing of the solutions results in a perturbation of the initial equilibrium states, and relaxation to the new equilibrium state is monitored as a function of time, usually by absorption or fluorescence spectroscopy.[24,25] The use of fluorescence or absorption requires that either the guest or host have different absorption or fluorescence emission properties when free in solution and when part of the supramolecular complex. Stopped-flow time resolution is generally 1–2 ms,[24] and is determined by the time required for mixing and stopping the flow.

Stopped-flow can be employed to study the association and dissociation processes of supramolecular systems, with rate constants for the processes determined from the analysis of the relaxation kinetics obtained following mixing. The simplest kinetic scheme is that for a 1:1 complex formed between a guest (G) and a host (H) (Scheme 39.1).

$$G + H \underset{k_-}{\overset{k_+}{\rightleftharpoons}} HG$$

$$K = \frac{[HG]}{[G][H]} = \frac{k_+}{k_-}$$

SCHEME 39.1 Formation of a 1:1 host-guest complex.

The following rate law (Equation 39.1) defines the relaxation kinetics after perturbation:

$$\frac{d[HG]}{dt} = k_{+}[H][G] - k_{-}[HG] \tag{39.1}$$

If one of the components for the bimolecular reaction is in excess (e.g., [H] ≫ [G]) and concentration changes due to the perturbation are small, the kinetics will follow an exponential function, with the observed rate constant (k_{obs}) given by Equation 39.2:

$$k_{obs} = k_{+}[H] + k_{-} \tag{39.2}$$

In general, the concentration of free host ([H]) is approximately equal to the total host concentration ($[H]_T$) and the analytical concentration of the host is used. Otherwise, a quadratic expression for the concentration is obtained from the equilibrium constant and the mass balance equations.

The observed rate constant is related to the sum of the rate constants for the pseudo-first-order association process and the rate constant for the dissociation process. The association process can be affected by changes in [H], but the dissociation rate constant is intrinsic to the system and cannot be manipulated by external factors.

Host-guest interactions involving coupled or sequential first-order or pseudo-first-order reactions can be analyzed using a sum of exponential functions. If the reactions are not first order or pseudo first order, more complex equations have to be derived.[26,27] In all cases, the rate law is related to both association and dissociation processes, and these processes can never be decoupled when measuring relaxation kinetics.

39.3.1.2 Supramolecular Dynamics from Stopped-Flow Experiments

Stopped-flow experiments have been used to study dynamics of binding to CDs for a number of guest molecules.[28–43] Several organic molecules, including azo dyes[34,40] and pyrene[30,42,43] have been studied, as well as the binding dynamics of some metal ions.[29,31,41] Generally, only dynamics that occur on time scales slower than milliseconds can be explored, which often results in the study of systems that involve multistep kinetic processes or higher order complexes.

A primary consideration when designing kinetic experiments to probe host-guest dynamics is to choose a guest molecule for which the photophysics are as different as possible for host-guest complexes with different stoichiometries. In the context of studying complexes with higher order stoichiometry, it is important to differentiate between complexes containing one guest and those containing two guest molecules. Guests that show prominent excimer emission, which is due to a complex between the singlet excited state and a ground state molecule, are ideally suited for such studies. Examples where pyrene excimer emission was used to study the dynamics of CDs or micelles follow.

Both 1:1 and 2:2 complexes are formed by pyrene (Scheme 39.2) and γ-CD.[30,42,43] The dynamics for the formation of the 1:1 pyrene: γ-CD complex occur within the time resolution of the stopped-flow

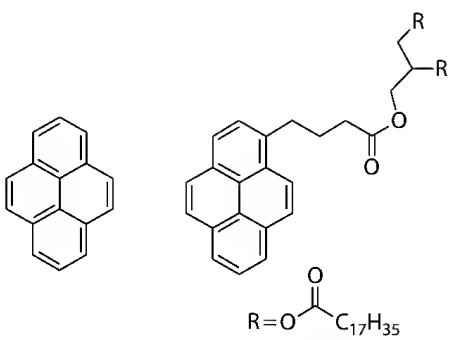

SCHEME 39.2 Structure of pyrene and a pyrene-substituted triglyceride.

equipment, but the formation of the higher order complex is much slower and suitable for stopped-flow studies. An excimer-like emission was observed for the 2:2 complex, which was redshifted in comparison to the pyrene monomer fluorescence observed for the 1:1 complex and pyrene in water. The excimer-like emission could be used to follow the formation of the 2:2 complex from two 1:1 complexes. The association constant for the 2:2 complex was found to be 6×10^7 M^{-1} s^{-1}, which is an order of magnitude smaller than the typical association rate constants for 1:1 complexes where the guest fits into the CD cavity (see the following text).[30] The dissociation rate constant for the 2:2 complex was 73 s^{-1}, which is up to five orders of magnitude slower than typical dissociation rate constants for a 1:1 complex.[30]

Exchange of guest molecules between micelles, such as Triton X-100 and SDS, has been studied using stopped-flow methods.[44–48] Triglyceride pyrene derivatives (Scheme 39.2) were used as water-insoluble probes, so that exit and reentry of the guest is unimportant, and exchange of a guest between micelles will only occur through fusion and fragmentation of two micelles. The concentration of the pyrene derivative employed was sufficient to ensure that a significant number of micelles contained two guest molecules. Pyrene excimer emission will occur when two pyrene moieties are located in the same micelle. The exchange processes could be monitored as a decrease in pyrene excimer fluorescence intensity when, in the stopped-flow experiment, a solution of guest/micelles was mixed with a solution of empty micelles. In this experiment, two relaxation processes were observed. One of these relaxations showed a dependence on the micelle concentration, and was assigned to micelle fusion, a bimolecular reaction involving the collision of two micelles. The other relaxation process was independent of micelle concentration and was assigned to micelle fragmentation, which is a unimolecular process. For the nonionic micelle Triton X-100, the rate constant for fusion was 1.47×10^6 M^{-1} s^{-1}, and the rate constant for fragmentation was 12.6 s^{-1}.[45] In the case of the anionic SDS micelles, the observed rate constants were much slower and showed a dependence on the salt concentration. When the concentration of sodium cations was 140 mM, the rate constant for fusion was 38 M^{-1} s^{-1}, while the rate constant for fragmentation was 0.037 s^{-1}.[44,48]

39.3.1.3 Fluorescence Correlation Spectroscopy

Fluorescence correlation spectroscopy (FCS) does not require a perturbation of the system's equilibrium to measure the host-guest dynamics on a wide range of time domains, from picoseconds to seconds.[49] This technique is based on the measurement of fluctuations in the fluorescence intensity of individual molecules.[50–52] A very small volume of the sample is continuously irradiated, and fluctuations in intensity occur because of events that affect the molecule's fluorescence efficiency, such as diffusion out of the detection volume or formation of a dark triplet excited state. Binding dynamics can be measured if the quantum yields for the free and complexed fluorophore are different, since in such a situation association to or dissociation from a supramolecular system would contribute to fluorescence intensity fluctuations.

Data are analyzed from autocorrelation functions, $G(\tau)$, which define the probability of detecting a photon emitted from the same molecule at time zero, and at time τ. A typical correlation curve (Figure 39.4) shows a growth at short times, called antibunching, which is related to the reexcitation of an individual fluorophore.[49] Decreases in the correlation curve occur due to events that change the probability of forming the molecule's singlet excited state, with an inflection point at a certain time corresponding to each event such as triplet formation or diffusion. Correlation completely disappears when the molecule diffuses out of the detection volume. Host-guest dynamics can be measured on time scales occurring between antibunching and diffusion events.

In order to develop appropriate models to analyze the correlation curve and obtain binding dynamics from the autocorrelation function various mechanistic assumptions have to be made. More comprehensive reviews of the relevant models and mathematical treatments have been recently published.[13,53] For a 1:1 host-guest complex, the correlation time associated with the host-guest dynamics has a time constant τ_R (Equation 39.3):

$$\tau_R = \frac{1}{k_{obs}} = \frac{1}{k_+[H] + k_-} \tag{39.3}$$

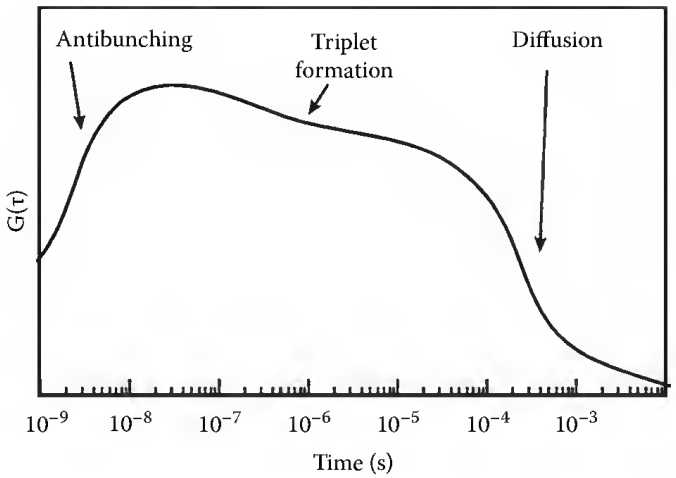

FIGURE 39.4 Representation of a typical FCS correlation curve showing various processes that occur on different time scales.

39.3.1.4 Supramolecular Dynamics from Florescence Correlation Spectroscopy

The binding of Pyronine Y and Pyronine B (Scheme 39.3) to β-CD has been examined by FCS.[53,54] A new correlation event was observed in the 1–10 μs region, with a correlation time that became shorter as the β-CD concentration was increased. This event corresponded to the dynamics of the host-guest complex. Additionally, the correlation time related to diffusion shifted to longer times as CD was added due to the increased molar mass of the host-guest complex compared to free guest. At the highest concentration of CD employed, there was still a significant contribution from the free guest to the diffusion term. Because of the contribution from free guest, the diffusion time of the complex could not be directly determined and the errors associated with fitting individual curves were high. Instead global analysis fits of the entire data set resulted in recovery of k_- values of 5.0×10^5 s^{-1} for Pyronine Y and 7.6×10^4 s^{-1} for Pyronine B.[53,54] The k_+ values of 2×10^8 M^{-1} s^{-1} for Pyronine Y and 1.5×10^8 M^{-1} s^{-1} for Pyronine B were then calculated from the equilibrium constants.[53,54]

Another system that has been studied by FCS is the binding of Rhodamine 123 cations (Scheme 39.4) to the nonionic surfactants Triton X-100 and Brij-35.[53,55] A cationic guest was used to ensure partition between the micelle and the aqueous phase, while nonionic surfactants were chosen to eliminate contributions from electrostatic interactions. Similar to the CD system discussed earlier, when micelles were present in solution changes were observed in the diffusion term, and a new correlation term, corresponding to the host-guest dynamics, was seen. An additional component had to be considered in this

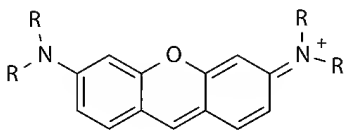

SCHEME 39.3 Structure of Pyronine Y (R = CH_3) and Pyronine B (R = CH_2CH_3).

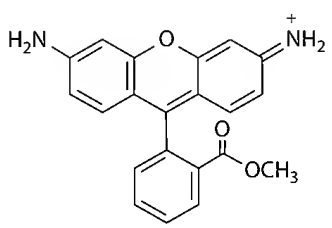

SCHEME 39.4 Structure of the Rhodamine 123 cation.

system as the Rhodamine 123 cation undergoes significant intersystem crossing to the triplet excited state. To differentiate the correlation term for triplet formation from the host-guest dynamics, a series of FCS curves at different excitation powers had to be analyzed. The triplet state population is dependent on excitation power, while host-guest dynamics are affected by micelle concentration. Values of k_- determined by global analysis of a concentration series of FCS correlation curves were $2.2 \times 10^5\ s^{-1}$ for Triton X-100 and $4 \times 10^5\ s^{-1}$ for Brij-35.[53,55] The values for k_+, $1.4 \times 10^{10}\ M^{-1}\ s^{-1}$ for Triton X-100 and $8 \times 10^9\ M^{-1}\ s^{-1}$ for Brij-35, were calculated from the equilibrium constants.[53,55] The calculated values for the association rate constants are the same as that for a diffusion-controlled process, which is in agreement with what has been observed in other micellar systems (see the following sections).

39.3.2 Photophysics as a Perturbation Method

Excited states and reactive intermediates are species with finite lifetimes. The fast formation of these species, generally by the use of lasers, can be used as the fast perturbation required for real-time kinetic studies. Using excited states adds an extra aspect to the treatment of the kinetic data since the lifetime of the excited state must be taken into account. The lifetimes of excited states can be shorter, longer, or of the same magnitude as the kinetic processes of interest. Each case will be considered later for the simplest host-guest system, with 1:1 binding stoichiometry (Scheme 39.1). It will be assumed that the guest is the species being excited; however, the same conceptual framework applies if the host is excited.

Changes in excited state concentration are generally monitored over time by either time-resolved fluorescence emission measurements, that is, single photon counting, or by transient absorption spectroscopy, that is, laser flash photolysis.

39.3.2.1 Time-Resolved Emission Measurements

Fluorescence is the most common type of emission from excited states of organic molecules. Kinetic data is obtained from time-resolved experiments, of which the most common method is single photon counting.[56] The fluorophore is excited using a high repetition excitation source and the time for emission of a single photon is measured. A histogram of the number of photons detected as a function of time is built, relying on the concept that the probability distribution for emission of a single photon follows the statistical distribution for all photons emitted as a result of excitation. A large dynamic range is obtained for the intensity, which helps in differentiation of fluorescence species with similar lifetimes.

Fluorescence decay functions are generally exponential or a sum of exponentials (Equation 39.4), where k_i is the decay rate constant of each fluorescent species, i, and its inverse value is equal to the singlet excited state lifetime of the emissive species ($\tau_i = 1/k_i$). A_i is the preexponential factor for each emissive species with a different lifetime, and the sum of all preexponential factors equals 1:

$$I(t) = I_o \sum_{1}^{i} A_i\, e^{-k_i t} \tag{39.4}$$

The preexponential factors are related to the concentration and the excitation efficiency of each species, and can only be related to absolute concentrations if the system is excited at an isosbestic point, or if the molar absorptivity is known for the supramolecular complex.

Time-resolved fluorescence can be used to obtain dynamic information when the lifetime of the excited state is similar to the time scale of the dynamics of interest. The longest time range accessible in time-resolved fluorescence is limited by the lifetime of the excited state being studied. In general, the singlet excited states of organic molecules have lifetimes that are shorter than 100 ns. Information on dynamics can therefore only be obtained from time-resolved fluorescence measurements if the association and dissociation rate constants are very fast, and in most cases the lifetime of the singlet excited state is too short for the guest to move between the bulk solution and the host system.

39.3.2.2 Laser Flash Photolysis

Laser flash photolysis (lfp) experiments use a pulsed laser to form the excited state guest.[56] Laser irradiation is orthogonal to a monitoring beam that is used to measure the absorption of the sample. Absorption is monitored before and after the laser pulse and changes are related to the difference in absorbance of the transient formed during the laser pulse and absorbance of the system prior to the laser pulse. In studies of supramolecular dynamics, the decays of triplet excited states are usually measured in lfp experiments. Triplet excited states are much longer lived than singlet excited states. Triplet lifetimes in aqueous solution can often be hundreds of nanoseconds or longer, and are generally long enough for relocation of the guest between the bulk solution and the supramolecular system to occur.

The time domains covered by most lfp systems are nanoseconds to hundreds of microseconds, though this can be extended to the millisecond time scale.[57,58] The longest time range accessible is dependent on the lifetime of the excited state being monitored.

39.3.3 Photophysics with Immobile Excited States

39.3.3.1 Short-Lived Excited States

When an excited state is short-lived, it does not have time to relocate between the host-guest complex and the bulk solution. The excited state acts as a probe for the environment in which it is located since the association and dissociation kinetics are slow in comparison to deactivation of the excited state (Figure 39.5). Each species can be separately identified when the lifetimes for the excited states of the free and bound guest are different.

39.3.3.2 Quenching of Short-Lived Excited States

The fact that most singlet excited state guests do not relocate during their lifetimes means that they can be used to examine the migration of the quencher, and rate constants can be measured for the association of the quencher with the host system (Figure 39.6).[56,59–64] Quenching is a bimolecular

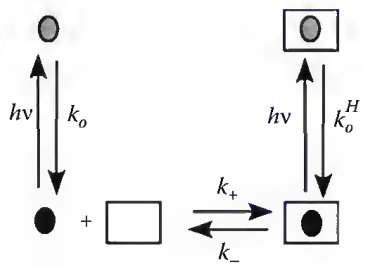

FIGURE 39.5 Schematic representation of the binding dynamics for a system where the excited state of the guest (gray circles) does not relocate between the bulk solution and the host during its lifetime.

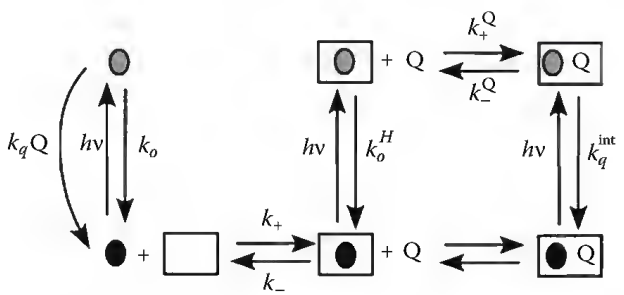

FIGURE 39.6 Schematic representation of the binding dynamics for a system where the excited state of the guest (gray circles) does not relocate between the bulk solution and the host during its lifetime. Quenching of the excited state can occur in the bulk solution or inside the host.

reaction between the excited state and a quencher molecule. It can be viewed as the formation of an encounter complex, followed by quenching, with intrinsic quenching rate constant, k_q^{int}. In general, there are two different quenching scenarios. In the first case, every encounter between the quencher and the excited state in the host leads to deactivation of the excited state ($k_q^{int} \gg k_-^Q$). This is most likely the case for smaller hosts, such as CDs, with a confined volume for binding. In the second, scenario the quencher has a finite probability of exiting the host before encountering the bound guest ($k_q^{int} \sim k_-^Q$ or $k_q^{int} \ll k_-^Q$). This is more likely the case for larger hosts, such as micelles, where the quencher and excited state guest can be incorporated in the same micelle at some distance from each other.

39.3.3.3 Deactivation of Every Encounter in the Host

The excited state lifetimes of the guest bound to the host and in the bulk solution are often different, with a longer lifetime usually observed for the guest in the host. In such a case, the fluorescence decay will be a sum of exponentials when appreciable amounts of guest are located in each environment (Equation 39.4). Quenching leads to an increase in the observed decay rate constant for each component (k_{obs}^i), and a linear relationship with respect to the quencher concentration is observed (Equation 39.5):

$$k_{obs}^i = k_o^i + k_q^i[\mathrm{Q}] \tag{39.5}$$

The quenching rate constant for the guest bound to the host is related to the association rate constant of the quencher with the host, k_+^Q, the intrinsic intra-micellar quenching rate constant, k_q^{int}, and the rate constant for the dissociation of the quencher from the host, k_-^Q (Equation 39.6):

$$k_q^H = \frac{k_+^Q k_q^{int}}{k_-^Q + k_q^{int}} \tag{39.6}$$

When every inclusion of quencher in the host leads to quenching, that is, k_-^Q is much smaller than k_q^{int}, the quenching rate constant of the guest in the host, k_q^H, is equal to the association rate constant of the quencher with the host, k_+^Q. It should be noted that time-resolved measurements cannot be used if static quenching occurs due to the guest and quencher being located in close proximity prior to excitation.

39.3.3.4 Competition between Quenching and Exit from the Host

Quenching efficiencies of less than 100% are observed when exit of the quencher from the host competes with quenching of the guest in the host. The simplest model that has been developed to analyze the fluorescence decay of an excited guest in the host assumes that all guest molecules are bound to the host, and that the rate constants for quencher association with and dissociation from a host are independent of guest population in the host. In the absence of quencher, the fluorescence decay follows an exponential function with a rate constant of k_o (Equation 39.4). In the presence of quencher, the decay is nonexponential (Equation 39.7), with parameters A to D defined in Equations 39.8 through 39.11[59,60–63]:

$$I(t) = Ae^{\left[-Bt - C\left(1 - e^{-Dt}\right)\right]} \tag{39.7}$$

$$A = I_o \tag{39.8}$$

$$B = k_o + \left[\frac{k_q^{\text{int}}\, k_+^Q}{\left(k_q^{\text{int}} + k_-^Q\right)\left(1 + K_Q[\text{H}]\right)}\right][\text{Q}] \tag{39.9}$$

$$C = \left[\frac{\left(k_q^{\text{int}}\right)^2 k_+^Q}{\left(k_q^{\text{int}} + k_-^Q\right)^2 k_-^Q \left(1 + K_Q[\text{H}]\right)}\right][\text{Q}] \tag{39.10}$$

$$D = k_q^{\text{int}} + k_-^Q \tag{39.11}$$

Parameters B and C are dependent on the quencher concentration, so measurements of the fluorescence decay at different quencher concentrations allows recovery of all relevant rate constants. This model has been expanded to describe more complex mechanisms, for example, inclusion of additional processes such as exchange of quencher or guest between micelles during the lifetime of the guest.[59]

39.3.3.5 Supramolecular Dynamics from Quenching Short-Lived Excited States

For the case in which every encounter in the host between quencher and excited state guest leads to quenching of the excited state, the quenching rate constant is equivalent to the association rate constant for the quencher with the host. This quenching methodology has been used in the study of singlet excited state guest molecules bound to bile salt aggregates.[65–67] In the presence of 10 mM sodium cholate (NaCh), some of the guest is bound to the aggregate, while some guest remains in the aqueous solution. Incorporation of the guest into the bile salt aggregate leads to a lengthening of its singlet excited state lifetime and the fluorescence decays were fit to the sum of two exponentials (Equation 39.4). The lifetime for the excited guest in water was shortened to a greater extent in the presence of iodide anions when compared to the lifetime for the guest in the aggregate, leading to an enhancement of the curvature in the semilog decay plot (Figure 39.7).

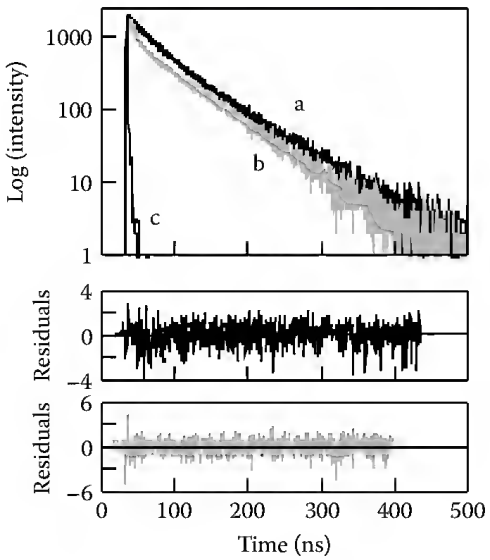

FIGURE 39.7 Fluorescence decays for 1-ethylnaphthalene in the presence of 10 mM NaCh in the absence of iodide anions (a, black) and in the presence of 20 mM iodide anion (b, gray) used as a quencher for the singlet excited state of 1-ethylnaphthalene. The instrument response function of the singlet photon counter is shown as c. The residual plot between the data and the fit to a sum of two exponentials in the absence of iodide anions is shown in the middle plot, while the residuals for the fit in the presence of iodide anions is shown in the lower plot. (Reprinted with permission from Li, R., Carpentier, E., Newell, E. D., Olague, L. M., Heafey, E., Yihwa, C., and Bohne, C., *Langmuir*, 25, 13800–13808, 2009. Copyright 2009 American Chemical Society.)

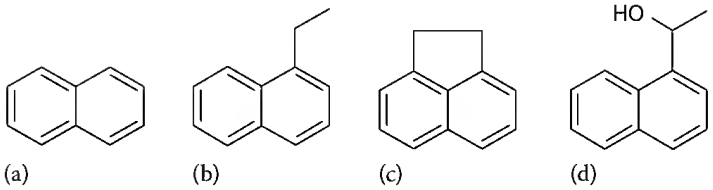

SCHEME 39.5 Structures of (a) naphthalene, (b) 1-ethylnaphthalene, (c) acenaphthene, and (d) 1-naphthyl-1-ethanol.

Values for the quenching rate constant for quenching by iodide anions were determined by analysis of the lifetime for the excited guest in the aggregate at different quencher concentrations using Equation 39.5. The quenching rate constants change with both the structure of the guest and of the host. These changes have been used to make inferences about the structure of the bile salt aggregates, as can be illustrated with the series naphthalene, 1-ethylnaphthalene, acenaphthene, and 1-naphthyl-1-ethanol (Scheme 39.5) in the presence of NaCh and NaDC bile salt aggregates (Table 39.1).[66] Naphthalene, 1-ethylnaphthalene, and acenaphthene all bind to the primary aggregate but significantly different quenching rate constants were obtained, suggesting that the primary aggregate structure is affected by the structure of the bound guest. The quenching rate constants for 1-naphthyl-1-ethanol, which resides in the secondary aggregate, were much greater than those for the other naphthalenes, showing that association of iodide anions to primary aggregates is much slower than association with secondary aggregates. Quenching rate constants were higher for the trihydroxyl bile salt (NaCh) than for the dihydroxyl bile salt (NaDC). This increased access of the iodide anions to the aggregates of the trihydroxyl bile salts indicates that they are more loosely packed than the dihydroxyl bile salts.

The extensive use of the model described in Equations 39.7 through 39.11 to study the binding dynamics of quenchers with micelles has been previously reviewed.[8,59] This model is employed when quenching of the guest inside the micelle is competitive with exit of the quencher from the micelle, and rate constants are recovered from the four-parameter fit of the fluorescence decay in the presence of quencher. At high micelle concentrations, deviations from this model have been seen, as parameter D (Equation 39.11) shows a dependence on micelle concentration.[68,69] However, comparison of rate constants obtained at low micelle concentrations should not be affected.

An illustrative example of this method is the quenching of pyrene (Scheme 39.2) in SDS micelles by alkyl iodides of different chain lengths.[70] The association rate constants recovered from the fit to Equation 39.7 were close to diffusion controlled for all chain lengths (Table 39.2). Chain length had a much greater effect on the dissociation rate constant, with a 20-fold decrease as the length of the chain was increased from ethyl to octyl (Table 39.2). The same trends are seen for most quencher/micelle systems: diffusion-controlled association rate constants are obtained whenever there is no electrostatic

TABLE 39.1 Quenching Rate Constants (k_q) for Quenching the Singlet Excited States of Guests by Iodide Anions in NaCh and NaDC (10 and 40 mM)

	$k_q/10^8\ M^{-1}\ s^{-1}$			
	NaCh		NaDC	
Guest	10 mM	40 mM	10 mM	40 mM
Naphthalene	2.2	1.77	0.34	0.34
1-Ethylnaphthalene	1.1	1.06	0.12	0.14
Acenaphthene	0.53	0.39	0.07	0.043
1-Naphthyl-1-ethanol	9	7	4	3.4

Source: Li, R. et al., *Langmuir*, 25, 13800, 2009.

TABLE 39.2 Association (k_+^Q), Dissociation (k_-^Q), and Intrinsic Intramicellar Quenching Rate Constants (k_q^{int}) for the Quenching of Pyrene by Alkyl Iodides in SDS Micelles (0.04 M)

Quencher	k_+^Q / 10^9 M^{-1} s^{-1}	k_-^Q / 10^6 s^{-1}	k_q^{int} / 10^9 s^{-1}
Ethyl iodide	9.7	8.3	2.9
Butyl iodide	8.8	1.4	4.8
Hexyl iodide	7.8	0.75	5.4
Octyl iodide	6.6	0.4	5.9

Source: Löfroth, J.E. and Almgren, M., *J. Phys. Chem.*, 86, 1636, 1982.

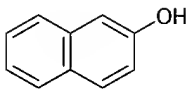

SCHEME 39.6 Structure of 2-naphthol.

interaction between the quencher and the micelle, and dissociation rate constants are determined by the hydrophobicity of the guest.[8,60,70,71]

This model has also been applied to bile salt aggregates by studying the access of the quencher *N,N*-dimethylaniline to pyrene in sodium taurocholate aggregates in the presence of 1.0 M NaCl.[72] An association rate constant of 1.4×10^9 M^{-1} s^{-1} and a dissociation rate constant of 3.8×10^6 s^{-1} were recovered for this quencher.[72] These rate constants are of the same magnitude as those obtained for quenching of pyrene by *N,N*-dimethylaniline in SDS micelles, suggesting that access of this neutral quencher is similar in bile salt aggregate and conventional micelles.

In some specific cases, global compartmental analysis can be used to recover association and dissociation rate constants from quenching studies, even when the excited state is short-lived in comparison to the binding dynamics. Such an analysis, for the quenching of 2-naphthol (Scheme 39.6) bound to β-CD by iodide anions, was possible because the observed lifetimes changed with host concentration.[73] The recovered association and dissociation rate constants were, respectively, 2.5×10^9 M^{-1} s^{-1} and 520 s^{-1}.[73] The k_- value obtained in this experiment is much smaller than has been observed for other guest molecules (see the following text).

39.3.4 Photophysics with Mobile Excited States

39.3.4.1 Excited States with Lifetime of Similar Magnitude to the Kinetics of Interest

Triplet excited states of organic molecules often have lifetimes of the same magnitude as the time scale for binding dynamics in host-guest systems. Triplet state kinetics are usually measured by following transient absorption in lfp experiments; the same conceptual framework can be applied to time-resolved fluorescence experiments, when long-lived singlet excited states occur.

Perturbation of the supramolecular system occurs when the excited state is formed. Excited states have different properties from their ground states, for example, different geometries or different dipole moments. These differences will lead to reequilibration of the host-guest system upon formation of the excited state. When the lifetime of the excited state is of the same order of magnitude as the dynamics of interest, that is, k_o, $k_o^H \sim k_+^*$, k_-^*, relocation of the excited state guest between the host and the bulk solution can occur. In this case, coupled kinetics are observed (Figure 39.8), and the observed rate constant, k_{obs}, will include the reequilibration of the excited state guest with the host and the decays of the excited state guest in the bulk solution and bound to the host.

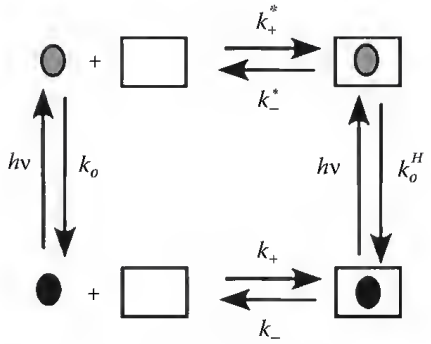

FIGURE 39.8 Schematic representation for the binding dynamics of an excited state guest (gray circles) when reequilibration of the excited guest between the bulk solution and the host is competitive with the decay of the excited state to the ground state.

If a property of the guest, for example, absorption, is different when free in bulk solution and when bound to the guest, then changes in relative concentration can be measured, and relocation of the guest can be followed directly. The kinetic decay can be fit to a sum of two exponentials (Equation 39.12) using a mathematical treatment that is equivalent to that developed for the dynamics of excimer emission[74]:

$$\Delta A = A_1 e^{-\gamma_1 t} + A_2 e^{-\gamma_2 t} \tag{39.12}$$

The two exponential factors, γ_1 and γ_2, are related to the intrinsic decay rate constants for the excited guest in bulk solution and in the host, and the association and dissociation rate constants for the excited state guest with the host (Equations 39.13 through 39.16)[74,75]:

$$\gamma_{1,2} = -\frac{1}{2}\left[(A+B) \pm \sqrt{(A-B)^2 + 4C}\right] \tag{39.13}$$

$$A = k_o + k_+^*[\mathrm{H}] \tag{39.14}$$

$$B = k_o^{\mathrm{H}} + k_-^* \tag{39.15}$$

$$C = k_- k_+^*[\mathrm{H}] \tag{39.16}$$

The sum and product of the exponential factors γ_1 and γ_2 are related to the individual rate constants by Equations 39.17 and 39.18[75]:

$$\gamma_1 + \gamma_2 = k_o + k_o^{\mathrm{H}} + k_-^* + k_+^*[\mathrm{H}] \tag{39.17}$$

$$\gamma_1\gamma_2 = k_o\left(k_o^{\mathrm{H}} + k_-^*\right) + k_o^{\mathrm{H}} k_+^*[\mathrm{H}] \tag{39.18}$$

39.3.4.2 Excited States with Lifetimes Longer Than the Kinetics of Interest

The formation of an excited state that has a lifetime that is much longer than the binding dynamics, that is, k_o, $k_o^{\mathrm{H}} \ll k_+^*$, k_-^*, simplifies the aforementioned treatment. In this case, the perturbation can be viewed as permanent, and the kinetics are only related to the reequilibration of the excited state. Under these conditions, γ_2 is zero and Equation 39.17 is simplified to Equation 39.19, which is equivalent to a relaxation process:

$$\gamma_1 = k_{\mathrm{obs}} = k_+^*[\mathrm{H}] + k_-^* \tag{39.19}$$

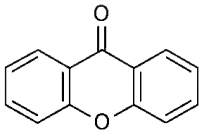

SCHEME 39.7 Structure of xanthone.

39.3.4.3 Supramolecular Dynamics from Long-Lived Excited States

Direct measurement of supramolecular dynamics using a long-lived triplet excited state requires that an observable property of the excited state change when bound and when free in solution. To date, xanthone (Scheme 39.7) is the only molecule for which relocation of the excited state has been directly monitored.[76,77] The xanthone triplet–triplet absorption spectrum shifts to shorter wavelengths on binding to CD because the spectrum is very sensitive to solvent polarity.[78,79] Additionally, the basicity[80] and dipole moment[76,79] of xanthone are higher for the triplet excited state, leading to significant relocation of this guest from the host following excitation. Kinetic measurements were made at various concentrations of β-CD. Since the triplet lifetime of xanthone is significantly longer than the binding dynamics, analysis of the kinetics could be carried out using the simplified Equation 39.19.[77,81,82] The recovered association and dissociation rate constants for the triplet excited state of xanthone with β-CD were respectively 5×10^8 M^{-1} s^{-1} and 8.1×10^6 s^{-1}.[82]

39.3.4.4 Quenching Studies with Long-Lived Excited States

Quenching experiments can also be employed with long-lived excited states.[7,8,83,84] A competitive deactivation pathway for the excited state is introduced when a quencher is added to the system (Figure 39.9). If the quenching rate constants for the excited state in bulk solution, k_q, and bound to the host, k_q^H, are different then information on binding dynamics can be elucidated even if the bound and free guest do not have different molar absorptivities. This greatly broadens the number of systems for which supramolecular dynamics can be studied.

Generally, quenchers that reside primarily in the bulk solution are employed so that the quenching efficiency of excited state guests in the aqueous phase is higher than that for guests bound to the host. If the concentration of free guest is small in comparison to the amount of bound guest, then the kinetics

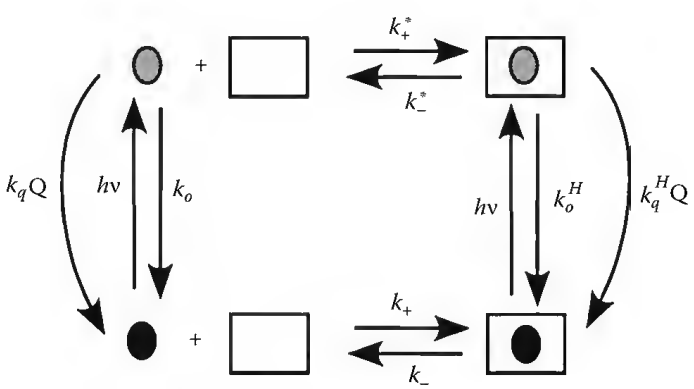

FIGURE 39.9 Schematic representation for the binding dynamics of an excited state guest (gray circles) when reequilibration of the excited guest between the bulk solution and the host is competitive with the decay of the excited state to the ground state. The lifetime of the excited state is shortened with the addition of a quencher.

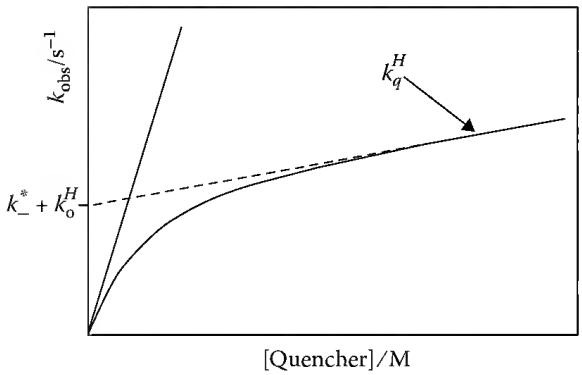

FIGURE 39.10 Linear quenching plot for the excited state guest in bulk solution and curved quenching plot for the excited state guest in the presence of host (Equation 39.20). At high quencher concentrations, the linear portion of the graph corresponds to the dissociation rate constant of the excited guest from the host (intercept of the dashed line) and the quenching rate constant for the guest bound in the host (slope). (Reprinted with permission from Li, R., Carpentier, E., Newell, E. D., Olague, L. M., Heafey, E., and Yihwa, C., *Langmuir*, 25, 13800–13808, 2009. Copyright 2009 American Chemical Society.)

are pseudo-first-order and follow a monoexponential decay, and the observed rate constant is given by Equation 39.20[83,84]:

$$k_{obs} = k_o^H + k_-^* + k_q^H[Q] - \frac{k_-^* k_+^* [H]}{k_o + k_q[Q] + k_+^*[H]} \tag{39.20}$$

The dependence of k_{obs} on quencher concentration is nonlinear. Conceptually, this arises when $k_q \gg k_q^H$ because, at higher quencher concentrations, the rate-limiting step for quenching becomes exit of the guest from the host or its intrinsic decay within the host. Qualitatively, larger differences between the linear quenching plots obtained in bulk solution and the curved plots obtained in the presence of host indicate slower binding dynamics for the host-guest system (Figure 39.10).

39.3.4.5 Supramolecular Dynamics from Quenching Long-Lived Excited States

Generally, the singlet excited state lifetime is too short for relocation of the excited state between the bulk solution and the binding site in the host. However, in special cases where the lifetime of the singlet excited state is quite long, time-resolved fluorescence experiments can be used to recover kinetic information related to complex formation. The singlet excited state of 2,3-diazabicyclo[2.2.2]oct-2-ene (DBO, Scheme 39.8) has a very long lifetime in aqueous and deuterated aqueous solutions (420 and 730 ns, respectively) and can be used to measure binding dynamics to CDs.[85,86] The lifetime of DBO is sensitive to the presence of abstractable hydrogens, as the DBO singlet excited state can be quenched by an "aborted" hydrogen abstraction.[85] When this guest binds to CDs, it is in close proximity to a number of abstractable hydrogens from the glucose units; the lifetime of the singlet excited state is greatly decreased, and exit of the excited state from the CD does not occur. The quenching rate constant of DBO by CD is therefore directly related to the association rate constant of singlet excited DBO with CDs, k_+^*. The k_+^* values were determined to be 1.9×10^8 M^{-1} s^{-1}, 4.0×10^8 M^{-1} s^{-1}, and 0.78×10^8 M^{-1} s^{-1} for α-, β-, and γ-CD, respectively.[86] Qualitatively these values parallel the trends observed for the ground state equilibrium constant (50 M^{-1}, 1100 M^{-1}, and 6 M^{-1} for α-, β-, and γ-CD, respectively).[86]

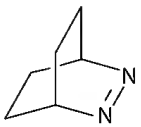

SCHEME 39.8 Structure of DBO.

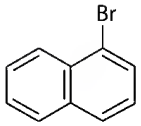

SCHEME 39.9 Structure of 1-bromonaphthalene.

Triplet excited states are typically much longer lived than singlet excited states and quenching methodologies can be more generally applied in the determination of binding dynamics for these excited states. The triplet quenching methodology (Equation 39.20) was developed originally to study the binding dynamics of polycyclic aromatic guests with SDS micelles.[83] The dissociation rate constant for 1-bromonaphthalene (Scheme 39.9) determined by analysis of the quenching plot ($2.5 \times 10^4\ s^{-1}$) was similar to the dissociation rate constant calculated from the equilibrium constant, assuming a diffusion-controlled rate constant for the association reaction.[83] The dissociation rate constants for other aromatic guests calculated in the same way were found to decrease as the hydrophobicity of the guest was increased.

A similar trend was seen in the investigation of a series of ketone guests with SDS micelles.[87,88] Quenching of these triplet excited state guests was carried out using γ-methylvalerophenone, which resides in the micelle, or nitrite anions, which reside in the aqueous solution. Binding dynamics were determined from quenching experiments; the association rate constants were diffusion controlled for all guests, while the dissociation rate constants varied and were faster for the more polar ketones.

The quenching methodology has been employed in the determination of binding dynamics of a number of guests with CDs.[7,84] The binding dynamics of the triplet excited states of xanthone (Scheme 39.7), chromone, flavone, and 2-naphthyl-1-ethanol (Scheme 39.10) with β-CD have been studied using metal cation quenchers.[89,90] Curved quenching plots were analyzed using Equation 39.20 to recover association and dissociation rate constants for the triplet excited states of these guests with β-CD (Table 39.3). Analysis of this data showed that binding mode and guest size have some effect on the binding dynamics.

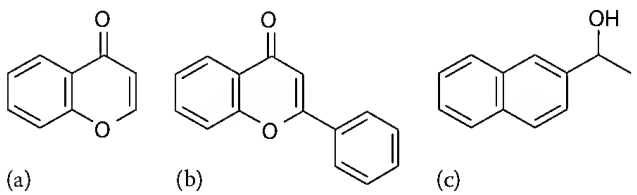

SCHEME 39.10 Structures for (a) chromone, (b) flavone, and (c) 2-naphthyl-1-ethanol.

TABLE 39.3 Values for Association (k_+^*) and Dissociation (k_-^*) Rate Constants for the Triplet Excited State Determined from the Triplet Quenching of Xanthone, Chromone, Flavone, and 2-Naphthyl-1-Ethanol by Metal Ions in the Presence of β-CD

Guest	$k_+^*/10^9\ M^{-1}\ s^{-1}$	$k_-^*/10^6\ s^{-1}$	K_{11}^T/M^{-1}	K_{11}/M^{-1}
Xanthone	1.1	12	90	1100
Chromone	3	21	140	240
Flavone	2.4	4.4	550	1090
2-Naphyl-1-ethanol	0.29	0.18	1600	1800

Sources: Barros, T.C. et al., *J. Phys. Chem. A, 102*, 5639, 1998; Christoff, M. et al., *J. Photochem. Photobiol. A Chem.*, 134, 169, 2000.

The triplet-state equilibrium constants (K_{11}^T) were calculated from the values of k_+^* and k_-^*, and the ground-state equilibrium constants (K_{11}) were determined from fluorescence or absorption experiments.

For instance, 2-naphthyl-1-ethanol is deeply included in the CD cavity,[91] and exhibits slower dynamics than xanthone, which is known to bind to the CD rim.[92] The association rate constants for xanthone, chromone, and flavone are of the same magnitude, but the dissociation rate constant for flavone is an order of magnitude smaller. It was proposed that the pendant phenyl ring of flavone is incorporated into the CD cavity, slowing down dissociation of the flavone: CD complex. The equilibrium constants for the triplet excited state, calculated from the ratio of rate constants (Scheme 39.1), are lower than the equilibrium constants for the ground state in the case of the ketones, while similar equilibrium constants were obtained for both electronic states of the naphthalene (Table 39.3). This analysis shows that equilibrium constants can be different depending on the nature of the excited state and care should be taken for calculations where rate constants and equilibrium constants for different electronic states are combined.

The association and dissociation rate constants for the triplet excited state of xanthone with β-CD recovered from these quenching experiments are higher than those determined using the direct method (see earlier). Reasons for this overestimation of the rate constants are unknown, but comparisons of binding dynamics for different guests can be made as long as the quencher used is similar.

The quenching methodology has also been employed to study the binding dynamics of a number of triplet excited state guests with bile salt aggregates.[65–67,93] Analysis of the obtained curved plots for nitrite quenching using Equation 39.20 allows recovery of k_-^* and k_q^H. Dissociation rate constants of 0.18×10^6 s^{-1} and 5.5×10^6 s^{-1} were obtained for the triplet excited states of 1-ethylnaphthalene and 1-naphthyl-1-ethanol (Scheme 39.5), respectively from NaCh aggregates.[66,93] The quenching plots for 1-naphthyl-1-ethanol showed no curvature at bile salt concentrations where primary aggregates are present, but secondary aggregates have not yet formed. This observation, and the notably faster dissociation rate constant for this guest led to the proposal that 1-naphthyl-1-ethanol binds in the secondary aggregate, while 1-ethylnaphthalene is bound in the primary aggregate.

The different dynamics for the binding of triplet naphthalene (Scheme 39.5) with NaCh and NaDC are exemplified by the different quenching plots observed when nitrite anions were used as quenchers (Figure 39.11).[66] The larger deviation of the quenching plot for NaDC from the quenching plot in water showed that the binding dynamics were slower for this bile salt than for NaCh, which is consistent with the larger dissociation rate constant of 1.4×10^6 s^{-1} in the case of NaCh when compared to that of 7×10^5 s^{-1} for NaDC.[66] In addition, the slopes for the quenching plots at high nitrite concentrations were different because the access of nitrite anions to triplet naphthalene was easier in the NaCh aggregate

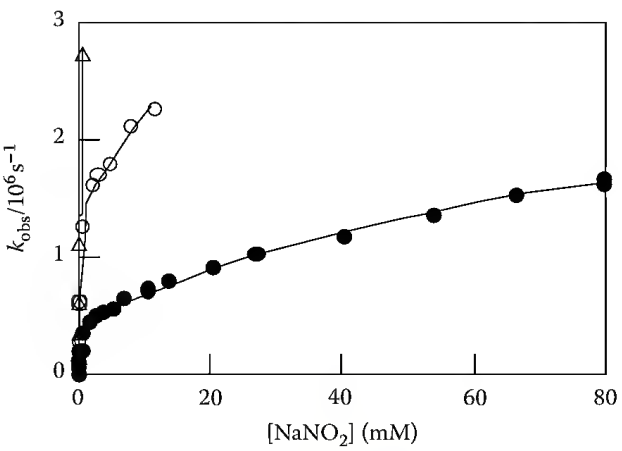

FIGURE 39.11 Quenching plots for triplet naphthalene quenching by nitrite anions in water (black triangles, only the points at low quencher concentration are shown for clarity; $k_q = 3.6 \times 10^9$ M^{-1} s^{-1}), in the presence of 10 mM NaCh (open circles) and in the presence of 10 mM NaDC (solid circles). The data in water were fit to Equation 39.5 and the data in the presence of both bile salts were fit to Equation 39.20. (Adapted with permission from Li, R., Carpentier, E., Newell, E. D., Olague, L. M., Heafey, E., and Yihwa, C., *Langmuir*, 25, 13800–13808, 2009. Copyright 2009 American Chemical Society.)

($k_q^H = 4 \times 10^7\ M^{-1}s^{-1}$) than the access in the NaDC aggregate ($k_q^H = 1.4 \times 10^7\ M^{-1}s^{-1}$).[66] These results are in agreement with the quenching studies of the singlet excited states where the quenching rate constant for iodide anions was smaller for the dihydroxyl bile salt NaDC compared to the trihydroxyl bile salt NaCh (see earlier).

39.4 Conclusions

Photophysics can be used in the determination of dynamics in supramolecular systems either as an analytical tool or as a source of perturbation in the system. This chapter outlined the fast kinetic techniques and the analysis methods necessary when applying photophysics to studies of supramolecular dynamics. Examples in CD, micelle, and bile salt aggregate systems were presented to highlight the potential applications of the various methods discussed.

Acknowledgments

CB would like to thank the Natural Sciences and Engineering Research Council of Canada (NSERC) for the continued support of her supramolecular dynamics research program in the form of discovery and equipment grants. TCSP would like to thank the University of Victoria and NSERC (CGS-D) for fellowships while in graduate school.

References

1. Atwood, J. L.; Davies, J. E. D.; MacNicol, D. D.; Vögtle, F.; Lehn, J.-M. *Comprehensive Supramolecular Chemistry*; Pergamon: New York, 1996; Vol. 1–11.
2. Lehn, J.-M. *Supramolecular Chemistry: Concepts and Perspectives*; VCH: Weinheim, Germany, 1995.
3. Lehn, J.-M. *Chem. Soc. Rev.* 2007, *36*, 151–160.
4. Whitesides, G. M.; Mathias, J. P.; Seto, C. T. *Science* 1991, *254*, 1312–1319.
5. Whitesides, G. M.; Simanek, E. E.; Mathias, J. P.; Seto, C. T.; Chin, D.; Hammen, M.; Gordon, D. M. *Acc. Chem. Res.* 1995, *28*, 37–44.
6. Montalti, M.; Credi, A.; Prodi, L.; Gandolfi, M. T. *Handbook of Photochemistry*; 3rd edn.; CRC Press: Boca Raton, FL, 2006.
7. Bohne, C. *Langmuir* 2006, *22*, 9100–9111.
8. Kleinman, M. H.; Bohne, C. In *Molecular and Supramolecular Photochemistry*; Ramamurthy, V., Schanze, K. S., Eds.; Marcel Dekker Inc.: New York, 1997; Vol. 1, p. 391–466.
9. Bhattacharyya, K. *Acc. Chem. Res.* 2003, *36*, 95–101.
10. Douhal, A. *Chem. Rev.* 2004, *104*, 1955–1976.
11. Nandi, N.; Bagchi, B. *J. Phys. Chem.* 1996, *100*, 13914–13919.
12. Vajda, S.; Jimenez, R.; Rosenthal, S. J.; Fidler, V.; Fleming, G. R.; Castner, Jr., E. W. *J. Chem. Soc. Faraday Trans.* 1995, *91*, 867–873.
13. Pace, T. C. S.; Bohne, C. *Adv. Phys. Org. Chem.* 2008, *42*, 167–223.
14. Aniansson, E. A. G.; Wall, S. N.; Almgren, M.; Hoffmann, H.; Kielmann, I.; Ulbricht, W.; Zana, R.; Lang, J.; Tondre, C. *J. Phys. Chem.* 1976, *80*, 905–922.
15. Hinze, W. L.; Hu, W.; Quina, F. H.; Mohammadzai, I. U. In *Organized Assemblies in Chemical Analysis*; Hinze, W. L., Ed.; JAI Press Inc.: Stamford, CT, 2000; Vol. 2: Bile Acid/Salt Surfactant Systems, p. 1–70.
16. Mazer, N. A.; Carey, M. C.; Kwasnick, R. F.; Benedek, G. B. *Biochemistry* 1979, *18*, 3064–3075.
17. O'Connor, C. J.; Wallace, R. G. *Adv. Colloid Interface Sci.* 1985, *22*, 1–111.
18. Small, D. M. In *The Bile Salts*; Nair, P. P., Kritchevsky, D., Eds.; Plenum Press: New York, 1971; Vol. 1, p. 249–256.

19. Small, D. M.; Penkett, S. A.; Chapman, D. *Biochim. Biophys. Acta* 1969, *176*, 178–189.
20. Szejtli, J. *Chem. Rev.* 1998, *98*, 1743–1753.
21. Szejtli, J.; Osa, T. In *Comprehensive Supramolecular Chemistry*; Atwood, J. L., Davies, J. E., MacNicol, D. D., Vögtle, F., Lehn, J.-M., Eds.; Elsevier Science Ltd.: New York, 1996; Vol. 3.
22. Connors, K. A. *Chem. Rev.* 1997, *97*, 1325–1357.
23. Rekharsky, M. V.; Inoue, Y. *Chem. Rev.* 1998, *98*, 1875–1917.
24. Berger, R. L.; Balko, B.; Borcherdt, W.; Friauf, W. *Rev. Sci. Instrum.* 1968, *39*, 486–493.
25. Robinson, B. H. In *Chemical and Biological Applications of Relaxation Spectrometry*; Wyn-Jones, E., Ed.; D. Reidel Publishing Co.: Boston, MA, 1974.
26. Bernasconi, C. F. *Relaxation Kinetics*; Academic Press, Inc.: New York, 1976.
27. Czerlinski, G. H. *Chemical Relaxation: An Introduction to Theory and Application of Stepwise Perturbation*; Marcel Dekker Inc.: New York, 1966.
28. Abou-Hamdan, A.; Bugnon, P.; Saudan, C.; Lye, P. G.; Merbach, A. E. *J. Am. Chem. Soc.* 2000, *122*, 592–602.
29. Demont, P. M.; Reinsborough, V. C. *Aust. J. Chem.* 1991, *44*, 759–763.
30. Dyck, A. S. M.; Kisiel, U.; Bohne, C. *J. Phys. Chem. B.* 2003, *107*, 11652–11659.
31. Mochida, K.; Matsui, Y. *Chem. Lett.* 1976, 963–966.
32. Okubo, T.; Maeda, Y.; Kitano, H. *J. Phys. Chem.* 1989, *93*, 3721–3723.
33. Saudan, C.; Dunard, F. A.; Abou-Hamdan, A.; Bugnon, P.; Lye, P. G.; Lincoln, S. F.; Merbach, A. E. *J. Am. Chem. Soc.* 2001, *123*, 10290–10298.
34. Seiyama, A.; Yoshida, N.; Fujimoto, M. *Chem. Lett.* 1985, 1013–1016.
35. Yoshida, N. *J. Chem. Soc. Perkin Trans. 2* 1995, 2249–2256.
36. Yoshida, N.; Fujimoto, M. *J. Phys. Chem.* 1987, *91*, 6691–6695.
37. Yoshida, N.; Fujita, Y. *J. Phys. Chem.* 1995, *99*, 3671–3677.
38. Yoshida, N.; Hayashi, K. *J. Chem. Soc. Perkin Trans. 2* 1994, 1285–1290.
39. Yoshida, N.; Seiyama, A.; Fujimoto, M. *Chem. Lett.* 1984, 703–706.
40. Yoshida, N.; Seiyama, A.; Fujimoto, M. *J. Phys. Chem.* 1990, *94*, 4246–4253.
41. Hersey, A.; Robinson, B. H.; Kelly, H. C. *J. Chem. Soc. Faraday Trans. 1* 1986, *82*, 1271–1287.
42. Hamai, S. *J. Phys. Chem.* 1989, *93*, 6527–6529.
43. Wright, P. J.; Bohne, C. *Can. J. Chem.* 2005, *83*, 1440–1447.
44. Rharbi, Y.; Chen, L. S.; Winnik, M. A. *J. Am. Chem. Soc.* 2004, *126*, 6025–6034.
45. Rharbi, Y.; Li, N.; Winnik, M. A.; Hahn, Jr., K. G. *J. Am. Chem. Soc.* 2000, *122*, 6242–6251.
46. Rharbi, Y.; Winnik, M. A. *Langmuir* 1999, *15*, 4697–4700.
47. Rharbi, Y.; Winnik, M. A. *Adv. Colloid Interface Sci.* 2001, *89*, 25–46.
48. Rharbi, Y.; Winnik, M. A. *J. Phys. Chem. B.* 2003, *107*, 1491–1501.
49. Felekyan, S.; Kühnemuth, R.; Kudryavtsev, V.; Sandhagen, C.; Becker, W.; Seidel, C. A. M. *Rev. Sci. Instrum.* 2005, *76*, 083104.
50. Thompson, N. L. In *Topics in Fluorescence Spectroscopy Volume 1 Techniques*; Lakowicz, J. R., Ed.; Plenum Press: New York, 1991, p. 337–378.
51. Webb, W. W. In *Fluorescence Correlation Spectroscopy*; Rigler, R., Elson, E. S., Eds.; Springer: Berlin, Germany, 2001, p. 305–330.
52. Widengren, J. In *Fluorescence Correlation Spectroscopy*; Rigler, R., Elson, E. S., Eds.; Springer: Berlin, Germany, 2001, p. 277–301.
53. Al-Soufi, W.; Reija, B.; Felekyan, S.; Seidel, C. A. M.; Novo, M. *Chem. Phys. Chem.* 2008, *9*, 1819–1827.
54. Al-Soufi, W.; Reija, B.; Novo, M.; Felekyan, S.; Kühnemuth, R.; Seidel, C. A. M. *J. Am. Chem. Soc.* 2005, *127*, 8775–8784.
55. Novo, M.; Felekyan, S.; Seidel, C. A. M.; Al-Soufi, W. *J. Phys. Chem. B* 2007, *111*, 3614–3624.
56. Bohne, C.; Redmond, R. W.; Scaiano, J. C. In *Photochemistry in Organized and Constrained Media*; Ramamurthy, V., Ed.; VCH Publishers: New York, 1991, p. 79–132.
57. Cosa, G.; Scaiano, J. C. *Photochem. Photobiol.* 2004, *80*, 159–174.

58. Mitchell, R. H.; Bohne, C.; Wang, Y.; Bandyopadhyay, S.; Wozniak, C. B. *J. Org. Chem.* 2006, *71*, 327–336.
59. Gehlen, M. H.; De Schryver, F. C. *Chem. Rev.* 1993, *93*, 199–221.
60. Infelta, P. P.; Grätzel, M.; Thomas, J. K. *J. Phys. Chem.* 1974, *78*, 190–195.
61. Reekmans, S.; De Schryver, F. C. In *Frontiers in Supramolecular Organic Chemistry and Photochemistry*; Schneider, H.-J., Dürr, H., Eds.; VCH Verlagsgesellschaft: Weinheim, Germany, 1992, p. 287–310.
62. Tachiya, M. *Chem. Phys. Lett.* 1975, *33*, 289–292.
63. Van der Auweraer, M.; Dederen, C.; Palmans-Windels, C.; De Schryver, F. C. *J. Am. Chem. Soc.* 2002, *104*, 1800–1804.
64. Yekta, A.; Aikawa, M.; Turro, N. *J. Chem. Phys. Lett.* 1979, *63*, 543–548.
65. Amundson, L. L.; Li, R.; Bohne, C. *Langmuir* 2008, *24*, 8491–8500.
66. Li, R.; Carpentier, E.; Newell, E. D.; Olague, L. M.; Heafey, E.; Yihwa, C.; Bohne, C. *Langmuir* 2009, *25*, 13800–13808.
67. Ju, C.; Bohne, C. *J. Phys. Chem.* 1996, *100*, 3847–3854.
68. Dederen, J. C.; Auweraer, M. V. D.; De Schryver, F. C. *Chem. Phys. Lett.* 1979, *68*, 451–454.
69. Dederen, J. C.; Auweraer, M. V. D.; De Schryver, F. C. *J. Phys. Chem.* 1981, *85*, 1198–1202.
70. Löfroth, J. E.; Almgren, M. *J. Phys. Chem.* 1982, *86*, 1636–1641.
71. Van der Auweraer, M.; Dederen, C.; Palmans-Windels, C.; De Schryver, F. C. *J. Am. Chem. Soc.* 1982, *104*, 1800–1804.
72. Hashimoto, S.; Thomas, J. K. *J. Colloid Interface Sci.* 1984, *102*, 152–163.
73. van Stam, J.; De Feyter, S.; De Schryver, F. C.; Evans, C. H. *J. Phys. Chem.* 1996, *100*, 19959–19966.
74. Birks, J. B. *Photophysics of Aromatic Molecules*; Wiley-Interscience: London, U.K., 1970.
75. Cheung, S. T.; Ware, W. R. *J. Phys. Chem.* 1983, *87*, 466–473.
76. Barra, M.; Bohne, C.; Scaiano, J. C. *J. Am. Chem. Soc.* 1990, *112*, 8075–8079.
77. Liao, Y.; Frank, J.; Holzwarth, J. F.; Bohne, C. *J. Chem. Soc. Chem. Commun.* 1995, 199–200.
78. Evans, C. H.; Prud'homme, N.; King, M.; Scaiano, J. C. *J. Photochem. Photobiol. A Chem.* 1999, *121*, 105–110.
79. Scaiano, J. C. *J. Am. Chem. Soc.* 1980, *102*, 7747–7753.
80. Ireland, J. F.; Wyatt, P. A. H. *J. Chem. Soc. Faraday Trans. I* 1972, *68*, 1053–1058.
81. Liao, Y.; Frank, J.; Holzwarth, J. F.; Bohne, C. *J. Chem. Soc. Chem. Commun.* 1995, 2435–2436.
82. Okano, L. T.; Barros, T. C.; Chou, D. T. H.; Bennet, A. J.; Bohne, C. *J. Phys. Chem. B* 2001, *105*, 2122–2128.
83. Almgren, M.; Grieser, F.; Thomas, J. K. *J. Am. Chem. Soc.* 1979, *101*, 279–291.
84. Turro, N. J.; Okubo, T.; Chung, C.-J. *J. Am. Chem. Soc.* 1982, *104*, 1789–1794.
85. Nau, W. M.; Greiner, G.; Rau, H.; Wall, J.; Olivucci, M.; Scaiano, J. C. *J. Phys. Chem. A* 1999, *103*, 1579–1584.
86. Nau, W. M.; Zhang, X. *J. Am. Chem. Soc.* 1999, *121*, 8022–8032.
87. Scaiano, J. C.; Selwyn, J. C. *Can. J. Chem.* 1981, *59*, 2368–2372.
88. Scaiano, J. C.; Selwyn, J. C. *Photochem. Photobiol.* 1981, *34*, 29–32.
89. Barros, T. C.; Stefaniak, K.; Holzwarth, J. F.; Bohne, C. *J. Phys. Chem. A* 1998, *102*, 5639–5651.
90. Christoff, M.; Okano, L. T.; Bohne, C. *J. Photochem. Photobiol. A Chem.* 2000, *134*, 169–176.
91. Murphy, R. S.; Barros, T. C.; Mayer, B.; Marconi, G.; Bohne, C. *Langmuir* 2000, *16*, 8780–8788.
92. Murphy, R. S.; Barros, T. C.; Barnes, J.; Mayer, B.; Marconi, G.; Bohne, C. *J. Phys. Chem. A* 1999, *103*, 137–146.
93. Rinco, O.; Nolet, M.-C.; Ovans, R.; Bohne, C. *Photochem. Photobiol. Sci.* 2003, *2*, 1140–1151.

40

Photostability of Drugs and Drug Products

Beverley Glass
James Cook University

40.1 Introduction

Drugs and drug products are exposed to a number of environmental elements such as heat, moisture, oxygen, and light with combinations of these stresses causing complex behavior. The photostability of drugs has been reviewed over the years by a number of authors [1–5]. For this chapter, the literature has been explored to review the photostability of drugs and drug products, published since 2005.

The photodegradation of drug substances has previously been the major focus of drug photostability studies, with structural elucidation of photoproducts providing information to allow photodegradation pathways to be proposed. However, much of this research in the past has been conducted in solution (methanolic or aqueous), with more recent studies focusing on the photostability of solid-state drug substances.

In drug products, the presence of excipients further complicates the stability profile of drug substances within these products, as they may increase, have no effect on, or decrease the inherent stability of the drug substances. This has prompted an investigation into excipients, such as cyclodextrins, which have been included into drug products to improve the photostability of drug substances. Delivery systems such as liposomes, nanocapsules, and solid lipid nanoparticles have also been researched because of their ability to not only improve the delivery of the drug but also alter its stability. In some cases, these formulations or formulation excipients may result in the appearance of different photoproducts and photodegradation pathways, making this an important consideration from a regulatory perspective.

Since human exposure to sunlight is associated with skin damage, the application of sunscreens is important to protect against the development of skin cancer. These sunscreens in the past have presented with unique formulations of ultraviolet (UV) absorbers to protect against UV-B-induced skin damage. Recent developments have indicated that protection against UV-A has the ability to delay the aging process and reduce photodamage. New formulation challenges include that sunscreens should contain not only ingredients that are effective against UV-B and UV-A damage but also UV absorbers that have antioxidant properties.

Recent developments in repackaging of drugs from original manufacturers' packaging have stimulated discussion on in-use photostability of drug substances and drug products, which is not accounted for in the International Committee on Harmonisation (ICH) Photostability Testing Protocol. An example includes the repacking of drugs into dose administration aids (DAAs), which is employed to improve compliance of patients worldwide. These new areas of photostability have shifted the focus from that of just photodegradation studies of drug substances more to that of drug products with the challenge to provide quality products that are stable, effective, and safe in-use for patients.

40.2 Photostability of Drug Substances

40.2.1 Introduction

Although drugs degrade on exposure to light, heat, moisture, and oxygen, it is a combination of these conditions, which may cause extremely complex behavior. Many studies have reported on the behavior of drugs in the presence of light, most commonly the photodegradation of drugs in aqueous solution, with photoreactions (Table 40.1) of drugs in the solid-state being even more complex.

Light-induced decomposition of drugs may result not only in a loss of potency and decreased therapeutic efficacy but also in the formation of toxic photodegradants, which have the potential to cause adverse effects in patients. It is thus important to determine the photostability of drugs in order to elucidate photodegradants and predict the potential for the occurrence of these adverse effects on patients. Photosafety [6] refers to a number of photobiological reactions caused by drugs in the presence of light: phototoxicity, photoallergy, photogenotoxicity, and photocarcinogenicity. Since the evaluation of photosafety is now a regulatory requirement for all drug substances, the focus on the absorption of light by drugs in the 290–700 nm region is a key factor, in addition to the presence of the drug in exposed tissue. However, the Q1B Photostability Protocol [7] focuses on overall photoinstability, packaging, labeling, and storage of photolabile drugs and not on photosafety. Measurement of a molar extinction coefficient (MEC) of known photosensitive compounds would then provide information to support thresholds, which could be utilized in risk assessments to evaluate the photosafety of drugs. Although this study puts forward a suggestion that drugs with MEC thresholds above 1000 L mol^{-1} cm^{-1} should be assessed for photosafety, a correlation between photolability and photosafety could not be established. Onoue and Tsuda [8] have reported on an effective screening method in order to predict the ability of a drug and/or its photodegradants to cause unwanted adverse effects on patients,

TABLE 40.1 Photoreactions of Drugs

Types of Photoreactions	
Cyclization	Photoreduction/photosubstitution
Rearrangement	Hydroxylation
Photooxidation	Decarbonylation
Isomerization	Dehalogenation
N-Dealkylation	Ring dealkylation
Polymerization	Dehydroxylation
Photohydrolysis	Decarboxylation

which may be broadly described as photosensitivity effects. Methodology involved UV spectral analyses and photostability studies of known photosensitive drugs and some weakly or nonphotosensitive drugs. Their ability to generate reactive oxygen species (ROS) and photooxidize linoleic acid was also monitored. The results of this study were a strong correlation between the ability to generate ROS and known photosensitivity, giving rise to a predictive model which could be used to recognize the potential for drugs to cause photosensitivity reactions. The concern that the ICH guidelines published in November of 1996 do not focus on photosafety has been confirmed by Baertschi et al., who make comment that although it has been a useful basic protocol, it fails to cover the photostability of drugs under conditions of patient use and should be revised [9].

40.2.2 Photodegradation of Nitrofurazone

Nitrofurazone's use as an antibacterial agent has declined over the years, and nowadays, it is mainly used topically as a local anti-infective. However, its use in topical preparations presents a problem due to its susceptibility to light and the potential loss of pharmacological activity as a result of exposure to light. Although the photodegradation of nitrofurazone has been previously studied [10,11], the mechanism of its photodegradation remains unclear. A study to describe the kinetic model of nitrofurazone photodegradation by hybrid hard–soft multivariate resolution (HS-MCR) was undertaken by De Luca et al. [12]. The authors applied the HS-MCR method to UV spectrophotometric data in order to interpret the complete kinetic pathway. The photodegradation of nitrofurazone is seen to occur through rapid isomerization to the syn-form (Figure 40.1) and subsequent further degradation to a series of unstable colored compounds, which in addition to arising from the parent drug can also result from the azine and hydrazone derivatives, themselves not detected in the final photoproducts. Despite the rapid photodegradation of nitrofurazone making characterization of photodegradants very difficult, the use of this modeling technique has allowed a photodegradation pathway to be proposed.

40.2.3 Photodegradation of Metoclopramide

A recent study [13] investigating the photodegradation of metoclopramide (Figure 40.2) has been undertaken to elucidate its photoproducts, not only because of potential adverse effects to patients but also because of importance of gaining insight into the fate of pharmaceuticals in the environment. Photolytic degradation using a photoreactor equipped with a 254 nm UV lamp showed that metoclopramide is highly susceptible to photodegradation, which followed first-order kinetics in solution. The major degradation pathway involved cleavage of the chlorine with subsequent hydroxylation and formation of high-molecular-weight products, which proved to be dimers and trimers of metoclopramide. Examples of drugs in the literature, which lose their chlorine substituent on exposure to light are many [14,15] and as mentioned, this occurs through homolysis resulting in the formation of dimers and heterolysis with the formation of hydroxylated products. However, in these previous studies, the photosubstituted and photoreduced products were reported to be the major degradation products with very little mention made of high-molecular-weight photoproducts.

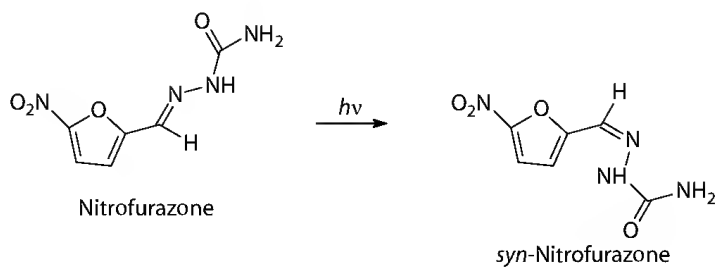

FIGURE 40.1 Photodegradation of nitrofurazone.

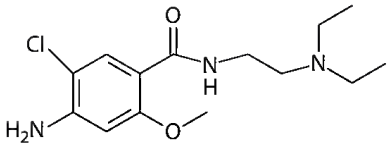

Metoclopramide

FIGURE 40.2 Chemical structure of metoclopramide.

40.2.4 Photodegradation of Pitavastatin

The reason for investigating the photostability of drug molecules is twofold: first to determine the effect of light on the stability of the drug substance and product in order to inform storage, packaging, and labeling, and second to determine possible biological effects, which may result in photosensitivity reactions in patients. Many of the statins used extensively in the treatment of elevated cholesterol levels have proved to be highly photochemically reactive [16–18]. Pitavastatin, a synthetic 3-hydroxy-3-methylglutaryl-coenzyme A (HMG-CoA) reductase inhibitor, used in the reduction of serum cholesterol in patients was studied to determine its photochemical transformation in solution to identify its main photoproducts. Pitavastatin [19] was found to degrade by first-order kinetics with the main photodegradation pathway (Figure 40.3) involving cleavage of the side chain at the double bound with subsequent photocyclization resulting in the formation of a tetracyclic photoproduct. The formation of these photoproducts is of significance due to the ability of such products to interact with biological molecules.

40.2.5 Photodegradation of Seratrodast

Although the photodegradation of seratrodast, a quinone derivative known to inhibit bronchoconstriction, has been previously reported by Ohta et al. [20], there was a lack of detail especially in respect of the photodegradation pathway as the study essentially focused on the high-performance liquid chromatography method (HPLC) of analysis. In a recent study [21], the authors have elucidated the major photoproducts and proposed a possible photodegradation pathway. Although seratrodast was found to be stable in the solid-state, photodegradation in solution occurred by first-order kinetics resulting in three main photoproducts 1, 2, and 3 (Figure 40.4). The formation of these three photoproducts is proposed to occur via a zwitterion–diradical, a spirocyclopropyl intermediate, and a zwitterion.

40.2.6 Photodegradation of Primaquine

The antimalarial drug, primaquine, an 8-aminoquinoline, is photolabile and decomposes to several photoproducts at physiological pH in the presence of oxygen [22–25]. Recent research [26] looked to gain further insight into the mechanism of photodecomposition of primaquine by characterizing primary excited states, which may be transient.

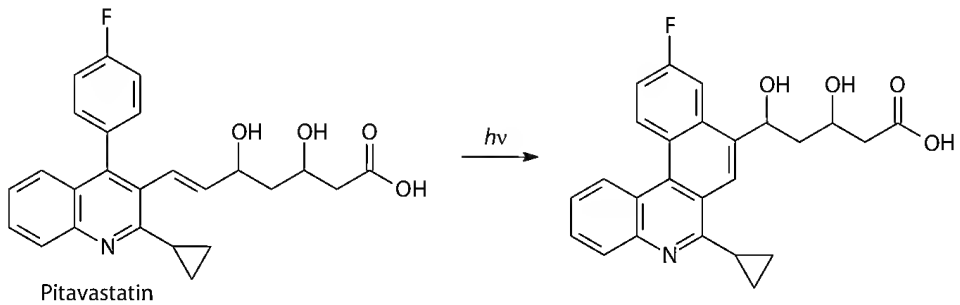

Pitavastatin

FIGURE 40.3 Photodegradation of pitavastatin.

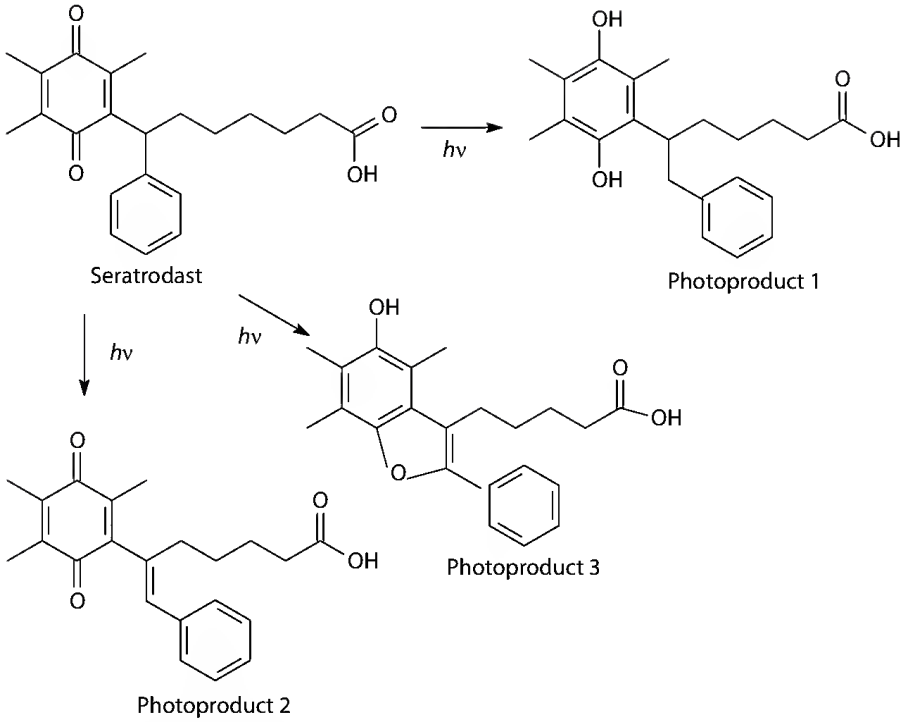

FIGURE 40.4 Photodegradation of seratrodast.

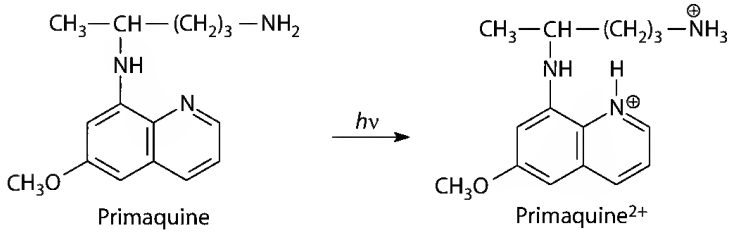

FIGURE 40.5 Photodegradation of primaquine.

The photochemical decomposition of primaquine is reported to occur by $^1O_2$ formed through a sensitized reaction with a synthetic impurity present in the bulk drug. Formation of primaquine^{2+} (Figure 40.5) is likely to occur *in vivo* in the presence of free radicals, and because of its relatively long lifetime, susceptibility to oxidative reactions is enhanced.

40.2.7 Photodegradation of Flurbiprofen

Flurbiprofen (Figure 40.6) belongs to the aryl propionic acid derivatives and is widely used as an analgesic, antipyretic, and anti-inflammatory agent. Because of the presence of the biphenyl moiety within the drug structure causing it to be highly lipophilic, the photoproducts formed in the skin after exposure to light have the potential to cause photoallergic contact dermatitis.

Because flurbiprofen [27] exists mainly in the deprotonated form at physiological pH, decarboxylation, which is likely to occur from the triplet excited state, will be the dominant initial degradation pathway (Figure 40.6). The interaction of the photoproduct with a biological membrane will result in abstraction of hydrogen from a lipid molecule with subsequent addition of molecular oxygen to a lipid radical causing radical damage to be propagated. With the occurrence of a number of photoreactions subsequent to decarboxylation, such as generating singlet oxygen and superoxide radicals, it is the formation of peroxyl radicals that explains the contact dermatitis, which occurs in patients taking flurbiprofen.

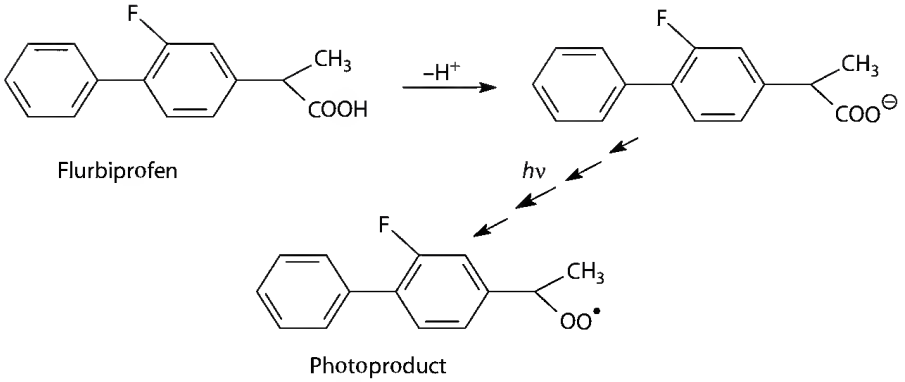

FIGURE 40.6 Photodegradation of flurbiprofen.

40.2.8 Photodegradation of Amlodipine

The photostability of the 1,4-dihydropyridines especially nifedipine [28] has been studied because of their ability to absorb UV-A light with photoreactions occurring with ease due to the presence of an hydrogen, which interacts with the nitro group. The photoreactivity of amlodipine [29] was studied due to the absence of the nitro group and the presence of a chloro group in this position in addition to an aliphatic amino group in the side chain. Irradiation of amlodipine resulted in the formation of the aromatized pyridine photoproduct (Figure 40.7) as the major degradant. In the case of amlodipine, the H-transfer has been facilitated by the presence of the amino group in the side chain, which was similarly observed in nicardipine [30] that also possesses this group in the side chain.

40.2.9 Photodegradation of Memoquin

The drug memoquin, a 1,4-benzoquinone (Figure 40.8) derivative, has been rationally designed for the treatment of Alzheimer's disease and neurodegeneration [31]. Quinones are known to be sensitive to light, and since memoquin has been designed to affect certain mechanisms relevant to Alzheimer's

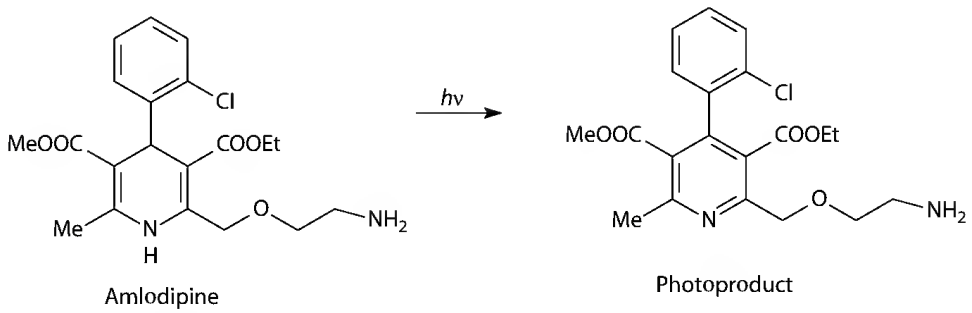

FIGURE 40.7 Photodegradation of amlodipine.

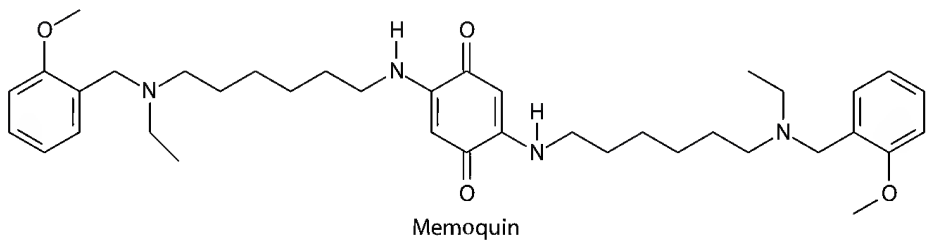

FIGURE 40.8 Chemical structure of memoquin.

disease such as the formation of ROS, it is important that exposure to light does not reduce its potency. It is however thought that the presence of two long, symmetric polyamine side chains may increase the stability and offer protection against light-induced decomposition.

Results show that memoquin degrades by first-order kinetics and that the photodegradation reactions involve the benzylamino groups in the side chains and not the antioxidant center (1,4-benzoquinone), which is important for its activity. This therefore illustrates the successful design of a light stable drug for the treatment of Alzheimer's disease.

40.2.10 Photodegradation of Montelukast

Montelukast, a light-sensitive drug, has been shown to be effective in the treatment of chronic asthma [32]. Montelukast in solution (methanol) is reported to degrade rapidly in daylight and UV light. About 30% of the drug was converted to the *cis*-isomer after only 15 min of exposure, increasing to 77% after 4 h. However, storage of the solution in amber flasks resulted in a reduction of the *cis*-isomer from 77% to 10% after 4 h. Since montelukast absorbs light at wavelengths over 400 nm, it was found to be more stable when exposed to sodium or neon lights (wavelength < 500 nm). Although most drugs in the solid-state are usually relatively stable to light, this was not the case for montelukast, which showed a 20% reduction in drug content after being exposed to daylight for 1 week, with the formation of the *cis*-isomer and the S-oxide as the major photoproducts (Figure 40.9). When tablets were exposed to daylight for 2 weeks, degradation to about 90% of the drug content occurred. This was however not observed with the film-coated tablets, indicating that the film coating was in fact providing some protection against its light degradation. Since the major photoproduct in solution is the *cis*-isomer as opposed to the S-oxide in the solid-state, it may be suggested that the solvents used are favoring photoisomerization rather than photooxidation. The predominance of the S-oxide as a thermal degradation product as well suggests that antioxidants may be used to stabilize montelukast against oxidation to facilitate better handling and storage.

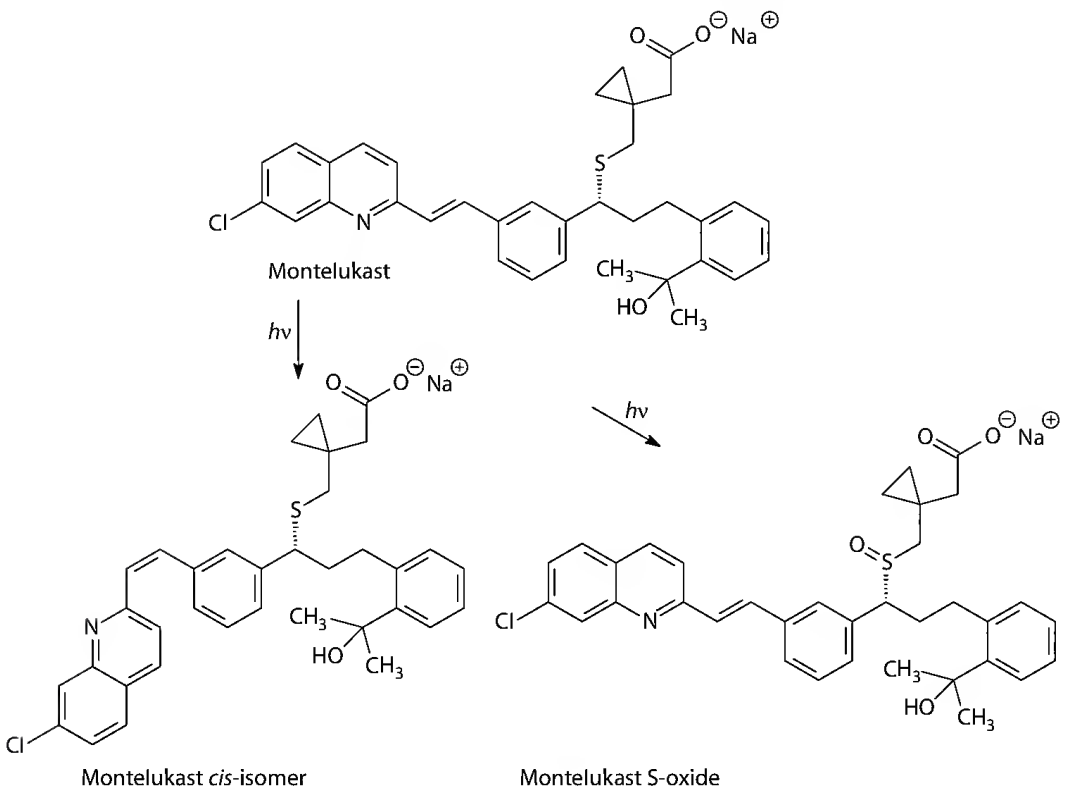

FIGURE 40.9 Photodegradation of montelukast.

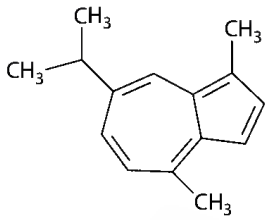

FIGURE 40.10 Chemical structure of guaiazulene.

40.2.11 Photodegradation of Guaiazulene

Guaiazulene (Figure 40.10), an alkyl derivative of azulene, is a natural product which is gaining popularity for inclusion into cosmetic products [33]. The rational for its inclusion is its ability to act as a skin conditioning product. Guaiazulene has been found to be photochemically reactive [34], being able to inhibit lipid peroxidation and scavenge free radicals. A more recent report [35] has also implicated guaiazulene in photomutagenicity in *Salmonella typhimurium* bacteria strains.

The photochemical stability of guaiazulene was assessed in an emollient cream exposed to simulated natural light. Results indicated that after 3 h exposure only 21% of guaiazulene remained, indicating the inability of the cream base to protect guaiazulene against photodegradation.

40.2.12 Photodegradation of Aloe Vera

Since exposure to UV-A light can cause the generation of ROS, the fact that aloe vera extract [36], containing anthraquinones also capable of generating ROS, is incorporated in many commercial products is cause for concern. This is especially the case since many of these products are applied as cosmetics to large areas of skin exposed to sunlight. Aloe vera-derived anthraquinones have shown photooxidative damage to both cellular RNA and DNA attributed to the generation of ROS and the formation of stable photoproducts.

40.2.13 Conclusions

The photostability of drug substances in recent years has focused on detecting the ability of photoproducts to cause adverse reactions in patients and on issues of photosafety, rather than drug content. New initiatives have involved the rational design of drugs such as memoquin, where the inclusion of polyamine side chains has offered protection against light and thus preserved potency.

40.3 Photostability of Drug Products

40.3.1 Introduction

The stability of a drug product is important to ensure safety and efficacy for patients because instability due to exposure to light may result not only in a loss of the potency of the active ingredient but also the potential presence of toxic photodegradants. During the preformulation stage, the selection of the solid form (polymorph) of the active pharmaceutical ingredient (API) is undertaken, so that transformation of polymorphs or pseudopolymorphs does not occur under storage conditions relating to temperature, light, and humidity. In addition to the choice of a polymorphic form of the drug for optimum photostability, cyclodextrins as formulation excipients have played a role in the photostabilization of drugs. The other excipient currently of interest is titanium dioxide because of its photocatalytic ability and routine inclusion in pharmaceuticals as a coating agent and in sunscreens as a physical blocker.

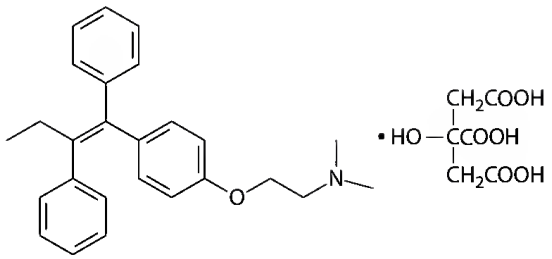

FIGURE 40.11 Chemical structure of tamoxifen citrate.

40.3.2 Polymorphism

Polymorphism has the ability to affect the physical and chemical stability of drug substances and thus drug products due to differences in the molecular arrangement. The photostability of drugs in the solid-state depends on surface area, irradiation conditions such as spectral irradiation energy and the type of the light source, and most importantly the photochemical properties of the sample drug, which may be different for different polymorphs. Although the relationship been crystal forms and photostability has been reported on [37–42], the exact nature of this relationship has not been fully elucidated. The solid-state photochemistry of tamoxifen citrate (Figure 40.11), an antiestrogenic agent for the treatment of breast cancer, has been investigated with a view to providing some insight into a potential relationship between the photostability and spectroscopic properties of the polymorphs A and B.

Polymorph A appeared to be photosensitive (Table 40.2), whereas B was quire resistant to photodegradation [43].

A ΔE value of 54.5 and 33.6 for A and B respectively on irradiation, indicated that form A discolored more than form B, with results also showing that penetration of light as greater for A than for B. Diffuse-reflectance solid-state UV data showed that form B absorbed mainly in the UV-B and UV-C regions, while A absorbed mainly in the UV-A region resulting in A absorbing more photoenergy than B and thus exhibiting greater photodegradation. This result is attributed to differences in the molecular arrangement of the crystal lattice of A and B and the resulting different energy states. Based on these photostability results, form B would be the polymorph of choice in drug product development.

40.3.3 Cyclodextrins

Cyclodextrins in drug formulations have been indicated not only to improve the physicochemical properties of drug substances but also to improve their pharmacological, pharmacokinetic, and/or adverse effect profiles. The most characteristic property of cyclodextrins is their ability to form inclusion complexes with a variety of guest molecules resulting in increased solubility and dissolution rates of poorly water-soluble drugs. Cyclodextrin inclusion complexation may influence drug stability in three ways: Depending on the inclusion mode of the drug in the cyclodextrin cavity, degradation may either be retarded, accelerated, or unchanged with the stereochemistry and/or stoichiometry of the guest–host interaction influencing the stabilizing/destabilizing effects of complexation. The photochemistry and photophysics within the cyclodextrin cavity involves features quite distinct from that of uncomplexed substances, since the interior of the cavity constitutes an isolated environment where

TABLE 40.2 Polymorphs A and B Remaining (%) on Photoirradiation (30,000 Lux)

Tamoxifen Citrate	0 Days	10 Days	20 Days	30 Days
A	100	94	92	87
B	100	99	99	100

included species are usually present as single molecules. The photochemistry is therefore generally restricted to intramolecular events except in cases of double or multiple occupancy. The effects of cyclodextrin inclusion complexation on drug photostability are in many ways similar to its impact on general drug stability in that it may increase, decrease, or have no effect on the rate of photodegradation [44]. Curcumin, a naturally occurring compound indicated in the treatment of a number of diseases including cancer, HIV infections, and cystic fibrosis is susceptible to photochemical degradation. In addition, curcumin has been used as a pharmaceutical excipient to stabilize photolabile drugs in solution and in topical preparations. Because of the susceptibility of curcumin to both alkaline hydrolysis and light degradation, inclusion complexation with cyclodextrins was investigated to stabilize curcumin toward these conditions. Although the hydrolytic stability of curcumin under alkaline conditions was improved, the photodecomposition was increased compared to a curcumin solution in organic solvents [45]. Recently, Tomren et al. have extended their study to the interaction of other curcuminoids with hydroxypropyl-beta-cyclodextrin, 2-*O*-methyl-beta-cyclodextrin, and hydroxypropyl-gamma-cyclodextrin, with the larger size of the hydroxypropyl-gamma-cyclodextrin cavity allowing a study on the effect of the cavity size. Results were again similar to those previously achieved, with decreased photostability observed [46].

Nicardipine (Figure 40.12), a calcium channel blocking agent like other 1,4-dihydropyridines, is poorly water soluble and susceptible to photochemical decomposition. The effect of cyclodextrins (including the natural cyclodextrins, alpha, beta, and gamma and the chemically modified hydroxypropyl, hydroxyethyl, and methyl-cyclodextrin) and complexation on photochemical decomposition has been investigated using capillary electrophoresis. This is due to the ability of this technique to be used to evaluate cyclodextrin-induced enantioselective effects in the photodegradation process.

Although a photoprotective effect was observed for some cyclodextrins, some did not affect the photostability, and in the case of gamma-cyclodextrin, photodegradation was increased. Cyclodextrin-mediated stereoselective photodegradation was seen only for the beta-cyclodextrin complex with different photodegradation profiles and kinetic constants observed for the two enantiomers [47].

Although sunscreens are effective in providing protection against solar radiation, they need to be applied prior to exposure to sun. Secondary photoprotective agents, such as the anti-inflammatory drug ibuprofen (Figure 40.13), have the ability to reduce the effects of solar radiation after sun exposure. Cyclodextrins such as hydroxypropyl-beta-cyclodextrin have the ability to alter not only the drug penetration into the skin but also its ability for secondary photoprotection. In this case, the cyclodextrin increased ibuprofen's aqueous solubility and flux across and accumulation in the skin to a maximum

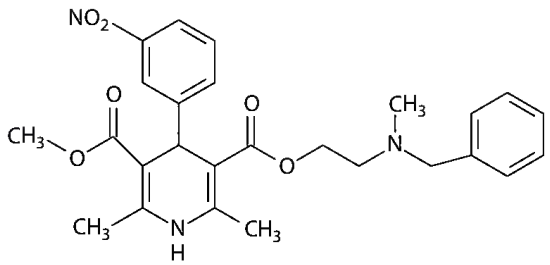

Nicardipine

FIGURE 40.12 Chemical structure of nicardipine.

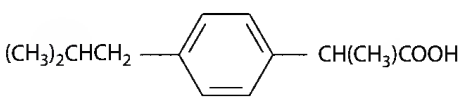

Ibuprofen

FIGURE 40.13 Chemical structure of ibuprofen.

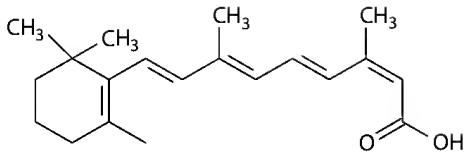

13-*cis*-retinoic acid

FIGURE 40.14 Chemical structure of 13-*cis*-retinoic acid.

at a 10% concentration of the cyclodextrin. This correlated with the greatest photoprotection being afforded by the ibuprofen–cyclodextrin formulation, which delivered the greatest amount of ibuprofen to the skin [48].

13-*cis*-Retinoic acid (isotretinoin) commonly used in the treatment of acne is very poorly water soluble and is highly photosensitive making it an excellent candidate for inclusion complexation with cyclodextrins. In a study by Yap et al. [49], the effect of selected cyclodextrins on the photostability of isotretinoin (Figure 40.14) was investigated. Hydroxypropyl-beta-cyclodextrin proved to be effective in retarding the photodegradation of isotretinoin in solution. This effect can be explained by the mode of inclusion of the isotretinoin molecule into the cavity of the cyclodextrin. The molecular modeling studies indicated that the alkyl chain which is susceptible to isomerization on exposure to light was included into the cavity, thus explaining the improved photostability.

Altered photodegradation pathways and different photodegradants in the presence of cyclodextrins were also observed in a study undertaken by Lebete et al. [50].

The effect of randomly methylated beta-cyclodextrin (RAMEB) as an excipient on the rate of photodegradation of midazolam and the nature of the photoproducts was determined. Results indicated that the kinetics of degradation could not be fitted to a specific order with the initial stages acceleratory, suggesting autocatalysis by the degradants. The rate constants determined by the application of the power law were found to be 0.137 and 0.154 h^{-1} in the absence and the presence of RAMEB, respectively. The photodegradation pathway (Figure 40.15) is altered in the presence of the cyclodextrin by the formation of a dimer (photoproduct 2) and an intermediate (photoproduct 1) not isolated in the absence of RAMEB due to its ability to provide conformational control and to stabilize free radicals.

These findings present an important consideration for pharmaceutical scientists to be aware of the presence of unexplained photodegradants if cyclodextrin and possibly other excipients are included in formulations.

40.3.4 Titanium Dioxide

The photostability of drugs may be altered in various formulations, whether they are suspensions, creams, tablets, or gels. This altered photostability, which may be increased or decreased, is often attributed to the effect of excipients within the formulation. It is therefore not surprising that interest has been focused on the effect of excipients on the photostability of drugs.

Titanium dioxide is a naturally occurring oxide of titanium, which is widely used as a filler and coating with range of applications from paint to sunscreens. Due to its high refractive index, it is often used as a physical blocker in sunscreens; however, the particles are often required to be coated with silica or alumina because of its ability to create radicals, which are carcinogenic in a photocatalytic reaction. The crystal structure determines its photocatalytic ability with the anastase form particularly photocatalytic to UV light [51]. Recently, there has been much said about the use of nanomaterials especially ultrafine titanium dioxide in cosmetics and sunscreens due to their transparent appearance and aesthetic appeal. The ultrafine titanium dioxide occurs in three different crystalline forms namely, rutile, anastase, and brookite, with the rutile and anastase forms being used commercially. Although these fine particles have the advantage in enhancing the photostability of sunscreens and preventing the discoloration of the pigment, there is some concern about their ability to form free radicals and thus cause oxidative

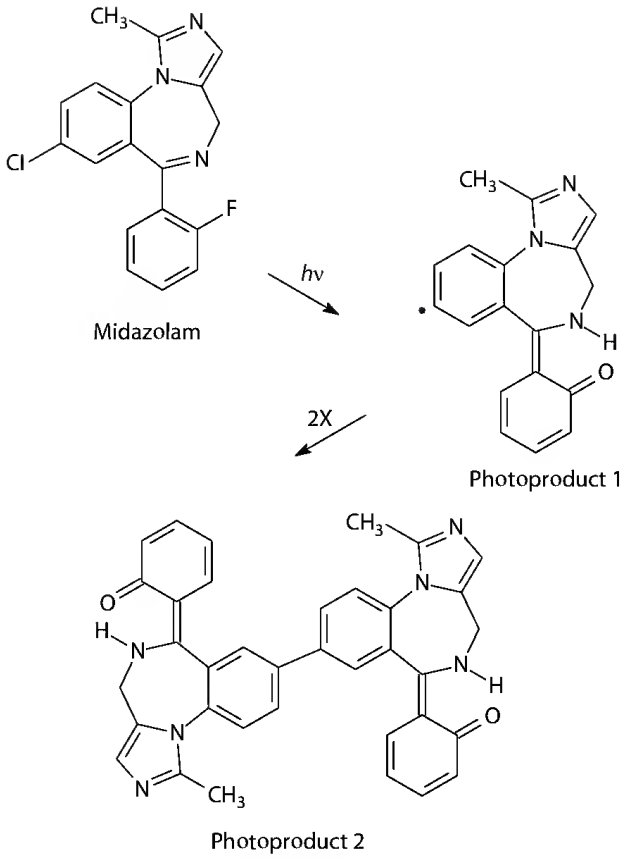

FIGURE 40.15 Photodegradation of midazolam in the presence of RAMEB.

damage to DNA. It is thought that the enhanced penetration of these ultrafine particles is responsible due to photocatalysis, DNA damage, and skin cancer following exposure to sunlight. This has however been refuted as it is doubtful whether penetration occurs beyond the stratum corneum. Theogaraj et al. investigated the photo-clastogenic potential of titanium dioxide using the Chinese hamster ovary and proved a lack of photochemical genotoxicity in this model [52].

Titanium dioxide has been used in pharmaceutical products as a coating material, with a required purity as specified by the United States Pharmacopoeia of 99.0%. Because of its known photocatalytic activity, it is important to evaluate its effect on the photodecomposition of drug substances to ensure the quality of the resulting drug products.

Researchers have focused on the solid-state reactions between titanium dioxide and selected drug substances. In a study on the H_2 blocker, famotidine (Figure 40.16) with titanium dioxide, discoloration was observed on exposure to light, and the photocatalytic activity of titanium dioxide was affected by the relative humidity (RH) of the environment. Therefore, it is important to take into account the exposure of pharmaceuticals to moisture in terms of storage and repackaging as this can affect the quality of pharmaceuticals delivered to patients [53].

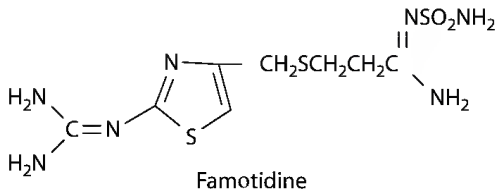

FIGURE 40.16 Chemical structure of famotidine.

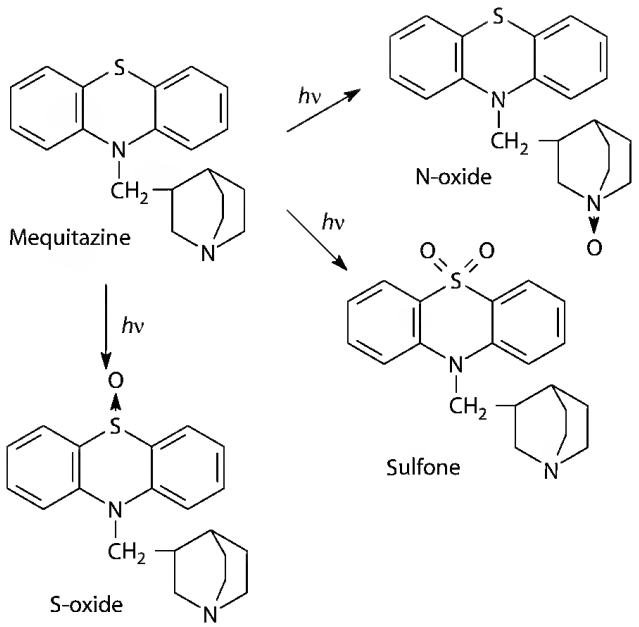

FIGURE 40.17 Chemical structure of mequitazine and its photodegradants.

It is therefore important during preformulation to determine whether there is any relationship between titanium dioxide and the photodecomposition of drug substances. Mequitazine [54], an H_1 receptor antagonist, presented as a good candidate due to its discoloration on exposure to light as it is possible that the presence of titanium dioxide might photocatalyze the degradation of the mequitazine. Results confirmed that the presence of titanium dioxide especially in the anatase form caused significant photodegradation of the drug. Although photodegradation occurred using a near-UV lamp as a light source, it is significant that degradation of the mequitazine also occurred on exposure to the D65 source, which is routinely used in photostability testing of pharmaceuticals. Similar to the results achieved with the famotidine, the degradation was accelerated with increasing RH.

The photodegradation resulted in the formation of three photodegradants: mequitazine-N-oxide, mequitazine-S-oxide, and mequitazine-sulfone (Figure 40.17). Photooxidation of mequitazine resulted in the N-oxide while the other two products were proven to be a result the photocatalytic effects of the titanium dioxide.

These findings present an important consideration for pharmaceutical scientists to be aware of the presence of unexplained photodegradants if titanium dioxide is included as an excipient or in the coating of tablets.

The photocatalytic activity of titanium dioxide on the photodegradation of the commonly used calcium channel blocker drug, nisoldipine [55], has also been examined. Results indicated that the differing photodegradation observed in the presence of titanium dioxide was attributed to its photocatalytic activity and that this activity is not only dependant on the crystal form of the titanium dioxide.

Although exposure of nisoldipine (Figure 40.18) to light results in two photodegradants: the nitropyridine and nitrosopyridine derivatives, the nitrosopyridine derivative arises from direct photooxidation on exposure to artificial daylight or white fluorescent light, while the nitropyridine derivative occurs even on exposure to light sources of low irradiation energy. This photodegradant results due to the photocatalytic effect of the titanium dioxide.

40.3.5 Photostability of Formulations

There are many reasons why drug substances are formulated in a dosage form. In general, this is to provide a mechanism for the safe, convenient delivery of accurate dosages to patients. Specifically, drug

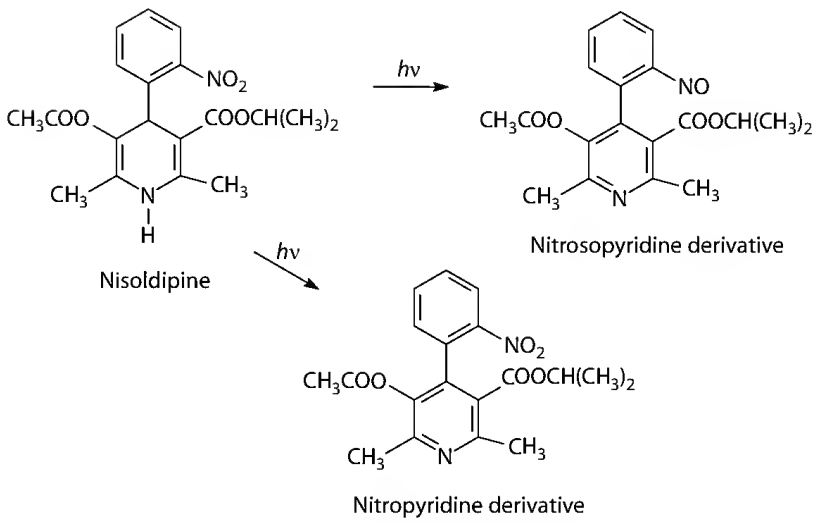

FIGURE 40.18 Chemical structure of nisoldipine and its photodegradants.

substances are formulated in dosage forms to provide protection from destructive influences such as atmospheric oxygen, moisture, heat, and light.

In recent years, a number of delivery systems have been developed not only to enhance the photostability of drug substances, but also to optimize their therapeutic efficacy. Examples of these include the inclusion of UV filters, nanoparticles, nanocapsules, solid lipid nanoparticles, liposomes, and lipid microparticles.

Although UV filters are most commonly associated with sunscreens, there are many other formulations which contain UV filters for the purpose of improving hydration of the skin and promoting antiaging. It is therefore important to evaluate the effect of these UV filters on the photostability of other active ingredients in these formulations. The role of antioxidants such as vitamins A, C, and E in topical formulations is to act as a photoprotectants and maintain a healthy skin barrier. Topical application has the advantage in that these antioxidants are targeted at the site of action. Gaspar and Maia Campos conducted a study evaluating the effect of UV filters (unstable—combination octyl methoxycinnamate, avobenzone, 4-methylbenzilidene camphor; *stable*—combination octyl methoxycinnamate, benzophenone, octocrylene) on the photostability of a formulation containing vitamins A, C, and E [56]. Although the UV filters did not influence the hydration and antiaging effects of the formulations, they played a role on the reduction of skin irritation attributed to both the protective effect of these lipid soluble molecules in the stratum corneum but also due to reduction in the conversion of vitamin A to isotretinoin, a skin irritant. In terms of the photostability study, only the stability of the vitamin A was improved by the UV filters especially the photostable UV filters.

Formulation of drug substances which are sensitive to UV radiation in topical dosage forms may in turn improve the photostability of the drug substance. Hydrocortisone acetate which is used both topically and systemically is susceptible to photodegradation. Exposure of hydrocortisone acetate to UV-B radiation resulted in the formation of a number of photoproducts. However, the photolysis of hydrocortisone acetate in a commercial topical cream resulted in 20% degradation with the formation of only one photoproduct, the 4-androstene-11β-ol-3,17 dione (Figure 40.19).

Hydrocortisone acetate [57] was more stable to light in the cream formulation than in solution, and this was attributed to the light-scattering properties of the cream base and/or the protecting effect of the excipients in the cream. Since any modification in corticosteroids especially in the side chain results in loss of anti-inflammatory activity, the photolability of the hydrocortisone acetate even in the cream base confirms the requirement for light protection of this drug.

Curcuminoids [58] are the yellow bioactive compounds of turmeric. Together with their lipophilicity and low bioavailability, there are also issues associated with the stability of the curcuminoids, namely,

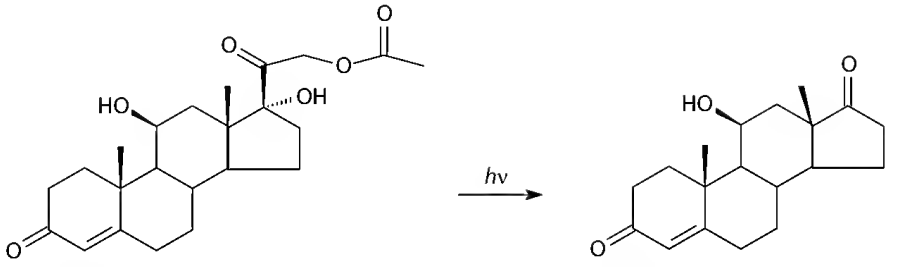

Hydrocortisone acetate 4-Androstene-11β-ol-3,17 dione

FIGURE 40.19 Chemical structure of hydrocortisone acetate and its photodegradant.

their alkaline degradation and instability to light. There have already been many studies to address the formulation and stability problems of the curcuminoids [45,58–62]. Mulik et al. [58] have loaded poly(butyl) cyanocrylate nanoparticles coated with poloxamer in order to improve the release profile and the photostability of these curcuminoids. The stability study revealed, that although the curcuminoids showed a good stability profile by remaining within the nanoparticles at 40°C/75% RH, in the absence of light the concentration range was between 87% and 93%, while in the presence of sunlight this was reduced to 79%–89%. However, when the stability of the curcuminoids in the nanoparticles was compared to curcuminoids solubilized in a surfactant solution, there was a 30% improvement in stability, both in the presence and in the absence of light. This highlights the role of the poly(butyl) cyanocrylate nanoparticles not only in improving the delivery of this lipophilic drug but also providing a much improved stability profile for the curcuminoids.

Both tretinoin and isotretinoin are degraded when exposed to light, with the UV-A in solar-simulated light largely responsible [63]. Since UV-A penetrates the skin, the adverse effects associated with this therapy such as photosensitivity reactions can therefore be attributed to this UV-A light. Therefore, any improvements in formulations as well as the use of UV-A sunscreens which eliminate this adverse effect will make a positive contribution to therapy. Since both tretinoin and isotretinoin are biologically active, their disappearance on exposure to light was monitored. Both of these two drugs underwent photoisomerization and photolysis on exposure to solar simulated light with greater degradation in a cream formulation than in ethanol occurring. The effect is thought to be due to the multiple components present in the cream, and a strategy for improvement would need problematic ingredients to be identified, removed, and replaced. This concurs with findings by another group of researchers [64]. While these studies suggest that the use of UV-A sunscreens might have a positive effect in reducing the adverse effects associated with this therapy. Brisaert and Plaizier-Vercammen [64] reported that although tretinoin had the highest efficacy when formulated as a lotion, photodegradation was rapid until an equilibrium called a photo stationary state, involving 80% isomerization, was achieved. Although the principal isomerization product isotretinoin is therapeutically active, 40% of the tretinoin is isomerized to inactive products. Selection of the various components of the cream involved the emulsifying agent; but very importantly the oil and a number of candidates, including castor oil, olive oil, maize oil, Miglyol 812, and isopropyl myristate, were chosen for their dissolving and penetration-enhancing properties. Results indicated that tretinoin was most soluble in castor oil and less soluble in isopropyl myristate, Miglyol 812, maize oil, and olive oil. There appears to be some relationship between this solubility and the photostability of tretinoin, which proved to be the highest in the castor oil. When tested in the cream formulation, the results achieved contradicted those in the oils with the olive oil and castor oil creams proving to be the most stable. These anomalous results achieved for the olive oil were explained by the presence of tretinoin crystals in the cream on microscopic examination and the obvious difference in degradation kinetics between the solid-state and the dissolved molecule. The conclusion drawn from this study is that castor oil is the chosen oil for the formulation of the cream both in terms of the solubility and the photostability of tretinoin. Other authors [65–67] concurred that incorporation of

tretinoin into vesicles, liposome, and liposome complexes results in slower photodegradation compared to tretinoin dissolved in methanol.

Kumar et al. [68] investigated the incorporation of tretinoin into solid lipid nanoparticles in a gel with a view not only of improving its delivery but also its photostability. Solid lipid nanoparticles are suggested as a delivery option in preference, for example, to liposomes due to enhanced physical stability and reduced costs compared to the phospholipids. The photostability of tretinoin in a methanolic solution resulted in initial rapid degradation, which then slowed but continued to only 12% remaining after 180 min. The photodegradation of tretinoin in this case was accompanied by a shift in the maximum peak from 344 to 360 nm. Inclusion of the tretinoin into the nanoparticles in comparison dramatically reduced the photodegradation with 71% remaining after the same time of exposure, without the shift in the maximum peak. Since it might be more appropriate to compare the photodegradation in the solid lipid nanoparticles to that of tretinoin in a cream, it was observed that a study conducted by Nighland et al. [69] reported 81% degradation in a commercial product after light exposure for 120 min. This confirms that tretinoin incorporated into solid lipid nanoparticles provides a good alternative to those existing tretinoin formulations not only in terms of patient acceptability but also photostability.

Polymeric nanocapsules, [70] in which drugs can be dissolved or dispersed, used as drug carriers are characterized by a lipophilic core surrounded by a polymeric layer. Two types of tretinoin-loaded nanocapsules (capric/caprylic triglyceride mixture/sunflower seed oil) have been prepared to improve both the delivery and photostability of tretinoin. Although the photodegradation profile of tretinoin in methanol (half-life 40 min) followed first-order kinetics, for the tretinoin-loaded nanocapsules (half-life 85–100 min) zero-order kinetics were observed. Although the photostability of tretinoin was improved in a nanoemulsion (half-life 69–82 min), it is obvious that the polymer in the nanocapsules is important in improving the photodegradation profile of tretinoin. This result is attributed to the crystallinity of the polymer reflecting and scattering UV light. These results achieved are independent of the type of oil used and present another option for the delivery of tretinoin.

Pantoprazole [71] is a proton pump inhibitor (Figure 40.20) used extensively for various gastric conditions. This drug is however unstable in solution, and therefore, it is important to compare its stability to light in solution and on microencapsulation using or a blend of poly(ε-caprolactone) or hydroxypropyl methylcellulose (HPMC). Photodegradation in a methanolic solution resulted in reduction in the concentration to only 1.7% after 120 min, with a resulting yellow coloration. Although solid-state photostability of pantoprazole was improved, the results were not significant with 27% drug remaining after 10 days. However, microencapsulation using Eudragit® S 100 showed increasing photostability for pantoprazole with 56% of the drug remaining after the same irradiation period, with no significant improvement resulting from the use of the polymer blends.

Lipid microparticles, using tristearin as lipid and phosphatidylcholine as emulsifier, have also been investigated to improve the stability of the photoprotective agent and antioxidant, quercetin (Figure 40.21) [72]. The study is important by virtue of the potential application of quercetin in the protection of the skin against oxidative damage. A comparative study was conducted on a cream containing nonencapsulated and encapsulated quercetin, which was irradiated for 2 h using a solar simulator maintained at 500 W m^{-2}. Results indicated that 23% of the unencapsulated quercetin was degraded, compared to 11.9% for the encapsulated quercetin, a 48.5% improvement.

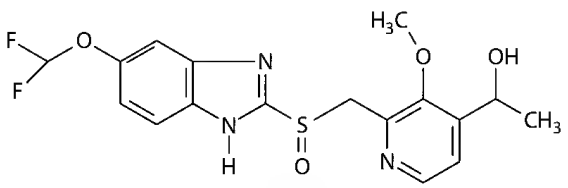

Pantoprazole

FIGURE 40.20 Chemical structure of pantoprazole.

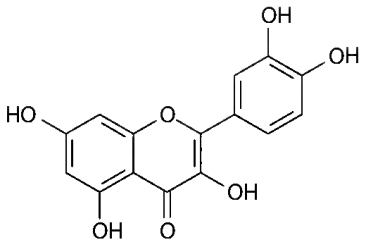

Quercetin

FIGURE 40.21 Chemical structure of quercetin.

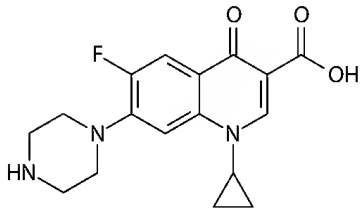

Ciprofloxacin

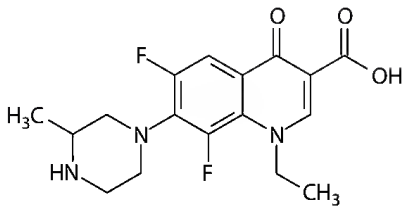

Lomefloxacin

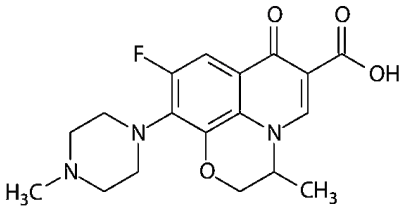

Ofloxacin

FIGURE 40.22 Chemical structures of ciprofloxacin, ofloxacin, and lomefloxacin.

Fluoroquinolone antibiotics (Figure 40.22) extensively used have the adverse side effect of an acute phototoxic reaction induced by light. These compounds are capable of undergoing a number of photochemical reactions, including generation of singlet oxygen and superoxide, in addition to those fluorinated quinolones undergoing defluorination on exposure to UV-A radiation. Liposomes have been used in order to increase the bioavailability of the fluoroquinolones but it was also thought important to investigate the ability of these liposomes to reduce the phototoxicity of these molecules. Although results indicated that lomefloxacin was the most photolabile drug, the most important findings were that the lipids did not increase the rate of degradation but altered the photodegradation pathway and the resulting photoproducts. In the α-L-dipalmitoylphosphatidylcholine liposomes, double defluorination occurred differently from the degradation in aqueous solution. Thus, the presence and the type of the lipids had an effect on the photodegradation process [73].

40.3.6 Photostability of Sunscreens

Sunscreens are designed to protect the skin from UV radiation. In the design of these drug products, molecules which both absorb and reflect light are included. However, there have been some developments to include substances in these products, which prevent, reduce, or repair sun-induced skin damage [74].

A sunscreen should be designed to fulfill the following criteria [75]:

- Provide protection against both UV-B and UV-A radiation. Initially, broad spectrum protection was achieved by chemical absorbers in the UV-B range, and for the UV-A, protection was achieved by using physical blockers such as titanium dioxide and zinc oxide. However, in recent years, the trend has been to include UV-A chemical absorbers into sunscreens. This increasing complexity has provided a challenge for the formulation scientist as well the regulatory authorities such as the Therapeutics Goods Administration (TGA) in Australia and the American Food and Drug Administration (FDA).
- Be stable to heat and light and be user friendly, cost-effective and allow for both ease of formulation and reapplication.

Recently, the role of free radical scavengers in delaying the aging process and reducing the damage caused by excessive exposure to sun has been investigated. It is suggested that new formulations contain both UV-B and UV-A absorbers, which also display antioxidant properties. This prompted Venditti et al. [76] to design a new derivative of one of the most commonly used sunscreens, ethylhexyl methoxycinnamate, attaching a nitroxide moiety to impart antioxidant activity (Figure 40.23).

This new compound posses the cinnamate group, which has UV-B absorbing properties and the ethylhexyl group, which confers solubility in oil and resistance to water, which is an important feature of all sunscreens. Replacement of the methoxy group by the pyrrolidine nitroxide is strategic in conferring the antioxidant activity in the design of sunscreens. Photostability of sunscreens is important not only to retain their activity but also because of the potential for their photodegradants to cause genotoxic reactions and photo aging.

While most UV-B absorbers are photostable to the UV-B wavelengths, there was some concern about their stability when exposed to the UV-A range. The fact that these compounds would then lose their photoprotective effect posed a safety hazard to their use. This study concluded that this designed sunscreen showed that it was photostable to UV-A radiation. Most important was its ability to scavenge free radicals with comparable antioxidant activity to that of vitamin E and butylated hydroxytoluene. The safety profile was good with proven noncytotoxicity to the human skin.

The sun protection factor (SPF) is widely accepted to measure sunscreen efficacy and has been defined as the sun radiation dose to produce a minimal erythemal dose after the application of 2 mg/cm^2 of sunscreen, for example, an SPF of 2 absorbs 50% of UV radiation [77]. However, in August 2007, this SPF was altered to stand for sunburn protection factor [78]. To account for the importance of sunscreens to protect against ROS in skin, a new SPF, the radical protection factor (RPF) has also been suggested.

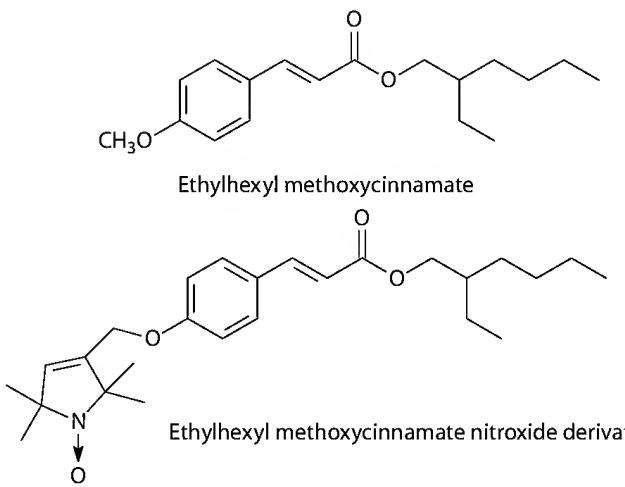

FIGURE 40.23 Chemical structures of ethylhexyl methoxycinnamate and the nitroxide derivative.

Inorganic sunscreens such as titanium dioxide and zinc oxide reflect and scatter UV and visible radiation, and they have the advantage in that they do not react with organic sunscreens. However, because of the fact that they are opaque and occlusive has caused some resistance to their use. This problem has been overcome in recent years by reduction in the particle size of these agents leading to a more aesthetically pleasing product. Concerns about the safety of these compounds due to their potential penetration deeper than the stratum corneum have been proven to be unfounded [77].

These findings were confirmed by Newman et al. [79] who investigated the use of nanosized particles of titanium dioxide and zinc oxide in sunscreens. Although it was discovered that there was no significant penetration beyond the stratum corneum, there is however concern that this might not be the case on the sunburned skin and under extreme UV conditions. In addition, it will be important to measure the penetration of ROS formed on the stratum corneum as a result of exposure of these nanosized particles to UV light on the surface of the skin. The photocatalytic effect of titanium dioxide involves an electron–hole pair photogeneration and a subsequent energy transfer process, which results in the generation of ROS. There is therefore a possibility that titanium dioxide included into commercial sunscreens may be photoactive. This is therefore the rationale for the inclusion of additional antioxidants, for example, vitamin E, ascorbic acid, or beta-carotene in these products [80]. Photoreactivity of titanium dioxide in three different products was compared to the whole product and phenalenone, which is an efficient singlet oxygen photosensitizer. There is an important question to be answered. Is titanium dioxide in commercial sunscreens responsible for singlet oxygen generation? The outcome has significant implications for the safety and efficacy of these commercial products. In order to assess the photocatalytic activity, the photodegradation of 4-chlorophenol and azur B (Figure 40.24) was monitored, and in addition, the photocatalytic oxidation of α-terpinene was determined. The photocatalytic oxidation in this case resulted in the formation of the endoperoxide ascaridol (Figure 40.25).

Although the photodegradation of the 4-chlorophenol and azur showed low efficiency in the generation of ROS, there appeared to be other reactions taking place, which can result in the production of singlet oxygen. A significant finding was that even when the rutile form, which is much less reactive than the anatase form, of titanium dioxide was used, photoactivity resulted, especially in the presence of zinc oxide. Thus, even though singlet oxygen scavengers are included in commercially products, it is recommended that the photoactivity of the titanium dioxide be evaluated.

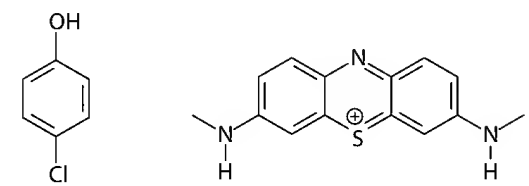

FIGURE 40.24 Chemical structures of 4-chlorophenol and azur B.

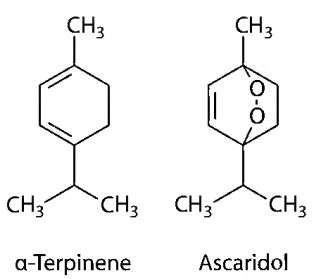

FIGURE 40.25 Chemical structures of α-terpinene and ascaridol.

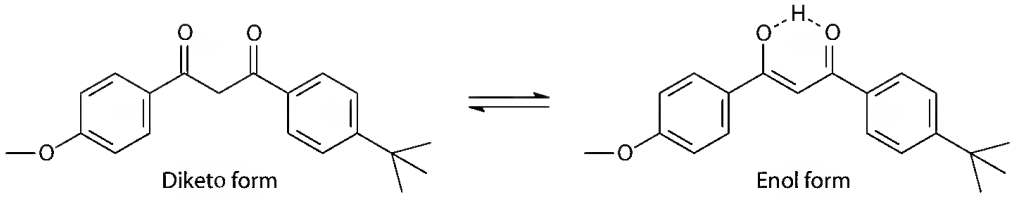

FIGURE 40.26 Chemical structure of butyl methoxy dibenzoylmethane, showing the diketo and enol forms.

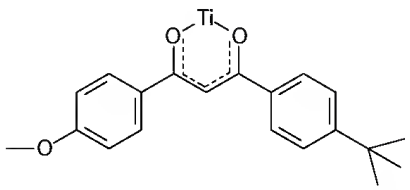

FIGURE 40.27 Butyl methoxy dibenzoylmethane–titanium dioxide complex.

Egerton et al. [81] evaluated the interaction between the organic UV absorber, butyl methoxy dibenzoylmethane (Figure 40.26), and nanoparticles of coated titanium dioxide.

The yellowing caused by the addition of butyl methoxy dibenzoylmethane to titanium dioxide was reduced by silica coatings deposited on the titanium dioxide, with the more uniform the coating the greater the reduction in the coloring. Infrared (IR) studies showed the enol form to predominate in solution and that the yellowing is caused by a complex which is formed (Figure 40.27).

Since the actual particle size of these inorganic agents is critical, it is important to be able to monitor the particle size and to ensure that this size remains the same in the formulations [82]. Both titanium dioxide raw material and finished products were evaluated for particle size and particle size distribution using scanning electron microscopy. Results indicated that the titanium dioxide particles maintain their size and size distribution in the sunscreen products, suggesting that the formulation process did not affect particle size.

Although the photostability of commercially sunscreens can be determined by conventional methods using a solar simulator followed by HPLC analysis, Scalia et al. [83] are proposing a comparative evaluation of polymethylmethacrylate plates and Transpore™ tape. On application of the sunscreen to the plates and the tape, factors such as SPF and UV-A protection factor were measured by transmission spectroscopy before and after irradiation. When compared with HPLC analysis of the ethylhexyl methoxycinnamate, the photo-unstable UV-B filter, the results from the polymethylmethacrylate plates compared favorably, whereas this was not the case for the Transpore™ plates.

40.4 Drugs and Drug Products: Repackaging

40.4.1 Introduction

The stability of a pharmaceutical product may be defined as the capability of a particular formulation, in a specific container to maintain its physical, chemical microbiological, therapeutic, and toxicological specifications [84]. The stability of manufactured dosage forms is routinely confirmed by the manufacturer as per regulatory requirements [85], where stability studies on packaged dosage forms are conducted by means of real-time, long-term tests and accelerated stability tests at specific temperatures and RHs representing storage conditions experienced in the various climatic zone(s). Manufacturers' packaging does not guarantee the stability of the drug substance and the drug product on removal, manipulation, and repackaging. Recently, Baertschi et al. [9] have critically assessed the

ICH Guideline on Photostability Testing, commenting on its usefulness as a protocol for testing new drug substances and products. However, now that the Pharmaceutical Industry has had considerable experience in photostability testing, the question is posed about the photostability of drugs under in-use conditions. Although the stability of a dosage form is often seen to be the responsibility of the manufacturer, this does not include removal from the original packaging. In electing to repackage a drug product, healthcare professionals must consider the implications on drug stability of the transfer to a nonmanufacturer pack.

Because of their known light instability, frusemide and prochlorperazine tablets have been investigated [47].

40.4.2 Frusemide

Frusemide (Figure 40.28) used in the treatment of cardiac events and hypertension is commonly repacked into DAAs. Because of the susceptibility of frusemide to photodegradation, Bowen et al. [86] evaluated both the chemical and physical stability of frusemide tablets repackaged into a DAA.

Frusemide tablets were repackaged into DAAs and evaluated for physicochemical stability over an 8 week period at a controlled room temperature (25°C ± 2°C) and other relevant in-use conditions. In addition, photostability studies were performed according to the ICH guidelines.

Chemical stability was confirmed for all storage conditions, including for those light ICH conditions. However, storage in a simulated pharmacy environment and exposure to ICH light conditions resulted in a yellow coloration of the tablets, with this discoloration being unacceptable.

40.4.3 Prochlorperazine

Prochlorperazine tablets [87] were stored repackaged in DAAs and in their original packaging for 8 weeks at ambient (25°C ± 1°C; 60% ± 1.5% RH), accelerated (40°C ± 1°C; 75% ± 1.5% RH), and *in-use* conditions encountered *in situ* both in a pharmacy and the patients' home. These tablets in the DAA were assessed for chemical stability, and photostability testing was undertaken under ICH conditions. Although their chemical and physical stability was confirmed, there were, however, noticeable organoleptic changes occurring in the tablets stored under *in-use* conditions with a progressive gray discoloration over the 8 week period. Because of the discoloration of the prochlorperazine (Figure 40.29) tablets, this needs to be taken into account in their repackaging and storage into DAAs.

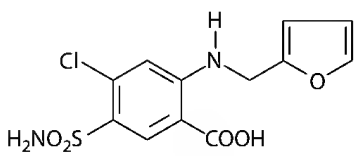

Frusemide

FIGURE 40.28 Chemical structure of frusemide.

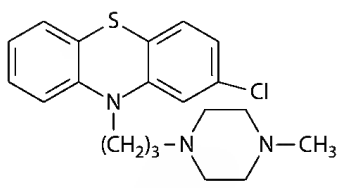

Prochlorperazine

FIGURE 40.29 Chemical structure of prochlorperazine.

40.5 Conclusions

The photostability of drug substances continues to be an important consideration, not only because of the drug content of dosage forms but also because the photodegradation of these substances may result in the formation of photoproducts, which cause adverse effects in patients. Although photostability testing focuses on the overall photoinstability, packaging, labeling, and storage of photolabile drugs, the challenge is to address the cause of the photoinstability in drug products and the role of excipients in this process. Photosafety especially related to the effect of toxic photoproducts on patients, including those that may arise from commercially available sunscreens also needs to be addressed. Recently, the issue associated with the in-use photostability of drugs and drug products has been reported on by Baertschi et al. [9] as an important challenge for the future.

The photodegradation of a number of drug substances has been described: nitrofurazone, metoclopramide, pitavastatin, seratrodast, primaquine, flurbiprofen, amlodipine, memoquin, montelukast, guaiazulene, and aloe vera, illustrating a diversity of photoreactions occurring on exposure to light. The effect of drug structure on photostability has been highlighted with the photodegradation of amlodipine occurring similarly to nicardipine because of the presence of an amino group in the side chain of both of these drugs.

The photostability of drugs in drug products has been complicated by not only the polymorphic forms of drug substances, but also the inclusion of excipients. Cyclodextrins, for example, have the ability to increase or decrease the rate of photodegradation in the addition to altering the photodegradation pathway. The appearance of photoproducts not isolated in the absence of the cyclodextrin provides a challenge to the pharmaceutical scientist in terms of analytical method development and validation and photostability studies. Drug formulations and delivery systems also play a role in improving the delivery of drug substances and their photostability. The inclusion of UV filters and the delivery of drug substances in nanoparticles, nanocapsules, solid lipid nanoparticles, liposomes, and lipid particles have to a large extent improved the photostability of drug substances, such as curcuminoids, tretinoin, and isotretinoin, pantoprazole, and selected fluoroquinolone antibiotics.

Sunscreens are required to provide protection against both UV-B and UV-A radiation and in addition often include antioxidants and physical blockers, such as titanium dioxide. Because of the complexity of these broad spectrum products and the known photocatalytic activity of titanium dioxide, it is important that photostability tests be conducted to ensure that these products are both safe and effective. Some recent formulations have involved the inclusion of nanoparticles of coated titanium dioxide in order to reduce the potential for interaction with the UV absorber, butyl methoxy dibenzoylmethane. Understanding the potential interaction has provided the information required to reduce its occurrence, highlighting the need for further research into sunscreen products.

Baertschi et al. [9] have reported on the need to revisit the ICH Photostability Guidelines with the view to including in-use testing. This has been confirmed by the research group of Glass and Haywood [86,87] in their investigations on the photostability of repackaged drugs. Since repackaging of drugs is on the increase worldwide, this suggests the need for further studies in the future into the in-use photostability of drugs and drug products.

References

1. Tonnesen, HH, Ed. *The Photostability of Drugs and Drug Formulations*; Taylor & Francis, London, U.K., 1996.
2. Albini, A; Fasani, E, Eds. *Drugs: Photochemistry and Photostability*; Royal Society of Chemistry, Cambridge, U.K., 1998.
3. Byrn, SR; Pfeiffer, RR; Stowell, JG, Eds. *Solid-State Chemistry of Drugs*; 2nd edn.; SSCI, Inc., West Lafayette, IN, 1999.
4. Carstensen, JT, Ed. *Drug Stability*; 3rd edn.; Marcel Dekker Inc., New York, 2000.

5. Glass, BD; Novak, C; Brown, ME. The thermal and photostability of solid pharmaceuticals—A review. *J. Therm. Anal. Cal.*, 2004, 77, 1013–1036.
6. Henry, B; Foti, C; Alsante, K. Can light and photostability data be used to access the photosafety risks in patients for a new drug molecule? *J. Photochem. Photobiol. B: Biol.*, 2009, 96, 57–62.
7. International Conference on Harmonization, Guidelines for photostability testing of new drug substances and products. *Federal Register*, 1997, 62, 27115–27122.
8. Onoue, S; Tsuda, Y. Analytical studies on the prediction of photosensitive/phototoxic potential of pharmaceutical substances. *Pharm. Res.*, 2006, 23, 156–164.
9. Baertschi, SW; Alsante, KM; Tonnesen, HH. A critical assessment of ICH guideline on photostability testing of new drug substances and products (Q1B): Recommendations for revision. *J. Pharm. Sci.*, 2010, 99, 2934–2940.
10. Shahjahan, M; Enever, RP. Photostability of nitrofurazone in aqueous solution I. Quantum yield studies. *Int. J. Pharm.*, 1996, 143, 75–82.
11. Shahjahan, M; Enever, RP. Photostability of nitrofurazone in aqueous solution II. Kinetic studies. *Int. J. Pharm.*, 1996, 143, 83–92.
12. De Luca, M; Mas, S; Ioele, G; Oliverio, F; Ragno, G; Tauler, R. Kinetic studies of nitrofurazone photodegradation by multivariate curve resolution applied to UV-spectral Data. *Int. J. Pharm.*, 2010, 386, 99–107.
13. Maquille, A; Habib Jiwan, J-L. LC-MS characterization of metoclopramide photolysis products. *J. Photochem. Photobiol. A: Chem.*, 2009, 205, 197–202.
14. Cuquerella, MC; Bosca, F; Miranda, MA. Photonucleophilic aromatic substitution of 6-fluoroquinolone in basic media: Triplet quenching by hydroxide anion. *J. Org. Chem.*, 2004, 69, 7256–7261.
15. Li, YN; Moore, DE; Tattam, BN. Photodegradation of amiloride in aqueous solution. *Int. J. Pharm.*, 1999, 183, 109–116.
16. Cermola, F; Dellagreca, M; Lesce, MR; Montanaro, S; Previtera, L; Temussi, F. Photochemical behaviour of the drug atorvastatin in water. *Tetrahedron*, 2006, 62, 7390–7395.
17. Cermola, F; Dellagreca, M; Lesce, MR; Montanaro, S; Previtera, L; Temussi, F; Brigante, J. Irradiation of fluvastatin in water: Structure elucidation of photoproducts. *J. Photochem. Photobiol. A: Chem.*, 2007, 189, 264–271.
18. Astarite, A; Cermola, F; Dellagreca, M; Lesce, MR; Montanaro, S; Previtera, L; Temussi, F. Polycyclic compounds by sunlight exposure of the drug rosuvastatin in water. *J. Photochem. Photobiol. A: Chem.*, 2007, 187, 263–268.
19. Grobelny, P; Viola, G; Vedaldi, D; DallAcqua, F; Gliszczynska-Swiglo, A; Mielcarek, J. Photostability of pitavastatin—A novel HMG-CoA reductase inhibitor. *J. Pharm. Biomed. Anal.*, 2009, 50, 597–601.
20. Ohta, R; Amano, K; Yamashita, M; Motohashi, M. High performance liquid chromatographic determination of seratrodast and its metabolites in human serum and urine. *J. Chromatogr. B*, 1997, 704, 325–331.
21. Xu, J; Zhang, Y; Hu, Y. Isolation and structure elucidation of major photodegradation products from seratrodast. *J. Pharm. Biomed. Anal.*, 2008, 48, 78–84.
22. Kristensen, S; Grislingaas, A-L; Greenhill, T; Skjetne, J; Karlsen, J; Tonnesen, HH. Photochemical stability of biologically active compounds: V. Photochemical degradation of primaquine in an aqueous medium. *Int. J. Pharm.*, 1993, 100, 15–23.
23. Kristensen, S; Grinberg, L; Tonnesen, HH. Photoreactivity of biologically active compounds. XI. Primaquine and metabolites as radical inducers. *Eur. J. Pharm. Sci.*, 1997, 5, 139–146.
24. Kristensen, S; Nord, K; Orsteen, A-L; Tonnesen, HH. Photoreactivity of biologically active compounds. XIV. Influence of oxygen on light induced reactions of primaquine. *Pharmazie*, 1998, 53, 98–103.
25. Kristensen, S. Photoreactivity of biologically active compounds. XVII. Influence of solvent interactions on spectroscopic properties and photostability of primaquine. *Pharmazie*, 2005, 60, 426–433.

26. Kristensen, S; Edge, R; Tonnesen, HH; Bisby, RH; Navaratnam, S. Photoreactivity of biologically active compounds. XIX. Excited states and free radicals from the antimalarial drug primaquine. *J. Photochem. Photobiol. B: Biol.*, 2009, 94, 147–157.
27. Musa, KAK; Eriksson, LA. Photochemical and photophysical properties and photodegradation mechanism of the non-steroidal anti-inflammatory drug, Flurbiprofen. *J. Photochem. Photobiol. A: Chem.*, 2009, 202, 48–56.
28. Fasani, E; Dondi, D; Ricci, A; Albini, A. Photochemistry of 4-(2-dinitrophenyl)-1,4-dihydropyridines. Evidence for electron transfer and formation of an intermediate. *Photochem. Photobiol.* 2006, 82, 225–230.
29. Fasani, E; Albini, A; Gemme, S. Mechanisms of photochemical degradation of amlodipine. *Int. J. Pharm.*, 2008, 352, 197–201.
30. Fasani, E; Fagnoni, M; Dondi, D; Albini, A. Intramolecular electron transfer in the photochemistry of some nitrophenyldihydropyridines. *J. Org. Chem.*, 2006, 71, 2037–2045.
31. Mancini, F; Bolognesi, ML; Melchiorre, C; Andrisano, V. Investigation of the photostability properties of memoquin, a quinone derivative for the treatment of Alzheimer's disease. *J. Pharm. Biomed. Anal.*, 2009, 50, 164–170.
32. Al Omari, MM; Zoubi, RM; Hasan, EI; Khader, TZ; Badwan, AA. Effect of light and heat on the stability of montelukast in solution and the solid state. *J. Pharm. Biomed. Anal.*, 2007, 45, 465–471.
33. Fiori, J; Gotti, R; Valgimigli, L; Cavrini, V. Guaiazulene in healthcare products: Determination by GC-MS and HPLC-DAD and photostability test. *J. Pharm. Biomed. Anal.*, 2008, 47, 710–715.
34. Selco, JI; Brooks, T; Chang, M; Trieu, MT; McDonald, JK; McManus, SP. Solution photochemistry of azulene. *J. Org. Chem.*, 1994, 59, 429–433.
35. Wang, L; Yan, J; Fu, PP; Parekh, KA; Yu, H. Photomutagenicity of the cosmetic ingredient chemicals azulene and guaiazulene. *Mutat. Res.*, 2003, 530, 19–26.
36. Xia, Q; Yin, JJ; Fu, PP; Boudreau, MD. Photo-irradiation of aloe vera by UVA—Formation of free radicals, singlet oxygen, superoxide and induction of lipid peroxidation. *Toxicol. Lett.*, 2007, 168, 165–175.
37. Akimoto, K; Inoue, K; Sugimoto, I. Photostability of several crystal forms of cianidanol. *Chem. Pharm. Bull.*, 1985, 33, 4050–4053.
38. Nord, K; Andersen, H; Tonnesen, HH. Photoreactivity of biologically active compounds. XII. Photostability of polymorphic modifications of chloroquine diphosphate. *Drug. Stab.*, 1997, 1, 243–248.
39. Teraoka, R; Otsuka, M; Matsuda, Y. Evaluation of the photostability of nicardipine hydrochloride polymorphs by using Fourier-transformed reflection-absorption infrared spectroscopy—Effect of grinding on the photostability of crystal form. *Int. J. Pharm.*, 2004, 286, 1–8.
40. Matsuda, Y; Akazawa, R; Teraoka, R; Otsuka, M. Pharmaceutical evaluations of carbamazepine modifications: Comparative study for photostability of carbamazepine polymorphs by using Fourier-transformed reflection absorption infrared spectroscopy and colorimetric measurement. *J. Pharm. Pharmacol.*, 1994, 46, 162–167.
41. De Villiers, MM; van der Watt, JG; Lotter, AP. Kinetic study of the solid state photolytic degradation of two polymorphic forms of frusemide. *Int. J. Pharm.*, 1992, 88, 275–283.
42. Matsuda, Y; Tatsumi, E. Physiochemical characterization of frusemide modifications. *Int. J. Pharm.*, 1990, 60, 11–26.
43. Kojima, T; Onoue, S; Fumie, K; Teraoka, R; Matsuda, Y; Kitagawa, S; Mitsutomo, T. Effect of the spectroscopic properties on the photostability of tamoxifen citrate polymorphs. *Int. J. Pharm.*, 2007, 336, 346–351.
44. Cal, K; Centkowska, K. Use of cyclodextrins in topical formulations: Practical aspects. *Eur. J. Pharm. Biopharm.*, 2008, 68, 467–478.
45. Tonnesen, HH; Masson, M; Loftsson, T. Studies of curcumin and curcuminoids. XXVII. Cyclodextrin complexation: Solubility, chemical and photochemical stability. *Int. J. Pharm.*, 2002, 244, 127–135.

46. Tomren, A; Masson, M; Loftsson, T; Tonnesen, HH. Studies of curcumin and curcuminoids. XXXI. Symmetric and asymmetric curcuminoids: Stability, activity and complexation with cyclodextrin. *Int. J. Pharm.*, 2007, 338, 27–34.
47. Pomponio, R; Gotti, R; Fiori, J; Cavrini, V; Mura, P; Cirri, M; Maestrelli, F. Photostability studies on nicardipine-cyclodextrin complexes by capillary electrophoresis. *J. Pharm. Biomed. Anal.*, 2004, 35, 267–275.
48. Godwin, DA; Wiley, CJ; Felton, LA. Using cyclodextrin complexation to enhance secondary photoprotection of topically applied ibuprofen. *Eur. J. Pharm. Biopharm.*, 2006, 62, 85–93.
49. Yap, KL; Liu, X; Thenmozhiyal, JC; Ho, PC. Characterization of 13-cis-retenoic acid/cyclodextrin inclusion complexes by phase solubility, photostability, physicochemical and computational analysis. *Eur. J. Pharm. Sci.*, 2005, 25, 49–56.
50. Lebete, M; Brown, ME; Glass, BD. The influence of methylated-beta-cyclodextrin on the photostability of midazolam in aqueous solution. MSc Thesis. Rhodes University, Grahamstown, South Africa, 2001.
51. Schiller, M; Muller, FW; Damm, C. Photo-physics of surface-treated titanium dioxides. *J. Photochem. Photobiol. A: Chem.*, 2002, 149, 227–236.
52. Theogaraj, E; Riley, S; Hughes, L; Maier, M; Kirkland, D. An investigation of the photo-clastogenic potential of ultrafine dioxide particles. *Mutat. Res.*, 2007, 634, 205–219.
53. Kakinoki, K; Yamane, K; Teraoka, R; Otsuda, M; Matsuda, Y. Effects of the relative humidity on the photocatalytic activity of titanium dioxide and the photostability of famotidine. *J. Pharm. Sci.*, 2004, 93, 582–589.
54. Kakinoki, K; Yamane, K; Yamamoto, M; Teraoka, R; Sugimoto, I; Matsuda, Y. Effect of titanium dioxide on photostability of solid-state mequitazine. *Chem. Pharm. Bull.*, 2005, 53, 1092–1096.
55. Kakinoki, K; Yamane, K; Igarashi, M; Yamamoto, M; Teraoka, R; Matsuda, Y. Evaluation of titanium dioxide as a pharmaceutical excipient for preformulation of a photo-labile drug: Effect of physicochemical properties on the photostability of solid-state nisoldipine. *Chem. Pharm. Bull.*, 2005, 53, 811–815.
56. Gaspar, LR; Maia Campos, PMBG. Photostability and efficacy studies of topical formulations containing UV filters combination and vitamins A, C and E. *Int. J Pharm.*, 2007, 343, 181–189.
57. Caffieri, S; Dall'Acqua, S; Castagliuolo, I; Brun, P; Miolo, G. UVB photolysis of hydrocortisone 21-acetate. *J. Pharm. Biomed. Anal.*, 2008, 47, 771–777.
58. Mulik, R; Mahadik, K; Paradkar, A. Development of curcuminoids loaded poly(butyl) cyanocrylate, nanoparticles: Physicochemical characterization and stability study. *Eur. J. Pharm. Sci.*, 2009, 37, 395–404.
59. Anand, P; Kunnumakkara, AB; Newman, RA; Aggarwal, BA. Bioavailability of curcumin: Problems and promises. *Mol. Pharm.*, 2007, 4, 807–818.
60. Ansari, MJ; Ahnmad, S; Kohli, K; Ali, J; Khar, RK. Stability-indicating HPTLC determination of curcumin in bulk drug and pharmaceutical formulations. *J. Pharm. Biomed. Anal.*, 2005, 39, 132–138.
61. Tiyaboonchaia, W; Tungpradita, W; Plianbangchang, P. Formulation and characterization of curcuminoid loaded solid nanoparticles. *Int. J Pharm.*, 2007, 337, 299–306.
62. Zhang, JF; Hou, SX; Liu, HL. Comparison of preparing two polylactide nanoparticles loaded lipophilic anti-cancer herb drug by nanoprecipitation method. *China J. Clin. Mater. Med.*, 2007, 32, 303–306.
63. Bassam, TM; Jacobsen, EL; Jacobsen, MK. UVA is the major contributor to the photodegradation of tretinoin and isotretinoin: Implications for development of improved pharmaceutical formulations. *Int. J. Pharm.*, 2008, 352, 123–128.
64. Brisaert, M; Plaizier-Vercammen, J. Investigation of the photostability of tretinoin in creams. *Int. J. Pharm.*, 2007, 334, 56–61.
65. Brisaert, M; Gabriels, M; Matthijs, V; Plazier-Vercammen, J. Liposomes with tretinoin: A physical and chemical evaluation. *J. Pharm. Biomed. Anal.*, 2001, 26, 909–917.

66. Ioele, G; Cione, E; Risoli, A; Genchi, G; Ragno, G. Accelerated photostability study of tretinoin and isotretinoin in liposome formulation. *Int. J. Pharm.*, 2005, 293, 251–260.
67. Manconi, M; Valenti, D; Sinico, C; Lai, F; Loy, G; Fadda, AM. Niosomes as carriers of tretinoin. II. Influence of vesicular incorporation on tretinoin photostability. *Int. J. Pharm.*, 2003, 260, 261–272.
68. Kumar, SA; Abhijt, DA; Medha, JD; Vandana, PB. Solid lipid nanoparticles (SLN) of tretinoin: Potential for topical delivery. *Int. J. Pharm.*, 2007, 345, 163–171.
69. Nighland, M; Yusuf, M; Wisniewski, S; Huddleston, K; Nyirady, J. The effect of simulated solar UV radiation on tretinoin in tretinoin gel microsphere (0.1%) and tretinoin gel (0.025%). *Cutis*, 2006, 77, 313–316.
70. Ourique, AF; Pohlmann, AR; Guterres, SS; Beck, RCR. Tretinoin-loaded nanocapsules: Preparation, physicochemical characterization and photostability. *Int. J. Pharm.*, 2008, 352, 1–4.
71. Raffin, RP; Colome, LM; Schapoval, EES; Pohlmann, AR; Guterres, SS. Increasing sodium pantoprazole photostability by microencapsulation: Effect of the polymer and the preparation technique. *Eur. J. Pharm. Biopharm.*, 2008, 69, 1014–1018.
72. Scalia, S; Mezzena, M. Incorporation of quercetin in lipid microparticles: Effect on photo- and chemical stability. *J. Pharm. Biomed. Anal.*, 2009, 49, 90–94.
73. Budai, M; Grof, P; Zimmer, A; Papai, K; Klebovich, I; Ludanyi, K. UV light induced photodegradation of liposome encapsulated fluoroquinolones: An MS study. *J. Photochem. Photobiol. A: Chem.*, 2008, 198, 268–273.
74. Gonzalez, S; Fernandez-Lorente, M; Gilaberte-Calzada, Y. The latest on skin photoprotection. *Clin. Dermatol. Dermatol.*, 2008, 26, 614–626.
75. Forestier, S. Rationale for sunscreen development. *J. Am. Acad. Dermatol.*, 2008, 58, S133–S138.
76. Venditti, E; Spadoni, T; Tiano, L; Astolfi, P; Greci, L; Littarru, GP; Damiani, E. In vitro photostability and photoprotection studies of a novel multi-active UV-absorber. *Free Radical Bio. Med.*, 2008, 45, 345–354.
77. Lautenschlager, S; Wulf, HC; Pittelkow, MD. Photoprotection. *Lancet*, 2007, 370, 526–537.
78. Wang, SQ; Stanfield, SW; Osterwalder, U. In-vitro assessments of UV-A protection by popular sunscreens available in the United States. *J. Am. Acad. Dermatol.*, 2008, 59, 934–942.
79. Newman, MD; Stotland, M; Jeffrey, EI. The safety of nanosized particles in titanium dioxide—and zinc oxide—based sunscreens. *J. Am. Acad. Dermatol.*, 2009, 61, 685–692.
80. Buchalska, M; Kras, G; Oszajca, M; Lasocha, W; Macyk, W. Singlet oxygen generation in the presence of titanium dioxide materials used as sunscreens in suntan lotions. *J. Photochem. Photobiol. A: Chem.*, 2010, 213, 158–163.
81. Egerton, TA; Everall, NJ; Mattinson, JA; Kessell, LM; Tooley, IR. Interaction of TiO_2 nanoparticles with organic UV absorbers. *J. Photochem. Photobiol. A: Chem.*, 2008, 193, 10–17.
82. Wokovich, A; Tyner, K; Doub, W; Sadrieh, N; Buhse, L. Particle size determination of sunscreens formulated with various forms of titanium dioxide. *Drug. Dev. Ind. Pharm.*, 2009, 35, 1180–1189.
83. Scalia, S; Mezzena, M; Bianchi, A. Comparative evaluation of different substrates for the in vitro determination of sunscreen photostability: Spectrophotometric and HPLC analyses. *Int. J. Cosmet. Sci.*, 2010, 32, 55–64.
84. United States Pharmacopeia. *National Formulary (USP 31-NF 26) <1191> Stability Considerations in Dispensing Practice*. United States Pharmacopeial Convention, Rockville, MD, 2008.
85. ICH Harmonised Tripartite Guideline. Stability Testing of New Drug Substances and Products Q1A (R2): ICH Steering Committee; 2003; ICH Harmonised Tripartite Guideline. Stability Testing: Photostability testing of new drug substances and products Q1B: ICH Steering Committee; 1996. www.ich.org specifically http://www.ich.org/products/guidelines/quality/article/quality-guidelines.html (accessed on 22 September 2011).
86. Bowen, L; Mangan, M; Haywood, A; Glass, B. Stability of Frusemide tablets repackaged into dose administration aids. *J. Pharm. Prac. Res.*, 2007, 37, 178–181.
87. Glass, BD; Mangan, M; Haywood, A. Prochlorperazine tablets repackaged into dose administration aids: Can the patient be assured of quality. *J. Clin. Pharm. Ther.*, 2009, 34, 161–169.

41

Computational Photochemistry and Photobiology

Patrick Z. El-Khoury
Bowling Green State University

Igor Schapiro
Bowling Green State University

Mark Huntress
Bowling Green State University

Federico Melaccio
Bowling Green State University

and

Università degli Studi di Siena

Samer Gozem
Bowling Green State University

Luis Manuel Frutos
Universidad de Alcalá

Massimo Olivucci
Bowling Green State University

and

Università degli Studi di Siena

41.1 Introduction

When a thermally equilibrated chromophore is promoted to an excited electronic state by light absorption, nuclear motion is triggered. The evolution of the original molecular and electronic structures determines the fate of the absorbed light energy that can either be released (via internal conversion/luminescence) or exploited to drive a change in the original chromophore structure (i.e., a photochemical reaction). Throughout these processes, the initially populated Franck–Condon (FC) active modes couple to other available normal modes, this coupling rendered even more effective by the anharmonicity of molecular vibrations.[1,2] Computational chemists view such events in terms of the evolution of the chromophore's nuclear coordinates on different 3N-6 dimensional potential energy surfaces, where N is the number of atoms. These are rigorously defined on the basis of the Born–Oppenheimer (BO) approximation,[3,4] which states that the relatively large mass of a nucleus, as compared to that of an electron, permits the separation of electronic and nuclear motions. A consequence of the BO approximation is that for any molecular system, there exists a different potential energy surface for each electronic state. Since in these processes, the initial excited state electronic structure ultimately evolves into a ground state electronic structure, the computational description of light-energy wastage and exploitation at the molecular level requires the mapping of different potential energy surfaces. Most importantly, one has to attain an understanding of *how and where potential energy surfaces connect*.

To describe the connection between potential energy surfaces, one has to be able to locate the points (i.e., the molecular and electronic structures) where the decay probability from an upper (excited state) surface to a lower (e.g., ground state) surface is largest. These points are termed "photochemical funnels,"[5] and their existence is required to explain the events occurring after the deactivation of an excited state. A funnel is a critical structure where species evolving on an excited state potential energy surface will hop to a lower surface (associated either with a different excited state or with the ground state) on a time scale shorter than the typical radiative decay times (ns). Such decay either initiates the formation of a transient/photoproduct or the relaxation to the original reactant. When considering organic reaction mechanisms, funnels provide a structurally (e.g., describing the reaction stereochemistry) and electronically (e.g., describing the homolytic or heterolytic nature of bond-breaking events) well defined *connection* between different electronic states of the reacting species.

More than 40 years ago, the aforementioned concepts were introduced in seminal papers by Van der Lugt and Oosterhoff[6] and later by Grimbert.[7] In their work, a minimum located on a spectroscopically forbidden singlet potential energy surface (see Figure 41.1a) was proposed to provide the funnel mediating the photochemical conversion of butadiene into cyclobutane. The minimum was found to be associated with an avoided crossing with the ground state. Therefore, the authors' conclusions seemed to be consistent with the idea that potential energy curves of electronic states of the same symmetry (such as the 1A and 2A electronic states of a butadiene with Cs symmetry) should obey the noncrossing rule.[8] However, at the time of the Van der Lugt and Oosterhoff calculation, the only quantity that could be computed was the potential energy of the relevant electronic states. No first or second derivatives of the potential energy surface (with respect to the nuclear coordinates) could be calculated. Since these quantities are instrumental for the numerical methods used to follow downhill paths along a potential energy surface and, therefore, to locate local minima (a process known as geometry optimization), the authors had to assume that the funnel was located along a linear path connecting reactant to product and consistent with the photochemically allowed (disrotatory) electrocyclic ring closure of the diene.

An excited state decay time corresponding to the avoided crossing energy gap (ca. 30 kcal mol^{-1}) estimated by Van der Lugt and Oosterhoff is on the order of nanoseconds, comparable to typical fluorescence lifetimes.[9] However, the weak or absent fluorescence observed in many chromophores[10] and, most importantly, the discovery of ultrafast photochemical reactions[11,12] indicate that the energy gap between excited and ground states is smaller than a few kilocalories per mole. Early versions of the theory of radiationless transitions were dominated by the application of Fermi's golden rule[13–15] and seemed to

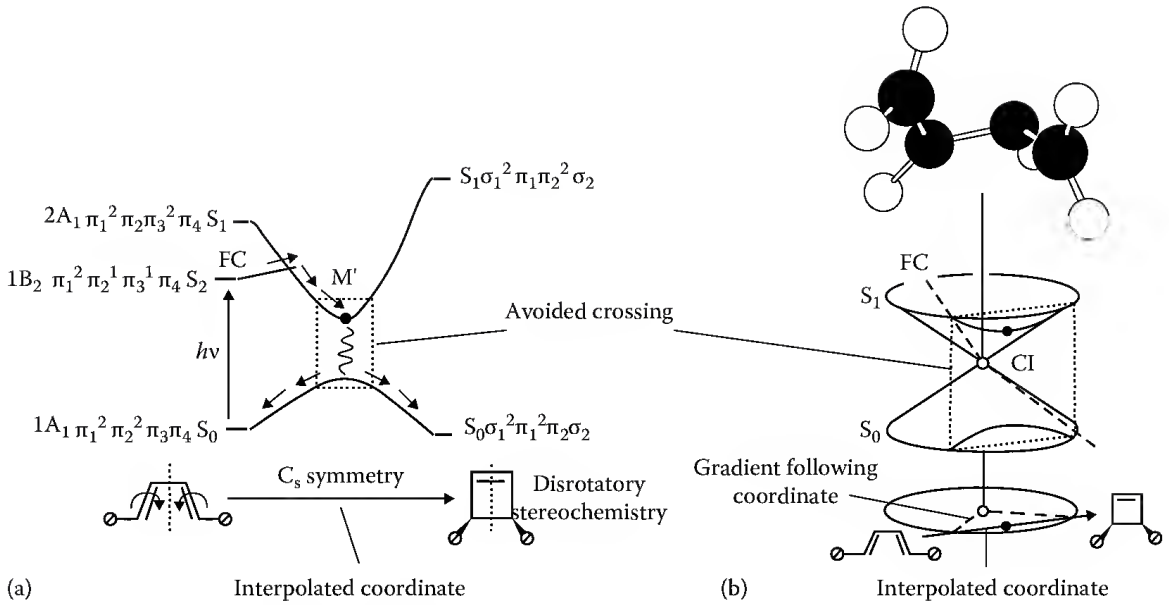

FIGURE 41.1 The Van der Lugt and Oosterhoff (i.e., avoided crossing) vs. the CI model. (a) Schematic representation of the Van der Lugt and Oosterhoff avoided crossing mechanism resulting from the calculations of Ref. [6]. (b) The Van der Lugt and Oosterhoff path appears as a 1D cross section of more complex potential energy surfaces, which has the shape of a double cone and a CI as the excited state minimum. The broken line represents the reaction path starting from the Franck-Condon point (FC) and going to the products via the CI. The computed and fully asymmetric structure of the CI [20] mediating the electrocyclic ring closure of butadiene is also shown.

provide a good description for the weak coupling cases where the time scales for internal conversion and fluorescence are comparable. However, such theoretical framework cannot explain ultrafast events.

The search for photochemical funnels that could explain the apparent selectivity of photochemical reactions led Zimmerman,[16] Michl,[17] and Salem[18] to independently suggest that the formation of photochemical products can be explained by the presence of *conical intersections* (CIs). Unlike an avoided crossing, a CI structure or point corresponds to an actual crossing of the potential energy surfaces associated with two electronic states of the same spin multiplicity. The concept had already been outlined by Teller[19] who proposed that (1) the noncrossing rule, which is valid for diatomic systems, fails in polyatomic molecules where two states, even when they have the same symmetry, are allowed to cross and (2) this crossing is conical rather than linear. Teller also suggested that radiationless decay in the vicinity of intersection spaces takes place within a single vibrational period.

Nowadays, we know that the photochemical conversion of butadiene to cyclobutene is mediated by a CI (see Figure 41.1b).[20,21] We also know that the CI is fully asymmetric and that the two intersecting states therefore belong to the same space and spin symmetry. These results have been produced after much progress in the development of *ab initio* multiconfigurational quantum chemistry methods. These methods currently allow for the computation of both potential energies and their first and second derivatives at a level of accuracy that makes them comparable with the observed spectroscopic data. Notice that this class of quantum chemical methods has been widely applied in photochemical studies. As we will explain later, this is due to the flexibility and unbiased nature of the associated wavefunctions. Techniques such as time-dependent density functional theory (TD-DFT)[22] have been used in photochemical studies[23] and successfully applied to the investigation of a number of spectroscopic problems in systems as large as porphyrins[24,25] and phthalocyanins.[26] However, the present TD-DFT functionals are accurate only for excited states dominated by single excitations, failing to correctly describe regions near CI.[27] Until these problems are solved by the development of new functionals, this method has very limited applications in the study of photochemical processes. Therefore, all the studies revisited in the present chapter will focus on the *ab initio* quantum chemical methods mentioned earlier with a special

emphasis on the complete active space self-consistent field (CASSCF) and complete active space second order perturbation theory (e.g., CASPT2) methodologies.

The relationship between the avoided crossing found by Van der Lugt and Oosterhoff and the computed butadiene/cyclobutene CI is schematically illustrated in Figure 41.1b. Constraining the reaction path to follow a linear coordinate is equivalent to slicing the potential energy surfaces along a specific one-dimensional cross section where the CI degeneracy appears to be lifted and is replaced by an avoided crossing. When this constraint is released, and the potential energy is minimized along all possible 3N-6 molecular modes, it is found that the local minimum corresponds to a real crossing (i.e., a CI). However, in the following, we will see that not all CIs mediating photochemical processes are readily accessible or correspond to local minima on the excited state potential energy surface.

While the existence of CIs was predicted by Teller,[28] Longuet-Higgins,[29] and Herzberg,[30] their importance for the control of photochemical reactivity was proposed later. In the 1970s, Salem[18,31] introduced state correlation diagrams that illustrate the occurrence of CIs at symmetric geometries along the photochemical reaction path of carbonyl compounds. Salem's work on photochemical reactions of carbonyl compounds was developed from Zimmerman's early qualitative notions.[16] Exchange of ideas between Salem, Turro, and Dauben[32] led to the development of a comprehensive classification of photochemical reactions soon after.[33] Using numerical computations and *ab initio* procedures, the geometries of a few CIs were subsequently computed for Schiff base cis–trans isomerization processes by Bonačić-Koutecký and Michl.[34] A model of biradicaloid electronic structures was also introduced to permit a qualitative prediction of the geometries at which S_1/S_0 CIs take place.[35,36] Although the presence of CIs seemed to account for ultrafast radiationless decay in at least a few polyatomic molecules, CIs were regarded as being "extremely rare" and/or "too high in energy" to be of practical value. However, as outlined earlier, advances in *ab initio* multireference quantum chemical methods and the implementation of analytical gradients of the CASSCF method allowed for a systematic mapping of the excited state potential energy surfaces of several organic chromophores. The results revealed that CIs are abundant and, similar to transition structures, their electronic and structural features explain the outcome of a variety of photochemical transformations.[5]

The ability to map excited state potential energy surfaces was influential in shaping the field of computational photochemistry.[37] Potential energy surfaces can only be computed numerically. This means that their mapping (e.g., the search for energy minima, transition structures, CIs, and the calculations of reaction paths and trajectories) relies on the independent or sequential calculation of a finite number of points of the potential energy surface and of their first derivatives (the gradient) and second derivatives (the hessian) with respect to the nuclear coordinates. Thus, the emergence of computational photochemistry cannot be solely attributed to the increase in availability of computing power. The coding of efficient and more accurate methods for computing the potential energy, the gradient, and the hessian of electronically excited states as well as the development of suitable geometry optimization methods[38] have rendered the computational investigations of excited state species practical. Nowadays, this technology is available in a variety of software packages including Gaussian,[39] Molcas,[40,41] Gamess US,[42,43] Columbus,[44] Molpro,[45] and Q-Chem,[46] among others.

41.2 Computational Photochemistry

As mentioned earlier one of the basic ideas behind the development of tools for *mapping* and *connecting* excited and ground state potential energy surfaces is that certain excited state critical structures prompt a surface hop. Since a hop involves the breaking of the BO approximation, this event is also referred to as a nonadiabatic transition. Potential energy surface crossings such as CIs (between states with the same spin multiplicity) and singlet–triplet crossings (an example of crossings between states of different spin multiplicity) represent "natural" loci for nonadiabatic transitions.

If a quantum mechanical (QM) method can be used to (a) evaluate excited state energies and (b) calculate excited state gradients with respect to nuclear coordinates, then it can be used to map the surface and locate crossing regions (the hessian is presently too expensive to be employed in systematic mapping and

is only used to get information—such as vibrational frequencies—for important points along the energy surfaces). However, such a method needs to be able to describe the change in the weights of the electronic configurations that describe the ground and excited state bonding character, as well as the bond-breaking and/or bond-forming processes. The wavefunction must thus be flexible enough to provide a balanced treatment of the different possible electronic configurations. The *ab initio* multiconfigurational self-consistent field (MCSCF) method and, more specifically, its variant the *ab initio* CASSCF method originally developed by Wahl and coworkers,[47] but implemented in a practical form by M. A. Robb[48] and B. O. Roos[49] independently, serve well in this regard. The CASSCF[50] method is one of the most commonly used multiconfigurational wavefunction methods in computational photochemistry. At the CASSCF level, static electron correlation is taken into account, allowing for the treatment of situations involving partially broken bonds and the development of diradical character. However, in order to reproduce the spectroscopic parameters (e.g., absorption and fluorescence maximum), the remaining electron correlation effects need to be treated. This can be achieved, for instance, using the CASPT2[51] method already mentioned. The CASPT2//CASSCF protocol, where one carries out the potential energy surface mapping at the CASSCF level and then corrects the energies of chemically meaningful points (e.g., energy minima and CIs) by running single-point CASPT2 calculations, has been extensively used in the past and has been shown to reproduce experimental observations within a few kilocalories per mole.[5,52]

The first application of the *ab initio* CASSCF method to a photochemical problem in organic reactivity was reported in the early 1990s.[53,54] The aim was to investigate photoinduced [2π + 2π] cycloaddition: a simple model for a variety of observed cycloaddition reactions with well-defined stereochemistry (Figure 41.2). It was demonstrated that excited state species are funneled to the product through a CI. The molecular structure of the characterized CI correlates well with the observed photoproduct

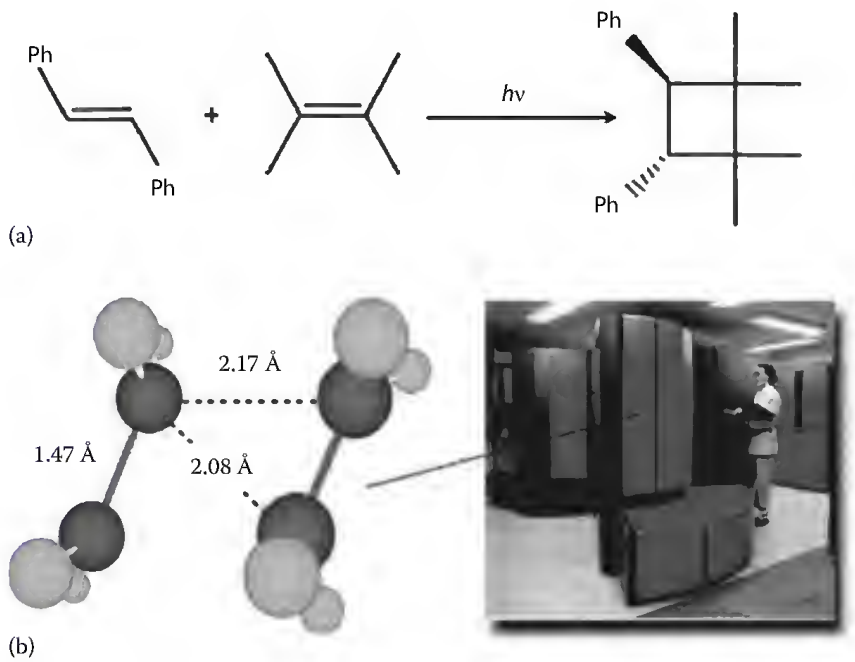

FIGURE 41.2 The first CI located for an organic [2π + 2π] photochemical cycloaddition reaction. (a) The cycloaddition reaction between *trans*-stilbene and tetramethylethylene (two substituted ethylenes). The structure of the photochemical funnel must be consistent with the observed *supra–supra* stereospecificity (demonstrated by the formation of a *trans* cyclobutane) of the reaction. (b) The computed molecular structure for the CI mediating the *supra–supra* cycloaddition of two ethylene molecules. This structure provides a connection between the $^2A_1$ and $^1A_1$ (i.e., ground state) potential energy surfaces, consistently with a hindered rotation along the two C–C bonds leading to the observed *supra–supra* stereochemistry. The University of London CRAY-XMP machine where the original calculation was carried out (Ref. [53]) is also shown.

stereochemistry and also with the fact that is possible to produce tetramethylene intermediates. At that time, the calculation (a scan of the first excited state along two different coordinates) required an unconventional computational effort that was carried out by M. A. Robb's group at King's College London, UK, using the CRAY X-MP operating at the University of London Computer Center.[55] This work provided strong support for the existence of Salem, Zimmerman, and Michl's photochemical funnels. Over the past few decades, different groups, including ours, employed the CASPT2//CASSCF approach to document the existence of low-lying CIs in different classes of organic chromophores and biological photoreceptors.[43,56,57] On the other hand, the rise of the field of femtochemistry at the experimental front[11,12] revealed that ultrafast radiationless deactivation channels are commonly encountered, and nowadays considered as a manifestation of decay through CIs.[5]

Radiationless deactivation at a CI implies that (a) ultrafast internal conversion processes may be up to 100% efficient (a Landau–Zener decay of unity),[58] (b) delayed internal conversion or slower reaction rates are indications of the presence of an excited state energy barrier that separates excited state species in the FC region from the CI region, and (c) in photochemical (as opposed to photophysical) transformations, the structure of the intersection point correlates with the structure of the photoproduct. As documented in recent photochemistry textbooks,[9,10] CIs in singlet reactions and singlet–triplet crossings in triplet reactions are as abundant as transition states (in thermal processes). Regrettably, the structural and electronic complexity of these features still hinders a prompt understanding of their fundamental role in the control of photochemical processes at the molecular level. More basic theoretical work is needed.

41.2.1 Photochemical Reaction Paths and the Branching Plane

A photochemical reaction path[59] is a minimum energy path (MEP) connecting the FC point on the potential energy surface of the light-absorbing state to one or more photoproduct minima on the ground state surface via one or more surface crossings. A basic photochemical reaction path (Figure 41.3a) involves an excited state MEP[60] connecting the FC point to two ground state MEPs through a CI, one

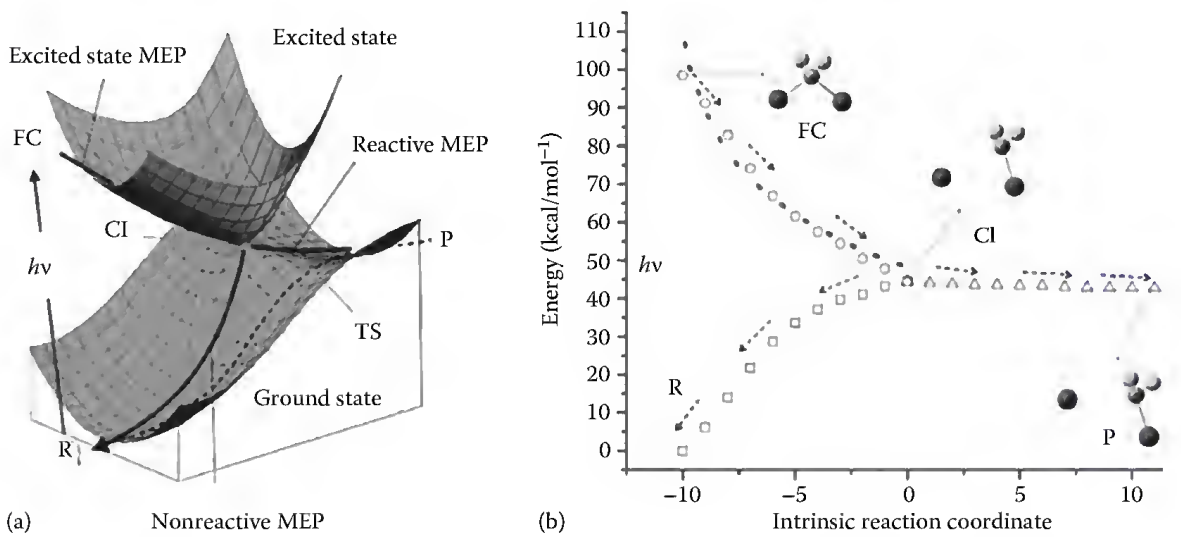

FIGURE 41.3 The photochemical reaction path. (a) Schematic representation of the photochemical reaction path (full lines) for an ultrafast photochemical reaction (i.e., with a barrierless excited state MEP). The dashed line represents a thermal path controlled by the transition state TS. (b) The computed photochemical reaction path (three different MEPs—open circles, open triangles, and open squares—computed in terms of IRCs) for the photofragmentation of CF_2I_2. The FC, the CI, the I.....CF_2I van der Waals complex (P), and the reactant (R) are connected by MEPs computed at the CAS(8,6)/3-21G** level of theory. The dotted line (showing an IRC computed at the superior CAS(12,8)/Sadlej-pvtz level) shows that the use of an approximate basis set and of a reduced active space does not affect the conclusions.

MEP describing the relaxation of the system back to the initial reactant (an aborted photochemical reaction) and another MEP describing the relaxation of the system to the photoproduct in a successful photochemical reaction. Notice that aborted photochemical reaction paths describe a form of far-from-equilibrium internal conversion, distinct from the traditional process controlled by FC factors in the weak coupling regime. A computed reaction path for the photolysis (involving the breaking of a C–I bond) of a simple halogenated compound[61] is given in Figure 41.3b.

While the regions of the excited state potential energy surface located far from intersections can be investigated using the same geometry optimization and MEP computation methods used for investigating (thermal) ground state reactions, the characterization of the CI region and of the associated relaxation path(s) require not only the location of the *photochemically relevant* CI point but also the calculation of the branching plane defined by the $\mathbf{X}_1$ and $\mathbf{X}_2$ vectors.[5,62,63] These vectors correspond to the only two molecular modes capable of splitting the energy degeneracy at the intersection (Section 2.2). They have chemical significance because they provide information on the bond-breaking/bond-forming processes mediated by the CI. $\mathbf{X}_1$ corresponds to the difference of the gradients of the upper and lower state potential energies and is called "gradient difference" or "g vector." $\mathbf{X}_2$ corresponds to the projection of the gradient of the upper state wavefunction on the lower state wavefunction and is called "derivative coupling" or "h vector."[63]

The decay from the CI can be understood by plotting the upper and lower state potential energies along the branching plane (i.e., along the plane defined by the suitably normalized $\mathbf{X}_1$ and $\mathbf{X}_2$ vectors), which yields a double cone shape (Figure 41.4). The results of the CF_2I_2 computation already seen in Figure 41.3b[61] are used to illustrate how the analysis of the branching plane can be used to locate the valleys (the exit channels A and B in Figure 41.4) collecting the reacting molecule immediately after the decay.

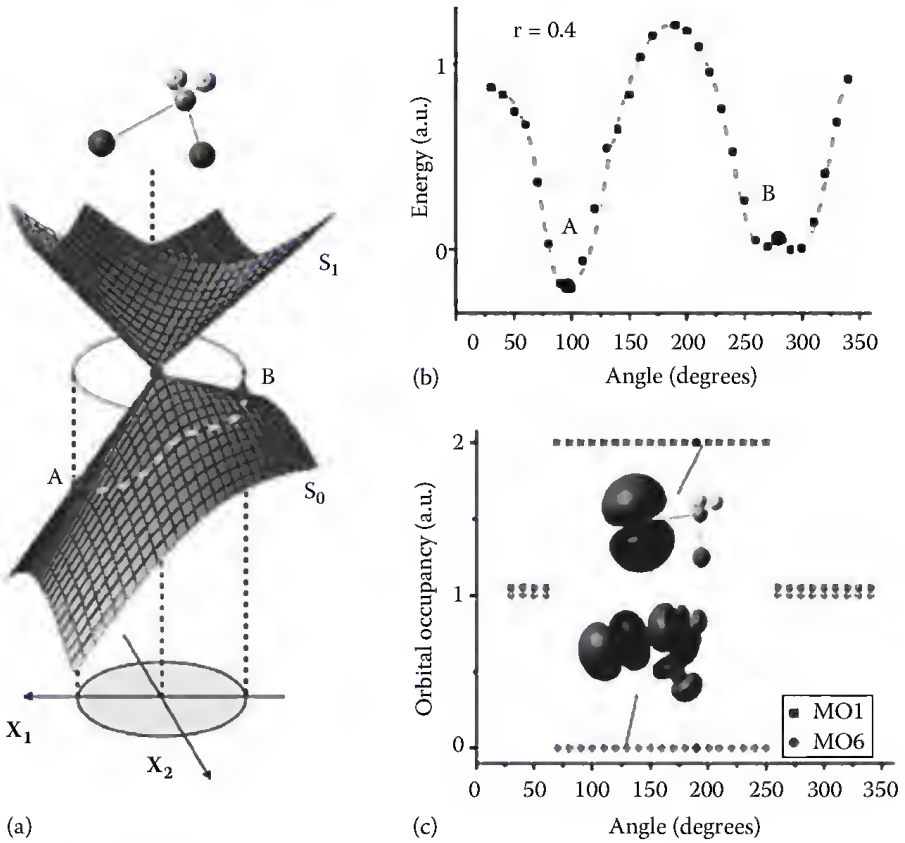

FIGURE 41.4 The branching plane. (a) Shape of an "elliptical" peaked CI. The structure on top refers to the CI driving the photofragmentation of CF_2I_2 (see also Figure 41.3b). (b) Ground state energy profile for a r = 0.4 Å loop centered at the CI. The exit channels A and B correspond to the energy minima along the profile. (c) The change in the wavefunction along the same loop described in terms of change in orbital occupancy.

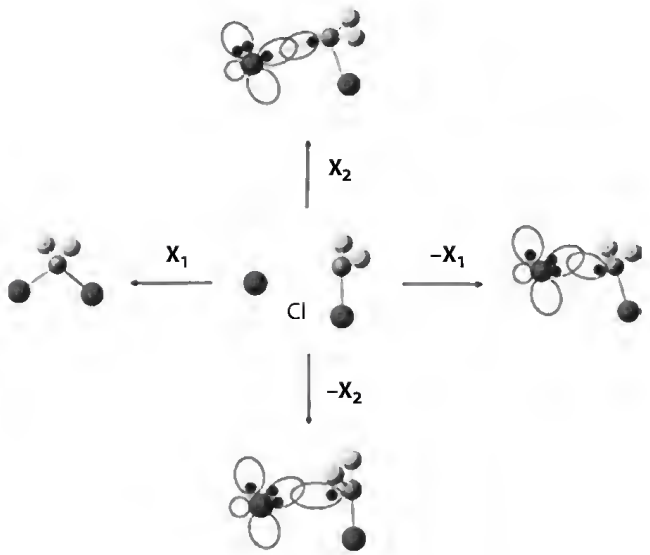

FIGURE 41.5 A branching diagram describing the chemical meaning of the derivative coupling and gradient difference vectors for the CI driving the photofragmentation of CF_2I_2. These vectors can be used to predict or rationalize the possible outcome of the photochemical reaction driven by the associated CI. This outcome can be described in term of both geometrical deformation and change in electronic structure and must be consistent with the results shown in Figure 41.4a and c.

As mentioned earlier, these valleys are ultimately computed in terms of ground state MEPs describing the ground state relaxation from a CI. A scan along a circular cross section centered at the CI and spanning the associated branching plane reveals two exit channels. The scan can be achieved, for example, using the Moplot graphical interface program[64] that reads the gradient difference and derivative coupling vectors computed with the program package Gaussian.[39] Single point calculations are then performed to determine the S_0 energy profile along the circular scan (Figure 41.4). In this particular case, two channels (channels A and B) were found at a radial distance of about 180°. At the CI, the MEP calculations yielding the reactive and nonreactive paths of Figure 41.3 are started along the direction connecting the CI to the cross-section energy minima. The actual $\mathbf{X}_1$ and $\mathbf{X}_2$ vectors for the CF_2I_2 case are pictorially shown in the branching plane diagram of Figure 41.5 in terms of both structural and electronic displacements.[61]

The changes in electronic wavefunction along the circular cross section can also be monitored. These reveal very rapid changes in electronic structure along the loop (for the theory associated with these changes and general properties of CIs, see Ref. 62). As shown in Figure 41.4, the changes are described by looking at the occupancy of the molecular orbital describing the reactive and excitation processes (an alternative approach is to plot the change in the weight of the electronic configurations along the loop). In this example, at an angle of 100° (corresponding to channel R), the electronic configuration is such that molecular orbital MO1 is doubly occupied and molecular orbital MO6 is empty. This reflects the ground state electronic configuration of the reactant R, and confirms that this channel leads to the reformation of the reactant. On the other hand, both orbitals are singly occupied at an angle of about 280° (corresponding to channel B) reflecting the electronic configuration of the excited state that is maintained along the ground state channel leading to the product. The change in occupancy along the loop of Figure 41.4 is consistent with the change in Lewis structures described in the branching diagram of Figure 41.5.

41.2.2 Minimum Energy Conical Intersections and the Intersection Space

Any CI structure is an element of a 3N-8 dimensional subspace (the intersection space) of the configuration space, which is formed by an infinite collection of CIs.[37,63] The intersection space is locally orthogonal to the branching plane. If the value of one branching plane vector (e.g., $\mathbf{X}_1$) at any CI point

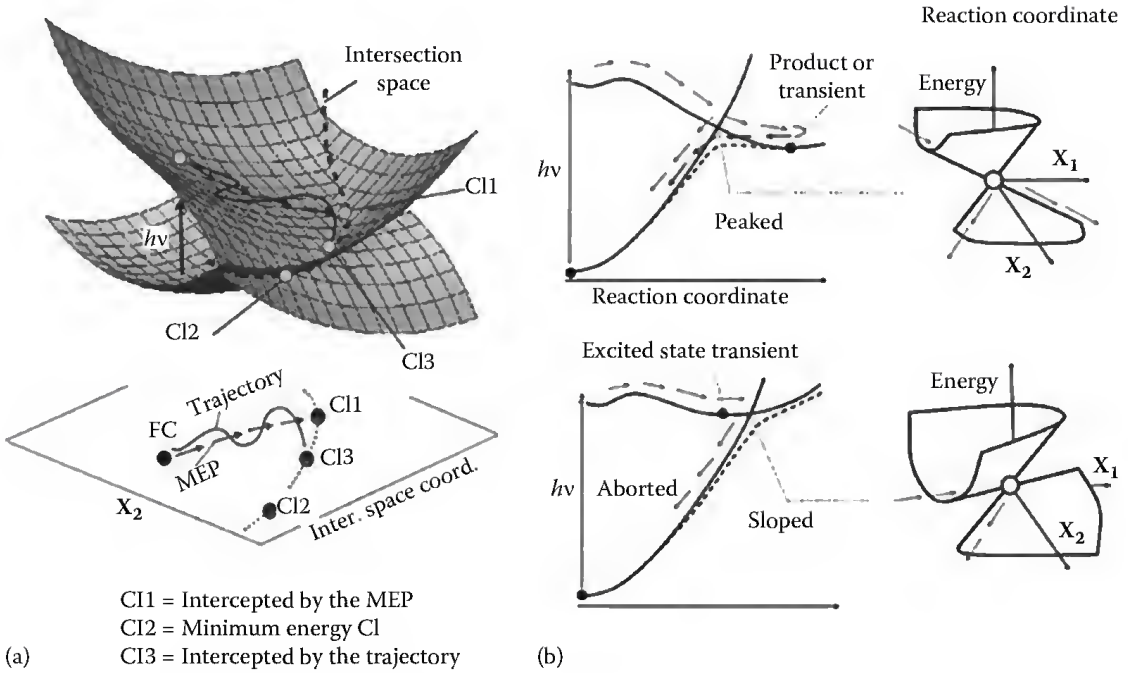

FIGURE 41.6 The intersection space. (a) A pictorial representation of the intersection space between two energy surfaces (see text). The CI1, CI2, and CI3 refer to the intersection space points located via excited state MEP calculation, CI optimization (the MECI), and with trajectory computation, respectively. (b) Shape of the photochemical reaction path and CI region for paths leading to peaked (a) and sloped (b) CIs.

is kept fixed and the energy is plotted along a plane formed by the other vector (e.g., $\mathbf{X}_2$) and by one of the remaining 3N-8 molecular modes then a plot of the upper and lower potential energy must display a seam of intersection points (Figure 41.6a). The decay to the lower potential energy surface may, in principle, occur from any point of the seam (which is a local representation of the intersection space).

The description of the photochemical funnel of a specific reaction requires the definition of the most chemically significant CI point belonging to the intersection space of the reacting system. One possibility is to assume that the excited state reactant is funneled to the ground state through the lowest energy point of the seam (the minimum energy conical intersection, MECI). Methods for locating MECI points[38,65–68] have been reported and are available in computer packages such as Gaussian,[39] Molcas,[41] and Columbus.[44] CI optimization and branching plane analysis reveal the widespread existence of qualitatively different MECIs (Figure 41.6b), which were initially predicted by Ruedenberg and coworkers on the basis of theoretical work.[62] In the case of a peaked CI, excited state species can be channeled to the ground state in two or even more directions. As a consequence, one or more photoproducts can be formed together with the original reactant. On the other hand, a sloped CI implies, almost exclusively, an internal conversion (i.e., nonchemical) event where the original reactant structure is reconstituted.

MECIs do not necessarily correspond to the point reached by a MEP starting at the FC point. This means that they may not be part of the photochemical reaction path even if they are computationally convenient. For this reason, when possible, meaningful CI points are defined as the first point of degeneracy intercepted by an excited state MEP (Figure 41.6a). This point may differ significantly from the MECI especially in those cases where the MEP is not orthogonal to the intersection space.

41.2.3 Complexity of Conical Intersections

This section focuses on a computationally well-documented case to illustrate the potential complexity of the processes mediated by a single CI. In particular, we show that CIs can describe fundamental processes such as intermolecular electron transfer, proton transfer, and H-atom transfer. We also show

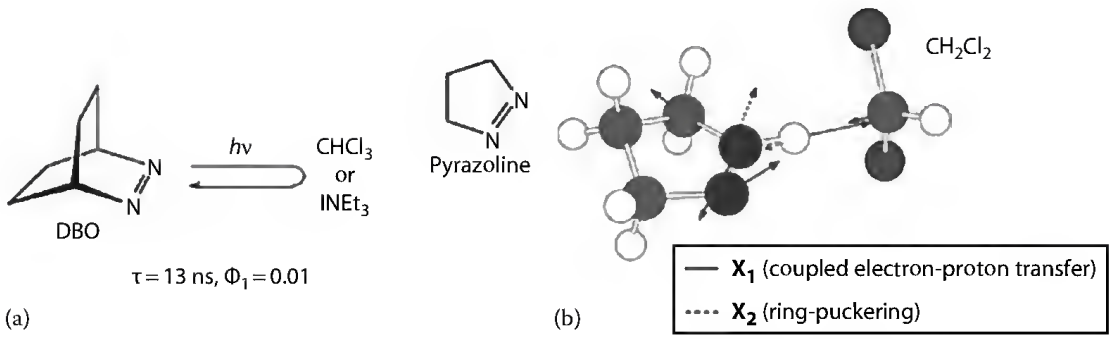

FIGURE 41.7 Fluorescence quenching in azoalkanes. (a) The measured fluorescence lifetime of DBO in contact with chloroform or triethylamine (i.e., the quenchers). (b) CI structure and branching plane vectors (full arrows and dashed arrows) of the CI responsible for the quenching of pyrazoline, a reduced model of DBO.

that the analysis of the wavefunction along a loop centered at the CI yields a level of understanding that is difficult to achieve with spectroscopic measurements.

We discuss the quenching of a "photochemically reluctant" azoalkane (reluctant because its singlet n,π* excited state is long-lived compared to those of other azoalkanes that rapidly denitrogenate). Upon photoexcitation, 2,3-diazobicyclo[2.2.2]oct-2-ene (DBO) becomes strongly fluorescent (Figure 41.7). However, the emission is rapidly quenched in the presence of electron or hydrogen donors.[69]

Structures corresponding to the fluorescent excited state minima, transition states, and MECIs for the interaction of an isolated n,π* pyrazoline molecule with methylene chloride (the hydrogen donor) and trimethylamine (the electron donor) have been optimized. This system provides a computationally effective model of DBO in the presence of chloroform[70] or trimethylamine.[71] For methylene chloride, an excited state reaction coordinate was found corresponding to a hydrogen atom transfer from a C–H bond of the chlorinated hydrocarbon to one of the nitrogens of pyrazoline. A transition structure separates the FC point from a CI, which clearly shows an almost completely transferred hydrogen. Indeed, at the CI (see Figure 41.7 for the molecular structure and associated branching plane vectors), the N–H bond is nearly formed (1.02 Å), but the N=N bond still has double bond character (1.30 Å), and the $CHCl_2$–H bond is still not completely broken (2.01 Å). The CI is peaked (Figure 41.7b) and the process can either be immediately aborted (leading to back formation of the reactant) or can proceed toward the production of a radical pair intermediate. It is found that the radical pair intermediate (assumed to be solvent caged) can revert back to the original reactant pair along a ground state path, thus completing the quenching process.

To understand the nature of this bimodal quenching (i.e., occurring via the aborted process and the radical pair intermediate), it is necessary to look at the ground state wavefunction (i.e., the electronic structure of the system) along a loop centered at the CI as done for the CF_2I_2 system in Figure 41.4. Starting from the radical pair side, one finds that after traversing a path spanning 180° along the loop, the wavefunction changes character, describing an ion pair with a protonated pyrazoline and a deprotonated methylene chloride (Figure 41.8). The behavior of the excited state wavefunction along the same loop is exactly reversed. The wavefunction is a biradical in the direction of the FC point but describes an ion pair at the primary photoproduct position. This analysis implies that at the CI, excited state systems that decay back to the ground state reactant produce initially a transient ion pair via a sudden electron transfer from the azoalkane to the CH_2Cl_2 (i.e., the CI mediates an electron transfer). During the following relaxation, the protonated azoalkane then transfers the proton back to the methylene chloride anion thus reconstituting the original reactant. (This mechanism is consistent with the established harpoon model proposed by Polanyi.[72]) In contrast, the excited state pair that evolves in the direction of the radical pair never experiences a change in its electron distribution (i.e., the wavefunction maintains its character moving adiabatically from the excited state to the ground state through the intersection). On the other hand, the radical pair returning to the original reactant through a ground state transition structure located in close proximity to the CI (dotted line in Figure 41.8) must undergo an electron transfer that generates the same transient ion pair.

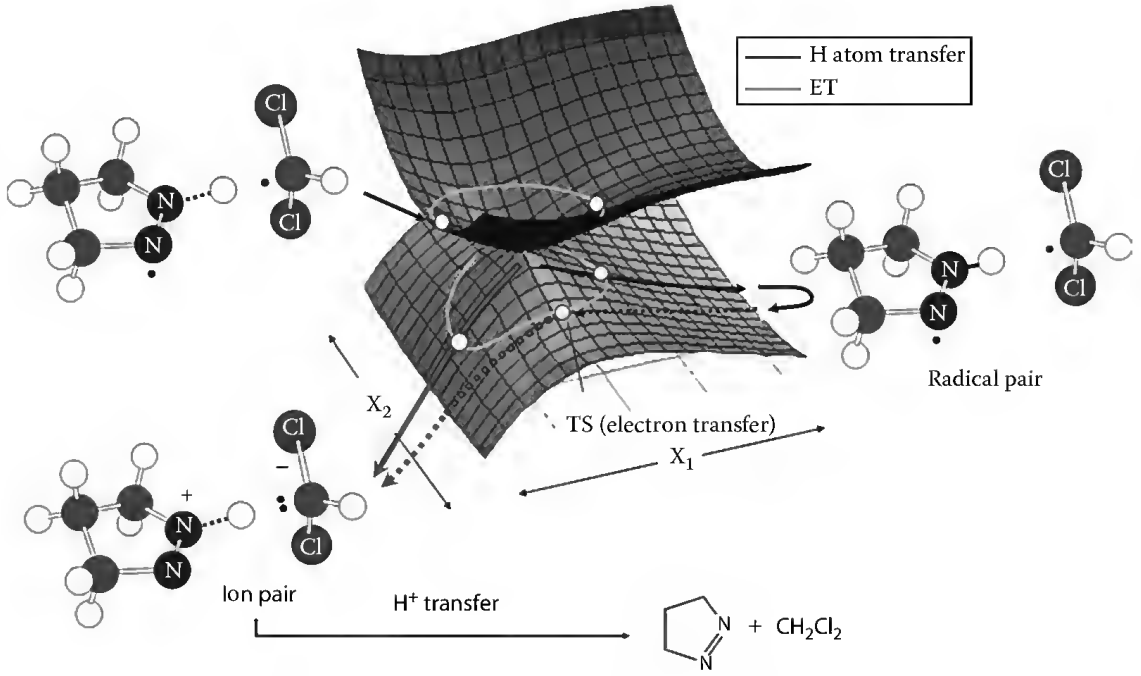

FIGURE 41.8 Relationship between hydrogen atom transfer and proton transfer during pyrazoline (a DBO model) quenching. Two different quenching mechanisms are described: direct, via decay through the intersection on the reactant side, and indirect, via formation of a transient diradical pair that then undergoes a thermal coupled electron/proton transfer.

The mechanism of trimethylamine quenching[73] is similar but simpler. It is shown that when trimethylamine moves close to n,π* pyrazoline, it forms an exciplex via partial excited state intermolecular electron transfer (i.e., the exciplex has an incipient radical cation/radical anion pair character). The exciplex is located in the vicinity of a sloped CI that corresponds to a structure where the electron transfer has been completed, and that mediates its return to the ground state via back electron transfer.

The aforementioned azoalkanes provide one example of deactivation, which took place via quenching. Among other fluorophores, temperature-dependent radiationless decay has been reported for closed-shell hydrocarbons such as benzene,[74] octatetraene,[75,76] indacene,[77] pentalene,[78] fulvene,[79] azulene,[80] annulene,[81] heterocycles (like chromene),[82] closed-shell cations (like cyanine dyes),[83] and even for biological chromophores such as cytosine[84] and the HBDI anion.[85] As for open-shell systems, the presence of CIs on the potential energy surfaces of radical cations was first detected and investigated by Bally and coworkers[86,87] using matrix isolation techniques as well as suitable quantum chemical calculations. Recently, Bearpark and colleagues have shown that ultrafast thermal deactivation of the excited states in such open-shell species as naphthalene[88] and pyrene[89] radicals happens via two consecutive sloped D_2/D_1 and D_1/D_0 CIs.

41.2.4 Photochemical Trajectories

Photochemical reaction path computations provide valuable information on the spectroscopy (excitation energies), energetics (reaction barriers and excess vibrational energy), and mechanisms of a photochemical reaction.[59] On the other hand, this information is only valid under the well-known assumption that the center of the excited state population (e.g., a laser generated vibrational wavepacket) would, on average, follow a path close to the MEP. This is considered to be a fair approximation in cases where the potential energy valleys are deep. However, photochemical reaction paths do not provide information on the time scale of ultrafast photochemical or internal conversion processes[59] that are characterized by

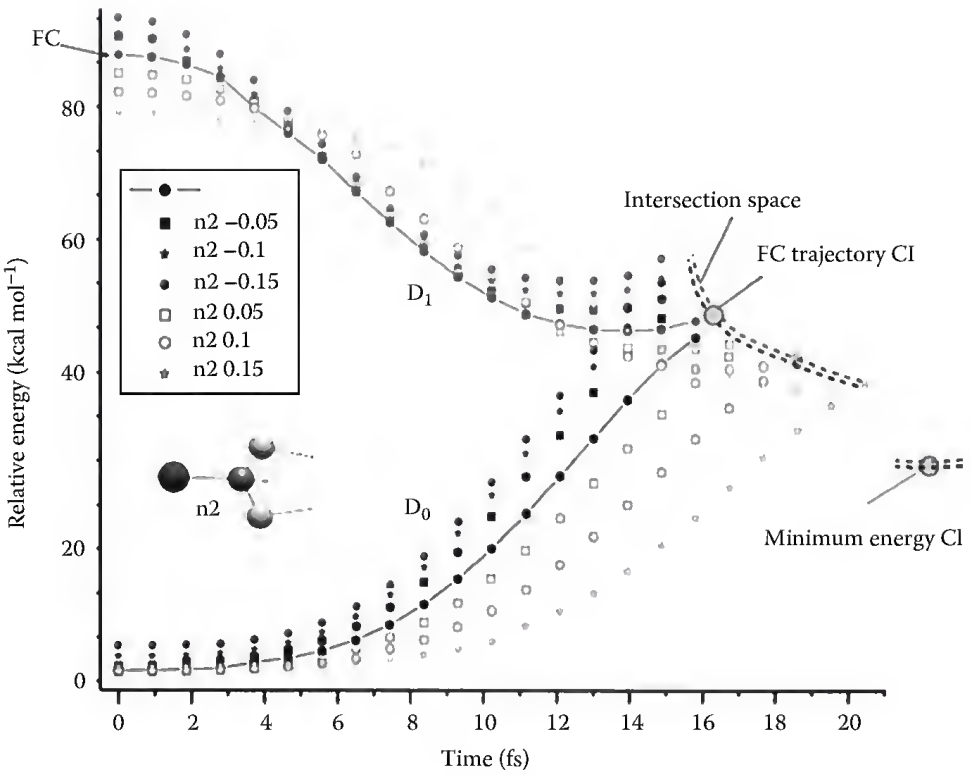

FIGURE 41.9 Energy profile along a set of seven CASPT2/ANO-RCC-VDZP trajectories released in the vicinity of the FC point of the CF_2I radical. Each trajectory corresponds to a different geometrical displacement along the n2 vibrational mode of the reactant. Since the n2 mode displacement is not orthogonal to the intersection space [it has minor components on the branching plane computed for the MECI (located ca. 28 kcal mol^{-1} above the ground state reactant)], the intersection space is visualized as a series of intersection points.

a very small excited state reaction barrier (or no barrier at all) to control the reaction kinetics. In these cases, the mechanism and dynamics of the process can be investigated by computing excited state classical or semiclassical trajectories.[90] Trajectory computations are still computationally demanding but they have been shown to provide predictions and rationalizations of observed time scales even for proteins. A single classical trajectory released from the FC point with no initial velocities (from now on called "FC trajectory") provides a better representation of the average motion of the center of the excited state population and, for this reason, is a tool superior to MEP computations. Moreover, this tool remains valid even when the upper and lower state potential energy valleys are shallow and the motion of the center of the vibrational wavepacket deviates significantly from the reaction path. In these cases, an FC trajectory represents a better way to locate the most chemically relevant CI point along the intersection space (CI3 in Figure 41.6b). An example is provided in Figure 41.9 where we show the results of several excited state trajectories computations exploring the photochemistry of the radical CF_2I.[91] The FC trajectory intercepts a CI point after 16 fs. This CI is about 20 kcal mol^{-1} higher in energy than the MECI and it displays a structure further from planarity. These classical trajectories can be used to explore and "visualize" the intersection space. For instance, a group of trajectories can be released from a set of structures that are displaced along a specific vibrational mode. In Figure 41.9, it can be seen that CF_2I trajectories released from points obtained by distorting the FC structure along the totally symmetric mode n2 intercept a segment of the intersection space higher in energy than the MECI. This result can be understood on the basis of the schematic representation of Figure 41.10. n2 is a vibrational mode with a large projection on the intersection space (since it is orthogonal to modes n1 and n3 that have significant projections on the branching plane). Therefore, a distortion along this mode is expected to "scan" the intersection space of the molecule.

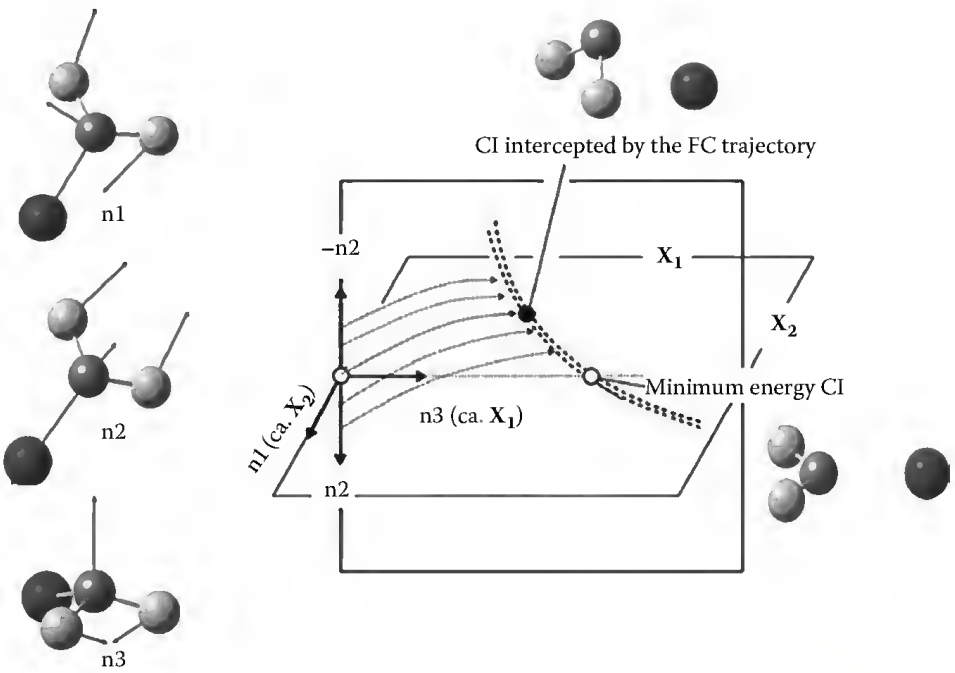

FIGURE 41.10 Three-dimensional pictorial interpretation of the calculation of Figure 41.9. The trajectories are released along the n2 mode and accelerate (roughly) along the branching plane vector $\mathbf{X}_1$ that has significant components along mode n3.

Another application of classical excited state trajectory computations focuses on the photoinduced double bond isomerization of a retinal chromophore embedded in a protein environment. The methodology required for computing the potential energy in large molecules featuring a small reactive part will be discussed in the next subsection that will deal with the simulation of biological photoreceptors. The excited state lifetimes of the visual receptor bovine Rhodopsin (Rh),[92] its reactive intermediate Bathorhodopsin (Batho-Rh),[93] and its isomer Isorhodopsin (Iso-Rh)[94] have been estimated by computing the time necessary to reach a CI starting from the FC point (Figure 41.11). This also corresponds to the time required for the excited state isomerization of the covalently attached chromophores (the 11-*cis*, all-*trans*, and 9-*cis* isomers of the protonated Schiff base of retinal, respectively) of these proteins. The ca. 100 fs observed lifetime of Rh has been reproduced while the trajectory for Iso-Rh is shown up to 450 fs with a decreasing energy gap. This is in agreement with the observed lifetime of 600 fs. Batho-Rh (Figure 41.11a, right) is predicted to have an extremely short lifetime (ca. 70 fs) consistently with the distorted nature of its all-*trans* chromophore. In Figure 41.11c, we report a comparison between the energy profiles along the FC trajectory of Rh and other excited state classical trajectories computed with different initial conditions where the initial geometry is displaced from the FC geometry in different ways. It is clear that the trajectories are all similar.

In the past, a number of groups,[95–106] including ours,[92] have reported nonadiabatic semiclassical trajectories computed using simple surface-hop methods.[107,108] This type of trajectory provides a description of the entire photoinduced molecular motion (within a certain time scale that is usually shorter than 1 ps) and simulates the hop from the upper to a lower potential energy surface that usually occurs in the vicinity of an intersection space. Not only do they simulate the decay but they also allow us to follow the evolution of the system along the lower potential energy surface toward a photoproduct or toward the original reactant. Thus, nonadiabatic trajectory calculations provide information not only on the excited state lifetime already provided by classical trajectories (see earlier) but also on the time scale for the formation of the product that may be compared with the observed photoproduct appearance time. One example of such a calculations is given in Figure 41.12 for the gas-phase 3-*cis* pentadieniminium cation (a minimal model of the retinal chromophore of Rh).[98]

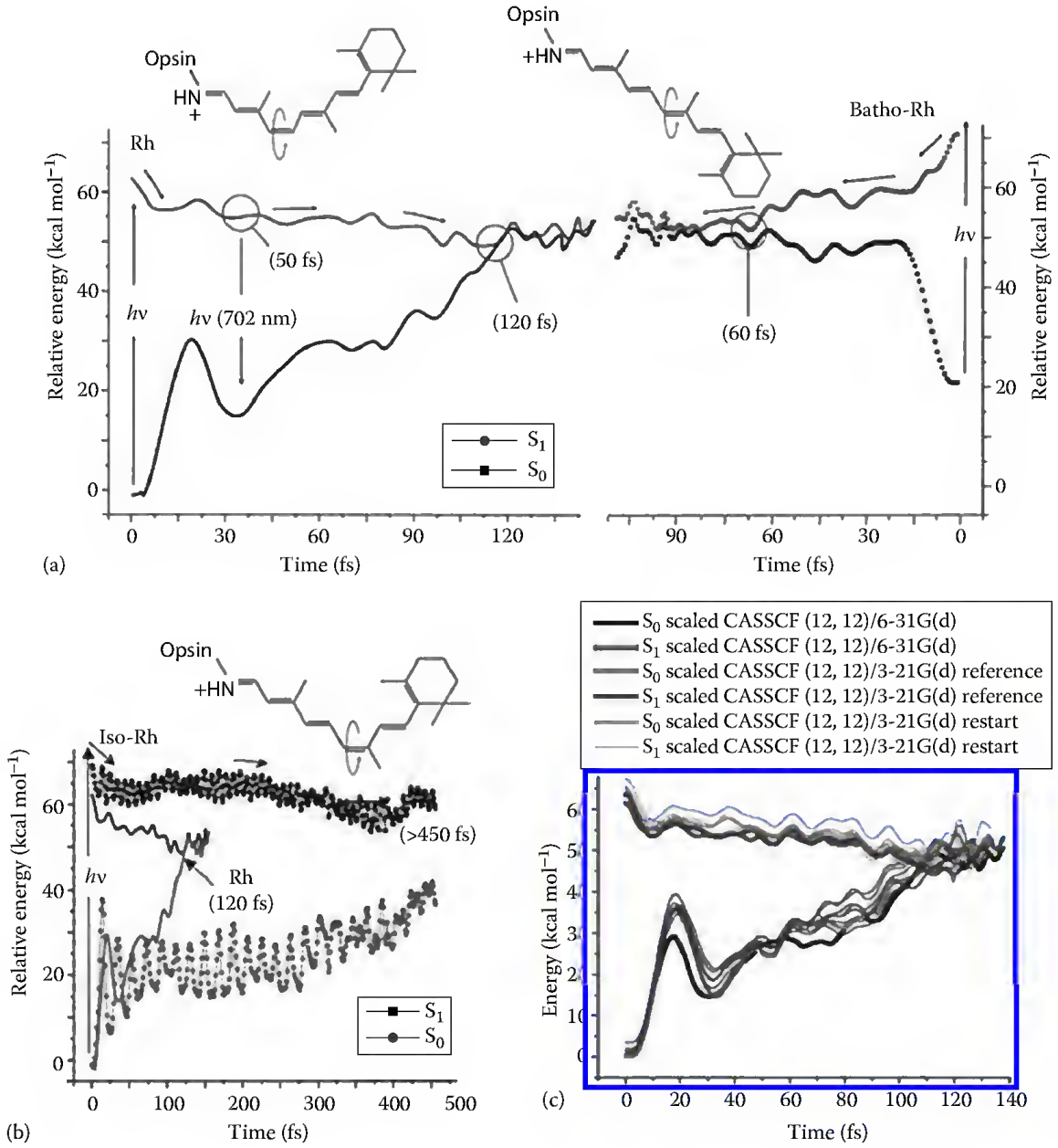

FIGURE 41.11 Rh and Batho-Rh form a photochromic system at 77 K, where the Batho-Rh intermediate (the first isolable intermediate in the Rh visual cycle) cannot undergo further conformational changes. (a) Excited state classical trajectories for the Rh→Batho-Rh (left) and Batho-Rh→Rh (right) photochemical interconversion. The trajectories are released from the corresponding FC point without initial velocities. The structures of the retinal chromophore in Rh and Batho-Rh are given. (b) Comparison of the excited state classical trajectory of Rh and Iso-Rh. The structure of the retinal chromophore in Iso-Rh is given. (c) Excited and ground state energy profiles for a set of excited state Rh trajectories computed with different initial conditions..

In the figure, the energy values at different surface-hopping points are reported for a set of trajectories defined by different initial conditions. It is apparent that the decay takes place at energies significantly above the lowest-lying cross section of the intersection space of the molecule (represented by the curve at the bottom of the diagram) and featuring an average torsional angle different from the one of the MECI. Such a cross section contains the MECI point ($CI_{90°}$) and also a low-lying CI point obtained via a constrained geometry optimization with a fixed 70° torsional angle about the isomerizing bond (the $CI_{70°}$ of Figure 41.12).

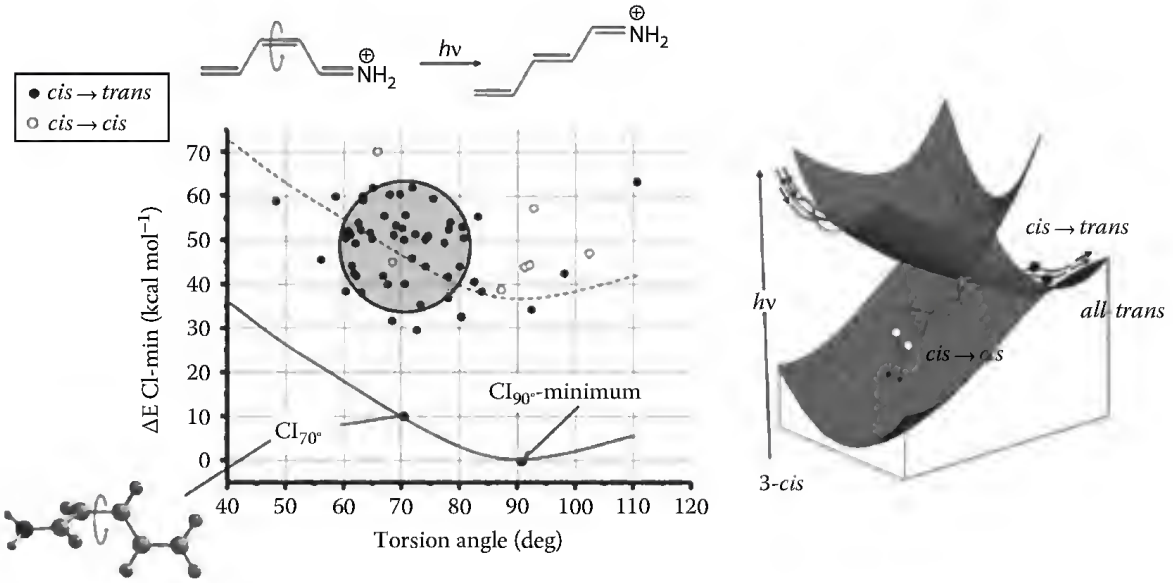

FIGURE 41.12 Energy and torsional angle distribution at the decay (hop) point for a set of 60 trajectories predicting a 80% quantum yield for gas-phase 3-*cis* pentadieniminium cation (a minimal model for the chromophore of Rh). Each trajectory is associated to a different set of initial conditions, and is released from the FC point region. A pictorial interpretation of the computational results is given on the right side where the corresponding successful (*cis*→*trans*) and unsuccessful (*cis*→*cis*) isomerizations are marked with full and opened circles, respectively.

We will discuss the use of single nonadiabatic trajectories in Section 41.3. Unfortunately, the calculation of a single nonadiabatic trajectory will not provide solid statistical information because the trajectory does not necessarily describe the average motion of the whole reacting population. This is especially true after the decay when the population may split into different directions as demonstrated in Figure 41.12.

As we will emphasize in the conclusion and perspective section, the increasing availability of multiprocessor facilities like parallel computers, clusters, and computer farms is presently paving the way for computations of statistically meaningful trajectory ensembles.[96,102,109] Therefore, the difficulties associated with the use of single trajectories could be, in principle, overcome by computing statistical properties (including quantum yields) over tens or hundreds of semiclassical trajectories.[110]

41.2.5 Photochemistry in Solution and in Proteins

While multiconfigurational quantum chemical methods have been successfully applied to sizable organic molecules, their computational cost renders the calculation of large and/or complex molecular systems impossible. These systems include chromophores in solution and chromophores embedded in a protein environment such as the visual photoreceptors discussed in Section 2.4. The underlying idea is to combine the accuracy of QM methods and the low computational cost of molecular mechanics (MM) methods. The methodology that has become increasingly popular is the hybrid QM/MM method.[111] The history of hybrid methods starts around 30 years ago with Warshel's work on lysozyme, where a MM method was coupled to semiempirical QM calculations.[112] This type of calculation was soon after applied to the study of visual pigments[113] and therefore to photobiology.

In a QM/MM setup, the part of the system (QM subsystem), which is responsible for the reactivity, spectroscopy, photophysics, and photochemistry, is described by a suitable quantum chemical method. The remaining part (MM subsystem), such as a box of solvent molecules or the protein hosting the QM

subsystem, is described in a computationally inexpensive way at the MM level (i.e., using parametrized classical force fields). The total (relative) potential energy of the system can be described by the additive relation[111]:

$$E_{Total} = E_{QM} + E_{MM} + E_{\frac{QM}{MM}}$$

While the first two terms account for the contributions coming from noninteracting QM and MM subsystems, the third term describes their interaction. Notice that there are different E_{QM} and $E_{QM/MM}$ terms for each electronic state while the E_{MM} remains the same. The general classification of QM/MM methods is based on the formulation of the $E_{QM/MM}$ term and on the scheme adopted to describe the boundary region between the QM part and the MM part. Depending on the way in which electrostatic interactions are treated, the QM/MM schemes can be divided into two classes: mechanical embedding (ME) and electrostatic embedding (EE).[114] In photochemical and photobiological studies, we need to use an EE method. In these methods, the QM computation is carried out in the presence of the MM subsystem by including the description of the electrostatic interactions between the two subsystems in the one-electron operators of the QM Hamiltonian. The remaining nonbonding (Van der Waals) interactions and bonding (stretching, bending, and torsional) interactions are treated at the MM level. It is usually convenient to represent the MM atoms by atomic-centered partial point charges for the purpose of calculating electrostatic interactions. Sets of these point charges have been calculated and incorporated into popular MM force fields, like Chemistry at Harvard Molecular Mechanics (CHARMM)[115] or Assisted Model Building with Energy Refinement (AMBER).[116] Some advantages of using these MM charges are that they have been validated extensively and have been parametrized to give accurate MM energies.

In cases where there is direct bonding between the QM and MM subsystems, such as when a chromophore is covalently linked to the protein (e.g., fluorescent proteins or visual pigments), the $E_{QM/MM}$ term also includes bond, angle, and torsional parameters accounting for the treatment of the frontier bond (the bond that connects the QM and MM moieties). The simplest and most popular approach to treat the frontier bond is the "link-atom"[117,118] scheme, where the free valencies of the "frontier atoms" are saturated with one or more hydrogen atoms that are included in the quantum chemical treatment of the QM fragment.

The parts of a QM/MM model for the microbial sensory receptor from the fresh water cyanobacterium *Anabaena* (*Nostoc*) sp. PCC 7120[119] are shown in Figure 41.13. The position of the frontier bond and link-atom is highlighted. The tube representation indicates the QM subsystem (the retinal chromophore of the Rh) and the covalently linked amino acid side chain included in the MM subsystem. These two regions are separated by a link-atom represented as a circle. The ball and stick representation highlights the backbone of the same residue. In computational photobiology studies, not all of the atoms of the photoreceptors (originally taken from the available crystallographic structure) are free to relax during the geometry optimization (i.e., to search for an excited state or ground state energy minimum). To make the optimization more effective without losing accuracy, only the QM subsystem and the part of the MM subsystem significantly interacting with it (including nearby residues, waters, or waters connected to the QM subsystem via hydrogen bonds) are incorporated in the set of nuclear coordinates allowed to be relaxed.

QM/MM models of an assortment of retinal proteins have been constructed and investigated by different research groups. As shown in Figure 41.13, these offer a good demonstration of the level of complexity that a QM/MM model can achieve. The information that the models provide has been partially discussed earlier for the photoreceptor Rh and will be further discussed in Section 41.3. A more complex model of a water soluble retinal protein mimic[120] is currently under investigation in our lab. On the basis of the available x-ray crystallographic structure, we have constructed (using a protocol similar to the one used to reproduce the spectra of the soluble protein monellin)[121] a QM/MM model of the KLE-CRABPII construct[120] in water solution. Figure 41.14a provides an overview of the complexity of the model. The protein (Figure 41.14b) is embedded in a large rectangular solvent (water) box. The model features 7040 waters, forming a $62 \times 58 \times 71$ Å^3 box that extends at least 10.0 Å from any atom of the

	ASR_{13C}	ASR_{AT}	AT-13C
Obs.	53.2	52.1	1.1
Model 1	53.3	50.9	2.4
Model 2	54.1	52.6	1.5

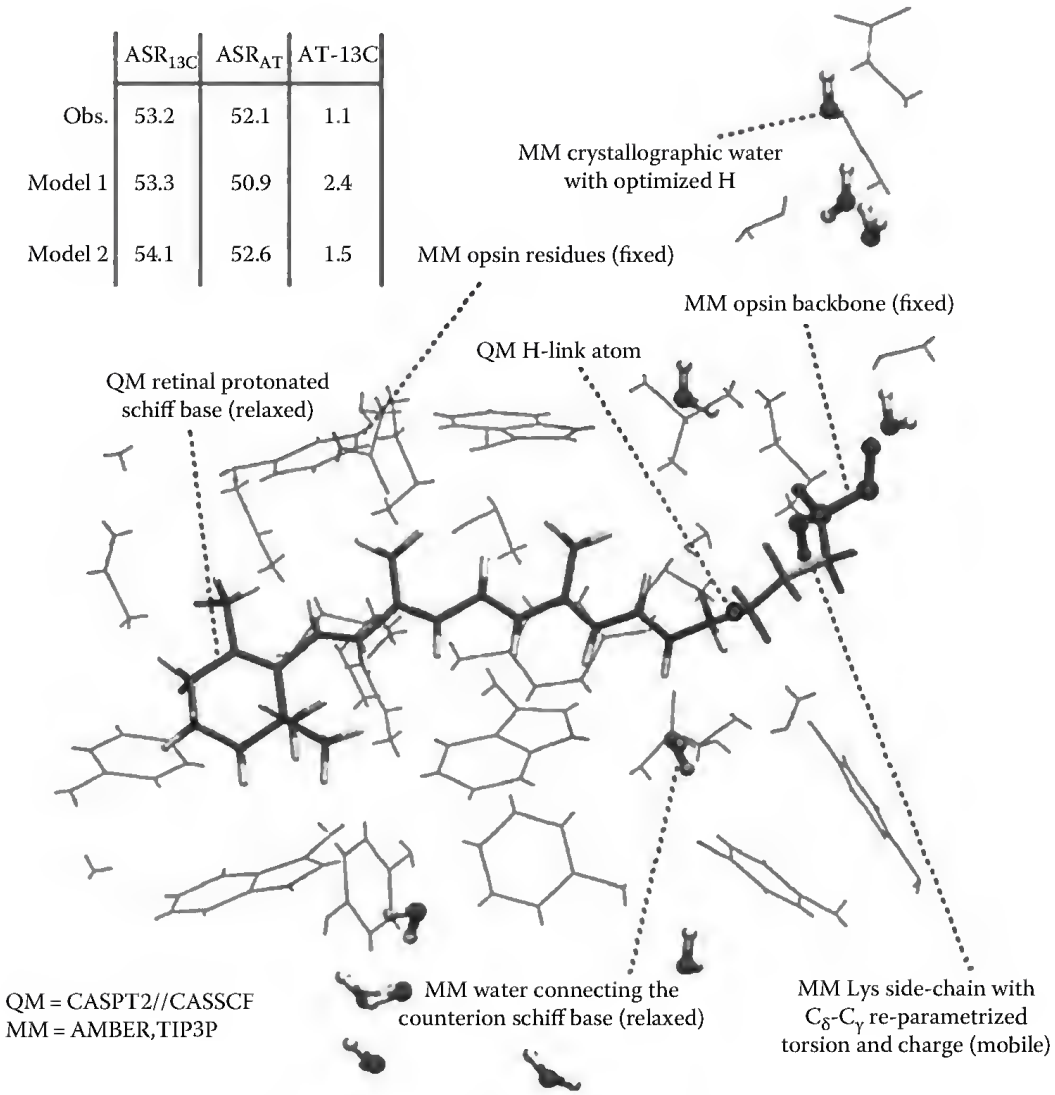

FIGURE 41.13 Partial view of the CASPT2//CASSCF/AMBER (QM/MM) model used for simulating the spectroscopy and photochemistry of a biological photoreceptor (e.g., the microbial sensory Rh from the cyanobacterium *Anabaena* displayed in the figure). The protein backbone and the cavity residues (the study of the photochemical step in these systems requires subpicosecond simulations that do not allow for important displacements of the cavity residues) are kept fixed at their crystallographic positions. The table reports the excitation energies in kcal/mol computed with a basic model with fixed water hydrogens (Model 1) and an improved model (Model 2) with relaxed water hydrogens (thus allowing a reorganization of the hydrogen bond network).

protein. To correctly account for the solvent, a 1 ns molecular dynamics (MD) simulation of all the water molecules was initially performed. Coordinates from the last (equilibrated) part of the simulation were used to build different QM/MM models. In turn, these were used to compute the system absorption maxima and for successive excited state reactivity studies. To accomplish this, for each chosen snapshot, a CASSCF/AMBER geometry optimization was performed, where CASSCF/AMBER method used to compute the equilibrium structure and AMBER indicates the MM force field used. The coordinates of the retinal chromophore (the QM subsystem), the glutamate counterion, and water molecules within 5 Å from any given QM atoms were relaxed. The rest of the protein is held fixed at the crystal structure. The achieved accuracy is illustrated in Figure 41.14c[122] that reports the computed absorption λ_{max} value. This is computed as an average of the predicted λ_{max} values for several minimum energy configurations generated with an MM based ground state molecular dynamics simulation (using a parametrized

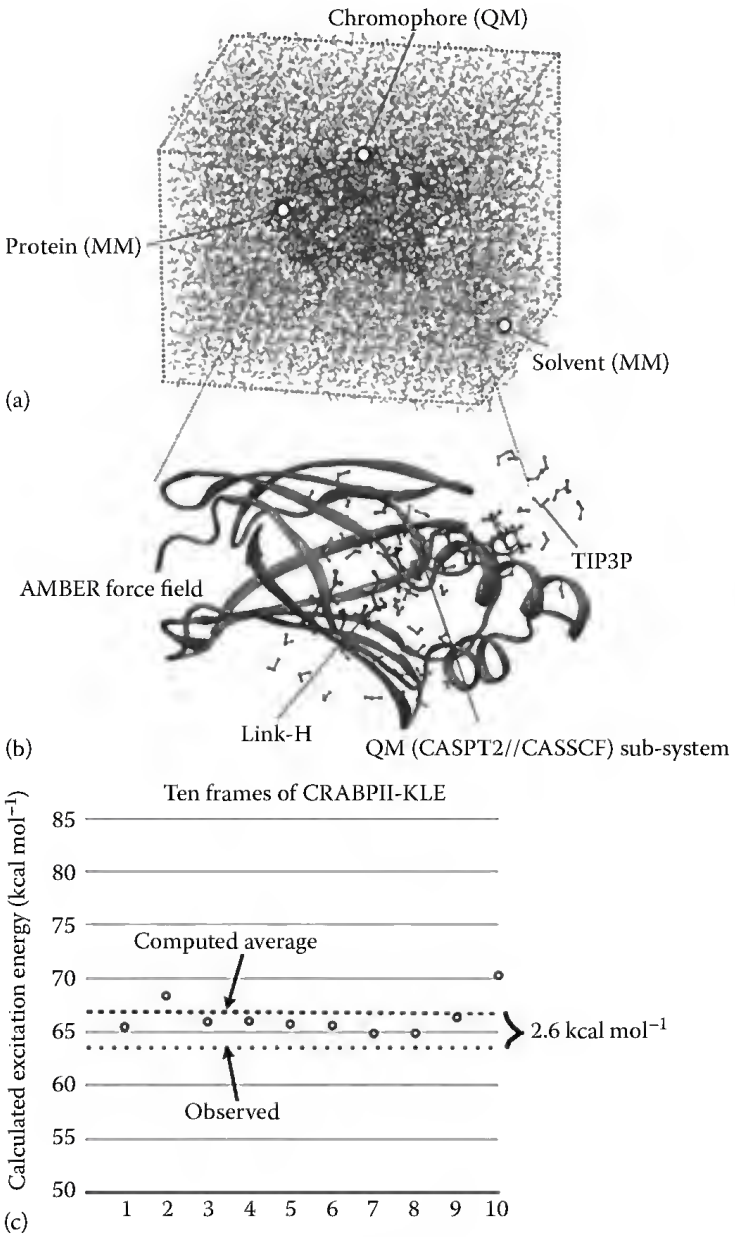

FIGURE 41.14 (a) QM/MM model for CRABPII-KLE in solution. (b) Parts of the protein model. (c) Prediction of the absorption maximum (see text) using MS-CASPT2//CASSCF/AMBER calculations. Each data point represents a different geometry sampled from the MD simulation with the chromophore and waters within 5.0 Å optimized at the QM/MM level.

retinal chromophore) and determined at the CASSCF/AMBER level. These values are computed via single point MS-CASPT2//CASSCF/AMBER computations. It is shown that the observed absorption λ_{max} is reproduced within 3 kilocalories per mole (less than a 20 nm error).

CASPT2//CASSCF/AMBER models can also be used for simulating or predicting spectroscopic and photochemical properties of organic chromophores in solution. A recent example is provided by an N-alkyl indanylidene-pyrroline (NAIP) molecular switch that has been shown to mimic different aspects of the photoisomerization of the retinal chromophore in Rh. In Figure 41.15, we show the core of a QM/MM model featuring a solvent box of methanol entrapping the chromophore unit.[123] Comparison of the computed and observed λ_{max} values for three electronic transitions shows that the model can reproduce the spectra correctly.

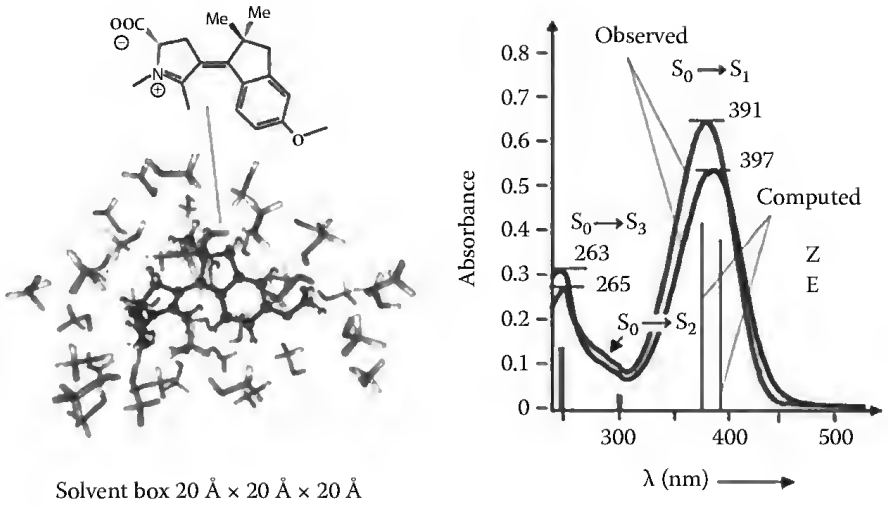

FIGURE 41.15 A low-energy CASSCF/AMBER configuration (only the first solvation shell is displayed) of a zwitterionic NAIP switch in methanol solution studied in Ref. [123]. Room temperature experimental absorption spectra of the Z isomer (λ_{max} 397 nm) and E isomer (λ_{max} 391 nm) of the same switch in MeOH.

41.3 Computational Photobiology

We have earlier seen that the mapping of the excited state potential energy surface[124] and CIs[37] requires methods that can deal with electronic structures featuring a changing mixture of open-shell and charge transfer characters. The aforementioned CASPT2//CASSCF method offers maximum flexibility for an unbiased description of the electronic and equilibrium structures of the ground and excited states of a molecule.

In the past, we have shown (Figure 41.16) that, when used as part of the QM/MM method described earlier, CASPT2//CASSCF quantum chemical computations allow to model the spectra of different proteins incorporating cationic, anionic, and neutral chromophores.[121,125–129] This method has already been mentioned earlier for the case of the visual pigment Rh, the soluble KLE-CRABPII Rh mimic, and the biomimetic NAIP switch in methanol solution. For the membrane protein Rh,[125,126,130] which is the visual pigment of vertebrates, the observed absorption maximum of its retinal chromophore embedded in the apoprotein opsin was reproduced with an error of less than 3 kcal mol^{-1} in excitation energy. Furthermore, we were able to reproduce[126] the λ_{max} values of one isomer and two mutants of Rh with less than 2 kcal mol^{-1} error. Similarly, the computed change in oscillator strength (f) at λ_{max} for those proteins has been found to be consistent with the corresponding experimental change in the extinction coefficients (ε). These results have been confirmed by others[131,132] and extended to microbial Rhs[133], to the retinal chromophore in solution[134-138] and to other photoactive systems, such as luciferase,[139] phytochrome,[140] and the GFP-like protein Dronpa.[141] While these studies have also prompted the investigation of different *ab initio* multiconfigurational quantum chemistry-based QM/MM protocols,[136,142] the CASPT2//CASSCF is arguably the only method allowing a description of spectra, excited state reaction paths, CIs, and trajectories on a consistent basis.[59,124,128] While CASPT2 geometry optimizations would be more accurate, they are unfeasible for a retinal chromophore due to the very high computational cost. That is why realistic trajectory computations (i.e., the double bond isomerization dynamics) are currently carried out at the scaled-CASSCF level[92] to account for the CASPT2 correction in an approximate way.

These studies have focused on different photoreceptor properties including spectra (for instance, as a function of mutations[126]), the structure of the CI (either obtained via geometry optimization, MEP computation,[124] and/or trajectory computation[98]), the topology of the intersection space, and, ultimately, reactivity using classical (Figure 41.11) and semiclassical trajectory computations. Most recently, as anticipated earlier, the use of whole sets of semiclassical trajectory computations has been used to tackle the problem of predicting photoisomerization quantum yields.[103,110]

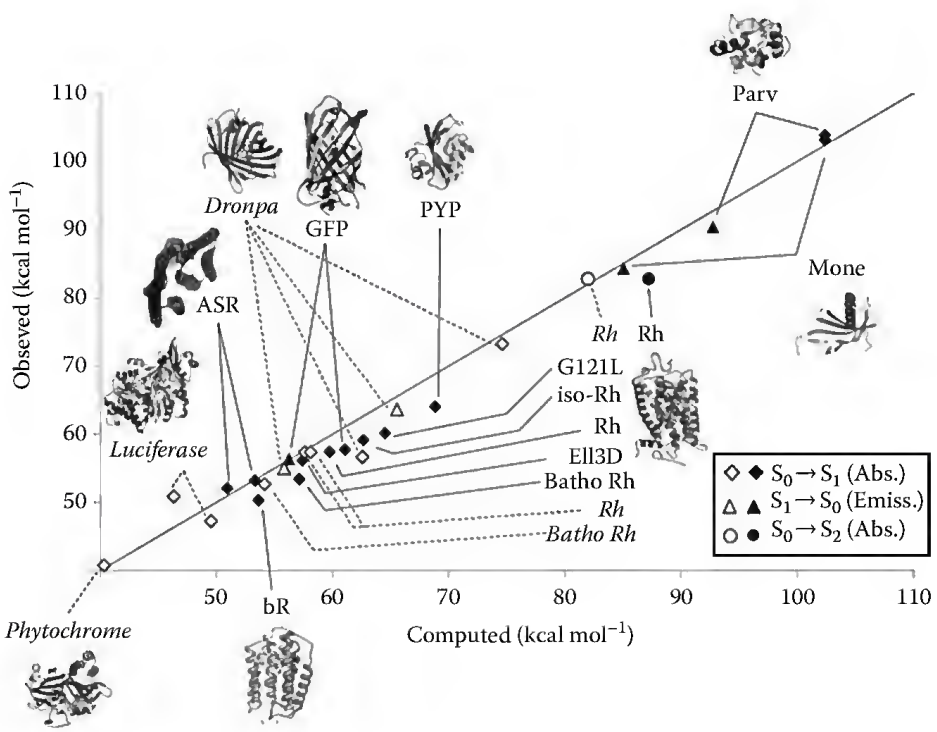

FIGURE 41.16 In our group the CASPT2/CASSCF//MM method (see text) has successfully reproduced the excitation energies of a set of pigments related to bovine Rh (Rh and related isomers and mutants), bacteriorhodopsin (bR), *Anabaena* sensory rhodopsin (ASR), the green fluorescent protein (GFP), the photoactive yellow protein (PYP), the tryptophan containing proteins parvalbumin (Parv), and monellin (Mone). These data are indicated with filled shapes and full lines. By using the same method, other groups have obtained the excitation energies of Rh-related proteins, along with luciferase, phytochrome and the GFP-like protein Dronpa. These data are indicated in the chart with empty shapes and broken lines.

In Figure 41.17, we schematically show the results of our study on the control of the absorption maxima in Rh[126] featuring a chromophore incorporated in a tight protein cavity. It is shown that the rationale behind the changes in λ_{max} value induced by a change in amino acid composition is based on the established difference[143–145] in singlet ground (S_0) and excited state (S_1) charge distributions. As reported[125] for bovine Rh (Figure 41.17a), upon excitation of the chromophore, the positive charge located on the Schiff base moiety is spread toward the β-ionone ring. This is due to the charge transfer nature of the S_1 state. Thus, polar residues located in the Schiff base region will affect the λ_{max} value stabilizing (or destabilizing) S_0 with respect to S_1, thus inducing a shortening (or lengthening) of the absorption wavelength. The direction of this effect depends on the sign of the *change* in electrostatic potential "projected" by the residues on the Schiff base region. Replacement with a residue increasing the positive potential will result in a destabilization of S_0 and stabilization of S_1 causing a red shift of the chromophore absorption. In contrast, a replacement imposing a decrease of the positive potential will yield a larger S_0–S_1 gap, thus causing a blue shift.

In Figure 41.18, we show a mapping of the excited state potential energy surface of Rh[124] produced using a relaxed scan approximating the MEP, driven by the twisting of the reactive 11-*cis* bond and ultimately leading to the production of Batho-Rh. It is shown that, in its last part, the MEP runs along a path that maintains the energy degeneracy. This suggests that, at the bottom of the excited state potential energy surface of the photoreceptor, there is a segment of the intersection space. This is also confirmed by the result of excited state trajectory computations. Indeed, as shown in Figure 41.11a, a classical trajectory (i.e., a trajectory that cannot computationally hop to the ground state) detects an intersection space segment in its last part. Similarly, the trajectory simulating the reverse isomerization reaction (i.e., from Batho-Rh to Rh) also detects a similar near degeneracy region that most probably belongs to the

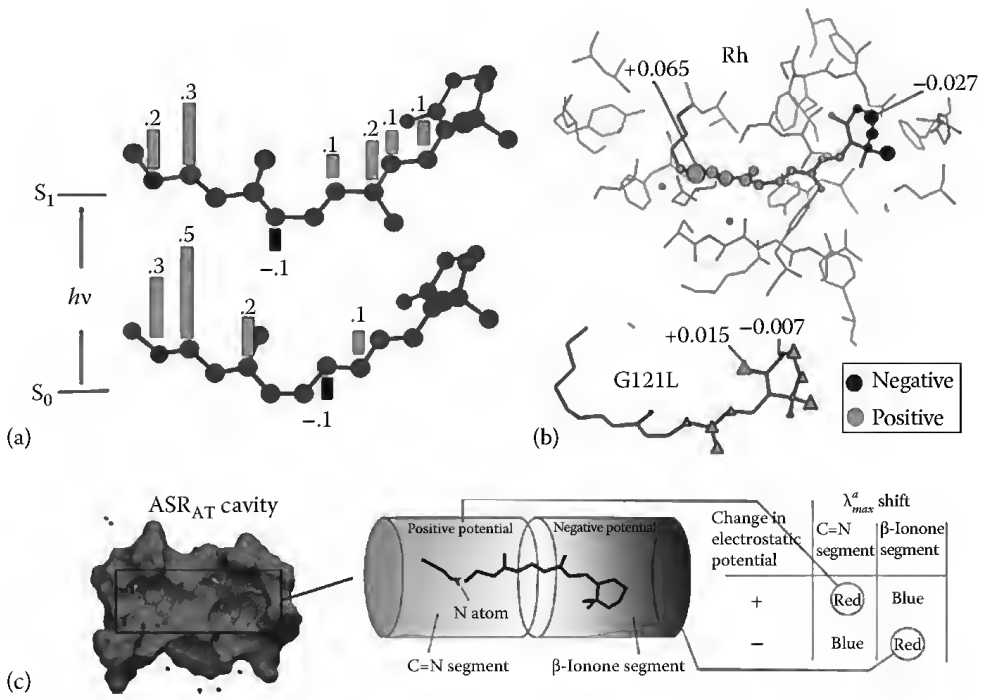

FIGURE 41.17 (a) Change in the charge distribution along the backbone of the 11-*cis* chromophore of Rh upon photoexcitation. It is shown that <30% shift of the positive charge occurs upon vertical transition to the first excited singlet state. (b) Electrostatic potential (numbers give the maximum and minimum values in atomic units) generated by the opsin partial charges (excluding the counterion) on the retinal chromophore centers of Rh. Bottom. Change in electrostatic potential (numbers give the maximum and minimum values in atomic units) on the atoms of the chromophores of the mutant G121L with respect to the wild type. (c) A mutated rhodopsin (e.g., ASR) cavity imposing a more positive potential on the chromophore C=N segment or a more negative potential on the β-ionone segment will red shift the λ^a_{max} value.

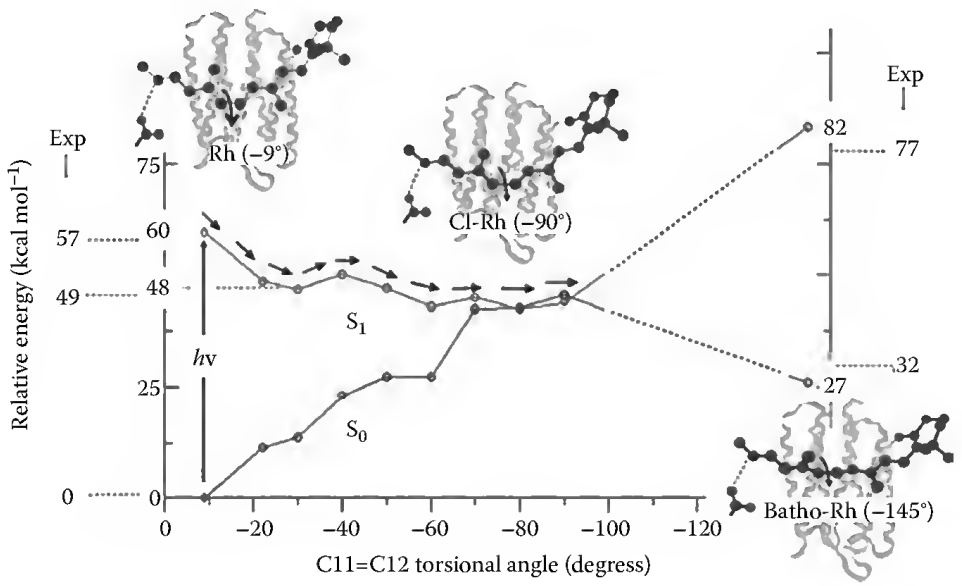

FIGURE 41.18 MEP along the excited state photoisomerization path of Rh. Notice that the excited and ground states are degenerate in the 70–90 region, suggesting that the reaction path is parallel to a small segment of the intersection space. The QM/MM Rh and Batho-Rh models used for these studies have been validated by comparing the computed excitation energies with the observed ones.

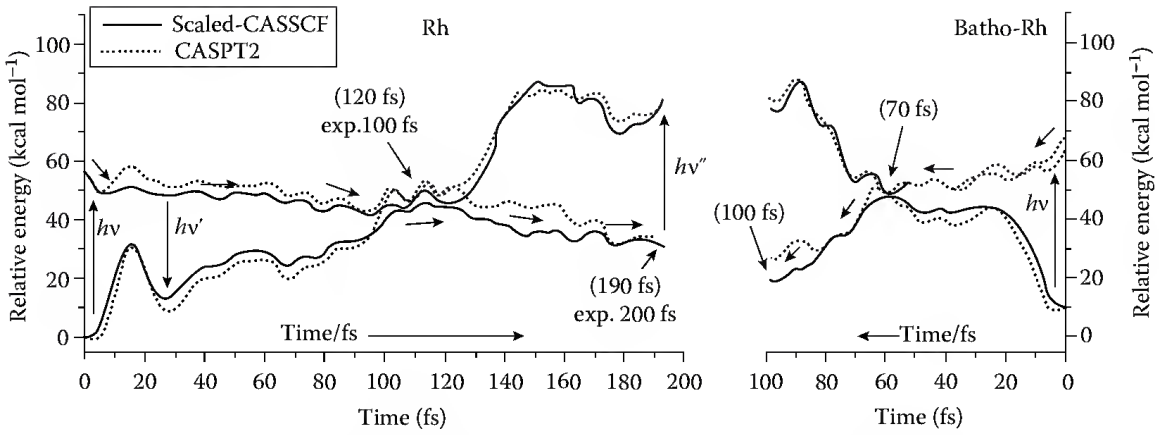

FIGURE 41.19 Scaled-CASSCF/Amber semiclassical trajectories for Batho-Rh and Rh. The S_1 and S_0 energy profiles along the trajectory of Rh are given on the left. The data for Batho-Rh are given on the right.

same intersection space. Indeed, in a recent work, we have shown that the same intersection space is also connected to the CI reached during the photoisomerization of Iso-Rh.[146]

The aforementioned results are useful to interpret the more realistic semiclassical trajectory computations. For instance, in Figure 41.19, we show that the semiclassical trajectories computed for Rh and Batho-Rh, and describing the low-temperature (77 K) photochromic interconversion of these receptors, clearly reach the intersection region as well as the region of their vibrationally hot photoproducts on a subpicosecond time scale. It is evident that in the case of Rh, the trajectories remain close to the intersection region immediately after its decay. This does not happen for Batho-Rh where the intersection space is immediately abandoned and the evolution on lower energy regions of the ground state potential energy surface is directly initiated. We believe that in the future, the understanding of these differences at the level of the single molecular vibrational modes driving the excited state dynamics and the hop event will become of great importance.

41.4 Conclusions and Perspectives

A correct formulation of the mechanism of a photochemical reaction requires the computation of real crossings, like CIs and singlet–triplet crossings, between different potential energy surfaces. In ultrafast reactions, these *critical* structures are reached by the excited state reactant on the time scale of a few vibrational periods. However, slower processes can also be mediated by CI channels. In fact, as documented in Section 2.3, there are cases where the access to a CI is controlled by a non-negligible excited state barrier. In other words, the involvement of CIs in chemistry may go considerably beyond the field of femtochemistry and comprise processes such as photoinduced electron transfer, quenching, and internal conversion. From this conclusion, it is evident that a growing need to effectively locate and calculate chemically meaningful CIs, and thus rigorously connect different potential energy surfaces, will drive further research.

We have earlier clarified that MECIs are, in general, crude representations of photochemical funnels. This is due to the fact that CI points are elements of complex intersection spaces. Two more effective strategies to locate meaningful photochemical funnels have been revised. These are photochemical reaction paths and trajectories. However, single (classical or semiclassical) trajectories only yield an approximation of the most meaningful CI. In fact, such a structure has a statistical meaning and can only be computed in terms of an average value that can be derived by analyzing a set of different trajectories. It is therefore apparent that the future of computational photochemistry and photobiology is associated with the development of efficient methods for the computation of entire sets of semiclassical trajectories. These methods are characterized by (1) the way in which the initial set of geometries and velocities are generated, (2) the way in which the hop decision is taken for each trajectory, and (3) the QM/MM protocol used for computing the potential energy and energy gradients.

For the formulation of the QM/MM protocol to be used in photochemical and photobiological studies, one would want to use quantitative methods such as the *ab initio* CASPT2 (or the more advanced MS-CASPT2) or MRCI methods. In principle, these methods will ensure that the forces acting on the nuclear coordinates and driving both the excited state dynamics and the following ground state relaxation are realistic. In this way, one could avoid non-negligible errors coming from the difficulties of parametrizing and validating semiempirical methods, scaling the energies and gradients of CASSCF, or formulating/parametrizing novel functionals for TD-DFT calculations. However, even these advanced methods need further performance improvements. In particular, CASPT2 analytical gradients are not available and both geometry optimizations and trajectory computations can only be performed for relatively small molecular systems.[91,147–149] Furthermore, the validity of CASPT2 energies and gradients in the strict vicinity of a CI requires a careful analysis. The more reliable MRCI method has, however, a much higher computational cost and it is presently of limited applicability to sizable organic systems.

The search for realistic and computationally effective QM/MM excited state force fields is perhaps the most important technical challenge that modern computational photochemistry and photobiology have to face. The availability of such force fields would make possible the exploitation of the constantly expanding computational facilities available for chemical research. In particular, facilities going from in-house computer clusters up to the extensive computer farms available at state or federal computer centers are particularly suited for the *simultaneous* investigation of large families of different molecular systems or for the *simultaneous* computations of statistically meaningful sets of trajectories of a given chromophore. It is apparent that this last target will have a significant impact in our understanding and future engineering of the light energy exploitation at the molecular level and, therefore, in the development of new functional materials.

The use of a computer farm for the simultaneous investigation of a chromophore or a family of related chromophores in solution or in a complex protein environment is reminiscent of the way in which one of the fathers of modern photochemistry used to carry out his research. In Figure 41.20, we see how Giacomo Ciamician used to expose entire sets of different organic compounds to sunlight on a balcony of his laboratory in Bologna (Italy).[150] In a sense, the opportunities described earlier are shifting this effective way of carrying out photochemical research to the virtual (*in silico*) world revealing, once again, the extraordinary link between the past and the future of photochemistry.

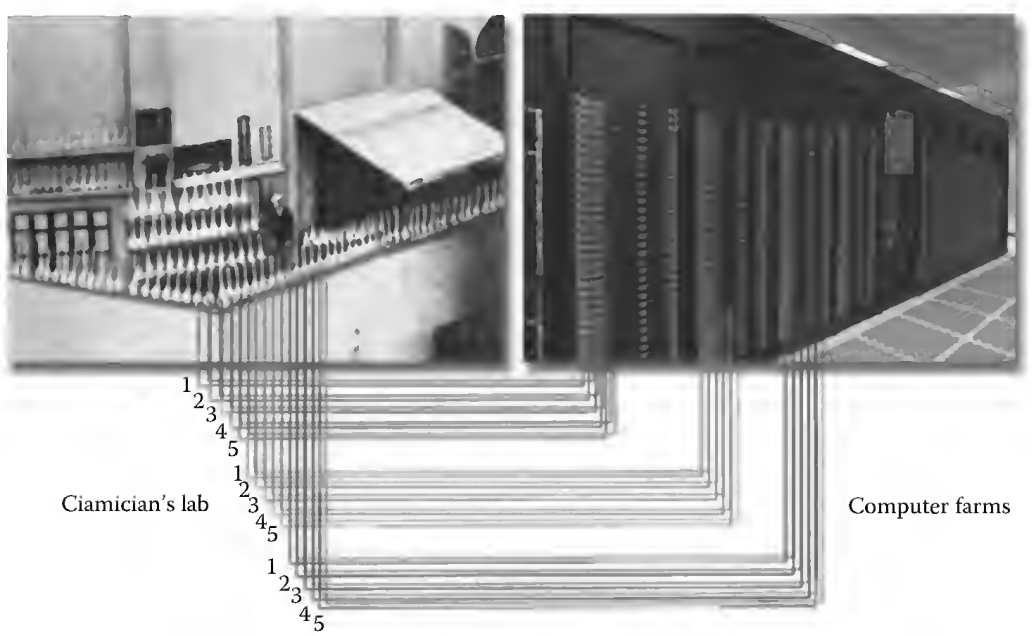

FIGURE 41.20 "Parallel" photochemical research in Giacomo Ciamician's lab (from 1889 to 1921) in Bologna, Italy, and a modern computer farm. In both cases, different sets of compounds are investigated simultaneously either experimentally or *in silico*.

References

1. M. Rini, A. Kummrow, J. Dreyer, E. T. J. Nibbering, T. Elsaesser, *Faraday Discuss.* 2003, *122*, 27.
2. P. Hamm, S. M. Ohline, W. Zinth, *J. Chem. Phys.* 1997, *106*, 519.
3. M. Born, R. Oppenheimer, *Ann. Phys.* 1927, *389*, 457.
4. C. Eckart, *Phys. Rev.* 1934, *46*, 383.
5. F. Bernardi, M. Olivucci, M. A. Robb, *Chem. Soc. Rev.* 1996, *25*, 321.
6. W. T. A. M. Van der Lugt, L. J. Oosterhoff, *J. Am. Chem. Soc.* 1969, *91*, 6042.
7. D. Grimbert, G. Segal, A. Devaquet, *J. Am. Chem. Soc.* 1975, *97*, 6629.
8. K. R. Naqvi, *Chem. Phys. Lett.* 1972, *15*, 634.
9. A. Gilbert, J. Baggott, *Essentials of Molecular Photochemistry*, CRC Press, London, U.K., 1991.
10. N. J. Turro, *Modern Molecular Photochemistry*, University Science Books, Sausalito, CA, 1991.
11. L. R. Khundkar, A. H. Zewail, *Annu. Rev. Phys. Chem.* 1990, *41*, 15.
12. A. H. Zewail, *Angew. Chem. Int. Ed.* 2000, *39*, 2587.
13. M. Bixon, J. Jortner, *J. Chem. Phys.* 1968, *48*, 715.
14. K. F. Freed, *Acc. Chem. Res.* 1978, *11*, 74.
15. W. M. Gelbart, K. F. Freed, S. A. Rice, *J. Chem. Phys.* 1970, *52*, 2460.
16. H. E. Zimmerman, *J. Am. Chem. Soc.* 1966, *88*, 1566.
17. J. Michl, *J. Mol. Phys.* 1972, *4*, 243.
18. L. Salem, *J. Am. Chem. Soc.* 1974, *96*, 3486.
19. E. Teller, *Isr. J. Chem.* 1969, *7*, 227.
20. P. Celani, F. Bernardi, M. Olivucci, M. A. Robb, *J. Chem. Phys.* 1995, *102*, 5733.
21. M. Garavelli, F. Ruggeri, F. Ogliaro, M. J. Bearpark, F. Bernardi, M. Olivucci, M. A. Robb, *J. Comput. Chem.* 2003, *24*, 1357.
22. E. Runge, E. K. U. Gross, *Phys. Rev. Lett.* 1984, *52*, 997.
23. E. Tapavicza, I. Tavernelli, U. Rothlisberger, C. Filippi, M. E. Casida, *J. Chem. Phys.* 2008, *129*, 19.
24. E. J. Baerends, G. Ricciardi, A. Rosa, S. J. A. van Gisbergen, *Coord. Chem. Rev.* 2002, *230*, 5.
25. O. Cramariuc, T. I. Hukka, T. T. Rantala, H. Lemmetyinen, *J. Phys. Chem. A* 2006, *110*, 12470.
26. K. A. Nguyen, R. Pachter, *J. Chem. Phys.* 2001, *114*, 10757.
27. B. G. Levine, C. Ko, J. Quenneville, T. J. Martínez, *Mol. Phys.* 2006, *104*, 1039.
28. E. Teller, *J. Phys. Chem.* 1937, *41*, 109.
29. H. C. Longuet-Higgins, *Proc. R. Soc. A* 1975, *344*, 147.
30. G. Herzberg, H. C. Longuet-Higgins, *Discuss. Faraday Soc.* 1963, *35*, 77.
31. L. Salem, W. G. Dauben, N. J. Turro, *J. Chim. Phys. Phys. Chim. Biol.* 1973, *70*, 694.
32. N. J. Turro, *THEOCHEM* 1998, *424*, 77.
33. W. G. Dauben, L. Salem, N. J. Turro, *Acc. Chem. Res.* 1975, *8*, 41.
34. V. Bonačić-Koutecký, J. Michl, *Theor. Chim. Acta* 1985, *68*, 45.
35. V. Bonačić-Koutecký, J. Koutecky, J. Michl, *Angew. Chem. Int. Ed.* 1987, *26*, 170.
36. J. Michl, V. Bonačić-Koutecký, *Electronic Aspects of Organic Photochemistry*, John Wiley & Sons Inc., New York, 1990.
37. A. Migani, M. Olivucci, in *Conical Intersections: Electronic Structure, Dynamics and Spectroscopy*, Vol. 15 (Eds.: W. Domcke, D. Yarkony, H. Koppel), World Scientific, River Edge, NJ, 2004.
38. M. J. Bearpark, M. A. Robb, H. Bernhard Schlegel, *Chem. Phys. Lett.* 1994, *223*, 269.
39. M. J. Frisch, G. W. Trucks, H. B. Schlegel, G. E. Scuseria, M. A. Robb, J. R. Cheeseman, G. Scalmani, V. Barone, B. Mennucci, G. A. Petersson, H. Nakatsuji, M. Caricato, X. Li, H. P. Hratchian, A. F. Izmaylov, J. Bloino, G. Zheng, J. L. Sonnenberg, M. Hada, M. Ehara, K. Toyota, R. Fukuda, J. Hasegawa, M. Ishida, T. Nakajima, Y. Honda, O. Kitao, H. Nakai, T. Vreven, J. A. Montgomery Jr., J. E. Peralta, F. Ogliaro, M. Bearpark, J. J. Heyd, E. Brothers, K. N. Kudin, V. N. Staroverov, R. Kobayashi, J. Normand, K. Raghavachari, A. Rendell, J. C. Burant, S. S. Iyengar, J. Tomasi, M. Cossi, N. Rega, N. J. Millam, M. Klene, J. E. Knox, J. B. Cross, V. Bakken, C. Adamo, J. Jaramillo,

R. Gomperts, R. E. Stratmann, O. Yazyev, A. J. Austin, R. Cammi, C. Pomelli, J. W. Ochterski, R. L. Martin, K. Morokuma, V. G. Zakrzewski, G. A. Voth, P. Salvador, J. J. Dannenberg, S. Dapprich, A. D. Daniels, Ö. Farkas, J. B. Foresman, J. V. Ortiz, J. Cioslowski, D. J. Fox, Revision A.1 ed., Gaussian, Inc., Wallingford, CT, 2009.

40. K. Andersson, F. Aquilante, M. Barysz, E. Bednarz, A. Bernhardsson, M. R. A. Blomberg, Y. Carissan, et al., Molcas 2009 edn., University of Lund, Lund, Sweden.
41. F. Aquilante, L. De Vico, N. Ferré, G. Ghigo, P. A. Malmqvist, P. Neogrady, T. B. Pedersen, M. Pitonak, M. Reiher, B. O. Roos, L. Serrano-Andres, M. Urban, V. Veryazov, R. Lindh, *J. Comput. Chem.* 2009, *31*, 224.
42. M. W. Schmidt, K. K. Baldridge, J. A. Boatz, S. T. Elbert, M. S. Gordon, J. H. Jensen, S. Koseki, N. Matsunaga, K. A. Nguyen, S. J. Su, T. L. Windus, M. Dupuis, J. A. Montgomery, *J. Comput. Chem.* 1993, *14*, 1347.
43. M. S. Gordon, M. W. Schmidt, G. Frenking, K. S. Kim, G. E. Scuseria, *Theory and Applications of Computational Chemistry: The First Forty Years*, Elsevier, Amsterdam, the Netherlands, 2005.
44. H. Lischka, R. Shepard, I. Shavitt, R. M. Pitzer, M. Dallos, T. Müller, P. G. Szalay, F. B. Brown, R. Ahlrichs, H. J. Böhm, A. Chang, D. C. Comeau, R. Gdanitz, H. Dachsel, C. Ehrhardt, M. Ernzerhof, P. Höchtl, S. Irle, G. Kedziora, T. Kovar, V. Parasuk, M. J. M. Pepper, P. Scharf, H. Schiffer, M. Schindler, M. Schüler, M. Seth, E. A. Stahlberg, J.-G. Zhao, S. Yabushita, Z. Zhang, M. Barbatti, S. Matsika, M. Schuurmann, D. R. Yarkony, S. R. Brozell, E. V. Beck, J.-P. Blaudeau, COLUMBUS, an ab initio electronic structure program, release 5.9.1 edn., 2006.
45. H.-J. Werner, P. J. Knowles, R. Lindh, F. R. Manby, M. Schütz, P. Celani, T. Korona, A. Mitrushenkov, G. Rauhut, T. B. Adler, R. D. Amos, A. Bernhardsson, A. Berning, D. L. Cooper, M. J. O. Deegan, A. J. Dobbyn, F. Eckert, E. Goll, C. Hampel, G. Hetzer, T. Hrenar, G. Knizia, C. Köppl, Y. Liu, A. W. Lloyd, R. A. Mata, A. J. May, S. J. McNicholas, W. Meyer, M. E. Mura, A. Nicklass, P. Palmieri, K. Pflüger, R. Pitzer, M. Reiher, U. Schumann, H. Stoll, A. J. Stone, R. Tarroni, T. Thorsteinsson, M. Wang, A. Wolf, MOLPRO, version 2009.1, a package of ab initio programs ed., University of Cardiff, Cardiff, U.K., 2009.
46. Y. Shao, L. F. Molnar, Y. Jung, J. Kussmann, C. Ochsenfeld, S. T. Brown, A. T. B. Gilbert, L. V. Slipchenko, S. V. Levchenko, D. P. O'Neill, R. A. DiStasio, R. C. Lochan, T. Wang, G. J. O. Beran, N. A. Besley, J. M. Herbert, C. Y. Lin, T. Van Voorhis, S. H. Chien, A. Sodt, R. P. Steele, V. A. Rassolov, P. E. Maslen, P. P. Korambath, R. D. Adamson, B. Austin, J. Baker, E. F. C. Byrd, H. Dachsel, R. J. Doerksen, A. Dreuw, B. D. Dunietz, A. D. Dutoi, T. R. Furlani, S. R. Gwaltney, A. Heyden, S. Hirata, C. P. Hsu, G. Kedziora, R. Z. Khalliulin, P. Klunzinger, A. M. Lee, M. S. Lee, W. Liang, I. Lotan, N. Nair, B. Peters, E. I. Proynov, P. A. Pieniazek, Y. M. Rhee, J. Ritchie, E. Rosta, C. D. Sherrill, A. C. Simmonett, J. E. Subotnik, H. L. Woodcock, W. Zhang, A. T. Bell, A. K. Chakraborty, D. M. Chipman, F. J. Keil, A. Warshel, W. J. Hehre, H. F. Schaefer, J. Kong, A. I. Krylov, P. M. W. Gill, M. Head-Gordon, *Phys. Chem. Chem. Phys.* 2006, *8*, 3172.
47. A. C. Wahl, G. Das, L. Per-Olov, in *Advances in Quantum Chemistry*, Vol. 5, Academic Press, New York, 1970, p. 261.
48. F. Bernardi, M. Olivucci, M. A. Robb, G. Tonachini, *J. Am. Chem. Soc.* 1986, *108*, 1408.
49. B. O. Roos, P. R. Taylor, P. E. M. Siegbahn, *Chem. Phys.* 1980, *48*, 157.
50. B. O. Roos, in *Ab Initio Methods in Quantum Chemistry* (Ed.: K. P. Lawley), Wiley, New York, 1987, p. 399.
51. K. Andersson, P. A. Malmqvist, B. O. Roos, A. J. Sadlej, K. Wolinski, *J. Phys. Chem.* 1990, *94*, 5483.
52. M. A. Robb, M. Garavelli, M. Olivucci, F. Bernardi, in *Reviews in Computational Chemistry*, Vol. 15, Wiley-VCH, Inc., New York, 2000, p. 87.
53. F. Bernardi, S. De, M. Olivucci, M. A. Robb, *J. Am. Chem. Soc.* 1990, *112*, 1737.
54. F. Bernardi, M. Olivucci, M. A. Robb, *Acc. Chem. Res.* 1990, *23*, 405.
55. X. Li, J. Paldus, *Mol. Phys.* 2006, *104*, 655.
56. W. Domcke, D. R. Yarkony, H. Koppel, in *Advanced Series in Physical Chemistry* (Ed.: N. Cheuk-Yiu), World Scientific Publishing Company, Incorporated, Singapore, 2004.

57. I. Schapiro, M. N. Ryazantsev, W. J. Ding, M. H. Huntress, F. Melaccio, T. Andruniow, M. Olivucci, *Aust. J. Chem.* 2010, *63*, 413.
58. M. Desouter-Lecomte, J. C. Lorquet, *J. Chem. Phys.* 1979, *71*, 4391.
59. M. Olivucci, A. Sinicropi, in *Computational Chemistry*, Elsevier, Oxford, U.K., 2005.
60. D. G. Truhlar, M. S. Gordon, *Science* 1990, *249*, 491.
61. P. Z. El-Khoury, A. N. Tarnovsky, I. Schapiro, M. N. Ryazantsev, M. Olivucci, *J. Phys. Chem. A* 2009, *113*, 10767.
62. G. J. Atchity, S. S. Xantheas, K. Ruedenberg, *J. Chem. Phys.* 1991, *95*, 1862.
63. D. R. Yarkony, *Rev. Mod. Phys.* 1996, *68*, 985.
64. R. V. Olkhov, S. Matzinger, T. Bally, 1.85 edn., University of Fribourg, Switzerland, 2005, *MoPlot* (Molecular Orbital Plotting program).
65. N. Koga, K. Morokuma, *Chem. Phys. Lett.* 1985, *119*, 371.
66. M. R. Manaa, D. R. Yarkony, *J. Chem. Phys.* 1993, *99*, 5251.
67. J. M. Anglada, J. M. Bofill, *J. Comput. Chem.* 1997, *18*, 992.
68. F. Sicilia, L. Blancafort, M. J. Bearpark, M. A. Robb, *J. Chem. Theory Comput.* 2008, *4*, 257.
69. W. M. Nau, G. Greiner, H. Rau, J. Wall, M. Olivucci, J. C. Scaiano, *J. Phys. Chem. A* 1999, *103*, 1579.
70. A. Sinicropi, R. Pogni, R. Basosi, M. A. Robb, G. Gramlich, W. M. Nau, M. Olivucci, *Angew. Chem. Int. Ed.* 2001, *40*, 4185.
71. A. Sinicropi, W. M. Nau, M. Olivucci, *Photochem. Photobiol. Sci.* 2002, *1*, 537.
72. M. Polanyi, *Atomic Reactions*, Williams and Norgate, London, U.K., 1932.
73. A. Sinicropi, U. Pischel, R. Basosi, W. M. Nau, M. Olivucci, *Angew. Chem. Int. Ed.* 2000, *39*, 4582.
74. I. J. Palmer, I. N. Ragazos, F. Bernardi, M. Olivucci, M. A. Robb, *J. Am. Chem. Soc.* 1993, *115*, 673.
75. P. Celani, M. Garavelli, S. Ottani, F. Bernardi, M. A. Robb, M. Olivucci, *J. Am. Chem. Soc.* 1995, *117*, 11584.
76. M. Garavelli, P. Celani, N. Yamamoto, F. Bernardi, M. A. Robb, M. Olivucci, *J. Am. Chem. Soc.* 1996, *118*, 11656.
77. M. J. Bearpark, P. Celani, F. Jolibois, M. Olivucci, M. A. Robb, F. Bernardi, *Mol. Phys.* 1999, *96*, 645.
78. M. J. Bearpark, F. Bernardi, M. Olivucci, M. A. Robb, *Int. J. Quantum Chem.* 1996, *60*, 505.
79. M. J. Bearpark, F. Bernardi, M. Olivucci, M. A. Robb, B. R. Smith, *J. Am. Chem. Soc.* 1996, *118*, 5254.
80. M. J. Bearpark, F. Bernardi, S. Clifford, M. Olivucci, M. A. Robb, B. R. Smith, T. Vreven, *J. Am. Chem. Soc.* 1996, *118*, 169.
81. M. J. Bearpark, F. Bernardi, S. Clifford, M. Olivucci, M. A. Robb, T. Vreven, *Mol. Phys.* 1996, *89*, 37.
82. A. Migani, P. L. Gentili, F. Negri, M. Olivucci, A. Romani, G. Favaro, R. S. Becker, *J. Phys. Chem. A* 2005, *109*, 8684.
83. A. Sanchez-Galvez, P. Hunt, M. A. Robb, M. Olivucci, T. Vreven, H. B. Schlegel, *J. Am. Chem. Soc.* 2000, *122*, 2911.
84. N. Ismail, L. Blancafort, M. Olivucci, B. Kohler, M. A. Robb, *J. Am. Chem. Soc.* 2002, *124*, 6818.
85. M. E. Martin, F. Negri, M. Olivucci, *J. Am. Chem. Soc.* 2004, *126*, 5452.
86. T. Bally, S. Matzinger, P. Bednarek, *J. Am. Chem. Soc.* 2006, *128*, 7828.
87. G. N. Sastry, T. Bally, V. Hrouda, P. Càrsky, *J. Am. Chem. Soc.* 1998, *120*, 9323.
88. K. F. Hall, M. Boggio-Pasqua, M. J. Bearpark, M. A. Robb, *J. Phys. Chem. A* 2006, *110*, 13591.
89. A. M. Tokmachev, M. Boggio-Pasqua, M. J. Bearpark, M. A. Robb, *J. Phys. Chem. A* 2008, *112*, 10881.
90. J. C. Tully, *J. Chem. Phys.* 1990, *93*, 1061.
91. P. Z. El-Khoury, L. George, A. Kalume, I. Schapiro, M. Olivucci, A. N. Tarnovsky, S. A. Reid, *Chem. Phys. Lett.* 2010, *496*, 68.
92. L. M. Frutos, T. Andruniow, F. Santoro, N. Ferré, M. Olivucci, *Proc. Natl. Acad. Sci. USA* 2007, *104*, 7764.
93. I. Schapiro, M. N. Ryazantsev, L. M. Frutos, N. Ferre, R. Lindh, M. Olivucci, *J. Am. Chem. Soc.* 2011, *133*, 3354.
94. M. Olivucci, in preparation.

95. F. Jolibois, M. J. Bearpark, M. A. Robb, *J. Phys. Chem. A* 2002, *106*, 4358.
96. B. G. Levine, T. J. Martínez, *Annu. Rev. Phys. Chem.* 2007, *58*, 613.
97. M. Ruckenbauer, M. Barbatti, T. Müller, H. Lischka, *J. Phys. Chem. A* 2010, *114*, 6757.
98. O. Weingart, A. Migani, M. Olivucci, M. A. Robb, V. Buss, P. Hunt, *J. Phys. Chem. A* 2004, *108*, 4685.
99. O. Weingart, I. Schapiro, V. Buss, *J. Phys. Chem. B* 2007, *111*, 3782.
100. M. Boggio-Pasqua, M. Ravaglia, M. J. Bearpark, M. Garavelli, M. A. Robb, *J. Phys. Chem. A* 2003, *107*, 11139.
101. M. Garavelli, F. Bernardi, M. Olivucci, M. J. Bearpark, S. Klein, M. A. Robb, *J. Phys. Chem. A* 2001, *105*, 11496.
102. S. Hayashi, E. Taikhorshid, K. Schulten, *Biophys. J.* 2009, *96*, 403.
103. S. Hayashi, E. Tajkhorshid, K. Schulten, *Biophys. J.* 2003, *85*, 1440.
104. M. Ben-Nun, T. J. Martínez, *Chem. Phys. Lett.* 1998, *298*, 57.
105. T. J. Martínez, R. D. Levine, *J. Chem. Phys.* 1996, *105*, 6334.
106. A. L. Kaledin, J. Seong, K. Morokuma, *J. Phys. Chem. A* 2001, *105*, 2731.
107. K. Drukker, *J. Comput. Phys.* 1999, *153*, 225.
108. J. R. Schmidt, P. V. Parandekar, J. C. Tully, *J. Chem. Phys.* 2008, *129*, 6.
109. G. Zechmann, M. Barbatti, H. Lischka, J. Pittner, V. Bonačić-Koutecký, *Chem. Phys. Lett.* 2006, *418*, 377.
110. A. M. Virshup, C. Punwong, T. V. Pogorelov, B. A. Lindquist, C. Ko, T. J. Martìnez, *J. Phys. Chem. B* 2008, *113*, 3280.
111. H. M. Senn, W. Thiel, *Angew. Chem. Int. Ed.* 2009, *48*, 1198.
112. A. Warshel, M. Levitt, *J. Mol. Biol.* 1976, *103*, 227.
113. A. Warshel, *Nature* 1976, *260*, 679.
114. D. Bakowies, W. Thiel, *J. Phys. Chem.* 1996, *100*, 10580.
115. B. Brooks, R. Bruccoleri, B. Olafson, D. States, S. Swaminathan, M. Karplus, *J. Comput. Chem.* 1983, *4*, 187.
116. W. D. Cornell, P. Cieplak, C. I. Bayly, I. R. Gould, K. M. Merz, D. M. Ferguson, D. C. Spellmeyer, T. Fox, J. W. Caldwell, P. A. Kollman, *J. Am. Chem. Soc.* 1995, *117*, 5179.
117. U. C. Singh, P. A. Kollman, *J. Comput. Chem.* 1986, *7*, 718.
118. M. J. Field, P. A. Bash, M. Karplus, *J. Comput. Chem.* 1990, *11*, 700.
119. K. H. Jung, V. D. Trivedi, J. L. Spudich, *Mol. Microbiol.* 2003, *47*, 1513.
120. C. Vasileiou, S. Vaezeslami, R. M. Crist, M. Rabago-Smith, J. H. Geiger, B. Borhan, *J. Am. Chem. Soc.* 2007, *129*, 6140.
121. S. Pistolesi, A. Sinicropi, R. Pogni, R. Basosi, N. Ferré, M. Olivucci, *J. Phys. Chem. B* 2009, *113*, 16082.
122. M. H. Huntress, in preparation.
123. A. Melloni, R. Rossi Paccani, D. Donati, V. Zanirato, A. Sinicropi, M. L. Parisi, E. Martin, M. Ryazantsev, W. J. Ding, L. M. Frutos, R. Basosi, S. Fusi, L. Latterini, N. Ferré, M. Olivucci, *J. Am. Chem. Soc.* 2010, *132*, 9310.
124. A. Migani, A. Sinicropi, N. Ferré, A. Cembran, M. Garavelli, M. Olivucci, *Faraday Discuss.* 2004, *127*, 179.
125. T. Andruniow, N. Ferré, M. Olivucci, *Proc. Natl. Acad. Sci. USA* 2004, *101*, 17908.
126. P. B. Coto, A. Strambi, N. Ferré, M. Olivucci, *Proc. Natl. Acad. Sci. USA* 2006, *103*, 17154.
127. P. B. Coto, S. Marti, M. Oliva, M. Olivucci, M. Merchan, J. Andres, *J. Phys. Chem. B* 2008, *112*, 7153.
128. A. Sinicropi, T. Andruniow, N. Ferré, R. Basosi, M. Olivucci, *J. Am. Chem. Soc.* 2005, *127*, 11534.
129. A. Strambi, P. B. Coto, N. Ferré, M. Olivucci, *Theor. Chem. Acc.* 2007, *118*, 185.
130. N. Ferré, M. Olivucci, *J. Am. Chem. Soc.* 2003, *125*, 6868.
131. G. Tomasello, G. Olaso-Gonzàlez, P. Altoè, M. Stenta, L. Serrano-Andrès, M. Merchàn, G. Orlandi, A. Bottoni, M. Garavelli, *J. Am. Chem. Soc.* 2009, *131*, 5172.
132. M. Schreiber, M. Sugihara, T. Okada, V. Buss, *Angew. Chem. Int. Ed.* 2006, *45*, 4274.

133. P. Altoè, A. Cembran, M. Olivucci, M. Garavelli, *Proc. Natl. Acad. Sci. USA* 2010, *107*, 20172.
134. A. Altun, S. Yokoyama, K. Morokuma, *J. Phys. Chem. B* 2008, *112*, 6814.
135. K. Bravaya, A. Bochenkova, A. Granovsky, A. Nemulkhin, *J. Am. Chem. Soc.* 2007, *129*, 13035.
136. M. Hoffmann, M. Wanko, P. Strodel, P. H. Konig, T. Frauenheim, K. Schulten, W. Thiel, E. Tajkhorshid, M. Elstner, *J. Am. Chem. Soc.* 2006, *128*, 10808.
137. A. Munoz-Losa, I. F. Galvan, M. A. Aguilar, M. E. Martin, *J. Phys. Chem. B* 2008, *112*, 8815.
138. M. Wanko, M. Hoffmann, P. Strodel, A. Koslowski, W. Thiel, F. Neese, T. Frauenheim, M. Elstner, *J. Phys. Chem. B* 2005, *109*, 3606.
139. I. Navizet, Y.-J. Liu, N. Ferré, H.-Y. Xiao, W.-H. Fang, R. Lindh, *J. Am. Chem. Soc.* 2009, *132*, 706.
140. P. Altoè, T. Climent, G. C. De Fusco, M. Stenta, A. Bottoni, L. Serrano-Andrès, M. Merchàn, G. Orlandi, M. Garavelli, *J. Phys. Chem. B* 2009, *113*, 15067.
141. X. Li, L. W. Chung, H. Mizuno, A. Miyawaki, K. Morokuma, *J. Phys. Chem. B* 2009, *114*, 1114.
142. K. Fujimoto, S. Hayashi, J. Hasegawa, H. Nakatsuji, *J. Chem. Theory Comput.* 2007, *3*, 605.
143. R. Mathies, L. Stryer, *Proc. Natl. Acad. Sci. USA* 1976, *73*, 2169.
144. V. Bonačić-Koutecký, J. Köhler, J. Michl, *Chem. Phys. Lett.* 1984, *104*, 440.
145. V. Bonačić-Koutecký, K. Schöffel, J. Michl, *Theor. Chem. Acc.* 1987, *72*, 459.
146. A. Strambi, P. B. Coto, L. M. Frutos, N. Ferré, M. Olivucci, *J. Am. Chem. Soc.* 2008, *130*, 3382.
147. H. Tao, B. G. Levine, T. J. Martínez, *J. Phys. Chem. A* 2009, *113*, 13656.
148. M. Barbatti, H. Lischka, *J. Am. Chem. Soc.* 2008, *130*, 6831.
149. C. Filippi, M. Zicchedu, F. Buda, *J. Chem. Theory Comput.* 2009, *5*, 2074.
150. V. Balzani, E. Marchi, M. Semeraro, *Rend. Fis. Acad. Lincei* 2010, *21*, 91.

42

DNA Fluorescence

Dimitra Markovitsi
Laboratoire Francis Perrin

Thomas Gustavsson
Laboratoire Francis Perrin

Akos Banyasz
Laboratoire Francis Perrin

42.1 Introduction

Talking about fluorescence with respect to DNA, one usually refers to fluorescent labels used extensively in biology and genetics. Yet DNA does emit fluorescence albeit with a low quantum yield, on the order of 10^{-4}. Such weak emission, which so far prevented large-scale technological applications, may be precious in many respects provided that its properties are well understood. For example, it can contribute to elucidate questions such as the following: How did the building blocks of the genetic code "survive" when intense ultraviolet (UV) radiation was reaching the earth? What are the primary events leading to photochemical reactions that induce carcinogenic mutations? This is possible because following the time behavior of fluorescence brings information about the singlet electronic excited states and their relaxation.

Although the first articles reporting room-temperature fluorescence of DNA components were published already in 1971,[1,2] a thorough study of the emitting states was limited by the time resolution. It is only during the past few years that the development of femtosecond techniques, mainly based on fluorescence upconversion (FU) and allowing excitation and detection in the UV spectral domain, gave an important impulse to this field.

Here, we tackle studies that have appeared since the turn of the twenty-first century. We mention that two recent reviews deal with the excited-state dynamics of nucleic acids with particular emphasis on transient absorption studies.[3,4] In the present chapter, we present the fluorescence behavior of these systems in more detail, and we address the main problems and outcomes related to such investigations.

We examine successively the monomeric building blocks (bases, nucleosides, nucleotides; Section 42.5) and then more complex systems (single, double, and quadruple strands; Section 42.6). As photon emission is strongly related to photon absorption, at least in the reported work, we also discuss the absorption spectra and the Franck–Condon excited states (Section 42.4).

Detecting very weak fluorescence signals with UV excitation is not a trivial task. Therefore, we describe experimental methods specially related to this type of measurements (Section 42.2). Finally, in the case of DNA strands, particular cautions are required due to their increased fragility versus UV radiation and the plasticity of their structure. This renders comparison of data obtained by various groups using different experimental conditions quite delicate and the definition of commonly accepted protocols is an urgent need (Section 42.3).

42.2 Experimental Methods and Setups

42.2.1 Steady-State Fluorescence Spectra

The following procedure was followed in order to record fluorescence spectra of DNA components over a large spectral domain and make a refined comparison of the emission spectra of various systems.[5]

Fluorescence spectra were recorded with a SPEX Fluorolog-2 spectrofluorimeter equipped with a 450 W arc xenon lamp. The calibration of emission monochromator was verified using a Hg low-pressure standard lamp whereas that of the excitation monochromator was confirmed by observing the scattered excitation light from water. The emission correction factor was performed by means of deuterium and tungsten lamps of standard irradiance and checked via the standard fluorescence spectrum of quinine sulfate.[6]

For fluorescence measurements, 1 cm × 1 cm and 0.2 cm × 1 cm quartz cells (QZS) were used for dilute and concentrated solutions, respectively. For dilute solutions ($<5 \times 10^{-5}$ M; 1 cm × 1 cm cells), the signal of solvent (in most cases the Raman line of water) was not negligible compared to the fluorescence intensity. Therefore, its contribution was subtracted from the fluorescence spectra. Each spectrum was recorded several times: (1) without any filter at the emission side and using (2) a Schott WG320 or (3) a Schott GG385 filter. In all cases, a Schott UG5 filter was used on the excitation side. The three spectra were normalized at appropriate wavelengths and then joined. Such a procedure allowed us to eliminate the second order of the scattered excitation light from water, Raman scattering and also the second order of the main fluorescence peak.

Fluorescence quantum yields (ϕ_s) were determined using quinine sulfate dihydrate in 0.1 M $HClO_4$ ($\phi_s = 0.59$).[6] As a control, the fluorescence quantum yield of 2,5-diphenyloxazole (PPO) in cyclohexane was determined and found to be 0.90 ± 0.02, in perfect agreement with the most recent value reported in the literature (0.89).[7]

42.2.2 Time-Resolved Techniques

As mentioned in Section 42.1, time-resolved fluorescence studies of DNA constituents require femtosecond resolution. Nevertheless, much longer-lived components are present in the fluorescence of DNA helices. In order to obtain a global picture, probing fluorescence over several decades of time is necessary. This can only be achieved by combination of different detection techniques.

Femtosecond time resolution is obtained by the use of femtosecond lasers together with optical gating detection: FU and optical Kerr gating (OKG). In FU, an intense laser (gate) pulse is mixed with the polarized fluorescence in a nonlinear optical crystal creating a sum-frequency light. The gate pulse defines a time window during which the fluorescence can be measured. By scanning the optical delay between the gating and excitation pulses, fluorescence intensity traces are recorded. The detection is performed by photon counting, favorable for high-repetition (MHz) laser sources,[8] but also amplified kHz systems are used.[9,10] In OKG, the polarized fluorescence is directed through a Kerr shutter consisting of two crossed polarizers between which a Kerr medium is positioned. Without a gating pulse, the fluorescence is extinguished by the Kerr shutter. However, when a highly intense laser pulse (gate) is focused into the Kerr medium, it induces a change of the fluorescence polarization, letting part of it to pass through to detection. An amplified kHz laser system is necessary in order to attain the gating pulse intensities needed.[11] Time-resolved fluorescence spectra of DNA were obtained by both FU[12–17] and OKG.[18,19]

Recent DNA fluorescence studies focusing on longer components relied on time-correlated single photon counting (TCSPC) using either femtosecond laser[20,21] or synchrotron radiation.[22]

The experimental setup developed in our laboratory for the time-resolved fluorescence measurements of DNA cited here gives the possibility to probe fluorescence over a large time domain from 100 fs to 100 ns using the same excitation source (267 nm, 120 fs). Two different detection techniques were used. On the one hand, FU detects emission associated with allowed electronic transitions with a resolution of ca. 100 fs after deconvolution. On the other hand, TCSPC probes emission from both bright and "dark" excited states with a time resolution of 10 ps after deconvolution.

We paid special attention to the determination of the fluorescence anisotropy. To this end, parallel $I_{par}(t)$ and perpendicular components $I_{per}(t)$ of the fluorescence signals were recorded by means of a half wave plate, positioned at the excitation side (FU) or by means of a Glan Thomson prism positioned at the detection side (TCSPC). Fluorescence decays F(t) and fluorescence anisotropy decays r(t) were determined as follows:

$$F(t) = I_{par}(t) + 2GI_{per}(t),$$

$$r(t) = \frac{I_{par}(t) - GI_{per}(t)}{I_{par}(t) + 2GI_{per}(t)}.$$

In the case of FU, the G factor was equal to 1, whereas in the case of TCSPC, it was determined by the tail-matching method using protonated guanosine (pH = 2.5).[23]

42.3 Protocols for the Study of DNA Helices

Spectroscopic studies of DNA helices present specific difficulties, which are not encountered in the experiments carried out with monomeric chromophores.[24] Indeed, the close proximity of the bases within a helix favors photoreactions leading to dimeric products, such as cyclobutane dimers and (6-4) adducts.[25–27] Moreover, base stacking increases their propensity to lose an electron upon photon absorption.[28–30] Thus, laser pulses are likely to provoke two-photon ionization of both the aqueous solvent as well as of the DNA helices. The produced radicals[31–33] are very reactive and they lead to oxidation products, such as 6-hydroxy-5,6-dihydrocytosine or 8-oxo-7,8-dihydroguanine. Further reactions may be induced by the hydrated electrons, which can attack the studied nucleic acids.

The various photoproducts may affect fluorescence measurements in two ways. On the one hand, some of them emit light. This is typically the case of the (6-4) adducts whose fluorescence quantum yield is higher by two orders of magnitude than that of DNA components.[34] On the other hand, photoproduct formation within a helix may alter its conformation, which, in turn, may modify the electronic coupling. Consequently, excited-state relaxation of damaged duplexes should be different compared to that of the initial duplexes, which are the objects under study. For example, we found that accumulation of photoproducts in $(dA)_n \cdot (dT)_n$, shortens its fluorescence lifetime recorded by FU and increases that determined by TCSPC.[24]

Analysis of the thymine dimers formed upon continuous irradiation at 267 nm of $(dA)_{20} \cdot (dT)_{20}$ using high-performance liquid chromatography coupled to mass spectrometry brought an important insight into the relation between spectral changes and photodamage.[35] It was demonstrated that changes in the steady-state absorption spectra result from two antagonistic effects: on the one hand, a decrease in the absorbance due to disappearance of the thymines which reacted and, on the other hand, an increase in the absorbance due to local denaturation of the adenines. Consequently, judging the amount of photodamage provoked by a laser experiment on the basis of absorption changes [36,37] may be misleading. To be more specific, the formation of one cyclobutane dimer within $(dA)_{20} \cdot (dT)_{20}$ corresponds to a destruction of 5% of the bases of the duplex but leads to only 0.6% decrease in the absorption maximum.[35]

In order to avoid contamination of the fluorescence signals with photons emitted from damaged helices, it is important to follow a few rules: keep the laser intensity as low as possible, use a sufficiently large ratio of molecules compared to that of the photons absorbed during the measurement and avoid local accumulation of photoproducts. In practice, FU experiments were performed using a flow cell allowing circulation of 20 mL of solution (ca. 2×10^{-3} M per base), the laser intensity at the surface of the sample being 2×10^8 W cm^{-2}. Much lower laser intensities (10^4 W cm^{-2}) were used in TCSPC measurements, which gave the possibility to work with smaller volumes: 0.6 mL (ca. 2×10^{-4} M per base) in a moving cell. However, the ultimate test is to check if successive signals recorded with the same solution are reproducible. Experimental procedures similar to ours were also followed by Schwalb and Temps.[38]

Besides the aforementioned cautions related to UV excitation of DNA helices, further problems are associated specifically with double strands. Polymers are produced biochemically, which insures efficient base pairing, whereas oligomers are prepared by annealing of the parent single strands. In the latter case, duplex formation depends both on the annealing conditions and on the base sequence. In particular, when repetitive simple base sequences are used, such as $(dA)_n \cdot (dT)_n$ or $(dAdT)_n \cdot (dAdT)_n$, slipping between the two complementary strands is possible. The degree of hyperchromism observed upon melting of a duplex should be used as a quality test for base pairing.[24]

42.4 Franck–Condon Excited States

42.4.1 Monomeric Chromophores

The absorption spectra of the nucleosides (dA: 2′-deoxyadenosine; dT: thymidine; dG: 2′-deoxyguanosine; dC: 2′-deoxycytidine), identical to those of the nucleotides (dAMP: 2′-deoxyadenosine 5′-monophosphate; TMP: thymidine 5′-monophosphate; dGMP: 2′-deoxyguanosine 5′-monophosphate; dCMP: 2′-deoxycytidine 5′-monophosphate) that constitute the monomeric DNA chromophores, are shown in Figure 42.1. The cytosine and thymine derivatives belong to the pyrimidine family, while adenines and guanines are denoted as purines.

The lowest in energy absorption band of dA/dAMP and dG/dGMP corresponds to two close-lying electronic transitions. This is suggested by a shoulder present in the dG spectrum. In the case of the adenine derivatives, the existence of two transitions was evidenced experimentally by means of linear dichroism and magnetic circular dichroism.[39] These observations are corroborated by quantum chemistry calculations, which have shown the existence of two close-lying $\pi\pi^*$ states, denoted by L_a and L_b,[40,41] in accordance with the Platt nomenclature.[42] Even if their relative ordering in gas phase is under debate, we can assume that for chromophores in aqueous solution, the more polar L_a is the first excited state. For the pyrimidines, the L_a and L_b are much further apart, so the first absorption band corresponds essentially to only one strong $\pi\pi^*$ transition.

In addition to the spectra of the nucleosides corresponding to the four major bases, we also present in Figure 42.1 that of 5-methylcytidine (5MedC). Methylation and demethylation at the five position of cytosine are natural processes playing an important biological role.[43] Methylated sites are strongly correlated with the occurrence of carcinogenic mutations.[44] The absorption spectrum of 5MedC is red-shifted with respect to that of dC.[12] This observation together with the fact that the intensity of the solar radiation reaching the earth increases with increasing wavelength could be a hint for the involvement of this rare base to the appearance of UV-induced DNA lesions.

42.4.2 DNA Helices

When going from monomeric chromophores to the DNA double strands, the absorption spectra are altered (Figure 42.2). The most striking change concerns the oscillator strength. The DNA hypochromism is used to characterize the stability of double strands via their melting curves, obtained by

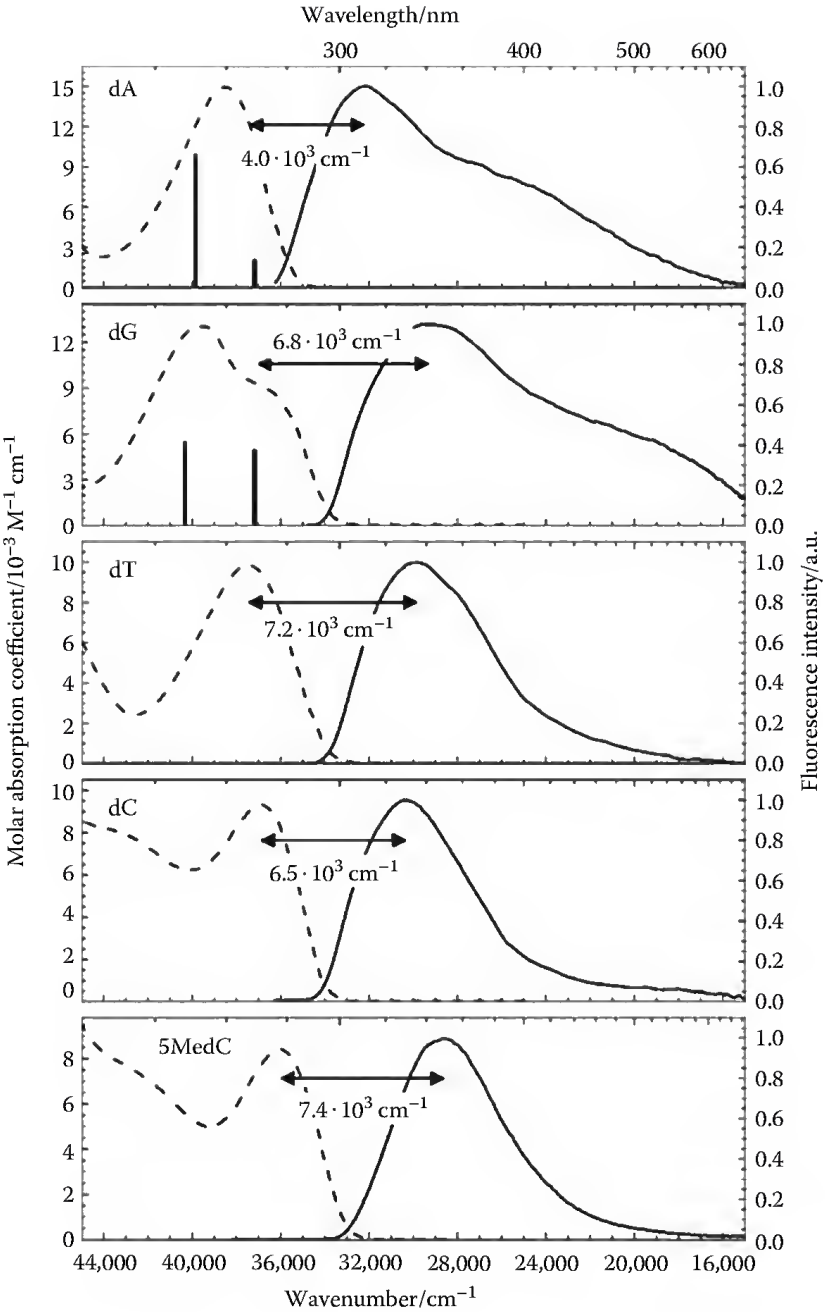

FIGURE 42.1 Steady-state absorption (dashed) and fluorescence (solid) spectra of dA, dG, dT, dC, and 5MedC in water. Arrows designate the Stokes shift. Vertical bars indicate the two lowest transitions of dA and dG; $\lambda_{exc} = 255$ nm.

following the absorbance at 260 nm as a function of temperature. Despite the extensive application of this phenomenological property, the underlying modifications of the electronic transitions remained unclear until recently. The study of base pairs and dimers of base pairs by quantum chemistry methods shed light on this question attributing the DNA hypochromism to charge transfer transitions between different bases.[45,46] It was also shown that simple coupling between bright and "dark" transitions may lead to the same effect.[47]

It can be seen in Figure 42.2 that the change in the molar absorption coefficient observed for the duplex with respect to an equimolar mixture of the constitutive nucleotides is not uniform over the

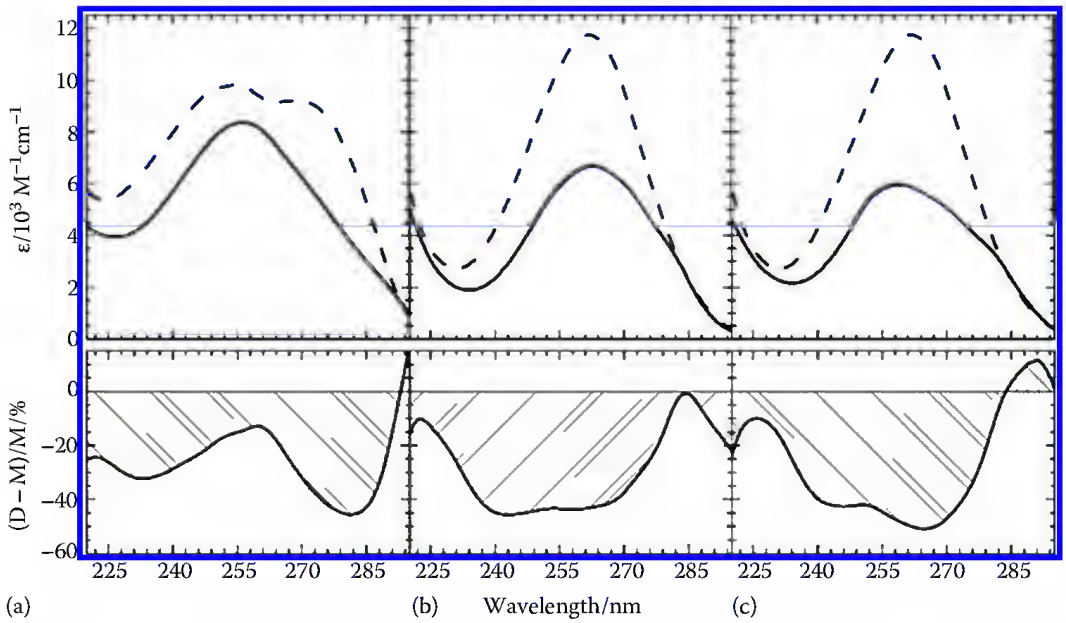

FIGURE 42.2 Comparison of the absorption spectra obtained for duplexes [D in solid lines: (a) poly(dGdC)·poly(dGdC); (b) poly(dA)·poly(dT); (c) poly(dAdT)·poly(dAdT)] and an equimolar mixture of the constitutive nucleotides (M in dashed lines). The shaded area in the lower part corresponds to (D − M)/M. The molar absorption coefficient is given per base.

whole spectrum and depends on the base sequence. Interestingly, an increase in the oscillator strength is observed at the red edge of the spectra of duplexes composed of homopolymeric adenine–thymine $(dA)_n \cdot (dT)_n$ and alternating guanine–cytosine $(dCdG)_n \cdot (dCdG)_n$ sequences. This is also known to occur in the case of four-stranded structures formed by self-association of guanines via Hoogsteen bonds (Figure 42.3) called G-quadruplexes.[48–50]

In addition to orbital overlap interactions, another type of electronic interactions is also operative within double strands: coupling between dipolar transitions of the monomeric chromophores, which gives rise to Frenkel excitons. According to the exciton theory, the excited states of a multichromophoric system are linear combinations of the excited states localized on each monomeric constituent.[51,52] The calculated properties of the eigenstates highly depend on the way that the exciton matrix is constructed. Recent calculations performed in this frame for duplexes composed of 10 base pairs marked a significant progress with respect to older studies.[53,54] The diagonal terms of the Hamiltonian matrix (dipolar coupling) were calculated using atomic transition charges derived from quantum chemistry data[55] and taking into account various conformations determined by molecular dynamics simulations.[56–58] These theoretical studies showed that, even in the presence of conformational disorder, the dipolar coupling alone is capable of inducing delocalization of the excitation over several bases. The number of coherently coupled bases in a given eigenstate *k* can be calculated by the participation ratio $PR = 1/L_k$,[59,60] where L_k is given by

$$L_k = \sum_{\text{monomer m}} \left[\sum_{\text{states i}} \left(C^i_{k,m} \right)^2 \right]^2 .$$

The sum within the square brackets represents the contribution to the eigenstate <k> of different electronic states (i) belonging to the same monomer (m). The participation ratio was determined for two limiting cases (Figure 42.4). First, in the absence of spectral broadening, considering that each electronic transition of the monomeric chromophores is a delta function. Then, spectral broadening was taken into account. As the homogeneous width is not known, diagonal disorder was represented by the inhomogeneous width derived from decomposition of the experimental spectra in solution (Figure 42.1)

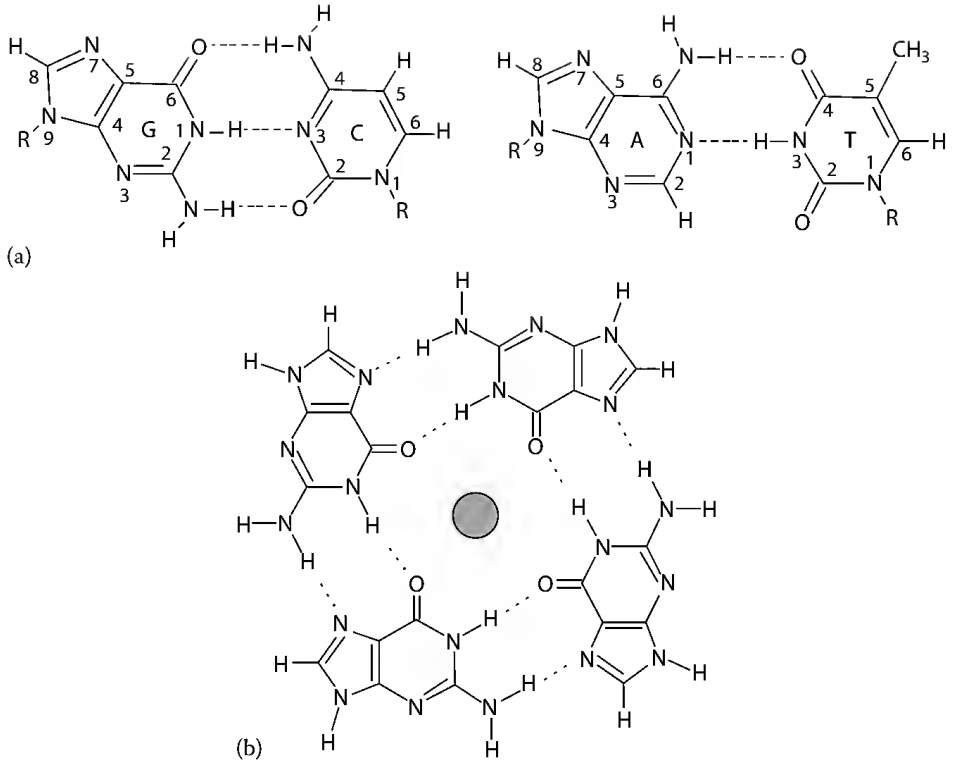

FIGURE 42.3 Schematic representation of (a) guanine–cytosine and adenine–thymine Watson–Crick base pairs and (b) a tetrad where guanines are linked via Hoogsteen hydrogen bonds and stabilized by a metal cation (gray circle).

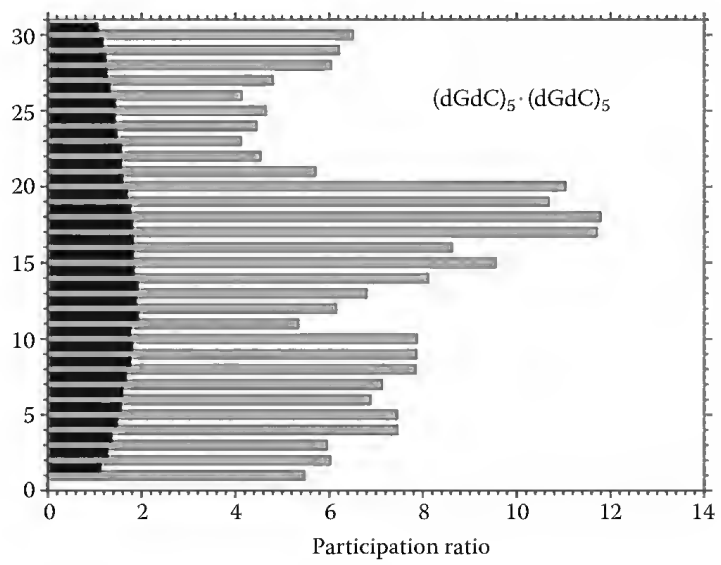

FIGURE 42.4 Average participation ratios calculated for the 30 eigenstates of $(dCdG)_5 \cdot (dCdG)_5$ within the frame of the exciton theory. Two extreme cases are shown: the diagonal terms are represented either by delta functions (gray) or by Gaussian curves whose width corresponds to the inhomogeneous width of the experimental absorption spectra of nucleotides in aqueous solution (black).

using lognormal functions.[55] Even in the latter case, where the diagonal disorder is overestimated, many of the excited states, in particular those located near the absorption maximum, remain delocalized over several bases.[57,58] The same theoretical studies showed that delocalization of the excitation does not induce large spectral shifts with respect to the spectra of noninteracting monomers.[57,58] Burin et al.[62] showed that the dipolar coupling within DNA hairpins composed of adenine–thymine pairs can be deduced from their absorption spectra.[62]

Finally, theoretical calculations performed by quantum chemical methods for smaller systems than those studied by the exciton theory, also reported delocalization of the $\pi\pi^*$ transitions over two or more bases as well as mixing among $\pi\pi^*$ and charge transfer excitons.[63–67]

42.5 Fluorescence of Monomeric Chromophores

42.5.1 Steady-State Measurements

Few studies have been consecrated to the steady-state fluorescence properties of the natural DNA bases in recent years. In 2002, we published refined room-temperature fluorescence spectra of the eight natural DNA nucleosides and nucleotides in water.[5] Those of dA, dG, dT, dC, and 5MedC in water are shown in Figure 42.1, and the corresponding peak positions are given in Table 42.1. In contrast to the spectra published up to 2000, which were restricted to the near UV and blue region, the spectra in Figure 42.1 are extended further into the visible.

We determined the quantum yields using the fluorescence spectra recorded over the whole visible spectral region and compared their values with earlier ones.[5] The fluorescence quantum yield values thus obtained were systematically higher than earlier ones and are given in Table 42.1.

Covalent substitutions have strong effects on the fluorescence properties. This is shown in a striking manner by methylation of the various bases. For 5MedC, the fluorescence peak value was found to be shifted by 14 nm to the red and the fluorescence quantum yield increased by a factor of six compared to dC.[12] The effect of methylation, as well as other substitutions, was also reported in a systematic study of various uracils in reference.[68] Uracil (Ura) itself has the lowest fluorescence quantum yield of all DNA/RNA bases.

TABLE 42.1 Fluorescence Maxima (λ_{fl}) and Quantum Yields (ϕ) of Monomeric Chromophores in Aqueous Solution

Compound	λ_{fl} (nm)[a]	$\phi \times 10^4$	r_0	References
dA	307	0.86 ± 0.15		5
dAMP	306	0.68 ± 0.10	0.24 ± 0.01	5
dG	334	0.97 ± 0.08		5
dGMP	334	1.09 ± 0.10	0.15 ± 0.04	5
Thy	329	1.02	≈0.4	68
dT	330	1.32 ± 0.07		5
TMP	330	1.54 ± 0.11	0.36 ± 0.01	5
dC	328	0.89 ± 0.10		5
dCMP	328	1.15 ± 0.06	0.34 ± 0.01	5
5MedC	342	5.6 ± 0.1		12
Ura	312	0.35	≈0.4	68
5FUra	335	2.21	≈0.4	68

Thy, Ura, 5FUra, 5MedC refer to the Thymine, Uracil, 5-fluorouracil and 5-methylcytidine, respectively; dX and XMP/dXMP refer to 2′-deoxynucleosides and 2′-deoxynucleotides respectively, where X corresponds to the first letter of the name of the base.

[a] Error: ±1 nm.

For 5-methyluracil (thymine), the quantum yield increases by a factor of 3 and for 5-fluorouracil (5FUra), it increases by another factor of two. Furthermore, the maxima of the emission spectra are correlated with the quantum yields; for uracil, it is blueshifted with regard to thymine, while for 5FUra it is redshifted. This indicates that the emitting state is deactivated faster than its energetic relaxation.[68]

42.5.2 Time-Resolved Measurements

42.5.2.1 Natural DNA Bases

Since 2000, numerous ultrafast spectroscopic studies in solution have contributed largely to characterize the fluorescence decays of the DNA monomeric chromophores. These studies have established that the excited-state decays are globally subpicosecond, even though there are differences from one system to another. In the large majority of cases, the decays have been measured close to the fluorescence maximum, that is, 330 nm in spite of the fact that, as mentioned earlier, the steady-state fluorescence extends well into the visible region. Visible wavelengths have only been probed in a few cases, showing that the fluorescence decays are ultrafast all over the spectral domain.

Peon and Zewail[9] were the first to publish femtosecond fluorescence measurements of DNA/RNA nucleosides and nucleotides in room-temperature water solution using FU.[9] They reported that all fluorescence decays are subpicosecond and monoexponential. The latter fact that was later revised.[69]

We have, in a series of papers, refined the study of fluorescence from DNA monomeric constituents using femtosecond FU.[5,8,17,68,70,71] A general feature for all molecules is that the fluorescence decay is strongly nonexponential. This is exemplified in Figure 42.5, where the fluorescence decay of TMP at 330 nm is shown over 7 ps, covering three decades in intensity. Also shown in this figure are the resulting curves from fitting with mono- and bi-exponential model functions.

Normalized fluorescence decays for the four mononucleotides at 330 nm are shown in Figure 42.6. In these experiments the apparatus function was 325 fs full width at half maximum (fwhm).

Regarding the two pyrimidine chromophores, there are only small variations between the fluorescence decays of the base, the nucleoside, and the nucleotide.[5,18,68,70,71] The nonexponential decays are all dominated by an ultrafast component, between 150 and 300 fs and a slower one of ca. 1 ps having much lower amplitude (Table 42.2). In their broadband femtosecond Kerr-gate study of thymidine, Kwok et al.[18] evoked the existence of a "doorway" state facilitating excited-state deactivation. This "doorway" state should mainly be $^1n\pi^*$ but mix with the close-lying $^1\pi\pi^*$ states.

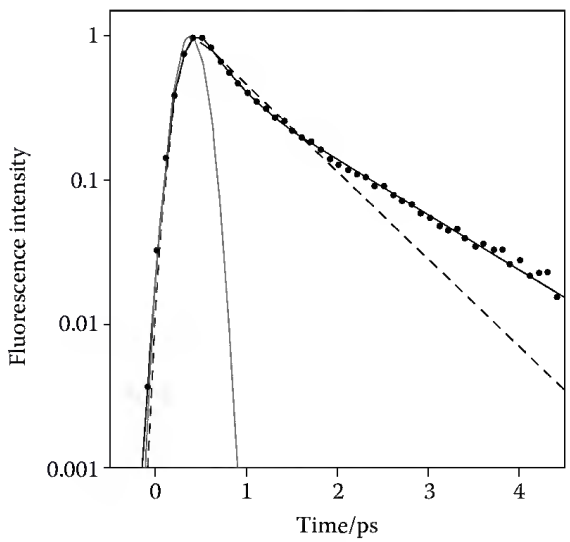

FIGURE 42.5 Fluorescence decay of TMP recorded by FU at 330 nm. Also shown the apparatus function (gray) and the fits with mono- and bi-exponential functions.

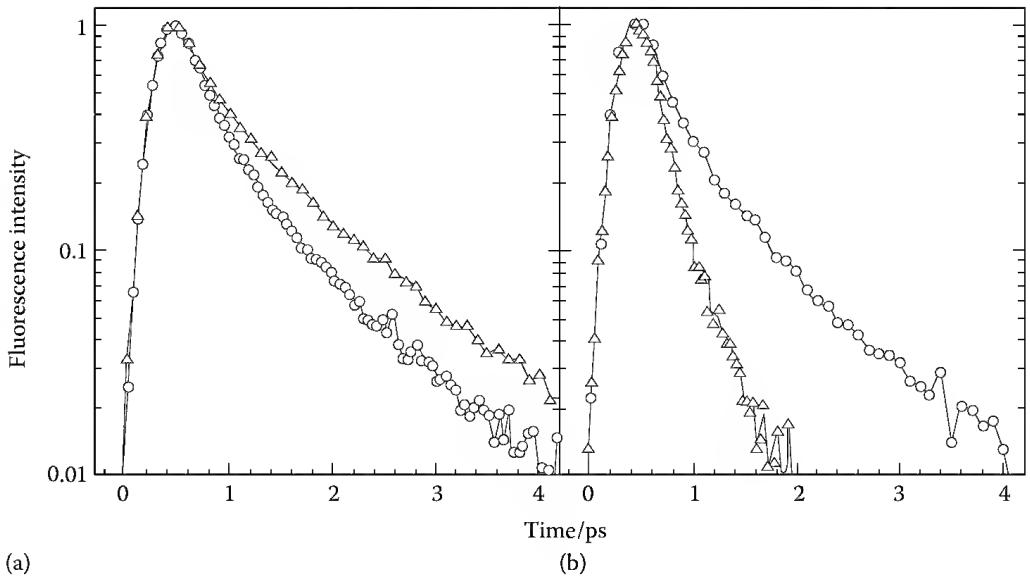

FIGURE 42.6 Fluorescence decays of (a) dCMP (circles) and TMP (triangles) and (b) dAMP (triangles) and dGMP (circles) recorded by FU at 330 nm.

The fluorescence decay of adenine is characterized by an exceptionally long component of about 8 ps and a faster one of about 0.2 ps.[5,8,72] The long component was assigned to the 7H tautomer, while the fast component was assigned to the canonical 9H tautomer. The simultaneous presence of two tautomers has only been observed in the case of adenine but not for dA and dAMP. The latter exist only in their 9H form and displays much faster fluorescence decays. Temps and coworkers studied adenine and adenosine by FU using a tunable excitation source.[72] For the 9H-adenine tautomer, they found the decays to vary significantly with the excitation wavelength. This was explained by the opening of an additional nonradiative decay channel with decreasing excitation wavelength, possibly involving a near-lying $n\pi^*$ state. For adenosine, on the other hand, they found a monoexponential decay for all excitation wavelengths. Kwok et al.[11] studied the adenosine fluorescence by a broadband femtosecond Kerr-gated technique. Analysis of the fluorescence decays gave two components with lifetimes of ~0.13 and ~0.45 ps, which were associated these with the L_b and L_a $^1\pi\pi^*$ excited states, respectively. The 0.13 ps time constant was proposed to correspond to the $L_b - L_a$ internal conversion. This is in line with an interpretation based on the Strickler–Berg equation, suggesting that both $^1\pi\pi^*$ excited states contribute to the fluorescence of these chromophores.[73] However, the very low initial value (0.25) and the lack of any rapid decay of fluorescence anisotropy[5] clearly show that the $L_b - L_a$ relaxation is too fast ($\ll$100 fs) for L_b to contribute to the emission of dA/dAMP. This is corroborated by the fact that the steady-state emission spectra are independent of the excitation wavelength.[5]

Regarding the guanine chromophore, there are only data for the nucleoside and the nucleotide since guanine itself is not soluble enough in water. As their steady-state fluorescence spectra are by far the broadest, extending beyond 700 nm,[5] we performed an extensive study of the dGMP fluorescence at various emission wavelengths.[17] The fluorescence decays were found to depend strongly on the wavelength, indicating important spectral shifts (Figure 42.7). Incompatible with solvation dynamics, a global analysis revealed that the spectral evolution can be explained by an ultrafast redshift and broadening, in accordance with a recent theoretical study.[74] As in the case of dAMP, dGMP emission originates only from the first excited state.

The nonexponentiality of the fluorescence decays was rationalized as arising from two different "regions" of the potential energy surface of the first $\pi\pi^*$ state.[68,74] The fast component should then correspond to the Franck–Condon region, while the longer one should be correlated with a "relaxed" geometry along the reaction coordinate toward a conical intersection (CI).

On Table 42.2, we have assembled fitted time constants from recent measurements of fluorescence decays at 330 nm of the four DNA bases and their nucleosides and nucleotides.

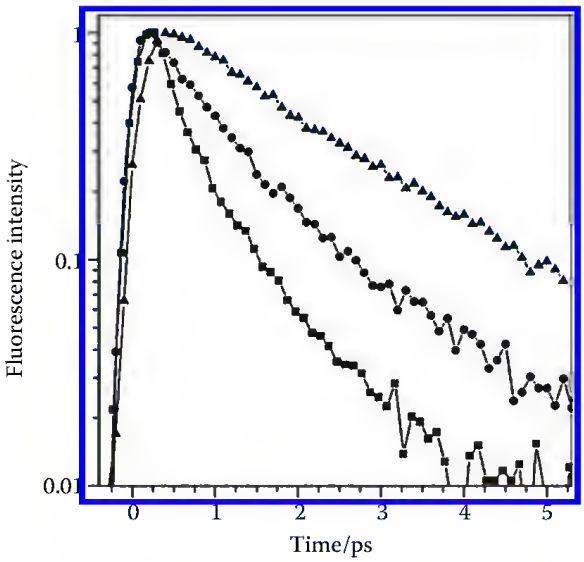

FIGURE 42.7 Fluorescence decays of dGMP recorded by FU at 330 (squares), 450 (circles), and 600 nm (triangles).

42.5.2.2 Role of Substituents

In addition to the natural DNA bases mentioned earlier, the fluorescence of various substituted bases has been studied by ultrafast spectroscopy. The objective was to elucidate conformational and electronic changes occurring during excited-state relaxation in close connection with theoretical studies. Among the possible substitutions, the most important one is without doubt methylation, which also occurs naturally. For example, thymine is just the 5-methylated form of the RNA base uracil.

The average fluorescence lifetime of 5MedC is about one order of magnitude longer than that of dC[12] (Figure 42.8b). Contrary to dC, the fluorescence decays of 5MedC depend strongly on the wavelength, indicating important spectral shifts.

We have paid special attention to the fluorescence of uracil and its derivatives.[68,75–77] The effect of methylation, halogenation as well as that of other substituents on the first excited $\pi\pi^*$ and $n\pi^*$ singlet states were investigated by combining femtosecond fluorescence spectroscopy and quantum chemistry calculations.[78] The analysis relied on time-dependent density functional theory (TD–DFT) calculations, described in the following. Uracil itself has the fastest fluorescence decay observed for any nucleic acid. It is shorter than the time resolution (100 fs) of the FU setup. In contrast to methylation at the five position, methylation of uracil at positions 1, 3, and 6 does not induce any observable change on the fluorescence decays.[78] An example is given in Figure 42.8a, where the fluorescence decays of uracil and thymine are compared. These results, obtained with femtosecond resolution, contrast with those obtained for a "blocked" uracil (5,6-trimethyleneuracil) by a TCSPC study combined with quantum chemistry calculations[79,80] indicating that the six substituent is also involved in the internal conversion mechanism. According to these studies, the five and six substituents flip out of the molecular plane in opposite directions forming a biradical state.

Focusing on the five substituent, it was found that the fluorescence lifetime depends on its chemical nature.[78] The longest lifetime was observed for 5FUra. A particular behavior was observed in the case of the amino group.[81] While amino substitution on the six position has no effect at all, amino substitution on the five position (5-aminouracil, 5AUra) causes a drastic increase in lifetime. The fluorescence decays of 5AUra depend strongly on the emission wavelength.

As noted in the preceding subsection, the adenine chromophore has the shortest fluorescence lifetime of the natural DNA constituents. However, slight structural changes may have enormous consequences on the electronic structure and thus the fluorescence properties. A striking example is provided by 2-aminopurine, which contrary to adenine (6-aminopurine) is highly fluorescent with a lifetime of

TABLE 42.2 Fluorescence Lifetimes (ps) Determined at 330 nm of DNA Monomeric Chromophores in Aqueous Solution Obtained from Fits with Monoexponential [$\exp(-t/\tau_0)$] or Biexponential Functions [$\alpha \exp(-t/\tau_1) + (1 - \alpha)\exp(-t/\tau_2)$]

Compound	τ_0	τ_1	τ_2	α	$<\tau>$[a]	References
Thy		0.20 ± 0.02	0.63 ± 0.02	0.56 ± 0.02	0.39 ± 0.02	68
T	0.70 ± 0.12					9
dT	0.47 ± 0.01	0.15 ± 0.02	0.72 ± 0.03	0.70 ± 0.02	0.32 ± 0.01	5
dT		0.15	0.76			18
TMP	0.98 ± 0.12					9
TMP	0.68 ± 0.02	0.21 ± 0.03	1.07 ± 0.06	0.67 ± 0.02	0.50 ± 0.02	5
Cyt	0.50 ± 0.02	0.20 ± 0.02	1.30 ± 0.07	0.85 ± 0.02	0.37 ± 0.01	71
C	0.76 ± 0.12					9
dC	0.40 ± 0.01	0.18 ± 0.02	0.92 ± 0.06	0.83 ± 0.02	0.30 ± 0.01	5
CMP	0.95 ± 0.12					9
dCMP	0.53 ± 0.02	0.27 ± 0.02	1.38 ± 0.11	0.84 ± 0.02	0.45 ± 0.02	5
Ade		0.23 ± 0.05	8.0 ± 0.3	0.65 ± 0.05	2.95	8
Ade		0.34 ± 0.07 −0.67 ± 0.14[b]	8.4 ± 0.8			10
A	0.53 ± 0.12					9
A	0.31 ± 0.02					10
A		0.13	0.45			11
dA	0.17 ± 0.01	0.10[c]	0.42 ± 0.10	0.91 ± 0.01	0.13 ± 0.01	5
AMP	0.52 ± 0.16					9
dAMP	0.16 ± 0.01	0.10[c]	0.52 ± 0.10	0.94 ± 0.02	0.13 ± 0.01	5
G	0.69 ± 0.10					9
dG	0.46 ± 0.01	0.16 ± 0.02	0.78 ± 0.05	0.73 ± 0.02	0.33 ± 0.01	5
GMP	0.86 ± 0.10					9
dGMP	0.47 ± 0.01	0.20 ± 0.02	0.89 ± 0.06	0.79 ± 0.02	0.34 ± 0.01	5
dGMP		0.16 ± 0.02 −0.29 ± 0.08[d]	0.94 ± 0.09 −4.0 ± 1.0[d]			17

Thy, Cyt and Ade refer to the nucleobases Thymine, Cytosine and Adenine, respectively; X, dX, XMP and dXMP refer to nucleosides, 2′-deoxynucleosides, nucleotide and 2′-deoxynucleotide respectively, where X corresponds to the first letter of the name of the base.

[a] $<\tau> = \alpha\tau_1 + (1 - \alpha)\tau_2$.

[b] Depending on the excitation wavelength (245–280 nm).

[c] Limited by the time resolution of the system, 0.10 ps after deconvolution.

[d] Depending on the emission wavelength (310–600 nm).

about 12 ns.[82,83] Being a structural analog to adenine, it can replace the latter in stacked structures and form Watson–Crick base pairs with thymines allowing incorporation in the DNA double helix. Zewail and coworkers studied 2-aminopurine in water and in ethanol by FU, focusing on the early time evolution.[69] They observed important dynamical spectral shifts assigned to solvation dynamics.

Schwalb and Temps[84,85] have published detailed FU studies of DMAdenine. This molecule presents dual fluorescence, covering the whole visible region. A global analysis of fluorescence decays between 290 and 650 nm enabled the authors to distinguish five different time constants from below 100 fs to 62 ps.

On Table 42.3, we have assembled fluorescence decays of substituted DNA bases.

42.5.2.3 Solvent Effects

Until recently, the solvent effects on the excited-state dynamics of DNA and its constituents were described as quite modest.[3] This statement was based on the fact that the excited state decays actually faster than the solvent response. This may be true for "slower" solvents such as alcohols, but for water,

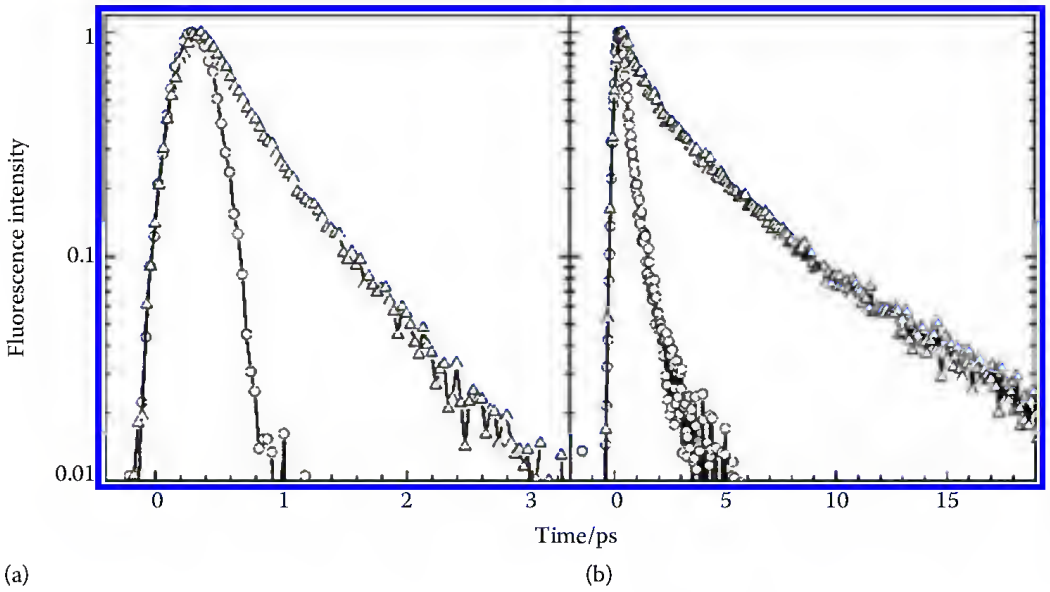

FIGURE 42.8 Fluorescence decays of (a) uracil (circles) and thymine (triangles) and (b) cytidine (circles) and 5MedC (triangles) recorded by FU at 330 nm.

TABLE 42.3 Fluorescence Lifetimes (ps) of Modified Monomeric Chromophores in Aqueous Solution Obtained from Fits with Monoexponential or Multiexponential Functions

Compound	τ_1	τ_2	τ_3	$\langle\tau\rangle$[a]	References
Ura	0.10 ± 0.01				[68]
5FUra	0.69 ± 0.06	1.74 ± 0.06		1.32 ± 0.05	[68]
5AUra[b]	0.15 ± 0.01	0.66 ± 0.07	2.78 ± 0.05		[81]
5MedC[c]	1.0 ± 0.1	5.4 ± 0.3		2.8	[12]
DMAde[d]	0.52 ± 0.03	3.0 ± 0.2	62.0 ± 1.0		[85]

[a] $\langle\tau\rangle$ is the average lifetime.
[b] Based on a global fit 330–465 nm.
[c] At 330 nm.
[d] Based on a global fit 350–510 nm.

the solvation dynamics is actually too fast for the time resolution available with existing experimental setups. For many modified bases, on the other hand, important spectral shifts have been observed. However, the role of the solvent is not limited to its dynamical response. It can also influence the energetic ordering of the excited states, and thus the intramolecular dynamics.

We studied solvent effects on the fluorescence properties of chosen uracils.[75–77,86] An example is given in Figure 42.9, where the fluorescence decays of 5FUra in acetonitrile, methanol, and water are compared. The fastest decays are observed in acetonitrile and the slowest in aqueous solution, while those observed in alcohols are intermediate.

In a FU study of isolated guanosine–cytosine base pairs in chloroform solution after 283 nm excitation, Schwalb and Temps[87] also gave lifetimes of the individual chromophores. Since these "nucleosides" were modified with a tert-butyldimethylsilyl group instead of the deoxyribose group, some caution has to be made when comparing with aqueous solution data. The measured decays are dominated by a subpicosecond component followed by a small amplitude longer component. The subpicosecond components, 0.67 ps for dC and 0.84 ps for dG are fairly close to the fluorescence lifetimes measured in water solution. The longer components were assigned to $n\pi^*$ state emission, since this state is less destabilized in chloroform than in aqueous solution, and thus may be on the same level as or below the directly excited $\pi\pi^*$

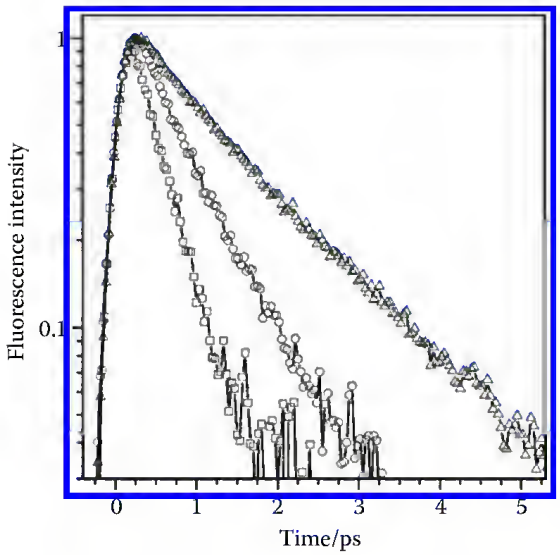

FIGURE 42.9 Fluorescence decays of 5FUra in acetonitrile (squares), methanol (circles), and water (triangles) recorded by FU at 330 nm.

state. In a subsequent study of DMAdenine,[84,85] they found that the lifetime of the intermolecular excited charge transfer state is much longer for dioxane solutions (1.4 ns) than that in aqueous solutions (62 ps).

42.5.3 Nonradiative Deactivation Mechanism

The ultrafast fluorescence decays of the DNA bases are due to highly efficient nonradiative processes occurring in the first excited singlet state. The detailed understanding of these nonradiative relaxation processes constitutes a major challenge from a theoretical point of view, and an increasing number of quantum chemistry calculations have addressed this problem for uracil/thymine,[68,78,80,88–96] cytosine,[79,91,97–105] adenine,[65,89,106–121] and guanine.[74,122–132]

The picture emerging is that the ultrafast decay of the excited state is due to highly efficient conical intersection between the first singlet $\pi\pi^*$ state and the ground state. These conical intersection are related to important geometrical changes occurring in the fluorescent $^1\pi\pi^*$ state, but the actual geometries involved differ from one molecule to the other. Complicating the picture even more is the fact that fluorescence only probes the first excited $^1\pi\pi^*$ state, but the calculated deactivation processes often involve near-lying dark states of $^1n\pi^*$ character. Most theoretical work has been performed for molecules in vacuo, while this chapter focuses on fluorescence of solutions. Evidently, the relative energy ordering of the $^1\pi\pi^*$ and $^1n\pi^*$ states is very sensitive to the environment, wherefore it is not always possible to compare theory and experiment. In general, the $^1n\pi^*$ states are strongly destabilized in aqueous solution and contribute less to the excited-state dynamics. An instructive comparison, from a theoretical point of view, of the nonradiative processes involved in the excited-state deactivation for the five DNA/RNA bases has recently been given by Serrano-Andrés and Merchán.[41]

Finally, it should be mentioned that transient absorption experiments probing from the UV to the infrared (IR) spectral domains have provided complementary information on the excited-state relaxation.[4,133–136]

42.6 Fluorescence of DNA Helices

The fluorescence properties change dramatically when we go from monomeric chromophores to multichromophoric systems. This is reflected in both the fluorescence decays and the fluorescence anisotropies. The latter were used to evidence transfer of the excitation energy among the bases of duplexes occurring

before conformational changes. Therefore, we first describe this aspect, taking place on the femtosecond timescale, and we continue with the fluorescence decays, which extend up to the nanosecond timescale.

42.6.1 Energy Transfer

We have seen in Section 42.4 that the electronic coupling is capable of inducing delocalization of the Frank–Condon excited states within DNA double helices. According to this model, each eigenstate has its own spatial characteristics determined by the electronic transitions of the bases participating to the eigenstate. In the studies performed in the frame of exciton theory,[55–58] the eigenstate topography was given by the square of the coefficients ($C^i_{k,m}$). The latter depend on the conformation of the duplex, which determines the strength of the electronic coupling. As an example, Figure 42.10 shows the topography corresponding to one eigenstate of $(dCdG)_5 \cdot (dCdG)_5$ averaged over 100 conformations.[58] Different eigenstates have different topographies.[56–58] Therefore, it is expected that population of an upper eigenstate and subsequent internal conversion will result in a transfer of the excitation energy within the helix, which is known as intraband scattering.

As the polarization of the electronic transitions associated with the various eigenstates of a duplex are also different, intraband scattering should lead to a loss of fluorescence anisotropy. But molecular motions may produce the same effect. Therefore, probing fluorescence anisotropy on early times, when molecular motions have not the time to occur, in particular for large systems, may provide information about energy transfer.

We determined the fluorescence anisotropy decays of DNA duplexes and G-quadruplexes using FU (Section 42.2) and compared them with the anisotropy decays corresponding to a stoichiometric mixture of noninteracting nucleotides.[13–16,20] Table 42.4 shows some typical anisotropy values obtained from these experiments. We found that the fluorescence anisotropy of all the studied duplexes decays more rapidly than that of noninteracting chromophores whose size is much smaller. These results reveal that energy transfer takes indeed place within the helices on the subpicosecond time domain.

More important, the anisotropy values detected for double helices are lower than that of the nucleotide mixture already at zero time, which means that the onset of energy transfer occurs at times shorter

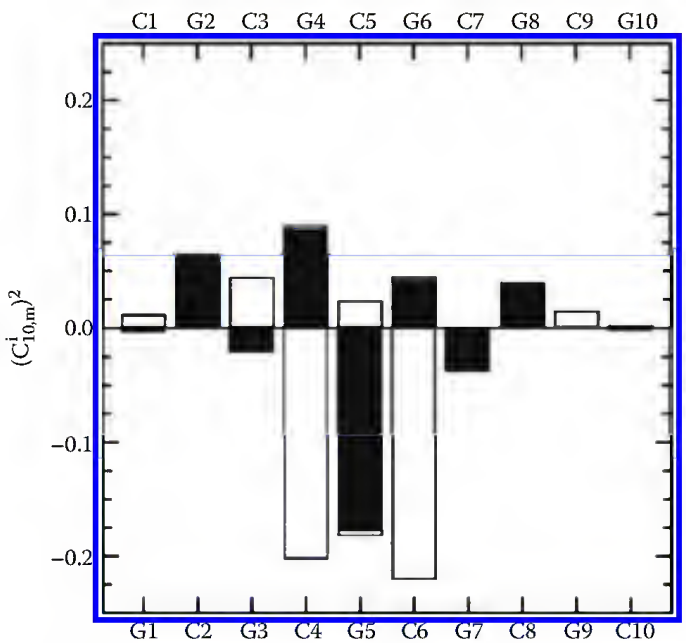

FIGURE 42.10 Topography of the eigenstate <10> determined for $(dCdG)_5 \cdot (dCdG)_5$. The coefficients ($C^i_{10,m}$) represent the contribution of the chromophore m in its i-th excited stated to the eigenstate <10>. The upper and lower parts of each histogram refer to chromophores located on each one of the strands. Average values obtained for 100 different conformations of the duplex in the absence of diagonal disorder.

TABLE 42.4 Fluorescence Anisotropy of DNA Strands r(t) Determined at Time t (in ps) from the Fits of the Experimental Decays Using Monoexponential Functions

Compound	λ (nm)	r(0)	r(0.5)	r(1)	r(3)
$(dA)_{20}\cdot(dT)_{20}$[13]	310	0.37	0.29	0.26	0.24
	330	0.31	0.29	0.27	0.23
	380	0.31	0.28	0.26	0.18
	420	0.28	0.24	0.21	0.12
poly(dA)·poly(dT)[13,20]	330	0.28	0.24	0.20	0.18
$(dAdT)_{10}\cdot(dAdT)_{10}$[14]	330	0.28	0.24	0.20	0.18
poly(dAdT)·poly(dAdT)[14]	330	0.28	0.25	0.23	0.18
	380	0.31	0.25	0.21	0.17
	420	0.22	0.16	0.1	−0.1
poly(dGdC)·poly(dGdC)[16]	330	0.25	0.15		
$d(TG_4T)_4$[50]	330	0.26	0.16	0.11	0.07
	360	0.25	0.16	0.11	0.07
	420	0.22	0.15	0.11	0.06

than the 100 fs, time resolution of our setup. Such an ultrafast energy transfer cannot take place via Förster transfer considering, in particular, the very large Stokes shift associated with the monomeric chromophores (Figure 42.1).

Ultrafast energy transfer takes also place in the case of self-associated guanines.[50] Figure 42.11 shows the anisotropy decay determined for self-associated triguanosine monophosphates, likely to form four-stranded structures[49] composed of only one type of chromophore. Their fluorescence anisotropy is already lower than that of dGMP at zero time. Moreover, at 1 ps, it dwindles down to 0.02 whereas that of the mononucleotides remains higher than 0.10.

Energy transfer, possibly assisted by conformational motions, may continue on longer timescales, until the whole population of the excited states relaxes to the ground state.

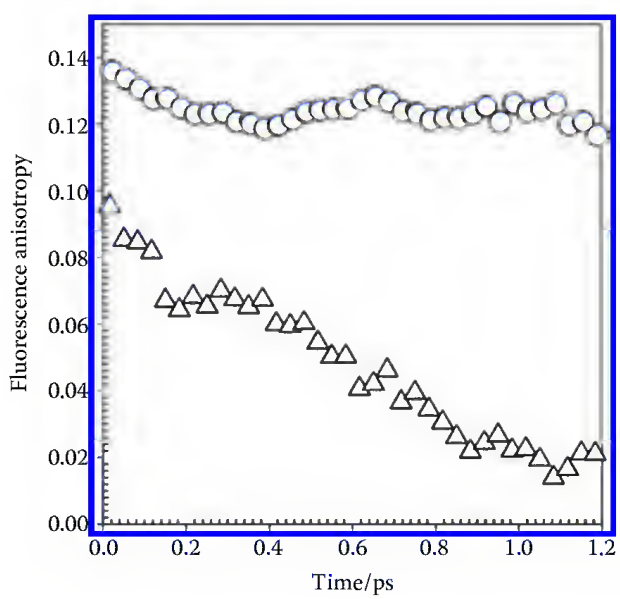

FIGURE 42.11 Fluorescence anisotropy determined for dGMP (circles) and self-associated triguanosine diphosphates (triangles) at 350 nm.

42.6.2 Fluorescence Decays

The fluorescence decays of DNA helices recorded by FU slow down upon increasing the emission wavelength. At least two time constants, whose values vary with the emission wavelength, are necessary in order to fit the decays with exponential functions. This is not surprising for such multichromophoric systems, knowing that even the fluorescence decays of the monomeric chromophores cannot be described by single exponentials (Section 42.5). Again here, the average lifetime $<\tau>$ is used in order to evaluate the sequence effect on the fluorescence decays. Table 42.5 shows the $<\tau>$ values determined for various model systems.

The lifetimes of the single strands containing only one type of base are all longer than those of the corresponding nucleotides. The most important lengthening is encountered in the case of adenine and, even more, of guanine strands. For these systems, the fluorescence decays slow down with increasing number of bases.[38] We recall that guanine single strands have the propensity to self-associate but so far only one system characterized by a well-defined quadruplex structure was studied. This is formed by association of four single strands d(TGGGGT); its FU decay is presented in Figure 42.12 together with those of TMP and dGMP.[50]

A noticeable size effect is also reported for homopolymeric duplexes composed of adenine–thymine pairs, the oligomer $(dA)_{20}\cdot(dT)_{20}$ and the polymer poly(dA)·poly(dT) (ca. 2000 base pairs).[13] Not only is the lifetime at the fluorescence maximum longer when going from the oligomer to the polymer, but the fluorescence anisotropy also decays faster indicating a more efficient energy transfer.

TABLE 42.5 Average Fluorescence Lifetimes $<\tau>$ (in ps) Determined for Various DNA Strands from FU Measurements

Compound	310 nm	330 nm	350 nm	360 nm	380 nm	420 nm
$(dG)_{10}\cdot(dC)_{10}$			2.07[38]			
$(dG)_{20}\cdot(dC)_{20}$			3.29[38]			
poly(dGdC)·poly(dGdC)	0.16[16]	0.2[16]		0.25[16]		
$(dA)_{20}\cdot(dT)_{20}$	0.75[13]	1.26[13]	2.73[38]		1.27[13]	1.57[13]
$(dAdT)_{10}\cdot(dAdT)_{10}$		0.50[14]				
poly(dA)·poly(dT)		2.1[15]			2.48[15]	2.99[15]
poly(dAdT)·poly(dAdT)		0.50[14]			1.14[14]	3.75[14]

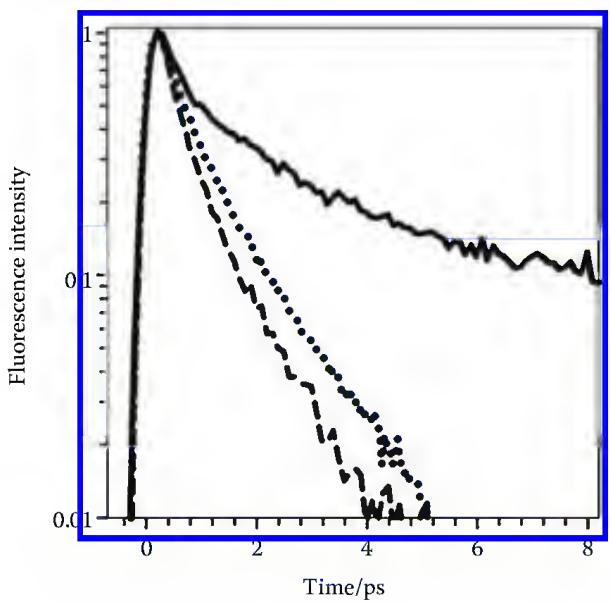

FIGURE 42.12 Fluorescence decays of dGMP (dashed line), TMP (dotted line), and $(TG_4T)_4$ (solid line) recorded by FU at 360 nm.

Moreover, the maxima of the steady-state absorption and emission spectra shift to slightly higher energies. All these effects are the fingerprints of a collective behavior becoming more pronounced as structural disorder diminishes with increasing size. The size effect on the fluorescence decays of alternating adenine–thymine duplexes is less pronounced.[14] However, even here the fluorescence anisotropy decays more rapidly for the polymer compared with the oligomer. For the latter, a combined broadband time-resolved fluorescence and transient absorption study suggested the existence of an intermediate weakly emitting species.[19]

Focusing on the polymeric duplexes, the FU decays exhibit a clear sequence effect.[137] The decays of poly(dA)·poly(dT), poly(dAdT)·poly(dAdT), and poly(dGdC)·poly(dGdC) are successively longer, equal, and shorter than those of an equimolar mixture of the constitutive nucleotides. An acceleration of the excited-state dynamics was also found upon formation of isolated Watson–Crick guanine–cytosine pairs dissolved in chloroform.[87] These data were correlated with theoretical calculations, which pointed out the role of interbase proton transfer.[138–140]

The introduction of guanine–cytosine pairs in homopolymeric purine–pyrimidine oligomeric duplexes leads to a decrease of the FU lifetimes.[38] Nevertheless, when the guanine/adenine ratio increases, a more complex behavior is observed, assigned to important structural changes.

In contrast to the monomeric chromophores, fluorescence emission of DNA helices contains long-lived components. Already described in earlier studies,[27,141] they have been revisited recently in combination of FU and TCSPC measurements. As in the case of FU, TCSPC signals exhibit strong wavelength and sequence dependence.[15,21] This is also true for the double strand poly(dG5MedC)·poly(dG5MedC).[22] For all the studied systems, fits of the fluorescence decays with multiexponential functions gave time constants amounting up to a few nanoseconds and contributing to the signal with weak amplitude.

Extended time-resolved investigations were carried out for the duplex poly(dA)·poly(dT). A nonlinear fitting/deconvolution procedure was performed by merging the data obtained by FU and TCSPC. Then, using the parameters derived from this global fit, the percentage of the emitted photons per decade of time was calculated for various wavelengths. Figure 42.13 shows the time distribution of the photons emitted at 330 and 420 nm up to 10 ns together with the steady-state fluorescence spectrum. We remark

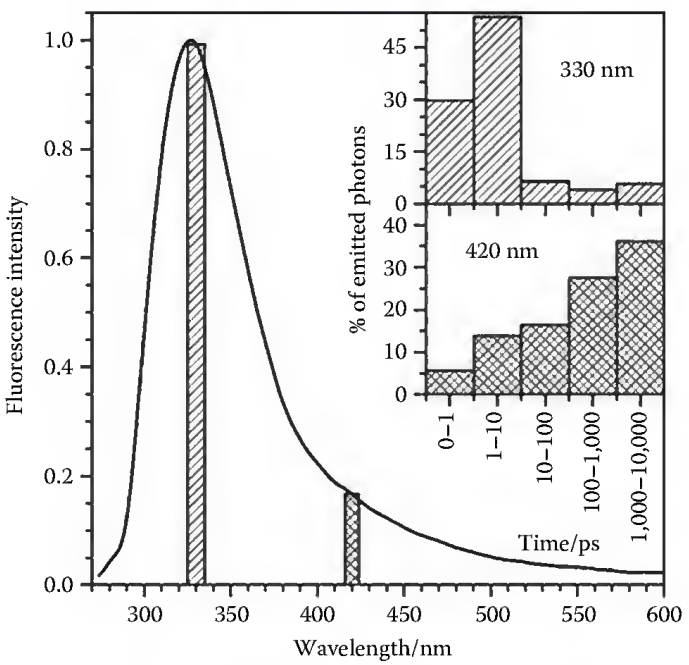

FIGURE 42.13 Fluorescence spectrum of poly(dA)·poly(dT). The inset shows the percentage of emitted photons per decade of time at 330 and 420 nm, resulting from a combined fit of the fluorescence decays recorded by FU and TCSPC using multiexponential functions.

that near the emission maximum most of the photons are emitted between 1 and 10 ps whereas the red tail of the spectrum is dominated by photons emitted at times longer than 1 ns.

The identification of the various emitting states of DNA helices is an intricate problem. The time constants derived from the fits with multiexponential functions, used in order to quantify the fluorescence decays, are not necessarily associated with precise excited states. As mentioned previously, a large multitude of excited states may exist for a given DNA helix, governed by electronic coupling and associated with the various conformations: $\pi\pi^*$ states localized on a single base, Frenkel excitons delocalized over a few bases, charge transfer states, $n\pi^*$ states,[134,142] as well as combinations among them. The situation becomes even trickier due to the excitation energy transfer processes. In this respect, it is important to stress that, when energy transfer takes place within a low-dimensional multichromophoric system, the time constants derived from fits with multiexponential functions do not have physical meaning.[143] However, the change of the fluorescence anisotropy decays as a function of the emission wavelength observed for the same excitation wavelength[13,14] clearly shows the existence of a variety of bright emitting states.

The great complexity of the fluorescence decays and fluorescence anisotropy decays observed for DNA helices contrasts with the relative simplicity of the transient absorption signals. In the latter case, only two time constants, assigned to localized $\pi\pi^*$ excited states and intrastrand excimers[4,36,37] were determined in most studies. Yet, the fingerprint of Frenkel excitons, living a few ps and depending of the size of the helix, was reported in a transient absorption study.[144]

42.7 Concluding Remarks

We have described earlier how sophisticated spectroscopic measurements have been performed during the past few years for DNA components despite the extremely weak fluorescence quantum yields. By following specific and rigorous experimental protocols, these measurements have started to unravel the very complex mechanisms that govern the excited-state dynamics.

Evidently, the experimental work has to be supported by theoretical calculations. This is relatively easier for the monomeric chromophores, even if modeling solvent effects correctly is not an easy task and more efforts are still needed. Modeling excited-state relaxation gets much trickier in the case of model helices for which two different approaches have been followed so far. On the one hand, quantum chemical calculations were performed for small systems taking into account orbital overlap and solvent.[65,66] On the other hand, calculations in the frame of the exciton theory, neglecting orbital overlap but studying larger systems.[145] Ideally, the combination of both methods is necessary and can be done properly only in close connection with the experiments.

Collecting detailed experimental data such as fluorescence decays, fluorescence anisotropy decays, and time-resolved fluorescence spectra recorded over several decades of time will be a decisive step. Needless to say this has not yet been realized for any DNA strand, but we are fairly optimistic that this is now within reach. Modification of various parameters such as the ionic strength, the size of the helix, or the base sequence, known to induce conformational changes, is expected to provide precious additional information. Finally, investigation of nucleosomes (DNA–histones complexes) will provide certainly a more biologically relevant picture. This poses many problems from experimental point of view and constitutes a real challenge. After submission of the present chapter, two important articles dealing with DNA fluorescence have been published. One of them describes the first photophysical study of UVA-induced fluorescence in DNA model helices[146] whereas the other reports on fluorescence of natural DNA.[147] Moreover, two perspectives, dedicated to monomeric DNA building blocks[148] and DNA helices,[149] have appeared.

References

1. P. Vigny, *C. R. Acad. Sci. Paris*, 1971, **272 D**, 3206–3209.
2. M. Daniels and W. Hauswirth, *Science*, 1971, **171**, 675–677.
3. C. E. Crespo-Hernàndez, B. Cohen, P. M. Hare, and B. C. R. Kohler, *Chem. Rev.*, 2004, **104**, 1977–2019.

4. C. T. Middelton, K. de La Harpe, C. Su, U. K. Law, C. E. Crespo-Hernàndez, and B. Kohler, *Ann. Rev. Phys. Chem.*, 2009, **60**, 13–47.
5. D. Onidas, D. Markovitsi, S. Marguet, A. Sharonov, and T. Gustavsson, *J. Phys. Chem. B*, 2002, **106**, 11367–11374.
6. R. A. Velapoldi and K. D. Mielenz, *A Fluorescence Standard Reference Material: Quinine Sulfate Dihydrate*, U. S. Government Printing Office, Washington, DC, 1980.
7. N. Nijegorodov and R. Mabbs, *Spectrochim. Acta Part A*, 2000, **56A**, 2157–2166.
8. T. Gustavsson, A. Sharonov, D. Onidas, and D. Markovitsi, *Chem. Phys. Lett.*, 2002, **356**, 49–54.
9. J. Peon and A. H. Zewail, *Chem. Phys. Lett.*, 2001, **348**, 255–262.
10. T. Pancur, N. K. Schwalb, F. Renth, and F. Temps, *Chem. Phys.*, 2005, **313**, 199–212.
11. W.-M. Kwok, C. Ma, and D. L. Phillips, *J. Am. Chem. Soc.*, 2006, **128**, 11894–11905.
12. A. Sharonov, T. Gustavsson, S. Marguet, and D. Markovitsi, *Photochem. Photobiol. Sci.*, 2003, **2**, 362–364.
13. D. Onidas, T. Gustavsson, E. Lazzarotto, and D. Markovitsi, *J. Phys. Chem. B*, 2007, **111**, 9644–9650.
14. D. Onidas, T. Gustavsson, E. Lazzarotto, and D. Markovitsi, *Phys. Chem. Chem. Phys.*, 2007, **9**, 5143–5148.
15. D. Markovitsi, T. Gustavsson, and F. Talbot, *Photochem. Photobiol. Sci.*, 2007, **6**, 717–724.
16. F. A. Miannay, A. Banyasz, T. Gustavsson, and D. Markovitsi, *J. Am. Chem. Soc.*, 2007, **129**, 14574–14575.
17. F. A. Miannay, T. Gustavsson, A. Banyasz, and D. Markovitsi, *J. Phys. Chem. A*, 2010, **114**, 3256.
18. W. M. Kwok, C. Ma, and D. L. Phillips, *J. Am. Chem. Soc.*, 2008, **130**, 5131–5139.
19. W. M. Kwok, C. S. Ma, and D. L. Phillips, *J. Phys. Chem. B*, 2009, **113**, 11527–11534.
20. D. Markovitsi, D. Onidas, T. Gustavsson, F. Talbot, and E. Lazzarotto, *J. Am. Chem. Soc.*, 2005, **127**, 17130–17131.
21. D. Markovitsi, F. Talbot, T. Gustavsson, D. Onidas, E. Lazzarotto, and S. Marguet, *Nature*, 2006, **441**, E7.
22. M. Daniels, L. P. Hart, P. S. Ho, J. P. Ballini, P. Vigny, and J. C. Brochon, *Photochem. Photobiol. Sci.*, 2007, **6**, 883–893.
23. T. Fujiwara, Y. Kamoshida, R. Morita, and M. Yamashita, *J. Photochem. Photobiol. B Biol.*, 1997, **41**, 114–121.
24. D. Markovitsi, D. Onidas, F. Talbot, S. Marguet, T. Gustavsson, and E. Lazzarotto, *J. Photochem. Photobiol. A Chem.*, 2006, **183**, 1–8.
25. H. Görner, *J. Photochem. Photobiol. B Biol.*, 1994, **26**, 117–139.
26. J. Cadet, M. Berger, T. Douki, B. Morin, S. Raoul, J. L. Ravanat, and S. Spinelli, *Biol. Chem.*, 1997, **378**, 1275–1286.
27. J. Cadet and P. Vigny, in *Bioorganic Photochemistry*, ed. H. Morrison, John Wiley & Sons, New York, 1990, pp. 1–272.
28. Q. Zhu and P. R. LeBreton, *J. Am. Chem. Soc.*, 2000, **122**, 12824–12834.
29. S. Marguet, D. Markovitsi, and F. Talbot, *J. Phys. Chem. B*, 2006, **110**, 11037–11039.
30. L. Colon, C. E. Crespo-Hernandez, R. Oyola, C. Garcia, and R. Arce, *J. Phys. Chem. B*, 2006, **110**, 15589–15596.
31. L. P. Candeias, P. O'Neill, G. D. D. Jones, and S. Steenken, *Int. J. Radiat. Biol.*, 1992, **61**, 15–20.
32. L. P. Candeias and S. Steenken, *J. Am. Chem. Soc.*, 1989, **111**, 1094–1099.
33. L. P. Candeias and S. Steenken, *J. Am. Chem. Soc.*, 1992, **114**, 699–704.
34. J. Blais, T. Douki, P. Vigny, and J. Cadet, *Photochem. Photobiol.*, 1994, **59**, 402–404.
35. A. Banyasz, S. Karpati, E. Lazzarotto, D. Markovitsi, and T. Douki, *J. Phys. Chem. C*, 2009, **113**, 11747–11750.
36. C. E. Crespo-Hernández, B. Cohen, and B. Kohler, *Nature*, 2005, **436**, 1141–1144.
37. K. de La Harpe, C. E. Crespo-Hernàndez, and B. Kohler, *ChemPhysChem*, 2009, **10**, 1421–1425.
38. N. K. Schwalb and F. Temps, *Science*, 2008, **322**, 243–245.
39. A. Holmén, A. Broo, B. Albinsson, and B. Nordén, *J. Am. Chem. Soc.*, 1997, **119**, 12240–12250.

40. A. C. Borin, L. Serrano-Andres, M. P. Fulscher, and B. O. Roos, *J. Phys. Chem. A*, 1999, **103**, 1838–1845.
41. L. Serrano-Andrés and M. Merchán, *J. Photochem. Photobiol. C Photochem. Rev.*, 2009, **10**, 21–32.
42. J. R. Platt, *J. Chem. Phys.*, 1949, **17**, 484–495.
43. W. Dean, F. Sandos, S. Miodrag, V. Zakhartchenko, J. Walter, E. Wolf, and W. Reik, *Proc. Natl. Acad. Sci. USA*, 2001, **98**, 13734–13738.
44. Y.-H. You and G. P. Pfeifer, *J. Mol. Biol.*, 2001, **305**, 389–399.
45. E. B. Starikov, *Modern Phys. Lett. B*, 2004, **18**, 825–831.
46. D. Varsano, R. Di Felice, M. A. L. Marques, and A. Rubio, *J. Phys. Chem. B*, 2006, **110**, 7129–7138.
47. F. Santoro, V. Barone, and R. Improta, *ChemPhysChem*, 2008, **9**, 2531–2537.
48. J. L. Mergny, A. De Cian, A. Ghelab, B. Sacca, and L. Lacroix, *Nucleic Acids Res.*, 2005, **33**, 81–94.
49. D. Markovitsi, T. Gustavsson, and A. Sharonov, *Photochem. Photobiol.*, 2004, **79**, 526–530.
50. F. A. Miannay, A. Banyasz, T. Gustavsson, and D. Markovitsi, *J. Phys. Chem. C*, 2009, **113**, 11760–11765.
51. E. I. Rashbah and M. D. Sturge, *Excitons*, North-Holland, Amsterdam, the Netherlands, 1982.
52. M. Kasha, H. R. Rawls, and M. A. El-Bayoumi, *Pure Appl. Chem.*, 1965, **11**, 371–392.
53. I. Tinoco Jr., *J. Am. Chem. Soc.*, 1960, **82**, 4785–4790.
54. W. Rhodes, *J. Am. Chem. Soc.*, 1961, **83**, 3609–3617.
55. B. Bouvier, T. Gustavsson, D. Markovitsi, and P. Millié, *Chem. Phys.*, 2002, **275**, 75–92.
56. B. Bouvier, J. P. Dognon, R. Lavery, D. Markovitsi, P. Millié, D. Onidas, and K. Zakrzewska, *J. Phys. Chem. B*, 2003, **107**, 13512–13522.
57. E. Emanuele, D. Markovitsi, P. Millié, and K. Zakrzewska, *ChemPhysChem*, 2005, **6**, 1387–1392.
58. E. Emanuele, K. Zakrzewska, D. Markovitsi, R. Lavery, and P. Millie, *J. Phys. Chem. B*, 2005, **109**, 16109–16118.
59. P. Dean, *Rev. Mod. Phys.*, 1972, **44**, 127–169.
60. M. Schreiber and Y. Toyosawa, *J. Phys. Soc. Jpn.*, 1982, **51**, 1537–1543.
61. D. F. Lewis, X. Liu, Y. Wu, and X. Zuo, *J. Am. Chem. Soc.*, 2003, **125**, 12729–12731.
62. A. L. Burin, J. A. Dickman, D. B. Uskov, C. F. F. Hebbard, and G. C. Schatz, *J. Chem. Phys.*, 2008, **129**, 091102.
63. E. B. Starikov, J. P. Lewis, and O. F. Sankey, *Int. J. Mod. Phys. B*, 2005, **19**, 4331–4357.
64. E. B. Starikov, G. Cuniberti, and S. Tanaka, *J. Phys. Chem. B*, 2009, **113**, 10428.
65. F. Santoro, V. Barone, and R. Improta, *Proc. Natl. Acad. Sci. USA*, 2007, **104**, 9931–9936.
66. F. Santoro, V. Barone, and R. Importa, *J. Am. Chem. Soc.*, 2009, **131**, 15232–15245.
67. A. W. Lange and J. M. Herbert, *J. Am. Chem. Soc.*, 2009, **131**, 3913.
68. T. Gustavsson, A. Banyasz, E. Lazzarotto, D. Markovitsi, G. Scalmani, M. J. Frisch, V. Barone, and R. Improta, *J. Am. Chem. Soc.*, 2006, **128**, 607–619.
69. S. K. Pal, J. Peon, and A. H. Zewail, *Chem. Phys. Lett.*, 2002, **363**, 57–63.
70. T. Gustavsson, A. Sharonov, and D. Markovitsi, *Chem. Phys. Lett.*, 2002, **351**, 195–200.
71. A. Sharonov, T. Gustavsson, V. Carré, E. Renault, and D. Markovitsi, *Chem. Phys. Lett.*, 2003, **380**, 173–180.
72. T. Pancur, F. Renth, F. Temps, B. Harbaum, A. Kruger, R. Herges, and C. Nather, *Phys. Chem. Chem. Phys.*, 2005, **7**, 1985–1989.
73. B. Cohen, C. E. Crespo-Hernández, and B. Kohler, *Faraday Discuss. Chem. Soc.*, 2004, **127**, 137–147.
74. V. Karunakaran, K. Kleinermanns, R. Improta, and S. A. Kovalenko, *J. Am. Chem. Soc.*, 2009, **131**, 5839–5850.
75. T. Gustavsson, N. Sarkar, E. Lazzarotto, D. Markovitsi, V. Barone, and R. Improta, *J. Phys. Chem. B*, 2006, **110**, 12843–12847.
76. T. Gustavsson, N. Sarkar, A. Banyasz, D. Markovitsi, and R. Improta, *Photochem. Photobiol.*, 2007, **83**, 595–599.
77. T. Gustavsson, N. Sarkar, E. Lazzarotto, D. Markovitsi, and R. Improta, *Chem. Phys. Lett.*, 2006, **429**, 551–557.

78. F. Santoro, V. Barone, T. Gustavsson, and R. Improta, *J. Am. Chem. Soc.*, 2006, **128**, 16312–16322.
79. M. Z. Zgierski, T. Fujiwara, W. G. Kofron, and E. C. Lim, *Phys. Chem. Chem. Phys.*, 2007, **9**, 3206–3209.
80. M. Z. Zgierski, S. Patchkovskii, T. Fujiwara, and E. C. Lim, *J. Phys. Chem. A*, 2005, **109**, 9384–9387.
81. A. Bányász, T. Gustavsson, E. Keszei, R. Improta, and D. Markovitsi, *Photochem. Photobiol. Sci.*, 2008, **7**, 765–768.
82. A. Holmén, B. Nordén, and B. Albinsson, *J. Am. Chem. Soc.*, 1997, **119**, 3114–3121.
83. R. K. Neely, S. W. Magennis, D. T. F. Dryden, and A. C. Jones, *J. Phys. Chem. B*, 2004, **108**, 17606–17610.
84. N. K. Schwalb and F. Temps, *Phys. Chem. Chem. Phys.*, 2006, **8**, 5229–5235.
85. N. K. Schwalb and F. Temps, *J. Phys. Chem. A*, 2009, **113**, 13113–13123.
86. T. Gustavsson, A. Bányász, N. Sarkar, D. Markovitsi, and R. Improta, *Chem. Phys.*, 2008, **350**, 186–192.
87. N. Schwalb and F. Temps, *J. Am. Chem. Soc.*, 2007, **129**, 9272–9273.
88. S. Matsika, *J. Phys. Chem. A*, 2004, **108**, 7584–7590.
89. S. Matsika, *J. Phys. Chem. A*, 2005, **109**, 7538–7545.
90. E. Epifanovsky, K. Kowalski, P. D. Fan, M. Valiev, S. Matsika, and A. I. Krylov, *J. Phys. Chem. A*, 2008, **112**, 9983–9992.
91. M. Merchán, R. Gonzalez-Luque, T. Climent, L. Serrano-Andres, E. Rodriguez, M. Reguero, and D. Pelaez, *J. Phys. Chem. B*, 2006, **110**, 26471–26476.
92. H. R. Hudock, B. G. Levine, A. L. Thompson, H. Satzger, D. Townsend, N. Gador, S. Ullrich, A. Stolow, and T. J. Martinez, *J. Phys. Chem. A*, 2007, **111**, 8500–8508.
93. R. Improta and V. Barone, *J. Am. Chem. Soc.*, 2004, **126**, 14320–14321.
94. R. Improta, V. Barone, A. Lami, and F. Santoro, *J. Phys. Chem. B*, 2009, **113**, 14491–14503.
95. G. Zechmann and M. Barbatti, *J. Phys. Chem. A*, 2008, **112**, 8273–8279.
96. J. J. Szymczak, M. Barbatti, J. T. S. Hoo, J. A. Adkins, T. L. Windus, D. Nachtigallova, and H. Lischka, *J. Phys. Chem. A*, 2009, **113**, 12686–12693.
97. M. Z. Zgierski, S. Patchkovskii, and E. C. Lim, *J. Chem. Phys.*, 2005, **123**, 081101–081104.
98. M. Z. Zgierski and S. Alavi, *Chem. Phys. Lett.*, 2006, **426**, 398–404.
99. L. Blancafort and M. A. Robb, *J. Phys. Chem. A*, 2004, **108**, 10609–10614.
100. L. Blancafort, B. Cohen, P. M. Hare, B. Kohler, and M. A. Robb, *J. Phys. Chem. A*, 2005, **109**, 4431–4436.
101. L. Blancafort, *Photochem. Photobiol.*, 2007, **83**, 603–610.
102. L. Blancafort and A. Migani, *J. Photochem. Photobiol. A Chem.*, 2007, **190**, 283–289.
103. K. A. Kistler and S. Matsika, *J. Phys. Chem. A*, 2007, **111**, 8708–8716.
104. K. A. Kistler and S. Matsika, *J. Phys. Chem. A*, 2009, **113**, 12396–12403.
105. H. R. Hudock and T. J. Martinez, *ChemPhysChem*, 2008, **9**, 2486–2490.
106. C. M. Marian, M. Kleinschmidt, and J. Tatchen, *Chem. Phys.*, 2008, **347**, 346–359.
107. C. M. Marian, *J. Chem. Phys.*, 2005, **122**, 104314.
108. C. Marian, D. Nolting, and R. Weinkauf, *Phys. Chem. Chem. Phys.*, 2005, **7**, 3306–3316.
109. S. B. Nielsen and T. I. Sølling, *ChemPhysChem*, 2005, **6**, 1276–1281.
110. S. Perun, A. L. Sobolewski, and W. Domcke, *Chem. Phys.*, 2005, **313**, 107–112.
111. S. Perun, A. L. Sobolewski, and W. Domcke, *J. Am. Chem. Soc.*, 2005, **127**, 6257–6265.
112. L. Blancafort, *J. Am. Chem. Soc.*, 2006, **128**, 210–219.
113. L. Serrano-Andres, M. Merchán, and A. C. Borin, *Chem. Eur. J.*, 2006, **12**, 6559–6571.
114. L. Serrano-Andres, M. Merchán, and A. C. Borin, *Proc. Natl. Acad. Sci. USA*, 2006, **103**, 8691–8696.
115. M. Barbatti and H. Lischka, *J. Phys. Chem. A*, 2007, **111**, 2852–2858.
116. W. C. Chung, Z. Lan, Y. Ohtsuki, N. Shimakura, W. Domcke, and Y. Fujimura, *Phys. Chem. Chem. Phys.*, 2007, **9**, 2075–2084.
117. S. Yamazaki and S. Kato, *J. Am. Chem. Soc.*, 2007, **129**, 2901–2909.
118. C.-H. Chin, A. M. Mebel, G.-S. Kim, K. Y. Baek, M. Hayashi, K. K. Liang, and S. H. Lin, *Chem. Phys. Lett.*, 2007, **445**, 361–369.

119. I. Conti, M. Garavelli, and G. Orlandi, *J. Am. Chem. Soc.*, 2009, **131**, 16108–16118.
120. R. Improta and V. Barone, *Theor. Chem. Acc.*, 2008, **120**, 491–497.
121. Y. B. Lei, S. A. Yuan, Y. S. Dou, Y. B. Wang, and Z. Y. Wen, *J. Phys. Chem. A*, 2008, **112**, 8497–8504.
122. H. Langer, N. L. Doltsinis, and D. Marx, *ChemPhysChem*, 2005, **6**, 1734–1737.
123. H. Langer and N. L. Doltsinis, *Phys. Chem. Chem. Phys.*, 2004, **6**, 2742–2748.
124. H. Langer and N. L. Doltsinis, *Phys. Chem. Chem. Phys.*, 2003, **5**, 4516–4518.
125. H. Chen and S. Li, *J. Chem. Phys.*, 2006, **124**, 154315.
126. M. Z. Zgierski, S. Patchkovskii, T. Fujiwara, and E. C. Lim, *Chem. Phys. Lett.*, 2007, **440**, 145–149.
127. C. M. Marian, *J. Phys. Chem. A*, 2007, **111**, 1545–1553.
128. L. Serrano-Andres, M. Merchán, and A. C. Borin, *J. Am. Chem. Soc.*, 2008, **130**, 2473–2484.
129. S. Yamazaki and W. Domcke, *J. Phys. Chem. A*, 2008, **112**, 7090–7097.
130. S. Yamazaki, W. Domcke, and A. L. Sobolewski, *J. Phys. Chem. A*, 2008, **112**, 11965–11968.
131. M. K. Shukla and J. Leszczynski, *J. Phys. Chem. B*, 2008, **112**, 5139–5152.
132. Z. G. Lan, E. Fabiano, and W. Thiel, *ChemPhysChem*, 2009, **10**, 1225–1229.
133. D. N. Nikogosyan, D. Angelov, B. Soep, and L. Lindqvist, *Chem. Phys. Lett.*, 1996, **252**, 322–326.
134. P. M. Hare, C. Crespo-Hernández, and B. Kohler, *Proc. Natl. Acad. Sci. USA*, 2007, **104**, 435–440.
135. P. M. Hare, C. E. Crespo-Hernández, and B. Kohler, *J. Phys. Chem. B*, 2006, **110**, 18641–18650.
136. D. A. McGovern, G. W. Doorley, A. M. Whelan, A. W. Parker, M. Towrie, J. M. Kelly, and S. J. Quinn, *Photochem. Photobiol. Sci.*, 2009, **8**, 542–548.
137. D. Markovitsi and T. Gustavsson, in *Energy Transfer Dynamics in Biomaterial Systems*, eds. I. Burghardt, V. May, D. A. Micha, and E. R. Bittner, Springer, Heidelberg/Berlin, Germany, 2009, p. 93. pp. 127–142.
138. A. L. Sobolewski and W. Domcke, *Phys. Chem. Chem. Phys.*, 2004, **6**, 2763–2771.
139. A. L. Sobolewski, W. Domcke, and C. Hättig, *Proc. Natl. Acad. Sci. USA*, 2005, **102**, 17903–17906.
140. G. Groenof, L. V. Schäfer, M. Boggio-Pasqua, M. Goette, H. Grubmüller, and M. A. Robb, *J. Am. Chem. Soc.*, 2007, **129**, 6812–6819.
141. R. Plessow, A. Brockhinke, W. Eimer, and K. Kohse-Höinghaus, *J. Phys. Chem. B*, 2000, **104**, 3695–3704.
142. G. W. Doorley, D. A. McGovern, M. W. George, M. Towrie, A. W. Parker, J. M. Kelly, and S. J. Quinn, *Ang. Chem. Int. Ed.*, 2009, **48**, 123–127.
143. A. Blumen, J. Klafter, and G. Zumofen, in *Optical Spectroscopy of Glasses*, ed. I. Zschokke, Reidel Publishing Co., Dordrect, the Netherlands, 1986, pp. 199–265.
144. I. Buchvarov, Q. Wang, M. Raytchev, A. Trifonov, and T. Fiebig, *Proc. Natl. Acad. Sci. USA*, 2007, **104**, 4794–4797.
145. E. R. Bittner, *J. Chem. Phys.*, 2006, **125**, 094909 (094901–094912).
146. A. Banyasz, I. Vayá, P. Changenet-Barret, T. Gustavsson, T. Douki, and D. Markovitsi, *J. Am. Chem. Soc.* 2011, **133**, 5163.
147. I. Vayá, T. Gustavsson, F. A. Miannay, T. Douki, and D. Markovitsi, *J. Am. Chem. Soc.* 2010, **132**, 11834.
148. T. Gustavsson, R. Improta, and D. Markovitsi, *J. Phys. Chem. Lett.* 2010, **1**, 2025.
149. D. Markovitsi, T. Gustavsson, and I. Vayá, *J. Phys. Chem. Lett.* 2010, **1**, 3271.

43

Action Spectroscopy: General Problems

Edward D. Lipson
Syracuse University

43.1 Introduction

Action spectroscopy is a general approach toward identifying the receptor pigment(s) for a particular photobiological response or effect. The early identification of major chromophores, such as rhodopsin and chlorophyll, depended on comparison of the action spectra for vision and photosynthesis, respectively, with the absorption spectra of candidate pigments.

It is remarkable how few chromophore types with intrinsic photochemistry are employed in photobiological systems (Delbrück 1976; Lipson and Horwitz 1991). A basic list consists of the following: (a) retinal pigments (in rhodopsins), (b) tetrapyrroles (including chlorophylls and phycobiliproteins including phytochromes), (c) flavin and pterin accessory chromophores (in cryptochrome and phototropin pigments; these are blue-light receptors in plants and microorganisms and, in the case of cryptochromes, in animals too), (d) hypericin pigments (Song 2005), and (e) the *p*-coumaric acid chromophore of the photoactive yellow protein (PYP) of *Ectothiorhodospira halophila* (Meyer et al. 1987; Schlichting and Berendzen 1997).

This chapter focuses on analytical methods for measuring action spectra, with emphasis on those derived from fluence–response data. For a set of examples, the reader can consult studies of *Phycomyces,* not only of its phototropism (Ensminger et al. 1990; Galland and Lipson 1985a,b) but also of the light-growth response (Ensminger and Lipson 1991; Ensminger et al. 1991), carotene synthesis

(Bejarano et al. 1990), and differentiation (Corrochano et al. 1988), as well as studies of other blue-light systems (Baskin and Iino 1987; De Fabo et al. 1976; Galland and Senger 1988; Presti and Galland 1987; Schmid et al. 1987). The later studies on *Phycomyces* employed formal data analysis methods—including error analysis with error propagation (Baird 1994) in the curve fitting and parameter estimation—as summarized elsewhere (Lipson 1991), so that error bars could be assigned to the points in the action spectra derived from the fluence–response raw data points and their error bars.

For other representative action spectra, the reader is referred to the following chapters in this volume and to the major photobiology journals: *Photochemistry and Photobiology*, the *Journal of Photochemistry and Photobiology, B: Biology*, and *Photochemical and Photobiological Sciences*. There are also a number of review articles that give various perspectives on action spectroscopy (Coohill 1991, 1992; Foster 2001; Galland 1987; Hartmann 1983; Jagger 1967; Lipson 1991; Schäfer and Fukshansky 1984; Schäfer et al. 1983; Shropshire 1972). For practical advice on light sources and radiometry, the reader should consult standard photobiology texts (Björn 2008; Häder and Tevini 1987; Smith 1989).

43.2 Alternative Types of Action Spectra

The most elementary type of action spectrum consists of a graph of some response or effect as a function of wavelength, under conditions where the photon fluence is maintained constant at all wavelengths. This convenient approach, however, can be confounded by the frequent circumstance that the response may depend nonlinearly on the fluence (or fluence rate). For example, if at some wavelengths the response is in a saturation region, then the action spectrum will be "clipped" (*viz.* peaks flattened) at those wavelengths; similarly, other types of nonlinearities will produce other distortions. Accordingly, a preferred way of obtaining an action spectrum—provided that the experimenter is willing and able to apply the additional effort needed—is to derive it from fluence–response curves (sometimes called dose–response curves, by analogy with pharmacology). In this way, one obtains essentially a graph of *sensitivity*, rather than response, as a function of wavelength. Operationally, one determines for each wavelength the photon fluence required to achieve a standard response level and then plots the reciprocal of that photon fluence as a measure of sensitivity. The graph so obtained is sometimes called an "equal-response action spectrum," which is not subject to the nonlinear distortions, and is therefore more likely to represent the absorption spectrum of the responsible chromophore (subject to various considerations specified in the following).

43.3 Photophysics

After a chromophore absorbs a photon, a number of alternative photophysical events may ensue. These can be represented graphically by a "Jablonski diagram" depicting transitions among the electronic, vibrational, and rotational states of the pigment molecule (Grossweiner 1989). Upon absorption of a photon, the molecule is promoted from the ground state (usually of singlet character and designated therefore as S_0) to an excited electronic state (also singlet and designated as S_1, S_2, etc.); the molecule generally becomes excited with respect to vibrational and rotational motions as well (the corresponding energy spacings among these states are progressively lower than those between electronic states). The molecule then de-excites rapidly by internal conversion and vibrational relaxation to the lowest excited singlet level S_1 before there is time for photochemistry to take place. Consequently, regardless of the wavelength of the incident photon that excited the molecule, the molecular excitation relaxes rapidly to the bottom vibrational levels based on S_1. Then the relevant photochemistry proceeds either directly from S_1 or else—following intersystem crossing from the singlet to the triplet manifold—from the lowest triplet state T_1 provided that the excitation energy has not been dissipated in the meantime by internal conversion or fluorescence.

43.4 Illumination Units

Fluence–response curves are sometimes measured using broadband rather than monochromatic light because (a) higher fluence rates are achievable with broadband filters and (b) unless one is trying to study the wavelength dependence of a particular response or effect, it may be more representative of natural illumination conditions to use broadband light covering the range of sensitivity. For example, in studies of photogravitropism "threshold curves" of *Phycomyces* wild-type and mutant strains (Galland and Lipson 1985a,b, 1987), it is customary to employ broadband-blue illumination at fluence rates extending over a 10 decade range. With broadband illumination, the units pertain to *energy* fluence rather than *photon* fluence. The energy units are J m^{-2} for fluence and J m^{-2} s^{-1} (or, equivalently, W m^{-2}) for fluence rate. In action spectroscopy, however, one must use monochromatic light (occasionally in *combination* with polychromatic background light; see chapter in this volume by T. Coohill). It is then preferable to use photon units: photons m^{-2} for fluence and photons m^{-2} s^{-1} for fluence rate.

43.5 Conditions for Measurement and Interpretation of Action Spectra

The shape of an action spectrum may be distorted significantly from the absorption spectrum of the responsible pigment. To obviate such distortions, the experimenter should strive to satisfy the following conditions insofar as possible (Jagger 1967; Shropshire 1972):

1. The quantum efficiency (or quantum yield)—defined as the probability that a particular type of event of photobiological or photochemical interest occurs as the result of absorption of a photon—should be independent of wavelength.
2. The absorption spectrum of the receptor pigment should be the same whether measured *in vivo* or *in vitro*.
3. Screening or shading pigments, as well as scattering effects, should not cause significant wavelength-dependent distortion. Scattering is generally stronger at shorter wavelengths, but the trend is a gradual one and normally would not obscure the key features of an action spectrum; instead, scattering tends to superpose a sloping baseline, which can be largely eliminated, if desired, by use of a suitable scattering reference.
4. When an action spectrum is derived from fluence–response curves, the condition of reciprocity should be valid over the range of fluence rates and exposure times used. In other words, the response should depend on the *product* of fluence rate and exposure time but should not otherwise depend on either factor.
5. Light should not be totally absorbed by the sample for any wavelength under study. More specifically, an ample fraction of the incident light (a practical guideline is 50%) should reach the receptor pigment region under all conditions.

43.6 Reciprocity

For measurements employing continuous illumination, the stimulus strength is given by the fluence rate itself. With pulse illumination, however, the fluence can be adjusted by varying the exposure time (pulse width) and/or the fluence rate. Considering the kinetics of photochemical and subsequent dark reactions, it is preferable in most circumstances to maintain the exposure time constant and vary the fluence rate. In general, though, one should establish the range of validity of reciprocity between exposure time and fluence rate (see the preceding text).

43.7 Fundamental Derivations

For action spectroscopy with pulse illumination, assume that the response R can be expressed as a function of the product of four variables:

$$R = R(\phi\sigma_1 I_1 \Delta t), \tag{43.1}$$

where

ϕ is the quantum efficiency (or quantum yield)
σ_1 is the cross section (see the following) at wavelength λ_1
I_1 is the fluence rate (*Note*: the traditional symbol I stands for "intensity," which is sometimes used informally in place of fluence rate; however, according to strict radiometric terminology, intensity is defined as the power per unit solid angle)
Δt is the exposure time (pulse duration)

The fluence is given by $F_1 = I_1 \Delta t$.

To derive an equal-response action spectrum from fluence–response curves, the first step is to specify a "criterion" response level. Then, for each wavelength, one determines the fluence (or fluence rate) needed to produce that standard response. Choices for the criterion response include (a) some fixed absolute level, (b) a percentage (typically 50%) of the maximum response level, which itself may depend on wavelength, (c) the maximum response (peak) level, for those instances where the response descends at high fluence after reaching a peak, or (d) the absolute threshold fluence rate (often extrapolated downward to the baseline from the linearly rising part of the fluence–response curve; note that an alternative approach that should be avoided would be to try to find the limiting fluence at which there just begins to be a perceptible response; the difficulty is that this measure is highly susceptible to experimental noise and subjective judgment); see the following for a further discussion of threshold measurements.

If both fluences $F_{\lambda 1}$ and $F_{\lambda 2}$ elicit the same response level—the criterion response—and if one assumes that Δt is the same in both experiments (or, if reciprocity applies, one can correct for the different values of Δt), then the argument of the function in Equation 43.1 is the same for both experiments at these two wavelengths, λ_1 and λ_2. If the quantum efficiency ϕ is assumed to be the same at both wavelengths, then

$$\frac{\sigma_{\lambda_1}}{\sigma_{\lambda_2}} = \frac{F_{\lambda_2}}{F_{\lambda_1}}. \tag{43.2}$$

It is assumed implicitly that the fluence–response curves are monotonic or at least that the corresponding criterion response points on the curves are chosen (otherwise, if the fluence–response curve were, e.g., bell shaped, there would be two values of fluence with the same response value, and one could conceivably err by choosing noncorresponding points on curves for different wavelengths). From Equation 43.2, it is evident that the cross section at any wavelength λ is inversely proportional to the applied fluence that produces the criterion response at that wavelength or $\sigma_\lambda \propto F_\lambda^{-1}$.

If, instead, the response is measured as a function of fluence rate rather than fluence, then a derivation similar to that mentioned earlier, starting from the equation

$$R = R(\phi\sigma_1 I_1) \tag{43.3}$$

leads to the relation

$$\frac{\sigma_{\lambda_1}}{\sigma_{\lambda_2}} = \frac{I_{\lambda_2}}{I_{\lambda_1}} \tag{43.4}$$

or

$$\sigma_\lambda \propto I_\lambda^{-1}.$$

43.8 Relationship between Extinction Coefficient and Cross Section

The extinction coefficient ε is used in conventional spectrophotometry and measured in the traditional units of L mol^{-1} cm^{-1}. It can be related by a conversion factor to a quantity from physics, the absorption cross section (introduced in Section 43.7), in traditional units of cm^2. The ratio between the fluence rate I transmitted through a spectrophotometric sample and the incident intensity I_0 can be derived from the following relations:

$$\frac{I}{I_0} = 10^{-\varepsilon cl} = e^{-\sigma nl}, \tag{43.5}$$

where

c is the molar concentration of the pigment
ℓ is the internal path length through the cuvet (usually 1 cm)
σ is the absorption cross section
n is the pigment concentration in units of molecules per cm^3

The expression in the first exponent, εcl, represents the absorbance, A.

The extinction coefficient and the cross section are therefore interrelated by the following conversion formula:

$$\varepsilon = 2.62 \times 10^{20}\, \sigma, \tag{43.6}$$

where

ε is in units of L mol^{-1} cm^{-1}
σ is in cm^2

As an example of applying this conversion formula, consider riboflavin (or other flavin), which has an extinction coefficient of 1.25×10^4 L mol^{-1} cm^{-1} (at ~450 nm), then $\sigma = 4.8 \times 10^{-17}$ cm^2. This represents the effective target area the chromophore presents for absorption of light. As another example, rhodopsin, with an extinction of 4×10^4 L mol^{-1} cm^{-1} (at ~500 nm), has $\sigma = 1.5 \times 10^{-16}$ cm^2.

43.9 Derivation of Action Spectrum from Fluence–Response Curves

Figure 43.1 shows a set of five idealized fluence–response curves. The following discussion will demonstrate how action spectra can be derived from such curves. The hypothetical response is presumed to be measured as a function of the photon fluence; alternatively, fluence rate could have been chosen as the independent variable. The fitting function of the form $ax/(x + b)$, where x stands for the fluence (or fluence rate), is plotted for the five wavelengths on both (a) logarithmic and (b) linear scales for x. In this example, wavelength λ_3 is the most effective one because the least amount of light is required to achieve the criterion response level, chosen here to be half of the maximum response. Conversely, λ_5 is the least effective. So, when this set of "data" is converted into an action spectrum, the ordinate representing the sensitivity, or effectiveness, will be high for λ_3 and low for λ_5.

In the semilogarithmic plot (Figure 43.1a), the curves all have the same sigmoidal shape and differ only by lateral displacement. The symmetrical sigmoidal shape is a property of the hyperbolic saturation

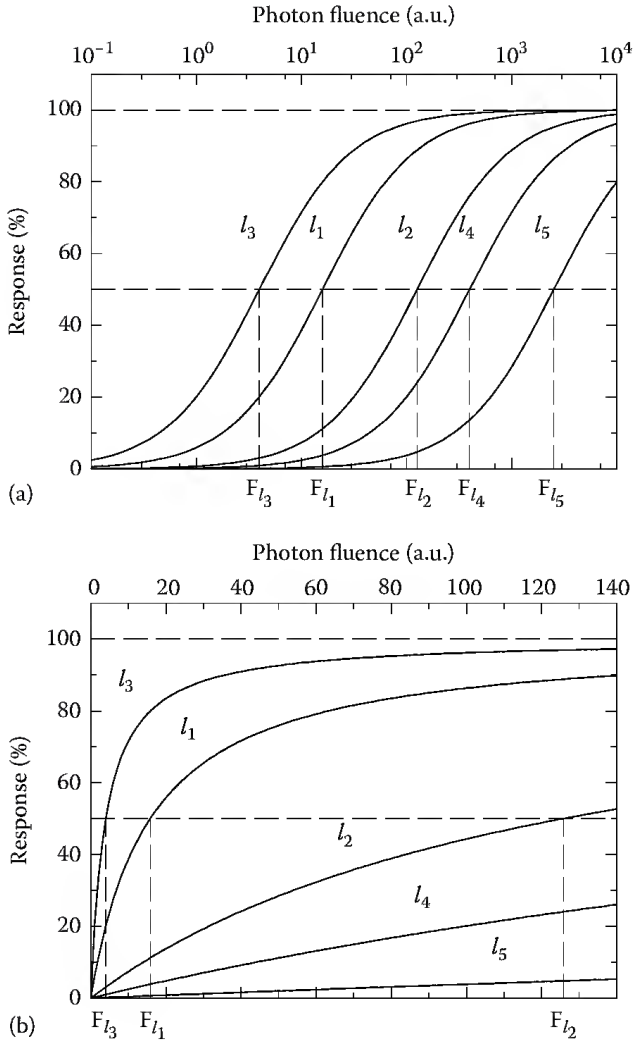

FIGURE 43.1 Generic fluence–response curves for five wavelengths (λ_1 through λ_5) shown on logarithmic (a) and linear (b) scales for photon fluence. The curves represent the hyperbolic saturation function of the form $ax/(x + b)$, where x is the fluence (also denoted in this chapter by the symbol F). On a semilogarithmic scale (a), the curves all have the same sigmoidal shape (see functions in rows 4 and 5 of Table 43.1). The fluence F needed to produce the standard criterion response (here chosen to be 50%) at each wavelength is shown by the vertical dashed lines. The designation of "arbitrary units" on the abscissa scales above each graph means that no importance should be given to the absolute numbers used in this example and, implicitly, that fluence rate could be used instead of fluence if continuous rather than pulse illumination were employed; the actual units of photon fluence would be mol m^{-2}. If photon fluence rate were used instead, the units would be mol m^{-2} s^{-1}.

function, which is frequently used to fit fluence–response curves and other types of stimulus–response relationships in sensory physiology (Naka and Rushton 1966; Williams and Gale 1978), in photochemical kinetics (Lipson and Presti 1980), and in other areas of biophysics and biology, including the well-known Michaelis–Menten enzyme kinetics.

The procedure for deriving the action spectrum (Figure 43.2) from these curves is straightforward. The action spectrum ordinate, often labeled as "relative quantum effectiveness" or just "effectiveness," is simply the reciprocal of the fluence required to produce a criterion response (see Equations 43.2 and 43.4). Some authors choose instead to label the ordinate in "relative units," for example, by normalizing several action spectra to the wavelength of maximal effectiveness of one of them. However, it is preferable to retain the proper physical units of m^2 mol^{-1}. If fluence rate–response curves are used instead as

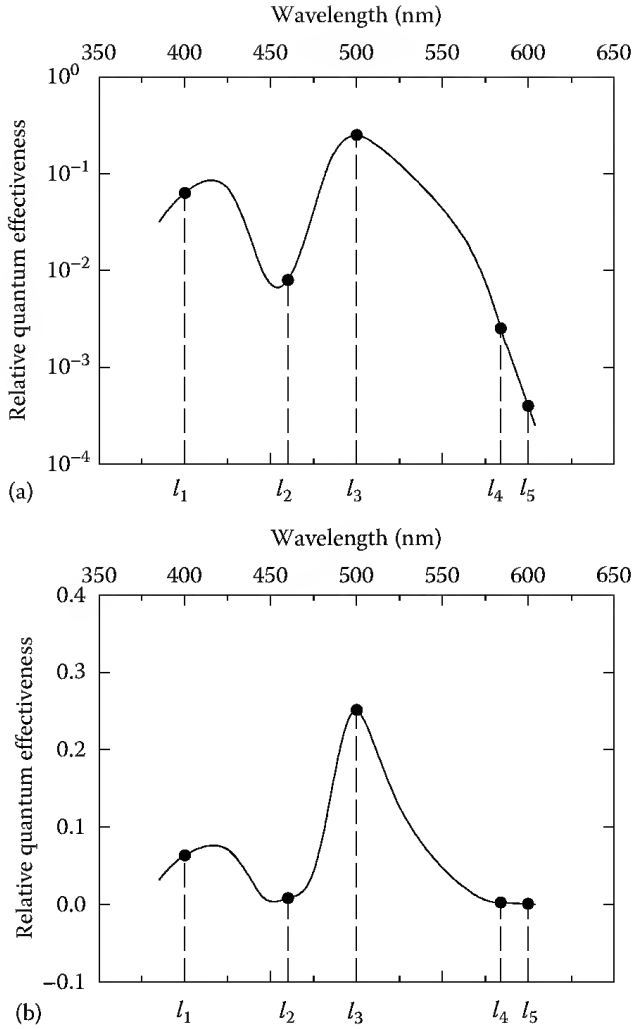

FIGURE 43.2 Five-point action spectrum derived from the fictitious fluence–response curves in Figure 43.1. The relative quantum effectiveness, shown on logarithmic (a) and linear (b) scales, is simply the reciprocal of the photon fluence F required at each wavelength to achieve the criterion response, as indicated in Figure 43.1.

the basis for the action spectra, then the corresponding reciprocal units for the "effectiveness" are m^2 s mol^{-1}. In the former case—based on fluence rather than fluence rate—the units of the action spectrum ordinate are reciprocal to the fluence units, which themselves are essentially m^{-2} (apart from dimensionless entities such as photons or moles of photons). Consequently, the action spectrum physical units are m^2, indicating that some kind of area quantity is involved. This dimensionality corresponds specifically to that of a *cross section* (see relationship, given earlier, between extinction coefficient and cross section).

For a given application, one has to decide between plotting the action spectrum on a logarithmic or linear ordinate. In *Phycomyces*, with a sensitivity range exceeding 10 decades, it is particularly appropriate to plot such action spectra on a logarithmic ordinate (Galland and Lipson 1985a,b, 1987). This choice is advantageous for comparing action spectra with one another or with absorption spectra of putative receptor pigments. Spectra that differ only by a scale factor will have identical shape on a logarithmic scale (and will be displaced by the logarithm of the scale factor). Now, if such spectra were truly identical, apart from a scale factor, they could be forced to have the same shape on a linear scale too, simply by normalizing them at any wavelength of choice (thereby superposing the spectra completely). The practical problem, however, is that in the usual case when spectra are similar but not identical, choosing one wavelength or another for normalization will lead to different relative shapes.

Such ambiguity and subjectivity are avoided by doing the comparison on a logarithmic scale. On the other hand, though, using a linear ordinate scale has the advantage that it is the more familiar way of viewing absorption spectra, for example, the chart records from traditional spectrophotometers.

The abscissa of an action spectrum is usually presented as a wavelength scale. On the basis of quantum mechanical principles, it would be preferable to use an energy rather than a wavelength scale; the two are related reciprocally according to the relation $E = hc/\lambda$, where E is the energy of a photon of wavelength λ, h is Planck's constant, and c is the speed of light. When an action or absorption spectrum is plotted as a function of energy, the positions of peaks are linearly related to transitions between the energy levels corresponding to molecular states (as on a Jablonski diagram; see the preceding text). This is particularly worthwhile in the case of rhodopsin-type pigments in animals—as well as in halophilic bacteria and algae—because such pigments have spectra of standard shape except for lateral shifts in the energy of maximum absorption and vertical shifts in the absolute extinction or effectiveness. Nevertheless, most action and absorption spectra are plotted customarily on a wavelength scale for the abscissa, in keeping with the usual display from spectrophotometers.

43.10 Additional Fitting Functions

The hyperbolic saturation function of the form $ax/(x + b)$ often arises in biophysical and biochemical applications. It is more obvious that this represents a hyperbola, if it is written in a double-reciprocal form as in the Lineweaver–Burk transformation of the Michaelis–Menten enzyme kinetics that employs this type of function. Other contexts where this function appears are monomolecular photochemical kinetics (Lipson and Presti 1980) and visual physiology (Naka and Rushton 1966; Williams and Gale 1978). In the present context of action spectroscopy, x would stand for the fluence or, in some cases, the fluence rate. When $x = b$, the function is at the half-maximum level that is often chosen to be the criterion response. So, when one performs least squares fits using such a function, the parameter b is the estimate of the fluence needed for the criterion response, and the effectiveness (action spectrum ordinate) is just b^{-1}.

Table 43.1 gives several functional forms that are useful for fitting fluence–response curves. These are all based on the hyperbolic saturation function given earlier and shown in the top row of the table. In certain cases, fluence–response curves have a two-component (biphasic) structure. The first component reaches a plateau as in Figure 43.1, and then, at high fluence, a second component appears that may or may not approach saturation at the maximum available fluence. For such a two-component curve, if saturation is reached for the second component, then the function in the second row of Table 43.1 may apply, perhaps with the addition of exponents n (often attributable to cooperativity) for each component, as in the Hill function in the third row. Otherwise, if saturation is not reached at some or all wavelengths, then the function in the last row of Table 43.1 may be useful. The second and third terms of that function together have the shape of a hyperbola when plotted on a semilogarithmic scale (i.e., with abscissa $\log x$). Note that this hyperbola, with a (rising) slant asymptote at high fluence, is unrelated to the hyperbola functions (for linear axes) in the first and second rows.

The functions in Table 43.1 depend nonlinearly upon their parameters (unlike the case of a polynomial, e.g., where the coefficients are linear parameters). Therefore, it is appropriate to use nonlinear least squares data analysis methods. These are widely available and are specifically incorporated in graphical packages such as Origin® (OriginLab Corporation). For applications, like the present one of deriving action spectrum values from fluence–response curves, that require error-propagation methods, it is important to have the *variance–covariance matrix* of the parameter estimates obtained by least squares methods. This matrix is made available in Origin. For those preferring to develop their own data analysis programs, a valuable resource is the *Numerical Recipes* series of books and software (http://www.nr.com), which includes source code in Fortran, Pascal, C, and C++ programming languages for various numerical analysis problems including nonlinear regression (nonlinear least squares), applicable here.

TABLE 43.1 Representative Functions for Fluence–Response Curve Fits

Description	Function	References
Hyperbola	$\frac{ax}{x+b}$	Corrochano et al. (1988)
Two hyperbolas plus a constant[a]	$\frac{ax}{x+b}+\frac{cx}{x+d}+h$	Corrochano et al. (1988); Galland et al. (1989)
Hill function	$\frac{ax^n}{x^n+b^n}$	Ensminger et al. (1990)
Sigmoid[b]	$\frac{a}{1+\exp[n(k-u)\ln 10]}$	Ensminger et al. (1990)
Sigmoid[b]	$\frac{a}{2}\left[1+\tanh\left\{n(u-k)\frac{\ln 10}{2}\right\}\right]$	Ensminger et al. (1990)
Hill plus hyperbola[c]	$\frac{ax^n}{x^n+b^n}+c\log\left(\frac{x}{d}\right)+\sqrt{c^2\log^2\left(\frac{x}{d}\right)+k^2}$	Bejarano et al. (1990); Trad and Lipson (1987)

Source: Lipson, E.D., Action spectroscopy, in *Biophysics of Photoreceptors and Photomovements in Microorganisms*, eds. F. Lenci, F. Ghetti, G. Colombetti, D.-P. Häder, and P.-S. Song, Plenum Press, New York and London, U.K.

[a] This function consists of a sum of two hyperbolas plus an optional constant, h. The coefficients a and c may be positive or negative for saturation components that rise or fall, respectively.

[b] These two equivalent functions are derivable from the Hill function (e.g., familiar in the context of ligand binding for hemoglobin) in the third row, with the substitutions $u = \log x$ and $k = \log b$. They represent the sigmoidal shape taken on by the Hill function when plotted on a semilogarithmic scale, that is, plotted against $\log x$ instead of x. In the special case with $n = 1$, these sigmoidal functions are equivalent to the hyperbola function in the top row (see Figure 43.1). In general, the Hill exponent need not be an integer.

[c] The last two terms together comprise a hyperbola when plotted on a *logarithmic* scale for x. Note that this usage of hyperbola is quite different from that in the top row function. The hyperbola here has a horizontal asymptote for small x and a slant asymptote with slope $2c$ for large x.

43.11 Null and Threshold Action Spectra

Another way to measure action spectra is to employ a balance or null method, in which the criterion response is zero, but without the need to work at absolute threshold levels. For example, two lights, one a fixed "reference" light and the other a variable "test" light could be applied, as appropriate, from opposite directions or in temporal alternation, in such a way that no net response occurs. Examples for action spectroscopy on *Phycomyces* are balance experiments on phototropism (Galland and Lipson 1985a,b) and null experiments on the light-growth response (Ensminger and Lipson 1991; Ensminger et al. 1991).

In general, when sigmoidal and other functions are fit to fluence–response curves for the purpose of action spectroscopy, there is another clear choice for criterion response besides the half-maximum (50%) level, namely, a "threshold" response level. However, as mentioned earlier, thresholds (defined as the highest fluence at which there is no apparent response) *per se* are difficult to measure because of signal-to-noise considerations at low response levels. A more practical measure of the threshold can be defined operationally as the fluence at which the tangent line at the inflection point (or midpoint) intersects the baseline. This level is generally somewhat higher than the actual threshold, but it has the advantages of being much better defined and easier to measure. For a fluence–response curve, or component thereof, described by the Hill function (third row of Table 43.1), the operational threshold fluence is smaller than the midpoint fluence by a factor of $e^{-2/n}$. In the special case when $n = 1$ (top two rows of Table 43.1), the factor is just e^{-2}. On a $\log_{10}$ scale, this threshold fluence is displaced to the left of the midpoint fluence by $0.869/n$ "log units."

43.12 Conclusion

This chapter on action spectroscopy, which has given some practical methodology for obtaining action spectra from fluence–response data, has not delved into action spectroscopy for photochromic receptors, such as phytochrome, a complex topic dealt with in many of the references on action spectroscopy cited in the introduction. Photochromic systems, and others with significant kinetic complexity, call for a mathematical approach termed "analytical action spectroscopy" by Hartmann (1983). Beyond the key recommendation of basing action spectra on fluence–response curves, readers are encouraged to apply formal data analysis techniques, including error analysis, for analyzing experimental results in action spectroscopy research. Details on such methods are available elsewhere (Lipson 1991).

References

Baird, D. C. 1994. *Experimentation: An Introduction to Measurement Theory and Experiment Design.* 3rd ed. Upper Saddle River, NJ: Prentice-Hall.

Baskin, T. I. and M. Iino. 1987. An action spectrum in the blue and ultraviolet for phototropism in alfalfa. *Photochem. Photobiol.* 46:127–136.

Bejarano, E. R., J. Avalos, E. D. Lipson, and E. Cerdá-Olmedo. 1990. Photoinduced accumulation of carotene in *Phycomyces. Planta* 183:1–9.

Björn, L. O., ed. 2008. *Photobiology: The Science of Life and Light.* 2nd ed. New York: Springer.

Coohill, T. P. 1991. Action spectra again. *Photochem. Photobiol.* 54 (5):859–870.

Coohill, T. P. 1992. Action spectra revisited. *J. Photochem. Photobiol. B* 13 (1):95–98.

Corrochano, L. M., P. Galland, E. D. Lipson, and E. Cerdá-Olmedo. 1988. Photomorphogenesis in *Phycomyces*: Fluence-response curves and action spectra. *Planta* 174:315–320.

De Fabo, E. C., R. W. Harding, and W. Shropshire. 1976. Action spectrum between 260 and 800 nanometers for the photoinduction of carotenoid biosynthesis in *Neurospora crassa. Plant Physiol.* 57 (3): 440–445.

Delbrück, M. 1976. Light and life III. *Carlsberg Res. Commun.* 41:299–309.

Ensminger, P. A., X. Y. Chen, and E. D. Lipson. 1990. Action spectra for photogravitropism of *Phycomyces* wild type and three behavioral mutants (L150, L152, and L154). *Photochem. Photobiol.* 51 (6): 681–687.

Ensminger, P. A. and E. D. Lipson. 1991. Action spectra of the light-growth response in three behavioral mutants of *Phycomyces. Planta* 184 (4):506–509.

Ensminger, P. A., H. R. Schaefer, and E. D. Lipson. 1991. Action spectra of the light-growth response of *Phycomyces. Planta* 184:498–505.

Foster, K. W. 2001. Action spectroscopy of photomovement. In *Photomovement*, edited by D.-P. Häder and M. Lebert. Amsterdam, the Netherlands: Elsevier.

Galland, P. 1987. Action spectroscopy. In *Blue Light Responses: Phenomena and Occurrence in Plants and Microorganisms*, edited by H. Senger. Boca Raton, FL: CRC Press.

Galland, P. and E. D. Lipson. 1985a. Action spectra for phototropic balance in *Phycomyces blakesleeanus*: Dependence on reference wavelength and intensity range. *Photochem. Photobiol.* 41 (3):323–329.

Galland, P. and E. D. Lipson. 1985b. Modified action spectra of photogeotropic equilibrium in *Phycomyces blakesleeanus* mutants with defects in genes madA, madB, madC, and madH. *Photochem. Photobiol.* 41 (3):331–335.

Galland, P. and E. D. Lipson. 1987. Light physiology of *Phycomyces* sporangiophores. In *Phycomyces*, edited by E. Cerdá-Olmedo and E. D. Lipson. Cold Spring Harbor, NY: Cold Spring Harbor Laboratory.

Galland, P., M. Orejas, and E. D. Lipson. 1989. Light-controlled adaptation kinetics in *Phycomyces*: Evidence for a novel yellow-light absorbing pigment. *Photochem. Photobiol.* 49:493–499.

Galland, P. and H. Senger. 1988. The role of flavins as photoreceptors. *J. Photochem. Photobiol. B Biol.* 1:277–294.

Grossweiner, L. I. 1989. Photophysics. In *The Science of Photobiology*, edited by K. C. Smith. New York: Plenum Press.

Häder, D.-P. and M. Tevini. 1987. *General Photobiology*. Oxford, U.K.: Pergamon Press.

Hartmann, K. M. 1983. Action spectroscopy. In *Biophysics*, edited by W. Hoppe, W. Lohmann, H. Markl, and H. Ziegler. Berlin/Heidelberg/New York: Springer-Verlag.

Jagger, J. 1967. *Introduction to Research in Ultraviolet Photobiology*. Englewood Cliffs, NJ: Prentice-Hall.

Lipson, E. D. 1991. Action spectroscopy. In *Biophysics of Photoreceptors and Photomovements in Microorganisms*, edited by F. Lenci, F. Ghetti, G. Colombetti, D.-P. Häder, and P.-S. Song. New York and London, U.K.: Plenum Press.

Lipson, E. D. and B. A. Horwitz. 1991. Photosensory reception and transduction. In *Sensory Receptors and Signal Transduction*, edited by J. Spudich and B. Satir. New York: Academic Press.

Lipson, E. D. and D. Presti. 1980. Graphical estimation of cross sections from fluence-response data. *Photochem. Photobiol.* 32:383–391.

Meyer, T. E., E. Yakali, M. A. Cusanovich, and G. Tollin. 1987. Properties of a water-soluble, yellow protein isolated from a halophilic phototrophic bacterium that has photochemical activity analogous to sensory rhodopsin. *Biochemistry* 26 (2):418–423.

Naka, K. I. and W. A. Rushton. 1966. S-potentials from colour units in the retina of fish (Cyprinidae). *J. Physiol.* 185 (3):536–555.

Presti, D. E. and P. Galland. 1987. Photoreceptor biology of *Phycomyces*. In *Phycomyces*, edited by E. Cerdá-Olmedo and E. D. Lipson. Cold Spring Harbor, NY: Cold Spring Harbor Laboratory.

Schäfer, E. and L. Fukshansky. 1984. Action spectroscopy. In *Techniques in Photomorphogenesis*, edited by H. Smith and M. G. Holmes. London, U.K.: Academic Press.

Schäfer, E., L. Fukshansky, and W. Shropshire, Jr. 1983. Action spectroscopy of photoreversible pigment systems. In *Photomorphogenesis*, edited by W. Shropshire, Jr., H. Mohr, and M. H. Zimmermann. Berlin, Heidelberg, New York: Springer-Verlag.

Schlichting, I. and J. Berendzen. 1997. Out of the blue: The photocycle of the photoactive yellow protein. *Structure* 5 (6):735–739.

Schmid, R., E.-M. Idziak, and M. Tuennermann. 1987. Action spectrum for the blue-light-dependent morphogenesis of hair whorls in *Acetabularia mediterrania*. *Planta* 171:96–103.

Shropshire, W., Jr. 1972. Action spectroscopy. In *Phytochrome*, edited by K. Mitrakos and W. Shropshire, Jr. London, U.K.: Academic Press.

Smith, K. C., ed. 1989. *The Science of Photobiology*. 2nd ed. New York: Plenum Press.

Song, P.-S. 2005. Hypericin-like photoreceptors. In *Handbook of Photosensory Receptors*, edited by W. R. Briggs and J. L. Spudich. Weinheim, Germany: Wiley-VCH.

Trad, C. H. and E. D. Lipson. 1987. Biphasic fluence-response curves and derived action spectra for light-induced absorbance changes in *Phycomyces* mycelium. *J. Photochem. Photobiol. B Biol.* 1:169–180.

Williams, T. P. and J. G. Gale. 1978. "Compression" of retinal responsivity: V-log I functions and increment thresholds. In *Visual Psychophysics and Physiology*, edited by J. C. Armington. New York: Academic Press.

44

Action Spectroscopy: Ultraviolet Radiation

Thomas P. Coohill
Siena College

Francesco Ghetti
Istituto di Biofisica

44.1 Introduction to Ultraviolet Radiation

Ultraviolet (UV) radiation is the portion of the electromagnetic spectrum that extends from the lower wavelength limit of human vision (usually defined as 380–400 nm) to wavelengths as short as about 10 nm, where it overlaps the x-ray region. In the natural environment, the shortest wavelength of sunlight that can be routinely measured at the earth's surface is about 290 nm, largely due to the absorption properties of ozone and other atmospheric gases. So, the only environmentally relevant UV region is from 290 to 380 nm. However, artificial UV sources such as certain fluorescent lamps, mercury and xenon arcs, and lasers are readily available and extend the possibility of exposure of biological specimens to UV down to wavelengths of about 190 nm. Below 190 nm, air (oxygen) and water begin to absorb UV heavily, making it difficult to expose biological samples except under extreme conditions (e.g., in a vacuum). Hence, UV photobiology is concerned mainly with the effects on biological processes due to exposure to photons in the wavelength range of 190–380 nm.[1]

44.2 Division of the UV Region for Photobiological Studies

44.2.1 Vacuum UV (10–190 nm)

Photons in the "vacuum" UV (VUV) are heavily absorbed by water and oxygen (in air), both of which become essentially transparent (more than 50% transmission, for a 1 cm path length) to UV at wavelength above 190 nm. Because of this limited penetration, VUV damage to cells is usually confined to a narrow region (a few micrometers) near the cell surface. The energies of single photons in this region are

above 6.5 eV, sufficient to ionize many biomolecules. Since the biological effects due to ionizing photons are different from those due to nonionizing photons, the VUV often causes different types of cellular and molecular damage. Thus, VUV effects can be qualitatively different from those of other UV regions.

44.2.2 UV-C (190–290 nm)

The shorter-wavelength end of the UV-C (190 nm) is the wavelength region where air and water become transparent. The longer-wavelength limit (290 nm) is the shortest solar UV wavelength easily measured at the earth's surface. Thus, all of the UV-C is environmentally irrelevant. However, research in the UV-C range was central in elucidating many important features of cell functioning. DNA, the genetic material, has a peak absorption near 260 nm that falls by a factor of 6 by 290 nm. This fact, combined with the readily available 254 nm "germicidal" UV fluorescent source, allowed for simple experimental molecular manipulation of DNA, and UV-C photobiology was central in establishing the then-new field of molecular biology.

44.2.3 UV-B (290–320 nm)

The shorter-wavelength limit (290 nm) of the UV-B region can be defined as the shortest UV wavelength routinely measurable at the earth's surface where it is about 1 million-fold less prevalent than 320 nm radiation. The longer-wavelength limit (320 nm) is where ozone and other atmospheric components begin to (more than 50%) attenuate sunlight appreciably. This absorption prevents much of the significant DNA damage that would result if no ozone layer existed. DNA absorption rapidly decreases by more than four orders of magnitude from 290 to 320 nm.[2] Nevertheless, absorption of UV-B photons by DNA contributes to a wide variety of bioeffects. The UV-B, which constitutes less than 0.3% of the total sunlight spectrum, is responsible for most of the damage inflicted on organisms by sunlight.

44.2.4 UV-A (320–380 nm)

The shorter-wavelength limit of the UV-A (320 nm) can be defined as that wavelength at which ozone becomes transparent. The longer-wavelength limit (380 nm) is where human vision begins and the UV ends. The UV-A region is also biologically effective and causes cellular death, mutation, and DNA damage, although the primary chromophores for these effects may be non-DNA sensitizers that are chemically matched to the photon energy and act as intermediates in relaying the absorbed energy to DNA.[3] UV-A exposures from sunlight are considerable, constituting about 8% of the total sunlight spectrum.

44.2.5 Terrestrial Solar UV (290–380 nm)

This region is easily defined as the wavelength bracket that is the limit of human vision (380 nm) at the long-wavelength end and the effective limit of the solar UV reaching the earth's surface at the short wavelength (290 nm) end. This is the environmentally relevant UV region and is, of course, just the UV-B plus the UV-A.

44.3 Absorption of UV by Cells

The responses of biological samples to UV can be greatly affected by their absorption properties. Beginning at the cellular level, it can be seen in Table 44.1 that 200 nm UV-C, for example, is absorbed only slightly by viruses (about 30%), more so by bacterial cells (about 70%), and entirely by mammalian cells (more than 90%). This absorption is due mainly to the presence of endogenous molecules that absorb heavily in the UV-C. At longer wavelengths, cell absorption decreases. The absorption of two important biomolecules, the genetic material DNA and protein, is compared in Figure 44.1. Both molecules begin

TABLE 44.1 Percent Transmission to the Center of Selected Cells and Viruses in the UV

		Wavelength (nm)			
Biological Sample	Diameter (μm)	200	250	300	350
Bacteriophage (T2)	0.1	74	86	100	100
Herpes simplex virus	0.15	66	80	100	100
Bacterial cell	1	33	78	98	100
Yeast cell	5	1.6	69	97	100
Mammalian cell (spherical)	20	10[a]	20	91	96
Mammalian tissue (100 μm thick)	—	—	10[b]	39	66

Note: All values are approximate. Values at λ above 300 nm can vary widely due to the presence of endogenous chromophores (Coohill, 1984).

[a] See also Coohill (1984).

[b] See also Coohill (1990).

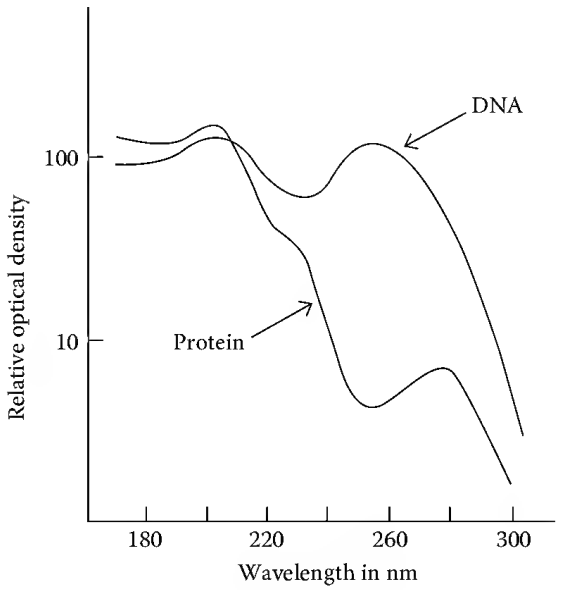

FIGURE 44.1 The absorption spectra of DNA and protein (bovine serum albumin). Both curves are for a 1% solution and 1 cm path length.

to absorb appreciably in the UV-B and substantially in the UV-C. On a weight-by-weight comparison, DNA absorbs about 20-fold as much 260 nm radiation as does protein. Therefore, the absorption of even homogenates of mammalian cells is similar in the wavelength range of 220–290 nm to that of DNA. The absorbance (a logarithmic function) of such homogenates is seven times higher at 240 nm compared to 300 nm. As the UV wavelength decreases below 220 nm, both proteins and nucleic acids contribute greatly to the total cellular absorption. At wavelengths below 190 nm, water and oxygen absorption prevails. In addition to these macromolecules, some cells contain certain pigments that can alter cellular absorption significantly, even at the longest UV wavelengths. Also, cellular particles and organelles can absorb and scatter UV radiation and, at some wavelengths, shield the center of the cell from a significant portion of the incident beam. Such cytoplasmic screening can alter measured bioeffects to a large degree, especially in the UV-C, and must be considered when cellular exposure is attempted.[4] Such concerns are important because biological cells and tissues will absorb radiation in a wavelength-dependent

manner and alter the exposure of the target accordingly. Therefore, the absorption properties of cells are not merely a summation of the individual absorptions of their component molecules.

44.4 Absorption by Tissue

Much of the direct absorption of UV by tissues such as human skin can be accounted for by the presence of endogenous pigments, especially melanin, hemoglobin, carotenes, and keratin, and exogenous pigments and drugs. Because skin is such a heterogeneous material, UV can be reflected, absorbed, scattered, and rescattered. This means that the direct component of the UV beam is augmented by additions from photons scattered and reflected back into the beam pathway. Hence, at any tissue depth, the sum of the total UV exposure is just the direct plus the diffuse. At wavelengths below 300 nm, absorption by tissue rapidly increases, making all but the first few cell layers of the skin essentially opaque to radiation below about 290 nm.

44.5 Action Spectroscopy

44.5.1 Differences in Effect with Wavelength

An action spectrum (AS) is simply defined as the measurement of a biological effect as a function of wavelength. Crude AS was first used in the nineteenth century to help identify chlorophyll as the chromophore most responsible for the growth of plants. In this century, more sophisticated methods refined the analysis of AS so that it is now possible, in some instances, to make a reasonable determination of the molecule that is likely to contain the chromophore(s) responsible for the response being studied (see Chapter 43). It is this latter usage that was among the first methods that pointed to DNA as the genetic material. This was possible because small unicellular organisms, such as bacteria, had relatively high transmission rates for UV and thus meet the rather stringent criteria[5] for a reliable analysis called an analytical action spectrum (AAS). An AAS can only be claimed if the AS corresponds closely to the absorption spectrum of the suspected molecule.

44.5.1.1 UV-C (190–290 nm) Action Spectra

Because some molecules absorb heavily in the UV, certain bioresponses are highly dependent on the wavelengths to which the cell is exposed. In 1930, Gates[6] (Figure 44.2) reported that the AS for bacterial cell death closely followed the absorption of nucleic acid, not proteins, which was then widely believed to be the genetic material. In retrospect, this was the first clear evidence that DNA was the genetic material. It should be remembered that an AS could not distinguish between DNA and RNA as the target molecules since both have similar absorption spectra. However, an AS for a photoproduct exclusive to DNA, such as the thymine dimer, can. Although AS utilizing small cells is somewhat simple, it is difficult to extend these studies to larger (e.g., mammalian) cells because of the substantial absorption of UV by large cells and tissues (Table 44.1). Two other AS's in the UV-C for cell death, one for mammalian tissue and one for individual mammalian cells, are shown in Figure 44.2.[5] Experiments utilizing hanging-drop mammalian tissue samples failed to produce an AS with the fine structure of those studies that utilized bacteria because the tissue was essentially opaque to radiation near the peak of DNA absorption (260 nm). Thus, the target molecule (DNA) was shielded to an extent such that the shape of the AS did not parallel the absorption spectrum of the target. The advent of single-cell mammalian culture techniques and the unique flattened geometry that mammalian cells assume when in monolayer culture allowed these studies to begin. Thus, AS for killing of cultured mammalian cells reported data similar to those with bacteria, but the peak was shifted to about 270 nm. This discrepancy can be accounted for by looking at the absorption properties of single mammalian cells and considering, as is the case in bacteria, that the likely target molecule for cell killing is also DNA that resides in the nucleus. This means that the UV beam has to traverse half of the cell on average to strike its target. In bacteria, this

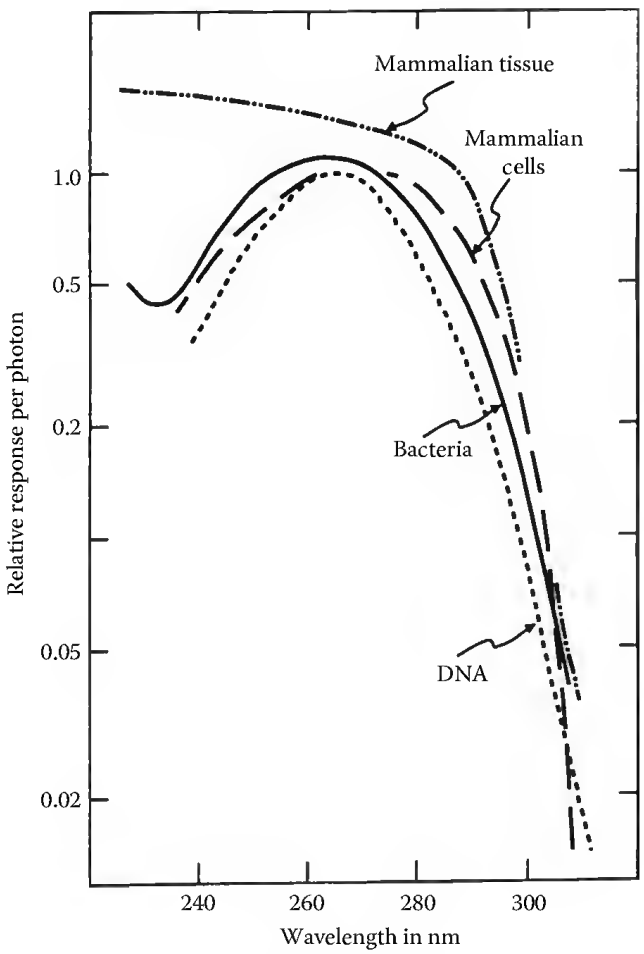

FIGURE 44.2 UV action spectra for the killing of bacteria, mammalian cells, and mammalian tissue. Also represented is the absorption spectrum for DNA. Note that the fine structure inherent in the AAS for bacteria and mammalian cells is absent in the case of the essentially opaque mammalian tissue.

distance is small enough to allow one to neglect absorption effects; in mammalian cells, the absorption is substantial. An AS for the production of pyrimidine dimers caused by UV exposure to the DNA in mammalian cells matched the AS for cell death. Therefore, DNA alone was considered responsible for mammalian cell lethality in the 220–290 nm region.[7] However, if a detailed knowledge of scattering and absorption events before the beam reaches the target is not known, or if the identification of the target is unsure, then any attempt to "correct" or interpret the data generated is suspect. In some cases, it may be useful to modify the incident beam such that the center of the cell, rather than the cell surface, always receives the same exposure.

Not all UV-C AS's follow DNA absorption. For example, the loss of saxitoxin binding to sodium channels in rodent cells, or sodium conduction loss in frog cells or lobster axons, or the UV-induced termination of beating by embryonic chick heart aggregates, all follow an AS similar to the absorption spectra of protein moieties.[7] In addition, UV-C AS's for highly pigmented tissues (such as plants) show little correspondence to the absorption of any chromophore. The latter is due to the high degree of absorption of UV-C, which essentially rules out useful AAS in this region for cells and tissues that absorb most of the incident radiation before it can reach the target molecule(s). Thus, UV-C AS's are very useful for small or relatively transparent cell studies, but are of very limited use for multicellular or highly pigmented samples. But even if a chromophore cannot be identified, an AS still shows the effect of separate wavelengths on a biological response, and as such is of some use in predicting the results due

to exposure. Studies of human skin exposure to UV-C (e.g., skin cancer or erythema) show on average, an essentially flat response in the UV-C, or in some cases a lessening of effect at shorter wavelengths, that is almost certainly due to limited penetration of the UV beam.

44.5.1.2 UV-B and UV-A (290–380 nm) Action Spectra

It was widely thought that experimental work in the UV-C and UV-B (wavelength range of 190–320 nm) could be extrapolated to predict photobiological responses in the UV-A (320–380 nm). This is not the case, and UV-A AS's are much more complex than had been predicted.[3] Here, even events such as cell mutation, which surely involve the genetic material, can be affected at fluences that appear to be below those necessary to affect DNA in these wavelength regions. Details of the divergence of several AS's for human cell photoresponses from the DNA absorption spectrum as the curves shift to longer wavelengths in the UV-A are given in Figure 44.3. In the UV-C, cell killing and mutagenesis follow the absorption spectrum of DNA, and carcinogenesis shows a decrease in effect at shorter wavelengths. The UV-B is a transition region from the highly damaging UV-C to the less damaging UV-A. In the UV-A, all of the biological parameters are affected at levels that are not fully explainable by the absorption properties of DNA. The absolute absorption of moieties in the DNA molecule itself is difficult to measure at wavelengths above 320 nm because of scattering and contamination by extraneous chromophores.[2] It is thought that if the absorption is not intrinsic to DNA, then an intermediate molecule may be involved that absorbs the incident UV-A photon and transfers the effect to DNA.

The motivation for focusing on studies of the effects of UV-A, UV-B, and the solar UV wavelength region is provided by three observations. First, many cells and tissues are more transparent to terrestrial solar UV than to UV-C, especially in the UV-A; thus, this region should be more amenable to AS analysis.

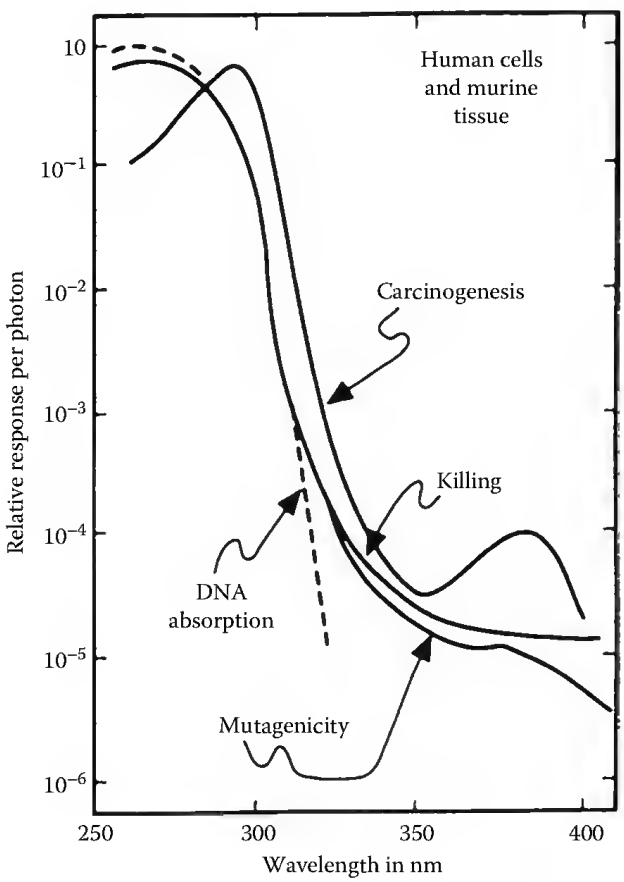

FIGURE 44.3 UV action spectra for human cell killing and mutagenesis and carcinogenic AS for mouse skin.

Second, research has suggested that the nature of the primary and secondary chromophores, photoproducts, and mechanisms for cellular response to solar UV appear in some cases to be very different from those elucidated for wavelengths shorter than about 300 nm. For example, in contrast to their marked sensitivity to UV-C, certain photosensitive human cell lines, such as xeroderma pigmentosum (XP) cells, exhibit the same sensitivity to UV-A as normal cells.[8] Third, solar UV impacts a large number of important bioresponses, such as skin cancer, plant growth, cellular survival, and mutagenesis. Research in this area should reveal ultimately the nature of biological responses to a portion of the radiation present in a normal environmental setting.[9,10]

44.6 Carcinogenesis/Erythema/Vitamin D

The role of solar UV in human skin cancer has been long established. Squamous and basal cell carcinomas are believed to be the result of chronic UV exposure. The expression of these cancers is highly dependent on skin type and individual predisposition. The carcinogenic data in Figure 44.3 are mainly a composite from the analysis of De Gruijl and van der Leun[11] and incorporate 12 separate studies utilizing mice. This AS shows major effects in the UV-C and UV-B, and falls off rapidly in the UV-A. But, there is about 35× more UV-A then UV-B in sunlight; therefore, the contribution of UV-A to carcinogenesis is significant. As shown, however, the major cause of UV-induced cancer is the UV-B component of sunlight.

An AS similar, but not identical to the AS for carcinogenesis, is that generated for the production of previtamin D_3 in human skin.[12] Both action spectra peak in the UV-B, but previtamin D_3 synthesis decreases by two orders of magnitude going from 320 to 330 nm (entering the UV-A), whereas the carcinogenic or human erythemal AS shows significant contributions in the UV-A. An analysis of the problems inherent in weighting these AS's to sunlight exposure is given by Pope et al.[13]

44.7 Polychromatic Action Spectra

Some scientists, perhaps realizing the futility of attempting to construct monochromatic AAS using multicellular organisms, have reported AS that employ polychromatic sources.[14] These studies vary from irradiating the affected system with additional single wavelengths that are added to an ambient background, or generating a set of data using polychromatic sources that employ cutoff filters at successively shorter wavelength. The polychromatic system is complex and tends to obscure individual chromophores, but it is the closest experimental setup to natural field conditions. A major advantage of using polychromatic radiation in the development of polychromatic action spectra (PAS) is that interactions of biological responses to different wavelengths (usually unknown) are empirically incorporated into the composite spectrum. In addition, highly pigmented tissues, such as those of plants, have a large variety of chromophores that interact to give a total effect. Here, PAS can give a composite view of the organism's response even for such complex parameters as "generalized plant response"[15] and many other field measurements.

In this regard, PAS play a central role in assessing the effects on the biosphere, and especially on plants, of the increase of solar UV-B irradiance at the Earth's surface caused by the depletion of the stratospheric ozone layer.[16]

Notwithstanding the complexity of experiments under natural radiation, various spectral studies have been performed either removing increasingly larger portions of the solar UV spectrum by means of different combinations of long-pass filters,[17–19] or supplementing UV radiation by means of appropriate fluorescent lamps.[20,21] Quite recently, a sophisticated irradiation system has been described, which uses both filters and supplementary UV lamps and can provide computer-controlled modulated changes in any radiation band between about 250 and 730 nm.[22–24]

Also sun simulators (also known as phytotrons) are very promising tools to overcome the difficulties of outdoor studies.[25–27] The employment of a wide range of modern lamp types and different filter

combinations allow obtaining the spectral quality and the intensity of natural global radiation and the appropriate shaping of the short-wave cutoff. Moreover, the appropriate irradiation conditions and climatic factors can be reproduced at any time, and disturbing agents can be excluded.[28,29]

Sutherland[30] describes mathematical procedures for calculating the biological effects from exposing samples to polychromatic (especially UV) radiation. His analysis includes a variety of fluence response functions and presents an approach for predicting total effect and analyzing subtle differences between classical AS analysis and biological weighting functions.

Two different approaches have been proposed for extracting an AS from experimental data obtained with polychromatic exposures in which UV irradiance is varied by means of filter combinations with progressively decreasing cutoff wavelength. Differential action spectroscopy (DAS) takes into account the spectral bands given by the difference in irradiance of two filter combinations with successive cutoff wavelength. Assuming that different spectral bands supplement one another in producing the observed effect, it is possible to estimate the weighted contribution of each band by dividing the differences in response to the treatment by the corresponding differential irradiances. Finally, the AS is derived by plotting the weighted effects as a function of the average wavelength of the corresponding band. As UV action spectra tend to exponentially increase with decreasing wavelength, the main limit of this method is given by the potentially large variability of the response in the range of each differential band, which could significantly alter the shape of the resulting AS.[31] This limit, however, is present also for monochromatic action spectroscopy, when using currently available interference filters. The differential method can be improved by using several irradiance levels for each differential band, thus reducing statistical errors and allowing a more correct shaping of the AS.[16]

If DAS reduces the problem to the monochromatic situation, the other approach proposed by Rundel[31] is a deconvolution technique in which it is assumed that the AS is an analytical continuous function $\varepsilon(\lambda)$ and the predicted system response R_i to the ith irradiation regime $E_i(\lambda, t)$ can be expressed as depending on the biologically active irradiance integrated over the irradiation time:

$$R_i = F\left[\iint_{t,\lambda} \varepsilon(\lambda)E_i(\lambda,t)d\lambda dt\right].$$

Once a functional form for $\varepsilon(\lambda)$ has been chosen in dependence of a given number of parameters, the latter can be determined by means of iterative calculations to minimize the differences between each R_i and the corresponding measured response. The limit of this method is that the *a priori* choice of both the form of $\varepsilon(\lambda)$ and the functional relationship F between response and exposure is critical for the correct determination of the AS. However, the use of multivariate statistical analysis (such as, e.g., principal component analysis) allows obtaining more detailed biological weighting functions.[32,33]

44.8 Effectiveness Spectra

It is also possible to estimate the damage to a biological system by exposure to UV by combining an AS for a given effect with a known ambient exposure.[15] These are called effectiveness spectra (ES's) and give at least a first approximation for the effects of UV on the studied system. One such ES is shown in Figure 44.4, which charts the AS for generalized plant damage[15] and the ambient solar UV. The product of these two curves is the solar plant damage ES. From this chart, one can see that the UV-B region is the most damaging, with a peak at about 308 nm. Although solar intensity increases by a factor of 10 from 310 to 330 nm, the biological response decreases more rapidly over the same wavelength range so that the overall effect is less.

Cullen and his coworkers,[34] using spectrally resolved model calculations of water column photosynthesis (and its inhibition by UV), have been able to generate simple mathematical functions that allow researchers to add in environmentally relevant variables and generate results that predict total yield that match field measurements.

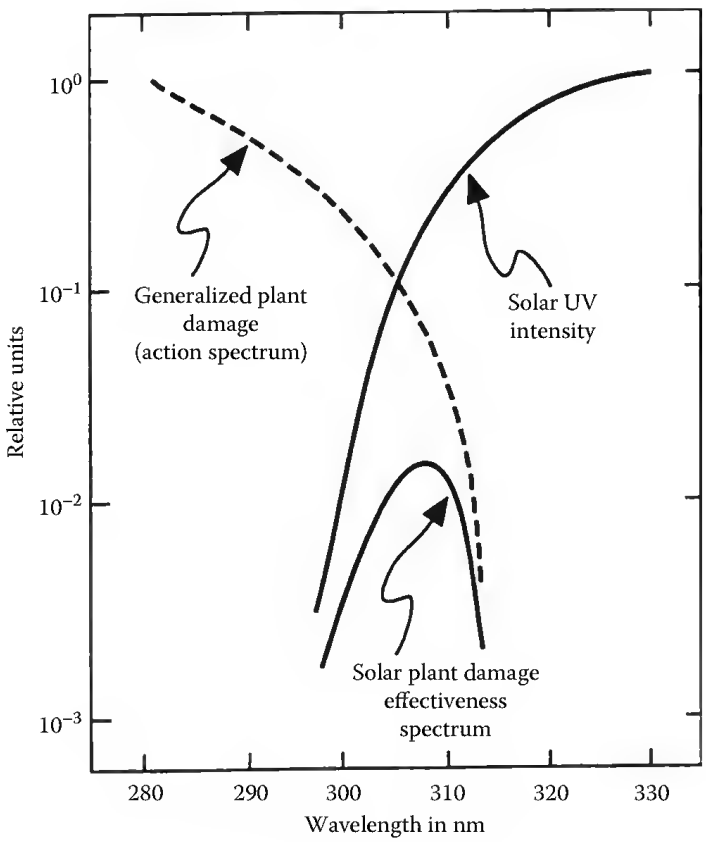

FIGURE 44.4 An AS for generalized plant damage, the terrestrial solar UV intensity spectrum, and a solar plant damage ES obtained by combining the previous two spectra.

44.9 Constraints

Finally, it should be pointed out that even if all the constraints necessary to produce a detailed AS are adhered to, experimental variables usually limit the reliability of any AS. These variables include, but are not limited to (1) the spectral purity of the radiation source (including the bandwidth of any "monochromate radiation"); (2) the accuracy of the dosimetry measurements; (3) the presence of endogenous or exogenous "nonparticipating" chromophores; (4) the ambient (even microenvironmental) condition; (5) the time in the life cycle (cellular) or growth cycle (developmental) of the exposed organism; (7) the geometry of the cell or tissue when irradiated; (8) the availability of proper nutrients; (9) water stress in plant studies; and (10) numerous other extraneous conditions.

References

1. Jagger, J., *Introduction to Research in Ultraviolet Photobiology*, Prentice-Hall, Englewood Cliffs, NJ, 1967.
2. Sutherland, J. C. and Griffin, K. P., Absorption spectrum of DNA for wavelengths greater than 300 nm, *Radiat. Res.*, 41, 399, 1981.
3. Coohill, T. P., Peak, M. J., and Peak, J. G., The effects of the ultraviolet wavelengths present in sunlight on human cells in vitro, *Photochem. Photobiol.*, 46, 1043, 1987.
4. Coohill, T. P., Knauer, D. J., and Fry, D. G., The wavelength dependence of changes in cell geometry on the sensitivity to ultraviolet radiation of mammalian cellular capacity, *Photochem. Photobiol.*, 30, 565, 1979.

5. Coohill, T. P., Action spectra again? *Photochem. Photobiol.*, 54, 859, 1990.
6. Gates, F. L., A study of the bactericidal action of ultraviolet light. III. The absorption of ultraviolet light by bacteria, *J. Gen. Physiol.*, 14, 31, 1930.
7. Coohill, T. P., Action spectra for mammalian cells in vitro, in *Topics in Photomedicine*, Smith, K. C., Ed., Plenum, New York, 1984, p. 1.
8. Keyse, S. M., Moss, S. H., and Davies, K. J. G., Action spectra for inactivation of normal and xeroderma pigmentosum human skin fibroblasts by ultraviolet radiations, *Photochem. Photobiol.*, 37, 307, 1983.
9. Jagger, J., *Solar-UV Actions on Living Cells*, Praeger, New York, 1985.
10. Peak, M. J. and Peak, J. G., Use of action spectra for identifying molecular targets and mechanisms of action of solar ultraviolet light, *Physiol. Plan.*, 58, 367, 1983.
11. de Gruijl, F. R. and van der Leun, J., Action spectra for photocarcinogenesis, in *Biological Responses to UV-A Radiation*, Urbach, F., Ed., Valdenmar, Overland Park, KS, 1991, p. 91.
12. CIE Technical Committee 6–54. CIE technical report CIE 174 action spectrum for production of previtamin D3 in human skin. *Commission Internationale de l'Eclairage (CIE)* Central Bureau, Vienna, Austria, 2006.
13. Pope, S. J., Holick, S. J., Mackin S., and Godar, D. E. Action spectrum conversion factors that change erythemally weighted to previtamin D3-weighted UV doses. *Photochem. Photobiol.*, 84, 1277, 2008.
14. Flint, S. D. and Caldwell, M. M., A biological weighting function for ozone depletion research with higher plants, *Physiol. Plant.*, 117, 137, 2003.
15. Coohill, T. P., Ultraviolet action spectra (280 to 380 nm) and solar effectiveness spectra for higher plants, *Photochem. Photobiol.*, 50, 451, 1989.
16. Holmes, M. G., Action spectra for UV-B effects on plants: Monochromatic and polychromatic approaches for analysing plant responses, in *Plant and UV-B: Responses to Environmental Change*, Lumsden, P. J., Ed., Cambridge University Press, Cambridge, U.K., 1997, p. 31.
17. Searles, P. S., Caldwell, M. M., and Winter, K., The response of five tropical dicoltyledon species to solar ultraviolet-B radiation, *Am. J. Bot.*, 82, 445, 1995.
18. Boucher, N. P. and Prézelin, B. B., Spectral modeling of UV inhibition of *in situ* Antarctic primary production using a field-derived biological weighting function, *Photochem. Photobiol.*, 64, 407, 1996.
19. Hermann, H., Häder, D.-P., and Ghetti, F., Inhibition of photosynthesis by solar radiation in *Dunaliella salina*: Relative efficiencies of UV-B, UV-A and PAR, *Plant Cell Environ.*, 20, 359, 1997.
20. Caldwell, M. M., Gold, W. G., Harris, G., and Ashurst, C. W., A modulated lamp system for solar UV-B (280–320 nm) supplementation studies in the field, *Photochem. Photobiol.*, 37, 479, 1983.
21. McLeod, A. R., Outdoor supplementation systems for studies of the effects of increased UV-B radiation, *Plant. Ecol.*, 128, 1, 1997.
22. Holmes, M. G., An outdoor multiple wavelength system for the irradiation of biological samples: Analysis of the long-term performance of various lamps and filter combinations, *Photochem. Photobiol.*, 76, 158, 2002.
23. Cooley, N. M., Truscott, H. M. F., Holmes, M. G., and Attrige, T. H., Outdoor ultraviolet polychromatic action spectra for growth responses of *Bellis perennis* and *Cynosurus cristatus*, *J. Photochem. Photobiol. B Biol.*, 59, 64, 2000.
24. Holmes, M. G. and Keiler, D. R., A novel phototropic response to supplementary ultraviolet (UV-B and UV-A) radiation in the siliquas of oilseed rape (*Brassica napus* L.) grown under natural conditions, *Photochem. Photobiol. Sci.*, 1, 890, 2002.
25. Ghetti, F., Hermann, H., Häder, D.-P., and Seidlitz, H. K., Spectral dependence of the inhibition of photosynthesis under simulated global radiation in the unicellular green alga *Dunaliella salina*, *J. Photochem. Photobiol. B Biol.*, 48, 166, 1999.
26. Ries, G., Heller, W., Puchta, H., Sandermann, Jr., H., Seidlitz, H. K., and Hohn, B., Elevated UV-B radiation reduces genome stability in plants, *Nature*, 406, 98, 2000.

27. Ibdah, M., Krins, A., Seidlitz, H. K., Heller, W., Strack, D., and Vogt, T., Spectral dependence of flavonol and betacyanin accumulation in *Mesembryanthemum crystallinum* under enhanced UV radiation, *Plant Cell Environ.*, 25, 1145, 2002.
28. Thiel, S., Döhring, T., Köfferlein, M., Kosak, A., Martin, P., and Seidlitz, H. K., A phytotron for plant stress research: How far can artificial lighting compare to natural sunlight? *J. Plant Physiol.*, 148, 456, 1996.
29. Döhring, T., Köfferlein, M., Thiel, S., and Seidlitz, H. K., Spectral shaping of artificial UV-B irradiation for vegetation stress research, *J. Plant Physiol.*, 148, 115, 1996.
30. Sutherland, J. C., Biological effects of polychromatic light, *Photochem. Photobiol.*, 76, 164, 2002.
31. Rundel, R. D., Action spectra and estimation of biologically effective UV radiation, *Physiol. Plant.*, 58, 380, 1983.
32. Cullen, J. J. and Neale, P. J., Biological weighting functions for the effects of ultraviolet radiation on aquatic systems, in *The Effects of Ozone Depletion on Aquatic Ecosystems*, Häder, D.-P., Ed., R.G. Landes Company, Austin, TX, 1997, p. 97.
33. Cullen, J. J., Patrick, J. N., and Lesser, M. P., Biological weighting function for the inhibition of phytoplankton photosynthesis by ultraviolet radiation, *Science*, 258, 646, 1992.
34. Cullen, J. J., Davis, R. F., Huot, Y., and Lehmann, M. K., Simple functions describing the effects of UV on daily water column photosynthesis, at *30th Annual Meeting of the American Society for Photobiology*, Quebec City, Canada, July 2002, Abrs. #205, p. 71.

45

Photosensitization: Basic Principles

Giulio Jori
University of Padova

45.1 Introduction

The first scientific documentation that sunlight or visible light can be detrimental for cells and more complex biological systems was provided by Marcacci in the late nineteenth century [1]; this investigator reported that the fermentation of plant alkaloids and amphibian eggs is drastically impaired under exposure to UV/visible light. Shortly thereafter, Raab [2], a medical student working in the laboratory of Prof. H. von Tappeiner in Munich, demonstrated that the presence of some exogenously added visible-light-absorbing compounds, for example, acridine orange, was necessary for sunlight to promote the death of paramecia. In a second paper, von Tappeiner [3] associated this property with fluorescence, postulating that the necrotic effects were consequent to the transfer of energy from the light-activated chemical compounds to other sites in their close surroundings. These photoactivatable substances were defined as photosensitizers. The overall scenario was completed by the observation [4] that the presence of oxygen is often a necessary requisite for photosensitization to occur. The combined effect of the three elements, namely, light, photosensitizer, and oxygen, has been termed "photodynamic action" [5]. Finally, von Tappeiner in collaboration with a dermatologist named Jesionek showed that the photodynamic processes could be quite useful in medicine by using topically applied eosin and visible light to positively treat skin tumors [6]. This finding prompted a wealth of studies aimed at defining the pharmacokinetic properties of photosensitizing agents *in vivo* and devising suitable strategies for promoting the selective or preferential localization of the photosensitizer in specific diseased tissues. The results thus obtained eventually paved the way to the development of the so-called photodynamic therapy (PDT) for several pathologies, including solid tumors, actinic keratosis, atheromas, rheumatoid arthritis, infectious diseases of microbial origin, sterilization of blood products, age-related macular degeneration, and a variety of skin diseases [7,8]. At the same time, photodynamic processes are now showing very promising features for addressing important problems connected with the protection of the environment and the preservation of biodiversity [9,10].

At present, it is generally recognized that a large number of near-UV or visible-light-absorbing dyes belonging to different categories of organic compounds exhibit interesting photosensitizing properties, whose control can lead to different types of damaging or beneficial effects on biological systems, including living organisms [11]. A particularly prominent role is played by porphyrins and their natural or synthetically prepared tetrapyrrolic analogues, including chlorophylls, porphycenes, purpurins, phthalocyanines, and naphthalocyanines. Porphyrins absorb essentially all the wavelengths included in the sun emission spectrum; hence, they are especially important for applications in natural environments where the sun represents the source of the photochemically useful light wavelengths. Historically, the first porphyrin to be isolated was hematoporphyrin, which was extracted from dried blood by treatment with concentrated sulfuric acid followed by solubilization with ethanol [12]. The name hematoporphyrin was assigned by Hoppe-Seyler in 1871 [13], and this porphyrin was first used as a photosensitizer in humans by Meyer-Betz in 1913 [14], who injected himself with hematoporphyrin and subsequently suffered a prolonged pain and swelling in light-exposed skin areas. A derivative of hematoporphyrin, known under the commercial name of Photofrin, was initially used as a photosensitizer for the PDT of tumors [7], whereas hematoporphyrin itself was proposed as an environmentally friendly photoinsecticidal agent [15]. Moreover, the tetrapyrrolic core of porphyrins can be chemically modified at different levels, such as the coordination of metal ions at the center of the macrocycle and axial ligands in the fifth and/or sixth coordination positions of the ion, as well as the introduction of substituents in the peripheral positions of the pyrrole rings or the meso inter-ring carbon atoms. In this way, the physical and chemical properties of the porphyrin photosensitizer can be tailored to orientate the molecule toward predetermined sites of a cell or tissue [16].

A few photosensitizers are naturally present in plants and animals, that have consequently developed appropriate protection or repair mechanisms to counteract the potentially noxious action of the wavelengths present in the solar spectrum. Otherwise, the photosensitizing agent can be introduced into the organism accidentally (e.g., through the diet or the uptake of drugs) or on purpose. The main photophysical, photokinetic, and photochemical characteristics of these photosensitizers will be briefly reviewed in the following.

45.2 Photodynamic Sensitization of Biological Systems: Photophysical Aspects

Upon absorption of a UV or visible photon, a photosensitizer P can be promoted to a variety of electronically excited states. Such higher energy states involve two systems, which are represented by the singlet (^{1}P) and the triplet (^{3}P) manifold. In general, the efficiency of the photosensitizing action in fluid media is dependent on the photophysical properties of the lowest excited triplet state, which is reached via intersystem crossing from the initially formed excited singlet state. The ^{3}P species is most often characterized by a lifetime in the microsecond to millisecond range; hence, it can play a major role in diffusion-controlled processes. The most effective photosensitizers are therefore those which give a long-lived triplet state with a high quantum yield. The primary photophysical and photochemical steps involved in photosensitized processes can be represented according to the scheme outlined in Figure 45.1.

In the figure, ^{0}P and ^{3}P indicate the ground state and the lowest triplet state of the photosensitizer, respectively; ^{0}Sub and ^{3}Sub represent the corresponding electronic states of a photosensitive substrate. R indicates a general reactant, $^3O_2$ and $^1O_2$ are ground-state oxygen (a triplet), $^1\Delta_g$ is singlet oxygen, O_2^- is the superoxide anion, and P_{ox} and Sub_{ox} are oxidized forms of the photosensitizer and the substrate.

As shown in Figure 45.1, the ^{3}P species can undergo deactivation to the ^{0}P species by radiative (luminescence) or nonradiative (largely thermal) modes or become involved in a photochemical reaction with oxygen or another constituent of the medium, accompanied by a loss of the absorption typical of

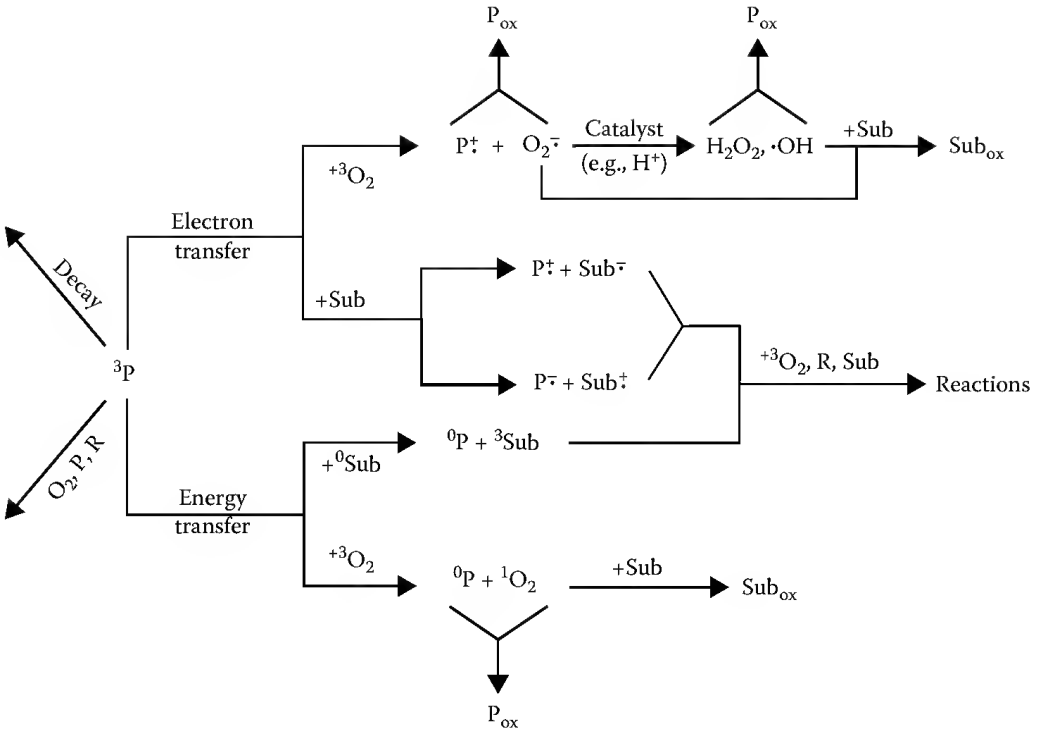

FIGURE 45.1 Schematic representation of the primary photophysical and photochemical steps typically involved in the photosensitized modification of biological substrates.

the photosensitizer in the visible spectral interval ("photobleaching"). For most photosensitizers, the quantum yield of photobleaching is around 10^{-4} to 10^{-5}. As regards the photosensitized modification of the substrate, two pathways are operative as follows:

1. *Electron transfer* between ^3P and a suitable acceptor, resulting in the formation of semireduced and semioxidized radical-type species. This pathway is termed as *Type I mechanism*: the direction of the electron transfer step is obviously dependent on the value of the redox potential for the triplet photosensitizer and the substrate. The initially formed radical intermediates can then undergo further reactions with other substrates, solvent molecules, or oxygen. A particular case occurs when oxygen acts as the electron acceptor with the generation of the superoxide anion; the latter derivative has a relatively low level of reactivity; however, it can be often converted to very reactive and cytotoxic species, such as the hydroxyl radical and hydrogen peroxide. The production of free radicals in the Type I process less frequently involves the transfer of one hydrogen atom from a reducing substrate RH to the photosensitizer.
2. *Energy transfer* to any substrate whose triplet state lies at a lower level compared with the ^3P species; this pathway is defined as a *Type II mechanism*. Most components of cells and tissues are not suitable acceptors of electronic energy from ^3P, since their triplet states are too energetic. One notable exception is represented by oxygen; this almost ubiquitous component of biological systems can be readily promoted to its excited singlet state $^1\Delta_g$, whose energy level lies at only 22.5 kcal above the triplet ground state of molecular oxygen and which is endowed with a high reactivity and cytotoxicity. In actual fact, the $^1\Delta_g$ oxygen has an empty orbital, which imparts a high electrophilicity to this intermediate; moreover, its return to the ground state is forbidden by the selection rules; hence, singlet oxygen has a long lifetime (3–4 μs in aqueous media, several tens of microseconds in lipid environments), which allows this species to diffuse over appreciably long distances before being deactivated [17].

The Type I and Type II pathways occur competitively; the reaction rates for the interaction of the triplet photosensitizer with the substrate and oxygen can be described by the following equations:

$$v_{sub} = k_{sub}[Sub][^3P] \quad \text{and} \quad v_{O_2} = k_{O_2}[^3O_2][^3P]$$

The value of k_{O_2} for typical photosensitizing agents is approximately 2×10^9 M^{-1} s^{-1}, and $[^3O_2]$ is about 0.3 mM in aqueous solutions. Therefore, in aerated solutions, the substrate can compete efficiently with the triplet photosensitizer only if the product $k_{sub}[Sub]$ is at least 5×10^5 s^{-1}. The competition between the Type I and Type II pathways could be significantly different in non-aqueous or inhomogeneous systems where the oxygen concentration generally increases while the local reactant concentrations and rate constants can be altered by the nature of the microenvironment.

On the other hand, the energy transfer reaction from ^3P to $^3O_2$ is much faster than the electron transfer; hence, the formation of singlet oxygen accounts for almost all the quenching steps of photosensitizer triplets by oxygen. The formation of the superoxide anion usually occurs on less than 1 in 100 deactivating collisions of oxygen with ^3P. Therefore, the singlet oxygen-involving pathway is of utmost importance for the photosensitized processes involving biological systems unless special situations obtain, as discussed in the following.

The intermediacy of singlet oxygen in photosensitized processes can be detected by a variety of techniques, out of which the most frequently used involve the following:

- Comparison of the photosensitized oxidation rates for a substrate in a given hydrogenated solvent and its deuterated analogue. It is well known that the lifetime of singlet oxygen is markedly longer in the deuterated medium (e.g., it is about 10-fold longer in D_2O as compared with H_2O), which must obviously favor a Type II, $^1\Delta_g$ oxygen-involving, mechanism.
- Direct spectroscopic determination of singlet oxygen through its luminescence emission at 1270 nm, namely, in the near-IR range.
- Use of specific acceptors, such as 9,10-dimethyl-anthracene (DMA), 2,5-dimethyl-furan (DMF), or 1,4-diazabicyclo[2,2,2]-octane (DABCO), which have the property to give 100% chemical quenching upon interaction with singlet oxygen.
- In some cases, the photooxidation products are at least partially different for Type I and Type II pathways; hence, the identification of such products can be a very helpful diagnostic tool for assessing the actual mechanism of the photoprocess (see Section 45.4).

Recently, the formation of singlet oxygen as a main intermediate of photosensitized processes has been detected also *in vivo* [18].

45.3 Kinetics of Photosensitized Reactions

The rate constants of the primary reactions, k_I and k_{II}, involved in the two processes are now well enough known, so that many of the factors which govern their competition can be stated definitely. The rate of the Type I process depends on the photosensitizer and the substrate and can vary over a rather wide range. Typical rates for a selected number of cell constituents are shown in Table 45.1. In general, triplet ketones and quinones are more powerful hydrogen abstractors than the common polycyclic organic dyes: for example, benzophenone abstracts hydrogen from a weak reductant, such as isopropanol, about 10^4 times more rapidly than does eosin. The scenario can change in the presence of powerful hydrogen or electron donors: thus, both eosin and benzophenone triplets react at similar rates with *N,N*-dimethylaniline. Notably, histidine differs from other amino acids, for the very poor tendency to undergo hydrogen/electron transfer with a very frequently used photosensitizer, such as methylene blue.

TABLE 45.1 Rate Constants (M^{-1} s^{-1}) for the Reaction of Different Triplet Photosensitizers with Selected Substrates

	Photosensitizer Triplet State		
Substrate	Benzophenone	Eosin	Methylene Blue
Aniline	4.8×10^9	1.4×10^9	0.8×10^9
N,N-Dimethyl-aniline	5.7×10^9	2.2×10^9	1.7×10^9
Isopropanol	1.8×10^6	ca. 10^2	n.a.
Tryptophan	n.a.	8.9×10^7	2.0×10^8
Methionine	8.8×10^8	1.0×10^7	3.5×10^7
Histidine	n.a.	2.7×10^5	3.3×10^6
Guanosine	5.6×10^8	1.1×10^9	2.4×10^9

n.a. = not available.

Riboflavin is an excellent promoter of Type I processes thanks to the presence of an internal hydrogen source in the poly-hydroxylated side chain, which predisposes it to complex radical reactions.

The types of molecular structures for the substrate that enhance the efficiency of a Type I process include those which are most readily oxidized, such as phenols and amines, or readily reduced, such as quinones. On the other hand, compounds belonging to the classes of olefins, polyenes, or aromatic compounds favor the occurrence of reaction pathways via singlet oxygen.

The rates of the Type II processes mainly depend on the oxygen concentration in the reaction medium, since the k_{II} rate constant with few exceptions falls in the $1–3 \times 10^9$ M^{-1} s^{-1} for a very large number of photosensitizing agents. Oxygen is known to be less soluble in water than in most organic solvents; therefore, the product $k_{II}[^3O_2]$ can be expected to be smaller in an air-saturated aqueous solution (ca. 5×10^5 s^{-1} as experimentally measured) than in oxygen-saturated organic solvents (ca. 3×10^7 s^{-1}). As a consequence, depending on the type of photosensitizer and substrate, as well as on the nature of the reaction medium, the mechanism of the photosensitized oxidation may change from Type I to Type II and vice versa. In particular, the binding of the photosensitizer to the substrate, as it often occurs in biological systems, is likely to favor Type I mechanisms.

Lastly, it is important to emphasize the role of another competition in determining the fate of a photosensitization process, namely, that between the decay rate of singlet oxygen (k_d) and the rate at which singlet oxygen reacts with a substrate ($k_{sub}[Sub]$). In case $k_{sub}[Sub]$ is $\ll k_d$, the major result of a Type II pathway is simply the quenching of the triplet photosensitizer with no or very little chemical modification of the substrate. A very important example is provided by β-carotene and other carotenoids with a chain length involving at least 11 conjugated double bonds, whose triplet state is of sufficiently low energy to accept electronic energy from singlet oxygen. The k_{sub} for this interaction is higher than 10^{10} M^{-1} s^{-1}, and these considerations explain the very efficient photoprotective action of carotenoids in plants, as well as in humans affected by porphyria:

$$^0\text{Car} + {}^1O_2 \rightarrow {}^3\text{Car} + {}^3O_2 \quad (k = 3 \times 10^{10}\ M^{-1}\ s^{-1})$$

$$^3\text{Car} \rightarrow {}^0\text{Car} \quad \text{(radiationless decay)}$$

Rate constants controlling the reaction between singlet oxygen and selected substrates of biological interest are given in Table 45.2.

TABLE 45.2 Rate Constants (M^{-1} s^{-1}) for the Reaction of Selected Substrates with Singlet Oxygen

Substrate	Rate Constant
2,5-Dimethyl-furan	1.4×10^8
Tryptophan	4.5×10^7
Methionine	2.9×10^7
Histidine	1.3×10^8
Guanosine	4.7×10^8
2-Methyl-pentene	1.1×10^6
Cyclohexene	3.3×10^3

45.4 Initial Photooxidation Products of Photodynamic Processes

The electrophilic nature of the photoreactive intermediates generated upon electronic excitation of photosensitizers explains why the most sensitive targets of such photoprocesses are represented by electron-rich sites or functional groups.

Type I chemistry proceeds through radical intermediates, which may involve the promotion of chain reactions, which are often characterized by high overall quantum yields. Since such processes can involve substrates with a truly large typology of chemical structures, a broad variety of reactions can take place. In some cases, the products of the Type I photosensitized oxidations are identical with those which are produced by classical oxidative procedures: a typical example is represented by the benzophenone-photosensitized oxidation of secondary alcohols, which lead to the formation of ketones as the end products. Analogously, photooxidation of olefins at the level of the unsaturated carbon–carbon bonds by a Type I route yields a mixture of allylic hydroperoxides, peroxides, and epoxides.

More frequently, the photosensitized oxidation follows a specific reaction pathway: thus, the anthraquinone-photosensitized oxidation of tertiary amines proceeds via electron transfer from the nitrogen atom; a common result of this kind of process is represented by dealkylation: the photoinduced radical intermediates appear to react with oxygen with the generation of peroxides, whose subsequent decomposition promotes a breakdown to dealkylated products.

Interestingly, Type I photosensitization can result in the modification of substrates which are not sensitive to Type II photosensitization, thereby amplifying the scope of this photoprocess. Thus, quinone or ketone photosensitization can induce the decarboxylation of substituted carboxylic acids: again, this reaction is believed to involve electron transfer as the key step.

On the other hand, the reactions of singlet oxygen with biological targets have been studied in great detail, also in view of the aforementioned predominant role of such reactions in photosensitization of isolated biomolecules and cells or tissues. Five classes of singlet oxygen-involving reactions have been identified as follows:

1. *Oxidation of thiols and thioethers.* The usual product is represented by sulfoxides, which means that two thioether molecules are oxidized per each molecule of oxygen taken up, or sulfonic acids. A persulfoxide intermediate has been detected for this type of process.
2. *Oxidation of phenols.* Phenols are eventually converted to quinone-type products, even though hydroperoxide products can be also isolated if the photoprocess is carried out under mild conditions. It has also been observed that the quinones often undergo a spontaneous polymerization to yield melanin-type products.
3. *1,4 Addition to dienes and heterocycles.* This reaction is typical of many dienes, as well as of aromatic molecules and heterocycles, which are highly substituted by electron-donating moieties. In general, endoperoxides are initially formed, which are stable only at low temperatures; at room

TABLE 45.3 Effect of Photosensitization on the Nature of the Photooxidation Products of Selected Biological Substrates

Substrate	Type I	Type II
Tryptophan	Hydroxy-indoles	*N*-formyl-kynurenine
Histidine	Mixture of amino and carboxyl derivatives	Endoperoxides gradually hydrolyzed to ketone-type compounds
Methionine	Methional	Methionine sulfoxide
Cysteine	Cystine	Cysteic acid
Guanosine	Dimeric polyketonic photoadducts	Endoperoxide/ketone derivatives
Cholesterol	7,α-Hydroperoxide	5,α-Hydroperoxide

temperature, the endoperoxides decompose and react with solvent molecules to yield stable peroxides or hydroperoxides.

4. *1,2 Addition to olefins.* Once again, this process occurs efficiently only in the presence of particularly electron-rich double bonds, for example, enamines or vinyl ethers. The photoproducts include fairly stable 1,2-dioxetanes; on mild warming, these cleave to carbonyl compounds, an event that is possibly characterized by the emission of light (chemiluminescence).
5. *Ene reaction with olefins.* Olefins with two or more alkyl substituents react with singlet oxygen to form allylic hydroperoxides. This photoprocess has been also observed for unsaturated fatty acids and steroids.

The different mechanisms which are involved in the Type I and Type II pathways often result in the formation of different end products. This circumstance can be taken advantage of for discriminating between the two mechanisms in a given system. This is exemplified in the case of the most highly photosensitive amino acids and cholesterol in Table 45.3.

45.5 Photosensitization in Complex Biological Systems

Cells are intrinsically nonhomogeneous and highly compartmentalized systems and thus provide a great variety of microenvironments for photosensitizers and potential targets of a photoprocess. Since the photophysical parameters of a photosensitizer and the lifetimes/reactivity of the possible intermediate species are strongly dependent on the nature of their surroundings, it is often difficult to extrapolate information obtained from photosensitization studies in homogeneous solutions to cells. In particular, cell-associated photosensitizers are frequently bound noncovalently in different sites of cells, thereby altering their photochemical behavior. Further, the cell environment is dynamic; this requires that diffusion of the photosensitizer to different subcellular loci as a consequence of the endocellular modifications brought about in the initial stages of the photoprocess be taken into account in developing accurate descriptions of the mechanisms involved in photosensitization of cells. Therefore, relevant model systems mimicking specific cellular situations have been tested in order to obtain some clues as to how selected factors influence the course of a photoprocess in cells and tissues.

Such approaches are based on the tendency of several cell constituents, such as proteins, nucleic acids, and polysaccharides to form stable complexes with a variety of photosensitizers [19]. In many cases, such binding increases the photophysical properties of the photosensitizer, including the fluorescence emission quantum yield and the triplet lifetime. These effects, of obvious importance in cell photosensitization, result from the reduced probability of collisional deactivation for bound electronically excited photosensitizer molecules; thus, dyes located in internal regions of three-dimensionally folded macromolecules exhibit phosphorescent emission at room temperature. The incorporation of photosensitizing agents in polymeric matrices is often leading to an increased steady-state triplet population, as might be expected from the typical bathochromic shift of the absorption peak of bound photosensitizers and the consequent smaller singlet-triplet splitting.

TABLE 45.4 Effect of the Mode of Photosensitizer Binding on the Photoinduction of Free Radicals in Calf-Thymus DNA

Substrate	Mode of Binding	Absorption Maximum (nm)	Molar Extinction Coefficient (M^{-1} cm^{-1})	Radical Yield (a.u.)
Chloroquine	Intercalation	329	19,700	620
9-Amino-acridine	Intercalation	398	10,825	325
Proflavine	Intercalation	444	33,500	1000
Ethidium bromide	Intercalation	480	5600	160
Pyronine	Stacking	538	13,650	175
Thiopyronine	Stacking	564	46,960	450
Acridine red	Stacking	549	8320	98

Photosensitizer concentration: 0.50 mM; DNA concentration: 1.56 mM; solvent: aqueous 0.1 M NaCl; light source: high-pressure Hg lamp ($\lambda < 320$ nm removed by a cutoff filter)

The enhanced photoactivity of bound photosensitizers is particularly evident in the case of nucleic acids. Illumination of calf thymus DNA in the presence of intercalating and nonintercalating photosensitizing agents shows that, with comparable light absorption, binding increases the extent of photodamage (Table 45.4). The efficiency of the photoprocess is favored by a tight and rigid environment for the photosensitizer as found in photooxidation studies with intercalated proflavine–DNA complexes: Supercoiled double-stranded DNA is approximately 10 times more photolabile than the corresponding double-stranded DNA [20].

The ground-state complexing of photosensitizers with macrobiomolecules can also influence the mechanism of the photoprocess, usually by enhancing the probability of a direct interaction between the triplet photosensitizer and the substrate through electron or hydrogen transfer. This is a consequence of the close spatial relationship between the bound photosensitizer and the photosensitive functional groups of the target. In some cases, the initially formed photosensitizer and substrate radicals can recombine with the formation of intramolecular cross-links in the macromolecule, dimeric substrate–substrate complexes, and covalent substrate–photosensitizer photoadducts [20].

Another class of model systems has been developed to address the problems connected with the abrupt phase changes and variations in medium polarity caused by the heterogeneous and compartmentalized structure typical of cells; this can appreciably affect the diffusibility and reactivity of the photogenerated oxidized agents inside cells. Toward this aim, aqueous dispersions of surfactant micelles and uni- or multi-lamellar liposomal vesicles are used to mimic biological assemblies that are characterized by the coexistence of hydrophobic and hydrophilic regions. This approach allows the availability of various combinations of photosensitizers and substrates solubilized in either the lipid or aqueous phase. As a result, several important advances as regards the mechanisms modulating the progress of photosensitized processes in complex biological systems have been achieved. The main conclusions can be summarized as follows:

- The observed high quantum yield of singlet oxygen generation inside micelles and liposomes and its rapid diffusion across phase boundaries support the hypothesis based on oxygen quenching of the fluorescence emitted by micellized aromatic compounds that oxygen diffuses through micelles in an essentially unrestricted fashion.
- In general, the reaction rate of singlet oxygen is at least as great with micelle- or liposome-incorporated targets as with the same substances in a homogeneous solution. Ionic micelles do not alter the lifetime of singlet oxygen appreciably, whereas neutral micelles (as prepared with Igepal CO-660 or Triton X) may reduce the singlet oxygen lifetime as a result of excitation transfer from its electronic levels to vibrational modes of the terminal hydroxyl groups of the surfactant.
- On the other hand, the reaction rate for a given pair of substrate–photosensitizer appears to depend on the micellar or liposomal outer charge. For example, the photooxidation of

1,3-diphenyl-isobenzofuran is most efficient when the substrate is embedded in anionic vesicles. With cationic photosensitizers, such as methylene blue, this may result from adsorption of the dye on the external shell of the micelle or liposome. Other factors which contribute to the modulation of the photosensitization rate are the dimension of the vesicle and the substrate distribution among the various endomicellar or endoliposomal districts, which could determine the accessibility of the target to the attacking agents.

- The outer charge also affects the rate and efficiency of electron transfer processes across the phase boundary. Thus, the forward e^- transfer step from a micellized donor to an external acceptor is usually favored in the presence of negatively charged sodium dodecyl sulfate (SDS) micelles as compared with homogeneous media: the negative charge of the micelle markedly decreases the rate of the back reaction. Conversely, the positive charge of cationic micelles (e.g., cetyltrimethylammonium bromide) or liposomes attracts the e^- toward the surface of the vesicle and extends the duration of the encounter, thus enhancing the overall efficiency of the photoprocess.
- Finally, it should be underlined that both singlet oxygen and electrons can diffuse from one micelle or vesicle through an aqueous medium and attack reactive targets localized in a different vesicle. The efficiency of the singlet oxygen-involving reaction is relatively little affected by both the external charge of the vesicle and the substrate accessibility, while the outer charge is of primary importance for the efficiency of electron-mediated photoprocesses.

45.6 Conclusions

On the basis of the discussions developed in the previous paragraph, it is apparent that the optimal utilization and fine control of a photosensitized process especially in *in vivo* systems require a carefully planned interplay among several different parameters, which can be operationally subdivided into physical–chemical, photophysical, photobiological, pharmacological, and phototherapeutic properties. An attempt at summarizing the main features which should characterize a biologically efficient photosensitizer is shown in Table 45.5.

TABLE 45.5 Main Features of an Efficient Photodynamic Sensitizer

Property	Related Structural and Biological Features
Physical–chemical	
High chemical purity	Preferentially lack of structural isomers or stereoisomers
Large molar extinction coefficient in the red	Extensive conjugation of π electrons in the macrocycle
Low tendency to aggregation in aqueous media	Electrically charged peripheral substituents in the macrocycle
Photophysical	
Long triplet lifetime	
High yield of $^1O_2$ generation or electron transfer to substrates	Easy accessibility to oxygen or close proximity to substrates with suitable redox potential
Pharmacological	
Efficient and selective targeting of diseased tissue	Association with suitable delivery or targeting systems
Fast clearance from serum and healthy tissues	Affinity for serum proteins responsible for transport from peripheral tissues to liver
Low systemic toxicity	Lethal dose (LD-50) greater than ca. 100 mg/kg body weight
Phototherapeutic	
Preferential damage/necrosis of diseased tissue	Large concentration difference between lesional/perilesional districts and/or fast healing of any damaged healthy tissue
Lack of side effects	Particular attention to avoid generalized photosensitivity
Lack of mutagenic effects	No involvement of genetic material in the photoprocess

It is obvious from Table 45.5 that the photosensitized processes of biological systems are characterized by a high degree of complexity. Thus, it is understandable that this chapter is not intended to be an exhaustive review, but presents a framework of basic facts and principles essential to understanding the main phenomena, illustrating them with a few of the more interesting and instructive examples. A more detailed and in-depth description of the various aspects of this subject can be found in the reviews indicated at the end of the references, namely, Refs. [21–32].

References

1. Marcacci, A. 1888. Sur l'action des alcaloids dans le règne végétale et animal. *Arch. Ital. Biol.* 9: 2–4.
2. Raab, O. 1900. Uber die wirkung fluoresceinder stoffe and infusorien. *Zeit. fur Biol.* 39: 524–546.
3. von Tappeiner, H. 1902. Uber die wirkung fluoresceinder stoffe and infusorien nach versuchen von O. Raab. *Munch. Med. Wochenschr.* 47: 5–6.
4. von Tappeiner, H. and A. Jodlbauer. 1904. Uber die wirkung der photodynamischen (fluoreszierenden) stoffe auf protozoan und enzyme. *Dtsch. Arch. Klin. Med.* 80: 427–487.
5. von Tappeiner, H. and A. Jodlbauer. 1907. *Die Sensibilisierende Wirkung Fluoreszierender Substanzer. Gesamme Untersuchungen Uber Die Photodynamische Erscheinung*. Leipzig, Germany: F.C.W. Vogel.
6. von Tappeiner, H. and A. Jesionek. 1903. Therapeutische versuche mit fluoreszierenden stoffen. *Munch. Med. Wochenschr.* 47: 2042–2044.
7. Dougherty, T.J., C.J. Gomer, G. Jori et al. 1998. Photodynamic therapy. *J. Natl. Cancer Inst.* 90: 889–905.
8. Patrice, T. 2003. *Photodynamic Therapy*. Cambridge, U.K.: Royal Society of Chemistry.
9. Almeida, A., A. Cunha, N.C.M. Gomes, E. Alves, L. Costa, and M.A.F. Faustino. 2009. Phage therapy and photodynamic therapy: Low environmental impact approaches to inactivate microorganisms in fish farming plants. *Mar. Drugs* 7: 268–313.
10. Magaraggia, M., F. Faccenda, A. Gandolfi, and G. Jori. 2006. Treatment of microbiologically polluted aquaculture waters by a novel photochemical technique of potentially low environmental impact. *J. Environ. Microbiol.* 8: 923–931.
11. Boyle, R.W. and D. Dolphin. 2006. Structure and biodistribution relationships of photodynamic sensitisers. *Photochem. Photobiol.* 14: 4253–4259.
12. Scherer, H. 1841. Chemisch-physiologischen untersuchungen. *Ann. Chem. Pharm.* 40: 1–2.
13. Hoppe-Seyler, F. 1871. *Medische Und Chemische Untersuchungen*. Berlin, Germany: Eberhard-Karls-Universitat.
14. Meyer-Betz, F. 1913. Untersuchungen uber die biologische (photodynamische) wirkung des haematoporphyrins und anderer derivative des blut- und galenfarbstoffs. *Dtsch. Arch. Klin. Med.* 112: 475–503.
15. Ben Amor, T., M. Tronchin, L. Bortolotto, and G. Jori. 1998. Porphyrins and related compounds as photoactivatable insecticides. I. Phototoxic activity of haematoporphyrin toward *Ceratitis capitata* and *Bactrocera oleae*. *Photochem. Photobiol.* 67: 206–211.
16. Bonnett, R. and M. Berenbaum. 1989. Porphyrins as photosensitisers. In *Photosensitising Compounds: Their Chemistry, Biology and Clinical Use*, eds. G. Bock and S. Harnett, pp. 40–59, Chichester, U.K.: Wiley.
17. Wasserman, H.H. and R.W. Murray. 1999. *Singlet Oxygen*. New York: Academic Press.
18. Niedre, M., M.S. Patterson, and B.C. Wilson. 2002. Direct near-infrared luminescence detection of singlet oxygen generated by photodynamic therapy in cells in vitro and tissues in vivo. *Photochem. Photobiol.* 75: 382–391.
19. Reddi, E. and G. Jori. 1988. Steady-state and time-resolved spectroscopic studies of photodynamic sensitisers: Porphyrins and phthalocyanines. *Rev. Chem. Interm.* 10: 241–268.

20. Jori, G. and J.D. Spikes. 1991. Photosensitised oxidations in complex biological systems. In *Oxygen and Oxy-Radicals in Chemistry and Biology*, eds. M.A.J. Rodgers and E.L. Powers, pp. 441–459, New York: Academic Press.
21. Jori, G. 1996. Tumour photosensitisers: Approaches to enhance the selectivity and efficiency of photodynamic therapy. *J. Photochem. Photobiol. B Biol.* 36: 87–93.
22. Ochsner, M. 1997. Photophysical and photobiological processes in photodynamic processes. *J. Photochem. Photobiol. B Biol.* 39: 1–18.
23. Jori, G. and J.D. Spikes. 1984. Photobiochemistry of porphyrins. In *Topics in Photomedicine*, ed. K.C. Smith, pp. 183–319. New York: Plenum Press.
24. Bonnett, R. 2000. *Chemical Aspects of Photodynamic Sensitisation*. Amsterdam, the Netherlands: Gordon and Breach Science Publishers.
25. De Rosa, M.C. and R.J. Crutchley. 2002. Photosensitised singlet oxygen and its applications. *Coord. Chem. Reviews* 233: 351–371.
26. Dolmans, D.E., D. Fukumura, and R.K. Jain. 2003. Photodynamic therapy for cancer. *Nature Rev. Cancer* 3: 380–387.
27. Moore, A.C.E., B. Ortel, and T. Hasan. 2003. Mechanisms of photodynamic therapy. In *Photodynamic Therapy*, ed. T. Patrice, pp. 19–57. Cambridge, U.K.: Royal Society of Chemistry.
28. Jori, G. and S.B. Brown. 2004. Photosensitised inactivation of microorganisms. *Photochem. Photobiol. Sci.* 3: 403–405.
29. Hamblin, M.R. and T. Hasan. 2004. Photodynamic therapy: A new antimicrobial approach to infectious diseases? *Photochem. Photobiol. Sci.* 3: 436–450.
30. Hatz, S., J.D. Lambert, and P.R. Ogilvy. 2007. Measuring the lifetime of singlet oxygen in a single cell. Addressing the issue of cell viability. *Photochem. Photobiol. Sci.* 6: 1106–1116.
31. Jori, G. and O. Coppellotti. 2007. Inactivation of pathogenic micro-organisms by photodynamic techniques: Mechanistic aspects and perspective applications. *Anti-infect. Agents in Med. Chem.* 6: 119–131.
32. Robertson, C.A., D. Hawkins Evans, and H. Abrahamse. 2009. Photodynamic therapy (PDT): A short review on cellular mechanisms and cancer research applications for PDT. *J. Photochem. Photobiol. B Biol.* 96: 1–8.

46

Photoecology and Environmental Photobiology

Donat-P. Häder
Möhrendorf, Germany

46.1 Introduction

In addition to gravity, light is one of the most important external factors, not only for photosynthetic organisms, to control their movement and position in their habitat. For photosynthetic bacteria, algae, and higher plants, solar radiation is an indispensable source of energy. During evolution, a number of light-harvesting pigments have been developed for collecting solar energy, most of which are based on cyclic tetrapyrroles. In addition, a number of different accessory pigments are being utilized to augment the amount of light absorbed by funneling the energy to the reaction centers for photosynthesis.

The light intensity and wavelength distribution of solar radiation vary considerably in dependence of the habitat, the geographic position, the time of day, and the season. At low light intensities, photosynthesis is suboptimal and results in reduced growth and biomass production. At intensities below the light compensation point, the respiratory oxygen uptake exceeds the photosynthetic oxygen production and biomass production is negative. This light compensation point is reached after dawn and before dusk. For different plant species, it is found at different intensities; it is lower for shade plants than for high-light-adapted plants [1].

Plants are adapted to the availability of light in their habitat. Sun-exposed and shade plants are extreme examples for this process [2], and within the same plant, different leaves can be adapted to high- or low-irradiation regimes [3]. Plants in a forest under a canopy of trees may be exposed to less than 10% of the radiation impinging on the surface of the canopy, but may be shortly exposed to full sunlight during phases of sunflecks, when direct solar radiation finds a gap between the tree leaves. The photosynthetic machinery of the shade plants on the forest floor needs to adapt to these sudden changes in irradiation [4]. Likewise extreme is the light climate for macroalgae growing in the tidal zone on

a rocky shore. During low tide, the algae are exposed to the unfiltered solar radiation. Depending on whether they grow in rock pools or on rocks they may also have to tolerate desiccation and high-salt concentrations. At high tide, these macroalgae may be covered by up to several meters of water, which in the coastal zone can be very turbid and transmit little light. Since the occurrence of high and low tides changes from day to day, the algae need to adapt to a very variable light scenario [5,6].

Light plays a major role in the zonation of macroalgae, which selects light- [and ultraviolet (UV)] resistant species in surface locations and sensitive species deeper down in the water column [7]. Adaptation processes to widely changing light intensities include changes in pigmentation [8,9] and morphology [10] as well as changes in the physiological processes such as the photosynthetic electron transport chain [11–13].

Completely independent from utilization of solar energy for photosynthesis, light serves as an external factor for habitat selection. For this purpose, organisms have developed a host of photoreceptor molecules during evolution. Higher plants use light to direct growth into areas in their habitats with sufficient irradiation. On a short-term basis, they adapt to changing light conditions during the day by movement responses of their leaves.

Motile microorganisms heavily depend on light-directed behavior mechanisms to move to and stay at depths in the water column with optimal light conditions. Often flagellated cells swim toward the water surface guided by the light direction and/or the gravitational field of the earth [14,15]. However, the unfiltered solar radiation at the water surface may be excessive and their sensitive photosynthetic apparatus may be affected and even destroyed by visible and especially UV radiation [16]. When confronted with this situation, many motile photosynthetic—but also nonphotosynthetic—organisms reverse their direction of movement, for example, by switching to an orientation pattern away from the light direction [17]. The constant antagonism between upward oriented movement at low light intensities and downward directed movement at high intensities results in a dynamic habitat selection with optimal light conditions [18].

46.2 Photocontrol of Development and Movement in Higher Plants

After sessile plants have selected a habitat, they are confined to growth and movement of their leaves and branches to optimize light harvesting [19]. This is instrumented by long-term growth responses and photomorphogenesis as well as by short-term light-mediated movement responses.

46.2.1 Photomorphogenesis: Light Control of Growth and Morphology

Phytochromes constitute a small protein family (phyA–phyE) with a linear bilin chromophore linked by an S–H bond to a 126 kDa protein and are derived from prokaryotic ancestors in bacteria and cyanobacteria. These pigments show photochromicity: They absorb light in the red region of the spectrum (660 nm) and are converted to a far-red absorbing (730 nm) form and vice versa. The far-red absorbing form is assumed to be the physiologically active one. Hundreds of functions are known to be mediated by the phytochrome system. It controls seed germination by preventing germination of seeds exposed to light (dark germinators) or induces germination of seed in the presence of light (light germinators) [20]. Phytochromes regulate the hypocotyl length by inducing increased growth under low light conditions in order to allow plants to eventually reach areas of higher light intensities in their habitat [21,22]. A drastic example of this process is the extreme growth of etiolated, leafless shoots in darkness, which can be observed in germinating potatoes, beans, and many other plants (Figure 46.1). Phytochromes control size, shape, and number of leaves [23] and affect leaf thickness as well as stomata and chloroplast density [24,25], regulate flowering [26] by measuring the length of day and night (photoperiodism) [27], and control circadian rhythms, for example, of leaf position and pigment content [28,29].

FIGURE 46.1 Etiolated leafless bean plants that have grown in darkness (left) as compared to light-grown plants. (Photo D.-P. Häder.)

46.2.2 Light-Mediated Movement Responses in Higher Plants

In contrast to long-term developmental processes such as growth and flowering, photomovement of plant organs, such as branches, leaves, flowers, or fruits, occur within minutes or hours.

According to the classical definition, organs of sessile plants can respond to light by photonasty or phototropism [30,31]. Photonastic movements are induced by light quantity and quality but they are independent of the light direction; rather they follow a predefined pattern. Therefore, they are also described as nondirectional movement. For example, flower opening or stomata movements are guided by the existing morphology and are elicited by changes in the light quality or quantity. Other external factors that can elicit nastic movements are darkness (nyctinasty), chemicals (nyctinasty), for example, water (hydronasty), temperature (thermonasty), gravity (gravinasty), and mechanical stimuli such as touch (thigmonasty) or seismic stimuli (seismonasty). Usually, the intensity of the response depends on the stimulus strength. The movement is realized by changes in turgor or growth of specific plant tissues. This has been studied in the fast movements of leaves in *Mimosa* or *Dionaea*, which move by releasing the turgor in specific motor tissues [32,33]. Stomata open and close in response to the light level, but their movements are also triggered by the CO_2 concentration in the leaf and the water availability. This is controlled by the phytohormones auxin and abscisic acid. Photonasty in the prayer plant (*Maranta leuconeura*) is manifested by the downward movement of leaves induced by the increasing light intensity during sunrise. Some *Gentiana* species close their flowers after an even slight decrease in light intensity caused by a cloud. Night-flowering plants, in contrast, open their flowers following a decrease in intensity, such as *Silene nutans*, which is pollinated by night-active moths. Also leaves of some plants respond photonastically; for example, some *Phaseolus* and *Impatiens* species lower their leaves in darkness by an increased growth of cells at the upper surface. Leaves, which have stopped growing, respond photonastically by changes in the turgor or motor tissues, such as in the leaf base (pulvinus) of *Mimosa* species. Both phytochrome and blue-light-absorbing flavoproteins are involved in photonastic reactions.

Phototropism, in contrast to photonasty, is a movement of plant organs with respect to the light direction [34,35]. Shoots show positive phototropism and usually bend toward the light source

(positive phototropism) at low fluence rates. At higher irradiances, grass coleoptiles display negative phototropism (bending away from the light direction) [36,37], while many dicots stop bending in this intensity range. At even higher fluence rates, both monocots and dicots show again positive phototropism. Roots either do not respond phototropically or show negative phototropism [38,39]. Leaves orient themselves perpendicular or at other angles with respect to the light direction (plagio- or diaphototropism). A special case of leaf movement is suntracking in which the leaves follow the sun to harvest an optimal amount of light energy [40,41]. This can also be seen in some flowers; however, in contrast to common belief, mature sunflowers do not follow the sun, but, for whatever reason, face their flower heads toward the southeast, at least in the northern hemisphere.

In the absence of light, a shoot of a higher plant orients itself by negative gravitropism and grows upward (away from the center of the earth) [42,43]. This can be seen impressively in the stems of a forest growing on a steep slope. The trees are oriented upward and not perpendicular to the sloping surface. When a shoot of a higher plant bends toward a lateral light source, it will automatically be stimulated gravitropically and try to bend upward again. The vectorial product of both stimuli (light and gravity) results in a bending angle between vertical and horizontal. This phenomenon has been termed photogravitropism [44].

The photoreceptors for phototropism in shoots and leaves of higher plants are blue-light-absorbing phototropins [45,46]. They are characterized by a light, oxygen, or voltage (LOV) domain, which is the binding site for the flavin mononucleotide (FMN) chromophore [47]. However, their action can be modulated by phytochromes [48]. Phototropins are also responsible for the movement responses of chloroplasts within the photosynthetic tissues [49,50]. To make the story even more complicated, in addition to five phytochromes, at least two phototropins and at least two cryptochromes are found in higher plants; their roles as photoreceptors and their interactions are still under discussion [51].

Positive and negative phototropism has also been found in mosses and ferns [52,53]. In the latter group, even polarotropic reactions have been observed. Both protonemata and chloroplasts, for example, of *Adiantum* and *Pteris*, respond to and orient with respect to polarized light [54,55]. Even though not photosynthetic, several fungi show pronounced phototropic reactions. The mold *Phycomyces* has an extremely sensitive photoreceptor and reacts to 10^{-10} W m^{-2} blue light [56,57]. The photoreceptor involved is still under discussion; pterins and flavins have been suggested as chromophoric group [58].

46.2.3 Effects of and Protection against Solar UV Radiation in Higher Plants

When exposed to high levels of solar irradiation, plants are simultaneously affected by solar UV radiation. Especially, the high-energetic photons within the UV-B band (280–315 nm) have been shown to affect the morphology of higher plants and mosses. In many species, increased UV radiation results in reduced leaf area and stem elongation [59,60]. Similar results have been found with artificial or supplementary UV-B radiation [61]. Even though UV-B radiation does not deeply penetrate into the soil, it has significant effects on root morphology and biomass production [62]. In other studies, reductions of fresh and dry weight as well as crop yield were found as a consequence of increased UV-B radiation [63]. Also germination [64], flower induction [65], and orientation with respect to light and gravity [66] are affected by increased UV-B radiation. However, there are marked differences between cultivars of the same species [67–69]. Therefore, it seems possible to select or breed UV-B resistant cultivars of crop plants to counter increased solar UV radiation. The manifold effects of increased solar UV-B radiation due to stratospheric ozone depletion, on higher plants, in conjunction with global climate change have been summarized [70,71].

Since species differ in their sensitivity toward short-wavelength radiation, an increase in solar UV-B radiation due to stratospheric ozone depletion can lead to changes in species distribution within terrestrial ecosystems [71]. Photosynthetic performance has been found to be affected in greenhouse studies with artificially increased UV-B radiation [72,73]; but it was rarely inhibited in field studies. Changes in the chemical composition of plant tissues have been often reported to be

induced by UV radiation. Some of the consequences are changes in herbivory, litter decomposition, and species composition of microbial communities [74].

Higher plants have developed a number of protective strategies against excessive solar UV radiation including the formation of epidermal hairs, cuticular waxes, and the synthesis of UV-absorbing substances [75,76]. In contrast to cyanobacteria, phytoplankton, macroalgae, and some animals, higher plants utilize flavonoids to reduce the penetration of solar UV. The synthesis of these substances, mostly in the epidermal layers, is induced by short-wavelength radiation [77–79]. Other defense strategies include the repair of UV-inflicted damage [80]. UV-B radiation causes the formation of cyclopyrimidine dimers (CPD) such as those of adjacent thymine bases. These can be removed by the enzyme photolyase, which uses long-wavelength UV-A radiation or blue light as energy source to break the dimer bond. Other options include nucleotide excision repair (NER) [81].

46.2.4 Photoinhibition

The photosynthetic electron transport is prone to damage by excessive radiation. One way of protecting it is downregulation at the site of the D1 protein in photosystem (PS) II; both algae and higher plants use this mechanism, called photoinhibition [82–84]. When exposed to excessive solar radiation, the quantum yield of PS II decreases. This is due to a kink of the D1 protein by high-intensity visible or UV radiation [12,85]. Subsequently, the damaged protein is removed. Regeneration is brought about by resynthesis of the damaged and cleaved D1 protein in a fast turnover mechanism [86]. After short-term exposure, photoinhibition may be reversible within minutes or hours (dynamic photoinhibition), while long-term exposure may result in irreversible damage. With pulse amplitude modulated (PAM) fluorescence, several fluorescence parameters can be determined.

In this technique a red light-emitting diode (LED), produces short (microseconds) pulses that are repeated at a high frequency (e.g., 20 kHz) and applied to a photosynthetic tissue by means of a glass fiber optics. A PIN diode detects the resulting fluorescence pulses via the same glass fiber. The actinic light is also applied to the leaf through the same glass fiber. In the beginning of an experiment, a weak red excitation light is provided to a dark adapted leaf, and a weak fluorescence radiation (F_0) is detected at this time all reaction centers are open (oxidized). Now a saturating pulse is applied, which reduces the photosynthetic electron transport chain and results in a peak of maximal fluorescence (F_m; Figure 46.2). The difference between F_o and F_m is denoted as F_v. From these parameters, the maximal quantum yield Y can be calculated [87]:

$$Y = \frac{F_m - F_o}{F_m} = \frac{F_v}{F_m}$$

After light adaptation of the leaf, a ground fluorescence higher than F_o is found (F_t) and a saturating light pulse results in a lower maximal fluorescence ($F_{m'}$). From these parameters, the effective quantum yield can be calculated [88,89]:

$$Y' = \frac{F_{m'} - F_t}{F_{m'}} = \frac{F_{v'}}{F_{m'}}$$

The decrease of F_m to $F_{m'}$ is due to the nonphotochemical quenching (qN) calculated as

$$qN = 1 - \frac{F_{m'} - F_{o'}}{F_m - F_o}$$

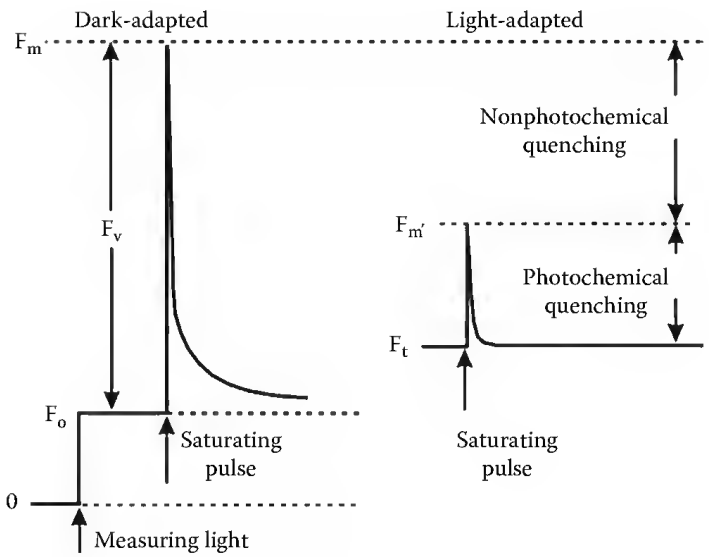

FIGURE 46.2 Parameters of PAM fluorescence. A weak red actinic light, which does not result in net photosynthesis, produces a weak fluorescence in a dark-adapted leaf (F_o). A saturating white light pulse induces F_m. After light adaptation, the ground fluorescence (F_t) is higher than F_o and the F_m after a saturating pulse ($F_{m'}$) is lower than F_m. From these parameters, qP and qN can be calculated.

while the difference between $F_{m'}$ and F_t is due to the photochemical quenching (qP) [90]

$$qP = \frac{F_{m'} - F_t}{F_{m'} - F_{o'}}$$

Simultaneous steady-state gas exchange measurements have proven the validity of this approach [91]. Modern versions of this technology include visualization of the quantum yield in an imaging PAM as well as multichannel chlorophyll fluorimeters [92,93].

Many plants show a typical midday decline in their photosynthetic yield around noon [94]. This pattern is believed to be mainly due to dynamic photoinhibition. Later in the afternoon, the photosynthetic yield increases again.

46.3 Habitat Selection in Microorganisms

Photosynthetic and nonphotosynthetic microorganisms are likewise affected by quality and quantity of solar radiation. Motile microorganisms use active propulsion to optimize their position in the water column. But even nonmotile microorganisms have been found to move up and down in the water column by changing their buoyancy in order to select a suitable habitat [95,96].

46.3.1 Orientation by Light

In addition to endogenous rhythms that govern vertical migration [97], motile microorganisms orient with respect to external factors to control their position in their habitat. Light and gravity are the major clues for orientation [98–100], but both flagellated and gliding microorganisms use chemical gradients (including organic molecules, dissolved oxygen or carbon dioxide) [101–103], temperature [104], the magnetic field of the earth [105,106], and even electric currents [107,108].

The reactions of microorganisms to quality and quantity of light, its direction, and spatial and temporal changes of light can be distinguished into several responses.

46.3.1.1 Photokinesis

Both prokaryotic and eukaryotic organisms show photokinetic reactions [109,110]. The term defines the locomotion velocity in dependence of the ambient irradiance [111]; it is independent of the direction of light. Not only photosynthetic microorganisms show this behavior, but also heterotrophic organisms such as the colorless *Astasia longa* [112]. In the flagellate *Euglena gracilis*, photokinesis saturates at low-intensity white light (about 300 lx) [113]. The photoreceptor for photokinesis absorbs in the blue light region but its chemical nature has not yet been identified [114].

46.3.1.2 Photophobic Responses or Photoshock Response

Engelmann [115] vividly described the behavior of photosynthetic bacteria, which reversed their swimming direction as if frightened when leaving the irradiated field under the microscope and entered a dark field. Phobic reactions at light/dark boundaries result in the accumulation of cells in dark or illuminated areas. This can be seen in, for example, flagellates, cyanobacteria, diatoms, and ciliates [116–118].

Photophobic responses are independent of the light direction and can also be elicited by a temporal change in light intensity. A sudden increase (step-up) or decrease (step-down) in the steady-state irradiance may cause a movement response, which may manifest itself as a sudden stop, a reversal of swimming or a tumble [119]. In the flagellate *Euglena*, step-down and step-up photophobic reactions occur at different irradiances [114]. The action spectra for both responses indicate the involvement of a blue light photoreceptor. Iseki et al. [120] have recently identified a novel photoreceptor [photoactivated adenylyl cyclase (PAC)], which belongs to the family of BLUF proteins and which they showed to be responsible for the step-down photophobic reaction, but interestingly not for the step-up response. BLUF proteins are also found in bacteria and cyanobacteria [121,122].

46.3.1.3 Phototaxis

Oriented movement with respect to the light direction is defined as phototaxis. Organisms move toward the light source (positive phototaxis), away from it (negative phototaxis), or at a given angle to the light direction (dia- or plagiophototaxis; Figure 46.3). Often the same organism shows positive phototaxis at low light intensities and a negative one at higher intensities. Most organisms use UV/blue light photoreceptors (300–550 nm). In addition to a light-absorbing pigment, the cells need an apparatus to identify the light direction. One option is to compare the readings from two or more receptors looking into different directions, the other is to scan the environment, for example, by rotation of the cell during forward locomotion [123]. Some ciliates have developed complicated cellular structures with a lens and a photosensitive layer of pigments, which resemble eyes in invertebrates even though the organisms are unicellular [124].

Phototaxis in the flagellate *Euglena* is mediated by the same PAC photoreceptor, which also governs step-down photophobic responses [125]. Other organisms use different classes of photoreceptors including cryptochromes, phototropins, phytochromes, and rhodopsins [126]. Several prokaryotic and eukaryotic organisms have been found to use photoactive yellow proteins (PYP), which contains a 4-hydroxycinnamate chromophore [127], chlorophylls, carotenoids, phycobilins, and pterins. Hypericin derivatives (e.g., blepharismin, stentorin) have been identified to mediate photoorientation of ciliates [128]. Phototaxis in cyanobacteria is currently intensively investigated. These organisms use a number of different photoreceptor pigments including bacterial phytochromes and BLUF proteins [129–131].

46.3.2 Defense Systems against Excessive Solar Radiation in Microorganisms

Vertical migration of motile phytoplankton organisms and protection in the shade of floating objects is an effective defense mechanism for motile microorganisms. Cyanobacteria were the earliest organisms with oxygenic photosynthesis [132]. They were responsible for releasing oxygen to the up-to-then anaerobic atmosphere. This was the prerequisite for the formation of the stratospheric ozone layer, which absorbs all of the solar UV-C and most of the detrimental UV-B radiation.

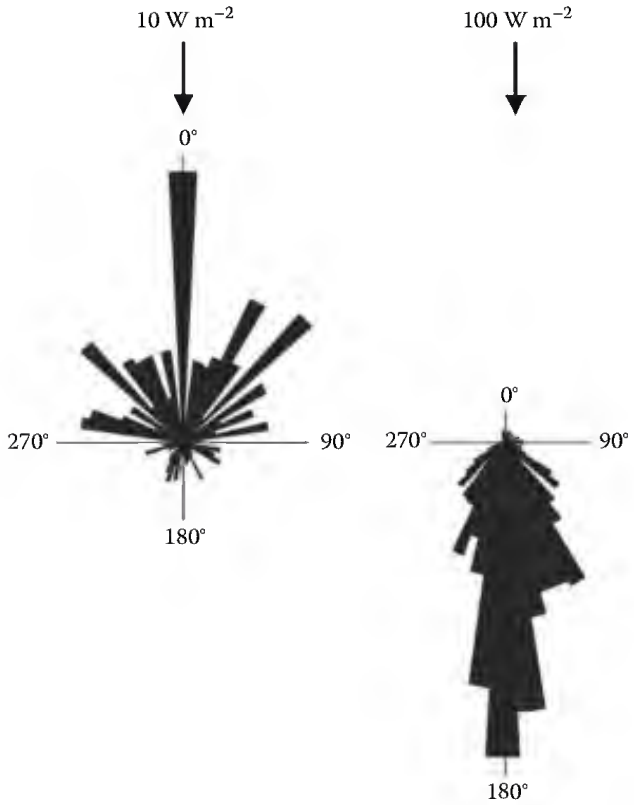

FIGURE 46.3 Circular histograms indicating positive (left) and negative phototaxis (right) of the flagellate *Euglena gracilis*. Light impinges from 0°. The length of the sectors indicate the percentage of cells moving in the respective direction.

Many organisms utilize protective pigments to absorb solar UV radiation before it can damage sensitive cellular targets. Since cyanobacteria evolved still under the influence of UV-C they have developed substances, which absorb in this wavelength range: scytonemins are yellow-brown lipid-soluble dimeric pigments (Figure 46.4), located in the extracellular sheath of certain cyanobacteria growing in extreme habitats such as on rocks or the bark of tropical trees exposed to intensive solar radiation [133,134]. In addition, these substances absorb in the UV-B and UV-A [135,136].

Other cyanobacteria, many eukaryotic phytoplankton and macroalgae produce mycosporine-like amino acids (MAAs), which are water-soluble substances [137,138] (Figure 46.4). These are characterized by a cyclohexenone or cyclohexenimine chromophore, which is conjugated with the nitrogen substituent of an amino acid (or its imino alcohol). They have absorption maxima ranging from 310 to 360 nm and an average molecular weight of around 300. Animals are believed not to synthesize MAAs but take them up with their food and use them likewise as UV protectants [138,139]. Up to now more than 20 different

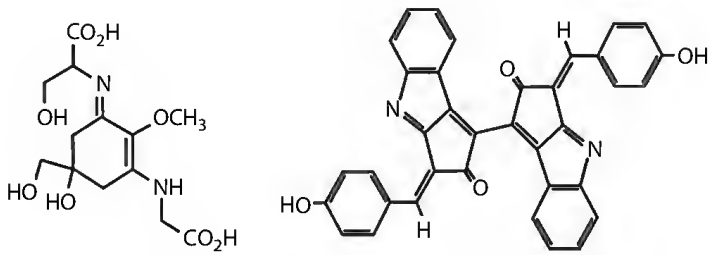

FIGURE 46.4 Chemical structures of scytonemin (right) and the mycosporine-like amino acid shinorine (left).

MAAs are known, but their synthesis is still elusive. It is thought that they are synthesized within the shikimate pathway; currently molecular genetic methods and genome mining are employed to elucidate their biosynthesis [140]. Comparison of MAA-producing and nonproducing cyanobacteria, with sequenced genomes, identified a combination of genes involved in MAA synthesis. YP_324358 is predicted to code for a DHQ (3-dehydroquinate) synthase and YP_324357 for an O-methyltransferase; both were found only in the MAA-producing *Anabaena variabilis* PCC 7937 and missing in other (non-MAA producing) cyanobacteria. Phylogenetic analysis showed that these two genes were also transferred from a cyanobacterial donor to dinoflagellates and finally to metazoa by lateral gene transfer. All other investigated cyanobacteria, which possess these two genes, also had a second copy of the DHQ synthase gene.

In most cases, biosynthesis of MAAs is induced by UV-B radiation. The action spectrum for MAA synthesis induction in the cyanobacterium *Anabaena* shows a peak at 290 nm [141]. The UV-B-dependent induction of MAA synthesis in *Anabaena* sp., *Nostoc commune*, and *Scytonema* sp. promoted the synthesis of a single MAA, shinorine, containing both a glycine and a serine with an absorption maximum at 334 nm [142]. A polychromatic induction spectrum for MAAs in the dinoflagellate *Gyrodinium* showed a pronounced peak at 310 nm [143] and that for the chlorophyte *Prasiola stipitata* a maximum at 300 nm [144].

An alternative to preventing UV damage in the first place is the repair of DNA damage after it has occurred. Basically, three mechanisms are known to repair damages of the DNA. Photoenzymatic repair (PER) uses the enzyme DNA photolyase that breaks cyclobutane dimers in the presence of UV-A or blue light. NER starts with the recognition of damaged DNA and continues with the excision and resynthesis of the damaged strand by DNA polymerase. Recombinational repair (postreplication repair) repairs DNA damage that has not been recognized by the replication mechanism [145]. If not repaired, UV-induced DNA damage can result in mutations and death of the cells.

46.4 Ecological Consequences of the Photoenvironment

Both habitat selection of higher plants and movement of microorganisms to areas of suitable growth conditions is governed to a large extent by light. In addition to the availability of water and permissive temperatures, seed germination is often triggered by the presence of light (light germination, e.g., *Amaranthus retroflexus*, *Betula pubescens*, *Chenopodium album*, *Lactuca sativa*, and *Pinus sylvestris*), while in other plants seed germination is prevented by light (dark germination, e.g., *Brassica juncea*, *Cucumis sativus*, *Phacelia tanacetifolia*, and *Raphanus sativus*) [146]. After germination, the success of growth and development largely depends on the quality and quantity of solar radiation. Shade plants are inhibited by unfiltered solar radiation. In contrast, many trees, for example, in tropical and subtropical rain forests, start as seedlings and are sustained in an early developmental phase with limited growth until the falling of a large tree opens up a gap in the canopy. Only then, and this may be decades after germination, the young seedling quickly starts growing to reach the top level of the canopy [147]. Plant development in the shade under a canopy is governed by the red/far red ratio in the impinging radiation as shown by the work of Harry Smith [148,149].

Light also controls the timing of flowering. They do that by measuring the length of the day with great precision [150]. Some plants flower in short days, which need to be shorter than a species-specific critical day length (e.g., *Xanthium*, *Primula*, *Fragaria*); as a consequence, they flower in spring or autumn. Other plants flower in long days, longer than the critical day length (e.g., *Spinacea*, *Lactuca*), which therefore flower in summer. This is the reason why lettuce forms heads in spring, but elongates and flowers in summer, no matter when it has been planted. Still other plants flower independently of the day length (e.g., *Helianthus*, *Oryza*, *Pisum*, *Zea*). Since the day length varies with the geographical latitude, the same species flower earlier or later depending on the latitude. Biannual plants have an even more complex flowering control mechanism: in the first year they form a rosette, subsequently they require low temperatures (vernalization), and in the following year they shoot (stem elongation) and flower when the critical day length is reached (e.g., *Hyoscyamus*).

The movement responses of motile microorganisms in aquatic habitats result in the accumulation of populations in favorable light environments. Positive phototaxis leads the organisms toward the water surface. Often negative gravitaxis supports the upward movement [15]. Graviorientation has the advantage that it allows the organisms to orient themselves in darkness or in murky waters to move to the surface even without light guidance [151]. As indicated earlier, excessive solar visible and UV radiation at the water surface may damage the organisms. In response to this detrimental radiation, they often invert their direction of movement. This can be achieved by switching to negative phototaxis [152,153] or positive gravitaxis [154], by stopping movement and relying on sedimentation or by changes in buoyancy [155,156]. Often various responses operate antagonistically. In the flagellate *Euglena*, negative gravitaxis and negative phototaxis guide the cells in opposite directions. As a result, the population accumulates at a specific depth in the water column, which changes dynamically with changing irradiation and cloud cover. In this flagellate, the preferred depth is at an irradiance of 30 W m^{-2}, which is also the optimum for its photosynthesis [157].

While phototaxis has been found in several cyanobacteria, photophobic responses seem to be more important for habitat selection in these prokaryotes. At low light intensities, gliding cyanobacteria cross dark/light boundaries without responding, however, when leaving the light field they reverse the direction of their gliding motility; this behavior causes filamentous cyanobacteria (but also other gliding microorganisms such as *Dictyostelium* amoebae) to accumulate in light fields [158,159]. At higher fluence rates, the opposite behavior may occur. Again an antagonism between opposite behavioral responses allows the organisms to fine-tune their movement and select optimal light conditions.

Photokinesis seems not be as important for habitat selection even though a higher swimming speed in light compared to darkness causes the organism to spend less time in irradiated areas and more time in darkness [160,161]. This behavior has been discussed for the light-sensitive ciliate *Stentor*, which is easily killed by excessive solar radiation [162]. Other ciliates have been found to rely on phototaxis to escape excessive solar and especially UV radiation [163–165].

46.5 Excessive Light Stress

At low light intensities, growth and photosynthetic biomass production are suboptimal. On the other hand, exposure to excessive intensities is a stress factor for most photosynthetic organisms. One of the molecular mechanisms involved is the production of reactive oxygen species (ROS) [166,167]. Solar energy absorbed by the photosynthetic antenna pigments and passed to the reaction centers excites chlorophyll to one of several possible excited singlet states. Under normal conditions, this energy is utilized to initiate an electron transport involving several redox systems, which finally results in the production of ATP and NADPH + H^+. If under excessive radiation the electron transport chain is saturated, the chlorophyll molecule may convert to the first excited triplet state. The energy level of this is close to that of oxygen, which, in the ground state, is also in the triplet state. By transfer of the excitation energy to oxygen the latter reaches the singlet state $^1O_2$, which is rather short-lived but can destroy proteins, lipids, and other biomolecules in its vicinity. In the chloroplasts of photosynthetic organisms, this reaction is prevented as much as possible by assembling carotenoids in direct contact to the chlorophyll-binding proteins. By this construction, any excess energy is transferred to the carotenoids, which release the excitation energy as heat. Higher plants and some algae use the xanthophyll cycle to improve this protective mechanism [168,169].

In addition to singlet oxygen, other ROS may be generated including superoxide radicals ($O_2^{\bullet -}$), hydroxyl radicals ($OH^{\bullet}$), hydrogen peroxide (H_2O_2), and other radicals, all of which can destroy cellular organelles and biomolecules. Cellular responses are the synthesis of several enzymes [170–172], including catalase, superoxide dismutase, glutathione peroxidases, and peroxiredoxins. Furthermore, ascorbic acid, tocopherol, or glutathione are used to scavenge ROS [173].

Especially aromatic amino acids within the proteins absorb short-wavelength UV radiation. By this mechanism UV-B can break down proteins. In addition, it can bleach chromoproteins, such as

chlorophylls, carotenoids, and phycobilins, which are important accessory pigments of cyanobacteria, cryptophytes, and rhodophytes [174,175]. Other targets of solar UV radiation are DNA and RNA both in the nucleus and the plastids. As indicated above, UV-B mainly induces the formation of cyclobutane. UV-C radiation (<280 nm) results in the formation of 6-4 photoproducts, pyrimidine hydrates, and DNA–protein cross links. But solar radiation with wavelengths below ~290 nm does not reach the earth's surface due to the absorption by stratospheric ozone [176].

References

1. Taiz, L. and Zeiger, E. *Plant Physiology*, Sinauer Associates, Inc., Sunderland, 2006.
2. Valladares, F., Dobarro, I., Sánchez-Gómez, D., and Pearcy, R. W., Photoinhibition and drought in Mediterranean woody saplings: Scaling effects and interactions in sun and shade phenotypes, *J. Exp. Bot.*, 56, 483, 2005.
3. Yano, S. and Terashima, I., Developmental process of sun and shade leaves in *Chenopodium album* L., *Plant Cell Environ.*, 27, 781, 2004.
4. Pearcy, R. W., Gross, L. J., and He, D., An improved dynamic model of photosynthesis for estimation of carbon gain in sunfleck light regimes, *Plant Cell Environ.*, 20, 411, 1997.
5. Häder, D.-P., Lebert, M., and Helbling, E. W., In situ effects of solar radiation on photosynthesis in the Patagonian rhodophyte, *Porphyra columbina* Montagne, *Recent Res. Dev. Biochem.*, 4, 931, 2003.
6. Häder, D.-P., Lebert, M., and Helbling, E. W., Variable fluorescence parameters in the filamentous Patagonian rhodophytes, *Callithamnion gaudichaudii* and *Ceramium* sp. under solar radiation, *J. Photochem. Photobiol. B Biol.*, 73, 87, 2004.
7. Wulff, C., Iken, K., Quartino, M. L., Al-Handal, A., Wiencke, C., and Clayton, M. N., Biodiversity, biogeography and zonation of benthic micro- and macroalgae in the Arctic and Antarctic, *Bot. Mar.*, 52(6), 491, 2009.
8. Sinha, R. P., Barbieri, E. S., Lebert, M., Helbling, E. W., and Häder, D.-P., Effects of solar radiation on phycobiliproteins of marine red algae, *Trends Photochem. Photobiol.*, 10, 149, 2003.
9. Helbling, E. W., Barbieri, E. S., Sinha, R. P., Villafañe, V. E., and Häder, D.-P., Dynamics of potentially protective compounds in *Rhodophyta* species from Patagonia (Argentina) exposed to solar radiation, *J. Photochem. Photobiol. B Biol.*, 75, 63, 2004.
10. Kim, G.-T., Yano, S., Kozuka, T., and Tsukaya, H., Photomorphogenesis of leaves: Shade-avoidance and differentiation of sun and shade leaves, *Photochem. Photobiol. Sci.*, 4, 770, 2005.
11. Niyogy, K. K., Grossman, A. R., and Björkman, O., *Arabidopsis* mutants define a central role for the xanthophyll cycle in the regulation of photosynthetic energy conversion, *Plant Cell*, 10, 1121, 1998.
12. Carr, H. and Björk, M., Parallel changes in non-photochemical quenching properties, photosynthesis and D1 levels at sudden, prolonged irradiance exposures in *Ulva fasciata* Delile, *J. Photochem. Photobiol. B Biol.*, 87, 18, 2007.
13. Okubo, T., Tomo, T., and Noguchi, T., Detection of the D0→D1 transition of β-carotene radical cation photoinduced in photosystem II, *Photochem. Photobiol. Sci.*, 8, 157, 2009.
14. Häder, D.-P. and Hemmersbach, R., Gravitational biology, *Protoplasma*, 229, I, 2006.
15. Häder, D.-P., Hemmersbach, R., and Lebert, M., *Gravity and the Behavior of Unicellular Organisms*, Cambridge University Press, Cambridge, New York, Melbourne, Madrid, Cape Town, Singapore, Sao Paulo, 2005.
16. Marcoval, M. A., Villafañe, V. E., and Helbling, E. W., Combined effects of solar ultraviolet radiation and nutrients addition on growth, biomass and taxonomic composition of coastal marine phytoplankton communities of Patagonia, *J. Photochem. Photobiol. B Biol.*, 91, 157, 2008.
17. Richter, P. R., Häder, D.-P., Gonçalves, R. J., Marcoval, M. A., Villafañe, V. E., and Helbling, E. W., Vertical migration and motility responses in three marine phytoplankton species exposed to solar radiation, *Photochem. Photobiol.*, 83, 810, 2007.

18. Lebert, M., Phototaxis of *Euglena gracilis*—Flavins and pterins, in *Photomovement*, Häder, D.-P. and Lebert, M., Eds., Elsevier, Amsterdam, London, New York, Oxford, Paris, Shannon, Tokyo, 2001, p. 297.
19. Fankhauser, C. and Chory, J., Light control of plant development, *Annu. Rev. Cell Dev. Biol.*, 13, 203, 1997.
20. Hennig, L., Stoddart, W. M., Dieterle, M., Whitelam, G. C., and Schäfer, E., Phytochrome E controls light-induced germination of *Arabidopsis*, *Plant Physiol.*, 128, 194, 2002.
21. Park, J.-E., Seo, P. J., Kee, A.-K., Jung, J.-H., Kim, Y.-S., and Park, C.-M., An *Arabidopsis GH3* gene, encoding an auxin-conjugating enzyme, mediates phytochrome B-regulated light signals in hypocotyl growth, *Plant Cell Physiol.*, 48, 1236, 2007.
22. von Arnim, A. and Deng, X.-W., Light control of seedling development, *Annu. Rev. Plant Physiol.*, 47, 215, 1996.
23. Pepper, A. E., Corbett, R. W., and Kang, N., Natural variation in *Arabidopsis* seedling photomorphogenesis reveals a likely role for *TED1* in phytochrome signalling, *Plant Cell Environ.*, 25, 591, 2002.
24. Weller, J. L., Beauchamp, N., Huub, L., Kerckhoffs, L. H. J., Platten, J. D., and Reid, J. B., Interaction of phytochromes A and B in the control of de-etiolation and flowering in pea, *Plant J.*, 26, 283, 2001.
25. Mazzella, M. A. and Casal, J. J., Interactive signalling by phytochromes and cryptochromes generates de-etiolation homeostasis in *Arabidopsis thaliana*, *Plant Cell Environ.*, 24, 155, 2001.
26. Moon, J., Lee, H., Kim, M., and Lee, I., Analysis of flowering pathway integrators in *Arabidopsis*, *Plant Cell Physiol.*, 46, 292, 2005.
27. Zheng, Z.-L., Yang, Z., Jang, J.-C., and Metzger, J. D., Phytochromes A1 and B1 have distinct functions in the photoperiodic control of flowering in the obligate long-day plant *Nicotiana sylvestris*, *Plant Cell Environ.*, 29, 1673, 2006.
28. Iwamoto, M., Higo, K., and Takano, M., Circadian clock- and phytochrome-regulated Dof-like gene, *Rdd1*, is associated with grain size in rice, *Plant Cell Environ.*, 32, 592, 2009.
29. Prombona, A. and Argyroudi-Akoyunoglou, J., Diverse signals synchronize the circadian clock controlling the oscillations in chlorophyll content of etiolated *Phaseolus vulgaris* leaves, *Plant Sci.*, 167, 117, 2004.
30. Iino, M., Phototropism in higher plants, in *Photomovement. Comprehensive Series in Photosciences*, Häder, D.-P. and Lebert, M., Eds., Elsevier Science B.V., Amsterdam, London, New York, 2001, p. 659.
31. Brauner, L., Tropisms and nastic movements, *Annu. Rev. Plant Physiol.*, 5, 163, 1954.
32. Turnquist, H. M., Allen, N. S., and Jaffe, M. J., A pharmacological study of calcium flux mechanisms in the tannin vacuoles of *Mimosa pudica* L. motor cells, *Protoplasma*, 176, 91, 1993.
33. Hodick, D. and Sievers, A., On the mechanism of trap closure of *Venus flytrap* (*Dionaea muscipula* Ellis), *Planta*, 179, 32, 1989.
34. Haupt, W., Bewegungen, *Fortschr. Bot.*, 23, 358, 1961.
35. Iino, M., Phototropism: Mechanisms and ecological implications, *Plant Cell Environ.*, 13, 633, 1990.
36. Macleod, K., Firn, R. D., and Digby, J., The phototropic responses of *Avena* coleoptiles, *J. Exp. Bot.*, 37, 542, 1986.
37. Salomon, M., Zacherl, M., and Rüdiger, W., Phototropism and protein phosphorylation in higher plants: Unilateral blue light irradiation generates a directional gradient of protein phosphorylation across the oat coleoptile, *Bot. Acta*, 110, 197, 1997.
38. Kiss, J. Z., Miller, K. M., Ogden, L. A., and Roth, K. K., Phototropism and gravitropism in lateral roots of *Arabidopsis*, *Plant Cell Physiol.*, 43, 35, 2002.
39. Molas, M. L. and Kiss, J. Z., PKS1 plays a role in red-light-based positive phototropism in roots, *Plant Cell Environ.*, 31, 842, 2008.
40. Vogelmann, T. C. and Björn, L. O., Response to directional light by leaves of a sun-tracking lupine (*Lupinus succulentus*), *Physiol. Plant.*, 59, 533, 1983.

41. Koller, D., Shak, T., and Briggs, W. R., Enhanced diaphototropic response to vectorial excitation in solar-tracking leaves of *Lavatera cretica* by an immediately preceding opposite vectorial excitation, *J. Plant Physiol.*, 135, 601, 1989.
42. LaMotte, C. E. and Pickard, B. G., Control of gravitropic orientation. II. Dual receptor model for gravitropism, *Funct. Plant Biol.*, 31, 109, 2004.
43. Soga, K., Wakabayashi, K., Kamisaka, S., and Hoson, T., Graviperception in growth inhibition of plant shoots under hypergravity conditions produced by centrifugation is independent of that in gravitropism and may involve mechanoreceptors, *Planta*, 218, 1054, 2004.
44. Galland, P., Tropisms of *Avena* coleoptiles: Sine law for gravitropism, exponential law for photogravitropic equilibrium, *Planta*, 215, 779, 2002.
45. Inoue, S.-I., Kinoshita, T., and Shimazaki, K.-I., Possible involvement of phototropins in leaf movement of kidney bean in response to blue light, *Plant Physiol.*, 138, 1994, 2005.
46. Christie, J. M. and Briggs, W. R., Blue light sensing and signaling by the phototropins, in *Handbook of photosensory receptors*, Briggs, W. R. and Spudich, J. L., Eds., Wiley-VCH, Weinheim, Germany, 2005, p. 277.
47. Christie, J. M., Salomon, M., Nozue, K., Wada, M., and Briggs, W. R., LOV (light, oxygen, or voltage) domains of the blue-light photoreceptor phototropin (nph1): Binding sites for the chromophore flavin mononucleotide, *Proc. Natl. Acad. Sci. USA*, 96, 8779, 1999.
48. Casal, J. J., Phytochromes, cryptochromes, phototropin: Photoreceptor interactions in plants, *Photochem. Photobiol.*, 71, 1, 2000.
49. Kagawa, T., Kasahara, M., Abe, T., Yoshida, S., and Wada, M., Function analysis of phototropin2 using fern mutants deficient in blue light-induced chloroplast avoidance movement, *Plant Cell Physiol.*, 45, 416, 2004.
50. Suetsugu, N., Kagawa, T., and Wada, M., An auxilin-like J-domain protein, JAC1, regulates phototropin-mediated chloroplast movement in *Arabidopsis*, *Plant Physiol.*, 139, 151, 2005.
51. Briggs, W. R. and Olney, M. A., Photoreceptors in plant photomorphogenesis to date. Five phytochromes, two cryptochromes, one phototropin, and one superchrome, *Plant Physiol.*, 125, 85, 2001.
52. Lamparter, T., Kagawa, T., Brücker, G., and Wada, M., Positive and negative tropic curvature induced by microbeam irradiation of protonemal tip cells of the moss *Ceratodon purpureus*, *Plant Biol.*, 6, 165, 2004.
53. Uenaka, H. and Kadota, A., Phototropin-dependent weak and strong light responses in the determination of branch position in the moss *Physcomitrella patens*, *Plant Cell Physiol.*, 49, 1907, 2008.
54. Wada, M., Kadota, A., and Furuya, M., Intracellular photoreceptive site for polarotropism in protonema of the fern *Adiantum capillus-veneris* L., *Plant Cell Physiol.*, 22, 1481, 1981.
55. Kadota, A., Kohyama, I., and Wada, M., Polarotropism and photomovement of chloroplasts in the protonemata of the ferns *Pteris* and *Adiantum*: Evidence for the possible lack of dichroic phytochrome in *Pteris*, *Plant Cell Physiol.*, 30, 523, 1989.
56. Cerdá-Olmedo, E. and Corrochano, L. M., Genetics of *Phycomyces* and its responses to light, in *Photomovement*, Häder, D.-P. and Lebert, M., Eds., Elsevier, Amsterdam, London, New York, Oxford, Paris, Shannon, Tokyo, 2001, p. 589.
57. Galland, P., Phototropism in *Phycomyces*, in *Photomovement*, Häder, D.-P. and Lebert, M., Eds., Elsevier, Amsterdam, London, New York, Oxford, Paris, Shannon, Tokyo, 2001, p. 621.
58. Hohl, N., Galland, P., Senger, H., and Eslava, A. P., Altered pterin patterns in photoreceptor mutants of *Phycomyces blakesleeanus* with defective *madI* gene, *Bot. Acta*, 105, 441, 1992.
59. Wargent, J. J., Moore, J. P., Ennos, R., and Paul, N. D., Ultraviolet radiation as a limiting factor in leaf expansion and development, *Photochem. Photobiol.*, 85, 279, 2009.
60. Hopkins, L., Bond, M. A., and Tobin, A. K., Ultraviolet-B radiation reduces the rates of cell division and elongation in the primary leaf of wheat (*Triticum aestivum* L. cv Maris Huntsman), *Plant Cell Environ.*, 25, 617, 2002.

61. Fagerberg, W. R. and Bornman, J. F., Modification of leaf cytology and anatomy in *Brassica napus* grown under above ambient levels of supplemental UV-B radiation, *Photochem. Photobiol. Sci.*, 4, 275, 2005.
62. Ballaré, C. L., Rousseaux, M. C., Searles, P. S., Zaller, J. G., Giordano, C. V., Robson, T. M., Caldwell, M. M., Sala, O. E., and Scopel, A. L., Impacts of solar ultraviolet-B radiation on terrestrial ecosystems of Tierra del Fuego (southern Argentina). An overview of recent progress, *J. Photochem. Photobiol. B Biol.*, 62, 67, 2001.
63. Al-Oudat, M., Baydoun, S. A., and Mohammad, A., Effects of enhanced UV-B on growth and yield of two Syrian crops wheat (*Triticum durum* var. *Horani*) and broad beans (*Vicia faba*) under field conditions, *Environ. Exp. Bot.*, 40, 11, 1998.
64. Tosserams, M., Bolink, E., and Rozema, J., The effect of enhanced ultraviolet-B radiation on germination and seedling development of plant species occurring in a dune grassland ecosystem, *Plant Ecol.*, 128, 138, 1997.
65. Saile-Mark, M. and Tevini, M., Effects of solar UV-B radiation on growth, flowering and yield of central and southern European bush bean cultivars (*Phaseolus vulgaris* L.), *Plant Ecol.*, 128, 114, 1997.
66. Holmes, M. G. and Keiller, D. R., A novel phototropic response to supplementary ultraviolet (UV-B and UV-A) radiation in the siliquas of oilseed rape (*Brassica napus* L.) grown under natural conditions, *Photochem. Photobiol. Sci.*, 1, 890, 2002.
67. Yanqun, Z., Yuan, L., Haiyan, C., and Jianjun, C., Intraspecific differences in physiological response of 20 soybean cultivars to enhanced ultraviolet-B radiation under field conditions, *Environ. Exp. Bot.*, 50, 87, 2003.
68. Zu, Y., Li, Y., Chen, J., and Chen, H., Intraspecific responses in grain quality of 10 wheat cultivars to enhanced UV-B radiation under field conditions, *J. Photochem. Photobiol. B Biol.*, 74, 95, 2004.
69. Núñez-Olivera, E., Martínez-Abaigar, J., Tomás, R., Otero, S., and Arróniz-Crespo, M., Physiological effects of solar ultraviolet-B exclusion on two cultivars of *Vitis vinifera* L. from La Rioja, Spain, *Am. J. Enol. Vitic.*, 57, 441, 2006.
70. Andrady, A. L., Aucamp, P. J., Bais, A. F., Ballaré, C. L., Björn, L. O., Bornman, J. F., Caldwell, M. M., Cullen, A. P., de Gruijl, F. R., Erickson, D. J., III, Flint, S. D., Häder, D.-P., Hamid, H. S., Ilyas, M., Kulandaivelu, G., Kumar, H. D., McKenzie, R. L., Longstreth, J., Lucas, R. M., Noonan, F. P., Norval, M., Paul, N. D., Smith, R. C., Soloman, K. R., Sulzberger, B., Takizawa, Y., Tang, X., Torikai, A., van der Leun, J. C., Wilson, S. R., Worrest, R. C., and Zepp, R. G., Environmental effects of ozone depletion: 2006 assessment: Interactions of ozone depletion and climate change. Executive summary, *Photochem. Photobiol. Sci.*, 6, 212, 2007.
71. Andrady, A., Aucamp, P. J., Bais, A. F., Ballaré, C. L., Björn, L. O., Bornman, J. F., Caldwell, M., Cullen, A. P., Erickson, D. J., de Gruijl, F. R., Häder, D.-P., Ilyas, M., Kulandaivelu, G., Kumar, H. D., Longstreth, J., McKenzie, R. L., Norval, M., Paul, N., Redhwi, H. H., Smith, R. C., Solomon, K. R., Sulzberger, B., Takizawa, Y., Tang, X., Teramura, A. H., Torikai, A., van der Leun, J. C., Wilson, S. R., Worrest, R. C., and Zepp, R. G., Environmental effects of ozone depletion and its interactions with climate change: Progress report, 2008. United Nations Environment Programme, Environmental Effects Assessment Panel, *Photochem. Photobiol. Sci.*, 8, 13, 2009.
72. Nogues, S. and Baker, N. R., Effects of drought on photosynthesis in Mediterranean plants grown under enhanced UV-B radiation, *J. Exp. Bot.*, 51, 1309, 2000.
73. Abdullaev, A., Djumaev, B., and Karimov, K. K., Influence of UV-radiation on the photosynthesis and photosynthetic carbon metabolism in high mountainous plants, *BMC Plant Biol.*, 5, S1, 2005.
74. Caldwell, M. M., Bornman, J. F., Ballaré, C. L., Flint, S. D., and Kulandaivelu, G., Terrestrial ecosystems, increased solar ultraviolet radiation, and interactions with other climate change factors, *Photochem. Photobiol. Sci.*, 6, 252, 2007.
75. Frohnmeyer, H. and Staiger, D., Ultraviolet-B radiation-mediated responses in plants. Balancing damage and protection, *Plant Physiol.*, 133, 1420, 2003.

76. Krause, G. H., Gallé, A., Gademann, R., and Winter, K., Capacity of protection against ultraviolet radiation in sun and shade leaves of tropical forest plants, *Funct. Plant Biol.*, 30, 533, 2003.
77. Rice-Evans, C., Flavonoids and isoflavones: Absorption, metabolism, and bioactivity, *Free Rad. Biol. Med.*, 36, 827, 2004.
78. Ruhland, C. T., Xiong, F. S., Clark, W. D., and Day, T. A., The influence of ultraviolet-B radiation on growth, hydroxycinnamic acids and flavonoids of *Deschampsia antarctica* during springtime ozone depletion in Antarctica, *Photochem. Photobiol.*, 81, 1086, 2005.
79. Gerhardt, K. E., Lampi, M. A., and Greenberg, B. M., The effects of far-red light on plant growth and flavonoid accumulation in *Brassica napus* in the presence of ultraviolet B radiation, *Photochem. Photobiol.*, 84, 1445, 2008.
80. Yoshihara, R., Imaki, T., Hori, M., Watanabe, C., Yamamoto, K., and Takimoto, K., CPD photolyase gene from *Spinacia oleracea*: Repair of UV-damaged DNA and expression in plant organs, *J. Radiat. Res.*, 46, 157, 2005.
81. Liu, Z., Hossain, G. S., Islas-Osuna, M. A., Mitchell, D. L., and Mount, D. W., Repair of UV damage in plants by nucleotide excision repair: *Arabidopsis* UVH1 DNA repair gene is a homolog of *Saccharomyces cerevisiae* Rad1, *Plant J.*, 21, 519, 2000.
82. Scheller, H. V. and Haldrup, A., Photoinhibition of photosystem I, *Planta*, 221, 5, 2005.
83. Häder, D.-P., Photoinhibition and UV response in the aquatic environment, in *Photoprotection, Photoinhibition, Gene Regulation, and Environment*, Demmig-Adams, B., Adams, W. W., III, and Mattoo, A. K., Eds., Springer, Dordrecht, the Netherlands, 2006, p. 87.
84. Sarvikas, P., Hakala, M., Pätsikkä, E., Tyystjärvi, T., and Tyystjärvi, E., Action spectrum of photoinhibition in leaves of wild type and *npq1-2* and *npq4-1* mutants of *Arabidopsis thaliana*, *Plant Cell Physiol.*, 47, 391, 2006.
85. Bouchard, J. N., Roy, S., and Campbell, D. A., UVB effects on the photosystem II-D1 protein of phytoplankton and natural phytoplankton communities, *Photochem. Photobiol.*, 82, 936, 2006.
86. Godde, D. and Hefer, M., Photoinhibition and light-dependent turnover of the D1 reaction-centre polypeptide of photosystem II are enhanced by mineral-stress conditions, *Planta*, 193, 290, 1994.
87. Björkman, O. and Demmig, B., Photon yield of O_2 evolution and chlorophyll fluorescence characteristics at 77 K among vascular plants of diverse origins, *Planta*, 170, 489, 1987.
88. Genty, B., Briantais, J.-M., and Baker, N. R., The relationship between the quantum yield of photosynthetic electron transport and quenching of chlorophyll fluorescence, *Biochim. Biophys. Acta*, 990, 87, 1989.
89. Klughammer, C. and Schreiber, U., Complementary PS II quantum yields calculated from simple fluorescence parameters measured by PAM fluorometry and the saturation pulse method, *PAN*, 1, 27, 2008.
90. Krause, G. H. and Weis, E., Chlorophyll fluorescence and photosynthesis: The basics, *Annu. Rev. Plant Physiol.*, 42, 313, 1991.
91. Schreiber, U. and Bilger, W., Progress in chlorophyll fluorescence research: Major developments during the past years in retrospect, in *Progress Botany*, Lüttge, U. and Ziegler, H., Eds., Springer Verlag, Berlin, Germany, 1993, p. 151.
92. Meyerhoff, O. and Pfündel, E., Photosynthesis in ripe strawberries (*Fragaria* x *ananassa*) recording by an IMAGING-PAM *M-Series* (MAXI-version), *PAN*, 1, 19, 2008.
93. Pfündel, E., Estimating epidermal UV-A and UV-B screening in leaves with a WALZ XE-PAM fluorometer, *PAM*, 1, 25, 2008.
94. Muraoka, H., Tang, Y., Terashima, I., Koizumi, H., and Washitani, I., Contributions of diffusional limitation, photoinhibition and photorespiration to midday depression of photosynthesis in *Arisaema heterophyllum* in natural high light, *Plant Cell Environ.*, 23, 235, 2000.
95. Kinsman, R., Ibelings, B. W., and Walsby, A. E., Gas vesicle collapse by turgor pressure and its role in buoyancy regulation by *Anabaena flos-aquae*, *J. Gen. Microbiol.*, 137, 1171, 1991.
96. Overmann, J. and Pfennig, N., Buoyancy regulation and aggregate formation in *Amoebobacter purpureus* from Mahoney Lake, *FEMS Microbiol. Ecol.*, 101, 67, 1992.

97. Round, F. E. and Palmer, J. D., Persistent, vertical-migration rhythms in benthic microflora. II. Field and laboratory studies on diatoms from the banks of the river Avon, *J. Mar. Biol. Ass. U.K.*, 44, 191, 1966.
98. Lenci, F., Ghetti, F., and Song, P.-S., Photomovement in ciliates, in *Photomovement*, Häder, D.-P. and Lebert, M., Eds., Elsevier, Amsterdam, London, New York, Oxford, Paris, Shannon, Tokyo, 2001, p. 475.
99. Häder, D.-P. and Lebert, M., Graviperception and gravitaxis in algae, *Adv. Space Res.*, 27, 861, 2001.
100. Armitage, J. P. and Hellingwerf, K. J., Light-induced behavioral responses ('phototaxis') in prokaryotes, *Photosynth. Res.*, 76, 145, 2003.
101. Manahan, C. L., Iglesias, P. A., Long, Y., and Devreotes, P. N., Chemoattractant signaling in *Dictyostelium discoideum*, *Annu. Rev. Cell Dev. Biol.*, 20, 223, 2004.
102. Wadhams, G. H. and Armitage, J. P., Making sense of it all: Bacterial chemotaxis, *Nat. Rev. Mol. Cell Biol.*, 5, 1024, 2004.
103. Govorunova, E. G. and Sineshchekov, O. A., Chemotaxis in the green flagellate alga *Chlamydomonas*, *Biochemistry (Moscow)*, 70, 717, 2005.
104. Maree, A. F. M., Panfilov, A. V., and Hogeweg, P., Migration and thermotaxis of *Dictyostelium discoideum* slugs, a model study, *J. Theor. Biol.*, 199, 297, 1999.
105. Frankel, R. B. and Blakemore, R. P., Magnetite and magnetotaxis in microorganisms, *Bioelectromagnetics*, 10, 223, 1989.
106. Delong, E. F., Frankel, R. B., and Bazylinski, D. A., Multiple evolutionary origins of magnetotaxis in bacteria, *Science*, 259, 803, 1993.
107. Korohoda, W., Mycielska, M., Janda, E., and Madeja, Z., Immediate and long-term galvanotactic responses of *Amoeba proteus* to dc electric fields, *Cell Motil. Cytoskeleton*, 45, 10, 2000.
108. Kišidayová, S. and Váradyová, Z., Potential of galvanotaxis to separation and cleaning of rumen ciliates, *J. Microbiol. Meth.*, 57, 65, 2004.
109. Iwatsuki, K., *Stentor coeruleus* shows positive photokinesis, *Photochem. Photobiol.*, 55, 469, 1992.
110. Cohn, S. A., Light dependent effects on diatom motility, *Mol. Biol. Cell*, 4, 168a, 1993.
111. Häder, D.-P., Photomovement, in *Encyclopedia of Plants*, Haupt, W. and Feinleib, M. E., Eds., Springer, Berlin, Heidelberg, 1979, p. 268.
112. Mikolajczyk, E. and Walne, P. L., Photomotile responses and ultrastructure of the euglenoid flagellate *Astasia fritschii.*, *J. Photochem. Photobiol. B Biol.*, 6, 275, 1990.
113. Wolken, J. J. and Shin, E., Photomotion in *Euglena gracilis*. I. Photokinesis. II. Phototaxis, *J. Protozool.*, 5, 39, 1958.
114. Diehn, B., Phototaxis and sensory transduction in *Euglena*, *Science*, 181, 1009, 1973.
115. Engelmann, T. W., Bakterium photometricum. Ein Beitrag zur vergleichenden Physiologie des Licht- und Farbensinnes., *Pflügers Arch.*, 30, 95, 1883.
116. Clayton, R. K., Patterns of accumulation resulting from taxes and changes in motility of microorganisms, *Arch. Microbiol.*, 27, 311, 1957.
117. Diehn, B., Feinleib, M., Haupt, W., Hildebrand, E., Lenci, F., and Nultsch, W., Terminology of behavioral responses of motile microorganisms, *Photochem. Photobiol.*, 26, 559, 1977.
118. Wenderoth, K., Photokinese und photophobische Reaktionen der Kieselalge *Navicula peregrina*, *Publikationen zu wissenschaftlichen Filmen*, 16, 3, 1983.
119. Diehn, B., Fonseca, J. R., and Jahn, T. R., High speed cinemicrography of the direct photophobic response of *Euglena* and the mechanism of negative phototaxis, *J. Protozool.*, 22, 492, 1975.
120. Iseki, M., Matsunaga, S., Murakami, A., Ohno, K., Shiga, K., Yoshida, C., Sugai, M., Takahashi, T., Hori, T., and Watanabe, M., A blue-light-activated adenylyl cyclase mediates photoavoidance in *Euglena gracilis*, *Nature*, 415, 1047, 2002.
121. Jung, A., Domratcheva, T., Tarutina, M., Wu, Q., Ko, W.-H., Shoeman, R. L., Gomelsky, M., Gardner, K. H., and Schlichting, I., Structure of a bacterial BLUF photoreceptor: Insights into blue light-mediated signal transduction, *Proc. Natl. Acad. Sci. USA*, 102, 12350, 2005.

122. Fukushima, Y., Okajima, K., Ikeuchi, M., and Itoh, S., Two intermediate states *I* and *J* trapped at low temperature in the photocycles of two BLUF domain proteins of cyanobacteria *Synechocystis* sp. PCC6803 and *Thermosynechococcus elongatus* BP-1, *Photochem. Photobiol.*, 83, 112, 2007.
123. Haupt, W., General review on phototactic microorganisms, in *Biophysics of Photoreceptors and Photobehaviour of Microorganisms*, Colombetti, G., Ed., Lito Felici, Pisa, 1975, p. 4.
124. Kuhlmann, H.-W., Bräucker, R., and Schepers, A. G., Phototaxis in *Porpostoma notatum*, a marine scuticociliate with a composed crystalline organelle, *Eur. J. Protistol.*, 33, 295, 1997.
125. Ntefidou, M. and Häder, D.-P., Photoactivated adenylyl cyclase (PAC) genes in the flagellate *Euglena gracilis* mutant strains, *Photochem. Photobiol. Sci.*, 4, 732, 2005.
126. Song, P.-S., Protozoan and related photoreceptors: Molecular aspects, *Annu. Rev. Biophys. Bio.*, 12, 35, 1983.
127. Hendriks, J., Gensch, T., Hviid, L., van der Horst, M. A., Hellingwerf, K. J., and van Thor, J. J., Transient exposure of hydrophobic surface in the photoactive yellow protein monitored with Nile Red, *Biophys. J.*, 82, 1632, 2002.
128. Matsuoka, T., Sato, M., and Matsuoka, S., Photoreceptor pigment mediating swimming acceleration of *Blepharisma*, a unicellular organism, *Microbios*, 99, 89, 1999.
129. Wilde, A., Fiedler, B., and Börner, T., The cyanobacterial phytochrome Cph2 inhibits phototaxis towards blue light, *Mol. Microbiol.*, 44, 981, 2002.
130. Okajima, K., Yoshihara, S., Fukushima, Y., Geng, X., Katayama, M., Higashi, S., Watanabe, M., Sato, S., Tabata, S., Shibata, Y., Itoh, S., and Ikeuchi, M., Biochemical and functional characterization of BLUF-type flavin-binding proteins of two species of cyanobacteria, *J. Biochem.*, 137, 741, 2005.
131. Montgomery, B. L., Sensing the light: Photoreceptive systems and signal transduction in cyanobacteria, *Mol. Microbiol.*, 64, 16, 2007.
132. Sinha, R. P., Rastogi, R. P., Ambasht, N. K., and Häder, D.-P., Life of wetland cyanobacteria under enhancing solar UV-B radiation, *Proc. Nat. Acad. Sci. India B*, 78, 53, 2008.
133. Sinha, R. P., Klisch, M., Vaishampayan, A., and Häder, D.-P., Biochemical and spectroscopic characterization of the cyanobacterium *Lyngbya* sp. inhabiting mango (*Mangifera indica*) trees: Presence of an ultraviolet-absorbing pigment, scytonemin, *Acta Protozool.*, 38, 291, 1999.
134. Rogoff, D., Rothschild, L. J., Bishop, J., and Carpenter, E. J., The ultraviolet (UV) protecting pigment in cyanobacteria, scytonemin: The effects of the external protectant, iron, and its implications for life on Mars, *Astrobiology*, 5, 317, 2005.
135. Garcia-Pichel, F., Sherry, N. D., and Castenholz, R. W., Evidence for an ultraviolet sunscreen role of the extracellular pigment scytonemin in the terrestrial cyanobacterium *Chlorogloeopsis* sp., *Photochem. Photobiol.*, 56, 17, 1992.
136. Hansucker, S. W., Tissue, B. M., Potts, M., and Helm, R. F., Screening protocol for the ultraviolet-photoprotective pigment scytonemin, *Anal. Biochem.*, 288, 227, 2001.
137. Richter, P. R., Klisch, M., Sinha, R. P., and Häder, D.-P., Mycosporine-like amino acids (MAAs) protect against UV-B-induced damage in *Gyrodinium dorsum*, in *Environmental UV Radiation: Impact on Ecosystems and Human Health and Predictive Models*, Ghetti, F., Checcucci, G., and Bornman, J. F., Eds., Springer, Dordrecht, the Netherlands, 2006, p. 283.
138. Sinha, R. P., Singh, S. P., and Häder, D.-P., Database on mycosporines and mycosporine-like amino acids (MAAs) in fungi, cyanobacteria, macroalgae, phytoplankton and animals, *J. Photochem. Photobiol. B Biol.*, 89, 29, 2007.
139. Carignan, M. O., Cardozo, K. H. M., Oliveira-Silva, D., Colepicolo, P., and Carreto, J. I., Palythine–threonine, a major novel mycosporine-like amino acid (MAA) isolated from the hermatypic coral *Pocillopora capitata*, *J. Photochem. Photobiol. B Biol.*, 94, 191, 2009.
140. Singh, S. P., Klisch, M., Sinha, R. P., and Häder, D.-P., Genome mining of mycosporine-like amino acid (MAA) synthesizing and non-synthesizing cyanobacteria: A bioinformatics study, *Genomics*, 95, 120, 2010.

141. Singh, S. P., Kumari, S., Rastogi, R. P., Singh, K. L., Richa, Sinha, R. P., and Häder, D.-P., Induction of mycosporine-like amino acids (MAAs) in a cyanobacterium *Anabaena doliolum* by ultraviolet (UV) radiation, 4th Asia Oceania Conference on Photobiology, Nov. 24–26, 2008, Varanasi, India, 39.
142. Sinha, R. P. and Häder, D.-P., UV-protectants in cyanobacteria, *Plant Sci.*, 174, 278, 2008.
143. Klisch, M. and Häder, D.-P., Mycosporine-like amino acids in the marine dinoflagellate *Gyrodinium dorsum*: Induction by ultraviolet irradiation, *J. Photochem. Photobiol. B Biol.*, 55, 178, 2000.
144. Gröniger, A. and Häder, D.-P., Induction of the synthesis of an UV-absorbing substance in the green alga *Prasiola stipitata*, *J. Photochem. Photobiol. B Biol.*, 66, 54, 2002.
145. Sinha, R. P. and Häder, D.-P., UV-induced DNA damage and repair: A review, *Photochem. Photobiol. Sci.*, 1, 225, 2002.
146. Bewley, J. D., Black, M., and Halmer, P., *The Encyclopedia of Seeds: Science, Technology and Uses*, CAB International, Wallingford, U.K.
147. Palomaki, M. B., Chazdon, R. L., Arroyo, J. P., and Letcher, S. G., Juvenile tree growth in relation to light availability in second-growth tropical rain forests, *J. Trop. Ecol.*, 22, 223, 2006.
148. McCormac, A. C., Whitelam, G. C., Boylan, M. T., Quail, P. H., and Smith, H., Contrasting responses of etiolated and light-adapted seedlings to red:far-red ratio: A comparison of wild type, mutant and transgenic plants has revealed differential functions of members of the phytochrome family, *J. Plant Physiol.*, 140, 707, 1992.
149. Shlumukov, L. R., Barro, F., Barcelo, P., Lazzeri, P., and Smith, H., Establishment of far-red high irradiance responses in wheat through transgenic expression of an oat phytochrome A gene, *Plant Cell Environ.*, 24, 703, 2001.
150. Raven, P. H., Evert, R. F., and Eichhorn, S. E., *Biology of Plants*, Freeman, New York, 2005.
151. Häder, D.-P., Lebert, M., Richter, P., and Ntefidou, M., Gravitaxis and graviperception in flagellates, *Adv. Space Res.*, 31, 2181, 2003.
152. Häder, D.-P., Negative phototaxis of *Dictyostelium discoideum pseudoplasmodia* in UV radiation, *Photochem. Photobiol.*, 41, 225, 1985.
153. Takahashi, T., Watanabe, M., Kamo, N., and Kobatake, Y., Negative phototaxis from blue light and the role of third rhodopsinlike pigment in *Halobacterium cutirubrum*, *Biophys. J.*, 48, 235, 1985.
154. Richter, P. R., Streb, C., Ntefidou, M., Lebert, M., and Häder, D.-P., High light-induced sign change of gravitaxis in the flagellate *Euglena gracilis* is mediated by reactive oxygen species, *Acta Protozool.*, 42, 197, 2003.
155. Reynolds, C. S., Oliver, R. L., and Walsby, A. E., Cyanobacterial dominance: The role of buoyancy regulation in dynamic lake environments, *N. Z. J. Mar. Freshw. Res.*, 21, 379, 1987.
156. Walsby, A. E., Mechanisms of buoyancy regulation by planktonic cyanobacteria with gas vesicles, in *The Cyanobacteria*, Fay, P. and Van Baalen, C., Eds., Elsevier Science Publishers, Amsterdam, the Netherlands, 1987, p. 385.
157. Häder, D.-P., Polarotaxis, gravitaxis and vertical phototaxis in the green flagellate, *Euglena gracilis*, *Arch. Microbiol.*, 147, 179, 1987.
158. Burkart, U. and Häder, D.-P., Phototactic attraction in light trap experiments: A mathematical model, *J. Math. Biol.*, 10, 257, 1980.
159. Häder, D.-P. and Poff, K. L., Light-induced accumulations of *Dictyostelium discoideum* amoebae, *Photochem. Photobiol.*, 29, 1157, 1979.
160. Nultsch, W., Schuchart, H., and Dillenburger, M., Photomovement of the red alga *Porphyridium cruentum* (Ag.) Naegeli. I. Photokinesis, *Arch. Microbiol.*, 122, 207, 1979.
161. Melkonian, M., Meinicke-Liebelt, M., and Häder, D.-P., Photokinesis and photophobic responses in the gliding flagellate, *Euglena mutabilis*, *Plant Cell Physiol.*, 27, 505, 1986.
162. Häder, D.-P. and Häder, M. A., Effects of solar radiation on motility in *Stentor coeruleus*, *Photochem. Photobiol.*, 54, 423, 1991.

163. Martini, B., Marangoni, R., Gioffre, D., and Colombetti, G., Effects of UV-B irradiation on the motility and photomotility of the marine ciliate *Fabrea salina*, *J. Photochem. Photobiol. B Biol.*, 39, 197, 1997.
164. Marangoni, R., Preosti, G., and Colombetti, G., Phototactic orientation mechanism in the ciliate *Fabrea salina*, as inferred from numerical simulations, *J. Photochem. Photobiol. B Biol.*, 54, 185, 2000.
165. Marangoni, R., Messina, N., Gioffré, D., and Colombetti, G., Effects of UV-B irradiation on a marine microecosystem, *Photochem. Photobiol.*, 80, 78, 2004.
166. Henmi, T., Miyao, M., and Yamamoto, Y., Release and reactive-oxygen-mediated damage of the oxygen-evolving complex subunits of PS II during photoinhibition, *Plant Cell Physiol.*, 45, 243, 2004.
167. Tominaga, H., Kodama, S., Matsuda, N., Suzuki, K., and Watanabe, M., Involvement of reactive oxygen species (ROS) in the induction of genetic instability by radiation, *J. Radiat. Res.*, 45, 181, 2004.
168. Goss, R., Oroszi, S., and Wilhelm, C., The importance of grana stacking for xanthophyll cycle-dependent NPQ in the thylakoid membranes of higher plants, *Physiol. Plant.*, 131, 496, 2007.
169. Schumann, A., Goss, R., Jakob, T., and Wilhelm, C., Investigation of the quenching efficiency of diatoxanthin in cells of *Phaeodactylum tricornutum* (Bacillariophyceae) with different pool sizes of xanthophyll cycle pigments, *Phycologia*, 46, 113, 2007.
170. Li, G.-B., Liu, Y.-D., Wang, G.-H., and Song, L.-R., Reactive oxygen species and antioxidant enzymes activity of *Anabaena* sp. PCC 7120 (Cyanobacterium) under simulated microgravity, *Acta Astronautica*, 55, 953, 2004.
171. He, Y.-Y., Klisch, M., and Häder, D.-P., Adaptation of cyanobacteria to UV-B stress correlated with oxidative stress and oxidative damage, *Photochem. Photobiol.*, 76, 188, 2002.
172. He, Y.-Y. and Häder, D.-P., Reactive oxygen species and UV-B: Effect on cyanobacteria, *Photochem. Photobiol. Sci.*, 1, 729, 2002.
173. Hensley, K., Robinson, K. A., Gabbita, S. P., Salsman, S., and Floyd, A. R., Reactive oxygen species, cell signaling, and cell injury, *Free Rad. Biol. Med.*, 28, 1456, 2000.
174. Sinha, R. P., Kumar, A., Tyagi, M. B., and Häder, D.-P., Ultraviolet-B-induced destruction of phycobiliproteins in cyanobacteria, *Physiol. Mol. Biol. Plants*, 11, 313, 2005.
175. Rinalducci, S., Hideg, É., Vass, I., and Zolla, L., Effect of moderate UV-B irradiation on *Synechocystis* PCC 6803 biliproteins, *Biochem. Biophys. Res. Commun.*, 341, 1105, 2006.
176. Björn, L. O., Stratospheric ozone, ultraviolet radiation, and cryptogams, *Biol. Conservat.*, 135, 326, 2007.

47

Photoactive Yellow Protein, the Prototype Xanthopsin

Johnny Hendriks
University of Amsterdam

Marijke Hospes
University of Amsterdam

Klaas J. Hellingwerf
University of Amsterdam

47.1 Introduction

47.1.1 Discovery and Biological Context of the Photoactive Yellow Protein

In 1985, several ferredoxins and other chromophoric proteins from the halophilic phototrophic bacterium *Ectothiorhodospira halophila* were isolated by T. E. Meyer in Tucson, Az.[1] One of the "other chromophoric proteins" he identified in this screen was yellow and was named "photoactive yellow protein" (PYP) in a subsequent study.[2] *E. halophila* was reclassified in 1996 to its current name *Halorhodospira halophila*.[3] *H. halophila* is a unicellular prokaryote, or more specifically, a phototrophic purple spirillum that deposits sulfur extracellularly. It was first isolated and classified from salt-encrusted mud taken from the shores of Summer Lake, Lake County, Oregon.[4,5] Later, it was also isolated from the extremely saline lakes of the Wadi el Natrun in Egypt.[6] Both locations are salt lakes, and indeed, *H. halophila* only thrives in extremely salty environments.

As a phototrophic organism, *H. halophila* exploits the free energy available from sunlight to survive. However, like most organisms, *H. halophila* is not immune to the effects of UV radiation. It is therefore essential for the organism to find a place to live where there is enough light to grow, but where the amount of UV radiation is at a minimum. Like most phototrophic organisms, *H. halophila* has mechanisms to perceive the available light climate. It is not only attracted by (infra)red (i.e., photosynthetic)

light, but it also has a blue-light response system which steers it away from potentially harmful places, rich in blue light. This blue-light repellent response has a wavelength dependence that fits the absorption spectrum of the PYP.[7] This observation provides evidence that PYP is the light sensor in the blue-light response of *H. halophila*. Further evidence for this function of PYP in *H. halophila* may be provided via genetic techniques. However, the application of these techniques in extremophilic prokaryotes like *H. halophila* is not well developed, which may be the reason why genetic proof for the function of PYP is not yet available.

Interestingly, the function of PYP is similar to that of the sensory rhodopsins, and in particular to sensory rhodopsin II, which is also a sensor for a negative tactile response to blue light (in *Halobacterium salinarum*, an archaebacterium that can also be found in salt lakes). The family of the rhodopsins is a large family. Its members are found in all kingdoms of life, from unicellular organisms to complex ones such as *Homo sapiens sapiens*. It is the most extensively studied family of photoactive proteins available. Its best known members are the visual rhodopsins, which allow *Homo sapiens sapiens* to see, and bacteriorhodopsin, which is a light-activated proton pump found in *Halobacterium salinarum*. Sensory rhodopsins are close relatives to bacteriorhodopsin and can be found in the latter organism too. In fact, the most notable difference between bacteriorhodopsin and the sensory rhodopsins is their function. Bacteriorhodopsin provides the cell with means of harvesting light energy, whereas the sensory rhodopsins are light detectors that make sure the organisms can find a niche in the environment in which bacteriorhodopsin can do its work safely and efficiently. Striking similarities between PYP and the sensory rhodopsins were already noted after the first characterization of PYP.[2] There is, however, one major difference with the sensory rhodopsins that has boosted the study of PYP: It is highly water soluble, whereas the rhodopsins, being membrane proteins, are not. As we shall see later, PYP and the sensory rhodopsins turned out to belong to two structurally very different families of proteins, which are only similar in function. For more information on the rhodopsins, the reader is referred to several excellent reviews on this topic.[8–12]

47.1.2 Xanthopsins: The Family of PYPs

H. halophila is not the only organism in which a PYP has been discovered. The family of PYPs has been named the Xanthopsin family.[13] Other Xanthopsins have been detected and biochemically characterized in *Rhodothalassium salexigens* (synonymous to *Rhodospirillum salexigens*),[14] *Halochromatium salexigens* (synonymous to *Chromatium salexigens*),[15] *Rhodobacter sphaeroides*,[13] *Rhodobacter capsulatus*,[16] *Rhodospirillum centenum*,[17] *Idiomarina loihiensis*,[17] *Thermochromatium tepidum*,[17] *Stigmatella aurantiaca*,[18] *Rhodopseudomonas palustris*,[18] *Burkholderia phytofirmans*,[18] and *Salinibacter ruber*.[18] From DNA sequence information, more PYPs are predicted to exist in *Methylobacterium* sp., *Allochromatium vinosum*, *Leptospira biflexa*, *Gemmatimonas aurantiaca*, *Haliangium ochraceum*, *Sorangium cellulosum*, *Acidithiobacillus caldus*, *Leptothrix cholodnii*, *Magnetospirillum gryphiswaldense*, *Curvibacter* (a putative symbiont of *Hydra magnipapillata*), and *Spirosoma linguale*. All corresponding reading frames have significant similarity ($<10^{-8}$) to PYP from *H. halophila* and contain at least two of the strongly conserved key residues: Tyr42, Glu46, and Cys69 (Figure 47.1).[19] All of these organisms are from the domain of the *Bacteria*, while most are *Proteobacteria*. *Salinibacter ruber* belongs to the subgroup of *Bacteroidetes* and *L. biflexa* is from the subgroup of *Spirochetes*. In the phylogenetic tree shown in Figure 47.2, the PYPs of these latter two organisms group together. Another member of the *Bacteroidetes* with a PYP is *S. linguale*, which however has only 30% identity with the Xanthopsin from *S. ruber*. The last non-*Proteobacterium* is *G. aurantiaca*, which is a member of the *Gemmatimonadetes*.

The length of all known Xanthopsins (domains) varies between 123 and 162 residues, which implies that this domain shows very few deletions or insertions (see Figures 47.1 and 47.2). Four of these Xanthopsins are the N-terminal domain of a multidomain protein. Significantly, these four PYP domains—from *Rhodospirillum centenum*, *T. tepidum*, *A. vinosum*, and *Methylobacterium* sp.—also cluster in the phylogenetic tree of the Xanthopsins (Figure 47.2). Also the Xanthopsin from *G. aurantiaca*, with a length

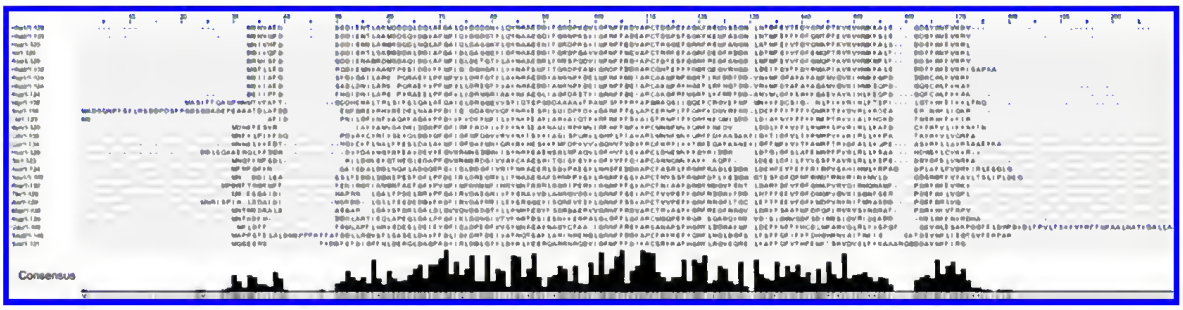

FIGURE 47.1 Sequence alignment of the Xanthopsins. An alignment of all currently known Xanthopsins is presented, where the following abbreviations stand for the organism in which the Xanthopsin was found with the strains in parentheses: Hha1, *H. halophila* (DSM 244/SL1); Hha3, *H. halophila* (DSM 244/SL1); Hsa, *H. salexigens*; Ilo, *I. loihiensis*; Rsa, *R. salexigens*; Hha2, *H. halophila* (DSM 244/SL1); Rsp1, *Rhodobacter sphaeroides* (strain ATCC 17023/2.4.1/NCIB 8253/DSM 158/ATCC 17029/ATH 2.4.9); Rsp2, *Rhodobacter sphaeroides* (KD131/KCTC 12085); Rca, *Rhodobacter capsulatus*; Mgr, *M. gryphiswaldense*; Sru, *Salinibacter ruber* (DSM 13855); Lbi, *L. biflexa* (Patoc 1/ATCC 23582/Paris/Ames); Bph, *B. phytofirmans* (DSM 17436/PsJN); Lch, *L. cholodnii* (ATCC 51168/LMG 8142/SP-6); Cur, *Curvibacter* (putative symbiont of *Hydra magnipapillata*); Hoc, *Haliangium ochraceum* (DSM 14365/JCM 11303/SMP-2); Sli, *Spirosoma linguale*; Aca, *A. caldus* (ATCC 51756); Sau1, *S. aurantiaca* (DW4/3-1); Rce, *Rhodospirillum centenum* (ATCC 51521/SW); Tte, *T. tepidum*; Avi, *A. vinosum* (DSM 180); Msp, *Methylobacterium* sp. (4–46); Rpa, *Rhodopseudomonas palustris* (BisB5); Gau, *G. aurantiaca* (T-27/DSM 14586/JCM 11422/NBRC 100505); Sau2, *S. aurantiaca* (DW4/3-1); Sce, *Sorangium cellulosum* (So ce56). Two slightly different Xanthopsins with one amino acid different are found in different *Rhodobacter sphaeroides* strains. In *H. halophila* and *S. aurantiaca,* two different Xanthopsins are found in the same organism. This figure was prepared with Jalview[20] (http://www.jalview.org/) using information obtained from alignment performed with ClustalW[21] (http://www.ebi.ac.uk/Tools/msa/clustalw2/).

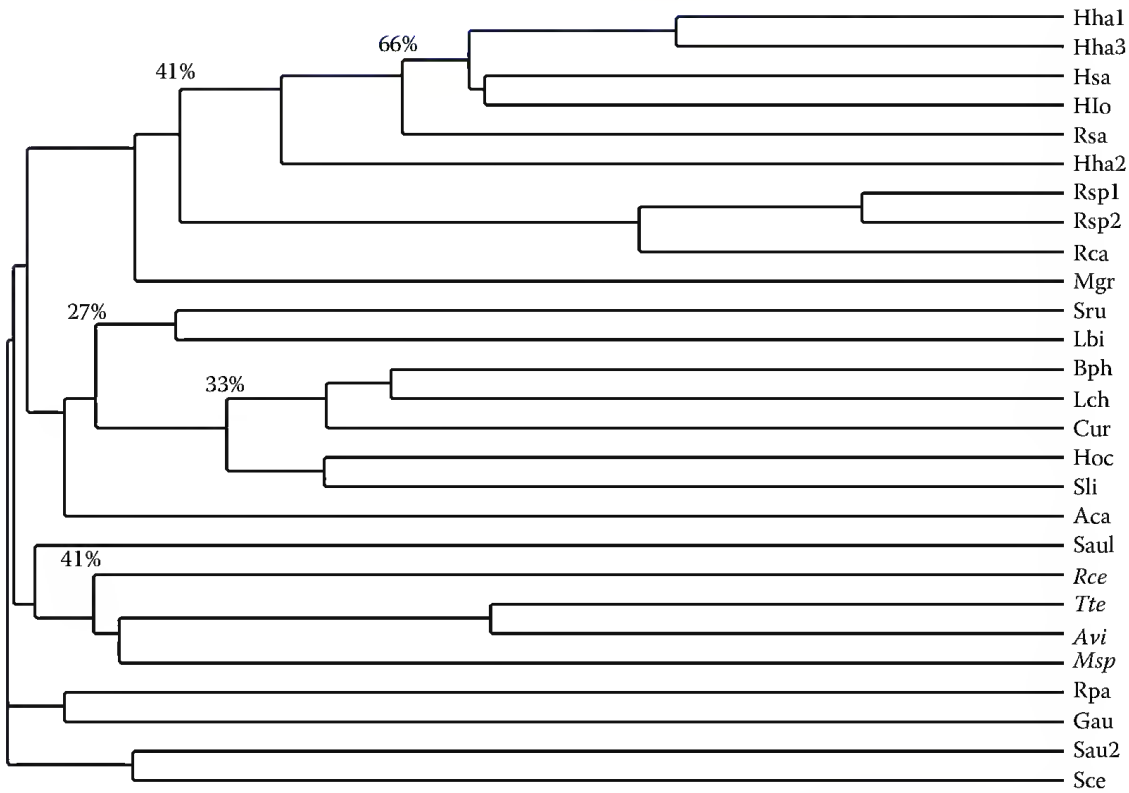

FIGURE 47.2 Phylogenetic tree of the 27 Xanthopsins from the alignment shown in Figure 47.1. The Xanthopsins from multidomain proteins are indicated in italics. Several percentages are placed for the lowest pair-wise identity for the set of PYP in that branch.

of 162 amino acids, may have a separate output domain, for example, in the form of a helix-turn-helix domain. Bioinformatics analysis of the secondary structure of this domain, however, only clearly showed one helical stretch in the carboxy-terminal 40 amino acids.

The biological function of the Xanthopsins in the various organisms may differ quite significantly. In *H. halophila*, PYP induces a photophobic tactile response.[7] For *Rhodobacter sphaeroides*, genetic evidence is available that indicates that the blue-light-induced photophobic tactile response in that organism is not mediated by the Xanthopsin present in that organism, provided no genetic redundancy exists.[22] The Xanthopsin found in *Rhodospirillum centenum* regulates chalcone synthase gene expression.[23] The PYP domains from *Methylobacterium* sp. and in the Ppr protein from *Rhodospirillum centenum* are followed by a bacteriophytochrome domain and a histidine kinase domain. For Ppr, it has been observed that blue light causes changes in autokinase activity.[23] In *T. tepidum* and *A. vinosum*, a PYP is present that is also part of a multidomain protein, but here the PYP and bacteriophytochrome domain is followed by a GGDEF/EAL domain, which may suggest that these photoreceptors have a function in biofilm formation. The function of only a limited number of members of the Xanthopsin family has so far been elucidated. However, it is reasonable to suggest that the members within the different subgroups of Xanthopsins, distinguished based on sequence similarity (see Figure 47.2), have a similar function, while these functions may differ between the subgroups.

47.1.3 Photoactive Yellow Protein: The Prototypical PAS Domain

As described earlier, PYP is part of a family of proteins named Xanthopsins. Nevertheless, PYP also shows striking similarities with the much larger family of PAS domains. These PAS domains have been identified in proteins from all three kingdoms of life, that is, in the *Bacteria*, the *Archaea*, and the *Eucarya*. PAS is an acronym formed from the names of the proteins in which the PAS motive was first recognized[24]: the *Drosophila* period clock protein (**P**ER), the vertebrate aryl hydrocarbon receptor nuclear translocator (**A**RNT), and the *Drosophila* single-minded protein (**S**IM).

Proteins containing PAS domains are predominantly involved in signal transduction. Over 21,000 PAS domains have been identified that contain (a) PAS domain(s).[25] Most of these are receptors, signal transducers, or transcriptional regulators present in the cytoplasm. PAS domains are usually present in proteins with a multidomain architecture. Furthermore, a single protein can have multiple PAS domains; in fact, proteins have been identified containing up to six. In contrast, the entire PYP from *H. halophila* can be considered a single PAS domain. As it is the first protein from the PAS domain family for which the 3D structure was elucidated, it was proposed that PYP is the structural prototype of the PAS domain fold.[26]

47.2 Structure

After an initial period of confusion, in which only the primary structure of PYP was solidly secured through gene sequencing,[27] the spatial structure of PYP was solved at a resolution of 1.40 Å with x-ray diffraction analysis in 1995 and deposited in the protein data bank (PDB).[28] Not much later, multidimensional NMR spectroscopy provided the structure of PYP in solution,[29] and the resolution in the structure of PYP was brought down to 0.82 Å.[30] Now, even a neutron diffraction–derived structure is available for PYP.[31] During the past 20 years, structural information on PYP has been secured through studies on wild-type PYP, nine site-specific and deletion mutants, one PYP-like protein (i.e., Ppr), crystallized in four different space groups (P63, P65, P21, and H) in the temperature range from 85 K[32] to ambient temperatures. Besides structures of the stable ground state of these proteins, of wild-type PYP, and the E46Q mutant thereof, also nine and four (mixtures of) intermediate states of these two proteins, respectively, populated through illumination of the respective proteins, have been deposited in the PDB (http://www.pdb.org/). This wealth of information has helped to acquire very detailed understanding, not only of the stable dark structure of PYP, but also of its functioning, in terms of the dynamical changes in its structure that are elicited by illumination. Part of this insight will be discussed in the following.

47.2.1 Secondary and Tertiary Structure of PYP

The protein backbone of PYP is folded in an α/β-fold, with a six-stranded antiparallel β-sheet as the central scaffold, flanked by five elements with α-helical secondary structure.[28] In addition, a short π-helix can be identified at the site where the chromophore is attached to the apo-protein.[33] The loops containing helices α3 and α4, and helix α5, fold on top of this central β-sheet to form the major hydrophobic core of the protein, which then forms a pocket in which the chromophore of PYP, *p*-coumaric acid[34] (or 4-hydroxy cinnamic acid), is incorporated. The N-terminus of the protein, which contains helices α1 and α2, folds at the back of the central β-sheet to form a second, smaller, hydrophobic core. This tertiary structure is shown more clearly in Figure 47.3 in two orientations: with the plane of the central β-sheet parallel and perpendicular to the plane of the paper, respectively. The latter view allows one to see how the different α-helical loops fold around the central β-sheet.

47.2.2 Xanthopsins Compared

From previous alignment with six Xanthopsins, the Xanthopsin family was divided into three subgroups, based on their primary structure. Subgroup I contains Xanthopsins found in *H. halophila*, *R. salexigens*, and *H. salexigens*. With the current alignment (Figure 47.1), the Xanthopsins from another *H. halophila* strain, a second PYP in *H. halophila* and *I. loihiensis*, are added to subgroup I. Previous subgroup II contains Xanthopsins found in *Rhodobacter sphaeroides* and *Rhodobacter capsulatus* and to this subgroup belongs also a PYP from another *R. sphaeroides* strain. The only member of subgroup III was the Xanthopsin found in *Rhodospirillum centenum*. This Xanthopsin has a low similarity with the Xanthopsins from subgroups I and II. From the currently known 27 Xanthopsins, 19 fall outside subgroups I and II. These Xanthopsins have less than 45% identity to PYP from *H. halophila*. Xanthopsin from *Rhodospirillum centenum* forms a subgroup with the three other Xanthopsins of multidomain proteins. A fourth subgroup can be made from Xanthopsins found in *B. phytofirmans*, *L. cholodnii*, *Curvibacter*, *Haliangium ochraceum*, and *Spirosoma linguale*. The rest of Xanthopsins are not divided into subgroups. The primary structures within subgroups I and II are very similar with identities around 75% in pair-wise alignments. Subgroups III and IV have identities around 42%. In a comparison of Xanthopsins from subgroup I or II with other Xanthopsins, the alignments become worse with identities around 30%. Several pair-wise comparisons of Xanthopsins have even poorer results with identities low as 14%. Beside the earlier mentioned functional important residues Tyr42, Glu46, and Cy69, the residues Gly29, Phe63, Ala67, and Pro68 are highly conserved.

Since the Xanthopsin subgroups were defined based on sequence similarity, these results should not be very surprising. However, by looking at subdomains of the sequence alignments, better insight is

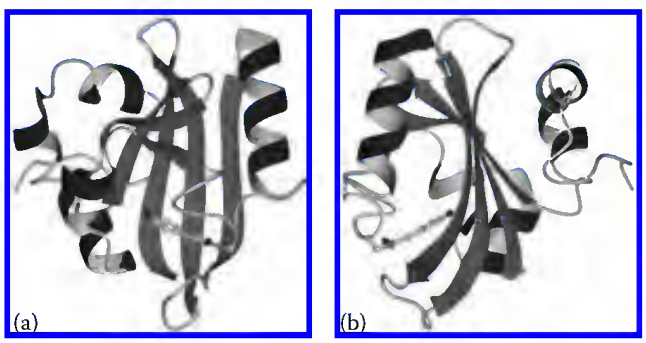

FIGURE 47.3 Tertiary structure of the PYP. Two orientations of a ribbon representation of the PYP from *H. halophila* are presented. Panel (a) clearly shows the β-sheet with the chromophore in front of it. Panel (b) is a side view, of the orientation in panel (a), visualizing both sides of the β-sheet. The figure was prepared using the program MOLMOL[35] using the structure coordinate file deposited at the Protein Data Bank[36] (http://www.pdb.org/) with PDB ID: 2PHY.[28] The program POV-Ray™ (http://www.povray.org) was used to render the images.

obtained on which domains make a Xanthopsin a Xanthopsin, and which domains are important for the function the Xanthopsin has in the organism it resides in. PYP was earlier proposed to be a prototype for the PAS domain. The family of PAS domains is very large and spans all three kingdoms of life. A PAS domain is not so much defined by its primary structure, but more by its secondary and tertiary structural elements. The PAS domain can be divided into four subdomains, the N-terminal cap, the PAS core, the helical connector, and the β-scaffold. In PYP from *H. halophila*, these subdomains comprise residues 1–28, 29–69, 70–87, and 88–125, respectively. Thus, the N-terminal cap contains helices α1 and α2; the PAS core contains the β-strands β1, β2, and β3, and the helices α3 and α4; the helical connector contains helix α5; and the β-scaffold contains the β-strands β4, β5, and β6. The residues that form the chromophore pocket are all contained within the PAS core and β-scaffold, which are sandwiched together.

The conservation in the Xanthopsin family is different for the four PAS subdomains. The similarity is high for the PAS core and low for the N-terminal cap. The edges of the PAS core, including residues 28–46 and 58–69, have the highest degrees of homology. However, the helical connector and the β-scaffold also have high similarity within the different Xanthopsin subgroups. Especially, the β-scaffold in subgroup I and the helical connector in subgroup III have high homology. This suggests that the PAS core is important for the general sensing function of the Xanthopsins, and the other subdomains determine the specific function of a particular Xanthopsin.

Most Xanthopsins are small single-domain proteins. Twenty-one of these single-domain Xanthopsins have length between 123 and 146 amino acids. Two other single-domain Xanthopsins from *Salinibacter ruber* and *G. aurantiaca* have longer lengths of 156 and 162 residues, respectively. PYP from *S. ruber* has a 31 residue N-terminal extension that appears to be important for dimerization.[37] Dimerization of PYP is only described in literature for the PYP from *S. ruber*. The PYP from *G. aurantiaca* has a 39 residue C-terminal extension. The primary structure of the extension suggests that it contains at least one α-helix. Indicating the C-terminal extension is involved in signal transduction.

There are more proteins similar to the Xanthopsin family than these 27. An unclassified Gammaproteobacteria (NOR5-3) contains a single protein of 115 residues with similarity 10^{-6} to PYP from *H. halophila*. Despite the low similarity with PYP, this protein contains the conserved residues Gly29, Tyr42, Glu46, Phe63, and Cys69, but not the two conserved residues Ala67 and Pro68. Therefore, the environment of the chromophore-binding place is different than in most Xanthopsins. Further, PYP-like domains are found in *Methylobacterium radiotolerans*, *Methylobacterium extorquens*, *Methylobacterium populi*, and *Methylobacterium chloromethanicum*. All these PYP-like domains are N-terminal domains of multidomain proteins and have similarity between 10^{-9} and 10^{-8} to PYP from *H. halophila*. However, these protein domains lack conserved residues Tyr42, Glu46, Ala67, and Cys69. These protein domains have a serine or glycine instead of Cys69. Therefore, it is not clear if these proteins function as photoreceptor without a cysteine for chromophore attachment. However, all these PYP-like domains contain the highly conserved Gly29, Phe63, and Pro68. In these multidomain proteins, the PYP-like domain is followed by a bacteriophytochrome domain and a histidine kinase domain. These are the same domains as the domains of the Ppr protein from *Rhodospirillum centenum* and the Xanthopsins domain-containing protein of *Methylobacterium* sp. This suggests a similar function for all these six proteins.

47.2.3 Chromophore and Its Binding Pocket

As amino acids do not significantly absorb visible light, functional activity of a photoreceptor protein depends on a covalently, or non-covalently, associated chromophore to the specific photoreceptor. The type of chromophore selected by evolution typically corresponds with the wavelength range in which the receptor protein is required to function.[38] Accordingly, the Xanthopsins use an aromatic chromophore, identified in *H. halophila* in 1994 as 4-hydroxy cinnamic acid, covalently linked to the apo-protein via a thiol ester bond to Cys69.[34,39] This chromophore plays a crucial role in the functional activation of PYP

via its sensitivity to *trans/cis* (or E/Z) isomerization upon absorption of a photon from the visible part of the electromagnetic spectrum. This chromophore is embedded in the protein in a pocket lined by the following amino acids (in the order in which they appear in the sequence): Ile31, Tyr42, Glu46, Thr50, Arg52, Phe62, Val66, Ala67, Cys69, Thr70, Phe96, Asp97, Tyr98, Met100, Val120, and Val122. These amino acids completely bury the chromophore in the major hydrophobic core of the protein and prevent direct contact of the former with solvent.

In the dark state of PYP, the chromophore is deprotonated.[39,40] The resulting negative charge of its phenolic oxygen is buried in the main hydrophobic core of the protein. This is possible only through stabilization of this negative charge by a dedicated hydrogen-bonding network.[28,41] The phenolate anion, of which part of the charge is delocalized over the large π-orbital system of the chromophore, interacts with Glu46, Tyr42, and Thr50, such that O_{η} from Tyr42 and $O_{\varepsilon,2}$ from Glu46 form very short hydrogen bonds with the chromophore. O_{η} from Tyr42 in turn hydrogen-bonds with $O_{\gamma,1}$ from Thr50; the latter amino acid, however, does not line the chromophore pocket. This hydrogen-bonding network is the main determinant of the spectral tuning of PYP.[41]

The recent neutron diffraction study of deuterated PYP[31] has revealed further specific detail of this hydrogen-bonding network: From the position of the deuteron relative to the two pairs of oxygen atoms that form the two hydrogen bonds, it has been deduced that Tyr42 and Glu46 form a short-ionic- and low-barrier hydrogen bond with the phenolate oxygen of the chromophore, respectively. The special character of these hydrogen bonds was recently confirmed with solid-state NMR spectroscopy.[42] The discovery of the special character of these hydrogen bonds is particularly relevant for computational analyses of the mechanism of photoactivation of PYP because the relative bond strength changes dramatically from a regular to a low-barrier hydrogen bond. The latter type of bond is also predicted to convey typical characteristics to the infrared spectrum of the protein,[43] which, however, have not been characterized yet. Nevertheless, the ultrafast changes in the infrared absorption of Glu46 are fully consistent with the results of the neutron diffraction experiment.

The structure of PYP in aqueous solution, determined via multidimensional NMR spectroscopy,[29] is very similar to the structure determined with x-ray and neutron diffraction. The elements of secondary structure identified in both of them are nearly identical, be it that they may start/end 1–2 residues earlier or later. Notably different are helix α2 and the π-helix, which are just below the cutoff for positive identification in the solution structure. Furthermore, there are three poorly defined regions in the solution structure, comprising residues 1–5, 17–23, and 113–117. This is caused by lack of structural constraints in the NMR dataset in those regions, which may be caused by high side-chain and/or backbone mobility.[29] In the crystal structure, these same regions have higher values for the B-factor, which expresses the mean-square fluctuations of atoms from their average position. Another difference is observed with respect to the position of Arg52: This residue is present in two conformations in the solution structure: One in which Arg52 is positioned 4 Å above the aromatic ring of the chromophore, and in the other, the guanidinium group of Arg52 is positioned about 4 Å above the aromatic ring of Tyr98,[29] which is suggestive of π-stacking.[44] These positions of both Arg52 and Tyr98 differ from those in the crystal structures. The position of Arg52 is particularly relevant because it has been proposed that it plays an important role in the primary photochemistry of PYP.[45] The results of site-directed mutagenesis, in combination with ultrafast UV/Vis spectroscopy, however, have failed to substantiate this proposal (A. Stahl et al., unpublished).

All this information available about the dark or ground state of PYP has formed a very fertile frame of reference for the interpretation of a large body of spectroscopic and biochemical data on a wide range of aspects of this photoreceptor protein. Nevertheless, its photosensory function requires that additional (transient) structural states exist. Such states have been identified and characterized; they will be discussed within the framework of the discussion of the photocycle of PYP in the following. However, in the characterization of these intermediates, it has turned out that there is a profound effect of the crystal lattice on the dynamics and extent of the structural transitions to which the PYP acquires access upon photoactivation.

47.2.4 Dynamical Changes in the Structure of PYP and the Confines of the Crystal Lattice

From an ensemble of structures, such as obtained with NMR spectroscopy or molecular dynamics simulations, it is possible to determine eigenvectors that describe the path along which the atoms of a protein may move.[46,47] Using these eigenvectors, or "modes of flexibility," it is possible to transform the solution structure into the crystal structure, indicating that the observed differences between the two structures are within the confines of the intrinsic flexibility of the protein. This is further corroborated by the fact that a transition of the structures of PYP, crystallized in the $P6_5$ and the $P6_3$ space group, respectively,[28] can also be performed within the confines of its intrinsic modes of flexibility.

Illumination of PYP crystals allows formation of transient intermediate states that spontaneously revert back into their stable ground state. While doing this, they may largely use the same "modes of flexibility," and therefore, initially such intermediates formed in a crystal lattice[48] were thought to show considerable similarity to corresponding states formed in aqueous solution.[49,50] Nevertheless, when PYP is activated in the latter type of medium, structural changes take place that go far beyond these modes. This conclusion was initially based on spectroscopic measurements that revealed that PYP shows non-Arrhenius type of kinetics and that this kinetics is strongly affected by the hydrophobicity of the medium.[51,52] This interpretation subsequently has been confirmed by molecular dynamics simulations[53] and multidimensional solution NMR spectroscopy,[54] be it that the latter experiments are complicated by the very high degree of disorder of a large part of the polypeptide backbone of PYP when the protein resides in its signaling state. Only recently has it turned out possible to record well-resolved spectra of the signaling state of PYP with ^{15}N,^{13}C-NMR spectroscopy in solution (H. Ippel et al., unpublished experiments).

To characterize the different photocycle pathways that PYP goes through upon photoactivation in a crystal lattice and in aqueous solution (both a room temperature), dedicated spectroscopic experiments were designed both with microcrystals and with crystals of a size suitable for diffraction studies.[55,56] These experiments have revealed that the crystal lattice does not only accelerate the thermal recovery of the ground state of PYP approximately 10-fold; it also allows various branching pathways to make a significant contribution to this recovery.[56] These studies have clearly shown that the presence of a crystal lattice confines the extent to which the PYP backbone reversible unfolds with respect to the degree of transient unfolding in solution.

In vivo, the PYP functions in the cytoplasm of *H. halophila*.[57] The freedom it experiences for dynamical alterations in its structure in this crowded bacterial cytoplasm is as yet unknown, but may be intermediate between that of an aqueous buffer and a crystalline lattice. Particularly, the precise nature of the interaction of PYP with downstream transducer proteins may tip the balance to either of these.

47.3 Photoactivity of the Xanthopsins

Photoactivity of the Xanthopsins expresses itself in the form of a photocycle. When a Xanthopsin in the ground state absorbs a photon of the proper wavelength, structural changes occur in the protein that lead to a signaling state that can be "read" by the organism it resides in. From the signaling state, the Xanthopsin spontaneously returns to its stable ground state. This self-regenerative cycle only requires the holoprotein to be in hydrated form and does not require the presence of a membrane, additional proteins, or cofactors, etc. Most Xanthopsin research is focused on this photocycle or a part of it. The best-studied Xanthopsin by far is PYP from *H. halophila*. Therefore, the photocycle of this protein will be discussed in detail in the following.

47.3.1 Basic Photocycle

Though models for the photocycle of the PYP have become more and more elaborate over the years, they still feature no more than the three basic intermediates that were initially described[51] (see Figure 47.4): (1) the ground or dark-adapted state, pG, in which the chromophore is deprotonated and the

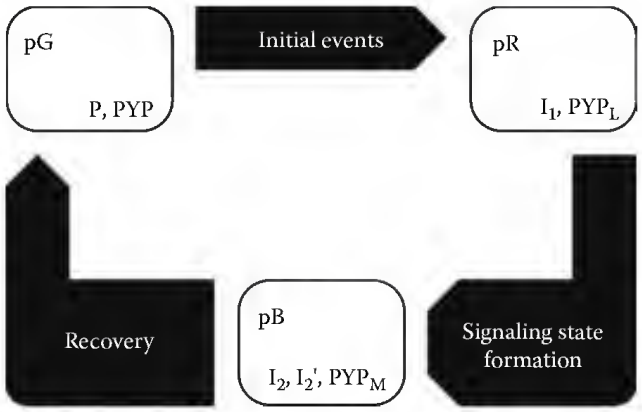

FIGURE 47.4 Basic photocycle model of PYP. Nomenclature used in this review is indicated in the top-left of the balloons. Alternative nomenclatures found in the literature are indicated bottom-right of the balloons.

isomerization state of the chromophore is *trans*; (2) pR, a spectrally red-shifted state (relative to pG), which is formed on a nanosecond timescale, in which the chromophore is still deprotonated but its configuration has changed to *cis*; and (3) pB, a spectrally blue-shifted state (relative to pG), which is formed on a microsecond timescale. This species is presumed to be the signaling state of the photoreceptor. It is stable enough to allow for a signal to be processed by the organism. In the pB state, the chromophore has become protonated while it retains the *cis* configuration. The holoprotein subsequently recovers to its ground state on the millisecond to second timescale.

These three major steps, isomerization, protonation change, and recovery, are also observed in the sensory rhodopsins, which have a similar cellular function as PYP, but are structurally very different. It is interesting to note that although the Xanthopsins and sensory rhodopsins have evolved separately, the photochemical mechanism they use to generate a signal from an absorbed photon is essentially the same.

47.3.2 Photocycle Interpretation

Over the years, several nomenclatures for the photocycle intermediates have been introduced. As the photocycle models become more and more complex, so does the nomenclature. Unfortunately, there is not a single nomenclature that is really able to handle all the new intermediates that meanwhile have been described. All the different nomenclatures contain the aforementioned three basic photocycle species and can therefore be compared using these three species as a reference (see Figure 47.4). Initially, these ground-, red-shifted, and blue-shifted states were called P, I_1, and I_2.[51] In 1995, the names pG, pR, and pB were introduced by Hoff et al.[58] Yet another nomenclature[59] was introduced in 1996, in which these species are called PYP, PYP_L, and PYP_M, a nomenclature based upon the photocycle nomenclature of bacteriorhodopsin. To add to the confusion, in 2005 the use of the name I_2' instead of I_2[60] was proposed, while I_2 is used to indicate an intermediate introduced in 1996 as pB′.[61] This nomenclature is becoming even more complicated by the use of various photocycle models that introduce "new" intermediates to describe results obtained under very specific reaction conditions.

Proteins are not static, but highly dynamic molecules. We therefore should see a photocycle intermediate as an ensemble of similar but individually different structures. The question is then of course what criterion is used to assign a structure to a specific intermediate ensemble. We have chosen to take the three main photocycle intermediates (pG, pR, and pB; see Figure 47.4) as anchor points. We then subdivided the ensembles representing the intermediates into sub-ensembles relevant to a specific analysis problem. Figure 47.5 shows an example for the pH dependence of the photocycle. Note that the intermediate ensembles are subdivided horizontally according to pH (left to right represents a change from low to high pH). In addition, several characteristics of interest (isomerization state, and

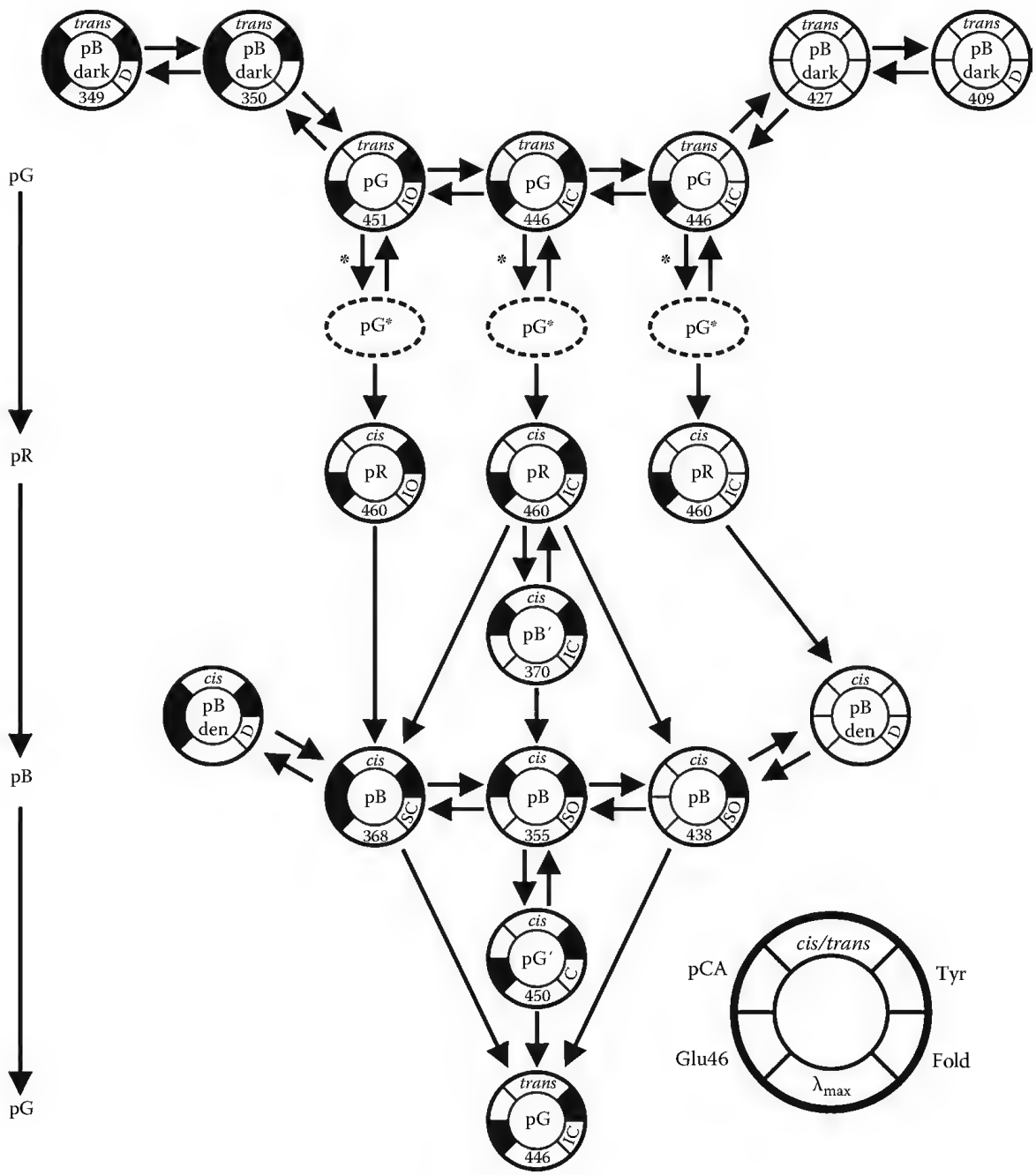

FIGURE 47.5 pH-dependent photocycle scheme for PYP. The scheme is an adaptation of the scheme presented in Ref. 62. The initial reactions are depicted in their most basic form, that is, light-induced formation of the excited state followed by formation of either pG or pR. Light-induced reactions are illustrated by a * next to the arrow. For each species in the scheme, several characteristics are depicted as indicated by the legend (bottom-right): *cis/trans*, the chromophore's isomerization state; pCA, Glu46, and Tyr, the protonation state of respectively the chromophore, of residue 46, and of tyrosine residues (black is protonated, white is deprotonated); Fold, the folding state of the protein; λ_{max}, the absorption maximum. Absorption maxima in italics are assumed. The following folding states are distinguished: IC and IO represent the closed and open form of the initial folding state of pG; SC and SO represent the closed and open form of the signaling state (pB); D represents an undefined denatured/unfolded state; C represents a hypothetical folded state that is able to catalyze chromophore isomerization.

protonation state of the chromophore and Glu46, folding state of the protein, and absorption maximum) are shown for each species. Of course, other characteristics may be chosen as well depending on the situation. A more detailed explanation of the pH dependence of the photocycle is given in the following. However, we would like to note two aspects of this photocycle: (1) There are five subspecies of pB indicated in the photocycle, with apparently quite different characteristics, such as the UV/Vis absorption maximum. Generally, one would try to think of different names for these species when depicted in a single figure. However, if one would have to describe them at a single pH, one would likely just use pB (or an equivalent from one of the other nomenclatures). (2) There is more than one route to step through the photocycle. The sample pH then will determine which route is the dominant route. Furthermore, depending on the physicochemical conditions of an experiment, one could construct additional routes when necessary. This partly explains the multitude of photocycle models for PYP that have been suggested in the literature.

47.3.3 Experimental Context

It is of crucial importance to take experimental context in consideration, when comparing different experiments. Four different experimental parameters are of basic importance: temperature, nature of the solvent, mesoscopic context (or phase), and illumination conditions. The first one, temperature, is obviously important in kinetic experiments. At very low (cryogenic) temperatures, certain photocycle species may be trapped,[59,63] while others cannot be formed. The second one, the nature of the solvent, is also very important and is usually different between different experiments. Though pH is probably the most important solvent feature that has an effect on, for example, the kinetics of the photocycle,[64,65] others such as hydrophobicity of the solvent,[51] type and concentration of solutes present,[50,51] and the nature of the solvent itself (e.g., water vs. deuterium oxide)[64] also can have their effect on the data. The third experimental parameter is the mesoscopic context or phase. In the crystalline phase (or lattice), no large structural change is observed in the protein upon formation of the signaling state, whereas when the protein is in solution such a significant overall structural change is observed.[55,56] Furthermore, illumination conditions can also have pronounced effects on the data, particularly, the color and intensity of the light are important. The choice of wavelength can already have an effect on which photocycle species are formed.[59,63] Also the duration of the excitation pulse can have an effect. Longer illumination allows the possibility of photoactivation of photocycle species other than the ground state[66] and may lead to hysteresis effects in the recovery (Gensch et al., unpublished). It should be kept in mind that in UV/Vis experiments the probe beam also contributes to illumination of the sample.

47.4 Photocycle of Photoactive Yellow Protein

The key element of the photocycle is the transition between the ground/dark state and the signaling state. In the signaling state, PYP interacts with a putative transducer protein to signal the cell that a blue photon has been absorbed. Therefore, this state needs to have a relatively long lifetime to allow for this communication. Since the interacting transducer protein has not been identified yet, all experiments have so far been performed with purified PYP itself. It is possible that certain characteristics of the signaling state will change when transducer protein is added. An example of the dramatic effect that a transducer protein can have on a photosensory protein can be observed in sensory rhodopsin I. Here, in the absence of the transducer protein, the sensor protein acts as a proton pump, while in the presence of the transducer protein the proton pump activity is lost.[67] Also, the pH dependence of the photocycle kinetics of sensory rhodopsin I changes upon removal of the transducer protein.[67] This does not imply that measurements on just the isolated photosensor are obsolete. On the contrary, any differences between the characteristics in the absence and the presence of the accompanying transducer may lead to a better understanding of how a signal might be transmitted.

47.4.1 pH-Dependence of the Photocycle

Before breaking down the photocycle into its elementary partial reactions, it is good to have a closer look at the pH-dependent aspects of the complete photocycle as illustrated in Figure 47.5. At first glance, this representation of the photocycle looks rather complicated. However, all species in a horizontal line have the same name (e.g., pG, pR, and pB) and the same basic structure (see Section 47.3.2). The point is that these species essentially are subspecies of the named species. It then depends on the pH which of these subspecies will dominate the mixture and the subspecies represent sub-ensembles of the main species. Depending on the absolute pH, the dominant route through the various (sub)species in the photocycle will vary. This to the point that some intermediates (like pB′ and pG′) may even be bypassed altogether under certain conditions. This explains some of the seemingly contradictory results that can be found in the literature.

The pH dependence of the photocycle in Figure 47.5 is illustrated via the equilibrium reactions between subspecies on a horizontal line, in which low to high pH is from left to right. Note that for any given pH, more than one subspecies may be present (dictated by the pKs involved) and consequently more than one route through the photocycle may be possible. The complexity that this introduces is in most cases not detected in the experimental data, which in most cases is (and should) to be analyzed with (highly) simplified models. This complexity can only be fully revealed if a series of measurements is analyzed in which specific conditions, such as pH, ionic strength, and temperature, are systematically varied. Regardless of the experiments, one might want to perform with PYP; this underlying complexity of its behavior should always be kept in mind, as the experimental conditions selected can have an important impact on results.

47.4.2 Initial Events

The initial photocycle events, studied in the science domain of biophysics, generally hold the key to important biological characteristics of a photosensory receptor, such as light sensitivity, and photocycle efficiency (or photocycle quantum yield). In its most basic form, the initial events can be depicted as the formation of a photon-induced excited state, which subsequently relaxes either back to the original dark state or to the first intermediate in the photocycle (see Figure 47.5). On the other hand, one can also try to describe all the different reactions in the initial photocycle step that leads to either formation of pR or pG. In both cases, the very first step, formation of an electronically excited sate, is the same. Assuming that every absorbed photon results in the formation of an electronically excited state, an equation can be derived for the rate with which the excited state is formed (see Equation 47.1).[62] In this equation, I_0 represents the light intensity (in $mmol \cdot cm^{-2} \cdot s^{-1}$) for a specific wavelength range; ε represents the molar extinction coefficient (in $M^{-1} \cdot cm^{-1}$) for the same specific wavelength range; l represents the light's path length (in cm) through the sample; [R] represents the concentration of the photon-absorbing species (in M). Note that in most cases, Equation 47.1 can be approximated by Equation 47.2. One can use these formulas to simulate the light-dependent reaction(s) of photocycles:

$$k = \frac{I_0(1-10^{-\varepsilon \cdot l \cdot [R]})}{l \cdot [R]}, \tag{47.1}$$

$$k \approx I_0 \varepsilon \ln(10). \tag{47.2}$$

Trying to deduce what exactly happens after formation of the excited state of pG is a difficult exercise. This is evidenced by the very different models for the initial events in the PYP photocycle that have been published over the years. Furthermore, only very few experiments have been performed to analyze how much the experimental context influences these initial events.

Light absorption by the chromophore of PYP induces primary photochemistry that leads to its *cis* configuration within a few picoseconds, with a quantum yield of 0.35.[68,69] The structural transition

underlying this E/Z isomerization can only be completed in a complex reaction in which also the hydrogen bond between the C=O group of the chromophore, and the nitrogen atom of the peptide bond between Pro68 and Cys69 is disrupted, to allow the C(9)=O group to rotate around the long axis of the chromophore to stabilize the isomerization of the C_7=C_8 ethylenic bond[45,70] so that the first *cis* ground-state intermediate (GSI) I_0 can be formed.

During the past few years, it has become clear that in parallel, a transient GSI[71] is formed, which may well also have an isomerized C_7=C_8 ethylenic bond but has its carbonyl group still hydrogen bonded to the nitrogen atom of the proteins' backbone.[72] This GSI is also formed with a quantum yield of approximately one-third (the remaining one-third fraction decays through internal conversion) and then rapidly (i.e., with a half-life of 6 ps) thermally relaxes back to the stable GSI. The I_0 intermediate converts with near 100% efficiency into the I_1 state (also denoted pR_1) and subsequently to the pR_2 intermediate, through additional configurational relaxation of the *cis*-chromophore. Discovery of this transient GSI (5) has been relevant not only for the proper understanding of the primary photochemistry of PYP, but also has resolved several controversies on this aspect, for example, related to quantum yields.

Recently, we have shown (A. Rupenyan et al., unpublished experiments) that the formation of the GSI is due to a fraction of molecules in which the hydrogen bond between the C(9)=O group of the chromophore, and the nitrogen atom of the peptide bond between Pro68 and Cys69 is not disrupted during the initial stages after photoexcitation. Whether or not the chromophore in this GSI state has a true *cis* configuration, or (still) is in a distorted *trans* configuration, remains to be established.

Considering that formation of the electronically excited singlet state in PYP is accompanied by a very large charge redistribution, as was demonstrated with Stark spectroscopy,[73] and that for several organic dyes with a pronounced donor/acceptor asymmetry across the ethylenic bond light absorption leads to the formation of a so-called twisted-intramolecular charge transfer (TICT) state,[74] the relevance of single-bond rotation has been discussed for PYP. Independently, this issue was addressed in Quantum Mechanics/Molecular Mechanics (QM/MM) calculations on a model system that simulates the primary photochemistry in PYP.[45] Our most recent experiments suggest that such single-bond rotation indeed is relevant; however, most surprisingly, not as an alternative to double-bond isomerization, but rather to facilitate it (A. Stahl et al., manuscript in preparation).

After (spectroscopic) identification, the next important issue for any intermediate is its spatial structure. Consensus exists on the view that the protein part shows very little structural change during the first step of the photocycle and that even the aromatic ring of the chromophore stays more or less at the same position.[75–77] The only way to facilitate isomerization of the chromophore under these conditions is by rotating the thiol ester carbonyl. This carbonyl flip can be interpreted as a double isomerization around the C_7=C_8 double bond and the C_9–S_γ single bond, that is, the chromophore configuration changes from C_7=C_8-*trans* C_9–S_γ-*cis* to C_7=C_8-*cis* C_9–S_γ-*trans*. This model was first introduced on the basis of low-temperature Fourier transform infrared spectroscopy (FTIR) spectroscopy[61] and later confirmed.[55,76,78]

The (free) energy content of PYP increases from 120 to 160 $kJ \cdot mol^{-1}$ upon formation of pR.[68,79] This means that about half the energy of an absorbed photon is stored in the holoprotein at this point (a photon with a wavelength of 446 nm has an energy content of 268 $kJ \cdot mol^{-1}$). This amount of energy should then be enough to drive the remainder of the photocycle. This also implies that half the energy of the absorbed photon is lost in, for example, thermal relaxations. FTIR analysis of the cryotrapped intermediates in the first step of the photocycle suggests that there is very little structural difference between these intermediates.[76] Thus, small movements induced by thermal relaxation may dictate the exact isomerization path of the chromophore.

47.4.3 Signaling State Formation

Much of the early work on the photocycle of PYP assumed a simple three-state photocycle model, that is, with the pG, pR, and pB state only. In these models, formation of the signaling state, that is, pB (from pR), has been described both as a kinetically biexponential and as a monoexponential event.

Actually, the first detailed analysis of the photocycle of PYP[50] postulated a photocycle containing an additional intermediate with similar spectral properties as pB, because of the observed biexponential kinetic character of pB formation. However, this model was refuted in a subsequent paper.[51] Later, the intermediate pB′ was introduced as an intermediate in the pR to pB photocycle step based on results obtained with FTIR spectroscopy.[55] A subsequent detailed laser-induced transient UV/Vis spectroscopic kinetic analysis of the photocycle confirmed the existence of this intermediate and showed it has spectroscopic properties very similar to those of pB.[64] Here, it was also revealed that the pB′ intermediate is in equilibrium with pR, which explains the previously observed biexponential character of the pR to pB photocycle step.[49,50]

47.4.3.1 Structural Relaxation of pR

After formation of pR, additional relaxation events occur in the protein.[80,81] Through the use of the transient grating and pulsed-laser photoacoustic methods, it was shown that a microsecond dynamic component exists during the lifetime of pR. This indicates that after the structural changes in and immediately around the chromophore are completed, additional structural changes occur in the protein, further away from the chromophore. Thus, pR can be decomposed into the intermediates pR_1 and pR_2. Though the transition from pR_1 to pR_2 initially was claimed to be spectrally silent, the transition presumably was already observed earlier in UV/Vis data.[49] However, as this transition contributed only very little to the total UV/Vis signal, no confident assignment could be made in those experiments. In a more recent analysis of UV/Vis data,[64] reaction kinetics were obtained that fit the pR_1 to pR_2 transition, observed via transient grating. Though the obtained spectra for both pR intermediates are very similar, pR_1 seems to have a slightly higher extinction coefficient than pR_2, whereas the λ_{max} values are indistinguishable.

47.4.3.2 Protonation Change upon pB′ Formation

One of the major events that have to occur in the transition from pR to pB is protonation of the chromophore. FITR measurements have shown that deprotonation of Glu46 and protonation of the chromophore are a single event, which is followed by structural change of the protein.[55] This interpretation led to the introduction of the pB′ intermediate, which then converts into the pB state. A photocycle model that included the pB′ intermediate was then used to analyze UV/Vis data in a study on the kinetic deuterium isotope effect in the photocycle of PYP.[64] From these analyses, it was evident that pR and pB′ exist in an equilibrium that shifts toward pB′ upon going to the extremes of pH (both low and high pH). The observed kinetic Deuterium isotope effect is in line with a proton transfer from Glu46 to the chromophore for the whole pH range that was investigated (pH 5–11). However, for the return reaction, the situation is more complex. Here, formation of pR from pB′ can occur via different routes, dependent on pH. The shift of the pR/pB′ equilibrium toward pB′, when going to the pH extremes, also explains the shift toward monoexponential behavior for the formation of pB at these latter pH values.

The UV/Vis spectroscopic properties of pB′ and pB are rather similar,[64] which explains why the first experimental evidence for the existence of this intermediate was obtained via FTIR measurements. The pB′ spectrum is most similar to the pB subspecies that dominates at low pH (see Figure 47.5). Incidentally, this is also the pB subspecies that shows the least structural change, and thus of all the pB subspecies presumably structurally resembles pB′ the most. However, pB′ typically transforms into either pR or the pB subspecies that dominates at medium pH. The latter has an absorption maximum blue shifted by 13 nm with respect to pB′.

47.4.3.3 Structural Change upon pB Formation

Another major event that occurs in the transition from pR to pB is structural change. From the strongly nonlinear Arrhenius kinetics of the pG recovery reaction,[52] it was concluded that the signaling state of PYP is at—least partly—unfolded. In a mutant with the first 25 N-terminal amino acids removed,[82] the deviation from normal Arrhenius behavior was largely gone. It therefore seems that the N-terminal

region of PYP is largely responsible for the large structural change upon formation of the signaling state. Several other methods, like, for example, CD, NMR, fluorescence, and FTIR spectroscopy have confirmed this partial unfolding.

Hydrogen-Deuterium exchange measurements in particular have contributed to the insight into the structural change that is at the basis of signaling state formation in PYP. Whereas a buried hydrogen atom may take days to exchange, an exposed hydrogen atom may be exchanged within seconds. PYP contains 235 potentially exchangeable hydrogen atoms, 42 of which are from (de)protonatable groups. In a study with electrospray ionization mass spectrometry,[83] it was shown that in the dark, less hydrogen atoms were exchanged for deuterium atoms compared to an experiment performed in the presence of light. Also, in apoPYP 29 potential exchange sites resist exchange, which can be interpreted as that 29 or less of the 42 (de)protonatable groups are deprotonated. Additionally, it may mean that apoPYP has a certain degree of structure, depending on the actual number of deprotonated groups. The light-induced hydrogen/deuterium exchange was independently confirmed using FTIR difference spectroscopy.[83] Though these experiments show that there is a difference between the ground and signaling state of PYP with respect to hydrogen/deuterium exchange protection, they do not pinpoint the areas of the protein responsible for the observed differences. However, it is possible to obtain more specific information with NMR spectroscopy.[84] Though it was only possible to obtain specific information for the backbone amide exchangeable hydrogen of 51 residues, 14 of these showed a significant change in protection (i.e., resistance against exchange) upon formation of the signaling state pB, that is, only two less than the number predicted by mass spectrometry, which was not limited to the backbone amide hydrogen atoms. The residues with the most significant loss in protection are Phe28, Glu46, and Thr70. The latter two are close to the chromophore, whereas Phe28 is close to Glu46. These results have been confirmed and extended by Brudler et al.[85]

In a solution NMR study of the pB intermediate, it was shown that pB exhibits structural and dynamic disorder with respect to the ground state.[86] Interestingly, a subsequent NMR study of pB_{dark} formation[84] showed that pB_{dark} and the photocycle intermediate pB are very similar. It was also made clear that upon formation of pB_{dark}, the protein can be divided into three parts, a relatively stable core (residues 32–41, 80–94, and 113–122) and two areas that display large structural perturbation: the N-terminus (residues 6–18 and 26–29) and the area around the chromophore-binding site (residues 42–58, 69–78, and 95–100). As discussed earlier, the structural perturbations of the N-terminus are largely responsible for the observed non-Arrhenius behavior of the photocycle kinetics. Furthermore, the NMR data suggest that the pB intermediate is a mixture of structurally perturbed forms and a form structurally similar to the ground state, or more specifically, similar to the pB crystal structure.[48]

The trigger for the major structural change upon formation of pB is the formation of a buried negative charge on Glu46 when it donates its proton to the chromophore.[55] After formation of pB′, the buried negative charge, initially located on the chromophore, is centered on Glu46. On the chromophore, the negative charge can be effectively neutralized by delocalization of the charge and the hydrogen-bonding network of the chromophore. On Glu46, the buried negative charge cannot be effectively neutralized. This leads to a stress situation within the protein, which can be relieved via several routes. One is return to the pR state, reflecting the reversible nature of pB′ formation (see earlier paragraphs). Other routes lead to the formation of pB. The extent of the structural change upon formation of the pB intermediate depends then on the route taken. One route to relieve the buried negative charge is to expose it to solvent, which requires structural change of the protein. Another route is to protonate the Glu46, but not via the chromophore since that would lead to the reformation of pR. Once Glu46 is protonated, the stress situation is relieved and a large structural change is no longer necessary. Since protonation changes play a key role, it is to be expected that these events are pH dependent. Thus, depending on the pH, one route may dominate over the other. In fact, a pH dependence of the extent of structural change has been observed to coincide with protonation of Glu46 (J. Hendriks and A. Xie et al., unpublished results). Of course, both routes to pB mentioned here assume that pB′ is formed as an intermediate. It is also possible that a direct, or alternative, route from pR to pB exists. In such a route, Glu46 may stay protonated, that is, it does not donate a proton to the chromophore. The chromophore then becomes protonated only after

exposure to the solvent, or via another residue (e.g., Tyr42). Such a route would require little structural change of the protein and might be preferred in the crystal environment. All mentioned routes are possibilities, and depending on the conditions one particular route may dominate. The key factor in all these routes is what happens to the protonation state of both Glu46 and the chromophore. In fact, it has been shown that for the Glu46Gln mutant in solution, the structural change upon formation of pB is significantly less compared to the wild-type protein.[55] In this mutant residue, 46 no longer can donate a proton to the chromophore, and thus, no buried negative charge is formed on residue 46, and hence less driving force for structural change is generated. Though residue 46 plays an essential role in the amount of structural change that takes place, other residues may also have influence. For example, His108 also has influence on the extent of structural change as it has been shown that the mutant His108Phe also exhibits less structural change compared to the wild-type protein.[87]

The pH dependence of structural change has also been shown to exist via transient probe binding,[88] showing less structural change at low pH. Together with experiments monitoring the pH-dependent net proton uptake/release of PYP during pB formation[89] and pH-dependent FTIR results (J. Hendriks and A. Xie et al., unpublished results), this leads to the conclusion that the pK_a of Glu46 in pB is 5.5, so that above pH 5.5 much more structural change occurs than below.

The structural change upon formation of pB is typically related to changes in the N-terminus. However, significant structural changes also occur on the other side of the central β-sheet, around the chromophore pocket. This was nicely demonstrated by NMR measurements on a mutant of PYP lacking the N-terminus.[54] Furthermore, these latter measurements showed that the N-terminus most likely is involved in stabilizing the helix containing residues Asn43 to Thr50 (helix α3). These NMR results were independently corroborated via parallel tempering simulations initiated to simulate the formation of pB.[53] Further simulations showed the importance of helix α3 for the successful recovery of the ground state.[90] These pioneering steps in trying to simulate events that take place on a millisecond timescale have since then been improved to the point that the mechanisms underlying the transition from pB′ to pB can be deduced.[91] Here, a salt-bridge between Asp20 and Lys55 appears to play an important role. As such, the effect of salt (or ionic strength) on the PYP photocycle may be linked to this salt-bridge.

47.4.4 Ground-State Recovery

Recovery of the ground state can be achieved either spontaneously in the dark or light induced via an accelerated path. In the latter, a photon absorbed by pB′ and/or pB photoisomerizes the chromophore, thereby allowing a 1000-fold increase in the rate of recovery, with respect to the rate of recovery in the dark.[92] The existence of this branching reaction can influence data in the presence of light that can be absorbed by any of the pB intermediates. This may allow recovery kinetics to appear faster than they really are in the absence of this light.[93] Such accelerated recovery with visible light can be exploited in the study of the very slow recovery variants, like M100A.

During the thermal recovery of the ground state of PYP, several events have to take place simultaneously. The chromophore has to reisomerize to the *trans* form; the protonation state of several residues and the chromophore have to be changed, and the protein needs to return to its original fold. Though these are seemingly distinct steps, until recently, they often were assumed to occur concertedly. However, it had already been suggested that prior to isomerization, the chromophore must first be deprotonated, and thus an intermediate must exist between pB and pG.[94] Confirmation of the existence of this intermediate was obtained in measurements of the kinetic deuterium isotope effect.[64] Here, it was shown that deprotonation of the chromophore occurs prior to its isomerization. Though deprotonation of the chromophore aids the reisomerization of the chromophore tremendously,[95] this reisomerization is still a rate-controlling step, in which the protein fold likely plays a crucial part. Only recently, the existence of such an intermediate was actually shown experimentally, in an extensive pH-dependent study on PYP recovery.[62] The new intermediate was named pG′ and appears to have a UV/Vis spectrum highly similar to pG, indicating that the chromophore is already deprotonated in this photocycle intermediate, as

suggested before. It also explains why pG′ was not noticed before. The pG′ intermediate is characterized by a deprotonated chromophore and a folding state that allows reisomerization of the chromophore. This latter characteristic is important, as this intermediate has an absorption spectrum that is similar to that of the ground state of PYP and not one that is similar to the pB intermediate at high pH, which also has a deprotonated chromophore but has its absorption maximum around 430 nm.[64,89]

Several studies have been done to study refolding of PYP. In a study utilizing the denaturants urea and guanidinium·HCl, refolding was studied in unfolded ground-state protein and in the unfolded signaling state.[96] The major difference between these two denatured forms of the protein is the isomerization state of the chromophore. Where refolding from the denatured ground state is a monoexponential event, refolding from the denatured signaling state is biexponential. Here, the fast component is identical to refolding from the denatured ground state, and the slow exponent has a rate similar to the photocycle ground-state recovery rate under similar conditions. This indicates that after the signaling state renatures, it recovers to the ground state through the regular photocycle pathway. Interestingly, extrapolation of the obtained refolding kinetics in the absence of denaturant shows close to a 1000-fold faster rate for refolding for the protein with the chromophore in the *trans* state compared to protein with the chromophore in the *cis* state. This is similar to the difference in rate observed between the ground-state recovery in the dark and photo activated ground-state recovery via the branching reaction.[92]

Similar experiments with the acid denatured state of PYP were also performed,[97] and similar results were obtained. Refolding from the acid denatured state with the chromophore in the *trans* state, that is, pB_{dark}, is 3–5 orders of magnitude faster with the chromophore in the *cis* state. Interestingly, it was shown with temperature denaturation that in the acid denatured state, the chromophore is in the *cis* state, the protein is more stable than when the chromophore is in the *trans* state. Furthermore, it was shown that the acid denatured state with the chromophore in the *cis* state is very similar to the photocycle intermediate pB.

For a few mutants of PYP, a dramatic decrease in recovery rate has been observed, that is, Glu46Asp,[98] Met100Ala,[99] and Met100Leu.[100] This indicates that Glu46 and Met100 are important for facilitating recovery. Met100 is important for the reisomerization of the chromophore, as indicated by the dramatic increase in rate of recovery when the chromophore is photochemically reisomerized in the Met100Ala mutant.[99] In a recent study, it was argued that the electron-donating character of the residue at position 100 influences the rate of recovery through interaction with another residue, most likely Arg52.[101] With the Glu46Asp mutant, such a dramatic increase in recovery rate was not observed upon photochemical reisomerization of the chromophore.[98] As such it is likely that Glu46 is important for refolding of the protein, though it may still be involved in dark reisomerization of the chromophore.

47.5 Future Perspective

Soon after its discovery, 26 years ago, PYP developed into a model system for biophysical research on protein structure and function. In retrospect, this development came quite rapidly after the initial confusion about its spatial structure. Its excellent physicochemical and photochemical stability, however, made it to an excellent tool with the introduction and calibration of new biophysical methodology, like various forms of ultrafast spectroscopy, time-resolved diffraction experiments, small-angle scattering, etc. Conversely, the application of this myriad of techniques has provided almost unprecedented insight into the dynamical and structural aspects of its function.

Nevertheless, these experiments are still ongoing and promise to provide even more intricate detail. A surprising aspect herein is that we know most of the initial and the final stages of the processes that underlie the functional photocycle of the protein. A key step in the central part of this cycle, the transfer of a proton from Glu46 to the chromophore, is still poorly understood with respect to its dynamics and the structure of the protein from which this transfer takes place in solution. Not even the extensive computational efforts, that have rationalized many aspects of the functioning of PYP, have provided this insight.

With respect to the biological aspects of functioning of PYP, little progress has been made beyond the initial studies of phototaxis in *E. halophila*. This is partly due to the difficulty of applying the methodology of molecular genetic to extremophilic bacteria. Nevertheless, an additional factor has been the rather restricted range of organisms in which a representative of the Xanthopsin family was discovered. In this light, the expansion of the Xanthopsin family as described in this review is very exciting. Furthermore, this recent expansion implies that the range of output domains to which PYP appears to be able to couple has increased to the extent that now also domain of unknown function (DUF) domains are included. This even more suggests that this photoreceptor family may have a role in biofilm formation.

Procedures for heterologous expression of the holoprotein form of PYP have been well-established. So far, applications of a Xanthopsin member in the exciting field of optogenetics have not yet been reported. But who knows what the future has in store.

References

1. Meyer, T. E., Isolation and characterization of soluble cytochromes, ferredoxins and other chromophoric proteins from the halophilic phototrophic bacterium *Ectothiorhodospira halophila*, *Biochimica et Biophysica Acta* 806 (1), 175–183, 1985.
2. McRee, D. E., Meyer, T. E., Cusanovich, M. A., Parge, H. E., and Getzoff, E. D., Crystallographic characterization of a photoactive yellow protein with photochemistry similar to sensory rhodopsin, *The Journal of Biological Chemistry* 261 (29), 13850–13851, 1986.
3. Imhoff, J. F. and Suling, J., The phylogenetic relationship among *Ectothiorhodospiraceae*: A reevaluation of their taxonomy on the basis of 16S rDNA analyses, *Archives of Microbiology* 165 (2), 106–113, 1996.
4. Raymond, J. C. and Sistrom, W. R., The isolation and preliminary characterization of a halophilic photosynthetic bacterium, *Archiv für Mikrobiologie* 59 (1), 255–268, 1967.
5. Raymond, J. C. and Sistrom, W. R., *Ectothiorhodospira halophila*: A new species of the genus *Ectothiorhodospira*, *Archiv für Mikrobiologie* 69 (2), 121–126, 1969.
6. Imhoff, J. F., Hashwa, F., and Trüper, H. G., Isolation of extremely halophilic bacteria from the alkaline Wadi Natrun, Egypt, *Archives of Hydrobiology* 84, 381–388, 1978.
7. Sprenger, W. W., Hoff, W. D., Armitage, J. P., and Hellingwerf, K. J., The eubacterium *Ectothiorhodospira halophila* is negatively phototactic, with a wavelength dependence that fits the absorption spectrum of the photoactive yellow protein, *Journal of Bacteriology* 175 (10), 3096–3104, 1993.
8. Balashov, S. P., Photoreactions of the photointermediates of bacteriorhodopsin, *Israel Journal of Chemistry* 35 (3–4), 415–428, 1995.
9. Hoff, W. D., Jung, K. H., and Spudich, J. L., Molecular mechanism of photosignaling by archaeal sensory rhodopsins, *Annual Review of Biophysics and Biomolecular Structure* 26, 223–258, 1997.
10. Spudich, J. L., Yang, C. S., Jung, K. H., and Spudich, E. N., Retinylidene proteins: Structures and functions from archaea to humans, *Annual Review of Cell and Developmental Biology* 16, 365–392, 2000.
11. Klare, J. P., Chizhov, I., and Engelhard, M., Microbial rhodopsins: Scaffolds for ion pumps, channels, and sensors, *Results and Problems in Cell Differentiation* 45, 73–122, 2008.
12. Sharma, A. K., Spudich, J. L., and Doolittle, W. F., Microbial rhodopsins: Functional versatility and genetic mobility, *Trends in Microbiology* 14 (11), 463–469, 2006.
13. Kort, R., Hoff, W. D., Van West, M., Kroon, A. R., Hoffer, S. M., Vlieg, K. H., Crielaand, W., Van Beeumen, J. J., and Hellingwerf, K. J., The xanthopsins: A new family of eubacterial blue-light photoreceptors, *The EMBO Journal* 15 (13), 3209–3218, 1996.
14. Meyer, T. E., Fitch, J. C., Bartsch, R. G., Tollin, G., and Cusanovich, M. A., Soluble cytochromes and a photoactive yellow protein isolated from the moderately halophilic purple phototrophic bacterium, *Rhodospirillum salexigens*, *Biochimica et Biophysica Acta* 1016 (3), 364–370, 1990.

15. Koh, M., Van Driessche, G., Samyn, B., Hoff, W. D., Meyer, T. E., Cusanovich, M. A., and Van Beeumen, J. J., Sequence evidence for strong conservation of the photoactive yellow proteins from the halophilic phototrophic bacteria *Chromatium salexigens* and *Rhodospirillum salexigens*, *Biochemistry* 35 (8), 2526–2534, 1996.
16. Jiang, Z. and Bauer, C. E., Genetic characterization of photoactive yellow protein from *Rhodobacter capsulatus*, 1998, GenBank, Accession No. AF064095.
17. Kyndt, J. A., Meyer, T. E., and Cusanovich, M. A., Photoactive yellow protein, bacteriophytochrome, and sensory rhodopsin in purple phototrophic bacteria, *Photochemical & Photobiological Sciences* 3 (6), 519–530, 2004.
18. Kumauchi, M., Hara, M. T., Stalcup, P., Xie, A. H., and Hoff, W. D., Identification of six new photoactive yellow proteins—Diversity and structure-function relationships in a bacterial blue light photoreceptor, *Photochemistry and Photobiology* 84 (4), 956–969, 2008.
19. Altschul, S. F., Gish, W., Miller, W., Myers, E. W., and Lipman, D. J., Basic local alignment search tool, *Journal of Molecular Biology* 215 (3), 403–410, 1990.
20. Waterhouse, A. M., Procter, J. B., Martin, D. M. A., Clamp, M., and Barton, G. J., Jalview version 2—A multiple sequence alignment editor and analysis workbench, *Bioinformatics* 25 (9), 1189–1191, 2009.
21. Thompson, J. D., Higgins, D. G., and Gibson, T. J., CLUSTAL W: Improving the sensitivity of progressive multiple sequence alignment through sequence weighting, position-specific gap penalties and weight matrix choice, *Nucleic Acids Research* 22 (22), 4673–4680, 1994.
22. Kort, R., Crielaard, W., Spudich, J. L., and Hellingwerf, K. J., Color-sensitive motility and methanol release responses in *Rhodobacter sphaeroides*, *Journal of Bacteriology* 182 (11), 3017–3021, 2000.
23. Jiang, Z., Swem, L. R., Rushing, B. G., Devanathan, S., Tollin, G., and Bauer, C. E., Bacterial photoreceptor with similarity to photoactive yellow protein and plant phytochromes, *Science* 285 (5426), 406–409, 1999.
24. Nambu, J. R., Lewis, J. O., Wharton, K. A., Jr., and Crews, S. T., The Drosophila single-minded gene encodes a helix-loop-helix protein that acts as a master regulator of CNS midline development, *Cell* 67 (6), 1157–1167, 1991.
25. Finn, R. D., Mistry, J., Schuster-Bockler, B., Griffiths-Jones, S., Hollich, V., Lassmann, T., Moxon, S., Marshall, M., Khanna, A., Durbin, R., Eddy, S. R., Sonnhammer, E. L. L., and Bateman, A., Pfam: Clans, web tools and services, *Nucleic Acids Research* 34, D247–D251, 2006.
26. Pellequer, J. L., Wager-Smith, K. A., Kay, S. A., and Getzoff, E. D., Photoactive yellow protein: A structural prototype for the three-dimensional fold of the PAS domain superfamily, *Proceedings of the National Academy of Sciences of the United States of America* 95 (11), 5884–5890, 1998.
27. Van Beeumen, J. J., Devreese, B. V., Van Bun, S. M., Hoff, W. D., Hellingwerf, K. J., Meyer, T. E., McRee, D. E., and Cusanovich, M. A., Primary structure of a photoactive yellow protein from the phototrophic bacterium *Ectothiorhodospira halophila*, with evidence for the mass and the binding site of the chromophore, *Protein Science* 2 (7), 1114–1125, 1993.
28. Borgstahl, G. E., Williams, D. R., and Getzoff, E. D., 1.4 Å structure of photoactive yellow protein, a cytosolic photoreceptor: Unusual fold, active site, and chromophore, *Biochemistry* 34 (19), 6278–6287, 1995.
29. Düx, P., Rubinstenn, G., Vuister, G. W., Boelens, R., Mulder, F. A., Hard, K., Hoff, W. D., Kroon, A. R., Crielaard, W., Hellingwerf, K. J., and Kaptein, R., Solution structure and backbone dynamics of the photoactive yellow protein, *Biochemistry* 37 (37), 12689–12699, 1998.
30. Getzoff, E. D., Gutwin, K. N., and Genick, U. K., Anticipatory active-site motions and chromophore distortion prime photoreceptor PYP for light activation, *Nature Structural Biology* 10 (8), 663–668, 2003.
31. Yamaguchi, S., Kamikubo, H., Kurihara, K., Kuroki, R., Niimura, N., Shimizu, N., Yamazaki, Y., and Kataoka, M., Low-barrier hydrogen bond in photoactive yellow protein, *Proceedings of the National Academy of Sciences of the United States of America* 106 (2), 440–444, 2009.
32. Kort, R., Hellingwerf, K. J., and Ravelli, R. B. G., Initial events in the photocycle of photoactive yellow protein, *The Journal of Biological Chemistry* 279 (25), 26417–26424, 2004.

33. Weaver, T. M., The pi-helix translates structure into function, *Protein Science* 9 (1), 201–206, 2000.
34. Hoff, W. D., Dux, P., Hard, K., Devreese, B., Nugteren-Roodzant, I. M., Crielaard, W., Boelens, R., Kaptein, R., van Beeumen, J., and Hellingwerf, K. J., Thiol ester-linked p-coumaric acid as a new photoactive prosthetic group in a protein with rhodopsin-like photochemistry, *Biochemistry* 33 (47), 13959–13962, 1994.
35. Koradi, R., Billeter, M., and Wuthrich, K., MOLMOL: A program for display and analysis of macromolecular structures, *Journal of Molecular Graphics* 14 (1), 51–55, 1996.
36. Berman, H. M., Westbrook, J., Feng, Z., Gilliland, G., Bhat, T. N., Weissig, H., Shindyalov, I. N., and Bourne, P. E., The protein data bank, *Nucleic Acids Research* 28 (1), 235–242, 2000.
37. Memmi, S., Kyndt, J., Meyer, T., Devreese, B., Cusanovich, M., and Van Beeumen, J., Photoactive yellow protein from the halophilic bacterium *Salinibacter ruber*, *Biochemistry* 47 (7), 2014–2024, 2008.
38. Hellingwerf, K. J., Hoff, W. D., and Crielaard, W., Photobiology of microorganisms: How photosensors catch a photon to initialize signalling, *Molecular Microbiology* 21 (4), 683–693, 1996.
39. Baca, M., Borgstahl, G. E., Boissinot, M., Burke, P. M., Williams, D. R., Slater, K. A., and Getzoff, E. D., Complete chemical structure of photoactive yellow protein: Novel thioester-linked 4-hydroxycinnamyl chromophore and photocycle chemistry, *Biochemistry* 33 (48), 14369–14377, 1994.
40. Kim, M., Mathies, R. A., Hoff, W. D., and Hellingwerf, K. J., Resonance Raman evidence that the thioester-linked 4-hydroxycinnamyl chromophore of photoactive yellow protein is deprotonated, *Biochemistry* 34 (39), 12669–12672, 1995.
41. Yoda, M., Houjou, H., Inoue, Y., and Sakurai, M., Spectral tuning of photoactive yellow protein. Theoretical and experimental analysis of medium effects on the absorption spectrum of the chromophore, *Journal of Physical Chemistry B* 105 (40), 9887–9895, 2001.
42. Sigala, P. A., Tsuchida, M. A., and Herschlag, D., Hydrogen bond dynamics in the active site of photoactive yellow protein, *Proceedings of the National Academy of Sciences of the United States of America* 106 (23), 9232–9237, 2009.
43. Brzezinski, B. and Zundel, G., Intramolecular easily polarizable charged and non-charged hydrogen-bonds—IR continua and hydrogen-bond length, *Journal of Molecular Structure* 72 (March), 9–15, 1981.
44. Scrutton, N. S. and Raine, A. R., Cation-pi bonding and amino-aromatic interactions in the biomolecular recognition of substituted ammonium ligands, *The Biochemical Journal* 319 (Pt 1), 1–8, 1996.
45. Groenhof, G., Schafer, L. V., Boggio-Pasqua, M., Grubmuller, H., and Robb, M. A., Arginine52 controls the photoisomerization process in photoactive yellow protein, *Journal of the American Chemical Society* 130 (11), 3250–3251, 2008.
46. van Aalten, D. M., Hoff, W. D., Findlay, J. B., Crielaard, W., and Hellingwerf, K. J., Concerted motions in the photoactive yellow protein, *Protein Engineering* 11 (10), 873–879, 1998.
47. van Aalten, D. M. F., Crielaard, W., Hellingwerf, K. J., and Joshua-Tor, L., Conformational substates in different crystal forms of the photoactive yellow protein—Correlation with theoretical and experimental flexibility, *Protein Science* 9 (1), 64–72, 2000.
48. Genick, U. K., Borgstahl, G. E., Ng, K., Ren, Z., Pradervand, C., Burke, P. M., Srajer, V., Teng, T. Y., Schildkamp, W., McRee, D. E., Moffat, K., and Getzoff, E. D., Structure of a protein photocycle intermediate by millisecond time-resolved crystallography, *Science* 275 (5305), 1471–1475, 1997.
49. Hoff, W. D., van Stokkum, I. H., van Ramesdonk, H. J., van Brederode, M. E., Brouwer, A. M., Fitch, J. C., Meyer, T. E., van Grondelle, R., and Hellingwerf, K. J., Measurement and global analysis of the absorbance changes in the photocycle of the photoactive yellow protein from *Ectothiorhodospira halophila*, *Biophysical Journal* 67 (4), 1691–1705, 1994.
50. Meyer, T. E., Yakali, E., Cusanovich, M. A., and Tollin, G., Properties of a water-soluble, yellow protein isolated from a halophilic phototrophic bacterium that has photochemical activity analogous to sensory rhodopsin, *Biochemistry* 26 (2), 418–423, 1987.

51. Meyer, T. E., Tollin, G., Hazzard, J. H., and Cusanovich, M. A., Photoactive yellow protein from the purple phototrophic bacterium, *Ectothiorhodospira halophila*. Quantum yield of photobleaching and effects of temperature, alcohols, glycerol, and sucrose on kinetics of photobleaching and recovery, *Biophysical Journal* 56 (3), 559–564, 1989.
52. van Brederode, M. E., Hoff, W. D., Van Stokkum, I. H., Groot, M. L., and Hellingwerf, K. J., Protein folding thermodynamics applied to the photocycle of the photoactive yellow protein, *Biophysical Journal* 71 (1), 365–380, 1996.
53. Vreede, J., Crielaard, W., Hellingwerf, K. J., and Bolhuis, P. G., Predicting the signaling state of photoactive yellow protein, *Biophysical Journal* 88 (5), 3525–3535, 2005.
54. Bernard, C., Houben, K., Derix, N. M., Marks, D., van der Horst, M. A., Hellingwerf, K. J., Boelens, R., Kaptein, R., and van Nuland, N. A. J., The solution structure of a transient photoreceptor intermediate: Delta 25 photoactive yellow protein, *Structure* 13 (7), 953–962, 2005.
55. Xie, A., Kelemen, L., Hendriks, J., White, B. J., Hellingwerf, K. J., and Hoff, W. D., Formation of a new buried charge drives a large-amplitude protein quake in photoreceptor activation, *Biochemistry* 40 (6), 1510–1517, 2001.
56. Yeremenko, S., van Stokkum, I. H. M., Moffat, K., and Hellingwerf, K. J., Influence of the crystalline state on photoinduced dynamics of photoactive yellow protein studied by ultraviolet-visible transient absorption spectroscopy, *Biophysical Journal* 90 (11), 4224–4235, 2006.
57. Hoff, W. D., Sprenger, W. W., Postma, P. W., Meyer, T. E., Veenhuis, M., Leguijt, T., and Hellingwerf, K. J., The photoactive yellow protein from *Ectothiorhodospira halophila* as studied with a highly specific polyclonal antiserum: (Intra)cellular localization, regulation of expression, and taxonomic distribution of cross-reacting proteins, *Journal of Bacteriology* 176 (13), 3920–3927, 1994.
58. Hoff, W. D., Matthijs, H. C. P., Schubert, H., Crielaard, W., and Hellingwerf, K. J., Rhodopsin(s) in eubacteria, *Biophysical Chemistry* 56 (1–2), 193–199, 1995.
59. Imamoto, Y., Kataoka, M., and Tokunaga, F., Photoreaction cycle of photoactive yellow protein from *Ectothiorhodospira halophila* studied by low-temperature spectroscopy, *Biochemistry* 35 (45), 14047–14053, 1996.
60. Borucki, B., Kyndt, J. A., Joshi, C. P., Otto, H., Meyer, T. E., Cusanovich, M. A., and Heyn, M. P., Effect of salt and pH on the activation of photoactive yellow protein and gateway mutants Y98Q and Y98F, *Biochemistry* 44 (42), 13650–13663, 2005.
61. Xie, A., Hoff, W. D., Kroon, A. R., and Hellingwerf, K. J., Glu46 donates a proton to the 4-hydroxycinnamate anion chromophore during the photocycle of photoactive yellow protein, *Biochemistry* 35 (47), 14671–14678, 1996.
62. Hendriks, J. and Hellingwerf, K. J., pH dependence of the photoactive yellow protein photocycle recovery reaction reveals a new late photocycle intermediate with a deprotonated chromophore, *The Journal of Biological Chemistry* 284 (8), 5277–5288, 2009.
63. Hoff, W. D., Kwa, S. L. S., van Grondelle, R., and Hellingwerf, K. J., Low temperature absorbance and fluorescence spectroscopy of the photoactive yellow protein from *Ectothiorhodospira halophila*, *Photochemistry and Photobiology* 56, 529–539, 1992.
64. Hendriks, J., van Stokkum, I. H. M., and Hellingwerf, K. J., Deuterium isotope effects in the photocycle transitions of the photoactive yellow protein, *Biophysical Journal* 84 (2), 1180–1191, 2003.
65. Genick, U. K., Devanathan, S., Meyer, T. E., Canestrelli, I. L., Williams, E., Cusanovich, M. A., Tollin, G., and Getzoff, E. D., Active site mutants implicate key residues for control of color and light cycle kinetics of photoactive yellow protein, *Biochemistry* 36 (1), 8–14, 1997.
66. Gensch, T., Hellingwerf, K. J., Braslavsky, S. E., and Schaffner, K., Photoequilibrium in the primary steps of the photoreceptors phytochrome A and photoactive yellow protein, *Journal of Physical Chemistry A* 102 (28), 5398–5405, 1998.
67. Spudich, E. N. and Spudich, J. L., The photochemical reactions of sensory rhodopsin I are altered by its transducer, *The Journal of Biological Chemistry* 268 (22), 16095–16097, 1993.

68. van Brederode, M. E., Gensch, T., Hoff, W. D., Hellingwerf, K. J., and Braslavsky, S. E., Photoinduced volume change and energy storage associated with the early transformations of the photoactive yellow protein from *Ectothiorhodospira halophila*, *Biophysical Journal* 68 (3), 1101–1109, 1995.
69. Groot, M. L., van Wilderen, L., Larsen, D. S., van der Horst, M. A., van Stokkum, I. H. M., Hellingwerf, K. J., and van Grondelle, R., Initial steps of signal generation in photoactive yellow protein revealed with femtosecond mid-infrared spectroscopy, *Biochemistry* 42 (34), 10054–10059, 2003.
70. Groenhof, G., Lensink, M. F., Berendsen, H. J., and Mark, A. E., Signal transduction in the photoactive yellow protein. II. Proton transfer initiates conformational changes, *Proteins: Structure, Function, and Genetics* 48 (2), 212–219, 2002.
71. Larsen, D. S., van Stokkum, I. H. M., Vengris, M., van der Horst, M. A., de Weerd, F. L., Hellingwerf, K. J., and van Grondelle, R., Incoherent manipulation of the photoactive yellow protein photocycle with dispersed pump-dump-probe spectroscopy, *Biophysical Journal* 87 (3), 1858–1872, 2004.
72. van Wilderen, L., Van der Horst, M. A., van Stokkum, I. H. M., Hellingwerf, K. J., van Grondelle, R., and Groot, M. L., Ultrafast infrared spectroscopy reveals a key step for successful entry into the photocycle for photoactive yellow protein, *Proceedings of the National Academy of Sciences of the United States of America* 103 (41), 15050–15055, 2006.
73. Premvardhan, L. L., van der Horst, M. A., Hellingwerf, K. J., and van Grondelle, R., Stark spectroscopy on photoactive yellow protein, E46Q, and a nonisomerizing derivative, probes photo-induced charge motion, *Biophysical Journal* 84 (5), 3226–3239, 2003.
74. Rettig, W., Photoinduced charge separation via twisted intramolecular charge-transfer states. In *Electron Transfer I.* Springer-Verlag, Berlin, Germany, Vol. 33, 1994, pp. 253–299.
75. Genick, U. K., Soltis, S. M., Kuhn, P., Canestrelli, I. L., and Getzoff, E. D., Structure at 0.85 Å resolution of an early protein photocycle intermediate, *Nature* 392 (6672), 206–209, 1998.
76. Imamoto, Y., Shirahige, Y., Tokunaga, F., Kinoshita, T., Yoshihara, K., and Kataoka, M., Low-temperature Fourier transform infrared spectroscopy of photoactive yellow protein, *Biochemistry* 40 (30), 8997–9004, 2001.
77. Ren, Z., Perman, B., Srajer, V., Teng, T. Y., Pradervand, C., Bourgeois, D., Schotte, F., Ursby, T., Kort, R., Wulff, M., and Moffat, K., A molecular movie at 1.8 Å resolution displays the photocycle of photoactive yellow protein, a eubacterial blue-light receptor, from nanoseconds to seconds, *Biochemistry* 40 (46), 13788–13801, 2001.
78. Brudler, R., Rammelsberg, R., Woo, T. T., Getzoff, E. D., and Gerwert, K., Structure of the I1 early intermediate of photoactive yellow protein by FTIR spectroscopy, *Nature Structural Biology* 8 (3), 265–270, 2001.
79. Takeshita, K., Hirota, N., and Terazima, M., Enthalpy changes and reaction volumes of photoisomerization reactions in solution: Azobenzene and p-coumaric acid, *Journal of Photochemistry and Photobiology A: Chemistry* 134 (1–2), 103–109, 2000.
80. Takeshita, K., Imamoto, Y., Kataoka, M., Mihara, K., Tokunaga, F., and Terazima, M., Structural change of site-directed mutants of PYP: New dynamics during pR state, *Biophysical Journal* 83 (3), 1567–1577, 2002.
81. Takeshita, K., Imamoto, Y., Kataoka, M., Tokunaga, F., and Terazima, M., Thermodynamic and transport properties of intermediate states of the photocyclic reaction of photoactive yellow protein, *Biochemistry* 41 (9), 3037–3048, 2002.
82. van der Horst, M. A., van Stokkum, I. H., Crielaard, W., and Hellingwerf, K. J., The role of the N-terminal domain of photoactive yellow protein in the transient partial unfolding during signalling state formation, *FEBS Letters* 497 (1), 26–30, 2001.
83. Hoff, W. D., Xie, A., Van Stokkum, I. H., Tang, X. J., Gural, J., Kroon, A. R., and Hellingwerf, K. J., Global conformational changes upon receptor stimulation in photoactive yellow protein, *Biochemistry* 38 (3), 1009–1017, 1999.
84. Craven, C. J., Derix, N. M., Hendriks, J., Boelens, R., Hellingwerf, K. J., and Kaptein, R., Probing the nature of the blue-shifted intermediate of photoactive yellow protein in solation by NMR: Hydrogen–deuterium exchange data and pH studies, *Biochemistry* 39 (47), 14392–14399, 2000.

85. Brudler, R., Gessner, C. R., Li, S., Tyndall, S., Getzoff, E. D., and Woods, V. L., PAS domain allostery and light-induced conformational changes in photoactive yellow protein upon I-2 intermediate formation, probed with enhanced hydrogen/deuterium exchange mass spectrometry, *Journal of Molecular Biology* 363 (1), 148–160, 2006.
86. Rubinstenn, G., Vuister, G. W., Mulder, F. A., Dux, P. E., Boelens, R., Hellingwerf, K. J., and Kaptein, R., Structural and dynamic changes of photoactive yellow protein during its photocycle in solution, *Nature Structural Biology* 5 (7), 568–570, 1998.
87. Kandori, H., Iwata, T., Hendriks, J., Maeda, A., and Hellingwerf, K. J., Water structural changes involved in the activation process of photoactive yellow protein, *Biochemistry* 39 (27), 7902–7909, 2000.
88. Hendriks, J., Gensch, T., Hviid, L., van Der Horst, M. A., Hellingwerf, K. J., and van Thor, J. J., Transient exposure of hydrophobic surface in the photoactive yellow protein monitored with Nile Red, *Biophysical Journal* 82 (3), 1632–1643, 2002.
89. Hendriks, J., Hoff, W. D., Crielaard, W., and Hellingwerf, K. J., Protonation/deprotonation reactions triggered by photoactivation of photoactive yellow protein from *Ectothiorhodospira halophila*, *The Journal of Biological Chemistry* 274 (25), 17655–17660, 1999.
90. Vreede, J., Hellingwerf, K. J., and Bolhuis, P. G., Helix formation is a dynamical bottleneck in the recovery reaction of photoactive yellow protein, *Proteins-Structure Function and Bioinformatics* 72 (1), 136–149, 2008.
91. Vreede, J., Juraszek, J., and Bolhuis, P. G., Predicting the reaction coordinates of millisecond light-induced conformational changes in photoactive yellow protein, *Proceedings of the National Academy of Sciences of the United States of America* 107 (6), 2397–2402, 2010.
92. Hendriks, J., van Stokkum, I. H., Crielaard, W., and Hellingwerf, K. J., Kinetics of and intermediates in a photocycle branching reaction of the photoactive yellow protein from *Ectothiorhodospira halophila*, *FEBS Letters* 458 (2), 252–256, 1999.
93. Miller, A., Leigeber, H., Hoff, W. D., and Hellingwerf, K. J., A light-dependent branching-reaction in the photocycle of the yellow protein from *Ectothiorhodospira-Halophila*, *Biochimica Et Biophysica Acta* 1141 (2–3), 190–196, 1993.
94. Demchuk, E., Genick, U. K., Woo, T. T., Getzoff, E. D., and Bashford, D., Protonation states and pH titration in the photocycle of photoactive yellow protein, *Biochemistry* 39 (5), 1100–1113, 2000.
95. Sergi, A., Gruning, M., Ferrario, M., and Buda, F., Density functional study of the photoactive yellow protein's chromophore, *Journal of Physical Chemistry B* 105 (19), 4386–4391, 2001.
96. Lee, B. C., Pandit, A., Croonquist, P. A., and Hoff, W. D., Folding and signaling share the same pathway in a photoreceptor, *Proceedings of the National Academy of Sciences of the United States of America* 98 (16), 9062–9067, 2001.
97. Lee, B. C., Croonquist, P. A., and Hoff, W. D., Mimic of photocycle by a protein folding reaction in photoactive yellow protein, *The Journal of Biological Chemistry* 276 (48), 44481–44487, 2001.
98. Devanathan, S., Brudler, R., Hessling, B., Woo, T. T., Gerwert, K., Getzoff, E. D., Cusanovich, M. A., and Tollin, G., Dual photoactive species in Glu46Asp and Glu46Ala mutants of photoactive yellow protein: A pH-driven color transition, *Biochemistry* 38 (41), 13766–13772, 1999.
99. Devanathan, S., Genick, U. K., Canestrelli, I. L., Meyer, T. E., Cusanovich, M. A., Getzoff, E. D., and Tollin, G., New insights into the photocycle of *Ectothiorhodospira halophila* photoactive yellow protein: Photorecovery of the long-lived photobleached intermediate in the Met100Ala mutant, *Biochemistry* 37 (33), 11563–11568, 1998.
100. Sasaki, J., Kumauchi, M., Hamada, N., Oka, T., and Tokunaga, F., Light-induced unfolding of photoactive yellow protein mutant M100L, *Biochemistry* 41 (6), 1915–1922, 2002.
101. Kumauchi, M., Hamada, N., Sasaki, J., and Tokunaga, F., A role of Methionine100 in facilitating PYP(M)-decay process in the photocycle of photoactive yellow protein, *The Journal of Biochemistry* 132 (2), 205–210, 2002.

48

Photomovements in Eukaryotic Microorganisms

Giovanni Checcucci
Istituto di Biofisica

Francesco Ghetti
Istituto di Biofisica

48.1 Introduction

Since solar radiation that reaches earth's surface can be both beneficial and harmful to living organisms, the large majority of them have developed mechanisms to perceive it as a signal to get information on the surrounding environment and behavioral strategies to expose themselves to radiation intensities suitable for their survival.

Also many motile microorganisms, despite their reduced dimensions and the absence of a neural system, use radiation as an environmental clue and are able to accumulate in areas where light is favorable to their viability and to disperse from areas where it is harmful. These behaviors mainly evolved because of the necessity of optimizing photochemical energy production or avoiding photoinduced damage; however, some microorganisms show photooriented movement for different reasons, since radiation may also be correlated with the presence of preys (e.g., photosynthetic algae)[1] or predators[2] or favor the possibility of reproducing.[3]

48.1.1 Historical Perspective

Despite the fact that unicellular organisms were described for the first time in 1675 by Anton van Leeuwenhoek, it is not until the beginning of the nineteenth century that the first references to a motile response elicited by a luminous stimulus in microorganisms appears in the scientific literature. In his paper of 1817, Treviranus describes the behavior of the algae *Draparnaldia glomerata* and *Ulothrix subtilis* under illumination, noting that they accumulate in the shadowy region of the vessel and interpreting this behavior as a mean to avoid harmful light irradiances.[4]

In the following years and especially at the end of the century, several authors began to study the effect of light on the movement of filamentous algae and cyanobacteria, debating on the mechanisms of photoorientation in microorganisms.[5,6] In those years, the foundations of the study of photomovement were laid, and it is interesting to note that many of the discussions initiated at that time have continued until few years ago, even if in a more modern way.

An important contribution to the study of photomovements was given by Engelmann, starting in 1879. Better known for his studies on the role of chlorophyll in photosynthesis, Engelmann was the first to describe the sudden change of motion of microorganisms when encountering a light-dark boundary (he named it "schreckbewegung," i.e., "phobic motion"), to correctly explain the mechanism of accumulation in a light trap in terms of single cell behavior, and to perform the first experiments on the localization of light sensitivity in particular areas of the cell body.[7]

At the beginning of the twentieth century, Jennings includes light among the stimuli affecting the behavior of microorganisms and reports the findings of several authors on the photomotile responses of unicellular organisms.[8] His hypotheses and suggestions, like those on the mechanisms of reaction in *Euglena* sp. later supported by Mast who repeated his experiments, are the basis of the modern research on photomovements.[9] The fact that the discoveries and ideas of Jennings were cited and considered fundamental for so many years is even more remarkable if we consider that all the experiments were carried out using an optical microscope with the aid of primitive techniques (e.g., he modulated the intensity of the actinic light by screening the light source with a hand).[8]

After these pioneer years, the study of photomovements benefited by a better control of the experimental conditions (such as temperature, salinity, and pH), by the collection of quantitative rather than qualitative data and by a more accurate description of the phenomena.

In 1977, an *ad hoc* Committee[10] revised the terminology of behavioral responses of motile microorganisms and indicated three basic movement patterns following an external stimulation: phobic response, taxis, and kinesis. These patterns, with the prefix "photo" to denote the light stimulation, have a sign according to the effect triggered by the perception of the stimulus (Figure 48.1): step-up and step-down photophobic reactions follow an increase or a decrease in light intensity, respectively; phototaxis can be positive or negative if the cells move toward or away from the light source; photokinesis is either positive or negative if the cell speed increases or decreases after the onset of the light stimulus (see Chapter 46 for the definition of the terms). Positive phototaxis, step-down photophobic responses, and negative photokinesis cause photoaccumulation, whereas negative phototaxis, step-up photophobic responses, and positive photokinesis result in photodispersal.

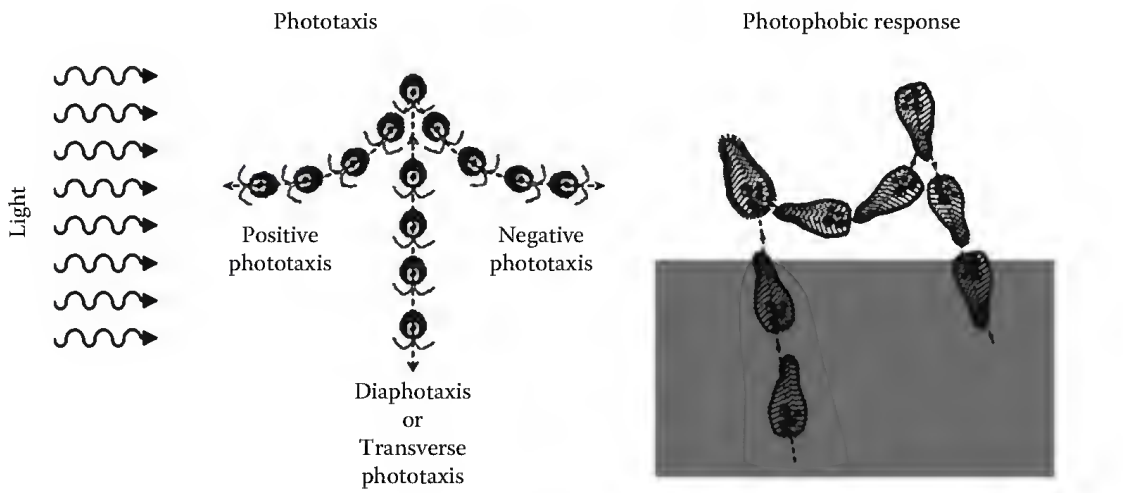

FIGURE 48.1 Schematic representation of the different types of phototaxis and of the step-up photophobic response.

Most eukaryotic microorganisms exhibit more than one of these photoresponses, which can be concurrent in producing photoaccumulation or photodispersal, or act separately depending on the level of light intensity and/or the presence of other signals from the environment.

48.2 Photoreceptor

While the eyes of metazoa share similar characteristics even when comparing organisms phylogenetically very distant, the photoreceptor apparatuses of different microorganisms show a significant richness in photoreceptive apparatuses, chromophores, and apoproteins.

Notwithstanding this high variability of structures and molecules, the flow from light perception to the motile reaction, that is the photoresponse, can be split into different stages characterized by similar features. In fact, the absorption of a photon induces molecular modifications of the photosensing chromophore that switches to the signaling state, which in turn activates the dark reaction of the transduction chain to eventually bring a signal to the motor apparatus. In the following, we will go through the different stages of the photomotile process, briefly discussing the main recent advancements and the still open questions in a few case examples.

48.2.1 Photoreceptor Organelles and Antennas

In many photosensitive eukaryotic microorganisms, the light perceiving apparatus is formed of two parts: the actual photosensing organelle, analogous to the metazoan retina, and other supramolecular structures (antennas) dedicated to modulate the signal reaching the photoreceptor molecules, either collecting and focalizing the light or screening it altogether.

The photosensing organelles are structures showing a wide range of complexity, from photoregulated channels embedded in a patch of the plasma membrane, such as in the case of the green alga *Chlamydomonas reinhardtii*[11] to the ordered 3D array of the paraxonemal body (PAB) of *Euglena gracilis*.[12] Some heterotrichous ciliates (like *Blepharisma japonicum*, *Stentor coeruleus*, and *Fabrea salina*) possess a high number of granules rich in pigment, diffused all over the cell body and arranged in rows below the plasma membrane; in the case of *B. japonicum*, electron microscopy showed an internal honeycomb-like structure.[13] These ciliate pigments, strong photosensitizers, are thought to have both a photosensing and a defensive function, and the pigment granules are supposed to work as photoreceptor organelles[13,14] and to be discharged as defensive barrage against predators if need be.[15]

Also the antennas modulating the light signal are rich in variety.[16–19] In the slime mold, *Dictyostelium discoideum* light is focused on the distal side of the pluricellular slug by means of a lens effect of the roughly cylindrical surface of the body.[20] Slightly more complex is the stigma of *E. gracilis*, whose function is simply to screen the light reaching the photosensor: because of the helicoidal swimming of this microorganism, light reaching the PAB is alternatively switched on and off, thus allowing *E. gracilis* to detect light direction comparing its intensity in two different instants.[21] In *C. reinhardtii* and in several dinoflagellates, the antenna, also known as eyespot, is constituted by one or more layers of globules containing carotenoids or melanoid pigments. Such layers are usually concave, and they work on one side as screening devices and on the other as reflectors, focusing the light on the photoreceptor organelle and possibly selecting the wavelength by means of a positive quarter-wave interference.[16] Also light-refractive devices show a wide range of complexity from the watchglass organelle of the Ophryoglenidae ciliates[17] up to the most elaborated eyespots found in Warnowiaceae dinoflagellates, a complex structure called ocelloid for its resemblance to a metazoan eye.[22,23]

48.2.2 Chromophore

Microorganisms are an artificial wide assembly of unicellular organisms belonging to several phyletic groups; it is therefore not surprising that different taxonomic groups have evolved different strategies to be able to extract information from solar radiation, beginning from the chromophore used as the

prosthetic group of the photoreceptor complex. For example, in unicellular eukaryotes at the moment the identified chromophores for motile photoresponses include retinoids (e.g., in green algae), pterins (in euglenoids), flavins (in euglenoids and Loxodida ciliates), porphyrins (in slime molds), and dianthronic molecules (in Heterotrichida ciliates) (Figure 48.2).

Even if belonging to different chemical groups, natural chromophores usually share similar features. In fact, a chromophore is usually characterized by broad absorption bands with high molar extinction coefficients in order to be able to detect light over a large range of the solar spectrum; in alternative, an assembly of different chromophores, absorbing in contiguous spectral ranges, could be spatially arranged in molecular frameworks in order to maximize the collective interaction and in the end the spectral sensitivity.

The direct identification of the chromophore is in most cases difficult because it is often present in extremely low amount, and the photoreceptor organelle is very tricky to isolate and in some cases even hard to identify.

Action spectroscopy allows to establish a direct link between the observed photoresponse and the functional absorption of photons in order to formulate hypotheses on the nature of the chromophore; in fact, the structure of the action spectrum is expected to be corresponding to that of the chromophore absorption spectrum. However, the shape of the action spectrum may be affected by the presence

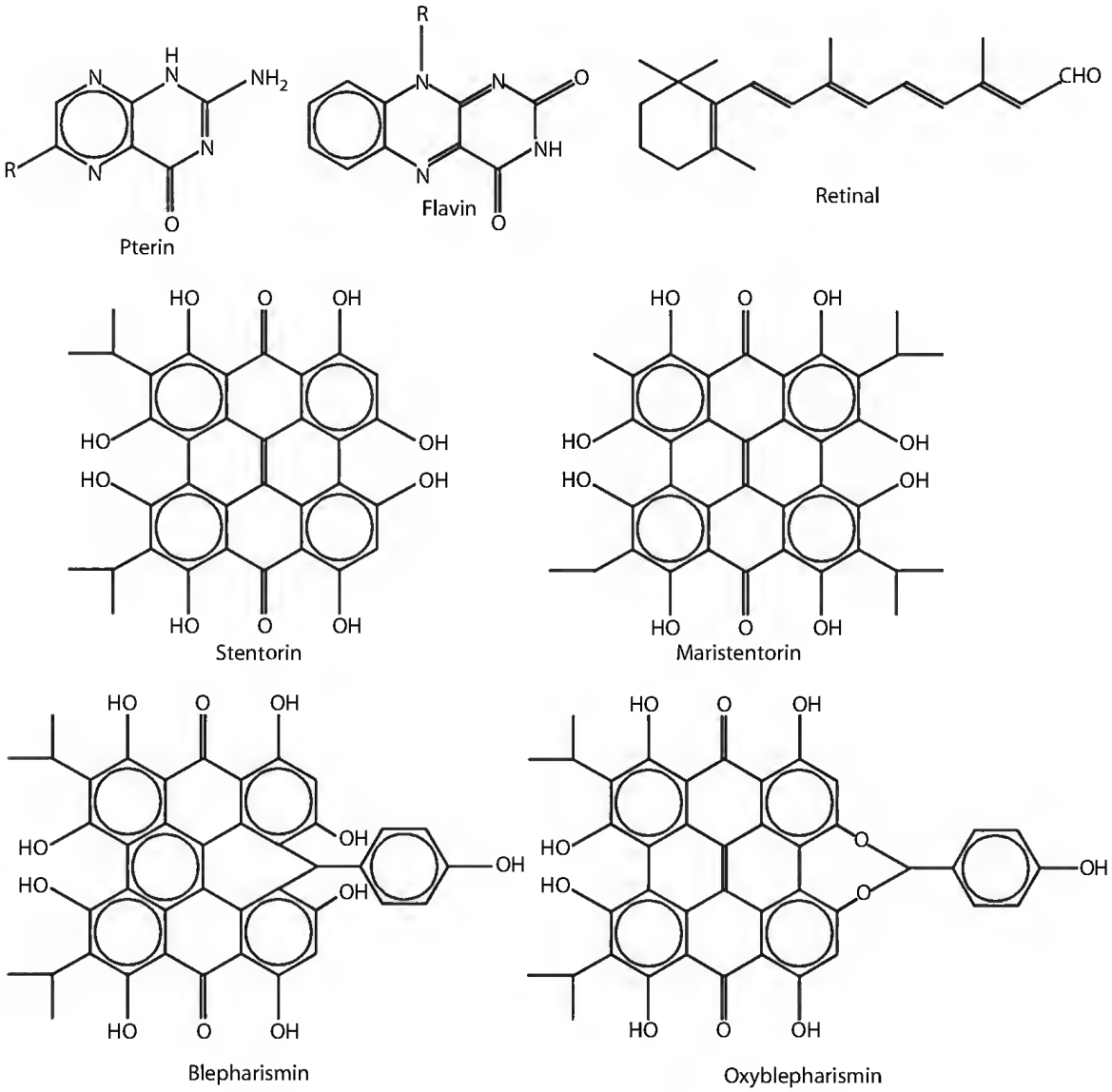

FIGURE 48.2 Determined molecular structures of chromophores for photomovements in eukaryotes.

either of screening pigments not involved in the photosensing process or of more than one chromophore absorbing in different spectral ranges and acting in parallel or in cascade (i.e., by means of energy transfer) (see Chapter 43).

Notwithstanding these limitations, in several cases, action spectroscopy proved to be a sufficiently sensitive technique. For example, Foster and Smyth, reinterpreting previous data by Nultsch et al.,[24] produced an action spectrum suggesting a rhodopsin-like photoreceptor for the phototactic response of the flagellated alga *C. reinhardtii*.[16] Later, this hypothesis was confirmed using a blind mutant, which exhibits photoresponse only at very high fluence rates: incorporating analogues of the retinal chromophore into the mutant cells, it was shown, in fact, that the photoresponse was restored also at lower fluence rates and that the maxima of the action spectra were shifted consistently with the absorption maxima of the different incorporated retinoids.[11]

Also in the case of the ciliate *B. japonicum*, several research groups identified by means of action spectroscopy the endogenous pigments blepharismin and oxyblepharismin (OxyBP) as the photosensing chromophores. This ciliate, when grown in dim light (less than about 30 W m^{-2}), is characterized by the fact that the endogenous red pigment blepharismin photoconverts to blue OxyBP and the absorption spectrum structure changes with a shift toward the red. However, OxyBP maintains the photosensing properties and the action spectra for step-up photophobic response of red and blue *B. japonicum* match blepharismin and OxyBP absorption spectra, respectively.[25,26] Also the action spectrum for the membrane receptor potentials of red cells correlated with the absorption spectrum of blepharismin.[27]

Also absorption and fluorescence microspectroscopy has been used to formulate hypothesis on the localization and the nature of the chromophore. For example, recent confocal microscopy measurements showed that in *B. japonicum*, the putative photoreceptor chromophore is located not only in the pigment granules, as thought before, but also in the cilia.[28] Moreover, by means of fluorescence lifetime imaging microscopy (FLIM), it has been found that the cilium chromophore shows a different fluorescence decay time pattern, thus allowing to formulate the hypothesis that it could be the functional photosensing chromophore, also due to its proximity to the motor apparatus. In the case of *E. gracilis*, the nature of the photoreceptor chromophore was a much debated issues also because *in vivo* microspectrofluorometry suggested that the PAB contains flavins,[29] whereas absorption studies on a single isolated PAB indicated the presence of rhodopsin.[30,31]

Chemical, biochemical, and physicochemical approaches have been used in the attempt to isolate the chromophore alone or bound to its apoprotein, characterize its structural and functional properties, and investigate the following stages of the transduction chain. By means of anion-exchange and gel filtration chromatography on *E. gracilis* isolated PABs, Iseki and co-workers[32] were able to separate a 400 kDa protein complex to which flavins were bound. Sodium dodecyl sulfate-polyacrylamide gel electrophoresis (SDS-PAGE) revealed that this protein complex is constituted by two pairs of similar subunits with different molecular mass (105 and 90 kDa) and therefore has a heterotetrameric structure. The presence of the 105 kDa subunit in the PAB was confirmed by means of immunostaining with the polyclonal antibody.

In the case of the hypericin-like endogenous pigments of the heterotrichous ciliates *S. coeruleus*,[33] *Maristentor dinoferus*,[34] and *B. japonicum* in its blue form,[35] high-performance liquid chromatography (HPLC) isolation and subsequent nuclear magnetic resonance (NMR) and mass spectrometry characterization highlighted differences in the molecular structure, which were not predictable from the absorption and fluorescence spectra.

Experiments with nonphotoresponsive mutants have been used to identify the chromophore, supplying the putative photoreceptor molecule to check whether the photoresponse is restored, and in general to study the phototransduction chain. In fact, one of the first evidences that the photoreceptor for phototaxis in *C. reinhardtii* is a rhodopsin-like molecule came from the observation that light-unresponsive mutants lacking carotenoids recovered orientation capability when incubated with retinal and other retinoids.[11]

Nowadays, molecular biology is becoming one the most powerful methods to study the different steps of the photoreception process, especially because the number of microorganism genomes completely

or partially determined is constantly increasing. The most used techniques in photomovement studies are gene sequencing of proteins characterized by biochemical methods and the subsequent search in DNA databanks of homologous sequences in other organisms; DNA and RNA inhibition by means of antisense DNA/RNA to block the expression of specific proteins; heterologous expression of selected proteins to study their functionality in host cell systems; DNA hybridization to build the philogenetic tree and to study the evolution of the photosensing apparatus.

The antisense approach has been used to identify the photoreceptor proteins of *C. reinhardtii*. Although several opsin proteins are encoded in its DNA,[36] only two of them, channelrhodopsin 1 and 2, have been shown to be involved in photomotile responses; reducing the content of one or the other channelrhodopsin, it was found that the light-generated flagellar currents are smaller, and consequently, a diminished photophobic response is observed.[37] These two chlamyrhodopsins and a rhodopsin from *Volvox carteri* have also been heterologously expressed in *Xenopus* oocytes, HEK and PC12 cells to study their functions by means of electrophysiological techniques.[38]

The amino acid sequence of the amino-terminal portion of the two subunits of the *E. gracilis* 400kDa flavin-binding protein was determined and used to synthesize degenerate primers for the amplification of the cDNAs by polymerase chain reaction (PCR). The analysis of the products evidenced in both polypeptides the presence of two regions homologous to flavin-binding domains already sequenced in various microorganisms (AppA in *Rhodobacter sphaeroides*, F403 in *Escherichia coli*, Slr1694 in *Synechocystis* sp.) and two regions homologous to catalytic domains from class III adenylyl cyclases (*Treponema pallidum* and *Anabaena cylindrica* adenylyl cyclases). Fluorescence investigation of the heat-denaturated protein complex seems to indicate that the chromophore is flavin adenine dinucleotide (FAD) not covalently bound, and it was proposed that each subunit binds two FAD molecules. In the PAB gel filtration chromatography, the adenylyl cyclase activity and fluorescence peaks were observed in the same fraction, and the activity in the light was 80-fold that measured in the dark, thus confirming the importance of photoactivation. The knockdown of the expression of the two subunits by means of RNA-mediated interference (RNAi) did not alter the vitality of the treated cells, but caused the PAB to diminish in size or disappear altogether and inhibited several responses to light, that is positive and negative phototaxis and step-up photophobic responses, but not step-down photophobic responses.[32] In this regard, it is interesting to note that, whereas phototaxis, step-up photophobic response and photokinesis are induced by the absorption of one or more photons, the signal for the step-down photophobic response is a decrease of the number of photons absorbed by the photoreceptor. Therefore, it is reasonable to suppose that a different photoreceptor triggers the step-down photoresponse.

48.2.3 Chromophore Primary Reactions and the Surrounding Environment

After the absorption of a photon, the photosensing chromophore undergoes molecular changes which depend on its physico-chemical properties and lead to the primary event of the sensory transduction chain. For the different chromophores, the proposed primary events are photoisomerization (retinal), photoinduced charge transfer (flavins, stentorins, and blepharismins), and energy transfer (from pterins to flavins, as proposed in *E. gracilis*[39]).

However, reliable hypothesis on the primary molecular event can be formulated only based on a deep knowledge of the surrounding microenvironment. In fact, the molecular pocket in which the chromophore is inserted affects the probability of radiationless and radiative transitions from the singlet and triplet excited states and the yields of charge and energy transfer processes from excited and metastable states.

As mentioned earlier, restoration of phototaxis by adding retinal analogues in blind mutants suggested retinal as photosensing chromophore of *C. reinhardtii*.[11] Like in animal vision, the photoperception of *C. reinhardtii* is based on the photoisomerization of retinal. However the molecular conformation of the chromophore and the molecular modifications it undergoes upon photon absorption are different in the

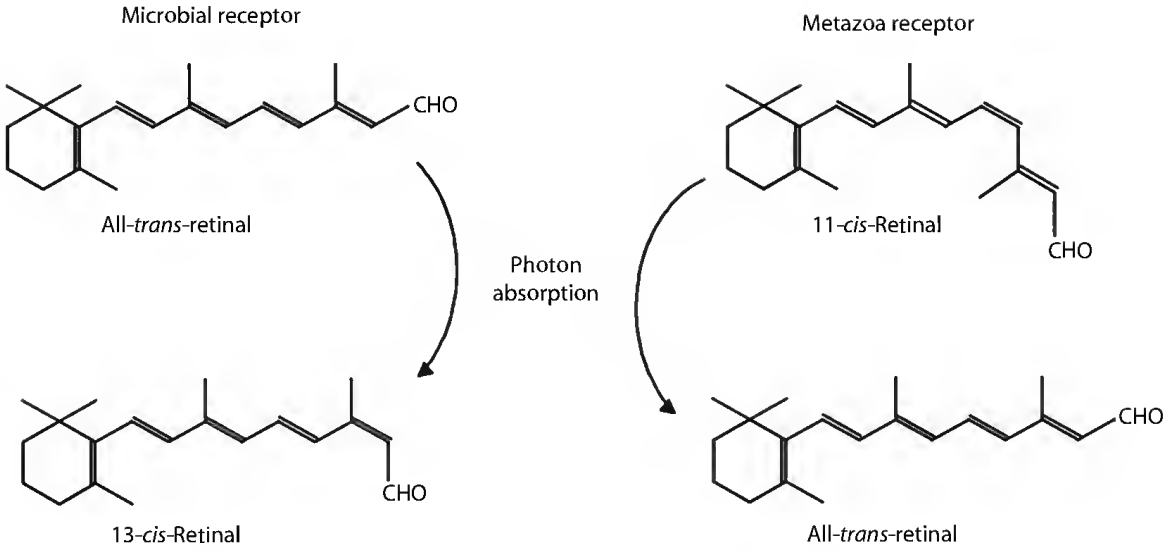

FIGURE 48.3 Comparison between retinal of microbial and metazoa photosensory receptors showing the molecular conformation before and after light absorption.

two cases. In fact, it has been demonstrated that in the green alga the photosensing chromophore is a microbial type all-*trans* retinal instead of a 11-*cis* retinal and that the isomerization involves the double bond in position 13 rather than that in position 11 (Figure 48.3).[40]

An OxyBP chromophore–protein complex has been extracted from the blue form of *B. japonicum*.[13,41] Both blepharismin and OxyBP are strong photosensitizers; however, red cells undergo photodamage when irradiated with strong light, whereas blue cells are resistant under the same irradiation condition.[42] The advantage of extracting from blue *B. japonicum* is that the complex is stable, contrary to what happens in the case of the red cells. The apoprotein has a molecular weight of about 200 kDa, is not water soluble, and not covalently bound to OxyBP, which is presumably inserted in a molecular pocket of the protein and free to rotate in all directions, even if about 10 times more slowly than in an ethanol solution due to a local higher microviscosity.[43]

This photoreceptor complex [OxyBP-binding protein (OBIP)] has been widely studied in buffer solution by means of steady-state, transient absorption and time-resolved fluorescence spectroscopy in order to verify the hypothesized involvement of a fast electron transfer in the first steps of the phototransduction chain. The interpretation of the most recent experimental data suggests the presence of two independent classes of chromoproteins: a reactive species rOBIP, undergoing fast dynamics, and a nonreactive one nrOBIP, behaving like the free chromophore in solution with a nanosecond decay.[44,45]

An important feature of rOBIP is the much faster kinetics of bound OxyBP compared to free OxyBP in dimethyl sulfoxide: in fact, OBIP displays a characteristic 675 nm absorption band occurring with a time constant of 0.54 ps and decaying with lifetimes of 3.7, 29, and 133 ps. This relaxation process could be interpreted as a reversible excited-state intermolecular electron transfer followed by electron recombination in the ground state. Brazard et al. hypothesized that OxyBP is involved in a hydrogen-bond interaction with a yet unknown electron acceptor within the apoprotein. However, these rOBIP dynamics seem too fast to generate any biologically useful signaling state, and it has been proposed that, rather than being the primary step of the transduction chain, it could be a fast efficient deactivation pathway of the OxyBP excited state, which could explain the resistance to photodamage showed by the blue cells. Therefore, the task of triggering the phototransduction chain remains for the moment assigned to the nrOBIP class of chromoprotein, hypothetically acting as a proton donor.[45]

48.3 Dark Steps of the Transduction Chain

Once the chromophore has undergone the molecular changes that constitute the primary event, the output signal from the photoreceptor travels to the motor apparatus to elicit the final cellular response. Although not directly dependent on the photic stimulus, the phases of the phototransduction chain connecting the photoreceptor to the effector, usually called "dark steps," are nonetheless important to fully understand the photoresponse, because in general this part of the transduction chain is used to amplify and modulate the signal without increasing the noise, to control the interaction with other transduction pathways, and in general to extend dynamic ranges, improve the accuracy, prevent overloads as well as signal reduction and uncontrolled fluctuations.[46]

The first models depicted the phototransduction chain to be made up of a small number of functional components spatially contiguous, with the photoreceptor directly influencing the state of ion channels, especially in the case of flagellated algae, where it was hypothesized that the vicinity of the photoreceptor to the motor apparatus, that is the flagella, was functional to the direct control of the photoreceptive protein on the nearby membrane channels. As a matter of fact, the more it has been studied, the more the transduction chain in unicellular eukaryotes has been found to involve secondary messengers and transduction pathways similar to those found in pluricellular organisms.

A typical example is given by the studies conducted on *E. gracilis*. Since its photoreceptor organelle exhibits a crystalline structure and a lattice-like morphology and it is strictly adjoining the emerging flagellum (hence the name PAB), it was hypothesized that a light-generated photoelectric signal, more precisely a long-range coherent displacement photocurrent, would propagate along the flagellar rod, finally causing flagella stiffening and therefore a change in swimming direction of the microorganism.[47] However, recent results of genetic analysis, demonstrating a photoactivated adenylyl cyclase activity of the flavin-carrying photoreceptor protein (see the preceding text), suggest that cAMP is somehow involved in the signaling pathway, as already shown for gravitaxis in the same microorganism.[48]

Similar considerations can be done on *C. reinhardtii*, where the presence of the two channelrhodopsins had suggested a direct control of this light-activated proteins on the influx of mono- and divalent ions and, consequently, on the membrane potential.[49] However, the presence of guanine nucleotide-binding proteins (G proteins) in the eyespot could suggest a more complex transduction mechanism,[50] as proposed in the closely related green alga *Spermatozopsis similis*. In eyespot preparations from this microorganism not only the presence of heterotrimeric G proteins was confirmed, but also specific, reversible green light modulation of at least one G_α subunit was demonstrated. Moreover, light-sensitive GTPase activity was completely abolished by antisera directed against G_q and G_i subunits as well as by an antiserum directed against the rhodopsin of *C. reinhardtii*, whereas corresponding control sera had no significant effect. This clearly indicates that in *S. similis*, there is a close coupling of at least one of the putative G proteins to the photoreceptor for phototaxis.[51]

Also in the case of *S. coeruleus* and *B. japonicum*, initial studies suggested a quite simple mechanism of phototransduction: an intracellular increase of the concentration of protons released by the photoreceptor could induce the opening of membrane calcium channels, the depolarization of the membrane, and consequently the stop of the ciliary beating. More recent pharmacological and biochemical results enrich and complicate this simple model, suggesting the involvement of secondary messengers (cGMP and IP_3) similar to those operating in the visual processes of metazoa.[52]

The fundamental role of G proteins has been demonstrated also in the photo- (and thermo-) transduction chain of the slime mold *D. discoideum*. This small soil amoeba (10–20 μm diameter), when undergoing nutritional stress, becomes aggregation-competent and capable of responding chemotactically to a specific pheromone. As a consequence, a few hundred thousand amoebae aggregate together to form a multicellular mass, called pseudoplasmodium or slug.[53] Both unicellular and multicellular forms react to photic and thermal stimuli with extremely high sensitivity. The two senses share most of the transduction chain and help the slug to reach the surface, where light and the concomitant drop in humidity induce culmination, i.e., the fruiting body formation.[54]

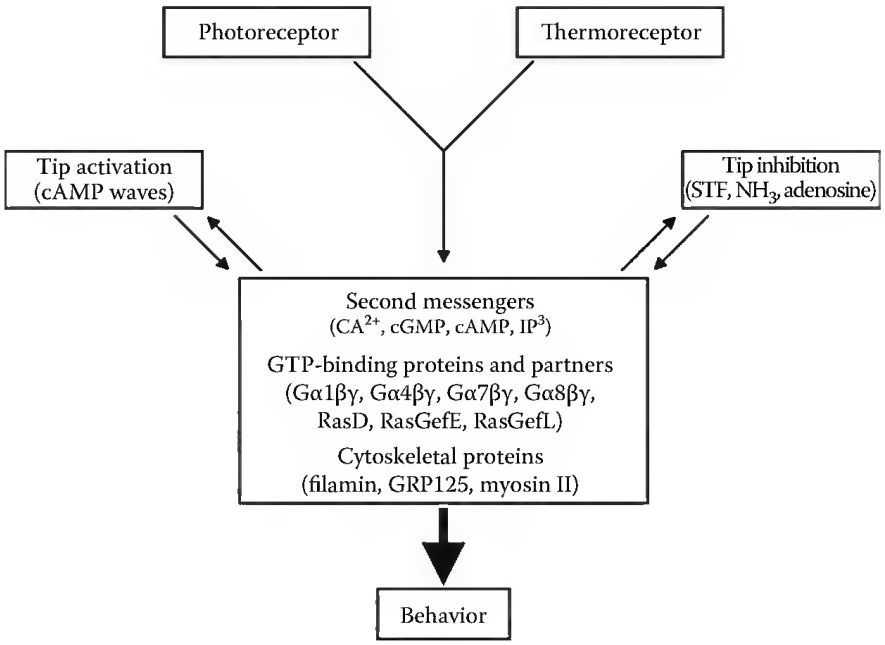

FIGURE 48.4 Simplified scheme of the known messenger molecules and proteins taking part in the transduction chain of *D. discoideum* slug phototaxis and thermotaxis. (Modified from Fisher, P.R. and Annesley, S.J., Methods in *Molecular Biology, Dictyostelium discoideum Protocols*, Eichinger, L. and Rivero, F., Eds., Vol. 346, Humana Press, New York, 2006, p. 137.)

The slug amoebae communicate among them by means of extracellular chemical signals, which are modulated by light and temperature gradients. The leading role in the slug is played by the anterior tip, which "chooses" the direction and is followed by the slug body. Slug turning is the result of the imbalance in the extracellular concentration of activating and inhibiting messengers produced by the slug tip: the activating signal is carried by cAMP waves, whereas the inhibiting signal is yet unknown (possibly one or more between NH_3, adenosine, and a small unidentified substance called slug turning factor). Light perception is supposed to alter the pacemaker frequency associated with the cAMP waves, which in turn are detected by four cAMP receptors coupled to heterotrimeric G proteins. At least two of these G proteins are known to be essential for normal slug phototaxis (and thermotaxis).[54] By means of molecular biology techniques, it has been found that also other proteins are essential for a correct phototaxis: monomeric GTP-binding proteins of the RAt Sarcoma (RAS) family, cAMP 7-transmembrane domain receptors, protein kinases, and even cytoskeletal proteins, like filamin (actin-binding protein ABP-120 or gelation factor) and GRP125 (gelsolin-related protein of 125 kDa), which are required to build a photoreceptor signaling protein complex, or myosin II (Figure 48.4). As a matter of fact, by genetic analysis it has been estimated that the number of genes that can be silenced without affecting cell viability and aggregation capacity, but are necessary for a correct photoorientation, is most probably around 20 and could be as high as 55.[55]

48.4 Concluding Remarks

This chapter is mainly focused on the photosensing and transducing systems of the most studied photomotile eukaryotic microorganisms, but not even in these few examples a full comprehension of the molecular machinery connecting the perception of the light stimulus to the motile response has been achieved. Many other microorganisms have been studied less intensively, and in these cases, the knowledge of the photosensory processes is even more fragmented and incomplete. However, the results of the last 30 years of research reveal the existence of a relatively wide variety of photoreceptor structures and transduction mechanisms for which it seems impossible to provide any unitary description.

Taking into account that light is not the only environmental signal influencing the motile behavior of microorganisms, which is also affected by chemical, thermal, mechanical, and gravitational stimuli, it is conceivable that some similarity exists between the various transduction pathways. Integrated studies of motile responses elicited by light in the presence of others of the aforementioned external signals might therefore offer clues for a deeper understanding of microbial sensory processes.

However, from the point of view of the photobiologist, the most interesting aspect is the primary mechanism of triggering the transduction chain by the chromophore–protein complex. Its knowledge should be the objective of future research, by unambiguously localizing the photoreceptor in the cell body, determining its structure, the kind of interaction between chromophore and apoprotein, and the first molecular events which initiate the transduction cascade.

In conclusion, further intensive and multidisciplinary studies, conducted on as many photomotile microorganisms as possible, are needed to understand the different steps of the photoreaction both as an isolated process and in relation to other external and internal stimuli.

Dedication

Dedicated to Francesco Lenci on the occassion of his 70th birthday.

References

1. Colombetti, G., Marangoni, R., and Machemer, H., Phototaxis in *Fabrea salina*, *Med. Biol. Environ.*, 20, 93, 1992.
2. Finlay, B.J. and Fenchel, T., Photosensitivity in the ciliated protozoon *Loxodes*: Pigment granules, absorption and action spectra, blue light perception and ecological significance, *J. Protozool.*, 33, 534, 1986.
3. Bialczyk, J., An action spectrum for light avoidance by *Physarum nudum* plasmodia, *Photochem. Photobiol.*, 30, 301, 1979.
4. Treviranus, L.C., Beobachtungen über die Bewegung der grünen Materie im Pflanzenreich, *Vermischte Schriften Anat. und Physiol. Inhalts*, 2, 71, 1817.
5. Fraenkel., S. and Gunn, D.L., *The Orientation of Animals*, Dover Publications, New York, 1961.
6. Colombetti, G. and Petracchi, D., Photoresponse mechanisms in flagellated algae, *Crit. Rev. Plant Sci.*, 8, 309, 1989.
7. Engelmann, Th.W., Über Reizung contraktilen Protoplasmus durch plötzliche Beleuchtung, *Pflügers Arch. Gesamte Physiol. Menschen Tiere*, 19, 1, 1879.
8. Jennings, H.S., *Behaviour of the Lower Organisms*, The Columbia University Press, New York, 1906.
9. Mast, S.O., *Light and the Behavior of Organisms*, John Wiley & Sons, New York, 1911.
10. Diehn, B., Feinleib, M.E., Haupt, W., Hildebrand, E., Lenci, F., and Nultsch, W., Terminology of behavioral responses of motile microorganisms, *Photochem. Photobiol.*, 26, 559, 1977.
11. Foster, K.W., Saranak, J., Patel, N., Zarilli, G., Okabe, M., Kline, T., and Nakanishi, K., A rhodopsin is the functional photoreceptor for phototaxis in the unicellular eukaryote *Chlamydomonas*, *Nature*, 311, 756, 1984.
12. Piccinni, E. and Mammi, M., Motor apparatus of *Euglena gracilis*: Ultrastructure of the basal portion of the flagellum and the paraflagellar body, *Boll. Zool.*, 45, 405, 1978.
13. Matsuoka, T., Tokumori, D., Kotsuki, H., Ishida, M., Matsushita, M., Kimura, S., Itoh, T., and Checcucci, G., Analyses of structure of photoreceptor organelle and blepharismin associated protein in unicellular eukaryote *Blepharisma*, *Photochem. Photobiol*, 72, 709, 2000.
14. Kim, I.-H., Rhee, J.S., Huh, J.W., Florell, S., Faure, B., Lee, K.W., Kahsai, T., Song, P.-S., Tamai, N., Yamazaki, T., and Yamazaki, I., Structure and function of the photoreceptor stentorins in *Stentor coeruleus*. I. Partial characterization of the photoreceptor organelle and stentorins, *Biochim. Biophys. Acta*, 1040, 43, 1990.
15. Harumoto, T., Miyake, A., Ishikawa, N., Sugibayashi, R., Zenfuku, K., and Iio, H., Chemical defense by means of pigmented extrusomes in the ciliate *Blepharisma japonicum*, *Eur. J. Protistol.*, 34, 458, 1998.

16. Foster, K.W. and Smyth, R.D., Light antennas in phototactic algae, *Microbiol. Rev.*, 44, 572, 1980.
17. Kuhlmann, H.-W., Do phototactic ciliates make use of directional antennas to track the direction of light? *Eur. J. Protistol.*, 34, 244, 1998.
18. Kreimer, W., Reflective properties of different eyespots types in dinoflagellates, *Protist*, 150, 311, 1999.
19. Kreimer, W., The green algal eyespot apparatus: A primordial visual system and more? *Curr. Genet.*, 55, 19, 2009.
20. Fisher, P.R., Genetic analysis of phototaxis in *Dictyostelium*, in *Photomovements*, Häder, D.-P. and Lebert, M., Eds., Comprehensive Series in Photosciences, Vol. 1, Elsevier, Amsterdam/New York, 2001, p. 193.
21. Lebert, M., Phototaxis of *Euglena gracilis*—Flavins and pterins, in *Photomovements*, Häder, D.-P. and Lebert, M., Eds., Comprehensive Series in Photosciences, Vol. 1, Elsevier, Amsterdam/New York, 2001, p. 297.
22. Gómez, F., López-García, P., and Moreira, D., Molecular phylogeny of the ocelloid-bearing dinoflagellates *Erythropsidinium* and *Warnowia* (Warnowiaceae, Dinophyceae), *J. Eukaryot. Microbiol.*, 56, 440, 2009.
23. Hoppenrath, M., Bachvaroff, T.R., Handy, S.M., Delwiche, C.F., and Leander, B.S., Molecular phylogeny of ocelloid-bearing dinoflagellates (Warnowiaceae) as inferred from SSU and LSU rDNA sequences, *BMC Evol. Biol.*, 9, 116, 2009.
24. Nultsch, W., Throm, G., and von Rimscha, I., Phototaktische untersuchungen an *Chlamydomonas reinhardtii* dangeard in homokontinuierlicher kultur, *Arch, Mikrobiol.*, 80, 351, 1971.
25. Checcucci, G., Damato, G., Ghetti, F., and Lenci, F., Action spectra of the photophobic response of the blue and red forms of *Blepharisma japonicum, Photochem. Photobiol.*, 57, 686, 1993.
26. Matsuoka, T., Matsuoka, S., Yamaoka, Y., Kuriu, T., Watanabe, Y., Takayanagi, M., Kato, Y., and Taneda, K., Action spectra for step-up photophobic response in *Blepharisma, J. Protozool.*, 39, 498, 1992.
27. Fabczak, S., Fabczak, H., and Song, P.-S., Photosensory transduction in ciliates. III. The temporal relation between membrane potentials and photomotile response in *Blepharisma japonica urn. Photochem. Photobiol.*, 57, 872, 1993.
28. Colombetti, G., Checcucci, G., Lucia, S., Usai, C., Ramoino, P., Bianchini, P., Pesce, M., Vicidomini, G., and Diaspro, A., Evidence for ciliary pigment localization in colored ciliates and implications for their photosensory transduction chain: A confocal microscopy study, *Microsc. Res. Techniq.*, 70, 1028, 2007.
29. Ghetti, F., Colombetti, G., Lenci, F., Campani, E., Polacco, E., and Quaglia, M., Fluorescence of *Euglena gracilis* photoreceptor pigment: An in vivo microspectrofluorometric study, *Photochem. Photobiol.*, 42, 29, 1985.
30. Gualtieri, P., Barsanti, L., and Passarelli, V., Absorption spectrum of a single isolated paraflagellar swelling of *Euglena gracilis, Biochim. Biophys. Acta*, 993, 293, 1989.
31. James, T.W., Crescitelli, F., Loew, E.R., and McFarland, W.N., The eyespot of *Euglena gracilis*: A microspectrophotometric study, *Vision Res.*, 32, 1583, 1992.
32. Iseki, M., Matsunaga, S., Murakami, A., Ohno, K., Shiga, K., Yoshida, K., Sugai, M., Takahashi, T., Hori, T., and Watanabe, M., A blue-light-activated adenylyl cyclase mediates photoavoidance in *Euglena gracilis, Nature*, 415, 1047, 2002.
33. Tao, N., Orlando, M., Hyon, J.-S., Gross, M., and Song, P.-S., A new photoreceptor molecule from *Stentor coeruleus, J. Am. Chem. Soc.*, 115, 2526, 1993.
34. Mukherjee, P., Fulton, D.B., Halder, M., Han, X., Armstrong, D.W., Petrich, J.W., and Lobban, C.S., Maristentorin, a novel pigment from the positively phototactic marine ciliate *Maristentor dinoferus*, is structurally related to hypericin and stentorin, *J. Phys. Chem. B*, 110, 6359, 2006.
35. Spitzner, D., Höfle, G., Klein, I., Pohlan, S., Ammermann, D., and Jaenicke, L., On the structure of oxyblepharismin and its formation from blepharismin, *Tetrahedon Lett.*, 39, 4003, 1998.

36. Fuhrmann, M., Stahlberg, A., Govorunova, E., Rank, S., and Hegemann, P., The abundant retinal protein of the *Chlamydomonas* eye is not the photoreceptor for phototaxis and photophobic responses, *J. Cell Sci.*, 114, 3857, 2001.
37. Sineshchekov, O.A., Jung, K.H., and Spudich, J.L., Two rhodopsins mediate phototaxis to low- and high-intensity light in *Chlamydomonas reinhardtii*, *Proc. Natl. Acad. Sci. USA*, 99, 8689, 2002.
38. Hegemann, P., Algal sensory photoreceptors, *Annu. Rev. Plant Biol.*, 59, 167, 2008.
39. Sineshchekov, V.A., Geiss, D., Sineshchekov, O.A., Galland, P., and Senger, H., Fluorometric characterization of pigments associated with isolated flagella of *Euglena gracilis*: Evidence for energy migration, *J. Photochem. Photobiol. B Biol.*, 23, 225, 1994.
40. Hegemann, P., Gärtner, W., and Uhl, R., All-*trans* retinal constitutes the functional chromophore in *Chlamydomonas reinhardtii*, *Biophys. J.*, 60, 1477, 1991.
41. Matsuoka, T., Murakami, Y., and Kato, Y., Isolation of blepharismin-binding 200 kDa protein responsible for behavior in *Blepharisma*, *Photochem. Photobiol.*, 57, 1042, 1993.
42. Ghetti, F., Checcucci, G., Lenci, F., and Heelis, P.F., A laser flash photolysis study of the triplet states of the red and the blue forms of *Blepharisma japonicum* pigment, *J. Photochem. Photobiol. B Biol.*, 13, 315, 1992.
43. Plaza, P., Mahet, M., Martin, M.M., Angelini, N., Malatesta, M., Checcucci, G., and Lenci, F., Spectroscopic study of the chromophore–protein association and primary photoinduced events in the photoreceptor of *Blepharisma japonicum*, *Photochem. Photobiol. Sci.*, 4,754, 2005.
44. Plaza, P., Mahet, M., Martin, M.M., Checcucci, G., and Lenci, F., Target analysis of primary photoprocesses involved in the oxyblepharismin-binding protein, *J. Phys. Chem. B*, 111, 690, 2007.
45. Brazard, J., Ley, C., Lacombat, F., Plaza, P., Martin, M.M., Checcucci, G., and Lenci, F., Primary photoprocesses involved in the sensory protein for the photophobic response of *Blepharisma japonicum*, *J. Phys. Chem. B*, 112, 15182, 2008.
46. Block, S.M., Biophysical principles of sensory transduction, in *Sensory Transduction*, The Rockfeller University Press, New York, 1992, p. 1
47. Bovee, E.C. and Jahn, T.L., A theory of piezoelectric activity and ion-movements in the relation of flagellar structures and their movements to the phototaxis of *Euglena*, *J. Theor. Biol.*, 35, 259, 1972.
48. Häder, D.-P. and Lebert, M., Photoorientation in photosynthetic flagellates, in *Methods in Molecular Biology "Chemotaxis,"* Jin, T. and Hereld, D., Eds., Vol. 571, Humana Press, New York, 2009, p. 51.
49. Deininger, W., Kröger, P., Hegemann, U., Lottspeich, F., and Hegemann, P., Chlamyrhodopsin represents a new type of sensory photoreceptor, *EMBO J.*, 4, 5849, 1995.
50. Korolkov, S.N., Garnovskaya, M.N., Basov, A.S., Chunaev, A.S., and Dumler, I.L., The detection and characterization of G-proteins in the eyespot of *Chlamydomonas reinhardtii*, *FEBS Lett.*, 270, 132, 1990.
51. Calenberg, M., Brohsonn, U., Zedlacher, M., and Kreimer, G., Light- and Ca^{2+}-modulated heterotrimeric GTPases in the eyespot apparatus of a flagellate green alga, *Plant Cell*, 10, 91, 1998.
52. Sobierajska, K., Fabczak, H., and Fabczak, S., Photosensory transduction in unicellular eukaryotes: A comparison between related ciliates *Blepharisma japonicum* and *Stentor coeruleus* and photoreceptor cells of higher organisms, *J. Photochem. Photobiol. B Biol.*, 83, 163, 2006.
53. Annesley, S.J. and Fisher, P.R., *Dictyostelium discoideum*—A model for many reasons, *Mol. Cell Biochem.*, 329, 73, 2009.
54. Fisher, P.R. and Annesley, S.J., Slug phototaxis, thermotaxis, and spontaneous behavior, in *Methods in Molecular Biology, Dictyostelium discoideum Protocols*, Eichinger, L. and Rivero, F., Eds., Vol. 346, Humana Press, New York, 2006, p. 137.
55. Darcy, P.K., Wilczynska, Z., and Fisher, P.R., Genetic analysis of *Dictyostelium* slug phototaxis mutants, *Genetics*, 137, 977, 1994.

49

Transport and Sensory Rhodopsins in Microorganisms

Yuki Sudo
Nagoya University
and
Japan Science and Technology Agency

49.1 Introduction

Rhodopsin molecules are photochemically reactive membrane-embedded proteins, with seven transmembrane α-helices which bind the chromophore retinal (vitamin A aldehyde).[1,2] Rhodopsins are classified into two groups, microbial (type 1) and mammalian (type 2).[3] Type 2 rhodopsins, such as visual pigments, are G-protein-coupled receptors (GPCRs) that are widespread in vertebrates and invertebrates.[2,4,5] This chapter reviews type 1 rhodopsins functioning as light-driven ion transporters or photosensory receptors in microorganisms. They are widespread in the microbial world in prokaryotes (bacteria and archaea) and in eukaryotes (fungi and algae).[3,6,7] A striking characteristic of these photoactive proteins is their wide range of seemingly dissimilar functions. Some are light-driven transporters, such as the proton pump bacteriorhodopsin (BR) and the chloride pump halorhodopsin (HR) (Figure 49.1).[3,8] Others are light sensors, such as the phototaxis receptors sensory rhodopsins I and II (SRI and SRII).[9] SRI and SRII relay signals by protein–protein interactions to integral membrane transducer proteins HtrI and HtrII, respectively, and SRI–HtrI and SRII–HtrII complexes control the flagellar motor rotation through kinases (Figure 49.1). The microbial rhodopsins have become a focus of interest, in part because of their importance to the general understanding of ion flux across membranes, and communication between integral membrane proteins, about which little is known.

BR was first identified in 1971 in the archaeon *Halobacterium salinarum* (also called *Halobacterium halobium*).[10] Subsequently, HR, SRI, and SRII were independently discovered in *H. salinarum* before 1985.[11–14] Those four archaeal rhodopsins have been well characterized over the past 40 years using various techniques from fields including photochemistry, biochemistry, and molecular biology.[15] At this

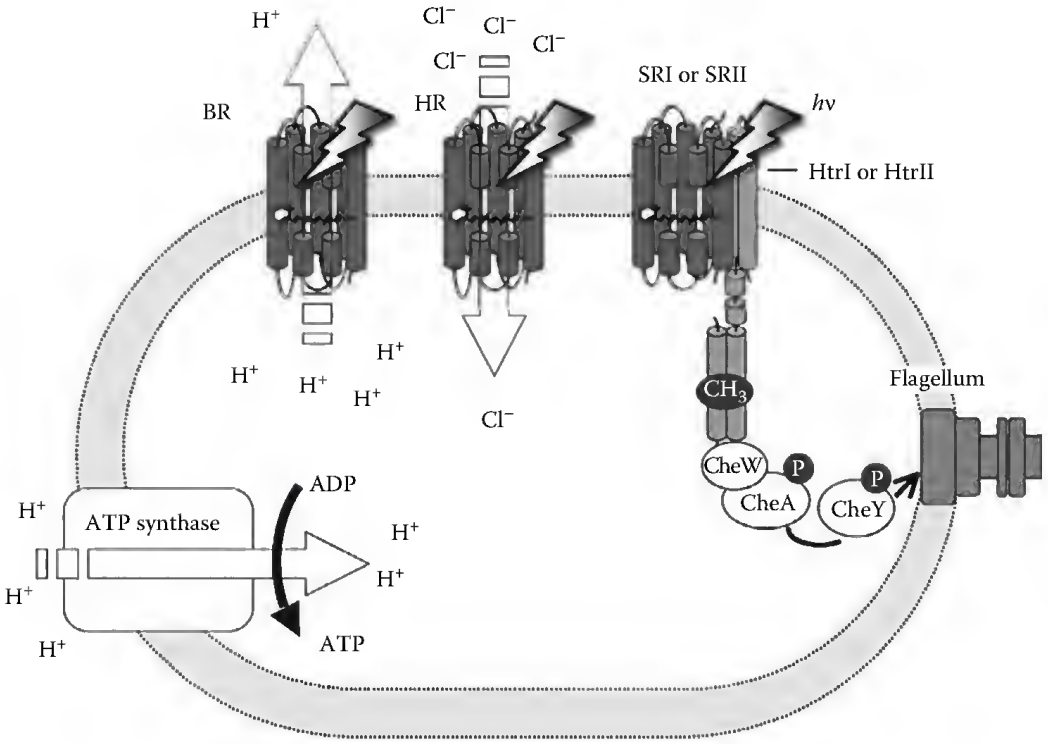

FIGURE 49.1 Microbial rhodopsins in microorganisms and their functions.

time, thousands of investigations concerning the structure and functional mechanisms of BR have been reported, and therefore, BR is one of the best-understood membrane proteins and photoactive proteins.[8] The proton gradient produced by BR is utilized by adenosine triphosphate (ATP) synthase, indicating that organisms having light-driven pumps can produce ATP under light illumination (Figure 49.1). It is well known that ATP is a multifunctional nucleotide, used in cells and organisms as a coenzyme, and is often called the molecular unit of currency of intracellular energy transfer. Since 2000, new types of microbial rhodopsins have been found in various microbes,[15] including the light-gated cation channelrhodopsins I and II (ChR1 and ChR2) from *Chlamydomonas*,[16–18] a light sensor *Anabaena* sensory rhodopsin (ASR) from algae,[19] BR homologues from fungi and algae [*Leptosphaeria* rhodopsin (LR) and *Gloeobacter* rhodopsin (GR)],[20,21] SRI homologues from eubacteria (*Salinibacter* sensory rhodopsin I: *Sr*SRI),[22] etc. In this review, the characteristics of new types of rhodopsins are also discussed.

49.2 Ion-Pumping Rhodopsins

49.2.1 BR and BR-Like Proton-Pumping Rhodopsins

In 1971, Oesterhelt and Stoeckenius identified a visual rhodopsin-like membrane-embedded protein having retinal (vitamin A aldehyde; see Figure 49.2) as a chromophore in the archaeon *H. salinarum* (*halobium*).[10] They named that protein BR. In the past four decades since then, BR has become a model for the simplest and most essential features necessary in an active proton transporter that is activated by a light stimulus. The mechanism of the proton pumping across the membrane is based on the stepwise reactions that accompany the photoisomerization from all-*trans* to 13-*cis* retinal upon formation of the K-photointermediate (Figure 49.2).[8]

A description of the transport mechanism, to a large extent at atomic resolution, has been elucidated due to the huge effort of many researchers on the spectroscopic, mutational, theoretical, and crystallographic aspects of the intermediates.[23,24] The structure and structural changes of the protein and the

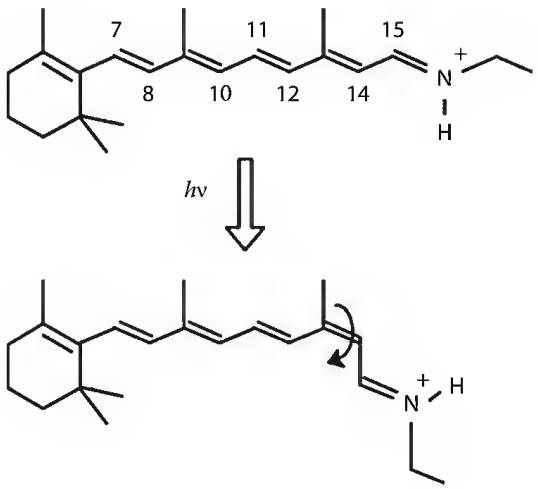

FIGURE 49.2 Retinal chromophore and its isomerization by light activation.

retinal in photointermediates are essential to understand the transport mechanism. However, in this chapter, they are only discussed in the context of the proton transfer reactions. The structure of BR is available from cryo-electron microscopy and x-ray diffraction at 1.55 Å resolution.[24–27] The retinal chromophore is linked to a specific lysine residue (Lys216) via a protonated Schiff base (PSB) (Figure 49.2). The active center is composed of deprotonated Asp85, deprotonated Asp212, protonated Arg82, water molecules, and their hydrogen bonds (Figure 49.3). It should be noted that x-ray crystallography does not report the charged states of these groups, and they have mainly been revealed by vibrational spectroscopic studies.[28] As shown in Figure 49.3, the membrane normally is roughly in the vertical plane of the image, and the top and bottom regions correspond to the cytoplasmic (CP) and extracellular (EC) sides, respectively. D85N and D212N mutant proteins lack the proton-pumping activity.[29] In addition, water 402 (Wat402) of BR forms an unusually strong hydrogen bond with Asp85,[30] indicating the importance of the pentagonal cluster for active transport. Using comprehensive low-temperature Fourier transform infrared (FTIR) spectroscopy, Kandori and coworkers showed that strongly hydrogen-bonded water molecules (water O–D stretching vibration in D_2O at <2400 cm^{-1}) are found in the proton-pumping rhodopsins (including BR) but not in the nonproton-pumping rhodopsins.[31] That suggests that a strongly hydrogen-bonded water molecule (Wat402) that bridges the Schiff base and its counterion Asp85 are essential for the proton-pumping function (Figure 49.3). The hydrogen bond becomes much weaker upon photoisomerization,[32] suggesting that the specialized hydrogen bond between Wat402 and Asp85

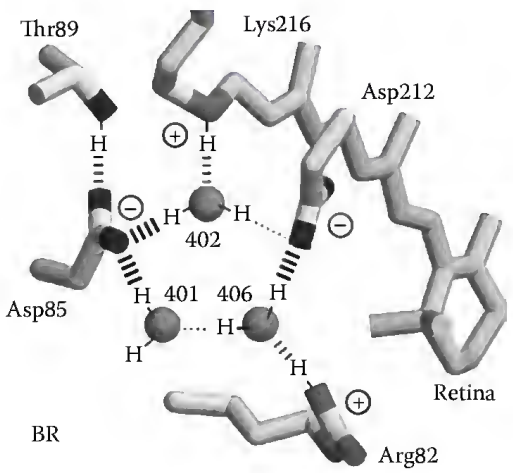

FIGURE 49.3 X-ray structure of the Schiff base region in BR.

carries the energy needed for the proton-pumping function. Water molecules exist not only in soluble proteins, but also in membrane-embedded proteins, and they play important roles in the functions of those proteins. One of the roles of internal water molecules is to occupy the sites inside the protein that may be energetically unfavorable. Proteins that actively pump ions across membranes must translocate these ions through hydrophobic regions inside proteins. In particular, such water molecules must participate in hydrogen-bonding networks inside proteins that constitute an ion flux pathway. Therefore, internal water molecules may assist the transport of ions inside proteins by raising the dielectric constant.

BR absorbs light at around 570 nm, and this photoexcitation results in the sequential appearance of various photointermediates (K_{590}, L_{550}, M_{410}, N_{560}, and O_{640}), followed by a return to the unphotolyzed form of the protein (Figure 49.4).[33] The numbers in Figure 49.4 denote wavelengths (in nm) of the maximum absorption, λ_{max}. This linear cyclic series of photochemical reactions is referred to as the photocycle. A schematic representation of the BR photocycle is shown in Figure 49.4, with the cascade of proton movements. During the photocycle of BR, proton movement occurs through the following steps: (1) upon formation of the M-intermediate, the proton of the PSB is transferred to the nearby deprotonated Asp85. (2) The pKa values of Glu204, an initially protonated residue located at the EC surface, and Asp85 are coupled in such a way that when Asp85 becomes protonated, the proton of Glu204, or the cluster of water molecules, is released to the EC surface. This is accompanied by the outward helix titling of the CP end of the sixth α-helix (F-helix) at the M-intermediate. This structural change leads to an accessibility change of the Schiff base from Asp85 on the EC side toward Asp96, an initially protonated residue on the CP side. (3) The proton of Asp96 is transferred to the Schiff base upon formation of the N-intermediate. (4) the deprotonated Asp96 is protonated upon formation of the O-intermediate. (5) consequently, during the recovery from the O to the BR state, the proton of Asp85 is transferred to Glu204. Thus, the one-photon accumulation of the BR molecule drives the active proton transport across the membrane. The detailed conformational changes of the protein and retinal chromophore during the photocycle have been discussed at length in numerous review articles elsewhere.[23,24,26–28,33,34]

So far, BR and related proteins capable of producing a chemiosmotic membrane potential in response to light have only been described in halophilic archaea. Recently, genome-sequencing projects, and environmental genomics, have revealed that proton-pumping rhodopsins also exist in eukarya and eubacteria.[15,35,36] In 2000, a type of rhodopsin derived from eubacteria was discovered through genomic analysis in marine bacterioplankton and was named "proteorhodopsin (PR)."[37] The recombinant PR,

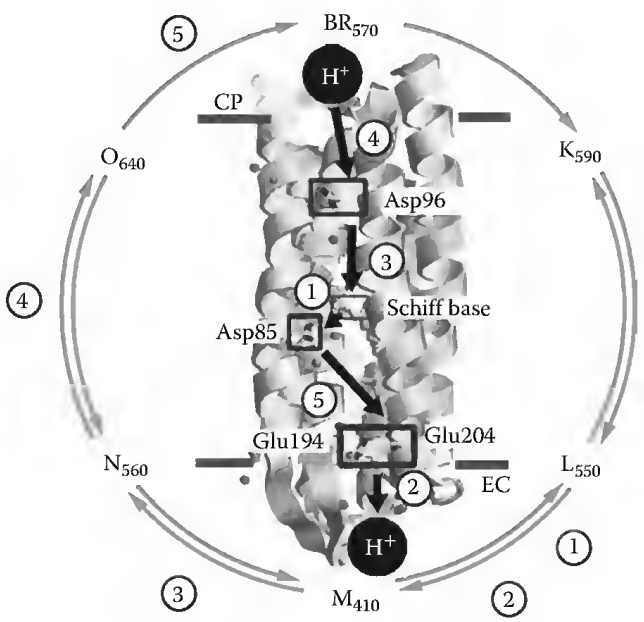

FIGURE 49.4 Proton movement during the photocycle in BR.

having retinal as a chromophore, showed active proton transport upon photoillumination, and exhibited a photocycle with intermediates and kinetics characteristic of BR. This implies that archaeal-like rhodopsins are broadly distributed among different taxa, including members of the domain Bacteria. This also indicates that a previously unsuspected mode of bacterially mediated light-driven energy production may commonly occur in oceanic surface waters worldwide.[38] In 2005, a fungal rhodopsin LR was cloned and heterologously expressed in *Phichia pastoris*.[20] LR turned out to be very similar to BR in its photochemical behavior. Interestingly, LR exhibits light-driven active proton transport and, consequently, LR is the first BR-like proton pump to be identified in a eukaryote. At present, microbial rhodopsins, *Acetabularia* rhodopsin (AR),[39] xanthorhodopsin (XR),[40] and GR[21] have been found in the genomes of various microbes, and they also function as light-driven proton pumps. It should be noted that most amino acid residues important for the proton pumping in BR (Arg82, Asp85, Asp96, Glu194, Glu204, and Asp212) are also conserved in LR, AR, and GR. Thus, it is now clear that BR and related proteins are very common for large taxonomic groups, implying that light-driven proton transport is considerably important for various organisms.

49.2.2 Halorhodopsin

A light-driven inward chloride pump, HR, was discovered in the archaeon *H. salinarum* in 1980, 9 years after the discovery of BR.[12] In contrast to the extensive studies on BR, the molecular mechanism of HR is less well understood. Functionally, HR is the mirror image of BR: an anion rather than a cation is transported, and the translocation is in the EC→CP direction.[41,42] In 1995, Sasaki et al. reported that replacement of Asp at position 85 to Thr converts BR from a proton to a chloride pump,[43] which implies that the essential features of the proton transport mechanism of BR are commonly conserved in the anion transport mechanism of HR. The absorption of light by the all-*trans* form of the retinal chromophore triggers a cyclic reaction in HR, as it does in BR. A schematic representation of the photocycle is shown in Figure 49.5. HR absorbs light at around 580 nm, and the photoexcitation results in the sequential appearance of various photointermediates (K_{600}, L_{520}, N_{520}, and O_{600}), followed by a return to the unphotolyzed form of the protein, as it does in BR, except for the lack of the M-intermediate.[44]

The retinal Schiff base of HR is protonated, as in BR, but the counterion Asp85, which is essential for the proton pump, is replaced by a Thr residue (Thr111) (Figure 49.6). As previously described for BR, the proton of the PSB is transferred to the nearby deprotonated counterion upon formation of the M-intermediate, and therefore, the photocycle of HR lacks the M-intermediate.[44] The high-resolution crystal structures of HR molecules from *H. salinarum* (*Hs*HR),[45] and from the related archaeon *Natronomonas pharaonis* (*Np*HR),[46] were reported in 2000 and 2010, respectively. Figure 49.6 shows the Schiff base region of *Hs*HR, which contains a quadrupole with positive charges located at the PSB and at Arg108, and counterbalancing negative charges located at the chloride ion and Asp238. Both in the crystal structures of *Hs*HR and *Np*HR, the Cl^- is only ~4 Å from the PSB, indicating a strong electrostatic interaction, as extrapolated previously from FTIR data and changes in the visible spectrum upon halide binding.[47] From the spectral shift, its affinity is determined as about 10 and 2.5 mM for *Hs*HR and

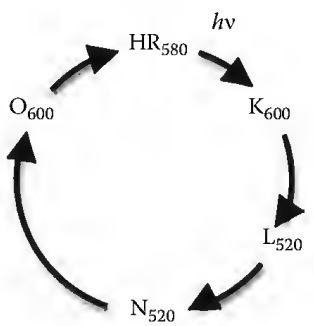

FIGURE 49.5 Photocycle of HR.

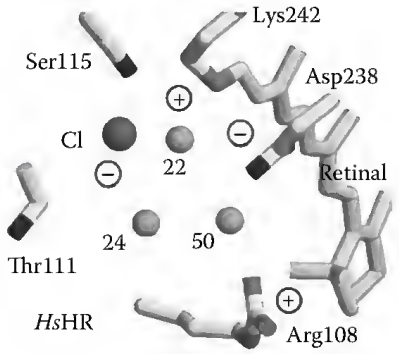

FIGURE 49.6 X-ray structure of the Schiff base region in *Hs*HR.

*Np*HR, respectively. The chloride ion also forms a direct hydrogen bond with a conserved Ser residue (Figure 49.6). Upon formation of the K-intermediate, the Cl^- follows the flipped dipole of the N–H Schiff base bond (see Figure 49.2) and forms a strong hydrogen bond with the PSB. The opening of an EC pathway from the CP release site toward the protein surface was attributed either to a spectroscopically silent transition between two L-like intermediates, L1 and L2, or to an L2↔O transition.[48] According to stopped-flow experiments on *Np*HR, Cl^- uptake itself is mostly ruled by passive diffusion through an EC pathway during later stages of the photocycle.[49] Other features of the transport site have not yet been defined. Thus, compared with BR, the ion transport mechanism of HR is still ambiguous. Of note, genes encoding a HR-like protein have also been found in the eubacterium *Salinibacter ruber*, and in other related species,[1,50] implying that anion pumps are distributed not only in archaea, but also in bacteria.

49.3 Photosensory Rhodopsins

Motile microorganisms, such as bacteria and archaea, sense and respond to EC stimuli to survive in the various environments in which they live, by changing their swimming mode to migrate toward more favorable habitats. This behavior, termed *taxis*, is achieved by a signaling system from membrane-embedded receptors (input) to the flagellar motor (output) (Figure 49.1).[51] Light is one of the most important signals providing critical information to biological systems, and therefore, many organisms utilize light, not only as an energy source, but also as a signal. Similar to vision in vertebrates, microorganisms can also sense light; they show avoidance or attractive behavior from or toward light. In spite of being nonspecific, the behavior is generally called phototaxis; when a cell moves toward a certain wavelength of light, this behavior is designated as positive phototaxis, while behavior in which a cell avoids a certain wavelength of light is designated as negative phototaxis (Figure 49.7). The phototaxis of *H. salinarum* (*halobium*) was the first to be described, and those cells show both positive and negative phototaxis.

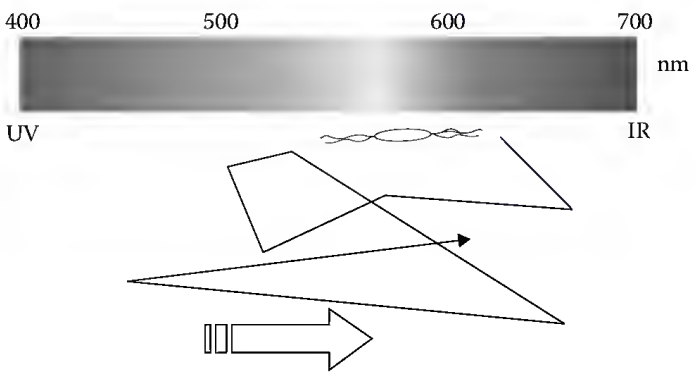

FIGURE 49.7 Phototaxis behavior of *H. salinarum*.

49.3.1 Sensory Rhodopsin I and Sensory Rhodopsin II

What are the receptors (sensors) for phototaxis? The first clue for the receptor was obtained by investigation using a BR minus mutant that was believed to express only HR at that time (in 1983); however, it has since been found that there are two independent (fast and slow) photocycles.[52] The pigment having the slow photocycle was identified as the receptor for phototaxis, and the receptor protein was named sensory rhodopsin I (SRI).[53] Interestingly, the original state of SRI functions as a sensor for the positive phototaxis, whose action maximum is located at ~587 nm, while the long-lived photointermediate, absorbing maximally at 373 nm, works as a sensor for negative phototaxis.[53] In 1985, a fourth retinal protein was discovered in *H. salinarum*, and it functions as a sensor of negative phototaxis, whose action maximum is located at ~500 nm.[14] This retinal protein was named sensory rhodopsin II (SRII) or phoborhodopsin (pR) after its function. Thus, *H. salinarum* is attracted to light with wavelengths longer than 520 nm, and avoids light shorter than 520 nm by SRI and SRII. Light of >520 nm can activate BR and HR to obtain the light-energy, and cells avoid the shorter wavelength light, which contains harmful near-UV (Figures 49.1 and 49.7).[9] Although the function is not yet identified, a third sensory rhodopsin molecule [named sensory rhodopsin III (SRIII)] has been recently found in the halophilic archaeon *Haloarcular marismortui*.[54,55]

In the cell membrane, SRI and SRII form a 2:2 signaling complex with their cognate transducer proteins HtrI and HtrII, respectively.[56,57] Light absorption by SRI and SRII triggers the *trans–cis* photoisomerization of retinal chromophores, leading to the photocycle. The essential photocycle of SRI is SRI (587)→SRI_K(620)→SRI_L(540)→SRI_M(373)→SRI (Figure 49.8).[9] Here, the P520 intermediate is produced by a second photon absorption by the near-UV light. The M- and P-intermediates are thought to be essential for the positive and negative phototaxis, respectively.[53] On the other hand, the essential photocycle of SRII is SRII(498)→$SRII_K$(540)→$SRII_L$(488)→$SRII_M$(390)→$SRII_O$(560)→SRII (Figure 49.8).[58] The M-intermediate of SRII is thought to be essential for the negative phototaxis.[59] During the photocycle, light signals are transmitted from the SRI–HtrI and SRII–HtrII complexes to the CP two-component signal transduction cascade, consisting of the kinases CheA and CheY, which regulates the rotational direction of the flagellar motor, resulting in positive or negative phototaxis.[9] Ion-pumping rhodopsins, such as BR and HR, have been optimized by nature to have relatively fast photocycling rates (~10 ms), making them efficient pumps, whereas the sensory rhodopsins SRI and SRII have slow photocycles, persisting for several seconds, which allow the transient accumulation of long-lived signaling states (M-intermediate) of the receptors to catalyze a sustained phosphorylation cascade. The slow photocycle of sensory rhodopsins is thought to be caused by the lack of Asp96 in BR,[60] which works as a proton donor at the M-state, as described earlier.

The close relationship between the transport and sensory signaling activities of microbial rhodopsins was revealed when SRI was separated from its tight complex with HtrI and was found to exhibit light-driven electrogenic proton transport across the membrane. The transport activity of SRI is blocked by HtrI binding.[61] Such a latent proton transport activity was also shown in SRII and similarly was

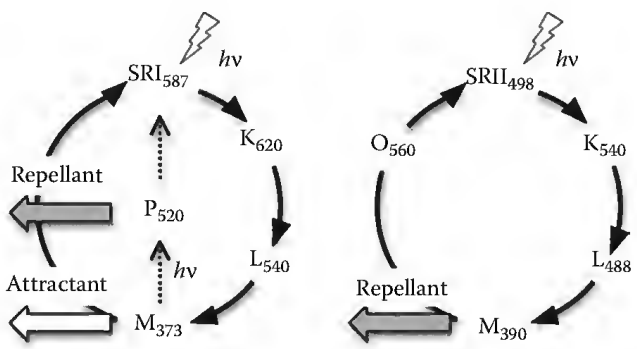

FIGURE 49.8 Photocycles of SRI and SRII.

blocked by HtrII binding.[62] These findings demonstrate that the essential features of the proton transport mechanism are conserved in the signal transduction mechanism of SRI and SRII. Phylogenetic analysis strongly supports the concept that rhodopsin photosensors, like SRI and SRII, evolved from light-driven proton pumps.[1] The pumps function as individual functional units, without the need for interaction with other proteins, and therefore, they readily undergo lateral gene transfer, duplication, and modification to develop a functional interaction with the signal transduction machinery of the new host. What changes would be required to convert a proton pump into a sensory receptor; in other words, how extensive need be the modifications to evolve the new sensory function? The answer to this was resolved by the site-specific mutagenesis of BR to confer the ability to transmit signals through HtrII, which normally exists as a subunit of the SRII–HtrII heterotetrameric complex. As a result, three distinct mutations converted BR into an SRII-like photosensor,[63] and this is discussed in the following.

49.3.2 Signal Transfer Mechanism of the SRII–HtrII Complex

In 2000, the crystal structure of SRII was reported by two independent research groups.[64,65] In their experiments, SRII from *N. pharaonis* (*Np*SRII) was used instead of *H. salinarum* SRII (*Hs*SRII) because *Np*SRII is much more stable than *Hs*SRII, especially in dilute salt solutions, and is much more resistant against detergents.[66,67] The solved atomic structure of *Np*SRII was superimposed on those of BR and *Hs*HR, as shown in Figure 49.9. Although ~74% of residues in *Np*SRII differ from those of BR and *Hs*HR, their crystal structures show close similarities in architecture, helix positions and locations of the retinal-binding pocket, indicating that functional differentiation is regulated by differences in the detailed structures including the amino acid side chain(s), ions, and water molecules. Thus, in spite of the structure being very similar, the question arises of how these proteins function differently? This issue will be discussed later.

The crystal structure of *Np*SRII, bound to an N-terminal fragment of HtrII, provided atomic details of the two proteins' interaction surface in the periplasm and within the membrane (Figure 49.10).[57] The crystal structure of the SRII/HtrII complex suggests the formation of two specific hydrogen bonds, between Tyr199–SRII and Asn74–HtrII, and between Thr189–SRII and Glu43–HtrII/Ser62–HtrII (Figure 49.10). To investigate the importance of these hydrogen bonds, the dissociation constants for the binding of various mutants of BR, HR, SRI, and SRII with HtrII were estimated using isothermal titration calorimetry

FIGURE 49.9 X-ray structure of *Np*SRII with those of BR and HR.

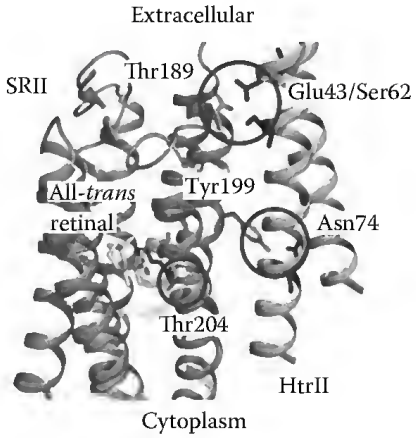

FIGURE 49.10 Interaction surface between SRII and HtrII.

(ITC) and spectroscopic techniques.[68–70] These studies concluded that these two specific hydrogen bonds play important roles in the binding between SRII and HtrII. In addition, an interaction of the HtrII membrane-proximal domain with the CP domain of SRII has been demonstrated by various biophysical and spectroscopic techniques.[71–75] From these experiments, the stoichiometry of the SRII–HtrII complex is estimated as 1:1, which is in accord with the 2:2 stoichiometry resolved by x-ray structure.

A clue about the signal relay mechanism from SRII to HtrII was obtained from the FTIR data. The dark minus K difference spectra of SRII possess positive and negative vibrational bands of SRII at 3479(–)/3369(+) cm^{-1}, which are observed only in the presence of HtrII.[76] Mutational studies showed that the bands originate from the O–H stretch of Thr204,[77] which indicates that a stronger hydrogen bonding alteration of Thr204 takes place upon the retinal photoisomerization (Figure 49.11, upper panel).

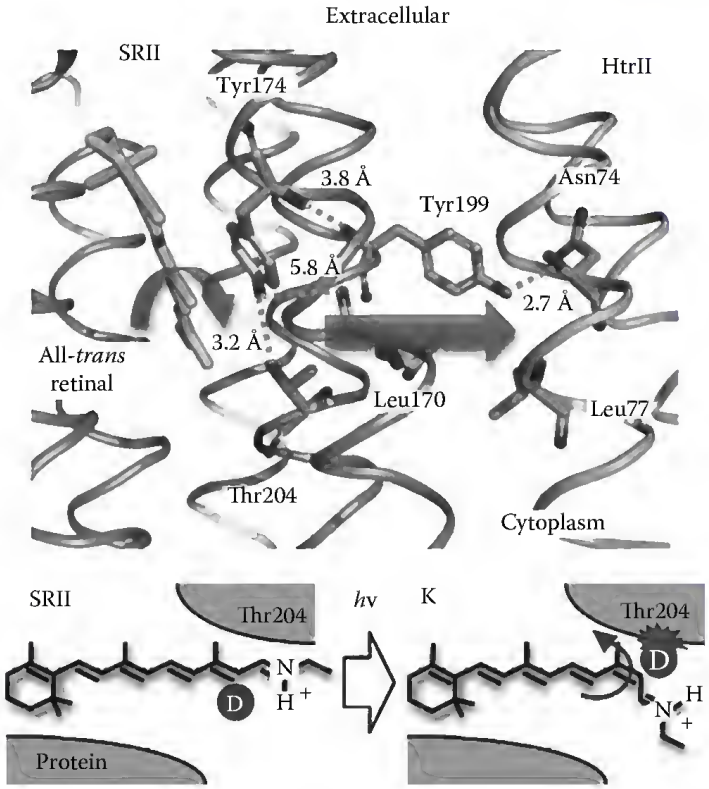

FIGURE 49.11 Structural changes upon formation of the K-intermediate of SRII.

The structural changes are important for the HtrII activation by SRII at the following intermediates. In fact, mutations of Thr204, and its hydrogen-bonding residue Tyr174, disrupt the negative phototaxis function.[78] In addition, using deuterated retinal analogs, it was demonstrated that a regiospecific steric hindrance between the C14–H group of the retinal (see Figure 49.2) and Thr204 occurs upon formation of the K-intermediate (Figure 49.11, lower panel).[79] Although $SRII_K$ is not considered to be an active state (signaling state), the A215T mutant of BR, which corresponds to Thr204 of SRII, confers weak phototaxis signaling activity, and structural changes, upon formation of the K-intermediate of the A215T, which are quite similar to the structural changes of SRII.[80] The signaling is greatly enhanced by two additional substitutions, P200T and V210Y, which correspond to Thr189 and Tyr199 of SRII, respectively, indicating that the BR triple mutant (BR-T) transmits light signals to the motility apparatus through the HtrII protein.[63] The interpretation of these findings is that the hydrogen bonds of Thr189–Glu43/Ser62 and Tyr199–Asn74 that pin the receptor to the transducer are important for aligning the two proteins, but do not necessarily participate significantly in the signal relay process. Therefore, remarkably, it appears that a single hydrogen bond (i.e., that between Thr204 and Tyr174 in SRII) determines the essential difference between a sensory receptor and a proton pump in the microbial rhodopsin family. These results suggest a chemical mechanism for the signaling that entails an initial storage of the energy of photoisomerization in SRII's hydrogen bond between Tyr174, which is in contact with retinal, and Thr204, which borders residues on the SRII surface in contact with HtrII. This is followed by the transfer of this chemical energy to drive structural transitions in the transducer helices. These results also demonstrate that the distinct functions of active transport and signaling can be produced by a small number of modifications of the same protein structure, and the nature of the changes needed to convert the proton pump BR into a signaling receptor provides insight into the essential core of the signal relay mechanism.

Although it has been concluded that the M-intermediate is one of the active (signaling) states from the studies of *Hs*SRII,[59] this is also considered valid for *Np*SRII. Upon formation of the $SRII_M$, the primary proton transfer occurs from the Schiff base to the proton acceptor, Asp75, which is a counterion of the PSB, as well as BR.[81] It is known that the photo-dependent structural changes of BR occur at the CP ends of helices F and G upon formation of the M-intermediate (and/or the N-intermediate). These movements open a narrow water-accessible channel in the protein,[33] which enables the transfer of a proton from the proton-donating Asp residue to the Schiff base nitrogen. Similar helix movements of SRII, an outward tilting of helix F, during the photocycle are also suggested by various studies,[82–84] and they are thought to be an essential step for the HtrII activation. Also the HAMP domain of HtrII, a 50 aminoacid segment which is conserved among histidine kinases, adenylyl cyclases, methyl accepting chemotaxis proteins (MCPs) and phosphatases, is thought to have a critical role in the signaling.

On the basis of these results, and other findings, a model for the signal transduction by the SRII–HtrII system was proposed as follows (Figure 49.12)[51]: (i) *trans–cis* photoisomerization of the retinal chromophore, (ii) steric hindrance between C14–H of retinal and Thr204, (iii) hydrogen bonding alteration between Thr204 and Tyr174, (iv) F-helix outward tilting of SRII, (v) TM-2 rotation of HtrII, (vi) dissociation of the HAMP domain of HtrII from SRII, (vii) structural changes of the highly conserved domain (HCD), and (viii) activation (phosphorylation) of CheA.

49.3.3 Signal Transfer Mechanism of the SRI–HtrI Complex

SRI has received considerable attention because of its function in mediating opposing signals (on/off switching of CheA), depending on different colors of light, by the photochromic reaction as described earlier. However, compared with SRII, little is known about the molecular mechanism(s) of interactions between SRI and HtrI, about structural changes, or about the signal relay mechanism of the phototaxis. One reason is that SRI from *H. salinarum* (*Hs*SRI) is unstable in various conditions, and its inherent instability hampers the elucidation of its molecular mechanism.[22] In fact, the x-ray crystal structures of BR, HR, SRII, and the SRII/HtrII complex have been solved over the past 10 years; however, almost no structural information at the atomic level has been obtained for SRI. Spudich and coworkers have

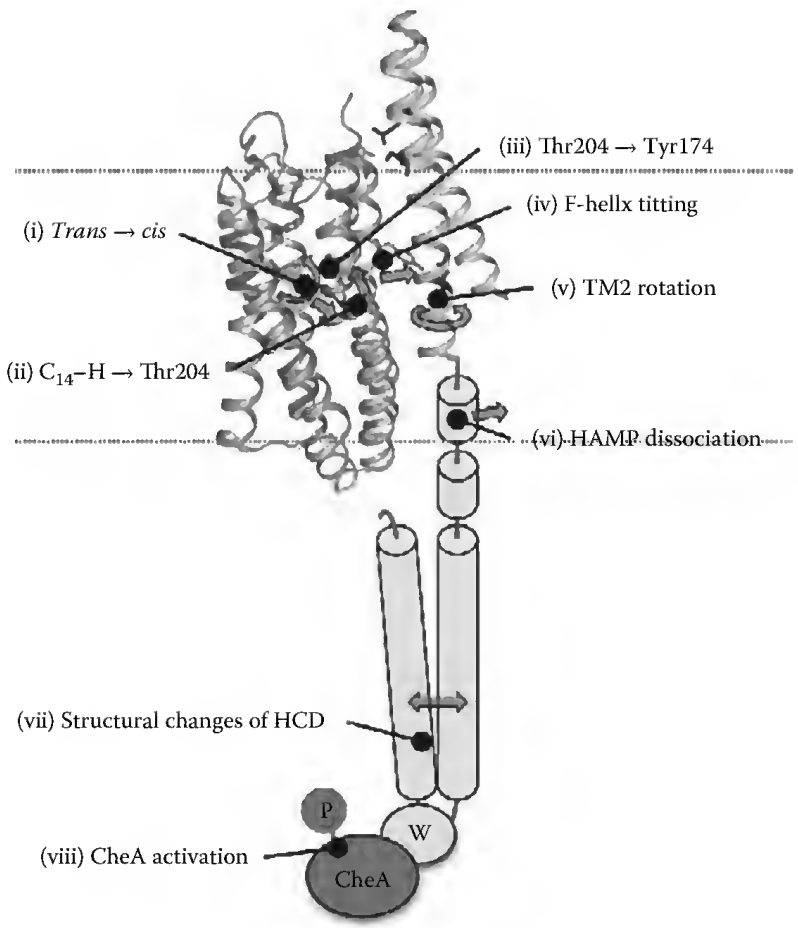

FIGURE 49.12 Model for signal transduction mechanism of SRII–HtrII complex.

proposed a model for the signal transduction by the SRI–HtrI system on the basis of experimental evidence (Figure 49.13).[85,86] As described earlier, the PSB plays an essential role in the functions of microbial rhodopsins, deprotonating in the first half of the photocycle, by transferring its proton to an Asp (counterion) residue in the EC half-channel, and reprotonating in the second half of the cycle from the Asp residue in the CP channel. In the ion-pumping rhodopsins, the key step, known as the "Schiff base connectivity switch," consists of a structural change of the photoactive site that occurs in the photocycle and changes the accessibility of the retinylidene Schiff base nitrogen from the EC to the CP channel. In the dark, the SRI–HtrI complex exists in two conformational states, which differ by their connection of the Schiff base in the SRI photoactive site to inner or outer half-channels. In single-quantum photochemical reactions, the conformer with the Schiff base connected to the CP half-channel generates an attractant signal, whereas the conformer with the Schiff base connected to the EC half-channel generates a repellent signal. The opposite signals from the two conformers are integrated in the downstream transduction pathways, leading to one or the other sign of the behavioral response. In the wild-type SRI–HtrI complex, the conformer equilibrium is poised strongly in favor of that with the CP-accessible Schiff base. The inverting mutations shift the equilibrium in favor of the EC-accessible Schiff base form, whereas the suppressor mutations shift the equilibrium back toward the CP-accessible Schiff base form, restoring the wild-type phenotype. This implies that the sign of the behavioral response directly correlates with the state of the connectivity switch.

In an effort to improve the stability of *Hs*SRI, a novel SRI protein from the eubacterium *S. ruber* (*Sr*SRI) was cloned and characterized with its transducer protein, *Sr*HtrI.[22] *Sr*SRI is the first eubacterial SRI identified as a functional protein, and it has all-*trans* retinal as a chromophore, with an absorption maximum

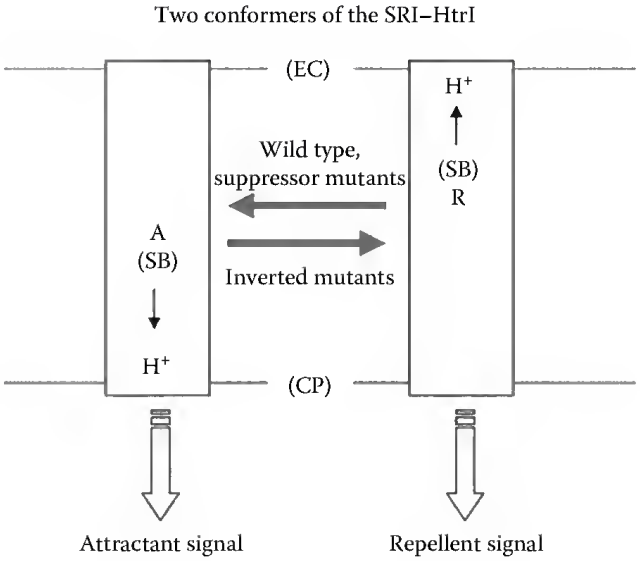

FIGURE 49.13 Model for signal transduction mechanism of SRI–HtrI complex.

at a longer wavelength (557 nm) than SRII (500 nm). It also has a slower photocycle than the light-driven ion-pumping rhodopsins,[22] indicating similarities to the prototypic SRI (*Hs*SRI). *Sr*SRI was expressed in *Escherichia coli* and shows high protein stability, even in various detergent micelles, making it possible to prepare large amounts of protein. This also allows new approaches to investigate the photo-signaling process in the SRI–HtrI system. In fact, it provided new information about structural changes[87] and Cl^- binding,[88] which are conserved in SRI from the archaeon *Haloarcula vallismortis* (*Hv*SRI).[89] In the original state, the absorption maximum of *Sr*SRI is shifted from 542 to 556 nm, in a Cl^--dependent manner, with a Kd of ~300 mM. The bathochromic spectral shift was caused not only by NaCl, but also by other salts (NaI, NaBr, and $NaNO_3$), implying that anion-binding (I^-, Br^-, and NO_3^-) site(s) exist in *Sr*SRI. A conserved residue, His131, was identified to be a residue involved in the Cl^--binding site.[88] It was assumed that a positive charge located on the Schiff base nitrogen moves to the β-ionone ring of the retinal chromophore by chloride ion binding to His131 (Figure 49.14). Although the high-resolution structure of SRI has not yet been solved, it is predicted that the space around His131 is significantly narrow for the Cl^- binding, suggesting large structural changes of *Sr*SRI upon Cl^- binding. Interestingly, *Hv*SRI exhibited similar alterations due to chloride ion binding.[89] The binding to *Sr*SRI is likely to be important for the function of the SRI protein family.

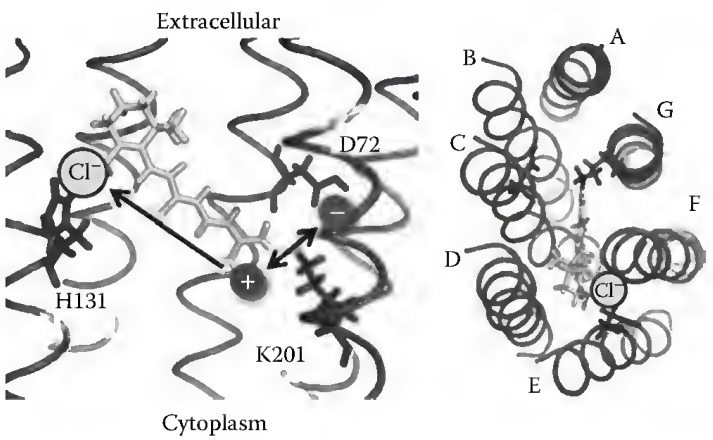

FIGURE 49.14 Structural model of SRI and its identified Cl^--binding site.

Recently, FTIR spectroscopy was performed with *Sr*SRI, and the spectral changes were compared with those of other archaeal rhodopsins (BR, HR, and SRII).[87] Briefly, in the K-intermediate, the extended chromophore distortion takes place in *Sr*SRI and *Hs*SRI, as well as in SRII and BR-T, as judged by the hydrogen-out-of plane (HOOP) vibrations of the retinal chromophore, whereas the distortion is localized in the Schiff base region in BR and HR. It appears that the sensor and pump functions are distinguishable from the spectral feature of the HOOP modes. The C14–HOOP band at 864 cm^{-1} for *Np*SRII, which is important for negative phototaxis in SRII, is absent in *Sr*SRI, suggesting that the changes of C14–H HOOP are a specific feature among sensors for negative phototaxis. This is reasonable because the counterpart of the C14 atom, Thr204 of SRII, is not conserved in other microbial rhodopsins, including SRIs. In the M-intermediate, the frequency shifts of amide-I and amide-A vibrations, which probe structural changes in the α-helix, were opposite between SRI and SRII, where a downshift and an upshift were observed, respectively. This indicates that the M formation accompanies a weakened hydrogen bond of the α-helix in SRI, but a strengthened hydrogen bond of the α-helix in SRII. In other words, activation of SRI or SRII may involve breakage or formation of the helical structure. The different modes in protein structural changes between SRI and SRII are consistent with a model proposed by Spudich and coworkers[86] and may correlate with their functional differences. Thus, as expected, *Sr*SRI can be a key protein to investigate the functions of SRI at the molecular level.

49.4 New Types of Microbial Rhodopsins

Since the discovery of BR, "rhodopsins" had been thought to be unique proteins, found only in extremely halophilic archaea, and in animal photoreceptors, for nearly three decades. It was concluded as merely a coincidence that these two groups of rhodopsins have common features because of their large differences in primary structure, and the lack of evolutionary evidence to link them. However, new discoveries started at the end of the last century when the techniques in mass genome sequencing and bioinformatics started to advance dramatically. Today, the number of rhodopsin genes identified is up to several thousand and keeps growing (Figure 49.15).[1] Most of them are found

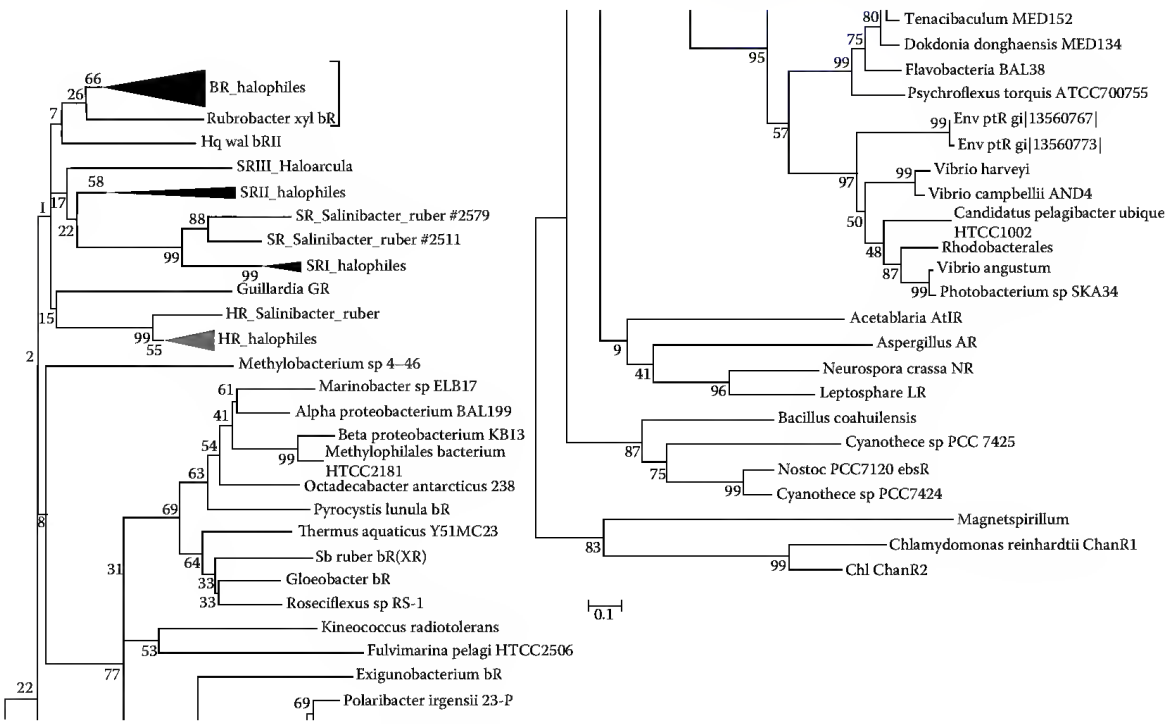

FIGURE 49.15 Microbial rhodopsins from various species.

in eubacteria and fungi, and are therefore of microbial origin, and are presumed to have some evolutionary relationship to the well-studied archaeal rhodopsins.

49.4.1 Fungal Rhodopsins

The first microbial rhodopsin discovered outside the archaea was identified as the *nop-1* gene of *Neurospora crassa*.[90] Nop-1 (NR) was successfully bound to retinal after heterologous expression in *Pichia pastries*, and its photocycle was characterized.[91] A homologous gene of *nop-1* was also found in another ascomycete *Leptosphaeria maculans*. This fungal rhodopsin, LR, has an aspartic acid in place of the proton donor of the PSB. Unlike NR, spectroscopic studies showed that reconstituted LR can transfer protons as efficiently as BR.[20,92] Replacement of the Asp residue (proton donor) of LR to Glu resulted in an NR-like conversion of LR.[93,94] Even though NR and LR are successful examples of spectroscopically characterized fungal rhodopsins, genome-sequencing projects, and bioinformatics, have identified several hundreds of other fungal rhodopsins.[35] According to the residue conservation at the proton donor position, and the Lys residue on the G helix, these fungal rhodopsin genes can be classified into three groups: NR-like rhodopsins, LR-like rhodopsins, and those without the capability of covalent bonding with retinal. So what are their functions? Since LR shows significant resemblance in photocycle and photokinetics with BR, LR-type rhodopsins are probably relevant in photosynthesis, as is BR in archaea. On the other hand, NR has a very slow photocycle, which suggests that maintenance of an intermediate state itself has relevance, as in the case of SRI and SRII. *nop-1* is not photoinducible and is negatively regulated by blue light, which NR does not absorb. Also, *nop-1* expression increases as conidiation proceeds, and the NR level influences some other conidiation genes.[6] This evidence supports the sensory role of NR and some kind of signal transduction in the conidiation gene cascade.

49.4.2 Proteorhodopsins

The first eubacterial rhodopsin discovered was identified in an uncultivated (or more precisely unculturable) gammaproteobacterium.[37] This protein demonstrates BR-like light-driven proton transport and is called PR. Later, the presence of PR was confirmed in a bacterioplankton membrane fraction, taken from oceanic surface water, and its density in the membrane was estimated to be similar to that of BR,[38] suggesting there is a significant physiological role for PR in the bacterium. PR has two aspartates, consisting of a proton donor, and an acceptor (homologs of Asp85 and Asp96 in BR), although the latter is replaced by glutamate, whereas EC glutamates constituting the proton-releasing complex in BR are missing. Biochemical and biophysical studies have been performed with PR over the past 10 years. Briefly, although there are several notable differences between PR and BR, it is concluded that the structure and structural changes of PR are very similar to those of BR, indicating that the proton gradient produced by PR is utilized by ATP synthesis, generating biochemical energy from light. The potential influence of PR-based light-driven energy flux in ocean ecosystems would be significant, but is still difficult to quantify directly. Of note, PR-like proteins are also found in eubacterial groups other than proteobacteria.[6]

49.4.3 Rhodopsins with Auxiliary Carotenoid Antenna

The extreme halophile *S. ruber* has been found to have a proton-pumping rhodopsin XR with an additional carotenoid, salinixanthin, as a light-harvesting antenna.[40] XR has similarity in its primary structure with both BR and PR, and attaching salinixanthin to XR almost doubles the flow of light quanta to energize proton transport.[40] The efficiency of energy transfer from salinixanthin to retinal has been calculated as approximately 45%.[40,95] The crystallographic structure of XR revealed that salinixanthin lies on the outer surface of the F-helix, with its keto-ring immobilized between the EC ends of the E and F helices, and placed within van der Waals distance of the retinal β-ionone (Figure 49.16).[96] The Schiff

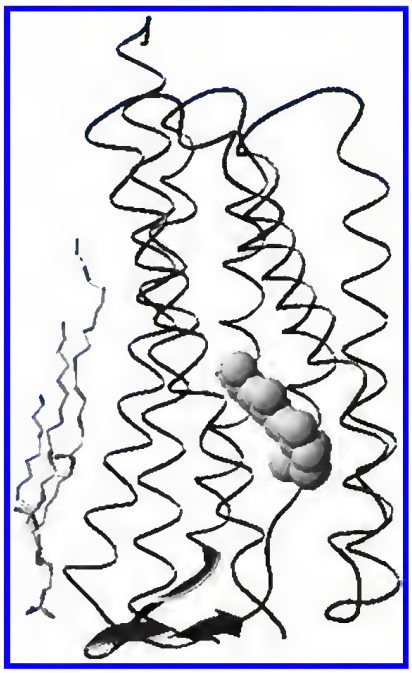

FIGURE 49.16 X-ray structure of XR, with salinixanthin as light-harvesting antenna.

base proton donor of XR is Glu (as in PR), but this Glu side chain does not make hydrogen bond coupling with the Ser residue (as does PR), but forms a hydrogen bond with a water molecule (Wat-502) that connects to the carbonyl of the retinal-bound Lys residue.[96]

In the sequence alignment, XR appears between BR and PR, but there is another rhodopsin from cyanobacterium *Gloeobacter violaceus* (GR), which has a significant sequence similarity with XR. In the dark state, GR contains primarily all-*trans* retinal, but replacement of the proton donor Glu residue significantly increases the 13-*cis* content, which had been seen for BR mutants, but not for the homologous mutant of PR.[21] The photocycle of GR over-expressed in *E. coli* is much like PR, having a low accumulation of the M-intermediate, and proton uptake preceding proton release.[21] The most interesting similarities with XR lie in the E and F helices, where salinixanthin docks on XR. In BR, the space where the keto-ring of salinixanthin, and the adjacent Tyr ring, is immobilized in XR is occupied by two Trp rings. GR has an almost identical feature for this with XR, and reconstitution of GR with salinixanthin was performed, and the change in action spectra was observed, which resembles that of XR.[97]

49.4.4 Anabaena Sensory Rhodopsin

In 2003, the first bacterial sensory rhodopsin was identified in the freshwater cyanobacterium *Anabaena* PCC7120 and was named ASR.[19] Sensory rhodopsin-like genes and Htr-like genes were also discovered in proteobacteria through the genome-sequencing projects, although the properties of those proteins have not yet been identified because of the difficulty of heterologously expressing them. ASR is encoded in an operon, along with a second gene that encodes a small soluble CP protein, named the ASR transducer (ASRT).[19] This is very different from the haloarchaeal phototaxis transducers, HtrI and HtrII, which are membrane-embedded proteins. Crystallographic analysis revealed the photochromic nature of ASR, and the water molecule network in its CP half region, where it possibly interacts with ASRT (Figure 49.17).[98,99] ASR accommodates both all-*trans* and 13-*cis* retinal in the original state, which can be interconverted by illumination with blue (480 nm) or orange (590 nm) light.[100] Such photochromic behavior has never been observed in other archaeal rhodopsins such as BR, HR, SRI, and SRII and is characteristic to ASR. Therefore, ASR is the first rhodopsin that exhibits a photochromic reaction, and now, it has been determined that all photochemical reactions of ASR are photochromic, and there is

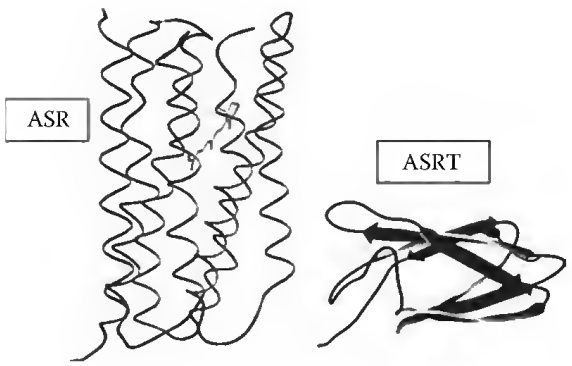

FIGURE 49.17 X-ray structures of ASR (left) and ASRT (right).

no photocycle such as those observed in all other microbial rhodopsins.[101] ASRT forms tetramers in solution, and the ASRT tetramer binds to ASR with a stoichiometry of one ASRT tetramer per one ASR with a dissociation constant of 8μM. What are the functional roles of ASR and ASRT? One possible possibility is the regulation of gene expression in response to light intensity and/or quality. This control could occur via direct transcriptional regulation by ASRT (making ASRT a transcription factor) or via transcription factors further downstream in an uncharacterized signaling cascade.[99]

49.4.5 Channelrhodopsins

Two rhodopsins (ChR1 and ChR2) that account for the phototactic behaviors of *Chlamydomonas* were identified in 2002.[16,17] Both rhodopsins function as direct light-gated cation-selective ion channels, but they differ in the saturating light intensity (e.g., ChR1 saturates with higher-intensity light).[17] Although both rhodopsins can conduct Na^+, K^+, and Ca^{2+} at a similar rate, the conductance of both rhodopsins for these ions is much smaller than that for protons,[18] that is, these two rhodopsins basically function as proton channels to quickly depolarize the plasma membrane, especially when illuminated with light intensity sufficient to saturate the ChR1 population. However, the delayed rise, and slower decay, of biochemically amplified current (or the photoreceptor current under lower-intensity light) is mediated by ChR2, and this long-lived conducting state is essential for low-intensity light excitation to cause any change in flagellar movement.[102] In addition, ChR1 consists of two isoforms with different absorption maxima that are in a pH-dependent equilibrium; thus, the photochemical nature of ChR1 is photochromic and protochromic.[103] By taking advantage of ChR2 producing a long half-life current, ChR2 has been widely utilized as a tool to control membrane potential, which seems to have potential to cure blindness, and to control synaptic activity.[104,105]

In conclusion, rhodopsins are widely spread in the microbial world, and despite showing close similarities in architecture, they display a large variety of different functions, including, but not limited to, ion transporters, photosensors, and ion channels.

Acknowledgment

This work was also supported by grants from the Japanese Ministry of Education, Culture, Sports, Science, and Technology.

References

1. Sharma, A.K., Spudich, J.L., and Doolittle, W.F., Microbial rhodopsins: Functional versatility and genetic mobility, *Trends Microbiol.*, 14, 463, 2006.
2. Hofmann, K.P., Scheerer, P., Hildebrand, P.W., Choe, H.W., Park, J.H., Heck, M., and Ernst, O.P., A G protein-coupled receptor at work: The rhodopsin model, *Trends Biochem. Sci.*, 34, 540, 2009.

3. Spudich, J.L., Yang, C.S., Jung, K.H., and Spudich, E.N., Retinylidene proteins: Structures and functions from archaea to humans, *Annu. Rev. Cell Dev. Biol.*, 16, 365, 2000.
4. Costanzi, S., Siegel, J., Tikhonova, I.G., and Jacobson, K.A., Rhodopsin and the others: A historical perspective on structural studies of G protein-coupled receptors, *Curr. Pharm. Des.*, 15, 3994, 2009.
5. Tsukamoto, H. and Terakita, A., Diversity and functional properties of bistable pigments, *Photochem. Photobiol. Sci.*, 9, 1435–1443, 2010.
6. Brown, L.S. and Jung, K.H. Bacteriorhodopsin-like proteins of eubacteria and fungi: The extent of conservation of the haloarchaeal proton-pumping mechanism, *Photochem. Photobiol. Sci.*, 5, 538, 2006.
7. Sharma, A.K., Zhaxybayeva, O., Papke, R.T., and Doolittle, W.F., Actinorhodopsins: Proteorhodopsin-like gene sequences found predominantly in non-marine environments, *Environ. Microbiol.*, 10, 1039, 2008.
8. Lanyi, J.K., Bacteriorhodopsin, *Annu. Rev. Physiol.*, 66, 665, 2004.
9. Hoff, W.D., Jung, K.H., and Spudich, J.L., Molecular mechanism of photosignaling by archaeal sensory rhodopsins, *Annu. Rev. Biophys. Biomol. Struct.*, 26, 223, 1997.
10. Oesterhelt, D. and Stoeckenius, W., Rhodopsin-like protein from the purple membrane of *Halobacterium halobium*, *Nat. New Biol.*, 233, 149, 1971.
11. Matsuno-Yagi, A. and Mukohata, Y., Two possible roles of bacteriorhodopsin; A comparative study of strains of *Halobacterium halobium* differing in pigmentation, *Biochem. Biophys. Res. Commun.*, 78, 237, 1977.
12. Lanyi, J.K., Light-driven primary sodium ion transport in *Halobacterium halobium* membranes, *J. Supramol. Struct.*, 13, 83, 1980.
13. Spudich, J.L. and Bogomolni, R.A., Spectroscopic discrimination of the three rhodopsinlike pigments in *Halobacterium halobium* membranes, *Biophys. J.*, 43, 243, 1983.
14. Takahashi, T., Tomioka, H., Kamo, N., and Kobatake, Y., A photosystem other than PS370 also mediates the negative phototaxis of *Halobacterium halobium*, *FEMS Microbiol. Lett.*, 28, 161, 1985.
15. Spudich, J.L., The multitalented microbial sensory rhodopsins, *Trends Microbiol.*, 14, 480, 2006.
16. Nagel, G., Ollig, D., Fuhrmann, M., Kateriya, S., Musti, A.M., Bamberg, E., and Hegemann, P., Channelrhodopsin-1: A light-gated proton channel in green algae, *Science*, 296, 2395, 2002.
17. Sineshchekov, O.A., Jung, K.H., and Spudich, J.L., Two rhodopsins mediate phototaxis to low- and high-intensity light in Chlamydomonas reinhardtii, *Proc. Natl. Acad. Sci. USA*, 99, 8689, 2002.
18. Nagel, G., Szellas, T., Huhn, W., Kateriya, S., Adeishvili, N., Berthold, P., Ollig, D., Hegemann, P., and Bamberg, E., Channelrhodopsin-2, a directly light-gated cation-selective membrane channel, *Proc. Natl. Acad. Sci. USA*, 100, 13940, 2003.
19. Jung, K.H., Trivedi, V.D., and Spudich, J.L., Demonstration of a sensory rhodopsin in eubacteria, *Mol. Microbiol.*, 47, 1513, 2003.
20. Waschuk, S.A., Bezerra, A.G., Jr., Shi, L., and Brown, L.S., *Leptosphaeria rhodopsin*: Bacteriorhodopsin-like proton pump from a eukaryote, *Proc. Natl. Acad. Sci. USA*, 102, 6879, 2005.
21. Miranda, M.R., Choi, A.R., Shi, L., Bezerra, A.G., Jr., Jung, K.H., and Brown, L.S., The photocycle and proton translocation pathway in a cyanobacterial ion-pumping rhodopsin, *Biophys. J.*, 96, 1471, 2009.
22. Kitajima-Ihara, T., Furutani, Y., Suzuki, D., Ihara, K., Kandori, H., Homma, M., and Sudo, Y., *Salinibacter* sensory rhodopsin: Sensory rhodopsin I-like protein from a eubacterium, *J. Biol. Chem.*, 283, 23533, 2008.
23. Cartailler, J.P. and Luecke, H., X-ray crystallographic analysis of lipid–protein interactions in the bacteriorhodopsin purple membrane, *Annu. Rev. Biophys. Biomol. Struct.*, 32, 285, 2003.
24. Hirai, T., Subramaniam, S., and Lanyi, J.K., Structural snapshots of conformational changes in a seven-helix membrane protein: Lessons from bacteriorhodopsin, *Curr. Opin. Struct. Biol.*, 19, 433, 2009.
25. Luecke, H., Schobert, B., Richter, H.T., Cartailler, J.P., and Lanyi, J.K., Structure of bacteriorhodopsin at 1.55 A resolution, *J. Mol. Biol.*, 291, 899, 1999.

26. Lanyi, J.K., Crystallographic studies of the conformational changes that drive directional transmembrane ion movement in bacteriorhodopsin, *Biochim. Biophys. Acta*, 1459, 339, 2000.
27. Lanyi, J.K., X-ray diffraction of bacteriorhodopsin photocycle intermediates, *Mol. Membr. Biol.*, 21, 143, 2004.
28. Kandori, H., Role of internal water molecules in bacteriorhodopsin, *Biochim. Biophys. Acta*, 1460, 177, 2000.
29. Mogi, T., Stern, L.J., Marti, T., Chao, B.H., and Khorana, H.G., Aspartic acid substitutions affect proton translocation by bacteriorhodopsin, *Proc. Natl. Acad. Sci. USA*, 85, 4148, 1988.
30. Shibata, M., Tanimoto, T., and Kandori, H., Water molecules in the schiff base region of bacteriorhodopsin, *J. Am. Chem. Soc.*, 125, 13312, 2003.
31. Furutani, Y., Shibata, M., and Kandori, H., Strongly hydrogen-bonded water molecules in the Schiff base region of rhodopsins, *Photochem. Photobiol. Sci.*, 4, 661, 2005.
32. Shibata, M. and Kandori, H., FTIR studies of internal water molecules in the Schiff base region of bacteriorhodopsin, *Biochemistry*, 44, 7406, 2005.
33. Lanyi, J.K., Proton transfers in the bacteriorhodopsin photocycle, *Biochim. Biophys. Acta*, 1757, 1012, 2006.
34. Kandori, H., Hydration switch model for the proton transfer in the Schiff base region of bacteriorhodopsin, *Biochim. Biophys. Acta*, 1658, 72, 2004.
35. Brown, L.S., Fungal rhodopsins and opsin-related proteins: Eukaryotic homologues of bacteriorhodopsin with unknown functions, *Photochem. Photobiol. Sci.*, 3, 555–565, 2004.
36. Jung, K.H., The distinct signaling mechanisms of microbial sensory rhodopsins in Archaea, Eubacteria and Eukarya, *Photochem. Photobiol.*, 83, 63, 2007.
37. Beja, O., Aravind, L., Koonin, E.V., Suzuki, M.T., Hadd, A., Nguyen, L.P., Jovanovich, S.B., Gates, C.M., Feldman, R.A., Spudich, J.L., Spudich, E.N., and DeLong, E.F., Bacterial rhodopsin: Evidence for a new type of phototrophy in the sea, *Science*, 289, 1902, 2000.
38. Beja, O., Spudich, E.N., Spudich, J.L., Leclerc, M., and DeLong, E.F., Proteorhodopsin phototrophy in the ocean, *Nature*, 411, 786, 2001.
39. Tsunoda, S.P., Ewers, D., Gazzarrini, S., Moroni, A., Gradmann, D., and Hegemann, P., H^+-pumping rhodopsin from the marine alga Acetabularia, *Biophys. J.*, 91, 1471, 2006.
40. Balashov, S.P., Imasheva, E.S., Boichenko, V.A., Anton, J., Wang, J.M., and Lanyi, J.K., Xanthorhodopsin: A proton pump with a light-harvesting carotenoid antenna, *Science*, 309, 2061, 2005.
41. Lanyi, J.K., Halorhodopsin: A light-driven chloride ion pump, *Annu. Rev. Biophys. Biophys. Chem.*, 15, 11, 1986.
42. Essen, L.O., Halorhodopsin: Light-driven ion pumping made simple? *Curr. Opin. Struct. Biol.*, 12, 516, 2002.
43. Sasaki, J., Brown, L.S., Chon, Y.S., Kandori, H., Maeda, A., Needleman, R., and Lanyi, J.K., Conversion of bacteriorhodopsin into a chloride ion pump, *Science*, 269, 73, 1995.
44. Varo, G., Analogies between halorhodopsin and bacteriorhodopsin, *Biochim. Biophys. Acta*, 1460, 220, 2000.
45. Kolbe, M., Besir, H., Essen, L.O., and Oesterhelt, D., Structure of the light-driven chloride pump halorhodopsin at 1.8 Å resolution, *Science*, 288, 1390–1396, 2000.
46. Kouyama, T., Kanada, S., Takeguchi, Y., Narusawa, A., Murakami, M., and Ihara, K., Crystal structure of the light-driven chloride pump halorhodopsin from *Natronomonas pharaonis*, *J. Mol. Biol.*, 396, 564, 2010.
47. Oesterhelt, D., The structure and mechanism of the family of retinal proteins from halophilic archaea, *Curr. Opin. Struct. Biol.*, 8, 489, 1998.
48. Haupts, U., Tittor, J., and Oesterhelt, D., Closing in on bacteriorhodopsin: Progress in understanding the molecule, *Annu. Rev. Biophys. Biomol. Struct.*, 28, 367, 1999.
49. Sato, M., Kubo, M., Aizawa, T., Kamo, N., Kikukawa, T., Nitta, K., and Demura, M., Role of putative anion-binding sites in cytoplasmic and extracellular channels of *Natronomonas pharaonis* halorhodopsin, *Biochemistry*, 44, 4775, 2005.

50. Mongodin, E.F., Nelson, K.E., Daugherty, S., Deboy, R.T., Wister, J., Khouri, H., Weidman, J., Walsh, D.A., Papke, R.T., Sanchez Perez, G., Sharma, A.K., Nesbo, C.L., MacLeod, D., Bapteste, E., Doolittle, W.F., Charlebois, R.L., Legault, B., and Rodriguez-Valera, F., The genome of *Salinibacter ruber*: Convergence and gene exchange among hyperhalophilic bacteria and archaea, *Proc. Natl. Acad. Sci. USA*, 102, 18147, 2005.
51. Suzuki, D., Irieda, H., Homma, M., Kawagishi, I., and Sudo, Y., Phototactic and chemotactic signal transduction by transmembrane receptors and transducers in microorganisms, *Sensors*, 10, 4010, 2010.
52. Hazemoto, N., Kamo, N., Terayama, Y., Kobatake, Y., and Tsuda, M., Photochemistry of two rhodopsinlike pigments in bacteriorhodopsin-free mutant of *Halobacterium halobium*, *Biophys. J.*, 44, 59, 1983.
53. Spudich, J.L. and Bogomolni, R.A. Mechanism of colour discrimination by a bacterial sensory rhodopsin, *Nature*, 312, 509, 1984.
54. Fu, H.Y., Lin, Y.C., Chang, Y.N., Tseng, H., Huang, C.C., Liu, K.C., Huang, C.S., Su, C.W., Weng, R.R., Lee, Y.Y., Ng, W.V., and Yang, C.S., A novel six-rhodopsin system in a single archaeon, *J. Bacteriol.*, 192, 5866, 2010.
55. Nakao, Y., Kikukawa, T., Shimono, K., Tamogami, J., Kimitsuki, N., Nara, T., Unno, M., Ihara, K., and Kamo, N., Photochemistry of a putative new class of sensory rhodopsin (SRIII) coded by xop2 of *Haloarcular marismortui*, *J. Photochem. Photobiol. B.*, 102, 45, 2011.
56. Chen, X. and Spudich, J.L., Demonstration of 2:2 stoichiometry in the functional SRI–HtrI signaling complex in *Halobacterium* membranes by gene fusion analysis, *Biochemistry*, 41, 3891, 2002.
57. Gordeliy, V.I., Labahn, J., Moukhametzianov, R., Efremov, R., Granzin, J., Schlesinger, R., Buldt, G., Savopol, T., Scheidig, A.J., Klare, J.P., and Engelhard, M., Molecular basis of transmembrane signalling by sensory rhodopsin II-transducer complex, *Nature*, 419, 484, 2002.
58. Kamo, N., Shimono, K., Iwamoto, M., and Sudo, Y., Photochemistry and photoinduced proton-transfer by pharaonis phoborhodopsin, *Biochemistry-Moscow*, 66, 1277, 2001.
59. Yan, B., Takahashi, T., Johnson, R., and Spudich, J.L., Identification of signaling states of a sensory receptor by modulation of lifetimes of stimulus-induced conformations: The case of sensory rhodopsin II, *Biochemistry*, 30, 10686, 1991.
60. Iwamoto, M., Shimono, K., Sumi, M., and Kamo, N., Positioning proton-donating residues to the Schiff-base accelerates the M-decay of pharaonis phoborhodopsin expressed in *Escherichia coli*, *Biophys. Chem.*, 79, 187, 1999.
61. Bogomolni, R.A., Stoeckenius, W., Szundi, I., Perozo, E., Olson, K.D., and Spudich, J.L., Removal of transducer HtrI allows electrogenic proton translocation by sensory rhodopsin I, *Proc. Natl. Acad. Sci. USA*, 91, 10188, 1994.
62. Sudo, Y., Iwamoto, M., Shimono, K., Sumi, M., and Kamo, N., Photo-induced proton transport of pharaonis phoborhodopsin (sensory rhodopsin II) is ceased by association with the transducer, *Biophys. J.*, 80, 916, 2001.
63. Sudo, Y. and Spudich, J.L., Three strategically placed hydrogen-bonding residues convert a proton pump into a sensory receptor, *Proc. Natl. Acad. Sci. USA*, 103, 16129, 2006.
64. Royant, A., Nollert, P., Edman, K., Neutze, R., Landau, E.M., Pebay-Peyroula, E., and Navarro, J., X-ray structure of sensory rhodopsin II at 2.1-A resolution, *Proc. Natl. Acad. Sci. USA*, 98, 10131, 2001.
65. Luecke, H., Schobert, B., Lanyi, J.K., Spudich, E.N., and Spudich, J.L., Crystal structure of sensory rhodopsin II at 2.4 angstroms: Insights into color tuning and transducer interaction, *Science*, 293, 1499, 2001.
66. Shimono, K., Iwamoto, M., Sumi, M., and Kamo, N., Functional expression of pharaonis phoborhodopsin in *Escherichia coli*, *FEBS Lett.*, 420, 54, 1997.
67. Sudo, Y., Yamabi, M., Iwamoto, M., Shimono, K., and Kamo, N., Interaction of *Natronobacterium pharaonis* phoborhodopsin (sensory rhodopsin II) with its cognate transducer probed by increase in the thermal stability, *Photochem. Photobiol.*, 78, 511, 2003.
68. Sudo, Y., Iwamoto, M., Shimono, K., and Kamo, N., Tyr-199 and charged residues of pharaonis Phoborhodopsin are important for the interaction with its transducer, *Biophys. J.*, 83, 427, 2002.

69. Hippler-Mreyen, S., Klare, J.P., Wegener, A.A., Seidel, R., Herrmann, C., Schmies, G., Nagel, G., Bamberg, E., and Engelhard, M., Probing the sensory rhodopsin II binding domain of its cognate transducer by calorimetry and electrophysiology, *J. Mol. Biol.*, 330, 1203, 2003.
70. Sudo, Y., Yamabi, M., Kato, S., Hasegawa, C., Iwamoto, M., Shimono, K., and Kamo, N., Importance of specific hydrogen bonds of archaeal rhodopsins for the binding to the transducer protein, *J. Mol. Biol.*, 357, 1274, 2006.
71. Yang, C.S., Sineshchekov, O., Spudich, E.N., and Spudich, J.L., The cytoplasmic membrane-proximal domain of the HtrII transducer interacts with the E-F loop of photoactivated *Natronomonas pharaonis* sensory rhodopsin II, *J. Biol. Chem.*, 279, 42970, 2004.
72. Sudo, Y., Okuda, H., Yamabi, M., Fukuzaki, Y., Mishima, M., Kamo, N., and Kojima, C., Linker region of a halobacterial transducer protein interacts directly with its sensor retinal protein, *Biochemistry*, 44, 6144, 2005.
73. Bergo, V.B., Spudich, E.N., Rothschild, K.J., and Spudich, J.L., Photoactivation perturbs the membrane-embedded contacts between sensory rhodopsin II and its transducer, *J. Biol. Chem.*, 280, 28365, 2005.
74. Taniguchi, Y., Ikehara, T., Kamo, N., Yamasaki, H., and Toyoshima, Y., Dynamics of light-induced conformational changes of the phoborhodopsin/transducer complex formed in the n-dodecyl β-D-maltoside micelle, *Biochemistry*, 46, 5349, 2007.
75. Doebber, M., Bordignon, E., Klare, J.P., Holterhues, J., Martell, S., Mennes, N., Li, L., Engelhard, M., and Steinhoff, H.J., Salt-driven equilibrium between two conformations in the HAMP domain from *Natronomonas pharaonis*: The language of signal transfer? *J. Biol. Chem.*, 283, 28691, 2008.
76. Furutani, Y., Sudo, Y., Kamo, N., and Kandori, H., FTIR spectroscopy of the complex between pharaonis phoborhodopsin and its transducer protein, *Biochemistry*, 42, 4837, 2003.
77. Sudo, Y., Furutani, Y., Shimono, K., Kamo, N., and Kandori, H., Hydrogen bonding alteration of Thr-204 in the complex between pharaonis phoborhodopsin and its transducer protein, *Biochemistry*, 42, 14166, 2003.
78. Sudo, Y., Furutani, Y., Kandori, H., and Spudich, J.L., Functional importance of the interhelical hydrogen bond between Thr204 and Tyr174 of sensory rhodopsin II and its alteration during the signaling process, *J. Biol. Chem.*, 281, 34239, 2006.
79. Sudo, Y., Furutani, Y., Wada, A., Ito, M., Kamo, N., and Kandori, H., Steric constraint in the primary photoproduct of an archaeal rhodopsin from regiospecific perturbation of C-D stretching vibration of the retinyl chromophore, *J. Am. Chem. Soc.*, 127, 16036, 2005.
80. Sudo, Y., Furutani, Y., Spudich, J.L., and Kandori, H., Early photocycle structural changes in a bacteriorhodopsin mutant engineered to transmit photosensory signals, *J. Biol. Chem.*, 282, 15550, 2007.
81. Furutani, Y., Iwamoto, M., Shimono, K., Kamo, N., and Kandori, H., FTIR spectroscopy of the M photointermediate in pharaonis phoborhodopsin, *Biophys. J.*, 83, 3482, 2002.
82. Wegener, A.A., Chizhov, I., Engelhard, M., and Steinhoff, H.J., Time-resolved detection of transient movement of helix F in spin-labelled pharaonis sensory rhodopsin II, *J. Mol. Biol.*, 301, 881, 2000.
83. Wegener, A.A., Klare, J.P., Engelhard, M., and Steinhoff, H.J., Structural insights into the early steps of receptor-transducer signal transfer in archaeal phototaxis, *EMBO J.*, 20, 5312, 2001.
84. Yoshida, H., Sudo, Y., Shimono, K., Iwamoto, M., and Kamo, N., Transient movement of helix F revealed by photo-induced inactivation by reaction of a bulky SH-reagent to cysteine-introduced pharaonis phoborhodopsin (sensory rhodopsin II), *Photochem. Photobiol. Sci.*, 3, 537, 2004.
85. Sineshchekov, O.A., Sasaki, J., Phillips, B.J., and Spudich, J.L., A Schiff base connectivity switch in sensory rhodopsin signaling, *Proc. Natl. Acad. Sci. USA*, 105, 16159, 2008.
86. Sineshchekov, O.A., Sasaki, J., Wang, J., and Spudich, J.L., Attractant and repellent signaling conformers of sensory rhodopsin-transducer complexes, *Biochemistry*, 49, 6696, 2010.
87. Suzuki, D., Sudo, Y., Furutani, Y., Takahashi, H., Homma, M., and Kandori, H., Structural changes of *Salinibacter* sensory rhodopsin I upon formation of the K and M photointermediates, *Biochemistry*, 47, 12750, 2008.

88. Suzuki, D., Furutani, Y., Inoue, K., Kikukawa, T., Sakai, M., Fujii, M., Kandori, H., Homma, M., and Sudo, Y., Effects of chloride ion binding on the photochemical properties of *Salinibacter* sensory rhodopsin I, *J. Mol. Biol.*, 392, 48, 2009.
89. Yagasaki, J., Suzuki, D., Ihara, K., Inoue, K., Kikukawa, T., Sakai, M., Fujii, M., Homma, M., Kandori, H., and Sudo, Y., Spectroscopic studies of a sensory rhodopsin I homologue from the archaeon *Haloarcula vallismortis*, *Biochemistry*, 49, 1183, 2010.
90. Bieszke, J.A., Braun, E.L., Bean, L.E., Kang, S., Natvig, D.O., and Borkovich, K.A., The *nop-1* gene of *Neurospora crassa* encodes a seven transmembrane helix retinal-binding protein homologous to archaeal rhodopsins, *Proc. Natl. Acad. Sci. USA*, 96, 8034, 1999.
91. Brown, L.S., Dioumaev, A.K., Lanyi, J.K., Spudich, E.N., and Spudich, J.L., Photochemical reaction cycle and proton transfers in *Neurospora rhodopsin*, *J. Biol. Chem.*, 276, 32495, 2001.
92. Sumii, M., Furutani, Y., Waschuk, S.A., Brown, L.S., and Kandori, H., Strongly hydrogen-bonded water molecule present near the retinal chromophore of *Leptosphaeria rhodopsin*, the bacteriorhodopsin-like proton pump from a eukaryote, *Biochemistry*, 44, 15159, 2005.
93. Furutani, Y., Sumii, M., Fan, Y., Shi, L., Waschuk, S.A., Brown, L.S., and Kandori, H., Conformational coupling between the cytoplasmic carboxylic acid and the retinal in a fungal light-driven proton pump, *Biochemistry*, 45, 15349, 2006.
94. Fan, Y., Shi, L., and Brown, L.S., Structural basis of diversification of fungal retinal proteins probed by site-directed mutagenesis of *Leptosphaeria rhodopsin*, *FEBS Lett.*, 581, 2557, 2007.
95. Balashov, S.P., Imasheva, E.S., Wang, J.M., and Lanyi, J.K., Excitation energy-transfer and the relative orientation of retinal and carotenoid in xanthorhodopsin, *Biophys. J.*, 95, 2402, 2008.
96. Luecke, H., Schobert, B., Stagno, J., Imasheva, E.S., Wang, J.M., Balashov, S.P., and Lanyi, J.K., Crystallographic structure of xanthorhodopsin, the light-driven proton pump with a dual chromophore, *Proc. Natl. Acad. Sci. USA*, 105, 16561, 2008.
97. Imasheva, E.S., Balashov, S.P., Choi, A.R., Jung, K.H., and Lanyi, J.K., Reconstitution of *Gloeobacter violaceus* rhodopsin with a light-harvesting carotenoid antenna, *Biochemistry*, 48, 10948, 2009.
98. Vogeley, L., Sineshchekov, O.A., Trivedi, V.D., Sasaki, J., Spudich, J.L., and Luecke, H., Anabaena sensory rhodopsin: A photochromic color sensor at 2.0 A, *Science*, 306, 1390, 2004.
99. Vogeley, L., Trivedi, V.D., Sineshchekov, O.A., Spudich, E.N., Spudich, J.L., and Luecke, H., Crystal structure of the *Anabaena* sensory rhodopsin transducer, *J. Mol. Biol.*, 367, 741, 2007.
100. Sineshchekov, O.A., Trivedi, V.D., Sasaki, J., and Spudich, J.L., Photochromicity of *Anabaena* sensory rhodopsin, an atypical microbial receptor with a *cis*-retinal light-adapted form, *J. Biol. Chem.*, 280, 14663, 2005.
101. Kawanabe, A., Furutani, Y., Jung, K.H., and Kandori, H., Photochromism of *Anabaena* sensory rhodopsin, *J. Am. Chem. Soc.*, 129, 8644, 2007.
102. Sineshchekov, O.A., Govorunova, E.G., and Spudich, J.L., Photosensory functions of channelrhodopsins in native algal cells, *Photochem. Photobiol.*, 85, 556, 2009.
103. Hegemann, P., Ehlenbeck, S., and Gradmann, D., Multiple photocycles of channelrhodopsin, *Biophys. J.*, 89, 3911, 2005.
104. Zhang, F., Aravanis, A.M., Adamantidis, A., de Lecea, L., and Deisseroth, K., Circuit-breakers: Optical technologies for probing neural signals and systems, *Nat. Rev. Neurosci.*, 8, 577, 2007.
105. Tomita, H., Sugano, E., Isago, H., and Tamai, M., Channelrhodopsins provide a breakthrough insight into strategies for curing blindness, *J. Genet.*, 88, 409, 2009.

50

Nonvisual Photosensitivity and Circadian Vision

Carlo Musio
Istituto di Biofisica
Fondazione Bruno Kessler

and

Istituto di Cibernetica

Silvia Santillo
Istituto di Cibernetica

50.1 Introduction

Our belief about visual system as functional tool providing only image formation, and in a common sense an interpretative depiction of the surrounding real world, has been drastically changed by recent (and old but revised) achievements on nonimage-forming vision, more widely termed as nonvisual photoreception or nonvisual photosensitivity (NVP for both). Classical studies in invertebrate and lower vertebrate species have described, namely, at time, extraocular or extraretinal photosensitive cells which exerted an ancillary role to obvious eye-like structures in mere detection of environmental irradiance (one for all the so-called third eye, i.e., the pineal gland, of lower vertebrate organisms). Such role assumes remarkable importance in those animals that lack obvious eyes or with poor optical apparatus.

Several stereotyped behaviors and vital functions, both strictly related to a precise temporal fluctuation, are strictly linked to nonvisual photoreception.

That adaptive role seemed restricted to primitive or phylogenetically old animal species until when in the 1990s a new kind of intrinsically photosensitive cells, and their photopigment melanopsin, has been identified in the vertebrate retina in addition to the rod and cone photoreceptor cells. Those findings unveil a fast-growing research field that has showed and confirmed by molecular, cellular, and physiological studies a new non-rod non-cone photoreception pathway that supplies nonimage-forming vision.

Therefore, an unconventional kind of light sensitivity that was trivially (and erroneously) considered as an evolutive residue typical of invertebrate species is present also in higher species of vertebrates, including mammals up to humans, retaining the same physiological role and value.

In the animal kingdom, nonvisual photoreception is a photosensory capability involved in the regulation of several expressions of temporal physiology such as photoperiodism, locomotion, neurogenesis, entrainment of circadian rhythms, and the timing of biological clocks (in addition to other functions of vital importance such as the sleep/wake cycle, the melatonin regulation, and the constriction of the pupil).[1,2] Photic information mediated by nonvisual photosensitivity parallels and integrates, to some extent, the function of canonical visual system, being involved in circadian vision (i.e., the measurement of daily environmental irradiance to serve photoentrainment of circadian rhythms).[3,4]

The ubiquity of circadian rhythms points to an earlier evolutive origin of their molecular machinery as adaptation to light/dark daily cycles in the external environment. Endogenously generated oscillation strictly linked to circadian rhythms evolved and "incorporated" in animals to time several vital functions. Analogously, nonvisual photic input driving and interacting with circadian rhythms has determined temporal features of several functions and behaviors.

This review, far to be comprehensive above all for what it concerns the molecular and genetic machinery of circadian clocks, summarizes the current state of art of NVP and its relationships with circadian vision. In particular, this chapter focuses on the molecular and functional properties of the so-called nonvisual opsins, which are the candidate photopigments of the novel retinal and extraretinal photosensitive cells in both vertebrates and invertebrates. The aim is to provide the reader with a sketch of the evolutionary course of the animal vision based on the comparative/phylogenetic analysis of the molecular and functional mechanisms of photoreception and of the regulation of circadian rhythms exerted by light input.

50.2 Biological Time and the Origin of Circadian Rhythmicity

The physiology and the behavior of all living forms on our planet have been influenced by light periodic changes due to seasonal and day/night cycles. During evolution, the endowment for an organism to develop mechanisms for irradiance measurement, to fine-tune its biological time according to environmental conditions, and to anticipate the light periodic changes have been developed as a whole to provide crucial adaptive responses.

Living organisms, in fact, have evolved different biological clocks, some, with an endogenous period of approximately 24 h (due to the daily rotation of the Earth) controlling circadian responses and other ones, with a longer photoperiod, regulating seasonal behaviors (migration, reproduction, hibernation, etc.).

Rhythms are not just a passive reaction to light, but they are programmed by endogenous mechanisms which are continuously synchronized by changes in quantity and quality of light at dawn and dusk.[5]

Light is the predominant *Zeitgeber* (from German, literally "time giver") for the resetting of this machinery, and photoreceptor proteins are the molecules responsible for its photoentrainment.[6]

A circadian system is often described as consisting of three parts: the rhythm generator that autonomously generates rhythmicity is continuously entrained to environmental signals by clock input components (such as photoreceptors) and relays to clock output components (the peripheral oscillators) present in all tissues throughout the body to drive rhythmicity (Figure 50.1a). Outside this system, light acts as *Zeitgeber*.[7] This scheme is not so simple because clock components can feedback on themselves generating multiple overlapping loops. In fact, important transcription/translation feedback loops of clock components intervene to fine-tune this complex machinery (Figure 50.1b).

Current literature depicts a comprehensive account of the molecular and genetic issues of the circadian system's machinery above all for what it concerns the clock genes and relative signal pathways in both vertebrates and invertebrates (e.g., mouse and drosophila, respectively). However, this complex topic deserves an exhaustive coverage that is not proper of this chapter due to space limitation; thus, we refer the reader to recent reviews for detailed results and references.[8,9]

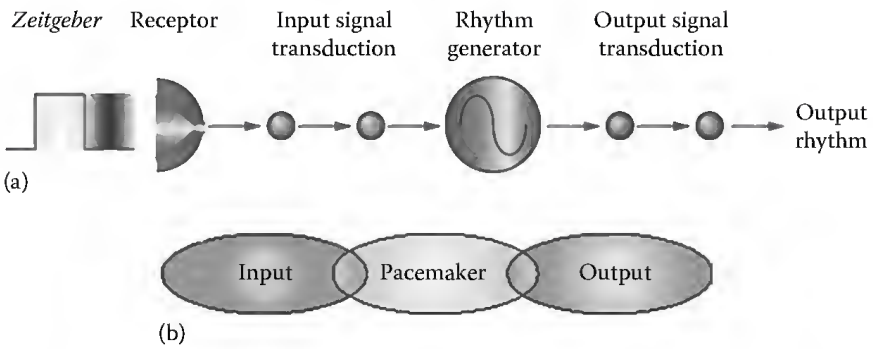

FIGURE 50.1 (a) Conceptual sketch of the circadian system pathway which includes three major components: the input receiving the signal from environmental *Zeitgeber*, the pacemaker generating the circadian rhythm, and the output producing the physiological rhythm. (Modified from Roenneberg, T. and Merrow, M., *Curr. Biol.*, 13, R198–R207, 2003.) (b) At any stage of the pathway, the entrainment may be varied and modulated due to an overlapping and a mutual relationship between the three major components. (Modified from Cermakian, N. and Sassone-Corsi, P., *Nat. Rev. Mol. Cell. Biol.*, 1, 59, 2000.)

50.3 Localization of Photoreceptorial Systems within Receptorial Clocks

In addition to the classical eye or eye-like structures performing image-forming functions by means of classical visual opsins, vertebrate and invertebrates have auxiliary photoreceptor systems committed to the measurement of daily environmental irradiance for the entrainment of circadian rhythms (Figure 50.2).[10] This auxiliary visual modality is named circadian vision and regulates the temporal and behavioral physiology of animals (e.g., photoperiodism in locomotion and reproduction, timing of circadian rhythms, the sleep/wake cycle; the melatonin inhibition and the constriction of the pupil) synchronizing peripheral clocks present in all tissues.[2–3,11–14]

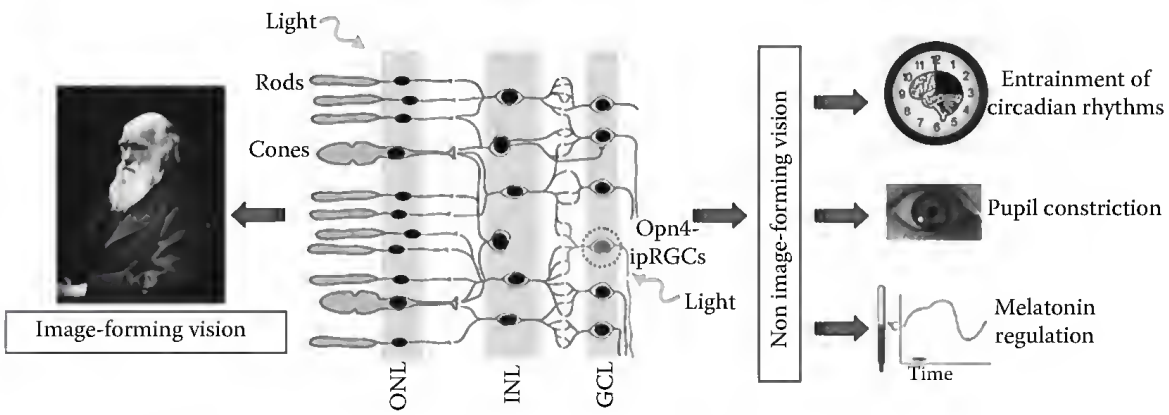

FIGURE 50.2 Schematic drawing of the three kinds of retinal photoreceptive systems in vertebrates. On the left, rod/cone pathway is the first step subserving image-forming vision (including color and spatial vision). On the right, melanopsin-containing intrinsically photosensitive retinal ganglion cells (Opn4-ipRGCs) constitute the building blocks of the nonimage-forming visual system (non-rod non-cone photoreception). Opn4-ipRGCs detect light directly and convey signals of irradiance to the brain triggering nonvisual responses like entrainment of circadian rhythms (including sleep function), the pupil reflex, the entrainment of melatonin suppression, and, in humans, the regulation of body temperature and mood. Abbreviations: ONL, outer nuclear layer; INL, inner nuclear layer; GCL, ganglion cell layer. (Right side images, adapted after Bailes, H.J. and Lucas, R.J., *Cell. Mol. Life Sci.*, 67, 99, 2010; left side image, Charles Darwin (1809–1882) in his later years, photo by J. Cameron, 1869, public domain via Wikimedia Commons.)

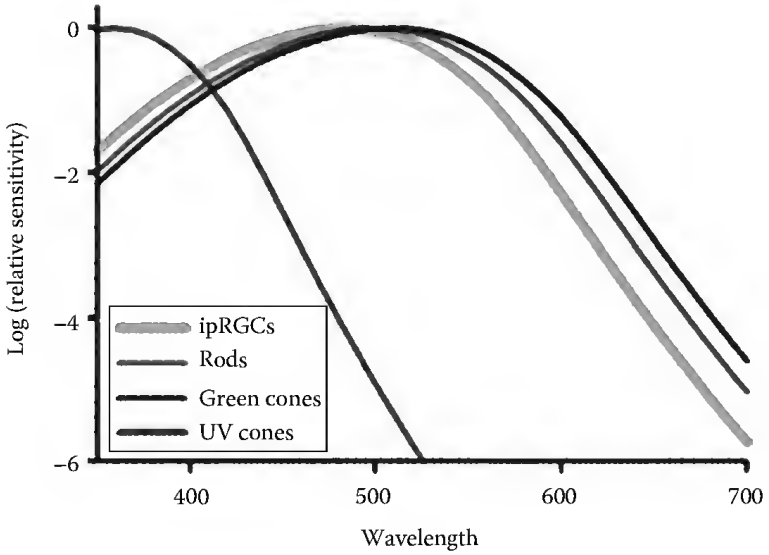

FIGURE 50.3 **(See color insert.)** Action spectrum of intrinsically photosensitive retinal ganglion cells (ipRGCs) compared with action spectra of other photoreceptors of the rat retina. The curve shapes indicate that each photopigment uses a vitamin A-based chromophore. Relative trends of the curves on the wavelength axis reflect differences in the opsin component of the photopigment. Wavelengths: ipRGCs (red), 484 nm; green cones (green), 510 nm; UV cones (purple), 359 nm; rods (blue), 500 nm. (Adapted from Berson, D.M., *Trends Neurosci.*, 26, 314, 2003.)

As shown in Figure 50.2, these photoreceptorial systems are indicated as receptorial component clocks and have been identified in the retina as well as in some cerebral extraocular structures and peripheral structures of vertebrate and invertebrates. Pineal complex, deep brain photoreceptors, dermal photosensitive cells, central nervous system photoneurons, peripheral organs, and obviously lateral eyes represent important photoreceptive sites that, sensing light, entrain rhythms.

The retina of lateral eyes (i.e., the obvious eyes) of mammalian and nonmammalian vertebrates processes light information by classical photoreceptors, rods, and cones in the outer layer and photosensitive cells containing novel opsins in the inner layer.[15]

Classical photoreceptors provide image-forming vision while the others, defined as non-rod non-cone photoreceptors, are involved in NVP (Figure 50.2). The latter, in vertebrates, include subsets of intrinsically photosensitive retinal ganglion cells (ipRGCs) (Figure 50.3), amacrine and horizontal cells, all expressing melanopsin,[16–19] teleost horizontal cells expressing vertebrate ancient (VA)-long opsin,[20] cyprinid horizontal cell expressing both melanopsin and VA,[21] and gecko retinal cell expressing pinopsin.[22]

Among vertebrates, the pineal complex has different structures and roles (Figure 50.4). In teleosts and lampreys, the intracranial pineal complex includes the pineal organ (*epiphysis cerebri*), and the parapineal organ and light penetrates throughout a translucent area of reduced pigmentation overlying the pineal. The parapineal organ becomes an extracranial third eye, named parietal body in reptiles and frontal organ in anuran amphibians; it is definitively lost in aves, which have only the pineal organ.

The pineal complex, like eyes, originates embryologically from evagination of dorsal diencephalon and represents important photosensitive pathways that in vertebrate nonmammals directly and locally control the melatonin neurosecretory function.

Only in mammals, the pineal organ, although showing opsin-like immunoreaction,[23] has a function exclusively secretory. In fact, light indirectly controls pineal melatonin synthesis by means of the hypothalamic suprachiasmatic nucleus (SCN), the central pacemaker of circadian rhythms, that once synchronized to the external light–dark cycle, relays to all peripheral clocks present in the body (Figure 50.4).[4]

Melatonin is synthesized in the dark phase of a diurnal cycle and acts as a signal of darkness to regulate circadian rhythms and photoperiodic responses.[24]

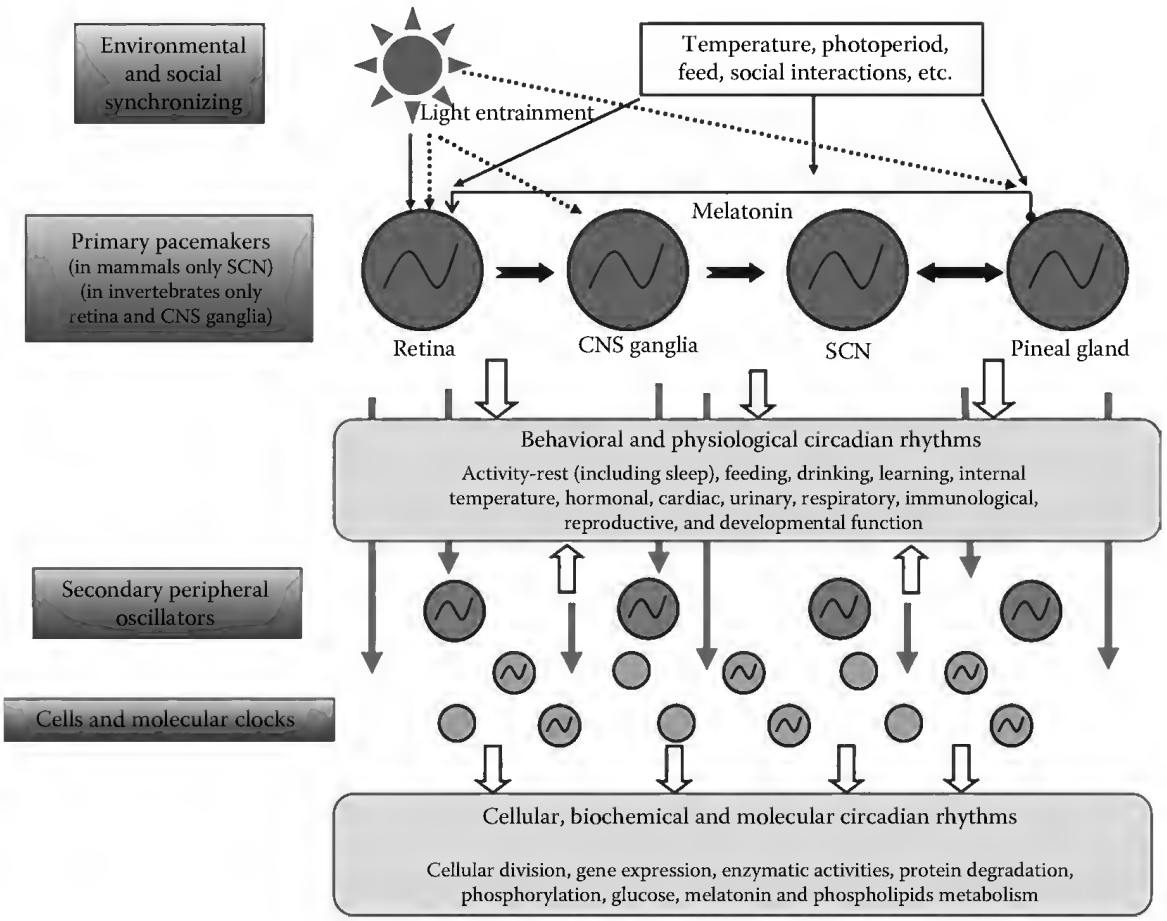

FIGURE 50.4 General scheme of the animal circadian system showing the three main components of the system in relation to the top-down/bottom-up organization of physiological processes and behavior. Entrainment pathways (above all environmental *Zeitgeber*), major pacemakers, and peripheral oscillators are reported with some indications typical of vertebrates and invertebrates. A system of cellular and molecular clocks is coupled to the output signals in order to express circadian rhythmicity at cellular level. See text for details. (Adapted and modified from Guido, M.E. et al., *Neurochem. Res.*, 27, 1473, 2002.)

Many nonvisual opsins have been identified in the pineal complex of various vertebrates: pinopsin from avian[25] and lizard,[26] exo-rhodopsin and VA opsin from teleosts,[27] parapinopsin from catfish[28] and lamprey,[29] and melanopsin from chicken.[30]

Circadian clocks are also located deeply in the brain of fish, amphibian, reptile, and bird (Figure 50.4). Light reaches opsins after having crossed neural tissue and helps to control various behaviors like negative phototaxis in European eel[31] or gonadal growth as demonstrated in blinded and pinealectomized bird.[32]

These neurons are intrinsically sensitive to light although lacking of any specialized structures of eye photoreceptors, such as the microvilli or cilia. Their opsin content has been characterized: encephalopsin from mammalian,[33] VA-long opsin from zebrafish,[20] neuropsin from mammalian,[34] and VA opsin from bird.[35]

Also in invertebrates, some ganglia present photoresponsive neurons (Figure 50.4): in dorsal ganglia of the mollusk *Onchidium*, they act as modulators of the nonphotoreceptive sensory inputs and of the motor response.[36] In the crayfish *Procambarus clarkia*, they contribute to the circadian locomotory activity,[37] and serotonin seems to produce a circadian phase shift in their electrical activity.[38]

In the cnidarian *Hydra*, the first metazoan that shows a nervous system, although primitive and structured as a nervous net, and being eyeless a rhodopsin-like protein has been identified and presumably

localized in epithelial sensory cells[39] ascribing the animal's photosensitivity to neuronal NVP instead of dermal light reception as early reported. In this prototypical animal model, the measurements of different phase response curves during light and darkness regimes, in addition to behavioral spectrum with two opposite peaks of responses around 450 and 550 nm, have demonstrated that the photic inputs exert a strong regulatory effect on the oscillatory animal's behavior that is characterized by alternating phases of contraction and elongation of the body column.[40]

In many nonmammalian vertebrates and invertebrates, the dermal photosensitivity controls the density of pigment granules in photosensitive dermal chromatophores,[41] the locomotory activity,[42] while in frog melanophores the pigment dispersion is regulated by the melanopsin photopigment.[43]

Finally, photosensitivity is ascertained in several peripheral organs of both vertebrates and invertebrates. In zebrafish, the teleost multiple tissue (tmt) opsin could entrain heart and kidney to light[44]; in addition, a direct muscle photosensitivity has been recently reported in the heart of the isopod *Ligia exotica*[45] and in the jellyfish *Cladonema* the expression of opsins in the gonads suggests a role in light-controlled releasing of gametes.[46]

In the crayfish, light-controlled rhythms are a primary regulator of neuronal proliferation, and hormonal influences on neurogenesis may represent secondary events in a multicomponent circadian control pathway (Figure 50.4).[47]

A comprehensive coverage of invertebrate behavioral and functional issues dealing with the NVP associated with the regulation of circadian rhythms is provided in Ref. [2].

50.4 Mammalian Receptor Clocks

In mammals, input clock components able to sense external lighting are located only in the retina. In fact, they have lost extraretinal photoreceptors and use their lateral eyes for both image detection and photic regulation of temporal physiology.[48]

Retina projects to the hypothalamic SCN, a structure located deeply in the brain, in the ventral part of the hypothalamus. Its neurons exhibit intrinsic circadian rhythmicity and coordinate daily cycles in behavior and physiology.[49]

The SCN appears to be the central pacemaker of the circadian timing system synchronizing peripheral clocks present in all tissues throughout the body.[50] Clocks are multioscillatory systems based on complex molecular feedback loops by means they regulate themselves and entrain SCN to external lightning. SCN directly relays on circadian rhythms by both neural efferents and diffusible mechanisms (Figure 50.4).[4]

The photoentrainment of circadian rhythms can occur in the absence of classical visual photoreceptors (rods and cones) but not in animals in which enucleation of the eyes abolishes all responses to light.[51]

As above reported, within the mammalian retina, rods and cones are not the only photosensitive cells. Retina also presents in its inner layer a subset of ipRGCs and amacrine and horizontal cells, all containing melanopsin,[16–19] which is considered a key opsin for circadian vision.

These cells are currently termed as nonimage-forming or nonvisual photoreceptors or, much better, non-rod non-cone photoreceptors to distinguish them from photoreceptors discovered in extraocular sites of vertebrates and invertebrates.[2]

The ipRGCs directly project to the SCN via the tact retinohypothalamic (RHT) as well as to the other diencephalic and midbrain regions,[18,52–54] including the olivary pretectal nucleus, the brain center controlling the pupillary light reflex.[18] Pupillary constriction is regulated by both rod and cones but also survive in mammals with photoreception degeneration.[55]

The ipRGCs represent the primary photoreceptors involved in circadian regulation,[16] as their destruction alters the effect of light on circadian rhythms.[56] Photic regulation of circadian rhythms is also influenced by the classical visual photoreceptors via the polysynaptic rod/cone pathway to ipRGCs as the 20% of the tract RHT is constituted of non-contained melanopsin RGC fibers.[52,57–59]

50.5 Timing by Opsins

Different experimental approaches conducted on vertebrates and invertebrates have identified for nonvisual responses several photopigments referred to as opsin-like proteins.[60] By now, a putative role for the blue-light flavoprotein cryptochrome (CRY) as the NVP photopigment in the light-regulated behavior of insects,[61] crustaceans,[62] and corals[63] is emerging. Nevertheless, a conserved photoreceptive role for CRY in vertebrate eyes has been discovered recently in chick iris, whose constriction to light *ex vivo* depends on CRY rather than on opsin activity.[64]

Despite inter- and intra-species functional differences, molecular genetic approaches have identified about 1000 opsins belonging to both vertebrates and invertebrates. The updated molecular phylogenetic tree of animal opsins (identified so far) shows seven subfamilies corresponding to a functional classification of opsins based on the specific G-protein type that links each proper opsin receptor.[60] The opsin subfamilies include (1) vertebrate visual (T-coupled) and nonvisual opsins, (2) encephalopsin/tmt-opsins, (3) G_q-coupled opsins/melanopsins, (4) G_o-coupled opsins, (5) neuropsins, and (6) peropsins and retinal G protein-coupled receptor (RGR) photoisomerase.

The functional diversity of opsins, and their localization, indicates that a high percentage (about 70%) of these proteins deals with nonimage-forming systems.

Recent findings on the molecular evolution of novel nonvisual opsins suggest a strict relationship of the NVP process with canonical vision, which could have occurred in lower organisms of the animal phylogenetic tree. In this regard, the identification of novel opsins suggests that the history of visual pigments is strictly connected with the evolution of photoreceptors and eyes.[65]

In particular, there is strong evidence that opsins evolved according to the main evolutionary lineages of animal visual cells, the ciliary and the rhabdomeric (or microvillar) photoreceptors.[65] However, although those aspects are not strictly related to the main topics of this chapter, some accounts related to NVP will be given.

More recently, Suga et al.[46] have reported in jellyfish as many as 18 opsins in *Cladonema* and 2 in *Podocoryne*. Their expression patterns suggest two possible functions: a role in vision by the eye, and the other involved in the timing control of oogenesis or spawning process, possibly in cooperation with CRY.

In the brain of four species of lepidopterans, three kinds of spectrally distinct opsins have been reported outside of the retina: ultraviolet (UV) and blue opsins, which are restricted to adult stemmata (where melatonin is expressed together with opsins), and long-wavelength (LW) opsins, which are specific for dorsal and ventral photosensitive neurons of the optic lobes.[66] These opsins provide the extraretinal detection of ambient light variations and are involved in the neuroendocrine output mediated by melatonin, underlying the entrainment of circadian and/or photoperiodic rhythms.

Arendt and coworkers[67] have found in the ragworm, *Platinereis*, the coexistence of rhabdomeric photoreceptors in the eyes (for phototaxis) and ciliary photosensitive cells in the brain (for entrainment of biological clocks). The latter (referred to as NVP cells) use an opsin closely related to vertebrate rod and cone opsins. A recent study in the honeybee, *Apis mellifera*, has revealed that a ciliary opsin, called pteropsin, is expressed in the brain of this species, indicating the presence of a vertebrate-like light-detecting system in insects.[68]

Indeed, in vertebrates, photoreception is not restricted to the rod/cone pathways but is extended to other neuronal districts of the central and the peripheral nervous system providing the nonvisual processes necessary for circadian vision.[1]

Also in those cellular districts, several opsins have been identified as candidate photopigments such as neuropsin, peropsin, and encephalopsin.[60] However, the corner stone of the field has been the discovery in ipRGCs of melanopsin as the novel photopigment triggering the nonvisual phototransduction (see Section 50.7 for details).

The functional mean of the colocalization of those opsins with other opsin subfamilies still remains unclear and, at same time, the role of deep brain opsins (e.g., encephalopsin, neuropsin) is far to be elucidated.

Interestingly, as reported for vertebrate rhodopsin, evidences for diurnal and circadian regulation of nonvisual opsin expression patterns have been reported in very few species of invertebrates, lower (nonmammalian) vertebrates, and only in mouse among mammals (see Section 50.6 for details). Unfortunately, although a key evolutionary trait is the adaptation to day/night alternation, and its impact on integrated physiology, the photic regulation of opsin gene expression remains rather neglected.

The interest in studying opsin expression has been enhanced by the finding in mouse of correlations between the amounts of expressed opsins with photoreceptor cell death. Light-dependent (diurnal and circadian) opsin expression could have potential clinical implications both with the condition improvements, which are under the circadian control, and in the timing of therapy.

50.6 Opsins as Oscillating Biomolecules

Opsin expression and retina physiology display a daily rhythm and, as previously reported, many opsin genes show a fluctuation in their mRNA pattern expression.

Various works give insights into possible interactions between sensory and circadian systems in the regulation of opsin expression in some species of invertebrates (*Limulus*[69] and Apis[70]), vertebrates (teleost fish,[71] zebrafish,[72] chicken,[30] and chick[73]), and mammals (mouse[74]).

In zebrafish pineal organ, exo-rhodopsin (*exorh*) is the putative opsin mediating the effects of environmental light on pineal rhythms and melatonin synthesis.[75] It is activated by a transcription factor (*Orthodenticle homeobox 5*) and repressed by a circadian clock component (*Period 3*). Furthermore, light contributes to this transcription rhythm as *exorh* is expressed with a daily rhythm which is higher at night than during the day.

Again, in teleost embryos, the expression of mRNA long-wavelength cone (LC) opsin shows a robust day–night cycle and is regulated by Clock, a core circadian gene that contributes to the central circadian pacemaker.[72] In the lizard, brain cone opsins seems to be the candidate in photic entrainment of behavioral rhythms.[76]

Also in the cnidarian *Hydra*, where an opsin-like photoreceptor protein has been already identified as candidate photopigment,[39] preliminary evidences speak in favor of a possible coexistence of putative visual and nonvisual opsins yet in a primitive animal.[77] In fact, quantitative RT-PCR has shown fluctuations with different trends for daily and circadian cycles of various opsin sequences expressed suggesting that rhythms could be endogenous and light could have a direct role in the regulation of the photopigment molecule supply.[78]

For melanopsin, the principal mediator of the circadian photoentrainment, a daily oscillating pattern has been reported with a peak in the transitional phase from day to night, while the minimum has been observed at the end of the night.[79] This rhythm appears to be influenced by rod/cone inputs, since melanopsin expression in rats lacking of rod and cone photoreceptors is lower and arrhythmic than in control rats.[80] Moreover, the elimination of dopamine in the rat retinic circuit alters the mRNA pattern profiling,[81] suggesting that also the aminergic neurotransmitter is involved in this daily oscillation.[82] Recently, two isoforms of melanopsin have been identified in the mammalian retina, a long (Opn4L) and a novel short isoform (Opn4S), differing each other in the length of their C-tail and in their expression which is higher for Opn4S. In addition, two distinct subpopulations of ipRGC, with different morphologies, functions, and projections, coexist in the inner retina, selectively expressing Opn4L and Opn4S or Opn4L only.[83]

50.7 Melanopsin: A Key Photopigment in Circadian Vision

The understanding of how nonvisual functions work has derived from the discovery of a novel opsin termed melanopsin.[84] It was first identified in frog dermal melanophores[43] and then in the inner retina of mammalian eye including mice, monkeys, and humans[58,85] and in retina, pineal, and brain of vertebrates nonmammals.[30,86]

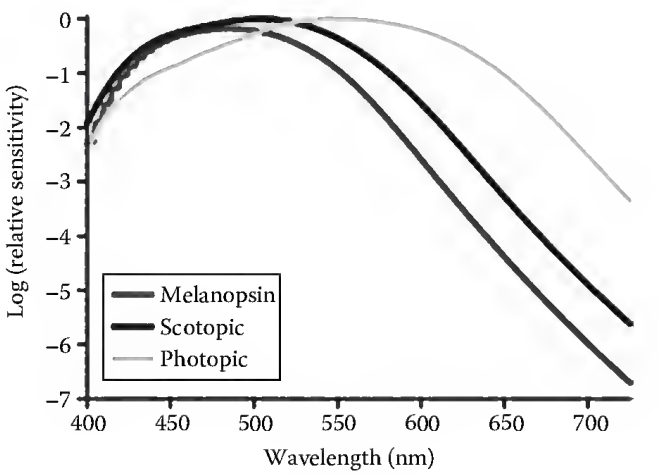

FIGURE 50.5 **(See color insert.)** Action spectrum of human melanopsin showing an optimal sensitivity to short-wavelength "blue" light at 480 nm. The spectral sensitivity profile indicates an opsin-based photopigment utilizing a vitamin A-based chromophore. The spectral sensitivity of scotopic (rod-based) and photopic (cone-based) vision is presented for comparison. Although melanopsin sensitivity peaks around 480 nm, it shows in addition a good responsiveness into the green/yellow portion of the spectrum. (Adapted from Bailes, H.J. and Lucas, R.J., *Cell. Mol. Life Sci.*, 67, 99, 2010.)

Melanopsin, a member of the G-protein-coupled receptor family, shares a seven-transmembrane domain. It presents many invertebrate opsins-like features, conversely to those showed by vertebrates, and for this reason, it probably represents, with other nonvisual opsins, a divergent line of photopigment evolved before vertebrates.[87]

Melanopsin, unlike vertebrate visual opsins, presents in counterion position a tyrosine instead of a glutamate[88] that, in addition to phenylalanine, is the most frequent counterion occurring in invertebrates. Moreover, its third cytoplasmatic loop is surprisingly long (as in *Hydra* melanopsin expressed sequences, Santillo and Musio, unpublished data) respect to the conventional opsins. The melanopsin spectral sensitivity is close to the short-wavelength blue light with peaks ranging from 459 to 484 nm; it overlaps the peak sensitivity for circadian responses and not the spectral sensitivity of rods and cones (Figure 50.5).

Surprisingly, it is a bistable photoreversing pigment[89,90] and like invertebrate photopigments[91] it requires photon absorption to drive both retinal activation and regeneration conversion of all-*trans*- back to 11-*cis*-retinal (retinoid cycle), a process resident in non-photoreceptor cells of retinal pigment epithelium (RPE). This distinctive aspect enables melanopsin to function as both photoisomerase and sensory photopigment.

Upon cladistic analysis, it segregates with the invertebrate opsins expressed in rhabdomeric cells, the typical invertebrate photoreceptor, and not with vertebrate ciliary ones.[43,90,92,93] Moreover, it exhibits the typical phototransduction signaling of invertebrate rhabdomeric opsins.[94,95] In the retinal ipRGCs, it generates a receptor potential difference in several important aspects from that in rod and cone photoreceptors.[96]

Recent studies indicate that melanopsin utilizes a rhabdomeric Gq-type phototransduction with a IP_3-mediated Ca_2 visual cascade[95] different from ciliary photoreceptors in which activation of transducin (Gi/o) and phosphodiesterase give rise to closure of cyclic nucleotide-gated (CNG) channels and membrane hyperpolarization.[15] As far as we know in ipRGCs and other melanopsin-containing cells, light response is coupled to an opening of a nonspecific cation channel that leads to a cellular depolarization.[94,97]

In various melanopsins of closely related species, the intracellular domains for G-protein specificity are poorly conserved, suggesting that they could activate multiple signaling pathways by means of multiple G-protein interactions (Gi/o, Gq/G11, and Gs).[93]

Recently, melanopsin has been identified in the cephalochordate amphioxus, an outlined vertebrate being the most primitive living chordate closest to invertebrates and ancestor of vertebrate lineage.[87,97]

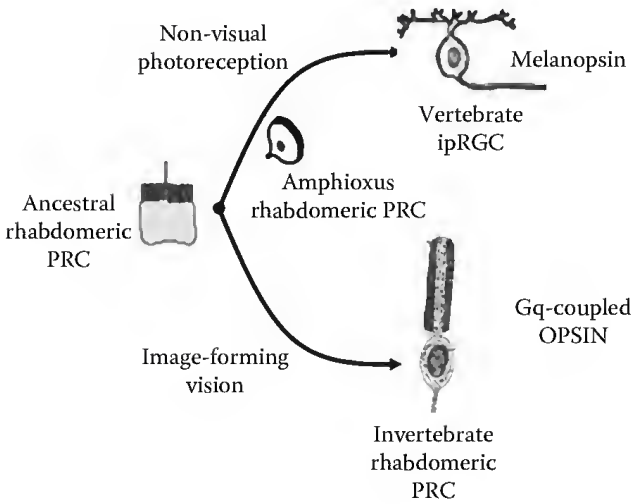

FIGURE 50.6 Sketch illustrating the evolutionary linkage between invertebrate rhabdomeric visual cells and vertebrate photosensitive retinal ganglion cells from a common ancestral rhabdomeric cell. See text for details. (Adapted and modified from Koyanagi, M. and Terakita, A., *Photochem. Photobiol.*, 84, 1024, 2008.)

The identification of melanopsin in the rhabdomeric photoreceptors of dorsal ocelli and not in frontal eyes and the identification of a Gq phototransductive pathway represent an evolutionary link between photoreceptor cells of higher invertebrates and photosensitive ganglion cells of vertebrates and place the origin of melanopsin before the vertebrate radiation (Figure 50.6).

During evolution, these rhabdomeric cells should have lost their morphology resulting in a photosensitive retinal ganglion cell controlling different light-sensitive signaling systems.[90,98–100]

50.8 Why Blue Light?

Among photopigments there exists a great diversity in their spectral sensitivity with absorption maxima for the image-forming visual system ranging from medium to long wavelengths. Shorter frequencies, corresponding to the blue monochromatic light, seem to prevail in nonvisual photoreception. Experiments demonstrating the direct effect of blue light on alertness and vigilance in humans[101] suggest that nonvisual photoreceptive systems could have had a primary role in animal adaptive response to the environmental changes in both terrestrial and aquatic species. Blue-light wavelength dominates at dawn and dusk, it also penetrates deeply in seawater, and consequently, both ocean and antarctic under-ice species are blue-light sensitive.

An ancestral nonvisual photoreceptor system should have evolved by means of a blue-light key *Zeitgeber* to develop such aquatic and terrestrial adaptive responses. Otherwise, no excitatory input and evolving responses should have obtained in deeply water with a light key *Zeitgeber* of a longer wavelength.[102] Many fishes are active near dawn and dusk[103]; indeed, it is possible that when marine vertebrates began to colonize terrestrial habitats, a blue photoreceptive clockwork had just evolved.

Interestingly, a hypothesis explaining possible coevolution between blue-light photoreceptor systems and circadian rhythms has been reported by Gehring and Rosbash.[104]

50.9 Conclusions

As a matter of fact, the achievements of the last decade on molecular, cellular, and functional properties of nonvisual photoreception have disclosed challenging and unexpected issues in this research field.

The study of the molecular evolution of novel nonvisual opsins is necessary to unveil the evolution of photoreceptors, and definitely of visual function. In addition, the comparative physiology of the

nonvisual photoreceptor may shed light on the events of the phototransduction cascade along the phylogenetic tree as showed by interesting scenarios recently proposed.[67,93]

The desirable identification of novel opsins in a wide number of animal species, their molecular evolution, and phylogenetic analysis will help to untangle the evolutionary relationship between invertebrate nonvisual cells and photosensitive ganglion cells, since it concerns the putative common molecular and photochemical strategies of phototransduction.

From the functional side, a crucial point is the cross talk between NVP and the image-forming visual system, and the resultant signal streaming to the circadian system. Accordingly, only some accounts are available about the merging of nonimage-forming vision and image-forming vision and the capability of NVP in sending both irradiance and color information, previously gathered by the rods and cones, to the brain.

Another key topic is the modulatory role of NVP on temporal physiology and photoentrainment of circadian rhythms. In addition, due to the close link between nonvisual extraocular photoreception and circadian regulation, the study of NVP could be extended to pharmacological and clinical aspects. In this regard, following the recent demonstration of a direct role of melanopsin in mediating the photic regulation of sleep,[105] the melanopsin signaling systems could potentially be a new pharmacological target for the selective manipulation of sleep and arousal states as recently reported.[106]

The study of the modulatory role of NVP could be extended also to those issues of visual system in which a clear link between circadian rhythm dysfunctions and pathological conditions has been ascertained.[107] In these terms, a sharp confirmation of NVP as possible regulatory player in the molecular clock machinery would be really challenging.

In summary, we can assert that nonvisual photoreception is a renewed and fast-growing area of photosensory biology and visual neuroscience. The study of NVP can provide crucial details on the evolution of visual systems and its relationships with chronobiology. Moreover, it can be a powerful tool to investigate important clinical implications for several pathological conditions (e.g., blindness and sleep/wake alterations) whose defects nowadays can be related to defects occurring in the nonvisual phototransduction pathway(s). Finally due to the close functional link between biological clocks and pathophysiology of several disorders, the study of NVP could provide novel indications concerning chronotherapy protocols.[108] Currently, it has been well ascertained that nonpharmacological (light therapy, sleep deprivation, and rhythm therapy) and pharmacological (lithium, antidepressants, etc.) therapies of several time-dependent disorders influence circadian rhythms.[109]

Acknowledgments

We are indebted to Cloe Taddei-Ferretti, who introduced us to this research field. Carlo Musio is sincerely grateful to Francesco Lenci for his friendly support and encouragement, and to the editor Francesco Ghetti for his kind patience and indulgence. Few parts of this chapter have been inspired from a previous review[2] and from lectures and discussions that took place in the Symposium "Classical and novel photoreceptors in circadian vision—Nonvisual photoreceptors" (of which Carlo Musio was the organizer and chair) held at the 13th Congress of the European Society for Photobiology (ESP), Wroclaw University, Poland, 5–10 September, 2009.

References

1. Foster, R.G. and Hankins, M.W. 2002. Non-rod, non-cone photoreception in the vertebrates. *Progr. Retin. Eye Res.* 21: 507–527.
2. Musio, C. and Santillo, S. 2009. Non-visual photoreception in invertebrates. In *Photobiological Sciences Online*, ed. K.C. Smith, pp. 1–32. American Society for Photobiology (ASP), Lawrence, KS. http://www.photobiology.info.

3. Fu, Y., Liao, H.-W., Tri, H., Do, M., and Yau, K.-W. 2005. Non-image-forming ocular photoreception in vertebrates. *Curr. Opin. Neurobiol.* 15: 415–422.
4. Morin, L.P. and Allen, C.N. 2006. The circadian visual system, 2005. *Brain Res. Rev.* 51: 1–60.
5. Roenneberg, T. and Foster, R.G. 1997. Twilight times: Light and the circadian system. *Photochem. Photobiol.* 66: 549–561.
6. Harmer, S.L., Panda, S., and Kay, S.A. 2001. Molecular bases of circadian rhythms. *Annu. Rev. Cell. Dev. Biol.* 17: 215–253.
7. Roenneberg, T. and Merrow, M. 2003. The network of time: Understanding the molecular circadian system. *Curr. Biol.* 13: R198–R207.
8. Cermakian, N. and Sassone-Corsi, P. 2000. Multilevel regulation of the circadian clock. *Nat. Rev. Mol. Cell. Biol.* 1: 59–67.
9. Nitabach, M.N. and Taghert, P.H. 2008. Organization of the *Drosophila* circadian control circuit. *Curr. Biol.* 18: R84–R93.
10. Peirson, S.N., Halford, S., and Foster, R.G. 2009. The evolution of irradiance detection: Melanopsin and the non-visual opsins. *Phil. Trans. R. Soc. Lond. B Biol. Sci.* 364: 2849–2865.
11. Bertolucci, C. and Foà, A. 2004. Extraocular photoreception and circadian entrainment in non-mammalian vertebrates. *Chronobiol. Int.* 21: 501–519.
12. Foster, R.G. and Hankins, M.W. 2007. Circadian vision. *Curr. Biol.* 17: R746–R751.
13. Guido, M.E., Carpentieri, A.R., and Garbarino-Pico, E. 2002. Circadian phototransduction and the regulation of biological rhythms. *Neurochem. Res.* 27: 1473–1489.
14. Musio, C. 1997. Extraocular photosensitivity in invertebrates. In *Biophysics of Photoreception: Molecular and Phototransductive Events*, ed. C. Taddei-Ferretti, pp. 245–262. World Scientific, Toh Tuck Link, Singapore.
15. Yau, K.-W. and Hardie, R.C. 2009. Phototransduction motifs and variation. *Cell* 139: 246–264.
16. Berson, D.M. 2003. Strange vision: Ganglion cells as circadian photoreceptors. *Trends Neurosci.* 26: 314–320.
17. Cheng, N., Tsunenari, T., and Yau, K.-W. 2009. Intrinsic light response of retinal horizontal cells of teleosts. *Nature* 460: 899–903.
18. Hattar, S., Kumar, M., Park, A. et al. 2006. Central projections of melanopsin-expressing retinal ganglion cells in the mouse. *J. Comp. Neurol.* 497: 326–349.
19. Paul, K.N., Saafir, T.B., and Tosini, G. 2009. The role of retinal photoreceptors in the regulation of circadian rhythms. *Rev. Endocr. Metab. Disord.* 10: 271–278.
20. Kojima, D., Mano, H., and Fukada, Y. 2000. Vertebrate ancient-long opsin: A green-sensitive photoreceptive molecule present in zebrafish deep brain and retinal horizontal cells. *J. Neurosci.* 20: 2845–2851.
21. Jenkins, A., Muñoz, M., Tarttelin, E.E., Bellingham, J., Foster, R.G., and Hankins, M.W. 2003. VA opsin, melanopsin, and an inherent light response within retinal interneurons. *Curr. Biol.* 13: 1269–1278.
22. Taniguchi, Y., Hisatomi, O., Yoshida, M., and Tokunaga, F. 2001. Pinopsin expressed in the retinal photoreceptors of a diurnal gecko. *FEBS Lett.* 496: 69–74.
23. Korf, H.W., Foster, R.G., Ekström, P., and Schalken, J.J. 1985. Opsin-like immunoreaction in the retinae and pineal organs of four mammalian species. *Cell Tissue Res.* 242: 645–648.
24. Thapan, K., Arendt, J., and Skene, D.J. 2001. An action spectrum for melatonin suppression: Evidence for a novel non-rod, non-cone photoreceptor system in humans. *J. Physiol.* 535: 261–267.
25. Okano, T., Yoshizawa, T., and Fukuda, Y. 1994. Pinopsin is a chicken pineal photoreceptive molecule. *Nature* 372: 94–97.
26. Kawamura, S. and Yokoyama, S. 1997. Expression of visual and nonvisual opsins in American chameleon. *Vis. Res.* 37: 1867–1871.
27. Mano, H., Kojima, D., and Fukada, Y. 1999. Exo-rhodopsin: A novel rhodopsin expressed in the zebrafish pineal gland. *Brain Res. Mol. Brain Res.* 73: 110–118.

28. Blackshaw, S. and Snyder, S.H. 1997. Parapinopsin, a novel catfish opsin localized to the parapineal organ, defines a new gene family. *J. Neurosci.* 17: 8083–8092.
29. Koyanagi, M., Kawano, E., Kinugawa, Y. et al. 2004. Bistable UV pigment in the lamprey pineal. *Proc. Natl. Acad. Sci. USA* 101: 6687–6691.
30. Chaurasia, S.S., Rollag, M.D., Jiang, G. et al. 2005. Molecular cloning, localization and circadian expression of chicken melanopsin (Opn4): Differential regulation of expression in pineal and retinal cell types. *J. Neurochem.* 92: 158–170.
31. Veen van, T., Hartwig, H.G., and Muller, K. 1976. Light-dependent motor activity and photonegative behaviour in the eel (*Anguilla anguilla* L.). *J. Comp. Physiol. A* 111: 209–219.
32. Yokoyama, K., Oksche, A., Darden, T.R., and Farner, D.S. 1978. The sites of encephalic photoreception in photoperiodic induction of the growth of the testes in the white-crowned sparrow, *Zonotrichia leucophrys gambelii. Cell Tissue Res.* 189: 441–467.
33. Blackshaw, S. and Snyder, S.H. 1999. Encephalopsin: A novel mammalian extraretinal opsin discretely localized in the brain. *J. Neurosci.* 19: 3681–3690.
34. Tarttelin, E.E., Bellingham, J., Hankins, M.W., Foster, R.G., and Lucas, R.J. 2003. Neuropsin (Opn5): A novel opsin identified in mammalian neural tissue. *FEBS Lett.* 554: 410–416.
35. Halford, S., Pires, S.S., Turton, M. et al. 2009. VA opsin-based photoreceptors in the hypothalamus of birds. *Curr. Biol.* 19: 1396–1402.
36. Gotow, T. and Nishi, T. 2008. Simple photoreceptors in some invertebrates: Physiological properties of a new photosensory modality. *Brain Res.* 1225: 3–16.
37. Sullivan, J.M., Genco, M.C., Marlow, E.D., Benton, J.L., Beltz, B.S., and Sandeman, D.C. 2009. Brain photoreceptor pathways contributing to circadian rhythmicity in crayfish. *Chronobiol. Int.* 26: 1136–1168.
38. Rodríguez-Sosa, L., Calderón-Rosete, G., Flores, G., and Porras, M.G. 2007. Serotonin-caused phase shift of circadian rhythmicity in a photosensitive neuron. *Synapse* 61: 801–808.
39. Musio, C., Santillo, S., Taddei-Ferretti, C. et al. 2001. First identification and localization of a visual pigment in *Hydra* (Cnidaria, Hydrozoa). *J. Comp. Physiol. A* 187: 79–81.
40. Taddei-Ferretti, C. and Musio, C. 2000. Photobehaviour of *Hydra* (Cnidaria, Hydrozoa) and correlated mechanisms: A case of extraocular photosensitivity. *J. Photochem. Photobiol. B Biol.* 55: 88–101.
41. Weber, W. 1983. Photosensitivity of chromatophores. *Am. Zool.* 23: 495–506.
42. Binder, T.R. and McDonald, D.G. 2008. The role of dermal photoreceptors during the sea lamprey (*Petromyzon marinus*) spawning migration. *J. Comp. Physiol. A Neuroethol. Sens. Neural Behav. Physiol.* 194: 921–928.
43. Provencio, I., Jiang, G., De Grip, W.J., Hayes, W.P., and Rollag, M.D. 1998. Melanopsin: An opsin in melanophores, brain, and eye. *Proc. Natl. Acad. Sci. USA* 95: 340–345.
44. Moutsaki, P., Whitmore, D., Bellingham, J., Sakamoto, K., David-Gray, Z.K., and Foster, R.G. 2003. Teleost multiple tissue (tmt) opsin: A candidate photopigment regulating the peripheral clocks of zebrafish? *Brain Res. Mol. Brain Res.* 112: 135–145.
45. Miyamoto, H., Horiguchi, H., Hariyama, T., Takano, S., and Yamagishi, H. 2006. Photosensitive neurogenic heart of the isopod crustacean *Ligia exotica. Proc. Biol. Sci.* 273: 2535–2540.
46. Suga, H., Schmid, V., and Gehring, W.J. 2008. Evolution and functional diversity of jellyfish opsins. *Curr. Biol.* 18: 51–55.
47. Goergen, E.M., Bagay, L.A., Rehm, K., Benton, J.L., and Beltz, B.S. 2002. Circadian control of neurogenesis. *J. Neurobiol.* 53: 90–95.
48. Foster, R.G. 1998. Shedding light on the biological clock. *Neuron* 20: 829–832.
49. Antle, M.C. and Silver, R. 2005. Orchestrating time: Arrangements of the brain circadian clock. *Trends Neurosci.* 28: 145–151.
50. Lee, H.S., Billings, H.J., and Lehman, M.N. 2003. The suprachiasmatic nucleus: A clock of multiple components. *J. Biol. Rhythm.* 18: 435–449.

51. Foster, R.G., Provencio, I., Hudson, D., Fiske, S., De Grip, W., and Menaker, M. 1991. Circadian photoreception in the retinally degenerate mouse (*rd/rd*). *J. Comp. Physiol. A* 169: 39–50.
52. Dacey, D.M., Liao, H.W., Peterson, B.B. et al. 2005. Melanopsin-expressing ganglion cells in primate retina signal colour and irradiance and project to the LGN. *Nature* 433: 749–754.
53. Gooley, J.J., Lu, J., Chou, T.C., Scammell, T.E., and Saper, C.B. 2001. Melanopsin in cells of origin of the retinohypothalamic tract. *Nat. Neurosci.* 4: 1165.
54. Hannibal, J., Hindersson, P., Knudsen, S.M., Georg, B., and Fahrenkrug, J. 2002. The photopigment melanopsin is exclusively present in pituitary adenylate cyclase-activating polypeptide-containing retinal ganglion cells of the retinohypothalamic tract. *J. Neurosci.* 22: RC191.
55. Lucas, R.J., Douglas, R.H., and Foster, R.G. 2001. Characterization of an ocular photopigment capable of driving pupillary constriction in mice. *Nat. Neurosci.* 4: 621–626.
56. Göz, D., Studholme, K., Lappi, D.A., Rollag, M.D., Provencio, I., and Morin, L.P. 2008. Targeted destruction of photosensitive retinal ganglion cells with a saporin conjugate alters the effects of light on mouse circadian rhythms. *PLoS One* 3: e3153.
57. Dkhissi-Benyahya, O., Gronfier, C., De Vanssay, W., Flamant, F., and Cooper, H.M. 2007. Modeling the role of mid-wavelength cones in circadian responses to light. *Neuron* 53: 677–687.
58. Hattar, S., Lucas, R.J., Mrosovsky, N. et al. 2003. Melanopsin and rod-cone photoreceptive systems account for all major accessory visual functions in mice. *Nature* 424: 76–81.
59. Sollars, P.J., Smeraski, C.A., Kaufman, J.D., Ogilvie, M.D., Provencio, I., and Pickard, G.E. 2003. Melanopsin and non-melanopsin expressing retinal ganglion cells innervate the hypothalamic suprachiasmatic nucleus. *Vis. Neurosci.* 20: 601–610.
60. Terakita, A. 2005. The opsins. *Genome Biol.* 6: 213.
61. Emery, P., Stanewsky, R., Helfrich-Förster, C., Emery-Le, M., Hall, J.C., and Rosbash, M. 2000. *Drosophila* CRY is a deep brain circadian photoreceptor. *Neuron* 26: 493–504.
62. Fanjul-Moles, M.L., Escamilla-Chimal, E.G., Gloria-Soria, A., and Hernández-Herrera, G. 2004. The crayfish *Procambarus clarkii* CRY shows daily and circadian variation. *J. Exp. Biol.* 207: 1453–1460.
63. Levy, O., Appelbaum, L., Leggat, W. et al. 2007. Light-responsive cryptochromes from a simple multicellular animal, the coral, *Acropora millepora*. *Science* 318: 467–470.
64. Tu, D.C., Batten, M.L., Palczewski, K., and Van Gelder, R.N. 2004. Nonvisual photoreception in the chick iris. *Science* 306: 129–131.
65. Nilsson, D.-E. 2005. Photoreceptor evolution: Ancient siblings serve different tasks. *Curr. Biol.* 15: R94–R96.
66. Lampel, J., Briscoe, A.D., and Wasserthal, L.T. 2005. Expression of UV-, blue-, long-wavelength-sensitive opsins and melatonin in extraretinal photoreceptors of the optic lobes of hawkmoths. *Cell Tissue Res.* 321: 443–458.
67. Arendt, D., Tessmar-Raible, K., Snyman, H., Dorresteijn, A.W., and Wittbrodt, J. 2004. Ciliary photoreceptors with a vertebrate-type opsin in an invertebrate brain. *Science* 306: 869–871.
68. Velarde, R.A., Sauer, C.D., Walden, K.K., Fahrbach, S.E., and Robertson, H.M. 2005. Pteropsin: A vertebrate-like non-visual opsin expressed in the honey bee brain. *Insect Biochem. Mol. Biol.* 35: 1367–1377.
69. Dalal, J.S., Jinks, R.N., Cacciatore, C., Greenberg, R.M., and Battelle, B.A. 2003. *Limulus* opsins: Diurnal regulation of expression. *Vis. Neurosci.* 20: 523–534.
70. Sasagawa, H., Narita, R., Kitagawa, Y., and Kadowaki, T. 2003. The expression of genes encoding visual components is regulated by a circadian clock, light environment and age in the honeybee (*Apis mellifera*). *Eur. J. Neurosci.* 17: 963–970.
71. Halstenberg, S., Lindgren, K.M., Samagh, S.P., Nadal-Vicens, M., Balt, S., and Fernald, R.D. 2005. Diurnal rhythm of cone opsin expression in the teleost fish *Haplochromis burtoni*. *Vis. Neurosci.* 22: 135–141.
72. Li, P., Chaurasia, S.S., Gao, Y., Carr, A.L., Iuvone, P.M., and Li, L. 2008. CLOCK is required for maintaining the circadian rhythms of opsin mRNA expression in photoreceptor cells. *J. Biol. Chem.* 283: 31673–31678.

73. Bailey, M.J. and Cassone, V.M. 2004. Opsin photoisomerases in the chick retina and pineal gland: Characterization, localization, and circadian regulation. *Investig. Ophthalmol. Vis. Sci.* 45: 769–775.
74. Schantz von, M., Lucas, R.J., and Foster, R.G. 1999. Circadian oscillation of photopigment transcript levels in the mouse retina. *Brain Res. Mol. Brain Res.* 72: 108–114.
75. Pierce, L.X., Noche, R.R., Ponomareva, O., Chang, C., and Liang, J.O. 2008. Novel functions for Period 3 and Exo-rhodopsin in rhythmic transcription and melatonin biosynthesis within the zebrafish pineal organ. *Brain Res.* 223: 11–24.
76. Pasqualetti, M., Bertolucci, C., Ori, M. et al. 2003. Identification of circadian brain photoreceptors mediating photic entrainment of behavioural rhythms in lizards. *Eur. J. Neurosci.* 18: 364–372.
77. Santillo, S., Orlando, P., De Petrocellis, L., Cristino, L., Guglielmotti, V., and Musio, C. 2006. Evolving visual pigments: Hints from the opsin-based proteins in a phylogenetically old eyeless invertebrate. *BioSystems* 86: 3–17.
78. Musio, C. and Santillo, S. 2009. Photic regulation of gene expression of classical and novel visual pigments. *Presented at 13th Congr. Europ. Soc. Photobiol. (ESP)*, Wroclaw Univ. (PL), September 5–10, 2009, invited lecture IL414, p. 103.
79. Hannibal, J., Georg, B., Hindersson, P., and Fahrenkrug, J. 2005. Light and darkness regulate melanopsin in the retinal ganglion cells of the albino Wistar rat. *J. Mol. Neurosci.* 27: 147–155.
80. Wan, J., Zheng, H., Hu, B.Y. et al. 2006. Acute photoreceptor degeneration down-regulates melanopsin expression in adult rat retina. *Neurosci. Lett.* 400: 48–52.
81. Sakamoto, K., Liu, C., Kasamatsu, M., Pozdeyev, N.V., Iuvone, P.M., and Tosini, G. 2005. Dopamine regulates melanopsin mRNA expression in intrinsically photosensitive retinal ganglion cells. *Eur. J. Neurosci.* 22: 3129–3136.
82. González-Menéndez, I., Contreras, F., Cernuda-Cernuda, R., and García-Fernández, J.M. 2009. Daily rhythm of melanopsin-expressing cells in the mouse retina. *Front. Cell. Neurosci.* 3: 3. doi:10.3389/neuro.03.003.2009.
83. Pires, S.S., Hughes, S., Turton, M. et al. 2009. Differential expression of two distinct functional isoforms of melanopsin (Opn4) in the mammalian retina. *J. Neurosci.* 29: 12332–12342.
84. Bailes, H.J. and Lucas, R.J. 2010. Melanopsin and inner retinal photoreception. *Cell. Mol. Life Sci.* 67: 99–111.
85. Provencio, I., Rodriguez, I.R., Jiang, G., Hayes, W.P., Moreira, E.F., and Rollag, M.D. 2000. A novel human opsin in the inner retina. *J. Neurosci.* 20: 600–605.
86. Bellingham, J., Chaurasia, S.S., Melyan, Z. et al. 2006. Evolution of melanopsin photoreceptors: Discovery and characterization of a new melanopsin in nonmammalian vertebrates. *PLoS Biol.* 4: e254.
87. Koyanagi, M., Kubokawa, K., Tsukamoto, H., Shichida, Y., and Terakita, A. 2005. Cephalochordate melanopsin: Evolutionary linkage between invertebrate visual cells and vertebrate photosensitive. *Curr. Biol.* 15: 1065–1069.
88. Ebrey, T. and Koutalos, Y. 2001. Vertebrate photoreceptors. *Prog. Retin. Eye Res.* 20: 49–94.
89. Rollag, M.D. 2008. Does melanopsin bistability have physiological consequences? *J. Biol. Rhythm.* 23: 396–399.
90. Terakita, A., Tsukamoto, H., Koyanagi, M., Sugahara, M., Yamashita, T., and Shichida, Y. 2008. Expression and comparative characterization of Gq-coupled invertebrate visual pigments and melanopsin. *J. Neurochem.* 105: 883–890.
91. Hillman, P., Hochstein, S., and Minke, B. 1983. Transduction in invertebrate photoreceptors: Role of pigment bistability. *Physiol. Rev.* 63: 668–772.
92. Arendt, D. 2005. Genes and homology in nervous system evolution: Comparing gene functions, expression patterns, and cell type molecular fingerprints. *Theor. Biosci.* 124: 185–197.
93. Koyanagi, M. and Terakita, A. 2008. Gq-coupled rhodopsin subfamily composed of invertebrate visual pigment and melanopsin. *Photochem. Photobiol.* 84: 1024–1030.
94. Isoldi, M.C., Rollag, M.D., Castrucci, A.M., and Provencio, I. 2005. Rhabdomeric phototransduction initiated by the vertebrate photopigment melanopsin. *Proc. Natl. Acad. Sci. USA* 102: 1217–1221.

95. Graham, D.M., Wong, K.Y., Shapiro, P., Frederick, C., Pattabiraman, K., and Berson, D.M. 2008. Melanopsin ganglion cells use a membrane-associated rhabdomeric phototransduction cascade. *J. Neurophysiol.* 99: 2522–2532.
96. Melyan, Z., Tarttelin, E.E., Bellingham, J., Lucas, R.J., and Hankins, M.W. 2005. Addition of human melanopsin renders mammalian cells photoresponsive. *Nature* 433: 741–745.
97. Gomez del Pilar, M., Angueyra, J.M., and Nasi, E. 2009. Light-transduction in melanopsin-expressing photoreceptors of Amphioxus. *Proc. Natl. Acad. Sci. USA* 106: 9081–9086.
98. Arendt, D. 2003. Evolution of eyes and photoreceptor cell types. *Int. J. Dev. Biol.* 47: 563–571.
99. Peirson, S. and Foster, R.G. 2006. Melanopsin: Another way of signaling light. *Neuron* 49: 331–339.
100. Hankins, M.W. and Foster, R.G. 2007. Microarray analysis and functional genomics identify novel components of melanopsin signalling. *Curr. Biol.* 17: 1363–1372.
101. Brainard, G.C., Sliney, D., Hanifin, J.P. et al. 2008. Sensitivity of the human circadian system to short-wavelength (420 nm) light. *J. Biol. Rhythm.* 23: 379–386.
102. Erren, T.C., Erren, M., Lerchl, A., and Meyer-Rochow, V.B. 2008. Clockwork blue: On the evolution of non-image-forming retinal photoreceptors in marine and terrestrial vertebrates. *Naturwissenschaften* 95: 273–279.
103. McFarland, W.N. 1991. The visual world of coral reef fishes. In *The Ecology of Fishes on Coral Reefs*, ed. P.F. Sale, pp. 16–37. Academic Press, New York.
104. Gehring, W. and Rosbash, M. 2003. The co-evolution of blue-light photoreception and circadian rhythms. *J. Mol. Evol.* 57: S286–S289.
105. Lupi, D., Oster, H., Thompson, S., and Foster, R.G. 2008. The acute light-induction of sleep is mediated by OPN4-based photoreception. *Nat. Neurosci.* 11: 1068–1073.
106. Tsai, J.W., Hannibal, J., Hagiwara, G. et al. 2009. Melanopsin as a sleep modulator: Circadian gating of the direct effects of light on sleep and altered sleep homeostasis in $Opn4^{-/-}$ mice. *PLoS Biol.* 7(6): e1000125.
107. Drouyer, E., Dkhissi-Benyahya, O., Chiquet, C. et al. 2008. Glaucoma alters the circadian timing system. *PLoS One* 3(12): e3931.
108. Schulz, P. and Steimer, T. 2009. Neurobiology of circadian systems. *CNS Drugs* 23(S2): 3–13.
109. Antoch, M.P. and Chernov, M.V. 2009. Pharmacological modulators of the circadian clock as potential therapeutic drugs. *Mutat. Res.* 680: 109–115.

51

The Essential Role of Retinoids as Ligands for Visual Pigment Formation in and Survival of Cone Photoreceptors

Peter H. Tang
Medical University of South Carolina

Rosalie K. Crouch
Medical University of South Carolina

51.1 Introduction

The retina is the crucial component of the eye that is responsible for converting environmental light into neuronal signals by a process called phototransduction. Photoreceptor cells are specialized phototransducing neurons within the retina and are divided into two families: rods and cones. Rods mediate low-light monochromatic vision, and cones mediate color and bright-light vision. Their patterns of distribution differ within the human retina; rods are found throughout, whereas cones are localized mainly within the fovea to mediate central vision. Although both rods and cones contribute to sight, humans, like other diurnal animals, exhibit a far greater dependence on cones for daily activity. Intrinsic to the phototransduction pathway are vitamin A derivatives called retinoids that are used to generate the chromophore for visual pigment formation within rods and cones [1,2]. After light excitation, the ligand/chromophore is recycled through a multistep enzymatic process called the visual cycle, with the retinal pigment epithelium 65 kDa protein (RPE65) playing an essential role as the isomerohydrolase. In the following chapter, we will explore the contributions of retinoids and RPE65 to cone function, as well as the pathogenesis of cone loss associated with RPE65 dysfunction.

51.2 Dietary Sources of Vitamin A

Retinoids have many important and diverse functions throughout the body including roles in vision [3], regulation of cell proliferation and differentiation [4], and immune function [5,6]. Retinal is the aldehyde derivative of retinol, commonly referred to as vitamin A, which naturally exists in the all-*trans* configuration (all-*trans* retinol). Along with retinoic acid, the oxidized form of retinal, the three compounds compose the three oxidized states of retinoids (Figure 51.1A).

All-*trans* retinol is one of the essential fat-soluble vitamins for humans and is obtained mainly through dietary consumption [7]. A major source is the enzymatic modification of β-carotene (Figure 51.1B) from plants [7,8]. Each molecule of β-carotene is converted into two molecules of all-*trans* retinal, through an irreversible oxidative cleavage mediated by either a monooxygenase or a dioxygenase enzyme. All-*trans* retinal can either be reduced to all-*trans* retinol by retinol dehydrogenases (RDH) or oxidized to all-*trans* retinoic acid by retinal dehydrogenases and retinal oxidases, depending on the requirements of each cell. The second source of all-*trans* retinol is derived from retinyl esters found in animals [7]. A retinyl ester is composed of retinol bound to a fatty acid (most commonly palmitate) through an ester linkage (Figure 51.1B). Retinyl esters are hydrolyzed in the intestinal lumen to yield free all-*trans* retinol and the corresponding fatty acid. After hydrolysis, all-*trans* retinol is taken up by enterocytes and released into the gastrointestinal circulation. The majority of dietary all-*trans* retinol from both sources is stored within the liver and adipose tissue for long-term use.

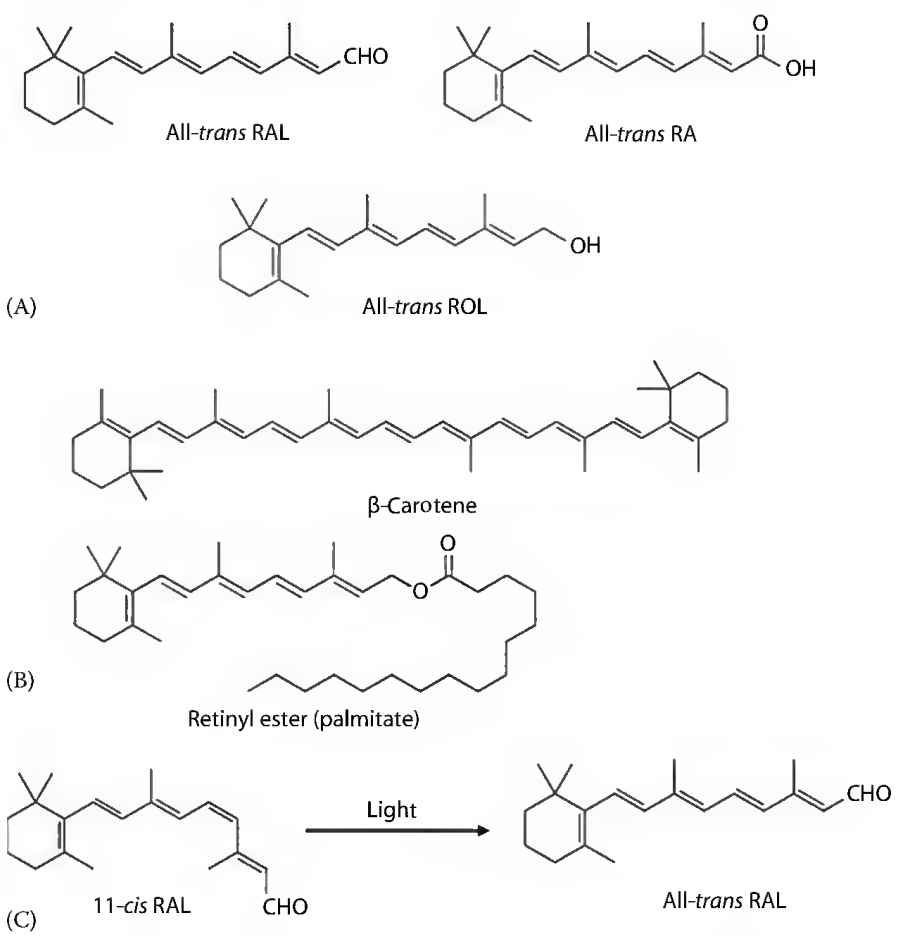

FIGURE 51.1 Structural characteristics of retinoids. (A) The three oxidized states of retinoids: RAL, retinal; RA, retinoic acid; ROL, retinol. (B) Dietary source of retinoids. β-Carotene is the main source from plants; retinyl palmitate and other esters are the major source from animals. (C) Photoisomerization of 11-*cis* retinal to all-*trans* retinal.

The 11-*cis* form of retinal (11-*cis* retinal) serves as the chromophore for visual pigment formation within both rods and cones. As 11-*cis* retinal is not synthesized *de novo* in the eye, its necessary substrate, all-*trans* retinol, is taken up by the RPE from circulation [9,10]. Transport of all-*trans* retinol through the blood is mediated by carrier proteins such as the family of retinol-binding proteins (RBPs) [10]. Once all-*trans* retinol enters the RPE cells, it is converted to 11-*cis* retinal through a series of enzymatic steps that is explained in further detail later in this chapter.

51.3 Structure and Function of Visual Pigments

The retina is organized into numerous layers, with the outer segment, nucleus, and synapse of the photoreceptor cell spanning the outer segment, outer nuclear, and outer plexiform layers, respectively (Figure 51.2A). 11-*cis* Retinal serves as the ligand for G-protein-coupled receptors called opsins in both rods (rod opsins) and cones (cone opsins). When 11-*cis* retinal and the various protein opsins are covalently

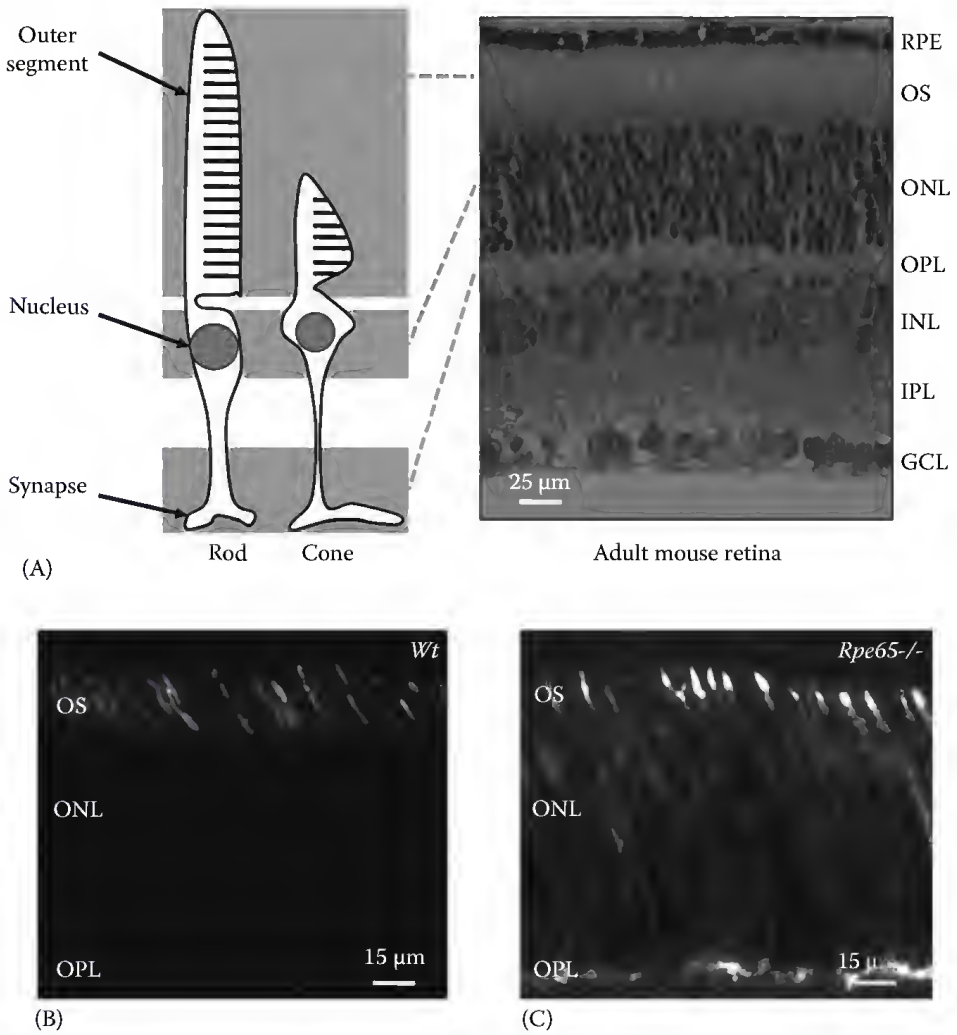

FIGURE 51.2 Retina morphology and cone visual pigment S-opsin distribution. (A) Morphology of mouse retina and epithelium (left); schematic diagram of photoreceptor cells (right). RPE, retinal pigment epithelium; OS, outer segment; ONL, outer nuclear layer; OPL, outer plexiform layer; INL, inner nuclear layer; IPL, inner plexiform layer; GCL, ganglion cell layer. (B, C) S-opsin distribution in *C57BL6* (*Wt*, B) and *Rpe65*$^{-/-}$ (C) mouse cones at 2 weeks of age. While the cone visual pigment S-opsin is properly localized to the outer segment of the *Wt* cone, it is mislocalized throughout the *Rpe65*$^{-/-}$ cone, including the soma and synapse. Immunofluorescence staining performed with antibody specific for S-opsin (1:500 dilution; Cat# sc-14363; Santa Cruz Biotech, Santa Cruz, CA).

bound, the resulting visual pigments have absorption in the UV-visible region (300–700 mm). Although differences exist between rod and cone opsins [11], there are numerous similarities. Opsins are integral membrane proteins located within the outer segment disks of photoreceptors and are composed of seven transmembrane helices linked by six loops of various lengths [12,13]. 11-*cis* Retinal binds to a lysine residue in helix VII via a protonated Schiff base linkage and acts as an inverse agonist to maintain the pigment in an inactive conformation [14]. Upon excitation with light, 11-*cis* retinal isomerizes to an all-*trans* arrangement (Figure 51.1C), inducing the pigment to change into an active conformation and triggering the phototransduction pathway that begins with activation of transducin, the opsin-associated G-protein, and ends with hyperpolarization of the photoreceptor cell to terminate synaptic release of the neurotransmitter, glutamate (for reviews, see Refs. [15–18]).

To mediate the spectral range of light detection, rhodopsin and cone pigments differ in their absorption spectra. In human and mice retina, rods express a single type of opsin; therefore, only one form of rhodopsin exists and absorbs maximally at 500 nm [11,19]. Cones can express numerous types of opsins, leading to cone types with pigments that absorb maximally at various wavelengths. For example, human cones can express three types of cone opsins to generate pigments that absorb maximally at 420 nm (S, short-wavelength), 530 nm (M, mid-wavelength), or 560 nm (L, long-wavelength) [11], and mouse cones can express two types of opsins (359 nm, S; 505 nm, M), depending upon its retinotopic location [20]. Distinctive visual function within the retina is dependent upon the spatial arrangements of these cone types, such as the high concentration of cones within the fovea of humans and the dorsoventral gradients of cone opsin expression in mice [21,22].

51.4 Classic and Cone-Specific Visual Cycles

Photoisomerization of the chromophore underlies the ability of the photoreceptor cell to convert light into neuronal signals to be processed by the visual cortex for vision. Regeneration of the chromophore relies upon the visual cycle. Although a large amount of information has been gathered about the "classic visual cycle," which is characterized by the interactions of both rods and cones with RPE cells for pigment regeneration, less is known about the proposed alternate visual cycle that specifically supports cone pigment regeneration (cone-specific visual cycle). Both visual cycles overlap at numerous enzymatic steps (Figure 51.3) and are explained in further detail in the following.

51.4.1 Classic Visual Cycle

The classic visual cycle has been mainly characterized as an interaction between RPE cells and rods (for reviews, see Refs. [2,3,23,24]); however, it is assumed to function similarly for cones. The main role of RPE cells within the classic visual cycle is to convert all-*trans* retinol to 11-*cis* retinal, and it obtains its substrate from two sources. The first source involves the delivery of RBP-bound all-*trans* retinol from the liver or adipose tissue through the circulation to RPE cells, where RBP docks with the RPE cell multitransmembrane domain protein STRA6 and releases all-*trans* retinol for uptake [9,10]. The second source involves recycling the all-*trans* retinal produced after excitation of the visual pigment by light. After 11-*cis* retinal is photoisomerized to all-*trans* retinal, it is released from opsin into the cytoplasm of the photoreceptor outer segment and reduced to all-*trans* retinol in a reaction that requires both an all-*trans*-specific RDH enzyme and nicotinamide adenine dinucleotide phosphate (NADPH) as a cofactor [25,26]. All-*trans* retinol is then shuttled across the extracellular interphotoreceptor matrix (IPM) to the RPE cell by interphotoreceptor retinoid-binding protein (IRBP) [27,28], which can also bind and shuttle 11-*cis* retinal [29–32].

Once all-*trans* retinol is released into the RPE cell, it is esterified by lecithin:retinol acyltransferase (LRAT) to form all-*trans* retinyl ester for storage [33]. RPE65 acts as the isomerohydrolase enzyme within RPE cells to catalyze the hydrolysis of all-*trans* retinyl ester and its subsequent isomerization to 11-*cis* retinol [1,34,35]. 11-*cis* Retinol can either be esterified again by LRAT to the storage form 11-*cis*

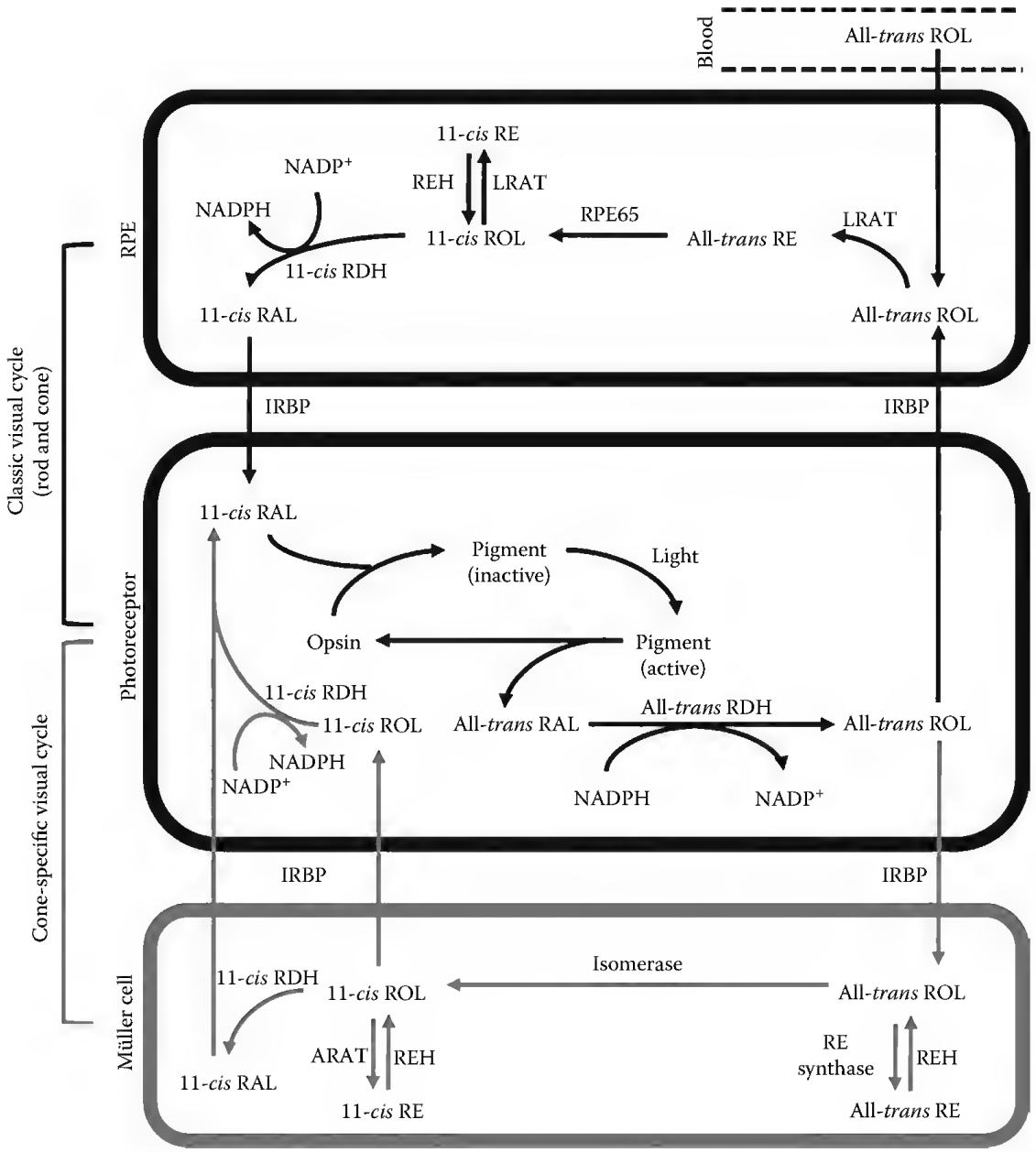

FIGURE 51.3 Diagram of classic and cone-specific visual cycles. RPE, retinal pigment epithelium; RAL, retinal; ROL, retinol; RDH, retinol dehydrogenase; REH, retinyl ester hydrolase; RE, retinyl ester; RPE65, retinal pigment epithelium-specific 65 kDa protein; LRAT, lecithin:retinol acyltransferase; ARAT, acyl CoA:retinol acyltransferase; IRBP, interphotoreceptor retinoid-binding protein.

retinyl ester [36] or oxidized to 11-*cis* retinal by an 11-*cis*-specific RDH [37,38]. IRBP mediates the shuttling of 11-*cis* retinal across the IPM to the photoreceptor outer segment, where it will once again serve as the chromophore to generate visual pigment in rods and cones.

51.4.2 Cone-Specific Visual Cycle

While the function of RPE65 has been well documented to support the classic visual cycle, there is a growing amount of evidence to suggest that there is a second isomerase enzyme that specifically supports rapid cone pigment regeneration (for reviews, see Refs. [24,39]). This alternate visual cycle

has been observed to exist entirely within the retina and functions in parallel with the classic visual cycle [40–43]. Salamander cones within retina that were isolated away from the RPE were observed to recover light sensitivity after photobleaching; however, this recovery disappeared in photobleached cones disassociated from the retina [40]. Previous work in the isolated frog retina produced similar results [44,45].

This second isomerase enzyme has yet to be identified, but studies have provided insight into its characteristics. There is evidence to suggest that RPE65 may be this second isomerase enzyme, and that it is expressed by cones in addition to the RPE. Isolated salamander cones have been shown to express RPE65 mRNA [46], and immunohistochemistry analysis of mouse retina has shown cones to express RPE65 protein [47]. Further studies are needed to clarify the expression of RPE65 in cones.

Further evidence was recently obtained in the cone-dominant chicken retina, where synthesis of 11-*cis* retinyl esters from all-*trans* retinol by retina microsomes required palm-CoA as an acyl donor, suggesting the dependence of the novel isomerase on acyl CoA:retinol acyltransferase (ARAT) instead of LRAT, as in RPE65 [41]. Together, these data implicate the existence of a novel isomerase within the retina that has different characteristics from RPE65, and that physical associations between cones and neighboring cells must be preserved in order for the alternate visual cycle to function.

Several important observations have implicated Müller cells to express the novel isomerase enzyme and to deliver the regenerated chromophore to cones. The ability of Müller cells to isomerize all-*trans* retinoids into 11-*cis* forms *in vitro* was confirmed, where cultured chicken Müller cells treated with all-*trans* retinol generated and released 11-*cis* retinol into the surrounding medium [48]. This was further supported by the observation that Müller cells express cellular retinol-binding protein (CRBP) and cellular retinal-binding protein (CRALBP), both of which are also found in RPE cells where they enhance the uptake of all-*trans* retinol and stabilize both 11-*cis* retinal and 11-*cis* retinol, respectively [49,50]. Within the intact isolated salamander retina, lesioning Müller cells with a Müller cell-specific gliotoxin inhibited the ability of photobleached cones to recover light sensitivity [40]. Additional work is needed to identify the specific isomerase protein within the Müller cell.

How does the alternate visual cycle mediate its specificity for supporting cone pigment regeneration? The previously mentioned observation that cultured Müller cells generate 11-*cis* retinol from all-*trans* retinol [48] may indicate its mechanism. While rods are only able to utilize 11-*cis* retinal for generating pigment, cones are capable of utilizing either 11-*cis* retinal or 11-*cis* retinol. This was shown through electrophysiologic recordings from isolated salamander rods and cones, where treatment with 11-*cis* retinal recovered light sensitivity in both rods and cones, but treatment with 11-*cis* retinol only recovered light sensitivity in cones [32]. Furthermore, 11-*cis* retinal could only restore light sensitivity in cones when specifically delivered to the cell body [51], coinciding with morphologic data showing that the Müller cell processes make numerous associations with the cone specifically at its cell body [40,52]. Finally, IRBP may play an essential role in shuttling 11-*cis* retinol and all-*trans* retinol between the Müller cell and the cone, as IRBP binds 11-*cis* retinol endogenously [53], is colocalized with Müller cell processes surrounding the cone cell body [54] and is found in high concentrations around cones [55,56]. Although IRBP has also been shown to function in the classic visual cycle between photoreceptor outer segments and RPE cells, knocking out the gene in mice appears to have the most detrimental effects on cone function [57]. Therefore, the cone-specific nature of the alternate visual cycle is dependent upon Müller cells generating and delivering 11-*cis* retinol to cones. The novel isomerase enzyme within the Müller cell is proposed to use all-*trans* retinol as a substrate. IRBP mediates the movement of both all-*trans* retinol and 11-*cis* retinol between Müller cell processes and the cone cell body. Once inside the cone, 11-*cis* retinol is oxidized to 11-*cis* retinal by an unidentified RDH, and it binds to cone opsin to form visual pigment. Rods apparently do not utilize the alternate visual cycle as 11-*cis* retinal is not oxidized within these cells and, indeed, is quite toxic [14].

51.5 RPE65 Dysfunction and Leber Congenital Amaurosis

The visual cycle is composed of numerous enzymes that function at various steps of an organized pathway to support pigment regeneration. Genetic defects leading to the disruption at any one of these steps can have a detrimental effect on the ability of the visual cycle to generate an adequate supply of chromophore, causing a subset of recessively inherited retinal diseases known as Leber congenital amaurosis (LCA) (for review, see Refs. [3,58]). LCA is rare (population frequency is between 1/30,000 [59] and 1/81,000 [60]), presents at a young age (around 6 weeks after birth), and is generally characterized by four clinical features including severe loss of vision, sensory nystagmus, amaurotic pupils, and absent electrical signals on electroretinography (ERG) [58]. Mutations in genes encoding for a wide variety of proteins that function within the retina can cause LCA, including those involved in photoreceptor morphogenesis (CRB1 and CRX), phototransduction (AIPL1 and GUCY2D), chromophore regeneration (LRAT, RDH12, and RPE65), guanine synthesis (IMPDH1), outer segment phagocytosis (MERTK), and intra-photoreceptor ciliary transport processes (CEP290, LCA5, RPGRIP1, and TULP1) [58]. Online Mendelian inheritance in man (OMIM) currently recognizes 13 forms of LCA, with the second form (LCA2) caused by a defect in the gene encoding for the isomerase protein RPE65 [34,61].

51.5.1 Early Onset of Cone Loss

The use of animal models for LCA2 has greatly enhanced our understanding of the mechanisms underlying this disease, as well as strategies for therapeutic development. In the rod-dominant human retina, cones compose around 3% of the total number of photoreceptors and are located mainly within the fovea, which is responsible for central vision. The symptoms of LCA2 are attributed to the loss of cones within this region of the retina beginning in the early years of life [61]. To develop an appropriate mouse model to further investigate this clinical feature, the gene encoding for RPE65 protein was knocked out (*Rpe65*$^{-/-}$). The lack of a rod photoresponse measured by ERG [62,63] and the accumulation of all-*trans* retinyl esters within the RPE [34] confirm the disruption of the classic visual cycle at the RPE65-mediated retinoid isomerization step within these mice. The mouse retina is also rod-dominant; however, its cones are uniformly distributed throughout the entire retina. To quantify the amount of cones present within an area, the whole mouse retina was fluorescein isothiocyanate (FITC)–conjugated peanut agglutinin (PNA), a marker for the cone outer segment sheath, and mounted flat onto a microscope slide for counting. Results indicated a dramatic and rapid loss of cones within the retinae of *Rpe65*$^{-/-}$ mice between 2 and 4 weeks of age. By 4 weeks of age, large areas of the central and ventral *Rpe65*$^{-/-}$ retina showed almost no positive PNA labeling [64]. The lack of chromophore generation in *Rpe65*$^{-/-}$ mice was confirmed to cause this rapid loss of cones, as the delivery of exogenous 11-*cis* retinal to the retina beginning at 2 weeks of age significantly decreased the rate of cone loss [64–66].

51.5.2 Cones Expressing High Levels of S-Opsin Are More Susceptible to Degeneration

While a significant proportion of cones within the fovea are lost at a young age in LCA2 patients, a residual amount survive well into later ages [61]. Assessing the functionality of specific subsets of cones within LCA2 patients of various ages, it was discovered that the earliest loss of function occurred in cones expressing S-opsin, while the function of cones expressing L-opsin was significantly reduced in later ages, but was still present [61]. Thus, it would appear that, within the LCA2 human retina, cones expressing S-opsins degenerate at a faster rate than those expressing L-opsins.

Although mouse cones differ from human cones in their opsin expression patterns within the retina, mouse models for LCA2 can be used to further investigate this clinical feature. Unlike human cones, mouse cones only express two types of cone opsins (S and M). Both opsins may be coexpressed within a

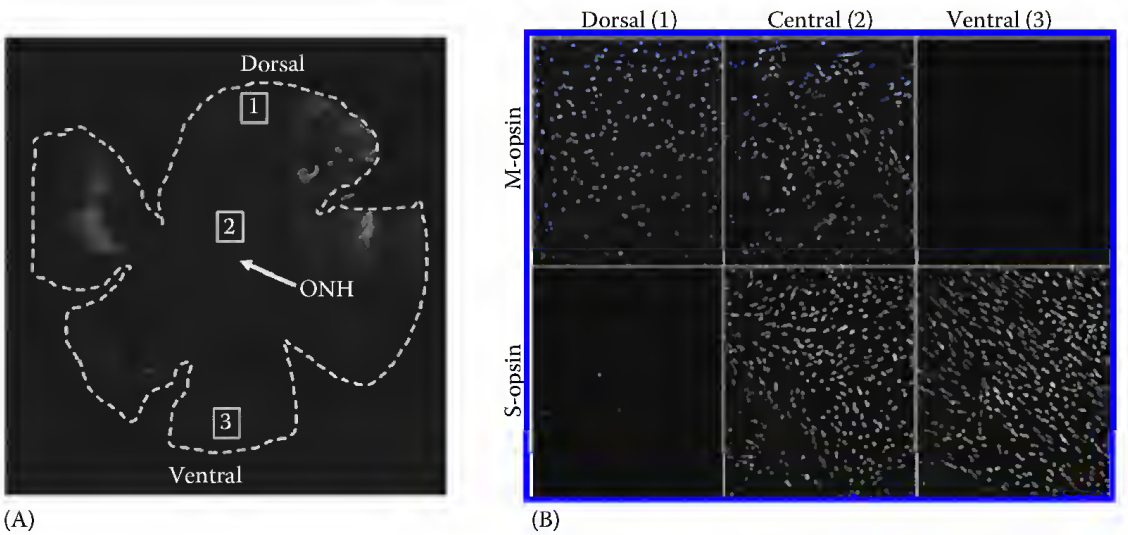

FIGURE 51.4 M/L- and S-opsin distribution along the dorsal–ventral axis of the mouse retina. (A) Low magnification of 2 week old *Wt* flat-mounted retina indicating three regions (1–3) analyzed for cone M/L- and S-opsin distribution. ONH, optic nerve head. (B) High magnification immunofluorescence images of M/L- (top panel) and S- (bottom panel) opsins from the dorsal (1), central (2), and ventral (3) regions of the retina. Immunofluorescence staining performed with antibodies specific for M/L-opsin (1:500 dilution; Cat# AB5405; Millipore, Billerica, MA) and S-opsin (1:500 dilution; Cat# sc-14363; Santa Cruz Biotech, Santa Cruz, CA).

single cone depending upon its retinotopic location [20]. While cones within the majority of the retina express M-opsin, those in the most ventral region do not. S-opsin distribution is in an opposite gradient, where cones within all but the most dorsal regions of the retina express it (Figure 51.4). Numerous developmental factors mediate this pattern of opsin expression, including thyroid hormone and the b2-isoform of its receptor (TRb2) [67,68]. This results in the establishment of unique M- to S-opsin ratios within cones along the dorsal–ventral axis of the mouse retina [20,22].

Data collected from the *Rpe65*$^{-/-}$ mouse retina support the clinical observation that cones expressing a high amount of S-opsin degenerate at a faster rate than those that do not. Using fluorescent PNA labeling as a general marker for cones to assess survival at various regions of the *Rpe65*$^{-/-}$ retina over time, it was observed that cones within the dorsal region of the retina, which express low amounts of S-opsin, exhibited a much slower rate of decline compared to cones within the central and ventral regions, which express high amounts of S-opsin [64–66]. This was confirmed through analysis of cone opsin mRNA expression in the *Rpe65*$^{-/-}$ retina, where the reduction of M-opsin mRNA expression progressed more slowly than that of S-opsin [64].

Morphological analysis of opsin distribution within the *Rpe65*$^{-/-}$ mouse cone provides insight into the correlation between a high level of S-opsin expression within the cone and its faster rate of degeneration in an environment of limited chromophore supply. Integral membrane proteins of the outer segment, such as opsins, are produced within the inner segment and subsequently trafficked through the connecting cilium to the outer segment [69] (Figure 51.2B). During the normal development of mouse cones, S-opsin expression begins immediately before birth and M-opsin expression begins at the end of the first postnatal week [65,66]. The mechanism for targeted transport of integral membrane proteins to the outer segment is active after the second postnatal week, as both opsins are localized indiscriminately throughout the normal mouse cone beforehand. 11-*cis* Retinal appears to play an important role in promoting this mechanism. In untreated *Rpe65*$^{-/-}$ mice, S-opsin appears to be more susceptible to mislocalization than M-opsin, and degeneration follows immediately afterward [66,70] (Figure 51.2C). Repeat 11-*cis* retinal supplementation at an early age is able to correct cone opsin mislocalization, restore function, and arrest degeneration [64–66,71].

The mechanism by which the mislocalization of cone opsin in *Rpe65*$^{-/-}$ retina triggers cone degeneration is not well understood; however, it may be due to the decreased amount of opsins that are properly trafficked in the absence of chromophore production [65,66,71]. As S-opsin constitutes the majority of the cone opsins expressed within the retina [20,64], its mislocalization plays a greater role in the early cone loss observed within the central and ventral retina of *Rpe65*$^{-/-}$ mice. With M-opsins less susceptible to mislocalization and the relatively low level of S-opsin expression, cones within the dorsal *Rpe65*$^{-/-}$ retina follow a slower degeneration rate and survive for much longer. This occurs in a manner similar to that observed in the rods of a mouse where the gene responsible for expressing rod opsin is mutated, with massive rod degeneration occurring afterward [72,73].

51.5.3 Treatments for LCA2

One of the exciting recent developments for treating congenital disorders has been the pioneering use of viral vectors to deliver functional genes to treat LCA2. The eye is ideally suited as a target organ for gene therapy, as its compartmentalized anatomy facilitates accurate delivery, the blood–retina barrier minimizes systemic side effects, and its relative ease of access and visualization facilitates the delivery process (for review, see Ref. [74]). Two clinical trials using adeno-associated viruses (AAV) to deliver *Rpe65* cDNA to adult LCA2 patients have been successfully completed with dramatic results [75,76]. A third clinical trial aiming to treat pediatric LCA2 patients using a similar approach is currently underway. The potential of AAV-mediated gene therapy for treating LCA2 and other congenital retinal diseases holds great promise and requires further validation to ensure safety and efficacy.

51.6 Conclusion

The intrinsic production of 11-*cis* retinal by the visual cycle is crucial for proper function of photoreceptor cells. RPE65 is a crucial enzyme in this multistep process, and its dysfunction is related to numerous congenital retinal diseases, which lead to early onset cone degeneration. The availability of animal models has allowed us to further investigate the mechanisms by which RPE65 dysfunction leads to cellular degeneration and has provided insights into developing novel treatment strategies such as gene therapy.

References

1. Moiseyev, G., Takahasi, Y., Chen, Y., Gentleman, S., Redmond, T.M., Crouch, R.K., and Ma, J.X., RPE65 is the isomerohydrolase in the retinoid visual cycle. *Proc Natl Acad Sci USA*, 2005. **102**(35): 12413–12418.
2. Crouch, R.K., Chader, G.J., Wiggert, B., and Pepperberg, D.R., Retinoids and the visual process. *Photochem Photobiol*, 1996. **64**(4): 613–621.
3. Travis, G.H., Golczak, M., Moise, A.R., and Palczewski, K., Diseases caused by defects in the visual cycle: Retinoids as potential therapeutic agents. *Annu Rev Pharmocol Toxicol*, 2007. **47**(8): 1–44.
4. Wolf, G., Retinoic acid as cause of cell proliferation or cell growth inhibition depending on activation of one or two different nuclear receptors. *Nutr Rev*, 2008. **66**(1): 55–59.
5. Moro, J.R., Iwata, M., and Von-Andriano, U.H., Vitamin effects on the immune system: Vitamins A and D take centre stage. *Nat Rev Immunol*, 2008. **8**(9): 685–698.
6. Pino-Lagos, K., Benson, M.J., and Noelle, R.J., Retinoic acid in the immune system. *Ann NY Acad Sci*, 2008. **1143**: 170–187.
7. Harrison, E., Mechanisms of digestion and absorption of dietary vitamin A. *Annu Rev Nutr*, 2005. **25**: 87–103.
8. Biesalski, H.K., Chichili, G.R., Frank, J., von-Lintig, J., and Nohr, D., Conversion of beta-carotene to retinal pigment. *Vitam Horm*, 2007. **75**: 117–130.

9. Kawaguchi, R., Yu, J., Honda, J., Hu, J., Whitelegge, J., Ping, P., Wiita, P., Bok, D., and Sun, H., A membrane receptor for retinol binding protein mediates cellular uptake of vitamin A. *Science*, 2007. **315**(5813): 820–825.
10. Wolf, G., Identification of a membrane receptor for retinol-binding protein functioning in the cellular uptake of retinol. *Nutr Rev*, 2007. **65**(8 Part 1): 385–388.
11. Carroll, J., Focus on molecules: The cone opsins. *Exp Eye Res*, 2008. **86**: 865–866.
12. Hargrave, P.A., McDowell, J.H., Curtis, D.R., Wang, J.K., Juszczak, E., Fong, S.L., Rao, J.K., and Argos, P., The structure of bovine rhodopsin. *Biophys Struct Mech*, 1983. **9**(4): 235–244.
13. Palczewski, K., Kumasaka, T., Hori, T., Behnke, C.A., Motoshima, H., Fox, B.A., Le-Trong, I., Teller, D.C., Okada, T., Stenkamp, R.E., Yamamoto, M., and Miyano, M., Crystal structure of rhodopsin: A G protein-coupled receptor. *Science*, 2000. **289**: 739–745.
14. Kono, M., Goletz, P.W., and Crouch, R.K., 11-cis and all-trans retinols can activate rod opsin: Rational design of the visual cycle. *Biochemistry*, 2008. **47**(28): 7567–7571.
15. Pugh, E.N. and Lamb, T.D., Phototransduction in vertebrate rods and cones: Molecular mechanisms of amplification, recovery, and light adaptation. *Molecular Mechanisms in Visual Transduction*, eds. Stavenga, D.G., de Grip, W.J., and Pugh, E.N., Jr., Vol. 3., pp. 183–255, 2000, Amsterdam, the Netherlands: Elsevier.
16. Wensel, T.G., Signal transducing membrane complexes of photoreceptor outer segments. *Vis Res*, 2008. **48**(20): 2052–2061.
17. Yau, K.W. and Hardie, R.C., Phototransduction motifs and variations. *Cell*, 2009. **139**(2): 246–264.
18. Fain, G.L., Matthews, H.R., Cornwall, M.C., and Koutalos, Y., Adaptation in vertebrate photoreceptors. *Physiol Rev*, 2001. **81**(1): 117–151.
19. Park, P.S.H., Sapra, K.T., Jastrzebska, B., Maeda, T., Maeda, A., Pulawski, W., Kono, M., Lem, J., Crouch, R.K., Filipek, S., Müller, D.J., and Palczewski, K., Modulation of molecular interactions and function by rhodopsin palmitylation. *Biochemistry*, 2009. **48**: 4294–4304.
20. Applebury, M.L., Antoch, M.P., Baxter, L.C., Chun, L.L., Falk, J.D., Farhangfar, F., Kage, K., Kryzstolik, M.G., Lyass, L.A., and Robbins, J.T., The murine cone photoreceptor: A single cone type expresses both S and M opsins with retinal spatial patterning. *Neuron*, 2000. **27**(3): 513–523.
21. Ahnelt, P.K. and Kolb, H., The mammalian photoreceptor mosaic-adaptive design. *Prog Retin Eye Res*, 2000. **19**: 711–777.
22. Szel, A., Rohlich, P., Caffe, A.R., and van-Veen, T., Distribution of cone photoreceptors in the mammalian retina. *Microsc Res Tech*, 1996. **35**: 445–462.
23. Rando, R., The biochemistry of the visual cycle. *Chem Rev*, 2001. **101**(7): 1881–1896.
24. Muniz, A., Villazana-Espinoza, E.T., Hatch, A.L., Trevino, S.G., Allen, D.M., and Tsin, A.T., A novel cone visual cycle in the cone-dominant retina. *Exp Eye Res*, 2007. **85**(2): 175–184.
25. Rattner, A., Smallwood, P.M., and Nathans, J., Identification and characterization of all-trans-retinol dehydrogenase from photoreceptor outer segments, the visual cycle enzyme that reduces all-trans-retinal to all-trans-retinol. *J Biol Chem*, 2000. **274**(15): 11034–11043.
26. Cideciyan, A.V., Haeseleer, F., Fariss, R.N., Aleman, T.S., Jang, G.F., Verlinde, C.L., Marmor, M.F., Jacobson, S.G., and Palczewski, K., Rod and cone visual cycle consequences of a null mutation in the 11-cis-retinol dehydrogenase gene in man. *Vis Neurosci*, 2000. **17**(5): 667–678.
27. Fong, S.L., Liou, G.I., Landers, R.A., Alvarez, R.A., and Bridges, C.D., Purification and characterization of a retinol-binding glycoprotein synthesized and secreted by bovine neural retina. *J Biol Chem*, 1984. **259**: 6534–6542.
28. Pepperberg, D.R., Okajima, T.L., Wiggert, B., Ripps, H., Crouch, R.K., and Chader, G.J., Interphotoreceptor retinoid-binding protein (IRBP). Molecular biology and physiological role in the visual cycle of rhodopsin. *Mol Neurobiol*, 1993. **6**: 61–85.
29. Ala-Laurila, P., Kolesnikov, A.V., Crouch, R.K., Tsina, E., Shukolyukov, S.A., Govardovskii, V.I., Koutalos, Y., Wiggert, B., Estevez, M.E., and Carter Cornwall, M., Visual cycle: Dependence of retinol production and removal on photo-product decay and cell morphology. *J Gen Physiol*, 2006. **128**: 153–169.

30. Wu, Q., Blakeley, L.R., Cornwall, M.C., Crouch, R.K., Wiggert, B.N., and Koutalos, Y., Interphotoreceptor retinoid-binding protein is the physiologically relevant carrier that removes retinol from rod photoreceptor outer segments. *Biochemistry*, 2007. **46**: 8669–8679.
31. Edwards, R.B. and Adler, A.J., IRBP enhances removal of 11-cis-retinaldehyde from isolated RPE membranes. *Exp Eye Res*, 2000. **70**: 235–245.
32. Jones, G.J., Crouch, R.K., Wiggert, B., Cornwall, M.C., and Chader, G.J., Retinoid requirements for recovery of sensitivity after visual-pigment bleaching in isolated photoreceptors. *Proc Natl Acad Sci*, 1989. **86**(23): 9606–9610.
33. Saari, J.C. and Bredberg, D.L., CoA- and non-CoA-dependent retinol esterification in retinal pigment epithelium. *J Biol Chem*, 1988. **263**: 8084–8090.
34. Redmond, T.M., Yu, S., Lee, E., Bok, D., Hamasaki, D., Chen, N., Goletz, P., Ma, J.X., Crouch, R.K., and Pfeifer, K., RPE65 is necessary for production of 11-cis-vitamin A in the retinal visual cycle. *Nat Genet*, 1998. **20**(4): 344–351.
35. Redmond, T.M., Poliakov, E., Yu, S., Tsai, J.Y., Lu, Z., and Gentleman, S., Mutation of key residues of Rpe65 abolishes its enzymatic role as isomerohydrolase in the visual cycle. *Proc Natl Acad Sci*, 2005. **102**: 13658–13663.
36. Saari, J.C., Bredberg, D.L., and Farrell, D.F., Retinol esterification in bovine retinal pigment epithelium: Reversibility of lecithin:retinol acyltransferase. *Biochem J*, 1993. **291** (Pt 3): 697–700.
37. Haeseleer, F., Jang, G.F., Imanishi, Y., Driessen, C.A., Matsumura, M., Nelson, P.S., and Palczewski, K., Dual-substrate specificity short chain retinol dehydrogenases from the vertebrate retina. *J Biol Chem*, 2002. **277**(47): 45537–45546.
38. Driessen, C.A., Janssen, B.P., Winkens, H.J., van-Vugt, A.H., de-Leeuw, T.L., and Janssen, J.J., Cloning and expression of a cDNA encoding bovine retinal pigment epithelial 11-cis retinol dehydrogenase. *Investig Ophthalmol Vis Sci*, 1995. **36**(10): 1988–1996.
39. Wolf, G., The visual cycle of the cone photoreceptors of the retina. *Nutr Rev*, 2004. **62**(7 Pt 1): 283–286.
40. Wang, J.S., Estevez, M.E., Cornwall, M.C., and Kefalov, V.J., Intra-retinal visual cycle required for rapid and complete cone dark adaptation. *Nat Neurosci*, 2009. **12**(3): 295–302.
41. Muniz, A., Betts, B.S., Trevino, A.R., Buddavarapu, K., Roman, R., Ma, J.X., and Tsin, A.T., Evidence for two retinoid cycles in the cone-dominant chicken eye. *Biochemistry*, 2009. **48**: 6854–6863.
42. Collery, R., McLoughlin, S., Vendrell, V., Finneagan, J., Crabb, J.W., Saari, J.C., and Kennedy, B.N., Duplication and divergence of zebrafish CRALBP genes uncovers novel role for RPE- and Muller-CRALBP in cone vision. *Investig Ophthalmol Vis Sci*, 2008. **49**(9): 3812–3820.
43. Fleisch, V.C., Schonthaler, H.B., von-Lintig, J., and Neuhauss, S.C., Subfunctionalization of a retinoid-binding protein provides evidence for two parallel visual cycles in the cone-dominant zebrafish retina. *J Neurosci*, 2008. **28**(33): 8208–8216.
44. Hood, D.C. and Hock, P.A., Recovery of cone receptor activity in the frog's isolated retina. *Vis Res*, 1973. **13**(10): 1943–1951.
45. Goldstein, E., Visual pigments and the early receptor potential of the isolated frog retina. *Vis Res*, 1968. **8**(8): 953–963.
46. Ma, J.X., Xu, L., Othersen, D.K., Redmond, T.M., and Crouch, R.K., Cloning and localization of RPE65 mRNA in salamander cone photoreceptor cells. *Biochim Biophys Acta*, 1998. **1443**: 255–261.
47. Znoiko, S.L., Crouch, R.K., Moiseyev, G., and Ma, J.X., Identification of the RPE65 protein in mammalian cone photoreceptors. *Investig Ophthalmol Vis Sci*, 2002. **43**: 1604–1609.
48. Das, S.R., Bhardwaj, N., Kjeldbye, H., and Gouras, P., Muller cells of chicken retina synthesize 11-cis-retinol. *Biochem J*, 1992. **285**(3): 907–913.
49. Bunt-Milam, A.H. and Saari, J.C., Immunocytochemical localization of two retinoid-binding proteins in vertebrate retina. *J Cell Biol*, 1983. **97**(3): 703–712.
50. Eisenfeld, A.J., Bunt-Milam, A.H., and Saari, J.C., Localization of retinoid-binding proteins in developing rat retina. *Exp Eye Res*, 1985. **41**(3): 299–304.

51. Jin, J., Jones, G.J., and Cornwall, M.C., Movement of retinal along cone and rod photoreceptors. *Vis Neurosci*, 1994. **11**(2): 389–399.
52. Sarantis, M. and Mobbs, P., The spatial relationship between Müller cell processes and the photoreceptor output synapse. *Brain Res*, 1992. **584**: 299–304.
53. Saari, J.C., Teller, D.C., Crabb, J.W., and Bredberg, L., Properties of an interphotoreceptor retinoid-binding protein from bovine retina. *J Biol Chem*, 1985. **260**: 195–201.
54. Uehara, F., Matthes, M.T., Yasumura, D., and LaVail, M.M., Light-evoked changes in the interphotoreceptor matrix. *Science*, 1990. **248**: 1633–1636.
55. Carter-Dawson, L. and Burroughs, M., Interphotoreceptor retinoid-binding protein in the cone matrix sheath. Electron microscopic immunocytochemical localization. *Investig Ophthalmol Vis Sci*, 1992a. **33**: 1584–1588.
56. Carter-Dawson, L. and Burroughs, M., Interphotoreceptor retinoid-binding protein in the Golgi apparatus of monkey foveal cones. Electron microscopic immunocytochemical localization. *Investig Ophthalmol Vis Sci*, 1992b. **33**: 1589–1594.
57. Parker, R.O., Fan, J., Nickerson, J.M., Liou, G.I., and Crouch, R.K., Normal cone function requires the interphotoreceptor retinoid binding protein. *J Neurosci*, 2009. **29**(14): 4616–4621.
58. den-Hollander, A.I., Roepman, R., Koenekoop, R.K., and Cremers, F.P., Leber congenital amaurosis: Genes, proteins and disease mechanisms. *Prog Retin Eye Res*, 2008. **27**(4): 391–419.
59. Koenekoop, R., An overview of Leber congenital amaurosis: A model to understand human retinal development. *Surv Ophthalmol*, 2004. **49**: 379–398.
60. Stone, E.M., Leber congenital amaurosis—A model for efficient genetic testing of heterogeneous disorders: LXIV Edward Jackson Memorial Lecture. *Am J Ophthalmol*, 2007. **144**: 791–811.
61. Jacobson, S.G., Aleman, T.S., Cideciyan, A.V., Heon, E., Golczak, M., Beltran, W.A., Sumaroka, A., Schwartz, S.B., Roman, A.J., Windsor, E.A., Wilson, J.M., Aguirre, G.D., Stone, E.M., and Palczewski, K., Human cone photoreceptor dependence on RPE65 isomerase. *Proc Natl Acad Sci*, 2007. **104**(38): 15123–15128.
62. Ekesten, B., Gouras, P., and Salchow, D.J., Ultraviolet and middle wavelength sensitive cone responses in the electroretinogram (ERG) of normal and Rpe65$^{-/-}$ mice. *Vision Res*, 2001. **41**: 2425–2433.
63. Seeliger, M.W., Grimm, C., Stahlberg, F., Friedburg, C., Jaissle, G., Zrenner, E., Guo, H., Remé, C.E., Humphries, P., Hofmann, F., Biel, M., Fariss, R.N., Redmond, T.M., and Wenzel, A., New views on Rpe65 deficiency: The rod system is the source of vision in a mouse model of Leber congenital amaurosis. *Nat Genet*, 2001. **29**: 70–74.
64. Znoiko, S.L., Rohrer, B., Lu, K., Lohr, H.R., Crouch, R.K., and Ma, J.X., Downregulation of cone-specific gene expression and degeneration of cone photoreceptors in the RPE65$^{-/-}$ mouse at early ages. *Investig Ophthalmol Vis Sci*, 2005. **46**(4): 1473–1479.
65. Fan, J., Rohrer, B., Frederick, J.M., Baehr, W., and Crouch, R.K., RPE65$^{-/-}$ and LRAT$^{-/-}$ mice: Comparable models of Leber congenital amaurosis. *Investig Ophthalmol Vis Sci*, 2008. **49**(6): 2384–2389.
66. Zhang, H., Fan, J., Li, S., Karan, S., Rohrer, B., Palczewski, K., Frederick, J.M., Crouch, R.K., and Baehr, W., Trafficking of membrane-associated proteins to cone photoreceptor outer segments requires the chromophore 11-cis-retinal. *J Neurosci*, 2008. **28**(15): 4008–4014.
67. Roberts, M.R., Srinivas, M., Forrest, D., Morreale-de-Escobar, G., and Reh, T.A., Making the gradient: Thyroid hormone regulates cone opsin expression in the developing mouse retina. *Proc Natl Acad Sci*, 2006. **103**(16): 6218–6223.
68. Applebury, M.L., Farhangfar, F., Glösmann, M., Hashimoto, K., Kage, K., Robbins, J.T., Shibusawa, N., Wondisford, F.E., and Zhang, H., Transient expression of thyroid hormone nuclear receptor TRb2 sets S opsin patterning during cone photoreceptor genesis. *Dev Dyn*, 2007. **236**: 1203–1212.
69. Insinna, C. and Besharse, J.C., Intraflagellar transport and the sensory outer segment of vertebrate photoreceptors. *Dev Dyn*, 2008. **237**: 1982–1992.

70. Avasthi, P., Watt, C.B., Williams, D.S., Le, Y.Z., Li, S., Chen, C.K., Marc, R.E., Frederick, J.M., and Baehr, W., Trafficking of membrane proteins to cone but not rod outer segments is dependent on heterotrimeric kinesin-II. *J Neurosci*, 2009. **29**(45): 14287–14298.
71. Rohrer, B., Lohr, H.R., Humphries, P., Redmond, T.M., Seeliger, M.W., and Crouch, R.K., Cone opsin mislocalization in RPE65$^{-/-}$ mice: A defect that can be corrected by 11-cis retinal. *Investig Ophthalmol Vis Sci*, 2005. **46**: 3876–3882.
72. Humphries, M.M., Rancourt, D., Farrar, G.J., Kenna, P., Hazel, M., Bush, R.A., Sieving, P.A., Sheils, D.M., McNally, N., Creighton, P., Erven, A., Boros, A., Gulya, K., Capecchi, M.R., and Humphries, P., Retinopathy induced in mice by targeted disruption of the rhodopsin gene. *Nat Genet*, 1997. **15**(2): 216–219.
73. Lem, J., Krasnoperova, N.V., Calvert, P.D., Kosaras, B., Cameron, D.A., Nicoló, M., Makino, C.L., and Sidman, R.L., Morphological, physiological, and biochemical changes in rhodopsin knockout mice. *Proc Natl Acad Sci*, 1999. **96**(2): 736–741.
74. Buch, P.K., Bainbridge, J.W., and Ali, R.R., AAV-mediated gene therapy for retinal disorders: From mouse to man. *Gene Ther*, 2008. **15**(11): 849–857.
75. Maguire, A., Simonelli, F., Pierce, E.A., Pugh, E.N., Mingozzi, F., Bennicelli, J., Banfi, S., Marshall, K.A., Testa, F., Surace, E.M., Rossi, S., Lyubarsky, A., Arruda, V.R., Konkle, B., Stone, E., Sun, J., Jacobs, J., Dell'Osso, L., Hertle, R., Ma, J.X., Redmond, T.M., Zhu, X., Hauck, B., Zelenaia, O., Shindler, K.S., Maguire, M.G., Wright, J.F., Volpe, N.J., McDonnell, J.W., Auricchio, A., High, K.A., and Bennett, J., Safety and efficacy of gene transfer for Leber's congenital amaurosis. *N Engl J Med*, 2008. **358**(21): 2240–2248.
76. Bainbridge, J.W., Smith, A.J., Barker, S.S., Robbie, S., Henderson, R., Balaggan, K., Viswanathan, A., Holder, G.E., Stockman, A., Tyler, N., Petersen-Jones, S., Bhattacharya, S.S., Thrasher, A.J., Fitzke, F.W., Carter, B.J., Rubin, G.S., Moore, A.T., and Ali, R.R., Effect of gene therapy on visual function in Leber's congenital amaurosis. *N Engl J Med*, 2008. **358**(21): 2231–2239.

52

Phytochrome: Molecular Mechanisms for Light Signaling in Plants

Jeong-Il Kim
Chonnam National University

Yun-Jeong Han
Chonnam National University

Pill-Soon Song
Jeju National University

52.1 Introduction

Phytochromes are photoreceptors that regulate many aspects of plant growth and development in response to red/far-red light signals from the environment.[1–3] Phytochromes in higher plants are encoded by small gene families.[4] For example, the completed whole genome sequences of *Arabidopsis thaliana* and *Oryza sativa* phytochromes reveal five (*PHYA* to *PHYE*) and three (*PHYA* to *PHYC*) genes, respectively.[5,6] Phytochromes are dimeric chromoproteins having covalently linked open tetrapyrrole phytochromobilin and exist in two photochromic species, red-light-absorbing Pr and far-red-light-absorbing Pfr forms. They are biosynthesized as the Pr form in the dark, which can be phototransformed into the Pfr form upon exposure to red light. The Pr-to-Pfr phototransformation of phytochromes induces the highly regulated signaling network for photomorphogenesis in plants.[7–9] Recent studies on the molecular mechanisms of the phytochrome-mediated light signaling reveal that phytochrome photoactivation impacts on the control of protein subcellular localization,[10,11] transcription,[12,13] protein stability,[14,15] and protein phosphorylation.[16] Here, we highlight the current knowledge about the molecular mechanisms of phytochrome function based on the recent advances.

52.2 Domain Structure of Phytochrome

The phytochrome molecule consists of two major structural domains, the globular N-terminal chromophore-binding domain (~65 kDa) and the structurally open or extended C-terminal domain (~55 kDa).[17] The two domains are connected via a flexible hinge region (Figure 52.1A). A domain swap experiment demonstrated that the N-terminal domains of phyA and phyB determine their photosensory specificity and differential light lability.[18] There are a few subdomains in the N-terminal photosensory domain, including N-terminal extension (NTE), bilin lyase domain (BLD), and phytochrome-specific domain (PHY). The NTE is dispensable for chromophore binding but necessary for a biological activity.[19] The BLD is composed of PAS (PER/ARNT/SIM) and GAF (cGMP phosphodiesterase/adenylate

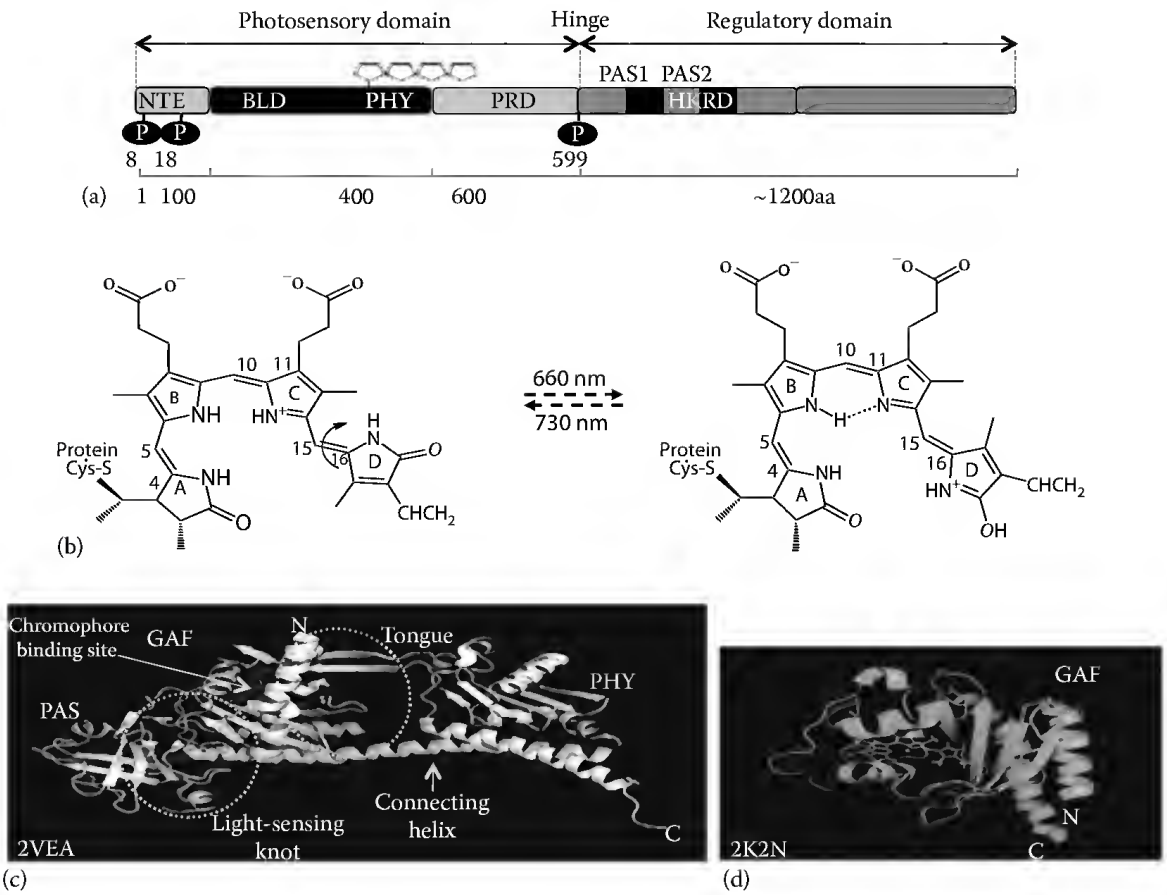

FIGURE 52.1 (**See color insert.**) Domain and protein structures of phytochrome. (a) Domain structure of phytochrome. Phytochrome has a two-domain structure, N-terminal photosensory domain and C-terminal regulatory domain. The photosensory domain contains both light sensor chromophore (phytochromobilin) and signaling motifs for phosphorylation and interactions with phytochrome-interacting factors (PIFs) (see text). NTE, N-terminal extension; BLD, bilin lyase domain consisting of PAS and GAF; PHY, phytochrome-specific GAF-related domain; PRD, PAS-related domain; PAS1 and PAS2, two PAS repeats; HKRD, histidine kinase–related domain. As examples, *Arabidopsis* phyA and phyB are composed of 1122 and 1172 amino acids, respectively. The four-connected pentagon in the BLD is the chromophore (i.e., phytochromobilin) that binds to the cysteine residue at 322. Three phosphorylation sites on oat phyA are also shown. (b) Photoisomerization of phytochromobilin during the Pr-to-Pfr phototransformation. (c) The N-terminal photosensory module structure (residues 1–514) of cyanobacterial phytochrome (Cph1).[21] The complete sensory module (PDB ID: 2VEA) consists of PAS, GAF, and PHY domains. Chromophore-binding site and connecting helix are indicated. The regions for light-sensing knot and the tongue are shown as circles. (d) The structure of the Cph1 GAF domain (PDB ID: 2K2N) assembled with phytocyanobilin.[34] N-terminus (N) and C-terminus (C) are labeled, and the chromophore is shown in white.

cyclase/FhlA) domains and is sufficient for chromophore attachment via a conserved cysteine residue that forms a thioester linkage with the A ring of phytochromobilin.[20] The PHY domain is a phytochrome-specific GAF-related domain adjacent to the BLD and has been suggested to directly interact with the D ring of the chromophore to maintain its open tetrapyrrole configuration (*ZZZ*) in the Pr form and to stabilize the Pfr form.[1,21]

Importance of the C-terminal regulatory domain is highlighted by numerous missense mutations affecting this part of the protein.[22,23] In the C-terminal domain, there are PAS-related domain (PRD) consisting of a pair of PAS repeats (PAS1 and PAS2) and histidine kinase–related domain (HKRD). The PRD has been reported to have regulatory roles for phytochrome dimerization,[24] nuclear localization,[25] and protein–protein interaction of phytochromes with their downstream components.[13,26,27] The HKRD is homologous to a histidine kinase domain, but is suggested to be a nonfunctional kinase domain because the key conserved residues within the histidine kinase domain are absent in the phytochrome HKRD.[16] This domain may play a regulatory role in the phytochrome signaling, because the domain interacts with downstream signaling components such as phytochrome kinase substrate 1 (PKS1)[28] and phytochrome-associated protein phosphatase 5 (PAPP5).[29] Furthermore, it has been reported that the phyB N-terminal domain by itself is functional *in vivo* when it could exist as dimers and be localized in the nucleus,[30,31] suggesting a model that the C-terminal domain is dispensable for phytochrome function except for dimerization and nuclear localization. However, phyA requires the C-terminal domain for its full activity in plants, suggesting a regulatory function of the C-terminal domain at least in the phyA-mediated light signaling.

52.3 Conformational Changes during Photoactivation

The striking characteristic of phytochromes is its reversible photochromism between the red- and the far-red-absorbing forms.[32] Phytochromes are synthesized in the Pr form (λ_{max} = 660 nm) which can be phototransformed into the Pfr from (λ_{max} = 730 nm) upon exposure to red light. The absorption of red light triggers a *Z*-to-*E* isomerization of the chromophore in the C_{15}–C_{16} double bond between the C and D rings of the linear tetrapyrrole (*ZZZ* to *ZZE*)[33] (Figure 52.1B). Contrary to the commonly held model for the photoisomerization, Ulijasz et al.[35] proposed a C_4–C_5 isomerization (*ZZZ* to *EZZ*) for the Pr-to-Pfr phototransformation based on the NMR-elucidated structure of Cph1 GAF domain. However, the configuration/conformation assigned to the presumed Pfr chromophore in the GAF domain does not possess the characteristic Pfr absorbance spectrum, so it remains to be seen if the C_4–C_5 isomerization occurs in native phytochromes. The photoisomerization of phytochromes leads to reversible conformational changes throughout the protein moiety of phytochrome,[17] which constitutes the first step of phytochrome signaling. Due to the promotive effect of the red light on most physiological responses, the Pfr form is considered as the active form. Once the Pfr form is formed, phytochrome moves into the nucleus and regulates the transcription of genes for photomorphogenesis and photosynthesis (see the following). Therefore, a basic molecular mechanism for the on/off switching of the phytochromes is driven by the photochromic transformation between the two forms.

Although the protein structure of plant phytochromes is not currently available, tertiary structures of eubacterial and cyanobacterial phytochrome fragments have been elucidated.[20,21,34,35] The 35 kDa N-terminal PAS/GAF domain structure (1ZTU) of a bacteriophytochrome DrBph1 from *Deinococcus radiodurans* illustrates how the chromophore buried in the chromophore-binding pocket formed in the N-terminal GAF domain, showing the light-sensing "knot" formed between PAS and GAF.[20] In the N-terminal PAS/GAF/PHY domain structure (2VEA) of a cyanobacterial phytochrome 1 (Cph1) from *Synechocystis* 6803, the PAS/GAF and the PHY domains are connected by a tongue-like structure protruding from the PHY domain[21] (Figure 52.1C and D). The structural information with phytochrome mutant analysis provides the basis to understand how the light signal is intramolecularly processed, in which the light-sensing knot is suggested to play a crucial role in the interaction of phytochrome with phytochrome-interacting factors (PIFs), and the tongue structure is suggested to be a modulator of the

phytochrome activity.[32,36,37] These structural analyses will be important for understanding how phytochromes perceive light signals and transmit them intramolecularly and intermolecularly with signal transducer proteins.

52.4 Molecular Mechanisms of Phytochrome Signaling

Phytochromes have been studied intensively by a broad range of experimental approaches since their first discovery in 1950s, but there is no definitive picture about how phytochromes transduce light signals into physiological responses so far. However, recent studies have resulted in several important advances in our understanding of phytochrome signaling.

52.4.1 Translocation of Phytochromes from Cytosol to Nucleus

Many plant proteins are known to change their localization in response to stimuli, and nucleocytoplasmic partitioning of proteins is a critical step in the regulation of gene expression.[10,38] Since phytochromes are biosynthesized as Pr forms and accumulate in the cytoplasm, it was once thought that phytochromes acted in the cytoplasm. However, analysis of phyB fused to β-glucosidase (GUS) demonstrated that phytochrome has nuclear localization activity,[39] and subsequent analysis of green-fluorescent-protein (GFP)-fused phytochromes showed that all phytochromes including phyA are translocated into the nucleus.[40,41] Therefore, the photoactivation of cytoplasmic Pr to Pfr causes translocation of phytochromes into the nucleus, which appears to be the early molecular event for phytochrome signaling. In the case of *Arabidopsis* phyB, the nuclear localization signal (NLS) is located in the PRD (amino acids 594–917), and the latter is both necessary and sufficient for nuclear localization.[25] It has been also known that the N-terminal photosensing GAF–PHY domain interacts with the PRD in a light-dependent manner, which provides a mechanistic link between light-dependent Pr-to-Pfr conformational changes and the unmasking of the NLS that regulates nuclear accumulation of phyB. This is consistent with the "intramolecular interdomain crosstalk" model that we previously proposed, based on the results of structural changes in NTE and PRD during phototransformation.[17] In the case of phyA, there is no putative NLS, but the nuclear accumulation of phyA is mediated by several plant-specific factors, including far-red elongated hypocotyl 1 (FHY1), FHY1-like (FHL), FHY3, and far-red impaired response 1 (FAR1).[11] FHY1 and FHL have a conserved C-terminal domain and N-terminal NLS and nuclear export signal (NES) sequences.[42,43] They directly interact with photoactivated phyA (i.e., the Pfr) in the cytoplasm through their conserved C-terminal domain, and the complex is imported into the nucleus.[44,45] FHY3 and FAR1 are transposase-derived transcription factors and indirectly control phyA nuclear accumulation by controlling the expression of FHY1 and FHL.[46] Therefore, the light-controlled translocation of the phytochromes from cytoplasm into the nucleus is a key regulatory step for phytochrome-mediated light signaling in plants.

52.4.2 Transcriptional Control of Light-Responsive Genes through Phytochromes

Photoactivation and nuclear localization of phytochromes trigger a transcription cascade that leads to the regulation of light-responsive genes. Recently, DNA microarray analyses have been applied to identify genome-wide set of phytochrome-regulated genes.[47] Approximately 10% of the genes in the *Arabidopsis* genome (2500 genes) are regulated by phytochromes under prolonged light exposure, whereas about 250 genes are affected at least twofold by continuous red light within 1 h.[48] Approximately 80% of the light-responding genes are induced, and about 20% repressed. The majority of these genes are strongly related to the various morphogenic changes observed during de-etiolation, including photosynthetic, hormone-pathway-related and metabolic genes, reflecting the transition from heterotrophic to autotrophic growth. To answer how phytochromes can mediate a global response to light at the transcriptional level, many downstream components in the phytochrome signaling have been identified and

characterized by genetic, biochemical, and molecular biological studies.[12,49] For the early search for the downstream components, yeast two-hybrid screens have identified a few proteins capable of interacting with phytochromes, such as PIF3,[50] nucleoside diphosphate kinase 2,[51] and PKS1.[28] Subsequently, a few other positively and negatively acting factors in the phytochrome signaling have been identified including blue/UV-A photoreceptor cryptochromes, Aux/IAA proteins, protein phosphatases, and F-box protein ZEITLUPE (see reviews, Refs. [2,52]). Among these components, a small set of PIFs are considered as the central players in the phytochrome-mediated light signaling.[13,53] PIFs are basic helix-loop-helix (bHLH) transcription factors among which PIF3 exhibits phytochrome-mediated and light-dependent binding to G-box promoter regions of various light-responsive genes, providing a plausible mechanism for direct photoregulation of gene expression by phytochromes.[54] The PIF or PIL (PIF3-like) proteins belong to subfamily 15 of the *Arabidopsis* bHLH superfamily,[26] and act to repress seed germination, promote seedling skotomorphogenesis, and shade avoidance through regulated expression of more than a 1000 genes.[13] Among them, several PIF/PIL proteins are involved in the phytochrome-mediated light signaling, for example, PIF1/PIL5 in chlorophyll biosynthesis and seed germination,[55,56] PIL1/PIF2 and PIL2/PIF6 in shade avoidance,[57] and PIL6/PIF5 in circadian rhythms,[58] as well as PIF3 and PIF4 in deetiolation.[59,60] These proteins appear to act as negative regulators in the phytochrome signaling,[61] and they are rapidly degraded by Pfr-induced proteasome.[62,63] In addition, photoactivated phytochromes induce rapid *in vivo* phosphorylation of PIF3 preceding degradation. Considering that phytochromes are known as atypical serine/threonine protein kinases,[64,65] the molecular mechanism of signal transfer from phytochromes to PIFs involves the degradation of PIFs through their phosphorylation by phytochromes.

52.4.3 Regulated Proteolysis in Phytochrome Signaling

Recent studies have shown that plants make extensive use of regulated proteolysis to modulate signal transduction pathways, including hormone and light signalings.[14,15,66] PhyA accumulates in etiolated seedlings and degrades rapidly upon light exposure via ubiquitin/26S proteasome-mediated protein degradation pathway.[67,68] Recently, phyB has been also shown to be degraded upon light treatment.[69] PIFs are also subject to regulated ubiquitination and subsequent degradation by the 26S proteasome. It appears likely that regulated proteolysis is an important molecular event in phytochrome signaling. Recently, we demonstrated that the autophosphorylation of phyA reduces the protein stability, thus desensitizing the phytochrome signaling.[65,70] These results are consistent with the previous report that the knockout plants of PAPP5 showed a decrease in photoresponsiveness and a decline in the stability of the phyA protein, while the protein stability increased in plants overexpressing PAPP5.[29] Further studies have shown that phosphorylated phyA preferentially associates with the COnstitutive Photomorphogenic 1/Suppressor of phyA-105 (COP1/SPA1) complex, the E3 ligase involved in the degradation of phyA.[71] The phosphorylated form of phyA increased in coimmunoprecipitation with COP1, suggesting that phyA phosphorylation is important for its interaction with the COP1/SPA1 complex. Therefore, the phosphorylation of phyA accelerates its degradation, whereas its dephosphorylation slows the degradation. Likewise, PIFs including PIF1, PIF3, and PIF5 undergo light-induced phosphorylation depending on their interaction with photoactivated phytochromes, which accelerates the proteasome-mediated degradation of the negative regulators in the phytochrome signaling.[63,72,73] These findings suggest that the levels of both photoreceptors and phytochrome-interacting proteins are regulated by 26S proteosomal degradation during the phytochrome-mediated light signaling in plants.

52.4.4 Phosphorylation and Dephosphorylation in Phytochrome Signaling

Phosphorylation and dephosphorylation of a protein often serve as a signal modulation mechanism in the regulation of cellular activities, and the involvement of protein phosphorylation has been known in almost all signaling pathways in plants.[74,75] Phytochromes are known as phosphoproteins by phosphate

analysis on purified phytochrome preparations.[76] The sites of phytochrome phosphorylation have been investigated with purified phyA from oat seedlings, and three serines, Ser8, Ser18, and Ser599, have been identified as the phosphorylation sites.[77] Phosphorylation at Ser599 in the hinge region prevents the interaction of phyA with its signal transducers such as nucleoside diphosphate kinase 2.[78] These data suggest that the hinge region of phytochrome serves as a phosphorylatable signal-modulating site which regulates protein–protein interactions between phytochrome and its signal transducers. Ser8 and Ser18 in the NTE have been identified as autophosphorylation sites of oat phyA, and the autophosphorylation provides a molecular mechanism for signal attenuation in phytochrome-mediated light signaling by accelerating the degradation of phyA.[65,70] Therefore, phosphorylation on phytochrome molecule is important for the regulation of phytochrome interaction with downstream signal transducers and for the regulation of protein stability, which might play an important role in fine-tuning phytochrome signaling. The observation that phytochromes are phosphoproteins also suggests the existence of protein kinase(s) that phosphorylate the phytochromes and protein phosphatase(s) that dephosphorylate them. However, despite extensive studies of phytochrome-interacting proteins, there is no report thus far of a protein kinase that can phosphorylate phytochromes. On the other hand, a few protein phosphatases have been reported as being able to interact with and dephosphorylate phytochromes, including flower-specific phytochrome-associated protein phosphatase (FyPP),[79] PAPP5,[29] and phytochrome-associated protein phosphatase type 2C (PAPP2C).[80] All these protein phosphatases act as positive regulators in the phytochrome signaling, suggesting that the phytochrome signaling is regulated by phosphorylation and dephosphorylation in which phytochrome is autophosphorylated and then dephosphorylated by FyPPs. Phytochrome autophosphorylation decreases its signaling flux by reducing the amounts of phytochrome proteins, while phytochrome dephosphorylation increases the signaling flux by enhancing phytochrome interaction with its signal transducers and increasing its protein stability.

52.4.5 Phytochromes as Serine/Threonine Protein Kinases

Plant phytochromes are known as autophosphorylating serine/threonine kinases.[64] It is possible that phytochromes exert their kinase activity to control the downstream signaling components as well as themselves. As mentioned earlier, the autophosphorylation by the intrinsic protein kinase activity of phytochromes provides a signal attenuation or desensitization mechanism for the phytochrome signaling. In addition, phytochromes can phosphorylate downstream signal transducers to regulate them for light signaling. These proteins include PKS1, Aux/IAA proteins, cryptochromes, and more.[16] The Pfr form of phytochromes induces rapid *in vivo* phosphorylation of PIFs preceding degradation,[63,72,73] suggesting the possible role of the phytochrome kinase activity in photomorphogenesis. We observed that phytochromes phosphorylated PIFs *in vitro* (Kim and Song, unpublished data). Also, phyA mediates rapid red light-induced phosphorylation of *Arabidopsis* FHY1 and FHL in a low-fluence response, probably regulating the protein stability of FHY1 and FHL.[81] Therefore, the phytochrome-induced phosphorylation of proteins such as PIFs may represent a primary intermolecular signal transduction for tagging a target protein for proteosomal degradation. However, the molecular mechanisms about how the phosphorylation of these proteins by phytochromes affects the light signaling are still unknown, so further studies will be necessary to elucidate the signaling pathways related to the phytochrome kinase activity.

52.5 Descriptive Model for Phytochrome Function in Plant Light Signaling

Recent advances in the study of molecular mechanisms for phytochrome functioning provide a plausible model for the regulation of phytochrome-mediated light signaling (Figure 52.2). In the dark, phyA proteins are synthesized and accumulate as the Pr form in the cytosol, composed of autophosphorylated and dephosphorylated phytochromes due to the action of kinases and phosphatases. Upon illumination,

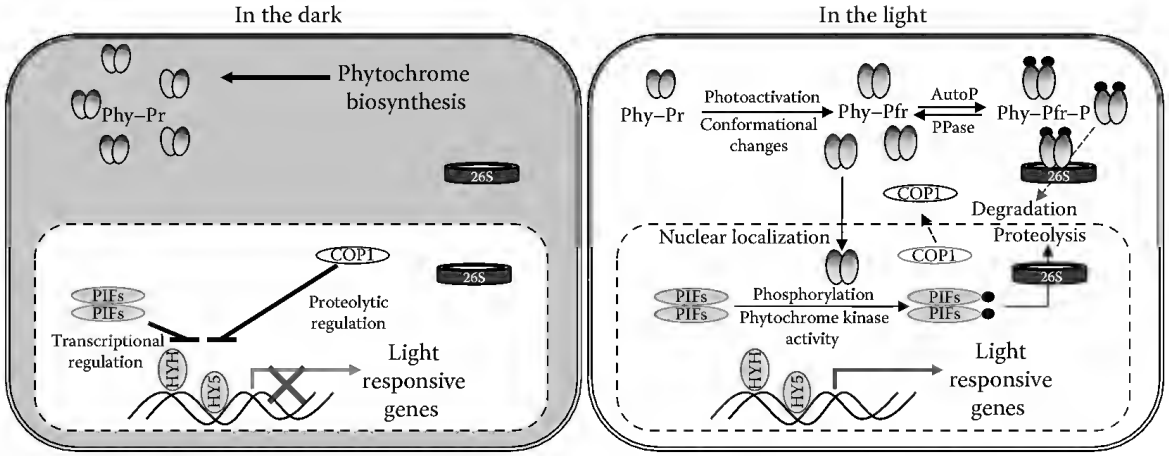

FIGURE 52.2 A model for the molecular mechanisms of phytochrome. Phy–Pr, the Pr form of phytochrome; Phy–Pfr, the Pfr form of phytochrome; Phy–Pfr–P, the phosphorylated Pfr form; AutoP, autophosphorylation; PPase, protein phosphatase; 26S, 26S proteasome. In the dark, phytochrome is synthesized and accumulates as the Pr forms in the cytosol (Phy–Pr). Light-responsive genes for photomorphogenesis are not expressed because the photomorphogenesis-promoting transcription factors such as HY5 and HYH are suppressed by PIFs and degraded by COP1. In the light, the Pr form is photoactivated to the Pfr form (Phy–Pfr), which translocates into the nucleus. The photoactivated phytochromes in the nucleus phosphorylate PIFs and thus PIFs' degradation are promoted, which release the suppression of the photomorphogenesis-promoting transcription factors. At the same time, COP1 is translocalized from the nucleus to the cytoplasm. These events finally induce photomorphogenesis in plants. Upon photoactivation, phosphorylated phytochromes (Phy–Pfr–P) are also rapidly degraded for the efficient desensitization of the phyA signal, which is necessary for responses to subsequent changes in fluctuating light environments.

the Pr form is photoactivated to the Pfr form that translocates from cytosol to the nucleus. At this point, the phosphorylated Pfr form is rapidly degraded via the ubiquitin/26S proteasome protein degradation pathway. The balance between the autophosphorylated and dephosphorylated phyA proteins is probably shifted to the autophosphorylated phyA, because the phosphorylated phyA proteins are efficiently degraded by the ubiquitin/26S proteasome through the COP1/SPA1 complex. This rapid phyA degradation mechanism involving autophosphorylation could facilitate the efficient attenuation of the phyA signal. On the other hand, phytochrome protein phosphatases insure the stability of phyA protein for an enhanced light response in photomorphogenesis, resulting from a decline in the autophosphorylated phyA level. If phyA-signaling activity is not modulated by light, plants could globally respond to light by overshooting photomorphogenic signaling events and/or could become desensitized to subsequent changes in light quality or quantity. We suggest that the posttranslational regulation of phyA plays an efficient role in rapidly controlling the number of active phyA photoreceptors available to elicit signaling events, and improve the response of plants to fluctuating light environments.

In the dark, COP1 is a nuclear protein that mediates light control of gene expression through proteasome-mediated targeted degradation of multiple photomorphogenesis-promoting transcription factors including two basic leucine zipper (bZIP) transcription factors long hypocotyl 5 (HY5) and HY5 homolog (HYH).[82,83] COP1 is also involved in the degradation of phytochromes. However, COP1 is known to be translocated from the nucleus to cytosol upon light illumination, which prevents the degradation of phytochromes and transcriptional factors for light-responsive genes. Once the photoactivated forms of phytochromes enter the nucleus, they could phosphorylate the substrate proteins such as PIFs that suppress the expression of light-responsive genes for photomorphogenesis and photosynthesis. Together with the translocation of COP1 from the nucleus to the cytoplasm, the removal of negative regulators for light signaling (i.e., PIFs) by photoactivated phytochromes turns on the transcription of light-responsive genes, which allows plants to grow and develop optimally in the light environment.

52.6 Conclusions

Understanding of the phytochrome-mediated light signaling has improved dramatically in recent years. Phytochrome migration to the nucleus followed by Pfr–PIF/PIL–DNA element interactions provides a shortcut between light signals and the target genes. The control of COP1 localization by phytochrome coupled to the role of COP1 in the proteolytic degradation of transcription factors for photomorphogenesis provides a second route to control the signaling. The regulation of phytochrome function by phosphorylation and dephosphorylation provides an early signaling mechanism to affect photomorphogenesis. A plausible model for the phytochrome function involves a network of the light signaling cascades with multiple points of convergence and divergence by controlling protein subcellular localization, transcription, protein stability, and protein phosphorylation. Although dramatic progress has been made during the past decade in understanding the molecular mechanisms of phytochrome signaling, largely owing to the use of molecular genetics in the model plant *Arabidopsis*, it is also clear that current information about the nature and extent of the phytochrome-mediated signaling network is still limited and fragmentary. Further research remains to be pursued to dissect the phytochrome signaling network with a better understanding of how the various nodes of the network interact to transmit the light signals.

Acknowledgments

This work was supported in part by Basic Science Research Program through the National Research Foundation of Korea (NRF) funded by the Ministry of Education, Science and Technology (grant no. 2010-0012628) and by the BioGreen 21 Program (Code no. 20080401034014), Rural Development Administration, Republic of Korea.

References

1. Rockwell, N.C., Su, Y.S., and Lagarias, J.C., Phytochrome structure and signaling mechanisms, *Annu. Rev. Plant Biol.*, 57, 837, 2006.
2. Bae, G. and Choi, G., Decoding of light signals by plant phytochromes and their interacting proteins, *Annu. Rev. Plant Biol.*, 59, 281, 2008.
3. Chory, J., Light signal transduction: An infinite spectrum of possibilities, *Plant J.*, 61, 982, 2010.
4. Mathews, S. and Sharrock, R.A., Phytochrome gene diversity, *Plant Cell Environ.*, 20, 666, 1997.
5. Takano, M., Inagaki, N., Xie, X., Kiyota, S., Baba-Kasai, A., Tanabata, T., and Shinomura, T., Phytochromes are the sole photoreceptors for perceiving red/far-red light in rice, *Proc. Natl. Acad. Sci. USA*, 106, 14705, 2009.
6. Mathews, S., Evolutionary studies illuminate the structural-functional model of plant phytochromes, *Plant Cell*, 22, 4, 2010.
7. Quail, P.H., Phytochrome photosensory signaling networks, *Nat. Rev. Mol. Cell Biol.*, 3, 85, 2002.
8. Chen, M., Chory, J., and Fankhauser, C., Light signal transduction in higher plants, *Annu. Rev. Genet.*, 38, 87, 2004.
9. Han, Y.J., Song, P.S., and Kim, J.I., Phytochrome-mediated photomorphogenesis in plants, *J. Plant Biol.*, 50, 230, 2007.
10. Nagatani, A., Light-regulated nuclear localization of phytochromes, *Curr. Opin. Plant Biol.*, 7, 708, 2004.
11. Fankhauser, C. and Chen, M., Transposing phytochrome into the nucleus, *Trends Plant Sci.*, 13, 596, 2008.
12. Jiao, Y., Lau, O.S., and Deng, X.W., Light-regulated transcriptional networks in higher plants, *Nat. Rev. Genet.*, 8, 217, 2007.
13. Leivar, P. and Quail, P.H., PIFs: Pivotal components in a cellular signaling hub, *Trends Plant Sci.*, 16, 19, 2011.

14. Hoecker, U., Regulated proteolysis in light signaling, *Curr. Opin. Plant Biol.*, 8, 469, 2005.
15. Henriques, R., Jang, I.C., and Chua, N.H., Regulated proteolysis in light-related signaling pathways, *Curr. Opin. Plant Biol.*, 12, 49, 2009.
16. Kim, J.I., Park, J.E., Zarate, X., and Song, P.S., Phytochrome phosphorylation in plant light signaling, *Photochem. Photobiol. Sci.*, 4, 681, 2005.
17. Kim, J.I. and Song, P.S., A structure-function model based on inter-domain crosstalks in phytochromes. In: *Light Sensing in Plants* (M. Wada, K. Shimazaki, and M. Iino, Eds.), Springer-Verlag, Tokyo, Japan, p. 53, 2005.
18. Wagner, D., Fairchild, C.D., Kuhn, R.M., and Quail, P.H., Chromophore-bearing NH_2-terminal domains of phytochromes A and B determine their photosensory specificity and differential light lability, *Proc. Natl. Acad. Sci. USA*, 93, 4011, 1996.
19. Cherry, J.R., Hondred, D., Walker, J.M., and Vierstra, R.D., Phytochrome requires the 6-kDa N-terminal domain for full biological activity, *Proc. Natl. Acad. Sci. USA*, 89, 5039, 1992.
20. Wagner, J.R., Brunzelle, J.S., Forest, K.T., and Vierstra, R.D., A light-sensing knot revealed by the structure of the chromophore-binding domain of phytochrome, *Nature*, 438, 325, 2005.
21. Essen, L.O., Mailliet, J., and Hughes, J., The structure of a complete phytochrome sensory module in the Pr ground state, *Proc. Natl. Acad. Sci. USA*, 105, 14709, 2008.
22. Quail, P.H., Boylan, M.T., Parks, B.M., Short, T.W., Xu, Y., and Wagner, D., Phytochromes: Photosensory perception and signal transduction, *Science*, 268, 675, 1995.
23. Krall, L. and Reed, J.W., The histidine kinase-related domain participates in phytochrome B function but is dispensable, *Proc. Natl. Acad. Sci. USA*, 97, 8169, 2000.
24. Kim, J.I., Bhoo, S.H., Han, Y.J., Zarate, X., Furuya, M., and Song, P.S., The PAS2 domain is required for dimerization of phytochrome A, *J. Photochem. Photobiol. A Chem.*, 178, 115, 2006.
25. Chen, M., Tao, Y., Lim, J., Shaw, A., and Chory, J., Regulation of phytochrome B nuclear localization through light-dependent unmasking of nuclear-localization signals, *Curr. Biol.*, 15, 637, 2005.
26. Toledo-Ortiz, G., Huq, E., and Quail, P.H., The Arabidopsis basic/helix-loop-helix transcription factor family, *Plant Cell*, 15, 1749, 2003.
27. Shen, Y., Kim, J.I., and Song, P.S., NDPK2 as a signal transducer in the phytochrome-mediated light signaling, *J. Biol. Chem.*, 280, 5740, 2005.
28. Fankhauser, C., Yeh, K.C., Lagarias, J.C., Zhang, H., Elich, T.D., and Chory, J., PKS1, a substrate phosphorylated by phytochrome that modulates light signaling in Arabidopsis, *Science*, 284, 1539, 1999.
29. Ryu, J.S., Kim, J.I., Kunkel, T., Kim, B.C., Cho, D.S., Hong, S.H., Kim, S.H., Fernandez, A.P., Kim, Y., Alonso, J.M., Ecker, J.R., Nagy, F., Lim, P.O., Song, P.S., Schafer, E., and Nam, H.G., Phytochrome-specific type 5 phosphatase controls light signal flux by enhancing phytochrome stability and affinity for a signal transducer, *Cell*, 120, 395, 2005.
30. Matsushita, T., Mochizuki, N., and Nagatani, A., Dimers of the N-terminal domain of phytochrome B are functional in the nucleus, *Nature*, 424, 571, 2003.
31. Oka, Y., Matsushita, T., Mochizuki, N., Suzuki, T., Tokutomi, S., and Nagatani, A., Functional analysis of a 450-amino acid N-terminal fragment of phytochrome B in Arabidopsis, *Plant Cell*, 16, 2104, 2004.
32. Nagatani, A., Phytochrome: Structural basis for its functions, *Curr. Opin. Plant Biol.*, 13, 565, 2010.
33. Rudiger, W., Thummler, F., Cmiel, E., and Schneider, S., Chromophore structure of the physiologically active form (P(fr)) of phytochrome, *Proc. Natl. Acad. Sci. USA*, 80, 6244, 1983.
34. Cornilescu, G., Ulijasz, A.T., Cornilescu, C.C., Markley, J.L., and Vierstra, R.D., Solution structure of a cyanobacterial phytochrome GAF domain in the red-light-absorbing ground state, *J. Mol. Biol.*, 383, 403, 2008.
35. Ulijasz, A.T., Cornilescu, G., Cornilescu, C.C., Zhang, J., Rivera, M., Markley, J.L., and Vierstra, R.D., Structural basis for the photoconversion of a phytochrome to the activated Pfr form, *Nature*, 463, 250, 2010.

36. Oka, Y., Matsushita, T., Mochizuki, N., Quail, P.H., and Nagatani, A., Mutant screen distinguishes between residues necessary for light-signal perception and signal transfer by phytochrome B, *PLoS Genet.*, 4, e1000158, 2008.
37. Kikis, E.A., Oka, Y., Hudson, M.E., Nagatani, A., and Quail, P.H., Residues clustered in the light-sensing knot of phytochrome B are necessary for conformer-specific binding to signaling partner PIF3, *PLoS Genet.*, 5, e1000352, 2009.
38. Merkle, T., Nucleo-cytoplasmic partitioning of proteins in plants: Implications for the regulation of environmental and developmental signaling, *Curr. Genet.*, 44, 231, 2003.
39. Sakamoto, K. and Nagatani, A., Nuclear localization activity of phytochrome B, *Plant J.*, 10, 859, 1996.
40. Kircher, S., Kozma-Bognar, L., Kim, L., Adam, E., Harter, K., Schafer, E., and Nagy, F., Light quality-dependent nuclear import of the plant photoreceptors phytochrome A and B, *Plant Cell*, 11, 1445, 1999.
41. Kircher, S., Gil, P., Kozma-Bognar, L., Fejes, E., Speth, V., Husselstein-Muller, T., Bauer, D., Adam, E., Schafer, E., and Nagy, F., Nucleocytoplasmic partitioning of the plant photoreceptors phytochrome A, B, C, D, and E is regulated differentially by light and exhibits a diurnal rhythm, *Plant Cell*, 14, 1541, 2002.
42. Desnos, T., Puente, P., Whitelam, G.C., and Harberd, N.P., FHY1: A phytochrome A-specific signal transducer, *Genes Dev.*, 15, 2980, 2001.
43. Zhou, Q., Hare, P.D., Yang, S.W., Zeidler, M., Huang, L.F., and Chua, N.H., FHL is required for full phytochrome A signaling and shares overlapping functions with FHY1, *Plant J.*, 43, 356, 2005.
44. Hiltbrunner, A., Tscheuschler, A., Viczian, A., Kunkel, T., Kircher, S., and Schafer, E., FHY1 and FHL act together to mediate nuclear accumulation of the phytochrome A photoreceptor, *Plant Cell Physiol.*, 47, 1023, 2006.
45. Genoud, T., Schweizer, F., Tscheuschler, A., Debrieux, D., Casal, J.J., Schafer, E., Hiltbrunner, A., and Fankhauser, C., FHY1 mediates nuclear import of the light-activated phytochrome A photoreceptor, *PLoS Genet.*, 4, e1000143, 2008.
46. Lin, R., Ding, L., Casola, C., Ripoll, D.R., Feschotte, C., and Wang, H., Transposase-derived transcription factors regulate light signaling in Arabidopsis, *Science*, 318, 1302, 2007.
47. Quail, P.H., Phytochrome-regulated gene expression, *J. Integr. Plant Biol.*, 49, 11, 2007.
48. Tepperman, J.M., Hwang, Y.S., and Quail, P.H., PhyA dominates in transduction of red-light signals to rapidly responding genes at the initiation of Arabidopsis seedling de-etiolation, *Plant J.*, 48, 728, 2006.
49. Wang, H. and Deng, X.W., Dissecting the phytochrome A-dependent signaling network in higher plants, *Trends Plant Sci.*, 8, 172, 2003.
50. Ni, M., Tepperman, J.M., and Quail, P.H., PIF3, a phytochrome-interacting factor necessary for normal photoinduced signal transduction, is a novel basic helix-loop-helix protein, *Cell*, 95, 657, 1998.
51. Choi, G., Yi, H., Lee, J., Kwon, Y.K., Soh, M.S., Shin, B., Luka, Z., Hahn, T.R., and Song, P.S., Phytochrome signaling is mediated through nucleoside diphosphate kinase 2, *Nature*, 401, 610, 1999.
52. Gyula, P., Schafer, E., and Nagy, F., Light perception and signaling in higher plants, *Curr. Opin. Plant Biol.*, 6, 446, 2003.
53. Castillon, A., Shen, H., and Huq, E., Phytochrome interacting factors: Central players in phytochrome-mediated light signaling networks, *Trends Plant Sci.*, 12, 514, 2007.
54. Martinez-Garcia, J.F., Huq, E., and Quail, P.H., Direct targeting of light signals to a promoter element-bound transcription factor, *Science*, 288, 859, 2000.
55. Huq, E., Al-Sady, B., Hudson, M., Kim, C., Apel, K., and Quail, P.H., Phytochrome-interacting factor 1 is a critical bHLH regulator of chlorophyll biosynthesis, *Science*, 305, 1937, 2004.
56. Oh, E., Kim, J., Park, E., Kim, J.I., Kang, C., and Choi, G., PIL5, a phytochrome-interacting basic helix-loop-helix protein, is a key negative regulator of seed germination in *Arabidopsis thaliana*, *Plant Cell*, 16, 3045, 2004.
57. Salter, M.G., Franklin, K.A., and Whitelam, G.C., Gating of the rapid shade-avoidance response by the circadian clock in plants, *Nature*, 426, 680, 2003.

58. Fujimori, T., Yamashino, T., Kato, T., and Mizuno, T., Circadian-controlled basic/helix-loop-helix factor, PIL6, implicated in light-signal transduction in *Arabidopsis thaliana*, *Plant Cell Physiol.*, 45, 1078, 2004.
59. Huq, E. and Quail, P.H., PIF4, a phytochrome-interacting bHLH factor, functions as a negative regulator of phytochrome B signaling in Arabidopsis, *EMBO J.*, 21, 2441, 2002.
60. Kim, J., Yi, H., Choi, G., Shin, B., and Song, P.S., Functional characterization of phytochrome interacting factor 3 in phytochrome-mediated light signal transduction, *Plant Cell*, 15, 2399, 2003.
61. Duek, P.D. and Fankhauser, C., bHLH class transcription factors take centre stage in phytochrome signaling, *Trends Plant Sci.*, 10, 51, 2005.
62. Bauer, D., Viczian, A., Kircher, S., Nobis, T., Nitschke, R., Kunkel, T., Panigrahi, K.C., Adam, E., Fejes, E., Schafer, E., and Nagy, F., Constitutive photomorphogenesis 1 and multiple photoreceptors control degradation of phytochrome interacting factor 3, a transcription factor required for light signaling in Arabidopsis, *Plant Cell*, 16, 1433, 2004.
63. Al-Sady, B., Ni, M., Kircher, S., Schafer, E., and Quail, P.H., Photoactivated phytochrome induces rapid PIF3 phosphorylation prior to proteasome-mediated degradation, *Mol. Cell*, 23, 439, 2006.
64. Yeh, K.C. and Lagarias, J.C., Eukaryotic phytochromes: Light-regulated serine/threonine protein kinases with histidine kinase ancestry, *Proc. Natl. Acad. Sci. USA*, 95, 13976, 1998.
65. Han, Y.J., Kim, H.S., Kim, Y.M., Shin, A.Y., Lee, S.S., Bhoo, S.H., Song, P.S., and Kim, J.I., Functional characterization of phytochrome autophosphorylation in plant light signaling, *Plant Cell Physiol.*, 51, 596, 2010.
66. Huq, E., Degradation of negative regulators: A common theme in hormone and light signaling networks? *Trends Plant Sci.*, 11, 4, 2006.
67. Clough, R.C. and Vierstra, R.D., Phytochrome degradation. *Plant Cell Environ.*, 20, 713, 1997.
68. Seo, H.S., Watanabe, E., Tokutomi, S., Nagatani, A., and Chua, N.H., Photoreceptor ubiquitination by COP1 E3 ligase desensitizes phytochrome A signaling, *Genes Dev.*, 18, 617, 2004.
69. Jang, I.C., Henriques, R., Seo, H.S., Nagatani, A., and Chua, N.H., *Arabidopsis* PHYTOCHROME INTERACTING FACTOR proteins promote phytochrome B polyubiquitination by COP1 E3 ligase in the nucleus, *Plant Cell*, 22, 2370, 2010.
70. Han, Y.J., Kim, H.S., Song, P.S., and Kim, J.I., Autophosphorylation desensitizes phytochrome signal transduction, *Plant Signal Behav.*, 5, 868, 2010.
71. Saijo, Y., Zhu, D., Li, J., Rubio, V., Zhou, Z., Shen, Y., Hoecker, U., Wang, H., and Deng, X.W., Arabidopsis COP1/SPA1 complex and FHY1/FHY3 associate with distinct phosphorylated forms of phytochrome A in balancing light signaling, *Mol. Cell*, 31, 607, 2008.
72. Shen, Y., Khanna, R., Carle, C.M., and Quail, P.H., Phytochrome induces rapid PIF5 phosphorylation and degradation in response to red-light activation, *Plant Physiol.*, 145, 1043, 2007.
73. Shen, H., Zhu, L., Castillon, A., Majee, M., Downie, B., and Huq, E., Light-induced phosphorylation and degradation of the negative regulator PHYTOCHROME-INTERACTING FACTOR1 from Arabidopsis depend upon its direct physical interactions with photoactivated phytochromes, *Plant Cell*, 20, 1586, 2008.
74. Watson, J.C., Light and protein kinases, *Adv. Bot. Res.*, 32, 149, 2000.
75. Luan, S., Protein phosphatases in plants, *Annu. Rev. Plant Biol.*, 54, 63, 2003.
76. Hunt, R.E. and Pratt, L.H., Partial characterization of undegraded oat phytochrome, *Biochemistry*, 19, 390, 1980.
77. Lapko, V.N., Jiang, X.Y., Smith, D.L., and Song, P.S., Mass spectrometric characterization of oat phytochrome A: Isoforms and posttranslational modifications, *Protein Sci.*, 8, 1032, 1999.
78. Kim, J.I., Shen, Y., Han, Y.J., Park, J.E., Kirchenbauer, D., Soh, M.S., Nagy, F., Schafer, E., and Song, P.S., Phytochrome phosphorylation modulates light signaling by influencing the protein–protein interaction, *Plant Cell*, 16, 2629, 2004.
79. Kim, D.H., Kang, J.G., Yang, S.S., Chung, K.S., Song, P.S., and Park, C.M., A phytochrome-associated protein phosphatase 2A modulates light signals in flowering time control in Arabidopsis, *Plant Cell*, 14, 3043, 2002.

80. Phee, B.K., Kim, J.I., Shin, D.H., Yoo, J., Park, K.J., Han, Y.J., Kwon, Y.K., Cho, M.H., Jeon, J.S., Bhoo, S.H., and Hahn, T.R., A novel protein phosphatase indirectly regulates phytochrome-interacting factor 3 via phytochrome, *Biochem. J.*, 415, 247, 2008.
81. Shen, Y., Zhou, Z., Feng, S., Li, J., Tan-Wilson, A., Qu, L.J., Wang, H., and Deng, X.W., Phytochrome A mediates rapid red light-induced phosphorylation of Arabidopsis FAR-RED ELONGATED HYPOCOTYL1 in a low fluence response, *Plant Cell*, 21, 494, 2009.
82. Hardtke, C.S., Gohda, K., Osterlund, M.T., Oyama, T., Okada, K., and Deng, X.W., HY5 stability and activity in arabidopsis is regulated by phosphorylation in its COP1 binding domain, *EMBO J.*, 19, 4997, 2000.
83. Holm, M., Ma, L.G., Qu, L.J., and Deng, X.W., Two interacting bZIP proteins are direct targets of COP1-mediated control of light-dependent gene expression in Arabidopsis, *Genes Dev.*, 16, 1247, 2002.

53

Blue Light Regulation in Plants and Microorganisms

Aba Losi
University of Parma

Wolfgang Gärtner
Max-Planck-Institute for Bioinorganic Chemistry

53.1 Introduction

Following many centuries of observation of plant orientation toward light [1], we have only quite recently become aware that phototropism is regulated by blue-light (BL) sensing photoreceptor proteins that were accordingly coined as phototropins (phot) [2]. Many more physiological processes have been ascribed to the presence of BL photoreceptors in plants, including stomata opening, chloroplast movements, leaf expansion, solar tracking, and circadian rhythms regulation [1,3,4]. The long-sought plant photoreceptors for BL, which represents a ubiquitous, subtle, and dominating (*vide infra*) environmental factor for the living world, presently comprise cryptochromes (Cry) [5,6], phot, Zeitlupe (ZTL), LOV Kelch Protein 2 (LKP2), and Flavin-binding Kelch F-box1 (FKF1) proteins [4]. All these photoreceptors host riboflavin (RB, vitamin B2) derivatives as chromophores, bound within defined protein domains or subdomains: a photolyase (PL)-like domain in Cry binds flavin-adenine dinucleotide (FAD) into an all-helix subdomain; the light, oxygen, voltage (LOV) domain of phot and ZTL/LKP2/FKF1, forming a small α/β unit, binds flavin mononucleotide (FMN) [2]. The blue-light sensing using FAD (BLUF) domain, the third type of flavin (FL)-based photosensing unit, is solely found in Euglenoids and Bacteria

and binds FAD. Cry and the phot-related, so-called LOV proteins appear to be ubiquitous, being widespread in prokaryotes, fungi, and lower plants [7,8]. Cry are present also in animals [6,9,10], whereas LOV proteins are the sole FL-based BL sensors occurring also in Archaea (see also Section 53.2) [8].

It is clear that not only plants, but all organisms have to detect and to respond to environmental stimuli in order to adjust their metabolic activities. Light is a major factor for the adaptation process, be it in relation to photosynthetic activities or for the entrainment of the circadian clock. The BL spectral region deserves particular attention, since light from this wavelength range not only penetrates deepest into a water column [11], but it also excites with high efficiency ubiquitous photosensitizers, for example, endogenous metal-free porphyrins and flavins [12]. From their excited state, these molecules readily form triplets that, decaying to the singlet ground state, generate singlet oxygen ($^1O_\Delta$) and other reactive oxygen species (ROS) with high quantum yield [12]. The same RB derivatives found in BL sensors are potentially very powerful photosensitizers for $^1O_\Delta$ (ca. 50% efficiency in aqueous solution for RB and FMN) [13,14]. At the same time, flavins are extremely versatile, that is, they can accomplish one- or two-electron transfer reactions, can function as electrophiles and nucleophiles, and are frequently involved in enzyme catalysis with the formation of covalent intermediates of flavin and substrates [15,16]. Light excitation obviously results in charge redistribution and a changed redox potential, giving rise to a variety of possible photochemical reactions, but also of potential danger: the high redox potential of the flavin triplet (ca. 1.7 V) accounts for the oxidation of several electron rich biological substrates, such as aromatic amino acids and DNA bases, and is responsible for a great part of food degradation in illuminated environments [17]. Flavin photoreceptors must therefore have evolved mechanisms to minimize the yield of potentially dangerous reaction intermediates and to maximize the requirements for signaling and for "beneficial" reactions (Section 53.2).

After the analysis of the basic requirements for BL sensing in FL-based receptors (Section 53.2), we will follow the molecular journey of signal transduction from the chromophore-binding cavity down to interacting partners, based on structural, functional, molecular biology, and cellular data (Section 53.3). Prominent examples of biological responses driven by BL sensors are presented in Section 53.4. Finally, in Section 53.5, we will illustrate some novel trends in this research area, notably the applicability of BL sensors in cellular studies and the uncovering of novel proteins by screening environmental samples.

53.2 "Sine Qua Non" of Flavin BL Receptors: Sensing Light

The first requirement of a photosensory protein is the presence of an absorbing chromophore that undergoes physicochemical and structural changes upon light absorption. The protein moiety hosting it modulates these photochemical aspects and at the same time constitutes the microenvironment that immediately responds to the photoinduced changes of the chromophore, having the important duty to carry this information to partner domains and/or proteins: namely, to carry out the first and essential step in the signal transduction process.

53.2.1 Chromophores: RB, FMN, FAD

RB, that is, 7,8-dimethyl-10-(1-deoxy-d-ribitol-1-yl)isoalloxazine, is biosynthesized by plants, fungi, bacteria, and archaea, whereas it is essential for mammalian cells (vitamin B2) and must be provided with diet [18–20]. RB kinase and FAD diphosphorylase convert RB to FMN (RB 5′-phosphate) and FAD, respectively, the two RB derivatives predominantly present in cells. FMN and FAD are cofactors of enzymes, mostly involved in biological redox systems. Mammalian cells contain approximately 50 different flavoproteins [21]. Cry bind FAD as an active chromophore (and co-adopts an antenna, see Section 53.2.2), LOV domains bind FMN, and BLUF proteins bind FAD. A scheme of the chromophores is depicted in Figure 53.1 together with the absorption spectrum of fully oxidized RB. The spectrum shows basically three major π–π^* electronic transitions, encompassing the UVB to BL region (Figure 53.1), and minor n–π^* transitions [22,23].

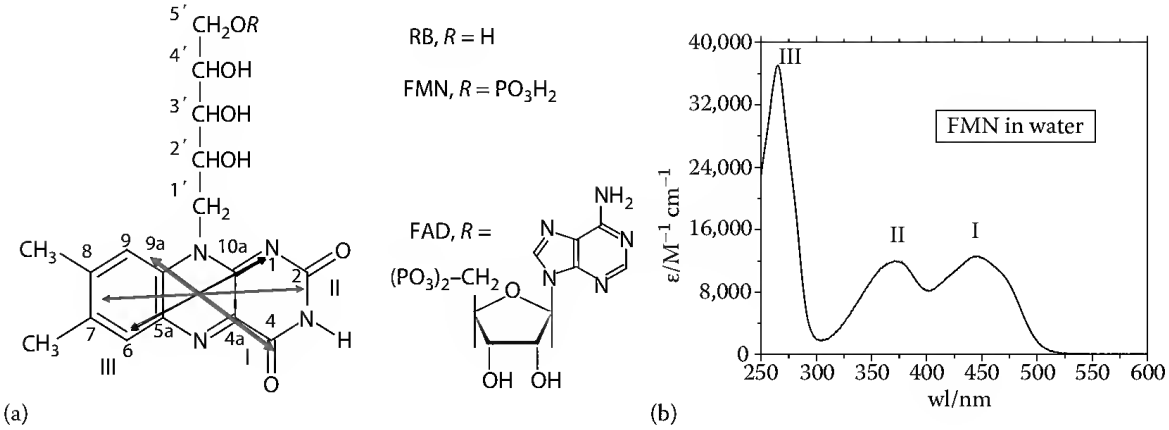

FIGURE 53.1 (a) The three flavin chromophores of BL sensors. RB consists of a 7,8-dimethyl-isoalloxazine ring linked to D-ribitol. FMN and FAD are the phosphorylated and adenosylated forms of RB, respectively. (b) Absorption spectrum of RB in water, scaled to show the absorption coefficients at the different wavelengths. This spectrum exemplifies a fully oxidized form of the chromophore and is basically the same for the three derivatives. I, II, and III indicate the three major electronic transitions in the visible, UVA, and UVB region, respectively, whose approximate transition dipoles are shown in (a). (From Schleicher, E. et al., *FEBS J.*, 276, 4290, 2009. With permission.)

In the spectral region of interest for this presentation, the maximum absorption coefficient is ca. 12,500 M^{-1} cm^{-1} at 450 nm [25,26]. In this form, RB and FMN are brightly fluorescent with a quantum yield of ca. 0.25–0.3 [25,27], and efficiently form triplets with a yield of ca. 0.6 [28–30]. A recent *ab initio* theoretical study on the flavin isoalloxazine ring suggests that, in solution, this high yield of intersystem crossing is related to spin-orbit vibronic coupling between the S_1 $^1(\pi-\pi^*)$ state (BL transition) and the triplet state T_2 $^3(\pi-\pi^*)$, and by the intersection of their potential energy hypersurfaces [23]. FAD in solution is a special case, such that the singlet excited state of the isoalloxazine ring is quenched by stacking interactions with the adenosine moiety [31], consequently rendering a much lower triplet and singlet oxygen yield (<0.1 [14]).

One electron reduction or triplet formation causes a shift to longer wavelengths (lower frequencies) for transition I, for example, around 600 nm for the FMN neutral radical of flavodoxin [32] and 660 nm for the FMN triplet in LOV domains [33,34]. Depending on the surrounding microenvironment, the semiquinone species can be stable on a timescale of several milliseconds or even longer [35], thus providing the possibility for a red-light-driven or secondary photochemistry. In fact, PL is normally purified with FAD in a stable semiquinone state [36]. The fully reduced (two-electron) form, with the loss of a double bond and conjugation, is non-fluorescent and absorbs very poorly in the visible region. Notwithstanding this fact, fully reduced FAD is the active chromophore for the BL-driven DNA repair carried out by PL [6,37]. One- or two-electron reduction can occur from the ground state or from the excited states (triplets or singlets), obviously with different redox potentials. The presence of dissociable protons on the ring (at N1 and N5) of fully reduced flavins accounts for the occurrence of anionic and neutral one-electron (flavin semiquinones) and two-electron (flavin hydroquinones) species, depending on the pH (see [32] and ref. therein). These are the basic facts about the chromophore that we need as a basis to understand how BL sensors become photoactivated.

53.2.2 Photosensing Units: Cry, LOV, and BLUF Domains

Of these three chromoprotein domains, Cry exhibit the most complex composition. They have basically the same structure of PL and are two-chromophore systems, where an antenna (e.g., 5,10-methenyl-tetrahydrofolate (MTHF), 8-hydroxy-8-dimethyl-5-deazariboflavin (8-HDF), FMN, or FAD is bound to the N-terminal α/β subdomain, and a FAD molecule is bound to an all-helix subdomain. The main

difference between PL and Cry is the presence in the latter of C-terminal or N-terminal extensions, of still poorly defined structure, which are considered to be responsible for signal transduction to protein partners [37–39]. The PL-like, bilobate core encompasses ca. 480 aa while the C-terminal tail is of variable length and aa composition (50–250 aa), but is absent in the Cry-DASH (*Drosophila*, *Arabidopsis*, *Synechocystis,* and *Homo*) family, originally identified in *Arabidopsis thaliana* (also called Cry 3) and *Synechocystis* [40]. The structure of Cry and PL has been recently reviewed [37]. The key photochemical event in PL is the transfer of an electron from the fully reduced $FADH^-$, excited directly or by energy transfer from the antenna, to the DNA lesion [41]. Conversely, the active form of the FAD chromophore in Cry is most probably fully oxidized, and light excitation promotes electron transfer events from a conserved chain of aromatic amino acids (W324, W377, and W400 in *A. thaliana, At*Cry1; W342, W397, and W420 in *Drosophila melanogaster Dm*Cry1) to FAD, to form the neutral ($FADH^{\bullet}$) or anionic ($FAD^{-\bullet}$) semi-reduced radical [39,42], thus forming radical pairs (RP) appearing to be the characteristic trait of at least the majority of these BL receptors after photoactivation. Up to now, it appears that some Cry proteins form the anionic semiquinone $FAD^{-\bullet}$ [43], whereas other Cry proteins form the neutral $FADH^{\bullet}$, *via* secondary proton transfer from an aspartic acid residue [42,44]. These electron transfer reactions are reversible, thus building a photocycle whose yield is still under debate [45], but generally low (e.g., ca. 0.02 for Cry1 [46]). The general photoreaction scheme of Cry, as presently understood, is depicted in Scheme 53.1. We note, nevertheless, that the recently discovered CryB from *Rhodobacter sphaeroides* lacks the Trp triad, but undergoes also a light-induced reduction of its FAD chromophore [47]. Also, animal-type 4 Cry form fully reduced $FADH_2$ or $FADH^-$ after photoexcitation [48].

Both LOV and BLUF domains are small photosensing modules of ca. 100 aa building up quite compact α/β structures. Their topology is depicted in Figure 53.2a. Following a recently proposed nomenclature (Figure 53.2), we assign the following secondary structure elements to the LOV core (from the N-terminal part): AβBβCαDαEαFαGβHβIβ, and for the BLUF core: $\beta_1\alpha_1\beta_2\beta_3\alpha_2\beta_3$ [51–57].

The photochemistry of LOV domains, first elucidated for phot and afterward for a variety of bacterial and fungal proteins (reviewed in [39]), involves the formation of the so-called FMN-Cys photoadduct, significantly blueshifted with respect to the dark state and non-fluorescent (referred to as LOV_{390}), which is generated *via* the short-microsecond decay of the FMN triplet state. In LOV_{390}, a covalent bond is formed between the carbon atom at position 4a and the thiol group of a conserved cysteine localized in the Dα-Eα loop. LOV_{390} reverts in the dark to the unphotolyzed state (LOV_{447}) on a timescale ranging from a few seconds to many hours at room temperature [39,60–62]. The quantum yield of LOV_{390} formation ranges from 0.3 to 0.6 after BL excitation, but drops dramatically for UVA excitation, for still poorly understood reasons [63,64]. Despite this well-established photocycle, the details both for LOV_{390} formation from the triplet state and for its reversion are still a matter of

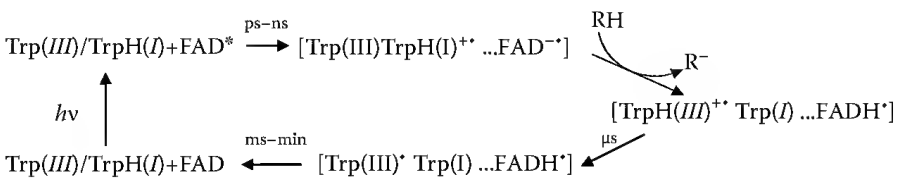

SCHEME 53.1 A general scheme for Cry photocycle. (Modified from Langenbacher, T. et al., *J Am. Chem. Soc.*, 131, 14274, 2009.) BL excitation of FAD withdraws an electron from the distal tryptophan (Trp(*I*)) of the conserved triad, a fast process occurring on the picosecond to nanosecond timescale. A subsequent proton transfer, most probably from a nearby aspartic acid, occurs on the microsecond timescale with concomitant electron and proton transfer from Trp(*I*) to the distal tryptophan Trp(*III*). The relatively stable RP thus formed decays back to the dark state during a multistep process, not yet entirely resolved, with full recovery of FAD to the oxidized state on the hundreds of seconds timescale [42]. This figure refers in particular to a plant Cry, but an RP as [W306• ⋯FADH•] has been also observed for a *Xenopus laevis* Cry [44]. Insect Cry by-pass the formation of the neutral semiquinone $FADH^{\bullet}$ and decay to the parent state directly from the anionic $FAD^{-\bullet}$ [43,49] (see also [50]).

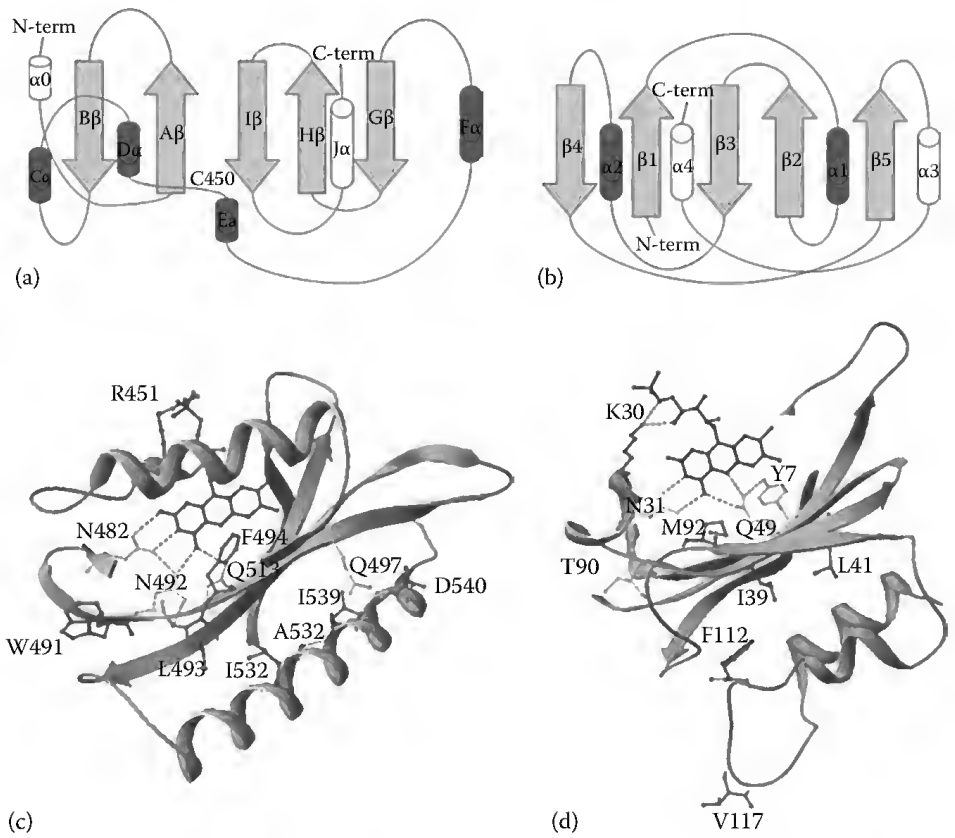

FIGURE 53.2 **(See color insert.)** Top: topology of (a) light oxygen voltage (LOV) and (b) blue light sensing using FAD (BLUF) domains. Secondary structure elements have been named after [57] and [58]. Arrows: strands, cylinders: helices. The caps at the N- or C-termini of the domain core are given without color. The caps may adopt different conformations/geometries in different proteins or/and in a different state (dark or lit). Relative size of loops, strands, and helices are not respected. In (a) the N-cap has been labeled α0. Bottom: structure of a (c) LOV (PDB 1V1A [59]) and of a (d) BLUF (PDB 3GFX [56]) domain, highlighting residues involved in signal propagation, in different LOV and BLUF proteins. Numbering is from *As*phot1-LOV2 and *Kp*BlrP1, respectively (*As* = *Avena sativa*, *Kp* = *Klebsiella pneumoniae*), see Tables 53.1 and 53.2 for details. We also show residues that are not known to be involved in signal transduction, but participate in the modification of the HB network around the flavin after photoexcitation (N482, N492, and R451 in (c); K30 and N31 in (d)). Some secondary structure elements, or part of them, have been cut to better show the chromophore cavity. Note that, from available data, signal transmission from the α/β light-sensing domain favors, in both cases, the β-sheet/helical cap mechanism (Section 53.3.1). (From Wu, Q. and Gardner, K.H., *Biochemistry*, 48, 2620, 2009. With permission.)

debate, as well as the molecular basis of the dramatically different photocycle kinetics in different proteins, even from the same organism [65,66].

BLUF domains respond to light excitation with a reversible redshift of the absorption spectrum [67,68], dictated by the rearrangement of the HB network involving N5 and O4, and by the flipping of a glutamine residue in the chromophore vicinity (Q49 in Figure 53.2b, protein *Kp*BlrP1, that is, *Klebsiella pneumoniae* BL-regulated phosphodiesterase [56] (for a comparative discussion see also [39]). This peculiar photocycle was first described for AppA, a BL receptor from *R. sphaeroides* [67], and afterward for a photoactivated adenylate cyclase (PAC) from *Euglena gracilis* [69] and several further bacterial proteins [51,70–72]. All the BLUF proteins up to now investigated show an AppA-like photocycle, with some differences in the dark state absorption maxima and in the magnitude of the redshift interval and the recovery lifetime, ranging from a few seconds to several minutes (for a comprehensive presentation of these parameters see [73]). Values between 0.24 and 0.9 have been reported for the photocycle

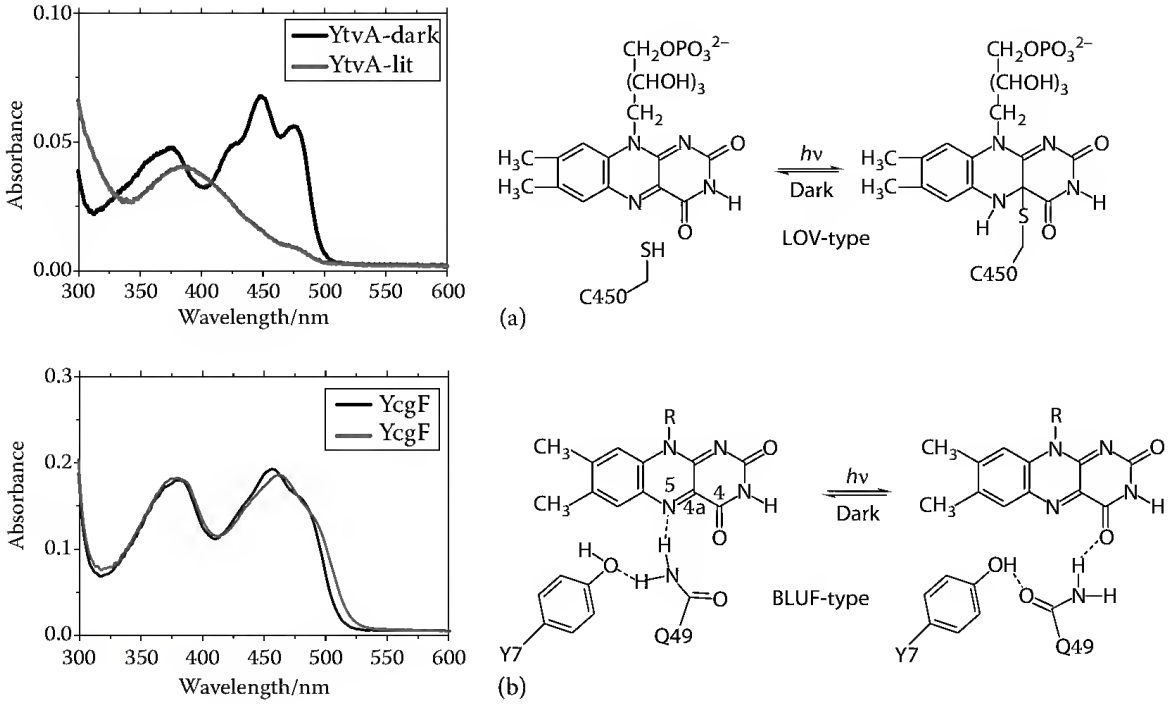

FIGURE 53.3 Steady-state absorption spectra and simplified reaction scheme of (a) LOV-protein-YtvA from *B. subtilis* and (b) BLUF protein-YcgF from *E. coli*. For clarity, the numbering of involved amino acids is the same as in Figure 53.2 (*As*phot1-LOV2 and *Kp*BlrP1, respectively).

quantum yield of BLUF proteins (rev. in [39]). Different to LOV domains, triplet formation is just a side reaction for the BLUF photocycle [74], but its yield can be increased by point mutagenesis: in the *Thermosynechococcus elongatus Te*PixD protein, the change Q50N (Q50 corresponds to Q49 of *Kp*BlrP1) results in a well detectable formation of a triplet state [75] and the I66C substitution, bringing an LOV-like cysteine in the vicinity of C4(a), permits the formation of an LOV_{390}-like photoadduct [76]. There is evidence that photoinduced electron transfer reactions occur in both LOV and BLUF domains prior to the formation of the photoactivated state, forming possible short-living radical intermediates [77,78]. For LOV domains, a time-resolved EPR study at low temperature proposed that after triplet formation an electron transfer step generates a RP in the form ^{3}[$FMN^{\bullet-}$ …$SH^{\bullet+}$], whose recombination would give a zwitterionic complex and then the final LOV_{390} observed at room temperature [79]. For BLUF domains, the signaling state formation seems to proceed *via* light-driven electron and proton transfer from the conserved tyrosine (Y7 in Figure 53.2) to FAD, followed by a hydrogen bond rearrangement and radical-pair recombination [78]. In Figure 53.3, the absorption spectra of an LOV and a BLUF protein are shown together with a simplified reaction scheme.

53.3 From BL to Signaling

The photosensing unit continues its work by passing the signal to partner domains (intraprotein pathways) or/and partner proteins. These steps are often the most difficult to be elucidated, given the general paucity of structural data. Furthermore, the soluble domains of BL sensors have the tendency to forms dimers or oligomers, whose function and regulation by light is only partially understood. Light-regulated phosphorylation is also emerging as an important aspect during signal transduction. Finally, partner proteins, often shared with other signaling pathways, have the duty to integrate the BL inputs within the cellular signal transduction networks.

53.3.1 Conveying Signals: Intraprotein Pathways of Signal Transduction

53.3.1.1 LOV Proteins

In phot, the activity of the effector S/T-kinase domain is enhanced after LOV photoactivation with BL, resulting in phot autophosphorylation [80–83], a key event in signaling [84]. The same effect is observed for bacterial LOV-HisKinases [85–87]. In other LOV proteins, the effector module can be represented by diverse functional motifs, for example, gene expression regulators, phosphodiesterases, phosphatases [8,88,89]. This poses the question whether LOV domains communicate with effector partners through the same or partially overlapping surfaces, such that the structural basis for light-to-signal transduction is basically the same in the different LOV proteins, with only few residues acting as specific signal transmitters within the different systems. There is increasing experimental evidence that this surface largely involves the β-scaffold of the LOV core (Figure 53.1), which on one side hosts residues directly interacting with the isoalloxazine ring of FMN [90,91] and on the other side communicates with helical regions flanking the LOV core [59,92–94]. In phot, a conserved glutamine on strand Iβ (Gln513 in *Avena sativa* phot1-LOV2) participates in light-driven conformational changes of LOV2 [94–98], and of the LOV protein VIVID [92] and in the light activation of phot self-phosphorylation [99]. In *Bacillus subtilis* YtvA, two acidic aa localized on strand Hβ (E105 and D109) are essential for conveying light-triggered conformational changes to the Guanosine-5′-triphosphate (GTP)/Adenosine-5′-triphosphate (ATP)-binding site on the sulfate transporter and anti-sigma factor antagonist (STAS) domain, considered a secondary switch or/and the effector module of the protein [100]. The same two residues are also essential for the *in vivo* light regulation of YtvA activity [101] (see Table 53.1 for a list of residues involved in signal transmission in several LOV proteins).

Autophosphorylation of phot is enhanced by the light-induced unfolding of the so-called Jα-linker helix that interacts in the dark with the β-scaffold of LOV2 and connects LOV2 to the kinase domain [58,102,103]. Phot2 also shows light-triggered conformational changes of the Jα-linker, although not as

TABLE 53.1 Residues Affecting Signal Propagation in LOV Domains

	Light-Driven Changes/Effects of Mutations	Location
*Ac*phy3-LOV2	F1010 [239]	Hβ
	F1010L impairs conformational changes [240]	
	Q1029 (flipping) [239]; Q1029L impairs conformational changes [95]	Iβ
*Bs*YtvA	W103, conformational changes [241]	Hβ
	E105L suppress interdomain signal transmission [93]; functionally locked in a pseudo-lit state [101]	Hβ
	L106F impairs interdomain transmission [100]	Hβ
	D109L suppress interdomain signal transmission [100]; functionally locked in a pseudo-dark state [101]	Hβ
	Q123 (flipping) [133]	Iβ
*As*phot1-LOV2	W491, conformational changes [59,242]	Hβ
	Removal of interactions for Leu493 with J-helix (I532E), constitutively activates the kinase [102]	Hβ
	Q513 (flipping) [59]; Q513L = impairs light-driven conformational changes, pseudo-dark state [96]	Iβ
	Q513N = impairs light-driven conformational changes, pseudo-lit state [96]	
*At*phot1-LOV2	F556L diminish light-driven conformational changes [243]	Hβ
	Q575 (flipping) [59]; Q575L: diminish light-driven conformational changes [243] and attenuates light-induced self-phosphorylation [99]	Iβ
*At*phot2-LOV2	Q489 (flipping) [94]	Iβ
VIVID	Q182 (flipping) [92]; Q182L impairs light-driven dimerization [92]	Iβ

dramatic as in phot1 [98]. An involvement of the Jα-linker in interdomain communication has been demonstrated also in the bacterial protein YtvA [100], but this function is not connected to light-driven unfolding [93]. As a whole, the scenario for the early signal propagation steps in LOV proteins point to a general involvement of the β-sheet/helical cap mechanism, as recently proposed also for BLUF proteins [57], with the involvement of specific residues depending on the different proteins. Also, it is now clear that a conserved "flipping" glutamine, located on strand Iβ and directly interacting with the chromophore, is important both in signal propagation and in the photochemical reactions (e.g., duration of the photocycle, see Table 53.1 and Figure 53.2) [59,92,94,96,99].

Still we had, until recently, only few hints about the significance of two tandem LOV domains in phot, given that only LOV2 photoexcitation plays a major role in regulating phot1 kinase activation by BL [83,104–106]. This issue was elegantly addressed by the Christie group by means of a domain-swapping strategy, which highlighted the constitutive (not light-regulated) activity of a phot1-LOV1+LOV1 protein and the need of having an LOV2 adjacent to the Jα-linker in order to inhibit the kinase [107]. Thus, although it is possible to exchange LOV domains and retain the photobiological function, even among different organisms [108,109], LOV1 is not able to replace LOV2 as inhibitor of the kinase, most probably due to a weaker binding of the β-sheet to the Jα-linker [82]. In addition, an involvement of LOV1 in arresting chloroplast accumulation at high light intensities was suggested, thus promoting an efficient transition from accumulation to avoidance movement [107].

BL-triggered enhancement of autophosphorylation activity in LOV kinases is obviously an important observation [80–82,84–87], but this reaction still needs to be linked to the photobiological activity mediated by the receptor. In a bacterial LOV kinase from *Pseudomonas syringae*, the end phosphoacceptor is a fused response regulator, denoting a typical bacterial two-component system [87]. For phot, a substrate other than phot itself is till date not known, but several phosphoacceptor sites have been identified [81,83]. *At*phot1is phosphorylated *in vivo* on multiple serine residues, localized in the N-terminus (S58 and S185) and in the linker region comprised between LOV1 and LOV2 (S350 and S410), with phosphorylation at S185, S350, and S410 being BL-induced [83]. Phosphorylation at these sites is not determinant for phototropism and leaf expansion, but may be necessary for maximizing stomatal performance, light-induced relocalization of phot1, and interactions with protein partners (see also Section 53.3.3) [83,107,110].

53.3.1.2 BLUF Proteins

A recent work dealing with the BLUF domain of *Kp*BlrP1 (see Figure 53.2) has summarized our current understanding about signal propagation within BLUF proteins [57]. Earlier work with the *Escherichia coli* YcgF protein, built of a BLUF domain and a C-terminal EAL domain (a putative phosphodiesterase for cyclic diguanylate, c-di-GMP [111]) and with *Sy*PixD (a short-BLUF protein) suggested that the helical region comprising α_3 and α_4 (Figure 53.2), C-terminal to the BLUF core, is important in signal propagation [112–114]. Although a phosphodiesterase activity of YcgF-EAL has been ruled out [115] (Section 53.3.3), the importance of the α_3–α_4 region for protein stability and conformational changes has been confirmed [116]. Similarly, the C-helical cap is necessary for the stability of *Kp*BlrP1-BLUF, and the $\alpha_3\alpha_4$ loop undergoes significant light-induced conformational changes, as detected by NMR experiments [57]. Other regions involved in signal propagation comprise the $\beta_4\beta_5$ loop and strand β_5 (see also Table 53.2). These elements host T90 and M92 (in *Kp*BlrP1-BLUF, see Figure 53.2) residues, which are the subject of intense debate regarding their roles in signal activation process for BLUF proteins.

In AppA-BLUF, the W104A mutation (W104 correspond to T90 in *Kp*BlrP1) impairs light-induced structural changes in the β-sheet, without appreciable effects on the photocycle [117]. In functional essays with full-length AppA, the W104A mutation locks the protein in a functionally lit-like state [118]. Recent spectroscopic studies led to the suggestion that light absorption by the flavin causes partial movement/uncovering of W104. However, dramatic changes were ruled out that would support a model of W104 movement as a key output signal [119] (the so-called Trp-in to Trp-out previously proposed on

TABLE 53.2 Residues Affecting Signal Propagation in BLUF Domains

	Light-Driven Changes/Effects of Mutations	Location
*Rs*Appa	Q63L Suppressed photocycle; light insensitivity *in vivo* [118]	β_3
	W104A biphasic and fast photocycle [119] (AppA1–126); light insensitivity *in vivo* [118]	$\beta_4\beta_5$ loop
	W104M/M106W much faster photocycle [117,119]	$\beta_4\beta_5$ loop
*Kp*BlrP1	L41V interrupts signal propagation [57]	β_3
	Q49, essential for flavin binding and photocycling, several mutations investigated [57]	β_3
	Mutations (e.g., T90W) alter conformational changes [57]	$\beta_4\beta_5$ loop
	M92, essential for flavin binding and photocycling, several mutations investigated [57]	$\beta_4\beta_5$ loop
	F112L, F112Y alter light-induced conformational changes; [57]	
	V117F, V117L alter conformational changes [57]	$\alpha_3\alpha_4$ loop
*Sy*Slr1694/*Sy*PixD	W91A, retains photobiological activity [145]	$\beta_4\beta_5$ loop
	M93A, suppress signal transmission and is functionally locked in a lit state [145]	$\beta_4\beta_5$ loop
*Te*Tll0078/*Te*PixD	Q50N, alters photocycle, formation of flavin triplet [75];	β_3
	I66C forms an LOV-like adduct [76]	$\alpha_2\beta_4$ loop
*Eg*PAC	Y60F (F1), loss of photo-stimulated cyclase activity; no effects for Y472F (F2) [244]	β_1?

the basis of alternative dark and light structures [53,120] state) [54,55,117,121,122]. In other words, the initial position of Trp104 in the dark state has no significant influence on the ability of the BLUF domain to undergo a photocycle, but has only an effect on the kinetics of the photocycle [119]. Instead, T90 and M92 appear essential for WT-like conformational changes, FAD binding and photocycling in *Kp*BlrP1-BLUF [57]. As a whole, the extensive work on *Kp*BlrP1-BLUF [57] raises the possibility that, after BL illumination, the C-terminal helical cap undergoes some kind of reorientation process, and that might be associated with the conformational changes of $\beta_4\beta_5$ and $\alpha_3\alpha_4$ loops, and strand β_5 [57].

53.3.1.3 Cry Proteins

A peculiarity of Cry signaling is related to the C-terminal tail (50–250 aa), present in all Cry proteins with the exception of Cry-DASH, and demonstrated to be important for signal transduction/regulation in several cases [38,123]. Transgenic plants overexpressing the C-terminal extension of either *At*Cry1 or *At*Cry2 exhibit a constitutive photomorphogenic phenotype in the dark, suggesting a main role of this protein region in mediating Cry interactions with COP1, the main interacting partner of Cry [124]. In *A. thaliana*, an 80 aa long peptide, referred to as NC80, was necessary and sufficient to confer the physiological function of Cry2 [123]. In *D. melanogaster Dm*Cry, the removal of the C-terminal end renders the protein constitutively active, and it was concluded that this protein region promotes repression of signaling, a repression alleviated by light activation [125]. A detailed analysis of the C-terminal end in *At*Cry1 and *Homo sapiens Hs*Cry2 showed that both are intrinsically disordered in solution, although they share little sequence homology, and that they interact with the PL core in the dark [126]. This interaction induces a stable tertiary structure that undergoes a transition to a more disordered state upon light activation of the protein [126], a feature surprisingly reminiscent of the Jα-linker unfolding in phot.

Like phot and bacterial LOV kinase, both plant- and animal-type Cry bind ATP and display intrinsic autokinase activity, in sharp difference to PL [123,127–130]. The significance of ATP binding and self-phosphorylation is still a matter of debate, but a recent study has suggested that ATP binding induces significant conformational changes, increases the yield of the photocycle, and slows it down, thus configuring as a regulatory factor, even in the absence of a of further self-phosphorylation

activity [131]. Furthermore, ATP renders *At*Cry1 more resistant to denaturation. ATP binding might modulate the structure and function of Cry *in vivo*, rather or besides supporting the observed self-phosphorylation activity [128–130,132]. This opens the possibility that ATP binding can regulate the biological effects of Cry, also in the absence of light. In this respect, we note that autokinase activity seems to be light regulated in plant Cry (*At*Cry1 and *Cr*Cry) [127,128,130], but not in *Hs*Cry1 [128,129].

A recently proposed model, based on data obtained for *At*Cry2, links phosphorylation to the C-terminal tail and Cry activation [123]. The PL domain and the C-terminal tail of an unphosphorylated Cry form a closed conformation in the dark to repress the NC80 (last portion of the C-terminal tail) motif from functioning. Upon BL absorption, the C-terminal tail is phosphorylated and electrostatically repelled from the negatively charged PL domain, resulting in an open conformation that derepresses the NC80 motif to trigger the physiological responses [123].

53.3.2 Dimers or More: When and Why?

53.3.2.1 LOV Proteins

Besides conveying signal transmission (Section 53.3.1), the β-scaffold is also involved in LOV–LOV dimerization, with or without the assistance or competition of the helical flanking regions [93,133,134]. In the fungal protein VIVID (a "short-LOV" protein), light activation induces dimerization through the helical N-cap, but dissociation or removal of the N-cap induces dimerization *via* a β-sheet–β-sheet contact [135]. In YtvA, the β-scaffold of the LOV core has been identified as a competitive interface for LOV–LOV dimerization and intraprotein domain interactions [93], and a recently crystal structure confirms the β-sheet-mediated contact within the YtvA–LOV dimer [133]. Dimerization of YtvA–LOV is also observed when both the N- and C-terminal flanking regions to the LOV core are present, and it is solely prevented in the full-length protein [93].

It is of course important to understand if and how LOV–LOV dimerization is relevant for the *in vivo* activity, and if and how dimerization (or oligomerization) is light regulated. Similarly, it has to be questioned whether the full-length LOV proteins are dimeric, in the dark or/and light-activated state. Phot-LOV domains show a tendency to dimerize, in general more prominent for LOV1 than for LOV2 [134,136–138]. By means of pulsed thermal grating, Terazima and coworkers detected a transient, light-induced dimerization in the phot1-LOV2-Jα-linker, suggesting a light regulation of dimerization; however, the functional significance remains unknown [139]. Bimolecular fluorescence complementation analysis has shown that *At*phot1 undergoes light-dependent dimerization *in vivo*, coinciding with a mechanism of light-driven autophosphorylation *in trans* [107]. LOV1 is not necessary for this dimerization, occurring also in a phot1 carrying two LOV2 domains. The site(s) of receptor dimerization still need to be defined, and the relevance of the trans phosphorylation for phot signaling remains to be assessed [107].

Finally, we note that fungal white-collar 1 (WC-1; see Figure 53.4), a Zn-finger photoreceptor LOV protein, is active as a dimer, where dimerization is mediated by the non-photosensing PAS domain [140].

53.3.2.2 BLUF Proteins

AppA-BLUF has been suggested to form a dimer in the dark state [141], in good agreement with gel filtration analysis [142]. Light excitation induces the transient formation of a tetrameric state [141], driven by hydrophobic interactions [143]. By gel filtration chromatography, an increase in the apparent molecular weight (MW) to 37 kD in the light-activated state of AppA-BLUF is also indicative of a sharp conformational change, but it is not compatible with the formation of a tetramer [142]. From the dimers within the crystal units, we have a good hint about the dimer interface of AppA-BLUF in solution, conceivably built by the hydrophobic β-scaffold surface [53,120], as recently confirmed by spectroscopic studies on W104 located on strand β_5 [119,120]. The full protein appears instead to be monomeric in solution, as it

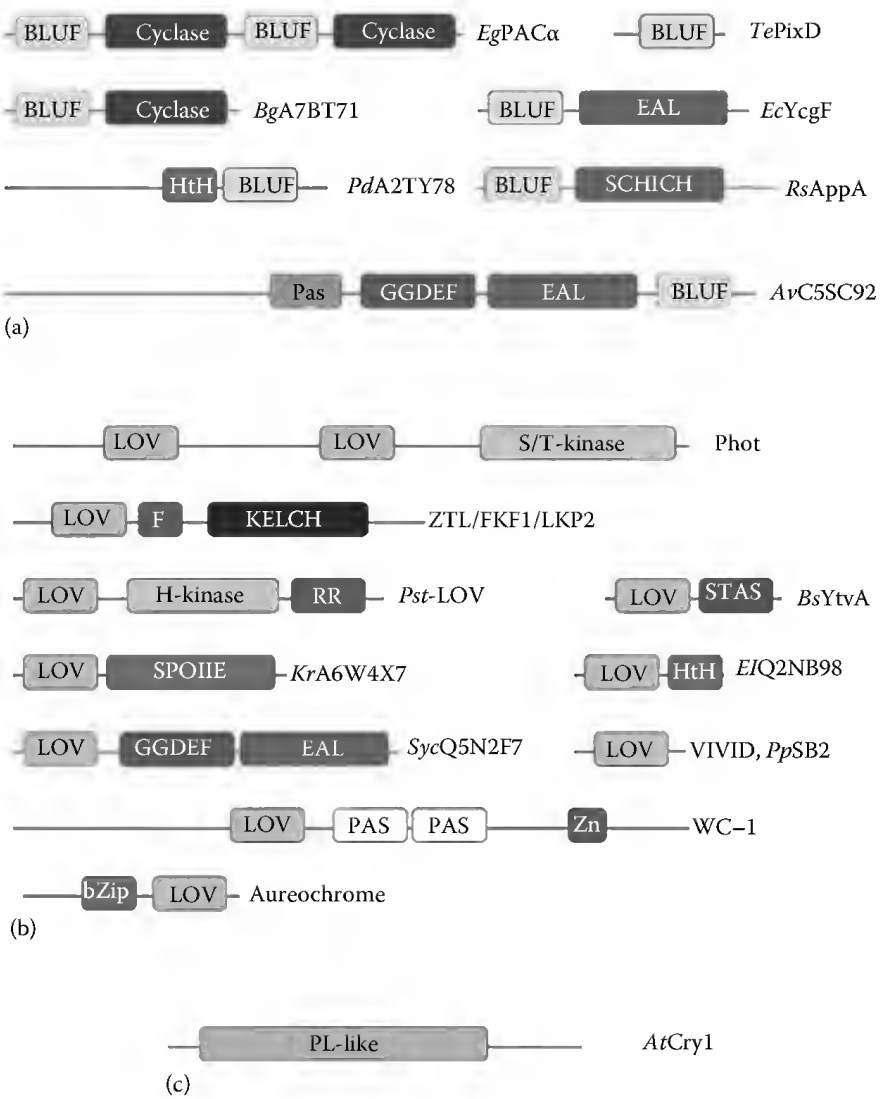

FIGURE 53.4 Domain architecture for a selected ensemble of BL sensors. Panel (a) BLUF proteins. The BLUF domain binds FAD as photoactive chromophore. *E. gracilis* (*Eg*) PAC is formed of two similar subunits (α and β) and has a counterpart in a bacterial cyclase from *Beggiatoa* sp. *PS* (*Bg*A7BT71). The GGDEF and EAL domains of *Av*C5SC92 (*Av, Allochromatium vinosum*) should act as cyclase and phosphodiesterase, respectively, for c-di-GMP, but note that the EAL domain of *Ec*YcgF (*Ec, E. coli*) is not a phosphodiesterase (see Section 53.3.1). The "short-BLUF" protein *Te*PixD from *T. elongatus*, without a linked output domain, is a prototype for the vast majority (ca. 80%) of bacterial BLUF proteins. *R. sphaeroides* (Rs) AppA binds additionally heme, as a redox sensor, in its SCHICH domain. Panel (b) LOV proteins. The LOV domain binds FMN as photoactive chromophore. Plant phot have a typical Ser/Thr kinase domain, C-terminally to the two LOV domains. The ZTL/FKF1/LKP2 family harbor an F-box and six Kelch repeats [159], suggesting that they act in light-regulated protein degradation [4]. WC-1 and VIVID are fungal proteins, the former bearing a DNA-binding Zn-finger region and two further PAS domains; VIVID is a prototype for "short-LOV" proteins, also well represented in bacteria, for example, the SB2 protein from *P. putida* (*Pp*) [8,65]. Other DNA-binding motives are present in AUREO from stramenopile algae (bZIP, basic region/leucine zipper) [157,158] and in *El*Q2NB98 (HtH, helix-turn-helix domain; *El, E. litoralis*). Besides the GGDEF–EAL domains, introduced for Panel (a) (shown here is a protein from *Synechococcus* sp. *PCC 6301, Syc*), we find also His-kinases and phosphatases of the SPOIIE family. Pst, *P. syringae pv. Tomato*; Kr, *Kineococcus radiotolerans*, RR, response regulator domain. Panel (c). Cry proteins are formed by a PL core, binding FAD as photoredox active chromophore and an antenna molecule absorbing in the UVA–blue spectral region (a flavin or a pterin derivative). A C-terminal end, an extension of variable length and poorly defined structure, is crucial for signal transduction (see Sections 53.3.1 and 53.3.3).

is also evident from the higher degree of exposure of W104 (T90 in Figure 53.2) with respect to AppA-BLUF alone, showing, as in the case of YtvA, that the same surface is involved in dimerization and intra-protein interactions [119,120]. The blue light receptor B (BLRB) protein, a short-BLUF protein, is dimeric in crystals, adopting a similar conformation as AppA-BLUF dimers [51], referred to as AB dimers. The two cyanobacterial short-BLUF proteins *Te*PixD and *Sy*PixD form that forms a 10-subunit complex comprised of two stacked pentameric rings [52,54]. These structures show another way how BLUF domains can dimerize: they form β-sheet interfaced, [AB] dimers between subunits from separate rings, while they form the so-called [AC] dimers within the same ring, stabilized *via* the α_3–α_4 helices [52,54]. From a recent analysis of the interactions of *Sy*PixD with the response regulator PixE, it was demonstrated that the latter drives aggregation of PixD dimers, the stable form in solution, into a *Sy*PixD$_{10}$–PixE$_5$ complex under dark conditions. Illumination of the bound flavin destabilizes the complex into monomers of PixE and dimers of *Sy*PixD [144]. The light-driven destabilization is most probably triggered by the conformational changes occurring at strand β_5 and at the β_4–β_5 loop, a region comprising the conserved W91 and M93 residues and comprising a significant portion of the [AB] type of dimer in the complex [144]. It is likely that light-induced disassembly of the PixD–PixE complex constitutes the "output signal" that regulates a signal transduction pathway that controls motility of *Synechocystis*. Indeed, it was recently shown that M93, but not W91, is essential for the biological response, that is, positive phototaxis, as well as for the light-driven destabilization of the *Sy*PixD$_{10}$–PixE$_5$ complex [145].

Information is also available for the *Kp*BlrP1-BLUF domain in solution, which appears to be a stable monomer [57], while full-length *Kp*BlrP1 is dimeric [56]. A crystal structure is now available for *Kp*BlrP1, and biochemical investigation reveals that photon absorption by the BLUF domain of one subunit of the antiparallel homodimer activates *in trans* the phosphodiesterase activity of the EAL domain of the second subunit *via* allosteric communication, transmitted through conserved domain–domain interfaces [56]. Interestingly, in the full-length protein, dimerization does not occur *via* BLUF–BLUF interactions, but rather *via* BLUF–EAL interactions *in trans* and mostly mediated by α_4, which is in turn clamped on the BLUF domain β-sheet [56].

Summarizing the data discussed in Sections 53.3.1 and 53.3.2 for LOV and BLUF domains, we can state in both cases (a) the β-sheet undergoes light-driven conformational changes, directly conveyed by interactions with the flavin chromophores; (b) the β-sheet can mediate dimerization, but is also able to interact, more or less tightly, with helical regions flanking the photosensing LOV or BLUF core and, most probably, directly interacting with an effector domain [93,100]; (c) the sequences flanking the photosensing LOV or BLUF core can in turn mediate an alternative dimerization and interactions with effector domains, thus mediating light-driven activation of the latter. Unfolding of the Jα-linker in phot might represent a limited case of a general β-sheet/helical cap mechanism [57].

53.3.2.3 Cry Proteins

*At*Cry1 has been reported to form homodimers in solution, mediated by the PHR core, and that dimerization is required for *At*Cry1 activity *in vivo* [5,146]. The same holds for *At*Cry2 [123]. A dimeric crystal structure also characterizes *At*Cry3, which is instead monomeric in solution [147]. This agrees with the fact that the interface is mostly polar and prone to dissociation in aqueous solution. It is thus likely that the crystallographically observed dimer of *At*cry3 is not representing an oligomer that is relevant *in vivo*.

53.3.3 Delivering Signals: Partners of BL Receptors during Signal Transduction

53.3.3.1 LOV Proteins

Up to now, much effort has been focused on elucidating the primary mechanisms underlying LOV proteins activation by light, but the downstream signaling processes remain largely elusive. Yet several targets have been identified, and in the following section some examples will be presented.

Several phot-interacting proteins have been identified. Phot1 from *Vicia faba* and *A. thaliana* has been shown to bind to 14-3-3, a family of conserved regulatory molecules expressed in all eukaryotic cells [84,110,148,149]. The binding to a defined 14-3-3 seems to be specific for phot1 and not phot2 [110]. The most prominent paradigms involving 14-3-3 proteins in plant regulatory events include regulation of plasma membrane H^+-ATPase activity, nitrate reductase, and sucrose phosphate synthase [150]. One of the targets for 14-3-3 family members is NONPHOTOTROPIC HYPOCOTYL-3 (NPH3), a phot1-interacting protein essential for phototropism [151]. Other phot1-interacting proteins include ROOT PHOTOTROPISM-2 (RPT2) that is closely related to NPH3 and mediates both phototropism and stomatal opening [152], and to phytochrome kinase substrate 1 (PKS1) that influences phototropic curvature [153]. Furthermore, PKS1 interacts with phot1 and NPH3 *in vivo* at the plasma membrane and *in vitro*, indicating that the PKS proteins may function directly with phot1 and NPH3 to mediate phototropism. We note that PKS proteins may provide a molecular link between these BL and red-light photoreceptor families and explain why phytochrome influences phototropism [153]. However, none of these three proteins is required for all the phot responses that were tested, for example, NPH3 is required for phototropism, but is dispensable for chloroplast positioning and stomatal opening (reviewed in [4]). A second example illustrating rapid branching in phot1 signaling is given by the rapid increase of cytosolic Ca_2 upon BL irradiation, required for phot1-dependent inhibition of hypocotyl elongation, but not for phototropism [154]. Growth responses such as phototropism require auxin and brassinosteroids but these two factors have been shown to be not involved in the control of chloroplast movements. Also, gene expression changes are essential for phototropism and are most probably induced following the asymmetric distribution of auxin that is required for directional growth [155].

Besides the indirect control of gene expression carried out *via* complex pathways by phot [4], some LOV proteins are equipped with effector modules predicted to directly interact with target genes [8,156], and at least for one class of them, the AUREOCHROMES (AUREO) from photosynthetic stramenopiles algae, such interaction has been demonstrated [157,158]. AUREO are built of an N-terminal, DNA-binding basic leucine zipper (bZIP) motif and a C-terminal LOV domain (Figure 53.4). BL treatment of AUREO1 from *Vaucheria frigida* triggers an LOV-type photocycle (Figure 53.3) and enhances binding of AUREO1 to its target DNA sequence, implying that AUREO1 functions as a BL-regulated transcriptional factor [157].

In the ZTL/LKP2/FKF1 family, the LOV domain is linked to an F-box and six Kelch (beta-propeller structures) repeats [159], suggesting that they may act in BL-regulated protein degradation, but interactions with components of ubiquitin-mediated protein turnover are not dependent on the LOV domain [4,160–162]. The main partner of ZTL and LKP2 is GIGANTEA (GI) that interacts directly with the LOV domain in a light-dependent way, ultimately leading to regulation of *CONSTANS* (*CO*) gene expression, which is necessary for day-length discrimination and photoperiodic flowering [163,164]. FKF1 binds to GI upon BL perception, forming then a complex with CDF1, a *CO* repressor GI, FKF1, and CDF1 proteins associate with *CO* chromatin. The FKF1–GI complex forms on the *CO* promoter in late afternoon to regulate *CO* expression, providing a mechanistic view of how the coincidence of light with circadian timing regulates photoperiodic flowering [163]. The level of ZTL protein in plant cells oscillates in time, and GI is essential to establish and sustain oscillations of ZTL by a direct protein–protein interaction that stabilizes ZTL. This interaction is enhanced by BL. Because the regulation of GI transcription is clock-controlled, consequent GI protein cycling confers a post-translational rhythm on ZTL protein [164].

For bacterial LOV proteins, we only have (limited) information. Yet, the best characterized protein function was found for *B. subtilis* YtvA [30]. The fused STAS domain shows light-modulated GTP binding *in vitro* [100,165]. During the environmental stress pathway, Ytva upregulates the alternative transcription factor σ^B through a cascade of Rsb proteins, organized in stressosomes, in a BL-regulated way [166–168]. This ability strictly depends on signal propagation from the LOV domain to the GTP-binding cavity on the STAS domain [100,101], demonstrating that nucleotide binding is physiologically relevant (see Figure 53.5 for details).

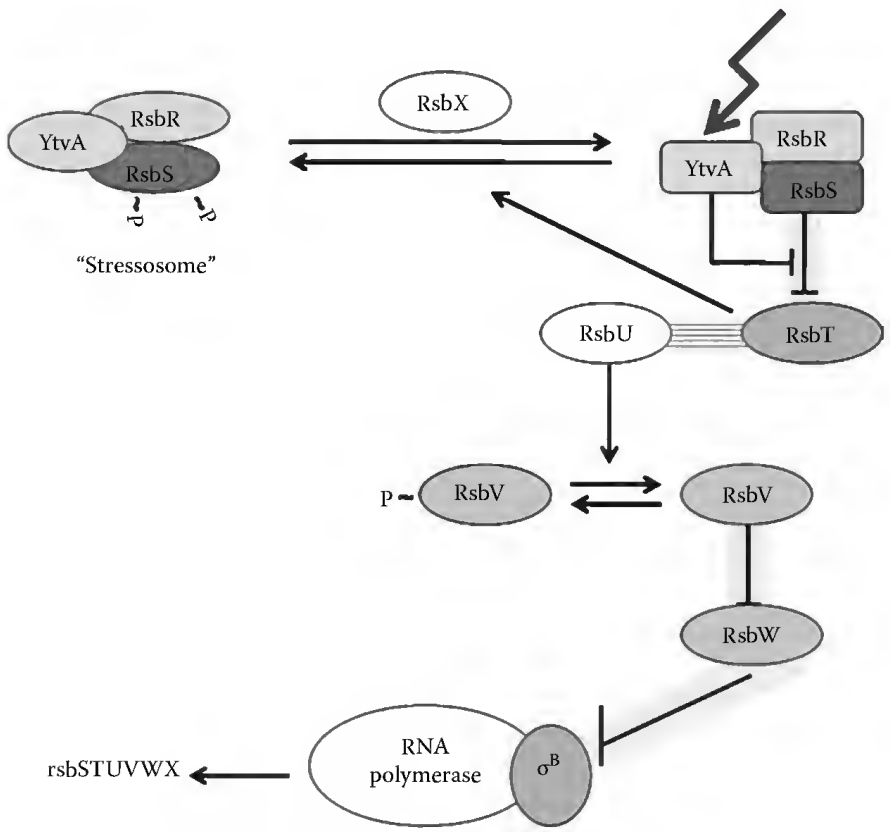

FIGURE 53.5 An example of a BL-regulated reaction pathway in a prokaryotic cell. *Bs*YtvA (*Bs*, *B. subtilis*), located in the stressosome, integrates a light signal in the environmental stress response centered on the alternative transcription factor σ^B and the kinase RsbT. Upon light stress, YtvA stimulates RsbT to phosphorylate RsbS. This releases RsbT that in turn stimulates the phosphatase RsbU to dephosphorylate RsbV. RsbV can now sequester RsbW, thus setting free σ^B. As a result, the RNA polymerase–σ^B complex transcribes the σ^B regulon rsbSTUVWX. The phosphatase RsbX is used to reset the system to a "prestress" status. YtvA bears a photoactivable LOV domain linked to a STAS domain. (Modified from van der Horst, M.A. et al., *Trends Microbiol.*, 15, 554, 2007; Losi, A. et al., *Biophys. J.*, 82, 2627, 2002. With permission.)

53.3.3.2 BLUF Proteins

The *E. coli* YcgF protein (Figure 53.4) carries an EAL domain, until recently being postulated to catalyze c-di-GMP hydrolysis in a light-regulated way [70,114,116]. Actually, it could be shown that YcgF does not hydrolyze or bind c-di-GMP, but rather acts by protein–protein interaction [115]. YcgF directly binds to the repressor YcgE, releasing it from its operator DNA upon BL irradiation. As a consequence, a distinct regulon of eight small proteins involved in biofilm formation is induced. Furthermore, BL and other stress signals are integrated at the level of the YcgF–YcgE system that is strongly induced at low temperature and starvation conditions, and may thus modulate biofilm formation when *E. coli* has to survive in an extrahost aquatic environment [115]. This work not only elucidated the molecular pathway leading to a BL response in *E. coli via* a BLUF protein, but also showed that in a protein possessing a degenerate EAL domain [111], BL can activate a function other than an enzymatic one. We should not forget that in the protein *Kp*BlrP1 from *K. pneumonia* (ortholog to *E. coli* YcgF, i.e., identically built with a BLUF+EAL architecture), the EAL domain shows a light-activated phosphodiesterase activity [56].

The way how YcgF works is reminiscent of AppA (Figure 53.4), one of the other few complex bacterial BLUF proteins (the majority of which (ca. 87%) are "short-BLUF" without a fused effector domain) [8,68]. Present in the facultative photosynthetic bacterium *R. sphaeroides*, AppA binds, at low oxygen tension,

constitutively the repressor protein PpsR, whereas under fully aerobic conditions PpsR is released from AppA and binds to the promoter of certain photosynthesis genes, repressing their transcription. These responses are light independent, but at intermediate oxygen concentration (~50% oxygen saturation) light determines whether AppA releases the repressor PpsR [170,171]. Thus, AppA integrates and transmits both redox and light signals, the former thanks to the heme-binding sensor containing heme instead of cobalamin (SCHICH) domain [172] and probably to a C-terminal cysteine-rich sequence. The function of the AppA/PpsR system is fully coordinated by the PrrB/PrrA system (based on bacteriochlorophyll absorbers) that, at low oxygen concentration, activates photosynthesis gene expression [171,173]. The work of these systems in *R. sphaeroides* is obviously aimed to the maximization of photosynthesis efficiency in conditions when oxidative heterotrophy is impaired, and to minimize waste of energy for the building of photosynthesis complexes and also to reduce photooxidative damages.

53.3.3.3 Cry Proteins

The signaling mechanism of Cry in *A. thaliana* is mediated through negative regulation of the constitutive photomorphogenic-1 (COP1) protein by direct CRY–COP1 interaction through the Cry C-terminal tail, with dimerization being an important factor of Cry functioning (Section 53.3.2) [5,174]. The COP1 protein is conserved in both higher plants and vertebrates. In plants, COP1 acts as an E3 ubiquitin ligase to repress light signaling by targeting photoreceptors and downstream transcription factors for ubiquitylation and degradation. In the dark, COP1 specifically targets the transcription factor HY5 for degradation through a 26S proteasome-dependent pathway. Upon BL activation, Cry proteins repress COP1 activity through a direct protein–protein contact, and this direct regulation is primarily responsible for the Cry-mediated BL regulation of seedling photomorphogenic development and genome expression profile [175,176]. Another transcription factor, HFR1, is required for both phytochrome A-mediated far-red and Cry1-mediated BL signaling. HFR1 is a short-lived protein in darkness and is also degraded through a 26S proteasome-dependent pathway, for which COP1 is required [177]. Light, blue or red, enhances HFR1 protein accumulation by promoting its stabilization. Light enhances HFR1 protein accumulation by abrogating COP1-mediated degradation of HFR1, which is necessary and sufficient for promoting light signaling [177]. For further information and other components of the signaling cascade, refer to recent reviews [3,178–180] (for Cry proteins that are able to repair and bind to DNA, see Section 53.4.1).

53.4 Physiological Photoresponses Mediated by Cry, LOV, and BLUF Proteins

Phototropism, photomorphogenesis, and circadian rhythms entrainment in plants have important counterparts in BL-regulated growth patterns and BL/redox regulation of photosynthesis or of infectivity in bacteria, and even in BL killing of pathogens.

53.4.1 Cry: From Photomorphogenesis to Single-Strand DNA Repair

Cry proteins regulate a variety of growth and adaptive processes in organisms from bacteria to humans [6,48,181]. In *A. thaliana*, *At*Cry1 and *At*Cry2 are nuclear proteins that mediate light control of stem elongation, leaf expansion, photoperiodic flowering, and the circadian clock by interacting with proteins such as phytochromes, COP1, and clock proteins, or/and chromatin and DNA [5]. Recently, it was shown that although phot and Cry mediate largely distinct responses, there exist some interactions among their regulated pathways [182]. For example, Cry exert a positive effect on phototropic curvature under long-term irradiation conditions, and phot exert a small promotive effect on such Cry-mediated responses as hypocotyl elongation and anthocyanin accumulation. Also, Cry exert a negative regulatory effect on phot1 levels [182].

The so-called Cry-DASH subclade includes the majority of bacterial Cry but is spread throughout the living world [39,183]. The Cry-DASH protein sll1629 from *Synechocystis* has been proposed to function as a transcriptional repressor [40]; *Vc*Cry1 from *Vibrio cholerae*, another Cry-DASH protein, acts as a specific PL for the repair of single-strand DNA lesions [184]. The ortholog protein *At*Cry3 from *A. thaliana* has been extensively studied from the structural and biochemical point of view [45,147,185], but its precise role *in vivo* remains elusive: *At*Cry3 is able to repair both single- and double-stranded DNA, although the interaction with cyclobutane pyrimidine dimers is not as optimal as for PL [186], and its N-terminal sequence mediates import of Cry3 into chloroplasts and mitochondria [187].

Finally, CryB from *R. sphaeroides*, an unusual protein with low sequence similarity to other Cry/PL, might have some role in photorepair of DNA and downregulates the expression of photosynthesis genes in a light-dependent way [47]. Last, but not least, the PtCPF1 protein from the marine diatom *Phaeodactylum tricornutum* shows BL-driven DNA repair activity and can act as a transcriptional repressor of the circadian clock and seems to have a dominant role in BL-regulated gene expression in diatoms. The protein might therefore represent a missing link in the evolution of the Cry/PL family [188].

53.4.2 LOV Proteins: From Phototropism to Infectivity Regulation

In eukaryotes, the major LOV protein groups are formed by phot and the ZTL/FKF/LKP2 family in plants [3,4], by WC-1 [189–191], VIVID [192,193], and ENVOY [194] in fungi, and by the recently discovered AUREO in stramenopiles [157,158]. In the following, we will focus on plant, stramenopiles, and bacterial receptors.

Phot act as BL-driven regulators for processes that aim to the optimization of photosynthesis, growing of plants under dim light conditions and minimization of photodamage [2,4]. In *A. thaliana*, two phot (phot1 and phot2) act redundantly during many responses (phototropism, stomatal opening, leaf expansion, and chloroplast accumulation at low light intensity), but are specifically active for others, for example, phot1 inhibits hypocotyl growth during photomorphogenesis while phot2 is responsible for chloroplast avoidance movement at high light intensities (see [2,4] and references therein).

Phototropism, or curvature response to directional light, has been recently reviewed [195]. The phenomenon is very easily observed in coleoptiles of a dark grown plant seedling exposed to unidirectional light: the curvature toward light is actually due to an accumulation of auxins phytohormones in the shadowed area. This lateral movement of hormones is possible with the aid of transporter proteins. Besides auxins, phototropism requires brassinosteroids [4]. The formed auxin gradient initiates function for another class of proteins (e.g., the transcription activator complex NPH4/ARF7), by which differential growth is promoted (see [2,4,195] and references therein). Under low fluence rates, phot1 is the principal photoreceptor regulating phototropism, whereas under high fluence rates, phototropism is regulated redundantly by phot1 and phot2 [196]. Stomatal opening and leaf flattening/positioning are also phot1–phot2 coregulated responses, whereas chloroplast accumulation under dim BL and avoidance under high BL are distinctly mediated by phot1 and phot2, respectively [4].

In the green alga *Chlamydomonas reinhardtii*, however, only one phot is present. This BL photoreceptor regulates the algal sexual lifecycle, namely, it is essential for the light-dependent step in gamete differentiation [197]. Furthermore, it modulates the expression of several photosynthesis genes [198]. Broadly speaking, the two-LOV-domain phot proteins regulate movements, growth, development, and reproduction patterns.

Proteins belonging to the ZTL/FKF/LKP2 family act mainly *via* their interaction with GI (see Section 53.3.3). ZTL and FKF1 form a complex with GI upon light activation, leading to derepression of *CO* expression, a central element of day-length-regulated flowering. Both proteins influence flowering time by affecting circadian rhythm-controlled gene expression, i.e., they are BL sensors that posttranslationally regulate the circadian clock and photoperiodic flowering [162]. The precise role of LKP2 is still to be clarified, but it is certainly involved in the circadian regulation of the central clock [4,161].

The LOV-bearing AUREO from the stramenopile *V. frigida* not only binds to target DNA as predicted from its domain organization, but also regulates gene expression in a BL-dependent way; in other words, it is a (directly) BL-regulated transcription factor. The physiological response regulated by AUREO1 is a photomorphogenetic growth pattern, namely, BL-induced branching, elegantly demonstrated by means of interference RNA experiments [156,157]. AUREO2 may instead act as a subswitch to initiate development of a branch.

Despite the large spread of LOV proteins in the prokaryotic world, including Archaea [88,89, 156,199,200], only for few of them a biological role has been established. YtvA from *B. subtilis* binds GTP and ATP within its C-terminal STAS domain. This nucleoside-5′-triphosphate (NTP)-binding capability is of special interest, since it has been shown that ATP and GTP are important signaling compounds during the sporulation process and nutritional stress responses of *B. subtilis* [201–203]. It has also been demonstrated that YtvA acts as a positive regulator for the general stress transcription factor σB, specifically within the environmental branch, apparently in a BL-regulated way [101,166–168]. BL upregulation of the stress pathway is suppressed by mutations that affect NTP binding or light-induced conformational changes within the NTP-binding site, thus establishing a link between *in vitro* and *in vivo* data [100,101].

Recently, a link has been established between an LOV kinase and the photoregulation of bacterial pathogenesis of the Gram-negative pathogen *Brucella abortus*: the LOV kinase is required for BL-dependent cellular proliferation in macrophages [86]. A similar LOV kinase modulates the capacity for cell adhesion in a BL-dependent way [85]. Since the ability of bacterial pathogens to adhere to host cells is often a critical determinant of virulence, this observation might represent an important feature during infection. Bioinformatic analysis of over 600 bacterial genomes reveals that at least one LOV domain protein is present in 13% of species, including a number of pathogens. However, the relation between BL receptors and pathogenicity cannot yet be considered as a general one [8,204].

53.4.3 BLUF Proteins: From Phototaxis to Biofilms

There are still few examples where physiological functions could be unambiguously ascribed to BLUF proteins. Important information has been collected for the PAC proteins of *E. gracilis*. PAC-α and PAC-β are large proteins, comprising each ca. 1000 aa. Each protein (α and β) consists of two BLUF-cyclase motifs arranged in tandem. They function in a PAC-α/PAC-β heterodimeric complex as BL-regulated adenylate cyclases, responsible for step-up (but not step-down) photophobic responses as well as both positive and negative phototaxis [205,206]. PAC proteins are conserved among euglenoids [207], but to our knowledge, BLUF proteins are not present in other eukaryotic phyla.

Also in bacteria, functional information for BLUF proteins is still sparse, with the notable exception of AppA from *R. sphaeroides*, whose role and photocycle have been described [67], and of YcgF from *E. coli*. AppA is a light and redox regulator for the expression of photosynthesis genes, built of a light-sensing BLUF module [67,208] and a redox sensing C-terminal domain, shown to bind heme (see also Figure 53.4) [172,209]. This light-dependent regulatory function of AppA is accomplished only at intermediate oxygen concentration (see Section 53.3.3), when BL excitation induces the release of the transcription factor PpsR [171]. Interestingly, a BLUF domain from a Euglena PAC protein fused to the C-terminus of AppA is fully functional in regulating light-dependent gene expression in *R. sphaeroides* [210]. This finding implies that a BLUF domain can convey signals to completely different output domains, and that a eukaryotic light-sensing module can fully replace its homologue in a prokaryotic cell, although the sequence similarity between PAC-BLUF and AppA-BLUF is lower than 30%.

YcgF from *E. coli* (Figure 53.4) carries out BL regulation of biofilm formation [115]. The EAL domain in YcgF neither hydrolyzes c-di-GMP nor binds it, but is rather active in protein–protein interaction. The molecular pathway leading to light-induced upregulation of a biofilm matrix component (colanic acid) and acid resistance genes, and to the downregulation of adhesive curli fimbriae has been illustrated in Section 53.3.3. The Slr1694 short-BLUF protein from *Synechocystis* sp. PCC 6803 has been identified to be involved in phototaxis [211,212], but its action appears to be integrated with that of other photoreceptors and its precise function remains elusive [213].

53.4.4 BL, a Dangerous Beauty?

At first glance, it is surprising to find a large number of positive hits for BL photoreceptor genes from GenBank surveys. In fact, ca. 13% of fully sequenced bacteria possess at least one LOV or a BLUF protein [8]. Obviously, BL represents an important environmental factor that penetrates deepest into a water column, compared to all other spectral ranges [11]. It is also potentially harmful photochemical reactions which have to be efficiently counteracted, making the initiation of physiological responses upon the detection of BL essential for survival. This assumption also explains the variation in signaling domains for one and the same detector domain in several microorganisms (e.g., *Erythrobacter litoralis* exposes three histidine kinases fused to LOV domains and one helix-turn-helix (HTH)—motif), allowing a wider set of BL-regulated physiological responses [7,8,86,169]. Alternatively, microorganisms are found (well studied in *B. subtilis*) where several stress factors are integrated in a "stressosome" to initiate a more stereotypical response, for example, activation of the σ^B regulon (Figure 53.5) [166,167]. BL represents an attracting light range allowing activation of the photosynthetic apparatus, and also it is essential for the function of light-activated DNA-repairing enzymes (PL, *vide supra*). On the other hand, porphyrinic compounds that are ubiquitous, for example, as cofactors in cytochromes, exhibit a strong absorption (ε_{max} ca. 10^5 M^{-1} cm^{-1}) in the blue region of the visible spectrum [214]. These compounds usually function *via* an iron atom bound in the center of the tetrapyrrole ring structure. In case, however, the central metal ion is absent, the porphyrins exhibit a high tendency to form triplets from their excited singlet state [12,214]. Triplet state porphyrins, in turn, convert with high yield the ever present triplet oxygen into its singlet state [12], which is outstandingly reactive and readily causes deleterious damage in its direct surrounding, eventually even causing cell death by photooxidative stress [214]. This photosensitization effect is presently being exploited in the photodynamic therapy of cancer [214], and as a potential killing device for bacteria: for example, antibiotic resistant *Staphylococcus aureus* can be killed, *in vitro*, with 470 nm light [215]. Interestingly, one finds in several cases genes encoding BL photoreceptors in vicinity to genes of the iron metabolism (e.g., encoding Fe chelatases and iron scavengers). Such increase in biosynthesis of iron scavengers (pyoverdins), which is upregulated selectively by BL, has recently been demonstrated for *Pseudomonas putida* [216].

In an aerobic environment, the deleterious oxidative effects rely on the same BL bio-absorbers that optimize both respiration and photosynthesis, that is, porphyrins and flavins, but living organisms have learnt how to take advantage of O_2 and BL, at the same time minimizing photodamages. One of the organisms that has best exploited this interplay between O_2 and BL is *R. sphaeroides*, a member of the cosmopolitan α-proteobacteria family (see Section 53.3.3). *R. sphaeroides* can switch between photosynthesis and aerobic respiration *via* a complex regulation mechanism that includes the AppA protein [171]. At high pO_2, photosynthesis genes are not expressed, no matter if BL is present: it would be useless, costly, and potentially dangerous. The contrary is true under anaerobic conditions. At low pO_2, it is BL that promotes the transcription of photosynthesis genes by triggering AppA photocycle [217].

53.5 Novel "Blue" Trends

BL flavo-photosensors definitely present novel concepts and can be exploited and engineered for a variety of biological and biomedical applications, notably for cellular studies and for the light-controlled level of important metabolites. One of the most discussed topics is the role of Cry proteins in magnetoreception and its connection with their role as photosensors. Besides these two aspects, BL photoreceptors are being explored within the emerging field of metagenomics.

53.5.1 Cry as "Photomagnetoreceptors"

This issue has its roots in the "radical-pair" model for magnetoreception in birds, suggesting that magnetoreception is based on spin-chemical processes in specialized photopigments [44,218,219], representing an alternative to magnetite-based receptors. Cry proteins have been proposed as good candidates

for accomplishing this role (reviewed in [220]). Basically, this model implies the formation of RP upon light absorption [218]. These RP may be in the singlet (^{1}RP) or in the triplet state (^{3}RP), with the portion of each state, and its products depending, among other circumstances, on the alignment of the molecule in the external magnetic field. Birds must be able to compare the amount of singlets or triplets in various spatial alignments. One prediction of this model is that oscillating magnetic fields in the MHz range would interfere with the singlet–triplet interconversion and thus should disrupt magnetic compass orientation [218,221]. This was experimentally confirmed for a variety of cases, also showing that this photo-magnetoreception is taking place in the eyes of migratory birds [220]. Two types of responses can be distinguished in birds: (1) compass orientation controlled by the inclination compass, a response restricted to a narrow functional window around the total intensity of the local geomagnetic field that requires light from the short-wavelength part of the spectrum. The compass is based on RP processes in the right eye and is observed under "white" and low-level monochromatic light from ultraviolet (UV) to about 565 nm. This observation would imply that a RP with the flavin in the semi-reduced state (Scheme 53.1) can accept a second photon in the green spectral region and (2) "fixed direction" responses occur under artificial light conditions and in total darkness mediated by iron-based receptors located in the beak. The influence of light conditions on the two types of response suggests complex interactions between magnetoreceptors in the right eye, those in the upper beak and the visual system [220].

Quite surprisingly, evidence supporting the Cry hypothesis has been obtained from a report of magnetic field responses in *A. thaliana*. Enhanced Cry-mediated inhibition of hypocotyl elongation in a 500 μT magnetic field, relative to controls in the ambient magnetic field (approx. 40 μT), was observed under BL irradiation, but not under red light or in total darkness. Also, no magnetic field effects were found in Cry1/Cry2-deficient Arabidopsis mutants [222]. Also other Cry-mediated responses were enhanced at 500 μT, that is, BL-induced degradation of Cry2 and BL-dependent anthocyanin accumulation, consistent with a magnetic field-induced increase in the sensitivity of the seedlings to BL. This was interpreted as the formation of a photoinduced flavin–Trp RP [46]. However, these data could not be reproduced by another group that argued "that plant growth responses to the imposed magnetic field treatments are highly variable" [223]. These authors also state on the basis of their own unpublished results that the magnetic responses of various members of the PL/Cry family *in vitro* are strongly dependent on experimental conditions, including solvent viscosity, suggesting that that the protein molecules must be both immobilized and aligned in order to show the anisotropic magnetic field effects essential for a compass detection mechanism [218,223].

53.5.2 BL Sensors as Tools for Cellular Studies: From Reporters to Engineered Regulators

The employment of flavins as chromophores in BL photoreceptors distinguishes these chromoproteins as promising tools for biotechnological applications. Whereas flavins are ubiquituous in practically all cell types (either endogenously generated or provided *via* dietary supplementation), chromophores for other photoreceptor types have to be added. In particular, the high fluorescence quantum yield of the LOV domain (in its dark state) makes applications possible such as those now common for the various green fluorescent protein (GFP) derivatives [224]. As fluorescence is lost upon the photochemical formation of the "signaling" photoadduct state, this process can be annihilated by exchanging the covalent bond-forming cysteine residue for an alanine or serine, yielding a permanently fluorescent molecule [225]. In fact, compared to GFPs, where the fluorescent chromophore forms *via* an intramolecular condensation of three amino acids, however, requiring the presence of oxygen, the LOV domains are advantageous for selected applications in anaerobic or microaerobic environments, where they outperform GFP since they exhibit an endogeneous fluorescence [225,226].

Beyond the inherent properties of the LOV domains, their combination with various signaling domains, as found by genome surveys (Figure 53.4) [8,88], has led to the emergence of an entirely new field of biomedical applications. The possibility to regulate intracellular physiological processes simply

by an external irradiation is definitely an intriguing aspect and has experienced an explosion in applications. Initially, retinal (vitamin A aldehyde)-based photoreceptors have opened this research field [227–229]; however, the earlier discussed PAC from *E. gracilis* (carrying as functional elements a combination of a BLUF and an adenosine monophosphate (AMP) cyclase) has made possible "optogenetic" research [230,231]. This function is based on the light-regulated cAMP-mediated activation of certain neurons upon functional expression of PAC, yielding light-induced changes in behavior *via* the BLUF domain activation of the cyclase [230,231]. The fast increase in cAMP in turn regulates, *via* a phosphorylation cascade, gene expression in eukaryotic cells; accordingly, this research has been coined as "optogenetics." Additional applications are expected to come including also the activation of other second messengers, for example, the specificity conversion of an AMP- into a GMP cyclase function by site-directed mutagenesis [232]. Recently, the first 3D structure for a GMP cyclase with an overall high similarity to the AMP cyclase has been published, making also this regulatory pathway a target for light-controlled activity [233].

One step further in this direction has been made by the combination of BL-sensing domains (LOV and BLUF) with enzymatic or regulatory functions from other proteins. The kinase domain of phot2 is constitutively active toward the heterologous substrate casein [234]. Adding *in vitro* the phot2-LOV2 domain enables a light control of this kinase activity, even in the absence of a covalent LOV2–kinase interaction [234]. Employing the building principle of many LOV domain proteins being fused to histidine kinases, the LOV domain of YtvA was fused to a histidine kinase from an oxygen-sensing pathway [109]. A direct light-regulated DNA binding was accomplished by a hybrid protein consisting of an LOV2 domain from *A. sativa* phot1 and the *E. coli trp* repressor [235]. These authors made use of the property of LOV2 to interrupt upon irradiation the interaction of the LOV core with its C-terminal extension (Jα-helix). Only in the light-activated, non-interacting state of the LOV domain, the trp repressor could form the active DNA-binding homodimer [235]. Extending this principle with transcription factors of different selectivity would open the path toward an irradiation-controlled gene expression. Recently, exciting results have been published, whereby Rho-like GTPases, Rac and Cdc42, caged with an LOV domain have been engineered: the proteins are activated upon irradiation, repeatedly and reversibly, in living cells to produce protrusions, filopodia, etc., and to probe signaling pathways [236].

53.5.3 From the Lab to Real World: The Wonder of Metagenomics in the BL World

The broad distribution of LOV domains in many prokaryotic genomes, documented by ongoing GenBank surveys [8], has initiated a novel activity to investigate even uncharacterized material for the presence of BL photoreceptors [237,238], assuming that the presence of BL photoreceptors would be similarly high as in genome-classified organisms. The rational for such an approach is the expectation that searching exotic or extreme environments, proteins with novel and unusual properties might be found. Such studies are readily performed on a sequence-based setup: assuming a distribution of LOV domains in metagenome material similar as in sequenced genomes, a set of oligonucleotides, encoding representative LOV domain regions within a highly conserved, canonical sequence region, is covalently attached to a solid support material (a glass or plastic slide or an electronic chip). This DNA microarray serves as bait for hybridization with fluorescence-labeled, unknown DNA (potentially cloned into bacterial artificial chromosome (BAC), plasmids, or cosmids). It will give rise to a positive fluorescent signal at positions, where hybridization to an oligonucleotide with known sequence took place. Moving out from the known sequence motif into the unknown DNA then allows to "harvest" the full-length gene encoding a novel protein. The intermediate cloning step of uncharacterized DNA even allows, after identification of the full-length gene, a heterologous expression and a functional characterization of the gene product [200]. Such approach reveals only sequences with a relatively high degree of similarity to the oligonucleotides used as bait. A function-based investigation, however, would enable us to identify a protein function irrespective of

the sequence. In case of LOV domain proteins, the recovery of the fluorescent parent state (LOV_{445}) could readily be followed in a high-throughput heterologous expression approach.

Also entirely in-silico-based investigations have recently been reported for both BLUF and LOV domains [237,238]. These studies, again based on sequence comparisons, revealed the presence of BLUF and also LOV domains in practically any environment, deriving from many locations in various oceans (Sargasso and Global Ocean Sampling Project), or from wastewater treatment plants or mine drainage.

The last decade has seen an enormous growth in our understanding of the function of BL photoreceptors, both with respect to their inherent photochemical reactivity and also related to their role in regulating physiological functions. This knowledge is now starting to be extended by investigations on the role of (blue) light as an important and regulatory function in environmental research and microbial communities, including screening data bases and metagenomes. Based on these developments, one can expect in near future that novel research directions, for example, the regulation of physiological processes by BL domains in naturally occurring photoreceptors or as parts of hybrid proteins will become a rapidly growing research area.

List of Acronyms and Abbreviations

AUREO	AUREOCHROME, a LOV protein from Stramenopiles
BL	blue light
BLUF	blue light-sensing using FAD (protein domain)
c-di-GMP	bis-(3′,5′)-cyclic dimeric guanosine monophosphate, a second messenger
Cry	cryptochrome
FAD	flavin-adenine dinucleotide
FKF1	flavin-binding Kelch F-box1, a LOV protein from plants
FMN	flavin mononucleotide
GGDEF, EAL	protein domains named after conserved sequences, involved in the turnover of c-di-GMP
HB	hydrogen bond
LKP2	LOV Kelch protein 2, a LOV protein from plants
LOV	light oxygen voltage, FMN binding photosensing protein domain
NTP	nucleoside triphosphate (e.g., ATP, GTP)
PAC	photoactivated adenylate cyclase, a BLUF protein from Euglenoids
PAS	PerArntSim (protein domain)
phot	phototropin, a plant LOV-kinase
PL	photolyase, a BL-activated protein for DNA repair, related to Cry
RB	riboflavin
RP	radical pair
RR	response regulator, a protein domain involved in signal transduction
SPOIIE	Stage II sporulation protein E
STAS	Sulphate Transporter/Anti-Sigma factor antagonist (protein domain)
VIVID	fungal LOV protein
YtvA	a LOV protein from *Bacillus subtilis*
ZTL	Zeitlupe, a LOV protein from plants

References

1. W. R. Briggs, in *Photomorphogenesis in Plants and Bacteria*, eds. E. Schäfer and F. Nagy, Springer, Dordrecht, the Netherlands, 2006, Chapter 10, pp. 171–197.
2. J. M. Christie, *Annu. Rev. Plant Biol.*, 2007, 58, 21–45.
3. R. Banerjee, A. Batschauer, *Planta*, 2005, 220, 498–502.

4. E. Demarsy, C. Fankhauser, *Curr. Opin. Plant Biol.*, 2009, 12, 69–74.
5. Q. H. Li, H. Q. Yang, *Photochem. Photobiol.*, 2007, 83, 94–101.
6. A. Sancar, *Adv. Protein. Chem.*, 2004, 69, 73–100.
7. W. R. Briggs, *J. Biomed. Sci.*, 2007, 14, 499–504.
8. A. Losi, W. Gärtner, *Photochem. Photobiol. Sci.*, 2008, 7, 1168–1178.
9. A. R. Cashmore, J. A. Jarillo, Y. J. Wu, and D. M. Liu, *Science*, 1999, 284, 760–765.
10. C. L. Partch, A. Sancar, *Methods Enzymol.*, 2005, 393, 726–45.
11. C. S. Cockell, *Orig. Life Evol. Biosphere*, 2000, 30, 467–499.
12. R. W. Redmond, J. N. Gamlin, *Photochem. Photobiol.*, 1999, 70, 391–475.
13. S. Y. Egorov, A. A. Krasnovsky, Jr., M. Y. Bashtanov, E. A. Mironov, T. A. Ludnikova, and M. S. Kritsky, *Biochem. Mosc.*, 1999, 64, 1117–1121.
14. J. Baier, T. Maisch, M. Maier, E. Engel, M. Landthaler, and W. Baumler, *Biophys. J.*, 2006, 91, 1452–1459.
15. V. Massey, *Biochem. Soc. Trans.*, 2000, 28, 283–296.
16. A. M. Edwards, in *Flavins Photochemistry and Photobiology*, eds. E. Silva and A. M. Edwards, Elsevier, Amsterdam, the Netherlands, 2006, Chapter 1, pp. 1–11.
17. A. M. Edwards, in *Flavins Photochemistry and Photobiology*, eds. E. Silva and A. M. Edwards, Amsterdam, the Netherlands, 2006, Chapter 6, pp. 115–130.
18. S. Roje, *Phytochemistry*, 2007, 68, 1904–1921.
19. M. Fischer, A. K. Schott, W. Romisch, A. Ramsperger, M. Augustin, A. Fidler, A. Bacher, G. Richter, R. Huber, and W. Eisenreich, *J. Mol. Biol.*, 2004, 343, 267–278.
20. V. Y. Yatsyshyn, D. V. Fedorovych, and A. A. Sibirny, *Appl. Biochem. Microbiol.*, 2009, 45, 115–124.
21. J. Velisek, K. Cejpek, *Czech J. Food Sci.*, 2007, 25, 49–64.
22. S. Salzmann, V. Martinez-Junza, B. Zorn, S. E. Braslavsky, M. Mansurova, C. M. Marian, and W. Gärtner, *J. Phys. Chem. A*, 2009, 113, 9365–9375.
23. S. Salzmann, J. Tatchen, and C. M. Marian, *J. Photochem. Photobiol. A Chem.*, 2008, 198, 221–231.
24. L. B. Johansson, A. Davidsson, G. Lindblom, and K. R. Naqvi, *Biochemistry*, 1979, 18, 4249–4253.
25. P. W. van den Berg, J. Widengren, M. A. Hink, R. Rigler, and A. G. Visser, *Spectrochim. Acta A*, 2001, 57, 2135–2144.
26. A. Losi, E. Ghiraldelli, S. Jansen, and W. Gärtner, *Photochem. Photobiol.*, 2005, 81, 1145–1152.
27. P. Drossler, W. Holzer, A. Penzkofer, and P. Hegemann, *Chem. Phys.*, 2002, 282, 429–439.
28. M. S. Grodowski, B. Veyret, and K. Weiss, *Photochem. Photobiol.*, 1977, 26, 341–352.
29. J. N. Chacon, J. McLearie, and R. S. Sinclair, *Photochem. Photobiol.*, 1988, 47, 647–656.
30. A. Losi, E. Polverini, B. Quest, and W. Gärtner, *Biophys. J.*, 2002, 82, 2627–2634.
31. S. D. M. Islam, T. Susdorf, A. Penzkofer, and P. Hegemann, *Chem. Phys.*, 2003, 295, 137–149.
32. Y. T. Kao, C. Saxena, T. F. He, L. J. Guo, L. J. Wang, A. Sancar, and D. P. Zhong, *J. Am. Chem. Soc.*, 2008, 130, 13132–13139.
33. T. E. Swartz, S. B. Corchnoy, J. M. Christie, J. W. Lewis, I. Szundi, W. R. Briggs, and R. A. Bogomolni, *J. Biol. Chem.*, 2001, 276, 36493–36500.
34. T. Kottke, J. Heberle, D. Hehn, B. Dick, and P. Hegemann, *Biophys. J.*, 2003, 84, 1192–1201.
35. M. J. Damiani, G. N. Yalloway, J. Lu, N. R. McLeod, and M. A. O'Neill, *Biochemistry*, 2009, 48, 11399–11411.
36. A. Sancar, *Chem. Rev.*, 2003, 103, 2203–2237.
37. M. Müller, T. Carell, *Curr. Opin. Struct. Biol.*, 2009, 19, 277–285.
38. C. B. Green, *Curr. Biol.*, 2004, 14, 847–849.
39. A. Losi, *Photochem. Photobiol.*, 2007, 83, 1283–1300.
40. R. Brudler, K. Hitomi, H. Daiyasu, H. Toh, K. Kucho, M. Ishiura, M. Kanehisa, V. A. Roberts, T. Todo, J. A. Tainer, and E. D. Getzoff, *Mol. Cell*, 2003, 11, 59–67.
41. S. Weber, *Biochim. Biophys. Acta Bioenerg.*, 2005, 1707, 1–23.
42. T. Langenbacher, D. Immeln, B. Dick, and T. Kottke, *J. Am. Chem. Soc.*, 2009, 131, 14274–14280.

43. A. Berndt, T. Kottke, H. Breitkreuz, R. Dvorsky, S. Hennig, M. Alexander, and E. Wolf, *J. Biol. Chem.*, 2007, 282, 13011–13021.
44. T. Biskup, E. Schleicher, A. Okafuji, G. Link, K. Hitomi, E. D. Getzoff, and S. Weber, *Angew. Chem. Int. Ed.*, 2009, 48, 404–407.
45. S. H. Song, B. Dick, A. Penzkofer, R. Pokorny, A. Batschauer, and L. O. Essen, *J. Photochem. Photobiol. B Biol.*, 2006, 85, 1–16.
46. B. Giovani, M. Byrdin, M. Ahmad, and K. Brettel, *Nat. Struct. Biol.*, 2003, 10, 489–490.
47. A. K. Hendrischk, S. W. Fruehwirth, J. Moldt, R. Pokorny, S. Metz, G. Kaiser, A. Jaeger, A. Batschauer, and G. Klug, *Mol. Microbiol.*, 2009, 74, 990–1003.
48. N. Ozturk, C. P. Selby, S. H. Song, R. Ye, C. Tan, Y. T. Kao, D. Zhong, and A. Sancar, *Biochemistry*, 2009, 48, 8585–8593.
49. N. Hoang, E. Schleicher, S. Kacprzak, J. P. Bouly, M. Picot, W. Wu, A. Berndt, E. Wolf, R. Bittl, and M. Ahmad, *PLoS Biol.*, 2008, 6, 1811.
50. E. Schleicher, R. Bittl, and S. Weber, *FEBS J.*, 2009, 276, 4290–4303.
51. A. Jung, T. Domratcheva, M. Tarutina, Q. Wu, W. H. Ko, R. L. Shoeman, M. Gomelsky, K. H. Gardner, and I. Schlichting, *Proc. Natl. Acad. Sci. USA*, 2005, 102, 12350–12355.
52. A. Kita, K. Okajima, Y. Morimoto, M. Ikeuchi, and K. Miki, *J. Mol. Biol.*, 2005, 349, 1–9.
53. A. Jung, J. Reinstein, T. Domratcheva, R. L. Shoeman, and I. Schlichting, *J. Mol. Biol.*, 2006, 362, 717–732.
54. H. Yuan, S. Anderson, S. Masuda, V. Dragnea, K. Moffat, and C. Bauer, *Biochemistry*, 2006, 45, 12687–12694.
55. J. S. Grinstead, S. T. Hsu, W. Laan, A. M. J. J. Bonvin, K. J. Hellingwerf, R. Boelens, and R. Kaptein, *ChemBioChem*, 2006, 7, 187–193.
56. T. R. M. Barends, E. Hartmann, J. J. Griese, T. Beitlich, N. V. Kirienko, D. A. Ryjenkov, J. Reinstein, R. L. Shoeman, M. Gomelsky, and I. Schlichting, *Nature*, 2009, 459, 1015–U150.
57. Q. Wu, K. H. Gardner, *Biochemistry*, 2009, 48, 2620–2629.
58. S. M. Harper, L. C. Neil, and K. H. Gardner, *Science*, 2003, 301, 1541–1544.
59. A. S. Halavaty, K. Moffat, *Biochemistry*, 2007, 46, 14001–14009.
60. M. Kasahara, T. E. Swartz, M. A. Olney, A. Onodera, N. Mochizuki, H. Fukuzawa, E. Asamizu, S. Tabata, H. Kanegae, M. Takano, J. M. Christie, A. Nagatani, and W. R. Briggs, *Plant Physiol.*, 2002, 129, 762–773.
61. M. Nakasako, D. Matsuoka, K. Zikihara, and S. Tokutomi, *FEBS Lett.*, 2005, 579, 1067–1071.
62. S. Kikuchi, M. Unno, K. Zikihara, S. Tokutomi, and S. Yamauchi, *J. Phys. Chem. B*, 2009, 113, 2913–2921.
63. A. Losi, T. Kottke, and P. Hegemann, *Biophys. J.*, 2004, 86, 1051–1060.
64. A. Penzkofer, L. Endres, T. Schiereis, and P. Hegemann, *Chem. Phys.*, 2005, 316, 185–194.
65. U. Krauss, A. Losi, W. Gärtner, K.-E. Jaeger, and T. Eggert, *Phys. Chem. Chem. Phys.*, 2005, 7, 2229–2236.
66. K. Jentzsch, A. Wirtz, F. Circolone, T. Drepper, A. Losi, W. Gärtner, K.-E. Jaeger, and U. Krauss, *Biochemistry*, 2009, 48, 10321–10333.
67. S. Masuda, C. E. Bauer, *Cell*, 2002, 110, 613–623.
68. M. Gomelsky, G. Klug, *Trends Biochem. Sci.*, 2002, 27, 497–500.
69. S. Ito, A. Murakami, K. Sato, Y. Nishina, K. Shiga, T. Takahashi, S. Higashi, M. Iseki, and M. Watanabe, *Photochem. Photobiol. Sci.*, 2005, 4, 762–769.
70. S. Rajagopal, J. M. Key, E. B. Purcell, D. J. Boerema, and K. Moffat, *Photochem. Photobiol.*, 2004, 80, 542–547.
71. S. Masuda, K. Hasegawa, A. Ishii, and T. A. Ono, *Biochemistry*, 2004, 43, 5304–5313.
72. Y. Fukushima, K. Okajima, Y. Shibata, M. Ikeuchi, and S. Itoh, *Biochemistry*, 2005, 44, 5149–5158.
73. P. Zirak, A. Penzkofer, T. Schiereis, P. Hegemann, A. Jung, and I. Schlichting, *J. Photochem. Photobiol. B Biol.*, 2006, 83, 180–190.

74. M. Gauden, S. Yeremenko, W. Laan, I. H. M. van Stokkum, J. A. Ihalainen, R. van Grondelle, K. J. Hellingwerf, and J. T. M. Kennis, *Biochemistry*, 2005, 44, 3653–3662.
75. K. Okajima, Y. Fukushima, H. Suzuki, A. Kita, Y. Ochiai, M. Katayama, Y. Shibata, K. Miki, T. Noguchi, and S. Itoh, *J. Mol. Biol.*, 2006, 363, 10–18.
76. H. Suzuki, K. Okajima, M. Ikeuchi, and T. Noguchi, *J. Am. Chem. Soc.*, 2008, 130, 12884–12885.
77. M. Gauden, I. H. M. van Stokkum, J. M. Key, D. C. Luhrs, R. van Grondelle, P. Hegemann, and J. T. M. Kennis, *Proc. Natl. Acad. Sci. USA*, 2006, 103, 10895–10900.
78. C. Bonetti, M. Stierl, T. Mathes, I. H. M. van Stokkum, K. M. Mullen, T. A. Cohen-Stuart, R. van Grondelle, P. Hegemann, and J. T. M. Kennis, *Biochemistry*, 2009, 48, 11458–11469.
79. E. Schleicher, R. M. Kowalczyk, C. W. M. Kay, P. Hegemann, A. Bacher, M. Fischer, R. Bittl, G. Richter, and S. Weber, *J. Am. Chem. Soc.*, 2004, 126, 11067–11076.
80. E. Huala, P. W. Oeller, E. Liscum, I. S. Han, E. Larsen, and W. R. Briggs, *Science*, 1997, 278, 2120–2123.
81. M. Salomon, E. Knieb, T. von Zeppelin, and W. Rüdiger, *Biochemistry*, 2003, 42, 4217–4225.
82. S. Tokutomi, D. Matsuoka, and K. Zikihara, *Biochim. Biophys. Acta*, 2008, 1784, 133–142.
83. S. Sullivan, C. E. Thomson, D. J. Lamont, M. A. Jones, and J. M. Christie, *Mol. Plant*, 2008, 1, 178–194.
84. S. Inoue, T. Kinoshita, M. Matsumoto, K. I. Nakayama, M. Doi, and K. Shimazaki, *Proc. Natl. Acad. Sci. USA*, 2008, 105, 5626–5631.
85. E. B. Purcell, D. Siegal-Gaskins, D. C. Rawling, A. Fiebig, and S. Crosson, *Proc. Natl. Acad. Sci. USA*, 2007, 104, 18241–18246.
86. T. E. Swartz, T. S. Tseng, M. A. Frederickson, G. Paris, D. J. Comerci, G. Rajashekara, J. G. Kim, M. B. Mudgett, G. A. Splitter, R. A. Ugalde, F. A. Goldbaum, W. R. Briggs, and R. A. Bogomolni, *Science*, 2007, 317, 1090–1093.
87. Z. Cao, V. Buttani, A. Losi, and W. Gärtner, *Biophys. J.*, 2008, 94, 897–905.
88. S. Crosson, S. Rajagopal, and K. Moffat, *Biochemistry*, 2003, 42, 2–10.
89. A. Losi, *Photochem. Photobiol. Sci.*, 2004, 3, 566–574.
90. S. Crosson, K. Moffat, *Proc. Natl. Acad. Sci. USA*, 2001, 98, 2995–3000.
91. R. Fedorov, I. Schlichting, E. Hartmann, T. Domratcheva, M. Fuhrmann, and P. Hegemann, *Biophys. J.*, 2003, 84, 2492–2501.
92. B. D. Zoltowski, C. Schwerdtfeger, J. Widom, J. J. Loros, A. M. Bilwes, J. C. Dunlap, and B. R. Crane, *Science*, 2007, 316, 1054–1057.
93. V. Buttani, A. Losi, T. Eggert, U. Krauss, K.-E. Jaeger, Z. Cao, and W. Gärtner, *Photochem. Photobiol. Sci.*, 2007, 6, 41–49.
94. A. Pfeifer, T. Majerus, K. Zikihara, D. Matsuoka, S. Tokutomi, J. Heberle, and T. Kottke, *Biophys. J.*, 2009, 96, 1462–1470.
95. D. Nozaki, T. Iwata, T. Ishikawa, T. Todo, S. Tokutomi, and H. Kandori, *Biochemistry*, 2004, 43, 8373–8379.
96. A. I. Nash, W. H. Ko, S. M. Harper, and K. H. Gardner, *Biochemistry*, 2008, 47, 13842–13849.
97. M. T. A. Alexandre, R. van Grondelle, K. J. Hellingwerf, and J. T. M. Kennis, *Biophys. J.*, 2009, 97, 238–247.
98. T. Koyama, T. Iwata, A. Yamamoto, Y. Sato, D. Matsuoka, S. Tokutomi, and H. Kandori, *Biochemistry*, 2009, 48, 7621–7628.
99. M. A. Jones, K. A. Feeney, S. M. Kelly, and J. M. Christie, *J. Biol. Chem.*, 2007, 282, 6405–6414.
100. Y. Tang, Z. Cao, E. Livoti, U. Krauss, K.-E. Jaeger, W. Gärtner, and A. Losi, *Photochem. Photobiol. Sci.*, 2010, 9, 47–56.
101. M. Avila-Perez, J. Vreede, Y. Tang, O. Bende, A. Losi, and W. Gärtner, *J. Biol. Chem.*, 2009, 284, 24958–24964.
102. S. M. Harper, J. M. Christie, and K. H. Gardner, *Biochemistry*, 2004, 43, 16184–16192.
103. X. Yao, M. K. Rosen, and K. H. Gardner, *Nat. Chem. Biol.*, 2008, 4, 491–497.
104. J. M. Christie, T. E. Swartz, R. A. Bogomolni, and W. R. Briggs, *Plant J.*, 2002, 32, 205–219.

105. H. Y. Cho, T. S. Tseng, E. Kaiserli, S. Sullivan, J. M. Christie, and W. R. Briggs, *Plant Physiol.*, 2007, 143, 517–529.
106. W. R. Briggs, T. S. Tseng, H. Y. Cho, T. E. Swartz, S. Sullivan, R. A. Bogomolni, E. Kaiserli, and J. M. Christie, *J. Integr. Plant Biol.*, 2007, 49, 4–10.
107. E. Kaiserli, S. Sullivan, M. A. Jones, K. A. Feeney, and J. M. Christie, *Plant Cell*, 2009, 21, 3226–3244.
108. P. Cheng, Q. He, Y. Yang, L. Wang, and Y. Liu, *Proc. Natl. Acad. Sci. USA*, 2003, 100, 5938–5943.
109. A. Moglich, R. A. Ayers, and K. Moffat, *J. Mol. Biol.*, 2009, 385, 1433–1444.
110. S. Sullivan, C. E. Thomson, E. Kaiserli, and J. M. Christie, *FEBS Lett.*, 2009, 583, 2187–2193.
111. A. J. Schmidt, D. A. Ryjenkov, and M. Gomelsky, *J. Bacteriol.*, 2005, 187, 4774–4781.
112. K. Hasegawa, S. Masuda, and T. A. Ono, *Biochemistry*, 2004, 43, 14979–14986.
113. K. Hasegawa, S. Masuda, and T. A. Ono, *Plant Cell Physiol.*, 2005, 46, 136–146.
114. K. Hasegawa, S. Masuda, and T. A. Ono, *Biochemistry*, 2006, 45, 3785–3793.
115. N. Tschowri, S. Busse, and R. Hengge, *Gene Dev.*, 2009, 23, 522–534.
116. C. Schroeder, K. Werner, H. Otten, S. Krätzig, H. Schwalbe, and L. O. Essen, *ChemBioChem*, 2008, 9, 2463–2473.
117. S. Masuda, K. Hasegawa, and T. A. Ono, *Plant Cell Physiol.*, 2005, 46, 1894–1901.
118. S. Masuda, Y. Tomida, H. Ohta, and K. I. Takamiya, *J. Mol. Biol.*, 2007, 18, 1223–1230.
119. V. Dragnea, A. I. Arunkumar, H. Yuan, D. P. Giedroc, and C. E. Bauer, *Biochemistry*, 2009, 48, 9969–9979.
120. S. Anderson, V. Dragnea, S. Masuda, J. Ybe, K. Moffat, and C. Bauer, *Biochemistry*, 2005, 44, 7998–8005.
121. J. S. Grinstead, M. Avila-Perez, K. J. Hellingwerf, R. Boelens, and R. Kaptein, *J. Am. Chem. Soc.*, 2006, 128, 15066–15067.
122. T. Domratcheva, B. L. Grigorenko, I. Schlichting, and A. V. Nemukhin, *Biophys. J.*, 2008, 94, 3872–3879.
123. X. Yu, D. Shalitin, X. Liu, M. Maymon, J. Klejnot, H. Yang, J. Lopez, X. Zhao, K. T. Bendehakkalu, and C. Lin, *Proc. Natl. Acad. Sci. USA*, 2007, 104, 7289–7294.
124. H. Q. Yang, Y. J. Wu, R. H. Tang, D. Liu, Y. Liu, and A. R. Cashmore, *Cell*, 2000, 103, 815–827.
125. S. Dissel, V. Codd, R. Fedic, K. J. Garner, R. Costa, C. P. Kyriacou, and E. Rosato, *Nat. Neurosci.*, 2004, 7, 834–840.
126. C. L. Partch, M. W. Clarkson, S. Özgür, A. L. Lee, and A. Sancar, *Biochemistry*, 2005, 44, 3795–3805.
127. D. Shalitin, H. Yang, T. C. Mockler, M. Maymon, H. Guo, G. C. Whitelam, and C. Lin, *Nature*, 2002, 417, 763–767.
128. J. P. Bouly, B. Giovani, A. Djamei, M. Mueller, A. Zeugner, E. A. Dudkin, A. Batschauer, and M. Ahmad, *Eur. J. Biochem./FEBS*, 2003, 270, 2921–2928.
129. S. Özgür, A. Sancar, *Biochemistry*, 2006, 45, 13369–13374.
130. D. Immeln, R. Schlesinger, J. Heberle, and T. Kottke, *J. Biol. Chem.*, 2007, 282, 21720–21728.
131. S. Burney, N. Hoang, M. Caruso, E. A. Dudkin, M. Ahmad, and J. P. Bouly, *FEBS Lett.*, 2009, 583, 1427–1433.
132. C. A. Brautigam, B. S. Smith, Z. Ma, M. Palnitkar, D. R. Tomchick, M. Machius, and J. Deisenhofer, *Proc. Natl. Acad. Sci. USA*, 2004, 101, 12142–12147.
133. A. Möglich, K. Moffat, *J. Mol. Biol.*, 2007, 373, 112–126.
134. M. Nakasako, K. Zikihara, D. Matsuoka, H. Katsura, and S. Tokutomi, *J. Mol. Biol.*, 2008, 381, 718–733.
135. B. D. Zoltowski, B. R. Crane, *Biochemistry*, 2008, 47, 7012–7019.
136. M. Salomon, U. Lempert, and W. Rüdiger, *FEBS Lett.*, 2004, 572, 8–10.
137. M. Nakasako, T. Iwata, D. Matsuoka, and S. Tokutomi, *Biochemistry*, 2004, 43, 14881–14890.
138. H. Katsura, K. Zikihara, K. Okajima, S. Yoshihara, and S. Tokutomi, *FEBS Lett.*, 2009, 583, 526–530.
139. Y. Nakasone, T. Eitoku, D. Matsuoka, S. Tokutomi, and M. Terazima, *Biophys. J.*, 2006, 91, 645–653.

140. P. Ballario, C. Talora, D. Galli, H. Linden, and G. Macino, *Mol. Microbiol.*, 1998, 29, 719–729.
141. P. Hazra, K. Inoue, W. Laan, K. J. Hellingwerf, and M. Terazima, *Biophys. J.*, 2006, 91, 654–661.
142. B. J. Kraft, S. Masuda, J. Kikuchi, V. Dragnea, G. Tollin, J. M. Zaleski, and C. E. Bauer, *Biochemistry*, 2003, 42, 6726–6734.
143. P. Hazra, K. Inoue, W. Laan, K. J. Hellingwerf, and M. Terazima, *J. Phys. Chem. B*, 2008, 112, 1494–1501.
144. H. Yuan, C. E. Bauer, *Proc. Natl. Acad. Sci. USA*, 2008, 105, 11715–11719.
145. S. Masuda, K. Hasegawa, H. Ohta, and T. Ono, *Plant Cell Physiol.*, 2008, 49, 1600–1606.
146. Y. Sang, Q. H. Li, V. Rubio, Y. C. Zhang, J. Mao, X. W. Deng, and H. Q. Yang, *Plant Cell*, 2005, 17, 1569–1584.
147. T. Klar, R. Pokorny, J. Moldt, A. Batschauer, and L. O. Essen, *J. Mol. Biol.*, 2007, 366, 954–964.
148. T. Kinoshita, T. Emi, M. Tominaga, K. Sakamoto, A. Shigenaga, M. Doi, and K. I. Shimazaki, *Plant Physiol.*, 2003, 133, 1453–1463.
149. P. Mhawech, *Cell Res.*, 2005, 15, 228–236.
150. J. M. DeLille, P. C. Sehnke, and R. J. Ferl, *Plant Physiol.*, 2001, 126, 35–38.
151. A. Motchoulski, E. Liscum, *Science*, 1999, 286, 961–964.
152. S. Inada, M. Ohgishi, T. Mayama, K. Okada, and T. Sakai, *Plant Cell*, 2004, 16, 887–896.
153. P. Lariguet, I. Schepens, D. Hodgson, U. V. Pedmale, M. Trevisan, C. Kami, M. de Carbonnel, J. M. Alonso, J. R. Ecker, E. Liscum, and C. Fankhauser, *Proc. Natl. Acad. Sci. USA*, 2006, 103, 10134–10139.
154. X. Chen, W. H. Lin, Y. Wang, S. Luan, and H. W. Xue, *Plant Cell*, 2008, 20, 353–366.
155. C. A. Esmon, A. G. Tinsley, K. Ljung, G. Sandberg, L. B. Hearne, and E. Liscum, *Proc. Natl. Acad. Sci. USA*, 2006, 103, 236–241.
156. A. Losi, and W. Gärtner, *Proc. Natl. Acad. Sci. USA*, 2008, 105, 7–8.
157. F. Takahashi, D. Yamagata, M. Ishikawa, Y. Fukamatsu, Y. Ogura, M. Kasahara, T. Kiyosue, M. Kikuyama, M. Wada, and H. Kataoka, *Proc. Natl. Acad. Sci. USA*, 2007, 104, 19625–19630.
158. M. Ishikawa, F. Takahashi, H. Nozaki, C. Nagasato, T. Motomura, and H. Kataoka, *Planta*, 2009, 230, 543–552.
159. M. A. Andrade, M. Gonzalez-Guzman, R. Serrano, and P. L. Rodriguez, *Plant Mol. Biol.*, 2001, 46, 603–614.
160. T. Mizoguchi, G. Coupland, *Trends Plant Sci.*, 2000, 5, 409–411.
161. D. E. Somers, S. Fujiwara, *Trends Plant Sci.*, 2009, 14, 206–213.
162. S. Fujiwara, *Plant Biotechnol.*, 2009, 25, 123–129.
163. M. Sawa, D. A. Nusinow, S. A. Kay, and T. Imaizumi, *Science*, 2007, 318, 261–265.
164. W. Y. Kim, S. Fujiwara, S. S. Suh, J. Kim, Y. Kim, L. Han, K. David, J. Putterill, H. G. Nam, and D. E. Somers, *Nature*, 2007, 449, 356–360.
165. V. Buttani, A. Losi, E. Polverini, and W. Gärtner, *FEBS Lett.*, 2006, 580, 3818–3822.
166. T. A. Gaidenko, T. J. Kim, A. L. Weigel, M. S. Brody, and C. W. Price, *J. Bacteriol.*, 2006, 188, 6387–6395.
167. M. Avila-Perez, K. J. Hellingwerf, and R. Kort, *J. Bacteriol.*, 2006, 188, 6411–6414.
168. N. Suzuki, N. Takaya, T. Hoshino, and A. Nakamura, *J. Gen. Appl. Microbiol.*, 2007, 53, 81–88.
169. M. A. van der Horst, J. Key, and K. J. Hellingwerf, *Trends Microbiol.*, 2007, 15, 554–562.
170. C. Bauer, S. Elsen, L. R. Swem, D. L. Swem, and S. Masuda, *Philos. T. R. Soc. B*, 2003, 358, 147–153.
171. S. Metz, A. Jager, and G. Klug, *J. Bacteriol.*, 2009, 191, 4473–4477.
172. Y. Han, M. H. F. Meyer, M. Keusgen, and G. Klug, *Mol. Microbiol.*, 2007, 64, 1090–1104.
173. L. Gomelsky, O. V. Moskvin, R. A. Stenzel, D. F. Jones, T. J. Donohue, and M. Gomelsky, *J. Bacteriol.*, 2008, 190, 8106–8114.
174. C. Lin, T. Todo, *Genome Biol.*, 2005, 6, 220.
175. H. Wang, L. G. Ma, J. M. Li, H. Y. Zhao, and X. W. Deng, *Science*, 2001, 294, 154–158.
176. C. Yi, X. W. Deng, *Trends Cell Biol.*, 2005, 618–625.
177. J. Yang, R. Lin, J. Sullivan, U. Hoecker, B. Liu, L. Xu, X. W. Deng, and H. Wang, *Plant Cell*, 2005, 17, 804–821.

178. J. A. Sullivan, X. W. Deng, *Dev. Biol.*, 2003, 260, 289–297.
179. Y. Jiao, O. S. Lau, and X. W. Deng, *Nat. Rev. Gen.*, 2007, 8, 217–230.
180. C. Y. Kang, H. L. Lian, F. F. Wang, J. R. Huang, and H. Q. Yang, *Plant Cell*, 2009, 21, 2624–2641.
181. A. R. Cashmore, *Cell*, 2003, 114, 537–543.
182. B. Kang, N. Grancher, V. Koyffmann, D. Lardemer, S. Burney, and M. Ahmad, *Planta*, 2008, 227, 1091–1099.
183. H. Daiyasu, T. Ishikawa, K. I. Kuma, S. Iwai, T. Todo, and H. Toh, *Gene. Cell.*, 2004, 9, 479–495.
184. E. N. Worthington, I. H. Kavakli, G. Berrocal-Tito, B. E. Bondo, and A. Sancar, *J. Biol. Chem.*, 2003, 278, 39143–39154.
185. Y. Huang, R. Baxter, B. S. Smith, C. L. Partch, C. L. Colbert, and J. Deisenhofer, *Proc. Natl. Acad. Sci. USA*, 2006, 103, 17701–17706.
186. R. Pokorny, T. Klar, U. Hennecke, T. Carell, A. Batschauer, and L. O. Essen, *Proc. Natl. Acad. Sci. USA*, 2008, 105, 21023–21027.
187. T. Kleine, P. Lockhart, and A. Batschauer, *Plant J.*, 2003, 35, 93–103.
188. S. Coesel, M. Mangogna, T. Ishikawa, M. Heijde, A. Rogato, G. Finazzi, T. Todo, C. Bowler, and A. Falciatore, *EMBO Rep.*, 2009, 10, 655–661.
189. P. Ballario, G. Macino, *Trends Microbiol.*, 1997, 5, 458–462.
190. R. Ambra, B. Grimaldi, S. Zamboni, P. Filetici, G. Macino, and P. Ballario, *Fungal Genet. Biol.*, 2004, 41, 688–697.
191. C. H. Chen, J. J. Loros, *Commun. Integr. Biol.*, 2009, 2, 448–451.
192. M. Elvin, J. J. Loros, J. C. Dunlap, and C. Heintzen, *Gene. Dev.*, 2005, 19, 2593–2605.
193. J. S. Lamb, B. D. Zoltowski, S. A. Palin, L. Li, B. R. Crane, and L. Pollack, *Biophys. J.*, 2009, 96, 524a.
194. M. Schmoll, L. Franchi, and C. P. Kubicek, *Eukaryot. Cell*, 2005, 4, 1998–2007.
195. J. J. Holland, D. Roberts, and E. Liscum, *J. Exp. Bot.*, 2009, 60, 1969–1978.
196. T. Sakai, T. Kagawa, M. Kasahara, T. E. Swartz, J. M. Christie, W. R. Briggs, M. Wada, and K. Okada, *Proc. Natl. Acad. Sci. USA*, 2001, 98, 6969–6974.
197. K. Huang, C. F. Beck, *Proc. Natl. Acad. Sci. USA*, 2003, 100, 6269–6274.
198. C. S. Im, S. Eberhard, K. Y. Huang, C. F. Beck, and A. R. Grossman, *Plant J.*, 2006, 48, 1–16.
199. U. Krauss, B. Q. Minh, A. Losi, W. Gärtner, T. Eggert, A. von Haeseler, and K.-E. Jaeger, *J. Bacteriol.*, 2009, 191, 7234–7242.
200. G. Pathak, A. Ehrenreich, A. Losi, W. R. Streit, and W. Gärtner, *Environ. Microbiol.*, 2009, 11, 2388–2399.
201. J. M. Scott, J. Ju, T. Mitchell, and W. G. Haldenwang, *J. Bacteriol.*, 2000, 182, 2771–2777.
202. P. J. Piggot, D. W. Hilbert, *Curr. Opin. Microbiol.*, 2004, 7, 579–586.
203. S. Zhang, W. G. Haldenwang, *J. Bacteriol.*, 2005, 187, 7554–7560.
204. A. Idnurm, S. Crosson, *PLoS Pathog.*, 2009, 5, e1000470.
205. M. Iseki, S. Matsunaga, A. Murakami, K. Ohno, K. Shiga, K. Yoshida, M. Sugai, T. Takahashi, T. Hori, and M. Watanabe, *Nature*, 2002, 415, 1047–1051.
206. M. Ntefidou, M. Iseki, M. Watanabe, M. Lebert, and D. P. Hader, *Plant Physiol.*, 2003, 133, 1517–1521.
207. Y. Koumura, T. Suzuki, S. Yoshikawa, M. Watanabe, and M. Iseki, *Photochem. Photobiol. Sci.*, 2004, 3, 580–586.
208. S. Braatsch, M. Gomelsky, S. Kuphal, and G. Klug, *Mol. Microbiol.*, 2002, 45, 827–836.
209. O. V. Moskvin, S. Kaplan, M. A. Gilles-Gonzalez, and M. Gomelsky, *J. Biol. Chem.*, 2007, 282, 28740–28748.
210. Y. Han, S. Braatsch, L. Osterloh, and G. Klug, *Proc. Natl. Acad. Sci. USA*, 2004, 101, 12306–12311.
211. S. Masuda, T. A. Ono, *FEBS Lett.*, 2004, 577, 255–258.
212. K. Okajima, S. Yoshihara, Y. Fukushima, X. Geng, M. Katayama, S. Higashi, M. Watanabe, S. Sato, S. Tabata, Y. Shibata, S. Itoh, and M. Ikeuchi, *J. Biochem.*, 2005, 137, 741–750.
213. B. Fiedler, T. Borner, and A. Wilde, *Photochem. Photobiol.*, 2005, 81, 1481–1488.
214. M. C. DeRosa, R. J. Crutchley, *Coord. Chem. Rev.*, 2002, 233, 351–371.

215. C. S. Enwemeka, D. Williams, S. K. Enwemeka, S. Hollosi, and D. Yens, *Photomed. Laser Surg.*, 2009, 27, 221–226.
216. Krauss, U., Bacterial Blue-Light Photoreceptors of the LOV Family, PhD dissertation, University of Düsseldorf, Düsseldorf, Germany, 2008.
217. B. Stephan, K. Gabriele, *Photosynth. Res.*, 2004, 79, 45–57.
218. T. Ritz, S. Adem, and K. Schulten, *Biophys. J.*, 2000, 78, 707–718.
219. I. A. Solov'yov, K. Schulten, *Biophys. J.*, 2009, 96, 4804–4813.
220. R. Wiltschko, K. Stapput, P. Thalau, and W. Wiltschko, *J. R. Soc. Interface*, 2009. doi:10.1098/rsif.2009.0367.focus
221. H. Mouritsen, T. Ritz, *Curr. Opin. Neurobiol.*, 2005, 15, 406–414.
222. M. Ahmad, P. Galland, T. Ritz, R. Wiltschko, and W. Wiltschko, *Planta*, 2007, 225, 615–624.
223. S. R. Harris, K. B. Henbest, K. Maeda, J. R. Pannell, C. R. Timmel, P. J. Hore, and H. Okamoto, *J. R. Soc. Interface*, 2009, 6, 1193–1205.
224. A. A. Pakhomov, V. I. Martynov, *Chem. Biol.*, 2008, 15, 755–764.
225. T. Drepper, T. Eggert, F. Circolone, A. Heck, U. Krauss, J.-K. Guterl, M. Wendorff, A. Losi, W. Gärtner, and K.-E. Jaeger, *Nat. Biotechnol.*, 2007, 25, 443–445.
226. S. Chapman, C. Faulkner, E. Kaiserli, C. Garcia-Mata, E. I. Savenkov, A. G. Roberts, K. J. Oparka, and J. M. Christie, *Proc. Natl. Acad. Sci. USA*, 2008, 105, 20038–20043.
227. G. Nagel, M. Brauner, J. F. Liewald, N. Adeishvili, E. Bamberg, and A. Gottschalk, *Curr. Biol.*, 2005, 15, 2279–2284.
228. C. D. Nichols, B. L. Roth, *Front. Mol. Neurosci.*, 2009, 2, Article 16.
229. A. B. Arrenberg, F. Del Bene, and H. Baier, *Proc. Natl. Acad. Sci. USA*, 2009, 106, 17968–17973.
230. T. Nagahama, T. Suzuki, S. Yoshikawa, and M. Iseki, *Neurosci. Res.*, 2007, 59, 81–88.
231. S. Schröder-Lang, M. Schwärzel, R. Seifert, T. Strünker, S. Kateriya, J. Looser, M. Watanabe, U. B. Kaupp, P. Hegemann, and G. Nagel, *Nat. Methods*, 2007, 4, 39–42.
232. A. Beuve, *Methods*, 1999, 19, 545–550.
233. A. Rauch, M. Leipelt, M. Russwurm, and C. Steegborn, *Proc. Natl. Acad. Sci. USA*, 2008, 105, 15720–15725.
234. D. Matsuoka, S. Tokutomi, *Proc. Natl. Acad. Sci. USA*, 2005, 102, 13337–13342.
235. D. Strickland, K. Moffat, and T. R. Sosnick, *Proc. Natl. Acad. Sci. USA*, 2008, 105, 10709–10714.
236. Y. I. Wu, D. Frey, O. I. Lungu, A. Jaehrig, I. Schlichting, B. Kuhlman, and K. M. Hahn, *Nature*, 2009, 461, 104–108.
237. A. H. Singh, T. Doerks, I. Letunic, J. Raes, and P. Bork, *J. Bacteriol.*, 2009, 191, 32–41.
238. G. Pathak, A. Losi, and W. Gärtner, *Photochem. Photobiol.*, 2011, in press.
239. S. Crosson, K. Moffat, *Plant Cell*, 2002, 14, 1067–1075.
240. A. Yamamoto, T. Iwata, S. Tokutomi, and H. Kandori, *Biochemistry*, 2008, 47, 922–928.
241. A. Losi, E. Ternelli, and W. Gärtner, *Photochem. Photobiol.*, 2004, 80, 150–153.
242. S. M. Harper, L. C. Neil, I. J. Day, P. J. Hore, and K. H. Gardner, *J. Am. Chem. Soc.*, 2004, 126, 3390–3391.
243. A. Yamamoto, T. Iwata, Y. Sato, D. Matsuoka, S. Tokutomi, and H. Kandori, *Biophys. J.*, 2009, 96, 2771–2778.
244. J. Looser, S. Schröder-Lang, P. Hegemann, and G. Nagel, *Biol. Chem.*, 2009, 390, 1105–1111.

54

Bioluminescence

Vadim R. Viviani
Federal University of São Carlos

54.1 Introduction

Bioluminescence, the emission of visible light by living organisms, has called the attention of humanity since ancient times. In a broad sense, bioluminescence includes all kinds of light emissions by living organisms, including biofluorescence, delayed luminescence, and ultraweak chemiluminescence. However, strictly speaking, bioluminescence is defined as an efficient enzyme-catalyzed chemiluminescence for biological purposes.

It occurs in a wide variety of organisms including bacteria, fungi, algae, coelenterates, mollusks, annelids, arthropods, and fishes (Harvey 1952), being used mainly for communication purposes. It results from the efficient conversion of potential energy of chemical bonds into photons of visible light, during exothermic oxidation of organic substrates generally called luciferins by oxygen or one of its derivatives, in reactions catalyzed by enzymes called luciferases (Scheme 54.1; Wilson and Hastings 1998). A special class of luciferases, in which the emitter is stably bound to the protein, are termed photoproteins because they apparently can emit light just once (Shimomura 2006). However, under specific conditions, photoproteins can also release the products, turning over like enzymes. Despite the fact that the chemical mechanism of bioluminescence is reasonably similar in most cases (Hastings 1983, 1995), the biochemical components of the bioluminescent systems in different organisms involve distinct and evolutionarily unrelated luciferases, luciferins, and cofactors (Table 54.1). Currently, the luciferases from bacteria, dinoflagellates, coelenterates, crustaceans, and beetles have been cloned, their primary sequences determined (Viviani 2007), and more recently their 3D structure was solved bringing new insights on the relationship between structure and function in this interesting class of enzymes.

$$\text{Luciferin} + O_2 \rightarrow \text{Peroxy-intermediate} \rightarrow CO_2 + \text{Oxyluciferin} + h\nu$$

SCHEME 54.1 Classical luciferin–luciferase bioluminescence reaction.

Many of these luciferases and the respective luciferins are currently used for bioanalytical purposes and their genes are used as efficient reporter tools in a wide range of biotechnological applications (Roda et al. 2009). In this chapter, my aim is to give a general overview of the field of bioluminescence, and it is not intended to make an in detail review of its several aspects; for such purpose several specialized reviews are recommended.

54.2 Biological Chemiluminescence: Light as a By-Product of Biochemical Reactions

Bioluminescence is the reverse process of photobiology. During photosynthesis, photons of visible light are absorbed by chlorophyll molecules, and their energy is ultimately stored as potential energy in the chemical bonds of reduced organic molecules. Eventually, this energy may leak again as photons of visible light during the breakdown of these bonds in reactions such as radical ion pair annihilation and peroxides cleavage, resulting in a variety of chemiluminescent processes. Although true bioluminescence is a rather rare phenomenon, all living cells, especially aerobic ones, produce an ultraweak chemiluminescence, which results from the generation of excited species during oxidative processes such as lipid peroxidation, generation of singlet oxygen, and organic molecules oxidations (Lee 1989). Generally, such excited species deactivate preferentially by other nonradiative mechanisms such as thermal inactivation and photobiochemistry (Figure 54.1). Thus, such processes produce a luminescence of the order of a few to thousand photons/s, which is not visible to most animal eyes, and therefore is not functional at least for communicative purposes. Although ultraweak chemiluminescence is considered a by-product of oxidative metabolic reactions, nevertheless it could be considered an interesting indicator of physiological state of living organisms. Attempts to use chemiluminescence to probe physiological condition is not new (Campbell 1988), but has been hampered by the lack of sufficient knowledge of the specific mechanisms underlying these reactions and by the lack of sensitive and convenient equipments for their measurement. More recently, however, with the development of very sensitive light detecting equipments for *in vivo* imaging, the use of chemiluminescence may become a reality.

54.3 Mechanisms of Bioluminescence

What differentiates bioluminescence from biological chemiluminescence is the efficiency and the intensity of such processes: in ultraweak chemiluminescence, the light efficiency is under 0.1 and the intensity is well below the detecting capacity of eye photoreceptors, whereas in bioluminescence the efficiency approaches the unity and intensity is of the order of 10^7 photons/s, being visible in dark environments. The basic requirements for an efficient bioluminescent reaction are as follows: (1) an exergonic reaction providing enough energy to yield a photon of visible light (38–71 kcal/mol for photons in the red–violet range of the spectrum); (2) a particular mechanism to channel the available chemical energy into visible photons, in the so-called chemiexcitation step; (3) an efficient radiative deactivation of the excited product. These requirements define the quantum yield of bioluminescence ($\theta_{BL} = \theta_C\theta_{EX}\theta_{FL}$), which is quite high for all bioluminescent reactions, ranging from 3% to 61%. The two first requirements are provided by the oxidation of organic compounds called luciferins and the intermediacy of peroxides, usually dioxetanones, whose cleavage yields electronic excited states with high efficiency (Wilson and Hastings 1998; Figure 54.2). The efficient emissive deactivation depends on the structure of the emitter, known as oxyluciferin, which is usually a fluorescent compound that provides preferential production of singlet excited species, which decay emitting fluorescence. Usually, the oxidation and cleavage of

TABLE 54.1 Biochemical Properties of the Main Bioluminescent Systems Investigated

Organism	Type	Function	MW (kDa)	Length (Residues)	Luciferin	Co-Substrate (Co-Factor)	λ_{max} (nm)	ϕ_{BL}
Bacteria	Luciferin–luciferase	Monooxygenase	36–38	354–363	Reduced flavin mononucleotide ($FMNH_2$) aldehyde	Long chain	490	0.2
			38–40	324–368				
Fungi	Luciferin–luciferase	Monooxygenase					520	
Algae								
Dinoflagellates	Luciferin–luciferase	Monooxygenase	140	1240	Tetrapyrrole		475	
Coelenterates								
Ctenophores	Photoprotein	Ca^{2+}-dependent monooxygenase			Coelenterazine	Ca^{2+}	460	
Hydrozoa	Photoprotein	Ca^{2+}-dependent monooxygenase	21–28	89	Coelenterazine	Ca^{2+}	465–495	0.2
Anthozoa	Luciferin–luciferase	Monooxygenase	21		Coelenterazine		460–610	0.05
Mollusks								
Bivalves	Photoprotein	Peroxidase	150		Pholasin	Cu^{2+}	490	0.09
Latia	Luciferin–luciferase	Monooxygenase	170(31)				536	
Squid	Luciferin–luciferase	Monooxygenase			Coelenterazine disulfate	ATP	470	
Annelids								
Diplocardia	Luciferin–luciferase	Peroxidase	300		*N*-Isovaleryl-3-amino-1-propanol	Cu^{2+}	500	
Polychaeta	Photoprotein		120			Fe^{2+}	460	
Echinoderms								
Arthropods								
Crustacea	Luciferin–luciferase	Monooxygenase	62	555	Imidazolpyrazine		460	
Diplopoda	Photoprotein		60		7,8 dihydropterin-6-carboxylic acid	ATP		
Insecta								
Diptera								
Arachnocampa	Luciferin–luciferase	Monooxygenase	57		Unknown	ATP	484	—
Orfelia	Luciferin–luciferase		140		Unknown	LBP, di thio threitol (DTT)	460	
Coleoptera	Luciferin–luciferase	AMP/CoA ligase/monooxygenase	60	542–550	Benzothiazole	ATP, CoA	530–623	0.15–0.61

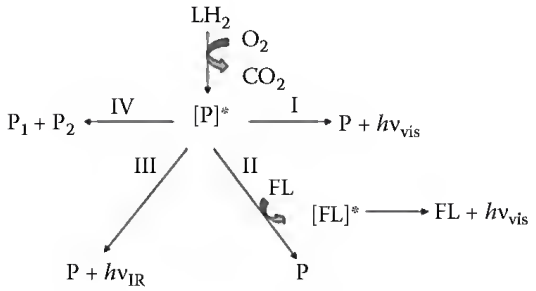

FIGURE 54.1 Basic mechanisms of electronic excited states deactivation in biological systems: (I) luminescence, (II) resonance energy transfer, (III) thermal inactivation, and (IV) photobiochemistry. (LH_2) luciferin, (P) product, (FL) fluorescent acceptor.

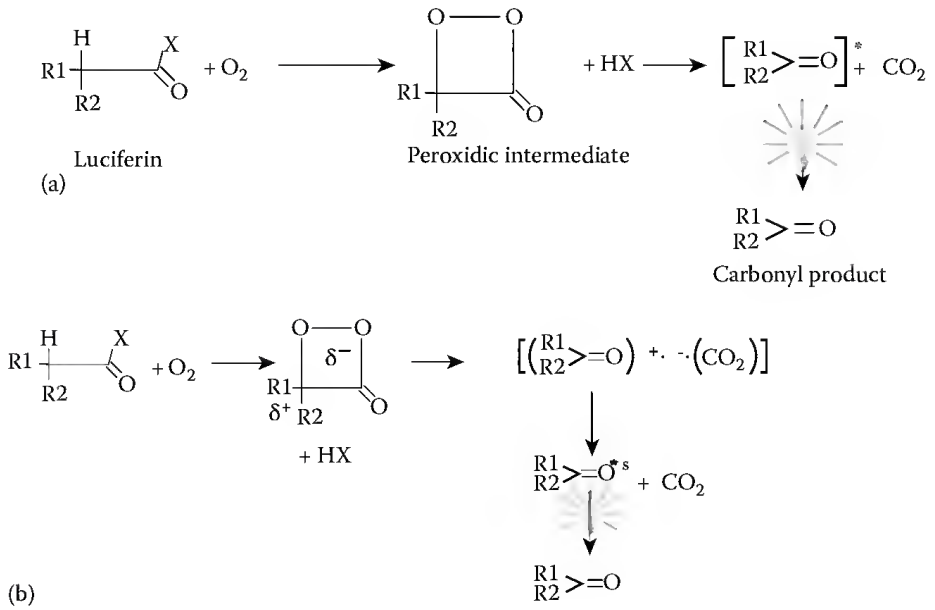

FIGURE 54.2 (a) General chemical mechanism of bioluminescent reactions: X is a good leaving group such as AMP and (b) CIEEL mechanism.

dioxetanones of aliphatic compounds produce high yield of triplet-excited species (Cilento and Adam 1988). Despite being potentially emissive in the absence of quenchers, the long lifetime of triplet-excited species provides a nonradiative route of deactivation through photochemical dark side reactions that compete with light emission. This is particularly important for triplet ketones, which are quenched by molecular oxygen. Nevertheless, triplet species are very important in biological systems for activating photobiochemical reactions in the absence of light. On the other hand, efficient production of excited singlet species can be achieved through the oxidation of cyclic peroxides with electron donating substituents. The mechanism of chemically initiated electron exchange luminescence (CIEEL; Figure 54.2b) was proposed to explain the efficient production of singlet species (Koo and Schuster 1978). According to this mechanism, the cleavage of the dioxetanone ring is activated by electron transfer from the electron donating substituent, followed by the cleavage and formation of radical ion pair. The back electron transfer from the radical anion intermediate results in the formation of the excited product, predominantly in the singlet state. Despite still considered an attractive mechanism, the involvement of CIEEL in bioluminescence has been subject of discussion (Tu and Mager 1995; Wilson and Hastings 1998). Luciferases may bring together all these three requirements: they are oxygenases providing favorable environments for the peroxides decomposition and excited state formation. Although the quantum

yields of bioluminescence are generally very high (0.05–0.61; Table 54.1), what turns a luciferase and its bioluminescence reaction so bright is the reaction rate. Light must be produced at a reasonable intensity to be detected by other organism. Therefore, luciferases function is to increase the rate of photon production to detectable levels through their catalytic activities.

54.3.1 Bioluminescence Colors

One of the most biologically relevant physical properties of bioluminescence is its spectrum or color. The bioluminescence color depends on the structure of the emitting molecule, oxyluciferin, its microenvironment affecting the energy gap between ground and excited states, and the presence of external factors such as the presence of filters and fluorescent acceptors that may modify the chromaticity of the primary emission.

Bioluminescence is thus classified in two groups according to the mechanism of emission (Figure 54.1): (1) the direct type, where the primary excited product formed during the luciferin–luciferase reaction is the actual emitter and (2) the type II or sensitized, where the excited product formed in the primary bioluminescence reaction transfers its energy via resonance to a fluorescent energy acceptor, which emits in another wavelength (Campbell 1988; Figure 54.1). The latter is well exemplified by green fluorescent protein (GFP) bioluminescence resonance energy transfer (BRET), which naturally occurs in jellyfish systems (Campbell 1988). In order for BRET to occur, the primary emitter and fluorescent acceptor in BRET must be in very close spatial proximity (<15 Å) and must display considerable emission and absorption spectral overlap.

The variety of luciferins and therefore oxyluciferin structures is followed by a wide range of colors spanning the entire visible spectrum. Coelenterazines usually emit in the violet–blue region, flavins emit in the green region and benzothiazolic luciferin usually emit in the yellow–green regions. But these spectra may also be considerably affected by the microenvironment in which the emitter is produced, through specific and nonspecific interactions with the excited molecule. Depending on the pH, the ionic forms of coelenteramide and firefly oxyluciferin can change their spectra. The most dramatic example of how the microenvironment can affect the bioluminescence color is provided by the active site of beetle luciferases that, although using the same biochemical reaction, can produce different colors ranging from green to red as well exemplified by railroad worms (Figure 54.3; Viviani 2002). The presence of filters narrowing down the spectral band is also found in several fishes (Haddock et al. 2010) and even insects (Viviani and Bechara 1997). Finally, fluorescent acceptors changing the color of light emission of a primary bioluminescent reaction is very well exemplified by fluorescent proteins, such as GFP in coelenterates and blue fluorescent protein (BFP) and yellow fluorescent protein (YFP) in some bioluminescent bacteria (Wilson and Hastings 1998).

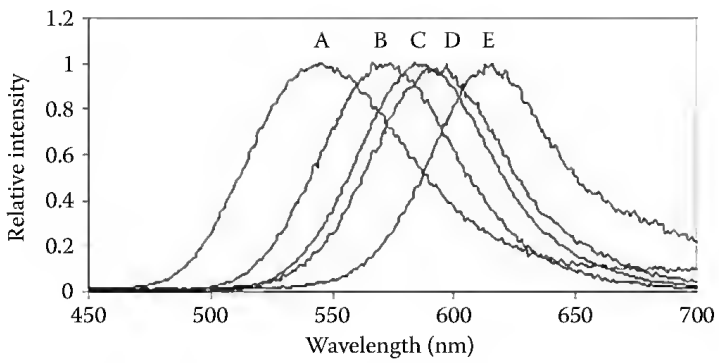

FIGURE 54.3 Bioluminescence spectra elicited by different beetle luciferases: A, *Pyrearinus termitilluminans* larval click beetle, B, *Phrixothrix viviani* railroad worm, C, *Macrolampis* sp firefly, D, engineered orange-emitting luciferase, and E, *Phrixothrix hirtus* red-emitting luciferase.

54.4 Diversity, Biological Functions, and Ecology of Bioluminescence

54.4.1 Biodiversity

Bioluminescence is found among bacteria, fungi, and several animal phyla, being absent in plants and higher vertebrates.

54.4.1.1 Marine Organisms

Bioluminescence is predominantly found in the marine environment, being found in bacteria, algae, Porifera, Cnidaria, Ctenophora, Nematoda, Annelida, Mollusca, Arthropoda, Echinodermata, Urochordata, fishes, and even sharks (Haddock et al. 2010; Figure 54.4). In the depths of the ocean, about 70% of the species and 95% of individuals were found to be luminescent (Herring 1987). Luminous bacteria are found in the genera *Vibrio*, *Photobacterium*, *Photorabdus* (*Xenorhabdus*), and *Shewanella* (Watanabe 2005). They are found in the environment either as endosymbionts in the light organs of some organisms like fishes and mollusks or as free living organisms. Dinoflagellate bioluminescence occurs in species of *Lingulodinium* (formerly *Gonyaulax*), *Noctiluca*, and *Pyrocystis*. In coelenterates, bioluminescence is found among Ctenophora, Hydrozoa (jellyfishes), and Anthozoa.

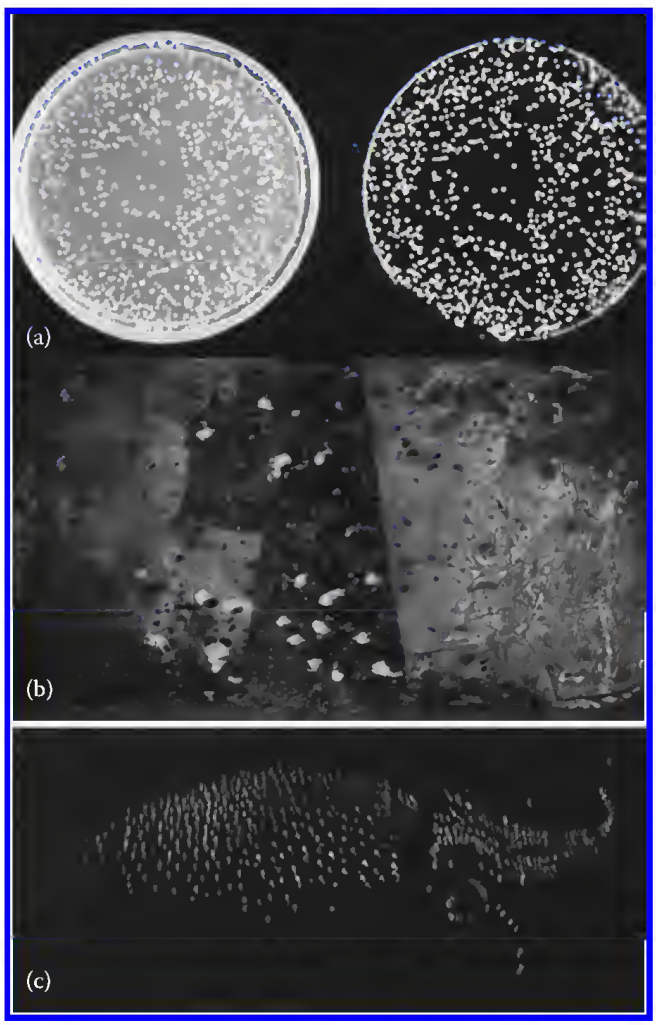

FIGURE 54.4 **(See color insert.)** Some marine bioluminescent organisms: (a) *Vibrio fischerii* bioluminescent bacteria, (b) sea firefly *Vargula hilgendorfii* (ostracod), and (c) firefly squid *Watasenia scintillans*.

Mollusks show various examples of luminescent species, such as the bivalve *Pholas dactylus*, the firefly squid *Watasenia scintillans*. Annelids have luminescent representatives in Polychaeta such as the tubeworm *Chaetopterus variopedatus*. Among marine arthropods, ostracods and decapods are found. Echinoderms (brittle stars) are also common. Finally, fishes include many representatives, either in shallow waters or in the depths.

54.4.1.2 Terrestrial Organisms

In the terrestrial environment, bioluminescence is apparently less common than in the marine environment, occurring in bacteria, fungi, nematodes, annelids and arthropods (Figure 54.5). Among bacteria, *Xenorhabdus luminescens* has been found infecting nematodes and insects, and eventually human wounds (Hosseini and Nealson 1995). In fungi, luminescence is found in the order Basidiomycetes, with 42 luminescent species in the genera *Armillaria*, *Mycena*, *Plerotus*, *Omphalotus*, and *Panellus* among others (Desjardin et al. 2008). Bioluminescent fungi or "foxfire" (Figure 54.2) are found over decayed logs and leaves in humid tropical and temperate forests around the globe. The bioluminescence is usually green and is emitted by the mycelium, pileum, and gills.

The arthropods constitute the richest group, with bioluminescent species being found in the classes of diplopods (millipides) and insects. In insects, luminescent species are found in Collembola, Diptera, and mainly Coleoptera (Viviani 2002) with around 2000 described species around the world in the superfamily Elateroidea, which includes fireflies (Lampyridae), click beetles (Elateridae), and railroad worms (Phengodidae) (Figure 54.5). Luminescent insects are found predominantly in tropical forests and temperate zones. Some species such as fungus gnats (Diptera: Mycetophilidae) are found in caves and along river banks in temperate regions (Viviani et al. 2002). Freshwater species are extremely rare; the only known organism is the freshwater snail.

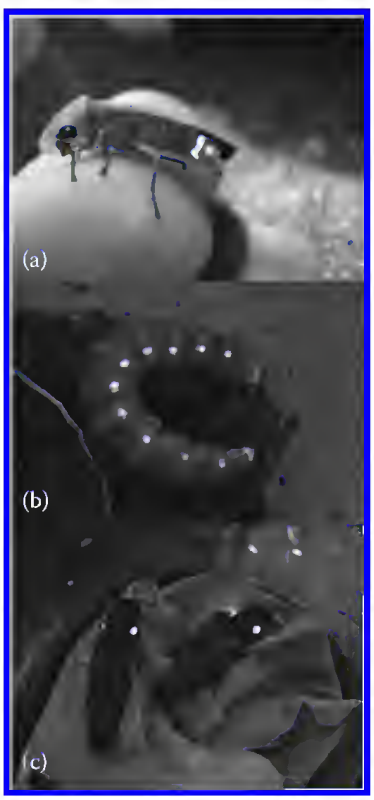

FIGURE 54.5 **(See color insert.)** Some bioluminescent beetles (a) *Cratomorphus concolor* firefly, (b) *Pyrophorus divergens* click beetle, and (c) *Phrixothrix* railroad worm.

54.4.2 Anatomy and Physiology

Bioluminescence can be produced by single-celled organisms such as bacteria and algae, secreted as in copepods and squids, or generated by complex light organs called photophores such as in several mollusks, fireflies, and fishes (Hastings 1983). Although the biochemical components are produced inside cells, bioluminescence can be intracellular or extracellular.

In single-celled organisms, bioluminescence can be produced in the cytoplasm or in specific organelles. Dinoflagellates have specific organelles called scintillons, which contain luciferin and luciferase, which react upon pH trigger. Fireflies have luciferase and luciferin inside peroxisomes (Gould et al. 1987).

Several organisms may secrete the bioluminescence components, which react outside of the body producing light. Bioluminescence in such cases can be produced as slimes and exudates, like in some annelids and diplopods (Shimomura 2006), or by ejection of luciferin and luciferase outside the body producing luminescent clouds like in some squids and ostracods (Haddock et al. 2010).

Light organs may assume variable degrees of complexity, from single cells to highly specialized photophores. In several cases, bioluminescence is neurally controlled, through the access of oxygen and the activation of photocytes. The simplest neural control is found in coelenterates. Some organisms like mollusks, fireflies, and fishes have more specialized light organs constituted by the photogenic tissue, reflector layers, lens, and developed neural control. Fireflies and other beetles exemplify such complexity at its utmost (Figure 54.6), with lanterns constituted by rosettes with thousands of photocytes, tracheolar end cells that control the access of oxygen upon neural control and an upper reflector layer (Ghiradella 1998).

54.4.3 Biological Functions

Bioluminescence is used mainly for communicative purposes, being divided in two main groups: interspecific and intraspecific functions. Among interspecific functions, bioluminescence may be used for defensive and for prey attraction purposes, whereas among intraspecific function, sexual attraction, group cohesion, and territoriality are the main functions.

54.4.3.1 Courtship

Among intraspecific functions, sexual attraction is especially common, being found in squids, polychaetes, ostracods, insects, brittle stars, and fishes like the lanternfish. Fireflies use an elaborate communication system where males and females emit species-specific signals during courtship. Formerly, two main communicative systems have been described (Lloyd 1978): In system I, females are stationary in the grass, broadcasting a specific signal that flying males recognize and answer. In system II, flying males broadcast a specific signal to which females in the grass answer. However, other communication systems are currently described (Branham and Wenzel, 2003; Lewis, 2010; De Cock 2010). Bioluminescence may also be used to advertise populational densities, to keep the integrity of groups, territoriality such as in fishes.

54.4.3.2 Defense

Among interspecific functions, defense against predators and attraction of preys are especially important. Usually sudden flashes may repel predator attacks by an effect of startling or frightening. Defense may assume different forms. In some fishes bioluminescence can be used for counter-illumination, turning the organism invisible against environmental background light (Haddock et al. 2010). Dinoflagellates may use their flashes as burglar alarm, advertising the presence of a predator to a higher rank predator. Some ostracods and squids secrete clouds of bioluminescent material, which may confuse a predator. Click beetles, as well as some bioluminescent beetle larvae, may display false eye-like spot lanterns upon touch, frightening potential predators. Luminescence can also be used as aposematic signals.

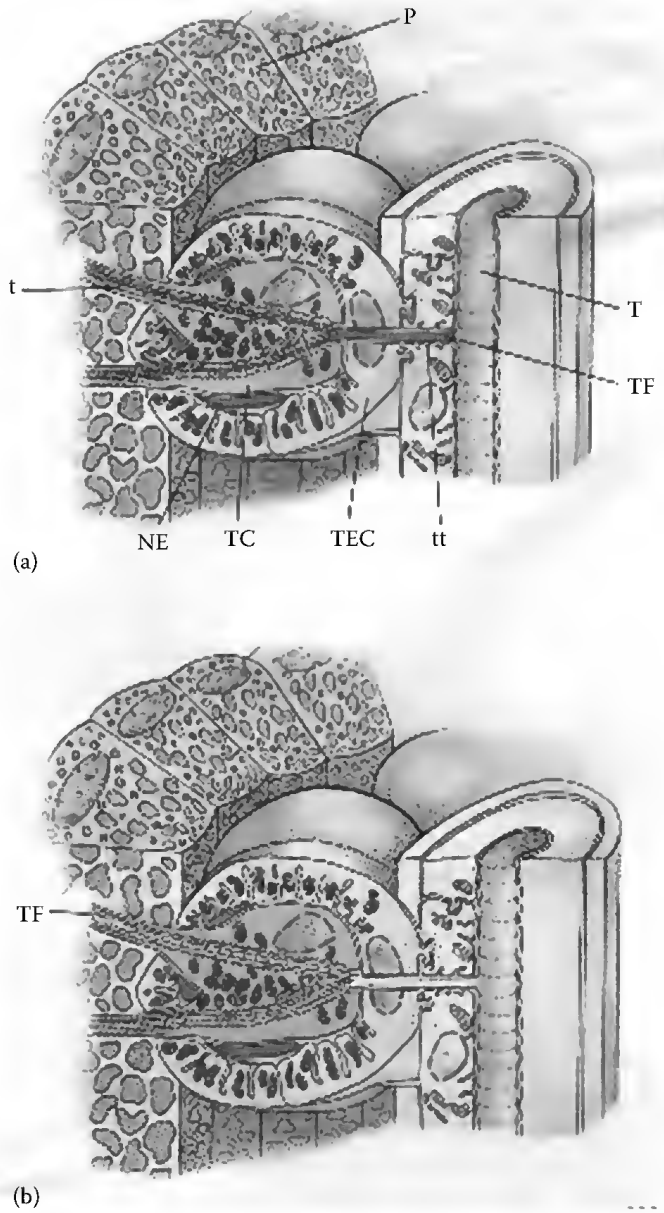

FIGURE 54.6 Firefly photophore: anatomical complexity at its utmost according to Ghiradella 1998. Oxygen access controlled by: (a) increased fluid length when lantern is off and (b) decreased fluid length when lantern is emitting. *Note:* P=photocytes; NE=nerve; T=trachea; t=tracheole; TF=tracheolar fluid; TEC=tracheal end cell. (From Ghiradella, H., The anatomy of light production: the fine structure of the firefly lantern, in *Microscopic Anatomy of Invertebrates*, eds. F. W. Harrison and M. Locke, Wiley-Liss, New York, 1998, pp. 363–381. With permission.)

Larval beetles such as glowworms and railroad worms may use their luminescence to advertise distastefulness to predators such as frogs and birds (Sivinsky 1981; DeCock 2004).

54.4.3.3 Prey Attraction

Continuous emissions may have the opposite effect of flashes, attracting the attention of other organisms. Several organisms such as siphonophores and the deep sea fishes such as the anglerfish use their lanterns as luminous traps to attract preys. Such behavior is also well known in the terrestrial mycetophilidae

larvae (fungus gnats) *Arachnocampa* spp. in New Zealand caves and *Orfelia fultoni* in the Appalachian stream banks in the United States, using their blue–green bioluminescence to attract flying insect preys in the caves and stream banks (Viviani et al. 2002). The larval click beetle *Pyrearinus termitilluminans* displays the wonderful phenomenon of luminous termite mounds in central Brazilian savannas, using its greenish-blue bioluminescence to attract flying insects (Bechara 1989).

54.4.3.4 Dispersion

The biological function of bioluminescence in bacteria and fungi is quite controversial because luminescence has no obvious intraspecific communication function. It has been suggested that their continuous luminescence plays an important role for the propagation and dispersal of species, by attracting positive phototropic organisms that feed on them, dispersing the species.

54.4.3.5 Illumination

Some organisms may also use their own light as a lantern to probe the environment during the search for preys. Such kind of behavior is found in the flashlight fish and dragonfishes and is apparently found in railroad worms, which use their head red bioluminescence to illuminate the environment during the search for preys (Sivinsky 1981; Viviani and Bechara 1997), in some fireflies and click beetle that use their abdominal lanterns during landing to illuminate the grass in front of them (Lall et al. 2009).

54.4.3.6 Physiological Functions

Another still poorly considered class of biological functions for bioluminescence is the physiological one. It is known that all bioluminescent systems require oxygen or one of its active species. It was originally suggested that bioluminescence systems evolved from such biochemical systems involved in removing or detoxifying oxygen (Seliger and McElroy 1965). Although unlikely in most cases, it is possible that at least in a few of them bioluminescence may aid in the removal and control the oxygen availability that may ultimately lead to reactive oxygen species (ROS) production, damaging the biological systems (Bechara 1989; Rees et al. 1998). This possibility has been proposed for bacteria, and also for bioluminescent click beetle larvae (Barros and Bechara 1998). Photobiochemistry mediated by bioluminescence is another possibility. In bacteria, bioluminescence was proposed to be used for the photoreactivation and repair of DNA damage caused by UV light, based on experiments in which UV damaged bacteria exposed to blue light, or bioluminescent bacteria, show higher rate of DNA repair (Czyz et al. 2003). Considering the photobiochemical reactions, it is even possible to wander whether bioluminescence could play a role in photoactivating certain metabolic pathways. Of course, it is hard to conceive such a hypothesis when considering organisms exposed to exceedingly higher environmental light doses, however, it could be a real possibility for organisms living in the darkness or for opaque tissues.

54.4.4 Photoecology

Thus, bioluminescence is adapted and optimized for specific biological functions under specific photic environments. In the marine environment, blue bioluminescence is predominant, because at depths below 10 m, most sunlight wavelengths have been absorbed and only blue light passes (Haddock et al. 2010). Therefore, the photoreceptors of most organisms are adapted to blue light. On the other hand, in the terrestrial environment, the incident sunlight has wide spectral range whereas the predominant reflectance color is green reflected from the foliage and blue from the skylight, therefore most visual systems are adapted to green and eventually blue (Lall et al. 2009). Indeed, most visual photoreceptors in terrestrial organisms display bands in the blue and green regions. Not surprisingly, the most predominant bioluminescence color among terrestrial organisms is green. Bioluminescent beetles usually emit light in the green–yellow range of the spectrum, though orange is also found, although much less common (Lall et al. 2009). Only the dipterans *Arachnocampa* spp. and *Orfelia fultoni* are known to produce blue bioluminescence (Viviani 2002). Even rarer is red

light, which is produced only in *Phrixothrix* genus and a few other railroad worm species (Viviani and Bechara 1997). In such cases, light is produced by head lanterns, which are likely to be used to illuminate the environment during the searching for preys. Although the function is not clear, red light in the case of railroad worms could be an adaptation to the reflectance of the soil where they live most of the time buried. In the case of blue light, bioluminescence could be an adaptation to blue skylight, attracting lost flying insects in the darkness.

The intensity and chromaticity of environmental light are important to modulate the activity of bioluminescence species. Fireflies and bioluminescent beetles become active at very specific times, usually at the twilight and during the night, which are triggered by the background environmental light (Lall et al. 2009). Full moon has been shown to affect the activity of bioluminescent organisms such as fireflies and scaleworms. Therefore, artificial night-lighting near urban areas may have disruptive effect on the occurrence of bioluminescent species. The impact of artificial illumination on bioluminescent species is just starting to be investigated in fireflies (Lloyd 2006), but it is almost unstudied for marine environment, where most of the bioluminescent diversity is found. Bioluminescent organisms, upon their dependence on light production for survival, could be good bioindicators of the impact of artificial night-lighting on nocturnal environment.

54.5 Biochemical and Molecular Diversity

Bioluminescent systems can be classified in several biochemical classes depending on the chemical nature of the luciferin. Luciferins have a wide variety of structures: bacterial luciferin is a flavin nucleotide, coelenterazine and cypridina luciferin are imidazolpyrazines, dinoflagellate and shrimp luciferin are a linear tetrapyrrols structurally similar to chlorophyll, some annelid luciferins are aldehydes, and firefly luciferin is a benzothiazole. Bioluminescence systems can also be classified in two basic subtypes depending on the protein responsible for light emission: classical luciferin–luciferase systems and photoprotein systems. Even within each of these two classes, the systems can be further split in different types according to the nature of the enzymatic reaction. In the case of most luciferin–luciferase systems, the luciferases are functionally classified as monooxygenases, which catalyze the insertion of an oxygen atom in the substrate and another in water or CO_2. In some cases, luciferases can be peroxidases (Viviani 2005), in which a transition metal within the protein, such as Fe^{2+} or Cu^{2+} or perhaps a heme group, catalyzes the abstraction of a labile proton from the substrate and use hydrogen peroxide as oxidizing agent, leading to the emissive step (Scheme 54.2). Peroxidase-like systems are found in bivalves and some annelids. Despite being isolated from a nonbioluminescent organism (horseradish), the widely used in immunoassays horseradish peroxide (HRP) exemplifies well the chemiluminescence mechanism of a peroxidase.

In the following sections, the main bioluminescent systems studied, those of bacteria, dinoflagellates, coelenterates, and beetles will be introduced and an overview of the other bioluminescent systems under investigation will be given.

54.5.1 Bacteria

The bioluminescent system of bacteria is one of the most well studied (Tu and Mager 1995; Watanabe 2005; Tu 2007). The luciferase is a flavin mononucleotide (FMN)-monooxygenase that co-oxidizes $FMNH_2$ and a long-chain aldehyde (>C8) using molecular oxygen (Scheme 54.3; Figure 54.7) producing blue–green bioluminescence (λ_{max} = 490–495 nm; Tu 2007). The reaction comprises the oxidation

$$H_2O_2 + X^- \rightarrow OX^- + H_2O$$

$$OX^- + H_2O_2 \rightarrow L\text{-}O + 2H_2O + h\nu$$

SCHEME 54.2 Peroxidase-catalyzed bioluminescence reaction.

$$FMNH_2 + O_2 \rightarrow PeroxyFMN$$

$$PeroxyFMN + RCHO \rightarrow R\text{-}COOH + FMN^* + H_2O + h\nu$$

SCHEME 54.3 Bacterial bioluminescence reaction.

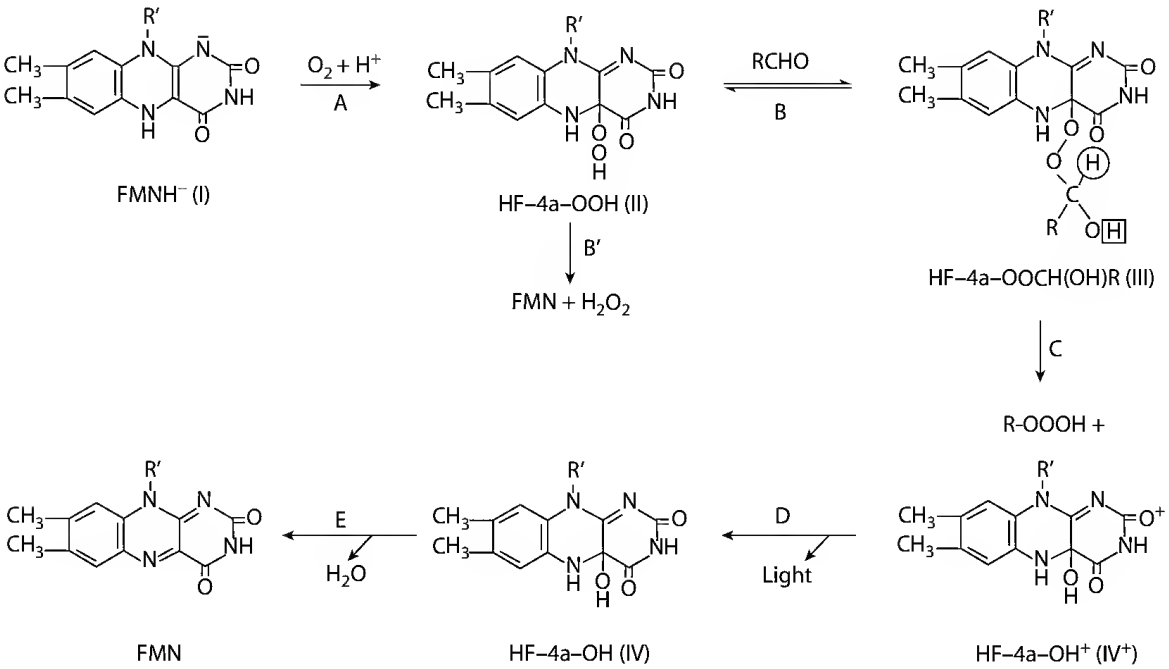

FIGURE 54.7 Bacterial bioluminescent reaction according to Tu (2007). (From Tu, S.C., Bacterial luciferase: structure-function relationships and protein engineering, in *Luciferases and Fluorescent Proteins: Principles and Advances in Biotechnology and Bioimaging*, eds. V. R. Viviani and Y. Ohmiya, Transworld Research Network, Kerala, 2007, pp. 1–18. With permission.)

of $FMNH_2$ forming a linear peroxide (intermediate II) which in the presence of a long-chain aldehyde forms a peroxyhemiacetal between the aldehyde and semi-reduced Flavin MonoNucleotide (FMNH) (intermediate III), which undergoes heterolytical cleavage forming excited 4a-hydroxy-FMNH intermediate, the light emitting species (Figure 54.7). Ground-state intermediate IV then suffers dehydration yielding FMN and thus completing the enzymatic cycle. FMN oxidoreductases participate on the reduction of FMN for luciferase reaction (Tu 2008). Accessory fluorescent proteins that modify the original emission into more blueshifted (BFP) or redshifted (YFP) colors and affect the rate of the reaction may participate in the reaction of some bacteria.

Bacterial luciferase is a heterodimer consisting of homologous α and β subunits with ca. 350 residues and ca. 40 kDa each, encoded by *Lux A* and *Lux B* genes of the operon Lux (Tu 2007), having a similar structure to triose phosphate isomerase consisting of a $(\beta/\alpha)_8$ barrel structure (Figure 54.8). Although the dimer is the active form, both subunits display orders of magnitude lower catalytic and bioluminescence activities than the dimer. The active site was proposed to be located in a pocket in the α subunit next to the *C*-terminal end of the β barrel. The loop between the residues 257–291 in the α subunit shields the catalytic intermediates and the emitter, providing a hydrophobic environment favorable for emissive decay (Tu 2007). The residues, αR107 interact with $FMNH_2$ phosphate group; αW250 with flavin isoalloxazine ring and aldehyde; and αH45 and αH44 are important for the formation of the catalytically active intermediate II and as a catalytic base participating in the proton abstraction from intermediate III.

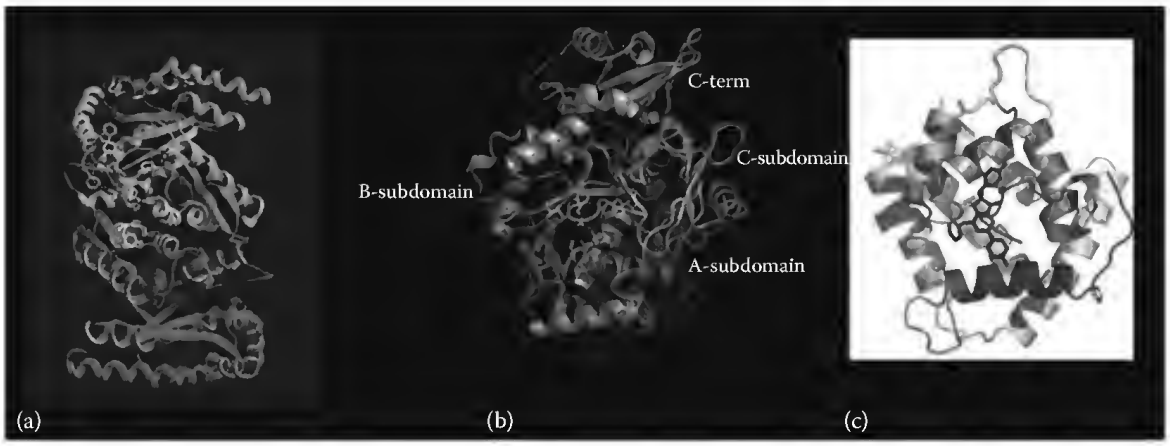

FIGURE 54.8 **(See color insert.)** 3D structures of luciferases and photoproteins: (a) bacterial luciferase according to Tu (2007), (b) firefly luciferase (*Photinus pyralis*), and (c) Obelin (coelenterate photoprotein) according to Vysotski and Lee (2004). (From Vysotski, E. and Lee, J., *Acc. Chem. Res.*, 37, 405, 2004. With permission.)

The operon Lux consists of the genes *ICDABEG* that code for proteins involved in the bioluminescent system and its regulation: gene *I* codes for the protein involved in production of autoinducer, homoserine lactone, the genes *C*, *D*, and *E* code for proteins involved in the luminescence-specific fatty acid reductase system. Once the autoinducer reaches a threshold level around 40 molecules/cell, gene expression is induced through the interaction with Lux R protein forming a complex, which facilitates association of RNA polymerase with the Lux operon activating transcription (Watanabe 2005). This autoinduction system, first discovered in luminous bacteria has been called "quorum sensing" to indicate a minimal population necessary to sense cell-to-cell communication.

54.5.2 Dinoflagellates

Their bioluminescent system contains a linear tetrapyrrolic luciferin, a 140 kDa luciferase and, in some species, a luciferin binding protein (LBP; Dunlap and Hastings 1981). The components of the bioluminescence occur inside organelles called scintillons. The reaction (Scheme 54.4) is triggered by pH changes: at acidic pH, the bioluminescent reaction is triggered whereas at alkaline ones the reaction is suppressed. The full-length luciferase displays maximum activity at pH 6.3 and no activity at pH 8. The LBP releases luciferin at acidic pH and sequesters it at pH 8. *Lingulodinium polyedra* luciferase has a 111 residue long *N*-terminal, followed by three conserved domains termed D1, D2, and D3, each one with proper catalytic activity (Liu et al. 2004). The individual domains are more conserved among different species than among themselves in the full-length luciferase, supporting their divergence by a gene duplication event prior to speciation. It was suggested that such repeated domains may result from a new evolutionary way to increase the catalytic efficiency of an enzyme. The full-length luciferase, as well as the independent domain luciferases, display maximal activity at pH 6.3 and no activity at pH 8. The removal of 50 *N*-terminal residues from each of the domains resulted in an increase of activity at pH 8. Site-directed mutagenesis showed that four conserved histidines are important for pH activity regulation (Liu et al. 2004):

$$\text{LBP} \rightarrow \text{LH}_2 + \text{Binding protein (BP)}$$

$$\text{LH}_2 + \text{O}_2 \rightarrow \text{Oxyluciferin} + \text{Light}$$

SCHEME 54.4 Dinoflagellate bioluminescence reaction: LBP and luciferin (LH_2).

54.5.3 Coelenterate Photoprotein System (Hydrozoa)

In the jellyfishes, the bioluminescent system includes coelenterazine, an imidazolpyrazine, as the luciferin, a photoprotein and calcium ion (Shimomura 2006). Some systems such as the jellyfish *Aequorea* may also contain a third component, a GFP that serves as an excitation energy acceptor from the primary bioluminescent product turning the bioluminescence color into green. The coelenterate photoproteins are calcium-binding proteins. Under reducing conditions, the apoprotein binds coelenterazine and oxygen forming a stable endoperoxy intermediate (Scheme 54.5). Upon calcium binding, the photoproteins undergo a conformational change leading to the breakdown of the peroxy-intermediate producing carbon dioxide and excited coelenteramide, which decays emitting a photon of blue light (λ_{max} = 464–495 nm) (Figure 54.9). Coelenteramide remains tightly and noncovalently bound to the active site of the photoprotein turning it into a temporary fluorescent protein. However, under reducing conditions, the coelenteramide product is released. The photoproteins aequorin, obelin, mitrocomin, and clytin are small polypeptides of 21–27 kDa homologous to other calcium-binding proteins such as calmodulin, parvalbumin, and troponin, displaying helices E and F (EF) hands calcium-binding sites (Vysotski and Lee 2007; Figure 54.8). The active site is highly hydrophobic, with the hydroperoxycoelenteramide intermediate being stabilized by hydrogen bonds with Y190 hydroxyl and other residues (Figure 54.9). Comparison between aequorin and obelin (Vysotski and Lee 2007) and site-directed mutagenesis studies showed that hydrogen bonding of coelenteramide hydroxyl groups with surrounding residues determine bioluminescence spectra. Fluorescence studies with coelenteramide and its analogues have also shown that differences in bioluminescence spectra among photoproteins are due to the activation of different ionic species in the active site: the neutral form has a fluorescence maximum at 400 nm, the monoanion at 450 nm, the phenolate between 465 and 495 nm, and the pyrazine-N(4) with a maximum between 530 and 565 nm.

$$\text{Apoprotein} + \text{Coelenterazine} + O_2 \rightarrow \text{Photoprotein}$$

$$\text{Photoprotein} + Ca^{2+} \rightarrow \text{Photoprotein} + \text{Light}$$

$$\text{Photoprotein} + \text{Mercaptoethanol} \rightarrow \text{Apoprotein} + \text{Coelenteramide}$$

SCHEME 54.5 Jellyfish photoprotein bioluminescence reaction.

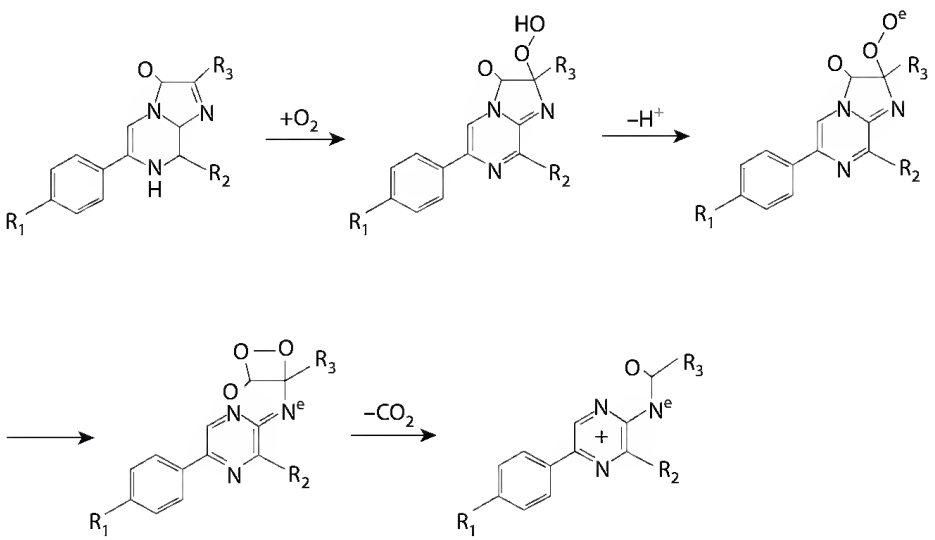

FIGURE 54.9 Mechanism of coelenterate photoprotein bioluminescence according to Vysotski and Lee (2004). (From Vysotski, E. and Lee, J., *Acc. Chem. Res.*, 37, 405, 2004.)

54.5.4 Beetles

The bioluminescent system of beetles involves the ATP-activated oxidation of a benzothiazolic luciferin (McElroy and DeLuca 1978; Wood 1995; Figure 54.10). Beetle luciferases are bifunctional enzymes, catalyzing a two step-reaction. In the first step, D-luciferin is activated by adenylation at expenses of ATP releasing pyrophosphate. The second step involves the addition of dioxygen to luciferyl-adenylate, followed by release of adenosine monophosphate (AMP) and concomitant formation of a dioxetanone, whose cleavage results in excited singlet oxyluciferin and carbon dioxide. The decay of excited oxyluciferin generates a photon usually in the green–yellow range of the spectrum with a reported efficiency of 15%–61% (Ando et al. 2008). Firefly luciferase can also catalyze the thioesterification of L-luciferin to Coenzyme A (CoA) but not of D-luciferin under aerobic conditions.

Despite extensive studies, the nature of the emitters involved in different bioluminescence colors is still unknown. It was originally proposed that the keto form of excited oxyluciferin was the red emitter and the enol form the green emitter (White et al. 1969): a tautomerization equilibrium under influence of a basic active site residue influencing the ratio between green and red emitters (White and Branchini 1975). However, recent studies (Branchini et al. 2004) showed that the polarization around the carbonyl and phenolate groups being major factors influencing the emission spectrum (Orlova et al. 2003; Hirano et al. 2009). Thus, three basic mechanisms have been proposed to explain bioluminescence color modulation by beetle luciferases: (1) nonspecific effects including the solvent effect and orientation polarizability (Ugarova and Brovko 2002); (2) specific interactions between active site residues and oxyluciferin functional groups, mainly acid–base and electrostatic interactions (Branchini et al. 2004; Hirano et al. 2009); and (3) the degree of rotational freedom of oxyluciferin thiazinic rings

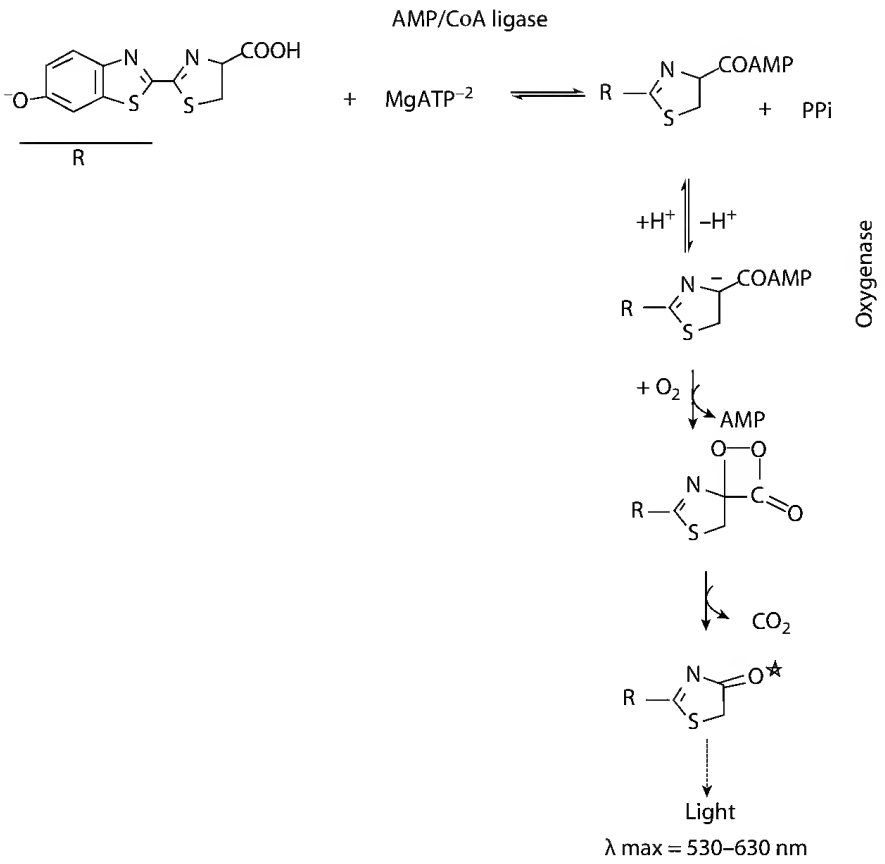

FIGURE 54.10 Beetle bioluminescence reaction.

under influence of active site geometry (McCapra et al. 1994); the two former hypothesis being supported theoretically and experimentally.

Bioluminescence colors in beetles are determined by different luciferases. Beetle luciferases can emit different colors using the same D-luciferin: firefly (Lampyridae) luciferases emit in the green–yellow region (545–575 nm); click-beetle (Elateridae) luciferases emit in the green–orange region (534–593 nm), and railroad worms (Phengodidae) in the green–red region (546–628 nm), the *Phrixothrix* railroad worms (Figure 54.8) being the only known terrestrial organisms to produce true red bioluminescence (Viviani and Bechara 1997).

Beetle luciferases are 542–550 long polypeptides with ca 60 kDa and a *C*-terminal peroxisomal targeting peptide, Ser–Lys–Leu, which drives them into peroxisomes (Gould et al. 1987). Beetle luciferases are homologous to the family of AMP-ligases, which include fatty acid CoA synthetases, aromatic acid CoA synthetases, coumarate CoA synthetases, and peptidyl synthetases (Schroeder 1989; Wood 1995; Viviani 2002).

The 3D structure of firefly luciferases show a main *N*-terminal domain bound by a hinge to a smaller *C*-terminal domain (Figure 54.8) (Conti et al. 1996; Nakatsu et al. 2006). The active site is located in a cavity in the *N*-terminal domain facing the *C*-terminal domain and consists of a luciferin and ATP binding sites. The *C*-terminal domain was found to play an essential role for efficient catalysis of the oxidative reaction and bioluminescence color (Branchini et al. 2004). Several mutations were found to affect the bioluminescence color of beetle luciferases. They fall into two main classes: those directly involved in the active site, probably affecting the microenvironment around the excited oxyluciferin, and those that affect the enzyme conformation indirectly affecting the active site microenvironment (Viviani et al. 2008). The pH-sensitive firefly luciferases were found to be especially prone to be affected by mutations outside the active site whereas the pH-insensitive ones were more resistant (Viviani et al. 2008).

54.5.5 Other Bioluminescent Systems

Several other bioluminescent systems that differ in their biochemistry (Table 54.1) and, therefore, in their evolutionary origin are partially investigated. In marine environment, most bioluminescent systems use imidazolpyrazines derivatives as luciferin, coelenterazine being the most common luciferin found in such environment. Coelenterazine can be acquired either from the diet, as in the case of fishes, or synthesized (Haddock et al. 2010). Differently from the jellyfish photoprotein systems of hydrozoans, anthozoans employ a typical luciferin–luciferase system with coelenterazine as luciferin, a luciferase which is unrelated to photoproteins, and, noteworthy, LBPs which are calcium-binding proteins evolutionarily related to the jellyfishes' photoproteins (Hastings and Wood 2001). Mollusks have a variety of bioluminescent systems: bivalves employ two proteins, pholasin that binds coelenterazine and displays weak chemiluminescence properties, and a peroxidase-like luciferase, which acts on pholasin to produce intense light; squids use a luciferase, coelenterazine disulfate and ATP activation; annelids may use photoprotein systems like in tubeworm *Chaetopterus variopedatus* (Shimomura 2006), peroxidase-like system involving aldehydes as luciferin such as in earthworm *Diplocardia longa*, and ATP-activated system. Marine crustaceans such as the copepods *Vargula* and *Gaussia* have luciferin–luciferase system with a glycosylated luciferase, which is secreted and cypridina luciferin, which is an imidazolpyrazine, or a porphyrin luciferin such as in decapods. Fishes may import their bioluminescent system from symbiotic bioluminescent bacteria, or have their own bioluminescent system, in the last case coelenterazine is the luciferin.

Terrestrial organisms are also quite diverse in their biochemistry. In fungi, the bioluminescence system has some resemblances with the bacterial system, including a nicotinamide adenine dinucleotide (NADH)-dependent reductase involved in reducing the luciferin. Although an enzymatic complex involving soluble and nonsoluble enzymes was found (Oliveira and Stevani 2009), no luciferase was

isolated yet. Furthermore, although several compounds have been correlated with fungal luciferin, its true identity is still unknown (Desjardin et al. 2008).

In arthropods, the millipede *Luminodesmus sequoiae* employs an ATP-activated photoprotein system. In insects, at least three different systems are known: the classical firefly luciferin–luciferase system, and two morphologically and biochemically distinct systems in Diptera: the system of *Arachnocampa*, which employs an ATP-activated luciferin–luciferase system, and the *Orfelia*'s bioluminescent system, which employs an unrelated dimeric luciferase, an LBP and a very unstable luciferin (Viviani et al. 2002). The system of Collembola and Staphylinid beetles remain unknown. *Latia neritoides*, the only freshwater snail uses an aldehyde as luciferin.

54.6 Origin and Evolution of Bioluminescent Systems

One of the most intriguing questions about bioluminescence is how such exotic processes originated during evolution. Bioluminescence may have arose about 40 independent times during the evolution (Haddock et al. 2010). It arose from the fortuitous encounter of a chemiluminescent substrate (luciferin) and an enzyme able to catalyze its chemiluminescent oxidation. The biosynthetic origin and functions of many luciferins remain unknown. In bacteria, the FMN is clearly involved in electron transport; in dinoflagellates luciferin may result from chlorophyll metabolism; in the case of coelenterazine, its imidazolpyrazine structure suggests it may arise from histidine biosynthetic pathway, its widespread occurrence in the marine environment and its antioxidant properties suggested that it may have played an antioxidant role analogous to α-tocopherol (Rees et al. 1998); in beetles, luciferin benzothiazoline ring may have originated from cysteine and quinone fusion, but its original function remains unknown.

Early reports suggested that bioluminescence arose as an accidental by-product of oxygen detoxification when photosynthetic oxygen started to rise in the atmosphere (Seliger and McElroy 1965). According to such a hypothesis, luciferases evolved from accidentally luminescent oxygenases, involved in the removal of the increasingly toxic oxygen. Later, Seliger (1975) suggested that luciferases may have arisen from mixed-function oxygenases involved with the oxidation of unsaturated and aromatic compounds, accumulated during early preaerobic life history, when the levels of oxygen started to rise. The new luminescent phenotype conferred a selective advantage in their survival. Whereas the origin from an early oxygenase could be valid for bacterial luciferases, it is unlikely that such a hypothesis applies to most other taxa since most of them originated after the oxygen pressure reached the current level. However, in some cases evidences suggest that bioluminescence plays an auxiliary role in oxygen detoxification (Barros and Bechara 1998). Hastings (1983) suggested that most luciferases evolved much later after the development of vision. Oxygenases are usually metalloproteins with prosthetic groups and no similarity with luciferases at the primary structure level (Rees et al. 1998). Thus, most luciferases did not originate from oxygenases but rather it was the accidental weak luminescent phenotype which drove the evolution of the new oxygenase functions (Hastings and Wood 2001). Indeed, recent experiments with bovine serum albumin (BSA) suggest that hydrophobic pockets of proteins increase the quantum yield of chemiluminescent reactions (Viviani and Ohmiya 2006a). In such a context, it is likely that upon the appearance of molecular oxygen in the atmosphere, several proteins providing hydrophobic pockets and even catalytic residues for oxidative reaction gave rise to protobioluminescent systems. Since bioluminescence is a specific case of the more general process of generation of excited states in biological systems, it may have evolved from other metabolic pathways generating excited species. Thus, some especially efficient reactions were selected from a milieu of chemiluminescent reactions. The recruitment of proteins for new biological functions during evolution is well exemplified by several proteins, which were independently recruited as structural proteins in invertebrate lens crystallins (Anke et al. 2000). Thus, calcium-binding proteins originated coelenterate photoproteins and LBPs, whereas AMP/CoA-ligases gave rise to beetle luciferases. The origin of many other luciferases remains unknown.

54.7 Bioluminescence Applications and Perspectives: Bioindication from the Molecular to the Global Level

Since the purification of the first bioluminescent systems almost 50 years ago, their luciferin and luciferases were used in a wide range of bioanalytical applications (Campbell 1988). Firefly luciferases have been extensively used for analytical detection and quantification of ATP, including biomass estimation, cell viability tests, enzymes assays, and signaling molecules in biological samples. Bacterial luciferases were used to measure $FMNH_2$ to monitor redox reactions. Coelenterate photoproteins were used as sensitive calcium indicators. With the advances of molecular biology two decades ago, the genes coding luciferases of bacteria, beetles, coelenterates, crustaceans among other organisms, and GFPs, have been cloned, sequenced, and used as reporter genes in many applications involving analysis of promoter activation and location of gene expression (Daunert and Deo 2006; Viviani 2007). Bacterial luciferases have the advantage that the full Lux operon was cloned, allowing the expression of all required components for bioluminescence without the need to exogenously provide luciferin or other cofactors. GFPs were the most popular reporter genes, due to their strong fluorescent signal and stability, allowing their use in diverse studies of gene expression *in situ* localization in biological and biomedical areas. Recently the Nobel prize was awarded to O. Shimomura, their discoverer, M. Chalfie for their heterologous expression in other cells, and R. Tsien, for their engineering, producing a variety of colors and for their application (http://www.nobelprize.org/nobel_prizes/chemistry/laureates/2008/press.html). On the other hand, luciferases as reporter genes have the desirable properties of being very sensitive and fast and not showing the disadvantage of unwanted background (Roda et al. 2009). Although luciferases are usually very unstable and for this reason they are not appropriate for *in situ* localization like GFPs, their instability associated with the high signal/background ratio make them the most versatile reporter genes for real time *in vivo* applications (Roda et al. 2009). Some of these genes are used for monitoring the progress and regress of bacterial and viral infections in animal models for drug screening purposes, for imaging brain structure and function, assessment of tumor metastasis (Figure 54.11), among others (Shinde et al. 2006). They are also used in sensitive cytotoxicity tests and in biosensors of toxic agents (Figure 54.11) and environmental disrupting agents such as heavy metals and halogenated aromatics (Feliciano et al. 2006; Roda et al. 2009). New luciferases emitting different bioluminescence colors such as *Phrixothrix* railroad worm and *Pyrearinus* click beetle luciferases, the only one that naturally produces red light, have been cloned (Viviani et al. 1999), engineered, and successfully expressed in mammalian cells (Nakajima et al. 2004a; Viviani and Ohmiya 2006b; Figure 54.11b). Dual and multicolor reporter systems employing luciferases emitting different bioluminescence colors are commercially available for simultaneously monitoring several genes expressions with the aim to better understand the cellular physiology and pathology, in studies such as circadian rhythms (Nakajima et al. 2004b). Systems involving BRET are currently available to study protein–protein interaction and agonist–receptor interactions (Shrestha and Deo 2006). Protease-sensitive biosensors have been developed to assess cellular and biochemical pathways (Shinde et al. 2006). And the range of applications keep increasing as new luciferases are cloned or engineered and new sensitive and affordable photodetecting systems are developed.

Whereas most applications of bioluminescence deal with its use as a bioindicator or biomarker at the molecular level, recently bioluminescent organisms themselves are beginning to be used as environmental indicators. Fireflies can be used as indicators of artificial night-lighting impact or to assess stream water quality, whereas bioluminescent bacteria and algae populations can be monitored by satellite giving global information about planktonic growth and oceanic currents (Figure 54.11c; Haddock et al. 2010), which are important for ecosystem assessment.

Many other bioluminescent systems such as those of fungi, Diptera, and many marine organisms remain poorly studied or not studied at all, therefore providing substrate for new scientific discoveries in the areas of biochemistry, evolution, and ecology, and the potential of new analytical tools. Bioluminescence will continue to provide important answers in different fields such as biophysics, enzymology, cell biology, evolution, and ecology.

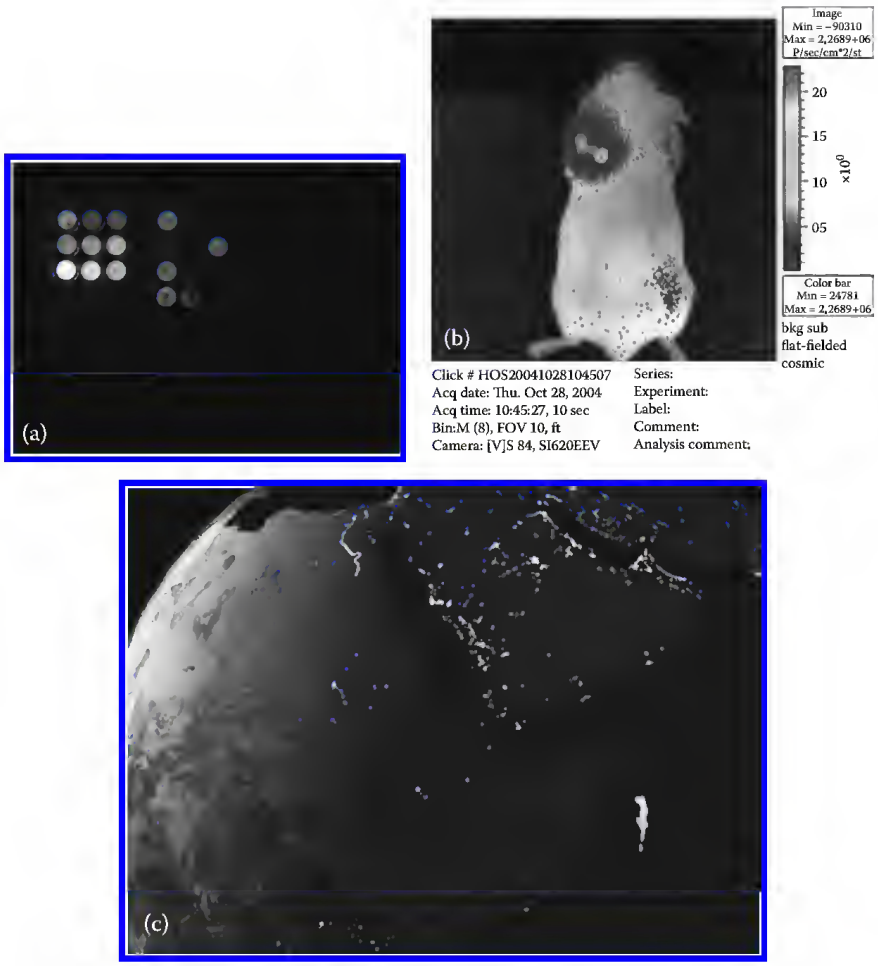

FIGURE 54.11 **(See color insert.)** Biotechnological and environmental applications of bioluminescence: (a) a whole cell biosensor in a 96-well plate format for toxicity based on bioluminescent *Escherichia coli* engineered with *Macrolampis* firefly luciferase gene; (b) real-time *in vivo* bioimaging of metastasis using cell line transformed with firefly luciferase gene (kindly donated by Y. Ohmiya); and (c) bioluminescent bacteria populational boom, a perspective for global level environmental biosensing. (From Haddock, S. et al., *Annu Rev. Mar. Sci.*, 2, 443, 2010.)

Acknowledgments

We thank Prof. S. Tu (Houston University) and Prof. E. Vysotski (Russian Academy of Sciences) for providing the pictures of 3D structure of bacterial luciferase and obelin, respectively, and Prof. Yoshihiro Ohmiya (AIST, Japan) and Rogilene Prado (UFSCAR) for their revision of this manuscript. This work was supported by a grants from Fundação de Amparo à Pesquisa do Estado de São Paulo (FAPESP, São Paulo, Brazil) and National Council of Research and Development (CNPq, Brazil).

References

Ando, Y., Niwa, K., Yamada, N. et al. 2008. Firefly bioluminescence quantum yield and colour change by pH-sensitive green emission. *Nat. Photon. (Lett.)* 2: 44–47.

Anke, F., Rijk, V., Hurk V., Renkema, W., Boelens, W. C., Wilfried, W. J., and Bloemendal, H. 2000. Characteristics of super A-crystallin, a product of in vitro exon shuffling. *FEBS Lett.* 480: 79–83.

Barros, M. P. and Bechara, E. J. 1998. Bioluminescence as a possible auxiliary oxygen detoxifying mechanism in elaterid larvae. *Free Radic. Biol. Med.* 24: 767–777.

Bechara, E. J. H. 1989. Luminescent elaterid beetles: Biochemical, biological and ecological aspects. In: *Advances in Oxygenated Process*, ed. A. L. Baumstark, pp. 123–178. London: JAI Press.

Branchini, B. R., Southworth, T. L., Murtiashaw, M. H. et al. 2004. An alternative mechanism of bioluminescence color determination in firefly luciferase. *Biochemistry* 43: 7255–7262.

Branham, M. A. and Wenzel, J. W. 2003. The origin of photic behavior and the evolution of sexual communication in fireflies (Coleoptera: Lampyridae). *Cladistics* 19: 1–22.

Campbell, A. K. 1988. *Chemiluminescence: Principles and Applications in Biology and Medicine*. Chichester, U.K.: Eliis Horwood.

Cilento, G. and Adam, W. 1988. Photochemistry and photobiology without light. *Photochem. Photobiol.* 48: 361–368.

Conti, E., Franks, N. P., and Brick, P. 1996. Crystal structure of firefly luciferase throws light on a superfamily of adenylate-forming enzymes. *Structure* 4: 287–298.

Czyz, A., Plata, K., and Wegrzyn, G. 2003. Stimulation of DNA repair as an evolutionary drive for bacterial luminescence. *Luminescence* 18: 140–144.

Daunert, S. and Deo, S. K. 2006. *Photoproteins in Bioanalysis*. Weinheim, Germany: Wiley-VCH.

De Cock, R. 2004. A field study on the bioluminescent activity of larval glow-worms, *Lampyris noctiluca* and *Phosphaenus hemipterus* (Coleoptera: Lampyridae) in relation to environmental factors and light pollution. PhD Thesis, Universiteit Antwerpen, Faculteit Wetenschappen, Chapter 3, pp. 43–74.

De Cock, R. 2010. Biology and behaviour of European Lampyrids. In: *Bioluminescence in Focus–A Collection of Illuminatings Essays*, ed. V. B. Meyer-Rochow, pp. 161–200. Kerala, India: Research Signpost.

Desjardin, D. E., Oliveira, A. G., and Stevani, C. V. 2008. Fungi bioluminescent revisited. *Photochem. Photobiol. Sci.* 7: 170–182.

Dunlap, J. C. and Hastings, J. W. 1981. Biochemistry of dinoflagellate bioluminescence: The purification and characterization of dinoflagellate luciferin from *Pyrocystis lunula*. *Biochemistry* 20: 983–989.

Feliciano, J., Xu, S., Lehmler, H. J., Bachas, L. G., and Daunert, S. 2006. Clc-based biosensing system in the detection of *cis*-dihydroxylated (chloro-) biphenyls. *Anal. Bioanal. Chem.* 385: 807–813.

Ghiradella, H. 1998. The anatomy of light production: The fine structure of the firefly lantern. In: *Microscopic Anatomy of Invertebrates*, eds. F. W. Harrison and M. Locke, pp. 363–381. New York: Wiley-Liss.

Gould, S. J., Keller, G. A., and Subramani, S. 1987. Identification of a peroxisomal targeting signal at the carboxy terminus of firefly luciferase. *J. Cell. Biol.* 105: 2923–2931.

Haddock, S. H. D., Moline, M. A., and Case, J. F. 2010. Bioluminescence in the sea. *Annu. Rev. Mar. Sci.* 2: 443–493.

Harvey, E. N. 1952. *Bioluminescence*. New York: Academic Press.

Hastings, J. W. 1983. Biological diversity, chemical mechanisms, and evolutionary origins of bioluminescence systems. *J. Mol. Evol.* 19: 309–321.

Hastings, J. W. 1995. Bioluminescence: Similar chemistries but many different evolutionary origins. *Photochem. Photobiol.* 62: 599–600.

Hastings, J. W. and Wood, K. V. 2001. Luciferases did not all evolve from precursors having similar enzymatic properties. In: *Photobiology*, eds. D. Valenzeno and T. Coohill, pp. 199–210. Overland Park: Valdenmar Publishing Company.

Herring, P. J. 1987. Systematic distribution of bioluminescence in living organisms. *J. Biolum. Chemilum.* 1: 147–163.

Hirano, T., Hasumi, Y., Ohtsuka, K. et al. 2009. Spectroscopic studies of the light-color modulation mechanism of firefly (beetle) bioluminescence. *J. Am. Chem. Soc.* 131: 2385–2396.

Hosseini, P. K. and Nealson, K. H. 1995. Symbiotic luminous soil bacteria: Unusual regulation for an unusual niche. *Photochem. Photobiol.* 62: 633–640.

Koo, J.-Y. K. and Schuster, G. B. 1978. Chemiluminescence of diphenoyl peroxide. Chemically initiated electron exchange luminescence. A new general mechanism for chemical production of electronically excited states. *J. Am. Chem. Soc.* 100: 4496–4503.

Lall, A., Cronin, T. W., Bechara, E. J. H., Costa, C., and Viviani, V. R. 2009. Visual ecology of bioluminescent beetles: Visual spectral mechanisms and the colors of optical signaling in Coleoptera, Elateroidea: Lampyridae, Elateridae and Phengodidae. In: *Bioluminescence in Focus. A Collection of Illuminating Assays*, ed. V. B. Meyer-Rochow, pp. 201–228. Kerala, India: Research Signpost.

Lee, J. 1989. Bioluminescence. In: *The Science of Photobiology*, ed. K. C. Smith, pp. 371–396. New York: Plenum Press.

Lewis, S. M. 2010. Bioluminescence and sexual signaling in fireflies. In: *Bioluminescence in Focus—A Collection of Illuminatings Essays*, ed. V. B. Meyer-Rochow, pp. 147–159. Kerala, India: Research Signpost.

Liu, L., Wilson, T., and Hastings, J. W. 2004. Molecular evolution of dinoflagellate luciferases, enzymes with three catalytic domains in a single polypeptide. *Proc. Natl. Acad. Sci. USA.* 94: 16555–16560.

Lloyd, J. E. 1978. Insect bioluminescence. In: *Bioluminescence in Action*, ed. P. J. Herring, pp. 241–272. London: Academic Press.

Lloyd, J. E. 2006. Stray light, fireflies, and fireflyers. In: *Ecological Consequences of Artificial Night Lighting*, eds. C. Rich and T. Longcore, pp. 345–364. Washington, DC: Island Press.

McCapra, F., Gilfoyle, D. J., Young, D. W., Church, N. J., and Spencer, P. 1994. The chemical origin of colour differences in beetle bioluminescence. In: *Bioluminescence and Chemiluminescence: Fundamental and Applied Aspects*, eds. A. K. Campbell, L. J. Kricka, and P. E. Stanley, pp. 387–389. Chichester, U.K.: John Wiley & Sons.

McElroy, W. D. and DeLuca, M. 1978. Chemistry of firefly bioluminescence. In: *Bioluminescence in Action*, ed. P. Herring, pp. 109–127. New York: Academic Press.

Nakajima, Y., Ikeda, M., Kimura, T., Honma, S., Ohmiya, Y., and Honma, K. 2004b. Bidirectional role of orphan nuclear receptor RORalpha in clock gene transcriptions demonstrated by a novel reporter assay system. *FEBS Lett.* 7: 122–126.

Nakajima, Y., Kimura, T., Suzuki, C., and Ohmiya, Y. 2004a. Improved expression of novel red- and green-emitting luciferases of *Phrixothrix* railroad worms in mammalian cells. *Biosci. Biotechnol. Biochem.* 68: 948–951.

Nakatsu, T., Ichiyama, S., Hiratake, J. et al. 2006. Structural basis for the spectral difference in luciferase bioluminescence. *Nature* 440: 372–376.

Oliveira, A. G. and Stevani, C. V. 2009. The enzymatic nature of fungal bioluminescence. *Photochem. Photobiol. Sci.* 8: 1416–1421.

Orlova, G., Goddard, J. D., and Brovko, L. Y. 2003. Theoretical study of the amazing firefly bioluminescence: The formation and structure of the light emitters. *J. Am. Chem. Soc.* 125: 6962–6971.

Rees, J. F., DeWergifosse, B., Noiset, O., Dubuisson, M., Janssens, B., and Thompson, E. M. 1998. The origins of marine bioluminescence: Turning oxygen defense mechanisms into deep-sea communication tools. *J. Exp. Biol.* 201: 1211–1221.

Roda, A., Guardigli, M., Michelini, E., and Mirasoli, M. 2009. Bioluminescence in analytical chemistry and *in vivo* imaging. *Trends Anal. Chem.* 28: 307–322.

Schroeder, S. 1989. Protein sequence homology between plant-4-coumarate: CoA ligase and firefly luciferase. *Nucl. Acid. Res.* 17: 460.

Seliger, H. H. 1975. The origin of bioluminescence. *Photochem. Photobiol.* 21: 355–361.

Seliger, H. H. and McElroy, W. D. 1965. Bioluminescence-enzyme catalyzed chemiluminescence. In: *Light: Physical and Biological Action*, eds. H. H. Seliger and W. D. McElroy, pp. 169–198. New York: Academic Press.

Shimomura, O. 2006. *Bioluminescence—Chemical Principles and Methods.* Singapore: World Scientific Publishing Co. Pvt. Ltd.

Shinde, R., Zhao, H., and Contag, C. 2006. Photoproteins as *in vivo* indicators of biological functions. In: *Photoproteins in Bioanalysis*, eds. S. Daunert and S. K. Deo, pp. 113–129, Weinheim, Germany: Wiley-VCH.

Shrestha, S. and Deo, S. K. 2006. Bioluminescence resonance energy transfer in bioanalysis. In: *Photoproteins in Bioanalysis*, eds. S. Daunert and S. K. Deo, pp. 95–111, Weinheim, Germany: Wiley-VCH.

Sivinsky, J. 1981. The nature and possible functions of luminescence in Coleoptera larvae. *Coleopt. Bull.* 35: 167–179.

Tu, S. C. 2007. Bacterial luciferase: Structure-function relationships and protein engineering. In: *Luciferases and Fluorescent Proteins: Principles and Advances in Biotechnology and Bioimaging*, eds. V. R. Viviani and Y. Ohmiya, pp. 1–18, Kerala, India: Transworld Research Network.

Tu, S. C. 2008. Activity coupling and complex formation between bacterial luciferase and flavin reductases. *Photochem. Photobiol. Sci.* 7: 183–188.

Tu, S. C. and Mager, H. I. X. 1995. Biochemistry of bacterial bioluminescence. *Photochem. Photobiol.* 62: 615–624.

Ugarova, N. N. and Brovko, L. Y. 2002. Protein structure and bioluminescent spectra for firefly bioluminescence. *Luminescence* 17: 321–330.

Viviani, V. R. 2002. The origin, diversity and structure function relationships in insect luciferases. *Cell Mol. Life Sci.* 59: 1833–1850.

Viviani, V. R. 2005. Luciferases: The light generating enzymes. In: *Recent Progress of Bio/Chemiluminescence and Fluorescence Analysis in Photosynthesis*, eds. N. Wada and M. Mimuro, pp. 1–22. Kerala, India: Research Signpost.

Viviani, V. R. 2007. Beetle luciferases: Origin, structure and function relationships, and engineering for biotechnological applications. In: *Luciferases and Fluorescent Proteins: Principles and Advances in Biotechnology and Bioimaging*, eds. V. R. Viviani and Y. Ohmiya, pp. 79–105. Kerala, India: Transworld Research Network.

Viviani, V. R., Arnoldi, F. G. C., Neto, A. J. S., Ohelmeyer, T. L., Bechara, E. J. H., and Ohmiya, Y. 2008. The structural origin and biological function of pH-sensitivity in firefly luciferases. *Photochem. Photobiol. Sci.* 7: 159–169.

Viviani, V. R. and Bechara, E. J. H. 1997. Bioluminescence and biological aspects of Brazilian railroad-worms (Coleoptera: Phengodidae). *Ann. Am. Soc. Entomol.* 90: 389–393.

Viviani, V. R., Bechara, E. J. H., and Ohmiya, Y. 1999. Cloning, sequence analysis, and expression of active *Phrixothrix* railroad-worm luciferases: Relationship between bioluminescence spectra and primary structures. *Biochemistry* 38: 8271–8279.

Viviani, V. R., Hastings, J. W., and Wilson, T. 2002. Two bioluminescent Diptera: The North American *Orfelia fultoni* and the Australian *Arachnocampa flava*. Similar niche, different bioluminescence systems. *Photochem Photobiol.* 75: 22–27.

Viviani, V. R. and Ohmiya, Y. 2006a. Bovine serum albumin displays luciferase-like activity in presence of luciferyl-adenylate: Insights on the origin of protoluciferase activity and bioluminescence colors. *Luminescence* 21: 262–267.

Viviani, V. R. and Ohmiya, Y. 2006b. Beetle luciferases: Colorful lights on biological processes and diseases. In: *Photoproteins in Bioanalysis*, eds. S. Daunert and S. Deo, pp. 49–60. Weinheim, Germany: Wiley-VCH.

Vysotski, E. and Lee, J. 2004. Ca^{2+}-regulated photoproteins: Structural insight into the bioluminescence mechanism. *Acc. Chem. Res.* 37: 405–415.

Vysotski, E. and Lee, J. 2007. Bioluminescence mechanism of Ca^{2+}-regulated photoproteins from three-dimensional structures. In: *Luciferases and Fluorescent proteins: Principles and Advances in Biotechnology and Bioimaging*, eds. V. R. Viviani and Y. Ohmiya, pp. 19–42. Kerala, India: Transworld Research network.

Watanabe, H. 2005. Bacterial bioluminescence. In: *Recent Progress of Bio/Chemiluminescence and Fluorescence Analysis in Photosynthesis*, eds. N. Wada and M. Mimuro, pp. 23–48. Kerala, India: Research Signpost.

White, E. H. and Branchini, B. R. 1975. Modification of firefly luciferase with a luciferin analog. Red light producing enzyme. *J. Am. Chem. Soc.* 97: 1243–1245.

White, E. H., Rapaport, E. Hopkins, T. A., and Seliger, H. H. 1969. Chemi- and bioluminescence of firefly luciferin. *J. Am. Chem. Soc.* 91: 2178–2180.

Wilson, T. and Hastings, J. W. 1998. Bioluminescence. *Annu. Rev. Cell Dev. Biol.* 14: 197–230.

Wood, K. V. 1995. The chemical mechanism and evolutionary development of beetle bioluminescence. *Photochem. Photobiol.* 62: 662–673.

55

Artificial Photosynthetic Systems

Péter Maróti
University of Szeged

Massimo Trotta
Istituto per i Processi Chimico-Fisici

55.1 Introduction

For millions of years, green plants have employed photosynthesis to capture energy from sunlight, to convert it into electrochemical energy, and finally to produce energy-rich (organic) compounds. Water is the key chemical component in this process: it supplies electrons to reduce carbon dioxide to carbohydrate and forms oxygen as by-product. The overall process is responsible for the majority of energy used by mankind during our evolution and is challenged only by nuclear processes highly debated by environmentalists [1–3].

Photosynthesis is deceptively a complex process and involves a large number of key photophysical, photochemical, and chemical steps. Photosynthesis (and respiration) employs catalysts that self-assemble, self-repair, use Mn, Cu, Fe, Ni, Ca (no noble metals), and operate at ambient temperature with essentially no overpotential. To a large degree, the underlying physics and chemistry are known and, in principle, could be used to devise artificial analogs suited to current energy and environmental demands. Nature has perfected the process of photosynthesis over billions of years but unfortunately it is not easily reproducible in laboratory since the natural components do not work properly outside their physiological environment. The unprecedented high degree of molecular connectivity in reaction center (RC)—antenna complexes of bacteria and plants—is well documented in the color insert. The alternative we are left with is replicating the natural parts in synthetic systems that—struggling through numerous trials and errors—aims to mimic photosynthesis. From energetic point of view, photosynthesis converts the free energy of (sun)light into redox potential, electrochemical potential of ions and protons through the membrane, and finally phosphate potential. The blueprint of a synthetic system mimicking these tasks should consist of parts that (1) efficiently absorb light and generate electron-excited states of suitable molecular moieties, (2) transfer the excitation energy to a donor/acceptor interface where it is trapped and converted into photochemical charge separation (CS), and

(3) neutralize the charges (removing excess electrons and filling holes) of the interface minimizing any wasteful internal charge recombination (CR) and eventually employ the final available free energy to (4a) generate protonmotive force (including membrane electric potential) by accumulation of charges in opposite sides of noncommunicating compartments or (4b) drive reversible proton pumps or (4c) couple the electron flow to appropriate catalysts to produce high-energy reduced species (fuels). A schematic representation of the four basic steps is given in Figure 55.1.

Plants use organic compounds that need to be continuously renewed. The D1 and D2 subunits of the RC of photosystem (PSII) of green plants (Figure 55.P2 in the color insert) exposed to strong UV-B irradiation suffer severe (photo-) damage but, depending on the degree of damage, recover very fast. By *de novo* synthesis of the subunits within short period of time (2–4 h), the function of the oxygen evolution of PSII is reestablished [4]. The effective repair mechanisms in natural systems present definite advantage compared to any man-made biomimetic constructions. Presently, much less requirements of operation of artificial systems are set as goals. Inorganic compounds are looked for that catalyze the needed reactions and are both efficient and widely available. Several artificial photosynthetic elements are designed and assembled them into energy converting systems. Carotenoid pigments and polymer polyenes can be incorporated into tetrapyrrole-based artificial RCs. In certain systems, the pigment is near 100% efficient. In more complex systems, liposome-based artificial ion pumps have been assembled that are based on Mitchellian redox loops and vectorial redox potential developed by either natural [5] or artificial RCs [6,7]. The direct conversion of light energy to chemical potential in similar biomimetic constructions will be surveyed in this work.

Synthetic photosystems have the advantage of manipulation of individual components at molecular and phenomenological levels and of direct test of theoretical considerations on thermodynamics and

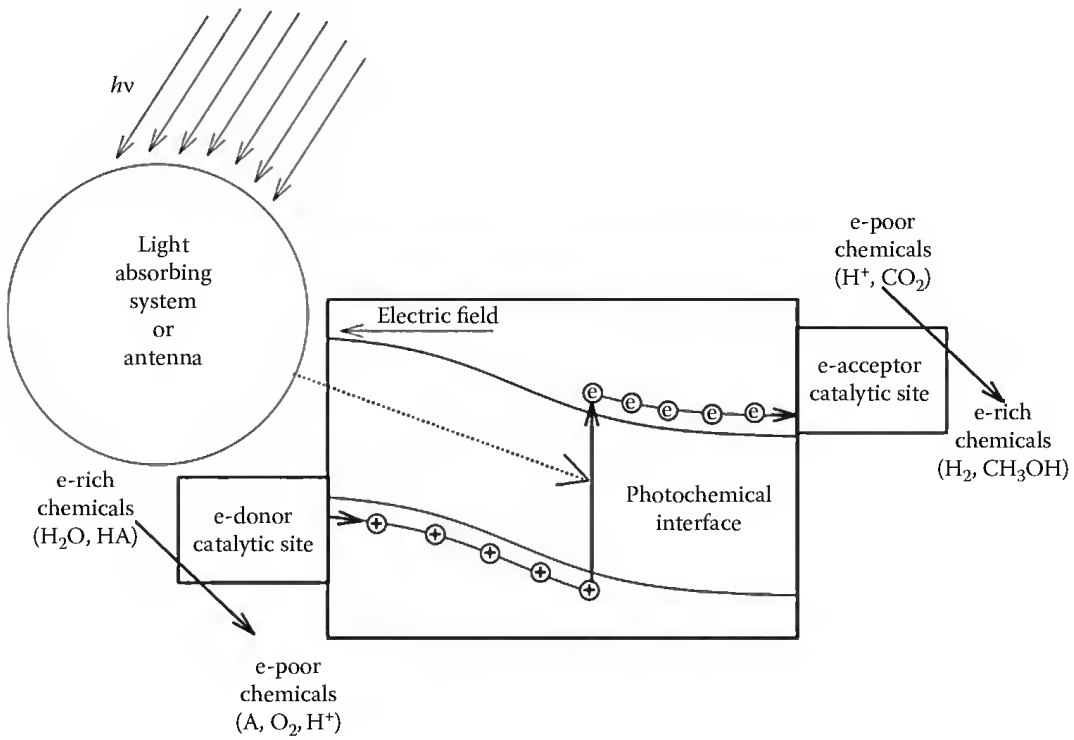

FIGURE 55.1 Key processes of oxygenic photosynthesis representing potential targets to establish artificial systems. The light energy is absorbed and collected by the large array of antenna pigments (circle) that surrounds the photochemical interface (RC, rectangular box) acting similarly as a semiconductor *p–n* junction. After the excitation energy is funneled to here (dotted line), CS (production of an electron (e)/hole (+) pair) takes place followed by consecutive ET processes (solid lines). The electrons emerging from the water-splitting process at the e-donor catalytic site (producing molecular oxygen and H^+ ions) fill the holes (vacancies of electrons) and drive reductive processes at the e-acceptor catalytic site (producing, e.g., molecular hydrogen or methanol from carbon dioxide).

reaction kinetics. As many of the essential parameters are not readily altered in the natural systems, trials on artificial systems have been helpful in understanding the principles of natural photosynthesis [8–11].

In artificial photosynthesis, the goal is to mimic the ability of green plants and other photosynthetic organisms to convert the free energy of sunlight into other forms of free energy including electrons (redox potential), ions (ion electrochemical potential), protons (protonmotive force), and high-energy chemicals (phosphate potential) [12]. Although the complexity of the structure and function of natural photosynthesis is unlimited, a number of promising approaches to artificial realization of some selected steps of the natural processes have appeared recently based on semiconductors, membranes, liposomes, nanoparticles, and (supra)molecular systems. Figure 55.2 demonstrates how the light energy can be utilized by photovoltaic (PV), electrochemical, and photocatalytic reactions designed by partial and/or combined processes of natural photosynthesis.

The first steps of photosynthesis including the absorption and collection of solar energy and its conversion into charge-separated state can be realized in silicon-based PV modules [13]. The photon is absorbed in the bulk silicon semiconductor, and the electron-excited state migrates to a *p–n* junction where CS occurs. The separated charges generate electromotive force (emf) that can drive electric current in an external wire connecting the two sides of the junction. The emf is produced by high yield as the intrinsic electric field of the *p–n* junction helps to prevent the recombination of the charges (see the direction of the electric field in Figure 55.1). Commercially available silicon PV cells convert sunlight to electricity with 14%–19% energy conversion efficiency [14,15]. Recent silicon PVs have even higher efficiencies that approach the Shockley–Quiesser limit of about 30%. Beside silicon PVs, alternative materials have been developed including dye-sensitized solar cells [16] and organic PVs [15]. Although these systems have presently significantly lower efficiency and stability compared to silicon PVs, they use lower cost materials.

Electrochemistry can be combined with PVs to convert electricity to chemical energy. If PVs is wired to a water electrolyzer, H_2 (fuel) is produced at $\Delta E^{0\prime} = -1.23$ V cell voltage according to the overall reaction of $2H_2O \leftrightarrow 2H_2 + O_2$. Typical alkaline electrolyzers operate in concentrated KOH, utilizing nickel or nickel-coated steel electrodes, and convert electricity to chemical energy in hydrogen with ~70% energy conversion

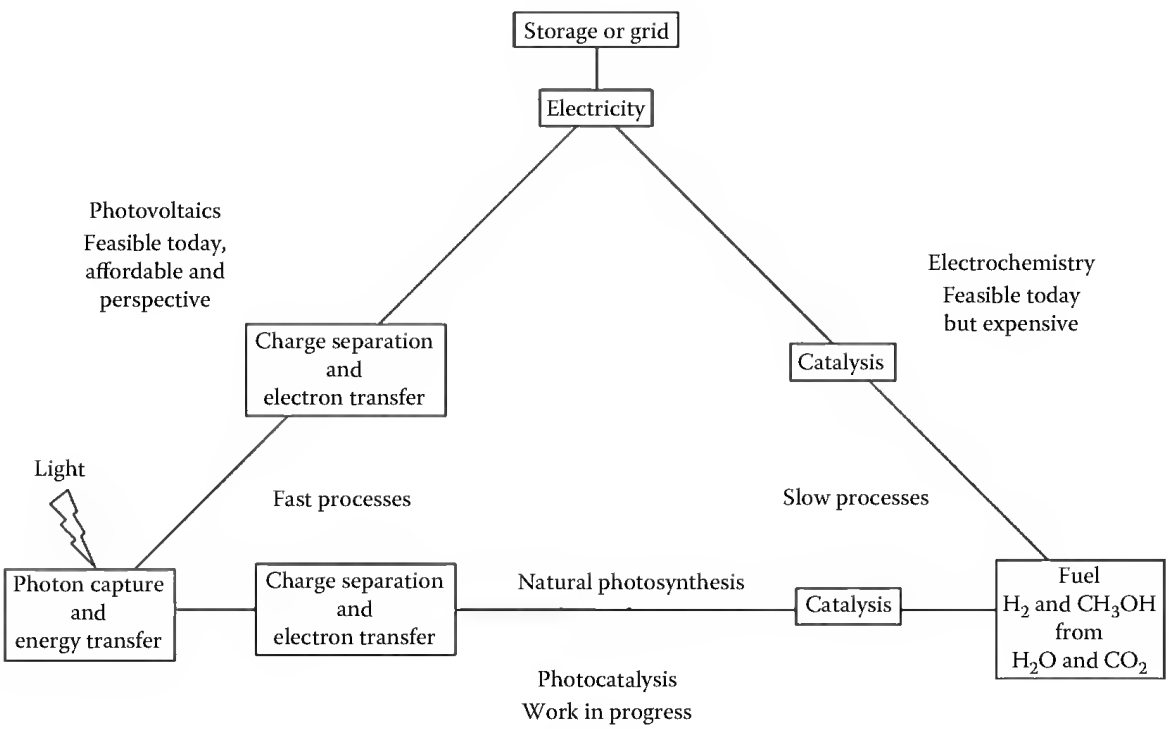

FIGURE 55.2 Possible ways of utilization of light energy in artificial photosystems based on photovoltaics, electrochemistry, and photocatalysis designed by natural processes of photosynthesis.

efficiency. Proton exchange membrane (PEM) electrolyzers operate near neutral pH, utilize noble metal catalysts, and convert sunlight to chemical energy with an energy conversion efficiency larger than 12% [17].

The photocatalytic ways of conversion of sunlight into chemical energy are implemented by the processes of natural photosynthesis. The final goal has been to develop an artificial version of photosynthesis that can be used to produce (liquid) fuels from carbon dioxide and water. The following sections will start with the introduction of the selected processes of natural photosynthesis followed by description of attempts to mimic the partial and/or overall natural reactions in artificial systems. While different manifestations of artificial photosynthesis work in the lab, they are not yet ready for mass consumption. The artificial photosynthesis should be a technology that would not only provide a green and renewable source of electrical energy, but could also help scrub the atmosphere of excessive carbon dioxide resulting from the burning of fossil fuels.

55.2 Harvesting the Light

55.2.1 Natural System

The photosynthesis is triggered by absorption of sunlight. Light harvesting is efficiently accomplished if performed by strongly absorbing and interacting molecules (usually pigments such as chlorophylls and bacteriochlorophylls *a*, *b*, *c* (Figure 55.3), *d*, and so forth, phycobilins, carotenoids). During the long-living electron-excited state of the pigment molecule, electron excitation energy can be transferred to unexcited pigments molecules before any detrimental decay processes take place. The intrinsic lifetime of the excited state of chlorophylls (τ_0) is 1–10 ns while the time required to transfer energy ($\tau = 1/k_T$) to neighboring pigment at distance of R is 2–3 orders of magnitude smaller (1–10 ps). This difference allows

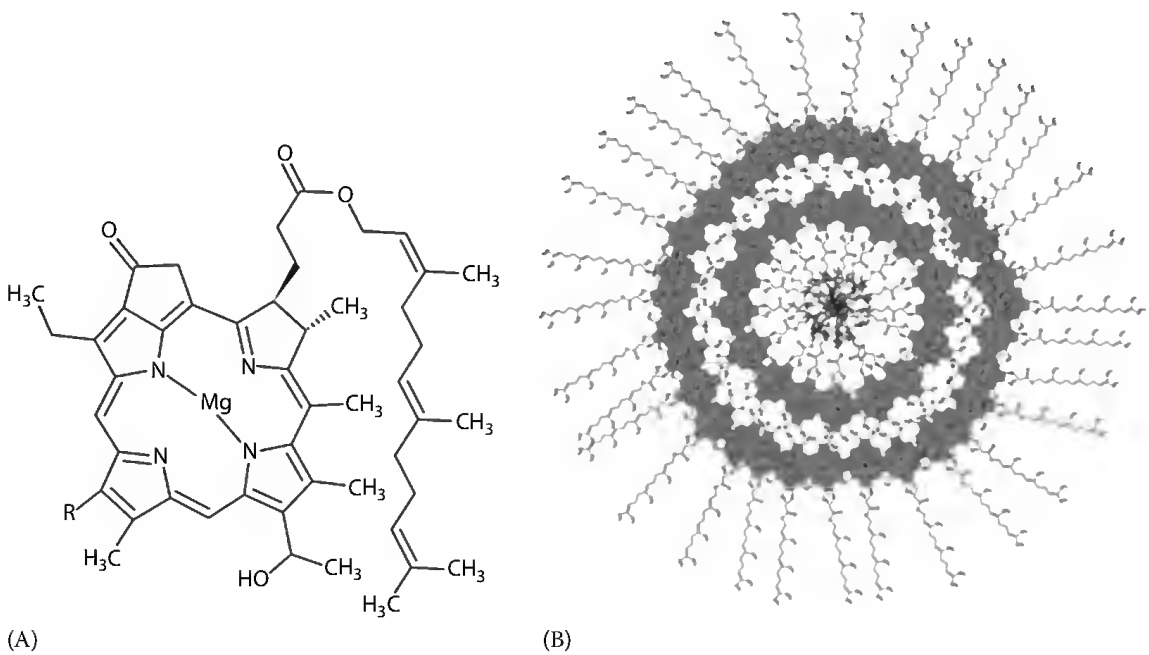

FIGURE 55.3 Chlorosomes, the peripheral antenna of green photosynthetic bacteria. Structure of bacteriochlorophyll *c*, the building block of the chlorosomes (A). The chlorin ring can have three naturally occurring different substitutes in *R*: ethyl, propyl, or iso-butyl moieties. The hydrophobic chain is formed by an unsaturated branched alcohol (farnesol, phytol, etc.) bound to the tetrapyrrole via ester formations. For more information, see Grimm et al. [139]. Cross-section view of the rod-shaped elements (B) of chlorosome with an average length of 100 nm and a diameter of 25–30 nm. The gray polar heads represent the chlorin macrocycle of the pigment. Within each chlorosome, a number of rod-shaped elements are formed by interconnected bacteriochlorophyll *c*.

excitation to travel by a biased random walk and to reach the RC much before the electron excitation energy of the pigment would dissipate. The rate of energy transfer between two (donor and acceptor) pigments (k_T) depends on the magnitude of interaction energy between the donor and acceptor molecules. If the coupling is very weak and is approximated by dipole–dipole interaction (as a rule of thumb, 1 nm < R < 10 nm), then the rate of energy transfer can be determined by the Förster's expression:

$$k_T = \frac{1}{\tau_0}\left(\frac{R_0}{R}\right)^6. \tag{55.1}$$

Here, R_0 is the Förster's distance (radius) at which the rate of energy transfer becomes equal to that of the intrinsic deactivation. R_0 depends upon the quantum yield of the donor fluorescence, the overlap integral between the emission spectrum of the donor and the absorption spectrum of the acceptor, the relative orientation of the donor and acceptor transition vectors, the so-called alignment or orientation factor and the refractive index of the medium. At smaller distance between the donor and the acceptor molecules (R < 1 nm), the electron wave functions may overlap and the Coulomb-type interactions are accompanied by several quantum effects (e.g., exchange interactions) [18]. Accordingly, the rate of energy transfer cannot be given by a simple, practical, and universal expression as Equation 55.1.

In native photosynthetic systems, the pigments form discrete structural and functional units to assure efficient harvest of the light. The first description of photosynthetic units (PSU) as supramolecular aggregates with a univocal purpose dates back to the research of Arnold and Emerson in the early 1930. In two pioneering articles [19,20], Emerson and Arnold found that the green alga *Chlorella* would produce, under optimal conditions, one molecule of oxygen every 2400 molecules of chlorophylls. Given that eight photons are needed to reduce one CO_2 molecule and evolve one molecule of O_2, the figure of 2400/8 = 300 chlorophylls represents the average number of pigment molecules that, without performing photochemistry, is anyway connected with the light phase of photosynthesis. It is clear today that chlorophylls and other pigments are organized within protein scaffoldings, and to present knowledge, we can conceive the PSU as a two-part assembled molecular machinery composed of a central unit dedicated to the conversion of (sun)light in CS (RC) and of an ancillary unit devoted to harvest the sun(light) (antenna). The antenna is organized in a peripheral part and a core antenna closely associated with the RC. The organizations of the supramolecular aggregates are illustrated in the color insert with atomic details in photosystem II in Figures 55.P1 and 55.P2 and in photosynthetic bacteria in Figures 55.B1 and 55.B2.

Antenna proteins offer perfect structural scaffolding for the efficient energy transfer among photosynthetic pigments. However, the scaffolding is not always required as in chlorosomes of green bacteria, where an array of light-harvesting pigments is organized without proteins (Figure 55.3). The chlorosomes are attached to the cytoplasm of the green bacteria and funnel the excitation energy to the RC by means of the so-called baseplate, a protein layer containing bacteriochlorophyll *a*. Because of the unusual organization (aggregates), the chlorosome structure has not been resolved and only models, in which BChl pigments are organized into large rods and lamellar structures are proposed on the basis of freeze-fracture electron microscopy and spectroscopic constraints [21]. According to a widely accepted model, the chlorosomes are formed by vesicles shaped as cigars, with an average length of 100 nm and a cross section of 25–30 nm. Within each chlorosome, a number of rod-shaped elements with a horizontal average cross section of 10 nm are formed by interconnected bacteriochlorophyll *c*. The bacteriochlorophyll *c* molecules are self-organized by extensive networks of hydrogen and coordinative bonding and by π– π interactions forming large supramolecular aggregates containing even thousands of BChls [22,23].

The chemical design of light-harvesting aggregates has taken more than 3×10^9 years to reach the actually unmatched efficiency both in terms of light capturing and of light conversion abilities, a goal

that artificial systems struggle to reach [24]. On the opposite side, the shelf life of these macromolecular aggregates outside their physiological environment does not allow to conjecture their direct use in any sort of device. As matter of examples, the various protective and repair mechanisms developed in oxygenic photosynthesis should be referred to [25–28]. In solution, one-third of the excited chlorophyll molecules populate triplet states, which may readily interact with the similar (triplet) state of the oxygen. Without protection of the carotenoids (whose triplet states are not sensitive to the attack of oxygen), the chlorophylls in the antenna or in RC would be exposed to significant photodestruction even under moderate light conditions [29,30]. Similarly, the D1 and D2 subunits of the PSII RC are subject to (photo-)damage but the entire photosynthetic process is not jeopardize since they can undergo to a very fast turnover by *de novo* synthesis ensuring the reestablishment of a fully active RC [31]. Not well operating heat dissipative pathways causing elevated temperature can be also harmful to RC [32,33]. The valuable protective and repair mechanisms in natural systems are based on very sophisticated processes accompanied by fine-tuning regulations but unfortunately are way out of any forecast in biomimetic systems. The present approach to mimic photosynthesis is to reproduce the physical phenomena (i.e., energy or electron transfer [ET]) without being diverted from the "useless" or "complicated" metabolic frills that evolution has put forward.

55.2.2 Artificial Model

Properly organized supramolecular arrays of molecules of large extinction coefficients can be synthesized to act as light-harvesting antenna. In recent years, the development of supramolecular chemistry, photophysics, and photochemistry enabled to design and assemble several of such arrays in which each molecular component can absorb the incident light effectively, transfer excitation to a nearby (unexcited) component before radiative or nonradiative deactivation, and funnel the excitation to a key component of the array interfaced with the photoconverter (see Figure 55.1).

55.2.2.1 Self-Organized Nanostructures for Artificial Light Harvest

In chlorosomes of green bacteria, the light-absorbing pigments form light-harvesting system by self-organization and without any protein scaffold. The strong interaction among pigments reduces the exciton–phonon coupling efficiently, which is mainly responsible for the optical dephasing and the localization of excitons on single chromophores. Due to the strong coupling, long-living coherent excitonic states are established even at room temperature. The coherence can be maintained over a range of about 100 chlorin molecules with duration of a few picoseconds. In this respect, the chlorosomes are extremely interesting objects as they may serve as artificial self-organized antenna system in artificial photosynthesis. The understanding the molecular interactions which control the self-aggregation of metallochlorins (BChl *c* or *d*, Figure 55.3) and the formation of supramolecular structures in natural systems and artificial aggregates is a great challenge and expectation.

Several principal structural models of the metallochlorin aggregates were proposed: (1) The rod model contains closely stacked chlorins based on a monomer basic unit. Some of these stacks combine at a higher level to single- or to double-rod structures [22]. (2) The lamellar structure model proposed from electron microscopy data uses chlorin dimers as basic building blocks and does not contain any rod elements. (3) The model of extended lamellar structure is based on solid-state nuclear magnetic resonance experiments [34]. The building block is dimeric chlorin but the structure contains rod elements, as well.

The ligation of the metal centers in chlorins has not been clearly attributed to a syn- or an anti-conformation [35,36]. The BChl *c* is rather unstable but can be modeled by Chl *a*, the main pigments of the photosynthetic apparatus of plants and algae, to which the magnesium of the chlorin ring is substituted by a zinc. The Zn-chlorophyll molecules associate with rod-shaped assemblies spontaneously as BChl *c* molecules do, but show much higher resistance to photodegradation. The drawback of such systems is the lack of any absorption peaks in the green part of the solar spectrum that diminishes

the light-harvesting capacity. This problem can be solved by preparation of rod-shaped structure with the use of a second chromophore—the green-absorbing naphthalene bisimide (NBI)—conjugated to Zn-Chl forming a dyad with 26% higher light absorption efficiency in the solar spectrum than Zn-Chl aggregates [37]. Such dyads can form aggregates longer than 200 nm with a horizontal section of few tens of nanometer. The energy transfer from the NBI chromophore to the chlorin aggregate is close to 100% efficient. By covalently attaching a third chromophore to this system, the solar coverage increases substantially and the absorption gap is practically closed.

Chlorosome-like artificial systems have been also obtained by using fluorescent chromophores as building blocks attached to a recombinant tobacco mosaic virus coat (TMVC) protein monomer functionalized with reactive cysteines [38]. Under appropriate buffer conditions, these monomers assemble into rods or stacks of disks that reach hundreds of nanometers in length. In these rods, several hundreds of chromophores can arrange every 100 nm of TMVC rods, with a spacing between neighboring chromophores averaging 2 nm in the horizontal and vertical dimensions. Donors and acceptor, chosen on the base of their large extinction coefficients ($\sim 10^5\ M^{-1}\ cm^{-1}$), have their excitation and emission maxima ranging between 495 and 612 nm, covering a large portion of the visible part of the solar spectrum. Energy transfer from donors (Oregon Green 488 and tetramethylrhodamine) to a single acceptor (Alexa Fluor 594) was observed, with an efficiency of 47%.

55.2.2.2 Dendrimers

The dendrimers (see an example in Figure 55.3) constitute a class of well-defined macromolecules exhibiting a treelike, nanometer-size architecture, reminiscent of the architecture of natural light-harvesting complexes [39]. Their structures are hence very attractive for the construction of artificial antennae since their convergent and/or divergent synthesis allows, in a few steps, the assembly of a large number of chromophores in a restricted space and with high topological control.

Photoactive units can be directly incorporated in or appended to different regions of a dendritic structure with covalent or coordination bonds or even caged into cavities formed within the structure such as void regions. Due to the proximity of the residues, the various functional groups of a dendrimer may easily interact with one another, a prerequisite for artificial antennas. The constitutive building blocks can be of different types among which porphyrins, a close analog of chlorophylls.

Photophysical investigations on porphyrin-based dendrimers have revealed [40] that (1) the singlet excited-state energy transfer from Zn-porphyrin to free-base porphyrin is extremely efficient (the yield is 95%–99%), (2) no competitive ET reactions are observed, (3) the predominant energy transfer mechanism involves through-bond communication via the linker, and (4) the energy transfer between two isoenergetic Zn-porphyrins is very fast. Hence, extended multiporphyrin arrays can be rationally designed with predictable photophysical features and efficient light-harvesting properties. By means of a modular approach and the use of an opportune linkers between aryl groups on adjacent tetraarylporphyrin macrocycles (typically ethyne groups), a variety of di-, tri-, tetra-, and pentameric porphyrin arrays have been synthetized [41]. Efficient excitation energy transfer has been shown to occur in giant dendrimer wheels (sizing about 7 nm in diameter) composed of 24 porphyrin units. In such system, the energy hopping between neighboring tetraporphyrin moieties takes place with a rate of 35 ps^{-1} [42]. Attempts to build up artificial antennae by self-assembling of porphyrin components have also been reported [22,37,43–46]. Recently, a series of dendritic multiporphyrin array systems were prepared to study singlet–singlet and triplet–triplet energy transfer from peripheral Zn-porphyrins to the focal core formed by a free-base porphyrin. In these systems, triplet–triplet annihilation has been detected [47].

The characteristics of light collection of the dendrimers dependent on morphology [48–50]. With the use of a free-base porphyrin as core, it is possible to connect up to four dendrons, originating from the four *meso* positions of the ring, generating four different shapes with different light-harvesting characteristics (see Figure 55.4 for the structure of the dendron). In the most substituted case, the four dendrons

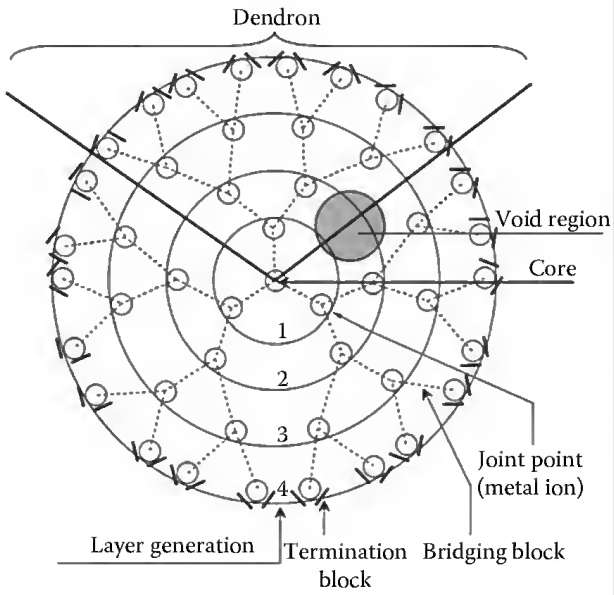

Joint blocks (O)	
Ru^{2+}	Ruthenium
Os^{2+}	Osmium
Bridging blocks (- - -)	
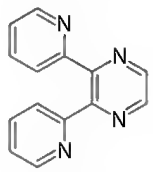	2,5 bis (2-Pyridyl)pyrazine (2,3 dpp)
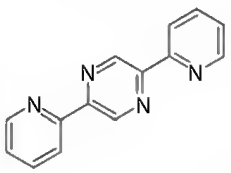	2,5 bis (2-Pyridyl)pyrazine (2,5 dpp)
Termination blocks (\ /)	
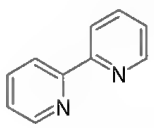	2,2′-Bipyridine (Bpy)
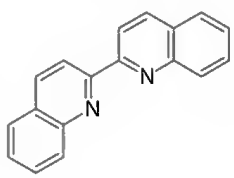	2,2′-Biquinoline (Biq)

FIGURE 55.4 General topology of a dendrite formed by the building (joint, bridging, and termination) blocks shown in the table. Each dendron, indicated by the curly bracket and limited by two thick black lines, is allowed to grow for four generations starting from a common core from which two other dendrons can layer up. The branching or (joint) points (O) are metal ions, ruthenium, and/or osmium, which coordinate three bridging units (- - -). These building blocks have two coordinative moieties on the opposite sides of the molecule, allowing the growth of a further layer. The growth of a dendron can be stopped by the termination blocks (\ /) having the coordinating nitrogen atoms only on one side of the molecule. A rather large void region (filled gray circle) wedging away from the core is formed between each couple of dendrons. (Redrawn from Balzani, V. et al., *ChemSusChem*, 1(1–2), 26, 2008.)

assume a star-like structure that incorporates 28 light-absorbing and interacting Zn-porphyrins able to efficiently gather light and funnel the absorbed energy to the core with a rate constant of $1.0 \times 10^9\ s^{-1}$ and 71% efficiency (Figure 55.5). In the case of monosubstitution, the conically shaped single dendron shows a 10-fold smaller rate of energy transfer with an efficiency as low as to 19%. In addition to suited morphology, the cooperative effects also improve the efficiency of the energy transfer within dendrons: the interaction increases with increasing number of chromophores but decreases with increasing conformational mobility (e.g., the efficiency of the energy transfer in a given dendron decreases with increasing temperature).

Thanks to the large number of chromophores, the suitable morphology and the compact scaffold of dendrimers they function efficiently in capture of visible photons and in transfer of the energy to the central core, mimicking natural photosynthetic systems, where energy migration within "wheels" of chromophoric groups (see Figures 55.B1 and 55.P1 in the color insert) results in an efficient energy transfer to the central RC.

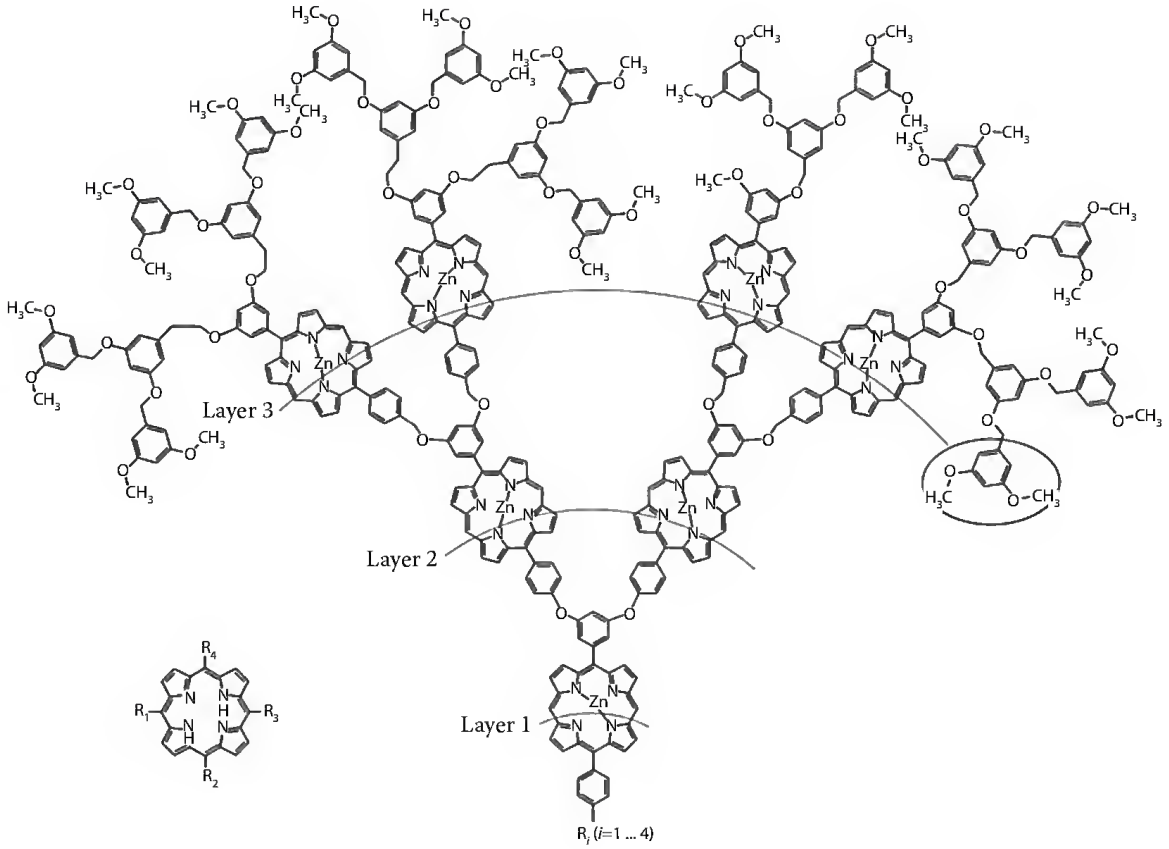

FIGURE 55.5 Building blocks of light-harvesting dendrimers based on porphyrins. A free-base porphyrin is in the core (left corner) and four dendrons (ligands) each constituting of seven Zn-porphyrin units (top) can be attached to R_1, R_2, R_3, and R_4. In these dendrons (see table in Figure 55.4), the bridging block is Zn-porphyrin while the termination block is 3,5 dimethoxy benzene (circled). The dendron has grown three layers before termination, and the core is formed by a free-base porphyrin. (Redrawn from Balzani, V. et al., *ChemSusChem*, 1(1–2), 26, 2008.)

55.3 Systems for Charge Separation and Electron Transfer

55.3.1 Biological Paragon

Once (sun)light is absorbed by the antenna of the photosynthetic organisms, the excitation is funneled to the photochemical core of the PSU, the RC. Here, a shallow energy trap catches the exciton: it cannot easily escape from the RC because of the lower excited energy state of the Chl dimer of the RC (P*) than those of the excited Chls in the antennae (Chl*). The excited state of the dimer has two possible deactivation routes: the first is to dissipate the electron excitation energy in the environment as fluorescence and the second is to generate a photoelectron that is transferred to a neighboring pigment, generating a biological hole–electron system. Similarly to what has been described in the case of energy transfer, the first possibility is a waist of energy (although can be utilized to characterize the photosynthetic states of the organisms [51,52]), while the second is a useful process that can take place only if the CS is faster than the dissipation. In RC, this is exactly the case, as illustrated in Figure 55.6 for purple photosynthetic bacteria, where the rate of the first ET step is faster by three orders of magnitude than the radiative decay of the excitation. This rule of thumb that forward reactions are at least two orders of magnitude faster than the competing wasteful reactions is true also for the following steps of the ET, in which the electron donation to the next acceptor is significantly faster than the back reaction and the CR [53–55]. Due to the well-organized architecture of the protein scaffolding and of

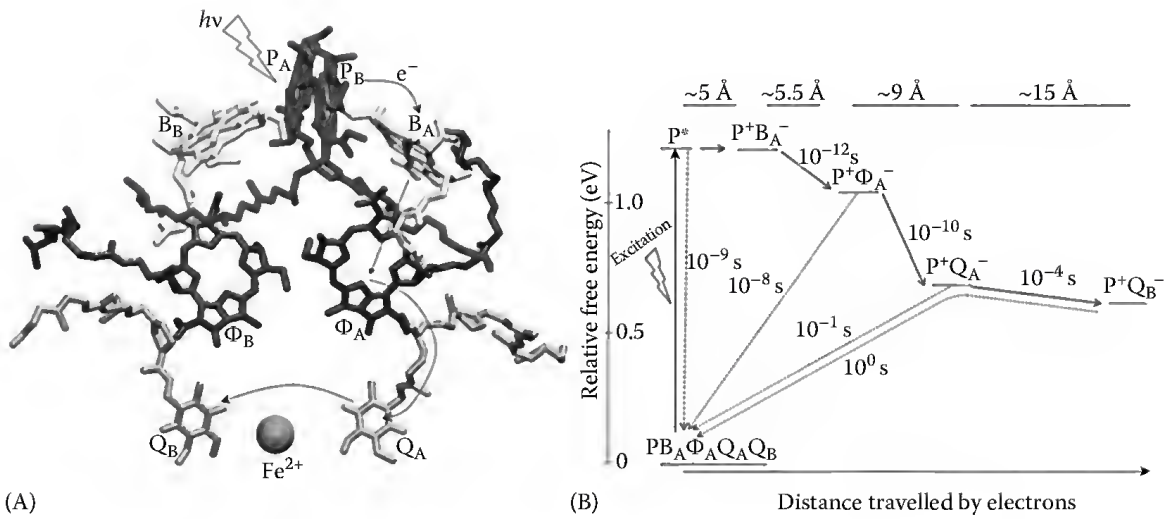

FIGURE 55.6 Organization of cofactors in two branches (A and B, left) and the free energies of redox states (right) in the RC of purple bacterium *Rba sphaeroides*. (Redrawn from Feher, G. et al., *Nature*, 339(6220), 111, 1989.) The dimer (P) formed by two partially overlapping molecules of bacteriochlorophyll *a* serves as trap for excitation energy and source of electron to the A (active) branch. The electron is transferred to the secondary ubiquinone electron acceptor (Q_B) via the bacteriopheophytin (Φ_A) and the primary ubiquinone (Q_A). The bridging bacteriochlorophyll monomer (B_A) and the nonheme iron ion facilitate but do not directly participate in ET. In the presence of external donor, reduced soluble cytochrome *c* (not shown), Q_B can accept up to two electrons and upon quinol (Q_BH_2) formation, it is replaced by exogenous quinone (quinone cycle). The closest distances between two neighboring pigments are as follows: P – B_A ~ 5 Å, B_A – Φ_A ~ 5.5 Å, Φ_A – Q_A ~ 9 Å, and Q_A – Q_B ~ 15 Å. The larger is the distance covered by the electron, the smaller are the free energy gaps and the rates of forward ET ($A_i \rightarrow A_{i+1}$) excluding $P^*B_A \rightarrow P^+B_A^-$ [140], backward ET ($A_i \leftarrow A_{i+1}$), and CR ($P^+A_i^- \rightarrow PA_i$). A_i and A_{i+1} denote neighboring electron acceptors.

the pigment localization, as shown in Figure 55.6 the arrangement is extremely efficient: 98% of the excitons caught by the dimer will generate CS [56] and subsequently semiquinone molecule [53,57]. In the presence of exogenous electron donors, the hole can be filled [58] and the RC is ready for a second cycle that terminates with the double reduction and double protonation of the quinone (refer to Figure 55.B3 in the color insert).

The successful competition between CS reactions and CR reactions is well explained by the Marcus theory of the ET reactions [59]. This theory predicts a parabolic relationship (see Figure 55.6) between the logarithm of the rate of the ET, k_{ET}, and the driving force of the reaction, $-\Delta G^\circ_{ET}$:

$$\ln k_{ET} = -\frac{\left(\Delta G^\circ_{ET} + \lambda\right)^2}{4\lambda k_B T} + \ln k_{max}, \tag{55.2}$$

where

k_BT is the Boltzmann term
λ is the reorganization energy
k_{max} is the maximum rate of ET

k_{max} is the product of the electron transmission coefficient, k (=1 for adiabatic reaction and ≪1 for nonadiabatic reactions) and the effective frequency of nuclear vibrations, ν_{nucl} (≈10^{13} s^{-1}): $k_{max} = k\nu_{nucl}$. In a couple formed by an electron donor and an electron acceptor, optimal conditions for forward ET are found for $-\Delta G^\circ_{ET} = \lambda_{CS}$ and the rate of charge-separated state formation corresponds to k_{max}, graphically found on the maximum of the CS parabola (see Figure 55.7). At this value of $-\Delta G^\circ_{ET}$, the highly exergonic

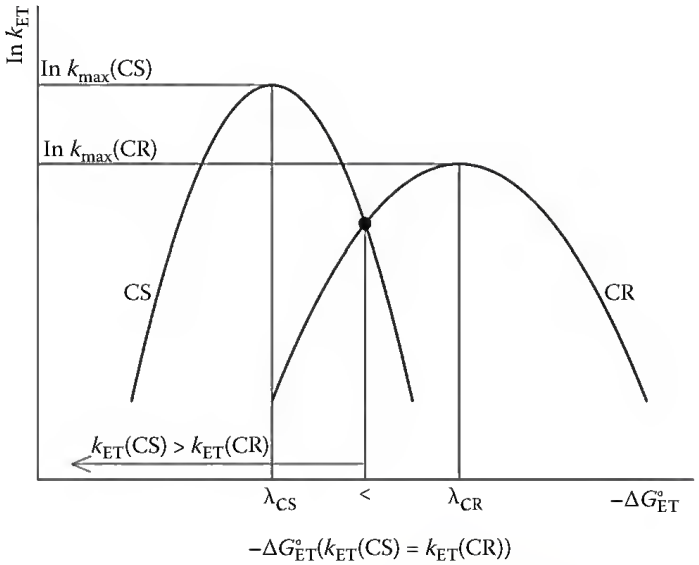

FIGURE 55.7 Marcus parabolas for CS and CR derived from Equation 55.2. At the peak of the parabola (the rate is at maximum), the driving force equals the reorganization energy, $-\Delta G^{\circ}_{ET} = \lambda$. Fast CS and slow CR are facilitated by small λ_{CS} and large λ_{CR}, respectively. The larger is the difference in reorganization energies (and in maximum rates), the wider is the range of driving force where the stabilization of the charges is effective.

and energy-wasting back ET process, found on the CR parabola in correspondence of the CS maximum, is much slower than the forward one and is shifted deeply into the inverted region of CS, leading to the formation of a charge-separated state with both high quantum yield and long lifetime.

This is the strategy adopted by natural photosynthesis. In bacterial RCs, the driving force $-\Delta G^{\circ}_{ET}$ ($P\Phi \rightarrow P^{+}\Phi^{-}$) of the donor–acceptor couple $P^{+}\Phi_{A}^{-}$ (≈1.2 eV) is lowered by roughly 0.2 eV compared to P* (1.38 eV) (Figure 55.6), which matches the CS reorganization energy optimizing the forward ET, but the CR process lies deep within the Marcus inverted region making it much slower.

The driving force at which the rates of the forward and back ET are equal (crossing point of the two parabolas in Figure 55.7) is obtained by applying Equation 55.2 to CS and CR and impose that $(\ln k_{ET})_{CS} = (\ln k_{ET})_{CR}$:

$$-\Delta G^{\circ}_{ET}\left(k_{CS} = k_{CR}\right) = \sqrt{\frac{\lambda_{CR} - \lambda_{CS} + 4k_{B}T \ln \dfrac{k_{max}(CS)}{k_{max}(CR)}}{\dfrac{1}{\lambda_{CS}} - \dfrac{1}{\lambda_{CR}}}}. \tag{55.3}$$

If the actual standard free energy change for ET reaction is smaller than this limit, the rate of the forward ET will exceed that of the competing reverse reaction. The larger is the difference between the reorganization energies ($\lambda_{CR} \gg \lambda_{CS}$) and the maximum rates ($k_{max}(CS) \gg k_{max}(CR)$) of the ET, the more favorable will be the CS and stabilization. The observed rate of ET is highly sensitive to the (network of) reaction pathways and consequently to the distance between donors and acceptors in proteins: a variation of 2 nm in the distance, the ET rate changes by 12 orders of magnitude [60,61]. The exact distance dependence of the rate of the ET is more complicated than that of the electronic excitation energy (Förster's expression, see Equation 55.1) but excellent empirical approximations are in use [61–63] which may serve also as ruler to determine distances between redox centers in biological systems [64].

55.3.2 Biomimetic Systems

Both artificial and natural light-harvesting systems would turn out useless in the absence of a molecular device able to induce photoelectron transfer and eventually to generate an electron–hole couple. It is hence vital the design and synthesis of artificial molecular systems provided with suitable organized electron donors and acceptors, which mimic photochemical CS and ET in photosynthetic proteins [8,65,66]. Many bioinspired systems employ photoactive transition metal complexes or chromophores with extended conjugated π-systems, such as porphyrins, which are often synthetically easier to incorporate into complex donor–acceptor systems than natural chlorophylls and bacteriochlorophylls. Porphyrins are frequently used as both donors and acceptors in these arrays, while aromatic amines and carotenoids serve as secondary electron donors. In addition, fullerenes, quinones, aromatic imides, and bis(imides) are common electron acceptors because of their low reduction potentials and stable anions. Oppositely to what happens in natural RCs, the artificial RCs do not need any further design for double ET as in the case of quinone reduction, but rather has to stabilize the photogenerated hole–electron couple as much as possible. Notwithstanding such simplification, the fight against wasteful CR reaction is much harder in bioinspired systems.

If CS occurs in a single step, the competition with CR will be extremely unfavorable. As in natural photosynthetic RC proteins, secondary electron donors and acceptors need to be attached to the artificial RC to further spatially separate the charge pair, thereby increasing the lifetime of the charge-separated state. Multicomponent donor–acceptor arrays performing multistep ET reactions are most useful for producing long-living charge-separated states. The importance of using a cascade of thermal ET steps following the initial photochemical event to increase CS lifetimes has been widely demonstrated [8,67–69].

Studies on the optimization of the free energy changes, distances, and orientations between the various donors and acceptors and minimizing the reorganization energy for ET have determined synthetic strategies for the development of novel molecular structures to tailor the CS and storage characteristics for specific applications. Relatively simple electron donor–acceptor ensembles linked by covalent and noncovalent bonds have been synthesized to attain fast CS with extremely slow CR of high-energy CS states provided by minimizing the reorganization energy of ET according to Marcus theory of ET [70,71]. Such simple electron donor–acceptor systems provide a variety of applications for photoinduced ET catalytic systems including radical coupling of radical ions produced by ET of electron donors and acceptors with the CS states and the photocatalytic hydrogen evolution.

55.3.2.1 Artificial Reaction Centers

The artificial RCs have to match the performance of the natural ones in terms of the fraction of photon energy conserved, the quantum yield of CS, and the lifetime of the photoinduced CS. In the synthesized molecule, the distance between electron donor and acceptor should not be too small in order to have much faster forward than backward ET. To follow this demand, a spacer that physically separates the donor and the acceptor should be inserted. The yield of light harvest would be increased if the spacer acted as sensitizer, as well. In addition, the introduction of secondary electron acceptors and donors would further stabilize the charge-separated state.

Figure 55.8 shows an example of an artificial photosynthetic RC formed by a molecular pentad, which is formally obtained by introducing a secondary acceptor and a secondary donor/chromophore in a triad [72,73]. The ZnP of the central dyad absorbs photons in the visible spectral range and becomes excited: C-ZnP*-P-Q_1-Q_2. The excitation energy is transferred to the neighbor porphyrin forming the singlet state C-ZnP-P*-Q_1-Q_2. From P, a photoelectron is shuttled toward the first electron acceptor, the quinone Q_1, forming the electron–hole system C-ZnP-P^+-$Q_1^{\bullet -}$-Q_2. The following step is performed by the secondary electron acceptor (Q_2) and electron donor (C) to establish the final charge-separated state $C^{\bullet +}$-ZnP-P-Q_1-$Q_2^{\bullet -}$. The relatively high quantum yield (0.83) and energy conversion efficiency (larger than 50%) make the assembly as promising candidate of photoconverter. The main drawbacks are the

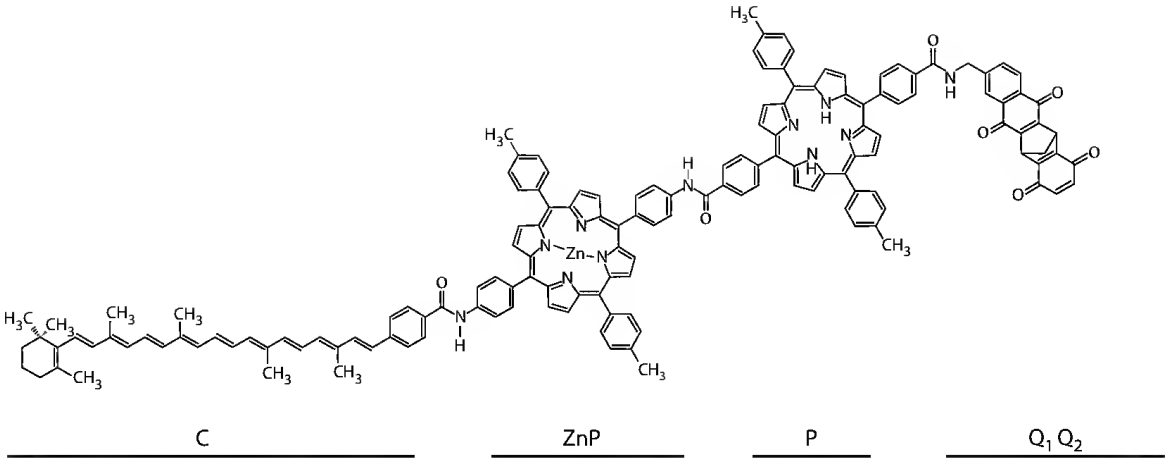

FIGURE 55.8 Molecular pentad as artificial RC. This molecule consists of a central tetraphenyl-porphyrin dyad (ZnP-P) connected by an amido group. The dyad is attached to a carotenoid moiety (C) on the ZnP side and to a diquinone moiety (Q_1–Q_2) on the P side via amido groups. With a molecular weight slightly above 2000 g/mol, this pentad has shown very interesting similarity (see text for details) with the photochemical behavior of bacterial RCs, whose molecular weight is well above 100.000 g/mol. (Redrawn from Gust, D. et al., Mimicking bacterial photosynthesis, in *Artificial Photosynthesis*, A.F. Collings and C. Critchley, Eds, Wiley-VCH Weinheim, Germany, 2005, pp. 187–210.)

high hydrophobicity of the molecules and the short-lived final state (the lifetime is 55 μs in chloroform) that is four orders of magnitude smaller than that of the bacterial RC (see Figure 55.6).

55.3.2.2 Porphyrin–Fullerene-Based Artificial Photosynthetic Systems

Porphyrins are excellent electron donors as well as sensitizers and the most frequently employed building blocks in artificial photosynthetic models. Although the quinones are the obligatory electron acceptors of native photosynthesis and frequently used also in artificial systems, buckminsterfullerene (C_{60}) [74] covalently linked to porphyrin appeared recently as novel type of attractive electron acceptor. The following basic characteristics of fullerenes can be utilized in artificial photoconverter systems: (1) the C_{60} consists solely of 60 carbon atoms and has a moderate size (with a molecular weight of 720 g/mol and a diameter of 8.8 Å) and round shape; (2) has moderate electron-accepting abilities [–300 ÷ –400 mV vs. standard calomel electrode (SCE)] and can reversibly accommodate up to six electrons; (3) the energy levels of the first excited singlet (2.0 eV) and triplet states (1.6 eV) are comparable to those of porphyrins; and (4) has a rigid framework in the ground, excited, and reduced states and high stability under severe environmental conditions.

Various porphyrin–fullerene systems have been synthesized to elucidate the intrinsic ET properties of fullerenes [71,75,76]. The C_{60} accelerated the photoinduced CS and the ET, but slowed down the CR. This is in sharp contrast to those of conventional planar acceptors such as quinones and imides. The distinctive ET properties of fullerene result from the small reorganization energies arising from the widely delocalized π system on the spherical structure accompanied with the rigid structure. This makes the long-lived charge-separated states with high quantum yield in donor–C_{60} systems. Porphyrin–fullerene systems display stepwise ET relay, and the lifetimes of the final charge-separated state in tetrads and pentads are comparable to those of the $P^+Q_B^{\bullet-}$ couple in bacterial RCs (see Figure 55.6).

Proper coupling of functions of antenna (light absorption) and RC (CS) in one artificial system is a crucial task [77–79]. Among the several attempts reported recently, only one will be demonstrated here (Figure 55.9). The CS (and recombination) module is represented by a porphyrin–fullerene dyad linked to a phenyl ring of an hexaphenylbenzene core bearing at the other positions five light-gathering moieties formed by bis(phenylethynyl)anthracene (for details see the legend of Figure 55.9).

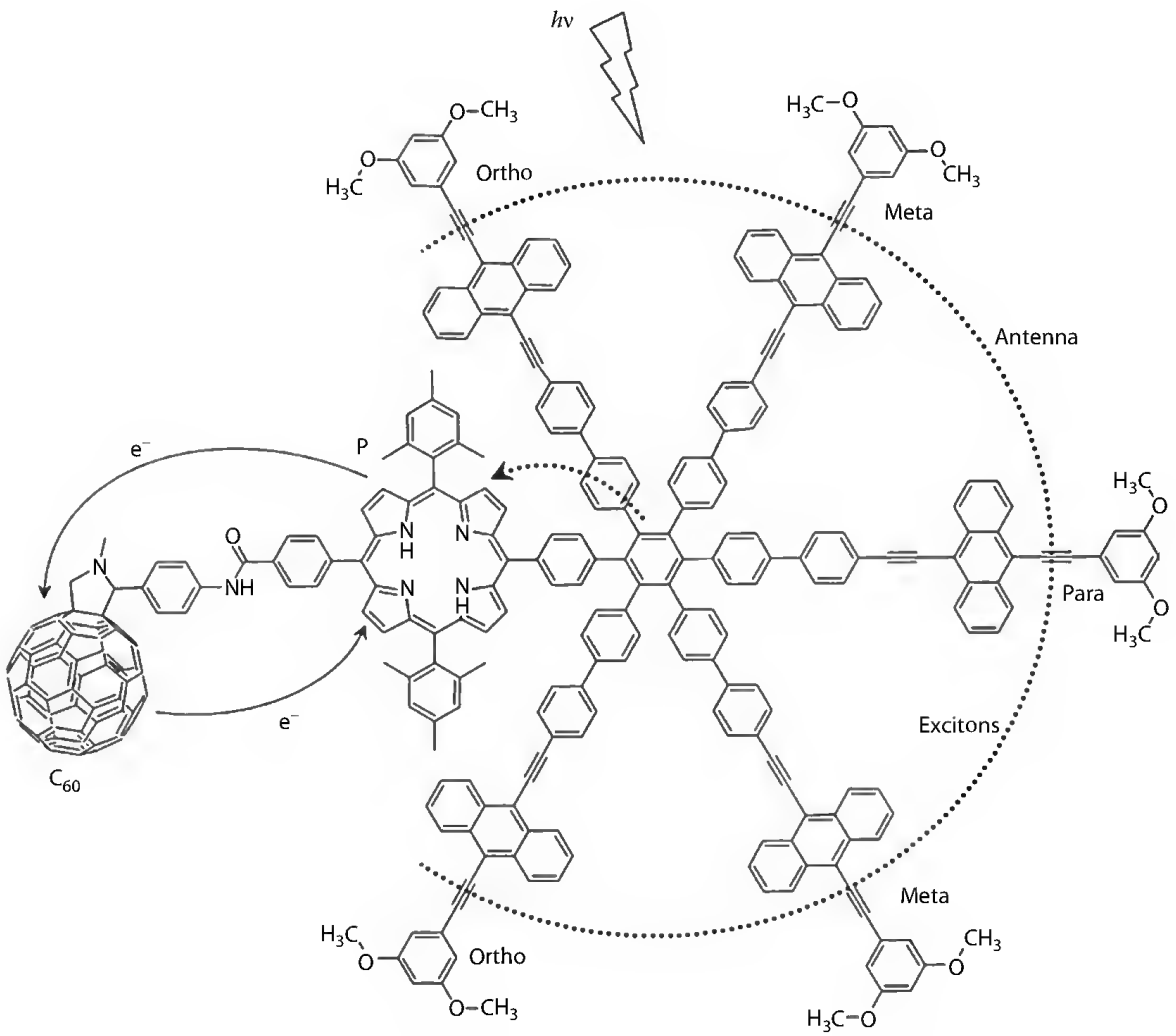

FIGURE 55.9 Coupling of energy and ET processes in a single biomimetic macromolecule with a porphyrin- (P) and fullerene (C_{60})-based macromolecular antenna–RC complex. The antenna moiety of the molecular system has very high extinction coefficient in the blue region of the visible spectrum (430 ÷ 475 nm), and the absorbed excitation energy is shared among the pigments (dotted open circle) with very high rate (2.5×10^{12} s^{-1}). The energy is funneled to the porphyrin via the ortho-, meta- and para-position of the central phenyl ring with somewhat less rates of 1.1×10^{12} s^{-1}, 1.3×10^{11} s^{-1}, and 2.5×10^{11} s^{-1}, respectively (dotted arrow). Resonance (Förster-type) mechanism dominates the energy transfer but through-bond and electron-exchange mechanisms may also contribute to the very high quantum yield of the process estimated to 80% for porphyrin and to 96% for Zn-porphyrin. From the first excited singlet state of the porphyrin (P^*C_{60}), one electron is donated to fullerene (the rate is 4.0×10^8 s^{-1}) forming the charge-separated state $P^+C_{60}^-$. The CR ($P^+C_{60}^- \rightarrow PC_{60}$) is four times slower (the rate is 1.1×10^8 s^{-1}). ETs are shown by solid arrows.

Highly efficient photoinduced energy and ET were achieved on gold and indium tin oxide (ITO) electrodes modified with self-assembled monolayers of the porphyrin–fullerene systems [71]. The internal quantum yield for photocurrent generation of the boron dipyrrin and ferrocene–porphyrin–C_{60} triad system has reached up to 50%. Supramolecular arrays of porphyrin with fullerene were linked to gold nanoparticles or to high-surface-area nanocrystalline TiO_2 films creating dye-sensitized solar cells [80]. The dye-sensitized bulk heterojunction photoelectrochemical cells possessed both characteristics of dye-sensitized and bulk heterojunction solar cells. These encouraging results show the advantages of fullerenes as electron acceptors in artificial photosynthetic models, photonic molecular devices and machines, and organic molecular electronics including solar cells.

55.4 Great Expectations: Oxygen and Hydrogen Gas Production

55.4.1 Oxygen Evolution

55.4.1.1 Native Oxygen-Evolving System

Through water oxidation, oxygen is continuously generated by oxygenic photosynthetic organisms (i.e., plants, algae, and cyanobacteria), which maintain the level of O_2 in the atmosphere presently around 21%. This paramount task is accomplished by use of a catalyst called oxygen-evolving complex (OEC, see the e-donor catalytic side in Figure 55.1). Due to its vital role in the development and maintenance of the present terrestrial conditions for life, its importance cannot be overestimated ("the most important catalyst on Earth"). The OEC is an extrinsic subunit of the PSII consisting of a cluster of four manganese ions, one calcium ion and one chloride ion. The latter is required in the oxygen evolution but the structural and chemical details are not yet clear.

The OEC is responsible for transfer of four electrons from water to the photo-oxidized chlorophyll dimer of the D1D2-RC. The extremely highly oxidizing P^+ is rereduced by a deprotonated tyrosine residue (Tyr_Z or Y_Z) that is subsequently rereduced by the OEC (see Figure 55.P3 in the color insert) in the color insert). The ET steps on the donor side of the PSII RC are very fast, much faster than the oxygen evolution. The observed period 4 damped oscillation of the oxygen evolution upon trains of saturating flashes was the first evidence that the Mn_4Ca cluster accumulated the oxidizing equivalents in five, so-called S (S_0, S_1, S_2, S_3, and S_4) states [81,82]. The values of the subscript of the S states indicate the oxidation state of the enzyme. In dark-adapted state, the OEC is found in a mixture of S_0 and S_1 states (usually in 25%–75% ratio) and, omitting the trivial waste processes of misses and double hits, the oxidation state of the enzyme increases stepwise after each saturating flashes of light (or ET steps) (Kok's clock). Finally, the S_4 state converts to S_0 state accompanied by splitting of the two water molecules ligated to the Mn_4Ca cluster resulting the release of one oxygen molecule and four H^+ ions.

Unrevealing the chemistry and the structure–function relationship is the key point to understand the function of the chemical core of the OEC and to attempt the mimicry of such indispensable enzyme [83].

55.4.1.2 Attempts to Artificial Water Splitting

The hardest but most wanted part of mimicking natural photosynthesis is splitting the water molecules to get the electrons and protons necessary to sustain additional chemical process including the reduction of CO_2. Under standard conditions, water can be reversibly electrolyzed at redox potential of +0.81 V – (–0.41 V) = +1.22 V (Figure 55.10). As splitting water requires energy input of about 2.5 eV, the oxidation of water requires a catalyst (e-donor catalytic site). Similarly, the reduction of proton needs catalyst, as well (e-acceptor catalytic site). The catalysts react with photons to initiate the chemical reactions. The e-acceptor site catalyst must be more negative than −0.41 V, the e-donor site catalyst must be more positive than 0.81 eV, and visible light ($\lambda > 400$ nm) should be applied.

In addition to the energy level requirements shown in Figure 55.10, it is important to suppress back ET by kinetic design of the ET reactions and/or by adoption of a heterogeneous phase to achieve unidirectional ET.

In construction of artificial systems, we have to face with additional difficulty that arises from coupling of photoinduced CS with oxygen evolution or reduction of CO_2 because different numbers of electrons are involved in these chemical reactions. CS is a one-photon and one-electron process whereas water splitting is a four-electron process. In natural photosynthesis, the problem is solved by the magnificent Mn_4Ca cluster that (1) releases electrons in a stepwise manner at constant potential and (2) oxidizes water molecules in a concerted way avoiding the formation of high-energy intermediates. Such multiple ET process is coupled to proton transfer (proton-coupled electron transfer [PCET]) and becomes thermodynamically favorable [84]. Unfortunately, such efficient catalyst cannot be used directly in artificial systems, and the design of specific multielectron redox catalysts remains a fascinating and challenging but yet unsolved problem.

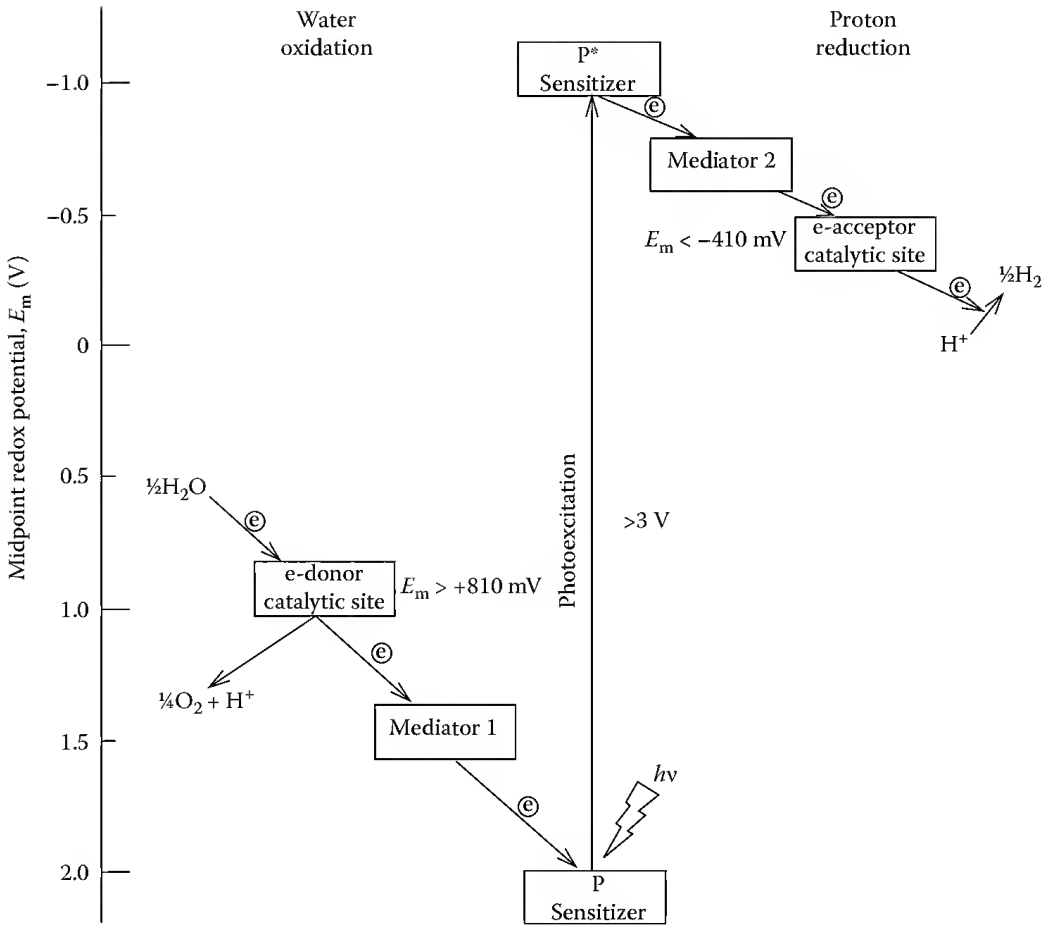

FIGURE 55.10 A schematic view of the electron flow and energy level requirements of sensitizer (P), catalytic sites, and mediators to oxidize water and to reduce proton (or CO_2). The minimum difference of the midpoint redox potentials between the two catalytic sites is $\Delta E_m = 1.23$ V. P can be a dye sensitizer (often metal complex), small bandgap semiconductor or dye-sensitized large bandgap semiconductor. Selection of appropriate catalysts and mediators is a key problem of current research.

55.4.1.3 Molecular Catalysts for Water Oxidation

Photooxidation of water molecules into oxygen, electrons, and protons (hydrogen ions) is one of the two essential half reactions of artificial photosynthetic systems—it provides the electrons needed to reduce carbon dioxide to a fuel. Effective photooxidation requires a catalyst that is both efficient in its use of solar photons and fast enough to keep up with solar flux in order to avoid wasting those photons.

The last 10 years have witnessed important advances in this area but we are still far away from our great expectation [85]. We will list here a few of the more successful catalysts.

55.4.1.3.1 Manganese

Manganese-based organometallic complexes have been employed to model off photosystem II, showing some promises as photocatalysts for water oxidation. However, the manganese that acts as a catalyst in plants does not work as well in a man-made setup, mostly because of the poor water solubility, easy degradation, and less robustness. Additional disadvantage is that the molecular geometry in plants is extraordinarily complex and exact and man-made setups cannot replicate that level of intricacy. Presently, the manganese-based artificial systems are inefficient and impractical.

55.4.1.3.2 Manganese–Ruthenium Complexes

Among the several multifunctional supramolecular complexes that are currently designing and synthesized hoping to achieve the light-driven oxidation of water, oligopyridine Ru(II) complexes are frequently chosen [86,87] because of their suited photochemical, photophysical, and electrochemical properties [88]. A variety of mono- and multinuclear Mn(II) complexes have been covalently linked to such complexes. Furthermore, inspired by the presence of tyrosine as a mediator in the photooxidation of the Mn cluster in PSII, tyrosines or another type of phenol moieties were introduced in the model systems. One example of such systems is given in Figure 55.11, where a dinuclear Mn complex linked to a Ru(II) complex is shown. The photogenerated excited state of the Ru(II) complex is quenched by ET to an external electron acceptor. Subsequently, the Ru(III) complex is rereduced by rapid intramolecular ET either from the Mn cluster ($k > 1 \times 10^7\ s^{-1}$) or from the tyrosine unit. The dinuclear Mn complex is oxidized to the Mn(II)–Mn(III) state, or a tyrosine radical is generated. The Mn cluster has appropriate redox properties and is capable of multiple ET needed for splitting water molecules. The model system closely mimics the primary reaction steps on the donor side of PSII, but as yet catalytic water oxidation has not been achieved.

Beside the almost overwhelming demand of splitting water with the aid of sunlight (artificial photosynthesis), the serious drawback associated with the formation of very aggressive substances in the process of water oxidation needs to be addressed. Plants solve this problem by constantly repairing and/or replacing a part of their green catalysts, but such evolved mechanism is far from being achieved

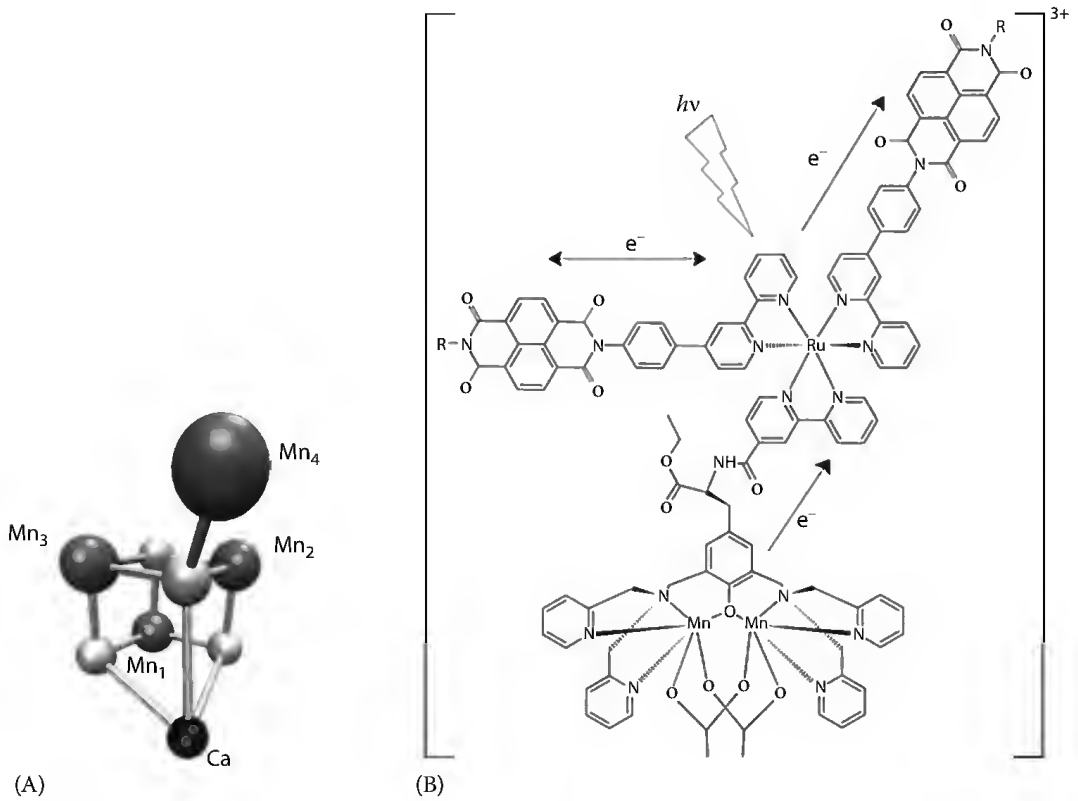

FIGURE 55.11 Manganese center in natural and artificial catalytic sites. (A) 3D structure of the OEC of PSII from the cyanobacterium *T. elongatus* at 3.5 Å resolution [141]. The white spheres represent the four oxygen atoms, the gray spheres the four manganese (Mn_i) atoms, and the black sphere the bivalent calcium (Ca) ion (in the front bottom corner). (B) Light-induced intramolecular ET in binuclear Mn(II) and Ru(II) complex as model system of the donor and acceptor sides of the PSII RC. The Ru(II) complex is photoexcited (Ru(II) → Ru(II)*), quenched, and oxidized by ET to an external electron acceptor (Ru(II)* → Ru(III)) and rapidly rereduced from the Mn cluster or from the tyrosine unit (Ru(III) → Ru(II)).

in artificial systems. Notwithstanding this, stable catalysts are being designed. Recently, tetraruthenium complexes were synthesized as stable catalyst for water oxidation [89]. The metal oxide cluster with a core of four ruthenium ions catalyzes the fast and effective oxidation of water to oxygen while remaining stable itself. This water-soluble complex—effective in water solution already at room temperature—does not contain any organic components, which presumably would explain its high stability. Presently, such catalyst has only being used with chemical oxidants, but the following step is its integration into photoactive system which efficiently converts solar energy into chemical energy.

55.4.1.3.3 Cobalt Oxide

One of the more recently discovered catalysts, clusters of nanosized cobalt oxide molecules (CoO) have been found to be a very stable and robust system and can be efficiently employed in artificial photosynthetic systems [90]. Cobalt oxide is currently a popular industrial catalyst. Rod-shaped nanocrystals of cobalt oxide were found effective in water-splitting molecules, with a turnover rate slightly higher than 1000 oxygen molecules produced per second per cluster cobalt oxide (Co_3O_4) which is commensurate with solar flux at ground level ($\sim 1\,kW \cdot m^{-2}$). Interestingly, the oxygen evolution yield of cobalt oxide clusters of micrometric size is 1600 times smaller than in nanostructured systems. While the catalytic efficiency of the cobalt metal itself was important, the size of the bundled clusters was the major factor behind the enhanced efficiency and rate. The comparatively very large internal area of the bundles (where catalysis takes place) was the cause of the increased efficiency. The efficiency, turnover rate, and size of the cobalt oxide nanocrystal clusters are comparable to the similar characteristics of photosystem II. Due to the abundance of cobalt oxide, the stability of the nanoclusters, the modest overpotential, and the mild pH and temperature conditions, it is believed a promising catalytic component of an artificial photosystem. The next big step, however, will be to integrate the water oxidation half reaction with the carbon dioxide reduction step in an artificial leaf type system.

A cheap and promising new catalyst that produces oxygen from water without the need for excessive driving potentials is being developed [91]. An inert ITO electrode is immersed in water containing Co^{2+} and potassium phosphate buffer in 2:1 ratio. The electric potential on the electrode will produce cobalt-based catalyst *in situ* that oxidizes the water to oxygen gas and hydrogen ions. On the opposite electrode, coated with platinum, protons are reduced to H_2 gas. During operation, the cobalt-based catalyst falls apart, but cobalt and potassium phosphate in the solution soon reaggregate replenishing the catalyst.

The discovery of the new catalyst earned wide public interest but much research and engineering work need to be done before it can be incorporated into commercial devices: (1) It should be revealed how the catalyst is driving the water oxidation reaction. (2) The rate of oxygen production by the catalyst is small and should be increased. (3) In strict sense, the process has nothing to do with photosynthesis *per se*, but involves an improved electrode for "splitting water" by electrolysis to generate oxygen at a lower potential than normal. A light-harvesting material has to be developed that absorbs sunlight and generates the electrons needed to power the water-splitting catalyst. (4) Although the catalyst does split water, it does not produce hydrogen gas (H_2). A second electrode and a different catalyst will be needed to combine the electrons and the hydrogen ions from water to make hydrogen gas.

In some devices, the primary problem is not the design and construction of the catalyst but the electrolyte solution that absorbs the protons from the split water molecules. It can cause essential problems in the current state-of-the-art dye-sensitized cells, where the electrolyte is made of volatile solvents that can erode other components in the system. Advances in the last few years are starting to address these issues. Cobalt oxide is a stable, fast and abundant metal oxide. Researchers have come up with a non-solvent-based solution to replace the corrosive stuff in dye-sensitized cells.

55.4.1.3.4 Dye-Sensitized Titanium Dioxide

Titanium dioxide (TiO_2) is a stable oxide that can act as an efficient catalyst. It is used in a dye-sensitized solar cell, also known as a Grätzel cell [92]. The TiO_2 is suspended in a layer of dye particles that captures the sunlight and then exposes it to the TiO_2 to start the reaction. The Grätzel cell as all other molecular

PVs has to face with the fundamental roadblock at nanoscale. How to build nanostructures that reconcile the short diffusion lengths of charge carriers (due to the dimension of the structure) with the long optical light path for visible light (expected for efficient absorption of the light excitation)? The Grätzel cell tries to solve this dilemma with a serpentine (and random) matrix.

55.4.2 Carbon Fixation

The light-driven reduction of CO_2 to organic compounds as principal bioenergetic process should have appeared long before the emergence of photosynthesis and might have played key role in origin of life on the Earth [93,94]. The primordial atmosphere dominated by carbon dioxide (similarly as presently on Mars and Venus, where CO_2 still makes 95% of the atmosphere) and ultraviolet (UV) light-driven reactions were capable to reduce CO_2 to organic compounds in solution or at semiconducting minerals, such as TiO_2, MnS, or ZnS [95]. While Fe^{2+}-catalyzed reduction of CO_2 in solution can occur with a quantum yield of 2%–3% only [96,97], the photoreduction of CO_2 to formate by colloidal ZnS particles shows much higher quantum yield of 80% [98]. The ability to store the solar energy and to drive CO_2 reduction is due to the depth of electron traps within the ZnS nanocrystals (nanoparticles) (see Figure 55.1).

55.4.2.1 Photosynthetic CO_2 Reduction, Native System

Natural photosynthesis by chlorophyll molecules involves the generation of carbohydrates and oxygen from the abundant raw materials CO_2 and H_2O at the expense of the driving force of the sun. On the other end, the photosynthesis is balanced by dark processes resulting in the oxidation of the reduced carbon compounds back to CO_2 and H_2O through combustion, decay, and cellular respiration. The two processes take place through a different sequence of chemical reactions and in different cellular compartments. Life on earth is sustained by maintaining the balance between the production and removal of atmospheric CO_2.

The dark reactions of photosynthesis in the chloroplast stroma are responsible for the biosynthesis of the carbohydrate that can occur even in the absence of photosynthetic electron transport. The biosynthetic reactions are catalyzed by a series of soluble enzymes, known collectively as the Calvin–Benson cycle. The enzyme RuBisCo (ribulose-1,5-bisphosphate carboxylase oxygenase) captures CO_2 from the atmosphere, and the cycle releases three-carbon sugars, which are later combined to form sucrose and starch. The overall equation is

$$6CO_2 + 12NADPH + 12H_2O + 18ATP \rightarrow C_6H_{12}O_6 + 12NADP^+ + 18ADP + 18P_i$$

that can be broken down into three major components:

1. Carbohydrate biosynthesis requires a source of electrons to ultimately reduce carbon dioxide to carbohydrate. The source is the oxidation of the NADPH produced during photosynthetic electron transport: $12NADPH + 12H^+ \rightarrow 12NADP^+ + 24H^+ + 24e^-$.
2. Utilization of atmospheric CO_2 for the synthesis of glucose using the electrons available from the oxidation of NADPH to $NADP^+$: $6CO_2 + 24e^- + 24H^+ \rightarrow C_6H_{12}O_6 + 6H_2O$.
3. Utilization of ATP produced during photosynthetic electron transport. Carbohydrate biosynthesis from carbon dioxide is an endergonic process. It is coupled to the hydrolysis of ATP, a highly exergonic reaction: $18ATP + 18H_2O \rightarrow 18ADP + 18P_i$.

By catalyzing the first major step of carbon fixation, RuBisCo is the key enzyme of the Calvin–Benson cycle. It is not only the major protein component of the chloroplast stroma but also considered to be the single most abundant protein on Earth [99,100]. It accounts for 50% of soluble leaf proteins in C3 plants (20%–30% of total leaf nitrogen) and 30% of soluble leaf proteins in C4 plants (5%–9% of total leaf nitrogen).

Although RuBisCo is one of the most important proteins in the nature, it is also one of the most inefficient as it reacts not only with carbon dioxide but also quite often with oxygen. This did not cause any problems to the protein developed three billion years ago. Back then, there was no oxygen present in the atmosphere. However, as more and more oxygen accumulated, RuBisCo could not adjust to this change. Nowadays, O_2 and CO_2 compete with similar affinities to the same active site of RuBisCo which decreases the efficiency of CO_2 fixation significantly. The carbon fixation by RuBisCo can be enhanced by increasing the carbon dioxide level in the compartment containing RuBisCo (chloroplast stroma). The use of oxygen as a substrate is an apparently puzzling process, since it seems to throw away the captured energy. However, it may be a mechanism for preventing overload during periods of high light flux. This weakness in the enzyme is the cause of photorespiration, such that healthy leaves in bright light may have zero net carbon fixation when the ratio of O_2 to CO_2 reaches a threshold at which oxygen is fixed instead of carbon.

RuBisCo is not only inefficient but also a slow enzyme, being able to "fix" only three CO_2 molecules each second. Nevertheless, because of its extremely large concentration, under most conditions, and, when light is not otherwise limiting photosynthesis, the reaction of RuBisCo responds positively to increasing CO_2 concentration; therefore, the concentration of carbon dioxide is limiting. The ultimate rate-limiting factor of the Calvin cycle is RuBisCo, which cannot be ameliorated in short time by any other factors.

Since RuBisCo is often rate limiting for photosynthesis in plants, it may be possible to improve photosynthetic efficiency by modifying RuBisCo genes in plants to increase its catalytic activity and/or decrease the rate of the oxygenation activity [101]. This could improve biosequestration of CO_2 and be an important climate change strategy. Approaches that have begun to be investigated include expressing RuBisCo genes from one organism in another organism, increasing the level of expression of RuBisCo subunits, expressing RuBisCo small chains from the chloroplast DNA, and altering RuBisCo genes so as to try to increase specificity for carbon dioxide or otherwise increase the rate of carbon fixation [102].

The protein RuBisCo is a large molecular complex consisting of 16 subunits, which made it impossible its reconstruction or artificial synthesis. The obstacle, however, is partly defeated as artificial production and modification of RuBisCo with the help of cellular chaperones were reported recently [103,104]. The correct folding of the enzyme was controlled by chaperons. The combination of this technique with genetic modification can create RuBisCo, which binds CO_2 stronger and metabolizes oxygen less frequently than the native enzyme.

55.4.2.2 Photocatalytic Reduction of CO_2, Artificial Systems

The CO_2 reduction process is thermodynamically uphill. The midpoint redox potentials, E^{o}_{m} (vs. a normal hydrogen electrode (NHE) at pH = 7), are –1.9 eV for the reduction of CO_2 to CO_2^- (one-electron process), –0.61 eV to formic acid (HCOOH), –0.53 eV to carbon monoxide (CO) (two-electron/proton processes), and –0.38 eV to methanol (CH_3OH) (six-electron/proton process). Economical CO_2 fixation is possible if solar energy is used as the free energy source. The fact that the proton-assisted and multielectron routes to these products require much less energy than the one-electron process suggests that it might have considerable advantage to employ multielectron transfer routes using transition metal complexes. Reduced metal centers, in which the oxidation number of the central metal is +1 and the ligand has four-coordinating atoms, typically have one or more vacant coordinate sites which can be used to bind and activate CO_2.

The artificial photocatalytic systems developed to reduce CO_2 have several common elements: they all contain photosensitizers (such as metalloporphyrins, ruthenium, or rhenium complexes with bipyridine), electron mediators or catalysts, and sacrificial electron donors (such as tertiary amines or ascorbic acid). Here, we will focus on artificial photosynthesis that is driven by photon absorption, CS through ET reactions, and energy storage in dark reaction, similar to the processes occurring in natural photosynthetic systems. From the development of artificial photochemical systems that carry out photocatalytic reduction of CO_2, one can expect the partial solution of the twin problem: the utilization of atmospheric CO_2 and the limited access to fossil fuel sources.

55.4.2.2.1 Ru–Re Photocatalyst

Several catalysts were tested and characterized in artificial photosystems which were able to reduce CO_2. Among these photocatalysts, the ruthenium–rhenium (Ru–Re) supramolecular complex has proved to be efficient to reduce CO_2 to CO by sunlight [105,106] (see Figure 55.12).

The Re complex has an excellent photocatalytic performance to reduce CO_2. The rhenium–diimine tricarbonium complex shows a quantum efficiency of 0.59 in an environment where a reductant such as amine coexists. However, it has absorption in the (ultra)violet region (shorter than 450 nm), not in the visible range. The Ru complex, which is an excellent photosensitizer, absorbs in the visible spectral range (longer than 500 nm) with a high quantum efficiency of 0.21. The combination of the Re complex, which has a high photocatalytic performance, with the Ru complex, which is an excellent sensitizer is a straightforward molecular design. There are many candidates for the compositions and structures to loosely combine the Re complex. The rhenium–trisdiimine complex with Ru complex demonstrated recently quantum efficiency as high as 0.34. The photocatalytic performance of the Re complex deteriorates when the two complexes are simply bonded. It turned out that the nonconjugated system is superior to the conjugated system. To develop a stable and practical supramolecular complex, the molecular design should be improved including the Re complex structure and the optimization of the length of the bridging ligand between the Re and Ru complexes in the nonconjugated system.

55.4.2.2.2 Carbon Nanotubes

As the synthesis of carbohydrates can only proceed when several energized electrons are available, you need to have multiple electrons in photosynthesis. A multiple electron system would comprise a donor molecule that can absorb visible light and release many electrons, and a receiver (acceptor) molecule capable of accepting and storing those electrons (Figure 55.13).

Single-walled carbon nanotubes (SWNTs) could act as the chemical heart of such a multiple electron system using isolated bacterial RC [107], Zn-porphyrin systems [67] (Figure 55.13), or phthalocyanine (PC) molecules [108]. A carbon nanotube can accept one electron for every 32 carbon atoms it contains,

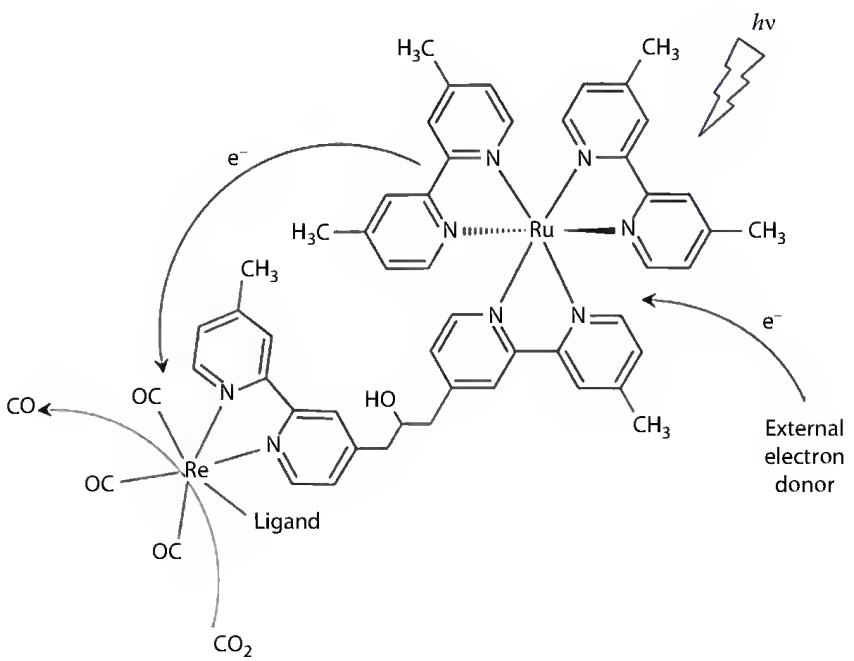

FIGURE 55.12 Ruthenium–rhenium (Ru–Re) supramolecular complex as photocatalyst of reduction CO_2 to CO by light. Electrons move from the light-excited ruthenium complex toward the rhenium complex where the CO_2 is reduced to CO at the Re catalytic site, in the presence of two alternative ligands (NCS^- and Cl^-). (Redrawn from Takeda, H. et al., *J. Am. Chem. Soc.*, 130(6), 2023, 2008.)

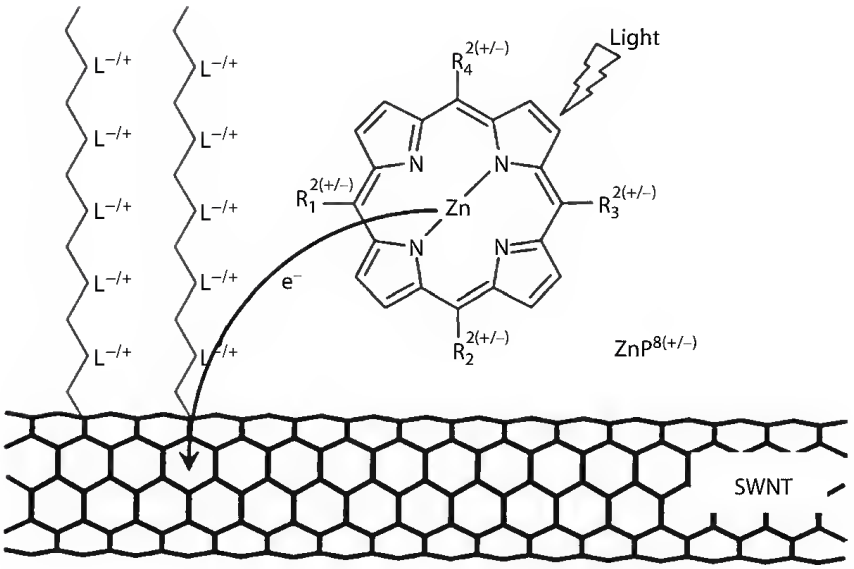

FIGURE 55.13 Building block of molecularly controlled integration of SWNT with Zn-porphyrin systems into nanostructured device. (Adapted from Guldi, D.M. and Imahori, H., *J Porphyr Phthalocyanines*, 8(7), 976, 2004.) The organization in solution is achieved by electrostatic interactions between linkers ($L^{-/+}$) attached to SWNT and $ZnP^{8(+/-)}$. While the SWNTs are good electron acceptors and, at the same time, 1D nanowires, the Zn-porphyrin acts as an excited-state electron donor. Their combination is a fundamental design consideration and signifies an innovative concept to harvest solar energy and to convert it into useful electricity.

and so even a short nanotube accepts many electrons. That means a carbon nanotube could act as the acceptor molecule in artificial photosynthesis. On the donor side, the PC molecule does release a single electron when it absorbs light, but by covalently bonding a large number of PCs to a carbon nanotube, they could create a multiple electron system activated by visible light. One hundred and twenty PC molecules can be bound to a nanotube just 1 μm long; thus, multiple electrons are simultaneously or sequentially transferred to the nanotube upon light absorption and multiple-CS states are formed. About 25% of the electrons donated from those PCs end up being stored in the nanotube. The extra electrons stored in the nanotubes could be used to convert NADP into NADPH. In the Calvin cycle, NADPH helps to fix carbon dioxide to form glucose, the end product of photosynthesis.

55.4.3 Hydrogen Production

55.4.3.1 Photosynthetic Hydrogen Production

Hydrogen can be produced from water by use of biological catalysts that have been optimized by nature: the process of water-splitting photosynthesis on one hand and hydrogen production via the catalyst hydrogenase on the other (Figure 55.14).

Indeed, under certain conditions, instead of reducing CO_2, a few groups of microalgae and cyanobacteria consume biochemical energy to produce molecular hydrogen [109]. The original discovery dates back to 1942, when Gaffron and Rubin reported that the green algae *Scenedesmus* produced molecular hydrogen upon illumination after being kept in darkness and under anaerobic conditions [110]. It was found recently that *Chlamydomonas reinhardtii* algae switched from the production of oxygen, as in normal photosynthesis, to the production of hydrogen if deprived of sulfur [111]. The key enzyme is the hydrogenase that catalyzes the most elementary reaction that can be imagined in biochemistry: it synthesizes one H_2 molecule from two protons (H^+ ions) and two electrons. The reducing power (electron donation) of hydrogenase does not always come from water, but may sometimes originate intracellularly from organic (carbon) compounds such as starch. The contribution of the fermentation pathway to

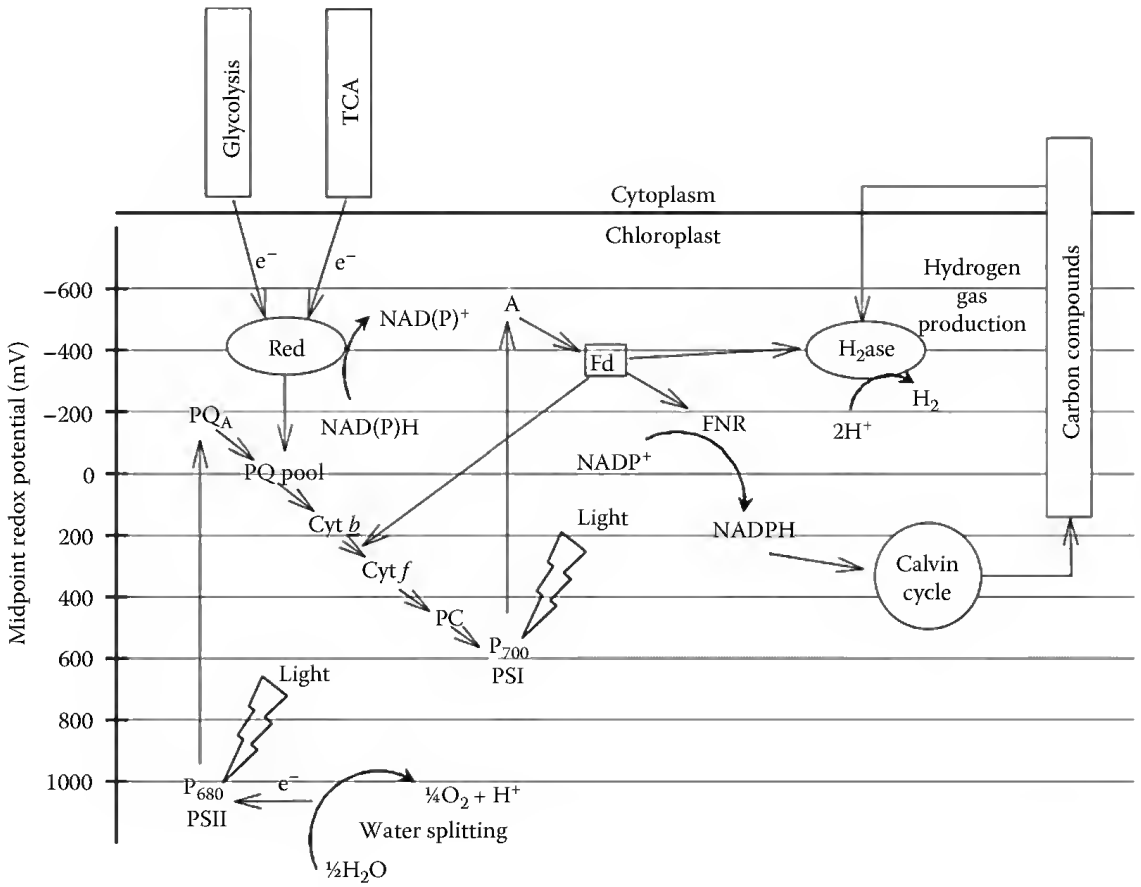

FIGURE 55.14 Coupling of photosynthetic electron transport and hydrogenase in green algae: H_2 gas production in expense of light and water splitting. Electrons (thin arrows) originate either at PSII upon photooxidation of water or at the PQ pool upon oxidation of cellular endogenous substrate (e.g., via glycolysis and the tricarboxylic acid cycle [TCA] through NAD(P)H oxidoreductase [Red]). Electrons are transported via PSI to ferredoxin (Fd), which plays a pivotal role in distribution of electrons among Fe-hydrogenase (H_2ase), cytochromes (Cyt *b* and Cyt *f*) of the Cyt b_6f complex (cyclic electron flow), and FNR. The other route of electrons to H_2ase is the fermentative pathway of carbon compounds in the Calvin cycle. Additional abbreviations: P680, RC of PSII; P700, RC of PSI; PQ_A, primary electron acceptor of PSII; A, primary electron acceptor of PSI; PQ, plastoquinone and PC, plastocyanin.

hydrogen production depends on the algal species and on culture conditions. The reason for hydrogenase inactivity in green algae under normal photosynthetic growth conditions is unclear. Hydrogenase is thought to become active in order to excrete excess reducing power under specific conditions, such as anaerobic conditions. The hydrogenase of green algae, however, is too oxygen-labile, and the light-dependent hydrogen production ceases within a few to several tens of minutes since photosynthetically produced oxygen inhibits or inactivates the enzyme.

Beside of hydrogenase, nitrogenase enzyme is also capable of hydrogen production. In 1974, Benemann and Weare demonstrated that a nitrogen-fixing cyanobacterium, *Anabaena cylindrica,* produced hydrogen and oxygen gases simultaneously in argon atmosphere for several hours [112]. Nitrogenase is responsible for nitrogen fixation by reduction of molecular nitrogen to ammonium with consumption of reducing power of ferredoxin and free energy of ATP. However, nitrogenase catalyzes proton reduction in the absence of nitrogen gas (i.e., in argon atmosphere). Hydrogen production catalyzed by nitrogenase occurs as a side reaction at a rate of one-third to one-fourth that of nitrogen fixation, even in 100% nitrogen gas atmosphere. Nitrogenase itself is extremely oxygen-labile. Unlike in the case of hydrogenase, however, cyanobacteria have developed mechanisms for protecting nitrogenase from oxygen gas and supplying it with energy (ATP) and reducing power.

In addition to cyanobacteria and green algae, some nonsulfur anoxygenic photosynthetic bacteria are also potent hydrogen producers, utilizing organic acids such as lactic, succinic, and butyric acids, or alcohols as electron donors. Since light energy is not required for water oxidation, the efficiency of light energy conversion to hydrogen gas by photosynthetic bacteria is in principle much higher than that by cyanobacteria. Hydrogen production by photosynthetic bacteria is mediated by nitrogenase activity, although hydrogenases may be active for both hydrogen production and hydrogen uptake under some conditions. Using *Rhodobacter* species, the maximum energy conversion efficiency (combustion energy of hydrogen gas produced/incident light energy) was 6%–8% in laboratory experiments [113].

55.4.3.2 Bioinspired Hydrogen Production

The potential combination of photosynthetic water oxidation and biophotolytic hydrogen production has been an enormous challenge to design photosynthesis-based artificial systems. Instead of complete treatment of the problem in one big step, several smaller steps have been made with partial solutions of related subproblems.

The self-organized platinization of the photosystem I nanoparticles from thermophilic cyanobacterium *Thermosynechococcus elongatus* allowed electron transport from sodium ascorbate to photosystem I via cytochrome c_6 and finally to the platinum catalyst, where hydrogen gas is formed upon illumination [114]. The maximum yield was ~5.5 μmol H_2 h^{-1} mg^{-1} chlorophyll that hoped to be improved by replacing the platinum catalyst with a renewable and covalently linked hydrogenase to the acceptor end of the PSI complexes.

Following the determination of the 3D structure of the active site of NiFe hydrogenases, a variety of nickel-based complexes as potential electrocatalysts for hydrogen production were synthesized [115,116]. These catalysts may provide an adequate alternative to platinum. This biomimetic structural approach, however, could not fulfill the expectations yet, as no activity was reported for dinuclear biomimetic nickel–iron complexes. The perspective of Ni–Ru complexes as functional models of [Ni–Fe] hydrogenases seems to be more encouraging as they are relatively easy to synthesize, stable in solution, and show high yield and turnover numbers of proton reduction to hydrogen at the expense of relatively high overpotentials (0.5–0.8 V) [117].

A further step of biomimetic approach of light-induced hydrogen production is the coupling of di-iron-(μ-dichlorobenzene-dithiolate)hexacarbonyl ([Fe–Fe] hydrogenase) as catalyst and ruthenium(II)tris-bipyridine as photosensitizer into ruthenium–diiron dyad (Swedish Consortium for Artificial Photosynthesis [1994–2010]). The dyad has rigid geometry, the Ru photosensitizer exhibits prolonged excited state lifetimes, and the catalysis can be tuned to mild potentials by attachment of aromatic dithiolate ligands to the diiron complex. Using ascorbic acid as both proton and electron donors, the dyad started to produce hydrogen at a rate of 4 μmol $H_2 \cdot h^{-1}$ but quitted to evolve H_2 after 100 turnovers (2.6 mL typical sample volume, H_2O:dimethylformamide 1:1 solvent, Ar atmosphere, pH 5.5, 0.1 M ascorbic acid, 140 μM sensitizer, 14 μM catalyst, 455 nm long-pass filter + infrared filter, and ~1 W light power). The chemical LEGO is supposed to be completed if the ascorbic acid is replaced by an Mn complex for water oxidation and linked to the Ru photosensitizer.

An alternative to the supramolecular (biomimetic) chemistry is the engineered natural systems including the (genetic) modification of the molecular machinery of living organisms (biophotolytic hydrogen production [37,118]). In special cells (heterocyst) of cyanobacterium *Nostoc*, hydrogen gas is formed from nitrogenase and electrons that enter the heterocyst from neighboring vegetative cells as a result of light-induced photosynthetic activity. The native nitrogenase is tried to be replaced by hydrogenase to get higher yield of hydrogen production [119].

The crucial step of water-splitting-based hydrogen production is the coupling of photosynthetic electron flow with hydrogenase. The key element is the ferredoxin that plays as the switching point for cyclic electron transport, CO_2 fixation (via ferredoxin, NADPH oxidoreductase [FNR], and NADPH) and hydrogen production (Figure 55.14). The main question of improvement of biosolar H_2 production is how to redirect the flux of electrons through PSI and ferredoxin into hydrogenase by downregulating the competing pathways.

Several pathways have been observed for light-induced H_2 production from water in natural photosynthetic microbes, and two pathways have proved to be encouraging candidates for realization in bioinspired systems (Figure 55.14). The first pathway, given by the overall stoichiometry of $H_2O \rightarrow H_2 + \frac{1}{2}O_2$, requires the two photosystems and complete electron transport chain to bring electrons from water to ferredoxin, the physiological electron donor to hydrogenase. This pathway requires four quanta per H_2 evolved and usually occurs concurrently with O_2 evolution in a single temporal stage with no gas separation. The pathway occurs in some cyanobacteria, but is inefficient and occurs appreciably in green algae only under conditions of sulfur deprivation, which significantly reduces PSII activity [120]. If this pathway was able to operate at full PSII capacity, it would require an O_2-tolerant hydrogenase, a promoter that enables gene expression in the presence of elevated O_2 levels, and a hydrogenase assembly process that is O_2 insensitive. This pathway is efficient in the use of photons, but results in the coevolution of H_2 and O_2 gases which are technically challenging to separate, economically unfeasible, and a safety hazard as mixture.

The second pathway for H_2 formation, which is currently favored, involves electron and proton flow to the plastoquinone (PQ) pool, from fermentation and oxidative carbon metabolism of photosynthetically stored carbon, mediated by a dehydrogenase, through PSI into ferredoxin and then to hydrogenase. The stoichiometry of the indirect two stage pathway is given by

$$H_2O + CO_2 \xrightarrow{\text{light}} [CH_2O]$$

$$\text{Hydrogenase} + \text{Dark} \xrightarrow{-\text{oxygen}} \text{Hydrogenase induction} \xrightarrow{\text{light}} H_2 + CO_2$$

and requires six quanta/H_2 (assuming all electrons are ultimately derived from water). This pathway is most efficient in two temporally resolved stages, a photosynthetic growth stage followed by an anaerobic stage in which hydrogenase expression is induced and PSI uses light to pump "fixed" electrons derived from stored reductants via the PQ pool to the potential needed to reduce ferredoxin, while the protons are pumped into the thylakoid lumen for use in ATP synthesis. The anaerobic stage requires O_2 to be substantially depleted (cyanobacteria) or virtually eliminated (green algae). The temporal separation of the H_2- and O_2-evolving steps is a major advantage for gas separation and safety. Suppression of O_2-induced inactivation of hydrogenase by attenuation of PSII activity is being implemented by several research teams. They have used sulfur deprivation of green algae to suppress the biosynthetic repair of an essential PSII subunit that is damaged during photoinhibition and requires replacement for recovery of O_2 evolution. Current rates of continuous H_2 photoproduction using the sulfur depletion strategy yield around 2.2 mL H_2 h^{-1} L^{-1} culture [121], while rates of 3.5 mL H_2 h^{-1} L^{-1} culture have been achieved using the *C. reinhardtii* mutant *Stm6* [122]. Diuron (DCMU) inhibition of PSII suggests that approximately 80% of the H_2 is reportedly being produced from water.

55.5 Protonmotive Force in Artificial Systems

In the biomimetic systems listed earlier, the free energy of the light was converted into energy of chemical products via several steps. The conversion is more direct if the system is capable to generate protonmotive force, which is defined as the sum (linear combination) of electric membrane potential, $\Delta\Psi$ and proton gradient, ΔpH: $pmf = \Delta\Psi + 60\,\text{mV} \cdot \Delta\text{pH}$ (at room temperature) and then to synthetize ATP. In natural systems, the light excitation moves an electron abruptly across the biological membrane resulting in transmembrane electric potential. The reverse effect is also operating: the local electric field within phospholipid membranes modulates the charge transfer reactions in RCs [123]. By coupling of proton binding/unbinding redox reactions to a sequence of slower ET steps [124,125], proton translocation takes place resulting in pH difference between the two sides of

the membrane. The organism (bacterium) uses the stored chemical energy in form of *pmf* to generate ATP, which can meet all its energy needs.

Several model systems which use light energy to generate *pmf* were prepared and studied based on theory [126] and experiments [127]. As the RC operates as half of a light-driven proton pump in natural photosynthesis [128,129], artificial system can be achieved by insertion of either isolated bacterial RC [130,131] or artificial triad [127,132] into the liposome (Figure 55.15). The heart of the proton pumping system is a liposome vesicle comprising a synthetic phospholipid bilayer, which should be sealed enough to let build up the proton gradient through the membrane [107]. The bilayer is spanned by isolated or artificial RC that undergoes photoinduced ET to generate transmembrane charge-separated state. Shuttle quinones use the CS to transport protons across the membrane and establish proton gradient. The systems effectively mimic the entire process of bacterial photosynthesis. The proton transport can be detected using a pH-sensitive fluorescence indicator dye inside the liposome [130,132]. A *pmf*-powered enzyme, F_0F_1-ATP synthase from spinach chloroplast (a nanomachine), has been also incorporated into the liposomal bilayer [127,133]. The illumination of the membrane with visible light leads to accumulation of sufficient *pmf* and to flow of protons through

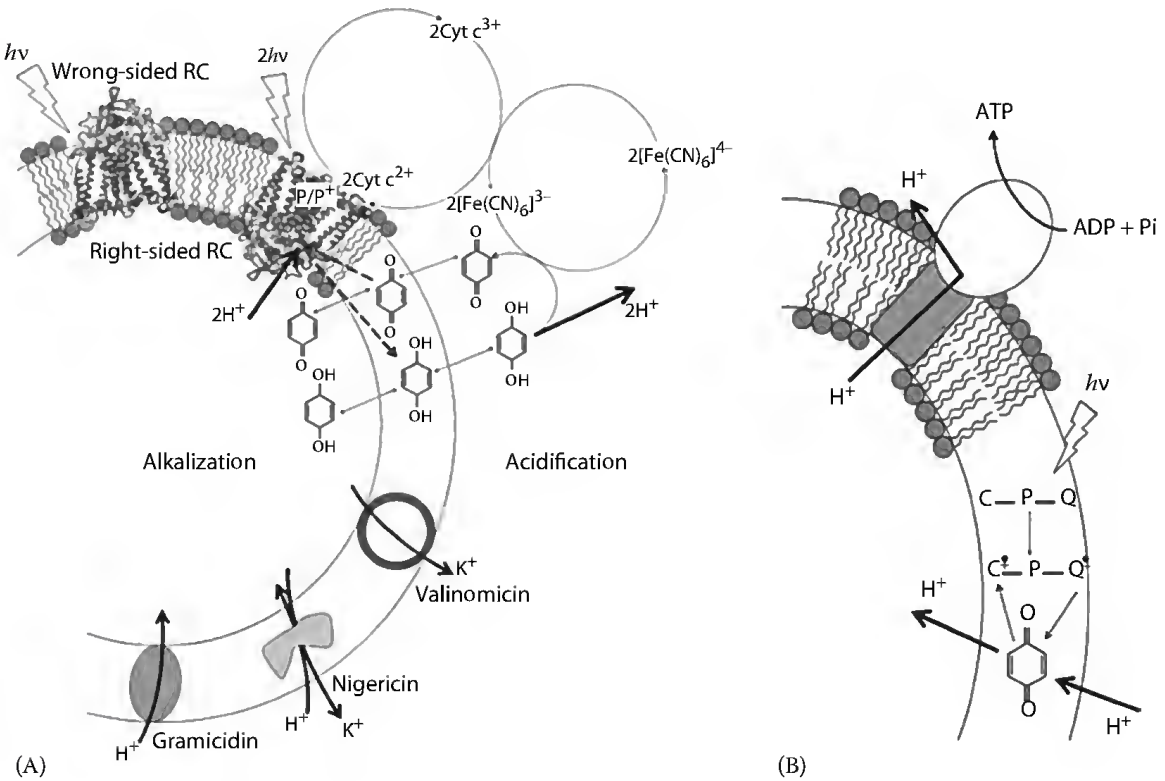

FIGURE 55.15 Generation of light-induced ΔpH by reconstituted bacterial RC [130] (A) and molecular triad [127] (B) in phospholipid vesicle. In (B), the ΔpH is used to drive ATP production. The liposome-based proton pumps are powered by photoinduced CS followed by proton-coupled ET reactions. Protons are taken up from one side (alkalization) and released to the other side (acidification) of the vesicle by a lipid soluble shuttle quinone which is part of the acceptor complex of the RC and undergoes to two-electron chemistry (A) or independent of the molecular triad (2,4-diphenyl benzoquinone) and undergoes to one-electron chemistry (B). Proton pumping results from the asymmetry of the system, ensured by cytochrome in RC vesicle (A). The proton gradient and protonmotive force depend on proton sealing of the vesicle that can be modified by protonophores (gramicidin and nigericin) and ionophore (valinomycin) (A) and by redox and diffusion properties of the shuttle quinone. Abbreviations: P, light-absorbing dimer (A) and tetraarylporphyrin (B); Q, quinone acceptor; C, carotenoid donor; $[Fe(CN)_6]^{3-}$ and $[Fe(CN)_6]^{4-}$, ferrocyanide and ferricyanide, respectively; Cyt, cytochrome.

the F_0F_1-ATP synthase producing ATP from ADP and Pi. As one molecule of ATP is synthesized per 14 absorbed photons of 633 nm light, up to 4% of the energy incident on the sample is stored by the system. The photocyclic system operates efficiently over a timescale of hours with a turnover rate of seven ATP molecules per F_0F_1 per second. This number is similar to that observed in bacteriorhodopsin/ATP synthase system.

55.6 Efficiency of Solar Energy Conversion

The primary purpose of research of photosynthesis-based artificial photosystems is to capture the solar energy efficiently. The efficiency of conversion of light energy is defined as the usable electrical or harvestable chemical energy output divided by the total solar energy incident on the organism or device. Its limitations are reviewed recently by Gust et al. [134] and Dau and Zaharieva [135]. The question is generally crucial in energy producing artificial photosystems but not so in natural photosynthesis. In several cases, light is not the limiting factor of the growth of the organisms. For example, the key enzyme of the Calvin cycle is RuBisCo that shows low turnover rate and poor affinity to CO_2 resulting in slow (generally rate limiting) step in the overall photosynthesis. Under high light intensity (full sunlight), the plant needs photoprotection against harmful illumination rather than using the absorbed energy for CO_2 fixation. Under this condition, the plant has no need to maximize the efficiency of solar energy conversion, and it can sustain even with relatively low yield of conversion. This leads to formulate a general warning: "The whole complex process of photosynthesis, not to mention the plant's way of life, is certainly not a target for chemical mimicry … mimick the photosynthesis, but just the best bits" [136].

The main efficiency-limiting factors are (1) the fraction of sunlight absorbed by the organism (or device), (2) the quantum yield of photoconversion, and (3) the photophysical–photochemical processes:

1. The photosynthetic organisms and simple PV devices such as silicon solar cells function as single-threshold systems with two obvious consequences. Photons below the threshold (i.e., having less energy than required for the lowest-energy absorption transition of the pigments [material]) will not be absorbed from the solar spectrum. Photons above the threshold will be absorbed but loose significant portion of their energy as heat during the electronic relaxation processes (internal conversion) that populate the lowest excited state of the chlorophyll (or the conduction band energy of a solar cell). The two opposite tendencies have an optimum value for the threshold (or bandgap) energy of about 1.3 eV (wavelength ≈ 910 nm). The photosynthetic bacteria approach this value (see Figure 55.6). The bandgap in water-oxidizing photosynthesis is about 1.8 eV, well on the high-energy side of the optimum which leads to a loss of about one-fourth of the absorbed energy. Although 90% of incident solar irradiation is absorbed up to 700 nm, the light-harvesting efficiency (LHE) can be maximum 34% of the incident solar irradiation: LHE < 0.34. The increase in chemical potential of the charge-separated state with increasing bandgap comes at the expense of the fraction of photons absorbed.
2. The quantum yield of CS (Φ_{quant}) from trapped electronic excitation state of the RC pigment ($P^* \rightarrow P^+Q_A^-$) is very high and approaches the unity: $\Phi_{quant} > 0.95$ [56].
3. The photochemical free energy conversion processes sacrifice some of the potentially available energy in order to slow CR reactions and drive desired chemical or electrical processes forward. As a result of these factors, a significant fraction of free energy must be lost as heat or delayed fluorescence in any conversion devices. The cost of the charge stabilization is a concomitant loss of stored free energy. In purple photosynthetic bacteria, the initial free energy of 1.38 eV stored in the electron excitation energy of the dimer, P^* (or in the initial charge-separated state $P^+\Phi_A^-$) is gradually decreased upon forward ET (see Figure 55.6). The rates of forward reactions are 2–3 orders of magnitude larger than those of the back reactions. The largest drop in stored

free energy relative to P* (860 meV) occurs when the electron is shifted to the primary quinone [52,55,137]. The fractional energy yield (FEY) values of the $P^+Q_A^-$ state is FEY = 38%. Depending on the S states, significantly larger FEY values (60%–75%) characterize the internal free energy conversion efficiencies in higher plants. In typical PV cells, the separated hole and electron are stabilized by an internal electric field at the junction of the *n*- and *p*-type semiconductor materials. The energy associated with separating the charges reduces the electrical energy available in the external circuit.

The total solar conversion energy efficiency (Φ_{total}) is the product of the three efficiencies: Φ_{total} = LHE · Φ_{quant} · FEY. The best single-threshold PV devices have efficiencies that approach the Shockley–Quiesser limit of $\Phi_{total} \approx 30\%$. The Si-based PV cells have $\Phi_{total} \approx 14.3\%$ efficiency. A new series of amphiphilic heteroleptic ruthenium(II) sensitizers self-assembled on TiO_2 surface from ethanol solution reveal Φ_{total} = 7.4% power conversion efficiency [138]. In contrast, the efficiency of natural photosynthesis is relatively small (maximum about 6% but usually observed to be about 0.3%–0.8%), although the initial steps of plant and bacterial photosynthesis have very high quantum yields. The apparent paradox of a high quantum yield, Φ_{quant} and low total efficiency, Φ_{total} in natural photosynthetic systems can be explained by small FEY that includes losses due to internal conversion, regulatory dissipation, production of NADPH and ATP, CO_2 assimilation, and the energy needed for growth and maintenance of the plant, resulting in a typical efficiency for land plants of 0.3%–0.8%. Interestingly, some algae and cyanobacteria have remarkably higher efficiencies (4.6%) than terrestrial plants. This is because some of the efficiency-limiting factors are more important for large land plants than they are for microalgae in aqueous environments. For example, CO_2 fixation in leaves is often limited by CO_2 diffusion, whereas uptake of inorganic carbon is much less limiting in small organisms with much larger surface/volume ratios. Moreover, because the solubility of CO_2 in water is much higher than that of O_2, the carbon fixation/carbon oxidation ratio of RuBisCo is much more favorable in aqueous environments. In addition, smaller organisms require less energy investment for chemical transport and for generation of a "skeleton," and they tend, overall, to have better efficiencies than terrestrial plants.

Water oxidation in photosynthesis is essentially also a single-threshold process and is therefore subject to the Shockley–Quiesser limit of about 30% efficiency. This value is further reduced to maximum Φ_{total} = 10% by taking the following values: two photosystems (two quanta per electron) are used, each with nonoptimal thresholds of 1.83 eV (PSII) and 1.77 eV (PSI), ΔE_m= 1.23 V per e^-/H^+ at 1 bar, FEY = 1.23 V/(1.83 V + 1.77 V) = 34%, LHE < 34% and $\Phi_{quant} \sim 90\%$. Similar value of about 10% describes the total solar energy conversion efficiency of H_2 production driven exclusively by PSII and PSI.

To explore the two-quanta-per-electron issue, artificial RCs are being used in conjunction with dye-sensitized semiconductor photoelectrodes (Grätzel-type photoanodes) to determine the overpotentials necessary to drive water oxidation and H_2 production at rates comparable to the solar photon flux, using biological and bioinspired catalysts. The interplay between natural and artificial constructs could lead to new materials or compounds. For example, the efficiency of the Grätzel PV cell would be substantially improved by a high-potential electron relay mimicking the tyrosine/histidine-based system used by nature in PSII.

55.7 Conclusions

Construction and study of biomimetic photosystems serve two reasons. They allow ready manipulation of individual components at molecular level and test of theoretical and practical suggestions, which are not readily feasible in the natural systems. The artificial systems are helpful in understanding the principles of natural photosynthesis. On the other end, artificial photosystems can be used as power supplies by conversion of sunlight into other useful forms of the free energy. In this field, efficiencies, powers, costs, and pollution are the determining factors whose control is occasionally beyond the capacity of the scientific community. Based on the present knowledge, and possible forecast for the next couple of years,

photosynthesis-mimicked artificial photosystems may have only limited (local) applications due to the not properly clarified principle of operation, the less robust constructions of the devices, and the relatively low total solar energy conversion efficiency. Photosynthesis-based oxygen evolution from water requires the absorption of four photons, at least. If the efficiency of water splitting could be increased to 50% by application of highly sophisticated catalysts (this would be a first ranked achievement in the science), then the quantum yield of O_2 evolution would be as low as 12% only. Semiconductor-based PV cells of higher efficiency, however, are already on the market and the stage is set for their widespread applications even on industrial level.

Although the free energy conversion efficiency of natural photosynthesis is low, it produces liquid fuel that is very convenient for human use. The solar cells have much higher efficiency, but they provide electricity "only." The goals are clear for a "bioinspired" technology of the future: to get more stable and higher energy conversion efficiency for photosynthesis-based artificial systems and/or to design PV systems with high solar energy conversion efficiency, but resulting in fuels.

Acknowledgments

The support of NKTH-OTKA (K-67850), COST Action on "Molecular machineries for ion translocation across biomembranes" (CM0902) and MTA-CNR bilateral agreement on "Bacterial photosynthesis: artificial photosystems and bioremediation" is acknowledged.

References

1. Kruse, O. and B. Hankamer, *Photosynthetic Hydrogen Production*, Brisbane, Queensland, Australia: The University of Queensland, 2005.
2. Barber, J., Biological solar energy, *Phil Trans Math Phys Eng Sci*, 365(1853), 1007–1023, 2007.
3. Barber, J., Photosynthetic energy conversion: Natural and artificial, *Chem Soc Rev*, 38(1), 185–196, 2009.
4. Sass, L., C. Spetea, Z. Máté, F. Nagy, and I. Vass, Repair of UV-B induced damage of photosystem II via *de novo* synthesis of the D1 and D2 reaction centre subunits in *Synechocystis* sp. PCC 6803, *Photosynth Res*, 54(1), 55–62, 1997.
5. van Rotterdam, B.J., H.V. Westerhoff, R.W. Visschers, D.A. Bloch, K.J. Hellingwerf, M.R. Jones, and W. Crielaard, Pumping capacity of bacterial reaction centers and backpressure regulation of energy transduction, *Eur J Biochem*, 268(4), 958–970, 2001.
6. Gust, D., T.A. Moore, and A.L. Moore, Solar fuels via artificial photosynthesis, *Accounts Chem Res*, 42(12), 1890–1898, 2009.
7. LaVan, D.A. and J.N. Cha, Approaches for biological and biomimetic energy conversion, *Proc Natl Acad Sci USA*, 103(14), 5251–5255, 2006.
8. Wasielewski, M.R., Photoinduced electron transfer in supramolecular systems for artificial photosynthesis, *Chem Rev*, 92(3), 435–461, 1992.
9. Gust, D., T.A. Moore, and A.L. Moore, Mimicking photosynthetic solar energy transduction, *Acc Chem Res*, 34(1), 40–48, 2001.
10. Gust, D., T.A. Moore, and A.L. Moore, Mimicking bacterial photosynthesis, in *Artificial Photosynthesis*, A.F. Collings and C. Critchley, Eds., Weinheim, Germany: Wiley-VCH, 2005, pp. 187–210.
11. Moore, T.A., D. Gust, P. Mathis, J.C. Mialocq, C. Chachaty, R.V. Bensasson, E.J. Land, D. Doizi, and P.A. Liddell, Photodriven charge separation in a carotenoporphyrinquinone triad, *Nature*, 307, 630–632, 1984.
12. Wiedenmann, A., P. Dimroth, and C. von Ballmoos, Deltapsi and DeltapH are equivalent driving forces for proton transport through isolated F(0) complexes of ATP synthases, *Biochim Biophys Acta*, 1777(10), 1301–1310, 2008.

13. Tiwari, G.N. and S. Dubey, *Fundamentals of Photovoltaic Modules and their Applications*. RSC Energy Series, J. Hunt, Ed., Cambridge, U.K.: The Royal Society of Chemistry, 2010, p. 411.
14. Schultz, O., A. Mette, R. Preu, and S.W. Glunz, Silicon solar cells with screen-printed front side metallization exceeding 19% efficiency, in *22nd European Photovoltaic Solar Energy Conference and Exhibition*, 2007, Milan, Italy.
15. Yang, F., K. Sun, and S.R. Forrest, Efficient solar cells using all-organic nanocrystalline networks, *Adv Mater*, 19(23), 4166–4171, 2007.
16. Grätzel, M., Photoelectrochemical cells, *Nature*, 414(6861), 338–344, 2001.
17. Lessing, P.A., Materials for water electrolysis cells, in *Materials for the Hydrogen Economy*, R.H. Jones and G.J. Thomas, Eds., Boca Raton, FL: CRC Press, 2008.
18. Maróti, P., G. Laczkó, and L. Szalay, Determination of the distance law of the transfer of electronic excitation energy, *J Theor Biol*, 86(4), 663–671, 1980.
19. Emerson, R. and W. Arnold, A separation of the reactions in photosynthesis by means of intermittent light, *J Gen Physiol*, 15, 391–420, 1932.
20. Emerson, R. and W. Arnold, The photochemical reaction in photosynthesis, *J Gen Physiol*, 16, 191–205, 1932.
21. Psencik, J., T.P. Ikonen, P. Laurinmaki, M.C. Merckel, S.J. Butcher, R.E. Serimaa, and R. Tuma, Lamellar organization of pigments in chlorosomes, the light harvesting complexes of green photosynthetic bacteria, *Biophys J*, 87(2), 1165–1172, 2004.
22. Balaban, T.S., H. Tamiaki, and A.R. Holzwarth, Chlorins programmed for self-assembly, in *Supramolecular Dye Chemistry—Topics in Current Chemistry*, F. Würthner, Ed., Dordrecht, the Netherlands: Springer, Vol. 258, 2005, p. 324.
23. Ganapathya, S., G.T. Oostergetel, P.K. Wawrzyniak, M. Reusc, A.G.M. Chew, F. Buda, E.J. Boekem, D.A. Bryant, A.R. Holzwarth, and H.J.M. de Groot, Alternating syn-anti bacteriochlorophylls form concentric helical nanotubes in chlorosomes, *Proc Natl Acad Sci USA*, 106(21), 8525–8530, 2009.
24. Nisbet, E. and N. Sleep, The habitat and nature of early life, *Nature*, 409(6823), 1083–1091, 2001.
25. Demmig-Adams, B. and W.W. Adams, The role of xanthophyll cycle carotenoids in the protection of photosynthesis, *Trends Plant Sci*, 1(1), 21–26, 1996.
26. Horton, P., A.V. Ruban, and R.G. Walters, Regulation of light harvesting in green plants (indication by nonphotochemical quenching of chlorophyll fluorescence), *Plant Physiol*, 106(2), 415–420, 1994.
27. Pascal, A.A., Z. Liu, K. Broess, B. van Oort, H. van Amerongen, C. Wang, P. Horton, B. Robert, W. Chang, and A. Ruban, Molecular basis of photoprotection and control of photosynthetic light-harvesting, *Nature*, 436(7047), 134–137, 2005.
28. Ventrella, A., L. Catucci, and A. Agostiano, Effect of aggregation state, temperature and phospholipids on photobleaching of photosynthetic pigments in spinach photosystem II core complexes, *Bioelectrochemistry*, 73(1), 43–48, 2008.
29. Maróti, P. and J. Lavorel, Intensity and time-dependence of the carotenoid triplet quenching under light flashes of rectangular shape in *Chlorella*, *Photochem Photobiol*, 29(6), 1147–1151, 1979.
30. Tandori, J., E. Hideg, L. Nagy, P. Maróti, and I. Vass, Photoinhibition of carotenoidless reaction centers from *Rhodobacter sphaeroides* by visible light. Effects on protein structure and electron transport, *Photosynth Res*, 70(2), 175–184, 2001.
31. Yokthongwattana, K., B. Chrost, S. Behrman, C. Casper-Lindley, and A. Melis, Photosystem II damage and repair cycle in the green alga *Dunaliella salina*: Involvement of a chloroplast-localized HSP70, *Plant Cell Physiol*, 42(12), 1389–1397, 2001.
32. Tandori, J., Z. Tokaji, K. Misurda, and P. Maróti, Thermodynamics of light-induced and thermal degradation of bacteriochlorins in reaction center protein of photosynthetic bacteria, *Photochem Photobiol*, 81(6), 1518–1525, 2005.
33. Tokaji, Z., J. Tandori, and P. Maróti, Light- and redox-dependent thermal stability of the reaction center of the photosynthetic bacterium *Rhodobacter sphaeroides*, *Photochem Photobiol*, 75(6), 605–612, 2002.

34. Egawa, A., T. Fujiwara, T. Mizoguchi, Y. Kakitani, Y. Koyama, and H. Akutsu, Structure of the light-harvesting bacteriochlorophyll c assembly in chlorosomes from *Chlorobium limicola* determined by solid-state NMR, *Proc Natl Acad Sci USA*, 104(3), 790–795, 2007.
35. de Boer, I., J. Matysik, M. Amakawa, S. Yagai, H. Tamiaki, A.R. Holzwarth, and H.J.M. de Groot, MAS NMR Structure of a microcrystalline Cd-bacteriochlorophyll d analogue, *J Am Chem Soc*, 125(44), 13374–13375, 2003.
36. Garcia-Martin, A., L.G. Kwa, B. Strohmann, B. Robert, A.R. Holzwarth, and P. Braun, Structural role of (bacterio)chlorophyll ligated in the energetically unfavorable β-position, *J Biol Chem*, 281(15), 10626–10634, 2006.
37. Röger, C., M.G. Müller, M. Lysetska, Y. Miloslavina, A.R. Holzwarth, and F. Wurthner, Efficient energy transfer from peripheral chromophores to the self-assembled zinc chlorin rod antenna: A bioinspired light-harvesting system to bridge the "green gap," *J Am Chem Soc*, 128(20), 6542–6543, 2006.
38. Miller, R.A., A.D. Presley, and M.B. Francis, Self-assembling light-harvesting systems from synthetically modified tobacco mosaic virus coat proteins, *J Am Chem Soc*, 129(11), 3104–3109, 2007.
39. Balzani, V., A. Credi, and M. Venturi, Photochemical conversion of solar energy, *ChemSusChem*, 1(1–2), 26–58, 2008.
40. Hsiao, J.-S., B.P. Krueger, R.W. Wagner, T.E. Johnson, J.K. Delaney, D.C. Mauzerall, G.R. Fleming, J.S. Lindsey, D.F. Bocian, and R.J. Donohoe, Soluble synthetic multiporphyrin arrays. 2. photodynamics of energy-transfer processes, *J Am Chem Soc*, 118(45), 11181–11193, 1996.
41. Holten, D., D.F. Bocian, and J.S. Lindsey, Probing electronic communication in covalently linked multiporphyrin arrays. A guide to the rational design of molecular photonic devices, *Acc Chem Res*, 35(1), 57–69, 2002.
42. Hori, T., N. Aratani, A. Takagi, T. Matsumoto, T. Kawai, M.C. Yoon, Z.S. Yoon, S. Cho, D. Kim, and A. Osuka, Giant porphyrin wheels with large electronic coupling as models of light-harvesting photosynthetic antenna, *Chemistry*, 12(5), 1319–1327, 2006.
43. Balaban, T.S., A. Eichhöfer, and J.-M. Lehn, Self-assembly by hydrogen bonding and π,π; interactions in the crystal of a porphyrin—Attempts to mimic bacteriochlorophyll *c*, *Eur J Org Chem*, 2000(24), 4047–4057, 2000.
44. Prodi, A., C. Chiorboli, F. Scandola, E. Iengo, E. Alessio, R. Dobrawa, and F. Wurthner, Wavelength-dependent electron and energy transfer pathways in a side-to-face ruthenium porphyrin/perylene bisimide assembly, *J Am Chem Soc*, 127(5), 1454–1462, 2005.
45. Prodi, A., C. Chiorboli, F. Scandola, E. Iengo, and E. Alessio, Electronic energy transfer in a multiporphyrin-based molecular box, *ChemPhysChem*, 7(7), 1514–1519, 2006.
46. Scandola, F., C. Chiorboli, A. Prodi, E. Iengo, and E. Alessio, Photophysical properties of metal-mediated assemblies of porphyrins, *Coord Chem Rev*, 250(11–12), 1471–1496, 2006.
47. Jang, W.-D., C.H. Lee, M.S. Choi, and M. Osada, Synthesis of multi-porphyrin dendrimer as artificial light harvesting antennae, *J Porphyr Phthalocyanines*, 13(7), 787–793, 2009.
48. Choi, M.S., T. Aida, T. Yamazaki, and I. Yamazaki, Dendritic multiporphyrin arrays as light-harvesting antennae: Effects of generation number and morphology on intramolecular energy transfer, *Chemistry*, 8(12), 2668–2678, 2002.
49. Choi, M.S., T. Yamazaki, I. Yamazaki, and T. Aida, Bioinspired molecular design of light-harvesting multiporphyrin arrays, *Angew Chem Int Ed Engl*, 43(2), 150–158, 2004.
50. Kozaki, M., A. Uetomo, S. Suzuki, and K. Okada, A light-harvesting array composed of porphyrins and rigid backbones, *Org Lett*, 10(20), 4477–4480, 2008.
51. Kocsis, P., E. Asztalos, Z. Gingl, and P. Maróti, Kinetic bacteriochlorophyll fluorometer, *Photosynth Res*, 105(1), 73–82, 2010.
52. Maróti, P., Kinetics and yields of bacteriochlorophyll fluorescence: Redox and conformation changes in reaction center of *Rhodobacter sphaeroides*, *Eur Biophys J*, 37(7), 1175–1184, 2008.
53. Feher, G., J.P. Allen, M.Y. Okamura, and D.C. Rees, Structure and function of bacterial photosynthetic reaction centres, *Nature*, 339(6220), 111–116, 1989.

54. Filus, Z., G. Laczkó, C.A. Wraight, and P. Maróti, Delayed fluorescence from the photosynthetic reaction center measured by electronic gating of the photomultiplier, *Biopolymers*, 74(1–2), 92–95, 2004.
55. Turzó, K., G. Laczkó, Z. Filus, and P. Maróti, Quinone-dependent delayed fluorescence from the reaction center of photosynthetic bacteria, *Biophys J*, 79(1), 14–25, 2000.
56. Wraight, C.A. and R.K. Clayton, The absolute quantum efficiency of bacteriochlorophyll photooxidation in reaction centres of *Rhodopseudomonas spheroides*, *Biochim Biophys Acta*, 333(2), 246–260, 1974.
57. Wraight, C.A., Proton and electron transfer in the acceptor quinone complex of photosynthetic reaction centers from *Rhodobacter sphaeroides*, *Front Biosci*, 9, 309–337, 2004.
58. Gerencsér, L., G. Laczkó, and P. Maróti, Unbinding of oxidized cytochrome c from photosynthetic reaction center of *Rhodobacter sphaeroides* is the bottleneck of fast turnover, *Biochemistry*, 38(51), 16866–16875, 1999.
59. Marcus, R.A. and N. Sutin, Electron transfers in chemistry and biology, *Biochim Biophys Acta*, 811(3), 265–322, 1985.
60. Lin, J., I.A. Balabin, and D.N. Beratan, The nature of aqueous tunneling pathways between electron-transfer proteins, *Science*, 310(5752), 1311–1313, 2005.
61. Moser, C.C., J.M. Keske, K. Warncke, R.S. Farid, and P.L. Dutton, Nature of biological electron transfer, *Nature*, 355(6363), 796–802, 1992.
62. Moser, C.C., C.C. Page, R. Farid, and P.L. Dutton, Biological electron transfer, *J Bioenerg Biomembr*, 27(3), 263–274, 1995.
63. Page, C.C., C.C. Moser, X. Chen, and P.L. Dutton, Natural engineering principles of electron tunnelling in biological oxidation-reduction, *Nature*, 402(6757), 47–52, 1999.
64. Maróti, P., Use of Marcus theory of electron transfer as an intramolecular ruler, *J Photochem Photobiol B Biol*, 19(3), 235–238, 1993.
65. Rybtchinski, B., L.E. Sinks, and M.R. Wasielewski, Combining light-harvesting and charge separation in a self-assembled artificial photosynthetic system based on perylenediimide chromophores, *J Am Chem Soc*, 126(39), 12268–12269, 2004.
66. Wasielewski, M.R., Energy, charge, and spin transport in molecules and self-assembled nanostructures inspired by photosynthesis, *J Org Chem*, 71(14), 5051–5066, 2006.
67. Guldi, D.M. and H. Imahori, Supramolecular assemblies for electron transfer, *J Porphyr Phthalocyanines*, 8(7), 976–983, 2004.
68. Gust, D. and T.A. Moore, Intramolecular photoinduced electron-transfer reactions of porphyrins, in *Electron Transfer*, K.M. Kadish, K.M. Smith, and R. Guilard, Eds., San Diego, CA: Academic Press, 2000, pp. 153–190.
69. Imahori, H., Porphyrin–fullerene linked systems as artificial photosynthetic mimics, *Org Biomol Chem*, 2(10), 1425–1433, 2004.
70. Fukuzumi, S., Development of bioinspired artificial photosynthetic systems, *Phys Chem Chem Phys*, 10(17), 2283–2297, 2008.
71. Imahori, H., Creation of fullerene-based artificial photosynthetic systems, *Bull Chem Soc Jpn*, 80(4), 621–636, 2007.
72. Gust, D., T.A. Moore, and A.L. Moore, Molecular mimicry of photosynthetic energy and electron transfer, *Accounts Chem Res*, 26(4), 198–205, 1993.
73. Gust, D., T.A. Moore, A.L. Moore, A.N. Macpherson, A. Lopez, J.M. DeGraziano, I. Gouni, E. Bittersmann, and G.R. Seely, Photoinduced electron and energy transfer in molecular pentads, *J Am Chem Soc*, 115(24), 11141–11152, 1993.
74. Kroto, H.W., J.R. Heath, S.C. O'Brien, R.F. Curl, and R.E. Smalley, C60: Buckminsterfullerene, *Nature*, 318(6042), 162–163, 1985.
75. Kobori, Y., S. Yamauchi, K. Akiyama, S. Tero-Kubota, H. Imahori, S. Fukuzumi, and J.R. Norris, Jr., Primary charge-recombination in an artificial photosynthetic reaction center, *Proc Natl Acad Sci USA*, 102(29), 10017–10022, 2005.

76. Maes, M., H. Sasabe, N. Kihara, Y. Araki, Y. Furusho, K. Mizuno, T. Takata, and O. Ito, Photoinduced electron and energy transfer processes in rotaxanes containing zinc porphyrin as pendant and [60] fullerene and ferrocene as axle ends, *J Porphyr Phthalocyanines*, 9(10), 724–734, 2005.
77. Kodis, G., Y. Terazono, P.A. Liddell, J. Andreasson, V. Garg, M. Hambourger, T.A. Moore, A.L. Moore, and D. Gust, Energy and photoinduced electron transfer in a wheel-shaped artificial photosynthetic antenna-reaction center complex, *J Am Chem Soc*, 128(6), 1818–1827, 2006.
78. Terazono, Y., G. Kodis, P.A. Liddell, V. Garg, T.A. Moore, A.L. Moore, and D. Gust, Multiantenna artificial photosynthetic reaction center complex, *J Phys Chem B*, 113(20), 7147–7155, 2009.
79. Terazono, Y., P.A. Liddell, V. Garg, G. Kodis, A. Brune, M. Hambourger, A.L. Moore, T.A. Moore, and D. Gust, Artificial photosynthetic antenna-reaction center complexes based on a hexaphenylbenzene core, *J Porphyr Phthalocyanines*, 9(10), 706–723, 2005.
80. Hasobe, T., Supramolecular nanoarchitectures for light energy conversion, *Phys Chem Chem Phys*, 12(1), 44–57, 2010.
81. Joliot, P., G. Barbieri, and R. Chabaud, Un nouveau modele des centres photochimiques du systeme II, *Photochem Photobiol*, 10, 309–329, 1969.
82. Kok, B., B. Forbush, and M. McGloin, Cooperation of charges in photosynthetic O_2 evolution. 1. A linear four step mechanism, *Photochem Photobiol*, 11, 457–475, 1970.
83. Meelich, K., C.M. Zaleski, and V.L. Pecoraro, Using small molecule complexes to elucidate features of photosynthetic water oxidation, *Phil Trans R Soc B*, 363, 1271–1281, 2008.
84. Chang, C.J., M.C. Chang, N.H. Damrauer, and D.G. Nocera, Proton-coupled electron transfer: A unifying mechanism for biological charge transport, amino acid radical initiation and propagation, and bond making/breaking reactions of water and oxygen, *Biochim Biophys Acta*, 1655(1–3), 13–28, 2004.
85. Yagi, M., A. Syouji, S. Yamada, M. Komi, H. Yamazaki, and S. Tajima, Molecular catalysts for water oxidation toward artificial photosynthesis, *Photochem Photobiol Sci*, 8(2), 139–147, 2009.
86. Burdinski, D., E. Bothe, and K. Wieghardt, Synthesis and characterization of tris(bipyridyl) ruthenium(II)-modified mono-, di-, and trinuclear manganese complexes as electron-transfer models for photosystem II, *Inorg Chem*, 39(1), 105–116, 2000.
87. Sun, L., L. Hammarström, B. Nkermark, and S. Styring, Towards artificial photosynthesis: Ruthenium-manganese chemistry for energy production, *Chem Soc Rev*, 30, 36–49, 2001.
88. Balzani, V., G. Bergamini, F. Marchioni, and P. Ceroni, Ru(II)-bipyridine complexes in supramolecular systems, devices and machines, *Coord Chem Rev*, 250(11–12), 1254–1266, 2006.
89. Geletii, Y.V., B. Botar, P. Kogerler, D.A. Hillesheim, D.G. Musaev, and C.L. Hill, An all-inorganic, stable, and highly active tetraruthenium homogeneous catalyst for water oxidation, *Angew Chem Int Ed Engl*, 47(21), 3896–3899, 2008.
90. Jiao, F. and H. Frei, Nanostructured cobalt oxide clusters in mesoporous silica as efficient oxygen-evolving catalysts, *Angew Chem Int Ed Engl*, 48(10), 1841–1844, 2009.
91. Kanan, M.W. and D.G. Nocera, In situ formation of an oxygen-evolving catalyst in neutral water containing phosphate and Co^{2+}, *Science*, 321(5892), 1072–1075, 2008.
92. O'Regan, B. and M. Grätzel, A low-cost, high-efficiency solar cell based on dye-sensitized colloidal TiO_2 films, *Nature*, 353(6346), 737–740, 1991.
93. Mulkidjanian, A.Y., On the origin of life in the zinc world: 1. Photosynthesizing, porous edifices built of hydrothermally precipitated zinc sulfide as cradles of life on Earth, *Biol Direct*, 4, 26, 2009.
94. Mulkidjanian, A.Y. and M.Y. Galperin, On the origin of life in the zinc world. 2. Validation of the hypothesis on the photosynthesizing zinc sulfide edifices as cradles of life on Earth, *Biol Direct*, 4, 27, 2009.
95. Halmann M, B. Aurian-Blajeni, and S. Bloch, Photoassisted carbon dioxide reduction and formation of two and three-carbon compounds, in *Third ISSOL Meeting and Sixth ICOL Meeting*, Jerusalem, Israel, Dordrecht, the Netherlands: D. Reidel Publishing Co., 1980.
96. Granick, S., Speculations on the origins and evolution of photosynthesis, *Ann NY Acad Sci*, 69(2), 292–308, 1957.

97. Mauzerall, D., Light, iron, Sam Granick and the origin of life, *Photosynth Res*, 33(2), 163–170, 1992.
98. Henglein, A., M. Gutierrez, and F. CH, Photochemistry of colloidal metal sulfides. 6. Kinetics of interfacial reactions at ZnS particles, *Ber Bunsen Phys Chem*, 88(2), 170–175, 1984.
99. Feller, U., I. Anders, and T. Mae, Rubiscolytics: Fate of Rubisco after its enzymatic function in a cell is terminated, *J Exp Bot*, 59(7), 1615–1624, 2008.
100. Portis, A.R., Jr. and M.A. Parry, Discoveries in Rubisco (Ribulose 1,5-bisphosphate carboxylase/oxygenase): A historical perspective, *Photosynth Res*, 94(1), 121–143, 2007.
101. Spreitzer, R.J. and M.E. Salvucci, Rubisco: Structure, regulatory interactions, and possibilities for a better enzyme, *Annu Rev Plant Biol*, 53, 449–475, 2002.
102. Parry, M.A., P.J. Andralojc, R.A. Mitchell, P.J. Madgwick, and A.J. Keys, Manipulation of Rubisco: The amount, activity, function and regulation, *J Exp Bot*, 54(386), 1321–1333, 2003.
103. Liu, C., A.L. Young, A. Starling-Windhof, A. Bracher, S. Saschenbrecker, B.V. Rao, K.V. Rao, O. Berninghausen, T. Mielke, F.U. Hartl, R. Beckmann, and M. Hayer-Hartl, Coupled chaperone action in folding and assembly of hexadecameric Rubisco, *Nature*, 463(7278), 197–202, 2010.
104. Saschenbrecker, S., A. Bracher, K.V. Rao, B.V. Rao, F.U. Hartl, and M. Hayer-Hartl, Structure and function of RbcX, an assembly chaperone for hexadecameric Rubisco, *Cell*, 129(6), 1189–1200, 2007.
105. Sato, S., K. Koike, H. Inoue, and O. Ishitani, Highly efficient supramolecular photocatalysts for CO_2 reduction using visible light, *Photochem Photobiol Sci*, 6, 454–461, 2007.
106. Takeda, H., K. Koike, H. Inoue, and O. Ishitani, Development of an efficient photocatalytic system for CO_2 reduction using rhenium(I) complexes based on mechanistic studies, *J Am Chem Soc*, 130(6), 2023–2031, 2008.
107. Dorogi, M., Z. Bálint, C. Miko, B. Vileno, M. Milas, K. Hernádi, L. Forro, G. Váró, and L. Nagy, Stabilization effect of single-walled carbon nanotubes on the functioning of photosynthetic reaction centers, *J Phys Chem B*, 110(43), 21473–21479, 2006.
108. Xian-Fu, Z., C. Xiaofeng, L. Qiang, and Z. Fushi, Multiple-charge separation in nanoscale artificial photosynthetic models, *ChemPhysChem*, 9(11), 1514–1518, 2008.
109. Melis, A. and T. Happe, Hydrogen production. Green algae as a source of energy, *Plant Physiol*, 127(3), 740–748, 2001.
110. Gaffron, H. and J. Rubin, Fermentative and photochemical production of hydrogen in algae, *J Gen Physiol*, 26(2), 219–240, 1942.
111. Melis, A., L. Zhang, M. Forestier, M.L. Ghirardi, and M. Seibert, Sustained photobiological hydrogen gas production upon reversible inactivation of oxygen evolution in the green alga *Chlamydomonas reinhardtii*, *Plant Physiol*, 122(1), 127–136, 2000.
112. Benemann, J.R. and N.M. Weare, Hydrogen evolution by nitrogen-fixing *Anabaena cylindrica* cultures, *Science*, 184(4133), 174–175, 1974.
113. Miyake, J. and S. Kawamura, Efficiency of light energy conversion to hydrogen by the photosynthetic bacterium *Rhodobacter sphaeroides*, *Int J Hydrogen Energ*, 12(3), 147–149, 1987.
114. Iwuchukwu, I.J., M. Vaughn, N. Myers, H. O'Neill, P. Frymier, and B.D. Bruce, Self-organized photosynthetic nanoparticle for cell-free hydrogen production, *Nat Nano*, 5(1), 73–79, 2010.
115. Canaguier, S., V. Artero, and M. Fontecave, Modelling NiFe hydrogenases: Nickel-based electrocatalysts for hydrogen production, *Dalton Trans* (3), 315–325, 2008.
116. Ichikawa, K., T. Matsumoto, and S. Ogo, Critical aspects of [NiFe]hydrogenase ligand composition, *Dalton Trans* 2009(22), 4304–4309, 2009.
117. Oudart, Y., V. Artero, J. Pecaut, and M. Fontecave, [Ni(xbsms)Ru(CO)2Cl2]: A bioinspired nickel-ruthenium functional model of [NiFe] hydrogenase, *Inorg Chem*, 45(11), 4334–4336, 2006.
118. Weetall, H. and L. Krampitz, Production of hydrogen from water using biophotolytic methods, *Appl Biochem Biotechnol*, 5(2), 115–124, 1980.
119. Cardona, T., N. Battchikova, P. Zhang, K. Stensjo, E.M. Aro, P. Lindblad, and A. Magnuson, Electron transfer protein complexes in the thylakoid membranes of heterocysts from the cyanobacterium *Nostoc punctiforme*, *Biochim Biophys Acta*, 1787(4), 252–263, 2009.

120. Tolstygina, I.V., T.K. Antal, S.N. Kosourov, T.E. Krendeleva, A.B. Rubin, and A.A. Tsygankov, Hydrogen production by photoautotrophic sulfur-deprived *Chlamydomonas reinhardtii* pre-grown and incubated under high light, *Biotechnol Bioeng*, 102(4), 1055–1061, 2009.
121. Kosourov, S., A. Tsygankov, M. Seibert, and M.L. Ghirardi, Sustained hydrogen photoproduction by *Chlamydomonas reinhardtii*: Effects of culture parameters, *Biotechnol Bioeng*, 78(7), 731–740, 2002.
122. Kruse, O., J. Rupprecht, K.P. Bader, S. Thomas-Hall, P.M. Scenk, G. Finazzi, and B. Hankamer, Improved photobiological H_2 production in engineered green algal cells, *J. Biol. Chem.* 280(40), 34170–34177, 2005.
123. Pilotelle-Bunner, A., P. Beaunier, J. Tandori, P. Maróti, R.J. Clarke, and P. Sebban, The local electric field within phospholipid membranes modulates the charge transfer reactions in reaction centres, *Biochim Biophys Acta*, 1787(8), 1039–1049, 2009.
124. Maróti, P. and C.A. Wraight, Flash-induced H^+ binding by bacterial photosynthetic reaction centers: Comparison of spectrophotometric and conductimetric methods, *Biochim Biophys Acta*, 934(3), 314–328, 1988.
125. Sebban, P., P. Maróti, and D.K. Hanson, Electron and proton transfer to the quinones in bacterial photosynthetic reaction centers: Insight from combined approaches of molecular genetics and biophysics, *Biochimie*, 77(7–8), 677–694, 1995.
126. Ghosh, P.K., A.Y. Smirnov, and F. Nori, Modeling light-driven proton pumps in artificial photosynthetic reaction centers, *J Chem Phys*, 131(3), 035102, 2009.
127. Steinberg-Yfrach, G., J.L. Rigaud, E.N. Durantini, A.L. Moore, D. Gust, and T.A. Moore, Light-driven production of ATP catalysed by F0F1-ATP synthase in an artificial photosynthetic membrane, *Nature*, 392(6675), 479–482, 1998.
128. Maróti, P. and C.A. Wraight, Kinetics of H^+ ion binding by the $P^+Q_A^-$ state of bacterial photosynthetic reaction centers: Rate limitation within the protein, *Biophys J*, 73(1), 367–381, 1997.
129. Nagy, L., F. Milano, M. Dorogi, A. Agostiano, G. Laczko, K. Szebenyi, G. Varo, M. Trotta, and P. Maroti, Protein/lipid interaction in the bacterial photosynthetic reaction center: Phosphatidylcholine and phosphatidylglycerol modify the free energy levels of the quinones, *Biochemistry*, 43(40), 12913–12923, 2004.
130. Milano, F., L. Gerencsér, A. Agostiano, L. Giotta, L. Nagy, M. Trotta, and P. Maróti, Kinetics of proton uptake during photocycle of reaction center of photosynthetic bacteria, in *Photosynthesis: Fundamental Aspects to Global Perspectives*, A. van der Est and D. Bruce, Eds., Lawrence, KS: Alliance Communication Group, 2005, pp. 213–215.
131. Steinberg-Yfrach, G., P.A. Liddell, S.-C. Hung, A.L. Moore, D. Gust, and T.A. Moore, Conversion of light energy to proton potential in liposomes by artificial photosynthetic reaction centres, *Nature*, 385(6613), 239–241, 1997.
132. Agostiano, A., F. Mavelli, F. Milano, L. Giotta, M. Trotta, L. Nagy, and P. Maróti, pH-sensitive fluorescent dye as probe for proton uptake in photosynthetic reaction centers, *Bioelectrochemistry*, 63(1–2), 125–128, 2004.
133. Hambourger, M., G.F. Moore, D.M. Kramer, D. Gust, A.L. Moore, and T.A. Moore, Biology and technology for photochemical fuel production, *Chem Soc Rev*, 38(1), 25–35, 2009.
134. Gust, D., D. Kramer, A.L. Moore, T.A. Moore, and W. Vermaas, Engineered and artificial photosynthesis: Human ingenuity enters the game, *MRS Bull*, 33, 383–387, 2008.
135. Dau, H. and I. Zaharieva, Principles, efficiency, and blueprint character of solar-energy conversion in photosynthetic water oxidation, *Acc Chem Res*, 42(12), 1861–1870, 2009.
136. Rutherford, A.W. and T.A. Moore, Mimicking photosynthesis, but just the best bits, *Nature*, 453(7194), 449, 2008.
137. Asztalos, E. and P. Maróti, Export or recombination of charges in reaction centers in intact cells of photosynthetic bacteria, *Biochim Biophys Acta*, 1787(12), 1444–1450, 2009.
138. Lagref, J.J., M.K. Nazeeruddin, and M. Grätzel, Artificial photosynthesis based on dye-sensitized nanocrystalline TiO_2 solar cells, *Inorg Chim Acta*, 361(3), 735–745, 2008.

139. Grimm, B., R.J. Porra, W. Rüdiger, and H. Scheer, Chlorophylls and bacteriochlorophylls: Biochemistry, biophysics, functions and applications, in *Advances in Photosynthesis and Respiration*, Govindjee, Ed., Dordrecth, the Netherlands Springer, 2006.
140. Arlt, T., B. Dohse, S. Schmidt, J. Wachtveitl, E. Laussermair, W. Zinth, and D. Oesterhelt, Electron transfer dynamics of *Rhodopseudomonas viridis* reaction centers with a modified binding site for the accessory bacteriochlorophyll, *Biochemistry*, 35(28), 9235–9244, 1996.
141. Ferreira, K.N., T.M. Iverson, K. Maghlaoui, J. Barber, and S. Iwata, Architecture of the photosynthetic oxygen-evolving center, *Science*, 303(5665), 1831–1838, 2004.
142. Roszak, A., T. Howard, J. Southall, A. Gardiner, C. Law, N. Isaacs, and R. Cogdell, Crystal structure of the RC–LH1 core complex from *Rhodopseudomonas palustris*, *Science*, 302(5652), 1969–1972, 2003.
143. Lancaster, C.R. and H. Michel, The coupling of light-induced electron transfer and proton uptake as derived from crystal structures of reaction centres from *Rhodopseudomonas viridis* modified at the binding site of the secondary quinone, Q_B, *Structure*, 5(10), 1339–1359, 1997.
144. Guskov, A., J. Kern, A. Gabdulkhakov, M. Broser, A. Zouni, and W. Saenger, Cyanobacterial photosystem II at 2.9-Å resolution and the role of quinones, lipids, channels and chloride, *Nat Struct Mol Biol*, 16(3), 334–342, 2009.
145. Müh, F., T. Renger, and A. Zouni, Crystal structure of cyanobacterial photosystem II at 3.0 Å resolution: A closer look at the antenna system and the small membrane-intrinsic subunits, *Plant Physiol Biochem*, 46(3), 238–264, 2008.

56

Fluorescent Proteins: Structural Determinants of Optical Response

Ranieri Bizzarri
The National Enterprise for nanoScience and nanoTechnology

and

Consiglio Nazionale delle Ricerche

Riccardo Nifosì
The National Enterprise for nanoScience and nanoTechnology

56.1 Introduction

The discovery of a fluorescent protein (FP) taking part in the bioluminescence system of jellyfish *Aequorea victoria* dates back to the early 1960s [1]. This protein was named green fluorescent protein (GFP), from its bright green fluorescence obtained by UV–blue light excitation; hereafter, it will be simply referred to as wild-type GFP or wtGFP to be consistent with the scientific nomenclature in use.

Thirty years later, with the cloning of the gene [2] and the demonstration that its expression in other organisms still produces fluorescence [3,4], the interest in wtGFP started to rise dramatically, eventually leading to a revolution in fluorescence microscopy bioimaging [5]. Soon after its cloning, many other fluorescent and nonfluorescent GFP homologues were discovered in a variety of organisms [6,7]. Additionally, protein engineering by sequence mutagenesis has produced a profusion of FPs with optical properties spanning most of the visible spectrum and beyond. Nowadays by the term FPs, it is customary to indicate all fluorescent variants of the original *A. victoria* wtGFP, notwithstanding their actual primary sequence homology. Many natural homologues of GFP are nonfluorescent, though they absorb visible light (chromoproteins or CPs). To provide the reader with some idea about the richness of FP world, Ref. [8] shows the phylogenetic tree of FPs, including some artificial mutants.

The mesmerizing success of FPs in bioimaging owes to the genetic encoding of fluorescence into their primary sequence without any additional help (enzymes, cofactors) from the host organism. This makes it possible to express fluorescent fusion chimeras of any FP with target proteins of relevant biochemical

interest in cells and follow their fate by real-time microscopy imaging. The fluorescent biomarker, coming from an unrelated organism, does not usually perturb the biological processes of the target protein. Hence, FPs represent a nearly perfect bionanodevice to unveil cell mechanisms.

Surprisingly, all known FPs show a remarkable structural similarity. A chromophore moiety, origin of fluorescence, is autocatalytically generated within the conserved β-barrel tertiary structure following a subsequential cyclization and oxidation of an internal tripeptide sequence; for many variants, further reactions can take place, increasing the variety of chromophore structures. A finer tuning originates from the noncovalent interactions of these chromophore structures with the surrounding molecular matrix. The structure-dependent variety of the optical response is surely one of the factors that have contributed to the success of FPs. Indeed, careful engineering of the protein sequence has enabled tailoring FPs to specific imaging techniques in cells. The tunability of FPs upon sequence engineering and careful sequence of the parent protein structure and chromophore represents a challenging, and very stimulating, field for all bioscientists interested in structure–property relationships in biomolecules.

It would be rather impossible to include in a single chapter the full list of developed FP variants together with the sheer number of their applications in molecular biology, biochemistry, and biophysics. For a more detailed overview on this general topic, the reader is referred to the complete reviews by Shaner, Chudakov, and Stepanenko on FPs as general molecular markers [9–11], Ibraheem on FP as general biosensors [12], Bizzarri on FPs as intracellular pH indicators [13], Takanishi and Masi on FPs to probe protein–protein interaction via FRET [14,15], and Lukyanov and Lippincott-Schwartz on photoactivatable FPs for high-resolution applications (including optical nanoscopy) [16,17].

Instead, adopting a physicochemical approach, this chapter focuses on how the protein structure influences the optical properties of FPs. Although it was the first FP to be cloned [2] and functionally expressed in other organisms [3], wtGFP has actually been replaced in most applications by its mutants and homologues. Nonetheless, being one of the best FPs characterized in terms of optical and photophysical properties, it is a suitable starting point to introduce the concepts recurring in this chapter. Hence, the reader is first presented with wtGFP, considered as the "photophysical" archetype of FPs. In Section 56.2.1, the structure and formation of wtGFP chromophore is presented, whereas Sections 56.2.2 and 56.2.3 dwell on the chromophore-related optical properties. Section 56.3 is devoted to the general description of FPs, addressing the chromophore structure and formation at Section 56.3.1, and the optical properties of FPs as derived by structure-induced spectral tuning. Note that FPs are grouped in five families on account of emission color. Finally, at Section 56.4, the role of chromophore protonation in determining the optical characteristics is discussed for FPs from *A. victoria* (*av*FPs), the protein class that include wtGFP.

56.2 Structure and Optical Properties of wtGFP

56.2.1 Structure and Chromophore Formation

wtGFP is constituted by a single peptide chain of 238 amino acids and 27 kDa molecular weight [5]. X-ray spectroscopy displayed that this sequence folds in a compact cylindrical 3D structure (referred to as β-barrel), whose lateral wall is an 11-stranded β-sheet, with a diameter of 24 Å and a height of 42 Å (Figure 56.1) [18]. Remarkably, all FPs share the β-barrel fold, regardless of the homology of their primary sequence [9]. Differences can be found in quaternary structure, as several natural FPs arrange as tightly bound tetramers or dimers, a feature that initially hampered their applications. Primary sequence mutagenesis, however, were able in most cases to reverse association and yield monomeric variants of the parent proteins.

The β-barrel of wtGFP (and, more generally, of FPs) is capped on both ends by short α-helical sections and run through by a α-helix, which contains the amino acids forming the chromophore. In wtGFP, the chromophore is a 4-(*p*-hydroxybenzylidene) imidazolinone, constituted by two conjugated aromatic rings, one being a six-member aromatic phenol and the other being a five-member imidazolidinone (Scheme 56.1) [5]. The chromophore originates from the posttranslational autocatalytic modification of three consecutive amino acids: Ser^{65}–Tyr^{66}–Gly^{67} [19,20]. Actually, the formation of the GFP

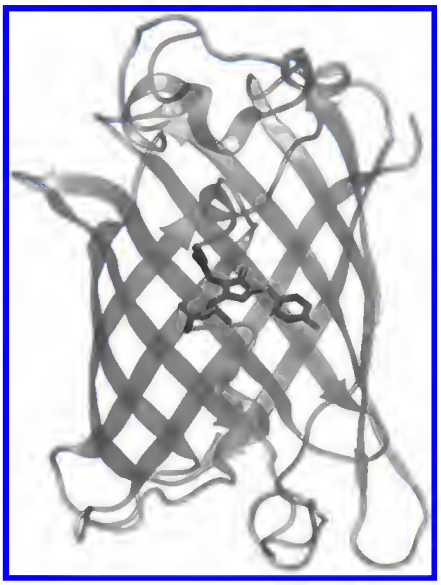

FIGURE 56.1 3D structure of wtGFP from x-ray analysis [18]. The protein chromophore buried at the center of the tertiary structure is pictured in darker colors.

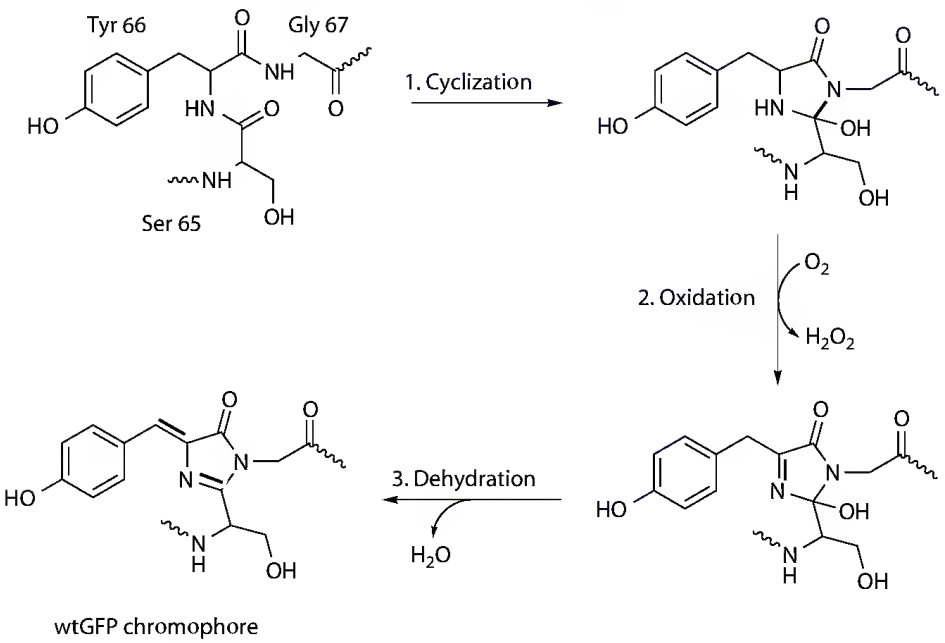

SCHEME 56.1 Formation of wtGFP chromophore from the cyclization–oxidation–dehydration posttranslational processing of the amino acid triplet Ser^{65}–Tyr^{66}–Gly^{67} [21].

chromophore comprises three distinct chemical processes and is triggered by the protein folding into the β-barrel tertiary structure [21,22]: in step 1, the tripeptide Ser^{65}–Tyr^{66}–Gly^{67} cyclizes (Scheme 56.1, Reaction **1**); in step 2, the cyclic intermediate is oxidized by molecular oxygen to yield a conjugated structure (Scheme 56.1, Reaction **2**); in step 3, a water molecule is released (Scheme 56.1, Reaction **3**). The oxidation reaction represents the rate-limiting step of the overall process, and it requires at least 30 min to occur [23]. As demonstrated by the heterologous expression of *Aequorea* GFP gene in other organisms leading to fluorescence, the posttranslational synthesis of the chromophore does not require any jellyfish-specific enzyme [3,4]. Exogenous oxygen is, however, required because in anaerobic conditions wtGFP does not develop fluorescence [4,20].

The imidazolinone five-member heterocyclic ring is a common feature of all known FP chromophores. In wtGFP, the alternating single and double bonds in the bridge region extend the electron delocalization from the phenolate to the carbonyl of the imidazolinone. Efficient visible-light absorption is ultimately determined by this π-conjugated system. It is worth noting that the phenol ring of the chromophore derives entirely from the lateral group of Tyr^{66}. This leaves room for the replacement of Tyr^{66} with other amino acids bearing aromatic side chains, such as phenylalanine, histidine, or tryptophan, in view of obtaining different optical properties; indeed, early mutagenesis studies showed that this is actually the case (see Section 56.3.1).

56.2.2 Optical Features of Chemical Model of wtGFP Chromophore

The *intrinsic* chromophore properties were thoroughly investigated by using several synthetic analogues. The established experimental model for the chromophore of wtGFP and many other FP variants derived therefrom is a *p*-hydroxybenzylidene-2,3-dimethlimidazolone or *p*-HBDI [24,25] (Scheme 56.2). Such a model encompasses the relevant π-conjugated system although it lacks the side chain of the first residue of the tripeptide, which is Ser in wtGFP.

p-HBDI bears two main protonation sites: the phenol group and the nonamide nitrogen in the imidazolinone ring (indicated in Scheme 56.2 and in general FP chromophore as N^1). Two protonation sites imply four protonation states, which we indicated as "protonated" ***P*** (protonated phenol and N^1, net charge: +1), "neutral" ***N*** (protonated phenol, deprotonated N^{66}, net charge: 0), "zwitterionic" ***Z*** (deprotonated phenol, protonated N^1, net charge: 0), and "anionic" ***An*** (deprotonated phenol and N^1, net charge: −1; Scheme 56.2). In *p*-HBDI, the ***P*** → ***N*** ionization has pK_a = 1.8–2.4,* whereas the ***N*** → ***An*** ionization has pK_a = 8.1–8.5. The pK_a of ***P*** → ***Z*** was determined to be around 6.5 by using a zwitterionic-mimicking *p*-HBDI analogue [26]. These three pK_a values allow for the full thermodynamic description of the protonation reactions for *p*-HBDI (Scheme 56.2). Importantly, this calculation shows that ***Z*** always accounts for less than 0.01% of its isoelectric counterpart ***N***. Hence, above pH = 3, the ***N*** → ***An*** ionization is overwhelming and residual presence of ***Z*** can be neglected.

In *p*-HBDI and similar structures, the four states have different optical properties (Figure 56.2a). The ***P***, ***N***, and ***An*** forms display absorption maxima at 387–393, 368–372, and 425–428 nm, respectively, in water [19,26,27]. The redshifted absorption of ***P*** and ***An*** states compared to ***N*** is attributed to extended electronic conjugation, which lowers the $S_0 \rightarrow S_1$ transition energy [28]. Owing to its negligible

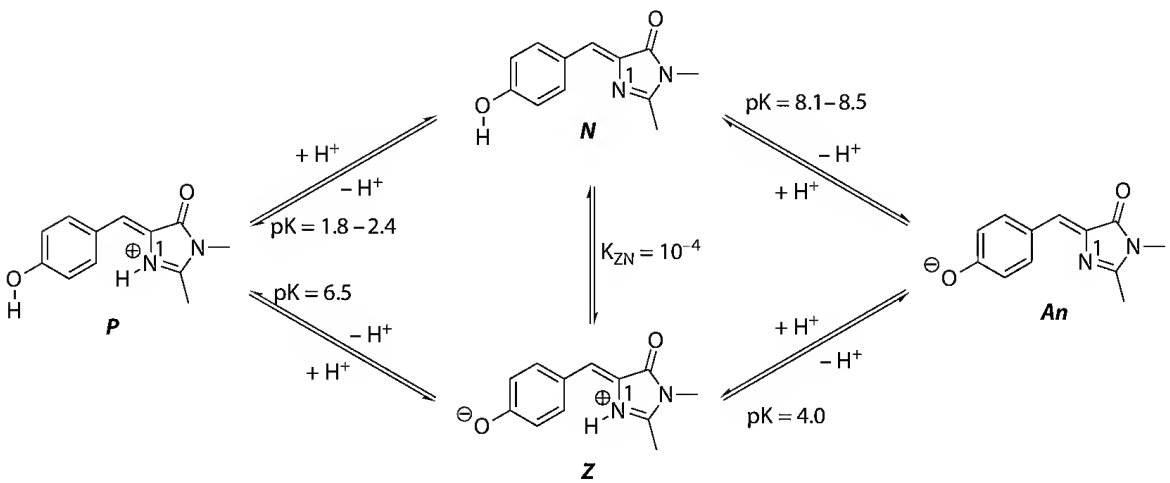

SCHEME 56.2 Protonation reaction of the wtGFP chromophore model *p*-HBDI. The four accessible protonation states ***P*** (protonated), ***N*** (neutral), ***Z*** (zwitterionic), and ***An*** (anionic) and their associated protonation reactions are reported together with the related pK_a values [26,27]. The nonamidic nitrogen of the imidazolinone ring is indicated as N^1.

* Minor variability depends on the addition of a small amount of methanol/ethanol to improve *p*-HBDI solubility.

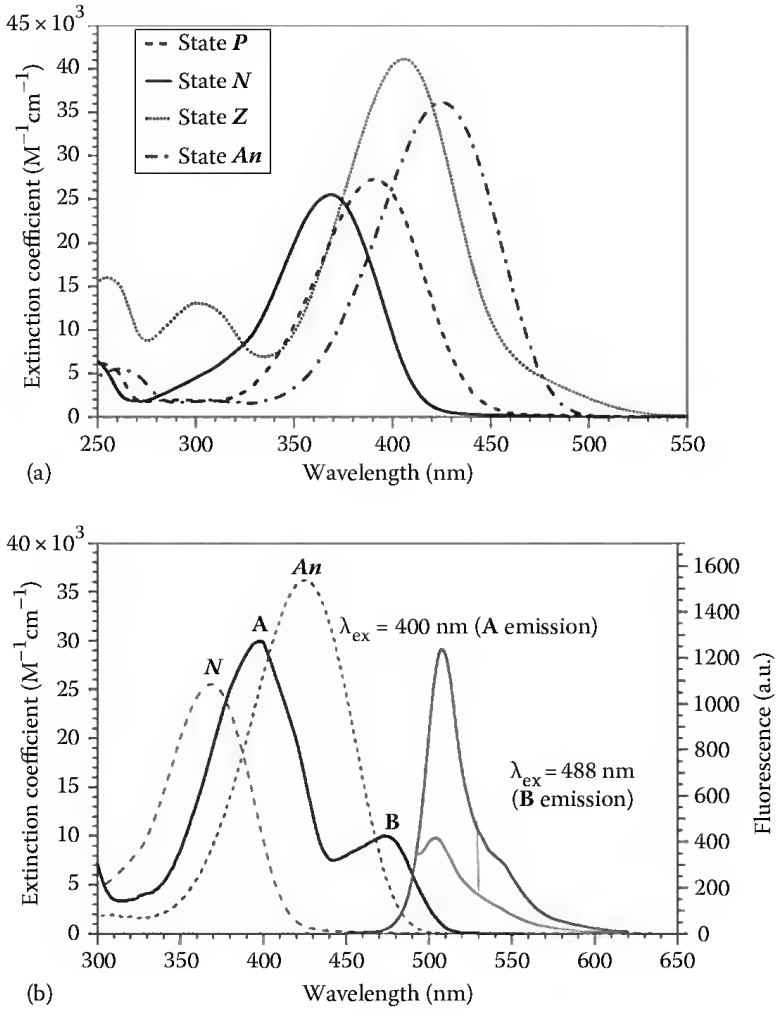

FIGURE 56.2 (a) Absorption spectra of the four protonation states of *p*-HBDI. (b) Absorption (left scale, green curve: states **A** and **B** are indicated) and emission (right scale, red and blue curves: emissions from each absorbing state are indicated) spectra of wtGFP at pH 7.4; the absorption spectra of **N** and **D** states in the denatured protein are added as reference. Note: For nomenclature and structural reference, see Schemes 56.2 and 56.3.

population at any pH, absorption of ***Z*** is not directly measurable. The aforementioned zwitterionic-mimicking derivative, however, was found to absorb at 406 nm in water (Figure 56.2a) [26].

The solvent sensitivity of ***An*** absorption (maximum shift from water taken as reference: +57 nm) has been highlighted by several authors [19,26,27]. By contrast, ***N*** and ***P*** chromophore states display a much narrower variation range (20 nm). Dong et al. were successful in interpreting these shifts by means of the Kamlet–Taft multivariant equation, indicating that acidic and basic properties of the solvent play a role comparable to that of solvent polarity [26]. The significant solvatochromic shift of the anionic state points to a marked sensitivity to the surrounding environment. As we shall see (Section 56.3), such sensitivity emerges also when the chromophore is embedded in the protein matrix: in different FPs, the absorption corresponding to the anionic chromophore of wtGFP shows a similar, if not larger, range of variation.

The four protonation states of *p*-HBDI display negligible fluorescence emission upon excitation at maximum wavelengths (quantum yields < 10^{-3}) [24]. Apparently, the poor emissivity is related to the presence of a fast and efficient deactivation channel that involves intramolecular *hula-twist* torsion of the chromophore in the excited state [29]. Consistently, indeed, *p*-HBDI fluorescence is restored when molecular mobility and the related torsional deactivation channel of the excited state is hampered, that is, at very low temperatures and in high-viscosity media [19,24,29–31].

The absorption and poor-emission properties of *p*-HBDI are mostly retained in the unfolded state of wtGFP, although the protein-corresponding ***N*** and ***An*** states are redshifted to 384 and 448 nm, respectively. Analogously to *p*-HBDI, the chromophore of the unfolded protein becomes emissive at 77 K [19]. Given this similarity, hereafter ***P***, ***N***, ***Z***, and ***An*** will generally denote the states of wtGFP chromophore when it is outside the protein fold in water solution.

56.2.3 Optical States and Mechanism of Fluorescence Emission in wtGFP

wtGFP is folded between pH 4 and 11; in this range only the neutral (i.e., protonated phenol and deprotonated N^1) and anionic (i.e., deprotonated phenol and N^1) states of the chromophore contribute to the optical properties of the protein. By using Raman spectroscopy, Bell et al. showed that the zwitterionic state has a negligible population also in the protein, suggesting that this form is always very unstable from a thermodynamic point of view. Following a long-standing tradition in the field of FPs, the neutral and anionic states of the wtGFP chromophore in the folded protein will be hereafter identified as state **A** and **B**, respectively. The use of nonitalic symbols helps distinguishing the states of the chromophore in folded proteins from those in artificial models such as *p*-HBDI and unfolded protein.

The room-temperature absorption and emission spectra of wtGFP in the visible region are reported in Figure 56.2b; absorption spectra of ***N*** and ***An*** are included in the same figure as benchmarks. Notably, the β-barrel fold of wtGFP proteins deeply affects the optical properties of the chromophore. Absorption of state **A** and **B** are redshifted by 30 and 50 nm compared to ***N*** and ***An***, respectively: **A** peaks at 398 nm, whereas **B** peaks at 475 nm (Figure 56.2b). As we shall try to highlight at Section 56.3, the observed optical changes likely stem from the complex network of interactions that take place into the protein fold between the chromophore and the nearby residues. X-ray data of wtGFP indicate that the chromophore is surrounded by four entrapped water molecules and several charged and polar residues such as Gln^{69}, Gln^{94}, Arg^{96}, His^{148}, Thr^{203}, Ser^{205}, and Glu^{222} [18,32–34]. Additionally, in **A** and **B** states, the chromophore environment is significantly different [32]. A proton network that connects the chromophore phenol to Glu^{222} is active in **A**, whereas it is hampered in **B** on account of the 120° rotation of Thr^{203} to establish a strong H-bond with the phenolate anion [32]. From the extinction coefficients of the two states, an **A**/**B** population ratio around 6/1 can be calculated. This ratio is nearly unaffected by changes of proton concentration in the 5–11 pH range [35]. This rather unexpected phenomenon, which suggests some additional contribution to simple phenol ionization, will be clarified at Section 56.4. It is worth mentioning that, beside the **A** and **B** bands, wtGFP display a strong peak at 278–280 nm attributable to the direct excitation of aromatic amino acids (10 Tyr and 1 Trp). This UV band is shared by all FPs.

The rigid folded structure of wtGFP is also responsible for the significant protein fluorescence emission compared to *p*-HBDI in water. The **A** state displays $\Phi_A = 0.78$ [36], whereas the **B** state has $\Phi_B = 0.79$ [37]. Fluorescence of both states is also unaffected by the presence of classical quenching agents [24,38]. **A** and **B** are characterized by minor differences of emission maxima and shapes, a rather unexpected property given their large difference in absorption maxima (Figure 56.2b). Pump–probe experiments targeting the excited-state depletion at short (ps) timescale highlighted that the emission similarity stems from a proton transfer mechanism occurring at the excited state [39,40]. Photon absorption by **B** leads to excited state **B*** that has a single emission channel at 503 nm. Conversely, upon excitation of **A**, two competing photoprocesses leading to emission are triggered: (1) direct emission from **A*** (at 440–480 nm) and (2) excited state proton transfer (ESPT) from **A*** to Glu^{222} through a proton wire of H-bonds involving one water molecule and Ser^{205} [39–41] eventually leading to 507 nm emission. ESPT takes place in a few picoseconds on account of the strongly increased acidity of the phenol group [28], and it represents a much more efficient depletion channel of **A*** than direct fluorescence emission [42]. In more details, upon ESPT **A*** evolves to **I***, an intermediate excited state where the chromophore is anionic like in **B*** but its surrounding residues are in the relaxed form typical of **A** owing to the very short timescale of **I** decay (a few ns) that does not allow for the rearrangement of the chromophore environment driven by phenol deprotonation (e.g., flipping of the lateral chain of Thr^{205}) [39,43]. This explains why **I*** emits at wavelengths similar, but not equal, to **B*** (Figure 56.2b). Upon emission, **I*** decays to **I**, which quickly evolves to **A**, which is more stable by

7.6 kJ mol^{-1} of free energy [44]. The **I** → **A** conversion seems to take place by reversing the internal proton wire associated with ESPT [32]. Some kinetic studies pointed out that **I** comprises two metastable intermediates $\mathbf{I}_1$ and $\mathbf{I}_2$, although $\mathbf{I}_1$ is very short-lived (3 ps) compared to $\mathbf{I}_2$ (0.4 ns) [45].

56.3 Structure and Optical Properties of Fluorescent Proteins

56.3.1 Chromophore Structure and Formation

Figure 56.3 summarizes both the chromophore structures and their proposed formation mechanism for most classes of known FPs.

The prechromophore tripeptide has a X_1–Tyr_2–Gly_3 sequence in all natural FPs discovered so far*; X_1 can be almost any amino acid, whereas no chromophore formation takes place upon mutation of the Gly_3 [21], suggesting that the peculiar conformational flexibility of glycine is necessary at that location. Conversely, the fluorescence is maintained by substitution of Tyr_2 with another aromatic amino acid (Phe, His, or Trp). The replacement of Tyr with Phe, His, or Trp leads to artificial mutants characterized by blueshifted excitation and fluorescence wavelengths with respect to the parent protein [20,46]. We shall refer to all chromophores originated by a tyrosine-based tripeptide as Y-chrom. Analogously, F-chrom, H-chrom, and W-chrom will denote tripeptides including Phe, His, or Trp, respectively.

The posttranslational processing around the X_1 α-carbon determines the ultimate chromophore structure (Figure 56.3). For several FPs, including wtGFP, no modifications of this site take place. By contrast, the oxidation of the C–N main chain bond of X_1, which leaves an acylimine substituent at the corresponding position of the imidazolinone ring, occurs in DsRed [47] and more generally for the class of red FPs (hereafter denoted as RFPs; Figure 56.3). It has been recently showed that the oxidation leading to the acylimine substituent actually precedes dehydrogenation of the bridging carbon [22]. From a photophysical point of view, formation of the acylimine moiety extends the π-conjugated system, and correspondently lowers the excitation energy, resulting in red–orange fluorescence.

In other FPs, additional reactions take place on the acylimine moiety, such as hydrolysis associated with backbone cleavage in asFP595 [48]† or side-chain cyclization by nucleophilic addition of the threonine (orange), cysteine (mKO), or lysine (zFP538) side chain, the latter reaction being followed by backbone cleavage [49–51]. In Kaede and related proteins (KikGR, EosFP, Dendra), UV excitation cleaves the backbone between main chain N and Cα of the Histidine at X_1. The cleavage is followed by double bond formation between Cα and Cβ (Figure 56.3) [52,53]. All these variants retain redshifted excitation/emission bands and therefore belong to the RFP family.

As already shown for wtGFP (Section 56.2.3), in all Y-chrom proteins, the phenol group on the chromophore can exist either as neutral (protonated phenol) or anionic (deprotonated phenol). The absorption of the neutral form is always significantly blueshifted with respect to the anionic form. In some FPs, the change of the external pH enables the reversible population shift from the neutral to the anionic states of the chromophore; this phenomenon, which will be thoroughly described for FPs from *A. victoria* (*av*FPs) at Section 56.4, is associated with a pH-titration curve clearly observable both in absorption and in fluorescence. Nonetheless, in most FPs, and particularly in RFPs, the anionic chromophore much more stable than its neutral counterparts in the 5–9 pH range. In RFPs, this effect stems from the increased phenol acidity brought about by the additional conjugated double bond(s).

According to some computational investigations, the zwitterionic form (with the imidazolinone nitrogen protonated) might be the emitting state in some FPs [54]. In addition, it is worth mentioning that the zwitterionic and other protonation state such as the cationic form (protonated phenol and imidazolinone) may be relevant to FP photophysics [55].

* Not all natural FPs are actually *fluorescent*. However, these nonfluorescent species (named chromoproteins) were eventually converted into fluorescent species by molecular engineering.

† As FP595 chromophore structure has been subject to debate, regarding the possible presence of an imino (NH) group in place of the ketone group at position 2 of the imidazolinone (see discussion in Ref. [48]).

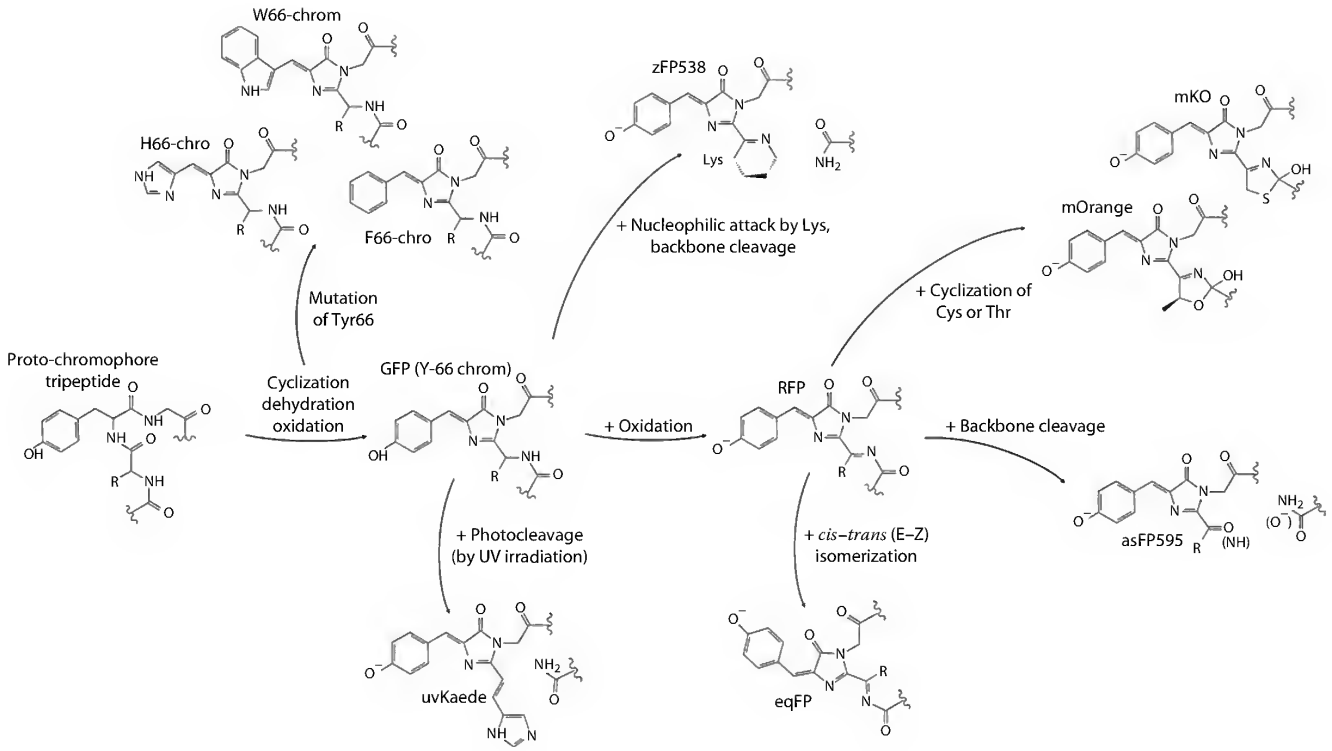

FIGURE 56.3 Formation and structures of FP chromophores.

56.3.2 Optical Properties of FPs: Mechanism of Spectral Tuning

Adopting a general perspective, rather than trying to exhaustively survey all FPs discovered and engineered so far, this section will focus on the structural mechanisms operating the observed spectral shifts in the main families of FPs: blue (BFPs), cyan (CFPs), green (GFPs), yellow (YFPs), and red (RFPs) emitting. Excitation and emission wavelengths in different representative FPs can be read in Table 56.1.

TABLE 56.1 Optical Properties of Representative FP Mutants

Protein Name	Chromophore	Excitation/ Absorption Peak (nm)	Emission Peak (nm)	Extinction Coefficient (10^3 M^{-1} cm^{-1})	QY	References
GFP Y66F	F66-chro	360	442	—	Low	[56]
EBFP	H66-chro	377	446	30	0.15	[56,57]
EBFP2	H66-chro	383	448	32	0.56	[58]
Azurite	H66-chro	384	450	26.2	0.55	[59]
mKalama1	Y66-chro (A)	385	456	36	0.45	[58]
mBlueberry2	RFP Y67F	402	467	51	0.48	[58]
Cerulean	W66-chro	433	475	43	0.62	[60]
ECFP	W66-chro	434	476	32.5	0.4	[61]
mTFP1-Y67W	W66-chro	424/440	461/482	13	0.02	[58]
cFP484 (tetr)	Y66-chro (B)	456	484	35.3	0.48	[62]
amFP486 (tetr)	Y66-chro (B)	458	486	40	0.24	[62]
mTFP1	Y66-chro (B)	462	492	64	0.85	[58]
EGFP	Y66-chro (B)	484	507	53	0.6	[37,57]
avGFP B state	Y66-chro (B)	477	508	9.5	0.72	[36]
avGFP A state	Y66-chro (A)	397	510 (espt)	25	0.78	[36]
T-sapphire	Y66-chro (A)	399	511 (espt)	44	0.60	[63]
Dronpa	Y66-chro (B)	503	518	95	0.85	[64]
EYFP	Y66-chro (B)	514	527	84	0.61	[65]
Venus	Y66-chro (B)	515	528	92.2	0.57	[66]
YPet	Y66-chro (B)	517	530	104	0.77	[67]
PhiYFP (dim)	Y66-chro (B)	525	537	115	0.60	[68]
zFP538 (dim)	zFP538	528	538	—	0.42	[62]
mKO	mKO	548	561	51.6	0.60	[69]
mHoneydew	RFP Y67W	487/504	537/562	17	0.12	[70]
mOrange	mOrange	548	562	71	0.69	[70]
Dendra photoc	uvKaede	557	575	20	0.72	[71]
EosFP photoc (tetr)	uvKaede	571	581	41	0.55	[53,72]
Kaede photoc (tetr)	uvKaede	572	582	60.4	0.33	[52,73]
DsRed (tetr)	RFP	558	583	57	0.79	[62]
asFP595	asFP	568	595	56.2	<0.001	[74,75]
mStrawberry	RFP	574	596	90	0.29	[70]
KFP1 (tetr) photoc	asFP	580	600	59	0.07	[76]
mRFP1	RFP	584	607	44	0.25	[77]
mCherry	RFP	587	610	72	0.22	[70]
eqFP611 (tetr)	eqFP	559	611	78	0.45	[78,79]
Rtms5 (tetr)	RFP	592	620	80	<0.001	[80]
mPlum	RFP	590	649	41	0.10	[81]
mNeptune	RFP	600	650	67	0.20	[82]
cjBlue	RFP	610	—	66.7	—	[83]

Note that the optical properties of any FP are the result of (1) the chromophore structure, particularly the nature of the aromatic ring and the presence of an additional double bond conjugated to the imidazolinone and (2) the interaction between chromophore and its immediate environment. The environment can act on the chromophore by (a) deforming some of its bond lengths through H-bonds, (b) distorting the planarity of the chromophore, and (c) differentially stabilizing the ground and excited states by electrostatic interactions.

The subtle chromophore–matrix interactions deserve some further observation, on account also of recent experimental [84] and theoretical [85] studies. Early Raman spectroscopy studies on the wtGFP model chromophore in solution and some *av*FPs revealed a tight correlation between the shift in absorption peak and the frequency of a specific Raman-active band [27]. This correlation was rationalized by invoking the selective stabilization of one of the two resonance structures of the chromophore (Scheme 56.3a) [86]. Indeed, variations of the Raman spectrum reflect a changing stabilization between a benzenoid-like resonance structure (Scheme 56.3a, **I**) and a quinonoid-like resonance structure (Scheme 56.3a, **II**). This effect is also at basis of the significant solvatochromism of the anionic Y-chrom. The neutral Y-chrom, indeed, evidences less environmental sensitivity, as the protonated phenol enforces a benzenoid-like structure thus decreasing the potential influence of nearby residues. Actually, in Y-chrom FPs, the optical properties principally stem from the anionic form of the chromophore in the

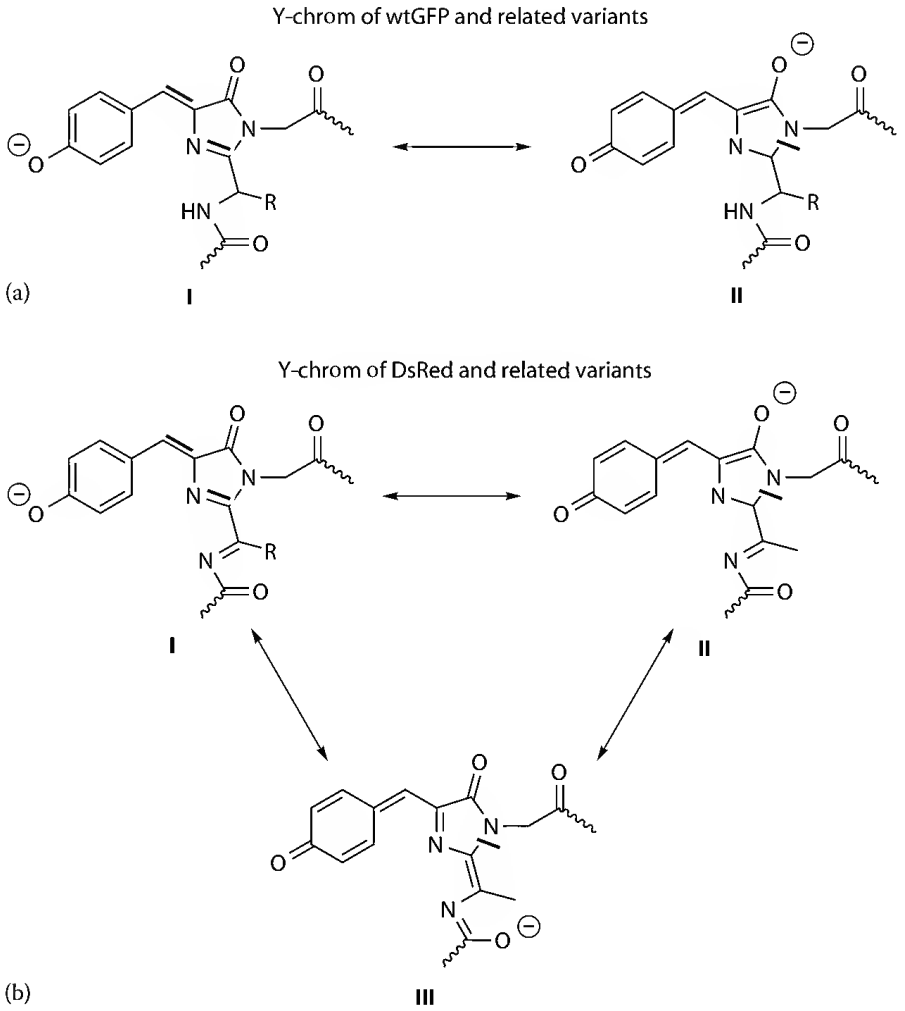

SCHEME 56.3 Resonance forms of the Y-chrom anionic state. (a) Chromophore of wtGFP and related proteins. (b) Chromophore of DsRed and related proteins. **I**: benzenoid structure, **II**: quinonoid structure, and **III**: extended enol structure.

physiological pH range. When present, the neutral absorption peak displays little variation in the 385–400 nm interval* [33,88–90]; emission from the neutral chromophore is generally very similar to that of the anionic state on account of the ESPT mechanism.

The ubiquitous hydrogen bond between the imidazolinone carbonyl and conserved Arg^{96} (in *av*GFP numeration) stabilizes the quinonoid form (Scheme 56.3a, **II**), thereby lowering the excitation energy. Vice versa, the establishment of H-bonds with chromophore phenolate (e.g., wtGFP) increases the contribution of the benzenoid form (Scheme 56.3a, **I**) in the anionic chromophore.

Other electrostatic interactions can be active and play a relevant role in determining the optical features of the protein. The interplay among all possible factors usually makes it difficult to predict the final outcome. Nonetheless, this general scheme is useful to decipher the mechanisms of spectral tuning. In the RFP chromophores, a third resonance structure is possible (Scheme 56.3, **III**). Hydrogen bonds to this additional site will tend to lower the excitation energy, stabilizing the excited-state charge displacement over the region [91].

Finally, the optical properties of the protein may be strongly related to protonation reactions and, in turn, by external pH. We shall describe this "chemical" effect (as complementary to the "electrostatic effects" described in this section) at Section 56.4.

56.3.2.1 Blue Fluorescent Protein (BFP) Family

Among the first *av*GFPs mutants to be produced, BFP were obtained by replacing Tyr^{66} with a His or a Phe. Model H-chro and F-chro in water display 17 nm [92]† and 21 nm [93] absorption blueshifts, respectively, compared to the neutral band of *p*-HBDI. Representative BFPs display absorption shifts from −37 to +5 nm, and emission shifts from the −68 to −43 nm, compared to the **A** state (neutral) of wtGFP (Table 56.1).

*av*BFP with F-chro was found to be extremely dim and it never found any biological application. Recently, however, Luin et al. suggested that the very low quantum yield of F-chro *av*BFP (named BFPF) stems from an efficient *cis–trans* photoisomerization of the chromophore [94]. The first "enhanced BFP" (EBFP) relied upon H-chro and included also other mutations to improve brightness and folding efficiency (F64L/S65T/Y145F) [92]. Even with those improvements, EBFP suffers from a low quantum yield (0.15) and is prone to fast photobleaching [95]. Recent mutagenesis efforts produced brighter and more photostable BFPs based on H-chro: Azurite [59], EBFP2 [58], and SBFP2 [96]. Two non-H-chro proteins also emit in the blue region, namely, mKalama1 [58], a *av*GFP mutant where the *neutral* chromophore is the stable state and is intrinsically fluorescent (i.e., ESPT is suppressed), and mBlueberry2 [58], a DsRed mutant with a F-chro with hyperconjugation.

56.3.2.2 Cyan–Teal Fluorescent Protein (CFP) Family

The most famous members of the cyan–teal family are artificial *av*GFPs where Tyr^{66} has been replaced by Trp. Model W-chro in water display 20 nm absorption blueshift compared to the anionic band of *p*-HBDI [93]. Representative CFPs display absorption shifts from −34 to −15 nm, and emission shifts from −32 to −16 nm, compared to the **B** state (anionic) of wtGFP (Table 56.1).

Enhanced CFP (ECFP, F64L/S65T/Y66W/N146I/M153T/V163A GFP) has been the first W-chro *av*FP to find large use in molecular biology studies, owing to its optical properties (main excitation/emission: 434/476 nm [5]) that makes it a good donor for fluorescence resonance energy transfer (FRET) when YFPs are selected as acceptors. Nonetheless, the medium-low brightness of ECFP and its multiexponential emission decay (due to multiple conformations of the W-chro [97]) early prompted for the engineering of improved mutants for FRET studies. In 2004, Rizzo et al. described *Cerulean*

* Somewhat redshifted value (415 nm) is observed in the S65T/H148D *av*GFP variant, where the D148 carboxyl oxygen forms a very tight hydrogen bond (distance 2.4 Å) with the chromophore hydroxyl group [87].

† No data about the absorption of model H-chrom has been ever reported. The shift is calculated considering unfolded enhanced BFP (EBFP) and wtGFP.

(S72A/Y145A/H148D ECFP), a 2.5-fold brighter variant of ECFP with monoexponential emission [60]. The x-ray structure of *Cerulean* and additional molecular modeling studies have clarified the origin of the peculiar optical properties of this protein [98–100]. Since 2004, *Cerulean* has mostly replaced ECFP in FRET experiments. Yet, Kremers et al. have engineered SCFP1, SCFP2, SCFP3a, and SCFP3b, which are similar to *Cerulean* concerning brightness but are characterized by larger lifetime variability (SCFP1 and SCFP3a can be used for dual-lifetime imaging although they have the same optical properties) [101].

The cyan–teal family also comprises FPs isolated from reef corals, such as *Discosoma striata* (dsFP483), *Anemonia majano* (amFP485), and *Clavularia* (cFP484), as well as two cFP484 mutants, mTFP0.7 and mTFP1. These cyan-emitting proteins are naturally tightly bound tetramers, but recently mTFPs were engineered to avoid oligomerization and exist as monomers [90]. The chromophore of these proteins is a Y-chrom, so the blueshifted spectral properties of this group originate from peculiar chromophore–protein interactions. Singling out the specific blueshifting interactions has proven rather puzzling, also because the broad absorption/excitation band hints at structural heterogeneity of either the chromophore or its close surroundings [102]. cFP484, amFP486, and mTFPs (but not dsFP483) display a quadrupole network of salt bridges underlying the chromophore and entailing Arg^{69}, one His, and two Glu. The His is presumably cationic, being hydrogen bonded on both sides to the glutamates [103]. Replacement of this His by Thr in amFP486 restores the optical properties typical of green mutants such as wtGFP (absorption and emission are redshifted from 454 to 470 nm and from 486 to 515, respectively), and is accompanied by a decline in fluorescence quantum yield and heterogeneity of chromophore structure [103]. Nonetheless, the quadrupole configuration is missing in dsFP483 [102] and is instead present in green-emitting Dronpa [64] and cmFP512 [104].

The general requirement for cyan fluorescence appears to be the presence of a positively charged residue underlying the chromophore (His in cFP484, amFP486, and the mTFPs and Lys70 in dsFP483), together with the arrangement of the three H-bond donors facing the chromophore phenolate. Indeed, a water molecule and serine are present in all examined structures, and at H-bonding distance to the phenolate. A histidine, again at H-bonding distance, is present in dsFP483 and in cFP484 and related mTFP mutants. amFP486 features an Ala at the equivalent position. Though Ala cannot donate a H-bond, its small bulk allows a water molecule to fill the cavity. Neither Dronpa nor cmFP512, though featuring the quadrupole arrangement, and hence the charged His, has all three H-bond donors.

56.3.2.3 Green Fluorescent Protein (GFP) Family

The proteins belonging to this class have optical properties similar to those displayed by wtGFP (Table 56.1), although in most cases only the bright anionic form of the chromophore is optically active. Indeed, the most popular green variant, Enhanced GFP (EGFP) (F64L/S65T GFP) owes its high brightness to a predominantly anionic Y-chrom above pH 6 [88,105].

Recent experiments on *p*-HBDI suggest that the Y-chrom is characterized by similar optical properties in gas phase and when embedded in folded protein [106]. This result is apparently in contrast with the experimental evidence of relevant interactions between the chromophore and its surrounding residues and water molecules in green FPs. However, a meaningful rationalization takes into account the mutual cancelation of the various contributions. Computational studies [86] point at a counteraction between the redshifting hydrogen bond with conserved Arg^{96} and the blueshifting of hydrogen bonds to the phenolate. This effect is supported by several experimental studies. Removal of Arg^{96} blueshifts the optical properties, because the H-bond stabilization of the phenolate becomes predominant. This effect is clearly observable in the R96M mutant (absorption/emission 466/490 nm) where the H-bond of Arg with the imidazolinone carbonyl group is replaced with a, somewhat weaker, hydrogen bond with a water molecule (donor–acceptor distance is 2.9 Å in protein data bank (PDB) structure 2AWK [107]). By contrast, removal of Thr^{203} abolishes the H-bond to the phenolate and induces optical redshift.

Indeed, in T203V and T203I, the anionic state peaks at 502 nm [33]. Proteins from other sea organisms, such as Dronpa and cmFP512, also belong to this family.

56.3.2.4 Yellow Fluorescent Protein (YFP) Family

Proteins belonging to the yellow family (YFPs) share an aromatic moiety (from Tyr, Phe, or His) π-stacked to Y-chrom. The T203Y mutation was introduced in *av*GFP under the assumption that Tyr^{203} would be π-stacked to the chromophore phenolate, thereby lowering the excitation energy by increasing the polarizability of the environment around the chromophore [65]. The mutation indeed resulted in yellow-emitting variants (Table 56.1) and x-ray studies confirmed the π-stacking configuration [65]. Similar redshift was observed in T203F *av*FP mutant [33]. Notably, nature played the same stratagem in a natural FP named phiYFP [68].

Although redshifted fluorescence to the yellow region should be totally ascribed to the π-stacked Tyr or Phe, π-stacking is only one of the causes underlying the *absorption* redshift. Additionally, the x-ray structure of EYFP show a peculiar hydrogen bond between Glu^{222} and the imidazolinone of the chromophore, which appears prodromic to redshift in other mutants [49].

Most notably, the π-stacking Tyr/Y-chrom of YFPs leads to the highest extinction coefficients (>75,000 M^{-1} cm^{-1}), emission quantum yields ($\Phi > 0.8$), and fluorescence lifetimes ($\tau > 3$ ns) that can be found in FPs. Indeed, YFPs are among the best candidates for high-resolution and single-molecule imaging studies [108,109]. The yellow absorption of YFPs makes this class the perfect partner for FRET with CFP variants. *Venus* YFP was engineered to overcome the maturation and optical drawbacks of earlier YFPs [66] and soon it was demonstrated to be a good acceptor partner for *Cerulean* CFP (Section 56.3.2.2) for intracellular FRET studies [110]. Additionally, the peculiar proton and chloride sensitivity of many YFPs prompted their use as intracellular pH/Cl^- indicators [13,111–114].

56.3.2.5 Red Fluorescent Protein (RFP) Family

As already stated, the strong redshift of RFPs compared to wtGFP is mainly attributable to the enlargement of the π-conjugated system by the additional double bond, regardless if the latter has acylimine structure (as in DsRed and its progeny) or not. Model anionic RFP (DsRed) chromophores in water is redshifted by 57 nm [115] compared to the anionic band of *p*-HBDI. Representative RFPs display absorption shifts from +71 to +133 nm and emission shifts from +54 to +142 nm, compared to the **B** state (anionic) of wtGFP (Table 56.1).

In spite of the main role of extended conjugation in RFP chromophore, the protein matrix plays a relevant role in tuning the final optical properties of the folded protein, especially for variants where Y-chrom is predominantly anionic. We should note that in some RFPs, the chromophore undergoes covalent modifications that alter its structure; when the x-ray data are not available, the assignment of the chromophore structure may be doubtful. For example, the chromophore of mOrange and mBanana contains a structural modification at the acylimine tail and the blueshifted optical properties of these FPs cannot be wholly attributed to the chromophore–protein interactions.

The archetype DsRed protein is amongst the most blueshifted RFPs. Its optical features can be redshifted by dislocating Lys^{70}, which in wtDsRed is in close contact with the chromophore bridging carbon (at 3.6 Å distance) [49,116]. This mechanism is at play in K83M DsRed variant as well as in mCherry and mStrawberry, both featuring the K83L mutation. In the latter two mutants, additional redshift is provided by the hydrogen bond between protonated E215 and the closest N in the chromophore imidazolinone. If pH is raised to 10, the absorption peak of mCherry and mStrawberry shifts from 584 to 566 nm and from 574 to 548 nm, respectively, likely owing to the deprotonation of E215. A third source of redshifting is achieved in mCherry/mStrawberry by the additional K163Q/K163M mutations that eliminate one hydrogen bond to the chromophore phenolate.

Much alike in YFPs, π-orbital stacking of the RFP chromophore with a Tyr residue results in a noticeable optical redshift, like in the protein mGrape3 characterized by I197Y (608 ex and 646 em).

Unfortunately, mGrape3 is characterized by low quantum yield (0.03) and complex photophysics possibly connected with *cis–trans* isomerization of the chromophore [117].

Variations in the surrounding environment of the acylimine group can also contribute to the optical properties of RFPs. For example, mPlum, a significantly redshifted DsRed variant, features a hydrogen bond between (presumably neutral) Glu16 and the acylimine oxygen, in addition to "redshifting" K163M mutation and the E215-imidazolinone hydrogen bond. Removal of the H-bond by replacing Glu16 with Leu shifts the emission peak from 649 to 630 nm [49]. Actually, mutation of Glu16 appears to affect strongly just the emission peak, while leaving the excitation band almost unchanged.

Similarly in mNeptune [117], a far-red FP derived from eqFP578 of *Entacmaea quadricolor* [118], the acylimine oxygen is H-bonded to a water molecule. As is the case with many FPs, the redshift of mNeptune is, however, the result of multiple entangled contributions. As a consequence, it may be difficult to predict the outcome of a mutation. The slightly blueshifted optical properties of mKate (another eqFP578 mutant) compared to mNeptune can be traced back to the absence of the H-bond entailing the acylimine oxygen, on account of the Met41-promoted displacement of the hydrogen-bonded water molecule.

Deviation from coplanarity of the two aromatic rings in the protein chromophore (quantified by the twist around τ and ϕ, or also including the tilt angle defined as the deviation of the phenol oxygen from the perfectly planar chromophore [119]) is another determinant of optical properties. In general, distorted chromophore structures are associated with poor quantum yield of fluorescence. As an example, mCherry is characterized by a particularly distorted chromophore and a rather low fluorescence quantum yield (0.22) [11].

56.4 pH Dependence of Optical Response in *av*GFP Mutants

As anticipated at Section 56.2.3, wtGFP shows detectable deviations from the 3:1 optical ratio between the **A** and **B** bands only at pH below pH 4.5 and above pH 10 [35]. Thus, no *net proton transfer* between wtGFP chromophore and the external solution takes place in the physiological pH range, although the concomitant presence of **A** and **B** states points to an *internal* proton equilibrium between the chromophore and surrounding residues. By this means, natural selection has engineered wtGFP to be almost unresponsive to external pH changes to prevent fluctuations of the jellyfish bioluminescence that could hamper its biological role.

In many other FPs with Y-chrom, however, the optical response of the protein is very sensitive to the external proton concentration in the 5–10 pH range, on account of the ionization reaction of the chromophore phenol [105,120,121]. In such cases, the β-barrel tertiary structure that protects the chromophore from the outside world is bypassed by "proton-wires" constituted by several residues networked by H-bonds connected to "proton-collecting antenna" systems, that is, several carboxylates within H-bond networks on the surface of proteins, which convey protons to the orifice of an internal proton wire leading to the protein's active site [122].

We shall restrict our discussion about the influence of pH on the optical protein response to *av*FPs with Y-chrom, owing to the much deeper comprehension of the protonation-related mechanism in this protein family. It seems likely, nonetheless, that similar mechanism hold also for other kinds of FPs as recently demonstrated for cmFP512 from *Cerianthus membranaceus* [104].

For many *av*FPs, the pH-dependent optical response follows that of *p*-HBDI or unfolded protein (Figure 56.4a and e), being characterized by the single-site protonation of Y-chrom phenol. Here, absorption spectra show the progressive interconversion of neutral state (absorbing at 390–420 nm) into anionic state (absorbing at 475–520 nm; Figure 56.4a). On account of a nearly pH-independent quantum yields of either chromophore forms, the fluorescence spectrum at each pH is determined by the relative populations of neutral and anionic Y-chrom; in the absence of ESPT, neutral Y-chrom is usually very dim, whereas anionic Y-chrom is always bright (Figure 56.4b). Notably, the pK_a of chromophore ionization usually ranges between 5 and 6 making anionic Y-chrom the most populated form at physiological pH.

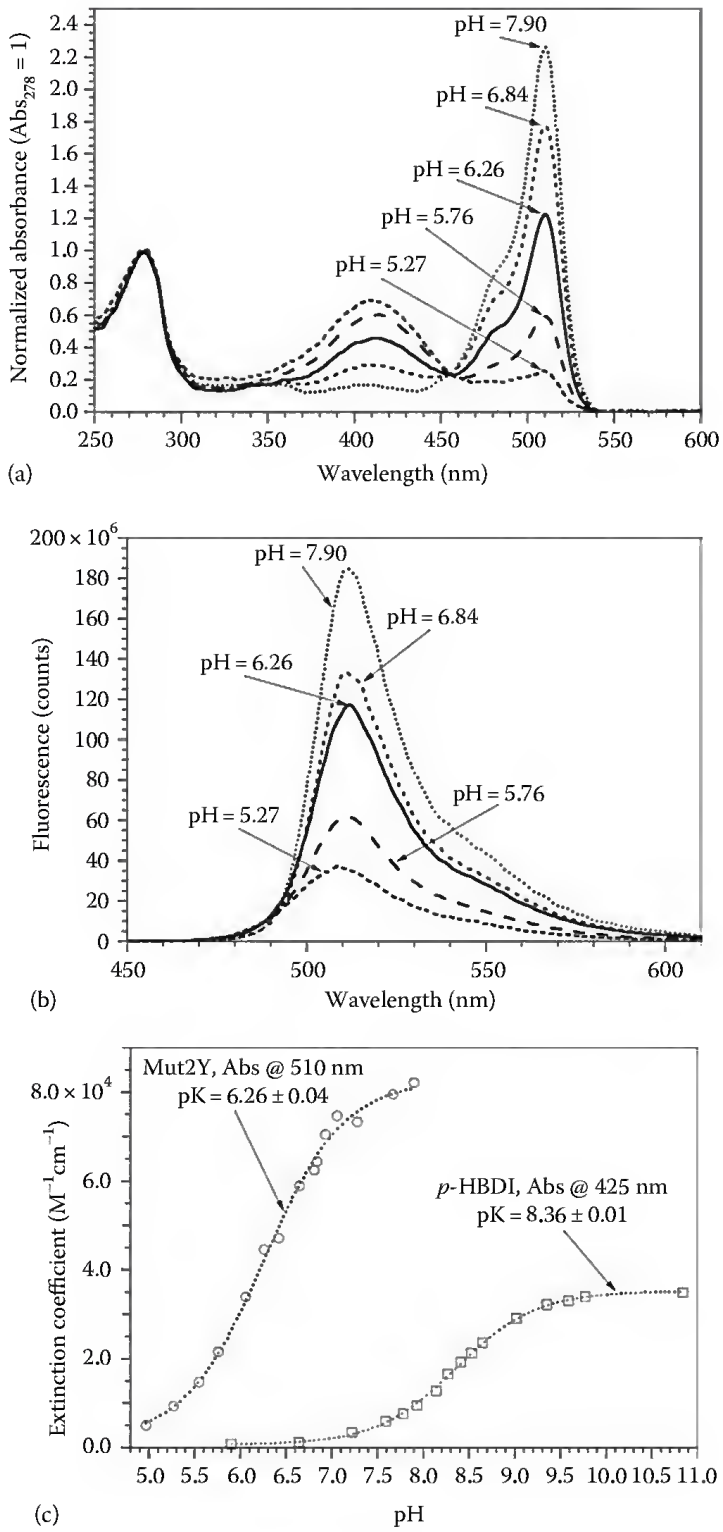

FIGURE 56.4 (a–c) pH-dependent optical features of S65A/V68L/S72A/T203Y GFP (Mut2Y [88]): (a) absorption spectrum, (b) emission spectrum (ex: 473 nm), and (c) pH plot of the extinction coefficient of the anionic chromophore (abs: 510 nm) and, for comparison, of *p*-HBDI (abs: 425 nm): data are fitted to the sigmoidal curve of Equation 56.2 representing the pH titration of a single ionization site (see text).

(*continued*)

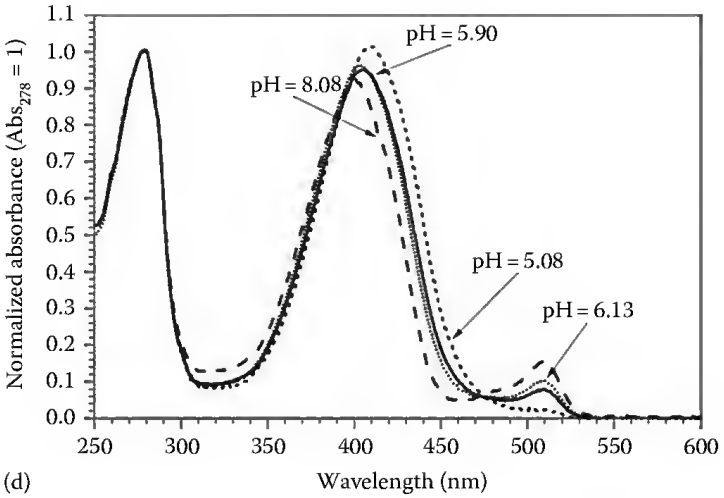

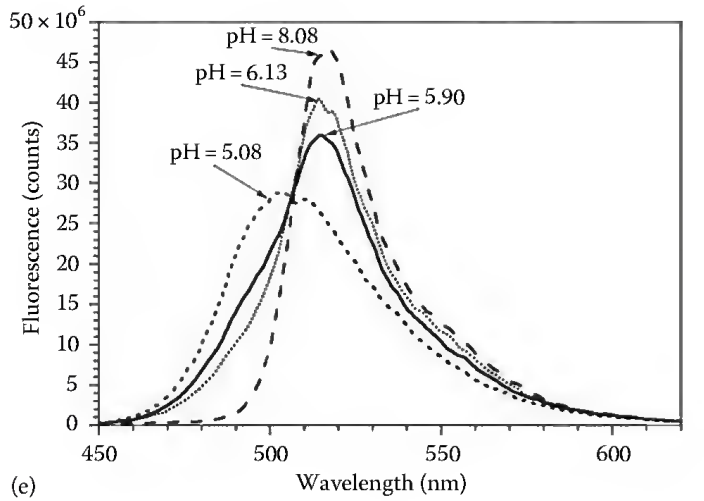

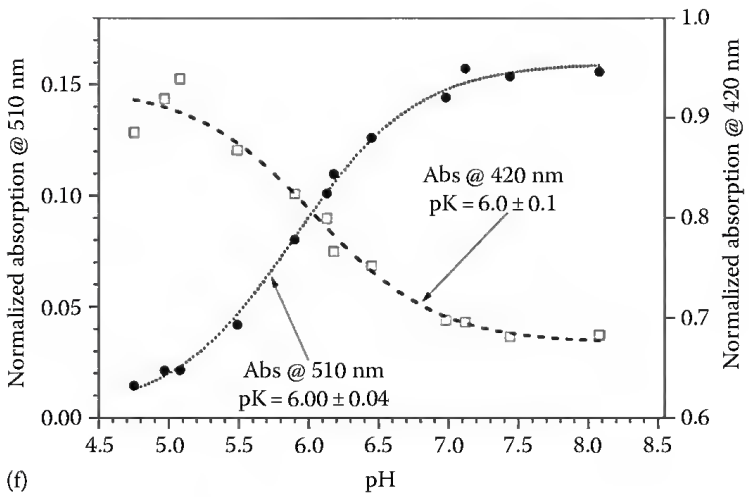

FIGURE 56.4 (cotninued) (d–f) pH-dependent optical features of F64L/T203Y (E^1GFP, [88]): (d) absorption spectrum, (e) emission spectrum (ex: 395 nm), and (f) pH plot of the extinction coefficient of the anionic (abs: 510 nm, full circles), and neutral (abs: 420 nm) chromophore: data are fitted to the sigmoidal curve of Equation 56.2 representing the pH titration of a single ionization site (see text).

In other mutants, the absorption spectra display a peculiar pH trend: a single-site ionization is inferred from optical pH-titration data [47,88,123] but at pH » pK_a, the absorption band corresponding to neutral Y-chrom is still intense, although blueshifted (Figure 56.4d and f). Obviously, neither this phenomenon can be accounted for by the simple ionization scheme of the phenol group nor the experimental pK_a can be attributed solely to the chromophore. Additionally, these mutants display detectable emission also from neutral state(s) [41]. This effect appears to be pH dependent, leading to emission spectra that are redshifted by raising the solution pH (Figure 56.4e).

We recently proposed a comprehensive model (named 2S model) that rationalizes both the observed photophysical behaviors [88]. The preliminary assumption in our model is that the optical response of Y-chrom reflect the pH-dependent ground state populations of neutral and anionic forms and their (almost) pH-independent intrinsic optical properties. We have not included in our treatment structurally/environmentally "nonrelaxed" anionic species **I** (if present), as they negligibly contribute to the protein absorption spectra owing to their metastable character and short lifetime. The central assumption in our model invokes the influence on the protein optical properties of a second *ionizable site* XH (henceforth, denoted as X when deprotonated), which resides on the lateral chain of a nearby residue to the chromophore. XH (or X) and the phenol group of Y-chrom are supposed to mutually exchange protons at ground state (and perhaps also at excited state), possibly through a few proton relays belonging to an internal H-bonding network. Actually, x-ray structures of *av*FPs show that many protonatable groups may exchange protons with the chromophore (e.g., His^{148}, Glu^{222}, Arg^{96}). Both Y-chrom and XH are supposed to be in direct proton communication with the external solution through some proton wire/proton antenna pathways such as those described by Agmon et al [122].

The two protonation sites generate four possible ground states: **A′**, **A**, **B**, and **B′** (Scheme 56.4). This notation follows the reported protonation scheme of wtGFP [32,39,40], where the **A** state is characterized by neutral chromophore and anionic Glu^{222} (the X residue in wtGFP and other *av*FPs, as we shall show in the following), while **B** has the opposite configuration. In the linear regime of the optical response, the absorption/fluorescence of the protein at a given pH is given by the sum of the fractional

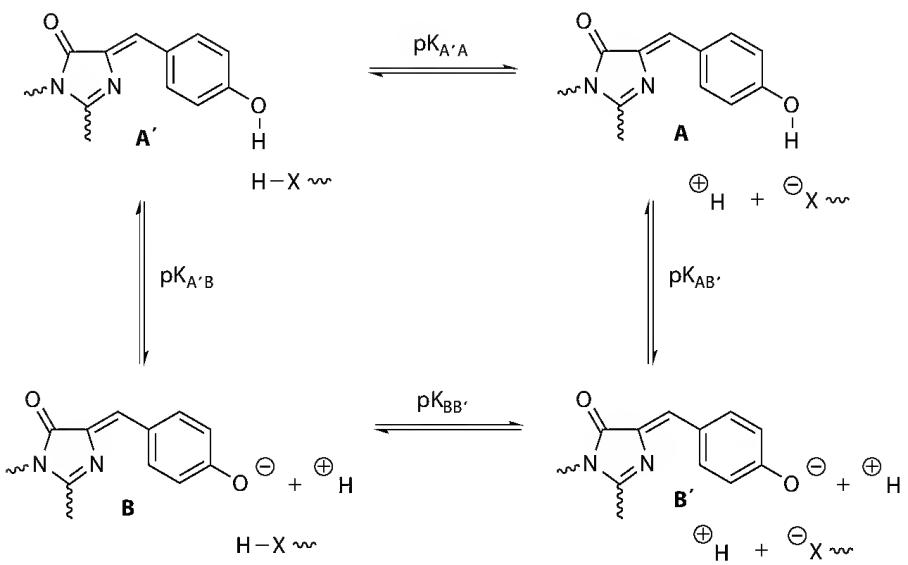

SCHEME 56.4 2S model of pH-dependent optical response in *av*FPs [88]. XH is an ionizable residue nearby Y-chrom. The two ionizable groups, phenol and XH, yield four possible ground states **A′**, **A**, **B**, and **B′**.

population of each state multiplied by its molar absorbance or fluorescence, respectively. Following Ullmann [124], we can write

$$R = C_0 \frac{R_{A'} + R_A 10^{(pH-pK_{A'A})} + R_B 10^{(pH-pK_{A'B})} + R_{B'} 10^{(2pH-pK_{A'A}-pK_{A'B}+W)}}{1+10^{(pH-pK_{A'A})}+10^{(pH-pK_{A'B})}+10^{(2pH-pK_{A'A}-pK_{A'B}+W)}}, \quad (56.1)$$

where

R is the protein optical response (absorbance or fluorescence) of the protein at a given observation (excitation) wavelength

C_0 is the protein concentration

$R_{A'}$, R_A, R_B, and $R_{B'}$ are the molar absorbance/fluorescence of each state at the observation (excitation) wavelength

$pK_{A'A}$ and $pK_{A'B}$ are the pK_a values pertaining to the **A′↔A** and **A′↔B** proton dissociation equilibria, respectively (Scheme 56.3)

W is the *interaction free energy* between the ionization reactions of Y-chrom and XH, assumed positive in sign when the coupling is *cooperative* (i.e., deprotonation of one site stabilizes the deprotonation of the other), whereas it is negative when the coupling is *anticooperative* (i.e., deprotonation of one site hampers the deprotonation of the other).

A first remarkable case occurs for $W = 0$, which imply complete decoupling between Y-chrom and XH/X and *Chro* (i.e., the ionization of the first *does not influence* the ionization of the other). Here, we can safely assume that the optical properties of the chromophore states depend only upon their protonation state and are not affected by the protonation state of HX group (i.e., $R_{A'} = R_A$ and $R_B = R_{B'}$). In this condition, Equation 56.1 becomes

$$R = C_0 \frac{R_{A'} + R_B 10^{(pH-pK_{A'B})}}{1+10^{(pH-pK_{A'B})}}. \quad (56.2)$$

Equation 56.2 describes the sigmoidal response typical of the pH titration of a single ionizable group with $pK_a = pK_{A'B}$. Indeed, Equation 56.2 holds also for *p*-HBDI in water at pH > 4 (below the N^1-protonation equilibrium must be included, Section 56.2.2). The simple, "chromophore-like," optical response upon external pH change is shared by many *av*FP mutants (e.g., some YFPs [34,125], citrine [126], Mut2 class [121]); $pK_{A'B}$, however, is usually 1–3 pH units lower than the pK_a of the isolated chromophore.

The second remarkable case occurs when $W \ll 0$, that is, the ionization of XH strongly hampers the deprotonation of phenol in Y-chrom. Apparently, this condition ensues in all *av*FPs, where Glu^{222} is not forced in a single protonation state by strong H-bonds with surrounding residues [88]. Here, the strong anticooperative coupling between X = Glu^{222} and the chromophore ionization presumably stems from the strong negative energy implied in the creation of two close negative charges on both groups upon concomitant deprotonation. In these mutants, the fully deprotonated **B′** state cannot be reached within the stability range of the protein [note that **B′** becomes significantly populated at $pH \approx i(pK_{A'A} + pK_{A'B} - W)$]. Neglecting **B′** in Equation 56.1 with $W \ll 0$, we have

$$R = C_0 \frac{R_{A'} + R_M 10^{(pH-pK_{A'M})}}{1+10^{(pH-pK_{A'M})}}, \quad (56.3)$$

where we have recast the original thermodynamic and optical parameters into the new ionization constant $K_{A'M} = K_{A'A} + K_{A'B}$ and molar absorption/fluorescence R_M, respectively:

$$R_M = \frac{R_A + R_B\left(K_{A'B}/K_{A'A}\right)}{1+\left(K_{A'B}/K_{A'A}\right)}. \tag{56.4}$$

Likewise Equations 56.2 and 56.4 describe the pH-dependent sigmoidal evolution of the optical response between the **A′** state (prevalent at pH < $pK_{A'M}$) and the new **M** state (prevalent at pH > $pK_{A'M}$). Differently to the case described by Equation 56.1, however, **M** state *does not coincide* with **B**, as **M** does not represent to the pure anionic phenolate of Y-chrom but a *mixed form* of **A** (neutral Y-chrom) and **B** (anionic Y-chrom) according to Equation 56.5 [88]. This explains the chemically puzzling observation, described at the beginning of this section, that some mutants display nonresidual presence of neutral chromophore in the absorption and/or fluorescence at pH well above the measured pK_a.

It is worth mentioning that also wtGFP belongs to the class of "coupled" *av*FPs, as previously suggested by Scharnagl [127]. Nonetheless wtGFP differs from other "coupled" mutants for a much lower $pK_{A'M}$, which is around 4.5–4.9 (other mutants display $pK_{A'M}$ from 5.5 up to 7.2) [88]. Hence, in wtGFP, the **M** state, that is, a constant mix of pure **A** and **B** spectra, is continuously observed from pH 5 to 11 (when **B′** and unfolding start to appear). Accordingly, the E222Q replacement has a dramatic effect in wtGFP: the optical response becomes strongly sensitive to external pH change in the physiological range [44,128].

Assuming $pK_{A'M}$ = 4.9 and a population ratio **B/A** = 6, Equation 56.5 and the trivial identity **B/A** = $K_{A'B}/K_{A'A}$ make us calculate $pK_{A'B}$ = 5.75 and $pK_{A'A}$ = 4.97 for wtGFP. This result indicates that the **M** state of wtGFP finds its origin in the ionization of Glu^{222} carboxylic group ($pK_{A'A}$ = 4.97) at rather low pH values. We can therefore conclude that Glu^{222} plays several pivotal roles in wtGFP: (1) it helps the maturation of chromophore [21]; (2) it "couples" anticooperatively with the phenol group of Y-chrom; (3) it deprotonates more easily than the chromophore lowering the optical pK_a (=$pK_{A'M}$) to a value outside the physiological range thereby stabilizing the protein emission; and (4) it is a good recipient for the *Chro's* proton upon ESPT, conferring significant emission to the neutral **A** state. The third and fourth properties definitely concur to the biological function of wtGFP: the pH-independent mixed neutral/anionic **M** state allows for the excitation of protein fluorescence in a very large wavelength range (390–500 nm, Figure 56.1d), thereby making wtGFP a very efficient FRET acceptor for the bioluminescence of its partner *Aequorin* (which bioluminescences between 400 and 550 nm [36]) in the jellyfish cells.

56.5 Conclusions

Nowadays, FPs are the best available probes to monitor in vivo biochemistry. This predominant role owes to the genetic encoding of fluorescence in the protein primary sequence. Almost any kind of protein can be fused and expressed with one or more FPs at intracellular level, with usually negligible perturbation of the biochemical pathways it is meant to undergo.

The optical properties of FPs stem largely from the structure of the chromophore, a conjugated moiety buried inside the protein β-barrel that originates from the spontaneous posttranslational modification of three amino acids. Natural selection has evolved FP chromophores from the triplet X_n–Tyr_{n+1}–Gly_{n+2}, where X is very variable; artificial FPs, however, bear also another aromatic amino acid instead of Tyr_{n+1}. Owing to the phenol group of Tyr, Tyr-based chromophores (Y-chrom) have access to two protonation states: neutral phenol and phenolate. The latter one displays always redshifted optical properties compared to the former, on account of the enhanced electronic conjugation. Modification of the external pH can shift the protonation equilibrium of Y-chrom, although additional ionizable residue(s) may deeply

affect the pH-dependent optical behavior of the protein. When the electronic conjugation of the chromophore is further extended by posttranslational modification at the main chain of X_n, FPs emitting in the orange–red spectral window are obtained. In spite of the relevant role of chromophore structure, the optical and photophysical properties of each mutant are determined also by the effect of the protein matrix surrounding the chromophore. Indeed, the protein matrix can act on the chromophore providing different electrostatic environments, by establishing H-bonds, and by distorting the molecular planarity; all these interactions can be at play in a given FP and need to be considered to account for the observed optical properties.

In this chapter, we reviewed the subtle interactions that cooperate to finely tune the optical response of representative FP homologues. Notably, understanding the structure–property relationships is the starting point for rational engineering of FPs tailored to specific applications in vivo.

Acknowledgments

This work was partially supported by the Italian Ministry for University and Research (MiUR) under the framework of the FIRB projects RBLA03ER38 and RBPR05JH2P and PRIN 2008JZ4MLB_002.

References

1. O. Shimomura, F. H. Johnson, and Y. Saiga, *J Cell Comp Physiol*, 1962, **59**, 223–239.
2. D. C. Prasher, V. K. Eckenrode, W. W. Ward, F. G. Prendergast, and M. J. Cormier, *Gene*, 1992, **111**, 229–233.
3. M. Chalfie, Y. Tu, G. Euskirchen, W. W. Ward, and D. C. Prasher, *Science*, 1994, **263**, 802–805.
4. S. Inouye and F. I. Tsuji, *FEBS Lett*, 1994, **341**, 277–280.
5. R. Y. Tsien, *Annu Rev Biochem*, 1998, **67**, 509–544.
6. M. V. Matz, A. F. Fradkov, Y. A. Labas, A. P. Savitsky, A. G. Zaraisky, M. L. Markelov, and S. A. Lukyanov, *Nat Biotechnol*, 1999, **17**, 969–973.
7. K. A. Lukyanov, D. M. Chudakov, A. F. Fradkov, Y. A. Labas, M. V. Matz, and S. Lukyanov, *Methods Biochem Anal*, 2006, **47**, 121–138.
8. A. Miyawaki, *Neuron*, 2005, **48**, 189–199.
9. O. V. Stepanenko, V. V. Verkhusha, I. M. Kuznetsova, V. N. Uversky, and K. K. Turoverov, *Curr Protein Pept Sci*, 2008, **9**, 338–369.
10. D. M. Chudakov, S. Lukyanov, and K. A. Lukyanov, *Trends Biotechnol*, 2005, **23**, 605–613.
11. N. C. Shaner, P. A. Steinbach, and R. Y. Tsien, *Nat Methods*, 2005, **2**, 905–909.
12. A. Ibraheem and R. E. Campbell, *Curr Opin Chem Biol*, 2010, **14**, 30–36.
13. R. Bizzarri, M. Serresi, S. Luin, and F. Beltram, *Anal Bioanal Chem*, 2009, **393**, 1107–1122.
14. C. L. Takanishi, E. A. Bykova, W. Cheng, and J. Zheng, *Brain Res*, 2006, **1091**, 132–139.
15. A. Masi, R. Cicchi, A. Carloni, F. S. Pavone, and A. Arcangeli, *Adv Exp Med Biol*, 2010, **674**, 33–42.
16. J. Lippincott-Schwartz and G. H. Patterson, *Trends Cell Biol*, 2009, **19**, 555–565.
17. K. A. Lukyanov, D. M. Chudakov, S. Lukyanov, and V. V. Verkhusha, *Nat Rev Mol Cell Biol*, 2005, **6**, 885–891.
18. M. Ormo, A. B. Cubitt, K. Kallio, L. A. Gross, R. Y. Tsien, and S. J. Remington, *Science*, 1996, **273**, 1392–1395.
19. H. Niwa, S. Inouye, T. Hirano, T. Matsuno, S. Kojima, M. Kubota, M. Ohashi, and F. I. Tsuji, *Proc Natl Acad Sci USA*, 1996, **93**, 13617–13622.
20. R. Heim, D. C. Prasher, and R. Y. Tsien, *Proc Natl Acad Sci USA*, 1994, **91**, 12501–12504.
21. R. M. Wachter, *Acc Chem Res*, 2007, **40**, 120–127.
22. R. M. Wachter, J. L. Watkins, and H. Kim, *Biochemistry*, 2010, **49**, 7417–7427.
23. L. Zhang, H. N. Patel, J. W. Lappe, and R. M. Wachter, *J Am Chem Soc*, 2006, **128**, 4766–4772.
24. N. M. Webber, K. L. Litvinenko, and S. R. Meech, *J Phys Chem B*, 2001, **105**, 8036–8039.

25. S. Kojima, H. Ohkawa, T. Hirano, S. Maki, H. Niwa, M. Ohashi, S. Inouye, and F. I. Tsuji, *Tetrahedron Lett*, 1998, **39**, 5239–5242.
26. J. Dong, K. M. Solntsev, and L. M. Tolbert, *J Am Chem Soc*, 2006, **128**, 12038–12039.
27. A. F. Bell, X. He, R. M. Wachter, and P. J. Tonge, *Biochemistry*, 2000, **39**, 4423–4431.
28. A. A. Voityuk, M. E. Michel-Beyerle, and N. Rosch, *Chem Phys*, 1998, **231**, 13–25.
29. A. Follenius-Wund, M. Bourotte, M. Schmitt, F. Iyice, H. Lami, J. J. Bourguignon, J. Haiech, and C. Pigault, *Biophys J*, 2003, **85**, 1839–1850.
30. K. L. Litvinenko, N. M. Webber, and S. R. Meech, *Chem Phys Lett*, 2001, **346**, 47–53.
31. K. L. Litvinenko, N. M. Webber, and S. R. Meech, *J Phys Chem A*, 2003, **107**, 2616–2623.
32. K. Brejc, T. K. Sixma, P. A. Kitts, S. R. Kain, R. Y. Tsien, M. Ormo, and S. J. Remington, *Proc Natl Acad Sci USA*, 1997, **94**, 2306–2311.
33. A. D. Kummer, J. Wiehler, H. Rehaber, C. Kompa, B. Steipe, and M. E. Michel-Beyerle, *J Phys Chem B*, 2000, **104**, 4791–4798.
34. R. M. Wachter, D. Yarbrough, K. Kallio, and S. J. Remington, *J Mol Biol*, 2000, **301**, 157–171.
35. G. J. Palm and A. Wlodawer, *Methods Enzymol*, 1999, **302**, 378–394.
36. H. Morise, O. Shimomura, F. H. Johnson, and J. Winant, *Biochemistry*, 1974, **13**, 2656–2662.
37. G. H. Patterson, S. M. Knobel, W. D. Sharif, S. R. Kain, and D. W. Piston, *Biophys J*, 1997, **73**, 2782–2790.
38. W. W. Ward and S. H. Bokman, *Biochemistry*, 1982, **21**, 4535–4540.
39. M. Chattoraj, B. A. King, G. U. Bublitz, and S. G. Boxer, *Proc Natl Acad Sci USA*, 1996, **93**, 8362–8367.
40. H. Lossau, A. Kummer, R. Heinecke, F. PollingerDammer, C. Kompa, G. Bieser, T. Jonsson, C. M. Silva, M. M. Yang, D. C. Youvan, and M. E. Michel-Beyerle, *Chem Phys*, 1996, **213**, 1–16.
41. T. B. McAnaney, E. S. Park, G. T. Hanson, S. J. Remington, and S. G. Boxer, *Biochemistry*, 2002, **41**, 15489–15494.
42. S. Bonsma, R. Purchase, S. Jezowski, J. Gallus, F. Konz, and S. Volker, *ChemPhysChem*, 2005, **6**, 838–849.
43. T. M. Creemers, A. J. Lock, V. Subramaniam, T. M. Jovin, and S. Volker, *Nat Struct Biol*, 1999, **6**, 557–560.
44. J. Wiehler, G. Jung, C. Seebacher, A. Zumbusch, and B. Steipe, *ChemBioChem*, 2003, **4**, 1164–1171.
45. J. T. Kennis, D. S. Larsen, I. H. van Stokkum, M. Vengris, J. J. van Thor, and R. van Grondelle, *Proc Natl Acad Sci USA*, 2004, **101**, 17988–17993.
46. R. Heim and R. Y. Tsien, *Curr Biol*, 1996, **6**, 178–182.
47. L. A. Gross, G. S. Baird, R. C. Hoffman, K. K. Baldridge, and R. Y. Tsien, *Proc Natl Acad Sci USA*, 2000, **97**, 11990–11995.
48. M. L. Quillin, D. M. Anstrom, X. Shu, S. O'Leary, K. Kallio, D. M. Chudakov, and S. J. Remington, *Biochemistry*, 2005, **44**, 5774–5787.
49. X. Shu, N. C. Shaner, C. A. Yarbrough, R. Y. Tsien, and S. J. Remington, *Biochemistry*, 2006, **45**, 9639–9647.
50. A. Kikuchi, E. Fukumura, S. Karasawa, H. Mizuno, A. Miyawaki, and Y. Shiro, *Biochemistry*, 2008, **47**, 11573–11580.
51. S. J. Remington, R. M. Wachter, D. K. Yarbrough, B. Branchaud, D. C. Anderson, K. Kallio, and K. A. Lukyanov, *Biochemistry*, 2005, **44**, 202–212.
52. H. Mizuno, T. K. Mal, K. I. Tong, R. Ando, T. Furuta, M. Ikura, and A. Miyawaki, *Mol Cell*, 2003, **12**, 1051–1058.
53. K. Nienhaus, G. U. Nienhaus, J. Wiedenmann, and H. Nar, *Proc Natl Acad Sci USA*, 2005, **102**, 9156–9159.
54. L. V. Schafer, G. Groenhof, A. R. Klingen, G. M. Ullmann, M. Boggio-Pasqua, M. A. Robb, and H. Grubmuller, *Angew Chem Int Ed Engl*, 2007, **46**, 530–536.
55. W. Weber, V. Helms, J. A. McCammon, and P. W. Langhoff, *Proc Natl Acad Sci USA*, 1999, **96**, 6177–6182.

56. A. B. Cubitt, R. Heim, S. R. Adams, A. E. Boyd, L. A. Gross, and R. Y. Tsien, *Trends Biochem Sci*, 1995, **20**, 448–455.
57. R. Heim, A. B. Cubitt, and R. Y. Tsien, *Nature*, 1995, **373**, 663–664.
58. H. W. Ai, N. C. Shaner, Z. Cheng, R. Y. Tsien, and R. E. Campbell, *Biochemistry*, 2007, **46**, 5904–5910.
59. M. A. Mena, T. P. Treynor, S. L. Mayo, and P. S. Daugherty, *Nat Biotechnol*, 2006, **24**, 1569–1571.
60. M. A. Rizzo, G. H. Springer, B. Granada, and D. W. Piston, *Nat Biotechnol*, 2004, **22**, 445–449.
61. A. B. Cubitt, L. A. Woollenweber, and R. Heim, *Method Cell Biol*, 1999, **58**, 19–30.
62. M. Matz, A. F. Fradkov, Y. Labas, A. Savitsky, A. Zaraisky, M. L. Markelov, and S. A. Lukyanov, *Nat Biotechnol*, 1999, **17**, 969–973.
63. O. Zapata-Hommer and O. Griesbeck, *BMC Biotechnol*, 2003, **3**, 5.
64. R. Ando, H. Mizuno, and A. Miyawaki, *Science*, 2004, **306**, 1370–1373.
65. R. M. Wachter, M. A. Elsliger, K. Kallio, G. T. Hanson, and S. J. Remington, *Structure*, 1998, **6**, 1267–1277.
66. T. Nagai, K. Ibata, E. S. Park, M. Kubota, K. Mikoshiba, and A. Miyawaki, *Nat Biotechnol*, 2002, **20**, 87–90.
67. A. W. Nguyen and P. S. Daugherty, *Nat Biotechnol*, 2005, **23**, 355–360.
68. D. A. Shagin, E. V. Barsova, Y. G. Yanushevich, A. F. Fradkov, K. A. Lukyanov, Y. A. Labas, T. N. Semenova, J. A. Ugalde, A. Meyers, J. M. Nunez, E. A. Widder, S. A. Lukyanov, and M. V. Matz, *Mol Biol Evol*, 2004, **21**, 841–850.
69. S. Karasawa, T. Araki, T. Nagai, H. Mizuno, and A. Miyawaki, *Biochem J*, 2004, **381**, 307–312.
70. N. Shaner, R. E. Campbell, P. A. Steinbach, B. N. G. Giepmans, A. E. Palmer, and R. Y. Tsien, *Nat Biotechnol*, 2004, **22**, 1567–1572.
71. N. G. Gurskaya, V. V. Verkhusha, A. S. Shcheglov, D. B. Staroverov, T. V. Chepurnykh, A. F. Fradkov, S. Lukyanov, and K. A. Lukyanov, *Nat Biotechnol*, 2006, **24**, 461–465.
72. J. R. Wiedenmann, S. Ivanchenko, F. Oswald, F. Schmitt, C. Rocker, A. Salih, K.-D. Spindler, and G. U. Nienhaus, *Proc Natl Acad Sci USA*, 2004, **101**, 15905–15910.
73. R. Ando, H. Hama, M. Yamamoto-Hino, H. Mizuno, and A. Miyawaki, *Proc Natl Acad Sci USA*, 2002, **99**, 12651–12656.
74. K. A. Lukyanov, A. F. Fradkov, N. G. Gurskaya, M. V. Matz, Y. A. Labas, A. P. Savitsky, M. L. Markelov, A. G. Zaraisky, X. Zhao, Y. Fang, W. Tan, and S. A. Lukyanov, *J Biol Chem*, 2000, **275**, 25879–25882.
75. Y. A. Tretyakova, A. A. Pakhomov, and V. I. Martynov, *J Am Chem Soc*, 2007, **129**, 7748–7749.
76. D. M. Chudakov, V. V. Belousov, A. G. Zaraisky, V. V. Novoselov, D. B. Staroverov, D. B. Zorov, S. Lukyanov, and K. A. Lukyanov, *Nat Biotechnol*, 2003, **21**, 191–194.
77. R. E. Campbell, O. Tour, A. E. Palmer, P. A. Steinbach, G. S. Baird, D. A. Zacharias, and R. Y. Tsien, *Proc Natl Acad Sci USA*, 2002, **99**, 7877–7882.
78. J. Wiedenmann, A. Schenk, C. Röcker, A. Girod, K.-D. Spindler, and G. U. Nienhaus, *Proc Natl Acad Sci USA*, 2002, **99**, 11646–11651.
79. J. Petersen, P. G. Wilmann, T. Beddoe, A. J. Oakley, R. J. Devenish, M. Prescott, and J. Rossjohn, *J Biol Chem*, 2003, **287**, 44626–44631.
80. M. Prescott, M. Ling, T. Beddoe, A. J. Oakley, S. Dove, O. Hoegh-Guldberg, R. J. Devenish, and J. Rossjohn, *Structure*, 2003, **11**, 275–284.
81. L. Wang, W. C. Jackson, P. A. Steinbach, and R. Y. Tsien, *Proc Natl Acad Sci USA*, 2004, **101**, 16745–16749.
82. M. Z. Lin, M. R. McKeown, H.-L. Ng, T. A. Aguilera, N. C. Shaner, R. E. Campbell, S. R. Adams, L. A. Gross, W. Ma, T. Alber, and R. Y. Tsien, *Chem Biol*, 2009, **16**, 1169–1179.
83. M. C. Y. Chan, S. Karasawa, H. Mizuno, I. Bosanac, D. Ho, G. G. Prive, A. Miyawaki, and M. Ikura, *J Biol Chem*, 2006, **281**, 37813–37819.
84. M. Drobizhev, S. Tillo, N. S. Makarov, T. E. Hughes, and A. Rebane, *J Phys Chem B*, 2009, **113**, 12860–12864.
85. J. Y. Hasegawa, T. Ise, K. J. Fujimoto, A. Kikuchi, E. Fukumura, A. Miyawaki, and Y. Shiro, *J Phys Chem B*, 2010, **114**, 2971–2979.

86. T. Laino, R. Nifosi, and V. Tozzini, *Chem Phys*, 2004, **298**, 17–28.
87. X. Shu, K. Kallio, X. Shi, P. Abbyad, P. Kanchanawong, W. Childs, S. G. Boxer, and S. James Remington, *Biochemistry*, 2007, **46**, 12005–12013.
88. R. Bizzarri, R. Nifosi, S. Abbruzzetti, W. Rocchia, S. Guidi, D. Arosio, G. Garau, B. Campanini, E. Grandi, F. Ricci, C. Viappiani, and F. Beltram, *Biochemistry*, 2007, **46**, 5494–5504.
89. S. Habuchi, P. Dedecker, J. Hotta, C. Flors, R. Ando, H. Mizuno, A. Miyawaki, and J. Hofkens, *Photochem Photobiol Sci*, 2006, **5**, 567–576.
90. H. W. Ai, J. N. Henderson, S. J. Remington, and R. E. Campbell, *Biochem J*, 2006, **400**, 531–540.
91. S. Olsen and S. C. Smith, *J Am Chem Soc*, 2007, **129**, 2054–2065.
92. R. M. Wachter, B. A. King, R. Heim, K. Kallio, R. Y. Tsien, S. G. Boxer, and S. J. Remington, *Biochemistry*, 1997, **36**, 9759–9765.
93. V. Voliani, R. Bizzarri, R. Nifosi, S. Abbruzzetti, E. Grandi, C. Viappiani, and F. Beltram, *J Phys Chem B*, 2008, **112**, 10714–10722.
94. S. Luin, V. Voliani, G. Lanza, R. Bizzarri, P. Amat, V. Tozzini, M. Serresi, and F. Beltram, *J Am Chem Soc*, 2009, **131**, 96–103.
95. T. T. Yang, P. Sinai, G. Green, P. A. Kitts, Y. T. Chen, L. Lybarger, R. Chervenak, G. H. Patterson, D. W. Piston, and S. R. Kain, *J Biol Chem*, 1998, **273**, 8212–8216.
96. G. J. Kremers, J. Goedhart, D. J. van den Heuvel, H. C. Gerritsen, and T. W. Gadella, Jr., *Biochemistry*, 2007, **46**, 3775–3783.
97. M. H. Seifert, D. Ksiazek, M. K. Azim, P. Smialowski, N. Budisa, and T. A. Holak, *J Am Chem Soc*, 2002, **124**, 7932–7942.
98. G. D. Malo, L. J. Pouwels, M. Wang, A. Weichsel, W. R. Montfort, M. A. Rizzo, D. W. Piston, and R. M. Wachter, *Biochemistry*, 2007, **46**, 9865–9873.
99. G. Vallverdu, I. Demachy, F. Merola, H. Pasquier, J. Ridard, and B. Levy, *Proteins*, 2010, **78**, 1040–1054.
100. M. Lelimousin, M. Noirclerc-Savoye, C. Lazareno-Saez, B. Paetzold, S. Le Vot, R. Chazal, P. Macheboeuf, M. J. Field, D. Bourgeois, and A. Royant, *Biochemistry*, 2009, **48**, 10038–10046.
101. G. J. Kremers, J. Goedhart, E. B. van Munster, and T. W. Gadella, Jr., *Biochemistry*, 2006, **45**, 6570–6580.
102. G. D. Malo, M. Wang, D. Wu, A. L. Stelling, P. J. Tonge, and R. M. Wachter, *J Mol Biol*, 2008, **378**, 871–886.
103. J. N. Henderson and S. J. Remington, *Proc Natl Acad Sci USA*, 2005, **102**, 12712–12717.
104. K. Nienhaus, F. Renzi, B. Vallone, J. Wiedenmann, and G. U. Nienhaus, *Biochemistry*, 2006, **45**, 12942–12953.
105. M. A. Elsliger, R. M. Wachter, G. T. Hanson, K. Kallio, and S. J. Remington, *Biochemistry*, 1999, **38**, 5296–5301.
106. M. W. Forbes and R. A. Jockusch, *J Am Chem Soc*, 2009, **131**, 17038–17039.
107. T. I. Wood, D. P. Barondeau, C. Hitomi, C. J. Kassmann, J. A. Tainer, and E. D. Getzoff, *Biochemistry*, 2005, **44**, 16211–16220.
108. T. B. McAnaney, W. Zeng, C. F. Doe, N. Bhanji, S. Wakelin, D. S. Pearson, P. Abbyad, X. Shi, S. G. Boxer, and C. R. Bagshaw, *Biochemistry*, 2005, **44**, 5510–5524.
109. J. S. Biteen, M. A. Thompson, N. K. Tselentis, G. R. Bowman, L. Shapiro, and W. E. Moerner, *Nat Methods*, 2008, **5**, 947–949.
110. P. Sarkar, S. V. Koushik, S. S. Vogel, I. Gryczynski, and Z. Gryczynski, *J Biomed Opt*, 2009, **14**, 034047.
111. R. Bizzarri, C. Arcangeli, D. Arosio, F. Ricci, P. Faraci, F. Cardarelli, and F. Beltram, *Biophys J*, 2006, **90**, 3300–3314.
112. D. Arosio, G. Garau, F. Ricci, L. Marchetti, R. Bizzarri, R. Nifosi, and F. Beltram, *Biophys J*, 2007, **93**, 232–244.
113. D. Arosio, F. Ricci, L. Marchetti, R. Gualdani, L. Albertazzi, and F. Beltram, *Nat Methods*, 2010, **7**, 516–518.

114. T. Kuner and G. J. Augustine, *Neuron*, 2000, **27**, 447–459.
115. X. He, A. F. Bell, and P. J. Tonge, *Org Lett*, 2002, **4**, 1523–1526.
116. G. S. Baird, D. A. Zacharias, and R. Y. Tsien, *Proc Natl Acad Sci USA*, 2000, **97**, 11984–11989.
117. M. Z. Lin, M. R. McKeown, H. L. Ng, T. A. Aguilera, N. C. Shaner, R. E. Campbell, S. R. Adams, L. A. Gross, W. Ma, T. Alber, and R. Y. Tsien, *Chem Biol*, 2009, **16**, 1169–1179.
118. D. Shcherbo, E. M. Merzlyak, T. V. Chepurnykh, A. F. Fradkov, G. V. Ermakova, E. A. Solovieva, K. A. Lukyanov, E. A. Bogdanova, A. G. Zaraisky, S. Lukyanov, and D. M. Chudakov, *Nat Methods*, 2007, **4**, 741–746.
119. A. A. Pakhomov and V. I. Martynov, *Chem Biol*, 2008, **15**, 755–764.
120. M. Kneen, J. Farinas, Y. Li, and A. S. Verkman, *Biophys J*, 1998, **74**, 1591–1599.
121. S. Abbruzzetti, E. Grandi, C. Viappiani, S. Bologna, B. Campanini, S. Raboni, S. Bettati, and A. Mozzarelli, *J Am Chem Soc*, 2005, **127**, 626–635.
122. A. Shinobu, G. J. Palm, A. J. Schierbeek, and N. Agmon, *J Am Chem Soc*, 2010, **132**, 11093–11102.
123. G. T. Hanson, T. B. McAnaney, E. S. Park, M. E. Rendell, D. K. Yarbrough, S. Chu, L. Xi, S. G. Boxer, M. H. Montrose, and S. J. Remington, *Biochemistry*, 2002, **41**, 15477–15488.
124. G. M. Ullmann, *J Phys Chem B*, 2003, **107**, 1263–1271.
125. S. Jayaraman, P. Haggie, R. M. Wachter, S. J. Remington, and A. S. Verkman, *J Biol Chem*, 2000, **275**, 6047–6050.
126. O. Griesbeck, G. S. Baird, R. E. Campbell, D. A. Zacharias, and R. Y. Tsien, *J Biol Chem*, 2001, **276**, 29188–29194.
127. C. Scharnagl, R. Raupp-Kossmann, and S. F. Fischer, *Biophys J*, 1999, **77**, 1839–1857.
128. G. Jung, S. Mais, A. Zumbusch, and C. Brauchle, *J Phys Chem A*, 2000, **104**, 873–877.

57

Formation and Repair of UV-Induced DNA Damage

Thierry Douki
INAC/SCIB UMR-E3
CEA/UJF CEA

57.1 Introduction

Ultraviolet (UV) radiation contained in sunlight may be considered as one of the most frequently encountered deleterious agent for DNA by living organisms. UV radiation has a few positive consequences like the production of vitamin D. It is very likely to have been a major driving force in the evolution on early earth. However, UV exposure results mostly in numerous harmful effects, including induction of skin cancer and skin aging in humans, but also impaired growing in plants or deleterious consequences in the environment. Consequently, UV-induced DNA damage has been a very active field of investigation for several decades. First identification of the cyclobutane pyrimidine dimers (CPDs) was reported in the late 1950s, followed a few years later by that of (6-4) photoproducts. The cellular response to UV radiation was likewise extensively investigated. DNA repair of UV-induced photoproducts was in particular the topic of numerous works, which led among other outstanding discoveries to the elucidation of the mechanism of nucleotide excision repair (NER) through the study of the xeroderma pigmentosum syndrome. The purpose of this review is to provide basic information on the photochemistry of DNA with emphasis placed on the most recent aspects. Information is also provided on the basic molecular mechanisms of DNA repair. More biological aspects of repair and other important topics like mutagenesis or translesion synthesis are not addressed because of space limitations.

57.2 UVC and UVB Photochemistry of DNA

DNA is the main cellular chromophore in the UVC (230–280 nm) and UVB (280–320 nm) ranges, sometimes referred to as far-UV radiations. At these wavelengths, only pyrimidine and purine bases absorb the incident photons. The resulting excited states undergo a number of transformations into final stable products. Although UVB is the relevant biological radiation because it is less blocked than UVC

by the ozone layer, numerous studies aimed at identifying DNA photoproducts used the latter photons (254 nm), the wavelength of which is close to the absorption maximum of DNA.

57.2.1 Excited States of DNA Bases

DNA exhibits a maximum absorption in the UVC range at 260 nm as the result of a strong $^1\pi\pi^*$ transition. At these wavelengths, only bases efficiently absorb the incident photons. Like all chromophores, bases first reach singlet excited states. From there, deactivation through fluorescence or nonradiative processes allows the molecule to return to the ground state. Alternatively, chemical reactions may take place from the singlet excited state. Another pathway involves intersystem crossing into a triplet state that again may deactivate or give rise to photoproducts. The excited states of DNA bases are under investigations for many years as reported in excellent early reviews [1–4]. However, a large amount of information was gathered in the last decade on both isolated monomers and double-stranded helices [5]. This increase in knowledge was made possible by the progress in time-resolved absorption and fluorescence spectroscopies that could provide information on very short time scales as low as 100 fs. Advances in theoretical approaches also made possible a better characterization of the excited states and of their deactivation processes.

57.2.1.1 Monomers

Numerous data have been gathered in the last decade on singlet excited states of monomeric bases, nucleosides and nucleotides. For purine free bases, both 7H and 9H tautomers are possible. However, only the former is relevant to DNA because of the presence of the 2-deoxyribose ring. No data on the 7H isomers will thus be discussed in the following. First, calculations provided information on the lowest vertical excitation energies of the bases that were found to be in the following order: Thy < Cyt < Gua < Ade at different levels of theory [6–13]. Second, time-resolved techniques allowed the accurate determination of the lifetimes of excited states of DNA bases that are known to be very short. Femtosecond time-resolved fluorescence and transient absorption spectroscopies showed that the lifetimes of the excited state of DNA bases monomers are below 1 ps. The decreasing order of lifetime was found to be Ade < Gua < Thy < Cyt with lifetimes ranging between 300 and 750 fs for the nucleosides [14–19]. No difference is observed between the 2′-deoxy- and the ribonucleosides but addition of a phosphate group at the C5′ position results in a slight increase in the lifetime [17,18]. These remarkable very short lifetimes of the singlet excited states could explain the poor photoreactivity of the DNA bases.

An additional interesting feature of DNA bases is their very low fluorescence quantum yield, indicative of a major contribution of nonradiative internal conversion in the relaxation processes. Evidence was obtained from transient absorption measurements in the UV region for the formation of hot ground states following relaxation of excited states [14,15]. Excess energy is then deposited in the solvent by vibrational cooling. Several hypotheses have been put forward to explain this photochemical behavior. First, proton transfer from the solvent and tautomerism has been proposed [12,13,20]. Thermodynamics considerations [21] and observation of limited solvent effects [19] seem to rule out this possibility. An alternative pathway that involves a coupling between the $^1\pi\pi^*$ and $^1n\pi^*$ states, which were reported by some authors to exhibit similar energy level, has been proposed [20,22–24]. This mechanism does not fully account for several experimental observations including solvent and methylation effects [5]. Therefore, a similar process involving conical intersections was proposed to take place for pyrimidine bases [5,25,26] and supported by the experimental observation of a long-lived excited states exhibiting lifetimes of tens of picosecond attributed to dark $^1n\pi^*$ states [27]. This excited state was proposed to lead to intersystem crossing into excited triplet states. In the case of adenine, spectroscopic data seem to favor a mechanism involving two $\pi\pi^*$ states [28].

57.2.1.2 Single- and Double-Stranded DNA

Like monomers, DNA is characterized by a rather poor photoreactivity in terms of quantum yield of products and a very low fluorescence that point to efficient relaxation pathways. However, the underlying processes differ from those in free bases and nucleoside as the result of stacking, base pairing, and

structural features of the DNA duplex. A first specificity of excited states in DNA is their delocalization along the strand that has been established by earlier works. The extent of this delocalization seems to be limited to a few base pairs [29]. Recent theoretical approaches based on spectroscopic observations have proposed that absorption of a UV photon by DNA populates numerous delocalized Frank–Condon states. Fast relaxation (<100 fs) then leads to the most stable ones [30–34]. Other authors have proposed a more localized initial excitation followed by energy transfer yielding excimers or exciplexes [35]. This hypothesis is supported by time- and wavelength-resolved studies in the case of an adenine polymer [28]. In order to get insights into this photochemistry in duplexes, time-resolved spectroscopy and theoretical studies have been conducted on model double-stranded systems that are mostly oligonucleotides bearing either A:T or G:C base pairs and of limited size (≤20 base pairs).

A rather lager amount of information has been gathered in the recent years on the deactivation pathways following UV excitation of adenine- and thymine-containing DNA models. As a general trend, excited states exhibiting longer lifetimes than the monomers were detected by time-resolved techniques in addition to monomeric-like transients. Lifetimes in the few picosecond range were observed by fluorescence up-conversion and found to be larger in homopolymers ($dA_n \cdot dT_n$) than in alternating sequences ($(dAdT)_n \cdot (dAdT)_n$) [36–38]. Additional decays larger than 100 ps were also observed [33]. Transient absorption measurement confirmed the existence of these excited states exhibiting a long lifetime, with a twofold lower value in alternating sequences with respect to homopolymers [38]. In spite of discrepancies on the interpretation of the experimental data obtained by these two techniques [39], it seems accepted that stacking of the bases along the DNA strands favors delocalization and stabilization of excited states, mostly through charge transfer states [33,35,40]. The link between the nature of these excited states and the formation of the final photoproducts remains poorly understood. The recent observation that formation of cyclobutane dimers in single-stranded dT_{18} is a very fast process suggests that only adjacent bases exhibiting the required orientation may yield stable photolesions [41].

The main features of the photochemical behavior of G:C-containing duplexes are different from those bearing only A:T base pairs. Indeed, deactivation of the excited state was found by fluorescence up-conversion to be faster in alternating poly(dG·dC)·poly(dG·dC) than in an equimolar mixture of guanine and cytosine nucleotides [42]. A similar result was obtained by the same technique for isolated G:C base pairs in chloroform [43] and confirmed by resonance-enhanced multiphoton ionization in the gas phase [44]. These results are in line with a number of calculations that show the possible role of base pairing between G and C in relaxation of excited state [45–47]. Indeed, excitation can lead to a charge-transfer excited state with electron transfer from G to C. The resulting species undergo very fast proton transfer from G to C to yield a biradical state that fast relaxes to the ground state via a conical intersection. However, this pathway was recently challenged by transient absorption measurements that show a longer lifetime for the excited stated of G:C polymers than for the corresponding monomers [48]. Involvement of nonemissive excited states in the deactivation pathway that cannot be detected by fluorescence-based techniques was put forward to explain these discrepancies. Understanding this process is of importance since substitution of a few A:T pairs by G:C pairs in double-stranded oligonucleotides leads to a sharp decrease in the fluorescence lifetimes [49].

57.2.1.3 Triplet States

The bulk of these recent data are related to the singlet excited state. Conversely, characterization of the triplet excited states of DNA has been less studied, although these transient species are well characterized in monomers [50,51]. Direct observation of the triplet state has been reported only in single-stranded thymine oligomers where its lifetime is 30 times shorter than in the monomer (150 vs. 4000 ps) while the intersystem crossing quantum is roughly similar (ca. 2×10^{-2}) [52]. To date, no evidence for the formation of triplet excited states in double-stranded DNA has been provided [53]. However, triplet energy transfer experiments from excited photosensitizers provide strong evidence for the high photoreactivity of this excited state. In these studies that involve various chromophores

such as aromatic ketones or quinolones, an efficient quenching of the triplet state of the photosensitizer by DNA is observed concomitant to the formation of CPDs [54,55]. This property was recently used to determine the energy level of the triplet state of thymine within double-stranded DNA that was found to be ca. 270 kJ/mol [56]. This value is 40 kJ mol^{-1} lower than for the free base or nucleoside showing that triplet energy transfer photosensitization is favored in DNA duplex. Whether triplet excited states of DNA are at the origin of photoproducts in addition to singlet species upon direct excitation by UV photons is still a matter of debate. Evidence has been provided for the sole involvement of singlet states [57–59] but theoretical works led to the conclusion of a possible role played by triplet states, at least for CPDs [60].

57.2.2 Structure and Properties of the Photoproducts

Final products induced by UVB and UVC radiation within DNA mostly involve adjacent pyrimidine bases, although some monomeric damage is produced as well as some purine photoproducts.

57.2.2.1 Cyclobutane Pyrimidine Dimers

CPDs were the first isolated DNA photoproducts, in 1958, following irradiation of thymine [61,62]. They arise from a concerted [2 + 2] cycloaddition between the C5–C6 double bonds of adjacent pyrimidine bases. The reaction is a very fast one and was reported to occur in less than 1 ps in single-stranded DNA [41]. CPDs can be produced between either two thymines (T<>T), two cytosine (C<>C), or a thymine and a cytosine (T<>C and C<>T, depending whether thymine is at the 5′- or the 3-OH end of DNA). In monomers such as the base thymine or the nucleoside thymidine, a large number of isomers can be produced [63] (Figure 57.1). First, the two pyrimidine rings can be either on the same or an opposite sides of the cyclobutane ring; this is the *cis, trans* isomery. In addition, the bases can be parallel with the C5 atoms linked to one another (as well as the two C6 atoms) or the C5 of a base linked to the C6 of the other. Such isomers define *syn, anti* isomery. The *anti* isomers cannot be produced between adjacent bases within DNA because bases are all parallel on a same strand. In addition, all pyrimidines are in the same orientation along the *N*-glycosidic bond in B-form DNA. Consequently, the *cis,syn* cyclobutane dimers are the major isomers found in double-stranded duplexes [64–67]. They are also the major isomer obtained upon irradiation of dinucleosides monophosphate [68–72], although some *trans, syn* are obtained in lower amounts.

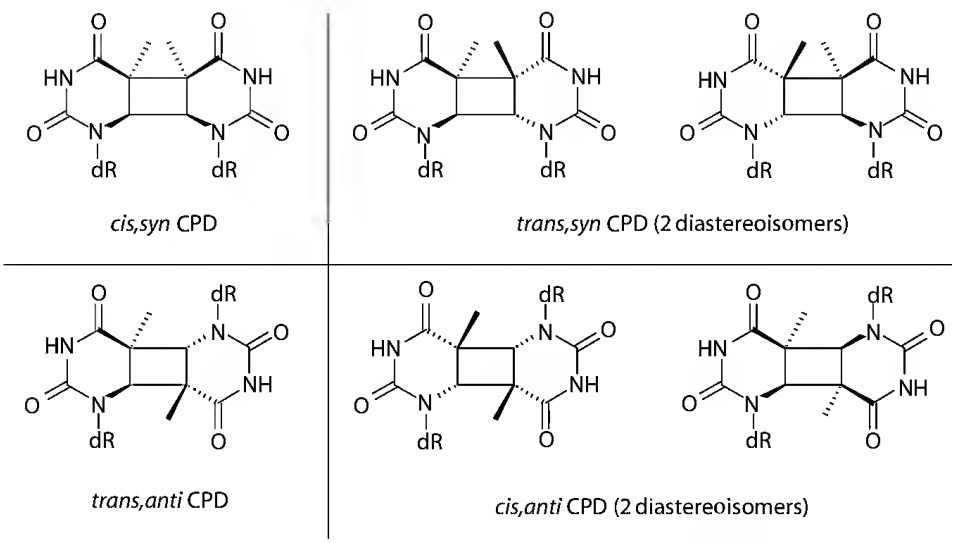

FIGURE 57.1 Diastereoisomers of the TT CPD. Only the *cis,syn* form is found in stable B-DNA.

57.2.2.2 Pyrimidine (6-4) Pyrimidone Photoproducts

The second main reaction taking place between adjacent pyrimidines is the formation of pyrimidine (6-4) pyrimidone photoproducts (64PPs) [73,74]. These lesions are proposed to arise from the decomposition of a heterocyclic intermediate, oxetane, or azetidine whether the 3′-end base is a thymine or a cytosine, respectively (Figure 57.2). This intermediate is expected to be the product of a Paterno–Büchi reaction [75], although an alternative pathway involving nucleophilic addition was also recently proposed [58]. The oxetane and azetidine intermediates have not been observed directly but a number of results strongly support the proposed mechanism. First, recent time-resolved studies showed that the (6-4) photoproducts appear only a few milliseconds after UV excitation, in agreement with the formation of a ground-state intermediate [53]. In addition, oxetanes are readily produced upon irradiation of thymine and specific ketones [76,77]. Finally, the corresponding thietane cyclic intermediate was isolated and characterized upon photolysis of a model system containing 4-thiothymidine [78]. The most characteristic features of 64PPs arise from the presence of the pyrimidone ring that exhibits strong absorption in the UVB range (315 nm for TC 64PP and CC 64PP; 325 nm for TT 64PP and CT 64PP) [70,79–81] and possesses fluorescence properties [82].

57.2.2.3 Secondary Photoreactions

Both types of photoproducts may undergo secondary photoreactions. CPDs have lost the aromaticity of the parent bases and thus the maximum absorption around 260–270 nm. Instead, a maximal absorption is observed around 220–230 depending whether thymine or cytosine is involved. Consequently, a residual absorption is still observed at 254 nm that should be taken into consideration in experiments with UVC. Indeed, upon excitation at this wavelength, CPDs undergo efficient photoreversion into the parent bases [71,83]. A consequence is that the formation of CPDs in DNA reaches a plateau at high doses while other photoproducts do not [66,67]. This may drastically modify the determination of the relative distribution of photoproducts like in a number of early studies that involved high doses because of the lack of sensitivity of the detection techniques. It is also worth mentioning that cytosine-containing CPDs undergo more efficient reversion than TT CPDs [67,71].

(6-4) Photoproducts also undergo secondary photoreactions in high quantum yield. Indeed, upon absorption in the 310–350 nm range, the pyrimidone ring undergoes intramolecular cycloaddition resulting in isomerization into a Dewar valence isomer [71,79,84,85] (Figure 57.3). These photoproducts do not exhibit absorption at wavelengths higher than 230 nm. Another UVC-induced secondary photoproduct of TT 64PP has been reported in the "locked nucleic acids" series but not in standard DNA [86]. Dewar isomers are detected upon UVB irradiation of DNA and cells [67,87] but high doses are required. The formation of these lesions is more efficient with simulated sunlight containing both UVB and UVA

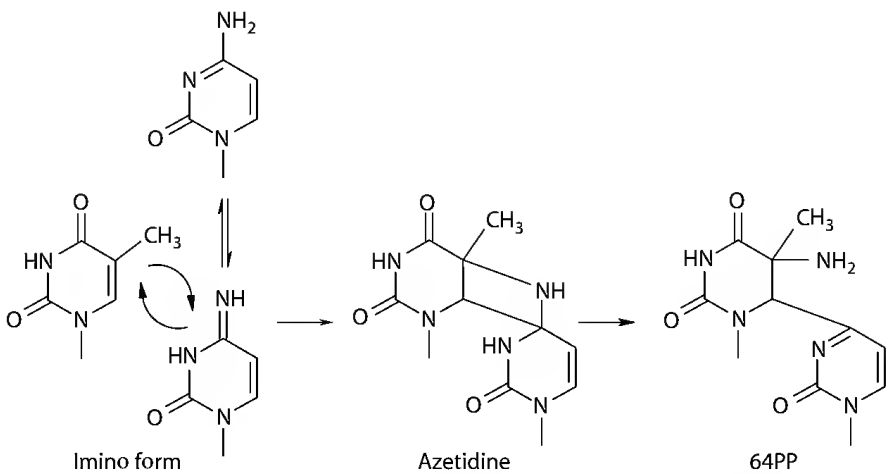

FIGURE 57.2 Formation of TC 64PP. A cycloaddition between the imino form of the 3′-end cytosine and the 5′-end thymine yields the cyclic intermediate azetidine. When the 3′-end base is a thymine, the NH group of the intermediate is replaced by an oxygen atom and the compound is an oxetane.

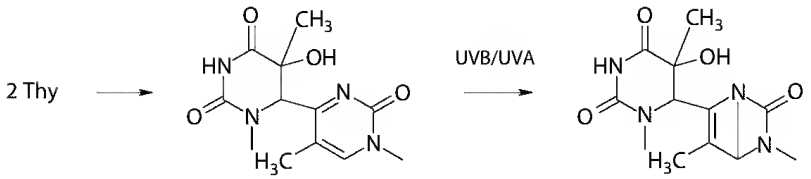

FIGURE 57.3 Structure of TT 64PP and its conversion into a Dewar valence isomer. For the pure photoproduct, the reaction is more efficient at the maximum of absorption around 320 nm. However, UVA is more efficient in DNA because of shielding by excess of normal bases.

[87,88], or by successive exposure to UVB and UVA [89]. This observation points to an efficient photoisomerization by the latter radiation. This result can be explained by the competitive absorption of normal bases in the UVB range that limits the absorption by 64PPs. Consequently, Dewar valence isomers are likely to be biologically relevant upon exposure to real sunlight.

57.2.2.4 Deamination

Spontaneous hydrolytic cytosine deamination is one of the most frequent reactions taking place within DNA [90]. This reaction involves substitution of the C4 exocyclic amino group by a hydroxyl group, leading to the enol form of uracil that rapidly evolves into the canonical form. Recent theoretical investigations have provided details on the mechanism that involves two water molecules [91,92]. This reaction is quite slow with a half-reaction time of 30,000 years [93]. However, saturation of the C5–C6 double drastically accelerates the deamination rate since the half-life of 5,6-dihydrocytosine is 3 h [94]. Interestingly, CPDs, 64PPs, and Dewar isomers all bare C5–C6 saturated pyrimidine rings. As could be expected, cytosine-containing photoproducts readily deaminate into the corresponding uracil derivative, although the structure significantly affects the reaction rate. *Cis,syn* cyclobutane dimers deaminate roughly as fast as 5,6-dihydrocytosine. Interestingly, the *trans,syn* isomers deaminate much more slowly [68,69,72,95]. 64PPs have also been shown to undergo deamination (Figure 57.4) but only for derivatives with the cytosine located at the 5′-end [68]. Indeed, the 3′-end base remains unsaturated and loses the C4 substituent upon formation of the lesion. The (6-4) photoproduct and the Dewar valence isomer of the dinucleoside monophosphate dCpT deaminate more slowly than the *cis,syn* cyclobutane dimer. It may be added that

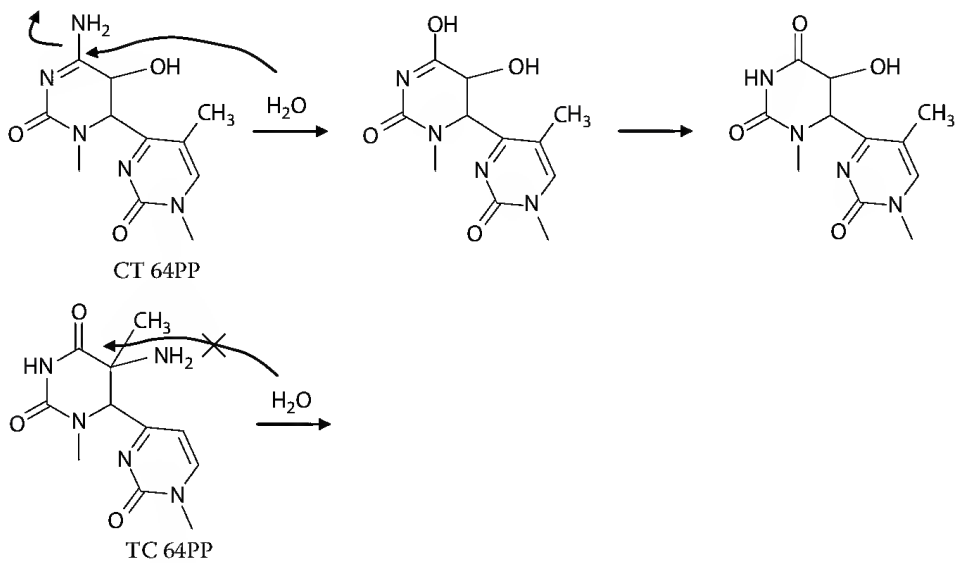

FIGURE 57.4 Deamination of the CT 64PP by nucleophilic addition of water on the C4 amino group. This reaction also takes place with cytosine-containing CPDs. However, it is not possible for TC 64PP because the C4 substituent is a carbonyl.

methylation of cytosine at the C5 position drastically reduces the deamination rate [96,97]. The rate of this reaction is increased by the presence of a guanine at the 5′-end in duplex DNA [98]. In addition, blockage of transcription machinery at the site of damage was found to accelerate the deamination rate.

Experiments involving synthetic oligonucleotides have shown that deamination of CPDs also takes placed in double-stranded DNA, although with a decreased rate [99–102]. The results provided evidence for an important role played by deamination in the mutagenic properties of UV radiation. Indeed, the UV-induced mutation spectrum is characterized by C→T mutations at TC dinucleotides and CC→TT tandem mutations [103–105]. These features are likely to be explained by the coding properties of uracil moiety in deaminated cytosine-containing dimers that efficiently pair with adenine.

57.2.2.5 Minor Photoproducts

Dimeric photoproducts are not only produced between adjacent pyrimidine. Data were obtained, mostly in oligonucleotidic models, for the formation of lesions involving adenine linked either to another adenine or to a thymine. The first lesion involves a [2 + 2] cycloaddition between the C5–C6 double bond of a tautomeric form of adenine to the C8–N9 double bond of a second adenine. A ring-opening reaction then takes place [106]. The adenine–thymine dimeric photoproduct arises from a similar mechanism involving a [2 + 2] cycloaddition of the two C5–C6 double bonds, followed by a ring-opening reaction [107,108]. Only limited information is available on the yield of formation of these adenine-containing dimers. Work on homopolymers showed that the quantum yield for the AA dimer is ca. two orders of magnitude lower than that of TT CPD [109].

Reactions leading to monomeric lesions also take place within DNA upon far-UV irradiation. A first example is hydration of cytosine that results from the addition of a water molecule to the C5–C6 double bond and yields the enantiomers of 6-hydroxy-5,6-dihydrocytosine. At the nucleoside level, 2′-deoxycytidine photohydrates are not stable and undergo two competitive decomposition pathways, namely, deamination and dehydration with respective rate constants of 0.0008 and 0.0105 min^{-1} [110,111]. Biochemical approaches based on the use of the repair enzyme endonuclease III showed that cytosine hydrates are 10 times more stable in double-stranded DNA and that deamination is favored over dehydration [112,113]. As a result, stable 2′-deoxyuridine hydrates accumulate within DNA. However, both enzymatic and chromatographic measurements showed that photohydrates are produced in a two orders of magnitude lower yield than CPDs [110,114]. A second class of monomeric far-UV-induced damage is oxidative lesions and particular guanine damage like 8-oxo-7,8-dihydroguanine (8-oxoGua). This lesion has been proposed to arise from reaction with singlet oxygen produced by DNA itself [115]. Another possibility is a one-electron oxidation process triggered by excitation of DNA. Although reported several times in isolated DNA, oxidation of guanine remains a minor lesion in UVB- and UVC-irradiated cells [116,117].

57.2.3 Formation of the Photoproducts within DNA

Study of the formation of pyrimidine dimers within double-stranded DNA strongly depends on the availability of appropriate techniques. Early works very mostly based on acidic hydrolysis of radiolabeled DNA and yielded only information on CPDs [118]. Sequencing methods such as ligation-mediated polymerase chain reaction (PCR) combined to T4 endonuclease V (T4endoV) provided information at the nucleotide resolution in targeted genes [119], although with limited sensitivity. Nevertheless, the major breakthrough in the field was the development of antibodies raised against the three classes of pyrimidine dimers [120–122]. More recently, chromatographic assays such as ^{32}P-post labeling [123] and high performance liquid chromatography (HPLC)–tandem mass spectrometry [66,67,124] yielded more detailed information on the individual yield of the four possible derivatives (TT, TC, CT, and CC) of each of the different classes of dimers.

57.2.3.1 Distribution of Dimeric Photoproducts in Isolated and Cellular DNA

In double-stranded DNA, CPDs are the main lesions. Only *cis,syn* isomers are detected in stable B-form duplexes [64,67,125,126]. Both UVB and UVC radiations lead to the same ratio between the yields of TT, TC, CT, and CC CPDs, namely, approximately 10:5:2:1 [67]. The quantum yield for TT CPDs has been

TABLE 57.1 Yield of Formation of Pyrimidine Dimers in Isolated Genomic DNA of Increasing GC Content upon Exposure to UVB Radiation

DNA Origin	*Clostridium perfringens*	Calf Thymus	*M. luteus*
%GC	25	41	72
TT CPD	49.8 ± 5.2 (59.2)	27.6 ± 1.8 (40.8)	2.8 ± 0.2 (8.7)
TT 64PP	2.7 ± 0.3 (3.3)	1.6 ± 0.1 (2.3)	0.2 ± 0.0 (0.5)
TC CPD	13.8 ± 1.3 (16.4)	15.0 ± 1.1 (22.2)	10.0 ± 0.8 (0.3)
TC 64PP	8.3 ± 0.8 (9.8)	11.3 ±.7 (16.7)	8.8 ± 0.7 (27.7)
CT CPD	7.4 ± 1.2 (8.7)	7.4 ± 0.5 (10.9)	3.7 ± 0.3 (11.5)
CC CPD	2.2 ± 0.3 (2.6)	4.7 ± 0.6 (7.0)	6.5 ± 0.4 (20.3)

Source: Matallana-Surget, S. et al., *Photochem. Photobiol. Sci.*, 7, 794, 2008.

Yields are expressed in photoproducts/10^4 bases per J/cm^2. The value in brackets represents the proportion of each photoproduct (expressed in %).

shown to be in the range of 2%–3% per TT sites [125–127]. This low value is in line with the very efficient relaxation of the excited states of DNA bases discussed in the "excited states" section. In cells, the yield of CPDs is around 0.2–0.5/10^6 bases per J/cm^2 upon exposure to UVB [87,89,116,128–130] while it ranges between 2 and 10 CPD per 10^6 bases per J/m^2 with UVC [66,114,131,132]. The (6-4) photoproducts are also readily produced in three- to fivefold lower amounts than CPDs [67,87–89,128,133]. The relative distribution of photoproducts is similar in cells and isolated DNA. However, it must be emphasized that this distribution is obtained in DNA of mammalian that contains 40%–42% G:C base pairs. The G + C content of DNA, which significantly varies in bacteria, was found to drastically affect the relative yield of the different photoproducts [134]. At high G + C content, TT CPD is a minor lesion, produced in lower yield than CC CPD (Table 57.1). This study also revealed that the TC dinucleotide exhibits the highest photoreactivity. Another interesting observation on UV-induced DNA damage in cells is related to Dewar valence isomers. These photoproducts are not detected upon exposure to biologically relevant doses of pure UVB but can be found in the DNA of cells exposed to simulated sunlight [67,87,88]. This emphasizes the role of UVA in the photoisomerization process. Quantitative information on whole skin is less frequent but the available one points to a drastic decrease in the yield of photoproducts in the UVB range.

The formation of dimeric photoproducts is not homogenous within DNA in cells. Indeed, sequencing techniques showed that CPDs are produced in higher yield at specific "hotspots" that correspond to more frequently mutated sites [135,136]. Another important modulation is related to methylation of cytosine. 5-Methylcytosine is a minor base of DNA representing a few percent of all cytosines and is generated at CpG islands in order to regulate gene expression. Interestingly, methylation drastically modifies the basic photochemical properties of cytosine [137,138] and significantly increases its photoreactivity [96,97]. As a consequence, methylated sites are hotspots for the formation of photoproducts [139,140]. Telomeres were also identified as sensitive parts of the chromosome [141]. Inhomogeneous distribution of dimeric photoproducts is also observed within skin where the cells of the upper layer of the epidermis are more damaged than those closer to the basal layer [142,143]. This trend is more pronounced with high (254 nm) than low-energy (UVB) radiation, in agreement with the different absorption properties of the tissue at these different wavelengths.

57.2.3.2 Structural Effects

Although often presented in its standard B-form, DNA exhibits a dynamic structure. The observation that formation of photoproducts is a reaction faster than the structural fluctuations of the biopolymer [38,41] suggested that only bases exhibiting the required orientation undergo dimerization with a high

efficiency, in agreement with theoretical works [144,145]. It is thus obvious that any structural modification is likely to affect the yield and/or the nature of the photoproducts. Such effects can be observed on small dimeric model systems in which the 2-deoxyribose rings are locked in a 3′-endo conformation and that yield only CPD at the expense of 64PP upon UVC irradiation [146]. Other chemical modifications leading to a favored 3′-endo conformation were found to increase the photoreactivity of thymine–thymine sequence models [147,148]. Numerous studies have reported a strong impact of the experimental conditions on the photochemistry of isolated DNA. A first example concerns *trans,syn* cyclobutane dimers that are not produced in B-form DNA. However, destabilization of the double-stranded structure by increased temperature or decreased ionic strength leads to their formation in a significant yield [64,149,150]. The same approach showed that at low temperature, the photoreactivity of single- and double-stranded DNA is similar. However, reduced stacking in single-stranded DNA at higher temperature results in a much lower yield of lesions [118,149]. Modulation of the ratio between CPDs and (6-4) photoproducts was also observed upon increasing the temperature and lowering the ionic strength [149,150].

More biologically relevant situations also illustrate the major impact of structure on the yield of photoproducts. A first example is the effect on the binding of transcription factors. These observations cannot be accounted for by shielding since, in a same DNA/protein complex, photoreactivity is enhanced at some sites and reduced at others [151]. Interestingly, strong sequence effects in promoters of human genes were observed *in vivo* in agreement with binding of transcription factors [152,153]. Another important aspect in cells is related to chromatin structure. Evidence has been obtained for a strong modulation of the formation of CPDs that is more efficient in the nucleosome core [154,155]. In contrast, 64PPs are preferentially produced in the linker DNA [156]. Conversely, the presence of dimeric photoproducts strongly impacts the stability of the nucleosomes [157,158]. It may finally be added that the difference in photoreactivity along sequences can also be explained by the rigidity of specific "steps," as illustrated by the different photochemistry at ATT and TTA sequences [159,160].

57.2.3.3 Interstrand Photoproducts

All dimeric photoproducts discussed earlier involve adjacent pyrimidine bases on a same DNA strand. Interestingly, studies in isolated DNA and oligonucleotidic probes have shown the possibility of formation of interstrand photoproducts under specific conditions. Formation of interstrand cross-links upon UV irradiation has been reported in single-stranded DNA [161,162], DNA loops [163], and in fragments of viral and plasmid DNA [164]. Unambiguous evidence for the actual involvement of a bipyrimidine dimer in such cross-links was recently obtained in an oligonucleotide at acidic pH [165]. The biological relevance of these results is strengthened by the observation of interstrand CPDs in models of the telomeres [166]. The characterization of these CPDs as *anti* derivatives definitively establishes that they are interstrand lesions because their formation requires an antiparallel orientation. Significant amounts of nonadjacent photoproducts were also obtained within isolated genomic DNA exposed to UVC either in the dry state or in aqueous solution containing 80% ethanol [167]. *Anti* isomers were also the major ones, together with *cis,syn* derivatives that were either produced between nonadjacent bases on a same strand or between bases belonging to two different helix turns. Interestingly, very low amounts of interstrand 64PPs were detected.

57.2.3.4 Photochemistry in Spores

Spores are dormant forms of a series of bacterial species (*Bacillus, Clostridium*) produced under unfavorable conditions such as drought, lack of nutriment, or external stresses. Bacterial spores exhibit a much higher resistance to a series of damaging agents including UV radiation [168]. This topic has been extensively studied with respect to UV-mediated sterilization procedures and in exobiology. Spores, which are produced by asymmetric division, are first characterized by the presence of several walls and membranes that surrender a highly dehydrated core. DNA is located in this part of the spore and bound to large amount of very specific small acid-soluble proteins (SASP) that modify its structure into an A-like form [169]. A last specific feature is the presence of large amounts of the calcium dipicolinate (DPA) [168]. These three parameters, namely, dehydration, SASP, and DPA, strongly modify the photochemistry of

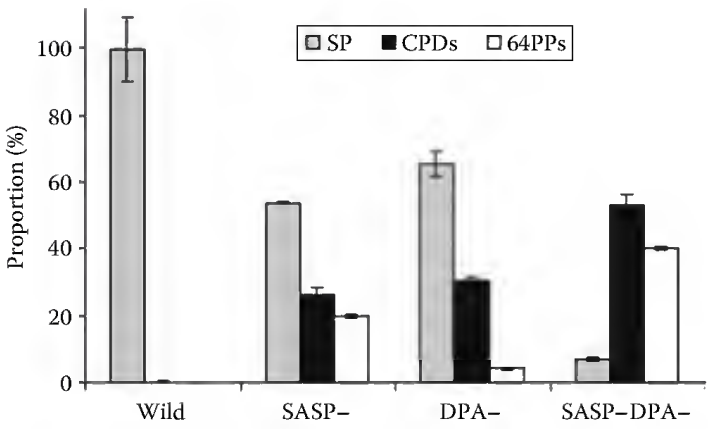

FIGURE 57.5 Relative distribution of SP, CPDs, and 64PPs in wild-type and mutant spore of *B. subtilis*.

DNA. A sole and specific lesion identified in 1965 [170] is produced upon exposure to far-UV radiation that arises from the formation of a link between the methyl group of a thymine with the C5 position of an adjacent one. This dimer 5-(α-thyminyl)-thymine is referred to as the "spore photoproduct" (SP).

Formation of SP has been shown by labeling experiment to involve a concerted mechanism [1] rather than a biradical recombination reaction as first proposed. Two sources of isomery have to be considered for SP. First, the methylene bridge may arise from the thymine located either at the 5′-OH or the 3′-OH end. In addition, the C5 atom of the saturated ring exhibits either a *S* or a *R* configuration. Structural configuration though suggested that the methylene arose from the 3′-end thymine and that the R isomer was the most likely configuration [171]. This hypothesis was only recently confirmed by a combine nuclear magnetic resonance (NMR)/density functional theory (DFT) study of SP under the form of the dinucleotide monophosphate released from DNA by enzymatic hydrolysis [172]. The main role of dehydration in the formation of SP is shown by its efficient formation in dry films of DNA [173,174]. In addition, the importance of the A-form was confirmed by the formation of SP in aqueous solutions of DNA containing large amounts of ethanol [64,167]. The role of SASP was shown by experiments carried out either on isolated DNA or in mutant spores. Lack of the SASP led to increased formation of the "classical" pyrimidine dimeric photoproducts at the expense of SP [175–177]. In a similar way, DPA was shown both *in vitro* and in whole spores to behave as a photosensitizer favoring formation of SP [178,179]. The major role of SASP and DPA in the very high specific formation of SP in spores is shown by the high similarity between the distribution of photoproducts in dry films of DNA and that in spores lacking SASP and DPA [174,179] (Figure 57.5). Interestingly, the overall yield of damage is the same in wild-type spores, and in this double mutant, the only difference being the nature of the photoproduct.

57.3 Photosensitization of DNA

In addition to photoproducts arising from direct excitation in the UVC and UVB ranges, photosensitized reactions also play a major role in cells and skin exposed to UVA and, to a lesser extent, visible light. The most widely studied photosensitization reactions in DNA involve oxidation processes. However, photosensitized triplet energy transfer may also take place and lead to the formation of cyclobutane dimers. It should be mentioned that the nature of the photosensitizers involved in these deleterious processes is not known, although compounds such as flavins, heme, and other biologically important chromophores are likely candidates [180].

57.3.1 Photooxidation

Several oxidative pathways are involved in UVA- and visible light–induced DNA damage. They are triggered by singlet oxygen (type II photosensitization), electron abstraction (type I photosensitization), or hydroxyl radicals. The two first arise from interaction of a photosensitizer in a

triplet excited state with molecular oxygen and DNA itself, respectively, while °OH radicals are by-products of metal-catalyzed reactions.

57.3.1.1 Singlet Oxygen

In its ground state, molecular oxygen is in a triplet state. Upon energy transfer from an excited photosensitizer in its triplet state, molecular oxygen is converted into a reactive excited singlet state. The $^1\Delta_g$ O_2 form of singlet oxygen ($^1O_2$) exhibits lifetimes in the microsecond range in pure solvents (2–3 µs in water and 20–50 µs in deuterium oxide), making it long-lived enough to react with biomolecules. $^1O_2$ reacts primarily with double bonds to yield oxetane, conjugate double bonds to produce endoperoxide and H atoms in α-position of a double bond through the ene reaction. In DNA, $^1O_2$ reacts only with guanine rings [181] and gives rise to a 4,8-endoperoxide as revealed by NRM studies carried out at low temperature [182]. This intermediate undergoes subsequent rearrangement into a C8 hydroperoxide that is reduced into 8-hydroxyguanine [183], a tautomeric form of 8-oxoGua (Figure 57.6). Interestingly, 8-oxoGua is the sole oxidation product in double-stranded DNA [184,185] but a minor one at the nucleoside level. Indeed, reaction of $^1O_2$ with 2′-deoxyguanosine rather yields the two diastereoisomers of a spiroiminodihydantoin (Sp) type lesion [186,187]. Sp is produced by successive dehydration and hydration of the hydroperoxide leading to the formation of 5-hydroxy-8-oxo-7,8-dihydro-2′-deoxyguanosine that then undergoes acyl shift. It may be added that singlet oxygen has sometimes been reported to induce strand breaks in DNA, in contrast with the total lack of reactivity of $^1O_2$ with the phosphodiester backbone [188]. These observations are most likely explained by the occurrence of secondary oxidation of 8-oxoGua that is much more prone to react with $^1O_2$ than the parent molecule [189]. The resulting lesions are quite unstable, in particular under mildly alkaline conditions. In agreement with this scheme, the formation of strand breaks in DNA is a second-order reaction that requires two $^1O_2$ molecules per cleavage site [190].

57.3.1.2 Electron Abstraction

Photosensitized oxidation of DNA may also involve direct electron abstraction from nucleic bases by an excited photosensitizer in its triplet state. As a result, a DNA radical cation is produced together with the radical anion of the sensitizer. This latter species reacts with molecular oxygen to yield superoxide anion ($O_2^{\bullet -}$) and ground-state sensitizer. Radical cations of DNA bases have been extensively studied at the nucleoside level. Two main reactions can take place, namely, hydration and deprotonation. In thymidine and 2′-deoxycytidine [191–193], hydration occurs at the C6 position, yielding a 6-hydroxy-5,6-dihydro-5-yl radical. This intermediate may then react with molecular oxygen and gives rise to a 6-hydroxy-5,6-dihydro-5-peroxyl radical that is then converted into 5-hydroperoxy-6-hydroxy-5,6-dihydropyrimidine [194]. This compound may be further reduced into thymidine or dCyd glycols (mixture of *cis* and *trans* diastereoisomers) or undergo ring-opening and cyclization to give rise to lesions such as the formamido residue and hydantoins. In thymidine, deprotonation takes place mostly at the methyl group and gives rise to a methyl-centered radical. This intermediate then reacts with oxygen and yield 5-(hydroxymethyl)-2′-deoxyuridine and 5-formyl-2′-deoxyuridine as final products. Deprotonation of cytosine involves mostly the C1′ position on the deoxyribose moiety and leads to the formation of the oxidized abasic site 2-deoxyribonolactone (Figure 57.7).

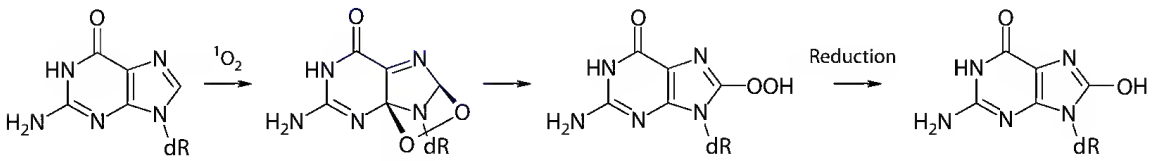

FIGURE 57.6 Formation of 8-oxodGuo by reaction of dGuo with singlet oxygen.

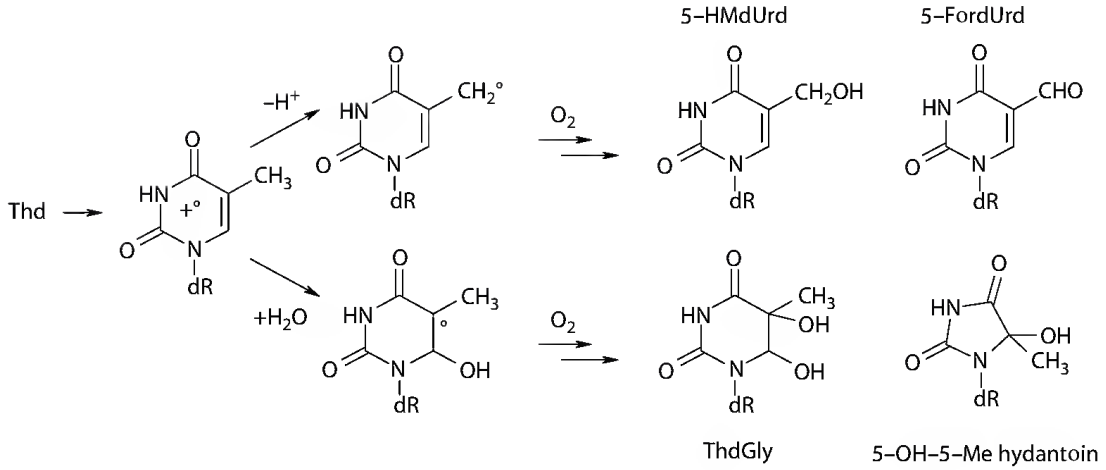

FIGURE 57.7 Final products upon one-electron oxidation of thymidine.

Guanine is more susceptible than pyrimidines to one-electron oxidation because it exhibits the lowest ionization potential among DNA bases [195–197]. Hydration of the guanine radical cation leads to the formation of a reducing 8-hydroxyl-guanyl-7-yl radical [198]. This radical (Figure 57.8) may be oxidized into 8-oxoGua or reduced into the ring-opened 2,6-diamino-4-hydroxy-5-formamidopyrimidine (FapyGua) [199–202]. Like for singlet oxygen, 8-oxoGua does not accumulate in solutions of the free nucleoside dGuo upon photosensitized one-electron oxidation [203]. Indeed, 8-oxoGua has a lower oxidation potential than guanine [204] and is readily further oxidized into Sp as well as guanidinohydantoin under acidic conditions [205–207]. Because of the availability of oligonucleotides containing these secondary oxidation products, large amounts of information on their repair and their mutagenic properties are available [208]. However, their biological relevance is likely to be limited because guanine is present in an at least six orders of magnitude excess over 8-oxoGua in cellular DNA [209]. Secondary oxidation of the latter modified base is thus very unlikely, in agreement with *in vitro* experiment showing that 8-oxoGua can accumulate to very larger extent in isolated DNA [210] and with the lack of detection of these secondary oxidation products in cells exposed to intense oxidative stress [211]. Another interesting feature of the reactivity of the guanine radical cation is its ability to react with nucleophiles other than water. In particular, a series of amino acid can undergo such reactions that could be at the origin of the formation of DNA–protein cross-links [212–214]. A last set of oxidation products of guanine involves deprotonation into an oxidizing radical and leads to the formation of a transient imidazolone derivative further hydrolyzed into oxazolone [215,216]. It was recently proposed that superoxide anion rather than molecular oxygen is involved in the formation of imidazolone [217].

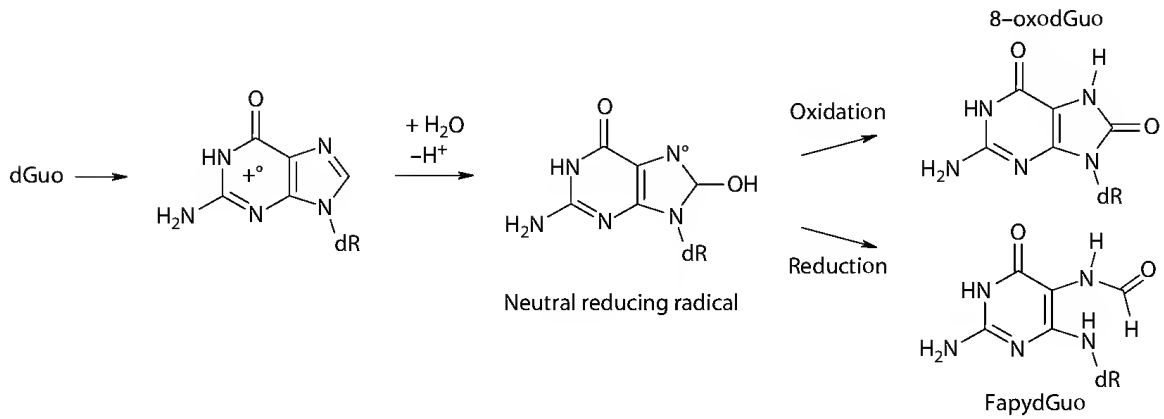

FIGURE 57.8 Final products arising from the reducing radical of guanine produced by electron abstraction.

TABLE 57.2 Distribution of Oxidized Bases within Isolates DNA Oxidized by Type I Photosensitizers and by G-Rays

Lesion	Benzophenone	Menadione	Riboflavin	γ-Rays
8-oxodGuo	80.3	77.5	86.9	37.4
FapyGua	8.1	4.4	7.4	10.8
5-OHdCyd	7.7	7.1	3.7	1.8
5-dUrd + dCydGly	0.5	2.2	1.2	9.8
5-HMdUrd	0.3	0.6	0.1	6.5
5-FordUrd	0.4	1.9	0.5	21.9
8oxo-dAdo	2.7	6.3	0.4	11.8

Source: Douki, T. and Cadet, J., *Int. J. Radiat. Biol.*, 75, 571, 1999.
All experiments were done under air bubbling. Results are expressed in %.

Like guanine, the radical cation of adenine undergoes hydration at the C8 position leading to the formation of 8-oxo-7,8-dihydroadenine and 2,4,6-triamino-5-formamidopyrimine (FapyAde) through the transient formation of a 8-hydroxy-7-yl radical. Deprotonation leads to an oxidizing radical that deaminates and yields inosine.

Although one-electron oxidation can take place with the four bases at the nucleoside level, guanine is by far the main target (Table 57.2) in double-stranded DNA. This is explained by its low oxidation potential that promotes efficient charge transfer through the double helix. The exact mechanism has been a matter of debate for almost a decade [218–222]. It appears that direct tunneling is involved on short distances while hoping is at the origin of long-range transfer. Evidence for predominant guanine oxidation upon one-electron oxidation has been mostly gathered from experiments involving photosensitizer tethered to double-stranded oligonucleotides [223–225]. The induction of guanine damage is monitored following conversion of the lesions into strand breaks by alkaline treatment. Such a strategy is only semi-quantitative because 8-oxoGua is not sensitive to such conditions [226]. It should also be emphasized that no direct strand breaks is observed before alkaline treatment, further supporting that the phosphodiester backbone is not a target of one-electron oxidation. Predominant oxidation of guanine has also been observed upon DNA ionization by high-intensity 193 nm laser pulses combined with biochemical analysis of the damage [227,228]. More specific chromatographic measurements confirmed the bulk of these results in isolated genomic DNA exposed to UVA light in the presence of type I photosensitizers [210] or upon biphotonic ionization triggered by a 266 nm laser beam [229].

57.3.1.3 Hydroxyl Radical Chemistry

Hydroxyl radical is a very reactive oxidizing species that reacts with 2-deoxyribose and with the four bases in double-stranded DNA [230–233]. In that respect, OH°-mediated DNA damage is very different from that triggered by singlet oxygen and type I photosensitization. Production of °OH is not a direct photochemical process but rather involves Haber–Weiss and Fenton chemistry. Indeed, UVA irradiation is at the origin of the release of significant amounts of superoxide anion in cells [234], either as a response of mitochondria or upon reaction of the radical anion of type I photosensitizers with molecular oxygen. Superoxide anion has the ability to dismutate into hydrogen peroxide, the precursor of hydroxyl radicals. These two last reactions are catalyzed by transition metals such as cuprous or ferrous ions. Interestingly, UVA has also been shown to induce the release of large amounts of iron from ferritin inside the cells [235]. Thus, irradiation leads to the simultaneous presence of excess $O_2^{\bullet -}$ and Fe^{2+}, making formation of •OH a likely reaction.

Observation that UVA leads to the formation of DNA strand breaks is a clear evidence of the production of •OH. Indeed, the other photooxidation pathways only damage the bases. Breaks in the phosphodiester backbone are accounted for by the abstraction hydrogen atom from the 2-deoxyribose ring by •OH,

mostly at 4′ and 5′ positions [236]. Addition of molecular oxygen to the resulting carbon-centered radicals followed by decomposition of the resulting peroxides leads to cleavage of the phosphodiester bonds associated with the formation of 2-deoxyribose oxidation products. Bases are also major targets of •OH within double-stranded DNA. Identification of the products was mostly performed with monomeric model systems. •OH radical was mostly found to add to double bonds. For instance, •OH adds to the C8 position of purine rings, yielding the 8-hydroxy-purin-7-yl radical precursor of 8-oxopurines and Fapys [198,199,202]. •OH also adds to the C6 and C5 positions of the double bonds of pyrimidines [237], leading to hydroxylated carbon-centered radical that reacts with oxygen like following one-electron oxidation. •OH may also abstract hydrogen atom from the methyl group of thymine, leading to 5-HMdUrd and 5-FordUrd. In summary, the bulk of the final lesions are similar to those produced by type I photosensitization, although in different proportions. For instance, methyl oxidation products of thymidine represent 30% of one-electron oxidation lesions while they account for only 5% with •OH. In isolated DNA exposed to •OH produced by γ-radiation in aerated aqueous solution, a wide variety of base oxidation products can be detected (Table 57.2). Interestingly, the ratio between 8-oxo and Fapy derivatives of purine decreases in the absence of oxygen, in agreement with the proposed redox chemistry of their common radical precursor [237].

57.3.1.4 Photooxidation in Cells

Direct chromatographic measurements by several groups have unambiguously shown the formation of 8-oxoGua in significant amounts in cells exposed to UVA [117,238,239]. In addition, traces amounts of Fapys were detected but in a ratio much lower than that obtained upon exposure to γ-radiation [240]. This observation rules out a major contribution of type I photosensitization processes triggered by endogenous chromophores. Information on other types of DNA damage can be inferred from assays involving purified repair enzymes used to cleave DNA at specific lesions. Formamidopyrimidine *N*-glycosylase (Fpg) recognizes oxidized purines while endonuclease III (endo III) reveals the presence of oxidized pyrimidines. The additional breaks produced by the enzymatic treatment are quantified by gel electrophoresis, comet assay, or alkaline elution. The same conclusion was obtained on the basis of these three different techniques, namely, that the most common UVA-induced oxidative lesions were oxidized purines, while breaks and oxidized pyrimidine were produced with a roughly threefold lower frequency [88,240,241]. This distribution is very different from that obtained for •OH (ionizing radiation) where breaks are produced in a twofold higher yield that oxidized bases. In sharp contrast, only oxidized purines corresponding to 8-oxodGuo were observed in cells exposed to UVA in the presence of exogenous type II sensitizers [240]. Altogether, these results suggest that singlet oxygen is the main mediator of oxidative damage to DNA in UVA-irradiated cells, with a small contribution of hydroxyl radical.

57.3.2 Formation of CPDs

Although considered as typical UVB-induced DNA photoproducts, CPDs are also involved in the genotoxicity of UVA. Indeed, they can be produced upon photosensitization by specific chromophores, but were also more recently shown to be induced in significant yield in mammalian cells and in skin in the absence of exogenous compounds.

57.3.2.1 Photosensitized Triplet Energy Transfer

The possibility of directly populating the triplet excited state of pyrimidine bases by energy transfer from a triplet excited sensitizer was established in the late 1960s [242,243]. Aromatic ketones were first used because they absorb in the UVA range, far from the maximum absorption of DNA, and exhibit a very high intersystem crossing yield. In addition, a requisite for the efficiency of the triplet energy transfer is an energy level higher for the sensitizer than the nucleic base. A number of other compounds were found to mediate this photosensitization process both in bases, nucleoside, and double-stranded DNA. The most studied include nonsteroidal anti-inflammatory drugs [55,244] that bare an aromatic ketone

motif and, more recently, fluoroquinolones [245–248]. Emphasis was placed on these molecules because they exhibit a high phototoxicity and photomutagenicity. Photosensitization of CPDs by exogenous molecule was found to take place in isolated DNA as well as in cultured cells. No (6-4) photoproduct is formed under these conditions, and TT CPDs represent ca. 90% of the CPDs [88], in higher predominance than upon UVC or UVB irradiation. This observation is in agreement with the lower energy of the triplet excited state of thymine with respect to that of the other bases, at the nucleoside level as well as in DNA. A number of basic studies have correlated the photophysical properties of the sensitizers with their ability at undergoing triplet energy transfer. It was observed for some of them that the results could not explain the induction of CPDs in DNA. It was actually found that photodecomposition products of the sensitizer could be the actual triplet energy transfer photosensitizers [249]. It was also shown that phosphate ions may exhibit drastic effect on the excited states of the sensitizers, maybe mimicking properties of DNA backbone [250].

57.3.2.2 UVA-Induced Formation of CPDs

UVA radiation alone also promotes the formation of CPDs in cells and skin in the absence of exogenous photosensitizer. This is a rather poorly efficient process with a yield roughly three orders of magnitude lower than UVB. However, its biological relevance cannot be neglected because the intensity of UVA is much higher than that of UVB in sunlight. The first observation of UVA-induced CPDs was reported after exposure of bacteria to narrowband 365 nm radiation [251]. It was then observed in mammalian cell lines [87,241,252,253] and in human skin [143,254]. Interestingly, recent quantitative chromatographic unambiguously showed that CPDs are produced in higher yield than oxidative damage (Table 57.3), in particular the most frequent one 8-oxoGua, in both cultured cells and whole human skin [88,116,255]. These results are in line with some mutagenic studies showing a large number of mutations at bipyrimidine sites in UVA-irradiated cells [256–258]. The distribution of CPDs is very similar to that observed after triplet energy transfer with a predominance of TT CPDs over the CT and TC derivatives, lack of formation CC CPD, 64PPs, and Dewar isomer. It was thus first proposed that a photosensitization process might be involved [88]. However, some reports have been made of the induction of CPDs upon UVA irradiation of isolated DNA, namely, in the absence of cellular sensitizers [239,259–262]. Unfortunately, these studies were based on biochemical approaches that do not provide an extensive distribution of the dimeric photoproducts. One interesting exception is a gel sequencing analysis that showed the predominance of TT CPDs, like in the DNA of UVA-irradiated cells [262]. More extensive chromatographic measurements showed the absence of 64PPs in UVA-irradiated isolated DNA and the same ratio between the yields of the different CPDs [263]. In addition, formation of CPDs was found to take place with a similar efficiency in isolated and cellular DNA [87,262,263]. Another similarity is the roughly constant yield of CPDs over the UVA range [241,263]. These results, combined with the observation of a weak but significant absorption of DNA in the UVA range [263,264], make a direct photochemical process like a plausible explanation of the UVA-induced formation of CPDs. However, the basic underlying photochemistry, such as the nature of the involved excited states, remains to be elucidated.

TABLE 57.3 Yield of 8-OxodGua and TT CPD in CHO Cells, Primary Culture of Human Fibroblasts and Keratinocytes, and in Human Skin upon Exposure to UVA

	CHO	Keratinocytes	Fibroblasts	Skin
8-oxodGuo	0.064 ± 0.020	0.015 ± 0.005	0.026 ± 0.019	0.007 ± 0.003
TT CPD	0.191 ± 0.010	0.089 ± 0.004	0.164 ± 0.008	0.066 ± 0.035
Ratio TT CPD/8-oxodGuo	3.0	5.9	6.4	9.3

Source: Douki, T. et al., *Biochemistry*, 42, 9221, 2003; Mouret, S. et al., *Proc. Natl. Acad. Sci USA*, 103, 13765, 2006; Courdavault, S. et al., *Mutat. Res.*, 556, 135, 2004.

Values are expressed in lesions/10^6 cells per J/cm^2.

57.4 DNA Repair

A series of DNA repair systems are based on the excision of the portion of the damaged strand around the lesion, followed by resynthesis using the undamaged strand as template and final ligation. Differences are mostly related to the size of the portion of DNA removed that can be a single nucleotide [base excision repair (BER) for small oxidized bases] or a short oligonucleotide (NER for bulky photoproducts). These two systems are conserved in all cell types, although the proteins can be structurally very different in eukaryotic and prokaryotic cells. In addition to these excision/synthesis mechanisms, some species possess repair enzymes that use radical reactions to restore unmodified bases from UV-induced photoproducts.

57.4.1 Nucleotide Excision Repair

NER is a versatile system that can remove from DNA a wide range of lesions inducing large structural modifications. NER is the major repair pathway for UV-induced dimeric pyrimidine photoproducts. In mammalian cells, more than 30 proteins are involved that act in a concerted way from the initial damage recognition to the restoration of the intact duplex. A large number of them were discovered in relationship with photosensitivity syndromes such as xeroderma pigmentosum, Cockayne syndrome, or trichothiodystrophy. Two subpathways have to be considered for NER. The first one is associated with blocking of the transcription [transcription-coupled repair (TCR)] and mostly removes damage from the transcribed strand of active genes [265–267]. The second NER subpathway removes bulky lesions from the rest of the genome and is referred to as global genome repair (GGR) [268]. The main difference in the two processes is related to the initial sensing of the damage.

57.4.1.1 GGR in Mammalian Cells

In GGR, lesions are recognized on the basis of local modification of the DNA structure. Consequently, lesions inducing larger distortion are more rapidly removed. For instance, CPDs only induce limited modifications with 10° unwinding and bending ranging between 9° [269] and 30° [270] and hardly perturb the hydrogen bonding. This is mostly explained by the parallel orientations of the bases. In contrast, the two pyrimidine rings adopt a perpendicular orientation in 64PPs resulting in a much more drastic distortion of the DNA helix and loss of base pairing [269]. The bending and unwinding angles of a duplex containing a TT 64PP opposite two adenines are 44° and 30°, respectively [271]. These strong differences in DNA-distorting properties of the two main classes of pyrimidine dimers are reflected in the repair kinetics. Indeed, it is now well established that GGR removes 64PPs much more rapidly than CPDs, with a half-lifetimes of 3–4 and 24 h, respectively [87,272–275]. Dewar isomers are repaired as efficiently as their (6-4) precursors [89]. It may be added that the nature of the two modified pyrimidines was recently shown to drastically impact the rate of removal of CPDs in the following order: CT > CC > TC > TT [276]. This observation points to a major impact of subtle structural differences on the recognition by the DNA damage-sensing proteins.

In GGR [268], this step is performed by the XPC–HR23B complex (Figure 57.9). In the case of CPDs, the DDB (DNA damage binding) complex acts as an key upstream sensor [277,278], possibly through the recognition of modifications of the chromatin structure [279]. The resulting increased DNA conformational modification is then recognized by XPC–HR23B. The next step in GGR involves recruitment of the TFIIH factor that contains among other proteins the two helicases XPB and XPD. These enzymes unwind DNA and verify the actual presence of a lesion in the repair complex. A preincision complex is then formed by assembly of RPA and XPA proteins, followed by XPG. The latter protein is believed to induce the release of XPC–HR23B. In a following step, ERCC1–XPF joins the complex. XPG and XPF perform incision of the single-stranded DNA at the 3′- and 5′-end, respectively. The produced 24–32 nucleotides long ssDNA piece containing the lesion is released. The proteins then leave the ssDNA with the exception of RPA that assists the DNA synthesis performed by Pol δ, RFC, and PCNA. The final nick is sealed by ligase I.

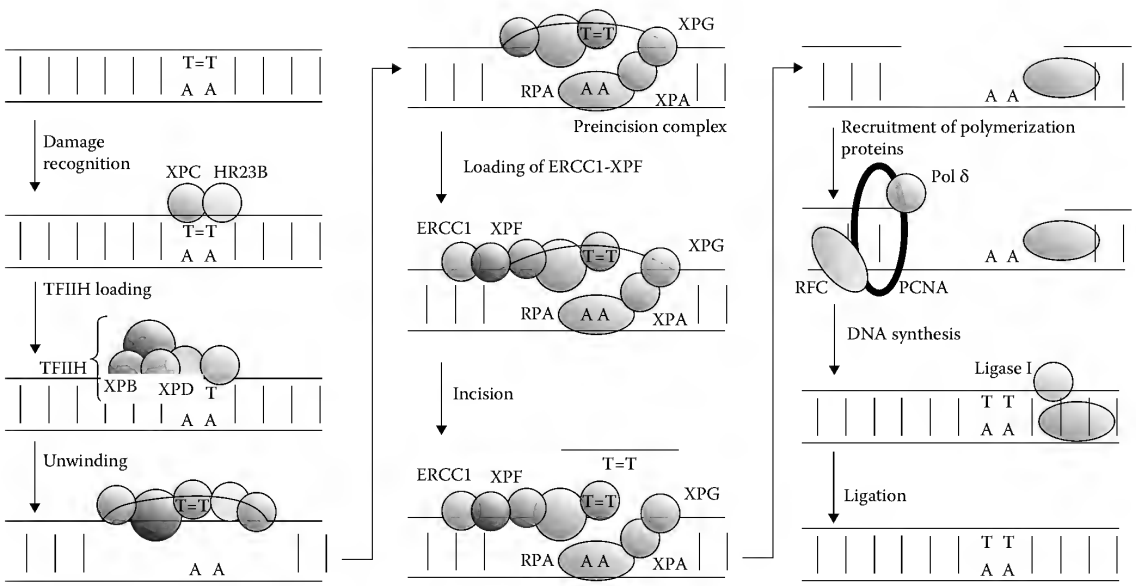

FIGURE 57.9 **(See color insert.)** Main steps in global genome repair (GGR) in eukaryotic cells.

57.4.1.2 TCR in Mammalian Cells

TCR differs from GGR in the damage recognition step that involves stalled RNA polymerase II (RNAPII) at the site of a lesion [265–267] (Figure 57.10). Because the signal for repair is not the lesion itself, CPDs and 64Ps are removed with equal rates by TCR. Although not completely established, it seems likely that RNAPII stays at the lesion site, possibly after backtracking in order to facilitate access of the repair proteins. Conformational changes induced by the Cockayne syndrome B protein (CSB) could also be involved in the latter process. CSB exhibits other key properties in TCR and appears as a central protein. Even in the absence of damage, CSB is in dynamic interaction with the transcription machinery. However, binding of CSB strongly increases upon UV irradiation as the result of the induction of DNA photoproducts. In a subsequent step, THFII localizes at the arrested complex. Another Cockayne syndrome A protein (CSA) is then loaded onto the complex, as well as XPG and chromatin remodeling factors such as HAT, p300, and HMGN1. The TCR complex then recruits the incision proteins involved in GGR, namely, RPA, XPA, and XPF–ERCC1. Excision of the oligonucleotide bearing the photoproduct is then carried out. DNA synthesis and ligation subsequently take place by likely using the same enzymes as during GGR. Disassembling of

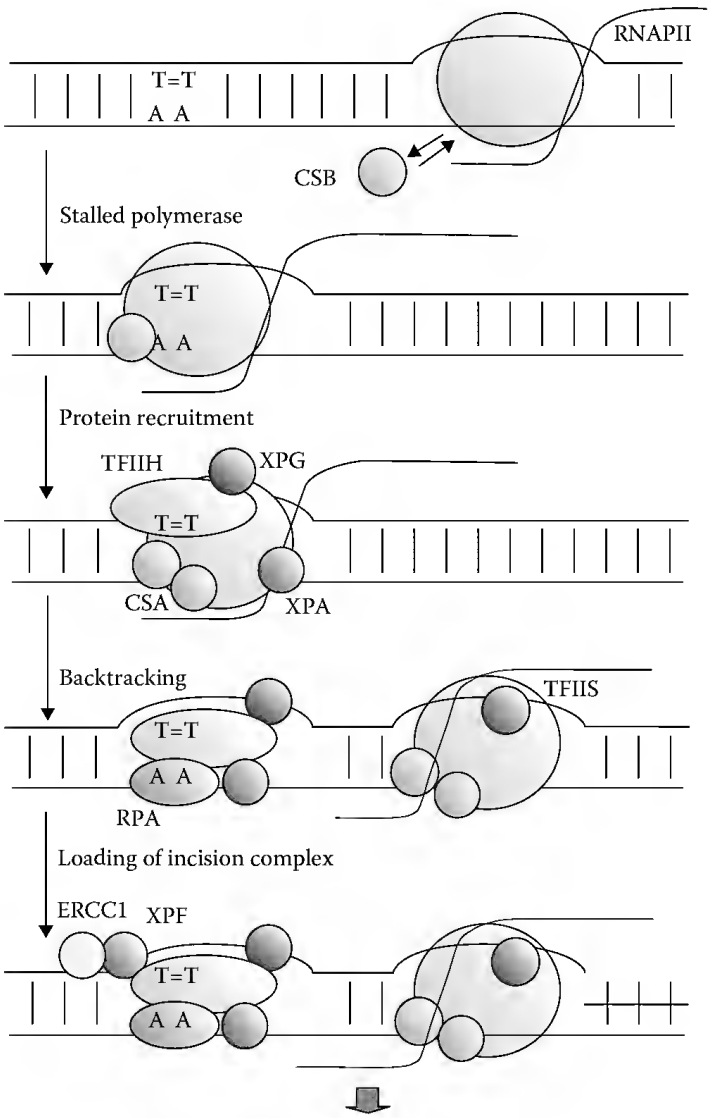

FIGURE 57.10 **(See color insert.)** Schematic representation of transcription-coupled repair (TCR) in eukaryotic cells.

the repair complex is initiated by CSA that ubiquitylates CSB that is further degraded. Restart of transcription involves the THIIS factor, recruited earlier in the process by CSB, which cleaves the 3′-end of the nascent RNA strand and restores its correct positioning in the active site of the RNA polymerase.

57.4.1.3 NER in Bacteria

NER is well-preserved process in evolution and is present in all cell types. In bacteria, GGR is performed by the UvrABC system [280,281]. The main steps are similar to those encountered in eukaryotic cells, namely, damage recognition, DNA unwinding, formation of the preincision complex, incision, release of the damaged ssDNA, DNA synthesis, and ligation. The main difference is that only six proteins are involved (UvrA, UvrB, UvrC, UvrD, Pol I, and ligase). Expression of *uvrA* and *uvrB* genes is controlled by the SOS response, a process triggered in bacteria by various stresses that block replication. The UvrA homodimer is the initial sensor for potentially damaged sites. The affinity of UvrA for damage DNA is 1000 times higher than for normal undamaged substrate. It then forms a complex with UvrB that first checks for the actual presence of a lesion. UvrB also exhibits helicase properties that permit DNA unwinding. UvrC is then recruited and cleaves the damage strand at the 8th nucleotide on the 5′-end and the 5th nucleotide on the 3′-end with respect to the photoproduct. The UvrD helicase facilitates oligonucleotide elimination. In a final step, UvrB is displaced from DNA by polymerase I that performs DNA synthesis prior to ligation. Bacteria also possess a system equivalent to TCR that involves the Mfd (TRCF) protein [282]. Mfd first removes RNA polymerases from the damaged site and then recruits UvrA in order to initiate repair. In that respect, TCR is different in eukaryotic cells where the polymerase remains close to the damaged site during repair.

57.4.2 Other Excision Enzymes for Dimeric Photoproducts

NER is a general repair process for CPDs and 64PPs present in all cells. In addition to NER, some unicellular systems possess additional repair enzymes for these photoproducts that also involve cleavage of DNA followed by resynthesis (Figure 57.11).

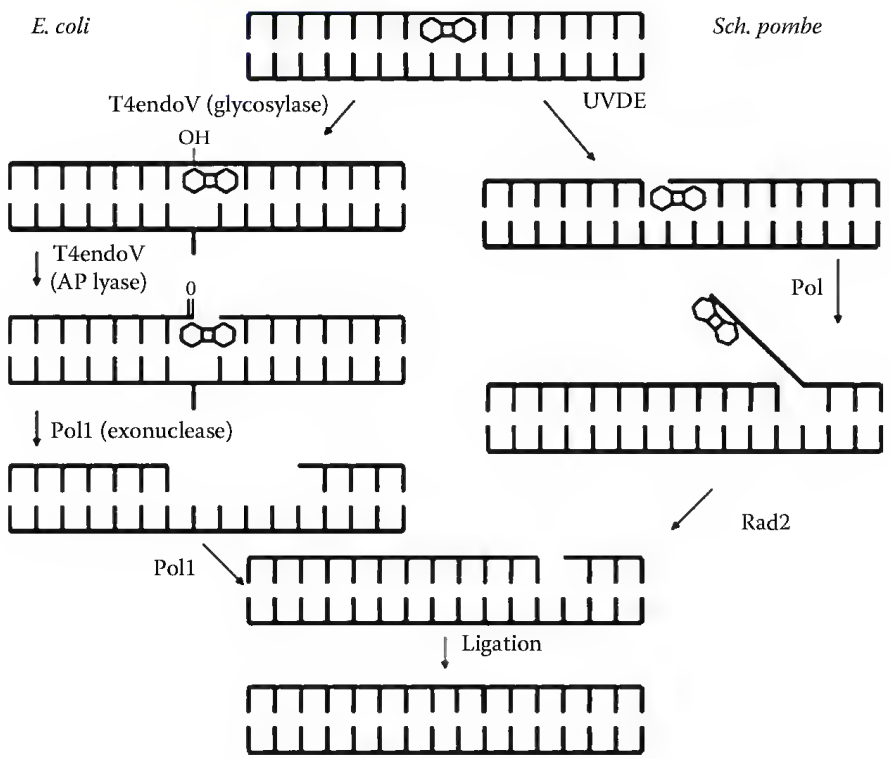

FIGURE 57.11 Excision repair of pyrimidine dimers by T4endoV and UVDE.

57.4.2.1 Thymine Dimer Glycosylases

A well-known protein is endonuclease V of bacteriophage T4 [283]. This enzyme specifically recognizes CPDs, but not 64PPs, and is widely used as a biochemical tool in order to convert CPDs into strand breaks detectable by electrophoresis techniques. T4endoV is actually a glycosylase rather than an endonuclease that catalyzes the cleavage of the *N*-glycosidic bond of the 5′-end pyrimidine nucleotide of the dimer (Figure 57.11) [284,285]. The nucleophilic group that attacks the C1′ atom is the α-NH_2 of the N-terminal end. It also exhibits an AP lyase activity that cleaves the 3′-phosphodiester bond of the abasic site, leaving a 5′-phosphorylated extremity and a 3′-end carrying an oxidized ring-opened 2-deoxyribose derivative. T4endoV exhibits an interesting repair mechanism. Upon binding to a damaged site, the enzyme induces a 60° kink to the DNA helix. In addition, the adenine opposite the 5′-pyrimidine of the dimer is flipped out from the duplex in order to let the catalytic amino acids localize close to the photoproduct. Followed cleavage of the DNA strand, the damaged nucleotide is then hydrolyzed together with three nucleotides by the exonuclease activity of the polymerase I of the infected bacteria. DNA synthesis and ligation then take place. Interestingly, enzymes exhibiting an activity identical to that of T4endoV were identified in several bacterial species including *Micrococcus luteus* [280,284]. With the exception of a single report in *Saccharomyces cerevisiae* [286], no cyclobutane dimer glycosylase activity was observed in eukaryotes.

57.4.2.2 UV Damage Endonuclease

Another series of enzymes involved in repair of UV-induced dimeric photoproducts are endonucleases. The first protein of this class, referred to as UV endonuclease (UVDE), was isolated from the yeast *Schizosaccharomyces pombe* [287–289], and later from bacteria such as *Deinococcus radiodurans*, *Bacillus subtilis*, and *Thermus thermophilus* [280]. A consequence of this alternative repair pathway for UV-induced pyrimidine dimers is the lower sensitivity of *S. pombe* with respect to *S. cerevisiae* to UV radiation. These proteins cleave the phosphodiester bond on the 5′-end of pyrimidine dimers, both the CPDs and the 64PPs, thereby introducing a nick in the strand (Figure 57.11). Polymerization of DNA induces the displacement of the damaged strand, leaving a single-stranded 5′-flap. This structure is resolved by rad2, the yeast homolog of FEN-1 that cleaves DNA at the single/double-strand junction. The resulting nick is then ligated. The role of *rad2* in UV excision repair is shown by the higher sensitivity of the corresponding mutant while the double *uvde rad2* mutant is less sensitive. This is explained by the accumulation of nicks produced by UVDE in the *rad2* mutant. However, a fraction of these endonucleotidic sites are repaired, in agreement with observation that DNA recombination proteins may be also involved in this alternative repair pathway.

57.4.3 Base Excision Repair

Modified bases that induce only limited structural deformation of the DNA duplex are mostly repaired by BER [290,291]. Most oxidized bases, as well as strand breaks and abasic sites, are repaired by BER, that, in contrast to NER, involves a series of repair enzymes exhibiting a define substrate specificity.

57.4.3.1 Specific Features of BER

N-glycosylases, which are responsible for the initial cleavage of the sugar-base bond in BER, can excise either oxidized pyrimidine [292–296] or oxidized purine [297–301], with some partial substrate overlapping [302,303]. Other largely expressed *N*-glycosylases recognize deaminated cytosine. Interestingly, all glycosidic activities are conserved in the different cell types, although the involved proteins are structurally very different (Table 57.4). It may be also emphasized that inhibition a single specific glycosylase does not seem to drastically affect cellular viability and genome integrity in knockout animal models [304–306]. This is mostly explained by the broad substrate specificity of these classes of enzymes that can back up the missing activities. A possible role of NER in these alternative pathways has been also

TABLE 57.4 The Main *N*-Glycosylases Involved in the Repair of Oxidized Bases

E. coli		Human	
Enzyme	Substrate	Enzyme	Substrate
UNG family, monofunctional			
Ung	Uracil	UNG	Uracil
		SMUG1	Uracil (+5-hydroxycytosine, 5-hydroxymethyluracil)
Nth family, bifunctional (β-elimination)			
*N*th (EndoIII)	Thymine and uracil glycols, cytosine hydrates, 5-OHCyt	NHT1	Thymine and uracil glycols, 5-formyluracil
MutY	Adenine in 8-oxoGua:Ade	MUTYH	Adenine in 8-oxoGua:Ade
		OGG1	8-OxoGua, FapyGua
Fpg family, bifunctional (βδ-elimination)			
Fpg	8-OxoGua, FapyGua, FapyAde (+5-OHCyt)		
Nei (EndoVIII)	Thymine and uracil glycols, 5-OHUra	NEIL1 (in ssDNA)	FapyAde, FapyGua, thymine glycols, 5-OHUra
		NEIL 2 (in ssDNA)	Hydantoin, 5-OHUra

proposed. One has also to emphasize the sophisticated systems aimed at preventing expression of the mutagenesis of 8-oxoGua. All cell types posses *N*-glycosylases that cleave 8-oxoGua paired with cytosine. In addition, proteins (MutY in bacteria and HMUY in human) are present that specifically remove adenine paired with 8-oxoGua to prevent mutation fixation [307]. Last, an enzyme (*Escherichia coli* MutT) is devoted to the hydrolysis of 8-oxodGuo triphosphate in the nucleotide pool that could be incorporated during DNA synthesis [308].

57.4.3.2 *N*-Glycosylases

BER events involve first a cleavage of the base-sugar link by an *N*-glycosylase (Table 57.4) followed by cleavage of the resulting abasic site (Figure 57.12). The last steps correspond to the synthesis and ligation of an undamaged DNA strand. Three main types of *N*-glycosylases have been identified [308]. The first one corresponds to monofunctional enzymes, and the nucleophile undergoing the *N*-glycosidic bond cleavage is an activated water molecule. The resulting abasic site is then cleaved in a second step by a pure AP lyase like APE1 present in large amounts in mammalian cells. The cleavage product is a gap that exhibits a 3′-OH and a 5′-deoxyribose-phosphate end. Typical proteins of this class are uracil *N*-glycosylases (UNG). Other *N*-glycosylases are bifunctional and perform both the excision of the base and the cleavage of the damage strand. A first type of bifunctional *N*-glycosylases is related to the bacterial endonuclease III (*N*th) enzyme [309]. The nucleophile is an internal lysine residue. It triggers a β-elimination reaction leading to the release of the base, and the formation of a one-nucleotide gap with an oxidized deoxyribose unit linked to the 3′-end while the 5′-end carries a phosphate group. Last, other bifunctional *N*-glycosylases belong to the Fpg family [310]. Their enzymatic reaction involves an N-terminal proline and catalyzes a β,δ-elimination. Their final product is a gap with both ends phosphorylated. It should be emphasized that for all *N*-glycosylases, the modified base is flipped out of the DNA duplex into the active of the enzyme after damage recognition [311].

57.4.3.3 End Cleaning and DNA Synthesis

The nature of the single-nucleotide gap produced by the two first steps of the BER process has a major impact on the subsequent DNA synthesis phase. Indeed, natural substrates for polymerases are gaps with 5′-phosphate and 3′-OH residues. End cleaning is thus required after the action of *N*-glycosylases

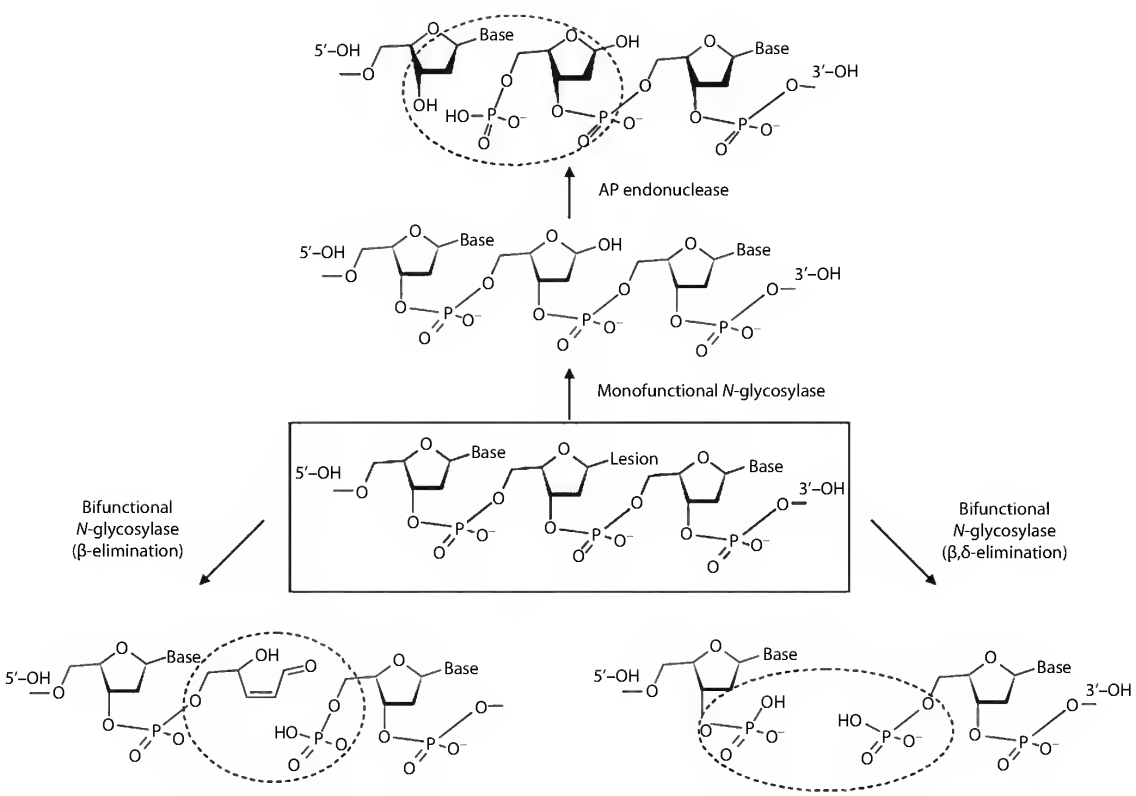

FIGURE 57.12 Chemical structure of the gap left in DNA after action of mono- or bifunctional *N*-glycosylases.

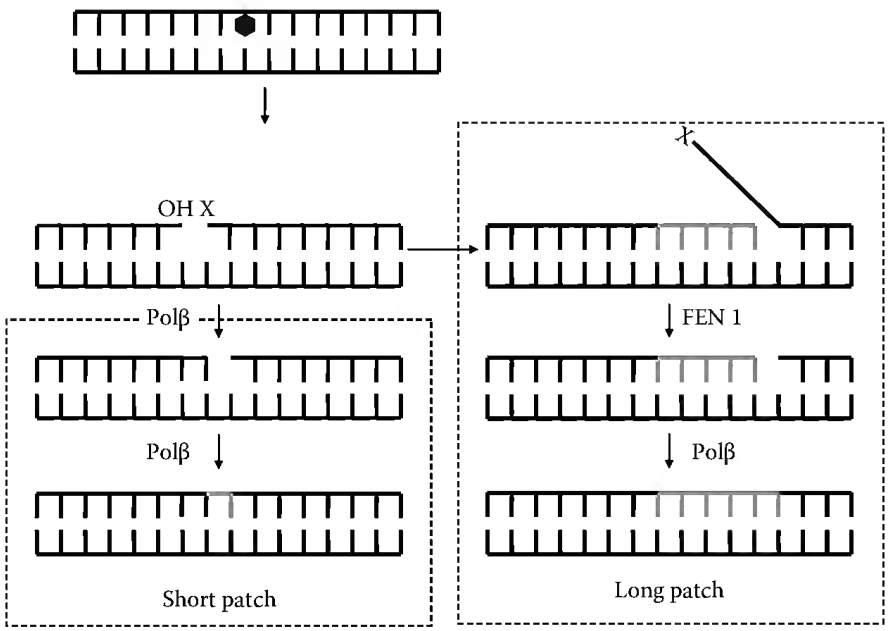

FIGURE 57.13 Schematic representation of the short-patch and long-patch synthesis pathways in BER. The selection of the process depends whether or not the 5′-end blocking group (X) can be efficiently processed.

and AP endonucleases before completion of repair. This is also true for the repair of single-strand breaks produced by oxidative stress, which exhibit a wide variety of structures frequently involving blocking ends. In mammalian cells, the 5′-deoxyribo-phosphate group produced by the action of APE1 on abasic sites is cleaved by Pol β that further adds the missing nucleotide [312]. The nick is then ligated. This pathway is referred to as short-patch repair (Figure 57.13). It is also involved after cleavage by polynucleotide kinase of the 3′-phosphate group [313] resulting from the action glycosylases with β,δ-elimination mechanism, and following cleavage of the unsaturated aldehyde produced by β-elimination. However, another synthesis pathway can take place, the long-patch repair. It involves strand invasion over 2–8 nucleotides by the polymerase followed by cleavage of the 5′-flap segment by FEN1 [314,315]. Long-patch repair occurs for instance when the 5′-end blocking group of an oxidative strand breaks [316,317] or a cleaved oxidized abasic site [318,319] cannot be processed. It is also triggered when polymerization is performed by Pol δ or Pol ε loaded onto PCNA instead of Pol β after cleavage of AP sites by APE1. It may be added that *N*-glycosylases, AP endonucleases, and polymerases are not the only proteins involved in BER. XRCC1 is a scaffold molecule [320,321] that interacts with PNK, Pol β, and XRCC1, and is thus a major player in short-patch repair. Poly(ADP-ribose) polymerase (PARP1 and 2) performs ADP-polyribosylation of numerous proteins at the site of strand breaks and thus induces early signaling and BER enzyme recruitment [322].

57.4.4 Radical Repair

Data presented in the photooxidation part unambiguously show that radical chemistry may be extremely harmful for DNA. Yet, some species possess enzymes that use specifically generated radicals in order to split UV-induced photoproducts back to the initial pyrimidines. The two main classes are the photolyases and the spore photoproduct lyase (SPL).

57.4.4.1 Photolyase

Photolyases are enzymes that use visible or near-UV radiation in a photoreactivation process [323,324]. By this strategy, cells are protected by using the genotoxic agent itself, sunlight, to repair the DNA damage it induces. Photolyases repair either CPDs or 64PPs. CPD photolyases are found in half of the

eubacteria [280], while both 64PPs and CPDs photolyases represent a major repair pathway in plant, especially in leaves where most cells are not dividing [325]. Photolyases have been also identified in some fishes, in drosophila, in some archaebacteria, and non-placental mammals (opossum) [326]. Humans do not possess photolyase but analog proteins, cryptochromes, are present and play a role in circadian rhythm. The photoenzymatic process of photolyases is now quite well understood, in particular for the CPDs photolyases. Recent advances mostly arose from state-of-the-art time-resolved measurements and crystallographic studies [326,327].

All CPD photolyases bare a fully reduced flavin adenine dinucleotide ($FADH^-$) cofactor (Figure 57.14). The reduction of the FAD cofactor into $FADH^-$ is catalyzed by light in a reaction that takes place independently of DNA repair, likely in order to keep the enzyme always functional. Three tryptophan residues are involved with the first one located at the surface of the protein and harvesting light energy [328,329]. The subsequent step is a series of electron transfer through the three tryptophans leading to the generation of $FADH^-$. During repair, the latter species is excited and cleaves the cyclobutane ring by initial injection of an electron into the photoproduct and formation of semi-reduced $FADH^•$. The resulting CPD radical anion undergoes intramolecular C5–C5 bond cleavage. The C6–C6 bond is broken in a subsequent step with formation of an intact pyrimidine at an end and of the radical anion of the pyrimidine at the other end. Oxidation of the latter species by $FADH^•$ regenerates $FADH^-$ and yields a second repaired pyrimidine. These reactions are quite fast, with decays around a few hundred picosecond for $FADH^-$ in the presence of CPDs while the C5–C5 and C6–C6 bonds were found to be broken in 60 ps and 1.5 ns, respectively [330]. The actual repair pathway is more complex because the photons are not directly absorbed by $FADH^-$. Indeed, photolyases possess another cofactor that behaves like an antenna and then transfers the absorbed energy to $FADH^-$. These compounds are either 5,10-methenyltetrahydrofolylpolyglutamate or 8-hydroxy-5-deazaflavin that exhibits respective absorption maximum in the 377–410 nm or the 430–460 nm range. The Förster-type energy transfer between light-harvesting cofactor and $FADH^-$ takes place within ca. 100 ps with high-quantum yield (0.6–1) [331,332]. It is facilitated by the proximity (15Å) of the interacting compounds.

In addition to CPD photolyase, a number of species also possess a similar enzyme specific for 64PPs [333–335]. Interestingly, such activity is not present in eubacteria. Because the enzyme exhibits a high degree of homology with CPD photolyase, a similar enzymatic reaction was postulated in both proteins. Yet, 64PPs do not exhibit a ring to be split upon repair. It is rather believed that electron is injected into their oxetane (or azetidine) derivatives, the species which are the intermediate in the formation of 64PPs.

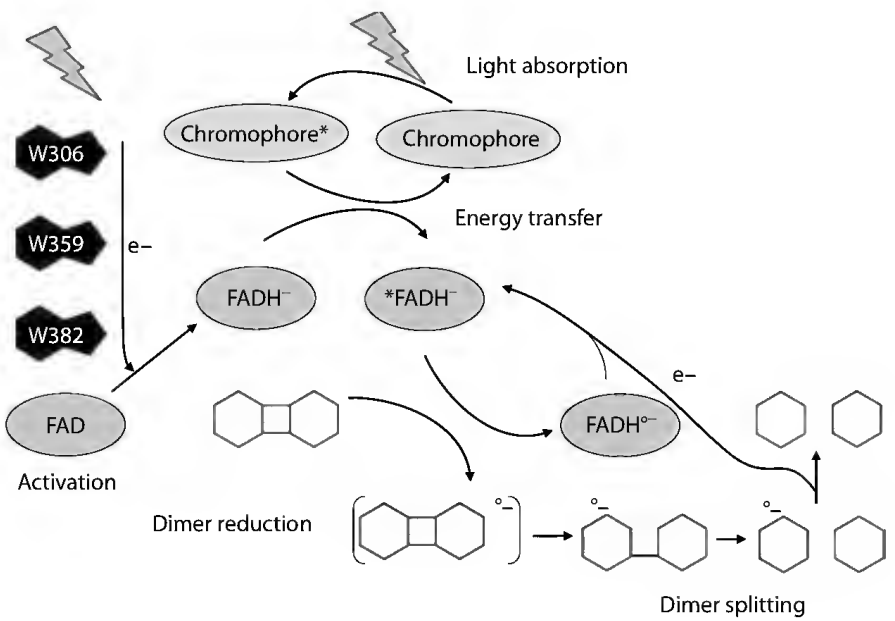

FIGURE 57.14 Scheme of the repair of CPDs by photolyases.

The likelihood of this mechanism was confirmed by model studies [336–338]. When free in aqueous solution, the oxetane (azetidine) derivative exhibits a very short lifetime. A key step in the enzymatic process is the induction of a drastic change in the balance between the pyrimidine (6-4) pyrimidone and the oxetane (azetidine) structure. Crystallographic studies strongly suggest that such a shift in the equilibrium results from the interaction of specific amino acids like glutamate 304 and aspartate 397 and 399 in the 64PPs photolyase of *Drosophila melanogaster* [339]. In contrast, histidine residues are more likely involved in the *Xenopus laevis* enzyme [340]. 64PPs photolyases seem to be less efficient than their CPD homolog as shown by their lower quantum yield (ca. 0.1). Surprisingly, 64PPs photolyases bind to Dewar isomer-containing DNA but do not cleave the photoproduct.

57.4.4.2 Spore Photoproduct Lyase

The peculiarity of the photobiology of spores has already been mentioned. This dormant form of some bacteria is highly resistant to UV radiation. In addition, SP is formed as the only photoproduct at the expense of CPDs and 64PPs. Understanding the repair of SP explains why such an evolutionary strategy has been selected. SP is reverted to the initial thymines by the SPL [341–343]. Because spores are dormant forms, UV-induced damage accumulates in their genome and has to be quickly repaired upon germination. This requirement is achieved through the fast repair of spore photoproducts by SPL that is more efficient than the repair of 64PPs and CPDs by NER. In order to make repair even faster upon germination, spores are loaded with SPL during sporulation. Another interest in SPL is that it does not need ATP, a source of energy almost absent from spores. Altogether, the UV resistance of spores can be explained by the voluntary accumulation of a very specific photoproduct easy to repair upon germination.

Like photolyase, SPL is a radical enzyme but it does not require light activation. SPL belongs to the radical S-Adenosyl-Methionine (SAM) superfamily where the initial radical is provided by the cleavage of *S*-adenosyl methionine into an adenosyl radical (Ado°) [344,345]. This last step is preformed in a [4Fe–4S] cluster located in the CXXXCXXC sequence specific for this class of proteins. Ado° then abstracts a hydrogen atom to the C6 position of the saturated thymine (Figure 57.15) [346]. A rearrangement leads to the cleavage of the methylene bridge with restoration of the 3′-thymine and formation of a methyl-centered radical on the 5′-thymine. Two pathways have been proposed for the completion of the process. First, the thymine radical may abstract H from AdoH and complete the cycle. Recent works with mutants also raised the possibility that a cysteine located out of the cluster (Cys 141 in SPL from *B. subtilis*) could be the final H donor [347], leading to the reversion of the second intact thymine. The observation that mutation of Cys 141 is as lethal as that of cysteines in the cluster supports the latter mechanism [348]. Another interesting issue is the stereoselectivity of SPL. The initial observation that the *S* enantiomer [349] was the favored substrate was surprising because the *R* isomer is expected to be the biologically relevant form. More recently, evidence were obtained that the *R* isomer of SP-TpT was a good substrate [350]. Moreover, the initial report of a favored repair of the *S* isomer of SP as a thymidine derivative was challenged [351].

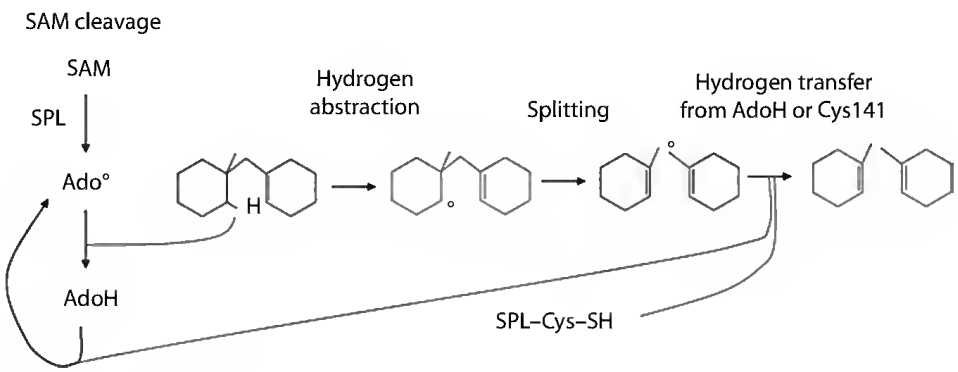

FIGURE 57.15 Principle of the repair of the SP by the SPL.

57.5 Conclusion

UVC and UVB photochemistry of DNA has been the topic of intense research for more than half a century, and large amounts of information have been gathered. The structure of the photoproducts and the relative contribution of the different lesions to UV genotoxicity are well established. Yet, questions remain open on the initial excited states involved in these photoreactions and how they can explain structural or sequence effects. In the UVA range, the photosensitized oxidation reactions are well described in model systems. However, the actual oxidative pathways in cells remain to be identified, although singlet oxygen seems to play a major role. DNA repair has also been extensively investigated, and the major repair enzymes or enzymatic complexes have been identified, as well as their substrate specificity. A large field of investigation remains open on molecular interaction between these proteins and damaged DNA. Other key questions are related to the interaction between the different repair pathways as well as between DNA repair protein and other major cellular functions. Altogether, the field of formation and repair of UV-induced DNA damage remains a very active one.

References

1. Cadet, J. and P. Vigny. 1990. Photochemistry of nucleic acids, in *Bioorganic Photochemistry*. New York: Wiley, pp. 1–272.
2. Ruzsicska, B. P. and D. G. E. Lemaire. 1995. DNA photochemistry, in *CRC Handbook of Organic Photochemistry and Photobiology*. Boca Raton, FL: CRC Press, pp. 1289–1317.
3. Daniels, M. 1983. Recent developments in the excited-states of nucleic acids. *Photochemistry and Photobiology* 37:691–693.
4. Callis, P. R. 1983. Electronic states and luminescence of nucleic acid systems. *Annual Review of Physical Chemistry* 34:329–357.
5. Crespo-Hernandez, C. E., B. Cohen, P. M. Hare, and B. Kohler. 2004. Ultrafast excited-state dynamics in nucleic acids. *Chemical Reviews* 104:1977–2019.
6. Broo, A., G. Pearl, and M. C. Zerner. 1997. Development of a hybrid quantum chemical and molecular mechanics method with application to solvent effects on the electronic spectra of uracil and uracil derivatives. *Journal of Physical Chemistry A* 101:2478–2488.
7. Fulscher, M. P. and B. O. Roos. 1995. Theoretical study of the electronic spectrum of cytosine. *Journal of the American Chemical Society* 117:2089–2095.
8. Fulscher, M. P., L. Serrano-Andres, and B. O. Roos. 1997. A theoretical study of the electronic spectra of adenine and guanine. *Journal of the American Chemical Society* 119:6168–6176.
9. Lorentzon, J., M. P. Fulscher, and B. O. Roos. 1995. Theoretical study of the electronic spectra of uracil and thymine. *Journal of the American Chemical Society* 117:9265–9273.
10. Merchan, M. and L. Serrano-Andres. 2003. Ultrafast internal conversion of excited cytosine via the lowest p-p* electronic singlet state. *Journal of the American Chemical Society* 125:8108–8109.
11. Mishra, S. K., M. K. Shukla, and P. C. Mishra. 2000. Electronic spectra of adenine and 2-aminopurine: An ab initio study of energy level diagrams of different tautomers in gas phase and aqueous solution. *Spectrochimica Acta Part A: Molecular and Biomolecular Spectroscopy* 56:1355–1384.
12. Shukla, M. K. and P. C. Mishra. 1999. A gas phase *ab initio* excited state geometry optimization study of thymine, cytosine and uracil. *Chemical Physics* 240:319–329.
13. Shukla, M. K., S. K. Mishra, A. Kumar, and P. C. Mishra. 2000. An *ab initio* study of excited states of guanine in the gas phase and aqueous media: Electronic transitions and mechanism of spectral oscillations. *Journal of Computational Chemistry* 21:826–846.
14. Pecourt, J.-M. L., J. Peon, and B. Kohler. 2000. Ultrafast internal conversion of electronically excited RNA and DNA nucleosides in water. *Journal of the American Chemical Society* 122:9348–9349.

15. Pecourt, J.-M. L., J. Peon, and B. Kohler. 2001. DNA excited-state dynamics: Ultrafast internal conversion and vibrational cooling in a series of nucleosides. *Journal of the American Chemical Society* 123:10370–10378.
16. Peon, J. and A. H. Zewail. 2001. DNA/RNA nucleotides and nucleosides: Direct measurement of excited-state lifetimes by femtosecond fluorescence up-conversion. *Chemical Physics Letters* 348:255–262.
17. Gustavsson, T., A. Sharonov, and D. Markovitsi. 2002. Thymine, thymidine and thymidine 5′-monophosphate studied by femtosecond fluorescence upconversion spectroscopy. *Chemical Physics Letters* 351:195–200.
18. Gustavsson, T., A. Sharonov, D. Onidas, and D. Markovitsi. 2002. Adenine, deoxyadenosine and deoxyadenosine 5′-monophosphate studied by femtosecond fluorescence upconversion spectroscopy. *Chemical Physics Letters* 356:49–54.
19. Cohen, B., P. M. Hare, and B. Kohler. 2003. Ultrafast excited-state dynamics of adenine and monomethylated adenines in solution: Implications for the nonradiative decay mechanism. *Journal of the American Chemical Society* 125:13594–13601.
20. Mennucci, B., A. Toniolo, and J. Tomasi. 2001. Theoretical study of guanine from gas phase to aqueous solution: Role of tautomerism and its implications in absorption and emission spectra. *Journal of Physical Chemistry A* 105:7126–7134.
21. Salter, L. M. and G. M. Chaban. 2002. Theoretical study of gas phase tautomerization reactions for the ground and first excited electronic states of adenine. *Journal of Physical Chemistry A* 106:4251–4256.
22. Broo, A. 1998. A theoretical investigation of the physical reason for the very different luminescence properties of the two isomers adenine and 2-aminopurine. *Journal of Physical Chemistry A* 102:526–531.
23. Marian, C. M., F. Schneider, M. Kleinschmidt, and J. Tatchen. 2002. Electronic excitation and singlet-triplet coupling in uracil tautomers and uracil-water complexes—A quantum chemical investigation. *European Physical Journal D* 20:357–367.
24. Mennucci, B., A. Toniolo, and J. Tomasi. 2001. Theoretical study of the photophysics of adenine in solution: Tautomerism, deactivation mechanisms, and comparison with the 2-aminopurine fluorescent isomer. *Journal of Physical Chemistry A* 105:4749–4757.
25. Ismail, N., L. Blancafort, M. Olivucci, B. Kohler, and M. A. Robb. 2002. Ultrafast decay of electronically excited singlet cytosine via pi,pi* to n(o)pi* state switch. *Journal of the American Chemical Society* 124:6818–6819.
26. Zechmann, G. and M. Barbatti. 2008. Photophysics and deactivation pathways of thymine. *Journal of Physical Chemistry A* 112:8273–8279.
27. Hare, P. M., C. E. Crespo-Hernandez, and B. Kohler. 2007. Internal conversion to the electronic ground state occurs via two distinct pathways for pyrimidine bases in aqueous solution. *Proceedings of the National Academy of Sciences of the United States of America* 104:435–440.
28. Kwok, W. M., C. Ma, and D. L. Phillips. 2006. Femtosecond time- and wavelength-resolved fluorescence and absorption spectroscopic study of the excited states of adenosine and an adenine oligomer. *Journal of the American Chemical Society* 128:11894–11905.
29. Buchvarov, I., Q. Wang, M. Raytchev, A. Trifonov, and T. Fiebig. 2007. Electronic energy delocalization and dissipation in single- and double-stranded DNA. *Proceedings of the National Academy of Sciences of the United States of America* 104:4794–4797.
30. Emanuele, E., K. Zakrzewska, D. Markovitsi, R. Lavery, and P. Millie. 2005. Exciton states of dynamic DNA double helices: Alternating dCdG sequences. *Journal of Physical Chemistry B* 109:16109–16118.
31. Emanuele, E., D. Markovitsi, P. Millie, and K. Zakrzewska. 2005. UV spectra and excitation delocalization in DNA: Influence of the spectral width. *ChemPhysChem* 6:1387–1392.
32. Bouvier, B., T. Gustavsson, D. Markovitsi, and P. Millie. 2002. Dipolar coupling between electronic transitions of the DNA bases and its relevance to exciton states in double helices. *Chemical Physics* 275:75–92.

33. Markovitsi, D., T. Gustavsson, and F. Talbot. 2007. Excited states and energy transfer among DNA bases in double helices. *Photochemical and Photobiological Sciences* 6:717–724.
34. Markovitsi, D., D. Onidas, T. Gustavsson, F. Talbot, and E. Lazzarotto. 2005. Collective behavior of Franck–Condon excited states and energy transfer in DNA double helices. *Journal of the American Chemical Society* 127:17130–17131.
35. Takaya, T., C. Su, K. de La Harpe, C. E. Crespo-Hernandez, and B. Kohler. 2008. UV excitation of single DNA and RNA strands produces high yields of exciplex states between two stacked bases. *Proceedings of the National Academy of Sciences of the United States of America* 105:10285–10290.
36. Onidas, D., T. Gustavsson, E. Lazzarotto, and D. Markovitsi. 2007. Fluorescence of the DNA double helices $(dAdT)_n$:$(dAdT)_n$ studied by femtosecond spectroscopy. *Physical Chemistry Chemical Physics* 9:5143–5148.
37. Onidas, D., T. Gustavsson, E. Lazzarotto, and D. Markovitsi. 2007. Fluorescence of the DNA double helix $(dA)_{20}$:$(dT)_{20}$ studied by femtosecond spectroscopy—Effect of the duplex size on the properties of the excited states. *Journal of Physical Chemistry B* 111:9644–9650.
38. Crespo-Hernandez, C. E., B. Cohen, and B. Kohler. 2005. Base stacking controls excited-state dynamics in A·T DNA. *Nature* 436:1141–1144.
39. Markovitsi, D., F. Talbot, T. Gustavsson, D. Onidas, E. Lazzarotto, and S. Marguet. 2006. Molecular spectroscopy: Complexity of excited-state dynamics in DNA. *Nature* 441:E7; discussion E8.
40. Lange, A. W. and J. M. Herbert. 2009. Both intra- and interstrand charge-transfer excited states in aqueous B-DNA are present at energies comparable to, or just above, the (1)pipi* excitonic bright states. *Journal of the American Chemical Society* 131:3913–3922.
41. Schreier, W. J., T. E. Schrader, F. O. Koller, P. Gilch, C. E. Crespo-Hernandez, V. N. Swaminathan, T. Carell, W. Zinth, and B. Kohler. 2007. Thymine dimerization in DNA is an ultrafast photoreaction. *Science* 315:625–629.
42. Miannay, F. A., A. Banyasz, T. Gustavsson, and D. Markovitsi. 2007. Ultrafast excited-state deactivation and energy transfer in guanine–cytosine DNA double helices. *Journal of the American Chemical Society* 129:14574–14575.
43. Schwalb, N. K. and F. Temps. 2007. Ultrafast electronic relaxation in guanosine is promoted by hydrogen bonding with cytidine. *Journal of the American Chemical Society* 129:9272–9273.
44. Abo-Riziq, A., L. Grace, E. Nir, M. Kabelac, P. Hobza, and M. S. de Vries. 2005. Photochemical selectivity in guanine–cytosine base-pair structures. *Proceedings of the National Academy of Sciences of the United States of America* 102:20–23.
45. Sobolewski, A. L., W. Domcke, and C. Hattig. 2005. Tautomeric selectivity of the excited-state lifetime of guanine/cytosine base pairs: The role of electron-driven proton-transfer processes. *Proceedings of the National Academy of Sciences of the United States of America* 102:17903–17906.
46. Sobolewski, A. L. and W. Domcke. 2004. *Ab initio* studies on the photophysics of the guanine–cytosine base pair. *Physical Chemistry Chemical Physics* 6:2763–2771.
47. Groenhof, G., L. V. Schafer, M. Boggio-Pasqua, M. Goette, H. Grubmuller, and M. A. Robb. 2007. Ultrafast deactivation of an excited cytosine–guanine base pair in DNA. *Journal of the American Chemical Society* 129:6812–6819.
48. Crespo-Hernandez, C. E., K. de la Harpe, and B. Kohler. 2008. Ground-state recovery following UV excitation is much slower in G x C-DNA duplexes and hairpins than in mononucleotides. *Journal of the American Chemical Society* 130:10844–10845.
49. Schwalb, N. K. and F. Temps. 2008. Base sequence and higher-order structure induce the complex excited-state dynamics in DNA. *Science* 322:243–245.
50. Gut, I. G., P. D. Wood, and R. W. Redmond. 1996. Interaction of triplet photosensitizers with nucleotides and DNA in aqueous solution at room temperature. *Journal of the American Chemical Society* 118:2366–2373.

51. Wood, P. D. and R. W. Redmond. 1996. Triplet state interactions between nucleic acid bases in solution at room temperature: Intramolecular energy and electron transfer. *Journal of the American Chemical Society* 118:4256–4263.
52. Kwok, W. M., C. Ma, and D. L. Phillips. 2008. A doorway state leads to photostability or triplet photodamage in thymine DNA. *Journal of the American Chemical Society* 130:5131–5139.
53. Marguet, S. and D. Markovitsi. 2005. Time-resolved study of thymine dimer formation. *Journal of the American Chemical Society* 127:5780–5781.
54. Kang, H. K., E. J. Shin, and S. C. Shim. 1992. Transient absorption-spectra and quenching of coumarin excited-states by nucleic-acid bases. *Journal of Photochemistry and Photobiology B: Biology* 13:19–28.
55. Lhiaubet-Vallet, V., J. Trzcionka, S. Encinas, M. A. Miranda, and N. Chouini-Lalanne. 2004. The triplet state of a *N*-phenylphthalimide with high intersystem crossing efficiency: Characterization of transient absorption spectroscopy and DNA sensitization properties. *Journal of Physical Chemistry B* 108:14148–14153.
56. Bosca, F., V. Lhiaubet-Vallet, M. C. Cuquerella, J. V. Castell, and M. A. Miranda. 2006. The triplet energy of thymine in DNA. *Journal of the American Chemical Society* 128:6318–6319.
57. Schreier, W. J., J. Kubon, N. Regner, K. Haiser, T. E. Schrader, W. Zinth, P. Clivio, and P. Gilch. 2009. Thymine dimerization in DNA model systems: Cyclobutane photolesion is predominantly formed via the singlet channel. *Journal of the American Chemical Society* 131:5038–5039.
58. Blancafort, L. and A. Migani. 2007. Modeling thymine photodimerizations in DNA: Mechanism and correlation diagrams. *Journal of the American Chemical Society* 129:14540–14541.
59. Boggio-Pasqua, M., G. Groenhof, L. V. Schafer, H. Grubmuller, and M. A. Robb. 2007. Ultrafast deactivation channel for thymine dimerization. *Journal of the American Chemical Society* 129:10996–10997.
60. Zhang, R. B. and L. A. Eriksson. 2006. A triplet mechanism for the formation of cyclobutane pyrimidine dimers in UV-irradiated DNA. *Journal of Physical Chemistry B* 110:7556–7562.
61. Rösch, A., R. Beukers, I. Ijistra, and W. Berends. 1958. The effect of U.V.-light on some components of the nucleic acids. I. Uracil, thymine. *Recueil des Travaux Chimiques des Pays-Bas* 77:423–429.
62. Beukers, R., A. P. M. Eker, and P. H. M. Lohman. 2008. 50 years thymine dimer. *DNA Repair* 7:530–543.
63. Varghese, A. J. 1970. Photochemistry of thymidine on ice. *Biochemistry* 9:4781–4787.
64. Patrick, M. H. and D. M. Gray. 1976. Independence of photoproduct formation on DNA conformation. *Photochemistry and Photobiology* 24:507–513.
65. Patrick, M. H. 1977. Studies on thymine-derived UV photoproducts in DNA-I. Formation and biological role of pyrimidine adducts in DNA. *Photochemistry and Photobiology* 25:357–372.
66. Douki, T., M. Court, S. Sauvaigo, F. Odin, and J. Cadet. 2000. Formation of the main UV-induced thymine dimeric lesions within isolated and cellular DNA as measured by high performance liquid chromatography-tandem mass spectrometry. *Journal of Biological Chemistry* 275:11678–11685.
67. Douki, T. and J. Cadet. 2001. Individual determination of the yield of the main-UV induced dimeric pyrimidine photoproducts in DNA suggests a high mutagenicity of CC photolesions. *Biochemistry* 40:2495–2501.
68. Douki, T. and J. Cadet. 1992. Far-UV photochemistry and photosensitization of 2′-deoxycytidylyl-(3′-5′)-thymidine: Isolation and characterization of the main photoproducts. *Journal of Photochemistry and Photobiology B: Biology* 15:199–213.
69. Freeman, K. B., P. V. Hariharan, and H. E. Johns. 1965. The ultraviolet photochemistry of cytidylyl-(3′-5′)-cytidine. *Journal of Molecular Biology* 13:833–848.
70. Johns, H. E., M. L. Pearson, J. C. LeBlanc, and C. W. Helleiner. 1964. The ultraviolet photochemistry of thymidylyl-(3′-5′)-thymidine. *Journal of Molecular Biology* 9:503–524.
71. Lemaire, D. G. E. and B. P. Ruzsicska. 1993. Quantum yields and secondary photoreactions of the photoproducts of dTpdT, dTpdC and dTpdU. *Photochemistry and Photobiology* 57:755–769.

72. Liu, F.-T. and N. C. Yang. 1978. Photochemistry of cytosine derivatives. 1 Photochemistry of thymidylyl-(3′-5′)-deoxycytidine. *Biochemistry* 17:4865–4876.
73. Varghese, A. J. and S. Y. Wang. 1967. Ultraviolet irradiation of DNA in vitro and in vivo produces a third thymine-derived product. *Science* 156:955–957.
74. Wang, S. Y. and A. J. Varghese. 1967. Cytosine–thymine addition product from DNA irradiated with ultraviolet light. *Biochemical and Biophysical Research Communications* 29:543–549.
75. Palmer, I. J., I. N. Ragazos, F. Bernardi, M. Olivucci, and M. A. Robb. 1994. An MC-SCF study of the (photochemical) Paterno–Büchi reaction. *Journal of the American Chemical Society* 116:2121–2132.
76. Charlier, M. and C. Helene. 1972. Photochemical reactions of aromatic ketones with nucleic acids and their components. I. Purine and pyrimidine bases and nucleosides. *Photochemistry and Photobiology* 15:71–87.
77. Encinas, S., N. Belmadoui, M. J. Climent, S. Gil, and M. A. Miranda. 2004. Photosensitization of thymine nucleobase by benzophenone derivatives as models for photoinduced DNA damage: Paterno-Büchi vs energy and electron transfer processes. *Chemical Research in Toxicology* 17:857–862.
78. Clivio, P., J.-L. Fourrey, and J. Gasche. 1991. DNA photodamage mechanistic studies: Characterization of a thietane intermediate in a model reaction relevant to "6-4 lesions." *Journal of the American Chemical Society* 113:5481–5483.
79. Douki, T., L. Voituriez, and J. Cadet. 1991. Characterization of the (6-4) photoproduct of 2′-deoxycytidylyl-(3′-5′)-thymidine and of its Dewar valence isomer. *Photochemistry and Photobiology* 27:293–297.
80. Franklin, W. A., P. W. Doetsch, and W. A. Haseltine. 1985. Structural determination of the ultraviolet light-induced thymine–cytosine pyrimidine-pyrimidone (6-4) photoproduct. *Nucleic Acids Research* 13:5317–5325.
81. Rycyna, R. E. and J. L. Alderfer. 1985. UV irradiation of nucleic acids: Formation, purification and solution conformational analysis of the "6-4" lesion of dTpdT. *Nucleic Acids Research* 13:5949–5963.
82. Blais, J., T. Douki, P. Vigny, and J. Cadet. 1994. Fluorescence quantum yield determination of pyrimidine (6-4) pyrimidone photoadducts. *Photochemistry and Photobiology* 59:402–404.
83. Johns, H. E., S. A. Rapaport, and M. Delbück. 1962. Photochemistry of thymine dimers. *Journal of Molecular Biology* 4:104–114.
84. Taylor, J.-S. and M. P. Cohrs. 1987. DNA, light, and Dewar pyrimidones: The structure and biological significance of TpT3. *Journal of the American Chemical Society* 109:2834–2835.
85. Taylor, J.-S., H.-L. Lu, and J. J. Kotyk. 1990. Quantitative conversion of the (6-4) photoproduct of TpdC to its Dewar valence isomer upon exposure to simulated sunlight. *Photochemistry and Photobiology* 51:161–167.
86. Thomas, M., D. Guillaume, J. L. Fourrey, and P. Clivio. 2002. Further insight in the photochemistry of DNA: Structure of a 2-imidazolone (5–4) pyrimidone adduct derived from the mutagenic pyrimidine (6-4) pyrimidone photolesion by UV irradiation. *Journal of the American Chemical Society* 124:2400–2401.
87. Perdiz, D., P. Grof, M. Mezzina, O. Nikaido, E. Moustacchi, and E. Sage. 2000. Distribution and repair of bipyrimidine photoproducts in solar UV-irradiated mammalian cells. Possible role of Dewar photoproducts in solar mutagenesis. *Journal of Biological Chemistry* 275:26732–26742.
88. Douki, T., A. Reynaud-Angelin, J. Cadet, and E. Sage. 2003. Bipyrimidine photoproducts rather than oxidative lesions are the main type of DNA damage involved in the genotoxic effect of solar UVA radiation. *Biochemistry* 42:9221–9226.
89. Courdavault, S., C. Baudouin, M. Charveron, B. Canghilem, A. Favier, J. Cadet, and T. Douki. 2005. Repair of the three main types of bipyrimidine DNA photoproducts in human keratinocytes exposed to UVB and UVA radiations. *DNA Repair* 4:836–844.
90. Lindahl, T. 1993. Instability and decay of the primary structure of DNA. *Nature* 362:709–715.
91. Labet, V., A. Grand, C. Morell, J. Cadet, and L. A. Eriksson. 2008. Proton catalyzed hydrolytic deamination of cytosine: A computational study. *Theoretical Chemistry Accounts* 120:429–435.

92. Labet, V., C. Morell, A. Grand, and A. Toro-Labbe. 2008. Theoretical study of cytosine deamination from the perspective of the reaction force analysis. *Journal of Physical Chemistry A* 112:11487–11494.
93. Frederico, L. A., T. A. Kunkel, and B. Ramsay Shaw. 1990. A sensitive genetic assay for the detection of cytosine deamination: Determination of rate constants and the activation energy. *Biochemistry* 29:2532–2537.
94. Green, M. and S. S. Cohen. 1957. Studies on the biosynthesis of bacterial and viral pyrimidines III. Derivatives of dihydrocytosine. *Journal of Biological Chemistry* 228:601–609.
95. Lemaire, D. G. E. and B. P. Ruzsicska. 1993. Kinetic analysis of the deamination reactions of cyclobutane dimers of thymidylyl-3′,5′-2′-deoxycytidine and 2′-deoxycytidine-3,5′-thymidine. *Biochemistry* 32:2525–2533.
96. Celewicz, L., M. Mayer, and M. D. Shetlar. 2005. The photochemistry of thymidylyl-(3′-5′)-5-methyl-2′-deoxycytidine in aqueous solution. *Photochemistry and Photobiology* 81:404–418.
97. Douki, T. and J. Cadet. 1994. Formation of cyclobutane dimers and (6-4) photoproducts upon far-UV photolysis of 5-methylcytosine containing dinucleoside monophosphates. *Biochemistry* 33:11942–11950.
98. Cannistraro, V. J. and J. S. Taylor. 2009. Acceleration of 5-methylcytosine deamination in cyclobutane dimers by G and its implications for UV-induced C-to-T mutation hotspots. *Journal of Molecular Biology* 392:1145–1157.
99. Barak, Y., O. Cohen-fix, and Z. Livneh. 1995. Deamination of cytosine containing photodimers in UV-irradiated DNA. *Journal of Biological Chemistry* 270:24174–24179.
100. Peng, W. and B. R. Shaw. 1996. Accelerated deamination of cytosine residues in UV-induced cyclobutane dimers leads to CC-TT transitions. *Biochemistry* 35:10172–10181.
101. Ruiz-Rubio, M. and R. Bockrath. 1989. On the possible role of cytosine deamination in delayed photoreversal mutagenesis targeted at thymine–cytosine dimers in *E. coli*. *Mutation Research* 210:93–102.
102. Tessman, I., M. A. Kennedy, and S. K. Liu. 1994. Unusual kinetics of uracil formation in single and double-stranded DNA by deamination of cytosine in cyclobutane pyrimidine dimers. *Journal of Molecular Biology* 235:807–812.
103. Brash, D. E., J. A. Rudolph, J. A. Simon, A. Lin, G. J. McKenna, H. P. Baden, A. J. Halperin, and J. Ponten. 1991. A role for sunlight in skin cancer: UV-induced p53 mutations in squamous cell carcinoma. *Proceedings of the National Academy of Sciences of the United States of America* 88:10124–10128.
104. Ziegler, A., D. J. Leffel, S. Kunala, H. W. Sharma, P. E. Shapiro, A. E. Bale, and D. E. Brash. 1993. Mutation hotspots due to sunlight in the p53 gene of nonmelanoma skin cancers. *Proceedings of the National Academy of Sciences of the United States of America* 90:4216–4220.
105. Dumaz, N., C. Drougard, A. Sarasin, and A. L. Daya-Grosjean. 1993. Specific UV-induced mutation spectrum in the p53 gene of skin tumors from DNA-repair-deficient xeroderma pigmentosum patients. *Proceedings of the National Academy of Sciences of the United States of America* 90:10529–10533.
106. Kumar, S., N. D. Sharma, R. J. H. Davies, D. W. Phillipson, and J. A. McCloskey. 1987. The isolation and characterization of a new type of dimeric adenine photoproduct in UV-irradiated deoxyadenylates. *Nucleic Acids Research* 15:1199–1216.
107. Koning, T. M. G., R. J. H. Davies, and R. Kaptein. 1990. The solution structure of the intramolecular photoproduct of d(TpA) derived with the use of NMR and a combination of distance geometry and molecular dynamics. *Nucleic Acids Research* 18:277–284.
108. Zhao, X. and J.-S. Taylor. 1996. The structure of d(TpA), the major photoproduct of thymidylyl-(3′5′)-deoxyadenosine. *Nucleic Acids Research* 24:1554–1560.
109. Sharma, N. D. and R. J. H. Davies. 1989. Extent of formation of a dimeric adenine photoproduct in polynucleotides and DNA. *Journal of Photochemistry and Photobiology B: Biology* 3:247–258.
110. Douki, T., G. Vadesne-Bauer, and J. Cadet. 2002. Formation of 2′-deoxyuridine hydrates upon exposure of nucleosides to gamma radiation and UVC-irradiation of isolated and cellular DNA. *Photochemical and Photobiological Sciences* 1:565–569.

111. Wierzchowski, K. L. and D. Shugar. 1957. Photochemistry of cytosine nucleosides and nucleotides. *Biochimica et Biophysica Acta* 25:355–364.
112. Boorstein, R. J., T. P. Hilbert, R. P. Cunningham, and G. W. Teebor. 1990. Formation and stability of repairable pyrimidine photohydrates in DNA. *Biochemistry* 29:10455–10460.
113. O'Donnell, R. E., R. J. Boorstein, R. P. Cunningham, and G. W. Teebor. 1994. Effect of pH and temperature on the stability of UV-induced repairable pyrimidine hydrates in DNA. *Biochemistry* 33:9875–9880.
114. Mitchell, D. L., J. Jen, and J. E. Cleaver. 1991. Relative induction of cyclobutane dimers and cytosine photohydrates in DNA irradiated *in vitro* and *in vivo* with ultraviolet-C and ultraviolet-B light. *Photochemistry and Photobiology* 54:741–746.
115. Mohammad, T. and H. Morrison. 1996. Evidence for the photosensitized formation of singlet oxygen by UVB irradiation of 2′-deoxyguanosine 5′-monophosphate. *Journal of the American Chemical Society* 118:1221–1222.
116. Mouret, S., C. Baudouin, M. Charveron, A. Favier, J. Cadet, and T. Douki. 2006. Cyclobutane pyrimidine dimers are predominant DNA lesions in whole human skin exposed to UVA radiation. *Proceedings of the National Academy of Sciences of the United States of America* 103: 13765–13770.
117. Douki, T., D. Perdiz, P. Grof, Z. Kulucsics, E. Moustacchi, J. Cadet, and E. Sage. 1999. Oxidation of guanine in cellular DNA by solar UV radiation: Biological role. *Photochemistry and Photobiology* 70:184–190.
118. Hosszu, J. L. and R. O. Rahn. 1967. Thymine dimer formation in DNA between 25°C and 100°C. *Biochemical and Biophysical Research Communications* 29:327–330.
119. Pfeifer, G. P., R. Drouin, and G. P. Holmquist. 1993. Detection of DNA adducts at the DNA sequence level by ligation-mediated PCR. *Mutation Research* 288:39–46.
120. Berg, R. J., F. R. de Gruijl, L. Roza, and J. C. van der Leun. 1993. Flow cytometric immunofluorescence assay for quantification of cyclobutyldithymine in separate phases of the cell cycle. *Carcinogenesis* 14:103–106.
121. Mitchell, D. L. and J. M. Clarkson. 1984. Use of synthetic polynucleotides to characterize an antiserum made against UV-irradiated DNA. *Photochemistry and Photobiology* 40:743–748.
122. Mori, T., M. Nakane, T. Hattori, T. Matsunaga, M. Ihara, and O. Nikaido. 1991. Simultaneous establishment of monoclonal antibodies specific for either cyclobutane pyrimidine dimer or (6-4) photoproduct from the same mouse immunized with ultraviolet-irradiated DNA. *Photochemistry and Photobiology* 54:225–232.
123. Bykov, V. J., R. Kumar, A. Forsti, and K. Hemminki. 1995. Analysis of UV-induced DNA photoproducts by ^{32}P-postlabeleing. *Carcinogenesis* 16:113–118.
124. Douki, T., M. Court, and J. Cadet. 2000. Electrospray-mass spectrometry characterization and measurement of far-UV induced thymine photoproducts. *Journal of Photochemistry and Photobiology B: Biology* 54:145–154.
125. Wang, S. Y. 1976. Pyrimidine bimolecular photoproducts, in *Photochemistry and Photobiology of Nucleic Acids*. New York: Academic Press 1:295–356.
126. Varghese, A. J. 1972. Photochemistry of nucleic acids and their constituents, in *Photophysiology*. New York: Academic Press 7:207–274.
127. Garcès, F. and C. A. Davila. 1982. Alterations in DNA irradiated with ultraviolet radiation-I. The formation process of cyclobutylpyrimidine dimers: Cross sections, action spectra and quantum yields. *Photochemistry and Photobiology* 35:9–16.
128. Courdavault, S., C. Baudouin, S. Sauvaigo, S. Mouret, S. Candéias, M. Charveron, A. Favier, J. Cadet, and T. Douki. 2004. Unrepaired cyclobutane pyrimidine dimers do not prevent proliferation of UVB-irradiated cultured human fibroblasts. *Photochemistry and Photobiology* 79:145–151.
129. Rosenstein, B. S. and D. L. Mitchell. 1991. The repair of DNA damages induced in normal human skin fibroblasts exposed to simulated sunlight. *Radiation Research* 126:338–342.

130. Thomas, D. C., D. S. Okumoto, A. Sancar, and V. A. Bohr. 1989. Preferential DNA repair of (6-4) photoproducts in the dihydrofolate reductase gene of Chinese hamster ovary cells. *Journal of Biological Chemistry* 264:1374–1378.
131. Dardalhon, M., L. A. Guillo, A. Moysan, P. Vigny, and D. Averbeck. 1994. Detection of pyrimidine dimers and monoadducts induced by 7-methylpyrido(3,4-c) psoralen and UVA in Chinese hamster V79 cells by enzymatic cleavage and high-pressure liquid chromatography. *Photochemistry and Photobiology* 59:423–429.
132. Swinton, D. C. and P. Hanawalt. 1973. The fate of pyrimidine dimers in ultraviolet-irradiated *Chlamydomonas*. *Photochemistry and Photobiology* 17:361–375.
133. Mitchell, D. L., J. P. Allison, and R. S. Nairn. 1990. Immunoprecipitation of pyrimidine(6-4)pyrimidone photoproducts and cyclobutane pyrimidine dimers in UV-irradiated DNA. *Radiation Research* 123:299–303.
134. Matallana-Surget, S., J. A. Meador, F. Joux, and T. Douki. 2008. Effect of the GC content of DNA on the distribution of UVB-induced bipyrimidine photoproducts. *Photochemical and Photobiological Sciences* 7:794–801.
135. Drouin, R. and J. P. Therrien. 1997. UVB-induced cyclobutane pyrimidine dimer frequency correlates with skin cancer mutational hotspots in p53. *Photochemistry and Photobiology* 66:719–726.
136. You, Y.-H., P. E. Szabo, and G. P. Pfeifer. 2000. Cyclobutane pyrimidine dimers form preferentially at the major *p53* mutational hotspot in UVB-induced mouse skin tumors. *Carcinogenesis* 21:2113–2117.
137. Sharonov, A., T. Gustavsson, S. Marguet, and D. Markovitsi. 2003. Photophysical properties of 5-methylcytidine. *Photochemical and Photobiological Sciences* 2:362–364.
138. Li, X. Y. and L. A. Eriksson. 2005. Influence of C5-methylation of cytosine on the formation of cyclobutane pyrimidine dimers. *Chemical Physics Letters* 401:99–103.
139. Tommasi, S., M. F. Denissenko, and G. P. Pfeifer. 1997. Sunlight induces pyrimidine dimers preferentially at 5-methylcytosine bases. *Cancer Research* 57:4727–4730.
140. You, Y.-H. and G. P. Pfeifer. 1999. Involvement of 5-methylcytosine in sunlight-induced mutagenesis. *Journal of Molecular Biology* 293:493–503.
141. Rochette, P. J. and D. E. Brash. 2010. Human telomeres are hypersensitive to UV-induced DNA damage and refractory to repair. *PLoS Genetics* 6:e1000926.
142. Chadwick, C. A., C. S. Potten, O. Nikaido, T. Matsunaga, C. Proby, and A. R. Young. 1995. The detection of cyclobutane thymine dimers, (6-4) photolesions and the Dewar valence photoisomers in sections of UV-irradiated human skin using specific antibodies, and the demonstration of depth penetration effects. *Journal of Photochemistry and Photobiology B: Biology* 28:163–170.
143. Young, A. R., C. S. Potten, O. Nikaido, P. G. Parsons, J. Boenders, J. M. Ramsden, and C. A. Chadmick. 1998. Human melanocytes and keratinocytes exposed to UVB or UVA *in vivo* show comparable levels of thymine dimers. *Journal of Investigative Dermatology* 111:936–940.
144. Johnson, A. T. and O. Wiest. 2007. Structure and dynamics of poly(T) single-strand DNA: Implications toward CPD formation. *Journal of Physical Chemistry B* 111:14398–14404.
145. Yarasi, S., P. Brost, and G. R. Loppnow. 2007. Initial excited-state structural dynamics of thymine are coincident with the expected photochemical dynamics. *Journal of Physical Chemistry A* 111:5130–5135.
146. Desnous, C., B. R. Babu, C. Moriou, J. U. Mayo, A. Favre, J. Wengel, and P. Clivio. 2008. The sugar conformation governs (6-4) photoproduct formation at the dinucleotide level. *Journal of the American Chemical Society* 130:30–31.
147. Moriou, C., M. Thomas, M. T. Adeline, M. T. Martin, A. Chiaroni, S. Pochet, J. L. Fourrey, A. Favre, and P. Clivio. 2007. Crystal structure and photochemical behavior in solution of the 3′-N-Sulfamate analogue of thymidylyl(3′-5′)thymidine. *Journal of Organic Chemistry* 72:43–50.
148. Ostrowski, T., J. C. Maurizot, M. T. Adeline, J. L. Fourrey, and P. Clivio. 2003. Sugar conformational effects on the photochemistry of thymidylyl(3′-5′)thymidine. *Journal of Organic Chemistry* 68:6502–6510.

149. Douki, T. 2006. Effect of denaturation on the photochemistry of pyrimidine bases in isolated DNA. *Journal of Photochemistry and Photobiology B: Biology* 82:45–52.
150. Douki, T. 2006. Low ionic strength reduces cytosine photoreactivity in UVC-irradiated isolated DNA. *Photochemical and Photobiological Sciences* 5:1045–1051.
151. Liu, X. Q., A. Conconi, and M. J. Smerdon. 1997. Strand-specific modulation of UV photoproducts in 5S rDNA by TFIIIA binding and their effect on TFIIIA complex formation. *Biochemistry* 36:13710–13717.
152. Pfeifer, G. P., R. Drouin, A. D. Riggs, and G. P. Holmquist. 1992. Binding of transcription factors creates hot-spots for UV photoproducts in vivo. *Molecular and Cellular Biology* 12:1798–1804.
153. Tornaletti, S. and G. P. Pfeifer. 1995. UV-light as a footprinting agent—Modulation of UV-induced DNA-damage by transcription factors bound at the promoters of 3 human genes. *Journal of Molecular Biology* 249:714–728.
154. Gale, J. M., K. A. Nissen, and M. J. Smerdon. 1987. UV-induced formation of pyrimidine dimers in nucleosome core DNA is strongly modulated with a period of 10.3 bases. *Proceedings of the National Academy of Sciences of the United States of America* 84:6644–6648.
155. Brown, D. W., L. J. Libertini, C. Suquet, E. W. Small, and M. J. Smerdon. 1993. Unfolding of nucleosome cores dramatically changes the distribution of ultraviolet photoproducts in DNA. *Biochemistry* 32:10527–10531.
156. Gale, J. M. and M. J. Smerdon. 1990. UV induced (6-4) photoproducts are distributed differently than cyclobutane dimers in nucleosome. *Photochemistry and Photobiology* 51:411–417.
157. Mann, D. B., D. L. Springer, and M. J. Smerdon. 1997. DNA damage can alter the stability of nucleosomes: Effects are dependent on damage type. *Proceedings of the National Academy of Sciences of the United States of America* 94:2215–2220.
158. Suquet, C. and M. J. Smerdon. 1993. UV damage to DNA strongly influences its rotational setting on the histone surface of reconstituted nucleosomes. *Journal of Biological Chemistry* 268:23755–23757.
159. Demidov, V. V. and V. N. Potaman. 1993. HPLC photofingerprinting of conformational peculiarities and transitions in oligonucleotide duplexes. *Nucleic Acids Research* 21:2691–2696.
160. Potaman, V. N., I. P. Chernov, and V. V. Demidov. 1993. High-performance liquid chromatography of the photoproducts of nucleic acid components. III Detection of the secondary structure differences in sequence isomeric self-complementary oligonucleotides. *Journal of Chromatography* 648:151–156.
161. Nguyen, H. T. and K. W. Minton. 1988. Ultraviolet-induced dimerization of non-adjacent pyrimidines. A potential mechanism for the targeted -1 frameshift mutation. *Journal of Molecular Biology* 200:681–693.
162. Nguyen, H. T. and K. W. Minton. 1989. Extensive photodimerization of non-adjacent pyrimidines. *Journal of Molecular Biology* 210:869–874.
163. Pehrson, J. R. and L. H. Cohen. 1992. Effects of DNA looping on pyrimidine dimer formation. *Nucleic Acids Research* 20:1321–1324.
164. Nejedly, K., R. Kittner, S. Pospisilova, and J. Kypr. 2001. Crosslinking of the complementary strands of DNA by UV light: Dependence on the oligonucleotide composition of the UV irradiated DNA. *Biochimica et Biophysica Acta* 1517:365–375.
165. Su, D. G., J. L. Kao, M. L. Gross, and J. S. Taylor. 2008. Structure determination of an interstrand-type *cis*-anti cyclobutane thymine dimer produced in high yield by UVB light in an oligodeoxynucleotide at acidic pH. *Journal of the American Chemical Society* 130:11328–11337.
166. Su, D. G. T., H. F. Fang, M. L. Gross, and J. S. A. Taylor. 2009. Photocrosslinking of human telomeric G-quadruplex loops by anti cyclobutane thymine dimer formation. *Proceedings of the National Academy of Sciences of the United States of America* 106:12861–12866.
167. Douki, T., G. Laporte, and J. Cadet. 2003. Inter-strand photoproducts are produced in high yield within A-DNA exposed to UVC radiation. *Nucleic Acids Research* 31:3134–3142.
168. Setlow, P. 2007. I will survive: DNA protection in bacterial spores. *Trends in Microbiology* 15:172–180.

169. Lee, K. S., D. Bumbaca, J. Kosman, P. Setlow, and M. J. Jedrzejas. 2008. Structure of a protein–DNA complex essential for DNA protection in spores of *Bacillus* species. *Proceedings of the National Academy of Sciences of the United States of America* 105:2806–2811.
170. Donnellan, J. E. and R. B. Setlow. 1965. Thymine photoproducts but not thymine dimers found in ultraviolet-irradiated bacterial spores. *Science* 149:308–310.
171. Kim, S. J., C. Lester, and T. P. Begley. 1995. Synthesis of the dinucleotide spore photoproduct. *Journal of Organic Chemistry* 60:6256–6257.
172. Mantel, C., A. Chandor, D. Gasparutto, T. Douki, M. Atta, M. Fontecave, P. A. Bayle, J. M. Mouesca, and M. Bardet. 2008. Combined NMR and DFT studies for the absolute configuration elucidation of the spore photoproduct, a UV-induced DNA lesion. *Journal of the American Chemical Society* 130:16978–16984.
173. Varghese, A. J. 1970. 5-Thyminyl-5,6-dihydrothymine from DNA irradiated with ultraviolet light. *Biochemical and Biophysical Research Communications* 38:484–490.
174. Douki, T. and J. Cadet. 2003. Formation of the spore photoproduct and other dimeric lesions between adjacent pyrimidines in UVC-irradiated dry DNA. *Photochemical and Photobiological Sciences* 2:433–436.
175. Nicholson, W. L., B. Setlow, and P. Setlow. 1991. Ultraviolet-irradiation of DNA complexed with alpha-beta-type small, acid-soluble proteins from spores of bacillus or clostridium species makes spore photoproduct but not thymine dimers. *Proceedings of the National Academy of Sciences of the United States of America* 88:8288–8292.
176. Nicholson, W. L., B. Setlow, and P. Setlow. 2002. UV photochemistry of DNA in vitro and in *Bacillus subtilis* spores at Earth-ambient and low atmospheric pressure: Implications for spore survival on other planets or moons in the solar system. *Astrobiology* 2:417–425.
177. Douki, T., B. Setlow, and P. Setlow. 2005. Effects of the binding of a/b-type small, acid-soluble spore proteins on the photochemistry of DNA in spores of *Bacillus subtilis* and *in vitro. Photochemistry and Photobiology* 81:163–169.
178. Setlow, B. and P. Setlow. 1993. Dipicolinic acid greatly enhances production of spore photoproduct in bacterial-spores upon UV irradiation. *Applied and Environmental Microbiology* 59:640–643.
179. Douki, T., B. Setlow, and P. Setlow. 2005. Photosensitization of DNA by dipicolinic acid, a major component of spores of *Bacillus* species. *Photochemical and Photobiological Sciences* 4: 951–957.
180. Wondrak, G. T., M. K. Jacobson, and E. L. Jacobson. 2006. Endogenous UVA-photosensitizers: Mediators of skin photodamage and novel targets for skin photoprotection. *Photochemical and Photobiological Sciences* 5:215–237.
181. Cadet, J. and R. Teoule. 1978. Comparative study of oxidation of nucleic acid components by hydroxyl radicals, singlet oxygen and superoxide anion radicals. *Photochemistry and Photobiology* 28:661–667.
182. Sheu, C. and C. S. Foote. 1993. Endoperoxide formation in a guanosine derivative. *Journal of the American Chemical Society* 115:10446–10447.
183. Sheu, C., P. Kang, S. Khan, and C. S. Foote. 2002. Low-temperature photosensitized oxidation of a guanosine derivative and formation of an imidazole ring-opened product. *Journal of the American Chemical Society* 124:3905–5913.
184. Ravanat, J.-L., C. Saint-Pierre, P. Di Mascio, G. R. Martinez, M. H. Medeiros, and J. Cadet. 2001. Damage to isolated DNA mediated by singlet oxygen. *Helvetica Chimica Acta* 84:3702–3709.
185. Ravanat, J. L., P. Di Mascio, G. R. Martinez, M. H. Medeiros, and J. Cadet. 2001. Singlet oxygen induces oxidation of cellular DNA. *Journal of Biological Chemistry* 276:40601–40604.
186. Niles, J. C., J. S. Wishnock, and S. R. Tannenbaum. 2001. Spiroiminodihydantoin is the major product of 8-oxo-7,8-dihydroguanosine reaction with peroxynitrite in the presence of thiols and guanosine photooxidation by methylene blue. *Organic Letters* 3:963–966.
187. Ye, Y., J. G. Muller, W. Luo, C. L. Mayne, A. J. Shallop, A. R. Jones, and C. J. Burrows. 2003. Formation of ^{13}C-, ^{15}N-, and ^{18}O-labeled guanidinohydantoin from guanosine oxidation with singlet oxygen. Implications for structure and mechanism. *Journal of the American Chemical Society* 125:13926–13927.

188. Nieuwint, A. W., J. M. Aubry, F. Arwert, H. Kortbeek, S. Herzberg, and H. Joenje. 1985. Inability of chemically generated singlet oxygen to break the DNA backbone. *Free Radical Research Communications* 1:1–9.
189. Sheu, C. and C. S. Foote. 1995. Reactivity toward singlet oxygen of a 7,8-dihydro-8-oxo-guanosine ("8-hydroxyguanosine") formed by photooxidation of a guanosine derivative. *Journal of the American Chemical Society* 117:6439–6442.
190. Di Mascio, P., H. Wefers, H.-P. Do-Thy, M. V. Lafleur, and H. Sies. 1989. Singlet oxygen causes loss of biological activity in plasmid and bacteriophage DNA and induces single-strand breaks. *Biochimica et Biophysica Acta* 1007:151–157.
191. Decarroz, C., J. R. Wagner, J. E. van Lier, K. C. Murali, P. Riesz, and J. Cadet. 1986. Sensitized photo-oxidation of thymidine by 2-methyl-1,4-naphtoquinone. Characterization of stable products. *International Journal of Radiation Biology* 50:491–505.
192. Decarroz, C., J. R. Wagner, and J. Cadet. 1987. Specific deprotonation reactions of the pyrimidine radical cation resulting from the menadione mediated photosensitization of 2′-deoxycytidine. *Free Radical Research Communications* 2:295–301.
193. Wagner, J. R., J. E. van Lier, C. Decarroz, M. Berger, and J. Cadet. 1990. Photodynamic methods for oxy radical-induced DNA damage. *Methods in Enzymology* 186:502–511.
194. Wagner, R. J., J. E. van Lier, M. Berger, and J. Cadet. 1994. Thymidine hydroperoxides: Structural assignment, conformational features and thermal decomposition in water. *Journal of the American Chemical Society* 116:2235–2242.
195. Crespo-Hernandez, C. E., D. M. Close, L. Gorb, and J. Leszczynski. 2007. Determination of redox potentials for the Watson–Crick base pairs, DNA nucleosides, and relevant nucleoside analogues. *Journal of Physical Chemistry B* 111:5386–5395.
196. Caruso, T., M. Carotenuto, E. Vasca, and A. Peluso. 2005. Direct experimental observation of the effect of the base pairing on the oxidation potential of guanine. *Journal of the American Chemical Society* 127:15040–15041.
197. Yang, X., X. B. Wang, E. R. Vorpagel, and L. S. Wang. 2004. Direct experimental observation of the low ionization potentials of guanine in free oligonucleotides by using photoelectron spectroscopy. *Proceedings of the National Academy of Sciences of the United States of America* 101:17588–17592.
198. Steenken, S. 1989. Purine bases, nucleosides, and nucleotides: Aqueous solution redox chemistry and transformation reactions of their radical cations and e- and OH adducts. *Chemical Reviews* 89:503–520.
199. Candeias, L. P. and S. Steenken. 2000. Reaction of HO° with guanine derivatives in aqueous solution: Formation of two different redox-active OH-adduct radicals and their unimolecular transformation reactions. Properties of G(-H)°. *Chemistry—A European Journal* 6:475–484.
200. O'Neill, P. 1983. Pulse radiolytic study of the interaction of thiols and ascorbate with OH adducts of dGMP: Implications for DNA repair processes. *Radiation Research* 96:198–210.
201. O'Neill, P. and P. W. Chapman. 1985. Potential repair of free radical adducts of dGMP and dG by a series of reductants. A pulse radiolysis study. *International Journal of Radiation Biology* 47:71–80.
202. Munk, B. H., C. J. Burrows, and H. B. Schlegel. 2007. Exploration of mechanisms for the transformation of 8-hydroxy guanine radical to FAPyG by density functional theory. *Chemical Research in Toxicology* 20:432–444.
203. Ravanat, J.-L., C. Saint-Pierre, and J. Cadet. 2003. One-electron oxidation of the guanine moiety of 2′-deoxyguanosine: Influence of 8-oxo-7,8-dihydro-2′-deoxyguanosine. *Journal of the American Chemical Society* 125:2030–2031.
204. Steenken, S., S. V. Jovanovic, M. Bietti, and K. Bernhard. 2000. The trap depth (in DNA) of 8-oxo-7,8-dihydroguanine as derived from electron-transfer equilibria in aqueous solution. *Journal of the American Chemical Society* 122:2373–2374.
205. Ye, Y., B. H. Munk, J. G. Muller, A. Cogbill, C. J. Burrows, and H. B. Schlegel. 2009. Mechanistic aspects of the formation of guanidinohydantoin from spiroiminodihydantoin under acidic conditions. *Chemical Research in Toxicology* 22:526–535.

206. Munk, B. H., C. J. Burrows, and H. B. Schlegel. 2008. An exploration of mechanisms for the transformation of 8-oxoguanine to guanidinohydantoin and spiroiminodihydantoin by density functional theory. *Journal of the American Chemical Society* 130:5245–5256.
207. Luo, W. C., J. G. Muller, and C. J. Burrows. 2001. The pH-dependent role of superoxide in riboflavin-catalyzed photooxidation of 8-oxo-7,8-dihydroguanosine. *Organic Letters* 3:2801–2804.
208. Kino, K. and H. Sugiyama. 2005. UVR-induced G-C to C-G transversions from oxidative DNA damage. *Mutation Research* 571:33–42.
209. Gedik, C. M. and A. Collins. 2005. Establishing the background level of base oxidation in human lymphocyte DNA: Results of an interlaboratory validation study. *FASEB Journal* 19:82–84.
210. Douki, T. and J. Cadet. 1999. Modification of DNA bases by photosensitized one-electron oxidation. *International Journal of Radiation Biology* 75:571–581.
211. Pang, B., X. Zhou, H. Yu, M. Dong, K. Taghizadeh, J. S. Wishnok, S. R. Tannenbaum, and P. C. Dedon. 2007. Lipid peroxidation dominates the chemistry of DNA adduct formation in a mouse model of inflammation. *Carcinogenesis* 28:1807–1813.
212. Perrier, S., J. Hau, D. Gasparutto, J. Cadet, A. Favier, and J.-L. Ravanat. 2006. Characterization of lysine-guanine cross-links upon one-electron oxidation of a guanine-containing oligonucleotide in the presence of a trilysine peptide. *Journal of the American Chemical Society* 128:5703–5710.
213. Xu, X. Y., J. G. Muller, Y. Ye, and C. J. Burrows. 2008. DNA–protein cross-links between guanine and lysine depend on the mechanism of oxidation for formation of C5 vs C8 guanosine adducts. *Journal of the American Chemical Society* 130:703–709.
214. Morin, B. and J. Cadet. 1995. Type-I benzophenone-mediated nucleophilic reaction of 5′-amino-2′, 5′-dideoxyguanosine—a model system for the investigation of photosensitized formation of DNA-protein cross-links. *Chemical Research in Toxicology* 8:792–799.
215. Cadet, J., M. Berger, G. W. Buchko, P. C. Joshi, S. Raoul, and J.-L. Ravanat. 1994. 2,2-Diamino-4-[(3,5-di-*O*-acetyl-2-deoxy-b-D-*erythro*-pentofuranosyl)amino]-5-(2*H*)-oxazolone: A novel and predominant radical oxidation product of 3′,5′-di-*O*-acetyl-2′-deoxyguanosine. *Journal of the American Chemical Society* 116:7403–7404.
216. Ravanat, J.-L., M. Berger, F. Benard, R. Langlois, R. Ouellet, J. E. van Lier, and J. Cadet. 1992. Phthalocyanine and naphthalocyanine photosensitized oxidation of 2′-deoxyguanosine: Distinct type I and type II products. *Photochemistry and Photobiology* 55:809–814.
217. Misiaszek, R., C. Crean, A. Joffe, N. E. Geacintov, and V. Shafirovich. 2004. Oxidative DNA damage associated with combination of guanine and superoxide radicals and repair mechanisms via radical trapping. *Journal of Biological Chemistry* 279:32106–32115.
218. Conwell, E. 2004. Polarons and transport in DNA, in *Long-Range Charge Transfer in DNA II*, Book Series *Topics in Current Chemistry.* Berlin: Springer-Verlag, pp. 73–101.
219. Shafirovich, V. and N. E. Geacintov. 2004. Proton-coupled electron transfer reactions at a distance in DNA duplexes, in *Long-Range Charge Transfer in DNA II*, Book, Series *Topics in Current Chemistry.* Berlin: Springer-Verlag, pp. 129–157.
220. Giese, B. 2004. Hole injection and hole transfer through DNA: The hopping mechanism, in *Long-Range Charge Transfer in DNA I*, Book Series *Topics in Current Chemistry.* Berlin: Springer-Verlag, pp. 27–44.
221. O'Neill, M. A. and J. K. Barton. 2004. DNA-mediated charge transport chemistry and biology, in *Long-Range Charge Transfer in DNA I*, Book Series *Topics in Current Chemistry.* Berlin: Springer-Verlag, pp. 67–115.
222. Schuster, G. B. and U. Landman. 2004. The mechanism of long-distance radical cation transport in duplex DNA: Ion-gated hopping of polaron-like distortions, in *Long-Range Charge Transfer in DNA I*, Book Series *Topics in Current Chemistry.* Berlin: Springer-Verlag, pp. 139–161.
223. Ly, D., L. Sanii, and G. Schuster. 1999. Mechanism of charge transport in DNA: Internally linked anthraquinone conjugates support phonon-assisted polaron hopping. *Journal of the American Chemical Society* 121:9400–9410.

224. Meggers, E., M. E. Michel-Beyerle, and B. Giese. 1998. Sequence dependent long range hole transport in DNA. *Journal of the American Chemical Society* 120:12950–12955.
225. Wan, C., T. Fiebig, S. O. Kelley, C. R. Treadway, and J. K. Barton. 1999. Femtosecond dynamics of DNA-mediated electron transfer. *Proceedings of the National Academy of Sciences of the United States of America* 96:6014–6019.
226. Cullis, P. M., M. E. Malone, and L. A. Merson-Davies. 1996. Guanine radical cations are precursors of 7,8-dihydro-8-oxo-2′-deoxyguanosine but are not precursors of immediate strand breaks. *Journal of the American Chemical Society* 118:2775–2781.
227. Melvin, T., S. Botchway, A. W. Parker, and P. O'Neill. 1995. Migration of photoinduced oxidative damage in models for DNA. *Journal of the Chemical Society—Chemical Communications* 653–654.
228. Melvin, T., S. Cunniffe, D. Papworth, T. Roldanarjona, and P. O'Neill. 1997. Irradiation of DNA with 193 nm light yields formamidopyrimidine-DNA glycosylase (Fpg) protein-sensitive lesions. *Photochemistry and Photobiology* 65:660–665.
229. Douki, T., D. Angelov, and J. Cadet. 2001. UV Laser photolysis of DNA: Effect of duplex stability on charge-transfer efficiency. *Journal of the American Chemical Society* 123:11360–11366.
230. Douki, T., T. Delatour, F. Paganon, and J. Cadet. 1996. Measurement of oxidative damage at pyrimidine bases in g-irradiated DNA. *Chemical Research in Toxicology* 9:1145–1151.
231. Douki, T., R. Martini, J.-L. Ravanat, R. J. Turesky, and J. Cadet. 1997. Measurement of 2,6-diamino-4-hydroxy-5-formamidopyrimidine and 8-oxo-7,8-dihydroguanine in isolated DNA exposed to gamma radiation in aqueous solution. *Carcinogenesis* 18:2385–2391.
232. Frelon, S., T. Douki, J.-L. Ravanat, C. Tornabene, and J. Cadet. 2000. High performance liquid chromatography—Tandem mass spectrometry measurement of radiation-induced base damage to isolated and cellular DNA. *Chemical Research in Toxicology* 13:1002–1010.
233. Swarts, S. G., D. Becker, M. Sevilla, and K. T. Wheeler. 1996. Radiation-induced DNA damage as a function of hydration.2. Base damage from electron-loss centers. *Radiation Research* 145:304–314.
234. Gniadecki, R., T. Thorn, J. Vicanova, A. B. Petersen, and H. C. Wulf. 2000. Role of mitochondria in ultraviolet-induced oxidative stress. *Journal of Cellular Biochemistry* 80:216–222.
235. Pourzand, C., R. D. Watkin, J. E. Brown, and R. M. Tyrrell. 1999. Ultraviolet A radiation induces immediate release of iron in human primary skin fibroblasts: The role of ferritin. *Proceedings of the National Academy of Sciences of the United States of America* 96:6751–6756.
236. Knapp Pogozelski, W. K. and T. D. Tullius. 1998. Oxidative strand scission of nucleic acids: Route initiated by hydrogen abstraction from the sugar moiety. *Chemical Reviews* 98:1089–1107.
237. Cadet, J., T. Delatour, T. Douki, D. Gasparutto, J.-P. Pouget, J.-L. Ravanat, and S. Sauvaigo. 1999. Hydroxyl radicals and DNA base damage. *Mutation Research* 424:9–21.
238. Rosen, J. E., A. K. Prahalad, and G. M. Williams. 1996. 8-Oxodeoxyguanosine formation in the DNA of cultured cells after exposure to H_2O_2 alone or with UVB or UVA irradiation. *Photochemistry and Photobiology* 64:117–122.
239. Zhang, X. S., B. S. Rosenstein, Y. Wang, M. Lebwohl, D. M. Mitchell, and H. C. Wei. 1997. Induction of 8-oxo-7,8-dihydro-2′-deoxyguanosine by ultraviolet radiation in calf thymus DNA and HeLa cells. *Photochemistry and Photobiology* 65:119–124.
240. Pouget, J.-P., T. Douki, M.-J. Richard, and J. Cadet. 2000. DNA damage induced in cells by gamma and UVA radiations as measured by HPLC/GC-MS, HPLC-EC and comet assay. *Chemical Research in Toxicology* 13:541–549.
241. Kielbassa, C., L. Roza, and B. Epe. 1997. Wavelength dependence of oxidative DNA damage induced by UV and visible light. *Carcinogenesis* 18:811–816.
242. Charlier, M. and C. Hélène. 1967. Photosensitized dimerization of orotic acid in aqueous solution. *Photochemistry and Photobiology* 6:501–504.
243. Lamola, A. A. 1970. Triplet photosensitization and the photobiology of thymine dimers in DNA. *Pure and Applied Chemistry* 24:599–610.

244. Lhiaubet, V., N. Paillous, and N. Chouini-Lalanne. 2001. Comparison of DNA damage photoinduced by ketoprofen, fenofibric acid and benzophenone via electron and energy transfer. *Photochemistry and Photobiology* 74:670–678.
245. Lhiaubet-Vallet, V., F. Bosca, and M. A. Miranda. 2009. Photosensitized DNA damage: The case of fluoroquinolones. *Photochemistry and Photobiology* 85:861–868.
246. Lhiaubet-Vallet, V., M. C. Cuquerella, J. V. Castell, F. Bosca, and M. A. Miranda. 2007. Triplet excited fluoroquinolones as mediators for thymine cyclobutane dimer formation in DNA. *Journal of Physical Chemistry B* 111:7409–7414.
247. Traynor, N. J. and N. K. Gibbs. 1999. The phototumorigenic fluoroquinolone lomefloxacin photosensitizes pyrimidine dimer formation in human keratinocytes in vitro. *Photochemistry and Photobiology* 70:957–959.
248. Sauvaigo, S., T. Douki, F. Odin, S. Caillat, J.-L. Ravanat, and J. Cadet. 2001. Analysis of fluoroquinolone-mediated photosensitization of 2′-deoxyguanosine, calf thymus and cellular DNA: Determination of type-I, type-II and triplet-triplet energy transfer mechanism contribution. *Photochemistry and Photobiology* 13:230–237.
249. Trzcionka, J., A. Noirot, P. L. Fabre, and N. Chouini-Lalanne. 2005. Comparative study of the photophysical properties of indoprofen photoproducts in relation with their DNA photosensitizing properties. *Photochemical and Photobiological Sciences* 4:298–303.
250. Lorenzo, F., S. Navaratnam, and N. S. Allen. 2008. Formation of secondary triplet species after excitation of fluoroquinolones in the presence of relatively strong bases. *Journal of the American Chemical Society* 130:12238–12239.
251. Tyrrell, R. M. 1973. Induction of pyrimidine dimers in bacterial DNA by 365 nm radiation. *Photochemistry and Photobiology* 17:69–73.
252. Besaratinia, A., T. W. Synold, H.-H. Chen, C. Chang, B. Xi, A. Riggs, and G. P. Pfeifer. 2005. DNA lesions induced by UV A1 and B radiation in human cells: Comparative analyses in the overall genome and in the *p53* tumor suppressor gene. *Proceedings of the National Academy of Sciences of the United States of America* 102:10058–10063.
253. Freeman, S. E. and S. L. Ryan. 1990. Wavelength dependence for UV-induced pyrimidine dimer formation in DNA of human peripheral blood lymphocytes. *Mutation Research* 235: 181–186.
254. Freeman, S. E., H. Hacham, R. W. Gange, D. J. Maytum, J. C. Sutherland, and B. M. Sutherland. 1989. Wavelength dependence of pyrimidine dimer formation in DNA of human skin irradiated *in situ* with ultraviolet light. *Proceedings of the National Academy of Sciences of the United States of America* 86:5605–5609.
255. Courdavault, S., C. Baudouin, M. Charveron, A. Favier, J. Cadet, and T. Douki. 2004. Larger yield of cyclobutane dimers than 8 oxo-7,8-dihydroguanine in the DNA of UVA-irradiated human skin cells. *Mutation Research* 556:135–142.
256. Kappes, U. P., D. Luo, M. Potter, K. Schulmeister, and T. M. Rünger. 2006. Short- and long-wave light (UVB and UVA) induce similar mutations in human skin cells. *Journal of Investigative Dermatology* 126:667–675.
257. Kappes, U. P. and T. M. Rünger. 2005. No major role of 7,8-dihydro-8-oxo-guanine in ultraviolet light-induced mutagenesis. *Radiation Research* 164:440–445.
258. Rochette, P. J., J.-P. Therrien, R. Drouin, D. Perdiz, N. Bastien, E. A. Drobetsky, and E. Sage. 2003. UVA-induced cyclobutane pyrimidine dimers form predominantly at thymine–thymine dipyrimidines and correlate with the mutation spectrum in rodent cells. *Nucleic Acids Research* 31:2786–2794.
259. Jiang, Y., M. Rabbi, M. Kim, C. H. Ke, W. Lee, R. L. Clark, P. A. Mieczkowski, and P. E. Marszalek. 2009. UVA generates pyrimidine dimers in DNA directly. *Biophysical Journal* 96:1151–1158.
260. Quaite, F. E., B. M. Sutherland, and J. C. Sutherland. 1992. Action spectrum for DNA damage in alfalfa lowers predicted impact of ozone depletion. *Nature* 358:576–578.

261. Schuch, A. P., R. D. Galhardo, K. M. de Lima-Bessa, N. J. Schuch, and C. F. M. Menck. 2009. Development of a DNA-dosimeter system for monitoring the effects of solar-ultraviolet radiation. *Photochemical and Photobiological Sciences* 8:111–120.
262. Kuluncsics, Z., D. Perdiz, E. Brulay, B. Muel, and E. Sage. 1999. Wavelength dependence of ultraviolet-induced DNA damage distribution: Involvement of direct or indirect mechanisms and possible artefacts. *Journal of Photochemistry and Photobiology B: Biology* 49:71–80.
263. Mouret, S., C. Philippe, J. Gracia-Chantegrel, A. Banyasz, S. Karpati, D. Markovitsi, and T. Douki. in press. UVA-induced cyclobutane pyrimidine dimers in DNA: A direct photochemical mechanism? *Organic and Biomolecular Chemistry* 8:1706–1711.
264. Sutherland, J. C. and K. P. Griffin. 1981. Absorption spectrum of DNA for wavelengths greater than 300 nm. *Radiation Research* 86:399–409.
265. Tornaletti, S. 2009. Transcription-coupled DNA repair: Directing your effort where it's most needed. *Cellular and Molecular Life Sciences* 66:1010–1020.
266. Hanawalt, P. C. and G. Spivak. 2008. Transcription-coupled DNA repair: Two decades of progress and surprises. *Nature Reviews Molecular Cell Biology* 9:958–970.
267. Fousteri, M. and L. H. Mullenders. 2008. Transcription-coupled nucleotide excision repair in mammalian cells: Molecular mechanisms and biological effects. *Cell Research* 18:73–84.
268. Gillet, L. C. J. and O. D. Scharer. 2006. Molecular mechanisms of mammalian global genome nucleotide excision repair. *Chemical Reviews* 106:253–276.
269. Kim, J.-K., D. Patel, and B.-S. Choi. 1995. Contrasting structural impacts induced by *cis–syn* cyclobutane dimer and (6-4) adduct in DNA duplex decamers: Implication in mutagenesis and repair activity. *Photochemistry and Photobiology* 62:44–50.
270. Park, H., K. J. Zhang, Y. J. Ren, S. Nadji, N. Sinha, J. S. Taylor, and C. H. Kang. 2002. Crystal structure of a DNA decamer containing a *cis–syn* thymine dimer. *Proceedings of the National Academy of Sciences of the United States of America* 99:15965–15970.
271. Lee, J.-H., G.-S. Hwang, and B.-S. Choi. 1999. Solution structure of a DNA decamer duplex containing the stable 3′ T.G base pair of the pyrimidine (6-4) pyrimidone photoproduct [(6-4) adduct]: Implications for the highly specific 3′ T-C transition of the (6-4) adduct. *Proceedings of the National Academy of Sciences of the United States of America* 96:6632–6636.
272. Mitchell, D. L., C. A. Haipek, and J. M. Clarkson. 1985. (6-4) Photoproducts are removed from the DNA of UV-irradiated mammalian cells more efficiently than cyclobutane pyrimidine dimers. *Mutation Research* 143:109–112.
273. Young, A. R., C. A. Chadwick, G. I. Harrison, J. L. Hawk, O. Nikaido, and C. S. Potten. 1996. The in situ repair kinetics of epidermal thymine dimers and 6-4 photoproducts in human skin types I and II. *Journal of Investigative Dermatology* 106:1307–1313.
274. Bykov, V. J., J. M. Sheehan, K. Hemminki, and A. R. Young. 1999. In situ repair of cyclobutane pyrimidine dimers and 6-4 photoproducts in human skin exposed to solar simulating radiation. *Journal of Investigative Dermatology* 112:326–631.
275. Riou, L., E. Eveno, A. van Hoffen, A. A. van Zeeland, A. Sarasin, and L. H. F. Mullenders. 2004. Differential repair of the two major UV-induced photolesions in trichothiodystrophy fibroblasts. *Cancer Research* 64:889–894.
276. Mouret, S., M. Charveron, A. Favier, J. Cadet, and T. Douki. 2008. Differential repair of UVB-induced cyclobutane pyrimidine dimers in cultured human skin cells and whole human skin. *DNA Repair* 7:704–712.
277. Fitch, M. E., S. Nakajima, A. Yasui, and J. M. Ford. 2003. In vivo recruitment of XPC to UV-induced cyclobutane pyrimidine dimers by the DDB2 gene product. *Journal of Biological Chemistry* 278:46906–46910.
278. Wakasugi, M., A. Kawashima, H. Morioka, S. Linn, A. Sancar, T. Mori, O. Nikaido, and T. Matsunaga. 2002. DDB accumulates at DNA damage sites immediately after UV irradiation and directly stimulates nucleotide excision repair. *Journal of Biological Chemistry* 277:1637–1640.

279. Groisman, R., J. Polanowska, I. Kuraoka, J. Sawada, M. Saijo, R. Drapkin, A. F. Kisselev, K. Tanaka, and Y. Nakatani. 2003. The ubiquitin ligase activity in the DDB2 and CSA complexes is differentially regulated by the COP9 signalosome in response to DNA damage. *Cell* 113:357–367.
280. Goosen, N. and G. F. Moolenaar. 2008. Repair of UV damage in bacteria. *DNA Repair* 7:353–379.
281. Truglio, J. J., D. L. Croteau, B. Van Houten, and C. Kisker. 2006. Prokaryotic nucleotide excision repair: The UvrABC system. *Chemical Reviews* 106:233–252.
282. Deaconescu, A. M., N. Savery, and S. A. Darst. 2007. The bacterial transcription repair coupling factor. *Current Opinion in Structural Biology* 17:96–102.
283. Seawell, P. C., C. A. Smith, and A. K. Ganesan. 1980. Den V gene of bacteriophage T4 determines a DNA glycosylase specific for pyrimidine dimers in DNA. *Journal of Virology* 35:790–796.
284. Lloyd, R. S. 2005. Investigations of pyrimidine dimer glycosylases—A paradigm for DNA base excision repair enzymology. *Mutation Research* 577:77–91.
285. Morikawa, K. and M. Shirakawa. 2000. Three-dimensional structural views of damaged-DNA recognition: T4 endonuclease V, *E-coli* Vsr protein, and human nucleotide excision repair factor XPA. *Mutation Research: DNA Repair* 460:257–275.
286. Hamilton, K. K., P. M. H. Kim, and P. W. Doetsch. 1992. A eukaryotic DNA glycosylase lyase recognizing ultraviolet light-induced pyrimidine dimers. *Nature* 356:725–728.
287. McCready, S. J., F. Osman, and A. Yasui. 2000. Repair of UV damage in the fission yeast *Schizosaccharomyces pombe. Mutation Research* 451:197–210.
288. Yonemasu, R., S. J. McCready, J. M. Murray, F. Osman, M. Takao, K. Yamamoto, A. R. Lehmann, and A. Yasui. 1997. Characterization of the alternative excision repair pathway of UV-damaged DNA in *Schizosaccharomyces pombe. Nucleic Acids Research* 25:1553–1558.
289. Bowman, K. K., K. Sidik, C. A. Smith, J. S. Taylor, P. W. Doetsch, and G. A. Freyer. 1994. A new ATP-independent DNA endonuclease from *Schizosaccharomyces pombe* that recognizes cyclobutane pyrimidine dimers and 6-4-photoproducts. *Nucleic Acids Research* 22:3026–3032.
290. Zharkov, D. O. 2008. Base excision DNA repair. *Cellular and Molecular Life Sciences* 65: 1544–1565.
291. Hegde, M. L., T. K. Hazra, and S. Mitra. 2008. Early steps in the DNA base excision/single-strand interruption repair pathway in mammalian cells. *Cell Research* 18:27–47.
292. Gasparutto, D., E. Muller, S. Boiteux, and J. Cadet. 2009. Excision of the oxidatively formed 5-hydroxyhydantoin and 5-hydroxy-5-methylhydantoin pyrimidine lesions by *Escherichia coli* and *Saccharomyces cerevisiae* DNA *N*-glycosylases. *Biochimica et Biophysica Acta* 1790:16–24.
293. Muller, E., D. Gasparutto, M. Jaquinod, A. Romieu, and J. Cadet. 2000. Chemical and biochemical properties of oligonucleotides that contain (5′S,6S)-cyclo-5,6-dihydro-2′-deoxyuridine and (5′S,6S)-cyclo-5,6-dihydrothymidine, two main radiation-induced degradation products of pyrimidine 2′-deoxyribonucleosides. *Tetrahedron* 56:8689–8701.
294. Gasparutto, D., M. Ait-Abbas, M. Jaquinod, S. Boiteux, and J. Cadet. 2000. Repair and coding properties of 5-hydroxy-5-methylhydantoin nucleosides inserted into DNA oligomers. *Chemical Research in Toxicology* 13:575–584.
295. D'Ham, C., J. L. Ravanat, and J. Cadet. 1998. Gas chromatography mass spectrometry with high-performance liquid chromatography prepurification for monitoring the endonuclease III mediated excision of 5-hydroxy-5,6-dihydrothymine and 5,6-dihydrothymine from gamma-irradiated DNA. *Journal of Chromatography B* 710:67–74.
296. Dizdaroglu, M., J. Laval, and S. Boiteux. 1993. Substrate-specificity of the *Escherichia-coli* endonuclease-III: Excision of thymine-derived and cytosine-derived lesions in DNA produced by radiation-generated free-radicals. *Biochemistry* 32:12105–12111.
297. Asagoshi, K., T. Yamada, H. Terato, Y. Ohyama, Y. Monden, T. Arai, S. Nishimura, H. Aburatani, T. Lindahl, and H. Ide. 2000. Distinct repair activities of human 7,8-dihydro-8 oxoguanine DNA glycosylase and formamidopyrimidine DNA glycosylase for formamidopyrimidine and 7,8-dihydro-8-oxoguanine. *Journal of Biological Chemistry* 275:4956–4964.

298. Girard, P. M., C. D'Ham, J. Cadet, and S. Boiteux. 1998. Opposite base-dependent excision of 7,8-dihydro-8-oxoadenine by the Ogg1 protein of *Saccharomyces cerevisiae*. *Carcinogenesis* 19:1299–1305.
299. Shinmura, K., H. Kasai, A. Sasaki, H. Sugimura, and J. Yokota. 1997. 8-Hydroxyguanine (7,8-dihydro-8-oxoguanine) DNA glycosylase and AP lyase activities of hOGG1 protein and their substrate specificity. *Mutation Research* 385:75–82.
300. Boiteux, S., E. Gajewski, J. Laval, and M. Dizdaroglu. 1992. Substrate-specificity of the *Escherichia coli* fpg protein (formamidopyrimidine DNA glycosylase)—Excision of purine lesions in DNA produced by ionizing-radiation or photosensitization. *Biochemistry* 31:106–110.
301. Tchou, J., H. Kasai, S. Shibutani, M. H. Chung, J. Laval, A. P. Grollman, and S. Nishimura. 1991. 8-Oxoguanine (8-hydroxyguanine) DNA glycosylase and its substrate-specificity. *Proceedings of the National Academy of Sciences of the United States of America* 88:4690–4694.
302. D'Ham, C., A. Romieu, M. Jaquinod, D. Gasparutto, and J. Cadet. 1999. Excision of 5,6-dihydroxy-5,6-dihydrothymine, 5,6-dihydrothymine, and 5-hydroxycytosine from defined sequence oligonucleotides by *Escherichia coli* endonuclease III and Fpg proteins: Kinetic and mechanistic aspects. *Biochemistry* 38:3335–3344.
303. Hatahet, Z., Y. W. Kow, A. A. Purmal, R. P. Cunningham, and S. S. Wallace. 1994. New substrates for old enzymes—5-Hydroxy-2′-deoxycytidine and 5-hydroxy-2′-deoxyuridine are substrates for *Escherichia coli* endonuclease III and formamidopyrimidine DNA *N*-glycosylase, while 5-hydroxy-2′-deoxyuridine is a substrate for uracil DNA *N*-glycosylase. *Journal of Biological Chemistry* 269:18814–18820.
304. Epe, B. 2002. Role of endogenous oxidative DNA damage in carcinogenesis: What can we learn from repair-deficient mice? *Biological Chemistry* 383:467–475.
305. Osterod, M., S. Hollenbach, J. G. Hengstler, D. E. Barnes, T. Lindahl, and B. Epe. 2001. Age-related and tissue-specific accumulation of oxidative DNA base damage in 7,8-dihydro-8-oxoguanine-DNA glycosylase (Ogg1) deficient mice. *Carcinogenesis* 22:1459–1463.
306. Klungland, A., I. Rosewell, S. Hollenbach, E. Larsen, G. Daly, B. Epe, E. Seeberg, T. Lindahl, and D. E. Barnes. 1999. Accumulation of premutagenic DNA lesions in mice defective in removal of oxidative base damage. *Proceedings of the National Academy of Sciences of the United States of America* 96:13300–13305.
307. Lu, A. L., H. B. Bai, G. L. Shi, and D. Y. Chang. 2006. MutY and MutY homologs (MYH) in genome maintenance. *Frontiers in Bioscience* 11:3062–3080.
308. Haghdoost, S., L. Sjolander, S. Czene, and M. Hanns-Ringdahl. 2006. The nucleotide pool is a significant target for oxidative stress. *Free Radical Biology and Medicine* 41:620–626.
309. Denver, D. R., S. L. Swenson, and M. Lynch. 2003. An evolutionary analysis of the helix-hairpin-helix superfamily of DNA repair glycosylases. *Molecular Biology and Evolution* 20:1603–1611.
310. Zharkov, D. O., G. Shoham, and A. P. Grollman. 2003. Structural characterization of the Fpg family of DNA glycosylases. *DNA Repair* 2:839–862.
311. Cao, C. Y., Y. L. Jiang, J. T. Stivers, and F. H. Song. 2004. Dynamic opening of DNA during the enzymatic search for a damaged base. *Nature Structural & Molecular Biology* 11:1230–1236.
312. Fortini, P., B. Pascucci, E. Parlanti, R. W. Sobol, S. H. Wilson, and E. Dogliotti. 1998. Different DNA polymerases are involved in the short- and long-patch base excision repair in mammalian cells. *Biochemistry* 37:3575–3580.
313. Wiederhold, L., J. B. Leppard, P. Kedar, F. Karimi-Busheri, A. Rasouli-Nia, M. Weinfeld, A. E. Tomkinson, T. Izumi, R. Prasad, S. H. Wilson, S. Mitra, and T. K. Hazra. 2004. AP endonuclease-independent DNA base excision repair in human cells. *Molecular Cell* 15:209–220.
314. Ranalli, T. A., S. Tom, and R. A. Bambara. 2002. AP endonuclease 1 coordinates flap endonuclease 1 and DNA ligase I activity in long patch base excision repair. *Journal of Biological Chemistry* 277:41715–41724.
315. Klungland, A. and T. Lindahl. 1997. Second pathway for completion of human DNA base excision-repair: Reconstitution with purified proteins and requirement for DNase IV (FEN1). *EMBO Journal* 16:3341–3348.

316. Caldecott, K. W. 2008. Single-strand break repair and genetic disease. *Nature Reviews Genetics* 9:619–631.
317. Wilson, D. M. 2007. Processing of nonconventional DNA strand break ends. *Environmental and Molecular Mutagenesis* 48:772–782.
318. Sung, J. S. and B. Demple. 2006. Roles of base excision repair subpathways in correcting oxidized abasic sites in DNA. *Febs Journal* 273:1620–1629.
319. Sung, J. S., M. S. DeMott, and B. Demple. 2005. Long-patch base excision DNA repair of 2-deoxyribonolactone prevents the formation of DNA–protein cross-links with DNA polymerase beta. *Journal of Biological Chemistry* 280:39095–39103.
320. Horton, J. K., M. Watson, D. F. Stefanick, D. T. Shaughnessy, J. A. Taylor, and S. H. Wilson. 2008. XRCC1 and DNA polymerase beta in cellular protection against cytotoxic DNA single-strand breaks. *Cell Research* 18:48–63.
321. Caldecott, K. W. 2003. XRCC1 and DNA strand break repair. *DNA Repair* 2:955–969.
322. Huber, A., P. Bai, J. M. de Murcia, and G. de Murcia. 2004. PARP-1, PARP-2 and ATM in the DNA damage response: Functional synergy in mouse development. *DNA Repair* 3:1103–1108.
323. Sancar, A. 2008. Structure and function of photolyase and in vivo enzymology: 50th anniversary. *Journal of Biological Chemistry* 283:32153–32157.
324. Essen, L. O. and T. Klar. 2006. Light-driven DNA repair by photolyases. *Cellular and Molecular Life Sciences* 63:1266–1277.
325. Kimura, S. and K. Sakaguchi. 2006. DNA repair in plants. *Chemical Reviews* 106:753–766.
326. Weber, S. 2005. Light-driven enzymatic catalysis of DNA repair: A review of recent biophysical studies on photolyase. *Biochimica et Biophysica Acta* 1707:1–23.
327. Kao, Y. T., C. Saxena, L. J. Wang, A. Sancar, and D. P. Zhong. 2007. Femtochemistry in enzyme catalysis: DNA photolyase. *Cell Biochemistry and Biophysics* 48:32–44.
328. Byrdin, M., A. P. M. Eker, M. H. Vos, and K. Brettel. 2003. Dissection of the triple tryptophan electron transfer chain in *Escherichia coli* DNA photolyase: Trp382 is the primary donor in photoactivation. *Proceedings of the National Academy of Sciences of the United States of America* 100:8676–8681.
329. Aubert, C., M. H. Vos, P. Mathis, A. P. M. Eker, and K. Brettel. 2000. Intraprotein radical transfer during photoactivation of DNA photolyase. *Nature* 405:586–590.
330. MacFarlane, A. W. and R. J. Stanley. 2003. *Cis–syn* thymidine dimer repair by DNA photolyase in real time. *Biochemistry* 42:8558–8568.
331. Kim, S. T., P. F. Heelis, and A. Sancar. 1992. Energy-transfer (deazaflavin -> FADH2) and electron-transfer ($FADH_2$ -> T<>T) kinetics in *Anacystis nidulans* photolyase. *Biochemistry* 31:11244–11248.
332. Kim, S. T., P. F. Heelis, T. Okamura, Y. Hirata, N. Mataga, and A. Sancar. 1991. Determination of rates and yields of interchromophore (folate->flavin) energy-transfer and intermolecular (flavin->DNA) electron-transfer in *Escherichia coli* photolyase by time-resolved fluorescence and absorption-spectroscopy. *Biochemistry* 30:11262–11270.
333. Todo, T., H. Ryo, A. Borden, C. Lawrence, K. Sakaguchi, H. Hirata, and T. Nomura. 1997. Non-mutagenic repair of (6-4) photoproducts by (6-4) photolyase purified from *Drosophila melanogaster*. *Mutation Research* 385:83–93.
334. Kim, S. T., K. Malhotra, J. S. Taylor, and A. Sancar. 1996. Purification and partial characterization of (6-4) photoproduct DNA photolyase from *Xenopus laevis*. *Photochemistry and Photobiology* 63:292–295.
335. Kim, S. T., K. Malhotra, C. A. Smith, J. S. Taylor, and A. Sancar. 1994. Characterization of (6-4)-photoproduct DNA photolyase. *Journal of Biological Chemistry* 269:8535–8540.
336. Asgatay, S., C. Petermann, D. Harakat, D. Guillaume, J. S. Taylor, and P. Clivio. 2008. Evidence that the (6-4) photolyase mechanism can proceed through an oxetane intermediate. *Journal of the American Chemical Society* 130:12618–12619.
337. Borg, O. A., L. A. Eriksson, and B. Durbeej. 2007. Electron-transfer induced repair of 6-4 photoproducts in DNA: A computational study. *Journal of Physical Chemistry A* 111:2351–2361.

338. Song, Q. H. H., X. M. Hei, Z. X. Xu, X. Zhang, and Q. X. Guo. 2003. Model studies of the (6-4) photoproduct photoreactivation: Synthesis and photosensitized splitting of uracil oxetane adducts. *Bioorganic Chemistry* 31:357–366.
339. Zhao, X. D., J. Q. Liu, D. S. Hsu, S. Y. Zhao, J. S. Taylor, and A. Sancar. 1997. Reaction mechanism of (6-4) photolyase. *Journal of Biological Chemistry* 272:32580–32590.
340. Hitomi, K., H. Nakamura, S. T. Kim, T. Mizukoshi, T. Ishikawa, S. Iwai, and T. Todo. 2001. Role of two histidines in the (6-4) photolyase reaction. *Journal of Biological Chemistry* 276:10103–10109.
341. Slieman, T. A., R. Rebeil, and W. L. Nicholson. 2000. Spore photoproduct (SP) lyase from *Bacillus subtilis* specifically binds to and cleaves SP (5-thyminyl-5,6-dihydrothymine) but not cyclobutane pyrimidine dimers in UV-irradiated DNA. *Journal of Bacteriology* 182:6412–6417.
342. Rebeil, R., Y. B. Sun, L. Chooback, M. Pedraza-Reyes, C. Kinsland, T. P. Begley, and W. L. Nicholson. 1998. Spore photoproduct lyase from *Bacillus subtilis* spores is a novel iron-sulfur DNA repair enzyme which shares features with proteins such as class III anaerobic ribonucleotide reductases and pyruvate-formate lyases. *Journal of Bacteriology* 180:4879–4885.
343. Fajardo-Cavazos, P., C. Salazar, and W. L. Nicholson. 1993. Molecular-cloning and characterization of the *Bacillus subtilis* spore photoproduct lyase (SPL) gene, which is involved in repair of UV radiation-induced DNA damage during spore germination. *Journal of Bacteriology* 175:1735–1744.
344. Rebeil, R. and W. L. Nicholson. 2001. The subunit structure and catalytic mechanism of the *Bacillus subtilis* DNA repair enzyme spore photoproduct lyase. *Proceedings of the National Academy of Sciences of the United States of America* 98:9038–9043.
345. Cheek, J. and J. B. Broderick. 2001. Adenosylmethionine-dependent iron-sulfur enzymes: Versatile clusters in a radical new role. *Journal of Biological Inorganic Chemistry* 6:209–226.
346. Cheek, J. and J. B. Broderick. 2002. Direct H atom abstraction from spore photoproduct C-6 initiates DNA repair in the reaction catalyzed by spore photoproduct lyase: Evidence for a reversibly generated adenosyl radical intermediate. *Journal of the American Chemical Society* 124:2860–2861.
347. Chandor-Proust, A., O. Berteau, T. Douki, D. Gasparutto, S. Ollagnier-De-Choudens, M. Fontecave, and M. Atta. 2008. DNA repair and free radicals, new insights into the mechanism of spore photoproduct lyase revealed by single amino acid substitution. *Journal of Biological Chemistry* 283:36361–36368.
348. Fajardo-Cavazos, P., R. Rebeil, and W. L. Nicholson. 2005. Essential cysteine residues in *Bacillus subtilis* spore photoproduct lyase identified by alanine scanning mutagenesis. *Current Microbiology* 51:331–335.
349. Friedel, M. G., O. Berteau, J. C. Pieck, M. Atta, S. Ollagnier-de-Choudens, M. Fontecave, and T. Carell. 2006. The spore photoproduct lyase repairs the 5S- and not the 5R-configured spore photoproduct DNA lesion. *Chemical Communications* 445–447.
350. Chandor, A., O. Berteau, T. Douki, D. Gasparutto, Y. Sanakis, S. Ollagnier-De-Choudens, M. Atta, and M. Fontecave. 2006. Dinucleotide spore photoproduct, a minimal substrate of the DNA repair spore photoproduct lyase enzyme from *Bacillus subtilis*. *Journal of Biological Chemistry* 281:26922–26931.
351. Chandra, T., S. C. Silver, E. Zilinskas, E. M. Shepard, W. E. Broderick, and J. B. Broderick. 2009. Spore photoproduct lyase catalyzes specific repair of the 5R but not the 5S spore photoproduct. *Journal of the American Chemical Society* 131:2420–2421.

58

The Biology of UVA Radiation

Rex M. Tyrrell
University of Bath

Evelyne Sage
Institut Curie-Centre de Recherche

58.1 Introduction

Even though there is a continuum of energies in the electromagnetic spectrum of radiations, the ultraviolet (UV) has been divided into UVC (below 290 nm, nonsolar), UVB (290–315 nm), and UVA (315–400 nm) for categorizing the main effects of solar exposure on human skin. Wavelengths below 290 nm are blocked by the stratospheric ozone. These wavelengths are of the highest energies (>4.4 eV) and coincide with maximal absorption by DNA and other biomolecules, and would be extremely damaging to genetic material and biological tissues in general if they reached the surface of the earth. The stratospheric ozone layer therefore protects life from UVC radiation, also called abiotic radiation.

Longer wavelength UVB ($\lambda >$ than approximately 290 nm) penetrates the ozone layer and constitutes about 5%–10% of the terrestrial solar UV radiation. It is absorbed by nucleic acids and has the ability to directly cause genotoxic damage to DNA and ultimately skin cancer. For many years, biologically nonrelevant UVC and, later, UVB focused most of the efforts of photobiologists to understand the phenomena underlying skin carcinogenesis. Although UVA radiation had been recognized as a powerful oxidant (Tyrrell 1991), wavelengths in this range had received relatively little attention until the 1990s, although they are by far the most abundant solar UV radiation that reaches the surface of the earth and they penetrate human skin more effectively than UVB.

Once thought to be relatively innocuous, UVA is now known as a damaging agent for DNA, proteins, and lipids, with harmful consequences that include skin aging and particularly carcinogenesis. In addition to these damaging effects, UVA is known to dramatically influence signal transduction and

thereby modify a myriad of cellular functions including cell death pathways through alterations in gene expression. While these may contribute to the deleterious effects of UVA such as preventing apoptosis of cancer cells or enhancing metastasis by increased metalloproteinase activity, they are not necessarily harmful and it is clear that UVA also has a potential protective role (reviewed recently by Tyrrell and Reeve 2006). UVA is also the basis for several types of therapy of diseases including atopic dermatitis and lupus erythematosus (see Krutmann 1998) where selective destruction of T helper cells has been postulated as an underlying mechanism. The purpose of this review is to provide a picture of the multiple and often opposing effects of UVA with particular focus on the explosion of studies in the last decade. We provide a synthetic view on DNA damage, inspect the numerous contradictory studies on UVA mutation spectra, and discuss recent advances in our understanding of the relevance of UVA effects on solar mutagenesis and skin cancer. Emphasis will also be placed on the potential role of protein damage on UVA effects. However, we will also consider how UVA can disrupt iron and heme homeostasis, alter cell cycle, and generate powerful signaling intermediates with dramatic effects on the balance of gene expression and biological outcomes. Not all aspects of UVA photobiology will be covered by the review. Mechanistic aspects of DNA damage (including that induced by UVA) will be considered by Douki (Chapter 57) elsewhere in this volume as will the crucial area of photoimmunology covered by Reeve (Chapter 63). The cellular and molecular responses to UVA in relation to skin carcinogenesis have recently been reviewed by Ridley et al. (2009). Given the oxidative nature of UVA damage, a very large literature has now emerged on agents that protect against UVA effects such as flavonoids and carotenoids, and a description of these many protective studies is beyond the scope of the current review.

Finally, we sound an obvious but sometimes overlooked note of warning when considering the UVA literature. Wavelengths shorter than 320 nm (i.e., not UVA) can have effects several orders of magnitude greater than those observed following irradiation at UVA wavelengths. For example, pyrimidine dimers are induced a 1000 times more efficiently at narrowband 313 nm radiation than at narrowband 365 nm radiation. Most studies employ broadband UVA sources for convenience and low cost. Short wavelengths that contaminate such sources have the potential to totally distort observations. We have tried to exclude work where we are aware that this is the case.

58.2 Chromophores

The biologically relevant cellular chromophore(s) that absorb UVA to generate reactive oxygen species (ROS) remain(s) a matter of debate. The photodynamic properties of porphyrins make them key candidates for generation of singlet oxygen. Of these, protoporphyrin IX, the immediate precursor to heme and a very strong photodynamic agent, merits particular consideration (Watkin and Tyrrell 2000). Other possible chromophores for UVA-generated ROS have been described by Wondrak et al. (2004, 2006) and include evidence for a role of 3-hydroxypyridine derivatives arising from a range of molecules occurring in skin (e.g., enzymatic collagen cross-links).

Baier et al. (2006) have studied singlet oxygen generation by time-resolved luminescence measurements at 1270 nm in various candidates and shown that UVA generates higher yields of singlet oxygen from riboflavin and flavin mononucleotide than from exogenous photosensitizers such as Photophrin. Beta-nicotinamide adenine dinucleotide and its phosphate (NADP) as well as cholesterol showed very low to undetectable levels of UVA-induced singlet oxygen.

58.3 UVA as an Oxidative Stress

Observations nearly 100 years ago demonstrated that UVA radiation inactivated enzymes such as amylase, catalase, trypsin, and tyrosinase and that the damage occurred in an oxygen-dependent fashion. Pioneering studies by Webb and co-workers (e.g., Webb and Lorenz 1970) demonstrated that the bacterium, *Escherichia coli*, showed a clear oxygen dependence for UVA inactivation and studies followed in several

microorganisms (reviewed in Tyrrell 1991) and in human cells (Danpure and Tyrrell 1976) where the oxygen dependence of inactivation of colony-forming ability was even more marked.

Work from several laboratories using components of cells *in vitro* demonstrated that UVA radiation at relevant fluences had the potential to generate various ROS in cells, and this, together with evidence for the oxygen dependence of most UVA-mediated biological events, provided the basis for concluding that UVA would generate a strong oxidative stress in cells and tissue (reviewed by Tyrrell 1991). Experiments with human fibroblasts demonstrated that reduction in the major source of cellular reducing equivalents (reduced glutathione) dramatically enhanced UVA-mediated events such as cell death (Tyrrell and Pidoux 1986) and gene activation (Lautier et al. 1992). Similarly, very strong evidence accumulated that singlet oxygen was the major ROS that mediated both UVA-induced cell death (Tyrrell and Pidoux 1989) and gene activation (Basu-Modak and Tyrrell 1993). Although this was first demonstrated with the heme oxygenase 1 (HO-1) gene, studies with other UVA-inducible genes reported a similar dependence (for reviews see Tyrrell 1996a; Grether-Beck et al. 1997). Many subsequent studies demonstrated the role of this species in UVA-mediated signaling (Ryter and Tyrrell 1998) so that UVA-generated singlet oxygen is now generally accepted as a primary signaling messenger.

More recently, Valencia and Kochevar (2008) have shown that nicotinamide adenine dinucleotide phosphate (NADPH) oxidase, an enzyme activated by UVA radiation, is a major source of ROS in human keratinocytes and that the generation of such ROS initiates rapid prostaglandin E2 (PGE2) synthesis. Importantly, these authors showed that knockout of the oxidase (*Nox1*) gene function completely prevents generation of these intermediates. In related studies comparing normal primary keratinocytes with cells knocked out for phagocyte oxidase (PHOX), He et al. (2005) concluded that the PHOX played only a limited role in both the induction of ROS and the increased apoptosis that follows UVA irradiation.

ROS have been measured in the skin of hairless rats (Yasui and Sakurai 2003) and in the stratum corneum of human skin after UVA (Herrling et al. 2003; Ou-Yang et al. 2004) (electron spin resonance [ESR] of nitroxides) with some evidence of ROS generation in deeper layers. Jain et al. (2010) have complemented these studies of the UVA radiation-induced chemiluminescence of human skin *in vivo* by following the decay characteristics of UVA-induced photon emission caused by different radiation doses.

In addition to the production of ROS, UVA radiation can influence the levels of pro-oxidant catalysts, particularly iron and heme (for reviews see Ryter and Tyrrell 2000; Tyrrell 2005). Iron plays a catalytic role via Fenton chemistry as a result of which peroxide is generated in cells, and although iron is not involved in the initial step of lipid peroxidation, it can play a catalytic role in the lipid peroxidation chain reaction. Reflecting these observations, there have been numerous examples where modulating free cellular iron levels by iron chelation has led to modulation of UVA-mediated effects (Tyrrell 2005). Importantly, a study by Pourzand et al. (1999) has shown that low-dose irradiation of human skin fibroblasts with UVA can increase the levels of labile iron in these cells by severalfold. This appears to result from UVA damage to the lysosomal membranes. Subsequent studies have confirmed these findings and shown that free iron is also increased in other skin cell types following UVA (Basu-Modak et al. 2006) and further implicated iron in necrotic cell death (Zhong et al. 2004).

Bystander effects whereby treatment of cells with a particular agent can lead to effects in untreated cells are well known in radiation biology. UVA radiation generally leads to an increase in excreted soluble cytokines, which may have effects including autocrine effects on other cells in the vicinity such as terms of gene activation, etc. For example, a recent study (An et al. 2010) showed that tumor necrosis factor (TNF)-alpha, interleukin (IL)-1 beta, and IL-10 were all upregulated in a c-Jun N-terminal kinase (JNK)-dependent pathway by UVA in cultured human keratinocyte (HaCaT) cells. On the other hand, Smit et al. (2009) observed that UVA inhibited calcineurin (Cn) in skin and skin cells as well as Jurkat cells and peripheral blood mononuclear cell (PBMC). In the latter two cell types, UVA also reduced the production of cytokines such as IL-2, gamma-interferon, IL-4, and IL-10 that are controlled by the Ca(2+)–Cn pathway. Although UVA irradiation has been reported to lead to release of histamine from human basophils (Monfrecola et al. 2003), other studies (Krönauer et al. 2001, 2003) indicated that UVA inhibits histamine release elicited by a variety of stimulants. UVA radiation has also been shown to decrease both basal and

cytokine-stimulated chemokine production in the specific case of the thymus and activation-regulated cytokine (TARC) in HaCaT cells (Zheng et al. 2003). All these factors may lead to effects on surrounding cells. However, long-lived ROS have received particular attention as agents of bystander effects. For example, UVA induces elevated mutation rates for several generations following UVA radiation by a proposed bystander effect, which can be abrogated by glutathione (Dahle et al. 2005a). In a classical bystander experiment by Whiteside and McMillan (2009), populations of keratinocytes (HaCaT) and fibroblasts (MRC5) were separated by a medium-permeable insert, and it was demonstrated that UVA (but not UVB) irradiation of one population leads to lethal damage in the untreated population.

Free heme can also play a catalytic role in the appropriate cellular environment and is a major UVA-absorbing chromophore. It has been known for some time that UVA can damage heme-containing proteins (e.g., catalase), and Kvam et al. (2000) have shown that following UVA damage to cells, free heme is released. The release of both labile iron and free heme by UVA radiation will further amplify the oxidative stress engendered by direct production of ROS.

58.4 UVA as a Damaging Agent

58.4.1 DNA Damage

Unlike UVB, the UVA component of solar radiation is very weakly absorbed by DNA (Sutherland and Griffin 1981) and acts by exciting other endogenous chromophores to generate ROS. Consequently, for many years, UVA was believed to generate mostly oxidative DNA damage. Indeed, Peak and Peak (1990) reported an induction of single-strand breaks (SSBs) by UVA, mediated by H_2O_2. In the 1990s, new and sensitive methods became available for the detection and measurement of various types of DNA lesions, for example, comet assays, commercially available specific antibodies and DNA repair enzymes, high performance liquid chromatography (HPLC) coupled with electrochemical detection to reveal 8-oxoguanine (8-oxoG), and more recently HPLC coupled with tandem mass spectrometry. This has led to new measurements of UVA-induced DNA damage.

58.4.1.1 UVA Induces Oxidative DNA Damage in Mammalian Cells

It is well established that UVA promotes photosensitization of DNA, triggered by singlet oxygen (type II photosensitization), electron abstraction (type I photosensitization), or hydroxyl radicals. The use of specific DNA repair proteins helped considerably in investigations of the different types of DNA lesions thus generated. The *E. coli* Fpg and *N*th proteins served to reveal oxidation products of purine (mainly 8-oxoG) and pyrimidine, respectively, and Nfo protein abasic sites. The additional breaks generated by the enzymes at the damaged sites were quantified by comet assay, alkaline elution, or alkaline gel electrophoresis. The 8-oxoG was more specifically measured by HPLC coupled with electrochemical detection. It has been shown that UVA radiation induces SSBs, oxidized pyrimidine, and oxidized purines in various mammalian cells (Zhang et al. 1997; Kvam and Tyrrell 1997; Douki et al. 1999; Besaratinia et al. 2005, 2008; Javeri et al. 2008), and that the most abundant oxidative DNA damage produced is 8-oxoG (Kielbassa et al. 1997; Pouget et al. 2000; Douki et al. 2003). The ratio SSB:oxidized pyrimidine:oxidized purine/8-oxoG is about 1:1:3. The low amounts of SSB and oxidized pyrimidines likely produced by hydroxyl radicals originated from the Fenton reaction and the predominance of 8-oxoG indicate a major contribution of singlet oxygen in the formation of oxidative DNA damage in cells by UVA (Cadet et al. 2009). Importantly, the human DNA *N*-glycosylase OGG1, which clears 8-oxoG, appears to be expressed more abundantly in the superficial than the basal layer of human skin (Javeri et al. 2008). This may lead to a lack of repair in the basal cells of the epidermis and therefore to accumulation of mutations due to 8-oxoG.

58.4.1.2 UVA Induces the Formation of Bipyrimidine Photoproducts in Mammalian Cells

Cyclobutane pyrimidine dimers (CPDs), pyrimidine (6-4) pyrimidone photoproducts (6-4PPs), and their Dewar valence isomers are produced by direct absorption of UVC or UVB radiation by DNA.

The inability of DNA to readily absorb in the UVA range means that these photoproducts are not expected to be formed by UVA. In fact, the first observation on CPDs induction by very pure narrowband 365 nm UVA was made by Tyrrell (1973) in bacteria. The quantum yield was 7×10^5 less at 365 nm than at 254 nm and the longer wavelength radiation induced predominantly thymine dimers, whereas at the shorter wavelength CPDs were induced in the ratio 5:4:1 (TT:CT:CC). CPDs were also observed in mammalian cells and human skin but it was a matter of debate because, unlike the original studies in bacteria, the protocols did not involve rigorous exclusion of short wavelengths (Enninga et al. 1986; Freeman et al. 1989; Hacham et al. 1990). In the late 1990s, the formation of CPDs by UVA has been reassessed in various laboratories with the help of more sensitive methods. Using denV protein from T4 phage to reveal CPDs or specific antibodies, CPDs were detected in mammalian cells, including in human skin (Chadwick et al. 1995; Kielbassa et al. 1997; Zhang et al. 1997; Young et al. 1998; Douki et al. 1999; Ley and Fourtanier 2000; Perdiz et al. 2000; Douki et al. 2003; Rochette et al. 2003; Courdavault et al. 2004; Besaratinia et al. 2005; Mouret et al. 2006). The yield of CPD formation by UVA is low in comparison to that produced by UVC or UVB. This may explain why cells from *xeroderma pigmentosum* patients who cannot repair bipyrimidine photoproducts and are thus extremely sensitive to sunlight and skin cancer, are not highly sensitive to UVA. Perdiz et al. (2000) found that CPDs were produced 10^3- and 10^5-fold less efficiently by UVA than by UVB and UVC, respectively. In addition, (6-4) photoproducts were barely detected after UVA (trace amount; Perdiz et al. 2000). Such yields of CPDs formation are in good agreement with the DNA absorption spectrum by Sutherland and Griffin (1981). Therefore, Perdiz et al. (2000) concluded that CPD formation by UVA could be compatible with direct absorption by DNA.

The formation of CPDs and 6-4PP can be analyzed with nucleotide resolution, either on the bulk DNA by HPLC–tandem mass spectroscopy (MS/MS) or at the gene level by ligation-mediated polymerase chain reaction (LM-PCR). In agreement with the original studies in bacteria (Tyrrell 1973) comparing induction at 365 and 254 nm, the distribution of CPDs induced by UVA drastically differs from that produced by UVC, UVB, or simulated sunlight. UVA-induced CPDs were predominantly formed at TT sites, while those produced at CC sites were poorly represented (Rochette et al. 2003). HPLC–MS/MS also revealed a predominance for TT CPDs over CT and TC CPDs, whereas CC CPDs and 6-4PPs were not detected (Douki et al. 2003; Mouret et al. 2006). The principal induction of CPDs at T-containing bipyrimidine sites, and mostly at TT sites, is similar to that observed when DNA was damaged by a photosensitization reaction with aromatic ketones (Lamola 1968; Charlier and Helene 1972). These data are consistent with an alternative hypothesis that most CPDs are formed through triplet energy transfer from photosensitizer to excited thymine which, in fact, has the lowest triplet state energy with regard to other bases. The hypothetical UVA-absorbing chromophore tightly bound to DNA to allow energy transfer remains to be identified.

58.4.1.3 CPDs May Be the Major DNA Lesions Induced by UVA in Mammalian Cells and Human Skin

Using the same method to measure 8-oxoG and CPDs in the same samples, either HPLC:MS/MS or DNA repair enzymes and alkaline agarose gel, it was shown that CPDs were roughly three times more efficiently produced than 8-oxoG. In skin biopsies, this ratio may vary depending on the donor (Douki et al. 1999, 2003; Courdavault et al. 2004; Mouret et al. 2006). The sensitivity of most DNA lesion detection methods requires high UVA dose exposure (above 750 kJm^{-2}). Nevertheless, CPDs have also been measured at environmentally relevant UVA doses (as low as 40 kJm^{-2}), and their formation increases linearly with dose (Sage and Douki unpublished). A conflicting publication (Besaratinia et al. 2008) claims a predominance of 8-oxoG lesion induction by UVA. This discrepancy can be partly explained by the use of less sensitive methods by the latter workers and the use of different irradiation conditions. Interestingly, in the yeast *Saccharomyces cerevisiae*, 8-oxoG is by far the major lesion produced by UVA, as revealed by mutation analysis of DNA repair mutants and alkaline agarose gel analysis (Kozmin et al. 2005).

58.4.1.4 Distribution of Damage Induced by UVA Is Similar in Plasmid/Isolated DNA and in Cells

A similar distribution of damaged induced by UVA in isolated DNA and cells was shown using various DNA repair enzymes (Kielbassa et al. 1997; Kuluncsics et al. 1999; Pouget et al. 2000; Douki et al. 2003; Jiang et al. 2009; Schuch et al. 2009) and more recently HPLC:MS/MS (Mouret et al. 2010). However, UVA irradiation of plasmid DNA should not lead to photosensitization reactions. This raises the question of the mechanism of DNA damage by UVA, and in particular that of CPDs formation. In addition, Schuch et al. clearly demonstrated that UVA radiation is able to induce 6-4PPs in plasmid DNA. However, 6-4PPs cannot be formed by photosensitization and are only produced by direct absorption. Thus, it could well be that in cells, the low energy of UVA photons is sufficient to directly excite DNA with subsequent formation of bipyrimidine photoproducts, both CPDs and 6-4PPs, yet at low level, whereas 8-oxoG is essentially formed by a photosensitization reaction mediated by singlet oxygen.

58.4.1.5 Does UVA Induce Other Types of DNA Lesions?

UVA is able to photoisomerize 6-4PPs produced by UVB in simulated sunlight into Dewar photoproducts (Perdiz et al. 2000; Douki et al. 2003). This is consistent with the observation that Dewar photoproducts are more frequently produced by natural and simulated sunlight, than by UVB, and conversely, the ratio 6-4PP to Dewar photoproduct is higher for UVB (Clingen et al. 1995; Perdiz et al. 2000). DNA–protein cross-links are expected to be produced by ROS and, indeed, have been reported to be formed upon UVA irradiation, even more efficiently than by ionizing radiation (Peak and Peak 1991; Arai et al. 2000). SSBs are induced in bacterial DNA by narrowband 365 nm radiation at yields approximately half that of CPDs, and the induction is totally dependent on the presence of oxygen (Tyrrell et al. 1974). Since DNA double-strand breaks (DSBs) are considered among the most deleterious DNA lesions, the question arose whether UVA induces DSBs, either directly or through processing of other types of DNA damage, such as at replication forks stalled at DNA photoproducts. DNA DSBs, revealed by neutral comet assay or γ-H2AX foci (phosphorylated H2AX variant histone), are not readily produced in human transformed fibroblasts or keratinocytes by direct UVA irradiation, but arise at low levels during the processing of DNA lesions (Girard et al. 2008; Wischermann et al. 2008). Long-lasting DSB may be responsible for the appearance of micronuclei and chromosomal aberrations in human HaCaT transformed keratinocytes (Wischermann et al. 2008). Interestingly, low doses of UVA induce ROS-mediated slowdown of DNA replication independently of cell cycle checkpoint activation and from the main DNA lesions such as CPDs, 8-oxoG, or delayed DSB (Girard et al. 2008). There may be biologically relevant DNA damage produced by UVA yet to discover.

58.4.2 Mutagenesis and Cancer

58.4.2.1 UVA Induces Mutations in Cultured Mammalian Cells

After long debate on whether or not UVA promotes the formation of bipyrimidine photoproducts, it is now recognized that the two major known photolesions induced by UVA radiation are 8-oxoG and CPDs, the ratio of which presumably depends on irradiation conditions, cell and skin types, and individuals. The UVB mutational signature, found in a large majority of nonmelanoma skin tumors, has been well established as C to T transitions at bipyrimidine sites and tandem CC to TT mutations (Brash et al. 1991), mostly mediated by CPDs in repair-proficient cells/individuals (Pfeifer et al. 2005). However, the relative contribution of bipyrimidine photoproducts or 8-oxoG to the mutagenic and cytotoxic effects of UVA exposure remains a topic of active debate. Moreover, the relative contribution of UVA radiation to solar mutagenesis and carcinogenesis is still an open question. The following reviews the types of mutations that have been reported to be induced by UVA over the last 15 years, with respect to the different DNA lesions induced and their repair rate (see the review by Rünger and Kappes (2008) for detailed discussion).

A first general observation from most of the studies is that UVA radiation is weakly mutagenic at environmentally relevant doses, while it is cytotoxic, in mammalian cells as well as in yeast and *Drosophila* larvae (Drobetsky et al. 1995; Negishi et al. 2001; Kozmin et al. 2005; Kim et al. 2007; Besaratinia et al. 2008). It has clearly been demonstrated in yeast that the cytotoxicity of UVA does not depend on DNA damage (Kozmin et al. 2005), but rather on damage to other constituents, particularly membrane lipids.

The first comprehensive work on mutagenesis induced by solar UV radiation of different wavelengths including the UVA range was by Drobetsky et al. (1995) in Chinese hamster ovary cells. It revealed that the UVA-induced mutation spectrum is dominated by AT to CG transversions, which, in fact, correlate with sites of UVA-induced TT CPDs (Rochette et al. 2003). However, such mutations could also be caused by incorporation of 8oxodGTP (from dNTP pool oxidized by UVA) opposite adenine by replicative DNA polymerase, or by another unknown process. The relative induction of C to T transitions is lower for UVA, in comparison with UVB or simulated sunlight, but their distribution is identical for the three radiation types and correlates well with sites of induced C-containing CPDs (Rochette et al. 2003). In the absence of repair of bipyrimidine photoproducts (in nucleotide excision repair-deficient cells), the mutation frequency is greatly increased (sevenfold) and the spectrum is largely dominated by C to T transitions after UVA (Sage et al. 1996). On the other hand, the G to T transversions, the so-called hallmark of 8-oxoG, represent no more than 4% of the total UVA-induced mutations. Among point mutations generated by UVA in an episomal plasmid transfected in transformed human embryonic kidney cells, C to T transitions are the predominant events, and mutations at AT base pairs are increased in comparison with UVB, whereas G to T mutations are barely recovered (Robert et al. 1996). The $OGG1^{-/-}$ mouse embryonic fibroblasts, that are unable to repair 8-oxoG, did not exhibit an increase in mutation induction in comparison with the $OGG1^{+/+}$ counterpart, after exposure to UVA or UVB (Kappes and Rünger 2005). Kappes et al. (2006) observed that in cultured primary human fibroblasts, UVA, like UVB, primarily induces C to T transitions at bipyrimidine sites. Interestingly, they also noticed that at similar cellular growth inhibition doses, UVA is more mutagenic than UVB in these skin cells. Since UVA also induced a much weaker and short-lived activation of p53 protein than UVB, the authors proposed that DNA damage induced in low amount by UVA relative to UVB does not elicit an effective protective response in human skin cells. Altogether, this series of data is not consistent with a prominent role for 8-oxoG in UVA-induced mutagenesis, but rather indicates CPDs as the culprit.

Pfeifer and collaborators (Besaratinia et al. 2005, 2008; Kim et al. 2007) using Big Blue mouse embryonic fibroblasts claim that promutagenic oxidative DNA damage, namely 8-oxoG, is the major cause for UVA mutagenesis. Indeed, in their hands, G to T transversions represented 26%–28% of the total mutations. Small deletions (about 10% of the mutations) also characterized the UVA-induced mutation spectra in the system used. All the small deletions comprised adjacent pyrimidines interrupted by a guanine, where CPDs (mainly TT CPDs) can potentially be formed. In addition, the most frequent events (30%–40% of total) were C to T transitions occurring at bipyrimidines. This class of mutation was excluded from the analysis by statistics, since they were also observed in unirradiated cells, albeit at a 2–3 times lower frequency. It is well known that spontaneous mutations occur primarily by deamination of methylcytosine in meCpG sequences, leading to C to T transitions. Due to the low relative induction of these mutational events by UVA, in comparison with UVB, it was legitimate to ask whether or not they originated from UVA-induced DNA lesions and were possibly caused by CPDs. Conversely, the distribution and sites of mutations are as important as the frequency. In addition, to assign a specific DNA lesion as the origin of a mutation at a given site is sometimes elusive. Nevertheless, reexamining the sites of mutations, it appeared that most of the C to T transitions induced by UVA, except for one hotspot (occurrence of four mutations that could be of spontaneous origin), occurred at sites different from that of the spontaneous C to T transitions. Moreover, part of them were recovered at sites which were also UVB mutational hotspots. Consequently, the latter data cannot be interpreted only as oxidative damage to guanine and points to a role for CPDs as premutagenic lesions. However, in contrast to all the other studies, cell irradiation was performed in the presence of culture medium that contained a well-known

photosensitizer, riboflavin, at high concentration so that the elevated frequency of G to T transversions may be explained by a prominent production of 8-oxoG by photosensitization via riboflavin (Besaratinia et al. 2007).

Altogether, the data may not be as conflicting as first thought and generally point to a role for CPDs. However, the relative contribution of 8-oxoG in UVA mutagenesis is not yet totally clear. The 8-oxoG is efficiently and quickly eliminated within 3–6 h by base excision repair in mammalian cells and is not expected to lead to extensive mutations in repair-proficient cells. The 6-4PPs are efficiently repaired by nucleotide excision repair and totally eliminated within 6 h, in contrast to CPDs, which are still partly present 24 h after exposure. In addition, UVA may compromise the repair of bipyrimidine photoproducts (Mouret et al. 2006). A still puzzling question concerns the role of TT CPDs, which largely predominate over C-containing CPDs, in UVA-induced mutagenesis. In mammalian cells and yeast, TT CPDs are supposed to be bypassed essentially in an error-free manner by the translesional DNA polymerase pol η (Johnson et al. 1999; Masutani et al. 1999), whereas they are more mutagenic in bacteria (Gibbs et al. 1993). It has also been proposed that beside CPDs, more complex DNA lesions play a role in UVA-induced mutagenesis, at least in hamster cells (Biverstål et al. 2008).

58.4.2.2 UVA Induces Mutation in Skin

Work on UVA-induced tumors in hairless mice showed a low incidence of p53 mutations in tumors (van Kranen et al. 1997). All of the p53 mutations were C to T transitions, mostly occurring at sites of UVB mutational hotspots. This indicates a role for CPDs in the formation of p53 mutation by UVA in mouse skin. The most extensive analysis of mutations induced in skin has been performed by Ikehata et al. (2008) in mice, using 364 nm UVA1 laser light, in comparison with UVB and sunlight. It was found that 65% of the total mutants recovered in the UVA-irradiated epidermis carried C to T transitions, 90% of which occurred at bipyrimidine sites. In contrast, G to T transversions, possibly generated by 8-oxoG, represented only 6% of total mutations, and no T to G transversions were found (Ikehata et al. 2008). The UVA-induced mutation spectrum differed somewhat from that induced by UVB. It is characterized by a high frequency of C to T mutations at 5′-TCG-3′ sequences where CpG is methylated at the cytosine residue, a feature which is less pronounced after UVB or sunlight exposure. As for UVA, 6% of the total mutations recovered in sunlight-irradiated epidermis were G to T transversions. As expected, UVB contributed much more than UVA to the sunlight-induced mutation spectrum (Ikehata et al. 2004). Remarkably, the authors calculated that the UVA component of sunlight would provoke a threefold induction of mutations after a whole day of sun exposure, while UVB or sunlight would cause 15-fold and 35-fold mutation induction after an hour exposure at noon. The genotoxicity of UVA is indeed much smaller than that of UVB. However, these results cannot be directly applied to the human situation to predict UVA genotoxicity and risk to health, since human skin is much thicker than mouse skin and, in reality, the human population is exposed to multiple doses rather than single doses of UVB or UVA.

Very limited data are available on the mutations induced by UVA in human skin. Persson et al. (2002) analyzed p53 mutation in individual human skin keratinocytes repeatedly exposed to UVA and found three p53-mutated cells, all with a G to T transversion. Engineered human skin was exposed four times to UVA, UVB, or a mixture, which resembled sunlight, and p53 mutations were recovered in all cases (Huang et al. 2009). UVA led to a predominance of mutations in the basal epidermis, which contains dividing keratinocytes and is thought to give rise to skin cancer. The low number of mutations observed and the presence of a strong mutational hotspot in UVA-irradiated samples do not allow further conclusions at the molecular level. However, the data did confirm an earlier report that UVA and UVB contribute to sunlight-induced p53 mutations in human skin tumors (Agar et al. 2004).

58.4.2.3 UVA Induces Delayed Mutations and Persistent Genomic Instability

There is increasing evidence for long-term consequences of UVA exposure. UVA-induced DNA damage may persist or continue to be generated not only during the postirradiation period in the irradiated cell, and its progeny, but also in surrounding cells. These long-term changes may lead to cells that can

eventually acquire a hypermutator phenotype and later carcinogenic potential. In particular, it has been shown in Chinese hamster fibroblasts that UVA produces fewer immediate mutations but more delayed mutations than UVB or x-rays (Dahle and Kvam 2003). ROS generated by UVA has been associated with such persistent genomic instability. Using a specific screen to reveal large gene alterations, Dahle et al. (2005b) observed that UVA is able to induce large deletion as both immediate and delayed mutations. Similarly, UVA exposure of human HaCaT transformed keratinocytes lead to a continuous reduction of cell survival, an increase in mutations and an increase in micronuclei formation up to 21 days postirradiation (Phillipson et al. 2002). It has also been proposed that long-lasting DSB may be responsible for the appearance of micronuclei and chromosomal aberrations in HaCaT keratinocytes and may confer tumorigenic phenotype (Wischermann et al. 2008). Notably, a dose-dependent telomere shortening has been reported in UVA-irradiated cells, which has been correlated with a targeting of 8-oxoG in the GC-rich telomeric sequences (Oikawa et al. 2001). This event could be one of the possible causes of skin aging.

58.4.2.4 Role for UVA in Human Skin Cancer?

UVA may play a role in solar mutagenesis and skin carcinogenesis that is manifested as mutations in tumor suppressor genes in melanoma and nonmelanoma skin cancers. A role of UVA in the promotion steps of carcinogenesis is beyond the scope of this chapter.

There are several lines of evidence but not absolute proof for a role of UVA in cancer: (1) UVA damages DNA, inducing CPDs, 8-oxoG, and other secondary lesions; (2) UVA is mutagenic at environmentally relevant doses, including to skin; (3) a UVA mutational signature has been observed in sunlight-induced mutation spectra in various biological systems, even though the UVB component largely predominates (Drobetsky et al. 1995; Kozmin et al. 2003, 2005; Ikehata et al. 2004, 2008; Besaratinia et al. 2008); and (4) the basal layer of the epidermis, where tumors originate, receives far more UVA than UVB radiation. UVA is likely involved in some of the skin cancers in the human population, at least in case of heavy exposure to UVA, that is, repeated and excessive use of sunbeds and sunlamps or misuse of sunscreens.

Based on the analysis of p53 mutations and on the presence of CPDs and 8-oxoG in biopsies from squamous cell carcinomas (SCCs) and excised premalignant solar keratosis (SK), Agar et al. (2004) reported that the basal layer in tumors harbors more UVA than UVB fingerprint mutations. The UVB fingerprints, C to T transitions at bipyrimidine sites, were located in keratinocytes in the stratum granulosum in SCC and SK, whereas the events chosen as UVA fingerprints, the T to G and G to T mutations, showed a bias toward basal layers. In addition, CPD detection occurred throughout the epidermis but was maximal in the upper layers, while 8-oxoG detection exhibited a bias toward basal layers in all SKs and SCCs. This is consistent with the ability of UVA to penetrate down to the basal epithelial layers and dermis, whereas the penetration of short-wavelength UVB is confined predominantly to the superficial epidermis. Even though the mutational specificity of UVA is not yet clearly established, in particular in skin cells and tissue, these data strongly suggest a role for UVA in human skin carcinogenesis (Halliday et al. 2005).

UVA and melanoma have been the subject of intense research activity and debate, since Setlow et al. (1993) discovered that UVA is susceptible to cause melanoma in pigmented backcross hybrids of the platyfish *Xiphophorus*. Among comprehensive reviews are those by Wang et al. (2001), Jhappan et al. (2003), and Bennett (2008). Briefly, suggestions for a role of UVA in the pathogenesis of cutaneous malignant melanoma can be summarized as follows: (1) Epidemiological studies tentatively suggest positive relationship between melanoma incidence and use of sunlamps; (2) the use of sunscreens which provide a better protection against UVB than against UVA may also be a melanoma risk factor; (3) UVA (and UVB) induces melanoma in the melanoma-prone pigmented fish *Xiphophorus*, through the generation of ROS from melanin (Wood et al. 2006); (4) prolonged UVA exposure, but not UVB, can induce melanocytic hyperplasia (melanoma precursor) in pigmented Opossum *Monodelphis domestica* (Ley 1997). In contrast, UVB, but not UVA, could induce malignant melanoma in engineered transgenic mice. In fact, virtually none of the animal models developed exhibits susceptibility to melanoma incidence by UVA.

Moreover, Mitchell et al. (2010) reexamined the induction of melanoma by UVA in a *Xiphophorus* hybrid model similar to that in Setlow's studies and could not confirm the original data. This recent and important report refutes the only direct evidence that UVA causes melanoma.

An important question yet to be resolved is to what extent melanin protects from skin cancer and in particular from melanoma. The fair-skinned population is far more prone to develop melanoma than darker-pigmented individuals. In addition to genetic predisposition of fair-skinned individuals, the pheomelanin present in fair skin may act as a photosensitizer and produce ROS, in contrast to eumelanin, which is more abundant in dark skin and exhibits a protective effect against solar radiation. Kvam and Tyrrell (1999) observed that human melanoma cells with high melanin content accumulated two times more 8-oxoG after UVA irradiation than cells with low melanin content. In addition, melanocytes have recently been shown to be deficient in repair of oxidative DNA damage and UVB photoproducts (Wang et al. 2010). Thus, UVA-induced melanoma could originate from melanocyte stem cells present in the basal layer of the epidermis. In contrast to what has been observed in the mutated genes p53 and patched homolog (Drosophila) (PTCH) in nonmelanoma skin tumors (Giglia-Mari and Sarasin 2003), no clear UV signature has been found in the genetic alterations found in melanoma. Meanwhile, the BRAF (gene encoding the serine/threonine-protein kinase B-Raf) missense mutation (V600E) present in 66% of melanoma has been tentatively attributed to CPDs, produced by UVB by an error-prone translesion synthesis (Thomas et al. 2006). Since the surrounding sequence is a T-rich region, it could also be produced by UVA. Even though some evidence from basic research argues for an involvement of UVA in skin cancer, we are far from being able to estimate the extent of it.

58.4.2.5 Mitochondrial Mutagenesis and Photoaging

The mutation frequency of mitochondrial DNA (mtDNA) is generally much higher than that observed in the nuclear genome. This is partly due to the lack of protective histones and the absence of nucleotide excision repair, but mainly to the deleterious effect of ROS issued from electron leak from the respiratory chain and reaction with oxygen. Large mtDNA deletions (3–10 kbp) have been detected in many human tissues, at high levels in nonreplicating tissues like muscle and brain, and at a lower extent in mixed replicating tissues. As a replicating tissue, normal human skin carries low content of mtDNA deletions that have been associated with cancer in many tissues. The accumulation of mtDNA deletions has been proposed as an underlying cause of the aging process. The use of mtDNA damage as a biomarker for cumulative sun exposure in human skin and skin photoaging is relatively recent (reviewed by Berneburg and Krutmann 2000; Birch-Machin and Swalwell 2010).

The most frequent deletion, a 4977 bp deletion known as the common deletion, has been observed at a higher frequency in chronically sun-exposed skin than in sun-protected skin or blood cells (Berneburg et al. 1997, 2004; Berneburg and Krutmann 1998). This common deletion and some others have been found with a higher frequency in the margin of nonmelanoma skin tumor of old patients, and age-related, but were typically absent from the tumors (Eshaghian et al. 2006). Furthermore, there was a greater frequency of mtDNA mutations (common deletion and tandem duplications) in "usually" sun-exposed compared to "occasionally" sun-exposed skin and none in sun-protected (i.e., rarely exposed) (Krishnan and Birch-Machin 2006). In addition, a rare 3895 bp mtDNA deletion observed in sun-exposed body sites and reproduced *in vitro* by in cultured HaCaT cells, repetitively, exposed to sublethal doses of UVA + UVB light has been proposed as a marker for cumulative sunlight exposure in human skin (Krishnan et al. 2004). UVA, in contrast to UVB, has long been known as an oxidative stress. Interestingly, earlier studies assessed the role of UVA and ROS in the process of mtDNA deletion, using normal human fibroblasts. They revealed that singlet oxygen mediates the UVA-induced generation of the photoaging-associated common deletion (Berneburg et al. 1999) and that such deletions can be prevented by supplementation with beta-carotene, a known ROS and singlet oxygen quencher, or with creatine, the adenosine triphosphate (ATP)-producing precursor (Berneburg et al. 2005). Recently, Schroeder et al. (2008) elegantly linked mtDNA deletions with photoaging by showing that gradual depletion of mtDNA from human skin fibroblasts causes a gene expression profile, which is reminiscent of

that observed in photoaged skin. In terms of DNA repair, mitochondria possess functional base excision repair, DSB repair, and mismatch repair, pathways that are essential to protect mtDNA from extensive damaging effect of ROS (Berneburg et al. 2006, see also Kamenisch et al. 2010).

The role of mitochondria and mtDNA mutagenesis in photoaging and photocarcinogenesis is related to mitochondrial functions in the bioenergetic system and in apoptosis. The ROS-mediated mtDNA damage causes mitochondrial misfunction which in turn favors ROS generation. Cancer cells may exhibit enhanced intrinsic ROS stress, partly because of increased metabolic activity and mitochondrial dysfunction. Indeed, ROS-mediated mtDNA damage may be a mechanism to amplify ROS stress in cancer cells (Birch-Machin and Swalwell 2010). Due to the current lifestyle favoring increased exposure to UVA and in order to limit the adverse effects of natural or artificial UV exposure, such as photoaging and photocarcinogenesis, protective effect of natural antioxidants such as beta-carotene (Eicker et al. 2003) or lycopene (Rizwan et al. 2008) is being proposed as potential protective agents.

58.4.3 Membrane Damage Effects on Fluidity and Lipid Oxidation Products

Pioneering studies by Hollaender (1943) demonstrated that the rate of UVA inactivation of bacterial populations was greatly enhanced as the salt content of the postirradiation incubation medium was raised, strongly indicating that UVA produced potentially lethal membrane damage. Many subsequent studies have demonstrated that UVA can peroxidize membrane lipids (for reviews see Tyrrell 1991; Girotti 2001; McMillan et al. 2008) and that the membrane damage arising can lead to many consequences including cell death, lysosomal rupture, and aberrant protein trafficking. UVA-mediated lipid oxidation involves iron, singlet oxygen, and hydroxyl radical (Vile and Tyrrell 1995; Dissemond et al. 2003) and, importantly, the lipid oxidation products are also key signaling intermediates (see the following).

Several studies have detected changes in cell membrane fluidity following UVA treatment, generally by using fluorescent probes. Gaboriau et al. (1993) showed that a UVA-induced change in fluidity was associated with increased lactate dehydrogenase (LDH) leakage, and since both were protected by the lipid antioxidant vitamin E, lipid peroxidation is likely to be the cause of the changes. Growing cells are more susceptible to such UVA-induced change than quiescent cells. A study of the effect of UVA on the membrane fluidity of human fibroblasts using electron paramagnetic resonance (after incorporation of spin-labeled stearic acids) indicated increased rigidity of the fibroblast membrane structure (Budai et al. 2004). Susceptibility of keratinocyte membranes to UVA-induced lipid oxidation can be influenced by substituting cholesterol by phytosterols (Mora-Ranjeva et al. 2006). Sitosterol is protective whereas stigmasterol dramatically increases lipid peroxidation (+70%) and increases prostaglandin release.

Fractionating UVA radiation with short intervals between doses can enhance cytotoxicity and oxidative damage (Merwald et al. 2005). However, allowing an interval of several hours between UVA irradiations can lead to a significant adaptive protection of human skin fibroblasts against oxidative membrane damage (Vile et al. 1994) and apoptosis (Yang et al. 2003). Although Vile et al. used antisense experiments to link this protection to the activation of heme oxygenase, repetitive low-dose UVA irradiation also leads to a substantial upregulation of manganese superoxide dismutase (MnSOD) activity (Poswig et al. 1999) and selenium-dependent upregulation of glutathione peroxidase (GPx) activity, and it has been suggested that this enzyme as well as inducible MnSOD is involved in protection against UVA (Meewes et al. 2001). Schneider et al. (2006) have also shown adaptive protection of human dermal fibroblasts against UVA radiation and demonstrated that the response is very variable from donor to donor and depends on glutathione content. Although these authors linked the protection to UVA activation of GPx, it should be noted that UVA upregulation of heme oxygenase is exquisitely sensitive to intracellular glutathione levels (Lautier et al. 1992), and it seems likely that the induced protection against membrane damage in cells and skin will be due to the combined activity of the inducible antioxidant enzymes.

Using guinea-pig ventricular monocytes, La et al. (2006) showed in whole-cell voltage clamp experiments that UVA caused a progressive increase in late (slowly inactivating) Na(+) current that

had been elicited by 200 ms depolarizations. This not only provides a cellular cardiac model but also injects a cautionary note for imaging studies since UVA wavelengths are commonly used for Ca(2+) imaging.

58.4.4 Heme and Iron Homeostasis

Both heme and iron are essential for synthesis of a variety of proteins but low levels must be maintained by tight homeostatic mechanisms to avoid cell and tissue damage resulting from an excess of these pro-oxidant catalysts (Tyrrell 2005). UVA radiation severely disturbs both heme and iron homeostasis. UVA irradiation of mammalian cells leads to a sharp increase in the levels of labile iron, and this occurs in all skin cell types tested (Pourzand et al. 1999; Zhong et al. 2004; Basu-Modak et al. 2006) and has been linked to UVA-mediated cell death (Zhong et al. 2004). The release appears to be primarily due to UVA disruption of lysosomal membranes, which leads to protease leakage and degradation of proteins that include the crucial iron storage protein ferritin. Iron homeostasis is largely controlled in mammalian cells by the state of the iron-responsive protein, which changes its capacity to bind to specific mRNAs as a function of labile iron levels (for recent review see Recalcati et al. 2010). Activation of this protein by binding to free iron results in downregulation of the transferrin receptor and upregulation of ferritin. The increase in ferritin levels observed 1 or 2 days following UVA radiation is likely to be due to both this immediate release of free iron and the activation of HO-1 (see the following), which breaks down heme to release iron (Vile and Tyrrell 1993).

As well as iron, free heme appears to be released in cultured fibroblasts following UVA irradiation and in a cyclooxygenase-dependent fashion (Kvam et al. 1999), and this disruption in heme homeostasis is likely to be the trigger for the dramatic increase in HO-1 transcription following relatively low fluences of UVA radiation (see the following).

58.4.5 Photooxidation of Proteins and Enzyme Damage

Proteins are highly susceptible to oxidation so it is not surprising that they will be damaged by the ROS and the pro-oxidant catalysts generated by UVA radiation. This is due in part to their abundance in cells but also to the fact that they include chromophores such as amino acids with aromatic rings (e.g., tryptophan) that give rise to the UV absorption of the proteins in the region 250–320 nm. As a result, direct photooxidation may occur and arises from absorption of radiation by the protein or the bound chromophores, thereby generating excited states or radicals through type I processes. In addition, some proteins bind prosthetic groups such as flavins and hemes, which absorb in the UVA and visible range. For example, catalase a crucial antioxidant enzyme containing heme is very susceptible to UVA (Zigman et al. 1996; Maresca et al. 2006). As a result, indirect photooxidation of proteins may also occur (type II mechanism), which involves singlet oxygen generated by energy transfer from either protein-bound or other endogenous chromophores to oxygen. All these processes have been detailed in Bensasson et al. (1993), Davies (2003), and Pattison and Davies (2006).

58.4.5.1 Protein Oxidation by Direct UV Absorption

The triplet states of Trp, Tyr, and Phe generated by absorption of radiation in the UVB range can undergo electron or hydrogen atom transfer reactions, including with disulfides of cystines and O_2. These reactions result in Trp and Tyr radical cations and then neutral indolyl and phenoxy radicals or benzyl radical in the case of Phe. A well-known end-product of such radicals is the dityrosine cross-link. Thiyl radicals and thiyl peroxyl radicals can further lead to sulfonic (RSO_3H) and sulfinic (RSO_2H) acids. Tyr is considered as the ultimate sink for one-electron oxidation, whereas cystine is the ultimate sink for one-electron reduction (Pattison and Davies 2006). Trp, Tyr, Phe, and His side chains, in the ground state, can also undergo direct photoionization processes.

58.4.5.2 Protein Oxidation by Singlet Oxygen

The main ROS produced in cells by UVA is singlet oxygen, which is generated via transfer of energy from an excited chromophore to molecular oxygen. As a result, the majority of UV-induced protein damage appears to be mediated by singlet oxygen (Pattison and Davies 2006). The interaction of singlet oxygen with proteins occurs mostly by reactions, which result in protein modification, rather than by quenching (relaxation to ground-state oxygen). Singlet oxygen reacts preferentially with Trp, His, Tyr, Met, Cys, and cystine side chains. Reaction with Trp gives rise to *N*-formylkynurenine, kynurenine, and 3α-hydroxypyrroloindole. The reaction of singlet oxygen with Tyr forms an unstable endoperoxide, which undergoes further reactions resulting in radical formation that may lead to dityrosine and protein cross-links. The products of His oxidation lead to His–His and His–Lys cross-links in free amino acid residues and very likely in proteins too. Disulfides are formed when free Cys reacts with singlet oxygen, probably along with cysteic acid (RSO_3H). UVA is also expected to produce intracellular protein peroxides probably localized on His, Trp, and Tyr residues (Pattison and Davies 2006). Photooxidation of proteins also commonly leads to high-molecular-weight aggregates, which may arise from dark reactions after the end of the light exposure. His residues may have a major role in the generation of these cross-linked proteins, since it has been reported that cross-links are absent from photooxidized proteins that lack His (Balasubramanian et al. 1990). Interestingly, the use of various photosensitizers in combination with UVA has helped in determining photooxidation products of His, either free or in peptides or proteins (Agon et al. 2006). Trp photoproducts have also been used as biomarkers for protein photooxidation and for establishing the molecular mechanism of photosensitization. For example, the pattern of Trp photoproducts differs for methylene blue, a predominant type II photosensitizer, and for naproxen, which belongs to the class of nonsteroidal anti-inflammatory drugs and produces photodamage supposedly through both type I and type II processes (Catalfo et al. 2009).

58.4.5.3 Protein Oxidation Induced by UVA and Biological Significance

Since proteins generally exist in multiple copies, biological effects will tend to be observed only at high doses. However, there is evidence dating back to studies in bacteria that damage to repair enzymes by UVA strongly influenced the biological outcome (Tyrrell and Webb 1973; Tyrrell et al. 1973). Indeed, this work led to a series of studies, which showed strong synergistic lethal interactions between UVA and various DNA damaging agents including shorter wavelength UV in bacteria and human cells (reviewed by Tyrrell 1978). Some years later, *in vitro* studies showed that irradiation of *E. coli lac* repressor with broadband UV (295–400 nm, centered at 325 nm) induces photooxidation of Trp and formation of *N*-formylkynurenine, which abolishes the inducer isopropyl β-D-1-thiogalactopyranoside (IPTG) binding (Spodheim-Maurizot et al. 1985). A continuous sublethal UVA irradiation administered to *E. coli* leads to a change in the activities of oxidative defense enzymes, hydroxyperoxidases, glutathione reductase, and manganese superoxide dismutase. This adaptative response resulted in an increased resistance to a lethal UVA irradiation challenge (Hoerter et al. 2005). Surprisingly, it did not confer increased protection against protein oxidation, as estimated by total carbonyl formation. In human skin cells, the addition of superoxide dismutase does not protect against oxidation of alcohol dehydrogenase and glyceraldehyde 3-phosphate dehydrogenase by UVA irradiation (Hu and Tappel 1992).

It was also shown in human skin cells that in addition to lipid peroxidation, UVA irradiation-induced sulfhydryl oxidation in proteins, which was dependent on iron, singlet oxygen, and hydrogen peroxide (Vile and Tyrrell 1995). Importantly, in melanoma cells, it was observed that UVA considerably increases L-isoaspartyl residues, a marker of protein damage, at doses lower than for induction of lipid peroxidation or DNA damage (D'Angelo et al. 2001). The same group showed that such protein damage is prevented by hydroxytyrosol, a natural antioxidant from olive oil (D'Angelo et al. 2005). In reconstituted epidermis of a different skin phototype, UVA was found more effective than UVB in impairing antioxidant enzyme activities (catalase and superoxide dismutase), and this inhibition correlated with the phototype of the melanocytes. In addition, it was shown that UVA induces a change in catalase levels

in epidermis reconstituted with low phototype melanocytes (Maresca et al. 2006). UVA has been shown to inactivate protein tyrosine phosphatase by a protease calpain-mediated degradation, and modification of tyrosine phosphatase is required to make it a calpain substrate (Gulati et al. 2004). It was later demonstrated that singlet oxygen inactivates protein tyrosine phosphatase-1B by oxidation of the active site cysteine (von Montfort et al. 2006).

Photoaging has been associated with protein oxidation in human skin (Sander et al. 2002) based on several observations. Firstly, the overall expression of antioxidant enzymes, catalase, copper–zinc superoxide dismutase, and manganese superoxide dismutase was elevated in the epidermis, but was low in the dermis. In photoaged skin, a depletion of expression of antioxidant enzymes was observed, as well as an accumulation of protein carbonyls, particularly in the upper dermis. UVA exposure also led to a dose-dependent protein oxidation. Proteosomal peptidases are involved in degrading oxidized proteins, and the activity of several of these peptidases was decreased in human keratinocyte cultures following UVA irradiation (Bulteau et al. 2002). Moreover, it was recently shown that the repair enzyme methionine-*S*-sulfoxide reductase (MSRA) was expressed in human epidermis and upregulated by low doses of UVA radiation (and H_2O_2), but not by UVB (Ogawa et al. 2006). Its expression was also increased by repetitive exposure of the human skin to simulated sunlight. MSRA reduces the methionine sulfoxide (MetO) to methionine, thus reversing the inactivation of proteins caused by oxidation of critical methionine residues. It is the only enzyme so far identified in human skin that is able to repair oxidative protein damage. Interestingly, MSRA knockout mice that exhibit an increased sensitivity to oxidative stress, leading to accumulation of oxidized proteins, also have a significantly shorter lifespan. Protein oxidation has clearly been correlated with solar elastosis and photoaging in human skin and also in the depigmentation disease, vitiligo. It could also be involved in degenerative disorders, such as cataract. Accumulation of oxidized protein is a hallmark of cellular aging.

Photodynamic cross-linking of proteins was first analyzed *in vitro*, using rose bengal and flavin mononucleotide as photosensitizers (Shen et al. 1996; Spikes et al. 1999). It was found that intermolecular dityrosine cross-linking involve a type I mechanism, whereas singlet oxygen generates His and/or Lys cross-links. An example of covalent photocross-linking is given by the replication and repair protein, proliferating cellular nuclear antigen (PCNA) homotrimer. High-molecular-weight PCNA forms were produced in human cells by photodynamic treatments, which generate singlet oxygen (Bae et al. 2008). PCNA oligomerization of at least tetramer lengths and cross-linking of PCNA with heterologous proteins were observed. Using a proteomic approach, the same authors showed that of the 300 protein spots, only seven were changed by the photodynamic treatment (proflavine plus fluorescent light). Similarly, cross-linking of PCNA trimers was observed in UVA-irradiated cells that have incorporated large amounts of 6-thioguanine (Montaner et al. 2007). UVA irradiation, in the absence of 6-thioguanine, is also able to induce covalent photocross-linking of PCNA, but to a lesser extent (Montaner et al. 2007; Girard and Sage unpublished). Notably, covalent PCNA trimers were found in the chromatin-associated fraction, and at active replication forks. It has not yet been demonstrated whether or not these fractions of cross-linked PCNA interfere with progression of replication. According to the 3D structure at the intersubunit region and the alignment of conserved residues, Montaner et al. proposed that the covalent cross-link involves His153 and Lys77.

Another repair protein that is sensitive to oxidation is the DNA *N*-glycosylase hOGG1, which removes 8-oxoG (Bravard et al. 2006). Interestingly, glutathione depletion of skin fibroblasts and melanoma cells, which increases oxidative stress, causes a strong retardation of repair of 8-oxoG after exposure to nontoxic doses of visible light or UVA radiation (Eiberger et al. 2008). Moreover, the cleavage activity at 8-oxoG residues measured in protein extracts from irradiated cells drops transiently after irradiation. A modification of hOGG1 is suspected, but it is not caused by critical oxidation of Cys such as reported by Bravard et al. (2006). It appears that the base excision repair of oxidized purines is surprisingly sensitive to oxidative stress, while the nucleotide excision that removes bipyrimidine photoproducts is not (Eiberger et al. 2008).

58.4.6 Cell Division, Cell Cycle, and Cell Migration Effects

Using synchronized murine fibroblasts (3T3), Bråthen et al. (2000) showed that cells were most photosensitive with respect to formation of multinucleated cells in G2 phase and that the delayed appearance of multinucleated cells in G2 and S phase was due to UVA impairment of cytokinesis. In a study with human transformed fibroblasts and other mammalian cells, Girard et al. (2008) demonstrated a UVA dose-dependent delay in S phase and showed that UVA-irradiated S-phase cells accumulated at the G2/M boundary. Although they confirmed that ataxia telangiectasia mutated (ATM)-, ATR (ATM and Rad3-related protein kinases)-, and p38-dependent signaling pathways are activated by UVA, they were not responsible for the cell cycle delay.

Thorn et al. (2001) showed no effect of UVA (in contrast to H_2O_2) on cell cycle or proliferation in HaCaT cells indicating that cells of epidermal origin may differ considerably from fibroblasts in their response to UVA. However, He et al. (2008) actually showed a UVA-mediated stimulation of cell cycle progression in HaCaT cells, which was dependent on cyclin D1. Inhibitor experiments indicated that UVA stimulated the AKt/cyclin D1 pathway, which in turn upregulated the epidermal growth factor receptor (EGFR) pathway. Interestingly, these authors also showed that the entire EGFR/Akt/cyclin D1 pathway was dependent on the activation of a metalloproteinase (Adam 17). UVA stimulation of growth was also seen by Jean et al. (2007) who showed that low-dose UVA actually reduced the G2/M arrest normally observed in human HaCaT keratinocytes and normal human keratinocytes. Their experiments indicated that following UVA exposure, the EGFR/Akt pathway subverts the G2/M checkpoint.

Shorrocks et al. (2004) compared UVA-mediated cell cycle effects in normal human fibroblasts with cells taken from patients heterozygotic for the breast cancer predisposing gene, *BRCA1*. Reentry into S phase was faster in the heterozygotes following G1 arrest indicative of an abnormal cell cycle checkpoint, which could lead to greater levels of unrepaired damage. However, no increases in micronuclei induction were observed following UVA, which would have been indicative of increased chromosomal instability.

Using dermal sheets derived from human skin, Furio et al. (2005) showed that UVA decreased the number of viable dendritic cells that moved out of the dermis and showed that this was related to increased apoptosis. Furthermore, UVA irradiation also prevented the maturation of migrating dendritic cells into antigen-presenting cells, which indicates an additional mechanism by which UVA is immunosuppressive (see also chapter by Reeve, this volume).

58.4.7 Cell Death: Necrosis and Apoptosis

UVA treatment leads to both necrotic and apoptotic cell death, and the relative importance of each pathway depends strongly on the cell type and dose level (reviewed by Pourzand and Tyrrell 1999; Godar 1999a). From a series of experiments, Godar (1999b) concluded that there are two pathways of UVA-induced apoptotic cell death. The primary pathway is an immediate triggering of apoptosis by opening of the cyclosporine A-sensitive mitochondrial megapore and involves singlet oxygen whereas superoxide anions appear to initiate a second cyclosporine A-insensitive final apoptotic pathway.

Apoptosis is believed to be the main pathway to eliminate sun-damaged keratinocytes in skin, and Fas accumulation (Bang et al. 2002) has been consistently observed in human skin epidermal cells following UVA (and UVB) treatment. Interestingly, *in vivo* studies in mice had shown that UVA could actually reduce UVB upregulation of FasL expression in mouse skin (Shen et al. 2000). UVA triggers the DNA damage-dependent ATM kinase activity and the ATM-dependent p53, and JNK pathways have been directly linked to UVA-induced apoptosis (Zhang et al. 2002). The involvement of signaling kinase in apoptosis is further described in Section 58.5.3.

ROS appear to be central to the UVA-induced apoptotic response. Thioredoxin levels increase following UVA irradiation of fibroblasts, and this antioxidant has been implicated in UVA apoptosis (Didier et al. 2001). Strong direct evidence that the sphingomyelin–ceramide signaling pathway is involved in UVA apoptosis was provided by Zhang et al. (2001a). They compared normal lymphoblasts with

lymphoblasts derived from patients genetically deficient in sphingomyelinase (SMase) and showed that UVA-induced acid SMase induction and apoptosis were inhibited in the latter cell type. These authors also linked SMase induction to the upstream activation of JNKs that lead to apoptosis. Induction of the lipid oxidation product and signaling molecule, 4-hydroxynonenal (4-HNE), also appears to be involved in the apoptotic pathway, at least in K562 cells (Yang et al. 2003).

Understanding the specific UV-mediated apoptotic pathways involved is crucial since apoptotic events are central to the carcinogenesis process. For example, the resistance to UVA apoptosis following chronic irradiation treatment of HaCaT cells involves increased Akt signaling and decreased phosphatase and TENsin homolog (PTEN) expression, and this process appears to be linked to malignant transformation (He et al. 2006). Inhibition of JNK leads to a dramatic increase in UVA-induced caspase-dependent apoptotic cell death in HaCaT cells (Silvers et al. 2006). Using mouse NIH 3T3 embryonic fibroblast cells as a model, Ibuki and Goto (2002) showed that unlike apoptosis induced by UVB, UVA apoptosis was independent of the PI3-kinase–Akt pathway. Hirota et al. (2005) showed that the Nrf2–Keap1 pathway is crucial to UVA-induced apoptosis in murine fibroblasts possibly via control of the anti-apoptotic heme oxygenase pathway (see the following).

Induction of singlet oxygen–mediated human T helper cell apoptosis is believed to be one of the central factors involved in UVA phototherapy (see Morita et al. 1997; Krutmann 1998). These authors showed that Malignant T-cell lines as well as CD4+ T cells derived from adult T-cell leukemia are very sensitive to UVA (but not UVB) radiation-induced early and late apoptosis compared with normal CD4+ T cells, and that this is related to the availability of caspases such as caspase 3 (Yamauchi et al. 2004). UVA-induced T-cell apoptosis also appears to be crucial to certain types of phototherapy. For example, phototherapy of atopic dermatitis and other T-cell-mediated inflammatory skin diseases appears to work by UVA-induced Fas ligand-independent activation of Fas death pathways in T helper cells (Zhuang and Kochevar 2003).

Interestingly, malignant human T cells appear to be more susceptible to UVA-induced apoptosis than nonmalignant cells, and this was related to higher levels of pro-caspase 3 activity (Yamauchi et al. 2004)

UVA-induced cell death in cultured human skin fibroblasts is primarily due to necrosis and correlated with intracellular ATP depletion (Zhong et al. 2004). Furthermore, these authors showed that the level of necrotic cell death in both fibroblasts and keratinocytes was directly linked to basal and induced levels of the labile iron pool.

58.5 UVA as a Modulator of Gene Expression

58.5.1 Introduction

UVA is well known to activate expression of a variety of genes at doses relevant to natural sunlight exposure (reviewed in Tyrrell 1996a,b). Of these, the largest and most studied effects are the activation of HO-1 (Keyse and Tyrrell 1987, 1989) and metalloproteinases (Herrmann et al. 1993). However, many other genes have been observed to be activated including intercellular adhesion molecule 1 (ICAM-1) (Krutmann and Grewe 1995) and cyclooxygenase 2 (COX-2) (Hanson and DeLeo 1989). Much has been learnt recently about the UVA-induced signaling intermediates involved and the complex cascades of signaling kinases and phosphatases. The pathways involved are very cell type dependent but a general picture emerges, which is described in the following.

58.5.2 UVA-Generated Signaling Intermediates

58.5.2.1 Singlet Oxygen

Singlet oxygen (see earlier section) was the first ROS to be clearly implicated in UVA activation of gene expression. This was first observed for HO-1 (Basu-Modak and Tyrrell 1993) but the species was soon implicated as a key intermediate in interstitial collagenase (Wlaschek et al. 1995) and ICAM-1 activation (Grether-Beck et al. 1996) by UVA. Singlet oxygen was also implicated in the UVA activation of IL-1 alpha and IL-6 (Wlaschek et al. 1997), both of which are known to activate HO-1 and interstitial collagenase.

58.5.2.2 Ceramide

Various ROS, including singlet oxygen, will lead to lipid peroxidation, and it is likely that lipid signaling intermediates are responsible for much of UVA modulation of gene expression. Among such intermediates is ceramide, which is known to be a key component of intracellular stress responses and is generated by UVA in a nonenzymatic singlet oxygen–dependent reaction (Grether-Beck et al. 2000). The ceramide is derived from sphingomyelin, and it was clearly demonstrated that this intermediate was involved in the AP-2 (transcription factor activator protein 2)-dependent activation of ICAM-1 expression in keratinocytes (Grether-Beck et al. 1996). Although another group failed to observe the direct (nonenzymatic) cleavage of ceramide (Mazière et al. 2001), Grether-Beck et al. (2005) later showed that both AP-2 activation and ICAM-1 activation were biphasic and the second more sustained peak most likely resulted from a ceramide-mediated autocrine loop since the latter involved activation of the key enzyme in ceramide synthesis, serine palmitoyltransferase. More recently, the same group (Grether-Beck et al. 2008) has shown that the UVA-mediated signaling response involved in ICAM-1 expression is entirely dependent on the ceramide composition of lipid rafts, which are well known to be involved in signaling responses.

58.5.2.3 Lipid Oxidation Products and 4-HNE

Lipid oxidation products have clearly been implicated in the activation of the HO-1 gene by UVA, and from studies using specific lipid antioxidants, it appears that the signaling molecules are derived from internal membrane lipids (Basu-Modak et al. 1996). An important nonenzymatic lipid peroxidation product induced by UVA irradiation of cells is 4-HNE. A role for 4-HNE in UVA effects was first suggested by Basu-Modak et al. (1996) who showed that 4-HNE was an extremely potent inducer of HO-1. 4-HNE production following UVA radiation has been linked to sustained activation of JNK and apoptosis (Yang et al. 2003) in a human myelogenous leukemia cell line (K562) although both are inhibited by a preconditioning dose of UVA. 4-HNE has also been implicated in other signal transduction pathways that affect cell cycle events as well as oxidant-induced apoptosis (Cheng et al. 2001). Cells that overexpress alpha class glutathione S-transferases (GSTs) show reduced intracellular levels of 4-HNE and resistance to apoptosis induced by UVA and other oxidants (Awasthi et al. 2004).

Oxidized phospholipids are known to stimulate a wide range of biological activities. It has been shown that UVA irradiation of fibroblasts can generate oxidized phospholipids from 1-palmitoyl-2-arachidonoyl-sn-glycero-3-phosphorylcholine (PAPC) in a singlet oxygen–dependent fashion and that these intermediates lead to strong expression of HO-1 in skin cells (Gruber et al. 2007). In very recent studies, Gruber et al. (2010) have shown that these oxidized phospholipids act by stimulating the accumulation of Nrf2, redox-regulated transcription factor, and therefore co-induce a series of antioxidant response genes including glutamate–cysteine ligase modifier subunit, aldo-keto reductases-1-C1 and -C2, and IL-8.

58.5.2.4 Phospholipase Metabolites

The phospholipase metabolites diacylglycerol and arachidonic acid were also shown to induce HO-1 mRNA accumulation three- to sixfold above basal levels (Basu-Modak et al. 1996). UVA irradiation of arachidonate-containing phospholipids generated lipid oxidation products including epoxyisoprostane-phosphatidylcholine, and these also induce HO-1 expression in dermal fibroblasts or keratinocytes (Gruber et al. 2007), and recently, Nrf2 has again been implicated in this phospholipid-mediated stress response (Gruber et al. 2010).

58.5.3 Protein Kinases and Phosphatases

Protein kinases are essential intermediates in many signaling pathways, which involve a cascade of protein phosphorylation reactions. Activation of a variety of protein kinases by UVA has been frequently observed but is skin cell type dependent and interpretation is often complex. This is further confounded

by laboratory variations in light source and protocols. For example, exquisitely small amounts of contaminating UVB in the broadband sources can cause kinase activation, and there is very often a narrow dose window of activation. Very often, there is no consideration of the target genes involved so that the biological significance is hard to assess. Nevertheless, there are strong arguments to support the notion that the activation of kinase-dependent signaling pathways is involved in skin tumor promotion and progression (Bachelor and Bowden 2004a). UVA radiation has been shown to activate protein kinase C (protein kinase C [PKC], phospholipid-dependent ser/thr kinase) in both murine fibroblasts (Matsui and DeLeo 1990), normal human epidermal keratinocytes (NHEK, Matsui et al. 1994), and rat myeloid leukemia cells (Leszczynski et al. 1995). Inhibitor studies have linked PKC signaling to the UVA activation of MMP-1 (Petersen et al. 1995 and see the following).

In studies by Klotz et al. (1997, 1999), evidence was presented that UVA could activate both p38 and JNK activity but not extracellular-regulated kinase (ERK) activity in human skin fibroblasts by a pathway involving singlet oxygen. However, many more studies have been undertaken in keratinocyte-derived cell lines than fibroblasts since these are considered a better model system for skin cancer. In contrast to the situation in human skin fibroblasts, UVA does activate ERK in mouse epidermal cells (He et al. 2004), and ERK activation by UVA is mediated by PKC in a Ras-dependent pathway. These authors showed that UVA activation of ERK occurs in an EGFR kinase-independent pathway (see the following) quite different to the observations of UVB and UVC activation of ERK. This sustained ERK activation by UVA may provide a cell survival signal crucial to cell transformation and carcinogenesis in human skin subject to sustained UVA irradiation.

Mitogen-activated protein kinases (MAPKs) are a group of phosphorylating enzymes that are activated in response to cytokines and stress. P38 kinases are a class of MAPKs that are involved in cell differentiation and apoptosis. In human dermal fibroblasts, UVA radiation was shown by Le Panse et al. (2003) to activate p38 MAPK but had no effect on ERKs or JNK–stress-activated protein kinase (SAPK). The pathway appears to involve singlet oxygen–dependent ligand–receptor activation or ribotoxic stress or both. In contrast, in HaCaT cells, UVA irradiation led to phosphorylation of both p38 protein and JNK (Bachelor et al. 2002; Silvers et al. 2003) although phosphorylation of ERK was significantly inhibited (Silvers et al. 2003). The activation was clearly linked to AP-1 transactivation and c-Fos expression. Activation of p38 in HaCaT cells has also been clearly implicated in stabilization of the COX-2 message and a consequent increase in COX-2 protein (Bachelor et al. 2002). COX-2, which generates pro-inflammatory intermediates (prostanoids), has been implicated in various pathways of tumorigenesis (e.g., Greenhough et al. 2009). COX-2 has also been heavily implicated in skin cancer, and recent phase 2 trials have indicated that celecoxib (a COX-2 inhibitor) is a potential chemopreventive agent in SCC. UVA activation of p38 mitogen-activated protein (MAP) kinase has also been linked to the UVA-induced expression of Bcl-XL, a crucial anti-apoptotic protein (Bachelor and Bowden 2004b) again highlighting the influence of UVA on cell survival pathways. This appears to occur via a posttranscriptional mechanism involving stabilization of the Bcl-XL messenger by binding of specific proteins to the 3′ untranslated region.

In addition to the activation of metalloproteinases (see the following), it has been shown that UVA may stimulate other proteases via activation of p38 kinase in human skin keratinocytes. For example, UVA activation of p38 MAPK in keratinocytes leads to granzyme B (a serine protease) induction via redox-dependent migration inhibitory factor (MIF) release, and this will facilitate degradation of extracellular matrix components (Hernandez-Pigeon et al. 2007). UVA irradiation is known to compromise gap junctional intercellular communication, and this has been associated with hyperphosphorylation and decreased levels of the highly expressed keratinocyte gap junction protein, Connexin 43 (Bellei et al. 2008). Although the authors showed that this was in part mediated by MAPK activation (at Ser 279 and Ser 282) and that this was correlated with the upstream activator of p38 MAPK, they did not directly demonstrate the involvement of p38 in UVA-mediated disruption of gap junctions due to the toxicity of the inhibitors.

Activation of JNK by UVA in both HaCaT cells and primary human keratinocytes has been linked to a cell survival pathway since inhibition of the kinase activity correlates with caspase 3, 8, and 9 activation; cleavage of the caspase substrate polyADP-ribose polymerase (PARP); and apoptotic cell death (Silvers et al. 2006).

58.5.3.1 ATM Kinase

Another important regulator of cell survival and cell cycle checkpoints, the DNA damage-inducible ATM kinase, has also been shown to be stimulated by UVA in an oxygen-dependent fashion (Zhang et al. 2002), and these authors also link ATM-dependent p53 and JNK pathways to UVA apoptosis.

58.5.3.2 PKR

Extracellular stress such as UVA irradiation of mouse epidermal cells (JB6 Cl41) can lead to phosphorylation (Thr 451) of PKR (double-stranded RNA-dependent protein kinase R) via ERK2 (or growth factor-regulated S6 kinase RSK2, p90 ribosomal S6 kinase) but not p38 kinase activation (Zykova et al. 2007). UVA-activated PKR can then cause protein synthesis inhibition by phosphorylating the alpha subunit of protein synthesis initiation factor eIF2, which is involved in both anti-viral and apoptotic pathways.

58.5.3.3 EGFR

The EGFR, a membrane surface receptor, is a member of the ErgB family of proteins, which are tyrosine kinases. It binds to specific ligands such as the epidermal growth factor (EGF) and transforming growth factor alpha (TGF-alpha) so that EGFR undergoes a transition from an inactive monomeric form to an active homodimer with tyrosine kinase activity. The subsequent autophosphorylation elicits downstream activation and signaling via SH2 domains, which in turn initiates several signal transduction pathways, principally the MAPK, Akt, and JNK pathways, leading to DNA synthesis and cell proliferation. Activation of the receptor is important for the innate immune response in human skin. Upregulation of EGFR can lead to various types of cancer, and it is therefore a much-studied oncogene. EGFR activation by UV is a critical event in keratinocyte transformation, but the mechanism that links the EGFR pathway and photocarcinogenesis remains unclear. It has been known for some time that UV and oxidants induce ligand-independent activation of numerous receptor tyrosine kinases including EGFR at the inner side of the plasma membrane (e.g., Devary et al. 1992; Sachsenmaier et al. 1994; Schieven et al. 1994; Coffer et al. 1995) and one pathway by which UVA achieves this is inhibition of tyrosine phosphatase activity (Knebel et al. 1996). Activation of EGFR leads to a cascade of downstream kinase activation. For example, UVA irradiation of EGFR in (murine epidermal) cells can lead to activation of p70(S6K)/p90(RSK) through phosphatidylinositol (PI)-3 kinase and extracellular receptor-activated kinases (ERKs). Results with $EGFR^{-/-}$ cells indicated that that UVA-induced EGFR signaling may be required for activation of p90(RSK)/p70(S6K), PI3 kinase, and ERKs but not JNKs or p38kinase in this mouse cell line (Zhang et al. 2001b). In contrast, Mazière et al. (2003) presented evidence that UVA could inhibit EGF signaling in human fibroblasts (MRC5) and that a high dose of UVA (9 J/cm^2) prevented the EGF-induced Tyr phosphorylation of the EGF receptor. However, in human HaCaT keratinocytes, exposure to UVA induces EGFR internalization and downregulation without receptor phosphorylation and ubiquitination (He et al. 2003). This indicates that unlike EGF, UVA can downregulate the receptor in the absence of kinase activity. In contrast to the situation with the EGF ligand, receptor kinase activity appears not to be required for receptor downregulation by UVA. Indeed, it has been considered that EGFR downregulation by UVA may play an important role in the execution of the cell suicide program by attenuating its anti-apoptotic function. Again using human HaCaT keratinocytes as well as normal human keratinocytes, Jean et al. (2007) observed that low doses of UVA irradiation led to EGFR-mediated Akt activation which in turn resulted in increased levels of checkpoint 1 kinase (Chk1) phosphorylation (Ser280). The consequent inhibition of G2/M arrest is again likely to be crucial in UVA photocarcinogenesis since damaged cells may replicate and mutate. He et al. (2008) also showed that low doses of UVA induce dose-dependent cell cycle progression in human HaCaT keratinocytes via PI3 (PI3-OH) kinase/Akt activation and linked it to UVA-induced cyclin D1 accumulation. Importantly, these authors also showed that the activation of the EGFR/AKt/cyclin D1 pathway and cell cycle progression to the S phase are mediated by an ADAM17 metalloproteinase and disintegrin pathway. Another potentially crucial factor in malignant transformation by UVA is that activation of EGFR by UVA irradiation of HaCaT cells potentiates anchorage-independent growth of the keratinocytes and that this is

abrogated by ErbB2 inhibition (Han et al. 2008). Low doses of UVA increases Erb 2 expression in both the skin of hairless mice and in HaCaT keratinocytes via cAMP- and protein kinase-dependent AP-2 alpha activation. Finally, a recent study by Jean et al. (2009) has linked UVA activation of EGFR with both loss of cell-to-cell contact as a result of beta-catenin/E-cadherin/alpha-catenin dissociation (via beta-catenin phosphorylation at the tyrosine Y654 residue) and the nuclear relocalization of beta-catenin to generate a beta-catenin/T-cell factor 4 (TCF4) complex, which mediates the activation of matrix metalloproteinase (MMP)-1. Both these events are likely to stimulate keratinocyte invasiveness following UVA.

Another protein tyrosine kinase, Abelson-related gene (Arg), is also highly upregulated by UVA in normal human keratinocytes (Klosner et al. 2008).

58.5.3.4 Phosphatases

UVA radiation is known to activate a specific protein tyrosine phosphatase (Keyse and Emslie 1992), which can downregulate protein kinases by dephosphorylation. However, UVA (and UVB) radiations can also degrade and irreversibly inactivate protein tyrosine phosphatases by the combined effect of substrate oxidation and calpain activation (Gulati et al. 2004).

58.5.4 Transcription Factors

58.5.4.1 Nuclear Factor-kappaB

Nuclear factor-kappaB (NFkappaB) is an ubiquitous transcriptional activator intimately involved in a variety of inflammation-related events and which was recognized as redox sensitive in pioneering studies by Bauerle and co-workers (Schreck et al. 1992).This factor would therefore be expected to be responsive to UVA, and indeed, it was shown that relatively low doses of UVA activate NFkB binding to DNA in human skin fibroblasts (Vile et al. 1995). Although activation of NFkB by UVC and UVB radiations has been reported, Vile et al. found that in human skin fibroblasts activation was only observed at very high doses or where there was evidence of significant membrane damage. It was later shown (Reelfs et al. 2004) that the kinetics of appearance of NFkB accumulation in the nucleus was slow and that this was related to labile iron-dependent nuclear membrane damage. Indeed, the work supported the concept that oxidized lipids are a crucial intermediate in UVA-mediated NFkB activation and may underlie the role of UVA in skin inflammation. UVA enhanced NFkB binding to DNA was also observed in keratinocytes (HaCaT, Shang et al. 2002) and a human epithelial cell line (Hellweg and Baumstark-Khan 2007). However, in normal human melanocytes, both negative (Shang et al. 2002) and positive (Larsson et al. 2006) results for activation of this transcription factor have been reported.

58.5.4.2 Signal Transducers and Activators of Transcription

Various extracellular polypeptides are able to activate the signal transducers and activators of transcription (STATs), and these play a crucial role in gene activation. The proteins include a single tyrosine phosphorylation site and, in a dimeric partner molecule, an Src homology 2 (SH2) phosphotyrosine-binding domain, a DNA interaction domain, and a number of protein–protein interaction domains (for review see Darnell 1997). They are now one of the most studied classes of transcription factors because they are often inappropriately activated in cancer and have been implicated in the carcinogenesis process since they regulate genes involved in cell proliferation, survival, differentiation, angiogenesis, and invasion. Many such target genes coding the oncogenic transcription factors are now known (Alvarez and Frank 2004). The promoter (DNA)-binding activity of STAT1 was enhanced by low UVA doses in a keratinocyte cell line (NCTC 2544) but higher doses caused inhibition (Mazière et al. 2000). Inhibitor studies indicated that phosphorylation by both serine/threonine kinases and mitogen-activated protein kinase kinase (MEK) was involved. These authors also observed nuclear transport of STAT 1 after UVA. Using a mouse epidermal cell line (JB6), Zhang et al. (2001c) showed that phosphorylation of STAT 3

(at Ser 727) occurs following UVA radiation, and that this occurs via MSK1 and JNKs but not ERKs or p38 kinase. These phenomena have not yet been linked directly to UVA carcinogenesis but the link between the signal transducers and activators of transcription (STAT) activation and cancer remains intensely studied (e.g., Behera et al. 2010).

58.5.4.3 Nrf2

Nuclear factor (erythroid-derived 2)-like 2 (Nrf2) is the most studied member of a transcription factor family involved in regulating genes involved in the cellular stress response and phase 2 proteins and has been strongly implicated in chemoprevention of carcinogenesis. The Nrf2 protein normally resides in the cytoplasm bound to Kelch-like-ECH-associated protein 1 (KEAP1) and is rapidly degraded by the ubiquitination pathway. Under stress conditions, the protein appears to be stabilized and move to the nucleus where it binds to small Maf proteins (typically MafK) to form a powerful activating transcription factor (ATF) that binds to the Maf-associated responsive element (MARE) present in a number of stress-activated genes. In a classical set of experiments, Gao and Talalay (2004) used retinal pigment epithelial cells derived from mice that had Nrf2 or the repressor KEAP1 (or both) disrupted and showed that these cells became photosensitive (300–400 nm). Hirota et al. (2005) demonstrated that UVA radiation could lead to nuclear accumulation of Nrf2 in human skin fibroblasts and that this appeared to have a protective role against UVA-induced apoptosis. Later, Zhong et al. (2010a) confirmed the UVA stabilization and nuclear accumulation of Nrf2 and using specific short interfering RNA (SiRNA) against Nrf2 demonstrated that this protein was involved in protection against UVA-induced membrane damage and that the response is dependent on heme levels. The UVA-mediated Nrf2 response is also correlated with the UVA generation of oxidized phospholipids (Gruber et al. 2010).

It should be noted that activation of Nrf2 by various agents (e.g., sulforafane and flavonoid antioxidants such as quercetin) has been implicated in photoprotection (e.g., Gao and Talalay 2004; Kimura et al. 2009).

58.5.4.4 Bach1

Bach1 (BTB and CNC homology 1, basic leucine zipper transcription factor 1) like Nrf2 forms a heterodimeric transcription factor by binding to Mafk but the Bach1/Maf complex acts as a negative regulatory protein and binds to the MARE site of HO-1 to prevent transcription (Sun et al. 2004). Heme is crucial to Bach1 activity since it loses DNA-binding activity when bound to heme (Ogawa et al. 2001), and heme also promotes its degradation (Zenke-Kawasaki et al. 2007) and nuclear transport (Suzuki et al. 2004). Bach1 bound to the HO-1 promoter prevents UVA activation of HO-1 under low heme conditions, and knockdown of Bach1 increases the resistance of keratinocytes to UVA-induced membrane damage (Zhong et al. 2010b).

58.5.4.5 ATF3

ATF3 is a member of the Ca2+- and cyclic adenosine monophosphate responsive element-binding protein (CREB) family of transcription factors, which are dependent on cyclic adenosine monophosphate (AMP). Transcription of this gene is substantially induced by relatively low (nonlethal) fluences of UVA radiation (Abe et al. 2003). Although the full significance in terms of the CREB-dependent genes has not been fully evaluated, ATF-dependent genes are involved both in immunity toll-like receptors and implicated in cancer biology.

58.5.5 Gene Induction and Significance

58.5.5.1 Heme Oxygenase 1

Induction of HO-1 by UVA radiation was first reported in human skin fibroblasts (Keyse and Tyrrell 1987, 1989) in work that identified a 32 kDa human stress protein that had also been shown to be induced by tumor promoters and heavy metals in various cell types. Lowering of cellular glutathione levels

strongly enhanced basal and induced levels of the gene (Lautier et al. 1992), and as had been shown previously for inactivation of skin fibroblast colony-forming ability, UVA-mediated HO-1 gene activation was shown to involve singlet oxygen (Basu-Modak and Tyrrell 1993). HO-1 induction remains the strongest general mammalian oxidative stress response observed to date (Applegate et al. 1991). It was recognized that the enzyme played an important role in protection against oxidative membrane damage (Vile et al. 1994), and as a crucial anti-apoptotic and anti-inflammatory protein, it has been implicated in numerous pathologies (Otterbein and Zuckerbraun 2005; Soares and Bach 2009).

Iron is one of the important by-products of heme catabolism by HO, and this, iron added to the direct release of labile iron in cells following UVA treatment, leads to a strong induction of the iron storage protein, ferritin (Vile and Tyrrell 1993). This immediate induction of HO-1 and delayed induction of ferritin are crucial to restoring heme and iron homeostasis in cells (see earlier section).

Considerable work in several laboratories has been devoted to elucidating the molecular mechanism of activation of the HO-1 protein. The HO-1 promoter of both the human and rodent gene contains two crucial *cis*-acting elements 4 and 10 Kb upstream of the start site known as Maf-activated response element (MARE) sites. Binding of a heterodimeric activator protein complex such as Nrf-2/MafK to these sites following stress replaces the inhibitory heterodimer, typically Bach1/MafK, to activate transcription (Sun et al. 2004). Recent work has shown that UVA stabilizes Nrf2 in a heme-dependent manner (Zhong et al. 2010a) and that both this pathway and the UVA-mediated heme-dependent release of the Bach1 heterodimer binding to the MARE site of the HO-1 promoter (Raval 2008; Zhong et al. 2010b) are crucial to UVA-mediated HO-1 gene activation.

Although the original observations concerning UVA-inducible HO-1 showed that the enzyme was strongly induced in skin fibroblasts (Keyse and Tyrrell 1989) and melanocytes (unpublished observations and Marrot et al. 2008), there was almost no induction in epidermal keratinocytes (Applegate et al. 1995). However, keratinocytes did express high levels of the constitutive enzyme HO-2, and it was postulated at the time that the lack of expression of induction of HO-1 reflected the low levels of free heme, a consequence of substantial levels of constitutive HO protein expression. It has now been shown that silencing of HO-2 expression (by specific siRNA knockdown) allows a strong basal and UVA-induced expression of HO-1 in epidermal keratinocytes (Zhong et al. 2010b). However, it is Bach1 itself that is the central factor suppressing HO-1 expression in fibroblasts since knockdown of Bach1 unlocks a strong constitutive expression of HO-1, which is not further enhanced by irradiation with UVA. These studies also strongly support the concept that it is the changing level of free heme that is the key to regulation of HO-1 expression and that the latter will be modified whenever HO is induced or constitutively expressed. This also explains the strong refractoriness to UVA induction of HO-1 by a second dose 24–48 h after the first one (Nöel and Tyrrell 1997) since at these times induced HO-1 levels will be high and free heme levels will be very low.

UVA radiation induces HO-1 in rodent skin, although quite unlike the human situation, the strongest response is seen in epidermal keratinocytes (Allanson and Reeve 2004).

58.5.5.2 Metalloproteinases

MMPs are a family of zinc-dependent proteinases (endopeptidases), which are involved in remodeling and degradation of the extracellular matrix proteins. The activity of MMPs is thought to be predominately posttranslationally regulated via proteolytic activation of precursor zymogens or via their naturally occurring endogenous inhibitors (Koch et al. 2009).

A phenomenon known as the "UV response" was first described in the late 1980s (for review see Herrlich et al. 2008) and involved the induction of a series of genes by short-wavelength UV. The earliest event detectable in the nucleus was the posttranslational modification of AP-1 (c-Jun/c-Fos), which was directly linked to the activation of the collagenase gene (MMP-1; Stein et al. 1989) via regulatory elements in the promoter. MMP-1 is known to initiate degradation of collagen type 1 and 2.The enzymes are crucial to cell proliferation, migration (adhesion/dispersion), differentiation, angiogenesis, apoptosis, and host defense and have been implicated in cancer metastasis. Importantly, UVA was shown to

induce both MMP-1 mRNA accumulation and protein synthesis following irradiation of human skin and human fibroblasts (Herrmann et al. 1993) and to mediate this via the generation of singlet oxygen (Wlaschek et al. 1995). Recently, the proteasome has been shown to be an integral part of the UVA stress response (Catalgol et al. 2009). Inhibition of the proteasomal system by UVA-induced protein oxidation led to c-jun phosphorylation and activation of AP-1, a transcription factor central to MMP-1 induction. Furthermore, overexpression of the proteasome or methionine sulfoxide reductase (MsrA), which repairs oxidized proteins, abrogated the UVA activation of MMP-1.

MMP-1 activation in skin fibroblasts has been shown to involve the UVA generation of organic peroxides and lipid peroxidation (Polte and Tyrrell 2004). Repeated (chronic) exposure of human skin fibroblasts to UVA radiation leads to a sustained overexpression of MMP-1 (Naru et al. 2005). In a recent study by Tanaka et al. (2009), UVA has been shown to downregulate the forkhead box gene, group O (FOXO) transcription factor (crucial in regulating insulin/insulin-like growth factor-1 signaling). Interestingly, interfering RNA knockdown of FOXO1A expression led to increased expression of MMP-1 and -2 implying a crucial role of this pathway in regulating metalloproteinase expression. As noted elsewhere, overexpression of phospholipid-hydroperoxide GPx can reduce UVA-induced MMP-1 expression (Wenk et al. 2004) by interfering with NFkB-mediated IL-6 release.

MMP-1 levels were slightly lowered by UVA treatment of epidermal keratinocytes (Scharffetter et al. 1991; Petersen et al. 1992) but later work with a SCC cell line (Ramos et al. 2004) and in HaCaT cells (Wertz et al. 2004, 2005) indicated significant induction of MMP-1 so that the cancer phenotype appears to have changed the induction pattern. Further support for the involvement of singlet oxygen in the response was obtained by Wertz et al. (2004) who modified the response using the natural singlet oxygen quencher, beta-carotene.

Metalloproteinases 1, 2, and 3 were all reported to be induced in human fibroblasts after UVA treatment (Herrmann et al. 1993). Activation of MMP-2 (and reduction in tissue inhibitors of matrix metalloproteinases (TIMPs)-2 activity) has been linked to increased secretion of thioredoxin following UVA treatment. One group (Kawaguchi et al. 1996) did not observe the induction of MMP-2 (type IV collagenase, gelatinase A) by UVA. Although other studies have independently reported UVA induction of MMP-2 in fibroblasts (e.g., Kut et al. 1997; Oh et al. 2004), a study in normal human keratinocytes (Steinbrenner et al. 2003) showed that UVA quite significantly lowered expression of both MMP-2 and MMP-9 (gelatinase B). No change in secretion of these proteins was seen by Onoue et al. (2003) but chronic (18 weeks) re-exposure of HaCaT cells to UVA treatment (He et al. 2006) actually led to increased secretion of MMP-9. In studies with human microvascular endothelial cells, UVA was shown to upregulate MMP-1 but downregulate MMP-2 (Cauchard et al. 2006), and this has been linked to impaired angiogenic phenotype of the dermal endothelial cells. The induction of MMP-3 (stromelysin 1) in fibroblasts by UVA has been the subject of (several) reports and appears to involve promoter activation through an AP-1 site (Sawamura et al. 1996). It is also induced in HaCaT cells (Wertz et al. 2005). Induction of MMP-10 (stromelysin-2) by UVA has been observed in a human SCC line by Ramos et al. (2004) and in HaCaT cells by Wertz et al. (2005).

Cytokines are intimately involved in the induction of MMP-1 by UVA since a rapid posttranslational activation of IL-1 has been shown to be linked to *de novo* IL-6 synthesis and both are involved in the early phase of MMP-1 induction (Wlaschek et al. 1994). Several studies (e.g., Wang et al. 2005) confirm a central role for IL-1 in MMP-1 activation, and this cytokine is excreted from keratinocytes following UVB radiation. Indeed, a second phase of induction of MMP-1 appears to be mediated via transcriptional activation of IL-1 through an autocrine loop. Indirect evidence implicates the UVA-mediated generation of singlet oxygen as the primary ROS involved in MMP-1 activation, and this was later linked to the singlet oxygen dependence of IL-1 and IL-6 activation (Wlaschek et al. 1995, 1997). Metalloproteinase inhibitors (e.g., TIMP-1 and -2) were not activated by UVA. Wlaschek et al. (1995) also directly demonstrated that singlet oxygen released by a thermolabile endoperoxide (disodium salt of 3,3′-(1,4-naphthylidene) dipropionate, NDPO2) strongly activated MMP-1 but not the metalloproteinase inhibitors. It should be noted that other ROS have been clearly demonstrated to activate MMP-1. For example,

Wenk et al. (1999) used fibroblasts overexpressing MnSOD, and these cells were shown to generate hydrogen peroxide as a result of the dismutation and lead to MMP-1 activation via the AP-1 site. More recently, it has been shown that macrophage MIF is involved in the upregulation of MMP-1 by UVA in dermal fibroblasts. Several protein kinase pathways (PKC, protein kinase A [PKA], Src family tyrosine kinase, MAPK, c-Jun, but not p38) have been implicated in this (Watanabe et al. 2004). Furthermore, experiments using MIF- and IL-1-deficient mice (Honda et al. 2008) have confirmed that the IL-1 beta/MIF cytokine network is involved in the upregulation of UVA-induced MMP-1 in dermal fibroblasts but in these studies there was an indication (using inhibitors) that p38 and JNK were also involved.

Ramos et al. (2004) showed involvement of MEK 1 and 2 and p38 in UVA-induced MMP-1 and MMP-10 activation in human SCC cells.

Among agents that have been shown to protect against MMP-1 activation by UVA are flavonoids (Basu-Modak et al. 2006). Beta-carotene can also prevent UVA-mediated MMP-1 activation in skin cells (Wertz et al. 2005), and dietary beta-carotene can suppress MMP-9 activation in mice (Minami et al. 2009). The authors conclude that this systemic effect is due to the prevention of cholesterol peroxidation, which is known to be mediated by UVA and to be a trigger for gene activation.

The influence of endogenous glutathione on UVA-induced gene activation was well established using the HO-1 model (see earlier section). Recently, new findings on redox regulation of MMP-1 have emerged. For example, the antioxidant oxidoreductase thioredoxin-1 (Trx) has been shown to inhibit UVA-induced MMP-1 activation (Buechner et al. 2008). Although these authors concluded that this was an effect on transcription, redox regulation of MMP-1 could occur at the posttranslational level. Koch et al. (2009) showed that reduced thiols such as cysteine or glutathione substantially reduced MMP-1 activity, and this effect was reversed by oxidizing radicals (e.g., the trolox radical). They concluded that these observations reflected redox control via derivatization or oxidation of a glutathione (GSH)–MMP-1 complex.

58.5.5.3 Intercellular Adhesion Molecule 1

ICAM-1 plays an important role in mediating leukocyte/keratinocyte adhesion and is therefore crucial to the inflammatory response. Although UVB radiation can prevent increased expression of ICAM-1 in murine epidermal Langerhans cells (LCs) as well as inhibiting LC function (Tang and Udey 1992), Krutmann and Grewe (1995) showed that both UVB and UVA could induce ICAM-1 in human skin keratinocytes, albeit by different mechanisms. Importantly, the activation of the AP-2 transcription factor on the ICAM-1 promoter of the human keratinocyte *ICAM-1* gene was shown to be the mechanism underlying this response (Grether-Beck et al. 1996), and this model system was used to show the crucial role of ceramide on UVA signaling (see earlier section). Interestingly, ICAM-1 (and E-selectin but not vascular cell adhesion molecule 1 [VCAM-1]) was induced by UVA but not UVB in human dermal microvascular epithelial cells (Heckmann et al. 1994) indicating an important role for these cells in skin inflammation. Further studies from this group (Heckmann et al. 1997) demonstrated that repeated exposure to UVA actually abrogated leukocyte adhesion to endothelial cells. Indeed, studies by Treina et al. (1996) indicated that UVA led to a decrease in ICAM-1 expression in both epidermis and epidermal keratinocytes, and although some increase in ICAM-1 was observed in dermal fibroblasts, ICAM-staining in the dermis was specific for vascular structures, a finding consistent with the data of Heckmann et al.

58.5.5.4 Cyclooxygenase-2

Cyclooxygenases generate the inflammatory mediators known as prostaglandins by breaking down arachidonate. Although such intermediates have been implicated in UVB erythema, studies using indomethacin (a cyclooxygenase inhibitor) indicated that prostaglandins were not involved in UVA erythema (Søndergaard et al. 1985). Nevertheless, cyclooxygenase activity was measured in human and murine skin fibroblasts (Hanson and DeLeo 1989) following UVA irradiation, and activation of COX-2 has been clearly demonstrated in HaCaT cells (Kvam et al. 1999) and in artificial human epidermis (Mahns et al. 2004). Although the latter authors reported that JNK rather than p38 signaling was

involved in COX-2 activation by solar-simulated light in this skin model, activation in keratinocytes appears to be mediated by p38 stabilization of the COX-2 mRNA (Bachelor et al. 2002). These authors conclude that MAPK's, JNK, and p38 are all involved in COX-2 stimulation by UVA activation, and AP-1 is a major factor.

58.5.5.5 NADPH Oxidase

UVA is now known to activate NADPH oxidase, and this is a primary source of UVA-induced ROS generation (primarily superoxide anion) in cells at sublethal doses (Valencia and Kochevar 2008). A direct consequence of this increase in ROS (as shown by Nox1 SiRNA knockdown experiments) is rapid initiation of PGE2 synthesis.

58.5.5.6 Methionine-*S*-Sulfoxide Reductase

The oxidized protein repair enzyme MSRA is expressed in human epidermis and upregulated by low doses of UVA radiation (and H_2O_2), but not by UVB (Ogawa et al. 2006). Its expression was also shown to be increased by repetitive exposure of human skin to simulate sunlight. MSRA reduces the methionine sulfoxide (MetO) to methionine, thus reversing the inactivation of proteins caused by oxidation of critical methionine residues. It is the only enzyme so far identified in human skin that is able to repair oxidative protein damage.

58.5.5.7 Modulation of Expression of Other Genes by UVA

An interesting preliminary report by Pastila and Leszczynski (2005a) indicated a UVA-mediated upregulation of N-cadherin and a downregulation of E-cadherin in a murine melanoma cell line. This was associated with a decrease in self-adhesion of melanoma cells and an increase in melanoma adhesion to epithelial cells with evident implications for metastatic potential. These authors also demonstrated the UVA-induced metastatic potential of these melanoma cells in mice (Pastila and Leszczynski 2005b). In a study of melanocyte proliferation in hairless SKH-2 mice, van Schanke et al. (2005) found that while a single (but not fractionated) doses of UVB led to a strong enhancement in proliferation, no change in proliferation rate was observed following any type of UVA dose regimen. In a study comparing UVA- and UVB-induced gene expression in primary human melanocytes (Zhang and Rosdahl 2003), proteins involved in cell growth (p73 and Nup88) were notably enhanced by UVA irradiation but induction of expression of these genes has not been noted in other cell types.

Grimbaldeston et al. (2003) showed that UVA irradiation of mouse epidermis or a murine keratinocyte cell line led to the induction of an oxidant-susceptible calcium-binding protein (S100A8) of significance in human psoriasis.

Finally, UVA has been shown (Breuckmann et al. 2004) to induce a reduction in neuron-specific enolase levels in acrosclerosis (a form of auto-immune rheumatic disorder). UVA has been used as an adjuvant treatment in moderately active systemic lupus erythematosus (Polderman et al. 2004). Such treatment has been associated with softening of sclerotic lesions but other UVA-mediated events such as T-cell apoptosis, metalloproteinase induction, and angiogenesis may all also be involved.

58.6 Disease and UVA Sensitivity

A human disease known to be uniquely sensitive to UVA radiation is Smith–Lemli–Opitz (SLO), an autosomal recessive mental retardation syndrome (Anstey and Taylor 1999). The greatest sensitivity was seen at 350 nm although in an examination of all known UK patients, no photosensitivity was observed in 10 out of the 23 people tested (Anstey et al. 1999). The genetic defect involves deficiency of the enzyme 7-dehydrocholesterol-7-reductase. Since cholesterol levels are reduced (and levels of 7-dehydrocholesterol increased), cholesterol supplementation has been used to treat the disease and has achieved limited success in alleviating some of the symptoms including photosensitivity (Azurdia et al. 2001; Starck et al. 2002). Unlike the short-wavelength UV sensitivity of cells from xeroderma pigmentosum

patients, sensitivity to UVA was not observed in skin cells derived from SLO patients. However, in a model system, exposing keratinocytes containing high 7-dehydrocholesterol levels and low cholesterol to UVA strongly enhanced ROS levels compared to nonsupplemented keratinocytes, and this was associated with enhanced UVA-induced cell death (Valencia et al. 2006; Valencia and Kochevar 2006). There is limited evidence that the extreme photosensitivity observed in Pellagra may be a UVA phenomenon (Wan and Anstey in preparation).

58.7 Conclusions

UVA has multiple effects on cells and tissues. In addition to causing damage to DNA which can lead to mutation, UVA damages other cellular macromolecules and triggers a series of stress responses indicative of wider damage. Damage to lipids in particular cannot only cause loss of membrane integrity at relatively low fluences but also lead to lipid intermediates, which have been heavily implicated in signaling and modulation of gene expression. UVA has been implicated as a human carcinogen for many years but it also plays a role in acute inflammatory skin damage as monitored by the dramatic HO-1 response. Furthermore, UVA activation of several types of proteinases causes both short- and long-term destruction of skin components that will contribute to the photoaging process. While we have not considered protection in the current review, the overwhelming evidence for the short- and long-term damaging consequences of UVA have already stimulated considerable scientific endeavor to find ways of preventing this damage and will continue to be a focus for the future.

References

Abe, T., Oue, N., Yasui, W., Ryoji, M. 2003. Rapid and preferential induction of ATF3 transcription in response to low doses of UVA light. *Biochem Biophys Res Commun* 310(4):1168–1174.

Agar, N.S., Halliday, G.M., Barnetson, R.S., Ananthaswamy, H.N., Wheeler, M., Jones, A.M. 2004. The basal layer in human squamous tumors harbors more UVA than UVB fingerprint mutations: A role for UVA in human skin carcinogenesis. *Proc Natl Acad Sci USA* 101:4954–4959.

Agon, V.V., Bubb, W.A., Wright, A., Hawkins, C.L., Davies, M.J. 2006. Sensitizer-mediated photooxidation of histidine residues: Evidence for the formation of reactive side-chain peroxides. *Free Radic Biol Med* 40:698–710.

Allanson, M., Reeve, V.E. 2004. Immunoprotective UVA (320–400 nm) irradiation upregulates heme oxygenase-1 in the dermis and epidermis of hairless mouse skin. *J Invest Dermatol* 122(4):1030–1036.

Alvarez, J.V., Frank, D.A. 2004. Genome-wide analysis of STAT target genes: Elucidating the mechanism of STAT-mediated oncogenesis. *Cancer Biol Ther* 3(11):1045–1050.

An, L., Dong, G.Q., Gao, Q., Zhang, Y., Hu, L.W., Li, J.H., Liu, Y. 2010. Effects of UVA on TNF-alpha, IL-1beta, and IL-10 expression levels in human keratinocytes and intervention studies with an antioxidant and a JNK inhibitor. *Photodermatol Photoimmunol Photomed* 26(1):28–35.

Anstey, A.V., Ryan, A., Rhodes, L.E., Charman, C.R., Arlett, C.F., Tyrrell, R.M., Taylor, C.R., Pearse, A.D. 1999. Characterization of photosensitivity in the Smith–Lemli–Opitz syndrome: A new congenital photosensitivity syndrome. *Br J Dermatol* 141(3):406–414.

Anstey, A.V., Taylor, C.R. 1999. Photosensitivity in the Smith–Lemli–Opitz syndrome: The US experience of a new congenital photosensitivity syndrome. *J Am Acad Dermatol* 41(1):121–123.

Applegate, L.A., Luscher, P., Tyrrell, R.M. 1991. Induction of heme oxygenase: A general response to oxidant stress in cultured mammalian cells. *Cancer Res* 51(3):974–978.

Applegate, L.A., Noël, A., Vile, G., Frenk, E., Tyrrell, R.M. 1995. Two genes contribute to different extents to the heme oxygenase enzyme activity measured in cultured human skin fibroblasts and keratinocytes: Implications for protection against oxidant stress. *Photochem Photobiol* 61(3):285–291.

Arai, S., Nakanishi, Y.H., Hayashi, M. 2000. Inhibitory effects of long-ultraviolet radiation of isolated chicken liver nuclei on the Mg^{2+}-dependent transition of chromatin structure. *J Vet Med Sci* 62:861–865.

Awasthi, Y.C., Yang, Y., Tiwari, N.K., Patrick, B., Sharma, A., Li, J., Awasthi, S. 2004. Regulation of 4-hydroxynonenal-mediated signaling by glutathione S-transferases. *Free Radic Biol Med* 37(5):607–619.

Azurdia, R.M., Anstey, A.V., Rhodes, L.E. 2001. Cholesterol supplementation objectively reduces photosensitivity in the Smith–Lemli–Opitz syndrome. *Br J Dermatol* 144(1):143–145.

Bachelor, M.A., Bowden, G.T. 2004a. UVA-mediated activation of signaling pathways involved in skin tumor promotion and progression. *Semin Cancer Biol* 14(2):131–138.

Bachelor, M.A., Bowden, G.T. 2004b. Ultraviolet A-induced modulation of Bcl-XL by p38 MAPK in human keratinocytes: Post-transcriptional regulation through the 3′-untranslated region. *J Biol Chem* 279(41):42658–42668.

Bachelor, M.A., Silvers, A.L., Bowden, G.T. 2002. The role of p38 in UVA-induced cyclooxygenase-2 expression in the human keratinocyte cell line, HaCaT. *Oncogene* 21(46):7092–7099.

Bae, S.I., Zhao, R., Snapka, R.M. 2008. PCNA damage caused by antineoplastic drugs. *Biochem Pharmacol* 76:1653–1668.

Baier, J., Maisch, T., Maier, M., Engel, E., Landthaler, M., Bäumler, W. 2006. Singlet oxygen generation by UVA light exposure of endogenous photosensitizers. *Biophys J* 91(4):1452–1459.

Balasubramanian, D., Du, X., Zigler, J.S.J. 1990. The reaction of singlet oxygen with proteins, with special reference to crystallins. *Photochem Photobiol* 52:761–768.

Bang, B., Rygaard, J., Baadsgaard, O., Skov, L. 2002. Increased expression of Fas on human epidermal cells after in vivo exposure to single-dose ultraviolet (UV) B or long-wave UVA radiation. *Br J Dermatol* 147(6):1199–1206.

Basu-Modak, S., Ali, D., Gordon, M., Polte, T., Yiakouvaki, A., Pourzand, C., Rice-Evans, C., Tyrrell, R.M. 2006. Suppression of UVA-mediated release of labile iron by epicatechin—A link to lysosomal protection. *Free Radic Biol Med* 41:1197–1204.

Basu-Modak, S., Lüscher, P., Tyrrell, R.M. 1996. Lipid metabolite involvement in the activation of the human heme oxygenase-1 gene. *Free Radic Biol Med* 20(7):887–897.

Basu-Modak, S., Tyrrell, R.M. 1993. Singlet oxygen. A primary effector in the UVA/near visible light induction of the human heme oxygenase gene. *Cancer Res* 53:4505–4510.

Behera, R., Kumar, V., Lohite, K., Karnik, S., Kundu, G.C. 2010. Activation of JAK2/STAT3 signaling by osteopontin promotes tumor growth in human breast cancer cells. *Carcinogenesis* 31(2):192–200.

Bellei, B., Mastrofrancesco, A., Briganti, S., Aspite, N., Ale-Agha, N., Sies, H., Picardo, M. 2008. Ultraviolet A induced modulation of gap junctional intercellular communication by P38 MAPK activation in human keratinocytes. *Exp Dermatol* 17(2):115–124.

Bennett, D.C. 2008. Ultraviolet wavebands and melanoma initiation. *Pigm Cell Melanoma Res* 21:520–524.

Bensasson, R.V., Land, E.J., Truscott, T.G. 1993. *Excited States and Free Radicals in Biology and Medicine: Contributions from Flash Photolysis and Pulse Radiolysis*. Oxford University Press, Oxford, U.K.

Berneburg, M., Gattermann, N., Stege, H., Grewe, M., Vogelsang, K., Ruzicka, T. et al. 1997. Chronically ultraviolet-exposed human skin shows a higher mutation frequency of mitochondrial DNA as compared to unexposed skin and the hematopoietic system. *Photochem Photobiol* 66:271–275.

Berneburg, M., Gremmel, T., Kürten, V., Schroeder, P., Hertel, I., von Mikecz, A., Wild, S., Chen, M., Declercq, L., Matsui, M., Ruzicka, T., Krutmann, J. 2005. Creatine supplementation normalizes mutagenesis of mitochondrial DNA as well as functional consequences. *J Investig Dermatol* 125(2):213–220.

Berneburg, M., Grether-Beck, S., Kürten, V., Ruzicka, T., Briviba, K., Sies, H., Krutmann, J. 1999. Singlet oxygen mediates the UVA-induced generation of the photoaging-associated mitochondrial common deletion. *J Biol Chem* 274(22):15345–15349.

Berneburg, M., Kamenisch, Y., Krutmann, J., Röcken, M. 2006. "To repair or not to repair—No longer a question": Repair of mitochondrial DNA shielding against age and cancer. *Exp Dermatol* 15(12):1005–1015. Review.

Berneburg, M., Krutmann, J. 1998. Mitochondrial DNA deletions in human skin reflect photo- rather than chronologic aging. *J Invest Dermatol* 111(4):709–710.

Berneburg, M., Krutmann, J. 2000. Photoageing-associated large-scale deletions of mitochondrial DNA. *Meth Enzymol* 319(34):366–376.

Berneburg, M., Plettenberg, H., Medve-König, K., Pfahlberg, A., Gers-Barlag, H., Gefeller, O., Krutmann, J. 2004. Induction of the photoaging-associated mitochondrial common deletion in vivo in normal human skin. *J Invest Dermatol* 122(5):1277–1283.

Besaratinia, A., Kim, S.I., Bates, S.E., Pfeifer, G.P. 2007. Riboflavin activated by ultraviolet A1 irradiation induces oxidative DNA damage-mediated mutations inhibited by vitamin C. *Proc Natl Acad Sci USA* 104:5953–5958.

Besaratinia, A., Kim, S., Pfeifer, G.P. 2008. Rapid repair of UVA-induced oxidized purines and persistence of UVB-induced dipyrimidine lesions determine the mutagenicity of sunlight in mouse cells. *FASEB J* 22:2379–2392.

Besaratinia, A., Synold, T.W., Chen, H.-H., Chang, C., Xi, B., Riggs, A., Pfeifer, G.P. 2005. DNA lesions induced by UV A1 and B radiation in human cells: Comparative analyses in the overall genome and in the *p53* tumor suppressor gene. *Proc Natl Acad Sci USA* 102:10058–10063.

Birch-Machin, M.A., Swalwell, H. 2010. How mitochondria record the effects of UV exposure and oxidative stress using human skin as a model tissue. *Mutagenesis* 25(2):101–107.

Biverstål, A., Johansson, R., Jenssen, D., Erixon, K. 2008. Cyclobutane pyrimidine dimers do not fully explain the mutagenicity induced by UVA in Chinese hamster cells. *Mutat Res* 648:32–39.

Brash, D.E., Rudolph, J.A., Simon, J.A., Lin, A., McKenna, G.J., Baden, H.P., Halperin, A.J., Ponten, J. 1991. A role for sunlight in skin cancer: UV-induced p53 mutations in squamous cell carcinoma. *Proc Natl Acad Sci USA* 88:10124–10128.

Bråthen, M., Bånrud, H., Berg, K., Moan, J. 2000. Induction of multinucleated cells caused by UVA exposure in different stages of the cell cycle. *Photochem Photobiol* 71(5):620–626.

Bravard, A., Vacher, M., Gouget, B., Coutant, A., de Boisferon, F.H., Marsin, S., Chevillard, S., Radicella, J.P. 2006. Redox regulation of human OGG1 activity in response to cellular oxidative stress. *Mol Cell Biol* 26:7430–7436.

Breuckmann, F., Appelhans, C., Bastian, A., Stuecker, M., Altmeyer, P., Kreuter, A. 2004. UVA1-induced decrease in dermal neuron-specific enolase (NSE) in acrosclerosis. *Arch Dermatol Res* 296(4):182–184.

Budai, M., Reynaud-Angelin, A., Szabó, Z., Tóth, S., Rontó, G., Sage, E., Gróf, P. 2004. Effect of UVA radiation on membrane fluidity and radical decay in human fibroblasts as detected by spin labeled stearic acids. *J Photochem Photobiol B* 77(1–3):27–38.

Buechner, N., Schroeder, P., Jakob, S., Kunze, K., Maresch, T., Calles, C., Krutmann, J., Haendeler, J. 2008. Changes of MMP-1 and collagen type Ialpha1 by UVA, UVB and IRA are differentially regulated by Trx-1. *Exp Gerontol* 43(7):633–637.

Bulteau, A.L., Moreau, M., Nizard, C., Friguet, B. 2002. Impairment of proteasome function upon UVA- and UVB-irradiation of human keratinocytes. *Free Radic Biol Med* 32(11):1157–1170.

Cadet, J., Douki, T., Ravanat, J.L., Di Mascio, P. 2009. Sensitized formation of oxidatively generated damage to cellular DNA by UVA radiation. *Photochem Photobiol Sci* 8:903–911.

Catalfo, A., Bracchita, G., de Guidi, G. 2009. Role of aromatic amino acid tryptophan UVA-photoproducts in the determination of drug photosensitization mechanism: A comparison between methylene blue and naproxen. *Photochem Photobiol Sci* 8:1467–1475.

Catalgol, B., Ziaja, I., Breusing, N., Jung, T., Höhn, A., Alpertunga, B., Schroeder, P., Chondrogianni, N., Gonos, E.S., Petropoulos, I., Friguet, B., Klotz, L.O., Krutmann, J., Grune, T. 2009. The proteasome is an integral part of solar ultraviolet a radiation-induced gene expression. *J Biol Chem* 284(44):30076–30086.

Cauchard, J.H., Robinet, A., Poitevin, S., Bobichon, H., Maziere, J.C., Bellon, G., Hornebeck, W. 2006. UVA-mediated down-regulation of MMP-2 and MT1-MMP coincides with impaired angiogenic phenotype of human dermal endothelial cells. *Biochem Biophys Res Commun* 345(2):681–687.

Chadwick, C.A., Potten, C.S., Nikaido, O., Matsunaga, T., Proby, C., Young, A.R. 1995. The detection of cyclobutane thymine dimers, (6–4) photolesions and the Dewar valence photoisomers in sections of UV-irradiated human skin using specific antibodies, and the demonstration of depth penetration effects. *J Photochem Photobiol B Biol* 28:163–170.

Charlier, M., Helene, C. 1972. Photochemical reactions of aromatic ketones with nucleic acids and their components. 3. Chain breakage and thymine dimerization in benzophenone photosensitized DNA. *Photochem Photobiol* 15:527–536.

Cheng, J.Z., Sharma, R., Yang, Y., Singhal, S.S., Sharma, A., Saini, M.K., Singh, S.V., Zimniak, P., Awasthi, S., Awasthi, Y.C. 2001. Accelerated metabolism and exclusion of 4-hydroxynonenal through induction of RLIP76 and hGST5.8 is an early adaptive response of cells to heat and oxidative stress. *J Biol Chem* 276:41213–41223.

Clingen, P.H., Arlett, C.F., Roza, L., Mori, T., Nikaido, O., Green, M.H.L. 1995. Induction of cyclobutane pyrimidine dimers, pyrimidine(6–4)pyrimidone photoproducts, and Dewar valence isomers by natural sunlight in normal human mononuclear cells. *Cancer Res* 55:2245–2248.

Coffer, P.J., Burgering, B.M., Peppelenbosch, M.P., Bos, J.L., Kruijer, W. 1995. UV activation of receptor tyrosine kinase activity. *Oncogene* 11(3):561–569.

Courdavault, S., Baudouin, C., Charveron, M., Favier, A., Cadet, J., Douki, T. 2004. Larger yield of cyclobutane dimers than 8 oxo-7,8-dihydroguanine in the DNA of UVA-irradiated human skin cells. *Mutat Res* 556:135–142.

Dahle, J., Kvam, E. 2003. Induction of delayed mutations and chromosomal instability in fibroblasts after UVA-, UVB-, and X-radiation. *Cancer Res* 63:1464–1469.

Dahle, J., Kvam, E., Stokke, T. 2005a. Bystander effects in UV-induced genomic instability: Antioxidants inhibit delayed mutagenesis induced by ultraviolet A and B radiation. *J Carcinog* 9(4):11.

Dahle, J., Noordhuis, P., Stokke, T., Svendsrud, D.H., Kvam, E. 2005b. Multiplex polymerase chain reaction analysis of UV-A- and UV-B-induced delayed and early mutations in V79 Chinese hamster cells. *Photochem Photobiol* 81:114–119.

D'Angelo, S., Ingrosso, D., Migliardi, V., Sorrentino, A., Donnarumma, G., Baroni, A., Masella, L., Tufano, M.A., Zappia, M., Galletti, P. 2005. Hydroxytyrosol, a natural antioxidant from olive oil, prevents protein damage induced by long-wave ultraviolet radiation in melanoma cells. *Free Radic Biol Med* 38:908–909.

D'Angelo, S., Ingrosso, D., Perfetto, B., Baroni, A., Zappia, M., Lobianco, L.L., Tufano, M.A., Galletti, P. 2001. UVA irradiation induces L-isoaspartyl formation in melanoma cell proteins. *Free Radic Biol Med* 31:1–9.

Danpure, H.J., Tyrrell, R.M. 1976. Oxygen-dependence of near-UV (365 nm) lethality and the interaction of near-UV and X-rays in two mammalian cell lines. *Photochem Photobiol* 23:171–177.

Darnell, J.E., Jr. 1997. STATs and gene regulation. *Science* 277(5332):1630–1635.

Davies, M.J. 2003. Singlet oxygen-mediated damage to proteins and its consequences. *Biochem Biophys Res Commun* 305:761–770.

Devary, Y., Gottlieb, R.A., Smeal, T., Karin, M. 1992. The mammalian ultraviolet response is triggered by activation of Src tyrosine kinases. *Cell* 71(7):1081–1091.

Didier, C., Kerblat, I., Drouet, C., Favier, A., Béani, J.C., Richard, M.J. 2001. Induction of thioredoxin by ultraviolet-A radiation prevents oxidative-mediated cell death in human skin fibroblasts. *Free Radic Biol Med* 31(5):585–598.

Dissemond, J., Schneider, L.A., Brenneisen, P., Briviba, K., Wenk, J., Wlaschek, M., Scharffetter-Kochanek, K. 2003. Protective and determining factors for the overall lipid peroxidation in ultraviolet A1-irradiated fibroblasts: In vitro and in vivo investigations. *Br J Dermatol* 149(2):341–349.

Douki, T., Perdiz, D., Grof, P., Kulucsics, Z., Moustacchi, E., Cadet, J., Sage, E. 1999. Oxidation of guanine in cellular DNA by solar UV radiation: Biological role. *Photochem Photobiol* 70:184–190.

Douki, T., Reynaud-Angelin, A., Cadet, J., Sage, E. 2003. Bipyrimidine photoproducts rather than oxidative lesions are the main type of DNA damage involved in the genotoxic effect of solar UVA radiation. *Biochemistry* 42:9221–9226.

Drobetsky, E.A., Turcotte, J., Chateauneuf, A. 1995. A role for ultraviolet A in solar mutagenesis. *Proc Natl Acad Sci USA* 92:2350–2354.

Eiberger, W., Volkmer, B., Amouroux, R., Dhérin, C., Radicella, J.P., Epe, B. 2008. Oxidative stress impairs the repair of oxidative DNA base modifications in human skin fibroblasts and melanoma cells. *DNA Repair* 7:912–921.

Eicker, J., Kürten, V., Wild, S., Riss, G., Goralczyk, R., Krutmann, J., Berneburg, M. 2003. Beta-carotene supplementation protects from photoaging-associated mitochondrial DNA mutation. *Photochem Photobiol Sci* 2(6):655–659.

Enninga, I.C., Groenendijk, R.T.L., Filon, A.R., van Zeeland, A.A., Simons, J.W.I.M. 1986. The wavelength dependence of U.V.-induced pyrimidine dimer formation, cell killing and mutation induction in human diploid skin fibroblast. *Carcinogenesis* 7:1829–1836.

Eshaghian, A., Vleugels, R.A., Canter, J.A., McDonald, M.A., Stasko, T., Sligh, J.E. 2006. Mitochondrial DNA deletions serve as biomarkers of aging in the skin, but are typically absent in nonmelanoma skin cancers. *J Invest Dermatol* 126:336–344.

Freeman, S.E., Hacham, H., Gange, R.W., Maytum, D.J., Sutherland, J.C., Sutherland, B.M. 1989. Wavelength dependence of pyrimidine dimer formation in DNA of human skin irradiated *in situ* with ultraviolet light. *Proc Natl Acad Sci USA* 86:5605–5609.

Furio, L., Berthier-Vergnes, O., Ducarre, B., Schmitt, D., Peguet-Navarro, J. 2005. UVA radiation impairs phenotypic and functional maturation of human dermal dendritic cells. *J Invest Dermatol* 125(5):1032–1038.

Gaboriau, F., Morlière, P., Marquis, I., Moysan, A., Gèze, M., Dubertret, L. 1993. Membrane damage induced in cultured human skin fibroblasts by UVA irradiation. *Photochem Photobiol* 58(4):515–520.

Gao, X., Talalay, P. 2004. Induction of phase 2 genes by sulforaphane protects retinal pigment epithelial cells against photooxidative damage. *Proc Natl Acad Sci USA* 101(28):10446–10451.

Gibbs, P.E., Kilbey, B.J., Banerjee, S.K., Lawrence, C.W. 1993. The frequency and accuracy of replication past a thymine–thymine cyclobutane dimer are very different in *Saccharomyces cerevisiae* and *Escherichia coli*. *J Bacteriol* 175:2607–2612.

Giglia-Mari, G., Sarasin, A. 2003. TP53 mutations in human skin cancers. *Hum Mutat* 21:217–228.

Girard, P.M., Pozzebon, M., Delacôte, F., Douki, T., Smirnova, V., Sage, E. 2008. Inhibition of S-phase progression triggered by UVA-induced ROS does not require a functional DNA damage checkpoint response in mammalian cells. *DNA Repair (Amst)* 7(9):1500–1516.

Girotti, A.W. 2001. Photosensitized oxidation of membrane lipids: Reaction pathways, cytotoxic effects, and cytoprotective mechanisms. *J Photochem Photobiol B.* 63(1–3):103–113.

Godar, D.E. 1999a. Light and death: Photons and apoptosis. *J Invest Dermatol Symp Proc* 4(1):17–23.

Godar, D.E. 1999b. UVA1 radiation triggers two different final apoptotic pathways. *J Invest Dermatol* 112(1):3–12.

Greenhough, A., Smartt, H.J.M., Moore, A.E., Roberts, H., Williams, A.C., Paraskeva, C., Kaidi, A. 2009. The COX-2/PGE2 pathway: Key roles in the hallmarks of cancer and adaptation to the tumour microenvironment. *Carcinogenesis* 30(3):377–386.

Grether-Beck, S., Bonizzi, G., Schmitt-Brenden, H., Felsner, I., Timmer, A., Sies, H., Johnson, J.P., Piette, J., Krutmann, J. 2000. Non-enzymatic triggering of the ceramide signalling cascade by solar UVA radiation. *EMBO J* 19(21):5793–5800.

Grether-Beck, S., Buettner, R., Krutmann, J. 1997. Ultraviolet A radiation-induced expression of human genes: Molecular and photobiological mechanisms. 1. *Biol Chem* 378(11):1231–1236.

Grether-Beck, S., Olaizola-Horn, S., Schmitt, H., Grewe, M., Jahnke, A., Johnson, J.P., Briviba, K., Sies, H., Krutmann, J. 1996. Activation of transcription factor AP-2 mediates UVA radiation- and singlet oxygen-induced expression of the human intercellular adhesion molecule 1 gene. *Proc Natl Acad Sci USA* 93(25):14586–14591.

Grether-Beck, S., Salahshour-Fard, M., Timmer, A., Brenden, H., Felsner, I., Walli, R., Füllekrug, J., Krutmann, J. 2008. Ceramide and raft signaling are linked with each other in UVA radiation-induced gene expression. *Oncogene* 27(35):4768–4778.

Grether-Beck, S., Timmer, A., Felsner, I., Brenden, H., Brammertz, D., Krutmann, J. 2005. Ultraviolet A-induced signaling involves a ceramide-mediated autocrine loop leading to ceramide de novo synthesis. *J Invest Dermatol* 125(3):545–553.

Grimbaldeston, M.A., Geczy, C.L., Tedla, N., Finlay-Jones, J.J., Hart, P.H. 2003. S100A8 induction in keratinocytes by ultraviolet A irradiation is dependent on reactive oxygen intermediates. *J Invest Dermatol* 121(5):1168–1174.

Gruber, F., Mayer, H., Lengauer, B., Mlitz, V., Sanders, J.M., Kadl, A. et al. 2010. NF-E2-related factor 2 regulates the stress response to UVA-1-oxidized phospholipids in skin cells. *FASEB J* 24(1):39–48.

Gruber, F., Oskolkova, O., Leitner, A., Mildner, M., Mlitz, V., Lengauer, B., Kadl, A., Mrass, P., Krönke, G., Binder, B.R., Bochkov, V.N., Leitinger, N., Tschachler, E. 2007. Photooxidation generates biologically active phospholipids that induce heme oxygenase-1 in skin cells. *J Biol Chem* 282(23):16934–16941.

Gulati, P., Markova, B., Göttlicher, M., Böhmer, F.D., Herrlich, P.A. 2004. UVA inactivates protein tyrosine phosphatases by calpain-mediated degradation. *EMBO Rep* 5(8):812–817.

Hacham, H., Freeman, S.E., Gange, R.W., Maytum, D.J., Sutherland, J.C., Sutherland, B.M. 1990. Does exposure of human skin *in situ* to 385 or 405 nm UV induce pyrimidine dimers in DNA? *Photochem Photobiol* 52:893–896.

Halliday, G.M., Agar, N.S., Barnetson, R.S., Ananthaswamy, H.N., Jones, A.M. 2005. UV-A fingerprint mutations in human skin cancer. *Photochem Photobiol* 81:3–8.

Han, C.Y., Lim, S.C., Choi, H.S., Kang, K.W. 2008. Induction of ErbB2 by ultraviolet A irradiation: Potential role in malignant transformation of keratinocytes. *Cancer Sci* 99(3):502–509.

Hanson, D.L., DeLeo, V.A. 1989. Long wave ultraviolet radiation stimulates arachidonic acid release and cyclooxygenase activity in mammalian cells in culture. *Photochem Photobiol* 49(4):423–430.

He, Y.Y., Council, S.E., Feng, L., Chignell, C.F. 2008. UVA-induced cell cycle progression is mediated by a disintegrin and metalloprotease/epidermal growth factor receptor/AKT/cyclin D1 pathways in keratinocytes. *Cancer Res* 68(10):3752–3758.

He, Y.Y., Huang, J.L., Block, M.L., Hong, J.S., Chignell, C.F. 2005. Role of phagocyte oxidase in UVA-induced oxidative stress and apoptosis in keratinocytes. *J Invest Dermatol* 125(3):560–566.

He, Y.Y., Huang, J.L., Chignell, C.F. 2004. Delayed and sustained activation of extracellular signal-regulated kinase in human keratinocytes by UVA: Implications in carcinogenesis. *J Biol Chem* 279(51):53867–53874.

He, Y.Y., Huang, J.L., Gentry, J.B., Chignell, C.F. 2003. Epidermal growth factor receptor down-regulation induced by UVA in human keratinocytes does not require the receptor kinase activity. *J Biol Chem* 278(43):42457–42465.

He, Y.Y., Pi, J., Huang, J.L., Diwan, B.A., Waalkes, M.P., Chignell, C.F. 2006. Chronic UVA irradiation of human HaCaT keratinocytes induces malignant transformation associated with acquired apoptotic resistance. *Oncogene* 25(26):3680–3688.

Heckmann, M., Eberlein-König, B., Wollenberg, A., Przybilla, B., Plewig, G. 1994. Ultraviolet-A radiation induces adhesion molecule expression on human dermal microvascular endothelial cells. *Br J Dermatol* 131(3):311–318.

Heckmann, M., Pirthauer, M., Plewig, G. 1997. Adhesion of leukocytes to dermal endothelial cells is induced after single-dose, but reduced after repeated doses of UVA. *J Invest Dermatol* 109(6):710–715.

Hellweg, C.E., Baumstark-Khan, C. 2007. Detection of UV-induced activation of NF-kappaB in a recombinant human cell line by means of enhanced green fluorescent protein (EGFP). *Radiat Environ Biophys* 46(3):269–279.

Hernandez-Pigeon, H., Jean, C., Charruyer, A., Haure, M.J., Baudouin, C., Charveron, M., Quillet-Mary, A., Laurent, G. 2007. UVA induces granzyme B in human keratinocytes through MIF: Implication in extracellular matrix remodeling. *J Biol Chem* 282(11):8157–8164.

Herrlich, P., Karin, M., Weiss, C. 2008. Supreme EnLIGHTenment: Damage recognition and signaling in the mammalian UV response. *Mol Cell* 29(3):279–290.

Herrling, T., Fuchs, J., Rehberg, J., Groth, N. 2003. UV-induced free radicals in the skin detected by ESR spectroscopy and imaging using nitroxides. *Free Radic Biol Med* 35(1):59–67.

Herrmann, G., Wlaschek, M., Lange, T.S., Prenzel, K., Goerz, G., Scharffetter-Kochanek, K. 1993. UVA irradiation stimulates the synthesis of various matrix-metalloproteinases (MMPs) in cultured human fibroblasts. *Exp Dermatol* 2(2):92–97.

Hirota, A., Kawachi, Y., Itoh, K., Nakamura, Y., Xu, X., Banno, T., Takahashi, T., Yamamoto, M., Otsuka, F. 2005. Ultraviolet A irradiation induces NF-E2-related factor 2 activation in dermal fibroblasts: Protective role in UVA-induced apoptosis. *J Invest Dermatol* 124(4):825–832.

Hoerter, J.D., Arnold, A.A., Kuczynska, D.A., Shibuya, A., Ward, C.S., Sauer, M.G., Gizachew, A., Hotchkiss, T.M., Fleming, T.J., Johnson, S. 2005. Effects of sublethal UVA irradiation on activity levels of oxidative defense enzymes and protein oxidation in *Escherichia coli*. *J Photochem Photobiol B* 81:171–180.

Hollaender, A. 1943. Effect of long ultraviolet and short visible radiation (3500 to 4900Å) on *Escherichia coli*. *J Bacteriol* 46(6):531–541.

Honda, A., Abe, R., Makino, T., Norisugi, O., Fujita, Y., Watanabe, H., Nishihira, J., Iwakura, Y., Yamagishi, S., Shimizu, H., Shimizu, T. 2008. Interleukin-1beta and macrophage migration inhibitory factor (MIF) in dermal fibroblasts mediate UVA-induced matrix metalloproteinase-1 expression. *J Dermatol Sci* 49(1):63–72.

Hu, M.L., Tappel, A.L. 1992. Potentiation of oxidative damage to proteins by ultraviolet-A and protection by antioxidants. *Photochem Photobiol* 56:357–363.

Huang, X.X., Bernerd, F., Halliday, G.M. 2009. Ultraviolet A within sunlight induces mutations in the epidermal basal layer of engineered human skin. *Am J Pathol* 174:1534–1543.

Ibuki, Y., Goto, R. 2002. Antiapoptotic effects induced by different wavelengths of ultraviolet light. *Photochem Photobiol* 75(5):495–502.

Ikehata, H., Kawai, K., Komura, J., Sakatsume, K., Wang, L., Imai, M., Higashi, S., Nikaido, O., Yamamoto, K., Hieda, K., Watanabe, M., Kasai, H., Ono, T. 2008. UVA1 genotoxicity is mediated not by oxidative damage but by cyclobutane pyrimidine dimers in normal mouse skin. *J Invest Dermatol* 128:2289–2296.

Ikehata, H., Nakamura, S., Asamura, T., Ono, T. 2004. Mutation spectrum in sunlight-exposed mouse skin epidermis: Small but appreciable contribution of oxidative stress-mediated mutagenesis. *Mutat Res* 556:11–24.

Jain, A., Rieger, I., Rohr, M., Schrader, A. 2010. Antioxidant efficacy on human skin *in vivo* investigated by UVA-induced chemiluminescence decay analysis via induced chemiluminescence of human skin. *Skin Pharmacol Physiol* 23(5):266–272.

Javeri, A., Huang, X.X., Bernerd, F., Mason, R.S., Halliday, G.M. 2008. Human 8-oxoguanine-DNA glycosylase 1 protein and gene are expressed more abundantly in the superficial than basal layer of human epidermis. *DNA Repair* 7:1542–1550.

Jean, C., Blanc, A., Prade-Houdellier, N., Ysebaert, L., Hernandez-Pigeon, H., Al Saati, T., Haure, M.J., Coluccia, A.M., Charveron, M., Delabesse, E., Laurent, G. 2009. Epidermal growth factor receptor/beta-catenin/T-cell factor 4/matrix metalloproteinase 1: A new pathway for regulating keratinocyte invasiveness after UVA irradiation. *Cancer Res* 69(8):3291–3299.

Jean, C., Hernandez-Pigeon, H., Blanc, A., Charveron, M., Laurent, G. 2007. Epidermal growth factor receptor pathway mitigates UVA-induced G2/M arrest in keratinocyte cells. *J Invest Dermatol* 127(10):2418–2424.

Jhappan, C., Noonan, F.P., Merlino, G. 2003. Ultraviolet radiation and cutaneous malignant melanoma. *Oncogene* 22:3099–3112.

Jiang, Y., Rabbi, M., Kim, M., Ke, C., Lee, W., Clark, R.L., Mieczkowski, P.A., Marszalek, P.E. 2009. UVA generates pyrimidine dimers in DNA directly. *Biophys J* 96:1151–1158.

Johnson, R.E., Prakash, S., Prakash, L. 1999. Efficient bypass of a thymine–thymine dimer by yeast DNA polymerase, Polη. *Science* 283:1001–1004.

Kamenisch, Y., Fousteri, M., Knoch, J., von Thaler, A.K., Fehrenbacher, B., Kato, H., Becker, T., Dollé, M.E., Kuiper, R., Majora, M., Schaller, M., van der Horst, G.T., van Steeg, H., Röcken, M., Rapaport, D., Krutmann, J., Mullenders, L.H., Berneburg, M. 2010. Proteins of nucleotide and base excision repair pathways interact in mitochondria to protect from loss of subcutaneous fat, a hallmark of aging. *J Exp Med* 207(2):379–390.

Kappes, U.P., Luo, D., Potter, M., Schulmeister, K., Rünger, T.M. 2006. Short- and long-wave UV light (UVB and UVA) induce similar mutations in human skin cells. *J Invest Dermatol* 126:667–675.

Kappes, U.P., Rünger, T.M. 2005. No major role for 7,8-dihydro-8-oxoguanine in ultraviolet light-induced mutagenesis. *Radiat Res* 164:440–445.

Kawaguchi, Y., Tanaka, H., Okada, T., Konishi, H., Takahashi, M., Ito, M., Asai, J. 1996. The effects of ultraviolet A and reactive oxygen species on the mRNA expression of 72-kDa type IV collagenase and its tissue inhibitor in cultured human dermal fibroblasts. *J Arch Dermatol Res* 288(1):39–44.

Keyse, S.M., Emslie, E.A. 1992. Oxidative stress and heat shock induce a human gene encoding a protein-tyrosine phosphatase. *Nature* 359(6396):644–647.

Keyse, S.M., Tyrrell, R.M. 1987. Both near ultraviolet radiation and the oxidizing agent hydrogen peroxide induce a 32-kDa stress protein in normal human skin fibroblasts. *J Biol Chem* 262(30):14821–14825.

Keyse, S.M., Tyrrell, R.M. 1989. Heme oxygenase is the major 32-kDa stress protein induced in human skin fibroblasts by UVA radiation, hydrogen peroxide, and sodium arsenite. *Proc Natl Acad Sci USA* 86(1):99–103.

Kielbassa, C., Roza, L., Epe, B. 1997. Wavelength dependence of oxidative DNA damage induced by UV and visible light. *Carcinogenesis* 18:811–816.

Kim, S.I., Pfeifer, G.P., Besaratinia, A. 2007. Mutagenicity of ultraviolet A radiation in the *lacI* transgene in Big Blue mouse embryonic fibroblasts. *Mutat Res* 617:71–78.

Kimura, S., Warabi, E., Yanagawa, T., Ma, D., Itoh, K., Ishii, Y., Kawachi, Y., Ishii, T. 2009. Essential role of Nrf2 in keratinocyte protection from UVA by quercetin. *Biochem Biophys Res Commun* 387(1):109–114.

Klosner, G., Varecka, R., Knobler, R., Trautinger, F. 2008. Ultraviolet-A and -B differentially modify the tyrosine-kinase profile of human keratinocytes and induce the expression of Arg+. *Photochem Photobiol* 84(2):261–265.

Klotz, L.O., Briviba, K., Sies, H. 1997. Singlet oxygen mediates the activation of JNK by UVA radiation in human skin fibroblasts. *FEBS Lett* 408 (3):289–291.

Klotz, L.O., Pellieux, C., Briviba, K., Pierlot, C., Aubry, J.M., Sies, H. 1999. Mitogen-activated protein kinase (p38-, JNK-, ERK-) activation pattern induced by extracellular and intracellular singlet oxygen and UVA. *Eur J Biochem* 260(3):917–922.

Knebel, A., Rahmsdorf, H.J., Ullrich, A., Herrlich, P. 1996. Dephosphorylation of receptor tyrosine kinases as target of regulation by radiation, oxidants or alkylating agents. *EMBO J* 15(19):5314–5325.

Koch, S., Volkmar, C.M., Kolb-Bachofen, V., Korth, H.G., Kirsch, M., Horn, A.H., Sticht, H., Pallua, N., Suschek, C.V. 2009. A new redox-dependent mechanism of MMP-1 activity control comprising reduced low-molecular-weight thiols and oxidizing radicals. *J Mol Med* 87(3):261–272.

Kozmin, S.G., Pavlov, Y.I., Kunkel, T.A., Sage, E. 2003. Roles of *Saccharomyces cerevisiae* DNA polymerases Polη and Polζ in response to irradiation by simulated sunlight. *Nucleic Acids Res* 31:4541–4552.

Kozmin, S., Slezak, G., Reynaud-Angelin, A., Elie, C., de Ryck, Y., Boiteux, S., Sage, E. 2005. Ultraviolet A radiation is highly mutagenic in cells that are unable to repair 7,8-dihydro-8-oxoguanine in *Saccharomyces cerevisiae. Proc Natl Acad Sci USA* 102:13538–13543.

Krishnan, K.J., Birch-Machin, M.A. 2006. The incidence of both tandem duplications and the common deletion in mtDNA from three distinct categories of sun-exposed human skin and in prolonged culture of fibroblasts. *J Invest Dermatol* 126:408–415.

Krishnan, K.J., Harbottle, A., Birch-Machin, M.A. 2004. The use of a 3895 bp mitochondrial DNA deletion as a marker for sunlight exposure in human skin. *J Invest Dermatol* 123:1020–1024.

Krönauer, C., Eberlein-König, B., Ring, J., Behrendt, H. 2001. Inhibition of histamine release of human basophils and mast cells in vitro by ultraviolet A (UVA) irradiation. *Inflamm Res* 50(Suppl 2):S44–S46.

Krönauer, C., Eberlein-König, B., Ring, J., Behrendt, H. 2003. Influence of UVB, UVA and UVA1 irradiation on histamine release from human basophils and mast cells in vitro in the presence and absence of antioxidants. *Photochem Photobiol* 77(5):531–534.

Krutmann, J. 1998. Therapeutic photoimmunology: Photoimmunological mechanisms in photo(chemo) therapy. *J Photochem Photobiol B* 44(2):159–164.

Krutmann, J., Grewe, M. 1995. Involvement of cytokines, DNA damage, and reactive oxygen intermediates in ultraviolet radiation-induced modulation of intercellular adhesion molecule-1 expression. *J Invest Dermatol* 105:67S–70S.

Kuluncsics, Z., Perdiz, D., Brulay, E., Muel, B., Sage, E. 1999. Wavelength dependence of ultraviolet-induced DNA damage distribution: Involvement of direct or indirect mechanisms and possible artefacts. *J Photochem Photobiol B Biol* 49:71–80.

Kut, C., Hornebeck, W., Groult, N., Redziniack, G., Godeau, G., Pellat, B. 1997. Influence of successive and combined ultraviolet A and B irradiations on matrix metalloelastases produced by human dermal fibroblasts in culture. *Cell Biol Int* 21(6):347–352.

Kvam, E., Hejmadi, V., Ryter, S., Pourzand, C., Tyrrell, R.M. 2000. Heme oxygenase activity causes transient hypersensitivity to oxidative UVA radiation dependent on release of iron from heme. *Free Radic Biol Med* 28:1191–1196.

Kvam, E., Noel, A., Basu-Modak, S., Tyrrell, R.M. 1999. Cyclooxygenase dependent release of heme from microsomal hemeproteins correlates with induction of heme oxygenase 1 transcription in human fibroblasts. *Free Radic Biol Med* 26(5–6):511–517.

Kvam, E., Tyrrell, R.M. 1997. Induction of oxidative DNA base damage in human skin cells by UV and near visible radiation. *Carcinogenesis* 18:2379–2384.

Kvam, E., Tyrrell, R.M. 1999. The role of melanin in the induction of oxidative DNA base damage by ultraviolet A irradiation of DNA or melanoma cells. *J Invest Dermatol* 113(2):209–213.

La, C., You, Y., Zhabyeyev, P., Pelzer, D.J., McDonald, T.F. 2006. Ultraviolet photoalteration of late NA+ current in guinea-pig ventricular myocytes. *J Membr Biol* 210(1):43–50.

Lamola, A.A. 1968. Excited state precursors of thymine photodimers. *Photochem Photobiol* 7:619–632.

Larsson, P., Ollinger, K., Rosdahl, I. 2006. Ultraviolet (UV)A- and UVB-induced redox alterations and activation of nuclear factor-kappaB in human melanocytes-protective effects of alpha-tocopherol. *Br J Dermatol* 155(2):292–300.

Lautier, D., Lüscher, P., Tyrrell, R.M. 1992. Endogenous glutathione levels modulate both constitutive and UVA radiation/oxidant-inducible expression of the human heme oxygenase gene. *Carcinogenesis* 13:227–232.

Le Panse, R., Dubertret, L., Coulomb, B. 2003. p38 mitogen-activated protein kinase activation by ultraviolet A radiation in human dermal fibroblasts. *Photochem Photobiol* 78(2):168–174.

Leszczynski, D., Leszczynski, K., Servomaa, K. 1995. Long-wave ultraviolet radiation causes increase of membrane-bound fraction of protein kinase C in rat myeloid leukemia cells. *Photodermatol Photoimmunol Photomed* 11(3):124–130.

Ley, R.D. 1997. Ultraviolet radiation A-induced precursors of cutaneous melanoma in *Monodelphis domestica*. *Cancer Res* 57(17):3682–3684.

Ley, R.D., Fourtanier, A. 2000. UVAI-induced edema and pyrimidine dimers in murine skin. *Photochem Photobiol* 72:485–487.

Mahns, A., Wolber, R., Stäb, F., Klotz, L.O., Sies, H. 2004. Contribution of UVB and UVA to UV-dependent stimulation of cyclooxygenase-2 expression in artificial epidermis. *Photochem Photobiol Sci.* 3(3):257–262.

Maresca, V., Flori, E., Briganti, S., Camera, E., Cario-André, M., Taïeb, A., Picardo, M. 2006. UVA-induced modification of catalase charge properties in the epidermis is correlated with the skin phototype. *J Invest Dermatol* 126(1):182–190.

Marrot, L., Jones, C., Perez, P., Meunier, J.R. 2008. The significance of Nrf2 pathway in (photo)-oxidative stress response in melanocytes and keratinocytes of the human epidermis. *Pigm Cell Melanoma Res* 21(1):79–88.

Masutani, C., Kusumoto, R., Yamada, A., Dohmae, N., Yokoi, M., Yuasa, M., Araki, M., Iwai, S., Takio, K., Hanaoka, F. 1999. The XPV (xeroderma pigmentosum variant) gene encodes human DNA polymerase η. *Nature* 399:700–704.

Matsui, M.S., DeLeo, V.A. 1990. Induction of protein kinase C activity by ultraviolet radiation. *Carcinogenesis* 11(2):229–234.

Matsui, M.S., Wang, N., MacFarlane, D., DeLeo, V.A. 1994. Long-wave ultraviolet radiation induces protein kinase C in normal human keratinocytes. *Photochem Photobiol* 59(1):53–57.

Mazière, C., Conte, M.A., Leborgne, L., Levade, T., Hornebeck, W., Santus, R., Mazière, J.C. 2001. UVA radiation stimulates ceramide production: Relationship to oxidative stress and potential role in ERK, JNK, and p38 activation. *Biochem Biophys Res Commun* 281(2):289–294.

Mazière, C., Dantin, F., Dubois, F., Santus, R., Mazière, J. 2000. Biphasic effect of UVA radiation on STAT1 activity and tyrosine phosphorylation in cultured human keratinocytes. *Free Radic Biol Med* 28(9):1430–1437.

Mazière, C., Floret, S., Santus, R., Morlière, P., Marcheux, V., Mazière, J.C. 2003. Impairment of the EGF signaling pathway by the oxidative stress generated with UVA. *Free Radic Biol Med* 34(6):629–636.

McMillan, T.J., Leatherman, E., Ridley, A., Shorrocks, J., Tobi, S.E., Whiteside, J.R. 2008. Cellular effects of long wavelength UV light (UVA) in mammalian cells. *J Pharm Pharmacol* 60(8):969–976.

Meewes, C., Brenneisen, P., Wenk, J., Kuhr, L., Ma, W., Alikoski, J., Poswig, A., Krieg, T., Scharffetter-Kochanek, K. 2001. Adaptive antioxidant response protects dermal fibroblasts from UVA-induced phototoxicity. 1. *Free Radic Biol Med* 30(3):238–247.

Merwald, H., Klosner, G., Kokesch, C., Der-Petrossian, M., Hönigsmann, H., Trautinger, F. 2005. UVA-induced oxidative damage and cytotoxicity depend on the mode of exposure. *J Photochem Photobiol B* 79(3):197–207.

Minami, Y., Kawabata, K., Kubo, Y., Arase, S., Hirasaka, K., Nikawa, T., Bando, N., Kawai, Y., Terao, J. 2009. Peroxidized cholesterol-induced matrix metalloproteinase-9 activation and its suppression by dietary beta-carotene in photoaging of hairless mouse skin. *J Nutr Biochem* 20(5):389–398.

Mitchell, D.L., Fernandez, A.A., Nairn, R.S., Garcia, R., Paniker, L., Trono, D., Thames, H.D., Gimenez-Conti, I. 2010. Ultraviolet A does not induce melanomas in a *Xiphophorus* hybrid fish model. *Proc Natl Acad Sci USA* 107(20):9329–9334.

Monfrecola, G., de Paulis, A., Prizio, E., Russo, I., Carfora, M., Santoianni, P., Marone, G. 2003. In vitro effects of ultraviolet A on histamine release from human basophils. *J Eur Acad Dermatol Venereol* 17(6):646–651.

Montaner, B., O'Donovan, P., Reelfs, O., Perrett, C.M., Zhang, X., Xu, Y.Z., Ren, X., Macpherson, P., Frith, D., Karran, P. 2007. Reactive oxygen-mediated damage to a human DNA replication and repair protein. *EMBO Rep* 8:1074–1079.

Mora-Ranjeva, M.P., Charveron, M., Fabre, B., Milon, A., Muller, I. 2006. Incorporation of phytosterols in human keratinocytes. Consequences on UVA-induced lipid peroxidation and calcium ionophore-induced prostaglandin release. *Chem Phys Lipids* 41(1–2):216–224.

Morita, A., Werfel, T., Stege, H., Ahrens, C., Karmann, K., Grewe, M., Grether-Beck, S., Ruzicka, T., Kapp, A., Klotz, L.O., Sies, H., Krutmann, J. 1997. Evidence that singlet oxygen-induced human T helper cell apoptosis is the basic mechanism of ultraviolet-A radiation phototherapy. *J Exp Med* 186(10):1763–1768.

Mouret, S., Baudouin, C., Charveron, M., Favier, A., Cadet, J., Douki, T. 2006. Cyclobutane pyrimidine dimers are predominant DNA lesions in whole human skin exposed to UVA radiation. *Proc Natl Acad Sci USA* 103:13765–13770.

Mouret, S., Philippe, C., Gracia-Chantegrel, J., Banyasz, A., Karpati, S., Markovitsi, D., Douki, T. 2010. UVA-induced cyclobutane pyrimidine dimers in DNA: A direct photochemical mechanism? *Org Biomol Chem* 8:1706–1711.

Naru, E., Suzuki, T., Moriyama, M., Inomata, K., Hayashi, A., Arakane, K., Kaji, K. 2005. Functional changes induced by chronic UVA irradiation to cultured human dermal fibroblasts. *Br J Dermatol* 153(Suppl 2):6–12.

Negishi, T., Nagaoka, C., Hayatsu, H., Suzuki, K., Hara, T., Kubota, M., Watanabe, M., Hieda, K. 2001. Somatic-cell mutation induced by UVA and monochromatic UV radiation in repair-proficient and -deficient *Drosophila melanogaster*. *Photochem Photobiol* 73:493–498.

Nöel, A., Tyrrell, R.M. 1997. Development of refractoriness of induced human heme oxygenase-1 gene expression to re-induction by UVA irradiation and hemin. *Photochem Photobiol* 66:456–463.

Ogawa, F., Sander, C.S., Hansel, A., Oehrl, W., Kasperczyk, H., Elsner, P., Shimizu, K., Heinemann, S.H., Thiele, J.J. 2006. The repair enzyme peptide methionine-S-sulfoxide reductase is expressed in human epidermis and upregulated by UVA radiation. *J Invest Dermatol* 126:1128–1134.

Ogawa, K., Sun, J., Taketani, S., Nakajima, O., Nishitani, C., Sassa, S., Hayashi, N., Yamamoto, M., Shibahara, S., Fujita, H., Igarashi, K. 2001. Heme mediates derepression of Maf recognition element through direct binding to transcription repressor Bach1. *EMBO J* 20(11):2835–2843.

Oh, J.H., Chung, A.S., Steinbrenner, H., Sies, H., Brenneisen, P. 2004. Thioredoxin secreted upon ultraviolet A irradiation modulates activities of matrix metalloproteinase-2 and tissue inhibitor of metalloproteinase-2 in human dermal fibroblasts. *Arch Biochem Biophys* 423(1):218–226.

Oikawa, S., Tada-Oikawa, S., Kawanishi, S. 2001. Site-specific DNA damage at the GGG sequence by UVA involves acceleration of telomere shortening. *Biochemistry* 40:4763–4768.

Onoue, S., Kobayashi, T., Takemoto, Y., Sasaki, I., Shinkai, H. 2003. Induction of matrix metalloproteinase-9 secretion from human keratinocytes in culture by ultraviolet B irradiation. *J Dermatol Sci* 33(2):105–111.

Otterbein, L., Zuckerbraun, B.S. (eds.). 2005. *Heme Oxygenase: The Elegant Orchestration of Its Products in Medicine*. Nova Science Publishers, New York.

Ou-Yang, H., Stamatas, G., Saliou, C., Kollias, N. 2004. A chemiluminescence study of UVA-induced oxidative stress in human skin in vivo. *J Invest Dermatol* 122(4):1020–1029.

Pastila, R., Leszczynski, D. 2005a. Ultraviolet A exposure alters adhesive properties of mouse melanoma cells. *Photodermatol Photoimmunol Photomed* 21(5):234–241.

Pastila, R., Leszczynski, D. 2005b. Ultraviolet A exposure might increase metastasis of mouse melanoma: A pilot study. *Photodermatol Photoimmunol Photomed* 21(4):183–190.

Pattison, D.I., Davies, M.J. 2006. Actions of ultraviolet light on cellular structures. In L.P. Bignold (ed.), *Cancer: Cell Structures, Carcinogens and Genomic Instability*, Birkhaüser Verlag, Switzerland, pp. 131–57.

Peak, M.J., Peak, J.G. 1990. Hydroxyl radical quenching agents protect against DNA breakage caused by both 365-nm UVA and by gamma radiation. *Photochem Photobiol* 51:649–652.

Peak, J.G., Peak, M.J. 1991. Comparison of initial yields of DNA-to-protein cross-links and single-strand breaks induced in cultured human-cells by far- and near-ultraviolet light, bluelight and X-rays. *Mutat Res* 246:187–191.

Perdiz, D., Grof, P., Mezzina, M., Nikaido, O., Moustacchi, E., Sage, E. 2000. Distribution and repair of bipyrimidine photoproducts in solar UV-irradiated mammalian cells. Possible role of Dewar photoproducts in solar mutagenesis. *J Biol Chem* 275:26732–26742.

Persson, A.E., Edström, D.W., Bäckvall, H., Lundeberg, J., Pontén, F., Ros, A.M., Williams, C. 2002. The mutagenic effect of ultraviolet-A1 on human skin demonstrated by sequencing the p53 gene in single keratinocytes. *Photodermatol Photoimmunol Photomed* 18:287–293.

Petersen, M., Hamilton, T., Li, H.L. 1995. Regulation and inhibition of collagenase expression by long-wavelength ultraviolet radiation in cultured human skin fibroblasts. *Photochem Photobiol* 62(3):444–448.

Petersen, M.J., Hansen, C., Craig, S. 1992. Ultraviolet A irradiation stimulates collagenase production in cultured human fibroblasts. *J Invest Dermatol* 99(4):440–444.

Pfeifer, G.P., You, Y.H., Besaratinia, A. 2005. Mutations induced by ultraviolet light. *Mutat Res* 571:19–31.

Phillipson, R.P., Tobi, S.E., Morris, J.A., McMillan, T.J. 2002. UV-A induces persistent genomic instability in human keratinocytes through an oxidative stress mechanism. *Free Radic Biol Med* 32:474–480.

Polderman, M.C., le Cessie, S., Huizinga, T.W., Pavel, S. 2004. Efficacy of UVA-1 cold light as an adjuvant therapy for systemic lupus erythematosus. *Rheumatology (Oxford)* 43(11):1402–1404.

Polte, T., Tyrrell, R.M. 2004. Involvement of lipid peroxidation and organic peroxides in UVA-induced matrix metalloproteinase-1 expression. *Free Radic Biol Med* 36(12):1566–1574.

Poswig, A., Wenk, J., Brenneisen, P., Wlaschek, M., Hommel, C., Quel, G., Faisst, K., Dissemond, J., Briviba, K., Krieg, T., Scharffetter-Kochanek, K. 1999. Adaptive antioxidant response of manganese-superoxide dismutase following repetitive UVA irradiation. *J Invest Dermatol* 112(1):13–18.

Pouget, J.-P., Douki, T., Richard, M.-J., Cadet, J. 2000. DNA damage induced in cells by gamma and UVA radiations as measured by HPLC/GC-MS, HPLC-EC and comet assay. *Chem Res Toxicol* 13:541–549.

Pourzand, C., Tyrrell, R.M. 1999. Apoptosis, the role of oxidative stress and the example of solar ultraviolet radiation. *Photochem Photobiol* 70:380–390.

Pourzand, C., Watkin, R., Brown, J., Tyrrell, R. 1999. UVA radiation induces immediate release of iron in human primary skin fibroblasts: The role of ferritin. *Proc Natl Acad Sci USA* 96:6751–6756.

Ramos, M.C., Steinbrenner, H., Stuhlmann, D., Sies, H., Brenneisen, P. 2004. Induction of MMP-10 and MMP-1 in a squamous cell carcinoma cell line by ultraviolet radiation. *J Biol Chem* 385(1):75–86.

Raval, C. 2008. The role of Bach 1 in ultraviolet-A mediated human heme oxygenase-1 gene regulation. PhD Thesis. University of Bath, England, U.K.

Recalcati, S., Minotti, G., Cairo, G. 2010. Iron regulatory proteins: From molecular mechanisms to drug development. *Antioxid Redox Signal* 13(10):1593–1616.

Reelfs, O., Tyrrell, R.M., Pourzand, C. 2004. Ultraviolet a radiation-induced immediate iron release is a key modulator of the activation of NF-kappaB in human skin fibroblasts. *J Invest Dermatol* 122(6):1440–1447.

Ridley, A.J., Whiteside, J.R., McMillan, T.J., Allison, S.L. 2009. Cellular and sub-cellular responses to UVA in relation to carcinogenesis. *Int J Radiat Biol* 85:177–195.

Rizwan, M., Rodriguez-Blanco, I., Harbottle, A., Watson, R., Birch-Machin, M., Rhodes, L. 2008. Lycopene protects against biomarkers of photodamage in human skin. *Br J Dermatol* 158:900.

Robert, C., Muel, B., Benoit, A., Dubertret, L., Sarasin, A., Stary, A. 1996. Cell survival and shuttle vector mutagenesis induced by ultraviolet A and ultraviolet B radiation in a human cell line. *J Invest Dermatol* 106:721–728.

Rochette, P.J., Therrien, J.-P., Drouin, R., Perdiz, D., Bastien, N., Drobetsky, E.A., Sage, E. 2003. UVA-induced cyclobutane pyrimidine dimers form predominantly at thymine-thymine dipyrimidines and correlate with the mutation spectrum in rodent cells. *Nucleic Acids Res* 31:2786–2794.

Rünger, T.M., Kappes, U.P. 2008. Mechanisms of mutation formation with long-wave ultraviolet light (UVA). *Photodermatol Photoimmunol Photomed* 24:2–10.

Ryter, S., Tyrrell, R.M. 1998. Singlet molecular oxygen ($^1O_2$): A possible effector of eukaryotic gene expression. *Free Radic Biol Med* 24:1520–1534.

Ryter, S.W., Tyrrell, R.M. 2000. The heme synthesis and degradation pathways: Role in oxidant sensitivity. *Free Radic Biol Med* 28:289–309.

Sachsenmaier, C., Radler-Pohl, A., Zinck, R., Nordheim, A., Herrlich, P., Rahmsdorf, H.J. 1994. Involvement of growth factor receptors in the mammalian UVC response. *Cell* 78(6):963–972.

Sage, E., Lamolet, B., Brulay, E., Moustacchi, E., Chateauneuf, A., Drobetsky, E.A. 1996. Mutagenic specificity of solar UV light in nucleotide excision repair-deficient rodent cells. *Proc Natl Acad Sci USA* 93:176–180.

Sander, C.S., Chang, H., Salzmann, S., Müller, C.S., Ekanayake-Mudiyanselage, S., Elsner, P., Thiele, J.J. 2002. Photoaging is associated with protein oxidation in human skin in vivo. *J Invest Dermatol* 118:618–625.

Sawamura, D., Ohta, T., Hanada, K., Ishikawa, H., Tamai, K., Yazima, H., Meng, X., Nomura, K., Hashimoto, I., Mauviel, A., Uitto, J. 1996. Involvement of the AP-1 site within the 5′-flanking region of the stromelysin-1 gene in induction of the gene expression by UVA irradiation. *Arch Dermatol Res* 288(10):628–632.

Scharffetter, K., Wlaschek, M., Hogg, A., Bolsen, K., Schothorst, A., Goerz, G., Krieg, T., Plewig, G. 1991. UVA irradiation induces collagenase in human dermal fibroblasts in vitro and in vivo. *Arch Dermatol Res* 283(8):506–511.

Schieven, G.L., Mittler, R.S., Nadler, S.G., Kirihara, J.M., Bolen, J.B., Kanner, S.B., Ledbetter, J.A. 1994. ZAP-70 tyrosine kinase, CD45, and T cell receptor involvement in UV- and H_2O_2-induced T cell signal transduction. *J Biol Chem* 269(32):20718–20726.

Schneider, L.A., Dissemond, J., Brenneisen, P., Hainzl, A., Briviba, K., Wlaschek, M., Scharffetter-Kochanek, K. 2006. Adaptive cellular protection against UVA-1-induced lipid peroxidation in human dermal fibroblasts shows donor-to-donor variability and is glutathione dependent. *Arch Dermatol Res* 297(7):324–328.

Schreck, R., Albermann, K., Baeuerle, P.A. 1992. Nuclear factor kappa B: An oxidative stress-responsive transcription factor of eukaryotic cells (a review). *Free Radic Res Commun* 17(4):221–237.

Schroeder, P., Gremmel, T., Berneburg, M., Krutmann, J. 2008. Partial depletion of mitochondrial DNA from human skin fibroblasts induces a gene expression profile reminiscent of photoaged skin. *J Invest Dermatol* 128(9):2297–2303.

Schuch, A.P., da Silva Galhardo, R., de Lima-Bessa, K.M., Schuch, N.J., Menck, C.F. 2009. Development of a DNA-dosimeter system for monitoring the effects of solar-ultraviolet radiation. *Photochem Photobiol Sci* 8:111–120.

Setlow, R.B., Grist, E., Thompson, K., Woodhead, A.D. 1993. Wavelengths effective in induction of malignant melanoma. *Proc Natl Acad Sci USA* 90:6666–6670.

Shang, J., Schwarz, C., Sanchez Ruderisch, H., Hertting, T., Orfanos, C.E., Tebbe, B. 2002. Effects of UVA and L-ascorbic acid on nuclear factor-kappa B in melanocytes and in HaCaT keratinocytes. *Skin Pharmacol Appl Skin Physiol* 15(5):353–359.

Shen, J., Bao, S., Reeve, V.E. 2000. UVA and UVB wavebands modulate expression of fasL in mouse skin epidermis. *Redox Rep* 5(2–3):154–155.

Shen, H.R., Spikes, J.D., Kopecková, P., Kopecek, J. 1996. Photodynamic crosslinking of proteins. II. Photocrosslinking of a model protein-ribonuclease A. *J Photochem Photobiol B* 35:213–219.

Shorrocks, J., Tobi, S.E., Latham, H., Peacock, J.H., Eeles, R., Eccles, D., McMillan, T.J. 2004. Primary fibroblasts from BRCA1 heterozygotes display an abnormal G1/S cell cycle checkpoint following UVA irradiation but show normal levels of micronuclei following oxidative stress or mitomycin C treatment. *Int J Radiat Oncol Biol Phys* 58(2):470–478.

Silvers, A.L., Bachelor, M.A., Bowden, G.T. 2003. The role of JNK and p38 MAPK activities in UVA-induced signaling pathways leading to AP-1 activation and c-Fos expression. *Neoplasia* 5(4):319–329.

Silvers, A.L., Finch, J.S., Bowden, G.T. 2006. Inhibition of UVA-induced c-Jun N-terminal kinase activity results in caspase-dependent apoptosis in human keratinocytes. *Photochem Photobiol* 82(2):423–431.

Smit, N., Musson, R., Romijn, F., van Rossum, H., van Pelt, J. 2009. Effects of ultraviolet A-1 radiation on calcineurin activity and cytokine production in (skin) cell cultures. *Photochem Photobiol.* 86(2):360–366.

Soares, M.P., Bach, F.H. 2009. Heme oxygenase-1: From biology to therapeutic potential. *Trends Mol Med* 15(2):50–58.

Søndergaard, J., Bisgaard, H., Thorsen, S. 1985. Eicosanoids in skin UV inflammation. *Photodermatol* 2(6):359–366.

Spikes, J.D., Shen, H.R., Kopecková, P., Kopecek, J. 1999. Photodynamic crosslinking of proteins. III. Kinetics of the FMN- and rose bengal-sensitized photooxidation and intermolecular crosslinking of model tyrosine-containing N-(2-hydroxypropyl)methacrylamide copolymers. *Photochem Photobiol* 70:130–137.

Spodheim-Maurizot, M., Charlier, M., Helene, C. 1985. Photochemical modifications of lac repressor: Effect of effectors binding on tryptophan photooxidation. *Photochem Photobiol* 42:353–359.

Starck, L., Lövgren-Sandblom, A., Björkhem, I. 2002. Cholesterol treatment forever? The first Scandinavian trial of cholesterol supplementation in the cholesterol-synthesis defect Smith–Lemli–Opitz syndrome. *J Intern Med* 252(4):314–321.

Stein, B., Rahmsdorf, H.J., Steffen, A., Litfin, M., Herrlich, P. 1989. UV-induced DNA damage is an intermediate step in UV-induced expression of human immunodeficiency virus type 1, collagenase, c-fos, and metallothionein. *Mol Cell Biol* 9(11):5169–5181.

Steinbrenner, H., Ramos, M.C., Stuhlmann, D., Sies, H., Brenneisen, P. 2003. UVA-mediated downregulation of MMP-2 and MMP-9 in human epidermal keratinocytes. *Biochem Biophys Res Commun* 308(3):486–491.

Sun, J., Brand, M., Zenke, Y., Tashiro, S., Groudine, M., Igarashi, K. 2004. Heme regulates the dynamic exchange of Bach1 and NF-E2-related factors in the Maf transcription factor network. *Proc Natl Acad Sci USA* 101(6):1461–1466.

Sutherland, J.C., Griffin, K.P. 1981. Absorption spectrum of DNA for wavelengths greater than 300 nm. *Radiat Res* 86:399–409.

Suzuki, H., Tashiro, S., Hira, S., Sun, J., Yamazaki, C., Zenke, Y., Ikeda-Saito, M., Yoshida, M., Igarashi, K. 2004. Heme regulates gene expression by triggering Crm1-dependent nuclear export of Bach1. *EMBO J* 23(13):2544–2553.

Tanaka, H., Murakami, Y., Ishii, I., Nakata, S. 2009. Involvement of a forkhead transcription factor, FOXO1A, in UV-induced changes of collagen metabolism. *J Invest Dermatol Symp Proc* 14(1):60–62.

Tang, A., Udey, M.C. 1992. Doses of ultraviolet radiation that modulate accessory cell activity and ICAM-1 expression are ultimately cytotoxic for murine epidermal Langerhans cells. *J Invest Dermatol* 99(5):71S–73S.

Thomas, N.E., Berwick, M., Cordeiro-Stone, M. 2006. Could BRAF mutations in melanocytic lesions arise from DNA damage induced by ultraviolet radiation? *J Invest Dermatol* 126:1693–1696.

Thorn, T., Gniadecki, R., Petersen, A.B., Vicanova, J., Wulf, H.C. 2001. Differences in activation of G2/M checkpoint in keratinocytes after genotoxic stress induced by hydrogen peroxide and ultraviolet A radiation. *Free Radic Res* 35(4):405–416.

Treina, G., Scaletta, C., Fourtanier, A., Seité, S., Frenk, E., Applegate, L.A. 1996. Expression of intercellular adhesion molecule-1 in UVA-irradiated human skin cells in vitro and in vivo. *Br J Dermatol* 135(2):241–247.

Tyrrell, R.M. 1973. Induction of pyrimidine dimers in bacterial DNA by 365 nm radiation. *Photochem Photobiol* 17:69–73.

Tyrrell, R.M. 1978. Radiation synergism and antagonism. In K.C. Smith (ed.), *Photochemical and Photobiological Reviews*, Vol. 3, Plenum Publishing Corporation, New York, pp. 35–113.

Tyrrell, R.M. 1991. UVA (320–380 nm) radiation as an oxidative stress. In H. Sies (ed.), *Oxidative Stress: Oxidants and Antioxidants*, Academic Press, London, U.K., pp. 57–83.

Tyrrell, R.M. 1996a. Activation of mammalian gene expression by the UV component of sunlight—From models to reality. *Bioessays* 18 139–148.

Tyrrell, R.M. 1996b. UV activation of mammalian stress proteins. In U. Feige, R.I. Morimoto, I. Yahara, B.S. Polla (eds.), *Stress-Inducible Cellular Responses*, Birkhäuser Verlag, Basel, Switzerland, pp. 255–272.

Tyrrell, R.M. 2005. Heme oxygenase—A crucial enzyme in iron and heme homeostasis. In L. Otterbein, B.S. Zuckerbraun (eds.), *Heme Oxygenase: The Elegant Orchestration of Its Products in Medicine,* Nova Science Publishers, New York, pp. 333–349.

Tyrrell, R.M., Ley, R.D., Webb, R.B. 1974. Induction of single-strand breaks (alkali-labile bonds) in bacterial and phage DNA by near UV (365 nm) radiation. *Photochem Photobiol* 20:395–398.

Tyrrell, R.M., Pidoux, M. 1986. Endogenous glutathione protects human skin fibroblasts against the cytotoxic action of UVB, UVA and near-visible radiations. *Photochem Photobiol* 44:561–564.

Tyrrell, R.M., Pidoux, M. 1989. Singlet oxygen involvement in the inactivation of cultured human fibroblasts by UVA (334 nm, 365 nm) and near-visible radiations. *Photochem Photobiol* 49:407–412.

Tyrrell, R.M., Reeve, V. 2006. Potential protection of skin by acute UVA irradiation—From cellular to animal models. (Overview paper: International workshop on UV exposure guidance 17th–18th Oct 2005, Munich, Germany). *Progr Biophys Mol Biol* 92:86–91.

Tyrrell, R.M., Webb, R.B. 1973. Reduced dimer excision in bacteria following near-ultraviolet (365 nm) radiation. *Mutat Res* 19:361–364.

Tyrrell, R.M., Webb, R.B., Brown, M.S. 1973. Destruction of the photoreactivating enzyme by 365 nm radiation. *Photochem Photobiol* 18:249–254.

Valencia, A., Kochevar, I.E. 2006. Ultraviolet A induces apoptosis via reactive oxygen species in a model for Smith–Lemli–Opitz syndrome. *Free Radic Biol Med* 40(4):641–650.

Valencia, A., Kochevar, I.E. 2008. Nox1-based NADPH oxidase is the major source of UVA-induced reactive oxygen species in human keratinocytes. *J Invest Dermatol* 128(1):214–222.

Valencia, A., Rajadurai, A., Carle, A.B., Kochevar, I.E. 2006. 7-Dehydrocholesterol enhances ultraviolet A-induced oxidative stress in keratinocytes: Roles of NADPH oxidase, mitochondria, and lipid rafts. *Free Radic Biol Med* 41(11):1704–1718.

van Kranen, H.J., de Laat, A., van de Ven, J., Wester, P.W., de Vries, A., Berg, R.J., van Kreijl, C.F., de Gruijl, F.R. 1997. Low incidence of p53 mutations in UVA (365-nm)-induced skin tumors in hairless mice. *Cancer Res* 57:1238–1240.

van Schanke, A., Jongsma, M.J., Bisschop, R., van Venrooij, G.M., Rebel, H., de Gruijl, F.R. 2005. Single UVB overexposure stimulates melanocyte proliferation in murine skin, in contrast to fractionated or UVA-1 exposure. *J Invest Dermatol* 124:241–247.

Vile, G.F., Basu-Modak, S., Waltner, C., Tyrrell, R.M. 1994. Heme oxygenase 1 mediates an adaptive response to oxidative stress in human skin fibroblasts. *Proc Natl Acad Sci USA* 91:2607–2610.

Vile, G.F., Tanew-Ilitschew, A., Tyrrell, R.M. 1995. Activation of NF-kappa B in human skin fibroblasts by the oxidative stress generated by UVA radiation. *Photochem Photobiol* 62(3):463–468.

Vile, G.F., Tyrrell, R.M. 1993. Oxidative stress resulting from ultraviolet A irradiation of human skin fibroblasts leads to a heme oxygenase-dependent increase in ferritin. *J Biol Chem* 268:14678–14681.

Vile, G.F., Tyrrell, R.M. 1995. UVA radiation-induced oxidative damage to lipids and proteins in vitro and in human skin fibroblasts is dependent on iron and singlet oxygen. *Free Radic Biol Med* 18:721–730.

von Montfort, C., Sharov, V.S., Metzger, S., Schöneich, C., Sies, H., Klotz, L.O. 2006. Singlet oxygen inactivates protein tyrosine phosphatase-1B by oxidation of the active site cysteine. *Biol Chem* 387:1399–1404.

Wang, X., Bi, Z., Chu, W., Wan, Y. 2005. IL-1 receptor antagonist attenuates MAP kinase/AP-1 activation and MMP1 expression in UVA-irradiated human fibroblasts induced by culture medium from UVB-irradiated human skin keratinocytes. *Int J Mol Med* 16(6):1117–1124.

Wang, H.T., Choi, B., Tang, M.S. 2010. Melanocytes are deficient in repair of oxidative DNA damage and UV-induced photoproducts. *Proc Natl Acad Sci USA* 107(27):12180–12185.

Wang, S.Q., Setlow, R.B., Berwick, M., Polsky, D., Marghooh, A.A., Kopf, A.W., Bart, R.S. 2001. Ultraviolet A and melanoma: A review. *J Am Acad Dermatol* 44:837–846.

Watanabe, H., Shimizu, T., Nishihira, J., Abe, R., Nakayama, T., Taniguchi, M., Sabe, H., Ishibashi, T., Shimizu, H. 2004. Ultraviolet A-induced production of matrix metalloproteinase-1 is mediated by macrophage migration inhibitory factor (MIF) in human dermal fibroblasts. *J Biol Chem* 279(3):1676–1683.

Watkin, R.D., Tyrrell, R.M. 2000. Study of the relationship between endogenous protoporphyrin IX concentration in human lymphoblastoid cells and inactivation by UVA radiation. *Radiat Protect Dosim* 91:85–88.

Webb, R.B., Lorenz, J.R. 1970. Oxygen dependence and repair of lethal effects of near ultraviolet and visible light. *Photochem Photobiol* 12:283–289.

Wenk, J., Brenneisen, P., Wlaschek, M., Poswig, A., Briviba, K., Oberley, T.D., Scharffetter-Kochanek, K. 1999. Stable overexpression of manganese superoxide dismutase in mitochondria identifies hydrogen peroxide as a major oxidant in the AP-1-mediated induction of matrix-degrading metalloprotease-1. 1. *J Biol Chem* 274(36):25869–25876.

Wenk, J., Schüller, J., Hinrichs, C., Syrovets, T., Azoitei, N., Podda, M., Wlaschek, M., Brenneisen, P., Schneider, L.A., Sabiwalsky, A., Peters, T., Sulyok, S., Dissemond, J., Schauen, M., Krieg, T., Wirth, T., Simmet, T., Scharffetter-Kochanek, K. 2004. Overexpression of phospholipid-hydroperoxide glutathione peroxidase in human dermal fibroblasts abrogates UVA irradiation-induced expression of interstitial collagenase/matrix metalloproteinase-1 by suppression of phosphatidylcholine hydroperoxide-mediated NFkappaB activation and interleukin-6 release. *J Biol Chem* 279(44):45634–45642.

Wertz, K., Hunziker, P.B., Seifert, N., Riss, G., Neeb, M., Steiner, G., Hunziker, W., Goralczyk, R. 2005. Beta-carotene interferes with ultraviolet light A-induced gene expression by multiple pathways. *J Invest Dermatol* 124(2):428–434.

Wertz, K., Seifert, N., Hunziker, P.B., Riss, G., Wyss, A., Lankin, C., Goralczyk, R. 2004. Beta-carotene inhibits UVA-induced matrix metalloprotease 1 and 10 expression in keratinocytes by a singlet oxygen-dependent mechanism. *Free Radic Biol Med* 37(5):654–670.

Whiteside, J.R., McMillan, T.J. 2009. A bystander effect is induced in human cells treated with UVA radiation but not UVB radiation. *Radiat Res* 171(2):204–211.

Wischermann, K., Popp, S., Moshir, S., Scharfetter-Kochanek, K., Wlaschek, M., de Gruijl, F., Hartschuh, W., Greinert, R., Volkmer, B., Faust, A., Rapp, A., Schmezer, P., Boukamp, P. 2008. UVA radiation causes DNA strand breaks, chromosomal aberrations and tumorigenic transformation in HaCaT skin keratinocytes. *Oncogene* 27:4269–4280.

Wlaschek, M., Briviba, K., Stricklin, G.P., Sies, H., Scharffetter-Kochanek, K. 1995. Singlet oxygen may mediate the ultraviolet A-induced synthesis of interstitial collagenase. *J Invest Dermatol* 104(2):194–198.

Wlaschek, M., Heinen, G., Poswig, A., Schwarz, A., Krieg, T., Scharffetter-Kochanek, K. 1994. UVA-induced autocrine stimulation of fibroblast-derived collagenase/MMP-1 by interrelated loops of interleukin-1 and interleukin-6. *Photochem Photobiol* (5):550–556.

Wlaschek, M., Wenk, J., Brenneisen, P., Briviba, K., Schwarz, A., Sies, H., Scharffetter-Kochanek, K. 1997. Singlet oxygen is an early intermediate in cytokine-dependent ultraviolet-A induction of interstitial collagenase in human dermal fibroblasts in vitro. *FEBS Lett* 413(2):239–242.

Wondrak, G.T., Jacobson, M.K., Jacobson, E.L. 2006. Endogenous UVA-photosensitizers: Mediators of skin photodamage and novel targets for skin photoprotection. *Photochem Photobiol Sci* 5(2):215–237.

Wondrak, G.T., Roberts, M.J., Jacobson, M.K., Jacobson, E.L. 2004. 3-Hydroxypyridine chromophores are endogenous sensitizers of photooxidative stress in human skin cells. *J Biol Chem* 279(29):30009–30020.

Wood, S.R., Berwick, M., Ley, R.D., Walter, R.B., Setlow, R.B., Timmins, G.S. 2006. UV causation of melanoma in *Xiphophorus* is dominated by melanin photosensitized oxidant production. *Proc Natl Acad Sci USA* 103:4111–4115.

Yamauchi, R., Morita, A., Yasuda, Y., Grether-Beck, S., Klotz, L.O., Tsuji, T., Krutmann, J. 2004. Different susceptibility of malignant versus non-malignant human T cells toward ultraviolet A-1 radiation-induced apoptosis. *J Invest Dermatol* 122(2):477–483.

Yang, Y., Sharma, A., Sharma, R., Patrick, B., Singhal, S.S., Zimniak, P., Awasthi, S., Awasthi, Y.C. 2003. Cells preconditioned with mild, transient UVA irradiation acquire resistance to oxidative stress and UVA-induced apoptosis: Role of 4-hydroxynonenal in UVA-mediated signaling for apoptosis. *J Biol Chem* 278(42):41380–41388.

Yasui, H., Sakurai, H. 2003. Age-dependent generation of reactive oxygen species in the skin of live hairless rats exposed to UVA light. *Exp Dermatol* 12(5):655–661.

Young, A.R., Potten, C.S., Nikaido, O., Parsons, P.G., Boenders, J., Ramsden, J.M., Chadmick, C.A. 1998. Human melanocytes and keratinocytes exposed to UVB or UVA *in vivo* show comparable levels of thymine dimers. *J Invest Dermatol* 111:936–940.

Zenke-Kawasaki, Y., Dohi, Y., Katoh, Y., Ikura, T., Ikura, M., Asahara, T., Tokunaga, F., Iwai, K., Igarashi, K. 2007. Heme induces ubiquitination and degradation of the transcription factor Bach1. *Mol Cell Biol* 27(19):6962–6971.

Zhang, Y., Dong, Z., Bode, A.M., Ma, W.Y., Chen, N., Dong, Z. 2001b. Induction of EGFR-dependent and EGFR-independent signaling pathways by ultraviolet irradiation. *DNA Cell Biol* 20(12):769–779.

Zhang, Y., Liu, G., Dong, Z. 2001c. MSK1 and JNKs mediate phosphorylation of STAT3 in UVA-irradiated mouse epidermal JB6 cells. *J Biol Chem* 276(45):42534–42542.

Zhang, Y., Ma, W.Y., Kaji, A., Bode, A.M., Dong, Z. 2002. Requirement of ATM in UVA-induced signaling and apoptosis. *J Biol Chem* 277(5):3124–3131.

Zhang, Y., Mattjus, P., Schmid, P.C., Dong, Z., Zhong, S., Ma, W.Y., Brown, R.E., Bode, A.M., Schmid, H.H., Dong, Z. 2001a. Involvement of the acid sphingomyelinase pathway in uva-induced apoptosis. *J Biol Chem* 276(15):11775–11782.

Zhang, H., Rosdahl, I. 2003. Ultraviolet A and B differently induce intracellular protein expression in human skin melanocytes—A speculation of separate pathways in initiation of melanoma. *Carcinogenesis* 24(12):1929–1934.

Zhang, X.S., Rosenstein, B.S., Wang, Y., Lebwohl, M., Mitchell, D.M., Wei, H.C. 1997. Induction of 8-oxo-7,8-dihydro-2′-deoxyguanosine by ultraviolet radiation in calf thymus DNA and HeLa cells. *Photochem Photobiol* 65:119–124.

Zheng, X., Nakamura, K., Tojo, M., Akiba, H., Oyama, N., Nishibu, A., Kaneko, F., Tsunemi, Y., Kakinuma, T., Saeki, H., Tamaki, K. 2003. Ultraviolet A irradiation inhibits thymus and activation-regulated chemokine (TARC/CCL17) production by a human keratinocyte HaCaT cell line. *Eur J Dermatol* 13(4):348–353.

Zhong, J.L., Edwards, G.P., Raval, C., Li, H., Tyrrell, R.M. 2010a. The role of Nrf2 in ultraviolet A mediated heme oxygenase 1 induction in human skin fibroblasts. *Photochem Photobiol Sci* 9(1):18–24.

Zhong, J.L., Holley, P., Tyrrell, R.M., Pourzand, C. 2004. Susceptibility of skin cells to UVA-induced necrotic cell death reflects the intracellular level of labile iron pool. *J Invest Dermatol* 123:771–780.

Zhong, J.L., Raval, C., Edwards, G.P., Tyrrell, R.M. 2010b. A role for Bach1 and HO-2 in suppression of basal and UVA-induced HO-1 expression in human keratinocytes. *Free Radic Biol Med* 48:196–206.

Zhuang, S., Kochevar, I.E. 2003. Ultraviolet A radiation induces rapid apoptosis of human leukemia cells by Fas ligand-independent activation of the Fas death pathways. *Photochem Photobiol* 78(1):61–67.

Zigman, S., Reddan, J., Schultz, J.B., McDaniel, T. 1996. Structural and functional changes in catalase induced by near-UV radiation. *Photochem Photobiol* 63(6):818–824.

Zykova, T.A., Zhu, F., Zhang, Y., Bode, A.M., Dong, Z. 2007. Involvement of ERKs, RSK2 and PKR in UVA-induced signal transduction toward phosphorylation of eIF2alpha (Ser(51)). *Carcinogenesis* 28(7):1543–1551.

59

Ultraviolet Radiation and Vitamin D

Lesley E. Rhodes
University of Manchester

Ann R. Webb
University of Manchester

59.1 Introduction

Vitamin D is a hormone, with a chemical structure closely related to that of cortisol. It is often called the "sunshine vitamin" as it is synthesized in the skin following exposure to the ultraviolet B (UVB) in solar radiation. There are two forms of vitamin D, with only vitamin D_3 (cholecalciferol) being photochemically produced in the skin, while vitamin D_2 (ergocalciferol) is formed from ergosterol in plants, through a similar process. Both require metabolism to produce the active hormone. Humans can obtain both vitamin D_3 and D_2 through diet, although several recent surveys confirm that the average diet contains low amounts. There is currently considerable controversy regarding the amounts of vitamin D required for human health and how these may best be obtained. While it is well known that vitamin D is essential for calcium metabolism and that deficiency causes the severe bone disorders of rickets and osteomalacia, there are also associations with systemic and malignant disorders where cause and effect are not firmly established.

59.2 Cutaneous Synthesis

59.2.1 Contribution of Sunlight to Vitamin D Levels

Vitamin D synthesis is the best known beneficial effect of ultraviolet radiation (UVR) on the skin. It is often quoted that around 90% of the body's source of vitamin D is obtained by this route, with only approximately 10% gained through diet. However, while sunlight is in most circumstances likely to be the larger contributor (Ashwell et al. in press), this statement is dependent on specific latitudinal, seasonal, and personal conditions and cannot be applied generally.

59.2.2 Biosynthetic Pathway

Precursor molecule, 7-dehydrocholesterol (7-DHC; provitamin D), is stored in the skin. On exposure of skin to UVB radiation, a photochemical reaction occurs, converting 7-DHC to pre-vitamin D_3. This is subsequently converted through a comparatively slower thermal isomerization step to vitamin D_3, which is released into the circulation where it is transported by vitamin D-binding protein. It is known that sunlight as well as initiating vitamin D_3 synthesis in the skin also regulates the process (Figure 59.1), and that this involves a role for ultraviolet A (UVA) wavelengths in addition to UVB (Norval et al. 2010). Prolonged sun exposure results in reversible photoconversion of pre-vitamin D_3 to alternative, inactive metabolites tachysterol and lumisterol, limiting the total amount of pre-vitamin D_3 that will form and be available for conversion to vitamin D_3. Sunlight (UVA) also degrades formed vitamin D_3 present in the skin to photoproducts 5,6-transvitamin D_3, suprasterol I, and suprasterol II (Webb et al. 1989). This photochemical regulation explains why hypervitaminosis D is only reported to occur when excess vitamin D is ingested, and not from sun exposure, and why short exposures to sunlight are most efficient in vitamin D production.

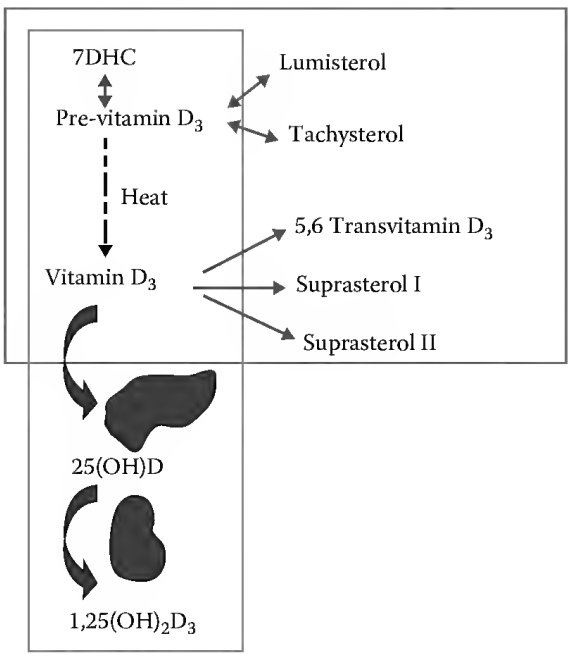

FIGURE 59.1 The formation of vitamin D and its metabolites. The long box (down the left side) shows the path from 7-DHC to the active metabolite $1,25(OH)_2D_3$. The top box indicates reactions that occur in the skin. Products outside the long box are inert isomers or degradation products. With the exception of the slow heat isomerization (dotted arrow), all reactions (continuous straight arrows) are driven by UVR, predominantly UVB for formation and UVA for degradation. Curved arrows indicate transport in the blood.

59.2.3 Action Spectrum

The wavelengths of radiation most effective in transforming 7-DHC to pre-vitamin D_3 were identified to fall between 295 and 300 nm, with a maximum around 297 nm (Figure 59.2; MacLaughlin et al. 1982). This and earlier works were examined by the Commission Internationale de L'Eclairage (CIE) in defining a standardized action spectrum for vitamin D synthesis (CIE 2006). However, *in vivo* studies are lacking and further research is required to confirm the action spectrum (Norval et al. 2010); as described in the preceding paragraph, the cutaneous processes prior to the release of vitamin D into the bloodstream are more complex than the initial production of pre-vitamin D_3, with the involvement of UVR at more than one step.

59.2.4 Latitude and Season

The quantity of UVB reaching the earth's surface is highly dependent on latitude, season, and time of day. The solar zenith angle (SZA), that is, the angle between the local perpendicular and the location of the sun in the sky, determines the path length of radiation through our attenuating atmosphere and

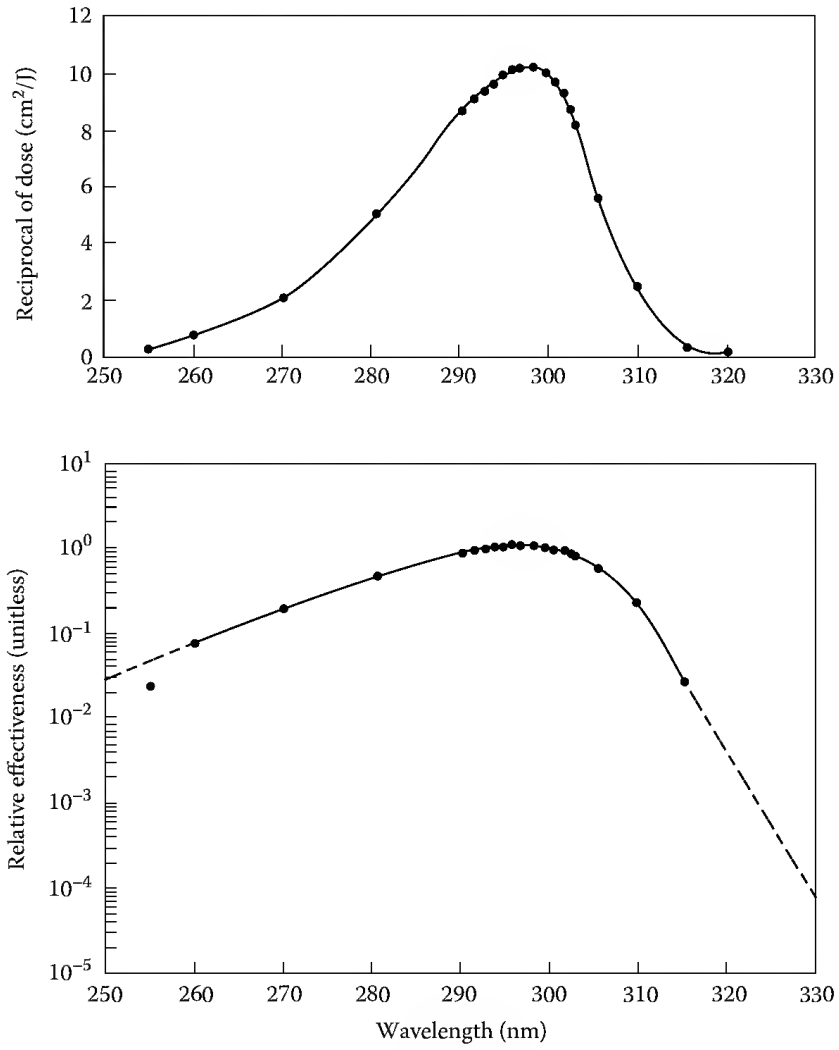

FIGURE 59.2 The action spectrum for the formation of pre-vitamin D_3 from 7-DHC. Top (linear scale): Data measured in human skin (MacLaughlin et al. 1982). Bottom (logarithmic scale): The CIE action spectrum based on the measured data (dots) and extrapolated (dashed line) to the regions with no data (CIE 2006).

also the angle at which radiation strikes the surface. As SZA increases, path length increases and the direct beam reaches the surface at a more oblique angle, both of which decrease the radiation at the surface. SZA increases with latitude, in autumn and winter, and outside noon hours. Maximum vitamin D production occurs at low latitudes, in the summer months and around midday, and there is no effective vitamin D production in winter time at higher latitudes such as in Northern Europe, Canada, and northern states of the United States (Webb et al. 1988; Webb and Engelsen 2006).

59.2.5 Atmospheric Factors

Cloud, pollution, and ozone affect the amount and type of UVR reaching the earth's surface (Webb and Engelsen 2006). Ozone changes result in spectral differences at the surface, since it absorbs most strongly at UVB (vitamin D producing) wavelengths. Low ozone therefore enhances potential vitamin D_3 production while having little effect on the rest of the solar spectrum. Cloud on the other hand generally decreases radiation at all wavelengths, by amounts that vary depending on cloud type, depth, and sky cover; in broken cloud conditions, radiation can even be enhanced for short periods of time. Pollution too results in overall reduction of solar radiation at the surface, though some pollutants absorb in particular wavebands, for example, sulfur dioxide, as well as ozone in the troposphere, absorbs at UV wavelengths.

59.2.6 Skin Pigmentation

Skin color affects vitamin D production as UVR is partially absorbed by melanin, reducing the amount reaching the chromophore 7-DHC (Webb and Holick 1988). Studies show that people with darker skin (skin phototypes V and VI) are capable of synthesizing vitamin D in their skins, but higher absolute UV doses are required (see Section 59.2.9). This puts people with darker skins living at higher latitudes at particular risk of low vitamin D status.

59.2.7 Age

Older people are in general at greater risk of low vitamin D levels, due to factors including lower 7-DHC levels in the skin and, potentially, decreased mobility reducing the time spent outdoors. In an *in vitro* study using skin samples from people aged 8–18 and 77–82 years, ability to produce pre-vitamin D_3 following UV exposure was decreased by more than twofold in the older group (MacLaughlin and Holick 1985), while an *in vivo* study showed a reduced seasonal boost in vitamin D levels in those living in nursing homes compared with independently living older people (Webb et al. 1990).

59.2.8 Impact of Photoprotective Measures

Shade, clothing, and sunscreens are employed to reduce the risk of sunburn and longer term hazards of UVR on the skin. Sunscreen, when applied according to the manufacturer's testing conditions, that is, an even application with surface density of $2\,mg/cm^2$, provides a barrier to UVB and to a lesser extent to UVA. Accordingly, it has been calculated that a sunscreen with sun protection factor (SPF) 15 could reduce vitamin D synthesis by up to 99.9% (Holick 2004). However, studies consistently show that in practice, sunscreen is applied less rigorously and in much lower densities, even by people with photosensitivity conditions (Azurdia et al. 2000; Thieden et al. 2005), and while sunscreens tend to be used to protect during the intense conditions of sunny holidays, they are less frequently used during outdoor pursuits at other times (Bourke et al. 1995). Shade can also be deceptive since much of our UV exposure is to diffuse or scattered radiation that is incident from all directions. Shade provides protection from the direct beam but not all the scattered radiation. Thus, unknowns regarding behavioral factors and UVB exposure patterns as well as target vitamin D status complicate this issue.

59.2.9 Artificial UVR Sources

Lamps emitting UVB, as used in the medical treatment of skin disorders, are known to raise vitamin D levels (Armas et al. 2007; Sayre et al. 2007). UVR lamps with peak emission at 310 nm fitted to the ceiling in a nursing home also increased vitamin D status in the elderly residents, in whom hands and face were exposed (Chuck et al. 2001). Elsewhere, people with both black and white skin responded to a 6 week course of total body irradiations with UVB, dosed according to their individual erythemal sensitivity, that is, their minimal erythema dose (MED) (Brazerol et al. 1988). Baseline vitamin D status was lower in the black subjects and remained lower following treatment. However, on the higher absolute UV dose regime (with longer irradiation times), the black subjects showed a similar gain in vitamin D status over the course. Commercial sunbeds, as used for indoor tanning, have been increasingly marketed as providing health benefit. Thieden et al. (2008) compared two groups of women given treatment courses with sunlamps containing primarily UVA with 0.5% or 1.4% UVB and a group given no intervention. The lower UVB group increased their circulating 25-hydroxyvitamin D (25(OH)D) by approximately 5 ng/mL while the increase was approximately double this in the higher UVB group, and no change was seen in the untreated group; however, the levels showed a plateau after four treatments. As the emission spectrum of commercial lamps varies, and the use of sunbeds increases the risk of skin cancer (IARC 2008), they are not recommended for use by the public for any perceived health gain. Thus, the U.S. Food and Drug Administration (FDA) states that sunbeds are for tanning purposes only and no health benefit claims can be made (Lim et al. 2005).

59.3 Dietary Sources

59.3.1 Natural and Fortified Foods

Few foods naturally contain significant amounts of vitamin D. Fatty fish, for example, herring and mackerel, contains the highest concentration, while meat, eggs, and dairy products (milk, butter, and cheese) contain moderate–low concentrations. Food fortification has enhanced the vitamin D content of some foods, particularly margarine, cereals, and milk, although countries vary in the degree to which this occurs. For example, in the United States, legislation has made milk fortification mandatory, although in the United Kingdom presently only margarine undergoes mandatory fortification and this is only to the (low) level found naturally in butter (Margarine Regulations 1967). Problems can occur with food fortification, for example, in controlling the dose within each portion when adding vitamin D to milk, resulting in overfortification of some portions and underfortification of others (Holick et al. 1992; Chen et al. 1993).

59.3.2 Recommended Intake

Guidelines on the daily oral requirement of vitamin D vary, but generally there has been an assumption that most is obtained via cutaneous exposure to sunlight and that relatively little is required orally. Some authorities are considering revising these recommendations upward in the light of recent reports of widespread low vitamin D status. The World Health Organisation (WHO 1998) currently recommends 5 μg (200 IU) per day for most adults, 10 μg for 50–65 years, 15 μg for >65 years, and 10 μg for pregnant and lactating women. In the United States and Canada, the Institute of Medicine, Food and Nutrition Board (1997) advised 5 μg for adults <50 years, 10 μg for 51–70 years, and 15 μg for 70+ years. Authorities in several European countries also recommend 5 μg per day for healthy adults (Doets et al. 2008). In the United Kingdom, there is no recommended nutrient intake for vitamin D for most adults and children aged 4–64 years, while older people, along with the housebound, pregnant, or lactating women, and those with pigmented skin, are identified as at risk and advised to take 10 μg daily, and children 0–6 months are recommended 8.5 μg daily, and 6 months–3 years, 7 μg daily (Department of Health, COMA 1998; Food Standards Agency 2003).

59.3.3 Actual Dietary Levels

Studies have revealed that the average dietary intake in Europe is low (Andersen et al. 2005). The U.K. National Diet and Nutrition Survey (NDNS) found that the mean daily intake from diet alone was only 2.8 μg in women and 3.7 μg in men. Fish and fish dishes were the main dietary sources, with most vitamin D provided by oily fish (Henderson et al. 2003). A survey in Ireland confirmed a daily vitamin D intake below 5 μg per day from all sources (diet and supplements) in the majority of men and women aged 18–64 years (Hill et al. 2004); however, the impact on bone health is currently unknown. Oily fish meals and use of fish oil supplements could explain the modestly higher vitamin D levels tending to be found in Scandinavia (Zittermann 2003). In Finland, the mean daily intake is 4.7 μg for women and 5.6 μg for men (Lamberg-Allardt et al. 2001).

59.4 Metabolism

Once in the circulation, vitamin D (both D_3 and D_2 forms) undergoes hydroxylation, first in the liver to form 25(OH)D, calcidiol, and second in the kidney to produce the active hormone, that is, 1,25 dihydroxyvitamin D (1,25$(OH)_2$D, calcitriol). Formation of 1,25$(OH)_2$D is tightly regulated and only small amounts occur in the bloodstream. Key target organs for the vitamin D hormone are those involved in calcium homeostasis and bone turnover, that is, the intestine, where vitamin D regulates the transport of calcium across the intestinal mucosa, and in the bone, kidney, and parathyroid glands (Shipley et al. 2002). However, many other organs including ovary, breast, and uterus are now known both to be able to synthesize 1,25$(OH)_2$D locally and to possess vitamin D receptors, thus accommodating wider biological roles of the hormone (Dokoh et al. 1983).

59.5 Role in Bone Health

59.5.1 Rickets and Osteomalacia

It is well known that severe vitamin D deficiency causes rickets in children, and osteomalacia in children and adults; these involve the development of severe bone deformity through a failure of bone mineralization (Lips 2006). Rickets was common particularly in cities at higher latitude in the nineteenth century, and it was discovered early in the twentieth century that this could be cured by sunlight exposure. However, it would be incorrect to regard rickets as a disease of previous times. Cases continue to be reported, particularly in the increasing populations of darker skinned people living at higher latitude, and in instances where total infant nutrition is through breast feeding, as breast milk can be a poor source of vitamin D, depending on the status of the mother (Specker et al. 1985; Kreiter et al. 2000; Hollis and Wagner 2004).

59.5.2 Other Aspects of Musculoskeletal Health

As well as the aforementioned severe bone disorders, relatively low vitamin D status is associated with the bone-thinning condition, osteoporosis, along with bone fracture and muscle weakness (Lips 2006). Low vitamin D status results in reduced resorption of intestinal calcium, and to a lesser extent, phosphorus. The parathyroid glands respond by increasing parathyroid hormone (PTH) secretion, with higher PTH levels resulting in increased calcium resorption from bone. Elevated levels of PTH also result in increased renal production of 1,25$(OH)_2$D, which then binds to and increases the activity of the bone-forming cells (osteoblasts) in the bone. However, phosphorous is lost, causing mobilization of minerals and matrix from bone and a negative effect on bone mineral density (Bischoff-Ferrari et al. 2004). These observations have led to expectations that higher vitamin D status may help achieve optimal bone health. Indeed, while studies are not completely consistent, results of a number of randomized

controlled intervention studies with vitamin D supplements suggest a reduction in bone fractures in those actively treated, and a protective effect of higher vitamin D levels is supported by biochemical and radiological data (Veith 2005; Bischoff-Ferrari et al. 2005; Wolpowitz and Gilchrest 2006).

59.6 Potential Role in Malignant and Systemic Disorders

59.6.1 Cellular Effects of Vitamin D

Evidence from experimental models supports that $1,25(OH)_2D$ has chemopreventive properties, including its role as a differentiating agent and modulator of apoptosis (Colston and Hansen 2002; Mehta and Mehta 2002; Ingraham et al. 2008). It is also an immunomodulatory agent, capable of influencing aspects of both innate and adaptive immunity (Deluca and Catorna 2001; Kamen and Tangpricha 2010). These roles could be facilitated by the presence of vitamin D receptors in many cells, with most tissues also capable of locally producing the active vitamin D hormone from circulating 25(OH)D. Thus, potentially low vitamin D status might contribute to increased risk of malignancy and disorders of immunity. Currently, while there is a wealth of evidence associating low vitamin D status or proxies for this with several malignancies, diabetes, multiple sclerosis, and other conditions, there is very little direct evidence to confirm cause and effect.

59.6.2 Malignant Conditions

Mortality from prostate, colon, and breast cancer is reported to be inversely associated with ambient UVB, and this has been attributed to low vitamin D status (Holick 2006). The expert panel of the International Agency for Research on Cancer reviewed multiple strands of evidence and supported a protective role for vitamin D in colon cancer, but found insufficient evidence for a protective effect in other malignancies (IARC 2008). In epidemiologic studies, ambient UVR data are used as a proxy for vitamin D status, but it is known that behavioral factors can confound this assumption. Moreover, comparisons of age-standardized incidence and mortality rates for colorectal and prostate cancers in Northern Europe with those in Australia and New Zealand reveal lower incidence of both cancers in Northern Europe, despite the lower ambient UVR (Ferlay et al. 2004; Diffey 2006). In the case of colon cancer, several studies do report a reduction in risk of colorectal cancer with higher circulating levels of 25(OH)D (Giovannucci 2005). Luscombe et al. (2001) examined the effect of UVR exposure on prostate cancer development by comparing recall of sun exposure levels in men with prostate cancer versus a control group with benign prostatic disease. They found that lower reported frequency of childhood sunburn, fewer foreign holidays, and low UV exposure correlated with the development of prostate cancer; however, this does not establish vitamin D as the protective factor. Epidemiological data conflict concerning potential protection in melanoma (Millen et al. 2004; Ingraham et al. 2008; Asgari et al. 2009).

59.6.3 Systemic Disorders

Further evidence exists of an association with beneficial effects in a range of other diseases, including multiple sclerosis, tuberculosis, diabetes, hypertension, and cardiac failure (Hypponen et al. 2001; Muray et al. 2003; Stene and Joner 2003; Zittermann et al. 2003), although confounding factors and data limitations frequently pose challenges in defining a clear link between vitamin D and reduced incidence of such diseases.

59.7 Defining Vitamin D Levels for Health

59.7.1 Vitamin D Status

The active hormone $1,25(OH)_2D$ is tightly regulated, and the measurement of its levels has limited value. On the other hand, 25(OH)D is the major circulating form of vitamin D and more responsive to the effects of sunlight exposure and dietary intake. Thus, there is international consensus that it is the most

appropriate marker of vitamin D status (Expert Group on Vitamins and Minerals 2003; Institute of Medicine 1997). However, there is much debate concerning the circulating 25(OH)D levels that should be reached.

59.7.2 Deficiency

It is well established that circulating levels of 25(OH)D below 5–10 ng/mL (12.5–25 nmol/L) can cause the severe bone conditions of rickets and osteomalacia, and hence, it is agreed that values below these levels are deficient (DoH, COMA 1998; NRPB 2002; Ashwell et al. in press). Some authors recently suggest regarding levels of <20 ng/mL (50 nmol/L) as being in the frankly deficient category (Holick 2009) but the evidence is weaker and the proposal is not generally accepted by investigators or government bodies (Ashwell et al. in press).

59.7.3 Sufficiency

Circulating 25(OH)D levels of above 20 ng/mL (50 nmol/L) are generally considered to be vitamin D sufficient, with good evidence for levels below this being associated with secondary hyperparathyroidism and increased risk of osteoporosis (Vieth 1999; Holick 2002). Many clinical biochemistry laboratories, including several in the U.K., regard 25(OH)D levels of 20 ng/mL and above as "normal." It was recently proposed that a level of 21–29 ng/mL is regarded as insufficient (Holick 2009), but this is based on biochemical rather than clinical evidence, including levels of 25(OH)D associated with maximal PTH suppression, which is not established to be beneficial to health.

59.7.4 Optimal Levels

Several researchers support that the optimal vitamin D level for bone health is much higher than previously thought, that is, 30–32 ng/mL (70–75 nmol/L) and above (Dawson-Hughes et al. 2005; Heaney 2005; Hollis 2005; Veith and El-Hajj Fuleihan 2005; Bischoff-Ferrari et al. 2006). Bishoff-Ferrari et al. (2006) reviewed evidence for optimal levels of vitamin D in multiple health parameters and concluded that these start at around 30 ng/mL. The optimal level of vitamin D for bone health might be defined as one providing maximal suppression of PTH level, peak intestinal calcium absorption, and maximum bone mineral density. However, there is no universal consensus, and others believe there is insufficient evidence that these high levels are physiological or required (Barger-Lux et al. 1998; Lim et al. 2005; Ashwell et al. in press).

59.7.5 Toxicity

Toxicity can occur through oral sources of vitamin D, that is, from an excessive dose of supplements and/or food fortification. However, quite high doses appear to be tolerated. The U.S. Food and Nutrition Board stated that the upper tolerable level for vitamin D is 2000 IU (50 μg) daily (1997), although this may be an underestimate (Heaney et al. 2003; Veith 2004). In a clinical setting, much higher doses are sometimes provided, for example, in treating osteoporosis, but this is different to regular self-administration of a supplement. Based on current evidence, vitamin D toxicity could be defined as a circulating 25(OH)D level of >150 ng/mL; this is accompanied by increased urinary excretion of calcium (hypercalciuria) and if prolonged there may also be increased blood levels of calcium (hypercalcemia), vomiting, weakness, and confusion (Veith 1999).

59.7.6 Vitamin D Status in the General Population

The groups particularly at risk of low vitamin D status were discussed earlier in this chapter. However, there is increasing evidence that low vitamin D status may occur across populations generally. A recent study examined a large cohort of white, British adults aged 45 years and found that around half the

study sample had 25(OH)D levels <40 nmol/mL (16 ng/mL) (Hypponen and Power 2007), and findings were broadly similar in the NDNS of British adults aged 19–64 years (Hirani et al. 2009). Furthermore, a recent partially published study indicated that 20%–25% women assessed in the north of Scotland had levels in the frankly deficient range (<10 ng/mL) in winter (Ashwell et al. in press).

59.8 Recommendations on Sunlight Exposure Levels

59.8.1 Skin Cancer Avoidance

Skin cancer has high incidence in countries with large populations of white Caucasians including in Northern Europe, the United States, and Australia, and the incidence continues to rise, with UVR the principal etiological agent in the majority of skin cancers (NRPB 2002; Elwood and Jopson 1997). Thus, national and international authorities advise summer sunlight limitation in these populations (Ziegelberger et al. 2006). Exposure to solar UVR is the principal cause in the majority of cases of the three main types of skin cancer, that is, basal cell carcinoma and squamous cell carcinoma [both are types of nonmelanoma skin cancer (NMSC)] and malignant melanoma. The NMSCs are the most commonly occurring, and while they infrequently cause death, they can cause high morbidity (NRPB 2002). Malignant melanoma occurs less frequently but is fatal in 25% of cases (http://www.sunsmart.org.uk/skin-cancer-facts/about-skin-cancer). People of the fairest skin coloring, freckled and with tendency to sunburn, that is, those in phototypes I and II, are the most prone to melanoma and NMSC.

59.8.2 Current Guidance

Policy recommendations and public health strategies to limit summer sunlight exposure in order to prevent skin cancer have generated considerable international debate in recent years. The "SunSmart" campaign originating in Australia has been emulated or paralleled elsewhere, with focus on providing the public, particularly those of phototypes I and II, with information on the relationship of skin cancer to sunlight and advice on how to reduce the risks. A particular emphasis is to avoid sunburn, as sunburn is a risk factor for both melanoma and NMSC (NRPB 2002). In Australia, the SunSmart campaign was associated with a slowing of the rate of rise of melanoma incidence in younger adults (Giles and Thursfield 1996), while elsewhere campaigns have generally not been running consistently for a sufficient period to assess impact on the longer term incidence of skin cancer. However, concerns have been raised, as advice to seek shade at noon hours, to cover up with clothing, and to use sunscreens may reduce opportunities for the skin to synthesize vitamin D, particularly at latitudes further from the equator. This concern is strengthened by the recognition that higher vitamin D levels may be required than previously realized for optimal health.

59.8.3 How Much Sunlight Is Needed?

Our group recently performed an *in vivo* study to examine the impact on vitamin D status of a casual summer's sunlight exposures, following an interpretation of the U.K. national recommendations on sun exposure levels (Rhodes et al. 2010). This national guidance is fairly general, with uncertainty regarding the specification and impact of following the recommendations, based as they are on data derived from *in vitro* and theoretical models (National Radiological Protection Board 2002; Ziegelberger et al. 2006). The U.K.'s SunSmart campaign is consistent with many countries in its recommendations to limit personal summer sunlight exposure levels (http://www.sunsmart.org.uk/skin-cancer-facts/about-skin-cancer), while the U.K.'s Health Protection Agency, in line with countries of similar latitude, advises that casual exposures to summer sunlight containing UVB are sufficient for attaining vitamin D (National Radiological Protection Board 2002) albeit at the levels required to avoid rickets. A population-justified sample of U.K. white Caucasians was given a simulated summer's UVR exposures of known dosage,

equivalent to <30 min exposure of unshaded skin to Manchester noon sun on a cloudless day. This was performed in the winter months, when ambient UVB could not confound the data, and to skin areas (35% total surface area) routinely exposed when wearing casual summer clothing (Rhodes et al. 2010). We showed this regime would produce a vitamin D sufficient status, that is, 25(OH)D of at least 20 ng/mL, in 90% of the population, whereas only approximately a quarter (26.2%) would reach the proposed optimal level, that is, 25(OH)D of at least 32 ng/mL. The findings were very similar to the vitamin D status acquired naturally following a British summer in the same population of white Caucasians (Webb et al. 2010). Thus, repeated sub-erythemal UV exposures while casually dressed can produce sufficiency at summer end. On the other hand, sufficiency (25(OH)D $\leq$ 20 ng/mL) was maintained during winter only in those reaching optimal levels (25(OH)D $\leq$ 32 ng/mL) at summer end, in the natural summer exposure study (Webb et al. 2010). These data can be utilized when considering how best to achieve and maintain vitamin D status, although clearly a consensus is required on the level of 25(OH)D that should be targeted for the population.

59.9 Future Directions

Human vitamin D requirements for optimal health may be greater than previously stated, when avoiding rickets was the main goal, and research is ongoing to both clarify the needs and establish feasible ways for attaining these. While vitamin D supplements could potentially satisfy needs and avoid health risks of UVR, questions to be addressed in this respect include: Will whole populations be prepared to take supplements? Are dietary sources handled in an equivalent manner to the cutaneous source? If high circulating 25(OH)D levels are required, should these be maintained year-round, thus removing the naturally occurring seasonal pattern seen at mid-high latitudes? Sunlight provides a natural, regulated source of vitamin D at sub-erythemal doses, and as people gain pleasure from this, they are likely to continue to expose their skin. However, sunlight appears more effective as a source in some individuals than others; hence, what biochemical and genetic differences influence vitamin D status gained? What factors influence effective storage of vitamin D into the winter months? An examination of the action spectrum for vitamin D synthesis *in vivo* may provide information regarding how to maximize benefits while avoiding the hazards of sun exposure. Research is also needed into other potential benefits of sunlight exposure, and how the overall optimal benefit/risk ratio for health can be gained in different population groups.

Acknowledgments

The authors thank Cancer Research U.K. (project no. C20668/A6808) for financial support.

References

Andersen R, Molgaard C, Skovgaard LT et al. (2005). Teenage girls and elderly women living in northern Europe have low winter vitamin D status. *Eur J Clin Nutr*, **59**: 1–9.

Armas LAG, Dowell S, Akhter M et al. (2007). Ultraviolet-B radiation increases serum 25-hydroxyvitmain D levels: The effect of UVB dose and skin color. *J Am Acad Dermatol*, **57** (4): 588–593.

Asgari MM, Maruti SS, Kushi LH, White E (2009). A cohort study of vitamin D intake and melanoma risk. *J Investig Dermatol*, **129**: 1675–1680.

Ashwell M, Stone EM, Stolte H, Cashman KD, Macdonald H, Lanham-New S, Hiom S, Webb AR, Fraser D (2010). UK Food Standards Agency Workshop Report: Investigation of the relative contributions of diet and sunlight to vitamin D status. *Br J Nutr*, **104**: 603–611.

Azurdia RM, Pagliaro JA, Rhodes LE (2000). Sunscreen application technique in photosensitive patients: A quantitative assessment of the effect of education. *Photodermatol Photoimmunol Photomed*, **16**: 53–56.

Barger-Lux MJ, Heaney RP, Dowell S, Chen TC, Holick MF (1998). Vitamin D and its major metabolites: Serum levels after graded oral dosing in healthy men. *Osteoporos Int*, **8**: 222–230.

Bischoff-Ferrari H, Dietrich T, Orav E, Dawson-Hughes B (2004). Positive association between 25(OH)D levels and bone mineral density: A population based study of younger and older adults. *Am J Med*, **116**: 634–639.

Bischoff-Ferrari HA, Giovannucci E, Willett WC, Dietrich T, Dawson-Hughes B (2006). Estimation of optimal serum concentrations of 25-hydroxyvitamin D for multiple health outcomes. *Am J Clin Nutr*, **84**: 18–28.

Bischoff-Ferrari HA, Willet WC, Wong JB, Giovanucci E, Dietrich P, Dawson-Hughes B (2005). Fracture prevention with vitamin D supplementation: A meta-analysis of randomised controlled trials. *JAMA*, **293**: 2257–2264.

Bourke JF, Healsmith MF, Graham-Brown RA (1995). Melanoma awareness and sun exposure in Leicester. *Br J Dermatol*, **132**: 251–256.

Brazerol WF, McPhee AJ, Mimouni F et al. (1988). Serial ultraviolet B exposure and serum 25 hydroxyvitamin D response in young adult American blacks and whites: No racial differences. *J Am Coll Nutr*, **7** (2): 111–118.

Chen TC, Shao A, Heath H, III, Holick MF (1993). An update on the vitamin D content of fortified milk from the US and Canada. *N Engl J Med*, **329**: 1507.

Chuck A, Todd J, Diffey B (2001). Subliminal ultraviolet-B irradiation for the prevention of vitamin D deficiency in the elderly: A feasibility study. *Photodermatol Photoimmunol Photomed*, **17**: 168–171.

CIE (2006). Action spectrum for the production of pre-vitamin D3 in human skin. Technical report **174**, Commission Internationale de L'Eclairage, Vienna.

Colston KW, Hansen C (2002). Mechanisms implicated in the growth regulatory effects of vitamin D in breast cancer. *Endocr Relat Cancer*, **9**: 45–59.

Dawson-Hughes B, Heaney RP, Holick MF, Lips P, Meunier PJ, Veith R (2005). Estimates of optimal vitamin D status. *Osteoporos Int*, **16**: 713–716.

Deluca HF, Catorna MT (2001). Vitamin D: Its role and uses in immunology. *FASEB J*, **15**: 2579–2585.

Department of Health report on Health and Social Subjects (1998). Nutrition and bone health: With particular reference to calcium and vitamin D. Report of the subgroup on bone health, working group on the nutritional status of the population of the Committee on Medical Aspects of Food and Nutrition (COMA) Policy. London: HMSO.

Diffey B (2006). Do we need a revised public health policy on sun exposure? *Br J Dermatol*, **154**: 1046–1051.

Doets E, de Wit L, Dhonukshe-Rutten R et al. (2008). Current micronutrient recommendations in Europe: Towards understanding their differences and similarities. *Eur J Nutr*, **47**: 17–40.

Dokoh S, Donaldson CA, Marion SL, Pike JW, Haussler MR (1983). The ovary: A target organ for 1,25-dihydroxyvitamin D_3. *Endocrinology*, **112**: 200–206.

Elwood JM, Jopson J (1997). Melanoma and sun exposure: An overview of published studies. *Int J Cancer*, **73**: 198–203.

Expert Group on Vitamins and Minerals (2003). Safe Upper Limits for Vitamins and Minerals. ©Crown copyright. Published by Food Standards Agency. ISBN 1-904026-11-7. (www.food.gov.uk/multimedia/pdfs/vitmin2003.pdf).

Ferlay J, Bray F, Pisani P, Parkin DM (2004). GLOBOCAN 2002: Cancer Incidence, Mortality and Prevalence Worldwide. IARC Cancer Database No. 5, version 2.0. Lyon: IARC Press.

Food Standards Agency, Expert Group on Vitamins and Minerals (2003). Vitamin D (online). Department of Health. www.eatwell.gov.uk/healthydiet/nutritionessentials/vitaminsandminerals/vitamind/#elem220582 (accessed October 22, 2007).

Giles GG, Thursfield VJ (1996). Trends in skin cancer in Australia. *Cancer Forum*, **20**: 188–191.

Giovannucci E (2005). The epidemiology of vitamin D and cancer incidence and mortality: A review (United States). *Cancer Causes Control*, **16**: 83–95.

Heaney RP (2005). The vitamin D requirement in health and disease. *J Steroid Biochem Mol Biol*, **97**: 13–19.

Heaney RP, Davies M, Chen TC, Holick MF, Barger-Lux MJB (2003). Human serum 25-hydroxycholecalciferol response to extended oral dosing with cholecalciferol. *Am J Clin Nutr*, **77**: 204–210.

Henderson L, Irving K, Gregory J et al. (2003). The national diet and nutrition survey: Adults aged 19 to 64 yrs. Vitamin and mineral intake and urinary analytes (online). http:www.food.gov.uk/multimedia/pdfs/ndnsv3.pdf (accessed October 26, 2007, November 11, 2009).

Hill TR, O'Brien MM, Cashman KD, Flynn A, Keily M (2004). Vitamin D intakes in 18–64-y-old Irish adults. *Eur J Clin Nutr*, **58**: 1509–1517.

Hirani V, Mosdøl A, Mishra G (2009). Predictors of 25-hydroxyvitamin D status among adults in two British national surveys. *Br J Nutr*, **101**: 760–764.

Holick MF (2002). Vitamin D: The underappreciated D-lightful hormone that is important for skeletal and cellular health. *Curr Opin Endocrinol Diab*, **9**: 87–98.

Holick MF (2004). Vitamin D: Importance in prevention of cancers, type I diabetes, heart disease and osteoporosis. *Am J Clin Nutr*, **79** (3): 362–371.

Holick MF (2006). Calcium plus vitamin D and the risk of colorectal cancer. *N Engl J Med*, **354**: 2287–2288.

Holick MF (2009). Vitamin D status: measurement, interpretation, and clinical application. *Ann Epidemiol*, **19**: 73–78.

Holick MF, Shao Q, Liu WW, Chen TC (1992). The vitamin D content of fortified milk and infant formula. *N Engl J Med*, **326**: 1178–1181.

Hollis BW (2005). Circulating 25-hydroxyvitamin D levels indicative of vitamin D sufficiency: Implications for establishing a new effective dietary intake recommendation for vitamin D. *J Nutr*, **135**: 317–322.

Hollis BW, Wagner CL (2004). Vitamin D requirements during lactation: High-dose maternal supplementation as therapy to prevent hypovitaminosis D for both the mother and the nursing infant. *Am J Clin Nutr*, **80** (suppl): 1752S–1758S.

Hypponen E, Laara E, Reunanaen A, Jarvelin MR, Virtanen SM (2001). Intake of vitamin D and risk of type 1 diabetes; a birth cohort study. *Lancet*, **358** (9292): 1500–1503.

Hypponen E, Power C (2007). Hypovitaminosis D in British adults at age 45 y: Nationwide cohort study of dietary and lifestyle predictors. *Am J Clin Nutr*, **85**: 860–868.

IARC (2008). Vitamin D and cancer. *International Agency for Research on Cancer Working Group Reports*, Vol. 5. Lyon: World Health Organisation.

Ingraham BA, Bragdon B, Nohe A (2008). Molecular basis of the potential of vitamin D to prevent cancer. *Curr Med Res Opin*, **24**: 139–149.

Institute of Medicine (1997). *Dietary Reference Intakes*. Washington, DC: National Academy Press.

Kamen DL, Tangpricha V (2010). Vitamin D and molecular actions on the immune system: Modulation of innate and autoimmunity. *J Mol Med*, **88**: 441–450.

Kreiter SR, Schwatrz RP, Kirkman HN, Charlton PA, Calikoglu AS, Davenport ML (2000). Nutritional rickets in African American breast-fed infants. *J Pediatr*, **137** (2): 153–157.

Lamberg-Allardt CJE, Outila TA, Karkkainen MUM, Rita HJ, Valsta LM (2001). Vitamin D deficiency and bone health in healthy adults in Finland: Could this be a concern in other parts of Europe? *J Bone Miner Res*, **16**: 2066–2073.

Lim HW, Gilchrest BA, Cooper KD et al. (2005). Sunlight, tanning booths and vitamin D. *J Am Acad Dermatol*, **52** (5): 868–876.

Lips P (2006). Vitamin D physiology. *Prog Biophys Mol Biol*, **92**: 4–8.

Luscombe CJ, Fryer AA, French ME et al. (2001). Exposure to ultraviolet radiation: Association with susceptibility and age at presentation with prostate cancer. *Lancet*, **358**: 641–642.

MacLaughlin JA, Anderson RR, Holick MF (1982). Spectral character of sunlight modulates photosynthesis of previtamin D_3 and its photoisomers in human skin. *Science*, **216**: 1001–1003.

MacLaughlin J, Holick MF (1985). Aging decreases the capacity of the skin to produce vitamin D3. *J Clin Investig*, **76**: 1536–1538.

Margarine Regulations (1967). *Statutory Instrument No. 1867 as Amended*. London: HMSO.

Mehta RG, Mehta RR (2002). Vitamin D and cancer. *J Nutr Biochem*, **13**: 252–264.

Millen AE, Tucker MA, Hartge P et al. (2004). Diet and melanoma in a case-control study. *Cancer Epidemiol Biomarkers Prev*, **3**: 1042–1051.

Muray S, Parisi E, Cardus A, Craver L, Fernandez E (2003). Influence of vitamin D receptor gene polymorphisms and 25-hydroxyvitamin D on blood pressure in apparently healthy subjects. *J Hypertens*, **21** (11): 2069–2075.

Norval M, Björn LO, de Gruijl FR (2010). Is the action spectrum for the UV-induced production of previtamin D3 in human skin correct? *Photochem Photobiol Sci*, **9**: 11–17.

NRPB (2002). Health effects of ultraviolet radiation. Report of an advisory group on non-ionizing radiation. *Documents of the National Radiological Protection Board*, **13**: 207–217.

Rhodes LE, Webb AR, Fraser HI et al. (2010). Recommended summer sunlight exposure levels can produce sufficient ($\geq$20 ng ml^{-1}) but not the proposed optimal ($\geq$32 ng ml^{-1}) 25(OH)D levels at UK latitudes. *J Invest Dermatol*, **130**: 1411–1418.

Sayre RM, Dowdy JC, Shepherd JG (2007). Reintroduction of a classic vitamin D ultraviolet source. *J Steroid Biochem Mol Biol*, **103**: 686–688.

Shipley M, Black CM, Compston J, O'Gradaigh D (2002). Chapter 10: Rheumatology and bone disease. Calcium homeostasis and it's regulation. In: Kumar P and Clark M (eds.), *Clinical Medicine*, 5th edn. U.K.: W.B. Saunders, pp. 576–577.

Specker B, Tsang RC, Hollis BW (1985). Effects of race and diet on human milk, vitamin D and 25-hydroxyvitamin D. *Am J Dis Child*, **139**: 1134–1137.

Stene LC, Joner G (2003). Use of cod liver oil during the first year of life is associated with lower risk of childhood-onset type 1 diabetes: A large population-based, case control study. *Am J Clin Nutr*, **78** (6): 1128–1134.

Thieden E, Jorgensen HL, Jorgensen NR, Philipsen PA, Wulf HC (2008). Sunbed radiation provokes cutaneous vitamin D synthesis in humans-A randomized controlled trial. *Photochem Photobiol*, **84**: 1487–1492.

Thieden E, Philipsen PA, Sandy-Moeller J, Wulf HC (2005). Sunscreen use related to UV exposure, age, sex and occupation based on personal dosimeter readings and sun-exposure behaviour diaries. *Arch Dermatol*, **141**: 967–973.

U.S. Food and Nutrition Board (1997). Standing committee on the scientific evaluation of dietary reference intakes, Institute of Medicine. *Dietary Reference Intakes for Calcium, Phosphorous, Magnesium, Vitamin D and Fluoride*. Washington, DC: National Academy Press, pp. 250–287.

Veith R (1999). Vitamin D supplementation, 25-hydroxyvitamin D concentrations, and safety. *Am J Clin Nutr*, **69**: 842–856.

Veith R (2004). Why the optimal requirement for vitamin D3 is probably much higher than what is officially recommended for adults. *J Steroid Biochem Mol Biol*, **20**: 575–579.

Veith R (2005). The role of vitamin D in the prevention of osteoporosis. *Ann Med*, **37**: 278–285.

Veith R, El-Hajj Fuleihan G (2005). There is no lower threshold level for PTH as 25-hydroxyvitamin D concentrations increase. *J Endocrinol Invest*, **28**: 183–186.

Webb AR, DeCosta BR, Holick MF (1989). Sunlight regulates the cutaneous production of vitamin D3 by causing its photodegradation. *J Clin Endocrinol Metab*, **68**: 882–887.

Webb AR, Engelsen O (2006). Calculated ultraviolet exposure levels for a healthy vitamin D status. *Photochem Photobiol*, **82**: 1697–1703.

Webb AR, Holick MF (1988). The role of sunlight in the cutaneous production of vitamin D3. *Ann Rev Nutr*, **8**: 375–399.

Webb AR, Kift R, Durkin MT, O' Brien SJ, Vail A, Berry JL, Rhodes LE (2010). The role of sunlight exposure in determining the vitamin D status of the UK white Caucasian adult population. *Br J Dermatol*, **163**: 1050–1055.

Webb AR, Kline L, Holick MF (1988). Influence of season and latitude on the cutaneous synthesis of vitamin D3: Exposure to winter sunlight in Boston and Edmonton will not promote vitamin D3 synthesis in human skin. *J Clin Endocrinol Metab*, **67** (2): 373–378.

Webb AR, Pilbeam C, Hanafin N, Holick MF (1990). An evaluation of the relative contributions of exposure to sunlight and of diet to the circulating concentrations of 25-hydroxyvitamin D in an elderly nursing home population in Boston. *Am J Clin Nutr*, **51**: 1075–1081.

WHO (1998). Vitamins and mineral requirements in human nutrition. Joint FAO/WHO expert consultation on human nutrition. World Health Organisation library cataloguing-in-publication data, Bangkok, Thailand.

Wolpowitz D, Gilchrest BA (2006). The vitamin D questions: How much do you need and how should you get it? *J Am Acad Dermatol*, **54**: 301–317.

Ziegelberger G, Repacholi M, McKinlay A (2006). International commission on non-ionizing radiation protection. *Prog Biophys Mol Biol*, **92**: 1–3.

Zittermann A (2003). Vitamin D in preventive medicine: Are we ignoring the evidence? *Br J Nutr*, **89**: 552–572.

Zitterman A, Schleihoff SS, Tenderich G, Berthold HK, Korfer R, Stetile P (2003). Low vitamin D status: A contributing factor in the pathogenesis of congestive heart failure? *J Am Coll Cardiol*, **41** (1): 105–12.

60

Endogenous Antioxidant Photoprotection and Its Enhancement in Human Skin

Maryam Afshar
King's College, London

Antony R. Young
King's College, London

60.1 Introduction

Terrestrial solar ultraviolet radiation (UVR) is a major environmental hazard and is the cause of the majority of skin cancers, especially in sun-sensitive white-skinned people. There is considerable evidence that nonmelanoma skin cancers are due to UVR-induced DNA damage (Ziegler et al., 1994). UVR also causes photoaging. The effects of UVR on the skin, whether acute such as sunburn or long term, are caused by damage to target molecules. This can be done in two ways: (1) Direct absorption of UVR by the target molecule such as DNA or urocanic acid. In such cases, the target molecule is the chromophore. One of the most important types of DNA damage formed in this way is the cyclobutane pyrimidine dimer (CPD), which has been implicated in erythema, immunosuppression, mutagenesis, and skin cancer (Yarosh, 2004). Alternatively (2) the target molecule can be damaged indirectly when UVR is absorbed by another chromophore, which generates reactive oxygen species (ROS), such as the superoxide anion, hydrogen peroxide, the hydroxyl radical, and singlet oxygen. ROS can interact with cellular proteins, membranes, and DNA to alter their functions. Consequently, excessive ROS may arrest the cell growth cycle and cause inflammation, immunosuppression, skin aging, DNA damage (Cadet et al., 2009), mutation, and cancer.

The specific chromophores that generate ROS are largely undefined. As an approximate rule of thumb, it can be said the minor ($\leq$5%) UVB (~295–320 nm) component of solar UVR is responsible for direct UVR effects and the majority ($\geq$95%) of UVA component (320–400 nm) is responsible for the indirect effects. However, there are many exceptions to this rule.

The skin has natural defense mechanisms against UVR. The most obvious is melanin, which attenuates UVR. The amount and type of melanin in the skin are genetically determined as is the melanogenic response to UVR. More important is DNA repair capacity, without which the skin is extremely prone to skin cancer. The classic example of this is in the genodermatoses xeroderma pigmentosum (XP), which lack nucleotide excision repair. The skin also has natural antioxidants.

60.2 Natural, Oral, and Topical Antioxidants

Low-molecular-weight antioxidants, naturally present in skin, provide endogenous protection by binding to and neutralizing ROS before oxidation can cause damage to healthy cells. These natural antioxidants are nonenzymic (e.g., ascorbic acid, α-tocopherol, ubiquinol, and glutathione) or enzymic (e.g., catalase, superoxide dismutase, thioredoxin reductase, glutathione peroxidase, and glutathione reductase) (Pinnell, 2003). Antioxidants are present in the epidermis and the dermis (Shindo et al., 1994); overall activities of the enzymatic antioxidants, and the concentrations of nonenzymatic antioxidants, are higher in the epidermis.

The majority of nonenymatic antioxidants are obtained through the diet and then transported to skin, where they may be depleted by UVR exposure. For example, in a model of human skin exposed to high doses of UVR, ubiquinol levels were reduced significantly, and α-tocopherol was depleted in a linear fashion with increasing UVR doses (Podda et al., 1998).

After UVR exposure, skin cannot protect itself as well against further ROS because of its diminished antioxidant levels. The excess ROS generated overwhelms the antioxidant system; the imbalance between ROS and endogenous protective mechanisms is known as "oxidative stress."

Since some of the adverse consequences of UVR are due to ROS production, it is logical to consider antioxidant supplementation as a defense against their generation, leading to a reduction in ROS's damaging effects. Moreover, since antioxidants are depleted as they shield the skin from oxidative stress, it would seem beneficial to add to the skin's supply. Antioxidants can be added to skin through diet, oral supplements, and topical application.

Direct application is advantageous because it adds antioxidants directly to skin surfaces which require defense and may also penetrate to the dermis. Oral antioxidants are appealing because they are simple and convenient and homogenously give the whole skin a basic UVR shield.

Much of the research on antioxidant photoprotection has been done on the mouse (Reeve et al., 2005, 2010) but this chapter will focus on human studies. Antioxidant micronutrients that enhance endogenous photoprotection in humans include carotenoids, vitamins E (a-tocopherol) and C (ascorbate), and polyphenols. A summary of these studies and their outcomes is given in Table 60.1.

60.2.1 Carotenoids

60.2.1.1 Structures and Characteristics

The carotenoids' antioxidant abilities are due to their structure: a long conjugated double bond chain. They efficiently quench ROS, especially excited singlet oxygen (Krinsky, 1998; Cantrell et al., 2003). Several carotenoids are precursors to Vitamin A. The two major carotenoids in humans are β-carotene and lycopene (Stahl et al., 1993), as shown in Figure 60.1.

60.2.1.2 β-Carotene

β-Carotene is a fat-soluble antioxidant commonly consumed from carrots, spinach, sweet potatoes, and cantaloupe.

60.2.1.2.1 Photoprotective Properties

A meta-analysis of the literature up to 2007 on oral supplementation with dietary β-carotene in humans showed that it effectively prevents sunburn (Kopcke and Krutmann, 2008), with a maximum sun protection factor (SPF) of 4. However, this photoprotection was only provided once the individual had been taking at least 24 mg β-carotene daily for over 10 weeks with the protective effect increased by 0.5 standard deviations with each extra month of taking supplements.

60.2.1.2.2 Mechanism of Action

The mechanism by which β-carotene provides photoprotection is unknown; it is presumed that this is due to its antioxidant properties, possibly by interfering with the cell signaling pathways through which UVB exerts its damaging effects (Kopcke and Krutmann, 2008).

TABLE 60.1 Summary of Photoprotective Effects of Antioxidants in Human Skin

Antioxidant	Daily Dose	Duration	ROA	UVR Source	Outcome	References
Carotenoid						
β-Car	24 mg/day	12 weeks	OS	SSR	a ↓ (~20%)	Heinrich et al. (2003)
	30–90 mg/day	24 weeks	OS	SSR	MED ↑ dose dependently (50% with 90 mg/day)	Lee et al. (2000)
	90 mg/day	3 weeks	OS	SSR	No protection: erythema or SBC	Garmyn et al. (1995)
	180 mg/day	10 weeks	OS	Sun	MED ↑ slightly	Mathews-Roth et al. (1972)
	15 mg/day	8 weeks	OS	Philips TL12	No protection: MED or oxidative stress	McArdle et al. (2004)
	16 mg/day	10 weeks	Tomato paste (40 g)	SSR	Δa ↓30%	Stahl et al. (2001)
Lyc	10.2 mg/day	12 weeks	Synthetic lyc capsules (2)	SSR	Δa ↓ not significant	Stahl et al. (2006)
	16 mg/day	12 weeks	Tomato paste (55 g)	Philips TL12	MED ↑ 16% (eye) and ~40% (reflectance), MMP-1 ↓. mtDNA damage	Rizwan et al. (2010)
β-Car + lyc	5.1 mg β-car + 10 mg lyc/day	12 weeks	Carrot juice (2 × 200 mL)	SSR	Δa ↓ 45%	Stahl et al. (2006)
	0.4 mg β-car + 9.8 mg lyc/day	12 weeks	OS	SSR	Δa ↓	Stahl et al. (2006)
	0.4 mg β-car + 8.2 mg lyc/day	12 weeks	Lyc drink (2 × 250 mL)	SSR	Δa ↓50%	Stahl et al. (2006)
β-Car + lyc + lutein	24 mg (8 mg each)/day	12 weeks	OS	SSR	a ↓ (~15%)	Heinrich et al. (2003)
Carotenoid mixture	150 mg β-car + canthaxin (2:3)/day	4 weeks	OS	UVA and UVB	No protection: MED and UDS with UVB	Wolf et al. (1988)
	25 mg (13.0 mg all-trans-β-car, 10.5 mg 9-*cis* β-car, 0.3 mg other *cis* isomers of β-car, 0.75 mg α-car, 0.18 mg cryptoxanthin, 0.15 mg zeaxanthin, 0.12 mg lutein)/day	12 weeks	OS	SSR	Δa ↓ 35%	Stahl et al. (2000)

(*continued*)

TABLE 60.1 (continued) Summary of Photoprotective Effects of Antioxidants in Human Skin

Antioxidant	Daily Dose	Duration	ROA	UVR Source	Outcome	References
β-Car + lycopene + α-toc + selenium	6 mg α- and β-car + 6 mg lyc + 10 mg α-toc + 75 μg selenium/day	7 weeks	OS	SSR	MED ↑ 20%, SBC, p53 and lipoperoxide ↓	Cesarini et al. (2003)
Carotenoids + α-toc	25 mg carotenoids (13.0 mg all-*trans*-β-car, 10.5 mg 9-*cis* β-car, 0.3 mg other *cis* isomers of β-car, 0.75 mg α-car, 0.18 mg cryptoxanthin, 0.15 mg zeaxanthin, 0.12 mg lutein) + 500 IU RRR-α-toc/day	12 weeks	OS	SSR	Δa ↓ 32%	Stahl et al. (2000)
α-Toc	400 IU/day	8 weeks	OS	Philips TL12	No protection: MED or oxidative stress	McArdle et al. (2004)
	400 IU/day	26 weeks	OS	Phototherapy lamp	No protection: MED and SBC	Werninghaus et al. (1994)
	1200 IU/day	1 week	OS	Phototherapy lamp	MED ↑ 8%	Mireles-Rocha et al. (2002)
	2000 mg/day	7 weeks	OS	SSR	No protection: MED	Fuchs and Kern (1998)
	2% Vitamin E	1 day	Topical	Westinghouse FS20	a ↓	Dreher et al. (1998)
Asc	3000 mg/day	7 weeks	OS	SSR	No protection: MED	Fuchs and Kern (1998)
	400 IU/day	8 weeks	OS	Philips TL12	No protection: erythema or oxidative stress	McArdle et al. (2002)
	2000 mg/day	1 week	OS	Phototherapy lamp	No protection: MED	Mireles-Rocha et al. (2002)
	5% Vitamin C	1 day	Topical	Westinghouse FS20	No protection: a	Dreher et al. (1998)

α-Toc + asc	1000 IU α-toc + 2000 mg asc/day	8 days	OS	Philips TL20	MED ↑ 20%, cutaneous blood flow ↓	Eberlein-Konig et al. (1998)
	1200 IU α-toc + 2000 mg asc/day	1 week	OS	Phototherapy lamp	MED ↑ 40%	Mireles-Rocha et al. (2002)
	2000 mg α-toc + 3000 mg asc/day	7 weeks	OS	SSR	MED ↑ ~80%	Fuchs and Kern (1998)
	2% Vitamin E + 5% vitamin C	1 day	Topical	Westinghouse FS20	a ↓	Dreher et al. (1998)
α-Toc + asc + ferulic acid	1% α-Toc + 15% L L-asc + 0.5% ferulic acid	4 days	Topical	SSR	Erythema ↓, CPD ↓, p53↓, cytokine mRNA ↓	Murray et al. (2008)
α-Toc + asc + melatonin	2% Vit E + 5% Vit C + 1%–2.5% melatonin	1 day	Topical	Westinghouse FS20	a ↓	Dreher et al. (1998)
Flavanols	3 mg EGCG/100 μL acetone/2.5 cm^2	1 day	Topical	Westinghouse FS20	Erythema ↓, leukocytes ↓, PG ↓	Katiyar et al. (1999)
	3 mg GTP/2.5 cm^2	1 day	Topical	Westinghouse FS20	Erythema ↓, CPD ↓	Katiyar et al. (2000)
	0.2 mL of GTPs dissolved in ethanol/water vehicle (0.25%–10%)	1 day	Topical	SSR	Erythema ↓ GTP dose dependent; LC ↑, SBC and DNA damage ↓	Elmets et al. (2001)
	326 mg flavanol dissolved in 100 mL water/day	12 weeks	Cocoa drink	SSR	a ↓ 25%	Heinrich et al. (2006)

Abbreviations: α-car, α-carotene; α-toc, α-tocopherol; asc, ascorbate; β-car, β-carotene; EGCG, epigallocatechin-3-gallate; GTP, green tea polyphenols; Lyc, Lycopene; CPD, cyclobutane pyrimidine dimer; MED, minimal erythema dose; MMP-1, matrixmetaloproteinase-1 (marker of photoaging); mtDNA, mitochondrial DNA; OS, oral supplement; PG, prostaglandins; ROA, route of administration; SBC, sunburn cell (marker of apoptosis/DNA damage); SSR, solar-simulated radiation; UDS, unscheduled DNA synthesis (a measure of DNA damage). In some cases, erythema was measured by a reflectance device where units are given as a ↓ or Δa ↓ values. The latter is the difference between a test and a control site.

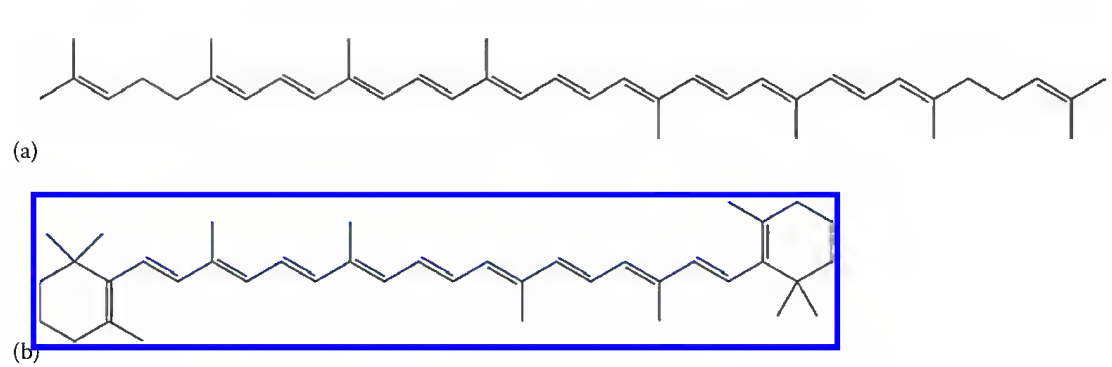

FIGURE 60.1 Structures of the major dietary carotenoids (a) lycopene and (b) β-carotene.

60.2.1.2.3 Side Effects

While β-carotene has significant photoprotective properties, for it to be marketed as an endogenous photoprotectant, it needs to be nontoxic at the recommended dose and over a long time period. However, two intervention trials have shown that β-carotene supplements given to individuals at a high risk for lung cancer increased their cumulative risk (Omenn et al., 1996; Alpha-Tocopherol Study, 1994; Goodman et al., 2004). Therefore, the use of β-carotene as an oral supplement may not be practical; further studies are required to determine the side effects of long-term use.

60.2.1.3 Lycopene

Lycopene is a major dietary carotenoid in tomatoes with the reddest strains having the highest levels; it is also present in apricots, guava, and watermelon (Stahl et al., 2006). Its bioavailability from tomato paste is greater than tomato juice or fresh tomatoes (Gartner et al., 1997). Of all the carotenoids, lycopene is the most efficient singlet oxygen quencher (Di et al., 1989).

The effectiveness of lycopene has been demonstrated (Stahl et al., 2001). Individuals who ingested 40 g of tomato paste (equivalent to 16 mg of lycopene) with 10 g of olive oil per day for 10 weeks had 40% less erythema exposure to a solar-simulated radiation (SSR) compared with controls who consumed olive oil only ($P = 0.02$). Individuals who consumed the test products with high lycopene content on a daily basis for 10–12 weeks had decreased skin erythema in response to UVR in comparison with the start of the study. These results have been confirmed in a more recent human study (Rizwan et al., 2010), which also found that oral lycopene could protect against UVR-induced dermal matrix metalloproteinase-1 (MMP-1) induction and mitochondrial DNA damage; the latter two endpoints have been implicated in photoaging. Overall, these data suggest that lycopene has potential as a photoprotecting agent.

60.2.1.4 Future Implications for Carotenoids

Should β-carotene's risks prove to be insignificant, sunscreen application and carotenoid supplementation could be used as complementary methods to provide photoprotection (Kopcke and Krutmann, 2008). The combination of carotenoid supplementation and topical sunscreens provides synergistic defense against UVR's damaging effects. β-Carotene intake would offer a complete, always present defense against UVR, while sunscreen would provide extra protection when the individual requires higher photoprotection requirements, such as while outdoors or on summer vacations.

Additionally, β-carotene should be combined with other oral antioxidants, thereby enabling lower β-carotene doses to be used and consequently decreasing the risk of β-carotene supplementation. A daily oral supplement consisting of β-carotene, lutein, and lycopene (8 mg each) efficiently reduces the degree of UVR-induced erythema at levels similar to those obtained with 24 mg daily β-carotene supplements (Heinrich et al., 2003).

60.2.2 Vitamin E (Tocopherols) and Vitamin C (Ascorbate)

The body already uses vitamins E and C for protection against UVR, making them ideal candidates for antioxidant supplementation (Pinnell, 2003). The main sources of dietary vitamin E are vegetable oils, cereal grains, green leaves, egg yolk, liver, milk fat, and nuts. Vitamin C is found in a wide variety of fruit and vegetables. Good sources include peppers, broccoli, Brussels sprouts, sweet potatoes, oranges and kiwi fruit.

60.2.2.1 Structures and Characteristics

Vitamin E is the generic name for a group of tocol and tocotrienol derivatives, that is, α-tocopherol. These compounds are lipophilic and present in cell membranes (Bendich and Machlin, 1988). Vitamin C is a water-soluble compound present in several tissues and is the most abundant antioxidant in the skin (Shindo et al., 1994). It acts as a cofactor in enzymatic reactions necessary for collagen synthesis; thereby, it helps in wound healing and maintenance of normal connective tissue. The structures for vitamin E and C are shown in Figure 60.2.

60.2.2.2 Photoprotective Properties

60.2.2.2.1 Oral Intake

High oral intake of α-tocopherol and ascorbate does not have serious side effects (Bendich and Machlin, 1988). One week of supplementation with 2000 mg/day of ascorbic acid and 1000–1200 IU/day of D-α-tocopherol reduced sunburn reaction (Eberlein-Konig et al., 1998; Mireles-Rocha et al., 2002). Oral combination therapy with a much lower dose of α-tocopherol and for a longer period—α-tocopherol (2 g/day) and ascorbate (3 g/day) for 50 days—also decreased the erythema produced from high doses of SSR (Fuchs and Kern, 1998). These studies resulted in an SPF of 1.4–2.

Several studies have determined that oral monotherapy with 400 IU α-tocopherol does not provide significant levels of photoprotection or affect the UVR-induced erythema response (Werninghaus et al., 1994; McArdle et al., 2004). However, minimal erythema dose (MED) was increased with 1200 IU α-tocopherol daily (Mireles-Rocha et al., 2002).

Numerous studies have illustrated that oral vitamin C supplementation does not have photoprotective properties (Fuchs and Kern, 1998; Mireles-Rocha et al., 2002; McArdle et al., 2002).

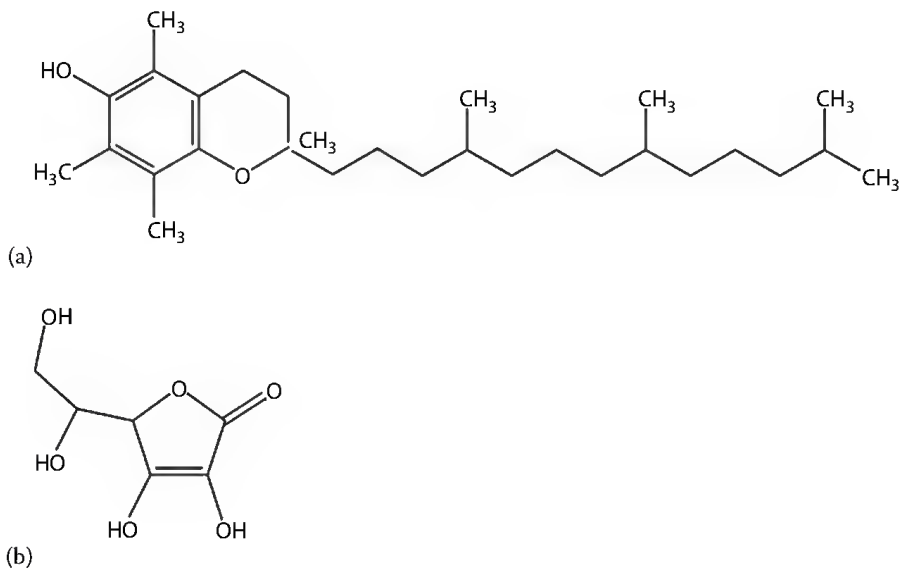

FIGURE 60.2 Structures of nonenzymatic antioxidants (a) α-tocopherol and (b) ascorbate.

60.2.2.2.2 Topical Application

Humans must obtain L-ascorbic acid from the diet. Since physiological mechanisms in the body restrict the amount of L-ascorbic acid that can be absorbed and transported to skin, topical L-ascorbic acid application is the sole method of further increasing skin concentrations (Pinnell, 2003). Vitamin E is appealing as a topical agent because its lipophilic nature enables easy absorption into skin.

Topical application of 2% vitamin E alone or 5% vitamin C alone 30 min before sun exposure provided modest or no inhibition of erythema, respectively (Dreher et al., 1998). However, topical application to swine skin of 15% L-ascorbic acid alone is photoprotective, as is 1% α-tocopherol (Lin et al., 2003). This suggests that topical application of vitamin C is not effective unless at high concentrations.

The combination of 15% L-ascorbic acid and 1% α-tocopherol over 4 days provides the best protection against erythema, and CPD in swine skin (Lin et al., 2003).

Because vitamins C and E are inherently unstable, modifications have been developed to increase their stability and effects. The addition of 0.5% ferulic acid, a potent antioxidant, to 1% α-tocopherol and 15% L-ascorbic acid was shown to improve the vitamins' stability and photoprotective properties (Murray et al., 2008). This combination reduced erythema, sunburn cells (SBC; apoptosis), and CPD as well as proinflammatory and immunosuppressive cytokines.

60.2.2.3 Mechanism of Action

Ascorbate scavenges ROS and protects the skin by neutralizing the superoxide radical anion, hydrogen peroxide, the hydroxyl radical, and singlet oxygen. Vitamin E inhibits oxidative damage to lipids and scavenges lipid peroxyl radicals. In the process, α-tocopherol is oxidized to the tocopheroxyl radical such that combination therapy is effective and synergistic because ascorbate regenerates α-tocopherol from its radical form (Packer et al., 1979; Fuchs and Kern, 1998).

60.2.2.4 Future Implications for Vitamins E and C

60.2.2.4.1 Oral Supplementation

The prevalence of melanoma has been found to be inversely correlated with serum α-tocopherol levels (Knekt, 1992). Additionally, individuals with basal cell carcinoma (BCC) have significantly lower ascorbic acid and α-tocopherol plasma levels (Vural et al., 1999). It has been suggested that regular consumption of supplemental vitamins, especially vitamins C and E, reduces the risk of BCC (Wei et al., 1994). Thus, systemic photoprotection with combination therapy may be a convenient adjunct to sunscreens in improving photoprotection.

60.2.2.4.2 Topical Application

Using a topical mixture containing vitamins E and C in addition to using sunscreen may provide effective protection against the adverse effects of UVR (Lin et al., 2003). In swine skin, combination therapy added to a UVA sunscreen (oxybenzone) provided greater than additive levels of photoprotection (Darr et al., 1996). Combining both antioxidants with ferulic acid and a broad-spectrum sunscreen is hypothesized to provide the most substantial photoprotection (Lin et al., 2005).

60.2.3 Polyphenols

Tea polyphenols are more potent than vitamins C and E (Pinnell, 2003). They are also the most common dietary antioxidants with intake as much as 1 g/day. They are found in tea, coffee, red wine, fruit juice, vegetables, cereals, chocolate, and dry legumes (Scalbert et al., 2005).

60.2.3.1 Structures and Classification

There are thousands of plant-derived molecules with the polyphenol structure; hydroxyl groups on aromatic rings (Manach et al., 2004). Based on their number of phenol groups, they are divided into

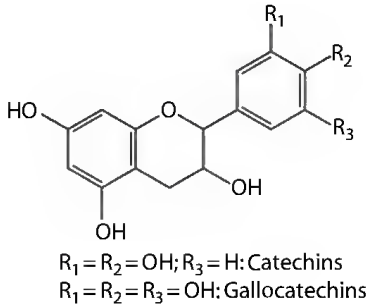

FIGURE 60.3 Structure of flavanols.

subgroups. The flavanoid subgroup has a structure of two aromatic rings united by three carbon atoms, which make up a heterocycle. Depending on the type of heterocycle in the structure, the flavonoids are further divided into different subclasses: flavonols, flavones, isoflavones, flavanones, anthocyanidins, and flavanols. The latter exist as monomers (catechins) and polymers (proanthocyanidins). Their structures are shown in Figure 60.3. While flavanols are abundant in numerous fruits and vegetables, the richest sources are green tea (GT) and chocolate.

60.2.3.2 Green Tea

GT produced through fermentation of fresh tea leaves, is one of the most commonly consumed drinks worldwide. The leaves of *Camellia sinensis* are fermented to produce GT such that the plant's polyphenols are not oxidized or polymerized (Yusuf et al., 2007). The chief polyphenols in GT are (–)-epicatechin (EC), (–)-epicatechin-3-gallate (ECG), (–)-epigallocatechin (EGC), and (–)-epigallocatechin-3-gallate (EGCG), as shown in Figure 60.4.

60.2.3.2.1 Photoprotective Properties

60.2.3.2.1.1 Oral Intake Chronic oral intake of green tea polyphenols (GTPs) (0.1%, w/v) significantly protects against developing UVR-induced skin cancer in mice in comparison with controls drinking normal water ($P < 0.01$) (Wang et al., 1991). This group also showed that treating mice with GT for 4–10 weeks caused partial regression or greater than 90% inhibition of growth of established skin papillomas,

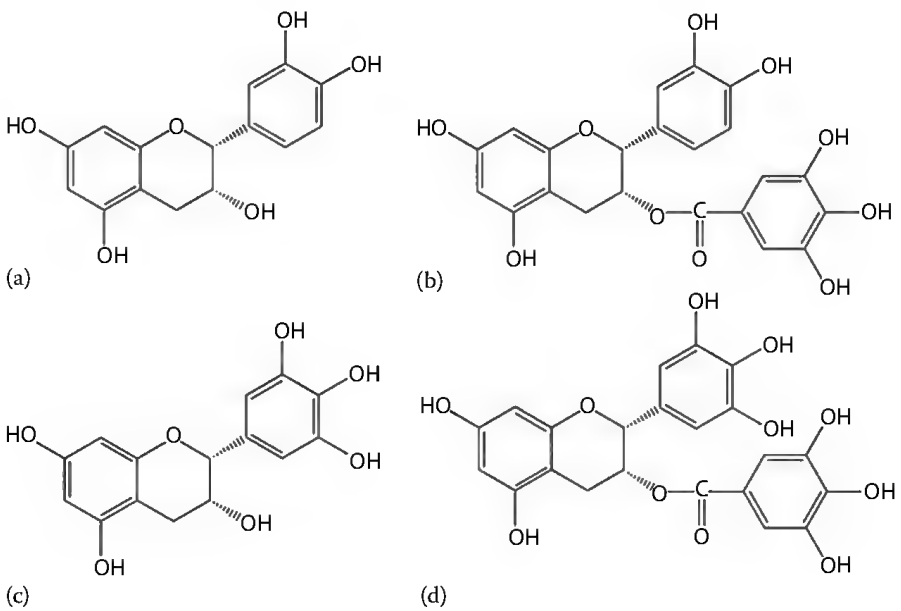

FIGURE 60.4 Structures of major polyphenols in GT (a) (–)-EC, (b) (–)-ECG, (c) (–)-EGC, and (d) (–)-EGCG.

and complete regression in 4% (Wang et al., 1992b). Further studies showed that a 1.25% GT extract as the only source of drinking water 10 days before and during UVB radiation, and for 7 days after, inhibited photocarcinogenesis (Wang et al., 1992a). Another study showed that GTPs in the drinking water (2 g/L) of mice decreased UVB-induced tumor incidence (35%), multiplicity (63%), and growth (55%) (Mantena et al., 2005). Furthermore, the intensity and area of red sunburn lesions in mice were decreased dose dependently with brewed GT consumption (at concentrations similar to human intake: 1.25% or 2.5%) for 2 weeks before and during UVB radiation (Wang et al., 1992a).

In humans, GT intake provided photoprotection: following exposure to 12 min of UVA radiation, peripheral blood cells taken after consumption of three cups of GT (totaling 540 mL) had less DNA damage (assessed by comet assay) in comparison with those taken before consumption (Morley et al., 2005). It has been suggested that drinking 5–6 cups (1 cup = 150 mL) of GT (1 g GT leaves/150 mL) daily may provide significant photoprotection (Mantena et al., 2005).

60.2.3.2.1.2 Topical Application

Tumor Formation, DNA Photodamage, and Apoptosis

Topical GTP application protected mice from UVB-induced tumors (Wang et al., 1991), as did EGCG in hydrophilic cream, which reduced tumor incidence (60%), multiplicity (86%), and growth (95%) ($P < 0.001$) (Mittal et al., 2003). In mice, topical application of GTPs in hydrophilic cream also prevented UVB-induced depletion of glutathione peroxidase, catalase, and glutathione (Vayalil et al., 2003).

Topical GTP application to human skin *in vivo* significantly inhibited CPD after UVR exposure (Katiyar et al., 2000; Elmets et al., 2001). Protection against DNA photodamage has also been demonstrated *in vitro*. Preincubation of human skin fibroblasts with 250 μM EGCG significantly reduced DNA damage, assessed by the comet assay, after UVR exposure (Morley et al., 2005). In addition, EGCG treatment to the human keratinocyte line (HaCaT) decreased UVA-induced single-strand DNA breaks assessed by the comet assay (Tobi et al., 2002). DNA damage is a trigger for apoptosis, observed as SBCs in the epidermis. Topical GTP application decreased SBC by 66% (Elmets et al., 2001). This was most effective when applied immediately before UVR but protection was still observed with application 4 h before UVR.

Lipid Peroxidation/Oxidative Stress

Application of EGCG (~1 mg/cm^2) to human skin before four MED inhibits UVR-induced oxidative stress, with decreased production of hydrogen peroxide, nitric oxide, epidermal lipid peroxidation, and inflammatory leukocyte infiltration (Katiyar et al., 2001). The latter may be due to the ability of EGCG to inhibit signaling pathways triggered by oxidative stress (Baliga and Katiyar, 2006). EGCG pretreatment also protected glutathione peroxidase and Langerhans cells in human skin (Elmets et al., 2001; Katiyar et al., 2001). The inhibition of the different adverse effects may inhibit photocarcinogenesis and photoaging (Baliga and Katiyar, 2006).

Erythema

Preapplication of GTPs to human skin (3 mg/2.5 cm^2) decreases UVB-induced erythema (Katiyar et al., 1999). In another study, skin treated with 0.2 mL GTP (concentrations ranging 1%–10%) immediately before UVR exposure dose dependently decreased the erythema response. A 10% solution provided nearly total protection at 48 and 72 h, while a 2.5% solution afforded excellent protection; even a 0.5% solution significantly protected some individuals from sunburn ($P < 0.01$). The polyphenols EGCG and ECG were much more effective than EGC and EC at inhibiting erythema (Elmets et al., 2001).

60.2.3.2.1.3 Oral vs. Topical Treatment

GTPs provide greater photoprotection when administered topically than orally, possibly because this allows for greater bioavailability, penetration, and absorption into skin (Vayalil et al., 2003). Despite this, oral GTPs' photoprotective effects are significant, and perhaps more relevant because GT is a popular drink (Mantena et al., 2005).

60.2.3.2.2 Modes of Action of the GTPs

Of the GTPs, EGCG is the most potent in preventing photocarcinogenesis in mouse. *In vitro* and *in vivo* experiments show that GTPs or EGCG are photoprotective via several mechanisms: GTP induces the immunoregulatory cytokine interleukin (IL)-12, inhibits UVR-induced immunosuppression and angiogenesis that supports tumor growth and metastasis, and promotes apoptosis of carcinogenic cells. Through these mechanisms, GTP therapy may prevent tumors and cause regression of existing tumors (Mantena et al., 2005; Katiyar et al., 2007).

60.2.3.3 Cocoa

The effect of regular consumption of cocoa containing high levels of the flavanol monomers epicatechin and catechin on human photoprotection has been studied. By the 12th week, those who drank the high flavanol drink had 25% less UVR-induced erythema after skin exposure to 1.25 MED compared with when they had begun the study (Heinrich et al., 2006). Another study found that better photoprotection was provided with consumption of high flavanol content chocolate in comparison with conventional dark chocolate (Williams et al., 2009). Both studies concluded that dietary flavanols increased endogenous photoprotection.

60.2.3.4 Future Implications for Polyphenols

Polyphenols in GT and cocoa/chocolate are ideal supplements because of their numerous photoprotective properties and because they are more pharmacologically safe, nontoxic, and easily obtained. For these reasons, the food and nutrition supplement companies have recently increased interest in promoting and producing polyphenol-rich products.

In addition to oral supplementation, GTP supplementation to sunscreens and skin care products is another strategy for reducing photocarcinogenesis and various skin disorders. In contrast to sunscreens, GTPs do not absorb UVR. Therefore, their addition to sunscreens should provide a synergistic photoprotection, stronger than the application of GTPs or sunscreens alone. Consequently, several companies have begun including *C. sinensis* plant extracts in their skin care products. GTPs may also be beneficial for individuals with sunscreen allergies or intolerance.

Clinical trials are required to determine the effectives of GTPS, both alone and in combination therapy, in preventing skin damage and cancer in high-risk individuals. Using GTPs should not be the only method of preventing photodamage but may be an effective adjunct to current strategies.

60.3 Conclusions

There is evidence that natural antioxidant defenses in humans can be enhanced by oral and topical supplementation. Table 60.1 shows that all studies have used erythema as an endpoint. It would be difficult to conclude a long-term benefit from these studies, and it is clear that more sophisticated techniques should be developed to assess long-term protection. Some groups have started to do this (Rizwan et al., 2010). The SPF provided by dietary and topical antioxidants is very much less than that provided by sunscreens, typically less than 2.

Many of the studies listed in Table 60.1 have used "SSR"; however, few authors have defined their UVR emission spectra, and it is quite likely that many sources, whether "SSR" or not, contained nonsolar UVR. This is important because some antioxidants, for example, vitamin E, absorb in the nonsolar and solar UVB range, which makes it impossible to exclude a small sunscreening effect (bearing in mind that photoprotection is typically very modest). This is an aspect that is often neglected by authors but has been considered in the case of GT polyphenols (Elmets et al., 2001), which do not absorb in the UVB range.

In general, oral route studies have required several weeks of daily intervention. While this may demonstrate a point of principle, it is unlikely to be of great use in practice where compliance is less likely. Nonetheless, it can be argued that systemic administration enhances photoprotection when sunscreens are not being worn. The topical route seems much more promising for the development of new intelligent

photoprotection strategies. Some studies have shown antioxidant protection against CPD (in particular thymine dimers). This is perhaps surprising because it is widely believed that CPD induced by solar UVR is formed by direct UVR absorption of UVB. However, there is some debate about the role of direct absorption or photosensitization reactions in the formation of UVA-induced CPD (Mouret et al., 2010).

References

Alpha-Tocopherol Study (1994). The effect of vitamin E and beta carotene on the incidence of lung cancer and other cancers in male smokers. The Alpha-Tocopherol, Beta Carotene Cancer Prevention Study Group. *New Engl J Med* **330**: 1029–1035.

Baliga MS, Katiyar SK (2006). Chemoprevention of photocarcinogenesis by selected dietary botanicals. *Photochem Photobiol Sci* **5**: 243–253.

Bendich A, Machlin LJ (1988). Safety of oral intake of vitamin E. *Am J Clin Nutr* **48**: 612–619.

Cadet J, Douki T, Ravanat JL, Di MP (2009). Sensitized formation of oxidatively generated damage to cellular DNA by UVA radiation. *Photochem Photobiol Sci* **8**: 903–911.

Cantrell A, McGarvey DJ, Truscott TG, Rancan F, Bohm F (2003). Singlet oxygen quenching by dietary carotenoids in a model membrane environment. *Arch Biochem Biophys* **412**: 47–54.

Cesarini JP, Michel L, Maurette JM, Adhoute H, Bejot M (2003). Immediate effects of UV radiation on the skin: Modification by an antioxidant complex containing carotenoids. *Photodermatol Photoimmunol Photomed* **19**: 182–189.

Darr D, Dunston S, Faust H, Pinnell S (1996). Effectiveness of antioxidants (vitamin C and E) with and without sunscreens as topical photoprotectants. *Acta Derm-Venereol* **76**: 264–268.

Di MP, Kaiser S, Sies H (1989). Lycopene as the most efficient biological carotenoid singlet oxygen quencher. *Arch Biochem Biophys* **274**: 532–538.

Dreher F, Gabard B, Schwindt DA, Maibach HI (1998). Topical melatonin in combination with vitamins E and C protects skin from ultraviolet-induced erythema: A human study in vivo. *Br J Dermatol* **139**: 332–339.

Eberlein-Konig B, Placzek M, Przybilla B (1998). Protective effect against sunburn of combined systemic ascorbic acid (vitamin C) and D-alpha-tocopherol (vitamin E). *J Am Acad Dermatol* **38**: 45–48.

Elmets CA, Singh D, Tubesing K, Matsui M, Katiyar S, Mukhtar H (2001). Cutaneous photoprotection from ultraviolet injury by green tea polyphenols. *J Am Acad Dermatol* **44**: 425–432.

Fuchs J, Kern H (1998). Modulation of UV-light-induced skin inflammation by D-alpha-tocopherol and L-ascorbic acid: A clinical study using solar simulated radiation. *Free Radical Bio Med* **25**: 1006–1012.

Garmyn M, Ribaya-Mercado JD, Russel RM, Bhawan J, Gilchrest BA (1995). Effect of beta-carotene supplementation on the human sunburn reaction. *Exp Dermatol* **4**: 104–111.

Gartner C, Stahl W, Sies H (1997). Lycopene is more bioavailable from tomato paste than from fresh tomatoes. *Am J Clin Nutr* **66**: 116–122.

Goodman GE, Thornquist MD, Balmes J, Cullen MR, Meyskens FL, Jr., Omenn GS et al. (2004). The beta-carotene and retinol efficacy trial: Incidence of lung cancer and cardiovascular disease mortality during 6-year follow-up after stopping beta-carotene and retinol supplements. *J Natl Cancer Inst* **96**: 1743–1750.

Heinrich U, Gartner C, Wiebusch M, Eichler O, Sies H, Tronnier H et al. (2003). Supplementation with beta-carotene or a similar amount of mixed carotenoids protects humans from UV-induced erythema. *J Nutr* **133**: 98–101.

Heinrich U, Neukam K, Tronnier H, Sies H, Stahl W (2006). Long-term ingestion of high flavanol cocoa provides photoprotection against UV-induced erythema and improves skin condition in women. *J Nutr* **136**: 1565–1569.

Katiyar SK, Afaq F, Perez A, Mukhtar H (2001). Green tea polyphenol (−)-epigallocatechin-3-gallate treatment of human skin inhibits ultraviolet radiation-induced oxidative stress. *Carcinogenesis* **22**: 287–294.

Katiyar S, Elmets CA, Katiyar SK (2007). Green tea and skin cancer: Photoimmunology, angiogenesis and DNA repair. *J Nutr Biochem* **18**: 287–296.

Katiyar SK, Matsui MS, Elmets CA, Mukhtar H (1999). Polyphenolic antioxidant (−)-epigallocatechin-3-gallate from green tea reduces UVB-induced inflammatory responses and infiltration of leukocytes in human skin. *Photochem Photobiol* **69**: 148–153.

Katiyar SK, Perez A, Mukhtar H (2000). Green tea polyphenol treatment to human skin prevents formation of ultraviolet light B-induced pyrimidine dimers in DNA. *Clin Cancer Res* **6**: 3864–3869.

Knekt P (1992). Vitamin E and cancer: Epidemiology. *Ann NY Acad Sci* **669**: 269–279.

Kopcke W, Krutmann J (2008). Protection from sunburn with beta-carotene—A meta-analysis. *Photochem Photobiol* **84**: 284–288.

Krinsky NI (1998). The antioxidant and biological properties of the carotenoids. *Ann NY Acad Sci* **854**: 443–447.

Lee J, Jiang S, Levine N, Watson RR (2000). Carotenoid supplementation reduces erythema in human skin after simulated solar radiation exposure. *Proc Soc Exp Biol Med* **223**: 170–174.

Lin FH, Lin JY, Gupta RD, Tournas JA, Burch JA, Selim MA et al. (2005). Ferulic acid stabilizes a solution of vitamins C and E and doubles its photoprotection of skin. *J Invest Dermatol* **125**: 826–832.

Lin JY, Selim MA, Shea CR, Grichnik JM, Omar MM, Monteiro-Riviere NA et al. (2003). UV photoprotection by combination topical antioxidants vitamin C and vitamin E. *J Am Acad Dermatol* **48**: 866–874.

Manach C, Scalbert A, Morand C, Remesy C, Jimenez L (2004). Polyphenols: Food sources and bioavailability. *Am J Clin Nutr* **79**: 727–747.

Mantena SK, Meeran SM, Elmets CA, Katiyar SK (2005). Orally administered green tea polyphenols prevent ultraviolet radiation-induced skin cancer in mice through activation of cytotoxic T cells and inhibition of angiogenesis in tumors. *J Nutr* **135**: 2871–2877.

Mathews-Roth MM, Pathak MA, Parrish J, Fitzpatrick TB, Kass EH, Toda K et al. (1972). A clinical trial of the effects of oral beta-carotene on the responses of human skin to solar radiation. *J Invest Dermatol* **59**: 349–353.

McArdle F, Rhodes LE, Parslew RA, Close GL, Jack CI, Friedmann PS et al. (2004). Effects of oral vitamin E and beta-carotene supplementation on ultraviolet radiation-induced oxidative stress in human skin. *Am J Clin Nutr* **80**: 1270–1275.

McArdle F, Rhodes LE, Parslew R, Jack CI, Friedmann PS, Jackson MJ (2002). UVR-induced oxidative stress in human skin in vivo: Effects of oral vitamin C supplementation. *Free Radic Biol Med* **33**: 1355–1362.

Mireles-Rocha H, Galindo I, Huerta M, Trujillo-Hernandez B, Elizalde A, Cortes-Franco R (2002). UVB photoprotection with antioxidants: Effects of oral therapy with D-alpha-tocopherol and ascorbic acid on the minimal erythema dose. *Acta Derm-Venereol* **82**: 21–24.

Mittal A, Piyathilake C, Hara Y, Katiyar SK (2003). Exceptionally high protection of photocarcinogenesis by topical application of (−)-epigallocatechin-3-gallate in hydrophilic cream in SKH-1 hairless mouse model: Relationship to inhibition of UVB-induced global DNA hypomethylation. *Neoplasia* **5**: 555–565.

Morley N, Clifford T, Salter L, Campbell S, Gould D, Curnow A (2005). The green tea polyphenol (−)-epigallocatechin gallate and green tea can protect human cellular DNA from ultraviolet and visible radiation-induced damage. *Photodermatol Photoimmunol Photomed* **21**: 15–22.

Mouret S, Philippe C, Gracia-Chantegrel J, Banyasz A, Karpati S, Markovitsi D et al. (2010). UVA-induced cyclobutane pyrimidine dimers in DNA: A direct photochemical mechanism? *Org Biomol Chem* **8**: 1706–1711.

Murray JC, Burch JA, Streilein RD, Iannacchione MA, Hall RP, Pinnell SR (2008). A topical antioxidant solution containing vitamins C and E stabilized by ferulic acid provides protection for human skin against damage caused by ultraviolet irradiation. *J Am Acad Dermatol* **59**: 418–425.

Omenn GS, Goodman GE, Thornquist MD, Balmes J, Cullen MR, Glass A et al. (1996). Risk factors for lung cancer and for intervention effects in CARET, the beta-carotene and retinol efficacy trial. *J Natl Cancer Inst* **88**: 1550–1559.

Packer JE, Slater TF, Willson RL (1979). Direct observation of a free radical interaction between vitamin E and vitamin C. *Nature* **278**: 737–738.

Pinnell SR (2003). Cutaneous photodamage, oxidative stress, and topical antioxidant protection. *J Am Acad Dermatol* **48**: 1–19.

Podda M, Traber MG, Weber C, Yan LJ, Packer L (1998). UV-irradiation depletes antioxidants and causes oxidative damage in a model of human skin. *Free Radic Biol Med* **24**: 55–65.

Reeve VE, Allanson M, Arun SJ, Domanski D, Painter N (2010). Mice drinking goji berry juice (*Lycium barbarum*) are protected from UV radiation-induced skin damage via antioxidant pathways. *Photochem Photobiol Sci* **9**: 601–607.

Reeve VE, Widyarini S, Domanski D, Chew E, Barnes K (2005). Protection against photoaging in the hairless mouse by the isoflavone equol. *Photochem Photobiol* **81**: 1548–1553.

Rizwan M, Rodriguez-Blanco I, Harbottle A, Birch-Machin MA, Watson RE, Rhodes LE (2010). Tomato paste rich in lycopene protects against cutaneous photodamage in humans in vivo: A randomized controlled trial. *Br J Dermatol* **164**(1): 154–162.

Scalbert A, Johnson IT, Saltmarsh M (2005). Polyphenols: Antioxidants and beyond. *Am J Clin Nutr* **81**: 215S–217S.

Shindo Y, Witt E, Han D, Epstein W, Packer L (1994). Enzymic and non-enzymic antioxidants in epidermis and dermis of human skin. *J Invest Dermatol* **102**: 122–124.

Stahl W, Heinrich U, Aust O, Tronnier H, Sies H (2006). Lycopene-rich products and dietary photoprotection. *Photochem Photobiol Sci* **5**: 238–242.

Stahl W, Heinrich U, Jungmann H, Sies H, Tronnier H (2000). Carotenoids and carotenoids plus vitamin E protect against ultraviolet light-induced erythema in humans. *Am J Clin Nutr* **71**: 795–798.

Stahl W, Heinrich U, Wiseman S, Eichler O, Sies H, Tronnier H (2001). Dietary tomato paste protects against ultraviolet light-induced erythema in humans. *J Nutr* **131**: 1449–1451.

Stahl W, Sundquist AR, Hanusch M, Schwarz W, Sies H (1993). Separation of beta-carotene and lycopene geometrical isomers in biological samples. *Clin Chem* **39**: 810–814.

Tobi SE, Gilbert M, Paul N, McMillan TJ (2002). The green tea polyphenol, epigallocatechin-3-gallate, protects against the oxidative cellular and genotoxic damage of UVA radiation. *Int J Cancer* **102**: 439–444.

Vayalil PK, Elmets CA, Katiyar SK (2003). Treatment of green tea polyphenols in hydrophilic cream prevents UVB-induced oxidation of lipids and proteins, depletion of antioxidant enzymes and phosphorylation of MAPK proteins in SKH-1 hairless mouse skin. *Carcinogenesis* **24**: 927–936.

Vural P, Canbaz M, Selcuki D (1999). Plasma antioxidant defense in actinic keratosis and basal cell carcinoma. *J Eur Acad Dermatol* **13**: 96–101.

Wang ZY, Agarwal R, Bickers DR, Mukhtar H (1991). Protection against ultraviolet B radiation-induced photocarcinogenesis in hairless mice by green tea polyphenols. *Carcinogenesis* **12**: 1527–1530.

Wang ZY, Huang MT, Ferraro T, Wong CQ, Lou YR, Reuhl K et al. (1992a). Inhibitory effect of green tea in the drinking water on tumorigenesis by ultraviolet light and 12-O-tetradecanoylphorbol-13-acetate in the skin of SKH-1 mice. *Cancer Res* **52**: 1162–1170.

Wang ZY, Huang MT, Ho CT, Chang R, Ma W, Ferraro T et al. (1992b). Inhibitory effect of green tea on the growth of established skin papillomas in mice. *Cancer Res* **52**: 6657–6665.

Wei Q, Matanoski GM, Farmer ER, Strickland P, Grossman L (1994). Vitamin supplementation and reduced risk of basal cell carcinoma. *J Clin Epidemiol* **47**: 829–836.

Werninghaus K, Meydani M, Bhawan J, Margolis R, Blumberg JB, Gilchrest BA (1994). Evaluation of the photoprotective effect of oral vitamin E supplementation. *Arch Dermatol* **130**: 1257–1261.

Williams S, Tamburic S, Lally C (2009). Eating chocolate can significantly protect the skin from UV light. *J Cosmet Dermatol* **8**: 169–173.

Wolf C, Steiner A, Honigsmann H (1988). Do oral carotenoids protect human skin against ultraviolet erythema, psoralen phototoxicity, and ultraviolet-induced DNA damage? *J Invest Dermatol* **90**: 55–57.

Yarosh DB (2004). DNA repair, immunosuppression, and skin cancer. *Cutis* **74**: 10–13.

Yusuf N, Irby C, Katiyar SK, Elmets CA (2007). Photoprotective effects of green tea polyphenols. *Photodermatol Photoimmunol Photomed* **23**: 48–56.

Ziegler A, Jonason AS, Leffell DJ, Simon JA, Sharma HW, Kimmelman J et al. (1994). Sunburn and p53 in the onset of skin cancer. *Nature* **372**: 773–776.

61

Acute and Chronic Effects of Ultraviolet Radiation, Visible Light, and Infrared

Saroj M. Verma
Beaumont Hospital

Gillian M. Murphy
Beaumont Hospital

61.1 Introduction

The term electromagnetic spectrum is used to encompass a broad range of radiation, from cosmic rays to radiowaves. Each type of radiation is made up of a range of wavelengths, and each wavelength comprises photons. Ultraviolet (UV) radiation, visible light, and infrared are specific terms for separate wavelength ranges within the electromagnetic spectrum and have been defined by Commission Internationale de l'Eclerage (CIE). In order to discuss the in vivo effects of radiation, it is necessary to understand one of the first principles of photobiology, that is, in order to have biological effect, a photon must be absorbed by a molecule termed "a chromophore" (Figure 61.1). Each chromophore has an individual absorption profile. The in vivo effects of radiation, or the "biological efficacy," depend on which wavelength is absorbed. This "action spectrum" has been defined for a number of different endpoints,

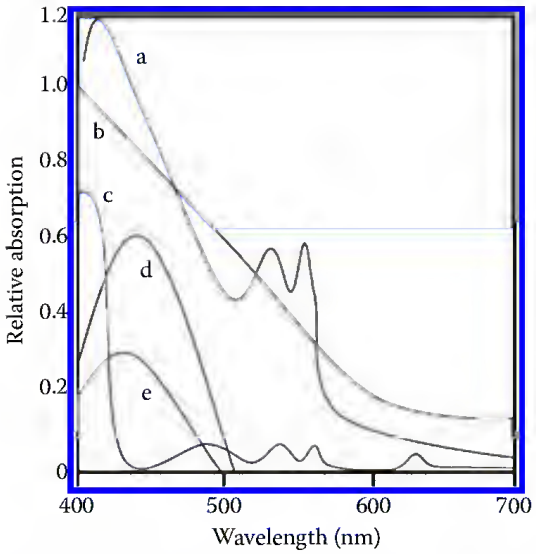

FIGURE 61.1 Absorption profile of chromophores in the skin. (a) oxyhaemoglobin, (b) melanin, (c) protoporphyrin IX, (d) bilirubin, and (e) riboflavin.

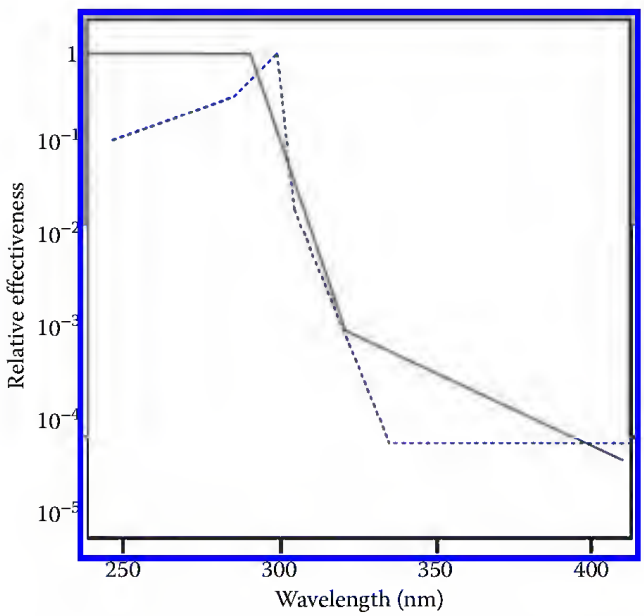

FIGURE 61.2 Action spectrum for erythema (continuous line) and photocarcinogenesis (broken line)—Commission Internationale de l' Eclairage (CIE).

which include erythema, thymine dimer formation, and skin cancers (Figure 61.2). UV radiation has both acute and chronic effects on the skin, the eye, and the immune system.

61.2 UV Radiation

The wavelengths of UV radiation can be subcategorized into UVC, UVB, UVA, and CIE has given definition to these wavelengths: UVC radiation includes wavelengths of less than 280 nm, UVB between 280 and 315 nm, and UVA ranging between 315 and 400 nm [1]. UVA can further be subdivided into UVA-1 (340–400 nm) and UVA-2 (315–340 nm). The difference between UVA-1 and UVA-2 being that

the shorter UVA wavelengths have been shown to have more photobiological activity, and therefore, UVA-2 and UVB are more closely related and exert a similar biological effect. Environmental factors can have a significant effect on solar UV exposure. Terrestrial UVR is derived from the sun and is scattered, reflected, or absorbed in the medium through which it travels. One's behavior, location (latitude and altitude), time of day, and the season all have an impact on the amount of ambient UV exposure to an individual [2]. It has been shown that a close proximity to the equator, a higher altitude, and the summer season all increase exposure to UV, as UVR is absorbed by the earth's atmosphere. Therefore, when the angle of the sun is high, the distance UVR travels through the earth's atmosphere is shortest, resulting in less UVR absorption. Conversely, when the angle of the sun is low, UVR travels a greater distance through the earth's atmosphere, and greater UVR is absorbed. White surfaces and rippling water reflect UVR in the earth's atmosphere, resulting in scatter. When the sky is blue, up to 50% of UV incident on the skin derives from scatter UVR. Thus, in light shade, a very significant amount of UVR may be received.

61.3 UV Effects on the Skin

UV radiation exerts its effects on the skin in one of two ways, either through direct DNA damage or indirectly through free radical formation. Epidermal DNA seems to be the most important chromophore in the skin resulting in inflammation, DNA photoproducts, and immunosuppression. DNA is only one of several endogenous chromophores that absorbs UV. Other chromophores include urocanic acid, melanin, protoporphyrins, and bilirubin. UVB and UVA act by forming pyrimidine dimers in DNA which, if not repaired, result in negative cutaneous effects that will be later discussed. There are also well-understood immunosuppressive effects due to UV, but is probably best to divide the effects of UVR, as well as those effects of visible light and infrared into acute and chronic photodamage.

61.4 Acute Effects on Normal Skin

Acute photoeffects broadly encompass inflammation and erythema, tanning, skin hyperplasia, immunosuppression, and vitamin D production. There are also acute abnormal photoeffects; namely the photodermatoses and phototoxic effects of drugs. The photodermatoses are skin conditions due to an abnormal immune-mediated response to UV radiation. This includes conditions such as polymorphous (polymorphic) light eruption (PLE), solar urticaria, actinic prurigo, chronic actinic dermatitis, and hydroa vacciniforme. Numerous other skin conditions, including atopic eczema, lupus erythematosus, rosacea, and bullous pemphigoid, can be aggravated by UV radiation [3]. Endogenous chemicals, the porphyrins, are also potent photosensitizers. In defects of porphyrin metabolism, that is, porphyrias, build up of excessive porphyrin products can result in cutaneous photosensitizing effects. Drugs can act as exogenous potent photosensitizers, such as seen with amiodarone and its hyperpigmentation effects [4]. Psoralens, a plant-derived photosensitizing agent, are frequently used in a therapeutic setting in combination with UVA to treat a variety of UV-sensitive skin conditions. The list of photosensitizing agents is extensive and will probably continue to grow.

61.5 Inflammation and Erythema

It has already been mentioned that DNA is a major chromophore for UVR. DNA damage occurs directly as a result of the effects of UVB and UVA [5] leading to cytokine production, inflammatory cell infiltration, and the release of inflammatory mediators such as interleukin-1 (IL-1) and tumor necrosis factor-alpha (TNF-α) from keratinocytes. The release of these cytokines results in the generation of reactive oxygen species (ROS), prostaglandins, and inflammatory mediators [6].

Studies carried out in vivo have demonstrated that ROS also develop secondary to UVB and UVA exposure [7]. Endogenous photosensitizers respond to both UVB and UVA and then react to form ROS such as superoxide anion radicals. The effects of UVA (particularly UVA-1) are mainly oxygen dependent but UVA (particularly UVA-2) also has the capacity to cause DNA photoproducts directly.

The CIE erythema action spectrum indicates that most sunburn is UVB induced as UVB is biologically 1000-fold more active than UVA. Erythema develops clinically as a result of inflammation causing vessel dilatation. UVA and visible light may also cause erythema [8]. The minimum dose of radiation to induce erythema is known as the minimal erythema dose (MED). The MED varies by wavelength, with shorter wavelengths being more biologically active [9]. The development of UVB-induced erythema has a delayed onset occurring hours (peaking at 24 h) and lasting up to days after the initial insult. The effects of this can be widely variable ranging from mild reddening of the skin to severe blistering. The histology of UVB erythema has been clearly delineated [10], with the molecular basis of UV-induced effects on human skin, in vivo, also being well described [11]. Apoptosis is an error free method of eliminating UV-induced DNA damage and will be discussed further in relation to its role in skin cancer.

61.6 Tanning

Tanning is triggered by DNA damage, which occurs as a response to UV radiation. It appears that not only are DNA photoproducts catalysts for tanning but formed DNA repair products, specifically the excised DNA fragments, so-called oligomers, are also able to induce tanning [12]. Endogenous pigmentation is a protective mechanism against skin cancer. The tanning response is an adaptive mechanism [13]. Tanning can be classified as immediate, persistent, and delayed [14]. Immediate tanning is of a rapid onset and has a short duration lasting only a few hours while persistent tanning is up to 24 h in duration [15]. Both immediate pigment darkening and persistent pigment darkening occur as a result of the oxidation and redistribution of preexisting melanin [14]. Both are the result of UVA exposure. Delayed tanning is mostly due to UVB, but UVA is also responsible to a lesser extent [16]. It occurs as a result of increased melanin synthesis and a redistribution of melanin in similar melanosomes [17]. Delayed tanning does not occur in the absence of DNA damage [12].

61.7 Skin Hyperplasia

Hyperplasia, much like tanning, occurs as a protective response mechanism to UV radiation. Hyperplasia of the epidermis leads to thickening of the stratum corneum layer, following UVB and UVC exposure. This happens due to an increase in cellular mitoses and occurs up to days to weeks after exposure. UVB induces transforming growth factor alpha production, which in turn leads to epidermal hyperplasia [18].

61.8 Immunosuppression

UV radiation is well known to be a potent immunosuppressant. Margaret Kripke demonstrated this phenomenon in a series of seminal experiments in mice. Kripke transplanted UV-induced tumors into the skin of mice that were either exposed to UV radiation or not. The tumors in the mice that were exposed to UVR continued to grow, and the tumors in the mice that were not exposed were rejected by the host. She also demonstrated that immunosuppression could also be transferred from the lymphocytes of irradiated mice into the nonirradiated mice by injection [19].

The mechanism of UV-induced immunusuppression is complex. One mechanism is the action of UVR on Langerhans cells. These Langerhans cells are both phagocytic and dendritic cells and specifically function as antigen-presenting cells (APCs) that play a role in the immune system. UV radiation has been demonstrated to deplete Langerhans cells, even at low doses [20]. There is a definite genetic

basis to this that determines the ability of UV radiation to deplete Langerhans cells, as this can be demonstrated in patients with the photodermatosis, PLE, who are genetically able to resist UV-induced Langerhan cell depletion [21].

The second major effect is on urocanic acid [22]. Urocanic acid is another major chromophore for UV within the stratum corneum where it is produced. The interaction of UVB induces isomerization of urocanic acid from a *trans* to *cis* formation, and this *cis*-isomer has a potent systemic immunosuppressant effect.

61.9 Vitamin D Production

The skin is a major source of vitamin D, which to a lesser extent can be derived from the diet [23]. The direct effects of specific UVB wavelengths on 7-dehydrocholesterol lead to cholecalciferol, or vitamin D3. This in turn is metabolized by both the liver and kidneys to its active form, 1α-hydroxyvitamin D. Vitamin D3 is more potent than the dietary form of vitamin D, ergocalciferol, and vitamin D2 [24]. Very little exposure to UVB leads to vitamin D formation—10 min seems sufficient as daily exposure for white skin [25].

61.10 Chronic Effects

61.10.1 Photoaging

The process of photoaging should be clearly distinguished from chronological aging. Photoaging refers to progressive degradation of the skin due to prolonged or repetitious UV exposure. Photoaging is superimposed on a background of natural degenerative skin changes, or chronological aging [26–28]. The extent and depth of UV penetration depend on the active wavelength, and both the epidermis and dermis are affected. UVA has longer wavelengths that penetrate deeply into the dermis and is most credited with photoaging [8]. UVA is also prevalent all year and for most of the day. Despite this, both UVB and UVA contribute to the effects, resulting in the degeneration of elastic tissue and the degradation of collagen. Collagen is a significant structural protein found in the dermis, by matrix metalloproteinases which are induced by the effects of UV radiation [29]. This manifests itself cutaneously with skin dryness, loss of tensile strength, wrinkles, skin laxity, as well as blotchy hyper and hypopigmentation and pseudoscarring [30–32].

61.10.2 Skin Carcinogenesis

UV radiation is a known cutaneous carcinogen. UV radiation when absorbed by DNA results in the formation of cyclobutane pyrimidine dimers [33]. There are several intrinsic repair mechanisms within the skin to combat UV-induced DNA damage. The primary intrinsic repair mechanism of the skin whereby DNA is uncoiled, the damaged DNA (a cross-linked thymine dimer) is excised, and the DNA is reinstated into its original shape [34]. This excision repair mechanism, known as nucleotide excision repair, is essential to maintain the integrity of the DNA helix. Without this, mutations within DNA occur, and errors in transcription of DNA result. Accumulation of mutations in damaged DNA ultimately results in carcinogenesis [35]. UVB is more effective at inducing carcinogenesis than UVA. UVA has also been shown to produce similar effects and has been shown to contribute between 10% and 20% of sunlight-induced carcinogenesis [36,37]. The effect of repeated exposures to both UVA-1 and visible light has also been studied and shown to increase the number of p53-positive cells, but this is only true to a lesser extent when referring to visible light [38]. The World Health Organization (WHO) has declared all UVR to be a Class I carcinogen [39]. Apoptosis, or programmed cell death, of heavily DNA-damaged cells is another protective mechanism against skin cancer [40]. This involves a complex cell signaling cascade that is most importantly regulated by p53 (referred to as the "guardian of the genome") and the caspase system. UV radiation has a dual effect

on the work of p53. UV radiation induces p53, which enables cell cycle arrest in the S1 phase and DNA repair occurs. Concomitantly, UV radiation also induces the MDM2 protein that paradoxically inhibits the function of p53 [11]. UV radiation also leads to mutations of p53 leading to alteration of its function from a tumor suppressor gene to a tumor-promoting protein, or oncogene.

61.11 Visible Light and Infrared

The range of visible light is from 400 to 800 nm; hence, visible light lies between UVA-1 and infrared radiation on the electromagnetic spectrum. Visible light has acute and chronic effects on the skin and eyes [41,42]. This is clinically relevant as visible light has been implicated in the pathogenesis of some diseases but has also been exploited therapeutically in the treatment of skin disease. Visible light is recognized to be responsible for adverse effects in several photodermatoses, including chronic actinic dermatitis, solar urticaria, porphyria, and pseudoporphyria. Conversely, visible light has a therapeutic role and is used in the treatment of actinic keratosis, Bowen's disease, and superficial forms of basal cell carcinomas when used in photodynamic therapy (PDT). PDT uses a chromophore derived from the heme biosynthetic pathway—protoporphyrin IX. Lasers utilize many wavelengths to produce very specific effects depending on the chromophore targeted (i.e., port wine stains—pulsed dye laser, ruby laser—pigmentation).

Infrared radiation has many effects on the skin [43]. A link between infrared radiation (heat, wavelength >800 nm) and carcinogenesis has also been demonstrated previously both in experiments and epidemiological models [44–46]. In recent years, this has been highlighted with particular significance in the context of climate change and ozone depletion. Both ozone depletion and the rising ambient temperature have been demonstrated to be linked to an increased risk of skin carcinogenesis [47].

61.12 Acute and Chronic Effects of Visible Light and Infrared Radiation

Visible light has a role in the development of erythemas and inflammation. Visible light has been shown to result in free radical formation [48]. Although we have described that most erythemas is due to UVR exposure, visible light can also produce vascular dilatation resulting in erythema within the deep dermis [8]. In a study by Porges et al., visible light was demonstrated to have effects of immediate tanning as well as delayed tanning [49]. The effect of repeated exposures to visible light has also been studied and shown to increase the number of p53-positive cells, but this is only true to a lesser extent when referring to visible light [38].

61.13 Effect of UVR and Visible Light on the Eye

Similar to the skin, ocular tissue is extremely sensitive and is also vulnerable to the effects of UV and visible light. The three main structures vulnerable to UV radiation and visible light are the cornea, lens, and the retina [50]. As with skin, the depth of penetration within the eye is dependent on the wavelength. The cornea transmits wavelengths only above 295 nm, with the anterior ocular structures of the eye absorbing most UV radiation. This limitation of transmission by the cornea means that in the adult eye, less than 1% UVR reaches the retina [50]. It is therefore the longer wavelengths of UV (>295 nm) that penetrates deeply into the eye reaching the lens [51]. Similarly, the longer wavelengths of visible light and infrared can also penetrate the retina [52].

61.14 Acute Ocular Effects

In terms of ocular exposure to UV, ground reflection is the major determinant of UVR exposure. Highly reflective ground surfaces include snow, while sand is moderately reflective and grass is of very low reflectance [53]. Rippling water acts as a mirror, reflecting the sun and skylight directly onto the cornea.

Both UVB and UVA play an important role in acute ocular effects. Epidemiologically, UVB has been shown to play a role in acute ocular damage [54]. The lens, as mentioned earlier, is exposed to significantly more UVA than UVB, although the effects of UVA on DNA damage are much less than that of UVB [50].

Photokeratitis describes the acute response of the cornea to UV radiation, with direct involvement of the corneal keratinocytes within the epithelium. It is also known as "snow blindness," "arc eye," or "welders flash." Symptoms of photokeratitis include gritty eyes, photophobia, and tearing. The onset of this is usually several hours after exposure but the cornea is able to reestablish itself and symptoms resolve within 48–72 h [55]. Both the angle of reflection and the highly reflective surface of snow explain why photokeratitis has such a high incidence of occurrence in skiers. Other acute responses of the cornea to UVR include transient haze, swelling, and corneal opacification [55]. The retina is relatively well protected from the effects of UVR, as most of it is filtered out by the lens, but acute injury from visible light can result in retinal burns. This usually occurs in the context of staring at the sun during an eclipse where macular burns may be sustained and even blindness may occur.

61.15 Chronic Ocular Effects

Chronic ocular effects include cataracts, pterygium, age-related macular degeneration (AMD), and pinguecula. The incidence of cataract and pterygium is much more prevalent at latitudes with greater UVB exposure [50]. Cortical cataract formation has been shown to be associated with UV radiation, particularly with exposure to UVB [54]. Visible light has not been shown to have this same association [42]. Structures like the cornea and conjunctiva are particularly vulnerable to direct UVR exposure due to their prominent anterior location.

Pterygium is another corneal response to chronic UVR exposure, and epidemiological studies have demonstrated a strong causal relationship linking pterygium to UVR [55–60]. In pterygium, there is formation of a fibrovascular tissue sheet that invades the corneal tissue. As pterygium is a disorder that is associated with sun exposure, it occurs commonly in tropical regions receiving more sun exposure. It has been linked to both UVB [57–60] and UVA [61,62], and strong associations between cumulative UVR exposure and the development of pterygium have also been shown [42]. Exposure to short-wavelength visible light, or blue light, has also been demonstrated to carry an increased risk in development of pterygium [42].

The development of other corneal disorders including climatic droplet keratopathy (CDK) is associated with both visible light (blue light) and UVR [42,59,63–65]. CDK is associated with intense climate conditions (i.e., Arctic). The prevalence of CDK also increases with age, similar to that of pterygium. Other corneal disorders worth mentioning include pinguecula and AMD. The development of pinguecula, a mass growing on the conjunctival surface adjacent to the cornea, is associated with UVR [60] but its association with UVR is much weaker than with pterygium. Taylor et al. found a strong association with the incidence of AMD and blue light or visible light exposure [42]. However, the causal relationship between AMD and both visible light and UVR remains a contentious issue. Acute intense light can cause macular damage, even blindness.

Ocular and periocular carcinomas have been associated with chronic UVR exposure. This includes an association between squamous cell carcinoma (SCC) of the eye, of both cornea and conjunctival surfaces, and UVR exists [55,56]. In addition to an association with SCC, basal cell carcinoma of the eyelid has also been demonstrated [66,67].

61.16 Photoprotection

The negative effects of UV radiation are clearly widespread and involve not only the skin but also the immune system and ocular tissue. The development of sunscreens has afforded protection against UV radiation, mostly against UVB, but the newer broad coverage sunscreens are also now affording

coverage against UVA. Sunscreens reflect or absorb UV radiation. However, the critical factor that affects how well a sunscreen works is the amount of sunscreen applied, the frequency of applying sunscreens, and the evenness of the application. It has been well demonstrated that most people who do not apply sufficiently meet these criteria [68].

Additional sun protection is afforded through the use of sunglasses and protective clothing. Sunglasses should be chosen to provide adequate protection against UV transmission to ocular structures while permitting normal vision [52]. European Standards have been formulated to act as guidelines in this [69]. The use of protective clothing, such as a brimmed hat, can provide additional ocular protection as well as protection to the scalp and ears, and to a lesser extent, the face and neck [70]. Clothing can be an excellent protectant against UVR. The UV protection factor (UPF) has been developed to provide guidelines to choose UV protective clothing. Fabric, thickness, weave, color, and composition all critically affect the amount of UV protection afforded by clothing [71–73]. Wet fabric can have a variable effect on the UPF of clothing [74,75]. The correct choice in clothing, hat, and sunglasses is crucial in providing optimal protection against UVR and its many consequences.

References

1. Commission Internationale de l'Eclairage, Vienna. CIE 132/2; TC 6–32 report: Action spectrum for photocarcinogenesis (non-melanoma skin cancers), 2000.
2. Diffey BL, Gies HP. The confounding influences of sun exposure in melanoma. *Lancet* 1998; *351*:1101–1102.
3. Murphy GM. Diseases associated with photosensitivity. *J Photochem Photobiol Sci* 2002; *1*:324–326.
4. Ferguson J. Photosensitivity due to drugs. *Photodermatol Photoimmunol Photomed* 2002; *18*(5):262–269.
5. Pillai S, Oresajo C, Hayward J. Ultraviolet radiation and skin aging: Roles of reactive oxygen species, inflammation and protease activation, and strategies for prevention of inflammation-induced matrix degradation—A review. *Int J Cosmet Sci* 2005; *27*(1):17–34.
6. Wood LC, Elias PM, Calhoun C, Tsai JC, Grunfeld C, Feingold KR. Barrier disruption stimulates interleukin-l alpha expression and release from a pre-formed pool in murine epidermis. *J Invest Dermatol* 1996; *106*(3): 397–403.
7. Wlaschek M, Tantcheva-Poór I, Naderi L, Ma W. Solar UV irradiation and dermal photoaging. *J Photochem Photobiol B* 2001; *63*(1–3):41–51.
8. Rottier PB, van der Leun JC. Hyperaemia of the deeper cutaneous vessels after irradiation of human skin with large doses of ultraviolet and visible light. *Br J Dermatol* 1960; *72*:256–260.
9. CIE Standard. Erythema reference action spectrum and standard erythema dose. CIE S 007/E-1998. Vienna: Commission International de l'Eclerairage, 1998.
10. Hawk JL, Murphy GM, Holden CA. The presence of neutrophils in human cutaneous ultraviolet-B inflammation. *Br J Dermatol* 1988; *118*(1):27–30.
11. Murphy M, Mabruk MJ, Lenane P, Liew A, McCann P, Buckley A, Billet P, Leader M, Kay E, Murphy GM. The expression of p53, p21, Bax and induction of apoptosis in normal volunteers in response to different doses of ultraviolet radiation. *Br J Dermatol* 2002; *147*(1):110–117.
12. Gilchrest BA, Eller MS. DNA photodamage stimulates melanogenesis and other photoprotective responses. *J Investig Dermatol Symp Proc* 1999; *4*(1):35–40.
13. Brown DA. Skin pigmentation enhancers. *J Photochem Photobiol B* 2001; *63*(1–3):148–161.
14. Rhodes LE, Lim HW. The acute effects of ultraviolet radiation on the skin. In *Photodermatology*; Lim HW, Hönigsmann H, and Hawk JL Eds.; Informa Healthcare USA Inc., New York, 2007; pp. 75–89.
15. Hönigsmann H. Erythema and pigmentation. *Photodermatol Photoimmunol Photomed* 2002; *18*:75–81.

16. Gange RW, Blackett AD, Matzinger EA, Sutherland BM, Kochevar IE. Comparative protection efficiency of UVA- and UVB-induced tans against erythema and formation of endonuclease-sensitive sites in DNA by UVB in human skin. *J Investig Dermatol* 1985; *85*:362–364.
17. Young AR, Sheehan JM. UV-induced pigmentation in human skin. In *Sun Protection in Man*; Giacomi PU Ed.; Elsevier, St Louis, MO, 2001; pp. 357–375.
18. Murphy GM, Quinn DG, Camp RD, Hawk JL, Greaves MW. In-vivo studies of the action spectrum and time course for release of transforming growth factor alpha by ultraviolet irradiation in man. *Br J Dermatol* 1991; *125*(6):566–568.
19. Fisher MS, Kripke ML. Systemic alteration induced in mice by ultraviolet light irradiation and its relationship to ultraviolet carcinogenesis. *Proc Natl Acad Sci U S A* 1977; *74*(4):1688–1692.
20. Murphy GM, Norris PG, Young AR, Corbett MF, Hawk JL. Low-dose ultraviolet-B irradiation depletes human epidermal Langerhans cells. *Br J Dermatol* 1993; *129*(6):482–486.
21. Lembo S, Fallon J, O'Kelly P, Murphy GM. Polymorphic light eruption and skin cancer prevalence: Is one protective against the other? *Br J Dermatol* 2008; *159*(6):1342–1347.
22. De Fabo EC, Noonan FP. Mechanism of immune suppression by ultraviolet irradiation in vivo. I. Evidence for the existence of a unique photoreceptor in skin and its role in photoimmunology. *J Exp Med* 1983; *158*(1):84–98.
23. Heaney RP, Davies KM, Chen TC, Holick MF, Barger MJ. Human serum 25-hydroxycholocalciferol response to extended oral dosing with cholecalciferol. *Am J Clin Nutr* 2003; *77*:204–229.
24. Armas LAG, Hollis BW, Heaney RP. Vitamin D2 is much less effective than vitamin D3. *J Clin Endocrinol Metabol* 2004; *89*:5387–5391.
25. Samanek AJ, Croager EJ, Gies P, Milne E, Prince R, McMichael AJ, Lucas RM, Slevin T. Estimates of beneficial and harmful sun exposure times during the year for major Australian population centres. *Med J Aust* 2006; *184*(7):338–341.
26. Herschenfeld RE, Gilchrest BA. The cumulative effects of ultraviolet radiation on the skin: Photoageing. In *Photodermatology*; Hawk, JLM Ed.; Arnold, Edward, London, 1999; pp. 69–89.
27. Krieg T, Hein R, Mauch C, Aumailley M. Molecular and clinical aspects of connective tissue. *Eur J Clin Investig* 1988; *18*:105–123.
28. Uitto J. Connective tissue biochemistry of the ageing dermis. Age related alteration in collage and elastin. *Dermatol Clin* 1986; *4*:433–446.
29. Fisher GJ, Kang S, Varani J et al. Mechanisms of photoaging and chronological skin aging. *Arch Dermatol* 2002; *138*:1462–1470.
30. Lavker RM. Structural alterations in exposed and unexposed aged skin. *J Investig Dermatol* 1979; *73*:559–566.
31. Lavker RM, Kilgman AM. Chronic heliodermatitis: A morphological evaluation of actinic dermal damage with emphasis on the role of mast cells. *J Investig Dermatol* 1988; *90*:325–330.
32. Gilchrest BA. Skin aging and photoaging: An overview. *J Am Acad Dermatol* 1989; *21*:610–613.
33. Young AR, Chadwick CA, Harrison GI, Nikaido O, Ramsden J, Potten CS. The similarity of the action spectra for thymine dimers in human epidermis and erythema suggests that DNA is the chromophore for erythema. *J Investig Dermatol* 1998; *111*(6):982–988.
34. Yarosh DB. DNA repair, immunosuppression, and skin cancer. *Cutis* 2004; *74*(Suppl):10–13.
35. Yamada M, Udono MU, Hori M, Hirose R, Sato S, Mori T, Nikaido O. Aged human skin removes UVB-induced pyrimidine dimers from the epidermis more slowly than young adult skin in vivo. *Arch Dermatol Res* 2006; *297*(7):294–302.
36. Mouret S, Baudouin C, Charveron M, Favier A, Cadet J, Douki T. Cyclobutane pyrimidine dimers are predominant DNA lesions in whole human skin exposed to UVA radiation. *Proc Natl Acad Sci U S A* 2006; *103*(37):13765–13770.
37. Kelfken G, de Grugli FR, van der Leun JC. Ozone depletion and increase in annual carcinogenesis by ultraviolet dose. *Photochem Photobiol* 1990; *52*:819–823.

38. Edström DW, Porwit A, Ros AM. Effects on human skin of repetitive ultraviolet-A1 (UVA1) irradiation and visible light. *Photodermatol Photoimmunol Photomed* 2001; *17*(2):66–70.
39. El Ghissassi F, Baan R, Straif K, Grosse Y, Secretan B, Bouvard V, Benbrahim-Tallaa L, Guha N, Freeman C, Galichet L, Cogliano V. On behalf of the WHO International Agency for Research on Cancer Monograph Working Group. A review of human carcinogens—Part D: Radiation. *Lancet Oncol* 2009; *10*(8):751–752.
40. Melnikova VO, Ananthaswamy HN. Cellular and molecular events leading to the development of skin cancer. *Mutat Res* 2005; *571*(1–2):91–106.
41. Mahmoud BH, Hexsel CL, Hamzavi IH, Lim HW. Effects of visible light on the skin. *Photochem Photobiol* 2008; *84*(2):450–462.
42. Taylor HR, West S, Munoz B, Rosenthal FS. The long-term effects of visible light on the eye. *Arch Opthalmol* 1992; *110*(1):99–104.
43. Schroeder P, Haendeler J, Krutmann J. The role of near infrared radiation in photoaging of the skin. *Exp Gerontol* 2008; *43*(7):629–632.
44. Bain JA, Rusch HP. Carcinogenesis with ultraviolet radiation of wave length 2800–3400 Å. *Cancer Res* 1943; *3*:425–430.
45. Bain JA, Rusch HP, Kline BE. The effect of temperature upon ultraviolet carcinogenesis with wave lengths 2800–3400 Å. *Cancer Res* 1943; *3*:610–612.
46. De Gruijl FR, van der Leun, JC. Estimate of wavelength dependency of ultraviolet carcinogenesis in humans and its relevance to the risk assessment of a stratospheric ozone depletion. *Health Phys* 1994; *67*:319–325.
47. Van der Leun JC, de Gruijl FR. Climate change and skin cancer. *Photochem Photobiol Sci* 2002; *1*:324–326.
48. Haywood R. Relevance of sunscreen application method, visible light and sunlight intensity to free radical protection: A study of ex vivo human skin. *Photochem Photobiol* 2006; *82*:1123–1131.
49. Porges SB, Kaidbey KH, Grove GL. Quantification of visible light-induced melanogenesis in human skin. *Photodermatology* 1998; *5*:197–200.
50. Sliney DH. How light reaches the eye and its components. *Int J Toxicol* 2002; *21*(6):501–509.
51. Weale RA. Age and the transmittance of the human crystalline lens. *J Physiol* 1988; *395*:577–587.
52. Tuchinda C, Srivannaboon S, Lim H. Photoprotection by window glass, automobile glass, and sunglasses. *J Am Acad Dermatol* 2006; *54*:845–854.
53. Sliney DH. Physical factors in cataractogenesis: Ambient ultraviolet radiation and temperature. *Investig Opthalmol Vis Sci* 1986; *27*:781–790.
54. Taylor HR, West SK, Rosenthal FS, Munoz B, Newland HS, Abbey H, Emmett EA. Effect of ultraviolet radiation on cataract formation. *N Eng J Med* 1988; *319*:1429–1433.
55. Cullen AP. Photokeratitis and other phototoxic effects on the cornea and conjunctiva. *Int J Toxicol* 2002; *21*:455–464.
56. Newton R, Ferlay J, Reeves G, Beral V, Parkin DM. Effect of ambient solar ultraviolet radiation on incidence of squamous-cell carcinoma of the eye. *Lancet* 1996; *347*(9013):1450–1451.
57. Anderson JR. A pterygium map. *Acta Opthalmol* 1954; *3*:1631–1642.
58. Cameron ME. Histology of pterygium: An electro microscopic study. *Br J Opthalmol* 1983; *67*:604–608.
59. Taylor HR. Aetiology of climate droplet keratopathy and pterygium. *Br J Opthalmol* 1980; *64*:154–163.
60. Moran DJ, Hollows FC. Pterygium and ultraviolet radiation: A positive correlation. *Br J Opthalmol* 1984; *68*:343–346.
61. Taylor HR, West SK, Rosenthal FS, Munoz B, Newland HS, Abbey H, Emmett EA. Corneal changes associated with chronic ultraviolet radiation. *Arch Opthalmol* 1989; *107*:1481–1484.
62. Tso MOM. Photic maculopathy in rhesus monkeys: A light and electron microscopic study. *Investig Opthalmol Vis Sci* 1973; *12*:14–34.

63. Klintworth GK. The cornea: Structure and macromolecules in health and disease. *Am J Pathol* 1977; *89*:717–808.
64. Johnson GJ, Ghosh M. Labrador keratopathy: Clinical and pathological findings. *Can J Opthalmol* 1975; *10*:119–135.
65. Johnson GJ, Overall M. Histology of spheroidal degeneration of the cornea in the Labrador. *Br J Opthalmol* 1978; *62*:53–61.
66. Sun EC, Fears TR, Goedert JJ. Epidemiology of squamous cell conjunctival cancer. *Cancer Epidemiol Biomarkers Prev* 1997; *6*:73–77.
67. Lindgren G, Diffey BL, Larko O. Basal cell carcinoma of the eyelids and solar ultraviolet radiation exposure. *Br J Opthalmol* 1998; *82*:1412–1415.
68. Diffey BL. People do not apply enough sunscreen for protection. *BMJ* 1996; *313*:942.
69. European Standards Organisation (CEN) 2005 EN 1836 Personal Eye Protection: Sunglasses and Sunglare Filters for General Use and Filters for Direct Observation of the Sun: EN 1836:2005. CEN; Brussels.
70. Carolyn B, Lyde R, Bergstrasser PR. Ultraviolet protection from sun avoidance. *Dermatol Ther* 1997; *4*:72–78.
71. Davis S, Capjack L, Kerr N, Fedosejevs R. Clothing as protection from ultraviolet radiation: Which fabric is most effective? *Int J Dermatol* 1997; *36*:374–379.
72. Crews PC, Kachmann S, Beyer AG. Influences on UVR of undyed woven fabrics. *Text Chem Color* 1999; *31*:17–26.
73. Wang SQ, Kopf AW, Marx J, Bogdan A, Polsky D, Bart RS. Reduction of ultraviolet transmission through cotton T-shirt fabrics with low ultraviolet protection by various laundering methods and dyeing: Clinical implications. *J Am Acad Dermatol* 2001; *44*:767–774.
74. Gambichler T, Altmeyer P, Hoffmann K. Role of clothes in sun protection. *Recent Results Cancer Res* 2002; *160*:15–26.
75. Gambichler T, Hatch KL, Avermaete A, Altmeyer P, Hoffmann K. Influences of wetness on UPF factor (UPF) of textiles: In vitro and in vivo measurements. *Photodermatol Photoimmunol Photomed* 2002; *18*:29–35.

62

Phototherapy and Photochemotherapy in Dermatology

Piergiacomo Calzavara-Pinton
University of Brescia

Mariachiara Arisi
University of Brescia

Bernhard Ortel
University of Chicago Medical Center

Mariateresa Rossi
University of Brescia

62.1 Introduction

Phototherapy is the use of nonionizing [ultraviolet (UV), visible, or infrared], electromagnetic radiation in the treatment of skin diseases. In dermatology, phototherapy commonly refers to UV phototherapy. Its goal is to suppress ongoing disease processes via the prevention, modulation, or abrogation of pathogenic mechanisms that cause the disease itself [1].

Natural UV from sunlight (heliotherapy) has been employed in the treatment of several dermatoses in Egypt and India since 2000–1200 B.C. In the present chapter, we will concentrate on clinical applications of artificial radiation sources. The carbon arc lamp was used as first man-made therapeutic UV source from the mid-1800s. At the beginning of the twentieth century, medium- and high-pressure mercury arc lamps became available. A variety of metal halides added to these mercury lamps improved their emission in certain regions of the UV and visible spectra. Fluorescent lamps became available in the late 1940s and, since then, multiple phosphors and envelope materials have been used to produce lamps with modified emission spectra in the UV region [2]. Finally, in the mid-1970s, the combination of artificial UVA (320–400 nm) radiation with psoralens (PUVA; photochemotherapy) was introduced into clinical practice [3,4]. In the following decades, phototherapies including photochemotherapy have been used at a constantly increasing rate in the management of multiple skin diseases and are an essential part of today's dermatologic therapeutic armamentarium. At the same time, advances in photoimmunology and molecular biology have improved our knowledge of many actions of UV radiation on the skin, although many aspects still remain to be clarified.

62.2 Light Sources and Dosimetry

Artificial light sources for phototherapy are characterized by three primary properties:

1. Irradiance is a radiometry term for the power per unit area of the total amount of electromagnetic radiation incident on a surface. The relevant SI unit is Watt per square meter ($W \cdot m^{-2}$) but in clinical practice $mW \cdot cm^{-2}$ is often used. The light dose is the irradiance multiplied by the application time, measured in $J \cdot m^{-2}$ (Joule = $W \cdot s$) or $mJ \cdot cm^{-2}$.
2. The emission spectrum, the plot of irradiance at each wavelength is measured in $W \cdot m^{-2} \cdot nm^{-1}$.
3. The 3D distribution of the emission field. Variations of light intensity at the skin level are caused by variations in the output along vertical and horizontal axes of the lamps as well as by their arrangement in the irradiation units.

Two main groups of radiation sources are used in phototherapy today: metal halide lamps and fluorescent lamps that emit variable proportions of UVA and UVB (290–320 nm) wavebands. The former contain mercury vapor at high or medium pressure within a quartz envelope. They have a high output throughout the whole UV spectrum, and the emission is confined to the desired range by suitable optical filters. Fluorescent tubes contain mercury vapor at low pressure, and the emission spectrum is modified by the inner phosphor coating of a thin glass tube.

Broadband UVB (BB-UVB; UV21) fluorescent lamps have a broad spectral emission (10%–20% of the total output) in the UVB range and some emission below 290 nm (i.e., within the UVC waveband). BB fluorescent UVB lamps with relatively little UVC emission (UV6) are available. Narrowband (NB) UVB lamps have more than 80% of the output concentrated in a narrow emission peak around 312 nm and only 0.1% below 290 nm. UVA sources for PUVA therapy have 98%–99% of the UV emission in the UVA waveband. For UVA-1 phototherapy, the high intensity emission of high-pressure metal halide lamps is strictly confined to the 340–400 nm range by special glass filters.

Recently, XeCl excimer lasers have become available for dermatological phototherapy. In such laser, a pseudo-molecule called an excimer is created, which can only exist in an energized state. Upon relaxation, monochromatic radiation at 308 nm is emitted, typically in 60 ns micropulses at a 200 Hz rate. Pulse trains (macropulses) deliver a fluence of 3–4 $mJ \cdot cm^{-2}$. The spot size is maximally 3.2 cm^2. Excimer lamps with a continuous emission at 308 nm at high energy are available at lower cost and offer the clinical advantage of a larger field of irradiation, but they are not monochromatic.

Careful dosimetry is essential to ensure efficacy and safety of phototherapy, because relatively small variations in the photophysical parameters may cause major changes in the biological activity. Irradiance in a given spectral range, for example, UVA or UVB, can be measured with inexpensive, practical BB dosimeters. However, their response spectrum must match the emission spectrum of the UV source and should be calibrated annually with a spectroradiometer, measuring the UV emission at 1–5 nm intervals.

62.3 BB- and NB-UVB Phototherapies

62.3.1 Action Mechanisms

Therapeutic effects of UVB phototherapy are caused by a cascade of biological events that begins with the absorption of a photon by an endogenous chromophore. The biologically most relevant target is DNA. Excited nucleotides give rise to various DNA photoproducts, notably cyclobutane-type pyrimidine dimers and (6-4) adducts. The amount of photoproducts is directly related to a decrease in synthesis of DNA, RNA, and proteins [5]. Oxidative damage to DNA (8-hydroxy-2′-deoxyguanosine) as well as to cellular membranes and surface receptors leads to activation of intracellular signaling pathways that contribute to the biological response. These effects are seen in all exposed cell populations. Until relatively recently, it was believed that UVB phototherapy improves hyperproliferative diseases,

such as psoriasis, mainly by interfering with keratinocyte proliferation and by inducing apoptosis. This assumption has been challenged by experimental evidence focusing on UVB effects on T lymphocytes [6]. Indeed, in vitro, UVB is antiproliferative and cytotoxic toward both T cells and keratinocytes, but T cells are 10 times more sensitive [1]. If UVB-induced DNA lesions are not repaired, C → T and CC → TT transitions can occur that are characteristic for UV exposure ("UVB signatures"). These DNA mutations may occur in biologically relevant genes such as tumor suppressor genes or oncogenes and thus represent initial events of the multistep UV carcinogenesis in keratinocytes and Merkel cells, whereas UV-induced cancers of other cutaneous cell populations have not been reported so far [7].

The depletion of the skin-resident T-cell population may be due to a combination of UVB-induced apoptosis (via direct activation of death receptor and upregulation of its ligand, CD95L on the keratinocytes) [1] and decreased recruitment from the circulation due to reduced expression of adhesion and homing molecules [6]. UVB upregulates transcription and release of anti-inflammatory interleukins (IL-3, IL-4, IL-6, IL-10, and IL-20), granulocyte macrophage colony-stimulating factor (GM-CSF), transforming growth factor-beta (TGF-β), nervegrowth factor (NGF), pro-opiomelanocortin (POMC), alfa-melanocyte stimulating hormone (α-MSH), and prostaglandins (PG)E_2 and $PGF_{2\alpha}$. UVB suppresses the Th1 (proinflammatory) axis as defined by IL-12, interferon (IFN)-γ, and IL-8, and other proinflammatory cytokines, that is, IL-1β, IL-2, IL-5, and tumor necrosis factor-alfa (TNF-α) [1,8,9]. The number and activity of Langerhans cells (LHC) and dendritic cells are downregulated [1,9]. In addition, the reduced expression by LHC of costimulatory molecules, such as CD86 and intercellular adhesion molecule-1 (ICAM-1), may result in a tolerogenic, rather than an immunogenic signal [1,9]. The induction of regulatory T cells [10] offers a mechanism to suppress the immune system in a rather specific fashion. UVB-induced isomerization of *trans*- to *cis*-urocanic acid in the stratum corneum plays an additional role in suppressing antigen presentation by LHC and complex immune responses such as contact hypersensitivity [1]. Vitamin D converted by UVB in the skin from 7-dehydrocholesterol has potent immunomodulatory properties as well. The active form of vitamin D has been shown to inhibit T-cell proliferation and major histocompatibility complex (MHC) class II expression on antigen-presenting cells, and to suppress LHC activity [11]. In addition, UVB stimulates keratinocytes and melanocytes to express α-MSH that besides its role in skin pigmentation also suppresses cutaneous inflammation [11]. Importantly, the suppression of delayed hypersensitivity reactions and immunosurveillance against skin tumors are seen already at UVB doses below the erythema threshold in human skin [6]. Finally, antimicrobial UV effects and alteration of the skin flora [12] may contribute to the therapeutic activity of UVB in some clinical applications.

62.3.2 Treatment Principles

Sensitivity of human skin to the erythemogenic activity of UVB can vary widely, and individual ranges are only roughly predictable by skin phototyping. The individual photosensitivity level may be determined by assessing the minimal erythema dose (MED). This is the lowest UVB dose that induces a well-defined perceptible redness of the skin 24 h after exposure. It is measured by exposing a set of small (1–4 cm^2) areas of untanned skin (e.g., on the buttocks) to an incremental series of UVB doses. A variable portion of the MED (35%–70%)—depending on the aggressiveness of the protocol—is used as starting dose [5]. Subsequent increments are determined according to the cutaneous reaction and, in most regimens, range from 10% to 40%. Some protocols use fixed dose increments rather than a relative portion of the previous exposure. The number of weekly treatments varies from two to five. Daily irradiations are possible because peak erythema occurs at 8–24 h following UVB exposure, and thus, cumulative toxicity can be avoided. A treatment cycle ends, when complete clearance (or improvement without further amelioration with 3–6 subsequent exposures) is obtained. A maximum number or cumulative dose of NB-UVB exposures has not been set so far. Repeated phototherapy usage depends not only on objective estimates of skin cancer risk but also on factors, such as whether or not the face is shielded during phototherapy, the frequency of repeated treatment courses, and each patient's attitude to the known risks of treatment [5]. Contraindications to UVB phototherapy are detailed in Table 62.1.

TABLE 62.1 Absolute and Relative Contraindications to UVB, UVA-1, PUVA and Bath-PUVA Phototherapy Treatments

	UVB	UVA-1	PUVA	Bath-PUVA
Absolute contraindications to treatment				
Pregnancy			Yes	
Breast feeding			Yes	
Lupus and autoimmune diseases	Yes		Yes	Yes
Xeroderma pigmentosum	Yes	Yes	Yes	Yes
Porphyrias	Yes	Yes	Yes	Yes
Albinism	Yes	Yes	Yes	Yes
Dysplastic nevus syndrome	Yes	Yes	Yes	Yes
Previous melanoma or nonmelanoma skin cancer (NMSC)	Yes	Yes	Yes	Yes
Severe cardiopathy	Yes	Yes	Yes	Yes
Liver or kidney insufficiency			Yes	
Therapy with phototoxic drugs	Yes	Yes	Yes	Yes
Relative contraindications (to be evaluated in the single case)				
Age less than 18 years	Yes	Yes	Yes	Yes
Melanoma in relatives	Yes	Yes	Yes	Yes
Anti nuclear (high titer) anti-extractable nuclear antigen (ENA) antibodies	Yes		Yes	Yes
High cumulative UV dosage	Yes	Yes	Yes	Yes
Therapy with ionizing radiation	Yes	Yes	Yes	Yes
Previous exposure to arsenic or nitrogen mustard	Yes	Yes	Yes	Yes
Cataract or aphakia			Yes	
Poor compliance	Yes	Yes	Yes	Yes

Note: Yes = Contraindicated.

62.3.3 Clinical Indications

62.3.3.1 Psoriasis

Both BB(UV21)-UVB and NB-UVB phototherapies have shown high efficacy in the treatment of psoriasis but the latter is associated with higher remission rates, lower number of exposures, lower cumulative UV dose (in terms of multiples of the MED), longer remission, and better tolerability with fewer phototoxic reactions [5]. Results are even better (fewer treatments, better long-term efficacy) when more aggressive protocols are used [13]. However, it is still a matter of discussion, whether NB-UVB is superior to BB(UV6)-UVB in clearing psoriasis [14]. Following clearance, the treatment cycle is terminated. In order to avoid high cumulative UVB doses, maintenance treatments are only suggested for selected patients, who are at high risk of early relapse. Combination therapies with other antipsoriatic agents proved effective to reduce cumulative UV doses and to enhance clearance of psoriatic lesions [7]. However, use of systemic corticosteroids is not favored because of adverse effects and risk of early relapse. Combinations with cyclosporin A or methotrexate should be avoided because of the risk of additive carcinogenesis. In contrast, the combination with acitretin improves efficacy, particularly in the treatment of thick plaques, erythrodermic, and pustular psoriasis, and potentially reduces long-term hazards [7]. A few sessions of UVB phototherapy before or during the first weeks of a treatment cycle with efalizumab or etanercept shorten the time to remission and increase clearing rates [15,16].

62.3.3.2 Atopic Dermatitis

NB-UVB phototherapy of atopic dermatitis (AD) of both childhood [17] and adulthood [18] is effective but, in comparison to protocols for psoriasis, more cautious dosimetry and prolonged maintenance are advisable. NB-UVB phototherapy was found as effective as bath-PUVA without differences in

the duration of remission [19]. In comparison to medium-dose UVA-1, NB-UVB is more effective for chronic AD but less effective to control acute flares [20].

62.3.3.3 Polymorphic Light Eruption and Solar Urticaria

Polymorphic light eruption (PLE) and solar urticaria (SU) represent an indication for photoprophylaxis, the prevention of recurrences by increasing the patient's tolerance to sunlight using controlled UV exposures. This effect is likely due to reduced UV penetration because of thickened epidermis, particularly stratum corneum, enhanced pigmentation, and immunomodulation. UVB hardening significantly promotes UV-induced LHC depletion, which is defective in patients with PLE [21]. Randomized controlled clinical trials have shown that BB-UVB is less effective than NB-UVB, and the latter is as effective as PUVA in managing photosensitive conditions [5,22,23]. UV treatment should be always preceded by photoprovocation testing to determine the pathogenic waveband and the minimal dose that triggers the disease. A treatment cycle should start at least 4 weeks before expected sun exposures.

Several case reports have also supported NB-UVB phototherapy in the treatment of other photosensitive disorders, such as erythropoietic protoporphyria, actinic prurigo, hydroa vacciniforme, and drug-induced photosensitivity (see for review Refs. [5,22]).

62.3.3.4 Vitiligo

NB- or BB-UVB are widely used for vitiligo in adults and children, with NB-UVB appearing more effective with up to 75% repigmentation in about two-thirds of patients after at least 1 year of treatment [7,24,25] (Figure 62.1a and b). Initial doses and increments are chosen cautiously to avoid excessive erythema. Response rates depend on anatomic location (face, neck, and trunk > distal extremities and genitals), duration (recent > older lesions), and skin type (darker > lighter phototypes) [5,7]. Phototherapy inhibits T-cell-mediated toxicity to melanocytes and stimulates by an unknown mechanism inactive melanocytes in the outer root sheath of hair follicles to proliferate and migrate into vitiligo patches.

62.3.3.5 Cutaneous T-Cell Lymphoma

BB-UVB and NB-UVB are effective for early stages of cutaneous T-cell lymphoma (CTCL), limited by the lesion thickness in relation to UVB penetration depth. Phototherapy is also a useful adjunct to other modalities such as IFNs, retinoids, and electron beam therapy. Induction of apoptosis of neoplastic T cells is the most likely therapeutic mechanism [26].

62.3.3.6 Other Indications

Open, uncontrolled studies, case series, and case reports have reported successful treatment with BB-UVB or NB-UVB of a broad range of dermatoses, including subcorneal pustular dermatosis (Sneddon–Wilkinson disease), acquired perforating disorder, pruritic folliculitis of pregnancy, prurigo

FIGURE 62.1 **(See color insert.)** Vitiligo of the face treated with NB-UVB: (a) before treatment and (b) after treatment.

nodularis, lichen planus, hand dermatitis, alopecia areata, granuloma annulare, pityriasis rubra pilaris, pigmented purpuric dermatosis (Schamberg's disease), mastocytosis, lymphomatoid papulosis, pityriasis lichenoides, eosinophilic folliculitis, scleromyxedema, and pruritus in polycythemia vera, hepatic, and renal disease (see for review Refs. 5, 7, 27). However, current evidence allows no definitive conclusions as to whether NB- or BB-UVB would be preferable to competing phototherapeutic options such as UVA-1 and PUVA.

62.3.4 Adverse Effects

Burns, dryness, pruritus, and reactivation of herpes simplex virus are common acute cutaneous side effects of UVB phototherapy. Lesional blistering of psoriatic plaques is uncommon, and the hazard of activation of HIV infection is still debated [28]. Data quantifying the carcinogenic risk of NB-UVB and BB-UVB are limited. Recently, a small increase in basal cell carcinoma among those NB-UVB patients also receiving PUVA was registered, without increase in squamous cell carcinoma (SCC) and melanoma rates [29]. One argument favoring NB-UVB was its hypothetically reduced carcinogenic risk compared to BB-UVB; this still remains to be demonstrated at the clinical level [5].

62.4 Excimer UVB Phototherapy (308 nm)

Excimer lasers or lamps deliver large fluences of 308 nm NB-UVB selectively to cutaneous lesions within reasonable time and without hazards to uninvolved skin. However, as it can only expose one small body area after the other, it is only practical for limited skin involvement. Biological and immunological effects are presumably the same as NB-UVB at 312 nm. Excimer light appears to be effective and safe for palmoplantar pustular psoriasis, vitiligo, plaque-type psoriasis, chronic atopic and non-AD of the hands, and alopecia [30].

62.5 UVA-1 Phototherapy

Unlike UVB and UVA-2 (320–340 nm), UVA-1 is poorly erythemogenic and penetrates into the dermis. Its biological effects are due to oxidative damage of proteins, lipids, and DNA (preferentially guanosine) [6,31]. UVA-1 induces apoptosis via the early (<20 min after the exposure) preprogrammed death pathway that depends on singlet-oxygen generation and is activated by the expression of Fas-ligand molecules on the cell surface. These mechanisms markedly differ from the delayed programmed pathway after anaerobic PUVA and UVB-induced DNA damage, and that is p53 dependent and requires synthesis of new proteins [32]. Apoptosis of normal and neoplastic T helper cells plays a central role in the therapeutic effects of UVA-1 [31,33]. In addition, UVA-1 radiation has the capacity to significantly increase mRNA and protein expression of IL-1, IL-6, IL-8, IL-10, and α-MSH, and to downregulate IFN-γ and TNF-α [26]. UVA-1-induced production of PG (prostaglandins), particularly PGE_2, in epidermal keratinocytes and dendritic cells may also contribute to immunosuppression by affecting costimulatory molecule expression on the surface of antigen-presenting cells and thereby preventing T-cell activation [26]. The number of LHC and dendritic cells is not changed by UVA-1, but their activity is downregulated. In fibroblasts, UVA-1 upregulates the synthesis of the collagen-degrading enzyme collagenase I (or matrix metalloproteinase I) [31,33].

62.5.1 Principles of Treatment

UVA-1 phototherapy may be delivered at low (10–30 J/cm^2), medium (40–60 J/cm^2), and high (80–120 J/cm^2) doses with 2–5 weekly exposures. Unlike other phototherapies, it is delivered at fixed dosages without further increments, and MED assessment is not required because even high doses are lower than the erythema thresholds.

62.5.2 Clinical Indications

62.5.2.1 Atopic Dermatitis

Several controlled studies indicate that UVA-1 is effective for AD of both adults and children. Medium-dose UVA-1 may be most cost-effective and safest when compared to low-dose and high-dose regimens. UVA-1 is more effective than BB-UVB and ultraviolet A-B but it is superior to NB-UVB and PUVA only for acute flares (see for review Ref. 20). Clinical improvement is accompanied by apoptosis of skin-infiltrating T cells, epidermal IgE bearing LHC, dermal mastocytes, and circulating eosinophils. In situ expression of IFN-γ, IL-2, and IL-4 is reduced, as are serum levels of the eosinophilic cationic protein [20,34].

62.5.2.2 Lupus Erythematosus

Controlled, randomized, double-blind studies suggest a beneficial effect of low-dose UVA-1 for skin lesions of acute and subacute lupus erythematosus. In addition, systemic symptoms such as arthralgia and malaise improve and elevated circulating inflammation markers and leukopenia normalize [35]. Nevertheless, uncritical treatment of this UV-sensitive disease may put patients at risk for systemic exacerbation [32].

62.5.2.3 Scleroderma and Other Sclerosing Conditions

UVA-1 softens localized scleroderma and cutaneous involvement in systemic scleroderma. Sonography shows a significant decrease in lesional skin thickness [31,36]. Activity on fibroblasts and stimulated apoptosis of autoreactive T cells are involved in the improvement of lichen sclerosus et atrophicus, polyneuropathy, organomegaly, endocrinopathy, monoclonal gammopathy, and skin changes (POEMS) syndrome, keloids, and hypertrophic scars [31,37].

62.5.2.4 CTCL and Other T-Cell-Mediated Diseases

Because of its proapoptotic effect on T lymphocytes, UVA-1 phototherapy has also been introduced successfully in the treatment of patients with early-stage CTCL, acute and chronic pityriasis lichenoides, and lymphomatoid papulosis [38].

62.5.2.5 Mastocytosis

Induction of apoptosis of mast cells infiltrating the skin has been postulated as mechanism of the beneficial effect of UVA-1 phototherapy on cutaneous mastocytosis. Moreover, serum and urine values of mast cell-derived mediators, such as histamine and serotonin, returned to normal levels [39].

62.5.2.6 Other Indications

Medium- and high-dose phototherapy was found effective for dyshidrotic hand eczema and a heterogeneous group of skin diseases characterized by dermal inflammatory infiltrates, including follicular mucinosis, sarcoidosis, granuloma annulare, and necrobiosis lipoidica. Its use for psoriasis in HIV+ patients remains controversial (see for review Ref. [31]). UVA-1 is useful for managing both lichenoid and sclerodermoid cutaneous graft-versus-host disease [37].

62.5.3 Adverse Events

Short-term adverse effects (erythema, pigmentation, induction of PLE or other UVA-sensitive photodermatoses, and herpes simplex reactivation) are uncommon and usually mild and transitory (less than 10% of patients). The major chronic side effects might be photoaging and skin cancer, although epidemiological studies do not support this concern so far [31,33].

62.6 PUVA Photochemotherapy

62.6.1 Mechanisms of Action

Biological effects of photochemotherapy are caused by a cascade of molecular effects triggered by the photoactivation of exogenous chromophores, usually psoralens.

8-Methoxypsoralen (8-MOP), 5-methoxypsoralen (5-MOP), and 4,5′,8-trimethylpsoralen (TMP) are bifunctional linear furocoumarins that are widely used worldwide. They have no systemic toxicity in the dark even at doses much higher than those used for PUVA therapy. Psoralens intercalate in the dark between DNA helices and induce their unwinding. Upon absorption of a photon, pyrone- and furan-side monoadducts are formed and, upon absorption of a second photon, the furan-side adduct only can further photoreact with a base of the opposite DNA strand to form an interstrand cross-link [40]. The DNA–psoralen cross-link blocks DNA polymerase progression and consequently DNA and RNA synthesis [22,40]. Psoralens also photoreact with proteins (DNA–protein cross-links, protein–protein cross-links), leading to damage of cell membranes and the microsomal P450 system, and inactivation of enzymes. Photoaddition of unsaturated fatty acids inhibits the activation of protein kinase C signaling [22]. In addition, activated psoralens may also modify proteins and lipids via generation of singlet oxygen, superoxide anion, or radicals and strongly decrease mitochondrial functions and activate caspase-3, -8, and -9 [41]. The significance of photochemical reactions other than DNA adducts in a clinical setting is unclear.

Cell death of CD4+ lymphocytes may be responsible for the anti-inflammatory effects of PUVA and for the beneficial therapeutic effects of PUVA in lymphoproliferative diseases, such as CTCL. Whether PUVA at clinical dose levels inhibits gene transcription, which ultimately results in a shutdown of cytokine release and expression of accessory surface molecules, is unclear at this point. Suppression by PUVA of the release of the proinflammatory cytokines IL-1, IL-6, IL-8, and TNF-α has been reported. These results were obtained in vitro at high 8-MOP concentrations and may not be therapeutically relevant [33]. Systemic PUVA in vivo suppressed the induction of contact hypersensitivity responses in a systemic fashion and also led to a marked increase in regulatory T-cell subpopulation (CD4 + CD25 + FoxP3 + Treg) in peripheral blood [42]. PUVA decreased the number of cutaneous T lymphocytes, macrophages, dendritic cells, and epidermal LHC with a diminished expression of CD86 and human leukocyte antigen-DR (HLA-DR) [43].

Keratinocytes are much more resistant to PUVA-induced apoptosis than T cells. Inhibition of cell proliferation, however, is observed at PUVA doses that do not affect cell viability. This indicates that the amount of DNA–psoralen photoadducts required for impairing cell replication and proliferation is much lower than that resulting in cell death [44]. An additional PUVA effect on keratinocytes is downregulation of ICAM-1 expression, while it has no significant effect on urocanic acid isomerization [33].

62.6.2 Principles of Treatment

Standard PUVA regimens consist of the psoralen ingestion followed by a delayed exposure to UVA. 8-MOP is administered at a standard dosage of 0.6–0.8 $mg \cdot kg^{-1}$ body weight and 5-MOP at 1.2 $mg \cdot kg^{-1}$ in partial compensation for its much lower intestinal uptake [22]. Low psoralen doses may be completely metabolized by the liver at first-pass and thus be nontherapeutic [45]. UVA exposures are given when the tissue psoralen concentration is highest. This happens after 2 h with pulverized or micronized crystalline preparations and after 1 h with liquid preparations in soft gelatin capsules [22]. Different irradiation protocols are available, and they vary in four parameters: the initial UVA dose, the frequency, the UVA dose increments, and maintenance therapy. The choice of the starting UVA dose has a crucial importance because of wide inter-individual variability in psoralen skin levels and photosensitivity following oral intake. UVA doses that are predetermined based on skin phototype may be too low and ineffective

or too high and hazardous. The initial UVA dose can be better determined by assessing the minimal phototoxic dose (MPD) via exposure of a series of small skin areas of untanned skin to incremental UVA doses after psoralen intake [45].

The number of weekly treatments ranges from 2 to 4 and is limited by the risk of cumulative phototoxicity because PUVA erythema peaks at 48–96 h. A high number of weekly treatments reduces the overall treatment duration but can only be delivered after careful MPD determination. UVA dose increments are necessary in order to maintain the therapeutic effect despite progressive pigmentation and thickening of the skin. Increments are calculated empirically either as fixed dose or as percentage of the previous irradiation [22,45]. Upon complete clearing, patients may discontinue the treatment or enter maintenance therapy with the latest UVA dose and gradually reduced frequency. Patients undergoing maintenance therapy remain longer in remission but prolonged maintenance is time consuming and carries higher risk of long-term adverse effects [22,45]. Unlike creams, ointments, or lotions, bath water delivery of psoralens results in uniform drug delivery, very low psoralen plasma levels, and quick elimination of unbound psoralens from the skin, thus reducing the hazard of accidental burns. Once a domain of TMP, bath-PUVA now largely includes 8-MOP. Bath-PUVA consists of 15–20 min whole body immersions in 0.5–10 mg of 8-MOP per liter of bath water. Photosensitivity increases in this dose range linearly with increasing psoralen concentrations, albeit to a lower extent, that is, a 10 times higher 8-MOP concentration resulted in a less than threefold stronger photosensitivity [46]. Dosimetry for bath-PUVA must take into account that—unlike in oral-PUVA—the phototoxic threshold declines during the early treatment phase [47].

Contraindications to both oral- and bath-PUVA are detailed in Table 62.1. It is noteworthy that bath-PUVA is more user-friendly because it lacks the hazards for internal organs and eye.

62.6.3 Clinical Indications

General treatment parameters are based on the response of psoriasis, where therapeutic effects can easily be quantified. No greater effort was spent on therapeutic development for any other indication. Thus, psoriasis is the model disease for dosimetry, and other indications follow similar regimens.

62.6.3.1 Psoriasis

There is no international consensus on the practical aspects of oral PUVA therapy. Protocols basing the initial irradiation on the individual MPD are preferable because they are as efficient in clearing psoriasis as protocols using a skin type-dependent fixed initial dose but the latter requires a 2.5-fold higher cumulative UVA dose until remission is achieved and therefore has a long-term safety disadvantage [22,30,45]. PUVA should be continued until complete remission or partial remission without any further improvement during the following 2 weeks. In general, maintenance therapy should be avoided [30,45]. Some authors argue that patients with recalcitrant disease should receive maintenance therapy once weekly for 2 months to avoid early relapses [22].

5-MOP is as effective as 8-MOP but at higher cumulative UVA doses because of its lower phototoxicity and higher melanogenic potential after ingestion [47]. The advantages of 5-MOP are its much better gastro-intestinal tolerability and reduced phototoxic side effects [22]. When comparing bath-PUVA with oral PUVA, similar clearing rates were found, but bath-PUVA achieved remissions with fewer treatment sessions and lower cumulative UVA doses [48] (Figure 62.2a and b).

Combination therapies may be useful in disease management. Topical vitamin D analogues enhance PUVA, whereas topical steroids have given conflicting results.

Acitretin is effective in treating hard-to-treat cases of psoriasis. The combination reduces cumulative UVA requirements and decreases long-term risks [30,45]. Combinations with cyclosporin A and methotrexate also work well, but they raise concerns of added carcinogenicity. In analogy, caution is advised for combination with biologicals, such as anti-TNF-α therapies.

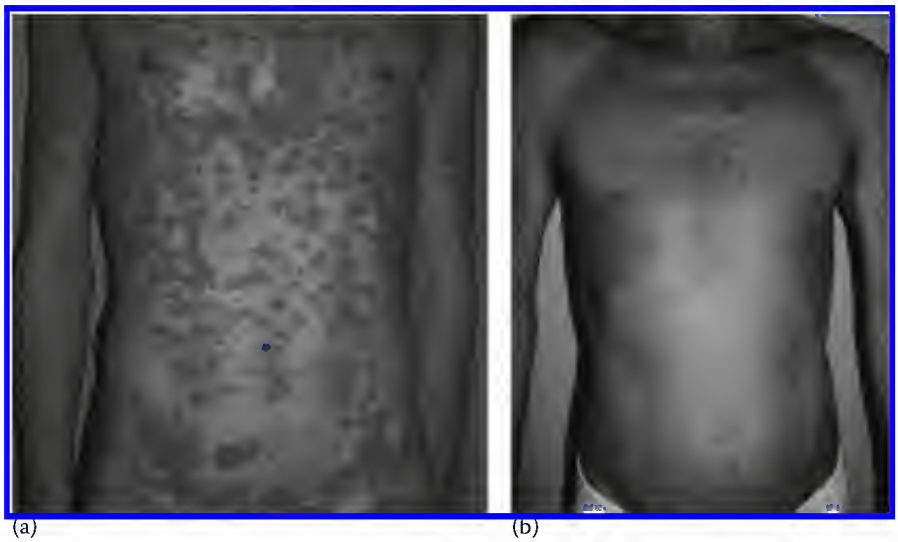

FIGURE 62.2 **(See color insert.)** Psoriasis of the trunk treated with PUVA: (a) before treatment and (b) after treatment.

In studies comparing PUVA and NB-UVB, PUVA seems to be more effective, particularly for the most severe cases, for palmoplantar pustulosis and pustular psoriasis [49,50]. However, considering the convenience of NB-UVB units and because no psoralen is required, NB-UVB can be considered the first choice in phototherapy [5].

62.6.3.2 Atopic Dermatitis

PUVA and bath-PUVA are effective in the treatment of AD of both children and adults, but the use in children and adolescents has to be carefully weighed. Low initial doses with cautious increments help prevent exacerbation, and prolonged maintenance is usually needed. Bath-PUVA was found to be as effective as NB-UVB (see for review Ref. [7]).

62.6.3.3 Vitiligo

PUVA is used for vitiligo because it stimulates migration of melanocytes and melanogenesis, and it has immunosuppressive effects. Low initial UVA doses and cautious increments are delivered until a faint erythema is attained in the vitiligo patches and then maintained by careful UVA dose adjustments.

In comparative trials, PUVA therapy has not been found superior to NB-UVB and due to a higher hazard ratio is now considered a second-line therapy [24]. PUVA seems to be safe in this indication with respect to photocarcinogenicity, as only two vitiligo patients have been reported so far, who developed SCC after prolonged PUVA therapy [7].

62.6.3.4 Cutaneous T-Cell Lymphoma

PUVA is considered a first-line therapy for patch- and plaque-stage CTCL. Long-term remissions have been reported. In the majority of cases, maintenance therapy was necessary. No consensus exists on the duration of treatment courses and frequency of exposures. Combinations of PUVA with IFN-α or bexarotene have shown to improve efficacy, safety, and tolerability for both early and advanced disease. PUVA is also a useful component for combined maintenance regimens [27].

62.6.3.5 Idiopathic Photodermatosis

PUVA can prevent relapses (photochemoprophylaxis) of idiopathic photodermatoses via the stimulation of pigmentation, thickening of the stratum corneum, and immunomodulation. Initial UVA doses are

given according to the MPD, and dose increments are cautious. Three weekly exposures for 4 weeks are sufficient in preventing relapses in up to 90% of patients with PLE.

PUVA is also quite useful for the photochemoprophylaxis of SU. The irradiations must be lower than the minimal urticarial dose (MUD) for UVA, and dose increments must be very small at least for the first few exposures. For accelerated regimens, two or more treatment sessions can be delivered on the same day. The first few exposures may be combined with oral antihistamines or corticosteroids to avoid complications from systemic histamine effects.

In order to speed up the achievement of a protection, a rush hardening protocol with multiple UVA (without psoralen) irradiations at 1 h intervals per day was proposed and allowed to achieve a good protection within 3 days [33]. For both, SU and PLE, the protective effect lasts generally during the whole summer as long as the "hardening" is maintained by repeated exposures to sunlight.

62.6.3.6 Other Indications

Oral PUVA and bath-PUVA have been used successfully in the treatment of a broad range of inflammatory skin diseases encompassing the indications that were listed above with UVB and UVA-1 (with the only exception of lupus erythematosus). However, for most indications, comparative clinical trials are unavailable (see for review Refs. [22,30,45]), and optimal treatment protocols are uncertain. The action mechanisms for different disorders may vary based on their pathogenesis and need further clarification.

62.6.4 Adverse Effects

Oral PUVA is generally well tolerated but one or more episodes of excessive phototoxic reactions and itching occur in 10%–20% of patients, who usually recover spontaneously. Gastrointestinal symptoms (nausea and vomiting) are not uncommon with 8-MOP but can be improved by intake of some food with the drug. Skin pain, blisters, acneiform eruptions, facial hypertrichosis, onycholysis, and subungual hemorrhages are uncommon. Increase of transaminases is rare unless there is preexisting liver damage. PUVA in the long term leads to photoaging with elastosis, poikiloderma, and prominent lentigines. PUVA-treated patients have a higher risk of nonmelanoma skin cancer, and the risk is higher for patients, who were previously treated with arsenic, BB-UVB, or methotrexate. It is uncertain if PUVA causes malignant melanoma [51,52]. However, patients with dysplastic nevus syndrome and those with a history of melanoma should not be treated. Because psoralens bind to the proteins in the ocular lens, there is a theoretical risk for accelerated cataract formation under PUVA therapy. However, PUVA does not increase cataract risk among persons using eye protection for at least 12 h after treatments [53]. Bath-PUVA has the same short-term cutaneous adverse effects as oral PUVA. However, because of minimal percutaneous absorption of psoralens, bath-PUVA has no systemic toxicity. In addition, hazards of skin cancers have not been reported with bath-PUVA so far.

References

1. Beissert, S., Schwarz, T. 2002. Role of immunomodulation in diseases responsive to phototherapy. *Methods* 28: 138–144.
2. Diffey, B.L., Farr, P.M. 1987. An appraisal of ultraviolet lamps used for the phototherapy of psoriasis. *Br. J. Dermatol.* 117: 49–56.
3. Parrish, J.A., Fitzpatrick, T.B., Tanenbaum, L., Pathak, M.A. 1974. Photochemotherapy of psoriasis with oral methoxsalen and longwave ultraviolet light. *N. Engl. J. Med.* 291: 1207–1211.
4. Wolff, K., Honigsmann, H., Gschnait, F., Konrad, K. 1975. Photochemotherapy of psoriasis: Clinical experiences with 152 patients (author's transl.). *Dtsch. Med. Wochenschr.* 100: 2471–2477, 1497.
5. Ibbotson, S.H., Bilsland, D., Cox, N.H. et al. 2004. An update and guidance on narrowband ultraviolet B phototherapy: A British Photodermatology Group Workshop Report. *Br. J. Dermatol.* 151: 283–297.

6. Weichenthal, M., Schwarz, T. 2005. Phototherapy: How does UV work? *Photodermatol. Photoimmunol. Photomed.* 21: 260–266.
7. Berneburg, M., Rocken, M., Benedix, F. 2005. Phototherapy with narrowband vs broadband UVB. *Acta Derm. Venereol.* 85: 98–108.
8. Sigmundsdottir, H., Johnston, A., Gudjonsson, J.E., Valdimarsson, H. 2005. Narrowband–UVB irradiation decreases the production of pro-inflammatory cytokines by stimulated T cells. *Arch. Dermatol. Res.* 297: 39–42.
9. Walters, I.B., Ozawa, M., Carindale, I. et al. 2003. Narrowband (312 nm) UV-B suppresses interferon and interleukin (IL) 12 and increases IL-4 transcripts: Differential regulation of cytokines at the single-cell level. *Arch. Dermatol.* 139: 155–161.
10. Schwarz, A., Beissert, S., Grosse-Heitmeyer, K. et al. 2000. Evidence for functional relevance of CTLA-4 in ultraviolet-radiation-induced tolerance. *J. Immunol.* 165: 1824–1831.
11. Lehmann, B., Querings, K., Reichrath, J. 2004. Vitamin D and skin: New aspects for dermatology. *Exp. Dermatol.* 13: 11–15.
12. Fluhr, J.W., Gloor, M. 1997. The antimicrobial effect of narrow-band UVB (313 nm) and UVA-1 (345–440 nm) radiation in vitro. *Photodermatol. Photoimmunol. Photomed.* 13: 197–201.
13. Kleinpenning, M.M., Smits, T., Boezeman, J., van de Kerkhof, P.C.M., Evers, A.W.M., Gerritsen, M.J.P. 2009. Narrowband ultraviolet B therapy in psoriasis: Randomized double-blind comparison of high-dose and low-dose irradiation regimens. *Br. J. Dermatol.* 161: 1351–1356.
14. Kirke, S.M., Lowder, S., Lloyd, J.J., Diffey, B.L., Matthews, J.N.S., Farr, P.M. 2007. A randomized comparison of selective broadband UVB and narrowband UVB in the treatment of psoriasis. *J. Invest. Dermatol.* 127: 1641–1646.
15. Zane, C., Capezzera, R., Venturini, M. et al. 2009. A short cycle of narrow-band UVB phototherapy in the early phase of long-term efalizumab can provide a quicker remission of moderate and severe psoriasis: A pilot study. *Dermatology* 218: 321–326.
16. Wolf, P., Hofer, A., Legat, F.J. et al. 2009. Treatment with 311-nm ultraviolet B accelerates and improves the clearance of psoriatic lesions in patients treated with etanercept. *Br. J. Dermatol.* 160: 186–189.
17. Collins, P., Ferguson, J. 1995. Narrow-band (TL-01) UVB air-conditioned phototherapy for atopic eczema in children. *Br. J. Dermatol.* 133: 653–655.
18. George, S.A., Bilsland, D.J., Johnson, B.E., Ferguson, J. 1993. Narrow-band (TL-01) UVB air-conditioned phototherapy for chronic severe adult atopic dermatitis. *Br. J. Dermatol.* 128: 49–56.
19. Der-Petrossian, M., Seeber, A., Honigsmann, H., Tanew, A. 2000. Half-side comparison study on the efficacy of 8-methoxypsoralen bath-PUVA versus narrow-band ultraviolet B phototherapy in patients with severe chronic atopic dermatitis. *Br. J. Dermatol.* 142: 39–43.
20. Gambichler, T. 2009. Management of atopic dermatitis using photo(chemo)therapy. *Arch. Dermatol. Res.* 301: 197–203.
21. Janssens, A.S., Pavel, S., Out-Luiting, J.J., Willemze, R., de Gruijl, F.R. 2005. Normalized ultraviolet (UV) induction of Langerhans cell depletion and neutrophil infiltrates after artificial UVB hardening of patients with polymorphic light eruption. *Br. J. Dermatol.* 152: 1268–1274.
22. Hönigsmann, H. 2003. Mechanisms of phototherapy and photochemotherapy for photodermatoses. *Dermatol. Ther.* 16: 23–27.
23. Bilsland, D., George, S.A., Gibbs, N.K. et al. 1993. A comparison of narrow band phototherapy (TL-01) and photochemotherapy (PUVA) in the management of polymorphic light eruption. *Br. J. Dermatol.* 129: 708–712.
24. Scherschun, L., Kim, J.J., Lim, H.W. 2001. Narrow-band ultraviolet B is a useful and well-tolerated treatment of vitiligo. *J. Am. Acad. Dermatol.* 44: 999–1003.
25. Njoo, M.D., Bos, J.D., Westerhof, W. 2000. Treatment of generalized vitiligo in children with narrow-band (TL-01) UVB radiation therapy. *J. Am. Acad. Dermatol.* 42: 245–253.
26. Krutmann, J., Morita, A. 1999. Mechanisms of ultraviolet (UV) B and UVA phototherapy. *J. Invest. Dermatol. Symp. Proc.* 4: 70–72.

27. McGinnis, K.S., Shapiro, M., Vittorio, C.C., Rook, A.H., Junkins-Hopkins, J.M. 2003. Psoralen plus long-wave UV-A (PUVA) and bexarotene therapy: An effective and synergistic combined adjunct to therapy for patients with advanced cutaneous T-cell lymphoma. *Arch. Dermatol.* 139: 771–775.
28. Breuer-McHam, J., Marshall, G., Adu-Oppong, A. et al. 1999. Alterations in HIV expression in AIDS patients with psoriasis or pruritus treated with phototherapy. *J. Am. Acad. Dermatol.* 40: 48–60.
29. Hearn, R.M.R., Kerr, A.C., Rahim, K.F., Ferguson, J., Dawe, R.S. 2008. Incidence of skin cancers in 3867 patients treated with narrow-band ultraviolet B phototherapy. *Br. J. Dermatol.* 159: 931–935.
30. Schneider, L.A., Hinrichs, R., Scharffetter-Kochanek, K. 2008. Phototherapy and photochemotherapy. *Clin. Dermatol.* 26: 464–476.
31. Mang, R., Krutmann, J. 2005. UVA-1 phototherapy. *Photodermatol. Photoimmunol. Photomed.* 21: 103–108.
32. Godar, D.E., Lucas, A.D. 2005. Ultraviolet-A1 (340–400 nm)-mediated receptor and cytokine changes of transformed lymphocytes. *Photodermatol. Photoimmunol. Photomed.* 21: 23–31.
33. Beissert, S., Winder, H., Schwarz, T. 2000. A rush hardening for the treatment of solar urticaria. *J. Am. Acad. Dermatol.* 42: 1030–1032.
34. Morita, A., Werfel, T., Stege, H. et al. 1997. Evidence that singlet oxygen-induced human T helper cell apoptosis is the basic mechanism of ultraviolet-A radiation phototherapy. *J. Exp. Med.* 186: 1763–1768.
35. McGrath, H., Jr. 1999. Ultraviolet A1 (340–400 nm) irradiation and systemic lupus erythematosus. *J. Investig. Dermatol. Symp. Proc.* 4: 79–84.
36. Gruss, C., Reed, J.A., Altmeyer, P., McNutt, N.S., Kerscher, M. 1997. Induction of interstitial collagenase (MMP-1) by UVA-1 phototherapy in morphea fibroblasts. *Lancet* 350: 1295–1296.
37. Calzavara Pinton, P.G., Porta, F., Izzi, T. et al. 2003. Prospects for ultraviolet A1 phototherapy as a treatment for chronic cutaneous graft-versus-host disease. *Haematologica* 88: 1169–1175.
38. Calzavara-Pinton, P.G., Venturini, M., Sala, R. 2005. Medium-dose UVA-1 therapy of lymphomatoid papulosis. *J. Am. Acad. Dermatol.* 52: 530–532.
39. Gabello, T., Mozzanti, C., Sordi, D. et al. 2003. Medium- versus high-dose ultraviolet A1 therapy for urticaria pigmentosa: A pilot study. *J. Am. Acad. Dermatol.* 49: 679–684.
40. Serrano-Pérez, J.J., Merchán, M., Serrano-Andrés, L. 2008. Photoreactivity of furocoumarins and DNA in PUVA therapy: Formation of psoralen–thymine adducts. *J. Phys. Chem. B* 112: 14002–14010.
41. Viola, G., Fortunato, E., Cecconet, L., Disaro, S., Basso, G. 2007. Induction of apoptosis in Jurkat cells by photoexcited psoralen derivatives: Implication of mitochondrial dysfunctions and caspases activation. *Toxicol. In Vitro* 21: 211–216.
42. Saito, C., Akira, M., Morita, A. 2009. Bath-PUVA therapy induces circulating regulatory T cells in patients with psoriasis. *J. Derm. Sci.* 53: 222–243.
43. Erkin, G., Ugur, Y., Gurer, C. et al. 2007. Effect of PUVA, narrow-band UVB and cyclosporin on inflammatory cells of the psoriatic plaque. *J. Cutan. Pathol.* 34: 213–219.
44. Lüftl, M., Röcken, M., Plewig, G., Degitz, K. 1998. PUVA inhibits DNA replication, but not gene transcription at nonlethal dosages. *J. Invest. Dermatol.* 111: 399–405.
45. British Photodermatology Group. 1994. British Photodermatology Group guidelines for PUVA. *Br. J. Dermatol.* 130: 246–255.
46. Vongthongsri, R., Konschitzky, R., Seeber, A., Treitl, C., Hönigsmann, H., Tanew, A. 2006. Randomized, double-blind comparison of 1 mg/L versus 5 mg/L methoxsalen bath-PUVA therapy for chronic plaque-type psoriasis. *J. Am. Acad. Dermatol.* 55: 627–631.
47. Calzavara-Pinton, P.G., Ortel, B., Carlino, A.M., Hönigsmann, H., De Panfilis, G. 1993. Phototesting and phototoxic side effects in bath-PUVA. *J. Am. Acad. Dermatol.* 28: 657–659.
48. Calzavara-Pinton, P.G., Ortel, B., Hönigsmann, H., Zane, C., De Panfilis, G. 1994. Safety and effectiveness of an aggressive and individualized bath-PUVA regimen in the treatment of psoriasis. *Dermatology* 189: 256–259.

49. Tanew, A., Radakovic-Fijan, S., Schemper, M., Hönigsmann, H. 1999. Narrowband UV-B phototherapy vs photochemotherapy in the treatment of chronic plaque-type psoriasis. *Arch. Dermatol.* 135: 519–524.
50. Yones, S.S., Palmer, R.Y., Garibaldinos, T.T., Hawk, J. 2006. Randomized double-blind trial of the treatment of chronic plaque psoriasis. Efficacy of psoralen–UV-A therapy vs narrowband UV-B therapy. *Arch. Dermatol.* 142: 836–842.
51. Stern, R.S. 1999. Malignant melanoma in patients treated for psoriasis with PUVA. *Photodermatol. Photoimmunol. Photomed.* 15: 37–38.
52. Wolff, K. 1997. Should PUVA be abandoned? *N. Engl. J. Med.* 336: 1090–1091.
53. Malanos, D., Stern, R.S. 2007. Psoralen plus ultraviolet A does not increase the risk of cataracts: A 25-year prospective study. *J. Am. Acad. Dermatol.* 57: 231–237.

63

Photoimmunology

Vivienne E. Reeve
The University of Sydney

63.1 Introduction

Photoimmunology has its origins in the landmark studies around 25 years ago that demonstrated the immunogenic nature of UV radiation–induced skin tumors taken from mice by the failure of their growth when fragments of these tumors were transplanted into naïve syngeneic recipient mice (Kripke 1974; Daynes and Spellman 1977). That the tumor rejection was immunological was shown by the reversal of the rejection by immunosuppressive drugs. Furthermore, if the recipient mice were pre-exposed to a subcarcinogenic dose of UV radiation, transplanted tumors again survived and grew, indicating for the first time that UV radiation could be immunosuppressive (Fisher and Kripke 1978). It was later observed that this inhibited anti-tumor immunity could be transferred to recipient mice with splenic T lymphocytes from such UV-irradiated donor mice, and thus, the dependence of the development of skin cancer on UV-induced defective T cell-mediated immunity was revealed (Fisher and Kripke 1982; Ullrich and Kripke 1984).

It is now understood that UV radiation is a complete carcinogen that not only mutates the DNA of epidermal cells to initiate cancer, but also suppresses the immunological recognition and rejection of this genetic damage in a specific manner that facilitates survival and progression of the initiated tumor cell. The early data arose from studies in mice, but all mammals appear to be susceptible to photoimmune suppression, including humans (Cooper et al. 1992; Kelly et al. 1998), with fair skin and sensitivity to sunburn in humans being associated with greater susceptibility to immune suppression by sunlight, measured by the contact hypersensitivity reaction (Kelly et al. 2000). Chronic overexposure

to sunlight is a universal precursor in otherwise healthy non-melanoma skin cancer patients and is reflected in their greater susceptibility to immune suppression by UVB radiation than normal subjects (Yoshikawa et al. 1990; Czarnecki et al. 1995). In addition, in patients receiving long-term immunosuppressive drug therapy such as organ transplant recipients, there is a highly significantly increased and often intractable metastatic skin cancer development that may prove to be manageable only by withdrawing the immunosuppressive drug (Berg and Otley 2002; Euvrard et al. 2006; Gutierrez-Dalmau and Campistol 2007; Veness et al. 1999).

The relentless increase in human skin cancers, particularly in fair-skinned populations worldwide, has made it urgent to understand the pathways by which solar UV radiation acquires its immunosuppressive property. Strategies for the protection of the immune system from UV damage are potentially helpful in preventing skin cancer development, but depend on the elucidation of the cutaneous photoreceptors that are activated to suppress immunity, and the relevant downstream cellular and molecular targets that result in the immunological defect. There has been much progress in identifying the mechanisms, gradually revealed to comprise a very complex multipathway network. Murine models have been a major contribution to this field, but important controversies currently persist that need clarification before the cutaneous immune response in humans can be targeted to advantage. Numerous excellent reviews have regularly charted the advances (Clydesdale et al. 2001; Ullrich 2005, 2007; Schade et al. 2005; Hanneman et al. 2006; Norval 2006; Loser and Beissert 2009; Schwarz 2008). In this chapter, the current state of knowledge will be summarized and updated with the newer observations.

63.2 Measurement of Immune Function

Photoimmune suppression is mediated primarily by T lymphocytes, and this arm of the immune system is conveniently modeled by the delayed-type or contact hypersensitivity (DTH or CHS) reactions. These T-cell-mediated reactions are relevant for laboratory rodents, marsupials (*Monodelphis domestica*), other mammals, and humans, and studies of these reactions in laboratory animals have been very fruitful in supplying the evidence for the critical pathways involved. The two reactions differ in the nature and route of administration of the sensitizing antigen, with sensitization for DTH usually being parenteral, whereas this is topical or epicutaneous for CHS (Reeve 2002). Commonly used sensitizers for DTH are injectable pathogens such as *Candida* or *Mycobacterium,* and for CHS are simpler topically applied chemicals such as oxazolone, 2,4-dinitrochlorobenzene, or 2,4-dinitrofluorobenzene. If sensitization is directly via UV-irradiated skin, the subsequently elicited reaction at a second site will reveal local UV-induced immune changes; if sensitization is via distant unirradiated skin, the elicited reaction at another site will reveal systemic UV-induced immune changes. Following sensitization, which is normally innocuous, the hypersensitivity reaction will be elicited by challenging the animal with the same sensitizing agent at another site, commonly the footpad (DTH) or the ear (CHS), resulting in an inflammation in the next 24–48 h that can be measured by the swelling. Local photoimmune suppression of CHS in the UVB-irradiated skin can be observed as soon as 24 h postirradiation, whereas systemic suppression develops more slowly and can be observed by 3–5 days postirradiation, but the UV dose to induce both defects is the same (Noonan and De Fabo 1990).

A well-used assay for photoimmune changes in humans is the elicitation of the nickel recall antigen response (Damian and Halliday 2002). The serendipitous prior sensitization to this metal in affected humans provides a population of potential human volunteers who will not require exposure to other chemical sensitizers, and the contact allergic reaction is readily elicited by topical application of a nickel salt solution. The suppressive effect of UV radiation will be measured by the local erythema and records the effect on the elicitation arm of the CHS response rather than on the primary sensitization.

In mice and humans, the immune defect after a single UV treatment is transient, and normal immune function will be restored within days or a few weeks. However, chronically repeated UV exposures result eventually in chronically suppressed skin immunity, when the animal or human can no longer be

successfully resensitized against the initial sensitizing agent, and this condition of immune tolerance is associated with the increased risk of carcinogenesis. The mechanisms underlying local and systemic suppression are different, as will be seen in the following.

63.3 Photoreceptors

63.3.1 DNA

The induction of a biological reaction to radiation requires a receptor that has an absorption spectrum matching the action spectrum for the biological reaction. The earliest attempt to produce an action spectrum for photoimmune suppression in mice was a heroic study (De Fabo and Kripke 1979) that indicated a peak in the UVB waveband between 290 and 320 nm. An immediately obvious potential receptor with UVB absorption encompassing this waveband was the DNA, and evidence began to accumulate showing that UVB-induced DNA lesions were the cause of the immunological dysfunction. Repair of the predominant UVB-induced DNA lesion, the cyclobutane pyrimidine dimer (CPD), either by switching on the endogenous photoreactivating enzyme pathway in the marsupial *M. domestica* (Applegate et al. 1989) or by treating mice with encapsulated T4N5 endonuclease to initiate nucleotide excision repair (Kripke et al. 1992; Yarosh et al. 1994) also repaired the immune defect. Furthermore, these strategies also resulted in a reduction in the photocarcinogenic outcome in both experimental species (Bito et al. 1995; Ley et al. 1991; Yarosh et al. 1992), emphasizing the connection between photoimmune suppression and the risk of skin cancer. Recently, patients with the hereditary disease *xeroderma pigmentosum*, who lack the DNA repair mechanism specific for UV-induced genetic damage and who suffer greatly exacerbated sunlight-induced immune suppression and skin cancer development, have been successfully treated with encapsulated DNA repair enzymes (Yarosh et al. 2001).

It has not been immediately clear in which cells the critical DNA damage with the immunosuppressive outcome occurs. The nuclei of all epidermal cell types are in the target range for genetic damage by UVB radiation, and there is good evidence that both the dendritic Langerhans cells (LCs) and the keratinocytes have roles to play. These will be addressed in the following.

63.3.2 *trans*-Urocanic Acid

DNA is not the only UVB-absorbing cutaneous molecule. It has transpired that a second potential photoreceptor for immune suppression is *trans*-urocanic acid (deaminated histidine). This molecule, the product of the enzyme histidase, is a catabolite of the amino acid histidine and is present in most body tissues where it is further degraded by urocanase activity, and is so-named for its original extraction from the urine of the dog, *Canis canis*. It occurs in relatively high concentrations in the upper epidermis and *stratum corneum*, due to the absence in the skin of urocanase. Urocanic acid has an UV absorption peak between 280 and 310 nm (McLoone et al. 2005), and the natural *trans* isomer is UV dose dependently photoisomerized to the *cis* form, equilibrating at the photostationary state of approximately equal concentrations of each isomer. *cis*-Urocanic acid, but not the *trans* isomer, is immunosuppressive, and many studies have tracked its actions in the skin, utilizing the ready responses of mice to topically applied or injected urocanic acid solutions (De Fabo and Noonan 1983; Noonan and De Fabo 1992). A neutralizing antibody to *cis*-urocanic acid prevents its immunosuppressive activity in mice (Moodycliffe et al. 1996), and more recently was shown to also inhibit photocarcinogenesis in the mouse (Beissert et al. 2001). This finding is consistent with an earlier demonstration that topically applied *trans*-urocanic acid daily to hairless mice during photocarcinogenesis induction resulted in an exacerbated tumorigenic outcome (Reeve et al. 1989). It is evident that the *cis* isomer is not the only urocanic acid photoproduct. A number of urocanic acid photooxidation products have been identified in UVB-irradiated human *stratum corneum*, which are also immunosuppressive in mice, and in combination may be more potently suppressive than *cis*-urocanic acid alone (Kammeyer et al. 2004). The contribution of such oxidized products to the immune defect in humans remains to be defined.

Urocanic acid has been isolated from the skin of many animals including reptiles, marsupials, rodents, and man, and the molecule appears to be very well conserved across the animal species (Ley et al. 2000). This suggests that it has a positive function of broader consequences in the skin than the immunosuppressive property of the *cis* isomer, perhaps in limiting the inflammatory immune reaction to photoantigens that could potentiate an autoimmune rejection of damaged skin cells. Several comprehensive reviews have followed the progress of understanding the activity of *cis*-urocanic acid (Gibbs et al. 2008; Mohammad et al. 1999; Norval et al. 1995; Norval and El-Ghorr 2002), but considerable uncertainty prevails as to its mode of action.

Because of its UVB absorption properties and location in the *stratum corneum*, it was originally thought that urocanic acid functioned as a natural endogenous sunscreen for the UV protection of the epidermal basal cells. However, calculations of its very low sun protection factor in humans from a cream containing more than 20 times the concentration of cutaneous *trans*-urocanic acid later seemed to rule out such a function (De Fine Olivarius et al. 1996). Nevertheless, cosmetic products were formulated with the inclusion of urocanic acid, but experimental application of one of these products was revealed to significantly increase the suppression of CHS in mice following their subsequent exposure to solar-simulated UV radiation (Reeve and Mitchell 1991). In contrast to these early experiments, a very recent report has provided evidence of significantly fewer CPDs induced in the skin of mice genetically deficient in histidase, and therefore deficient in *stratum corneum* urocanic acid, indicating that a photoprotective action for endogenous urocanic acid remains a possibility (Barresi et al. 2011).

The molecular and functional dissimilarity between the two molecules, DNA and urocanic acid, proposed as the receptors for photoimmune suppression led initially to much controversy. The possibility that *cis*-urocanic acid might bind to DNA or produce CPD-like dimers was examined and later refuted (IJland et al. 1998; Morrison et al. 1983), leading to the conclusion that two separate pathways to photoimmune suppression must exist. Today, the downstream targets of *cis*-urocanic acid remain somewhat controversial, and the critical cell population(s) bearing the immunosuppressive DNA damage are only recently becoming apparent.

63.3.2.1 Downstream Targets of *cis*-Urocanic Acid

Early evidence that histamine receptor antagonists could inactivate the immunosuppressive effects of urocanic acid indicated a role of the H1 and H2 histamine receptors (Gilmour et al. 1993), but as the cells involved did not appear to be the keratinocytes (Mitra et al. 1993), the relevant cell population, whether cutaneous or distantly localized, remains unclear. It has since been reported that UV irradiation clinically results in an approximately fivefold increase in the *cis/trans* ratio of urocanic acid in the urine, strongly indicative of a systemic distribution of this photoproduct (Kammeyer et al. 1997; Sastry et al. 2005). Therefore, it is relevant that oral, rather than topical, treatment of hairless mice with the H2 receptor antagonist cimetidine during photocarcinogenesis induction significantly reduced the skin tumor outcome (Matheson and Reeve 1991), and in a model of allergic respiratory inflammation in mice, suppression by UVB radiation has implicated a mediating role for histamine H2 receptors in the lung-draining lymph node (McGlade et al. 2007). Obviously, distant organ effects of *cis*-urocanic acid via this pathway remain a possibility.

More recent evidence based on its molecular structural similarity with 5-hydroxytryptamine (5-HT; serotonin) reports that the 5-HT(2A) receptor functions as the *cis*-urocanic receptor and is supported by studies in mice treated with various receptor antagonists (Walterscheid et al. 2006). *cis*-Urocanic acid, but not the *trans* isomer, was found to be a competitive inhibitor of 5-HT for this receptor (Shen and Ji 2009); a selective 5-HT receptor antagonist blocked the binding of *cis*-urocanic acid, and furthermore, the neutralizing antibody to *cis*-urocanic acid or blockade of the 5-HT(2A) receptor both prevented the suppression of DTH by UV radiation, *cis*-urocanic acid, or 5-HT. It was therefore consistent to find that 5-HT(2A) receptor blockade also reduced the photocarcinogenic outcome in chronically irradiated mice (Sreevidya et al. 2008). In contrast to these studies have been reports that do not find that *cis*-urocanic acts via the 5-HT(2A) receptor in either primary human keratinocytes (Kaneko et al. 2009)

or in peripheral human blood monocytes (Woodward et al. 2006). Whether human keratinocytes actually express the 5-HT(2A) receptor is controversial, since the mRNAs of several 5-HT receptors were identified in these cells by Slominski et al. (2003), but not in the later study (Kaneko et al. 2009). Further research is needed to clarify this issue.

Another target for *cis*-urocanic acid consists of the peripheral sensory nerves, which have been shown to release neuropeptides in response to this photoproduct, but not to the *trans* isomer (Khalil et al. 2001). Both substance P and calcitonin gene-related peptide (CGRP) were released, compounds that are known to induce the degranulation of mast cells to release many mediators, particularly histamine, which then can activate prostaglandin synthesis by the keratinocytes. The neuropeptides may also bind to the LCs and induce immunosuppressive interleukin (IL)-10 production (Lambert and Granstein 1998).

63.3.3 Cell Membrane Lipids

UV irradiation of the skin results in oxidative stress that indirectly damages additional epidermal molecules. Cell membrane lipids are oxidizable targets and provide a source of the potent phospholipid mediators, platelet-activating factor (PAF) and related compounds, that are now known to have inflammatory and immune modulating activity via the PAF receptor on keratinocytes (and various other cell types). The synthesis of PAF is believed to be one of the first responses to UV irradiation and can be detected within minutes (Barber et al. 1998; Marathe et al. 2005). Activation of the PAF receptor results in a cascade of cytokine and eicosanoid release that contributes to the inflammatory sunburn response (Pei et al. 1998; Ullrich et al. 2007), and this reaction is independent of any genomic or nuclear events (Simon et al. 1994). Significantly, PAF receptor antagonists in mice inhibit photoimmune suppression as well as *cis*-urocanic acid suppression of DTH (Walterscheid et al. 2002), and these actions were confirmed in the failure to induce photoimmune suppression in PAF receptor gene knockout mice (Wolf et al. 2006). Furthermore, PAF receptor antagonism in mice was demonstrated to inhibit photocarcinogenesis (Sreevidya et al. 2008).

On the other hand, more recent studies in primary human keratinocytes provide conflicting data (Kaneko et al. 2009). Treatment with *cis*-urocanic acid was reported to activate the secretion of relevant immunosuppressive factors, but this was not inhibited by a PAF receptor antagonist, nor was there evidence of *cis*-urocanic acid binding to the PAF receptor. It was earlier shown that *cis*-urocanic acid induced oxidative stress in primary human keratinocytes that could be anticipated to stimulate the PAF receptor (Kaneko et al. 2008), and antioxidants were found by others to inhibit *cis*-urocanic acid immunosuppression in mice (Steenvoorden and van Beijersbergen 1999). Nevertheless, the human keratinocyte does not appear to be the cell in which PAF signaling mediates photoimmune suppression, and further studies are needed to identify the role of alternate cell populations.

63.4 UV-Responsive Mediators

63.4.1 Cellular

63.4.1.1 LCs and T Lymphocytes

LCs are dendritic antigen-presenting cells that form a suprabasal interdigitating network in the epidermis, thus providing the surveillance against environmental and invading pathogens in order to protect the susceptible basal cells below. Their role is to capture and process exogenous antigens, to migrate to the regional lymph node, and there to present the processed antigen to T helper-1 (Th-1) lymphocytes. A population of specifically activated T cells is then generated, sensitized to that antigen. However, in the case of UV irradiation, this sequence fails to occur, and the failure can be partially attributed to the UV-induced DNA damage of the resident LC (Schwarz 2005). Increased numbers of LC with identifiable UV-DNA damage accumulate in the regional lymph nodes (Schwarz et al. 2005), viable but unable to present antigen normally, and instead causing the generation of a population of

regulatory T cells (Treg cells) associated with Th-2 function and immunological tolerance. Meanwhile, in the LC-depleted epidermis, it has been suggested that antigens can be taken up by nonspecific antigen-presenting cells like macrophages, thus avoiding specific sensitization and also resulting in the development of an aberrant population of T cells subsequently unable to recognize the antigen. Either mechanism may be involved; however, recent studies in which the reversal of the immunosuppressed state in mice was achieved by injecting IL-12 indicated that this cytokine both prevented the UV-depletion of the epidermal LC and unexpectedly also resulted in repair of their DNA lesions, apparently by stimulating the endogenous nucleotide excision repair (NER) enzymes (Schwarz et al. 1996, 2005; Schwarz 2005).

The target T cells were originally known as T suppressor cells (Ts cells), and populations of lymph node or splenic cells that included these Ts cells could adoptively transfer the defective immunosuppressed response to naïve recipient mice (Fisher and Kripke 1978, 1982; Elmets et al. 1983). For some years, the actual existence of the Ts cell was much debated, as it proved impossible to purify or clone such a cell population, but more recently their role in modulating the skin immune system has been confirmed, and they are now known as Treg cells and have been characterized as CD4+CD25+ (reviewed in Schwarz 2008). Another population of UV-induced suppressor T cells that plays a critical role in tumor rejection, while present in small numbers, is the unique natural killer T cell (NKT cell) that is CD3+CD4+ (Moodycliffe et al. 2000).

The photoantigenic defect induced by UV radiation in the skin cells may be the altered DNA, RNA, protein, or lipid components of the epidermal cells. UVB radiation is known to induce specific lesions directly in the DNA, predominantly the CPD, as well as alterations in the aromatic amino acids, and oxidation products of cell membrane lipids. These primary lesions have each been demonstrated to result from the initial interaction of the UV radiation with epidermal photoreceptors that results in the immune suppression and, as will be seen in the following, suggest that there are multiple pathways that can be activated by UV radiation to produce the immunosuppressed state. Treg cells in the periphery are important under normal conditions in tissues as they are required to terminate active immune responses when the antigen has been sequestered and removed, and provide important protection against the development of autoimmunity. Their continued presence is dependent on the expression of costimulatory molecules such as CD80 and CD86 of the B7 family (Loser et al. 2005), and receptor activator of NF-κB ligand (RANKL) of the tumour necrosis factor (TNF) family (Loser et al. 2006). When activated by the specific antigen, the Treg cells release the immunosuppressive cytokine IL-10, which then enables general immune suppression that can be local or systemic because of the soluble and systemically dispersible nature of this cytokine, and can be directed nonspecifically to other unrelated antigens encountered by the body at that time.

63.4.1.2 Mast Cells

The degranulation of mast cells in UV-irradiated skin releases many inflammatory and immune modulating factors that can contribute to UV-induced erythema and immune suppression, but TNFα and histamine have been identified as the critical molecules for immune suppression and involve the synthesis of inflammatory prostaglandins like PGE2. Degranulation is not mediated directly by *cis*-urocanic acid, but is dependent on neuropeptides such as CGRP released from sensory dermal fibers, that is, *cis*-urocanic acid dependent (Hart et al. 2001, 2002).

There is a correlation between dermal mast cell prevalence and susceptibility to immune suppression by UV radiation or *cis*-urocanic acid in mice, and mouse strains have been categorized according to their mast cell numbers for the dose of UV radiation, high or low, by which they can be photoimmune suppressed experimentally (Hart et al. 1999). In humans, mast cell numbers in chronically sun-exposed skin sites are significantly greater than in protected skin (Grimbaldeston et al. 2003) and may lead to predisposition for basal cell carcinoma (Grimbaldeston et al. 2006). Mast cell-depleted mice proved to be unresponsive for systemic immunosuppression by either UVB or *cis*-urocanic acid; therefore, these cells infiltrating the UV-irradiated skin sites are contributors to photoimmune suppression.

63.4.1.3 Macrophages/Monocytes

It has long been recognized that there is an inflammatory cellular infiltrate that appears in the UV-irradiated skin 3–4 days after exposure that includes macrophages, neutrophils, and mast cells. Because activated human macrophages can be potent sources of IL-10, it was consistent to find that CD11b+ macrophages appearing in the UV-irradiated skin of humans contained elevated levels of IL-10 protein (Kang et al. 1994). The macrophage is now recognized as a major contributor to epidermal IL-10 and photoimmune suppression. Furthermore, enhanced UV-induced tumor growth in mice could be attributed to the influx of CD11b+ and other inflammatory cells into the epidermis (Sluyter and Halliday 2000). In more recent studies, dendritic cells including macrophages from UV-irradiated mice were shown to be unable to secrete functional immunoprotective IL-12 (IL-12p70), but instead secreted an IL-12p40 homodimer that acts as an antagonist of biologically active IL-12, thus suppressing the Th1 cell inflammatory and immunological activity (Schmitt and Ullrich 2000).

63.4.1.4 B Cells

Studies of the crucial lymph nodes draining the UV-irradiated skin have provided new evidence that not only activated dendritic cells were present, but a population of B cells also responded by increasing in size and expressing antimajor histocompatibility complex II but not costimulatory molecules, a phenotype suggestive of immune suppression (Byrne and Halliday 2005). The B cells inhibited antigen presentation by the dendritic cells and could transfer the UVB-induced immunosuppression to naïve recipient mice in a manner that was inhibited by a PAF receptor antagonist (Matsumura et al. 2006). Furthermore, UV-stimulated infiltrating mast cells were attracted to the lymph node B cells by an upregulated ligand on the B cell specific for the CXCR4 receptor on the mast cell. Treatment with a CXCR4 antagonist prevented photoimmune suppression, confirming the immunoregulatory importance of the lymph node B cells (Byrne et al. 2008).

63.4.2 Molecular

63.4.2.1 Cytokines and Eicosanoids

The release of specific cytokines by different cell populations in response to the UV damage plays an important role in photoimmune suppression. The balance of Th-1/Th-2 cytokines becomes deranged in UV-irradiated skin, with an abnormal predominance of the suppressive Th-2 cytokines, primarily IL-4 and IL-10 at the expense of the pro-inflammatory Th-1 molecules IL-2, IL-12, and IFN-γ (El-Ghorr and Norval 1997; Rivas and Ullrich 1994). Immunohistochemical staining reveals these soluble mediators are present diffused throughout the UV-irradiated mouse epidermis (Shen et al. 1999), and it is thought that they are released from the UV-damaged keratinocytes, which have been described as "bags of cytokines" susceptible to environmental damage. The repertoire may include IL-12, IL-10, IL-7, IL-15, IL-18, as well as several costimulatory molecules, which contribute to the direction of either Th-1 or Th-2 helper cell responses, but whether human skin responses are the same as those observed in mouse skin remains unclear at present (reviewed in Halliday and Rana 2007).

It is not clear whether *cis*-urocanic acid itself can affect cytokine production in the skin. In murine keratinocytes, there was no evidence of cytokine induction at the protein level by *cis*-urocanic acid, although mRNA for IL-10 and TNFα was induced (Redondo et al. 1996; Zac-Prelich et al. 2001). Certainly, *cis*-urocanic acid has been shown to initiate the transcription of genes for TNFα, IL-6, IL-8, as well as the pro-inflammatory transcription factor NFκB, and enzymes of lipid peroxidation, in primary human keratinocytes (Kaneko et al. 2008). Serum levels of various cytokines are also modulated following UV exposure in mice, although this may not be true for humans (McLoone et al. 2004; Shreedhar et al. 1998).

The hallmark of the photoimmune suppressed state is the upregulated Th-2 cytokine IL-10 (Rivas and Ullrich 1992, 1994). This cytokine is known to mediate immune suppression in many tissues and

to play an important natural role in the conclusion of inflammatory reactions in the body. However, when overexpressed, or not counterbalanced by Th-1 expression such as functional IL-12, immune suppression prevails. It is relevant that exogenous IL-12 can prevent photoimmune suppression in mice (Schmitt et al. 2000; Schwarz et al. 1996). Importantly, it is also apparent that IL-12 can induce DNA repair (Schwarz et al. 2002), and this is via nucleotide excision repair because it does not occur in NER-deficient mice (De Vries et al. 1995; Schwarz et al. 2005). Possibly, the LCs are the targets for IL-12, because DNA-damaged LC numbers migrating to the regional lymph nodes were reduced by IL-12 injection in mice (Schwarz et al. 2005).

In addition to the altered cytokine profile, there is a major contribution to photoimmune suppression by the inflammatory prostaglandins such as PGE2. Synthesis of such eicosanoids is activated by UV irradiation, following the rapid production of the oxidized phospholipid product and inflammatory mediator PAF, the upregulation of phospholipase A, and the release of the precursor arachidonic acid from cutaneous cell membrane phospholipids. The production of IL-4 and IL-10 follows with the outcome of immunosuppression from this cascade (Shreedhar et al. 1998). In mice, treatment with PAF antagonists, or with nonsteroidal anti-inflammatory drugs that inhibit the cyclooxygenase that catalyzes PGE2 synthesis from arachidonic acid, also inhibits immunosuppression by UVB or *cis*-urocanic acid (Jaksic et al. 1995; Walterscheid et al. 2002), and reduces the severity of photocarcinogenesis induced in mice (Fischer et al. 1999; Pentland et al. 1999; Reeve et al. 1995; Sreevidya et al. 2008).

63.4.3 Convergence of DNA Damage and *cis*-Urocanic Acid Pathways

It has been pointed out (Sreevidya et al. 2010) that repairing UV-induced CPDs with exogenous T4N5 endonuclease, neutralizing *cis*-urocanic acid, blocking the PAF receptor, and blocking *cis*-urocanic acid binding to the 5-HT receptor, all prevent photoimmune suppression in mice. In contrast, treating mice with PAF, 5-HT, or *cis*-urocanic acid, each induces immunosuppression. When PAF or 5-HT pathways were blocked with receptor antagonists in UV-irradiated mice, and the major DNA lesions induced by the UV were assessed, it was found that there was a delayed and significant reduction in the numbers of CPDs, in the second most relevant DNA lesion, the 6,4-photoproduct, and in the oxidized lesion 8-oxo-dG. This finding was the first evidence that UV-induced immunosuppressive factors, PAF and *cis*-urocanic acid, can inhibit DNA repair, apparently by inducing oxidative stress, and it also provides a mechanism for the established protection against photocarcinogenesis by the inhibition of *cis*-urocanic acid activity. However, these new data must be considered together with the also new but contrary evidence that endogenous urocanic acid may photoprotectively inhibit epidermal DNA damage in the mouse (Barresi et al. in press). Obviously, there is a need for clarification here.

63.5 Wavelength Dependence

63.5.1 UVA versus UVB

Terrestrial solar UV radiation has been arbitrarily divided into the UVB (290–320 nm) and UVA (320–400 nm) wavebands, with UVA further defined as UVAI (340–400 nm) and UVAII (320–340 nm). Experimental UV sources can be used to produce selected spectral regions by the use of optical filters, and even narrow bandwidth regions that have been used to establish action spectra, or the critical wavelengths, for various UV-induced pathologies like erythema, DNA damage, and cancer induction. However, defining the wavelengths responsible for photoimmune suppression remains a controversial issue. While there is no argument that the UVB waveband is immunosuppressive, the role of the longer wavelength UVA is less clear. In mice and humans, there is much conflicting evidence as to whether UVA is immunosuppressive, and several reviews have attempted to rationalize the data but without overall success (Damian et al. 2001; Halliday et al. 2004; Phan et al. 2006; Reeve and Tyrrell 2007; Ullrich 2005). The issue for humans is important from a sun protection perspective, since the design

of an ideal sunscreen depends on the knowledge not only of the inflammatory burning wavelengths (agreed to be UVB), which do match the action spectrum for cancer induction at least in mice, but also those causing immunosuppression. Many studies in mice and humans have compared photoimmune responses after irradiation through sunscreens of different UV-absorbing properties, and there is general consensus that sunscreen protection from UVA as well as UVB radiation is necessary for optimal inhibition of immunosuppression (Damian et al. 1997; Fourtanier et al. 2008; Moyal and Fourtanier 2008). However, there exists significant contrary evidence from mice and humans that, in fact, UVA may not be immunosuppressive.

The recall antigen responses in nickel-sensitive UV-irradiated humans were reported to differ according to waveband, UVB being dose dependently suppressive, while UVA suppression was detected only transiently (Damian et al. 2001). In mice, the UVA content of minimally erythemogenic solar-simulated UV radiation did not suppress CHS or DTH, although fractionating the UVA dose unexpectedly acquired suppressive properties that are difficult to explain (Byrne et al. 2002, 2006). Interestingly, when the activation of lymph node B cells was the measure of immune response in mice, UVB was suppressive but UVA remained innocuous (Byrne et al. 2005). Recent mouse studies attribute UVA immunosuppression to the UVAII band and claim that the longer wavelength UVAI is immunologically innocuous (Ullrich 2007). This observation is consistent with evidence in human volunteers showing that while UVB suppressed LC-mediated antigen presentation, UVAI was innocuous (Dittmar et al. 1999), and these studies raise the question of the accuracy of experimental divisions into UVA and UVB regions of what is a continuous solar UV spectrum. Further problems arise from the demonstrated genetic dependence in wavelength-dependent immune response observed between mouse strains (Byrne et al. 2002), and the different methods for assessing immune function, which may target different phases of the immune response that need not all be affected in the same manner.

63.5.2 UVA/UVB Interactions

Interesting waveband interactions have been observed in mice to modulate the photoimmune response. In an early report in haired C3H mice, it was observed that the power of different broadband laboratory UV radiation sources to suppress CHS was reduced as the UVA content of these sources increased (Roberts et al. 1996). The UVA and UVB wavebands were separately shown to induce the expression of different cytokines in human keratinocytes (Kondo 1999) and also in the hairless mouse epidermis, in which an immunohistochemical study found that the UVB-induced upregulation of IL-10 was reversed if an exposure to UVA followed (Shen et al. 1999). This was later correlated with the modulation of immune function by UVA radiation, which was shown to provide a dose-dependent protective effect against UVB- or *cis*-urocanic acid–induced suppression of CHS (reviewed in Reeve and Tyrrell 2007). Furthermore, immunologically innocuous exposure to UVA in haired mice was found to protect against UVB-induced immune tolerance (Byrne et al. 2002, 2006), and this was associated with the UVA inhibition of the UVB-increased expression of IL-10 mRNA (Stapelberg et al. 2009).

63.5.3 Role of Heme Oxygenase-1

The powerful induction of the stress protein heme oxygenase-1 (HO-1) in UVA-irradiated primary human skin fibroblasts (Tyrrell 1991) suggested that HO-1 might have immunological relevance. It was found that the photoimmune protective doses of UVA radiation also induce HO-1 activity in mouse skin (Reeve and Tyrrell 1999; Allanson and Reeve 2004), and at least one of its enzymatic products, gaseous carbon monoxide, plays a major role in the mouse skin in protecting against photoimmune suppression (Allanson and Reeve 2005). A pathway of UVA-induced cutaneous biochemistry has been revealed showing that the HO-1-produced carbon monoxide acts via the enzyme soluble guanylyl cyclase. Its product, cyclic guanosine monophosphate (cGMP), accumulates in UVA-irradiated skin, and the levels in the skin dose dependently determine the photoimmune protection. Inhibition of the

normal phosphodiesterase (PDE)-catalyzed degradation of cGMP in the skin by topical application of the PDE-5 inhibitor sildenafil was photoimmune protective. Furthermore, mimicking the UVA-induced enzymatic production of carbon monoxide by topical application of a carbon monoxide-releasing molecule to the irradiated skin of mice reduced the severity of photocarcinogenesis (Allanson and Reeve 2007). Since HO-1 induction is a response not only to UVA radiation, but many endogenous and environmental stressors, it is of interest that treating mice with short-term physiological stress (involuntary restraint) during a photocarcinogenesis induction protocol was also recently reported to reduce the severity of the tumor outcome in an immune-protected manner (Dhabar et al. 2010).

The UVA photoimmune protective effect is active in solar-simulated radiation by its UVA component and is UVA dose dependent (Allanson et al. 2006) within a dose window equivalent to the UVA component of approximately 1–6 h of sunlight. Larger UVA doses then become immunosuppressive additively with the UVB (Reeve et al. 2006). The UVA content has been shown to attenuate cutaneous DNA damage and apoptosis in a HO-dependent manner in hairless mice (Ibuki et al. 2007). It remains to be seen whether such waveband interactions also apply to humans, who are prone to prolong their recreational sunlight exposure after using topical sunscreens and thus to absorb disproportionately high amounts of UVA radiation. Waveband interactions will have an important input into future sunscreen design if the UVA waveband is found to have the same advantageous properties that might protect not only mice but humans against sunlight-induced skin cancer development.

63.6 Photoimmune Protection (Non-Sunscreen)

63.6.1 Repair of DNA Damage

It has been demonstrated that treatment of UV-damaged skin with liposomally encapsulated DNA repair enzymes can reverse photoimmune suppression. Both the T4N5 endonuclease and the photolyase photoreactivating enzyme have been used successfully in humans in this way, with considerable advantage particularly for *xeroderma pigmentosum* patients who are genetically deficient in these pathways (Ke et al. 2008; Kuchel et al. 2005; Stege et al. 2000; Wolf et al. 2000).

63.6.2 Bioactive Phytochemicals

Many plant-derived extracts, or purified single phytochemicals, often substances long recognized in traditional medicine, have been reported to have photoimmune protective characteristics, and in numerous reports also to reduce the development of skin cancers. Most frequently, such extracts have powerful antioxidant potential, and their photoimmune protective properties have been demonstrated to be a function of these properties. The active compounds are commonly but not exclusively polyphenolic flavonoids like *Camellia* sp. (green tea), or isoflavones (genistein and daidzein) or proanthocyanidins (grape seed) that possess innate antioxidant activity due to their polyhydroxy molecular structure, but other extracts rich in sulfhydryl groups as in *Allium* sp. (garlic), or in glycated polysaccharides (tamarind and goji berry; Strickland 2001) have shown immunoprotective activity. The antioxidant vitamins C and E have also been demonstrated to protect against photoimmune suppression (Nakamura et al. 1997; Yuen and Halliday 1997), and recently, a further vitamin, nicotinamide (vitamin B3), has also shown photoimmune protection from topical or oral administration in mice and humans (Damian 2010). A number of comprehensive reviews have been written (Afaq et al. 2005; Katiyar 2005, 2007; Katiyar et al. 2001; Nichols and Katiyar 2010; Reeve 2001). Traditional Chinese medicine provided historic evidence for multiple health benefits in humans of *Lycium barbarum*, the goji berry, and a new report describes the photoimmune protection of goji berry juice consumption in mice (Reeve et al. 2010). This effect may be related to the report of photoimmune protection in humans supplemented with oral probiotic bacteria (Peguet-Navarro et al. 2008), since glycated cell wall polysaccharides appear to be common ingredients to each and have been shown to have relevant health benefits from at least the goji berry.

Complex extracts such as Pycnogenol, a standardized extract from the bark of the French maritime pine *Pinus pinaster,* and Propolis, the waxy honey-bee product, have also been found to afford photoimmune protection in mice from topical application (Cole et al. 2010; Sime and Reeve 2004).

63.6.3 Inducible Antioxidant Pathways

The skin, like other tissues, is well protected against moderate oxidative stress by radical scavenging molecules and enzymes like glutathione, glutathione peroxidase and reductase, catalase, and superoxide dismutase. In addition, two significant inducible responders have been shown to be important photoimmune regulators.

63.6.3.1 Metallothionein

This cysteine-rich protein, best known for its heavy metal chelating properties, also responds robustly to inflammatory cytokines and reactive oxygen and nitrogen species (Hanada et al. 1992). In the skin of mice and humans, it is induced by UVB radiation in the basal and suprabasal epidermal keratinocytes and also in dermal fibroblasts (Ablett et al. 2003; Nishimura et al. 2000). Its photoimmune protective role was shown in metallothionein gene knockout mice, which displayed an exacerbated suppression of CHS by either UV radiation or *cis*-urocanic acid (Reeve et al. 2000). Furthermore, the photoimmune properties of isoflavones or of goji berry juice in mice were reduced in the metallothionein-deficient mice, indicating the significant protective role of this molecule (Reeve et al. 2010; Widyarini et al. 2006a).

63.6.3.2 Heme Oxygenase-1

This stress enzyme, also recognized as heat shock protein-32 in humans, is highly inducible by UVA, but not UVB, in the skin. The gene is activated under many stressful conditions such as hyperoxia, hypoxia, heat, inflammation, heavy metal toxicity, by signaling via transcription factors Nrf2 and AP-1, or by its enzymatic substrate heme. Its inducibility particularly by the UVA waveband has been shown to inhibit photoimmune suppression in mice, as discussed in Section 63.5.3. The immediate products of the enzymatic activity are equimolar amounts of biliverdin, carbon monoxide, and ferrous iron. The fate of the free iron may be important, particularly in conditions of overexpression constitutively, but lack of inducibility, of HO-1 activity, such as have been reported in IL-6-deficient mice, and also in Er-β gene knockout mice (Reeve et al. 2008, 2009).

63.6.4 Estrogen Receptor (Er) Signaling

An interesting series of studies in mice treated topically with an isoflavone, equol, which is related to the primary isoflavone genistein, reported dose-dependent protection from photoimmune suppression of CHS and from photocarcinogenesis (Widyarini et al. 2001, 2005), and supportive evidence for photoimmune protection by equol in humans followed (Friedmann et al. 2004; Widyarini et al. 2006a). It was assumed that this compound, like most flavonoids, was acting as an antioxidant. However, the class of isoflavones is also recognized as phytoestrogenic, and it transpires that equol's photoimmune protective effect could be abrogated by Er blockade in mice (Widyarini et al. 2006b). Thus, a natural photoimmune regulatory role for Er signaling was revealed. Further studies have reported that it is the nonclassical Er-β that plays this role (Cho et al. 2008), and that modulation of the epidermal cytokine pattern is consistent with the protection of the CHS response from UV radiation by Er-β signaling. In Er-β gene knockout mice, there is exacerbated sensitivity to UV-induced erythema, suppression of CHS, and accelerated growth of transplanted skin tumors (Cho et al. 2010). Recent supportive evidence describes significant protection against photocarcinogenesis induction in hairless Skh:hr-1 mice by topical treatment with an Er-β agonist, which also inhibited malignant progression of the tumors, reduced the UV-activation of the mitogen activated protein kinase (MAPK) pathway, and repressed the expression of the proliferation markers proliferating cell nuclear antigen (PCNA), cyclin D1, and vascular endothelial growth factor (VEGF) (Singh et al. 2010).

In a further study, it has been found that the Er-β gene knockout mice have lost the capacity for HO-1 induction in response to UVA irradiation. This indicates that the photoimmune protective Er-β signaling relies on the UVA-inducibility of HO-1, the stress enzyme already established as contributing importantly to photoimmune suppression (Reeve et al. 2009). The mechanisms that underlie these interdependent protective pathways now await definition.

63.6.5 Gender Bias

Consistent with the evidence of photoimmune protection afforded by the Er-β, a gender bias in UV responses has been sought in mice and humans. Male mice have been reported to be more susceptible than females to photoimmune suppression (Hiramoto et al. 2004). Male Skh:hr-1 mice have also been reported to be more susceptible than females to photocarcinogenesis induction (Thomas-Ahner et al. 2007), with apparent estrogen protection against tumor progression from benign papilloma to malignant squamous cell carcinoma that was associated with an increase in the Er-α/Er-β ratio and upregulation of cyclin D1 (Mancuso et al. 2009), consistent with the findings of Singh et al. (2010) noted earlier.

These studies have been conducted in mice; however, whether humans also have a gender bias in immune responses to UV radiation remains uncertain. Photoimmune suppression was observed to be greater in men than women volunteers when elicitation of the Mantoux reaction was the immune test (Damian et al. 2008), although a gender bias was not found in a retrospective study that used dinitrochlorobenzene as a contact sensitizer, thus assessing both sensitization and elicitation reactions, but avoiding testing women within 5 days of their menstrual period (Morrissey et al. 2008). In addition, the level of cutaneous urocanic acid, anticipated to indicate the level of photoimmune susceptibility, when restricted by a polymorphism of the cutaneous histidase gene, appears to be associated with development, rather than inhibition, of squamous cell carcinoma particularly in women, and in women taking oral contraceptives (Welsh et al. 2008). This adds complexity to the human data by suggesting an anticancer function for urocanic acid as proposed for mice by Barresi et al. (in press), but in a manner modulated by estrogenic activity.

Nevertheless, substantial epidemiological data indicate that non-melanoma skin cancers (Armstrong and Kricker 2001; Foote et al. 2001; Graelis 2004; Hayes et al. 2007; Ramachandran et al. 2003; Scrivener et al. 2002; Staples et al. 2006), and possibly melanomas (Molife et al. 2001), are more prevalent in men than in women. It is therefore apparent that the potential gender bias in the role of the immune system response to UV radiation needs to be clarified.

63.7 Temporal UV Irradiation Studies

63.7.1 Neonatal UV Exposure

Migrant studies and epidemiological reports have demonstrated that childhood overexposure to sunlight is a major risk factor for skin cancer development later in life (Cooke and Fraser 1985; Khlat et al. 1992; Kricker et al. 1991; Whiteman et al. 2001). Therefore, it has been of interest to examine the neonatal immune response to UV irradiation, as neonatal immunity is relatively immature and is known to be prone to tolerance induction and to the generation of antigen-specific Treg cells that are long-lived and are detectable in the adult. Furthermore, the neonatal skin is resistant to inflammation, and even in response to large UVB doses, fails to develop an acute inflammatory reaction (Wolnicka-Glubisz et al. 2007). Studies of the LC responses to UV exposure in neonatal mice have identified that these cells differ from adult LC, do not express DEC-205 or langerin, have fewer dendrites, and are less efficient in transporting antigen to the draining lymph node (reviewed in Muller et al. 2008). When the draining lymph node cells were analyzed in adult mice after neonatal UV irradiation, an increase in the percentage of Treg cells and B cells was found compared with controls (McGee et al. 2009), consistent with the photoimmune suppressed state. Thus, neonatal UV irradiation results in a tolerogenic phenotype in the adult, and this immune deficit may account for the increased risk of skin cancers developing in adults.

63.7.2 Chronic UV Exposure

Much of our understanding of photoimmunology has come from acute or short-term UV irradiations in mice and humans. Less is known about immune status in chronically UV-irradiated skin. There is evidence in mice and humans that a form of photoadaptation occurs with repeated UV exposures that might be a reflection of the developed epidermal hyperplasia and thickened *stratum corneum* providing a greater physical barrier against the radiation. This adaptive response can then provide enhanced photoprotection against erythema development from a larger UV exposure. However, whether the immune system can also be primed for resistance in such a way remains improbable. An excellent review has summarized the current available evidence (Norval et al. 2008) and shows that only the induction of epidermal DNA damage and erythema, and possibly the infiltration into the skin of macrophages bringing immunosuppressive cytokines, are reduced by continuing UV exposures. Other markers of the photoimmune response such as urocanic acid levels or isomerization, LC persistence, mast cell numbers, or the CHS and DTH reactions have not shown photoadaptation in chronically irradiated skin.

However, in patients who suffer from the common "sun allergy" or polymorphic light eruption (PLE), a resistant photoimmune suppressive reaction to UV radiation has been identified. PLE patients reveal a combination of a dramatic persistence of the epidermal LC after a UVB exposure (Kolgen et al. 1999), a much reduced infiltration of CD11b+ macrophages/monocytes that are contributing producers of immunosuppressive IL-10 (Kang et al. 1994), and a resistance to photoimmune suppression of CHS (reviewed in De Gruijl 2008; Palmer and Friedmann 2004; Van de Pas et al. 2004). The usual therapy for PLE, "UV hardening," consists of a series of mild UV exposures over several weeks in Spring that result in resistance against activation of the PLE symptoms by summer sun exposure, and has been shown not only to increase the patients' resistance against erythema but also to restore the UVB-induced depletion of the LC and the infiltration of the macrophage population (Janssens et al. 2005). Thus, in this disease state, there is evidence that a normalization or photoadaptation of immune function can be induced. It may be significant that females predominate among PLE patients, consistent with their potentially more resistant photoimmune responses.

63.8 Conclusions

As our understanding of photoimmunology has progressed, rather than simplification, increasingly complex pathways and their interactions that regulate this important reaction of the skin to UV radiation have come to light. Multiple cell populations are now known to play a role—LC, T and B cells, mast cells, macrophages, keratinocytes, and more. Multiple modulatory pathways are also now known—DNA lesions, urocanic acid, cytokines, eicosanoids, oxidized lipids, stress proteins, steroid hormone receptors, and enzymes. The challenge now is to clarify whether and how these converge, and which mechanisms predominate for ultimate importance.

Photoimmune suppression is such a well-conserved function of the skin that it has always seemed as if it must have some form of biological advantage. This is now believed to be a protective role against the development of autoimmune responses against self-antigens induced by the UV radiation. However, this comes with the disadvantageous facilitation of the survival and growth of UV-initiated skin tumors. When the balance between these two outcomes is interrupted, either dermatological eruptions occur as in PLE, which can be treated by reinstating the photoimmune suppressive response, or the risk of skin cancer increases. This is well illustrated by the observation that PLE incidence is strongly reduced among skin cancer patients, and that skin cancer is reduced in patients with PLE (Lembo et al. 2008). Thus, the best mode of protection against both skin damage and cancer development might not be by totally inhibiting photoimmune suppression, but by maintaining a healthy balance, were it possible to determine exactly what that might be.

References

Ablett, E., Whiteman, D.C., Boyle, G.M., Green, A.C., and Parsons, P.G. 2003. Induction of metallothionein in human skin by routine exposure to sunlight: Evidence for a systemic response and enhanced induction at certain body sites. *J. Investig. Dermatol.* 120: 318–324.

Afaq, F., Adhami, V.M., and Mukhtar, H. 2005. Photochemoprevention of ultraviolet B signalling and photocarcinogenesis. Review. *Mutat. Res.* 571: 153–173.

Allanson, M., Domanski, D., and Reeve, V.E. 2006. Photoimmunoprotection by UVA (320–400 nm) radiation is determined by UVA dose and is associated with cutaneous cyclic guanosine monophosphate. *J. Investig. Dermatol.* 126: 191–197.

Allanson, M. and Reeve, V.E. 2004. Immunoprotective UVA (320–400 nm) irradiation upregulates heme oxygenase-1 in the dermis and epidermis of hairless mouse skin. *J. Investig. Dermatol.* 122: 1030–1036.

Allanson, M. and Reeve, V.E. 2005. Ultraviolet A (320–400 nm) modulation of ultraviolet B (290–320 nm)-induced immune suppression is mediated by carbon monoxide (CO). *J. Investig. Dermatol.* 124: 644–650.

Allanson, M. and Reeve, V.E. 2007. Carbon monoxide signalling is anti-carcinogenic in the hairless mouse. *Cancer Immunol. Immunother.* 56: 1807–1815.

Applegate, L.S., Ley, R.D., Alcalay, J., and Kripke, M.L. 1989. Identification of the molecular target for the suppression of contact hypersensitivity by ultraviolet radiation. *J. Exp. Med.* 170: 1117–1131.

Armstrong, B.K. and Kricker, A. 2001. The epidemiology of UV-induced skin cancer. *J. Photochem. Photobiol. B Biol.* 63: 8–18.

Barber, L.A., Spandau, D.F., Rathman, S.C. et al. 1998. Expression of the platelet-activating factor receptor results in enhanced ultraviolet B radiation-induced apoptosis in a human epidermal cell line. *J. Biol. Chem.* 273: 18891–18897.

Barresi, C., Stremnitzer, C., Mlitz, V. et al. 2011. Increased sensitivity of histidinemic mice to ultraviolet B radiation suggests a crucial role of endogenous urocanic acid in protection. *J. Investig. Dermatol.* 131: 188–194.

Beissert, S., Ruhlemann, D., Mohammad, D. et al. 2001. IL-12 prevents the inhibitory effects of *cis*-urocanic acid on tumor antigen presentation by Langerhans cells: Implications for photocarcinogenesis. *J. Immunol.* 167: 6232–6238.

Berg, D. and Otley, C.C. 2002. Skin cancer in organ transplant recipients. Epidemiology, pathogenesis and management. *J. Am. Acad. Dermatol.* 47: 1–17.

Bito, T., Ueda, M., Nagano, T., Fujii, S., and Ichihashi, M. 1995. Reduction of ultraviolet-induced skin cancer in mice by topical application of DNA excision repair enzymes. *Photodermatol. Photoimmunol. Photomed.* 11: 9–13.

Byrne, S.N., Ahmed, J., and Halliday, G.M. 2005. Ultraviolet B but not A radiation activates suppressor B cells in draining lymph nodes. *Photochem. Photobiol.* 81: 1366–1370.

Byrne, S.N. and Halliday, G.M. 2005. B cells activated in lymph nodes in response to ultraviolet irradiation or by interleukin-10 inhibit dendritic cell induction of immunity. *J. Investig. Dermatol.* 124: 570–578.

Byrne, S.N., Limon-flores, A.Y., and Ullrich, S.E. 2008. Mast cell migration from the skin to the draining lymph nodes upon ultraviolet irradiation represents a key step in the induction of immune suppression. *J. Immunol.* 180: 4648–4655.

Byrne, S.N., Spinks, N., and Halliday, G.M. 2002. Ultraviolet A irradiation of C57BL/6 mice suppresses systemic contact hypersensitivity or enhances secondary immunity depending on dose. *J. Investig. Dermatol.* 119: 858–864.

Byrne, S.N., Spinks, N., and Halliday, G.M. 2006. The induction of immunity to a protein antigen using an adjuvant is significantly compromised by ultraviolet A radiation. *J. Photochem. Photobiol. B Biol.* 84: 128–134.

Cho, J.-L., Allanson, M., Domanski, D., Arun, S.J., and Reeve, V.E. 2008. Estrogen receptor-beta signaling protects epidermal cytokine expression and immune function from UVB-induced impairment in mice. *Photochem. Photobiol. Sci.* 7: 120–125.

Cho, J.-L., Allanson, M., and Reeve, V.E. 2010. Oestrogen receptor-beta signaling protects against transplanted tumour growth in the mouse. *Photochem. Photobiol. Sci.* 9: 608–614.

Clydesdale, G.J., Dandie, G.W., and Muller, H.K. 2001. Ultraviolet light-induced injury: Immunological and inflammatory effects. *Immunol. Cell Biol.* 79: 547–568.

Cole, N., Sou, P.W., Ngo, A. et al. 2010. Topical "Sydney" Propolis protects against UV radiation-induced inflammation, lipid peroxidation and immune suppression in mouse skin. *Int. Arch. Allergy Immunol.* 152: 87–97.

Cook, K.R. and Fraser, J. 1985. Migrants and death from malignant melanoma. *Int. J. Cancer* 36: 175–178.

Cooper, K.D., Oberhelman, L., Hamilton, T.A. et al. 1992. UV exposure reduces immunization rates and promotes tolerance to epicutaneous antigens in humans—Relationship to dose, CD1a-DR+ epidermal macrophage induction and Langerhans cell depletion. *Proc. Natl. Acad. Sci. USA.* 89: 8497–8501.

Czarnecki, D., Zalcberg, J., Kulinskaya, E., and Kay, T. 1995. Impaired cell-mediated immunity of apparently normal patients who had multiple skin cancers. *Cancer* 76: 228–231.

Damian, D.L. 2010. Photoprotective effects of nicotinamide. *Photochem. Photobiol. Sci.* 9: 578–585.

Damian, D.L., Barnetson, R.S., and Halliday, G.M. 2001. Effects of low-dose ultraviolet radiation on in vivo human cutaneous recall responses. Review. *Australas. J. Dermatol.* 42: 161–167.

Damian, D.L. and Halliday, G.M. 2002. Measurement of ultraviolet radiation-induced suppression of recall contact and delayed-type hypersensitivity in humans. *Methods* 28: 25–33.

Damian, D.L., Halliday, G.M., and Barnetson, R.S. 1997. Broad-spectrum sunscreens provide greater protection against ultraviolet radiation-induced suppression of contact hypersensitivity to a recall antigen. *J. Investig. Dermatol.* 109: 146–151.

Damian, D.L., Patterson, C.R.S., Stapelberg, M. et al. 2008. Ultraviolet radiation-induced immunosuppression is greater in men and prevented by topical nicotinamide. *J. Investig. Dermatol.* 128: 447–454.

Daynes, R.A. and Spellman, C.W. 1977. Evidence for the generation of suppressor cells by UV radiation. *Cell. Immunol.* 31: 182–187.

De Fabo, E.C. and Kripke, M.L. 1979. Dose-response characteristics of immunologic unresponsiveness to UV-induced tumors produced by UV irradiation of mice. *Photochem. Photobiol.* 30: 385–390.

De Fabo, E.C. and Noonan, F.P. 1983. Mechanism of immune suppression by UV irradiation *in vivo*. Evidence for the existence of a unique photoreceptor in skin and its role in photoimmunology. *J. Exp. Med.* 158: 84–98.

De Fine Olivarius, F., Wulf, H.C., Crosby, J., and Norval, M. 1996. The sunscreening effect of urocanic acid. *Photodermatol. Photoimmunol. Photomed.* 12: 95–99.

De Gruijl, F.R. 2008. UV-induced immunosuppression in the balance. *Photochem. Photobiol.* 84: 2–9.

De Vries, A., van Oostrom, C.T., Hofhuis, F.M. et al. 1995. Increased susceptibility to ultraviolet-B and carcinogens of mice lacking the DNA excision repair gene XPA. *Nature* 377: 169–173.

Dhabar, F.S., Saul, A.N., Daugherty, C., Holmes, T.H., Bouley, D.M., and Oberyszyn, T.M. 2010. Short-term stress enhances cellular immunity and increases early resistance to squamous cell carcinoma. *Brain Behav. Immun.* 24: 127–137.

Dittmar, H.C., Weiss, J.M., Termeer, C.C. et al. 1999. In vivo UVA-1 and UVB irradiation differentially perturbs the antigen presenting function of epidermal Langerhans cells. *J. Investig. Dermatol.* 112: 322–325.

El-Ghorr, A.A. and Norval, M. 1997. The role of interleukin-4 in ultraviolet B light-induced immunosuppression. *Immunology* 92: 26–32.

Elmets, C.A., Bergstresser, P.R., Tigelaar, R.E., Wood, P.J., and Streilein, J.W. 1983. Analysis of the mechanism of unresponsiveness produced by haptens painted on skin exposed to low dose ultraviolet radiation. *J. Exp. Med.* 158: 781–794.

Euvrard, S., Kanitakis, J., Decullier, E. et al. 2006. Subsequent skin cancers in kidney and heart transplant recipients after the first squamous cell carcinoma. *Transplantation* 81: 1093–1100.

Fischer, S.M., Lo, H.H., Gordon, G.B. et al. 1999. Chemopreventive activity of celecoxib, a specific cyclooxygenase-2 inhibitor, and indomethacin against ultraviolet light-induced skin carcinogenesis. *Mol. Carcinog.* 25: 231–240.

Fisher, M.S. and Kripke, M.L. 1978. Further studies on the tumor-specific suppressor cells induced by ultraviolet radiation. *J. Immunol.* 121: 1139–1144.

Fisher, M.S. and Kripke, M.L. 1982. Suppressor T-lymphocytes control the development of primary skin cancers in UV-irradiated mice. *Science* 216: 1133–1134.

Foote, J.A., Harris, R.B., Giuliano, A.R. et al. 2001. Predictors for cutaneous basal and squamous cell carcinoma among actinically damaged adults. *Int. J. Cancer* 95: 7–11.

Fourtanier, A., Moyal, D., and Seite, S. 2008. Sunscreens containing the broad-spectrum UVA absorber Mexoryl SX prevent the cutaneous detrimental effects of UV exposure: A review of clinical study results. Review. *Photodermatol. Photoimmunol. Photomed.* 24: 164–174.

Friedmann, A.C., Halliday, G.M., Barnetson, R.S.C. et al. 2004. The topical isoflavonoid NV-07 alpha reduces solar simulated UV-induced suppression of Mantoux reactions in humans. *Photochem. Photobiol.* 80: 416–421.

Gibbs, N.K., Tye, J., and Norval, M. 2008. Recent advances in urocanic acid photochemistry, photobiology and photoimmunology. *Photochem. Photobiol. Sci.* 7: 655–667.

Gilmour, J.W., Norval, M., Simpson, T.J., Neuvonen, K., and Pasanen, P. 1993. The role of histamine-like receptors in immunosuppression induced by *cis*-urocanic acid. *Photodermatol. Photoimmunol. Photomed.* 9: 250–254.

Graelis, J. 2004. The risk and risk factors of a second non-melanoma skin cancer: A study in a Mediterranean population. *J. Eur. Acad. Dermatol. Venereol.* 18: 142–147.

Grimbaldeston, M.A., Finlay-Jones, J.J., and Hart, P.H. 2006. Mast cells in photodamaged skin: What is their role in skin cancer? *Photochem. Photobiol. Sci.* 5: 177–183.

Grimbaldeston, M.A., Simpson, A., Finlay-Jones, J.J., and Hart, P.H. 2003. The effect of ultraviolet radiation exposure on the prevalence of mast cells in human skin. *Br. J. Dermatol.* 148: 300–306.

Gutierrez-Dalmau, A. and Campistol, J.M. 2007. Immunosuppressive therapy and malignancy in organ transplant recipients: A systematic review. *Drugs* 67: 1167–1198.

Halliday, G.M., Byrne, S.N., Kuchel, J.M., Poon, T.S., and Barnetson, R.S. 2004. The suppression of immunity by ultraviolet radiation: UVA, nitric oxide and DNA damage. Review. *Photochem. Photobiol. Sci.* 3: 736–740.

Halliday, G.M. and Rana, S. 2007. The effects of solar radiation on the immune response in humans. In *Biophysical and Physiological Effects of Solar Radiation on Human Skin*, ed. P.U. Giacomoni, pp. 127–163. Cambridge, U.K.: Royal Society of Chemistry.

Hanada, K., Baba, T., Hashimoto, I., Fukui, R., and Watanabe, S. 1992. Possible role of cutaneous metallothionein in protection against photo-oxidative stress—Epidermal localization and scavenging activity for superoxide and hydroxyl radicals. *Photodermatol. Photoimmunol. Photomed.* 9: 209–213.

Hanneman, K.K., Cooper, K.D., and Baron, E.D. 2006. Ultraviolet immunosuppression: Mechanisms and consequences. *Dermatol. Clin.* 24: 19–25.

Hart, P.H., Grimbaldeston, M.A., and Finlay-Jones, J.J. 2001. Sunlight, immunosuppression and skin cancer: Role of histamine and mast cells. Review. *Clin. Exp. Pharmacol. Physiol.* 28: 1–8.

Hart, P.H., Grimbaldeston, M.A., Swift, G.J., Hosszu, E.K., and Finlay-Jones, J.J. 1999. A critical role for dermal mast cells in *cis*-urocanic acid-induced systemic suppression of contact hypersensitivity responses in mice. *Photochem. Photobiol.* 70: 802–812.

Hart, P.H., Townley, S.L., Grimbaldeston, M.A., Khalil, Z., and Finlay-Jones, J.J. 2002. Mast cells, neuropeptides, histamine and prostaglandins in UV-induced systemic immunosuppression. *Methods (Duluth)* 28: 79–89.

Hayes, R.C., Leonfellner, S., Pilgrim, W., Liu, J., and Keeling, D.N. 2007. Incidence of nonmelanoma skin cancer in New Brunswick, Canada, 1992 to 2001. *J. Cutan. Med. Surg.*11: 45–52.

Hiramoto, K., Tanaka, H., Yanagihara, N. et al. 2004. Effect of 17-beta-estradiol on immunosuppression induced by ultraviolet B irradiation. *Arch. Dermatol. Res.* 295: 307–311.

Ibuki, Y., Allanson, M., Dixon, K.M., and Reeve, V.E. 2007. Radiation sources providing increased UVA/UVB ratios attenuate the apoptotic effects of the UVB waveband UVA dose-dependently in hairless mouse skin. *J. Investig. Dermatol.* 127: 2236–2244.

IJland, S.A., Noonan, F.P., Ceryak, S. et al. 1998. Urocanic acid does not photobind to DNA in mice irradiated with immunosuppressive doses of UVB. *Photochem. Photobiol.* 67: 222–226.

Jaksic, A., Finlay-Jones, J.J., Watson, C.J., Spencer, L.K., Santucci, I., and Hart, P.H. 1995. *Cis*-Urocanic acid synergizes with histamine for increased PGE2 production by human keratinocytes: Link to indomethacin-inhibitable UVB-induced immunosuppression. *Photochem. Photobiol.* 61: 303–309.

Janssens, A.S., Pavel, S., Out-Luiting, J.J., Willemze, R., and de Gruijl, F.R. 2005. Normalized ultraviolet (UV) induction of Langerhans cell depletion and neutrophil infiltrates after artificial UVB hardening of patients with polymorphic light eruption. *Br. J. Dermatol.* 152: 1268–1274.

Kammeyer, A., Gaarsen, J., Sleijffers, A. et al. 2004. Suppression of different phases of systemic contact hypersensitivity by urocanic acid oxidation products. *Photochem. Photobiol.* 80: 72–77.

Kammeyer, A., Pavel, S., Asghar, S.S., Bos, J.D., and Teunissen, B.M. 1997. Prolonged increase of *cis*-urocanic levels in human skin and urine after single total-body ultraviolet exposures. *Photochem. Photobiol.* 65: 593–598.

Kaneko, K., Smetana-Just, U., Matsui, M. et al. 2008. *Cis*-Urocanic acid initiates gene transcription in primary human keratinocytes. *J. Immunol.* 181: 217–224.

Kaneko, K., Travers, J.B., Matsiu, M.S., Young, A.R., Norval, M., and Walker, S.L. 2009. *Cis*-Urocanic acid stimulates primary human keratinocytes independently of serotonin or platelet-activating factor receptors. *J. Investig. Dermatol.* 129: 2567–2573.

Kang, J., Hammerberg, C., Meunier, L., and Cooper, K.D. 1994. CD11b+ macrophages that infiltrate human epidermis after in vivo ultraviolet exposure potently produce IL-10 and represent the major secretory source of epidermal IL-10 protein. *J. Immunol.* 153: 5256–5264.

Katiyar, S.K. 2005. Silymarin and skin cancer prevention: Anti-inflammatory, antioxidant and immunomodulatory effects. *Int. J. Oncol.* 26: 169–176.

Katiyar, S.K. 2007. UV-induced immune suppression and photocarcinogenesis: Chemoprevention by dietary botanical agents. Review. *Cancer Lett.* 255: 1–11.

Katiyar, S.K., Bergamo, B.M., Vyalil, P.K., and Elmets, C.A. 2001. Green tea polyphenols: DNA photodamage and photoimmunology. Review. *J. Photochem. Photobiol. B Biol.* 65: 109–114.

Ke, M.S., Camouse, M.M., Swain, F.R. et al. 2008. UV protective effects of DNA repair enzymes and RNA lotion. *Photochem. Photobiol.* 84: 180–184.

Kelly, D.A., Walker, S.L., McGregor, J.M., and Young, A.R. 1998. A single exposure to solar simulated radiation suppresses contact hypersensitivity responses both locally and systemically in humans: Quantitative studies with high frequency ultrasound. *J. Photochem. Photobiol. B Biol.* 44: 130–142.

Kelly, D.A., Young, A.R., McGregor, J.M., Seed, P.T., Potten, C.S., and Walker, S.L. 2000. Sensitivity to sunburn is associated with susceptibility to ultraviolet radiation-induced suppression of cutaneous cell-mediated immunity. *J. Exp. Med.* 191: 561–566.

Khalil, Z., Townley, S.L., Grimbaldeston, M.A., Finlay-Jones, J.J., and Hart, P.H. 2001. *Cis*-Urocanic acid stimulates neuropeptide release from peripheral sensory nerves. *J. Investig. Dermatol.* 117: 886–891.

Khlat, M., Vail, A., Parkin, M., and Green, A. 1992. Mortality from melanoma in migrants to Australia: Variation by age at arrival and duration of stay. *Am. J. Epidemiol.* 135: 1103–1113.

Kolgen, W., Van Weelden, H., Den Hengst, S. et al. 1999. CD11b+ cells and ultraviolet B-resistant CD1a+ cells in skin of patients with polymorphic light eruption. *J. Investig. Dermatol.* 113: 4–10.

Kondo, S. 1999. The role of keratinocyte-derived cytokines in the epidermis and their possible responses to UVA-irradiation. *J. Investig. Dermatol. Symp. Proc.* 4(2): 177–183.

Kricker, A., Armstrong, B.K., English, D.R., and Heenan, P.J. 1991. Pigmentary and cutaneous risk factors for non-melanocytic skin cancer—A case-control study. *Int. J. Cancer* 48: 650–662.

Kripke, M.L. 1974. Antigenicity of murine skin tumors induced by UV light. *J. Natl. Cancer Inst.* 53: 1333–1336.

Kripke, M.L., Cox, P.A., Alas, L.G., and Yarosh, D.B. 1992. Pyrimidine dimers in DNA initiate systemic immunosuppression in UV-irradiated mice. *Proc. Natl. Acad. Sci. USA.* 89: 7516–7520.

Kuchel, J.M., Barnetson, R.S.C., and Halliday, G.M. 2005. Cyclobutane pyrimidine dimer formation is a molecular trigger for solar-simulated ultraviolet radiation-induced suppression of memory immunity in humans. *Photochem. Photobiol. Sci.* 4: 577–582.

Lambert, R.W. and Granstein, R.D. 1998. Neuropeptides and Langerhans cells. *Exp. Dermatol.* 7: 73–80.

Lembo, S., Fallon, J., O'Kelly, P., and Murphy, G.M. 2008. Polymorphic light eruption and skin cancer prevalence: Is one protective against the other? *Br. J. Dermatol.* 159: 1342–1347.

Ley, R.D., Applegate, L.A., Fry, R.J., and Sanchez, A.B. 1991. Photoreactivation of ultraviolet radiation-induced skin and eye tumors of *Monodelphis domestica. Cancer Res.* 51: 6539–6542.

Ley, R.D., Reeve, V.E., and Kusewitt, D.F. 2000. Photobiology of *Monodelphis domestica. Dev. Comp. Immunol.* 24: 503–516.

Loser, K. and Beissert, S. 2009. Regulation of cutaneous immunity by the environment: An important role for UV irradiation and vitamin D. *Int. Immunopharm.* 9: 587–589.

Loser, K., Mehling, A., Loser, S. et al. 2006. Epidermal RANKL controls regulatory T-cell numbers via activation of dendritic cells. *Nat. Med.* 12: 1372–1379.

Loser, K., Scherer, A., Krummen, M.B.W. et al. 2005. An important role of CD80/CD86-CTLA-4 signaling during photocarcinogenesis in mice. *J. Immunol.* 174: 5298–5305.

Mancuso, M., Gallo, D., Leonardi, S. et al. 2009. Modulation of basal and squamous cell carcinoma by endogenous estrogen in mouse models of skin cancer. *Carcinogenesis* 30: 340–347.

Marathe, G.K., Johnson, C., Billings, M.D. et al. 2005. Ultraviolet B radiation generates platelet activating factor-like phospholipids underlying cutaneous damage. *J. Biol. Chem.* 280: 35448–35457.

Matheson, M.J. and Reeve, V.E. 1991. The effect of the antihistamine cimetidine on ultraviolet radiation-induced tumorigenesis in the hairless mouse. *Photochem. Photobiol.* 53: 639–642.

Matsumura, Y., Byrne, S.N., Ngheim, D.X., Miyahara, Y., and Ullrich, S.E. 2006. A role for inflammatory mediators in the induction of immunoregulatory B cells. *J. Immunol.* 177: 4810–4817.

McGee, H.M., Dharmadasa, T., and Woods, G.M. 2009. Solar simulated ultraviolet radiation damages murine neonatal skin and alters Langerhans cell development, but does not induce inflammation. *Photochem. Photobiol. Sci.* 8: 881–886.

McGlade, J.P., Gorman, S., Lenzo, J.C. et al. 2007. Effect of both ultraviolet B irradiation and histamine receptor function on allergic responses to an inhaled antigen. *J. Immunol.* 178: 2794–2802.

McLoone, P., Man, I., and Yule, S. et al. 2004. Whole body UVB (TL-01) or UVA-1 irradiation does not alter the levels of immunomodulatory cytokines in the serum of human volunteers. *Photodermatol. Photoimmunol. Photomed.* 20: 76–80.

McLoone, P., Simics, E., Barton, A., Norval, M., and Gibbs, N.K. 2005. An action spectrum for the production of *cis*-urocanic acid in human skin in vivo. *J. Investig. Dermatol.* 124: 1071–1074.

Mitra, R.S., Shimizu, Y., and Nickoloff, B.J. 1993. Histamine and *cis*-urocanic acid augment tumour necrosis factor-alpha mediated induction of keratinocyte intercellular adhesion molecule-1 expression. *J. Cell Pathol.* 156: 348–357.

Mohammad, T., Morrison, H., and Hogenesch, H. 1999. Urocanic acid photochemistry and photobiology. *Photochem. Photobiol.* 69: 115–135.

Moodycliffe, A.A., Bucana, C.D., Kripke, M.L., Norval, M., and Ullrich, S.E. 1996. Differential effects of a monoclonal antibody to *cis*-urocanic acid on the suppression of delayed and contact hypersensitivity following ultraviolet irradiation. *J. Immunol.* 157: 2891–2899.

Moodycliffe, A.M., Ngheim, D., Clydesdale, G., and Ullrich, S.E. 2000. Immune suppression and skin cancer development: Regulation by NKT cells. *Nat. Immunol.* 1: 521–525.

Molife, R., Lorigan, P., and MacNeil, S. 2001. Gender and survival in malignant melanoma. *Cancer Treat. Rev.* 27: 201–209.

Morrison, H., Bernasconi, C., and Pandey, G. 1983. Urocanic acid photobiology. Photocycloaddition of *N,N*-dimethylthymine to urocanic acid. *Photochem. Photobiol.* 38: 23–27.

Morrissey, K., Xue, W., Cooper, K., and Baron, E. 2008. Age and gender effects on contact sensitization and photoimmune suppression in young and middle-aged adults. *Photodermatol. Photoimmunol. Photomed.* 24: 46–48.

Moyal, D. and Fourtanier, A. 2008. Broad-spectrum sunscreens provide better protection from solar ultraviolet-simulated radiation and natural sunlight-induced immunosuppression in human beings. Review. *J. Am. Acad. Dermatol.* 58 (suppl.): S149–S154..

Muller, H.K., Malley, R.C., McGee, H.M., Scott, D.K., Wozniak, T., and Woods, G.M. 2008. Effect of UV radiation on the neonatal skin immune system—Implications for melanoma. *Photochem. Photobiol.* 84: 47–54.

Nakamura, T., Pinnell, S.R., Darr, D. et al. 1997. Vitamin C abrogates the deleterious effects of UVB radiation on cutaneous immunity by a mechanism that does not depend on TNF-alpha. *J. Investig. Dermatol.* 109: 20–24.

Nichols, J.A. and Katiyar, S.K. 2010. Skin photoprotection by natural polyphenols: Anti-inflammatory, antioxidant and DNA repair mechanisms. Review. *Arch. Dermatol. Res.* 302: 71–83.

Nishimura, N., Reeve, V.E., Nishimura, H., Satoh, M., and Tohyama, C. 2000. Cutaneous metallothionein induction by ultraviolet B irradiation in interleukin-6 null mice. *J. Investig. Dermatol.* 114: 343–348.

Noonan, F.P. and De Fabo, E.C. 1990. Dose-response curves for local and systemic immunosuppression are identical. *Photochem. Photobiol.* 52: 801–810.

Noonan, F.P. and De Fabo, E.C. 1992. Immunosuppression by ultraviolet B radiation: Initiation by urocanic acid. *Immunol. Today* 13: 250–254.

Norval, M. 2006. The mechanisms and consequences of ultraviolet-induced immunosuppression. *Prog. Biophys. Mol. Biol.* 92: 108–118.

Norval, M. and El-Ghorr, A. 2002. Studies to determine the immunomodulating effects of *cis*-urocanic acid. *Methods* 28: 63–70.

Norval, M, Gibbs, N.K., and Gilmour, J. 1995. The role of urocanic acid in UVR-induced immunosuppression: Recent advances (1992–1994). *Photochem. Photobiol.* 62: 209–217.

Norval, M., McLoone, P., Lesiak, A., and Narbutt, J. 2008. The effect of chronic ultraviolet radiation on the human immune system. Review. *Photochem. Photobiol.* 84: 19–28.

Palmer, R.A. and Friedmann, P.S. 2004. Ultraviolet radiation causes less immunosuppression in patients with polymorphic light eruption than in controls. *J. Investig. Dermatol.* 122: 291–294.

Peguet-Navarro, J., Dezutter-Dambuyant, C., Buetter, T. et al. 2008. Supplementation with oral probiotic bacteria protects human cutaneous immune homeostasis after UV exposure—Double blind randomized placebo controlled clinical trial. *Eur. J. Dermatol.* 18: 504–511.

Pei, Y., Barber, L.A., Murphy, R.C. et al. 1998. Activation of the epidermal platelet-activating factor receptor results in cytokine and cyclooxygenase-2 biosynthesis. *J. Immunol.* 161: 1954–1961.

Pentland, A.P., Schoggins, J.W., Scott, G.A., Khan, K.N.M., and Han, R.J. 1999. Reduction of UV-induced skin tumors in hairless mice by selective COX-2 inhibition. *Carcinogenesis* 20: 1939–1944.

Phan, T.A., Halliday, G.M., Barnetson, R.S., and Damian, D.L. 2006. Spectral and dose dependence of ultraviolet radiation-induced immunosuppression. Review. *Front. Biosci.* 11: 394–411.

Ramachandran, S., Fryer, A.A., Lovatt, T.J. et al. 2003. Combined effects of gender, skin type and polymorphic genes on clinical phenotype: Use of rate of increase in numbers of basal cell carcinomas as a model system. *Cancer Lett.* 189: 175–181.

Redondo, P., Garcia-Foncillas, J., Cuevillas, F., Espana, A., and Quintanilla, E. 1996. Effects of low concentrations of *cis*- and *trans*-urocanic acid on cytokine elaboration by keratinocytes. *Photoderm. Photoimmunol. Photomed.* 12: 237–243.

Reeve, V.E. 2001. Chemoprevention of photocarcinogenesis. In *Photobiology for the 21st Century*, eds. T.P. Coohill and D.P. Valenzeno, pp. 41–51. Overland Park, KS: Valdenmar Publishing.

Reeve, V.E. 2002. Ultraviolet radiation and the contact hypersensitivity reaction in mice. *Methods* 28: 20–24.

Reeve, V.E., Allanson, M., Arun, S.J., Domanski, D., and Painter, N. 2010. Mice drinking goji berry juice (*Lycium barbarum*) are protected from UV radiation-induced skin damage via antioxidant pathways. *Photochem. Photobiol. Sci.* 9: 601–607.

Reeve, V.E., Allanson, M., Cho, J.-L., Arun, S.J., and Domanski, D. 2009. Interdependence between heme oxygenase-1 induction and estrogen receptor-β signaling mediates photoimmune protection by UVA radiation in mice. *J. Investig. Dermatol.* 129: 2702–2710.

Reeve, V.E., Domanski, D., and Slater, M. 2006. Radiation sources providing increased UVA/UVB ratios induce UVA dose-dependently increased photoprotection in hairless mice. *Photochem. Photobiol.* 82: 406–411.

Reeve, V.E., Greenoak, G.E., Canfield, P.J., Boehm-Wilcox, C., and Gallagher, C. H. 1989. Topical urocanic acid enhances UV-induced tumour yield and malignancy in the hairless mouse. *Photochem. Photobiol.* 49: 459–464.

Reeve, V.E., Matheson, M.J., Bosnic, M., and Boehm-Wilcox, C. 1995. The protective effect of indomethacin on photocarcinogenesis in hairless mice. *Cancer Lett.* 95: 213–219.

Reeve, V.E. and Mitchell, L.A. 1991. Hazards of urocanic acid as a cosmetic ingredient. *Photoderm. Photoimmunol. Photomed.* 8: 176–180.

Reeve, V.E., Nishimura, N., Bosnic, M., Michalska, A.E., and Choo, K.H. 2000. Lack of metallothionein-I and -II exacerbates the immunosuppressive effect of ultraviolet B radiation and *cis*-urocanic acid in mice. *Immunology* 100: 399–404.

Reeve, V.E. and Tyrrell, R.M. 1999. Heme oxygenase induction mediates the photoimmunoprotective activity of UVA radiation in the mouse. *Proc. Natl. Acad. Sci. USA* 96: 9317–9321.

Reeve, V.E. and Tyrrell, R.M. 2007. UVA and inducible protection. In *Biophysical and Physiological Effects of Solar Radiation on Human Skin*, ed. P. Giacomoni, pp. 293–310. Cambridge, U.K.: Royal Society of Chemistry.

Reeve, V.E., Tyrrell, R.M., Allanson, M., Domanski, D., and Blyth, L. 2008. The role of interleukin-6 in UVA protection against UVB-induced immunosuppression. *J. Investig. Dermatol.* 129: 1539–1546.

Rivas, J.M. and Ullrich, S.E. 1992. Systemic suppression of DTH by supernatants from UV-irradiated keratinocytes: An essential role for keratinocyte-derived interleukin-10. *J. Immunol.* 149: 3865–3871.

Rivas, J.M. and Ullrich, S.E. 1994. The role of IL-4, IL-10 and TNF-α in the immune suppression induced by ultraviolet radiation. *J. Leukoc. Biol.* 56: 769–775.

Roberts, L.K., Beasley, D.G., Learn, D.B., Giddens, L.D., Beard, J., and Stanfield, J.W. 1996. Ultraviolet spectral energy differences affect the ability of sunscreen lotions to prevent ultraviolet radiation-induced immunosuppression. *Photochem. Photobiol.* 63: 874–884.

Sastry, C.M., Whitmore, S.E., Breysse, P.N., Morison, W.L., and Strickland, P.T. 2005. The effect of clinical UVA/B exposures on urinary urocanic acid isomer levels in individuals with Caucasian (type II/III) skin types. *Dermatol. Online J.* 11: 1.

Schade, N., Esser, C., and Krutmann, J. 2005. Ultraviolet B radiation-induced immunosuppression: Molecular mechanisms and cellular alterations. *Photochem. Photobiol. Sci.* 4: 699–798.

Schmitt, D.A. and Ullrich, S.E. 2000. Exposure to ultraviolet radiation causes dendritic cells/macrophages to secrete immune-suppressive IL-12p40 homodimers. *J. Immunol.* 165: 3162–3167.

Schmitt, D.A., Walterscheid, J.P., and Ullrich, S.E. 2000. Reversal of ultraviolet radiation-induced immune suppression by recombinant IL-12: Suppression of cytokine production. *Immunology* 101: 90–98.

Schwarz, T. 2005. Regulatory T cells induced by ultraviolet radiation. *Int. Arch. Allergy Immunol.* 137: 187–193.

Schwarz, T. 2008. 25 years of UV-induced immunosuppression mediated by T cells—From disregarded T suppressor cells to highly respected regulatory T cells. Review. *Photochem. Photobiol.* 84: 10–18.

Schwarz, A., Grabbe, S., Aragane, Y. et al. 1996. Interleukin-12 prevents ultraviolet B-induced local immunosuppression and overcomes UVB-induced tolerance. *J. Investig. Dermatol.* 106: 1187–1191.

Schwarz, A., Maeda, A., Kernebeck, K., van Steeg, H., Beissert, S., and Schwarz, T. 2005. Prevention of UV radiation-induced immunosuppression by IL-12 is dependent on DNA repair. *J. Exp. Med.* 201: 173–179.

Schwarz, A., Stander, S., Berneburg, M. et al. 2002. Interleukin-12 suppresses ultraviolet radiation-induced apoptosis by inducing DNA repair. *Nat. Cell Biol.* 4: 26–31.

Scrivener, Y., Grosshans, E., and Cribier, B. 2002. Variations of basal cell carcinomas according to gender, age, location and histopathological subtype. *Br. J. Dermatol.* 147: 41–47.

Shen, J., Bao, S., and Reeve, V.E. 1999. Modulation of IL-10, IL-12 and IFN-gamma in the epidermis of hairless mice by UVA (320–400 nm) and UVB (290–320 nm) radiation. *J. Investig. Dermatol.* 113: 1059–1064.

Shen, L. and Ji, H.F. 2009. Molecular basis for *cis*-urocanic acid as a 5-HT(2A) receptor agonist. *Bioorg. Med. Chem. Lett.* 19: 5307–5309.

Shreedhar, V., Giese, T., Sung, V.W., and Ullrich, S.E. 1998. A cytokine cascade including prostaglandin E2, IL-4 and IL-10 is responsible for UV-induced systemic immune suppression. *J. Immunol.* 160: 3783–3789.

Sime, S. and Reeve, V.E. 2004. Protection from inflammation, immunosuppression and carcinogenesis induced by UV radiation in mice by topical Pycnogenol. *Photochem. Photobiol.* 79: 193–198.

Simon, M.M., Aragane, Y., Schwarz, A., Luger, T.A., and Schwarz, T. 1994. UVB light induces a nuclear factor κ (NF-κB) activity independently from chromosomal DNA damage in cell-free cytosolic extracts. *J. Investig. Dermatol.* 102: 422–427.

Singh, T., Kapur, P., Chaudhary, S.C., Elmets, C.A., Kopelovich, L., and Athar, M. 2010. ERB-041, an estrogen receptor beta agonist, inhibits skin photocarcinogenesis in SKH-1 hairless mice. *J. Investig. Dermatol.* 130 (suppl.): S23, abstract 134.

Slominski, A., Pisarchik, A., Zbytek, B., Tobin, D.J., Kauser, S., and Wortsman, J. 2003. Functional activity of serotoninergic and melatoninergic systems expressed in the skin. *J. Cell Physiol.* 196: 144–153.

Sluyter, R. and Halliday, G.M. 2000. Enhanced tumor growth in UV-irradiated skin is associated with an influx of inflammatory cells into the epidermis. *Carcinogenesis* 21: 1801–1807.

Sreevidya, C.S., Fukunaga, A., Khaskhely, N.M. et al. 2010. Agents that reverse UV-induced immune suppression and photocarcinogenesis affect DNA repair. *J. Investig. Dermatol.* 130: 1428–1437.

Sreevidya, C.S., Khaskhely, N.M., Fukunaga, A., Khaskina, P., and Ullrich, S.E. 2008. Inhibition of photocarcinogenesis by platelet-activating factor or serotonin receptor antagonists. *Cancer Res.* 68: 3978–3984.

Stapelberg, M.P., Williams, R.B., Byrne, S.N., and Halliday, G.M. 2009. The alternate complement pathway seems to be a UVA sensor that leads to systemic immunosuppression. *J. Investig. Dermatol.* 129: 2694–2701.

Staples, M.P., Elwood, M., Burton, R.C., Williams, J.L., Marks, R., and Giles, G.G. 2006. Non-melanoma skin cancer in Australia: The 2002 national survey and trends since 1985. *Med. J. Aust.* 184: 6–10.

Steenvoorden, D.P. and van Beijersbergen, H.G. 1999. Protection against UV-induced systemic immunosuppression in mice by a single topical application of the antioxidant vitamins C and E. *Int. J. Radiat. Biol.* 75: 747–755.

Stege, H., Roza, L., Vink, A.A. et al. 2000. Enzyme plus light therapy to repair DNA damage in ultraviolet-B-irradiated human skin. *Proc. Natl. Acad. Sci. USA* 97: 1790–1795.

Strickland, F.M. 2001. Immune regulation by polysaccharides: Implications for skin cancer. *J. Photochem. Photobiol. B Biol.* 63: 132–140.

Thomas-Ahner, J.M., Wulff, B.C., Tober, K.L. et al. 2007. Gender differences in UVB-induced skin carcinogenesis, inflammation and DNA damage. *Cancer Res.* 67: 3468–3474.

Tyrrell, R.M. 1991. UVA (320–380 nm) radiation as an oxidative stress. In *Oxidative Stress: Oxidants and Antioxidants*, ed. H. Sies, pp. 57–83. London: Academic Press.

Ullrich, S.E. 2005. Mechanisms underlying UV-induced immune suppression. Review. *Mutat. Res.* 571: 185–205.

Ullrich, S.E. 2007. Sunlight and skin cancer: Lessons from the immune system. *Mol. Carcinog.* 46: 629–633.

Ullrich, S.E. and Kripke, M.L. 1984. Mechanisms in the suppression of tumor rejection produced in mice by repeated UV irradiation. *J. Immunol.* 133: 2786–2790.

Ullrich, S.E., Ngheim, D.X., and Khaskina, P. 2007. Suppression of an established immune response by UVA—A critical role for mast cells. *Photochem. Photobiol.* 83: 1095–1100.

Van de Pas, C.B., Kelly, D.A., Seed, P.T., Young, A.R., Hawk, J.L., and Walker, S.L. 2004. Ultraviolet radiation-induced erythema and suppression of contact hypersensitivity responses in patients with polymorphic light eruption. *J. Investig. Dermatol.* 122: 295–299.

Veness, M.J., Quinn, D.I., Ong, C.S. et al. 1999. Aggressive cutaneous malignancies following cardiothoracic transplantation. The Australian experience. *Cancer* 85: 1758–1764.

Walterscheid, J.P., Ngheim, D.X., Kazimi, N. et al. 2006. *Cis*-Urocanic acid, a sunlight-induced immunosuppressive factor, activates immune suppression via the 5-HT2A receptor. *Proc. Natl. Acad. Sci. USA* 103: 17420–17425.

Walterscheid, J.P., Ullrich, S.E., and Ngheim, D.X. 2002. Platelet-activating factor, a molecular sensor for cellular damage, activated systemic immune suppression. *J. Exp. Med.* 195: 171–179.

Welsh, M.M., Karagas, M.R., Applebaum, K.M., Spencer, S.K., Perry, A.E., and Nelson, H.H. 2008. A role for ultraviolet radiation immunosuppression in non-melanoma skin cancer as evidenced by gene-environment interactions. *Carcinogenesis* 29: 1950–1954.

Whiteman, D.C., Whiteman, C.A., and Green, A.C. 2001. Childhood sun exposure as a risk factor for melanoma: A systematic review of epidemiologic studies. *Cancer Causes Control* 12: 69–82.

Widyarini, S., Allanson, M., Gallagher, N.L. et al. 2006a. Isoflavonoid photoprotection in mouse and human skin is dependent on metallothionein. *J. Investig. Dermatol.* 126: 198–204.

Widyarini, S., Domanski, D, Painter, N., and Reeve, V.E. 2006b. Estrogen receptor signaling protects against immune suppression by UV radiation exposure. *Proc. Natl. Acad. Sci. USA* 103: 12837–12842.

Widyarini, S., Husband, A.J., and Reeve, V.E. 2005. Protective effect of the isoflavonoid equol against hairless mouse skin carcinogenesis induced by UV radiation alone or with a chemical co-carcinogen. *Photochem. Photobiol.* 81: 32–37.

Widyarini, S., Spinks, N., Husband, A.J., and Reeve, V.E. 2001. Isoflavonoid compounds from red clover (*Trifolium pratense*) protect from inflammation and immune suppression induced by UV radiation. *Photochem. Photobiol.* 74: 465–470.

Wolf, P., Maier, H., Mullegger, R.R. et al. 2000. Topical treatment with liposomes containing T4 endonuclease-V protects human skin in vivo from ultraviolet-induced upregulation of interleukin-10 and tumor necrosis factor-alpha. *J. Investig. Dermatol.* 114: 149–156.

Wolf, P., Ngheim, D.X., Walterscheid, J.P. et al. 2006. Platelet-activating factor is crucial in psoralen and ultraviolet A-induced immune suppression, inflammation and apoptosis. *Am. J. Pathol.* 169: 795–805.

Wolnicka-Glubisz, A., Damsker, J., Constant, S., Corn, S., De Fabo, E., and Noonan, F. 2007. Deficient inflammatory response to UV radiation in neonatal mice. *J. Leukoc. Biol.* 81: 1352–1361.

Woodward, E.S., Prele, C.M., Finlay-Jones, J.J., and Hart, P.H. 2006. The receptor for *cis*-urocanic acid remains elusive. *J. Investig. Dermatol.* 126: 1191–1193.

Yarosh, D., Alas, L.G., Yee, V. et al. 1992. Pyrimidine dimer removal enhanced by DNA repair liposomes reduces the incidence of UV skin cancer in mice. *Cancer Res.* 52: 4227–4231.

Yarosh, D., Bucana, C., Cox, P., Kitibel, J., and Kripke, M.L. 1994. Localization of liposomes containing a DNA repair enzyme in murine skin. *J. Investig. Dermatol.* 103: 461–468.

Yarosh, D., Klein, J., O'Connor, A., Hawk, J., Rafal, E., and Wolf, P. 2001. Effect of topically applied T4 endonuclease V in liposomes on skin cancer in xeroderma pigmentosum: A randomised study. Xeroderma Pigmentosum Study Group. *Lancet* 357: 926–929.

Yoshikawa, T., Rae, V., Bruins-Slot, W., van den Berg, J.W., Taylor, J.R., and Streilein, J.W. 1990. Susceptibility to effects of UVB radiation on contact hypersensitivity as a risk factor for skin cancer in humans. *J. Investig. Dermatol.* 95: 530–536.

Yuen, K.S. and Halliday, G.M. 1997. Alpha-tocopherol, an inhibitor of lipid peroxidation, prevents ultraviolet radiation from suppressing the skin immune system. *Photochem. Photobiol.* 65: 587–592.

Zac-Prelich, M., Norval, M., Venner, T.J. et al. 2001. *Cis*-Urocanic acid does not induce the expression of immunosuppressive cytokines in murine keratinocytes. *Photochem. Photobiol.* 73: 238–244.

64

Photodynamic Therapy

Clare Conway
Photopharmica Ltd.

Stanley B. Brown
University of Leeds and Photopharmica Ltd.

64.1 Introduction and Background

Photodynamic therapy (PDT) is a clinically approved modality that utilizes a photosensitizing compound in conjunction with light and molecular oxygen to produce a localized cytotoxic effect. The photosensitizer is nontoxic in the absence of light. PDT has gained greatest acceptance in the fields of oncology (especially oncological dermatology) and ophthalmology, although other non-oncological and antimicrobial applications have recently begun to be exploited. Specific illumination of the photosensitizer results in the local formation of reactive oxygen species, primarily singlet oxygen, causing a variety of direct and indirect cytotoxic effects on the cellular targets, discussed in more detail in Section 64.2.

Clinical approval has been achieved in the treatment of skin, bladder, lung, head and neck, and esophageal cancers and in certain precancerous conditions (Brown et al., 2004); and the fluorescent properties of photosensitizers can also be used in cancer diagnosis (photodiagnosis). The potential benefits of PDT as an anticancer therapy include its unique targeting mechanisms and the fact that it is relatively noninvasive, induces minimal side effects, is capable of leaving no permanent scarring, and can be administered without lengthy hospital stays. Recent research in the field of oncology has focused on the development of methods by which photosensitizers can be actively targeted to

tumor tissue. PDT is also emerging as an option in the antimicrobial field, for a number of indications, where the potential for a rapid and painless treatment, to which the bacteria are unable to generate resistance, makes it an attractive alternative to antibiotics.

The first reported study of photodynamic action was carried out by Oscar Raab, a German medical student in 1897. He studied the effect of acridine on paramecia and found that light played a role in toxicity. The research group then carried out a number of experiments on photosensitization and discovered that oxygen was also necessary for an effect (described by Moan and Peng, 2003). The first report of human photosensitization was by Friedrich Meyer–Betz in 1913 who tested the effect of hematoporphyrin (on himself) and observed erythema and edema in light-exposed areas. The observation (from fluorescence) that porphyrins exhibit weak selectivity to tumor tissue led to PDT being used as an anticancer treatment, and attention was focused on the identification and purification of suitable photoactive compounds. Hematoporphyrin itself was shown to be a poor PDT agent as it is not effectively retained in tumor tissue. Acetylation and alkaline hydrolysis of hematoporphyrin produces a complicated mixture of mono- and di-acetylated porphyrins and a number of dehydration products. Neutralization of the mixture produces an even more complex mixture of monomers, dimers, and oligomers. This mixture [hematoporphyrin derivative (HpD)] was used in the majority of the early clinical PDT studies including the diagnosis and treatment of bladder cancers. Partial purification and analysis of HpD revealed that the most photoactive component was the oligomeric fraction and an oligomeric-rich HpD preparation was thus produced. This mixture was still complex, consisting of various number of porphyrin molecules linked by ester, ether, and carbon–carbon bonds but it was shown to have improved PDT activity. The mixture was named Photofrin® and, in Canada on April 19, 1993, it became the first photosensitizing compound to receive regulatory approval for clinical use.

A wide variety of conditions have now been successfully treated with Photofrin® including cancers of the bladder and lung. However, Photofrin® has several serious drawbacks as a photosensitizer. The complex mixture is difficult to reproduce exactly. It also shows limited selectivity for tumor tissue and has a low absorption coefficient at tissue-penetrating wavelengths. Patients can also exhibit cutaneous phototoxicity for several weeks after treatment with Photofrin® and so have to avoid strong sunlight. These disadvantages of Photofrin® as a photosensitizer have led to concentrated research into a number of second- and third-generation photosensitizers, discussed further in Section 64.4. Research is aimed at developing pure compounds that exhibit higher selectivity and have greater extinction coefficients at longer wavelengths (to maximize light penetration through tissue and reduce UV sensitivity).

Despite the intense research undertaken with the aim of optimizing PDT as a cancer therapy, perhaps the greatest clinical success to date is that achieved in the field of age-related macular degeneration (AMD). The success of Visudyne in targeting the abnormal blood vessels in AMD patients is discussed further in Section 64.9.

64.2 Photochemistry of PDT

For successful photodynamic treatment, a photon of visible light emitted from a suitable illumination source must be absorbed by a photosensitizer. The photosensitizer is transformed from its ground state (^{0}S) to a short-lived excited singlet state (^{1}S*) (Figure 64.1). The ^{1}S* molecule is very short-lived and rapidly loses its additional energy by either fluorescence, loss of heat (internal conversion) or by undergoing intersystem crossing to form the triplet state (^{3}S*). The photosensitizer in the triplet state is a much longer living molecule and can react in two ways:

- The ^{3}S molecule can react via a type 1 reaction with a cellular substrate. Electron or hydrogen transfer forms a photosensitizer radical (S$^{\bullet}$) and a substrate radical (X$^{\bullet}$). The radicals can then react with each other, further substrates or molecular oxygen to propagate the reaction and form reactive oxygen species including the superoxide anion radical ($O_2^{\bullet -}$).

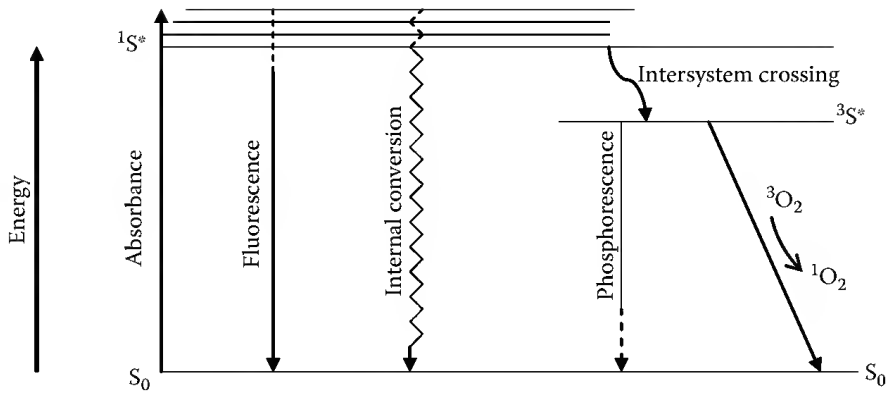

FIGURE 64.1 Simplified Jablonski diagram. The photosensitizer in the ground state (^0S) absorbs light to become excited ($^1S^*$). This energy can be lost via fluorescence, or the molecule can undergo intersystem crossing to form the longer lasting triplet state ($^3S^*$) molecule, which then reacts with oxygen or cellular substrates to form cytotoxic reactive oxygen species.

- A type 2 reaction can occur between the excited triplet photosensitizer and molecular oxygen. This direct energy transfer results in the formation of singlet oxygen ($^1O_2$), which is not a free radical and re-formation of the ground-state photosensitizer.

In the type 2 reaction, the photosensitizer does not itself undergo any chemical change, but simply cycles between different electronic energy states. Thus, once the triplet state photosensitizer has lost its energy and returned to the ground state, further illumination allows further excitation. Type 1 and type 2 reactions can occur simultaneously within a single cell, although it is thought that it is the formation of singlet oxygen via type 2 reactions, which is responsible for the majority of the cytotoxic damage in PDT. Further discussion surrounding the actions of the newly formed reactive oxygen species, and the consequences for the affected cells and tissues, can be found in Section 64.6.

64.3 Requirements for PDT to Become Clinically Successful

The key requirements for any novel therapy to become clinically successful are centered around treatment efficacy and economic viability. Clearly commercial development is essential for the wide use of PDT and, in this regard, the two key components required for a PDT treatment are the photosensitizer and the light source.

Much debate around the properties of an "ideal" photosensitizer can be found in the literature. Clearly a high level of PDT activity is required, usually measured by the quantum yield of singlet oxygen. A high specific absorption coefficient at wavelengths above 600 nm is desirable as light penetration through tissue increases with wavelength. There are many indication-specific requirements for photosensitizers, for example, only cationic photosensitizers can achieve a broad-spectrum antibacterial effect as anionic (and neutral) compounds are unable to efficiently cross the cell wall of Gram-negative organisms. Similarly, photosensitizers can be chosen for their ability to localize to certain areas of tumor cells or tissues.

From a pharmaceutical development point of view, photosensitizers must meet the same criteria as any other drug candidate: the drug should be able to be reproducibly and easily manufactured with a high level of purity. Complete toxicology packages are required: the compound must be nonmutagenic, noncarcinogenic, and minimally toxic in the absence of light. The compound should show optimal absorption, distribution, metabolism, and excretion (ADME) characteristics for the chosen route of administration and should not yield any toxic metabolites. Commercially, the intellectual property position is critical, along with a robust formulation and drug delivery system.

Light sources for PDT need to be simple to use and as inexpensive as possible. Much PDT is laser-based and lasers are essential for illumination of internal lesions. For superficial treatments however (e.g., of skin cancer), lasers are not required, and recent developments in LED technology have led to this option becoming economically favorable. The penetration of light through tissue is key to treating the complete depth of the lesion; therefore, light at a wavelength of greater than 600 nm is desirable. Further consideration of light sources is given in Section 64.7.2.

64.4 Photosensitizers

A vast array of molecules has been found to have photosensitizing abilities, but only a small proportion of those have been used in PDT beyond the laboratory. Several classes of photosensitizer are currently under study including porphyrins, chlorins, bacteriochlorins, phthalocyanines, and phenothiazinium salts.

64.4.1 Porphyrins

The general porphyrin structure is comprised of four pyrrole rings connected by methylene bridges, producing a highly delocalized structure. The side-chain composition gives each porphyrin its unique biological properties. Porphyrins are naturally occurring molecules and have a characteristic absorbance spectrum with maximal absorbance occurring at the Soret band (around 400 nm) and further absorbance peaks (Q bands) at higher wavelengths. For PDT, the Q band at around 630 nm is used to activate the porphyrins, as longer wavelengths of light penetrate the tissue more effectively. HpD and Photofrin are first generation porphyrin photosensitizers and were key to the development of PDT as a treatment modality. Despite being a complex mixture of oligomers, Photofrin is the most widely approved photosensitizer and is currently approved for the treatment of esophageal cancer, lung cancer, gastric and papillary bladder cancer, and cervical cancer/dysplasia. However, the prolonged skin photosensitization and suboptimal tissue penetration have limited its clinical success and have driven research into second- and third-generation photosensitizers.

64.4.2 ALA–PDT

A number of porphyrins play a key role in the heme biosynthetic pathway (Figure 64.2). In this process, 5-aminolevulinic acid (ALA) is synthesized from glycine and succinyl CoA by ALA synthase. This is followed by sequential reactions forming porphobilinogen, hydroxymethylbilane, uroporphyrinogen III, coproporphyrinogen III, protoporphyrinogen IX, and protoporphyrin IX. The addition of Fe^{2+} to protoporphyrin IX by ferrochelatase is the final step in the pathway and produces heme. Protoporphyrin IX is a highly efficient photosensitizer and manipulation of this physiological process gives rise to one of the most successful methods of PDT treatment, ALA–PDT.

ALA is widely used as a prodrug in dermatological PDT. ALA itself has no photosensitizing properties but, when given exogenously to tumor cells, the porphyrin biosynthesis pathway becomes overloaded and ferrochelatase cannot immediately convert all the protoporphyrin formed to heme. An accumulation of protoporphyrin IX can thus be induced and, upon illumination, a strong PDT effect is seen.

Levulan is the commercial name given to formulated ALA, and this was approved by the FDA for the topical treatment of actinic keratoses (AKs) in 1999. It has also been shown to successfully treat other nonmelanoma skin cancer (NMSC; Clark et al., 2003). The methyl ester of ALA (Metvix) has also been approved for topical PDT in NMSC. Metvix has similar photochemical and photophysical properties to Levulan but a higher lipophilicity allows greater penetration through skin. Metvix has been approved for the treatment of AK and basal cell carcinoma (BCC) in Europe. The major limitations of Levulan and Metvix therapy are the depth of penetration through tissue (which limits the treatable lesion depth) and

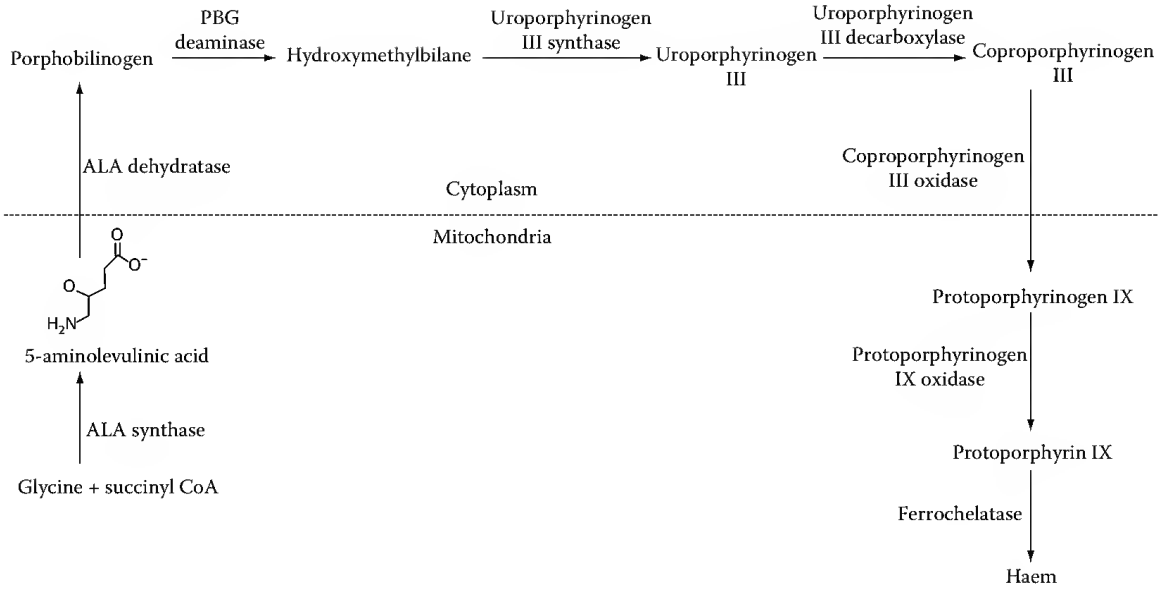

FIGURE 64.2 The heme biosynthetic pathway.

the pain associated with treatment (thought to be due to the accumulation of photosensitizer in nerve tissue). Comparisons between Levulan and Metvix have suggested a similar level of efficacy in AK, with Metvix having an advantage in deeper malignant lesions and also possibly causing less pain (Moloney and Collins, 2007).

64.4.3 Chlorins and Bacteriochlorins

Reduction of the porphyrin chromophore at a pyrrole ring produces a chlorin. This results in a wavelength shift out to the red region and an increase in the molar absorption coefficient, both desirable properties for increasing photosensitizer PDT efficiency. It also may improve the ability of the compounds to effectively penetrate tissue. Benzoporphyrin derivative (BPD) is a complex chlorin preparation but has been further developed to produce BPD monoacid ring A (verteporfin). This compound has shown much promise as a PDT agent and has a high molar extinction coefficient at 686 nm. It is taken up into cells via low density lipoprotein (LDL) receptor–mediated endocytosis and has a significantly damaging effect on tumor vasculature, although the specificity for tumor tissue is not very high. The compound has been used in the treatment of skin cancer, rheumatoid arthritis, endometrial ablation, and especially in AMD (as Visudyne™). Visudyne's use in AMD is the most commercially successful non-oncological use of PDT.

The chlorin, meta-tetra(hydroxyphenyl)chlorin (mTHPC, Foscan) has much greater photoactivity than Photofrin. It was developed for the treatment of cancers of the head, neck, esophagus, and lung and was clinically approved for use in Europe in 2001. Superior photophysical properties and a higher singlet oxygen yield allow much lower drug doses and light intensities to be used to achieve a comparable clinical effect to that seen with Photofrin. However, prolonged skin photosensitization remains an issue, as does the long drug-to-light time interval required.

Further reduction of the chlorin ring produces a bacteriochlorin. This results in a significant red shift in the longest wavelength Q band and an increase in the molar absorption coefficient. Reduction of mTHPC produces the bacteriochlorin, mTHPBC, which has been shown to have potential in the treatment of liver metastases, causing tumor necrosis in all patients taking part in a Phase I clinical trial (van Duijnhoven et al., 2005). Bacteriochlorins are the subject of active research in PDT (Huang et al., 2010), and the bacteriochlorin derivative Tookad is in clinical trials for focal ablation of prostate cancer (Huang et al., 2007; Trachtenberg et al., 2008).

64.4.4 Phenothiazinium Salts

Phenothiazinium salts are planar, aromatic blue dyes with a tricyclic ring structure and an overall cationic charge, allowing the molecule to form a complex with an anionic counter ion. Originally used in the dyeing industry, the phenothiazinium salt methylene blue has long been used as a tumor marker and is an effective *in vitro* photosensitizer, although its *in vivo* use has been limited due to low photodynamic activity, relatively high dark toxicity and subcellular localization to the nucleus, causing significant potential mutagenicity. Other drawbacks include the hydrophilic structure, which makes it very inefficient at entering cells.

Analogs of methylene blue have been synthesized with the aim of increasing the hydrophobicity of the compounds to allow easier delivery of the drug to tumor tissue and reducing the dark toxicity and nuclear accumulation. Particular emphasis has been placed on characterizing a series of symmetrical and asymmetrical methylene blue derivatives for use in PDT. These compounds have maximal absorbance peaks at a good tissue-penetrating wavelength, typically around 680 nm (Mellish et al., 2002; Walker et al., 2004) and have demonstrated excellent antibacterial and antiparasitic activity (Akilov et al., 2007; Akilov et al., 2009). Phenothiazinium salts are now in clinical trials for antimicrobial PDT (see Section 64.10)

64.5 Targeted PDT

As with other cancer therapies, much research has recently been put into developing methods, which will allow specific targeted delivery of photosensitizers to tumor tissue and into developing methods to prevent photosensitizer accumulation in non-target tissue. Ideally, the photosensitizer would be able to specifically accumulate within the target tumor tissue without any accumulation in healthy tissue. This absolute localization of the cytotoxic effect would allow greater light doses to be used clinically and may increase treatment efficacy without the side effects associated with systemic phototoxicity. The use of an active targeting mechanism may also increase the usefulness of many compounds, which show good photodynamic properties but are currently of limited use because they do not enter tumor cells effectively.

A complete review of the strategies employed in an attempt to actively target photosensitizers to tumor cells is outside the scope of this chapter. Liposome constructs, antibody conjugates, nanotechnology, specific ligand–receptor interactions, and a variety of other approaches have been tested *in vitro* and some *in vivo*, but none have currently achieved regulatory approval for clinical use. The technologies vary in their approach. Liposome constructs are easily taken up by the cell, once inside they are lysed and their photosensitizer contents released to allow local intracellular photodynamic activation. It has been shown that a liposome:BPD conjugate accumulates within tumor tissue slightly faster and to a higher level than free photosensitizer (Richter et al., 1993). Liposome preparations have also been used to target tumor neovasculature with some success. However, this method of targeting is complicated by difficulties in delivering liposome constructs to tumor cells via irregular and disorganized blood vessels.

The first example of antibody-mediated photosensitizer delivery was reported in 1983. HpD was conjugated to a tumor-specific antibody, and an increased PDT effect was observed, compared to HpD alone (Mew et al., 1983). More recently, a phage-derived L19 antibody has been shown to specifically bind fibronectin on newly formed blood vessels. The accumulation of L19-conjugated photosensitizer in neovasculature allows targeted damage to these vessels. This interaction could be exploited in the treatments of many diseases characterized by new blood vessel formation such as cancers and ocular disorders. A range of photosensitizers has been conjugated to antibodies, including mTHPC, $AlPcS_4$, and chlorin e_6.

Natural ligand–receptor interactions have also been exploited to enhance specific photosensitizer uptake. Tumor cells have been shown to upregulate LDL and estrogen receptors, effectively internalizing appropriately coupled photosensitizers (Allison et al., 1994; Swamy et al., 2002). Very recent advances in nanotechnology have been applied to PDT, with the conjugation of methylene blue to nanoparticles (Hah et al., 2011).

It is also possible to actively target photosensitizers to the tumor vasculature, with the aim of destroying the blood vessels that feed the tumor to give a more long-term response. This can be achieved via the use of specific peptide sequences that bind molecular targets specifically expressed in the rapidly expanding tumor neovasculature. The upregulation of one such target, integrin $\alpha_v\beta_3$, in tumor neovasculature allows macromolecules to be targeted to these vessels via the conjugation of small arginine–glycine–aspartic acid (RGD) containing peptides such as c(RGDfK) (Conway et al., 2008). It has been recently suggested that targeting the tumor vasculature potentiates the stimulation of the immune system, which would assist with long-term tumor control, but studies in the area are ongoing (Preise et al., in press).

64.6 Mechanism of Action of PDT In Vitro and In Vivo

Upon PDT treatment, several processes occur and combine to damage or destroy the target cells. The formation of reactive oxygen species by the processes discussed in Section 64.2 allows direct damage to both prokaryotic and eukaryotic cellular components. In some therapeutic indications, indirect mechanisms such as tumor vasculature ablation or the activation of the host immune system are also critical for long-term disease control.

64.6.1 Direct Cytotoxicity

A direct cytotoxic response to PDT is observed when the reactive oxygen species generated are able to damage tumor cellular components and induce an apoptotic or necrotic response. This response is dependent upon the subcellular localization of the photosensitizer and the availability of oxygen in the target tissue. Reactive oxygen species, particularly singlet oxygen ($^1O_2$), have a very small diffusion distance (i.e., they react before they can travel very far). The exact measurement of the singlet oxygen lifetime has been a topic of much debate; most recently, the lifetime has been calculated at 3 μs in a metabolically active cell (Hatz et al., 2008), with a resulting diffusion coefficient of $2–4 \times 10^{-6}$ cm^2 s^{-1} suggesting that the spatial domain of intracellular singlet oxygen will have a spherical radius of about 100 nm. Although these values are significantly greater than reported earlier (Moan and Berg, 1991), the ability of singlet oxygen to diffuse through the cell is still highly limiting and means that the site of primary intracellular damage is always very close to the photosensitizer location.

Many cellular components are susceptible to oxidative attack during PDT including proteins, lipids, and nucleosides. All but the very earliest photosensitizers are designed not to localize to the nucleus, making PDT very unlikely to induce DNA damage or have a carcinogenic effect. Mitochondrial localization of photosensitizers can cause depolarization or permeation of the mitochondrial membranes and induce a rapid apoptotic response via the release of cytochrome *c* and caspase cascade activation. Hydrophobic photosensitizers can localize to the plasma membrane. Here, the oxidation of unsaturated lipids causes a lipid peroxidation cascade and damage to the phospholipid bilayer. Such membrane damage can cause an alteration of membrane permeability and transport or a loss of membrane integrity resulting in rapid cell lysis, a necrotic pattern of death, and often the release of cellular contents inducing an inflammatory response. The induction of necrosis *in vitro* has been shown to be more dependent upon the PDT dose than the individual photosensitizer used; a more intensive PDT regimen gives rise to more necrotic changes and less apoptosis (Vantieghem et al., 1998).

The induction of apoptosis by PDT has been very well studied and recently reviewed (Ortel et al., 2009; Robertson et al., 2009; Reiners et al., 2010). This physiological process for the removal of redundant or potentially damaging cells can be activated by PDT, most often by photosensitizers that localize to the mitochondria of cells and, *in vitro*, under low-dose PDT conditions. The target cells undergo a series of carefully controlled chemical and physiological changes, which result in cell shrinkage and efficient phagocytosis by neighboring cells. As the changes that accompany apoptosis are common to

many different cell types responding to a variety of stimuli, it has been concluded that there is a common underlying program to cause cell death, and that PDT is able to stimulate the initiation of this process in various ways.

Photosensitizers that localize to lysosomes, such as methylene blue and aluminum phthalocyanine disulfonate ($AlPcS_2$), can cause lysosomal membrane rupture upon illumination and the release of cytotoxic components, such as the proteolytic cathepsin family, into the cytoplasm. However, the induction of apoptosis subsequent to lysosomal bursting is generally slower than after mitochondrial bursting, and it has also been reported that the lysosomal enzymes can be photoinactivated during PDT, which further limits the speed and extent of any cell damage. The observation that PDT with certain photosensitizers can result in lysosome degradation has led to the development of a technique for the intracellular delivery of therapeutic macromolecules known as photochemical internalization (PCI), discussed elsewhere in this book.

During and after PDT *in vivo*, both apoptotic and necrotic events can be seen, and both forms of cell death contribute to treatment success. Much research has illustrated that apoptosis can be initiated by PDT at various points of the signaling cascade and that the point of activation is dependent upon the subcellular localization of the photosensitizer. This most commonly occurs from the mitochondria via cytochrome *c* release or from the plasma membrane via death domain activation. Although apoptosis is an efficient form of cell death, the importance of the necrotic response to PDT should not be underestimated. Phagocytosis of apoptotic cell debris does not cause an immune response but the recruitment of leukocytes into tumor tissue is essential for complete tumor ablation and long-term tumor control. Under tightly controlled *in vitro* conditions, photosensitizers can be shown to cause almost exclusively one form of cell death or the other. However, *in vivo*, the situation is much more complicated, and a balance between apoptosis, necrosis, and other indirect effects of PDT is likely to exist.

Pertinently, only eukaryotic cells are capable of undergoing the complex apoptotic form of cell death. In antibacterial applications of PDT, cell death is generally induced much more quickly by simple lysis of the target bacterial cells. This causes rapid induction of an immune response, which is likely to be essential for long-term infection control.

64.6.2 Indirect Vascular Effects

For anticancer applications, the direct cytotoxic effects of PDT are often not sufficient for complete tumor ablation, and indirect effects on the tumor vasculature and induction of an immune response can be critical. Tumor vasculature can be destroyed via photooxidative damage to endothelial cells: manipulation of the treatment regime such as maximizing photosensitizer accumulation in the vasculature by having a short drug–light interval can potentiate the effect. Endothelial cell rupture is followed by the activation of the coagulation cascade, vessel occlusion, and starvation of the downstream tumor cells. Tumor cell necrosis can also have a stimulatory effect on the coagulation cascade. These indirect effects do not necessarily occur significantly more slowly than the direct effects discussed earlier—vasoconstriction of tumor blood vessels and thrombus formation have been shown to occur within 3 h post-illumination (Dolmans et al., 2002).

64.6.3 Indirect Immune System Effects

Immunological consequences of PDT have been much studied by Korbelik and coworkers and reviewed by Korbelik (2006). Upon PDT treatment, the host immune system becomes activated via the release of cellular constituents and cytokines into the bloodstream. Cytokine signaling causes rapid accumulation of neutrophils and macrophages into the treated tissue, which assist in tumor cell kill and release proteases to destroy the noncellular components of the tumor architecture. Further endothelial cell damage amplifies the inflammatory response. Phagocytosis of tumor cell debris by macrophages allows the maturation of antigen-presenting cells, which can then form part of the "acquired" immune system.

This response plays a critical role in the "mopping up" of any remaining tumor cells. This immunostimulatory action gives PDT a significant advantage over traditional cancer therapies such as chemotherapy and radiotherapy, which require concurrent suppression of the immune system. It is also essential for long-term tumor control and the prevention of disease resurgence as acquired antitumor immunity can slow down (or prevent) the regrowth of tumor at the same site or different sites. There is growing interest in the use of PDT in producing cancer vaccines (Korbelik, 2011).

In antibacterial applications of PDT, the stimulation of the immune system is equally important. Complete sterilization of the target tissue is an unrealistic aim; the objective of most PDT treatments is to significantly reduce the bacterial load, as discussed further in Section 64.10, and simultaneously stimulate the host immune system.

64.7 Clinical PDT: Rationale, Technologies, and Challenges

64.7.1 Rationale for Clinical Use of PDT

PDT is limited to producing a local cytotoxic effect since, although the photosensitizing drug may often be delivered systemically, a therapeutic effect is only possible precisely where the light and drug interact with tissue and there is no current means of whole-body illumination. This has advantages for targeting, and means that PDT is not associated with the kind of systemic toxicity experienced by patients receiving chemotherapy but, conversely, means that PDT cannot produce the same systemic efficacy as chemotherapy or molecular-targeted therapy. PDT is much more analogous to surgery or radiation therapy than to chemotherapy, but a major potential advantage of PDT is that it can potentially achieve selective targeting by two independent, but mutually reinforcing, mechanisms. The primary mechanism uses physical or mechanical targeting via the control of light delivery. The second mechanism is molecular targeting, where the photosensitizer can potentially be delivered selectively to the target lesion, rather than to healthy tissue. In principle, therefore, PDT has the potential to be highly selective for target tissue rather than healthy tissue and therein lies much of its appeal for applications in medicine. It also appears that any PDT damage to healthy tissue which does occur heals very easily without scarring, thought to be due to the preservation of connective tissue following PDT. This normal tissue healing is, in effect, another contributor to the selectivity observed following PDT.

There is ongoing debate as to the extent to which photosensitizing drugs used in clinical PDT are selectively present in target lesion versus normal tissue at the time of light application. This is very dependent on the drug, the tissue, the mode of drug delivery, and the drug-to-light time interval. That there is some selective targeting is certain, because there are many examples where tumors that have been exposed to photosensitizers clearly show much increased fluorescence compared with surrounding healthy tissue. This is especially so for the local administration of ALA or its methyl ester (Metvix), in NMSC or in bladder cancer *in situ* and is the basis of the growing use of photodetection in the clinic. However, there is less evidence for the selective accumulation of systemically administered photosensitizers in tumors.

64.7.2 Light Sources

The targeting of lesions by light has developed substantially in the past 25 years, as has the understanding of the behavior of light in human tissues and organs. By using lasers, optical fibers, and endoscopy, light appropriate for stimulating PDT can be delivered accurately and effectively to most internal organs, and PDT is now rarely rejected because of difficulties in delivering the light. In the early days of PDT development, lasers were extremely large, inconvenient, and expensive, in part because of the need for tunability to different wavelengths as researchers studied different photosensitizers. Developments in laser technology have greatly increased the convenience of PDT application in the clinic, and several watts of power are readily available from fixed wavelength diode lasers,

which are relatively inexpensive and easily transportable in the clinical environment. This is sufficient power to carry out most PDT applications in a clinically convenient timescale (e.g., 10–20 min of illumination).

For superficial PDT, for example, of NMSC or chronic wounds, lasers are not necessary and many non-laser sources have been developed. Among these, light-emitting diodes (LEDs) have now assumed a dominant role. LED-based light sources for PDT are simple to use, very reliable, and long-lasting and can provide sufficient power to allow relatively short treatment times. However, they are relatively inefficient in terms of conversion of electrical energy to light energy (typically around 10%), with the excess energy being released as heat, which means that LED devices for PDT require an integrated cooling system. Using LED technology, it is not yet possible to channel the light into an appropriate optical fiber efficiently, and so lasers are still required where PDT is to be performed internally.

64.7.3 Drugs Approved for PDT

Research on the various families of photosensitizers has been summarized in Section 64.4. Of the hundreds of compounds tested in the laboratory, relatively few have undergone clinical evaluation and only a handful has been approved for routine clinical use. Some of these are listed in Table 64.1, along with the applications for which they are approved.

64.7.4 Challenges in Clinical Development of PDT

One of the significant challenges in the development of clinical PDT is the determination of optimal dosimetry for the application is question. The number of dosing parameters to be optimized is approximately three times that of a drug-only therapy, since there are all of the usual drug-associated parameters (e.g., total dose, frequency of dosing, formulation) coupled with light-associated parameters (e.g., wavelength, total light dose, light dose rate, fractionation, or continuous) and then parameters associated with the combination of light and drug (e.g., drug-to-light time interval). It is practicable to optimize only a very small number of these parameters in clinical trials, and more reliance must be placed on preclinical studies than in clinical development of most therapies. Hence, it is likely that even in approved applications, the recommended protocols may be suboptimal.

In systemic PDT, the induction by the early photosensitizers, Photofrin and Foscan of a lengthy period of cutaneous photosensitivity (up to several weeks following drug administration), has been seen as a major challenge to widespread adoption. In those cases where PDT can be used either curatively or for long-term palliation, this may be acceptable. But for the many short- and medium-term palliative uses of PDT, where life expectancy may be measured in months, induction of lasting photosensitivity may be an unacceptable patient burden. Certainly, the elimination or reduction of cutaneous sensitivity following PDT must be a major aim of future development.

TABLE 64.1 Some Drugs Approved for PDT in the United States and the European Union

Chemical Name	Generic Name	Trade Name	Indications
HpD, polyhematoporphyrin	Porfimer sodium	Photofrin™	Advanced and early lung cancer, esophageal adenocarcinoma, bladder cancer, and Barrett's esophagus
mTHPC	Temoporfin	Foscan™	Head and neck cancer
5-ALA	ALA	Levulan™	AKs
Methyl 5-aminolevulinate	Methyl aminolevulinate	Metvix™	AKs, BCC
BPD	Verteporfin	Visudyne™	AMD

Another significant challenge is securing acceptability of a two-component modality, which may often be seen by practitioners as overly complex. This very much depends on the parameters applying to the photosensitizer being used. In the cases of Photofrin and Foscan, drug-to-light intervals of 3 and 4 days, respectively, have been commonly used, with the need for careful patient management to protect from photosensitivity during the long drug-to-light interval. On the other hand, the most successful PDT approach to date using systemic drug administration (Visudyne in macular degeneration, see Section 64.9) uses a drug-to-light interval of just 15 min. In terms of clinical convenience, this is comparable to MRI using intravenous image enhancement.

64.8 Clinical PDT: Developments in Cancer Treatment

64.8.1 Introduction

There is an extensive literature describing clinical studies of PDT in a large variety of cancers, including the Phase III studies that have led to regulatory approval for some photosensitizing drugs. Detailed considerations are beyond the scope of this chapter, which is restricted to a brief outline of the current clinical scene in PDT. However, reviews are available (e.g., Brown et al., 2004; Fayter et al., 2010). The most recent and extremely thorough systematic review of precancerous skin conditions, Barrett's esophagus, and cancers of the biliary tract, brain, head and neck, lung, esophagus, and skin is especially comprehensive and well-researched (Fayter et al., 2010).

64.8.2 Nonmelanoma Skin Cancer

NMSC includes a group of skin cancers and precancerous lesions, which are generally nonlife threatening if treated. They include BCC that can exist in nodular or superficial forms, and actinic (or solar) keratoses (AKs) and Bowen's disease, which are considered to be precancerous forms of squamous cell carcinoma (SCC). Melanoma is currently not treated by PDT, in part because pigmentation may limit light penetration, but largely because of the high risk of metastasis if removal is incomplete.

NMSC is extremely common in Caucasian populations. For example, the lifetime risk of developing AK is greater than 50% in Australia and the United States (Fayter et al., 2010). If not treated, NMSC may be locally invasive and, in the case of AK, may develop into invasive SCC, which can metastasize. Prompt diagnosis and either surveillance or treatment are therefore indicated.

Treatment of NMSC by PDT using either ALA (Levulan) or methyl aminolevulinate (MAL) (Metvix) is now well-established and widely practiced. While protocols vary, the general approach is to apply the ALA or MAL in a vehicle (solution or cream) to the lesion, allow a drug-to-light interval of between 3 and 10 h and then apply light. Depending on the type of lesion, debridement may be carried out before application of drug. In some applications for nodular BCC, a repeat treatment after 7 days is applied. Broadly, efficacy of PDT in treating NMSC is comparable with other modalities, but cosmetic results are superior with PDT. The safety profile of the treatment is favorable, with no serious adverse events or systemic photosensitivity (Fayter et al., 2010). The most characteristic adverse event is local pain or burning sensation when the light is administered, which usually quickly resolves when the light is switched off.

64.8.3 Barrett's Esophagus and Early, Localized Cancer

Since PDT is able to completely ablate superficial or early lesions, it is potentially curative for a variety of precancerous conditions and for early, localized cancer. In this sphere, it therefore competes with curative surgery, but PDT may have advantages in special niche areas where surgery is difficult or produces more serious sequelae. One such niche area is Barrett's esophagus.

Barrett's esophagus is considered a precursor of adenocarcinoma of the esophagus and is increasing in incidence (Brown et al., 2004). It is caused by acid reflux into the esophagus which damages the

normal esophageal lining, which may be replaced by dysplastic tissue. There are several grades of dysplasia ranging from low to high, with the latter at greatest risk of developing esophageal cancer. Clinical studies have used either Photofrin or Foscan given intravenously or ALA given orally. PDT is currently approved as a first-line treatment for patients with high-grade dysplasia using Photofrin. On the basis of systematic review of several trials, Fayter et al. (2010) concluded that PDT might be beneficial beyond proton pump inhibitors alone. However, there is some concern that after PDT with ALA, there may be submucosal islands of remaining Barrett's epithelium, which might act as foci for the development of future disease (Brown et al., 2004). This is probably due to incomplete uptake of drug and formation of photosensitizer and is less likely with systemic photosensitizers. There were no serious adverse events reported in trials of PDT in Barrett's esophagus suggesting an acceptable safety profile, though further evidence is needed.

There is increasing interest in focal treatment for localized prostate cancer. Currently, patients are offered either surveillance (which carries the risk of undertreatment and anxiety) or radical treatment, which is associated with debilitating side effects. Although still in the early phase of development, PDT is showing promise for focal treatment that involves destroying the cancer focus in order to offer patients the potential of combining cancer control with minimal side effects (Lecornet et al., 2010). Such an approach could avoid both over- and undertreatment. For PDT, such treatment would probably involve interstitial therapy whereby several optical fibers would be inserted into the lesion to ensure adequate light dosimetry.

Other localized cancers which should, in principle, be appropriate for the treatment with PDT include carcinoma *in situ* of the bladder, early non-small cell lung cancer, and intraepithelial neoplasias such as those of cervix and vulva (Brown et al., 2004). In the case of bladder, early treatments caused bladder shrinkage sometimes requiring cystectomy, and currently, PDT is little used in this indication. However, this may change with the introduction of improved photodetection of bladder carcinoma *in situ* using hexyl ALA (Hexvix) (Jocham et al., 2008). There are also recent reports of potential improvement in the treatment of cervical intraepithelial neoplasia by PDT using methyl ALA and hexyl ALA (Soergel et al., 2010).

64.8.4 Advanced Cancers

Photofrin is licensed for reduction of obstruction and palliation of symptoms for patients with completely or partially obstructing endobronchial non-small cell lung cancer, but it is difficult to find evidence on how often it is currently used in this indication. The trials that underpinned this approval were carried out before 2002 and generally did not include any recognized quality of life (QoL) assessment. Indeed, this appears to be a common failing of many PDT trials in the advanced cancer setting. More recently, QoL end points have become much more common and validated in cancer clinical studies in general, though not in PDT trials. This is unfortunate since there is certainly anecdotal evidence that QoL during and following PDT treatments may be better than in alternative treatment modalities.

Photofrin is also licensed for palliation of patients with completely obstructing esophageal cancer or for patients with partial obstruction of the esophagus who cannot be treated satisfactorily with NdYAG laser therapy (Brown et al., 2004). Again it is difficult to assess how frequently this procedure is used. There is a report that PDT is used with curative intent in early esophageal cancer (Gray and Fullarton, 2007). Trials have generally provided evidence of improvement of function (swallowing), with a conclusion that PDT is an effective treatment for palliation of advanced cancer at the gastroesophageal junction (Heier et al., 1995). Interestingly, two studies investigating the addition of hyperbaric oxygen to PDT concluded that patients receiving PDT plus hyperbaric oxygen had significantly longer survival than patients receiving PDT alone, 12 versus 7 months, $p = 0.01$; 13.8 versus 8.7 months, $p = 0.021$ (Maier et al., 2000a,b).

Treatment of head and neck cancer with Foscan has been licensed in Europe since 2001 as a local treatment for patients with advanced head and neck cancer unresponsive to previous therapies and

unsuitable for radiotherapy or chemotherapy. Again, the extent of its use is difficult to establish, but is not likely to be extensive. This is unfortunate as PDT has high potential in this indication (Fayter et al., 2010), especially in palliative treatment, in repeat treatments to control local regrowth (unlike radiotherapy and surgery, PDT can be repeated without safety concerns) and, ultimately, in the treatment of early cancers.

Biliary tract cancer is rare, but difficult to treat. Promising data have been achieved using PDT in cholangiocarcinoma (e.g., see Ortner et al., 2003). Most studies have been palliative in intent, and more extensive, controlled studies are required. Pancreatic cancer is similarly difficult to treat, and there is evidence from small studies that PDT may have a role in the treatment of this indication (Bown et al., 2002). Again, larger more rigorous trials are needed.

Treatment of glioma in the brain by PDT has been considered for many years, and progress has been made in adequate light delivery (Muller and Wilson, 1996). However, only two small trials have been reported (Krishnamurthy et al., 2000; Eljamel et al., 2008) and, yet again, larger more rigorous studies are needed to properly assess the potential of PDT in this indication.

64.9 Clinical PDT: Ophthalmology

AMD is the leading cause of registrable blindness in the Western world (Jager et al., 2008). The macula is the central part of the retina and contains the greatest concentration of photoreceptors, allowing a person to see fine details, to read, and to recognize faces (Jager et al., 2008). The most common form of AMD is the dry form, responsible for about 90% of AMD. However, this can progress into the less common, but much more damaging wet form of AMD, which is characterized by choroidal neovascularization beneath the fovea, with exudation, which leads to vision loss. Until recently, this loss in central vision was considered irreversible and progressive. It may occur in one or both eyes. The successful development of the chlorin verteporfin (under the name Visudyne™) in the late 1990s, represented a major breakthrough, both in the treatment of this disease and in the acceptance of PDT as a mainstream therapy (Mellish and Brown, 2001). The approach has been very successful, being widely applied throughout the world. It involves intravenous administration of Visudyne in a liposomal formulation over a period of 10 min. Five minutes after completion of drug administration, laser light at 690 nm is applied for precisely 83 s, during that time the patient feels no pain. This completes a single treatment, which can be repeated as indicated by fluorescein angiography, which gives an image showing the extent of neovascularization and exudation. On the basis of extensive Phase III studies, Visudyne was widely approved by regulatory authorities and became a commercial success.

Though it has now been largely superseded by targeted therapies, the success of Visudyne points the way for other PDT-based therapies. Not only does it work in the required indication, but it is also extremely convenient clinically, with very short treatment times. Part of the reason for its rapid uptake was due, at least in part, to the familiarity of ophthalmologists with laser technology. This has lessons for the acceptance of other modes of PDT by the clinical community.

64.10 Clinical PDT: Antimicrobial Therapy

There is now a large and expanding literature on the antimicrobial effects of PDT *in vitro*. Almost any photosensitizer and light will inactivate Gram-positive bacteria, including those used in PDT for cancer, but negatively charged and neutral photosensitizers have little effect on Gram-negative bacteria, due to their nonporous cell wall structure, which consists of an inner cytoplasmic membrane and an outer membrane, separated by the peptidoglycan-containing cytoplasm. Neutral and anionic photosensitizers can be made effective against Gram-negative bacteria if used in conjunction with a disrupting agent such as polymixin. However, in order to obtain true broad spectrum antimicrobial activity, photosensitizers need to be cationic (Merchat et al., 1996; Minnock et al., 1996), and there is a large variation in PDT efficacy depending upon the chemical structure of the cationic molecule. For example, methylene

blue, while being an excellent photosensitizer, has a relatively poor efficacy in bacterial inactivation, while its tetrabutyl analog (3,7-bis[*N*,*N*-dibutylamino] phenothiazin-5-ium bromide) demonstrates very high antimicrobial activity against both Gram-positive and Gram-negative organisms, as well as fungal species. Using such high activity photosensitizers *in vitro*, it is possible to achieve typically 5–7 logs of cell kill with comparatively very low photosensitizer and light doses.

A number of experimental animal model systems for tissue infection and for acute wounds have now been developed (e.g., Hamblin et al., 2002). Perhaps the most immediate impact of these models is that the high log kills seen by PDT regimes *in vitro* are not easily reproduced *in vivo*, where much higher photosensitizer and light doses are needed and lower log kills are typically achieved. Nevertheless, such models are valuable in establishing the most appropriate parameters to be used in clinical studies.
Antimicrobial PDT works by a completely different mechanism to antibiotics and is multi-targeted, since many types of biomolecule are degraded during antimicrobial PDT, any one of which could prove lethal to the cells. This imparts two key properties to antimicrobial PDT:

- Since it is multi-targeted, development of resistance to PDT is unlikely. Indeed, many attempts to deliberately induce resistance through repeated generations have proved unsuccessful.
- Since bacterial cells have no protection against singlet oxygen, antimicrobial PDT is able to inactivate cells of antibiotic-resistant bacterial strains.

Antimicrobial PDT has potential application across a variety of conditions including dental disease, acute and chronic wounds, parasitic lesions, nasal carriage of MRSA, acne, and superficial skin conditions. Although to date there have been very few reported clinical studies using antimicrobial PDT, this is likely to change as several clinical studies are underway. In a case study, Clayton and Harrison (2006) treated with PDT a 72-year-old woman with chronic recalcitrant venous ulceration of her right lower leg, persisting for more than 12 months and complicated by cellulitis and colonization with methicillin-resistant *Staphylococcus aureus* (MRSA). The PDT was well-tolerated with minimal discomfort to the patient, even without the use of topical local anesthesia (unlike the use of 5-ALA in the treatment of NMSC, where pain is frequently experienced), and significant improvement was subsequently observed in the ulcer.

The use of PDT to treat dental infection has been led by Wilson and coworkers and developed by Ondine. In 33 subjects with moderate to advanced periodontal disease, it was shown that there was a significant advantage (in terms of reduction in probing pocket depths) in combining PDT with scaling and root planing, compared with scaling and root planing alone (Andersen et al., 2007).

Following extensive preclinical safety and toxicology testing, Photopharmica Ltd is developing the photosensitizer PPA 904 (3,7-bis[*N*,*N*-dibutylamino] phenothiazin-5-ium bromide) for the treatment of chronic leg ulcers. This photosensitizer has several key advantages for antimicrobial PDT as follows:

- Very high, broad-spectrum antimicrobial activity compared with many other photosensitizers (e.g., methylene blue)
- Strong light absorption at 680 nm
- Easily manufactured and purified as good manufacturing practice (GMP) material (no isomers)
- Small molecular size compared with porphyrins and phthalocyanines
- Excellent preclinical safety profile

In a small antimicrobial PDT pilot study using broad-spectrum light, eight patients with bacterially colonized chronic ulcers, four with diabetic foot ulcers, and four with venous leg ulcers, a single PDT treatment with PPA 904 was well tolerated, and in each of the patients, there was a decrease in total bacterial load immediately after the treatment compared to pretreatment (median 2.5 $\log_{10}$ reduction) and this was statistically significant ($p = 0.0078$) as determined by the Wilcoxon rank nonparametric test. This was the first demonstration of a clinically significant reduction in bacterial load by a PDT treatment in this indication, and both Gram-positive and Gram-negative microorganisms were susceptible to the treatment. This was followed up by a Phase IIa, randomized, placebo-controlled trial in 32 patients, 16 each with chronic diabetic foot ulcers and venous leg ulcers. All patients received standard wound

therapy (compression bandaging for venous leg ulcers and standard dressing for diabetic foot ulcers) as well as a single treatment of either PPA 904 plus light or placebo plus light. The data showed a strongly significant reduction in bacterial load following PDT and a trend toward accelerated healing in the PPA 904 group compared with the placebo group. The study showed the therapy to be safe and without treatment-induced pain. A repeat dose study is now in progress, powered to detect significance in reduction of microbiological load, but also assessing healing.

64.11 Future of PDT

It is more than 30 years since PDT was first used in oncology and many thousands of patients have been treated. It cannot be described as a new therapy and yet its rightful place in the cancer armamentarium remains unclear. Why has PDT not achieved a more sustained place in cancer management and what is its future? This question was asked and tentative answers put forward in 2004 (Brown et al., 2004). Those responses bear repetition now and include the difficulty in establishing optimum treatment parameters, clinician and hospital resistance to a two-component approach, and the capital cost of setting up a PDT center. However, the chief reason is likely to be that the drugs in current use (with their inherent challenges of long drug-to-light intervals, coupled with prolonged skin photosensitivity) have not shown sufficient advantage over alternative treatments in large, randomized, controlled trials. Such trials are expensive and have been difficult to perform because of the lack of strong commercial support from the large oncology companies and from national agencies. New improved drugs are, however, entering clinical trials, such as Tookad for prostate cancer. As stated in the recent systematic review of PDT in oncology, while further research is needed to develop the field of PDT for cancer, appraisal of all the available trial evidence leads to the conclusion that PDT appears to be a promising treatment in the majority of conditions reviewed (Fayter et al., 2010), but the potential place of PDT among the range of other treatments available for each condition is not yet clearly defined.

Those who have been closely associated with clinical PDT programs in oncology have been impressed by patient feedback. Where alternatives are available, PDT is widely preferred by patients. Until now, QoL and patient preference studies have been largely anecdotal, but more sophisticated instruments are now available and such qualitative research must be part of future PDT trials.

We have much to learn from the success of Visudyne PDT, where treatment is very simple (at least to patients), there is no sustained photosensitivity and treatment times are extremely short. These advantages also apply to antimicrobial PDT, where there is a building momentum in the product pipeline moving from discovery through the clinical trial pathway and into products.

References

Akilov, O. E., Kosaka, S., O'Riordan, K., Hasan, T. 2007. Photodynamic therapy for cutaneous leishmaniasis: The effectiveness of topical phenothiaziniums in parasite eradication and Th1 immune response stimulation. *Photochem Photobiol Sci* 6: 1067–1075.

Akilov, O. E., Yousaf, W., Lukjan, S. X., Verma, S., Hasan, T. 2009. Optimization of topical photodynamic therapy with 3,7-bis(di-n-butylamino)phenothiazin-5-ium bromide for cutaneous leishmaniasis. *Laser Surg Med* 41: 358–365.

Allison, B. A., Pritchard, P. H., Levy, J. G. 1994. Evidence for low-density lipoprotein receptor-mediated uptake of benzoporphyrin derivative. *Br J Cancer* 69: 833–839.

Andersen, R., Loebel, N., Hammond, D., Wilson, M. 2007. Treatment of periodontal disease by photodisinfection compared to scaling and root planing. *J Clin Dent* 18: 34–38.

Bown, S. G., Rogowska, A. Z., Whitelaw, D. E., Lees, W. R., Lovat, L. B., Ripley, P. et al. 2002. Photodynamic therapy for cancer of the pancreas. *Gut* 50: 549–557.

Brown, S. B., Brown, E. A., Walker, I. 2004. The present and future role of photodynamic therapy in cancer treatment. *Lancet Oncol* 5: 497–508.

Clark, C., Bryden, A., Dawe, R., Moseley, H., Ferguson, J., Ibbotson, S. H. 2003. Topical 5-aminolaevulinic acid photodynamic therapy for cutaneous lesions: Outcome and comparison of light sources. *Photodermatol Photoimmunol Photomed* 19: 134–141.

Clayton, T. H., Harrison, P. V. 2006. Photodynamic therapy for infected leg ulcers. *Br J Dermatol* 156: 384.

Conway, C. L., Walker, I., Bell, A., Roberts, D. J., Brown, S. B., Vernon, D. I. 2008. In vivo and in vitro characterisation of a protoporphyrin IX-cyclic RGD peptide conjugate for use in photodynamic therapy. *Photochem Photobiol Sci* 7: 290–298.

Dolmans, D. E., Kadambi, A., Hill, J. S., Waters, C. A., Robinson, B. C., Walker, J. P. et al. 2002. Vascular accumulation of a novel photosensitizer, MV6401, causes selective thrombosis in tumor vessels after photodynamic therapy. *Cancer Res* 62: 2151–2156.

Eljamel, M. S., Goodman, C., Moseley, H. 2008. ALA and photofrin fluorescence-guided resection and repetitive PDT in glioblastoma multiforme: A single centre phase III randomised controlled trial. *Laser Med Sci* 23: 361–367.

Fayter, D., Corbett, M., Heirs, M., Fox, D., Eastwood, A. 2010. A systematic review of photodynamic therapy in the treatment of precancerous skin conditions, Barrett's oesophagus and cancers of the biliary tract, brain, head and neck, lung, oesophagus and skin. *Health Technolo Assess NIHR HTA Progr* 14: 37.

Gray, J., Fullarton, G. 2007. The current role of photodynamic therapy in oesophageal dysplasia and cancer. *Photodiagn Photodyn Ther* 4: 151–159.

Hah, H. J., Kim, G., Lee, Y. E., Orringer, D. A., Sagher, O., Philbert, M. A. 2011. Methylene blue-conjugated hydrogel nanoparticles and tumor-cell targeted photodynamic therapy. *Macromol Biosci* 11: 90–99.

Hamblin, M. R., O'Donnell, D. A., Murthy, N., Contag, C. H., Hasan, T. 2002. Rapid control of wound infections by targeted photodynamic therapy monitored by in vivo bioluminescence imaging. *Photochem Photobiol* 75: 51–57.

Hatz, S., Poulsen, L., Ogilby, P. R. 2008. Time-resolved singlet oxygen phosphorescence measurements from photosensitized experiments in single cells: Effects of oxygen diffusion and oxygen concentration. *Photochem Photobiol* 84: 1284–1290.

Heier, S. K., Rothman, K. A., Heier, L. M., Rosenthal, W. S. 1995. Photodynamic therapy for obstructing esophageal cancer: Light dosimetry and randomized comparison with Nd:YAG laser therapy. *Gastroenterology* 109: 63–72.

Huang, Z., Chen, Q., Dole, K. C., Barqawi, A. B., Chen, Y. K., Blanc, D. et al. 2007. The effect of Tookad-mediated photodynamic ablation of the prostate gland on adjacent tissues—In vivo study in a canine model. *Photochem Photobiol Sci* 6: 1318–1324.

Huang, Y. Y., Mroz, P., Zhiyentayev, T., Sharma, S. K., Balasubramanian, T., Ruzié, C. et al. 2010. In vitro photodynamic therapy and quantitative structure-activity relationship studies with stable synthetic near-infrared-absorbing bacteriochlorin photosensitizers. *J Med Chem* 53: 4018–4027.

Jager, R. D., Mieler, W. F., Miller, J. W. 2008. Age-related macular degeneration. *New Engl J Med* 358: 2606–2617.

Jocham, D., Stepp, H., Waidelich, R. 2008. Photodynamic diagnosis in urology: State-of-the-art. *Eur Urol* 53: 1138–1148.

Korbelik, M. 2006. PDT-associated host response and its role in the therapy outcome. *Laser Surg Med* 38: 500–508.

Korbelik, M. 2011. Cancer vaccines generated by photodynamic therapy. *Photochem Photobiol Sci* 10(5): 664–669.

Krishnamurthy, S., Powers, S. K., Witmer, P., Brown, T. 2000. Optimal light dose for interstitial photodynamic therapy in treatment for malignant brain tumors. *Laser Med Sci* 23: 361–367.

Lecornet, E., Ahmed, H. U., Moore, C., Emberton, M. 2010. Focal therapy for prostate cancer: A potential strategy to address the problem of overtreatment. *Arch Esp Urol* 63: 845–852.

Maier, A., Anegg, U., Fell, B., Tomaselli, F., Sankin, O., Prettenhofer, U. 2000b. Effect of photodynamic therapy in a multimodal approach for advanced carcinoma of the gastro-esophageal junction. *Laser Surg Med* 26: 461–466.

Maier, A., Tomaselli, F., Anegg, U., Rehak, P., Fell, B., Luznik, S. et al. 2000a. Combined photodynamic therapy and hyperbaric oxygenation in carcinoma of the esophagus and the esophago-gastric junction. *Eur J Cardio Thorac Surg* 18: 649–654.

Mellish, K. J., Brown, S. B. 2001. Verteporfin: A milestone in ophthalmology and photodynamic therapy. *Expert Opin Pharmacother* 2: 351–361.

Mellish, K. J., Cox, R. D., Vernon, D. I., Griffiths, J., Brown, S. B. 2002. In vitro photodynamic activity of a series of methylene blue analogues. *Photochem Photobiol* 75: 392–397.

Merchat, M., Bertoloni, G., Giacomini, P., Villanueva, A., Jori, G. 1996. Meso-substituted cationic porphyrins as efficient photosensitizers of gram-positive and gram-negative bacteria. *J Photochem Photobiol B Biol* 32: 153–157.

Mew, D., Wat, C. K., Towers, G. H., Levy, J. G. 1983. Photoimmunotherapy: Treatment of animal tumors with tumor-specific monoclonal antibody-hematoporphyrin conjugates. *J Immunol* 13: 1473–1477.

Minnock, A., Vernon, D. I., Schofield, J., Griffiths, J., Parish, J. H., Brown, S. B. 1996. Photoinactivation of bacteria. Use of a cationic water-soluble zinc phthalocyanine to photoinactivate both gram-negative and gram-positive bacteria. *J Photochem Photobiol B Biol* 32: 159–164.

Moan, J., Berg, K. 1991. The photodegradation of porphyrins in cells can be used to estimate the lifetime of singlet oxygen. *Photochem Photobiol* 53: 549–553.

Moan, J., Peng, Q. 2003. An outline of the hundred-year history of PDT. *Anticancer Res* 23: 3591–3600.

Moloney, F. J., Collins, P. 2007. Randomized, double-blind, prospective study to compare topical 5-amino-laevulinic acid methylester with topical 5-aminolaevulinic acid photodynamic therapy for extensive scalp actinic keratosis. *Br J Dermatol* 157: 87–91.

Muller, P. J., Wilson, B. C. 1996. Photodynamic therapy for malignant, newly diagnosed supratentorial gliomas. *J Clin Laser Med Surg* 14: 263–270.

Ortel, B., Shea, C. R., Calzavara-Pinton, P. 2009. Molecular mechanisms of photodynamic therapy. *Front Biosci* 14: 4157–4172.

Ortner, M. E., Caca, K., Berr, F., Liebetruth. J., Mansmann, U., Huster, D. et al. 2003. Successful photodynamic therapy for nonresectable cholangiocarcinoma: A randomized prospective study. *Gastroenterology* 125: 1355–1363.

Preise, D., Scherz, A., Salomon, Y. 2011. Antitumor immunity promoted by vascular occluding therapy: Lessons from vascular-targeted photodynamic therapy (VTP). *Photochem Photobiol Sci* 10: 681–688.

Reiners, J. J., Agostinis, P., Berg, K., Oleinick, N. L., Kessel, D. 2010. Assessing autophagy in the context of photodynamic therapy. *Autophagy* 6: 7–18.

Richter, A. M., Waterfield, E., Jain, A. K., Canaan, A. J., Allison, B. A., Levy, J. G. 1993. Liposomal delivery of a photosensitizer, benzoporphyrin derivative monoacid ring A (BPD), to tumor tissue in a mouse tumor model. *Photochem Photobiol* 57: 1000–1006.

Robertson, C. A., Evans, D. H., Abrahamse, H. 2009. Photodynamic therapy (PDT): A short review on cellular mechanisms and cancer research applications for PDT. *J Photochem Photobiol B Boil* 96: 1–8.

Soergel, P., Loehr-Schulz, R., Hillemanns, M., Landwehr, S., Makowski, L., Hillemanns, P. 2010. Effects of photodynamic therapy using topical applied hexylaminolevulinate and methylaminolevulinate upon the integrity of cervical epithelium. *Laser Surg Med* 42: 624–630.

Swamy, N., James, D. A., Mohr, S. C., Hanson, R. N., Ray, R. 2002. An estradiol–porphyrin conjugate selectively localizes into estrogen receptor-positive breast cancer cells. *Bioorg Med Chem* 10: 3237–3243.

Trachtenberg, J., Weersink, R. A., Davidson, S. R., Haider, M. A., Bogaards, A., Gertner, M. R. et al. 2008. Vascular-targeted photodynamic therapy (padoporfin, WST09) for recurrent prostate cancer after failure of external beam radiotherapy: A study of escalating light doses. *BJU Int* 102: 556–562.

van Duijnhoven, F. H., Rovers, J. P., Engelmann, K., Krajina, Z., Purkiss, S. F., Zoetmulder, F. A. et al. 2005. Photodynamic therapy with 5,10,15,20-tetrakis(m-hydroxyphenyl) bacteriochlorin for colorectal liver metastases is safe and feasible: Results from a phase I study. *Ann Surg Oncol* 12: 808–816.

Vantieghem, A., Assefa, Z., Vandenabeele, P., Declercq, W., Courtois, S., Vandenheede, J. R. et al. 1998. Hypericin-induced photosensitization of HeLa cells leads to apoptosis or necrosis. Involvement of cytochrome *c* and procaspase-3 activation in the mechanism of apoptosis. *FEBS Lett* 440: 19–24.

Walker, I., Gorman, S. A., Cox, R. D., Vernon, D. I., Griffiths, J., Brown, S. B. 2004. A comparative analysis of phenothiazinium salts for the photosensitisation of murine fibrosarcoma (RIF-1) cells in vitro. *Photochem Photobiol Sci* 3: 653–659.

65

Photodynamic Drug Delivery

Julie Tzu-Wen Wang
University College London

Josephine H. Woodhams
University College London

Alexander J. MacRobert
University College London

Stephen G. Bown
University College London

Kristian Berg
Oslo University Hospital
and
Norwegian Radium Hospital

65.1 Introduction

Photodynamic therapy (PDT) is considered to be a site-specific cancer therapy because the therapeutic effects only take place in the area exposed to light. With the rapid expansion of PDT, many new drugs either chemically or endogenously synthesized have been developed and exploited in various ways. Among them, there is a group of photosensitizers with a unique intracellular distribution pattern observed under fluorescence microscopy.

These photosensitizers enter cells through endocytosis and localize at the membrane of endocytic vesicles instead of being diffusely localized in the cytosol. Upon irradiation, the generated cytotoxic agents destroy the endocytic membranes and release the content inside these organelles (e.g., lysosomal enzymes) [1,2]. Moreover, the redistribution of these sensitizers (i.e., an increase of fluorescence intensity and the change of distribution phenomenon to become diffuse) was also observed. This particular lysosomal photosensitization and the membrane disruption accompanying the release of content led to the concept of photochemical internalization (PCI)—a novel photochemical technology for inducing the release of macromolecules from endocytic vesicles [3].

Macromolecules generally refer to oligo- and polynucleotides, peptides, proteins, and polymers whose sizes are normally larger than 1 kDa. They can serve as alternatives to traditional drugs (e.g., low-molecular-weight chemotherapeutics) but their bioavailabilities are usually limited [4]. First of all, the cell membrane is normally impermeable to the aforementioned large molecular complexes, whereas

small molecules such as glucose, ions, or amino acids can quickly diffuse into cells. Secondly, even though macromolecules still can enter cells through various active internalization mechanisms called endocytosis, escaping from endocytic vesicles to reach the intracellular targets is another problem [5]. Thirdly, degradation of these macromolecules within acidic lysosomes, which contain proteolytic enzymes, is a further factor that limits efficient delivery. There is therefore growing awareness of the need to develop drug delivery systems, which can efficiently release therapeutics accumulated in endosomes and lysosomes.

The fact that macromolecules retain in intracellular vesicles and remain inactive is not ultimately a hindrance. If their biological effects can be manipulated by a delivery system, these macromolecular drugs will be superior to traditional chemotherapeutics in terms of specificity. In this regard, PCI that causes the rupture of endo/lysosomal membranes during photosensitization can provide a site-specifically light-induced delivery of macromolecules.

The aim of PCI is to relocalize the therapeutics—escape from the barrier of endo/lysosomal membrane and ability to reach their targets. In other words, the principal considerations are the drug delivery effects and the cytotoxicity from macromolecules after PCI. The light and sensitizer doses required for PCI are much lower than the ones for PDT treatment whose ultimate goal is to kill the whole cell. Moreover, because the therapeutics used for PCI are normally potent drugs but not bioavailable without efficient delivery system, the drug dose can be reduced to extremely small (compared to its LD_{50} dose) using PCI technology. For these reasons, synergistic effects are expected for PCI strategy where individual treatment (i.e., PDT and drug alone) exhibits minor effect but an enhanced killing effect can be achieved when these macromolecules are activated after photosensitization.

This is different from most of the combination therapies, which combines PDT with another treatment modality (e.g., hyperthermia, radiation therapy, antibody therapy, or chemotherapy). Although a synergistic response can be obtained if one mechanism influences the other, additive effects are often the results of these combined strategies where treatments are working independently.

PCI has been established to enhance the intracellular delivery of a large variety of macromolecules including peptides, protein toxins, and genes [6]. It has been shown to be effective for release of these therapeutics both *in vitro* and *in vivo* [7]. However, some details of PCI remain to be investigated such as the exact mechanism of membrane rupture at molecular scale and the optimization of PCI in terms of the balance of photochemical treatment and drug toxicity.

65.2 Mechanisms of Action

65.2.1 Photosensitizers and Their Subcellular Localization

To date, meso-tetraphenylporphine ($TPPS_{2a}$) and aluminum phthalocyanine disulfonate ($AlPcS_{2a}$) are the most efficient photosensitizers for PCI with two sulfonate groups on adjacent phthalate/phenyl rings (Figure 65.1). After being taken up by cells through endocytosis, these sensitizers localize specifically at the membrane of endo/lysosomes, with a hydrophobic part inserted into the membranes and a hydrophilic part free inside the vesicle matrix. This amphiphilic feature ensures their membrane localization and inhibits further penetration.

It is not expected that all endo/lysosome-localized photosensitizers are suitable to be used for PCI. The selection of PCI sensitizers is based on the property of "membrane" localization at these endocytic vesicles. The reason for this requisition is simply to limit the photochemical destruction to the membrane and therefore minimize the possible photo-damage to the delivered macromolecules in the lumen compartment. As the reactive oxygen species, particularly singlet oxygen, generated from photochemical reactions have a short diffusion distance [8,9], amphiphilic sensitizers are desirable to fulfill this certain criteria.

Evidence has also been shown that the exact lysosomal membrane localization is crucial to an efficient PCI effect [10]. To study the impact of intracellular localization of photosensitizers for PCI, several photosensitizers were examined for their ability to induce polylysine-mediated gene transfection.

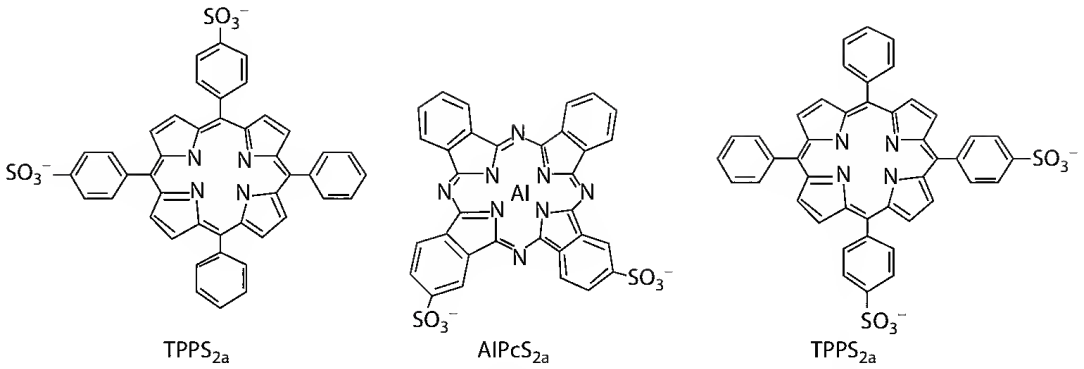

FIGURE 65.1 The structures and molecular weights of three PCI photosensitizers—(from the left) $TPPS_{2a}$, $AlPcS_{2a}$, and $TPCS_{2a}$.

This study showed that photosensitizers that are localized at the endo/lysosomal membrane (e.g., $AlPcS_{2a}$ and $TPPS_{2a}$) have the greatest effects on the transfection of plasmid encoding enhanced green fluorescent protein (EGFP). In contrast, transfection was not significantly stimulated after photoactivation of non-lysosomally localized photosensitizers (e.g., meso-tetrahydroxyphenyl porphin (3THPP) and 5-aminolevulinic acid (5-ALA)). Moreover, other hydrophilic sensitizers, such as $TPPS_4$ and Nile blue A, which localize within endocytic vesicles displayed only weak or negligible EGFP expression after exposure to light. As a result, the physical property of photosensitizers determines their intracellular localizations and amphiphilic sensitizers are the best photosensitizing compounds for PCI applications.

Amphiphilic sensitizers also exhibit some advantageous photodynamic properties [11]. The cell uptake of amphiphilic photosensitizers was detected as good as hydrophobic ones but the tendency to aggregate was lower. This is an important feature as dimerized photosensitizers are less effective in inducing photochemical reactions.

The absorbance spectrum should also be considered, especially in clinical practice, since near-infrared is preferable for deeper tissue penetration of light. Phthalocyanines have a porphyrin-based macrocycle with four benzo rings on the pyrrole units, which results in a strong absorption in the far-red region of spectrum (>670 nm) [12]. In this regard, $AlPcS_{2a}$ may be preferable to $TPPS_{2a}$ for *in vivo* or in clinic utilization.

Tetraphenylchlorin disulfonate adjacent ($TPCS_{2a}$, Amphinex®) is a new chlorin-based amphiphilic photosensitizer (PCI Biotech, Norway), which is designed for PCI (Figure 65.1). The chemical synthesis of Amphinex is rather simpler than $AlPcS_{2a}$, and it is proposed to be as efficient as the well-known chlorin sensitizer, m-THPC, regarding the photodynamic ability.

65.2.2 Light-Induced Macromolecule Delivery

Figure 65.2 depicts the principle mechanism of PCI. It contains three processes: the uptake of photosensitizer and macromolecules, the illumination and induced membrane rupture, and finally the release of macromolecules. After diffusing into the cytosol, macromolecules can thereby perform their pharmacological action when reaching their targets. The key step is the photochemically induced membrane rupture. As PCI also utilizes the same photochemical reactions as PDT, the fundamental requirements, such as the presence of oxygen and sufficient photosensitizers, are also essential to PCI.

It should be noted that the whole PCI process is dynamic, and therefore, the efficacy is highly dependent on the timing of drug (both sensitizers and macromolecules) administration and light exposure. Ideally, illumination should be carried out when sensitizers are sufficiently localized at the biomembranes, and the macromolecules have been internalized in endocytic vesicles but before being degraded

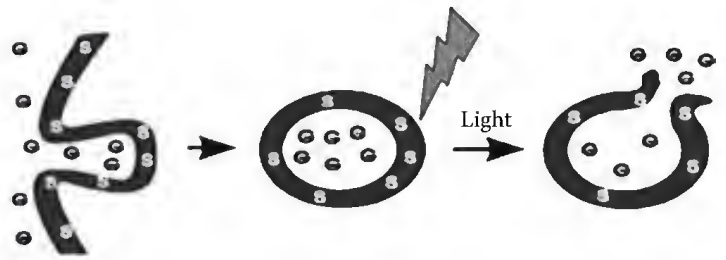

FIGURE 65.2 The principle of PCI. S: photosensitizer; G: molecules to be delivered. (From Hogset, A. et al., *Drug Deliv. Rev.*, 56, 95, 2004.)

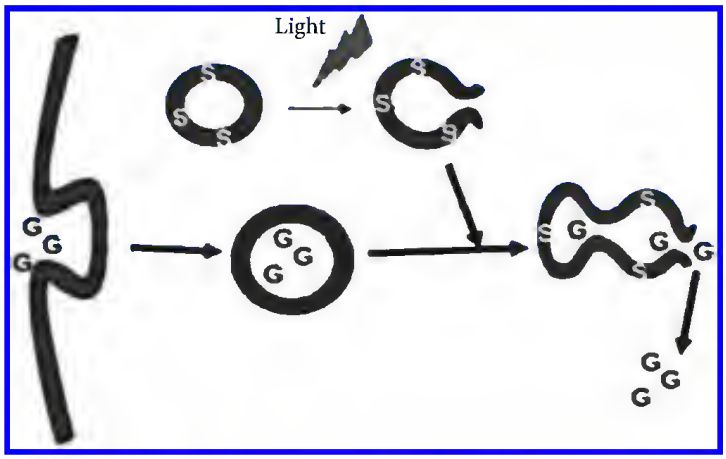

FIGURE 65.3 Possible mechanism for "light before" PCI. S: photosensitizer; G: molecules to be delivered. (Modified from Hogset, A. et al., *Drug Deliv. Rev.*, 56, 95, 2004.)

by the lysosomal enzymes. As a result, understanding the kinetics of the endocytosis of both sensitizers and macromolecules is very important.

In contrast to the conventional concept of PCI as described earlier, another strategy called "light before" PCI has been found to be as effective as or even better than "light after PCI" in some cases *in vitro* [13]. The possible mechanism is shown in Figure 65.3. Irradiation is performed after photosensitizers have been localized at the membrane of endocytic vesicles but before the administration of the macromolecules. It is suggested that the molecules will be taken up through endocytosis as well but can leak out immediately once the vesicles fuse with the ones damaged by light treatment. The foremost advantage is that the possible photochemical effects on the therapeutics should therefore be diminished since those drugs are delivered after illumination.

65.3 *In Vitro* Applications in Macromolecule Delivery

65.3.1 Peptides and Proteins

PCI has been employed to release some peptides or small proteins efficiently. It was reported that more than 60% of endocytosed horseradish peroxidase (HRP) can be released into cytosol using $TPPS_{2a}$ PCI. Similar findings were also obtained when it was shown that fluorescein-labeled ras peptide ($p21^{ras}$), a cancer-specific peptide, was colocalized granularly with $AlPcS_{2a}$ in cells but became diffuse in cytosol after light exposure [3].

The studies of PCI-induced delivery of protein have mainly focused on ribosome-inactivating proteins (RIPs), a group of protein toxins that inhibit protein synthesis by damaging ribosomes

catalytically. RIPs from plants are usually divided into two groups: Type II RIPs consist of an enzymatically active A chain (approximately 30 kDa) linked to a B chain (approximately 35 kDa), which contains a binding domain. Type I RIPs, however, which only consist of the A chain, are hardly take up by cells.

The absence of a B chain with a binding domain indeed limits the entry of type I RIPs into cells and justifies their very low toxicity to cells and to animals compared to type II RIPs, with LD_{50} for mice of 40–75 mg/kg [14]. However, if they are delivered into cells, they can induce efficient inhibition of protein synthesis. Several strategies have been employed to improve the cellular delivery of type I RIPs including enclosing them in drug carriers [15], subjecting cells to shock waves [16], and conjugating to antibodies [17]. These protein toxins are ideal model proteins to evaluate and demonstrate PCI effects.

Gelonin and saporin are two type I RIP toxins, which are mostly used in PCI strategy. The effect of PCI-induced delivery of gelonin has been investigated using several photosensitizers in a large number of cell lines of various origins [18]. The best results were found using $TPPS_{2a}$ PCI of gelonin in NHIK 3025 cells where protein synthesis was significantly reduced by more than a factor of 300 compared to each treatment alone [3].

Saporin is another type I RIP, which exerts a higher toxicity than gelonin [19]. Lai et al. investigated the PCI effect using $AlPcS_{2a}$ in combination of saporin *in vitro* [20]. In addition, the introduction of polyamidoamine (PAMAM) dendrimer to saporin showed an increased cellular uptake and cytotoxicity using PCI.

Bleomycins are a family of water-soluble glycopeptidic antibiotics with at least four functional domains mediating DNA breakage, ion binding, and O_2 activation [21]. Since first isolated by Umezawa in 1966, bleomycins have been used in combination with several anticancer agents for a number of cancer chemotherapies, notably squamous cell carcinomas and malignant lymphomas [22].

With a very high cytotoxicity, as few as 500 bleomycin molecules translocated to cytosol are sufficient to kill a cell in combination with electroporation *in vitro* [23,24]. However, due to its hydrophilic property, bleomycin penetrates membrane structures poorly and therefore accumulates in endocytic vesicles. The sensitivity of tumor cells to this drug is accordingly variable. Although many fundamental properties of bleomycin are still unknown, its therapeutic potential could be activated if delivered and exported sufficiently into cytosol.

PCI has demonstrated enhanced cell growth inhibition in combination with bleomycin *in vitro* using different cell lines [25]. Further *in vivo* studies of PCI of bleomycin will be described later.

65.3.2 Targeted Macromolecules: Immunotoxins

The targeting strategy was developed due to the demand of specific and efficient drug delivery system, especially in the *in vivo* studies. Immunotoxins are one of the designs that link antibodies with specific binding function to therapeutics which are mainly bacteria or plant protein toxins. The aims of combining targeting ligands are to achieve tumor specificity and a favorable biodistribution between normal and tumor tissues. The conjugates should meet several criteria to be used in clinical practice for cancer treatment: Because the number of receptors presenting on the cell surface is usually less than 10^5 molecules per cell, it is important to have very high toxicity to kill targeted cells efficiently. Moreover, most toxins enter the cell through the endocytic pathway; therefore, the toxin must be able to survive from the acidic compartments of endo/lysosomes and the proteolytic process [26].

Since cooperation of PCI and RIPs has inactivated protein synthesis efficiently, the use of immunotoxins—monoclonal antibody conjugated type I RIP—is believed to be able to increase the drug uptake and specificity. The first studies of PCI in combination with immuno-RIP conjugates were introduced by Selbo et al. coupling of monoclonal antibody MOC31 with gelonin [27,28]. This conjugation enables gelonin to directly bind to epithelial glycoprotein-2 (EGP-2), which is expressed on most carcinoma cells, resulting in increased uptake of the conjugates. The cell viability was significantly reduced using

$TPPS_{2a}$, $AlPcS_{2a}$, and ALA PCI compared to immunotoxins alone. Moreover, the results also show that there was no difference between immunotoxin and toxin alone in the case of using PCI in a EGP-2 negative cell line. The specificity might be very useful for *in vivo* application.

Epidermal growth factor receptor (EGFR) involves in regulating cell proliferation, metastasis, angiogenesis and is overexpressed in a variety of tumor cell lines [29], and targeting EGFR is one of the most common strategies to achieve specific cancer therapies. The EGFR inhibitor, C225, has been used as an anticancer drug in Phase-I to Phase-III trials for several malignant diseases and is approved for treatment of head and neck squamous cell carcinoma and colorectal cancer. It may therefore be a good combination employing EGFR-targeting system to PCI. Weyergang et al. established an EGF–saporin affinity toxin (biotin–streptavidin linkage) to investigate the PCI effects [30]. PCI of EGF–saporin enhanced the cytotoxicity about 1000-fold in EGFR overexpressing cells. Researchers from the same group later demonstrated increased cytotoxicity using PCI in combination with saporin-C225 complex (via the same linking method) in EGFR-positive cells [31]. The efficacy and selectivity of this combination of PCI and EGFR-targeting system indicate it can be of benefit for cancer therapies in clinic.

65.3.3 Multiple Drug Resistance (MDR)

Since PCI has been employed for enhancing the cellular uptake of drugs, which have difficulties in entering the cell, it is predicted that PCI might have the potential to deal with multiple drug resistance, which is a serious problem affecting many chemotherapy drugs. Two main mechanisms for MDR: The overexpression of p-glycoprotein (p-gp) efflux pumps leads to the extrusion of drugs from cytosol. The entrapment of anticancer drugs in endosome/lysosomes induces the degradation of drugs by lysosomal enzymes [32]. It was firstly established by Lou et al. that successful reversal of drug resistance can be induced by PCI [33]. Doxorubicin, a weak base chemotherapeutics, is often trapped in endocytic vesicles due to the increased acidification of these intracellular compartments. After $TPPS_{2a}$ PCI treatment, doxorubicin (administered after irradiation) was observed in the nuclei of MCF-7/ADR cells (a breast cancer cell line which is resistant to doxorubicin), and the drug dose required for 50% inhibition of cell survival was reduced to 10 times lower.

Another study using similar concepts also indicated the PCI effects on the improvement of drug resistance. The cytotoxicity of mitoxantrone (a chemotherapy agent) against its drug-resistant cancer cells sensitized with hypericin (a photosensitizer) was enhanced after illumination [34]. The mobilization of mitoxantrone to cell nuclei was also found after light exposure.

As pointed out earlier, there are many different phenotypes of drug resistance and some mechanisms may not be affected by PCI treatment. Selbo et al. reported that $TPPS_{2a}$ PCI has no influence in reducing the level of resistance to doxorubicin for MES-SA/Dx5 cells, a MDR cell line [35]. However, PCI of gelonin successfully reduced the cell survival. The results suggest that PCI may not be able to adjust the drug sensitivity for some MDR cells, but it still can be useful as a cancer treatment when in combination with other macromolecules.

65.3.4 Oligonucleotides

Oligonucleotides are a group of macromolecules with recognized therapeutic potential. Some of these molecules exhibit antisense effects, resulting in site-specific gene silencing in the host cell through steric blocking of gene expression or degradation of mRNA. Peptide nucleic acids (PNAs) are examples of the former action, which are DNA mimics with a pseudopeptide backbone [36]. Small interfering RNA (siRNA) molecules are the example for the latter mechanism, which are able to control gene expression through the process of RNA interference [37]. The inefficient cellular uptake is the major obstacle for both therapeutic agents [38] and, as a result, several strategies, including PCI, have been explored to enhance the drug delivery.

Recent studies have clearly shown that PCI represents an efficient delivery system for naked PNA conjugated with the catalytic component of human telomerase reverse transcriptase (hTERT-PNA) [39] and various cell-penetrating peptides (CPPs-PNA) [40]. As for siRNA molecules, substantial gene silencing was induced by PCI-mediated gene transfection of siRNA molecules against S100A4, a protein associated with the invasive and metastatic phenotype of cancer cells [41]. These promising *in vitro* results open the future applications using PCI technology for activating the biological antisense effects of oligonucleotides on animals or humans.

65.3.5 Gene Therapy

The basic principle of gene therapy is that insertion of corrective genetic material into cells alleviates the symptoms of disease. However, there are some obstacles, and consequently few successes in gene therapy. One of the main problems of gene therapy is the lack of efficient delivery systems [42] and PCI, as a novel technology for releasing macromolecules from endosomes to cytosol could provide efficient delivery for gene therapy.

Recent studies have shown encouraging results in gene transfection via either viral or nonviral vectors. $AlPcS_{2a}$-based PCI-induced EGFP/polylysine complex delivery was tested and the transfection efficiency reached above 50% of surviving cells [43]. PCI using different photosensitizers has also been examined to induce EGFP transfection, and a light-dependent transfect efficacy was found [10].

In addition, various delivery agents have been evaluated in PCI-mediated gene transfection where transfection can be enhanced using polycationic vectors [e.g., polylysine or polyethylenimine (PEI)], but was inhibited by cationic lipid vector-mediated transfection [e.g., dioleoyltrimethylammoniumpropane (DOTAP)] [44]. One possible explanation suggested was that the photochemical treatment might perturb the dissociation of DNA/DOTAP complex and cause DNA inactivation.

PCI-mediated delivery requires administration of both photosensitizers and candidate drugs or genes. There is a new design devised a complex composed of a core DNA packaged with cationic peptides and enveloped in the anionic dendrimer phthalocyanine (DPc) [45]. The concept was to reduce the administration of photosensitizers and drugs into one and was thought to be more suitable for *in vivo* application due to the integration of photosensitizers and DNA/polymer complex. After irradiation, an enhancement in transfection but with lowered photocytotoxicity was established *in vitro* compared to the results using unconjugated $AlPcS_{2a}$. This study is also the first success in PCI-mediated gene delivery *in vivo* with transgene expression in conjunctival tissues of rats.

Gene delivery through viral vectors is usually regarded as a very efficient process because of the natural occurrence of virus infections [46]. However, after being taken up into cells through endocytosis (mostly) [47], virus–DNA complex may still be trapped inside the endocytic system in cases of some virus vectors or in certain cell lines [48].

PCI-mediated gene transfection by adenoviral vectors was firstly introduced by Hogset et al. using β-galactosidase-encoding adenovirus [49]. Pronounced transduction efficiency was obtained, and the amount of virus dose was significantly lowered to achieve the same results using PCI compared with conventional adenovirus transfection (no illumination). A later study investigated the transfection efficacy of PCI-induced transduction of polycation-complexed adenovirus using several cell lines [50]. The efficacy was found to be cell type dependent but positive transgene expression was observed in all cell lines including cells with low or without the receptors to adenovirus on the cell surface.

65.4 *In Vivo* PCI Studies

Most of the *in vivo* PCI studies have been carried out using $AlPcS_{2a}$ in transplanted xenograft tumor models in nude mice. $AlPcS_{2a}$ PCI of gelonin delayed the tumor growth significantly compared to animals treated with PDT alone [51,52].

Bleomycin has been employed for *in vivo* PCI with $AlPcS_{2a}$ in four different xenograft tumors in mice [25,53]. A synergistic delay in the tumor growth was found in all models. The histological examination on the samples 7 days after surgery showed that the tumor regrowth in the peripheral zone was inhibited by PCI treatment. A further study also indicated that PCI treatment could act as an adjunct to surgery, resulting in the delay of tumor growth [54]. It is thus suggested that PCI may be suitable for treating residual tumor cells after incomplete surgical resection from the clinical point of view.

Another combination strategy was investigated using $AlPcS_{2a}$ PCI of bleomycin and radiotherapy. The time to tumor progression was increased when ionizing radiation was carried out after PCI compared to PDT or bleomycin combined with radiotherapy [55].

None of these studies quantified the effects of PCI compared with PDT other than by tumor growth delay. However, this has now been done in a normal tissue, liver. The therapeutic efficacies between AlS_2Pc PDT and PCI of gelonin were compared by measuring the necrosis induced in healthy rat liver in three dimensions [56]. The influence of drug doses and drug administration intervals to light delivery was investigated: the greatest enhancement in tissue damage was observed when gelonin was injected 1 h before irradiation and the effect was independent of the gelonin dose under a range of 5–50 μg/kg. In other words, significant treatment response can be induced with a very low dose of gelonin (5 μg/kg, 10,000 times lower than the LD_{50}). This study demonstrated the dependence of the drug–light intervals on the treatment effects and emphasized the importance of optimization of the treatment conditions. In addition, the PCI-induced relocalization of gelonin *in vivo* was established for the first time using immunohistochemistry (Figure 65.4).

Another study further compared the PCI effects of different drugs on different tissues. Experiments were undertaken using $TPCS_{2a}$ PCI in combination with saporin and bleomycin in normal rat liver/colon and a transplanted syngeneic rat fibrosarcoma model (Wang et al., unpublished). Significantly enhanced necrosis was induced in combination with saporin in liver and tumor but not colon, and with bleomycin in each case. The lack of enhanced tissue damage in colon after PCI with saporin is due to the fact that saporin does not accumulate significantly in colon, in contrast to liver and tumor. This study demonstrates that the uptake of the individual drugs in different organs can strongly affect the treatment response to PCI.

Altogether, the consistency between *in vitro* and *in vivo* experiments indicates the benefits of the PCI approach, which enhances PDT treatments and displays synergistic effects in combination with other therapeutic agents.

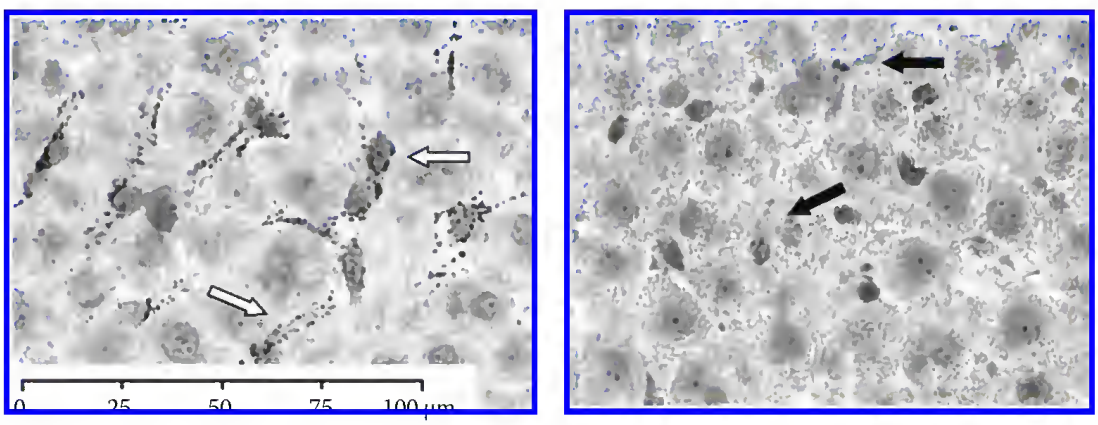

FIGURE 65.4 **(See color insert.)** PCI-induced relocalization of gelonin in rat liver. Tissues were stained with the primary antibody against gelonin and counterstained with hematoxylin. Animals were treated with 25 J light delivered 48 h after 1 mg/kg AlS_2Pc and 1 h after 500 μg/kg gelonin, examined 30 min after irradiation. (a) Area of liver not exposed to light (inset white arrows: distribution of gelonin in liver). (b) Areas exposed to light (inset black arrows: redistribution of gelonin).

65.5 Concluding Remarks and Clinical Applications

PCI is attracting interest as a novel technology for improving macromolecule delivery to cells. The key advantage of PCI is the site specificity due to the light-dependent activation of a photosensitizer, which is coadministered with the macromolecule. Additionally, PCI has the potential to approach different cancer treatments when in combination with different therapeutic agents since various macromolecules have been shown to be released by PCI and their size can range from small peptides to genetic materials. The combination with drugs coupled with specific targeting ligands may also improve the specificity of PCI treatment *in vivo* by directing drugs to the tumor cells. A recently published study demonstrated the use of a fusion toxin for PCI, which was recombinant fusion protein composed of gelonin and a single-chain Fv antibody fragment against a marker protein associated with a large number of cancer cells [57]. This construct was able to inhibit tumor growth significantly.

The uptake of photosensitizers and macromolecules varies between cell lines and so does the light sensitivity [6]. In fact, these are all factors, which relate to the optimization of PCI treatment conditions. The killing effect originating from the photochemical reaction is beneficial to cancer therapy where the final goal is to kill the malignant cells, whereas it might be a disadvantage for gene therapy of other diseases. Toward this point, optimizing the treatment conditions should therefore be emphasized again.

Collectively, PCI is a promising technology to improve a cytosolic delivery of macromolecules *in vitro* and *in vivo*. Despite the unclear mechanism, the significant release of large particles such as viral vectors indicates that PCI provides a remarkable drug delivery platform. A successful PCI should be well planned, and the photochemical reaction has to be efficient, precise, and well timed, in respect to the incorporated therapeutics.

It is important to point out that PCI is in the stage of its first clinical trial using $TPCS_{2a}$ PCI in combination with bleomycin for head and neck cancers in University College London Hospital. As a cancer treatment, the challenges will be the same as what PDT faces: the benefit of its therapeutic effects against the conventional well-established therapies, such as chemotherapy, radiation therapy, and surgery. The fact that PCI seems flexible for delivering a variety of anticancer drugs certainly broadens the future applications of PCI in clinic to deal with different cancers.

References

1. Berg, K. and J. Moan (1994) Lysosomes as photochemical targets. *Int. J. Cancer* **59**, 814–822.
2. Moan, J., K. Berg, H. Anholt, and K. Madslien (1994) Sulfonated aluminum phthalocyanines as sensitizers for photochemotherapy—Effects of small light doses on localization, dye fluorescence and photosensitivity in V79 cells. *Int. J. Cancer* **58**, 865–870.
3. Berg, K., P. K. Selbo, L. Prasmickaite, T. E. Tjelle, K. Sandvig, J. Moan, G. Gaudernack, O. Fodstad, S. Kjolsrud, H. Anholt, G. H. Rodal, S. K. Rodal, and A. Hogset (1999) Photochemical internalization: A novel technology for delivery of macromolecules into cytosol. *Cancer Res.* **59**, 1180–1183.
4. Bareford, L. M. and P. W. Swaan (2007) Endocytic mechanisms for targeted drug delivery. *Adv. Drug Deliv. Rev.* **59**, 748–758.
5. Lloyd, J. B. (2000) Lysosome membrane permeability: Implications for drug delivery. *Adv. Drug Deliv. Rev.* **41**, 189–200.
6. Hogset, A., L. Prasmickaite, P. K. Selbo, M. Hellum, B. O. Engesaeter, A. Bonsted, and K. Berg (2004) Photochemical internalisation in drug and gene delivery. *Adv. Drug Deliv. Rev.* **56**, 95–115.
7. Berg, K., A. Høgset, L. Prasmickaite, A. Weyergang, A. Bonsted, A. Dietze, P. J. Lou, S. Bown, O. J. Norum, H. M. T. Møllergård, and P. K. Selbo (2006) Photochemical internalization (PCI): A novel technology for activation of endocytosed therapeutic agents. *Med. Laser Appl.* **21**, 239–250.
8. Moan, J. and K. Berg (1991) The photodegradation of porphyrins in cells can be used to estimate the lifetime of singlet oxygen. *Photochem. Photobiol.* **53**, 549–553.

9. Niedre, M. J., M. S. Patterson, A. Giles, and B. C. Wilson (2005) Imaging of photodynamically generated singlet oxygen luminescence in vivo. *Photochem. Photobiol.* **81**, 941–943.
10. Prasmickaite, L., A. Hogset, and K. Berg (2001) Evaluation of different photosensitizers for use in photochemical gene transfection. *Photochem. Photobiol.* **73**, 388–395.
11. Allen, C. M., R. Langlois, W. M. Sharman, M. C. La, and J. E. van Lier (2002) Photodynamic properties of amphiphilic derivatives of aluminum tetrasulfophthalocyanine. *Photochem. Photobiol.* **76**, 208–216.
12. Spikes, J. D. (1986) Phthalocyanines as photosensitizers in biological systems and for the photodynamic therapy of tumors. *Photochem. Photobiol.* **43**, 691–699.
13. Prasmickaite, L., A. Hogset, P. K. Selbo, B. O. Engesaeter, M. Hellum, and K. Berg (2002) Photochemical disruption of endocytic vesicles before delivery of drugs: A new strategy for cancer therapy. *Br. J. Cancer* **86**, 652–657.
14. Battelli, M. G. (2004) Cytotoxicity and toxicity to animals and humans of ribosome-inactivating proteins. *Mini. Rev. Med. Chem.* **4**, 513–521.
15. Barbieri, L., M. G. Battelli, and F. Stirpe (1993) Ribosome-inactivating proteins from plants. *Biochim. Biophys. Acta* **1154**, 237–282.
16. Delius, M. and G. Adams (1999) Shock wave permeabilization with ribosome inactivating proteins: A new approach to tumor therapy. *Cancer Res.* **59**, 5227–5232.
17. Thorpe, P. E., A. N. Brown, J. A. Bremner, Jr., B. M. Foxwell, and F. Stirpe (1985) An immunotoxin composed of monoclonal anti-Thy 1.1 antibody and a ribosome-inactivating protein from *Saponaria officinalis*: Potent antitumor effects in vitro and in vivo. *J. Natl. Cancer Inst.* **75**, 151–159.
18. Berg, K., K. Sandvig, and J. Moan (1996) Transfer of molecules into the cytosol of cells. Patent no. PCT/NO95/00149.
19. Bolognesi, A., L. Polito, P. L. Tazzari, R. M. Lemoli, C. Lubelli, M. Fogli, L. Boon, B. M. de, and F. Stirpe (2000) In vitro anti-tumour activity of anti-CD80 and anti-CD86 immunotoxins containing type 1 ribosome-inactivating proteins. *Br. J. Haematol.* **110**, 351–361.
20. Lai, P. S., C. L. Pai, C. L. Peng, M. J. Shieh, K. Berg, and P. J. Lou (2008) Enhanced cytotoxicity of saporin by polyamidoamine dendrimer conjugation and photochemical internalization. *J. Biomed. Mater. Res. A* **87**, 147–155.
21. Hecht, S. M. (2000) Bleomycin: New perspectives on the mechanism of action. *J. Nat. Prod.* **63**, 158–168.
22. Sikic, B. I., M. Rozencweig, and S. K. Carter (1985) *Bleomycin Chemotherapy*. Academic Press, Orlando, FL.
23. Poddevin, B., S. Orlowski, J. Belehradek, Jr., and L. M. Mir (1991) Very high cytotoxicity of bleomycin introduced into the cytosol of cells in culture. *Biochem. Pharmacol.* **42**(Suppl), S67–S75.
24. Pron, G., N. Mahrour, S. Orlowski, O. Tounekti, B. Poddevin, J. Belehradek, Jr., and L. M. Mir (1999) Internalisation of the bleomycin molecules responsible for bleomycin toxicity: A receptor-mediated endocytosis mechanism. *Biochem. Pharmacol.* **57**, 45–56.
25. Berg, K., A. Dietze, O. Kaalhus, and A. Hogset (2005) Site-specific drug delivery by photochemical internalization enhances the antitumor effect of bleomycin. *Clin. Cancer Res.* **11**, 8476–8485.
26. Johannes, L. and D. Decaudin (2005) Protein toxins: Intracellular trafficking for targeted therapy. *Gene Ther.* **12**, 1360–1368.
27. Selbo, P. K., G. Sivam, O. Fodstad, K. Sandvig, and K. Berg (2000) Photochemical internalisation increases the cytotoxic effect of the immunotoxin MOC31-gelonin. *Int. J. Cancer* **87**, 853–859.
28. Selbo, P. K., O. Kaalhus, G. Sivam, and K. Berg (2001) 5-Aminolevulinic acid-based photochemical internalization of the immunotoxin MOC31-gelonin generates synergistic cytotoxic effects in vitro. *Photochem. Photobiol.* **74**, 303–310.
29. El-Rayes, B. F. and P. M. LoRusso (2004) Targeting the epidermal growth factor receptor. *Br. J. Cancer* **91**, 418–424.
30. Weyergang, A., P. K. Selbo, and K. Berg (2006) Photochemically stimulated drug delivery increases the cytotoxicity and specificity of EGF–saporin. *J. Control. Release* **111**, 165–173.

31. Yip, W. L., A. Weyergang, K. Berg, H. H. Tonnesen, and P. K. Selbo (2007) Targeted delivery and enhanced cytotoxicity of cetuximab–saporin by photochemical internalization in EGFR-positive cancer cells. *Mol. Pharm.* **4**, 241–251.
32. Gottesman, M. M., T. Fojo, and S. E. Bates (2002) Multidrug resistance in cancer: Role of ATP-dependent transporters. *Nat. Rev. Cancer* **2**, 48–58.
33. Lou, P. J., P. S. Lai, M. J. Shieh, A. J. Macrobert, K. Berg, and S. G. Bown (2006) Reversal of doxorubicin resistance in breast cancer cells by photochemical internalization. *Int. J. Cancer* **119**, 2692–2698.
34. Adigbli, D. K., D. G. Wilson, N. Farooqui, E. Sousi, P. Risley, I. Taylor, A. J. Macrobert, and M. Loizidou (2007) Photochemical internalisation of chemotherapy potentiates killing of multidrug-resistant breast and bladder cancer cells. *Br. J. Cancer* **97**, 502–512.
35. Selbo, P. K., A. Weyergang, A. Bonsted, S. G. Bown, and K. Berg (2006) Photochemical internalization of therapeutic macromolecular agents: A novel strategy to kill multidrug-resistant cancer cells. *J. Pharmacol. Exp. Ther.* **319**, 604–612.
36. Pooga, M., T. Land, T. Bartfai, and U. Langel (2001) PNA oligomers as tools for specific modulation of gene expression. *Biomol. Eng.* **17**, 183–192.
37. Dykxhoorn, D. M., C. D. Novina, and P. A. Sharp (2003) Killing the messenger: Short RNAs that silence gene expression. *Nat. Rev. Mol. Cell Biol.* **4**, 457–467.
38. Koppelhus, U., S. K. Awasthi, V. Zachar, H. U. Holst, P. Ebbesen, and P. E. Nielsen (2002) Cell-dependent differential cellular uptake of PNA, peptides, and PNA-peptide conjugates. *Antisense Nucleic Acid Drug Dev.* **12**, 51–63.
39. Folini, M., K. Berg, E. Millo, R. Villa, L. Prasmickaite, M. G. Daidone, U. Benatti, and N. Zaffaroni (2003) Photochemical internalization of a peptide nucleic acid targeting the catalytic subunit of human telomerase. *Cancer Res.* **63**, 3490–3494.
40. Shiraishi, T. and P. E. Nielsen (2006) Photochemically enhanced cellular delivery of cell penetrating peptide-PNA conjugates. *FEBS Lett.* **580**, 1451–1456.
41. Boe, S., A. S. Longva, and E. Hovig (2007) Photochemically induced gene silencing using small interfering RNA molecules in combination with lipid carriers. *Oligonucleotides* **17**, 166–173.
42. Verma, I. M. and N. Somia (1997) Gene therapy—Promises, problems and prospects. *Nature* **389**, 239–242.
43. Hogset, A., L. Prasmickaite, T. E. Tjelle, and K. Berg (2000) Photochemical transfection: A new technology for light-induced, site-directed gene delivery. *Hum. Gene Ther.* **11**, 869–880.
44. Prasmickaite, L., A. Hogset, T. E. Tjelle, V. M. Olsen, and K. Berg (2000) Role of endosomes in gene transfection mediated by photochemical internalisation (PCI). *J. Gene Med.* **2**, 477–488.
45. Nishiyama, N., A. Iriyama, W. D. Jang, K. Miyata, K. Itaka, Y. Inoue, H. Takahashi, Y. Yanagi, Y. Tamaki, H. Koyama, and K. Kataoka (2005) Light-induced gene transfer from packaged DNA enveloped in a dendrimeric photosensitizer. *Nat. Mater.* **4**, 934–941.
46. Anderson, W. F. (1998) Human gene therapy. *Nature* **392**, 25–30.
47. Greber, U. F., M. Willetts, P. Webster, and A. Helenius (1993) Stepwise dismantling of adenovirus 2 during entry into cells. *Cell* **75**, 477–486.
48. Hansen, J., K. Qing, H. J. Kwon, C. Mah, and A. Srivastava (2000) Impaired intracellular trafficking of adeno-associated virus type 2 vectors limits efficient transduction of murine fibroblasts. *J. Virol.* **74**, 992–996.
49. Hogset, A., B. O. Engesaeter, L. Prasmickaite, K. Berg, O. Fodstad, and G. M. Maelandsmo (2002) Light-induced adenovirus gene transfer, an efficient and specific gene delivery technology for cancer gene therapy. *Cancer Gene Ther.* **9**, 365–371.
50. Bonsted, A., B. O. Engesaeter, A. Hogset, G. M. Maelandsmo, L. Prasmickaite, O. Kaalhus, and K. Berg (2004) Transgene expression is increased by photochemically mediated transduction of polycation-complexed adenoviruses. *Gene Ther.* **11**, 152–160.
51. Dietze, A., Q. Peng, P. K. Selbo, O. Kaalhus, C. Muller, S. Bown, and K. Berg (2005) Enhanced photodynamic destruction of a transplantable fibrosarcoma using photochemical internalisation of gelonin. *Br. J. Cancer* **92**, 2004–2009.

52. Selbo, P. K., G. Sivam, O. Fodstad, K. Sandvig, and K. Berg (2001) In vivo documentation of photochemical internalization, a novel approach to site specific cancer therapy. *Int. J. Cancer* **92**, 761–766.
53. Norum, O. J., J. V. Gaustad, E. Angell-Petersen, E. K. Rofstad, Q. Peng, K. E. Giercksky, and K. Berg (2009) Photochemical internalization of bleomycin is superior to photodynamic therapy due to the therapeutic effect in the tumor periphery. *Photochem. Photobiol.* **85**, 740–749.
54. Norum, O. J., K. E. Giercksky, and K. Berg (2009) Photochemical internalization as an adjunct to marginal surgery in a human sarcoma model. *Photochem. Photobiol. Sci.* **8**, 758–762.
55. Norum, O. J., O. S. Bruland, L. Gorunova, and K. Berg (2009) Photochemical internalization of bleomycin before external-beam radiotherapy improves locoregional control in a human sarcoma model. *Int. J. Radiat. Oncol. Biol. Phys.* **75**, 878–885.
56. Woodhams, J. H., P. J. Lou, P. K. Selbo, C. A. Mosse, D. Oukrif, A. J. Macrobert, M. Novelli, Q. Peng, K. Berg, and S. Bown (2010) Intracellular relocalisation by photochemical internalisation enhances the cytotoxic effect of gelonin—Quantitative studies in normal rat liver. *J. Control. Release* **142**(3), 347–353.
57. Selbo, P. K., M. G. Rosenblum, L. H. Cheung, W. Zhang, and K. Berg (2009) Multi-modality therapeutics with potent anti-tumor effects: Photochemical internalization enhances delivery of the fusion toxin scFvMEL/rGel. *PLoS One* **4**, e6691.

66

Phototoxicity of Drugs

Virginie Lhiaubet-Vallet
Universidad Politécnica de Valencia-CSIC

Miguel Angel Miranda
Universidad Politécnica de Valencia-CSIC

66.1 Introduction

Photosensitizing effects of xenobiotics are of increasing concern in dermatology since modern lifestyle often associates sunlight exposure with the presence of chemical substances in the skin. Photosensitization is defined by the development of abnormal cutaneous reactions triggered by sunlight doses regarded as harmless, most often in the UVA range (320–400 nm). The photosensitizing compound, generally not toxic by itself, becomes reactive under irradiation. An important number of chemicals like perfumes, sunscreen components, or therapeutic agents have been reported as photosensitizers [1–5].

In this context, a number of efforts have been made to design a model system for photosafety assessment. Indeed, screening for phototoxicity is necessary at the early phase of drug discovery process, even before introducing drugs and chemicals into clinical therapy, to prevent undesired photoreactions in humans. In the case of new pharmaceutical or cosmetic compounds, their phototoxic potential has to be tested when they absorb in the regions corresponding to the solar spectrum, that is, for wavelengths >290 nm. So, there is an obvious need for a screening strategy based on *in vitro* experiments. Until now, the 3T3 neutral red uptake (NRU) test is the only validated *in vitro* method for phototoxicity assessment [6]. In spite of its advantages, it also shows some limitations. Thus, it addresses on phototoxicity and does not provide any information on photogenotoxicity, photocarcinogenicity, photoallergy, etc. Moreover, the large number of "false positives" might rule out some useful highly active therapeutic substances.

In this chapter, the attention will be focused on photosensitization by drugs and especially on two well-established photoactive families: the arylpropionic acid derivatives acting as nonsteroidal anti-inflammatory drugs (NSAIDs) and the fluoroquinolone (FQ) antibiotics [7–26]. First, a summary of clinical reports and *in vitro* assessment of phototoxicity by the 3T3 NRU test over the 10 last years is provided. Then, a mechanistically based strategy is presented in order to get insights into the molecular mechanism of drug photosensitization.

66.2 Clinical and Experimental Data on Humans

A systematic approach including pertinent patient history, physical examination, phototesting, and laboratory investigation is essential for evaluating a photosensitive patient. Photosensitivity induced by exogenous agents can be divided into two phenomena: phototoxicity and photoallergy.

Phototoxicity can be elicited by a wide range of pharmaceutical agents (but also by their metabolites or photoproducts). The reaction is essentially immediate and resembles an exaggerated sunburn. It is dependent on the photosensitizer concentration in the skin and on the light dose received. Phototoxic reactions are much more prevalent than photoallergic ones; they exhibit a maximum intensity early after ultraviolet (UV) exposure, followed by a decrescendo evolution within 24–72 h. Eruptions occur on exposed skin areas, giving a clear delineation of shading caused by clothing. The lesions are characterized by erythema, infiltration, edema, or blisters, followed by desquamation and hyperpigmentation. It has also been suggested that repeated phototoxic reactions have the potential to increase the already high risk of skin cancer from sunburn [4].

By contrast, photoallergy is uncommon and immunologically mediated requiring previous exposure to the photosensitizing agent and an induction period. In some cases, sensitization may be provoked by a structurally related chemical, a phenomenon that is called cross-reactivity. Clinically, it is very similar to plain contact allergic reactions, with a delayed onset and a crescendo reaction pattern. Photoallergic contact dermatitis may generally affect well-defined areas exposed to sunlight. However, it may extend to other parts of the body, sometimes distant from the initially affected area. The corresponding skin lesions are erythema, infiltration, papulovesicles, erosions, or bullae. The molecular mechanism completely differs from that of phototoxicity; the irradiated drug (metabolite or photoproduct) plays the role of a photohapten, which may covalently bind to a carrier protein (photobinding), giving rise to a photoantigen able to trigger the immunological process.

Diagnosis of drug-induced photosensitization can be clinically made by photopatch testing. Nevertheless, the methodology is not fully standardized; this could result in variations of the results from studies performed in different laboratories. Photopatch testing consists of topical application of the suspected agent (epicutaneous administration) on the upper back of the patient in duplicate; one area is then exposed to UV lamps (at suberythematogenic dose), whereas the other one is kept covered. Both, the UV shielded and nonshielded areas, are evaluated immediately, after 24 h, and up to 72 h after testing. The photosensitizing character of a chemical is positively established when its presence results in reduction of the minimal erythemal dose (MED, leading to the first faint reddening of the skin). Reactions are generally graded to a 4-point scale: 0, no reaction; 1, erythema; 2, erythema and dermal infiltrate; 3, erythema and blisters or erosions.

Arylpropionic acid derivatives are NSAIDs widely used for their analgesic and antirheumatic properties. Their photosensitive potential has largely been reported over the years, with the first photoallergic contact dermatitis to ketoprofen (KP) published in 1985 [27]. As shown in Table 66.1, KP, tiaprofenic acid, suprofen, naproxen, piketoprofen, and carprofen induce skin photosensitivity (Figure 66.1) [1,2,7–20]. Among these drugs, KP is by far the most frequently reported causing photoallergic contact dermatitis [2,16,17,28,29]. KP is administered in more than 70 countries in various forms of systemic or topical application: poultice, gel, tape, cream, oral medicine, suppository, and injection. However, the largest number of photosensitive disorders reported for this drug might be associated with its topical use, a formulation that is available in many countries without medical prescription (over the counter). An overview of photosensitivity disorders induced by topical drugs has shown that KP represents the majority of cases (i.e., 82%) although it is less used than diclofenac [17]. Severe skin dermatitis was reported as pruritic and papulovesicular, bullous, and edematous lesions, often leading to residual pigmentation (Table 66.1). Treatment of these skin symptoms required systemic corticotherapy [7,9,14] and eventually hospitalization [7,9]; KP was also found to induce prolonged photosensitivity in some cases [8,9,28].

In addition, cross-reactivity to KP has frequently been evidenced. It is now recognized that the benzophenone moiety, rather than the arylpropionic acid side chain, is responsible for the photoallergy triggered by this drug, which explains the cross-reactions elicited by suprofen, tiaprofenic acid, fenofibrate,

TABLE 66.1 Photosensitization Cases Reported during the Last 10 Years for Arylpropionic Acid NSAIDs or FQ Antibiotics

Family	Drug	Reference (No. of Patients in the Study)	Observed Effects (No. of Cases)	Photopatch or Phototest +/− (No. of Cases)	Cross-Reactivity
NSAIDs	Ketoprofen	[7] (42)	Pruritic and papulovesicular (42)/ bullous (21)/ edematous (28)	+ (38)	Etofenamate Suprofen
		[8] (18)	Pruritic and papulovesicular (13)/ bullous (5)	+ (18)	Fenofibrate Tiaprofenic acid Chlorproethazine Chlorpromazine Promethazine Chlorhexidine Triclosan Fentichlor Hexachlorophene
		[9] (18)	Pruritic papulovesicular dermatitis (10)/ bullous lesions (6)/ marked edema mimicking erysipelas (2)	+ (16)	Diclofenac[a]
		[10] (4)	Itchy erythema, bulla and swelling, vesicles (4)		Tiaprofenic acid Suprofen
		[11][b]	Pruritic erythema and blister, residual pigmentation	+	Piketoprofen
		[12] (3)	Eczematous lesions	+ (3)	Fentichlor[a] Promethazine Tetrachlorosalicylanilide
		[13] (6)	Strong eczematous with bullous lesions (6)	+ (6)	
		[14](5)	Severe acute dermatitis (5)	+ (5)	Tiaprofenic acid Suprofen
		[15] (2)[b]	Acute eczema, dermatitis	+ (2)	
		[16] (391)	*N.R.* (19)		
		[17] (139)		+ (68)	
		[18] (35)		+ (35)	Fenofibrate Fentichlor Tetrachlorosalicylanilide Chlorpromazine Bithionol Promethazine
		[1] (83)		+ (2)	
		[2] (1082)		+ (110)	
	Tiaprofenic acid	[3] (1600)		+	

(*continued*)

TABLE 66.1 (continued) Photosensitization Cases Reported during the Last 10 Years for Arylpropionic Acid NSAIDs or FQ Antibiotics

Family	Drug	Reference (No. of Patients in the Study)	Observed Effects (No. of Cases)	Photopatch or Phototest +/− (No. of Cases)	Cross-Reactivity
	Carprofen	[3] (1600)		+	
		[19] (2)	Itchy, erythematous facial skin severe dermatitis	+ (2)	
		[20] (1)	Pruritic erythematous eczematous eruption	+	
	Piketoprofen	[17] (139) [16] (391)	*N.R.* (2)	+ (4)	Ketoprofen
	Naproxen	[16] (391)	*N.R.* (3)		
	Ibuprofen	[16] (391)	*N.R.* (1)		
FQs	Grepafloxacin	[16] (391)	*N.R.* (14)		
	Ciprofloxacin	[16] (391)	*N.R.* (7)		
		[21] (12)		+[c]	
		[22] (99)	+ (48) Cystic fibrosis		
		[23] (1)	Exanthematous pustulosis		
	Trovafloxacin	[16] (391)	*N.R.* (2)		
		[24] (8)	(Sub)acute eczema, sunburn-like	+ (1)	
		[21] (12)		+[c]	
	Enoxacin	[25] (8)		+[c]	
	Sparfloxacin	[25] (4)		+[c]	
		[26] (371)	Solar erythema, blisters (23%), hyperpigmentation/ scarring and recurrent phototoxicity		
	Sitafloxacin	[25] (8)		+[c]	
	Lomefloxacin	[21] (12)		+[c]	

N.R. not reported.
[a] Possibility of a cosensitization process.
[b] Use of the enantiomerically pure (S)-KP, also known as dexketoprofen.
[c] Phototesting performed after systemic administration of the drug.

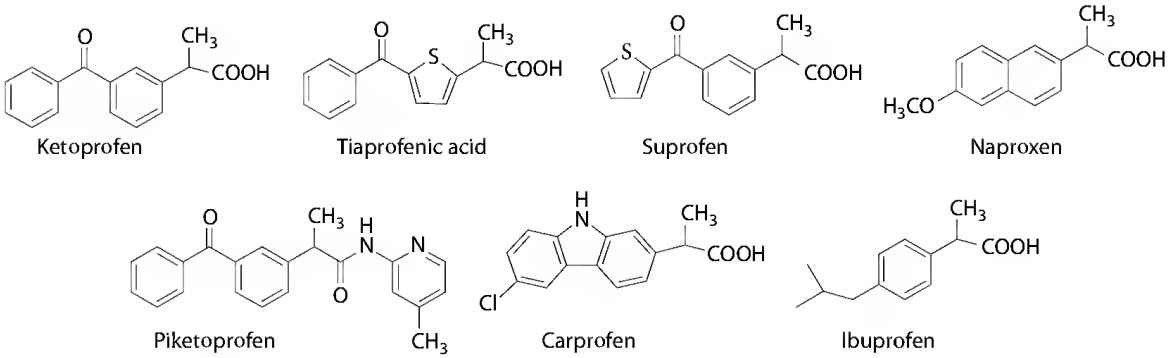

FIGURE 66.1 Structure of the phototoxic NSAIDs.

or piketoprofen [7,10,11,14,17]. Qualitative structure-activity relationships are clear for this series of compounds, bearing a diaryl ketone moiety. Nevertheless, some positive reactions to the photopatch test have been interpreted as resulting from potential cosensitization (i.e., fentichlor) [8,12,17].

It is noteworthy that notification of a large number of photosensitivity reactions to topical KP has modified its conditions of use in some countries. In France, topical preparations containing KP have been recently withdrawn from the market, waiting for a reevaluation of the risk/benefit ratio by the European Medicine Agency (EMEA) [30].

FQs are antibacterial agents with activity against a variety of Gram-positive and Gram-negative organisms. Cutaneous photosensitivity is relatively uncommon, but characteristic side effects of FQs are recognized to be caused by either a phototoxic or a photoallergic mechanism [16,17,21–26]. A related drug, nalidixic acid, has been registered as a photosensitizer since 1964 in Europe [24]. Phototoxicity cases have been described for most FQs (Figure 66.2). Interesting data from the French drug monitoring system reveal that the rate of treated patients suffering phototoxicity were 0.4% for sparfloxacin, 0.12% for lomefloxacin, 0.005% for pefloxacin, 0.0003% for ofloxacin, and 0.0001% for ciprofloxacin and norfloxacin (NFX) [26,31]. Thus, it is evident that FQs with two halogen substituents at positions 6 and 8 have a greater photosensitizing potential (i.e., lomefloxacin, sparfloxacin, fleroxacin) [21,25,26].

Interestingly, it has been shown that 8-halogenated FQs induce severe skin reaction in comparison with the low phototoxicity exhibited by 8-methoxy derivatives [32]. This can be correlated with the higher photostability of the latter, as compared with the efficient dehalogenation of the former, which gives rise to highly reactive carbene intermediates.

Phototosensitivity induced by FQs shows a spectrum from moderate reactions, that is, erythema, edema, desquamation, and hyperpigmentation, to more severe cases of blistering and scarring that might require hospitalization (Table 66.1). Systemic administration of ciprofloxacin provoked a case of photoinduced acute exanthematous pustulosis characterized by the rapid onset of photodistributed cutaneous pustules, fever, and leukocytosis [23].

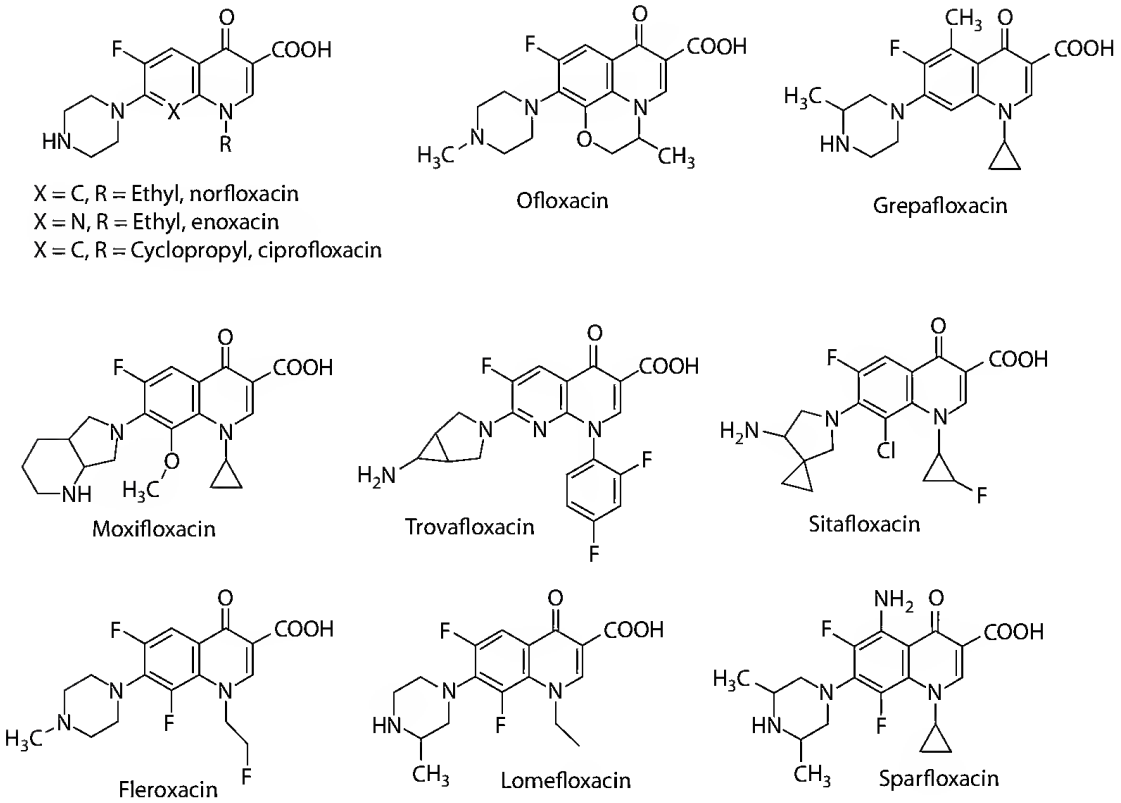

FIGURE 66.2 Structure of the phototoxic FQs.

It is remarkable that FQ photosensitization, in addition to induce skin photoreactions, is also suspected to be responsible for cutaneous photocarcinogenicity, as revealed by *in vivo* studies on mice [33–35].

66.3 *In Vitro* Phototoxicity Testing

The current protocol for phototoxicity testing is based on the *in vitro* 3T3 NRU assay. This is now recommended by the European Union Commission and member states for all compounds showing significant absorption of UVA and visible light. It is based on a protocol validated in 1998 by the European Centre for the Validation of Alternative Methods (ECVAM) and the European Cosmetic, Toiletry and Perfumery Association (COLIPA) and later in 2004 at a worldwide level by the Organization for Economic Cooperation and Development (OECD) [6,36,37].

The principle of this assay is to compare the cytotoxic potential of the considered chemicals to Balb/c 3T3 mouse fibroblasts when tested with and without UV irradiation (dose of $5\,J \times m^{-2}$). Viability is assessed 24 h after treatment by spectroscopic measurements of the vital dye neutral red (NR) uptake by the cell, as dead and damaged cells are unable to take up and retain NR. Cytotoxicity is expressed as a dose-dependent reduction of the growth rate of cells in the presence and in the absence of UV irradiation. The EC_{50} values are obtained from the concentrations of the test compounds causing a 50% reduction in NR dye. Then, the photoirritation factor (PIF) is calculated as the ratio between EC_{50} with and without UV light. A cutoff value of PIF = 5 for predicting the phototoxic potential of a chemical has been established, thus any chemical with a higher value is defined as having a potential phototoxic hazard.

In spite of its proved usefulness, it is now well established that a high number of compounds reported as positive in the 3T3 NRU assay are negative when tested *in vivo* using animal models. The important occurrence of these "false positives" (over predicting the human hazard) has encouraged the development of new strategies to assess and understand the phototoxic potential of drugs. Nevertheless, it should be underlined that this assay predicts negatives with excellent fidelity.

Another limitation of the 3T3 NRU test is that it has been designed to assess the photoirritant potency of compounds, and thus, it does not allow prediction of other important adverse photobiological effects, such as photogenotoxicity, photocarcinogenicity, or photoallergenic potential.

Table 66.2 summarizes the 3T3 NRU test results obtained with arylpropionic acids active as NSAIDs and with the antimicrobial FQ [38–40]. The high PIF values reported for KP and tiaprofenic acid are in agreement with the clinical data discussed earlier.

TABLE 66.2 PIF Values of Arylpropionic Acids (NSAIDs) and FQ Antibiotics Obtained during 3T3 Assays

Family	Drug	3T3 NRU Test	Reference
NSAIDs	Ketoprofen	PIF > 488	[38]
	Tiaprofenic acid	PIF 714.5	[38]
FQs	Ciprofloxacin	PIF 1.7	[39]
		PIF 5.35	[40]
	Sparfloxacin	PIF 10	[39]
		PIF 8.44	[40]
	Lomefloxacin	PIF 4	[39]
		PIF 6.88	[40]
	Ofloxacin	PIF > 6.5	[38]
	Norfloxacin	PIF > 25.5	[38]
		PIF 5.17	[40]
	Moxifloxacin	PIF 1	[39]
	Nadixilic acid	PIF 13.6	[40]

Literature data recovered from the last 10 years.

In the case of FQs, moxifloxacin and ciprofloxacin appear to be nonphotoirritant drugs with PIF values <2, whereas the other tested FQs exhibited a higher phototoxic potential.

66.4 Mechanistically Based Studies

66.4.1 General Reaction Scheme

A mechanistically based strategy taking into account the sensitizer's photophysical and photochemical properties has to be considered for a deeper understanding of the molecular processes involved in the photosensitivity side effects. In this way, study of well-established phototoxic drugs provides helpful information on the mechanisms. This knowledge can then be applied in the drug development process to design new pharmaceutics with a higher photosafety.

Such a strategy should include not only the study of photophysical and photochemical properties of the drug alone but also in the presence of biomolecules like lipids, proteins, DNA, and their simple building blocks.

The primary characteristic for a compound to be considered a potential photosensitizing agent is absorption in the UVA–UVB and visible range (i.e., at $\lambda > 290$ nm). After photon absorption, the molecule reaches a singlet excited state (Scheme 66.1). This generally short-lived state (in the nanosecond timescale) decays by different processes: (1) fluorescence, (2) intramolecular reactions generating reactive intermediates and/or photoproducts formation, (3) nonradiative processes like internal conversion, and (4) intersystem crossing leading to the population of the triplet excited state. It has been recognized that triplet states (with lifetimes of 10^{-6} to 10^{-3} s) are the key intermediates responsible for intermolecular reactions. Indeed, these states are considered as the biologically active species, due to their central role in the photosensitization of biomolecules. Generally, photosensitized reactions are classified into two processes. Type I mechanisms including H-abstraction or electron transfer processes result in the production of radical species that can further lead to oxidation of biomolecules. On the other hand, in type II mechanisms, energy transfer to molecular oxygen gives rise to the formation of reactive singlet oxygen, which in turn reacts with biological substrates.

To illustrate this concept, the results available for two relevant photosensitizing drugs, namely KP and NFX, will be considered for type I and type II processes, respectively.

66.4.2 Ketoprofen

66.4.2.1 Photophysical and Photochemical Properties

KP shows a maximum of absorption at 260 nm with an extended spectrum reaching the UVA region up to 350 nm. Its photochemistry in neutral aqueous media is dominated by an efficient photodecarboxylation ($\phi = 0.75$) triggered by intramolecular electron transfer from the carboxylate group to the

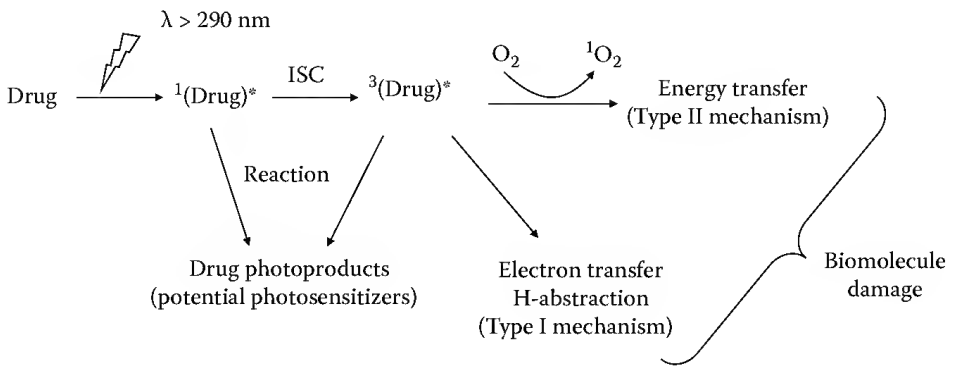

SCHEME 66.1 Mechanistic pathways involved in photosensitization by drugs.

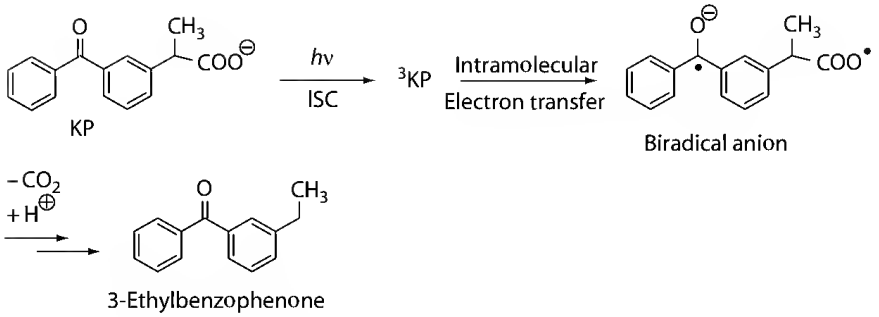

SCHEME 66.2 Mechanism of KP photodecomposition resulting in formation of the major product, 3-ethylbenzophenone.

excited carbonyl [41]. Steady-state irradiation gives rise to a variety of photoproducts, the major one being 3-ethylbenzophenone (Scheme 66.2).

From a photophysical point of view, KP exhibits an intersystem crossing quantum yield of unity, which results in quantitative population of its triplet state. Phosphorescence experiments show the typical characteristics of benzophenone-derived emission with an $n\pi^*$ nature and a triplet excited state energy of 69.3 kcal × mol^{-1}. Picosecond laser flash photolysis studies reveal formation of several transients, including a very short-lived triplet state (λ = 526 nm and lifetime of ca. 250 ps) and a biradical anion (λ = 570 nm and lifetime ca. 120 ns) [42,43].

Moreover, it has been shown that such photodecarboxylation process is retarded by a simple modification based on keeping away the carboxylate from the ketone carbonyl group and maintaining intact the arylpropionic part of KP. In this context, derivatization of KP with glycine results in a remarkable decrease of the photodecarboxylation quantum yield ($\phi < 0.06$); thus, it allows its photophysical study and determination of excited triplet state quenching rate constants by amino acids and nucleosides in phosphate buffer saline solution (PBS) [44].

Reactive oxygen species (ROS), that is, singlet oxygen, superoxide anion, and hydroxyl radical are formed during KP photolysis [41,45]. However, the high photolability of the drug renders it a poor candidate for ROS generation. A potentially superior photosensitizer is its main photoproduct, 3-ethylbenzophenone, which exhibits a singlet oxygen quantum yield of 0.29.

It is important to underline that photophysical and photochemical characteristics are dependent on the medium, in such a way that results obtained in PBS can only provide an approximation of drug behavior in a biological environment. As an example, laser flash photolysis studies of NSAIDs showed a remarkable increase of triplet excited state lifetimes when the drug is complexed with human or bovine serum albumin (HSA or BSA) [46,47]. In the case of KP, such increase represents more than three orders of magnitude (from 250 ps in PBS to 500 ns in HSA) [48,49]. It has been hypothesized that interaction of the negatively charged carboxylate group with positively charged amino acids disfavors intramolecular reactivity, thus enhancing the relatively slower intermolecular processes.

66.4.2.2 Interactions with Biomolecules

The strong photosensitizing properties of KP have been assigned to its benzophenone chromophore with a lowest lying $n\pi^*$ triplet excited state. Accordingly, it should exhibit an important reactivity as H-acceptor compound, and in fact a major contribution of type I processes has been observed in KP photosensitization.

66.4.2.2.1 Lipid Peroxidation

Hydrogen abstraction from target biomolecules appears to be the main process responsible for KP-induced phototoxicity, playing a key role in photodynamic lipid peroxidation, which is in the

origin of cell membrane lysis. Indeed, radical-mediated photohemolysis of red blood cells by KP has been described [41,50]. For a better understanding of the chemical mechanisms, studies were performed with linoleic acid and cholesterol, two structural components of cell membrane that may be oxidized by type I and/or type II mechanisms.

After irradiation in the presence of KP, lipid-derived dienic hyperoxides are produced. A type I mechanism initiated by abstraction of the double allylic hydrogen by the excited benzophenone moiety has been shown to occur, as the key step in radical chain oxygenation [41]. The KP ability to induce lipid peroxidation can be correlated with its potential to produce cell membrane lysis.

Further mechanistic studies have been performed on model diastereoisomeric bichromophoric model compounds containing KP tethered to cholesterol, but also to tetrahydrofuran, 1,4-cyclohexadiene, or isopropylbenzene derivatives as hydrogen donors. For the KP–cholesterol model, intramolecular hydrogen abstraction from the 7-allyl cholesterol position by the benzophenone moiety was established by laser flash and steady-state photolysis. This was based on detection of a transient species assigned as a ketyl–allyl biradical and, on the isolation and characterization of macrocyclic photoproducts arising from C–C coupling [51,52]. Similar results were obtained for KP tethered to the other H-donors [53–56]. Interestingly, chiral discrimination was demonstrated not only in the photoreactivity of the dyads but also in their very short triplet excited state lifetimes.

66.4.2.2.2 DNA Damage

DNA damage is not directly linked with phototoxicity; nevertheless, it is now well established that lethal, mutagenic, and/or carcinogenic effects might be the result of photochemical modification of DNA.

KP photosensitization of supercoiled ϕX174 DNA induces single-strand breaks (ssb) formation. A type I mechanism has been assessed by the use of radical scavengers [41]. On the basis of gel sequencing experiments, an electron transfer mechanism between the guanine nucleobase and the excited drug has been proposed. Indeed, after alkali-labile treatment of ^{32}P-labeled oligonucleotide, selective DNA strand break at the 5′-G of a –GG– site is observed as a hallmark of electron transfer process. Accordingly, negative values of free energy changes have been determined by the Rehm Weller equation [45]. These results are in agreement with the bimolecular rate constant of $1 \times 10^9\ M^{-1} \times s^{-1}$ obtained by laser flash photolysis for the interaction between triplet excited state of KP and 2′-deoxyguanosine [57]. A recent mechanistic study of KP–purine dyads also supports an intramolecular electron transfer from the nucleobase to KP. This initial step is followed by subsequent deprotonation of the C1′ purine radical cation leading to the generation of 2-deoxyribonolactone [58].

Moreover, formation of cyclobutane thymine dimers has been evidenced by the use of T4 endonuclease V, a DNA repair enzyme that specifically recognizes this lesion [41,45]. Thymine dimers are mutagenic damages formed by a triplet-triplet energy transfer mechanism from the excited state of the photosensitizer to the thymine triplet state. Indeed, this process is thermodynamically favored for KP, as its triplet state energy is $5\,kcal \times mol^{-1}$ higher than that of thymine in DNA, a value recently established at $64\,kcal \times mol^{-1}$ [59].

The ability of KP to induce DNA damage in the more complex environment of the whole cell has been assessed by the alkaline comet assay [60]. However, the major role of the 3-ethylbenzophenone photoproduct has been hypothesized from the observation of a delayed mechanism.

66.4.3 Norfloxacin

FQs have been reported to produce phototoxic, photoallergic, photomutagenic, and phototumorigenic effects, both *in vitro* and *in vivo* [34,61,62]. The photoreactivity of the 6,8-dihalogenated drugs has been associated with an efficient dehalogenation that results in the generation of highly reactive intermediates, able to attack biological components. By contrast, the phototoxic potential of some monohalogenated FQs has been related to type II processes.

66.4.3.1 Photophysical and Photochemical Studies

It is now well established that the excited state properties of FQs are strongly dependent on the pH as expected from the presence of both a carboxylic group and 7-amino substituent in their structures (pKa_1 5.5–6.5 and pKa_2 ca. 8.5). For biological studies, the experiments are generally performed in neutral aqueous solutions, where the prevailing FQ species is the zwitterionic form.

In phosphate buffer, NFX absorption spectrum is characterized by an intense absorption band that peaks at 275 nm, a weaker band centered at 340 and a long tail extending until 380 nm [63]. Under the same conditions, a fluorescence emission at λ_{max} = 410 nm, with a quantum yield of ca. 0.1 and a lifetime of 1.5 ns has been reported [63–66]. The singlet excited state is not significantly reactive, and an important deactivation channel is intersystem crossing to the triplet manifold. This excited state is detected by laser flash photolysis as a triplet-triplet transition centered at 620 nm and characterized by a lifetime of 3.5 μs, a molar absorption coefficient of $\varepsilon = 7900\ M^{-1} \times cm^{-1}$, and an intersystem crossing quantum yield of 0.52 [59]. Moreover, NFX triplet excited state energy has been determined at room temperature by applying Sandros' equation to the rate constants of energy transfer to a series of acceptors. The obtained value, estimated at 64.3 kcal × mol^{-1}, is close to that observed by low temperature phosphorescence measurements [64]. A particular property of FQs is their dynamic triplet state quenching by phosphate; a rate constant of $k_q = 8 \times 10^7\ M^{-1} \times s^{-1}$ has been determined for NFX [64].

The main photoreaction observed is heterolytic defluorination from the triplet state manifold [66,67]. However, important changes are induced by phosphate both in the decomposition quantum yields and in photoproduct distribution. Photolysis of NFX in neat water has a quantum yield of 0.5 and leads essentially to a single compound, the corresponding 6-hydroxyquinolone (Scheme 66.3). By contrast, in neutral sulfite or phosphate buffer, the decomposition quantum yield is two orders of magnitude lower ($\phi = 0.004$) and reductive defluorination is the main reaction pathway [63,68].

Production of ROS has also been reported. NFX generates both singlet oxygen (quantum yield < 0.1 in PBS) and superoxide anion [69].

66.4.3.2 Membrane Damage

A microspectrofluorometric study of skin fibroblasts has shown that NFX is localized in various cytoplasmic structures, especially in lysosome and mitochondria. Irradiation of the cells in the presence of NFX induces damage to these subcellular components, which results in membrane destabilization [69,70].

Photohemolysis of red blood cells has been reported, together with lipid peroxidation, estimated as the amount of species reactive to the thiobarbituric acid reactive substances (TBARS) assay [71,72].

66.4.3.3 DNA Damage

Formation of DNA strand breaks upon irradiation in the presence of NFX has been observed in plasmid and in cellular DNA [33]. In order to obtain more information on the nature of DNA

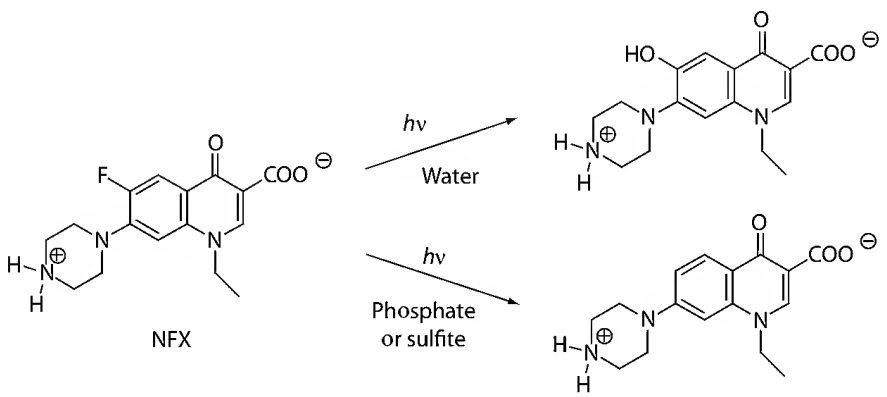

SCHEME 66.3 Photolysis of NFX in water and in phosphate or sulfite buffer.

photoproducts, formation of oxidized purines and pyrimidines has been studied by using the specific DNA repair enzymes *E. coli* formamidopyrimidine DNA glycosylase and endonuclease III, respectively. Only lesions on purine bases are observed. Accordingly, formation of 8-oxo-7,8-dihydro-2′-deoxyguanosine (8-oxodGuo) has been evidenced both in cellular and naked DNA. Nevertheless, this lesion does not give any information on the mechanism of the photodynamic process involved, as it can be obtained both by type I and type II guanine oxidation. To address this issue, a quantitative determination of the photoproducts of free dGuo nucleoside is necessary. This DNA component is the only one that can suffer both type I and type II processes, leading to mechanistically relevant photoproducts. On the one hand, the oxazolone derivative (2,2-diamino-4-[(2-deoxy-β-D-erythro-pentofuranosyl)amino]-2,5-dihydrooxazol-5-one) is considered as a hallmark of type I processes; it is obtained from the guanine radical cation initially generated by electron abstraction from dGuo. On the other hand, the diastereoisomeric spiroiminodihydantoins (dSp) are diagnostic of a singlet oxygen mechanism. The relatively high ratio between the yields of dSp and oxazolone formation found for NFX reveals its ability to act mainly as type II photosensitizer [33].

Other studies have shown that NFX is one of the few photosensitizers able to induce formation of T<>T cyclobutane dimers in cellular and isolated DNA. This result, attributed to energy transfer from NFX triplet excited state to the thymine bases, is in agreement with the triplet state energies of both compounds [59,73].

66.5 Conclusions

Photosensitization by drugs is an important issue as demonstrated by the large number of compounds involved in phototoxic and photoallergic reactions. Indeed, evaluation of drug photosensitizing potential relies on a series of *in vivo* and *in vitro* investigations. The photosensitizing history of a drug encompasses clinical observation in patients, photopatch tests but also 3T3 NRU assay and, fundamental studies taking into account its photophysical and photochemical properties. In this chapter, such an overview has been presented for KP and NFX; it demonstrates that a complete photophysical, photochemical, and photobiological study is fundamental to understand the key molecular mechanisms involved in the photosensitization process.

References

1. Cardoso, J. C., Canelas, M. M., Gonçalo, M., and Figueiredo, A., Photopatch testing with an extended series of photoallergens: A 5-year study, *Contact Dermatitis*, 60, 325, 2009.
2. Pigatto, P. D., Guzzi, G., Schena, D. et al., Photopatch tests: An Italian multicentre study from 2004 to 2006, *Contact Dermatitis*, 59, 103, 2008.
3. Neumann, N. J., Hölzle, E., Plewig, G. et al., Photopatch testing: The 12-year experience of the German, Austrian, and Swiss photopatch test group, *J. Am. Acad. Dermatol.*, 42, 183, 2000.
4. Moore, D. E., Drug-induced cutaneous photosensitivity, *Drug Safety*, 25, 345, 2002.
5. Quintero, B. and Miranda, M. A., Mechanisms of photosensitization induced by drugs: A general survey, *Ars Pharm.*, 41, 27, 2000.
6. Spielmann, H., Balls, M., Dupuis, J. et al., The international EU/COLIPA in vitro phototoxicity validation study: Results of phase II (blind trial). Part 1: The 3T3 NRU phototoxicity test, *Toxicol. In Vitro*, 12, 305, 1998.
7. Devleeschouwer, V., Roelandts, R., Garmyn, M., and Goossens, A., Allergic and photoallergic contact dermatitis from ketoprofen: Results of (photo) patch testing and follow-up of 42 patients, *Contact Dermatitis*, 58, 159, 2008.
8. Durbize, E., Vigan, M., Puzenat, E. et al., Spectrum of cross-photosensitization in 18 consecutive patients with contact photoallergy to ketoprofen: Associated photoallergies to nonbenzophenone containing molecules, *Contact Dermatitis*, 48, 144, 2003.

9. Matthieu, L., Meuleman, L., Van Hecke, E. et al., Contact and photocontact allergy to ketoprofen. The Belgian experience, *Contact Dermatitis*, 50, 238, 2004.
10. Sugiura, M., Hayakawa, R., Kato, Y., Sugiura, K., and Ueda, H., 4 Cases of photocontact dermatitis due to ketoprofen, *Contact Dermatitis*, 43, 16, 2000.
11. Lopez-Abad, R., Paniagua, M. J., Botey, E., Gaig, P., Rodriguez, P., and Richart, C., Topical dexketoprofen as a cause of photocontact dermatitis, *J. Investig. Allergol. Clin. Immunol.*, 14, 247, 2004.
12. Hindsen, M., Isaksson, M., Persson, L., Zimersson, E., and Bruze, M., Photoallergic contact dermatitis from ketoprofen induced by drug-contaminated personal objects, *J. Am. Acad. Dermatol.*, 50, 215, 2004.
13. Goday-Bujan, J. J., Rodriguez-Lozano, J., Martinez-Gonzalez, M. C., and Fonseca, E., Photoallergic contact dermatitis from dexketoprofen: Study of 6 cases, *Contact Dermatitis*, 55, 59, 2006.
14. Matsushita, T. and Kamide, R., Five cases of photocontact dermatitis due to topical ketoprofen: Photopatch testing and cross-reaction study, *Photodermatol. Photoimmunol. Photomed.*, 17, 26, 2001.
15. Gonzalez-Perez, R., Trebol, I., Garcia-Rios, I., Arregui, M. A., and Soloeta-Arechavala, R., Photocontact dermatitis due to dexketoprofen. Report of 2 cases, *Actas Dermosifiliogr.*, 97, 456, 2006.
16. de la Cuadra-Oyanguren, J. and Navarro Gosalbez, M., Fotosensibilidad a medicamentos en el Sistema Español de Farmacovigilancia, Boletin de la XVII Reunion del Grupo Español de Fotobiología en Bilbao (Bulletin of the Spanish Photobiology Group), p. 14, 2003.
17. Diaz, R. L., Gardeazabal, J., Manrique, P. et al., Greater allergenicity of topical ketoprofen in contact dermatitis confirmed by use, *Contact Dermatitis*, 54, 239, 2006.
18. Hindsen, M., Zimerson, E., and Bruze, M., Photoallergic contact dermatitis from ketoprofen in southern Sweden, *Contact Dermatitis*, 54, 150, 2006.
19. Kerr, A. C., Muller, F., Ferguson, J., and Dawe, R. S., Occupational carprofen photoallergic contact dermatitis, *Br. J. Dermatol.*, 159, 1303, 2008.
20. Walker, S. L., Ead, R. D., and Beck, M. H., Occupational photoallergic contact dermatitis in a pharmaceutical worker manufacturing carprofen, a canine non steroidal anti-inflammatory drug, *Br. J. Dermatol.*, 154, 569, 2006.
21. Ferguson, J., McEwen, J., Al-Ajmi, H., Purkins, L., Colman, P. J., and Willavize, S. A., A comparison of the photosensitizing potential of trovafloxacin with that of other quinolones in healthy subjects, *J. Antimicrob. Chemother.*, 45, 503, 2000.
22. Tolland, J., Davies, J., Elborn, S., and McKenn, K. E., Ciprofloxacin-induced phototoxicity: In vivo and in vivo data, *Br. J. Dermatol.*, 159(Suppl 1), 128, 2008.
23. Knoell, K. A. and Lynch, J. M., Photoinduced acute exanthematous pustulosis caused by ciprofloxacin and sunlight exposure, *Int. J. Dermatol.*, 48, 1134, 2009.
24. Oliveira, H. S., Gonçalo, M., and Figueiredo, A. C., Photosensitivity to lomefloxacin. A clinical and photobiological study, *Photodermatol. Photoimmunol. Photomed.*, 16, 116, 2000.
25. Dawe, R. S., Ibbotson, S. H., Sanderson, J. B., Thomson, E. M., and Ferguson, J., A randomized controlled trial (volunteer study) of sitafloxacin, enoxacin, levofloxacin and sparfloxacin phototoxicity, *Br. J. Dermatol.*, 149, 1232, 2003.
26. Pierfitte, C., Royer, R. J., Moore, N., and Begaud, B., The link between sunshine and phototoxicity of sparfloxacin, *Br. J. Clin. Pharmacol.*, 46, 609, 2000.
27. Alomar, A., Ketoprofen photodermatitis, *Contact Dermatitis*, 12, 112, 1985.
28. Goossens, A., Photoallergic contact dermatitis, *Photodermatol. Photoimmunol. Photomed.*, 20, 121, 2004.
29. de la Cuadra-Oyanguren, J., Perez-Ferriols, A., Lecha-Carrelero, M. et al., Results and assessment of photopatch testing in Spain: Towards a new standard set of photoallergens, *Actas Dermosifiliogr.*, 98, 96, 2007.
30. Chaboissier A., Hatinguais, E., and Rodde, M., Suspension d' autorisation de mise sur le marché des gels contenant du ketoprofine. Report (communiqué de presse) of 18 December 2009 by Afssaps (Agence française de sécurité sanitaire des produite de santé). http://www.afssaps.fr/Infos-de-securite/Communiques-de-presse

31. Royer, R. J., Adverse drug reactions with fluoroquinolones, *Therapie*, 51, 414, 1996.
32. Marutani, K., Matsumoto, M., Otabe, Y. et al., Reduced phototoxicity of a fluoroquinolone antibacterial agent with a methoxy group at the 8 position in mice irradiated with long-wavelength UV light, *Antimicrob. Agents Chemother.*, 37, 2217, 1993.
33. Lhiaubet-Vallet, V., Bosca, F., and Miranda, M. A., Photosensitized DNA damage: The case of fluoroquinolones, *Photochem. Photobiol.*, 66, 368, 2009.
34. Johnson, B. E. J., Gibbs, N. K., and Ferguson, J., Quinolone antibiotic with potential to photosensitize skin tumorigenesis, *J. Photochem. Photobiol. B Biol.*, 37, 171, 1997.
35. Klecak, G., Urbach, F., and Urwyler, H., Fluoroquinolone antibacterials enhance UVA-induced skin tumours, *J. Photochem. Photobiol. B Biol.*, 37, 174, 1997.
36. Spielmann, H. and Liebsch, M., Lessons learned from validation of in vitro toxicity test: From failure to acceptance into regulatory practice, *Toxicol. In Vitro*, 15, 585, 2001.
37. Spielmann, H., Grune, B., Liebsch, M., Seiler, A., and Vogel, R., Successful validation of in vitro methods in toxicology by ZEBET, the National Centre for Alternatives in Germany at the BfR (Federal Institute for Risk Assessment), *Exp. Toxicol. Pathol.*, 60, 225, 2008.
38. Jones, P. A. and King, A. V., High throughput screening (HTS) for phototoxicity hazard using the in vitro 3T3 neutral red uptake assay, *Toxicol. In Vitro*, 17, 703, 2003.
39. Neumann, N. J., Blotz, A., Wasinska-Kempka, G. et al., Evaluation of phototoxic and photoallergic potentials of 13 compounds by different in vitro and in vivo methods, *J. Photochem. Photobiol. B Biol.*, 79, 25, 2005.
40. Zhang, T., Li, J.-L., Ma, X.-C., Xin, J., and Tu, Z.-H., Reliability of phototoxic tests of fluoroquinolones in vitro, *Acta Pharmacol. Sin.*, 24, 453, 2003.
41. Bosca, F., Marin, M. L., and Miranda, M. A., Photoreactivity of the non steroidal anti-inflammatory 2-arylpropionic acids with photosensitizing side effects, *Photochem. Photobiol.*, 74, 637, 2001.
42. Martinez, L. J. and Scaiano, J. C., Transient intermediates in the laser flash photolysis of ketoprofen in aqueous solutions: Unusual photochemistry for the benzophenone chromophore, *J. Am. Chem. Soc.*, 119, 11066, 1997.
43. Monti, S., Sortino, G., De Guidi, G., and Marconi, G., Photochemistry of 2-(3-benzoylphenyl) propionic acid (ketoprofen). Part 1. A picosecond and nanosecond time resolved study in aqueous solution, *J. Chem. Soc. Faraday Trans.*, 93, 2269, 1997.
44. Lhiaubet-Vallet, V., Belmadoui, N., Climent, M. J., and Miranda, M. A., The long-lived triplet excited state of an elongated ketoprofen derivative and its interactions with amino acids and nucleosides, *J. Phys. Chem. B*, 111, 8277, 2007.
45. Lhiaubet, V., Paillous, N., and Chouini-Lalanne, N., Comparison of DNA damage photoinduced by ketoprofen, fenofibric acid and benzophenone via electron and energy transfer, *Photochem. Photobiol.*, 74, 670, 2001.
46. Lhiaubet-Vallet, V., Bosca, F., and Miranda, M. A., Stereodifferentiating drug-biomolecule interactions in the triplet excited state: Studies on supramolecular carprofen/protein systems and on carprofen–tryptophan model dyads, *J. Phys. Chem. B*, 111, 423, 2007.
47. Vaya, I., Bueno, C. J., Jimenez, M. C., and Miranda, M. A., Use of triplet excited states for the study of drug binding to human and bovine serum albumins, *ChemMedChem*, 1, 1015, 2006.
48. Monti, S., Manet, I., Manoli, F., Morrone, R., Nicolosi, G., and Sortino, S., Diastereoselective and site dependency in the photochemistry of ketoprofen in the bovine serum albumin matrix, *Photochem. Photobiol.*, 82, 13, 2006.
49. Monti, S., Manet, I., Manoli, F., and Sortino, S., Binding and photochemistry of enantiomeric 2-(3-benzoylphenyl)propionic acid (ketoprofen) in the human serum albumin environment, *Photochem. Photobiol. Sci.*, 6, 462, 2007.
50. De Guidi, G., Ragusa, S., Cambria, M. T., Belvedere, A., Catalfo, A., and Cambria, A., Photosensitizing effect of some nonsteroidal antiinflammatory drugs on natural and artificial membranes: Dependence on phospholipid composition, *Chem. Res. Toxicol.*, 18, 204, 2005.

51. Andreu, I., Morera, I. M., Bosca, F., Sanchez, L., Camps, P., and Miranda, M. A., Cholesterol-diaryl ketone stereoisomeric dyads as models for "clean" type I and type II photooxygenation mechanisms, *Org. Biomol. Chem.*, 6, 860, 2008.
52. Andreu, I., Bosca, F., Sanchez, L., Morera, I. M., Camps, P., and Miranda, M. A., Efficient and selective photogeneration of cholesterol-derived radicals by intramolecular hydrogen abstraction in model dyads, *Org. Lett.*, 8, 4597, 2006.
53. Bosca, F., Andreu, I., Morera, I. M., Samadi, A., and Miranda, M. A., Chiral discrimination in the intramolecular abstraction of allylic hydrogens by benzophenone triplets, *Chem. Commun.*, 1592, 2003.
54. Miranda, M. A., Martinez, L. A., Samadi, A., Bosca, F., and Morera, I. M., Stereoselective intramolecular hydrogen abstraction by a chiral benzophenone derivative, *Chem. Commun.*, 280, 2002.
55. Abad, S., Bosca, F., Domingo, L., Gil, S., Pischel, U., and Miranda, M. A., Triplet reactivity and regio-/stereoselectivity in the macrocyclization of diastereomeric ketoprofen-quencher conjugates via remote hydrogen abstractions, *J. Am. Chem. Soc.*, 129, 7407, 2007.
56. Pischel, U., Abad, S., Domingo, L. R., Bosca, F., and Miranda, M. A., Diastereomeric differentiation in the quenching of excited states by hydrogen donors, *Angew. Chem. Int. Ed.*, 42, 2531, 2003.
57. Lhiaubet-Vallet, V., Encinas, S., and Miranda, M. A., Excited state enantiodifferentiating interactions between a chiral benzophenone derivative and nucleosides, *J. Am. Chem. Soc.*, 127, 12774, 2005.
58. Paris, C., Encinas, S., Belmadoui, N., Climent, M. J., and Miranda, M. A., Photogeneration of 2-deoxyribonolactone in benzophenone-purine dyads. Formation of ketyl-C1′ biradicals, *Org. Lett.*, 10, 4409, 2008.
59. Lhiaubet-Vallet, V., Cuquerella, M. C., Castell, J. V., Bosca, F., and Miranda, M. A., Triplet excited fluoroquinolones as mediators for thymine cyclobutane dimer formation in DNA, *J. Phys. Chem. B*, 111, 7409, 2007.
60. Vinette, A. L., McNamee, J. P., Bellier, P. V., McLean, J. R. N., and Scaiano, J. C., Prompt and delayed nonsteroidal anti-inflammatory drug–photoinduced DNA damage in peripheral blood mononuclear cells measured with the comet assay, *Photochem. Photobiol.*, 77, 390, 2003.
61. Ball, P. and Tillotson, G., Tolerability of fluoroquinolone antibiotics, *Drug Safety*, 13, 343, 1995.
62. Ferguson, J., Fluoroquinolone photosensitization: A review of clinical and laboratory studies, *Photochem. Photobiol.*, 62, 954, 1995.
63. Monti, S., Sortino, S., Fasani, E., and Albini, A., Multifaceted photoreactivity of 6-fluoro-7-aminoquinolones from the lowest excited states in aqueous media: A study by nanosecond and picosecond spectroscopic techniques, *Chem. Eur. J.*, 7, 2185, 2001.
64. Albini, A. and Monti, S., Photophysics and photochemistry of fluoroquinolones, *Chem. Soc. Rev.*, 32, 238, 2003.
65. Cuquerella, M. C., Miranda, M. A., and Bosca, F., Role of excited state intramolecular charge transfer in the photophysical properties of norfloxacin and its derivatives, *J. Phys. Chem. A*, 110, 2607, 2006.
66. Cuquerella, M. C., Bosca, F., and Miranda, M. A., Photonucleophilic aromatic substitution of 6-fluoroquinolones in basic media: Triplet quenching by hydroxide anion, *J. Org. Chem.*, 69, 7256, 2004.
67. Fasani, E., Profumo, A., and Albini, A., Structure and medium-dependent photodecomposition of fluoroquinolone antibiotics, *Photochem. Photobiol.*, 68, 666, 1998.
68. Fasani, E., Barberis Negra, F. F., Mella, M., Monti, S., and Albini, A., Photoinduced C–F bond cleavage in some fluorinated 7-amino-4-quinolone-3-carboxylic acids, *J. Org. Chem.*, 64, 5388, 1999.
69. Martinez, L. J., Sik, R. H., and Chignell, C. F., Fluoroquinolone antimicrobials: Singlet oxygen, superoxide and phototoxicity, *Photochem. Photobiol.*, 67, 399, 1998.

70. Ouedraogo, G., Morliere, P., Bazin, M., Santus, R., Kratzer, B., Miranda, M. A., and Castell, J. V., Lysosomes are sites of fluoroquinolone photosensitization in human skin fibroblasts: A microspectrofluorometric approach, *Photochem. Photobiol.*, 70, 123, 1999.
71. Condorelli, G., De Guidi, G., Giuffrida, S., Miano, P., Sortino, S., and Velardita, A., Membrane and DNA damage photosensitized by fluoroquinolone antimicrobial agents: A comparative screening, *Med. Biol. Environ.*, 24, 103, 1996.
72. Yamamoto, T., Tsurumaki, Y., Takei, M., Hosaka, M., and Oomori, Y., In vitro method for prediction of the phototoxic potential of fluoroquinolones, *Toxicol. in Vitro*, 15, 721, 2001.
73. Bosca, F., Lhiaubet-Vallet, V., Cuquerella, M. C., Castell, J. V., and Miranda, M. A., The triplet energy of thymine in DNA, *J. Am. Chem. Soc.*, 128, 6318, 2006.

67

Photodynamic Approaches to Water Disinfection

Michela Magaraggia
University of Padova

Giulio Jori
University of Padova

67.1 Introduction

The question of water supply and distribution is becoming of utmost importance worldwide from both a social and a scientific point of view. Actually, a growing number of countries around the world, especially developing countries but also several Mediterranean countries, face increasingly difficult situations concerning the availability of irrigation, industrial, and drinking water from both surface and groundwater stocks. Many water sources are heavily polluted by hazardous chemicals, which are known to be harmful to humans and a variety of animal and vegetal ecosystems, as well as by several kinds of pathogenic microorganisms, such as bacteria, fungi, molds, viruses, and parasitic protozoa. Potential contaminants include agricultural runoff, landfill leachates, and industrial activities [1,2]. Therefore, there is an urgent need for the definition of efficacious and environmentally safe techniques yielding an efficient water purification and disinfection. Currently, the most commonly adopted approaches are based on physical methods (e.g., filtration, heating, or irradiation with ultraviolet [UV] light or x-rays), even though reliance is mainly placed on chemical treatments with oxidizing species, such as chlorine, chlorine dioxide, or ozone [3]. However, such methods often exhibit a number of negative aspects, in particular the formation of endoperoxides or trihalomethanes as by-products of the reaction between the chemical disinfectant and organic matter, or the selection of multidrug resistant microbial strains upon repeated treatment of waters characterized by a large microbial flora [4,5]. Moreover, chlorine is often phytotoxic [6], while the use of ozone proved to be moderately expensive and involve a high consumption of energy, thereby making its implementation on a large scale a not very attractive endeavor. The evolvement of resistance by microbial cells represents a particularly challenging problem as a consequence of the truly large variety of mechanisms, which have been found to be developed by pathogenic agents in order to increase their defensive strategies against external insults: these include a thickening of their outer wall, encoding of new proteins that prevent the penetration of drugs, onset of mutants deficient in those porin channels allowing the influx of externally added chemicals, etc. [7]. The transfer of such resistance to human pathogens represents a potentially serious threat to public health [8]. Therefore, it is by now apparent how difficult it is to identify a comprehensive strategy.

The use of photochemical techniques for the treatment of chemically or microbiologically contaminated waters has been operative for many years with so far contrasting results. Thus, the effectiveness of UV light is often limited by the reduced penetration power (<1 cm) of wavelengths shorter than 350 nm into natural water [9]; moreover, the direct absorption of UV-C and UV-B wavelengths by nucleic acids is a main cause of the onset of mutagenic processes leading to the selection of possibly dangerous new kinds of microbial strains [10]. To address these problems, novel photochemical pathways for water purification have been devised, including (a) the direct irradiation with full sunlight spectrum using specifically designed apparatuses in order to take advantage of the significantly deeper penetration of visible light wavelengths even into water samples characterized by relatively high levels of turbidity [11] and (b) the introduction of photoassisted reactions via semiconductors (e.g., TiO_2 or ZnO), which can be electronically excited by light wavelengths in the UV-A spectral range giving raise to the formation of strongly oxidizing and highly cytotoxic species, *in primis* the OH radical and hydrogen peroxide [6,12].

In actual fact, the disinfection of drinking water affected by an unusually high population of the Gram-negative bacterium *Escherichia coli* by means of solar reactors equipped with parabolic collectors has been obtained, even though the efficiency of the overall process was markedly enhanced by the presence of TiO_2 as a photocatalyst [13]. The addition of the semiconductor also yields an extensive destruction of a variety of organic micropollutants [14]. However, in spite of the intrinsic and experimentally demonstrated high efficiency of such approaches, their usefulness is presently confined to small-scale water treatment, mainly owing to the reduced water volumes that can be illuminated in a homogeneous way by using light wavelengths in the UV-A spectral range, as well as to the relatively high costs associated with the operation of this technology. Furthermore, the oxidizing intermediates normally involved in such photoprocesses display an appreciable reactivity against most nucleotides, hence there is again a high probability of promoting mutagenic effects [15].

Recently, a novel approach has been proposed, which appears to be of low cost and minimal impact on environment, namely, the use of photodynamic sensitizers, which can be activated by irradiation with selected intervals of visible light wavelengths. This methodology appears to be particularly useful for the decontamination of waters, which are characterized by a large level of microbial pathogens [16].

67.2 Photodynamic Sensitization of Biological Systems

67.2.1 Photodynamic Processes: Basic Mechanisms

The term "photodynamic effect" refers to a process that involves the combined action of three factors, namely, light of an appropriate wavelength, oxygen, and a photosensitizer to induce a biological damage [17]. A simplified mechanistic scheme of photosensitized processes is shown in Figure 67.1. The electronic excitation of the photosensitizer is generally achieved via a one-photon transition from the ground state $Sens^0$ to a more energetic singlet state Sens*.

Relaxation of Sens* through vibrational decay modes yields the lowest excited singlet state $Sens^1$. Several deactivation pathways are open to the $Sens^1$ species; the critical step from the point of view of the photodynamic process is represented by the intersystem crossing from $Sens^1$ to the first excited triplet state $Sens^3$, whose lifetime is in the order of the micro- to millisecond range, so that this intermediate can play a major role in diffusion-controlled processes. Actually, $Sens^3$ can promote two reaction mechanisms (Figure 67.1). The type I pathway involves hydrogen or electron transfer between $Sens^3$ and a nearby substrate with generation of radical species; the direction of the transfer is controlled by the relative redox potentials of the triplet photosensitizer and the electron acceptor or donor. In particular, electron transfer to oxygen yields the superoxide radical anion $O_2^{(-)}$, which under suitable experimental conditions can be converted to the hydroxyl radical OH· via the Haber–Weiss reaction. In the type II mechanism, the $Sens^3$ can give raise to the electronically excited oxygen species known as singlet oxygen ($^1O_2$) through electronic energy transfer to ground state molecular oxygen (which is a triplet). All the activated oxygen derivatives thus produced are highly electrophilic

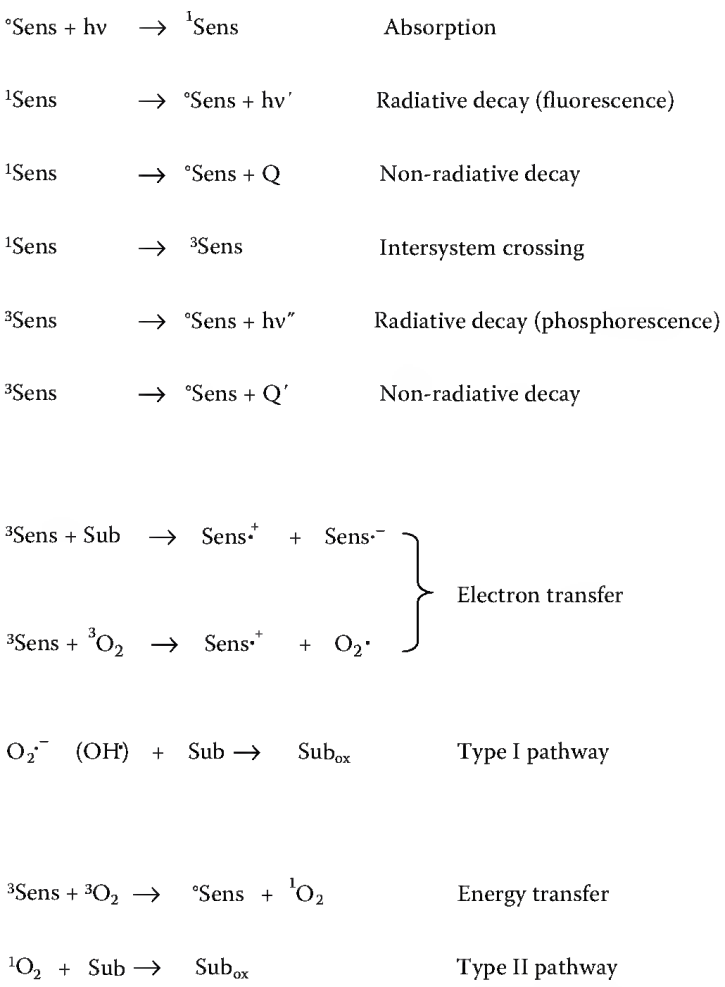

FIGURE 67.1 Schematic representation of the photophysical and photobiological steps involved in photodynamic sensitization processes.

moieties, hence they can rapidly react with electron-rich sites of a cell or tissue causing the formation of photooxidized products. A detailed description of the mechanisms controlling the fate and efficiency of photodynamic sensitization can be found in Ref. [18].

The biomolecules that are most sensitive to the photodynamic processes are listed in Table 67.1. Clearly, the side chains of aromatic- or sulfur-containing amino acids, guanosine nucleotides, and unsaturated lipids and steroids represent potential targets for attack by OH· or $^1O_2$. In general, such compounds are almost ubiquitously present in various subcellular compartments. Therefore, if such activated oxygen species are generated by a cell-bound photosensitizer, the overall process has a very high probability to be confined within a sphere with a diameter no greater than 1–2 nm around the Sens-binding site [19]. For example, the intracellular diffusion distance of $^1O_2$ has been estimated to be $2–4 \times 10^{-6}$ cm^2 s^{-1} [20] In some cases, one can distinguish between the two competing type I and type II mechanisms on the basis of the final photooxidation products, as outlined in Table 67.1.

As a general minor alternative to the type I and type II mechanisms, electronically excited sensitizers often undergo a chemical reaction, which results in the irreversible modification of their chemical structure [21]. The process is defined as "*photobleaching*" since it involves the loss of absorption and fluorescence intensity, so that with very few exceptions the photodegradation products do no longer contribute to the photosensitized process. In general, the quantum yields for the photobleaching of most photodynamic sensitizers are in the 10^{-4} to 10^{-5} range, namely, only a tiny fraction of the absorbed visible light photons eventually induce photobleaching of the sensitizer molecule. While some degree of

TABLE 67.1 Main Biological Targets of Photosensitized Processes

Cell Constituent	Target	Modified Functional Group	Main Biological Effects
Proteins	Tryptophan Tyrosine Histidine Methionine Cysteine	Indole Phenol Imidazole Thioether Thiol	Loss of enzymic activities; formation of protein–protein cross-links; inhibition of K^+ pump; impairment of DNA synthesis
Unsaturated lipids steroids	Oleic, linoleic, linolenic acid Cholesterol	Carbon–carbon double bond	Blockade of metabolic processes; alteration of membrane potential and fluidity
Nucleic acids	Guanosine	Purine	Alteration of chromatin; disturbed synthesis of membrane and cell wall

reduced efficacy of the photodynamic agent as the irradiation progresses can have some positive consequences in clinical antineoplastic applications [22], it is usually highly preferable to have active principle concentrations that remain at the maximal possible level throughout the exposure of the target system to light [23].

The biological consequences of the photoinduced chemical damage described are multiform and include protein denaturation, impairment of DNA replication, inhibition of transport processes across the cytoplasmic membrane, and loss of integrity of several subcellular organelles. If the alterations caused to cell metabolism and homeostasis are sufficiently extensive, then the cells can enter a death process via necrosis, apoptosis, or autophagia [24,25].

67.2.2 Photodynamic Inactivation of Microbial Cells

The possibility to kill microorganisms by the combined action of visible light and a photosensitizing dye was discovered at the very beginning of the twentieth century [26]. However, the use of this methodology to treat infectious diseases of microbial origin was not developed for several decades owing to two main reasons [27]: (a) the discovery of antibiotics raised the feeling that such diseases could be efficaciously controlled and counteracted even though this expectation was rapidly disappointed by the worldwide outbreak of antibiotic resistance and (b) microbial pathogens typically exhibit a very broad variety of cellular organization and defense strategies, so that it appeared quite problematic to devise a therapeutic approach, which could simultaneously achieve the death of bacterial, fungal, and parasitic cells. Thus, some porphyrin derivatives, such as hematoporphyrin, Photofrin, or tetrasulfonated porphyrins, which are known to be very active as antitumor photosensitizing agents [28], are ineffective against Gram-negative bacteria, whereas they still promote an extensive killing of Gram-positive bacteria [29,30]. The differences in the photoantimicrobial activity displayed by these porphyrin derivatives were ascribed to the anionic nature of the porphyrins used in photodynamic therapy (PDT) of neoplastic lesions; this feature precludes their close or stable interaction with the array of negatively charged moieties (largely, teichoic and teichuronic acids), which are present at the surface of the outer wall surrounding the cells of Gram-negative bacteria and several yeasts or fungi [30,31].

A significant change in the overall scenario of antimicrobial PDT occurred as a consequence of the discoveries independently made by three research groups showing that visible light-activated cationic photosensitizers belonging to the family of phenothiazines [32], porphyrins [33], and phthalocyanines [34] induce a fast and extensive killing of typical Gram-negative bacteria, such as *E. coli* and *Pseudomonas aeruginosa*, in addition to the inactivation of fungi and Gram-positive bacteria. Mechanistic investigations demonstrated that such positively charged photosensitizing agents are taken up by microbial cells via the so-called "self-promoted uptake pathway" [31,35], whose essential steps are schematically illustrated in Figure 67.2. A similar pathway has been observed for some cationic peptides, which can

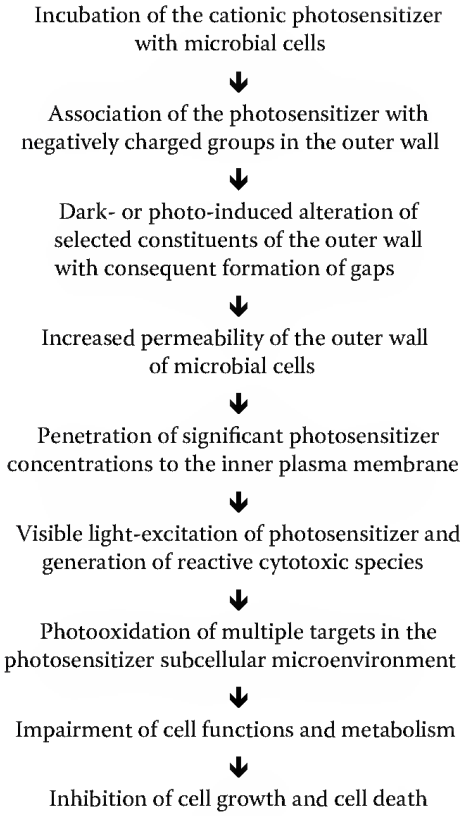

FIGURE 67.2 Schematic mechanism involved in the photosensitized inactivation of microbial cells.

displace divalent cations, such as Mg^{2+} or Ca^{2+}, from their binding sites on the cell surface owing to their 2–4 orders of magnitude larger affinity. The consequent reorganization of the outer membrane structure has been found to facilitate the penetration of various antibiotics and hydrophobic molecules to inner cellular compartments. Moreover, the close proximity of the photosensitizer to potentially sensitive targets in the outer wall (e.g., lipoproteins) can induce their preferential photooxidative modification, thus further enhancing the alteration of the compact native structure.

The initial binding of the photosensitizing agent is driven by an electrostatic interaction between the positively charged groups in its molecule and the negative charges at the cell surface, hence the process occurs at a very fast rate and is completed within 5–10 min. incubation. As a consequence, the visible light irradiation of the photosensitizer-loaded bacterial cells can start after very short incubation times and in the presence of photosensitizer dosages in the micromolar range: under these experimental conditions, very little, if any, amounts of photosensitizer are accumulated by mammalian cells, which guarantees a high selectivity of microbial cell damage as compared with the host tissue. In particular, the significant hydrophobic contribution of the large aromatic macrocycle typical of phenothiazine and porphyrinoid compounds favors the localization of the photosensitizer in the plasma membrane, which is the main site of the photoprocess. The genetic material becomes involved only in the later stages of the photosensitized process, which minimizes the risk for the onset of mutagenic processes [30,31].

A very similar scenario obtains for the photosensitized inactivation of fungi and yeasts, whose photosensitivity is less strictly dependent on structural factors as compared with Gram-negative bacteria [35]. In general, the stepwise scheme previously detailed for the photosensitized inactivation of bacteria (Figure 67.2) can be accepted also for this class of microbial cells. Thus, negatively charged photosensitizers, such as protoporphyrin [35,36], and mono- or tetra-sulfonated Al(III)-phthalocyanines [3] are accumulated by *Candida* spp. and photosensitize an extensive killing of this microorganism. On the other hand, also in the case of yeasts, cationic phthalocyanines are taken up

TABLE 67.2 Effect of the Porphyrin Photosensitization on the Survival of Selected Gram-Positive (*Enterococcus seriolicida*), Gram-Negative (*E. coli*) Bacteria, and Fungi (*Candida albicans*)

	Irradiation Time (min)		
Photosensitizer	1	5	10
E. seriolicida	2.3	4.9	5.8
E. coli	1.9	3.1	4.5
C. albicans	3.1	5.7	>6.5

Bacterial cells were irradiated with 600–700 nm light at a fluence rate of 40 mW cm^{-2} after 5 min incubation with 5 μM porphyrin (TMPyP). The photosensitivity is expressed as log decrease in cell survival.

in larger concentrations and display a more pronounced photosensitizing activity than their neutral or anionic analogues [37]. Interestingly, yeasts are also sensitive to the photodynamic action of cationic dyes even at the stage of biofilms [37]. Typical examples of the time-dependent photosensitized killing of selected bacterial and fungal cells in the presence of tetra-meso(*N*-methyl-pyridyl)porphine (TMPyP) are reported in Table 67.2.

Lastly, photodynamic sensitization can play a useful role for the efficient inactivation of parasitic protozoa. Thus, a cationic porphyrin bearing four positively charged meso-*N*-methyl-pyridyl peripheral substituents at 1–10 μM concentrations, upon visible light irradiation, induces an extensive damage of cystic cultures of *Colpoda inflata*, a soil and freshwater-dwelling ciliate, as well as of the free-living opportunistic *Acanthamoeba palestinensis*; in addition, the porphyrin photosensitizes the inhibition of excystment to produce vegetative cells [38]. The phototoxic activity is markedly enhanced by the replacement of at least one methyl group with a longer hydrocarbon chain. Analogously, a tetracationic Zn(II)-phthalocyanine can efficiently inactivate cultures of *A. palestinensis* in both the cystic and vegetative stages upon illumination with 600–700 nm light [39,40]: the two forms exhibit a comparable dependency on the photosensitizer concentration; however, cysts require a significantly longer irradiation time to give a similar degree of inactivation. A phthalocyanine concentration as low as 0.5 μM, followed by 20 min irradiation, induces 50% inhibition of excystment in vegetative cells after the addition of fresh culture medium.

Similarly, a variety of parasites such as the blood-borne pathogens *Plasmodium falciparum* and *Babesia divergens*, the protozoan responsible for Chagas disease *Trypanosoma cruzi*, or the agent causing visceral leishmaniasis *Leishmania donovani infantum* undergo an extensive inactivation upon irradiation with visible light wavelengths in the presence of selected photosensitizers (see for a recent review Ref. [41]).

67.3 Use of Photodynamic Processes for Decontamination of Water

67.3.1 General Features of the Approach

Water resources are suffering from a progressive and sometimes dramatic reduction in quantity and quality worldwide, as specified in the introductory paragraph. The situation is largely determined by the steady increase in environmental pollution and the lack of safe and efficient technologies for wastewater treatment. Therefore, there is an urgent need for the development of novel, convenient, and low cost methods for combating water contamination, especially that caused by biological agents that can originate dangerous epidemic diseases. In this connection, the results so far obtained on the

antimicrobial properties of photodynamic sensitizers clearly suggest that the combination of cationic porphyrins and visible light (or even sunlight under specific climatically favorable situations) could represent a viable and environmentally friendly alternative for the control of the population of potential pathogens in waters of different origin. The main favorable features of this technique can be summarized as follows:

1. The photosensitizing and cytocidal activity of positively charged porphyrins appears to be characterized by a broad spectrum, since an extensive drop in the population of a variety of microorganisms can be achieved, such as Gram-positive and Gram-negative bacteria, typically including aggressive and antibiotic-resistant bacteria, for example, methicillin-resistant *Staphylococcus aureus* (MRSA), a variety of fungal pathogens, viruses, and parasitic protozoa in both the cystic and vegetative stage. Such a behavior is typical of several photosensitizing agents bearing cationic functional groups: however, as regards the antimicrobial activity, porphyrins appear to be superior to other families of polycyclic compounds [42]. In particular, the presence of peripheral substituents with a relatively long hydrocarbon chain ($C > 10$) appreciably enhances the cytotoxic effect: this chain acts as a hydrophobic arm, which penetrates into lipid and protein domains of the cytoplasmic membrane, thereby altering its permeability [43]. This allows the use of lower dosages of photosensitizer to achieve a satisfactory extent of pathogen cell killing.
2. The multitarget nature of the mode of action typical of porphyrins (see Table 67.1) makes it very unlikely that photoresistant strains of bacterial and fungal cells are selected. Thus, up to 10 consecutive generations of bacteria have been exposed to the photosensitizing action of cationic porphyrins with no detectable modification of their degree of photosensitivity [44].
3. At the same time, the presence of the flat aromatic macrocycle favors the partitioning of porphyrin derivatives in the cell membranes or their stable association with a variety of proteins [21,41]; as a consequence, exogenously administered porphyrins have a high probability to be "intercepted" before significant concentrations reach the genetic material. All the evidences available so far indicate that photoprocesses promoted by porphyrins have a very low mutagenic potential. This feature is important for the safety of the procedure in the case of repetitive treatments.
4. Most porphyrins display no significant toxicity toward the normal constituents of animal or vegetal ecosystems at doses which are photochemically active and induce a marked mortality of microbial pathogens. This finding is in agreement with previous observations dealing with the effect of porphyrins on a variety of higher organisms, which justifies their increasing utilization as food additives or phototherapeutic agents [28,45]. Several porphyrins and their chlorine analogues are widespread in numerous ecosystems and their toxicity to cells and tissues becomes important only at millimolar concentrations [21], namely, for dosages that are 2–3 orders of magnitude larger than those yielding a satisfactory antimicrobial effect.
5. The intense absorption band of porphyrins in the 420–430 nm spectral region allows a very efficient interaction with blue light wavelengths, which are endowed with maximum penetration power into natural waters out of the wavelengths that are present in the solar spectrum [46]. On the basis of the Beer–Lambert law, one can estimate that for a porphyrin concentration of 0.5 μM, which exhibits a high photoantimicrobial activity (Table 67.2) and a molar extinction coefficient ε value of 194,000 M^{-1} cm^{-1} in the blue spectral region, the absorption A of the incident light will be around 0.085 cm^{-1}; since total light absorption by a system corresponds with $A = 2.0–2.2$, the illumination can be assumed to be sufficiently uniform to a water depth of about 25 cm. Less efficiently absorbed wavelengths (e.g., those in the green and red spectral regions, where porphyrins possess weaker absorption bands) will allow the illumination of even larger water volumes, even though the smaller probability of porphyrin photoexcitation by such wavelengths may require longer light exposure times.

6. The overall treatment time is further reduced by the short incubation, which is required in order to achieve a significantly large association of the porphyrin photosensitizer with the microbial cells. Such a fast kinetics is determined by the fact that the binding is of electrostatic nature, namely, it is promoted by the real time interaction between the positively charged peripheral substituents in the tetrapyrrolic macrocycle of the porphyrin molecule and the large number of negatively charged functional groups (e.g., lipopolysaccharides, lipoteichoic, and teichuronic acids), which are present in the outer wall of many microbial cells. Thus, previous investigations showed that prolonging the incubation of porphyrin-type derivatives with microbial cells from a few minutes to 1–2 h brings about no measurable increase in the amount of cell-bound antimicrobial agent [30,33]. The close proximity between the porphyrin and the potential targets of the photosensitized process represents an important factor for enhancing the efficacy of the treatment, since several photosensitive sites will be within the normal endocellular diffusion range (<0.1 μ) of the photogenerated reactive oxygen species, such as singlet oxygen [47].
7. The water disinfection can be successfully obtained by using a simple and inexpensive technology. In actual fact, an extensive decrease in microbial population is achieved by using low light intensities, of the order of 50 mW cm^{-2}, which can be easily reached by irradiation with halogen or incandescent filament lamps, that is, light sources of low cost, which have a long life span (a few thousand hours) and require no protective measures for the operators, the ecosystems and humans. Moreover, the low fluence rate causes no detectable thermal effect, thus avoiding any problems related with the possible increase in water temperature.
8. Lastly, the proposed methodology appears to be environmentally friendly, since it is based on the use of sunlight or sunlight simulators in combination with antimicrobial agents of natural origin. In any case, the accumulation of porphyrins in the various ecosystems is unlikely owing to their gradual photobleaching under the action of ambient light, as shown by studies from our laboratory and as repeatedly reported in the literature [21,48]. Moreover, the ready water solubility of cationic porphyrins should guarantee their fast dilution in the ground to levels that are below any risk threshold. In any case, the photobleaching products of these porphyrins also show no major toxic effects [41].

67.3.2 Photodynamic Treatment of Water from Fish-Farming Plants

Photodynamic sensitization appears to be endowed with a particularly great potential for the disinfection of waters from aquaculture systems. Such waters are often characterized by the presence of a large population of microbial pathogens owing to the often large density of fish in the farming structures, as well as to the high concentration of food residues, organic debris, and defecation products. In actual fact, several bacterial and fungal species, which are known to infect fish-farming waters, have been shown to be rapidly and efficiently inactivated upon visible light irradiation in the presence of porphyrin-type photosensitizers: these include *Vibrio anguillarum* [33,49], *Vibrio vulnificus* [50], *Bacillus* endospores [51], *Saprolegnia parasitica* [52], and several fecal coliforms and fecal enterococci isolated from wastewater samples [53]. The latter authors also propose a simple and expeditious method to evaluate the rate and extent of bacteria photoinactivation in wastewater; the method is based on the analysis of β-galactosidase activity and leucine incorporation as a function of the irradiation time. Moreover, preliminary studies performed in our laboratory using aquaria as model systems mimicking a variety of fish microenvironments clearly pointed out that the combined action of a tetracationic porphyrin, that is TMPyP, and visible light emitted by the aquaria-incorporated fluorescent lamps induces the regression or cure of several bacterial or fungal infections of different fish without any parallel (photo)toxic effect on the fish, as well as on other constituents of the aquaria ecosystem, such as invertebrates, algae, or green plants (see Table 67.3).

TABLE 67.3 Effect of Porphyrin and Visible Light Treatment on Aquaria Fish Affected by Bacterial or Parasitic Infections

Species	Pathology	Protocol	Results
Grammaloretus	White spots on a darkened skin	0.6 mg L^{-1} for 3 days	Disappearance of white spots
Lysmata	Black spots throughout the body	0.3 mg L^{-1} for 3 days	Disappearance of black spots
Megalamphodus	White spots on the skin	0.6 mg L^{-1} for 3 days	Fast spot disappearance
Symphysodon discus	Opaque and worn fins	0.6 mg L^{-1} for 3 days	Clear and reactive fins
Cheirodon axelrodi	Bleaching of skin color	0.6 mg L^{-1} for 6 days	Regression of infection
Colisa golden	Extensive lethality	0.6 mg L^{-1} for 6 days	Blockage of lethality
Discus	Mucous secretion and cotton-type outgrowth	0.6 mg L^{-1} for 2 days	Disappearance of pathologies

In all cases, the irradiations (400–800 nm light) were performed by using the light sources, which are naturally incorporated into the aquaria.

On the basis of such findings, the feasibility of this procedure for the disinfection of microbiologically polluted waters from fish-farming ponds was tested in pilot aquaculture plants involving either spontaneously or artificially *Saprolegnia*-infected rainbow trouts (*Oncorhynchus mykiss*) [52]. Actually, mycotic infections caused by members of *Saprolegnia* species, as well as by their close water mold relatives, represent a major challenge to a number of freshwater fishes and their eggs. Prevention and control of saprolegniasis are especially difficult, even under precisely established fish-farming conditions, owing to the ubiquitous nature and the rapid spreading of such fungi. The problem is further aggravated by various concomitant factors, such as (a) different stages of the fish life cycle are susceptible to saprolegniasis and in particular a marked increase in infection risk is observed during sexual maturation; (b) several forms of environmental stress, leading to a decreased water quality (e.g., increased average temperatures, high organic loads), act as predisposing agents for the outbreak of the disease, often by weakening the innate defense systems of the fish; (c) many fungicides that are effective against higher fungi exhibit a low activity against oomycetes; (d) spores of the pathogen can successfully locate in the fish epidermis and, while the majority are removed or inactivated during quarantine in clear water, a significant number of viable fungal units persist on the body surface [54]. *Saprolegnia*-induced mycotic infections have been traditionally treated by the application of malachite green, a triarylmethane dye. However, recent concerns about the safety of this aromatic derivative led to the banning of its use as a fisheries chemotherapeutant in many parts of the world. Even formalin, a 24% aqueous solution of formaldehyde, which has been introduced to replace malachite green, does not eliminate the risk for acute impact on ecosystems and potential harmful effects on human health [55].

On the other hand, the use of TMPyP and visible light proved to represent an efficacious technique for an environmentally friendly treatment of *Saprolegnia* infections. Two protocols were developed: a *preventive treatment* based on the irradiation of artificially infected trout (about 4×10^{11} zoospores deposited on a 2 cm^2 area of scraped skin) for 1 h day^{-1} and for 10 consecutive days after addition of 0.3 mg L^{-1} TMPyP; and a *curative treatment* where trout that had already developed a marked infection by *Saprolegnia*, as shown by the presence of cottony-like patches of the mycelium, were exposed to visible light (1 h day^{-1} for 6 consecutive days) in the presence of 0.6 mg L^{-1} TMPyP. The results unequivocally showed that the outlined procedures were very successful in both inhibiting the formation of the fungal infection and causing a complete disappearance of the preexisting infection with no detectable damage in correspondence of the perilesional tissue districts. Quite interestingly, such important effects were obtained by using fluence rates of the order of 50 mW cm^{-2}, which suggests that even sunlight in cloudy days can be used to disinfect waters in open-air fish-farming systems, thus further reducing the overall cost of the procedure and meeting the recommendations to increase the use of natural resources for energy-saving reasons. In actual fact, the killing of *Deinococcus radiodurans* by the use of sunlight-activated cationic Zn(II)-porphyrin derivatives [56], as well as of *E. coli* by sunlight-activated tetracationic meso-substituted porphyrins [57] has been demonstrated.

Recent investigations from our laboratory also showed that tetracationic porphyrins at doses as low as 0.3–0.6 mg L^{-1} efficiently protect trout eggs against infections by *Saprolegnia*. In this case, the irradiation by visible light needs to be carried out on the potentially polluted water before it flows through the container of trout eggs. The direct irradiation of eggs by full-spectrum 400–800 nm light provokes irreversible toxic effects on the trout eggs, since a broad number of visible wavelengths are directly absorbed by carotenoid pigments, which are present in the eggs, and these once photoexcited in turn promote photochemical damage in their surrounding leading to egg death (Magaraggia and Jori, unpublished results). The preventive efficiency of specific cationic porphyrins against saprolegniasis of trout eggs is comparable with that found for some commercially used chemical disinfectants, such as formalin or bronopol, which represent a serious threaten for fish and environment.

These findings can be correlated with experimental observations by other authors pointing out that cationic porphyrins can efficiently and extensively photosensitize the destruction of fecal bacteria [42,53], helminth eggs [58], and sewage bacteriophage [59]. Therefore, the photodynamic methodology appears to represent a very flexible and reliable tool for the decontamination of microbiologically polluted waters of different origins.

67.3.3 Future Perspectives

In spite of the favorable features that appear to presently characterize the use of porphyrin photosensitization for the control of microbial population in water, several approaches can be explored in order to enhance the efficiency, the economic convenience, and the safety of the technique.

So far, tetracationic porphyrins have been most frequently utilized as antimicrobial photosensitizing agents with a broad spectrum of activity. However, there are at least preliminary evidences suggesting that the number of positively charged functional groups and the distribution of the charges at the periphery of the tetrapyrrolic macrocycle can appreciably modulate both the interaction of the porphyrin with the microbial cells and the efficacy of the photosensitized killing of such cells [60,61]. Therefore, more studies are needed in order to gather a detailed understanding of the relationship between the chemical structure and the photoantimicrobial activity of porphyrins. In this connection, it is worthwhile taking into consideration the information provided by scattered reports that suggest that the overall photophysical properties and photosensitizing efficiency of porphyrins are enhanced by the introduction of fluorine atoms [62,63] or conjugation with saccharides [64] and poly-peptides, especially those of cationic nature, such as poly-lysine or poly-ornithine [30,65]. In particular, the positively charged poly-peptide acts as a destabilizing agent for the compact 3D organization of the outer wall, which surrounds several types of microbial cells, thereby enhancing their degree of photosensitivity [66,67]. Last, some photosensitizing agents that are structurally unrelated with porphyrins, such as phenothiazinium salts [68] and fullerenes derivatized to give them a cationic character [69], also display important antimicrobial properties. In all cases, the photoantimicrobial activity is by far superior for the positively charged compounds as compared with their neutral or anionic counterparts; one essential requirement is a high water solubility for the photosensitizer, since previous studies demonstrated [49] that the incorporation of a hydrophobic compound into various types of delivery vehicles (e.g., liposomes [49] or cyclodextrins [70]) results in a significant drop of the photocidal efficacy, especially toward Gram-negative bacteria.

From the economic point of view, a major progress for the future of environmental application of photodynamic antimicrobial methodologies is represented by the possibility to utilize photosensitizing agents, which are immobilized in inert matrices. This possibility was explored by a number of authors [71] at least for those photosensitizers that act via the production of singlet oxygen as the main cytotoxic agent: this hyperreactive oxygen species has a relatively long natural lifetime, especially in nonpolar media, hence it can diffuse to distances of up to almost 1 mm before undergoing deactivation to the ground state. As a consequence, the killing of bacteria physically separated from the immobilized photosensitizers has been observed [72,73]. The use of photosensitizers bound to solid particles of approximately micrometer size would allow their recovery from the water system at the end of the treatment

and even the irradiation of water prior to its introduction into (for example) the fish-farming ponds, thus avoiding any direct contact between the photoreactive species and the fish or other nontarget organisms. In addition, such complexes between the photosensitizing agent and the supporting matrix have been often found to be endowed with a significantly long shelf life, which facilitates their storage and reuse [56]. In this connection, porphyrins [74,75], phthalocyanines [76], and Ru(II) coordination complexes [77] immobilized on a variety of supports have been successfully tested for killing of microbial cells and proposed for the disinfection of water specimens, which are characterized by the presence of a significant flora of microbial pathogens.

In conclusion, photoactivated porphyrins and their analogues appear to possess a large scope and potential for addressing problems of high social interest, such as the disinfection of waters, with particular emphasis on aquaculture. The widespread application of this technique could provide a viable alternative to the currently adopted pharmaceutical or biological agents, whose continuous accumulation in the environment will inevitably result in an unbearable burden for a variety of ecosystems and human health [78].

References

1. Droste, R.L. 1997. *Theory and Practice of Water and Waste Water Treatment*. New York: John Wiley & Sons.
2. Bitton, G. 2005. *Wastewater Microbiology*. New York: John Wiley & Sons.
3. Tomas, C.R. 1990. Wastewater engineering and treatment: Problems and solutions. In *Chemical Engineering Techniques in Biotechnology*, ed. M.A. Winkler, 23–94. Amsterdam, the Netherlands: Elsevier.
4. Twort, A.C., F.M. Law, and F.W. Croley. 2005. *Water Supply*. London, U.K.: Arnold Publishing Co.
5. Doré, M. *Chimie des Oxydants et Traitment des Eaux: Techniques et Documentation*. Paris, France: Lavoisier.
6. Sioi, M., A. Bolosis, E. Kostopoulou, and I. Poulios. 2006. Photocatalytic treatment of coloured wastewater from medical laboratories. *J. Photochem. Photobiol. B Biol.* 184: 18–25.
7. Smith, T.L., M.L. Pearson, K.R. Wilcox et al. 1999. Emergence of vancomycin resistance in *Staphylococcus aureus*: Glycopeptide-intermediate *Staphylococcus aureus* working group. *New Engl. J. Med.* 340: 493–501.
8. Cabello, F.C. 2006. Heavy use of prophylactic antibiotics in aquaculture: A growing problem for human and animal health and for the environment. *Environ. Microbiol.* 8: 1137–1144.
9. Baker, K.S. and R.C. Smith. 1982. Spectral irradiance penetration in natural waters. In *The Role of Solar Ultraviolet Radiation in Marine Ecosystems*, ed. J. Calkins, 233–246. New York: Plenum Press.
10. Mitchell, D.L. and D. Kerentz. 1993. The induction and repair of DNA photodamage in the environment. In *Environmental UV Photobiology*, eds. A.R. Young, L.O. Bjorn, J. Moan, and W. Nultsch, 345–378. New York: Plenum Press.
11. Boyle, R.W. and D. Dolphin. 2006. Structure and biodistribution relationships of photodynamic sensitisers. *Photochem. Photobiol.* 14: 4253–4259.
12. Percherancier, J.P., R. Chapelon, and B. Pouyet. 1995. Semiconductor-sensitised photodegradation of pesticides in water. *J. Photochem. Photobiol. A Chem.* 87: 261–266.
13. Sichel, C., J. Blanco, S. Malato, and P. Fernandez-Ibanez. 2007. Effects of experimental conditions on *Escherichia coli* survival during solar photocatalytic water disinfection. *J. Photochem. Photobiol. A Chem.* 189: 239–246.
14. Amalric, L., C. Guillard, and P. Pichat. 1995. The photodegradation of 2,3-benzofuran and its intermediates, 2-coumarone and salicylaldehyde, in TiO_2 aqueous suspensions. *J. Photochem. Photobiol. A Chem.* 85: 239–246.
15. Bahnemann, D., J. Cunningham, M.A. Fox, E. Pelizzetti, P. Pichat, and N. Serpone. 1994. *Aquatic and Surface Photochemistry*. Boca Raton, FL: Lewis Publishing Co.

16. Almeida, A., A. Cunha, N.C.M. Gomes, E. Alves, L. Costa, and M.A.F. Faustino. 2009. Phage therapy and photodynamic therapy: Low environmental impact approaches to inactivate microorganisms in fish farming plants. *Mar. Drugs* 7: 268–313.
17. von Tappeiner, H. and H. Jesionek. 1903. Therapeutische versuche mit fluoreszierenden stoffen. *Munch. Med. Wochenschr.* 47: 2042–2044.
18. De Rosa, M.C. and R.J. Crutchley. 2002. Photosensitised singlet oxygen and its applications. *Coord. Chem. Rev.* 233: 351–371.
19. Pervaiz, S. and M. Olivo. 2006. Art and science of photodynamic therapy. *Clin. Exp. Pharmacol. Physiol.* 33: 551–556.
20. Hatz, S., J.D. Lambert, and P.R. Ogilvy. 2007. Measuring the lifetime of singlet oxygen in a single cell. Addressing the issue of cell viability. *Photochem. Photobiol. Sci.* 6: 1106–1116.
21. Jori, G. and J.D. Spikes. 1984. Photobiochemistry of porphyrins. In *Topics in Photomedicine*, ed. K.C. Smith, 183–319. New York: Plenum Press.
22. Roberts, J.E. and J. Dillon. 1993. Improvement of photodynamic therapy by selective protection of normal tissue. In *Biological Effects of Light*, ed. E.G. Jung and M.F. Holick, 393–399. Berlin, Germany: Gruyer & Co.
23. Dolmans, D.E., D. Fukumura, and R.K. Jain. 2003. Photodynamic therapy for cancer. *Nature Rev. Cancer* 3: 380–387.
24. Robertson, C.A., D. Hawkins Evans, and H. Abrahamse. 2009. Photodynamic therapy (PDT): A short review on cellular mechanisms and cancer research applications for PDT. *J. Photochem. Photobiol. B Biol.* 96: 1–8.
25. Kessel, D. and N.L. Oleinick. 2009. Initiation of autophagy by photodynamic therapy. *Methods Enzymol.* 453: 1–16.
26. Raab, O. 1900. Uber die wirkung fluoreszierender stoffe auf infusorien. *Z. Biol.* 39: 524–526.
27. Jori, G. and S.B. Brown. 2004. Photosensitised inactivation of microorganisms. *Photochem. Photobiol. Sci.* 3: 403–405.
28. Dougherty, T.J., C.J. Gomer, G. Jori et al. 1998. Photodynamic therapy. *J. Natl. Cancer Inst.* 90: 889–905.
29. Durantini, E.N. 2006. Photodynamic inactivation of bacteria. *Curr. Bioact. Compounds* 2: 127–142.
30. Jori, G., C. Fabris, M. Soncin et al. 2006. Photodynamic therapy in the treatment of microbial infections: Basic principles and perspective applications. *Lasers Surg. Med.* 38: 468–481.
31. Hamblin, M.R. and T. Hasan. 2004. Photodynamic therapy: A new antimicrobial approach to infectious diseases? *Photochem. Photobiol. Sci.* 3: 436–450.
32. Wilson, M. and C. Yanni. 1995. Killing of methicillin-resistant *Staphylococcus aureus* by low-power laser light. *J. Med. Microbiol.* 42: 62–66.
33. Merchat, M., G. Bertoloni, P. Giacomoni, A. Villanueva, and G. Jori. 1996. Meso-substituted cationic porphyrins as efficient photosensitisers of Gram-positive and Gram-negative bacteria. *J. Photochem. Photobiol. B Biol.* 32: 153–157.
34. Minnock, A., D.I. Vernon, J. Schofield, J. Griffiths, J.H. Parish, and S.B. Brown. 1996. Photoinactivation of bacteria: Use of a cationic water-soluble zinc phthalocyanine to photoinactivate both Gram-negative and Gram-positive bacteria. *J. Photochem. Photobiol. B Biol.* 32: 159–164.
35. Bliss, J.M., C.E. Bigelow, T.H. Foster, and C.G. Haidaris. 2004. Susceptibility of *Candida* species to photodynamic effects of Photofrin. *Antimicrob. Agents Chemother.* 48: 2000–2006.
36. Bertoloni, G., F. Rossi, G. Valduga, G. Jori, H. Ali, and J.E. van Lier. 1992. Photosensitising activity of water- and lipid-soluble phthalocyanines on prokaryotic and eukaryotic microbial cells. *Microbios* 71: 33–46.
37. Wilson, M. and N. Mia. 1993. Susceptibility of oral bacteria biofilms to antimicrobial agents. *J. Oral Pathol. Med.* 22: 354–357.
38. Kassab, K., T. Ben Amor, G. Jori, and O. Coppellotti. 2002. Photosensitisation of *Colpoda inflata* cysts by meso-substituted cationic porphyrins. *Photochem. Photobiol. Sci.* 1: 560–564.

39. Kassab, K., D. Dei, G. Roncucci, G. Jori, and O. Coppellotti. 2003. Phthalocyanine-photosensitised inactivation of a pathogenic protozoan, *Acanthamoeba palestinensis. Photochem. Photobiol. Sci.* 2: 668–672.
40. Ferro, S., O. Coppellotti, G. Roncucci, T. Ben Amor, and G. Jori. 2006. Photosensitised inactivation of *Acanthamoeba palestinensis* in the cystic stage. *J. Appl. Microbiol.* 101: 206–212.
41. Jori, G. and O. Coppellotti. 2007. Inactivation of pathogenic micro-organisms by photodynamic techniques: Mechanistic aspects and perspective applications. *Anti-infect. Agents Med. Chem.* 6: 119–131.
42. Jemli, M., Z. Alouini, S. Sabbahi, and M. Gueddari. 2002. Destruction of faecal bacteria in wastewater by three photosensitisers. *J. Environ. Monit.* 4: 511–516.
43. Reddi, E., M. Ceccon, G. Valduga et al. 2002. Photophysical properties and antibacterial activity of meso-substituted cationic porphyrins. *Photochem. Photobiol.* 75: 462–470.
44. Soncin, M., C. Fabris, A. Busetti, D. Dei, G. Roncucci, and G. Jori. 2002. Approaches to selectivity in the Zn(II)-phthalocyanine-photosensitised inactivation of wild-type and antibiotic-resistant *Staphylococcus aureus. Photochem. Photobiol. Sci.* 1: 815–819.
45. Certified Colour Industry Committee. 1988. *Food Technol.* 22: 15–16.
46. Hader, D.P., R.C. Worrest, and H.D. Kumar. 1989. Ozone reduction and increased solar radiation: Effects on aquatic ecosystems. In *United Nations Environmental Panel Report*, ed. J.C. van der Leun, 233–246. Nairobi, Kenya: UNEP.
47. Moore, A.C.E., B. Ortel, and T. Hasan. 2003. Mechanisms of photodynamic therapy. In *Photodynamic Therapy*, ed. T. Patrice, 19–57. Cambridge, U.K.: Royal Society of Chemistry.
48. Bonnett, R. and G. Martinez. 2001. Photobleaching of sensitisers used in photodynamic therapy. *Tetrahedron* 57: 9513–9547.
49. Merchat, M., J.D. Spikes, G. Bertoloni, and G. Jori. 1996. Studies on the mechanism of bacteria photosensitisation by meso-substituted cationic porphyrins. *J. Photochem. Photobiol. B Biol.* 35: 149–157.
50. Wong, P.N., S.K. Mak, M.W. Lo et al. 2005. *Vibrio vulnificus* peritonitis after handling of seafood in a patient receiving CAPD. *Am. J. Kidney Dis.* 46: 87–90.
51. Demidova, T.N. and M.R. Hamblin. 2005. Photodynamic inactivation of *Bacillus* endospores mediated by phenothiazinium dyes. *Appl. Environ. Microbiol.* 71: 6918–6925.
52. Magaraggia, M., F. Faccenda, A. Gandolfi, and G. Jori. 2006. Treatment of microbiologically polluted aquaculture waters by a novel photochemical technique of potentially low environmental impact. *J. Environ. Microbiol.* 8: 923–931.
53. Carvalho, C.M.B., A.T.P.C. Gomes, S.C. Fernandes et al. 2007. Photoinactivation of bacteria in wastewater by porphyrins. Bacterial β-galactosidase activity and leucine-uptake as methods to monitor the process. *J. Photochem. Photobiol. B Biol.* 88: 112–118.
54. Alderman, D.J. 1998. *Salmon Saprolegniasis.* Portland, Oregon: USDOE, Bonneville Power Administration.
55. Gieseker, C.M., S.G. Serfling, and R. Reimschuessel. 2006. Formalin as a chemotherapeutant for prophylaxis of finfish eggs and fry. *Aquaculture* 253: 120–129.
56. Faust, D., K.H. Funken, G. Horneck et al. 1999. Immobilized photosensitisers for solar photochemical applications. *Sol. Energy* 65: 71–74.
57. Carvalho, C.M.B., J.P.C. Tomé, M.A.F. Faustino et al. 2009. Antimicrobial photodynamic activity of porphyrin derivatives: Potential application on medical and water disinfection. *J. Porphyr. Phthal.* 13: 574–577.
58. Alouini, Z. and M. Jemli. 2001. Destruction of helminth eggs by photosensitised porphyrin. *J. Environ. Monit.* 3: 548–551.
59. Costa, L., E. Alves, C.M.B. Carvalho et al. 2008. Sewage bacteriophage photoinactivation by cationic porphyrins: A study of charge effect. *Photochem. Photobiol. Sci.* 7: 415–422.

60. Lazzeri, D., M. Rovera, L. Pascual, and E.N. Durantini. 2004. Photodynamic studies and photoinactivation of *Escherichia coli* using meso-substituted cationic porphyrin derivatives with asymmetric charge distribution. *Photochem. Photobiol.* 80: 286–293.
61. Cormick, M.P., M.G. Alvarez, M. Rovera, and E. Durantini. 2009. Photodynamic inactivation of *Candida albicans* sensitised by tri- and tetra-cationic porphyrin derivatives. *Eur. J. Med. Chem.* 44: 1592–1599.
62. Caminos, D.A., M.B. Spesia, and E.N. Durantini. 2005. Photodynamic inactivation of *Escherichia coli* by novel meso-substituted porphyrins by 4-(3-*N*,*N*,*N*-trimethylammoniumpropoxy)phenyl and 4-(trifluoromethyl)phenyl groups. *Photochem. Photobiol. Sci.* 5: 56–65.
63. Grancho, J.C.P., M.M. Pereira, M.D.G. Miguel, A.M.R. Gonçalves, and H.D. Burrows. 2002. Synthesis, spectra and photophysics of some free base tetrafluoroalkyl and tetrafluoroaryl porphyrins. *Photochem. Photobiol.* 75: 249–256.
64. Mikata, Y., Y. Onchi, K. Tabata et al. 1998. Sugar-dependent photocytotoxic properties of tetra- and octa-glycoconjugated tetraphenylporphyrins. *Tetrahedran. Lett.* 39: 4505–4508.
65. Maisch, T. 2007. Anti-microbial photodynamic therapy: Useful in the future? *Lasers Med. Sci.* 22: 83–91.
66. Polo, L., A. Segalla, G. Bertoloni, G. Jori, K. Schaffner, and E. Reddi. 2000. Poly-lysine porphycene conjugates as efficient photosensitisers for the inactivation of microbial pathogens. *J. Photochem. Photobiol. B Biol.* 59: 152–158.
67. Tome, J.P.C., M.G.P.M.S. Neves, A.C. Tome et al. 2004. Synthesis and antibacterial activity of new poly-L-lysine-porphyrin conjugates. *J. Med. Chem.* 47: 6649–6652.
68. Wainwright, M. 2000. Methylene blue derivatives—Suitable photoantimicrobials for blood product disinfection. *Int. J. Antimicrob. Agents* 16: 381–394.
69. Mroz, P., G.P. Tegos, H. Gali, T. Wharton, T. Sarna, and M.R. Hamblin. 2007. Photodynamic therapy with fullerenes. *Photochem. Photobiol. Sci.* 6: 1139–1149.
70. Bautista-Sanchez, A., A. Kasselouri, M.C. Desroches et al. 2005. Photophysical properties of glucoconjugated chlorins and porphyrins and their associations with cyclodextrins. *J. Photochem. Photobiol. B Biol.* 81: 154–162.
71. Bonnett, R., M.A. Krysteva, I.G. lalov, and S.V. Artarsky. 2006. Water disinfection using photosensitisers immobilized on chitosan. *Water Res.* 40:1269–1275.
72. Dahl, T.A., W.R. Midden, and P.E. Hartman. 1987. Pure singlet oxygen cytotoxicity for bacteria. *Photochem. Photobiol.* 46: 345–352.
73. Valduga, G., G. Bertoloni, E. Reddi, and G. Jori. 1993. Effect of extra-cellularly generated singlet oxygen on Gram-positive and Gram-negative bacteria. *J. Photochem. Photobiol. B Biol.* 21: 81–86.
74. Krouit, M., R. Granet, P. Branland, B. Verneuil, and P. Krausz. 2006. New photoantimicrobial films composed of porphyrinated lipophilic cellulose esters. *Bioorg. Med. Chem. Lett.* 16: 1651–1655.
75. Caminos, D. and E. Durantini. 2006. Photodynamic inactivation of *Escherichia coli* immobilized on agar surfaces by a tricationic porphyrin. *Bioorg. Med. Chem. Lett.* 14: 4253–4259.
76. Artrasky, S., S. Dimitrova, R. Bonnett, and M. Krysteva. 2006. Immobilization of zinc phthalocyanines in silicate matrices and investigation of their photobactericidal effect on *Escherichia coli. Sci. World J.* 6: 374–382.
77. Jimenez-Hernandez, M.E., F. Manjon, D. Garcia-Fresnadillo, and G. Orellana. 2006. Solar water disinfection by singlet oxygen photogenerated with polymer-supported Ru(II) sensitisers. *Sol. Energy* 80: 1382–1387.
78. Shao, Z.J. 2001. Aquaculture pharmaceuticals and biologicals: Current perspectives and future possibilities. *Adv. Drug Deliv. Rev.* 50: 229–243.

Index

B

C

E

F

G

H

I

K

N

O

P

S

T

U

V

W

X

Y

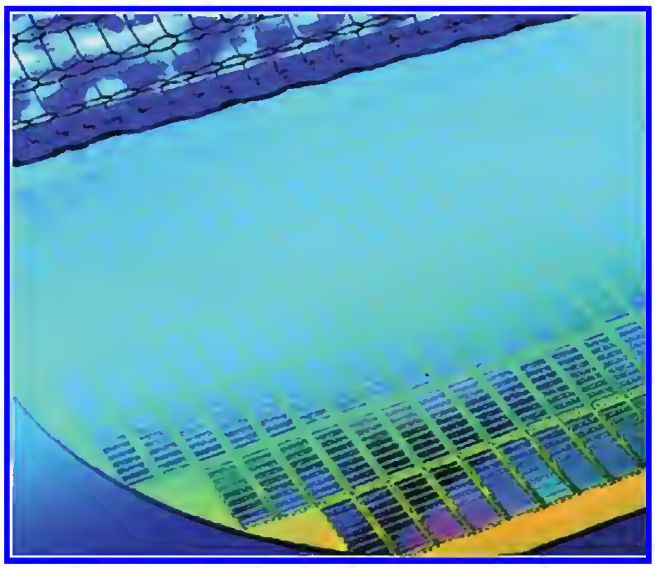

FIGURE 1.1 Photochemical surface treatment in wafer manufacturing. (From Heraeus Noblelight GmbH, *Ultraviolet, High Power Cold UV*, Hanau, Germany, 2005. With permission.)

FIGURE 1.4 Xe_2 excimer radiation source (Xeradex, 20 W, Radium, Wipperfürth, Germany) used for the surface functionalization of polystyrene films.

FIGURE 1.9 Photochemical mini-(thin-film) reactors of a production unit installed in a ventilated closet. (Picture shown with the kind permission of Heraeus, owner of IP rights of the pictured installation.)

FIGURE 2.6 The emission characteristics of a cylindrical and outward radiating DBD-driven XeCl* excilamp exhibiting thin micro- and homogeneous discharges. (Photo by B. Müller, Augsburg, Germany. Courtesy of Hochschule Furtwangen University.)

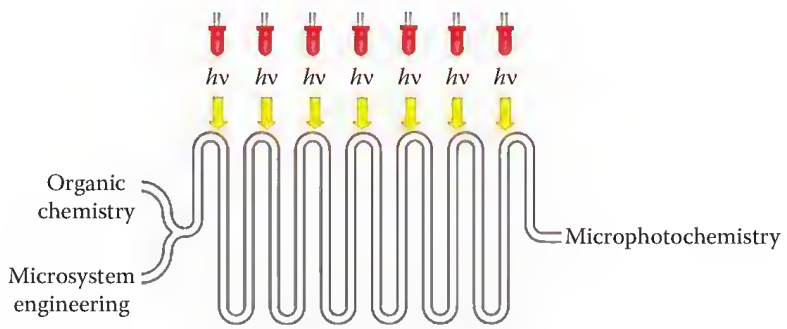

FIGURE 3.1 The concept of microphotochemistry.

FIGURE 3.2 Immersion well reactor (with courtesy of UV-consulting Peschl), chamber reactor (Rayonet) with Schlenk flask, and top-irradiation chamber reactor (Luzchem) with petri dishes.

FIGURE 3.3 Dwell device (Microglas), KeyChem-Lumino system (with courtesy of YMC), and falling-film reactor (IMM).

FIGURE 3.4 Photochemical production plant. (Courtesy of Heraeus.)

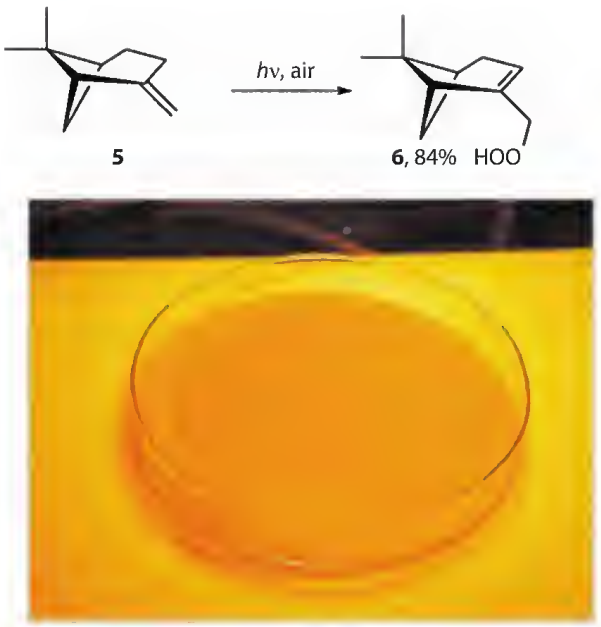

SCHEME 9.4 Photosensitized oxidation of β-pinene **5**. (From Griesbeck, A.G. and Bartoschek, A., *Chem. Commun.*, 1594, 2002. With permission.)

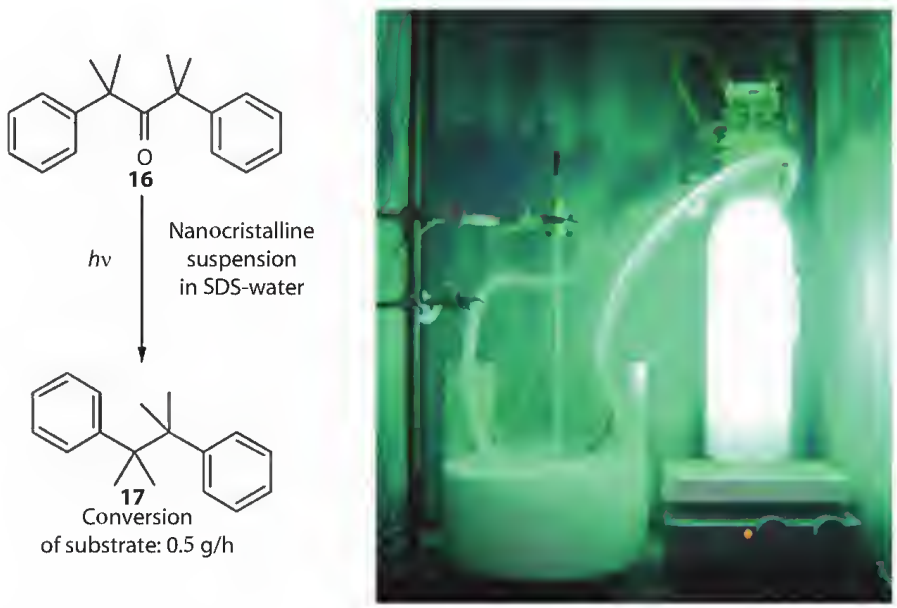

SCHEME 9.8 Solid-state photo-decarbonylation of dicumylketone **16** in a photochemical flow reactor. (From Veerman, M. et al., *Org. Lett.*, 8, 2615, 2006. With permission.)

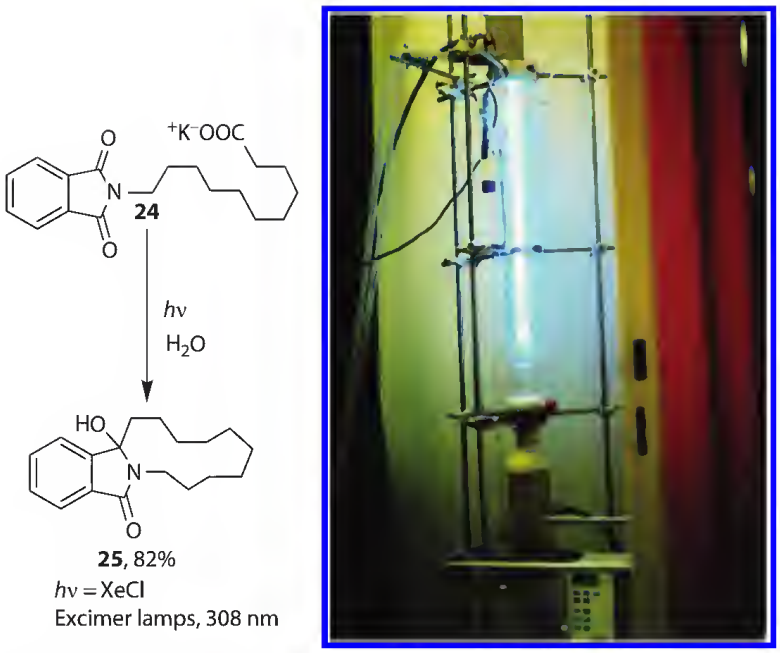

SCHEME 9.13 Photochemical cyclization of potassium carboxylate **24** carried out in a 3 kW XeCl excimer lamp equipped photoreactor. (From Griesbeck, A.G. et al., *Green Chem.*, 1, 205, 1999. With permission.)

SCHEME 9.26 Sunlight-induced photosensitized *cis–trans* isomerization of dinitrile **46.** (From Zhao, Y.P. et al., *Green Chem.*, 10, 1038, 2008; Zhao, Y.P. et al., *Green Chem.*, 11, 837, 2009. With permission.)

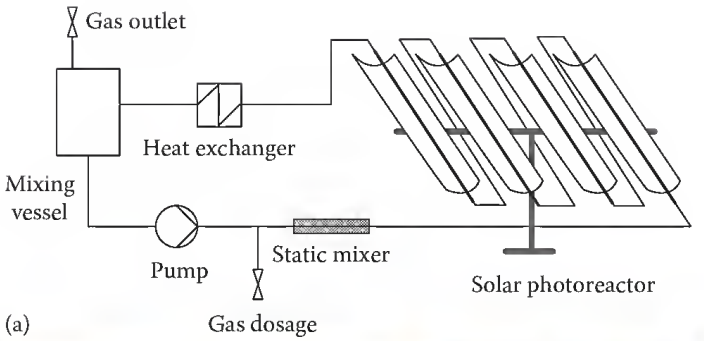

SCHEME 9.29 (a) The PROPHIS plant scheme, projected by German Aerospace center (DLR) in Cologne; (b) an image of the PROPHIS plant equipped by four parabolic troughs as light collector. (From Schiel, C. et al., *J. Green Chem.*, 3, 224, 2001. With permission.)

FIGURE 10.1 Flatbed and tube reactors at the DLR in Cologne.

FIGURE 10.2 Parabolic trough reactor for laboratory-scale experiments and the PROPHIS loop at the DLR in Cologne.

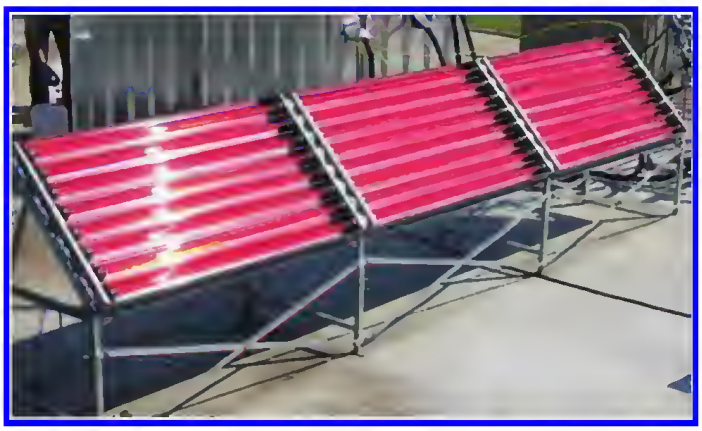

FIGURE 10.3 Compound parabolic collector.

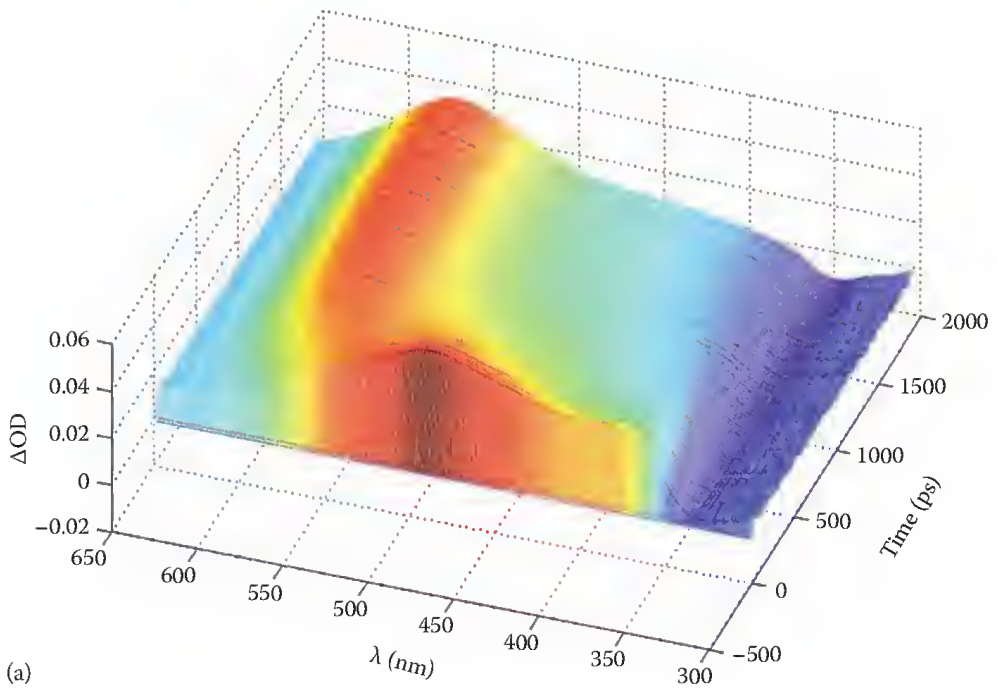

FIGURE 18.3 (a) Three-dimensional representation of transient absorption spectra of **51c** in methanol recorded after excitation at 260 nm.

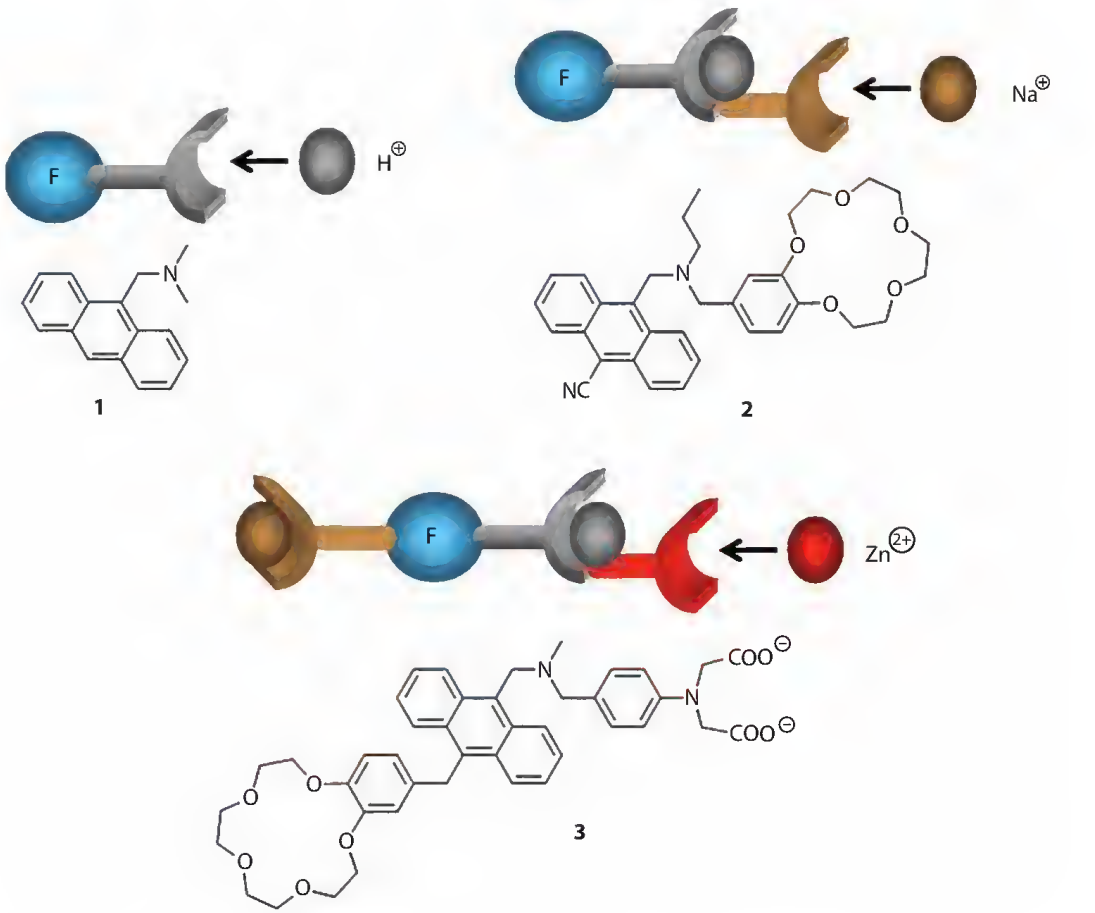

SCHEME 38.2 Family of fluorescent PET switches with one receptor (IDENTITY gate, **1**), two receptors (two-input AND gate, **2**), and three receptors (three-input AND gate, **3**).

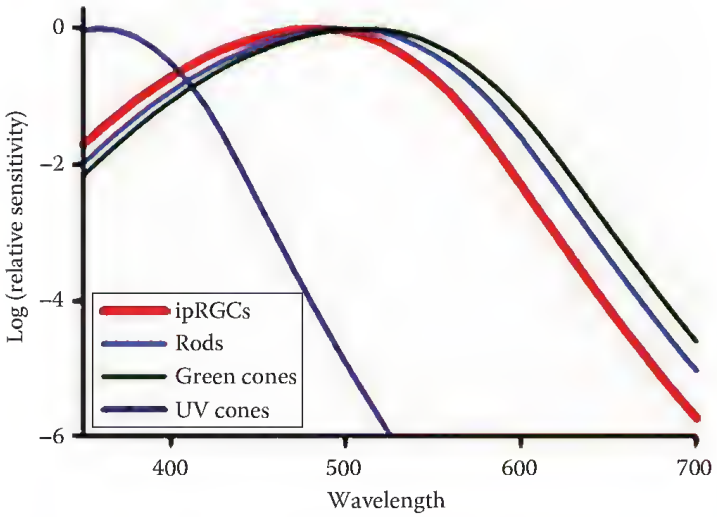

FIGURE 50.3 Action spectrum of intrinsically photosensitive retinal ganglion cells (ipRGCs) compared with action spectra of other photoreceptors of the rat retina. The curve shapes indicate that each photopigment uses a vitamin A-based chromophore. Relative trends of the curves on the wavelength axis reflect differences in the opsin component of the photopigment. Wavelengths: ipRGCs (red), 484 nm; green cones (green), 510 nm; UV cones (purple), 359 nm; rods (blue), 500 nm. (Adapted from Berson, D.M., *Trends Neurosci.*, 26, 314, 2003.)

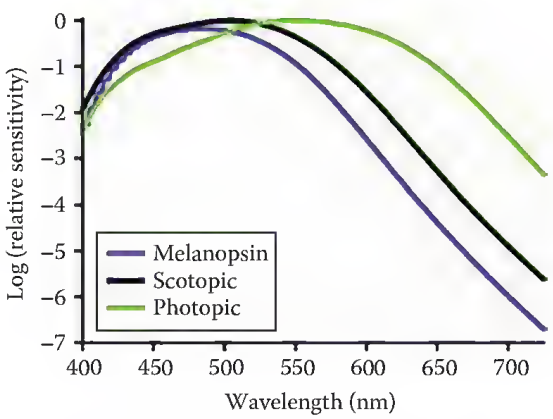

FIGURE 50.5 Action spectrum of human melanopsin showing an optimal sensitivity to short-wavelength "blue" light at 480 nm. The spectral sensitivity profile indicates an opsin-based photopigment utilizing a vitamin A-based chromophore. The spectral sensitivity of scotopic (rod-based) and photopic (cone-based) vision is presented for comparison. Although melanopsin sensitivity peaks around 480 nm, it shows in addition a good responsiveness into the green/yellow portion of the spectrum. (Adapted from Bailes, H.J. and Lucas, R.J., *Cell. Mol. Life Sci.*, 67, 99, 2010.)

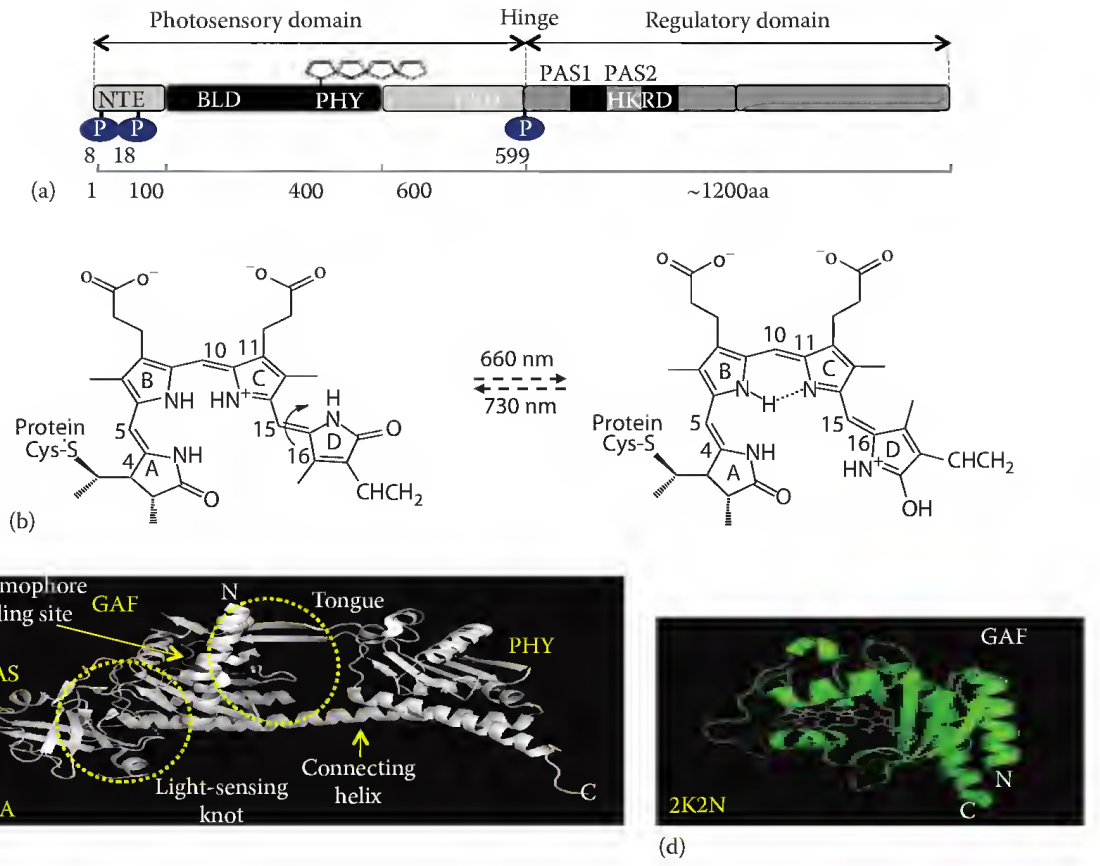

FIGURE 52.1 Domain and protein structures of phytochrome. (a) Domain structure of phytochrome. Phytochrome has a two-domain structure, N-terminal photosensory domain and C-terminal regulatory domain. The photosensory domain contains both light sensor chromophore (phytochromobilin) and signaling motifs for phosphorylation and interactions with phytochrome-interacting factors (PIFs) (see text). NTE, N-terminal extension; BLD, bilin lyase domain consisting of PAS and GAF; PHY, phytochrome-specific GAF-related domain; PRD, PAS-related domain; PAS1 and PAS2, two PAS repeats; HKRD, histidine kinase–related domain. As examples, *Arabidopsis* phyA and phyB are composed of 1122 and 1172 amino acids, respectively. The four-connected pentagon in the BLD is the chromophore (i.e., phytochromobilin) that binds to the cysteine residue at 322. Three phosphorylation sites on oat phyA are also shown. (b) Photoisomerization of phytochromobilin during the Pr-to-Pfr phototransformation. (c) The N-terminal photosensory module structure (residues 1–514) of cyanobacterial phytochrome (Cph1).[21] The complete sensory module (PDB ID: 2VEA) consists of PAS, GAF, and PHY domains. Chromophore-binding site and connecting helix are indicated. The regions for light-sensing knot and the tongue are shown as circles. (d) The structure of the Cph1 GAF domain (PDB ID: 2K2N) assembled with phytocyanobilin.[34] N-terminus (N) and C-terminus (C) are labeled, and the chromophore is shown in white.

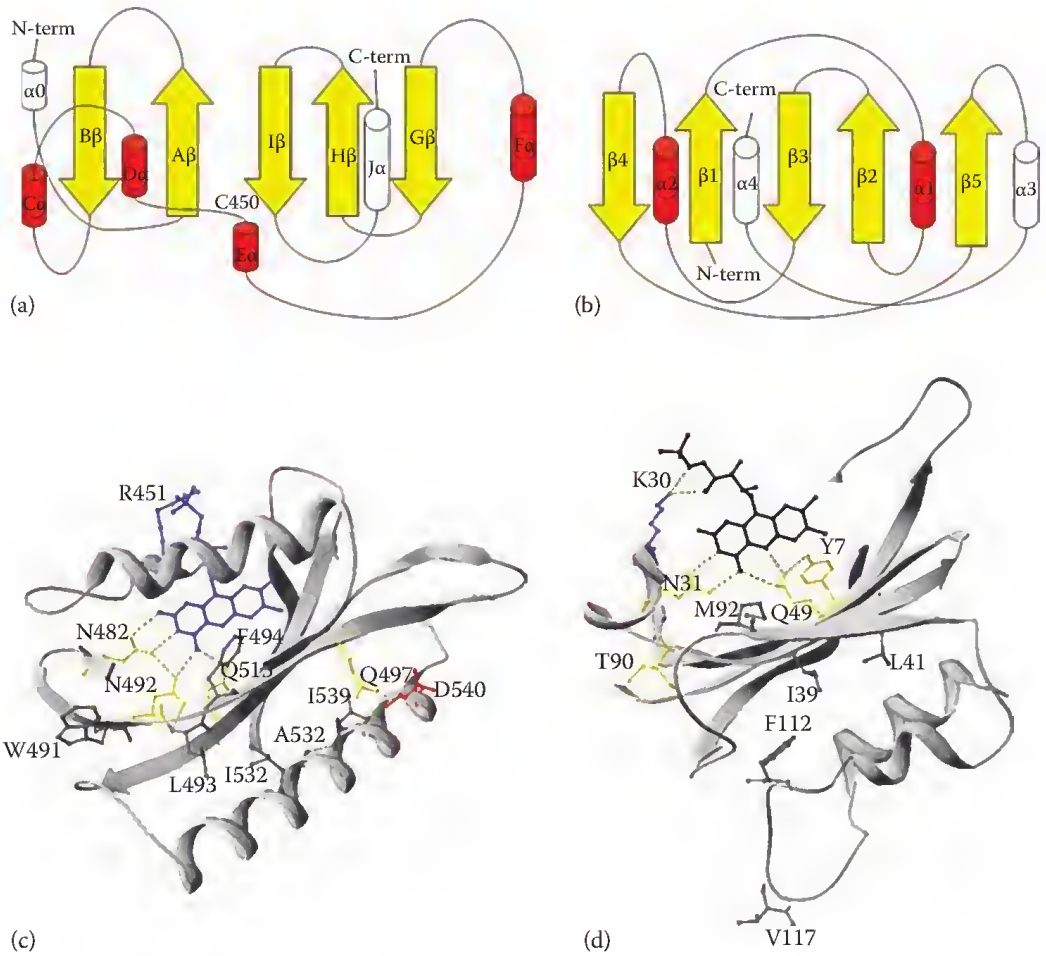

FIGURE 53.2 Top: topology of (a) light oxygen voltage (LOV) and (b) blue light sensing using FAD (BLUF) domains. Secondary structure elements have been named after [57] and [58]. Arrows: strands, cylinders: helices. The caps at the N- or C-termini of the domain core are given without color. The caps may adopt different conformations/geometries in different proteins or/and in a different state (dark or lit). Relative size of loops, strands, and helices are not respected. In (a) the N-cap has been labeled α0. Bottom: structure of a (c) LOV (PDB 1V1A [59]) and of a (d) BLUF (PDB 3GFX [56]) domain, highlighting residues involved in signal propagation, in different LOV and BLUF proteins. Numbering is from *As*phot1-LOV2 and *Kp*BlrP1, respectively (*As* = *Avena sativa, Kp* = *Klebsiella pneumoniae*), see Tables 53.1 and 53.2 for details. We also show residues that are not known to be involved in signal transduction, but participate in the modification of the HB network around the flavin after photoexcitation (N482, N492, and R451 in (c); K30 and N31 in (d)). Some secondary structure elements, or part of them, have been cut to better show the chromophore cavity. Note that, from available data, signal transmission from the α/β light-sensing domain favors, in both cases, the β-sheet/helical cap mechanism (Section 53.3.1). (From Wu, Q. and Gardner, K.H., *Biochemistry*, 48, 2620, 2009. With permission.)

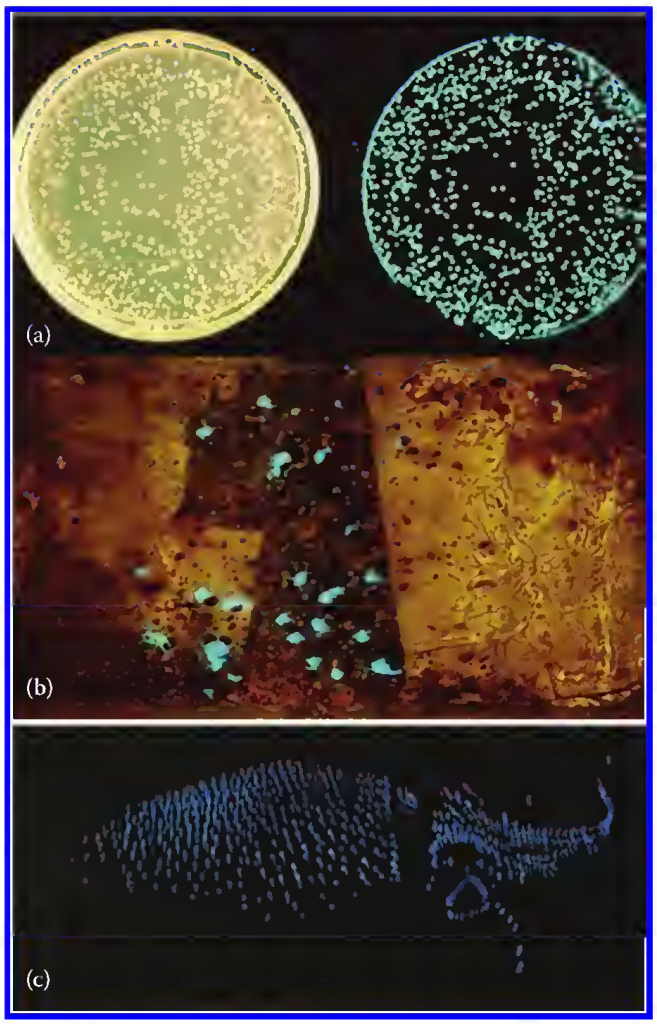

FIGURE 54.4 Some marine bioluminescent organisms: (a) *Vibrio fischerii* bioluminescent bacteria, (b) sea firefly *Vargula hilgendorfii* (ostracod), and (c) firefly squid *Watasenia scintillans*.

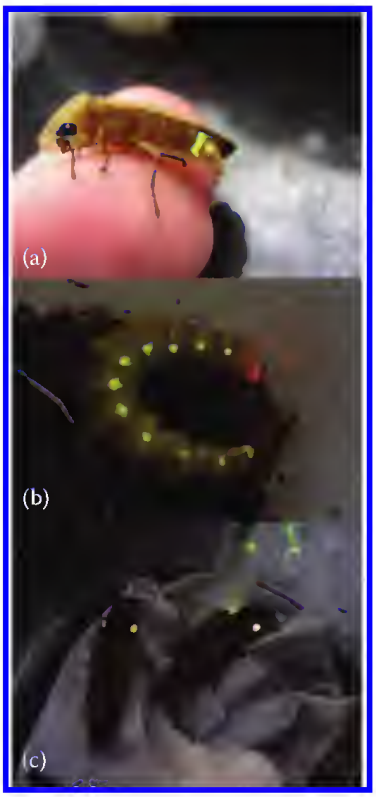

FIGURE 54.5 Some bioluminescent beetles (a) *Cratomorphus concolor* firefly, (b) *Pyrophorus divergens* click beetle, and (c) *Phrixothrix* railroad worm.

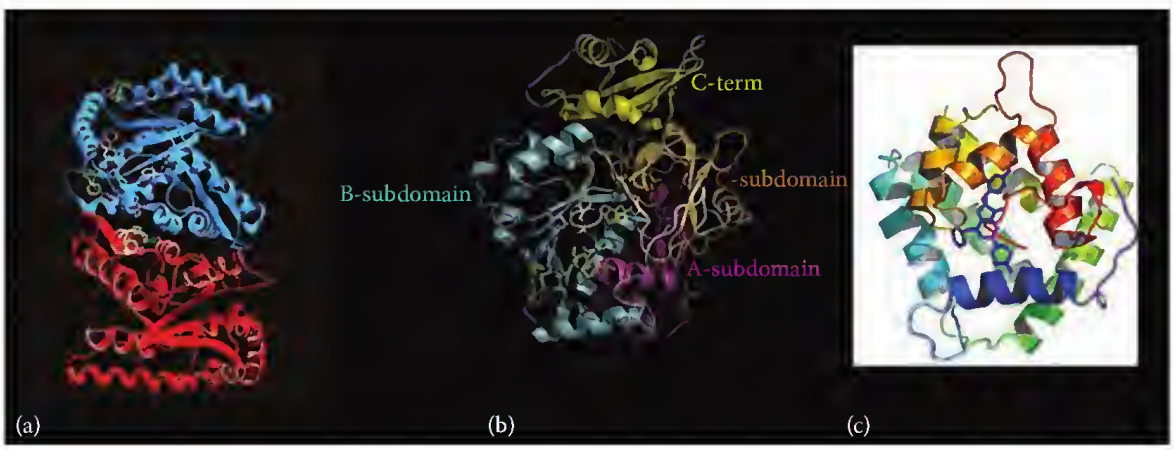

FIGURE 54.8 3D structures of luciferases and photoproteins: (a) bacterial luciferase according to Tu (2007), (b) firefly luciferase (*Photinus pyralis*), and (c) Obelin (coelenterate photoprotein) according to Vysotski and Lee (2004). (From Vysotski, E. and Lee, J., *Acc. Chem. Res.*, 37, 405, 2004. With permission.)

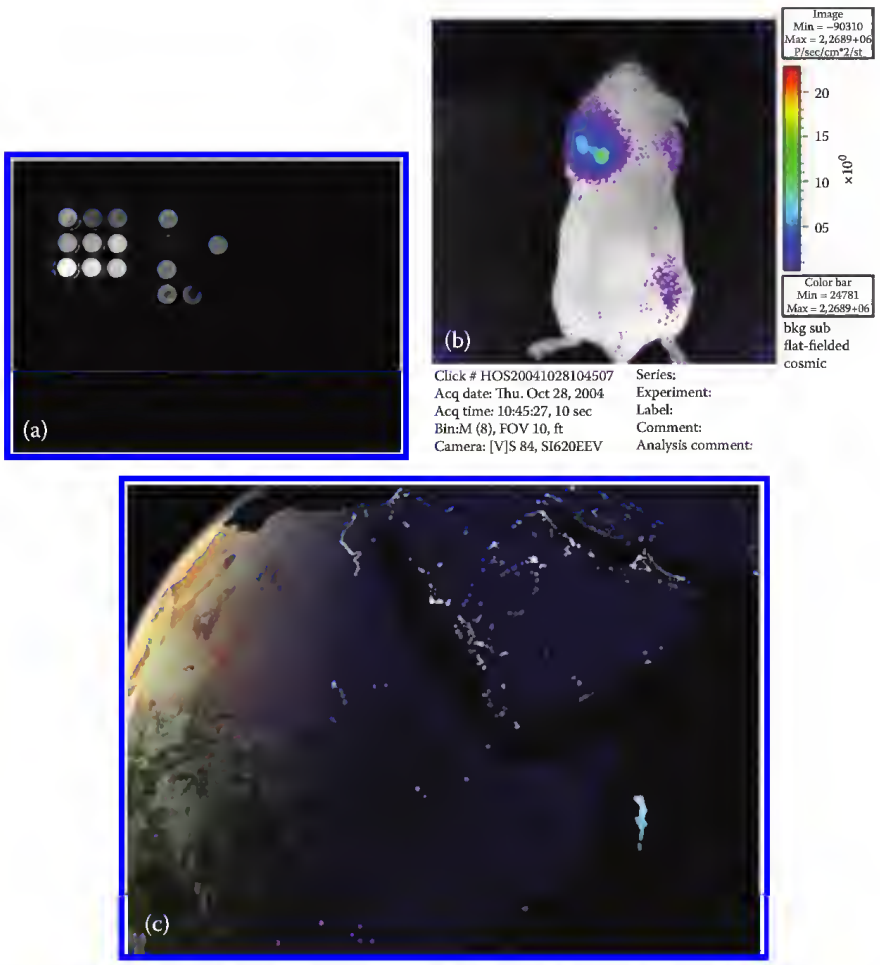

FIGURE 54.11 Biotechnological and environmental applications of bioluminescence: (a) a whole cell biosensor in a 96-well plate format for toxicity based on bioluminescent *Escherichia coli* engineered with *Macrolampis* firefly luciferase gene; (b) real-time *in vivo* bioimaging of metastasis using cell line transformed with firefly luciferase gene (kindly donated by Y. Ohmiya); and (c) bioluminescent bacteria populational boom, a perspective for global level environmental biosensing. (From Haddock, S. et al., *Annu Rev. Mar. Sci.*, 2, 443, 2010.)

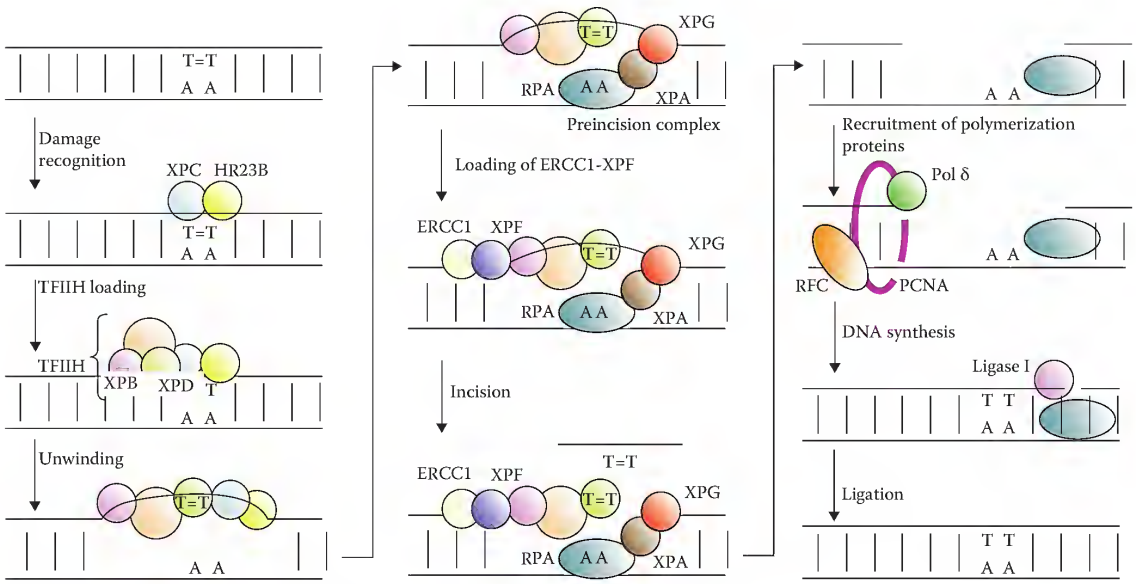

FIGURE 57.9 Main steps in global genome repair (GGR) in eukaryotic cells.

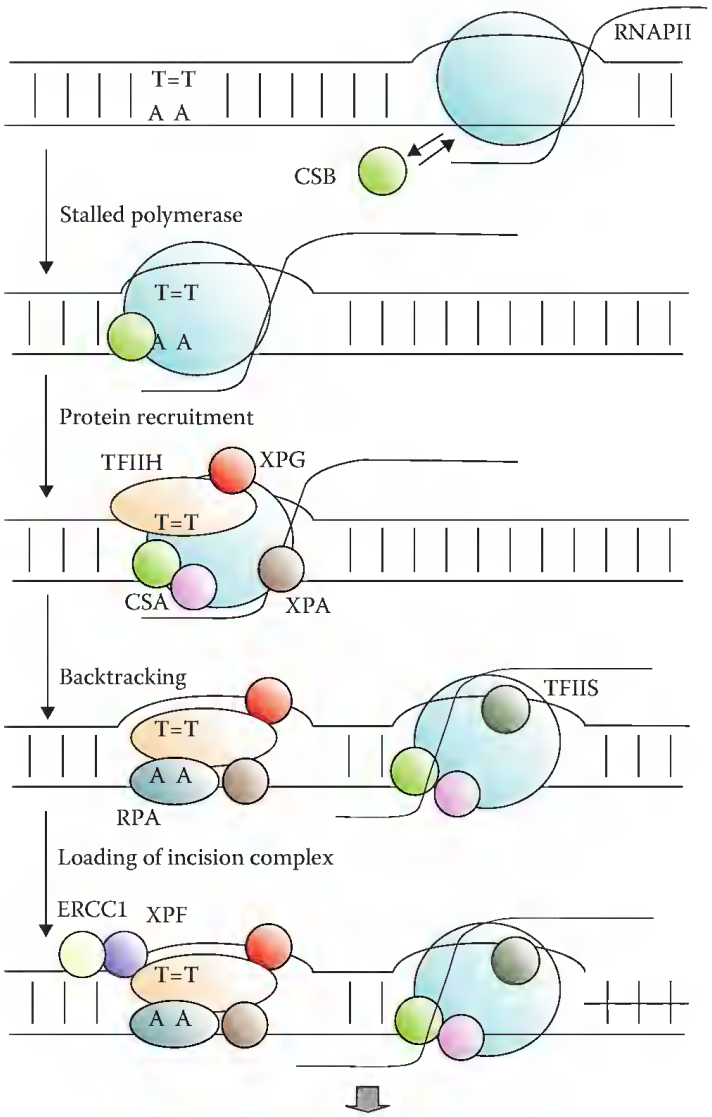

FIGURE 57.10 Schematic representation of transcription-coupled repair (TCR) in eukaryotic cells.

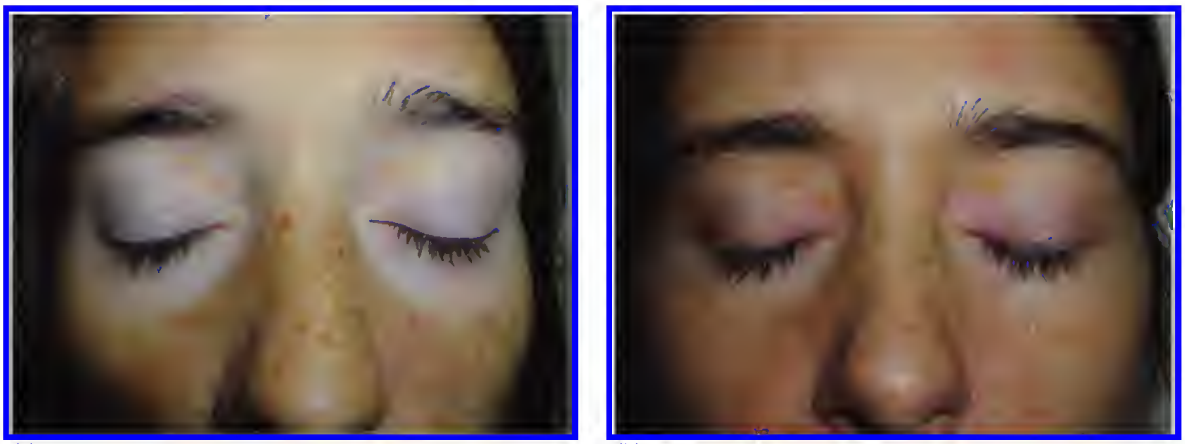

FIGURE 62.1 Vitiligo of the face treated with NB-UVB: (a) before treatment and (b) after treatment.

FIGURE 62.2 Psoriasis of the trunk treated with PUVA: (a) before treatment and (b) after treatment.

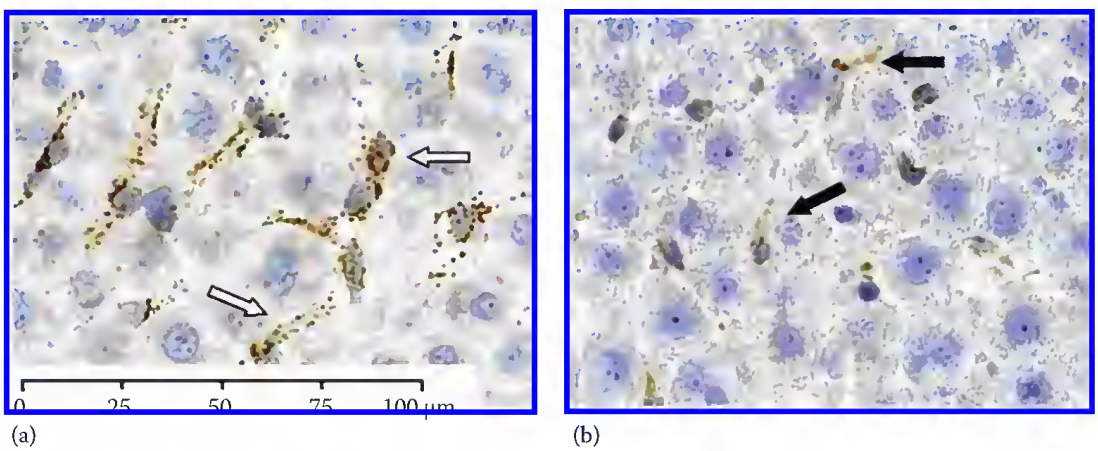

FIGURE 65.4 PCI-induced relocalization of gelonin in rat liver. Tissues were stained with the primary antibody against gelonin and counterstained with hematoxylin. Animals were treated with 25 J light delivered 48 h after 1 mg/kg AlS_2Pc and 1 h after 500 μg/kg gelonin, examined 30 min after irradiation. (a) Area of liver not exposed to light (inset white arrows: distribution of gelonin in liver). (b) Areas exposed to light (inset black arrows: redistribution of gelonin).

3D structures of antenna and RC complexes in bacteria (B, left side) and plants (P, right side).

Bacteria	Plants
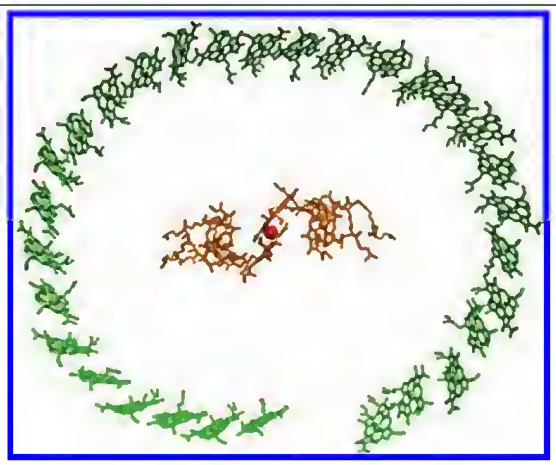	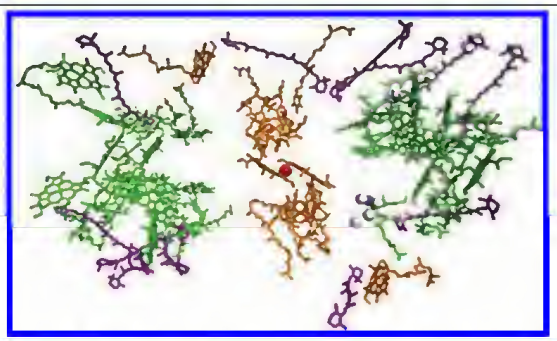
FIGURE 55.B1 Top view of the pigments and ions of the RC–LH1 complex from *Rhodopseudomonas palustris*. Note the highly symmetric arrangement of LH1 pigments around the RC [142]. The bacteriochlorophylls and the bacteriopheophytins of the RC are orange, the nonheme iron is red, and the bacteriochlorophylls of the LH1 complex are green. The average distance between the central magnesium ions of two consecutive pigments in the outer green circle is 9.13 Å with a minimum of 6.71 Å and a maximum of 11.31 Å.	**FIGURE 55.P1** Top view of the pigments and the ions in the PSII core complex at 3.50 Å resolution [141]. Protein Data Bank code 1s5l.pdb. The chlorophylls, the pheophytins, and the PQs of the D1 and D2 subunits are shown in orange. The central red sphere represents the nonheme iron of the RC. The chlorophylls of the core antenna subunits CP43 and CP47 are shown in green. The carotenoids are shown in violet. The white and the blue spheres represent the manganese and calcium ions of the OEC. In this representation, the OEC sticks out of the plane toward the reader in the cytoplasm.
	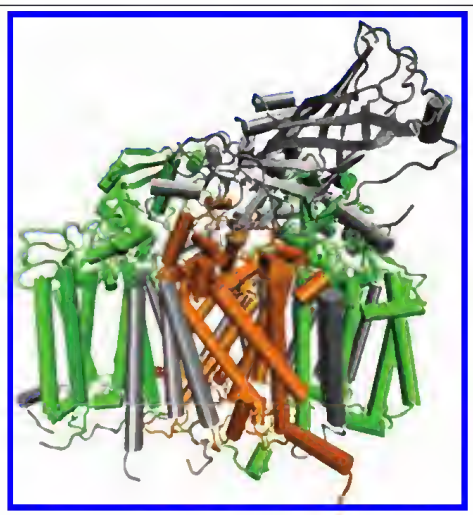
FIGURE 55.B2 3D structure of the RC–LH1 core complex from *R. palustris* at 4.8 Å resolution [142].Protein Data Bank code 1PYH.pdb. The transmembrane domain is formed by the almost parallel set of alpha helices. The hydrophobic part is formed by the sole H subunit of the RC that protrudes toward the cytoplasm. The three subunits forming the RC (L, M, and H) are shown in orange while the 15 couples of alpha and beta subunits of the light-harvesting 1 (LH1) complex are shown in green. The structure is much simpler than the PSII core complex shown in (P2). In contrast to PSII, the antenna ring and the central RC are not connected in the bacterial RC–LH1 core complex, as seen on the top view (B1).	**FIGURE 55.P2** 3D structure of photosystem II core complex from *T. elongatus* at 2.9 Å resolution [144]. Protein Data Bank codes 3BZ1.pdb and 3BZ2.pdb. The transmembrane domain is formed by the almost parallel set of alpha helices, while the hydrophilic part is formed by a number of randomly distributed short alpha helices and by an organized structure of beta sheets protruding toward the periplasm. The two central polypeptides (D1 and D2) form the RC (orange), CP47 and CP43 are the two peripheral core antenna polypeptides (green), and the other 16 polypeptides (gray) are also shown (for more details see [145]).

3D structures of antenna and RC complexes in bacteria (B, left side) and plants (P, right side).	
Bacteria	Plants
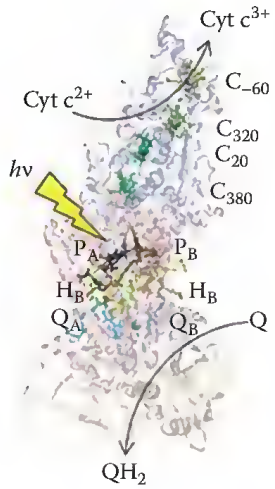	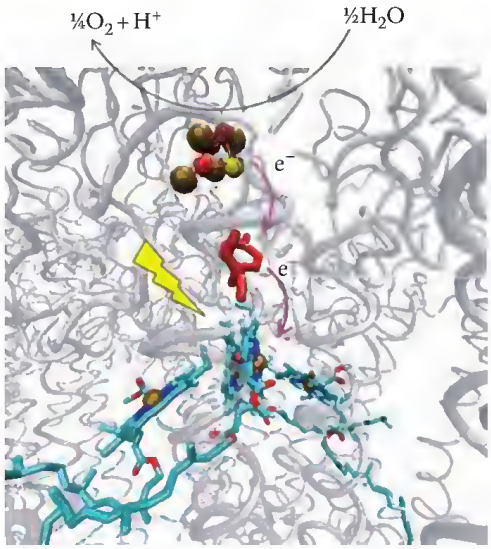
FIGURE 55.B3 Catalytic sites of the RC with internal cytochrome subunit of *Blastochloris viridis* at 2.45 Å resolution [143]. Protein Data Bank code 2prc.pdb. Color codes of the polypeptides: light red (L subunit), light orange (H subunit), light gray (M subunit), and light blue (C subunit). The iron is shown as a green sphere; the four hemes of the C subunit are green. Cofactors, catalytic reactions of quinone reduction and cytochrome oxidation initiated by light, are indicated in figure by arrows.	**FIGURE 55.P3** Catalytic donor site of photosystem II at 3.50 Å resolution [141]. Protein Data Bank code 1s5l. pdb. The ET started by light absorption is directed from water troughs the OEC (oxygen, red; manganese, brown; calcium, yellow) and the tyrosine Y_Z (red) to the chlorophyll dimer (cyan). The final by-products (oxygen and protons) are released.